Peptide Revolution

Genomics, Proteomics & Therapeutics

Peptide Revolution:
Genomics, Proteomics & Therapeutics

Peptide Revolution

Genomics, Proteomics & Therapeutics

Proceedings of the Eighteenth American Peptide Symposium

Edited by
Michael Chorev
and
Tomi K. Sawyer

American Peptide Society

Peptide Revolution: Genomics, Proteomics & Therapeutics

Proceedings of the
Eighteenth American Peptide Symposium
July 19-23, 2003, Boston, MA, U.S.A.

Edited by

Michael Chorev
Beth Israel Deaconess Medical Center &
Harvard Medical School
Harvard Institute of Medicine (HIM-944)
4 Blackfan Circle
Boston, MA 02115
Michael_Chorev@hms.harvard.edu

and

Tomi K. Sawyer
ARIAD Pharmaceuticals Inc.
26 Landsdowne Street
Cambridge, MA 02139
SawyerKRT@aol.com

American Peptide Society
San Diego

A C.I.P. Catalogue record for this book is available from the Library of Congress.

ISBN 0-9715560-1-6

Published by American Chemical Society,
2033 San Elijo Ave. #421
Cardiff, CA 92007, U.S.A.

Sold and distributed by American Peptide Society
2033 San Elijo Ave. #421
Cardiff, CA 92007, U.S.A.

and by Kluwer Academic Publishers
101 Philip Drive, Norwell, MA 02061, U.S.A.
(in North, Central and South America)
P.O.Box 322, 3300 AH Dordrecht,
The Netherlands
(in all other countries)

Copyright ©2004 American Peptide Society

All rights reserved. No part of the material protected by this copyright notice may be reproduced or utilized in any form or by any means, electronic or mechanical, including photocopying, recording or by any information storage and retrieval system, without written permission from the copyright owner.

Produced by Prompt Scientific Publishing,
www.promptpublishing.com, San Diego, U.S.A.
Printed in the Czech Republic

We dedicate this book to our beloved wives, Miri Chorev and Constance Sawyer, and our extraordinary children for their support and encouragement.

Preface And Epilogue

As co-chairs of the 18th American Peptide Symposium and co-editors of this Proceedings of the 18th American Peptide Symposium, we are very pleased to share both experiences with all participants and contributing authors, respectively. Indeed, the "Peptide Revolutions" was a success in many ways. These are summarized in a recent American Peptide Society newsletter (Autumn 2003) that commemorates "A Peptide Revolution in Boston" and includes our perspectives and pictures taken on-site at the beautiful Boston Marriott Copley Place.

This book includes more than 400 articles covering all key topics involving peptide science thus providing a snapshot of the state-of-the art for our interdisciplinary field of research and drug discovery. In addition, it provides special acknowledgements to our sponsors, exhibitors, committees, and all individuals who were recipients of awards and special recognition. We thank the Session Chairs and all who helped us with organizing this event and making it stand amongst the most successful of our long-lived tradition of American Peptide Symposia.

As time passes, we reflect on memories of the symposium and the Society which has undergone significant transitions since July 19, 2003, the kickoff day of the 18th American Peptide Symposium. Roger Freidinger became the new President and his support to us throughout the symposium and preparation of this book is highly appreciated. Murray Goodman, the immediate past President of our Society, was a powerful advocate of our many endeavors to organize this symposium and will be remembered as one of the most significant forces to support our work to ensure success. His recently passing comes with genuine sorrowfulness, and our lives and those of a plethora of individuals throughout the world of peptide science will not be the same in his absence. We are most pleased to give tribute in this Proceedings to his memory and in honor of a legendary peptide scientist. We thank Fred Naider for sharing his thoughts of Murray in his special commemoration which appears in this book.

Weeks before the opening of the 18th American Peptide Symposium, we were shocked with the untimely passing of our friend and Secretary of our Society, Arno Spatola. We truly missed his spirited presence at the symposium. The memories of many kind acts, speeches and a tribute keynote lecture (by Charlie Deber) to honor Arno was one of the most memorable of our last minute changes to the program and on-site activities at the symposium. These painful and untimely departures remind us that while science is our great quest for knowledge, it is our relationships with wonderful individuals such an important part of the fabric and passion of our lives.

Our outstanding young investigators who actively participated in the symposium will always be a special part of our memories as well as our investment and hopes for the future of our field of peptide science. Congratulations again to all who were recipients of awards and participants in the many on-site events, including the Bert Schram Young Investigators' Mini-Symposium (organized by Lila Gierasch and Kenneth Rotondi), the Young Investigator's Poster Competition (organized by DeAnna Long), and the Travel Grants (organized by Sylvie Blondelle). We wish you all the very best in your future careers.

To all, we hope that you enjoyed the symposium from the Welcome Reception and Revolutionary kickoff of the program (especially the procession of Revolutionary Flag bearers, drummers and bagpipe blowers) to the last lectures and Symposium Banquet. Relative to the program, we recall the visionary talk of Dr. Charles Deber of University

of Toronto as the Symposium's first canon blast, and a series of excellent Keynote lectures delivered by Drs. Tom Muir of The Rockefeller University, Janet Thornton of the European Bioinformatics Institute, Lewis Cantley of Harvard Medical School, and Robert Langer of Massachusetts Institute of Technology. In addition, the traditional and most highly esteemed Merrifield Award Lecture was delivered by the awardee Dr. William DeGrado of the University of Pennsylvania. Furthermore, the newly instituted Rao Makineni Lecture was delivered by Dr. James Tam of Vanderbilt University. Special acknowledgments are further given to Dale Mierke and Ziwei Huang for organizing two successful workshops on GPCRs and protein-protein/peptide interactions, respectively.

We thank our symposium coordinator Luciana Lavallee, the staff of the American Peptide Society, especially Donna Freher-Lyons, and the incredible team from Professional Conference Management Inc. led by Cass Jones for their many efforts in making this a successful symposium.

We thank Michal Lebl, Eileen Silva and Ellen Brenner for their many efforts in the editing and preparation of this book.

Lastly, we wish to give special tribute to our wives, Miri Chorev and Constance Sawyer, and our children for their steadfast love and support throughout the times that we devoted to organizing the 18th American Peptide Symposium and preparing the Proceedings of the 18th American Peptide Symposium.

Sincerely,

Michael Chorev and Tomi K. Sawyer
June 20, 2004

Message from the President of the American Peptide Society

The 18th American Peptide Symposium was a very successful addition to the American Peptide Society's series of biennial symposia. An international group of 1,080 registrants contributed to a high quality scientific program which is documented in this volume. Thank you to all lecturers and poster presenters for your excellent contributions. I congratulate co-chairs Michael Chorev and Tomi Sawyer along with their staff and the organizing and program committees for a terrific meeting, and I thank them for all of their hard work and dedication. Thank you also to all of our sponsors and exhibitors. Finally, thank you to Immediate Past President Murray Goodman for his oversight of this effort.

There were several special events in the Symposium which I will highlight. The American Peptide Society's Bruce Merrifield Award, which recognizes outstanding career achievements in peptide science, was presented to Bill DeGrado of the University of Pennsylvania. Bill's award lecture described his exciting work on "De novo Design of Proteins and Protein Mimetics". The inaugural Makineni Lecture, which honors long time peptide science supporter Rao Makineni, was presented by James Tam of Vanderbilt University. The Bert Schram Young Investigators Mini-Symposium again provided an excellent scientific program to start off the meeting on the opening Saturday. The Bert Schram Young Investigator Awards were presented to Amit Galande (University of Louisville, Arno Spatola, mentor), Agnes Jaulent (Imperial College, Robin Letherbarrow, mentor), and Roshni Sundaram (Ohio State University, Pravin Kaumaya, mentor). The scientific quality was high and the competition was keen in the Young Investigators Poster Competition. Several workshops and special plenary sessions proved to be popular with attendees. Symposium social events provided enjoyable opportunities to meet colleagues.

We were all saddened by the untimely death of Arno Spatola of the University of Louisville just two weeks before the Symposium. Arno was the Secretary of the American Peptide Society and a well known contributor to peptide science and American Peptide Symposia. There were several tributes to Professor Spatola during the meeting including lectures by Charles Deber and Victor Hruby. Arno will be greatly missed by his colleagues and friends.

I will now make a few comments about the American Peptide Society, which is committed to advancing and promoting the knowledge of the chemistry and biology of peptides and proteins. I invite you to visit our web site at www.ampepsoc.org to learn more about the Society and the benefits of membership. The Society has a dedicated Council of 15 individuals elected by Society members. Society officers are also elected by the membership. There are several active committees which administer areas such as awards, membership, publications, and student affairs. The official journal of the Society is *Biopolymers – Peptide Science*, and all members receive a subscription. The new editor of the journal is Lila Gierasch who succeeded Charles Deber at the beginning of 2004. The journal publishes original research and review articles. A well-received initiative was the publication of the abstracts of the 18th American Peptide Symposium in *Peptide Science* just prior to the meeting. Dr. Gierasch and I encourage you to submit your best work to our journal. The American Peptide Society also actively participates in activities of the broader research community through our associate membership in the Federation of American Societies for Experimental Biology (FASEB).

My term as President of the Society runs from July, 2003 to June, 2005. During this period, one of my priorities is to increase the membership of the Society and enhance the benefits to members. The Council is working to consolidate the improvements to the Society web site and make it a valuable source of information and contacts for peptide scientists. A new initiative involves developing a relationship with the Protein Society. The initial step will be the sponsorship by the American Peptide Society of a one day symposium on "Synthetic and Semisynthetic Proteins" on the opening day (August, 14, 2004) of the Protein Society annual meeting in San Diego. The 7 speakers will be American Peptide Society members who are the leaders in this area of research. In turn, the Protein Society is planning to sponsor a symposium during the 19th American Peptide Symposium. I welcome the participation of more members in our activities. Please contact me if you would like to get involved.

The American Peptide Society is already planning for future symposia. The 19th American Peptide Symposium will be held June 18 - 23, 2005 in San Diego. Co-chairs Jeff Kelly and Tom Muir are actively assembling the scientific program based on the theme "Understanding Biology Using Peptides". The 20th American Peptide Symposium is planned for June 22 - 27, 2007 in Montreal, and co-chairs are Bill Lubell and Emanuel Escher. The theme of this meeting is "Peptides for Youth".

It was a pleasure to interact on a scientific and personal level with many of you at the Symposium in Boston. I look forward to working with you in American Peptide Society activities and to seeing you in San Diego in 2005. My best wishes for success in your peptide activities.

Roger M. Freidinger
Merck Research Laboratories
April 6, 2004

Murray Goodman

Teacher, Mentor, Friend

Professor Murray Goodman passed away in Germany on June 1, 2004 at the age of 75 after a very brief illness. Murray, as he was known to thousands of peptide chemists world wide, was the immediate past president of our society. He was an incisive and influential force in the field of peptide chemistry and remained active, dedicated and enthusiastic until the end.

Murray Goodman received his Bachelor's degree from Brooklyn College and went on to earn his doctorate in the laboratory of the Nobel Laureate, Melvin Calvin. After postdoctoral studies at MIT and Cambridge University, he began his career at the Polytechnic Institute of Brooklyn in 1956. There he quickly rose to the rank of Full Professor and became Director of the Polymer Research Institute. In 1970 Murray moved to the University of California, San Diego as Professor of Chemistry. He served the University as Chair of the Chemistry Department for six years and as acting Provost of Revelle College from 1972-1974. He was recently honored by the endowment of the Goodman Chair in Chemistry at UCSD.

Dr. Goodman was the author of nearly 500 journal articles and served as the Editor-in-Chief of the recently published 5 volume compendium entitled *Synthesis of Peptides and Peptidomimetics* that will serve as a source material for our field for the foreseeable future. He was the founding Editor for Biopolymers and served this journal until his untimely passing. He also was the founding Editor of the Journal of Peptide Science, which is currently the official journal of the American Peptide Society. He was an inspiring teacher and during his more than 50 years in academia enlightened undergraduates and graduate students about the intricacies of organic chemistry and polymer chemistry. He mentored some 85 doctoral students and more than 200 postdocs many of whom became leaders in peptide chemistry in countries throughout the world. His excellence in pedagogy was recognized with the UCSD's Chancellor's Associates Recognition Award for Excellence in Graduate Teaching. He served on, and chaired, NIH Study Sections and was a member of many national and international review panels including IUPAC, AAAS, and the World Health Organization. He was the recipient of numerous prizes including The Scoffone Medal, The Humboldt Professorship, The Max Bergmann Award, The Ralph Hirschmann Prize in Peptide Chemistry, The Herman F. Mark Polymer Chemistry Award, The Arthur C. Cope Scholar Award and the Pierce (Merrifield) Prize sponsored by our Society. In 1999 he was inducted as a foreign member of the Russian Academy of Sciences.

Murray's research evolved in parallel to the field of peptide chemistry. His early work examined poly-α-amino acids and oligopeptides as models to understand fundamental aspects of protein secondary structure. His laboratory established methodologies that were adopted throughout the world and he determined the critical chain lengths for α-helix formation of a variety of amino acids. He did fundamental work on racemization during coupling reactions and on the mechanism of N-carboxyanhydride polymerization. Later studies from his laboratory turned to biologically relevant peptides and polypeptides. He was a pioneer in the field of peptidomimetics and was a leader in studies on retro-inverso peptides. His studies on depsipeptides provided basic insights into the contribution of the peptide bond to secondary structure and his recent work on template based polypeptides led to stable collagen models that

formed the triple helix at very short chain lengths. Difficulties encountered in the synthesis of novel analogs led him to develop urethane protected N-carboxy anhydrides for use in coupling reactions. These reagents are now used in the synthesis of valine-acyclovir, an important antiviral agent. His laboratory did seminal work on peptide sweeteners and he developed a model that could be used for the design of sweet peptidomimetics. Some of his analogs rank among the sweetest peptides ever synthesized. His interest in receptors led to work on the opioids and very recently he initiated studies on the structure of GPCRs and their interaction with peptide hormones. The breadth of his research and his ability to contribute to such diverse areas of peptide science were the hallmark of his career. He was a leader in his field and could be truly called a "peptide scientist".

However, Murray was not a man who can be captured on paper, his spirit and essence reached far beyond his scientific record and that of his laboratory. Who can forget Murray sitting through a scientific meeting? His breadth of knowledge was enormous. He was interested in the entire range of presentations from the strictly synthetic, to the biophysical, to the biological. He contributed unique and astute comments on almost every presentation and attended nearly every session from early in the morning until the last after dinner lecture. I recall how disturbed he was at the last Gordon Conference when people didn't stay until the lights were turned off.

Murray Goodman was a passionate man who was a fervent advocate for peptide science. He could never understand why peptide chemists didn't give the full support to peptide chemistry proposals at NIH Study Sections and he was as excited about our field today as he was on the first day I met him in 1966. His eclectic interests allowed him to see the great potential for peptide science and he tirelessly advocated for the next generation of peptide chemists who were pushing forward the frontiers of our field.

Perhaps most of all Murray will be remembered as an international ambassador for peptide chemistry. I remember his around the world three week jaunts when he traveled to the West Coast, Japan, India, Israel, Europe and returned to Brooklyn Poly energized with the peptide science he had encountered. His home was always open and scientists from nearly every country were frequently his guests. They all considered him to be their friend and came to him for advice. He was a man of vision and projected the value of peptide chemistry into both applied and fundamental research. His energy was boundless and he provided leadership in both academic and industrial settings. He was an outstanding role model for his students and his colleagues and he was highly respected at UCSD as an elder statesman.

It is difficult to write about Murray Goodman without personalizing the description. In doing so I represent not myself but the myriad individuals that Murray touched during his career. Murray was an outstanding teacher and mentor. He was highly supportive of his students and followed their careers long after they left his group. In my own case, he arranged for my postdoctoral appointment and helped to secure funding. We stayed in regular contact and continued collaborating over a nearly forty year period. We called each other regularly and he often helped my graduate students find industrial positions. His group reunions at peptide symposia were truly international events that grew in size from year to year. He was a man with a big heart and his inclusive spirit resulted in friendships that reached to nearly every corner of the globe. The outpouring of condolences upon his untimely passing testifies to the revered place he held in our discipline. He was a wonderful husband who, with his beloved wife Zelda, raised three sons to whom he was completely devoted. He was my teacher, my mentor and my friend. I miss him already.

Dr. Fred Naider
College of Staten Island
City University New York
June 6, 2004

In Memoriam: Arno F. Spatola

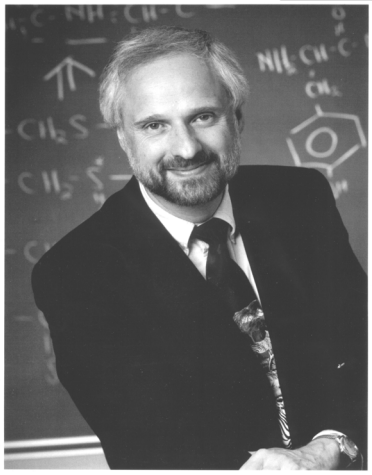

The sudden death of Arno F. Spatola at age 59 on July 5, 2003, of heart failure was a shock to the peptide community worldwide, particularly coming as it did on the eve of the 18th American Peptide Symposium, July 19-23, in Boston. Arno was a much beloved and respected member of the scientific community for his contributions to peptide chemistry and biology, his warm and infectious enthusiasm for science and scientists, and his love of life and international cooperation. During the course of the symposium there were many personal and group tributes to Arno the person, and Arno the scientist. A few words of reflection on his life and science is most fitting in the Proceedings of this meeting to which he has contributed for so many years.

Arno was born in upstate New York to Italian parents, and had a robust love of good food, good wine, and warm and generous friendship. He received his undergraduate training in chemistry at Cornell University, his Ph.D. in chemistry at the University of Michigan with Professor Daniel T. Longone, and then did a postdoctoral in my laboratory where be began his creative and productive career in peptide science.

Arno joined the Department of Chemistry at the University of Louisville in 1973 where he had an outstanding career practicing interdisciplinary science which had a major impact on the University of Louisville and the larger scientific community. At the time of his death, Arno was Professor of Chemistry and Biochemistry, a member of the Cancer Center, and Founder and Director of the Institute for Molecular Diversity and Design at the University, and President and CEO of Peptides International, Inc., the company he founded in 1983.

Arno's name is synonymous with pseudopeptides (peptide derivatives and analogues in which one or more peptide bond have been replaced with an isosteric bond with varying chemical structural and conformational properties. He made numerous contributions to the organic chemistry, structural chemistry and biological chemistry of these and related compounds, applying them to a wide variety of biologically active compounds, including peptide hormones and neurotransmitters, proteases, and other biological receptor/acceptors. His seminal reviews and overviews of amide bond replacements and pseudopeptides, and his own contributions in this area had a major impact worldwide. He developed not only synthetic strategies for these compounds, but also pointed to their advantages in producing derivatives and analogues of bioactive peptides which were resistant to proteolysis, modified their hydrophobic character, and provided molecules with unique conformational properties. In addition, he made important contributions to peptide and peptide mimetic synthetic methodology, design and synthesis of cyclic peptides with novel structures, in the development of combinatorial libraries to explore chemical biology and medicinal chemistry, and innovative contributions to many areas of peptide synthesis.

A major passion of Arno's was his dedication to excellence in teaching and mentorship. He developed unique chemistry courses which promulgated the latest

development in organic chemistry, in medicinal chemistry, and in peptide science to provide his students with a sense of the excitement about science that he felt. He personally trained and mentored numerous graduate students, postdoctoral fellows, and undergraduates who have gone on to distinguished academic and scientific careers.

Arno also participated worldwide in scientific conferences, grant reviews, editorial boards of several journals, and as a proactive member of the scientific community. At the time of his death, he was the Secretary of the American Peptide Society, and had served in one capacity or another in the national and international affairs of the Society since its inception. He traveled extensively, often with his adored wife, Jacquelyn, and daughter, Kimberley, and always with a great enthusiasm for life, friends, social intercourse and science. He was truly an ambassador of peptide science, and we will sorely miss him.

Victor J. Hruby
Regents Professor
University of Arizona
June 20, 2004

18th AMERICAN PEPTIDE SYMPOSIUM

July 19-23, 2003
Boston, Massachusetts

Co-Chairs

Michael Chorev
Beth Israel Deaconess Medical Center &
Harvard Medical School
Harvard Institute of Medicine (HIM-944)
4 Blackfan Circle
Boston, MA 02115
Michael_Chorev@hms.harvard.edu

Tomi K. Sawyer
ARIAD Pharmaceuticals Inc.
26 Landsdowne Street
Cambridge, MA 02139
tomi.sawyer@ariad.com

Scientific Program Committee

Fernando Albericio, Ph.D., University of Barcelona
Jean Chmielewski, Ph.D., Purdue University
Michael Chorev, Ph.D., Beth Israel Deaconess Medical Center
Emanuel Escher, Ph.D., University of Sherbrooke
Roger Freidinger, Ph.D., Merck Research Laboratories
Lila Gierasch, Ph.D., University of Massachusetts
Carrie Haskell-Luevano, Ph.D., University of Florida
Jeff Kelly, Ph.D., SCRIPPS Research Institute
Peter Lansbury, Ph.D., Brigham & Women's Hospital
William Lubell, Ph.D., University of Montreal
Dale Mierke, Ph.D., Brown University
Barry Morgan, Ph.D., PRAECIS Pharmaceuticals
Fred Naider, Ph.D., College of Staten Island, CUNY
Robin Offord, Ph.D., University of Geneva
Lynne Regan, Ph.D., Yale University
Tomi Sawyer, Ph.D., ARIAD Pharmaceuticals
Gregory Verdine, Ph.D., Harvard University

Symposium Organizing Committee

Michael Chorev, Ph.D., Beth Israel Deaconess Medical Center
Lila Gierasch, Ph.D., University of Massachusetts
Peter Lansbury, Ph.D., Brigham & Women's Hospital
Tomi Sawyer, Ph.D., ARIAD Pharmaceuticals, Inc.
Gregory Verdine, Ph.D., Harvard University

The Student Affairs Committee

DeAnna Wiegandt Long, Ph.D. (Chair), Peptides International
Richard Agnes, University of Arizona
Bret Beyer, University of Florida
Audrey Kelleman, University of California, San Diego
Natali Richter, University of Louisville

The Travel Award Committee

Sylvie E. Blondelle, Ph.D., (Chair), Torrey Pines Institute for Molecular Studies
Mibel Aguilar, Ph.D., Monash University
David Andreu, Ph.D., Universitat Pompeu Fabra
Phil Dawson, Ph.D., The Scipps Research Institute
Kit S. Lam, Ph.D., University of California, Davis

List of 18th American Peptide Symposium Sponsors

Gold Level Sponsor
Bachem

Silver Level Sponsors
Eli Lilly and Company
PolyPeptide Laboratories, Inc.
UCB Bioproducts, Inc.

Mercury Level Sponsors
Abgent
Advanced ChemTech
Gryphon Therapeutics
Merck Research Laboratories
Midwest Bio-Tech, Inc.
Rohm & Hass Advanced Biosciences
Senn Chemicals

Copper Level Sponsors
Amgen Inc.
Amylin Pharmaceuticals
Bristol-Myers Squibb Pharmaceutical Research Institute
Cambridge Research Biochemicals Ltd.
ESCOM Science Foundation
Genzyme Corporation
GL Biochem (Shanghai) Ltd.
Morre-Tec Industries
Multiple Peptide Systems
Novo Nordisk
Neosystem SA
PepTech Corp.
Peptide Institute, Inc.
Peptides International
Pfizer Global Research & Development
SynPep Corporation
SYNTHETECH, Inc.

Contributors
BioTechniques
Chemica Oggi
Genetic Engineering News
Fluka

List of 18th American Peptide Symposium Exhibitors

Advanced ChemTech
Akzo Nobel/Eka Chemicals
American Peptide Company, Inc.
AnaSpec, Inc.
Applied Biosystems
Bachem
Bentham Science Publishers Ltd.
Bio-Synthesis, Inc.
BioSource
C S Bio Inc.
C.A.T. GmbH & Co.
Cambridge Research Biochemicals Ltd.
CBL-PATRAS
CEM Corporation
Centerchem, Inc./Pentapharm Ltd.
Chem-Impex International, Inc.
Chemspeed Inc.
EMD Biosciences, Inc. (Calbiochem & Novabiochem)
Fluka
Genzyme Corporation
Georg Thieme Verlag
Groupe SNPE
(Neosystem & Multiple Peptide Systems & Isochem)
Intavis Bioanalytical Instruments
John Wiley & Sons
Jupiter Bioscience Limited
Luxembourg Industries (Pamol) Ltd.
Mallinckrodt, Inc.
New England Peptide, Inc.
ORPEGEN Pharma
Peptide Scientific, Inc.
Peptides International
Peptisyntha SA
Polycarbon Industries Inc.
Polymer Laboratories, Ltd.
PolyPeptide Laboratories
Protein Technologies, Inc.
Rapp Polymere GmbH
Reanal Fine Chemical Co.
Rohm and Haas
Senn Chemicals
Synasia Fine Chemical
SynPep Corporation
SYNTHETECH, Inc.
Tianjin Nankai Hecheng Sci. & Tech. Co., Ltd.
UCB Bioproducts, Inc.
Waters Corporation
YMC Co., Ltd.
Zinsser Analytic GmbH

The American Peptide Society

The American Peptide Society (APS), a nonprofit scientific and educational organization founded in 1990, provides a forum for advancing and promoting knowledge of the chemistry and biology of peptides. The approximately one thousand members of the Society come from North America and from more than thirty other countries throughout the world. Establishment of the American Peptide Society was a result of the rapid worldwide growth that has occurred in peptide-related research, and of the increasing interaction of peptide scientists with virtually all fields of science.

A major function of the Society is the biennial American Peptide Symposium. The Society also sponsors the Journal of Peptide Research and Biopolymers (Peptide Science), recommends awards to outstanding peptide scientists, works to foster the professional development of its student members, interacts and coordinates activities with other national and international scientific societies, sponsors travel awards to the American Peptide Symposium, and maintains a website at www.ampepsoc.org.

The American Peptide Society is administered by Officers and Councilors who are nominated and elected by members of the Society. The Officers are: Roger Freidinger, Merck Research Laboratories, President; Jane Aldrich, University of Kansas, President Elect; Robin Offord, University of Geneva, Secretary and Richard A. Houghten, Torrey Pines Institute for Molecular Studies, Treasurer. The councilors are: Fernando Albericio, University of Barcelona; Sylvie E. Blondelle, Torrey Pines Institute; Jean Chmielewski, Purdue University; Michael Chorev, Harvard Medical School; Ben Dunn, University of Florida; Kit S. Lam, University of California Davis; William D. Lubell, l'Universite de Montreal; Fred S. Naider, College of Staten Island, CUNY; Thomas J. Lobl, NeuroSystec and James P. Tam, Vanderbilt University.

Membership in the American Peptide Society is open to scientists throughout the world who are engaged or interested in the chemistry or biology of peptides and small proteins. Categories of membership include Active Member, Associate Member, Student Member, Emeritus Member and Honorary Member. For application forms or further information on the American Peptide Society, please visit the Society web site at www.chem.umn.edu/orgs/ampepsoc or contact Donna M. Freher-Lyons, APS Membership Coordinator, 2033 San Elijo Ave. #421, Cardiff, CA 92007, U.S.A., tel (858) 455-4752; fax (858) 455-2545; e-mail “APS_Member@tpims.org”.

American Peptide Symposia

Symposium	*Year*	*Chair (s)*	*Location*
1st	1968	Saul Lande *Yale University* Boris Weinstein *University of Washington-Seattle*	Yale University New Haven, CT
2nd	1970	F. Merlin Bumpus *Cleveland Clinic*	Cleveland Clinic Cleveland, OH
3rd	1972	Johannes Meienhofer *Harvard Medical School*	Children's Cancer Research Foundation, Boston, MA
4th	1975	Roderich Walter *University of Illinois Medical Center-Chicago*	The Rockefeller University and Barbizon Plaza Hotel New York, NY
5th	1977	Murray Goodman *University of CaliforniaSan Diego*	University of California-San Diego, San Diego, CA
6th	1979	Erhard Gross *National Institutes of Health*	Georgetown University Washington, DC
7th	1981	Daniel H. Rich *University of Wisconsin-Madison*	University of Wisconsin-Madison, Madison, WI
8th	1983	Victor J. Hruby *University of Arizona*	University of Arizona Tucson, AZ
9th	1985	Kenneth D. Kopple *Illinois Institute of Technology* Charles M. Deber *University of Toronto*	University of Toronto Toronto, Ontario, Canada
10th	1987	Garland R. Marshall *Washington University School of Medicine*	Washington University St. Louis, MO
11th	1989	Jean E. Rivier *The Salk Institute for Biological Studies*	University of California-San Diego, San Diego, CA
12th	1991	John A. Smith *Massachusetts General Hospital*	Massachusetts Institute of Technology, Cambridge, MA
13th	1993	Robert S. Hodges *University of Alberta-Edmonton*	Edmonton Convention Center Edmonton, Alberta, Canada
14th	1995	Pravin T.P. Kaumaya *The Ohio State University*	The Ohio State University Columbus, OH
15th	1997	James P. Tam *Vanderbilt University*	Nashville Convention Center Nashville, TN
16th	1999	George Barany *University of Minnesota* Gregg B. Fields *Florida Atalantic University*	Minneapolis Convention Center Minneapolis, MN
17th	2001	Richard A. Houghten *Torrey Pines Institute for Molecular Studies* Michal Lebl *Spyder Instruments and Illumina*	Town and Country Resort Hotel San Diego, CA
18th	2003	Michael Chorev *Beth Israel Deaconess Medical Center* Tomi K. Sawyer *ARIAD Pharmaceuticals*	Marriott Copley Place Boston, MA

The Merrifield Award
(previously the Alan E. Pierce Award)

Endowed by Rao Makineni (1997)
Sponsored by the Pierce Chemical Company (1977-1995)

William F. DeGrado

Dr. William F. DeGrado is congratulated as winner of the 2003 Merrifield Award. He officially received the highest recognition from the American Peptide Society on Thursday July 22, 2003, at the 18th American Peptide Symposium at which he gave a Merrifield Award Lecture that was entitled "De novo design of proteins and protein mimetics"

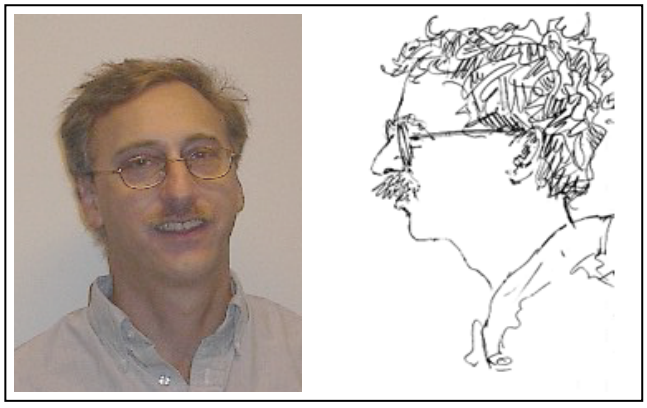

Dr. DeGrado is George W. Raiziss Professor of Biochemistry and Biophysics at the University of Pennsylvania School of Medicine. Professor DeGrado received a B.S. (chemistry) from Kalamazoo College and a Ph.D. (chemistry) from the University of Chicago. He has held industrial positions at DuPont Central Research & Development as well as DuPont Merck Pharmaceutical Company with his last position being Senior Director of Medicinal Chemistry. In 1996, Dr. DeGrado transitioned to academia to join the University of Pennsylvania School of Medicine as Professor of Biochemistry and Biophysics.

Professor DeGrado has a distinguished record of scientific contributions to peptide research and drug discovery. A comprehensive summary of his work is available at his website (http://www.med.upenn.edu/~biocbiop/faculty/pages/degrado.html). His publication record includes >130 articles and reviews. Professor DeGrado's research focuses on protein design as an approach to understanding macromolecule structure and function. His primary research interest is in the de novo design, in which one designs proteins beginning from first principles. This approach critically tests our understanding of protein folding and function, while also laying the groundwork for the design of proteins and biomimetic polymers with properties unprecedented in nature. The *de novo* design of proteins has proven to be a useful approach for understanding the features in a protein sequence that cause them to fold into their unique three-dimensional structures. In addition, it has been possible to design

functionally interesting proteins, which bind redox-active cofactors, DNA, and transition metals. Finally, this approach has been extended to the design of membrane-active proteins, including ion channels, antibiotics and fusogenic agents.

Dr. DeGrado has a eminent record of awards, including the Du Vigneaud Award for Young Investigators in Peptide Research (1988), the Protein Society Young Investigator Award (1989), the Eli Lilly Award in Biological Chemistry (1992), DuPont Merck Summit Award (1993), Fellow of American Association for the Advancement of Science (1995), Member of the National Academy of Sciences (1998), and the Merrifield Award of the Peptide Society (2003). He has been highly active in scientific societies, including most recently being President of the Protein Society (2001-2003). In the American Peptide Society, Dr. DeGrado has served as a member of Council and the Publications Committee, and as Associate Editor of the Journal of Peptide Research. He has also be actively involved in the Protein Society, the American Chemical Society, the American Association for the Advancement of Science as well as an organizer of Keystone Meetings and Gordon Conferences. Furthermore, Dr. DeGrado has served on many editorial boards and as guest editor, including *Chemical Reviews, Current Opinion in Structural Biology, Current Research in Protein Chemistry, Biopolymers, Current Opinion in Chemical Biology, Journal of Combinatorial Chemistry, Accounts of Chemical Research, Structure, Current Protein and Peptide Science, Protein and Peptide Letters, Biochemistry, Protein Science, Protein Engineering, Journal of Peptide Research, Journal of Molecular Recognition, Journal of the American Chemical Society and Proteins, Structure, Function, Genetics.*

2003 – William F. DeGrado, University of Pennsylvania
2001 – Garland R. Marshall, Washington University Medical School
1999 – Daniel H. Rich, University of Wisconsin-Madison
1997 – Shumpei Sakakibara, Peptide Institute, Inc.
1995 – John M. Stewart, University of Colorado-Denver
1993 – Victor J. Hruby, University of Arizona
1991 – Daniel F. Veber, Merck Sharp & Dohme
1989 – Murray Goodman, University of California-San Diego
1987 – Choh Hao Li, University of California-San Francisco
1985 – Robert Schwyzer, Swiss Federal Institute of Technology
1983 – Ralph F. Hirschmann, Merck Sharp & Dohme
1981 – Klaus Hofmann, University of Pittsburgh, School of Medicine
1979 – Bruce Merrifield, The Rockefeller University
1977 – Miklos Bodansky, Case Western Reserve University

The Makineni Lecture Award

Sponsored by the American Peptide Society (2003)

James P. Tam

Dr. James P. Tam is congratulated as winner of the 2003 Makineni Award Lecture. He officially received this special recognition from the American Peptide Society on Tuesday July 20, 2003, at the 18th American Peptide Symposium at which he gave a Makineni Award Lecture that was entitled "Protein mimetics as HIV therapeutics and vaccines prepared by tandem ligation".

Dr. Tam is Professor in the Department of Microbiology and Immunology, and Professor of Biochemistry at the Vanderbilt University Medical Center in Nashville, Tennessee. He also serves as Dean of School of Biological Sciences and Director of Biosciences Research Centre of Nanyang Technological University. Dr. Tam was born in Hong Kong, and received his B.S., and Ph.D. in Medicinal Chemistry from the University of Wisconsin, U.S. Over the past 25 years, Dr. Tam has established himself as a internationally renowned scientist in the fields of microbiology, immunology and biochemistry. He is particularly well known for his research achievements in peptide and protein chemistry with innovative applications to human biology. Dr. Tam's interdisciplinary contributions to research involving AIDS, autoimmune diseases and tumor biology are well recognized, including the development of novel approaches such as macromolecular assemblage (e.g., the MAP method) for the design of synthetic vaccines for AIDS and other infectious diseases, autoimmune diseases and cancer. His work on design and synthesis of modified growth factor analogs provides promise to the development of novel therapeutic agents for wound healing and cancer. Dr. Tam is recipient of numerous awards and honors, including the Vincent du Vigneaud Award for Outstanding Achievement in Peptide Research (1986), the Cathy Award for Peptide Chemistry (1996), and the Rao Makineni Lecture Award (2003). He has been highly active in the American Peptide Society, including serving as Councilor and Chair of the Fifteenth American Peptide Symposium. Dr. Tam has authored over 250 peer-reviewed scientific articles, and he holds more than a dozen patents, including several for the multiple antigen peptide system (MAPS) that is commonly used by many laboratories. Dr. Tam serves as an adviser to the National Science Foundation and the National Institute of Health in the U.S., and the Network Centres of Excellence of the Medical Research Council of Canada. He is current Associate Editor of the Journal of Peptide Research.

Peptide Society Travel Grants

Lori Anderson, Washington University
Matthew Anderson, Washington University
Jorg Auernheimer, Technical University of Munich
Lioudmika Baidakova, Russian Academy of Sciences Shemyakin & Ovchinnikov
Attila Borics, Creighton University
Minying Cai, University of Arizona
Eric Chang, Purdue University
Yuxin Chen, University of Alberta
Daniel Cline, University of Delaware
Ralf David, University of Leipzig
Mark Del Borgo, Howard Florey Institute University of Melbourne
Juan Del Valle, University of California San Diego
Amanda Enstrom, University of California Davis Cancer Center
Khee Dong Eom, Vanderbilt University
Racha Estephan, College of Staten Island
Marcus Etienne, Louisiana State University
Lukasz Frankiewicz, Warsaw University
Amit Galande, University of Louisville
Sharon Gazal, Hebrew University of Jerusalem
Xuyuan Gu, University of Arizona
Krisztina Heredi-Szabo, Creighton University
Jonathan Hodges, University of Wisconsin Madison
Heidi Huttunen, University of British Columbia
You Seok Hwang, Purdue University
Agnes Jaulent, Imperial College London
Christine Joseph, University of Florida
Adrian Kalaszi, Eotvos Lorand University
Joseph Kappel, University of Minnesota
Leena Khullar, Eastern Michigan University
Juliana Kretsinger, University of Delaware
Mohanraja Kumar, University of South Florida
Stanley Kwok, University of Colorado Health Sciences Center
Rafal Latajka, Wroclaw University of Technology
Hsien-Ming Lee, Purdue University
Kyung Lee, University of Delaware
Matthew Leighty, University of Kansas
Wenwu Li, University of Freiburg
Xianggun Li, Purdue University
Jose Lozano, Colombian Institute of Immunology Foundation
Alessandra Machado, University of Sao Paulo
Rosa Melendez, University of Montreal
Christopher Micklitsch, University of Delaware
Piotr Mroz, University of Louisville
Markus Muller, Max-Planck Institute of Biochemistry
Assunta Napolitano, University of Salerno
John Ndungu, University of Arizona

Bradley Nilsson, University of Wisconsin Madison
Francesca Nuti, University of Florence
Umut Oguz, Louisiana State University
Shinya Oishi, Kyoto University
Davide Pantarotto, University of Trieste
Elisa Peroni, University of Florence
Vi Pham, Howard Florey Institute University of Melbourne
Karthikan Rajagopal, University of Delaware
Kenny Roberts, State University of New York Stony Brook
Kristen Sadler, Vanderbilt University
Olga Sazonova, Russian Academy of Sciences Shemyakin & Ovchinnikov
Markus Schutt, Max-Planck Institute of Biochemistry
Jaroslav Sebestik, Institute of Chemical Technology Prague
Emily Seo, University of British Columbia
Youhei Sohma, Kyoto Pharmaceutical University
Magda Stankova, University of Arizona
Tanaji Talele, Louisiana State University
Meritxell Teixido, University of Barcelona
Stefania Terracciano, University of Salerno
Catherine Thomas, Louisiana State University
Georgette Thumshirn, Technical University of Munich
Yu Tian, Rutgers University
Aleksandar Todorovic, University of Florida
Haim Tsubery, Weizmann Institute of Science
Sylvia Van Cauwenberghe, Vrije University of Brussels
Miquel Vila-Perello, Pompeu Fabra University
Judit Villen, Pompeu Fabra University
Jia Wang, Louisiana State University
Xin Wang, University of Kansas
John Whitehead, Louisiana State University
Jinfa Ying, University of Arizona
Renata Zbozien-Pacamaj, University of Wroclaw
Junyi Zhang, University of Arizona
Lei Zhao, Purdue University

Bert Schram Young Investigators' Mini-Symposium

Co-Chairs
Lila Gierasch and Kenneth Rotondi (University of Massachusetts)

Keynote Speaker
Tom Muir (Rockefeller University)

Award Winners

Amit Galande (University of Louisville)
Agnes Joulent (Imperial College London)
Roshni Sundaram (The Ohio State University)

Participants

R.S. Agnes (University of Arizona)
L.L. Anderson (Washington University School of Medicine)
M. P. Del Borgo (University of Melbourne)
A.K. Galande (University of Louisville)
J.R. Holder (University of Florida)
A. Joulent (Imperial College London)
A. Krebs (University of Frankfurt)
K. Lee (NCI, NIH, NCI-Frederick)
R. Meléndez (Université de Montréal)
R. Melnyk (University of Toronto at Hospital for Sick Children)
E. Peroni (University of Florence)
K. Sadler (Vanderbilt University)
R. Sundaram (The Ohio State University)
M. Tada (Toyama Medical and Pharmaceutical University)

Young Investigators' Poster Competition

Chair
DeAnna Wiegandt Long

Award Winners

First Place:
Rosa Melendez (Université de Montréal)

Second Place:
Agnès Jaulent (Imperial College of London)
Roman Melnyk (University of Toronto)
Nicole Smith (University of California-San Diego)

Third Place:
Amit Galande (University of Louisville)
Jonathon Hodges (University of Wisconsin-Madison)

Honorable Mention:
Richard Agnes (University of Arizona)
Wenwu Li (Albert-Ludwigs-Universität Freiburg)
Chris Neidre (Scripps Research Institute)

Participants

R. S. Agnes (University of Arizona, USA)
L. L. Anderson (Washington University, USA)
M. A. Anderson (Washington University, USA)
B. Beyer (University of Florida, USA)
A. Borics (Creighton University School of Medicine, USA)
A. Capasso (University of Salerno, Italy)
Y. Che (Washington University, USA)
M. Del Borgo (University of Melbourne, Australia)
J. Del Valle (University of California–San Diego, USA)
L. P. Frankiewicz (Warsaw University, Poland)
A. K. Galande (University of Louisville, USA)
Xuyuan Gu (University of Arizona, USA)
K. Herédi-Szabó (Creighton University School of Medicine, USA)
J. A. Hodges (University of Wisconsin-Madison, USA)
J. R. Holder (University of Florida, USA)
L. K. Iwai (University of São Paulo Medical School, Brazil)
A. M. Jaulent (Imperial College London, United Kingdom)
C. G. Joseph (University of Florida, USA)
A. Krebs (Johann Wolfgang Goethe-Universität, Germany)
K. Lee (National Cancer Institute, NIH, USA)

W. W. Li (Albert-Ludwigs-Universität Freiburg, Germany)
M. W. Leighty (University of Kansas, USA)
R. E. Melendez (Université de Montréal, Canada)
R. A. Melnyk (Hospital for Sick Children, University of Toronto, Canada)
B. Mulinacci (Università di Firenze, Italy)
C. Neidre (Scripps Research Institute, USA)
B.L. Nilsson (University of Wisconsin–Madison, USA)
F. Nuti (Università di Firenze, Italy)
E. Peroni (Università di Firenze, Italy)
V. Pham (Melbourne University, Australia)
G. Sabatino, (Università di Firenze, Italy)
K. Sadler (Vanderbilt University, USA)
E. C. Schwartz (The Rockefeller University, USA)
F. Sicherl (Johann Wolfgang Goethe-Universität, Germany)
N. D. Smith (University of California–San Diego, USA)
M. Stankova (University of Arizona, USA)
R. Sundaram (The Ohio State University, USA)
M. Tada (Toyama Medical and Pharmaceutical University, Japan)
A. Todorovic (University of Florida, USA)
P. Wadhwani (Forschungszentrum Karlsruhe, Germany)
X. Wang (University of Kansas, USA)
Y. Yu (Torrey Pines Institute for Molecular Studies, USA)
S. Xie (Isco, Inc., USA)
J. Zou (University of Missouri, USA)

Abbreviations

μ	hydrophobic moment
[θ]	mean residue ellipticity
ααAAs	α,α-disubstituted amino acids
βA	β-amyloid peptides
a2AP	α2-antiplasmin
Aβ	amyloid β-protein
AβPP	amyloid β-precursor protein
Abc	4'-aminomethyl-2,2'-bipyridine-4-carboxylic acid
Abh	azabicyclo[2.2.1]heptane-2-carboxylic acid
Abl	Abelson kinase
Abu	α-amino-*n*-butyric acid
Abz	2-amino-benzoic acid;2-aminobenzoyl
AC	adenylyl cyclase
Ac	acetyl; acyl
Aca	adamantanecarboxyl-
Ac_nc	1-aminocycloalkane-1-carboxylic acid
ACHC	2-aminocyclohexanecarboxylic acid
AChE	acetylcholinesterase
ACHPA	4-amino-5-cyclohexyl-3-hydroxypentanoic acid
Acm	acetamidomethyl
ACTH	corticotropin
AD	Alzheimer's disease
Adc	10-aminodecanoic acid
Ado	12-aminododecanoic acid
ADP	aza-dipeptide
Adr	adriamycin
AEDANS	5-[(2-aminoethyl)amino]-naphthalene-1-sulfonic acid
AEDI	aminoethyldithio-2-isobutyric acid
AFM	atomic force microscopy
AGH	androgenic gland hormone
Agl	aminoglycine
AGRP	Agouti-related protein
Ahd	2-aminohexadecanoic acid
Ahp	2-amino-heptanoic acid
AHPPA	4-amino-3-hydroxy-5-phenylpentanoic acid
Δ^6Ahp	6-dehydro-2-amino-heptanoic acid
Ahx	6-aminohexanoic acid
Aib	α-aminoisobutyric acid
AIBN	2,2'-azobisisobutyronitrile
AIDS	aquired immune deficiency syndrome
AII	angiotensin II
Aka	3-(9-oxo-9,10-dihydroacridin-2-yl)-alanine
Al	allyl
Alloc	allyloxycarbonyl
ALS	amyloid lateral sclerosis
AKAP	A-kinase anchoring proteins
AM	alveolar macrophage
3-AMB	3-aminomethyl-benzoic acid
AMBER	assisted model building and energy refinement
AMC	aminomethylcoumaride
Amc	4-(aminomethyl)cyclohexane-carboxylic acid; aminomethylcoumarin
AMCA	7-amino-4-methylcoumarin-3-acetic acid
Amh	aminohomoserine
Amn	8-(aminomethyl)naphth-2-oic acid
AMPs	cationic antimicrobial peptides
AMPA	*o*-aminomethylphenylacetic acid
AMPB	4-aminomethyl)phenylazobenzoic acid
AngII	angiotensin II
ANP	atrial natriuretic peptide brain/ventricular and C-type NPs, BNP/VNP and CNP
ANS	8-anilino-l-naphthalenesulfonic acid
AnxA2	annexin A2
Aoc	8-aminooctanoic acid
APB	(4-amino)phenylazobenzoic acid
APC	antigen presenting cell
Apn	5-aminopentanoic acid
ApoA-I	apolipoprotein A-I
APP	amyloid precursor protein
APTT	activated partial thromboplastin time
AQN	anthraquinone moiety
Arg-al	argininal
Arg-ol	argininol
ARM	arginine rich motif
ASP	Agouti signal protein
AT_1	AngII receptor
ATL	adult T-cell leukemia
Atmp	4-amino-2,2,6,6-tetramethylpiperidine
ATP	adenosine triphosphate
AUC	area under the curve
Aun	11-aminoundecanoic acid
Ava	5-aminovaleric acid
AVP	vasopressin
Aze	azetidine-2-carboxylic acid
BA	bioavailability
BAL	backbone amide linker
BApG	*N,N*-bis(3-aminopropyl)-glycine
BBB	blood brain barrier
BBEC	bovine brain endothelial capillary
BBI	Bowman Birk Inhibitors
BCD	bicyclic decapeptide
BCIP	5-bromo-4-chloro-3-indolyl phosphate
BDNF	brain derived neurotrophic factor
Bes	*N,N*-bis[2-hydroxyethyl]-2-aminoethanesulfonic acid
BHA	benzhydrylamine

BHMT	betaine-homocysteine methyl-transferase
Bhoc	benzhydryloxycarbonyl
Bicine	*N,N*-bis[2-hydroxyethyl]glycine
Bid	1H-benzimidazole-2-yl
Biot	biotinyl
Bip	biphenylalanine, 4-phenyl-phenylalanine
BK	bradykinin
BMAP	bovine myeloid antimicrobial peptide
BME	β-mercaptoethanol
Bn	benzyl
BNP/VNP	brain/ventricular atrial natriuretic peptide and C-type NPs (and CNP
Boc	*tert*-butyloxycarbonyl
Boc-ON	2-*tert*-butyloxy-carbonylamino-2-phenylacetonitrile
Boc_2O	di-*tert*-butyl dicarbonate
Bom	benzyloxymethyl
BOP	(benzotriazol-1-yloxy)-tris(dimethylamino)phosphonium-hexafluorophosphate
Bpa	*p*-benzoylphenylalanine
BPTI	bovine pancreatic trypsin inhibitor
Bpy	2,2'-bipyridine
Brop	bromotris(dimethylamino)-phosphonium hexafluorophosphate
BRS-3	bombesin receptor subtype 3
BSE	bovine spongiform encephalopathy
Bsmoc	1,1-dioxobenzo[b]thiophene-2-ylmetholoxycarbonyl
BTD	β-turn dipeptide
BTIB	*I,I*-bis(trifluoroacetoxy)iodo]-benzene
BU	building unit
Bu^t, tBu	t-butyl
Bz	benzoyl
BZD	1,4-benzodiazepine
Bzl	benzyl
CaM	calmodulin
CAM	chorioallantoic membrane
CAMM	computer assisted molecular modeling
CAT	chloramphenicol acetyltransferase
Cba	2-amino-4-cyanobutanoic acid
o-CBA	*o*-chlorobenzoic acid
CBD	chitin binding domain
Cbz	carbobenzoxy;benzyloxycarbonyl
CCK	cholecystokinin
CD	circular dichroism
β-CD	β-cyclodextrin
CDI	*N,N'*-Carbonyldiimidazole
CE	capillary electrophoresis
CED3	*Cenorhabditis elegans* cell-death protein
CF	5(6)-carboxyfluorescein; cystic fibrosis
CFA	complete Freund's adjuvant
CFTR	cystic fibrosis transmembrane conductance regulator
CFU	colony forming units
CGRP	calcitonin gene related peptide
Cha	cyclohexylalanine
CHA	cyclohexylamine
CHAPS	3-[(3-cholamidopropyl)dimethyl-ammonio]-l-propanesulfonate
CHC	central hydrophobic cluster
ChAT	choline acetyl transferase
cHex	cyclohexyl
Chg	α-cyclohexylglycine
cHpa	cycloheptylalanine
Cht	chloro-*β*-hydroxytyrosine
CID-MS	collision-induced dissociation MS
CID	chemotherapy-induced diarrhea
CIDP	chronic inflammatory demyelinating polyneuropathy
Cit	2-amino-5-ureido-n-valeric acid
CJD	Creutzfeldt-Jacob disease
CLA	cyclolinopeptide A
Clt	2-chlorotrityl
Cl-Z	2-chlorobenzyloxycarbonyl
cmc	critical micelle concentrations
CNP	C-type natriuretic peptide
CNS	central nervous system
CNTs	carbon nanotubes
CNV	choroidal neovascularisation
Cpa	4-chlorophenylalanine; 4-carboxyphenylalanine
Cpg	α-cyclopentylglycine
CpG	α-cyclopentylglycine
CPPs	cyclopentapeptides; cell penetrating peptides
CPS	conditional protein splicing
CRF	corticotropin releasing Factor
CsA	cyclosporin A
CsC	cyclosporin C
CSDs	chemical shift deviations
CSLM	confocal scanning laser microscopy
CSPPS	convergent SPPS
CSPS	classical solution-phase synthesis
CT	calcitonin; carboxy terminal
CTACl	cetyltrimethylammonium chloride
CTL	cytotoxic T-lymphocyte
CTQ	cysteine tryptophylquinone
CTR	calcitonin receptor
CXCR	chemokine receptor
CZE	capillary zone electrophoresis
d.e.	diastereomeric excess
Da	Dalton
Dab	2,4-diaminobutyric acid
Dabcyl	(4-[4-(dimethylamino)phenylazo]-benzoyl
Dap	2,3-diaminopropionic acid
Dau	daunomycin
DB[DMAP]	2,6-di-*tert*-butyl-4-(dimethylamino)-pyridine
DABCO	1,4-diazabicyclo[2.2.2]octane

DBF	dibenzofulvene
Dbg	dibenzyl glycine
DBU	1,8-diazabicyclo[5.4.0]-undec-7-ene
DCC	dicyclohexylcarbodimide
DCHA	dicyclohexylamine
DCL	dynamic combinatorial libraries
DCM	dichloromethane
DDD	dodecanedioyl
Dde	1-(4,4-dimethyl-2,6-dioxocyclohexylidene)ethyl
Ddp-OH	3-[*N,N*-dimethylaminophenyl-4'-diazenyl]phenylacetic acid
DDQ	2,3-dichloro-5,6-dicyano-1,4-benzoquinone
Ddz	2–(3,5-dimethoxyphenyl)-propyl[2]oxycarbonyl
2DE	2-dimensional gel electrophoresis
DEA	diethylamine
DEAD	diethyl azodicarboxylate
Deg	diethylglycine
Dfm-AA	α-difluoromethyl amino
DHFR	dihydrofolate reductase
DhHP-9	deuteroheamin-His-peptide amide
Dhp	2,6-dimethyl-4-hydroxyphenyl)-propanoic acid
DHP	3,4-dihydro-2H-pyran
DHPC	dihexanoyl phospholcholine
DIAD	diisopropyl azodicarboxylate
Dibal-H	diisobutylaluminium hydride
Dibg	diisobutylglycine
DIC	diisopropy1carbodiimide; disseminated intravascular coagulation
DIEA	*N,N*-diisopropylethylamine
Dip	diphenylalanine
DIPCDI	*N,N'*-diisopropylcarbodiimide
DKPs	2,5-diketopiperazines
DMA	*N,N*-dimethylacetamide
DMAP	4-(dimethylamino)pyridine
Dmcp	*N*-dimethylcyclopropylmethyl
DME	dimethoxyethane, glyme
DMER-Plot	difference minimum energy Ramachandran plot
DMF	*N,N*-dimethylformamide
Dmob	2,4-Dimethoxybenzyl
DMPC	dimyristotl phosphocholine
DMPG	dimyristoyl phosphatidylglycerol
DMPU	1,3-dimethyl-3,4,5,6-tetrahydro-pyrimidin-2(1*H*)-one
DMS	dimethyl sulfide
DMSO	dimethyl sulfoxide
Dmt	2',6'-dimethyltyrosine
Dnp	2,4-dinitrophenyl
DOPA	3,4-dihydroxy-phenylalanine
DOPC	dioleoyl-DL-3-phosphatidylcholine
DOR	δ-opioid receptor
DOTA	dodecanetetraacetic acid
DOTAP	1,2-dioleoyl-3-trimathylamonium-propane
DPC	dodecylphospho-choline
DPDPB	[(1,4-di-[3'-(2'-pyridyldithio)-propionamido]butane
DPDS	2,2-dipyridyl disulfide
Dpg	di-n-propylglycine or 3,5-dihydroxyphenylglycine
DPH	phenytoin
Dpm	diphenylmethyl
DPP	dipeptidyl peptidase
DPPA	diphenylphosphoryl azide
DPPC	1,2-dipalmitoyl-sn-glycero-3-phosphatidylcholine
Dpr	diaminopropionic acid
DQF-COSY	double-quantum filtered-correlated spectroscopy
DRG	dorsal root ganglion
DS	dextran sulfate
DTT	dithiothreitol
DVB	divinylbenzene
Dyn	dynorphin
E_2	estradiol
EADI	(*E*)-alkene dipeptide isostere
EAE	experimental allergic encephalomyelitis
EBP	erytropoietin binding protein
EBV	Epstein-Barr-virus
ECD	extracellular domain
ECL	extended chemical ligation; extracellular loop
ECM	cell-extracellular matrix
ED_{50}	median effective dose
Eda	ethylenediamine
EDC	1-(3-dimethylaminopropyl)-3-ethyl carbodiimide hydrochloride
EDDnp	ethyldiamine-*N*-(2,4-dinitrophenyl)
EDOT	3,4-ethylenedioxythiophene
EDT	1,2-ethanedithiol
EDTA	ethylenediamine-tetraacetic acid
EGF	epidermal growth factor
EGFR	EGF receptor
EGS	ethylene glycol *bis*-succinyl-
ELISA	enzyme linked immunosorbance assay
EM	electron microscopy
EMP	erythropoietin mimetic protein; estrogen mimetic peptide
EMSA	electrophoretic mobility shift assays
EPL	expressed protein ligation
EPO	erythropoietin
EPR	electron paramagnetic resonance
ER	estrogen receptor
ERE	estrogen receptor element
ERK	extracellular signal-regulated protein kinase
ES-MS	electrospray mass spectrometry
ESI	electrospray ionization
ESR	electron spin resonance
ESTs	expressed sequence tags
ET	electron transfer
ET-1	endothelin-1
ET R	endothelin-A receptor

F_2Pmp	difluorophosphonomethyl phenylalanine
F5c	2,3,4,5,6-pentafluorocinnamoyl
FAB-MS	fast atom bombardment mass spectrometry
FceRI	IgE-receptor
FACS	fluorescence-activated cell sorting
FAD	familial Alzheimer's disease
FBS	fetal bovine serum
FceRIα	IgE-receptor-α-subunit
FFI	fatal familial insomnia
FGF	fibroblast growth factor
FITC	fluorescein isothiocyanate
FKBP	FK506 binding protein
FLIPR	fluorometric imaging plate reader
Flp	4-fluoroproline
Fm	9-fluorenylmethyl
FMDV	foot-and-mouth disease virus
fMLP	formyl-Met-Leu-Phe
Fmoc	9-fluorenylmethoxycarbonyl
Fmoc-Cl	9-fluorenylmethoxy chloroformate
For	formyl
FP	fusion peptide
FPLC	fast [erformance liquid chromatography
FRB	FKBP–rapamycin binding domain
FRET	fluorescence resonance energy transfer
FSH	follicle-stimulating hormone
FTICR-MS	Fourier-transform ion cyclotron resonance-mass spectrometry
FTIR	Fourier transform infrared
FTMS	Fourier transform mass spectrometry
FT-PGSE-NMR	Fourier transform pulsed-gradient spin-echo NMR
FXa	factor Xa
GA	genetic algorithm
GalR	galanin receptor
GAPDH	glyceraldehyde 3-phosphate dehydrogenase
GAS	group A *streptococci*
GBP	growth-blocking peptide
GC-C	guanylate cyclase C
GdnHCl	guanidinium hydrochloride
GFC	gel filtration chromatography
GGNs	gaegurins
GI	gastro-intestinal
GIF	growth inhibition factor
GITC	guanidinium thiocyanate
Glc	glycosyl
GlcNAc	*N*-acetylgalactosamine
GLP-1	glucagon-like peptide 1
GMEC	global minimum energy conformation
GMO	glycerol monooleate
GnRH	gonadotropin-releasing hormone
GPCR	G-protein-coupled receptor
GFP	green fluorescent protein
GpIIb/IIIa	glycoprotein IIb/IIIa
GPI	guinea pig ileum
Grb2	growth factor receptor-bound protein 2
GRF	growth hormone releasing factor
GS	gramicidin S
GSH	reduced glutathione
GSS	Gerstmann-Straussler-Scheinker syndrome
GSSG	oxidized glutathione
GST	glutathione S-transferase
GTT	glucose tolerance test
hA	human amylin
β-HA	β-hexosaminidase
HAART	highly active anti-retroviral therapy
HABPs	high activity binding peptides
Har	homoarginine
HAT	histone acetyl transferase
HATU	*N*-[(dimethylamino)-1*H*-1,2,3-triazolo[4,5-*b*]pyridin-1-yl-methylene]-*N*-methylmethanaminium hexafluorophosphate *N*-oxide
HBTU	*O*-benzotriazolyl-*N,N,N',N'*-tetramethyluronium hexafluorophosphate
HBV	hepatitis B virus
HCG	human chorionic gonadotropin
HCMV	human Cytomegalovirus
HCTU	1*H*-Benzotriazolium 1-[bis(dimethylamino)methylene]-5-chloro-3-oxide hexafluorophosphate
HCV	hepatitis C virus
Hcy	homocysteine
HDAC	histone deacetylase
HDIs	hydroxyethylamine dipeptide isosteres
HDL	high-density lipoprotein
HDV	hepatitis delta virus
Heppso	*N*-[2-hydroxyethyl]piperazine-*N'*-[2-hydroxypropane]sulfonic acid
HER-2	human epidermal growth factor receptor
HFBA	heptafluorobutyric acid
HFIP	hexafluoroisopropanol
HG	human gastrin
HGP	hairless guinea pig
Hib	*H. influenzae* type b
HILIC	hydrophilic interaction chromatography
HIMBA	4-hydroxymethylbenzoic acid
HIMPA	4-hydroxymethylphenoxyacetic acid
HIV	human immunodeficiency virus
HLA	human leukocyte antigen
Hma	hexahydromandelic acid
HMC	hydroxymethylcarbonyl
HMFS	*N*-[(9-hydroxymethyl)-2-fluorenyl] succinamic acid
HMPA	*p*-hydroxymethylphenoxyacetic acid
HMPA	hexamethylphosphoramide

HMPB	4-(4-hydroxymethyl-3-methoxyphenoxy)-butyric acid
^{1}H-NMR	proton nuclear magnetic resonance
HO-1	hemeoxygenase
Hoc	cyclohexyloxycarbonyl
HOAt	1-hydroxy-7-azabenzotriazole
HOBt	1-hydroxybenzotriazole
HONp	*p*-nitrophenol
HOOBT	3-Hydroxy-1,2,3-benzotriazin-4(3*H*)-one
HOPfp	pentafluorophenol
HOSu	*N*-hydroxysuccinimide
HP	hot plate
Hpg	4-hydroxyphenylglycine
HPLC	high performance liquid chromatography
HPV	human papilloma virus
HPLC	high performance liquid chromatography
Hpp	3-(4-hydroxyphenyl)proline
HPV	human papilloma virus
HSBOtU	(2-mercaptobenzoxazol-2-yl)-1,1,3,3-tetramethyluronium hexafluorophosphate
HSBtU	2-(1-mercaptobenzoxazol-1-yl)-1,1,3,3-tetramethyluronium hexafluorophosphate
HSDNPtU	2-(1-mercapto-2,4-dinitrophenyl-1-yl)-1,1,3,3-tetramethyluronium hexafluorophosphate
Hse	homoserine
HSF	hematopoietic synergistic factor
hSIE	high-affinity c-fos sis-inducible element
HSNPtU	2-(1-mercapto-4-nitrophenyl-1-y1)-1,1,3,3-tetramethyluronium hexafluorophosphate
Hsp	heat shock protein
HSPG	heparan sulfate proteoglycan
HSQC	heteronuclear single-quantum coherence
Htc	[3S]-1,2,3,4-tetrahydroisoquinoline-7-hydroxy-3-carboxylic acid
HTLV	human T cell leukemia virus
Htyr	homotyrosine
Hyp	hydroxyproline
Hyv	γ-hydroxyvaline
i.v.	intravenous
ivDde	1-(4,4-dimethyl-2,6-dioxocyclohex-1-ylidene)-3-methylbutyl
IAPP	ilet amyloid polypeptide
IBoc	isobutyloxycarbonyl
IC_{50}	50% inhibition concentration
ICE	interleukin-1β converting enzyme
icv	intracerebroventricular
IDA	isotope dilution assay
IDL	intermediate density lipoprotein
IFN	interferon
Ig	immunoglobulin
Igl	α-(2-indanyl)glycine
IL-1β	interleukin-1β
IN	HIV-1 integrase
Indo	indomethacin
INF	interferon
iNOS	inducible nitric oxide synthetase
Inp	isonipecotic acid
IP_3	inositol trisphosphate
IPA	isopropyl alcohol
IPE	isopropyl ether
IPTG	isopropyl-β-D-thiogalactopyranoside
ITC	isothermal titration calorimetry
ITAM	immunoreceptor tyrosine-based activation motif
Iva	isovaline
KHMDS	potassium hexamethyldisilazane
KLH	key hole limpet hemocyanin
Kyn	kynurenine
LAH	lithium aluminum hydride
LAT	linker for activation of T cells
LCFA	long chain fatty acids
LCP	lipid-polylysine core-peptide
LDA	lithium diisopropylamide
LDL	low density lipoprotein
LF	lactoferrin
LGA	L-glufosinate also L-homoalanine-4-yl-(methyl)phosphinic acid
LH	luteinizing hormone
LHR	lutropin receptor
LHRH	luteinizing hormone releasing hormone
LiHMDS	lithium bis(trimethylsilyl)amide/-lithium hexamethyl disilazide
LLOD	lower limit of detection
LLOQ	lower limit of quantification
LNC	lymph node cells
LPAP	lysophosphatidic acid
β-LPH	lypotropin hormone
LPPS	liquid phase peptide synthesis
LPS	lipopolysaccharide
LTS	low throughput screening
LUV	large unilamelar vesicle
mAb	monoclonal antibody
MAdCAM-1	mucosal addressin cell adhesion molecule-1
MAGI	multinuclear activated β-galactosidase indicator
MALDI	matrix-assisted laser desorption/ionization
MALDI-TOF	MALDI time-of-flight mass spectrometry
MAP	multiple antigenic peptide
MAPK	mitogen-activated protein kinase
Matp	4-(methylamino)-2,2,6,6-tetramethylpiperidine
Mbc	4'-methyl-2,2'-bipyridine-4-carboxylic acid
MBHA	*p*-methylbenzhydrylamine
MBP	myelin basic protein

Mbzl	4-methoxybenzyl
mCPBA	3-chloroperbenzoic acid
MC	melanocortin
MCR	melanocortin receptor
MCo	*Momordica cochinchinensis*
MD	molecular dynamics
Mdp	C^{α}-methyl DOPA; 3-methyl-3-(2,6-dimethyl-4-hydroxyphenyl)-propanoic acid
MDP	muramyl dipeptide
MDR	multi-drug resistance
Me	methyl
MeCN	acetonitrile
MED	minimum effective dose
MeIm	methylimidazole
MEK	mitogen-activated protein kinase
MeOBzl	*p*-methoxybenzyl
MeOH	methanol
MeOSuc	methoxysuccinyl
Mes	2-[*N*-morpholino]ethanesulfonic acid
MESNA	sodium 2-mercaoptoethanesulfonate
MER-Plot	minimum energy Ramachandran plot
MHC	major histocompatibility complex
MIC	minimum inhibitory concentration
MIF	macrophage migration inhibitory factor
MIPs	molecularly imprinted polymers
MLT	melatonin
MM	molecular modeling
MMA	*N*-methylmercaptoacetamide
MMP	matrix metalloproteinase
Mmt	4-methoxytrityl
MO	molecular orbital
MOG	myelin oligodendrocyte glycoprotein
MOM	methoxymethyl
Mop	1-methyl-2-oxo-2-phenyl
MOP	modular proteins
Mos	momosertatin
MPA	methionine proximity assay
Mpm	ethoxyphenylmethyl
MRI	magnetic resonance imaging
MRSA	methicillin-resistant *Staphylococcus aureus* strains
MS	mass spectrometry; multiple sclerosis
Msc	beta-methylsulfonylethoxycarbonyl
MsCI	methanesulfonyl chloride
MSH	melanocyte stimulating hormone melanotropin
MSNT	2,4,6-mesitylene-sulfonyl-3-nitro-1,2,4-triazolide
MTBD	7-methyl-1,5,7-triazabicyclo-[4.4.0]dec-5-ene
MTP	molecular transporter peptide
Mtr	2,3,6-trimethyl-4-methoxybenzenesulfonyl
MTS	methanethiosulfonyl
Mts	mesitylene-2-sulfonyl
MTSEA	methane thiosulfonylethylamine
MTSL	1-oxo-2,2,5,5-tetramethylpyrroline 3-methylmethane thiosulfonate
Mtt	4-methyltrityl
MTT	3-[4,5-dimethylthiazol-2-yl]-2,5-diphenyltetrazolium bromide
MVD	mouse vas deferens
NVOC	nitroveratryloxycarbonyl
NAChR	nicotinic acetylcholine receptors
NADPH	nicotinamide adeninedinucleotide phosphate, reduced form
Nal	naphthylalanine
NADP	nicotinamide adenine dinucleotide phosphate
NBD	7-nitro-2,1,3-benzoxadiazole norbornadiene
NBS	*N*-bromosuccinimide
NC	nociceptin
NCL	native chemical ligation
N-ECD	*N*-terminal extracellular domain
NECA	5'-*N*-ethylcarboxamidoadenosine
NED	neuroendocrine differentiation
NEM	*N*-ethylmorpholine; *N*-ethylmaleimide
NGF	nerve growth factor
NHL	non-Hodgkin's lymphoma
Nic	nicotinyl
NILIA	non-immobilized ligand interaction assay
Nip	nipecotic acid
NIR-FT	near-infrared, Fourier-transform
NK-1	neurokinin-1 receptor (substance P receptor)
NKA	neurokinin A
NKB	neurokinin B
NKR cells	normal rat kidney cells
NLS	nuclear localization sequence
NMePhe	*N*-methyl phenylalanine
NMM	*N*-methylmorpholine
NMMO	*N*-methylmorpholine-*N*-oxide
NMP	*N*-methylpyrrolidinone
NMR	nuclear magnetic resonance
NO	nitric oxide
nOct	*n*-octanoyl
NOE	nuclear overhauser effect
NOESY	nuclear overhauser enhanced spectroscopy
N/OFQ	nociceptin/orphanin FQ
NOP	nociceptin/orphanin FQ receptor
NPG	neopentylglycine
NPRA	natriuretic peptide receptor A
Nps	2-nitrophenylsulfenyl
NPY	neuropeptide Y
Npys	5-nitro-2-pyridinesulfenyl
NSAIDs	non-steroidal anti-inflammatory drugs
Nsc	2-(4-nitrophenylsulfonyl)ethoxy-carbonyl
NSG	*N*-substituted glycine

NT	amino-terminal; neurotrophin
NTA	nitrilo-triacetic acid
Ntc	nortropane-3-carboxylic acid
NTHI	nontypeable *Haemophilus influenzae*
Nva	norvaline
O	defined sequence position in peptide libraries
O/X_{10}	the complete set of 220 sublibraries
OBOC	one-bead one-compound
OC2Y	*O*-(2,6-dichlorobenzyl)-tyrosine
OChx	cyclohexyl ester
OHA	octahydroacridine
OHx	hexyl ester
Oic	octahydroindolyl-2-carboxylic acid
OMCA	methyloxazetidine-carboxylic acid
ON	oligonucleotides
ONp	4-nitrophenyl ester
OPA	*o*-phthaldehyde
OPCP	pentachlorophenyl ester
Opfp	pentafluorophenyl ester
OPhe	phenyl ester
OPT	oligopeptide transport
ORL-1	opioid receptor-like
Orn	ornithine
Osu	*N*-hydroxysuccinimide ester
OT	oxytocin
OTA	oxytocin antagonist
OVT	vasotocin
OVX	ovariectomy
Oxac	2-oxo-oxazolidineacetic acid
Oxd	4-methyl-5-carboxybenzyloxazolidin-2-one
Pab	4-aminomethyl-benzamidine
PAC	peptide acid linker, *p*-alkoxybenzyl ester; phenacyl
Pac	phenylacetyl
PACAP	pituitary adenylate cyclase-activating polypeptide
PAF-AH	platelet-activating factor acetylhydrolase
PAGE	polyacrylamide gel electrophoresis
Pal	(3-pyridinyl) alanine
PAL	peptide amide linker, 5-(4-Fmoc-aminomethyl-3,5-dimethoxyphenoxy)valeric acid
Pam	palmitoyl
PAM	phenylacetamidomethyl
PAO	*p*-aminophenyl arsenoxide
PAS	photoaffinity scanning
Pbf	2,2,4,6,7-pentamethyl-dihydrobenzofurane-5-sulfonyl
PBMC	peripheral blood mononuclear cells
PBS	phosphate-buffered saline
PC	phosphatidylcholine
PCs	precursor convertases; proprotein convertases
PCC	pyridinium chlorochromate
PCR	polymerase chain reaction
Pd/C	palladium on carbon
PDC	pyridinium dichromate
PDGF	platelet derived growth factor
PDI	protein disulfide isomerase
PEG	polyethylene glycol
PEGA	polyethylene glycol acrylamide copolymer
PEG-PS	polyethylene glycol-polystyrene copolymer
Pen	penicillamine
Pen-napAla	*N*-pentenoyl-L-2-naphthylalanine
PERMs	peptidomimetic estrogen receptor modulators
PET	positron emision tumography
pGlu	pyroglutarnic acid
Pfp	pentafluorophenyl ester
PFPA	pentafluoropropionic acid
ΔPhe	α,β-dehydrophenylalanine
PhF	9-(9-phenylfluorenyl
Phg	phenylglycine
Pht	phthaloyl
pHtc	phospho-Htc
PI	phosphatidylinositol
PICUP	cross-linking of unmodified proteins
Pip	pipecolic acid
PIP2	phosphoinositol 4,5-bisphosphate
PISA	protein *in situ* arrays
PK	pharmacokinetics
PKA	cAMP-dependent kinase A
PLC	phospholipase C
PLE	pig liver esterase
PLN	phospholamban
PLP	proteolipid protein
PLV	pulsed laser vaporization
PM	plasma membranes
$Pmb\text{-}NH_2$	4-methoxybenzylamine
PMBN	polymyxin B nonapeptide
Pmc	2,2,5,7,8-pentamethylchroman-6-sulfonyl
PMD	Pelizaeus Merzbacher disease
pMeBzl	*p*-methylbenzyl
PMMA	polymethylmethacrylate
PMN	polymorphonuclear leucocyte
Pmp	4-phosphonomethylphenylalanine
pNA	*p*-nitroaniline
PNA	peptide nucleic acid
*p*NBS	*p*-nitrobenzenesulfonyl
po	per os
PO	phenoloxidase
POI	phenoloxidase inhibitor
POMC	pro-opiomelanocortin
POPC	1-palmitoyl-2-oleoyl-*sn*-glycero-3-phosphocholine
POPG	1-palmitoyl-2-oleoyl-*sn*-3-[phospho-rac-(1-glycerol)]
Por	porphyrin
PP	pancreatic polypeptide
PPCE	post-proline cleaving enzyme
PPO	(2-oxo-4-[(hydroxy)(methyl)-phosphinoyl]butyric acid
PR	protease

PrP^{Sc}	scrapie prion protein
PrP^{C}	cellular prion protein
PrRP	prolactin releasing peptide
pS	phosphoserine
PS	polystyrene
PSAO	*p*-succinylamidephenyl arsenoxide
PSD/CID	post source decay/collision-induced dissociation
Pse	phenylsulfonylethyl
PS-SCL	positional scanning SCL
Pta	4-pyridylthioacetic acid
PTAMB	pinanyl *N,N,N*-trimethylamino-methane boronate
PTD	protein transduction domain
PTH	parathyroid hormone
PTHR	parathyroid hormone receptor
PTHrP	parathyroid hormone related protein
PTK	protein tyrosine kinase
PTM	post translational modifications
PTP	protein tyrosine phosphatase
PTR	peptide transport
PTX	pertussis toxin
pTyr	phosphotyrosine
PVDF	polyvinydene fluoride
PWR	plasmon wavelength resonance
PyAOP	(7-azabenzotriazol-1-yloxy)-tris(pyrrolidino)phosphonium hexafluorophosphate
PyBOP	(benzotriazol-1-yloxy)-tris(pyrrolidino)phosphonium hexafluorophosphate
PyBrOP	bromo-tris(pyrrolidino)phosphonium hexafluorophosphate
pY	phosphotyrosine
PYY	peptide YY
QSAR	quantitative structure-activity relationships
Rb	retinoblastoma gene product
RBC	red blood cells
RCM	ring-closing metathesis
Ret	trans-retinoyl
RGD	Arg-Gly-Asp
r.i.	retro-inverso
RMD	restrained molecular dynamics
RMSD	root mean square deviation
RNA	ribonucleic acid
RNAP	RNA polymerases
RNP	ribonucleopeptide
ROESY	rotating frame nuclear Overhauser enhanced spectroscopy
ROP	retinopathy
RP	reversed-phase
RP-HPLC	reversed-phase HPLC
RRE	rev response element
RR-MS	relapsing-remitting MS
rt/RT/r.t.	room temperature
RT-PCR	reverse transciptase-polymerase chain reaction
RTI	respiratory tract infections
$RuCl_2(dmso)_4$	dichlorotetrakis(dimethyl sulfoxide) ruthenium(II)
SANS	small-angle neutron scattering
SAPS	sequence assisted peptide synthesis
Sar	sarcosine
SAR	structure activity relationships
sc	subcotaneous
SCAM	substituted cysteine accessibility method
SCLC	small cell lung cancer
SCLs	synthetic combinatorial libraries
SD	standard deviation
SDF-1	cell-derived factor-1 or stromal-derived cell growth factor 1
SDS	sodium dodecyl sulfate
SDSL	site-directed spin labeling
SEM	scanning electron microscopy
SERMs	selective estrogen receptor modulators
serpin	serine protease inhibitor
SFTI-1	sunflower trypsin inhibitor-1
SH2	src homology domain 2
SH3	src homology domain 3
SIOM	7-spiroindoyloxymorphone
Sip	silaproline
siRNA	small interfering RNA
Smad	mothers against decapentaplegic
SN	secretoneurin
SP	substance P
SPECT	single photon emission computed tomography
SPOC	solid phae organic chemistry
SPPS	solid-phase peptide synthesis
SPR	surface plasmon resonance
SRB	sulforhodamine B
SRIF	somatostatin also somatotropin release-inhibiting factor
SS	Sjogren's Syndrome
SSA	senile systemic amyloidosis
sst	somatostatin receptor
Sta	statine, 2-amino-3-hydroxy-6-methylheptanoic acid
STa	heat-stable enterotoxin
Stat3	signal transduction and activator of transcription 3
StBu	*t*-butylthio
STD-NMR	saturation transfer difference NMR
SUIM	suberimidyl
Suc	succinyl
SUV	small unilamellar vesicle
SWNTs	single-walled carbon nanotubes
SynJ	synthetic J protein
T	temporin
TAEA	tris(2-aminoethyl) amine
TAMB	trimethylaminomethane boronate
TANDEM	triostin A tetra-*N*-demethylated
TAP	5,10,15,20-tetrakis(4-aminophenyl)-porphyrin
TAR	transactivating region

TASP	template-assembled synthetic protein(s)
TAT	transactivating transcriptional activator
TBA	*t*-butylammonium salt
TBAF	tetra-n-butylammonium fluoride
TBDMS	*tert*-butyldimethylsilyl
TBS-Cl	*t*-Butyldimethylsilyl chloride
TBTU	2-(1H-benzotriazol-yl)-1,1,3,3-tetramethyluronium tetrafluoroborate
*t*Bu	*tert*-butyl
Tce	2,2,2-trichloroethyl
TCEP	tris(carboxyethyl)phosphine
tCip	trans-1-cinnamylpiperazine
TCR	T cell receptor
TCTU	1-*H*-Benzotriazolium-1-[bis(dimethylamino)methylene]-5-chloro, 3-oxide tetrafluoroborate
Tdf	*p*-(3-trifluoromethyl-diazirin-3-yl)-phenylalanine
TEA	triethylamine
TEM	transmission electron microscopy
TEMP	2,3,5,6-tetramethylpyridine
TEMPO	2,2,6,6-tetramethylpiperidinyloxy
TEOF	triethylorthoformate
TES	triethylsilane
TF	tail-flick
TFA	trifluoroacetic acid
TFE	trifluoroethanol
TFFH	tetramethylfluoro-formamidiniumhexafluoro-phosphate
Tfm-AA	α-trifluoromethylamino acid
TFMSA	trifluoromethanesulfonic acid
TfOH	triflic acid
TGFα	transforming growth factor alpha
THF	tetrahydrofuran
Thi	β-(2-thienyl)-alanine
THP	triple-helical peptide
ThT	thioflavin T
Thz	thiazolidine-4-carboxylic acid, thioproline
Tic	1,2,3,4-tetrahydroisoquinoline-3-carboxylic acid
TIPS or TIS	triisopropyl silane
TLC	thin layer chromatography
Tle	*tert*-leucine/C-*tert*-butyl glycine
TMAO	trimethylamine *N*-oxide
TMH	transmembrane helix
Tmob	2,4,6-trimethoxybenzyl
TMP	2,4,6-trimethylpyridine
TMR	tetramethylrhodamine
TMS-Cl	trimethylsilyl chloride
TMSOTf	trimethylsilyloxy trifluoromethanesulfonate
TM	transmembrane domain
TMT	β-methyl-2,6'-dimethyltyrosine
TNF	tumor necrosis factor
TOAC	2,2,6,6-tetramethylpiperidine-1-oxyl-4-amino-4-carboxylic acid
TOCSY	total correlation spectroscopy
Tos	*p*-toluenesulfonyl
tPA	tissue-type plasminogen activator
TPTU	2-(2-oxo-1(2H)-pyridyl)-1,1,3,3-tetramethyluroniumtetrafluorophosphate;2-(2-pyridon-1-yl)-1,1,3,3-tetramethyluronium fluoroborate
TRH	thyrotropin-releasing hormone
Tris	tris(hydroxymethyl) aminomethane
TRLIF	time resolved laser-induced fluorescence
TrNOE	transferred nuclear verhauser effect
TRPV1	transient receptor potential vanilloid receptor 1
Trt	trityl
TSGs	tumor suppressor genes
TSH	thyroid stimulating hormone
TsOH	*p*-toluenesulfonic acid
TSS	toxic shock syndrome
TSTU	*O*-(*N*-succinimidyl)-1,1,3,3-tetramethyluronium tetrafluoroborate
TT	thrombin time
TTR	transthyretin
Tyr(NO_2)	3-nitrotyrosine
U-II	urotensin-II
UK	urokinase
uPA	urokinase plasminogen activator
uPAR	receptor of urokinase plasminogen activator
UTI	urinary tract infection
VCD	vibrational circular dichroism
VEGF	vascular endothelial growth factor
VesCPs	*Vespa* chemotactic peptides
VIP	vasoactive intestinal peptide
VLDL	very low density lipoprotein
vMIP-II	viral macrophage inflammatory protein II
VP	vasopressin
VRE	vancomycin-resistant enterococci
VSV	vesicular stomatitis virus
WHHL	Watanabe heritable hyperlipidemic
WT	wild type
X	randomized sequence position in peptide libraries
XAL	5-(9-aminoxanthen-2-oxy)valeric acid
Xan	9*H*-xanthen-9-yl
YFP	yellow fluorescent protein
Z, Cbz	benzyloxycarbonyl

Contents

Preface and Epilogue ix

Message from the President of the American Peptide Society xi

Murray Goodman, Teacher, Mentor, Friend xiii

In Memoriam: Arno Spatola xv

People Behind Symposium xvii

Symposium Sponsors and Exhibitors xix

American Peptide Society xxi

American Peptide Symposia xxii

The Merrifield Award: William F. DeGrado xxiii

The Makineni Lecture Award: James P. Tam xxv

Peptide Society Travel Grants xxvi

Bert Schram Young Investigators' Mini Symposium xxviii

Young Investigators' Poster Competition xxix

Abbreviations xxxi

Contents xli

Merrifield Award Lecture

De Novo Design of Peptides, Proteins, and Protein Mimetics 3
William F DeGrado

Amino Acid and Peptide Synthetic Chemistry

An Efficient Microwave-Assisted Synthesis of 2,5-Diketopiperazines Libraries 17
Maria C. Alcaro, Pietro Campiglia, Paolo Grieco, Ettore Novellino, Mario Chelli and Anna M. Papini

4-Fluoro-Phenylglycine and 3-Fluoro-Alanine: Labels for ^{19}F-Solid State NMR Structure Analysis of Membrane-Active Peptides 19
Parvesh Wadhwani, Sergii Afonin, Marina Berditchevskaja, Ralf W. Glaser and Anne S. Ulrich

Synthesis of 5-FAM-SSSSSSSSSS-OH: Comparison of Fmoc-Ser(Trt)-OH and Fmoc-Ser(tBu)-OH 21
Xiao-He Tong, Kabun Ichihara, Qing Tian and Anita Hong

Synthesis and Photophysical Properties of Acridonylalanine, a New Fluorescent Amino Acid 23
Aneta Szymańska, Katarzyna Wegner, Zbigniew Grzonka and Leszek Łankiewicz

Synthesis of PEG-Inhibitor Conjugates for Affinity Separation of Serine Proteases 25
Shin Ono and Makiko Umezaki

N-Methylation at the C-Terminus in Solid Phase Peptide Synthesis 27
Yun Wu, Yuan Gao, Wei-Jun Zhang and Garland R. Marshall

Stereospecific Synthesis of α-Alkyl α,α-Diamino-α-Carboxylates as Core Structural Units for Novel HIV-1 Protease Inhibitors 29
Tanaji T. Talele and Mark L. McLaughlin

Amino Acid and Peptide Labeling 31
Susana M.B. Fraga, M. Sameiro T. Gonçalves and Hernâni L.S. Maia

The 1,1-Dioxobenzo[b]thiophene-2-ylmetholoxycarbonyl (Bsmoc) Amino-Protecting Group 33
Nayan Amin, John Giantsidis, Ted Appleby, Sukhamaya Bain and Ed Price

Facile Synthesis of a Constrained Aza-Dipeptide (ADP) 35
Umut Oguz and Mark L. McLaughlin

Synthesis of Azapeptides using *N*-Boc-Aza[1]-dipeptide Building Blocks 37
Rosa E. Melendez and William D. Lubell

Efficient Synthesis of Fused Tetracyclic Benzimidazole Systems 39
Cornelia E Hoesl, Richard A Houghten and Adel Nefzi

Light-Induced Two-State Structural Transition of a Cyclic PDI-Related Azobenzene-Peptide 41
Markus Schütt, Alexander G. Milbradt, Luis Moroder and Christian Renner

Novel Gly Building Units for Backbone Cyclization: Synthesis and Incorporation into Model Peptides 43
Sharon Gazal, Gary Gellerman and Chaim Gilon

Application of Aspartic Acid in the Synthesis of Bicyclic Dipeptide Mimetics 45
John M. Ndungu, Xuyuan Gu, Dustin E. Gross, Jinfa Ying and Victor J. Hruby

Unique Biocatalytic Approach for the Synthesis of Chirally Pure Unnatural a- and b-amino Acids Using Novel Transaminases 47
Mohit Bhatia, Eric Law, Craig Lewis, George Matcham, Richard Nelson, Hemlata Rana, Bhavani Stout and Alice Wang

Assessment of 6Cl-HOBt-Based Coupling Reagents in Solid-Phase Cyclopeptide Synthesis 49
Giuseppina Sabatino, Maria Claudia Alcaro, Maria de la Cruz Pozo-Carrero, Mario Chelli, Paolo Rovero and Anna Maria Papini

Synthesis and Conformational Study of Peptides Based on Crowned C^a-Methyl L-DOPA 51
K. Wright, F. Melandri, M. Wakselman, J.-P. Mazaleyrat, F. Formaggio, S. Oancea, M. Crisma and C. Toniolo

Solid-phase Synthesis of des-*N*-tetramethyl Triostin A (TANDEM) 53
John P Malkinson and Mark Searcey

Total Solid-Phase Synthesis of Differentiation Factor from HL-60 Cells and Related Peptide Fragments 55
Lioudmila K. Baidakova, Igor L. Rodionov, Irina A. Kostanyan, Valery M. Lipkin and Vadim T. Ivanov

DioRaSSP [å]: Diosynth Rapid Solution Synthesis of Peptides 57
Ivo F. Eggen, Frits T. Bakelaar, Annet Petersen and Paul B.W. Ten Kortenaar

CLEAR-OX^{TM}: A New Polymer-Supported Reagent for the Preparation of Disulfide-Bridged Peptides 59
Krzysztof Darlak, Andrzej Czerwinski, Miroslawa Darlak, DeAnna W. Long, Francisco Valenzuela, Arno F. Spatola and George Barany

Predicting Lead Compounds Using Libraries of Flexible Molecules 61
Adrian Kalászi and Ödön Farkas

Parallel Solid-Phase Synthesis of Difluorinated Dipeptide Analogs 63
Agnès Vidal, Richard A. Houghten and Adel Nefzi

Synthetic Peptides as Certified Analytical Standards 65
Henriette A. Remmer, Nicholas P. Ambulos, Lynda F. Bonewald, John J. Dougherty, Edward Eisenstein, Elisabeth Fowler, Jinny Johnson, Ashok Khatri, Mark O. Lively, Nadine Ritter0 and Susan T. Weintraub

A Novel Approach for the Hydrophobic Peptides Synthesis and Purification through *O–N* Intramolecular Acyl Migration Reaction 67
Youhei Sohma, Masato Sasaki, Zyta Ziora, Naoko Takahashi, Tooru Kimura, Yoshio Hayashi and Yoshiaki Kiso

An Efficient Asymmetric Synthesis of Fmoc-*L*-Cyclopentylglycine Using a Chiral Auxillary 69
Satendra Singh and Michael W. Pennington

Thiazolidine as Protection for N^{α}-(1-Phenyl-2-Mercaptoethyl) Glycine in Extended Chemical Ligation of Three or More Fragments 71
Matteo Villain, Hubert Gaertner and Paolo Botti

Solid-Phase Synthesis of *C*-Terminal Thio-Linked Glycopeptides 73
John P. Malkinson and Robert A. Falconer

Isolation and Characterization of Autoantibodies in Multiple Sclerosis Patients' Sera: Towards a Novel Apheresis Treatment 75
Elisa Peroni, Francesco Lolli, Benedetta Mazzanti, Marta Pazzagli, Bruno Bonetti, Johan Hoebeke, Mario Chelli, Paolo Rovero and Anna M. Papini

Small Focused Library of CSF114-type Glycopeptides for the Characterization of Autoantibody Recognition in Multiple Sclerosis 77
Francesca Nuti, Ilaria Paolini, Barbara Mulinacci, Maria de la Cruz Pozo-Carrero, Benedetta Mazzanti, Marta Pazzagli, Francesco Lolli, Mario Chelli, Franca Maria Cordero, Alberto Brandi and Anna Maria Papini

O-Glycopeptide Synthesis Made Easy 79
Beechanahalli P. Gangadhar, Seetharama D. Jois, Sulaiman Sheriff, William T. Chance and Ambikaipakan Balasubramaniam

Synthesis of Guanidine Compounds Using Resin-Bound Guanidinylating Reagents 81
Markus M. Mueller, Hans J. Musiol and Luis Moroder

Facile Synthesis of Protected Hydrazino Amino Acids 83
Umut Oguz and Mark L. McLaughlin

Dialkyl Imidazolinones from α, α -Dialkyl Glycines 85
S.P.G. Costa, H.L.S. Maia and S.M.M.A. Pereira-Lima

A Methionine-Based Linker Strategy for Solid-Phase Synthesis of Lysine-Containing Cyclic Peptides 87
Joseph C. Kappel and George Barany

Synthesis of Isotopomers of the MHC II Antagonist AZD2315 89
H. Booth, J. R. Harding and D. P. Woodhouse

A Versatile Method for Fast and Selective Introduction of Multiple Probes into Peptides Using Solid Phase Synthesis — Application to Biophysical Models 91
Inbar Rofman, Elisha Haas, Varda Ittah and Gerardo Byk

An Efficient Peptide Synthesis in Solution Using Nsc-Amino Acids 93
Hyun Jin Lee, Weonu Chweh, Young-Deug Kim , Hyuk-Kwang Jung and Hack-Joo Kim

A Novel Post-Translational Modification: A Conopeptide From *Conus gladiator* Provides the First Example of γ-Hydroxyvaline (Hyv) Within a Polypeptide Chain 95
David Mora, Fred C. Pflueger, Katarzyna Pisarewicz, Gregg B. Fields and Frank Marí

Induced Axial Chirality in the Conformationally Labile, Atropoisomeric $C^{a,a}$-Disubstituted Glycine Bip in Peptides 98
J.-P. Mazaleyrat, K. Wright, N. Toulemonde, A. Gaucher, M. Wakselman, Q. B. Broxterman, F. Formaggio, S. Oancea, M. Crisma and C. Toniolo

Preparation and Use of Magnetic Solid Phase Synthesis Supports 100
Jan Mařík, Derick H. Lau and Kit S. Lam

Rapid Microwave-Assisted Solid Phase Peptide Synthesis 102
Máté Erdélyi, and Adolf Gogoll

Regioselective MCR4 Reaction: One Pot Synthesis of Spiro Heterobicyclic Aliphatic Rings Generated from Natural Amino Acids 104
Gerardo Byk and Eihab Kabha

Effective Peptide Synthesis Applying Thioesters in the Presence of Metal Ions 106
Raffaele Ingenito, Dijana Drezniak, Stefan Guffler and Holger Wenschuh

A Highly Acid-Labile Thiophene Backbone Amide Linker: T-BAL 108
Ulrik Boas, Mikkel Jessing, Jørn B. Christensen and Knud J. Jensen

A New Method for the Preparation of Peptide C-Terminal a-Thioesters Compatible with Fmoc-Solid-Phase Peptide Synthesis 111
Julio A. Camarero, Benjamin J. Hackel, James J. de Yoreo and Alexander R. Mitchell

Peptide $^{\alpha}$Thiol Ester Formation Using Standard Fmoc-Chemistry 113
Regula von Eggelkraut-Gottanka, Annerose Klose, Michael Bienert, Annette G. Beck-Sickinger and Michael Beyermann

Fluorophilic Tagging Reagents for Solid Phase Peptide Synthesis 115
Dmitri V. Filippov, Dirk J. van Zoelen, Peter C. de Visser, Marcel van Helden, Steven P. Oldfield, Daan Noort, Gijs A. van der Marel, Hermen S. Overkleeft, Jan W. Drijfhout and Jacques H. van Boom

Novel Targeting Strategy Based on Multimeric Ligands for Drug Delivery and Molecular Imaging: Homo-oligomers of α-MSH 117
Josef Vagner, Heather L. Handl, Robert J. Gillies and Victor J. Hruby,

P-BOP, a New Polymer-Supported Peptide Coupling Reagent 119
Sorin V. Filip, Valérie Lejeune, Jean-Pierre Vors, Jean Martinez and Florine Cavelier

New Approach for Peptide Ligation 121
Nan-Hui Ho, Ralph Weissleder and Ching-Husan Tung

Comparison of Effect of Anionic Ion-Pairing Reagents on Capillary Electrophoresis and Reversed-Phase Chromatography of Cationic Random Coil Peptides 123
T.V. Popa, Colin T. Mant and Robert S. Hodges

Synthesis of Peptide Thioesters by Masking as Trithioortho Esters in a Fmoc Backbone Amide Linker (BAL) Strategy 125
Jesper Brask, Fernando Albericio and Knud J. Jensen

Multiple Condensations of Peptide Thioesters Prepared by the “Safety-Catch” Resin Approach: Synthesis of p53 (303-393) 127
Kenta Teruya, Sharlyn Mazur and Ettore Appella

Base-Assisted Desulfurization: Synthetic Applications and Mechanistic Studies 129
Amit K Galande and Arno F Spatola

Stereospecific Synthesis of a Carbene-Generating Diazirine Phenylalanine: Non-Selective Photoaffinity Labeling of Angiotensin II Receptors AT_1 and AT_2 131
D. Fillion, M. Deraët and E. Escher

ESR-Solvation Study of Different Amine Loaded and Cross-Linked Resins: Implication for Peptide Synthesis and Liquid Chromatography 133
Elias H. Silva, Erick F. Poletti, Marcia A. F. S. Neves, Fernanda M. B. Coutinho, Shirley Schreier and Clovis R. Nakaie

Asymmetric Syntheses of Enantiomerically Pure α,α-Dialkylated Glycines as Core Structural Units for Novel HIV-1 Protease Inhibitors 135
Tanaji T. Talele and Mark L. McLaughlin

Preferred Conformation of C^{α} Methyl, C^{α} Cyclohexylglycine 137
Claudio Toniolo, Marco Crisma, Fernando Formaggio, Quirinus B. Broxterman and Bernard Kaptein

Side Reactions During Peptide Cyclization 139
Haim Tsubery, Tali Scherf and Mati Fridkin

Specificity of PDZ Interaction Using NMR Spectroscopy and Spot Synthesis 141
Prisca Boisguérin, Rainer Leben, Rudolf Volkmer-Engert, Jens Schneider-Mergener and Hartmut Oschkinat

NMP is Unsuitable as a Solvent for the Rapid Solid Phase Synthesis of $CGRP_{8-37}$ Using *in situ* Neutralization 143
Christopher K. Taylor, Peter W. Abel and D. David Smith,

Isocratic Reversed-Phase Chromatography Separation and Purification of Peptides 145
A.R. Mehok, C.T. Mant, B. Tripet and R.S. Hodges

New Technology Automates Sorting of Large, Bead-Based Combichem Libraries 147
K. Ver Donck, L. Bols, R. Bongaarts, P. Van Osta, A.J. Brouwer, R.M. J. Liskamp, D. Perrault, K. Kalutkiewicz, J.Geysen and R. Pulak

Monitoring Self-Association of Small Amphipathic Molecules by Temperature Profiling in Reversed-Phase Chromatography 149
Darin L. Lee, Colin T. Mant and Robert S. Hodges

Effect of Secondary Structure on Selectivity of Reversed-Phase Chromatography for Peptide Separations at Varying Temperatures 151
Yusin Chen and Robert S. Hodges

Controlling “Easy” and “Difficult” Fmoc-Deprotections 153
Phillip W. Banda and Mary Frances Leopold

The Effect of Trp on UV- and Vibrational Circular Dichroism of Helical Peptides 155
Attila Borics, Chibawanye Ene, Laszlo Otvos Jr, Richard F. Murphy and Sándor Lovas

Improved Automated Waste Handling for the Applied Biosystems 433 Peptide Synthesizer 157
David H. Singleton, Robert T. Suleske and J. Carter Courtney

X-Cys Ligation 159
Yi-An Lu and James P Tam

Orthogonally Protected Sugar Diamino Acids as Building Blocks for Oligosaccharide Mimetics 161
Frank Sicherl and Valentin Wittmann

Comparison Between NMR And CD Data Of Synthetic Peptides 163
Fanny Guzmán, Julio C. Calvo, Claudia Reyes, Angela G. Torres, Luz M. Salazar, José M. Lozano and Manuel E. Patarroyo

Molecular Design of Functional Peptides by Utilizing Unnatural Amino Acids that can Coordinate with Metal Ions 165
Hitoshi Ishida, Masato Kyakuno, Takahiro Nakazato, Mina Fujii and Shigero Oishi

Total Synthesis of Uroguanyline 167
Yoshitaka Nemoto, Jing Xu, Shawn Lee and Baosheng Liu

Synthesis of Prokineticin 2 Employing a Convergent Solid-Phase Strategy Performed in a Chloroform-Phenol Mixed Solvent 169
Masanori Ishimaru, Yuji Nishiuchi, Hideki Nishio and Terutoshi Kimura

Peptidomimetic and Pseudopeptide Synthetic Chemistry

3-Aminopiperidones as Dipeptide Constrained Surrogates in Biologically Relevant Compounds 173
Mònica Garcia, Xavier del Río, Rachid El Hafi, Patricia López, Eulàlia Pinyol, Jordi Piró, Pilar Forns, Mario Rubiralta, Ernest Giralt, and Anna Diez,

Synthesis of Aminopyrrole Carboxylate Analogs for Peptide Mimicry 176
Guillaume Jeannotte, Karl A. Hansford, Félix-Antoine Marcotte, Frederik Rombouts, Valeria Zanzarova and William D. Lubell

Advances in a Structure Activity Study of the Aureobasidin Peptide Antibiotics: Synthesis of L-*N*-Boc-*N*-Methyl-*β*-Hydroxyvaline 179
James E. Dettwiler, Laurent Bélec and William D. Lubell

Backbone Cyclic Peptidomimetic Superantigen Antagonists: Synthesis and Biological Activity 181
Evgenia Glukhov, Gila Arad, Revital Levy, Karina Hazan, Sharon Gazal, Raymond Kaempfer and Chaim Gilon

Transition Metal Complexes of Linear, Dimeric and Cyclic Pseudopeptides 183
Siegmund Reissmann, Sebastian Kuenzel, Georg Greiner, Inge Agricola, Sylvia Mueller, David Pretzel, Matthias Schmidt, Raiker Witter and Ullrich Sternberg

Cyclic Peptides from Plants of Genus Linum 186
B. Picur, P. Ruchala, M. Lisowski, M. Cebrat, A. Pasternak, R. Zbozień Pacamaj, P. Stefanowicz, T. Goszczyński and Ł. Tarnawski

Peptide Mimic Synthesis with Cyclic Sulfamidates 188
Fabrice Galaud, Priscille Laborde and William D. Lubell

Studies of Photoswitchable *β*-Hairpin Mimetics 190
Máté Erdélyi, Anders Karlén and Adolf Gogoll

Lactam Bridge Formation at High Temperature 192
Alessandra Machado, Giuliano C. Xavier, Giselli H. Lima, Antonio Miranda and M. Terêsa M. Miranda

Microwave-Assisted Solid-Phase Synthesis of γ[CH_2NH] Amide Bond Surrogate 194
Luigi Longobardo, Pietro Campiglia , Isabel Gomez-Monterrey, Ettore Novellino and Paolo Grieco

Metal-Pentaazacrown Peptidomimetics: RGD and WRY 196
Wei-Jun Zhang, Yun Wu, Yuan Gao, Amruta Poreddy, Urszula Slomczynska, Liwei Chang, Michelle E. Weber and Garland R. Marshall

Enhancing Selectivity, Stability, and Bioavailability of Peptidomimetic Estrogen Receptor Modulators 198
Arno F. Spatola, Amit K. Galande, Florence M. Brunel, Kelly S. Bramlett, Thomas P. Burris, John O. Trent and James L. Wittliff,

Stereoselective Synthesis of 4, 8-Disubstituted Azabicyclo[4.3.0]nonane Amino Acid Esters: Dipeptide β-Turn Mimetics for Melanocortin Peptide Receptors 200
Junyi Zhang, Chiyi Xiong and Victor J. Hruby

Novel Building Blocks for Peptidomimetic Chemistry 202
Murray Goodman, Juan R. Del Valle and Nicole D. Smith

Solid Phase Syntheses of Monovalent and Bivalent Peptidomimetics of the Neurotrophins 205
Kevin Burgess

The Sulfonamide Moiety in Peptidomimetics and Peptidomimetic-Peptide Hybrids 210
Rob M. J. Liskamp, Wilna J. Moree, Dries B. A. De Bont, Dennis W. P. M. Löwik, Arwin J. Brouwer, Menno C. F. Monnee, Remco De Jong and Dirk T.S. Rijkers

Peptoid-Peptide Hybrids as Potent Novel Melanocortin Receptor Ligands 213
John A.W. Kruijtzer, Wouter A.J. Nijenhuis, Willem Hendrik Gispen, Roger A.H. Adan and Rob M.J. Liskamp

New Methodology for Syntheses of Bicyclic β-Turn Dipeptides (BTD) on Solid Phase Supports 215
Xuyuan Gu, Josef Vagner, Danice Andrus, Magda Stankova and Victor J. Hruby

Search for Biologically Active Peptidomimetics of beta-Turns and beta-strands. Designed Scaffolds and Serendipitous Observations 217
Ralph Hirschmann and Amos B. Smith, III

Liquid-Phase Synthesis and Conformational Analysis of Pseudoproline-Containing Turn Mimics 223
C. Tomasini, G. Luppi, D. Lanci, M. Garavelli, A. Garelli and V. Trigari

Pseudo-Proline as Reversible Solubilizing Entity in Cyclosporin C 225
Olivier Turpin, Angela Wittelsberger, Manfred Mutter and Luc Patiny

Synthesis of Modified Prolines for Peptidomimetic Use 227
Eric Chang, Debra A. Roberts, Yannick Fillon and Jean Chmielewski

Synthetic a-Amino Acids as Building Blocks for Novel RNA Ligands 229
Andreas Krebs, Oliver Boden, Verena Ludwig and Michael W. Göbel

Protein Mimicry, Engineering, Synthetic Chemistry and Structure-Function

Locally Stable Native-Like Fragments in the Denatured State of PapD Chaperone 233
James G. Bann, Jeff L.-K. Kao, Yun Wu and Gregory V. Nikiforovich

Chemical Synthesis of Proteins Through Native and Extended Chemical Ligation 235
Paolo Botti, Matteo Villain, Sonia Manganiello and Hubert Gaertner

Combination of the Convergent and Native Chemical Ligation Methods in the Total Synthesis of Proteins 240
Dimitrios Gatos, Spyros Goulas and K. Barlos

Chemical Synthesis and Folding/Stability Studies of the Hydrophobic Protein, Crambin 242
Duhee Bang, Neeraj Chopra and Stephen.B.H. Kent

De Novo Four-Helix Bundle Proteins 244
Heidi K. Huttunen and John C. Sherman

Cavitand Based Four-Helix Bundles 246
Emily S Seo and John S Sherman

Using NMR and Segmental Isotopic Labeling to Elucidate the Role of the N-Terminal Region of s70-like Factors in Regulating Binding of Bacterial RNA Polymerase to DNA Promoter 248
Julio A Camarero, James J de Yoreo and David Fushman

G protein a-Subunit: Conformation and Dynamics of the C-Terminal Domain 250
Fabio Casallanovo, Clovis R Nakaie, Antonio CM Paiva and Shirley Schreier

A Biophysical Approach to the Structure of the Rhodopsin:Transducin Interface 252
Lori L. Anderson, Thomas J. Baranski, Wayne L. Hubbell, Ned Van Eps, Steven O. Smith and Garland R. Marshall

Chemically Modified hIL-8 for Biological Studies 254
Ralf David, Zuzana Machova and Annette G. Beck-Sickinger

Environmentally Sensitive Hydrogelation Via Designed Peptides 256
Karthikan Rajagopal, Juliana Kretsinger, Darrin J. Pochan and Joel P. Schneider

Peptide Microarrays Using Structure-Based Peptide Libraries for Protein Chips 258
Kenji Usui, Mizuki Takahashi, Tetsunori Ojima, Masato Suzuki, Kiyoshi Nokihara, Eiichi Tamiya and Hisakazu Mihara

A Rationally Designed CD4 Mimic Useful in HIV Inhibition and Vaccine Design 260
François Stricher, Loïc Martin, Philippe Barthe, Alain Mechulam, Claude Vidaud, Laurent Bellanger, Bernard Maillère, André Ménez, Francisco Veas, Christian Roumestand and Claudio Vita

Engineering New Metal Binding Specificity in Calmodulin Peptides 263
Loïc Le Clainche, Véronique Monjardet and Claudio Vita

Design and Synthesis of Electron Transfer Proteins with Flavin, Heme, and Quinone 265
Wenwu Li, Thomas Carell, and Wolfgang Haehnel

Photo-Control of the Activity of Proteins Via Caging of Their C-Terminus 267
Jean-Philippe Pellois, Michael E. Hahn and Tom W. Muir

The Chemical Biology of Protein Splicing 269
Elyse S. Blum, Henning D. Mootz, Izabela Giriat, Alessandra Romanelli, Alexander Shekhtman and Tom W. Muir

The Semisynthesis of the Potassium Channel KcsA 276
M. Sekedat, F. Valiyaveetil, R. MacKinnon and T. W. Muir

Protein Assembly Using the Staudinger Ligation 278
Bradley L. Nilsson, Matthew B. Soellner and, Ronald T. Raines

Rao Makineni Lecture 280

Protein Mimetics as HIV Therapeutics and Vaccines Prepared by Tandem Ligation
James P Tam

Three-Helix Bundles of HIV Mimics Fusion State and Blocks M- and T-Tropic HIV-1 Entry into Host Cells 290
Jin-Long Yang, Qitao Yu, Hua Li and James P. Tam

Manipulating the Hydrophobic Core of a Coiled Coil Peptide Self Replicator 292
Xiangqun Li and Jean Chmielewski

Synthetic Expansion of the Central Dogma: Chemical Aminoacylation, 4-Base Codons and Nonnatural Mutagenesis 294
Masahiko Sisido

Cytoplasmic Domain Of *E. coli* ProP Forms an Antiparallel Coiled-Coil as Determined by NMR Spectroscopy 301
David L. Zoetewey, Brian Tripet, Tatiana G. Kutateladze, Michael J. Overduin, Janet M. Wood and Robert S. Hodges

De novo Design, Synthesis and Properties of Model Quinoproteins 303
Wenwu Li, Michaela Ritter, Petra Hellwig, Jürgen Heinze and Wolfgang Haehnel

Protease and Enzyme Substrate/Inhibitor Structure-Function

Different Approaches to Inhibit the Chymotrypsin-Like Activity of the 20S Proteasome 307
Pascal Furet, Patricia Imbach, Carlos García-Echeverría, Marc Lang, Johannes Roesel, Maria Noorani, Johann Zimmermann, Peter Fuerst and Vito Guagnano

Synthesis and Evaluation of Phosphonopeptide Cathepsin C Inhibitors 310
Paweł Kafarski, Marcin Drąg, Łukasz Berlicki and Małgorzata Pawełczak

Cyclic Peptide Inhibitors of α-Amylase Based on Tendamistat 313
Leena Khullar, Steve M. Fernandes, James M. Waner, Elizabeth J. Blaney, Dennis A. Brown and Deborah L. Heyl

Betaine: Homocysteine Methyltransferase from Rat Liver: Purification and Inhibition by a Boronic Acid Substrate Analog 315
Payman Amiri, Mark Cava, Kyung-Hee Lee, Robert N. Lindquist and Tom Ottoboni

Activity and Refolding of Partially Folded Analogues of BPTI 317
George Barany, Irina V. Getun, Judit Tulla-Puche and Clare Woodward

Solid-Phase Synthesis of Amidoketones:Towards Caspase Inhibitors 319
Jesús Vázquez, and Fernando Albericio,

Synthesis and Biological Evaluation of Dipeptde Boronic Acids as Potent DPP IV Inhibitors 321
J.H. Lai, W. Wu, H. Maw, Y. Zhou and W.W. Bachovchin

Cyclic Tetrapeptides Containing a Zinc Ligand as Novel Histone Deacetylase Inhibitors 323
Binoy Jose, Tamaki Kato, Yuko Sumida, Minoru Yoshida, and Norikazu Nishino,

In Vivo Imaging of Thrombosis-Associated Enzyme Using Fluorescence Peptide Probes 325
Ching-Hsuan Tung, Nan-Hui Ho, Qing Zeng and Ralph Weissleder

A Fluorescence Resonance Energy Transfer Substrate (FRETS) Library for Determining Protease Specificity 327
Katsumi Takada, Masahiko Tsunemi, Yuji Nishiuchi and Terutoshi Kimura

Synthesis and Biological Activity of Dimeric HIV-1 Integrase Inhibitory Peptides 329
Krzysztof Krajewski†, Ya-Qiu Long, Christophe Marchand, Yves Pommier and Peter P. Roller

Peptide-lead Nonpeptidic Protease Inhibitor Targeting Multi-drug Resistant Strains of HIV 331
Nobutaka Fujii, Hirokazu Tamamura, Tomonori Yamasaki, Akira Otaka, Yasuhiro Koh, Manabu Aoki, Kenji Maeda, Kazuhisa Yoshimura and Hiroaki Mitsuya

Molecular Dynamics of the Caspase-3 Cleaved N-Half of Gelsolin 333
Inta Liepina, Paul Janmey, Cezary Czaplewski and Adam Liwo

Synthesis of Glutathione Peptidomimetics 335
Tunde Matola and Istvan Jablonkai

Aib Modified Dimerization Inhibitor of HIV-1 Integrase 337
Lei Zhao and Jean Chmielewski

HIV-1 Protease Dimerization Inhibitors: Reversing the Southern Peptide 339
You Seok Hwang and Jean Chmielewski

CD Analysis of Structure and Lipid Interacting Property of Inhibitors of Proprotein Convertases 341
A. Basak, K. Beking, M. Chrétien and S. Basak

Cellular Delivery and Design of Cell Transportable Inhibitors of Proprotein Convertases 343
A. Basak, F. Dong and S. Basak

Immobilized Bivalent Inhibitors as Tools for the Affinity-based Isolation of Human Mast Cell Tryptases 346
Norbert Schaschke, Dusica Gabrijelcic-Geiger, Andreas Dominik and Christian P. Sommerhoff

Cyclic Biphenyl Ether Tripeptides as Proteasome Inhibitors 348
Markus Kaiser, Alexander G. Milbradt, Christian Renner, Irmgard Assfalg-Machleidt, Michael Groll, Robert Huber and Luis Moroder

Triple-Helical Peptide Ligand Dissection of Unique Melanoma Cell Signaling Pathways 350
Janelle L. Lauer-Fields, Mohammad Al-Ghoul, Diane Baronas-Lowell, Jeffrey A. Borgia and Gregg B. Fields

Synthesis of $(Ac\text{-}XFRSLK)_2$-Rhodamine 110 353
Xiao-He Tong and Anita Hong

Synthesis and Activity of a Novel Peroxidase Mimetic Peptide 355
Yali Liu, Lili Guo, Hui Yang, Jingming Zhang, Roger W. Roeske and Wei Li

Novel Potent Peptides That Regulate Phenoloxidase Activity 357
Takashi Sato, Chihiro Awada and Yoshimi Ogata

Methanethiosulfonyl Derivatives of Linear and Cyclic Peptides as Novel Reagents to Study Topology of Active Center Gorge of Acetylcholinesterase 359
Peteris Romanovskis, Terrone L. Rosenberry, Bernadette Cusack and Arno F. Spatola

Peptide Anticoagulants in a Rat Model of Disseminated Intravascular Coagulation 361
Sándor Bajusz, Éva Barabás, Irén Fauszt, Gabriella Szabó and Attila Juhász

Solution Structure of a Cyclic Peptide, Subtilosin A, With Unusual Post-translational Modifications 363
Tara Sprules, Karen E. Kawulka, Ryan T. McKay, Pascal Mercier, Christopher M. Diaper, Peter Zuber and John C. Vederas

Synthesis and Biological Evaluation of Dimeric uPAR Antagonists and Aomatostatin Analogs 365
A. Modlinger, M. Sukopp, M. Buergle, K. Wosikowski and H. Kessler

Peptide-Based Near Infrared Opitical Probes Specific For Matrix Metalloproteinases Activity Detection 367
Wellington Pham, Ralph Weissleder and Ching-Husan Tung

Peptide Structure-Conformation-Function And Molecular Modeling

2D NMR Studies of Dynorphin A(1-13) in Solution: Potent κ Opioid Receptor Agonist 371
V. Renugopalakrishnan, Shaw-Guang Huang and M. Prabhakaran

Effects of Arsenic(III) Binding on α-Helicity 373
Daniel J. Cline, Colin Thorpe and Joel P. Schneider

3_{10}-Helix in Aib-Rich Peptides Containing Lactam-Bridged Side-Chains: Spectroscopic Characterization in TFE by CD and NMR 375
Elisabetta Schievano, Katiuscia Pagano, Stefano Mammi and Evaristo Peggion

Amphipathic α-Helix Apolipoprotein A-I Peptide Models as Atheroprotective Probes: Design, Construction and Phospholipid/Cholesterol Interactions 377
Charalampos Alexopoulos, John Mitsios, Alexandros Tselepis, Maria Sakarellos-Daitsiotis and Constantinos Sakarellos

Receptor-Bound Characteristics of MiniANP Analyzed by NMR, MM/MD, and the Use of Unusual Amino Acids 379
K. Sugase, M. Horikawa and M. Ishiguro

α,α-Dialkylated β-Hairpin Peptides: Design, Synthesis, and Conformational Analysis 381
Catherine L. Thomas, Marcus A. Etienne, Jia Wang, Vladimir Setnicka, Timothy A. Keiderling and Robert P. Hammer

Computational Design and Chemical Synthesis of a β-Sandwich Protein 383
Kai Fritzemeier and Wolfgang Haehnel

Design and Conformational Analysis of Peptides Containing α,α-Disubstituted Amino Acid 386
Jia Wang, Yanwen Fu, Martha M. Juban and Robert P. Hammer

An Encoding Method for One-bead One-compound Beta-turn Peptide and Peptidomimetic Libraries 388
Ruiwu Liu, Xiaobing Wang, Jan Marik and Kit S. Lam

Synthetic Bivalent Inhibitors Based on the Bowman Birk Inhibitors: The BiKK Inhibitor 390
Agnès M Jaulent and Robin J Leatherbarrow

Understanding b-Structure in Peptides and Proteins 392
Andrea G. Cochran, Nicholas J. Skelton and Melissa A. Starovasnik

Molecular Dynamic Investigation of the β-Turn Forming Nature of Tetra- and Hexapeptides 400
Attila Borics, Richard F. Murphy and Sándor Lovas

Discovery and Applications of the Cyclotides: Circular Proteins from Plants 402
David J. Craik, Norelle L. Daly, Michelle L. Colgrave and K. Johan Rosengren

Design of Novel Template Peptides to Mimic the Coiled Coil Conformation of the gp21 Envelope Subunit of HTLV-1 for the Induction of Neutralizing Antibodies 407
Roshni Sundaram, Sharad V. Rawale, Yiping Sun and Pravin T.P. Kaumaya,

Importance of Hydrophobic Clusters on Protein Folding and Stability 409
Stephen M. Lu, Stanley C. Kwok and Robert S. Hodges

Visual Molecular Recognition of cAMP with Azo-Bridged Cyclic Peptide Libraries 412
Martina Čížková, Martin Šafařík, Jaroslav Šebestík, Jan Hlaváček and Ivan Stibor

Organic Functionalization of Carbon Nanotubes with Peptides 414
D. Pantarotto, C. D. Partidos, J. Hoebeke, J. -P. Briand, M. Prato and A. Bianco

Structural and Biological Studies of a Penetratin-Linked Gas C-Terminal peptide 416
Anna M. D'Ursi, S. Albrizio, L. Giusti , M. Mazzoni, E. Novellino and P. Rovero

Structural Analysis of Nanomolar Quantities of Marine Neuropeptides Using 2D-NMR Methods 418
Elena Matei, Fred Pflueger, Aldo Franco, Herminsul Cano, David Mora and Frank Mari,

Solution Structure of α-Conotoxin OmIA, a Neuronal Toxin Specific for the a4b4 Subunit Interface of Neuronal Nicotinic Acetylcholine Receptor 420
Seung-Wook Chi, Do-Hyoung Kim and Kyou-Hoon Han

Cyclic Proline Peptides as Privileged Reverse-Turn Templates 422
Ye Che and Garland R Marshall

Synthesis and Ca^{2+} Interactions of Model Amphipathic Cyclic Peptides in Detergents 424
Day Gates, Jack Rostas, Victor Bailey and Maria Ngu-Schwemlein

Conformational Preferences and Biological Activity of Short Peptides Containing (E)-Dehydrophenylalanine 426
Rafal Latajka, Michal Jewginski, Malgorzata Pawelczak, Maciej Makowski and Pawel Kafarski,

Controlled Assembly of Carbon Nanotubes in Aqueous Solution with Designed Peptides 428
Gregg R. Dieckmann, Alfonso Ortiz-Acevedo, Alan B. Dalton, Joselito Razal, Jian Chen, Edgar Muñoz, Inga H. Musselman, Ray H. Baughman, and Rockford K. Draper

Role of Disulfide Bonds in the Folding of Prouroguanylin and Heat-stable Enterotoxin 431
Yuji Hidaka, Len Ito and Hiroshi Yamaguchi

Pseudopeptide Foldamers. The Homo-oligomers of 4(*S*)-Oxazolidineacetic Acid, 2-Oxo (Oxac) 433
C. Tomasini, G. Luppi, S. Oancea, F. Formaggio and C. Toniolo

C^{α} Methyl Norvaline Foldamers 435
Fernando Formaggio, Marco Crisma, Claudio Toniolo, Quirinus B. Broxterman, Bernard Kaptein, Catherine Corbier, Michele Saviano, Pasquale Palladino and Ettore Benedetti

Structure-Activity Studies of *cis*-γ-Amino-L-Proline Oligomers: Probing the Relationship between Conformational Stability and Cellular Internalization Capacity 437
Josep Farrera-Sinfreu, Ernest Giralt, Miquel Pons, Susana Castel, Fernando Albericio and Miriam Royo

Helix Formation in Oligomers of γ-Amino Acids (γ-Peptides) 439
Carsten Baldauf, Robert Günther and Hans-Jörg Hofmann

Vinylogous g-Amino Acids as Building Blocks for Foldamers 441
Carsten Baldauf, Robert Günther and Hans-Jörg Hofmann

Role of Intramolecular Hydrogen Bonds on the Electron Transfer Rate in Structurally Defined Peptides 443
Fernando Formaggio, Alessandro Moretto, Sabrina Antonello, Flavio Maran and Claudio Toniolo

A Structural Study of a Series of Conformationally Restricted Hexapeptides 445
Basilio Pispisa, Lorenzo Stella, Mariano Venanzi, Antonio Palleschi, Michel Wakselman, Jean-Paul Mazaleyrat, Ferdinando Fomaggio and Claudio Toniolo

Solution Structure of Daptomycin 447
Kenneth S. Rotondi and Lila M. Gierasch,

One Good Turn Deserves Another: Regular Turns in Peptide and Nucleic Acid Templates 450
Christian Lehmann

Molecular Modeling of Opioidmimetics Containing the Dmt-Tic-Bid Pharmacophores and Docking with the δ-Opioid Receptor 453
Sharon D. Bryant, Severo Salvadori, Remo Guerrini, Gianfranco Balboni, Yunden Jinsmaa and Lawrence H. Lazarus

Molecular Dynamics Simulations of BNP Binding to the NPRA Receptor Dimer 455
B.C. Wilkes, A. De Léan and P.W. Schiller,

The Symmetries in Changes of Conformational Equilibria Thermodynamic Parameters made by Structure Modifications in Peptides 457
Boleslaw Picur

Tripeptides as Model Systems to Understand the Random Coil Conformation of Peptides and Proteins: Ionized Tri-aspartate and Tri-Glutamate in Water 459
Reinhard Schweitzer-Stenner, Fatma Eker, Cao Xiaolin and Laurence Nafie

Analysis of Peptide β-Sheet Models Using Chemical Shift Deviations 462
Niels H. Andersen, R. Matthew Fesinmeyer and F. Michael Hudson

Photodimerization in Peptides for High-Density Optical Data Storage 464
Rolf H Berg and P S Ramanujam

Segmental Isotopic Labeling of RNA Polymerase for NMR Studies 466
Edmund C. Schwartz, Alexander Shekhtman, Seth A. Darst, David Cowburn and Tom W. Muir

Role of Aromatic Residues in the Structure and Biological Activity of the Small Cytokine, Growth-Blocking Peptide (GBP) 468
Masahito Tada, Tomoyasu Aizawa, Mineyuki Mizuguchi, Katsutoshi Nitta, Yoichi Hayakawa and Keiichi Kawano

Analysis of Structure and Metal Binding Properties of Secretoneurin and Related Peptides by CD and MALDI-MS 470
Ajoy Basak, Jane MacAulay and Vance Trudeau

Effect of 4-Fluoroproline in the X-Position on the Stability of the Collagen Triple Helix 472
Jonathan A Hodges and Ronald T Raines

Synthesis and Calcium Binding of Oligomeric Tropoelastin Analogs 474
Hiroaki Kodama, Shuhei Ueno, Satoshi Osada, Iori Maeda, Kouji Okamoto and Michio Kondo

Unique Structural Elements Profoundly Influence the Conformation of SOM230 476
Lukas Oberer, Gianluca Interlandi, Amedeo Caflisch, Günter Bovermann, Claus Ehrhardt and Ian Lewis

Venom Proteomics & Drug Discovery 478
Reto Stöcklin, Sophie Michalet, Laure Menin, Philippe Bulet, and Philippe Favreau

Fusion of Small Dimerizer Sequence at The Terminal Ends of a Linear Random Coil Peptide Induces Conformational Switch 480
Tarikere L. Gururaja, Donald G. Payan and D.C. Anderson

Conformational Conversion of Prion Proteins: Role Synthetic PRP 173-195 Fibrillogenic Peptide 482
Barbara Tizzano, Daniela Marasco, Ettore Benedetti, Antonia De Capua, Pasquale Palladino, Carlo Pedone, Giuseppe Perretta, Filomena Rossi, Raffaele Ragone and Menotti Ruvo

NMR Structure Investigation of α-MSH using TOAC Labeling 484
Renata de Freitas F. Vieira, Katya Sousa, Clóvis R. Nakaie, Shirley Schreier, Paulo M. Bisch, Fábio C. L. Almeida and Ana P. Valente

Antimicrobial and Insecticidal Effects of Crude Extract Momosertatin from *Momordica cochinchinensis* 486
Dung Le Nguyen, Annie Heitz, Laurent Chiche, Jean-François Hernandez, Thi Ha Phan and Tran Chau Pham

Effects of NOOPEPT in the Photochemically Induced Stroke Model 488
Galina A. Romanova, Tatjana A. Gudasheva, Rita U. Ostrovskaya and Fatima M. Shakova

Effect of Chain Length on Coiled-Coil Stability: Decreasing Stability with Increasing Chain Length 490
Stanley C. Kwok and Robert S. Hodges

Intracellular Signaling, Metabolism and Gene Regulation Structure-Function

Inhibition of HuPrP106-26 Aggregation in Presence of dsDNA by Peptide Libraries 495
Jaroslav Šebestík, Lenka Borovičková, Jan Hlaváček and Ivan Stibor

Development of Peptides Able to Modulate the Interaction of AKAP121 with Mitochondria 497
Michele Saviano, Laura Zaccaro, Ettore Benedetti, Carlo Pedone, Annarita del Gatto, Antonio Feliciello, Adele Affaiatati and Enrico V. Avvedimento

Synthesis of Heterodimeric Glycopeptide Hormone Containing Four Disulfide Bonds 499
H. Hojo, H. Nagasawa and Y. Nakahara

Peptidomimetic Design of Cyclic Grb2-SH2 Domain Antagonists not Relying on pTyr or its Mimics 501
Peter P. Roller, Peng Li, Manchao Zhang, Xiaodong Zhang, Ya-Qiu Long, Megan L. Peach, Marc Nicklaus, Hongpeng Liu and Dajun Yang

The Structure of a Cyclic Peptide Inhibitor of pp60$^{c\text{-}src}$ 504
K. Kaluarachchi, J.W. Rice, W. Wang and J.S. McMurray

Synthetic Approaches to the Bioactive Marine Cyclodepsipeptide Halipeptin A 506
Assunta Napolitano, Ines Bruno, Luigi Gomez-Paloma, Raffaele Riccio, Nakia Maulucci, Carmela Della Monica, Irene Izzo and Francesco De Riccardis

Toward the Synthesis of New Designed Analogues of the Marine Cyclodepsipeptide Jaspamide 508
Stefania Terracciano, Ines Bruno, Giuseppe Bifulco, Luigi Gomez-Paloma and Raffaele Riccio

Direct Translocation of Histone Molecules Across Cell Membrane 510
Elana Hariton-Gazal, Joseph Rosenbluh, Chaim Gilon and Abraham Loyter and

Peptides as A New Family of Compounds with Estrogen-Like Activity 512
Roni Kasher, Batya Gayer, Tikva Kulik, Natarajan Venkatesh, Dalia Somjen, Mati Fridkin, Ephraim Katchalski-Katzir and Fortune Kohen

Macrocyclization in the Design of Tetrapeptide Mimetics that Display Potent Inhibition of Grb2 SH2 Domain Binding in Whole Cell Systems 515
Z.-D. Shi, C.-Q. Wei, X. Wang, K. Lee, H. Liu, M. Zhang, J. Vasselli, L. R. Roberts, K. M. Worthy, M. J. Fivash, R. J. Fisher, D. P. Bottaro, W. M. Linehan, D. Yang and T. R. Burke, Jr.

Potent Grb2-SH2 Domain Antagonists Discovered by Extensive SAR Studies 518
Peng Li, Megan L. Peach, Manchao Zhang, Hongpeng Liu, Dajun Yang, Marc Nicklaus and Peter P. Roller

Protein P2 from *Haemophilus influenzae*: The Role of its Surface Exposed Loops on the Mitogen-Activated Protein Kinase Cascade 520
Stefania Galdiero, Domenica Capasso, Mariateresa Vitiello, Marina D'Isanto, Erminia Di Niola, Simona Monti, Menotti Ruvo, Carlo Pedone, and Massimiliano Galdiero

RDP58, A Rationally Designed Peptide, Inhibits Multiple Forms of Pathogenic Inflammation Through the Inhibition of p38MAPK and JNK 522
Suhasini Iyer, Ricardo Gonzalez, Jingsong Zhao, Mirella Lazarov, Ajith Welihinda, Roland Buelow, Alexis Te and Timothy Fong

Endeavors Toward a Specific Inhibitor for HDAC6 524
Tamaki Kato, Binoy Jose, Shinji Okamura, Yuko Sumida, Minoru Yoshida, and Norikazu Nishino,

The Proteome and the Metabolome - A Structural Perspective 526
Irene Nobeli and Janet M Thornton

Synthesis and Application of Large Phosphopeptides from the Linker for Activation of T Cells (LAT) Protein 534
Hiroshi Yamaguchi, Jon C.D. Houtman, Lawrence E. Samelson and Ettore Appella

Binding Interactions of Phospho-Htc Peptide to c-Fgr SH2 Domain 536
Paolo Ruzza, Alessio Osler, Silvia Del Piero, Arianna Donella-Deana, AnnaMaria Brunati, Giuliano Siligardi, Rohanah Hussain, Andrea Calderan, Andrea Guiotto, Lorenzo A. Pinna and Gianfranco Borin

Fluorescence Detection of Conformationally-Restricted Oxy-Peptide Nucleic Acids/DNA hybrids 538
Mizuki Kitamatsu, Mamoru Saito, Takashi Nakai and Masahiko Sisido

Preparation of Fluorescent and Radiolabeled Peptide-PNA Conjugates for Imaging *bcl-2* Expression 540
Fabio Gallazzi, Fang Jia, Linda A. Landon, Nalini Shenoy, Geethapriya Sivaguru, Mark Hannink, Susan Z. Lever, and Michael R. Lewis,

Solid Phase Synthesis of Tri-Peptide Derivatives of Kojic Acid Used as Tyrosinase Inhibitor 542
Hanyoung Kim, Jaehee Choi and Yoon-Sik Lee

Tripeptide Inhibitors of *Yersinia* Protein-Tyrosine Phosphatase as Potential Leads for Therapeutic Development Against Plague 544
Kyeong Lee, Sang Uk Kang, Yang Gao, Zhu-Jun Yao, Jason Phan, Li Wu, Jiao Liang, David S. Waugh, Zhong-Yin Zhang and Terrence R. Burke, Jr.

Interference with Protein-Protein Interactions in Signal Transduction 546
Frank J. Dekker, Nico J. de Mol, Marcel J.E. Fischer and Rob M.J. Liskamp

Testing and Characterizing Focused Tyrosine Kinase Inhibitory Libraries 548
Györgyi Bökönyi, Eszter Schäfer, Edit Várkondi, Edit Z. Szabó, Frigyes Wáczek, Zsolt Székelyhidi, Péter G.Bánhegyi, György Mészáros, Dániel Erős, László Őrfi, Ákos Pap, Richárd E. Schwab and György Kéri,

The Development of Peptide-Based Inhibitors of Stat3alpha 550
Zhiyong Ren, David R. Coleman, Larry A. Cabell and John S. McMurray

Novel Neutrophil-Activating Peptides: Physiological Roles of Direct Activation of GTP-Binding Regulatory Proteins by These Peptides 553
Hidehito Mukai, Yuko Matsuo, Rie Kamijo and Kaori Wakamatsu

Ribonucleopeptide Receptors 556
Masaki Hagihara, Tetsuya Hasegawa, Shin-ichi Sato, Susumu Yoshikawa, Katsutoshi Ohkubo and Takashi Morii,

Deformation of One a-Helix Leads to S-S Bond Formation of YhhP 559
Toshimasa Yamazaki, Etsuko Katoh, Shizue Katoh, Yuki Tsunoda and Takeshi Mizuno

Receptor and Ion Channel Agonist/Antagonist Structure-Function

Structure and Function Studies of a Bicyclic Agouti-Related Protein (AGRP) Melanocortin-4 Receptor Antagonist 565
Andrzej Wilczynski, Xiang S. Wang, Rayna M. Bauzo, R. Thirumoorthy, Zhimin Xiang, Arthur S. Edison, Nigel G. J. Richards and Carrie Haskell-Luevano

NMR Structure-Based Design of a-MSH Peptide Analogues 567
Jinfa Ying, Katalin E. Kövér, Xuyuan Gu, Guoxia Han, Josef Vagner, Minying Cai, Christopher M. Cabello, Chiyi Xiong, Junyi Zhang, Dev B. Trivedi, Malcolm J. Kavarana and Victor J. Hruby

Design and Synthesis of Novel Antihypertensive Drugs 569
Panagiotis Zoumpoulakis, Ioanna Kyrikou, Nektarios Giatas, Demetrios Gatos, Maria-Eleni P. Androutsou, I. Papanastasiou, Anastasia Zoga, P.M. Minakakis, G. Kokotos, Demetrios Vlahakos, Eustathios Iliodromitis and John Matsoukas

Novel Angiotensin II Lactam Bridge Cyclic Analogues 571
Vani X. Oliveira Jr., Alessandra Machado, Marcos A. Fázio, João B. Pesquero, Edson L. Santos, Cláudio M. C. Neto and Antonio Miranda

Shortcuts to Receptor Structures with Peptide Photoprobes: Angiotensin Receptors 573
Emanuel Escher, Maud Deraët, Jacqueline Pérodin, Marie-Ève Beaulieu, Lenka Rihakova, Martin Clément, Antony A. Boucard, Gaétan Guillemette, Richard Leduc and Pierre Lavigne

Synthesis and Evaluation of Substituted Benzophenone Photolabeling Amino Acids for the Methionine Proximity Assay 578
Martin Clément, Maud Deraët, Marie-Ève Beaulieu, Lenka Rihakova, Marie-Thérèse Bawolak, Gaétan Guillemette, P. Lavigne, R. Leduc and Emanuel Escher

The Name Game: Use of Words Composed of Letters of the English Alphabet as a Source of Novel Bioactive Peptides 580
David Wade

Beta-Methyl Substitution of the Cha Residue in Dmt-Tic-Cha-Phe Peptides Provides Highly Potent Delta Antagonists 582
Dirk Tourwe, Geza Toth, Gunter Carlens, Csaba Tomboly, Antal Péter, and Peter W Schiller

BKM-570 and Its New Acyl-Amino Acid Amide Analogs for Lung and Prostate Cancer 584
Lajos Gera, Daniel C. Chan, Eunice J. York, V. Simkeviciene, Adomas Vagonis, D. Bironaite, P. A. Bunn, Jr., Laimute Taraseviciene-Stewart and John M. Stewart,

Identification of a Direct Interaction Between Calcitonin Peptide and its Receptor 586
Vi Pham, John D. Wade, Brooke W. Purdue and Patrick M. Sexton

A Cyclic and Branched Peptide as a New Selective Ligand for the CCK_A Receptor 588
Ettore Benedetti, Giancarlo Morelli, Raffaella Della Moglie, Stefania De Luca, Michele Saviano and Luigi Aloj

Interhelical Side Chain-Side Chain Hydrogen Bonds in Membranes: Capture Potential of Aspartic Acid vs. Glutamic Acid 590
Charles M. Deber, Mei Y. Choi, and Lia Cardarelli

A Simplified Model of the Interaction Between SDF-1 Chemokine and the CXCR4 Receptor 597
Pasquale Palladino, Antonia De Capua, Carlo Pedone, Raffaele Ragone, Filomena Rossi, Cristina Limatola, Davide Ragozzino and Ettore Benedetti

Synthetic Unnatural Chemokines: Probes of Receptor-Ligand Interactions and Inhibitors of HIV-1 Entry 599
Ziwei Huang, Santhosh Kumar, Chang-Zhi Dong, Dongxiang Liu, Shaomin Tian, Won-Tak Choi, Youli Wang, Vitaly Stepensky, Ying Li, Jing An, Navid Madani, Mark Cayabyab and Joseph G Sodroski

Enhanced Hepatic Clearance of Plasma Cholesterol and Inhibition of Atherosclerosis by an Apolipoprotein E-mimetic Peptide 601
David W. Garber, Himanshu Gupta, Shaila Handattu, Geeta Datta, Manjula Chaddha, M. N. Palgunachari, C. Roger White and G. M. Anantharamaiah

Development of CRF-R2 Selective Peptide Ligands 604
Doreen Wietfeld, Angelika Ehrlich, Reinhard Seifert, Klaus Fechner, Eberhard Krause, Michael Bienert and Michael Beyermann

Discovery of a Novel CXCR4 Antagonist Using Two Orthogonal Cyclic Peptide Libraries 606
Shinya Oishi, Ayumu Niida, Kenichi Hiramatsu, Satoshi Ueda, Takanobu Araki, Hirokazu Tamamura, Akira Otaka, Shuichi Kusano, Shigemi Terakubo, Hideki Nakashima, Zi-xuan Wang, Stephen C. Peiper and Nobutaka Fujii

Design, Synthesis and Pharmacological Evaluation of Potential CXCR4 Chemokine Antagonist Peptides on Breast Cancer Cells 609
Xin Wang, Yan Wang, J.-P. Perchellet and Sandra C. Vigil-Cruz

Synthesis of Branched Cyclic Peptide Analogs of Angiotensin II 611
Yuan Gao, Yun Wu, Wei-Jun Zhang and Garland R. Marshall

QSAR Analysis of Ring-Substituted Tyrosine Replacements at the N-Terminus of a Nonselective Deltorphin Analog 613
Deborah L. Heyl, Kutralanathan Renganathan, Malika N. Jayamaha, David W. Rodgers and Stephen E. Schullery

New Paradigm For Drug Design: Overlapping Pharmacophores of Opioid And Cholecystokinin Ligands In The Design Of New Compounds For The Treatment Of Neuropathic Pain 615
Richard S. Agnes, Yeon S. Lee, Shou W. Ma, Peg Davis, Todd Vanderah, Jinfa Ying, Katalin Kövér, Josephine Lai, Frank Porreca and Victor J. Hruby

A New Series of Endothelin Receptor Antagonists 617
Ke-Liang Liu, Jun-Jun Dong, Bo Geng, Yuan-Jun Liang, Han Han Ping Wu, Mu-Gen Chi and Ze-Hui Gong

An Unexpected Modification of Histidine During the Preparation of Ghrelin 619
David L. Smiley, Steven Afendis, Melvin G. Johnson, Joseph V. Manetta, Xiliang Wang, Derrick R. Witcher and Lianshan Zhang

Misfolded Therapeutic Peptides Give Rise To Caspase-Mediated Cytotoxicity 621
Satomi Onoue, Keiichi Ohshima, Kazuhiro Debari, Keitatsu Koh, Takehiko Yajima and Kazuhisa Kashimoto

Long Acting Peptide (LAP^{TM}) Analogues of Glucagon-Like Peptide-1 623
Abdelkrim Habi, Daniel Abran, Krishna G. Peri, Patricia Brubaker and Thierry Abribat

Design and Synthesis of Novel GLP-1 Analogs that have Significantly Improved *In Vivo* Activities 625
Jesse Z. Dong, Yeelana Shen, Jundong Zhang, John E. Taylor, Chee-Wai Woon, Barry Morgan, S. Skinner, M. Cawthorne, M. Culler and Jacques-Pierre Moreau

The Role of Residues 5-8 of Lamprey Gonadotropin-Releasing Hormone III in the Inhibition of Cancer Cell Growth 628
Krisztina Herédi-Szabó, Jeremiah Lubke, Richard F. Murphy and Sándor Lovas

Native Chemical Ligation of Transmembrane Receptor Fragments of Ste2p 630
Vommina V. Suresh Babu, Jeffrey M. Becker and Fred Naider

Development of Highly Potent and Selective Low Molecular Weight Agonists for the Human Orphan Receptor BRS-3 632
Horst Kessler, Dirk Weber and Jochen Antel

Synthesis and Cross-Linking of Photoactivateable Biotinylated Ligands of G Protein-Coupled Receptors 635
Hasmik Sargsyan, Cagdas D. Son, Jeffrey M. Becker and Fred Naider

Cyclic Melanocortin-4 Receptor Ligands: Conformational Analysis Using 1H-NMR Spectroscopic Methodologies 637
Jerry Ryan Holder, Arthur S. Edison, Zhimin Xiang, Joseph W. Scott and Carrie Haskell-Luevano

Stereochemical Inversion Studies of Monocyclic hAGRP(103-122) Peptide 639
Christine G. Joseph, Xiang S. Wang, Joseph W. Scott, Rayna Bauzo, Zhimin Xiang, Nigel G. Richards and Carrie Haskell-Luevano

Long Chain Fatty Acid (LCFA) N-Acyl Derivatives of Melanocortin X-His-DPhe-Arg-Trp-NH2 Tetrapeptides: Potency and Selectivity Alteration at mMCR System 641
Aleksandar Todorovic, Jerry R. Holder, Rayna M. Bauzo, Joseph W. Scott and Carrie Haskell-Luevano

Structurally Related Peptides, Peptoids, and Peptide-Peptoid Hybrids: Comparison of Agonist Activity at the Melanocortin MC4 Receptor 643
Jerry Ryan Holder, Rayna M. Bauzo, Joseph W. Scott, Zhimin Xiang and Carrie Haskell-Luevano

A Novel AGRP-Melanocortin Peptide Chimeric Library 645
Krista R. Wilson, Andrzej M. Wilczynski, Joseph W. Scott, Rayna M. Bauzo and Carrie Haskell-Luevano

Structural Requirements for the Human MC4 Receptor Selectivity of Novel Cyclic MT-II Analogues 647
Alexander V. Mayorov, So-Yeop Han, Matthew R. Hammer, Minying Cai, Dev Trivedi and Victor J. Hruby

Novel Ligands for Human Melanocortin Receptor Subtypes: Design, Synthesis and Structure-Activity Relationships 649
Magda Stankova, Minying Cai, Chris Cabello, Bridgette DeCot, Victor Krchnak Jr. and Victor J. Hruby

Novel α-MSH/γ-MSH Hybrid Analogues that Lead to Selective Ligands for the Human MC1R and Human MC3R 651
Minying Cai, Magda Stankova, Christopher Cabello, Bridgette Decot, Alexander Mayorov, Dev Trivedi, and Victor J. Hruby

Synthesis and Evaluation of Leu-Enkephalin Analogues Containing Substituted b-Turn Bicyclic Dipeptide Mimetics 653
Chiyi Xiong, Junyi Zhang, Jinfa Ying and Victor J. Hruby

Using Diverse Topographical and Conformational Privileged Structures to Explore Selectivity in Melanocortin Receptors 655
Victor J. Hruby, Preeti Balse-Srinivasan, Paolo Grieco, Guoxia Han, Minying Cai, Dev Trivedi, Alexander Mayorov, Jinfa Ying and Magda Stankova

Studies on Synthetic Analogs of the TM VI Segment of the MT1 Melatonin Receptor 657
Andrea Calderan, Paolo Ruzza, Barbara Biondi, Andrea Guiotto, Alessio Osler and Gianfranco Borin

Opioid Peptide Analogues: Conformation and Pharmacological Properties of Synthetic Dermorphin and Deltorphin 1 Peptide-Peptoid Hybrids 659
Laura Biondi, Elisa Giannini, Fernando Filira, Marina Gobbo, Mauro Marastoni, Lucia Negri, Barbara Scolaro, Roberto Tomatis and Raniero Rocchi

A Potent Cyclic Opioid Peptide Antagonist Lacking an N-terminal Amino Group 661
Grazyna Weltrowska, Yixin Lu, Carole Lemieux, Nga N. Chung and Peter W. Schiller

Dimerization of NPY-Receptors by Fluorescence Resonance Energy Transfer (FRET) in Living Cells 663
Annette G. Beck-Sickinger, Michaela Dinger, Robert Rennert, Ilka Böhme and Karin Mörl

Replacement of the Tic Residue by Benzo-1,2,3,4-Tetrahydroisoquinoline-3-Carboxylic Acids in TIPP Peptides 665
Sylvia Van Cauwenberghe, José Martins, Mylene Gosselin, Lejla Hodzic, Sylvain Caron, Joanne Butterworth and Dirk Tourwé

Synthesis, Purification, and Stabilization of a Myc/His Epitope Tagged Human d Opioid Receptor 667
Scott M. Cowell, Isabel Alves, Eva Varga, Tadashi Okura, Padma Nair, Henry I. Yamamura and Victor J. Hruby

Potent Antinociceptive Activity by a Novel Opioid, 3-(3'-Dmt-aminopropyl)-6-(4'-Dmt-aminobutyl)-5-methyl-2(1*H*)-pyrazinone 669
Yunden Jinsmaa, Yoshio Okada, Yuko Tsuda, Yusuke Sasaki, Akihio Ambo, Sharon D. Bryant and Lawrence H. Lazarus

ORL1 Receptor Agonists and Antagonists 671
A.K. Judd, D.J. Tuttle, A. Kaushanskaya, R.W. Jones, A. Sanchez, W. Polgar, T. Khroyan and L. Toll

Bioactive N-terminal Undecapeptides Derived from Parathyroid Hormone: The Role of a-helicity 673
Alessandra Barazza, Nereo Fiori, Elisabetta Schievano, Stefano Mammi, Evaristo Peggion, Joseph M. Alexander, Michael Rosenblatt and Michael Chorev

Carboxy Terminal Modifications of PTH-(1-34) that Confer Skin Protease Resistance and Retain Biological Potency 675
Krishna G. Peri, Annie Bergeron, Thuy Lam, Kim High and Thierry Abribat

Synthesis of Conformationally Constrained PTH(1-14) Analogs 677
Ashok Khatri, Xiang-Chen Huang, Naoto Shimizu, and Thomas J. Gardella

Interactions of the Mid-Region of Parathyroid Hormone (1-34) with the Receptor Orient the Hormone for Receptor Activation 679
Angela Wittelsberger, Martina Corich, Byung-Kwon Lee, Alessandra Barazza, Dale F. Mierke, Michael Rosenblatt, and Michael Chorev

Hydrazide Linked Bifunctional Peptides for the Treatment of Pain 682
Yeon Sun Lee, Richard S. Agnes, Peg Davis, Shou-wu Ma, Josephine Lai, Frank Porreca and Victor J. Hruby

Assembly of High-Affinity Insulin Agonists and Antagonists from Peptide Building Blocks 684
Lauge Schäffer, Søren Østergaard, Jane C. Spetzler, Thomas Hoeg-Jensen, Jakob Brandt, Gillian M. Danielsen, Renuka C. Pillutla, Renee E. Brissette, Ulla Ribel, Asser S. Andersen and Neil I. Goldstein

Restoring a Functionally Important Loop in MAdCAM-1, the Primary Ligand of a_4b_7 Integrins 687
Gregory V. Nikiforovich and Garland R. Marshall

Synthesis of Membrane Active Peptides with a b-Helical Structure 689
Jyothi Thundimadathil, Lili Guo and Roger W. Roeske

Structure-Activity Relationships of a Novel Cyclic Dynorphin A Analog with Kappa Opioid Receptor Antagonist Activity 691
Matthew W. Leighty, Thomas F. Murray and Jane V. Aldrich

Multimeric Cyclic RGD Peptides with Improved Tumor Uptake for Tumor Targeting 693
G. Thumshirn, U. Hersel, T. Poethko, F. Rau, R. Haubner,M. Schwaiger, H.-J. Wester and H. Kessler

Conformational Study of Na^+ Channel Inactivation Gate Peptides Interacting with Local Anesthetic Diphenyl Drugs Using NMR and Molecular Modeling 695
Bih-Show Lou, Ta-Hsien Lin and Chi-Zen Lou

Comparative Conformational Analysis of Neurokinin B and Selective NK3 Receptor Agonist. 698
Gulshen A Agaeva

Novel PACAP Analogs that Selectively Bind to PACAP-I Receptor 700
Jesse Z. Dong, Yeelana Shen, John E. Taylor, Michael Culler and Jacques-Pierre Moreau

N-Methylated Analogs of the Receptor-Binding Region of Human Parathyroid Hormone (hPTH) 702
Jean-René Barbier, Susanne MacLean, James F Whitfield and Gordon E Willick

Are Neuropeptides of the NPY Family Recognized from the Membrane-Bound State? 704
M. Lerch, R. Bader and O. Zerbe

Chemical Synthesis of a Membrane Protein 707
Takeshi Sato, Yasuhiro Saito and Saburo Aimoto

Effect of RGD Peptides in *In Vivo* Model for Diabetic Retinopathy 709
Ralph-Heiko Mattern, Sergio Caballero, Amanda Omlor, Juerg F. Tschopp, Michael D. Pierschbacher and Maria B. Grant

Synthesis of Unusual RGD Cyclic Peptides Incorporating C $^{\alpha}$-Fluoromethylamino Acids, as Selective Inhibitors of $\alpha_v\beta_3$ Integrin 711
Alma DalPozzo, Minghong Ni and Laura Muzi

Plasmon Waveguide-Resonance Spectroscopy: A New Method to Study GPCR Signal Transduction 713
Isabel D. Alves, Zdzislaw Salamon, Gordon Tollin, and Victor J. Hruby

Novel, Potent, ORL-1 Receptor Agonist Peptides Containing a-Helix Promoting Conformational Constraints 715
Chongwu Zhang, Paul R. Blake, Shen Shan, K. J. Valenzano and Donald J. Kyle

Synthesis and Pharmacological Activity of Novel Peptide Ligands for the NOP Receptor 717
Severo Salvadori, Remo Guerrini, Marina Zucchini, Giacomo Carrà, Daniela Rizzi, Domenico Regoli and Girolamo Calo

The Peptide Complementarity 719
Renata Zbozien-Pacamaj, Piotr Stefanowicz, Alicja Kluczyk, Marek Cebrat, Marek Lisowski and Ignacy Z. Siemion

The Superior Therapeutic Potential of SOM230 Originates from Unique Structural Elements 721
Ian Lewis, Wilfried Bauer, Rainer Albert, Nagarajan Chandramouli, Janos Pless, Gisbert Weckbecker and Christian Bruns

Sst_4-selectivity is Induced by L-Configuration at Position 8 in Somatostatin (SRIF) Octapeptides 723
Judit Erchegyi, Sandra Wenger, Beatrice Waser, Jean-Claude Schaer, Renzo Cescato, Christy R.R. Grace, Carl Hoeger, Steven C. Koerber, Roland Riek, Jean Claude Reubi and Jean E. Rivier

Design of Oxytocin Antagonists that are Strikingly more Potent and Selective in Human Receptor Assays than Atosiban 725
LingLing Cheng, Stoytcho Stoev, Maurice Manning, Nga C. Wo, W.Y. Chan, Hazel H. Szeto, Thierry Durroux, Bernard Mouillac and Claude Barberis

Design, Synthesis and Analysis of Single Chain Mimetics of Relaxin and Relaxin-Like Factor (INSL3) 727
Mark P. Del Borgo, Richard A. Hughes and John D. Wade

Relaxin 3, a Novel Member of the Insulin Superfamily of Peptide Hormones 729
Ross A. Bathgate, Nicky F. Hanson, Feng Lin, Geoffrey W. Tregear and John D. Wade

Non-Peptidic RGD Mimetics for Stimulated Cell Adhesion on Biomaterials 732
C. Dahmen, A. Meyer, B. Jeschke, A. Enderle, S. L. Goodman, B. Nies and H. Kessler

Using Plasmon Waveguide Resonance (PWR) Spectroscopy to Directly Examine the Effects of Ligands on G-Protein Binding to Delta Opioid Receptors 734
Victor J. Hruby, Isabel Alves, Zdzislaw Salamon and Gordon Tollin

Silylated Amino Acid Containing Substance P Analogues 737
F. Cavelier, D. Marchand, J. Martinez, S. Lavielle and S. Sagan

Synthesis and Pharmacological Activity of Human Urotensin II Analogues Modified in Position 8 740
Remo Guerrini, Girolamo Calo, Marina Zucchini, Valeria Camarda, Domenico Regoli and Severo Salvadori

Mapping the N-terminal Contact of Urotensin II with its Receptor Using Peptide Photoprobes 742
Brian J. Holleran, Antony A. Boucard, Adrian Häberli, Klaus Klarskov, Richard Leduc and Emanuel Escher

3D Structural Analysis of Urotensin-II Analogues in Membrane Mimetic Environment 744
Alfonso Carotenuto, Paolo Grieco, Pietro Campiglia, Ettore Novellino and Paolo Rovero

Development of New Urotensin-II Receptor Ligands 746
Pietro Campiglia, Alfonso Carotenuto, Riccardo Patacchini, Carlo A. Maggi, Ettore Novellino, Paolo Rovero and Paolo Grieco

Molecular Modeling of the Urotensin-II Receptor Complex 748
Paolo Grieco, Antonio Lavecchia, Pietro Campiglia, Teresa Lama, Paolo Rovero, Alfonso Carotenuto, Riccardo Patacchini, Carlo A. Maggi and Ettore Novellino

Structure-Activity Relationship and Bioactive Conformation of Prolactin Releasing Peptides (PrRPs), Ligand for a Potential Obesity Target 750
Waleed Danho, Joseph Swistok, Wajiha Khan, Theresa Truitt, Grazyna Kurylko, David Fry, David Greeley, Hongmao Sun, Mark Dvorozniak, Garry Mackie, Cheryl Spence and Robert Goodnow, Jr.

Synthesis and Conformational Behavior of the First Extracellular Loop Peptide of a GPCR 752
Sanjay K. Khare, Boris Arshava, Jeffery M. Becker and Fred R. Naider

Biosynthesis of the Sixth Transmembrane Domain of the S*accharomyces cerevisiae* a-Factor Receptor 754
Racha Estephan, Enrique Arevalo, Jeffrey M. Becker and Fred Naider

Studies on the Cross-reactivity of Synthetic Oxytocin Receptors Prepared by Molecular Imprinting 756
Maria Kempe

Does a p-Cation Interaction Stabilize the Rhodopsin-Bound Conformation of Transducin's Alpha-Subunit? 758
Matthew A. Anderson, Rieko Arimoto, Wei Sha and Garland R. Marshall

Novel Peptide Therapeutic Approaches For Immune Tolerance 760
Stephanie D. Allen, Heike Bernert, Sharad V. Rawale, Anne M. VanBuskirk and Pravin T.P. Kaumaya

Protein Aggregation Substrate/Inhibitor Structure-Function

Primary–Quaternary Structure Relationships Controlling Early Ab Oligomerization 765
Gal Bitan, Marina D. Kirkitadze, Hilal A. Lashuel, Sabrina S. Vollers and David B. Teplow

Conversion of a Natively Amyloidogenic Sequence into an Inhibitor of Amyloid Formation and Cytotoxicity Via Conformational Restriction 768
Aphrodite Kapurniotu, Andreas Buck, Marco Weber, Anke Schmauder, Thomas Hirsch, Jürgen Bernhagen and Marianna Tatarek-Nossol

Cu (II) Interaction with Amylin's Peptide Fragments 771
Angela Amoresano, Angela Flagiello, Giuseppe Impellizzeri, Antonio Magrì, Giuseppe Pappalardo, Piero Pucci and Enrico Rizzarelli,

Inhibition of Amyloid Formation of Human Amylin 773
Dirk T.S. Rijkers, Jo W.M. Höppener, George Posthuma, Cornelis J.M. Lips and Rob M.J. Liskamp

Modulation of b-Amyloid 1-42 Aggregation by Other Aggregating Peptides 775
Lukasz P Frankiewicz and Aleksandra Misicka

Inhibition of β-Amyloid Aggregation with $C^{\alpha,\alpha}$Disubstituted Amino Acid Containing Peptides 777
Marcus A. Etienne, Jed P. Aucoin, Yanwen Fu, Robin L. McCarley and Robert P. Hammer

Amyloid-Like Fibrils of Laminin-1 Peptides 779
Motoyoshi Nomizu, Shingo Kasai, Yukiko Ohga, Mayumi Mochizuki, Masanori, Yamada, Yuichi Kadoya and Norio Nishi

Mass Spectrometric Elucidation of an Amyloid Plaque-specific Epitope: Molecular Basis for Probing the Proteolytic Mechanism of Alzheimer's Amyloid Precursor Protein 782
Michael Przybylski, Roxana Cecal, Xiaodan Tian , JoAnne McLaurin , Marilena Manea , Raluca Stefanescu and Peter St.George-Hyslop

Expression of a Synthetic Gene Encoding Human Transthyretin in *Escherichia coli* 785
Kimiaki Matsubara, Mineyuki Mizuguchi and Keiichi Kawano

Peptide Drug Delivery, Targeting And Biomaterials

Interactions between Lipid Bilayer and pH-Triggered Amphiphilic Peptides 789
Hsienming Lee and Jean Chmielewski

Application of Oligoarginine for the Delivery of Protein Complexes into Living Cells 791
Shiroh Futaki, Ikuhiko Nakase, Miki Niwa, Tomoki Suzuki, Daisuke Nameki, Ei-ichi Kodama, Masao Matsuoka and Yukio Sugiura

In Silico Investigation of LogP Parameters of Amino Acids and Peptides Tethered to C-Alkylated Sugar Bioconjugates 793
Piotr A Mroz, Florence M. Brunel, K. Grant Taylor and Arno F. Spatola

Are Alkylated C-Sugars Useful as Solubility Buffers? 795
Florence M. Brunel, Amit K. Galande, Piotr A. Mroz, K. Grant Taylor and Arno F. Spatola

Conformation and Bioactive Properties of Novel Osteoblast-Adhesive Peptides for Biomaterial Design 797
Manuela Vacatello, Gabriella D'Auria, Lucia Falcigno, Romina Oliva, Carmen Bevilacqua, Monica Dettin, Maria T. Conconi, Roberta Gambaretto, Carlo Di Bello and Livio Paolillo

Evolutionary Combinatorial Chemistry, a Novel Tool for SAR Studies on Peptide Transport across the Blood-Brain Barrier 1. Design, *In Silico* Validation and First Peptide Generation 800
Meritxell Teixidó, Ignasi Belda, Sonia González, Míriam Fabre, Senén Vilaró, Josep M. Garrell, Xavier Roselló, Fernando Albericio, and Ernest Giralt,

Structural Requirements for Non-Covalent Peptide-Mediated Cellular Delivery of siRNAs 802
Sébastien Deshayes, Nicole Van Mau, May C. Morris, Gilles Divita and Frédéric Heitz

Development of Bioavailable Water-Soluble Prodrugs of Peptidomimetics: Importance of the Conversion Time for Higher Gastrointestinal Absorption of Prodrugs based on Spontaneous Chemical Cleavage 805
Youhei Sohma, Yoshio Hayashi, Tomoko Ito, Hikaru Matsumoto, Tooru Kimura and Yoshiaki Kiso

Cyclic RGD-Peptides with Acidic-Anchors for Stimulated Cell Adhesion on Biomaterials 807
Jörg Auernheimer, Ulrich Hersel, Claudia Dahmen, Martin Kantlehner, Brigitte Jeschke, Anja Enderle, Berthold Nies, Simon L. Goodman and H. Kessler

Lipid and Carbohydrate Based Macromolecules in Drug and Vaccine Delivery 809
Istvan Toth, Aniko Horvath, Joanne Blanchfield, Colleen Olive, Michael Good, Norbert Wimmer and P. Elizabeth Rakoczy

Liposaccharides in Peptide Drug Delivery 811
Joanne Blanchfield, O. Paul Gallagher, Yasuko Koda, Paul Alewood, Richard Lewis and Istvan Toth

In Vivo Pharmacokinetic and Metabolic Studies of Peptide Drugs by MS and MS/MS 813
Reto Stöcklin, Philippe Favreau, Laure Menin, Philippe Bulet and Sophie Michalet

Peptide Targeting of Daunomycin into Sensitive and Multidrug Resistant Tumors 815
Ferenc Hudecz, Judit Reményi, Tamás Hegedűs, Péter Kovács, Barbara Szabó, Balázs Sarkadi and Dezső Gaál

Characterization of Multicomponent Aggregate Containing a Bioactive Peptide and a Gd Complex 818
Antonella Accardo, Diego Tesauro, Paola Roscigno, Luigi Paduano, Eliana Gianolio, Giancarlo Morelli and Ettore Benedetti

Synthesis and Application of Functional Peptides for the Therapy of HPV Type 18 Positive Cervix Cancer Cells 820
Rüdiger Pipkorn, Klaus Braun, Waldemar Waldeck, Mario Koch and Jürgen Debus

Tat Peptide-Mediated Vectorization Of Nucleic Acids 822
Eric Vivès, Thibault Michel, Françoise Debart, Jean-Philippe Richard, Kamran Melikov, Leonid Chernomordik, Jean-JacquesVasseur and Bernard Lebleu

Peptide Combinatorial Libraries, Proteomics And Screening Methods

A Reassessment of the Role of Cys^8 in Annexin A2-tPA Interaction 827
Oriol Roda, Mari-Luz Valero, Cristina Chiva, Sandra Peiró, Francisco X. Real, Pilar Navarro and David Andreu

Application of Topologically Segregated Bifunctional Beads to Construct Unique Combinatorial Bead Libraries 829
Xiaobing Wang, Li Peng, Ruiwu Liu and Kit S. Lam

Minimalism Applied To A Hit To Lead Program 831
Marc Vendrell, Rubén Ventura, Fernando Albericio, Rosario González-Muñiz, Laura García de Diego, Cristina Carreño, A. Ferrer-Montiel, and Miriam Royo

Is it Possible to Minimize the Toxicity of a Hit Compound Without Reducing its Activity? 833
Rubén Ventura, Marc Vendrell, Fernando Albericio, Rosario González-Muñiz, Laura de Diego, Cristina Carreño, Antonio Ferrer-Montiel, and Miriam Royo

The Combined Solid and Solution-Phase Synthesis of Small Molecular Libraries: The Evolution of the "Libraries from Libraries" Concept 835
Yongping Yu, John M. Ostresh and Richard A. Houghten

Combinatorial Neoglycopeptide Arrays for the Study of Peptide Resistance to Proteolysis 837
Michael R. Carrasco, Matthew D. Bernardina, Ryan T. Brown and Katherine A. Rawls

Solid-Phase Synthesis of 1,3,4-Thiadiazolium-2-Aminides 839
Joseph C. Kappel, T. Scott Yokum and George Barany

Synthesis, Folding and Deconvolution of Combinatorial Peptide Libraries Based on a-Conotoxins: Generation of a Novel Ligand for α7 Nicotinic Acetylcholine Receptors 841
M. Ellison, J. Nielsen, B. Green, P. Buczek, M.J. McIntosh, B.M. Olivera and G. Bulaj

A Novel Encoding Method for "One-Bead One-Compound" Peptidomimetic and Small Molecule Combinatorial Libraries 843
Aimin Song, Jinhua Zhang, Carlito B. Lebrilla and Kit S. Lam

Characterizations of Peptides That Selectively Bind Neuroendocrine Differentiated Prostate Cancer Cells 845
Amanda M Enstrom and Kit S Lam

Increasing Diversity of One-bead One-compound Combinatorial Peptide Libraries Using Side-chain Derivatization 847
Ruiwu Liu and Kit S. Lam

A Novel Encoded High-Density Chemical Microarray Platform for Proteomics and Drug Development 849
Jan Marik, Qingchai Xu, Xiaobing Wang, Li Peng and Kit S. Lam

Highly Flexible Assembly of Large Peptide Arrays Using a Novel Fully Automated SPOT-Robot 854
Johannes Zerweck, Thomas Ast, Stefan Guffler, Karsten Schnatbaum and Holger Wenschuh

Peptide Libraries as a Tool for Studying Proteolytic Enzymes 856
Benjamin E. Turk and Lewis C. Cantley

Novel Tools And Applications In Parallel Peptides Synthesis 864
O.J. Kreuzer, M. Birringer, K. Zarse, J. Henkel, F. Bier, M. Thürkand W. Zinsser

Design, Synthesis, and Study of Peptides Able to Recognize Hydrophilic Protein-Surface Patches 866
Marc Martinell, Xavier Salvatella, Ignasi Belda, Xavier Llorà, Jose J. Pastor, Marta Vilaseca, Margarida Gairí and Ernest Giralt

Chirality-Based Isotope Labeling in Library of Substrates (CHILLS) to Screen for Enzyme Preference by Mass Spectrometry 869
Laszlo Prokai, Stanley M. Stevens, Jr. and Katalin Prokai-Tatrai

Peptide Antibiotic, Anticancer, Antiviral and Antifungal Structure-Function

Membrane Binding and Antibacterial Activity of Cecropin-Mellitin Hybrid Peptides 873
Kalpana Bhargava and Jimmy B Feix

Interaction of Cationic Antimicrobial Peptides with Vesicles Mimicking the Outer Membrane of Gram-Negative Bacteria 875
Marina Gobbo, Laura Biondi, Fernando Filira, and Raniero Rocchi

Structure-Function Studies of Antimicrobial and Endotoxin Neutralizing Peptides 877
Sylvie E. Blondelle, Roman Jerala, Marta Lamata, Ignacio Moriyon, Klaus Brandenburg, Jörg Andrä, Massimo Porro and Karl Lohner

Fluorescent Analogs of Trichogin GA IV: A New Insight into the Mechanism of Membrane Permeabilization 879
Basilio Pispisa, Emanuela Gatto, Claudia Mazzuca, Antonio Palleschi, Lorenzo Stella, Mariano Venanzi, Fernando Formaggio and Claudio Toniolo

SAPD: Synthetic Antibiotic Peptides Database 881
David Wade and Jukka Englund

Generation of Novel Vancomycin–Type Glycopeptide Antibiotics by Mutasynthesis 883
Stefan Weist, Bojan Bister, Oliver Puk, Daniel Bischoff, Stefan Pelzer, Wolfgang Wohlleben and Roderich D. Süssmuth

Solution Structure of an Antifungal Peptide, Scarabaecin, from the Rhinoceros Beetle 886
Hikaru Hemmi, Jun Ishibashi, Tetsuya Tomie and Minoru Yamakawa

Small Analogues of Lysozyme with Antibacterial Properties 888
Xavier Doisy, Dan Ifrah, Trine S. Neerup and Paul R. Hansen

Effects of Glycine and Alanine Substitutions on Activity and Selectivity in Amphipathic β-Sheet Antimicrobial Peptides 890
Jack Blazyk, Yi Jin, Janet Hammer, Michelle Pate, Adam Bobbey, Jessica Mellinger and Erik Zmuda

Structure of Horseshoe Crab Antimicrobial Peptide, Tachyplesin I in Dodecylphosphocholine Micelles 892
Mineyuki Mizuguchi, Shinichi Kamata, Shun-ichiro Kawabata and Keiichi Kawano

From Innate Immunity to *De Novo* Designed Antimicrobial and Anticancer Diastereomeric Peptides 895
Yechiel Shai

Putative Intracellular Targets of the PR-rich Antimicrobial Peptide Bac7 900
Elena Podda, Marco Scocchi, Giuseppina Mignogna, Donatella Barra, Fulvio Micali, Andrea Mazzoli and Renato Gennaro

Pyrularia pubera Thionin: a Single Residue Mutation Enhances Antimicrobial Activity 902
Miquel Vila-Perelló, Andrea Sánchez-Vallet, Antonio Molina and David Andreu

Development of Orally Active Antibacterial Peptide Derivatives That Kill Resistant Urinary and Respiratory Tract Pathogens 904
Laszlo Otvos, Jr., Daniel J. Weiner, David E. Johnson and Mare Cudic,

Super Adhesive Peptides and Bacterial Adhesion 907
Yanlei Liu, Kit S. Lam, Xiaobing Wang, Ruiwu Liu, Frank Ventimiglia, and Joseph W. Leung

The Anti-HIV-1 Activity of Cyclic a-Defensins is Not Affected by Deleting Cystine 909
Hua Li, Qitao Yu, Jin-Long Yang and James P. Tam

Identification of T-Cell Epitopes Using SPOT-Synthesized Peptides 911
Mathias Streitz , Bernhard Aÿ , Florian Kern and Rudolf Volkmer-Engert

Approaches to the Reconstruction of a Discontinuous Binding Site 913
Judit Villén, Ricard A. Rodríguez-Mias, Ernest Giralt, Francisco Sobrino, and David Andreu

Inhibition of Antimicrobial Peptides by Exopolysaccharides of Lung Pathogens 915
Monica Benincasa, Maura Mattiuzzo, Yury Herasimenka, Paola Cescutti, Roberto Rizzo and Renato Gennaro

Structural Study of the HIV-1 gp160 Cleavage Site by Native and Modified Sequences: Role of Site Specific Mutations 917
Lucia Falcigno, Romina Oliva, Gabriella D'Auria, Massimiliano Maletta, Manuela Vacatello, Monica Dettin, A. Pasquato, Carlo Di Bello and Livio Paolillo

Structural Investigation of the HIV-1 Envelope Glycoprotein gp160 Cleavage Site: Solution Conformation of a 41-mer Peptide 919
Romina Oliva, Lucia Falcigno, Gabriella D'Auria, Diego Gargiulo, Monica Dettin, Antonella Pasquato, Carlo Di Bello and Livio Paolillo

Dendrimeric e-Peptides: A Novel Design of Antimicrobials 922
Qitao Yu, Chengwei Wu, Jin-Long Yang and James P. Tam

Membrane Permeable e-Peptides 924
Khee Dong Eom, Jin-Long Yang and James P. Tam

Structure-Activity Relationship Study of the Fragment 33-61 of a-Chain Bovine Hemoglobin 926
Alessandra Machado, Maurício L. Sforça, Sirlei Daffre, Antonio Miranda, Alberto Spisni, Thelma A. Pertinhez and M. Terêsa M. Miranda

Conformational Studies of Gomesin Analogues 928
Marcos A. Fázio, Sirlei Daffre, M. Terêsa M. Miranda and Antonio Miranda

Small l- and d-Amino Acid Peptides Antagonize HIV-1 Replication 930
César Boggiano and Sylvie E. Blondelle

Structure-function Relationship of Peptide Analogues of Gaegurin 4, an Antimicrobial Peptide Isolated from a Korean Frog 933
Hyung-Sik Won and Bong-Jin Lee

Fragments of HIV GAG Polyproteins Expressing Affinity to Opioid Receptors 935
Andrzej W. Lipkowski, Piotr Kosson, Aleksandra Misicka, Daniel B. Carr, Victor J. Hruby, Masaaki Yoshikawa, Fanni Toth and Geza Toth

Dimeric Analogs of The Immunosuppressory Fragment of HLA-DR 938
Zbigniew Szewczuk, Monika Biernat, Marcin Dyba and Michal Zimecki

Indolicidin Analogs with Potent Antibacterial Activity 940
Trine S. Neerup, Xavier Doisy, Dan Ifrah and Paul R. Hansen

MS PepKit: The First Diagnostic Test to Follow-up Multiple Sclerosis 942
Anna M. Papini, Barbara Mulinacci, Alfonso Carotenuto, Bruno Bonetti, Giuseppina Sabatino, Elisa Peroni, Francesca Nuti, Maria C. Alcaro, Maria C. Pozo-Carrero, Benedetta Mazzanti, Marta Pazzagli, Luca Massacesi, Luca Battistini, Mario Chelli, Paolo Rovero and Francesco Lolli

Structural Studies and Sequence Homology Investigations of the Guinea Pig Myelin Basic Protein (MBP) Epitope 74-85 Analogues 945
Andreas G. Tzakos, Patrick Fuchs, Nico A.J. van Nuland, Anastasios Troganis, Theodore Tselios, Spyros Deraos, George Deraos, Dimitrios Gatos, Ioannis P. Gerothanassis, Alexandre M.J.J. Bonvin and John Matsoukas

Peptide Strategies for Suppression of EAE 947
Stephanie D. Allen, Sharad V. Rawale, Caroline C. Whitacre and Pravin T.P. Kaumaya

The Temporin/VesCP (T/V)-Like Family of Bioactive Peptides 949
David Wade

Tissue Specific Peptide Pools: Fine Tuning of Cell Proliferation Rate in Cell Cultures and Tissues 952
Olga V. Sazonova, ElenaYu. Blishchenko, Konstantin V. Leontiev, S. V. Khaidukov, Evgeny I. Amchislavsky, Ella A. Starikova, Dmitry I. Sokolov, Irina S. Freidlin, Oleg N. Yatskin, Marina M. Philippova, Andrei A. Karelin and Vadim T. Ivanov

Metastin: Synthesis and Distribution in the Rat Medulla Oblongata and Spinal Cord 955
Jun Yang, G. Cristina Brailoiu, Siok L. Dun, Jaw-Kang Chang and Nae J. Dun

Peptide Dendrimer, Epitope and Vaccine Structure-Function

An Irreversible Inhibitor of a VIP-Hydrolyzing Antibody 961
Gita Bhatia, Yogesh Bangale, Hiroaki Taguchi, Robert Dannenbring, Stephanie Planque, Sangeeta Karle, Sudhir Paul and Yasuhiro Nishiyama

Bacterial and Mammalian Cell Penetration of Polycationic Antibacterial Peptides: Potential Utility as Drug Delivery Vehicles 963
Mare Cudic, Georgia Deliyannis, David C. Jackson and Laszlo Otvos Jr.

Synthetic Peptides in the Form of Dendrimers Retain Biological Activity and Become Resistant to Proteases 965
Luisa Bracci, Maria G De Montis, Chiara Falciani, Barbara Lelli, Luisa Lozzi, Paolo Neri, Alessandro Pini, Ylenia Runci and Alessandro Tagliamonte

Design and Synthesis of Porphyrin Centered Dendritic Poly(L-Lysine) 968
Louis A. Watanabe, Katsunori Kontani, Tamaki Kato and Norikazu Nishino

Property and Antibacterial Activity of Dendritic and Linear Cationic Peptides 970
Haruhiko Aoyagi, Akira Hirano, Takuro Niidome and Tomomitsu Hatakeyama

Introduction of Disulfide Bond Pairing into a HER-2 B-Cell Epitope Improves Tumor Cell Binding and Antitumor Activities of Peptide Antibodies 972
Kenneth D. Lute, Naveen Dakappagari, Shard Rawale and Pravin T.P. Kaumaya

Conformational and Conserved Epitope of gp120 Exposed During Viral Fusion in HIV-Vaccine Design 974
Kristen Sadler, Yi-An Lu, Khee Dong Eom, Ying Zhang and James P. Tam

Multiepitope Analysis of the HIV-1 gp41-Specific Immune Response Using a Panel of Constrained and Unconstrained Peptides 976
Elisabetta Bianchi, David Opalka, Paolo Ingallinella, William Schleif, Michael McElhaugh, Renee Danzeisen, Romas Geleziunas, Michael Miller, Debra Eckert, David Bramhill, Joseph Joyce, James Cook, William Magilton, Gennaro Ciliberto, John Shiver, Mark Esser and Antonello Pessi

Structural Analysis of the Epitope of the Anti-HIV-1 mAb 2F5 Yields Insights into the Mechanism of Neutralization and into the HIV-1 Fusion Process 978
Antonello Pessi, Gaetano Barbato, Paolo Ingallinella, William H. Hurni, Michael D. Miller, Gennaro Ciliberto, Riccardo Cortese, Renzo Bazzo, John W. Shiver and Elisabetta Bianchi

Novel Design of Thiol-Containing Lactam-Bridge Constraints for Immune Presentation of the ELDKWAS Epitope from gp41 in the Type-I β-Turn Conformation Recognized by mAb 2F5 981
Yu Tian, Edward Arnold, Gail F. Arnold, and John W. Taylor

Induction of Protective CTL Responses in HLA-A*0201 Transgenic Mice against HTLV-1 Recombinant Vaccinia Virus Using a Multivalent CTL Epitope Peptide Construct 983
Roshni Sundaram, Sharad V Rawale, Naveen Dakappagari, Don Young, Christopher M Walker, Steven Jacobson and Pravin T.P. Kaumaya

Totally Synthetic Lipopeptides as Self-adjuvanting Contraceptive Vaccines 985
Weiguang Zeng, Yuk Fai Lau, Lorena E. Brown and David C. Jackson

The Matrix-Scan: A Micro Array of Peptide Constructs Mimicking Discontinuous Sites 987
Wim M. M. Schaaper, Jerry W. Slootstra, Wouter C. Puijk, Evert van Dijk, Johannes P. M. Langedijk, Rob H. Meloen and P. Timmerman

Synthetic Peptide Vaccine Strategies for the Enhancement of Cytotoxic T-Cell Responses 989
Naveen K. Dakappagari, Roshni Sundaram, Sharad Rawale, and Pravin T. P. Kaumaya

Effects of a Specific Peptide Bond Replacement on a *Plasmodium falciparum* Protein Primary Processing 991
José Manuel Lozano, Diana R. Tovar, Luz M. Salazar, Marisol Ocampo, Fanny Guzmán and Manuel Elkin Patarroyo

Phosphorylated Antigenic Determinants of the La/SSB Autoantigen and Their Contribution as Potential Targets of the Autoimmune Response in Patients with Sjogren's Syndrome 994
Dimitrios Rokas, Eugenia Panou-Pomonis, Constantinos Sakarellos, Nicolas Coudevylle, Manh-Thong Cung, Athanassios G. Tzioufas, Haralampos M. Moutsopoulos and Maria Sakarellos-Daitsiotis

Ligand Binder Arrays 996
Michael J Taussig

T Cell Immunogenecity of Synthetic Oligopeptides with 91-105 Epitope Core and Ala Flanks of 16 kDa Protein of Mycobacterium Tuberculosis 1001
Szilvia Bosze, Nadia Caccamo, Zsuzsa Majer, Francesco Dieli, Gábor Mezo and Ferenc Hudecz

Solubility and CTL Activity of Elongated Hydrophobic Peptide Epitopes 1003
Christine Klinguer-Hamour, Liliane Goetsch, Maryline Lokteff, Marie-Claire Bussat, Aline Blaecke, Alexandra Gonzales, Jean-François Haeuw, Nathalie Corvaia and Alain Beck

Identification of Potential Vaccine T Cell Epitopes Based on Computer Selected Sequences 1005
Leo Kei Iwai, Márcia Yoshida, M. A. Shikanai-Yasuda, Maria A. Juliano , Jurgen Hammer, Luiz Juliano, Jorge Kalil, Luiz R. Travassos and Edecio Cunha-Neto

Structure-Activity Relationship Study of Glycopeptide Antigens Recognizing Specific Autoantibodies in Multiple Sclerosis 1007
Barbara Mulinacci, Francesca Nuti, Giuseppina Sabatino, Mario Chelli, Alfonso Carotenuto, Paolo Rovero, Benedetta Mazzanti, Marta Pazzagli, Francesco Lolli and Anna M. Papini

Author Index 1011

Subject Index 1021

Merrifield Award Lecture

Professor William F. DeGrado

Peptide Revolution: Genomics, Proteomics & Therapeutics
Michael Chorev & Tomi K. Sawyer (Editors)
American Peptide Society, 2003

De Novo Design of Peptides, Proteins, and Protein Mimetics

William F. DeGrado

Department of Biochemistry & Biophysics, & the Department of Chemistry,
University of Pennsylvania, Philadelphia, PA, 19104-6059, USA

Introduction

It is indeed an honor to receive the Merrifield Award given by the American Peptide Society. This award represents a very high point in my professional career. Bruce Merrifield's development of solid phase synthesis [1,2] first revolutionized peptide chemistry, and ultimately most aspects of organic synthesis and drug discovery. I first learned of Bruce Merrifield's invention in 1976, from a lecture in an organic chemistry class at Kalamazoo College. I was enchanted by the idea, and my lab partner and I decided to focus on this subject when we learned that we would be able to design our own laboratory in the final weeks of a biochemistry class. We spent days reading everything we could find about solid phase synthesis, ordering catalogues, devising glassware, and planning the synthesis. Much to our chagrin, the lab was not approved, but we wrote a lengthy, and somewhat irreverent lab report, about what we would have *liked* to have done. Not to be deterred by this first experience, most of my subsequent scientific work has revolved around synthetic peptides, proteins, and peptide mimetics, most synthesized by solid phase synthesis. The following manuscript will trace a few of these studies.

Peptide Chemistry In 1977 I began graduate studies at the University of Chicago with Emil T. (Tom) Kaiser, who suggested that I look into oxime esters as supports for solid phase synthesis. The basic idea was that the oxime ester might be cleaved by nucleophiles without affecting sidechain protecting groups, providing segments that subsequently could be stitched together. Earlier students and postdocs in the lab had attempted to use polymeric oxime esters, but had failed. Reading their reports identified three major problems that would have to be overcome. First, the support would have to be stable enough to treatment with strong acids (e.g., TFA) used for the repetitive removal of Boc groups. Systematic studies clearly showed that the 4-nitro-benzophenone oxime (Scheme 1) possessed sufficient stability towards acids [3].

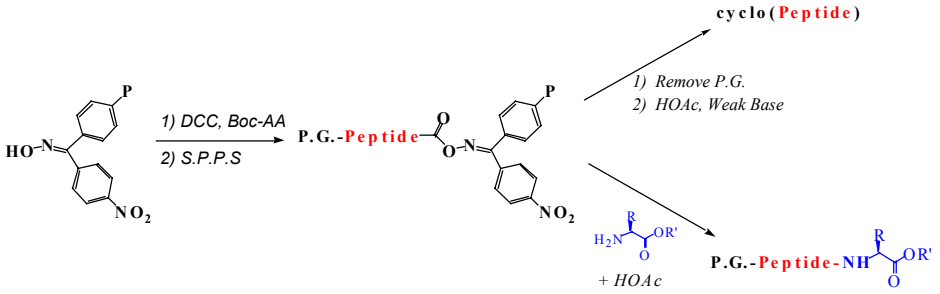

Scheme 1. Synthesis of linear and cyclic peptides on the Kaiser oxime resin.

However, the 4-nitro group aggravated an already troublesome problem; intramolecular and inter-site nucleophilic reactions between the N-terminal α-amine

and the peptide carbonyl group of the oxime ester. The problem was particularly problematic when a dipeptide was attached to the resin, in which case a diketopiperazine was rapidly formed. Fortunately, we found that this side reaction could be almost entirely suppressed by skipping the neutralization step typically employed in solid phase synthesis, and instead adding a tertiary base to the coupling mixture to neutralize the trifluoroacetate salt of the α-amine. The final problem involved cleaving the peptide from the resin with mild nucleophiles. We found that weak carboxylic acids such as acetic acid served as outstanding catalysts, enhancing the reactivity by at least one order of magnitude, and essentially eliminating epimerization of the peptide [3,4]. Subsequently, John Taylor's group [5] showed that the oxime was particularly well suited for the synthesis of cyclic peptides (Scheme 1). Years later, our group made extensive use of this procedure for the synthesis of template-constrained cyclic analogues of RGD with extremely high affinity and specificity for the integrins αIIbβ3 and αvβ3 [6,7]. Also, Mark Scialdone introduced a phosgenated derivative of the oxime ester, which provided a particularly convenient synthesis of asymmetric ureas, allowing efficient synthesis of peptide mimetics [8,9].

In 1981, I took a position at DuPont's Department of Central Research where I established a core facility for peptide synthesis. This position gave me the opportunity to interact with a large number of scientists, exposing me to a broad spectrum of biochemistry, molecular biology, and virology. During this period I collaborated with Jim Kauer to develop the amino acid *p*-benzoyl-phenylalanine (Bpa). Upon irradiation with approximately 320 nm light this amino acid forms a diradical, which reacts with C-H bonds in a net insertion reaction. The advantage of this probe is that it is essentially non-reactive towards water, assuring that it is not "wasted" by side reactions with solvent. As expected from its mechanism (Scheme 2), Bpa preferentially labels sidechains with reactive hydrogen atoms, particularly Met.

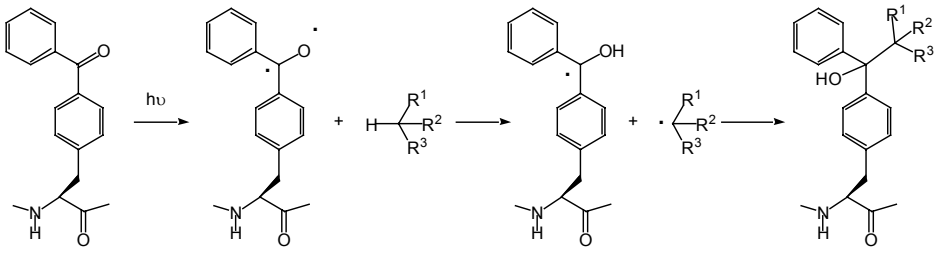

Scheme 2. Reaction of Bpa.

To test the utility of Bpa we introduced it into a series of calmodulin-binding peptides [10,11]. We were particularly interested in determining how calmodulin recognizes its target enzymes. Calmodulin recognizes a conserved structural feature – a positively charged, amphiphilic α-helix – rather than a precise amino acid sequence in these proteins [12]. Photolabeling identified hydrophobic pockets rich in Met residues in calmodulin's N-terminal and C-terminal domains, which interact with apolar residues in the bound peptides. Subsequent NMR structural studies of CaM-peptide complexes [13-15] confirmed and extended our photolabeling studies. Presumably the Met residues define a flexible binding site, which allows CaM to conform to the detailed surface topologies of its various targets. Independently, Kaiser and coworkers developed Bpa and used it to label the catalytic subunit of cyclic-AMP-dependent protein kinase [16].

Design of mimics of membrane-active antimicrobial peptides Another project that I engaged in while still a graduate student with Tom Kaiser and Ferenc Kèzdy involved the determination of the mechanism of action of melittin [17,18], a lytic peptide from bee venom. We hypothesized that this 26-residue peptide formed amphiphilic α-helices which bound to and disrupted the membranes of its targets [19,20]. According to our prediction, the N-terminal 20 residues formed a kinked helix with hydrophobic and neutral, polar residues segregated on opposite faces of the structure. A highly basic C-terminal hexapeptide also appeared to be important for activity. To test this hypothesis, we designed an analogue of this peptide, which idealized the amphiphilic secondary structure of the N-terminal helix, but had minimal sequence homology to melittin. The resulting peptide was even more potent than melittin, providing strong support for the guiding hypothesis [19,20].

Shortly after we completed these studies, Boman and coworkers reported the sequence of two antimicrobial peptides from cecropa moths, designated cecropins A and B. Unlike melittin, these peptides killed bacteria without affecting mammalian cells; they were the first examples in what was to become a large family of peptides that provide a first line of protection against bacterial infections. As was the case for melittin, the cecropins appeared to form amphiphilic helices. However, the positively charged residues were located on the polar face of the α-helix, rather than occuring in a separate C-terminal domain. After moving to DuPont, I prepared peptides that idealized the basic amphiphilic helix at the N-terminal region of cecropins A [21,22], and found that these peptides replicated the essential properties of the natural peptides. At this point I was just starting my own independent research career, and I learned that Bruce Merrifield was also working on the subject; he was soon to make many important contributions to the understanding of the activity of the cecropins [23-25]. Feeling greatly out-gunned, I dropped work on this subject for the next 15 years.

In the intervening years, hundreds of antimicrobial defense peptides were discovered in a variety of multicellular organisms including humans [26]. Their selectivity for lysing bacterial cells was found to be a result of the fact that bacterial cells lack cholesterol and generally bear more negatively charged lipids than mammalian cells [26]. A wealth of information clearly showed that the overall charge and amphiphilicity of the peptides – and not their precise sequences, secondary structures, or even chirality [27-29] – were required for activity. Also, a variety of highly potent antimicrobial peptides were designed based on these principles [26,30,31].

I again became interested in this subject following the groundbreaking work of Gellman [32,33] and Seebach [34], who showed that peptides composed of β-amino acids were capable of forming stable secondary structures. Gellman's group initially focused on β-peptides containing the conformationally constrained cyclic amino acid, 2-aminocyclohexanecarboxylic acid (ACHC), while Seebach's group studied β-peptides prepared from acyclic residues with a diverse collection of side chains. Both classes of compounds adopt an $\mathbf{L}_{+2}$ helix, which is also referred to as a 14-helix [33]. These helices appeared to provide an ideal scaffold for testing further whether the overall physicochemical properties of antimicrobial peptides are essential for their biological activities.

The 14-helix has an approximate 3-residue geometric repeat. Thus, if polar and apolar sidechains are arranged with precise three-residue periodicity in the sequence of a β-peptide, they will segregate to opposite sides of the helix. To test this hypothesis, two series of repeating tripeptides were prepared with β^3-hLeu and/or β^3-hVal chosen

as a hydrophobic residue and β^3-hLys as a polar, positively charged amino acid (Scheme 3) [35].

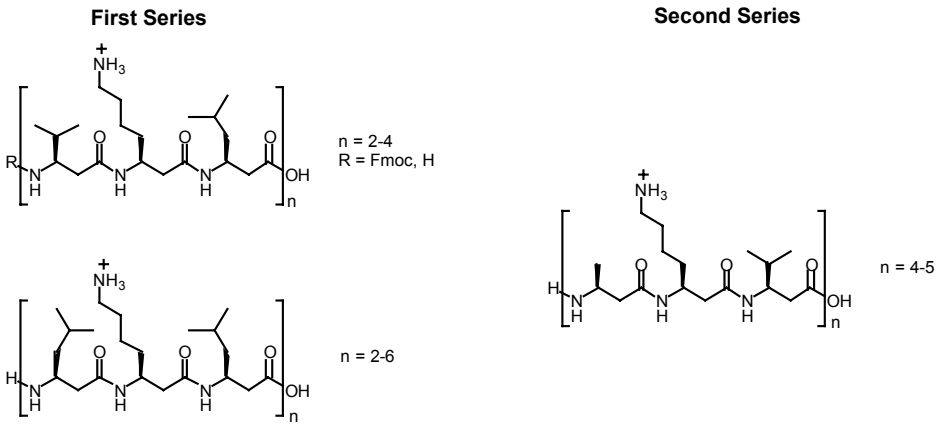

Scheme 3. Structures of antimicrobial β-peptides.

The biological activities of the peptides were measured using *E. coli* as a model for bacteria and human erythrocytes as a model for mammalian cells. The compounds were shown to have highly potent cell-lytic activity, with the longest peptides showing IC_{50} values in the nM range. As is the case for α-helical antimicrobial peptides, the β-peptides appeared to adopt largely unfolded conformations in aqueous solution, but well-defined secondary structures upon binding to phospholipid bilayers and micelles. For these β-peptides, the minimal length for the formation of a 14-helix was 9 – 12 residues, which also coincided with the minimal length required for biological activity.

Although these peptides were highly potent antimicrobial agents, they generally showed poor discrimination between bacteria versus red cells. Often, selective binding to bacterial membranes requires a careful balance of not only the charge, but also the secondary structure-forming potential and hydrophobicity [26,30]. Analogues of antimicrobial peptides that are too hydrophobic tend to have poor selectivity for bacteria versus mammalian cells [30,36]. Therefore, a second series of peptides was prepared, in which the hydrophobic β^3-hLeu or β^3-hVal was replaced with a less hydrophobic residue, β^3-hAla [37]. The resulting peptides showed potencies and selectivities comparable to those of natural antimicrobial peptides such as magainin. They also showed a strong tendency to bind to and disrupt the integrity of acidic, but not neutral phospholipid membranes.

Simultaneously and independently, Gellman and coworkers demonstrated the design of antimicrobial β-peptides that adopt 12-helical rather than 14-helical structures [38]. The 12-helix is an alternate secondary structure that is formed by β-amino acids composed of 2-amino-cyclopentane-carboxylic acid. This β-peptide was highly potent and highly specific toward bacteria, showing excellent activity against four species (including both gram positive and gram negative organisms**)** and minimal lytic activity against human erythrocytes. It is interesting to note that this compound is much more rigid than β-peptides composed of β^3-mono-substituted amino acids. Thus, there appears to be no *a priori* requirement for flexibility or rigidity, so long as the hydrophobicity-charge balance and length are appropriately optimized within a given class of compounds.

Although these studies were mechanistically revealing, β-peptides are expensive to prepare and difficult to produce on large scale, limiting their applications. We therefore set out to design inexpensive polymers and oligomers that adopt amphiphilic secondary structures. Such polymers could then be used either as pharmaceuticals or in antimicrobial materials and surfaces [39]. Our initial attempts to design facially amphiphilic structures focused on AB arylamide polymers typified by **1** (Scheme 4).

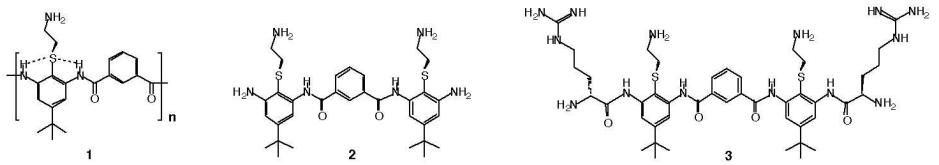

Scheme 4. Structures of antimicrobial β-peptides.

The diamine was chosen for its ease of synthesis, and its expected conformational properties. The choice of a thioether was based on the expectation that the methylene bonded to the thioether group would prefer to lie out of the plane of the ring, allowing weak hydrogen bonding to both amide protons. This interaction should constrain the conformation and help to eliminate the formation of intermolecular hydrogen-bonded aggregates with low solubility. Molecular dynamics simulations indicated that oligomers based on this repeat would adopt amphiphilic conformations at apolar-water interfaces, and the crystal structure of a short oligomer based on this substitution pattern indicated that the thioether group successfully constrained the amide bond to lie in the plane of the aryl group of the diamine.

Polymers and oligomers based on this repeat unit showed activity against a broad spectrum of bacteria, comparable to natural antimicrobial peptides. However, although these oligomers had potencies comparable to host defense peptides, they were toxic towards human red blood cells. A short triarylamide, **2** (Scheme 4), which showed reasonable potency, served as the starting point for optimizing the selectivity of this series of oligomers [40]. Amino acids appeared to be good candidates to append to this template; their amino groups would introduce an additional positively charged center, while their sidechains would provide a ready source of diversity.

Examination of a small collection of amino acids revealed two means of increasing activity [40]: Compounds with hydrophobic sidechains showed good activity against both Gram-negative and Gram-positive bacteria (MIC = 6 to 12 μg/ml versus both *E. coli* and *S. aureus*), but were also toxic towards human red blood cells. By contrast the introduction of sidechains with more polar sidechains led to oligomers with significantly lower toxicity towards erythrocytes. Compound **3** (Scheme 4), which features the dibasic Arg substituent, was the most active of the series. This compound displays antibacterial activity (MIC = 6 to 12 μg/ml versus both *E. coli* and *S. aureus*) similar to the potent magainin analogue MSI-78 [41] and significantly lower toxicity towards red blood cells.

These studies demonstrate that it is possible to design small, highly potent mimics of antimicrobial peptides. The oligomers are significantly smaller than comparable antimicrobial oligomers, which might provide significant advantages in terms of tissue distribution as well as cost of production.

De Novo Protein Design De novo design refers to the construction of a protein, intended to fold into a precisely defined 3-dimensional structure, with a sequence that

is not directly related to that of any natural protein. In early studies the motivation for work in this area was to test the rules governing protein folding; in more recent studies, proteins are increasingly being designed to serve specific functions. De novo design of proteins is an important endeavor because it critically tests our understanding of protein folding and function, while simultaneously laying the groundwork for the design of macromolecules with properties not precedented in nature. Many groups have contributed significantly to the de novo design of proteins, and there are a number of comprehensive reviews of the subject [42-60] The following account is a brief review of some our own accomplishments in this area.

When we began our studies in this area the design of proteins had not been convincingly demonstrated, and appeared to be largely impossible for several reasons: The stability of the native fold of a protein relative to the unfolded form is small, generally 5 to 10 Kcal/mol, and represents the difference between much larger favorable and unfavorable terms, making it very difficult to accurately compute the stable structures of proteins. The number of possible sequences for even a short protein of 100 residues (20^{100}) is larger than the number of atoms in the universe, precluding the possibility of trying all possible sequences. Indeed, it would not be possible to find a specific sequence by a random search, even if a protein could be mutated every femtosecond for the age of the universe! Similarly, the number of possible backbone conformations for a protein of this size represents an astronomically large number (10^{100}), indicating that folding cannot occur by a random search of conformational space [61]. How then might proteins have evolved? Relatively short peptide sequences of 10 to 20 residues in length are able to self-associate to form well defined helical bundles or β-sheets, depending on the order of polar and non-polar amino acids in the sequence [49,62,63]. Thus, early proteins might have been formed by the non-covalent self-assembly of relatively short peptide sequences. Gene duplication of such a sequence would provide a monomolecularly folded protein, allowing the individual segments to mutate independently, resulting in a highly complex protein. Indeed, the individual domains of many small globular proteins show residual approximate symmetry [64], indicative of gene duplication of a primordial precursor.

We have adopted a similar biomimetic approach to the design of functional four-helix bundle proteins [58,65]. The four-helix bundle is a common folding motif found in functionally diverse proteins such as myohemrythrin, cytochrome C', and TMV coat protein. This motif was an excellent target for molecular engineering because of its structural simplicity and natural tendency to produce cavities that accommodate prosthetic groups. Our strategy involved the design of a single-chain peptide (α_1) that would self-assemble into a four-helix bundle [66,67]. In collaboration with David Eisenberg, we designed a peptide with Glu and Lys residues along one face of the helix, and Leu sidechains on the opposite face to form a hydrophobic core. Previously Hodges and coworkers had used a similar strategy to probe the features required for the formation of coiled coils [68]. While they found that a chain length of approximately 30 residues was required for the formation of two-stranded coiled coils, we found a chain length of only 16 residues was sufficient to direct formation of a four-helix bundle [67], most probably because of the larger number of helices per aggregate as well as the more extensive hydrophobic core.

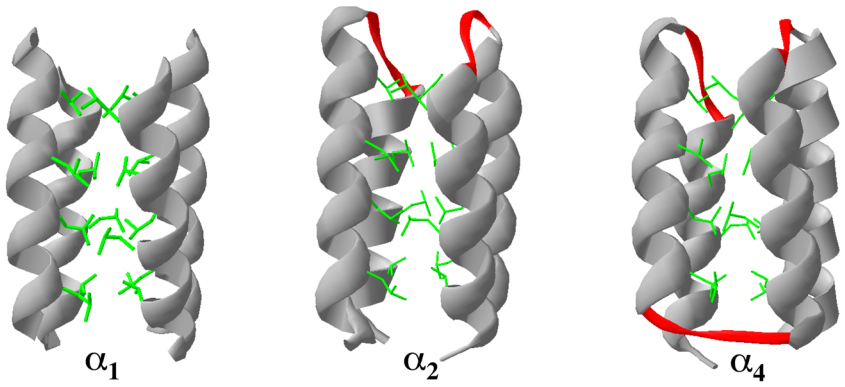

Fig. 1. Designed four-helix bundle proteins, beginning with a tetrameric bundle of α_1 (left). Addition of one or three loops provides the dimeric and monomolecularly folded proteins, α_2 and α_4, respectively.

The next stage in the design involved linking two adjacent α_1 helices by inserting a single Pro residue between N- and C-terminal Gly residues of this peptide [67]. However, the resulting peptide formed an unforeseen trimeric aggregate rather than the desired dimer of helical hairpins. This illustrates the importance of "negative design" [69]; the sequences of natural proteins have evolved not only to stabilize a desirable three-dimensional structure, but to destabilize all other possible alternatives. A successfully designed protein must do the same. The inappropriate aggregation was alleviated by introducing two Arg residues after the Pro residue in the link sequence to provide additional flexibility for loop formation, and to electrostatically destabilize a likely conformation of the trimer [67]. Finally, a gene directing the synthesis of the complete α_4 protein (Figure 1) with four helices connected by three Pro-Arg-Arg links was expressed in *E. coli* [70].

The α_1, α_2, and α_3 proteins showed some of the characteristics of four-helix bundle proteins: they were compact and globular, and their backbone was structurally well defined and helical as assessed by NMR [71]. However, between the conception of a designed protein and its realization lies the molten globule. Molten globules are non-native states of proteins with dynamically averaging conformations and poorly defined tertiary structures [72,73]. More native-like behavior could be induced by including a more diverse selection of sidechains in the interior of the protein [74-76], extending the lengths of the helices [77,78], changing some of the hydrophobic residues to polar residues that can engage in structure-defining hydrogen-bonded interactions [79-82], or through the introduction of metal ion binding sites [83-85].

As the principles and methods for de novo protein design have matured, it has recently become possible to design structurally defined models for metalloproteins. In collaboration with Dutton and coworkers, we designed a series of bundles containing between one and four heme groups [86,87], and these proteins provided excellent frameworks for determining how the protein matrix and heme-heme interactions affect electrochemical midpoint potentials of non-covalently associated cofactors. More recently, we have turned our attention to the diiron class of proteins [88-93]. This class of proteins is structurally and functionally quite diverse, and includes the radical-forming subunit of *E. coli* ribonucleotide reductase [94-96] and methane

monooxygenase [97]. We therefore sought to design minimal models for these large, highly complex proteins to address how the amino acid sequence modulates the type of chemistry performed.

A geometric analysis of six natural diiron proteins suggested that they all may have evolved from a dimer of helix-loop-helix motifs [98,99]. Each of the helices donates a single Glu residue. Additionaly, the second helix of each helix-loop-helix donates a single His residue to the diiron site. In the diferrous form, the ligands often show approximate two-fold symmetry with two bridging Glu residues, two Glu residues that bind a single metal ion, and two His residues. The ligands are arranged in an approximate square pyramidal array, with the His sidechains trans to the empty sites (which presumably bind oxygen). Based on this analysis, we designed a model diiron protein with four Glu residues and two His residues projecting towards the center of the bundle [99]. The backbone structure was dictated by a mathematical parameterization of the structures of natural diiron proteins, thus allowing the design process to proceed in an objective manner that is consistent with fully automated approaches to protein design [51]. Hydrogen-bonded interactions were introduced to stabilize the ligands in the proper orientation for binding to iron. In particular, an Asp residue was introduced to serve as a hydrogen bond acceptor for the buried His, and a hydrogen bond was also modeled between a buried Tyr and the non-bridging Glu residue in the core of the structure. The remaining positions in the core were chosen to stabilize the geometry of the active site, and the interfacial and exposed sidechains to uniquely stabilize the desired fold [78].

The crystal structures of the di-Zn(II) form of the resulting protein, designated DF1, conform precisely to the design, with an RMSD of approximately 1.0 Å between the model and the structure (Figure 2). DF1 has a well-defined dimetal-binding site with two bridging Glu carboxylates, two chelating Glu carboxylates, and two His ligands. Furthermore, the intended second shell ligands form hydrogen bonds with the first-shell ligands. The protein also folds in solution in the absence of metal ions, and the NMR solution structure of the protein indicated both the tertiary structure as well as the metal-binding site are largely preorganized in the apo-protein [100].

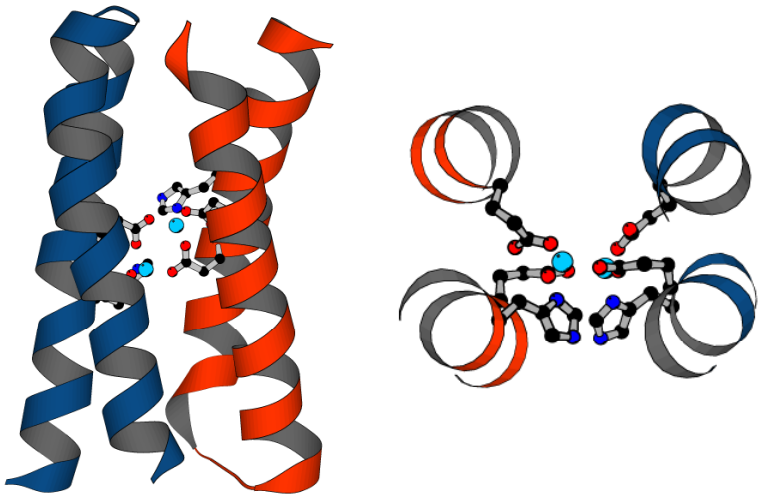

Fig. 2. Structure of DF1.

Having demonstrated that DF1 folded to the desired structure, we turned our attention to the design of substrate-binding sites and the understanding how the protein affected the reactivity of the diiron site, with the ultimate goal being to design new catalysts. The starting structure did not bind substrates, because a pair of Leu sidechains blocked access to the dimetal site. These residues were changed to Ala and Gly, giving rise to a protein that now bound exogenous ligands to the diferric form of the protein. Also, crystal structures of the di-Mn(II) form of the protein showed a cavity leading to the active site, with a water molecule or the sulfoxide group of a DMSO molecule bridging the metal ions in these variants of DF1.

We would now like to evaluate how systematic changes to the structure of DF1 affect its metal-binding, substrate-binding and catalytic properties. To be general, it would be useful to examine both natural as well as unnatural amino acids at a large number of positions. However, even if only five or six positions within the protein are substituted with a restricted number of sidechains, a very large number of combinations is generated. Furthermore, we would like to examine thoroughly the reaction of each one of these variants with a number of small molecule ligands and substrates. Such an extensive study would require the generation and purification of significant quantities of hundreds to thousands of variants.

To advance this goal, we designed a tetramer consisting of four disconnected helices, which could be separately synthesized, purified, and then combinatorially assembled to create an array of the desired helical bundles. By engineering the electrostatic interactions between the individual helices, we were able to prepare a two-component A_2B_2 heterotetramer [101] as well as a three-component $A_A{\cdot}A_B{\cdot}B_2$ heterotetrameric complex [102]. Using this construction, we are now screening a panel of variants for interesting metal-ion dependent activities.

In conclusion, it is now possible to design proteins in which fine-tuned geometric details are controlled at will. It will now be of considerable interest to apply the methods of de novo design to problems in catalysis, peptide-protein interactions, and protein-protein interaction.

Acknowledgments

I wish to thank my wife, Christine Tyma DeGrado, for support throughout this work, my Ph.D. advisors Emil T. Kaiser and Frenec Kèzdy for setting me on this research path, and all my collaborators and group members who have contributed so significantly to this work.

References

1. Merrifield, R. B. *J. Am. Chem. Soc.* **85**, 2149-2151 (1963).
2. Merrifield, R. B. *Adv. Enzymol. Relat. Areas Mol. Biol.* **32**, 221-296 (1969).
3. DeGrado, W. F. and Kaiser, E. T. *J. Org. Chem.* **40**, 1295-1230 (1980).
4. DeGrado, W. F. and Kaiser, E. T. *J. Org. Chem.* **42**, 3257-3281 (1982).
5. Ösapay, G., Profit, A. and Taylor, J. W. *Tetrahedron Lett.* **31**, 6121-6124 (1990).
6. Jackson, S., DeGrado, W. F., Dwivedi, A., Parthasarathy, A., Higley, A., Krywko, J., Rockwell, A., Markwalder, J., Wells, G., Wexler, R., Mousa, S. and Harlow, R. *J. Am. Chem. Soc.* **116**, 3220-3230 (1994).
7. Bach, A. C. I., Espina, J. R., Jackson, S. A., Stouten, P. F. W., Duke, J. L., Mousa, S. A. and DeGrado, W. F. *J. Am. Chem. Soc.* **118**, 293-294 (1996).
8. Scialdone, M. A. *Tetrahedron. Lett.* **37**, 8141-44 (1996).
9. Scialdone, M. A., Shuey, S. W., Soper, P. D., Hamuro, Y. and Burns, D. M. *J. Org. Chem.* **63**, 4802 - 4807 (1998).
10. Kauer, J. C., Viitanen, S. and DeGrado, W. F. *J. Biol. Chem.* **261**, 10695-10700 (1986).

11. O'Neil, K. T., Erickson-Viitanen, S. and DeGrado, W. F. *J. Biol. Chem.* **264**, 14571-14578 (1989).
12. O'Neil, K. T. and DeGrado, W. F. *Trends in Biochem. Sci.* **15**, 59-64 (1990).
13. Osawa, M., Tokumitsu, H., Swindells, M. B., Kurihara, H., Orita, M., Shibanuma, T., Furuya, T. and Ikura, M. *Nat. Struct. Biol.* **6**, 819-824 (1999).
14. Lee, A. L., Kinnear, S. A. and Wand, A. J. *Nat. Struct. Biol*. **7**, 72-77 (2000).
15. Ikura, M., Barbato, G., Klee, C. B. and Bax, A. *Cell Calcium* **13**, 391-400 (1992).
16. Miller, W. T. and Kaiser, E. T. *Proc. Natl. Acad. Sci. U.S.A.* **85**, 5429-5433 (1988).
17. Habermann, E. and Jentsch, J. *Hoppe Seylers Z. Physiol. Chem.* **348**, 37-50 (1967).
18. Habermann, E. and Reiz, K. G. *Biochem. Z.* **343**, 192-203 (1965).
19. DeGrado, W. F., Kèzdy, F. J. and Kaiser, E. T. *J. Amer. Chem. Soc.* **103**, 679-681 (1981).
20. DeGrado, W. F., Musso, G. F., Lieber, M., Kaiser, E. T. and Kézdy, F. J. *Biophys. J.* **37**, 329-338 (1982).
21. DeGrado, W. F. *Adv. Prot. Chem.* **39**, 51-124 (1988).
22. DeGrado, W. F. In Hruby V. J. and Rich D. H. (Eds.), *Peptides: Structure and Function (Proceedings of the eighth American Peptide Symposium)*, Pierce Chemical Company, Rockford, IL, p. 195 (1983).
23. Merrifield, R. B., Merrifield, E. L., Juvvadi, P., Andreu, D. and Boman, H. G. *Ciba Found. Symp.* **186**, 5-20 (1994).
24. Merrifield, E. L., Mitchell, S. A., Ubach, J., Boman, H. G., Andreu, D. and Merrifield, R. B. *Int. J. Pept. Protein Res.* **46**, 214-220 (1995).
25. Merrifield, R. B., Juvvadi, P., Andreu, D., Ubach, J., Boman, A. and Boman, H. G. *Proc. Natl. Acad. Sci. U.S.A.* **92**, 3449-3453 (1995).
26. Zasloff, M. *Nature* 415, 389-395 (2002).
27. Wade, D., Boman, A., Wahlin, B., Drain, C. M., Andreu, D., Boman, H. G. and Merrifield, R. B. *Proc. Natl. Acad. Sci. U.S.A.* **87**, 4761-4765 (1990).
28. Shai, Y. and Oren, Z. *Peptides* **22**, 1629-1641 (2001).
29. Shai, Y. *Biopolymers* **66**, 236-248 (2002).
30. Lee, D. L. and Hodges, R. S. *Biopolymers* **71**, 28-48 (2003).
31. Fernandez-Lopez, S., Kim, H. S., Choi, E. C., Delgado, M., Granja, J. R., Khasanov, A., Kraehenbuehl, K., Long, G., Weinber, D. A., Wilcoxen, K. M. and Ghadiri, M. R. *Nature* **412**, 452-455 (2001).
32. Appella, D. H., Christianson, L. A., Karle, I. L., Powell, D. R. and Gellman, S. H. *J. Am. Chem. Soc.* **118**, 13071-13072 (1996).
33. Gellman, S. H. *Acc. Chem. Res.* **31**, 173-180 (1998).
34. Seebach, D., Overhand, M., Kuhnle, F. N. M., Martinoni, B., Oberer, L., Hommel, U. and Widmer, H. *Helv. Chim. Acta* **79**, 913 (1996).
35. Hamuro, Y., Schneider, J. P. and DeGrado, W. F. *J. Amer. Chem. Soc.* **121**, 12200-12201 (1999).
36. Tossi, A., Sandri, L. and Giangaspero, A. *Biopolymers* **55**, 4-30 (2000).
37. Liu, D. and DeGrado, W. *J. Am. Chem. Soc.* **123**, 7553-7559 (2001).
38. Porter, E. A., Wang, X., Lee, H. S., Weisblum, B. and Gellman, S. H. *Nature* **404**, 565 (2000).
39. Tiller, J. C., Liao, C. J., Lewis, K. and Klibanov, A. M. *Proc. Natl. Acad. Sci. U.S.A.* **98**, 5981-5985 (2001).
40. Liu, D., Choi, S.-W., Chen, B., Doerkson, R., Clements, D., Winkler, J., Klein, M. L. and DeGrado, W. F. *Angew. Chem. Intl. Ed. Engl*. **43**, 1158-1162 (2004).
41. Maloy, W. L. and Kari, U. P. *Biopolymers* **37**, 105-122 (1995).
42. Lau, S. Y. M., Taneja, A. K. and Hodges, R. S. *J. Biol. Chem.* **259**, 13253-13261 (1984).
43. Hodges, R. S. *Biochem. Cell Biol.* **74**, 133-154 (1996).
44. Richardson, J., Richardson, D. C., Tweedy, N. B., Gernert, K. M., Quinn, T. P., Hecht, M. H., Erickson, B. W., Yan, Y., McClain, D., M. E. and Surles, M. C. *Biophys. J.* **63**, 1186-1209 (1992).

45. Balaram, P. *J. Pept. Res.* **54**, 195-199 (1999).
46. Baltzer, L., Nilsson, H. and Nilsson, J. *Chem. Rev.* **101**, 3153-3163. (2001).
47. Baltzer, L. and Nilsson, J. *Curr. Opin. Biotechnol.* **12**, 355-360 (2001).
48. Kamtekar, S. and Hecht, M. H. *Faseb. J.* **9**, 1013-1022 (1995).
49. Beasley, J. R. and Hecht, M. H. *J. Biol. Chem.* **272**, 2031-2034 (1997).
50. Schafmeister, C. E. and Stroud, R. M. *Curr. Opin. Biotechnol.* **9**, 350-353 (1998).
51. Street, A. G. and Mayo, S. L. *Structure Fold Des.* **7**, R105-109 (1999).
52. Regan, L. *Trends Biochem. Sci.* **20**, 280-285 (1995).
53. Muller, K. M., Arndt, K. M. and Alber, T. *Methods Enzymol.* **328**, 261-282 (2000).
54. Gibney, B. R., Rabanal, F. and Dutton, P. L. *Curr. Opin. Chem. Biol.* **1**, 537-542 (1997).
55. Mutter, M. and Tuchscherer, G. *Cell. Mol. Life Sci.* **53**, 851-863 (1997).
56. Schneider, J. P. and Kelly, J. W. *Chem. Rev.* **95**, 2169-2187 (1995).
57. Lombardi, A., Nastri, F. and Pavone, V. *Chem. Rev.* **101**, 3165-3189 (2001).
58. DeGrado, W. F., Wasserman, Z. R. and Lear, J. D. *Science* **243**, 622-628 (1989).
59. DeGrado, W. F., Summa, C. M., Pavone, V., Nastri, F. and Lombardi, A. *Ann. Rev. Biochem.* **68**, 779-819 (1999).
60. Betz, S. F., Bryson, J. W. and DeGrado, W. F. *Curr. Opin. Struct. Biol.* **5**, 457-463 (1995).
61. Dill, K. A. and Chan, H. S. *Nature Struct. Biol.* **4**, 10-19 (1997).
62. DeGrado, W. F. and Lear, J. D. *J. Amer. Chem. Soc.* **107**, 7684 (1985).
63. Wang, W. and Hecht, M. H. *Proc. Natl. Acad. Sci. U.S.A.* **99**, 2760-2765 (2002).
64. McLachlan, A. D. *Cold Spring Harbor Symp. Quant. Biol.* LII (1987).
65. Bryson, J. W., Betz, S. F., Lu, H. S., Suich, D. J., Zhou, H. X., O'Neil, K. T. and DeGrado, W. F. *Science* **270**, 935-941 (1995).
66. Eisenberg, D., Wilcox, W., Eshita, S. M., Pryciak, P. M., Ho, S. P. and DeGrado, W. F. *Proteins* **1**, 16-22 (1986).
67. Ho, S. P., DeGrado, W. F. *J. Am. Chem. Soc.* **109**, 6751-6758 (1987).
68. Talbot, J. A. and Hodges, R. S. *Acc. Chem. Res.* **15**, 224-230 (1982).
69. Richardson, J. S. and Richardson, D. C. *Proc. Natl. Acad. Sci. U.S.A.* **99**, 2754-2759 (2002).
70. Regan, L. and DeGrado, W. F. *Science* **241**, 976-978 (1988).
71. Osterhout, J. J., Handel, T., Na, G., Toumadje, A., Long, R. C., Connolly, P. J., Hoch, J. C., Johnson, W. C., Live, D. and DeGrado, W. F. *J. Am. Chem. Soc.* **114**, 331-337 (1992).
72. Kuwajima, K. *Proteins* **6**, 87-103 (1989).
73. Ptitsyn, O. B., Pain, R. H., Semisotnov, G. V., Zerovnik, E. and Razgulyaer, O. L. *Febs Lett* 262, 20-24 (1990).
74. Raleigh, D. P. and DeGrado, W. F. *J. Amer. Chem. Soc.* 114, 10079-10081 (1992).
75. Hecht, M. H. *Proc. Natl. Acad. Sci. U.S.A.* **91**, 8729-8730 (1994).
76. Roy, S. and Hecht, M. H. *Biochemistry* **39**, 4603-4607. (2000).
77. Betz, S. F. and DeGrado, W. F. *Biochemistry* **35**, 6955-6962 (1996).
78. Betz, S. F., Liebman, P. A. and DeGrado, W. F. *Biochemistry* **36**, 2450-2458 (1997).
79. Hill, R. B., Hong, J.-K. and DeGrado, W. F. *J. Amer. Chem. Soc.* **122**, 746-747 (1999).
80. Hill, R. B. and DeGrado, W. F. *J. Am. Chem. Soc.* **120**, 1138-1145 (1998).
81. Hill, R. B. and DeGrado, W. F. *Structure Fold Des.* **8**, 471-479 (2000).
82. Hill, R. B., Raleigh, D. P., Lombardi, A. and DeGrado, W. F. *Acc. Chem. Res.* **33**, 745-754 (2000).
83. Regan, L. and Clarke, N. D. *Biochemistry* **29**, 10878-10883 (1990).
84. Handel, T. and DeGrado, W. F. *J. Am. Chem. Soc.* **112**, 6710-6711 (1990).
85. Handel, T. M., Williams, S. A. and DeGrado, W. F. *Science* **261**, 879-885 (1993).
86. Robertson, D. E., Farid, R. S., Moser, C. C., Urbauer, J. L., Mulholland, S. E., Pidikiti, R., Lear, J. D., Wand, A. J., DeGrado, W. F. and Dutton, P. L. *Nature* **368**, 425-432 (1994).
87. Choma, C. T., Lear, J. D., Nelson, M. J., Dutton, P. L., Robertson, D. E. and DeGrado, W. F. *J. Amer. Chem. Soc.* **116**, 856-865 (1994).
88. Nordlund, P. and Eklund, H. *Curr. Opin. Struct. Biol.* **5**, 758-766 (1995).
89. Lange, S. J. and Que, L., Jr. *Curr. Opin. Chem. Biol.* **2**, 159-172 (1998).

90. Waller, B. J. and Lipscomb, J. D. *Chem. Rev.* **96**, 2625-2657 (1996).
91. Feig, A. L. and Lippard, S. J. *Chem. Rev.* **94**, 759-805 (1994).
92. Yocum, C. F. and Pecoraro, V. L. *Curr. Opin. Chem. Biol.* **3**, 182-187 (1999).
93. Dismukes, G. C. *Chem. Rev.* **96**, 2909-2926 (1996).
94. Stubbe, B. G., Horkay, F., Amsden, B., Hennink, W. E., De Smedt, S. C. and Demeester, J. *Biomacromolecules* **4**, 691-695 (2003).
95. Stubbe, J., Nocera, D. G., Yee, C. S. and Chang, M. C. *Chem. Rev.* **103**, 2167-2201 (2003).
96. Eklund, H., Uhlin, U., Farnegardh, M., Logan, D. T. and Nordlund, P. *Prog. Biophys. Mol. Biol.* **77**, 177-268 (2001).
97. Merkx, M., Kopp, D. A., Sazinsky, M. H., Blazyk, J. L., Müller, J. and Lippard, S. J. *Angew. Chem. Int. Ed.* **40**, 2782-2807 (2001).
98. Summa, C. M., Lombardi, A., Lewis, M. and DeGrado, W. F. *Curr. Opin. Struct. Biol.* **9**, 500-508 (1999).
99. Lombardi, A., Summa, C. and DeGrado, W. F. *Proc. Natl. Acad. Sci. U.S.A.* **97**, 6298-6305 (2000).
100. Maglio, O., Nastri, F., Pavone, V., Lombardi, A. and DeGrado, W. F. *Proc. Natl. Acad. Sci. U.S.A.* **100**, 3772-3777 (2003).
101. Summa, C. M., Rosenblatt, M. M., Hong, J. K., Lear, J. D. and DeGrado, W. F. *J. Mol. Biol.* **321**, 923-938 (2002).
102. Marsh, E. N. and DeGrado, W. F. *Proc. Natl. Acad. Sci. U.S.A.* **99**, 5150-5154. (2002).

Amino Acid and Peptide Synthetic Chemistry

Peptide Revolution: Genomics, Proteomics & Therapeutics
Michael Chorev & Tomi K. Sawyer (Editors)
American Peptide Society, 2003

An Efficient Microwave-Assisted Synthesis of 2,5-Diketopiperazine Libraries

Maria C. Alcaro[1], Pietro Campiglia[2], Paolo Grieco[2], Ettore Novellino[2], Mario Chelli[1] and Anna M. Papini[1]

[1]Laboratory of Peptide Chemistry & Immunology, Dipartimento di Chimica Organica "Ugo Schiff" and CNR-ICCOM, Università di Firenze, I-50019 Sesto Fiorentino (FI), Italy; [2]Dipartimento di Chimica Farmaceutica e Tossicologica, Università di Napoli "Federico II", I-80131 Napoli, Italy

Introduction

Small heterocyclic compounds, such as 2,5-diketopiperazines (DKPs), are widely used scaffolds in combinatorial chemistry, as they can provide, around a rigid core, diverse functionalities with a predictable spatial geometry. The cyclization step leading to DKPs occurs by intramolecular aminolysis at the dipeptide level, and is catalyzed by weak acids or bases. DKPs bound to the solid support, and then accessible to further on-resin modifications, can be obtained by two solid-phase strategies anchoring the first amino acid by: (a) reductive amination to a Backbone Amide Linker resin [1] or to an aldehyde peptide [2]; and (b) its side-chain to a resin [3]. However, on-resin cyclizations of difficult dipeptide sequences often leads to racemic products.

To optimize the DKP cyclization reaction we studied the reactivity of the different residues, anchoring the side chain of Fmoc-Xaa-OAl (Xaa = Asp, His) to a trityl resin and synthesizing two libraries of DKPs c[Xaa-Yaa] (Yaa = 20 natural amino acid).

Results and Discussion

The two building blocks, Fmoc-Asp(trityl-resin)-OAl (**1**) (Scheme 1), and Fmoc-His(trityl-resin)-OAl (**4**) (Scheme 2), were used for the synthesis of the linear dipeptide libraries **2** and **5** respectively, by a standard cycle of parallel SPPS.

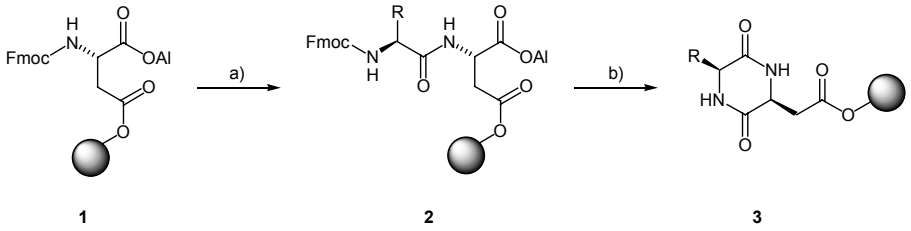

Scheme 1. Synthesis of c[Asp-Xaa] DKP. a) SPPS; b) piperidine, r.t.

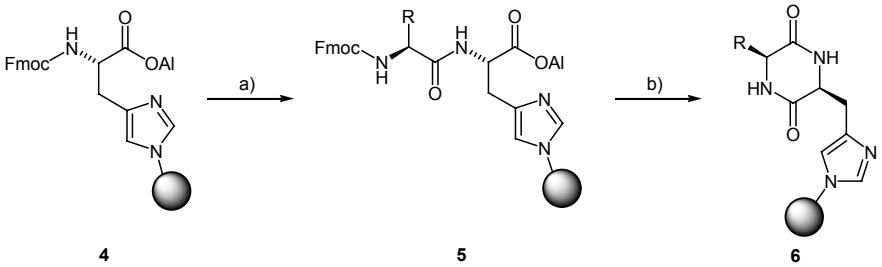

Scheme 2. Synthesis of c[His-Xaa] DKP. a) SPPS; b) piperidine.

To evaluate the reactivity of the different Xaa amino acids in the ring-closure reaction, cyclization was performed treating the resin with piperidine, modifying the base concentration and the temperature in order to drive reactions to completion. A scale of reactivity was thus determined (Figure 1), demonstrating the dependence of the intramolecular cyclization on the amino acid sequence. In fact, His-containing dipeptides **5** were less reactive than the Asp-containing ones **2**, and after 2 h in 20% piperidine in DMF, only the Pro-containing DKPs were formed. Moreover, for the DKPs c[His-Xaa], with Xaa = Glu, Gln, Gly, Ile, Lys, Met, Phe, Thr, Trp, Tyr, and Val, it was necessary to heat the reaction at 40-50 °C in pure piperidine. However, these conditions led, in some cases, to the epimerisation of the final compounds.

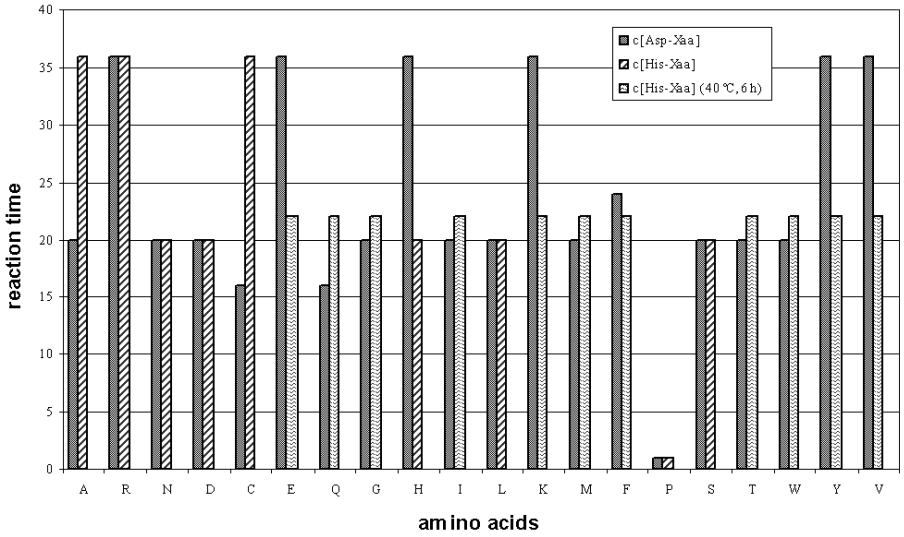

Fig. 1. Reactivity scale of the amino acids involved in DKP formation.

To optimize the reaction conditions for DKPs formation, shortening the reaction times and avoiding the use of pure piperidine, a microwave-assisted solid-phase strategy was applied. The on-resin microwave-assisted DKP formation was performed with 20% piperidine in DMF, in closed reactors at 150 W. In addition, the effects of temperature (50-80 °C), reaction time, and solvent (DMF, *N*-methylformamide) on the cyclization reaction, and on the extent of racemization of the final products were evaluated. By the on-resin microwave-assisted approach, DKPs were obtained with higher purity, and a significantly lower level of racemization.

Acknowledgments
The authors thank the University of Florence for the Progetto Giovani Ricercatori 2000 funds.

References

1. Del Fresno, M., Alsina, J., Royo, M., Barany, G. and Albericio, F. *Tetrahedron Lett.* **39**, 2639-2642 (1998).
2. Groth, T. and Meldal, M. *J. Comb. Chem.* **3**, 45-63 (2001).
3. (a) Bianco, A., Furrer, J., Limal, D., Guichard, G., Elbayed, K., Raya, J., Piotto, M. and Briand, J. P. *J. Comb. Chem.* **2**, 681-690 (2000); (b) Bianco, A., Sonksen, C. P., Roepstorff, P. and Briand, J. P. *J. Org. Chem.* **65**, 2179-2187 (2000).

Peptide Revolution: Genomics, Proteomics & Therapeutics
Michael Chorev & Tomi K. Sawyer (Editors)
American Peptide Society, 2003

4-Fluoro-Phenylglycine and 3-Fluoro-Alanine: Labels for ^{19}F-Solid State NMR Structure Analysis of Membrane-Active Peptides

Parvesh Wadhwani[1], Sergii Afonin[1], Marina Berditchevskaja[2], Ralf W. Glaser[3] and Anne S. Ulrich[1,2]

[1]Institute for Instrumental Analysis, Forschungszentrum Karlsruhe, Postfach 3640, 76021 Karlsruhe, Germany; [2]Institute for Organic Chemistry, Fritz-Haber-Weg 6, University of Karlsruhe, 76128 Karlsruhe, Germany, [3]Institute for Molecular Biology, Winzerlaer Strasse 10, Friedrich-Schiller-University, 07745 Jena, Germany

Introduction

Investigating the mode of action of membrane-active peptides is of prime importance in structural biology. Very often the activity of such peptides is related to their interactions with the lipids and orientation within the lipid membranes. There exist a variety of methods, including electron paramagnetic resonance, fluorescence spectroscopy, and solid state NMR, to study such peptide-lipid interactions [1]. The only requirement of this highly informative latter technique is the use of selective labels such as ^{2}H, ^{13}C or ^{15}N, and a relatively large amount of sample. To enhance sensitivity, the ^{19}F nucleus offers a much better choice, with no natural background and nearly as sensitive as ^{1}H, thus reducing the measurement time considerably. This approach has been previously used to determine the orientation and inter-fluorine distances in the well known antimicrobial peptide gramicidin S [2]. Incorporation of a ^{19}F label into peptides and proteins can be accomplished by a variety of methods. Here, we have incorporated the non-natural amino acids 4-fluoro-phenlyglycine (4F-Phg) and 3-fluoro-alanine (3F-Ala) into the membrane-associated peptide sequences summarized in figure 1. The advantage of 4F-Phg over the more commonly used fluorinated amino acids (such as F-Phe, F-Tyr, F-Trp, F-Leu) lies in the stiff connection of the 4-fluorophenyl side chain to the backbone, thus allowing us to directly monitor the structure and dynamics of the peptide backbone in the lipid environment. 3F-Ala on the other hand is closer to natural alanine and serine.

Three distinctly different membrane-active peptides were studied here: (1) An antimicrobial α-helical cationic peptide, PGLa; this 21-residue peptide from the magainin family is unfolded in aqueous solution but converts into an amphiphilic α-helix upon membrane binding. (2) The second peptide, Gramicidin S, is a cyclic antimicrobial β-sheet peptide produced by *Bacillus brevis*. (3) Finally B18 is a fully conserved 18-residue sequence derived form the sea urchin sperm protein "bindin", which mediates fertilization by triggering membrane fusion. Both PGLa and the B18 were singly labeled at several hydrophobic positions, one at a time, and gramicidin S was doubly labeled in two symmetric positions.

PGLa	GMASKAG**A**I**A**GK**I**AKVALKAL-NH_2
Gramicidin S	(P**V**O**L**^{D}F)$_2$
B18	**L**G**LLL**RH**L**RHHSN**LLA**N**I**

Fig. 1. Sequences of PGLa, Gramicidin S and B18. The residues shown in bold were substituted (usually one at a time) with 4F-Phg.

Results and Discussion

Synthetic peptides with a single 4F-Phg substitution were synthesized using standard Fmoc chemistry [3] on an Applied Biosystems 433A peptide synthesizer. Gramicidin S was synthesized manually. The N-terminal Fmoc deprotection was performed with 20% piperidine in DMF. The synthesis was carried out in an automated manner up to the desired residue, followed by the manual coupling of the fluorinated amino acid, and then the remaining sequence was continued in the automated manner. The cleavage of the peptide from the resin was achieved with reagent K. A higher percentage of triisopropylsilane was used for the gramicidin S cleavage in order to avoid the radical-derived side reactions. Incorporation of 4F-Phg and 3F-Ala was always accompanied by racemization at Cα. A variety of coupling agents was tried including HOBt/HBTU, Tetramethylfluoroformamidinium (TFFH), and cyanuric fluoride in order to suppress the racemization. TFFH/collidine was able to suppress the racemization only in case of 3F-Ala [4]. The additional problem was encountered for 3F-Ala, as the acidic α-H caused a substantial "HF" elimination during the basic conditions employed in the Fmoc-synthesis. Replacing this α-H by a deuterium afforded the desired peptide in appreciable yield with minimal elimination resulting from the primary kinetic isotope effect. The epimeric peptides containing D- and L-4F-Phg were readily separated on an C_{18} RP-HPLC (Vydac 218TP1010) column. Trifluoroacetic acid, a commonly used ion pairing agent in HPLC, was avoided and HCl was used instead, to obtain the peptide free of ^{19}F-background for solid state NMR. Marfey's derivatization was used to identify the epimeric peptides [5].

Antibacterial assays (agar diffusion tests and Minimum Inhibitory Concentration) and fusogenic activity (via a fluorescence dequenching assay) of the 4F-Phg labeled peptides were carried out (not shown). All the L-4F-Phg containing analogues of PGLa and gramicidin S showed a very similar pattern of activity. The stereoisomers of PGLa containing D-4F-Phg were found to be consistently less active. This could be related to the inability of such peptides to form an α-helix upon membrane binding which is known for such peptides. Doubly substituted gramicidin S, which could easily accommodate the D- and L-4F-Phg side chains, shows no difference in the activity of DL- and LL-epimeric peptides. However the DD- stereoisomer was found to be inactive presumably due to a distorted amphiphilic profile. The fusogenic peptide B18 tolerated both D- and L-4F-Phg and the fusogenic activity was retained, even when the conserved N- and C-terminal residues were substituted for 4F-Phg. These results show that 4F-Phg can be substituted for a hydrophobic amino acid without altering the fundamental mode of action of the peptide, thus it can be used as a sensitive ^{19}F-NMR label to study the lipid-peptide interactions [6]. The incorporation of 3F-Ala is now under active investigation.

Acknowledgments

The work was supported by Deutsche Froschungsgeminschaft (SFB 197).

References

1. Ketchem, R. R., Lee, K. C., Huo, S. and Cross, T. A. *J. Biomol. NMR.* **8**, 1-14 (1996).
2. Grage, S. L., Wang, J., Cross., T. A. and Ulrich, A. S. *Biophys. J.* **83**, 3336-335 (2002).
3. Fields, G. B. and Nobel, R. L. *Int. J. Peptide Protein Res.* **35**, 161-214 (1990).
4. Carpino, L. A. and El-Faham, A. *J. Am. Chem. Soc.* **117**, 5401-5402 (1995).
5. Marfey, P. *Carlsberg Res. Commun.* **49**, 591-596 (1984).
6. Afonin, S., Glaser, R. W., Berditchevskaia, M., Wadhwani, P., Gührs, K. H., Möllmann, U., Perner, A. and Ulrich, A. S. *ChemBioChem.* **4**, 1151-1163 (2003).

Peptide Revolution: Genomics, Proteomics & Therapeutics
Michael Chorev & Tomi K. Sawyer (Editors)
American Peptide Society, 2003

Synthesis of 5-FAM-SSSSSSSSSS-OH: Comparison of Fmoc-Ser(Trt)-OH and Fmoc-Ser(tBu)-OH

Xiao-He Tong, Kabun Ichihara, Qing Tian and Anita Hong

AnaSpec Inc., 2149 O'Toole Ave. # F, San Jose, CA 95131, USA

Introduction

The application of Fmoc/Trt-amino acid in peptide synthesis has led to more complete coupling and "deFmoc" than Fmoc/tBu-amino acid [1,2]. The comparison has been made based on the purity of the peptides obtained using Fmoc/Trt-amino acid and Fmoc/tBu-amino acid. It was found that using Fmoc/Trt-amino acid resulted in purer peptides [3].

Recently, we found that the 5-carboxyfluorecein-decaserine peptide, 5-FAM-SSSSSSSSSS-OH (1), can be synthesized with high purity by using Fmoc-Ser(Trt)-OH, but not by using Fmoc-Ser(tBu)-OH.

Results and Discussion

Initially, when we used Fmoc-Ser(tBu)OH to synthesize 5-FAM-SSSSSSSSSS-OH (1), we obtained a mixture containing 1 and several truncated peptides (Figure 1B) with multiple MALDI-*tof*-MS peaks (Figure 2B). The structures of truncated peptides are 5-FAM-S_n-OH with n = 3-9. In contrast, using Fmoc-Ser(Trt)-OH under similar synthetic conditions, crude 1 was obtained in >95% purity (Figure 3A). MALDI-*tof*-MS showed only one peak corresponding to the desired peptide (Figure 2A, $M+H^+$ 1248.2).

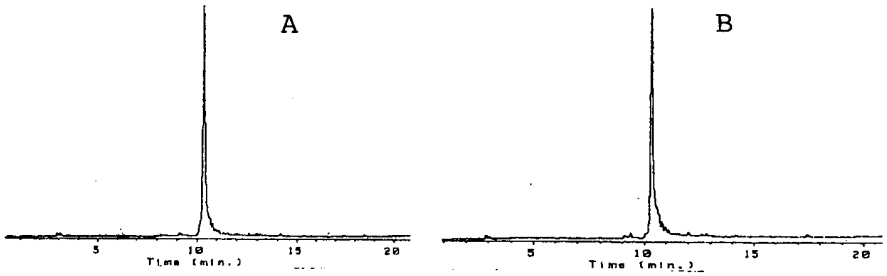

*Fig. 1. HPLC profiles of crude **1**: (A) **1** from **4**; (B) **1** using Fmoc-Ser(tBu)-OH**, Analysis: A-0.1% TFA/H_2O, B-0.09% TFA/MeCN; 1mL/min, 0-60% B for 20 min.*

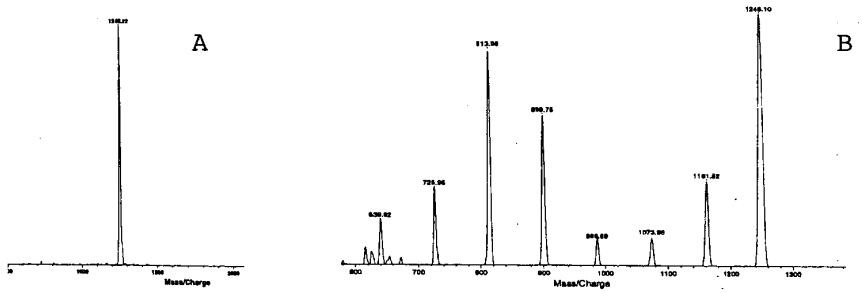

Fig. 2. MALDI-tof-MS of the 1: (A) 1 using Fmoc-Ser(Trt)-OH; (B) 1 using Fmoc-Ser(tBu)-OH.

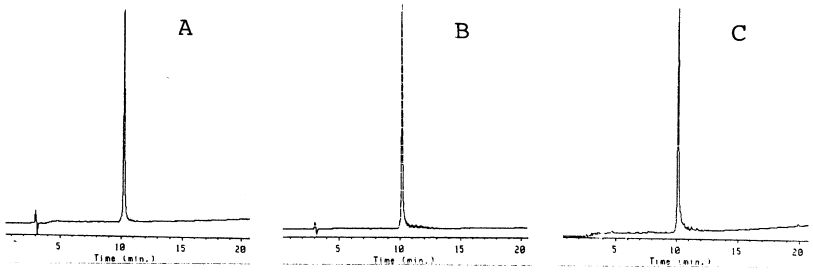

Fig. 3. HPLC profiles of crude 1: (A) 1 using Fmoc-Ser(Trt)-OH; (B) 1 from 2; (C) 1 from 3, Analysis: A-0.1% TFA/H_2O, B-0.09% TFA/MeCN; 1mL/min, 0-60% B for 20 min.

Furthermore, we studied the effect of partial replacement of the side-chain tBu protecting groups with Trt groups. We synthesized three protected peptides, 5-FAM-SSSSS-SSS (2), 5-FAM-SSSSSSSSS (3), and 5-FAM-SSSSSSSSSS (4) where S=Ser(Trt) and S=Ser(tBu), using the same synthetic protocol. After cleavage, 1 was obtained in >90%, and 80% purity from 2 and 3 respectively (Figure 3B and 3C), with the correct major MS peak. 1 was obtained in 50% purity from 4 (Figure 1A) with several MS peaks and the structures of truncated peptides are 5-FAM-S_n-OH with n = 5-9.

From this work, we think that the structural conformation of a peptide sequence containing more than three consecutive Ser(tBu) residues hindered the coupling or "deFmoc" reaction. Total or partial (three or less consecutive Ser(tBu) residues) replacement of Ser(tBu) residue with Ser(Trt) residue provides a more favorable peptide conformation for the coupling or "deFmoc" reaction.

References

1. Gausepohl, H., Behn, C., Schopfer, R. and Frank, R. W. In Epton, R. (Ed.) *Innovation and Perspectives in Solid Phase Synthesis & Combinatorial Libraries,* Mayflower Scientific, Kingswinford, U.K., p. 87-92 (1996).
2. Bloomberg, G., Mawby, W. and Tanner, M. In Epton, R. (Ed.) *Innovation and Perspectives in Solid Phase Synthesis & Combinatorial Libraries,* Mayflower Scientific, Kingswinford, U.K., p. 323-326 (1996).
3. Barlos, K., Gatos, D. and Koutsogianni, S. *J. Peptide Res.* **51**, 194-200 (1998).

Peptide Revolution: Genomics, Proteomics & Therapeutics
Michael Chorev & Tomi K. Sawyer (Editors)
American Peptide Society, 2003

Synthesis and Photophysical Properties of Acridonylalanine, a New Fluorescent Amino Acid

Aneta Szymańska, Katarzyna Wegner, Zbigniew Grzonka and Leszek Łankiewicz

Department of Organic Chemistry, Faculty of Chemistry, University of Gdańsk, Sobieskiego 18, 80-952 Gdańsk, Poland

Introduction

Synthesis of non-natural amino acids has been a major goal of many research groups. Such compounds are used for biological, biochemical and medicinal studies, both in their own right and as components of synthetic peptides and peptidomimetics. Non-coded amino acids, functionalized in the side chain with a chromophoric probe, can also serve as a very useful analytical tools, suitable e.g. for conformational studies of peptides and investigations of their interactions with other molecules.

In our own endeavor we focused on the synthesis of non-natural fluorescent amino acids, which can be used as energy donors in peptide studies based on measurements of fluorescence resonance energy transfer (FRET) [1,2]. Encouraged by excellent photophysical properties of 9-acridone derivatives substituted by alkylcarboxyl group in position 2 of aromatic ring [3] we decided to obtain amino acid bearing this chromophore in the side chain, determine its photophysical profile and design the appropriate donor-acceptor pairs applicable in peptide investigations by means of FRET technique.

Results and Discussion

3-(9-oxo-9,10-dihydroacridin-2-yl)-L-alanine (H-Aka-OH) was obtained from L-(*p*-nitro)phenylalanine in a multi-step reaction [4] (Scheme 1). The key steps of the synthesis were: catalytic reduction of the nitro group, modified Ullmann–Jourdan condensation of the obtained amine with *o*-chlorobenzoic acid (*o*-CBA) in the presence of activated cupper powder and K_2CO_3 [5] and final cyclodehydration of such obtained diphenylamine using hot polyphosphoric acid yielded the 9-acridone derivative [3,6]. This compound was next converted into Boc- or Fmoc- derivatives, useful in peptide synthesis.

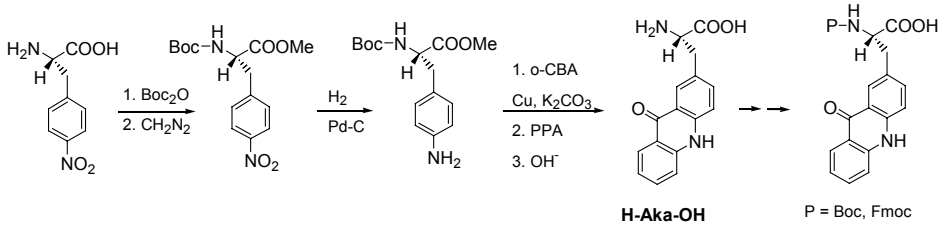

Scheme 1. Synthesis of H-Aka-OH and its derivatives.

The optical purity of the final compound was assessed by means of chromatographic method (RP-HPLC) with use of 1-fluoro-2,4-dinitrophenyl-5-L-

alanine amide (Marfey's reagent) as a differentiation agent. No racemization was observed.

As was expected, the photophysical properties of the synthesized compound are similar to those observed for 9-acridone substituted in position 2 with alkylcarboxyl group. The longwave absorption band, interesting from a point of view of further application of the chromophore in peptide studies, is located at λ=360-420 nm range. In the case of emission spectra strong influence of the solvent used is observed. In THF the quantum yield of fluorescence is strongly decreased (QY=0.21), probably due to non-specific interaction of the chromophore with the solvent. In other solvents used, the quantum yield of the fluorescence compound is very high (from QY=0.74 in MeOH to 0.94 in H_2O), which makes the acridonylalanine a very promising fluorescent probe, useful in many kinds of peptide investigations.

To confirm the utility of the obtained amino acid we have designed the donor-acceptor pairs, fulfilling the rules for the D-A pairs, engaged in a Förster type of interaction [1]. As the appropriate acceptor we have chosen two compounds: Dabcyl (4-[4-(dimethylamino)phenylazo]benzoyl) and lysine substituted in the side chain with anthraquinone moiety (H-Lys(AQN)-OH). The synthesis of the Dabcyl-like chromophore was previously reported by our laboratory [7]. The calculated values of the Förster distance were as follows: for Aka-Dabcyl pair R_0=44.3 Å and for Aka-Lys(AQN) pair R_0=36.4 Å. The Aka - Lys(AQN) pair was next incorporated into the model peptide, which sequence shows high tendency to adopt stable helical conformation [8]. In this compound strong quenching of the Aka emission was observed, as the result of very effective energy transfer to anthraquinone acceptor (E_T=0.89 for TFE, E_T=0.94 for H_2O). It confirms excellent properties of the obtained fluorescent amino acid and makes it a valuable tool for peptide investigations.

Acknowledgments

The work was supported by State Committee for Scientific Research (KBN, Poland) – grant 298/P04/2001/21.

References

1. Wu, P. and Brand, L. *Anal. Biochem.* **218**, 1-13 (1994).
2. Chirio-Lebrun, M.-Ch. and Prats, M. *Biochem. Edu*. **26**, 320-323 (1998).
3. Szymańska, A., Łankiewicz, L. and Wiczk, W. *Chem. Heterocycl. Comp*. **7**, 914-921 (2000).
4. Szymańska, A, Wegner, K. and Łankiewicz, L. *Helv. Chim. Acta* – accepted.
5. Pellon, R. F, Carrasco, R., Marquez, T. and Mamposo, T. *Tetrahedron Lett.* **38**, 5107-5110 (1997).
6. Taraporewala, I. B. and Kauffman, J. M. *J. Pharm. Sci.* **79**, 173-178 (1990).
7. Szymańska, A, Ossowski, T. and Łankiewicz L. *LIPS* **9**, 193-196 (2003).
8. Marqusee, S., Robbins, V. H. and Baldwin, R. L. *Proc. Natl. Acad. Sci. U.S.A.* **86**, 5286-5290 (1989).

Peptide Revolution: Genomics, Proteomics & Therapeutics
Michael Chorev & Tomi K. Sawyer (Editors)
American Peptide Society, 2003

Synthesis of PEG-Inhibitor Conjugates for Affinity Separation of Serine Proteases

Shin Ono and Makiko Umezaki

Biomolecular Function Design, Faculty of Engineering, Toyama University, Gofuku 3190, Toyama 930-8555, Japan

Introduction

Diphenyl α-aminoalkylphosphonates are known to irreversibly and specifically inactivate serine proteases [1]. Since diphenyl α-aminoalkylphosphonates are relatively stable in aqueous solution, Powers et al. succeeded in the synthesis of their conjugates with biotin [2] or fluorescent compounds [3] useful for investigation of localization of intracellular serine proteases. Legendre et al. developed a selection strategy for phage-displayed enzymes using a biotinylated phosphonate inhibitior and a streptoavidin coated support [4]. Moreover, we recently prepared a Phe-type diphenyl α-aminoalkylphosphonate derivative that irreversibly inactivated chymotrypsin-like serine proteases and immobilized it on sepharose gel, and we demonstrated that chymotrypsin could be separated from a solution containing chymotrypsin and trypsin by using the obained inhibitor-immobilized gel [5].

In this study, the Phe-type phosphonate inhibitor moiety (diphenyl 1-amino-2-phenylethylphosphonate) was introduced into poly(ethylene glycol)s (PEGs) with different average molecular weights of 300, 400 and 600 to give PEG-inhibitor conjugates (Figure 1), and then the binding abilities of chymotrypsin and trypsin to the otained PEG-inhibitor conjugates were evaluated. PEGs are hydrophilic and water-soluble, whereas the Phe-type phosphonate inhibitor moiety is hydrophobic and water-insoluble. Thus PEG-inhibitor conjugates are expected to be water-insoluble but adequately hydrophilic, resulting in an enhancement of their accessbility to enzymes.

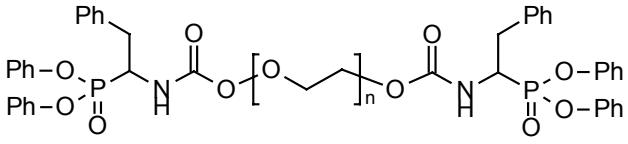

Fig. 1. Structural formula of PEG-inhibitor conjugate.

Results and Discussion

The PEG-inhibitor conjugates were synthesized in two steps. In the first step, carbamoyl groups were introduced into the teminal hydroxy groups in PEGs to give the PEG carbamates as previously described [6]. For the preparation of the PEG300-inhibitor conjugate, PEG300 and sodium cyanate were mixed in tetrahydrofuran. Trifluoroacetic acid was then gently added and the reaction was allowed to proceed overnight at room temperature. The produced PEG300 carbamate was extracted with chloroform. In the second step, the Phe-type phosphonate inhibitor moiety was introduced into the PEG300 carbamate, according to the α-amidoalkylation method of triphenyl phosphite described by Oleksyszyn et al [7]. The PEG300 carbamate was reacted with triphenyl phosphite and phenylacetaldehyde in acetic acid. After partial

purification by silica gel chromatography, the obtained product was treated with water to give the desired water-insoluble PEG300-inhibitor conjugate. Other water-insoluble PEG400- and PEG600-inhibitor conjugates were also prepared by a similar procedure.

To examine whether the PEG300, 400 and 600-inhibitor conjugates can selectively separate serine proteases, these conjugates were mixed with chymotrypsin for 20 min in a buffer. After the reaction mixtures were centrifuged to separate insoluble components, soluble components in the supernatants were analyzed by gel-filtration HPLC. Under these conditions, almost all of the chymotrypsin peak disappeared after reaction with the PEG600-inhibitor conjugate, indicating chymotrypsin can be separated from the solution due to formation of the precipitate with the water-insoluble PEG600-inhibitor conjugate, while other inhibitor conjugates gave only partial separation (26-43%).

Since the PEG600-inhibitor conjugate revealed the most excellent separation ability for chymotrypsin, selectivity in the separation was examined. In a similar manner to that described above, the PEG600-inhibitor conjugate was added to a sample solution containing chymotrypsin and trypsin, and the remaining components in the supernatant were analyzed by RP-HPLC. The chymotrypsin peak clearly disappeared but the trypsin peak remained after mixing with the PEG600-inhibitor conjugate, indicating that chymotrypsin was selectively precipitated with the conjugate. In addition, chymotryptic activity in the supernatant was not detected, but 90% of tryptic activity remained. These results indicate that chymotrypsin can be selectively separated by the PEG600-inhibitor conjugate.

Moreover, components in the precipitate formed by mixing of the PEG600-inhibitor conjugate with chymotrypsin were analyzed by gel-filtration HPLC and MALDI-TOF-MS. The precipitate was dissolved in DMSO and gel-filtration HPLC analysis of the components was directly carried out. The precipitate was found to contain two components related to chymotrypsin from the HPLC analysis. Two molecular mass peaks were detected at 25,288 and 50,670 m/z in MALDI-TOF-MS analysis of the precipitate. This result suggests that one component of the precipitate is a dimeric chymotrypsin cross-linked by the PEG600-inhibitor conjugate containing two phosphonate moieties and another is a monomeric chymotrypsin bound to the conjugate.

In conclusion, we succeeded in the preparation of water-insoluble PEG-inhibitor conjugates useful for affinity separation of chymotrypsin using the Phe-type diphenyl α-aminoalkylphosphonate [8]. The synthetic route of these PEG-inhibitor conjugates can be applied to preparation of other PEG-inhibitor conjugates with various substrate specificities by changing the aldehydes used in the amidoalkylation reaction of triphenyl phosphite. Our separation method can be also used for separation and screening of unknown serine proteases.

References

1. Oleksyszyn, J. and Powers, J. C. *Method in Enzymology* **244**, 423-441 (1994).
2. Woodard, S. L., et al. *J. Immumol.* **153**, 5016-5025 (1994).
3. Abuelyaman, A. S., et al. *Bioconjugate Chem.* **5**, 400-405 (1994).
4. Legendre, D., et al. *J. Mol. Biol.* **296**, 87-102 (2000).
5. Ono, S., et al. *Biosci. Biotechnol. Biochem.* **66**, 1111-1115 (2002).
6. Loev, B. and Kormendy, M. F. *J. Org. Chem.* **28**, 3421-3426 (1963).
7. Oleksyszyn, J., Subotkowska, L. and Mastalerz, P. *Synthesis* 985-986 (1979).
8. Umezaki, M., et al. *Biosci. Biotechnol. Biochem.* **67**, 2273-2276 (2003).

Peptide Revolution: Genomics, Proteomics & Therapeutics
Michael Chorev & Tomi K. Sawyer (Editors)
American Peptide Society, 2003

N-Methylation at the C-Terminus in Solid Phase Peptide Synthesis

Yun Wu, Yuan Gao, Wei-Jun Zhang and Garland R. Marshall

Department of Biochemistry and Molecular Biophysics, Washington University in St Louis, School of Medicine, 660 S Euclid, St Louis, MO 63110, USA

Introduction

Tripeptides are important model substances for exploring the initial steps of secondary structure formation in protein folding. Trialanine is of particular importance due to the high helical propensity of its amino acid residues [1]. In 1991, Brooks and co-workers preformed molecular dynamics calculation on Ac-Ala-Ala-Ala-NHMe and Ac-Val-Val-Val-NHMe in water [2]. For the alanine peptide, they found an extended β-sheet structure at only slightly lower energies than the helical conformation. For the valine peptides, the authors obtained a significant stabilization of the β-sheet structure. We introduced an "Aib-scan" method in the Ala tripeptide (Figure 1), to facilitate the use of polarized Raman and FTIR spectroscopy in investigating which position was more important for stabilization of β-sheet structures [3].

1. Ac-Aib-Ala-Ala-NHMe
2. Ac-Ala-Aib-Ala-NHMe
3. Ac-Ala-Ala-Aib-NHMe

Fig. 1. Target molecules with NHMe as the carboxy-terminal blocking group.

Results and Discussion

For the synthesis of similar peptides, solution methods have usually been the method of choice. Though site-selective N-methylation on solid phase emerged in 1997, the method of Miller and Scanlon was used at the N-terminus or within the peptide chain [4]. Here, we report a solid phase approach to prepare Aib-containing tripeptides with an NHMe-capped carboxy terminal.

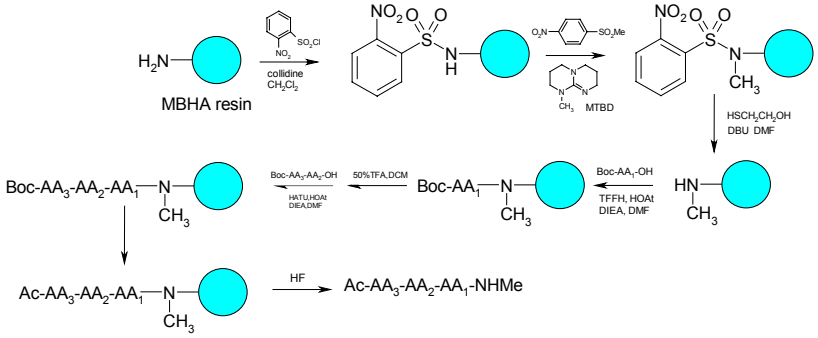

Fig. 2. Synthetic scheme of tripeptides with NHMe-capped carboxy terminal.
Sequences: Ac-Ala-Ala-Aib-NHMe, Ac-Ala-Aib-Ala-NHMe, Ac-Aib-Ala-Ala-NHMe.

Following Miller's procedure, the amino resin was protected at the *o*-nitrobenzenesulfonamide by treatment with the corresponding sulfonyl chloride in CH_2Cl_2 containing collidine for 2h. Deprotonation of the sulfonamide with MTBD and

alkylation with methyl *p*-nitrobenzenesulfonate in DMF for 30min gave us a methylated material, which was further treated with β-mercaptoethanol and DBU in DMF for 30min to provide a methylated amino resin. Loading of the first amino acid was residue-dependent. Though Boc-Ala-OH could be linked onto the resin conveniently, only repeated coupling with TFFH/HOAt gave us Aib-loaded resins. After deprotection of Boc-AA_2-AA_1-N(Me)-resin, the ninhydrin test was only pale blue. If we repeated the deprotection, it remained pale blue with ninhydrin. HF treatment at this stage didn't give us H_2N-AA_2-AA_1-NHMe, indicating a possible sequence deletion by diketopiperazine formation during the deprotection step of Boc-AA_2-AA_1-N(Me)-resin. We prepared the dipeptide Boc-AA_3-AA_2-OH first, and linked the dipeptide segment onto H_2N-AA_1-N(Me)-Resin.

We have thus demonstrated a useful method to prepare Aib-containing tripeptides with an NHMe-capped carboxy terminal. In addition to the Fmoc strategy Miller has used for N-methylation at the N-terminus or within the peptide skeleton, our experiment indicated that the Boc strategy was also compatible.

Acknowledgments
The work was funded by NIH grant GM53630.

References

1. Chou, P. Y. and Fassman, G. D. *Adv. Enzymol.* **47**, 45 (1978).
2. Tobias, D. J. and Brooks III, C. L. *Biochemistry* **30**, 6059-6070 (1991).
3. Schweitzer-Stenner, R., Eker, F., Huang, Q. and Griebenow, K. *J. Am. Chem. Soc.* **123**, 9628-9633 (2001).
4. Miller, S. C. and Scanlan, T. S. *J. Am. Chem. Soc.* **119**, 2301-2302 (1997).

Peptide Revolution: Genomics, Proteomics & Therapeutics
Michael Chorev & Tomi K. Sawyer (Editors)
American Peptide Society, 2003

Stereospecific Synthesis of α-Alkyl α,α-Diamino-α-Carboxylates as Core Structural Units for Novel HIV-1 Protease Inhibitors

Tanaji T. Talele and Mark L. McLaughlin*

Department of Chemistry, University of South Florida, Tampa, FL 33620, USA

Introduction

Rare and non-natural α-substituted and α,α-disubstituted amino acids have received considerable attention due largely to their important role in the design of conformationally restricted peptides with enhanced properties, sukch as resistance to hydrolysis and enzyme cleavage processes. The difficulty in asymmetric synthesis of the chiral α,α-disubstituted amino acids, which bear a chiral quaternary carbon, restricts the available chiral α,α-disubstituted amino acids for the conformational study of peptides containing such residues. Hydrolytic enzymes are one of the most useful groups of enzymes from the asymmetric synthetic point-of-view, with the pig liver esterase (PLE) having emerged as an especially useful catalyst for resolution and the creation of the chiral synthons.

Herein we report our studies of five different approaches to synthesize differentially protected geminal diamino acids. This investigation involves two major concerns: a) scope of the PLE for stereospecific hydrolysis of one of the esters of diethyl malonate, and b) application of Curtius rearrangement on the half esters.

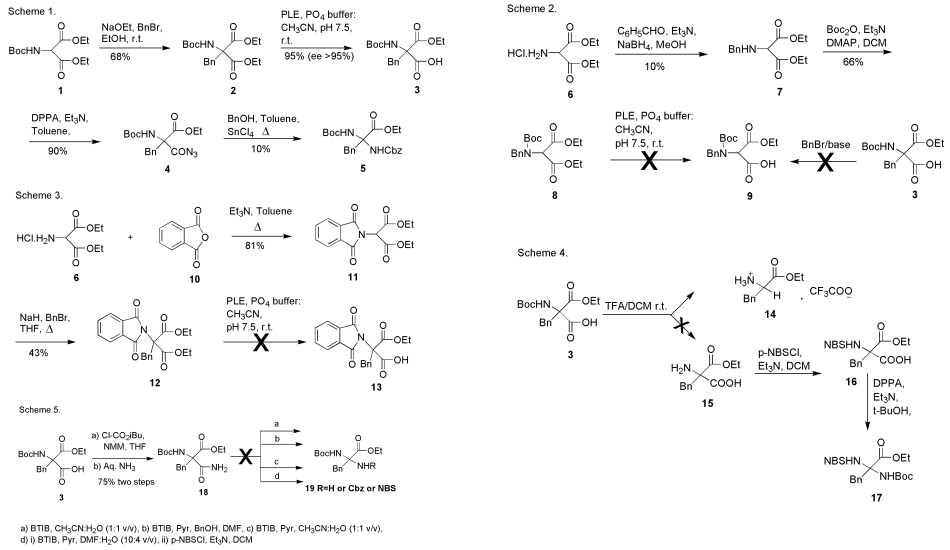

Schemes 1-5. Synthetic routes to differentially protected geminal diamino acids.

Results and Discussion

One of the most potentially direct routes to highly functionalized α,α-disubstituted amino acids is via alkylations, followed by stereospecific enzymatic hydrolysis and azide rearrangement. The first retrosynthetic route for the synthesis of target molecules is shown in Scheme 1. Synthesis starts with Boc protected amino diethyl malonate.

Alkylation of this derivative with benzyl bromide gave compound **2** in an excellent % yield. Treatment of compound **2** with PLE in acetonitrile/PO_4 buffer system (pH 7.5) afforded compound **3** in 95% yield with >95 enantiomeric excess (ee). Boc protected amino function in compound **2** seems appropriate not only for quantitative hydrolysis by PLE but also for stereospecificity of the hydrolytic cleavage of one of the ester groups. Based on the Jones PLE model [1], we propose that the benzyl substituent in compound **2** might be occupying H_L site while Boc amino substituent fills the H_S site of the enzyme. The absolute stereochemistry of the half ester **3** remains to be defined. However, derivatization of the acid group in compound **3** into chiral amide by coupling with R(+)-α-methylbenzylamine showed the presence of only one enantiomer. The acyl azide group in compound **4** would be expected to undergo Curtius rearrangement in high boiling solvents to corresponding free amines or protected amines. This reaction, however was found to be very sluggish. After investigations we concluded that nucleophilicity of the -NH- moiety might be the cause of complications at the Curtius rearrangement step. Thus, we decided to convert -NHBoc into fully protected -N(Bn)(Boc) functionality (see Scheme 2). Unfortunately, several attempts of reductive benzylation were very daunting (many spots by TLC and lots of unreacted benzaldehyde in spite of equimolar ratio of amine to aldehyde). The compound **7** was benzylated to form product **8** in good yields. Product **8** was treated with PLE at pH 7.5. This reaction failed to hydrolyze perhaps due to excess steric bulk at the N atom.

In our next approach (Scheme 3), we protected the amino group of compound **6** by phthalic anhydride, followed by alkylation and enzymatic hydrolysis. Enzymatic hydrolysis of compound **12** failed. Again we expect the excess steric bulk at H_L site of the enzyme could be responsible.

Next, we decided to revisit the first approach with some modifications at amine function. Compound **3** was deprotected with TFA/DCM to obtain compound **15**, instead we obtained compound **14** as an exclusive product (see Scheme 4). The decarboxylated compound **14** was unambiguously assigned based on its ^{13}C NMR and single crystal X-ray diffraction data.

Based on information obtained previously, we further attempted Hofmann rearrangement (direct oxidative conversion of amide to amines) through modified reagent [*I,I*-Bis(trifluoroacetoxy)iodo]benzene (BTIB). The amide **18** obtained from acid **3** via mixed anhydride intermediate was subjected to different reaction conditions to obtain free or protected amine function (see Scheme 5). Unfortunately, none of these attempts were successful. We believe milder methods are needed to synthesize α,α-diaminopropionic acids.

Acknowledgments
We acknowledge financial support from PHS grants AG19981, AG1983, and AI054246.

References

1. Toone, E. J. and Jones J. B. *Tetrahedron: Asymmetry* **2**, 1041-1052 (1991).
2. Salgado, A., Huybrechts, T., Eeckhaut, A., Eycken J. V., Szakonyi, Z., Fulop, F., Tkachev, A. and Kimpe, N. *Tetrahedron* **57**, 2781-2786 (2001).

Peptide Revolution: Genomics, Proteomics & Therapeutics
Michael Chorev & Tomi K. Sawyer (Editors)
American Peptide Society, 2003

Amino Acid and Peptide Labeling

Susana M.B. Fraga, M. Sameiro T. Gonçalves and Hernâni L.S. Maia

Department of Chemistry, University of Minho, Gualtar, P-4710-057 Braga, Portugal

Introduction

In the last two decades the sensitive detection, identification and quantification of amino acids has been achieved by using dyes in simple and fast analytical methods. Although fluorometric methods are potentially much more sensitive than colorimetric methods, the use of non-fluorescent dyes is also important. Examples of applications of non-fluorescent dyes include the use of amino acid N-derivatizing groups, such as 5-formyl-1-*H*-pyrrole-2-carboxylic acid, which can be colored on demand by treatment with hydrocinnamoyl [1] and 4[(*N,N*-dimethylaminophenyl)-4'-diazenyl]benzenesulfonyl chloride for amino acid analysis by HPLC [2], capillary [3] and polyacrylamide gel [4] electrophoresis. The use of chromophoric reagents in peptide chemistry also includes the synthesis of colored peptide libraries labeled with mono carboxylic blue anthraquinone and red azo dyes [5]. The synthesis of new fluorogenic substrate probes for HIV protease based on resonance energy transfer has also been reported [6]. The method uses a fluorescent donor placed near one end of the substrate and a chromophoric acceptor placed near the other end. The most effective donor/acceptor pair used was 5-(2'-aminoethyl)aminonaphthalene sulfonic acid and 4-[(*N,N*-dimethylaminophenyl)-4'-diazenyl] benzoic acid. Having this in mind we used an azo carboxylic dye for labeling lysine and serine amino acids at their side chain and also for the synthesis of several peptides colored at their amine group.

Results and Discussion

Following our previous work [7] using 3-[*N,N*-dimethylaminophenyl-4'-diazenyl]phenylacetic acid (**1**) in labeling amino acids at their N-terminus, an alternative acylation at a lysine ω-amine group was investigated. Thus, the methyl ester of *N*- benzyloxycarbonyl lysine was reacted with **1** in DMF by a DCC/HOBt coupling, to give the expected colored derivative (**2a**) in a yield of 70% (Scheme 1). The product of saponification of **2a** was obtained in a yield of 98% and then coupled with alanine methyl ester and phenylalanine ethyl ester to produce **3a** and **3b** in high yields (98 and 91%, respectively).

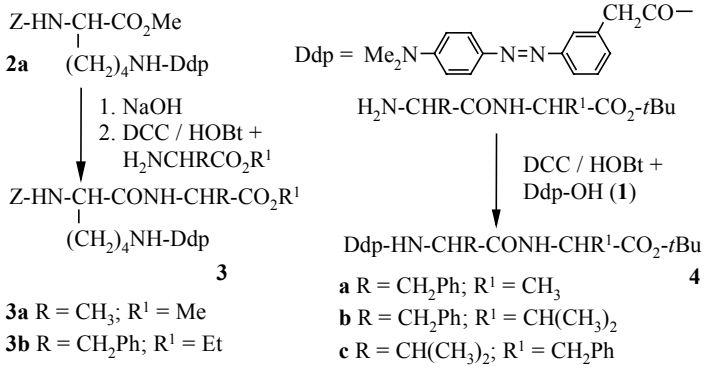

Scheme 1. Ddp-labeling of Lys at the ω-amine and amino acids at the N-terminus.

Another approach for side chain labeling was undertaken by reacting *tert*-butyloxycarbonyl serine methyl ester with dye **1** to yield 86% of the corresponding orange ester derivative **2b**. Labeled dipeptides (**4**) were also obtained by acylation (DCC/HOBt) at their N-terminus with chromophore **1** in yields ranging from 66 to 94%.

*Table 1. Physical and analytical data of compounds **2**, **3** and **4**.*

Compound	Yield/ %	m.p./ °C	λ_{max}/nm (ε) (in MeOH)
Z-Lys(ω-Ddp)-OMe (**2a**)	70	130.0-132.0	410 (28 430)
Boc-Ser(Ddp)-OMe (**2b**)	86	95.6-96.6	415 (23 643)
Z-Lys(ω-Ddp)-Ala-OMe (**3a**)	98	152.6-154.6	414 (22 069)
Z-Lys(ω-Ddp)-Phe-OEt (**3b**)	91	142.7-144.7	412 (18 704)
Ddp-Ala-Phe-O*t*Bu (**4a**)	84	119.7-120.4	410 (27 967)
Ddp-Val-Phe-O*t*Bu (**4b**)	66	187.5-188.8	414 (29 146)
Ddp-Phe-Val-O*t*Bu (**4c**)	94	124.7-126.0	411 (25 029)

All compounds were obtained as solid materials and were characterized by elemental analyses, NMR (^{1}H and ^{13}C) and visible spectroscopy. The visible spectra of labeled dipeptides showed absorption peaks between 410 (**4a**) and 414 (**3a**, **4b**) with ε values ranging from 18 704 (**3b**) to 29 146 (**4b**) (Table 1). All products were stable on storage in the air and at room temperature.

Acknowledgments
We thank the Foundation for Science and Technology (Portugal) for financial support to the Institute of Biotechnology and Fine Chemistry (University of Minho).

References

1. Abell, D. C., et al. *Tetrahedron Lett.* **43**, 3673-3675 (2002).
2. Jansen, E. H. J. M., et al. *J. Chromatogr.* **553**, 123-133 (1991).
3. Garner, T. W. and Yeung, E. S. *Anal. Chem*. **62**, 2193-2198 (1990).
4. Parkinson, D. and Redshaw, J. D. *Anal. Biochem*. **14**, 121-126 (1984).
5. Sebestyén, F., et al. *J. Peptide Sci*. **4**, 294-299 (1998).
6. Wang, G. T., et al. *Tetrahedron Lett.* **31**, 6493-6496 (1990).
7. Fraga, S. M. B., Gonçalves, M. S. T. and Maia, H. L. S. In Benedetti, E. and Pedone, C. (Eds.), *Peptides 2002* (Proceedings of the 27th European Peptide Symposium), Edizioni Ziino, Napoli, 2002, pp. 110-111.

Peptide Revolution: Genomics, Proteomics & Therapeutics
Michael Chorev & Tomi K. Sawyer (Editors)
American Peptide Society, 2003

The 1,1-Dioxobenzo[b]thiophene-2-ylmetholoxycarbonyl (Bsmoc) Amino-Protecting Group

Nayan Amin, John Giantsidis, Ted Appleby, Sukhamaya Bain and Ed Price

PolyCarbon Ind., 88 Jackson Road, Devens, MA 01432 USA

Introduction

Prof. Louis Carpino developed the Bsmoc (1,1-Dioxobenzo[b]thiophene-2-ylmethyl-oxycarbonyl) amino-protecting group in 1997 [1]. Realizing the advantages of using the Bsmoc group over the more traditional Fmoc group in peptide synthesis, Carpino and co-workers began developing strategies to utilize the Bsmoc amino acid protecting group for solid- phase, solution-phase and rapid, continuous solution-phase synthesis of peptides. This methodology represent a significant improvement over corresponding Fmoc-based synthesis methods since one can use either water or salt solutions rather than an acidic phosphate buffer to remove all by products that are formed after deprotection. Consequently, by employing this methodology one can achieve cleaner phase separations and higher yields of the desired peptide. PolyCarbon Industries has completed significant work in order to promote the use of Bsmoc over Fmoc in peptide synthesis as well as develop and perfect the commercial-scale production methods of Bsmoc protected amino acids. Base sensitive amino-protecting groups such as Fmoc (fluorenylmethoxycarbonyl) and related species owe their reactivity to a facile β-elimination process. Certain peptide segments founder when resins bearing cyclic secondary amino functions are found to be inefficient scavenging agents for the facile β-elimination byproduct dibenzofulvene (DBF). The dibenzofulvene is in fact an insoluble polymer material. In order to avoid the troublesome purification problems due to the formation of this byproduct a search for a different type of amino-protecting group (in which the deblocking event is simultaneously a scavenging event) was undertaken.

Results and Discussion

Typically peptide syntheses are carried out by either solution-phase (rapid or continuous solution) or solid-phase. Some examples of peptides synthesized by each of these three methods are described below.

Rapid solution-phase synthesis. The BSMOC technique has been utilized in the synthesis of several short peptides [2] such as: Bsmoc-Tyr(t-Bu)-Ile-Asp(o-t-Bu)-Gly-O-t-Bu (87%), Bsmoc-Tyr(t-Bu)-Gly-Gly-Phe-Leu-O—t-Bu(49%), Bsmoc-Phe-Phe-Val-Gly-Leu-Met-Obn (37%), and Fmoc-Ile-Thr-(t-Bu)-Arg(Pbf)-Gln(Trt)-Arg(Pbf)-Tyr(tBu)-Odcmp. These examples demonstrate the applicability of using BSMOC for solution phase synthesis.

Rapid, continuous solution phase synthesis: One of the best means of employing the Bsmoc strategy would be what Carpino has described to be rapid, continuous solution-phase peptide synthesis [3] for longer peptides. This method incorporates the Bsmoc/TAEA [tris(2-aminoethyl) amine] means of production that is applicable from gram to scale synthesis. Rapid, continuous solution-phase peptide synthesis avoids the isolation and purification steps frequently associated with classical solution methods as well as not requiring expensive resins or excess reagents that are associated with solid-phase peptide synthesis. The other major benefits to utilizing Bsmoc and the rapid,

continuous solution-phase peptide synthesis technique results in the formation of only water soluble by-products (TAEA) and that sophisticated or expensive equipment is not required. For example a nine amino acid segment of human growth hormone releasing factor, hGRF(21-29) was produced using this methodology [3].

Solid-phase syntheses. Solid phase peptide synthesis is based on the sequential addition of alpha amino and side–chain protected amino acid residues to an insoluble polymeric support. Several peptides have been made using Bsmoc protected amino acids with coupling agents such as HATU [4]. The deblocking step was routinely carried out with 2,3,or 5% piperidine rather than the 20 % piperidine commonly used for Fmoc removal. This allows the reduction or elimination of base catalyzed side reactions. The following peptide has been made utilizing this technique [2]: Bz-Val-Lys-(Boc)- β-Asp(α--t-Bu)-Gly-Tyr(t-Bu)-Ile-OH, H-Tyr-Aib-Aib-Phe-Leu-OH.

Application of Bsmoc chemistry. Some examples in which application of Bsmoc has been shown to be favored over Fmoc chemistry are described below.

In a first case, the assembly of a 5-mer peptide H-Tyr-Aib-Aib-Phe-Leu-NH_2 includes the very difficult Aib-Aib sequence for peptide bond formation. If one were to run Bsmoc versus Fmoc using the same conditions, the difficult Aib-Aib peptide bond is formed more readily via Bsmoc chemistry than via Fmoc.

In the formation of an octapeptide the assembly was started with the C-terminal function of tryptophan amide modified as the N-dimethylcyclopropylmethyl (Dmcp) derivative. In order to maintain the solubility of the growing peptide a nonpolar, water immiscible solvent (dichloromethane) was used in the extraction process. This was needed to achieve complete byproduct removal. Two different methods were used to assemble the chain and both worked equally well. In one case isolated amino acid fluorides were used throughout for coupling. In a second run, the HATU reagent was used for the first seven coupling steps, and then the switch was made from TAEA to piperazino silica as the deblocking agent.

A recently published paper by Greenwald [5] used one equivalent of 4-piperidinopiperidine to easily deblock the Bsmoc group during the synthesis of 2`-paclitaxel glycinate that was obtained in high yield (98%) and good quality. However, clean products were not obtained in reasonable yield when FMOC synthesis technique was used. This is an excellent example of where a lower concentration of base can be used to achieve both higher yields and much improved quality.

References

1. Carpino, L. A., et al. *J. Am. Chem. Soc.* **119**, 9915-9916 (1997).
2. Carpino, L. A., et al. *J. Org. Chem.* **64**, 4324-4338 (1999).
3. HATU is manufactured and sold by Polycarbon Inds.
4. Carpino, L. A. *Org. Pro. Res. Dev.* **7**, 28-37 (2003).
5. Greenwald, R. B. *J. Org. Chem*. **68**, 4894-4896 (2003).

Peptide Revolution: Genomics, Proteomics & Therapeutics
Michael Chorev & Tomi K. Sawyer (Editors)
American Peptide Society, 2003

Facile Synthesis of a Constrained Aza-Dipeptide (ADP)

Umut Oguz and Mark L. McLaughlin*

Department of Chemistry, University of South Florida, Tampa, FL, 33620, USA

Introduction

Herein, we report a very efficient way of synthesizing a constrained aza-dipeptide (ADP). A general retrosynthetic analysis of this compound shows two possible synthetic routes to the target dipeptide (Figure 1). The key intermediate in each route is a hydrazino amino acid derivative [1].

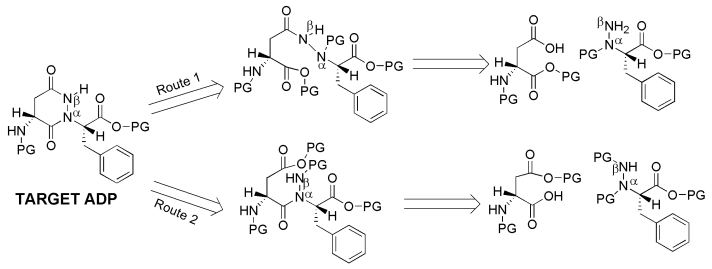

Fig 1. Retrosynthetic analysis of ADP.

Results and Discussion

In Route 1, after the removal of benzyl groups, compound **4** was ready to be cyclized to the corresponding ADP by intramolecular amide bond formation (Figure 2). Compound **4** has two nucleophilic nitrogens, and the coupling of N_α to the free carboxyl group would give the desired six-membered ring **6**. Coupling of the N_β to free carboxyl group would give five-membered ring **5**. Surprisingly, the five-membered ring forms faster than the six-membered ring, in spite of the N_β being much less nucleophilic than N_α. The product was easily crystallized from DCM/hexanes after introducing a more rigid protecting group, *p*-nitrobenzenesulfonyl (*p*NBS-) and five-membered ring **7** was the only product (Figure 3).

One way to avoid five-membered ring formation over six-membered ring formation is to protect the amide nitrogen, N_β, of **3** before the hydrogenation step, which would diminish its already low nucleophilicity. N_β is protected with a Boc- group and cyclization of the fully protected compound still yields the five-membered ring, which indicates that during the reaction, the Boc-group on the N_β comes off to give the five-membered ring as the only product. As a conclusion, it is not possible to get the desired six-membered ring from Route 1.

Unlike Route 1, Route 2 does not have any intermediate compounds with the possibility of giving five-membered rings (Figure 2). The key reaction step in the synthesis is the very effective coupling of the D-aspartic acid derivative with the N_α of the intermediate **8** by symmetrical anhydride method [2]. Coupling reactions of sterically hindered amino acid derivatives generally give very low yields and require harsh conditions. Some of these traditional coupling methods interfere with the protecting groups of the amino acids. This method is proven to be very advantageous for our synthesis, and the lack of base effectively prevented a variety of side reactions.

After coupling it was not possible to separate the unreacted starting material **8** from the product **10**. During purification, the presence of the unreacted starting material was not seen on TLC plates in many different solvent systems where only one spot was present. The results of ^{1}H and ^{13}C NMR spectra verified the presence of the unreacted hydrazine **8.** The reaction conditions were optimized to make the reaction go to completion without any remaining unreacted **8**. To our surprise, the extended reaction times had more significant effect on the yield than the equivalents of the anhydride used.

Cyclization of **11** with PyOAP and HATU gave very low yield. Formation of a side product as the major product is seen, which we think is a result of a reaction between **11** and the coupling reagent according to ^{1}H and ^{13}C NMR spectra. High yields in cyclization are obtained with DCC/HOBt/DIEA without any racemization. The overall yield in the ADP **12** synthesis is 93%. The overlapping broad multiplets observed for compound **10** are resolved into sharper well-resolved multiplets in the ^{1}H NMR spectrum of compound **12**.

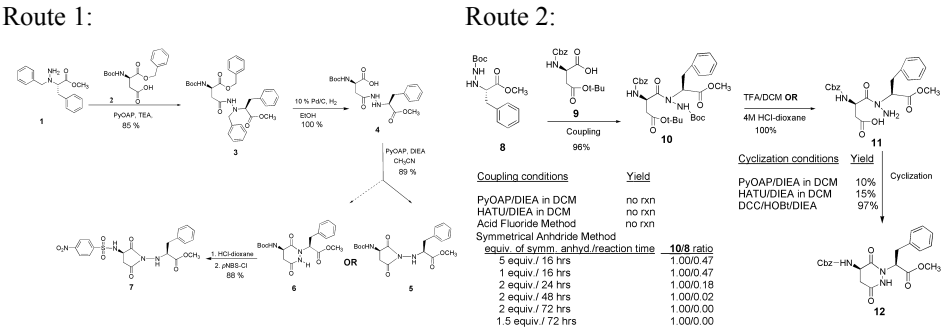

Fig. 2. Synthetic Route 1 and Route 2 for the synthesis of ADP.

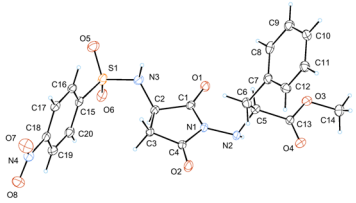

Fig. 3. X-ray crystal structure of 7.

Acknowledgments

We acknowledge financial support from PHS via AG-19981, AG-1983, and AI-054246.

References

1. Oguz, U., Guilbeau, G. G. and McLaughlin, M. L.,*Tetrahedron Lett.* **43,** 2873 (2001).
2. Fu, Y. and Hammer, R. P. *Org. Lett*. **4**, 237 (2002).

Peptide Revolution: Genomics, Proteomics & Therapeutics
Michael Chorev & Tomi K. Sawyer (Editors)
American Peptide Society, 2003

Synthesis of Azapeptides using *N*-Boc-Aza[1]-dipeptide Building Blocks

Rosa E. Melendez and William D. Lubell

Département de Chimie, Université de Montréal, C.P. 6128, Succursale Centre-Ville, Montréal, Québec H3C 3J7, Canada

Introduction

Azapeptides are peptide analogues in which the α-carbon of one or more of the amino acid residues is replaced with a nitrogen atom [1]. The elimination of the chiral carbon maintains the side-chain and hydrogen bond functionality that may contribute to recognition. Having demonstrated the synthesis of azapeptides without racemization in solution by the preparation of Boc-azaPhe-Ala-Phe-OMe [2], we present a general strategy for the synthesis of *N*-Boc-aza[1]-dipeptides and their introduction into peptide chains by solid-phase synthesis (Figure 2). Three azapeptide analogs of the C-terminus fragment of human calcitonin gene related peptide **1** (α-hCGRP) have been synthesized for evaluation as potential antagonists (Figure 1). α-hCGRP is a 37 amino acid neuropeptide that is characterized by a disulfide loop between residues 2-7, an α-helix between residues 8-18 and an aminated C-terminus (Figure 1) [3]. Structure activity studies have found that C-terminus fragments exhibit antagonist activity as well as turn secondary structures. Because azapeptides have been shown to adopt the *i*+1 and *i*+2 positions of β-turns [4], control peptides **2** and **3** and their azapeptide counterparts **4**-**6**, all have been synthesized to study the importance of turn regions around the aromatic residues for antagonist activity.

Results and Discussion

Previous syntheses of azapeptides on solid-phase have suffered from intramolecular hydantoin formation [5]. By incorporation of aza-amino acids as *N*-Boc-aza[1]-dipeptides, hydantoin formation was avoided during the synthesis of **4**-**6** (Figure 2). *N*-Benzyl *t*-butylcarbazate **7** was synthesized by condensation of *t*-butylcarbazate with benzaldehyde followed by hydrogenation over Pd/C in methanol. Isocyanates of alanine and valine benzyl esters reacted with **7** in DCM to yield azadipeptide esters **8**. Hydrogenolysis of benzyl esters **8** was carried out over Pd/C in ethanol to obtain **9a** and **b** in 71% and 80% overall yield respectively from **7**.

(**1**) α-hCGRP ACDTATCVTHRLAGLLSRSGGVVKNNFVPTNVGSKAF-NH_2

	Sequence	MS	HPLC purity
(**2**)[D^{31}, P^{34}, F^{35}]$CGRP_{29-37}$	PTDVGPFAF-NH_2	948	94
(**3**)[D^{31}, P^{34}, F^{35}]$CGRP_{27-37}$	FVPTDVGPFAF-NH_2	1194	94
(**4**) [D^{31}, P^{34}, $AzaF^{35}$]$CGRP_{29-37}$	PTDVGP**F**AF-NH_2	949	90
(**5**) [$AzaF^{27}$, D^{31}, P^{34}, F^{35}]$CGRP_{27-37}$	**F**VPTDVGPFAF-NH_2	1195	94
(**6**) [D^{31}, P^{34}, $AzaF^{35}$]$CGRP_{27-37}$	FVPTDVGP**F**AF-NH_2	1195	89

Fig. 1. Sequence of α-hCGRP and potential azapeptide antagonists.

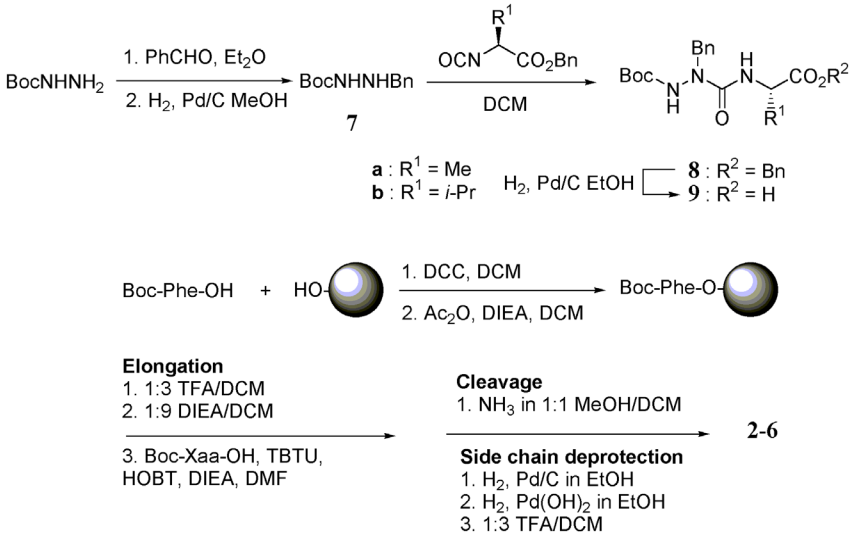

*Fig. 2. Synthesis of N-Boc-aza[1]-dipeptides **9a-b** and their incorporation into **4-6**.*

Dipeptides **9a** and **9b** were incorporated into peptides **4-6** using a Boc protection strategy on oxime resin [6]. Removal of Boc groups was carried out using 25% TFA in DCM (30 min) and neutralization was done in 10% DIEA in DMF (10 min). Peptide couplings were carried out with 5 eq. each of the appropriate Boc protected amino acid, TBTU, HOBT, DIEA in DMF (2 h). Final cleavage of the peptide from the resin was performed using a 1:1 mixture of a saturated NH_3 solution in MeOH:DCM. Removal of the side chain protecting groups [Thr(OBn) and Asp(OBn)] was carried out by hydrogenolysis over $Pd(OH)_2$ and Pd/C in ethanol, respectively. The Boc group of the final peptide was removed using 25% TFA in DCM. After purification peptides **2-6** were obtained in 10-20 % yields calculated from an initial loading of 0.3 mmol/g.

Acknowledgments

The research was supported in part by the Natural Sciences and Engineering Research Council (NSERC) of Canada and the Ministère de l'Éducation du Québec. REM would like to thank FQRNT for a postdoctoral fellowship.

References

1. Gante, J. *Synthesis* 405-413 (1989).
2. Melendez, R. E. and Lubell, W. D. In Benedetti, E. and Pedone C. (Eds.) *Peptides 2002, Proc. 27th Eur. Pept. Symp.),* Edizioni Ziino, Napoli, pp. 204-205 (2002).
3. Breeze, A. L., Harvey, T. S., Bazzo, R. and Campbell, I. D. *Biochemistry* **30**, 575-582 (1991).
4. André, F., Boussard, G., Bayuel, D., Didierjean, C., Aubry, A. and Marraud, M. *J. Peptide Res.* **49**, 556-562 (1997); Benatalah, Z., Aubry, A., Boussard, G. and Marraud, M. *Int. J. Peptide Protein Res.* **38**, 603-605 (1991); André, F., Vincherat, A., Boussard, G., Aubry, A. and Marraud, M. *J. Peptide Res.* **50**, 372-381 (1997); Zouikri, M., Vicherat, A., Aubry, A., Marraud, M. and Boussard, G. *J. Peptide Res.* **52**, 19-26 (1997).
5. Quibell, M., Turnell, W. G. and Johnson, T. *J. Chem. Soc., Perkin Trans.* **1**, 2843-2849 (1993).
6. DeGrado, W. F. and Kaiser, E. T. *J. Org. Chem.* **45**, 1295-1300 (1980).

Peptide Revolution: Genomics, Proteomics & Therapeutics
Michael Chorev & Tomi K. Sawyer (Editors)
American Peptide Society, 2003

Efficient Synthesis of Fused Tetracyclic Benzimidazole Systems

Cornelia E. Hoesl, Adel Nefzi and Richard A. Houghten

Torrey Pines Institute for Molecular Studies, 3550 General Atomics Court, San Diego, CA 92121, USA

Introduction

An efficient one-pot procedure for the solid phase synthesis of new tetracyclic 1,3,5-triazino[1,2-*a*]benzimidazolium derivatives starting from resin-bound benzimidazoles is described (Figure 1). The synthetic strategy involves an unprecedented one-pot Aza-Wittig/heterocyclization/substitution reaction sequence using halogenoalkyl isocyanates. The structure of the tetracyclic ring system was determined by two-dimensional NMR experiments and x-ray analysis.

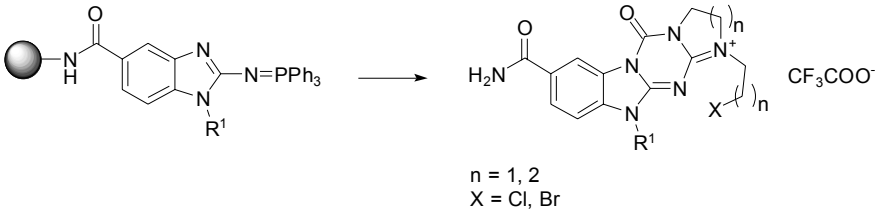

Fig. 1. Solid phase synthesis of tetracyclic 1,3,5-triazino[1,2-a]benzimidazolium derivatives.

Results and Discussion

We previously reported a solid phase tandem Aza-Wittig/annulation reaction starting from resin-bound benzimidazoles for the synthesis of 2-imino-4-oxo-1,3,5-triazino[1,2-*a*]benzimidazoles [1]. Using halogenoalkyl isocyanates, an Aza-Wittig/heterocyclization/substitution sequence occurred providing a fused tetracyclic benzimidazole system (Scheme 1). Both the imino nitrogen atom 2 and the triazino nitrogen 1 in compound **1** display nucleophilic properties and may substitute a halogeno functionality introduced by halogeno isocyanates (R^2 = $(CH_2)_nCH_2X$) thereby leading to new tetracyclic benzimidazolium derivatives **2** and **3**. Benzimidazoles are known for their biological properties including anthelmintic, antiviral, antiallergic and antineoplastic activity. The preparation of all compounds described was carried out utilizing Houghten's "tea-bag" method. Different amines were used to synthesize the solid-supported benzimidazoles.

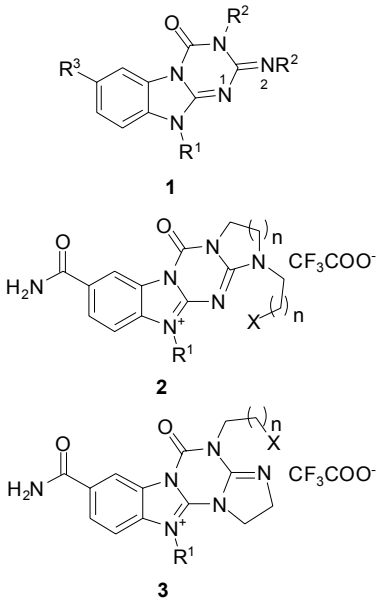

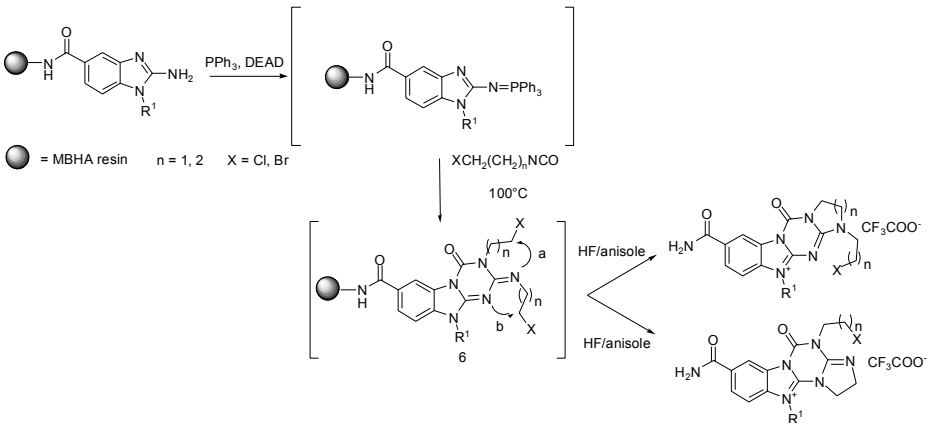

Scheme 1. Synthesis of fused tetracyclic benzimidazoles from resin-bound benzimidazoles.

Acknowledgments
The work was funded by Mixture Sciences.

References

1. Hoesl, C. E., Nefzi, A. and Houghten, R. A. *J. Comb. Chem.* ***5***, 155-170 (**2002)**.
2. Molina, P. and Vilaplana, M. J. *Synthesis* 1197 **(1994)**.

Peptide Revolution: Genomics, Proteomics & Therapeutics
Michael Chorev & Tomi K. Sawyer (Editors)
American Peptide Society, 2003

Light-Induced Two-State Structural Transition of a Cyclic PDI-Related Azobenzene-Peptide

Markus Schütt, Alexander G. Milbradt, Luis Moroder and Christian Renner

Max-Planck-Institut für Biochemie, 82152 Martinsried, Germany

Introduction

In the search for small model peptide systems that allow the photo-control of conformational states and correspondingly of biological properties, we have selected cyclic bis(cysteinyl)peptides related to the active sites of thiol/disulfide oxidoreductases of the thioredoxin family and light-switchable azobenzene derivatives as backbone constituents [1]. The fully reversible *cis/trans* photoisomerization of the azobenzene group results in significant changes of the conformational states which, as expected, in compound **1** (Figure 1) led to strong effects on the redox properties (E'_0) of the bis(cysteinyl)peptide and thus to a photocontrol of its catalytic efficiency in oxidative refolding of proteins [2]. From mutagenesis studies it is known that the redox potentials of enzymes of the thioredoxin family are decisively affected by the amino acid composition of the active-site Cys-Xaa-Yaa-Cys sequence motif [3]. By imparting conformational restraints on these active-site sequences via cyclization into hexapeptides, the impact of conformational constraints on the bis-cysteinyl motif was fully confirmed leading in the case of the PDI active-site Cys-Gly-His-Cys to a strongly oxidizing E'_0 value which was in the range of the parent enzyme [4]. Based on these results, in the present study the cyclic peptide **2** (Figure 1) was synthesized, where high water-solubility was induced by incorporation of Lys residues adjacent to the PDI active-site tetrapeptide.

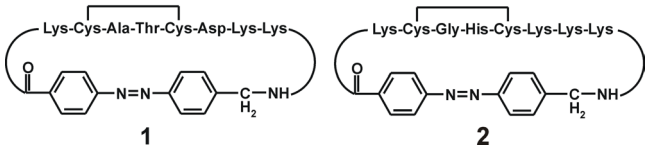

*Fig. 1. Structure of cyclic peptides containing (4-aminomethyl)phenylazobenzoic acid (AMPB) as backbone constituent and the Cys-Xaa-Yaa-Cys active-site sequence motifs of thioredoxin reductase (**1**) and PDI (**2**).*

Results and Discussion

Similar to previous studies [5], the cyclic peptide was synthesized with Cys(Trt) derivatives on chlorotrityl-resin, cleaved from the resin by mild acid treatment and cyclized in solution by the PyBOP/HOBt procedure. To avoid partial reduction of the azo group during acidic cleavage of the *S*-Trt groups, aqueous TFA was applied in absence of mercaptanes or trialkylsilanes as scavengers. Upon air-oxidation, the bicyclic compound **2** was isolated by HPLC as homogeneous material. NMR conformational analysis of the cyclic peptide in water clearly revealed that in contrast to peptide **1**, the PDI-related peptide **2** assumes both as *trans* and *cis* isomers well-defined, but differentiated conformational states. This is evidenced by the high convergence of the structural ensembles derived from the NMR data (Figure 2). Both

isomers display a distorted β-turn for the bis-cysteinyl motif that is fixed in its geometry by the disulfide bridge. In the *cis* isomer the second part of the sequence again exhibits a distorted β-turn linked to the first turn by a quite regular γ-turn centered on Lys-6 and twisted by 90° with respect to the plane of the first turn. In the *trans* isomer the peptide backbone is more extended. The γ-turn centered on Lys-6 is distorted as the three lysines are in an extended β conformation. Surprisingly, the middle lysine inserts its side chain between peptide backbone and chromophore. A flip-flop of the backbone between various conformational states, as in the case of peptide **1**, could not be observed, a fact that would suggest that the conformational preferences of peptide **2**, even as *cis* isomer, are well compatible with the constraints imposed by backbone cyclization. The reduced monocyclic peptide **2** is even more relaxed since no pronounced conformational preferences could be detected by NMR. Therefore, cyclization of the PDI octapeptide did not afford the expected conformational restriction. In fact, an E'_0 of -230 mV was determined with GSH/GSSG as reference redox pair, a value which is close to that of the linear active-site octapeptide (E'_0 = -205 mV [6]).

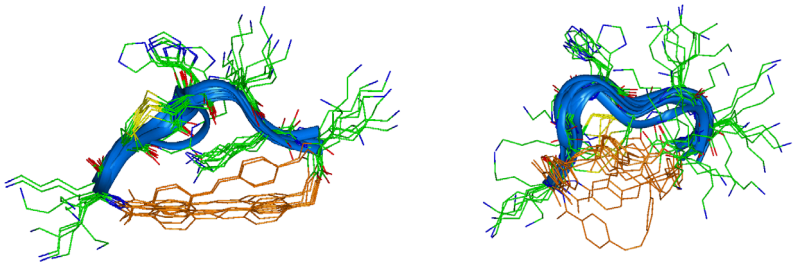

Fig. 2. Lowest energy structures of cyclic peptide ***2*** *as* trans *(left) and* cis *isomer (right) as determined by NMR.*

Although with peptide **2** the expected modulation of redox properties was not obtained, its well-defined structures in both the *trans* and *cis* isomeric state should be ideally suited for studying the earliest events of light-induced conformational transitions by ultrafast UV and IR spectroscopy.

Acknowledgments
This study was supported by SFB 533 of the Ludwig-Maximilians-University of Munich (grant A8).

References

1. Behrendt, R., Renner, C., Schenk, M., Wang, F., Wachtveitl, J., Oesterhelt, D. and Moroder, L. *Angew. Chem. Int. Ed. Engl.* **38**, 2771-2774 (1999).
2. Cattani-Scholz, A., Renner, C., Cabrele, C., Behrendt, R., Oesterhelt, D. and Moroder, L. *Angew. Chem. Int. Ed*. **41**, 289-292 (2002).
3. Huber-Wunderlich, M. and Glockshuber, R. *Fold. Des*. **3** 161-171 (1998).
4. Cabrele, C., Fiori, S., Pegoraro, S. and Moroder, L. *Chem. Biol.* **9**, 731-740 (2002).
5. Behrendt, R., Schenk, M., Musiol, H,-J., Moroder, L. *J. Pept. Sci*. **5**, 519-529 (1999).
6. Siedler, F., Rudolph-Böhner, S., Doi, M., Musiol, H-.J. and Moroder, L. *Biochemistry* **32** 7488-7495 (1993).

Peptide Revolution: Genomics, Proteomics & Therapeutics
Michael Chorev & Tomi K. Sawyer (Editors)
American Peptide Society, 2003

Novel Gly Building Units for Backbone Cyclization: Synthesis and Incorporation into Model Peptides

Sharon Gazal[1], Gary Gellerman[2] and Chaim Gilon[1]

[1]Department of Organic Chemistry, the Hebrew University of Jerusalem, Jerusalem 91904, Israe; [2]Peptor Ltd., Kiryat Weizmann, Rehovot, 76326 Israel

Introduction

Backbone cyclization [1] is a concept that enables the design conformationally constrained peptidomimetics [2] and proteinomimetics [3] that posses improved biological and pharmacological properties such as selectivity and metabolic stability. Since backbone cyclic peptides are obtained by linking two N^{α} atoms, cyclization is attained without affecting or using the side chain of the amino acid (Xaa) residue, which may be crucial for the biological properties of the original peptide or protein. In order to obtain backbone cyclic peptides, special N-alkylated, ω-functionalized orthogonally protected Xaa termed building units (BU) were prepared. However, the preparation of "non Gly" BU (BU based on Xaa other than Gly) requires a considerable synthetic effort which is time consuming. This is a major limiting step which hampers the preparation of backbone cyclic peptide libraries for preliminary biological screening. In contrast to "non Gly" building units (BUs), the preparation of Gly BU is simple and rapid. However, using Gly BU is efficient only when these BUs replace Gly residues; the biological activity might be lost if Gly BU are used to replace non Gly residues. In order to overcome this difficulty, we report the preparation of a novel class of building units, in which the side chain of the desired Xaa is preserved. Since these BUs are based on Gly BUs, less synthetic effort is needed for their preparation than in the traditional "non Gly" BUs. Yet, they conserve the side chain of the original residue. The incorporation of these BU's into model peptides is also presented.

Results and Discussion

The BUs **1(a-f)**, containing the different side chains (Figure 1) were easily prepared by reductive alkylation of the appropriate Xaa allyl esters with glyoxilic acid. The in situ reduction of the imine took place in the presence of $NaBH_3CN$. Introduction of Fmoc was achieved by reaction with Fmoc-Cl in the presence of DIEA. The crude product was easily purified by flash chromatography. However, the incorporation of these novel BUs into model peptides, shown in Figure 2, demanded a different strategy than usual SPPS, since two major problems arose throughout the peptide assembly. The

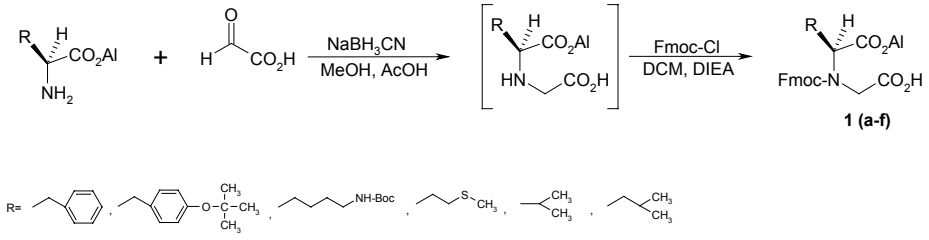

Fig. 1. Synthesis of building units.

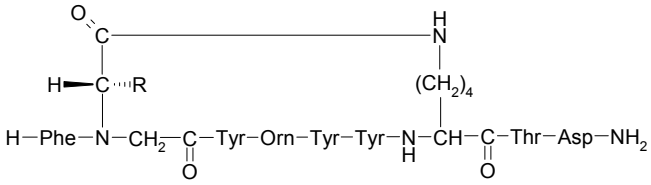

Fig. 2. The general structure of the backbone cyclic model peptides.

first was the difficult coupling to the sterically hindered secondary amine of the BU. The utilization of PyBrOP, which efficiently couples Fmoc-AA-OH to N alkyl glycine failed to yield the desired product. This difficult coupling was successfully achieved using triphosgene as a coupling reagent [4]. Another major obstacle was formation of diketopiperazine during the assembly. This obstacle was avoided by cyclization of the peptide following the coupling of the Fmoc protected BU (prior to the coupling of the preceding Xaa). Overcoming the above synthetic obstacles resulted in crude peptides of high quality.

We have demonstrated the preparation of novel type of BUs for backbone cyclization as well as their incorporation in backbone cyclic model peptides. These BUs may be suitable for rapid screening of backbone cyclic libraries since their preparation requires minimal synthetic effort. Peptides containing this type of BUs comprise an R group located between the backbone amide (α position) and the ring's lactame bridge (Figure 2). Hence, further conformational constraint is gained (in addition to N-alkylation and cyclization). The possibility to obtain a free amine branching from the ring enables labeling the peptide in the endocyclic part without utilizing essential side chains. This mode of labeling could be superior since the endocyclic part of the peptide is more resistant to degradation than the exocyclic part traditionally used for labeling (e.g., amino terminus or a terminal Cys residue).

References

1. Gilon, C., Halle, D., Chorev, M., Selinger, Z. and Byk, G. *Biopolymers* **31**, 745-750 (1991).
2. Altstein, M., Ben Aziz, O., Daniel, S., Schefler, I., Zeltser, I. and Gilon, C. *J. Biol. Chem.* **274**, 17573-17579 (1999).
3. Kasher, R., Oren, D. A., Barda, Y. and Gilon, C. *J. Mol. Biol.* **292**, 421-429 (1999).
4. Falb, E., Yechezkel, T., Salitra, Y. and Gilon, C. *J. Pep. Res.* **53**, 507-5031 (1999).

Peptide Revolution: Genomics, Proteomics & Therapeutics
Michael Chorev & Tomi K. Sawyer (Editors)
American Peptide Society, 2003

Application of Aspartic Acid in the Synthesis of Bicyclic Dipeptide Mimetics

John M. Ndungu, Xuyuan Gu, Dustin E. Gross, Jinfa Ying and Victor J. Hruby

Department of Chemistry, University of Arizona, Tucson, AZ 85721, USA

Introduction

The need to elucidate the bioactive conformation(s) in peptides and also improve their metabolic stability, bioavailability and selectivity towards different receptors and receptor subtypes has necessitated the synthesis of novel peptides and peptide mimetics. One of the strategies we are examining is the synthesis of peptides containing bicyclic dipeptide mimetics which constrain the conformation(s) adopted by a particular peptide to a β-turn. Azabicycloalkane amino acids have been shown to have unique potential advantages, and numerous bicyclic derivatives of this general class have been synthesized [1]. In our efforts towards the synthesis of bicyclic dipeptide mimetics for the CCK receptor, Nle-Gly and Asp-Phe dipeptide mimetics were designed using modified synthetic methodologies recently developed in our labs [2]. Both the targets would require the synthesis of β-allyl substituted aspartic acids, while the latter also requires β-phenyl substituted cysteines which have been synthesized in our labs [3].

Results and Discussion

Alkylation of aspartic acid [4] with allyl bromide in the presence of LHDMS and HMPA gave the (2*S*, 3*R*) and (2*S*, 3*S*) β-allyl substituted aspartic acids in a ratio of 3:1 respectively (Figure 1). The aminal group was then protected as a trifluoroacetamide to prevent the spontaneous cyclization of aldehydes to hemiaminals associated with oxidation of carbamate protected β-allyl aspartic acids [5]. Each of the N^{α}-trifluoroacetyl β-allyl substituted aspartic acid was oxidized to the aldehyde, and in a one pot reaction coupled with *L*-Cys to form a thiazolidine followed by bicyclization and methylation. The (2*S*,3*R*) isomer gave two bicyclic products in a ratio of 2:1 while the (2*S*, 3*S*) isomer gave only one bicyclic dipeptide mimetic **3c** (Figure 1). The ^{1}H-NMR spectra were assigned by DQF-COSY, while the stereochemistry of the three bicyclics was assigned by 1D transient nOe experiments. This protocol is being used to synthesize the Asp-Phe bicyclic dipeptide mimetics.

To synthesize the Nle-Gly dipeptide mimetic, **2a** was deprotected by hydrogenation and the resultant carboxylic acid reduced by $NaBH_4$ in the presence of BOP [6] to give the alcohol **4** contaminated by a small amount of the lactone. The alcohol was subjected to Swern oxidation, and the crude aldehyde coupled with *L*-Cys as previously described to give a bicyclic dipeptide mimetic for Nle-Gly. This bicyclic dipeptide mimetic has being incorporated in CCK-7 (**Tyr-Nle-Gly-Trp-Nle-Asp-Phe-NH_2**). Attempts to reduce **2b** to the alcohol failed since only the lactone was obtained. In order to fully study the topographical requirements for the CCK receptor, efforts are in progress to synthesize other isomers of the Nle-Gly bicyclic dipeptide mimetic by utilizing the Kazmaier–Claisen rearrangement reaction [7].

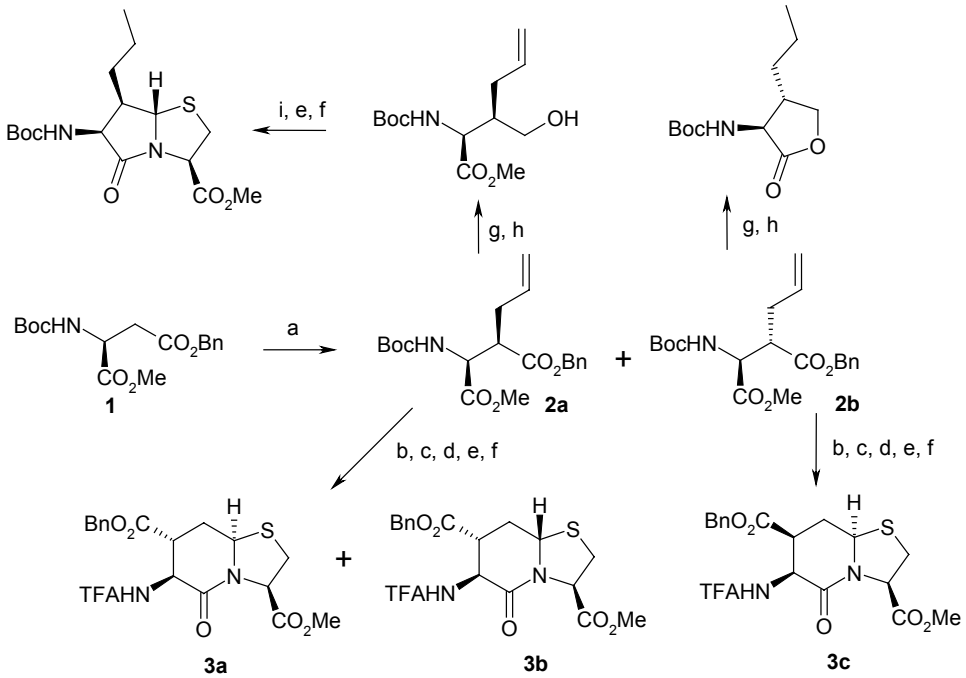

a) LHDMS, HMPA, THF, CH_2=$CHCH_2Br$, -42 °C b) i) TFA, CH_2Cl_2 ii) (trifluoroacetyl) benzotriazole iii) OsO_4, $NaIO_4$ iv) *L*-Cys, Mol. sieves, pyr, RT, 4h: pyr, 50 °C, 4 days v) CH_2N_2, CH_2Cl_2 c) H_2, Pd/C ii) BOP, DIPEA, $NaBH_4$ d) $(COCl)_2$, DMSO, DIPEA, CH_2Cl_2, -78 °C

Fig.1. Synthesis of [5,5] and [6,5] azabicycloalkane dipeptide mimetics.

Acknowledgments

This work was supported by US Public Health Service (DA 12394, DA 13449 and DA 06284). NMR was acquired using a DRX 500MHz spectrometer obtained by a grant from the NSF(9729350).

References

1. Hanessian, S., Smith-McNaughton, G., Lombart, H. G. and Lubell, W. D. *Tetrahedron* **53**, 12789-12854 (1993).
2. Qiu, W., Gu, X., Soloshonok, V. A., Carducci, M. D. and Hruby, V. J. *Tetrahedron Lett*. **42**, 145-148 (2001).
3. Xiong, C., Wang, W. and Hruby, V. J. *J. Org. Chem*. **67**, 3514-3517 (2002).
4. Cotton R., Johnstone, A. N. C. and North, M. *Tetrahedron* **51**, 8525-8544 (1995).
5. Gu, X., Tang, X., Cowell, S., Ying, J. and Hruby, V. J. *Tetrahedron Lett*. **43**, 6669-6672 (2002).
6. McGeary, R. P. *Tetrahedron Lett.* **39**, 3319-3322 (1998).
7. Kazmaier, U. *Synlett*. 1138-1140 (**1995**).

Peptide Revolution: Genomics, Proteomics & Therapeutics
Michael Chorev & Tomi K. Sawyer (Editors)
American Peptide Society, 2003

Unique Biocatalytic Approach for the Synthesis of Chirally Pure Unnatural α- and β-amino Acids Using Novel Transaminases

Mohit Bhatia*, Eric Law, Craig Lewis, George Matcham, Richard Nelson, Hemlata Rana, Bhavani Stout and Alice Wang

Celgro Division of Celgene Corporation, 661 Route 1 South, North Brunswick, NJ 08902, USA

Introduction

The introduction of unusual α– and β–unnatural amino acids into peptides can profoundly modify the physical properties and biological activity of such peptides. With that in mind, we have developed proprietary technology [1,2] for the economical large-scale production of a broad spectrum of enantiomerically pure (R and S) α– and β–unnatural amino acids.

Our biocatalytic technology employs a unique transamination reaction providing high keto acid conversion (99%) and chiral purity (99.9%) with high product concentration (300 g/L). Key to high performance in our biocatalysis reactions is our approach to "rational enzyme design" and screening. Here we demonstrate our approach and technology as applied to L-glufosinate (LGA; L-homoalanine-4-yl-(methyl)phosphinic acid) an unnatural amino acid and the active ingredient in a commercial herbicide [3]. L-glufosinate is a component of a natural tripeptide **Bialaphos** from *Streptomyces hygroscopicus* with herbicidal and antibiotic activity.

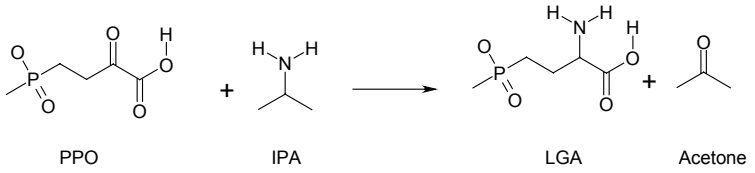

Fig.1. Example of transaminase reaction using IPA as amine donor.

As shown in Figure 1, the transamination of the keto acid PPO (2-oxo-4-[(hydroxy)(methyl)phosphinoyl]butyric acid is carried out using isopropylamine (IPA) as the amine donor, rather than an amino acid [3]. Isopropylamine is an inexpensive (~$1.00/lb) achiral molecule forming acetone upon transamination. This reaction has a favorable equilibrium constant (K_{EQ}) of about 1000 and acetone can be stripped from the reaction using vacuum and high temperature (50°C), allowing for a complete conversion (>99%) of the keto acid substrate to the amino acid product.

Methods

At Celgro, we have extensive experience in (and biocatalysts adapted to) the use of isopropylamine as the amino donor. The challenge is to adapt these biocatalyst(s) to also use new unnatural keto acids. We do this via a stepwise tailoring approach that combines a thorough understanding of reaction kinetics and process limitations, and a sequential screening of error-prone PCR generated random libraries of biocatalysts to identify mutants which overcome these limitations. Candidates are typically identified using an agarose plate or liquid reaction screens based on the transaminase reaction. After each round of improvement, the best enzyme is subjected to kinetic and process

analysis to redefine limitations, followed by a new round of mutagenesis and screening. This iterative process allows us to continuously raise the ceiling of product concentration/biocatalyst use, until a process meeting economic targets is achieved.

Results and Discussion

In the case of PPO, the example reported here, no activity was observed with existing enzymes. Starting with a thermally stable biocatalyst as the parent candidate enzyme, we conducted a series of screens with PPO analogs to develop a biocatalyst with low level PPO activity (90 mM LGA in 24 hrs). Reaction kinetic showed a high K_M (465 mM) for PPO, and IPA induced substrate inhibition (K_I = 218 mM). In the process of being tailored for PPO activity, the biocatalyst had also sacrificed thermal stability ($T_{1/2}$ = 0.75 hrs). In two rounds of mutagenesis and screening, the K_M for PPO was reduced to 192 mM, IPA inhibition eliminated (K_I = 650 mM) and thermal stability enhanced ($T_{1/2}$ > 8 hrs). In process reactions, this biocatalyst, designated GEN-2, reached a product concentration of 500 mM in 24 hrs.

Table I. Activities of biocatalysts.

	K_M (mM)		V_{MAX}	K_I (mM)		$T_{1/2}$ (hrs)	[Product]
	PPO	IPA	mM/hr/mg/mL	LGA	IPA	50°C	mM/8hrs
GEN-0	465	30	4	>500	218	0.75	90 mM
GEN-2	192	99	7	>500	615	>8	350 mM
GEN-4	53	89	12	300	>900	>8	700 mM
GEN-6	68	73	14	469	>900	>8	900 mM
GEN-7	57	63	16	600	>900	>8	1250 mM

Subsequent rounds of mutagenesis further reduced the K_M for PPO (~50 mM) and increased reaction rate. The low K_M for PPO allowed high conversion of substrate and the high reaction rate afforded reduced biocatalyst usage. The final biocatalyst, GEN-7, used for scale-up, produced 1.25 M LGA with 99% keto acid conversion in 7 hrs.

Our biocatalysis reaction can be carried out in conventional stirred tank reactors and easily up-scaled. With acetone stripping and near complete conversion of keto acid substrate, downstream processing is simplified. Using rational biocatalyst design, we have developed enzymes to cover a broad spectrum of α– and β–unnatural amino acids and other chiral amines. Our biocatalysts are easily tailored for new and unusual molecules. We have also designed new transaminase biocatalysts that can withstand solvents and a wide range of pH (5-11) and temperature (25-70°C).

Acknowledgements

Technical contributions are acknowledged from W. Lang, C. Lugo and C. Pegram.

*Corresponding author. All communications to *mbhatia@celgro.com*

References

1. US Patent 4,950,606 (*Celgene Corp., U.S.A.*) 1990.
2. WO Patent 99/46398A1 (*Celgro U.S.A.*) 1999.
3. Schultz, A., Taggeselle, P., Tripier, D. and Bartsch, K. *Appl. Env. Microbiol.* **56**, 1-6 (1990).

Peptide Revolution: Genomics, Proteomics & Therapeutics
Michael Chorev & Tomi K. Sawyer (Editors)
American Peptide Society, 2003

Assessment of 6Cl-HOBt-Based Coupling Reagents in Solid-Phase Cyclopeptide Synthesis

Giuseppina Sabatino[1], Maria Claudia Alcaro[1], Maria de la Cruz Pozo-Carrero[1,2], Mario Chelli[1], Paolo Rovero[3] and Anna Maria Papini[1]

[1]Laboratory of Peptide Chemistry & Immunology, Dipartimento di Chimica Organica "Ugo Schiff" and CNR-ICCOM, Università di Firenze, I-50019 Sesto Fiorentino (FI), Italy; [2]CSF S.r.l., I-50124 Firenze, Italy; [3]Dipartimento di Scienze Farmaceutiche, Università di Salerno, I-84080 Fisciano (SA), Italy

Introduction

We recently described a comparative study [1,2] on the efficiency of the 6Cl-HOBt-based coupling reagents TCTU, and HCTU (Luxembourg Industries Ltd, Tel Aviv, Israel) synthesizing a difficult peptide sequence, ACP(65-74), and a longer peptide, rMOG(35-55). We demonstrated, using a multiple peptide synthesizer (Advanced ChemTech APEX 396), that these coupling reagents were efficient in both cases.

Due to the great interest in SAR studies of cyclic peptides, presenting a restricted conformation, we compared TCTU and HCTU with other aminium coupling reagents (TBTU, in a first instance) in the solid-phase on-resin cyclization of head-to-tail cyclopeptides [3], by anchoring the side chain of Fmoc-Asp-OAl to the Wang resin [4,5].

Results and Discussion

In order to undertake a comparative study between the efficiency of different coupling reagents in the solid-phase cyclization reaction, as model peptides we chose three RGD containing sequences (biologically interesting) [5]. In particular, we synthesized the cyclotetrapeptide cyclo(FRGD), the cyclopentapeptide cyclo(VFRGD) and the cyclohexapeptide cyclo(SVFRGD), in which hindered amino acids are present (Phe, Val). Moreover, the cyclohexapeptide also contains a Ser residue, a well-known amino acid, to induce extensive racemization during the coupling reaction [2].

Starting from Fmoc-Asp(Wang resin)-OAl (0.24 mmol/g), we synthesized the linear peptides Fmoc-FRGD(Wang resin)-OAl, Fmoc-VFRGD(Wang resin)-OAl and Fmoc-SVFRGD(Wang resin)-OAl by the standard SPPS protocol. After deprotection of the C-terminal carboxyl function of Asp (anchored to the resin via its side chain) with a solution of $PhSiH_3/Pd(PPh_3)_4$ (20 equiv./0.25 equiv. in dry DCM, under Ar), the Fmoc group was removed with piperidine (25% in DMF). The comparative study was undertaken performing the solid-phase on-resin head-to-tail cyclizations in parallel, on a multiple peptide synthesizer, using 1 equiv. of one of the three different aminium coupling reagents, TBTU, TCTU or HCTU, in the presence of DIPEA (2 equiv.).

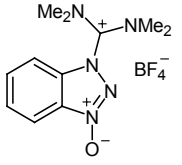

TBTU

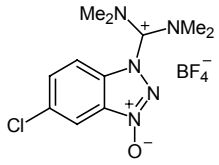

TCTU

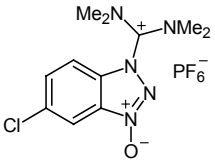

HCTU

During the synthesis of the cyclohexapeptide cyclo(SVFRGD), we carried out microcleavages at different cyclization times (45 min, 90 min, 3 h, overnight), in order to evaluate the effectiveness of the different coupling reagents for the on-resin cyclization reaction. The synthesis of cyclo(VFRGD) and cyclo(FRGD) was performed using HCTU or TCTU as coupling reagents and 2 h of cyclization time. The cleavage from the resins (and contemporary deprotection of the amino-acids side chains) were carried out in 2h, at room temperature, with TFA/TIS/H_2O (95 :2.5:2.5). The crude products were precipitated with diethyl ether, centrifuged, re-dissolved in H_2O and lyophilized. The cyclization yield (%) on the crude products was determined by RP-HPLC on a ThermoFinnigan Surveyor system (equipped with a diode array detector) coupled to the ESI-MS (ESI Ion Trap LCQ Advantage ThermoFinnigan), using a Phenomenex Aqua C18 column (5µm, 150×2.0 mm) (flow rate: 200µL/min) with a gradient of 5–30% CH_3CN/H_2O with 0.1% TFA for cyclo(SVFRGD) and 5–30% CH_3CN/H_2O with 0.1% HCOOH for cyclo(FRGD), and cyclo(VFRGD).

Preliminary data (Figure 1) concerning the cyclization step to obtain cyclo(SVFRGD) showed that both HCTU and TCTU are very efficient after only 45 min of reaction time, while a lower cyclization percentage with TBTU was reached only after 3 hours. The cyclization yields (%) were determined as a ratio between the cyclopeptide and the corresponding linear peptide concentrations.

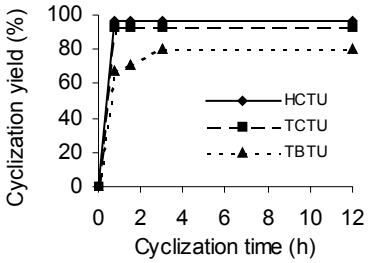

Fig. 1. Comparison of three coupling reagents (HCTU, TCTU, and TBTU) at different cyclization times in the synthesis of cyclo(SVFRGD).

We obtained good cyclization yields also in the more difficult synthesis of the constrained cyclopeptides cyclo(FRGD) and cyclo(VFRGD), both with HCTU and TCTU (Table 1).

Interestingly, in the synthesis of the cyclopentapeptide cyclo(VFRGD) no dimer was detected. The evaluation of racemization and other side reactions [6] is under investigation.

Table 1. Cyclization yield after 2 h.

Cyclopeptide	HCTU	TCTU
cyclo(VFRGD)	90%	90%
cyclo(FRGD)	75%	87%

Acknowledgments

The coupling reagents HCTU and TCTU were kindly provided by Luxembourg Industries Ltd, Tel Aviv, Israel.

References

1. Sabatino, G., et al. *Lett. Pept. Sci*. **9**, 119–123 (2002).
2. Di Fenza, A., Rovero, P. *Lett. Pept. Sci*. **9**, 125–129 (2002).
3. Rovero, P., In: Kates, S. A. and Albericio, F. (Eds.) *Solid-Phase Synthesis: A Practical Guide*, M. Dekker, New York, 2000, p. 331.
4. Sabatino, G., et al. *Tetrahedron Lett.* **40**, 809–812 (1999).
5. Alcaro, M. C., et al. *J. Pept. Sci.* **9**, 218-228 (2004).
6. Arttamangkul, S., et al. *Lett. Pept. Sci*. **3**, 357–370 (2002).

Peptide Revolution: Genomics, Proteomics & Therapeutics
Michael Chorev & Tomi K. Sawyer (Editors)
American Peptide Society, 2003

Synthesis and Conformational Study of Peptides Based on Crowned C^{α}-Methyl L-DOPA

K. Wright[1], F. Melandri[1], M. Wakselman[1], J.-P. Mazaleyrat[1], F. Formaggio[2], S. Oancea[2], M. Crisma[2] and C. Toniolo[2]

[1]SIRCOB, UMR CNRS 8086, Bât. Lavoisier, University of Versailles, F-78000 Versailles, France; [2]Institute of Biomolecular Chemistry, CNR, Department of Organic Chemistry, University of Padova, 35131 Padova, Italy

Introduction

In connection with the pioneering studies of Voyer *et al*. [1] who have explored the use of peptide frameworks based on crowned *(L)*-DOPA residues for the construction of molecular receptors and devices, we exploited the catechol function of C^{α}-methyl *(L)*-DOPA (Mdp) to prepare a new series of $C^{\alpha,\alpha}$-disubstituted glycines with α-carbon chirality, carrying various crown-ether receptors on their side-chain: [15-C-5]-*(L)*-Mdp, [18-C-6]-*(L)*-Mdp and [benzo-24-C-8]-*(L)*-Mdp (Figure 1) [2].

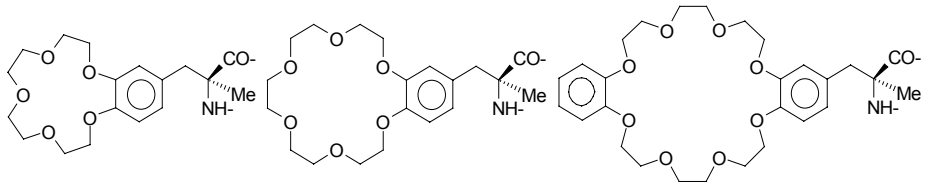

Fig. 1. Chemical structures of the crowned $C^{\alpha,\alpha}$-disubstituted glycines [15-C-5]-(L)-Mdp, [18-C-6]-(L)-Mdp and [benzo-24-C-8]-(L)-Mdp.

Results and Discussion

Peptides based on these new amino acids, combined with either *(L)*-Ala, or Aib/*(L)*-Ala, or Aib/Gly, up to hexamer level in which two crowned-Mdp residues are at the *i* and *i*+3 positions of the main chain, were synthesized by solution methods. For the synthesis of the tripeptides Boc-Aib-[15-C-5]-(*L*)-Mdp-(*L*)-Ala-OMe, Boc-Aib-[15-C-5]-(*L*)-Mdp-Gly-OMe, Fmoc-(*L*)-Ala-[18-C-6]-(*L*)-Mdp-(*L*)-Ala-OMe, Boc-Aib-[18-C-6]-(*L*)-Mdp-(*L*)-Ala-OMe and Boc-Aib-(Benzo-24-C-8)-*(L)*-Mdp-(*L*)-Ala-OMe, the N-carboxyanhydrides Fmoc-*(L)*-Ala-NCA and Boc-Aib-NCA were used for the difficult couplings at the N-terminus of the crowned-Mdp residues, while couplings of both H-Gly-OMe and H-*(L)*-Ala-OMe at their C-terminus were performed by the EDC/HOAt method. From Fmoc-(*L*)-Ala-[18-C-6]-(*L*)-Mdp-(*L*)-Ala-OMe, stepwise coupling at the deprotected N-termini finally gave the hexapeptide Fmoc-[(*L*)-Ala-[18-C-6]-(*L*)-Mdp-(*L*)-Ala]$_2$-OMe. On the other hand, the hexapeptides Boc-[Aib-(15-C-5)-(*L*)-Mdp-(*L*)-Ala]$_2$-OMe, Boc-[Aib-(15-C-5)-(*L*)-Mdp-Gly]$_2$-OMe, Boc-[Aib-(18-C-6)-(L)-Mdp-(L)-Ala]$_2$-OMe and Boc-[Aib-(Benzo-24-C-8*)-(L)*-Mdp-(*L*)-Ala]$_2$-OMe, were all obtained by 2+4 segment coupling.

Conformational analysis of these peptides was performed using FT-IR absorption, NMR and CD techniques. By comparing the FT-IR absorption spectra in the N-H stretching region of the five peptide series in $CDCl_3$ solution, it is clear that the

contribution of the crowned (*L*)-Mdp residues to intramolecular H-bonding is much more significant than that of either (*L*)-Ala or Gly. The $CDCl_3$/DMSO ^{1}H NMR titrations of the five hexapeptides are, in all cases, those expected for a 3_{10}-helical structure. Finally, the CD spectra of all crowned (*L*)-Mdp series as a function of increasing peptide main-chain length tend to a pattern characterized by a weak negative Cotton effect at 225-230 nm followed by a very intense negative Cotton effect centered near 205 nm (Figure 2). This dichroic spectrum is typically exhibited by a right-handed 3_{10}-helical peptide structure.

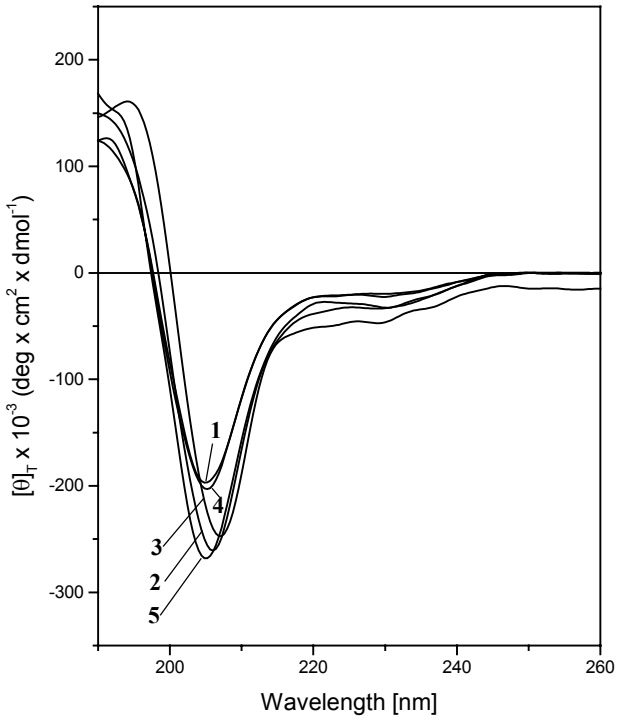

*Fig. 2. CD spectra of Boc-[Aib-(15-C-5)-(L)-Mdp-(L)-Ala]$_2$-OMe (**1**), Boc-[Aib-(15-C-5)-(L)-Mdp-Gly]$_2$-OMe (**2**), Fmoc-[(L)-Ala-(18-C-6)-(L)-Mdp-(L)-Ala]$_2$-OMe (**3**), Boc-[Aib-(18-C-6)-(L)-Mdp-(L)-Ala]$_2$-OMe (**4**), Boc-[Aib-(Benzo-24-C-8)-(L)-Mdp-(L)-Ala]$_2$-OMe (**5**) in methanol solution.*

In conclusion, the results of our combined FT-IR absorption, ^{1}H NMR and CD analyses strongly favor our contention that the C^{α}-tetrasubstituted, crowned (*L*)-Mdp residues have a remarkable bias for right-handed β-turn and 3_{10}-helix structure formation, much more significant than that exhibited by the (*L*)-Ala or Gly residue.

References

1. (a) Voyer, N. and Lamothe, J. *Tetrahedron* **51**, 9241-9284 (1995). (b) Voyer, N. *Topics in Current Chemistry* Vol. 184, Springer, Berlin, 1996, pp. 1-37.
2. Wright, K., Melandri, F., Cannizzo, C., Wakselman, M., and Mazaleyrat, J.- P. *Tetrahedron* **58**, 5811-5820 (2002).

Peptide Revolution: Genomics, Proteomics & Therapeutics
Michael Chorev & Tomi K. Sawyer (Editors)
American Peptide Society, 2003

Solid-Phase Synthesis of Des-*N*-Tetramethyl Triostin A (TANDEM)

John P. Malkinson and Mark Searcey

Department of Pharmaceutical and Biological Chemistry, The School of Pharmacy, University of London, 29-39 Brunswick Square, London, WC1N 1AX, UK

Introduction

The quinoxaline antibiotics are a class of structurally related bicyclic depsipeptides isolated from *Streptomyces* sp. [1] and are typified by triostin A (**1**) and its synthetic analogue TANDEM (*T*riostin *A* tetra-*N*-*DEM*ethylated; **2**) [2]. Each consists of a two-fold symmetrical cyclic octadepsipeptide, cross-linked by a disulfide bridge, with two 2-quinoxalinecarbonyl chromophores attached to the amino groups of the D-serine residues. These depsipeptides demonstrate both anti-bacterial and anti-tumour activity, binding to DNA via a bis-intercalative mechanism [3]. Both chromophores insert themselves between adjacent base pairs of a specific DNA sequence, forming a two base pair sandwich and orienting the cyclic depsipeptide in the minor groove. This long-lived complex has fatal consequences for the cell, possibly via the inhibition of recognition by RNA polymerase [4].

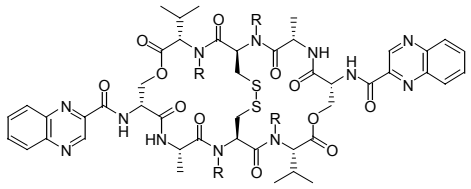

1 R=Me Triostin A
2 R=H TANDEM

Solution-phase syntheses of the quinoxaline antibiotics have been developed [2,5,6]. Such syntheses are often protracted and low yielding, requiring extensive washing, isolation and purification steps after each coupling/deprotection. We were interested in developing solid-phase methodology for the synthesis of analogues such as TANDEM.

Results and Discussion

N^{α}-Fmoc protected alanine immobilized on a Wang resin (**3**) was deprotected, followed by coupling of Fmoc-DSer(Trt)-OH to generate resin-bound protected dipeptide **4**.

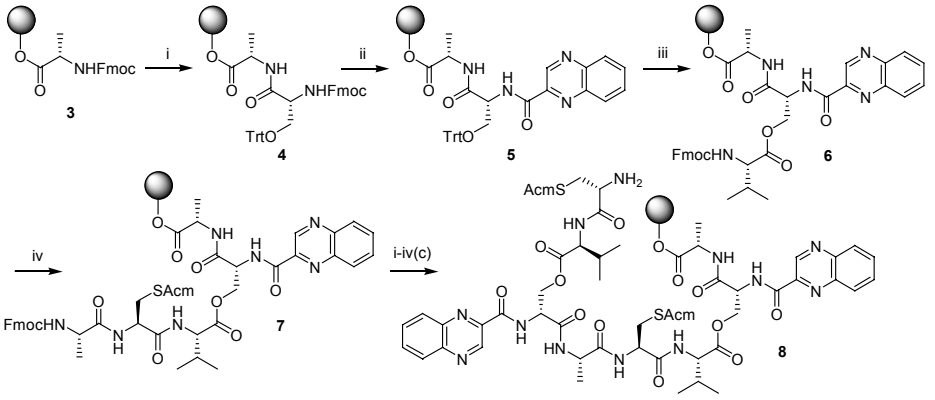

Scheme 1. Reagents and conditions: (i)(a) 20% piperidine; (b) Fmoc-DSer(Trt)-OH, HBTU, HOBt, iPr_2NEt; (ii)(a) 20% piperidine; (b) 2-quinoxaloyl chloride, iPr_2NEt; (iii)(a) 1% TFA, iPr_3SiH, CH_2Cl_2; (b) Fmoc-Val-OH, DIC, DMAP; (iv)(a) 20% piperidine; (b) Fmoc-Cys(Acm)-OH, HBTU, HOBt, iPr_2NEt; (c) 20% piperidine; (d) Fmoc-Ala-OH, HBTU, HOBt, iPr_2NEt.

After N^{α}-deprotection, the first 2-quinoxalinecarboxylic acid chromophore was introduced using the acyl chloride. The D-serine *O*-trityl protection was then removed by mild acidolysis. A variety of reagents and conditions were investigated for *in situ* depsipeptide bond formation. Activation of N^{α}-Fmoc protected valine as the symmetrical anhydride derivative in the presence of a catalytic amount of DMAP gave generally superior coupling efficiencies compared to either the OBt active ester method, or MSNT/4-methylimidazole-mediated coupling. The peptide chain of resin-bound depsipeptide **6** was then extended using standard N^{α}-Fmoc-based SPPS, coupling Fmoc-Cys(Acm)-OH and Fmoc-Ala-OH in turn. As a consequence of the two-fold symmetrical nature of the depsipeptide, steps i-iv(c) were then repeated resulting in the resin-bound bis-Acm protected linear precursor **8** (Scheme 1).

Treatment of the resin-bound linear precursor **8** with iodine generated the intramolecular disulphide. After cleavage, however, attempts to prepare TANDEM via solution-phase macrolactamization were largely unsuccessful, most likely as a result of unfavorable steric constraints. Consequently, the linear precursor **8** was removed from the solid support, with subsequent lactam ring closure using EDCI/HOAt under high-dilution conditions. The bis-Acm protected cyclic depsipeptide **9** was then oxidized using iodine to give TANDEM in good yield (Scheme 2).

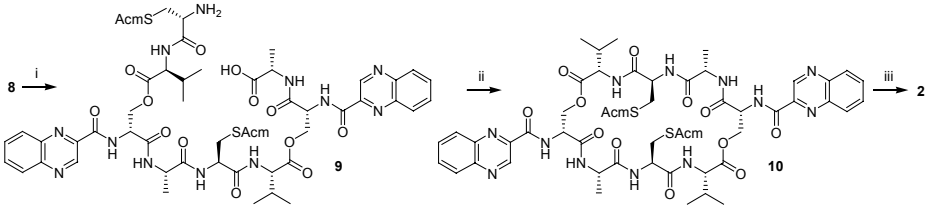

Scheme 2. Reagents and conditions: (i) TFA/iPr_3SiH/H_2O 95:2.5:2.5, 2 h; (ii) EDCI, HOAt, THF/DMF 4:1, 24 h; (iii) I_2, MeOH, 2 h.

Conclusions

The bicyclic octadepsipeptide TANDEM was synthesized rapidly and in good yield on the solid-phase. The key features of the synthesis are the use of large excesses of reagents to drive coupling reactions to completion, the isolation of resin-bound intermediates by simple filtration and washing, the introduction of both chromophores and the formation of both depsipeptide bonds on the solid-phase, and the completion of both ring closure reactions in solution after removal from the solid support.

This method allows one or both chromophores, or one or more of the amino acids to be replaced easily, allowing straightforward access to a large variety of structural analogues. Such analogues will allow a more thorough investigation of the mechanism of action of the quinoxaline antibiotics to be carried out. The method is also applicable to the synthesis of other depsipeptides in the class, and lends itself well to the synthesis of libraries using a combinatorial approach.

Acknowledgments

This work was supported by a School of Pharmacy fellowship for JM.

References

1. Shoji, J. and Katagiri, K. *J. Antibiot.* **14**, 335-339 (1961).
2. Ciardelli, T. L., *et al. J. Am. Chem. Soc.* **100**, 7684-7690 (1978).
3. Waring, M. and Wakelin, L. P. G. *Nature* **252**, 653-657 (1974).
4. Waring, M., *et al. Mol. Pharmacol.* **10**, 214-224 (1974).
5. Shin, M., *et al. Bull. Chem. Soc. Jpn.* **57**, 2203-2210 (1984).
6. Boger, D. L., *et al. J. Am. Chem. Soc.* **123**, 561-568 (2001).

Peptide Revolution: Genomics, Proteomics & Therapeutics
Michael Chorev & Tomi K. Sawyer (Editors)
American Peptide Society, 2003

Total Solid-Phase Synthesis of Differentiation Factor from HL-60 Cells and Related Peptide Fragments

Lioudmila K. Baidakova[1], Igor L. Rodionov[1], Irina A. Kostanyan[2], Valery M. Lipkin[2] and Vadim T. Ivanov[2]

[1]Branch of Shemyakin-Ovchinnikov Institute of Bioorganic Chemistry, Pushchino, 142290 Moscow Region; [2]Shemyakin-Ovchinnikov Institute of Bioorganic Chemistry, 117997 Moscow, Russian Federation

Introduction

The HLDF-54 (Figure 1, I) is a differentiation factor previously isolated at our Institute from the HL-60 cells treated with retinoic acid [1]. Total SPS of I was carried out because all attempts to produce this 54-mer polypeptide in different prokaryotic systems were unsuccessful.

```
                                  RRWHRL
                                  RRWHRLKE  (IV)
                                  RRWHRLKELLTGENHR
                                 YRRWHRLKELLTGENHR
                                 PRRWHRLKELLTGENHR
AGLMASLKLMLSAGPFVGWVSQMIPFSDWPRRWHRLKELLTGENHRCGIFVINK (I)
AGLMASLKLMLSAGPFVGWVSQMIPFSDWPRPMASSQKLLTGENHRCGIFVINK(II)
                                  RRWHRLKELLTGENHRCGIFVINK
                                            TGENHRCGIFVINK
                                            TGENHR  (III)
                                           YTGENHR
                                            YGENHR
                                            AAEAHR
                                            TGENHA
                                            TGENAR
                                            TGDNHR
                                             GENHR
                                              ENHR
                                               NHR
```

Fig. 1. Sequences of HLDF-54 (I), its putative full-length analog (II) and related fragments.

Results and Discussion

HLDF-54 and its full-length analog II were synthesized in parallel as follows. C-terminal 16-mer was synthesized, the peptide-resin was partitioned and the internal segments were assembled in separate continuous-flow reactors. Then, the reactors were joined and the N-terminal parts of the sequences were synthesized simultaneously. Continuous-flow Boc/Bzl technique with real-time swellographic monitoring [2] was employed in the syntheses of all peptides listed above. Double coupling protocol was followed by Kaiser ninhydrine test and conditional third coupling. All couplings were performed with Boc-AA-OH:TBTU:HOBt:NMM at a ratio of 4:3.8:4:6 equivalents with respect to peptide-resin. "Low-high" HF cleavage procedure [3] was employed in

the final step. Crude synthetic I was separated from low molecular weight by-products by ultra-filtration, refolded from 6 M guanidine hydrochloride and subjected to preparative RP FPLC (Pharmacia C_8-ProRPC). HLDF-54 was obtained in a homogeneous form on a 100 mg scale. It was characterized by a correct molecular weight and showed the expected functional activity (Figure 2). SAR studies performed on shorter segments of HLDF-54 revealed that the TGENHR (HLDF-6) is the minimal segment possessing cell-differentiation activity, and all amino acids forming this hexapeptide are essential for its high functional activity (see Figure 2).

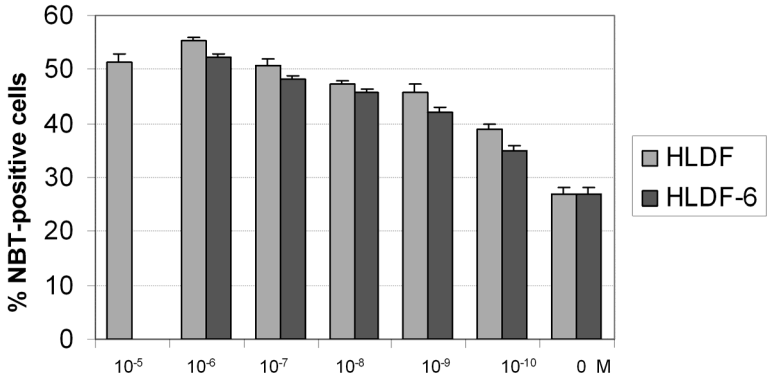

Fig. 2. HLDF-54 and HLDF-6 (III) influence on HL-60 differentiation.

The other interesting aspect of our studies is that the RRWHR pattern was recognized as a potential nucleic acid binding site due to its marked homology to a number of DNA/RNA binding and hydrolyzing proteins. Experimental evidence for this conjecture was provided by the studies of functional properties of HLDF-54 and related peptides. It was found that, in addition to inducing cell differentiation, HLDF-54 exhibits the properties of unspecific nuclease. Moreover, pronounced RNA and DNA binding/hydrolyzing properties were demonstrated for peptide RRWHRLKE (IV) and some other segments, harboring this remarkable cluster. Peptide IV (10^{-6} M) cleaves *in vitro* matrix and ribosomal RNA, linear and all forms of plasmid DNA at low ionic strength, at pH below 4.5 and in the presence of bivalent transition metals, Zn^{2+} and Mn^{2+}. It was also demonstrated that treatment of the HL-60 cell culture with this peptide (10^{-6} M) results in an increase in the number of apoptotic cells which suggests that HLDF-54 is involved in processes of apoptosis.

Acknowledgments
This work was funded by an ISTC grant #1554 and a Wellcome Trust BRC Grant #059823. L. K. B.'s participation in the 18th APS was supported by travel grants from the APS organization and the Russian Foundation for Basic Research, which is gratefully acknowledged.

References
1. Kostanyan, I. A., Astapova, M. V., et al. *Russ. J. Bioorgan. Chem.* **21**, 243-8 (1995).
2. Rodionov, I. L., Baru, M. B. and Ivanov, V. T. *Peptide Res.* **5**, 119-125 (1992).
3. Heath, W. F., Tam, J. P. and Merrifield, R. B. *Int. J. Pept. Protein Res.* **28**, 498-507 (1986).

Peptide Revolution: Genomics, Proteomics & Therapeutics
Michael Chorev & Tomi K. Sawyer (Editors)
American Peptide Society, 2003

DioRaSSP®: Diosynth Rapid Solution Synthesis of Peptides

Ivo F. Eggen, Frits T. Bakelaar, Annet Petersen and Paul B.W. Ten Kortenaar

Diosynth bv, P.O. Box 20, NL-5340 BH Oss, the Netherlands

Introduction

An ever-increasing pressure is imposed upon the pharmaceutical industry to reduce time-to-market for new drugs. The time-to-market from the API-manufacturer's point of view comprises the development of synthesis routes for new compounds, the scale-up of the ensuing processes and their validation *c.q.* registration. An additional challenge lies in the eventual manufacturing of API's of increasingly higher and reproducible purity in a commercially competitive way, which is environment-friendly and compatible with ever more stringent guidelines regarding GMP. These incentives prompted Diosynth's R&D Peptides Department to a thorough re-evaluation of the two classical approaches of peptide synthesis, *i.e.* classical solution-phase synthesis (CSPS) and solid-phase synthesis (SPPS), taking into account the extensive knowledge of impurity profiles built up by Diosynth in the course of 50 years of peptide manufacturing experience. The results of this study summarized in Table 1.

Results and Discussion

Based on the re-evaluation of the classical methods for peptide synthesis, Diosynth's R&D Peptides Department has developed a new and patented method for the synthesis of peptides in solution, called DioRaSSP - Diosynth Rapid Solution Synthesis of Peptides, which combines the advantages of both classical methods. The features of DioRaSSP are also included in Table 1. In the DioRaSSP approach, the growing peptide is essentially anchored in a permanent organic phase by means of its hydrophobic C-terminal and side-chain protecting groups. A synthesis according to the DioRaSSP protocol is completely homogeneous and its intermediates are not isolated. Excess reagents and by-products are intermittently removed by aqueous extractions. No organic waste streams are generated during the performance of the synthesis.

One cycle of the DioRaSSP protocol consists of a coupling step, quenching of residual activated carboxylic compound, aqueous extractive work-up, deprotection of the N-terminal amino function, and finally another aqueous extractive work-up. The benzyloxycarbonyl (Z) function is applied for temporary amino protection, whereas *tert*-butyl-type functions or functions of similar lability are applied for the semi-permanent protection of functional side-chains. The former is removed by hydrogenolysis in each cycle of a DioRaSSP process. The applied protection scheme in the DioRaSSP protocol justifies the commercial viability of its application on a manufacturing scale. Moreover, on account of its homogeneous character, reagents and amino acid derivatives may be applied in low molar excess.

After completion of a coupling, residual activated carboxylic compound, if hydrophobic, is quenched using an anion-forming amine such as benzyl β-alaninate. This approach allows the completely quantitative removal of quenched compounds before the coupling step of the next cycle of the synthesis by basic aqueous (*i.e.,* active) extraction. Consequently, the application of an anion-forming amine in the quenching step of the DioRaSSP protocol followed by the appropriate work-up procedures accounts for absolute impediment of formation of insertion sequences. Deletion

sequences are avoided in the DioRaSSP protocol, since all reactions can be minutely monitored. Functional side-chains on the growing peptide, being shielded by protecting groups, are not modified during the assembly of the sequence.

Syntheses according to DioRaSSP proceed by a generic and fast protocol. In the last two years, a considerable number of protected peptides have thus been synthesized at Diosynth, varying from tripeptides to a dodecapeptide. Purities and yields are generally high, as exemplified by the synthesis of a protected human Insulin octapeptide fragment, which was obtained in 98% purity and 85% yield in a first seven days' trial. Several DioRaSSP processes have been directly scaled-up after a preliminary feasibility study on a laboratory scale, achieving reproducible results in terms of both yield and purity. Accordingly, Diosynth aims at a process time of 2-4 days per residue for the synthesis of a first 10-gram scale sample of a protected peptide, 3-6 days per residue for the synthesis of a 500-gram scale development batch, and 3-6 days per residue for the synthesis of a multi-kg scale validation batch. Moreover, Diosynth is currently dealing with the implementation of the first fully automated solution-phase peptide synthesizer, which will result in another reduction of timespans.

DioRaSSP evidently offers substantial benefits concerning time-to-market, manufacturing efficiency, quality assurance and environment and thence meets all specifications for peptide manufacturing of the 21st century.

Table 1. Comparison of methods for peptide synthesis.

Aspect	Determined by	CSPS	SPPS	DioRaSSP
Time-to-market				
Route development	Generic protocol	–	+	+
Scale-up & Validation	Homogeneous synthesis	+/–	–	+
Manufacturing efficiency				
Cycle times	No isolations	–	+	+
	Automation	–	+	+
Materials	Small excess reagents	+	–	+
	No solid support	+	–	+
	Minimal side-chain protection	+	–	+/–
Product quality assurance				
High purity	No insertion sequences	–	+	+
	No deletion sequences	+	–	+
	No side-chain reactions	–	+	+
Reproducibility	Reproducible isolations	–	n.a.	n.a.
	Reproducible supports	n.a.	–	n.a.
Environmental demands				
Organic waste streams	No solvent changes	–	+	+
	No organic washings	+	–	+

Peptide Revolution: Genomics, Proteomics & Therapeutics
Michael Chorev & Tomi K. Sawyer (Editors)
American Peptide Society, 2003

CLEAR-OX™: A New Polymer-Supported Reagent for the Preparation of Disulfide-Bridged Peptides

Krzysztof Darlak[1], Andrzej Czerwinski[1], Miroslawa Darlak[1], DeAnna W. Long[1], Francisco Valenzuela[1], Arno F. Spatola[1] and George Barany[2]

[1]Peptides International, Inc., 11621 Electron Drive, Louisville, KY 40299 USA; [2]University of Minnesota, Department of Chemistry, 207 Pleasant Street SE, Minneapolis, MN 55455 USA

Introduction

Disulfide bridges represent an important evolutionarily conserved structural motif for many biologically significant peptides and proteins. Formation of disulfide bonds in synthetic peptides is one of the more challenging transformations to achieve in peptide chemistry, in view of possible formation of oligomeric by-products and other side reactions, as well as occasional insolubility problems in aqueous oxidizing media [1]. Polymer-supported reagents are increasing in popularity since they combine the advantages of solid-supported chemistry with the versatility of solution-phase reactions, allowing clean reactions and easy removal of contaminating by-products by simple filtration [2]. One solution, proposed in 1995, involved the use of a polymer-supported oxidant (Ekathiox™) [3], but that product is no longer commercially available. In 1998, Annis et al. [4] reported that a solid-phase Ellman's reagent, bound through two sites of a solid support, is an effective oxidizing agent promoting disulfide formation of peptides in solution. Solid supports used included PEG-PS™, controlled-pore glass and a modified Sephadex [4]. In principle, a polymer that is also water compatible would be advantageous for various biochemical applications and for increasing the versatility of conditions for solubilizing peptides. The chemistry proposed by Annis et al. [4] was extended to the use of CLEAR resin [5,6] as the ideal support for this application, due to its twin organic/aqueous compatibility. The initial results concerning the use of this newly developed polymer-bound oxidant are reported here. Model peptides were selected to demonstrate the effectiveness of this new reagent as a mild oxidant, and results were compared to solution oxidation data.

Results and Discussion

CLEAR-OX was prepared starting with Fmoc-Lys(Fmoc)-CLEAR resin (0.2 meq/g amino groups), using chemistry described previously [4]. The model peptides selected as synthetic targets for oxidation are shown in Table 1. The first three examples represent common, naturally occurring peptides or their analogues. An artificial construct (**4**) incorporates two of the most troublesome residues, Trp and Met, that are prone to side reactions during solution oxidation. The last peptide (**5**) is a very potent urotensin II analogue [7] that contains a sterically hindered penicillamine residue.

All peptide sequences used in oxidation studies were prepared via manual or automated solid phase synthesis (Milligen 9050), using Fmoc/*t*Bu strategies on either polystyrene or CLEAR resins. Peptides were cleaved from the resins with TFA: phenol:H_2O:TIS (88:5:5:2, v/v/v/v) for 2 h at 25°C. Solution oxidations were performed in 0.1 M ammonium acetate buffer at pH 7-8 with peptide concentrations of 0.5 mg/mL, using $K_3Fe(CN)_6$ (0.01 M) as the oxidant. Oxidations with CLEAR-OX resin were performed in MeCN:0.1 M ammonium acetate buffer solution (1:1, v/v), with a peptide concentration of 6.7 mg/mL and 3-fold molar excess of CLEAR-OX at

Table 1. Mass spectral and purity results of oxidation products obtained using CLEAR-OX™ and solution oxidation methods.

	Mass Spectral Analysis	HPLC Purity[a] (%)		
(#) Peptide Sequence	*MW Found Oxidized*	*CLEAR-OX Resin pH=4.6*	*CLEAR-OX Resin pH=6.8*	*Solution Oxidation pH=7-8*
1 H-c[CYFQNC]-PRG-NH_2	1084.46	56.6	51.4	27.8
2 H-GG-c[CRIGPITWVC]-GG-NH_2	1372.68	25.6	28.1	32.8
3 H-ETPD-c[CFWKYC]-V-OH	1388.59	54.3	43.6	28.1
4 H-c[CWAMC]-K-NH_2	809.34	49.9	43.0	42.1
5 H-D-c[Pen-FWKYC]-V-OH	1089.47	41.6	37.5	20.9

[a]*Purity of crude peptide after oxidation.*

two different pH levels. Oxidation products were analyzed by RP-HPLC and ES-MS (Table 1).

In the majority of tested examples, oxidations mediated by CLEAR-OX gave good product yields, while the purities of the crude cyclic oxidized products were generally higher than those oxidized in solution. Moreover, oxidations using CLEAR-OX were carried out at much higher concentrations than solution oxidations (6.7 vs 0.5 mg/mL). In general, oxidations with CLEAR-OX were complete within 1-2 h, even in the case of the sterically-hindered penicillamine residue (**5**). CLEAR-OX was found to be compatible with wide ranges of pH (2-8) used in typical oxidation reactions, and solubility problems were overcome by addition of acetonitrile to CLEAR-OX cyclization mixtures. Most significantly, reactants were separated from the polymer-bound oxidant by simple filtration. In summary, CLEAR-OX resin was successful in all test cases and should prove to be a valuable new tool for the preparation of disulfide-bridged peptides.

Acknowledgments
CLEAR-OX studies were funded by an SBIR Grant 1R43 GM 58987-01A2.

References

1. Andreu, D., Albericio, F., Solé, N. A., Munson, M. C., Ferrer, M., Barany, G. In Pennington, M. W. and Dunn, B. M. (Eds.) *Methods in Molecular Biology, Vol. 35: Peptide Synthesis Protocols*, Humana Press Inc., Totowa, N.J., 1994, pp. 91-169.
2. Ley, S. V., Baxendale, I. R., Bream, R. N., Jackson, P. S., Leach, A. G., Longbottom, D. A., Nesi, M., Scott, J. S., Storer, R. I. and Taylor, S. J. *J. Chem. Soc. Perkin Trans*. 3815-4195 (2000).
3. Clark, B. R. and Pai, M. WO9607676 (1996).
4. Annis, I., Chen, L. and Barany, G. *J. Am. Chem. Soc*. **120**, 7226-7238 (1998).
5. Kempe, M. and Barany, G. *J. Am. Chem. Soc*. **118**, 7083-7093 (1996).
6. CLEAR resins are protected under US Patents 5,910,554 and 5,656,707.
7. Grieco, P., Carotenuto, A., Campiglia, P., Zampelli, E., Patacchini, R., Maggi, C. A., Novellino, E. and Rovero, P., *J. Med. Chem.* **45**, 4391-4394 (2002).

Peptide Revolution: Genomics, Proteomics & Therapeutics
Michael Chorev & Tomi K. Sawyer (Editors)
American Peptide Society, 2003

Predicting Lead Compounds Using Libraries of Flexible Molecules

Adrian Kalászi and Ödön Farkas

Department of Organic Chemistry, Eötvös Loránd University, 1/A Pázmány Péter sétány, Budapest, H-1117, Hungary

Introduction

The purpose of the present method is to ease the search for lead compounds in cases of drug discovery when no acceptable candidate is available yet. Flexible molecules are not widely expected to be lead compounds, due to the unlikelihood of their specific activity, however, they may show some activity more easily. A library of flexible molecules can provide a wide range of different activities. We use the different activity and different conformational behavior of the individual molecules to choose the lead conformers which are responsible for the binding or biological activity. Lead conformers may help us to find the less flexible lead structures and then drug molecules. Important to note, that lead conformers can also be obtained in situations when no *a priori* 3D structure information but quantitative binding or biological activity data are available. The present method can also be extended into studies on generic libraries of flexible molecules but oligopeptide libraries are naturally good candidates.

Molecules with low flexibility can be described by a discrete structure and well-defined properties in QSAR based analysis. Flexible molecules, on the other hand, may provide detectable binding affinity easier due to the wider range of spatial arrangement of their functional groups. The wider range of spatial arrangements may prevent applying regular QSAR methods on flexible molecules. The correlation between conformational flexibility and bioactivity has already been examined in previous studies [1-3]. In these studies the region of the conformational space, responsible for the bioactivity, was previously defined by a native binder or a less flexible cyclic molecule (R_{bio}). The size of the overlap between the conformational space of the selected flexible molecules and R_{bio} was found to correlate well in many cases with the biological binding results.

Based on that correlation the active conformers, the lead conformers, can be located in the conformational space of the flexible molecules. Our present method [4] automatically calculates the conformational distribution for each member of a selected library of flexible molecules and collects all the regions, which correlates well with the experimental binding results. We call the conformers associated with these regions, lead conformers. Reducing the flexibility of the lead conformer either by performing chemical modifications or carrying out similarity searches on 3D structure databases, can provide lead molecules or lead compounds. The resulting set of lead conformers can also supply the necessary spatial information for further QSAR studies to find an acceptable lead compounds (Scheme 1).

Results and Discussion

For testing our method, we have chosen the active members of the TQTXT (X = all amino acids except C) pentapeptide library [5]. The members of the peptide library represent epitope candidates to prospective tumor marker antibody mAb 994. The IC_{50} values of the members were obtained from competitive ELISA experiments. The amino

acids Thr_1 Thr_3, and Thr_5 were identified as groups essential for binding. Six members had considerable inhibition activity: X=A,F,P,S,Y,W.

We used our conformational search method to gain low energy conformers for six pentapeptides [6,7]. Molecular dynamics simulations [8,9] including explicit solvent on room temperature were executed from these structures.

The correlation of the conformational distribution and binding data resulted in a set of bins for the backbone dihedral angles. This set of intervals can be mapped on any of the library members to obtain the lead conformers. However, it is advisable to map them on the most active candidate, on the TQTPT pentapeptide.

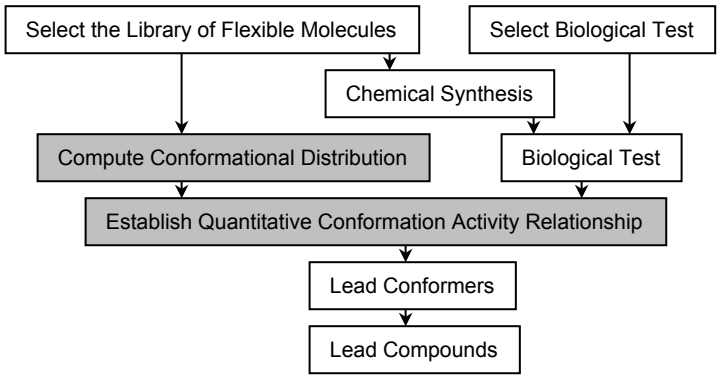

Scheme 1. Outline of the proposed role of the present method in finding lead compounds. This work elaborates on the parts denoted with gray.

Acknowledgments

This work has been supported by Gaussian, Inc., Hungarian Research Foundation (OTKA D-29446) and Gedeon Richter Ltd. The authors would also like to thank NSF, MTA and OTKA for an international collaboration grant. The computations have been performed in part using the facilities of the Hungarian Supercomputer Center and the High Performance Computing Center of the Eötvös Loránd University.

References

1. Becker, O. M., Levy, Y. and Ravitz, O., *J. Phys. Chem. B.* **104,** 2123-2135 (2000).
2. Payne, J. W., Marshall, N. J., Grail, B. M. and Gupta, S., *Curr. Org. Chem.* **6,** 1221 (2002).
3. Marshall, N. J., Andruszkiewicz, R., Gupta, S., Milewski, S. and Payne, J. W. *J. Antimicrob. Chemoth.* **51,** 821-831(2003).
4. Kalászi, A. and Farkas, Ö., *THEOCHEM* 666-667 & 645-649 (2003).
5. E. Windberg, F. Hudecz, A. Marquardt, F. Sebestyen, A. Kiss, S. Bosze, H. Medzihradszky-Schweiger and M. Przybylski, *Rapid Commun. Mass Spect.* **16**, 834-239 (2002).
6. A. Kalászi, G. Mező, F. Hudecz, Ö. Farkas, in E. Benedetti and C. Pedone, (Eds.), *Peptides 2002, (Proc 27th Eur. Pept. Symp.),* Edizioni Ziino, Napoli, p.774 (2002).
7. A. Kalászi, G. Mező, F. Hudecz and Ö. Farkas *J. Pept. Sci.* **8,** S194, P D28 (2002).
8. Berendsen, H. J. C., van der Spoel, D. and van Drunen, R. *Comp. Phys. Comm.* **91,** 43-56 (1995).
9. Lindahl, E., Hess, B. and van der Spoel, D., *J. Mol. Mod*. **7,** 306-317 (2001).

Peptide Revolution: Genomics, Proteomics & Therapeutics
Michael Chorev & Tomi K. Sawyer (Editors)
American Peptide Society, 2003

Parallel Solid-Phase Synthesis of Difluorinated Dipeptide Analogs

Agnès Vidal, Richard A. Houghten and Adel Nefzi

Torrey Pines Institute for Molecular Studies, 3550 General Atomics Court, San Diego, CA 92121, USA

Introduction

The solid-phase synthesis of a novel class of fluorinated dipeptide analogs featuring an α,α-difluoromethyl amide bond as potential bioactive analogs is described. MBHA resin was engaged in a Reformatsky reaction with ethyl bromodifluoroacetate. The generated resin-bound α,α-difluoroamino acids can be coupled with amines or amino esters with the aim of producing peptidomimetic combinatorial libraries.

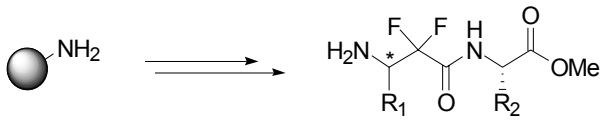

Results and Discussion

The alteration of peptides to peptidomimetics is a very efficient way to improve the pharmacological properties of biologically active peptides (bioavailability, solubility, stability against enzymes etc.). Due to the unique physical and biological properties imparted by fluorine, a large number of therapeutic agents containing fluorine at a strategic position are currently widely used. In particular, the incorporation of an α,α-difluoro carbonyl unit into substrate analogs in place of the scissile amide bond has led to the discovery of potent inhibitors of serine and aspartyl proteases [1]. Because the fluorine atoms activate the neighboring electrophilic carbonyl group, this carbonyl can readily react with active site nucleophiles (hydroxyl groups, thiol groups or water) to produce transition-state analogues in the active site. We became interested in the potential effect caused by the incorporation of a difluoromethylene unit in the α position of the amide bond.

Our study is based on the preparation of di- and tripeptide analogues that contain one α,α-difluoro-β-amino acid and one or two α-amino acids. We recently reported the solid-phase synthesis of α,α-difluoro-β-carbamoylalkylamino acids **4** via a Reformatsky reaction of a resin-bound *N*-carbamoylalkylamino benzotriazole derivative with ethyl bromodifluoroacetate (Scheme 1). Following formation of the *N*-aminoalkylbenzotriazole **2** from an aldehyde and benzotriazole in refluxing benzene, subsequent Reformatsky reaction with ethyl bromodifluoroacetate and zinc, saponification of the resulting ethyl ester and cleavage from the resin in presence of HF, yielded compounds **4** in good yields and excellent purities. In order to extend the chain, an α-amino ester was introduced using BOP activation and diisopropylamine (DIEA) in DCM. Numerous reactions can be achieved to allow the derivatization of its terminal carboxylic function. In this synthesis, the main difficulty lies in the preparation of the substrate **3** without incorporation of a second Reformatsky reagent or intramolecular cyclization into the imidazolidinone derivative, which can also potentially regenerate the free amino acid. Consequently, optimal conditions have to be carefully determined in order to prepare libraries of peptide analogues **4** [2].

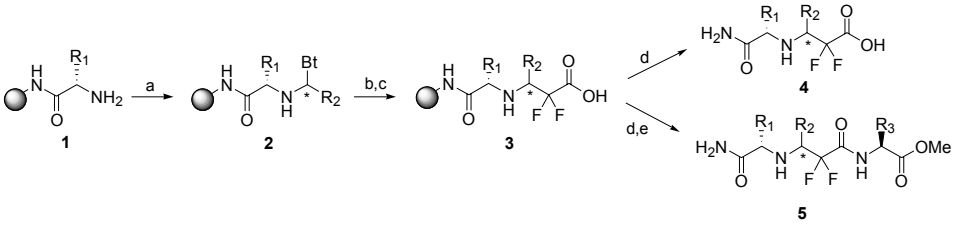

Scheme 1. (a) BtH (10 eq), R_1CHO (10 eq), benzene, reflux; (b) $BrZnCF_2CO_2Et$ (10 eq), TMSCl, THF, reflux; (c) $LiOH.H_2O$, THF, r.t.; (d) HF/Anisole; (e) H_2N-CH(R_3)-CO_2Me (5 eq); BOP (5 eq), DIEA (10 eq); DCM.

Direct functionalization of the *p*-methylbenzhydrylamine resin offers the advantage of preventing possible cyclization (Scheme 2). Moreover, surprisingly, no products of over-addition have been detected using 10 to 15 equivalents of Reformatsky reagent as was the case using the resin-bound amino acid. The reaction leads to the incorporation of two distinct amino acids (alpha and beta), while in the compound **1**, they were sharing the same nitrogen atom. Eight different aldehydes were selected for the preparation of compounds **7**, **8** and **9**. The key step of the synthesis is the preparation of the supported α,α-difluoro-β-amino acids **6**.

Yields obtained for amino acids **6** range from 21 to 85% indicating a difficulty for hindered aldehydes to react with the bulky methylbenzhydrylamine resin. Benzylamine and L-phenylalanine methyl ester were condensed using BOP and DIEA in DCM to give compounds **8** and **9** respectively. In a separate experiment, not reported here, the carboxylic acid was condensed with *N*-Boc-piperazine and, after deprotection of the Boc group in the presence of 55% TFA in DCM, the generated secondary amine was coupled with an amino acid. Following HF cleavage, the resulting compounds were obtained in up to 10% yield. Unlike the resin-bound α,α-difluoro-β-carbamoylalkyl-amino acids **4**, corresponding α,α-difluoro-β-*p*-methylbenzhydrylamino acids appear to be sensitive to strong acidic conditions and therefore allow fewer transformations.

In conclusion, we presented a convenient method for the rapid generation of a large diversity of primary α,α-difluorinated β-amino acids **7** and amides **8**, as well as dipeptide analogues **9**. The cleavage from the resin releases the free primary amine, which can then be functionalized in solution.

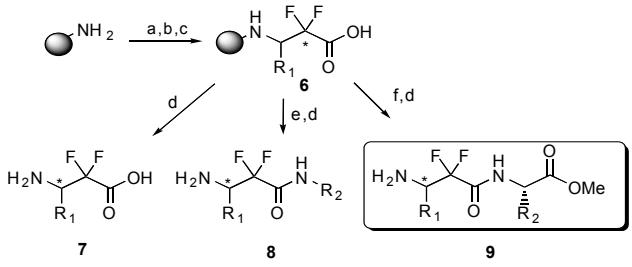

Scheme 2. a to e: same as Scheme 1. (f) H_2N-CH(R2)-CO_2 Me (5 eq); BOP (5 eq), DIEA (10 eq); DCM.

References

1. Hageman, J. J. M., Wanner, M. J., Koomen, G. J. and Pandit, J. *J. Med. Chem*. **20**, 1677-1679 (1977).
2. Vidal, A., Nefzi, A. and Houghten, R. A. *J. Org. Chem.* **66***,* 8268-71 (2001).

Peptide Revolution: Genomics, Proteomics & Therapeutics
Michael Chorev & Tomi K. Sawyer (Editors)
American Peptide Society, 2003

Synthetic Peptides as Certified Analytical Standards

Henriette A. Remmer[1], Nicholas P. Ambulos[2], Lynda F. Bonewald[3], John J. Dougherty[4], Edward Eisenstein[5], Elisabeth Fowler[6], Jinny Johnson[7], Ashok Khatri[8], Mark O. Lively[9], Nadine Ritter[10] and Susan T. Weintraub[11]

[1]The University of Michigan, Ann Arbor, MI 48109, USA; [2]University of Maryland, Baltimore, MD 21201, USA; [3]University of Missouri, Kansas City, MO 64108, USA; [4]Eli Lilly and Company, Indianapolis, IN, 46285, USA; [5]Center for Advanced Research in Biotechnology, Rockville, MD 20850, USA; [6]Millennium Pharmaceuticals, Cambridge, MA 02139, USA; [7]Texas A&M University, College Station, TX 77843, USA; [8]Massachusetts General Hospital Charlestown, MA 02129, USA; [9]Wake Forest University, Winston-Salem, NC 27157, USA; [10]NMRbiotech, Germantown, MD 20874, USA; and [11]The University of Texas Health Science Center at San Antonio, San Antonio, TX 78229, USA

Introduction

The goal of the Peptide Standards Project is the production and establishment of three synthetic peptides as registered and certified peptide reference standards. This project is being conducted by the Peptide Standards Project Committee of the Association of Biomolecular Resource Facilities (ABRF) in collaboration with the National Institute of Standards and Technology (NIST). The Peptide Standards Project is the first ABRF endeavor funded by NIST. This project entails: large-scale production of three high-purity peptides; packaging in 1-mg portions; collaborative analysis by the committee and ABRF member laboratories; stability testing; generation of Certificates of Analysis and storage of the peptide vials at NIST.

The Peptide Standards Project was originally initiated by the joint interactions between the Quality Compliance Committee and Peptide Synthesis Research Group of the ABRF. Together they designed, synthesized and qualified the three synthetic peptide sequences (Figure 1) as suitable peptide reference standards based on the following considerations: coverage of a range of molecular weights, charge and hydrophobicity; avoidance of Met, Cys or Trp to facilitate synthesis and improve stability; incorporation of Tyr to allow quantification by UV spectrophotometry; inclusion of protease cleavage sites; avoidance of acid-labile amino acids and sequences resistant to acid hydrolysis; and susceptibility of the *C*-terminus to carboxypeptidases. Multiple analyses were performed, including mass spectrometry, reversed-phase and ion exchange HPLC, amino acid composition analysis, UV spectrophotometry, *N*- and *C*-terminal sequence analysis, and enzymatic hydrolysis [1].

Peptide A	H-DAEPDILELATGYR-OH
Peptide B	H-KAQYARSVLLEKDAEPDILELATGYR-OH
Peptide C	H-RQAKVLLYSGR-OH

*Fig. 1. Sequences of **Peptides A**, **B** and **C**.*

Results and Discussion

Initially, small-scale syntheses were performed using Fmoc chemistry on a Symphony synthesizer (0.1 mmol scale) to test suitability of synthesis conditions and choice of resin (Fmoc-Arg(Pbf)-Wang resin and Fmoc-Arg(Pbf)-PEG resin). It was found that the Arg-Wang and Arg-PEG resins yielded products of comparable quality. The Arg-

Wang resin was chosen for large-scale synthesis due to its higher substitution level. Subsequently, large-scale synthesis (7.5 mmol) of **Peptide C** was performed on the Sonata Synthesizer (Protein Technologies Inc.) using Fmoc-Arg(Pbf)-Wang resin (substitution level 0.43 mmol/g). The synthesis conditions were: solvents, DCM/DMF (1:1); deprotection, 20% piperidine in DMF/0.1M HOBt for 3x30 min; coupling, HBTU/Fmoc-amino acid/ NMM (1:1:1.5) in 4-fold molar excess. The coupling steps were monitored for completion by qualitative ninhydrin testing. After synthesis, the peptides were cleaved with Reagent B (TFA/water/phenol/TIS (88:5:5:2) for 10 hr at RT. Crude peptide was analyzed by HPLC-MS which indicated three major components: **Peptide C**, des-[Gly^{10},Arg^{11}]-Peptide C and des-[Ser^{9},Gly^{10},Arg^{11}]-Peptide C. Deletion of the *C*-terminal Arg was confirmed by MS/MS analysis. Subsequently, the synthesis was repeated using Fmoc-Arg(Pbf)-PEG resin (substitution level 0.21 mmol/g) at the same scale using quantitative ninhydrin monitoring and 6-fold molar excess during the coupling steps. The crude peptide (12.5 g) contained one main component, **Peptide C** (36.5%). which was purified by cation exchange chromatography followed by reversed phase HPLC. The final **Peptide C** (yield 1.5 g) was 92% pure as confirmed by RP-HPLC and capillary zone electrophoresis. **Peptides A** and **B** were synthesized analogously on 10 mmol scale using a 4-fold (**Peptide A**) or 8-fold (**Peptide B**) molar excess of Fmoc-amino acids and coupling reagents. The target peptides were the major components in each crude mixture (**A**, 54.3% pure, 15 g; **B**, 36.6% pure, 16 g). After purification (anion exchange chromatography and RP-HPLC for **Peptide A** and two steps of RP-HPLC for **Peptide B**), each peptide was 99% pure, in yields of 1.8 g (**Peptide A**) and 1.0 g (**Peptide B**).

In conclusion, **Peptides A**, **B**, and **C** have been successfully synthesized in gram quantities in academic core laboratories. The high purity (99%, **A** and **B**; 92%, **C**) was achieved in a two-step purification using either RP HPLC or the combination of ion exchange and RP-HPLC. Multiple analytical techniques were used to confirm the identity and purity of the peptides. The purified peptides were obtained in sufficient quantities to prepare 1000 – 2000 vials of each reference standard packaged at 1 mg per vial.The research community has long needed peptide standards for comparisons among laboratories and for validation purposes. Availability of a standard peptide will also greatly enhance efforts for quality control and compliance in both industry and academia. Possible applications for peptide reference standards are instrument qualification, method verification/validation, system suitability, and analyst certification. **Peptides A**, **B** and **C** will be the first set of peptides available as standard reference material from NIST.

Acknowledgments

The work was funded by the National Institute of Standards and Technology (NIST) and the Association of Biomolecular Resource Facilities (ABRF). We thank the staff of the Biopolymers Core Facility of the University of Maryland for large-scale synthesis of the peptides and purification of **Peptides A** and **C** as well as Vasanti Vallurupalli (Protein Structure Facility, The University of Michigan) and Anaspec Inc. for purification of **Peptide B**.

Reference

1. Fowler, E., Angeletti, R., Canova-Davis, E., Cohrs, M., Dougherty, J., Hayes, T., Ritter, N. and Smith, A. *J. Biomol. Tech.* **11**, 103-105 (2000).

Peptide Revolution: Genomics, Proteomics & Therapeutics
Michael Chorev & Tomi K. Sawyer (Editors)
American Peptide Society, 2003

A Novel Approach for the Hydrophobic Peptides Synthesis and Purification through *O–N* Intramolecular Acyl Migration Reaction

Youhei Sohma, Masato Sasaki, Zyta Ziora, Naoko Takahashi, Tooru Kimura, Yoshio Hayashi and Yoshiaki Kiso

Department of Medicinal Chemistry, Center for Frontier Research in Medicinal Science, Kyoto Pharmaceutical University, Yamashina-Ku, Kyoto 607-8412, Japan

Introduction

The synthesis of peptides containing "difficult sequences" is one of the most troublesome matters in peptide chemistry, and the peptides are often afforded with low yield and purity in the SPPS. It is known that the difficult sequences are generally hydrophobic and promote the peptide aggregation in solvent during synthesis and purification [1]. This aggregation, normally produced during the sequential assembly of amino acids, is attributed to intermolecular hydrophobic interaction and hydrogen bond formation among the resin-bound peptide chains, resulting in the formation of extended secondary structures such as a β-sheet [2].

In our previous studies regarding new water-soluble prodrugs of HIV-1 protease inhibitors having a α-hydroxy-β-amino acid [3], we synthesized prodrugs based on the *O–N* intramolecular acyl migration reaction which is well-known in the synthesis of Ser- or Thr-containing peptides. These prodrugs increased water-solubility with a newly formed and ionized amino group, and conversion to the parent drugs could be controlled by pH and realized in a short time with no side reactions under physiological conditions. Based on these findings, we conceived the idea that the *O–N* intramolecular acyl migration reaction could be applied to the synthesis of difficult sequence-containing peptides (Figure 1).

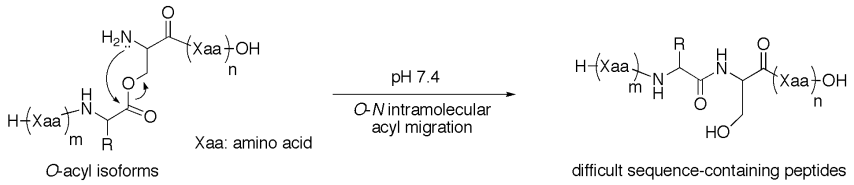

Fig. 1. Conversion of O-isoforms to parent peptides with a difficult sequence through O–N intramolecular acyl migration reaction.

Results and Discussion

As a model peptide with a difficult sequence, Ac-Val-Val-Pns-Val-Val-NH_2 (**1**, Pns: phenylnorstatine, (2*R*,3*S*)-3-amino-2-hydroxy-4-phenylbutyric acid) was selected and synthesized by standard Fmoc-based SPPS (Route A) or through its *O*-isoform **5** followed by *O–N* intramolecular acyl migration (Route B, Scheme 1). Pns in **1** is an α-hydroxy-β-amino acid possessing the hydroxymethylcarbonyl (HMC) isostere required for aspartyl protease inhibition [4].

In Route A, a major by-product, Fmoc-Val-Val-Pns-Val-Val-NH_2, in which the N-terminal Fmoc group was not deprotected by a 20% piperidine treatment, was produced in a similar amount to the desired product **1** (Figure 2A), suggesting that the high hydrophobicity in **1** prevented access of the base to the Fmoc group, probably forming insoluble micro-aggregates on the resin. Further purification of **1** was difficult in preparative HPLC due to the extreme low solubility of the products, since the solubility of **1** in H_2O and MeOH was 0.008 and 0.065 mg mL^{-1}, respectively.

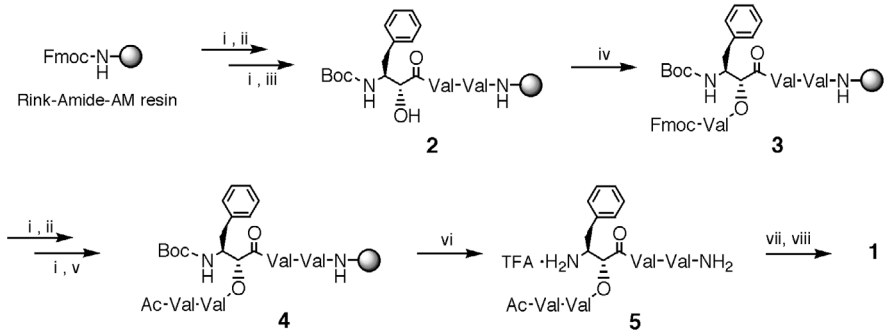

Scheme 1. Reagents in Route B: i) 20% piperidine/DMF, 20 min; ii) Fmoc-Val-OH, DIPCDI, HOBt, DMF; iii) Boc-Pns-OH, DIPCDI, HOBt, DMF; iv) Fmoc-Val-OH, DIPCDI, DMAP, CH_2Cl_2; v) Ac_2O, TEA, DMF; vi) TFA/m-cresol/thioanisole/H_2O (92.5/2.5/2.5/2.5); vii) preparative HPLC (a linear gradient of CH_3CN in 0.1% TFA aq); viii) PBS, pH 7.4, rt.

In Route B, after final cleavage, *O*-isopeptide **5** was detected as the major product (Figure 2B), indicating that the protected peptide resin **4** is efficiently synthesized with no obstruction due to its high hydrophobicity. This suggests that the branched ester structure in **4** modifies the property of difficult sequence in **1**. In addition, **5** showed higher H_2O- and MeOH-solubility, with values of 59.4 (7500-fold) and 277.3 mg mL^{-1} (4300-fold), respectively, than the *N*-acyl peptide **1**. Hence, it could be purified easily by HPLC using 0.1% aqueous TFA-CH_3CN system as an eluant.

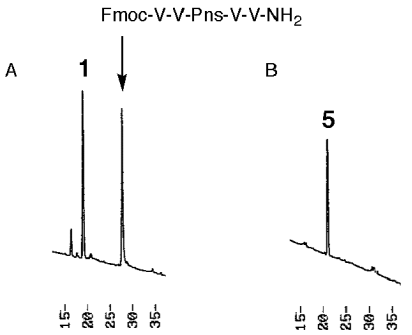

Fig. 2. HPLC profiles of crude deprotected peptide; (A) Route A, (B) Route B purification of peptides containing difficult sequences.

Finally, in Route B, the purified **5** was dissolved in PBS (pH 7.4) and completely converted to the corresponding parent peptide **1** via *O–N* intramolecular acyl migration at rt with no side reactions, resulting in the precipitation of pure **1**. This migration was rapid with a half-life of < 1 min. Consequently, the overall yield of **1** in Route B was higher (54%) than that in Route A (1.3%). Thus, these results suggest that this novel strategy based on *O–N* intramolecular acyl migration would overcome the problems in the synthesis and purification.

References

1. (a) Wöhr, T., et al. *J. Am. Chem. Soc.* **118**, 9218-9227 (1996). (b) Howe, J., et al. *Tetrahedron Lett.* **41**, 3997-4001 (2000).
2. (a) Live, D. H. et al. In Hruby, V. J. and Rich, D. H. (Eds.) *Peptides: Structure and Function (Proceedings of the 8th American Peptide Symposium)* Pierce Chemical: Rockford, pp 65-68 (1984). (b) Tam, J. P. and Lu, Y. A. *J. Am. Chem. Soc.* **117**, 12058-12063 (1995).
3. (a) Hamada, Y., et al. *Bioorg. Med. Chem.* **10**, 4155-4167 (2002). (b) Hamada, Y., et al. *Bioorg. Med. Chem. Lett.* **13**, 2727-2730 (2003).
4. Mimoto, T., et al. *Chem. Pharm. Bull.* **39**, 2465-2467 (1991).

Peptide Revolution: Genomics, Proteomics & Therapeutics
Michael Chorev & Tomi K. Sawyer (Editors)
American Peptide Society, 2003

An Efficient Asymmetric Synthesis of Fmoc-*L*-Cyclopentylglycine Using a Chiral Auxillary

Satendra Singh and Michael W. Pennington

BACHEM Bioscience, Inc., 3700 Horizon Drive, King of Prussia, PA 19406, USA

Introduction

Nature has afforded us 22 naturally occurring coded amino acids commonly found in proteins isolated from eukaryotic and prokaryotic sources. A host of enzymes are present in nature to extend this repertoire much further by utilizing post-translational modification [1]. A variety of synthetic means have also been established to produce a plethora of non-proteinogenic amino acids as tools to investigate enzymatic mechanisms, extend biological half-life, establish a specific conformational determinant or increase potency of therapeutically interesting peptides [2].

Cyclopentylglycine (Cpg) is a competitive inhibitor of isoleucine uptake in *E. coli* [3] and also has been used in designing angiotensin II antagonists [4]. It has been synthesized via S_N2 displacement of bromoglycinate with an organometallic reagent followed by epimerization [5]. Syntheses of racemic 2-cyclopentenylglycine [6], cyclopentylglycine [3], and 2-cyclopentadieneylglycine [7] have been reported as shown in Scheme 1.

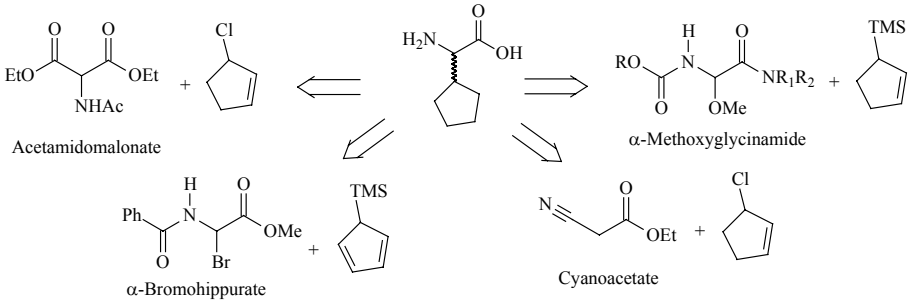

Scheme 1. Synthesis of racemic 2-cyclopentylglycine from various routes.

In this paper, we wish to report a short and efficient asymmetric synthesis of Fmoc-*L*-cyclopentylglycine (5) by using benzyl (*2R,3S*)-(-)-6-oxo-2,3-diphenyl-4-morpholinecarboxylate (1) as a template. The reasons behind choosing this chiral auxiliary were: 1) commercial availability; 2) excellent optical purity of the final product; 3) high reactivity towards unactivated electrophiles; and 4) scalability.

Results and Discussion

As shown in Scheme 2, chiral auxiliary **1** was alkylated with cyclopentyl iodide in the presence of lithium bis(trimethylsilyl)amide base. Enolate generation at –78 ^{0}C followed by quenching with alkylating agent at the same temperature did not result in any reaction. Optimum conditions utilized dissolving **1** and cyclopentyl iodide in THF/HMPA (10:1) by heating to ~35 ^{0}C, generating enolate at –78 ^{0}C and allowing the reaction mixture to warm to room temperature for 2 hrs. Under these conditions, alkylated product **3** was obtained in 60% yield [8].

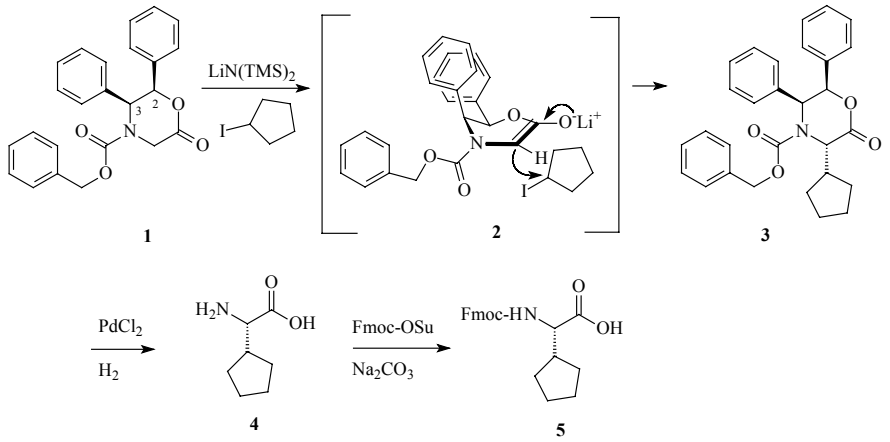

Scheme 2. Asymmetric synthesis of Fmoc-L-cyclopentylglycine.

Variations in experimental conditions, such as longer reaction time, increasing the amount of base (>1.5 equiv.) or cyclopentyl iodide (>5 equiv.) and substituting the solvating agent HMPA with DMPU either did not result in any improvements or lowered the yield of the alkylation product **3**. Since cyclopentyl iodide is an unactivated electrophile, raising the reaction temperature to 40 ^{0}C was expected to improve the yield of alkylation product **3**. However, reaction at 40 ^{0}C for 1 hr resulted in the formation of more side products, in addition to alkylation product **3** [8].

Cleavage of the auxiliary ring system **3** was performed using H_2 and $PdCl_2$ as a catalyst in THF/MeOH (2:1) solvent mixture at 60 psi for 48-60 hrs. After removing the catalyst (pyrophoric), the solvent was removed and the residue was triturated with ether to afford Cpg **4** in almost quantitative yield. The contaminating byproduct, 1,2-diphenylethane was easily removed by extracting the dilute aqueous HCl solution of **4** with EtOAc. Removal of aqueous solvent followed by crystallization of the syrup from MeOH/EtOAc afforded **4** in 84% yield [8].

Protection of the α-amino function of Cpg **4** was accomplished by treating it with Fmoc-OSu in the presence of Na_2CO_3 overnight in dioxane/H_2O (1.5:1) solvent mixture. Fmoc-Cpg-OH (**5**) was obtained in quantitative yield after crystallization from EtOAc/hexane [8].

Thus, an efficient asymmetric synthesis of Fmoc-Cpg-OH (**5**) from a commercially available chiral auxiliary was successfully accomplished on multigram scale. Synthesis was easy to perform, as no chromatographic purification was required at any step. Furthermore, excellent optical purity (>99%) and high yield (50% overall) was obtained.

References

1. Atkins, J. F. and Gesteland, R. *Science* **296,** 1409-1410 (2002).
2. Duthaler, R. O. *Tetrahedron* **50,** 1539-1650 (1994).
3. Harding, W. M. and Shire, W. J. *J. Biol. Chem.* **206,** 401-410 (1954).
4. Nyeki, O., *et al. J. Med. Chem.* **30,** 1719-1724 (1987).
5. Williams, R. M., *et al. J. Am. Chem. Soc.* **110,** 1547-1557 (1988).
6. Dennis, R. L., *et al. J. Am. Chem. Soc.* **77,** 2362-2364 (1955).
7. Dialer, H., Steglich, W. and Beck, W. *Tetrahedron* **57,** 4855-4861 (2001).
8. Singh, S. and Pennington, M. W. *Tetrahedron Lett.* **44**, 2683-2685 (2003).

Peptide Revolution: Genomics, Proteomics & Therapeutics
Michael Chorev & Tomi K. Sawyer (Editors)
American Peptide Society, 2003

Thiazolidine as Protection for N^{α}-(1-Phenyl-2-Mercaptoethyl) Glycine in Extended Chemical Ligation of Three or More Fragments

Matteo Villain, Hubert Gaertner and Paolo Botti

GeneProt Inc., Geneva Branch, 2, Pré-de-la–Fontaine, 1217 Meyrin, Switzerland

Introduction

Synthesis of large polypeptides by native chemical ligation typically requires the assembly by chemical ligation of three or more unprotected peptide segments of 30 or more amino acids. In the C-to-N direction synthesis, a key issue is the potential reactivity of the middle segments, which would bear both an N-terminal cysteine and a C-terminal thioester. We recently introduced a new approach for protecting N terminal cysteine in the intermediate fragments using a thiazolidine cyclic structure as the N terminal protection [1]. With the recent introduction of the extended chemical ligation (ECL) method [2, 3], ligations are no longer restricted to N-terminal cysteines. A peptide fragment presenting an N-terminal glycine functionalized with the auxiliary group N^{α}-(1-phenyl-2-mercaptoethyl) readily generates with a C-terminal thioester peptide fragment a natural amide bond after auxiliary removal with HF or TFA.

We extended the concept of cyclization of a 1-2 amino thiol with formaldehyde to protect the N-terminal auxiliary-glycine moiety on an intermediate peptide fragment. Also in this case, the thiazolidine ring is stable to ligation conditions. After ligation the ring is readily opened using mild acid and O-ethylhydroxylamine.

Results and Discussion

The first requirement for our strategy was the modification of the thiol protection present on the auxiliary, from the initially proposed *p*-methylbenzyl, to the Boc orthogonal trityl group. This protection allowed, after incorporation of the auxiliary on a bromoacetylpeptidyl thioester resin, and trityl removal, thiazolidine formation on solid phase, using formaldehyde and acetic acid in DMF for 12 hrs (Scheme 1).

A test peptide with the sequence YAKYAKL, functionalized at the N terminus with *N*-[4-(4-methoxyphenyl)-1,3-thiazolidin-3-yl]acetyl, was used to test the stability of the thiazolidine ring in ligation conditions (0.1 M $NaHPO_4$, 6 M guanidine hydrochloride, 1 % thiophenol, pH 7.4), proving to be stable for more then 50 hrs. The same peptide was tested for thiazolidine opening, employing 0.5 M O-ethylhydroxyl amine and pH 3.5. Ring opening was completed in two hours.

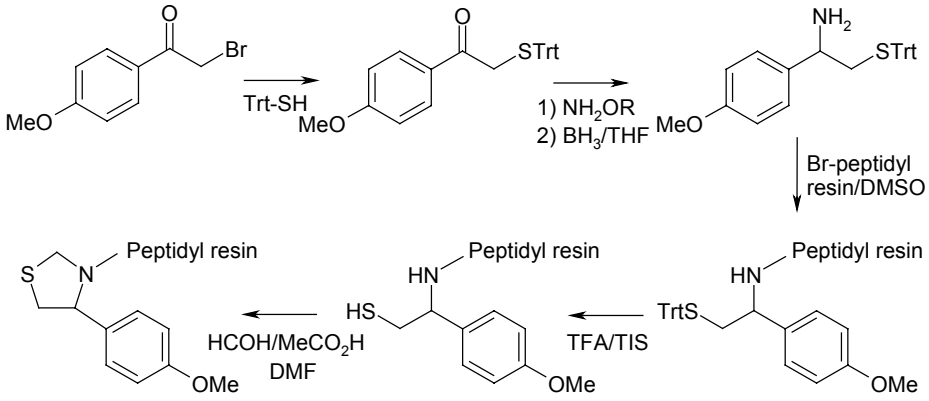

Scheme 1. Synthetic route to N-*[4-(4-methoxyphenyl)-1,3-thiazolidin-3-yl]acetyl thioester peptides.*

Using a three fragments approach, with the middle fragment functionalized at the N-terminous with *N*-[4-(4-methoxyphenyl)-1,3-thiazolidin-3-yl]acetyl, and at the C-terminus with the thioester MALP, we synthesized with two consecutive ligations, the following sequence:

KWGVCRPQKCASPGAKSEPKCSDFQKRLYKCKPCPKCGDQST*G(N$^{\alpha}$Aux)PGDP SMLYDKVAPNNLPKSKVNFGKNIM*CYAKYAKL.

Auxiliary removal from the purified full-length sequence was achieved after treating the peptide for three hours with TFA/TIS/H_2O (95/2.5/2.5).

Thiazolidine is a convenient temporary protection of the N-terminal cysteine in peptide segments with a C-terminal thioester. In this communication, we show that a thiazolidine ring is also a suitable protection for the recently introduced N$^{\alpha}$-(1-phenyl-2-mercaptoethyl) glycine. Ring opening is achieved at acidic pH in the presence of O-alkyl-oxy amine as for cysteine, and no side reaction was observed. The one pot deprotection procedure proposed here permits a considerable reduction in the handling losses common to peptide ligation synthesis during HPLC purification. The presented Nα-(1-trityl-2-mercaptoethyl) amine can find a further application in Fmoc chemistry, since it is perfectly suited for the synthesis of C-terminal fragment using this technique.

Acknowledgments

We would like to acknowledge Nicolas Dafflon, Benoit Depresle, Marianne Paolini and Sylvain Raimondi for their excellent technical assistance and useful discussions.

References

1. Villain, M., Vizzavona, J., Gaertner, H., In Lebl, M. and Houghten, R. A. (Eds.) *Peptides: the Wave of the Future (Proceedings of 17th American Peptide Symposium)*, American Peptide Society, 2001, pp. 107–108.
2. Botti, P., Carrasco, M. and Kent, S. B. *Tetrahedron Lett.* **42**, 1831-1833 (2001).
3. Low, D. W., Hill, M. G., et al. *Proc. Natl. Acad. Sci. U.S.A*. **98**, 6554-6559 (2001).

Peptide Revolution: Genomics, Proteomics & Therapeutics
Michael Chorev & Tomi K. Sawyer (Editors)
American Peptide Society, 2003

Solid-Phase Synthesis of *C*-Terminal Thio-Linked Glycopeptides

John P. Malkinson and Robert A. Falconer

Department of Pharmaceutical and Biological Chemistry, The School of Pharmacy, University of London, 29-39 Brunswick Square, London WC1N 1AX, UK

Introduction

The synthesis of modified glycopeptides is a strategy to improve the absorption and distribution of poorly bioavailable therapeutic peptides, increasing resistance to enzymatic degradation, enhancing physicochemical properties and providing the potential to exploit active transporters.

The assembly of *S*-linked glycopeptides on a solid support is complicated by the need to anchor a sugar moiety to the resin and by the requirement for a selectively removable thiol protecting group that is compatible with standard Fmoc solid phase synthesis protocols. Potential protecting groups include triphenylmethyl (Trt) and 9-fluorenylmethyl (Fm). Each, however, presented problems in our hands both with introduction (low yields) and removal.

Results and Discussion

The recently reported 9*H*-xanthen-9-yl (Xan) protecting group [1], used as a temporary cysteine *S*-protecting group in the synthesis of α-conotoxin [2], has been successfully utilized here as a temporary thio-protection compatible with other carbohydrate protecting groups [3].

The xanthenyl protecting group was introduced in quantitative yield by reaction of 1-thiosugars **1a-c** (glucose, *N*-Acetylglucosamine and mannose, respectively) with 9-hydroxyxanthene in the presence of TFA (Figure 1).

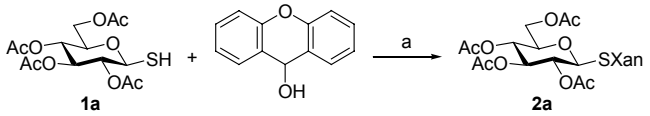

Fig. 1. Reagents and Conditions: (a) TFA 2:50 CH_2Cl_2 (97%).

Following de-*O*-acetylation of the Xan-protected thiosugar (**3a-c**), a silyl (TBDMS) protecting group was selectively introduced to the primary alcohol (**4a-c**). After re-*O*-acetylation (**5a-c**), the TBDMS group could be selectively cleaved with tetra-butylammonium fluoride (TBAF) to give **6a-c** [3]. Due to difficulties in anchoring **6a-c** directly, succinate derivatives **7a-c** were immobilized onto an MBHA derivatized polystyrene resin (Figure 2).

Following removal of the *S*-Xan protection, the first amino acid, with its carboxylic acid reduced to the alcohol, was attached to the resin-bound mannose derivative (used for this study) by a Mitsunobu reaction [4,5]. The reaction conditions were varied and are reported below (Table 1).

The optimum conditions for the Mitsunobu reaction were found to be: (i) anhydrous THF, which promoted good solvation of the polystyrene polymer network; (ii) diethyl azodicarboxylate (DEAD) (added dropwise to a cooled solution of *N*-Fmoc protected amino alcohol) and triphenylphosphine (the solution was cooled during addition of the DEAD in order to prevent potential decomposition and subsequent undesirable ethyl thioether formation); (iii) a two-fold excess of alcohol over DEAD and phosphine, to

minimize the possibility of any remaining unreacted DEAD being alkylated by the thiol; (iv) a reaction time of 1-3 h.

After washing and *N*-Fmoc deprotection, the peptide chain was extended using standard N^{α}-Fmoc based SPPS (Figure 2).

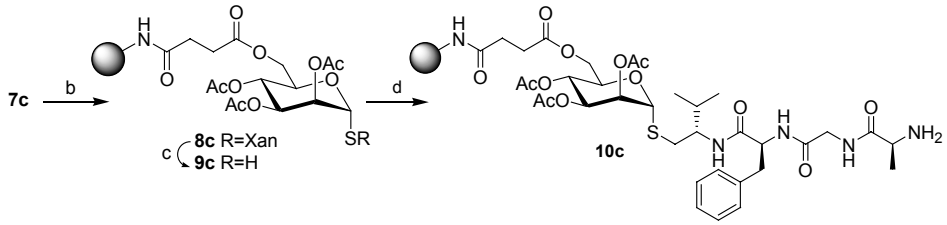

Fig. 2. Reagents and Conditions: (b) MBHA resin, HBTU, HOBt, iPr_2NEt, DMF (99%); (c) CH_2Cl_2:TFA:Et_3SiH 97:2:1 [1h] then CH_2Cl_2:TFA:Et_3SiH 89:10:1 [2x0.5h]; (d) (1) Fmoc-Val-ol, Mitsunobu reaction, see Table 1; (2) 20% v/v piperidine, DMF, rt, [2x10min]; (3) Fmoc-Phe-OH, HBTU, HOBt, iPr_2NEt, DMF, rt, [2x0.5h]; 20% v/v piperidine, DMF, rt, [2x10min]; repeat for Fmoc-Gly-OH then Fmoc-Ala-OH.

Table 1. Investigation of conditions for Mitsunobu reaction.

Entry	Solvent	Equivalents			Time (h)	Yield[#], %
		Alcohol	PPh_3	DEAD		
1	THF	10	5	5*	3	62
2	THF	10	5	5	3	66
3	THF	10	5	5	1	70
4	THF	5	5	5	3	27
5	THF	5	2.5	2.5	3	47
6	THF	10	5	5	5	60
7	CH_2Cl_2	10	5	5	3	40

**DIAD used in place of DEAD; [#]Isolated yield.*

The resin-bound model glycopeptide **10c** was removed from the solid support (with simultaneous deprotection of the carbohydrate *O*-acetyl protecting groups) by nucleophilic cleavage with methanolic ammonia [5] to give the desired thio-linked peptide in very good yield (Table 1).

In summary, the utility of the Mitsunobu reaction for the solid-phase assembly of *C*-terminal thioether-linked glycopeptides has been demonstrated. Conditions for the Mitsunobu reaction have been investigated.

Acknowledgments

The work was funded by a C. W. Maplethorpe fellowship (JPM) and a School of Pharmacy fellowship (RAF).

References

1. Han, Y. and Barany, G. *J. Org. Chem.* **62**, 3841-3848 (1997).
2. Hargittai, B. and Barany, G. *J. Peptide Res.* **54**, 468-479 (1999).
3. Falconer, R. A. *Tetrahedron Lett.* **43**, 8503-8505 (2002).
4. Falconer, R. A., Jablonkai, I. and Toth, I. *Tetrahedron Lett.* **40**, 8663-8666 (1999).
5. Malkinson, J. P. and Falconer, R. A. *Tetrahedron Lett.* **43**, 9549-9552 (2002).

Peptide Revolution: Genomics, Proteomics & Therapeutics
Michael Chorev & Tomi K. Sawyer (Editors)
American Peptide Society, 2003

Isolation and Characterization of Autoantibodies in Multiple Sclerosis Patients' Sera: Towards a Novel Apheresis Treatment

Elisa Peroni[1], Francesco Lolli[3], Benedetta Mazzanti[1], Marta Pazzagli[1,2], Bruno Bonetti[4], Johan Hoebeke[5], Mario Chelli[1], Paolo Rovero[6] and Anna M. Papini[1]

[1]Dipartimento di Chimica Organica "Ugo Schiff" and CNR-ICCOM, Università di Firenze, I-50019 Sesto Fiorentino (FI), Italy; [2]CSF S.r.l I-50122 Firenze, [3]Azienda Ospedaliera Careggi and Dipartimento di Scienze Neurologiche e Psichiatriche, Università di Firenze, I-50134 Firenze, Italy; [4]Azienda Ospedaliera di Verona, Dipartimento di Neurologia, I-37134 Verona, Italy; [5]UPR 9021, IBMC F-67084 Strasbourg Cedex, France; [5]Dipartimento di Scienze Farmaceutiche, Università di Salerno, I-84084 Fisciano (SA), Italy

Introduction

Apheresis is a biotechnological procedure to remove basic components from blood (red cells, white cells, platelets and plasma). The use of immunoadsorbents for extra-corporeal treatment of plasma in various diseases is a recent application of affinity chromatography. Therefore, affinity separation by antibody-antigen interaction is one of the most promising applications, in which either the antigen (Ag) or the Ab is immobilized to various matrices for the purification or removal of the corresponding Ab or Ag. Peptide affinity ligands have been used to develop immunoadsorption therapies in autoimmune diseases [1].

Multiple sclerosis is an inflammatory demyelinating disease of the central nervous system and is the most common cause of neurological disability in young adults. There is consistent evidence that distinct pathogenic mechanisms lead to the formation of MS lesions, suggesting a pathophysiological hetereogeneity of the disease. In particular an antibody-mediated disease pattern seems to correlate with the typical relapsing-remitting MS form. In this context, we previously demonstrated [2,3] that the structure-based designed glycopeptide CSF114(Glc) is able to detect specific Abs by a solid phase non-competitive indirect ELISA on sera of MS patients. CSF114(Glc) was selected as the first synthetic Ag because of its binding properties to auto-Abs putatively involved in the pathogenesis of MS. These properties prompted us to use CSF114(Glc) as a synthetic ligand for purification of Abs (correlating with the disease activity) present in sera of MS patients. Up to now no selective apheresis technique for MS was set up, particularly because no selective Ag was identified for this disease. Our aim is to study the feasibility of antigen-specific immunotherapies based on CSF114(Glc).

Results and Discussion

We selected CNBr-Sepharose as a biocompatible activated immunoadsorbent. The glycopeptide CSF114(Glc) was coupled to the matrix obtaining CSF114(Glc)-sepharose. By this glycopeptide affinity column, we tested the recognition properties of CSF114(Glc) and its ability to isolate the auto-Abs from MS patients' sera. CSF114(Glc)-positive sera (diluted 1:10 in PBS) were loaded onto the column. We demonstrated that auto-Abs [present in CSF114(Glc) MS positive serum] were immobilized onto the immunoaffinity column by measuring the Ab titre, by SP-ELISA, before and after the loading. Adsorbed Abs were then eluted by a buffer change (0.1 M

glycine, pH 2.6). The efficiency of this immunoadsorption was confirmed by SP-ELISA performed on the collected fractions. No Abs could be separated using the inert Sepharose matrix (Gly-sepharose). CSF114(Glc)-based affinity column proved to be useful for a very convenient one-step purification of auto-Abs, directly from MS patients' serum. In order to analyze the affinity of purified IgGs for CSF114(Glc), we performed Biomolecular Interaction Analysis with a BIACORE instrumentation. The BIACORE uses surface plasmon resonance (SPR) to monitor, with a microfluidic system, on a sensor surface, binding interactions between molecular partners. The sensor surface was prepared by immobilizing the Ag to a streptavidin coated CM5 chip. CSF114(Glc) was biotinylated in SPPS by *N*-biotinyl-6-aminohexanoic acid. The dissociation rate constant, $k_d = 1.3 \pm 0.12 \times 10^{-3}$ s^{-1}, is the slope obtained from the linear fitting of the dissociation sensorgrams. By the fitting, on a half logarithmic scale, of the inhibition sensorgrams, we evaluated the affinity constant $K_A = 3.9 \pm 1.8 \times 10^9$ M^{-1} and the association rate constant $k_a = K_A \times k_d = 5.1 \pm 2.6 \times 10^6$ M^{-1} s^{-1}.

In order to assess whether anti-CSF114(Glc) auto-Abs recognized CNS structures *in situ*, sera from patients with either high Ab titers (5 MS) or no reactivity to CSF114(Glc) [5 MS and 5 CIDP (chronic inflammatory demyelinating polyneuropathy)] were tested by immunohistochemistry on sections from normal human CNS [4]. All five CSF114(Glc)-positive MS patients' sera showed diffuse IgM immunostaining of CNS white matter, particularly concentrated on myelin sheaths and glial cells morphologically resembling oligodendrocytes. Sera from all ten CSF114(Glc)-negative cases gave no detectable immunoreactivity in CNS sections. We then explored which Ab fraction in CSF114(Glc)-positive sera was responsible for CNS immunostaining; for this purpose, we used CSF114(Glc)-specific IgM, IgG, and biotinylated-IgG isolated from two CSF114(Glc)-positive MS sera. The immunostaining with CSF114(Glc)-specific IgG or IgM was comparable to that of respective sera. Double immunofluorescence with isolated anti-CSF114(Glc) IgG/IgM and lineage specific glial cell markers were then performed to assess the precise cellular distribution of the CNS Ags recognized by these auto-Abs from MS patients. Both CSF114(Glc)-specific IgM, IgG and biotinylated-IgG co-localized with MBP on myelin sheaths and at the surface of mature oligodendrocytes.

Considering the pathophysiological hetereogeneity of MS, the Abs isolated from MS patients reactive to myelin and oligodendrocytes could help to characterize the MS subtype associated with antibody-mediated demyelination. This result could have an important impact in the development of a specific immunotherapy based on apheresis biotechnology.

Acknowledgments
This research was supported by PRIN-COFIN 2002-2004, MIUR, Italy.

References

1. Wallukat, G., Muller, J. and Hetzer, R. *N. Engl. J. Med.* **347**, 1806 (2002).
2. Papini, A. M., Rovero, P., Chelli, M. and Lolli, F. "Glycopeptides, their preparation and use in the diagnosis or therapeutic treatment of multiple sclerosis," Eur. Pat. Appl. (2002), EP02-06767 20020619. Priority: IT 2001-FI114 20010622.
3. Lolli, F., Mulinacci, B., Carotenuto, A., Bonetti, B., Sabatino, G., Zipoli, V., Mastrangelo, E., Mazzanti, B., Pazzagli, M., Alcaro, M. C., Peroni, E., Marconi, S., Pozo-Carrero, M. C., Nuti, F., Battistini, L., Chelli, M., Rovero, P. and Papini., A. M. "A glycopeptide designed to identify, isolate, and characterize autoantibodies in Multiple Sclerosis", submitted.
4. Valdo, P., Stegagno, C., Mazzucco, S., Zuliani, E., Zanusso, G. L., Moretto, G., Raine, C. S. and Bonetti, B. *J. Neuropathol. Exp. Neurol.* **61**, 91-98 (2002).

Peptide Revolution: Genomics, Proteomics & Therapeutics
Michael Chorev & Tomi K. Sawyer (Editors)
American Peptide Society, 2003

Small Focused Library of CSF114-type Glycopeptides for the Characterization of Autoantibody Recognition in Multiple Sclerosis

Francesca Nuti[1], Ilaria Paolini[1], Barbara Mulinacci[1], Maria de la Cruz Pozo-Carrero[1,2], Benedetta Mazzanti[1,2], Marta Pazzagli[2], Francesco Lolli[3], Mario Chelli[1], Franca Maria Cordero[1], Alberto Brandi[1] and Anna Maria Papini[1]

[1]Laboratory of Peptide Chemistry & Immunology, Dipartimento di Chimica Organica "Ugo Schiff", and CNR-ICCOM, Università di Firenze, I-50019 Sesto Fiorentino (FI), Italy; [2]CSF S.r.l., I-50124 Firenze; [3]Azienda Ospedaliera Careggi, and Dipartimento di Scienze Neurologiche e Psichiatriche, Università di Firenze, I-50134 Firenze, Italy

Introduction

To study the role of the glycosyl moiety in autoantibody (auto-Ab) recognition in Multiple Sclerosis (MS), we designed and developed the glycopeptide CSF114(Glc) as the first synthetic antigen (Ag) recognized by specific auto-Abs in MS patients sera. No Abs could be identified by the corresponding unglycosylated peptide sequence. Therefore, we could determine that the specific auto-Ab recognition is most likely driven by direct interactions of the Abs with the Asn-linked sugar moiety [1]. These results demonstrate for the first time the possibility of identifying auto-Abs by post-translationally modified peptides as synthetic Ags in solid-phase noncompetitive indirect ELISA (SP-ELISA), leading to potential new approaches to MS diagnosis and prognosis, and more specific therapeutic treatments. In order to assess that the minimal epitope recognized by MS patients sera must contain Asn(Glc), we synthesized a small focused library of CSF114-type glycopeptides, based on glyco-amino acid diversity.

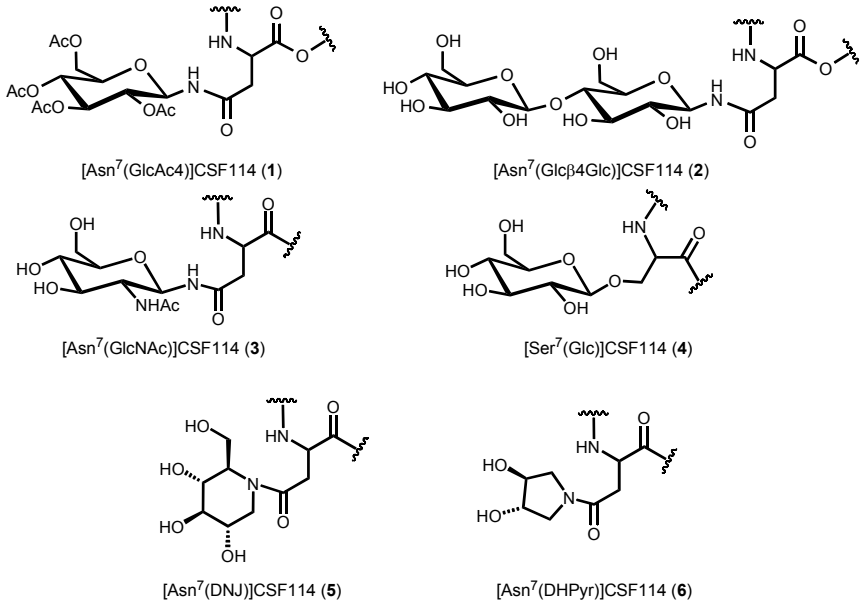

Fig. 1. CSF114-type glycopeptides.

Results and Discussion

To study the role of glycosylation in auto-Ab recognition in patients affected by MS, we developed a small focused library of CSF114-type glycopeptides containing different sugar residues (Figure 1). Significant to our objective were the glycopeptides characterized by the CSF114 sequence bearing the Asn-7 residue modified with different glycosyl moieties linked by an N- or an O-glycosidic bond. In particular, we used tetraacetylated glucose (GlcAc4) [2], cellobiose (Glcβ4Glc) [2], acetylglucosamine (GlcNAc) (Bachem, Switzerland), and the glyco-amino acid Ser(Glc) [3] to obtain [Asn^7(GlcAc4]CSF114 (**1**), [Asn^7(Glcβ4Glc)]CSF114 (**2**), [Asn^7(GlcNAc)]CSF114 (**3**), and [Ser^7(Glc)]CSF114 (**4**), respectively. Moreover, because it is known that alkaloidal sugar mimics, particularly glycosidases or mannosidases inhibitors, have therapeutic potential in many diseases, we synthesized new Fmoc-protected amino acids bearing polyhydroxylated azasugars. Our aim was to investigate the influence on antibody recognition in MS of a different bond, introducing on the Asn-7 side chain in the CSF114 sequence, deoxynojirimycin (DNJ), an iminosugar [4] with the same number of hydroxyl functions and the same glucose configuration, and 3,4-dihydroxypyrrolidine (DHPyr) [5,6], to study the effect of a constrained ring. With these new Fmoc-protected sugar-amino acids we obtained [Asn^7(DNJ)]CSF114 (**5**), and [Asn^7(DHPyr)]CSF114 (**6**).

Auto-Ab recognition by the glycopeptides of the small focused library was evaluated by SP-ELISA and competitive ELISA. In SP-ELISA, only CSF114(Glc) detected increased IgG Abs in MS patients sera compared to control negative sera. In competitive experiments, the results showed that all the glycopeptides **1**–**5** displayed inhibitory activity only at higher concentration, while the glycopeptide [Asn^7(DHPyr)]CSF114 (**6**) showed no activity. To date, none of the CSF114-type glycopeptides of the focused library was able to inhibit anti-CSF114(Glc) Abs. In conclusion, Asn(Glc) is the minimal epitope, present in CSF114(Glc), recognized by specific auto-Abs in MS [7].

References

1. Papini, A. M., Rovero, P., Chelli, M., Lolli, F. "Glycopeptides, their preparation and use in the diagnosis or therapeutic treatment of multiple sclerosis". Eur. Pat. Appl. (2002); EP02-06767 20020619. Priority: IT 2001-FI114 20010622.
2. Meinjohanns, E., Meldal, M., Paulsen, H., Dwek, R. A. and Bock, K. *J. Chem. Soc. Perkin Trans. 1,* 549-560 (1998).
3. Reimer, K. B., Meldal, M., Kusumoto, S., Fukase, K. and Bock, K. *J. Chem. Soc. Perkin Trans.* **1***,* 925-932 (1993).
4. Matos, C. R. R., Lopes, R. S. C. and Lopes, C. C. *Synthesis* **4**, 571-573 (1999).
5. Nagel U., Kinzel, E., Andrade, J. and Prescher, G., *Chem. Ber.* **119**, 3326-3343 (1986).
6. Nuti, F., Cicchi, S., Peroni, E., Pozo-Carrero, M. C., Mazzanti, B., Pazzagli, M., Lolli, F., Chelli, M., Papini, A. M., Brandi, A. In: Benedetti, E. and Pedone, C. (Eds.) *Peptides 2002*, Editions Ziino, Napoli, Italy, 238-239 (2002).
7. Lolli, F., Mulinacci, B., Carotenuto, A., Bonetti, B., Sabatino, G., Zipoli, V., Mastrangelo, E., Mazzanti, B., Pazzagli, M., Alcaro, M. C., Peroni, E., Marconi, S., Pozo-Carrero M. C., Nuti, F., Battistini, L., Chelli, M., Rovero, P., Papini, A. M. "A glycopeptide designed to identify, isolate, and characterize autoantibodies in Multiple Sclerosis", manuscript submitted.

Peptide Revolution: Genomics, Proteomics & Therapeutics
Michael Chorev & Tomi K. Sawyer (Editors)
American Peptide Society, 2003

O-Glycopeptide Synthesis Made Easy

Beechanahalli P. Gangadhar[1], Seetharama D. Jois[2], Sulaiman Sheriff[1], William T. Chance[1] and Ambikaipakan Balasubramaniam[1]

[1]Department of Surgery, University of Cincinnati Medical Center, Cincinnati, OH 45267, USA;
[2]Department of Pharmacy, National University of Singapore, Singapore

Introduction

Carbohydrate moieties in glycoproteins play a crucial role in a number of biological process, including cell recognition, cell adhesion, infection and tumor metastasis [1]. Glycosylation of peptides has also been shown to increase proteolytic stability, and promote blood brain barrier (BBB) permeability [2, 3]. Moreover, glycosylation enhances solubility, and may also contribute to the stabilization of peptide structures. The latter may impart differential receptor selectivity. Thus glycopeptides have attracted much attention in recent years. It is therefore desirable that a convenient and high yield method is available for the routine synthesis of glyocopeptides. In this regard a significant advancement has been made in the solid and solution phase glycopeptide synthesis during the last decade [1-3]. However, stereospecific synthesis of protected glycosylated amino acid derivatives required solid and solution glycopeptide synthesis still remains challenging, and expensive. To overcome these difficulties, we have devised a method for the rapid, high yield and stereoslective synthesis of glycopeptides.

Results and Discussion

Several methods have previously been reported for the synthesis of O-glycopeptides [1-3]. Our investigations towards improvising these methodologies revealed that O-glycopeptides could easily be synthesized using the Fmoc-X[β-D-Glc$(OAc)_4$]-OPfp (X = Tyr, Ser, Thr or Hyp) generated in solution, thus eliminating the tedious procedures involved in the isolation and purification of this building block. This is illustrated for the solid phase synthesis of model tripeptides X(β-D-Glc)-Gly-Ala-NH_2 (Scheme 1). As judged by TLC, glycosylation reaction of Fmoc-X-OPfp with β-D-Glc$(OAc)_5$ in the presence of $BF_3.Et_2O$ at room temperature was complete within 1-2 h. The reaction mixture was then washed repeatedly to remove the excess of $BF_3.Et_2O$, dried and concentrated, and the solution containing the Fmoc-X[β-D-Glc$(OAc)_4$]-OPfp was used directly for the acylation of α-amino group of the peptide resin without further purification or isolation. At the end of step wise solid phase synthesis, OAc-protection of the glucose was removed with 6 mM NaOMe in 85% DMF-MeOH. This solvent composition was found optimal for resin swelling and complete deprotection. Finally, the free peptide was obtained by the standard TFA cleavage. Alternatively, direct treatment of the fully protected peptide resin with TFA gave the tetra-acetyl glycosylated peptide. RP-HPLC indicated that the crude products contained greater than 90% of the target glycosylated peptides. Moreover, 500 MHz proton NMR analysis revealed that all the glycopeptides thus obtained contained > 97% of the β-anomer, suggesting that glycosylation under these conditions is nearly stereoselective. We have also successfully extended this strategy for the synthesis of lactosylated peptides.

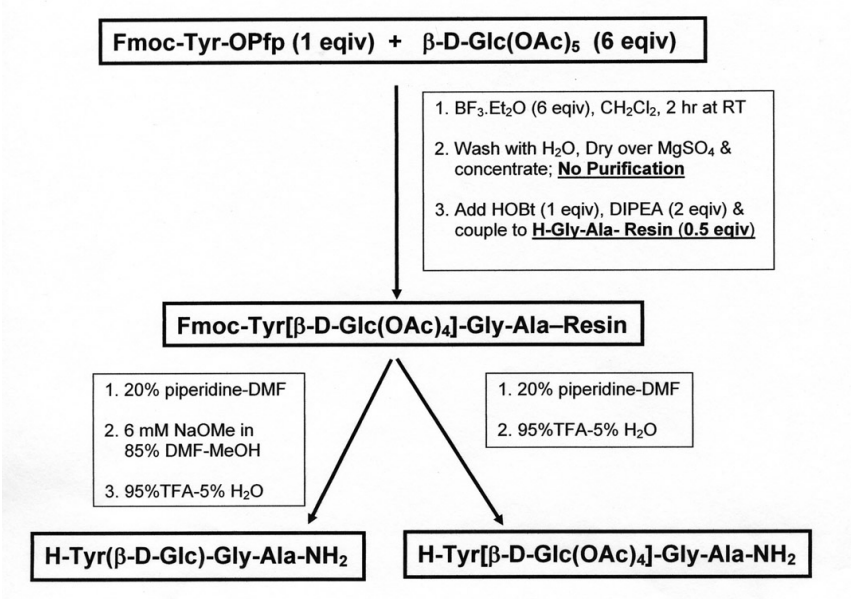

Scheme 1. SPPS of model O-glycosylated tripeptides.

O-glycosylation of peptides have previously been reported to enhance BBB passage [2-4]. Therefore, we used this strategy to synthesize the O-glycopeptide analog, N-α-Ac-Trp-Arg-Tyr(β-D-Glc)-NH_2, of a Neuropeptide Y (NPY) Y_5 receptor antagonist monomer [5]. Systemic administration of this peptide (4 mg/rat) significantly inhibited the food intake in Schedule-Fed rats over 8 h ($p < 0.05$ vs. saline). However, at this time we do not know whether the entry of this peptide into the brain is by diffusion or mediated by glucose transporters in the BBB capillaries [4].

In summary, we have a devised a rapid, economical and convenient method for the stereoselective synthesis of O-glycopeptides. This method may be exploited for the synthesis of various glycopeptides required for SAR studies as well as other applications [1, 2].

Acknowledgments

This work was supported in part by a NIH grant GM47122.

References

1. Hojo, H. and Nakahara, Y. *Curr. Prot. Pept. Sci.* **1**, 23-48 (2000).
2. Polt, R. and Palian, M. M. *Drugs of the Future* **26**, 561-576 (2001).
3. Polt, R., Porreca, F., Szabo, L. Z., Bilsky, E. J., Davis, P., Abbruscato, T. J., Davis, T. P., Horvath, R., Yamamura, H. I. and Hruby, V. J. *Proc. Natl. Acad. Sci. U.S.A.* **91**, 7114-7118 (1994).
4. Egleton, R. D., Mitchell, S. A., Huber, J. D., Palian, M. M., Polt, R. and Davis, T. P. *J. Pharmacol. Exp. Ther*. **299**, 967-972 (2001).
5. Balasubramaniam, A. unpublished results.

Peptide Revolution: Genomics, Proteomics & Therapeutics
Michael Chorev & Tomi K. Sawyer (Editors)
American Peptide Society, 2003

Synthesis of Guanidine Compounds Using Resin-Bound Guanidinylating Reagents

Markus M. Mueller, Hans J. Musiol and Luis Moroder

Max-Planck-Institut für Biochemie, 82152 Martinsried, Germany

Introduction

For the synthesis of trypsin-like enzyme inhibitors arginine mimetics are commonly applied as P1 residues. The synthesis of such guanidine compounds could be significantly facilitated with efficient and traceless resin-bound guanidinylating reagents that allow recovery of the final products from the resin under mild conditions. For this purpose, so far, a urethane-protected triflyl guanidine attached to resin via an acid-labile carbamate linker [1] and *N*-*tert*-butoxycarbonyl-1*H*-pyrazole-1-carboxamidine *N´*-linked to the resin via *p*-alkoxybenzyl carbamate (Figure 1, resin **1**) were proposed [2]. In a previous comparative study *N,N´*-di-*tert*-butoxycarbonyl-1*H*-benzotriazole-1-carboxamidines proved to be significantly more reactive than the related pyrazole-1-carboxamidines, particularly, when applied for guanidinylation of less nucleophilic amines such as aniline [3]. These results compelled us to attempt the use of benzotriazole as the better leaving group even for resin-bound reagents. For this purpose the reagent **2** (Figure 1, resin **2**) was synthesized and compared to **1** in terms of its reactivity.

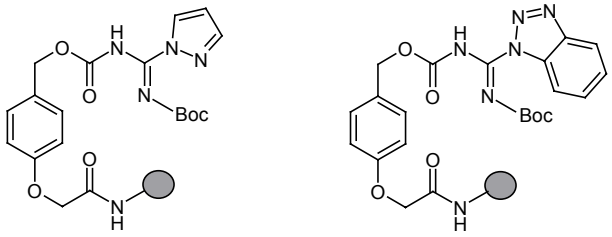

1 **2**

*Fig. 1. Structure of the resin-bound guanidinylating reagents **1** and **2** containing pyrazole and benzotriazole as leaving groups, respectively.*

Results and Discussion

The resin **1** was synthesized according to published procedures [2]. In analogous manner the synthesis of the intermediate *N*-(allyl 4-oxyacetate)benzyloxycarbonyl)-1*H*-benzotriazole-1-carboxamidine proceeded smoothly; however, its mono-*tert*-butoxycarbonylation with $(Boc)_2O$ was achieved only in the presence of DMAP instead of NaH, and small amounts of contaminating di-Boc derivative were removed by flash chromatography. In the final allyl ester cleavage with Pd(0), again according to the reported procedure [2], rather unexpectedly an allyl transfer to the carboxamidine moiety is taking place which results in *N*-allyl-guanidine derivatives as minor contaminants in the final products. Similarly, coupling of the carboxy-functionalized linker to NovaSyn TG amino resin by DIC/HOBt is accompanied by guanidinylation of the resin-bound amino groups as evidenced by the Sakaguchi positive test upon acidic treatment of the resin. Because of the use of larger HOBt excesses this side reaction

*Table 1. Guanidinylating efficiencies of reagents **1** and **2**.*

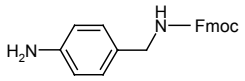	Resin **1**		Resin **2**	
	[mmol/g]	*[%]*	*[mmol/g]*	*[%]*
THF, 25 °C, 16 h	0	0	0.06	21
THF, 60 °C, 16 h	0.15	52	0.09	31

occurs only to a minor extent, as determined by almost quantitative TFA-mediated recovery of benzotriazole-1-carboxamidine.

The guanidinylating efficiencies of reagents **1** and **2** were compared using *N*-Fmoc-(4-amino)benzylamine as the amine (Table 1). The reaction yields were determined spectroscopically upon piperidine-mediated cleavage of the resin-linked *N*-Fmoc-(4-guanidino)benzylamine. Although reagent **2** proved to be more reactive at room temperature than **1**, an increase of the temperature to enhance reaction yields, leads with both the reagents **1** and **2** to a 5 : 1 and 6 : 1 mixture of product **3** and side product **4**, respectively (Figure 2). The side product results at higher temperature from conversion of the *N*-Boc-carboxamidine into the isocyanate by loss of *tert*-butanol; it then reacts competitively with the aromatic amine to form *N*-(amidino)urea derivatives as well evidenced by LC-MS. This side reaction which is known to occur with *N*,*N′*-di-*tert*-butoxycarbonyl-guanidines at higher temperature [4] has been deliberately exploited for the synthesis of *N*-(amidino)ureas [5].

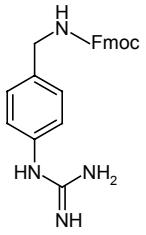

3

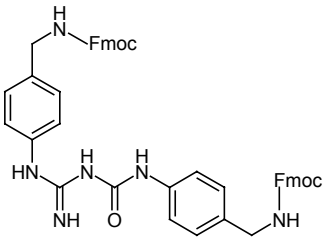

4

*Fig. 2. Structures of product **3** and side product N-(amidino)urea **4**.*

These results clearly show that higher reactivities at room temperature with sterically hindered or poorly nucleophilic amines are required for an efficient use of resin-bound guanidinylating reagents based on pyrazole or benzotriazole as leaving groups.

Acknowledgments

The work was supported by Wilex AG, Munich and by the SFB 469 (grant A2) of the Ludwig-Maximilians-University of Munich.

References

1. Zapf, C. W., Creighton, C. J., Tomioka, M. and Goodman, M. *Org. Lett*. **3**, 1133-1136 (2001).
2. Pátek, M., Smrčina, M., Nakanishi, E. and Izawa, H. *J. Comb. Chem.* **2**, 370-377 (2000).
3. Musiol, H.- J. and Moroder, L. *Org. Lett.* **3**, 3859-3861 (2001).
4. Miel, H. and Rault, S. *Tetrahedron Lett*. **39**, 1565-1568 (1998).
5. Sun, C.- M. and Shey, J.- Y. *J. Comb. Chem.* **1**, 361-363 (1999).

Peptide Revolution: Genomics, Proteomics & Therapeutics
Michael Chorev & Tomi K. Sawyer (Editors)
American Peptide Society, 2003

Facile Synthesis of Protected Hydrazino Amino Acids

Umut Oguz and Mark L. McLaughlin*

Department of Chemistry, University of South Florida, Tampa, FL, 33620, USA

Introduction

Previously reported syntheses of optically pure hydrazino amino acids with orthogonally protected N_α- and N_β- involve expensive reagents, laborious methods or harsh reaction conditions. We report a general route from L-α-amino esters to L-α-hydrazino esters using inexpensive reagents and in excellent overall yield. The overall synthesis is shown in Figure 1.

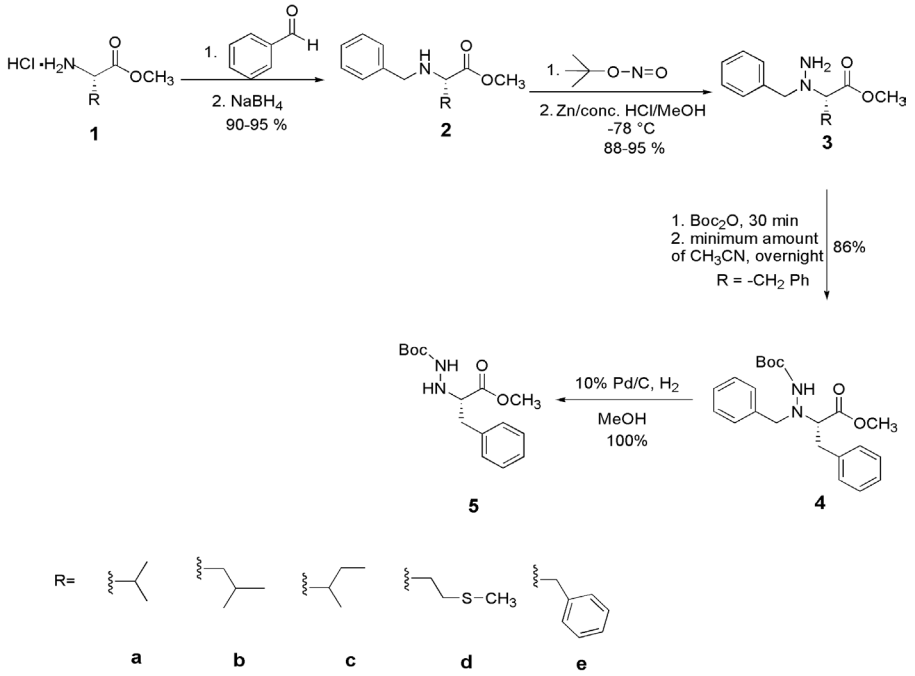

Fig. 1. Synthesis of α-hydrazino esters from α-amino esters.

Results and Discussion

One of the key steps in the overall synthesis is the reduction of the nitrosoamines to the corresponding hydrazines [1]. The best results were obtained with Zn/conc. HCl/MeOH/-78 °C. It is important to activate the Zn powder, which dramatically increases the efficiency of the reaction. One way to activate Zn is to wash several times with 5% HCl, and to wash in turn with water, methanol and ether and then dry under high vacuum.

We investigated the nitrosation of the amino acids and found placement of an acyl group on the nitrogen was not as practical. Acyl protected amino acids require stronger nitrosating agents such as $NOBF_4$ and give very low to no yield in the reduction step. In addition, nitrosoamines of α-amino esters with acyl protecting groups on the α-

nitrogen are relatively unstable and could not be stored over a long period of time even at low temperatures.

Another key step in the synthesis is the protection of the N_β- with a Boc- group. Dissolving the hydrazines in a solvent such as DCM or CH_3CN followed by the addition of the Boc-anhydride results primarily in the methylation of the N_β along with some Boc- protected hydrazine. This is probably due to the more favorable sterics of the small methyl group of the methyl ester over the bulky acyl group. The yield was increased by adding solid Boc-anhydride directly to the hydrazine **5**, as an oil, and the mixture was stirred at room temperature for 30 min without any solvent present [2]. The Boc-anhydride melts at room temperature easily and the mixture becomes homogenous. After 30 min, a very small amount of acetonitrile is added and the reaction is stirred overnight giving the desired fully protected hydrazine in 86%. The presence of the product was verified by FAB MS (385, $M+H^+$), ^1H and ^{13}C NMR. ^1H NMR shows the disappearance of the broad singlet for the N_β protons around 3.20 ppm and the appearance of a singlet at 1.35 ppm for *tert*-butyl protons and a broad singlet around 6.68 ppm for the proton on N_β.

To remove the benzyl group on N_α, compound **4** is dissolved in MeOH, a catalytic amount of 10% Pd/C is added and hydrogenated at 45 psi in a Paar Hydrogenator for 3 hrs. For large-scale reactions, it might be necessary to add additional Pd/C during the reaction due to the fact that the amine product would poison the catalyst. We have observed that the N-N bond of the hydrazino amino acid derivatives is stable to hydrogenation when N_β is protected; otherwise the N-N bond easily cleaves to give the corresponding amine. The presence of the product is verified by FAB MS (295, $M+H^+$), ^1H and ^{13}C NMR. ^1H NMR shows the appearance of a new broad triplet at 4.24 ppm for the N_α proton.

Acknowledgments
We acknowledge financial support from PHS via AG-19981, AG-1983, and AI-054246.

References

1. Oguz, U., Guilbeau, G. G. and McLaughlin, M. L. *Tetrahedron Lett.* **43,** 2873-2875 (2001).
2. Mäeorg, U., Grehn, L. and Ragnarsson, U. *Angew. Chem. Int. Ed. Engl.* **35,** 2626-2627 (1996).

Peptide Revolution: Genomics, Proteomics & Therapeutics
Michael Chorev & Tomi K. Sawyer (Editors)
American Peptide Society, 2003

Dialkyl Imidazolinones from α, α -Dialkyl Glycines

S.P.G. Costa, H.L.S. Maia and S.M.M.A. Pereira-Lima

Department of Chemistry, University of Minho, Gualtar, Braga, P-4710-057, Portugal

Introduction

Peptides containing residues of α, α-dialkyl glycines have been known since the 1960s and lately have been widely used in modification of natural peptides and in peptidomimetics [1]. Nevertheless, most of the reports found in the literature refer to the simplest representative of this class of compounds, i.e., α, α-dimethyl glycine (Aib), which is certainly due to the discouraging difficulties usually met during synthesis. In fact, usually α, α -dialkyl glycines are not readily available compounds, their synthesis being most commonly carried out by hydrolysis of specially prepared hydantoins or Schiff bases, but, owing to steric crowding, these reactions are slow and often lead to low yields. Furthermore, most methods of peptide synthesis are of little use to handle these compounds [2].

Ugi's four-component condensation reaction is known to be a complement or even an alternative to classical peptide synthesis but it is difficult to find any such application in literature. This is due to two inherent drawbacks: (i) peptide isonitriles, required for the reaction, racemise above –20ºC and (ii) an unavoidable *N*-alkyl group must be cleaved from the reaction product [3]. In recent years, we have studied the application of Ugi's reaction to the synthesis of several α, α -dialkylglycines. Using 4-methoxybenzylamine (Pmb-NH_2) as the amine component, we were able to remove the *N*-alkyl group by TFA cleavage and, during this process, the *C*-terminal amide bond of the resulting Ugi adducts was cleaved by a mechanism involving an oxazolinium-type intermediate (see Figure 1) [4]. This intermediate allows *in situ* functionalization of the C-terminus by reaction with several nucleophiles (HO^-, MeO^- and amines), thus affording different derivatives such as free acids, esters and amides [5]. We report here the results obtained to date in the attempt of *in situ* formation of peptide bonds.

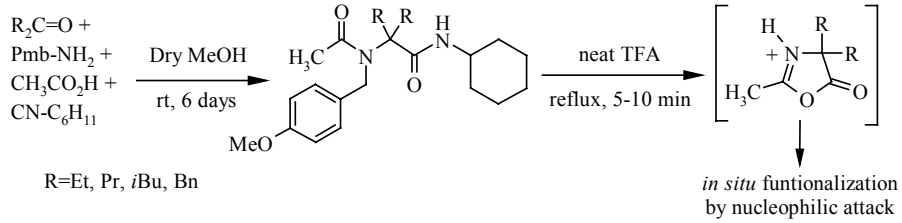

Fig. 1. Schematic representation of the intermediate formed during TFA cleavage of Ugi adducts.

Results and Discussion

Our previous findings suggested that a dipeptide could be obtained if an amino acid ester was used as the nucleophile. We started out with usual treatment of the Ugi reaction product (diethyl and dibenzyl glycine derivatives) with neat TFA in order to obtain the corresponding oxazolinium intermediates. After removal of excess TFA, a solution with 2 eq of glycine *tert*-butyl ester and 3 eq of NEt_3 was added to the residue.

Although a small amount of the required dipeptides (2) (<15% yield) was formed, the major products were 5,5-dialkyl-imidazolin-4-ones (1) (>75% yield) (see Figure 2), resulting from competitive attack at the less hindered C-2 of the oxazolinium intermediate, followed by rearrangement. Furthermore, the presence of a positive charge at the oxazolinium nitrogen atom renders the adjacent carbon more prone to nucleophilic attack than that at the carbonyl group.

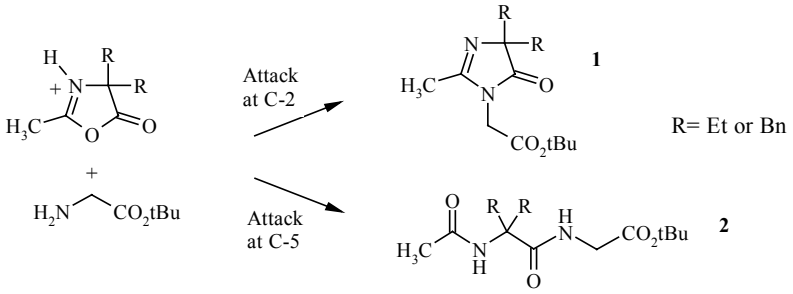

Fig. 2. Schematic representation of competitive nucleophilic attack at the oxazolinium salt.

Next, we neutralized the oxazolinium salt by adding 20 eq of NEt_3 in acetonitrile to the residue obtained after TFA evaporation, so that the coupling reaction could proceed via the corresponding oxazolone by nucleophilic attack at C-5. Although some imidazolinone was still obtained, we were able to improve dipeptide formation (83 and 49% yield for diethyl and dibenzyl glycine dipeptide, respectively).

These results, combined with previous findings [5], suggest that the bulkiness of the nucleophile and α-alkyl groups and the positive charge at N-3, directs nucleophilic attack either to C-2 or C-5. Therefore, *in situ* formation of peptide bonds can be accomplished; reaction conditions, however, have to be carefully controlled.

References

1. a) Faust, G. and Lange, H. *J. Prakt. Chem*. **11**, 153 (1960). b) Toniolo, C. *Janssen Chim. Acta* **11**, 10 (1993). c) Mazeleyrat, J.- P. K., *et al. Eur. J. Org. Chem.* 1821 (2001).
2. a) Goodson, L., et al. *J. Org. Chem*. **25**, 1920 (1960). b) Lygo, B., et al. *Tetrahedron Lett.* **40**, 8671 (1999). c) Jones, D. S., et al. *J. Chem. Soc.* 6227 (1965).
3. Gokel, G., et al. In *Isonitrile Chemistry*, Ugi, I. (Ed.), Academic Press, 1971, New York and London, p. 201.
4. a) Costa, S. P. G., Maia, H. L. S. and Pereira-Lima, S. M. M. A. *Org. Biomol. Chem.* **1**, 1475 (2003). b) Creighton, C. J., et al. *J. Am. Chem. Soc.* **121**, 6786 (1999).
5. Costa, S. P. G., Maia, H. L. S. and Pereira-Lima, S. M. M. A. In Benedetti, E. and Pedone, C. (Eds.), *Peptides 2002: Proceedings of the 27th European Peptide Symposium*, Edizioni Ziino, Naples, 2002, p. 250.

Peptide Revolution: Genomics, Proteomics & Therapeutics
Michael Chorev & Tomi K. Sawyer (Editors)
American Peptide Society, 2003

A Methionine-Based Linker Strategy for Solid-Phase Synthesis of Lysine-Containing Cyclic Peptides

Joseph C. Kappel and George Barany

Department of Chemistry, University of Minnesota, Minneapolis, MN 55455, USA

Introduction

Cyclic peptides are often challenging targets for chemical synthesis [1]. These constrained structures may have increased metabolic stability, receptor selectivity, and bioavailability, all of which may lead to useful medicinal qualities [2]. The present study reveals a solid-phase strategy for the synthesis of lysine-containing cyclic peptides, featuring side-chain anchoring to a methionine residue. This strategy is demonstrated in the synthesis of *cyclo*(Val-Phe-Sar-Tyr-D-Trp-Lys) [3].

Results and Discussion

Our method takes advantage of the selective, orthogonal reaction between cyanogen bromide and the side-chain of methionine, which results in the formation of an amine and a homoserine lactone [4]. The following steps are carried out sequentially: (i) inverse coupling of a suitably protected methionine residue to the solid support; (ii) side-chain anchoring of a partially protected lysine derivative; (iii) stepwise solid-phase assembly of the linear sequence; (iv) deprotection of the C^{α}-carboxyl group of lysine; (v) activation of the free carboxyl and head-to-tail cyclization to generate the desired product; and (vi) final cleavage to release the cyclic peptide into solution.

The methionine linkage, from which synthesis would proceed, was prepared by reacting amino functionalized PEG-PS resin with succinic anhydride, followed by coupling of HCl·H-Met-OFm. After Fm removal with piperidine–DMF (1:4), Fmoc-Lys(HCl)-OAl was coupled through its side-chain to give the protected intermediate **1** (Scheme 1).

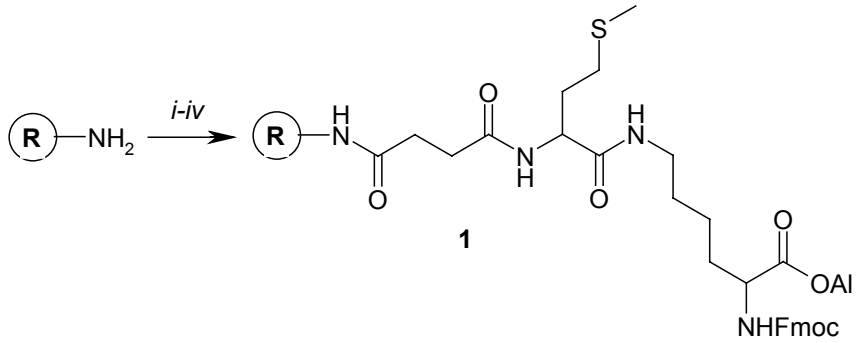

Scheme 1. Preparation of methionine linker. Reagents and conditions: (i) succinic anhydride (10 equiv), DIEA (20 equiv), CH_2Cl_2, 0.5 h; (ii) HCl·H-Met-OFm (5 equiv), HATU (5 equiv), DIEA (10 equiv), CH_2Cl_2–DMF (1:1), 0.5 h; (iii) piperidine–DMF (1:4) (3 × 5 min); (iv) Fmoc-Lys-OAl·HCl (5 equiv), HATU (5 equiv), DIEA (10 equiv), CH_2Cl_2–DMF (1:1), 0.5 h. All reactions were conducted at 25 °C.

Manual assembly of the peptide sequence was performed in the $C \rightarrow N$ direction using standard Fmoc/*t*Bu protocols [Tyr was incorporated as a *t*Bu ether]. Following allyl group removal with $Pd(PPh_3)_4$ (5 equiv) in $CHCl_3$–HOAc–NMM (37:2:1), and Fmoc removal with piperidine–DMF (1:4), the peptide was cyclized with BOP/HOAt/DIEA in DMF. Treatment of the resin-bound protected cyclic peptide with CNBr in CH_3CN–HOAc–H_2O (5:4:1) generated the cyclic product with *t*Bu protection intact (**2**), which was observed as the major component (79% purity) by analytical HPLC (Scheme 2, Route A).

A two-step deprotection/cleavage sequence was used to prepare the free cyclic peptide **3**. The *t*Bu side-chain protecting group of Tyr was first removed from the resin-bound peptide with TFA–thioanisole–1,2-ethanedithiol–anisole (90:5:3:2). Following that, the usual CNBr cleavage released peptide **3**, which was observed as the major component (85% purity) by analytical HPLC (Scheme 2, Route B).

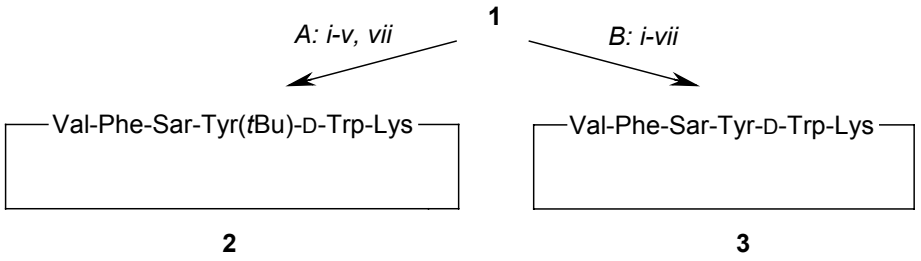

*Scheme 2. Synthesis of cyclo(Val-Phe-Sar-Tyr(tBu)-D-Trp-Lys) (**2**) and cyclo(Val-Phe-Sar-Tyr-D-Trp-Lys) (**3**). Reagents and conditions: (i) piperidine–DMF (1:4); (ii) Fmoc-AA-OH, DIPCDI, HOAt, DMF / piperidine–DMF (1:4) / repeat × 4; (iii) $Pd(PPh_3)_4$ (5 equiv), $CHCl_3$–HOAc–NMM (37:2:1); (iv) piperidine–DMF (1:4); (v) BOP (5 equiv), HOAt (5 equiv), DIEA (10 equiv), DMF; (vi) TFA–thioanisole–1,2-ethanedithiol–anisole (90:5:3:2); (vii) CNBr (60 equiv), CH_3CN–HOAc–H_2O (5:4:1).*

Acknowledgments
The work was supported by the National Institutes of Health (GM 42722).

References

1. (a) Blackburn, C. and Kates, S. A. *Methods Enzymol.* **289**, 175-198 (1997). (b) Kates, S. A., Solé, N. A., Johnson, C. R., Hudson, D., Barany, G. and Albericio, F. *Tetrahedron Lett.* **34**, 1549-1552 (1993). (c) Nambert, J. N., Mitchell, J. P. and Roberts, K. D. *J. Chem. Soc., Perkin Trans. I*, 471-484 (2001).
2. (a) Hruby, V. J. and Bonner, G. G. *Methods Mol. Biol.* **35**, 201-240 (1994). (b) Rizo, J. and Gierasch, L. M. *Annu. Rev. Biochem.* **61**, 387-418 (1992).
3. Veber, D. F., Saperstein, R., Nutt, R. F., Freidinger, R. M., Brady, S. F., Curley, P., Perlow, D. S., Paleveda, W. J., Colton, C. D., Zacchei, A. G., Tocco, D. J., Hoff, D. R., Vandlen, R. L., Gerich, J. E., Hall, L., Mandarino, L., Cordes, E. H., Anderson, P. S. and Hirschmann, R. *Life Sci.* **34**, 1371-1378 (1984).
4. Gross, E. *Methods Enzymol.* **11**, 238-255 (1967).

Peptide Revolution: Genomics, Proteomics & Therapeutics
Michael Chorev & Tomi K. Sawyer (Editors)
American Peptide Society, 2003

Synthesis of Isotopomers of the MHC II Antagonist AZD2315

H. Booth[1], J. R. Harding[1] and D. P. Woodhouse[2]

[1]Isotope Chemistry, Drug Metabolism and Pharmacokinetics Department, AstraZeneca UK Limited, Mereside, Alderley Park, Macclesfield, Cheshire, SK10 4TG, UK; [2]Cambridge Research Biochemicals Limited, Billingham, Cleveland, TS23 4AZ, UK

Introduction

AZD2315 (1) is a major histocompatibility class II (MHC II) antagonist being developed primarily for the treatment of rheumatoid arthritis. Several isotopomers of AZD2315 were prepared in order to progress the compound to clinical studies (Figure 1). Thus, ^{14}C and ^{3}H labelled forms were used to investigate the metabolism and pharmacokinetics in animals and man, and a ^{2}H labelled form was used as a mass labelled internal standard for a mass spectrometry based clinical assay. The synthesis of these labelled forms of AZD2315 is described.

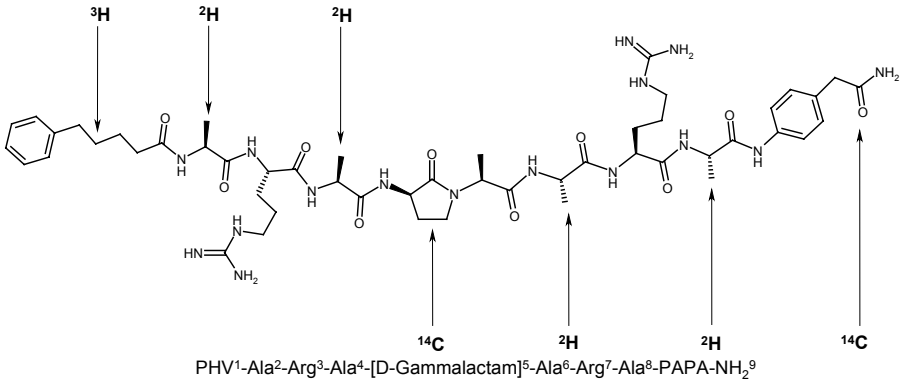

*Fig. 1. AZD2315 and Isotopomers: (**1**) AZD2315; (**2**) [D-[Ring carbonyl-^{14}C]gammalactam]^{5} AZD2315; (**3**) [[Carboxyl-^{14}C]PAPA]^{9} AZD2315; (**4**) [3,3,3-^{2}H-Ala]^{2,4,6,8} AZD2315; (**5**) [2,3,4,5-^{3}H-Phenylvaleryl]^{1} AZD2315.*

Synthetic Procedures

Peptides were prepared using standard Fmoc solid-phase synthesis techniques. All peptides were assembled on a Rink type linker and amino acids were coupled as their N-Fmoc derivatives with the guanidine function of the side chain additionally protected using the Pdf group. The protected amino acids were coupled using TBTU and DIPEA. The progress of couplings was monitored using a ninhydrin colour test where appropriate. After coupling of the Fmoc amino acid derivative, the N-terminal Fmoc group was removed by treatment with 20% v/v piperidine in dimethylformamide. Peptides were cleaved from the solid support with TFA containing scavengers (typically water, phenol and triisopropylsilane) and purified by reverse-phase HPLC using TFA buffered solutions of water and acetonitrile.

Preparation of [D-[ring carbonyl-^{14}C]gammalactam][5] AZD2315 (2)
A synthesis of AZD2315 was undertaken using Fmoc-D-[ring carbonyl-^{14}C]gammalactam (250mCi, 56mCi/mmol; 4.46mmol) (**6**, see Figure 2). After cleavage and purification, 35.3mCi of (**2**) was isolated with radiochemical purity in excess of 95%.

Preparation of [[carboxyl-^{14}C]PAPA][9] AZD2315 (3)
A synthesis of AZD2315 was undertaken using Fmoc-[carboxyl-^{14}C]PAPA-OH (250mCi, 57mCi/mmol; 4.39mmol) (**7**, see Figure 2). After cleavage and purification, 25mCi of (**3**) was isolated with radiochemical purity in excess of 95%.

Preparation of [3,3,3-^{2}H-Ala][2,4,6,8] AZD2315 (4)
A synthesis of AZD2315 was undertaken using Fmoc-[3,3,3-^{2}H-Ala]-OH prepared from 3,3,3-^{2}H-alanine (**8**, see Figure 2). The crude peptide after cleavage had a purity of 77%. Following HPLC purification, 800mg of (**4**) was isolated with a chemical purity in excess of 98%.

Preparation of [2,3,4,5-^{3}H-phenylvaleryl][1] AZD2315 (5)
A synthesis of [5-phenyl-2,4-pentadienoyl][1] AZD2315 was undertaken using 5-phenyl-2,4-pentadienoic acid. Following cleavage and purification the [5-phenyl-2,4-pentadienoyl][1] AZD2315 (3.5mg) was dissolved in dimethylformamide (200µL) and 10% Pd/C added (5.8mg). The mixture was freeze-degassed under vacuum and then tritium gas introduced (9.1Ci) and the mixture stirred at room temperature for 5 hours. Excess tritium gas was removed and the catalyst removed by filtration. The filtrate was evaporated in vacuo and the residue redissolved in methanol (1mL) then further evaporated to remove labile tritium. Following HPLC purification, 107mCi of (**5**) was isolated with radiochemical purity in excess of 99%. The specific activity was 107Ci/mmol, as determined by amino acid analysis.

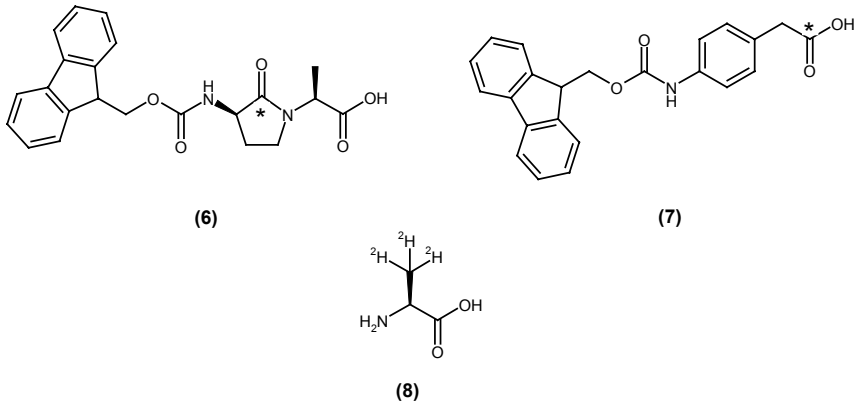

Fig. 2. Amino acid derivatives used in the synthesis of isotopomers of AZD2351.

Conclusion
The Fmoc solid-phase method has been successfully used to synthesise several isotopomers of the peptide derivative AZD2315 at high isotopic abundance.

Peptide Revolution: Genomics, Proteomics & Therapeutics
Michael Chorev & Tomi K. Sawyer (Editors)
American Peptide Society, 2003

A Versatile Method for Fast and Selective Introduction of Multiple Probes into Peptides Using Solid Phase Synthesis — Application to Biophysical Models

Inbar Rofman[1], Elisha Haas[2], Varda Ittah[2] and Gerardo Byk[1]

[1]Department of Chemistry and [2]Faculty of Life Sciences, Bar Ilan University, Ramat Gan - 52900, Israel

Introduction

Analysis of conformation, flexibility and dynamics of a peptide present a range of challenging problems both experimentally and conceptually. Small peptides of less than 30 amino acids will generally be flexible and their conformation will depend on their concentration, the solvent, pressure, temperature and on other molecules in solution. Fluorescence resonance energy transfer (FRET) can be used as a spectroscopic ruler and determine the conformational distributions of peptides in solution. The lack of information on the distances between specific positions in peptide sequences makes the choice of a donor-acceptor pair difficult. Using currently available techniques, the entire peptide sequence must be re-synthesized when a new donor-acceptor pair is needed for a given (or assumed) end-to-end peptide distance.
This research simplifies the labeling process using a methodology based on *in-situ* conjugation of probes to solid-supported peptide though thiol modifications of multiple cysteines (Figure 1). This method also allows for the synthesis of parallel libraries of donor-acceptor pairs using the same batch of a given peptide sequence.

Results and Discussion

There is great interest to develop a disulfide bridge cleavage on solid support since the reaction conditions are orthogonal to many other cysteine protecting groups. This research focused on developing tButhio protecting group cleavage reaction using (Bu)3P. For this study a tri-peptide prototype was used. The probe was imitated using iodoacetamide (the reactive groups of the probes is iodoacetyl). Once the reaction conditions for the disulfide cleavage and the coupling of iodo-acetamide were found, the method was applied on longer peptides and a series of "real" probe-pairs were introduced for FRET measurements. The general method is shown in Figure 1. Briefly, the orthogonal groups on the cysteine residues to be labeled are s-tert-buthio at the N extremity and p-methoxy-trityl (Mmt) at the C-terminal position. Both groups can be cleaved on solid support followed by a labeling with iodo-acetamido-fluorescent probe.

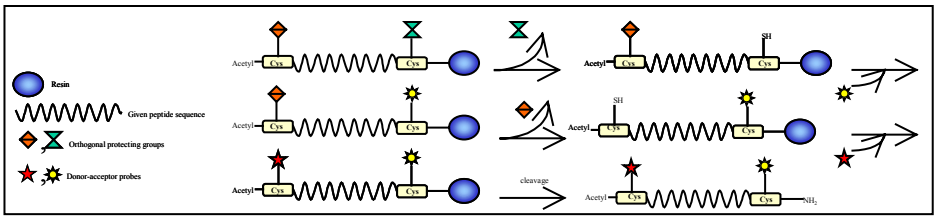

Fig. 1. New selective method for the introduction of multiple molecular probes into peptides fully performed on solid phase.

We have found that the cleavage of t-Buthio was not efficient when the cysteine was at the C-terminus of longer peptides (results not shown). Thus, the strategy was to use the t-Buthio at the N-terminus and p-methoxyltrityl at the C-terminus near the solid support. We have also found that when cysteine(tBu-\thio) was at N-terminus, the tButhio deprotection conditions for long peptides (and probably some sequences) were difficult and more extreme conditions were used. No difficulties were found when cleaving the Mmt at any position of the peptide. The labeling can be also performed using the tea-bag method (results not shown).

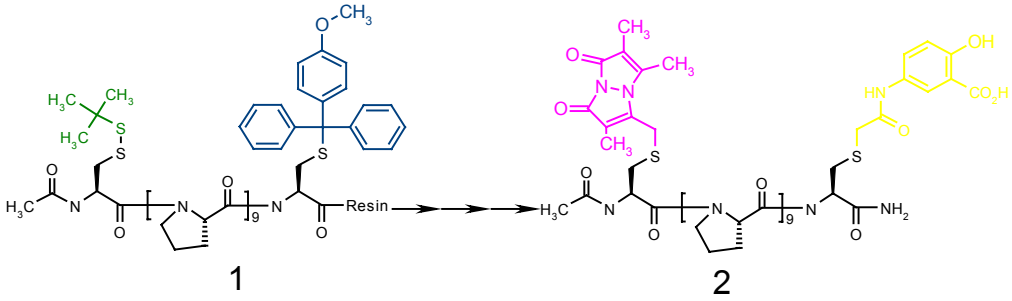

*Fig. 2. Example of labeling procedure: Polyproline labeling. The tButhio protecting group was cleaved from **1** using 10 eq. (Bu)3P in DMF at 40°c. After washing with DMF and DCM the first probe (5-IASA) was inserted on the cysteine. The Mmt protecting group was cleaved using 1% TFA in DCM and TIS. After washing with DMF and DCM the second probe (mBBr) was inserted on the cysteine. The peptide was then cleaved from the resin and HPLC purified (MS (H+)=1523).*

1. CH_3CO-Cys(Bimane)-$(Pro)_9$-Cys(salicylic acid)-NH_2
2. CH_3CO-Cys(pyrene)-$(Pro)_8$-Cys(Bimane)-NH_2
3. CH_3CO-Cys(pyrene)-$(Pro)_{14}$-Cys(coumarine)-NH_2
4. CH_3CO-Cys(salicylic acid)-$(Pro)_{14}$-Cys(fluorecein)-NH_2
5. CH_3CO-Cys(IEADAS)-$(Pro)_{18}$-Cys(fluorecein)-NH_2

Fig. 3. Labeled peptides obtained in this study.

We have developed a versatile procedure for double labeling of peptides based on a solid support strategy (Figure 2). The labeling probes were exclusively introduced into the peptides on the solid support. The protective groups developed here for the orthogonal strategy were t-Buthio and p-Methoxy-trityl. The labels can be also introduced using the tea-bag strategy. The new method is especially recommended for protein folding studies using fluorescently labeled peptides by means of FRET. Folding studies on the synthesized peptides reported here (Figure 3) will be presented elsewhere.

Acknowledgments
This work was financed by an internal fund of Bar Ilan University**,** the Ygal Alon Foundation and the "Marcus Center for Medicinal Chemistry". We are indebted to Dr. Miriam Cojocaru, Dr. Igor Ulanovsky and Dr. Hugo Gotlieb from the Structural Analysis Department of Bar-Ilan University for MS and NMR analyses of products.

Peptide Revolution: Genomics, Proteomics & Therapeutics
Michael Chorev & Tomi K. Sawyer (Editors)
American Peptide Society, 2003

An Efficient Peptide Synthesis in Solution Using Nsc-Amino Acids

Hyun Jin Lee, Weonu Chweh, Young-Deug Kim, Hyuk-Kwang Jung and Hack-Joo Kim

A&Pep Inc., 6-15B/L, Wolsan Industrial Zone, Nam-myeon Yeongi-gun, Chungnam, 339-824, Korea

Introduction

In contrast to the Fmoc, the cleavage of the Nsc group with secondary amines leads to the formation of 4-nitrophenyl vinyl sulfone, which is trapped very rapidly and irreversibly [1]. The tertiary amine trapped as 4-nitrophenyl vinyl sulfone-amine adduct could be directly used for the subsequent coupling step. Tertiary amines that remain are always used to maintain the basicity of the medium in the next coupling reaction and to promote the acylation reaction as already existing molar equivalent amine. Due to this fact, the Nsc chemistry in solution phase peptide synthesis was successfully employed [2]. For example, we used this principle to the efficient the liquid phase peptide synthesis (LPPS) of leuprolide using the Nsc-amino acids.

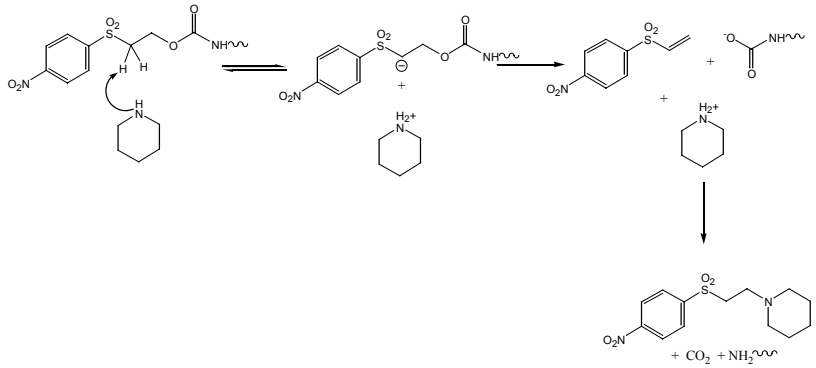

Fig. 1. Nα-Nsc-Cleavage mechanism.

Results and Discussion

For introducing C-terminal N-ethyl amide of leuprolide [(Des-Gly^{10}, D-Leu^{6}, Pro-NHEt^{9})-LHRH] synthesis using the LPPS, ethylammonium HOBt salt was prepared by adding an equimolar ethylamine solution to the HOBt suspension. The obtained solution was lyophilized and the salt dried over KOH in vacuum. The 1.5-fold excess of Nsc-Pro-OH was coupled with ethylammonium HOBt for 8h with DIC method in DCM/DMF. The resulting reaction mixture was diluted with DCM, carefully washed with water and dried over sodium sulfate. The Nsc-Pro-NHEt was readily obtained after evaporation and triturated with diethyl ether.

As shown in scheme 1, the removal of the Nsc group was treated by 20% piperidine in DMF and the condensation of the peptide chain was performed by using BOP/HOBt. The final cleavage was performed by the treatment of fully protected leuprolide with TFA:TIS:H_2O (95:2.5:2.5). The prepared crude leuprolide was determined by HPLC and Maldi-Tof Mass (Fig. 2). With respect to each coupling steps using Nsc-amino acids, we could obtain the good purity and yields (up to 90%).

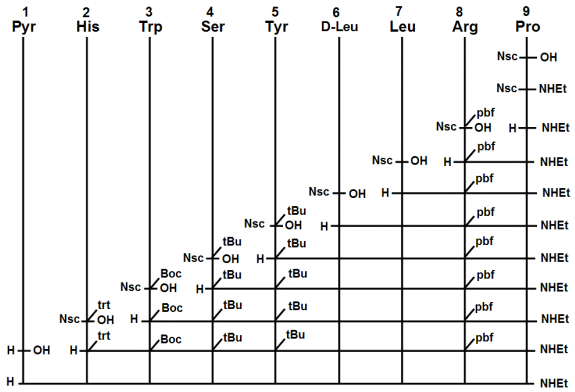

Scheme 1. Synthesis scheme of Leuprolide.

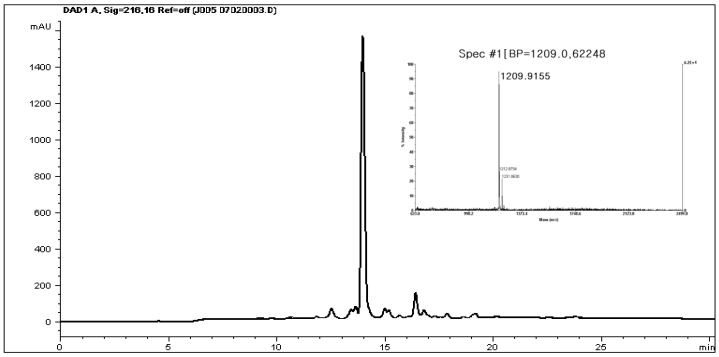

Fig. 2. HPLC & Maldi-Tof Mass profile of crude Leuprolide. Synthesis: Solution phase synthesis, Coupling: 1.06eq Nsc-amino acids, 1.2eq Bop/1.5eq HOBt, 2eq NMM in DMF, rt, 1~2h, Deprotection: 20% Piperidine/DMF, 10min, Cleavage: 95% TFA/2.5% TIS/2.5% H_2O, 2h, Analysis: A-0.1% TFA/H_2O, B-0.1% TFA/AcCN, 1ml/min, 0-100% B for 50min.

In conclusion, the Nsc-amino acids could be successfully applied to the liquid phase peptide synthesis (LPPS) in contrast to the Fmoc. because the urethane cleavage product, Nsc vinyl sulfone, is trapped very rapidly and irreversibly when an excess of piperidine is employed in deblocking condition. Due to these results, the LPPS using the Nsc-amino acids could be regarded as a useful technology for bulk peptide synthesis, and the Nsc chemistry as a suitable for developing for more applications.

References

1. Sabirov, A. N., Kim Y.- D., Kim H.- J. and Samukov, V. V. *Protein Peptide Lett*. **4**, 307 (1997).
2. Samukov, V. V., Pozdnyakov, P. I., Karpyshev, N. N., Lebedeva, D. V. and Kim H.- J. In Benedetti, E. and Pedone C. (EDs.), *Peptides 2002 (Proceedings of the 27th Eur. Peptide Symp.),* Edizioni Ziino, Napoli, Italy, p. 274 (2002).

Peptide Revolution: Genomics, Proteomics & Therapeutics
Michael Chorev & Tomi K. Sawyer (Editors)
American Peptide Society, 2003

A Novel Post-Translational Modification: A Conopeptide from *Conus gladiator* Provides the First Example of γ-Hydroxyvaline (Hyv) within a Polypeptide Chain

David Mora, Fred C. Pflueger, Katarzyna Pisarewicz, Gregg B. Fields and Frank Marí*

Department of Chemistry & Biochemistry, Florida Atlantic University, 777 Glades Rd., Boca Raton, Fl, 33431, USA

Introduction

Proteins and peptides are often modified post-translationally to impart them with characteristics that define their specific functions. This is the case for peptides found in the venom of predatory marine mollusks belonging to the genus *Conus*. The *Conus* venom is a complex mixture of peptides (conopeptides) that elicit a wide range of neurophysiological responses [1,2]. Several conopeptides have been shown to be valuable therapeutic agents for the treatment of a variety of neurologically related conditions [3-5]. Conopeptide precursors are ribosomally-expressed proteins that subsequently undergo proteolytic cleavage and post-translational modifications to form the mature conopeptide. Conopeptides inherently contain a high degree of modified amino acids that confer them with unique stability and exquisite specificity towards their neuronal targets [6-8]. Several modified or unusual amino acids, such as cystines, hydroxyproline, γ-carboxyglutamate, Br-Trp, D-amino acids, pyro-Glu, glycosylated Ser/Thr, C-terminal amidation and sulphonated Tyr are found in conopeptides [7,9,10] and are part of the neurochemical arsenal used by cone snails to capture their prey. Hydroxylated amino acids are an important class of modified amino acids and several examples have been isolated from non-animal sources [11-13]; however, γ-hydroxyvaline (Hyv=V*) has never been found within a polypeptide chain [14-15]. Here we report the isolation and characterization of novel conopeptide from *Conus gladiator*, gla-1, that contains γ-hydroxyvaline. While γ-hydroxyvaline was first described [11] as a novel amino acid isolated from plants, it would be an unexpected post-translational modification in proteins and peptides, as its hydroxyl group would readily cleave the peptide bond by intraresidue cyclization to form a lactone.

Results and Discussion

We have isolated two novel conopeptides, gla-1 and gla-2, from the venom of *Conus gladiator* (species code gla), a widespread cone snail species that inhabits the tropical Eastern Pacific region and preys upon marine worms.

Their nano-NMR spectra (Figure 1) revealed similar compositions for these octapeptides (2A, 2S, W, N, O, an unusual amino acid for gla-1 and V for gla-2). The mass spectra of gla-1 and gla-2 gave molecular ions of 863.3 Da and 847.3 Da, respectively. Edman degradation sequence analysis of gla-1 resulted in AOANS, which is smaller than indicated by NMR and MS results. Combined ESI-MS/MS (Figure 3) and NMR analysis revealed that the sequences of these octa-conopeptides are the following:

gla-1 **AOANSV*WS**
gla-2 **AOANSV WS**
V*=γ-hydroxyvaline; W=D-Trp
O=trans-γ-hydroxyproline

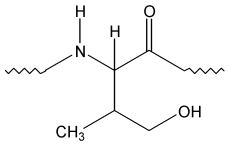

≡ Hyv, V*

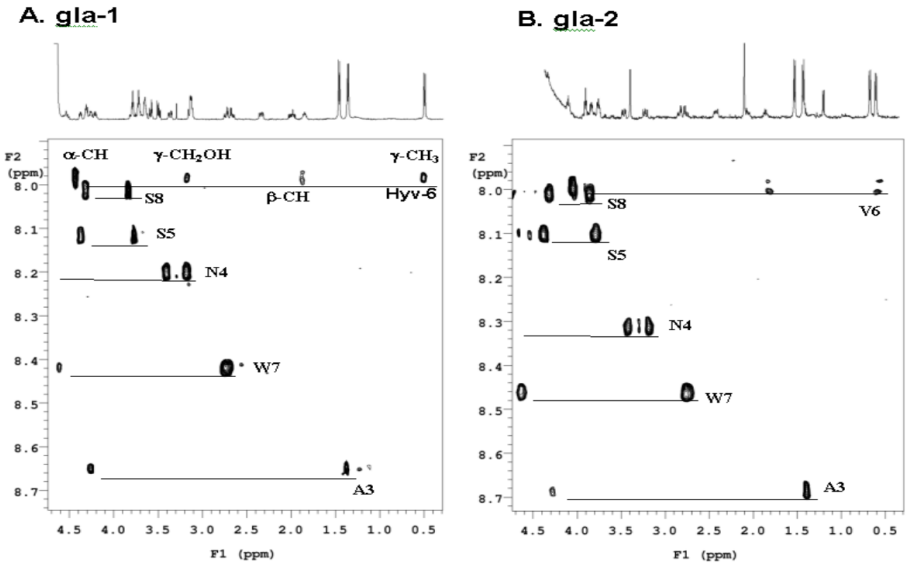

Fig. 1. NMR spectra of the gla peptides. A) 1D proton spectrum along with its corresponding 2D-TOCSY spectrum of 35 nanomoles of gla-1 recorded at 25°C using a gHX HR-MAS probe [18,19] on a Varian Inova 500MHz spectrometer. The resonance assignments were carried out using standard biomolecular NMR procedures [20]. The NMR assignments of the γ-hydroxyvaline (HN: d 7.99, 8Hz; αH: 4.45, m; γCH_2.m 3.15; βCH m 1.89, 6.9Hz; γCH_3: d 0.52, 7.1Hz) correspond to the to stereochemistry of the synthetic 2S,4S isomer[13]. B) 1D and the corresponding 2D-TOCSY spectra of gla-2, putative precursor of gla-1. The stereochemistry of the tryptophan residue was determined by comparing the NMR and MS/MS spectra of gla-2 with synthetic peptides made using L-Trp and D-Trp amino acids, respectively.

γ-hydroxylated amino acids (except for trans-γ-hydroxyproline) are unlikely to be observed in proteins since their side chains would have the tendency to undergo intraresidue cyclization and cleave the polypeptide chain. This tendency would explain why the Edman degradation of gla-1 yielded its sequence only up to the residue preceding γ-hydroxyvaline.

The presence of γ-hydroxyvaline in gla-1 as opposed to valine in gla-2 suggests the existence of a corresponding enzyme capable of Val oxidation. This putative enzyme could be using gla-2, or its precursor protein, as a substrate to modify the specified Val to generate the final form of the toxin. The relative stability of gla-1 may be attributed to presence of the D-Trp residue following the γ-hydroxyvaline modification. Molecular models of gla-1 suggest that this changed configuration of the Trp residue is required to disfavour the intraresidue cleavage of the peptide bond by the γ-hydroxyl group. Conopeptides are known to incorporate D-Trp in their sequence [16,17]. This

double modification of the polypeptide chain in contiguous residues, γ-OH-Xaa-D-Trp, is a novel structural motif that defines a new class of conopeptides that we have termed γ-Hydroxy-Conophans; whereas their corresponding precursors, such as gla-2, are termed Conophans.

These gla conopeptides (conophans) are unusual because: (i) they are not constrained like the conotoxin family, (ii) they are short in length, (iii) they have a high content of hydroxylated residues, and (iv) their primary structure has no close match in the sequence databases. Conophans are novel conopeptides that add further diversity to the known neurochemical strategies used by cone snails to capture their prey.

Acknowledgments

We thank J. Lauer-Fields for synthesis of peptides; A. Franco for collection of specimens; M. Crawford for peptide sequencing; K. Stone for mass spectrometry analysis. We thank to government of the Republic of Costa Rica for providing the permits to collect the necessary specimens. This work was supported by the Florida Sea Grant College Program (R/LR-MB-18) and the NIH (CA 77402).

References

1. Mari, F. and Fields G. B., *Chimica Oggie* **21**, 43-48 (2003).
2. Jones, R. M. and Bulaj, G. *Current Pharm. Design* **6**, 1249-1285 (2000).
3. Adams, D. J., Alewood, P. F., Craik, D. J., Drinkwater, R. D. and Lewis, R. J. *Drug Develop. Res.* **46**, 219-234 (1999).
4. McIntosh, J. M. and Jones, R. M. *Toxicon.* **39**, 1447-1451 (2001).
5. Shen, G. S., Layer, R. T. and McCabe, R. T. *Drug Discov. Today* **5**, 98-106 (2000).
6. McIntosh, J. M., Olivera, B. M. and Cruz, L. J. *Methods in Enzymology* **294**, 605-624 (1999).
7. Craig, A. G., Bandyopadhyay, P. and Olivera, B. M. *Eur. J. Biochem.* **264**, 271-275 (1999).
8. Myers, R. A., Cruz, L. J., Rivier, J. E., Olivera, B. M. *Chemical Reviews* **93**, 1923-1936 (1993).
9. Craig, A. G., Norberg, T., Griffin, D., Hoeger, C., Akhtar, M., Schmidt, K., Low, W., Dykert, J., Richelson, E., Navarro, V., Mazella, J., Watkins, M., Hillyard, D., Imperial, J., Cruz, L. J. and Olivera, B. M. *J. Biol. Chem.* **274**, 13752-13759 (1999).
10. Craig, A. G., Park, M., Fischer, W. H., Kang, J., Compain, P. and Piller, F. *Toxicon*. **39**, 809-815 (2001).
11. Pollard, J. K., Sondheimer, E. and Steward, F. C. *Nature* **182**, 1356-1358 (1958).
12. Ariza, J., Font, J. and Ortuno, R. M. *Tetrahedron* **46**, 1931-1942 (1990).
13. Easton, C. J. and Merrett, M. C. *Tetrahedron* **53**, 1151-1156 (1997).
14. Hernandez, I. L. C., Godinho, M. J. L., Magalhaes, A., Schefer, A. B., Ferreira, A. G. and Berlinck, R. G. S. *J. Nat. Prod.* **63**, 664-665 (2000).
15. Krishna, R. G.; Wold, F. In Angeletti, R.H. (Ed.) *Proteins: Design and Analysis*, Academic Press, San Diego, 1998, pp 121-206.
16. Jimenez, E. C., Olivera, B. M., Gray, W. R. and Cruz, L. J. *J. Biol. Chem.* **271**, 28002-28005 (1996).
17. Jacobsen, R., Jimenez, E. C., Grilley, M., Watkins, M., Hillyard, D., Cruz, L. J. and Olivera, B. M. *Journal of Peptide Research* **51**, 173-179 (1998).
18. Barbara, T. M. *Journal of Magnetic Resonance Series A* **109**, 265-269 (1994).
19. Barbara, T. M. and Bronnimann, C. E. *J. Magnetic Resonance* **140**, 285-288 (1999).
20. Wuthrich, K. *NMR of Proteins and Nucleic Acids* Wiley & Sons: New York, 1986.

Peptide Revolution: Genomics, Proteomics & Therapeutics
Michael Chorev & Tomi K. Sawyer (Editors)
American Peptide Society, 2003

Induced Axial Chirality in the Conformationally Labile, Atropoisomeric $C^{\alpha,\alpha}$-Disubstituted Glycine Bip in Peptides

J.-P. Mazaleyrat,[1] K. Wright,[1] N. Toulemonde,[1] A. Gaucher,[1] M. Wakselman,[1] Q. B. Broxterman,[2] F. Formaggio,[3] S. Oancea,[3] M. Crisma[3] and C. Toniolo[3]

[1]SIRCOB, UMR CNRS 8086, Bât. Lavoisier, University of Versailles, F-78000 Versailles, France; [2]DSM Research, Life Sciences, Advanced Synthesis and Catalysis, P. O. Box 18, 6160 MD Gelen, The Netherlands; [3]Institute of Biomolecular Chemistry, CNR, Department of Organic Chemistry, University of Padova, 35131 Padova, Italy

Introduction

The Bip residue, selected peptides of which have recently been investigated by our groups, is a conformationally labile, atropoisomeric $C^{\alpha,\alpha}$-disubstituted glycine with interconverting, non isolable *(R)* and *(S)* enantiomers (rotational energy barrier of about 14 kcal mol^{-1}) [1]. For peptides of the type X-Bip-Y (Figure 1), in which the X and/or Y groups are amino acid residues (Xaa*), the presence of extra chiral element(s) results in the onset of an equilibrium between two diastereoisomeric conformers with unequal populations: X-*(R)*-Bip-Xaa* and² X-*(S)*-Bip-Xaa* or Xaa*-*(R)*-Bip-Y and Xaa*-*(S)*-Bip-Y, in a manner similar to that recently investigated by Rosini *et al*. in the case of biphenyl-dioxolanes derived from chiral 1,2- and 1,3-diols [2]. We expanded the synthesis of a small series [3] to a much larger series of Boc(Z)/OMe terminally protected di- and tripeptides with Xaa* = C- or N-protected *(L)*- and/or *(D)*-α-amino acids: Ala, Val, Leu, Phe, (αMe)Val, (αMe)Leu, and X,Y = protecting group or Xaa*.

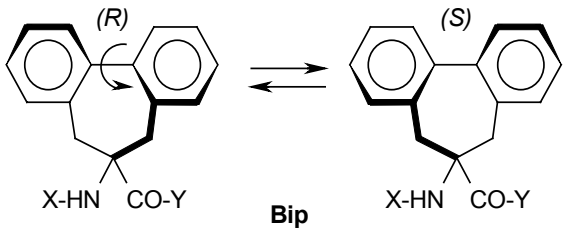

Fig. 1. Conformational equilibrium of the X-Bip-Y peptides.

Results and Discussion

^{1}H NMR experiments at low temperature allowed determination of the diastereomeric excesses of the Bip/Xaa* pairs of isomers exchanging slowly on the NMR time scale. The diastereomeric ratio (d.r.) was determined at 233 K by integration of the best separated sets of signals. The d.r. was found to be strongly dependent *(i)* on the nature of the solvent, with much lower values in $CDCl_3$ than in CD_3CN or CD_3OD, and *(ii)* on the C-terminal (higher d.r.) or N-terminal (lower d.r.) position of the Xaa* residue, especially in the latter solvents. Our CD analysis in MeOH solution of the terminally protected Bip di- and tripeptides allowed us to conclude that –Bip-(*L*)[or (*D*)-] Ala-dipeptides give a clear information on the Xaa* configuration. However, the CD spectra of the -(*L*)[or (*D*)-] Ala-Bip- dipeptides are not informative enough (too weak).

Obviously, the spectra of the enantiomeric -Bip-(*L*)-Ala-/-Bip-(*D*)-Ala- and -(*L*)-Ala-Bip/-(*D*)-Ala-Bip- dipeptides are mirror images. The conclusions discussed above for the -Bip-(*L*)-Ala- dipeptides can be extended to all protein Xaa* residues with an aliphatic side chain. The same conclusion applies to the corresponding C^{α}-methylated α-amino acids, even if in these cases the CD signal is generally weaker. This is not surprising in view of the reduced difference in the number of carbon atoms between the two side chains of the C^{α}-methylated residues compared to their protein counterparts. In the tripeptides with a central Bip residue the signs of the CD bands are governed by the configuration of the Xaa* residue following Bip, not by that of the residue preceding it.

The X-ray diffraction analysis of Boc-Bip-*(D)*-Ala-OMe confirmed the stereochemical correlation between the Ala configuration and the induced *M* twist [*(R)* configuration] of the biphenyl moiety of Bip (Figure 2).

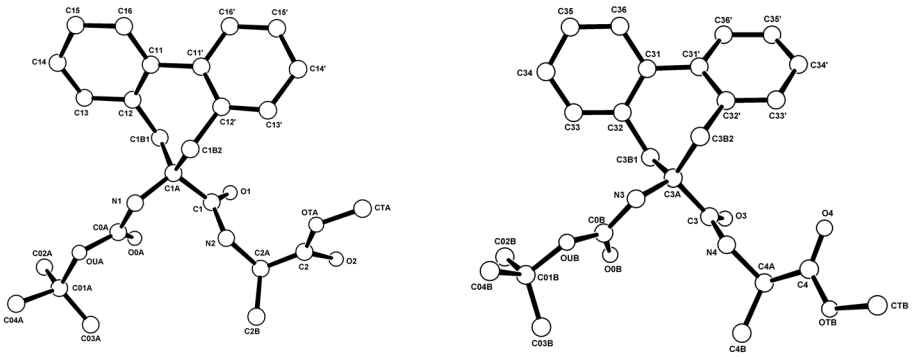

MOLECULE A MOLECULE B

Fig. 2. X-Ray diffraction structures of the two independent molecules (A and B) in the asymmetric unit of the dipeptide of Boc-Bip-(D)-Ala-OMe. The two molecules differ only in the conformation (folded versus extended) of the Ala residue. In both molecules the configuration of Bip is (R) and its conformation is helical.

In conclusion, both CD and ^{1}H NMR spectra highlighted the induced chirality of the single Bip residue, which was always higher in the -Bip-Xaa*- sequences than in the poorly informative -Xaa*-Bip- sequences. The CD response correlated with the absolute configuration of Xaa*: *(L)*-Xaa* and *(D)*-Xaa* induced *P* and *M* torsions in the biphenyl chromophore, respectively, with the *(SS)*-or *(RR)*-Bip-Xaa* isomers favored over the *(RS)*-or *(SR)*-Bip-Xaa* isomers.

References

1. Formaggio, F., Crisma, M., Toniolo, C., Tchertanov, L., Guilhem, J., Mazaleyrat, J. P., Gaucher, A., Wakselman, M. *Tetrahedron* **56**, 8721-8734 (2000).
2. Superchi, S., Casarini, A., Laurita, A., Bavoso, A. and Rosini, C. *Angew. Chem. Int. Ed.* **40**, 451-454 (2001).
3. Oancea, S., Formaggio, F., Gaucher, A., Wright, K., Toulemonde, N., Wakselman, M., Mazaleyrat, J. -P., Toniolo, C. In *Peptides 2002*, Benedetti, E., Pedone, C. eds., Edizioni Ziino, Naples, 2002, pp 392-393.

Peptide Revolution: Genomics, Proteomics & Therapeutics
Michael Chorev & Tomi K. Sawyer (Editors)
American Peptide Society, 2003

Preparation and Use of Magnetic Solid Phase Synthesis Supports

Jan Mařík, Derick H. Lau and Kit S. Lam

Division of Hematology and Oncology, Department of Internal Medicine, University of California Davis Cancer Center, 4501 X Street, Sacramento CA 95817, USA

Introduction

Over two decades ago, Mosbach and Anderson were the first to describe the application of magnetized 5'-AMP-Sepharose in affinity chromatography for isolation of NADP-dependent enzymes. The use of affinity magnetic beads to isolate mRNA, DNA, proteins, and cells from biological samples is now a routine in many laboratories. Typically, these magnetic beads, with diameters of less than 10 μm, are made of agarose or polyurethane coated with polystyrene and conjugated with a biological or chemical agent of interest. Iron nanoparticles coated with dextran and affinity reagents have also been used. However none of these supports are suitable for solid phase synthesis.

There have been several attempts to prepare a magnetic solid support for solid phase synthesis. Magnetic polymer has been prepared by polymerization of 1% DVB-PS followed by nitration and reaction with ferrous sulfate to form the magnetic moiety magnetite [1]. Encapsulation of preformed magnetite with polystyrene polymer to form paramagnetic support for solid phase organic synthesis has been reported [2]. Direct incorporation of magnetite particles into polystyrene beads during polymerization has also been published [3]. A simpler method of precipitating a mixture of ferrous chloride and ferric chloride inside polymer beads to form magnetite has been patented [4]. We have found that this latter approach can be used to magnetize commercially available solid supports that are suitable for peptide synthesis. The procedure of magnetization could be performed on beads already with covalently linked peptides, or on blank beads that can be used for subsequent peptide synthesis.

Results and Discussion

To magnetize TentaGel resins, we have modified the preparative procedure of ferrofluids [5]: One gram of the TentaGel peptide beads was swollen in dimethylformamide (DMF) and washed with water one time to allow hydration. After water was drained, a freshly prepared mixture of 2 ml of 2 M $FeCl_2$ and 8 ml of 1 M $FeCl_3$ in 2 M HCl was added to the beads. With continuous stirring in a hood, 100 ml of aqueous ammonia (0.7 M) was added drop-wise in 20 min. It was important to add the ammonia slowly to achieve precipitation of magnetite (Fe_3O_4) particles within the

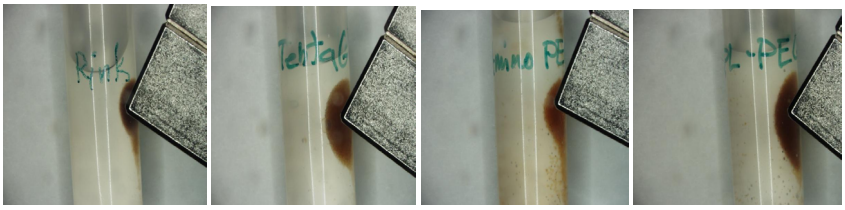

Fig. 1. Magnetic solid phase synthesis supports concentrated by a magnet placed next to the tube (from left to right): Rink, TentaGel, Amino-PEGA and PL-PEGA.

beads. The liquid and precipitate were drained from the beads in a column. The beads were washed briefly with 25% trifluoroacetic acid (TFA) and then 3 times with distilled water. The beads were sterilized by washing and stored in 70% ethanol. By applying a magnetic field, we demonstrated that these beads indeed were magnetized (Figure 1).

To demonstrate that the magnetized resins can be used for the solid phase peptide synthesis, we synthesized LHPQF pentapeptide on the magnetized Rink MBHA resin with standard Fmoc methodology. HPLC analysis of the crude product revealed over 95% purity, and the identity of the desired product was confirmed by MALDI MS (Calc: 639.4 Found: 640.4). The stability of magnetic solid supports towards 95% TFA was tested and we found no significant loss of magnetic properties after 4hrs treatment in the case of magnetized TentaGel resin (Table 1). LHPQF peptide, without a cleavable linker was also synthesized on magnetized TentaGel beads. We were able to demonstrate that these magnetized LHPQF beads could be stained by Streptavidin-alkaline phosphatase in an enzyme-linked colorimetric assay. We have also prepared magnetized peptide beads that bind to $\alpha 3\beta 1$ integrin of non-small cell lung cancer. Using the cell-growth-on-bead assay with these affinity magnetic beads, we were able to retrieve the rare A549 cancer cells added to human whole blood (1 cancer cell in 5×10^4 blood cells) [6].

Table 1. Stability of the magnetic properties of resins in 95% TFA.

	0 min	30 min	1 hour	2 hours	4 hours	20 hours
TentaGel	+	+	+	+	+	-
PL PEGA	+	+	+	+	-	-
Amino PEGA	+	+	+	-	-	-

+ magnetic property retained, - magnetic property lost.

In this report, we have described a simple and very reproducible method for direct deposition of the magnetite nanoparticles into four selected polymer supports: Rink (GL Biochem), TentaGel (Rapp Polymere), Amino-PEGA (Nova Biochem) and PL-PEGA (Polymer Laboratories) that can be used in solid phase organic chemistry. We found these magnetized supports to be compatible with Fmoc based peptide synthesis methodology and subsequent bead assays.

Acknowledgments
This work has been supported by NIH grant R21-CA094519, R33-CA86364 and R33-CA-89706.

References

1. Szimonifka, M. J. and Chapman, K. T. *Tetrahedron Lett.* **36**, 1597 (1995).
2. Sucholeiki, I. and Perez, J. M. *Tetrahedron Lett.* **40**, 3531 (1999).
3. Rana, S., White, P. and Bradley, M. *Tetrahedron Lett.* **40**, 8137 (1999).
4. Ugelstadt. G., Ellingsten, T., Berge, A. and Helgee, O. B. *US Patent #4,774,265* (1988).
5. Berger, P., Nicholas, B., Adelman, N. B., Beckman, K. J., Campbell, D. J. and Ellis, B. A. *J. Chem. Educ.* **76**, 943 (1999).
6. Mařík, J., Lau, D. H., Song, A., Wang, X., Liu, R. and Lam, K. S. *J. Magnet. Magn. Mater.* **264**, 153-157 (2003).

Peptide Revolution: Genomics, Proteomics & Therapeutics
Michael Chorev & Tomi K. Sawyer (Editors)
American Peptide Society, 2003

Rapid Microwave-Assisted Solid Phase Peptide Synthesis

Máté Erdélyi[1,2] and Adolf Gogoll[1,*]

[1]*Department of Organic Chemistry, Uppsala University, Box 599, S-751 24 Uppsala, Sweden*
[2]*Department of Medicinal Chemistry, Uppsala University, Box 574, S-751 23 Uppsala, Sweden*

Introduction

The development of combinatorial chemistry has caused a renaissance and growth of interest in SPPS. In recent years, it has been shown that the use of microwave heating can be advantageous in a large variety of organic reactions [1]. However, there are few reports on the use of microwave heating in combination with solid-phase synthesis [2], possibly due to the requirement of special heavy-walled vials for microwave irradiation that makes resin handling rather complicated, and problems in controlling reaction conditions. In general, peptide chemistry is today limited to room temperature conditions, originating from the general belief of the heat sensitivity of peptide coupling reagents and practical difficulties. The enhancement of SPPS by the use of microwave heating has so far received little attention. Here, we present a microwave-enhanced (110-130°C), rapid procedure for the coupling of sterically hindered amino acids on solid phase. The optimized conditions for a variety of common coupling reagents yielded a significant rate increase [3].

Results and Discussion

Single mode microwave irradiation with an automatic power control to keep the reaction temperature constant was used throughout. Pressure, temperature and irradiation power versus time were monitored. A unique, modified Smith Process vial was used that provided the possibility of both simplified resin handling and microwave heating. The vial (see Figure 1) was equipped with a polypropylene frit and screw cap at one end, and was sealed with an aluminum crimp cap fitted with a silicon septum at the other end.

Fig. 1 Modified Smith Process Vial for microwave promoted solid phase synthesis.

We investigated the compatibility of HATU, TBTU, PyBOP and Mukaiyama's reagent mediated couplings with high temperatures. Reaction conditions for the synthesis of a small tripeptide containing the three most hindered natural amino acids (Fmoc-Thr-Val-Ile-NH_2), and the Fmoc-Ala-Ile-NH_2 or Fmoc-Thr-Ile-NH_2 dipeptides were optimized. The coupling of Fmoc-protected amino acids on polystyrene resin using Rink amide linker was performed. No degradation of the solid support was observed. Fast piperidine mediated Fmoc-deprotection steps (15 min) were conducted at room temperature, and the coupling steps were performed using microwave

Table 1. Coupling times and temperatures for peptide synthesis on Rink's amine resin employing a variety of coupling reagents. The average pressure for reactions performed in DMF and CH_2Cl_2 were 1-2 bar and 6-8 bar, respectively.

Coupling reagents	PyBOP	Mukaiyama's reagent	TBTU	HATU
Reaction time (min)	20	10	10	1.5
Temperature (°C)	110	130	110	110
Solvent	DMF	CH_2Cl_2	DMF	DMF

irradiation. All coupling steps were monitored by qualitative ninhydrin test and by LC-MS investigation of peptides cleaved from small amounts of the resin. Using this procedure, completion of coupling was obtained in a few minutes after a single coupling step. Our optimized conditions are shown in Table 1.

The absence of racemization during the high temperature treatment of amino acids in the presence of a base (*i*-Pr_2NEt) was confirmed by LC-MS and ^1H NMR. The presence of only one peak on the chromatogram of the synthesized peptides suggested the absence of diastereomeric compounds. The ^1H NMR spectrum of this material containing a single set of signals of the oligopeptide confirmed the presence of only one diastereomer.

We have also shown the compatibility of the *t*-BOC protecting schedule with high temperature treatment, as well as the suitability of the modified microwave vial for organometallic reactions [4].

Our microwave promoted procedure will be of interest for incorporation of sterically hindered and deactivated non-natural amino acids in peptide synthesis. The speed of this method may also accelerate the production of peptide libraries.

Acknowledgments

We would like to thank Personal Chemistry AB for access to the Smith Synthesizer™ and modified Smith process vials. We also thank the Swedish Pharmaceutical Society (IF:s stiftelse) for providing financial support for participation at the 18th APS.

References

1. Lindström, P., Tierney, J., Wathey, B. and Westman, J. *Tetrahedron* **57**, 9225 (2001).
2. Lew, A., Krutzik, P. O., Hart, M. E., Chamberlin, A. R. *J. Comb. Chem.* **4**, 95 (2002).
3. Erdélyi, M., Gogoll, A. *Synthesis* **11**, 1592 (2002).
4. Erdélyi, M., Gogoll, A. *J. Org. Chem.* **68**, 6431-6434 (2003).

Peptide Revolution: Genomics, Proteomics & Therapeutics
Michael Chorev & Tomi K. Sawyer (Editors)
American Peptide Society, 2003

Regioselective MCR4 Reaction: One Pot Synthesis of Spiro Heterobicyclic Aliphatic Rings Generated from Natural Amino Acids

Gerardo Byk and Eihab Kabha

Bar Ilan University, Department of Chemistry, Laboratory of Peptidomimetics and Genetic Chemistry, 52900-Ramat Gan/ISRAEL

Introduction

In a previous work [1] we have found that a special family of β-keto esters (five member ring beta-ketolactone) reacts with urea and two equivalents of aldehyde to give a new family of spiro heterobicyclic aliphatic rings in good yields and in a single step. In the present work we have extended the scope of this MCR4 to β-ketolactams of natural amino acids and different ureido-analogs. Interestingly, the reaction proceeds regioselectively and is directed by the substituents on the heterocyclic ring. We demonstrate that this new reaction can be significantly extended and performed in parallel arrays by the use of chiral β-keto lactams derived from α-amino acids as starting compounds using the Radley's parallel platform.

Results and Discussion

The β-ketolactams are easily obtained by a method previously reported [2] using N-protected amino acids and Meldrum acid as starting compounds and DCC as C-C coupling agent. As prototype syntheses we have reacted lactams derived from Gly, Ala and Phe with a series of aromatic and aliphatic aldehydes and urea. The reactions were performed in a parallel array using the Radley's carrousel (see Figure 1).

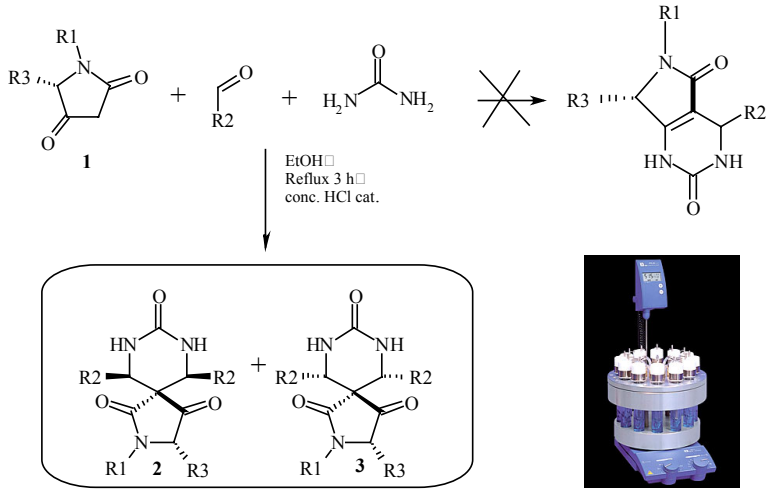

Fig. 1. Synthesis of new spiro-bicyclic lactams from β-ketolactams derived from amino acids.

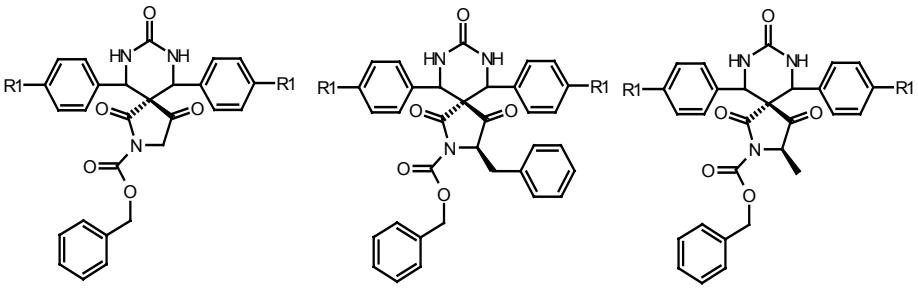

Fig. 2. New spiro-bicyclic lactams obtained in this study: R_1= H, CH_3, OCH_3, NO_2, F, Cl.

In a representative experiment, 2.4 mmol of aromatic aldehyde, 2.4 mmol of urea and 1 mmol of β-ketolactam derived from Gly, Ala or Phe were dissolved in 2 ml of acetic acid and reacted at 78 °C for 3h. Crude products precipitated upon cooling the reactors. The mean yields were between 60-85% after HPLC purification. Products were characterized by H- and C-NMR and by high-resolution mass spectroscopy (see Figure 2).

The efficiency of the reaction depends on the nature of the aldehydes. While aromatic aldehydes generated the anticipated products in good yields aliphatic aldehydes resulted in poor yields of the desired products (results not shown). These variable yields were also observed by others in the classical Biginelli reaction. We have found that aliphatic aldehydes generate Schiff bases with urea that can undergo isomerization to relatively more stable enamides. These enamides do not react in the desired multicomponent reaction or in the regular Biginelli reaction, but form six member ring as final side-product by cyclization between a double shiff-base/enamide (formed between urea and two equivalents of the aldehyde). This side reaction can also be explained as a reaction between a Knovenagel-self addition of two aldehydes and urea.

Conclusions

A novel ψMCR4 extension of the Biginelli reaction previously demonstrated for tetronic acid was extended to lactam derived from glycine, phenylalanine and valine. The reaction can be performed in a combinatorial array using Radley's Carrousel. We noted anomalous HNMR signals due to shielding of the methylene protons by the π electrons. A regiospecificity is clearly observed toward one of the syn isomers in the case of glycine derivatives. In the case of phenylalanine analogs, the regiospecificity, favoring one of the syn isomers, seems to be lower as compared to Gly, suggesting that the benzyl from the Phe has an opposite effect from the Z group on regioselectivity.

Acknowledgments

This work was financed by the Israel Science Foundation Grant # 694/1, the Ygal Alon Foundation and the "Marcus Center for Medicinal Chemistry." A grant from "The Council for Higher Education of Israel" supported Eihab Kabha's PhD fellowship.

References

1. Byk, G., Gottlieb, H. E., Herscovici, J. and Mirkin, F. *J. Comb. Chem.* **2**, 732-735 (2000).
2. Jouin, P. and Castro, B. *J. Chem. Soc. Perkin Trans.* **1**, 1177 (1987).

Peptide Revolution: Genomics, Proteomics & Therapeutics
Michael Chorev & Tomi K. Sawyer (Editors)
American Peptide Society, 2003

Effective Peptide Synthesis Applying Thioesters in the Presence of Metal Ions

Raffaele Ingenito, Dijana Drezniak, Stefan Guffler and Holger Wenschuh

Jerini Peptide Technologies, a Division of Jerini AG, Invalidenstrasse 130, D-10115 Berlin, Germany

Introduction

Thioesters of carboxylic acids have been introduced as acylation reagents for amines many years ago [1]. Although their application for the stepwise synthesis of peptides is limited, their use as key intermediates for fragment condensations has become increasingly important. Convergent peptide synthesis (CPS) as introduced by Blake [2] and later improved by Aimoto [3], applies peptide thioesters as building blocks to form native amide bonds, thus assembling long peptides and proteins not readily accessible before by conventional peptide synthesis methods [4].

Optimized CPS protocols apply partially protected peptide thioesters in the presence silver ions and HOOBt, which can be directly reacted with any amino group of a second partially protected peptide fragment [5]. Herein we describe an extension of this method to the use of copper salts as additives to accelerate the reaction between peptide thioesters and a second peptide fragment to form native amide bonds in both solution and solid phase approaches.

Results and Discussion

Initially, a model peptide thioester Msc-LYRAG-COSR was synthesized according to previously published methods [6]. It was subsequently coupled to the resin bound peptide H-FY(OtBu)GK(Boc)A-resin in the presence of various copper based additives. Additionally, the reaction was conducted only with sodium thiophenate added to the thioester to increase the reactivity via conversion into the more reactive aromatic thioester. The fastest reactions were observed with ($Cu(OBt)_2$/TMP and CuCl/Thiophenate/TMP), respectively (Table 1).

Table 1. Acylation yields for various additives on solid support.*

Additive	Yield (%)	Additive	Yield (%)
Thiophenate	25	$CuCl_2$/TMP/HOBt	10
$CuCl_2$/TMP	0	CuCl/TMP	45
Thiophenate/$CuCl_2$	25	Thiophenate/CuCl/TMP	85
$Cu(OBt)_2$/TMP	90	CuCl/HOBt/TMP	80

**5 eq. thioester, 5 eq. additives in DMF, c= 0.2 M, 40°C, 16 h.*

In order to extend the most effective procedures to more hindered systems, the same model reaction was used applying two N-terminal peptide fragments carrying C-terminal Ala and Leu thioesters, respectively. It was found that the same reaction conditions yielded similarly high amounts of coupling product compared to the less hindered junction point Gly/Phe (Table 2).

Since epimerization at the activated C-terminal amino acid of the N-terminal fragment is one of the main drawbacks in fragment condensation processes, the question of chiral integrity also needed to be addressed for the new procedure. In order to detect the racemization values during the condensation reaction, the Leu-thioester peptide was synthesized having both the L-Leu and D-Leu respectively at the C-terminal ends to obtain the corresponding stereoisomeric standards for HPLC comparison of the full length peptides after reaction with the resin bound peptide (Table 2).

Table 2. Acylation yields and racemization values obtained for Ala-Phe and Leu-Phe ligation points using different methods on solid support.

Thioester	Additive	Yield (%)	D,L-Isomer (%)
Msc-LYRAA-COSR	$Cu(OBt)_2$/TMP	80	-
	Thiophenate/CuCl	85	-
Msc-LYRAL-COSR	$Cu(OBt)_2$/TMP	80	2.6
	Thiophenate/CuCl	82	2.0
	AgCl/HOOBt/DIEA	34	20

Relatively low values of racemization were detected compared to the approach using silver ions. The results obtained for reactions on solid support could be verified for reactions carried out in solution with regard to both acceleration of reaction speed and suppression of racemization.

In conclusion, it has been shown that the amide bond formation between a thioester and a primary amine can be accelerated by the addition of copper-based additives. In addition to the increased reaction rates a suppression of racemization was observed.

Acknowledgments

This work was supported by the FITE program of the European EFRE fund and the Senate of Berlin.

References

1. Wieland, T., Bokelmann, E. and Bauer, L. *Liebigs Ann. Chem*. **573,** 129 (1951).
2. Blake, J. *Int. J. Peptide Protein Res.* **17**, 273 (1981).
3. Aimoto, S. *Biopolymers* **51**, 247 (1999).
4. Blake, J., Yamashiro, D., Ramasharma, K. and Li, C. H. *Int. J. Peptide Protein Res.* **28**, 468 (1986).
5. (a) Kawakami, T., Kogure, S., Aimoto, S *Bull. Chem. Soc. Jpn.* **69**, 3331 (1996). (b) Kawakami, T., Hasegwa, K., Teruya, K., Akaji, K., Hotiuchi, M., Inagaki, F., Kurihara, Y., Uesugi, S. and Aimoto, S. *J. Peptide Sci.* **7**, 474 (2001).
6. (a) Ingenito, R., Bianchi, E., Fattori, D., Pessi, A. *J. Am. Chem. Soc.* **121**, 11369 (1999). (b) Ingenito, R., Dreznjak, D., Guffler, S. and Wenschuh, H. *Org. Lett.* **4**, 1187 (2001).

Peptide Revolution: Genomics, Proteomics & Therapeutics
Michael Chorev & Tomi K. Sawyer (Editors)
American Peptide Society, 2003

A Highly Acid-Labile Thiophene Backbone Amide Linker: T-BAL

Ulrik Boas[1,2], Mikkel Jessing[1,2], Jørn B. Christensen[2] and Knud J. Jensen[1]

[1]Department of Chemistry, Royal Veterinary and Agricultural University, DK-1871 Frederiksberg, Denmark; [2]Department of Chemistry, University of Copenhagen, DK-2100 Copenhagen, Denmark

Introduction

The backbone amide linker (BAL) has, since the first reports in the mid-1990's, become a widely used concept in solid-phase synthesis [1,2]. In the BAL approach, the growing peptide chain can be anchored through a backbone amide, giving easy access to *C*-terminal modified and cyclic peptides. The BAL concept was first implemented in a tris(alkoxy)benzyl system, which allowed release of final products by treatment with concentrated TFA. Highly acid-labile BAL type handles, which can release amides, e.g. peptides, while retaining *tert*-butyl based protecting groups, are very desirable. They would provide ready access to selectively protected, C-terminal modified peptides, such as for use in iterative chemoselective ligations.

Thiophene BAL is a new handle based on a 3,4-ethylenedioxythiophene (EDOT) core structure. EDOT has found use as an electron-donating monomer in conducting materials[3] and is commercially available. The electron-richness of EDOT makes it a promising candidate as carbocation stabilizing core in acid-labile linkers, especially of the BAL-type.

The first step in the synthesis of T-BAL was Vilsmeier-Haack formylation of EDOT under mild conditions. The thiophene aldehyde was α-iodinated using NIS and acetic acid (Figure 1). The alkyl spacer was introduced by a chemoselective Negishi coupling on the thiophene iodide, creating a carbon-carbon bond without affecting the unprotected aldehyde or the ethyl ester moieties [4,5]. Hydrolysis of the ester was mediated by aqueous LiOH in DMF to afford T-BAL. The linker was anchored to amino-functionalized resins using standard protocols.

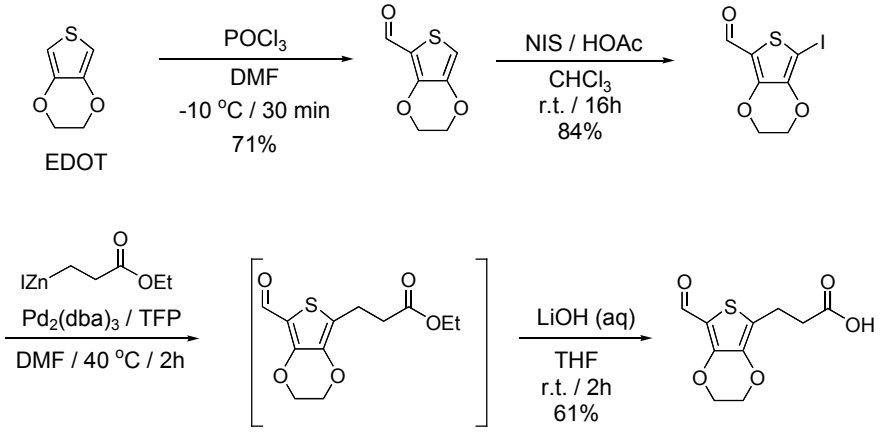

Fig. 1. Synthesis of the T-BAL handle.

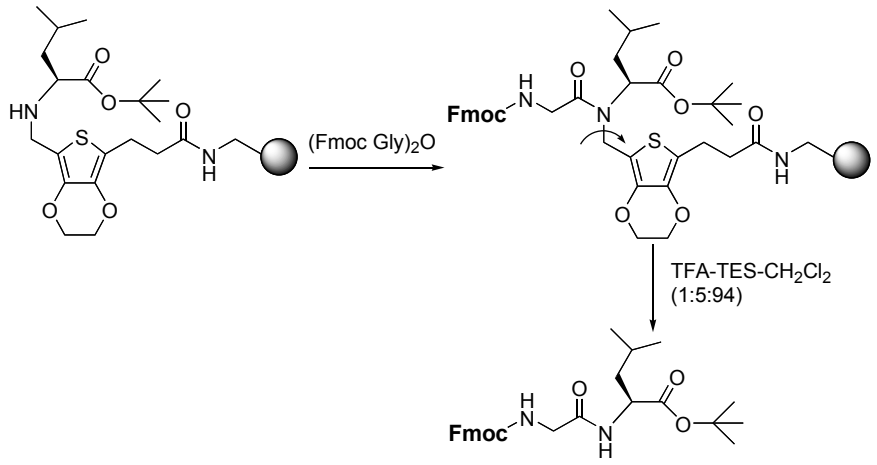

Fig. 2. Synthesis of a peptide tert-butyl ester using a T-BAL approach.

Reductive amination in the presence of $NaBH_3CN$ anchored the first residue through the amine; also sterically more demanding amino acids such as Val were anchored efficiently. The second amino acid was coupled as the Fmoc-protected symmetrical anhydride. Peptide chain assembly then continued following standard Fmoc protocols. Fully deprotected peptides were released using high-TFA conditions (TFA-CH_2Cl_2 1:1 or TFA-H_2O 95:5). With the aim of establishing conditions for

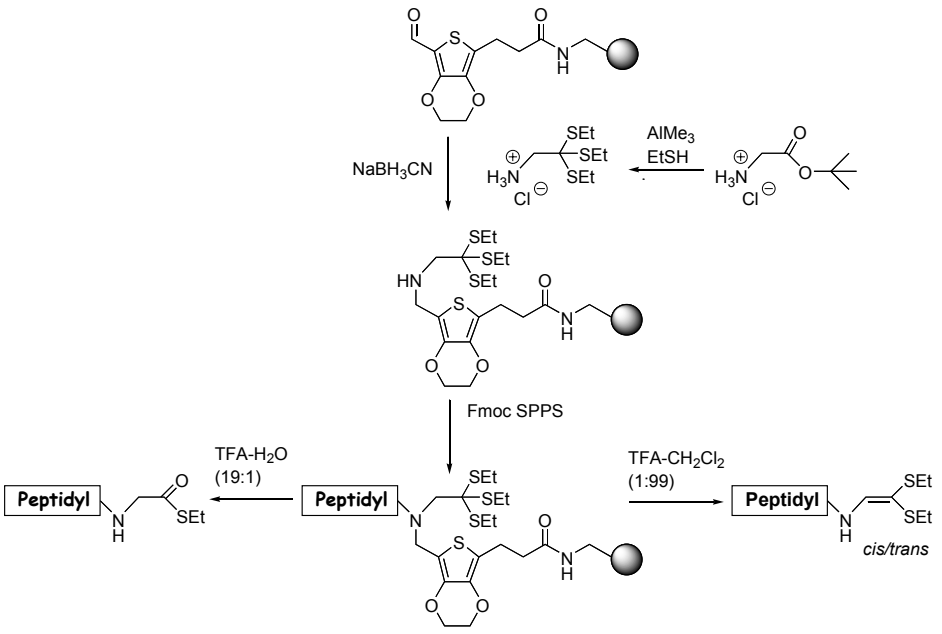

Fig. 3. Synthesis of peptide thioester and peptide ketene dithioacetal.

release of partially protected peptides, low-TFA cleavage conditions were studied. We found that as low as 1% TFA efficiently released peptides from the handle. This allowed the synthesis of peptides while retaining tert-butyl based protecting groups (Figures 2 and 3). Also, a peptide ketene dithioacetal was prepared from the corresponding trithioortho ester [6]; high-acid conditions (TFA-H_2O 95:5) gave the peptide thioester (Figure 4).

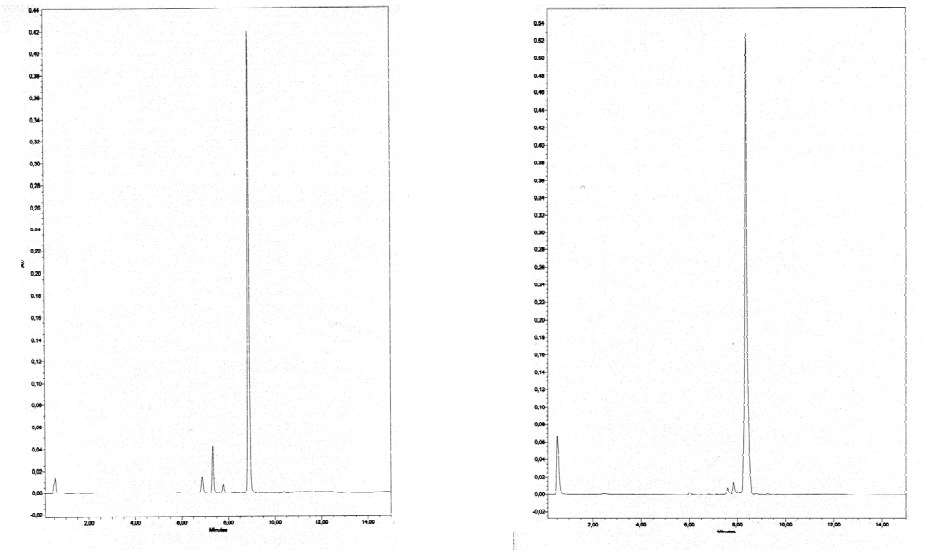

Fig. 4. Analytical HPLC chromatograms of Fmoc-Gly-Leu-O^{t}Bu (left) and Fmoc-Phe-Gly-Gly-SEt (right).

Acknowledgments
We are grateful to Ms. Jette Petersen for assistance with AAA analyses, and thank the Leo Foundation and Lundbeck Foundation for financial support to UB. MJ thanks Novo for a stipend.

References

1. Jensen, K. J., Alsina, J., Songster, M. F., Vágner, J., Albericio, F. and Barany, G. *J. Am. Chem. Soc.* **120**, 5441-5452 (1998).
2. For a review see: Alsina, J., Jensen, K. J., Albericio, F. and Barany, G. *Chem. Eur. J.* **5**, 2787-2795 (1999).
3. Groenendaal, L., Jonas, F., Freitag, D., Pielartzik, H. and Reynolds, J. R. *Adv. Mater.* **12**, 481-494 (2000).
4. For chemoselection between thiophene iodides and bromides by Negishi coupling, see: Boas, U., Dhanabalan, A., Greve, D. R. and Meijer, E. W. *Synlett.* 634-636 (2001).
5. Boas, U. *Studies in Polymer Assisted Organic Chemistry* Ph.D. Thesis, Department of Organic Chemistry, University of Copenhagen, (2002).
6. Brask, J., Albericio, F. and Jensen, K. J. *Org. Lett.* **5**, 2951-2953 (2003).

Peptide Revolution: Genomics, Proteomics & Therapeutics
Michael Chorev & Tomi K. Sawyer (Editors)
American Peptide Society, 2003

A New Method for the Preparation of Peptide C-Terminal α-Thioesters Compatible with Fmoc-Solid-Phase Peptide Synthesis

Julio A. Camarero, Benjamin J. Hackel, James J. de Yoreo and Alexander R. Mitchell

Chemical Biology and Nuclear Sciences Division, Lawrence Livermore National Laboratory, University of California, Livermore, CA 94550, USA

Introduction

C-terminal peptide thioesters are key intermediates for the synthesis/semisynthesis of proteins and for the production of cyclic peptides by native chemical ligation [1]. These mildly activated species are also valuable for the construction of proteins containing non-natural backbones and for the synthesis of peptide dendrimers.

Peptide C-terminal thioesters can be prepared by standard solid-phase peptide synthesis (SPPS) using Boc methodology, or for larger polypeptide domains and protein domains, using intein-based bacterial expression systems. Unfortunately, the Boc methodology requires the use of HF which is extremely toxic and not well suited for synthesis of phospho- and glycopeptides.

The Fmoc–based methodology does not employ such a hazardous reagent. Therefore, synthetic methods compatible with this widely used methodology would greatly complement these approaches, especially in peptides containing functionalities incompatible with Boc-chemistry (i.e. glycopeptides and phosphopeptides). However, the poor stability of the thioester functionality to strong nucleophiles such as piperidine, used for the deprotection of the N^{α}-Fmoc group, seriously limits the use of this methodology. So far, several approaches have been used to overcome this problem [2-5]. Unfortunately all of them have limitations such as poor yields for long peptides [2], epimerization of the C-terminal residue [3], aspartimide formation [4] and alkylation of Met residues [6] which limit their potential use.

In the present work, we describe a totally new method for the SPPS of C-terminal peptide thioesters by using the Fmoc/*t*-Bu methodology that addresses all of the problems mentioned above. Our approach is based on the use of the aryl hydrazide linker [7], which is totally stable to Boc- and Fmoc-SPPS protocols.

Results and Discussion

The principle of our approach is to employ a base- and acid- stable hydrazine linker, (the commercially available 4-Fmoc-hydrazinobenzoyl AM resin) for peptide assembly via the Fmoc-strategy (Scheme 1).

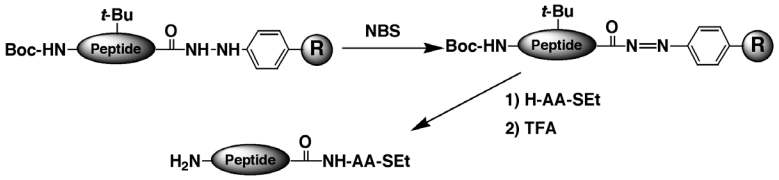

Scheme 1. Solid phase synthesis of C-terminal thioesters on 4-Fmoc-hydrazinobenzoyl resin.

Once the synthesis is complete, the hydrazide linker is oxidized with 2 equiv. of *N*-bromosuccinimide (NBS) for 10 min to give an acyl diazene derivative. This acyl diazene reacts with α-amino ethylthioesters (H-AA-SEt) cleaving the peptide from the

resin and yielding the corresponding Boc/*t*-butyl-protected peptide thioesters. Finally the remaining protecting groups are removed (when necessary) by acidolytic treatment with trifluoroacetic acid (TFA) thus giving the desired α-thioester peptides. Our method was initially tried in two model peptides Th-1 and Th-2 (see Table 1) showing that the corresponding α-thioesters could be obtained relatively quickly (reaction was complete in 30 min.) and efficiently (cleavage yield was ≈65%), as is shown in Figure 1. Racemization of the *C*-terminal amino acid after oxidation of the hydrazide to form the diazene was also investigated. LL and LD Phe-Ala peptides were assembled on a hydrazine resin, oxidized with NBS and the diazene derivatives reacted with propyl amine. The HPLC analysis of both propylamide peptide diastereomers revealed that racemization had not occurred (≤0.5%). Furthermore, we also investigated the compatibility of this oxidative method with sensitive residues (Tyr, Met, Trp and Cys,). Several model peptides containing these residues were synthesized (see Table 1) and their compatibility with the oxidative step was checked. The results (Figure 1) showed that Tyr(t-Bu), Trp(Boc) and Cys(Npys) residues were not affected by the NBS treatment. Met-containing peptide Th-4 was oxidized to the corresponding sulfoxide by NBS, but during the TFA cleavage was reduced if 5% EtSH was added to the cleavage cocktail. Finally this method was used to generate Th-7 peptide, a 22-mer thioester peptide derived from the c-Crk *N*-t SH3 domain, which was used to prepare a synthetic SH3 domain by native chemical ligation.

Table 1. Peptides prepared for this study.

Name	Sequence
Th-1	Ac-IAFG-SEt
Th-2	Ac-IAFA-SEt
Th-3	H-LYKAG-SEt
Th-4	H-LMYKAG-SEt
Th-5	H-LWAG-SEt
Th-6	H-CYAVTGKGDSPAAG-SEt
Th-7	Ac-AEYVRALFDFNGNDEEDLPFKKG-SEt

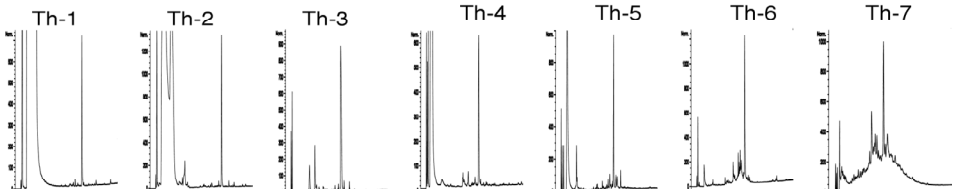

Fig.1. RP-HPLC traces of the crude cleavage products for the thioester peptides shown in Table 1 (the major peak denotes in each case the expected thioester peptide product).

Acknowledgments

This work was performed under auspices of the U.S. Department of Energy by the University of California, Lawrence Livermore National Laboratory (LLNL) under contract W-7405-Eng-48. J. A. C is a Distinguished Lawrence Fellow at the LLNL.

References

1. Dawson, P. E. et al. *Science* **260**, 776 (1994).
2. Li, X., et al. *Tet. Lett*. **39**, 8669 (1998); Clippingdale, A. B., et al. *J. Pept. Sci.* **6**, 225 (2000).
3. Alsina, J., Yokum, T. S., Albericio, F. and Barany, G. *J. Org. Chem*. **64**, 8761-8769 (1999).
4. Swinnen, D. and Hilvert, D. *Org. Lett*. **2**, 2439-2442 (2000); Sewing, A. and Hilvert, D. *Angew. Chem. Int. Ed.* **40**, 3395-3396 (2001).
5. Ingenito, R. et al. *J. Am. Chem. Soc.* **121**, 11369-11374 (1999); Shin, Y. *et al*., *J. Am. Chem. Soc*. **121**, 11684-11689 (1999).
6. Flavell, R. R. et al. *Org. Lett*. **4**, 165-168 (2002).
7. Milne, H. B., Most, C. F. *J. Org. Chem*. **33**, 169 (1968); Wieland, T., et al. *Liebigs Ann. Chem*. **740**, 31 (1970); Millington, C. R., et al. *Tetrahedron Lett*. **39**, 7201 (1998).

Peptide Revolution: Genomics, Proteomics & Therapeutics
Michael Chorev & Tomi K. Sawyer (Editors)
American Peptide Society, 2003

Peptide $^{\alpha}$Thiol Ester Formation Using Standard Fmoc-Chemistry

Regula von Eggelkraut-Gottanka[1], Annerose Klose[2], Michael Bienert[2], Annette G. Beck-Sickinger[1] and Michael Beyermann[2]

[1]Institut für Biochemie, Universität Leipzig, D-04103 Leipzig, Germany; [2]Forschungsinstitut für Molekulare Pharmakologie, Berlin, D-13125, Germany

Introduction

C-terminal peptide thiol esters can be used for chemical synthesis of proteins particularly since the development of the native chemical ligation method. Expanding the applicability of the chemical ligation via thiol esters requires effective methods for their preparation. Whereas the intein technology enables the molecular biological access to protein thiol esters, peptide thiol esters may be better obtained by chemical synthesis. The preparation by SPPS using Fmoc-strategy has been limited by the susceptibility of thiol ester linkages to strong nucleophiles such as the piperidine used for the removal of Fmoc groups. Several strategies for solving the problem have been reported, but all of them either require special agents/linker or are reported to cause undesirable side-reactions. An attractive route results from an Fmoc-based synthesis of protected peptide acids on commercially available Cl-trityl-resin followed by a direct conversion of the C-terminal carboxylic group to the corresponding thiol ester. Peptide thiol esters are sufficiently stable towards acidic conditions which allows deprotection in TFA and even a following chromatographic purification in acetonitrile/water systems. So far, application of this approach was complicated by the use of either a high excess (DIPCDI, 20 eq) of the activating agent [1], which requires an extra purification step before the deprotection, or the level of epimerization [2]. We have investigated conditions for the $^{\alpha}$thiol ester formation using a very low or no excess of activating agent. Different activating agents (PyBOP, BOP, DIPCDI, and TBTU) and thiols (thiophenol, *p*-acetamidothiophenol, 3-mercapto-propionic acid ethyl ester) have been tested with respect to the rate of thiol ester formation and epimerization.

Results and Discussion

Initial studies were performed with Z-Gly-Ala-OH and different activating agents; the corresponding agent (0.01 mmol) was added to Z-Gly-Ala-OH (0.01 mmol) and *p*-acetamidothiophenol (0.01 mmol) dissolved in 0.5 ml of DCM. In the case of TBTU, BOP or PyBOP reactions were started by addition of DIEA (0.01 mmol). Progress of the reaction was monitored by analytical RP-HPLC. The product peaks were collected and identified with MALDI-MS. Activation by phosphonium salts and carbodiimide, with or without HOBt, resulted in a fast thiol ester formation; the highest rate was achieved by PyBOP. After 16 h (overnight) all reactions had run to completion with PyBOP or DIPCDI/HOBt, respectively. In contrast, TBTU could hardly activate Z-Gly-Ala-OH, a fact that can be attributed to a fast reaction between TBTU and the thiol prior to the activation of Z-Gly-Ala-OH. Comparing *p*-acetamidothiophenol (HSAatp) with thiophenol or 3-mercaptopropionic acid ethyl ester, the SAatp-ester is formed most rapidly and, additionally, without the typical thiol malodor. In order to determine whether epimerization takes place during the thiol ester formation. The resulting Z-Gly-Ala-S-acetamidophenyl esters (0.005 mmol) were ligated to H-Cys-OEt x HCl (0.005 mmol) in 1 mL of 0.1 M TRIS buffer (pH 7.7) containing 3 M urea and β-mercaptoethanol (2 vol-%). An aliquot of the reaction mixture was applied to analytical

RP-HPLC (t_R(LL): 19.7 min, t_R(DL): 20.3 min). According to the HPLC data, we observed <3.5% stereomutation for PyBOP-activation and <1% for DIPCDI/HOBt-activation. The Z-Gly-Ala-OH used for the studies was optically pure (> 99.9%) as checked by a control experiment.

Applying the method to biologically interesting peptides, we prepared the thiol ester of an N-terminal segment of urocortin, acetyl-urocortin(1-21) (Figure 1): ac-DDPPLSIDLTFHLLRTLLELA, to couple it later on via chemical ligation to a peptide library, yielding urocortin analogs with several C-terminal modifications. The crude protected peptide, after synthesis on Cl-Trt-resin using a standard protocol for Fmoc-chemistry (final linker cleavage with AcOH/TFE/DCM), was treated with DIPCDI (1.5 eq.) and HSAatp (15 eq.) in DCM overnight. After TFA deprotection we obtained the corresponding thiolester in a yield of 47 %. Epimerization of the C-terminal alanine was found to be very low (0.2 %) [3].

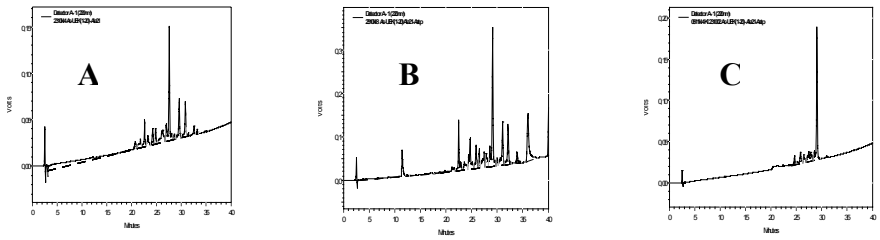

Fig. 1. Thiol ester formation of ac-urocortin(1-21): (A) crude peptide after SPPS (deprotected sample), (B) crude peptide thiol ester, and (C) thiol ester after prep. RP-HPLC on C-18.

In another approach we wanted to prepare a carboxyfluorescein(CF)-labeled proNPY analogue by chemical ligation using the N-terminal segment of pro-neuropeptide Y (proNPY 1-40) as thiol ester. ProNPY(1-40) thiol ester of the protected peptide acid obtained by Fmoc-based SPPS was formed with PyBOP (3 eq), HSAatp (3 eq) and DIEA (3 eq) dissolved in DCM [3]. The peptide thiol ester was formed with a yield of > 95 % and obtained, with respect to the peptide content in the crude product, with a final yield of 70 %. For the C-terminal amino acid of the proNPY(1-40)-SAatp a very little epimerization was found (1.39% D-serine). Native chemical ligation of the thiol ester fragment of proNPY(1-40) and the carboxyfluorescein(CF)-labeled [Cys^{41},K68(CF)]proNPY(41-69) was performed in γ-morpholinopropanesulfonate buffer (0.1 M), pH 7.5, containing 6 M guanidine x HCl, thiophenol (2 %) and benzyl mercaptan (2 %) for 8 hs. The ligation product was purified by semi-preparative RP-HPLC and analyzed by MALDI-MS ($[M+H]_{calc.}$: 8425.4, $[M+H]_{found}$: 8425.4).

In conclusion, the preparation method presented here provides a highly efficient, fast and low-cost way for the generation of peptide thiol esters by Fmoc-based solid phase strategy. We have shown that phosphonium salt-based reagents in the presence of thiol are very suitable for an excellent thiol ester formation.

Acknowledgments

The work was funded by a DFG grant (SFB 610/A1 and the Fond der Chemischen Industrie.

References

1. Futaki, S. *et al*. *Tetrahedron Lett.* **38**, 6237-6240 (1997).
2. Biancalana, S. *et al*. *Lett. Pept. Sci.* **7**, 291-297 (2001).
3. v. Eggelkraut-Gottanka, R. *et al*. *Tetrahedron Lett.* **44**, 3551-3554 (2003).

Peptide Revolution: Genomics, Proteomics & Therapeutics
Michael Chorev & Tomi K. Sawyer (Editors)
American Peptide Society, 2003

Fluorophilic Tagging Reagents for Solid Phase Peptide Synthesis

Dmitri V. Filippov[1], Dirk J. van Zoelen[1], Peter C. de Visser[1], Marcel van Helden[1], Steven P. Oldfield[1], Daan Noort[2], Gijs A. van der Marel[1], Hermen S. Overkleeft[1], Jan W. Drijfhout[3] and Jacques H. van Boom[1]

[1]Department of Organic Chemistry, Gorlaeus Laboratories, Leiden Institute of Chemistry, Leiden University, P.O. Box 9502, 2300 RA Leiden, The Netherlands;
[2]TNO Prins Maurits Laboratory, P.O. Box 45, 2280 RA, Rijswijk, The Netherlands,
[3]Department of Immunohematology and Blood Transfusion, Leiden University Medical Center, P.O. Box 9600, 2300 RC Leiden, The Netherlands

Stepwise solid-phase peptide synthesis (SPPS), originally devised by Merrifield, has been improved over the past years by the introduction of automation and new chemical methodologies (*i.e.* protective groups, resin supports as well as condensing and capping agents). Despite these advances it became evident that the occurrence of unwanted truncated and deletion sequences could not be prevented. The latter is mainly due to the fact that the efficacy of a condensation step strongly depends on the secondary structure of the growing peptide chain. Consequently, routine SPPS of polypeptides may lead to the accumulation of impurities that can only be removed by a laborious and time-consuming purification procedure. It has been reported [1] that the separation of chromatographically similar impurities can be facilitated by the incorporation of a reversible chromatographic tag at the H_2N-terminus of an immobilized target peptide obtained in the final stage of a stepwise SPPS protocol. Cleavage of the tagged peptide from the solid support will afford, after a tag-defined specific purification procedure and subsequent removal of the tag, the target peptide.

It was envisaged that the implementation of a reversible probe derivatized with a suitable fluorophilic tail would be a powerful tool in the purification by fluorous chromatography [2] of target sequences obtained via a stepwise SPPS approach. We here present a convenient route to the synthesis of three Z-based acid labile fluorine-tagged reagents [*i.e.* **1** (FZ-Cl), **2** (FMZ-Cl) and **3** (FEZ-Cl) in Scheme 1] as well as FMsc group cleavable with diluted base (e. g. 1% aq. ammonia)[3, 4].

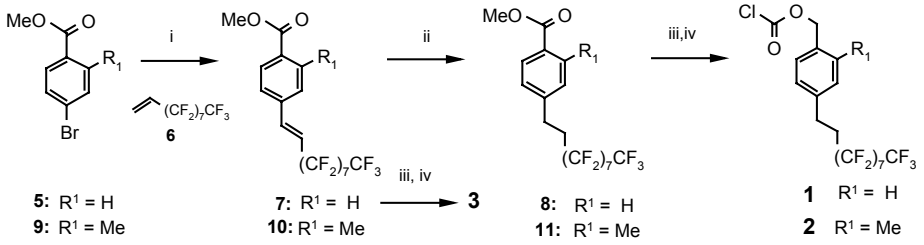

Scheme 1. (i) ***6****, Herrmann-Beller cat., NaOAc, DMF, 125ºC, 14 h (72%); (ii) Pd/C 10%, H_2, 3 bar, 3 h (88%); (iii) $LiAlH_4$, Et_2O, 0ºC, 2 h (90%); (iv) $COCl_2$ toluene/THF, 3 h (100%).*

The route of synthesis of the three fluorophilic reagents **1**-**3** is presented in Scheme 1 and is based on a Heck cross-coupling of 4-bromobenzoic acid derivatives (**5, 9**) with commercially available [1H,1H,2H]-perfluoro-1-decene (**6**). The tagging reagent **4** was obtained in a high-yielding three-step sequence (see Scheme 2) starting from commercially available [1H,1H,2H,2H]-perfluorodecyl iodide **12** [5].

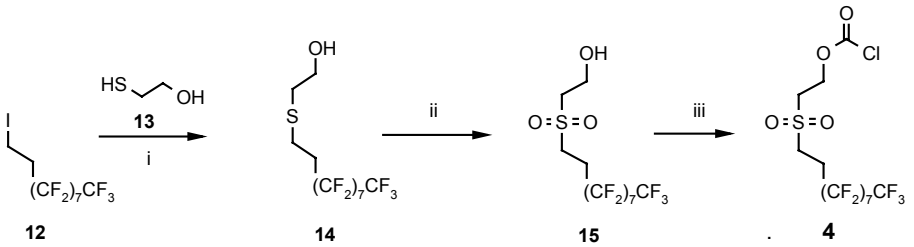

Scheme 2. (i) NaOH, t-BuOH, reflux (91%); (ii) AcOOH/H_2O (30% in AcOH); (iii) $COCl_2$ toluene/THF, 16 h (97%, 2 steps).

The potential usefulness of **1** (FZ-Cl) in the purification of synthetic peptides was explored by the purification of hydrophobic nonadecamer **16** (Figure 1) and docosameric peptide **17**. For example, FZ-tagged **17** could be readily separated from capped truncated sequences on Fluophase HPLC column (Figure 2) and detagged by TFA treatment (10 h). The same purification protocol applied to **16** furnished pure product in 35% yield. In turn, FMsc-Cl (**4**) could be used to purify 35-meric peptide **18** (Figure 1). The latter was isolated in 21% yield after fluorous HPLC and detagging (1% aq. NH_3).

19-mer H-GVWPLPLLLLALPPKAYAG-OH (**16**)
22-mer H-GAYKGLPAKKPTAPTIEGAKKG -OH (**17)**
35-mer H-LSELDDRADALQAGFSQFESSAAKLKRKYWWKNLK-NH_2(**18)**

Fig. 1. Sequences of peptides used in the tagging experiments.

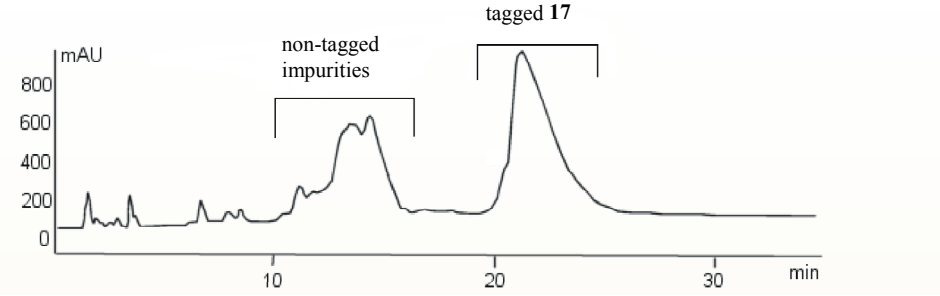

*Fig. 2. Chromatogram obtained by eluting crude FZ-tagged **17** (0.5 mg), loaded on a Fluophase™ column, with a gradient of trifluoroethanol in 0.05 % aq. TFA. MS analysis showed that the product eluted as a broad peak at 21 min is FZ-tagged peptide **17**.*

References

1. For tagging concepts in purification of synthetic peptides see: Mascagni, P. In Chan W. C. and White P. D. (Eds.) *Fmoc Solid Phase Peptide Synthesis: A practical Approach* Oxford University Press, New York. p. 265-276 (2000) and the references cited.
2. Zhang, W., et al. *Tetrahedron* **58**, 3871-3875 (2002) and the references cited.
3. Filippov, D. V., van Zoelen, D. J., Oldfield, S. P., van der Marel, G. A., Overkleeft, H. S. and van Boom, J. H. *Tetrahedron Lett*. **43**, 7809-7812 (2002).
4. de Visser, P. C., van Helden, M., Filippov, D. V, Noort, D., van der Marel, G. A., Overkleeft, H. S., Drijfhout, J. W. and van Boom, J. H *manuscript in preparation*.
5. A reagent to introduce FZ-tag and advanced intermediates for the preparation of fluorous tagging reagents can be obtained from Fluorous Technologies Inc. (www.fluorous.com).

Peptide Revolution: Genomics, Proteomics & Therapeutics
Michael Chorev & Tomi K. Sawyer (Editors)
American Peptide Society, 2003

Novel Targeting Strategy Based on Multimeric Ligands for Drug Delivery and Molecular Imaging: Homo-oligomers of α-MSH

Josef Vagner[1], Heather L. Handl[2], Robert J. Gillies[2] and Victor J. Hruby[1,2]

[1]Department of Chemistry, University of Arizona, Tucson, AZ 85721 USA; [2]Department of Biochemistry and Molecular Biophysics, University of Arizona HSC, Tucson, AZ 85724 USA

Introduction

Multivalent interactions are characterized by the simultaneous binding of an entity that displays multiple copies of a molecular recognition element to multiple receptors contained on another entity. Multivalent ligands are important features of molecular recognition, as cells often encounter naturally ocurring multiple arrays [1]. By combining multiple specific ligands into a single molecule, it is possible to create compounds that will selectively bind to cells bearing the appropriate mix of complementary receptors [2]. Representative examples of multimeric interactions are pentavalent ligands that target the enterotoxin LT-1 [3], and peptide ligands ([Nle^4, DPhe^7]α-MSH), dynorphin and substance P attached to polyvinylalcohol [4].

Results and Discussion

We describe here the stepwise, solid-phase synthesis and characterization of MSH-fragment homomultimers. To initiate a systematic study of multimeric interactions, we chose to evaluate binding of α-melanocyte stimulating hormone (α-MSH) to the human melanocortin receptor [5]. Residues in the β-turn region 6-9 (His-Phe-Arg-Trp) are critical for agonist activity. By replacing the Met with Nle and the Phe with a DPhe, potent analogs were obtained [6]. We selected the tetrapeptide and the hexapeptide (Tables 1 and 2); these compounds have low nanomolar binding activity while still maintaining the opportunity to detect enhancement of avidity through oligomerization.

Individual ligands were tethered with various spacers of different length and rigidity, and the influence of spacers on the binding was studied. The spacer should not interfere with the binding, and preferably should be both hydrophilic and small. As an obvious choice we included PEG-diamine succinic acid spacers (PEG-Su-19, $H_2NCH_2[CH_2CH_2O]_3CH_2CH_2CH_2NHCOCH_2CH_2COOH$ and similar PEG-Su-14, $H_2N[CH_2CH_2O]_2CH_2CH_2NHCOCH_2CH_2COOH$). The combination of PEG with polyamide chains may serve as a tool for fine-tuning spacer properties.

Binding assays were performed on Hek293 cells transfected with hMC4R. As expected, the binding affinities of the hexapeptides were greater than those of the tetrapeptides. Compound **4** displayed a low EC_{50} value, indicating that a rigid linker with a length of **7** atoms is optimal for this set of dimers. The AMB family of linkers provides interesting results in terms of linker rigidity and its effects on ligand binding. Compounds **6** and **7** both have a linker length of 14 atoms, but compound **7**, with its more rigid AMB linker, has a binding affinity about two-fold greater than **6**, containing a flexible PEG linker. In agreement with this trend, compound **10**, with the longer AMB linker has enhanced affinity compared to compounds **9** and **11**, both of similar length.

Evaluation of the Hill coefficients resulting from ligand binding provides added evidence that our multimeric ligands bind with cooperative affinity.

*Table 1. Binding affinities of Ac-His-DPhe-Arg-Trp-**Spacer**-His-DPhe-Arg-Trp-NH_2.*

Compound	Spacer[a]	Length[b]	EC_{50} (nM)	Hill Coeff.
1	No spacer	0	264	0.9
2	βAla	4	119	1.39
3	AMB[c]	7	38	1.05
4	Pro-Gly-Pro	9	14	0.84
5	βAla-Gly-βAla	11	143	0.99
6	PEG-Su-14	14	234	1.10
7	$(AMB)_2$	14	123	1.12
8	$(βAla\text{-}Gly)_2$-βAla	18	231	1.09
9	PEG-Su-19	19	662	1.83
10	$(AMB)_3$	21	164	1.05
11	$(βAla\text{-}Gly)_3$-βAla	25	571	0.88

*Table 2. Binding affinities of Ac-Nle-Glu-His-DPhe-Arg-Trp-**Spacer**-Nle-Glu-His-DPhe-Arg-Trp-NH_2.*

Compound	Spacer[a]	Length[b]	EC_{50} (nM)	Hill Coeff.
12	βAla-Gly-βAla	11	7	0.91
13	PEG-Su-14	14	9	1.23
14	PEG-Su-19	19	33	1.59
15	(PEG-Su-19)	38	122	0.97

Table 3. Binding Affinities of Homotrimers of α-MSHTetrapetides.

Ac-His-DPhe-Arg-Trp-**Spacer**-Lys(Ac-His-DPhe-Arg-Trp)-**Spacer**-His-DPhe-Arg-Trp-NH_2

Compound	Spacer[a]	Length[b,d]	EC_{50} (nM)	Hill Coeff.
16	βAla	11-11-11	15	1.13
17	βAla-Gly-βAla	18-25-18	24	1.56

[a]Spacer is incorporatee via amide bond. [b]Length of spacer in atoms. [c]4-aminobenzoic acid. [d]Linker length in Table 3 are expressed as atom length between L1-L2.L1-L3. and L2-L3.

On average, the Hill coefficient for the tetrapeptide dimers is 1.12, while that for the trimers is 1.35. For the hexapeptide dimers, the average Hill coefficient is 1.18. The average Hill coefficient for monomers was 0.78. These oligoligands bind with enhanced affinity and apparent cooperativity compared to the monomers. The oligomeric ligands were synthesized by solid-phase technology [7].

Acknowledgements
This research was supported by NIH grant R21 CA95944 (RJG) and DK 17420 (VJH).

References

1. Mammen, M., Choi, S. K., Whitesides, G. M. *Angew. Chem. Int. Ed*. **37**, 2755–2794 (1998).
2. Gillies, R. J. and Hruby, V. J. *Expert Opinion on Therapeutic Targets* **2003**, **7**, 137–139.
3. Fan, E. K., Zhang, Z. S. et al. *J. Am. Chem. Soc.***122**, 2663–2664 (2000).
4. Sharma, S. D., Jiang, J. et al. *Proc. Natl. Acad. Sci. U.S.A.* **93**, 13715-13720 (1996).
5. Sawyer, T. K., et al. *Proc. Natl. Acad. Sci. U.S.A.* **77**, 5754-5758 (1980).
6. Hruby, V. J., Han, G. In Cone, R. D., Ed., *The Melanocortin Receptors* Humana Press Inc.: Totowa, Chapter 8, pp 239–261 (1997).
7. Krchnak, V. and Vagner, J. *J. Peptide Res.* **3**, 182 (1990).

Peptide Revolution: Genomics, Proteomics & Therapeutics
Michael Chorev & Tomi K. Sawyer (Editors)
American Peptide Society, 2003

P-BOP, a New Polymer-Supported Peptide Coupling Reagent

Sorin V. Filip[1], Valérie Lejeune[1], Jean-Pierre Vors[2], Jean Martinez[1] and Florine Cavelier[1]

[1]*University of Montpellier II, LAPP, UMR-CNRS 5810, CC19, 34095 Montpellier, France;*
[2]*Bayer CropScience, La Dargoire Research Centre, 14-20 rue Pierre Baizet, 69009 Lyon, France*

Introduction

In recent years, the benefits of performing organic synthesis using polymer-supported reagents have been fully recognized. Peptide synthesis also takes advantage of the emerging supported reagents, especially in those aspects regarding the formation of the amide bond.

BOP reagent (Castro's reagent) [1] has been reported as ideally suited for solid phase peptide synthesis and especially for the difficult coupling of α,α-dialkyl amino acids (*e.g.* Aib) [2]. In connection with our research directed towards developing new methodologies for the automated synthesis of peptides, we wish to report the synthesis and the use of a new polymer-supported peptide coupling reagent P-BOP (**2**).

Results and Discussion

P-BOP (**2**) was prepared by the reaction of commercially available P-HOBt (**1**) with 5 equiv. of bromotris(dimethylamino)phosphonium hexafluorophosphate (Brop) (Scheme 1).

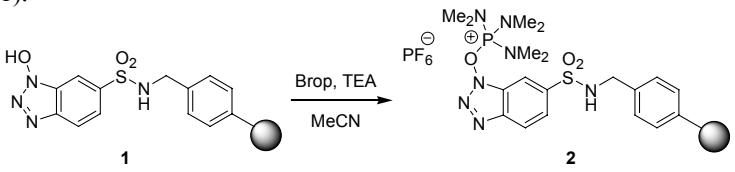

Scheme 1. Synthesis of the polymer-supported reagent P-BOP (2).

IR spectra of the resulting resin displays three new strong bands at 843 cm^{-1} (assigned to P-F), 1064 cm^{-1} and 1320 cm^{-1}, both corresponding to P-NMe_2. Gel Phase ^1H NMR of the resin in CD_2Cl_2 as solvent, shows the appearance of a broad single peak at 2.90 ppm, which was attributed to the N-Me groups. The elemental analysis indicates an increase of ca. 24% in nitrogen content, relative to the starting P-HOBt (**1**). The calculated N:S mol ratio for P-BOP (**2**) is 6.78:1, while for the P-HOBt (**1**) the N:S mol ratio is 3.98:1. The efficient resin loading was determined based on the synthesis of Fmoc-βAla-NHiPr (Scheme 2) and proved to be solvent dependent and slightly influenced by the nature of the base (Table 1).

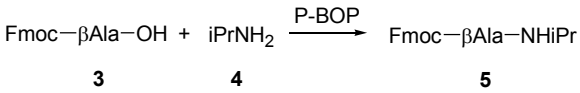

Scheme 2. Reaction used for loading determination of P-BOP (2).

*Table 1. Determination of P-BOP (**2**) loading.*

Entry	*Solvent*	*Base*	*Loading, mmol/g*
1	MeCN	Py	0.61
2	MeCN	TEA	0.60
3	DCM	Py	0.76
4	DCM	TEA	0.72

A series of dipeptides were prepared using P-BOP (**2**) as coupling reagent (Table 2), starting from *N*-protected amino acids and amino acid ester hydrochlorides, in the presence of an organic base.

*Table 2. Peptides prepared using P-BOP (**2**) as coupling reagent.*

Entry	*Peptide* [a]	*Solvent*	*Base*	*Yield, %* [b]
1	BocGly-PheOEt	MeCN	TEA	74
2	BocGly-PheOEt	MeCN	Py	68
3	BocGly-PheOEt	DCM	TEA	80
4	BocGly-PheOEt	DCM	Py	78
5	BzLeu-GlyOEt [c]	DCM	DIPEA	82
6	ZGlyPhe-ValOMe [d]	DCM : MeCN = 1 : 1	DIPEA	80
7	BocAib-PheOEt	DCM	TEA	75
8	BocAib-ValOMe	DCM	TEA	76

a) The reactions were performed at rt for 18 h. b) Isolated pure peptides.
c) Young's test: e.e. = 53%. d) Ateunis's test: no detectable epimerization (^{1}H NMR.)

The choice of DCM proved best with regard to resin swelling. The yields of isolated peptides were good and the levels of epimerization in Young's and Ateunis's tests (Table 2, Entries 5 and 6) were comparable to those reported in the literature [3]. Pyridine and TEA were tested as bases, and the last one afforded better yields. Contrary to the results reported with the polymer-supported TBTU reagent [3], good yields were obtained in reactions involving the sterically hindered Aib (Table 2, Entries 7 and 8).

In conclusion, P-BOP (**2**) is a promising new polymer-supported peptide coupling reagent, showing an acceptable degree of epimerization based on standard tests. Moreover, these preliminary results indicate that P-BOP (**2**) is also a suitable activating reagent for difficult peptide coupling reactions involving α,α-dialkyl amino acids.

References

1. Castro, B., Dormoy, J. R., Evin, G. and Selve, C. *Tetrahedron Lett.* **14**, 1219-1222 (1975).
2. Frérot, E., et al. *Tetrahedron* **47**, 259-270 (1991).
3. Chinchilla, R., et al. *Tetrahedron Lett.* **41**, 2463-2466 (2000).

Peptide Revolution: Genomics, Proteomics & Therapeutics
Michael Chorev & Tomi K. Sawyer (Editors)
American Peptide Society, 2003

New Approach for Peptide Ligation

Nan-Hui Ho, Ralph Weissleder and Ching-Husan Tung

Center for Molecular Imaging Research, Massachusetts General Hospital,
Harvard Medical School, Charlestown, MA 02129, USA

Introduction

Peptides and polypeptides have been widely used as diagnostic and therapeutic agents. It's well known that Tat peptide is an effective molecular transporter to carry drugs, such as peptide substrates, proteins or small molecules, across plasma membrane [1]. Solid-phase peptide synthesis has been proven to be useful in synthesizing such peptides, but there are still some limitations. Long peptides are typically challenging. Here we report a facile peptide ligation method to prepare functional active polypeptides. Peptide with bromo-reactive group was first synthesized using standard Fmoc chemistry. The peptide was then cleaved and deprotected simultaneously using TFA/anisole. The deprotected thiol-bearing peptide can be ligated efficiently with the bromoacetyl containing peptide in neutral aqueous condition. Using this approach, protease substrates with a membrane penetrating signal peptide were synthesized to study protease activity.

Results and Discussion

The polyarginine molecular transporter peptide (MTP), GRRRRRRRK, was synthesized using standard Fmoc chemistry. During solid phase synthesis, the bromoacetyl group was attached to the amino group on the C-terminal lysine side chain using symmetric anhydride of bromoacetic acid [2]. The bromoacetylated peptide appears to withstand the cleavage and deprotection condition with TFA/anisole (9:1, 2hrs). The major product is the desired bromoacetylated peptide, confirmed by RP-HPLC and MALDI-MS analysis. For model study of chemical ligation, the bromoacetylated MTP was rapidly coupled to a cysteine-bearing peptide, GSGRSLSRLTAGK(FITC)GGC-NH_2, to form stable thioether linkage in 0.1M $NaHCO_3$ at pH 8.3 characterized by RP-HPLC. To study the biological effect on chemical ligation, a coumarin analog, 7-amino-4-carbamoylmethylcoumarin (Acc) [3], was used as a fluorescence reporter. The first caspase-3 substrate peptide (Figure 1A) was synthesized using normal SPPS, and the second one was prepared using the ligation approach (Figure 1B). For both approaches, the bifunctional Acc was first attached to the Rink amide resin using standard Fmoc chemistry and followed with other standard amino acids. The probe **2** was prepared by

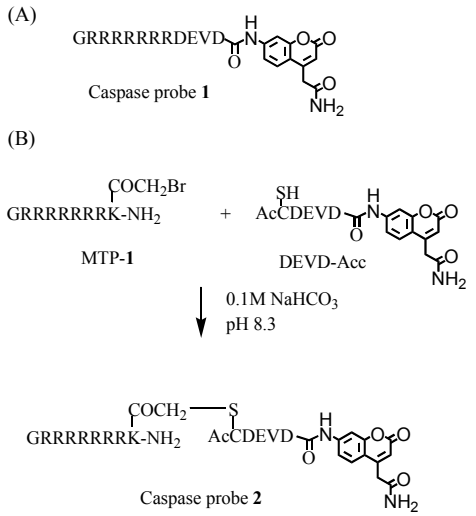

Fig. 1. Sequences and preparation of caspase probes.

ligating bromoacetylated peptide, MTP-1, and the cysteine containing caspase-3 substrate peptide, DEVD-Acc. The ligation reaction was complete in 2h as shown in RP-HPLC (Figure 2). After purification and characterization, the caspase-3 enzyme activity was measured by the release of Acc, with a 380 excitation and 450 nm emission. The caspase-3 substrate probes in assay buffer were incubated with 50 ng of active caspase-3. In 5 min, the fluorescence signal increased 24-fold with both probes. This experiment indicates that the rate of enzymatic hydrolysis of the ligated substrate is comparable to that of the analog prepared by conventional SPPS method.

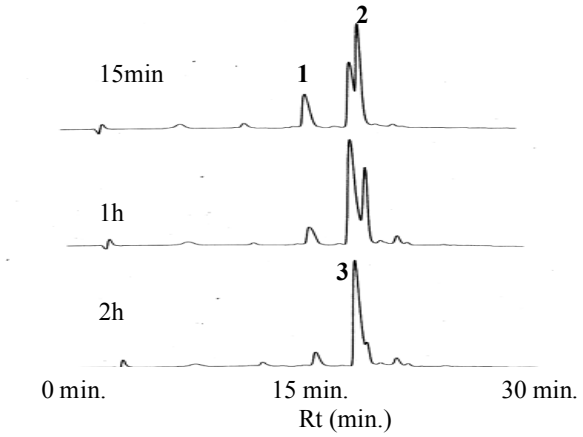

*Fig. 2. HPLC profiles monitoring the ligation between MTP **1** (peak 1) and DEVD-Acc (peak 2) to produce product Caspase probe **2** (peak 3) in the time course of 15 mins to 2h.*

In conclusion, we described a facile method of peptide ligation for preparing functional active cell-permeable peptide. The bromoacetylated peptide was prepared with conventional automated syntheses in good yield. This pre-prepared and shelf ready thio-reactive MTP can be rapidly coupled to any thio-bearing peptide. The reaction is site-specific and the thioether bond did not interfere with the biological activity of functional peptide module. To extend the utility of the method, investigation into preparation a polypeptide with three functionalized, unprotected peptide segments by a sequential thioether ligation is in progress.

References

1. Wender, P. A. et al. *Proc. Natl. Acad. Sci. U.S.A.* **97,** 13003-13008 (2000).
2. Robey, F. A. and Field, R. L. *Anal. Biochem.* **55**, 4-30 (2000).
3. Ellman, J. A. et al. *J. Org. Chem.* **67** (3), 910-915 (2002).

Peptide Revolution: Genomics, Proteomics & Therapeutics
Michael Chorev & Tomi K. Sawyer (Editors)
American Peptide Society, 2003

Comparison of Effect of Anionic Ion-Pairing Reagents on Capillary Electrophoresis and Reversed-Phase Chromatography of Cationic Random Coil Peptides

T.V. Popa[1], Colin T. Mant[2] and Robert S. Hodges[2]

[1]Department of Biochemistry, University of Alberta, Edmonton, Alberta T6G 2H7, Canada;
[2]Department of Biochemistry and Molecular Genetics, University of Colorado Health Sciences Center, Denver, CO 80262, USA

Introduction

The goal of complete characterization of complex mixtures of peptides and proteins, frequently a requirement of proteomics applications, depends on the availability of very powerful methods for peptide separations such as capillary electrophoresis (CE) [1] and RP-HPLC [2]. In addition, we believe a thorough assessment of the comparative utility of these techniques for peptide/protein analysis requires a comprehensive examination of the effect of varying conditions on the resolution of a mixture of peptides specifically designed for such a purpose (Table 1).

Table 1. Characteristics of synthetic peptide standards used in this study[1].

Peptide[2]	Peptide sequence	Mass	Nominal Charge
3a	*NH_2-*Arg-Gly-Gly-Gly-Gly-Leu-Gly-Leu-Gly-*Lys-amide	871	+3
3b	*NH_2-*Arg-Gly-Ala-Gly-Gly-Leu-Gly-Leu-Gly-*Lys-amide	885	+3
3c	*NH_2-*Arg-Gly-Val-Gly-Gly-Leu-Gly-Leu-Gly-*Lys-amide	913	+3
3d	*NH_2-*Arg-Gly-Val-Val-Gly-Leu-Gly-Leu-Gly-*Lys-amide	955	+3
2a	Ac-*Arg-Gly-Gly-Gly-Gly-Leu-Gly-Leu-Gly-*Lys-amide	913	+2
2b	Ac-*Arg-Gly-Ala-Gly-Gly-Leu-Gly-Leu-Gly-*Lys-amide	927	+2
2c	Ac-*Arg-Gly-Val-Gly-Gly-Leu-Gly-Leu-Gly-*Lys-amide	955	+2
2d	Ac-*Arg-Gly-Val-Val-Gly-Leu-Gly-Leu-Gly-*Lys-amide	997	+2
1a	Ac-Gly-Gly-Gly-Gly-Gly-Leu-Gly-Leu-Gly-*Lys-amide	814	+1
1b	Ac-Gly-Gly-Ala-Gly-Gly-Leu-Gly-Leu-Gly-*Lys-amide	828	+1
1c	Ac-Gly-Gly-Val-Gly-Gly-Leu-Gly-Leu-Gly-*Lys-amide	856	+1
1d	Ac-Gly-Gly-Val-Val-Gly-Leu-Gly-Leu-Gly-*Lys-amide	898	+1

*[1] The peptide order in the table is the same with peptide migration order in all electrophoretic separations, the group 3 peptide migrating first, and the group 1 peptides migrating last. The charged residues are marked by * and the substitutions relative to the --Gly-Gly-- sequence are underlined. Ac denotes Nα-acetyl; amide = Cα-amide.*

[2] The number in the peptide denotions refers to nominal positive charge; within each group of identically charged peptides, the letters "a", "b", "c" and "d" represent the same substitutions relative to the --Gly-Gly-- sequence at positions 3 and 4 of the sequence. In addition, within each peptide group, the hydrophobicity of the analogs increases in the order a<b<c<d.

Results and Discussion

From Table 1, each group of four peptides has the same positive charge (+1, +2 and +3) and length and differs only subtly in hydrophobicity within the four peptides. All three groups of peptides have just two properties by which a separation may be achieved by either CE or RP-HPLC: positive charge(s) that are independent of acido-

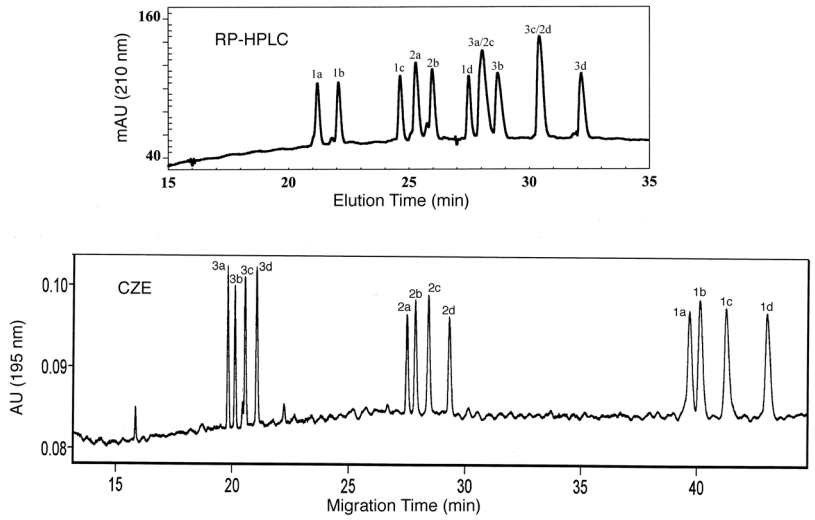

Fig. 1. Comparison of CE and RP-HPLC for separation of cationic peptide standards in the presence of hydrophobic anionic ion-pairing reagent. CE conditions: capillary, uncoated, 60.2 cm (50 cm effective length) x 50 μm I.D.; background electrolyte, 300 mM aq. HFBA, adjusted to pH 2.0 with LiOH; applied voltage, 25kV (direct polarity) with 5-min voltage ramp; temperature, 15°C; detection, UV absorption at 195 nm. RP-HPLC conditions: linear AB gradient (1% B/min) at a flow-rate of 0.3 ml/min on a Zorbax 300SB-C_8 column (150 x 2.1 mm I.D.; 5-μm particle size; 300-Å pore size), where eluent A is 25 mM aq. HFBA and eluent B is 25 mM HFBA in acetonitrile; temperature, 25°C; detection, UV absorption at 210 nm.

basic equilibria; and hydrophobic characteristics unable to induce charge variations (via pKa changes).

The peptide standards were subjected to CE, specifically capillary zone electrophoresis (CZE), and RP-HPLC in the presence of varying concentrations of trifluoroacetic acid (TFA), pentafluoropropionic acid (PFPA) and heptafluorobutyric acid (HFBA), a series of anionic ion-pairing reagents generally used for RP-HPLC peptide separations and increasing in hydrophobicity of the perfluorinated anion in the order $TFA^- < PFPA^- < HFBA^-$. Figure 1 represents the best separation achieved by either CZE or RP-HPLC. Clearly, for this mixture of peptide standards, RP-HPLC (with the separation based mainly on peptide hydrophobicity) could not match the excellent peak capacity achieved by CZE in the presence of HFBA (with separations based on both peptide charge and hydrophobicity).

Acknowledgments

This work was supported by NIH grant RO1GM61855 to R.S. Hodges.

References

1. Hu, S. and Dovichi, N. J. *Anal. Chem.* **74**, 2833-2850 (2002).
2. Mant, C. T., Hodges, R. S., in Gooding, K. M., Regnier, F. E. (Eds.), *HPLC of Biological Macromolecules,* Marcel Dekker, New York, NY, U.S.A., p. 433-511 (2002).

Peptide Revolution: Genomics, Proteomics & Therapeutics
Michael Chorev & Tomi K. Sawyer (Editors)
American Peptide Society, 2003

Synthesis of Peptide Thioesters by Masking as Trithioortho Esters in a Fmoc Backbone Amide Linker (BAL) Strategy

Jesper Brask[1,2,3], Fernando Albericio[2] and Knud J. Jensen[1]

[1]Department of Chemistry, Royal Veterinary and Agricultural University, 1871 Frederiksberg, Denmark; [2]Barcelona Science Park, University of Barcelona, 08028 Barcelona, Spain; [3]Department of Chemistry, Technical University of Denmark, 2800 Kgs. Lyngby, Denmark

Introduction

The development of efficient methods for covalent coupling of unprotected peptides (referred to as chemoselective ligation) has dramatically extended the reach of total chemical synthesis of proteins. In 'native chemical ligation,' originally developed by Kent and co-workers, a peptide thioester is reacted with a peptide carrying an *N*-terminal Cys moiety to provide a native amide bond connecting the two peptide segments. The often favored Fmoc/^{t}Bu strategy includes repeated treatment with piperidine which will aminolyze thioesters. Recently, several strategies for overcoming this obstacle to Fmoc based synthesis of peptide thioesters have been reported [1-6]. However, all these methods have inherent limitations (e.g., use of harsh alkylating agents, poor nucleophiles to remove the Fmoc group). Backbone amide linker (BAL) strategies provide general approaches to the synthesis of C-terminal modified peptides; a BAL strategy for the synthesis of C-terminal peptide thioesters has been reported [7]. Although this approach was successful in many cases, its scope was somewhat limited.

Corey reported in the 1970s that lactones could be masked as dithioortho esters to prevent nucleophilic attack on the carbonyl and that alkyl esters could be converted to thioesters or trithioortho esters [8,9]. Recently, Hilvert and co-workers reported an application of Corey's chemistry to the synthesis of peptide thioesters, starting from ester linked peptidyl resins [10,11].

Here we present a novel and safe strategy which, after standard Fmoc/^{t}Bu solid-phase synthesis and TFA deprotection/release, directly provides the peptide thioester (Scheme 1). The key element is anchoring of an amino trithioortho ester derived from Gly through an *o*-BAL handle to a solid support in the first step of the synthesis. Two tactics were developed: (*i*) synthesis of the Gly trithioortho ester in solution followed by anchoring through *o*-BAL [12], or (*ii*) first anchoring of a Gly ester to *o*-BAL followed by formation of the trithioortho ester on-resin. An additional advantage is that the trithioortho ester is not susceptible to nucleophilic attack and thus that formation of DKP at the dipeptide stage is avoided.

Results and Discussion

The trithiortho ester $H_2NCH_2C(SEt)_3$ HCl (**2**) was readily synthesized from a Gly ester. Reductive amination of *o*-PALdehyde-Tentagel resin with **2** proceeded with only 2 equiv in the presence of $NaBH_3CN$. Using standard protocols, the target sequence H-Phe-Val-Lys(Boc)-Glu(^{t}Bu)-Tyr(^{t}Bu)-Ala-N[$CH_2(SEt)_3$]-BAL-Ile-TG was obtained. Treatment with TFA-H_2O (19:1) released peptide thioester H-Phe-Val-Lys-Glu-Tyr-Ala-Gly-SEt (**2**) into solution (42% yield after prep. HPLC purification).

In the alternative approach, entirely on solid phase, the synthesis commenced with reductive amination of resin-bound *o*-PALdehyde with H-Gly-OMe HCl in DMF in the presence of $NaBH_3CN$. Next, the resin was treated with the aluminum reagent, preformed from $AlMe_3$ and EtSH, in CH_2Cl_2 under Ar for 18 h to give the BAL

anchored trithioortho ester. After chain assembly, peptide thioester **2** was obtained after acidolytic release from the support with either TFA-H_2O (19:1) or Reagent B. It is noteworthy that this approach was compatible with a variety of peptide side-chain functionalities, including ester moieties, as the on-resin reaction with the aluminum reagent was at the beginning of the synthesis and not on the fully protected peptide after chain-assembly.

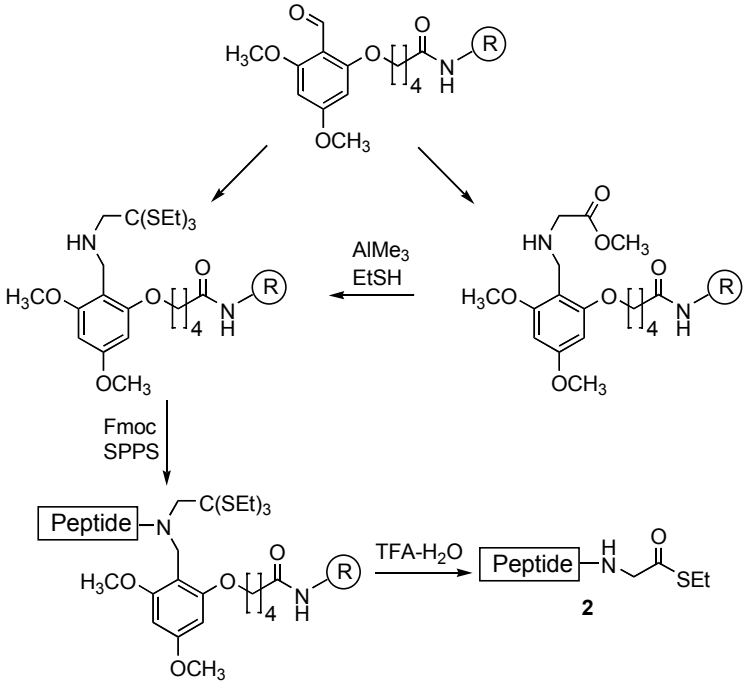

Scheme 1. Synthesis of peptide thioesters by masking as trithioortho esters.

References

1. Biancalana, S., Hudson, D., Songster, M. F. and Thompson, S. A. *Lett. Pept. Sci.* **7**, 291-297 (2001).
2. Ingenito, R., Bianchi, E., Fattori, D., Pessi, A. *J. Am. Chem. Soc*. **121**, 11369-11374 (1999).
3. Shin, Y., Winans, K. A., Backes, B. J., Kent, S. B. H., Ellman, J. A. and Bertozzi, C. R. *J. Am. Chem. Soc*. **121**, 11684-11689 (1999).
4. Li, X., Kawakami, T. and Aimoto, S. *Tetrahedron Lett.* **39**, 8669-8672 (1998).
5. Futaki, S., Sogawa, K., Maruyama, J., Asahara, T. and Niwa, M. *Tetrahedron Lett.* **38**, 6237-6240 (1997).
6. Jensen, K. J., Alsina, J., Songster, M. F., Vágner, J., Albericio, F. and Barany, G. *J. Am. Chem. Soc.* **120**, 5441-5452 (1998).
7. Alsina, J., Yokum, T. S., Albericio, F. and Barany, G. *J. Org. Chem*. **64**, 8761-8769 (1999).
8. Corey, E. J. and Beames, D. J. *J. Am. Chem. Soc.* **95**, 5829-5831 (1973).
9. Corey, E. J. and Kozikowski, A. P. *Tetrahedron Lett.* **38**, 925-928 (1975).
10. Swinnen, D. and Hilvert, D. *Org. Lett*. **2**, 2439-2442 (2000).
11. Sewing, A. and Hilvert, D. *Angew. Chem. Int. Ed.* **40**, 3395-3396 (2001).
12. Boas, U., Brask, J., Christensen, J. B. and Jensen, K. J. *J. Comb. Chem.* **4**, 223-228 (2002).

Peptide Revolution: Genomics, Proteomics & Therapeutics
Michael Chorev & Tomi K. Sawyer (Editors)
American Peptide Society, 2003

Multiple Condensations of Peptide Thioesters Prepared by the "Safety-Catch" Resin Approach: Synthesis of p53 (303-393)

Kenta Teruya, Sharlyn Mazur and Ettore Appella

National Cancer Institute, NIH, Bethesda, MD 20892, USA

Introduction

The tumor suppressor protein p53 plays a central role in the regulation of the cellular response to DNA damage through transcriptional activation or repression of specific genes and through specific protein-protein interactions [1]. These functions are potentiated by a complex signal transduction network that regulates phosphorylation and acetylation of at least 18 distinct sites on p53. p53 is regarded as a modular protein, consisting of transactivation, SH3, DNA binding, tetramerization and regulatory domains. The C-terminal domain corresponding to p53 (303-393), which contains the tetramerization and regulatory domains, also has the potential to bind specific DNA structures, such as supercoiled DNA [2]. The C-terminal domain contains seven sites of post-transcriptional modifications, including phosphorylation and acetylation. To investigate the effects of post-transcriptional modifications on the structure-specific DNA binding ability of the domain, we designed a chemical synthesis based on Fmoc chemistry [3, 4]. A synthesis of the p53 C-terminal domain was reported previously employing Boc-SPPS [5]. Recent investigations, however, revealed that some side reactions occurred during the cleavage step, especially for peptide thioester containing a phosphoryl group [6]. Because changes in amino acid sequence of p53 may affect its function and stability [7], we chose the thioester method, as it does not restrict, in principle, the residues that can be used for the condensation [8]. Multisegment coupling, involving two or more thioester condensations to construct the target protein, requires that the N-termini of internal segments be protected by a group orthogonal to the group used for side chain protection. For this purpose, the Fmoc group has been utilized in a Boc-SPPS based peptide thioester preparation [6]. However, the "safety-catch" linker approach [3], which is an Fmoc-SPPS based peptide thioester preparation method, exposes the intermediate to basic conditions during the cleavage step from the resin. We observed elimination of the Fmoc group in a preliminary experiment. Thus, an alternative protection strategy was required for the synthesis of p53 (303-393) in order to combine the thioester condensation with the "safety-catch" resin approach for peptide thioester preparation.

Results and Discussion

In this work, p53 (303-393) (Figure 1) was synthesized from three building blocks. A photolabile protecting group, 3,4-dimethoxy-6-nitrobenzyloxycarbonyl (NVOC) group [9], was used for the N-terminus protection of the middle block. Thus the three building blocks, Boc-[Lys(Boc)^{305,319,320,321}]-p53(303-325)-SBzl (**1**), NVOC-[Lys(Boc)^{351,357}]-p53(326-360)-SBzl (**2**) and [Lys(Boc)^{370,372,373,381,382,386}]-p53(361-393) (**3**), were prepared employing Fmoc chemistry [3]. The three segments correspond to the linker to DNA binding domain, the tetramerization domain and the regulatory domain, respectively.

Peptide thioester **2** and peptide **3** were condensed in the presence of silver nitrate, 3,4-dihydro-3-hydroxy-4-oxo-1,2,3-benzotriazine, and N,N-diisopropylethylamine to

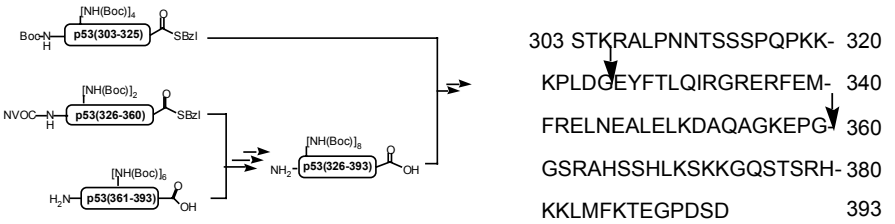

Fig. 1. Schematic drawing for the synthesis and the amino acid sequence of p53 (303-393). The two arrows in the sequence indicate the sites of segment condensation.

give NVOC-[Lys(Boc)^{351,357,370,372,373,381,382,386}]-p53(326-393), which was treated with trifluoroacetic acid and purified on RP-HPLC. After the purification, the side chain amino groups again were protected with the Boc group. The NVOC group was eliminated by UV irradiation (365nm, 1.3 mW/cm^2) for 90 min. in the presence of dithiothreitol to produce the building block for the last coupling. Peptide thioester **1** and peptide [Lys(Boc)^{351,357,370,372,373,381,382,386}]-p53(326-393) were condensed with the same procedure described above following TFA treatment to give the coupling product p53 (303-393).

C-terminal domains containing post-transcriptional modified p53 (303-393), [Ser^{315}(PO_3H_2)]-, [Lys^{320}(Ac),]- and [Ser^{378}(PO_3H_2)]-p53 (303-393), were also successfully synthesized following the procedure described above. Competition gel shift assay and Western blot analysis show specific binding of the peptide p53 (303-393) and its derivatives to supercoiled DNA. Phosphorylation of Ser378 enhances specific binding of the 326-393 peptide to supercoiled DNA.

In conclusion, p53 (303-393) and its derivatives were successfully synthesized from peptide thioesters prepared by Fmoc-based SPPS following successive thioester condensations. The NVOC group was stable during the preparation, condensation and side chain deprotections. In addition, no significant side reaction of the phosphoryl group during UV irradiation was observed.

References

1. Appella, E. and Anderson, C. W. *Eur. J. Biochem.* **268**, 2764-2772 (2001).
2. (a) Mazur, S. J., Sakaguchi, K., Appella, E., Wang, X. W., Harris, C. C. and Bohr, V. A. *J. Mol. Biol.* **22**, 241-249 (1999). (b) Brázdová, M., Palecek J., Cherny, D. I., Billová, S., Fojta, M., Pecinka, P., Vojtesek, B., Jovin T. M. and Palecek, E. *Nucleic Acid Res.* **30**, 4966-4974 (2002).
3. (a) Ingenito. R., Bianchi, E., Fattori, D. and Pessi, A. *J. Am. Chem. Soc.* **121**, 11369-11374 (1999). (b) Ingenito, R., Dreznjak, D., Guffler, S. and Wenshuh, H. *Org. Lett.* **4**, 1187-1188 (2002).
4. Hofmann, R. M. and Muir, T. W. *Curr. Opinion in Biotech.* **13**, 297-303 (2002).
5. (a) Hernandez-Boussard, T. Rodriguez-Tome, P., Montesano, R. and Hainaut P. *Hum. Mutat.* **4**, 1-8 (1999). (b) Davison, T. S., Nie, X., Ma, W., Lin, Y., Kay, C., Benchimol, S. and Arrowsimth C. H. *J. Mol. Biol.* **307**, 605-617 (2001).
6. (a) Hojo, H. and Aimoto, S. *Bull. Chem. Soc. Jpn.* **64**, 111-117 (1991). (b) Aimoto, S. *Biopolymers (Peptide Sci.)* **51**, 247-265 (1999).
7. Sakamoto, H., Kodama, H., Higashimoto, Y. Kondo, M., Lewis, M. S., Anderson, C. W., Appella, E. and Sakaguchi, K. *Int. J. Pept. Sci. Res.* **64**, 429-442 (1996).
8. Hasegawa, Sha, Y. L., Bang, J. K., et al. *Lett. in Pep. Sci.* **8**, 277-284 (2002).
9. Amit, B., Zehave, U. and Patchornik, A. *J. Org. Chem.* **39**, 192-196 (1974).

Peptide Revolution: Genomics, Proteomics & Therapeutics
Michael Chorev & Tomi K. Sawyer (Editors)
American Peptide Society, 2003

Base-Assisted Desulfurization: Synthetic Applications and Mechanistic Studies

Amit K. Galande and Arno F. Spatola˙

Department of Chemistry and the Institute for Molecular Diversity and Drug Design, University of Louisville, Louisville, KY 40292, USA, ˙deceased

Introduction

Constriction of a disulfide bridge under basic conditions in an aqueous environment is a long known but not a well investigated reaction. In the early 19th Century, desulfurization was observed in sulfur-rich proteins [1]. In most cases, a product of this desulfurization was a thioether containing amino acid, which in 1941 was termed 'Lanthionine' [2]. Interestingly, later it was realized that several sulfur-rich proteins undergo facile desulfurization but there are no reported examples of facile thioether formation from the action of alkali on small organic disulfides such as free cystine or its analogs [3]. No systematic study has been carried out in the case of peptides to determine whether the disulfide bond in short sequences can be transformed into thioether linkages under mild alkaline conditions. Accordingly, we have studied the effect of mild alkaline treatment (0.3% aqueous ammonium hydroxide) on a series of disulfide-bridged peptides and have realized synthetic utility and mechanistic details of this seemingly simple reaction.

Results and Discussion

We observed facile sulfur extrusion from a few disulfide-bridged peptides under mild alkaline conditions in an aqueous solution [4]. We postulated that this transformation goes through a β-elimination mechanism followed by Michael-addition, thus accomplishing thioether macrocyclization. Herein we have further explored the scope of this reaction using several different models of disulfide-bridged peptides. This reaction has been applied to peptides containing cysteine, homocysteine, and penicillamines to yield unusual amino acids: lanthionine, cystathionine, and penthionine, respectively (Figure 1).

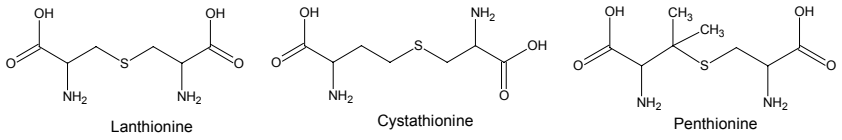

Fig. 1. Unusual thioether-bridged amino acids that can be incorporated into peptide chains using base-assisted desulfurization.

Initially we examined regioselectivity of the proton abstraction and stereoselectivity of the Michael-addition involved in this transformation. The stereochemical analysis (as assessed by TOCSY, HSQC and amino acid analysis experiments) revealed that in the case of lanthionine formation, the reaction shows lack of regioselectivity in proton abstraction as well as the lack of stereoselectivity in Michael-addition. Such an indiscriminate transformation yields three diastereomeric lanthionine peptides in the product mixture.

However, a significant synthetic application of this reaction emerges when one of the cysteines is replaced by a homocysteine. Such a Cys-Homocys disulfide combination shows not only regioselective proton abstraction, but also a stereoselective Michael-addition [5], yielding a single cystathionine containing peptide as a product (Figure 2). Cystathionine has been shown to be an isostere of a cystine disulfide bridge. Using the desulfurization reaction, we successfully incorporated cystathionine in several biologically active disulfide-bridged peptides such as enkephalin, RGD, and peptodomimetic estrogen receptor modulator (PERM) analogs.

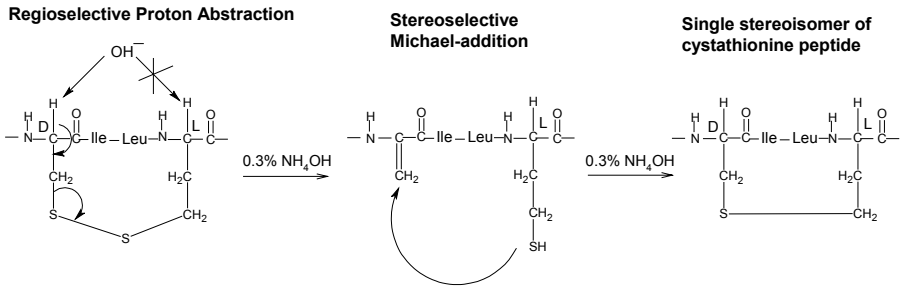

Fig. 2. Stereospecific cystathionine formation using base-assisted desulfurization.

Significantly, i, i+3 spaced cystathionine peptides, synthesized using base-assisted desulfurization showed higher helicity and bioactivity as compared to their disulfide counterparts. When one of the cysteines is replaced by penicillamine, the product peptide contains a β,β-dimethyl lanthionine analog, which we refer to as 'penthionine' (Figure 1). Presence of D amino acids (particularly D-Cys) facilitates desulfurization. Bulky residues within the disulfide bridge tend to hinder macrocyclization yielding dehydroamino acid containing products. Dehydroamino acids such as dehydroalanine and dehydrovaline have also been found from i, i+2 cystine and i, i+3 penicillamine containing disulfide-bridged peptides, respectively. The desulfurization reaction was successful for i, i+2 to i, i+4 disulfide bridges, but no upper limit was established. Amino acid configuration, disulfide ring size, position of the disulfide bridge, amino acids adjacent to and incorporated into the disulfide bridge, and peptide conformation are among the factors determining the product distribution and the facility of this reaction. Synthetically, the reaction can be used for making cyclic peptides incorporating redox stable thioether linkages and for making cyclic helical peptides.

References

1. Mulder, G. J. *Ann*. **28**, 73 (1838).
2. Horn, M. J., Jones, D. B. and Ringel, S. J. *J. Biol. Chem*. **138**, 141 (1941).
3. Danehy, J. P. (Ed.) *The Chemistry of Organic Sulfur Compounds*, Pergamon Press, NY,1966.
4. Galande, A. K. and Spatola, A. F. *Lett. Pept. Sci*. **8**, 247 (2001).
5. a.) Burrage, S., et al. *Chem. Eur. J*. **6**, 1455 (2000). b.) Okeley, N. M., et al. *Org. Lett*. **2**, 3603 (2000). c.) Polinsky, A., et al. *J. Med. Chem*. **35**, 4185, (1992). d.) Toogood, P. L. *Tetrahedron Lett.* **34**, 7833 (1993).

Peptide Revolution: Genomics, Proteomics & Therapeutics
Michael Chorev & Tomi K. Sawyer (Editors)
American Peptide Society, 2003

Stereospecific Synthesis of a Carbene-Generating Diazirine Phenylalanine: Non-Selective Photoaffinity Labeling of Angiotensin II Receptors AT_1 and AT_2

D. Fillion, M. Deraët and E. Escher

Department of Pharmacology, Université de Sherbrooke, Sherbrooke, Qc, J1H 5N4, Canada

Introduction

Photoaffinity labeling is the most widely used technique for direct mapping of ligand-receptor interfaces. This technique provides essential constraints for molecular modeling and applications ranging from rational drug design to analysis of metabolic and signal transduction networks. In the case of peptidergic G protein-coupled receptors (GPCR) such as the angiotensin II (AngII) receptors AT_1 and AT_2, which are not yet amenable to either NMR or X-ray analysis, photoaffinity and chemical labeling are among the only approaches for this purpose.

p-Benzoyl-*L*-phenylalanine (Bpa) is one of the most widely used photoprobes in receptor mapping [1]. Two important drawbacks of Bpa are: 1) relative bulky size which gives full antagonistic properties to ^{125}I[Sar^1,Val^5,Bpa^8]AngII on hAT_1 [2], thus reducing its pertinence for analysis of activated receptor structures; and 2) pronounced photolabeling selectivity for thiomethyl and thiomethylene moieties of Met residues in the receptor binding pocket, thus reducing considerably the precision of the photoprobe since Bpa photolabels selectively Met residues in a range of ~ 6-8 Å instead of the commonly accepted 3.1 Å [3]. Therefore, there is a need for less bulky and non Met-selective photoprobes, such as carbene-generating aryl-diazirines, for the purpose of investigating the exact contact point of activated hAT_1 receptor.

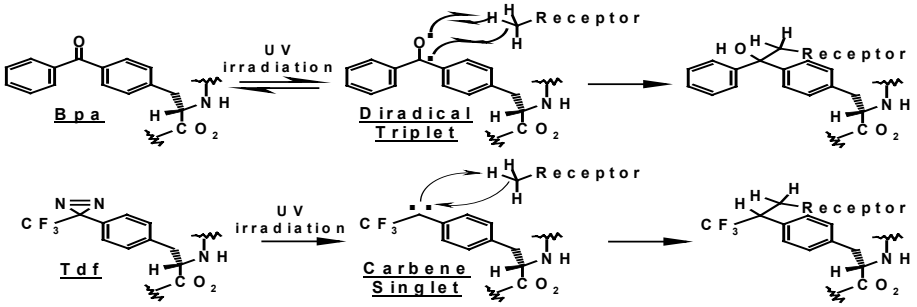

Scheme 1. Photolysis and photo-insertion of Bpa and Tdf.

Results and Discussion

Since prior litterature indicates that aryl-diazirinophenylalanine synthesis is not effective [4,5] and expensive [6], we have developed a total stereospecific synthesis of *N*-(9-fluorenyl)methoxycarbonyl-*p*-(3-trifluoromethyl-diazirin-3-yl)-L-phenylalanine (Fmoc-Tdf) in 10 convergent steps with an overall yield of 13%. Fmoc-Tdf was then incorporated by SPPS into AngII and radioiodinated to form pure ^{125}I[Sar^1,Val^5,Tdf^8]AngII.

The resulting synthetic peptide was used in a binding assay on transiently transfected COS-7 cells with the hAT_1-WT, hAT_2-WT, hAT_2-M128,138A and hAT_2-

M128,138L receptors. The peptide showed affinities of ~1 nM for all four transfected receptors which were similar to ^{125}I[Sar^1,Val^5,Bpa^8]AngII and to the endogenous AngII. Functional assays demonstrated the partial agonistic properties on hAT_1 of the Tdf analogue whereas the Bpa analogue was a pure antagonist [2]. To compare the labeling efficiency and the non Met-selectivity of ^{125}I[Sar^1,Val^5,Tdf^8]AngII with the previously utilized ^{125}I[Sar^1,Val^5,Bpa^8]AngII, we calculated the photoaffinity labeling yields of specific ligand-receptor interaction (Figure 1). Photoaffinity labeling experiments were carried out on the same four receptors. In hAT_1, the labeling contact is of non-Met nature (F^{293} and N^{294}) [7], whereas on hAT_2 it is on M^{128} and M^{138} [8].

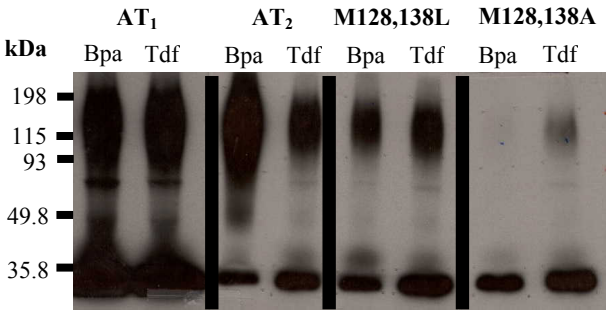

Fig. 1. Comparative Photo-affinity labeling of ^{125}I[Sar^1,Val^5,Bpa^8]AngII and ^{125}I[Sar^1,Val^5,Tdf^8]AngII on hAT_1-WT (AT_1), hAT_2-WT (AT_2), hAT_2-M128,138L (M128,138L) and hAT_2-M128,138A (M128,138A) receptors.

Both Bpa and Tdf photoprobes photolabel control hAT_1 with similar efficiency, whereas for hAT_2, Bpa has a photolabeling yield three times higher than Tdf, showing the Met-selectivity of Bpa. On the isosteric, non-Met mutant hAT_2-M128,138L, both photoprobes again have similar photolabeling yields, but for the second mutant hAT_2-M128,138A, Tdf has a photolabeling yield two-fold higher than Bpa, showing a more indiscriminate photolabeling behavior of the highly reactive carbene.

In conclusion, both Bpa and Tdf photolabels display comparable labeling efficiencies and, most importantly, Tdf labeling appears to be more reactive and free of Met-selectivity. This difference in reactivity and Met-selectivity can be explained by the Bpa diradical triplet forming a charge–transfer complex with thioether, thus stereochemically favoring γCH_2 or εCH_3 insertion in Met residue [9]. On the other hand, Tdf's highly reactive carbene appears not to form such a charge–transfer complex with the thioether. This greatly enhances Tdf's precision for exact contact point determination in peptide-receptor interactions, and renders possible the analysis of activated receptor structures such as in the AngII receptors AT_1 and AT_2.

Acknowledgments
The work was funded by the Canadian Institutes of Health (E. Escher).

References

1. Weber, P. J. A. et al. *J. Peptide Res.* **49**, 375-383 (1997).
2. Laporte, S. A. et al. *R. Mol. Pharmacol.* **49**, 89-95 (1996).
3. Rihakova, L., et al. *J. Recept. Signal. Transduct. Res.* **22**, 297-313 (2002).
4. Nassal M. *J. Am. Chem. Soc.* **106**, 7540-7545 (1984).
5. Shih, L. B., et al. *Anal. Biochem.* **144**, 132-141 (1985).
6. Fishwick, C. W. G., et al. *Tet. Lett*. **35**, 4611-4614 (1994).
7. Perodin, J. et al. *Biochemistry* **41**, 14348-14356 (2002).
8. Deraët, M., et al. *Can. J. Physiol. Pharmacol.* **80,** 418-425 (2002).
9. Bobrowski, K., et al. *J. Am. Chem. Soc.* **114**, 10279-10288 (1992).

Peptide Revolution: Genomics, Proteomics & Therapeutics
Michael Chorev & Tomi K. Sawyer (Editors)
American Peptide Society, 2003

ESR-Solvation Study of Different Amine Loaded and Cross-Linked Resins: Implication for Peptide Synthesis and Liquid Chromatography

Elias H. Silva[1], Erick F. Poletti[1], Marcia A. F. S. Neves[2], Fernanda M. B. Coutinho[2], Shirley Schreier[3] and Clovis R. Nakaie[1*]

[1]Department of Biophysics, Universidade Federal de São Paulo, Rua 3 de Maio 100, 04044-020, São Paulo; [2] Institute of Macromolecules-Universidade Federal do Rio de Janeiro; [3]Department of Biochemistry – Institute of Chemistry, Universidade de São Paulo, Brazil

Introduction

Following with our strategy for examining potentials of different polymeric materials, we have initially evaluated some physicochemical characteristics of benzhydrylamine-resin (BHAR) attaching different degrees of cross-linkage (divinylbenzene) and amine group content. Solvation properties of these BHAR batches, with amine function in deprotonated and protonated forms, were investigated through microscopic swelling measurement of beads sizes. The plot of swelling versus polarity of the medium using the alternative and more accurate amphoteric polarity scale [1,2] was determined aiming at search for the more appropriate solvation systems for each type of resin. In complement, the motion degree throughout the polymer network was also accessed through the EPR spectroscopy approach as previously reported [3-5], using the spin label amino acid TOAC (2,2,6,6-tetramethyl-1-oxyl-4-amino-4-carboxylic acid) [6]. The correlation between these properties and the applicability of these resins for use in peptide synthesis and anion exchange chromatography is described.

Results and Discussion

Starting from 1, 3, 8 and 12% divinylbenzene-containing copolymer of styrene, the corresponding BHAR batches were synthesized in forceful conditions to achieve as high as possible amine group incorporation. The corresponding substitution degrees obtained were 2.61, 2.44, 1.24, and 0.17 mmol/g, respectively for those copolymers, thus depicting that the yield of the benzhydrylamine incorporation varied inversely to the cross-linking degree of the polymer. The correlation between solvation of beads and the amphoteric (AN+DN) solvent polarity term [1] showed that when containing deprotonated amine groups, BHAR batches displayed maximum solvation region in apolar solvents characterized by solvents with (AN+DN) values lower than 20. Moreover, the lower the cross-linkage of resin, the higher the maximum swelling values achieved (about 80-90% of bead volume occupied by solvent). In contrast, the more rigidly structured 8% and 12% cross-linked BHAR presented maximum swelling values not higher than about 60%. Conversely and revealing potential for alternative use as anion exchanger resin, BHAR batches attaching high amount of positively charged ammonium groups (those with low cross-linkage degree) displayed maximum solvation region shifted to more polar region, i.e., solvents with (AN+DN) values higher than 40. Therefore, these resins should solvate reasonably well also in aqueous solution, thus permitting their test as anion exchange resins.

EPR experiments with TOAC-labeled 1% and 8% cross-linked BHAR showed different mobility patterns when solvated in diverse solvent systems. Owing to the higher rigidity of its matrix, the backbone mobility of the 8% cross-linked BHAR was

comparatively lower, estimated by the larger linewidth values of the mid-field peak in the EPR spectra. In addition, and stressing the relevance of copolymer matrix structural details for convenient application of innovative polymeric materials, a 2% cross-linked BHAR batch (2.45 mmol/g) was synthesized specifically to contain much larger beads than usual (diameters of about 300 μm). Preliminary studies depicted that this resin displays about 5-fold higher backbone mobility in comparison with the aforementioned BHAR batches.

In terms of biotechnological application, the 1 and 8% cross-linked BHAR were used for assembling model octapeptide angiotensin II (AII). Much higher synthesis yield (about 85%) was obtained with the 1% cross-linked BHAR, thus emphasizing the positive influence of the solvation characteristics of the resin matrix for this type of complex chemical process. Figure 1 reveals the HPLC profiles of crude AII synthesized in 1 and 8% cross-linked BHAR. In the latter resin, the synthesis yield was 35%.

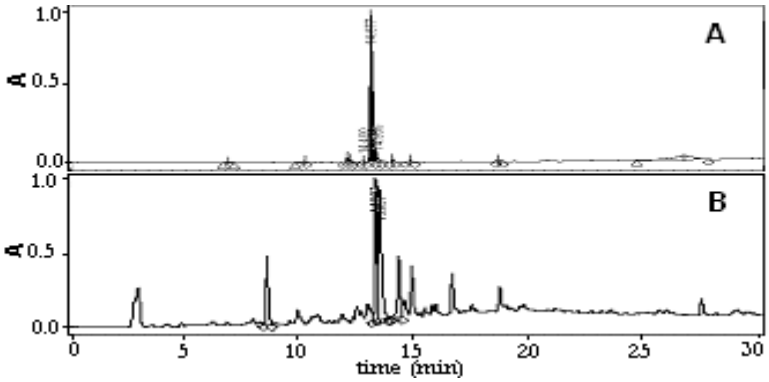

Fig. 1. HPLC profiles of AII synthesized in 1% (A) and 8% (B) cross-linked BHAR.

Comparative potentials for use as anion exchanger resin were also evaluated with the two cross-linked BHAR (1 and 8%). As expected, the former BHAR batch, attaching higher amount of positively charged amine groups (2.61 mmol/g) presented improved swelling in aqueous media (72%), in contrast to lower value measured for the 8% BHAR (42%). In agreement with these solvation values, the purification yield of negatively charged DEVYEHPF-amide (-1) and DEVYEDPF-amide (-3) peptides indicated that the 1% cross-linked BHAR functioned as a good anion exchanger resin, with chromatographic property equivalent to commercial anion exchanger supports. Amazingly, these findings demonstrate that peptide sequences can be synthesized and further purified in the same type of resin (*eg.,* 2.6 mmol/g 1% BHAR). And according to its poorer solvation and structural rigidity/porosity characteristics, the 8% BHAR did not show acceptable anion exchange capacity for 1 KDa peptide solutes.

Acknowledgments
This work was supported by FAPESP, CNPq and CAPES.

References

1. Cilli, E. M., Oliveira, E., Marchetto R. and Nakaie C. R. *J. Org. Chem.* **61**, 8992 (1996).
2. Malavolta, L., Oliveira, E., Cilli, E. M. and Nakaie, C. R. *Tetrahedron* **58**, 4383 (2002).
3. Cilli, E. M., Marchetto R., Schreier, S. and Nakaie C. R. *Tetrahedron Lett.* **38**, 715 (1997).
4. Cilli, E. M., Marchetto R., Schreier, S. and Nakaie C. R. *J. Org. Chem.* **64**, 9118 (1999).
5. Oliveira, E., Cilli, E. M., Miranda, A., et al. *Eur. J. Org. Chem*. 3686 (2002).
6. Marchetto R., Schreier, S. and Nakaie C. R. *J. Am. Chem. Soc.* **115**, 11042 (1993).

Peptide Revolution: Genomics, Proteomics & Therapeutics
Michael Chorev & Tomi K. Sawyer (Editors)
American Peptide Society, 2003

Asymmetric Syntheses of Enantiomerically Pure α,α-Dialkylated Glycines as Core Structural Units for Novel HIV-1 Protease Inhibitors

Tanaji T. Talele and Mark L. McLaughlin*

Department of Chemistry, University of South Florida, Tampa, FL 33620, USA

Introduction

The α,α-disubstituted glycines represent an important group of modified amino acids. In spite of the recent progress in the field of α,α-disubstituted amino acids, convenient and inexpensive preparative methods for enantiopure synthesis of these compounds are currently not available. Among the various methods available for the preparation of enantioenriched α-amino acids, those employing chiral glycine derivatives have been particularly successful. We were motivated by the work of Belokon and co-workers [1], who demonstrated the efficiency of Gly-Ni-BPB chiral auxiliary to produce α,α-dialkylated glycines. However, these authors including others [2,3] have maintained one of the alkyl groups as methyl in all of the published papers. Here we exploit this strategy for preparing enantiomerically pure sterically demanding α,α-dialkylated glycines.

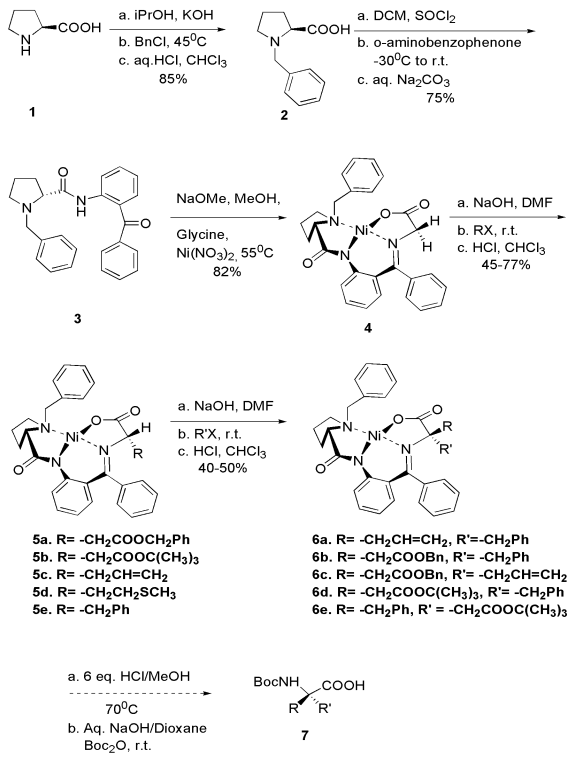

Scheme 1. Asymmetric sythesis of α,α-dialkylated glycines.

Results and Discussion

We report here the results of the use of Gly-Ni-BPB as chiral auxiliary for the synthesis of bulkier α,α-disubstituted amino acids. The Gly-Ni-BPB **4** was selected as a chiral equivalent for a nucleophilic glycine for the following reasons: a) –CH acidity of glycine methylene, which allows the use of bases like K_2CO_3, NaOH, and KOH for enolate formation, b) multigram scale availability, c) easy chromatographic separation of diastereomeric products, and d) simple recovery of chiral auxiliary. With these points in mind, we synthesized Gly-Ni-BPB template. It was successfully synthesized in three steps following the combined methodology discussed by Belokon *et al* [1] and Nadvornik *et al* [4]. Use of 1 eq of nickel nitrate afforded clean complex **4** in excellent yields as

compare to 2 eq of nickel salt (see Scheme 1). Next we replaced both of the glycine methylene protons with R groups with variable bulk in two steps. The results of alkyl halide addition to glycine enolate generated with strong bases such as potassium *tert*-butoxide, LiHMDS or LDA were discouraging. The highly acidic nature of the glycine methylene protons allowed us to carry out both alkylations using milder bases such as NaOH or KOH in DMF and results were excellent with these bases. The representative compound **6a** was obtained in 50% yields with greater than 90% diastereomeric excess (de) (Table 1). The diastereomeric excesses in the case of compounds **6b-e** ranged from 60 to 85%. Single-crystal X-ray analysis of the major diastereomer of allyl-benzyl-Ni-BPB **6a** confirmed its (R) absolute configuration (see Figure 1).

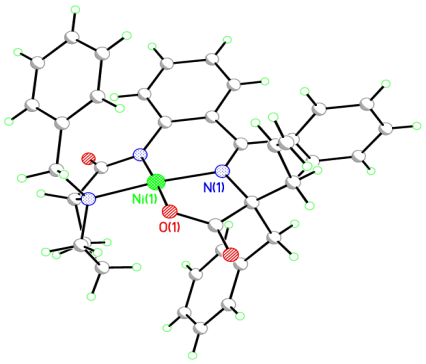

Fig. 1. X-ray crystal structure of complex 6a.

Table 1. Alkylation reactions with complex 4.

Compound	R	R'	yield (%)[a]
5a	$-CH_2COOBn$	H	55
5b	$-CH_2COOt$-But	H	52
5c	$-CH_2CH=CH_2$	H	77
5d	$-CH_2CH_2SCH_3$	H	45[b]
5e	$-CH_2Ph$	H	75
6a	$-CH_2CH=CH_2$	$-CH_2Ph$	50
6b	$-CH_2COOBn$	$-CH_2Ph$	46
6c	$-CH_2COOBn$	$-CH_2CH=CH_2$	40
6d	$-CH_2COOt$-But	$-CH_2Ph$	41
6e	$-CH_2Ph$	$-CH_2COOt$-But	Not isolated

[a]*Yields were based on isolated major diastereomer as minor diastereomers were obtained in insignificant amount as determined by TLC.* [b]*This compound was obtained by reaction of methionine with compound* ***3***.

Acknowledgement

We acknowledge financial support from PHS grants AG19981, AG1983, and AI054246.

References

1. Belokon, Y. N., et al. *Tetrahedron:Asymmetry* **9**, 4249-4252 (1998).
2. Nadvornik, M. and Popkov, A. *Green Chemistry* **4**, 71-72 (2002).
3. Soloshonok, V. A., Tang, X., Hruby, V. J. and Meervelt, L. V. *Org. Lett.* **3**, 341-343 (2001).
4. Qiu, W., Soloshonok, V. A., Cai. C., et al. *Tetrahedron* **56**, 2577-2582 (2000).

Peptide Revolution: Genomics, Proteomics & Therapeutics
Michael Chorev & Tomi K. Sawyer (Editors)
American Peptide Society, 2003

Preferred Conformation of C^{α}-Methyl, C^{α}-Cyclohexylglycine

Claudio Toniolo[1], Marco Crisma[1], Fernando Formaggio[1], Quirinus B. Broxterman[2] and Bernard Kaptein[2]

[1]Institute of Biomolecular Chemistry, CNR, Department of Organic Chemistry, University of Padova, 35131 Padova, Italy; [2]DSM Research, Life Science, Advanced Synthesis and Catalysis, P.O. Box 18, 6160 MD Geleen, The Netherlands

Introduction

Non-coded α-amino acids (in particular C^{α}-methylated α-amino acids) have increasingly attracted the attention of chemists interested in designing and synthesizing novel constituents of potentially bioactive, conformationally constrained peptides [1]. To gain a deeper understanding of the sub-class of C^{α}-methylated, C^{β}-branched (C^{β}-*tri*substituted) α-amino acids [1] [we have already investigated the (αMe)Val and (αMe)Dip residues], and to offer new tools to peptide chemists for the control of conformation we embarked on a program directed toward the first 3D-structural characterization of peptides based on (αMe)Chg. More specifically, we examined a homo-oligomeric series (to the tetramer level) and oligopeptides in which L-(αMe)Chg, produced by DSM Research, is combined with either Aib or Gly (to the pentamer level).

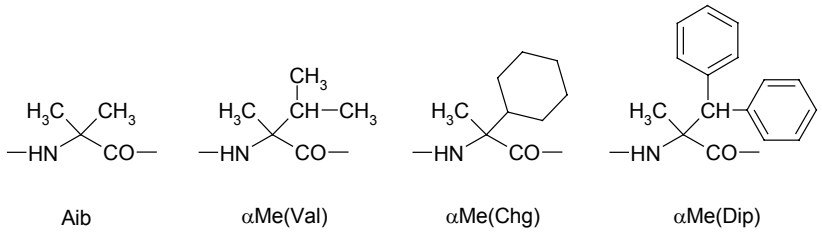

Results and Discussion

In this work we have been able to synthesize step-by-step in solution, either by the acyl fluoride or the EDC/HOAt C-activation method, oligopeptides based on the sterically demanding (αMe)Chg residue. We have also shown that in tri- and longer peptides in a structure supporting solvent ($CDCl_3$) by FT-IR absorption and ^1H NMR, as well as in the crystal state by X-ray diffraction, this C^{α}-methylated, C^{β}-trisubstituted α-amino acid is an efficient β-turn and 3_{10}-helix promoter, as strong as the structurally related (αMe)Val residue (Figure 1). Furthermore, both *L*-(αMe)Val and *L*-(αMe)Chg residues tend to favour *right*-handed turns and helices, analogous to the stereopropensity of protein amino acids. However, these conformational conclusions are partially at variance with the tendency of the aromatic (αMe)Dip, also a C^{α}-methylated, C^{β}-trisubstituted residue, known to extensively promote both folded and fully-extended structures to a remarkable extent. As this latter conformational versatility is shared by C^{α}-methyl, C^{α}-phenylglycine [1], an aromatic, C^{α}-methylated, C^{β}-*tetra*substituted amino acid, the results described here confirm the hypothesis that it is the aromatic character and/or its related steric hindrance, not the degree of C^{β}-substitution, that directs the structural bias of this class of C^{α}-methylated α-amino acids.

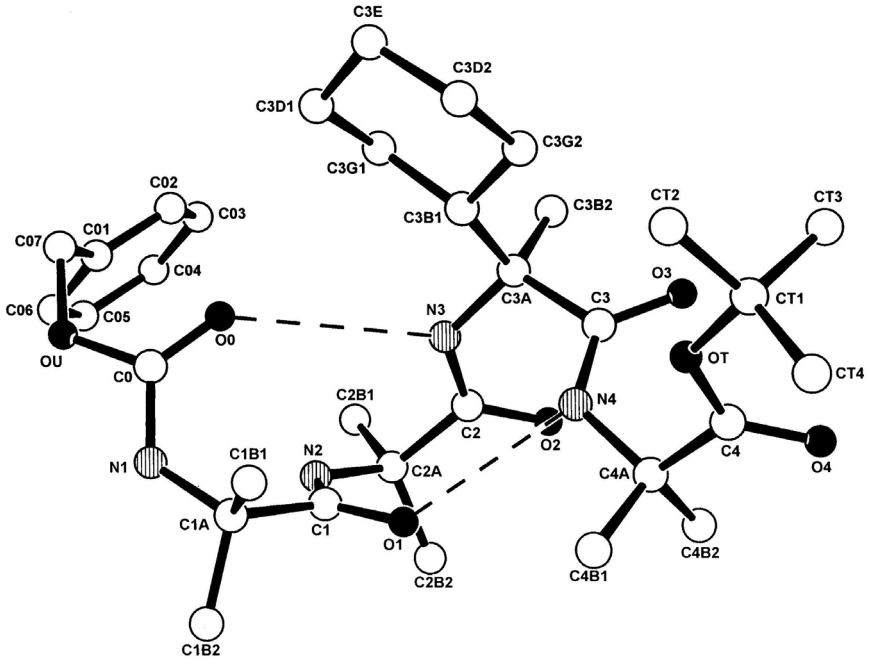

Fig. 1. X-Ray diffraction structure of Z-(Aib)$_2$-L-(αMe)Chg-Aib-OtBu [only the most populated of the two positions for the L-(αMe)Chg side chain is shown]. The terminally protected tetrapeptide is folded in a right-handed, incipient 3_{10}-helical structure.

Bearing in mind the quite limited conformational space explorable by *L*-(αMe)Chg, it is our contention that its homo-peptide foldameric series undoubtely represents one of the best rigid (but easily tunable) molecular ruler systems for physico-chemical investigations.

References

1. For a recent review-article, see: Toniolo, C., Crisma, M., Formaggio, F. and Peggion, C. *Biopolymers (Pept. Sci.)* **60**, 396-419 (2001).

Peptide Revolution: Genomics, Proteomics & Therapeutics
Michael Chorev & Tomi K. Sawyer (Editors)
American Peptide Society, 2003

Side Reactions During Peptide Cyclization

Haim Tsubery[1], Tali Scherf[2] and Mati Fridkin[1]

[1]Department of Organic Chemistry; [2]Department of Chemical Research Support, The Weizmann Institute of Science, Rehovot, 76100, Israel

Introduction

Polymyxin B nonapeptide (PMBN, Figure 1) is a cyclic antimicrobial peptide obtained from Polymyxin B by proteolytic removal of its terminal amino acyl residue. PMBN is composed of a positively charged cyclic peptide ring and a short linear tail. The cyclic part is a seven-member amino acids ring containing four α,γ-diaminobutyric acid residues (Dab), one Thr residue and a hydrophobic segment of dPhe-Leu. Thus, the C-terminal Thr^9 is forming an amide bond with the γ-amino group of Dab^3. The linear N-terminal region is composed of Thr-Dab moiety. In order to establish a convenient, general, efficient and rapid method for the synthesis of PMBN analogs, three routes for the synthesis of PMBN have been evaluated. Here we describe the occurrence of two side reactions; one involves the amino moiety in an intermolecular reaction and the other occurs on the carboxyl moiety through an intramolecular reaction.

H-Thr^1-Dab^2-*cyclo*[Dab^3-Dab^4-$dPhe^5$-Leu^6-Dab^7-Dab^8-Thr^9]

Fig. 1. The sequence of PMBN.

Results and Discussion

Three synthetic routes were evaluated for the synthesis of PMBN. One of the synthetic routes (Figure 2, A) involved linear chain assembly on a solid support followed by solution cyclization, whereas the second (Figure 2, C) was based on cyclization on the solid support. The first method afforded the expected PMBN, characterized by the desired calculated mass and amino acid contents (Table 1, A) and by HPLC-identity with PMBN obtained via proteolysis of natural polymyxin B. However, a major by-product, presumably a result of β-elimination reaction of the C-terminal Thr(tBu)-OH residue (i.e., α-amino crotonic acid derivative **1**, Figure 2, A) accompanied the desired product [2]. An alternative route (not shown) in which the tBu protecting groups were removed prior to the cyclization reaction step minimized the β-elimination reaction and afforded the desired PMBN in high yield (Table 1, B) [1].

In an attempt to confirm our observation, a two-dimensional ^{1}H-NMR study was performed. The fingerprint region of two-dimensional TOCSY spectra of the two products (PMBN and **1**) was measured in H_2O/D_2O (90/10; v/v) at pH 4.98, 298K on Bruker DMX-500. A comparison of the spectra reveals a major change in the chemical shift of the amide proton of Thr^9 of the peptides (7.8 and 8.5 ppm for PMBN and **1**, respectively), implying a significant change in its chemical environment i.e. modification at the Thr residue side chain. Further NMR study is currently being performed.

An additional synthetic route in which peptide cyclization was performed on the solid support (Figure 2, C) was initiated by coupling a dipeptide, i.e., Fmoc-Dab-Thr(tBu)OtBu, to benzylchloroformate resin. The final cyclization reaction was performed on the resin-bound peptide using either HATU or PyBOP as reagents. Cyclization with HATU afforded, in addition to PMBN, a by-product identified as a

tetramethylguanidinium (Tmg) derivative of Dab[3] resulting from a transfer of Tmg moiety from HATU to the γ-amine of Dab[3] (Table 1, C) [3]. However, cyclization with PyBOP led to the desired PMBN product (Table 1, C).

Table 1. Analysis of PMBN synthesis products.

Route	Cyclization coupling reagent	Yield (%)[a]	t_R.[b] (min)	ESMS found (calcd)	Amino acid composition [c]
A	PyBOP/HOBT	30	24.5	963.6 (962.8)	T 1.7, L 1, X 4.7, F 0.9
		54	24.9	963.6 (962.8)	T 0.9, L 1, X 4.7, F 0.9
B	PyBOP/HOBT	90	24.5	963.6 (962.8)	T 1.8, L 1, X 4.9, F 0.9
C	PyBOP/HOBT	95	24.5	963.6 (962.8)	T 1.7, L 1, X 4.9, F 0.9
	HATU/HOBT	55	24.1	1080.5 (1079.7)	T 1.8, L 1, X 4.1, F 0.9
		41	24.5	963.6 (962.8)	T 1.8, L 1, X 4.9, F 0.9

[a]*According to analytical HPLC.* [b]*Retention time according to analytical HPLC on RP-18 column.* [c]*Observed values for calculated: T (2), L (1), X=Dab (5), F (1).*

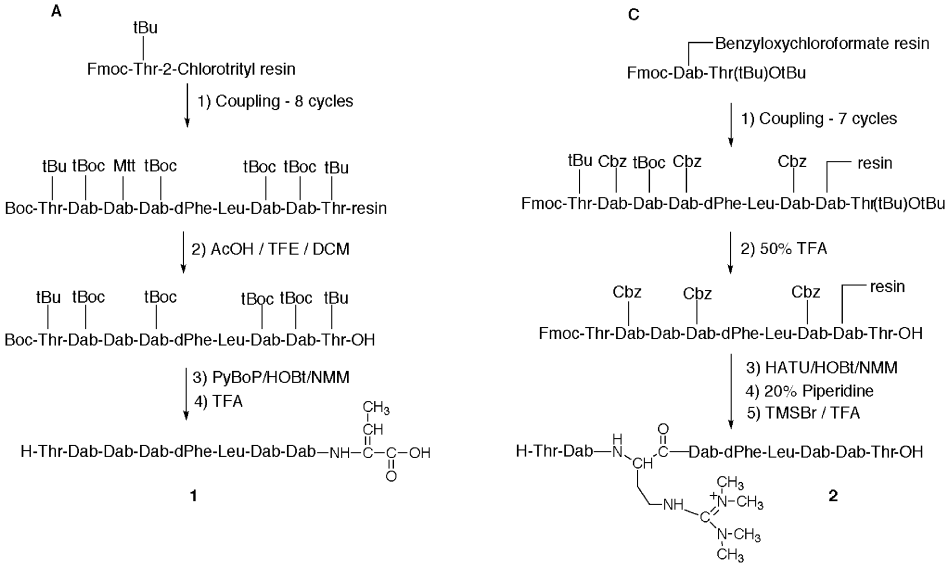

*Fig. 2. Major products α-amino crotonic acid derivative (**1**) and Tmg peptide derivative (**2**) obtained in two synthetic routes for PMBN.*

References

1. Tsubery, H., Ofek, I., Cohen, S. and Fridkin, M. *J. Med. Chem.* **43**, 3085-3092 (2000).
2. Chino, N., Kimura, T. and Sakakibara, S. *The 1st Akabori Conference, Max Planck Institute for Biochemistry, Martinsried, Germany* (1985).
3. Story, S. C. and Aldrich, J. V. *Int. J. Pept. Protein Res.* **43**, 292-296 (1994).

Peptide Revolution: Genomics, Proteomics & Therapeutics
Michael Chorev & Tomi K. Sawyer (Editors)
American Peptide Society, 2003

Specificity of PDZ Interaction Using NMR Spectroscopy and Spot Synthesis

Prisca Boisguérin[1], Rainer Leben[1], Rudolf Volkmer-Engert[1], Jens Schneider-Mergener[1] and Hartmut Oschkinat[2]

[1]Institute of Medical Immunology, University Clinic Charité, Humboldt University of Berlin, Berlin, 10117, German; [2]Institute of Molecular Pharmacology, Berlin, 13125, Germany

Introduction

PDZ domains are modular protein interaction domains that bind to short C-terminal peptides [1] as well as to internal peptides folded as a finger in a sequence-specific manner. The protein AF6 contains a single PDZ domain and has been described first as a fusion protein of ALL-1 in acute myeloid leukemia [2]. It has been demonstrated that the PDZ domain of AF6 interacts with several members of the Eph receptor family of tyrosine kinases (RTKs) via their C-termini [3].

PDZ domains are classified into two major categories based on their target sequence specificity. Class I domains bind to peptides with the consensus motif X-[S,T]-X-Φ_{COOH}, whereas class II domains recognize the motif X-Φ-X-Φ_{COOH}. The residues at position 0 and -2 of the peptide (position 0 referring to the carboxyl-terminal residue) play a critical role in the specificity and the affinity of the interaction. However, the structural determinants of ligand selectivity by PDZ domains are more complex than initially thought, suggesting an intrinsic flexibility in these modules to accommodate both polar and non-polar side chain at position -2.

Spot synthesis [4] with the method of the inverted peptides [5] allowed the characterization of the amino acids positions of the AF6 PDZ domain ligands. Substitutional analyses of the four different peptides, in which each position was exchanged by all 20 natural amino acids, reveals that the four C-terminal positions are key residues for binding.

The NMR measurements (e.g. ^{15}N-HSQC) enable the mapping of the PDZ-binding sites for the four same peptides used in the substitutional analyses. The successive titration of the peptides to the ^{15}N labelled PDZ domain showed chemical shifts of the PDZ domain amino acids that are involved in the interaction with the ligand.

Both methods suggest that the AF6 PDZ domain bind as well to ligand class I (X-[S,T]-X-Φ_{COOH}) as to class II (Φ-X-Φ_{COOH}).

Results and Discussion

In order to determine the binding specificity of the AF6 PDZ domain we examine the interactions of four different synthetic peptides with free C-termini using NMR spectroscopy and spot synthesis. We choose EPB2 [AQMNQIQSVEV$_{COOH}$] and EPA7 [MLHLHGTGIQV$_{COOH}$] with a hydrophobic amino acid at position -2 (class II) and two peptides with a serine / threonine at this position (class I), like CIN4 [TVRPGVKESLV$_{COOH}$] and FXI1 [GVLYPREGTEV$_{COOH}$].

From the substitutional analyses we can deduce the consensus motif [A, G, P, S, E]-[I, L, T, V]-X-V$_{COOH}$, preferring small amino acids at position -3. E is only allowed near a small amino acid like S at position -2. At the PDZ class specific location (position -2) hydrophobic amino acids are required to make contacts with A (αB:705) and M (αB:708). But also T and S are allowed at this position. They are able to form hydrophobic contacts with their methylen group whereas their hydroxyl group point out

of the solvent. These results are in agreement with the NMR measurements and the resulting surface mapping of the PDZ domain which show similar chemical shifts in the same binding region. The strongest chemical shifts are located in the typical binding pocket of the PDZ domain formed by the GLGF-loop, the αB-helix and the βB-strand. Also the Kd values, which are all in a micromolar range, indicate no special preference for one of the four ligands.

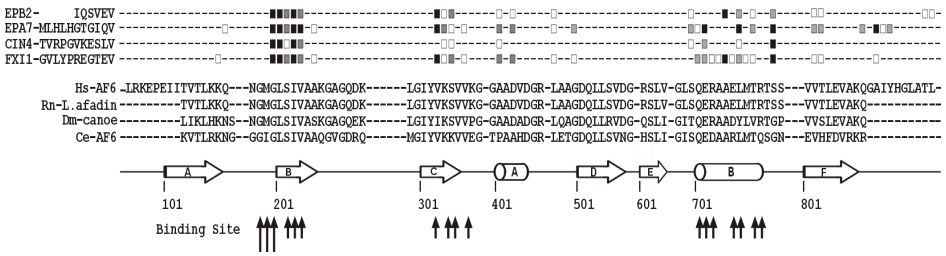

Fig. 1. Comparison of sequence of AF6 PDZ domain with homologous proteins and chemical shift changes results. Residues undergoing intermediate exchange upon peptide binding are indicated with black rectangles, strong chemical shift changes ($\Delta\delta$ > 0,140 ppm) are indicated with gray rectangles and moderate chemical shift changes ($\Delta\delta$ > 0,100 ppm) by white rectangles. The strongest chemical corresponding to the typical binding site of a PDZ domain.

The AF6 protein has no enzymatic activity and its PDZ domain only acts as an adaptor, bringing together receptors and signaling molecules in large molecular complexes. For this reason it is necessary that the PDZ domain is able to recognize a large scale of different ligands without being unspecific.

References

1. Songyang, Z., Fanning, A. S., Fu, C., Xu, J., Marfatia, S. M., Chishti, A. H., Crompton, A., Chan, A. C., Anderson, J. M. and Cantley, L. C. *Science* **275**; 73-77 (1997).
2. Prasad, R., Gu, Y., Alder, H., Nakamura, T., Canaani, O., Saito, H., Huebner, K., Gale, R. P., Nowell, P. C., Kuriyama, K., Miyazaki, Y., Croca, C. M. and Canaani, E. *Cancer. Res*. **53**, 5624 (1993).
3. Buchert, M., Schneider, S., Meskenaite, V., Adams, M. T., Canaani, E., Baechi, T., Moelling, K. and Hoven, C. M. *J. Cell. Biol.* **144** (2), 361-371 (1999).
4. Frank, R. *Tetrahedron* **48**, 9217-9232 (1992).
5. Licha, K., Bhargava, S., Rheinlaender, C., Becker, A., Schneider-Mergener, J. and Volkmer-Engert, R. *Tetrahedron Let.* **41**; 1711-1715 (2000).

Peptide Revolution: Genomics, Proteomics & Therapeutics
Michael Chorev & Tomi K. Sawyer (Editors)
American Peptide Society, 2003

NMP is Unsuitable as a Solvent for the Rapid Solid Phase Synthesis of $CGRP_{8-37}$ Using *in situ* Neutralization

Christopher K. Taylor[1], Peter W. Abel[1] and D. David Smith[1,2]

[1]Department of Pharmacology; [2]Department of Biomedical Sciences, Creighton University Medical Center, Omaha, NE 68178, USA

Introduction

Calcitonin Gene-Related Peptide (CGRP) is a 37-amino acid residue vasodilatory peptide that is produced from tissue-specific alternative splicing of the primary RNA transcript of the calcitonin gene. CGRP has a seven-residue N-terminal ring structure that includes a disulfide bridge between Cys^2 and Cys^7. Removal of the seven-residue N-terminal ring structure produces $CGRP_{8-37}$, a 30-amino acid residue competitive antagonist of CGRP (Figure 1). CGRP receptors have been classified into $CGRP_1$ and $CGRP_2$ subtypes on the basis of different potency of the competitive antagonist $CGRP_{8-37}$. $CGRP_1$ receptor-mediated responses are antagonized with high potency by $CGRP_{8-37}$ (K_B<100 nM), whereas $CGRP_2$ receptor-mediated responses are antagonized with low potency (K_B>1 mM). In the present studies we have examined the feasibility of rapid peptide synthesis method of Kent using Boc-chemistry and *in situ* neutralization of the growing resin-bound peptide chain [1] to synthesize $CGRP_{8-37}$. We report here the solvent requirements to achieve acceptable coupling yields.

CGRP ACDTACTVTHRLAGLLSRSGGVVKNNFVPTNVGSKAF-NH_2
$CGRP_{8-37}$ VTHRLAGLLSRSGGVVKNNFVPTNVGSKAF-NH_2

Fig. 1. Sequence of CGRP and $CGRP_{8-37}$.

Results and Discussion

We examined the effect of the solvents NMP, NMP/DMSO (8:2), DMSO, DMA and DMF on coupling yields for the rapid synthesis of $CGRP_{8-37}$. $CGRP_{8-37}$ was synthesized on a 0.1mmol scale using an MBHA resin (88.0 mg, 1.16 mmol/g). Boc-Phe (0.4 mmol) was activated for 2 minutes by addition of a 0.38 M solution of HBTU in the solvent used for synthesis (1.0 mL, 0.38 mmol) and DIEA (0.105 mL, 6.0 mmol) and coupled to the resin for 10 minutes. The Boc-protecting group was removed with neat TFA and subsequent amino acids were coupled to the resin in a similar manner. Coupling yields were determined by the quantitative ninhydrin test [2]. Peptides were cleaved from the resin, and side chain protecting groups simultaneously removed, using TFMSA by the method of Tam [3]. A sample of the crude cleavage product was dissolved in 5% acetic acid and analyzed by C_{18} RP-HPLC.

Surprisingly, low coupling yields were obtained using the solvents NMP, NMP/DMSO (8:2), DMSO and DMA. Using NMP, the lowest yield observed was 42% for the coupling of R^{20} to S^{21} (Figure 2) and the average coupling yield was 78.1% resulting in a failed synthesis (Table 1). Interestingly, extending the activation time to 5 minutes resulted in an average coupling yield of 61.9% and increasing the coupling time to 20 minutes resulted in an average coupling yield of 83.1%. In contrast, improved yields were obtained throughout the whole synthesis when DMF was used as the solvent. The lowest yield was 97.4% for coupling of L^{26} to R^{27} and the average coupling yield was >99%. In conclusion, DMF appears to be the only suitable solvent

for the rapid synthesis of $CGRP_{8-37}$ using Boc-chemistry and *in situ* neutralization solid phase peptide synthesis.

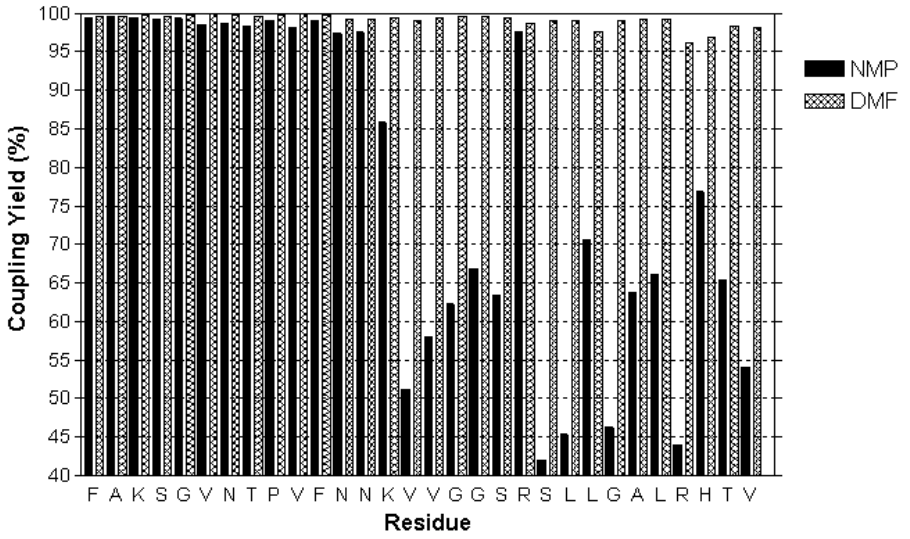

Fig. 2. Coupling yields per residue for the synthesis of $CGRP_{8-37}$ using the solvents NMP and DMF.

Table 1. Average coupling yields for the synthesis of $CGRP_{8-37}$ using various solvents as well as increased activation and coupling times.

Solvent System	Average Coupling Yields (%)
NMP	78.1
NMP, 5 minute Activation Time	61.9
NMP, 20 minute Coupling Time	83.1
NMP/DMSO (8:2)	88.9
DMSO	91.8
DMA	98.0
DMF	99.3[a], 99.5[b]

[a]*HBTU,* [b]*HCTU.*

Acknowledgments

The work was funded in part by an American Heart Association Pre-Doctoral Fellowship to C. K. Taylor.

References

1. Schnolzer, M., Alewood, P., Jones, A., Alewood, D. and Kent, S. B. H. *Int. J. Peptide Protein Res*. **40**, 180-193 (1992).
2. Sarin, V. K., Kent, S. B., Tam, J. P. and Merrifield, R. B. *Anal. Biochem*. **117**, 147-157 (1981).
3. Tam, J. P., Heath, W. F. and Merrifield, R. B. *J. Am. Chem. Soc*. **108**, 5242-5251 (1986).

Peptide Revolution: Genomics, Proteomics & Therapeutics
Michael Chorev & Tomi K. Sawyer (Editors)
American Peptide Society, 2003

Isocratic Reversed-Phase Chromatography Separation and Purification of Peptides

A.R. Mehok, C.T. Mant, B. Tripet and R.S. Hodges

Department of Biochemistry and Molecular Genetics, University of Colorado Health Sciences Center, Denver, CO 80262, USA

Introduction

The present study describes initial RP-HPLC approaches to purify two 25-residue peptides, identical in sequence except for methionine (Met) in one peptide and methionine sulfoxide (MetO) in the other. Such a mixture reflects a particularly difficult purification problem, which we encountered following peptide synthesis, since oxidation of Met to MetO is a relatively common undesirable side-reaction.

Results and Discussion

From Figure 1, the MetO-containing peptide represents an impurity of the native Met-containing peptide. Under these standard RP-HPLC conditions, the peptides are co-eluted. Under isocratic conditions of 31.5% aq. acetonitrile (6% below that of the elution concentration under gradient conditions), the peptides are first seen to be baseline resolved. Lowering the concentration to 29.5% aq. acetonitrile was deemed a good compromise between a reasonable run time and sufficient separation between the two peptides for scale-up purposes.

Ac - DEALLKRYRK EI **M** DLKKQLE EVSLE - Amide
Ac - DEALLKRYRK EI **M(o)** DLKKQLE EVSLE - Amide

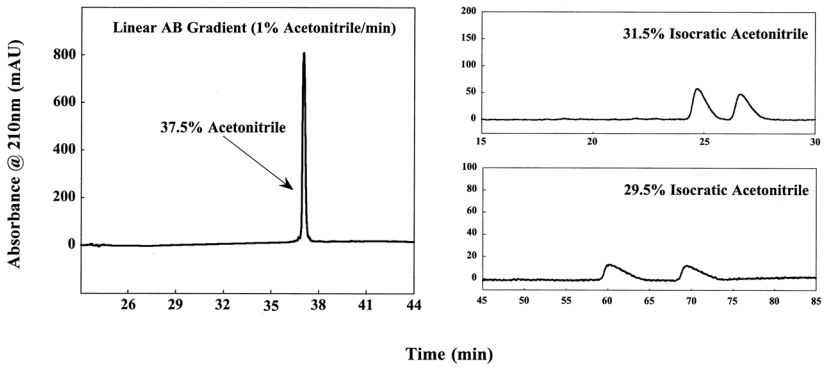

Fig. 1. Top: sequences of Met-containing native peptide and MetO-containing peptide. Left panel: analytical RP-HPLC profile of 1:1 mixture of the two peptides on a Kromasil C_{18} column (250 x 4.6 mm I.D.; 5-μm particle size; 300-Å pore size) using a linear AB gradient (1% B/min) at a flow-rate of 1 ml/min, where eluent A is 0.1% aq. trifluoroacetic acid (TFA), pH 2.0, and eluent B is 0.1% TFA in acetonitrile. Right panels: isocratic elution of 1:1 peptide mixture (25 μg) on the Kromasil column at 1 ml/min with 31.5% or 29.5% aq. acetonitrile containing 0.1% TFA, pH 2.0.

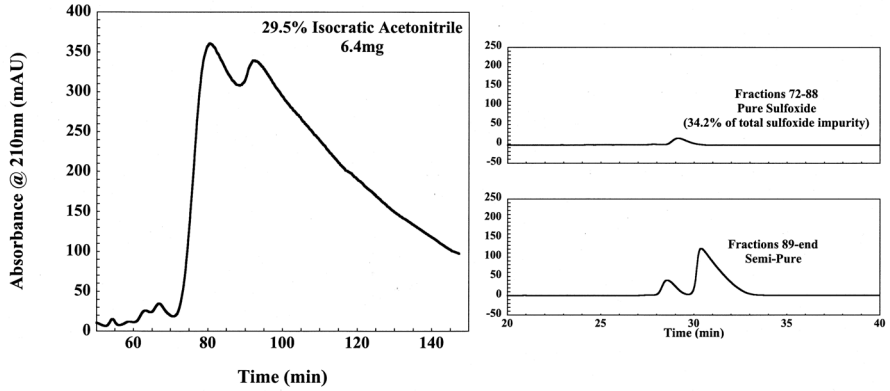

Fig. 2. Left panel: preparative isocratic elution at 2 ml/min of 6.4 mg of two-peptide mixture (1:3; MetO:Met) on a Zorbax SB300-C_8 column (250 x 9.4 mm I.D.; 5-μm particle size; 300-Å pore size) with 29.5% aq. acetonitrile containing 0.1% TFA. Right panels: analytical runs of purified sulfoxide-containing peptide (top) and semi-purified native peptide (bottom) (see Fig. 1, left panel, for conditions).

However, from Figure 2, even a relatively modest scale-up to 6.4 mg on a larger diameter column resulted in rapid loss of peptide resolution, with just 34.2% of the impurity being removed from the two-peptide mixture.

Due to the relatively low sample loads available, a multi-column sample displacement approach, with the major separation process taking place in the absence of organic modifier [1], was adjusted to effect a separation in the presence of an optimum acetonitrile concentration to enhance the partition rate and sample displacement effects at the sample loads available. At a loading of 15 mg of the two-peptide mixture (1:3, MetO:Met), a 20% acetonitrile concentration for 10 hours at 0.5 ml/min was still unable to separate the components through displacement with all the sample bound to the first (inlet) of three linked columns (4.6 mm I.D. x 50 mm x 3 Zorbax SB300-C_8 columns). Clearly, the correct combination of sample load and acetonitrile concentration (between 20%-29.5% in the present example) is critical for such difficult separations, and is presently under investigation.

Acknowledgments

The work was supported by an NIH grant RO1GM61855 to R.S. Hodges.

References

1. Hodges, R. S., Burke, T. W. L. and Mant, C. T. *J. Chromatogr*. **548**, 267-280 (1991).

Peptide Revolution: Genomics, Proteomics & Therapeutics
Michael Chorev & Tomi K. Sawyer (Editors)
American Peptide Society, 2003

New Technology Automates Sorting of Large, Bead-Based Combichem Libraries

K. Ver Donck[1], L. Bols[1], R. Bongaarts[1], P. Van Osta[1], A.J. Brouwer[2], R.M. J. Liskamp[2], D. Perrault[3], K. Kalutkiewicz[3], J.Geysen[1] and R. Pulak[3]

Union Biometrica, [1]Geel, BE, [3]Somerville, MA USA; [2]Utrecht University, Utrecht, NL

Introduction

Bead-based libraries in the drug discovery process are now more practical due to technology advances, including: increased sensitivity of single bead analysis with MS and NMR; availability of high capacity biocompatible beads; and the COPAS instrument for high speed analysis and sorting of a continuous flow of beads [1].

We used the COPAS flow sorting technology with a chemically synthesized random peptide library on beads in a binding assay. The purpose was to identify short peptides that bind the carboxyl-terminal target of proteoglycan-precursors that form the bacterial cell wall [2]. A fluorescently-tagged target peptide was used to identify those beads, with peptides synthesized on the bead surface, that bind to this target (peptide-peptide interactions). The selected beads were individually dispensed by the instrument into multi-well plates for further validation, retesting and subsequent peptide analysis. Different beads bound to different amounts of target under the tested conditions as determined by their levels of fluorescence, which was quantified by the COPAS instrument. Edman degradation of the peptide on each selected bead revealed the binding sequence.

This work was focused on determining the usefulness and increased speed of the COPAS™ flow sorter for this peptide-peptide binding assay. The COPAS technology platform brings these qualities to other bead-based assays and allows for the reconsideration of using these approaches to biomedical research.

Results and Discussion

The target of these studies was the dipeptide sequence of peptidoglycan precursor. Specifically, tripod chains were designed to encapsulate peptidoglycan end termini. Libraries were prepared that consist of variable tripeptide constituents on tripod fingers on Argogel (160 mm). Such tripeptide sequences could be determined relative to weak interactions to bind the proteoglycan precursor and block cross-linking (Figure 1). Batch incubations were conducted using 0.1N phosphate, pH 7.0, buffer to test three concentrations (i.e., 0.5, 5, and 50 µM) of the target. Testing was based on approximately 8000 beads /experiment overnight at 20°C, and analysis was achieved using on-bead fluorescence analysis and sorting of fluorescently-labeled beads using the COPAS instrumentation.

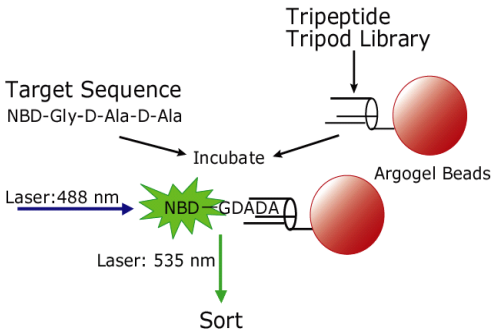

Fig. 1. Mode of action of binding.

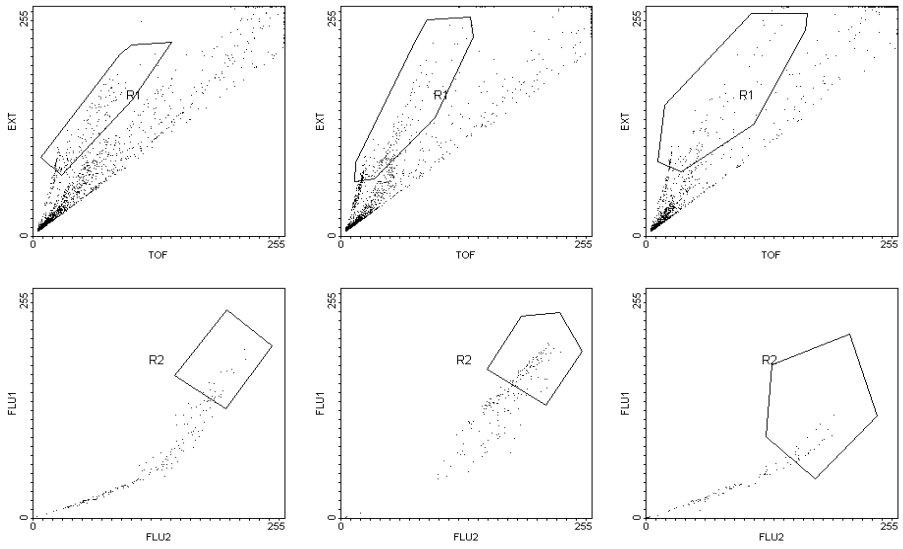

9	10	11
Library + NBD-Gly-Ala-Ala 50 μM (washed)	Library + NBD-Gly-Ala-Ala 5 μM (washed)	Library + NBD-Gly-Ala-Ala 0.5 μM (washed)

Fig. 2. Lower panels indicate the relative distribution of fluorescence amounts for the library beads at each target concentration. Polygon regions in lower panels indicate the sorted region of the distribution for each target concentration.

Assays were designed to identify protein-protein interactions synthesized on the surface of small resin beads. Binding was detected using COPAS bead sorting and analysis technology. Control experiments indicate that resin used is not inherently fluorescent however, the fluorescently labeled target does bind to these Argogel beads, albeit weakly, as mild washing with buffer removes the binding. Data from resins carrying the peptide library indicate beads possess a greater amount of binding activity to the target protein than do the "naked" Argogel beads. Washing conditions that completely remove target from Argogel beads only reduces the level of binding to the peptide library beads. The nature of this binding is not understood. Selecting and collecting by sorting of beads with the highest levels of fluorescence after washing identified the tightest binders. Sorting is fast – approximately 15 minutes per analysis. Fluorescence level values can be determined in a number of ways. For example, using fluorescence image analysis instrumentation (microscope with CCD camera and appropriate software) or from the data collected by the COPAS instrument to allow the initial ranking of the strength of the binding interactions. Peptide sequences have been determined and will be described elsewhere (Brouwer and Liskamp, Utrecht University).

References

1. Smith, H. K., and Bradley, H. *J. Combi. Chem.* **4**, 326-32 (1999).
2. Williams D. H., and Kalman J. *J. Am. Chem. Soc.* **99**, 2768-74 (1977).

Peptide Revolution: Genomics, Proteomics & Therapeutics
Michael Chorev & Tomi K. Sawyer (Editors)
American Peptide Society, 2003

Monitoring Self-Association of Small Amphipathic Molecules by Temperature Profiling in Reversed-Phase Chromatography

Darin L. Lee, Colin T. Mant and Robert S. Hodges

Department of Biochemistry & Molecular Genetics, University of Colorado Health Sciences Center, 4200 East Ninth Avenue, Denver, CO 80262, USA

Introduction

We describe here a novel, sensitive method with no upper or lower molecular size limits that indicates self-association of molecules driven together by the hydrophobic effect under aqueous conditions. Temperature profiling in reversed-phase chromatography analyzes the retention behavior of a sample over the temperature range of 5-80°C during gradient elution RP-HPLC.

We demonstrate the utility of this technique with 14-residue cyclic and linear cationic peptides (<2000 Da) based on the sequences of the *de novo*-designed peptide, GS14 (Figure 1), and analogs with D-lysine substitutions at various sequence positions.

GS14	cyclo-VKLKV<u>Y</u>PLKVKL<u>Y</u>P
GS14K2	cyclo-V<u>K</u>LKV<u>Y</u>PLKVKL<u>Y</u>P
GS14K4	cyclo-VKL<u>K</u>V<u>Y</u>PLKVKL<u>Y</u>P
GS14K9	cyclo-VKLKV<u>Y</u>PL<u>K</u>VKL<u>Y</u>P
GS14K11	cyclo-VKLKV<u>Y</u>PLKV<u>K</u>L<u>Y</u>P
GS14K2K4K9K11	cyclo-V<u>K</u>L<u>K</u>V<u>Y</u>PL<u>K</u>V<u>K</u>L<u>Y</u>P
GS14K4 A6 lin	H_2N-AKA<u>K</u>A<u>Y</u>PAKAKA<u>Y</u>P-COOH

Fig. 1. Sequences of GS14 and related peptides [1, 2]. D-amino acids are underlined.

Results and Discussion

GS14 is a cytolytic 14-residue cyclic β-sheet molecule that contains six aliphatic residues (3 Val and 3 Leu) on the nonpolar face and four basic (Lys) residues on the polar face (Figure 2A). The segregation of the nonpolar and charged residues on opposite sides of the molecule makes it an extremely amphipathic peptide. It is known to aggregate in solution at concentrations above 50 μM (84 μg/ml), while the analogs containing D-Lys displayed increased solubility and no aggregation up to the highest concentration tested, 175 μM (292 μg/ml) [3]. The NMR solution structures of GS14 and GS14K4 show that the improved solubility of GS14K4 is due to the placement of the D-Lys on the nonpolar face, which decreases peptide amphipathicity (Figure 2B).

GS14 displayed the highest degree of self-association, as indicated by the largest change in retention time (Δt_R=4.2 min at 55°C) relative to retention time at 5°C (Figure 2C). From the behavior of the GS14 analogs, single D-Lys substitutions at positions 2 and 9 appear to disrupt self-association to a similar extent, while positions 4 and 11 disrupt self-association to an even greater extent. The four D-Lys substitutions in GS14K2K4K9K11 almost completely abolished self-association, as its temperature profile approached that of the unstructured linear control peptide, GS14K4 A6 lin, which exists in only a monomeric form in solution [1].

Among these cationic membrane-active peptides, the highest therapeutic value is achieved with a degree of self-association that is neither too high nor too low. GS14 (high self-association) exerted strong activity towards red blood cells but had little

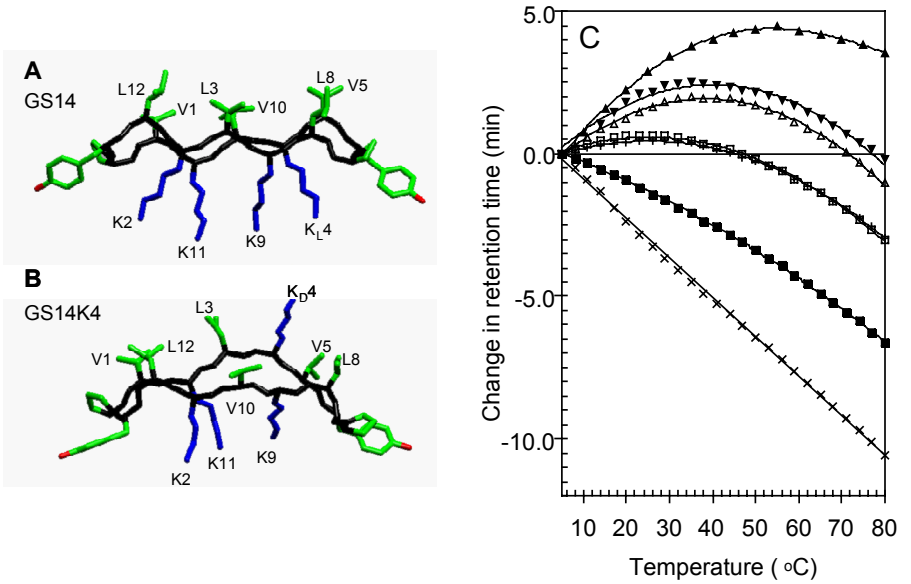

Fig. 2. NMR structures and temperature profiles of GS14 peptides. GS14 (Panel A) and GS14K4 (Panel B) structures were obtained in 30% trifluoroethanol [4]. Panel C: Temperature profiles of peptides normalized to retention times obtained at 5℃. Peptides were GS14 (closed triangles), GS14K9 (closed inverted triangles), GS14K2 (open triangles), GS14K4 (open squares), GS14K11 (+), GS14K2K4K9K11 (closed squares), and GS14K4 A6 lin (X). Runs were performed on a Zorbax 300-SB C8 column (2.1 I.D. x 150 mm) at 0.5%B/min, a flow-rate of 0.35 ml/min, where solvent A was 0.05% aqueous trifluoroacetic acid and solvent B was 0.05% trifluoroacetic acid in acetonitrile. Runs were performed in 3° or 5° increments from 5℃ to 80℃.

antimicrobial activity, while GS14K2K4K9K11 (low self-association) had neither antimicrobial nor hemolytic activity. Peptides GS14K4 and GS14K11, which displayed nearly superimposable temperature profiles and an intermediate degree of self-association (Figure 2C), had the greatest specificity for microbial membranes versus human red blood cell membranes [2]. It is clear that peptide self-association measurements by chromatographic temperature profiling may be a useful marker in the *de novo* design of small, biologically active amphipathic molecules.

Acknowledgments

The work was funded by NSERC and AHFMR student fellowships to D. Lee, and an NIH grant RO1-GM61855 to R. S. Hodges.

References

1. Lee, D. L., Mant, C. T. and Hodges, R. S. *J. Biol. Chem.* **278**, 22918-22927 (2003).
2. Kondejewski, L. H., Jelokhani-Niaraki, M., et al. *J. Biol. Chem.* **274**, 13181-13192 (1999).
3. Jelokhani-Niaraki, M., Prenner, E. J., et al. *J. Pept. Res.* **58**, 293-306 (2001).
4. McInnes, C., Kondejewski, L. H., Hodges, R. S. and Sykes, B. D. *J. Biol. Chem.* **275**, 14287-14294 (2000).

Peptide Revolution: Genomics, Proteomics & Therapeutics
Michael Chorev & Tomi K. Sawyer (Editors)
American Peptide Society, 2003

Effect of Secondary Structure on Selectivity of Reversed-Phase Chromatography for Peptide Separations at Varying Temperatures

Yusin Chen[1] and Robert S. Hodges[2]

[1]Department of Biochemistry, University of Alberta, Edmonton, AB, T6G 2H7, Canada;
[2]Department of Biochemistry and Molecular Genetics, University of Colorado Health Sciences Center, Denver, CO 80262, USA

Introduction

RP-HPLC has emerged as the main method in the development of separation protocols for peptide and protein mixtures. Temperature has been utilized as an important parameter to optimize peptide separations during RP-HPLC [1]; in addition, RP-HPLC of peptides and proteins at varying temperatures has also provided insight into the role of conformation in the retention behavior of peptides and proteins [2].

Thus, the present study examines the effect of secondary structure on selectivity of RP-HPLC for peptide separations at varying temperatures, based on model amphipathic α-helical peptides and random coil peptides with 19 single L- or D-amino acid substitutions (Figure 1). We believed that the study of the temperature effect on retention behavior of such peptide models would have implications, not only for the rational development of separation/optimization protocols, but also for the understanding of the hydrophobic interactions between RP-HPLC stationary phases and peptides with conformational differences.

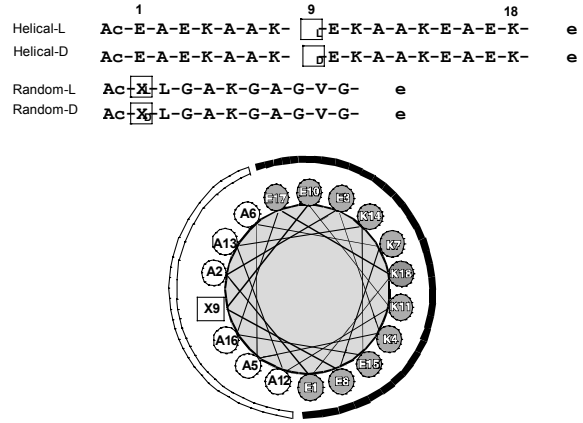

Fig. 1. Model synthetic peptides with conformational differences. Top: sequences of the model amphipathic helical and random coil peptides with L- or D-amino acid substitutions at position X (boxed X_L or X_D). Bottom: helical wheel representation of the model amphipathic α-helical peptide. The closed arc denotes the hydrophilic face; the open arc denotes the hydrophobic face.

Results and Discussion

In this study, in spite of the tremendous structural difference between model helical and random coil peptides, all peptides became less retentive at higher temperature, due to the general effects of increasing temperature resulting in increased solubility of the solute in the mobile phase, as well as a decrease in solvent viscosity and an increase in mass transfer between the mobile and stationary phases. We demonstrated that the

separations of peptide analogs during RP-HPLC can be obtained based on two temperature effects as follows: (i) temperature influences the retention behavior of different α-helical peptides or random coil peptide analogs to different degrees; (ii) temperature has a greater effect on helical peptide analogs than unstructured random coil peptides during the temperature increase, due to the change in peptide secondary structure. Optimum separations of peptide mixtures, including random coil and α-helical peptides, can be obtained by slight adjustments of temperature within a fairly narrow range, indicating the validity of the temperature-based optimization protocol.

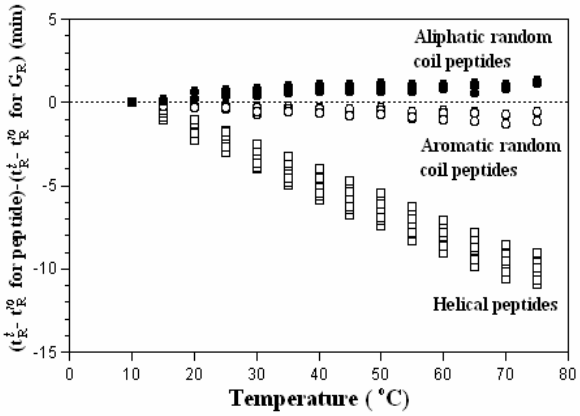

Fig. 2. Effect of temperature on RP-HPLC of helical and random coil peptides: normalization to retention behavior of random coil Gly peptide. The retention behavior of the peptides was normalized to that of random coil Gly peptide through the expression (t^t_R-t^{10}_R) minus (t^t_R-t^{10}_R for Gly peptide), where t^t_R is the retention time at a specific temperature of a helical or random coil peptide, and t^{10}_R is the retention time at 10 °C.

From Figure 2, the method of temperature profiling shows the power RP-HPLC temperature studies to identify the peptides with varying secondary structures. The steep negative profiles of α-helical peptides indicate considerable unfolding of the α-helices with increasing temperature. The slightly positive and negative profiles of the aliphatic and aromatic random coil peptides show the dramatic effect of temperature on peptides of different conformations. In conclusion, we believe that varying temperature during RP-HPLC not only aids the rational development of peptide separation/optimization protocols, but also can be used as a sensitive and practical probe to distinguish peptide conformations, which should prove valuable for peptide/protein structure studies.

Acknowledgments
The work was supported by an NIH grant R01GM61855 to R.S.Hodges.

References

1. Mant, C. T., Kondejewski, L. H., Cachia, P. J., Monera, O. D. and Hodges, R. S. *Methods Enzymol*. **289**, 426-469 (1997).
2. Purcell, A. W., Aguilar, M. I. and Hearn, M. T. W. *Anal. Chem*. **65**, 3038-3047 (1993).

Peptide Revolution: Genomics, Proteomics & Therapeutics
Michael Chorev & Tomi K. Sawyer (Editors)
American Peptide Society, 2003

Controlling "Easy" and "Difficult" Fmoc-Deprotections

Phillip W. Banda[1] and Mary Frances Leopold[2]

[1]Protein Research & Development; [2]Chemical Development & Manufacturing,
Applied Biosystems, Foster City, CA 94404, USA

Introduction

The beta-chemokines, MCP1 and Rantes, have similar 3D solution structures [1] but display distinctly different patterns of Fmoc-deprotection during SPPS via UV monitoring on the Applied Biosystems 433A peptide synthesizer [2]. Specifically, the MCP1 sequence runs into difficult (overtime) deprotections at a string of hydrophobic amino acids starting 34 residues from the C-terminus, while the corresponding hydrophobic string in Rantes shows easy deprotections during SPPS. This report at the 17th APS has also shown that an exchange of hydrophobic strings between the two beta-chemokines converts the "difficult" MCP1 string into "easy" and the "easy" Rantes string into "very difficult" deprotections [2]. The latter substitution, Rantes AVVFV into MCP1, is herein called the hybrid sequence. The present communication explores the changes in the UV deprotection patterns and in the NMR spectra of the peptide-resins for three hybrid peptides, as the preceding C-terminal sequence of MCP1 increases in length.

Results and Discussion

Figure 1, displayed in the C- to N-direction of SPPS, is a simplified representation of the UV deprotection profiles from the 433A. The three hybrid sequences (10-mer, 15-mer, 30-mer) have the Rantes hydrophobic string at the N-terminus and increasing MCP1 C-terminal chain length. The easy deprotections are represented as short bars and the difficult deprotections as tall bars in order to focus attention on the start/stop positions of the overtime deprotections. As the C-terminal MCP1 chain length increases, both the extent of difficult deprotections and their position of onset change

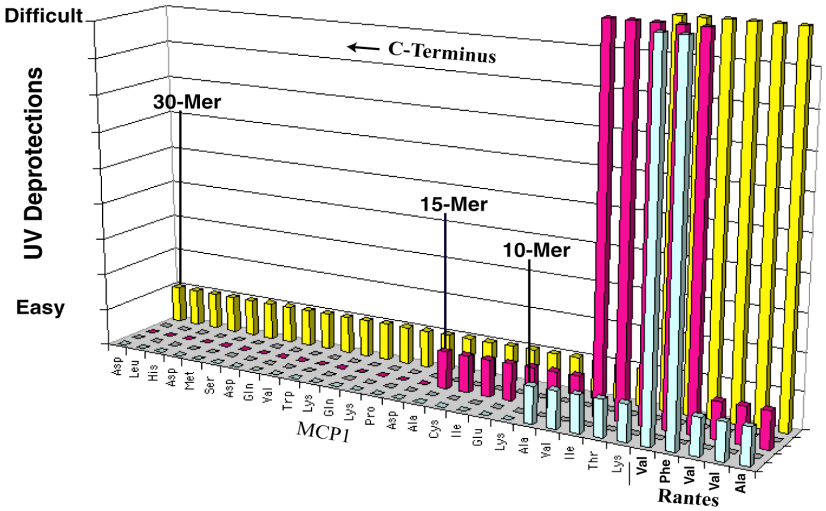

Fig. 1. The start and the extent of difficult deprotections depend on the MCP1 chain length.

significantly. It is clear that the deprotection difficulty of the hybrid sequences depends on the preceding residues of MCP1. Note that varying the preceding C-terminal sequence of Rantes alone exerts no influence on the deprotection of AVVFV, i.e. the Rantes sequence is easy to deprotect [2].

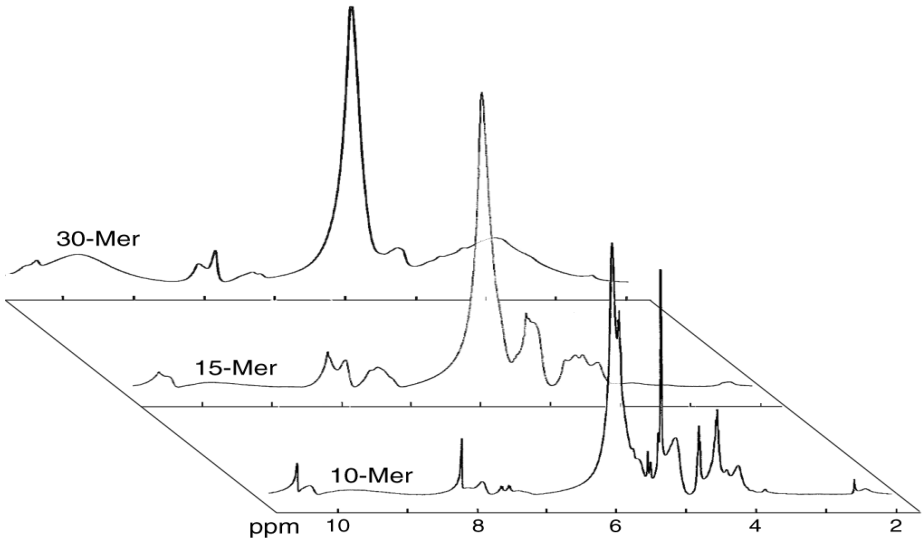

Fig. 2. 1H-NMR spectra of the three peptide-resins (Fig. 1) are shown in an overlay diagram.

Figure 2 is a composite of the 400 MHz 1H-NMR spectra for the three peptide-resins whose UV deprotections are represented in Figure 1. As the chain length and the deprotection difficulty increase, the details of the NMR spectra lose definition. The broader peaks of the more difficult sequences are signifying a more condensed state of the peptide-resin. The three NMR spectra reflect different structural states of the peptide-resins just as the three sequences display distinctly different UV deprotection patterns. Note that peptide-resins of long (easy deprotection) sequences exhibit a different type of NMR spectrum [3]. The details of the peptide-resin structures for the three sequences remain to be studied but it is clear that as the easy vs. difficult UV deprotection patterns change, so do the NMR spectra of the peptide-resins in this chemokine model system. UV monitoring of Fmoc-deprotection on the 433A reveals changes in peptide-resin structure during SPPS. The easy vs. difficult deprotections are being controlled by the sequence of the MCP1 residues.

References

1. Handel, T. M. and Domaille, P. J. *Biochem.* **35**, 6569-6584 (1996).
2. Banda, P. W., In Lebl, M. and Houghton, R. A. (Eds.) *Peptides: The Wave of the Future*, American Peptide Society, San Diego, p. 81-82 (2001).
3. Banda, P. W. and Leopold, M. F., In Martinez, J. and Fehrentz, J.- A. (Eds.) *Peptides 2000*, EDK, Paris, p. 191-192 (2001).

For research use only. Not for use in diagnostic procedures. Applied Biosystems is a registered trademark of Applera Corporation. All rights reserved.

Peptide Revolution: Genomics, Proteomics & Therapeutics
Michael Chorev & Tomi K. Sawyer (Editors)
American Peptide Society, 2003

The Effect of Trp on UV- and Vibrational Circular Dichroism of Helical Peptides

Attila Borics[1], Chibawanye Ene[1], Laszlo Otvos Jr[2], Richard F. Murphy[1] and Sándor Lovas[1]

[1]Department of Biomedical Sciences, Creighton University, Omaha, NE 68128, USA;
[2]The Wistar Institute, Philadelphia, PA 19104 USA

Introduction

Interpretation of the UV-CD spectra of helical peptides containing aromatic residues can be difficult because the contribution of the UV absorption of aromatic side chains has to be taken into account [1]. Neglecting this contribution can lead to inaccurate structure assignment and false conclusions about the helix-stabilizing or destabilizing effect of aromatic residues. A quantitative model of aromatic contributions with which these problematic spectra could be corrected has not yet been proposed. Alternatively, VCD spectroscopy can be used because aromatic side chains do not contribute significantly to VCD spectra in the frequency region of interest. It was, thus, shown previously that Tyr in different positions does not affect helicity in 12-residue Ala-based peptides in 50% (v/v) TFE/H_2O [2]. In this study, a set of Ala-based model peptides with Trp in different positions (Figure 1) was synthesized and analysed using UV-CD and VCD spectroscopy. Molecular dynamics (MD) studies were also performed to better understand the effect of Trp residues on conformation.

Peptides were synthesized, purified and characterized as described elsewhere [2]. UV-CD spectra of peptides were recorded on a Jasco J810 spectropolarimeter using a 0.08 mm path length cell. Peptides were dissolved in 50% (v/v) TFE/H_2O at approximately 0.5 mg/ml. Final concentrations of peptide solutions were determined following RP-HPLC by comparing peak areas to those for standard solutions. For VCD studies, peptides were added to 50% (v/v) TFE/D_2O (10 mg/ml), centrifuged and the clear supernatants were used for further studies. VCD measurements were performed with a BOMEM-Biotools Chiralir FT-VCD spectrometer, at 10 °C and 8 cm^{-1} resolution, using a CaF_2 cell with 75 μm path length. MD simulations in the presence of 50% (v/v) TFE/SPC H_2O were carried out using the GROMOS96 force field. Input structures were generated with the Φ and Ψ angles set to -57 and -47 degrees respectively, and 20.1 ns MD was performed at constant temperature (300 K) and pressure (1 bar). For Coulomb interactions, a twin range cut-off with reaction-field correction was used. Trajectories were analyzed by the DSSP secondary structure-recognizing algorithm.

Results and Discussion

The signal intensity in the UV-CD spectra (Figure 2) of Trp-containing peptides was lower than of the template peptide. Since Trp residues are known to contribute

W0	Ac-AAAAAAAEAAKA-NH_2	**W3**	Ac-AA**W**AAAAEAAKA-NH_2
W1	Ac-**W**AAAAAAEAAKA-NH_2	**W4**	Ac-AAA**W**AAAEAAKA-NH_2
W2	Ac-A**W**AAAAAEAAKA-NH_2	**W5**	Ac-AAAA**W**AAEAAKA-NH_2
W6	Ac-AAAAA**W**AEAAKA-NH_2		

Fig. 1. Sequences of model peptides.

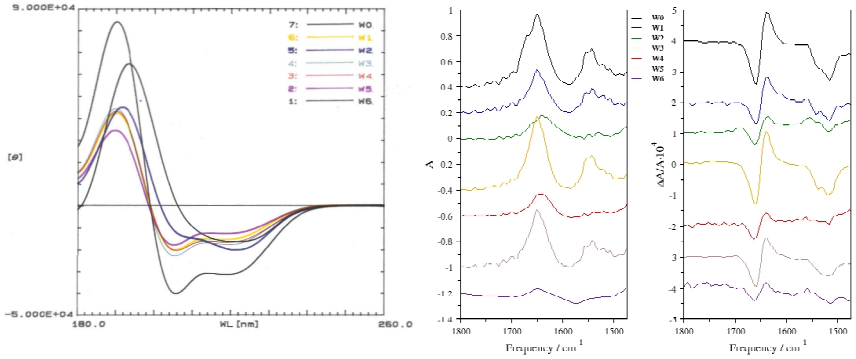

Fig. 2. UV-CD, IR and VCD spectra of the model peptides (left to right, respectively).

positively to helical signal intensity in UV-CD spectra of peptides, this result can be attributed to the slight decrease of helicity caused by the Trp residue. Poor solubility of **W2** and **W6** was also observed and their UV-CD spectra showed significant loss of helicity compared to other Trp-containing peptides.

The low solubility of Trp-containing peptides became a problem for VCD spectroscopic studies since this technique requires much higher concentration than does UV-CD. Both the IR and VCD signal intensities of **W1**, **W2**, **W4** and **W6** are significantly lower than those of the others (Figure 2). The lowest intensity was observed for **W6**, in agreement with the results of the UV-CD experiments. All VCD spectra, however, show helical features to some extent, despite their low signal to noise ratio. It still can not be concluded that intensity differences are caused only by low sample concentrations. The UV-CD and VCD results suggest that Trp disrupts helical structure with variable effectiveness depending on its position.

MD simulations of the model sequences and trajectory analysis showed that all peptides, except **W1** and **W4**, retain helical structure for 20 ns in 50% (v/v) TFE/H_2O. These results, however, can not be correlated completely with experimental results. It is still possible that spectral differences are not due only to low sample concentrations, especially in the case of VCD experiments. The dependence of helix stability on the position of Trp and the low peptide solubility might both be explained by aromatic side chain-backbone amide interactions [3]. When a particular position allows the Trp side chain to interact with the backbone amide, better solubility of the peptide could result, because the hydrophobic indolyl group would be less exposed to the solvent. On the other hand, this interaction could hinder the intramolecular hydrogen bond formation between amide groups, thereby destabilizing the helix.

Acknowledgments

This work was supported by NIH-BRIN (1 P20 RR16469-01) and NSF-EPScOR-(EPS-0091900) grants.

References

1. Chakrabartty, A., Kortemme, T., et al. *Biochemistry* **32**, 5560-5565 (1993).
2. Borics, A., Murphy, R. F. and Lovas, S. *Biopolymers* **72**(1), 21-24 (2003).
3. Tóth, G., Kövér, K. E., Hirst, J., Murphy, R. F. and Lovas, S. In Lebl M. and Houghten R. A. (Eds.) *Peptides: The Wave of the Future*, *(Proceedings of the 2nd International and 17th American Peptide Symposium)* American Peptide Society, San Diego, 2001, pp. 303-305.

Peptide Revolution: Genomics, Proteomics & Therapeutics
Michael Chorev & Tomi K. Sawyer (Editors)
American Peptide Society, 2003

Improved Automated Waste Handling for the Applied Biosystems 433 Peptide Synthesizer

David H. Singleton, Robert T. Suleske and J. Carter Courtney

Pfizer Global Research and Development, Eastern Point Road, Groton, CT 06340 USA

Introduction

Automated peptide synthesis on the Applied Biosystems (ABI) 433 (Foster City, CA) requires careful operator attention to detail. Much effort is expended when setting up the synthesizer focusing on cycle programming, resin and monomer selection and instrument performance, easily overlooking the waste-generating component. The ability to intervene during a synthesis due to failure of the waste system assures that a catastrophic failure resulting in synthesis failure and instrument service is avoided. Also, waste disposal from the polyethylene carboy container typically used requires pouring of the waste into a container deemed adequate by environmental regulations for waste disposal. Potential spillage and waste handling of this nature are best avoided when possible.

The waste container typically provided with the synthesizer is not rugged enough for handling in environmental waste disposal systems. The Justrite™ (VWR Scientific) brand waste container is the preferred container of our health and safety group for chemical waste comprised largely of solvents containing little else (typical of peptide synthesizer waste). Modification of this container by plumbing waste to flow directly into and hooded exhaust directly out of was accomplished by drilling two access holes and plumbing with two CPC™ poly propylene quick disconnect fittings secured with O-rings at the interface. Tubing is connected with the male portion of the fitting.

Since our synthesizers are located on lab benches with closed cabinetry beneath, it becomes imperative to know the status of the waste container. Our goal was to devise a system to fill the waste container to an optimal level (70-80% capacity) by remote monitoring. Given that peptide synthesizer waste is uniform in density, this is simply accomplished by container weight. We chose a large footprint, relatively inexpensive balance for this task (O-Haus Champ™ Model B50S10). This balance provides the adequate weight range and RS-232 communications capability for our alarm system.

Results and Discussion

One could simply read the weight from the remote balance controller to determine the waste status. However, exploiting the capability of the RS-232 communication and interface with the synthesizer adds a level of fail-safe security. The heart of the monitoring system lies in the communications and alarm box.

The alarm system is composed of a computer board, RS232 interface board, a sound generating device, a push button and a light. The computer board, a Parallax Basic Stamp II® (Parallax Inc, Rocklin, CA) module is programmed to flash the light and interrogate the balance for the current weight through the RS232 board (Pfizer design using max232 integrated circuit) about once every two seconds. The standard Ohaus "print" command monitors the weight from the balance and flashes a light indicating proper operation. Once the pre-programmed trip point is reached, the computer turns on the sound generating device, and an analog output of 1 volt is generated across a 10000-ohm potentiometer, signaling the synthesizer that waste storage is full. A reset button reinitializes the computer for the next cycle.

This 1V signal is delivered to channel 3 input on the rear panel of the synthesizer and monitored similarly to any analog signal. Simple lines of programming are added to the first module of the synthesis cycle to determine if error state has been reached. Using function 141 ((Interrupt Channel 3 above X) with X=5% full scale to deter false positives)) and function 58 (Interrupt conditional), the synthesizer polls the alarm ready / fail status and continues or interrupts synthesis accordingly. Once the interrupt condition is satisfied (waste emptied), manual intervention on the front panel continues synthesis. This interrupt is strategically placed where the synthesis has added the incoming amino acid, the resin has been washed and the amino terminal protecting group is still in place — in essence, the synthesis is dormant here.

Return of cost outlay for the system is quick. The system cost was $1356 USD. Given the fact that the costs of one cycle of peptide synthesis using ABI reagents is approximately $31.77, payoff is achieved the first time the alarm system is activated. Therefore, without this system in place, once 43 cycles are lost due to failure (not quite two containers of waste), the system has paid for itself. This simple cost benefit analysis ignores productivity enhancements and service visit reductions, which makes implementation even more attractive.

Peptide Revolution: Genomics, Proteomics & Therapeutics
Michael Chorev & Tomi K. Sawyer (Editors)
American Peptide Society, 2003

X-Cys Ligation

Yi-An Lu and James P. Tam

Department of Microbiology and Immunology, Vanderbilt University,
Nashville, TN 37232 USA

Introduction

Cysteine thioester ligation is a robust method to couple unprotected peptides and proteins to form a peptide bond in an aqueous solution without coupling reagents. It is thought that an amino-terminal Cys is obligatory for the Cys ligation.

Here, we report the development of X-Cys ligation in which the Cys nucleophile is placed 1 to 3 residues proximal to the N-terminus (Figure 1). X-Cys ligation provides alternatives in choosing ligation sites. It also permits development of new approaches for tandem or combinatorial ligation of multiple segments without a protecting scheme. A new method is presented that uses parallel peptide array synthesis on cellulose membranes to evaluate the X-Cys ligation. The ligation was studied directly on cellulose membrane to determine the ligation yield as measured by scanning each spot color density (UN-SCAN-it software, Silk Scientific, Inc. Orem, UT, USA).

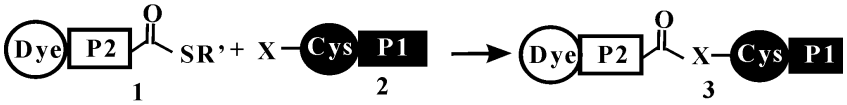

Fig. 1. Scheme of X-Cys ligation.

Results and Discussion

The mechanism of X-Cys ligation is similar to Cys-ligation [1,2] in which the X-Cys nucleophile reacts with a thioester through a thiol-thioester exchange to form a covalent thioester, and spontaneously rearranges by an S, N-acyl migration, to form an amide bond through an 8-, 11, or 14-member ring intermediate (Figure 1). However, the S, N-acyl migration in X-Cys ligation is significantly slower than the Cys-ligation and is highly dependent on the X-residue(s) preceding Cys.

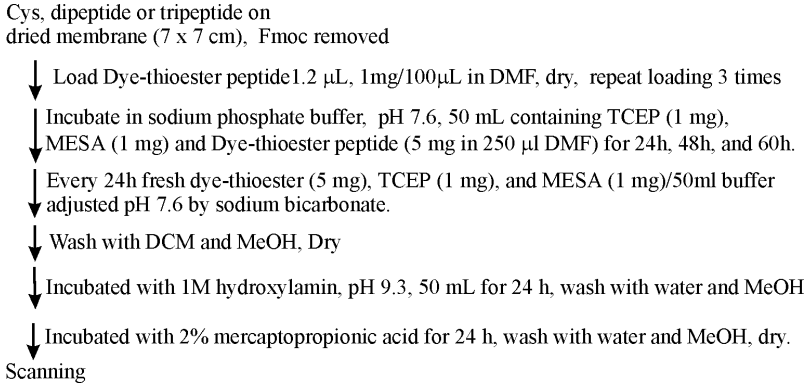

Fig. 2. Spot-synthesis approach to determine X-Cys ligation scheme of X-Cys ligation.

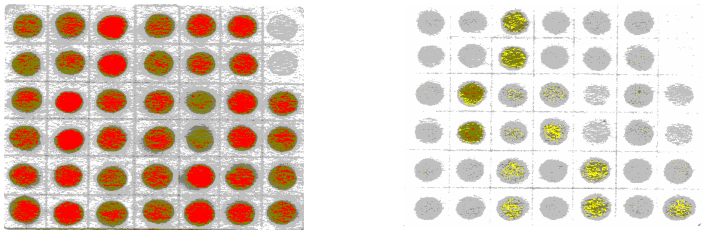

AC 21 AC	NC 25 NC	**GC 92** **GC**	LC 22 LC	FC 32 FC	TC 38 TC	-SR' -SR'
RC 25 RC	**CG 100** **CG**	HC 46 HC	KC 64 KC	PC 9 PC	WC 49 WC	Ac-C Ac-C
DC 29 DC	EC 30 EC	IC 59 IC	MC 28 MC	**SC 90** **SC**	YC 33 YC	VC 35 VC

Fig. 3. Upper left panel X-Cys ligation for 24 h. Upper right panel ligated products treated with NH_2OH solution, pH 9.2, then 2% mercaptopropionic acid in DCM for 24 h to remove thioester side products. Table shows corresponding sequence of each spot. The ligation yield is an average of two experiments.

Three peptide-thioester were synthesized by SPPS on a thioester resin:

(1) dye-Ser-Leu-Arg-Arg-Ser-$SCH_2CH_2CONH_2$,

(2) dye-Ser-Leu-Arg-Arg-Ser-Gly-$SCH_2CH_2CONH_2$

(3) dye-Gly-Glu-Arg-Gly-Ala-Leu-SCH_2CH_2CO-Gly.

No significant difference in the X-Cys ligation yields was observed. Figure 2 shows the X-Cys ligation procedure.

We tested X-Cys ligation on all 20 L-amino acids using a large excess of thioester and long reaction time. Two sequences GC and SC showed > 90% ligation yield (Figure 3). Other sequences such as KC afforded > 60%. In N-tripeptide, low ligation yields were obtained except that GGC and SSC > 80%. In X = 3 amino acids no satisfactory ligation yield resulted

The results provide new insights that cysteine is not obligatory at N-terminal for Cys-ligation. X-Cys ligation, especially GC- or SC- on N-terminal will be particularly useful.

Acknowledgments

This work was funded by US Public Health Service NIH CA36544 and AI46164.

References

1. Tam, J. P., Lu, Y.- A., Liu, C.- F. and Shao, J. *Proc. Natl. Acad. Sci. U.S.A.* **92**, 12485-12489 (1995).

2. Dawson, P. E., Muir, T. W., Clark-Lewis, I. and Kent, S. B. *Science* **266**, 776-779 (1994).

3. Frank, R. *J. Immunol. Methods* **267**, 13-26 (2002).

4. Tam, J. P., Rao, C., Liu, C.-F. and Shao, J. *Int. J. Pept. Protein Res.* **45**, 209-216 (1995).

Peptide Revolution: Genomics, Proteomics & Therapeutics
Michael Chorev & Tomi K. Sawyer (Editors)
American Peptide Society, 2003

Orthogonally Protected Sugar Diamino Acids as Building Blocks for Oligosaccharide Mimetics

Frank Sicherl and Valentin Wittmann

Institut für Organische Chemie und Chemische Biologie, Johann Wolfgang Goethe-Universität, Marie-Curie-Str. 11, 60439 Frankfurt am Main, Germany and Fachbreich Chemie, Universität Konstanz, 78457 Konstanz, Germany

Introduction

Sugar amino acids (SAAs) [1] have received considerable interest as building blocks for oligosaccharide and peptide mimetics and as pharmacophor-presenting scaffolds. Used as monomers with a rigid pyran ring, functional pharmacophoric groups attached to the hydroxy, amino, and carboxyl groups can be presented in a distinct spatial arrangement following seminal studies by Hirschmann et al. [2]. Linear and cyclic oligomers of SAAs have been synthesized taking advantage of well-established peptide chemistry, and in certain cases adopting defined secondary structures [1, 3]. Branched structures employing sugar diamino acids, however, are not known.

Here we introduce the protected derivative **1** of 2,6-diamino-2,6-dideoxy-β-D-glucopyranosyl carboxylic acid, the first example of a sugar diamino acid (SDA) amenable to solid-phase synthesis (Figure 1). Compared to SAAs, the additional amino group can be used to increase diversity by selective functionalization and to form branched oligomers. Oligomeric SDAs with unprotected amino groups, on the other hand, are potential aminoglycoside mimetics.

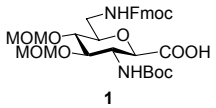

Fig. 1. Orthogonally protected sugar diamino acid (SDA).

Results and Discussion

The synthesis of **1** started from glycosyl cyanide **2** which was prepared according to a published procedure [4]. After deacetylation the obtained triol was regioselectively tosylated at the 6 position followed by azide substitution to give **3** (Figure 2). Hydrolysis of both the nitrile and acetamide under acidic conditions led to the free amino acid. To facilitate isolation, methyl ester **4** was formed by treatment with 2,2-dimethoxypropane and concentrated HCl. First attempts to obtain the free amino acid by basic hydrolysis of **3** ($Ba(OH)_2$, H_2O, reflux) were, however, not successful. Under these conditions the reaction stopped at the acetamido carboxylate stage.

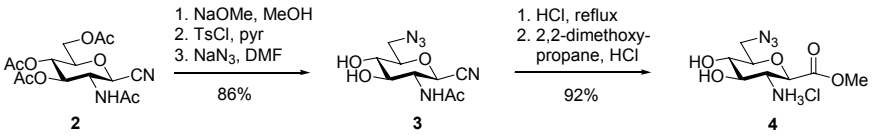

*Fig. 2. Formation of azido amino ester **3**.*

The amino group of **4** was protected by the Boc group with concomitant cleavage of the methyl ester. Methoxymethyl (MOM) groups were introduced by treatment with dimethoxymethane and P_2O_5 in order to circumvent toxic MOM-Cl to give **5** (Figure 3). The MOM ester contained in **5** was cleaved with NaOH. Finally, hydrogenation of the azide and subsequent Fmoc protection of the amine gave SDA building block **1**.

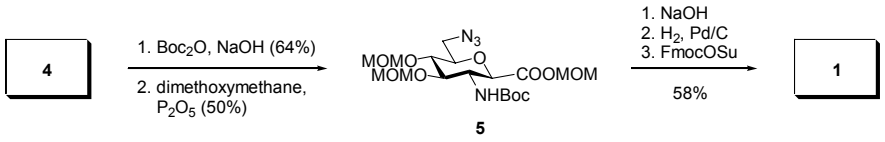

*Fig. 3. Synthesis of SDA building block **1**.*

Building block **1** is suited for peptide coupling reactions in solution and on solid support using the Fmoc strategy as demonstrated in Figure 4. Diphenylmethyl protected β-alanine amide **6** served as a model for a solid-phase linked amino acid. Stepwise coupling of **1** using HATU/HOAt as coupling reagents followed by complete deprotection led to β-alanine-linked pseudo disaccharide **8** within 5 steps (Figure 4).

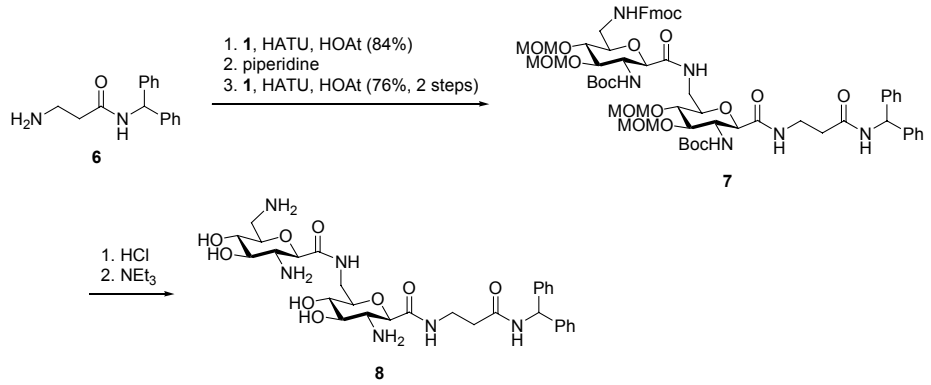

*Fig. 4. Application of SDA building block **1** in peptide coupling reactions.*

Acknowledgments

This work was funded by the Deutsche Forschungsgemeinschaft (SFB 579).

References

1. Gruner, S. A. W., Locardi, E., Lohof, E. and Kessler, H. *Chem. Rev.* **102**, 491-514 (2002).
2. Hirschmann, R, Nicolaou, K. C., Pietranico, S., Leahy, E. M., Salvino, J., Arison, B., Cichy, M. A., Spoors, P. G., Shakespeare, W. C., Sprengler, P. A., Hamley, P., Smith, A. B., III, Reisine, T., Raynor, K., Maechler, L., Donaldson, C., Vale, W., Freidinger, R. M., Cascieri, M. R. and Strader, C. D. *J. Am. Chem. Soc.* **115**, 12550-12568, (1993).
3. Smith, M. D., Claridge, T. D. W., Fleet, G. W. J., Tranter, G. E. and Sansom, M. S. P. *Chem. Commun.* 2041-2042 (1998).
4. Carrière, D., Meunier, S. J., Tropper, F. D., Cao, S. and Roy, R. *J. Mol. Catal. A: Chem.* **154**, 9-22 (2000).

Peptide Revolution: Genomics, Proteomics & Therapeutics
Michael Chorev & Tomi K. Sawyer (Editors)
American Peptide Society, 2003

Comparison Between NMR and CD Data of Synthetic Peptides

Fanny Guzmán, Julio C. Calvo, Claudia Reyes, Angela G. Torres, Luz M. Salazar, José M. Lozano and Manuel E. Patarroyo

Fundación Instituto de Inmunología de Colombia, FIDIC,
Carrera 50 No. 26-00, Bogota, D.C., Colombia

Introduction

Although X-ray diffraction and NMR are definitive structural techniques, they are limited because of the time reuired to obtain protein structures. In addition, NMR fails when the molecules are too flexible or too large, or insoluble, and X-ray diffraction fails when crystals cannot be grown. While NMR and X-ray require high quantities of protein or peptide, other spectroscopic techniques that provide less complete, but still valuable, structural information, such as circular dichroism (CD), require small quantities of protein or peptide. The main use of CD measurements is in the characterization of the secondary structure and the assessment of its magnitude [1].

Groups of 20-mer peptides from *P. falciparum*, including a native sequence and some discreet substitution analogues, were analysed by NMR and CD. Monkeys *Aotus nancymaae* were immunized to correlate immunogenicity with the 3-D structural features [2-4].

While monomer peptides were easy to analyse by NMR, analysis of the complex mixture of species obtained after oxidation of Cys-containing peptides was not possible. In this paper we describe our efforts to improve the structural characterization by CD and compare it with results obtained from NMR. We show for the first time the similarity in structural features between monomeric and polymeric peptides.

Results and Discussion

It is common to use the polymer form of antigens in immunization, while the monomer is used in NMR studies. It has been difficult to analyze by NMR the complex product obtained after the polymerization process. Cysteine-containing peptides form linear and cyclic monomers, dimers and more complex cyclic polymers. Until now there was no evidence that monomer and polymer of the same peptide can have the same structure. In this work we found by CD that both cysteine-containing monomer and polymer (Table 1) presenting the same antigen had the same the CD spectra profile (Figure 1).

Short and long helix. Peptides 6762, 12755 (Figure 1, b), 14043 and 13813 have a helical tendency their molar ellipticities are different and increase in value going from the smallest helical content (peptide 140430) to the largest one (peptide 12755).

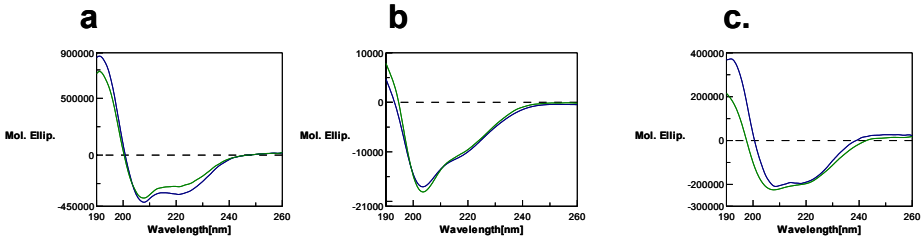

Fig. 1. Comparison between monomer and polymer CD spectra; (a) helix 12755; (b) turn 13767; (c) insoluble peptide 1779.

Table 1. Sequence and identification number of peptides.

Peptide	Monomer/Polymer Sequence [a]	Structural features (NMR/CD)
6762	CG-NEVSERVHVYHILKHIKDGK-GC	Helix (2-17)
12755	CG-VINSERVHVYHILKHIKDGK-GC	Helix (2-20)
13813	CG-YSEMKRASMTTPVLMEKPYY-GC	Helix (3-9)
14043	CG-YSEMKRASLTTPVLKEKPYY-GC	Helix (5-10)
13785	CG-MSYGSDDNDDKNKSLDHKHN-GC	Turn Type III' distorted
13999	CG-MVYGSDDNNDKNKSLNHKHN-GC	Turn Type III' distorted
13479	CG-DAEVAGTQWFLPSGKSPVFG-GC	Turn Type III' distorted
13767	CG-DAEVAGTQWFNPSGKSPVFG-GC	Turn Type III distorted
1779	CG-NIDRIYDKNLLMIKEHILAI-GC	Helix (only by CD)

[a] *Polymers have CG in N- and C-termini.*

Turn type III. Peptides 13999, 13785, 13479 and 13767 (Figure 1, b) showed a low maximum at 198 nm and a wider deep ellipticity (200-205 nm and 215-220 nm) which is found in some peptides identified as β-turns by NMR.

Insoluble peptides. Peptide 1779, NIDRIYDKNLLMIKEHILAI, is slightly soluble in water/TFE. Insoluble peptides cannot be analysed by NMR. Based on the agreement we found between NMR and CD data, we used this insoluble peptide as an example to test the possibility in determining its structural tendency by CD. From our experience in peptide synthesis, many peptides have very low solubility and therefore do not undergo conformational analysis. Peptide 1779 showed a helical tendency by CD in both the monomeric and polymeric presentation forms (Figure 1, c).

Acknowledgments
This work was funded by the Colombian President's Office and the Ministry of Public Health.

References

1. Sreerama, N., Venyaminov, S. Y. and Woody, R. W. *Anal. Biochem.* **287**, 243-251 (2000).
2. Salazar, L. M. et al. *FEBS Lett.* **527**, 95-100 (2002).
3. Guzman, F. et al. *Life Sci.* **71**, 2773-2785 (2002).
4. Purmova, J. et al. *Biochim. Biophys. Acta* **1571**, 27-33 (2002).

Peptide Revolution: Genomics, Proteomics & Therapeutics
Michael Chorev & Tomi K. Sawyer (Editors)
American Peptide Society, 2003

Molecular Design of Functional Peptides by Utilizing Unnatural Amino Acids that Can Coordinate with Metal Ions

Hitoshi Ishida, Masato Kyakuno, Takahiro Nakazato, Mina Fujii and Shigero Oishi

Department of Chemistry, School of Science, Kitasato University, Kitasato, Sagamihara, Kanagawa 228-8555, Japan

Introduction

Unnatural amino acids have become increasingly attractive for their properties of adding unique functions to the peptide and/or controlling peptide conformation [1]. We have introduced 3-aminobenzoic acid as an unnatural amino acid into peptides, and succeeded in designing functional cyclic peptides [2, 3]. We have further designed functional peptides attached to ruthenium tris(bipyridine) complex, which is emissive and carries out photo-induced electron/energy transfer [4].

We designed novel peptides by incorporating 5'-amino-2,2'-bipyridyl-5-carboxylic acids, expecting that the modified peptide will fold by coordinating with metal ions (Figure 1). If ruthenium is used as the metal, the core metal complex is ruthenium tris(bipyridine), which should be photo-functional. In order to predict the photochemical properties and functions of those peptides, we have synthesized the model complexes, ruthenium tris(2,2-bipyridine) bear-ing amide groups at 5,5'-positions (Figure 2). Here we report the synthesis, crystal structures, photo-chemical properties, and functions of these model complexes, and further discuss the design of artificial proteins with photochemical functions.

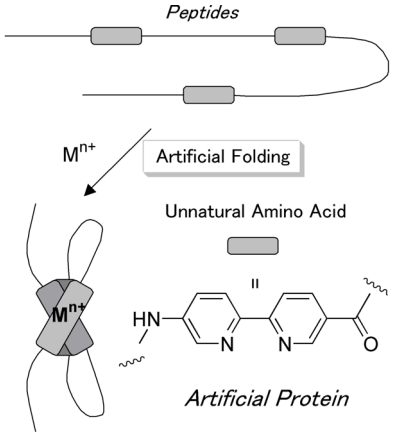

Fig. 1. Molecular design of artificial proteins utilizing unnatural amino acids.

Results and Discussion

Abbreviation for ligands, **5RNHCO-bpy**, **5RCONHbpy**, and **RCO-5bpy-NHR**, express the direction of amide groups as shown in Figure 2. 5,5'-Diamino-2,2'-bipyridine [5] and **H-5bpy-OH** [6] were prepared according to the literature. The ruthenium complexes were synthesized by heating or microwave irradiation to the ethylene glycol solution of $RuCl_3$ and the ligand (3 eq.), and were obtained as PF_6 salts.

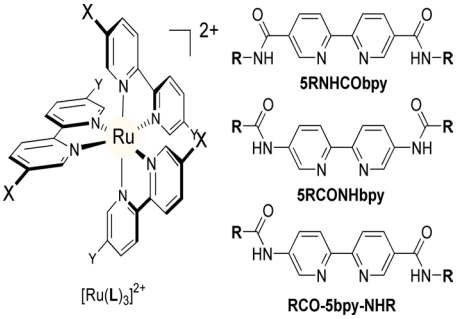

Fig. 2. Ruthenium model complexes and the ligands.

The photochemical properties of these ruthenium model complexes were examined in acetonitrile. As observed in the parent ruthenium complex $[Ru(bpy)_3]^{2+}$ (λ_{abs} = 451 nm; λ_{em} = 611 nm; τ = 1.00 μs), these ruthenium tris(bipyridine) complexes bearing amide groups at 5,5'-positions in the ligands maintained the basic photo-physical properties of the parent one. However, they were strongly dependent on the direction of amide groups: the absorption maximum wavelength (λ_{abs}) for $[Ru(\mathbf{5RNHCObpy})_3]^{2+}$ was 482 nm, which was longer than that for $[Ru(\mathbf{5RCONHbpy})_3]^{2+}$ (441 nm). The maximum wavelength (λ_{em}) and life time (τ) in the emission spectrum were 662 nm and 0.37 μs for the former complex, while 591 nm and 1.72 μs for the latter, respectively. For the significant effect of the direction of amide groups, we were interested in the photo-physical properties for $[Ru(\mathbf{RCO\text{-}5bpy\text{-}NHR})_3]^{2+}$ which had different directions of amide groups in the ligand. We synthesized $[Ru(\mathbf{MeCO\text{-}bpy\text{-}N(}\mathit{c}\mathbf{Hex)_2})_3]^{2+}$ (*c*Hex means cyclohexyl) because we considered that the bulky groups such as cyclohexyl promoted selective synthesis of the *mer* isomer, which was an isomer for octahedral metal complexes with three unsymmetrical bidentate ligands. *mer*-$[Ru(\mathbf{MeCO\text{-}bpy\text{-}N(}\mathit{c}\mathbf{Hex)_2})_3]^{2+}$ showed similar photo-physical properties to $[Ru(bpy)_3]^{2+}$.

In the course of pursuing the function, we investigated the anion binding abilities of these ruthenium complexes. The emission of the complexes in acetonitrile or methanol under air decreased in intensity upon adding tetrabutylammonium salts of Cl^-, Br^-, and I^-. The ruthenium complexes with the symmetrical ligands, **5RNHCObpy** and **5RCONHbpy** were found to bind to these anions with the ratio ($Ru:X^-$) of 1:2. The binding constants were quite large, for example, the values of log β_1 and log β_2 for $[Ru(\mathbf{5MeNHCObpy})_3]^{2+}$ to Cl^- were 5.03 and 9.08 in acetonitrile, respectively. These binding constants increased in the order of $Cl^- > Br^- > I^-$. Although the binding to phosphate anion ($H_2PO_4^-$) was of interest, it gave precipitates in solution and the exact binding constants could not be evaluated.

Peptides into which the unnatural amino acid **H-bpy-OH** was introduced could not be synthesized by the common solid phase synthetic procedure due to poor reactivity of the amino group in the unnatural amino acid. Therefore, we initially synthesized dipeptides, Fmoc-AA-**bpy**-OH (AA denotes a natural amino acid), which could be introduced into the solid phase peptide synthesis. We are currently synthesizing peptides into which two or more unnatural amino acids can be introduced, and we plan to construct artificial proteins with photo-functions based on such model studies.

Acknowledgments

This work was supported, in part, by the Grant-in-Aid for Scientific Research from the Ministry of Education, Culture, Sports, Science, and Technology, Japan (14380292).

References

1. Ishida, H. and Inoue, Y. *Rev. Heteroatom Chem.* **19**, 79-142 (1999).
2. Ishida, H., Suga, M., Donowaki, K. and Ohkubo, K. *J. Org. Chem*. **60**, 5374-5375 (1995).
3. Ishida, H., et al. *J. Org. Chem*. **66**, 2978-2989 (2001).
4. Ishida, H. and Inoue, Y. *Biopolymers (Peptide Science),* **55**, 469-478 (2000).
5. C. P. Whittle, *J. Heterocyclic Chem*. **14**, 191-194 (1977).
6. G. R. Newkome, Gross, J. and Patri, A. K. *J. Org. Chem.* **62**, 3013-3014 (1997).

Peptide Revolution: Genomics, Proteomics & Therapeutics
Michael Chorev & Tomi K. Sawyer (Editors)
American Peptide Society, 2003

Total Synthesis of Uroguanyline

Yoshitaka Nemoto, Jing Xu, Shawn Lee and Baosheng Liu

American Peptide Company, Inc., 777 E. Evelyn Ave., Sunnyvale, CA, USA

Introduction

Guanylin and uroguanylin are peptide ligands for membrane-bound guanylate cyclase C (GC-C) that are located in the intestine, kidney, adrenal gland, pancreas and airway tract [1]. In the literature [2], the yield of these peptides prepared by solid-phase methodology using Fmoc/HBTU chemistry was significantly low. As part of our on-going work on the synthesis of these peptides, we tried to enhance the yield of the peptide by using combination of solid-phase and solution-phase synthesis.

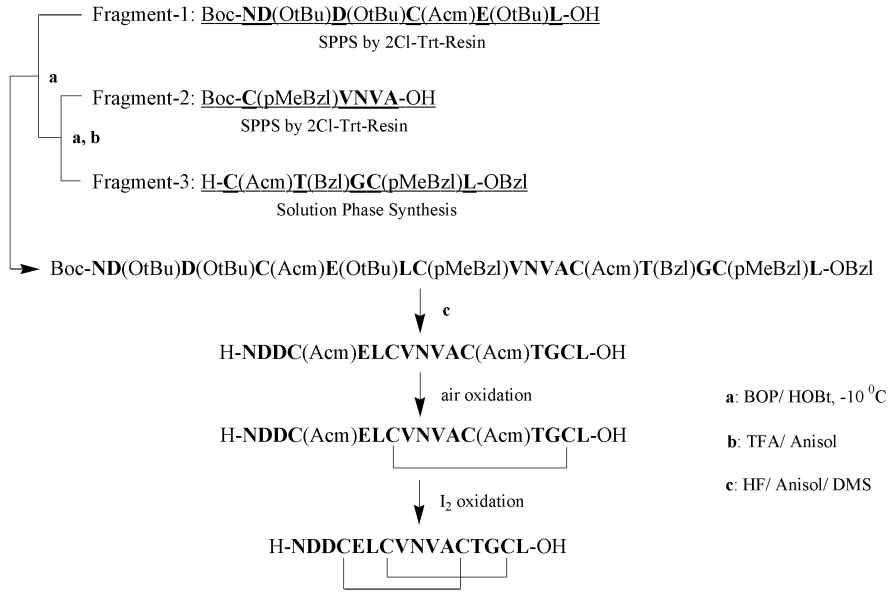

Fig. 1. Synthesis Scheme of Uroguanyline.

Results and Discussion

The synthesis of uroguanylin was achieved by fragment condensation as shown in Figure 1. Fragment 1 and 2 were prepared by solid-phase methodology using 2Cl-Trt-Resin. Fragment 3 was prepared by Boc-based stepwise solution-phase synthesis. BOP/HOBt was used for each fragment coupling at -10 ºC and HF was used for final deprotection (Figure 2). The first disulfide bond (Cys7-Cys15) was introduced by air oxidation. To obtain final product with high purity, HPLC purification of the monocyclic Acm2-peptide was performed (Figure 2). The second disulfide bond was introduced by iodine treatment of Cys(Acm) residues. The bicyclic product was purified by preparative C18 HPLC (Figure 2). Over all yield was 15% (purity >95%). This yield is much higher than that obtained from SPPS (3% yield) using Fmoc/HBTU chemistry (Table 1).

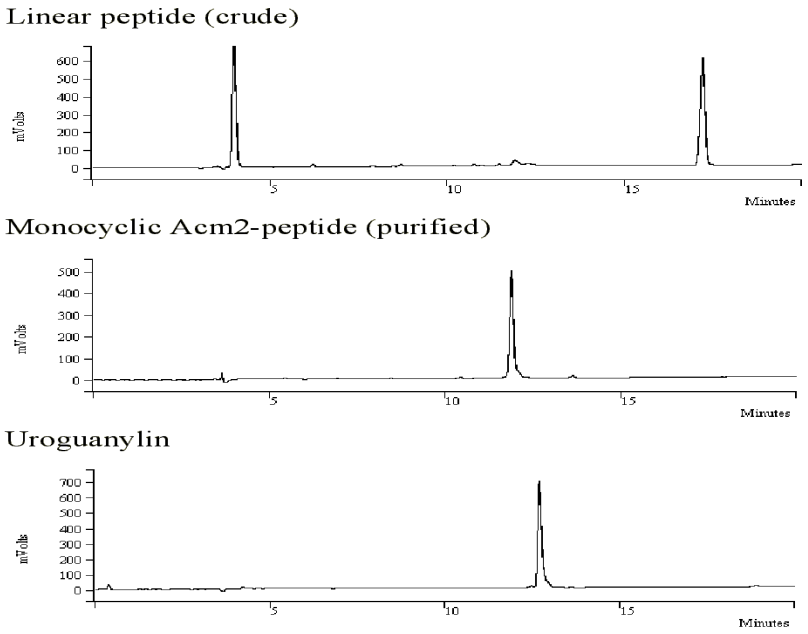

Fig. 2. Reverse-phase HPLC of crude peptide intermediates and purified Uroguanylin (97-112).

Table 1. The Comparison of the Yield between SPPS and Combination of SPPS and Solution Phase Synthesis.

Method	Overall yield
Solid-phase synthesis	3%
Combination of solid-phase and solution-phase synthesis	15%

References

1. Forte, L. R., Eber, S. L., Turner, J. T., Freeman, R. H., Fok, K. F and Currie, M. G. *J. Clin. Invest.* **91**, 2423-2428 (1993).
2. Klodt, J., Kuhn, M., Marx, U. C., Martin, S., Rosch, P., Forssmann, W. G. and Adermann, K. *J. Peptide Res*. **50**, 222-230 (1997).

Peptide Revolution: Genomics, Proteomics & Therapeutics
Michael Chorev & Tomi K. Sawyer (Editors)
American Peptide Society, 2003

Synthesis of Prokineticin 2 Employing a Convergent Solid-Phase Strategy Performed in a Chloroform-Phenol Mixed Solvent

Masanori Ishimaru, Yuji Nishiuchi, Hideki Nishio and Terutoshi Kimura

Peptide Institute Inc., Protein Research Foundation, Minoh-shi, Osaka 562-8686, Japan

Introduction

A chloroform and phenol mixed solvent system (v/v, 3/1) proved to be essential for coupling sparingly soluble protected segments without danger of epimerization and of phenyl ester formation, if the EDC/HOOBt-mediated coupling reaction was performed in the solution phase [1]. This solvent system possesses a much higher solubilizing potential than those of the commonly used organic solvents, including a mixture of chloroform and TFE. We successfully applied this system to a combined solid-phase and solution approach for the synthesis of green fluorescent protein (238 AAs) and human leptin (146 AAs). This procedure is based on performing the segment condensation reaction in solution employing a maximum protection strategy with Boc chemistry. Each segment used in the subsequent segment condensation is prepared by solid-phase assembly on a base-labile *N*-[9-(hydroxymethyl)-2-fluorenyl]succinamic acid (HMFS) linker, which is cleaved by treatment with 20% morpholine in DMF to release fully protected segments with a free α-carboxyl group. In this context, base-resistant side-chain protecting groups such as the cyclohexyloxycarbonyl (Hoc) group for Trp and the 3-pentyl (Pen) group for Tyr are indispensable for preparing highly homogeneous protected segments [2]. In the present study, to grasp the scope and limitations of the chloroform-phenol mixed solvent as a coupling medium in peptide synthesis, we used it for convergent SPPS (CSPPS) involving the coupling of protected peptide segments on a solid support.

Results and Discussion

The solvent employed for CSPPS must possess a solubilizing potential for achieving high concentrations of protected segments as well as effective solvation of the peptide resin, both of which are the most crucial conditions for efficient chain assembly on a solid support. First, we examined the swelling properties of peptide-resin in chloroform-phenol (v/v, 3/1) by comparing them with those in commonly used organic solvents. This solvent system could help maintain the swelling of the peptide-resin matrix to approximately 1.5- to 2-fold the volume of that in DCM or NMP, even in the case of a relatively highly substituted resin with more than 50% of the weight content of the peptide-resin being the protected peptide. Next, we examined the coupling conditions suitable for CSPPS by a model coupling reaction of Boc-Phe-Ile onto the Phe-Gly-HMFS resin. After detachment of the resulting tetrapeptide by treatment with 20% morpholine in DMF, the purity and yield of the product were assessed by RP-HPLC. The diisopropylcarbodiimide (DIC)/HOAt method using chloroform-phenol was determined to be the most efficient for CSPPS, although HOOBt appeared to surpass HOAt with regard to the suppressive effect on epimerization and phenyl ester formation (Table 1). However, the carbodiimide-mediated coupling in the presence of HOOBt was accompanied by a considerable amount of azidebenzoyl derivative (0.4-1.2%) due to Lossen's rearrengement, whereas the formation of this by-product was negligible in the solution phase (< 0.1%). When the EDC·HCl/HOAt or HOOBt method was used, as in the case of the solution phase, the extent of epimerization was

Table 1. Effects of solvents and additives on the yield and epimerization with Ile in the coupling mediated by DIC (1 eq) between Boc-Phe-Ile-OH (1 eq) and H-Phe-Gly-O-HMFS resin.

Solvent	Additive	Yield[a]	Epimerization[a]	Ester formation[a]
DMF	HOBt	94.8	7.4	-
	HOAt	96.8	3.6	-
	HOOBt	92.0	1.8	-
$CHCl_3$-TFE (v/v, 3/1)	HOBt	89.5	1.2	8.9
	HOAt	94.6	0.7	0.9
	HOOBt	93.9	0.4	0.5
$CHCl_3$-phenol (v/v, 3/1)	HOBt	83.5	1.1	16.1
	HOAt	94.1	0.3	1.1
	HOOBt	94.2	0.2	0.8

[a]*Values (%) assessed by HPLC (220 nm).*

found to increase by one order of magnitude in every solvent system, compared with that obtained by using DIC. Furthermore, the use of HATU resulted in the same tendency with epimerization. This may be related to the basicity of EDC·HCl or HATU itself, which would be critical for the slow coupling process in CSPPS.

In order to demonstrate the utility of CSPPS performed in chloroform-phenol with the aid of the DIC/HOAt method, this procedure was applied to the synthesis of prokineticin 2, an 81 residue-peptide having five intramolecular disulfide bonds (AVITGACDKD-SQCGGGMCCA-VSIWVKSIRI-CTPMGKLGDS-CHPLTRKVPF-FGRRMHHTCP-CLPGLACLRT-SFNRFICLAQ-K), which was identified as a selective mitogen for endocrine gland endothelial cells [3]. The molecule was divided into eight parts, i.e. seven segments (1-14), (15-26), (27-35), (36-43), (44-52), (53-64) and (65-78), and one resin-bound C-terminal segment (79-81). The protected segments were synthesized on HMFS resin using Boc chemistry, except for the C-terminal one, which was elongated on a PAM resin. The protected segments detached from the HMFS resin were purified by reprecipitation and/or silica-gel chromatography. The homogeneity of each segment, determined by amino acid analysis, TLC, HPLC and ESI MS, was found to be more than 95% pure. Next, the molecule was constructed by sequential assembly of seven segments in chloroform-phenol onto the resin-bound C-terminal segment. Each segment condensation reaction proceeded smoothly when 1.5-2 eq of the respective segment, DIC and HOAt were used, except for the coupling of segment (53-64) onto the resin-bound segment (65-81). This was incomplete even after the double coupling procedure was performed, since the formation of phenyl ester preferentially occurred in chloroform-phenol. It was recognized that the His(Bom)-containing segment enhances its own ester formation in the coupling reaction due to the catalytic effect of the unprotected τ-nitrogen of His(Bom). The extent of ester formation in the corresponding coupling, however, was much higher than we had expected. This may have been due to two consecutive His(Bom) residues on segment (53-64). To avoid this issue, we are now carrying out the synthesis using His(DNP), which is expected to possess less basicity in the imidazol moiety than His(Bom).

In conclusion, the present synthetic strategy used with the chloroform-phenol mixed solvent permits facile synthesis of large peptides using the solid-phase method.

References

1. Inui, T., et al. *Lett. in Pept. Sci*. **8**, 319-330 (2002).
2. Nishiuchi, Y., et al. *J. Pept. Sci*. **6**, 84-93 (2000).
3. Bullock, M. Li. C. M. et al. *Mol. Pharmacol*. **59**, 692-698 (2001).

Peptidomimetic and Pseudopeptide Synthetic Chemistry

Peptide Revolution: Genomics, Proteomics & Therapeutics
Michael Chorev & Tomi K. Sawyer (Editors)
American Peptide Society, 2003

3-Aminopiperidones as Dipeptide Constrained Surrogates in Biologically Relevant Compounds

Mònica Garcia[1,2], Xavier del Río[1], Rachid El Hafi[1], Patricia López[1], Eulàlia Pinyol[1], Jordi Piró[2], Pilar Forns[2], Mario Rubiralta[1,2], Ernest Giralt[1,3] and Anna Diez[1,2*]

[1]IRBB-Parc Científic de Barcelona, c/ Josep Samitier, 1-5. 08028-Barcelona, Spain; [2]Laboratori de Química Orgànica, Facultat de Farmàcia, Universitat de Barcelona, 08028-Barcelona, Spain; [3]Departament de Química Orgànica, Facultat de Química, Universitat de Barcelona, 08028-Barcelona, Spain

Introduction

We have prepared a series of 3-aminopiperidones to be used as constrained surrogates of dipeptides. Three applications of some of these scaffolds are presented:

1. As β-turn mimetics in the synthesis of potential inhibitors of HIV-1 protease dimerization (**1**).
2. As β-turn mimetics in the synthesis of ψ-Stylostatins as potential anticancer agents (**2**).
3. In the synthesis of a targeted library of potential tryptase inhibitors (**3**).

1. Inhibitors of HIV-1 protease dimerization in anti-AIDS therapy

Human immunodeficiency virus type 1 (HIV-1) RNA encodes an aspartate protease which is responsible for the processing of gag-pol polyproteins to mature structural proteins and functional enzymes required in the viral life cycle.

Dimerization of HIV-1 protease is essential to attainment of the mature structure, an enzymatically active C_2-symmetric homodimer. The dimerization interface is largely composed of interdigitated *N*- and *C*-terminal portions of the protease, which thus form a four-stranded antiparallel β-sheet (Figure 1). The X-ray structure shows that the interface directly involves the *N*-terminal residues 1-4 and *C*-terminal residues 96-99 [1]. By targeting this β-sheet portion of the protease, a region which is highly conserved among HIV-1 isolates, it may be possible to generate agents which block the assembly of the homodimer or disrupt the dimeric interface, and so lead to loss of biological activity.

Dimerization inhibitors being developed in the context of this research are based on the structure composed of the native sequences of HIV-1 protease *N*- and *C*-termini. The two peptides need to be connected by an alkyl chain to ensure the correct interaction distance (Figure 2) [2].

Our objective is to substitute pseudopeptides with restricted conformation (Figure 2) for some of the dipeptides in these structures, to enable the study of their activity as inhibitors of HIV-1 protease dimerization.

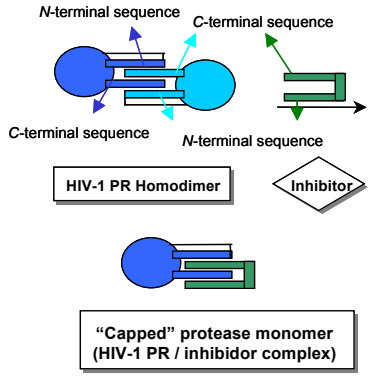

Fig. 1. Schematic of the HIV-1 protease dimer and its disruption by an inhibitor.

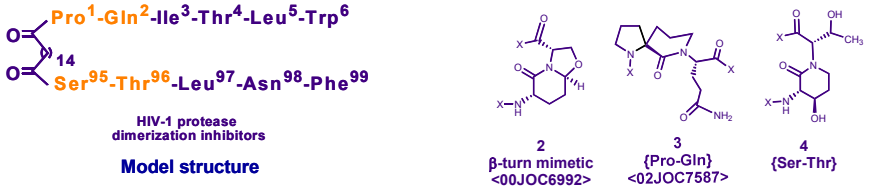

Fig. 2. Model of HIV-1 dimerization inhibitor (left panel) and conformationally constrained pseudodipeptides as potential building blocks.

2. Analogs of stylostatin 1 as anticancer agents [3]

Stylostatin 1 (**5**), a marine cycloheptapeptide isolated and characterized in 1992, was reported to have antileukemic properties [4]. X-Ray crystallographic analysis reveals two β-turns, one centered on Ile-Pro, the other on Ser-Leu (Figure 3) [4]. The structural characteristics of stylostatin 1 make it a good model for evaluating the lactam {Ser-Leu} pseudopeptide **6** as a β-turn mimetic, and for studying the biological activity of the conformationally restricted sequence.

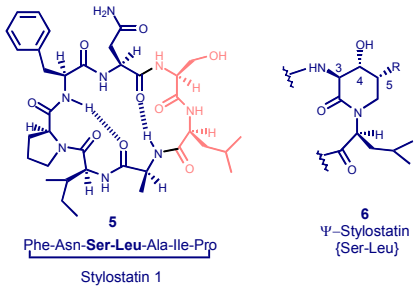

Fig. 3. Stylostatin 1 and a pseudo{Ser-Leu} mimetic.

The synthesis of the native peptide and of ψ-stylostatins has been achieved by macrocyclization through both the Ile-Pro [5] and the Pro-Phe ω bonds. In both cases the linear precursors were prepared manually on solid phase (Fmoc protocol using HBTU/HOBt/DIPEA), and cyclized in solution.

The first approach (Ile-Pro) also yields epimerized derivatives that contain D-*allo*-Ile. However, a parallel experiment (monitored by HPLC) demonstrated that the cyclization rate is 15 times faster for the pseudopeptide, which indicates that the lactam ring induces a turned conformation of the linear precursor.

Macrocyclization through the Pro-Phe bond gave the target compounds as the only products, and in good yields (HPLC analysis and purification).

NMR studies of the ψ-stylostatins and their epi-derivatives (5 compounds total) showed that the lactam ring profoundly modifies the secondary structure of the cyclopeptide. Thus, stylostatin 1 shows only one conformation in which the Ile-Pro ω bond is *cis*, whereas the presence of D-*allo*-Ile induces a *trans* conformation of the X-Pro amide bond. The non-epimerized ψ-stylostatins show a mixture of two conformers, which happen to be *cis* and *trans* about the Ile-Pro amide bond.

The more flexible ψ-cyclopeptides appear to be less active than stylostatin 1 against a number of cancer cell lines. New derivatives with potential antibiotic activity are being developed.

3. Targeted library of potential tryptase inhibitors

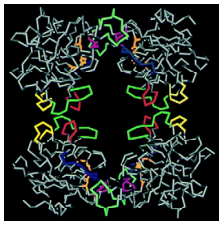

Tryptase is a homotetrameric serine protease (Figure 4), secreted by lung mast cells, that has been implicated in the pathogenesis of asthma and other allergic and inflammatory conditions. Recent approaches to developing selective inhibitors of tryptase have focused on symmetric molecules presenting bivalent amidino or guanidino moieties (Figure 5) [6].

Fig. 4. Human tryptase.

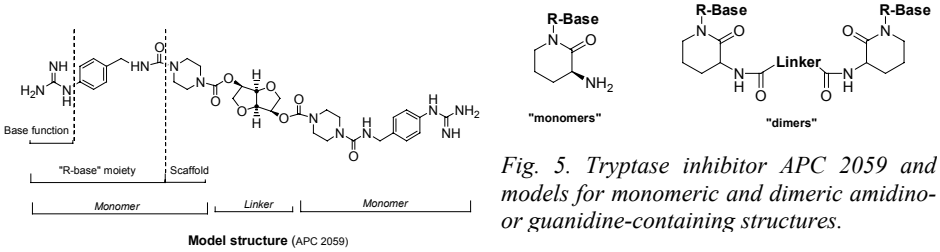

Fig. 5. Tryptase inhibitor APC 2059 and models for monomeric and dimeric amidino- or guanidine-containing structures.

Our research group is working on the design and synthesis of a small library of potential tryptase inhibitors of mono- and dimeric structure, related to the molecule APC 2059 (presently in phase II clinical trials). We are developing strategies for both solution and solid phase syntheses, with the aim of optimizing the yield and purity of the final products.

Acknowledgments

This research is funded by the Spanish government through grant BQU2001-3228, and by the Catalan government through grant SGR2001-00082. We also thank Pharma Mar, S.A. and Almirall-Prodesfarma, S.A. for performing the biological tests.

References

1. a. Todd, M. J., Semo, N. and Freire, E. *J. Mol. Biol*. **283**, 475-488 (1998). b. Song, M., Todd, M. J., Semo, N. and Freire, E. *J. Mol. Biol*. **283**, 475-488 (1998). c. Zutshi, R., Shultz, D., Luckner, U., Lutgring, R., Bishop. P., Schweitzer, B., Vogel, K., Franciskovich, J., Wilson, M. and Chmielewski, J. *Synth. Lett.* 1040-1044 (1998).
2. a. Bouras, A., Boggetto, N., Benatalah, Z., de Rosny, E., Sicsic, S. and Reboud-Ravaux, M. *J. Med. Chem*. **42**, 957-962 (1999). b. Schultz, M. D., Bowman, M. J., Ham, Y.-W., Zhao, X., Tora, G. and Chmielewski, J. *Angew. Chem. Int. Ed*. **39**, 2710-2713 (2000). c. Zutshi, R. and Chmielewski, J. *Bioorg. Med. Chem. Lett.* **10**, 1901-1903 (2000). d. Song, M., Rajesh, S., Hayashi, Y. and Kiso, Y. *Bioorg. Med Chem Lett*. **11**, 2465-2468 (2001).
3. Forns, P., Piró, J., Cuevas, C., García, M., Rubiralta, M., Giralt, E. and Diez, A. *J. Med. Chem*. **46**, 5825-5833 (2003).
4. Pettit, G. R., Srirangam, J. K., Herald, D. L., Erickson, K. L., Doubeck, D. L., Schmidt, J. M., Tackett, L. P. and Bakus, G. J. *J. Org. Chem*. **57**, 7217-7220 (1992).
5. For a precedent using this strategy, see: Bourne, G. T., Meutermans, W. D. F., Alewood, P. F., McGeary, R. P., Scanlon, M., Watson, A. A. and Smythe, M. L. *J. Org. Chem*. **64**, 3095-3101 (1999).
6. a. Sommerhoff, C. P., Bode, W., Matschiner, G., Bergner, A. and Fritz, H. *Biochim & Biophys*. *Acta* **1477**, 75-89 (2000). b. Sommerhoff, C. P., Söllner, C., Mentele, R., Piechottka, G. P., Auerswald, E. A. and Fritz, H. *Biol. Chem*. **375**, 685-694 (1994).

Peptide Revolution: Genomics, Proteomics & Therapeutics
Michael Chorev & Tomi K. Sawyer (Editors)
American Peptide Society, 2003

Synthesis of Aminopyrrole Carboxylate Analogs for Peptide Mimicry

Guillaume Jeannotte, Karl A. Hansford, Félix-Antoine Marcotte, Frederik Rombouts, Valeria Zanzarova and William D. Lubell

Département de Chimie, Université de Montréal, C.P. 6128, Succursale Centre-Ville, Montréal, Québec H3C 3J7, Canada

Introduction

Aminopyrrole 2-carboxylates **1**, pyrrolo-prolines **2** and pyrrolopyrimidine-6-carboxylates **3** may all be considered as flattened prolines possessing respectively functionality at the β-, γ- and δ-carbons (Figure 1). The high presence of proline in secondary structures involved in recognition events in protein chemistry bears well for heterocyclic amino acids like **1**-**3** to serve as useful scaffolds for orienting various pharmacophores in ways that mimic natural biologically active peptides. For example, 4-amino-pyrrole-2-carboxylates **1** has been frequently employed in the synthesis of oligomeric amides that bind to the minor groove of DNA and exhibit antibiotic activity [1]. In model dipeptides, pyrroloprolines **2** have shown potential for β-turn mimicry [2]. Pyrrolopyrimidines **3** share structural homology with thienopyrimidines, a class of mimics that have found use as non-peptide antagonists for the h-LHRH receptor [3]. In addition, aminoazole carboxylates, such as **4**, act as rigid *cis*-amide surrogates that may serve as type VI β-turn mimics [4,5]. Protocols for the diversity-oriented synthesis of peptide mimic libraries from pyrroles **1**-**4** may thus provide promising candidates for studying protein receptor chemical biology.

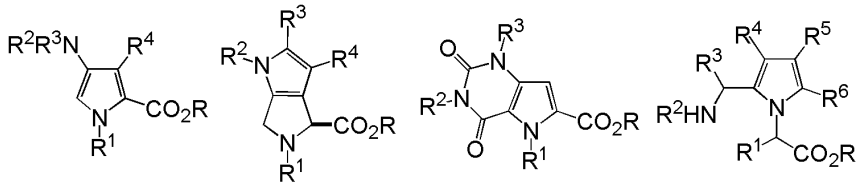

1 **2** **3** **4**

*Fig. 1. Representative aminopyrrole carboxylates **1-4** for peptide mimicry.*

Results and Discussion

Recently, we demonstrated that 4-aminopyrrole 2-carboxylates **1** can be effectively obtained by reacting 4-oxo-*N*-(PhF)prolinate **5** with primary and secondary amines and catalytic acid in a polar solvent (PhF = 9-(9-phenylfluorenyl)) [6] (Figure 2). This method has provided various 4-aminopyrrole-2-carboxylates possessing diverse substituents at the 4-position. An effective means for preparing pyrrolo[3,2-d]pyrimidine 6-carboxylates **3** with various substituents at the pyrimidine nitrogens was next developed using three additional steps from aminopyrrole **1** by reacting it with an isocyanate, acylation of the resulting urea with trichloroacetyl chloride in acetonitrile and stirring with Cs_2CO_3. Crystallization from toluene gave the desired deazapurines in 37-55 % overall yields from proline **5** [7].

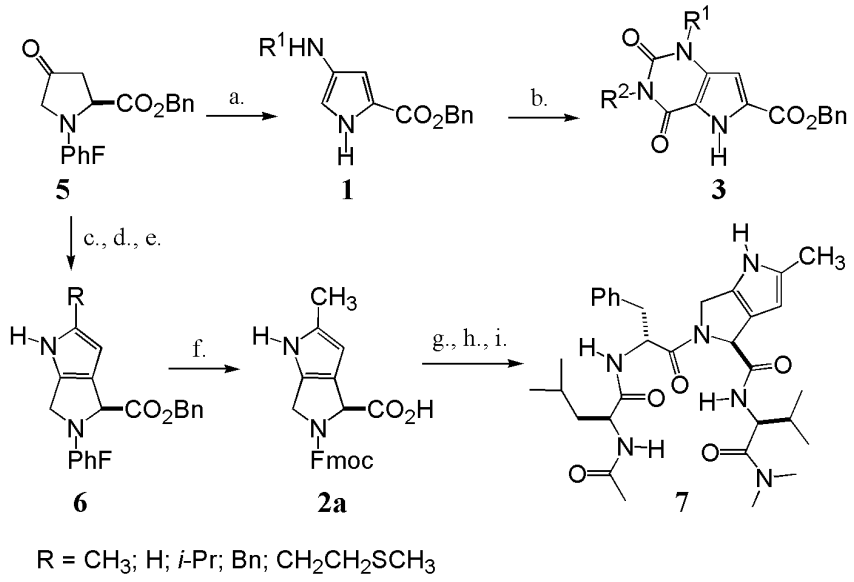

*Fig. 2. Synthesis of aminopyrrole carboxylates **1-3** and tetrapeptide **7**: a. ref. 6; b. ref. 7; c. n-BuLi, THF, –78°C; RCH(NHBoc)CHO; d. conc. HCl, CH_2Cl_2; e. 180°C, neat; f. H_2, $Pd(OH)_2$, MeOH:THF; Fmoc-OSu, $NaHCO_3$, dioxane:H_2O; g. Val-N(Me)$_2$, TBTU, DIEA, CH_2Cl_2; h. $N(CH_2CH_2NH_2)_3$, CH_2Cl_2; i. Ac-Leu-D-Phe, TBTU, DIEA, CH_2Cl_2.*

A series of protected pyrrolprolines **2** have been synthesized from *N*-PhF-4-oxoproline benzyl ester **5** by a process featuring enolization with *n*-BuLi in THF at –78°C, aldol condensation with *N*-(Boc)aminoaldehyde and acid catalyzed cyclization to the pyrrole [2]. After chromatography to remove **5**, the aldol intermediates were isolated as diastereomeric mixtures contaminated with starting aldehyde. The mix was treated with conc. HCl in DCM to afford *N*-(Boc)pyrroles, which were deprotected by thermolysis at 180°C to give pyrroles **6** in 8-32% yields from **5**. Hydrogenation of **6a** (R = Me) with $Pd(OH)_2$ as catalyst in THF:MeOH at 5 atm of H_2 effected cleavage of the PhF and benzyl groups. Acylation of the pyrrolidine nitrogen with Fmoc-OSuc and $NaHCO_3$ in a H_2O:dioxane solution affords Fmoc-protected amino acid **2a** in 76% yield from **6a**. Model tetrapeptide **7** was synthesized from **2a** by coupling Val-N(Me)$_2$ using TBTU and DIEA in CH_2Cl_2 for 24 h. After aqueous workup and chromatography eluting with 3% MeOH in $CHCl_3$, the corresponding dipeptide was isolated in 70% yield. Removal of the Fmoc group was accomplished in 39% yield using tris(2-aminoethyl)amine in CH_2Cl_2, followed by aqueous workup and chromatography with 1:1:18 MeOH:Et_3N:$CHCl_3$ as eluant. Tetrapeptide **7** was obtained in 67% yield on coupling Ac-Leu-D-Phe to the pyrrolidine nitrogen using the same TBTU procedure and chromatography eluting with 5% MeOH in $CHCl_3$. Examination of the COSY NMR spectrum of **7** in $CDCl_3$ showed a predominant isomer in which the Val, D-Phe and Leu amide protons were respectively assigned to signals at 6.66, 7.43 and 7.74 ppm. This pattern, and the J_{NH} coupling constants for these residues, resembled closely that of the related Leu-D-Phe-Pro-Val region of the cyclic-peptide gramicidin S which adopts a type II' β-turn [8]. In DMSO, peptide **7** existed as a 60:40 mixture of conformational isomers.

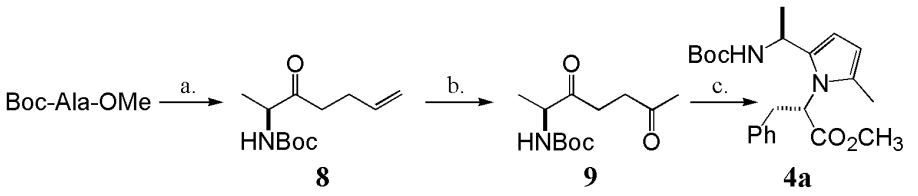

*Fig. 3. Synthesis of aminopyrrole carboxylate **4**: a. 500 mol% H_2C=CHMgBr, 50 mol% Cu(OAc)$_2$, THF –40°C - rt; b. 10 mol % $PdCl_2$, 100 mol% CuCl, O_2, DMF:H_2O; c. 500 mol% Phe-OMe, 150 mol% 1:1 NaOAc:AcOH, toluene, 65°C.*

Finally, a novel approach for synthesizing pyrrole dipeptide surrogate **4** is under development to facilitate its application (Figure 3). *N*-(Boc)Alanine methyl ester was reacted with 500 mol% of vinyl magnesium bromide and 50 mol% of Cu(OAc)$_2$ in THF at –40°C to rt to afford homoallylic ketone **8** in 65 % yield. The mechanism of this reaction is presumed to involve nucleophilic attack with elimination of methoxide to form an enone intermediate that undergoes 1,4-addition to furnish the enolate that on work-up gives homoallylic ketone **8**. Because no epimer was detected when using this reaction on Boc-Thr-OMe and Boc-HyPro-OMe, we assume that **8** is significantly enantiomerically enriched in the *S*-isomer. Olefin oxidation of ketone **8** with 10 mol% $PdCl_2$ and 100 mol% CuCl in a 7:1 DMF:H_2O solution stirred under a balloon of oxygen overnight provided 1,4-diketone **9** in 83% yield. Knorr condensation of **9** with benzylamine, NaOAc, AcOH and 4Å molecular sieves in toluene gave the desired pyrrole in 30 min and 73 % yield. Under similar conditions, Phe-OMe reacted slower with diketone **9** such that the rigid dipeptide surrogate **4a** was obtained in 30% yield after 36 h. Integration of the diastereotopic signals in the ^{1}H NMR spectrum demonstrated that epimerization had occurred and that **4a** was only 20% diastereomerically pure. This rapid access to azole dipeptide surrogates **4** was thus compromised by the configurational lability of the amino ketone and imino carboxylate intermediates. Our investigation is presently targeted on conditions to form pyrrole **4** without epimerization. In sum, we have introduced four new diversity-oriented synthesis methods for preparing aminopyrrole carboxylates for use in peptide mimicry.

Acknowledgments
This research was supported by NSERC (Canada) and FQRNT (Québec).

References

1. Wang, C. C. C. and Dervan P. B. *J. Am. Chem. Soc*. **123**, 8657 (2001).
2. Jeannotte, G. and Lubell, W. D. In Benedetti, E. and Pedone, C (Eds.) *Peptides 2002 (Proceedings of the 27th Eur. Peptide Symp.),* Edizioni Ziino, Napoli, Italy, p. 206-207 (2002).
3. Sasaki, S., Cho, N., Nara, Y., Harada, M., Endo, S., Suzuki, N., Furuya, S. and Fujinor, M. *J. Med. Chem.* **46**, 113-124 (2003).
4. Zabrocki, J., Smith, G. D., Dunbar, J. B. Jr., Marshall, K. W., Iijima, H. and Marshall, G. R. *J. Am. Chem. Soc.* **110**, 5875 (1988).
5. Abell, A. D., Hoult, D. A. and Jamieson, E. J. *Tetrahedron Lett*. **33**, 5831-5832 (1992).
6. Marcotte, F.-A. and Lubell, W. D. *Org. Lett*. **4**, 2601 (2002).
7. Marcotte, F.-A., Rombouts, F. and Lubell, W. D. *J. Org. Chem*. **68**, 6984-6987 (2003).
8. Bach, II, A. C., Markwalder, J. A. And Ripka, W. C. *Int. J. Peptide Protein Res*. **38**, 314 (1991).

Peptide Revolution: Genomics, Proteomics & Therapeutics
Michael Chorev & Tomi K. Sawyer (Editors)
American Peptide Society, 2003

Advances in a Structure Activity Study of the Aureobasidin Peptide Antibiotics: Synthesis of L-*N*-Boc-*N*-Methyl-*β*-Hydroxyvaline

James E. Dettwiler, Laurent Bélec and William D. Lubell

Département de chimie, Université de Montréal, C.P. 6128, Succursale Centre Ville, Montréal, QC H3C 3J7, Canada

Introduction

Aureobasidins are a family of ~20 related potent antifungal antibiotic cyclic depsi-nonapeptides produced by black yeast [1-4]. The L-*N*-methyl-*β*-hydroxyvaline residue has been suggested to play a central role in their activity based on limited SAR data from the natural peptides. The biological activity of the aureobasidins is likely mediated by an equilibrium involving amide isomerization *N*-terminal to Pro-5 [3] such that they adopt both *trans*-amide type II' and *cis*-amide type VI *β*-turn conformations (Figure 1) [4]. Exploring the importance of turn geometry on activity, we are pursuing the synthesis of analog **1** possessing an indolizidin-2-one amino acid [5] as a constrained mimic of the type II' isomer. We report herein an effective protocol for the construction of a protected form of the prerequisite L-*N*-methyl-*β*-hydroxyvaline building block [6].

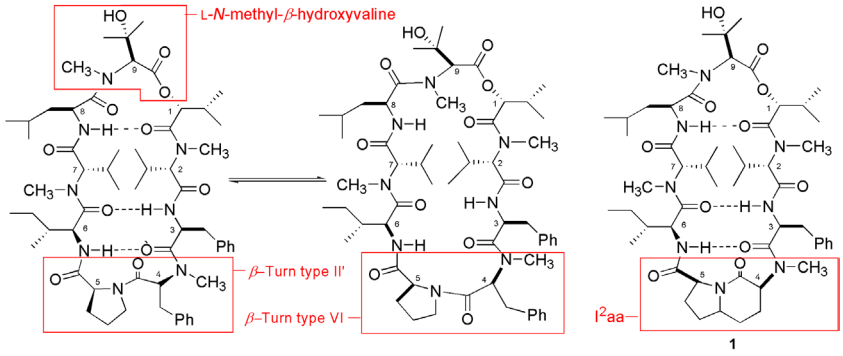

*Fig. 1. Trans- and cis-amide isomers of aureobasidin B, and constrained trans-amide analog **1**.*

Results and discussion

Recently, we reported syntheses of enantiopure *N*-protected *β*-hydroxyvaline in two steps and 75-80% overall yield from *N*-protected serine methyl ester, featuring MeMgBr addition followed by TEMPO oxidation [7]. Because *N*-methylation of *N*-Boc-*β*-hydroxyvaline was unsuccessful using various methods, we have examined an alternative route to L-*N*-Boc-*N*-methyl-*β*-hydroxyvaline (**2**) (Figure 2). D-*N*-(PhF)Serine methyl ester [8] was converted to its oxazolidine carboxylate **3** in 93% yield [9] with formaldehyde and catalytic *p*-TsOH [10] in THF. The addition of MeLi to a solution of ester **3** in THF at 0°C produced oxazolidine alcohol **4** in 91% yield as a mixture of equilibrating geometric isomers, as shown by NMR experiments in different solvent. Treatment of **4** with $NaBH_3CN$ and HCl in anhydrous dioxane afforded **5** *N*-methyl aminodiol in 86% yield [10]. Attempts to selectively oxidize **5** failed; however, hydrogenation of **5** in the presence of $(Boc)_2O$ gave in 82% yield the corresponding Boc protected diol **6** [11], which was oxidized to L-*N*-Boc-*N*-methyl-*β*-hydroxyvaline

(**2**) in 87% yield using TEMPO free radical, $NaOCl_2$ and NaOCl in a sodium phosphate buffered acetonitrile solution [7]. To assess for racemization, protected acid **2** was converted to diastereomeric dipetides **7** by coupling respectively to L- and D-Phe-OMe·HCl using TBTU, HOBt and DIEA in acetonitrile. After removal of the *N*-Boc group with HCl(g) in CH_2Cl_2, observation of the ^1H NMR spectra of crude samples of **7** in MeOD and integration of the signals for the diastereotopic methyl amine singlets at 2.04 and 2.52 ppm demonstrated dipeptide **7** to be of >99% diastereometric purity. *N*-L-Boc-*N*-Methyl-*β*-hydroxyvaline (**2**) is thus assumed to be of similarly high enantiomeric purity. In conclusion, toward the synthesis of constrained aureobasidin analogs, such as **1**, an efficient synthesis of enantiopure L-*N*-Boc-*N*-methyl-*β*-hydroxyvaline has been achieved in 52% overall yield and 5 steps from D-*N*-(PhF)serine methyl ester.

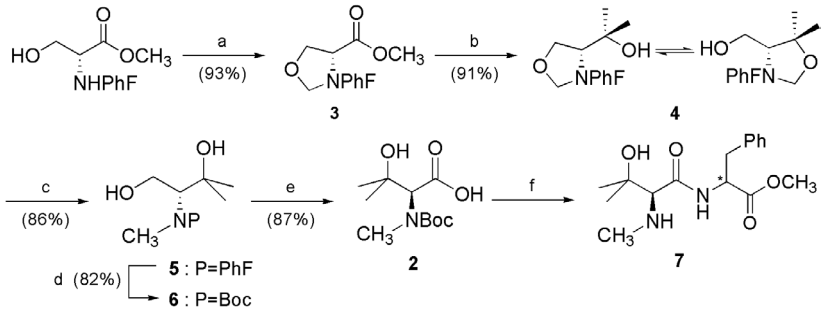

(a) aq. CH_2O, p-TsOH, THF; (b) 250 mol% CH_3Li (1.4 M in ether), THF, 0°C; (c) $NaBH_3CN$, HCl g. dioxane; (d) $(Boc)_2O$, H_2 (5 atm), Pd/C, THF; (e) TEMPO, $NaOCl_2$, NaOCl, CH_3CN, phosphate buffer; (f) D- or L-Phe-OMe·HCl, TBTU, HOBt, DIEA, CH_3CN; HCl, CH_2Cl_2

*Fig. 2. Synthesis and enantiomeric purity of L-N-Boc-N-methyl-β-hydroxyvaline valine (**2**).*

Acknowledgments

This research was supported in part by the Natural Sciences and Engineering Research Council (NSERC) of Canada and the Ministère de l'Éducation du Québec.

References

1. Takesako, K., Kuroda, H., Inoue, T., Haruna, F., Yoshikawa, Y., Haruna, F., Yoshikawa, Y. and Kato, I. *J. Antibiot.* **46**, 1414-1420 (1993).
2. Awazu, N., Ikai, K., Yamamoto, J., Nishimura, K., Mizutani, S., Takesako, K. and Kato, I *J. Antibiot.* **48**, 525-527 (1994).
3. Ishida, T., In, Y., Inoue, M., Fujikawa, A., Urata, H., Inoue, M., Katsushige, I., Ikai, K., Takesako, K. and Kato, I. *J. Chem. Soc., Chem. Commun.* 1231-1233 (1992).
4. Fujikawa, A., In, Y., Inoue, M., Ishida, T., Nemoto, N., Kobayashi, Y., Kataoka, R., Ikai, K., Takesako, K. and Kato, I. *J. Org. Chem.* **59**, 570-578 (1994).
5. Lombart, H.-G. and Lubell, W. D. *J. Org. Chem*. **61**, 9437-9446 (1996).
6. Methods for the synthesis of protected *N*-methyl-*β*-hydroxyvaline are reviewed in reference 7.
7. Dettwiler, J. E. and Lubell, W. D. *J. Org. Chem.* **68**, 177-179 (2003).
8. Lubell, W. D. and Rapoport, H. *J. Org. Chem*. **54**, 3824-3831 (1989).
9. Yields are given for product obtained after chromatography on silica gel.
10. Lubell, W. D., Jamison, T. F. and Rapoport, H. *J. Org. Chem.* **55**, 3511-3522 (1990).
11. Sharma, R. and Lubell, W. D. *J. Org. Chem.* **61**, 202-209 (1996).

Peptide Revolution: Genomics, Proteomics & Therapeutics
Michael Chorev & Tomi K. Sawyer (Editors)
American Peptide Society, 2003

Backbone Cyclic Peptidomimetic Superantigen Antagonists: Synthesis and Biological Activity

Evgenia Glukhov[1], Gila Arad[2], Revital Levy[2], Karina Hazan[1], Sharon Gazal[1], Raymond Kaempfer[2] and Chaim Gilon[1]

[1]Department of Organic Chemistry; [2] Department of Molecular Virology, The Hebrew University of Jerusalem, Jerusalem, Israel

Introduction

Toxic shock syndrome (TSS) is an acute onset illness caused by bacterial production of protein exotoxins called superantigens. TSS of staphylococcal origin is now estimated to have a case fatality rate of 5% [1]. At least 24 different types of toxins were identified (SEA, SEB, SEE, *etc*). In addition to the sequence homology, these bacterial superantigenes also share common 3D structures. The SEB segment (150-161), TNKKKVTAQELD, was found to inhibit SEB superantigenic activity *in vitro* [2]. The above sequence is well conserved and located outside of the known binding domains in the superantigen family. Linear dodecapeptide, termed p12A (aYNKKKATVQELDa), a variant of the sequence (150-161), has a broad spectrum of protective activity in mice against lethal challenge with staphylococcal and streptococcal superantigens [2].

Results and Discussion

In order to increase metabolic stability and efficacy of p12A, we designed two spatial libraries (SEB-1 and SEB-2) consisting of 34 proteinomimetic backbone to backbone, backbone to side chain or side chain to side chain cyclic peptides. The design of these libraries was accomplished by applying the cycloscan [3] methodology to this conserved dodecapeptide segment (150-161) of SEB (PDB file 3SEB, Figure 1).

We have noticed that Lys152 and Glu159 form an intramolecular H-bond that stabilizes the β-sheet-turn-helix motif of the segment. We covalently attached these residues *in-silico* and designed 20 regular and extended backbone cyclic peptides for library SEB-1 (Figure 2). Two modes of peptide cyclization were used: through the side chains of the original amino acids (4 peptides), and by extended backbone cyclization. All 20 peptides have the same sequence, but differ by their modes of cyclization, ring size and ring chemistry. The design of SEB-2 library (Figure 2) was based on the biological results of the SEB-1 library. The SEB-2 library consists of 14 regular and reverse-extended backbone cyclic dodeca- and deca-peptides. The design of the library included: changing of the direction of the amide bond in the linker and the ring positions to alter the location of the positive charge, shortening the peptides by removal of exocyclic amino acids, and introduction of additional positive charge.

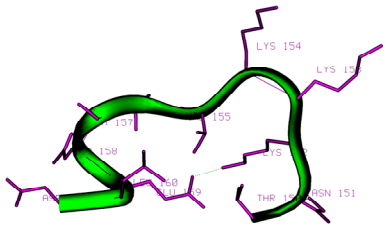

Fig. 1. X-ray structure of the region of SEB(150-161).

Peptides from both libraries were synthesized by the "tea bag" simultaneous multiple peptide synthesis methodology [4] in combination with manual solid phase peptide synthesis in case of SEB-1.

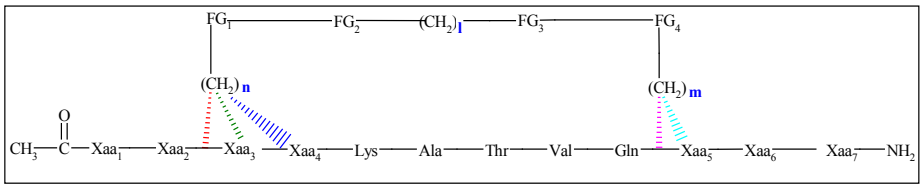

Fig. 2. Structure of SEB-1 and SEB-2 libraries. Xaa represent amino acid or Gly building unit or nothing. FG are N-H or C=O or nothing.

Three types of orthogonal protecting groups (Boc, Allyl/Alloc and Fmoc) were used during the synthesis to obtain the desirable products. Peptides were cleaved from the resin with concomitant deprotection and purified by HPLC. The desired peptides were characterized by ES-MS and amino acid analysis.

Peptides were tested for their ability to inhibit SEB triggered cytokine gene expression (IL-2 and INFγ) by quantitative dot blot method on blood cells of healthy human donors [2].

Cyclic peptides were used in 70 μM (SEB-1) and 0.7mM (SEB-2) concentrations, p12A in 0.7mM and SEB was used in concentration of 100 ng/ml. Data processing was accomplished using arbitrary normalized scoring units. The average scores of SEB13 and SEB18 were three times greater than of p12A (Figure 3). The lead from SEB-2 library was SEB32, which has the N^{α}(1-(4-aminobutyl)1-carboxy)Gly building unit at the N-terminus. Structure-activity relationships of the cyclic peptides indicated that the inhibition activity depends on all conformational parameters used. In conclusion, biological cellular screening led to the discovery of new cyclic peptides that are potentially more effective blockers of TSS exerted by SEB and other superantigens than the parent linear peptide p12A. Moreover, exocyclic amino acids at positions 150 and 151 are not essential for inhibitory activity. The numbers m ,n and l, in figure 2, represent chain lengths at positions 152, 159 and lengths of the bridge between these two positions, respectively, influence inhibitory activity. The best value of n is 6. The best value of m is 2. The best values of l are 1 or 2. We assume that the improved activity of the cyclic peptides SEB18 and SEB32 is due to their enhanced metabolic and conformational stability.

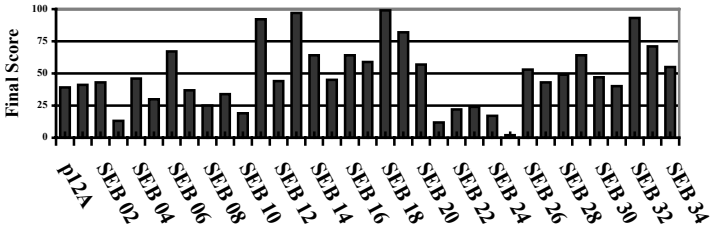

Fig. 3. Relative inhibitory activity of peptides from libraries SEB-1 & 2 (experimental in [2]).

References

1. Stevens, D. et al. *N. Engl. J. Med*. **321**, 1-7 (1989).
2. Arad, G., Levy, R., Hillman, D. and Kaempfer, R. *Nat. Med.* **6**, 414-421 (2000).
3. Gilon, C. et al. In Ramage, R. and Epton, R. (Eds.) *Peptides 1996, Proceedings of the 24th Eur. Peptide Symp.,* Mayflower Scientific, Kingswinford, West Midlands, 1998, p. 423-424.
4. Houghten R. *Proc. Natl. Acad. Sci. U.S.A.* **82**, 5131-5135 (1985).

Peptide Revolution: Genomics, Proteomics & Therapeutics
Michael Chorev & Tomi K. Sawyer (Editors)
American Peptide Society, 2003

Transition Metal Complexes of Linear, Dimeric and Cyclic Pseudopeptides

Siegmund Reissmann[1], Sebastian Kuenzel[1], Georg Greiner[1], Inge Agricola[1], Sylvia Mueller[1], David Pretzel[1], Matthias Schmidt[1], Raiker Witter[2] and Ullrich Sternberg[2]

[1]Institute of Biochemistry and Biophysics; [2]Institute of Optics and Quantum Electronics, Friedrich-Schiller-University Jena, 07743 Jena, Germany

Introduction

Interactions of proteins and peptides with metal ions are in many cases important for their biological activities. To get more insight into specific metal complexation by proteins and into catalytic mechanism of metallo enzymes we synthesized linear and cyclic pseudopeptides as mimetics. We used pseudopeptides with N-alkylated amide groups because of the higher flexibility induced by *cis-trans* isomerism. For our studies we used only those transition metal ions that have a high incidence in metallo enzymes, the bivalent ions of Zn, Ni, Co, Cu and Mn. For a deeper understanding of the complexation motifs we estimated the complex formation tendencies and searched for ligands with a high selectivity [1-4]. Because many metallo enzymes are dinuclear complexes we synthesized cyclic and dimeric ligands with two complexation centers, capable to forming homo- or heterodinuclear complexes.

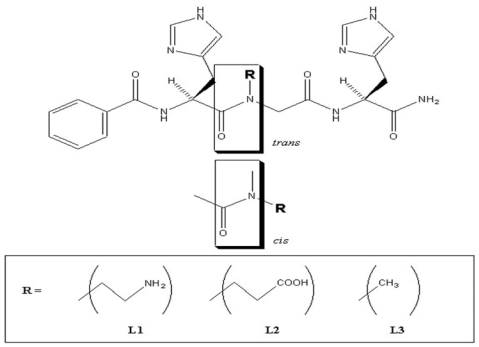

Fig. 1. Common stucture of pseudotripeptides.

Results and Discussion

We applied different methods to estimate the complex formation tendencies. Comparison of pairs by MS methods allows an estimation of the rank order of complexation tendency of one ligand with different metal ions and requires the least amount of substance. Other methods applied, such as potentiometric titration, capillary electrophoresis and circular dichroism provided additional information on structural properties of the formed complexes; however they either required too much pseudopeptide ligand or were not applicable for all transition metal ions used in this study.

Table 1. Ion selectivity of mono- and dinuclear ligands.

No.	Structure	Selectivity
1	Bz-His-N[CH_2-CH_2-NH_2]Gly-His-NH_2	***Cu > Ni*** > Zn ~ Co > Mn
2	Bz-His-N[CH_2-CH_2-CH_2-NH_2]Gly-His-NH_2	***Cu > Co*** > Ni > Zn ~ Mn
3	Bz-His-Sar-His-NH_2	Cu ~ Ni > Zn ~ Co > Mn
4	Bz-Asp-Sar-His-NH_2	Cu ~ Co ~ ***Mn*** > Ni ~ Zn
5	Bz-Glu-Sar-His-NH_2	Cu ~ Ni > Co > Zn ~ Mn
6	Bz-His-Sar-Asp-NH_2	***Co ~ Ni*** > Zn, Cu, Mn
7	Bz-His-Npig-His-NH_2	Cu > Zn > Ni ~ Co ~ Mn
	Structure	Detected dinuclear complexes
8	Bz-His-Sar-His-***(Ala)$_4$***-His-Sar-His-NH_2	Mn2, Zn2,Ni2,Cu2,***NiZn,CoNi,CoZn,CuZn***
9	Bz-His-Sar-Asp-***(Ala)$_4$***-His-Sar-His-NH_2	Zn2,Ni2,Cu2,***CuMn,CuCo,CuNi CuZn***
10	Bz-His-Sar-His-***Gly***-His-Sar-His-NH_2	Zn2,Cu2,***CuZn***
11	Bz-Asp-Sar-His-***Gly***-His-Sar-His-NH_2	Cu2,***CoMn***
12	Bz-His-Naeg -His-***Pro***-His-Sar-His-NH_2	Zn2,Cu2,Ni2,Co2,***CoNi***
13	Bz-His-Npig-His-***Pro***-His-Npig-His-NH_2	Zn2,Cu2,Ni2

Naeg: N[CH_2-CH_2-NH_2]Gly ; Npig: N(1-propylimidzole)Gly.

Some pseudotripeptides (1,3,5,7) do not differ much in terms of selectivity for the metal ions. Since ligands with a high selectivity would be the *sine qua non* condition for the synthesis of heterodinuclear peptide metal complexes, we searched for small, affine and selective metal chelating sequences. For this purpose we systematically replaced the two histidine residues in pseudotripeptide ligand L3 by all possible combinations of His, Lys, Asp and Glu. Some of these tripeptides show good affinity towards transition metal ions and a preference for only one or two of them.

We synthesized dinuclear ligands by bridging the same or different pseudotripeptides by an amino acid or by peptide linkers and also studied the influence of the ligands and of the linkers on the formation of homo- and heterodinuclear complexes. Table 1 shows that not all possible combinations of metal ions in the dinuclear ligands were found. We compared our dinuclear Cu-complexes with the dinuclear Cu-enzyme catecholoxidase. Solomon et al. [5] proposed an enzymatic mechanism involving both copper ions. In our complexes the involvement of both Cu^{2+} becomes evident by the higher catalytic activity of the dinuclear com- plexes compared to the monomeric complexes of the corresponding tripeptide ligands.

Table 2. Kinetic parameters of oxidation of 4-Methylcatechol with Cu^{2+}-complexes at 35 °C.

Ligand	k_{kat} [s^{-1}]	K_m [M]	k_{kat}/K_m [$M^{-1}s^{-1}$]
3	$(7.3 \pm 0.5) * 10^{-4}$	$(2.4 \pm 0.4) * 10^{-4}$	3.9 ± 0.9
8	$(3.2 \pm 0.1) * 10^{-3}$	$(1.8 \pm 0.2) * 10^{-4}$	18 ± 1
10	$(2.5 \pm 0.1) * 10^{-3}$	$(1.4 \pm 0.1) * 10^{-4}$	18 ± 1
Tyrosinase	*$1.0 * 10^{3}$*	*$2.5 * 10^{-4}$*	*$4.0 * 10^{6}$*

The calculated kinetic parameters (Table 2) show that the Km values for all estimated complexes, including the native enzyme tyrosinase, is nearly the same indicating that the affinity to the substrate is nearly the same. But, the pseudomonomolecular rate constants of our complexes are some orders of magnitude lower than for the enzyme. On the other hand the constants are strongly increased for dinuclear complexes compared to the mononuclear ones. Based on our results with dinuclear complexes we propose a catalytic mechanism, which corresponds well with the assumed mechanism for catecholoxidase.

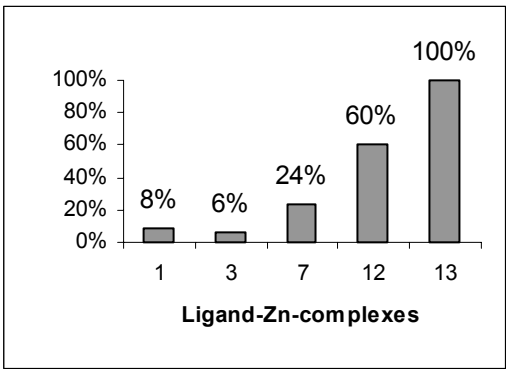

Ligand	k_{BNP}^- [10^{-5} $s^{-1}M^{-1}$]
1	7.2
3	5.3
7	*23.0*
12	51.5
13	83.4

Fig. 2. Hydrolysis of Bis(p-nitrophenyl)phosphate by monomeric and dimeric Zn-Complexes.

Similar results were obtained with dinuclear Zn^{2+}-complexes of dimeric pseudopeptide ligands. The hydrolysis of Bis(p-nitrophenyl)phosphate was strongly enhanced by dinuclear complexes compared to mononuclear complexes (Figure 2). This finding can be explained by the cooperative involvement of both complex bound Zn-ions similar to the enzymatic mechanism of phosphodiesterase.

We studied the influence of cyclization on complex formation with cyclic peptides. The complexation motifs for the cyclic peptides were derived from protein database. Their conformation was designed by the force field program COSMOS®. The results with the cyclic peptides were disappointing because of the low affinity and the low catalytic activity. The results show that prediction methods for 3-D-structures of transition metal complexes of cyclic pseudopeptides still remain a challenge. Thus, our more experimental approach to estimate binding motifs and especially selective complexation motifs for forming heterodinuclear complexes seems to be superior to the modeling, untill now. On the other hand, the conformation of the Zn^{2+} complex of the smaller pseudotripeptide ligand L1 was more successfully designed by the same program and correlates best with experimental data verified by COSMOS®-NMR force field and by density functional theory calculations.

Acknowledgements
We thank the Deutsche Forschungsgemeinschaft for financial support (SFB 436).

References

1. Greiner, G. et al. *Lett. Pept. Sci.* **7**, 133-141 (2000).
2. Seyfarth, L. et al. *Lett. Pept. Sci.* **8,** 13-20 (2002).
3. Witter, R. et al. *J. Biomol. NMR* **24**, 277-289 (2002).
4. Kuenzel, S. et al. *Lett. Pept. Sci.* in press (2003).
5. Kuenzel, S. et al. *J. Pept. Sci.* **9**, 502-509 (2003).
6. Solomon, E. I., Sundaram, U. M., Machonkin, T. E. *Chem. Rev.* **96**, 2563-2605 (1996).

Peptide Revolution: Genomics, Proteomics & Therapeutics
Michael Chorev & Tomi K. Sawyer (Editors)
American Peptide Society, 2003

Cyclic Peptides from Plants of Genus Linum

B. Picur[1], P. Ruchala[2], M. Lisowski[1], M. Cebrat[1], A. Pasternak[1], R. Zbozień Pacamaj[1], P. Stefanowicz[1], T. Goszczyński[1] and Ł. Tarnawski[1]

[1]Faculty of Chemistry, University of Wroclaw, 14 F. Joliot-Curie Street, 50-383 Wroclaw Poland;
[2]Department of Medicine, Harvard Medical School, Boston, MA 02215, USA

Introduction

Over millennia the peoples of Europe and Asia exploited flax as an effective plant producing strong fibers and eatable oil. The linseed is still applied in folk medicine for digestive malfunction treatment. The oil and seed are used in the therapy of wounds and in skin problems. The whole as well as milled linseed is still used as an additive in bakery. The above properties of this plant are reflected in its Latin name -*Linum ussitatissimum* what means *Linum "the most needed"*. Lastly, the great interest in flaxes is observed because of appearance in these plants of cyclic peptides containing nonproteinaceous amino acids [1,2]. These compounds reveal many biological activities [3]. Above discoveries make flaxes, the "most needed" plants, producing not only eatable oils and natural fibers but also potential pharmaceuticals.

Results and discussion

As an example we present here the structure of bicyclic decapeptide appearing in *Linum perenne* as well as in *Linum rubrum*. The amino acid analysis of this peptide is 2F, 2L, 1V, 1W, 1R, 1E and 1A*, where A* is 2-methylalanine. The MS/MS experiment revealed the sequence of bicyclo[G(RE)A*FWLVL], which was previously presented [2]. We have proved using chemical synthesis of α-methylalanine and synthetic dipeptides containing this amino acid that this residue is present in the bicyclic decapeptide (BCD). It has been already shown [4] that the structure of CLX (isolated from *Linum ussitatissimum*) corresponds to cyclo(XPPFFILL), where X is [2S,4R] N-methyl-4-aminoproline, after oxygen induction converts itself to a new cyclic hexapeptide of the sequence cyclo (X*PPILL) and linear dipeptide containing aromatic residues. The X* is the product of oxidative opening of the X pyrrolidine ring - [2S,4R] 4-amino-N-methylglutamic acid. This discovery encouraged us to search for similar processes in respect to other unstable peptides present in flaxes. It has been found that extracts from seeds of *Linum rubrum* contain components with masses of BCD (372 and 900 Da). We found fraction with dipeptide H-FW-OH (MW=372 Da corresponding to the sodium complex of this dipeptide). The second mass (900 Da corresponds to a component of an octapeptide) was not found in the collected fractions. This suggests that BCD reveal similar tendencies to decomposition and polycondensation as those observed for CLX. The similarities of BCD and CLX are shown in Figure 1. The ability to specifically transform the initial cyclic peptide (after the formation of the core including a set acidic and basic groups) including the exclusion of two aromatic residues and the formation of the new peptide bond generating a new cyclic peptide smaller by two residues. Generating the insoluble polycondensate of general topology depicted in Figure 2 concludes the process.

Conclusions

1. The different plants from *Genus Linum* are producing different cyclic peptides.

2. The BCD and CLX both contain nonproteinaceous amino acids α-methylalanine (A*) and γ-amino-N-methylproline (X), respectively.
3. The similarity between of BCD and CLX molecules includes the center core with free basic and acidic groups, a transformation in which two aromatic residues are excluded followed by a tendency to undergo polycondensation.

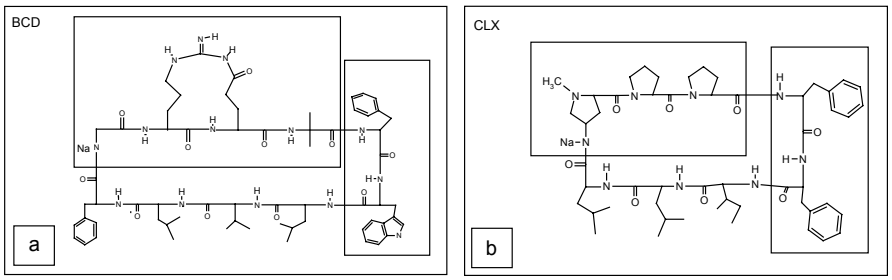

Fig. 1. The comparison of the structure decapeptide BCD (a) to the CLX (b).

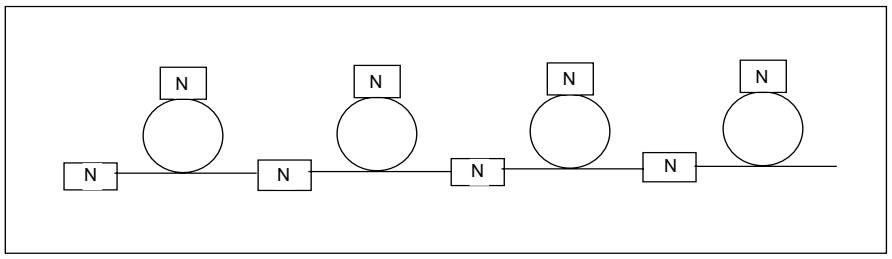

Fig. 2. The topology of finally insoluble polycondensate generated by converting the BCD or CLX natural peptides. The main chain of the polycondensate as well as cyclic elements contain new peptides bonds not present in precursore peptides (marked here by N in boxes).

Acknowledgements

This work was financially supported by a KBN grant No. 3T09A03618. The Jelfa Pharmaceutical Company S.A. is greatly appreciated for support this presentation. We thank Novartis Company for 0.5g of reference cyclosporine A.

References

1. Picur, B., Lisowski, M. and Siemion, I. Z. *Lett. Pept. Sci.* **5**, 183-187 (1998).
2. Picur B., Brzezicka A., Chliszcz P., Cebrat M., Lisowski M., Olejarnik M., Ruchala P., Spiewak K. and Siemion I. Z., In Benedetti, E. and Pedone, C. (Eds.) *Peptides 2002 - Proceedings of the 27th European Peptide Symposium,* Edizioni Ziino, Napoli, Italy, pp. 396-967 (2002).
4. Picur B., In Benedetti, E. and Pedone, C. (Eds.) *Peptides 2002 - Proceedings of the 27th European Peptide Symposium,* Edizioni Ziino, Napoli, Italy, pp. 258-259 (2002).
3. Bell, A., McSteen, P. M., Cebrat, M., Picur, B. and Siemion, I. Z. *Acta Pol.Pharm*. **57**, 134-136 (2000).

Peptide Revolution: Genomics, Proteomics & Therapeutics
Michael Chorev & Tomi K. Sawyer (Editors)
American Peptide Society, 2003

Peptide Mimic Synthesis with Cyclic Sulfamidates

Fabrice Galaud, Priscille Laborde and William D. Lubell

Département de Chimie, Université de Montréal, C.P. 6128, Succursale Centre Ville, Montréal, QC H3C 3J7, Canada

Introduction

Serine- and homoserine-derived cyclic sulfamidates have served as useful building blocks for the synthesis of β- and γ-substituted amino acid analogs, respectively [1,2]. For example, opening of homoserine-derived cyclic sulfamidate **1** with amine nucleophiles has provided a set of enantiopure α, γ-diamino acid analogs [2]. 6-Membered cyclic sulfamidates have now been reacted with different amino esters to prepare a series of 1,3-diamines **5a-h** for use in peptide mimicry. Employing aspartate-derived cyclic sulfamidate **2** in this route, we have provided a novel entry for synthesizing α-amino γ-lactams, commonly named Freidinger lactams, which have been used to study conformation-activity relationships of a variety of biologically active peptides [3,4].

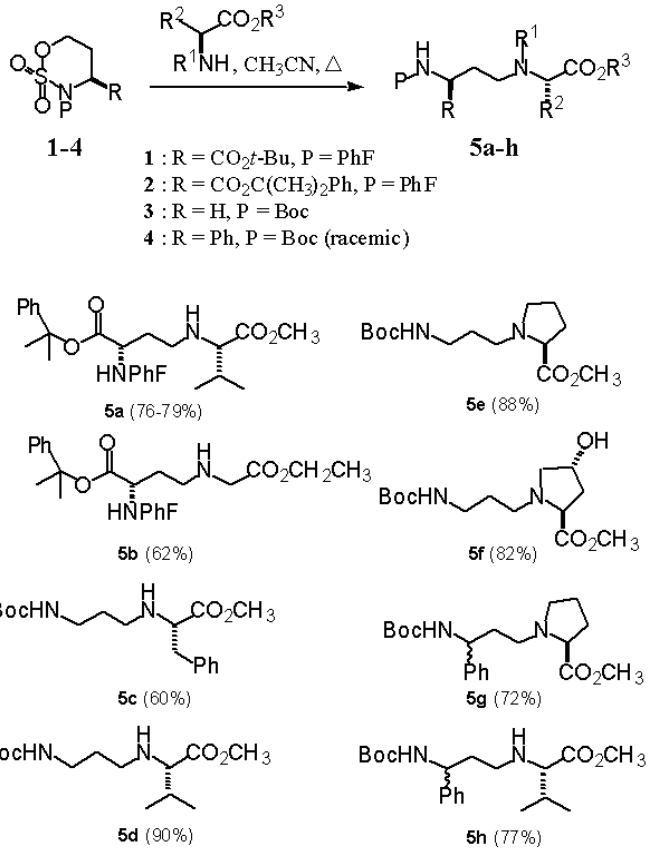

Fig. 1. 6-Membered cyclic sulfamidate ring opening with amino esters.

Results and Discussion

The synthesis of homoserine-derived cyclic sulfamidate cumyl ester **2** was performed from *N*-(PhF)aspartate β-methyl ester in a similar way as its *tert*-butyl ester counterpart **1** in 46% overall yield [2]. Cyclic sulfamidate **3** was synthesized in 58% overall yield from *N*-(Boc)-γ-aminopropanol by treatment with thionyl chloride followed by oxidation of the sulfamidite with catalytic $RuCl_3 \bullet H_2O$ and $NaIO_4$ in acetonitrile/water [2]. 3-Phenylpropanol was converted to 6-membered cyclic sulfamidate **4** by acylation with sulfamoyl chloride ($ClSO_2NH_2$) and pyridine in dichloromethane followed by C-H insertion using $PhI(OAc)_2$, MgO and $Rh_2(OAc)_4$ in CH_2Cl_2 at 40°C [5]. Amino esters were liberated from their corresponding HCl salts by partitioning between $CHCl_3$ and aq. K_2CO_3, and reacted with cyclic sulfamidates **2-4** in acetonitrile at 75°C to provide the corresponding 1,3-diamines **5** in 60-90% yields (Figure 1) [2]. The synthesis of α-amino γ-lactams **6** was achieved by selective removal of the cumyl ester with HCl in EtOAc [6] and lactam cyclization with TBTU and DIEA in DCM, which afforded **6a** (73% yield) and **6b** (44% yield) from diamines **5a** and **b**, respectively. After removal of the PhF group with 50% TFA in DCM, coupling of **6b** to *N*-(Boc)-proline with TBTU, HOBt, DIEA in DCM provided **7** in 90% overall yield from **6b**. Lactam **7** is designed to serve in the synthesis of an analog of PLG, which has exhibited modulating activity at the D_2 dopamine receptor (Figure 2) [7]. Proof of concept that α-amino γ-lactams can be synthesized from the homoserine-derived cyclic sulfamidates has thus been demonstrated and the development of this method is now in progress.

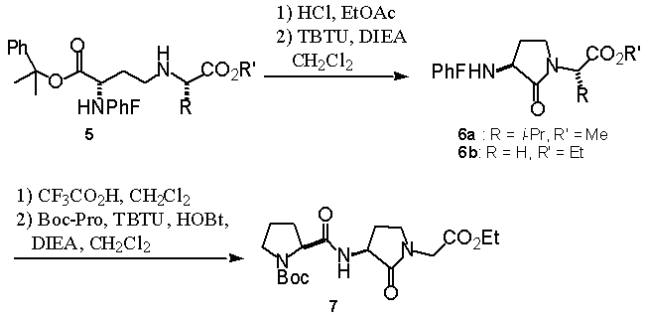

Fig. 2. Synthesis of Freidinger lactams.

Acknowledgments

This research was supported by NSERC (Canada) and FQRNT (Québec).

References

1. Melendez, R. E. and Lubell, W. D. *Tetrahedron* **59**, 2581-2616 (2003).
2. Atfani, M., Wei, L. and Lubell, W. D. *Org. Lett*. **3**, 2965 (2001).
3. Freidinger, R. M., Veber, D. F., et al. *Science* **210**, 656 (1980).
4. Aubé, *J. Adv. Amino Acid Mimetics Peptidomimetics* Abel, A. Ed.; JAI Press: Greenwitch; **1**, 193-232 (1997).
5. Espino, C. G., Wehn, P. M., Chow, J. and Du Bois, J. *J. Am. Chem. Soc*. **123**, 6935 (2001).
6. Bergmeier, S. C., Cobas, A. A. and Rapoport, H. *J. Org. Chem*. **58**, 2369 (1993).
7. Dolbeare, K., Pontoriero, G. F., Gupta, S. K., et al. *J. Med. Chem.* **46**, 727 (2003).

Peptide Revolution: Genomics, Proteomics & Therapeutics
Michael Chorev & Tomi K. Sawyer (Editors)
American Peptide Society, 2003

Studies of Photoswitchable β-Hairpin Mimetics

Máté Erdélyi[1,2], Anders Karlén[2] and Adolf Gogoll[1,*]

[1]*Department of Organic Chemistry, Uppsala University, Box 599, S-751 24 Uppsala, Sweden;*
[2]*Department of Medicinal Chemistry, Uppsala University, Box 574, S-751 23 Uppsala, Sweden*

Introduction

β-Hairpins are involved in a large variety of physiological processes. Recently, it has been shown that the biological activity of some β-hairpins can be correlated to the thermodynamic stability of their folded conformation [1].

We investigate β-hairpin mimetics that incorporate a photoswitchable structural element that can be used to externally control the conformational behavior of a peptide. Incorporating a turn mimetic capable of light-triggered *cis-trans* isomerization, the peptidomimetic can be forced to switch between two distinct tertiary structures (Figure 1). If one of the isomers forms a stable β-hairpin, while the other does not, the physiological activity of the peptidomimetic may be photochemically regulated. Motivated by the promising results of our computational studies, stilbene type turn-mimetics were incorporated into a known β-hairpin mimetic [2].

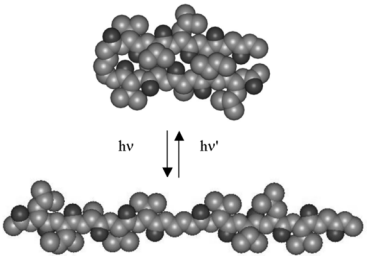

Fig. 1. Photoswitchable β-hairpin mimetic.

Results and Discussion

Amongst other factors, the rigidity of the β-turn, the hydrophobicity of the amino acid side chains and the distance between the antiparallel strands have been shown to play a key role in β-hairpin stability. Therefore, meta-substituted stilbene type turn-mimetics **4**-**6** (Figure 2) containing $(CH_2)_n$ (n=0, 1, 2) linkers allowing various degrees of flexibility were investigated. Since peptides containing a rigid ^{D}P-G type II' turn mimetic [2], or a diphenylacetylene type turn mimetic [3] are known to fold in well-defined β-hairpin conformations, mimetics **1**-**3** were prepared as reference compounds.

Monte Carlo/Molecular Mechanics simulations performed using OPLS-AA all atom force field and the GB/SA solvation model for chloroform predicted a tendency for hairpin folding for all investigated compounds (Table 1).

Table 1. Results of MCMM calculations. Predicted relative amount of β-hairpin conformations for the mimetics 1-3 and for the cis-isomers of the mimetics ***4-6*** *identified among all conformations within 25 kcal/mol.*

Peptide	**1**	**2**	**3**	*cis*-**4**	*cis*-**5**	*cis*-**6**
Hairpin conformations	20%	16%	31%	16%	50%	34%

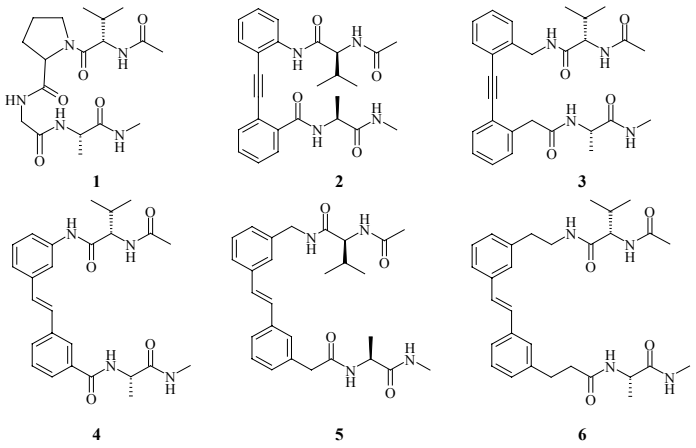

Fig. 2. The investigated β-hairpin mimetics.

Compounds **1**, **3**, **5** and **6** were prepared by incorporation of the Boc-protected diphenylacetylenic *trans*-stilbene type dipeptide mimics into PyBOP mediated SPPS on Kaisers resin and were cleaved with methylamine in THF. The less peptide-like mimetics **2** and **4** were prepared in solution. Following conformational studies of the *trans*-stilbene type mimetics, the *cis*-isomers of mimetics **4**-**6** were obtained by irradiation of acetonitrile solutions of the corresponding *trans*-isomers at 300 nm for 90 minutes.

NMR investigations (NOE, $\Delta\delta_{NH}/\Delta T$, $\Delta\delta_{NH,solv}$) revealed, that the ^{D}P-G nucleated peptide **1** folded into a stable *β*-hairpin in methanol and chloroform solutions, however in DMSO or D_2O:H_2O (1:2) solutions no interchain NOEs were observed. The rigid diphenylacetylenic mimetic **2** formed a *β*-hairpin in both $CDCl_3$, DMSO and methanol solutions. In opposite to our expectations, in the methanol and DMSO solutions of the *cis* isomers of **4**-**6**, similarly to the relatively flexible **3** no hairpin folding could be observed. This fact can be explained by the increased flexibility of the turn part of **3**-**6**, a factor allowing the antiparallel peptide strands to align themselves in optimal distance for intramolecular hydrogen bonding, however, simultaneously having a negative impact on the rigidity of the turn part.

The stability of *β*-hairpins is known to be affected by the length of the antiparallel peptide chains [4]. The *β*-hairpin mimetics studied here will therefore be incorporated into larger model systems, in which the flexibility of the turn mimics may be compensated by the increased number of favorable interchain hydrogen bonding and hydrophobic interactions.

Acknowledgments

Johanna Nurbo, Ida Niklason and Åsa Persson are gratefully acknowledged for their contributions to the synthesis. We also thank the Swedish Pharmaceutical Society (IF:s stiftelse) for providing financial support for participation at the 18th APS.

References

1. Lai, J. R., Huck, B. R., Weisblum, B. and Gellman, S. H. *Biochemistry* **41**, 12835 (2002).
2. Erdélyi, M., Langer, V., Karlén, A. and Gogoll, A. *New J. Chem.* **26**, 834 (2001).
3. Ragothama, S. R., Awasthi, S. K. and Balaram, P. *J. Chem. Soc. Perkin Trans. 2.* 137 (1998).
4. Stanger, H. E., Syud, F. A., et al. *Proc. Natl. Acad. Sci. U.S.A.* **98**, 12015 (2001).

Peptide Revolution: Genomics, Proteomics & Therapeutics
Michael Chorev & Tomi K. Sawyer (Editors)
American Peptide Society, 2003

Lactam Bridge Formation at High Temperature

Alessandra Machado[1], Giuliano C. Xavier[1], Giselli H. Lima[1], Antonio Miranda[2] and M. Terêsa M. Miranda[1]

[1]Depto. de Bioquímica, Instituto de Química, Universidade de São Paulo, 05508-900; [2]Depto. de Biofísica, Universidade Federal de São Paulo, 04044-020, São Paulo, SP, Brazil

Introduction

The benefits of using elevated temperatures to perform chemical reactions that are difficult drive to completion at room temperature (RT) are well known. It is also recognized that the cyclization of a growing peptide by the formation of a lactam bridge is not always an easy task. Indeed, this can be very slow and troublesome since it depends on the peptide sequence, bridgehead elements, size of the lactam ring and chemical environment. We have studied different aspects of stepwise solid-phase peptide synthesis (SPPS) at high temperature [1]. Due to difficulties encountered during lactam bridge formation in DMF at RT, we recently examined the possibility to improve this synthetic step at 60°C. The choice of this temperature was based on former studies [1,2]. cyclo(30-33)[Glu^{30},Lys^{33},Nle^{38}]r/$hCRF_{28-41}$ [3], cyclo(2-15)[Asp^{2},Orn^{15}]- and cyclo(2-15)[Glu^{2}, Lys^{15}]-Gm [4] were used as peptide models. CRF is a peptide that plays a key role within the brain, especially during stress [3]. Gomesin (Gm) is a potent antimicrobial peptide isolated from a Brazilian spider [5].

Results and Discussion

The MBHA-bound protected peptides were synthesized manually using solid-phase customized protocols and the t-Boc strategy. Amino acid analysis confirmed their composition. The swelling properties of the peptidyl-resins were determined by measuring volume variations in the absence (peptidyl-resins prewashed with MeOH) and in presence of DCM, DMF, NMP, DMSO, 20% DMSO/NMP or 25% DMSO/toluene at RT and 60°C using a water-jacketed glass vessel connected to a heated water bath circulator. OFm and Fmoc were selectively removed by treatment of the peptidyl-MBHA with 20% piperidine in DMF. Lactam bridge formation was carried out at RT and 60°C in different chemical environments. Reaction progress was monitored by the ninhydrin test every one or two hours. After cyclization was completed, the dry peptidyl-resin was treated with HF/scavengers to release the cyclized crude peptide. This was analyzed by RP-HPLC and LC-ESI/MS.

Generally, the peptidyl-MBHA presented similar swelling properties at RT and 60°C in the solvents or mixtures tested. Higher solvation degrees were observed in NMP or 20% DMSO/NMP. Table 1 shows the experimental conditions employed for lactamization. Either the recoveries of the crude peptides from MBHA or their chemical complexities were in agreement with those expected for medium size peptides built by stepwise SPPS and cyclized by lactam bridge formation. Cyclization of [Glu^{30},Lys^{33},Nle^{38}]r/$hCRF_{28-41}$-MBHA in DMF containing BOP or TBTU at RT indicated that BOP was more efficient. This finding concurs with the fact that such coupling reagent has often been used to mediate lactamization at RT [3]. Based on these findings, we employed BOP in the subsequent reactions. Cyclization time for [Glu^{30},Lys^{33},Nle^{38}]r/$hCRF_{28-41}$-MBHA in 25% DMSO/toluene at 60°C was significantly shorter than that in DMF at RT. In contrast, lactamizations carried out in 20% DMSO/NMP and DMSO at 60°C were clearly faster. Besides, and oppositely to

that performed in NMP, the resulting crude peptides were equivalent to those resulting from cyclization in DMF at RT. Thus, both organic media were used for cyclization of [Asp^2,Orn^{15}]-Gm-MBHA and [Glu^2,Lys^{15}]-Gm-MBHA. The best results were found in 20% DMSO/NMP. Slightly higher product quality was achieved using EDC, suggesting that in such cases this carbodiimide was more efficient than BOP.

Table 1. Lactamization of peptidyl-resins.

Peptidyl-MBHA	Coupling reagent	Solvent or mixture	Temperature	Time for negative ninhydrin test
[Glu^{30},Lys^{33},Nle^{38}]r/hCRF$_{28-41}$-	TBTU	DMF	room	48
	BOP	DMF	room	24
	BOP	DMF	60°C	16
	BOP	DMSO	60°C	3
	BOP	NMP	60°C	3
	BOP	20%DMSO/NMP	60°C	3
	BOP	25%DMSO/toluene	60°C	10
[Asp^2,Orn^{15}]-Gm-	BOP	DMF	room	12
	BOP	DMF	60°C	10
	BOP	DMSO	60°C	8
	BOP	20%DMSO/NMP	60°C	6
	EDC	20%DMSO/NMP	60°C	6
[Glu^2,Lys^{15}]-Gm-	BOP	DMF	room	12
	BOP	DMF	60°C	12
	BOP	DMSO	60°C	10
	BOP	20%DMSO/NMP	60°C	8
	EDC	20%DMSO/NMP	60°C	6

BOP, TBTU or EDC: equimolar amount with the peptide + DIPEA needed for apparent pH 9-10.

Collectively, our data show that elevated temperature can abbreviate lactam bridge formation in peptidyl-MBHA with preservation of product quality and saving of organic solvents and chemical reagents. A high solvation of the peptidyl-resin is required. Nevertheless, this is not the only parameter that determines the efficiency of lactamization. In fact, the gomesinyl analogues-MBHA studied presented similar swelling properties in 20% DMSO/NMP and DMF, but quite different cyclization rates. Among the solvents and mixtures tested, 20% DMSO/NMP was found to be the most suitable. BOP and EDC were the best coupling reagents.

Acknowledgments
The authors are grateful to FAPESP and CNPq for the grants and fellowships.

References

1. Varanda, L. M. and Miranda, M. T. M. *J. Pept. Res.* **50**, 102-108 (1997).
2. Rivier, J. and Miranda, M.T.M., *Synthesis of Peptides and Peptido-mimetics –Commemorating 100 Years of Peptide Research.* Chapter 4, Subchapter 4.3.4, 806-813 (2001).
3. Miranda, A., Lahrichi, S. L., Gulyas, J., Koerber, S. C., Craig, A. G., Corrigan, A., Rivier, C., Vale, W. and Rivier, J. *J. Med. Chem.* **40**, 3651-3658 (1997).
4. Fázio, M. A., Daffre, S., Miranda, M. T. M., Bulet, P., Miranda, A. In Lebl, M. and Houghten, R.A. (Eds) *Peptides: The Wave of the Future* (Proceedings of the 17th American Peptide Symposium), American Peptide Society, San Diego, 2001, pp. 495-496.
5. Silva Jr., P. I., Daffre, S. and Bulet, P., *J. Biol. Chem.* **275***,* 33464-33470 (2000).

Peptide Revolution: Genomics, Proteomics & Therapeutics
Michael Chorev & Tomi K. Sawyer (Editors)
American Peptide Society, 2003

Microwave-Assisted Solid-Phase Synthesis of ψ[CH_2NH] Amide Bond Surrogate

Luigi Longobardo[1], Pietro Campiglia[2], Isabel Gomez-Monterrey[1], Ettore Novellino[2] and Paolo Grieco[2]

[1]Dip. Scienza degli Alimenti and [2]Dip. Chimica Farmaceutica e Toss., University of Naples "Federico II", Naples, Italy

Introduction

The amide bonds in peptides constitute a major site of enzymatic attachment and limit the use of peptides as drugs. This has led to a extensive studies aimed at replacing the amide bond of biologically active peptides with a variety of isosteric groups. Amine bond surrogates include the reversed amide (NHCO), Thiomethylene (CH_2S) methyleneoxy (CH_2O), methyleneamino (CH_2NH), ketomethylene ($COCH_2$) or trans-olefin (CH=CH). These modifications have been used in an attempt to achieve metabolically stable peptides. Pseudopeptides containing a ψ[CH_2NH] amide bond surrogates have been used in the design of enzyme inhibitors, in the development of antagonists against several receptors, and recently as potential agents for gene delivery. Here, we report the progress in the study of an alternative approach for the direct solid-phase synthesis of ψ[CH_2NH] amide bond surrogates, based on use of enantiopure *N*-Protected β-Iodoamines, PNH-CH(R)-CH_2-I and microwave irradiation.

Results and Discussion

The synthesis of the methyleneamino ψ[CH_2NH] [1-2] surrogate is currently conducted through the condensation of *N*-protected amino aldehydes with resin-bound protonate amines in presence of a reducing agent, as $NaBH_3CN$. This method has been used for the synthesis of the ψ[CH_2NH] pseudopeptide analogs of various biologically active peptides. However *N*-protected amino aldehydes are difficult to prepare, particularly in enantiomeric pure form. In addition, undesirable side reactions such as the double alkylation and the formation of pseudopeptide diastereomers during the synthesis have often been observed. We have initiated the study of an alternative approach for solid-phase synthesis characterized by use of a chiral *N*-protected β-iodoamines**,** easily available in two steps from α-amino acids [3], in a solid-phase SN_2 reaction on resin-bound amines under conventional and microwave conditions. The new building blocks are prepared from *N*-protected β-amino, already employed in the solid-phase synthesis of thiomethylene amide bond surrogates [4]. The solid-phase amine alkylation has been studied on a series of tetrapeptide models prepared on different supports, such as Wang, PEG-PS and Rink resin. The tetrapeptides on support carrying an aliphatic (Leu), an aromatic (Phe), Proline and Glycine residue at *N*-terminal position, were assembled under standard Fmoc solid-phase strategy. The *N*-Protected β-Iodoamines used were prepared from Phenylalanine, Leucine and Proline with Boc and Fmoc protection. Each peptide on polymeric support was subject to reaction in a Milestone Ethos CombiChem microwave synthesizer (Figure 1). The reactions were performed on 100 mg scale using 4 eq. of *N*-Protected β-Iodoamines and 1 eq. of base (DIPEA) in order to minimize the Fmoc deprotection. The mixture was maintained for 2h at 80°C and irradiated with microwave at 250 Watt. Under these conditions we observed a clear improvement in yield and reaction time as compared to the conventional procedure.

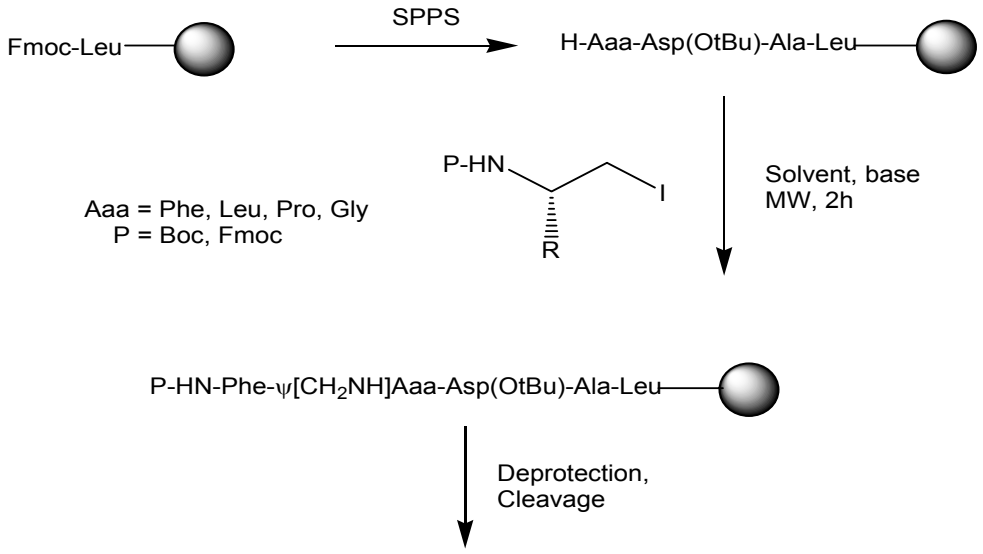

Fig. 1. General scheme of new synthetic procedure.

The preliminary data obtained in this study showed that the *N*-Boc-protected β-Iodoamines are generally more reactive with respect to the corresponding Fmoc derivatives. Tetrapeptides containing the Glycine at *N*-terminal position are alkylated almost in quantitative yield, indicating that microwave irradiation combined with the solid-phase peptide synthesis represents a powerful technique for accelerating thermal organic reactions to synthesize peptidomimetics. Further experiments are in progress to clearly determine the role of support and of solvent employed. In conclusion, the synthetic method described here could be of considerable interest for the development of solid phase synthesis of peptides containing a ψ[CH_2NH] amide surrogate bond.

References

1. Spatola, A. F. In Weinstein, B. (Ed.) *Chemistry and Biochemistry of Amino Acids, Peptides and Proteins*, Vol. VII, Marcel Dekker, New York, 1983, p. 267.
2. Wen, J. J. and Spatola, A. F. *J.Peptide Res.* **49**, 3-14 (1997).
3. Caputo, R., Cassano, E., Longobardo, L. and Palumbo, G. *Tetrahedron* **51**, 12337 (1995).
4. Longobardo, L., Fierro, G., and Molinaro, G. In Benedetti, E., and Pedone, C. (Eds), *Peptides 2002* (*Proceedings of the 27th European Peptide Symposium),* Edizioni Ziino, Napoli, p. 200.

Peptide Revolution: Genomics, Proteomics & Therapeutics
Michael Chorev & Tomi K. Sawyer (Editors)
American Peptide Society, 2003

Metal-Pentaazacrown Peptidomimetics: RGD and WRY

Wei-Jun Zhang[1], Yun Wu[1], Yuan Gao[1], Amruta Poreddy[2], Urszula Slomczynska[2], Liwei Chang[1], Michelle E. Weber[1] and Garland R. Marshall[1,2]

[1]Department of Biochemistry and Molecular Biophysics, Washington University, St Louis, MO 63110; [2]MetaPhore Pharmaceuticals, Inc., St. Louis, MO 63117, USA

Introduction

A metal-complex of a chiral pentaazacrown (MAC) [1] was designed to mimic the proposed receptor-bound conformation of the RGD motif of the cyclic pentapeptide c[RGDfMeV] [2] that was recently confirmed by the crystal structure of the complex with the $\alpha_v\beta_3$ integrin receptor (Figure 1) [3]. Another MAC was designed to mimic the α-amylase-bound conformation of a WRY motif from tendamistat (crystal structure of complex, PDB = 1BVN, 2.5 Å resolution) analogous to studies on cyclic peptides and copper complexes [4]. These efforts were stimulated by Reaka *et al*. [5] who showed that MACs fixed chiral side chains in orientations comparable to those of ideal ß-turns.

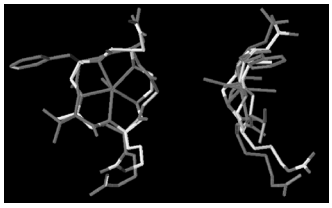

Fig. 1. Orthogonal view of overlap of the suggested receptor-bound conformer of the RGD triad deduced from c(RGDFv) and c(RGDfV) with one of possible modifications of the MAC. The metal is shown in center of left figure with axial chloride ligands. Asp at top; Arg at bottom.

Results and Discussion

Originally, we prepared the RGD and WRY MACs by reduction of cyclic pentapeptides (CPP) [1] containing the RGD and WRY motifs. The cyclic pentapeptide, c(aARGD) was prepared by attachment to PAM resin through the β-carboxyl of Asp of Boc-Asp(OH)-OFm, followed by chain elongation and on-resin cyclization to give the CPP linked through the β-carboxyl. Reduction with BH_3/THF at 60° for 40 hours apparently reduced all five amides to the pentaazacrown; approximately 50% of the ester, however, was reductively cleaved from the support as c[aAR(Tos)GS]. Treatment of the remaining azacrown support with HF gave the desired pentaazacrown containing the side-chains of RGD as the diborane complex (clearly identified by MS of the borane isotopes). Oxidation of the diborane complex with I_2 gave the desired chiral pentaazacrown. Unfortunately, complete reduction of all five amides without side reactions was rare, isolated yields were often low, and reactions difficult to reproduce. Despite considerable effort, a reliable approach to combinatorial libraries was not obvious.

We have abandoned the cyclic pentapeptide approach in favor of metal-templated cycloaddition of *bis*-dialdehydes to chiral tetraamines (tripeptide amides with all peptide bonds reduced) (Figure 2), prepared by reductive amination or Mitsunobu reactions. As examples, for both RGD and WRY MAC series, the scheme in Figure 2 was followed to give high yields of MACs after the appropriate protected chiral tetraamines were prepared in solution (Figure 3).

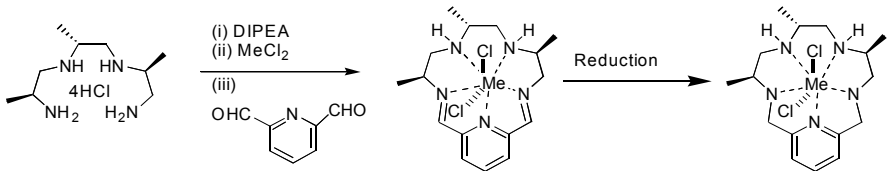

Fig. 2. Synthesis of chiral tetraamines from amino acid aldehydes and metal-templated cycloaddition with chiral tetraamines to form chiral MACs.

In the synthesis of a WRY analog, the protected MAC was isolated in 83% overall yield starting from the protected chiral tetraamine through the metal-templated cycloaddition reaction illustrated in Figure 2.

Conclusions

Metal complexes of chiral pentaazacrowns provide a novel approach to peptido-mimetics mimicking reverse-turn motifs. Two examples of MACs, where the receptor bound conformation has been previously determined by X-ray crystallography of peptide/receptor complexes, have been designed and prepared to demonstrate proof of concept. Both the RGD and WRY MACs will be complexed with a variety of metals and bioassayed as appropriate with integrin receptors and as inhibitors of α-amylase to determine the effects of subtle conformational constraints introduced by different metals. The metal-templated cycloaddition has allowed a facile synthetic preparation of pure MACs in excellent yields. Adaptation to a solid phase organic chemistry (SPOC) equivalent is under investigation in our laboratory.

Fig. 3. Synthesis of the protected chiral tetraamines in solution.

Acknowledgments

The work was funded in part by NIH grant GM53630 to GRM and by NIH training grant support to MEW.

References

1. Aston, K. W., *et al*. *Tetrahedron Lett.* **35**, 3687-3690 (1994).
2. Nikiforovich, G. V., *et al*. *J. Am. Chem. Soc.* **122**, 3262-3273 (2000).
3. Xiong, J. P. *et al*. *Science* **296**, 151-155 (2002).
4. Tian, Z. Q. and Bartlett, P. A. *J. Am. Chem. Soc.* **118**, 943-949 (1996).
5. Reaka *et al*. *J. Comput.-Aided Mol. Des.* **16**, 585-600 (2002).

Peptide Revolution: Genomics, Proteomics & Therapeutics
Michael Chorev & Tomi K. Sawyer (Editors)
American Peptide Society, 2003

Enhancing Selectivity, Stability, and Bioavailability of Peptidomimetic Estrogen Receptor Modulators

Arno F. Spatola,[1,2] Amit K. Galande,[1,2] Florence M. Brunel,[1,] Kelly S. Bramlett,[4] Thomas P. Burris,[4] John O. Trent[2] and James L. Wittliff[2,3]

[1]Department of Chemistry; [2]The Institute of Molecular Diversity and Drug Design,
[3]Department of Biochemistry, University of Louisville, Louisville, KY, 40292, USA;
[4]Lilly Research Laboratories, Indianapolis, IN 46285, USA ˙deceased

Introduction

Estrogen receptor proteins (ERα & ERβ), members of the type I nuclear hormone receptor superfamily, are involved in tissue development including intracellular signaling. Estrogens are implicated in various disease states including breast and endometrial cancers, cardiovascular disease, osteoporosis and Alzheimer's disease [1]. More than 50% of breast cancers express ERα protein, which binds the mitogen, estrogen, with high affinity [2]. Anti-estrogens, e.g., Tamoxifen, bind ER and block estrogen action, inhibiting cell growth in many cancers. Upon binding an agonist, 4 of the 12 α helices that constitute the ligand binding domain of ERα are rearranged to form a hydrophobic cleft with docking sites for coactivator proteins (via the LXXLL motif) important for AF-2 function. Norris et al. [3] provided compelling evidence that inhibition of this crucial interaction between ER and coactivator disrupts the AF-2 mediated transcriptional activation, subsequently inhibiting cell growth. Thus, peptidomimetic estrogen receptor modulators (PERMs) designed to inhibit this crucial protein-protein interaction may lead to a drug against breast cancer. Design of such peptide-based molecules requires mimicry of the coactivator protein docking site. Mutational mapping and X-ray related studies pointed to a specific LXXLL sequence motif and its conformational feature (helicity) as elements important in mediating interaction of coactivators. Previous SAR studies from our laboratory based on this information gave a potent disulfide-bridged peptide (PERM-1) containing the LXXLL motif, which binds to the ER with the Ki of 25nM (4). We have now conducted further SAR of PERMs to obtain more bioactive, stable, and selective analogs. Additionally, we synthesized cell-permeable PERMs to study their effectiveness in cell-based assays. Development of optimized peptidomimetics presents an alternative cancer therapy, complementary to standard treatment with steroid antagonists such as Tamoxifen.

Results and Discussion

We investigated various types of side chain to side chain cyclic peptides to stabilize the helical conformation while retaining the inhibitory activity of some linear parent coactivator peptides. We found that disulfide bridged peptides were more active than lactams, and the best appear to contain D-Cys^{i} to L-Cys^{i+3} bridges. In fact, one of our most effective inhibitors, a disulfide bridged octapeptide, displayed a K*i* of 11 nM, compared to a K*i* of 720 nM for a standard linear 14-mer peptide (Table 1). Additional SAR studies have been performed in which ring size was varied using homocysteines in place of cysteine, or by examining *i, i*+2 and *i, i*+4, along with *i, i*+3 disulfide linkages. Conformational constraints were introduced through D and L penicillamine replacements. Such a constrained peptide showed a significant selectivity towards ERα as shown in Table 1.

We have reported application of base-assisted desulfurization to prepare lanthionine derivatives from our disulfide bridged peptides [5]. This reaction has been extended to the preparation of cystathionine derivatives by replacing one cysteine with homocysteine. The resulting stabilized thioether derivative is also our most potent lead analog with a Ki value of 7nM. More importantly, thioether-bridged PERMs exhibit biostability. Disulfide-bridged PERMs targeted to ER can easily be reduced because of the high concentrations (mM) of glutathione present in mammalian cells. The redox stable thioether linkage not only improves the helical character of PERMs (and hence bioactivity) but also imparts additional stability in the intracellular environment.

In the design of such PERMs, we also considered the bioavailability aspect. Targets of these PERMs (the ER & coactivator proteins) are located in the cell nucleus. Hence we designed cell permeable conjugates of PERMs by attaching moieties (decanoic acid and a polyarginine peptide, R7) via an interstrand disulfide bridge. We utilized a novel solid-phase reaction for making these permeable bioconjugates [6].

Table 1. Selectivity of cyclic disulfide LXXLL peptides relative to ERα and ERβ coactivator inhibition.[a]

#	Compound	K*i* (μM) ERα	K*i* (μM) ERβ	β/α
1	H-Lys-cyclo(Glu-Ile-Leu-Arg-Lys)-Leu-Leu-Gln-NH_2	0.22	4.8	21.8
2	H-Lys-cyclo(Cys-Ile-Leu-Arg-Cys)-Leu-Leu-Gln-NH_2	0.17	1.2	6.6
3	H-Lys-cyclo(D-Cys-Leu-D-Cys)-Arg-Leu-Leu-Gln-NH_2	1.8	5.2	2.9
4	Ac-Lys-cyclo(D-Cys-Ile-Leu-Cys)-Arg-Leu-Leu-Gln-NH_2	0.12	7.7	64
5	Aib-Lys-cyclo(D-Cys-Ile-Leu-Cys)-Arg-Leu-Leu-Gln-NH_2	0.13	1.4	10.8
6	H-Lys-cyclo(D-Cys-Ile-Leu-Cys)-Arg-Leu-Leu-Gln-NH_2	0.025	0.39	15.6
8	H-Arg-cyclo(D-Cys-Ile-Leu-Cys)-Arg-Leu-Leu-Gln-NH_2	0.011	0.077	7.0
10	H-D-Lys-cyclo(D-Cys-Ile-Leu-Cys)-Arg-Leu-Leu-Gln-NH_2	0.22	1.9	8.6
11	H-Lys-cyclo(D-Cys-Ile-Leu-D-Cys)-Arg-Leu-Leu-Gln-NH_2	0.93	3.9	4.2
12	H-Lys-cyclo(Cys-Ile-Leu-D-Cys)-Arg-Leu-Leu-Gln-NH_2	2.4	7.2	3.0
13	H-Lys-cyclo(Cys-Ile-Leu-Cys)-Arg-Leu-Leu-Gln-NH_2	0.42	1.8	4.3
17	LTERHKILHRLLQEGSPSD (SRC-1 NR2)	0.39	-	-

[a] *Displacement assays using LXXLL linear peptides from coactivators against ERα and ERβ.*

References

1. Korach, K. *Science* **266**, 1544-1527 (1994).
2. Wittliff, J. L., Pasic, R., Bland, K. I. *In*: K. I. Bland and E. M. Copeland III, Eds., *The Breast: Comprehensive Management,* pp. 458-498, Philadelphia, PA: W. B. Saunders Co., 1998.
3. Norris, J. D., Paige, L. A., Christensen, D. J., et al. *Science* **285**, 744-746 (1999).
4. Leduc, A. M., et al. In Lebl, M. and Houghten, R. A., Eds., *Peptides: The Wave of the Future*, 136 (2001).
5. Galande, A. K. and Spatola, A. F. *Lett. Pept. Sci.* **8**, 247 (2001).
6. Galande, A. K. and Spatola, A. F. *Org. Lett*. **5**, 3431 (2003).

Peptide Revolution: Genomics, Proteomics & Therapeutics
Michael Chorev & Tomi K. Sawyer (Editors)
American Peptide Society, 2003

Stereoselective Synthesis of 4, 8-Disubstituted Azabicyclo[4.3.0]nonane Amino Acid Esters: Dipeptide β-Turn Mimetics for Melanocortin Peptide Receptors

Junyi Zhang, Chiyi Xiong and Victor J. Hruby

Department of Chemistry, University of Arizona, Tucson, AZ 85721, USA

Introduction

As part of our ongoing program for the design of novel melanotropin peptide mimetics, we have identified the core bioactive sequence of melanotropin peptides as His-(D/L)Phe-Arg-Trp [1] and found a β-turn structural feature that includes the Phe and Arg residues [2]. Based on these findings, we have initiated a program to examine the structure-activity relationship of melanocyte stimulating hormone (MSH) peptides by replacing the dipeptide Phe-Arg with β-turn dipeptide mimetics, such as azabicyclo[4.3.0]nonane amino acids **1** (Scheme 1).

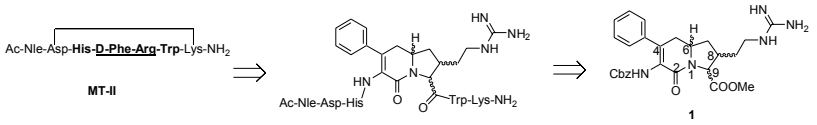

Scheme 1. Melanotropin peptide mimetic dipeptide analogues.

In our efforts to implement this plan, we need to develop a flexible synthetic approach to such dipeptide mimetics as **1** (Scheme 1). Some successful methodologies have been reported for the synthesis of unsubstituted indolizidinone amino acids. However, little success has been reported in the synthesis of indolizidinone amino acids with appropriate side-chain functionalities, which correspond to the side chains of natural amino acids. Many studies have shown that amino acid side chain moieties are involved directly in interactions between peptide ligands and receptors/acceptors that are critical for their biological activities and receptor selectivities [3]. Herein, we report the first synthesis of indolizidinone amino acid esters with appropriate amino acid side-chain functionalities at both C4 and C8 positions.

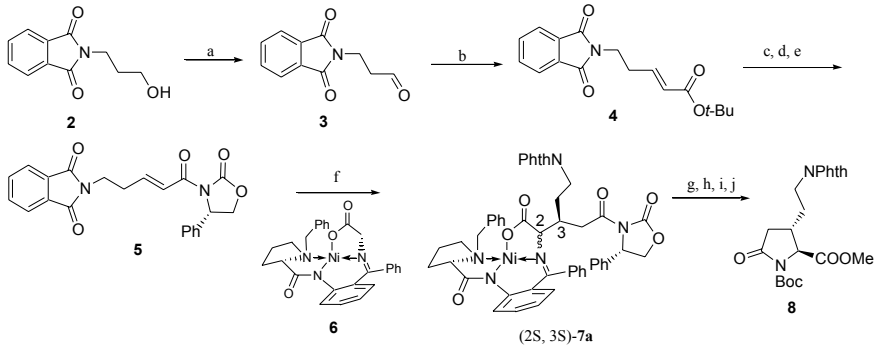

[a]Reagent: (a) PCC, silica gel, DCM; (b) *t*BuOCOCH$_2$PPh$_3$Br, NaOH, TEA, CH_2Cl_2, H_2O; (c) TFA (50% in CH_2Cl_2); (d) *t*BuCOCl, TEA, THF, -78 ^oC; (e) (S)-4-phenyl-2-oxazolidinone, *n*BuLi, THF, -78 ^oC; (f) DBU(15 mole%), DMF, rt;(g) 3N HCl, MeOH; (h) NH_4OH; (i) $SOCl_2$, MeOH; (j) $(Boc)_2O$, DMAP, acetonitrile.

Scheme 2. Preparation of β-substituted pyroglutamate.

Results and Discussion

Aldehyde **3** was prepared in good % yield by PCC oxidation of alcohol **2** (Scheme 2). Wittig olefination of aldehyde **3** gave **4** in excellent yield. The *t*-butyl protecting group was removed and *S*-4-phenyl-2-oxazolidinone was coupled to deprotected **4** as the chiral auxiliary for asymmetric functionalization of the β-position in the next step. Michael acceptor **5** underwent asymmetric Michael addition with the Ni(II) complex **6** [4] to give a mixture of (2S, 3S)-**7a** and (2R, 3S)-**7b**. Hydrolysis of the Ni(II) complex **7a** afforded the corresponding β-functionalized pyroglutamic acid, which was protected directly to give the N^{α}-Boc-pyroglutamate **8** [5].

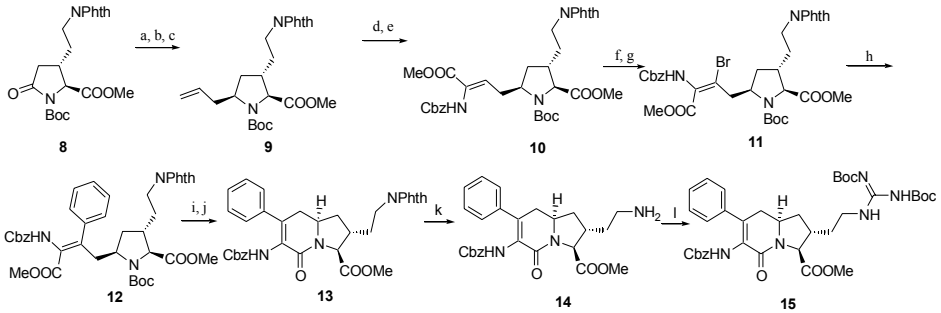

(a) DIBAL-H, THF, -78 °C; (b) Ts-OH, MeOH; (c) BF_3-Et_2O, $Me_3SiCH_2CH{=}CH_2$, Et_2O; (d) OsO_4, $NaIO_4$;(e) DBU, $(MeO)_2P(O)CH(NHCbz)COOCH_3$, CH_2Cl_2, rt; (f)NBS; (g) Dabco; (h) $PhB(OH)_2$,$Pd(OAc)_2$, P(*o*-tolyl)$_3$, Na_2CO_3, DME, 80 °C; (i) 20% TFA,CH_2Cl_2, rt; (j) $CHCl_3$, rt, 24 hr; (k) NH_2NH_2, EtOH, CH_3Cl; (l) *N, N*'-Bis-(*tert*-butoxycarbonyl)-*N*''-triflylguanidine, TEA, CH_2Cl_2.

Scheme 3. Preparation of Dipeptide Mimetics.

The reduction of **8** followed by allylation afforded **9**, which underwent osmylation and Horner-Emmons olefination to give **10** (Scheme 3). Treatment of **10** with NBS and DABCO afforded the (*Z*)-β-bromo-α,β-dehydroamino acid **11** [6]. Suzuki coupling of **11** introduced the phenyl side-chain at the β position. The crude **12** was deprotected and then cyclized to furnish **13** in good yield. Deprotection of phthalimide protecting group was accomplished by treatment with hydrazine. The crude **14** was directly guanidinated to give **15**.

In conclusion, we have developed an efficient approach to the synthesis of dipeptide β-turn mimetics **1**, which can serve as mimetics of the dipeptide Phe-Arg in our α-MSH program. The incorporation of these mimetics into melanocortin peptides and the study of their structure-activity relationships are under investigation.

Acknowledgments

This work was supported by U.S. Public Health Service Grants DK 17420 and DA 13449.

References

1. Hruby, V. J. et al. *J. Med. Chem.* **30***,* 2126 (1987).
2. Sawyer, T. K. et al. *Proc. Natl. Acad. Sci. U.S.A.* **79**, 1751 (1982).
3. Hruby, V. J. *Life Sci.* **31**, 189 (1982).
4. Chiral Ni(II) complex (S)-**6** was prepared according to a literature procedure, see: Belokon, Y. N. et al. *J. Am. Chem. Soc.* **107**, 4252 (1985).
5. Soloshonok, V. A., Cai, C. and Hruby, V. J. *Org. Lett.* **2**, 747 (2000).
6. Zhang, J., Xiong, C., Wang, W., Ying, J. and Hruby, V. J. *Org. Lett.* **4**, 4029 (2002).

Peptide Revolution: Genomics, Proteomics & Therapeutics
Michael Chorev & Tomi K. Sawyer (Editors)
American Peptide Society, 2003

Novel Building Blocks for Peptidomimetic Chemistry

Murray Goodman, Juan R. Del Valle and Nicole D. Smith

Department of Chemistry and Biochemistry, University of California
San Diego, La Jolla, CA 92093-0343, USA

Introduction

The synthesis and incorporation of novel building blocks into biologically relevant peptides is a fundamental aspect of peptidomimetic chemistry. Some of the most instructive research in this field has made use of a vast array of modified amino acid building blocks such as chimeric residues, β-amino acids, non-proteinogenic side-chains, and various cyclic amino acid analogs. The rational design of novel non-proteinogenic amino acids and constrained building blocks continues to be an invaluable resource for drug design.

In efforts toward the synthesis of biologically interesting peptidomimetics with enhanced potencies and selectivities, our laboratory maintains an ongoing interest in the design and synthesis of novel, constrained amino acid building blocks. In this presentation we briefly describe some of our most recent advances, which include: (1) the development of a divergent, substrate-directed hydrogenation strategy for the synthesis of 4-alkylprolines and (2) the asymmetric synthesis of α-methyl-D-cysteine and its incorporation into cyclic enkephalin peptides.

Results and Discussion

Diastereoselective synthesis of 4-alkylproline building blocks: In connection with our studies on bioactive and highly ordered peptides, we recently undertook the synthesis of both stereoisomers of 4-trifluoromethyl-L-proline [1]. Our divergent approach towards Boc-protected-4-trifluoromethylprolines utilized the protecting group on the hydroxymethyl substituent to dictate the facial selectivity of the hydrogenations. When protected as the silyl ether, delivery of hydrogen from the less hindered face of pyrroline 2 primarily provides the *cis*-substituted pyrrolidine (d.r. = 16:1) under heterogeneous conditions. Conversely, reduction of the deprotected hydroxymethyl moiety affords the *trans*-isomer with a diastereomeric ratio > 99:1 via homogenous, hydroxyl-directed hydrogenation (Scheme 1). These building blocks are currently being incorporated into thyrotropin-releasing hormone analogs, single-chain collagen mimetics, and cyclic somatostatin peptides.

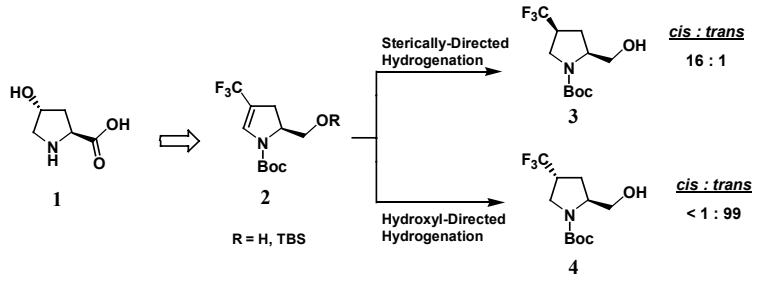

Scheme 1. Substrate-directed hydrogenations in the synthesis of 4-trifluoromethylprolines.

With the successful synthesis of 4-trifluoromethylprolines in hand, our focus turned to the preparation of other 4-substituted prolines by the above mentioned hydrogenation strategy. Beyond a general investigation of this methodology, we required a facile preparation of novel 4-arylalkylprolinols and prolines for use in our somatostatin research programs. By performing Wittig-type reactions on (2*S*)-*N*-(Boc)-*O*-(TBS)-2-hydroxymethylpyrrolidin-4-one **5** (derived from *trans*-4-hydroxyproline), we were conveniently able to prepare a number of functionalized olefins suitable for hydrogenation (Scheme 2).

An investigation of exocyclic olefin hydrogenations (carried out on the deprotected hydroxymethyl pyrrolidines) revealed that the Crabtree catalyst [2] consistently exhibits excellent diastereoselectivity in hydroxyl-directed reductions. In addition, the iridium catalyst is tolerant of a variety of functionalized olefins and the reactions are high yielding.

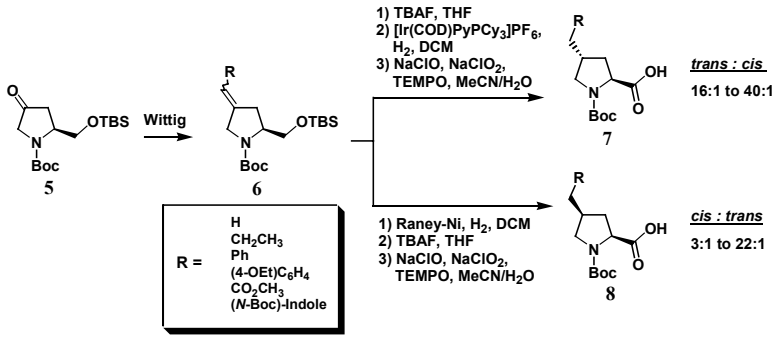

Scheme 2. General synthesis of 4-alkylprolines.

Sterically-directed hydrogenations of the silyl-protected olefin intermediates (**6**) with Raney-nickel generally showed high preference for the *cis* substituted products. The facial selectivities observed were superior to those obtained with Pd/C. Only in the case of the terminal exocyclic olefin of the 4-methyleneprolinol derivative did Raney-nickel fail to give better than a 13:1 diastereomeric ratio. Currently, our strategy is being applied to the large-scale synthesis of aralkyl-substituted proline building blocks for incorporation into various peptides and peptidomimetics [3].

Synthesis of α-methyl cysteines and lanthionine building blocks and their incorporation into disulfide enkephalin analogs: In our opioid research program, we are interested in the synthesis of α-methyl cysteine disulfide and lanthionine enkephalin analogs to develop drug candidates. As a result, we required an efficient, stereoselective synthesis of α-methyl cysteines (11) and their corresponding lanthionine building blocks (12) [4]. These analogs are useful in refining our model for the "bioactive" conformation of cyclic enkephalin opioids.

The asymmetric synthesis of α-methyl D-cysteine (Scheme 3) was achieved via regioselective ring-opening of serine lactone **10**. This key lactone intermediate was, in turn, synthesized in 7 steps from methacrylic acid **9** utilizing Sharpless asymmetric dihydroxylation and intramolecular Mitsunobu reactions. Opening of the lactone at the β-methylene carbon (*O*-alkyl fission) with 4-methoxy-α-toluenethiol in the presence of

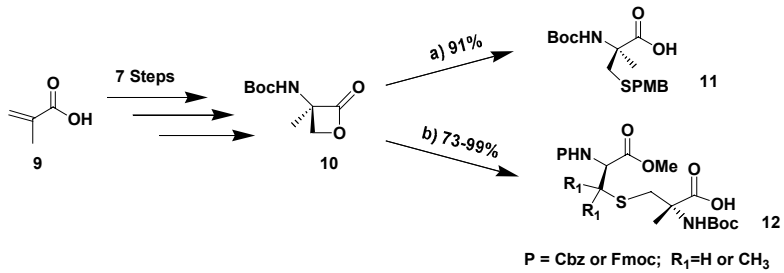

Scheme 3. Synthesis of α-Me-D-Cys and lanthionine building blocks a) PMBSH, Cs_2CO_3, DMF b) Protected Cys or Pen derivatives, Cs_2CO_3, DMF.

cesium carbonate occurs in 91% yield to give Boc protected α-methyl D-cysteine **11**. This intermediate also reacts efficiently with Cbz and Fmoc protected cysteine and penicillamine derivatives to afford the orthogonally protected lanthionine building blocks **12**.

The α-methyl cysteine building blocks were incorporated into a family of disulfide enkephalins. The family was designed to probe the steric and stereochemical requirements of the δ-opioid receptor. Listed in Table 1 is a representative group of the disulfide enkephalins and their biological data. Disulfide enkephalin analog [D-Cys^2, α-Me-D-Cys^5] is one of the most potent δ-agonists synthesized to date.

Table 1. Biological data of α-Me-D-Cys containing disulfide enkephalins.

Compounds	GPI IC_{50} [nM]	MVD IC_{50} [nM]	GPI/MVD IC_{50} ratio	*In vivo* ED_{50} [nM]
[D-Cys^2, α-Me-D-Cys^5]	1.25	0.022	57	0.042
[D-Cys^2, α-Me-Cys^5]	3.7	0.48	7.64	---
[α-Me-D-Cys^2, Cys^5]	9.4	3.7	2.55	1.59
[D-Pen^2, a-Me-D-Cys^5]	642	5.3	121	---
[D-Pen^2, D-Pen^5]	7300	4.10	1800	130
Morphine	58.6	644	0.09	15.0

Acknowledgments

We gratefully acknowledge Elisabetta Bosa, Antonia DeCapua and Chiara Perazzolo for NMR studies and the National Institutes of Health (NIH DK 15410, NIH DA07315) for financial support.

References

1. Del Valle, J. R. and Goodman, M. *Ang. Chem. Intern. Ed. Engl.* **41**, 1600-1602 (2002).
2. Crabtree, R. H., Felkin, H. and Morris, G. E. *J. Organometal. Chem.* **141**, 205-215 (1977).
3. Del Valle, J. R. and Goodman, M. *J. Org. Chem.* **68**, 3923-3931 (2003).
4. Smith, N. D. and Goodman, M. *Org. Lett.* **5**, 1035-1037 (2003).

Peptide Revolution: Genomics, Proteomics & Therapeutics
Michael Chorev & Tomi K. Sawyer (Editors)
American Peptide Society, 2003

Solid Phase Syntheses of Monovalent and Bivalent Peptidomimetics of the Neurotrophins

Kevin Burgess

Department of Chemistry, Texas A & M University, Box 30012,
College Station, TX 77841-3012, USA

Introduction

Key contact points, or "hot-spots", in protein-protein interactions can involve any element of secondary structure including helices, sheets, and loops. Chemists wishing to design molecules to mimic or disrupt these interactions may be attracted to β-turns because these are easiest to mimic small molecules [1]. Many β-turn analogs have been reported, but most, like **A** and **B**, were designed to orient the *N*- and *C*-termini in the correct directions to form a sheet, and do not allow easy introduction of pharmacophores in parallel syntheses [2].

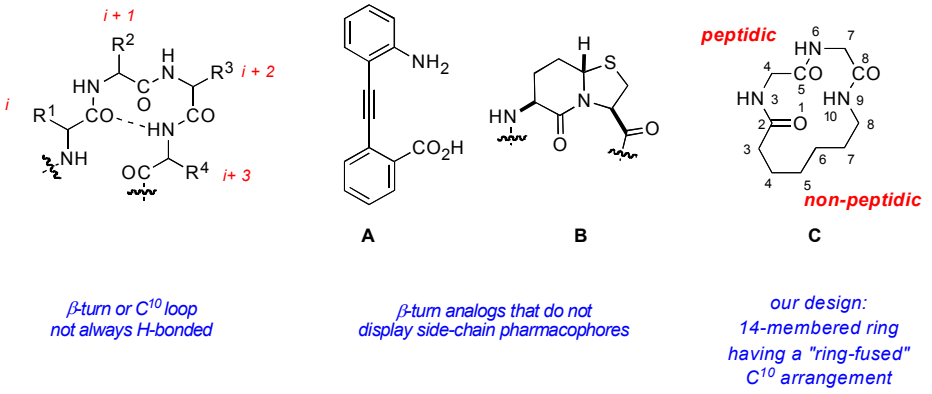

At the onset of this project, we sought to design a small molecule structure that would resemble the shapes of β-turns in solution, and allow the incorporation of any amino acid side-chain via parallel syntheses. The goal of this study was to produce focused libraries of turn mimics that have exactly the same side-chains as those found in targeted hot-spots that involve C^{10} loops. Consequently, the compound type **C** was conceived. This could contain any dipeptide fragment constrained by some organic molecular fragment. Models indicate that when the organic part has the correct number of atoms to also form a C^{10} conformation, then the dipeptide tends to adopt β-turn conformations, thus the whole molecule has two C^{10} arrangements that share an edge. Further, the organic part could be varied to allow easy syntheses of the molecules and to modify their pharmacokinetic properties. This presentation focuses on molecules that have 14-membered ring structures as illustrated in structure **C**.

Results and Discussion

Syntheses of the Turn Mimics. Members of our group have shown that various chemistries can be used to give turn mimics like those illustrated in structure **C**. Typically, the framework is prepared via modified solid-phase peptide syntheses in which a linear precursor is capped by some organic functionality, ring closure is

performed on the resin, then the peptidomimetic is cleaved from the support and unmasked in the final step. Polystyrene-based resins are used for this, the couplings are performed via the FMOC approach, and most of the side-chain protections are characteristic of that strategy. We have focused on structures that can be formed via ring closure reactions featuring S_NAr reactions, as in structure types **1** – **3**, but other chemistries may also be used for this key step [3].

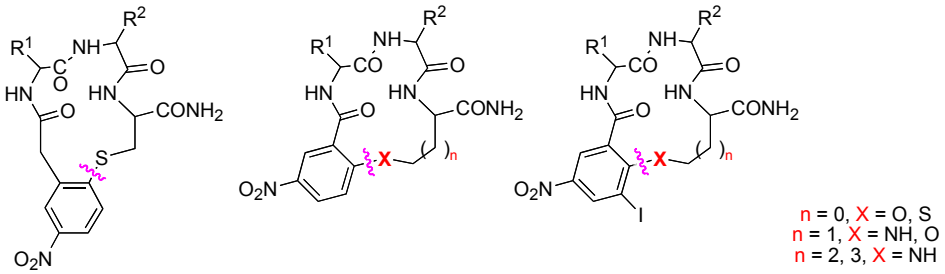

1 **2** **3**

formed via S_NAr reactions

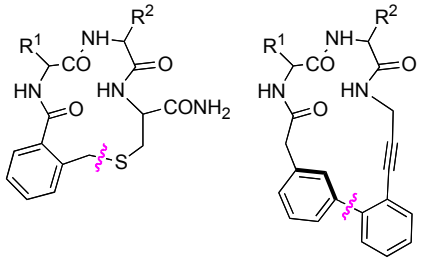

4 **5**

S_N2 *Suzuki*

Do These Compounds Really Have Turn Conformations? A representative number of compounds for each of turn mimic has been studied via a variety of NMR techniques to obtain ROE connectivities, *NH* temperature coefficients and deuterium exchange, coupling constants, and chemical shift data. CD spectra of the compounds have also been recorded. Simultaneously, the conformations of the compounds have been simulated *without using any constraints from physical data*. In most cases there was a good correspondence between the real and virtual structures. Compound types **1** - **5** tend to be good mimics of type I β-turns though type II structures are sometimes evident [3].

Sometimes interesting correlations between structure and conformation emerge. For instance, the homocysteine derivative **6** does not tend to adopt turn conformations, whereas the corresponding sulfone **7** and one epimer of the sulfoxide, the *S*-form **8**, have clear preferences towards type I β-turn conformations. We attribute it to the stabilization of the C^{10} conformations via *NH* to *OS* transannular H-bonds, but only for the sulfone and one of the sulfoxide epimers.

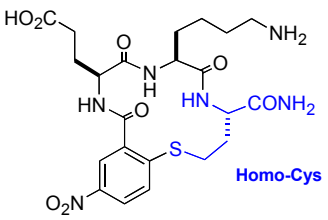

6

little or no tendency to rest in β-turn conformations

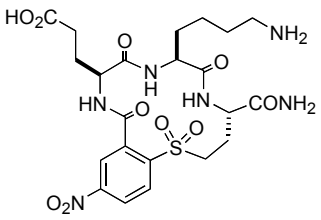

7

clear type I β-turn conformation

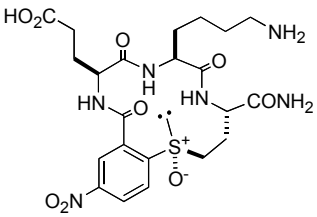

8

S-sulfoxide: type I turn

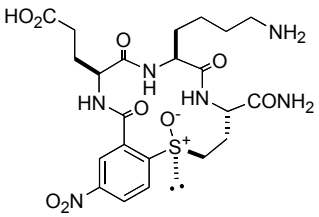

9

R-sulfoxide: not a turn

Some Biological Activities of the Compounds as Neurotrophin Mimics. So far we have only targeted a few protein-protein interactions using this approach, and the one we have worked on most is the nerve growth factor (NGF) and its extracellular receptor TrkA. Interactions of NGF with cells that express the TrkA receptor tend to cause cell-division and growth. As the name implies, most cell types that overexpress TrkA are involved with the nervous system, hence agonists of the NGF•TrkA interaction can be potential therapeutics in the treatment of neurodegenerative diseases and traumatic injuries to the head and spinal cord. Antagonists may be useful in treatment of some forms of cancer, including neuroblastoma and breast cancer (breast cancer cells express more TrkA than healthy breast cells). Use of NGF in clinical trials has failed for several reasons. These include the expense of expressing the protein in quantity, immune response, poor half-life, and interaction of NGF with other receptors that cause significant undesirable side-effects. Thus, there is a need for a small molecule mimic of NGF that interacts selectively with the TrkA receptor (and not with the other Trk receptors, or the p75 receptor that interacts with all the neurotrophins). When we started this research there were no credible reports of small molecules mimics of NGF that act via docking with the Trk receptors.

In fact, NGF is the most widely studied of a series of neurotrophins that include neurotrophin-3 (NT-3) and brain derived neurotrophic factor (BDNF). NT-3 is particularly interesting from a medicinal chemistry standpoint because its interaction with TrkC (another tyrosine kinase receptor) is implicated in potential treatments of amyloid lateral sclerosis (ALS). Prior to our work there were no reports of functional small molecule NT-3 mimics.

There is no structural data available for the neurotrophins binding with complete Trk receptors. However, we believe that the β-turn regions of the neurotrophins are involved at some of the critical hot-spots. This is consistent with simple homology modeling for the neurotrophins: they tend to share very similar primary sequences for

the core sheet regions, but differ at the turns (Figure 1). We believe these differences at least partially explain the selectivities of these growth factors for the different Trk receptors.

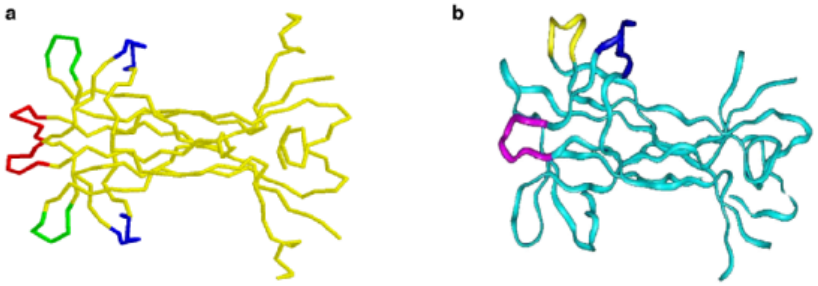

Fig. 1. Structures of ***a*** *the NGF homodimer and* ***b*** *NT-3/BDNF heterodimer from crystallographic data. In the latter diagram, the β-turns in the NT-3 molecule are highlighted.*

The compounds prepared in our group are tested for neurotrophin-like activities by Professor H. Uri Saragovi and his group at McGill University in Montreal [4]. Two of the earliest hits we found are compounds **D3** and **MPT18**. Compound **D3** acts at the TrkA receptor [5], while **MPT18** targets the TrkC receptor [6]. Neither are true agonists in cell survival assays, but they synergize with suboptimal concentrations of the corresponding growth factors to enhance the functional response. Uri's group has a range of assays to investigate the activities of the compounds, and some key findings are given below.

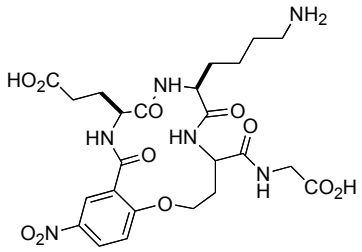

D3

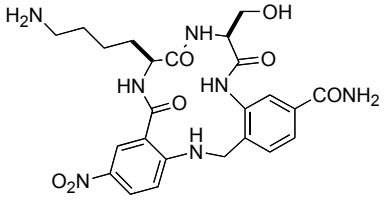

MPT18

Compound **D3**:

- Binds to immobilized TrkA with a K_d of ~4 μM.
- Binds to TrkA expressing cells with a K_d of ~4 μM.
- Potentiates the effects of sub-optimal NGF in cell survival assays in a dose dependent way.
- Potentiates the effects of sub-optimal NGF in assays to monitor production of choline acetyl transferase (ChAT).
- Induces differentiation of neurons (fetal DRG and septal neurons).
- Stabilizes TrkA-TrkA homodimers.
- Stable to trypsin and papain (indicating proteolytic stability).

Compound **MPT18**:

- Binds to TrkC expressing cells with a K_d of 0.5 μM.

- Potentiates the effects of sub-optimal NT-3 in cell survival assays (using TrkC expressing cells) in a dose dependent way.
- Causes intracellular phosphorylation of TrkC (at 50 μM conc. this effect is comparable with that caused by 0.1 nM NT-3).

A troubling feature of the data indicated above is that the compounds have agonist-like activities. The dogma in the field of extracellular receptors has been that dimeric ligands like NGF bring together molecules of receptors like TrkA to form dimers on the surface, and this initiates intracellular tyrosine phosphorylation and cell signaling. If this were true, **D3** and **MPT18** should really behave as antagonists since they cannot bridge two cell surface receptor molecules. However, recent evidence from several groups around the world indicates that the dimerization hypothesis for this type of receptor is at least an over-generalization. We propose that the TrkA receptor is pre-organized as a dimer (and there is experimental evidence from others to support this) [7], and that our small molecules act by relatively rapid binding to the oligomer, make its dimeric structure more open, and allow the growth factors to permeate in more easily.

Despite the arguments presented above, we believe that molecules that incorporate two peptidomimetics like **D3** and/or **MPT18** could have fascinating biological activities. Consequently, our current focus is to develop methodology that allows efficient construction of such "bivalent" molecules in a format that allows for the production of large number of compounds. This requires solution-phase coupling in the presence of reactive unprotected side-chains (like Lys-amines) and without coupling reagents.

Acknowledgments

I thank my group, H. Uri Saragovi, and members of his group for obtaining the data that made it possible to write this summary. Financial support for this project was provided by the National Institutes of Health (CA82642), The Texas Advanced Technology Program, and the Robert A. Welch Foundation.

References

1. Conte, L. L., Chothia, C. and Janin, J. *J. Mol. Biol.* **285**, 2177-2198 (1999).
2. Hanessian, S., McNaughton-Smith, G., Lombart, H.-G., Lubell, W. D. *Tetrahedron* **53**, 12789-12854 (1997).
3. Burgess, K. *Acc. Chem. Res.* **34**, 826-835 (2001).
4. Saragovi, H. U. and K. Burgess, WO 01/52843, United States (2001).
5. Maliartchouk, S., Feng, Y., Ivanisevic, L., Debeir, T., Cuello, A. C., Burgess, K. and Saragovi, H. U. *Mol. Pharm.* **57**, 385-391 (2000).
6. Pattarawarapan, M., Zaccaro, M. C., Saragovi, U. and Burgess, K. *J. Med. Chem.* **45**, 4387-4390 (2002).
7. Mischel, P. S., Umbach, J. A., Eskandari, S., Smith, S. G., Gundersen, C. B. and Zampighi, G. A. *Biophys. J.* **83**, 968-976 (2002).

Peptide Revolution: Genomics, Proteomics & Therapeutics
Michael Chorev & Tomi K. Sawyer (Editors)
American Peptide Society, 2003

The Sulfonamide Moiety in Peptidomimetics and Peptidomimetic-Peptide Hybrids

Rob M. J. Liskamp, Wilna J. Moree, Dries B. A. De Bont, Dennis W. P. M. Löwik, Arwin J. Brouwer, Menno C. F. Monnee, Remco De Jong and Dirk T.S. Rijkers

Department of Medicinal Chemistry, Utrecht Institute for Pharmaceutical Sciences, Utrecht University PO Box 80082,3508 TB Utrecht, The Netherlands

Introduction

The peptide-amide bond is the recurring central structural element of peptides and proteins. Not only is it virtually the only relatively rigid structural moiety because of the double bond character of the amide bond, but it also plays a crucial role in bio-recognition and bio-interactions because of its ability to form hydrogen bonds. This stable linkage between amino acid residues is nevertheless easily cleaved by appropriate proteases. Therefore, replacement of this moiety has been widely exploited for the development of protease inhibitors. Especially interesting with respect to this are replacements of the amide by isosteric groups mimicking both shape and electronic environment of the transition state of its hydrolysis. By virtue of its complementarity with the active site of a protease, strong binding and powerful inhibitors can be obtained. We have introduced the sulfonamide moiety as potential protease transition state isosteres, and decided to explore and investigate its synthesis and incorporation into peptides, as well as its properties.

Results and Discussion

Our research in this area began with realization that α-amino sulfonamides are not stable because they can easily undergo a fragmentation reaction. However, fragmentation can be circumvented by having an additional carbon atom between the amino group and the sulfonic acid moiety, so that we are dealing with β-amino sulfonic acids and the corresponding amides [1,2].

Two approaches for the synthesis of amino sulfonamides were investigated. The first approach, exemplified by the preparation of the sulfonamide derived from lysine (Scheme 1), featured the preparation of a sulfinylchloride followed by coupling to an amine originating from an amino acid or peptide—either in solution or on the solid phase—followed by oxidation of the resulting sulfinamide to the sulfonamide. [3,4,5].

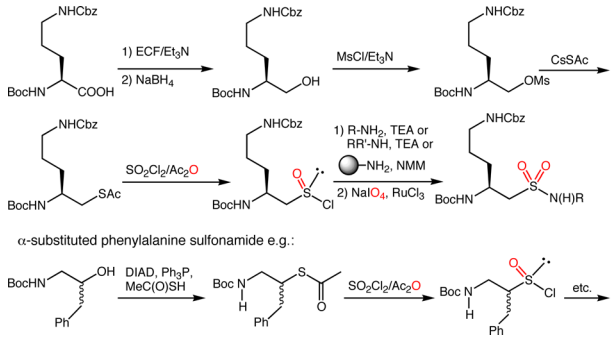

Scheme 1. Introduction of the sulfonamide moiety using the sulfinylchloride approach.

The advantage of this approach is that relatively reactive sulfinylchorides can be used in coupling reactions. However, the disadvantage is their limited stability. In this way a variety of α- and β- substituted sulfonamides could be prepared also derived from amino acids containing functional groups in their side chains (e.g. lysine, Scheme 1) [5].

The sulfinylchloride approach was used for introduction of the sulfonamide as a protease transition state isostere in potential HIV-protease inhibitors, thermolysin and thrombine inhibitors as well as haptens for generation of catalytic antibodies. Unfortunately, all so far with negative results.

The tetrahedral character of sulfonamide moiety in oligopeptidosulfonamides is apparent from X-ray structures. From these structures it is also clear that unlike amides *cis-trans* isomerism is absent in the sulfonamide [3,6].

Another important structural characteristic is the relatively acidic N-H in a sulfonamide moiety as compared to the amide. As a result hydrogen bonds involving the sulfonamide N-H will be stronger. Moreover, such a N-H can be easily deprotonated (*vide infra*). We have taken advantage of the former property in the design and synthesis of peptido sulfonamide tweezer molecules capable of binding peptides and acting as ligands in catalysis [7-9].

Although so far we have no evidence that the sulfonamide is a protease transition state isostere, the replacement of the peptide amide bond by a sulfonamide led to an improved stability towards degradation by proteases. Thus, half-lives of peptides may be prolonged by introducing sulfonamide moieties at one or several positions while maintaining a satisfactory biological activity [10,11].

The solid phase of these β-peptidosulfonamide-peptide hybrids, β-peptido-sulfonamide tweezers and moreover the solid phase synthesis of oligo β-peptido-sulfonamide foldamers required the development of a robust second approach for the sulfonamide building blocks, which led to the efficient synthesis of N-protected β-aminoethanesulfonyl chlorides (Scheme 2) [12].

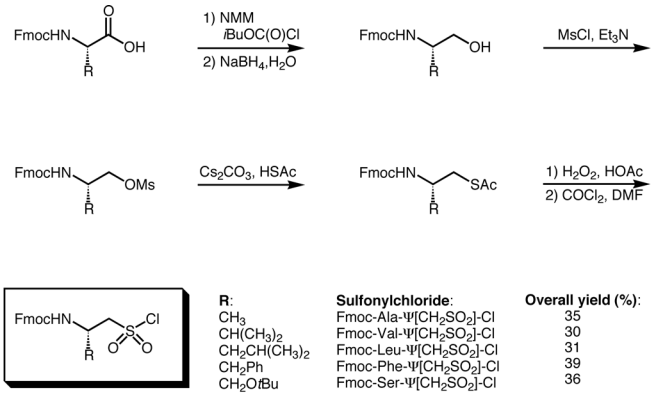

R:	Sulfonylchloride:	Overall yield (%):
CH_3	Fmoc-Ala-Ψ[CH_2SO_2]-Cl	35
$CH(CH_3)_2$	Fmoc-Val-Ψ[CH_2SO_2]-Cl	30
$CH_2CH(CH_3)_2$	Fmoc-Leu-Ψ[CH_2SO_2]-Cl	31
CH_2Ph	Fmoc-Phe-Ψ[CH_2SO_2]-Cl	39
CH_2OtBu	Fmoc-Ser-Ψ[CH_2SO_2]-Cl	36

Scheme 2. Synthesis of N-protected β-aminoethanesulfonyl chlorides.

The synthesis and structural investigation of these oligo β-peptidosulfonamides and β-peptidosulfonamide-peptide hybrids showed that the sulfonamide moiety is a powerful breaker of the helical structure displayed by β-peptides and that a single β-aminoethane sulfonamide residue was capable of disordering their foldamer behavior (Figure 1) [13,14].

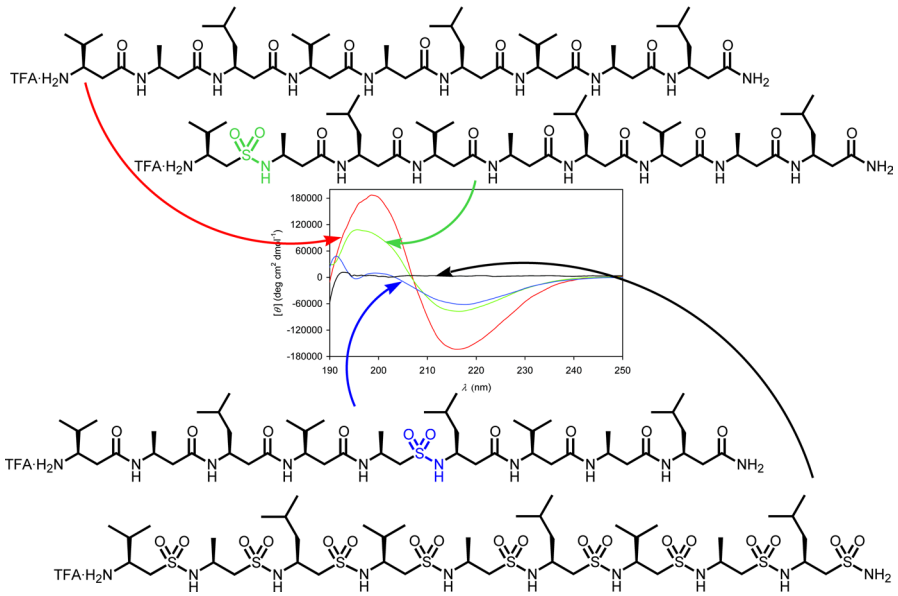

Fig. 1. CD-spectra of the nonameric β-peptide and the corresponding β-peptidosulfonamide, as well as β-peptidosulfonamide-β-peptide hybrids.

Finally, the increased acidity of the sulfonamide N-H was explored in further functionalization by alkylation leading to precursors which could be employed in the synthesis of cyclic peptidosulfonamides by ring closing metathesis [15].

Acknowledgments

These investigations were supported by the council for Chemical Sciences of The Netherlands—Organization for Scientific Research (CW-NWO), the Technology Foundation (STW), the AIDS Fund and Solvay Pharmaceuticals.

References

1. Moree, W. J., Van Der Marel, G. A. and Liskamp, R. M. J. *Tetrahedron Lett.* **32**, 409 (1991).
2. Moree, W. J., Van Gent, L. C., et al. J. *Tetrahedron* **49**, 1133 (1993).
3. Moree, W. J., Van Der Marel, G. A. and Liskamp, R. M. J. *J. Org. Chem.* **60**, 5157 (1995).
4. De Bont, D. B. A., Moree, W. J. and Liskamp, R. M. J. *Bioorg. Med. Chem.* **4**, 667 (1996).
5. Löwik, D. W. P. M. and Liskamp, R. M. J. *Eur. J. Org. Chem.* **2000**, 1219.
6. Moree, W. J., Schouten, A., Kroon, J. and Liskamp, R. M. J. *Int. J. Pept. Prot. Res.* **45**, 501 (1995); Moree, W. J., Schouten, A., Kroon, J., Liskamp, R. M. J. *unpublished results*.
7. Löwik, D. W. P. M., Mulders, S. J. E., et al. *Tetrahedron Lett.* **37**, 8253 (1996).
8. Löwik, D. W. P. M., Weingarten, M. D., et al., *Angew. Chem. Int. Ed. Engl.* **37**, 1846 (1998).
9. Brouwer, A. J., Van Der Linden, H. J. and Liskamp, R. M. J. *J. Org. Chem.* **65**, 1750 (2000).
10. De Bont, D. B. A., Dijkstra, G. D. H., et al. J. *Bioorg. Med. Chem. Lett* **6**, 3035 (1996).
11. De Bont, D. B. A., Sliedregt, K. M., et al. J. *Bioorg. Med. Chem.* **7**, 1043 (1999).
12. Brouwer, A. J., Monnee, M. C. F. and Liskamp, R. M. J. *Synthesis* **2000**, 1579.
13. Monnee, M. C. F., Marijne, M. F., et al. *Tetrahedron Lett.* **41**, 7991 (2000).
14. De Jong, R., Rijkers, D. T. S. and Liskamp, R. M. J. *Helv. Chim. Acta* **85**, 4230 (2002).
15. Brouwer, A. J. and Liskamp, R. M. J. *Manuscript in preparation*.

Peptide Revolution: Genomics, Proteomics & Therapeutics
Michael Chorev & Tomi K. Sawyer (Editors)
American Peptide Society, 2003

Peptoid-Peptide Hybrids as Potent Novel Melanocortin Receptor Ligands

John A.W. Kruijtzer[1], Wouter A.J. Nijenhuis[2], Willem Hendrik Gispen[2], Roger A.H. Adan[2] and Rob M.J. Liskamp[1]

[1]Department of Medicinal Chemistry, Utrecht Institute for Pharmaceutical Sciences, Utrecht University, P.O. Box 80082, 3508 TB Utrecht, The Netherlands;
[2]Department of Medical Pharmacology, Rudolf Magnus Institute for Neurosciences, University Medical Center, P.O. Box 80040, 3508 TA Utrecht, The Netherlands

Introduction

Peptoid-peptide hybrids are oligomeric peptidomimetics that contain one or more N-substituted glycine residues. In these hybrids, the side chains of one or several amino acids are "shifted" from the α-carbon atom to the amide nitrogen atom. The method of a peptoid scan using peptoid-peptide hybrids appears to be very useful to explore to what extent a peptide sequence can be transformed into a peptoid while retaining its affinity.

Recently we described the discovery and *in vivo* evaluation of a potent Melanocortin-4-receptor-selective ligand Ac-Nle-Gly-Lys-*D*-Phe-Arg-Trp-Gly-NH_2 also denoted as [Nle[4], Gly[5], Lys[6],*D*-Phe[7]] α-MSH(4-10) [1]. The melanocortin-4 receptor (MC4-r) is an excellent drug target for obesity. Here we report the transformation of the former ligand to peptoid-peptide hybrids, in order to better understand the structural requirements for receptor activation [2].

JK1 Ac-Nle[4]-Gly[5]-Lys[6]-*D*-Phe[7]-Arg[8]-Trp[9]-Gly[10]-NH_2
JK2 Ac-*NNle*-Gly-Lys-*D*-Phe-Arg-Trp-Gly-NH_2
↓↓↓
JK32 Ac-*NNle*-Gly-*NLys*-*NPhe*-*NArg*-*NhTrp*-Gly-NH_2

Fig. 1. Peptide transformation of Ac-Nle-Gly-Lys-D-Phe-Arg-Trp-Gly-NH_2 (JK1).

Results and Discussion

Peptoid-peptide hybrids were synthesized on a MultiSynTech Syro II Robot Synthesizer employing the "monomer" approach, in which Fmoc-protected N-substituted glycine monomers and amino acids are coupled [3]. A peptoid-peptide hybrid library JKB1 (Figure 1) containing 32 ligands based on ligand JK1 was synthesized. Peptoid-peptide hybrids were analyzed for activation of and binding to the hMC3, hMC4 and mMC5 receptors as described in Nijenhuis et al. [1].

First the activity of these peptoid-peptide hybrids was determined in a reportergene assay measuring MC receptor activity (Table 1). Two general trends are apparent from this library. First, the peptoid-peptide hybrids ligands still showed selectivity for the hMC4-receptor but the selectivity is decreased compared to that of the parent peptide JK1. Second, replacing the D-Phe residue in position 7 by the corresponding peptoid monomer (NPhe) greatly reduced the potency of the resulting ligand. This was not unexpected in view of the importance of the chirality of the Phe residue for agonistic properties of MC4-ligands and the fact that the NPhe residue is not chiral.

Sequential replacement of *one* amino acid residue in JK1 by the corresponding N-substituted glycine (peptoid) residue resulted in peptoid-peptide hybrids (e.g. JK3)

which have a lower activity than the peptide ligand JK1. When all combinations of *two* amino acids in JK1 were substituted by peptoid residues a satisfactory degree of potency is retained if amino acids in both positions 8 and 9 are substituted by peptoid residues. The potency of this ligand is even greater than the analogues in which either residue 8 or 9 is replaced by a peptoid residue. Replacement of *three*, *four* and *five* amino acid residues with peptoid residues led to hybrids displaying a further reduction of the binding potency. To a certain extent JK25 was an exception to this trend, in which in addition to residues 8 and 9 also residue 4 was substituted by a peptoid residue.

Table 1. EC_{50} and K_i values of the most active peptoid-peptide hybrids.

Compound	hMC3		hMC4		mMC5	
	EC_{50} (nM)	K_i (nM)	EC_{50} (nM)	K_i (nM)	EC_{50} (nM)	K_i (nM)
NDP α-MSH	1.20	3.7	12.2	27	0.57	2.26
JK1: Ac-Nle-Gly-Lys-D-Phe-Arg-Trp-Gly-NH_2	8.47	213	1.11	2.35	31	268
JK3: Ac-Nle-Gly-*NLys*-D-Phe-Arg-Trp-Gly-NH_2	350	159	18	7.77	570	61
JK7: Ac-*NNle*-Gly-*NLys*-D-Phe-Arg-Trp-Gly-NH_2	2000	1289	67	41.1	8500	910
JK16: Ac-Nle-Gly-Lys-D-Phe-*NArg*-*NhTrp*-Gly-NH_2	162	3094	52.9	89	35.3	1132
JK25: Ac-*NNle*-Gly-Lys-D-Phe-*NArg*-*NhTrp*-Gly-NH_2	242	3866	84	192	463	1778
JK33: Ac-Nle-Gly-Lys-D-Phe-Arg-*NTrp*-Gly-NH_2	300	1065	160	339	260	773
JK34: Ac-Nle-Gly-Lys-D-Phe-*NArg*-*NTrp*-Gly-NH_2	640	9643	160	510	90	2008
JK35: Ac-*NNle*-Gly-*NLys*-D-Phe-Arg-*NTrp*-Gly-NH_2	-	4185	4400	1149	-	2203
JK36: Ac-*NNle*-Gly-Lys-D-Phe-*NArg*-*NTrp*-Gly-NH_2	960	13608	470	1529	1000	4615

Upon replacement of a Trp residue by the corresponding peptoid residue a 'homo' peptoid derivative was used in which two carbon atoms were present between the amide nitrogen atom and the indole aromatic nucleus. A more closely related replacement of a Trp residue by a peptoid-NTrp residue would be with only one carbon atom between the amide nitrogen and the indole aromatic nucleus. For this purpose the required peptoid monomer was synthesized and subsequently incorporated, leading to peptide-peptoid hybrids JK33-36 (Table 1). However, introduction of this NTrp derivative as compared to the NhTrp derivatives led to lower EC_{50} and K_i values.

Acknowledgments
Financial support by Quadrant Healthcare plc (Nottingham, UK) and NWO/NDRF-STIGO is gratefully acknowledged.

References

1. Nijenhuis, W. A. J., Kruijtzer, J. A. W., et al. *Peptides* **24**, 271-280 (2003).
2. Kruijtzer, J. A. W., Nijenhuis, W. A. J., Gispen, W. H., Adan, R. A. H. and Liskamp, R. M. J *manuscript in preparation*.
3. Kruijtzer, J. A. W., Hofmeyer, L. J. F., Heerma, W., Versluis, C. and Liskamp, R. M. J. *Chem. Eur. J.* **4**, 1570-1580 (1998).

Peptide Revolution: Genomics, Proteomics & Therapeutics
Michael Chorev & Tomi K. Sawyer (Editors)
American Peptide Society, 2003

New Methodology for Syntheses of Bicyclic β-Turn Dipeptides (BTD) on Solid Phase Supports

Xuyuan Gu, Josef Vagner, Danice Andrus, Magda Stankova and Victor J. Hruby

Department of Chemistry, The University of Arizona, Tucson, AZ, 85721, USA

Introduction

Peptidomimetics has been an emerging area in drug discovery [1]. Special focus has been given to β-turn mimetics since these structures are important parts of proteins and many biologically active peptides. Although the design and synthesis of the simple bicyclic β-turn dipeptide (BTD) goes back to the early 1980s [2], these studies have been limited due to the difficulty in generating functionalized BTD scaffolds, and all possible diastereomers. We have recently developed chiral sidechain functionalized BTD mimetics [3]. However, we still have problems in synthesis of all isomers systematically. Here, we report a novel methodology we have recently developed. The strategies are illustrated by the total syntheses of [3,3,0]-, [4,3,0]-, and [5,3,0]-examples of BTD[2,3]-Leu-enkephalin analogues using Fmoc-based nonconventional solid-phase synthesis.

Results and Discussion

The synthetic strategy involves two unnatural amino acids. The first one is N^{α}-Fmoc-Cys-S(Fm)-OH, which was synthesized by modified methods [4]. We have chosen Fm protection for sulfur because both Fm and Fmoc can be deprotected at the same time. The second amino acids are ω-aldehyde amino acids, which are synthesized *via* Ni(II)-complex alkylations followed by osmylation [5]. Solid-phase synthesis was initiated on N^{α}-Fmoc-Leu-Wang-resin, and attachment of Fmoc-Phe-OH and Fmoc-Cys-S(Fm)-OH were accomplished as depicted in Scheme 1. The *N,S*-acetal formation was optimized in DMF in the presence of 2 eq of DIPEA, and the intramolecular cyclizations occurred very rapidly. In the [4,3,0]- and [5,3,0]-bicyclic strategy, the N^{α}- at position-2 has to be double protected so that the hemiaminal, a dead end reaction, would not be a problem. The N^{α}-methyl-N^{α}-Fmoc ω-unsaturated amino acids were prepared by a modified method [6]. After synthesis on the solid phase support, the peptides analogues were cleaved from the resin by treatment with a cocktail of TFA/H_2O/TIPS (0.90:0.05:0.05). These eleven-step total syntheses of BTD[2,3]-Leu-enkephalins were accomplished with total yields of 43-68% (Scheme 1).

The bridgehead hydrogens can exist in two configurations due to nonspecific thiazolidine formation. We were able to isolate two peptides each time in different ratios. *D*-Amino acids also were incorporated at position-2, thus four isomeric peptides were generated. The peptides stereochemistries were assigned by TOCSY and ROESY unambiguously (Figure 1). Peptides have been submitted for binding assays and functional assays. Their biological activities and structure conformational relationships will be further examined by modeling studies and NMR nOe studies.

In summary, we have developed a novel strategy for the synthesis of different sized BTDs, which represent different types of β-turns. Because both β-substituted ω-unsaturated amino acids [3b] and β-substituted cysteine derivatives [7] have been developed in our group, the methodology is general for introduction of functional groups at β- and β'-positions of BTDs.

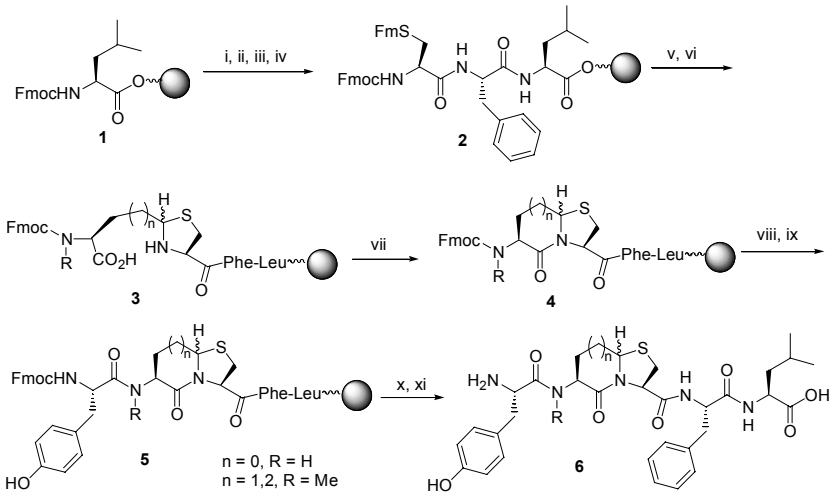

i. 25% piperidine in DMF; ii. Fmoc-Phe-OH, HBTU, HOBT, DIEA; iii. Same to i; iv. Fmoc-Cys-S(Fm)-OH, DCM/DMF, HBTU, HOBT, DIEA; v. 50% piperidine, 5% TIPS, DMF; vi. L-Fmoc-ω-Oxo-glycine, DMF, DIEA; vii. HBTU, HOBT, DIEA; viii. Same to i; ix. Fmoc-Tyr-(OBu^t)-OH, HBTU, HOBT, DIEA; x. same to i; xi. 90%TFA, 5%H_2O, 5%TIPS.

Scheme 1. The total syntheses of BTD$^{[2,3]}$-Leu-enkephalin on solid phase.

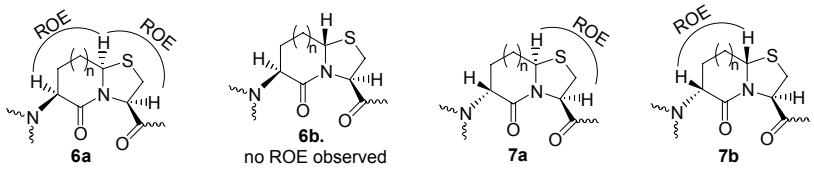

Fig. 1. ROE studies of the bridgehead H.

Acknowledgments This work was supported by grants from the U.S. Public Heath Service and NIDA DK 17420, DA 13449, and DA 06284.

References

1. Sawyer, T. K. and Chorev, M. *BioTechniques* **34**, 598 (2003).
2. Nagai, U., Sata, K., Nakamura, R. and Kato, R. *Tetrahedron* **49**, 3577 (1983).
3 (a). Qiu, W., Gu, X., Solshonok, V. A., Carducci, M. D. and Hruby, V. J. *Tetrahedron Lett*. **42**, 145 (2001); (b). Gu, X., Cowell, S., Ying, J., Tang, X. and Hruby, V. J. *Tetrahedron Lett*. **44**, 5863 (2003).
4. Albericio, F., Nicolas, E., Rizo, J., Ruiz-Grag, M., Pedroso, E. and Giralt, E. *Synthesis* 119, (1990).
5. Gu, X., Tang, X., Cowell, S., Ying, J. and Hruby, V. J. *Tetrahedron Lett*. **43**, 6669 (2202).
6. Freidinger, R. M., et al. *J. Org. Chem*. **48**, 77 (1983).
7 (a). Xiong, C., Wang, W., Cai, C. and Hruby, V. J. *J. Org, Chem*. **67**, 1399 (2002); (b). Xiong, C., Wang, W. and Hruby, V. J. *J. Org, Chem*. **67**, 3514 (2002).

Peptide Revolution: Genomics, Proteomics & Therapeutics
Michael Chorev & Tomi K. Sawyer (Editors)
American Peptide Society, 2003

Search for Biologically Active Peptidomimetics of β-Turns and β-Strands. Designed Scaffolds and Serendipitous Observations*

Ralph Hirschmann and Amos B. Smith, III

Department of Chemistry, University of Pennsylvania, 231 South 34th Street, Philadelphia, PA 19104-6323, USA

Introduction

The importance of proteins such as proteolytic enzymes and receptors in pathophysiology made low molecular weight peptidal enzyme inhibitors and receptor ligands of great pharmacologic interest. The pharmacokinetic shortcomings of peptides gave impetus to the search for peptidomimetics. The discovery by Hughes et al. [1] in 1975 that morphine is a ligand for the receptor which binds two endogenous pentapeptides, the enkephalins, was pivotal, but gave no clues how to exploit nature's achievement.

Design-based Pseudopeptidal Mimetics of Peptidal β-strands

Spatola [2] therefore designed peptidomimetics stable to proteolytic enzymes by replacing one or more peptidal amide bonds by isosteres, generating pseudopeptides. The broad application of this attractive approach proved to be challenging, because of both the chemical complexity and the unpredictability of the biological outcome.

Building on earlier work by Szelke [3], Rich [4] recognized statine as a dipeptide mimicking transition state analog, a breakthrough in the design of pseudopeptidal inhibitors of aspartic acid proteases, later applied also to nonpeptidal inhibitors.

Random Screening: An Early Approach to Peptidomimetics

Random screening of sample collections provided a reasonable approach to the discovery of peptidomimetics which, like morphine, bear no recognizable structural resemblance to biologically relevant peptides. Screening proved to be successful and in 1991 led to Losartan, an angiotensin II receptor antagonist widely used as an antihypertensive [5]. Sample collections remain an important source of nonpeptidal lead structures that can bind the growing number of protein targets.

Use of "Privileged Structures"

Ten years after the discovery of the enkephalins, screening of fermentation broths led to the isolation of asperlicin, a weak nonpeptidal cholecystokinin (CCK) antagonist [6]. The recognition that asperlicin contains "elements of the 1,4-benzodiazepine (BZD) ring system found in diazepam [7a], led to the suggestion that the 5-phenyl-1,4-benzodiazepine ring system might have broad utility. It thus became the basis for the discovery of potent, selective CCK and gastrin antagonist, and of ligands for other peptide receptors, establishing the concept of privileged structures [7b]. We have attributed the success of such designed screening in the discovery of ligands for G-protein coupled receptors (GPCRs) in part to the fact that there are common binding motifs inherent to the receptors themselves, making them complementary to the privileged platforms [8]. To be sure, the promiscuity (used here in a complimentary

* Ralph Hirschmann dedicates this lecture to the memory of Arno Spatola, a good friend, distinguished scientist, and a gentle person.

sense) of the benzodiazepines extends well beyond GPCRs. Fortunately medicinal chemists can generally incorporate specificity as long as the desired effect and the side effect are mediated via different proteins. Later, the facile screening of nonpeptidal libraries, which incorporate such privileged structures, was made possible by Merrifield's invention of solid phase peptide chemistry and by the ever-increasing sophistication of both modeling and screening technologies.

Design-Based Biologically Active Nonpeptidal Mimetics of Peptidal β-Strands and β-Turns: A Novel Approach

During the late 1980s chemists began to search for peptidomimetics by attaching relevant amino acid side chains and other substituents to scaffolds chosen to ensure the proper projection of these side chains in three-dimensional space. The resulting chemical entities would, therefore exhibit structural similarities with their peptidal progenitors, but be free of the unwanted amide backbone.

The concept was first suggested by Farmer [9] in 1980, who proposed cyclohexane as the scaffold. The first successful implementation was reported in 1986 in an elegant paper by Bélanger [10], generally overlooked until 1993 [11]. The Canadian group made use of the bicyclo[2.2.2]octane scaffold, to which they attached a phenol, a benzyl group and a dimethylaminomethyl substituent. The compound was a potent ligand for the opiate receptor for which it had been designed.

Olson and collaborators at Roche [12] reported in 1989 the design of a mimic of the tripeptide thyrotropin releasing hormone (TRH) which binds the low-affinity TRH receptor in the CNS and exhibits cogenitive dysfunction in animals. Cyclohexane served as the scaffold. Neither group pursued their studies further.

Research at the University of Pennsylvania

At about the same time (1987), Hirschmann, Smith, and - until his move to the Scripps Institute in 1989 - Nicolaou initiated extended research to learn whether scaffolds that mimic β-turns and scaffolds that mimic β-strands could be designed to generate compounds possessing diverse, predetermined biological activities. We recognized that the scaffolds required to mimic β-turns would have to differ in kind from those mimicking β-strands because H-bonding interaction with the protein target is important only for the latter.

Glycoside Scaffold-Based Peptidomimetics

The specific goal was the search for a peptidomimetic of the hormone/ neuro-transmitter somatostatin (SRIF-14), a tetradecapeptide isolated, characterized chemically and biologically and synthesized at the Salk Institute. The bioactive conformation (**1**) was established by Veber and his collaborators at Merck [13] and validated by the design and synthesis of the cyclic hexapeptide c(Phe-Pro-Phe-D-Trp[8]-Lys-Thr) [L-363,301] (**2a**) [14] and a highly potent congener, MK-678 [15]. Taken together their work confirmed the importance of the *i*, *i* + 1 and *i* + 2 positions of the β-turn of SRIF,

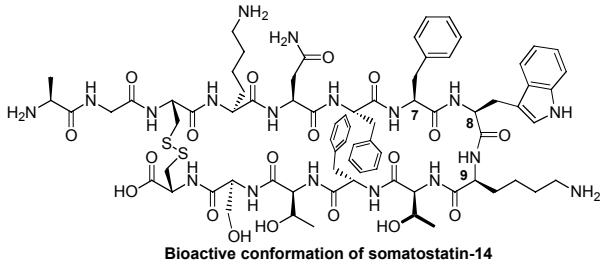

Bioactive conformation of somatostatin-14

comprising -Phe^7-Trp^8-Lys^9- for both binding and signal transduction. We speculated that the C2, C1 and C6 positions of β-D-glucose would permit the attachment of the three critical side chains of the turn with proper projection in three dimensional space. The β-D-glucoside **3**, synthesized by Cichy-Knight and Spoors, proved indeed to be a weak SRIF-14 mimetic agonist [11]. Shakespeare showed that the structure activity relationships are the same for the peptide **2a** as for the glycoside **3** [11], enabling us to synthesize compounds with increasingly better affinity, culminating in an analog with a K_i of 53 nM (see below) [16].

The Glycoside Scaffolds are Privileged: Although there has been no systematic effort to carry out broad screening of **3** and even less so of its congeners, **3** was found to be an SRIF agonist, an NK1 receptor antagonist, and a β-adrenergic blocking agent; one of the congeners of **3** inhibits a protein-protein interaction, remarkable for a small molecule [17]. We concluded that the glucoside scaffold is privileged, which we attribute in part to the fact that β-D-glucose, like c-peptides, incorporates a turn. In addition, and unlike c-hexapeptides, the glycosides display radial symmetry.

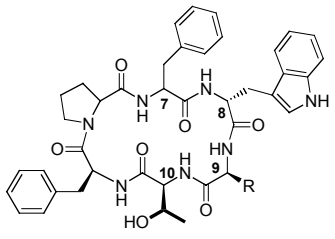

2a R = $-(CH_2)_4-NH_2$
2b R = *p*–F–Phe

The Concept of Radial Symmetry

Glucosides display radial symmetry because there are ten possible ways whereby one pyranoside can present $i + 1$ and $i + 2$ mimicking positions to a hypothetic GPCR binding pocket. In contrast there are only four possible ways in which a c-hexapeptide can insert $i + 1$ and $i + 2$ positions into the cleft of a GPCR [18].

We encountered evidence for the radial symmetry of **3** early in our research, with the discovery that the analog **4**, wherein the critical indole substituent is replaced by a methyl group, has an affinity at SRIF receptors comparable to that of **3**. Pietranico and Sprengeler proposed that this unexpected result is due to the fact that **3** can rotate in the SRIF receptor binding pocket, placing the 4-benzyl group into the Trp^8 binding pocket of SRIF [19] and the 3-benzyl group into the Phe^7 binding pocket of SRIF [11]. Because cyclic peptides lack radial symmetry, they do not allow the replacement of Trp^8 by Ala^8 [18].

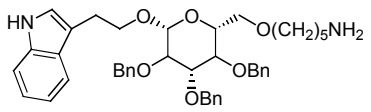

3

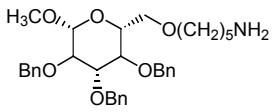

4

Additional evidence that the glycosides, but not the c-hexapeptides, display radial symmetry derives from the divergent SARs of sugars and peptides at the NK1 receptor. The serendipitous discovery that **3** can also bind the NK1 receptor of substance P (SP) was totally unexpected [19]. We reasoned that since **3** binds both receptors we might be able to use **2a** as a point of departure for the discovery of a c-hexapeptide that binds the NK1 receptor. Indeed **2b** has an IC_{50} of 28 nM as a SP antagonist and fails to recognize the SRIF receptors [20]. We soon recognized, however, that the SARs of **3** differ dramatically from those of **2b**. This paradoxical observation was resolved when we realized that although **2a** and **2b** both bind their respective receptors via the $i + 1$ and $i + 2$ positions of their β-turns, **3** binds its two receptors via different side chains of a

single chemical entity. Radial symmetry thus explains why *one* glycoside can bind both SRIF and NK1 receptors, but peptides **2a** and **2b** each bind only one receptor.

The Application of Spartan 3-21G(*) Molecular Orbital Analyses of Aromatic Electrostatic Potentials to Medicinal Chemistry

We have recently reported that congeners of **3**, in which the 4-Bn group is replaced by heterocyclic isosteres, display enhanced affinity at the SRIF receptor subtype 4 via H-bond formation with the receptor [16]. By contrast the Trp^8 binding pocket of the SRIF receptor does not bind these heterocyclic substituents [16]. Spartan 3-21G(*) molecular orbital analysis, carried out by E. Thornton of this department, provides an explanation for these results [16]. Calculations reveal significant negative electrostatic potential of the π-clouds for the benzene and indole, but not for the heterocyclic aromatic rings. The data suggest moreover that Trp^8 shields an aromatic amino acid in the hydrophobic receptor pocket, producing an important interaction, whereas the same receptor aromatic amino acid apparently cannot generate a comparable π-π interaction with the position 8 (SRIF numbering) heterocyclic amino acid substituents. We are exploring the broader significance of these observations.

3,5-Linked Pyrrolin-4-one Scaffold-Based Peptidomimetics

The goal of this research was to design a scaffold that would be broadly complementary to β-strands found in proteins such as proteolytic enzymes, and in class II MHC Protein HLA-DR1 [21], forming antiparallel β-pleated sheets with such target proteins. Pyrrolinones met our objectives very well because they (a) mimic amide bonds, (b) are stable to proteases, (c) permit the critical H-bonding interaction with their protein targets, and (d) are less solvated than amide bonds, thereby reducing the desolvation energy required for oral bioavailability and transport into infected cells.

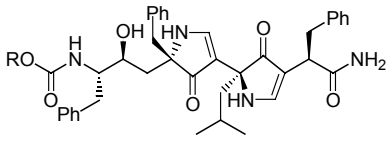

5a R = *t*-Bu

5b R = 3S-THF

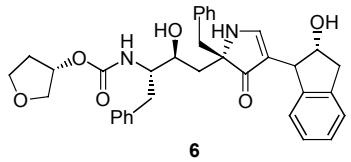

6

The side chains and other substituents to be attached to the 3,5-linked pyrrolin-4-ones were taken from those previously found to be effective in peptidal protease inhibitors. The biological results obtained with bispyrrolinone **5a** [22], were of interest because it was less potent than the peptide model, but displayed better activity in the important cellular assay, doubtless due to its diminished solvation. Its congener **5b** had an IC_{50} of 1.3 nM comparable to the peptidal inhibition (IC_{50} of 0.6 nM). Inhibitor **6**, of reduced molecular weight, was orally bioavailable in the dog (F=13%) and displayed a half-life of 35 min [23]. Its reduced potency compared to the relevant peptide is due in part to an entropically unfavorable inclusion of a water molecule in the active site.

The broad applicability of the pyrrolin-4-ones was demonstrated by the desired biological activity and the crystal structure of a pyrrolinone-peptide hybrid ligand bound to the human class II MHC protein HLA-DR1 [24], and by the synthesis of a matrix metalloprotease inhibitor [25].

Current research is exploring the observation that pyrrolinones can be designed to generate turns in addition to β-strands [26].

Conclusion

We have designed monosaccharide and pyrrolin-4-one scaffolds for β-turns and β-strands, respectively. X-ray crystallography, a tool available only to the latter project, fully demonstrates the validity of the design while disclosing also some differences between the peptidal and peptidomimetic inhibitors that could not have been predicted.

Acknowledgments

The work was funded by NIH Grants GM45611, AI-42010 and GM-41821. The authors also acknowledge with great pleasure the many superb intellectual and experimental contributions made by our students and postdoctoral associates, by the expert execution of biological experiments and of computational and molecular modeling efforts.

References

1. Hughes, J., Smith, T. W., Kosterlitz, H. W., Fothergill, L. A., Morgan, B. A., Morris, H. R. *Nature* **258**, 577-579 (1975).
2. Spatola, A. F. In Weinstein, B. (Ed.) *Chemistry and Biochemistry of Amino Acids, Peptides and Proteins* Marcel Dekker: New York (1983) Vol. VII, pp267-357.
3. Szelke, M., Leckie, B., Hallett, A., Jones, D. M., Sueiras, J., Atrash, B. and Lever, A. F. *Nature* **299**, 555-557 (1982).
4. Rich, D. H. *J. Med. Chem.* **28**, 263-273 (1985).
5. Carini, D. J., Duncia, J. V., Aldrich, P. E., Chiu, A. T., Johnson, A. L., Pierce, M. E., Price, W. A., Santella, J. B., III, Wells, G. J., *et al. J. Med. Chem.* **34**, 2525-2547 (1991).
6. Goetz, M. A., Lopez, M., Monaghan, R. L., Chang, R. S. L., Lotti, V. J. and Chen, T. B. *J. Antibiot.* **38**, 1633-1637 (1985).
7. (a) Evans, B. E., Bock, M. G., Rittle, K. E., DiPardo, R. M., Whitter, W. L., Veber, D. F., Anderson, P. S. and Freidinger, R. M. *Proc. Natl. Acad. Sci. U.S.A.* **83**, 4918-4922 (1986); (b) Evans, B. E., Rittle, K. E., Bock, M. G., DiPardo, R. M., Freidinger, R. M., Whitter, W. L., Lundell, G. F., Veber, D. F., Anderson, P. S., *et al. J. Med. Chem.* **31**, 2235-2246 (1988).
8. Liu, J., Underwood, D. J., Cascieri, M. A., Rohrer, S. P., Cantin, L.-D., Chicchi, G., Smith, A. B., III, and Hirschmann, R. *J. Med. Chem.* **43**, 3827-3831 (2000).
9. Farmer, P. S., In Ariëns, E.J. (Ed.) *Drug Design*, Academic: New York, (1980) Vol. X, p. 119.
10. Bélanger, P. C. and Dufresne, C. *Can. J. Chem.* **64**, 1514-1520 (1986).
11. Hirschmann, R., Nicolaou, K. C., Pietranico, S. Leahy, E. M., Salvino, J. Arison, B., Cichy, M. A., Spoors, P. G., Shakespeare, W. C., *et al. J. Am. Chem. Soc.* **115**, 12550-12568 (1993).
12. Olson, G. L., Cheung, H.-C., Voss, M. E., Hill, D. E., Kahn, M., Madison, V. S., Cook, M., *et al.* In *Proc. Biotechol. (U.S.A.)*, Conference Management Corp: Norwalk, CT, (1989) pS.348.
13. Veber, D. F., Holly, F. W., Nutt, R. F., Bergstrand, S. J., Brady, S. F., Hirschmann, R. Glitzer, M. S. and Saperstein, R. *Nature* **280**, 512-514 (1979).
14. Veber, D. F., Freidinger, R. M., Perlow, D. S., Paleveda, W. J., Holly, F. W., Strachan, R. G., Nutt, R. F., Arison, B. H., Hirschmann R. *et al. Nature* **292**, 55-58 (1981).
15. Veber, D. F. Saperstein, R., Nutt, R. F., Freidinger, R. M., Brady, S. F., Curley, P., Perlow, D. S., Paleveda, W. J., Colton, C. D., Zacchei, A. G., *et al. Life Sci.* **34**, 1371-1378 (1984).
16. Prasad, V., Birzin, E. T., McVaugh, C. T., van Rijn, R. D., Rohrer, S. P., Chicchi, G., Underwood, D. J., Thornton, E. R., Smith, A. B., III, and Hirschmann, R. *J. Med. Chem.* **46**, 1858-1869 (2003).
17. Prasad, V. K. Ph.D. Thesis, University of Pennsylvania (2001).
18. McVaugh, C. T., Hirschmann, R. *et al. manuscript in preparation.*
19. Hirschmann, R., Nicolaou, K. C., Pietranico, S., Salvino, J., Leahy, E. M., Sprengeler, P. A., Furst, G., Smith, A. B., III, Cascieri, M. A., *et al. J. Am. Chem. Soc.* **114**, 9217-9218 (1992).

20. Hirschmann, R., Yao, W., Cascieri, M. A., Strader, C. D., Maechler, L., Cichy, M. A., Hynes, J., Jr., van Rijn, R. D., Sprengeler, P. A. and Smith, A.B., III *J. Med. Chem.* **39**, 2441-2448 (1996).
21. Smith, A. B., III, Benowitz, A. B., Guzman, M. C., Sprengeler, P. A., Hirschmann, R., *et al. J. Am. Chem. Soc.* **120**, 12704-12705 (1998).
22. Smith, A. B., III, Hirschmann, R., Pasternak, A., Akaishi, R., Guzman, M. C., Jones, D. R., Keenan, T. P. and Sprengeler, P. A. *J. Med. Chem.* **37**, 215-218 (1994).
23. Smith, A. B., III, Hirschmann, R., Pasternak, A., Yao, W., Sprengler, P. A., Holloway, M. K., Kuo, L. C., Chen, Z., Darke, P. L. and Schleif, W. A. *J. Med. Chem.* **40**, 2440-2444 (1997).
24. Lee, K. H., Olson, G. L., Bolin, D. R., Benowitz, A. B., Sprengler, P. A., Smith, A. B., III, Hirschmann, R. and Wiley, D. C. *J. Am. Chem. Soc.* **122,** 8370-8375 (2000) and references cited.
25. Smith, A. B., III, Nittoli, T., Sprengler, P. A., Duan, J. J.-W., Liu, R.-Q. and Hirschmann, R. *Org. Lett.* **2**, 3809-3812 (2000).
26. Smith, A. B., III, Wang, W., Sprengler, P. A. and Hirschmann, R. *J. Am. Chem. Soc.* **122**, 11037-11038 (2000).

Peptide Revolution: Genomics, Proteomics & Therapeutics
Michael Chorev & Tomi K. Sawyer (Editors)
American Peptide Society, 2003

Liquid-Phase Synthesis and Conformational Analysis of Pseudoproline-Containing Turn Mimics

C. Tomasini, G. Luppi, D. Lanci, M. Garavelli, A. Garelli and V. Trigari

Department of Chemistry "G. Ciamician", Alma Mater Studiorum, University of Bologna, 40126 Bologna, Italy

Introduction

We have recently described the synthesis of oligomers of (4*S*,5*R*) 4-methyl 5-carboxybenzyl oxazolidin-2-ones (L-Oxd) [1, 2] and L-pyroglutamic acid (L-pGlu) [3] and have demonstrated that these molecules fold in ordered structures characterized by a *semi*-extended helical conformation, analogous to polyproline II and do not exhibit the amide *cis-trans* dynamic equilibrium typical of the related poly $(L\text{-}Pro)_n$ I ⇆ II helices. This effect is due to the presence of an imidic bond which always adopts only the *trans* conformation, even in the dimer. A typical effect of this behaviour is that the H_α chemical shift of the amino acid nearby is strongly deshielded by the *N*-acyl derivative. We have demonstrated that the anomalous chemical shift value is associated with the occurrence of a weak α-CH…O=C hydrogen bond.

Results and Discussion

The liquid-phase synthesis and the conformational analysis of a small library of fully protected tetramers containing L-pyroglutamic acid (L-pGlu), (4*S*,5*R*) 4-methyl 5-carboxybenzyl oxazolidin-2-one (L-Oxd), (4*R*,5*S*) 4-methyl 5-carboxybenzyl oxazolidin-2-one (D-Oxd) or 4(*S*)-oxazolidineacetic acid, 2-oxo (D-Oxac) as residue *i+1* are reported, to test the tendency of these oligomers to assume a β-hairpin conformation [4-7].

The general sequence of our library is Boc-L-Val-X-Y-L-Ala-Obzl (Scheme 1), where X is a heterocycle which mimics a constrained amino acid: (D-Oxd, L-Oxd, D-Oxac or L-pGlu), while Y is Gly or Aib (aminoisobutiric acid).

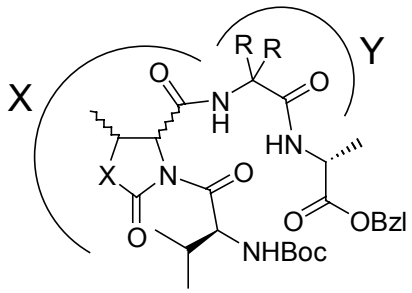

X	Y
L-pGlu	Gly
L-pGlu	Aib
L-Oxd	Gly
D-Oxd	Gly
D-Oxd	Aib
D-Oxac	Gly
D-Oxac	Aib
L-Pro	Gly
L-Pro	Aib

Scheme 1. Tetrapeptide library.

All these tetrapeptides have been analysed by IR, ^1H NMR and ESI-MS. The molecules containing D-Oxd showed a good propensity to the formation of a β-hairpin conformation. Among them Boc-L-Val-D-Oxd-Gly-L-Ala-OBzl assumed a preferential

β-turn conformation in chloroform and a preferential γ-turn conformation in DMSO, while its epimer Boc-L-Val-L-Oxd-Gly-L-Ala-OBzl showed a minor propensity to assume ordered conformations. On the other hand, the introduction of Aib moiety as residue *i+2* enhanced the propensity for the β-turn conformation in the L-series while restraining it in the D-series.

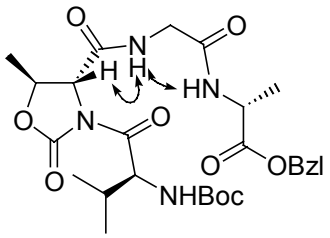

Boc-L-Val-D-Oxd-Gly-L-Ala-OBzl

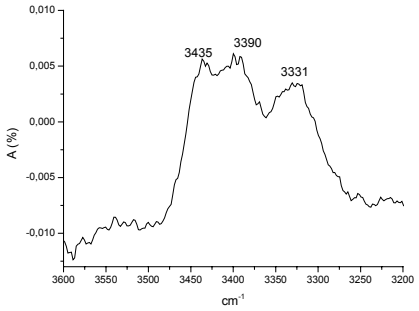

Fig. 1. Conformational studies of Boc-L-Val-L-Oxd-Gly-L-Ala-OBzl.

These findings have been confirmed by DFT calculations (Figure 2), which provide an interpretation for the available experimental data, and agree with the reported observations.

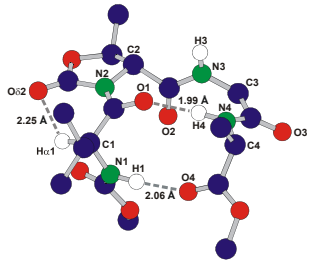

E_{rel} = 0 Kcal.mol^{-1}

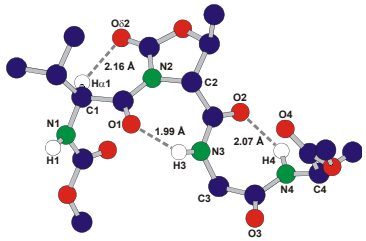

E_{rel} = +0.85 Kcal.mol^{-1}

Fig. 2. Computational studies of Boc-L-Val-L-Oxd-Gly-L-Ala-OBzl.

References

1. Lucarini, S. and Tomasini, C. *J. Org. Chem.* **66**, 727 (2001).
2. Tomasini, C., Trigari, V., Lucarini, S., Bernardi, F., Garavelli, M., Peggion, C., Formaggio, F. and Toniolo, C. *Eur. J. Org. Chem.* 259 (2003).
3. Bernardi, F., Garavelli, M., Scatizzi, M., Tomasini, C., Trigari, V., Crisma, M., Formaggio, F., Peggion, C. and Toniolo, C. *Chem. Eur. J.* **8**, 2516 (2002).
4. Tomasini, C. and Villa, M. *Tetrahedron Lett.* **42**, 5211 (2001).
5. Luppi, G., Lanci, D., Trigari, V., Garavelli, M., Garelli, A. and Tomasini, C. *J. Org. Chem.* **68**, 1982 (2003).
6. Tomasini, C. and Villa, M. *Tetrahedron Lett.* **42**, 5211 (2001).
7. Luppi, G., Villa, M. and Tomasini, C. *Org. Biomol. Chem.* **1**, 247 (2003).

Peptide Revolution: Genomics, Proteomics & Therapeutics
Michael Chorev & Tomi K. Sawyer (Editors)
American Peptide Society, 2003

Pseudo-Proline as Reversible Solubilizing Entity in Cyclosporin C

Olivier Turpin, Angela Wittelsberger, Manfred Mutter and Luc Patiny

Institute of Molecular and Biological Chemistry, Ecole Polytechnique Fédérale de Lausanne, CH-1015 Lausanne, Switzerland

Introduction

Cyclosporin C (CsC) differs from the well-known immunosuppressive analogue Cyclosporin A (CsA) by the presence of a trifunctional amino acid at position 2, i.e. a threonine (Thr^2) residue replacing 2-amino butyric acid (Abu^2) in CsA. While the biological and pharmacokinetic properties of CsC and CsA are very similar [1], the presence of the OH group of Thr^2 together with a non-methylated amide bond between residues 1 and 2 renders CsC a most attractive candidate for applying the pseudo-proline (ΨPro) concept [2] that was developed in our laboratory for enhancing the conformational effects of Pro.

Here we present the direct and selective insertion of pseudo-proline (ΨPro) systems into CsC featuring different 2-C-substituents at the oxazolidine ring. The presence of this five-membered ring not only exerts drastic effects upon the backbone conformation but also allows the introduction of solubilizing groups at the 2C position.

Results and Discussion

The reaction of dimethylketal with CsC in the presence of catalytic amounts of pyridinium-*p*-toluenesulfonate yields the corresponding ΨPro containing CsC in acceptable yields (Table 1). In the case of 2C-monosubstituted ΨPro, 2 diastereoisomers may be formed. For aromatic substituted ΨPro-systems, the R configuration is favored under thermodynamic conditions (100°C, 24h) while the S configuration is obtained preferentially under kinetic conditions (50°C, 3h).

The stability of the products towards hydrolysis was probed by dissolving 5 mg of Cs derivative in 500µL of acetonitrile and 500µL of 0.1M HCl (pH 1) or 500µL of phosphate buffer (pH 7). Most of the products proved to be stable at pH 7 while half-times ranging from less than 1min to 27.5h are observed at pH 1. In general 2C-disubstituted derivatives are more stable towards hydrolysis than 2C-monosubstituted derivatives; for monosubstituted ΨPro-systems the R epimer is more stable than the S epimer. Most notably, the modification of the group present at 2C allows one to tune the half-time of hydrolysis; i.e. donor groups, stabilize a cation at 2C and destabilize the ΨPro entity.

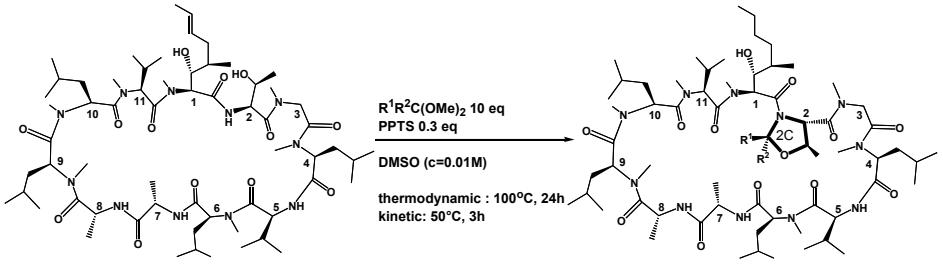

CsC — $Thr^2(\Psi^{R1,R2}pro)Cs$

Table 1. Direct insertion of ΨPro and stability towards hydrolysis at pH 1 and pH 7.

R^1	R^2		Yield (%)	$t_{1/2}$	
				pH 1	pH 7
CH_3	H	Dia S	33	7h	n.d.
*i*Pr	H	Dia S	19	9.5h	n.d.
Ph	H	Dia S	61	1h45	Stable (>15d)
		Dia R	39	49h	Stable (>15d)
	H	Dia S	55	< 1mn	30h
		Dia R	48	3h	1 month
CH_3	CH_3		26	17h	Stable (>30d) (bovine serum)
*n*Pr	*n*Pr		12	27h	n.d.
Ph	Ph		9	27.5h	n.d.

In order to convert CsC to a water-soluble compound, the introduction of a ΨPro containing a functionalizable group at position 2C have been probed. For example, the reaction of CsC with syringaldehyde dimethylketal results in the corresponding ΨPro in ~50% yield. Subsequently, this derivative can be converted to the corresponding phosphate using phosphorous oxychloride followed by hydrolysis (Scheme 1).

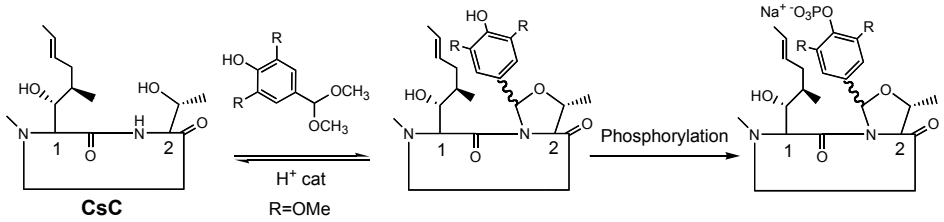

Scheme 1. Direct insertion of ΨPro followed by phosphorylation.

In summary, the direct-insertion of ΨPro-systems into a cyclic peptide proved to be feasible in acceptable yields. The presence of a five-membered ring not only exerts drastic effects upon the backbone conformation converting a bioactive drug to a biologically inactive compound, but also allows the introduction of solubilizing groups at the 2-C position. The reversibility of this reaction under conditions similar to the digestive tract suggests the possibility of using ΨPro-systems as reversible water solubilizing building blocks.

Acknowledgments

This work was supported by the Swiss National Science Foundation and Debiopharm S. A., Lausanne.

References

1. (a) Dreyfuss, M., Harri, E., Hofmann, H., et al. *Eur. J. Appl. Microbiol.* **3**, 125-133 (1976). (b) Kobel, H. and Traber, R. *Eur. J. Appl. Microbiol. Biotechnol.* **14**, 237-240 (1982).
2. (a) Wöhr, T., et al. *J. Am. Chem. Soc.* **118,** 9218-9227 (1996). (b) Wittelsberger, A., et al. *Angew. Chem. Int. Ed. Engl.* **39,** 1111-1115 (2000). (c) Keller, M., et al. *J. Med. Chem.* **44**, 3896-903 (2001). (d) Keller, M., et al. *Chem. Eur. J.* **6,** 4358-4363 (2000).

Peptide Revolution: Genomics, Proteomics & Therapeutics
Michael Chorev & Tomi K. Sawyer (Editors)
American Peptide Society, 2003

Synthesis of Modified Prolines for Peptidomimetic Use

Eric Chang, Debra A. Roberts, Yannick Fillon and Jean Chmielewski

Department of Chemistry; Purdue University, West Lafayette, IN 47906, USA

Introduction

The use of modified proline in the fields of chemistry and biochemistry has gained much interest in the recent decades. The importance of β-turns in protein folding and recognition has inspired the design of conformationally restricted mimics of β-turns. Halab L. et al. prepared 5-tert-butylproline to generate conformationally rigid mimics of the type VIa β-turn [1]. Modified proline has also been used in the design of enzyme inhibitors. Cheng et al. designed their inhibitors from cis-hydroxy-D-proline where the C-4 center was oxidized to form an sp^2 center [2]. In this paper, 4-hydroxyproline was used as a template for modification. Different side chains were added to the hydroxy group to mimic the side chains of natural occurring amino acids. These modified amino acids can potentially be used in the design of peptidomimetics.

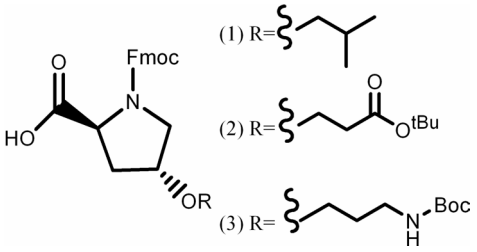

Results and Discussion

Herein we describe the synthetic pathways used to obtain modified proline residues in order to build unnatural oligopeptides of proline. New chemical functionalities were added via O-alkylation to hydroxyproline (Hyp, O) in order to obtain products **1**-**3**. These compounds were designed to mimic leucine (1), glutamic acid (2) and lysine (3).

The synthesis of the leucine mimic, **1,** was begun using Cbz-protected hydroxyproline, **4**, and the organic base potassium bis-(trimethylsilyl)amide (KHMDS). An S_N2' reaction was realized with 3-bromo-2-methyl-propene to provide the desired ether **5** after purification. Compound **5** was treated with hydrogen and palladium on activated carbon to remove the Cbz protecting group and reduce the double bond. The free amine was used without purification in the final Fmoc protection reaction to provide **1** (Scheme 1).

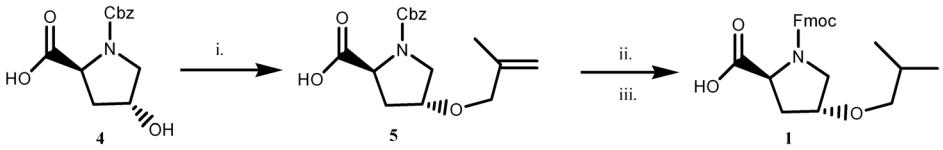

i. KHMDS, 3-Bromo-2-methyl propene, THF, -40°C to RT, 3 hrs; ii, Pd/C, H_2, MeOH, 12 hrs;
iii. FmocOSu, $NaHCO_3$, H_2O/$(CH_3)_2CO$, 0°C, 4 hrs.

*Scheme 1. Synthesis of novel Leu mimic **1**.*

The synthesis of the glutamic acid mimic, **2**, was also initiated with Cbz-protected hydroxyproline, **4**. Treatment of **4** with DMAP and t-butyl-propiolate results in a Michael addition without the need of a strong base [3]. The product **6** was treated with hydrogen and palladium on activated carbon to remove the Cbz protecting group and reduce the double bond. The free amine was used without purification in the final Fmoc protection reaction to provide **2** (Scheme 2).

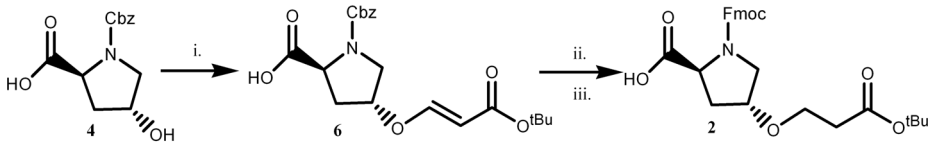

i. DMAP, t-butyl propiolate, THF 0°C, 30 min; ii. Pd/C, H_2, MeOH, 12 hrs
iii. FmocOSu, $NaHCO_3$, $H_2O/(CH_3)_2CO$, 0°C, 4 hrs.

*Scheme 2. Synthesis of Glu mimic **2**.*

The synthesis of the lysine mimic, **3**, was initiated with a Michael addition reaction between the anion of **4** and acrylonitrile (Scheme 3). This reaction was followed by benzyl protection of the carboxylic acid to provide ester **7**. The reduction of the nitrile proceeded with $NaBH_4$ and cobalt chloride in the presence of di-tert-dicarbonate. This procedure protected the free amine *in situ* [4]. Compound **8** was hydrogenated followed by Fmoc protection to provide compound **3**.

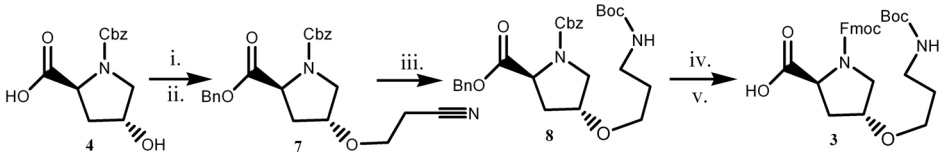

i. NaH, THF, 0°C, acrylonitrile, 24 hrs; ii. BnBr, Na_2CO_3, DMF, 2 hrs; iii. $CoCl_2$ $6H_2O$, Boc_2O, $NaBH_4$, MeOH, 0°C to r.t., 4 hrs; iv. Pd/C, H_2, MeOH, 12 hrs; v. FmocOSu, $H_2O/(CH_3)_2CO$, 4 hrs.

*Scheme 3. Synthesis of Lys mimic **3**.*

The synthesis of proline analogs be easily accomplished using these procedures. Compound **1**-**3** were synthesized in good overall % yield and they are currently being used in the synthesis of peptidomimetics.

Acknowledgments
The work was funded by a grant from the Indiana Elks.

References
1. Halab, L. and Lubell, W. D. *J. Org. Chem.* **64**, 3312-3321 (1999).
2. Cheng, M. et al. *J. Med. Chem.* **42**, 5426-5436 (1999).
3. Ariza, X., Costa, A. M., Faja, M., Pineda, O. and Vilarrasa, J. *Org Lett* **2**, 2809-2811 (2000).
4. McGeary, R. et al. *Tetrahedron* **57**, 8733-8742 (2001).

Peptide Revolution: Genomics, Proteomics & Therapeutics
Michael Chorev & Tomi K. Sawyer (Editors)
American Peptide Society, 2003

Synthetic α-Amino Acids as Building Blocks for Novel RNA Ligands

Andreas Krebs, Oliver Boden, Verena Ludwig and Michael W. Göbel

Institute of Organic Chemistry and Chemical Biology, Marie-Curie Straße 11, 60439 Frankfurt/Main, Germany

Introduction

In the last couple of years it became clear that many (if not most) mRNAs contain regulatory elements [1]. Complex formation of the TAR-RNA and the tat protein, for instance, is crucial for the efficient transcription of HIV genes [2]. The goal of our work is the synthesis of peptidic tat antagonists. Apart from electrostatic interactions, stacking was found to be fundamental for the molecular recognition of RNA. Because of the limited number of aromatic amino acids given by nature, we focused on the synthetic access to a broad scope of aromatic and heteroaromatic analogues. This project implemented two synthetic approaches to making glycine analogues with different linker lengths and aromatic substituents accessible in gram scales. Amino acids containing C_2 linkers can be prepared by chemical modification of (*S*)-methionine, hydroboration and subsequent Suzuki coupling with aryl halides (scheme 1) [3].

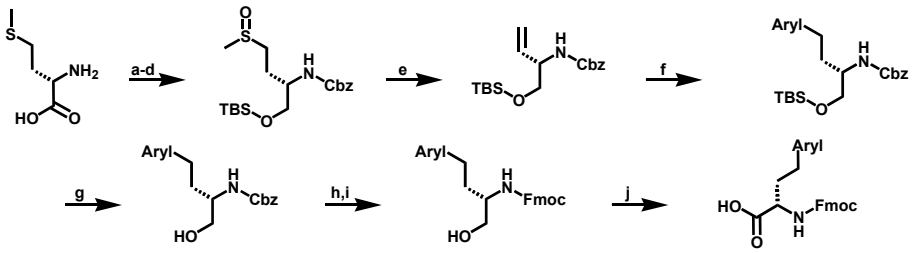

(a) $LiAlH_4$, THF, 76 % (b) Cbz-Cl (c) TBS-Cl, imidazole (d) $NaIO_4$, 94 % (over three steps) (e) o-Dichlorobenzene, 180°C, 88 % (f) 1. 9-BBN 2. Aryl-Br, CsF, $Pd[dppf]Cl_2$, 83-97 % (g) TBAF, 68-84% (h) 1,4-Cyclohexadiene, $Pd(OH)_2$ (i) Fmoc-Suc, 57-84 % (over two steps) (j) PDC, DMF, 56-86 %

Scheme 1. Synthesis of non-natural amino acids with C_2 linker starting from S-methionine.

Results and Discussion

Using the Myers-alkylation of glycine followed by hydroboration and Suzuki coupling conveniently leads to heteroaromatic amino acids with a C_3 linker (scheme 2) [4].

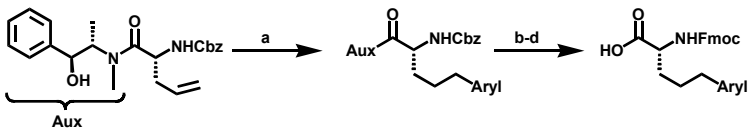

(a) 9-BBN, THF then K_3PO_4, Aryl-X, $Pd[PPh_3]_4$ 5 mol%, 27-90 % (b) MeOH, H_2, Pd/C (c) H_2O, reflux, 60 % (over two steps) (d) TMS-Cl, DCM then DIPEA, Fmoc-Cl, 70 %

Scheme 2. Synthesis of non-natural amino acids with C_3 linker by Myers-Alkylation.

The advantage of these approaches is the use of enantiopure common intermediates, resistant to racemization in the following synthetic steps. In addition, both enantiomers of the amino acids are available depending on the starting material initially used.

To proof the applicability of the new amino acids for solid phase synthesis, we generated tripeptides following the pattern Arg-X-Arg [5]. Peptides, surviving even

drastic acidic condition (including electrophilic intermediates) during cleavage, should fulfill the criteria required for library synthesis.

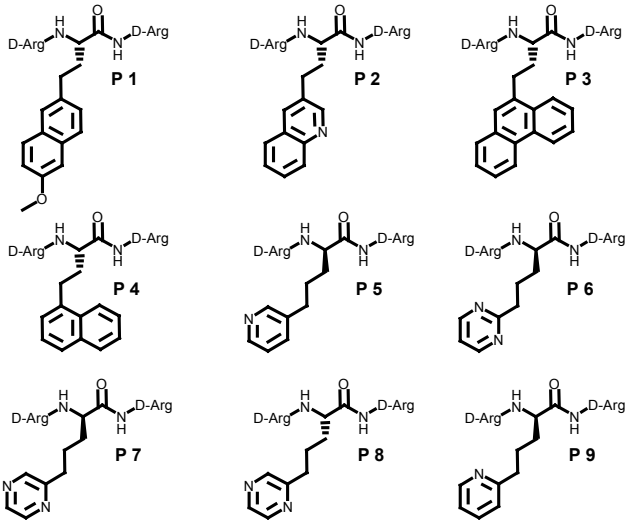

Scheme 3. Tripeptides synthesized by solid phase peptide synthesis.

The tripeptides were also tested for their binding affinity to HIV-1 TAR-RNA by a *FRET* assay [6] and compared with naturally occurring ligands. The new peptides showed IC_{50} values between 80 and 2 μM.

Table 1. IC_{50} values of tripeptides measured by FRET.

Tripeptide	IC_{50} [μM]	Tripeptide	IC_{50} [μM]
P 1	15	P 7	80
P 2	30	P 8	80
P 3	3	P 9	80
P 4	60	Argininamide	2000
P 5	23	Neomycin	7
P 6	2	Streptomycin	150

Acknowledgments
Financial support by the Deutsche Forschungsgemeinschaft (SFB 579) is gratefully acknowledged. A. K. thanks the Fonds der Chemischen Industrie for predoctoral fellowship.

References

1. Zaman, G. J. R., et al. *Drug Discov. Today* **8**, 297 (2003); Krebs, A., et al. *ChemBioChem*, **4**, 972-978 (2003).
2. Weeks, K. M. and Crothers, D. M. *Cell* **66**, 577, (1991).
3. Krebs, A., Ludwig, V., Pfitzer, J., Dürner, G. and Göbel, M. W. *Chem. Eur. J.* submitted.
4. Myers, A. G., Schnider, P., Kwon S. and Kung D. W. *J. Org. Chem.* **64**, 3322 (1999).
5. Chan, W. C., White, P. D. *Fmoc Solid Phase Peptide Synthesis* 2000, Oxford University Press. pp. 41-76.
6. Matsumoto, C., et al. *Bioorg. Med. Chem. Lett.* **10**, 1857 (2000).

Protein Mimicry, Engineering, Synthetic Chemistry and Structure-Function

Peptide Revolution: Genomics, Proteomics & Therapeutics
Michael Chorev & Tomi K. Sawyer (Editors)
American Peptide Society, 2003

Locally Stable Native-Like Fragments in the Denatured State of PapD Chaperone

James G. Bann[1], Jeff L.-K. Kao[2], Yun Wu[1] and Gregory V. Nikiforovich[1]

[1]Department of Biochemistry and Molecular Biophysics; [2]Department of Chemistry, Washington University, St. Louis, MO 63110, USA

Introduction

The computational search of the native-like hexapeptide fragments in the unfolded structure of proteins [1] may influence the early stages of protein folding [2], has been applied to the 218-residue two-domain PapD chaperone with the known native 3D structure (the PDB entry 1PDK). It was found, in agreement with the experimental data of ^{19}F-NMR spectroscopy of PapD [3], that the relative propensities of the fragments in the C-terminal domain 128-218 to form the native 3D structure are, as an average, higher than those in the N-terminal domain 1-118. The propensities to adopt the native-like 3D structure of PapD were also very high for hexapeptides KTRPNE and TRPNEV, which together comprise the link region 121-127 connecting the two domains of PapD. This specific structure is stabilized by the presence of Pro and interactions of the Glu side chain with the peptide backbone of Thr-Arg-Pro and with the side chain of Arg. The same search performed for the PapD mutants P124A and P124A/E126A showed that the propensities to adopt the native-like 3D structure of fragment PapD 121-126 dramatically decrease in the mutants compared to the wild type PapD (from 1.0 to 0.48 and 0.26, respectively). Energy calculations for the isolated "wild type" hexapeptide KTRPNE and for the "mutated" hexapeptides KTRANE and KTRANA showed distinct differences in their 3D structures; if validated by spectroscopic evidence, these computational predictions may open the way for rational design of the PapD mutants with the altered folding properties.

Results and Discussion

Energy calculations for the acetyl N-methylamides of KTRPNE, KTRANE and KTRANA were performed employing the standard ECEPP/2 force field with rigid valence geometry and planar *trans*-configurations of all peptide bonds [1]. All combinations of the local energetic minima in the Ramachandran map were considered as the starting points for energy minimization procedure. The sets of low-energy conformers of the peptide backbone (those with the relative energies $\Delta E \leq 6$ kcal/mol) were found to consist of 18 structures for KTRPNE, 155 for KTRANE and 115 for KTRANA.

All low-energy structures of KTRPNE form one single cluster as to their geometrical similarity (here and below an accepted criterion for geometrical similarity was the rms cut-off of 2 Å, C^{α}-atoms only; the same cut-off was used in [1]). All structures in the cluster are also similar to the X-ray structure of fragment PapD 121-126. Moreover, values of all variable proton-proton distances averaged over the cluster structures (assuming that all structures possess the same statistical weights) tightly correlate with the same distances in PapD 121-126, the correlation coefficient being 0.90. These findings clearly showed that the energy calculation results for the isolated KTRPNE hexapeptide can be interpreted as an indication of conformational behavior of the same hexapeptide included in the PapD protein chain.

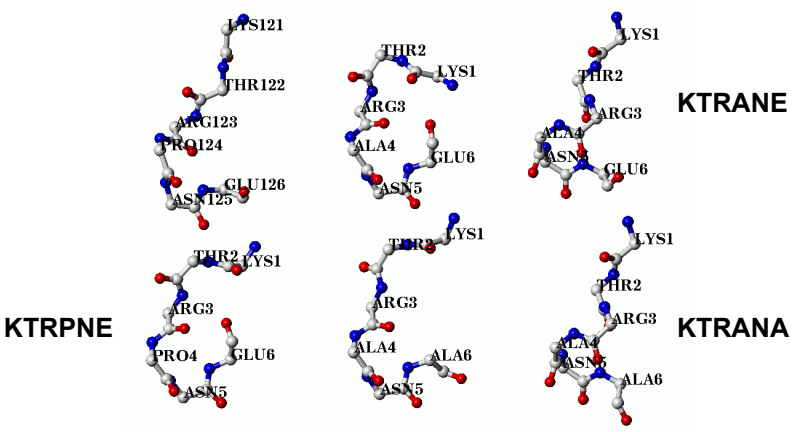

Fig. 1. Sketches showing 3D structure of PapD 121-126 (upper left) compared to the average 3D structures from the low-energy clusters in KTRPNE (lower left), KTRANE (upper center and upper right) and KTRANA (lower center and lower right). Only backbone atoms are shown; all hydrogens are omitted.

About 90% of all low-energy structures of KTRANE and KTRANA fall into two distinct clusters that are almost equally populated for each hexapeptide. One of the clusters in both KTRANE and KTRANA is geometrically similar to the cluster of low-energy conformations of KTRPNE (Figure1, central structures); the remaining clusters of KTRANE and KTRANA are similar to each other (Figure 1, structures at the right).

The acetyl N-methylamides of KTRPNE, KTRANE and KTRANA were synthesized by standard methods of solid-phase peptide synthesis. The NMR studies (TOCSY and NOESY spectra) were performed in water at two temperatures, 25º C and 1º C. No non-sequential NOEs were found in either peptide, which is consistent with calculations of the proton-proton distances averaged over all low-energy structures, assuming that all structures possess the same statistical weights. Since some NH signals were overlapped in the NOE spectra, not all possible NH_i-NH_{i+1} cross-peaks were observed and/or resolved; however, the observed NH_1-NH_2 cross-peaks were of less volume than others in KTRPNE and KTRANA, which is also in accordance with the calculation results. CD spectra in water at 5º C in the wavelength range 180-260 nM showed pronounced similarity of the two spectra for KTRANE and KTRANA, which, in turn, were distinctly different from the spectrum for KTRPNE (disappearance of a peak at *ca.* 215 nM). In summary, the obtained spectroscopic studies are in agreement with the calculation results; experimental studies on folding of the PapD mutants P124A and P124A/E126A will follow.

Acknowledgments

The work was supported by NIH grant GM53630.

References

1. Nikiforovich, G. V. and Frieden, C. *Proc. Natl. Acad. Sci. U.S.A.* **99**, 10388-10393 (2002).
2. Nikiforovich, G. V. and Frieden, C. in *Peptides 2002. Proceedings of the Twenty-Seventh European Peptide Symposium* (Benedetti, E., and Pedone, C., Eds.) pp 234-235, Edizioni Ziino, Napoli (2002).
3. Bann, J. G., et al. *Proc. Natl. Acad. Sci. U.S.A.* **99**, 709-714 (2002).

Peptide Revolution: Genomics, Proteomics & Therapeutics
Michael Chorev & Tomi K. Sawyer (Editors)
American Peptide Society, 2003

Chemical Synthesis of Proteins Through Native and Extended Chemical Ligation

Paolo Botti, Matteo Villain, Sonia Manganiello and Hubert Gaertner

GeneProt Inc., Geneva Branch, 2, Pré de-la–Fontaine, 1217 Meyrin, Switzerland

Introduction

Peptide fragments up to ~70 residues can be nowadays routinely synthesized in a high degree of homogeneity by SPPS [1]. Therefore, to synthesize proteins of small and medium size (larger than 100 residues) it is necessary to join together 2 or more fragments. During the last decade Native Chemical Ligation (NCL) [2] has been extensively demonstrated to be uniquely effective for the rapid preparation of small and medium size proteins with a high level of homogeneity. We present here an overview of the most recent advances in the field, including multi-step ligation strategies, ligation at non-cysteine site, ligation at special residues that require a protecting group strategy and a novel strategy to synthesize thioester fragments via Fmoc-based chemistry.

Results and Discussion

Native chemical ligation [2] is emerging as a powerful tool in protein chemistry, which enables the chemical synthesis of proteins of small to medium size. Such methodology exploits a chemoselective reaction between two unprotected fragments, a C-terminal thioester and a N-terminal cysteine, in aqueous solution at neutral pH. In the first step of this reaction transthioesterification occurs at pH 6-8 by thiol exchange between the free thiol of the N-terminal cysteine and the thioester moiety on the other molecule. The newly generated thioester then undergoes an S to N acyl shift due to the proximity of the amino group to the thioester functionality, thus generating a native amide bond at the ligation site. During the last few years several innovations improved NCL. In the three or more fragments ligation strategy a key issue is the reactivity of the middle segment, which bears both N-terminal cysteine and C-terminal thioester reacting sites. In such cases, the N-terminal cysteine must be protected to avoid cyclization [3]. The Acm [4] and Msc [5] groups have been exploited respectively as S and N protecting group, neither being totally satisfactory. To overcome the limitations of these two approaches, the use of the thiazolidine cyclic structure as the N terminal protection modality [6] (Scheme 1) has been successfully exploited in the synthesis of a fully native folded protein of over 18kD [7]. The thiazolidine ring [8,9] represents a convenient temporary protection for the N-terminal Cys especially for peptide segments with a C-terminal thioester and the "one pot" deprotection procedure. Facile ring opening in the presence of methoxamine under acidic conditions directly in the post-ligation mixture permits a considerable reduction in losses related to multistep purifications associated with solution syntheses.

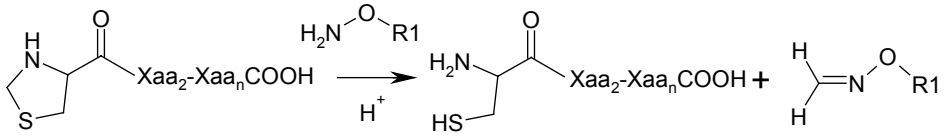

Scheme 1. Re-opening of thiazolidine ring by O-alkyl hydroxylamine derivatives.

The requirement for cysteine at the site of peptide ligation is an intrinsic restriction of the NCL strategy. In proteins, Cys occurs with a relatively low frequency; many protein sequences do not have suitably disposed cysteines for the NCL strategy and some lack Cys residues entirely. Recently, a novel and practical method that extends NCL to peptide segments at a Glycine site has been presented [10] (Scheme 2).

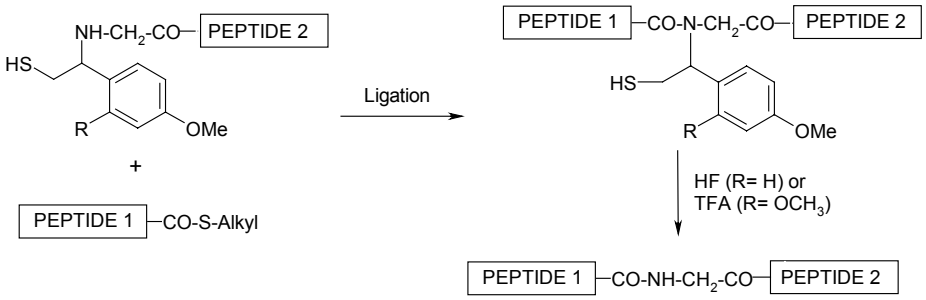

Scheme 2. General ligation strategy with 1-phenyl-2-mercaptoethyl auxiliaries.

With the recent introduction of Extended Chemical Ligation (ECL) ligations are no longer restricted to N-terminal cysteines. A peptide fragment presenting an N-terminal glycine functionalized with the auxiliary group N^{α}-(1-phenyl-2-mercaptoethyl) readily reacts with a C-terminal thioester peptide fragment generating a natural amide bond at the ligation site after auxiliary removal with HF or TFA. The key aspect of this strategy is that the 1-Phenyl substitution of the 2-mercaptoethyl auxiliary on the N^{α}-terminus of the fragment results in benzylamine derivative that is stable to the strong acidic conditions used to cleave the peptide from the resin. However, the same group present on the corresponding amide formed after the completion of the ligation reaction is easily cleaved under similar or less strong acidic conditions. Proteins devoid of natural cysteine residues have been then synthesized using this new methodology [11] thus greatly expanding the applicability of NCL.

An extensive study [12] with all the 20 naturally occurring amino acids had been conducted to demonstrate the feasibility of NCL at the Xaa-Cys ligation site. However, no further investigation was carried out to identify potential side reactions at the C-terminal thioester residue. Our attention focused on aspartic and glutamic acid residues, since the proximity of the β- or γ-carboxyl to the thioester moiety could cause a migration of the thioester onto the carboxylic acid side-chain. In this case the consequence would result in the formation of the unnatural β (for the Asp) or γ (for the Glu) amide bond between the Asp/Glu and the Cys residue (Scheme 3). Our work [13] proved that ligation at Asp/Cys and Glu/Cys, when conducted with an unprotected functionality at the ligation site, results in the generation of 20-30% non-natural backbone isoforms. Characterization of this side reaction was easy on a small peptide but could be challenging on a larger fragment suggesting prudence in the interpretation of an apparently perfect ligation. We investigated the existing protecting groups for both glutamic and aspartic acid side-chains (Figure 1). We proved that for glutamic acid the use of OPse side-chain protection, although not ideal, is the best solution, since OPse removal can be achieved with milder conditions than for OFm removal.

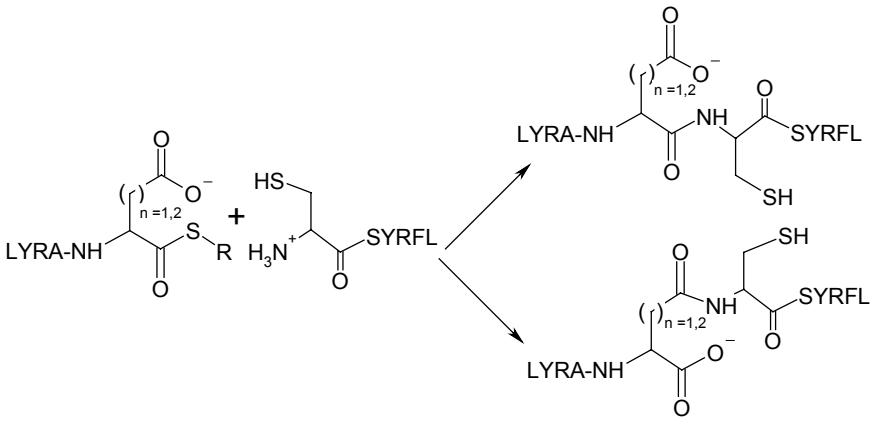

Scheme 3. Ligation at Asp (n =1) and Glu (n =2) residues.

Aspartic acid ligation was more problematic, since use of the available side-chain protecting groups enhanced the generation of the non-natural isoform. For this amino acid (and probably also for glutamic acid), the best solution lies in protecting groups removed by reduction with Zn and acetic acid. The classical phenacyl ester unfortunately proved to be unstable in the ligation reaction. A sterically hindered version, 1-methyl-2-oxo-2-phenyl ester (OMop) perfectly withstands long ligation reaction conditions, and generates only the expected natural compound at the ligation site.

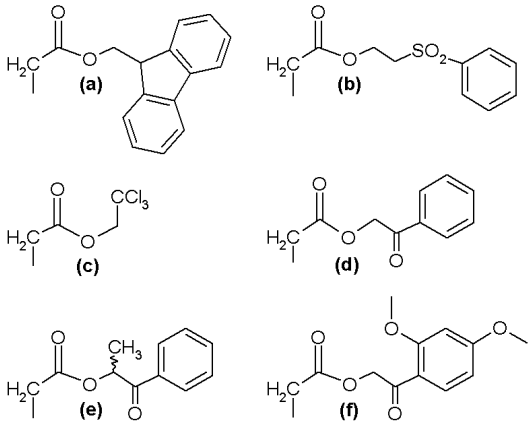

Fig. 1. Protecting groups tested for Glu or Asp side-chain protection: (a) OFm, (b) OPse, (c) OTce, (d) OPac, (e) OMop and (f) OdiMeOPac.

In our opinion, use of OMop protection is imperative when approaching a ligation at an aspartic acid site. Considering the advantage of avoiding basic conditions for the deprotection step, we suggest further exploration of OMop also for glutamic acid protection.

Presently, the synthesis of the oligopeptide thioester intermediates is carried out primarily by Boc-based chemistry and less so by Fmoc-based chemistry. This is due to

the instability of the thioester groups to the nucleophilic reagents used to remove the protecting groups in Fmoc-based approaches. On the other hand, the extremely strong acidic conditions, like HF or TFMSA used in Boc-based SPPS are generally incompatible with Post Translational Modifications (PTM), which are often necessary for biological activity. Therefore, a simple and practical strategy, which allows the generation of thioester fragments under conditions compatible with PTM dramatizations, is essential for the preparation of polypeptides with high biological value. The aim of our work was to design a strategy to generate peptide-C^{α}-thioesters via standard Fmoc chemistry that does not require any additional step after the first FmocAA is coupled to the appropriate resin.

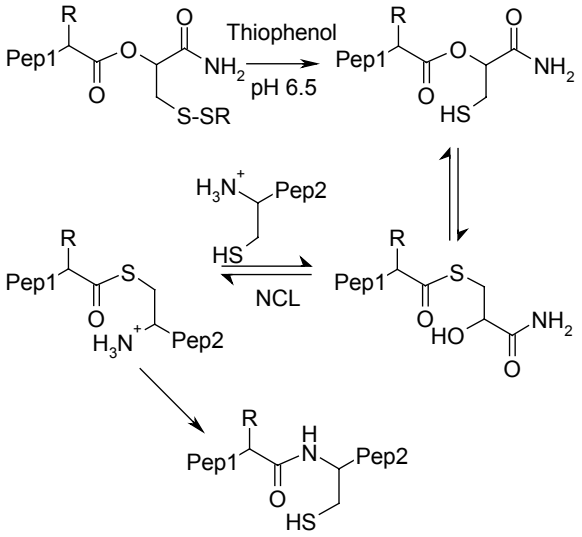

Scheme 4. Native chemical ligation through in situ O to S acyl shift.

In such methodology the first FmocAA of the sequence is attached to the template through a carboxyester linkage, a routine Fmoc SPPS synthesis and cleavage should then be performed. The generation of the thioester moiety using standard NCL reaction conditions occurs only prior to or during ligation.

Our group developed a new methodology [14] to obtain thioester intermediates through *in situ* O to S acyl shift (Scheme 4). We envisaged that a peptide-C^{α}-carboxyethylester bearing a free mercaptan in the β position might be in equilibrium with its thioester isomer through an O to S acyl shift via a five-member ring intermediate. It is known that the sulfhydryl group of a mercaptan is more acidic than the hydroxyl group of the corresponding alcohol. Therefore, at the pH required for NCL the sulfhydryl group is more dissociated than its corresponding hydroxyl isomer making the O to S acyl equilibrium unfavorable. If however an electron-withdrawing group is introduced adjacent to the oxygen occupied in the ester bond, activation of the carboxyester occurs making the hydroxyl moiety a better leaving group and allowing a more favorable O to S acyl equilibrium between the two isomers. Only under ligation conditions, namely neutral pH and in presence of mild reducing reagents like phosphines or appropriate nucleophiles like thiophenol, is the free active thiol slowly liberated and the O to S acyl shift is taking place. The newly formed thioester

intermediate is then immediately captured by the excess of the N-terminal cysteine fragment present in solution thus driving the overall process to completion. Once the transthioesterification reaction with the C-terminal fragment has occurred, the "classical" S to N acyl shift takes place resulting in an amide bond formation that drives the whole process to completion. Model peptides of sequence LYRAX-C^{α}OOCH-(CH_2SStBut)-$CONH_2$ where X=Gly, Phe and Lys were synthesized by standard Fmoc-based SPPS. When ligated under standard NCL conditions with a model fragment CYAKYAKL, the only side product detected was the hydrolyzed ester, which amount to 10-15% of the ligated product as measured by HPLC with UV detection at 214 nm. Using this novel methodology the linear precursor of a 68-residues chemokine protein and the Spermatid Nuclear Transition Protein 1 (SPT1) phosphorylated at position 8 (Ser), employing the phosphorylated protected residue FmocSer(PO(OBzl)OH)OH during SPPS, have been synthesized in high yield.

Conclusion

Small and medium-size proteins up to ~20 kD can be rapidly synthesized in high degree of purity via multi-step Native or Extended Chemical Ligation using either Boc or Fmoc chemistry to prepare the peptide fragments necessary for the assembly of the desired protein. Furthermore PTMs can be now easily incorporated into proteins further broadening the application of Native Chemical Ligation.

Acknowledgments

We would like to acknowledge Nicolas Dafflon, Benoit Depresle, Marianne Paolini and Sylvain Raimondi for the excellent technical assistance and useful discussions.

References

1. Schnolzer, M., Alewood, P., Jones, A., Alewood, D. and Kent, S. B. H. *Int. J. Pept. Protein Res*. **40**, 180-193 (1992).
2. Dawson, P. E., Muir, T. W., Clark-Lewis, I. and Kent, S. B. H. *Science* **266**, 776-779 (1994).
3. Zhang, L. and Tam, J. P. *J. Am. Chem. Soc*. **119**, 2363-2370, (1997).
4. Canne L, Botti P., Simon R. J., Chen Y., Dennis E. A. and Kent S. B. H. *J. Am. Chem. Soc*. **121,** 8720-8727 (1999).
5. Yamashiro, D. and Li, C. H. *Int. J. Pept. Protein Res*. **31**, 322-334 (1988).
6. Villain, M., Vizzavona, J. and Gaertner, H. In Lebl, M. and Houghten, R. A. (Eds.) *Peptides: The Wave of Future, Proceedings, 2nd International and 17th American Peptide Symposium,* American Peptide Society, San Diego, p.107–108 (2001).
7. Villain, M., Vizzavona, J. and Gaertner, H. In Epton R. (Ed.) *Collected Papers of the Seventh Symposium of Innovation and Perspectives in Solid Phase Synthesis*, Mayflower Worlwide Ltd., Kingswinford, UK, p. 39–42 (2002).
8. King, F. E., Clark-Lewis, J. W., Smith, G. R. and Wade, R. *J. Chem. Soc*. 2264 (1959).
9. Wöhr, T., Rohwedder, B., Wahl, F. and Mutter, M. *J. Am. Chem. Soc*. **118**, 9218-9224 (1994).
10. Botti, P., Carrasco, M. and Kent, S. B. *Tetrahedron Lett.* **42**, 1831-1833 (2001).
11. Low D. W., Hill M. G., Carrasco M. R., Kent S. B. and Botti P. *Proc. Natl. Acad. Sci. U.S.A*. **98**(12), 6554-6559 (2001).
12. Hackeng T. M., Griffin J. H., and Dawson P. E. *Proc. Natl. Acad. Sci. U.S.A*. **96**, 10068-73 (1999).
13. Villain, M., Gaertner, H. and Botti P. *Eur. J. Org. Chem.* **68**, 3267-3272 (2003).
14. Botti, P., Villain, M., Manganiello, S. and Gaertner, H. *Manuscript in preparation* (2003).

Peptide Revolution: Genomics, Proteomics & Therapeutics
Michael Chorev & Tomi K. Sawyer (Editors)
American Peptide Society, 2003

Combination of the Convergent and Native Chemical Ligation Methods in the Total Synthesis of Proteins

Dimitrios Gatos, Spyros Goulas and K. Barlos

Department of Chemistry, University of Patras, Patras, Greece

Introduction

The sequential condensation of fully protected peptide fragments either in solution or on solid phase (Convergent Synthesis) has been proven to be a very successful approach for the preparation of large or difficult peptides and proteins. Recently, this approach has been adapted for the production of the viral fusion inhibitor T-20 at the ton scale. Despite its considerable success, in some cases the application of the convergent method cannot be easily realized, due to fragment solubility problems and/or slow condensations at certain peptide regions. These problems could be overcome by combination of the convergent method with the chemoselective ligation of unprotected peptide fragments, such as the Native Chemical Ligation method. The successful combination of the two strategies would also expand the range of protein targets accessible to chemical synthesis. To investigate these possibilities we used hirudin variant 1 (HV1), consisting of 65 amino acid residues, as a model protein.

Results and Discussion

For the preparation of the peptide C-terminal thioesters, which are the necessary intermediates for the application of the ligation technique, we developed a new method based on the post-assembly thioesterification of peptide fragments attached on trityl-type resins, via an amino acid side-chain (two-directional synthesis approach [1]). Thus, the 19-27 protected fragment of hirudin variant 1, synthesized by conventional Fmoc-SPPS on 2-chlorotrityl resin, was selectively deprotected at Cys^{22} side-chain by removal of the S-4-methoxytrityl (Mmt) group with 2% TFA in DCM/TES (97:3) for 20 min at RT. This partially protected fragment was then attached onto Mmt-resin, via the thiol function, by reacting with Mmt-Cl resin in DCM/DMF (9:1) for 3 h at RT. Under these conditions, no attachment via the free C^{α}-carboxyl group occurred. The resin-bound peptide was then converted to the corresponding C-thioester by reacting with a 5-fold

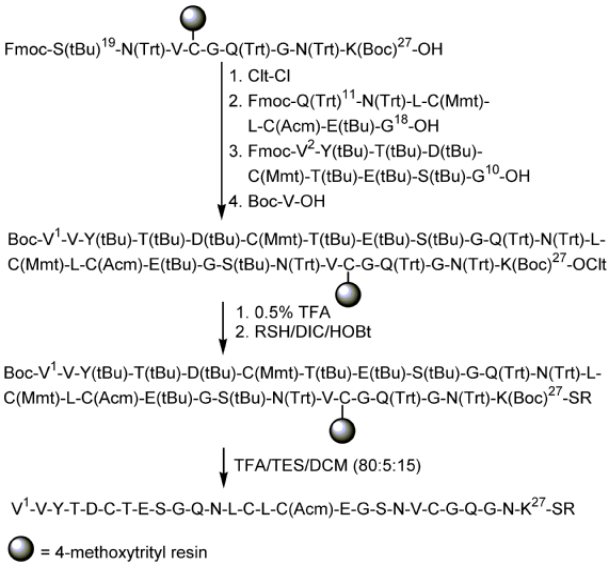

Fig. 1. Convergent synthesis of hirudin 1-27 thioester.

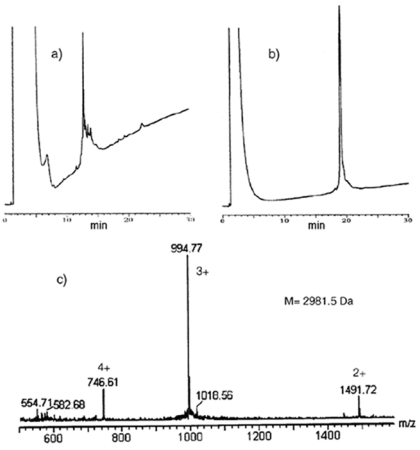

Fig. 2. HPLC analyses of crude (a) and purified (b) hirudin 1-27 thioester, (c) ES-MS.

molar excess of methyl mercaptoacetate using DIC/HOBt as condensing agent. Thioesterification reaction was complete in 2 h at RT, as revealed by the HPLC analysis of the obtained product after cleavage from the resin and total deprotection with TFA/DCM/TES (80:15:5) for 2 h at RT. Besides the thioester, the spontaneous formation of thiolactone, due to the presence of internal Cys residues, and oxidized S-S dimer, after dissolving the product in DMF or aqueous solvents, was also detected. Similar results were obtained when thiophenol was used instead of methyl mercaptoacetate.

In order to obtain longer peptide thioesters, the resin-bound fragment 19-27 was first esterified with a ten-fold molar excess of 2-chlorotrityl chloride (Clt-Cl) and DIPEA and then extended to the *N*-terminal direction by the solid phase sequential condensation of fragments 11-18, 2-10 and Boc-Val-OH (Figure 1). The Clt-group was selectively removed by a 5 min treatment with 0.5% TFA in DCM, and thioesterification with methyl mercaptoacetate was performed as described above. The C^{α}-thioester of the hirudin 1-27 fragment was thus obtained in good yield and purity, after cleavage from the resin and simultaneous total deprotection with TFA/DCM/TES (80:15:5) for 2 h at RT (Figure 2).

This peptide thioester was applied in the synthesis of the hirudin 1-34 fragment and the full-length hirudin 1-65, by the Native Chemical Ligation method.

In conclusion, peptide thioesters can be efficiently prepared by on-resin thioesterification of side-chain attached peptide fragments. Besides Cys-containing peptides, this method also could be easily applied to peptide fragments attached through the side-chain of His, Ser and Lys, or through the N^{α}-terminal, on trityl-type resins. Long thioesters can be obtained by chain extension applying convergent methods. Combination of this approach with the Native Chemical Ligation method constitutes a very advantageous strategy for the synthesis of large proteins.

Acknowledgments

This work was supported by CBL-Patras.

References

1. Barlos, K. and Gatos, D. In Chan, W. and White, P. D. (Eds.) *Fmoc Solid Phase Peptide Synthesis: A Practical Approach,* Oxford University Press, UK, p. 215 (2000).

Peptide Revolution: Genomics, Proteomics & Therapeutics
Michael Chorev & Tomi K. Sawyer (Editors)
American Peptide Society, 2003

Chemical Synthesis and Folding/Stability Studies of the Hydrophobic Protein, Crambin

Duhee Bang[1], Neeraj Chopra[2] and Stephen B. H. Kent[1,2]

Institute for Biophysical Dynamics; [1]Department of Chemistry; [2]Department of Biochemistry & Molecular Biology, The University of Chicago, Chicago IL 60637 USA

Introduction

Crambin is a small (46 amino acid) protein isolated from the seeds of the plant *Crambe abyssinica* [1]. Crambin has been extensively used as a model protein for the development of advanced crystallography and NMR techniques, and for computational folding studies. Previously, Crambin had been produced with extreme difficulty in only microgram amounts by rec-DNA expression [2]. We set out to establish efficient synthetic access to Crambin and to use it as a model system for experimental studies of protein folding. We have successfully synthesized the 46-amino acid polypeptide by native chemical ligation [3] of two peptide segments (15+31 residues). The synthetic polypeptide chain folded in good yield to give native Crambin containing three disulfide bonds. The chemically synthesized Crambin was characterized by LC-MS, CD and 2D NMR. However, the 31-residue peptide segments were difficult to purify, and this caused an overall low yield for the synthesis. To overcome this problem, we synthesized Crambin by the native chemical ligation of three segments (15+16+15 residues); this gave a 10-fold increase in yield and a protein product of exceptionally high purity. We are now using this efficient synthesis to apply the tools of modern chemistry to the study of this globular protein whose folding, unusually, causes the surface of the molecule to become more hydrophobic.

Results and Discussion

Crambin isolated from nature has two forms: one has Ser22 and Ile25 ('SI' form) and the other has Pro22 and Leu25 ('PL' form). We have chemically synthesized both the SI and PL forms; the SI form by ligation of Cram[1-31] and Cram[32-46], and the PL form by ligation of Cram[1-V15A] and Cram[16-46]. The synthetic polypeptide folded in good yield to give native Crambin containing three disulfide bonds. The chemically synthesized Crambin was characterized by LC-MS, CD and 2D-NMR (Figure 1). However, both Cram[1-31] and Cram[16-46] were difficult to purify even with multiple applications of RP-HPLC, because of a des-Thr impurity eluting very close to the desired product.

To overcome the problems associated with the synthesis of the 31-residue peptide segments, we synthesized Crambin by the native chemical ligation of three peptide segments. The peptide segments, Cram[1-V15A]-thioester, Cram[Acm16-31]-thioester, and Cram[32-46], were synthesized by stepwise SPPS. For the Cram[1-V15A] and Cram[32-46], one-step RP-HPLC gave good yields. However, the crude peptide Cram[Acm16-31] turned out to be comparable to the problematic crude peptide Cram[16-46], and the major des-Thr impurity eluted almost at the same time as the product peak. LC-MS^2 was used to determine the nature of the major impurity; Thr at position 21 turned out to be missing in the des-Thr coproduct. Triple coupling of Thr^{21} produced crude peptide devoid of des-Thr impurity; one-step RP-HPLC gave a good

purification yield. With this adjustment, each of the three purified peptide segments was obtained with typical yields of 49%-56%, based on starting amino acid-resin.

Ligation reaction of Cram[Acm16-31] and Cram[32-46] was complete in 6 hours, and Acm group removal was performed using mercury acetate ($Hg(OAc)_2$) and quenching with β-mercaptoethanol. To improve the yield of Acm-group removal, we examined the use of silver acetate, and optimized conditions gave a significantly improved yield. Ligation of Cram[1-V15A] and Cram[16-46] was complete in 24 hours. Folding of the purified 46 residue polypeptide was very efficient and was complete in one hour. The mass of folded Crambin showed a 6Da decrease, reflecting formation of three disulfide bonds. Preparative RP-HPLC gave highly purified Crambin in good yield. The chemically synthesized Crambin was characterized by LC-MS, CD, and by 2D-NMR (Figure 1). Based on the amount of Cram(31-46) used in the synthesis, highly purified Crambin was obtained with an overall yield of 25%.

This yield was increased more than 10-fold by the ligation of three highly purified peptide segments, instead of the two segment ligations. The facile chemical synthesis of Crambin will be useful for studying the high stability of this protein and its folding, by use of a variety of biophysical probes, as well as for the development of advanced structure determination methods.

Abbreviations for peptides. Cram[1-V15A]: TTCCPSIVARSNFNA-SCH_2CH_2CO-Leu;
Cram[16-31]: CRLPGTPEALCATYTG-SCH_2CH_2CO-Leu;
Cram[32-46]: CIIIPGATCPGDYAN

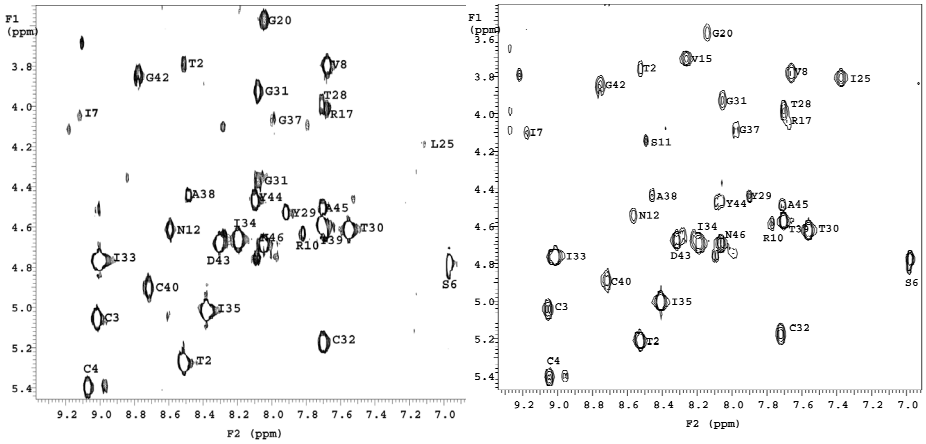

Fig. 1. 1H 2D-TOCSY NMR spectra fingerprint region of folded synthetic Crambin. Left; PL-Crambin[V15A]. Right; SI-Crambin.

Acknowledgments
We thank Josh Kurutz and Shohei Koide for instructions for NMR usage.

References

1. Teeter, M., Mazer, J.A., L'Italien, J. *Biochemistry* **20**, 5437 (1981).
2. Lobb, L., Stec, B., Kantrowitz, E., Yamano, A., Stojanoff, V. Markman, O., Teeter, M. *Protein Engneering* **9** 1996 (1223).
3. Dawson, P., Muir, T., Clark-Lewis, I. and Kent, S. *Science* **266**, 776 (1994).

Peptide Revolution: Genomics, Proteomics & Therapeutics
Michael Chorev & Tomi K. Sawyer (Editors)
American Peptide Society, 2003

De Novo Four-Helix Bundle Proteins

Heidi K. Huttunen and John C. Sherman

Department of Chemistry, University of British Columbia, Vancouver, BC V6T 1Z1, Canada

Introduction

One approach used to illustrate the interactions that govern protein structure is to design and characterize simple *de novo* proteins [1-2], which retain the crucial interactions of natural proteins, but lack their complexity. The use of templates [3] to assist in the organization of peptides to form pre-determined three-dimensional structures has emerged as a useful tool in this area of research. In our group, cavitands [4], which are rigid organic macrocycles with an enforced cavity, are used as a template in the formation of four-helix bundle proteins [5],[6],[7]. Two main goals in our research are to design, synthesize and characterize native-like Template Assembled Synthetic Proteins (TASPs; Figure 1) from first principles, and to create proteins with specific applications (e.g., non-natural catalysts).

To date this research has included the investigation of native-like structures through the design, synthesis and characterization of TASPs having nor-leucine amino acids at the hydrophobic positions, compared to those containing leucine residues. Since norleucine amino acids have unbranched side chains, the hypothesis is that the nor-leucine TASPs should manifest less native-like properties, such as broad ^{1}H NMR signals with low dispersion.

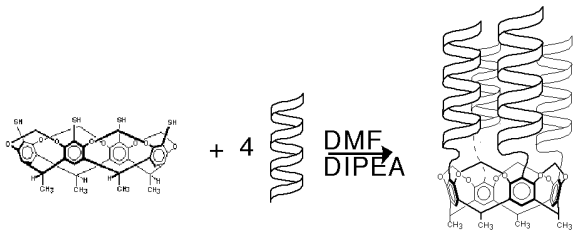

Fig. 1. TASP synthesis.

Furthermore, recent efforts toward the synthesis and characterization of TASPs containing two different peptide sequences within one bundle will be presented. This provides an opportunity to create a variety of de novo proteins, previously limited to having only one type of peptide sequence attached.

Results and Discussion

The ability to create native-like *de novo* proteins is hampered by the lack of information available to diagnose them. Previously in our lab, LG2 and LG3 have been studied, and have shown some native-like characteristics, but this character remains nebulous. We sought to perturb the putative native-like structure of LG2 and LG3 to determine this loss in conformational specificity in the synthesis and characterization of NG2 and NG3.

LG2 = [GG] – EELLKKLEELLKKG
LG3 = [GGG] – EELLKKLEELLKKG
NG2 = [GG] – EEXXKKXEEXXKKG where X = Norleucine
NG3 = [GGG] – EEXXKKXEEXXKKG where X = Norleucine

Fig. 2. Peptide sequences used for the synthesis of corresponding TASPs.

These TASPs were analyzed by CD and ^{1}H NMR spectroscopy, by GuHCl denaturation, and by analytical ultracentrifugation (AUC) experiments. NG2, LG2, NG3 and LG3 exhibited concentration independent CD spectra, and curves characteristic of alpha-helical secondary structure. The four caviteins were monomeric in solution according to the analysis of the AUC data. ^{1}H NMR spectroscopy is the most useful tool in identifying native-like character, and the spectra for LG2, LG3, NG2 and NG3 are shown in the Figure 3 below.

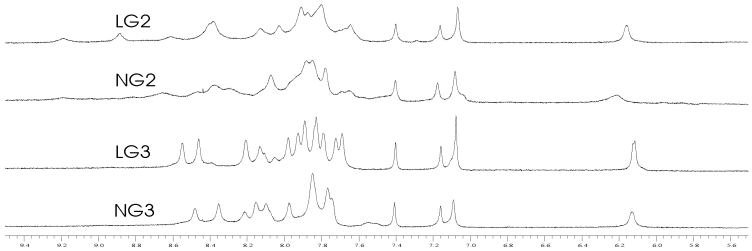

Fig. 3. ^{1}H NMR spectra of the amide region of the TASPs on 600 MHz spectrometer.

NG2 is as dispersed as LG2 but more broad. The ΔG^o_f's for NG2 and LG2 were comparable, suggesting that the tertiary structure of LG2 was not greatly affected by the substitution of residues to norleucine units. This observation is also consistent with their similar CD and NMR spectra.

LG3 is slightly more sharp than NG3. An interpretation is that the side chains in LG3 are packed well, characteristic of native-like structure. NG3, on the other hand, may have more motion in its core leading to averaged signals. Thus, similar spectra may result from different dynamics, as the ΔG^o_f for these two proteins were very different.

The synthesis of TASP **4** (Figure 4) with two different peptide sequences attached within one bundle has been successful, and its mass confirmed by MALDI-MS.

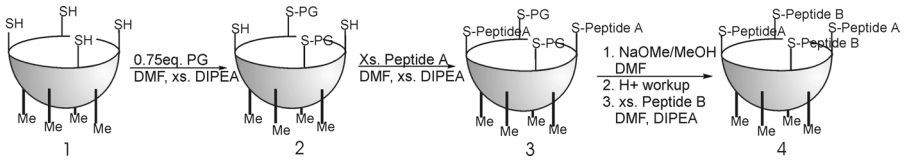

*Fig. 4. Synthesis of disubstituted TASP **4.***

This project will continue with the synthesis of variety of caviteins, the study of their dimers, and by attempting to encapsulate a guest molecule within the template.

Acknowledgments

The work was funded by NSERC and NIH grants, and by the University of British Columbia.

References

1. Degrado, W. F. *Adv. Prot. Chem.* **39**, 51-124 (1988).
2. Hecht, M. H., Richardson, J. S. and DeGrado, W. F. *Biochemistry* **36**, 2450-2458 (1997).
3. Mutter, M. and Vuilleumeir, S. *Angew. Chem. Int. Ed. England* **28**, 535-553.(1989).
4. Moran, J. R., Karbach, S., and Cram, D. J. *J. Am. Chem. Soc.* **104**, 5826-5828 (1982).
5. Causton, A. S. and Sherman, J. C. *J. Peptide Sci.* **8**, 275-282 (2002).
6. Mezo, A. R. and Sherman, J. C. *J. Am. Chem. Soc.* **121**, 8983 - 8993 (1999).
7. Gibb, B. C., Mezo, A. R. and Sherman, J. C. *Tetrahedron Lett.* **36**, 7587-7590 (1995).

Peptide Revolution: Genomics, Proteomics & Therapeutics
Michael Chorev & Tomi K. Sawyer (Editors)
American Peptide Society, 2003

Cavitand Based Four-Helix Bundles

Emily S. Seo and John C. Sherman

Department of Chemistry, University of British Columbia, Vancouver, BC V6T 1Z1, Canada

Introduction

A challenge in *de novo* protein design involves the investigation of elements that contribute to synthesizing precisely defined tertiary structures [1-2]. The template approach has proven to be a useful technique in directing peptides into desired folds [3]. Our group uses cavitands as the template, which are rigid organic macrocycles that possess an enforced cavity [4]. Four-helix bundles are widely studied because of their common occurrence in nature [5-6]. The latest efforts toward studying the linkage between the template and peptide, and exploring the attachment point will be presented. As protein folding becomes better understood, more complex structures with specific function can be designed and studied.

Recently, there has been a growing interest in dynamic combinatorial libraries (DCLs) [7]. DCLs differ from other libraries in that the individual members of the library are constantly interconverting, and therefore its composition is controlled thermodynamically. Disulfide bond linkages [8] can be used to examine this concept.

Results and Discussion

Our four-helix bundles are called caviteins (cavitand + proteins). The peptides were designed to be amphiphilic α-helices with intrahelical salt bridges. The cavitand template offers advantages such as providing stability, controlling the orientation of the helices, and overcoming the entropic barrier of bringing four peptide strands together (Figure 1).

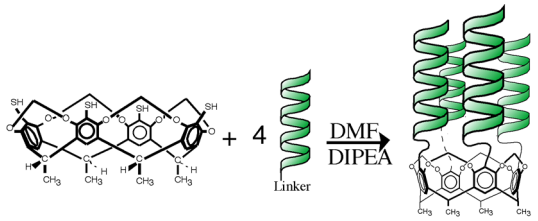

Fig. 1. Cavitein Synthesis.

Previous studies have shown that the type and length of the linker between the template and the peptides have a significant effect on the overall structure of the proteins [5]. A new sequence was designed to improve the inner core packing, and ultimately enhance the native-like character of the four-helix bundles (Figure 2).

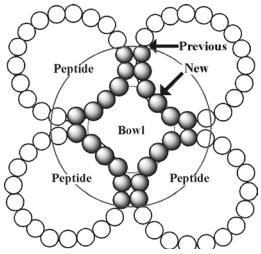

Previous sequence S0 = EELLKKLEELLKKG
New sequence S2 = AEELLKKLEELLKKG

The caviteins are named with the number in front of the sequence denoting the number of glycine linkers between the peptide and the template (i.e. 2GS2 cavitein has 2 glycine linker for every S2 peptide).

Fig. 2. Helical wheel of a cavitein showing the previous and new linkage points.

Circular dichroism (CD) spectroscopy, ^{1}H NMR spectroscopy and sedimentation equilibria studies have been used to probe the protein structures. Denaturation studies were conducted to determine the stability of the caviteins. Sharp, well dispersed peaks of ^{1}H NMR spectra are characteristic of native-like proteins. Comparing both sequences (S0 and S2), and the various linker lengths, the 2GS2 cavitein seems to be the most well defined species (stable, most native-like and monomeric). The reversed maximum/minimum trend in the near UV region of the CD spectrum may be an indication of opposite helical supercoiling effects (Figure 3). The enhanced signals displayed by the 2GS2 cavitein in the near UV region may be due to tighter supercoiling, which may indicate better packing, and therefore may contribute to its high stability and native-like character.

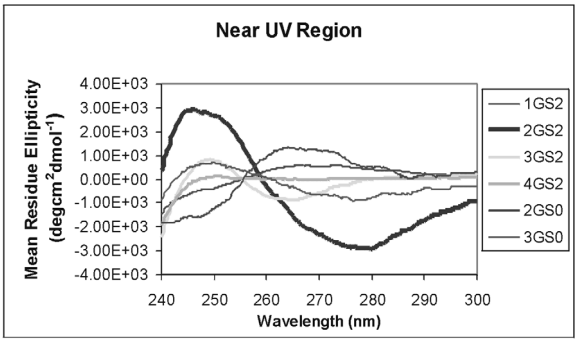

Fig. 3. Near UV region of a CD spectrum.

A more general approach toward creating native-like proteins is to synthesize the caviteins under reversible conditions. In other systems, disulfide bonds have previously been shown to form reversibly in water [7], and therefore these bonds will be used to form linkages between the template and the peptides. In principle, the most stable proteins, which are more likely to be native-like, should be obtained under reversible conditions. The amino acids within a sequence can be systematically changed to create a mixture of peptides, and then reacted with the template. Thus, this reversible assembly approach should provide an efficient screen for stable native-like de novo proteins.

A long-term goal would be to study catalysis using these template assembled proteins. Future studies include the design a cavitein that is more stable than natural enzymes but with the same selectivity. Our caviteins are suitable for this purpose because they are very robust, and thus can withstand higher temperatures and a wider pH range.

Acknowledgments

The work was funded by NSERC and NIH grants and by the University of British Columbia.

References

1. DeGrado, W. F., Wasserman, Z. R. and Lear, J. D. *Science* **243**, 622-628 (1989).
2. Bryson, J. W., Betz, S. F., Lu, H. S., Suich, D. J., Zhou, H. X., O'Neil, K. T. and DeGrado, W. F. *Science* **270**, 935-941 (1995).
3. Mutter, M., and Vuileumeir, S. *Angew. Chem. Int. Ed. Engl*. **28**, 535-554 (1989).
4. Moran, J. R., Karbach, S., and Cram, D. J. *J. Am. Chem. Soc.* **104**, 5826-5828 (1982).
5. Mezo, A. R. and Sherman, J. C. *J. Am. Chem. Soc.* **121**, 8983-8993 (1999).
6. Gibb, B. C., Mezo, A. R. and Sherman, J. C. *Tetrahedron Lett.* **36**, 7587-7590 (1995).
7. Otto, S., Furlan, R. L. and Sanders, J. K. *J. Am. Chem. Soc.* **122**, 12063-12064 (2000).
8. Causton, A. S. and Sherman, J. C. *J. Peptide Sci.* **8**, 275-282 (2002).

Peptide Revolution: Genomics, Proteomics & Therapeutics
Michael Chorev & Tomi K. Sawyer (Editors)
American Peptide Society, 2003

Using NMR and Segmental Isotopic Labeling to Elucidate the Role of the N-Terminal Region of σ^{70}-like Factors in Regulating Binding of Bacterial RNA Polymerase to DNA Promoter

Julio A. Camarero[1], James J. de Yoreo[1] and David Fushman[2]

[1]Chemical Biology and Nuclear Sciences Division, Lawrence Livermore National Laboratory, University of California, Livermore, CA 94550, USA; [2],Dept. of Chemistry & Biochemistry, University of Maryland, College Park, MD 20742, USA

Introduction

Prokaryotic core RNA polymerases (RNAPs) are complex enzymes made up of multiple polypeptide subunits called α, β, β', and σ. The σ subunit is relatively weakly bound to and can be separated from the other subunits, yielding a core polymerase consisting of two α, one β and one β' subunits. This core enzyme is fully capable of catalyzing the formation of RNA from a DNA template. However, it is unable to bind specifically to the DNA promoter sequence and initiate transcription. Specific initiation of transcription at the DNA promoter sequence depends on the binding of the corresponding σ subunit to the core RNAP to form the RNAP holoenzyme. The most abundant σ factor in *E. coli* is σ^{70}. Sequence comparisons among different σ^{70}-like factors have shown that they are comprised of four highly homologous regions. Although Regions 2 and 4.2 have been shown to interact with the –10 and –35 box of the promoter region, respectively, free σ^{70}-like subunits are unable to recognize the promoter DNA sequence. Region 1.1 has been shown to inhibit the ability of σ^{70}-like factors to recognize the promoter DNA region. However, recent NMR studies show that Region 1.1 does not interact directly with Region 4.2 [1]. Despite the importance of Region 1.1 in regulating transcription, the elucidation of its structure has remained elusive so far [2-4]. In the present work we will present the ongoing efforts to solve the structure of Region 1.1 of σ^A (a σ^{70}-like factor from *T. maritima*) as an independent domain and also in the context of the whole σ factor. This will be accomplished by using heteronuclear NMR in combination with isotopic segmental labeling techniques [1,5].

Results and Discussion

In order to study the structure of Region 1.1 in the context of the whole σ subunit, Region 1.1 was specifically labeled with ^{15}N and/or ^{13}C. To accomplish this, the N-terminal fragment (Region 1.1, residues 1-129) was readily expressed as a C-terminal fusion protein with a modified intein (expression vector pTXB1 from New England Biolabs) in a medium culture artificially enriched with ^{13}C and/or ^{15}N sources. After affinity purification, the isotopically labeled fusion protein was then treated with a soluble thiol to yield the corresponding σ^A Region 1.1 α-thioester. This precursor was characterized by ES-MS, UV-CD and 2D-NMR (Figure 1). The $^1H\{^{15}N\}$-HSQC and the UV-CD spectra showed that the σ^A Region 1.1 alone adopts a folded structure consistent with a high helical content.

On the other hand, the C-terminal fragment was expressed as a N-terminal His-tag fusion protein using the expression vector pET28 (commercially available from Novagen). By using PCR-driven mutagenesis the C-terminal fragment (Δ1.1-σ^A residues, 131-397) was linked via the linker sequence -Ile-Glu-Gly-Arg-Cys- to the poly-His affinity tag. Following expression and affinity purification, treatment with a specific protease (i.e. Factor Xa) provided the σ^A C-terminal fragment containing the

required *N*-terminal Cys. The C-terminal fragment was characterized by ES-MS (Figure 2) and UV-CD confirming the high helical character of $\Delta 1.1\text{-}\sigma^A$. Furthermore, the ability of $\Delta 1.1\text{-}\sigma^A$ to specifically bind T7 DNA promoter was also checked by fluorescence (Figure 2), thus confirming the fragment was correctly folded.

The segmental labeled σ^A construct was obtained by reacting the labeled *N*-terminal (1.5 equiv.) and the unlabeled C-terminal (1 equiv.) fragments in a PBS at pH 7.2 containing traces of a suitable thiol. As shown in Figure 3, the ligation reaction was very clean and it was completed after 18 h. The ligated product was purified by filtration on a semi-permeable membrane with a 30 kDa cut-off and characterized by ES-MS. Preliminary 2D-NMR analysis (data not shown) of the ligated sample revealed that Region 1.1 in the context of the whole σ^A is also folded and its spectrum was consistent with a high helical content.

Future work will involve a more detailed analysis by 2D-NMR of the structure of Region 1.1 in the context of the whole σ protein.

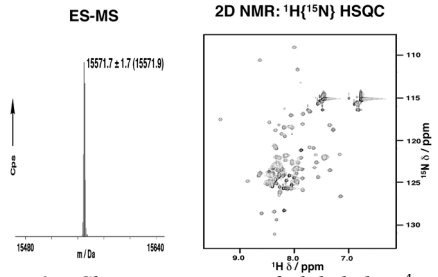

Fig. 1. Characterization of labeled σ^A Region 1.1.

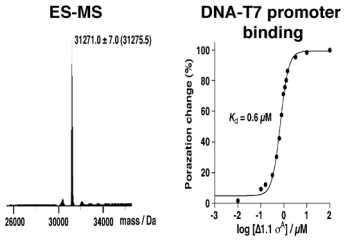

Fig. 2. Characterization of Cys-$\Delta 1.1\text{-}\sigma^A$.

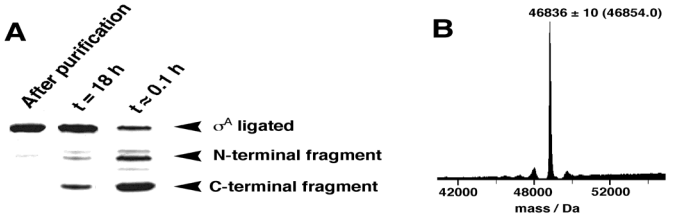

Fig. 3. A. Ligation reaction followed by 4-20% SDS-PAGE. B. ES-MS analysis of the purified ligated σ^A product.

Acknowledgments

This work was performed under auspices of the U.S. Department of Energy by the University of California, Lawrence Livermore National Laboratory (LLNL) under contract W-7405-Eng-48. J.A.C is a Distinguished Lawrence Fellow at the LLNL.

References

1. Camarero, J. A., et al. *Proc. Natl. Acad. Sci. U.S.A.* **99**, 8536 (2002).
2. Murakami, K. S., et al. *Science* **296**, 1280 (2002).
3. Murakami K. S., et al. *Science* **296**, 1285 (2002).
4. Campbell, E. A. et al. *Mol. Cell* **9**, 527 (2002).
5. Xu, R., et al. *Proc. Natl. Acad. Sci. U.S.A.* **96**, 388 (1999).

Peptide Revolution: Genomics, Proteomics & Therapeutics
Michael Chorev & Tomi K. Sawyer (Editors)
American Peptide Society, 2003

G protein α-Subunit: Conformation and Dynamics of the C-Terminal Domain

Fabio Casallanovo[1], Clovis R. Nakaie[2], Antonio C.M. Paiva[2] and Shirley Schreier[1]

[1]Department of Biochemistry, Institute of Chemistry, University of São Paulo, C.P. 26077, 05513-970; [2]Department of Biophysics, Federal University of São Paulo, São Paulo, Brazil

Introduction

The interaction between G protein-coupled receptors (GPCRs) and G proteins has been extensively studied [1]. GPCR cytosolic loops and C-terminal domain are proposed to be involved in this interaction [2]. G proteins are trimeric polypeptides consisting of G_α, G_β, and G_γ subunits; the N- and C-terminal domains of G_α are thought to participate in receptor-G protein contact sites [3]. These domains adopt α-helical conformation in the protein´s crystal structure [4]. Studies of synthetic peptides corresponding to the C-terminus have shown binding to GPCR and competition with G_α [5,6]. NMR studies of C-terminal sequences have been performed [7-9].

Here we present CD and fluorescence studies of a peptide from the C-terminus of a G_α subunit (FAAVKDTILQLNLKEYNLV, residues 341-359, CG). CG secondary structure prediction shows a great propensity for α-helical conformation. The conformational properties of CG were examined as a function of pH, ionic strength, in the presence of trifluorethanol (TFE), and upon interaction with micelles.

Results and Discussion

Studies in solution. The conformation of CG is pH and ionic strength-dependent. At low pH CG adopts an unordered conformation. At pH 4.0 and above, the peptide undergoes a significant conformational change, acquiring a more folded structure. Its fluorescence intensity decreases with increasing pH. Above pH 8.0 tyrosinate and bityrosine emission bands are seen. With regard to ionic strength. low salt concentrations induce significant conformational changes that saturate around 50 mM NaCl. At this salt concentration CG´s CD spectra are suggestive of the formation of turns.

The effect of TFE depends on the method of sample preparation. In samples prepared by mixing TFE and aqueous CG stock solutions, the peptide aggregates at low TFE concentration; it tends to become monomeric and α-helical at higher TFE content. Otherwise, concentrated CG stock solutions were prepared in 100 % TFE and the desired solvent concentration was obtained by dilution with water. Under these conditions, the peptide is monomeric and in α-helical conformation.

Studies in the presence of detergent. The conformation of CG was examined in the presence of detergent micelles. Samples were prepared by two methods: the detergent solution was added either to an aqueous solution of the peptide (A) or to a film of the peptide (B). In most cases, the CD spectra of CG revealed turns and peptide aggregation for samples prepared according to A, but they corresponded to α-helices and monomeric peptide for samples prepared according to B. Fluorescence spectra showed that the fluorescence intensity increase upon binding was larger for samples prepared from films. In agreement with the CD data, the largest increase in fluorescence intensity occurred for samples prepared by method B in the presence of lysophosphatidylcholine, LPC. The accessibility of the peptide to the water soluble

fluorescence quencher acrylamide decreased in the presence of micelles, confirming the binding of CG to the model membranes.

pK shifts are expected to occur due to the proximity of neighboring charged groups or binding to interfaces; pH variation and binding-induced conformational changes can also induce pK shifts. pH titrations of CG in water and in samples prepared according to method A showed that the most striking pH effects (pK shifts) took place upon interaction with LPC.

Theoretical predictions and structural homology with the crystal structure of transducin indicate that CG should display a high α-helical content. Indeed, the present findings provide evidence for this event. Nevertheless, in view of its tendency to aggregate, the peptide did not show α-helical conformation under all conditions. Thus, the conformation and aggregation state of CG are modulated by pH, ionic strength, TFE, and binding to model membranes. In addition, different detergents interact with CG in different manners, LPC being more effective in leading to monomer formation and inducing α-helical conformation. It is noteworthy that LPC is derived from a natural, membrane-forming phospholipid. The fact that the conformation of CG can be modulated by medium conditions could be related to different conformational states during the events of signal transduction.

Acknowledgments

This work was funded by FAPESP grants to CRN, ACMP, and SS. CRN, ACMP, and SS are CNPq research fellows. FC was recipient of a FAPESP Ph.D. fellowship.

References

1. Oliveira, L., Paiva, A. C. M. and Vriend, G. *Protein. Eng.* **12**, 1087-1095 (1999).
2. Okamoto, T., Murayama, Y., Hayashi, Y., Inagaki, M., Ogata, E., and Nishimoto, I. *Cell* **67**, 723-730 (1991).
3. Denker, B. M., Boutin, P. M. and Neer, E. V. *Biochemistry* **34**, 5544-5553 (1995).
4. Sondek J., Lambright, D. J., Noel, J. P., Hamm, H. E. and Siegler, P. B. *Nature* **372**, 276-279 (1994).
5. Martin, E. L., Rens-Domiano, S., Schatz, P. J. and Hamm, H. E. *J. Biol. Chem*. **271**, 361-366 (1996).
6. Hamm. H. E., Deretic, D., Arendt, A., Hargrave, P. A., Koenig, B. and Hofmann, K. P. *Science* **241**, 832-835 (1988).
7. Albrizio, S., D'Ursi, A., Fattorusso, C., Galoppini, G., Mazzoni, M. R., Novellino, E. and Rovero, P. *Biopolymers* **54**, 186-194 (2000).
8. Kisselev, O. G., Kao, J., Ponder, J. W., Fann, Y. C., Gautam, N. and Marshall, G. R. *Proc. Natl. Acad. Sci. U.S.A.* **95**, 4270-4275 (1998).
9. Dratz E. A., Furstenau, J. E., Lambert, C. G., Thireault, D. L., Rarick, H., Schepers, T., Pakhlevaniants, S. and Hamm, H. E. *Nature* **363**, 276-281 (1993).

Peptide Revolution: Genomics, Proteomics & Therapeutics
Michael Chorev & Tomi K. Sawyer (Editors)
American Peptide Society, 2003

A Biophysical Approach to the Structure of the Rhodopsin:Transducin Interface

Lori L. Anderson[1,2], Thomas J. Baranski[2], Wayne L. Hubbell[3], Ned Van Eps[3], Steven O. Smith[4] and Garland R. Marshall[1]

[1]Department of Biochemistry and Molecular Biophysics and [2]Department of Pharmacology, Washington University School of Medicine, St. Louis, MO 63110, USA; [3]University of California, Los Angeles, CA 90095, USA; [4]SUNY at Stony Brook, Stony Brook, NY 11794, USA

Introduction

Heterotrimeric G-proteins mediate signal cascades between G-protein-coupled receptors and a variety of intracellular messengers. Understanding the conformational changes which G-proteins undergo at the receptor:G-protein interface will provide an understanding of nucleotide exchange and subsequent G-protein activation and signal transduction. Although crystal structures of G-proteins have identified contact sites between G-protein subunits, the surfaces through which G-proteins bind to GPCRs have yet to be revealed. Alanine-scanning mutagenesis coupled with binding studies identified two distinct Gα surfaces: a receptor-interacting surface and a βγ-binding surface [1]. In chemical cross-linking studies, it was shown that the C-terminus of Gtα positions within the α4-β6 loop at residues 310-313 and residues 19-28 at the N-terminus are putative rhodopsin-interacting sites [2,3].

The structure of the interface between photoactivated rhodopsin and the α-peptide of Gt was solved using transferred nuclear Overhauser effect (TrNOE) NMR spectroscopy [4]. Results demonstrate that upon light activation, Gtα(340-350) shifts from a highly disordered conformation into an ordered continuous helix terminated by a C-terminal capping motif, with the formation of a unique clustering of hydrophobic residues. This is consistent with the structuring of the C-terminal 11 residues as observed in the crystal structure of RGS4 bound to AlF_4^--activated Gαi1 [5].

Although extensive studies have provided a structural model of rhodopsin upon photoactivation, there is still a general lack of structural data associated with the conformational changes transducin undergoes relative to receptor activation. In this study, we use expressed protein ligation to incorporate isotopically labeled amino acids into the C-terminus of Gα in order to gain insight into the structural mechanism, through NMR studies, by which rhodopsin activates transducin.

Results and Discussion

A series of peptides containing biophysical probes were manually synthesized by Fmoc chemistry on Wang resin, released from resin, purified by C18 RP-HPLC, and analyzed by mass spectroscopy. Ability to stabilize light-activated rhodopsin was measured using a MII rhodopsin-binding assay in which the EC_{50} of these peptides is compared to the ability of native Gtα(340-350) to stabilize this active intermediate of rhodopsin. These peptides were ligated to a recombinantly expressed, C-terminal truncated Gαi-thioester using intein-mediated protein ligation (See [6] for review). This strategy yields semi-synthetic Gα subunits in which recombinant expressed Gα-thioester proteins are modified at their C-terminal tail with synthetic peptides. Expression of the Gα-intein-chitin-binding-domain fusion protein was achieved by transformation into *E. coli* BL21(DE3) cells, followed by growth in T7 media (tryptone, yeast extract, sodium chloride, glycerol and potassium phosphate, pH 7.2) until an optical density at 600nm

was between 0.5 and 0.8 absorbance units. Cells were induced with 50mM IPTG for 5 hours and harvested. Following protein purification over a chitin column, formation of the protein thioester was induced by the addition of 1% MESNA followed by addition of 1mM synthetic peptide to yield semi-synthetic protein. EPL was complete after 24 hours at 4°C, as observed by western blotting with an antibody to the C-terminus of Gα. Functionality of the semi-synthetic α-subunit was confirmed by (1) [^{35}S]GTPγS binding, demonstrating the ability of the semi-synthetic protein to exchange nucleotide; and (2) a rhodopsin-binding and release assay, which demonstrated the ability of the ligated protein to form a reconstituted heterotrimer with βγ, associate with rhodopsin upon light activation, and dissociate from the complex upon nucleotide exchange.

Analysis of a semi-synthetic Gα-subunit, containing ^{13}C-labeled amino acids at its C-terminus (Leu344[U-^{13}C], Gly348[2-^{13}C], Phe350[ring-^{13}C]), by 2D ^{1}H-^{13}C HSQC NMR revealed that the C-terminus is highly mobile, but becomes structured upon titration with AlF_4^-. Titration with 2 and 4 molar equivalents of AlF_4^- resulted in a loss in intensity in all resonances observed in the HSCQ spectrum for the ^{13}C-LGF protein (Figure 1). The increase in line width, corresponding to loss of signal intensity, observed with the α-subunit can be attributed to the C-terminus becoming ordered and immobile, since its rotational correlation time would be on the same order as the overall tumbling rate of the protein. A proton spectrum of the α-carbon region of the protein before and after addition of AlF_4^- did not show any significant changes in proton line widths, indicating that the loss in intensity is due to large changes in the mobility of the C-terminal tail, but not as a result of global motion of the protein.

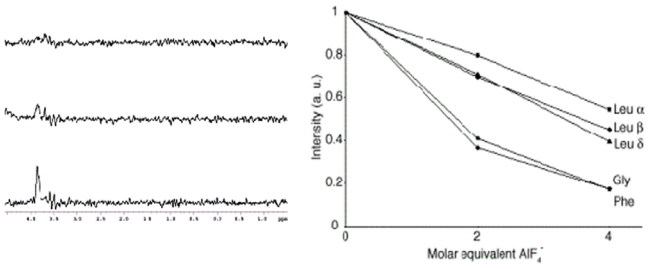

Fig. 1. Effect of AlF_4^- addition on ^{13}C-LGF α-subunit. (left) Representative spectra for the α-carbon of Leu344 with no AlF_4^- (lower scan) and increasing AlF_4^-. (right) Intensity of HSQC NMR resonances as a function of AlF_4^- addition.

Acknowledgments

The work was funded by NIH Grant EY12113 (GRM) and Chemistry-Biology Interface Training Grant T32 GM08785 (LLA).

References

1. Onrust, R., *et al. Science* **275**, 381-384 (1997).
2. Cai, K., Itoh Y. and Khorana G. *Proc. Natl. Acad. Sci. U.S.A.* **98**, 4877-4882 (2001).
3. Itoh, Y., Cai, K. and Khorana G. *Proc. Natl. Acad. Sci. U.S.A.* **98**, 4883-4887 (2001).
4. Kisselev, O. G., *et al. Proc. Natl. Acad. Sci. U.S.A.* **95,** 4270-4275 (1997).
5. Tesmer, J. J., *et al. Cell* **89**, 251-261 (1997).
6. Muir, T. W. *Annu. Rev. Biochem*. **72**, 249-289 (2003).

Peptide Revolution: Genomics, Proteomics & Therapeutics
Michael Chorev & Tomi K. Sawyer (Editors)
American Peptide Society, 2003

Chemically Modified hIL-8 for Biological Studies

Ralf David, Zuzana Machova and Annette G. Beck-Sickinger

Institute of Biochemistry, Faculty of Biosciences, Pharmacy and Psychology,
University of Leipzig, 04103 Leipzig, Germany

Introduction

Chemotactic cytokines (chemokines) play an important role in activation and regulation of the immune system and in the pathogenesis of a large number of inflammatory diseases. Chemokines are divided into four different families according to the position of the first two conserved cysteines: CC, CXC, C and CX3C chemokines [1]. Human interleukin-8 (hIL-8, also CXCL8) belongs to the CXC-family and activates neutrophils [2]. Its action is mediated through two specific G-protein coupled seven transmembrane helical receptors [3] isolated from neutrophils, but a;sp found in other cell types. CXCR1 shows high affinity to hIL-8 and low affinity to other CXC-chemokines, CXCR2 on the other hand exhibits high affinity to further CXC-chemokines. A 72 amino acid protein and an N-terminally extended 77 amino acid variant of hIL-8 are predominantly produced by different cell types. The structure of hIL-8 solved by NMR and X-ray methods [4] showed a homodimer, but the monomer is able to bind at the receptor as well. The amino terminal ELR motif is necessary for receptor-binding and activation. The structure of hIL-8 is stabilized by two intramolecular disulfide-bridges (Cys^{12} and Cys^{39}; Cys^{14} and Cys^{55} in the 77-mer protein). We performed the semisynthesis of the 77-amino acid hIL-8 and its carboxy-fluorescein-labelled analogue using expressed protein ligation [5] (see Figure 1).

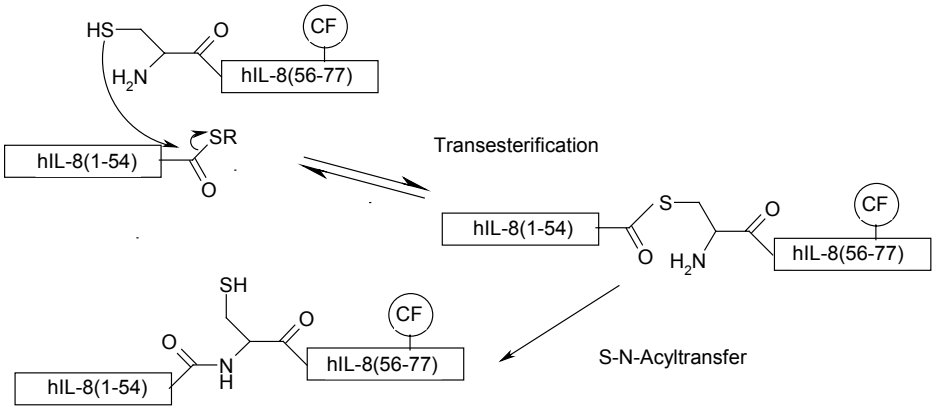

Fig. 1. Ligation of hIL-8(1-54) thioester with synthetic peptides possessing N-terminal cysteine led to the formation of hIL-8(1-77) and the site-specifically labelled [K^{69}(CF)]hIL-8(1-77).

Results and Discussion

The ligation site was chosen at the position of the naturally occurring Cys^{55}. Accordingly, hIL-8(1-54) was expressed using the IMPACT system (Intein Mediated Purification with an Affinity Chitin-binding Tag) [6]. hIL-8(1-54)-intein-CBD fusion protein was bacterially produced in insoluble inclusion bodies. We successfully isolated the recombinant thioester by applying slightly denaturing conditions.

Following affinity purification on chitin beads and thiol-induced intein cleavage hIL-8(1-54) thioester was obtained. The thioester was ligated to hIL-8(55-77) or [K^{69}(CF)]hIL-8(55-77), which both were obtained by solid-phase peptide synthesis. The ligation reactions proceeded under slightly denaturating conditions and the final products were characterized by RP-HPLC and MALDI mass spectrometry. Biological activity of [K^{69}(CF)]hIL-8(1-77) was evaluated in assays on human promyelotic HL60 cells naturally expressing CXCR1 and CXCR2 receptors.

Accordingly, by using expressed protein ligation we were able to generate hIL-8(1-77) and its CF-labelled analogue [K^{69}(CF)]hIL-8(1-77). The full agonistic activity of the CF-labelled variant of hIL-8 was demonstrated by the inhibition of forskolin-stimulated cAMP accumulation in HL60-cells. Binding of [K^{69}(CF)]hIL-8(1-77) was tested by fluorescence measurement on non-lysed HL60 cells in the absence or presence of different concentrations of non-labelled hIL-8(1-77) (Figure 2B). Furthermore, the internalization of the ligand-receptor complex was investigated with fluorescent-labelled ligand (Figure 2A). Both applications proved the usefulness of fluorescent labelled analogues for biological investigations. Current ligations focus on the introduction of non-natural amino acids, chemical labels or isotopic labelling for protein structure/function relationship studies.

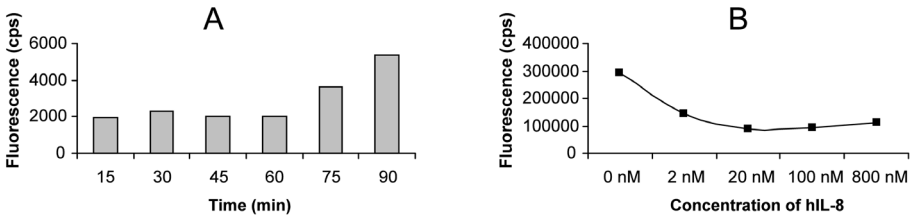

Fig. 2. Internalization of [K^{69}(CF)]hIL-8(1-77) (A). Cells were incubated with 20 nM of [K^{69}(CF)]hIL-8(1-77) for 15-90 min. After acidic wash, fluorescence spectra were recorded and subtracted from background fluorescence of the cells to obtain specific fluorescence at 520 nm. Competitive binding assay (B). Cells were incubated with 20 nM of [K^{69}(CF)]hIL-8(1-77) and different concentrations of non-labelled hIL-8(1-77) for 1 hour. Fluorescence spectra were recorded and subtracted from background fluorescence of the cells to obtain specific fluorescence.

References

1. Zlotnik, A., Morales, J., and Hedrick, J. A. *Crit. Rev. Immunol.* **19**, 1-47 (1999).
2. Baggiolini, M., Dewald, B. and Moser, B. *Adv. Immunol.* **55**, 97-179 (1994).
3. Wu, D., LaRosa, G. J. and Simon, M. I. *Science* **261**, 101-103 (1993).
4. Baldwin, E. T., Weber, I. T., St Charles, R., Xuan, J.C., Appella, E., Yamada, M., Matsushima, K., Edwards, B. F., Clore, G. M., Gronenborn, A. M., et al. *Proc. Natl. Acad. Sci. U.S.A.* **88**, 502-506 (1991).
5. Muir, T. W., Sondhi, D. and Cole, P. A. *Proc. Natl. Acad. Sci. U.S.A.* **95**, 6705-6710 (1998).
6. Chong, S., Mersha, F. B., Comb, D. G., Scott, M. E., Landry, D., Vence, L. M., Perler, F. B., Benner, J., Kucera, R. B., Hirvonen, C. A., Pelletier, J. J., Paulus, H. and Xu, M. Q. *Gene* **192**, 271-281 (1997).

Peptide Revolution: Genomics, Proteomics & Therapeutics
Michael Chorev & Tomi K. Sawyer (Editors)
American Peptide Society, 2003

Environmentally Sensitive Hydrogelation via Designed Peptides

Karthikan Rajagopal[1], Juliana Kretsinger[1], Darrin J. Pochan[2] and Joel P. Schneider[1]

[1]Department of Chemistry and Biochemistry; [2]Department of Materials Science and Engineering
University of Delaware, Newark DE 19716 USA

Introduction

Hydrogels are 3-dimensional water-filled porous structures. As biomaterials they have potential to be used as scaffolds for tissue engineering and in drug delivery applications [1]. Supra-molecular self-assembly leading to viscoelastic network structure formed by physical cross linking is one of the techniques employed for forming hydrogels. Physically cross linked gels have an added feature—when properly designed, they show responsive behavior to external stimuli. Herein, we investigate the potential of *de novo* designed peptides as building blocks in hydrogel construction to overcome current limitations in hydrogel technology.

Results and Discussion

In general, peptides are designed to undergo self-assembly into hydrogel material only after they are correctly folded into targeted conformations. We can controll the intramolecular folding of a class of hairpin peptides with distinct stimuli. The folding event can be designed to be totally reversible and as a result, self-assembled materials are fully responsive. MAX 1 a 20 amino acid peptide folds into a β-hairpin structure under alkaline conditions [2]. The design features incorporate factors that facilitate intramolecular folding as well as self-assembly. The sequence of MAX 1 has high β-sheet propensity for valine and lysine residues flanking an intermittent tetra peptide (-V^DPPT-) designed to adopt type II' turn [3], Figure 1. When the peptide is folded it presents an amphiphilic structure such that one face is hydrophobic and the other is hydrophilic. The folding of MAX 1 in response to pH changes (3 to 9) is caused by eliminating unfavorable electrostatic interactions between charged side chains. The folded structure is further stabilized by intramolecular hydrogen bonding and hydrophobic Van der Waals contacts. Also important to material formation is the burial of hydrophobic surfaces during self-assembly.

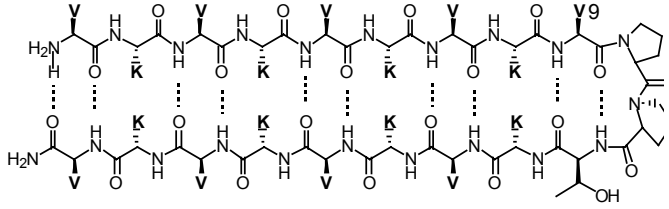

Fig. 1. Structure of MAX.

Results and Discussion

We have determined that intramolecular β-hairpin folding is an essential prerequisite for subsequent self-assembly by CD, IR, and rheology. In addition peptides can be designed that undergo reversible folding transitions leading to responsive materials. For example, Figure 2a shows the reversibility of β-sheet formation with pH for 300 μM solutions of MAX1. Folding and self-assembly is also monitored by measuring the visco-elastic properties of the material during hydrogel formation. Figure 2b shows an

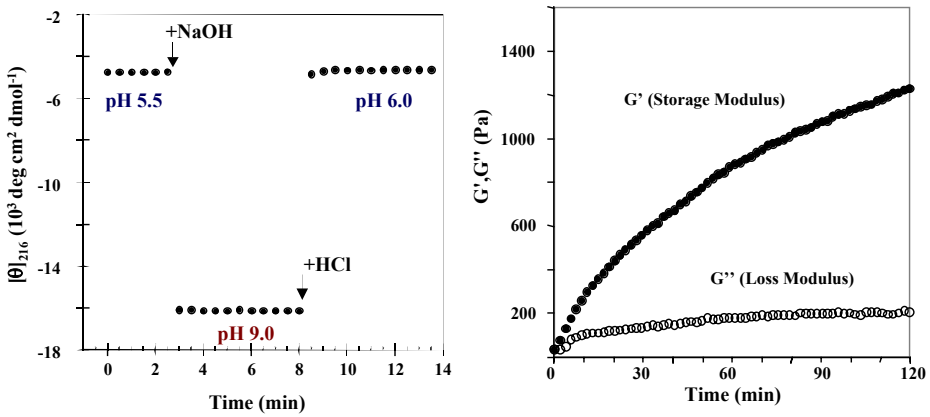

Fig. 1. left: Reversibility of b-sheet conformation of MAX as a function of pH; right: Increase of storage modulus versus time.

increase of the storage modulus (G', a measure of sample rigidity) versus time after folding has been initiated for a 1 wt% preparation. This degree of rigidity is sufficient for use in tissue engineering applications. Importantly, lowering the pH back to 3, results in the unfolding of individual peptides comprising the hydrogel material and as a result the material dissolves. In addition, Laser Scanning Confocal Microscopy and Cryo-TEM have shown that under folding conditions, the resultant hydrogel is highly porous on both the nano- and micro- length scales. This is a key requirement of successful hydrogel scaffolds used in tissue engineering. Current efforts to design temperature responsive hydrogels from peptides whose folding can be triggered by heat are underway, further increasing the processibility of these materials for medical applications.

We have shown that responsive materials can be prepared by linking the intramolecular folding of designed peptides to their ability to self-assemble into hydrogels.

Acknowledgments

The work was funded by NIH Grant 1-P20-RR17716-01.

References

1. Lee, K.Y. and Mooney, D. J. *Chem. Rev*. **101**, 1869-1879 (2001).
2. Schneider, J.P., Pochan,D.J., Ozbas, B., Rajagopal, K., Pakstis, L. and Kretsinger, J. *J. Am. Chem. Soc.* **124,** 1530-15037 (2002).
3. Stanger, H. E. and Gellman, S.H. *J. Am. Chem. Soc*. **120,** 4236-4237 (1998).

Peptide Revolution: Genomics, Proteomics & Therapeutics
Michael Chorev & Tomi K. Sawyer (Editors)
American Peptide Society, 2003

Peptide Microarrays Using Structure-Based Peptide Libraries for Protein Chips

Kenji Usui[1], Mizuki Takahashi[1], Tetsunori Ojima[1], Masato Suzuki[1], Kiyoshi Nokihara[2], Eiichi Tamiya[3] and Hisakazu Mihara[1]

[1]Graduate School of Bioscience and Biotechnology, Tokyo Institute of Technology, Yokohama 226-8501, Japan; [2]HiPep Laboratories, Kyoto 602-8158, Japan; [3]Japan Advanced Institute of Science and Technology, Ishikawa 923-1292, Japan

Introduction

As improvement on genome-wide sciences, the development of protein-chips/microarrays has been highly significant for the technology providing a high-throughput parallel detection method of target proteins. Small peptides may be useful as capturing agents for protein chips, because they can be easily designed and synthesized with suitable secondary and/or tertiary structures. In this study, designed peptide arrays consisting of α-helix, β-strand, or β-loop peptides were constructed to realize a practical protein-detection system.

Results and Discussion

Construction of a novel protein-detection system was carried out using a designed peptide library with fluorescent labels based on secondary and/or tertiary structures such as α-helix, β-strand, or β-loop [1]. At first, we selected model peptides known to interact with a structured protein to establish the synthetic and detection methods. In the case of an α-helix structure, a model combination is calmodulin (CaM) and a cationic amphiphilic α-helix peptide, which binds to CaM [2]. In the case of a β-loop, a peptide has been derived from the active site of tendamistat [3], an inhibitor of α-amylase. In the case of a β-strand, a model protein is β-lactoglobulin and a model β-strand peptide having an alkyl group. Phosphopeptides with secondary structures were also constructed to detect a protein kinase. The detection methods for proteins with immobilized peptides as well as peptides in solution have been successfully established. We describe here the development of a peptide array using a peptide library with an α-helix structure (Figure 1).

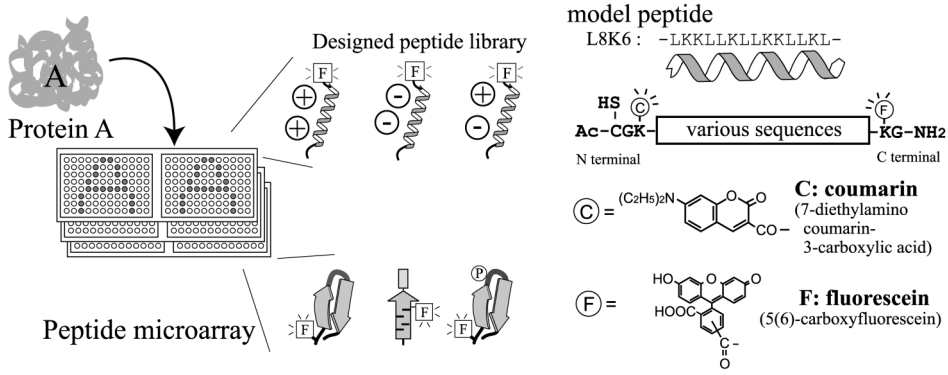

Fig. 1. Peptide microarrays using designed peptide libraries and α-helix peptide structures.

Initially, the fluorescent probes for the effective detection of a protein were selected, and the detection methods were established in solution and also in an immobilized manner using α-helix peptide L8K6 and CaM. The response of the peptide with FRET between two probes at both termini was several times higher than that of the peptide with a single probe. It was also found that fluorescein was an effective fluorophore in this system, because of its high fluorescence intensity. Then the peptides were immobilized on a solid support such as a 96-well plate and a glass plate. The target protein was detectable using the fluorescence increments of these peptides upon addition of the protein.

Furthermore, a small library of 112 α-helix peptides with systematic replacement of residues carrying specific charges and/or hydrophobicities was prepared for peptide microarrays. Using this library, various proteins including CaM and myosin were characterized effectively to give their own 'protein fingerprint' patterns (Figure 2). The resulting 'protein fingerprints' correlated with the recognition properties of the proteins.

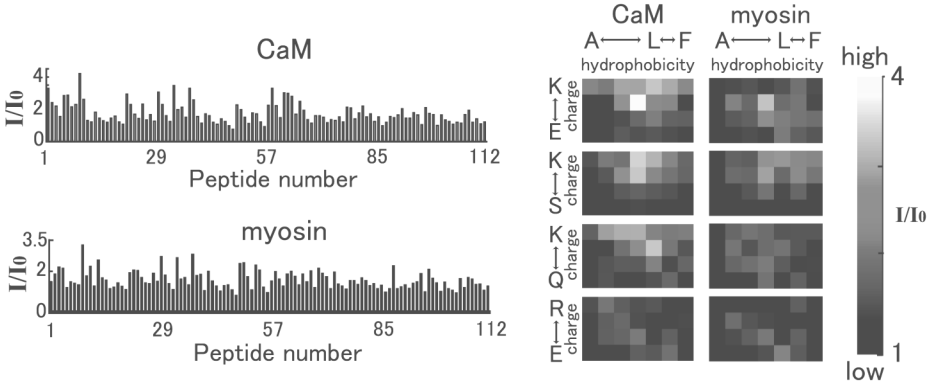

Fig. 2. Fluorescence responses of the α-helix peptide library by addition of various proteins and their 'protein fingerprints'.

Thus, it is demonstrated that the present microarray with designed synthetic peptides as the capturing agents is promising for the development of protein detection chips. With further improvement on sensitivity of detection, as well as the number of peptides, a practical and high-throughput protein chip technology will be established.

Acknowledgments

This study was, in part, supported by a grant from the Millennium Project of the Ministry of Education, Culture, Sports, Science and Technology (MEXT), and the COE21 program of Tokyo Institute of Technology.

References

1. Takahashi, M., Nokihara, K. and Mihara, H. *Chem. Biol.* **10** 53-60 (2003).
2. Cox, J. A., Comte, M., Fitton, J. E. and DeGrado, W. F. *J. Biol. Chem.* **260** 2527-2534 (1985).
3. Ono, S., Umezaki, M., Tojo, N., Hashimoto, S., Taniyama, H., Kaneko, T., Fujii, T., Morita, H., Shimasaki, C., Yamazaki, I., Yoshimura, T. and Kato, T. *J. Biochem.* **129** 783-790 (2001).

Peptide Revolution: Genomics, Proteomics & Therapeutics
Michael Chorev & Tomi K. Sawyer (Editors)
American Peptide Society, 2003

A Rationally Designed CD4 Mimic Useful in HIV Inhibition and Vaccine Design

François Stricher[1], Loïc Martin[1], Philippe Barthe[2], Alain Mechulam[3], Claude Vidaud[1], Laurent Bellanger[1], Bernard Maillère[1], André Ménez[1], Francisco Veas[3], Christian Roumestand[2] and Claudio Vita[1]

[1]Department of Protein Engineering and Research, CEA Saclay, 91191 Gif-sur-Yvette; [2]Structural Biochemistry Center, University of Montpellier, 34093 Montpellier; [3]Retroviral and Molecular Immunology Laboratory, IRD/CNRS, 34094 Montpellier, France

Introduction

Crystallographic studies on the HIV-1 gp120 envelope protein in complex with the cellular receptor CD4 and the Fab fragment of a neutralizing antibody [1], together with mutagenesis studies, have elucidated structural details of the first steps of the mechanism of HIV-1 entry and explained some of the fundamental tricks used by HIV-1 to avoid immune surveillance. This structure shows that the exposed HIV-1 envelope surfaces are hypervariable and hyperglycosylated, while conserved structures used for receptor binding are located in recessed cavities (e.g., the CD4 binding site) or exposed only after the first CD4 binding step (e.g., the chemokine receptor binding site). These hidden structures represent strategic targets for the development of entry inhibitors and neutralizing antibodies.

In a previous study [2], we have shown that the "hot spot" of the CD4 CDR2-like loop could be reproduced onto the structurally equivalent β-hairpin of a small disulfide-stabilized structural scaffold, scyllatoxin. The resulting miniprotein (CD4M9, 28 residues) inhibited gp120 binding to soluble CD4 at micromolar concentrations, which are more than 2-logs higher than those required by native CD4 to bind gp120, suggesting a sub-optimal miniprotein-gp120 interaction. Taking advantage of the available structural information on the CD4:gp120 complex [1], and the conformational stability and sequence permissiveness of the scaffold protein [3], we redesigned the CD4M9 miniprotein binding surface in order to optimize gp120 binding interactions, producing a potent CD4M33 miniprotein with *bona fide* CD4-like properties [4]. CD4M33 binds a variety of HIV-1 envelopes and viral particles, inhibits infection of primary HIV-1 isolates at nanomolar concentrations, and exposes conserved viral envelope epitopes to neutralization antibodies [4]. Here we report the results of a structural and functional study illustrating the mode of CD4M33 binding to gp120. These data may greatly help in the design of new small size HIV-1 inhibitors and vaccine preparations.

Results and Discussion

The structure of CD4M33 was solved by ^{1}H-NMR. Analysis of the final 30 low energy structures showed that the 18-27 β-hairpin of the CD4M33 was well defined and its average structure closely mimicked the corresponding CD4 38-47 region, which is central in gp120 binding, with only 0.69 Å RMS deviation between the two backbone atoms. On the basis of this structural similarity and using the CD4:gp120 complex structure as a template, the CD4M33 miniprotein was modeled in complex with gp120. In this structure, CD4M33 binds to the same gp120 depression where CD4 also binds, with 715 and 1068 Å^2 surfaces buried upon complex formation by the miniprotein and

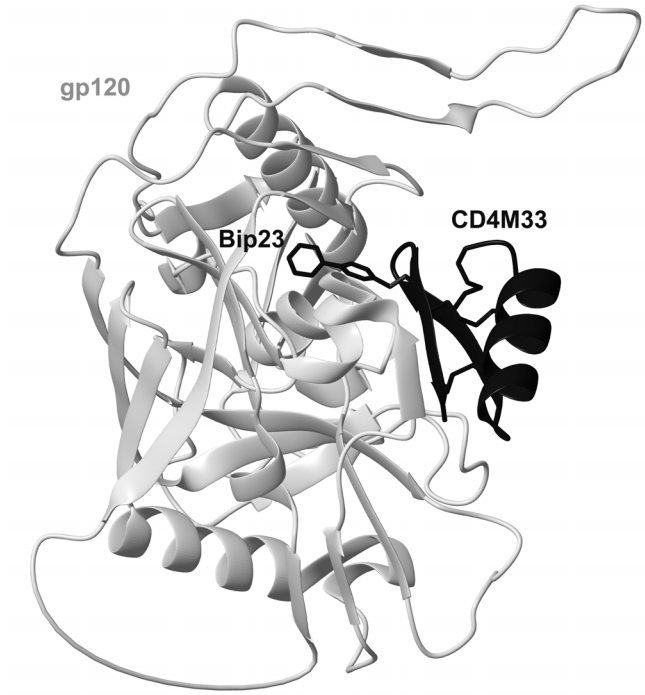

Fig. 1. The modeled structure of CD4M33:gp120 complex. Light and dark gray ribbons represent gp120 and CD4M33 backbones, respectively. The CD4M33 important functional side chain of biphenylalanine(Bip)-23 is represented in sticks.

CD4, respectively. Futhermore, CD4M33 binds gp120 in a manner similar to the equivalent region of CD4, experiencing CD4-like main-chain and side-chain interactions. In particular, the CD4M33 unnatural amino acid biphenylalanine(Bip)-23, which mimics the CD4 Phe-43, projects its longer hydrophobic side chain deeper into the gp120 "Phe-43 cavity" (Figure 1), thus supporting high binding affinity. These interactions have been confirmed in binding assays with specific gp120 and CD4M33 mutants, such as the [Ser375Trp]gp120YU2 mutant, which presents the "Phe43 cavity" partially filled by the larger tryptophan side chain, and the [Phe23]CD4M33 mutant, which contains a less protruding phenylalanine side chain. As shown Figure 2, ELISA experiments show that CD4M33, which carries a bulky Bip23, binds the [Ser375Trp]gp120YU2 mutant with about 3 log decreased affinity as compared to CD4 or [Phe23]CD4M33. In contrast, when the gp120YU2 wt (which presents an empty "Phe43 cavity") was tested in ELISA, CD4M33, [Phe23]CD4M33 and CD4 bound with similar affinity (Figure 2). These results have been also confirmed by using surface plasmon resonance (Biacore) technology.

When injected in rats, CD4M33 induced a poor antibody response, since only one of six injected rats elicited an anti-CD4M33 response. Most importantly, no anti-CD4 specificity was detected in the rat sera in ELISA. Furthermore, CD4M33 does not contain HLA class II restricted T-cell epitopes and did not significantly bind HLA class II in specific binding assays. This strongly suggests that the small-sized CD4 mimic might be poorly immunogenic in mammals.

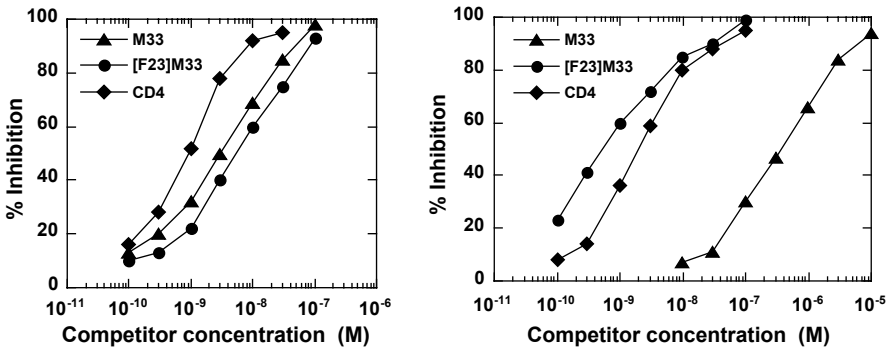

Fig. 2 Binding of CD4M33, [Phe23]CD4M33 and CD4 to gp120YU2 wt (left) and [Ser375Trp]gp120 mutant (right) in ELISA.

Interestingly, CD4M33, like CD4, upon gp120 binding, induces envelope conformational changes that expose gp120 conserved antigenic epitopes, which are targets of neutralization antibodies, such as MAb 48d, 17b, X5. These epitopes overlap the chemokine coreceptor binding sites. As detected by surface plasmon resonance technology, gp120 from different isolates were found to bind 48d MAb in the presence of CD4M33 as efficiently as in the presence of sCD4 (calculated K_d values for gp120HXB2 with CD4M33 or CD4 are 3.2 ± 0.5 nM or 1.3 ± 0.1 nM, respectively). In contrast, in the presence of the inactive [Ala23]CD4M33 variant or alone, this gp120 showed very little, if any, binding to 48d.

In conclusion, this non-immunogenic CD4 mimic represents a prototype of new HIV inhibitors blocking virus attachment to cells. It also represents a precious component to be included in new immunogen preparations—potential HIV-1 vaccine candidates. The advantage of using this CD4 mimic in the place of CD4 in vaccine preparation is that its low epitope sharing with CD4 prevents an anti-CD4 response, which was detected when envelope-CD4 was used, thus avoiding potential anti-immune responses, which is of fundamental importance in the development of HIV vaccines. The structure of the CD4M33:gp120 complex presented here may greatly help in the design of new small-sized inhibitors of HIV-1 entry and immunogens useful to induce neutralizing antibodies in new vaccine formulations.

Acknowledgments

The work was funded by an ANRS grant to C. Vita.

References

1. Kwong, P. D. et al. *Nature* **393**, 648-659 (1998).
2. Vita, C., Drakopoulou, E., Vizzavona, J., Rochette, S., Martin, L., Ménez, A., Roumestand, C., Yang, Y. S., Ylistagui, L., Benjouad, A. and Gluckman J. C. *Proc. Natl. Acad. Sci. U.S.A.* **96**, 13091-13096 (1999).
3. Martin, L., Barthe, P., Combes, O., Roumestand, C. and Vita, C. *Tetrahedron* **56**, 9451-9460 (2000).
4. Martin, L. Stricher, F., Misse, D., Sironi, F., Pugniere, M., Barthe, P., Prado-Gotor R., Freulon, I., Magne, X., Roumestand, C., Menez, A., Lusso, P., Veas, F. and Vita, C. *Nature Biotechnol.* **21**, 71-76 (2003).

Peptide Revolution: Genomics, Proteomics & Therapeutics
Michael Chorev & Tomi K. Sawyer (Editors)
American Peptide Society, 2003

Engineering New Metal Binding Specificity in Calmodulin Peptides

Loïc Le Clainche, Véronique Monjardet and Claudio Vita

Department of Protein Engineering and Research, CEA Saclay, 91190 Gif-sur-Yvette, France

Introduction

Heavy metals represent a source of important environmental pollution in our industrialized society. In particular, nuclear power plants may become a source of toxic metals, such as those coming from the nuclear fuel (uranium, plutonium, …), the fission products (strontium, selenium, technetium, iodine, …) or the activation products and liquid or gas wastes in nuclear reactors (cobalt, cesium, tritium, …). Thus, it would be extremely useful to develop specific analytical methods to monitor the presence of such toxic metals, as well as effective strategies for metal remediation of contaminated soils and waters. Engineering proteins with increased metal binding capability in bacterial and plant cells should increase the metal accumulation capability of such cells [1] and will enhance the applicability of biosorption over alternative metal removing techniques [2, 3]. In addition, engineering new metal chelating structures may also help the development of specific metal biosensors. In order to develop new proteins that bind such toxic metals, we envisage changing the calcium specificity of protein calmodulin, which coordinates four calcium ions in a bi-pyramidal geometry at the center of a helix-loop-helix motif, called EF-hand.

Herein, we report the synthesis of calmodulin derived peptides corresponding to the isolated helix-loop-helix motif, their specific affinities for different metal ions, including uranium, and how a few mutations can affect metal specificity, emphasizing the potential use of calmodulin structures in toxic metal binding.

Results and Discussion

We synthesized a 33-amino acid peptide, CaM-M1, spanning region 7-39 of calmodulin (CaM) from *Paramecium tetraurelia* (Figure 1) and corresponding to an isolated helix-loop-helix (EF-hand) motif. Since this linear peptide was unable to acquire an ordered structure in the presence of calcium ions, molecular simulation was used to design a disulfide bond that, by bridging positions 13 and 29, could stabilize the isolated metal binding site. The resulting cyclic peptide, CaM-M1c (Figure 1), also contained a Tyr-20, as a spectroscopic sensitive probe of metal binding, and was obtained by solid phase peptide synthesis. Analyzed by electrospray mass spectrometry (ES-MS), circular dichroism (CD) (Figure 2A) and fluorescence, the CaM-M1c peptide was found to bind calcium, cadmium, terbium and europium ions with native-like affinity (30 ± 1 μM dissociation constants for calcium). Metal binding induces an ordered conformation in the peptide, resembling that of the calmodulin site I. Interestingly, uranium, in the uranyl form, bound this peptide, as revealed by ES-MS, CD and time resolved laser induced fluorescence (TRLIF) spectroscopy.

```
            7                                   39
CaM-M1:     EQIAEFKEAFALFDKDGDGTITTKELGTVMRSL
CaM-M1c :   EQIAEFKEAFALCDKDGDGYITTKELGTCMRSL
CaM-M2c :   EQIAEFKEAFALCDKDGDGYITTKDLGTCMRSL
CaM-M3c:    EQIAEFKEAFALCTKTGDGYITTKELGTCMRSL
```

Fig. 1. Amino acid sequence of the calmodulin peptides synthesized.

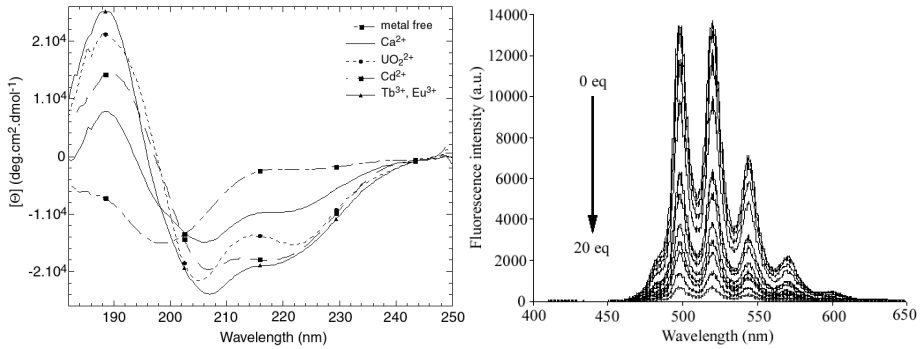

Fig. 2. A. Circular dichroism (CD) spectra of CaM-M1c (50 μM in 10 mM MES buffer, pH 6.5) in the absence and presence of 200 μM of various divalent and trivalent metal ions. B. Time resolved laser-induced fluorescence (TRLIF) of uranyl ions (2.0 μM in 1 mM phosphate buffer, pH 6.6), in the presence of increasing concentration of CaM-M3c peptide (from 0 to 40 μM).

Interestingly, by introducing the E31D sequence mutation, aiming at increasing the loop binding cavity in the CaM-M2c peptide (Figure 1), we suppressed the binding of calcium, cadmium and uranium ions, but preserved binding of lanthanide ions [4]. Then, we introduced the D20T, D22T neutral mutations in the chelating loop and synthesized a CaM-M3c peptide (Figure 1). As revealed by time resolved laser induced fluorescence (TRLIF) (Figure 2B), this peptide no longer bound calcium and terbium, but only uranyl ions with 18 μM Kd, Other mutations in the chelating loop, which reduced its negative charge, also produced similar effects and a specificity for uranyl ions.

Our studies demonstrate the potential of the structure-based approach in the engineering of metal binding specificity in EF-hand structures. This study suggests new avenues for obtaining specific metal-binding peptides and calmodulin proteins to be used to monitor metal pollution in biosensor systems or to augment metal binding capability of bacterial and plant cells in bioremediation strategies.

Acknowledgments

We thank the Nuclear Toxicology program of the French *Commissariat à l'Energie Atomique* (CEA) for financial support and a post-doctoral fellowship to V. Monjardet.

References

1. Sousa, C., Kotrba, P., Ruml, T., Cebolla, A. and De Lorenzo, V. *J. Bacteriol.* **180**, 2280-2284 (1998).
2. Raskin, I., Smith, R. D. and Salt, D. E. *Curr. Opin. Biotechnol.* **8**, 221-226 (1997).
3. Stephen, J. R. and Macnaughton, S. J. *Curr. Opin. Biotechnol.* **10**, 230-233 (1999).
4. Le Clainche, L., Plancque, G., Amekraz, B., Moulin, C., Pradines-Comte, C., Peltier, G. and Vita. C. *J. Biol. Inorg. Chem.* **8**, 334-340 (2003).

Peptide Revolution: Genomics, Proteomics & Therapeutics
Michael Chorev & Tomi K. Sawyer (Editors)
American Peptide Society, 2003

Design and Synthesis of Electron Transfer Proteins with Flavin, Heme and Quinone

Wenwu Li[1], Thomas Carell[2] and Wolfgang Haehnel[1]

[1]Institut für Biologie II / Biochemie, Albert-Ludwigs-Universität Freiburg, Schänzlestr. 1, D-79104 Freiburg, Germany; [2]Philipps-Universität Marburg, Fachereich Chemie, Hans-Meerwein Strasse, D-35032 Marburg, Germany

Introduction

Electron transfer (ET) in proteins plays a key role in living organisms. Nature uses a series of redox cofactors for catalysis, electron and energy transfer. Flavin is a very common cofactor with versatile redox chemistry in hundreds of flavoproteins. It also acts as an efficient photoreceptor and mediator in DNA photolyase for DNA repair and the blue light photoreceptors-cryptochromes and phototropins [1]. In addition, flavin is often used as a flash-activatable source of electrons for investigating protein-mediated electron transfer [2]. Quinones are ubiquitous for electron transfer reactions in nature. They also serve as covalent cofactors for electron transfer and catalysis in quinoenzymes [3]. Heme is often an important electron carrier in a number of cytochromes and enzymes. Recently, de novo design of redox proteins has become an attractive approach to investigate the factors involved in electron transfer and to create proteins with novel functions. For example, a photoactivatable flavocytochrome molecule maquette with two flavins and hemes was constructed by Dutton and coworkers [2]; a ruthenium complex and heme [4], and a Zn-Protoporphyrin IX and quinones [5] were attached by our group to four-helix bundle proteins to support light-induced electron transfer.

In this report we describe further attempts to include and combine the three native-like cofactors: flavin, heme and quinone into four-helix bundle proteins using a Template Assembled Synthetic Protein (*TASP*) approach [6] to mimic long range electron transfer through a triad. Peptide synthesis and chemical ligation methods enabled the construction of such proteins.

Results and Discussion

The protein scaffold of choice is an antiparallel four-helix bundle protein based on *TASP* (Figure 1a). Three different helices H1, H2 and H3 (sequences with helical net presentation are designed according to [4] and shown in Figure 1b) are modified by 3-maleimidopropionic acid (Mp) at either the N-terminal or the ε-amino group of a C-terminal lysine to achieve the antiparallel orientation. H2 is used twice as shielding helix. H1 and H3 are used as cofactor binding helices. H1 with Acm protected Cys-4 for covalent binding of quinone and H3 with flavin at position 18 both contain a histidine at position 11 for coordination of heme. Flavin is incorporated into H3 by use of a Fmoc protected Lys converted to a flavin amino acid [7], with the advantage of maintaining the native flavin structure instead of using its analogue 7-acetyl-10-methylisoalloaxine [2]. The template is a cyclic decapeptide [4] with an antiparallel β-sheet induced by type II turn structure containing four cysteines with orthogonal protecting groups. The assembly of a four-helix bundle protein with flavin (Flavin-MOP) was accomplished similarly to that of previous MOPs [4]. After Acm cleavage from H1 in the protein, ubiquinone (0) is covalently bound to yield a protein with flavin and ubiquinone (Flavin-UQ-MOP). The intermediate and final four-helix bundle

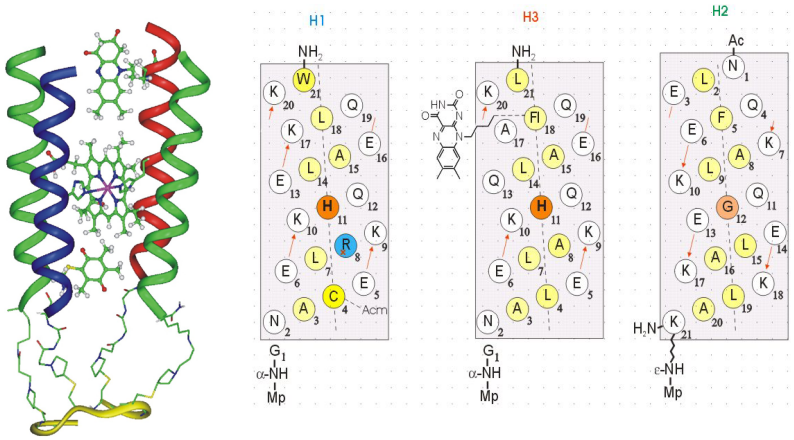

Fig. 1a (left). Model of the de novo protein Flavin-heme-UQ-MOP. 1b(right). Helical net representation of three different helices.

proteins were purified by HPLC and identified with correct structures by ESI-MS. Finally, heme is incorporated into Flavin-MOP and Flavin-UQ-MOP by *bis*-histidine coordination to yield a protein with flavin and heme (flavin-Heme-MOP, a dyad) similar tp flavocytochrome [2] and a protein with three native-like cofactors: flavin, heme and ubiquione (flavin-heme-UQ-MOP, a triad) (Figure 1), respectively.

The UV-vis spectrum of Flavin-MOP shows the characteristic absorption as that of free flavin. The covalent attachment of UQ only increases the absorption at 276 and 354 nm slightly, and the final incorporation of heme yields a typical *bis*-histidine ferric-*b*-heme spectrum. On reduction of sodium dithionate, the typical ferrous *b*-heme spectrum is obtained. Size exclusion chromatography shows the flavin-MOP and flavin-UQ-MOP mainly as the monomers in buffer and the triad as mainly the monomer as well as a minor fraction of dimer. Their CD spectra show the characteristic α-helical pattern.

Laser flash photolysis indicates the electron transfer from flavin to heme both in the dyad and triad systems after irradiation of flavin in the presence of EDTA as an extra electron donor (unpublished results by Leif Hammarström, Uppsala). The synthesis of a new Fmoc protected Dab carrying flavin amino acid with less rotamers has recently been accomplished, which will be used to possibly restrict the conformation of flavin in proteins. The future protein design is to rearrange the heme and ubiquinone and to extend the helices to produce a novel triad, flavin-UQ-heme-MOP protein system to facilitate light-induced electron transfer.

References

1. Sancar, A. *Chem. Rev*. **103**, 2203-2237 (2003).
2. Sharp, R. E., et al. *Proc. Natl. Acad. Sci. U.S.A*. **95**, 10465-10470 (1998).
3. Datta, S., et al. *Proc. Natl. Acad. Sci. U.S.A*. **98**, 14268-14273 (2001).
4. Rau, H. K., et al. *Proc. Natl. Acad. Sci. U.S.A*. **95**, 11526-11531 (1998).
5. Li, W., et al. *in* Benedetti, E. and Pedone, C. (Eds.) *Peptides 2002* (Proceedings of 27th European Peptide Symposium), Edizioni Ziino, Napoli, Italy, pp. 192-193 (2002).
6. Mutter, M. and Vuilleumier, S. *Angew. Chem. Int. Ed. Engl*. **28**, 535-554 (1989).
7. Carell, T., Schmid, H. and Reinhard, M. *J. Org. Chem*. **63**, 8741-8747 (1998).

Peptide Revolution: Genomics, Proteomics & Therapeutics
Michael Chorev & Tomi K. Sawyer (Editors)
American Peptide Society, 2003

Photo-Control of the Activity of Proteins Via Caging of Their C-Terminus

Jean-Philippe Pellois, Michael E. Hahn and Tom W. Muir

Laboratory of Synthetic Protein Chemistry, The Rockefeller University, New York, NY 10021, USA

Introduction

Many areas of biology can benefit greatly from methods to spatially and temporally control protein activity *in vitro* as well as *in vivo*. The synthesis of proteins containing photochemical groups that can be cleaved or modified upon simple light irradiation is an ideal approach to conveniently achieve such control [1]. For this purpose, we have developed a general method involving expressed protein ligation (EPL) [2] to selectively cage proteins at their C-termini. Here we describe the synthesis and caging of Smad2, a protein central to the transforming growth factor-β (TGF-β) signal transduction pathway (Figure 1).

TGF- β signaling is involved in various cellular processes, including cell proliferation, differentiation, recognition, and apoptosis [3]. Signaling from the cell membrane to the nucleus is mediated by Ser/Thr kinase and the Smad family of proteins. In particular, the binding of a specific cytokine to a pair of transmembrane receptors leads to the phosphorylation of Smad2, a receptor-regulated Smad, at the last two serine residues of the C-terminal sequence SSMS. The crystal structure of a phosphorylated Smad2 prepared by semi-synthesis revealed the formation of a homotrimer directly mediated by the phosphoserines [4]. The C-terminal carboxylic acid contributes significantly to the stabilization of the trimer by making several hydrogen bonds with neighboring residues. This group was therefore targeted as a potential caging site for protein inactivation. With this particular design, caging of the C-terminal carboxylate would maintain the chemically modified protein in an inactive monomeric state, while irradiation with UV light and subsequent cleavage of the caging group would produce the active trimeric Smad2. Thus, a photochemical trigger can be obtained that mimics the critical biochemical event of serine phosphorylation involved in the signaling pathway.

Results and Discussion

Caged Smad2 was obtained by EPL, with Cys463 as a convenient ligation site between a recombinantly expressed Smad2 thioester and the caged peptide CSpSMpS. 4-[4-(1-Hydroxyethyl)-2-methoxy-5-nitrophenoxy]butanoic acid (photolinker, pl) was chosen as a bifunctional caging group [5]. The peptide CspSMpS-pl-K was synthesized using Fmoc solid-phase peptide synthesis and purified by reversed-phase HPLC. A C-terminally-truncated Smad2 was cloned into the pTXB1 expression vector (New England Biolab) upstream of the GyrA intein and a chitin binding domain. The protein was expressed in *E. coli* and purified by affinity chromatography. The amide linkage between Smad2 and the GyrA intein is in equilibrium with a thioester bond, thus transthioesterification with 2-mercaptoethanesulfonic acid yields a Smad2 thioester required for native chemical ligation [6]. The ligation reaction was monitored by a combination of HPLC, SDS-PAGE and mass spectrometry analyses and was found to be quantitative after 24 hours.

The protein Smad2-CSSMS was synthesized as a control molecule. This unphosphorylated protein exists as a monomer, as judged by gel filtration analysis. Irradiation at 365 nm did not affect the physical state of the protein and no side-products were detected by HPLC and mass spectrometry analysis. The caged protein Smad2-CspSMpS-pl-K, although phosphorylated, was also detected as a monomeric species by gel filtration analysis. Upon irradiation at 365 nm, the caging group was cleaved and the activated protein formed an apparent homotrimer.

These results demonstrate that Smad2 can successfully be caged and photoactivated using the described approach. We are currently in the process of using this caged protein to study the physical behavior of Smad2 and the kinetics of the TGF-β signaling pathway inside of a cell. Furthermore, the general scheme presented is applicable to a wide range of protein modifications with photochemical groups and should prove particularly useful in cell biology.

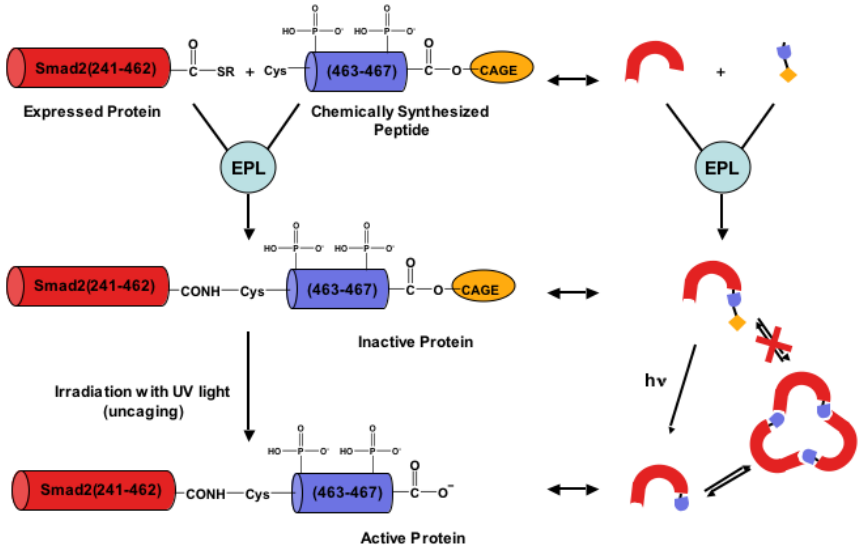

Fig.1. A schematic representation of the design, synthesis and photoactivation of caged Smad2.

Acknowledgments

This work was funded by the National Institutes of Health.

References

1. Curley, K. and Lawrence, D. S. *Curr. Opin. Chem. Biol.* **3**, 84-88 (1999).
2. Muir, T. W., Sondhi, D. and Cole, P. A. *Proc. Natl. Acad. Sci. U.S.A.* **95**, 6705-6710 (1998).
3. Shi, Y. and Massagué, J. *Cell* **113**, 685-700 (2003).
4. Wu, J.-W. *et al*. *Mol. Cell* **8**, 1277-1289 (2001).
5. Holmes, P. C. *et al*. *J. Org. Chem.* **60**, 2318-2319 (1995).
6. Dawson, P. E. *et al*. *Science* **266**, 776-779 (1994).

Peptide Revolution: Genomics, Proteomics & Therapeutics
Michael Chorev & Tomi K. Sawyer (Editors)
American Peptide Society, 2003

The Chemical Biology of Protein Splicing

Elyse S. Blum, Henning D. Mootz, Izabela Giriat, Alessandra Romanelli, Alexander Shekhtman and Tom W. Muir*

The Rockefeller University, 1230 York Avenue, New York, NY 10021, USA

Introduction

Understanding protein function is at the heart of experimental biology. This requires a full description of the posttranslational modifications of a protein and how they affect intrinsic structure and function, as well as interactions with other molecules. To achieve this at the level of a proteome is an unnerving proposition, yet the assembly of this encyclopedia is one of the long-term goals of biology. The size of this task is fueling considerable interest in the development of new technologies that allow the acquisition of protein function information to be accelerated relative to traditional genetic or biochemical approaches. The emergence of new fields such as *Proteomics, Structural Genomics, Bioinformatics* and *Chemical Biology*, illustrates how this problem is attracting the attention of researchers from a broad spectrum of disciplines. Although all these new areas will have significant roles to play, it is important to remember that the more traditional fields of peptide and protein chemistry are, in many ways, the best equipped to meet the challenges of proteomics. [Indeed, many of the current approaches used in proteomics and chemical biology have their origins in peptide chemistry.]

To fully understand how native proteins work, we need tools that allow protein function to be perturbed. Traditional genetic approaches are powerful in this regard, however, they do have limitations both in terms of the type of changes that can be made, and in terms of the temporal control one has over the modification being made. In the last decade, a suite of approaches have been developed that allow peptide chemistry and molecular biology to be wedded together, thereby allowing essentially any protein to be manipulated in a manner analogous to a small synthetic peptide. Moreover, these semisynthetic proteins can be generated both in the test-tube and in living cells, thereby allowing protein function to be studied using the toolbox of chemistry at both the biochemical and cell biological levels. What makes all of this possible is the discovery of the natural process, *protein splicing*, a post-translational editing event that is heaven sent for translating peptide chemistry into the world of proteins. We believe that technologies derived from protein splicing, such as *expressed protein ligation* and *conditional protein splicing,* will have an important impact in the broad area of proteomics. This article will give an overview of some of the ongoing developments in this area within my laboratory.

Results and Discussion

Protein Splicing and Trans-splicing. Protein splicing is an autocatalytic process in which an intervening sequence, termed the intein, excises itself out of a precursor protein with concomitant linking of the flanking sequences, termed the exteins, by a native peptide bond (Figure 1A) [1]. In protein trans-splicing the intein domain is split into two pieces and the splicing occurs only when the two polypeptides are reconstituted (Figure 1B). The first intein was discovered in 1990 and well over a 100 members of this protein domain family have now been identified in all three branches of life (see *www.neb.com/neb/inteins.html*). The basic splicing mechanism has been

elucidated and this has allowed the rational design of mutant inteins for biotechnology applications [2]. For example, mutation of the C-terminal Asn residue in the intein allows arrest of the splicing process at an intermediate step [3]. Fusing a protein of interest to such an intein mutant allows the generation of the corresponding recombinant protein α-thioester following a thiolysis step [4] (Figure 2). In addition, it is also possible to generate recombinant polypeptides possessing an N-terminal cysteine group by directed proteolysis of appropriate fusion proteins [4] (Figure 2). Thus, it is possible to generate both the necessary classes of building blocks for the well-known native chemical ligation reaction [5] by recombinant means. The process by which a recombinant protein is ligated, via native chemical ligation, to another recombinant or synthetic polypeptide, is known as Expressed Protein Ligation [4].

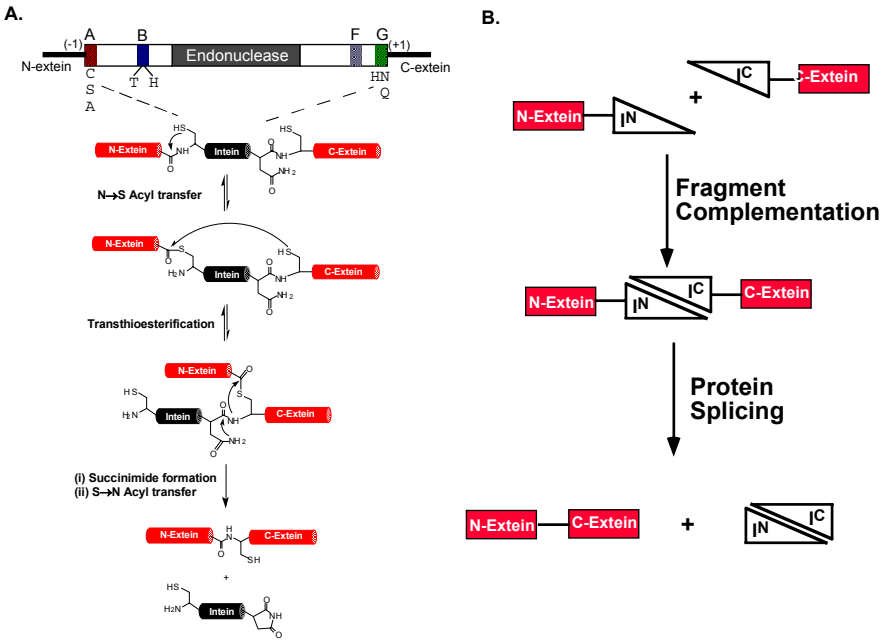

Fig. 1. Protein Splicing and Trans-splicing. ***A.*** *Top; the intein domain highlighting the conserved boxes and key residues. Bottom; the mechanism of protein splicing.* ***B****. The principle of protein trans-splicing. The N- and C-terminal halves of the intein are labeled* I^N *and* I^C*, respectively.*

Expressed Protein Ligation (EPL). Since its introduction in 1998 [6], EPL has been applied to many dozens of proteins. These include ion channels, polymerases, antibodies, transcription factors, nucleases, kinases, and various classes of signaling proteins [reviewed recently in ref. 4]. A wide-variety of groups have been site-specifically introduced into these proteins using EPL, for example; post-translational modifications, fluorophores, isotopic labels and unnatural amino acids. I will illustrate the utility of EPL with one recent example from our own work in which we were interested in studying how inteins catalyze the first step in the protein splicing process.

As illustrated in Figure 1A, the first step in the standard protein splicing mechanism involves an N→S (or N→O) acyl shift in which the N-extein unit is transferred to the side-chain SH or OH group of a Cys/Ser residue, located at the immediate N-terminus of the intein. On first analysis, this rearrangement is thermodynamically unfavorable

since it breaks an amide bond and forms a high energy (thio)ester linkage. What the driving force for this chemical rearrangement might be, remains an open question. There have been several high-resolution crystal structures of inteins and related proteins (reviewed in ref. 7) and these have provided useful insights into the structure-activity relationships underlying the first step. Perhaps, the most remarkable feature of these structures relates to the scissile peptide bond at the amino-terminal splice junction (-1 amide). This bond has been found in a variety of conformations ranging from normal *trans* to a *cis*-configuration. This has led to the hypothesis that the scissile bond is activated by distortion away from the normal *trans*-geometry, the strain being imposed by specific tertiary interactions involving conserved intein residues. Although attractive, there are a number of caveats to this model; firstly, the twisted amide geometry is not found in all intein crystal structures, and secondly, all the structures involved inteins inactivated through mutation of conserved residues. Conceivably, these mutations could have affected the –1 amide conformation. It should all also be pointed out that there is currently no information available regarding the solution conformation of the –1 amide bond.

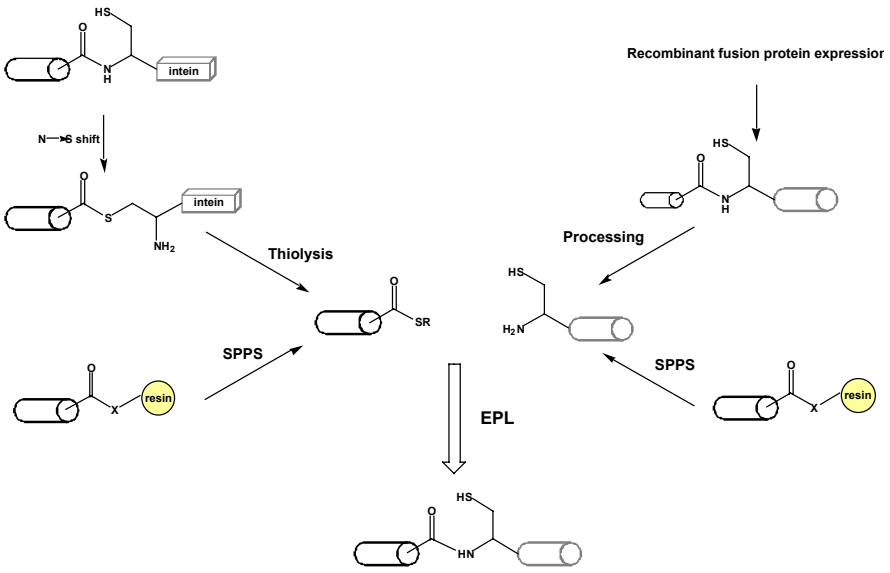

Fig. 2. Expressed protein ligation (EPL) is a semisynthetic version of native chemical ligation involving the chemoselective reaction of a peptide α-thioester and a peptide bearing an N-terminal cysteine to form a normal peptide bond. In EPL, at least one of the building blocks is recombinant in origin.

To study the solution conformation of the –1 amide bond, we used EPL to prepare the isotopically labeled protein shown in Figure 3A in which a uniformly ^{15}N labeled *Mxe* GyrA intein was ligated to a short synthetic peptide corresponding to the native N-extein residues and which contained a single ^{13}C isotope at the carboxy-terminus. The ligation reaction was performed in the presence of 6M GdmCl in order to prevent *in situ* thiolysis of the product during the ligation reaction. Following purification by HPLC, the ligation product, AAMRF[F5 ^{13}C', U-^{15}N]-GyrA, was refolded by stepwise dialysis into phosphate buffer at pH 7. Treatment of this material with DTT resulted in

quantitative thiolysis of the –1 amide bond. Moreover, the 1° order rate constants obtained for this reaction were the same for the refolded intein as for a control intein that had not be denatured, confirming that the former corresponded to a homogenous population of natively folded intein. We were able to prepare this folded material in multi-milligram amounts, which allowed us to perform a series of multidimensional heteronuclear NMR experiments including $^{1}H\{^{15}N\}$ HSQC spectroscopy (Figure 3B) and HNCO spectroscopy (Figure 3C). Importantly, the dual-isotopic labeling pattern in the sample allowed the unequivocal assignment of the scissile amide resonance from the HNCO spectrum. This information was then used to measure the $^{1}J(^{13}C_{i-1}\text{-}^{15}N_i)$ coupling constant by fitting the time evolution of the normalized peak intensities extracted from the series of HNCO type according to the method of Bax *et al.* [8]. Accordingly, the $^{1}J_{NC'}$ coupling constant for the (-1) scissile bond was found to be 12.3 ± 0.3 Hz, which is significantly lower than that expected for a normal planar peptide bond geometry, ~15 Hz [9]. Based on the lower coupling constant, it appears that the scissile amide has less π character than a normal *trans* or *cis* peptide bond, most likely because the peptide bond is twisted from planarity (i.e. ω < 180°). Thus, we propose that the intein catalyzes the first step in splicing by raising the energy of the scissile amide bond (ground state destabilization mechanism). Further, studies are underway to identify the residues within the intein required for this amide bond distortion.

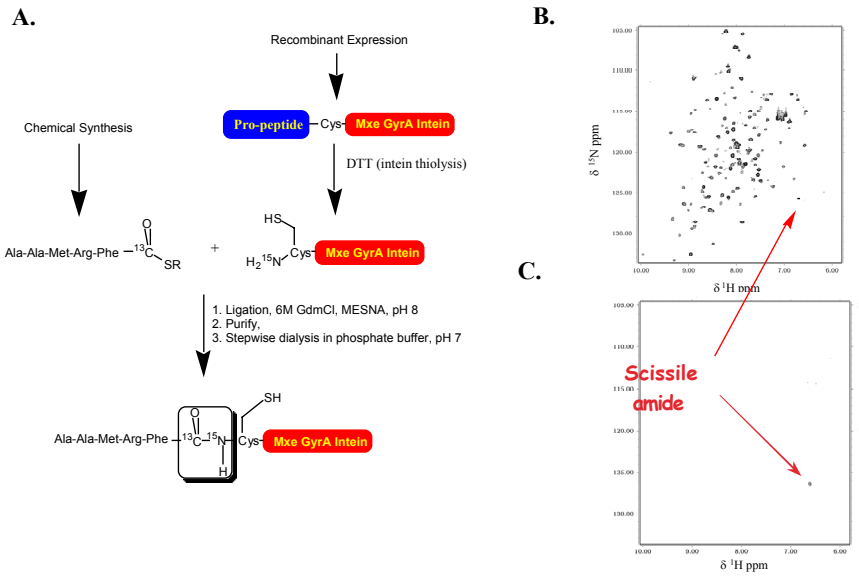

Fig. 3. A. Semisynthesis of AAMRF[F5 $^{13}C'$, U-^{15}N]-GyrA by EPL. B. $^{1}H\{^{15}N\}$ HSQC spectrum of the 200 μM sample in 20mM potassium phosphate buffer, pH 6.5, 0.1M NaCl, 10% D_2O, 0.01% NaN_3. C. (^{1}H, ^{15}N) projection of the HNCO spectrum of the same sample. The data sets were collected at 4° C on a Bruker DMX spectrometer operating at a ^{1}H frequency of 800 MHz. This data represents the work of Alessandra Romanelli and Alex Shekhtman.

In Vivo Protein Semisynthesis. Expressed protein ligation is extremely powerful for the biochemical (i.e. *in vitro*) analysis of protein function. However, there are many questions and systems that can only be studied in a cellular context, for example,

signaling networks in general, protein translocation, cell cycle. The prospect of endowing cellular proteins with the myriad structures available through chemical synthesis is very exciting, and is an active area of research. Recently, we introduced an approach that allows an externally synthesized molecule to be delivered into a mammalian cell and ligated to a target recombinant protein within [10]. As illustrated in Figure 4A, the protein of interest is expressed as a fusion to one half of the naturally split *Ssp* DnaE intein (I_N). The synthetic probe is appended, using EPL, to the other half of the split intein (I_C) and this construct is in turn attached to a protein transduction domain (PTD) peptide via a disulfide. The PTD delivers the I_C-probe into the cells whereupon reduction removes the peptide and simultaneously activates the I_C component. The split inteins then associate within the cell, triggering protein splicing. This results in the removal of the intein and ligation of the probe to the protein of interest through a peptide bond.

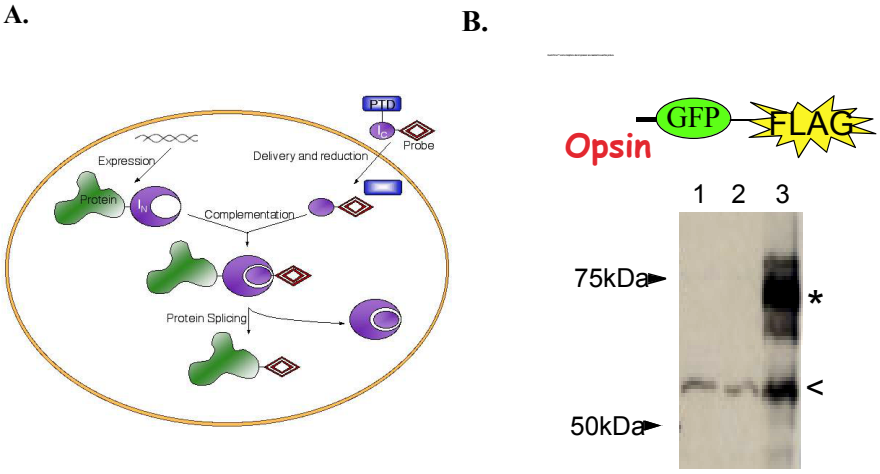

*Fig. 4. Protein semisynthesis in cells. A. Principle of the approach. B. Ligation of a synthetic peptide, FLAG, to the integral membrane protein, opsin, in CHO cells. Anti-FLAG IP, Anti-GFP Western blot of a 7.5% SDS-PAGE gel of un-transfected and untreated cells (lane 1), cells transfected with pOpsin-GFP-I_N left untreated (lane 2) and cells transfected with pOpsin-GFP-I_N treated with PTD-I_C-FLAG peptide (lane 3). The ligation product (Opsin-GFP-FLAG) is denoted by *, background bands are denoted by <, and the smearing in the band is due to the glycosylation of Opsin. The expected molecular weight of Opsin-GFP-FLAG is ~70 kDa. This is the work of Izabela Giriat.*

An example of protein semisynthesis in living cells is shown in Figure 4B. In this case we ligated a short synthetic peptide corresponding to the FLAG epitope to a GFP fusion of the G-protein coupled receptor, opsin. A band of the expected molecular weight is observed only when transfected cells are exposed to the PTD-I_C-FLAG peptide. Importantly, this band cross-reacts with antibodies against GFP and FLAG, thereby confirming that the desired product is generated. The ability to attach synthetic molecules to integral membrane proteins such as opsin, opens up a variety of opportunities for studying cellular function using, for example, fluorescent microscopy approaches.

Conditional Protein Splicing (CPS). Recently, we reported an approach, CPS, which allows protein trans-splicing to be triggered by the addition of the small molecule rapamycin, or non-toxic analogs thereof [11,12]. CPS starts with the observation that trans-splicing between artificially split inteins is not spontaneous, but rather requires a denaturation/renaturation step. This is likely because the affinity of artificially split inteins for each other is rather low. Thus, if we can change the effective molarity of the

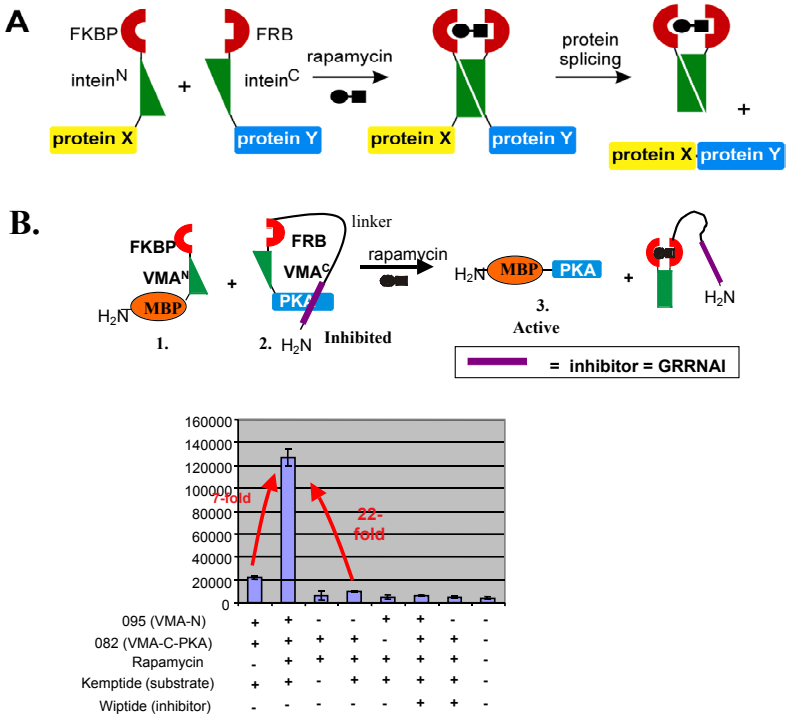

Fig. 5. A. Principle of Conditional Protein Splicing. B. CPS strategy for activation of a protein kinase. Top: Design of an autoinhibited version of the catalytic domain of cAMP-dependent kinase (PKA). A low affinity inhibitor sequence is cloned N-terminal to the FRB-VMA^C-PKA fusion construct via a short peptide linker. The inhibitor inhibits the kinase via an intramolecular interaction. Addition of rapamycin triggers CPS, leading to cleavage of the peptide bond between PKA and the VMA^C. Accordingly, the inhibitor is also removed and can no longer inhibit the kinase due to its low K_i. The bottom panel shows the results of an in vitro kinase assay using ^{32}P-ATP and peptide substrate (Kemptide). Consistent with the design principle, the PKA is autoinhibited, but can be turned on via the addition of rapmycin which triggers the protein splicing reaction. This is the work of Henning Mootz and Elyse Blum.

fragments in a *conditional* manner, it might be possible to induce splicing under physiological conditions. CPS does just that; by fusing the halves of a split *Sce* VMA intein to the FKBP/FRB rapamycin-mediation heterodimerization system, we can selectively induce trans-splicing with the resulting ligation of the associated exteins (Figure 5A). We have shown that approach works both *in vitro* [11] and *in vivo* [12]. Moreover, background splicing (i.e. without the drug) in cells is undetectable, and that

the amount of product formed is controllable either by adjusting the time of reaction or the amount of drug added to the cells.

Given the promiscuity of inteins with regard to the flanking exteins, CPS can, in principle, be used to selectively regulate the activity of any protein with great temporal precision; for example by ligating together two inactive pieces or domains of a protein. One application of CPS is shown in Figure 5B. In this case, we exploited the bond breaking steps (i.e. between the intein and the exteins) rather than the ligation step. This has allowed us to design a 'zymogenic' version of a protein kinase, specifically PKA, by generating a CPS construct containing the kinase and a substrate based peptide inhibitor. By incorporating suitable linker sequences, the system can be set up such that the kinase is in an autoinhibited state. CPS triggers the cleavage of the inhibitor from the kinase. If one chooses an inhibitor with just the right affinity, then inhibition will no longer occur following splicing (i.e. in an intermolecular fashion). Thus, one can control the activity of the kinase using rapamycin.

Conclusions

Protein splicing and trans-splicing are proving to be enormously useful for translating the principles and tools of peptide chemistry into the world of proteins. In the years to come we can look forward to the continued development of new chemical biology approaches based on protein splicing as well as the application of these to biological problems.

Acknowledgments

The work was funded by grants from the NSF and NIH grants.

References

1. Paulus, H. *Ann. Rev. Biochem.* **69**, 447-495 (2000).
2. Giriat, I., Muir, T. W. and Perler, F. B. *Genet. Eng.* **23**, 171-199 (2001).
3. Chong, S. et al. *Gene* **192**, 271-281 (1997).
4. Muir, T. W. *Ann. Rev. Biochem.* **72**, 249-289 (2003).
5. Dawson, P. E. and Kent, S. B. H. *Ann. Rev. Biochem.* **69**, 923-960 (2000).
6. Muir, T. W., Sondhi, D. and Cole, P. A. *Proc. Natl. Acd. Sci. U.S.A.* **95**, 6705-6710 (1998).
7. Noren, C. J., Wang, J. and Perler, F. B. *Angew. Chem. Int. Ed. Engl.* **39**, 450-455 (2000).
8. Cornilescu, G. Hu, J-S. and Bax, A. *J. Am. Chem. Soc.* **121**, 2949-2950 (1999).
9. Juranic, N., Ilich, P., Macura, S. *J. Am. Chem. Soc.* **117**, 405-410 (1995).
10. Giriat, I. and Muir, T. W. *J. Am. Chem. Soc.* **125**, 7180-7181 (2003).
11. Mootz, H. D. and Muir, T. W. *J. Am. Chem. Soc.* **124**, 9044-9045 (2003).
12. Mootz, H. D. Blum, E. S., Tyszkiewicz, A. B. and Muir, T. W. *J. Am. Chem. Soc.* **125**, 10561-10569 (2003).

Peptide Revolution: Genomics, Proteomics & Therapeutics
Michael Chorev & Tomi K. Sawyer (Editors)
American Peptide Society, 2003

The Semisynthesis of the Potassium Channel KcsA

M. Sekedat[1], F. Valiyaveetil[2], R. MacKinnon[2] and T. W. Muir[1]

[1]The Laboratory of Synthetic Protein Chemistry; [2]The Howard Hughes Medical Institute, The Laboratory of Molecular Neurobiology and Biophysics; [1,2]The Rockefeller University, Box 223, 1230 York Avenue, New York, New York, 10021, USA

Introduction

The potassium channel KcsA is a membrane spanning tetramer found in *Streptomyces lividans*. Each subunit is 160 amino acids long and comprises an N-terminal outer helix, a pore helix, a selectivity filter and a C-terminal inner helix (Figure 1). The selectivity filter consists of the sequence TVGYG, which is conserved in all potassium channels. Interactions between potassium ions and the selectivity filter involve mainly the backbone carbonyl oxygens [1], and are responsible for the ionic selectivity and conductance of potassium channels. Conventional mutational analysis offers no insight into the mode of selectivity in KcsA because it involves the peptide backbone. Expressed protein ligation is therefore an ideal method for modifying the backbone of the selectivity filter in order to study these interactions.

The N-peptide (residues 1-68) of KcsA was expressed as an α-thioester using an intein-fusion strategy [2]. The C-peptide (residues 69-122) was synthesized using optimized Boc solid-phase peptide synthesis techniques with a N-terminal cysteine. After purification of the fragments the peptides were ligated together and refolded in the presence of lipid vesicles. Folding was verified by measuring the protein's affinity towards agitoxin-2 [2].

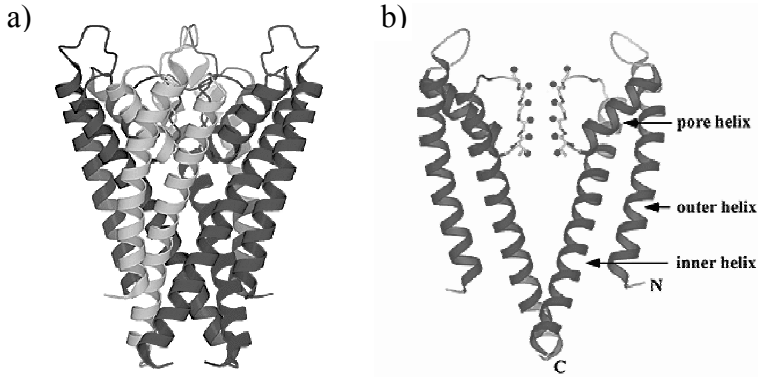

Fig. 1. a). Structure of the KcsA tetramer. Each subunit is gray-shaded differently. b). Two opposite subunits of the KcsA tetramer. Residues 74-79 comprising the selectivity filter are shown in ball-and-stick representation [1].

Results and Discussion

The recombinant N-peptide was expressed in *E. coli* as a double fusion with GST on the N-terminus and the GyrA intein on the C-terminus. The GST tag was used to aid in expression and was cleaved with thrombin. The GyrA intein was cleaved with MESNA leaving a C-terminal α-thioester. Analysis of the crude cleavage on a C_4 RP-HPLC column (Vydac) indicated that the thiolysis reaction had gone to >90% completion. The peptide was purified by RP-HPLC and analyzed by ES-MS. This procedure yielded

~2mg of purified N-peptide α-thioester per liter of bacterial culture. The 54 residue C-peptide was synthesized on a pre-loaded Pam resin (Applied Biosystems). All the amino acids were single-coupled using HBTU in DMF, except for β-branched amino acids, which were double coupled. Furthermore, consecutive β-branched amino acids were double-coupled using HBTU in DMSO [2]. The resulting peptide was cleaved by HF, dissolved in 1:1 TFE/H_2O, 0.1%TFA, and the crude material was analyzed on a C_4 RP-HPLC column (Figure 2a) and ES-MS (Figure 2b). The crude was of a very high quality and after purification by RP-HPLC, ~20mg of purified peptide was recovered from 400mg of resin.

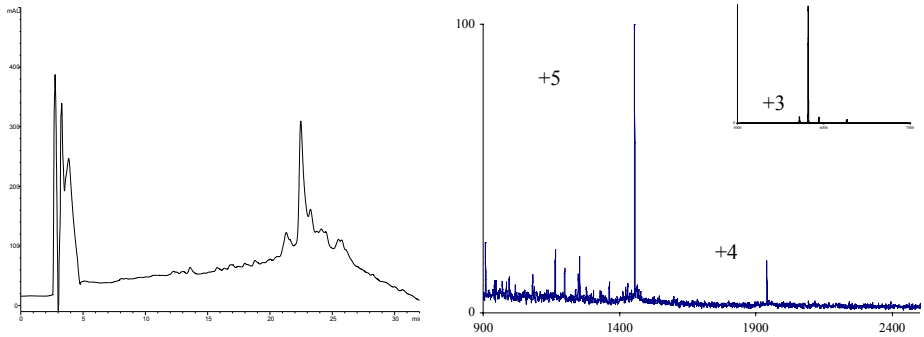

Fig. 2. a). RP-HPLC of the crude C-peptide cleavage. b). ES-MS of the purified C-peptide (inset, reconstructed mass). Expected m/z=5817.8.

The two fragments were chemically ligated together and the resulting polypeptide was folded to its tetrameric state through incorporation into lipid vesicles and purified [2]. The resulting semisynthetic KcsA is a truncated version that is similar to that used in crystallographic studies. This version contains the entire membrane-spanning region of KcsA, however single-channel measurements are unobtainable when using this construct because it has a higher closed state probability.

Mutational analysis revealed that an alanine to glycine mutation in the "gated-hinge" region (A98G) of the inner helix increases the open state probability of the truncated KcsA. This mutation allows for single channel measurements on the molecule, and therefore functional analysis of the truncated KcsA. Future studies will include single-channel measurements on KcsA channels containing ester bonds in place of amide bonds in the selectivity filter. This will alter the electronegativity of the carbonyl oxygens and affect the movement of potassium through the channel.

References

1. Doyle, D., Cabral, J., Pfuetzner, A., Gulbis, J., Cohen, S., Chait, B. and MacKinnon, R. *Science* **280**, 69-77 (1998).
2. Valiyaveetil, F., MacKinnon, R. and Muir, T., *J. Amer. Chem. Soc.* **124**, 9113-9120 (2002).

Peptide Revolution: Genomics, Proteomics & Therapeutics
Michael Chorev & Tomi K. Sawyer (Editors)
American Peptide Society, 2003

Protein Assembly Using the Staudinger Ligation

Bradley L. Nilsson[1], Matthew B. Soellner[1] and Ronald T. Raines[1,2]

[1]Department of Chemistry; [2]Department of Biochemistry;
University of Wisconsin–Madison, Madison, WI 53706, USA

Introduction

New methods are facilitating the total chemical synthesis of proteins. In particular, the chemical ligation of synthetic peptides provides a convergent route to proteins. Currently, the most common ligation method is "native chemical ligation" [1]. In native chemical ligation, the thiolate of an *N*-terminal cysteine residue of one peptide attacks the *C*-terminal thioester of a second peptide. An amide linkage forms after S→N acyl transfer. "Expressed protein ligation" is an extension of native chemical ligation in which the *C*-terminal thioester is produced by recombinant DNA (rDNA) technology rather than chemical synthesis [2].

A limitation of native chemical ligation is its intrinsic reliance on having a cysteine residue at each ligation juncture. Cysteine is uncommon, comprising only 1.7% of all residues in proteins. Modern peptide synthesis is typically limited to peptides of ≤40 residues [3]. Hence, most proteins cannot be prepared by any method that requires peptides to be coupled only at cysteine residues.

The removal of the cysteine limitation by the development of a more general ligation reaction would greatly expand the scope and utility of total protein synthesis. We have developed such a reaction. Specifically, we have used the Staudinger reaction to unite two peptides, one with a *C*-terminal phosphinothioester and the other with an *N*-terminal azide [4–6]. A putative mechanism for this version of the 'Staudinger ligation' is shown in Figure 1. The reaction of a phosphinothioester with a peptide azide leads to the formation of the reactive iminophosphorane. Attack of the iminophosphorane nitrogen on the thioester leads to an amidophosphonium salt. Hydrolysis of the amidophosphonium salt produces the desired amide bond and a phosphine oxide. Significantly, no residual atoms remain in the amide product.

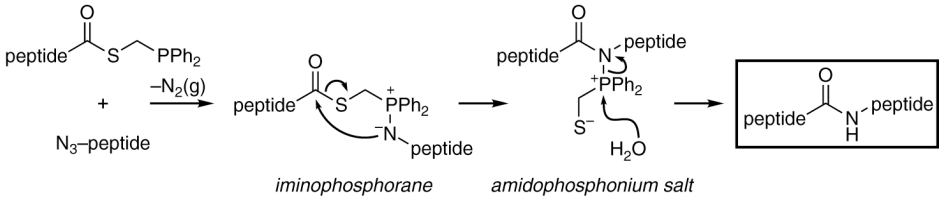

Fig. 1. Putative mechanism for the Staudinger ligation of peptides.

Results and Discussion

The Staudinger ligation of protected peptide fragments on a solid support is an orthogonal method to form an amide bond. Having demonstrated the efficacy of $HSCH_2PPh_2$ in mediating the Staudinger ligation [4–6], we sought to exploit this new synthetic methodology in the assembly of a protein [7]. As a model system for semisynthesis, we chose ribonuclease A (RNase A). The 123 amide bonds in our semisynthetic RNase A were formed by using four distinct amide-bond forming methods. Fragment 1–109 was prepared as a *C*-terminal thioester by rDNA techniques [2]. The amide bonds in this segment were formed by *m*RNA translation by the

ribosome. Fragment 110–124 was prepared by combining two methods. The amide bonds between residues 110–111 and 113–124 were formed by standard solid-phase peptide synthesis utilizing HATU activation. The protected fragment 110–111 was elaborated as a phosphinothioester of $HSCH_2PPh_2$. The protected fragment 113–124 was elaborated as an *N*-terminal azide while immobilized to a solid support. The phosphinothioester of 110–111 was coupled to the 113–124 fragment on the solid support by using the Staudinger ligation. Finally, fragment 110–124 was liberated from the resin, deprotected, and coupled to fragment 1–109 via native chemical ligation to give the semisynthetic protein. The k_{cat}/K_M value for catalysis by this semisynthetic RNase A was nearly identical to that of biosynthetic RNase A, as was its mass.

A promising application for the Staudinger ligation is in the total chemical synthesis of proteins. In our semisynthesis of RNase A we demonstrated the use of the Staudinger ligation to couple protected peptide fragments on a solid support. We envision expanding this methodology to assemble entire proteins on a solid support in an iterative and convergent manner (Figure 2). Our strategy is to divide a target protein into fragments of 20–30 residues. The *C*-terminal fragment is capped with an α-azido acid, and remains immobilized to the support. The remaining fragments are synthesized as protected peptides, and elaborated as *C*-terminal thioesters of $HSCH_2PPh_2$. The fragments are then coupled in turn to the growing polypeptide chain. After each Staudinger ligation, the nascent polypeptide is capped with an α-azido acid, preparatory for the next cycle. When the synthesis is complete, the polypeptide is deprotected and folded while still attached to the resin (to prevent aggregation), and then liberated from the support. Hence, protein assembly using the Staudinger ligation could facilitate access to the proteins encoded by the human genome.

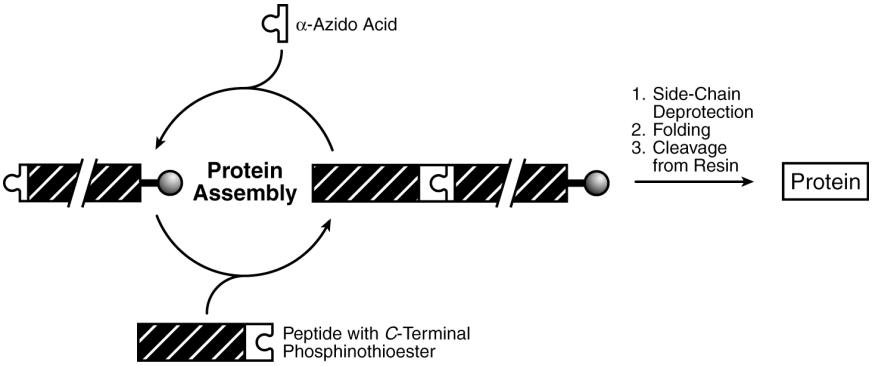

Fig. 2. Scheme for the total chemical synthesis of proteins using the Staudinger ligation.

Acknowledgments

This work was supported by grant GM44783 (NIH). B.L.N. was supported by the Abbott Laboratories Fellowship in Synthetic Organic Chemistry.

References

1. Dawson, P. E. and Kent, S. B. H. *Annu. Rev. Biochem.* **69**, 923–960 (2000).
2. Muir, T. W. *Annu. Rev. Biochem.* **72**, 249–289 (2003).
3. Bray, B. L. *Nat. Rev. Drug. Discov.* **2**, 587–593 (2003).
4. Nilsson, B. L., Kiessling, L. L. and Raines, R. T. *Org. Lett.* **2**, 1939–1941 (2000).
5. Nilsson, B. L., Kiessling, L. L. and Raines, R. T. *Org. Lett.* **3**, 9–12 (2001).
6. Soellner, M. B., Nilsson, B. L. and Raines, R. T. *J. Org. Chem.* **67**, 4993–4996 (2002).
7. Nilsson, B. L., Hondal, R. J., et al. *J. Am. Chem. Soc.* **125**, 5268–5269 (2003).

Peptide Revolution: Genomics, Proteomics & Therapeutics
Michael Chorev & Tomi K. Sawyer (Editors)
American Peptide Society, 2003

Makineni Lecture

Protein Mimetics as HIV Therapeutics and Vaccines Prepared by Tandem Ligation

James P. Tam

Department of Microbiology and Immunology, Vanderbilt University, Nashville, TN 37323, USA and School of Biological Sciences, Nanyang Technological University, Singapore

Introduction

Over the past 20 years, an interest of my laboratory is to develop tools to understand the pathogenesis and treatment of infectious diseases. One of our programs involves the design and synthesis of protein-like therapeutics to inhibit, and vaccines to prevent, the entry of HIV-1 into host cells. These pre-entry anti-HIV biologicals, differing in forms from the naturally occurring peptides and proteins, are synthetically challenging targets. Because they possess protein-like characters that are generally insoluble in organic solvents, it was necessary for us to develop new synthetic approaches. These include selective ligation methods based on aqueous chemistries, using building blocks of unprotected peptides, proteins, biopolymers and small chemicals [1,2]. Herein, I describe our development of specific amino-terminal (NT) ligation methods and their application for preparing pre-entry HIV-1 inhibitors and vaccines.

Results and Discussion

Selective ligation. An unmistakable advantage of selective ligation reactions is its efficiency that eliminates the need for coupling reagents as well as protection and deprotection schemes (Figure 1). Thus, they require far fewer steps than the conventional convergent methods, particularly those involving tandem ligation schemes that link multiple peptide segments. In addition, they employ building blocks of unprotected peptides and proteins derived from chemical, biochemical or recombinant synthesis. This, in turn, eliminates the size limitation restricted by the conventional synthetic methods.

Selective ligation methods in literature are referred interchangeably as chemoselective, orthogonal ligation and native ligation. For our purposes, we define chemoselective ligation as a site-specific method for forming non-amide bonds and orthogonal ligation for forming amide bonds, irrespective whether the ligation site is a native or non-native amino acid. We propose these distinctions based on their mechanistic consideration and from the perspective of the pioneering work of Kemp and his coworkers [3]. Since several orthogonal ligation methods routinely generate native peptides, we shall group native ligation under orthogonal ligation.

Chemoselective ligation is a one-step reaction that requires only a mutually reactive nucleophile-electrophile pair. In contrast, all known orthogonal ligation methods are two-step reactions requiring a combination of two nucleophile-electrophile pairs, the first pair to undergo a chemoselective capture reaction to link two segments covalently, and the second pair involving a proximity-driven acyl transfer reaction to an NT^{α}-amine.

Unlike chemoselective ligation, the requirement of forming a specific amide bond in orthogonal ligation was an obstacle because the presence of other reactive amines,

notably the other NT$^{\alpha}$-amine and ε-amines of Lys in the ligating peptide pairs. During the 1980s, Kemp and his coworkers found a clever solution to overcome this obstacle to distinguish these amines by a proximity-driven O,N-acyl transfer reaction using a rigid template through a "Prior Capture" strategy to link covalently two peptide segments [3].

The current orthogonal ligation schemes retain the Kemp's conceptual framework without the use of a rigid template. Figure 1 shows a scheme to prepare peptides or proteins: the nucleophile-electrophile pairs are placed at the appropriate ends of two peptides, an electrophile (Y) at the carboxyl terminal (CT) as an O- or S-ester (thioester) and a nucleophile (X) at the amino-terminal (NT) as a heteroatomic amine. In this regard, orthogonal ligation is a coupling reaction that distinguishes an orthogonal pair of NT-amines.

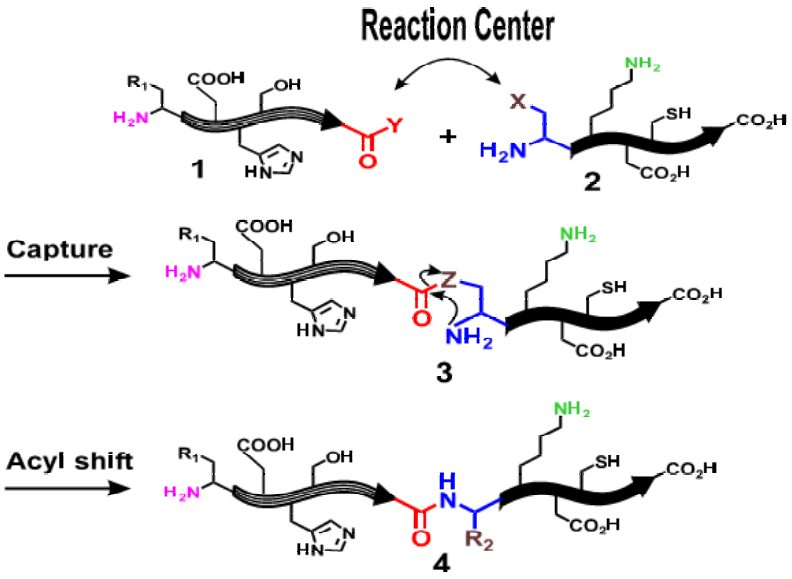

Fig. 1. A general scheme of orthogonal ligation. X and Y are mutually reactive nucleophile-electrophile and Z is its intermediate. For Cys ligation, X=SH, Y=SR, Z=S and R_2=SH. For Cys ligation through thioacid capture, X=SSR, Y=SH, Z=SS, and R_2=SH.

The acyl transfer reactions to α-amines in orthogonal ligation reactions are invariable, belonging to one of three types, O, S, or N^{Im} to N-transfers. They are proximity driven, and often involving a favorable 5- or 6-member ring transition. In contrast, captures are variable, linking two segments covalently as first of the two-step orthogonal ligation schemes. In part, this is contributed by the diverse reactivity of the 20 or more genetic-coded and modified amino acids as well as different approaches developed over the past decade. We can generalize the current capture methods in two categories: imine and thiol captures. Other capturing schemes are still evolving. A promising example is the metal ion capture developed by our laboratory using Ag+ ion to capture NT-Ser, Asn and Asp [1,4].

Ligation by imine capture. Imine capture mediates three types of selective ligation reactions [5-12]. They include orthogonal ligation forming ψPro (ψPro ligation),

Staudinger ligation with NT-azido acids, and chemoselective ligation to form dipeptide mimetics as heterocycles. A clever method based on phosphorane imines capture is the Staudinger ligation developed by the laboratories of Bertozzi [11] and Raines [12]. This ligation reaction requires modifications of an NT-amino acid to an azido moiety and the CT-O- or S-ester as a phosphino derivative. Phosphino capture of the α-azido group forms the phosphorane imine that isomerizes to permit the acyl shift. Subsequent hydrolysis releases the pendant N-phosphino moiety to generate the aliphatic amino acids such as Gly or Ala at the ligation sites.

a. ψPro at the ligation site. The ψPro ligation forms a Pro-like peptide with six NT-amino acids (Cys, Ser, Thr, Trp, His, and Asn) that incorporates their side chains into a Pro-containing heterocyclic ring [5-10]. The imine capture of the CT-glycoaldehyde with their α-amines starts the reaction, followed by a rapid ring-chain tautomerization to heterocycles through the addition of the side-chain nucleophiles to the imines, linking the amino and acyl segments covalently (Figure 2). The imine capture is a second-order reaction and often rate determining. The resulting heterocycles such as

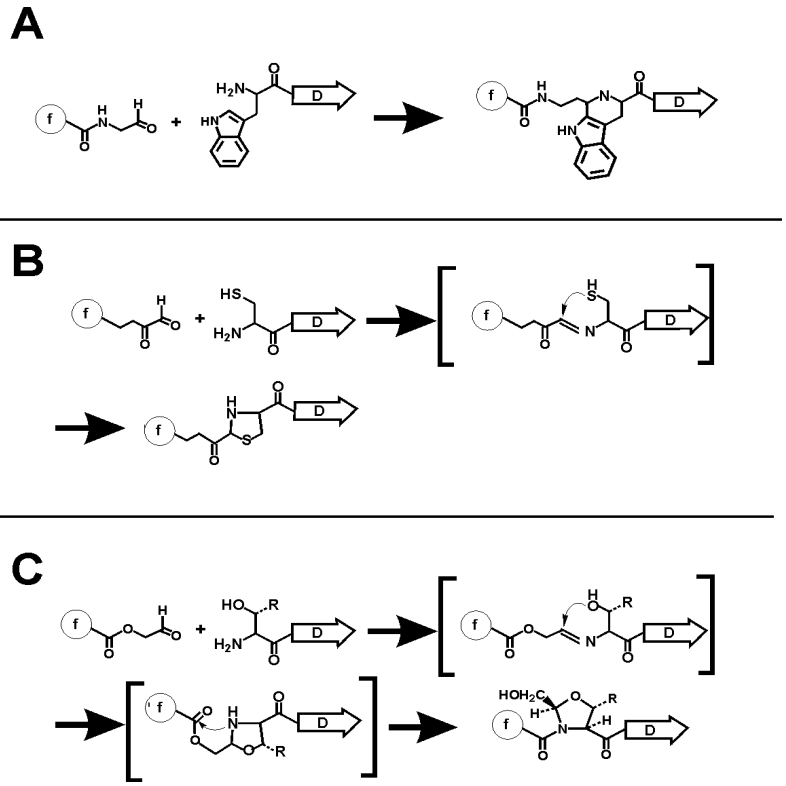

Fig. 2. Imine-capture chemoselective and orthogonal ligation methods. (A). N-to-C Trp ligation in 100% HOAc, (B). N-to-N Thz ligation in aqueous solution buffered pH 3-5, and (C). N-to-C ψPro ligation of NT-Ser in pyridine-HOAc (1:1, mol/mol). f = free and unprotected peptide or protein, D = free or unprotected/protected peptide segment in solution or solid phase.

thiazolidine (Thz) from Cys, oxazolidine (Oxz) from Ser or Thr, and tetrahydrocarboline (THC) from Trp not only convert their imines to the reactive secondary amines but also positioning them close to the acyl moiety to enable a

favorable O,N-acyl transfer reaction to form a ψPro peptide bond (Figure 2C). Of these six, the monocyclic ψPro ligation of NT-Cys (SPro), NT-Ser (OPro) and NT-Thr ($OPro^{Me}$) have been well studied [5-10]. In these imine captures, the heterocyclic ring formation creates a new asymmetric carbon at position 2 of the ψPro ring. The C2 stereochemistry for L-amino acids as determined by NMR indicates that the C2 stereocenter is an R epimer [7]. Thus, the oxaproline and thiaproline ligations are regiospecific as well as stereospecific.

Several approaches to prepare CT-glycoaldehyde have been developed using CT-thioester or an unprotected peptide as a precursor [1]. However, a convenient method to prepare the CT-glycoaldehyde ester is the $HOCH_2$-acetal resin [7-9]. This functionalized resin provides a CT-glyceric ester in which a diol serves as precursor for the CT-glycoaldehyde ester. The glyceric ester is converted by sodium periodate at pH 4-7 to a C-terminal glycoaldehyde ester.

b. Chemoselective heterocyclic ligation. The imine capture of the ψPro ligation has been used for the chemoselective ligation affording a heterocycle as a ψ-peptide bond without undergoing an acyl shift. Two examples are shown in Figure 2. In the N-to-C Trp ligation (Figure 2A), the CT-ester glycoaldehyde is replaced by a CT-glycoaldehyde (O replaces by N). Without the CT-ester, the acyl shift cannot occur and the heterocycle becomes a part of the peptide backbone. In the N-to-N Thz ligation, an α-acyl aldehyde is placed in the NT of another peptide segment (Figure 2B). Similar to ψPro ligation, the ring size of 5 or 6-member ring transition is favored in the tautomerization by the β-substituted heteroatomic side chains of Cys, Ser, Thr, Trp, His and Asn yielding a variety of mono-, bi- and tri-cyclic side chains at the ligation site. Heterocyclic ligation such as Thz with NT-Cys and THC with NT-Trp are fast whereas those in NT-Asn are exceedingly slow at ambient temperature. The Oxz formed by NT-Ser is unstable, but could be exploited for other applications. Chemoselective ligation with NT-His involving two or more nucleophilic sites affords a mixture of isomers. We have extended chemoselective ligation reactions of Thz from NT-Cys, Oxz from NT-Thr and THC from NT-Trp into solid-phase synthesis of dipeptidomimetics containing peptides [8,9].

Ligation by thiol capture. Ligation reactions by the thiol capture involves a thiol to form a covalent intermediate of two peptide segments to permits an acyl shift to occur (Figure 1). Discovered by Wieland in the 1950s (13) and conceptually similar to Kemps' Prior Capture in the 1980s [3], thiol capture has been extensively developed by our group [1,15], Kent and his coworkers [14] and many others in the past decade. Various thiol moieties of the NT-Cys, Cys mimetics, Hcy (homocysteine and CT-thioacid have been exploited as capture devices. Thiol capture method has also been extended to selenocysteine (reviewed in 1). The NT-Cys mimetics with a cleavable thiol handle linked directly at the α-amine as a capturing moiety further broaden its scope to non-cysteine-containing amino acids. We also include His ligation by the imidazole capture in this category because the principle of its capture mechanism is similar to the thiol capture-mediated ligation. The imidazole capture to link covalently two segments provided the first example of an N^{Im},N^{α}-acyl transfer reaction to form His at the ligation site.

a. Cysteine and methionine at the ligation site. Cys ligation possesses two ideal elements in the orthogonal ligation strategy. First, Cys bearing a thiol as an NT-supernucleophile readily undergoes a thiol-thioester exchange reaction with a CT-thioester that, after the acyl migration, regenerates the thiol moiety on the NT-nucleophile amino acid. This preserves the integrity of the side chain functional group of the NT-nucleophile amino acid at the ligation site. Second, the thioester as a CT-

electrophile contains the covalently linked thioester and a primary α-amine as the nucleophile. As a result, the S,N-arrangement is spontaneous and Cys ligation by thioester capture has been extensively exploited in chemical and, more recently, semi-syntheses of proteins [1]. The principle of thiol capture to afford homologs or analogs of Cys is an obvious extension. For example, we have exploited NT-homocysteine (Hcy) for Met ligation [1,2]. The latent thiol moiety of Hcy at the ligation after capture by transthioesterification and S,N-acyl shift with an acyl segment bearing a CT-thioester is methylated selectively to give Met at the ligation site. We have also extended the Cys ligation for end-to-end cyclization of peptides and proteins as well as linear and cyclic dehydropeptides, a family of peptides that are difficult to prepare by the conventional methods [16-18].

Several approaches have been developed for preparing CT-thioesters. A direct approach is to functionalize a resin support with a cleavable thiolate handle so that an unprotected peptide is released as a CT-thioester or CT-thioacid using either Boc or Fmoc chemistry. Recent developments of preparing the CT-thioester segments from a biosynthetic source through recombinant methodologies by two independent laboratories of Muir and Xu represent an exciting expansion of the scope of orthogonal ligation for semi-synthesis [1].

b. Thiol capture by CT-thioacid. The thiol of a CT-thioacid has been exploited for the Cys ligation with several variations. An early approach is to functionalize the NT-amino acid as an NT-bromoalanine [13]. The thiol capture by a CT-thioacid of the bromoalanine forms a thioester intermediate similar to the thioester in the Cys ligation. An improved variation involves an acyl disulfide intermediate in the capture step in which the thiol of the NT-Cys is activated as a mixed disulfide for a thiol-thiol exchange reaction with the CT-thioacid [1]. The mixed acyl disulfide (perthioester) then rapidly undergoes an intramolecular S, N-acyl transfer through a six-member ring intermediate (Figure 1). Thiolytic reduction of the resulting hydrodisulfide (S-SH) gives a Cys residue at the ligation site. A characteristic of the perthioester reaction is that the capture and S, N-acyl migration occurs under very acidic pH (pH< 4). The acyl transfer is spontaneous and 90% complete in 5 min even at acidic pH<4. The efficiency of this acyl transfer step is attributed to the activated acyl disulfide and proximity of the CT-acyl and α-amine in a six-member ring intermediate. This Cys ligation and disulfide reduction is a one-pot process that does not require isolation of the intermediates.

c. X-Cys ligation. In Kemp's thiol capture scheme using a tricyclic template, the O,N-acyl shift undergoes a medium-size transition consisting of 12- to 14-member rings. Based on Kemp's work, we reasoned that the thiol capture in Cys ligation must not necessarily be an NT-amino acid. To test our hypothesis, we tested the XCys ligation in which the Cys was placed at the second position at the N-terminus. To determine the optimal placement in the XCys ligation, we prepared a library of (Xaa)n-Cys segments with a Cys placed at various positions proximal to the N-terminals to perform XCys ligation reactions with a dye-linked N-segment screening through a library synthesis. No observable XCys ligation of (Xaa)n-Cys segments was found in 60 h when n>4, but ligation yields increased in the order of 1 > 2 >> 3 >>4, and were satisfactory when n = 1 or 2, involving S,N-acyl migrations through an 8 or 11-member transition. The S,N-acyl migrations involving the larger 14- or 17-ring transition (when n is 3 or 4) are likely too slow to be practical for XCys ligation and provides an explanation for the high reactivity of the NT-Cys ligation. Overall, these results show that the rate differences of acyl migrations with a Cys at the amino terminus may be optimal for the Cys ligation, but is not obligatory.

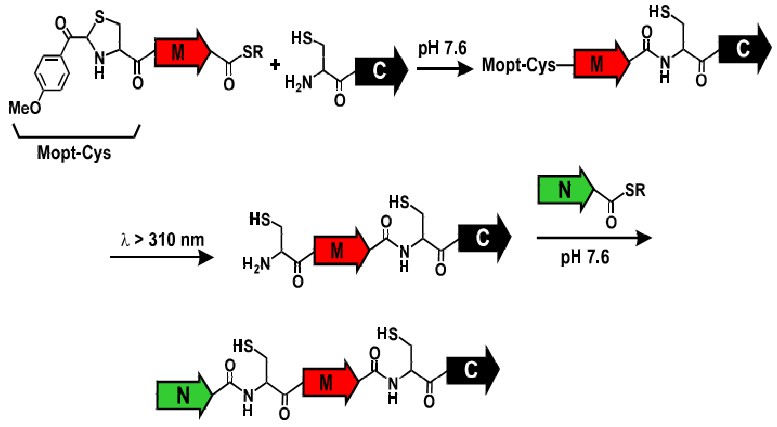

Fig. 3. Sequential Cys ligation using a photolabile phenacyl protecting group.

Sequential and tandem ligation strategies for proteins and protein mimetics. The repertoire of chemoselective and orthogonal ligation methods specific for different NT-amino acids permits the development of various sequential or tandem ligation strategies. In sequential ligation, the NT-amino acids are protected to avoid polymerization and the segments are ligated sequentially [1,2]. An example is the sequential Cys ligation using a removable Cys protecting group (Figure 3). We have developed two such protecting groups for the NT-Cys using a photolabile dione (phenacyl aldehyde) and a thiol-sensitive trione (ninhydrin). In contrast, tandem ligation strategies, one can successively ligate multiple peptide segments or proteins without the need for a protection scheme (Figures 4 and 5). We have developed and utilized tandem ligation schemes that employ orthogonal, chemoselective, or both ligation methods for the consecutive coupling of three or more peptide segments to prepare proteins, complex multipartite peptide and protein biologicals. Because a protecting group scheme is not necessary, tandem ligation is, perhaps, the most efficient convergent approach with the fewest synthetic steps.

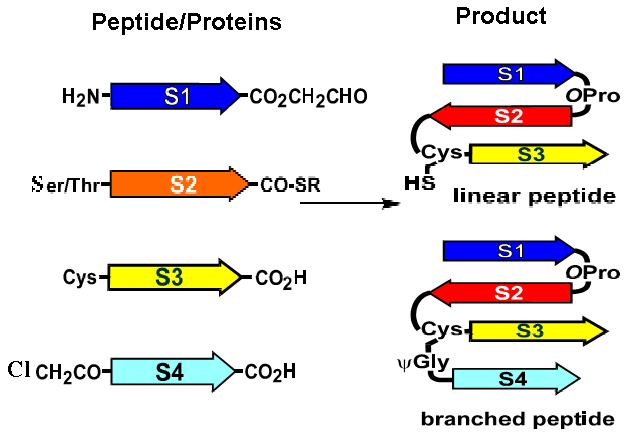

Fig. 4. Four-segment tandem ligation of linear and branched peptides and protein mimetics in the order of S4-S2 (Cys ligation)-S1 (ψPro ligation)-S3 (ψGly ligation).

a. Tandem ψPro ligation. The tandem ψPro ligation forms a thiaproline (SPro) and an oxaproline (OPro) bond to couple three unprotected peptide segments in tandem [19]. It exploits the large rate differences the imine capture of NT-Cys and NT-Ser or NT-Thr in forming two ψPro bonds. The SPro ligation of NT-Cys peptides is orthogonal to NT-Ser under aqueous conditions, followed by the OPro ligation of NT-Ser or NT-Thr peptides in nonaqueous pyridine-acetic acid solutions to complete the tandem ψPro ligation. This strategy is illustrated in the synthesis of a proline-rich helical antimicrobial and antitumor protein, the 59-residue bactenecin. Because of the presence of ψPro bonds in our preparation, they are more aptly called protein mimetics.
b. Tandem ψPro and Cys ligation. The tandem Cys and OPro ligation of three peptide segments exploits the orthogonality of the OPro and Cys ligation [20]. Cys ligation through a thiol capture to a CT-thioester is performed in aqueous buffers at pH 7 to 8, a condition NT-Ser or NT-Thr is not reactive to the CT-thioester (S2+S3 in Figure 4, S2+S4 in Figure 5). The oxaproline ligation is then achieved in pyridine or methylimidazole-acetic acid solutions to complete the tandem Cys and OPro ligation scheme (S2/3 + S1 in Figure 4). Similarly, a tandem SPro and Cys ligation scheme has been achieved by exploiting the semi-orthogonality of an N-terminal Cys to two different C-terminal electrophiles, a glycoaldehyde ester and a thioester, in forming a SPro and a Cys bond in tandem [21]. Again, this tandem ligation scheme exploits the rate differences of imine and thiol captures SPro under acidic conditions in which imine dominates over thiol capture to form the SPro bond.
c. Tandem chemoselective and orthogonal ligation. Schemes for tandem orthognal chemoselective ligation have also been developed for protein mimetics [1,2,18-21]. For example, NT-Trp-containing peptides based on the Pictet-Spengler reaction is orthogonal to the ψPro and Thz ligation of NT-Cys, Ser and Thr ligation when performed in nonaqueous acetic acid solutions. A combination of chemoselective and orthogonal schemes enable tandem ligation of four or more segments. An extension of the tandem Cys and OPro ligation to link four segments to form the single-chain and branched-chain peptides has been achieved [22]. This scheme exploits not only the orthogonalities of two N-terminal specific OPro and Cys ligation, but also a ψGly

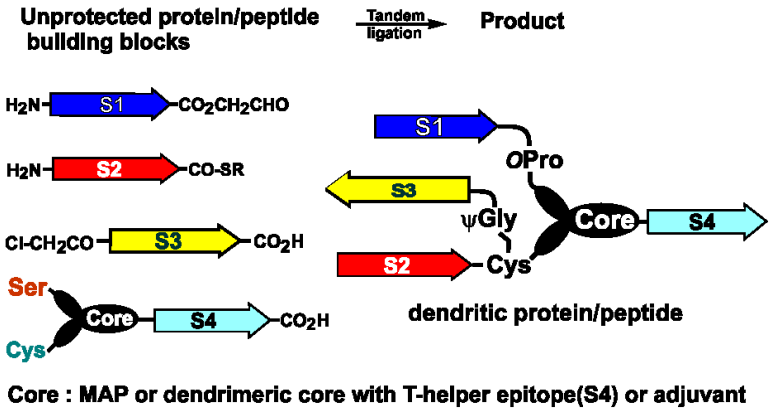

Fig. 5. Four-segment tandem ligation of dendrimers and protein mimetics in the order of S4-S2 (Cys ligation)-S1 (ψPro ligation)-S3 (ψGly ligation). The core is a branched trilysine scaffold.

ligation that mimics a Gly-Gly dipeptide between the chloroacetylated amino group and the newly generated thiol group from the Cys ligation (Figure 4 and 5). Cysteine and pseudoglycine ligation can be performed in aqueous buffers at pH 7 to 8, while oxaproline ligation can be achieved in pyridine or methylimidazole-acetic acid solutions.

Many functionally active peptides or motifs contain continuous sequences embedded in proteins. These peptides vary in lengths that range from 3 to >20 amino acids. They are found in cell adhesion molecules, and sequences specific for signal transduction, phosphorylation, sulfation, and nuclear localization. However, most of these peptides target intracellular proteins and will require a transportant or cell-permeable peptide for intracellular delivery that has the advantage of being non-invasive. We have used the tandem ligation approach to prepare multipartite peptides and protein mimetics for synthetic biologicals as vaccines and therapeutics. Some of these contain branch architectures carrying a novel transportant peptide to permit their cargoes to be translocated across membranes to probe protein-protein interactions in various intracellular compartments [21-23].

Application in pre-entry inhibitors and synthetic vaccines against HIV-1. The HIV envelope glycoprotein consists of two noncovalently associated subunits, gp120 and gp41 that play critical roles in the viral entry and infection. HIV gp120 directs target-cell recognition and viral tropism through interaction of the cell-surface receptor CD4 and a chemokine receptor. The membrane-anchored gp41 then promotes fusion of the viral and cellular membranes, resulting in the release of viral contents into the host cell. These entry events mediated by envelope glycoprotein gp120 and gp41 offer opportunities for intervention as pre-entry therapeutics and synthetic vaccines.

The crystal structures of gp120 and gp41 strongly suggest that they are trimeric in their quaternary structures. We have exploited these structural leads to design the conformational and conserved epitopes known as α3 and β4 mimetics as synthetic HIV vaccines. The α3 protein mimetics are covalently linked 3-helix bundles of three parallel α-helical peptides derived from various lengths of the coil-coil regions of gp41.

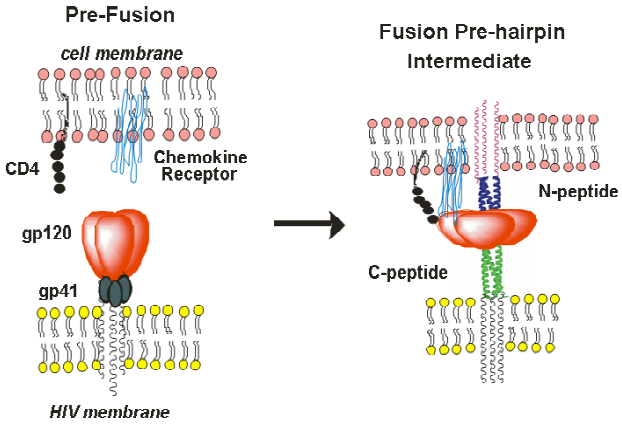

Fig. 6. A schematic representation of HIV entry and fusion to host cell. The prefusion state shows the trimeric structure of gp120/gp41. The fusion prehairpin shows the binding of gp120 to the CD4 and chemokine coreceptor to expose the 3-helix bundles of the N- and C-peptide of gp41 that mediates membrane fusion.

The β4 mimetics contain four cystine-stabilized β strands consisting of two discontinuous anti-parallel strands, β2/β3 and β20/β21 that represent the bridging region of the inner and outer domains of gp120. To elicit high-quality antibodies as synthetic vaccines, they must maintain their conformations. We show that they display protein-like characters. Circular dichroism measurements show that the α3 peptides are helical and the β4 peptides are β stranded. These ordered structures are immunogenic in guinea pigs and their antisera show the desirable properties to block viral entry. Since both α3 and β4 mimetics elicit antibody responses directing to the conserved sequences of the HIV envelope protein, they hold promise as vaccine candidates.

An ideal immunogen should be multipartite, containing several types of peptides to enhance its function, perhaps its structure as a protein mimetic. This may include a transportant for intracellular delivery, one or more helper peptide epitopes to boost immunogenicity and an additional peptide for providing extracellular specificity to target the relevant immune cells. Putting these peptides as a multipartite molecule is challenging. At present, most multipartite peptides are constructed as single-chain peptides that link different motifs in tandem because they are convenient to be prepared by stepwise solid-phase or recombinant methods. We reasoned that a branched design with various peptides antigens tethered onto a core might be as effective as the single-chain design because the biological activity of each peptide immunogen is largely dependent on the content of its sequence and conformation. Furthermore, tandem ligation methods would provide the most direct method for assembling branched multipartite peptides. Toward this end, we have developed tandem ligation methods to prepare multipartite branched peptides as protein mimetics with two to four chain arrangements [2].

For developing pre-entry anti-IV-1 therapeutics, we focus on the fusion active intermediates of gp41. The 3-dimensional structures of gp41 have been determined to be trimers-of-hairpins commonly involved in the final step of membrane fusion. This fusion-active prehairpin intermediate is exposed after gp120-binding with cell surface receptors. In this fuseogenic state, the prehairpin cross-links two different membranes, exposing an amino- and carboxyl-homotrimeric α-helical coiled ectodomain (N- and C-region) that eventually forms a hairpin structure of a six-helix bundle bringing the amino- and carboxyl-terminal regions of the gp41 ectodomains into close proximity enabling membrane fusion. Synthetic N-peptides such as N36 or C-peptides such as DP178 targeting these domains are effective fusion inhibitors and constitute a new class of HIV pre-entry therapeutics. However, the first-generation peptidyl drug candidate based on a C-peptide DP178 has limitations that include high dosage and poor stability. Thus, we have focused on developing novel protein mimetics of gp41as second-generation fusion inhibitors to improve the potency and stability of the peptide-based therapeutics.

To mimic an intermediate fusion-active state in which the heptad-repeat domains form 3-helix bundles, we have synthesized trimeric DP178 and N36 as 3-helix bundles using a thiazolidine and THC ligation of unprotected peptide segments on a peptide scaffold [10]. The 3-helix DP178 and 3-helix-N36 are protein mimetics and display protein-like characters. CD spectra show both 3-helix bundles are 100% α-helical and stable to thermal denaturation >95^{o}C. More importantly, they inhibited HIV-1 mediated cell-cell fusion as measured in a syncytium formation assay in a dose-dependent manner. Inhibition of viral infection of 3-helix DP178 was <1 nM and orders of magnitude higher than that of monomeric DP178. The 3-helix N36 also exhibited viral inhibition about 50-fold higher than the monomeric N36. The 3-helix DP178 and N36 were more active in blocking M-tropic HIV-1 entry into CCR5+ indicator cells than the

T-tropic strains on indicator cells. These 3-helix protein mimetics are nontoxic to human cell lines as determined by the MTT assay using 1,000 times concentrations of the effective doses that inhibit 50% fusion. Overall, our results show that the 3-helix DP178 and N36 are protein mimetics that act as pre-entry inhibitors to block HIV entry to host cells and are promising candidates as immunogens to elicit antibodies to block viral entry. The protein mimetic design using ligation methods provide a potential avenue for development of anti-HIV drugs and vaccines.

Conclusions

We have been able to solve difficult synthetic problems to prepare complex peptides and proteins with normal or unusual architectures by developing a repertoire of new selective ligation methods based on either imine or thiol captures. We have applied these methods to produce potent pre-entry anti-HIV therapeutics and vaccine candidates. One of our ongoing programs is to couple selective ligation with the combinatorial process to generate synthetic antibodies for biochemical and therapeutic applications.

Acknowledgments

I thank all my colleagues, past and present, who have contributed to this work. I am particularly indebted to Drs. C. F. Liu, L. S. Zhang, Y-A Lu, Q. Yu, Z. Miao, K. D. Eom, and J. L. Yang for their substantial contributions. I regret that there are omissions in our citations of other laboratories. This work was in part supported by NIH grants CA36544 and AI 46164.

References

1. Tam, J. P., Yu, Q. and Miao, Z. *Peptide Sci*. **51**, 311-332 (1999).
2. Tam, J. P., Yu, Q. and Lu, Y.-A. *Develop. Biologicals* **29**, 189-96 (2001).
3. Kemp, D. *J. Org. Chem.* **54**, 2803 (1989).
4. Zhang, L. S. and Tam, J. P. *J. Am. Chem. Soc.* **121**, 3311-3320 (1999).
5. Liu, C.-F., Shao, J., Rao, C. and Tam, J. P. In Hodges, R. S. and Smith, J. A. (Eds.), *Peptides: Chemistry, Structure and Biology, Proceedings of the 13th American Peptide Symposium*, ESCOM, Leiden, p. 218-220 (1994).
6. Liu, C.-F. and Tam, J. P. *J. Am. Chem. Soc.* **116**, 4149 (1994).
7. Tam, J. P. and Miao, Z. *J. Am. Chem. Soc.* **121**, 9013-9022 (1999).
8. Li, X.-F., Zhang, L.-S., Hall, S. E. and Tam, J. P. *Tetrahedron Lett.* **41**, 4069-4073 (2000).
9. Li, X.-F. Zhang, L., Zhang, W., Hall, S. E. and Tam, J. P. *Org. Lett.* **2**, 3075-3078 (2000).
10. Tam, J. P. and Yu, Q. *Org. Lett.* **4**, 4167-4170 (2002).
11. Saxon, E. and Bertozzi, C. R. *Science* **287**, 2007-2010 (2000).
12. Nilsson, B. L., Kiessling, L. L. and Raines, R. T. *Org. Lett.* **2**, 1939-1941 (2000).
13. Wieland, T. and Schneider, G. *Liebigs Ann. Chem.* **583**, 159 (1953).
14. Dawson, P. E., Muir, T. W., et al. *Science* **266**, 776-779 (1994).
15. Tam, J. P. Lu, Y.-A., et al. *Proc. Natl. Acad. Sci. U.S.A.* **92**, 12485-12489 (1995).
16. Tam, J. P. and Lu, .Y-A. *Protein Sci.* **7**, 1583-1592 (1998).
17. Tam, J. P., Lu, Y.-A. and Yu, Q. *J. Am. Chem. Soc.* **121**, 4316-4324 (1999).
18. Tam, J. P., et al. *Proc. Natl. Acad. Sci. U.S.A.* **96**, 8913-8918 (1999).
19. Miao, Z. and Tam, J. P. *J. Am. Chem. Soc.* **122**, 4253-5260 (2000).
20. Tam, J. P., Yu, Q. and Yang, J.-L. *J. Am. Chem. Soc.* **123**, 2487-2494 (2001).
21. Eom, K. D., Miao, Z., Yang, J.-L. and Tam, J. P. *J. Am. Chem. Soc.* **125**, 73-82 (2003).
22. Chang, M., Zhang, L. S., et al. *J. Biol. Chem.* **275**, 7021-7029 (2000).
23. Sadler, K. and Tam, J. P. *Rev. Mol. Biotechnol.* **90**, 195-229 (2001).

Peptide Revolution: Genomics, Proteomics & Therapeutics
Michael Chorev & Tomi K. Sawyer (Editors)
American Peptide Society, 2003

Three-Helix Bundles of HIV Mimics Fusion State and Blocks M- and T-Tropic HIV-1 Entry into Host Cells

Jin-Long Yang, Qitao Yu, Hua Li and James P. Tam

Department of Microbiology and Immunology, Vanderbilt University, Nashville, TN 37232, USA

Introduction

The envelope proteins gp41-gp120 of human immunodeficiency viruses (HIV-1) forms a nonconvalent complex that mediates membrane fusion during viral entry. The gp41 exists as a trimer with two leucine/Isoleucine-heptad domains that form coiled-coil α-helical trimers. During the membrane fusion between the viruses and host cells the trimeric helix C-terminal heptad-repeat domain (C-helix) interacts with the N-terminal helix (N-helix) to form a six-helix bundle structure [1]. Compounds that prevent the N- and C-helix pairing inhibit HIV-1 infection. Two synthetic peptides, T20 (DP178) and N36, respectively derived from the C- and N-region, inhibit gp41-mediated membrane fusion. The IC_{50} values of T20 and N36 are 2 ng/ml and about 1 μg/ml, respectively, against M-tropic strain HIV-1 viruses [2]. Crystallographic studies have revealed an intermediate fusion-active state in which the heptad-repeat domains form three-helix bundles. To mimic such a fusion-active intermediate, we have synthesized trimeric (three-helix) T20 and N36 using a thiazolidine ligation of unprotected peptide segments on a peptide scaffold [3]. The 3-helix bundles containing three parallel srands of C- or N-peptides mimic a truncated C- or N-helix. CD spectra that confirmed both trimers displayed stable α-helices. Antiviral assays revealed that the anti-HIV activity of 3-helix bundles of T20 and N36 were significantly higher than that of their monomeric peptides.

Results and Discussion

The design of the peptide scaffold was centered on the dipeptide Lys^3-Lys^4 to provide three amino groups for tethering helical N- or C-peptides. Unprotected peptides T20 and N36 with a Cys at their N-terminals were prepared by Fmoc chemistry using O-

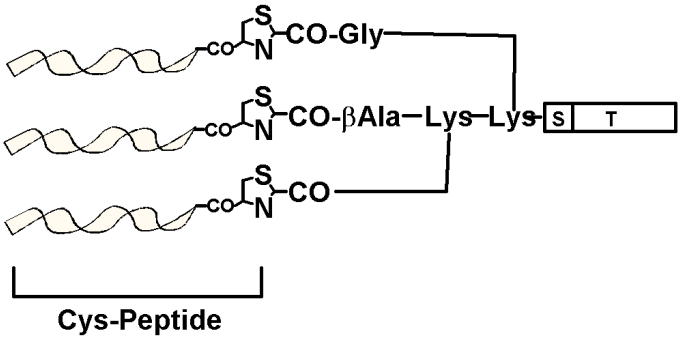

Fig. 1. Sequences of trimeric T20 and N36 peptides. T, T-helper sequence; S, spacer sequence. Cys-Peptide = T20 (YTSLIHSLIEESQNQQEKNEQELLELDKWASLWNWF) or N36 (SGIVQQQNNLLRAIEAQQHLLQLTVWGIKQLQARIL).

benzotriazole-N,N,N',N'-tetramethyl-uronium hexafluorophosphate and DIEA as coupling reagents. Two 3-helix bundle fusion-state protein mimetics, 3-helix T20 and 3-helix N36, were synthesized using this ligation method (Figure 1).

The inhibitory activity of three-helix T20 and N36 on HIV-1 infection was determined by a single-cycle MAGI assay [4]. Two virus strains were employed in this study. R9 viruses are T-cell-tropic, which display syncytium-inducing phenotype. R9BAL viruses are macrophage-tropic strain. P4R5 cells were transactivated by the HIV-1 tat protein induced expression of the *Escherichia coli* β-galactosidase gene from the HIV-1 long-termminal repeat [5]. The 3-helix T20 significantly inhibited infection by HIV-1 viruses R9 in P4R5 cells at 1-10 nM. The infected cell number was significantly decreased. In contrast, the viruses and cells treated with the same concentrations of T20 did not show inhibition. The 3-helix T20 was 47-fold more potent than the monomeric T20 agaomst HIV-1 infection. The 3-helix N36 at 500 nM also produced significant inhibition against infection by R9 viruses, but N36 did not show anti-HIV-1 activity.

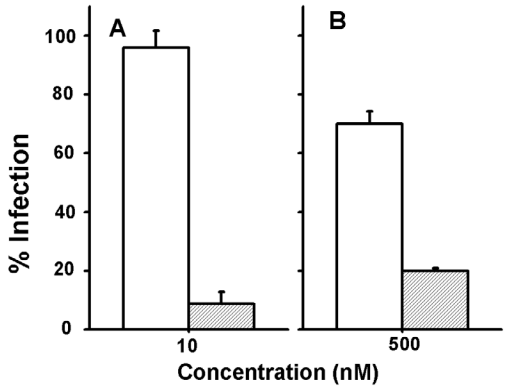

Fig. 2. Comparsion of anti-HIV activity of monomer (open bars) and three-helix (hatched bars) of T20 (A) and N36 (B) on HIV-1 virus infection in P4R5 cells.

These three-helix peptides were nontoxic to human cell lines using 1000 times the concentration of the effective doses. Three-helix bundles display protein-like characteristics. These peptides are soluble and stable without aggregation in physiological conditions as determined by HPLC. Our results show that three-helix T20 and N36 may mimic a fusion-state intermediate to block HIV entry to host cells and provide a potential avenue for development of anti-HIV drugs.

Acknowledgments
The work was funded by NIH Grants CA36544 and AI46164.

References

1. Chan, D. C. and Kim, P. S. *Cell* **93**, 681-684 (1998).
2. Wild, C. T., Shugars, D. C. and Matthews, T. J. *AIDS Res. Hum. Retroviruses* **9**, 1051-1053.
3. Tam, J. P. and Yu, Q. *Organic Letters* **4**, 4167-4170 (2002).
4. Pirounake, M., Heyden, N. A. and Ratner, L. *J. Virological Methods* **85**, 151-161 (2000).
5. Eckert, D. M., Malashkevich, V. N., et al. *Cell* **99**, 103-115 (1999).

Peptide Revolution: Genomics, Proteomics & Therapeutics
Michael Chorev & Tomi K. Sawyer (Editors)
American Peptide Society, 2003

Manipulating the Hydrophobic Core of a Coiled Coil Peptide Self Replicator

Xiangqun Li and Jean Chmielewski

Department of Chemistry, Purdue University, West Lafayette, IN 47907, USA

Introduction

The development of self-replicating peptides capable of high catalytic efficiency is a major challenge in the design of self-replicating peptides [1]. Modulation of coiled-coil stability by shortening the peptide to the minimum length necessary for coiled coil formation resulted in a highly efficient self-replicating peptide [2]. Incorporation of a proline kink within a coiled-coil peptide was also found to produce high catalytic efficiency [3]. Here we describe an alternative pathway to reduce the stability of coiled coils by modifying the residues present at the hydrophobic interface.

Results and Discussion

Because of its small side chain, locating Ala at the hydrophobic core would reduce the stability of the coiled coil peptide. For instance, Tanaka and coworkers destabilized a triple-stranded coiled coil peptide, IZ, to an almost random coil structure by replacing a Leu at the hydrophobic core with an Ala [4]. We employed this replacement strategy to decrease the stability of the self-replicating peptide E1E2 (Figure 1). In the overall design, it was envisioned that this modification, E1E2-A, would have less effect on the stability of the ternary complex of template and peptide fragments because the mutation position was near the N-terminus of E2.

E1E2-A and its two fragments were synthesized, one containing a C-terminal thioester (E1) and one containing an N-terminal cysteine (E2-A) (Figure 1). Circular dichroism (CD) was used to evaluate the helical content of the peptides. The helical content of the peptide fragments of E1E2-A increased upon addition of template; the fragments E1/E2-A increased by 17% and 39%, respectively (Figure 1). These data indicate the ability of E1E2-A to act as a template to organize the fragments for ligation.

Analytical ultracentrifugation was used to analyze the self-assembly of E1E2-A. E1E2-A was found to aggregate as a tetramer, whereas E1E2 was found to form a dimeric coiled-coil [5]. The stability of E1E2-A was compared to E1E2 using thermal denaturation. The melting temperature of E1E2-A was 91°C, whereas E1E2 remained greater than 55% folded at 98°C. These data confirm that the replacement of Leu with an Ala residue in the hydrophobic core of E1E2 decreases the overall stability of the coiled-coil.

To determine if E1E2-A had self-replicating properties, ligation of the fragments (E1 and E2-A) in the presence of different amounts of the template E1E2-A was performed. The reaction was accelerated by the presence of template; increasing the amount of E1E2-A in the reaction mixture increased the initial rate of E1E2-A formation. The data were analyzed with the program SimFit [6]. This analysis provided an apparent autocatalytic rate constant, k_a, of 2.1 ± 0.1 $M^{-1.65}s^{-1}$, and a noncatalytic rate constant, k_b, of 8.9 ± 0.4 x 10^{-4} $M^{-1}s^{-1}$. This corresponds to a catalytic efficiency ($\varepsilon=k_a/k_b$) of 2.4 x 10^3, 20-fold greater than that obtained for E1E2. This improved catalytic efficiency was mainly achieved by a decrease in the background

reaction rate. This difference is most likely due to the presence of fewer hydrophobic interactions between the two fragments, which resulted in reduced binding.

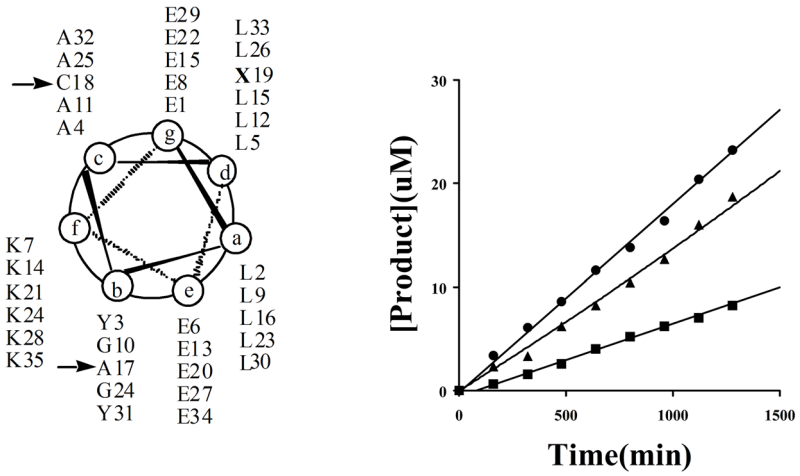

E1: Ac-ELYALEKELGALEKELA-COSR

E2: C**X**EKEEELGALEKELYALEK-$CONH_2$

E1E2-**X**: Ac-ELYALEKELGALEKELA C**X**EKEEELGALEKELYALEK-$CONH_2$

X=L(E1E2); X=A(E1E2-**A**)

Fig. 1. (left) Helical wheel diagram and sequence of peptides E1E2(X), where X = L or A. Peptide fragments used in the replication reactions are shown. (right) E1E2-A formation as a function of reaction time in the presence of different concentration of template: no template (square), 25μM (triangle), 50μ M (circle). The concentration of the fragments was 500μM each and the buffer contained 100 mM MOPS at pH 4.0.

In this study, we have demonstrated a strategy to design self-replicating peptides with high efficiency by modifying the residue at the hydrophobic interface.

Acknowledgments

We would like to acknowledge financial support from NSF.

References

1. Li, X. and Chmielewski, J. *Org. Biomol. Chem.* **1**, 901-904 (2003).
2. Issac, R. and Chmielewski, J. *J. Am. Chem. Soc.* **124**, 6808-6809 (2002).
3. Li, X. and Chmielewski, J. *J. Am. Chem. Soc*. **125**, 11820-11821 (2003).
4. Kashiwada, A., Hiroki, H., Kohda, D., Nango, M. and Tanaka, T. *J. Am. Chem. Soc.* **122**, 212 (2000).
5. Yao, S., Ghosh, I., Zutshi, R., Chmielewski, J. *J. Am. Chem. Soc.* **119**, 10559-10560 (1997).
6. von Kiedrowski, G. *Bioorg. Chem. Front.* **3**, 113-146 (1993).

Peptide Revolution: Genomics, Proteomics & Therapeutics
Michael Chorev & Tomi K. Sawyer (Editors)
American Peptide Society, 2003

Synthetic Expansion of the Central Dogma: Chemical Aminoacylation, 4-Base Codons and Nonnatural Mutagenesis

Masahiko Sisido

Department of Bioscience and Biotechnology, Okayama University,
3-1-1 Tsushimanaka, Okayama 700-8530, Japan

Introduction

The mechanism of protein biosynthesis can be divided into two routes: one for the flow of information from DNA to mRNA, the other for the flow of materials from amino acids to aminoacyl tRNA. The two routes encounter on a ribosome, where aminoacyl tRNAs are bound onto a mRNA with codon/anticodon pairing bringing the new amino acid close to the growing polypeptide chain. Since the process is common to every living organism on the earth and the molecules involved are so sophisticated, the biosynthetic mechanism has been thought to be an inaccessible process and was treated as the central dogma of biology. Until recently, only few researchers had been considering it realistic to expand the central dogma to include synthetic analogs of amino acids, nucleobases, and other components. During the past decade, however, the situation changed altogether. We have several types of DNA analogs that bind more strongly and more precisely to DNA of specific base sequences than the native DNA itself. We have an artificial pair of nonnatural nucleobases that are orthogonal to the existing pairs. We can charge a large variety of nonnatural amino acids onto the 3' end of tRNA by using chemical, biochemical, and biological ways. We can assign positions of nonnatural amino acids by artificial codon/anticodon pairs. Finally, we can expand protein functions by the introduction of specialty amino acids. These expansions made the central dogma an accessible and modifiable target by organic chemists who want to create new molecular systems in the living organisms.

In this paper, we will introduce our recent approaches along this line. Those include, (1) non-enzymatic aminoacylation of nonnatural amino acids onto tRNA molecules, (2) use of 4-base codon/anticodon pairs for assigning positions of nonnatural amino acids, and (3) examples of the nonnatural mutants that show specialty functions.

Non-Enzymatic and tRNA-Nonspecific Aminoacylation in Micellar Solutions

Aminoacylation of tRNA is the first key step for incorporation of a nonnatural amino acid into proteins. Hecht and coworkers have reported the first successful approach in early 1980's [1]. A revised version of the Hecht's method [2] consists of a chemical synthesis of a pdCpA dinucleotide that is aminoacylated with a specific amino acid, followed by the ligation the aminoacyl pdCpA with a tRNA that lacks 3'-terminal CA dinucleotide unit [tRNA(-CA)]. Although this is an excellent method that is applicable to any types of amino acids, it requires sophisticated organic synthesis for preparation and aminoacylation of pdCpA. Furthermore, we have recently found that the ligation of tRNA(-CA) with aminoacyl pdCpA with T4 RNA ligase gives cyclic tRNA(-CA) as a by-product and the latter works as an inhibitor in the *in vitro* protein synthesis [3]. Therefore, a simple and easy alternative has to be found for the non-enzymatic aminoacylation of tRNA.

Direct coupling of tRNAs with amino acid activated esters is the simplest route for aminoacylation. Since tRNA is not soluble in any organic solvents including ethanol,

and amino acid activated esters are soluble only in organic solvents, a special medium has to be found for the direct aminoacylation. Cationic micellar solution will be a promising medium for the aminoacylation because the cationic charges will increase local concentration of negatively charged tRNAs at the micelle surface and the micelle core may keep high local concentration of activated amino acid esters (Figure 1).

First we have examined aminoacylation of a model dinucleotide, pdCpA in a cetyltrimethylammonium chloride (CTACl) solution that solubilized N-pentenoyl-L-2-naphaylalanine cyanomethyl ester (Pen-napAla-OCM) [4]. When a mixture of pdCpA (2.5 mM), Pen-napAla-OCM (10 mM), and CTACl (18 mM) at pH8.0 was shaken for 1h at room temperature, more than 90% of pdCpA was aminoacylated. HPLC analysis indicated that the coupling took place specifically at the OH groups of A unit and not on the amino groups of the nucleobases. The aminoacyl pdCpA could be used as an intermediate for the aminoacylation by Hecht's method.

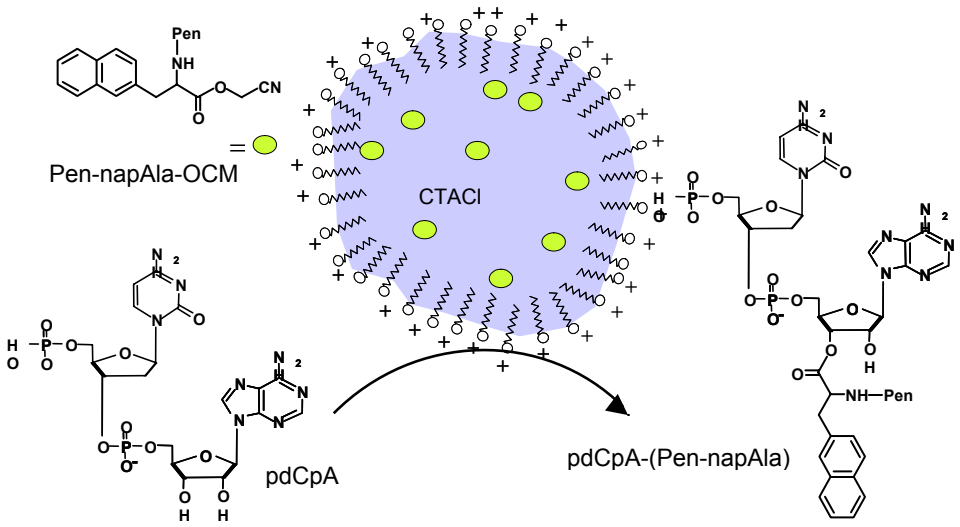

Fig. 1. Aminoacylation of pdCpA with an N-protected amino acid activated ester in cationic micellar solution.

Aminoacylation was also attempted in micellar solution of tRNA (Figure 2) [5]. When a mixture of tRNA (10 μM), Pen-napAla-OCM (5 mM), and CTACl (18 mM) was mechanically shaken at room temperature for 5 min, more than 50% of tRNA was aminoacylated. When the shaking was inefficient, no reaction took place. In this case, however, HPLC analysis did not give detailed information on the coupling positions. After removal of Pen-napAla-OCM, Pen-napAla-OH, and CTACl by extraction with phenol and chloroform, the tRNA was precipitated with ethanol. Then the latter was treated with nuclease S1 to decompose phosphodiester linkages. The resulting mixture was analyzed on HPLC to find the product distribution. More than 80% of the product was 3'(2')-N-pentenoyl-L-2-naphthylalanyladenosine monophosphate [AMP-(Pen-napAla)]; a digested product of successful aminoacylation of tRNA. About 10% of the product was CMP-(Pen-napAla) that must come from misaminoacylation of 2'-OH

group of C units of tRNA. Only very small amount of GMP-(Pen-napAla) and UMP-(Pen-napAla) was detected.

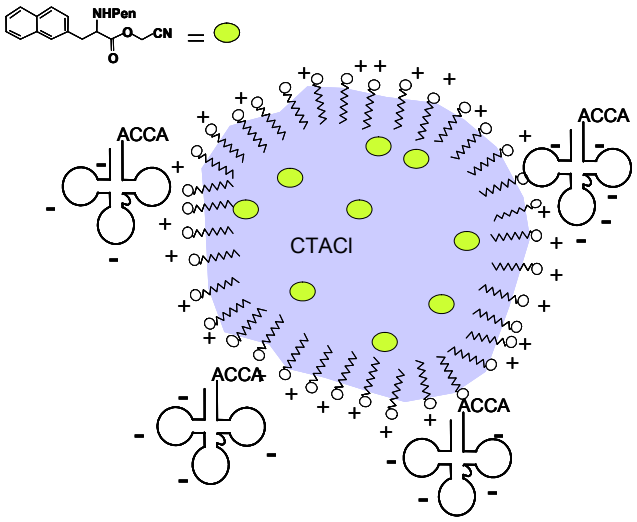

Fig. 2. Direct aminoacylation of tRNA with an N-protected amino acid activated ester in cationic micellar solution.

The HPLC analysis indicated that a major product of the direct coupling of tRNA with amino acid cyanomethyl ester in micellar solution was a correctly aminoacylated tRNA. Indeed, the aminoacyl tRNA gave a napAla mutant of streptavidin when it was added to an *E. coli in vitro* protein synthesizing system.

The direct aminoacylation in micellar solution is easy and reliable. The yields and the regio-selectivity to the 3'(2')-position of the terminal A unit will be improved by further optimization of the types of detergents, types of activated esters, and reaction conditions.

Non-Enzymatic but tRNA-Specific Aminoacylation through tRNA/DNA/PNA Ternary Hybrid

Aminoacylation in micellar solution is applicable only to isolated tRNAs in the test tube, because the micellar system cannot distinguish different types of tRNA molecules. If we want to carry out non-enzymatic aminoacylation in the *in vitro* and *in vivo* system where different types of tRNAs coexist, we have to distinguish tRNA molecules by some RNA-recognizing molecule. In nature, well-designed 3D structures of polypeptide chains bind specific tRNA molecules with high enough selectivity. But it is not easy, if not impossible, to screen new protein molecules that recognize a specific tRNA for a nonnatural amino acid.

We have adopted a complementary DNA molecule as the tRNA-recognizing molecule. Kanda and coworkers reported that a 23-mer DNA, which is complementary to the 3'-terminal region of tRNA, is long enough to recognize a specific tRNA molecule in the *E. coli* protein synthesizing system [6]. In our study, the 5'-end of the 23-mer DNA was extended by a 9 base sequence that is complementary to a 9-mer

peptide nucleic acid (PNA). At the N-terminal of the PNA, a nonnatural amino acid (2-naphthylalanine=napAla) is linked by a thioester linkage (tga) [7]. The base sequences of the tRNA, DNA, and PNA and the structure of ternary hybrid are shown in Figure 3. The ternary hybrid was actually detected in a gel-shift assay.

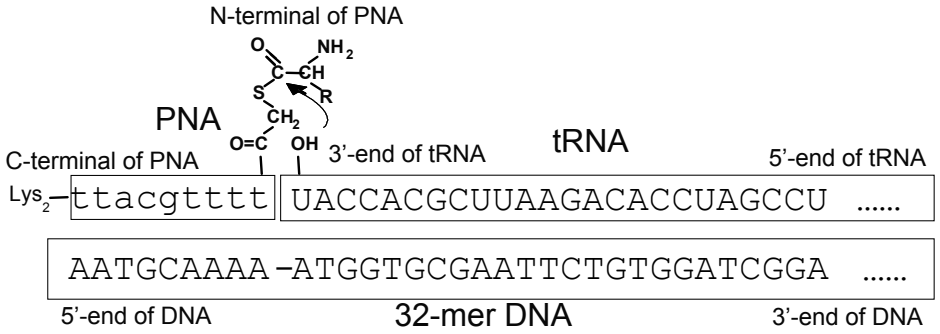

Fig. 3. Base sequences of tRNA, PNA, and bridging DNA that form a ternary hybrid.

The ternary hybrid in a mixture of tRNA (15 μM), the template DNA(22.5μM), and napAla-tga-PNA (22.5μM) was stored at pH7.5 at 20˚C for 1 h. Then the mixture was extracted twice with phenol and twice with chloroform to remove PNA. The RNA component was precipitated with 3 volume of ethanol at -30˚C. The yield of aminoacylation was about 9%. The aminoacylation took place only to OH groups at the 3' end. Indeed, the product of the aminoacylation worked to introduce a napAla unit into streptavidin (Figure 4).

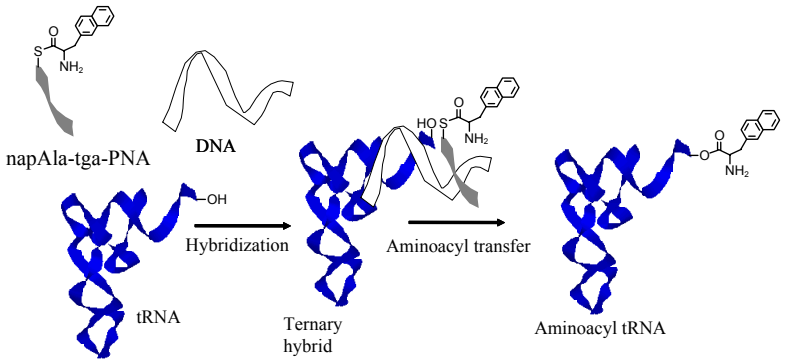

Fig. 4. Non-enzymatic aminoacylation through tRNA/DNA/PNA ternary hybrid.

Although the yield has to be improved, the non-enzymatic and tRNA-specific aminoacylation will find applications towards *in vivo* expression of mutant proteins that contain nonnatural amino acids at specific positions.

Four-Base Codon/Anticodon Pairs for Assigning Nonnatural Amino Acids

To introduce a nonnatural amino acid into a specific position on a protein, a unique codon/anticodon pair that is orthogonal to the existing codon/anticodon pairs is needed. Schultz's group and Chamberlin's group have been using amber stop codon (UAG) for this purpose. A disadvantage of the amber suppression method is that only single type

of nonnatural amino acid can be introduced into a single protein. An alternative way is to use 4-base codon/anticodon pairs that work in the *in vitro* system [8,9]. The principle of the 4-base strategy is illustrated in Figure 5. So far, CGGG, GGGU and AGGU have been found effective enough to produce high yields of the nonnatural mutants. Furthermore, they are orthogonal to the existing 3-base codon/anticodon pairs and to each other. This means that we can introduce, at least, up to three different types of amino acids into single proteins.

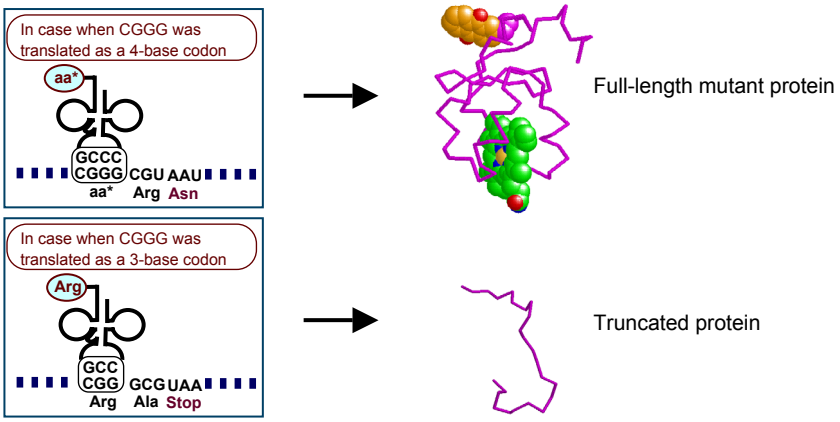

Fig. 5. Principle of 4-Base codon/anticodon strategy.

Efficient Synthesis of Nonnatural Mutant through *In Vitro* Protein Synthesizing System of *E. Coli*

In vitro (cell-free) protein synthesis is a simple, quick and versatile technique that enabled proteins synthesis within a few ten minutes. Efficiency of the protein production has been largely improved recently by optimizing reaction conditions and eliminating inhibitory factors. However, the protein yields of nonnatural mutants are still lower than the yields of proteins from the 20 naturally occurring amino acids. In particular, yields of nonnatural mutants that contain bulky amino acids are much lower than the wild-type protein. We have searched for factors that work as inhibitors of *in vitro* protein synthesis, especially, in the presence of aminoacyl tRNAs that were synthesized according to Hecht's method, i.e., ligation of aminoacyl pdCpA with tRNA(-CA) [3].

We found that protein synthesis was inhibited when a mixture of tRNA(-CA) and ligase was added to the *in vitro* system. The inhibitory effect was caused by a cyclic tRNA that was formed by an intramolecular ligation between the 5' phosphoryl end and the 3' hydroxyl end of tRNA(-CA). The same cyclic tRNA must be formed as a byproduct of the chemical aminoacylation of tRNA(-CA) with pdCpA-aa*. The inhibitory effect of cyclic tRNA became prominent about 10 min after the start of the *in vitro* synthesis, suggesting that the inhibitor accumulates onto ribosomes or other components in the protein synthesizing system.

Since the inhibition starts after 5 min, a practical way to increase yields of nonnatural mutants is to add fresh aminoacyl tRNA about 5 min after the start of the *in vitro* synthesis. As demonstrated in Figure 6, this was indeed effective to increase the yield of nonnatural mutants.

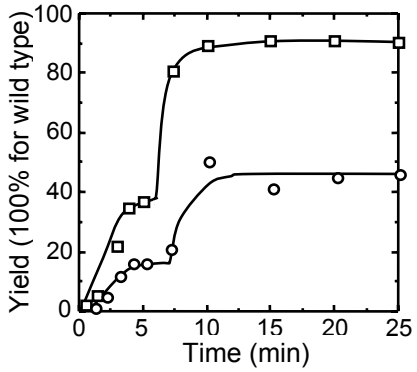

Fig. 6. Effect of the addition of fresh aminoacyl tRNAs at the early stage of E. coli in vitro protein synthesis of ^{83}2napAla mutant (open squares) and ^{83}1napAla mutant (open circles) of streptavidin.

Under the optimized conditions, we can synthesize about 1 μg quantity of a nonnatural mutant of streptavidin from 20 μL of commercial *E. coli* lysate (Promega). The yield is about 80% of the wild-type protein. As an example, TOF-mass spectra of wild-type and 83napAla-streptavidin are shown in Figure 7.

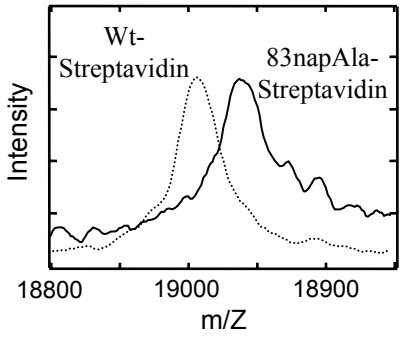

Fig. 7. TOF mass spectra of wild-type and ^{83}2napAla-streptavidin synthesized in E. coli in vitro protein synthesizing system.

Example of Nonnatural Mutagenesis: Introduction of a Fluorophore-Quencher Pair into a Single Protein

A pair of fluorescent amino acid (anthraniloyl-L-diaminopropionic acid = atnDap) and a quencher amino acid (*p*-nitrophenylalanine = ntrPhe) has been introduced by using orthogonal codon/anticodon pairs, CGGG/CCCG and GGGC/GCCC [10]. AtnDap was charged onto a $tRNA_{CCCG}$ and ntrPhe onto a $tRNA_{GCCC}$. Full length protein was produced when a mRNA that contain 54GGGC and 84CGGG 4-base codons was translated in the presence of atnDap-$tRNA_{CCCG}$ and $ntrPhe_{GCCC}$ (Figure 8). No full-length protein was detected when either of the two tRNAs was absent in the mixture.

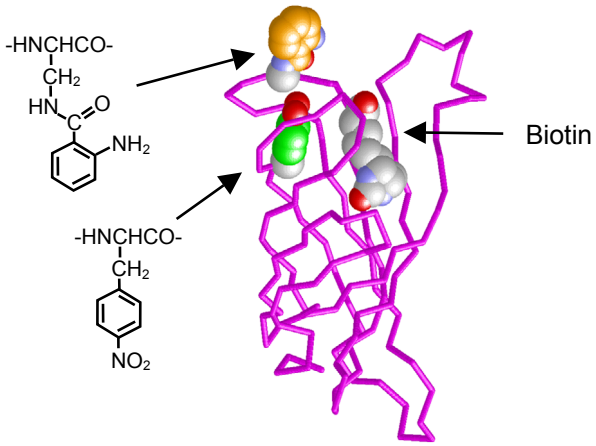

Fig. 8. Computer-predicted conformation of 54ntrPhe, 84atnDap-streptavidin with biotin.

The fluorescence of 84atnDap unit was quenched when an ntrPhe unit was introduced at position 54. Also fluorescence decay of anthraniloyl fluorescence was accelerated by the nitrophenyl group. The double mutant retained biotin-binding activity. These facts indicate that the double mutant takes conformation as predicted in Figure 8.

Conclusion

Easy and reliable aminoacylation and the 4-base codon/anticodon strategy combined with the efficient *in vitro* synthesis will make nonnatural mutagenesis a common tool for every chemist and biochemist. In particular, position-specific incorporation of fluorescent amino acids will find wide applications in the field of pharmaceutical chemistry.

Acknowledgment

This work has been supported by a Grand-in-Aid for Specially Promoted Research from the Ministry of Education, Science, Sports and Culture, Japan (No.11102003).

References

1. Heckler, T. G., Chang, L. H., Zama, Y., Naka, T., Chorghade, M. S. and Hecht, S. M. *Biochemistry* **23**, 1468 (1984).
2. Robertson, S.A., Ellman, J.A. and Schultz, P.G. *J. Am. Chem. Soc.* **113**, 2722 (1991).
3. Yamanaka, K, Hohsaka, T. and Sisido, M. *in preparation* (2003).
4. Ninomiya, K., Kurita, T., Hohsaka, T. and Sisido, M. *Chem. Commun*. 2242-2243 (2003).
5. Ninomiya, K., Endo, T., Hashimoto, N. and Sisido, M. *in preparation*.
6. Kanda, T., Takai, K., Yokoyama, S. and Takaku, H. *FEBS Lett.* **440**, 273 (1998).
7. Ninomiya, K., Suzuki, M., Hohsaka, T. and Sisido, M. *in preparation*.
8. Hohsaka, T., Ashizuka, Y., et al. *J. Am. Chem. Soc*. **118**, 9778 (1996).
9. Hohsaka, T., Ashizuka, Y., Taira, H., et al. *Biochemistry* **40**, 11060 (2001).
10. Taki, M., Hohsaka, T. and Sisido, M. *J. Am. Chem. Soc*. **124**, 14586 (2002).

Peptide Revolution: Genomics, Proteomics & Therapeutics
Michael Chorev & Tomi K. Sawyer (Editors)
American Peptide Society, 2003

Cytoplasmic Domain Of *E. coli* ProP Forms an Antiparallel Coiled-Coil as Determined by NMR Spectroscopy

David L. Zoetewey[1], Brian Tripet[2], Tatiana G. Kutateladze[2], Michael J. Overduin[2], Janet M. Wood[3] and Robert S. Hodges[1]

[1]Department of Biochemistry and Molecular Genetics and [2]Department of Pharmacology; University of Colorado Health Sciences Center, Denver, CO 80262, USA; [3]Department of Microbiology, University of Guelph, Guelph, ON N1G2W1, Canada

Introduction

Bacteria sense and respond to the osmolarity of their media through a variety of different proteins that can import and/or export inorganic ions or organic zwitterions to help adjust cellular osmolarity. One such protein used by *Escherichia coli* is ProP, which imports proline and glycine betaine [1]. The cytoplasmic extension was shown to be necessary for the ability of ProP to respond to osmotic up-shifts *in vivo* and to form a coiled-coil *in vitro* with some unusual properties [2]. In particular, the mutation R488I within the coiled-coil at a heptad **a** position in the hydrophobic core was destabilizing, in contrast to the stabilizing effect that was seen in model parallel coiled-coils [3]. This led to the prediction that the coiled-coil formed by the ProP cytoplasmic domain was in an antiparallel orientation rather than parallel. We used nuclear magnetic resonance (NMR) to determine the structure of the synthetic peptide corresponding to residues 468-497 of ProP and showed that this region does indeed form an antiparallel coil-coil. We also showed that the critical R488 plays an important role in specifying antiparallel orientation by the formation of stabilizing salt-bridges and that the topology created by the antiparallel orientation may be important in the role of osmosensing by ProP.

Results and Discussion

The antiparallel coiled-coil formed by the cytoplasmic domain of ProP contains some interesting features. First, R488 was shown to make salt bridges to two different Asp residues in the opposite strand, D478 and D475. Arginine has a relatively hydrophobic side-chain that is in the hydrophobic core and a charged guanidinium group that comes out of the core to make the charge-charge interactions and is more solvent-exposed (as seen in Figure 1).

Second, in an antiparallel coiled-coil there are two distinct surfaces. One is formed by residues in positions **b**, **e**, **b'**, and **e'** (**b**/**e** surface) and the other by residues in

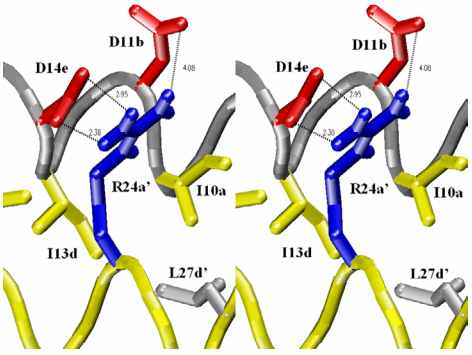

Fig. 1. Cross-eyed stereo view of critical R488a' and the putative hydrogen bonds made between it and residues D478e and D475b in the averaged structure. Only the protons of the guanidinium group of the arginine residue are shown. The nearby core residues, I477d, I474a and L491d' are also shown.

positions **c**, **g**, **c**', and **g**' (**c**/**g** surface). The ProP antiparallel coiled-coil contains a row of polar residues along the **b**/**e** surface (Figure 2b)) that may interact with polar solutes such as PEGs[4]. The **c**/**g** surface (Figure 2c)) contains three clusters of charges that may interact with various ionic solutes [4]. Furthermore, the unusual bent shape (Figure 2a)) may be a result of an unusual charge distribution caused by the high number of polar residues on the **b**/**e** surface compared to the charged **c**/**g** surface. We conclude that these features mentioned above may account for why ProP responds to osmolarity rather than any particular solute, and why the coiled-coil is necessary for the activation of ProP *in vivo* [2].

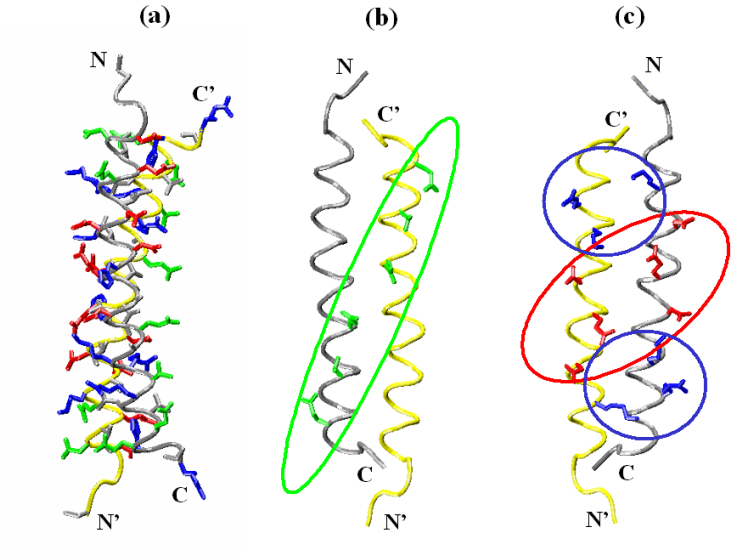

Fig. 2. Structural views of ProP cytoplasmic coiled-coil domain. (a) Side view of ProP peptide. Backbone atoms are colored as gray and yellow to distinguish between the two α-helices. Gray helix is labeled N and C while the yellow helix is labeled N' and C' throughout. Sidechains are colored by residue type: non-polar (gray), polar (green), basic (blue) and acidic (red). (b) View from (a) rotated 90° clockwise to show the prominent row of polar residues along the b/e surface. (c) View from (a) rotated by 90° counterclockwise along the coiled-coil axis to show the c/g surface. Basic residues (blue) and acidic residues (red) along this face that form three clusters with high local charge are highlighted.

Acknowledgments

This work was funded by the NIH-RO1GM61855 grant to R. S. Hodges and support from the University of Colorado Health Sciences Center.

References

1. Wood, J. M., Bremer, E., Csonka, L. N., Kraemer, R., Poolman, B., van der Heide, T., Smith, L. T., *Comp. Biochem. Physiol. A. Mol. Integr. Physiol*. **130**, 437-460 (2001).
2. Culham, D, E., Tripet, B., Racher, K. I., Voegele, R. T. Hodges, R. S., Wood, J. M., *J. Mol. Recognit.* **13**, 309-322 (2000).
3. Wagschal, K., Tripet, B., et al. *Protein Sci.* **8**, 2312-2329 (1999).
4. Culham, D. E., Henderson, J., Crane, R. A., Wood, J. M. *Biochemistry* **42**, 410-420 (2003).

Peptide Revolution: Genomics, Proteomics & Therapeutics
Michael Chorev & Tomi K. Sawyer (Editors)
American Peptide Society, 2003

De novo Design, Synthesis and Properties of Model Quinoproteins

Wenwu Li[1], Michaela Ritter[2], Petra Hellwig[2], Jürgen Heinze[3] and Wolfgang Haehnel[1]

[1]Institut für Biologie II / Biochemie, Albert-Ludwigs-Universität Freiburg, Schänzlestr. 1, D-79104 Freiburg, Germany; [2]Institut für Biophysik, Johann Wolfgang Goethe-Universität Frankfurt, Germany; and [3]Institut für Physikalische Chemie, Albert-Ludwigs-Universität Freiburg, Germany

Introduction

Quinones are ubiquitous in bacteria, plants and animals, with a wide variety of functions. The three classes of *p*-quinone, ubiquinone, menaquinone and plastoquinone, are essential components in membrane bound electron transfer reactions and conversion of redox energy to a H^+ gradient for ATP synthesis. Important redox cofactors of a newly discovered kind for electron transfer and catalysis in quinoenzymes are *o*-quinones including the non-covalently bound pyrroloquinoline quinone and the covalently bound topaquinone, lysine tyrosylquinone, tryptophan tryptophylquinone, and cysteine tryptophylquinone (CTQ) [1]. In addition, some quinones play important roles in medical use, in contrast, some other quinones exert cytotoxic effects because of their covalent binding to cellular thiols [2].

In order to mimic the functions of natural quinones in a protein matrix and to study the interaction between quinones and amino acids, it is of considerable interest and challenge to construct model quinone-protein systems. Recent advances in *de novo* design and synthesis of proteins have opened new directions in the creation of working models for proteins [3]. Most of the *de novo* proteins are based on the hydrophobic association of amphiphilic helices. Four-helix bundles have been successfully used for the incorporation of biological redox cofactors [3]. Template assembled synthetic proteins (TASP) [4] have been used to construct antiparallel four-helix bundle proteins with different cofactors [5]. The TASP or *modular proteins* (MOP) should also provide a suitable scaffold for an incorporation of the cofactor quinone. In a similar manner as natural CTQ of the quinoenzyme [1], we have bound a single molecule of ubiquinone 0 (UQ_0) or menaquinone 0 (MK_0) to a cysteine positioned within the hydrophobic core of the four-helix bundle protein. Here we present the design, synthesis, and properties of these quinoproteins.

Results and Discussion

The strategy of binding quinones to proteins is important to create quinoproteins. Although quinone binding sites in respiratory and photosynthetic systems [6] are known, to mimic such a pocket for stable quinone binding is not yet possible by de novo design. We turn to covalently binding quinones as those in quinoenzymes. We have tried several approaches to bind quinones to peptides or proteins; finally only the thiol addition and substitution to quinones which was attributed to the mechanisms for the toxicity of quinones [2] allows us to create model quinoproteins.

The scaffold of protein is a four-helix bundle based on TASP. The assembly of four antiparallel amphipathic α-helices [two shielding helices H2 of the same kind (N→C), and two different binding helices, H1 and H3 (both with C→N orientation)] on a cyclic decapeptide template was designed as previous MOPs [5]. The sequences of the template and the three different helices are as follows:

Template: $T(StBu)_2(Trt)(Acm)$, cyclo[C(Acm)-A-C(StBu)-P-G-C(Trt)-A-C(StBu)-P-G-]
H1: Mp-G-N-A-C(Acm)-E-E-L-A-K-K-H-Q-E-L-A-E-K-L-Q-K-W-$CONH_2$;
H2: Ac-N-L-E-Q-F-E-K-A-L-K-Q-G-E-E-L-A-K-K-L-A-K(Mp)-$CONH_2$;
H3: Mp-G-N-A-L-E-E-L-A-K-K-H-Q-Q-L-A-E-A-L-Q-K-L-$CONH_2$.
(Abbreviations: Mp, 3-maleimidopropionyl; Sp, 3-succinimidopropionyl)

The Cys-4 of H1 protected by Acm for covalently binding natural quinone analogues is positioned at the hydrophobic face in order to locate the quinones within the hydrophobic core of the four-helix bundle proteins. The synthesis of building blocks and assembly of four-helix bundle $T(Sp\text{-}H2)_2(Sp\text{-}H3)(Sp\text{-}H1\text{-}Acm)$ was accomplished in a similar manner as previous MOPs [5]. After cleavage of the Acm group from Cys-4 of H1 to give MOP with one free thiol group, UQ_0 and MK_0 added in excess were chemoselectively coupled to form UQ-MOP and MK-MOP, respectively (Figure 1). The detected masses by ESI-MS of the quinoproteins verify the correct primary structures and the spectra show the high purity of the proteins.

The UV-vis absorption spectra show the binding of quinones to proteins. The CD spectra of UQ-MOP and MK-MOP are consistent with the helical structure as designed. The ^{1}HNMR of UQ-MOP indicates the interaction and effect between quinone and the protein. Size exclusion chromatography demonstrates the presence of only monomer of UQ-MOP and 80 % MK-MOP as monomer as well as 20% as dimer. This difference may result from the larger group of MK in comparison with UQ. The redox potentials of quinones and their model N-acetyl cysteine or N-acetyl cysteine methyl ester bound quinones have been compared by the means of cyclic votammetry in both organic solvents and aqueous buffers. They show the similar redox mechanism and minor difference in redox potentials. The redox induced FT-IR spectra of these model quinones and quinoproteins also show the interactions between the quinone molecules and protein matrix.

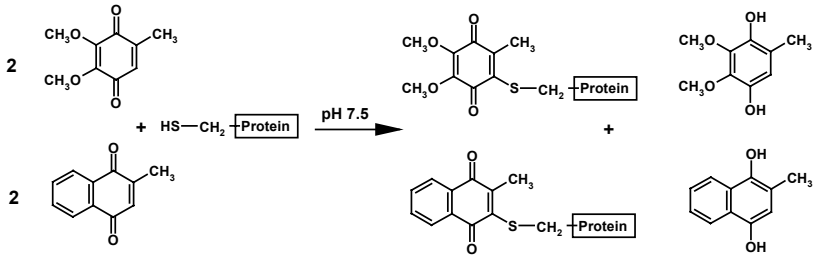

Fig. 1. A scheme of reaction between quinones and proteins.

Acknowledgements
Support from the Volkswagen-Stiftung is gratefully acknowledged. We thank Patric Hörth for the measurements of the mass spectra and Christa Reichenbach for technical assistance.

References

1. Datta, S., et al. *Proc. Natl. Acad. Sci. U.S.A*. **98**, 14268-14273 (2001).
2. Guo, Q., et al. *J. Biol. Chem*. **277**, 6104-6110 (2002).
3. DeGrado, W. F. *Chem. Rev*. **101**, 3025-3232 (2001).
4. Mutter, M., et al. *Helv. Chim. Acta* **71**, 835-847 (1988).
5. Rau, H. K. and Haehnel, W. *J. Am. Chem. Soc.* **120**, 468-476 (1998).
6. Iwata M., Abramson J., Byrne B. and Iwata S. *Adv. Protein Chem*. **63**, 151-176 (2003).

Protease and Enzyme Substrate/Inhibitor Structure-Function

Peptide Revolution: Genomics, Proteomics & Therapeutics
Michael Chorev & Tomi K. Sawyer (Editors)
American Peptide Society, 2003

Different Approaches to Inhibit the Chymotrypsin-Like Activity of the 20S Proteasome

Pascal Furet, Patricia Imbach, Carlos García-Echeverría, Marc Lang, Johannes Roesel, Maria Noorani, Johann Zimmermann, Peter Fuerst and Vito Guagnano

Oncology Research, Novartis Institute for Biomedical Research, CH-4002 Basel, Switzerland

Introduction

The 20S proteasome is an *N*-terminal threonine protease that exhibits at least three distinct peptidase activities: chymotrypsin-like, trypsin-like, and post-glutamyl-peptide hydrolytic activities. This multicatalytic protease complex is involved in the degradation and turnover of a variety of intracellular proteins, and inhibitors of this enzyme are currently being explored as therapeutic agents applicable as anti-inflammatory agents and for the treatment of cancer and autoimmune diseases.

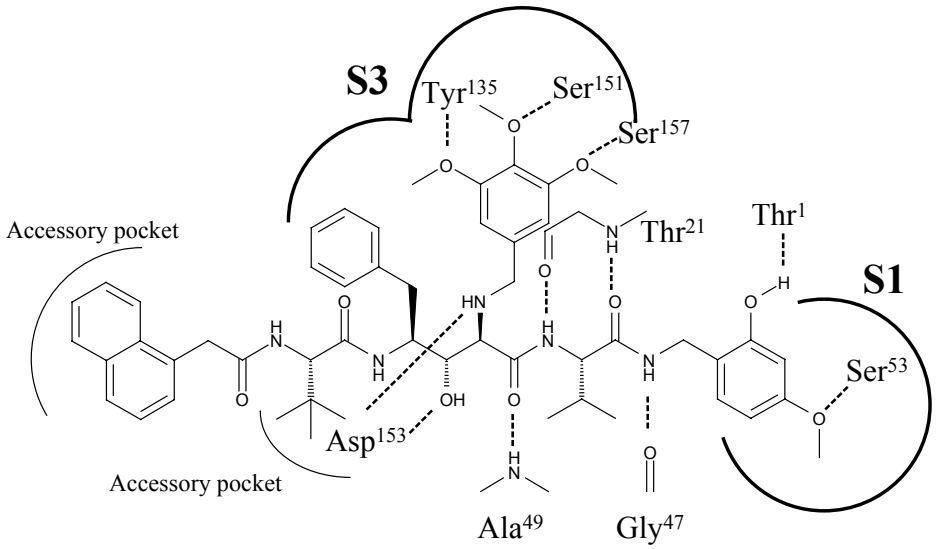

Fig. 1. A representative example of a structural class of non-covalent inhibitors of the 20S proteasome. This 2-aminobenzylstatine derivative inhibits the chymotrypsin-like activity of the 20S proteasome with an IC_{50} value of 7 nM, and shows at least 200-fold selectivity over the trypsin-like and post-glutamyl-peptide hydrolytic activities [2]. This figure also shows the most relevant interactions of the inhibitor with the enzyme as determined by molecular modeling.

Our specific target in the search for novel cytotoxic and antiproliferative agents is the chymotrypsin-like activity of the 20S proteasome. Recently, we have reported the identification and optimization of non-covalent inhibitors of the preceding hydrolytic site (Figure 1) [1-3]. To identify other potential classes of inhibitors, we have exploited our structural model of the human proteasome [4] to design covalent and non-covalent

inhibitors. These compounds show high potency and selectivity against the chymotrypsin-like activity of the 20S proteasome in *in vitro* enzyme assays, and inhibit the proliferation of different tumour cell lines with IC_{50} values in the low nanomolar range. We describe herein the *in vitro* and *in vivo* characterization of a new series of boronic acid derivatives.

Results and Discussion

Peptide boronic acids have been extensively used as serine protease inhibitors. In these enzymes, the active-site serine forms a covalent, nearly tetrahedral adduct with the boronic acid of the inhibitor [5]. This war-head group has also been used by different groups to block the 20S proteasome [6], and one of these inhibitors (bortezomib, Millenium Pharmaceutical Inc.) [7] has recently received approval from the U.S. FDA for the treatment of multiple myeloma. To expand our ongoing activities with non-covalent inhibitors of the 20S proteasome, we also decided to explore the possibility of using boronic acids in our drug discovery endeavor for this therapeutic target.

The optimization of the 2-aminobenzylstatine template highlighted the importance of a set of hydrophobic and hydrogen bond interactions with key amino acids of the 20S proteasome (Figure 1). The SAR data obtained during this work [1-3] was exploited to guide the structure-based design of boronic acid derivatives. A representative example of the compounds identified following this strategy is shown in Figure 2. According to our homology model of the X/HC5 binding site of the human 20S proteasome [4], the leucine side-chain of compound 1 occupies the S1 pocket and the phenylalanine moiety fills the S3 pocket. The *N*-terminal biphenyl group was designed to reach an accessory hydrophobic binding pocket formed by residues Pro-131, Pro-154 and Val-155. The van der Waals contacts mediated by these groups are complemented by a set of hydrogen bond interactions. The amide bonds flanking the valine residue of the inhibitor form in a β-sheet manner hydrogen bonds with the backbone of residues Thr-21, Gly-47 and Ala-49, while the 4-methoxy group of phenylalanine interacts with the side-chain of Ser-151 at the bottom of the S3 pocket. These interactions together with the covalent bond between the *C*-terminal boronic acid and the catalytic threonine residue account for the ability of compound 1 (Figure 2) to potently inhibit the 20S proteasome (IC_{50}= 3.1 ± 0.4 nM, 165 ± 24 nM and 93 ± 22 nM for the chymotrypsin-like, trypsin-like, and post-glutamyl-peptide hydrolytic activities, respectively). The larger size of the S3 pocket of the chymotrypsin-like site in comparison with the other catalytic sites was exploited to further modulate the β-subunit enzymatic selectivity of these covalent inhibitors. Replacement of 4-methoxy-phenylalanine by 3,4-dimethoxy-phenylalanine and 3,4,5-trimethoxyphenylaline did not affect the chymotrypsin-like 20S proteasome inhibitory activity of this class of compounds (IC_{50}= 3.6 ± 0.3 nM and 2.4 ± 0.2 nM, respectively), but improved its selectivity profile against the other two proteolytic sites (IC_{50}= 4.4 ± 1.2 μM and 6.3 ± 0.5 μM for the trypsin-like activity, and IC_{50}= 0.18 ± 0.04 μM and 2.44 ± 0.02 μM for the post-glutamyl-peptide hydrolytic activity, respectively).

To determine its *in vitro* selectivity profile, compound 1 was also tested against a panel of proteolytic enzymes. In these biochemical assays, the IC_{50} values for compound 1 were generally at least 300-fold higher than those for 20S proteasome [e.g., IC_{50} values of: > 1 μM for cathepsin K; > 10 μM for cathepsin L/S and complement activating enzyme (C1s); > 25 μM for thrombin; > 100 μM for post-proline cleaving enzyme (PPCE) and peptidyl peptidase IV (DPP-IV)]. However, it should be noted that compound 1 is also a potent inhibitor of calpain (IC_{50}= 15 ± 2 nM) and chymotrypsin (IC_{50}= 0.2 ± 0.05 μM).

Compound 1 blocked the intracellular 20S proteasome chymotrypsin-like activity of PC3 tumour cells with an IC_{50} value of 1.3 ± 0.5 nM, and inhibited the proliferation of lung (e.g., A549, NCI-H460), colon (e.g., HCT116, HCT15), prostate (e.g. Du145, PC3M) and breast (e.g., MBA-MD231, MCF7) tumour cells with IC_{50} values in the range between 17 nM (HCT116) to 220 nM (HCT15).

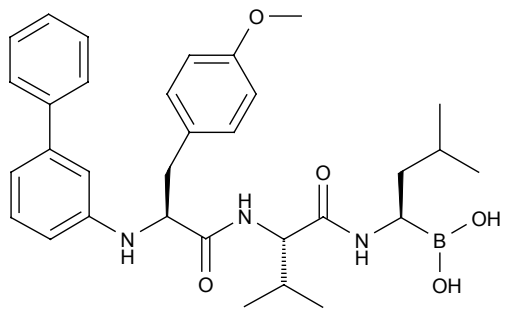

Compound 1

Fig. 2. A representative example of a new class of covalent-inhibitors of the 20S proteasome.

The *in vivo* efficacy of compound 1 was studied using a subcutaneous xenograft model. After implantation into the hind flank region of athymic mice (male BALB/c mice), PC3 tumours were allowed to grow to a size of ≅ 100 mm^3 before starting treatment. Compound 1 was administered i.v. (5 mg/Kg, 2x/week) for 21 days. On the basis of caliper measurements, compound 1 shows a statistically significant antitumour effect with a T/C value of 27 %. *Ex-vivo* analyses of tumour tissues after this efficacy study showed a statistically significant reduction (≅ 70 %) of the intracellular 20S proteasome proteolytic activity.

Acknowledgments
The authors thank M. D'Addio, S. Kläusler, J.-M. Groell, C. Radoch, L.-K. Phng, D. Arz, R. Wille, V. von Arx, W. Beck and E. Boss for their technical assistance.

References

1. García-Echeverría, C., Imbach, P., et al. *Bioorg. Med. Chem. Lett.* **12**, 1317 (2001).
2. Furet, P., Imbach, P., Fuerst, P., Lang, M., Noorani, M., Zimmermann, J. and Garcia-Echeverria, C. *Bioorg. Med. Chem. Lett*. **12,** 1331 (2002).
3. García-Echeverría, C., Imbach, P., Roesel, J., Fuerst, P., Lang, M., Guagnano, V., Noorani, M., Zimmermann, J. and Furet, P. *Chimia* **57**, 179 (2003).
4. Furet, P., Imbach, P., Fuerst, P., Lang, M., Noorani, M., Zimmermann, J. and García-Echeverría, C. *Bioorg. Med. Chem. Lett.* **11**, 1321 (2001).
5. For a representative example, see: Coutts, S. J., Kelly, T. A., Snow, R. J., Kennedy, C. A., Barton, R. W., Adams, J., et al. *J. Med. Chem.* **3.**
6. García-Echeverría*,* C. *Mini Rev. Med. Chem.* **2**, 247 (2002).
7. Adams, J. *Drug Disc. Today* **8**, 307 (2003).

Peptide Revolution: Genomics, Proteomics & Therapeutics
Michael Chorev & Tomi K. Sawyer (Editors)
American Peptide Society, 2003

Synthesis and Evaluation of Phosphonopeptide Cathepsin C Inhibitors

Paweł Kafarski[1,2], Marcin Drąg[1], Łukasz Berlicki[1] and Małgorzata Pawełczak[2]

[1]Institute of Organic Chemistry, University of Technology, Wybrzeże Wyspiańskiego 27, 50-370 Wrocław, Poland; [2]Institute of Chemistry, University of Opole, ul. Oleska 48, 45-052 Opole, Poland

Introduction

Cathepsin C (EC 3.4.14.1), known also as dipeptidyl aminopeptidase I (DPPI), dipeptidyl transferase or cathepsin J, is a lysosomal cysteine peptidase belonging to papain family [1]. It has been found in a variety of tissues in the human body, with the richest sources of this enzyme being spleen and kidney [2]. Cathepsin C catalyzes the removal of dipeptides from the unblocked N-terminus of proteins and peptides showing significant specificity towards PheGly and PheAla dipeptidyl fragment. Cathepsin C plays a key role in the activation of granule serine peptidases, which are involved in inflammation, cell-mediated apoptosis and tissue remodelling [3]. Thus, it is believed that inhibitors of this enzyme might be useful as possible drugs against rheumatoid arthritis and muscular dystrophy, as well as inhibitors of certain tumour metastases [4]. In addition, it is involved in neuroamidase activation and platelet factor XIII activation [5,6].

Tetrahedral geometry of pentavalent phosphorus is widely exploited as mimicking the tetrahedral intermediate in peptide bond hydrolysis, and thus organophosphonates serve as transition-state analogues of proteases. In many cases peptides containing phosphonate or phosphinate groups in the place of scissile peptide bond rank among the best inhibitors. To our best knowledge there are only two literature reports on the use of organophosphonates as inhibitors of cysteine proteases, namely on moderate inhibitory activity of simple phosphono peptides against cathepsin C and on moderate inhibitors of calpain I by dipeptides containing C-terminal dimethyl 2-amino-1-oxophoalkanesphonates (designed as bioisosteres of peptide ketones) [7,8]. Here we report the first succesful example of the use of this approach for the synthesis of potent inhibitors of cysteine proteases. Our strategy is based on the synthesis of phenylalanylglycine analogues and encompasses all requirements for competitive inhibitors of dipeptidyl aminopeptidase I reported earlier, namely the presence of N-terminal L-amino acids (stereochemical specificity), a free amino group at N-terminus the inhibitor-protein interaction of the peptide, and blocked C-terminal carboxyl group. In our case the latter one was replaced by phosphonate moiety.

Results and Discussion

The representative synthetic route for dipeptidyl 1-amino-2-hydroxyphosphonates is outlined in Scheme 1. The obtained compounds were mixtures of two diastereomers: (SSS) and (SSR) in the case of derivatives of 2-(L-phenylalanyl)amino-1-hydroxyetahnephosphonic acid and (SS) and (SR) in the case of derivatives of 2-(L-phenylalanyl)amino-1-hydroxymethanephosphonic acid. During addition of dialkyl phosphite to aldehydes 1 derived from L-phenylalanyl-L-alanine the formation of (SSS) diastereomer was privileged (72-92% de), whereas in the case of reaction with

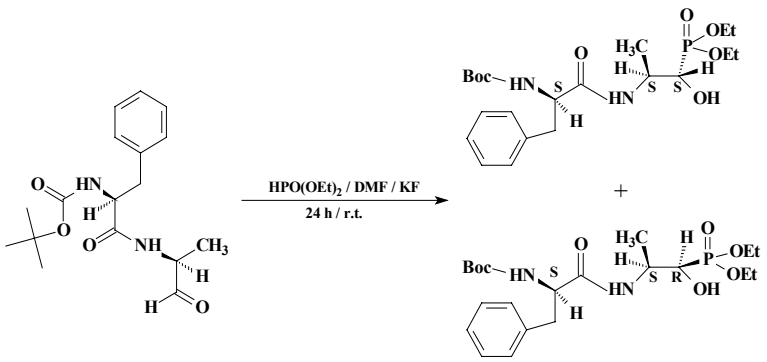

Scheme 1. Synthetic route for dipeptidyl 1-amino-2-hydroxyphosphonates.

L-phenylalanylglycinal the formation of equimolar mixture of both diastereomers was observed.

As shown in Scheme 2, the blocking groups were removed by a combination of standard methods and used in phosphonopeptide chemistry, affording the desired phosphonopeptide inhibitors of cathepsin C.

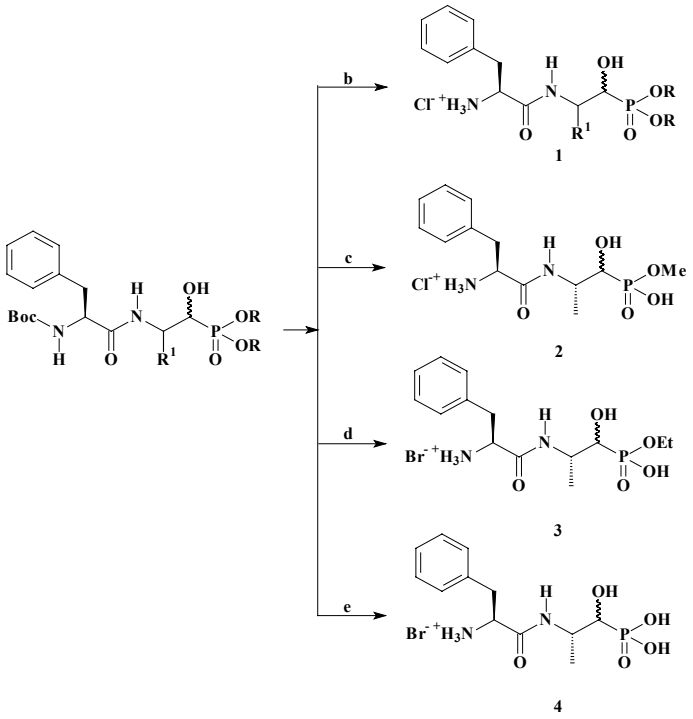

Reagents: (a) DMF/KF; (b)HCl/MeOH; (c) KI/acetone, HCl/MeOH;
(d) 1 eq. (CH3)3BrSi/CH_2Cl_2, MeOH; (e) 8 eq. $(CH_3)_3BrSi/CH_2Cl_2$, MeOH.

Scheme 2. Methods to deprotect phosphonate esters.

Table 1. The binding affinities of phosphonopeptides towards cathepsin C.

Phosphonopeptide	Ratio of stereoisomers	K_i (μM)
1; R = Et; R^1 = H	50:50	0.023
1; R = Me; R^1 = CH_3	50:50	174
1; R = Et; R^1 = CH_3	80:20	250
2	78:22	0.051
3	92:8	54.9
4	90:10	87.1
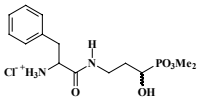	50:50	416
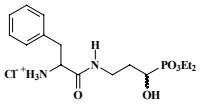	50:50	20

K_m for the synthetic substrate, GlyPhe-p-nitroanilide, is equal 2.24 mM.

The obtained compounds appear to be a new class of very promising inhibitors of cathepsin C from bovine spleen (Table 1). They also seem to be reversible, competitive and slow binding inhibitors of the enzyme, with the equilibrium in the inhibitor binding reached within several minutes after addition of cathepsin C to the mixture of inhibitor and substrate. To our best knowledge the binding affinities of the two strongest inhibitors towards the enzyme rank amongst the highest, if considering all low-molecular compounds. This suggests that the application of compounds containing phosphorus atom mimicking the transition state of the reaction catalysed by cysteine proteases might be considered as a promising method for designing new inhibitors of these enzymes. Molecular modelling of the inhibitor-protein interaction by application of the method implemented in the Ludi program [9] indicated that there is practically no stereochemical preference towards α-hydroxyl group of the inhibitor.

Acknowledgments
The work was supported by Komitet Badań Naukowych.

References

1. Rawlings, N. D. and Barrett, A. J. *Biochem. J.* **290**, 205-218 (1993).
2. Dahl, S. W. et al. *Biochemistry* **40**, 1671-1678 (2001).
3. Pham, C. T. and Ley, T. J. *Proc. Natl. Acad. Sci. U.S.A.* **96**, 8627-8632 (1999).
4. Katanuma, N. and Kominami, E. *Rev. Physiol. Biochem. Pharmacol.* **108**, 1-20 (1987).
5. D'Agrosa, R.M. and Calalhan, J.W. *Biochem. Biophys. Res. Commun.* **157**, 770-775 (1988).
6. Lynch, G.W. and Pfueller, S.L. *Thromb. Haemost*. **59,** 372-377 (1988).
7. Pawelczak, M. et al. *Phosphorus, Sulfur and Silicon* **132**, 65-71 (1998).
8. Tao, M. et al. *Biochemistry* **14**, 5249-5252 (1975).
9. Bohm, H. J. *J. Comput. Aided Mol. Des.* **6**, 593-606 (1992).

Peptide Revolution: Genomics, Proteomics & Therapeutics
Michael Chorev & Tomi K. Sawyer (Editors)
American Peptide Society, 2003

Cyclic Peptide Inhibitors of α-Amylase Based on Tendamistat

Leena Khullar, Steve M. Fernandes, James M. Waner, Elizabeth J. Blaney, Dennis A. Brown and Deborah L. Heyl

Department of Chemistry, Eastern Michigan University, Ypsilanti, MI 48197, USA

Introduction

Tendamistat is a tight-binding, pseudo-irreversible inhibitor of mammalian α-amylases with a K_I value of 9 x 10^{-12} M [1,2]. The crystal structure of the α–amylase-Tendamistat complex has been elucidated by X-ray techniques and nuclear magnetic resonance spectroscopy [3, 4], revealing that only 15 of the 74 amino acids in the inhibitor, in 4 segments, actually interact directly with the enzyme binding site via hydrogen bonding and hydrophobic and electrostatic forces [5]. The triplet of segment one, Tyr^{15} Trp^{18} Arg^{19} Tyr^{20}, forms a β-turn, with the positively charged side chain of Arg sandwiched between the aromatic side chains of Trp and Tyr and projected outward where it can interact with the active site. K_I values in the micromolar range have been reported for analogues consisting of various-sized pieces of Tendamistat containing the Trp-Arg-Tyr triplet, capped at either end with a Cys and cyclized via a disulfide bond [6,7]. Our goal was to design small conformationally restricted analogues of Tendamistat containing the essential segment one residues, which might be less immunogenic than the large protein.

Results and Discussion

The sequences of analogues I-VI are shown in Figure 1. Analogues II, III, V and VI were conformationally restricted via disulfide bond formation between Cys or Pen residues flanking the triplet, which replaced Ser residues of the natural sequence. Oxidation/cyclization was accomplished by treatment with 5% carbon tetrachloride in dichloromethane in the presence of tetrabutylammonium fluoride (TBAF) [8]. These were compared to the analogous linear Ser-containing peptides (I and IV). *D*-Pro was included in IV-VI to induce a bend in the structure. The ends were capped to avoid interaction of unnatural proximate charges.

I: Ac-YQSWRYSQ-NH_2
II: Ac-YQCWRYCQ-NH_2 disulfide
III: Ac-YQCWRY-Pen-Q-NH_2 disulfide
IV: Ac-YQSWRY-*D*-Pro-SQ-NH_2
V: Ac-YQCWRY-*D*-Pro-CQ-NH_2 disulfide
VI: Ac-YQCWRY-*D*-Pro-Pen-Q-NH_2 disulfide

Fig. 1. Sequences of peptide inhibitors I-VI; Pen=penicillamine (β,β-dimethylcysteine).

Mean V_{max} and K_m values for α-amylase in our assay system were 1.65 x 10^{-5} M/min and 12.1 mM, respectively. For I, IV, V and VI, visual observation provided clear qualitative evidence of enzyme inhibition, as tubes containing the inhibitor were distinctively less yellow in color than the tubes without inhibitor. These analogues generally inhibited the enzyme weakly with K_I values in the 100 to 300 micromolar range and exhibited 24-30% inhibition when [S]~K_m (Table 1). The mode of inhibition appeared to be competitive, indicating that the analogues interact at the

Table 1. Physicochemical and kinetic data[a] for peptide inhibitors.

Compound	Mol. Wt.	Purity[b] (%)	K_I (μM)	Mean Percent Inhibition[c]
I	1158	99	322	23
II	1188	99	---[d]	-24[d]
III	1216	99	---[d]	-2[d]
IV	1255	99	106	30
V	1285	99	237	24
VI	1313	99	753	9

[a]Determined from rate of cleavage of p-nitrophenyl-α-D-maltoside by porcine pancreatic α-amylase, monitored at 405 nm over 5 min.; HEPES buffer, pH 7.2; 30°C. [b]Purity of final product peptide as assessed by RP-HPLC peak integration at 214 nm. [c]% inhibition=1-(rate of inhibited reaction/rate of uninhibited reaction) when [S]=10 mM. [d] Increase in enzymatic rate observed.

active site of the enzyme. Results suggest that there is no advantage afforded by cyclization of inhibitors in this series. In fact, preliminary data indicate that cyclic analogues II and III (which do not contain *D*-Pro) are ineffective as inhibitors and, unexpectedly, reaction rates were slightly higher in the presence of these compounds. This effect is under investigation. Inclusion of *D*-Pro in the sequence resulted in better inhibitory activity over corresponding analogues lacking this amino acid. In addition, analogues in which Pen was incorporated at one position rather than Cys showed lower activity, perhaps due to the additional steric constraint imposed by the β-methyl groups. Studies with these and related analogues are underway at several different inhibitor, substrate and enzyme concentrations to further characterize the nature of the enzyme-inhibitor interaction.

Acknowledgments

This work was supported by PRF Grant 34911-B4 from the American Chemical Society, an EMU Faculty Research Fellowship and Graduate School Support Awards.

References

1. Aschauer, H., Vertesy, L., Nesemann, G. and Braunitzer, G. *Hoppe-Seyler's Z. Physiol. Chem*. **364**, 1347-1356 (1983).
2. Vertesy, L., Odeing, V., Bender, R., Zepf. K. and Nesemann, G. *Eur. J. Biochem*. **141**, 505-512 (1984).
3. Pflugrath, J.W., Wiegand, G., Huber, R. and Vertesy, L. *J. Mol. Biol.* **189**, 383-386 (1986).
4. Kline, A.D., Braun, W. and Wuthrich, K. *J. Mol. Biol*. **204**, 675-724 (1988).
5. Wiegand, G., Epp, O. and Huber, R. *J. Mol. Biol*. **247**, 99-110 (1995).
6. Ono, S., Umezaki, M., Tojo, N., Hashimoto, S., Taniyama, H., Kaneko, T., Fujii, T., Morita, H., Shimasaki, C., Yamazaki, I., Yoshimura, T. and Kato, T. *J. Biochem*. **129**, 783-790 (2001).
7. Ono, S., Hirano, T., Yasutake, H., Matsumoto, T., Yamaura, I., Kato, T., Morita, H., Fujii, T., Yamazaki, I., Shimasaki, C. and Yoshimura, T. *Biosci. Biotechnol. Biochem*. **62**, 1621-1623 (1998).
8. Maruyama, T., Ikeo, T. and Ueki, M. *Tet. Lett*. **40**, 5031-5034 (1999).

Peptide Revolution: Genomics, Proteomics & Therapeutics
Michael Chorev & Tomi K. Sawyer (Editors)
American Peptide Society, 2003

Betaine-Homocysteine Methyltransferase from Rat Liver: Purification and Inhibition by a Boronic Acid Substrate Analog

Payman Amiri, Mark Cava[1], Kyung-Hee Lee, Robert N. Lindquist and Tom Ottoboni

San Francisco State University, Department of Chemistry and Biochemistry, 1600 Holloway, San Francisco, California 9413; [1]RSP Amino Acids LLC, 87 Squannacook Road, Shirley, MA, 01464, USA

Introduction

Betaine-homocysteine methyltransferase (BHMT, EC 2.1.1.5) [1] and 5-methyltetrahydrofolate-homocysteine transmethylase (methionine synthetase, EC 2.1.1.13) catalyze the biosynthesis of methionine from homocysteine and betaine. The interconversion of homocysteine and methionine has been shown to be one of the key reactions at a major regulatory locus for methionine metabolism in rat liver. Methionine, while a key methyl donor in the biosynthesis of S-adenosylmethionine also serves as a precursor to cysteine via transsulfurization pathways. In addition to the role of BHMT in methionine biosynthesis, the utilization of betaine by BHMT is obligatory in the catabolism of choline in mammalian tissues [2].

Since a purified preparation of rat liver BHMT is desirable for enzyme kinetic and mechanistic studies, one of the goals of this study was to develop an efficient purification of the enzyme using FPLC chromatofocusing. A second goal was to synthesize a boronic acid analog of betaine as an inhibitor for BHMT. Because of the long history of the boronic acid group as an effective inhibitor and the reported synthesis of trimethylamine (N-B)-borane carbohydroxamic acids, compounds with significant pharmacological activity [3], we synthesized the boronic acids of N-methylated glycines for kinetic and inhibition studies of the purified BHMT.

Results and Discussion

A 170-fold purification was achieved by FPLC chromatofocusing of size exclusion fractions (Table 1). The most active form was dialyzed and used for kinetic studies.

Table 1. Purification of betaine-homocysteine methyltransferase from rat liver.

Step	Protein (mg)	Spec. Activity (units/mg)	Total Activity (units)	Purification Factor	% Recovery
Rat LH	4050	6.8	2.8×10^4	1	100
Heat Treat	640	27	1.7×10^4	4	61
Gel Filtration	67	170	1.1×10^4	25	40
Chromatofocusing	0.83	1120	9.3×10^2	170	3.4

The stability of purified BHMT was enhancement by the addition of 1 mM dimethylglycine and 1 mM homocysteine (Table 2). It was found that there was virtually no loss of activity during the first 2 weeks of storage at -20ºC. These results indicate that including dimethylglycine and homocysteine in the purification would be beneficial.

A new enzyme assay was developed based on HPLC detection of the *o*-phtalaldehyde derivatives of methionine as an alternative to standard radiochemical assays (e.g., unlabeled betaine, homocysteine and methyl[^{14}C]betaine incubated with BHMT to measure [^{14}C]-methionine and [^{14}C]-dimethylglycine generation). BHMT can be quantitated in the picomole range using this new assay as indicated by a linear response of enzyme activity to protein concentration.

Table 2. Stability of betaine-homocysteine methyltransferase.

Sample	Homocysteine (1mM) Dimethylglycine (1mM)	Glycerol 10%	2 weeks %	4 weeks %	10 weeks %
1	-	Neg -	65	20	0
2	-	Neg -	60	50	15
3	+	Neg -	105	60	30
4	+	Pos +	80	40	0

Sythesis of the pinanyl esters of betaine and dimethylglycine were achieved through reaction of the intermediate, phenylthiomethane boronate with pinanediol. Subsequent generation of pinanyl iodomethaneboronate followed by treatment with trimethylamine yielded the desired betaine analog, pinanyl N,N,N-trimethylaminomethane boronate as the iodide salt (PTAMB). The boronate analog of dimethylglycine was also generated as its pinanyl ester for kinetic and inhibition studies.

BHMT kinetic inhibition studies used the radiochemical assay with methyl[^{14}C]-betaine and a read-out of [^{14}C]-methionine and [^{14}C]-dimethylglycine. Trimethyl-aminomethane boronate (TAMB) was generated from PTAMB at pH 7. NaI was added as a control for the PTAMB counterion. We found that the K_m for betaine with the pure enzyme is 0.1 mM compared to 0.048 mM for rat liver homogenate and 0.1 mM for purified human enzyme. In the presence of high substrate concentration (7 mM homocysteine and 2 mM betaine), TAMB caused 30% inhibition at low concentration of the enzyme, 0.01 mM BHMT. The inhibition constant K_i for TAMB was 45 μM, calculated from the double reciprocal plot obtained when the concentration of betaine was varied from 50 to 500 μM. In this instance, homocysteine concentration was held constant at 7 mM. The inhibition of BHMT by TAMB appears to be competitive. Unlike other tight-binding boronic acid inhibitors, TAMB's micromolar inhibition shows that it binds more tightly to BHMT than betaine. In the absence of specific structural or crystallographic information, the magnitude of the difference between the binding TAMB and that of betaine suggests that the inhibitor is acting as a substrate style analog devoid any significant covalent interaction with BHMT. We also concluded that TAMB does not donate a methyl group to homocysteine when substituted for betaine in the enzyme reaction. Evidence for this was substantiated by substitution of TAMB for betaine in the new enzyme assay without concomitant generation of the OPA-methionine peak.

Acknowledgments
This study was sponsored in part by NIH Grant GM-42020.

References

1. Lee, K.-H., Cava, M., et al. *Arch. Biochem. Biophy.* **292**, 77-86 (1992).
2. Finkelstein, J. D. and Martin, J. J. *J. Biol. Chem.* **261**, 1582-1587 (1986).
3. Spielvogel, B. F., Wojnowich, L., et al. *J. Am. Chem. Soc.* **98**, 5702-5703 (1976).

Peptide Revolution: Genomics, Proteomics & Therapeutics
Michael Chorev & Tomi K. Sawyer (Editors)
American Peptide Society, 2003

Activity and Refolding of Partially Folded Analogues of BPTI

George Barany[1], Irina V. Getun[1], Judit Tulla-Puche[1] and Clare Woodward[2]

[1]Department of Chemistry, University of Minnesota, Minneapolis, MN 55455, USA;
[2]Department of Biochemistry, Molecular Biology, and Biophysics, University of Minnesota, St. Paul, MN 55108, USA

Introduction

Partially folded proteins are considered to be models of metastable forms transiently populated during folding. Their properties may also be relevant to understanding natively denatured proteins [1] and/or pathogenic, aggregating proteins [2]. Previously, we described the chemical synthesis and structural characterization of two β-turn analogues of $[14\text{-}38]_{Abu}$, the partially folded variant of bovine pancreatic trypsin inhibitor (BPTI) with only the disulfide between Cys 14 and Cys 38 left intact while Cys 5, 30, 51, and 55 are replaced by α-amino-*n*-butyric acid (Abu) [3]. In BPTI, a type I β-turn between core strands of antiparallel sheet (A25K26A27G28) is thought to be the main site for initiation of folding. The P26D27$[14\text{-}38]_{Abu}$ analogue involves two replacements by amino acids with a higher propensity for type I β-turns. In the N26G27K28$[14\text{-}38]_{Abu}$ variant, replacements in the turn favor a type I' turn, the most common in β-hairpins.

CD and one-dimensional ^{1}H NMR indicate that the parent $[14\text{-}38]_{Abu}$ strongly favors a native-like structure in the core β-hairpin, and has minor populations of ordered conformations in regions outside the core. Both new analogues have >75% reduction of signal at 277 nm in the near UV CD, indicating that much of the tertiary structure is lost, compared to $[14\text{-}38]_{Abu}$. P26D27$[14\text{-}38]_{Abu}$ has a small population of native-like conformations observed by NMR, but analogue N26G27K28$[14\text{-}38]_{Abu}$ has no ordered structure observable by CD or NMR [3].

To further characterize β-turn analogues of $[14\text{-}38]_{Abu}$, their trypsin inhibitor activity has been measured, and structure induced by the osmolyte trimethylamine *N*-oxide (TMAO) has been probed. As controls, partially folded $[14\text{-}38]_{Abu}$, as well as $[R]_{Abu}$, the unfolded protein with all six Cys residues replaced by Abu, have been used.

Results and Discussion

The inhibitor activity of partially folded and unfolded BPTI analogues is difficult to measure, as they are readily digested by the biological ligand, a serine proteinase. To remedy this, trypsin inhibition assays were carried out using a modified rat trypsin missing the conserved C191-C220 disulfide bond. This trypsin mutant is ineffective at cleaving unfolded peptides. By comparison to wild-type BPTI, partially folded $[14\text{-}38]_{Abu}$ has 14-fold weaker affinity for C191A/C220A trypsin (Table 1). Relative to $[14\text{-}38]_{Abu}$, affinity for trypsin is decreased by only 4-fold for P26D27$[14\text{-}38]_{Abu}$, and 28-fold for N26G27K28$[14\text{-}38]_{Abu}$. For $[R]_{Abu}$, no inhibition is detected, even when present in great excess (up to 500 molar equivalents) over trypsin.

Organic osmolytes protect proteins from denaturation, induce folding in otherwise destabilized proteins, and restore biological activity of partially folded proteins [4]. In the presence of TMAO, $[14\text{-}38]_{Abu}$ and both β-turn analogues fold to an ensemble with much higher helical content, as monitored by CD. In the absence of TMAO, increasing temperature induces in P26D27$[14\text{-}38]_{Abu}$, N26G27K28$[14\text{-}38]_{Abu}$, and $[R]_{Abu}$ a linear

Table 1. Inhibition of C191A/C220A trypsin by BPTI analogues[a].

Protein	K_i (nM)
BPTI	0.32 ± 0.07[b]
$[14\text{-}38]_{Abu}$	4.46 ± 0.19
$P26D27[14\text{-}38]_{Abu}$	16.9 ± 1.26
$N26G27K28[14\text{-}38]_{Abu}$	127 ± 4

[a]*Assays were performed in 50 mM Hepes, pH 8.0, 100 mM NaCl, and 10 mM $CaCl_2$ at 25 °C.*
[b]*The wild type data are taken from [5].*

decrease in CD ellipticity at 220 nm characteristic of peptides with a high degree of disorganization (data not shown). In contrast, in the presence of TMAO, $[14\text{-}38]_{Abu}$ and both β-turn analogues exhibit a cooperative thermal unfolding transition. Midpoint temperatures are around 10 °C for both analogues, and the T_m of $[14\text{-}38]_{Abu}$ increases from 19 °C in the absence of TMAO to 26 °C in the presence of TMAO (Figure 1).

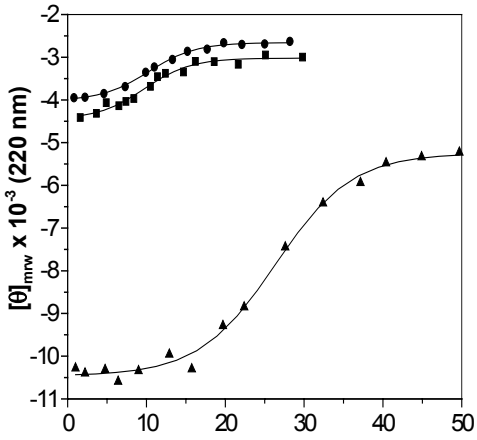

Fig. 1. Temperature dependence of molar ellipticity at 220 nm in the presence of 2 M TMAO, monitored at pH 4.6. Variants examined: $[14\text{-}38]_{Abu}$ (▲▲); $P26D27[14\text{-}38]_{Abu}$ (■); and $N26G27K28[14\text{-}38]_{Abu}$ (●).

Acknowledgments

This work was supported by NIH Grant GM 51628 (G.B. and C.W.).

References

1. Gunasekaran, K., et al. *Trends Biochem. Sci*. **28**, 81-85 (2003).
2. Dobson, C. M. *Trends Biochem. Sci.* **24**, 329-332 (1999).
3. Tulla, J., Woodward, C. and Barany, G., In Lebl, M. and Houghten R. (Eds.) *Peptides: The Wave of the Future (Proceedings of the 17th American Peptide Symposium).* San Diego, CA, 2001, p. 409.
4. Bolen, D. W. and Baskakov, I. V. *J. Mol. Biol.* **310**, 955-963 (2001).
5. Wang, E. C. W., Hung, S.-H., Cahoon, M. and Hedstrom, L. *Protein Eng*. **10,** 405-411 (1997).

Peptide Revolution: Genomics, Proteomics & Therapeutics
Michael Chorev & Tomi K. Sawyer (Editors)
American Peptide Society, 2003

Solid-Phase Synthesis of Amidoketones: Towards Caspase Inhibitors

Jesús Vázquez[1,2] and Fernando Albericio[1,2]

[1]Barcelona Biomedical Research Institute, Barcelona Science Park; [2]Department of Organic Chemistry, University of Barcelona, 08028-Barcelona, Spain

Introduction

Caspases are a family of cysteine proteases [1] that are implicated in both apoptosis, where they act as signal amplifiers, and in inflammatory processes [2]. To date, a total of eleven human caspases have been characterized. All of them present similarities in sequence of amino acids and in their substrate specificity. Thus, they are cleaved at the carboxyl terminal of an aspartic residue. The cleavage is specified by three or more amino acids immediately preceding the aspartic residue. Their implication in cell death is critical and varied: inactivation of proteins that protect live cells from apoptosis, disorganization of cell structures or deregulation of proteins, separating regulatory from catalytic domains. They have self-regulation (positive or negative feedback) but also through inhibitors (small molecules). They therefore constitute attractive objectives as therapeutic targets. Some of the caspase inhibitors described in the literature present a modified aspartyl residue with electrophilic groups, such as ketones, replacing the carboxyl group. Herein, the first results towards a new family of caspase inhibitors are discussed.

Results and Discussion

An optimal strategy for the preparation of these inhibitors would involve a solid-phase approach starting by the incorporation of an Fmoc-protected amino ketone onto a resin. Therefore, a convenient method for the preparation of Fmoc-derivatives of the modified aspartic acid would be necessary. The strategy used for the ketone formation should leave unaltered both the Fmoc and the *t*-butyl groups. After several trials, it was found that organocuprates, which are weak bases and compatible with the presence of the Fmoc group, react with thioesters to render cleanly the corresponding ketones [3]. Thus several Fmoc-amino ketones were prepared using the synthetic scheme showed in Figure 1.

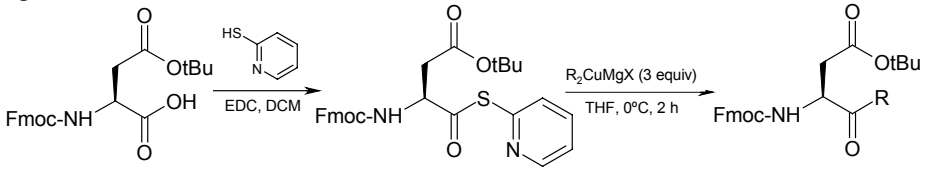

Fig. 1. Synthetic strategy for the preparation of Fmoc-aspartyl ketones.

The quality of the final product was superior when CuCN was used instead of CuI for the *in situ* preparation of organocuprates from the Grignard reagent.

Fmoc-aspartyl ketones can be incorporated onto a resin either through the β-carboxyl group (using Wang or Barlos resin) or the ketone (using carbazide resin). Although results obtained with both methods were satisfactory, the second was preferred because the incorporation step will serve as "auto-purification" of crude products (just those molecules containing a ketone will be anchored to the resin).

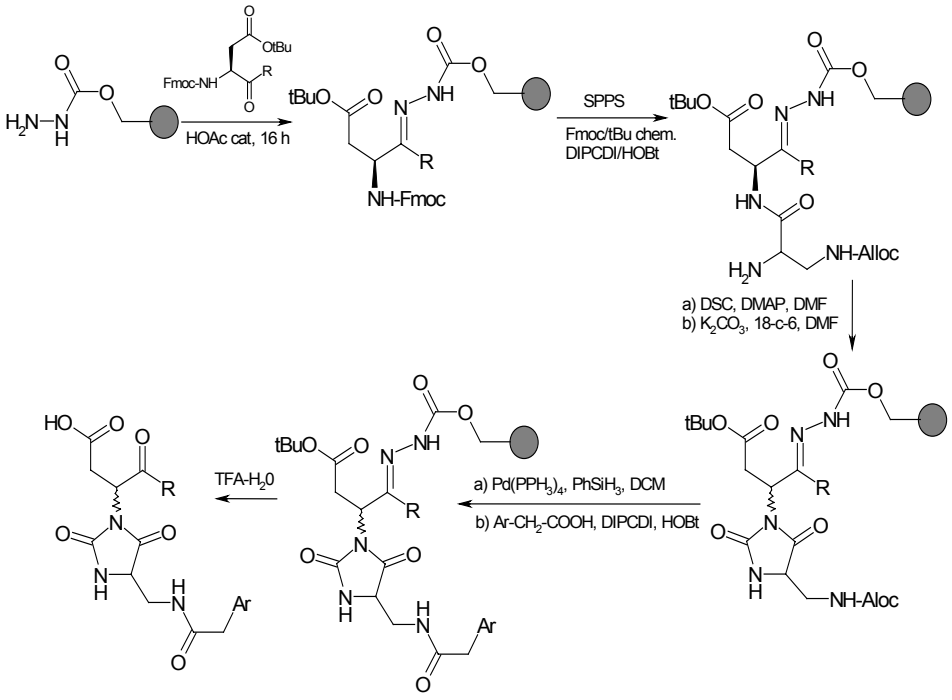

Fig. 2. Synthetic strategy for the preparation of hydantoin-aspartyl ketone based compounds.

The first family of compounds synthesized presents a hydantoin structure to confer rigidity. The hydantoin is formed from the aspartyl ketone and a diaminopropionic acid residue and serves also as a linker between the aspartyl ketone and derivatives of the acetic acid containing aromatic rings (Figure 2).

Although solutions of K_2CO_3 in the presence of 18-c-6 gave better results than DBU in DMF, the epimerization at the α-carbon of the aspartyl residue could not be avoided. Other steps of the synthetic scheme took place smoothly and without any important side reaction.

In conclusion, a general and straightforward methodology to prepare Fmoc-aspartyl ketones and hydantoins containing those derivatives has been developed. This has allowed the preparation of a first library of these compounds that is presently being evaluated as caspase inhibitors.

Acknowledgments
The work was funded by CICYT (BQU2000-0235) and Generalitat de Catalunya.

References

1. Otto, H. H. and Schirmeister, T. *Chem. Rev.* **97**, 133-171 (1997).
2. Thornberry, N. A. and Lazebnick, Y. *Science* **281**, 1312–1316 (1998).
3. Vázquez, J. and Albericio, F. *Tetrahedron Lett.* **43**, 7499-7502 (2002).

Peptide Revolution: Genomics, Proteomics & Therapeutics
Michael Chorev & Tomi K. Sawyer (Editors)
American Peptide Society, 2003

Synthesis and Biological Evaluation of Dipeptide Boronic Acids as Potent DPP IV Inhibitors

J.H. Lai, W. Wu, H. Maw, Y. Zhou and W.W. Bachovchin

Department of Biochemistry, Tufts University School of Medicine, 136 Harrison Ave., Boston, MA 02111, USA

Introduction

Dipeptidyl peptidase IV (DPP IV) is a proline-specific serine peptidase that cleaves Xaa-Pro or Xaa-Ala dipeptides from the N-terminus of oligo- and polypeptides. The *in vivo* introduction of DPP IV specific inhibitors has been shown to enhance the levels of intact endogeneous peptides (e.g. GLP-1), creating a new therapeutic paradigm in diabetes treatment [1]. In this study, we report the synthesis and biological activities of a series of boronic acid dipeptides containing unnatural amino acids with tertiary or quaternary aliphatic β-carbon side chains at the N-terminus (**5a-d** and **5a'-d'**).

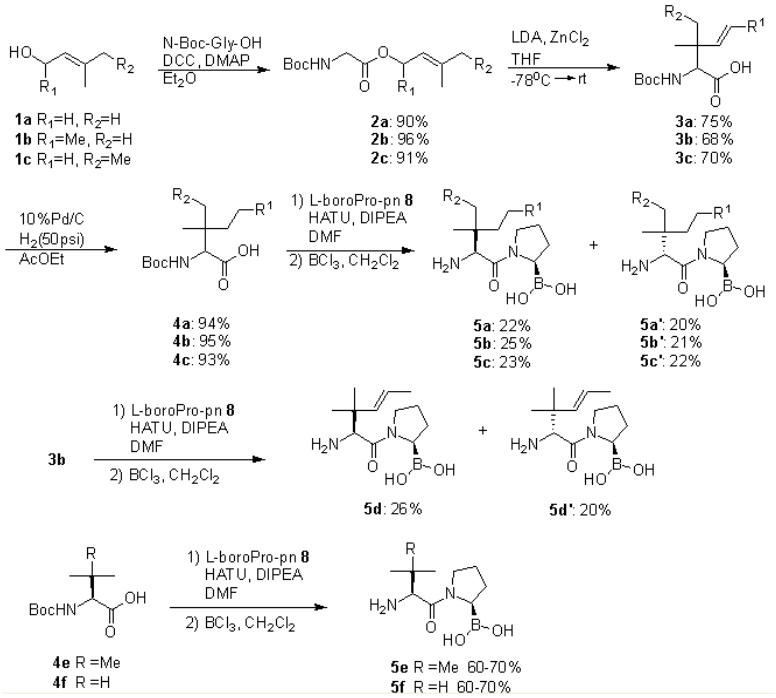

Fig. 1. Synthesis of dipeptide boronic acid derivatives.

Results and Discussion

The key to the synthesis of amino acids with quaternary β-carbon side chains **4a-c** is the ester enolate Claisen rearrangements, which convert allylic esters **2a-c** (Figure 1) to their corresponding acids **3a-c.** First, allylic esters **2a-c** were prepared by coupling of *N*-Boc-Gly-OH with allylic alcohols **1a-c** using DCC and DMAP. The Claisen rearrangements of **2a-c** to **3a-c** were achieved by treatment of the former with 2.2 equiv of LDA and 1.1 equiv $ZnCl_2$ following a previously reported method [2]. The

unsaturated acids **3a-c** were then reduced to **4a-c** by palladium catalyzed hydrogenation. The dipeptide derivatives **5a-d** were prepared by coupling the enantiomerically pure L-boroPro-pn **8** [3] to the racemic Boc protected *tert*-leucine derivatives (**4a-c** and **3b**) using HATU as the coupling reagent, followed by concurrent removal of the Boc and pinandiol protecting groups by BCl_3. The compounds **5e** and **5f** were prepared directly from **4e** and **4f** with a similar method. The diastereomeric Xaa-boroPro were separated into their component L,L (**5a-d**) and D,L (**5a'-d'**) diastereomers using RP-HPLC.

We have previously reported that the conformation of proline boronic acid dipeptides can adapt the open and cyclic forms at low and high pH values [4-5]. Consequently, inhibitors were fully equilibrated at pH 2 and pH 8 prior to addition to the enzyme. It is assumed that the IC_{50} value obtained with inhibitor pre-incubated at pH 2 approximates the value for a fully active inhibitor. In this report, we demonstrate that the size of the alkyl substituents does not significantly affect the activity (Table 1) where the N-terminal amino acids were set to the active configuration (L) and the β-carbon is either tertiary or quaternary centered. This finding is consistent with the recent crystal structure of DPP IV in a complex with its substrate analog, showing that the L- side chain of N-terminus amino acid points into a large cavity and does not make specific contacts with DPP IV [6].

Table 1. Inhibition of DPP IV by dipeptide boronic acids.

No.	Config.	IC50 (nM)[a]	± S.E. (nM)	IC50 (nM)[b]	± S.E. (nM)
5a	L,L	4.4	0.43	860	82
5b	L,L	3.4	0.36	670	44
5c	L,L	9.8	1.2	1400	168
5d	L,L	4.0	0.32	910	112
5e	L,L	3.5	0.47	680	56
5f	L,L	2.5	0.37	1800	112
5a'	D,L	970	66	-	-
5b'	D,L	740	82	-	-
5c'	D,L	7200	1600	-	-
5d'	D,L	1700	130	-	-

[a]Inhibitors were pre-incubated in the pH 2 buffer for 18 hrs before the assay. [b]Inhibitors were pre-incubated in the pH 8 buffer for 18 hrs before the assay.

References

1. Holst, J.J. and Deacon, C.F. *Diabetes* **47**, 1663-1670 (1998).
2. Kazmaier, U. *J. Org. Chem*. **61**, 3694-3699 (1996).
3. Kelly, T. A., Fuchs, V. U., Perry, C. W. and Snow, R. J. *Tetrahedron* **49**, 1009-1016 (1993).
4. Coutts, S. J., Kelly, T. A., Snow, R. J., et al. *J. Med. Chem*. **39**, 2087-2094 (1996).
5. Snow, R. J., Bachovchin, W. W., Barton, R. W., Campbell, S. J., Coutts, S. J., Freeman, D. M., Gutheil, W. G., Kelly, T. A., Kennedy, C. A. *J. Am. Chem. Soc*. **116**, 10860-10869 (1994).
6. Rasmussen, H. B., Branner, S., Wiberg, F. C. and Wagtmann, N. *Nature Struct. Biol*. **10**, 19-25 (2003).

Peptide Revolution: Genomics, Proteomics & Therapeutics
Michael Chorev & Tomi K. Sawyer (Editors)
American Peptide Society, 2003

Cyclic Tetrapeptides Containing a Zinc Ligand as Novel Histone Deacetylase Inhibitors

Binoy Jose[3], Tamaki Kato[1], Yuko Sumida[3], Minoru Yoshida[2,3] and Norikazu Nishino[1,3]

[1]Graduate School of Life Science and Systems Engineering, Kyushu Institute of Technology, Kitakyushu, Japan; [2]RIKEN, Saitama 351-0198, Japan; [3]CREST Research Project, Japan Science and Technology Corp., Saitama, 332-0012, Japan

Introduction

Post-translational modification of the *N*-terminal tails of histone proteins is achieved by reversible acetylation with histone acetyl transferase (HAT) and histone deacetylase (HDAC) enzymes involved in chromatin remodeling, and plays a crucial role in gene expression. The inappropriate recruitment of HDACs has been clearly linked to carcinogenesis and the inhibition of HDACs results in transcriptional reactivation, cell-cycle arrest and terminal differentiation of transformed cells. HDAC inhibitors have demonstrated potential for the prevention and treatment of cancer and emerged as an attractive target for anticancer drugs [1]. A number of structurally diverse natural and synthetic compounds have been reported exhibiting HDAC inhibitory activity. In our previous work, we synthesized cyclic hydroxamic acid-containing peptides (CHAPs) and found that they have very high HDAC inhibitory activity [2]. Many of these compounds have potent antitumor effect *in vivo* in tumor bearing animals, and some of them are currently in clinical trials. However, the potential for clinical drug development could be limited due to many reasons such as low potency, lack of selectivity, cytotoxicity, low solubility in aqueous vehicle and low stability in cell culture. In this work, we explored the possibility of other zinc binding ligands for cyclic tetrapeptides in order to develop more pharmaceutically desirable HDAC inhibitors.

Results and Discussion

Phosphonate containing molecules include potent inhibitors of many proteases. We synthesized cyclic tetrapeptides containing a phosphonate in the side chain as HDAC inhibitor (Figure 1). For this deprotected tripeptide, H-D-Tyr(Me)-L-Ile-D-Pro-OBzl was coupled with Boc protected L-2-amino-7-(dimethoxyphosphoryl)heptanoic acid to give the tetrapeptide. After deprotection, the linear tetrapeptide was cyclized to yield phosphonate **1**.

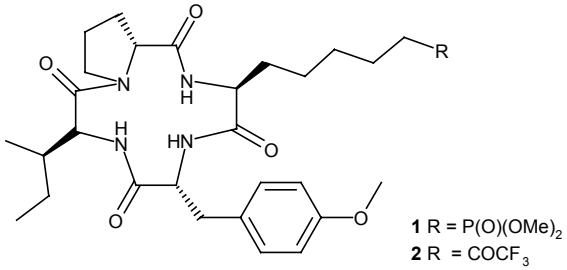

Fig. 1. Structures of the synthesized HDAC inhibitors.

Trifluoromethyl ketones and pentafluoroethyl ketones are potent inhibitors of aspartyl, serine and cysteine proteases and zinc-dependent enzymes by forming stabilized hemiketals and hemithioketals at the active site. Therefore we designed and synthesized cyclic tetrapeptides containing trifluoromethyl ketone and pentafluoromethyl ketone as HDAC inhibitors. The cyclic tetrapeptide *Cyclo*(L-Asu(OBzl)-D-Tyr(Me)-L-Ile-D-Pro) was synthesized usinga previously reported procedure [3]. The benzyl group was deprotected by hydrolysis using lithium hydroxide; next the lithium salt was treated with trifluoroacetic anhydride to give the trifluoromethyl ketone **2** in 40% yield. Using the same method with pentafluoroacetic anhydride, cyclic tetrapeptide containing pentafluoroethyl ketone **3** was also synthesized.

The results of HDAC inhibitory activity and P21 promoter assay of the compounds are shown in Table 1. The inhibitory activity of phosphonate **1** was very weak. It seems that the phosphonate ester hydrolysis does not occur in the cell. On the other hand, trifluoromethyl ketone **2** and pentafluoroethyl ketone **3** have high inhibitory activity. The higher activity of **2** for P21 promoter assay may be due to the higher degree of hydration of trifluoromethyl ketone **2** than pentafluoroethyl ketone **3**. The results indicate that cyclic tetrapeptides **2** and **3** have potential as anti-cancer drugs.

Table 1. HDAC inhibitory activity[a].

Compound	IC_{50} (μM)				P21 promoter assay EC_{50} (μM)
	HDAC1	*HDAC2*	*HDAC6*	*HDAC8*	
1	>500	>500	>500	>500	>100
2	0.72	2.04	1.44	0.37	3.09
3	0.85	12.63	5.70	0.78	31.1

[a]*HDAC inhibitory activity was evaluated using HDACs prepared from 293T cells.*

Acknowledgments

The work was funded by a research grant from the CREST Research Project, Japan Science and Technology Corporation.

References

1. Yoshida, M., Furumai, R., Nishiyama, M., Komatsu, Y., Nishino, N. and Horinouchi S. *Cancer Chemother. Pharmacol.* **48**, S20-S26 (2001).
2. Komatsu, Y., Tomizaki, K., Tsukamoto, M., Kato, T., Nishino, N., Sato, S., Yamori, T., Tsuruo, T., Furumai, R., Yoshida, M., Horinouchi S. and Hayashi, H. *Cancer Res.* **61**, 4459-4466 (2001).
3. Furumai, R., Komatsu, Y., Nishino, N., Khochbin, S., Yoshida, M. and Horinouchi S. *Proc. Natl. Acad. Sci. U.S.A.* **98**, 87-92 (2001).

Peptide Revolution: Genomics, Proteomics & Therapeutics
Michael Chorev & Tomi K. Sawyer (Editors)
American Peptide Society, 2003

In Vivo Imaging of Thrombosis-Associated Enzyme Using Fluorescence Peptide Probes

Ching-Hsuan Tung, Nan-Hui Ho, Qing Zeng and Ralph Weissleder

Center for Molecular Imaging Research, Massachusetts General Hospital, Harvard Medical School, Charlestown, MA 02129, USA

Introduction

Thrombosis is the pathological hallmark of cardiovascular diseases such as myocardial infarction, stroke, and pulmonary embolism. Rapid lysis of thrombi leads to improved clinical outcome, however many thrombi are resistant to fibrinolytic therapy with agents such as plasminogen activators. Recently, it has been demonstrated that activated blood coagulation factor XIII (FX13) is an important mediator of fibrinolytic resistance [1]. FX13, a plasma transglutaminase, is a key player in the final stages of blood coagulation. It is activated by thrombin and confers fibrinolytic resistance by covalently cross-linking plasmin inhibitors such as α2-antiplasmin (α2AP) to fibrin. This provides the clot with sufficient stiffness and the necessary resistance against thrombolytic enzymes by incorporating plasmin inhibitors to the crosslinked clot.

Although FX13 can be elegantly studied *in vitro*, direct visualization of FX13 activity *in vivo* is limited. Localized imaging of FX13 activity in thrombi could further elucidate its mechanism of fibrinolytic resistance and allow unique evaluation of anti-FX13 therapies. Furthermore, as FX13 is a hallmark of acute thrombi, specific imaging of FX13 activity may offer a new diagnostic method to detect biologically active acute thrombi. Molecular imaging is a new paradigm based on imaging specific cellular and molecular targets. Recently, our laboratory has developed a series of near-infrared fluorescence (NIRF) molecular probes for the *in vivo* detection of specific disease-associated enzymes [2], including a thrombin sensitive probe [3,4]. The rationale for using NIR fluorochromes rather than visible light fluorochromes is that NIR light travels though tissue most efficiently at 700-900 nm as blood does not strongly absorb NIR energy. In this study, we designed new thrombosis specific diagnostic probes based on the FX13 transglutaminase activity.

Results and Discussion

A specific peptide sequence, N_{13}QEQVSPLTLLK_{24}, corresponding to the amino terminus of α2AP, the primary inhibitor of plasmin-mediated fibrinolysis, was used as the template for imaging probe synthesis. This peptide is known to crosslink with fibrin clot in a specific manner [5]. Specifically, FX13 catalyzes the formation of covalent bond between the glutamine residue at position 14 and the ε-amino group of a lysine residue in different fibrin chains. The glutamine residue at position 16 was significantly less reactive than glutamine 14.

To prepare the NIR fluorescence probe (A15), an acetyl-glycine group was added to the N-terminus of the selected α2AP fragment for capping. In addition, a tryptophan residue and a cysteine residue were added to the C-terminus for quantitation and conjugation purposes, respectively (Figure 1). The peptide was synthesized by solid phase peptide synthesis, characterized by MS (Calcd. M+1=1701.9, found 1701.6), and then reacted with a sulfhydryl reactive fluorochrome, Alexa Fluor 680 C2 maleimide (Molecular probe, Eugene, OR), through the C-terminal cysteine sidechain in sodium acetate buffer, pH 6.5 (Figure 1). The HPLC purified final product, A15, had an

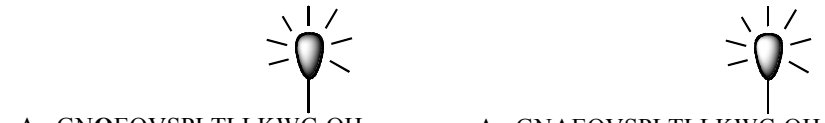

A15 **CA15**

Fig. 1. Sequences and structures of FX13 probe (A15) and control probe (CA15).

excitation and emission at 679 and 702 nm, respectively. A control probe (CA15) with only the glutamine residue at position 14 replaced with an alanine residue was also synthesized.

Incorporating NIR fluorescence probe to blood clot was studied with the use of mouse blood. After incubating the A15 probe (1 μM) with the freshly withdrawn mouse blood for 2 hrs, the clot was homogenized and washed extensively with PBS. The clots were then imaged using a homebuilt imaging system with 630±15 nm excitation and 700±20 nm emission. Intense fluorescence signal was observed from the clot, 10-fold higher than the background blood (n=3) (Figure 2). In comparison, the clot incubated with CA15 probe showed a significantly less fluorescent signal and only less than 3-fold signal enhancement could be observed. This result suggested that the glutamine residue at position 14 is critical for FX13 crosslinking reaction. Once the amide group on the glutamine sidechain was eliminated, the amount of probe attached to the fibrin was significantly dropped.

In conclusion, we have developed an effective imaging probe potentially can be applied to *in vivo* imaging of blood coagulation. The specific peptide derived from α2AP labeled with various reporter groups can be covalently attached to fibrin by FX13 blood coagulation factor, and imaged by different modalities, such as NMR and optical imaging. In addition, the same approach may be applied to other transglutaminases which are widely found in generic tissue stabilization and also contribute to a variety of disease, such as cancer, neurodegenerative diseases and celiac disease.

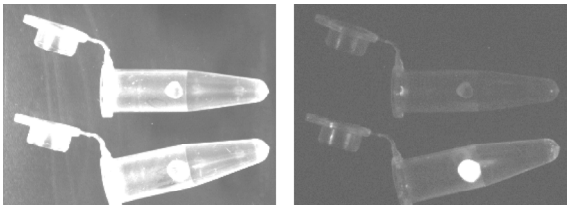

Fig. 2. Light and NIRF images of blood clot and blood clot with A15. The clot gave 10 fold difference in NIR fluorescence signal.

Acknowledgments

The authors would like to thank Drs. F. Jaffer and G. Reed for the technique suggestion. This research was supported by NIH Grants P50 CA86355, R33 CA88365 and RO1 CA99385.

References

1. Lorand, L. *Ann. N. Y. Acad. Sci.* **936**, 291-311 (2001).
2. Weissleder, R. and Ntziachristos, V. *Nat. Med.* **9**, 123-8 (2003).
3. Tung, C. H., et al. *ChemBioChem* **3**, 207-211 (2002).
4. Jaffer, F. A., et al. *Arterioscler. Thromb. Vasc. Biol.* **22**, 1929-35. (2002).
5. Robinson, B. R., Houng, A. K. and Reed, G. L. *Circulation* **102**, 1151-7 (2000).

Peptide Revolution: Genomics, Proteomics & Therapeutics
Michael Chorev & Tomi K. Sawyer (Editors)
American Peptide Society, 2003

A Fluorescence Resonance Energy Transfer Substrate (FRETS) Library for Determining Protease Specificity

Katsumi Takada, Masahiko Tsunemi, Yuji Nishiuchi and Terutoshi Kimura

Peptide Institute Inc., Protein Research Foundation, Minoh-shi, Osaka 562-8686, Japan

Introduction

Certification of the substrate specificity of proteolytic enzymes is indispensable for a better understanding of the biological function(s) as well as the rational design of inhibitors. To determine the specificity, there are a wide variety of techniques available such as those using synthetic peptides, phage display libraries and combinatorial peptide libraries. Well-established among them is the use of fluorescence resonance energy transfer substrate (FRETS) to determine protease specificity. In the present study, we describe the preparation and use of FRETS libraries (FRETS-25 Xaa series) to rapidly identify the specificity of proteases.

Results and Discussion

The hydrolytic cleavage of peptides by a protease can be monitored using fluorescence with an appropriate couple of fluorophore and quencher such as 2-(*N*-methylamino)benzoyl (Nma) and 2,4-dinitrophenyl (Dnp), respectively [1]. Therefore, FRETS allows positional scanning at both the N- and the C-terminal sides of the scissile bond of proteases. Positional-scanning peptide libraries are generally composed of several sub-libraries in which one position is defined by an amino acid, and the remaining positions contain a mixture of amino acids [2]. This strategy appears to be a powerful tool for rapidly and accurately assessing protease specificity, although an extensive effort is required to prepare such large libraries. To facilitate the preparation of FRETS libraries, we designed the FRETS-25 Xaa series (Figure 1) in which the scanning point is fixed at the P1 position, and other positions (e.g. P2 and P3 in the present study) to be substituted are restricted to five amino acids representing the acidic, basic, aromatic, aliphatic and bulky residues. Each substrate in the FRETS-25 Xaa series contains a highly fluorescent Nma group linked to the side chain of the N-terminal D-diaminopropionic acid (A_2pr). This group is efficiently quenched by a Dnp group linked to the ε-amino function of Lys. The D-amino acids located in both N- and C-termini are expected to avoid the degradation by exopeptidases. Furthermore, the two consecutive D-Arg residues improve the solubility in buffers used for the assay. Xaa represents a fixed position of each of the 19 natural amino acids excluding Cys. A mixture of five amino acids (K, D, Y, P and I) is at the Yaa position along with a

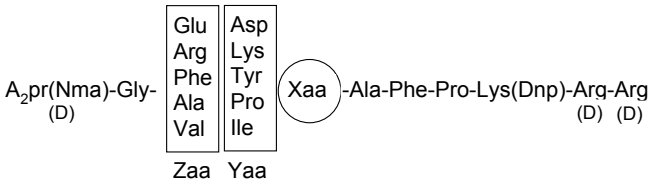

Fig. 1. Structure of the FRETS-25 Xaa series.

Table 1. Amino acid preferences of proteases determined using the FRETS-25 Xaa series.

Protease		Preferred Xaa	Amino acid preferences[a]
serine protease	trypsin	Arg	Val-Pro-Arg↑
	chymotrypsin	Tyr	Val-Pro-Tyr↑
	elastase	Ala	Val-Pro-Ala↑
	thrombin	Arg	Phe-Pro-Arg↑
	kex2	Arg	Arg-Lys-Arg↑
thiol protease	papain	Tyr	Arg-Ile-Tyr↑
acid protease	pepsin	Ile	Val-Tyr↑Ile
metallo protease	thermolysin	Phe	Phe-Lys-Phe↑
			Gly-Arg/Ala-Tyr↑Phe

[a]*Arrows indicate the scissile bonds for each protease employed.*

mixture of five amino acids (R, E, F, A and V) at the Zaa position for each fixed Xaa. This provides a peptide mixture of 25 combinations of each Xaa series resulting in a combinatorial library totaling 475 peptide substrates.

The assay procedure is composed of a primary screening for selection of the favored Xaa and a secondary one for identification of the specificity of the enzyme. In the latter screening, the LC MS analysis with the aid of fluorescence (at λex = 340 nm and λem = 440 nm) is performed to determine the degraded peptides preferentially generated from 25 substrates of the favored Xaa series. Although the FRETS-25 Xaa series does not include the comprehensive libraries of 20 proteinogenic amino acids, it efficiently offers a common measure of protease specificity by using a combination of five representative amino acids for substituents. To validate this approach, we applied it to determine the amino acid preferences of proteases such as serine proteases (trypsin, chymotrypsin, elastase, thrombin, kex2), a thiol protease (papain), an acid protease (pepsin) and a metallo protease (thermolysin) as summarized in Table 1. The results obtained by using the FRET-25 Xaa series are consistent with the assignments in the literatures.

In conclusion, our approach using the FRETS-25 Xaa series has proven to be an efficient and rapid method for providing a reliable measure of protease specificity. We are now extending this approach to determine the substrate specificities for some uncharacterized proteases.

References

1. Chagas, J. R., Juliano, L. and Prado, E. S. *Anal. Biochem*. **192**, 419-425 (1990).
2. Pinilla, C., Appel, J. R., Blanc, P. and Houghten, R. A. *BioTechniques* **13**, 901-905 (1992).

Peptide Revolution: Genomics, Proteomics & Therapeutics
Michael Chorev & Tomi K. Sawyer (Editors)
American Peptide Society, 2003

Synthesis and Biological Activity of Dimeric HIV-1 Integrase Inhibitory Peptides

Krzysztof Krajewski[1†], Ya-Qiu Long[1], Christophe Marchand[2], Yves Pommier[2] and Peter P. Roller[1]

[1]Laboratory of Medicinal Chemistry, NCI, NIH, Frederick MD 21702, USA;
[2]Laboratory of Molecular Pharmacology, NCI, NIH, Bethesda, MD 20892 USA

Introduction

The HIV-1 integrase (IN) is essential for HIV replication cycle, furthermore IN is a key enzyme for ability of the virus to infect nondividing cells [1]. It is thus a good target for HIV antiviral chemotherapy, in addition to reverse transcriptase and protease. IN is also an attractive target because it has no counterpart in mammalian cells, therefore, there is a possibility that selective inhibitors of integrase will not produce any side effects. The overall integration process occurs in three steps, and IN is involved in the first two. First, the enzyme removes two nucleosides from each of the viral DNA ends (3'-end processing) then, after migration of the DNA-protein complex into the nucleus, IN catalyzes the insertion of the viral DNA through its 3'-end into the cellular chromosome (strand transfer, also referred to as integration or 3'-end joining). Progress with the design of effective inhibitors of HIV-IN is slower than in the case of other HIV enzymes, such as reverse transcriptase or protease [2].

During our structure-activity studies of analogs of the hexapeptide IN inhibitor, His-**Cys**-Lys-Phe-Trp-Trp-NH_2 **1** [3], we found that a disulfide covalent dimer **4** (Table 1) was more potent than **1**. To explore the generality of this approach we synthesized and tested several dimeric analogs of **1** with a variety of linkers (peptides **5-9**), including the non-reducible thioether linkers (Scheme 1, peptides **6-9**).

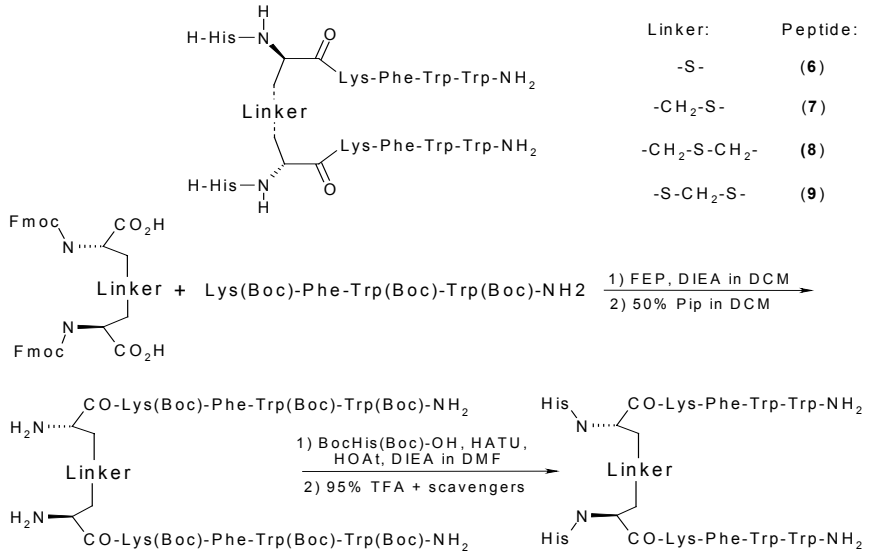

*Scheme. 1. Structures of thioether linked peptide dimers (**6-9**) and scheme of dimeric peptides synthesis.*

Table 1. HIV-1 Integrase inhibitory activity of synthetic peptides.

	Peptide	Linker	IC_{50} (μM)	
			3'-Processing	Strand Transfer
1	H-HCKFWW-NH_2	Monomer	102	97
2	(all-D)-H-HCKFWW-NH_2	Monomer	21	34
3	H-KFWW-NH_2	Monomer	>333	>333
4	S-S dimer of H-HCKFWW-NH_2	-S-S-	81	58
5	S-S dimer of (all-D)-H-HCKFWW-NH_2	-S-S-	15	15
6	Thioether dimer (**6**)	-S-	67	19
7	Thioether dimer (**7**)	-CH_2-S-	77	87
8	Thioether dimer (**8**)	-CH_2-S-CH_2-	59	63
9	Thioether dimer (**9**)	-S-CH_2-S-	**5**	**7**
10	(all-D)-H-HCKFWWW-NH_2	Monomer	59	80
11	S-S dimer of (all-D)-H-HCKFWWW-NH_2	-S-S-	**5**	**7**

Results and Discussion

Peptides **1**, **2**, **3**, and **10** were synthesized using Fmoc chemistry on Rink amide resins with an ABI 433A peptide synthesizer. Following cleavage (2.5% EDT, 2.5% H_2O, 1% TIS in TFA), the crude peptides were dissolved in water/acetonitrile solution and lyophilized, then purified by RP-HPLC (Vydac 218TP1022, fractions containing disulfide dimers were also collected) with a gradient of 20-70% acetonitrile in aq. 0.05% TFA. The H-Lys(Boc)-Phe-Trp(Boc)-Trp(Boc)-NH_2 tetrapeptide, used for syntheses of dimeric peptides **6-9**, (Scheme 1) was synthesized manually using Fmoc chemistry on Sieber amide resin. Peptides **6-9** were purified using the same method as for monomers.

The synthesized peptides were tested for inhibition of HIV-1 IN activity in both 3'-end processing and strand transfer steps, assay conditions are described in [4]. These data suggest (Table 1) that the selected covalently dimerized peptides are more potent inhibitors of both 3'-processing and strand transfer steps, than the monomers. The mechanistic implications of this data suggest that the dimeric peptide may act as a bivalent inhibitor, simultaneously occupying two neighboring catalytic sites in the multimeric IN complex. This is consistent with the suggestion that at least an IN tetramer is required to accomplish integration process [5]. Currently we are testing if dimerization of other known IN inhibitory peptides will increase their inhibitory potency.

† *Permanent address: Faculty of Chemistry, Wroclaw University, 50-383 Wroclaw, Poland.*

References

1. Vodicka, M. A. *Somat. Cell. Mol. Genet.* **26**, 35-49 (2001).
2. Pommier, Y., Marchand, C. and Neamati, N. *Antiviral Res.* **47**, 139-148 (2000).
3. Lutzke, R. A. P., Eppens, N. A., et al. *Proc. Natl. Acad. Sci. U.S.A.* **92**, 11456- 11460 (1995).
4. Marchand, C., Neamati, N. and Pommier, Y. *Methods Enzymol*. **340**, 624-633 (1999).
5. Cherepanov, P., Maertens, G., Proost, P., Devreese, B., Van Beeumen, J., Engelborghs, Y., De Clercq, E. and Debyser, Z. *J. Biol. Chem.* **278**, 372-381 (2003).

Peptide Revolution: Genomics, Proteomics & Therapeutics
Michael Chorev & Tomi K. Sawyer (Editors)
American Peptide Society, 2003

Peptide-lead Nonpeptidic Protease Inhibitor Targeting Multi-drug Resistant Strains of HIV

Nobutaka Fujii[1], Hirokazu Tamamura[1], Tomonori Yamasaki[1], Akira Otaka[1], Yasuhiro Koh[2], Manabu Aoki[2], Kenji Maeda[2], Kazuhisa Yoshimura[3] and Hiroaki Mitsuya[2,4]

[1]Graduate School of Pharmaceutical Sciences, Kyoto University, Kyoto 606-8501, Japan; [2]Department of Internal Medicine II, Kumamoto University School of Medicine, Kumamoto 860-8556, Japan; [3]Center for AIDS Research, Kumamoto University, Kumamoto 862-0976, Japan; [4]Experimental Retrovirology Section, Medicine Branch, Division of Clinical Sciences, NCI, NIH, Bethesda, MD 20892, USA

Introduction

Discovery and development of novel potent HIV protease inhibitors that are valid against multi-drug resistant (MDR) viral strains and have excellent bioavailability, are required for multiple drug-combination chemotherapy, "highly active anti-retroviral therapy (HAART)". We have derived novel potent inhibitors that are effective even against MDR viruses by combining substructure units of known HIV protease inhibitors (Figure 1). Subsequently, in order to improve bioavailability by developing inhibitors that contain no amide bonds, an (*E*)-alkene dipeptide isostere (EADI) was introduced into the above inhibitors.

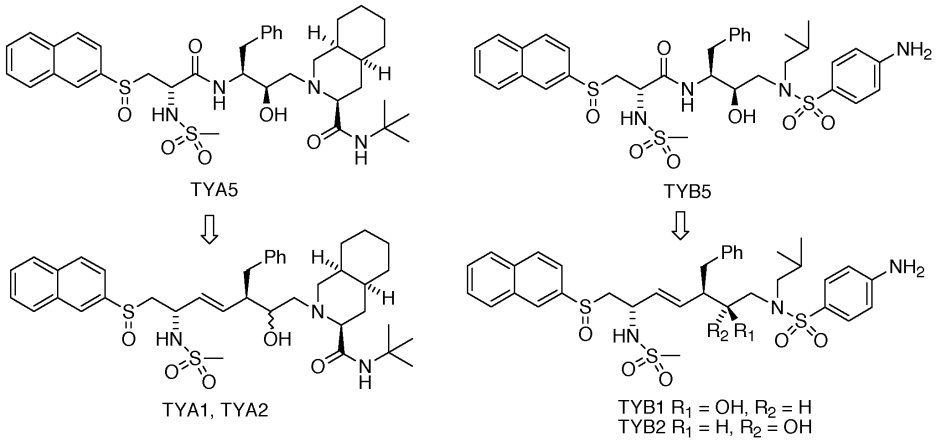

Fig. 1. Reduction of peptide character of HIV protease inhibitors that are valid against MDR HIV strains.

Results and Discussion

The efficacy of hydroxyethylamine dipeptide isosteres (HDIs) as the enzyme-substrate transition state mimic structure of aspartyl protease inhibitors has been well reported. Several target compounds containing an HDI were designed based on structural information derived from reported inhibitors [1-4] and synthesized using general procedures. Among them, TYA5 and TYB5 showed potent anti-HIV activity (IC_{50} = 9.5 nM and 66 nM, respectively, in the MTT assay) [5]. The potency of TYA5 was

Table 1. Anti-HIV activity of TYA5, TYB5 and TYB1 against HIV-1 clinical isolates.

Compound	wild type	IC_{50} (nM) (fold change)[a] MDR		
	HIV_{104pre}	HIV_{MM}	HIV_{JSL}	HIV_{TM}
TYA5	15 ± 2	32 ± 4 (2X)	220 ± 40 (15X)	34 ± 4 (2X)
TYB5	31 ± 3	36 ± 8 (1X)	25 ± 6 (1X)	43 ± 6 (1X)
TYB1	180 ± 30	520 ± 120 (3X)	340 ± 30 (2X)	> 1,000 (>6X)
AZT	2.5 ± 0.7	37 (15X)	64 (26X)	43 (17X)
saquinavir	19 ± 4	320 ± 2 (17X)	550 (29X)	230 ± 20 (12X)
amprenavir	20 ± 3	530 (27X)	800 (40X)	480 (24X)

[a] *IC_{50} values are based on the inhibition of HIV p24 antigen expression in PBMC.*

greater than those of saquinavir (IC_{50} = 17 nM) and amprenavir (IC_{50} = 36 nM). Next, the anti-HIV activities of TYA5 and TYB5 were investigated against MDR strains as measured by the inhibition of HIV p24 antigen expression in peripheral blood mononuclear cells (PBMC). As shown in Table 1, TYA5 and TYB5 are effective against MDR strains, while saquinavir and amprenavir exhibited low efficacy. As a result, combination of structural subunits from known inhibitors led to the development of protease inhibitors with high anti-HIV activity, including against MDR HIV-1.

Subsequently, target compounds, in which the amide bonds at the P_1-P_2 position of TYA5 and TYB5 were replaced by EADI, were synthesized to reduce the peptide character of TYA5 and TYB5. TYB1, an EADI-containing compound based on TYB5, having *syn* geometry as in TYB5, showed moderate anti-HIV activity (IC_{50} = 160 nM). Alternatively, TYA1 and TYA2, based on TYA5, did not show significant activity (IC_{50} > 1 μM). (Either TYA1 or TYA2 is the same *syn* isomer as TYA5.) It is reasonable that the *anti* isomer, TYB2, did not show significant activity (IC_{50} > 1 μM), whereas it was not readily explainable why the anti-HIV activities of compounds having EADIs are less than those of the corresponding amide-containing compounds. This suggested either that insertion of an EADI at the P_1–P_2 position or an increase in hydrophobicity is not suitable. Significant or complete loss of anti-HIV activity of TYB1 or TYA1 (TYA2), respectively, might underline the importance of the P_1–P_2 amide bond for interaction with the protease. Nonetheless, the anti-HIV activity of TYB1 was noted. TYB1 is a novel, purely nonpeptidic HIV protease inhibitor that possesses significant activity. TYB1 also exhibits effective activity (a third to one-half potency) against MDR strains, except for HIV_{TM} (Table 1) [6].

In conclusion, HDI-containing HIV protease inhibitors, which are highly active even against MDR strains, have been found by combination of substructure units of reported inhibitors. Furthermore, a purely nonpeptidic inhibitor, has been developed.

References

1. Roberts, N. A., et al. *Science* **248**, 358-361 (1990).
2. Kaldor, S. W., et al. *J. Med. Chem.* **40**, 3979-3985 (1997).
3. Jungheim, L. N., et al. *J. Med. Chem.* **39**, 96-108 (1996).
4. Ghosh, A. K., et al. *Bioorg. Med. Chem. Lett.* **8**, 687-690 (1998).
5. Munroe, J. E., et al. *Bioorg. Med. Chem. Lett.* **5**, 2897-2902 (1995).
6. Tamamura, H., et al. *J. Med. Chem.* **46**, 1764-1768 (2003).

Peptide Revolution: Genomics, Proteomics & Therapeutics
Michael Chorev & Tomi K. Sawyer (Editors)
American Peptide Society, 2003

Molecular Dynamics of the Caspase-3 Cleaved N-Half of Gelsolin

Inta Liepina[1], Paul Janmey[2], Cezary Czaplewski[3] and Adam Liwo[3]

[1]Latvian Institute of Organic Synthesis, Aizkraukles str. 21, Riga, LV1006, Latvia; [2]Institute for Medicine and Engineering, University of Pennsylvania, Philadelphia, PA 19104, USA; [3]Faculty of Chemistry, University of Gdansk, 80-952 Gdansk, Poland

Introduction

Gelsolin is an actin-severing protein, the activity of whichi is regulated by its conformation modulators: calcium, phosphoinositol 4,5-bisphosphate (PIP2) and caspase-3. The position of the caspase-3 cleavage site of horse gelsolin is not known; horse gelsolin is the only gelsolin for which the crystal structure has been determined. Caspase-3 cleaves murine, porcine, and human gelsolin at the sequence Asp-Gln-Thr-Glu-Gly. Specifically, murine gelsolin is cleaved at the peptide bond between the Asp^{352} and Gly^{353} residues [1]. For human gelsolin, there also is an alternative caspase-3-cleavage sequence at residues Ser^{585}-Glu^{586}-Pro^{587}-Asp^{588}-Gly^{589}, the cleavage taking place at the peptide bond between Asp^{588} and Gly^{589} [2]. Taking into account the fact that horse gelsolin has 94% sequence homology with human gelsolin, which suggests that the three-dimensional structure of human gelsolin is similar to that of the horse gelsolin, and based on the information regarding caspase-3-cleavage sequence in human gelsolin, it can be inferred that the cleavage site is located in the long linker between domains S3 and S4. The similar candidate sequence for caspase-3 cleavage Asp^{373}-Gln^{374}-Thr^{375}-Glu^{376}-Gly^{377} was found in horse gelsolin, and it was assumed that horse gelsolin is cleaved at the peptide bond between Glu^{376} and Gly^{377}. It has been suggested [3] that residues 23, 24, 69, 77, 78, 80, 81, 83, 84, 92, 94 of domain S1 are involved in actin binding, thus, after conformational changes of gelsolin, these residue should not be covered by domain S3.

Results and Discussion

To model the structural changes following caspase-3 cleavage, molecular dynamics (MD) simulations were carried out on the N-terminal part of horse gelsolin comprising domains S1-S3 (until the Glu^{376} residue) taken from the 1D0N crystal structure of horse gelsolin. Using the program CION from the AMBER 5.0 package, 15 sodium and 13 chloride ions were added to maintain zero overall charge of the system. The protein was placed in a periodic water box constructed to surround the molecule with at least 10 Å thick water layer from each side. The procedure of carrying out the MD run was as in previous simulations [4,5] (energy minimization and short low-temperature MD runs to relax the system, followed by the production MD simulation). The AMBER 5.0 force field and the NPT scheme with T=298 K, p=1 atm were used. The duration of the run was 3700 ps.

After 2227 ps of MD simulation, the S1-S3 structure still showed conformational stability, and only a slight opening of the structure was observed. Domain S3 moved away from domains S1 and S2, which remained at approximately the initial distance. Apart from N-and C-terminal flexibility of S1-S3, the most conformational lability was manifested by the string connecting domains S2 and S3, which comprises residues 248-270. The β-sheet between residues 117-122 of domain S2 and residues 323-328 of domain S3 after 2227 ps has a tendency to be disrupted, leading to conformational freedom for domain S3. During simulation time of 2751 ps it is possible to observe

how the β-sheet, which connects domains S1 and S3, loosens its structure and domains S1 and S3 become free. The process of disrupting of the β-sheet demonstrates how gelsolin could change from a globular structure to an open structure.

After 3770 ps of molecular dynamics were run domain S3 partly lost its α-helical and β-sheet structure, but still had two hydrogen bonding contacts with domain S1 via actin binding residue 94, and together with residue 92, were still covered by domain S3. Actin binding residues 81, 83, 84 were fully uncovered however, and residue 80 partly uncovered. It should be noted that residues 23, 24, 69, 77, 78 are placed on the protein surface already in the structure 1DON.

These results show that the S1-S3 latch in the N-half of gelsolin could release without the presence of calcium, and caspase-3 cleaved gelsolin could sever actin without calcium regulation. As shown in our previous work [5] however, some basic calcium concentration could contribute to the stability of separate gelsolin domain and to the maintenance of gelsolin secondary structure. The biggest conformational changes are likely to occur on S1-S3 binding with actin. It is possible that domain S3 separates from domain S1 before gelsolin N-half S1-S3 binding to actin.

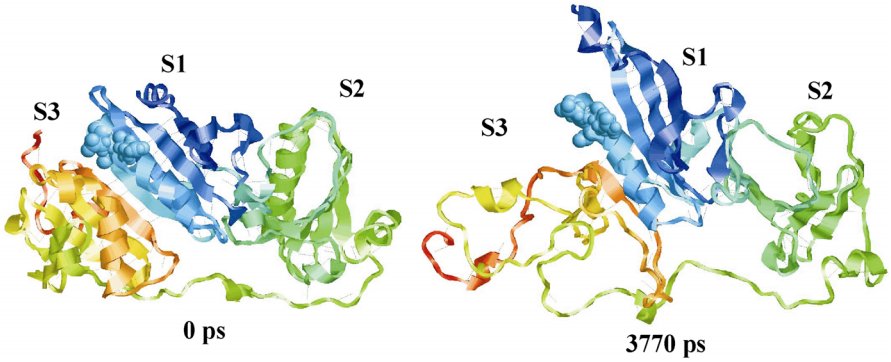

Fig. 1. Gelsolin S1-S3 at the start and after 3770ps of MD run. Actin binding residues 81,83,84, which were disclosed during the MD run, are represented in space fill mode.

Acknowledgments

The work was supported by NATO linkage grant LST.CLG.979807 and TASK computer center of Gdansk Technical University.

References

1. Kothakota, S., Azuma, T., Reinhard, C., Klippel, A., Tang, J., Chu, K., McGarry, T. J., Kirschner, M. W., Koths, K., Kwiatkowki, D. J. and Williams, L. T. *Science* **278**, 294-298 (1997).
2. Ohtsu, M., Sakai, N., Fujita, H., Kashiwagi, M., Gasa, S., Shimizu, S., Eguchi, Y., Tsujimoto, Y., Sakiyama, Y., Kobayashi, K. and Kuzumaki, N. *EMBO J.* **16**, 4650-4656 (1997).
3. Robinson, R. C., Mejillano, M., Le, V. P., Burtnick, L. D., Yin, H. L. and Choe, S. *Science* **286**, 1939-1942 (1999).
4. Liepina, I., Czaplewski, C., Janmey, P. and Liwo, A. *Biopolymers (Pept. Sci.)* **71**, 49-70 (2003).
5. Liepina, I., Czaplewski, C., Janmey, P. and Liwo, A. *J. Mol. Struct. THEOCHEM* **630,** 309-313 (2003).

Peptide Revolution: Genomics, Proteomics & Therapeutics
Michael Chorev & Tomi K. Sawyer (Editors)
American Peptide Society, 2003

Synthesis of Glutathione Peptidomimetics

Tunde Matola and Istvan Jablonkai

Department of Applied Organic Chemistry, Institute of Chemistry, Chemical Research Center, Hungarian Academy of Sciences, H-1025 Budapest, Hungary

Introduction

Alkylating agents are a class of clinically useful anticancer drugs. They can alter DNA replication by causing single- or double stranded DNA breaks and/or crosslinking [1]. A major limitation of their use in chemotherapy is the development of drug resistance due to multiple factors such as impaired cellular uptake, altered levels of tripeptide glutathione (GSH) and elevation of glutathione S-transferase (GST) activities leading to enhanced detoxication of chemotherapeutic agents [2]. GST isozymes are ubiquitous phase II detoxication enzymes catalyzing the conjugation of electrophilic cytotoxic chemicals with the biological nucleophile GSH yielding less toxic and water-soluble molecules. Overexpression of GSTs in tumor cells and emergence of drug resistance in chemotherapy resulted in an initiative for preparation of GST inhibitors [2].

Since the GSH-conjugates were found to be inhibitors of GSTs, a great number of esterified S-alkyl-glutathione analogues were synthesized. However, the use of inhibitory GSH-conjugates is limited due to their sensitivity towards peptidase-mediated breakdown. In contrast, only a few of non-peptidic GSH analogues were prepared [3, 4]. Non-peptide GSH bioisosters mercaptomethyl-alkane-dioic acids were inhibitory when the carbon skeleton was similar to that of GSH, which is an undecane carbon chain with the carboxylic acid groups at terminal positions [3]. However, undecene derivatives with isosteric *E* double bond were not inhibitors. Moreover, the N-methyltryptophan dehydrobutyrine diketopiperazine, a natural product, was not inhibitory to human GST-π, which is mostly related to tumour resistances [4].

Our objective was to prepare a new GSH isoster, 2-amino-7-mercaptomethyl-undecanedioic acid mimicking the GSH structure in which the sensitive peptide bonds were replaced by isosteric carbon-carbon bonds.

Results and Discussion

The initial strategy for the preparation of the undecane chain substituted with a mercaptomethyl group at position 5 was based on the synthesis of a decanealdehyde acetal intermediate constructed from two correspondingly functionalized five-carbon chain synthons. One-carbon homologation using the Strecker syntheses would have provided the required chain length. Starting from 1,2,6-trihydroxyhexane and 5-bromovaleric acid, 6-benzyloxy-1-methoxymethoxy-hexan-2-one and 5-bromo-1,1-dimethoxy-pentane [5] were prepared in multistep syntheses. However, both Grignard and Wittig reactions carried out with these reactants yielded the required 10-benzyloxy-1,1-dimethoxy-6-methoxymethoxymethyl-decan-5-ol and (10,10-dimethoxy-5-methoxymethoxymethyl-dec-5-enyloxymethyl)-benzene in very low yields (7% and 12%, respectively).

Due to the low yield of the key reaction step, the synthetic strategy was modified and started from dimethyl malonate as shown in Figure 1. The alkylation of malonic ester sequentially with 5-bromo-1,1-dimethoxy-pentane and 4-bromo-1-butene gave diester 1 in 60% yield. Decarbmethoxylation of diester 1 gave the corresponding monoester which was reduced to an alcohol and then converted to the

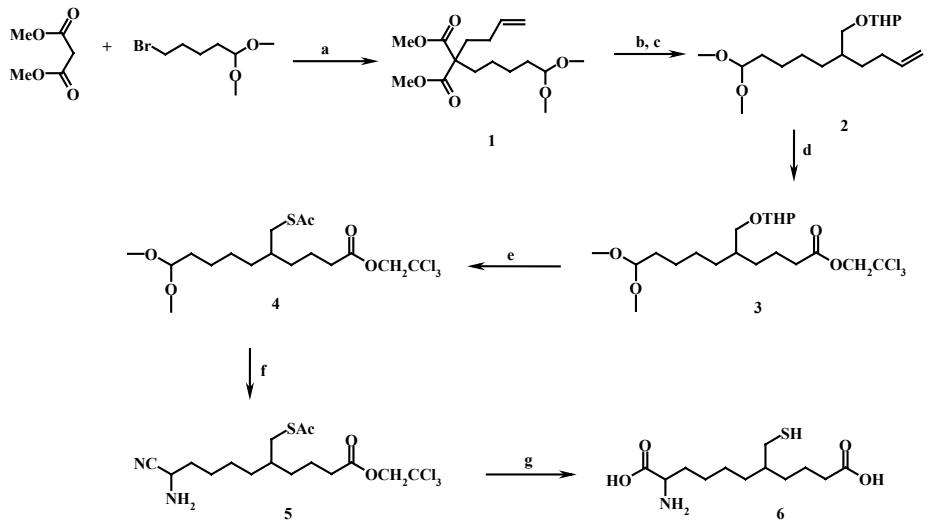

a: (1) NaH, DMF, 80º, (2) NaH, $BrCH_2CH_2CH=CH_2$, DMF, 60º, **b**:(1) NaCN, DMF, 150º, (2) $LiALH_4$, THF, **c**:dihydropyran, PPTS, **d**: (1) $HBBr_2{\cdot}SMe_2$, CH_2Cl_2, 40º, (2) PDC, DMF, (3) $HOCH_2CCl_3$, DCC, Pyr, **e**: (1) PPTS, EtOH/$CHCl_3$, (2) CH_3COSH, DEAD, PPh_3, **f**:(1) TsOH, acetone, (2) Strecker reaction, NH_4Cl, NaCN, **g**:NaOH, N_2

*Fig. 1. Synthesis of a GSH isosteric 2-amino-7-mercaptomethyl-undecanedioic acid (**6**).*

tetrahydropyranyl ether in 70% overall yield. Intermediate 2 containing a terminal double bond was converted to a carboxylic acid (72%) via the oxidation of the organoborane obtained by hydroboration using dibromoborane-methylsulfide reagent [6]. The carboxylic acid was protected as 2,2,2-trichloroethyl ester 3. Deprotection of the tetrahydropyranyl ether 3 followed by a Mitsunobu reaction afforded the acetylated thiol 4 (77%). The Strecker synthesis carried out with the aldehyde obtained after acidic deprotection of the dimethyl acetal resulted in α-amino nitrile 5 in good yield (87%). Hydrolysis of the nitrile under basic conditions also removed both 2,2,2-trichloroethyl and acetyl protections in one step, yielding the required glutathione peptidomimetic 2-amino-7-mercaptomethyl-undecanedioic acid (6) as a mixture of diastereomers (68%). A protein affinity chromatography will be used to evaluate the binding properties of 6 and its more cell-permeable carboxylic acid esters as well as N- and S-acyl and alkyl derivatives.

References

1. Hansson, J., *et al. Cancer Res.* **51**, 94-98 (1991).
2. Schultz, M., Dutta, S. and Tew, K. D. *Adv. Drug Deliv. Rev.* **26**, 91-104 (1997).
3. Klotz, P., *et al. J. Med. Chem.* **41**, 2278-2288 (1998).
4. Santamaria, A., Cabezas, N. and Avendano, C. *Tetrahedron* **55**, 1173-1186 (1999)
5. Trost, B. M. and Chen, W. C. D. *J. Am. Chem. Soc.* **118**, 12541-12554 (1996).
6. Brown, H. C. *et al. J. Org. Chem.* **57**, 6173-6177 (1992).

Peptide Revolution: Genomics, Proteomics & Therapeutics
Michael Chorev & Tomi K. Sawyer (Editors)
American Peptide Society, 2003

Aib Modified Dimerization Inhibitor of HIV-1 Integrase

Lei Zhao and Jean Chmielewski

Department of Chemistry, Purdue University, West Lafayette, IN 47907, USA

Introduction

A subset of interfacial peptides derived from HIV-1 integrase was found to be moderately potent inhibitors of the HIV-1 integrase 3'-processing activity [1]. The most potent inhibitors (α1, α5 and α6) of integrase activity were also able to disrupt the crosslinking of integrase dimer [1]. Since the inhibitors all adopt a random coil conformation in aqueous solution, extensive work to improve their helical propensity was undertaken to improve their potency. Peptide α5 was chosen for the study because the addition of 20% TFE was found to promote its helical conformation to 50%. As the residue Aib (α-aminosiobutyric acid) is known to limit ϕ and ψ values ($\pm$ 57° and $\pm$ 47°, respectively) and induce a helical conformation [2-3], it was introduced into the sequence of α5.

Results and Discussion

We designed five peptides with one or two residues replaced by Aib (Table 1). All the mutation sites are away from the dimerization interface (see Figure 1), and only hydrophobic residues were chosen for mutation. Agents α5(Aib_6) and α5(Aib_{10}) both have Val to Aib mutation, whereas α5(Aib_9) and α5(Aib_{12}) have mutations at Ala and Ile residues, respectively. A double mutant, α5($Aib_{6,10}$), was also designed to investigate the effect of two Aib residues. The peptides were prepared on the Rink resin [4] using an Fmoc-based synthetic strategy. The peptides were cleaved from the resin and purified to homogeneity by reverse phase HPLC. Each peptide was characterized by mass spectrometry and amino acid analysis, and evaluated for secondary structure by circular dichroism. The integrase assay of Craigie and coworkers was used to monitor 3'-endonuclease activity with a ^{32}P-labeled, double stranded oligonucleotide 21-mer probe [5].

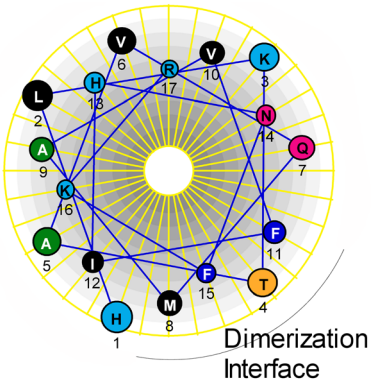

Fig. 1. Helical wheel representations of α5 of HIV-1 integrase.

According to the study, all peptides with a single mutation were found to adopt a random coil conformation in aqueous solution, indicating that a single Aib introduction

Table 1. Sequence and activity of peptides.

Peptide	Sequence	Conformation	IC_{50}
α5	HLKTAVQMAVFIHNFKR-$CONH_2$	Random coil	3 μM
α5(Aib_6)	HLKTA**Aib**QMAVFIHNFKR-$CONH_2$	Random coil	250 μM
α5(Aib_{10})	HLKTAVQMA**Aib**FIHNFKR-$CONH_2$	Random coil	125 μM
α5(Aib_9)	HLKTAVQM**Aib**VFIHNFKR-$CONH_2$	Random coil	125 μM
α5(Aib_{12})	HLKTAVQMAVF**Aib**HNFKR-$CONH_2$	Random coil	200 μM
α5($Aib_{6,10}$)	HLKTA**Aib**QMA**Aib**FIHNFKR-$CONH_2$	3_{10} helix	1 mM

to the sequence of α5 is not enough to induce helix formation. α5($Aib_{6,10}$) contains two Aib residues in the sequence. The CD spectrum showed that it adopted a 3_{10}-helix [6] conformation, instead of an α-helix. This result is not surprising since Aib is known to induce either α- or 3_{10}-helix [7].

Because α5($Aib_{6,10}$) was restricted to a 3_{10}-helix conformation and an α-helix conformation is presumed to be required for the interaction with HIV-1 integrase, its inhibition potency was very low (Table 1). For all the other peptides with a single mutation, their structure might be induced to form an α-helix upon binding to HIV-1 integrase, and their potencies were correspondingly higher than α5($Aib_{6, 10}$) (Table 1). But upon comparison to α5, the peptides with a single mutation were less potent, indicating the essential nature of the mutant residues.

In this study, we have demonstrated that introduction of Aib into the sequence of α5 favors a 3_{10}-helix, and decreases its inhibitory propensity. Other methods are currently underway to stabilize the α-helical conformation of the most potent inhibitors of HIV-1 integrase.

Acknowledgments
The authors are grateful to the National Institutes of Health for support of this work, and to the NIH AIDS Research Reagent Program for plasmid pINSD.His.Sol.

References

1. Zhao, L., O'Reilly, M. K., Shultz, M. D. and Chmielewski, J. *Bioorg. Med. Chem. Lett.* **13**, 1175-1177 (2003).
2. Marshall, G. R. and Bosshard, H. E. *Circ. Res*. **30/31**, *Suppl.* II, 143-150 (1972).
3. Fox, R. O. Jr. and Richards, F. M. *Nature (London)* **300,** 325-330 (1982).
4. Rink, H. *Tet. Lett.* **28**, 3787-3790 (1987).
5. Bushman, F. D. and Craigie, R. *Proc. Natl. Acad. Sci. U.S.A.* **88**, 1339–1343 (1991).
6. Yokum, T. S., Gauthier, T. J., Hammer, R. P. and McLaughlin, M. L. *J. Am. Chem. Soc.* **119**, 1167 (1997).
7. Karle, I. L. and Balaram, P. *Biochemistry* **29**, 6747-6756 (1990).

Peptide Revolution: Genomics, Proteomics & Therapeutics
Michael Chorev & Tomi K. Sawyer (Editors)
American Peptide Society, 2003

HIV-1 Protease Dimerization Inhibitors: Reversing the Southern Peptide

You Seok Hwang and Jean Chmielewski

Purdue University, Department of Chemistry, 560 Oval Dr.,West Lafayette, IN 47907-2038, USA

Introduction

The role of HIV protease in post-translational processing of the HIV gag/pol polypeptides has been established [1]. Due to its essential activity for the maturation and continued infectivity of HIV, the protease enzyme has been the target of a large number of therapeutic agents [2]. Although the currently approved FDA inhibitors are potent, the number of mutations that arise near the active site engenders viral resistance to many of the protease inhibitors [3]. These problems demonstrate the need for the development of an alternate method of protease inhibition.

The focus of our studies has been to target the dimerization interface of HIV-1 protease (PR) because disruption of the dimer will inhibit enzymatic activity [4]. The sequence of this region is also highly conserved through a number of HIV-1 isolates [5]. The initial strategy began with crosslinked peptides derived from the interface of HIV protease. Since the development of HIV-1 PR dimerization inhibitor **1**, extensive work to improve upon this class of inhibitors has been performed [6-7]. When smaller inhibitors such as **2** were developed the inhibitor lost potency against HIV-1 PR, and changed its mode of action from dimerization inhibition to competitive inhibition. One of our developments to overcome these drawbacks is to incorporate 12-aminododecanoic acid (12-Ado) as a tether to crosslink the interfacial peptides. This strategy enables us to change the directionality of the southern peptide from N → C to C → N in which the terminal amine can be used to incorporate various functional groups (Figure 1). Furthermore, fast screening for each amino acid residue is feasible because of its sequential solid phase synthesis. Compound **2** required a convergent synthesis, as it was not a continuous peptide.

Results and Discussion

The desired agents were synthesized using Fmoc chemistry on the Rink resin [8]. The resin-bound peptides were cleaved with 95 % TFA, 2.5 % water and 2.5% TIPS, and

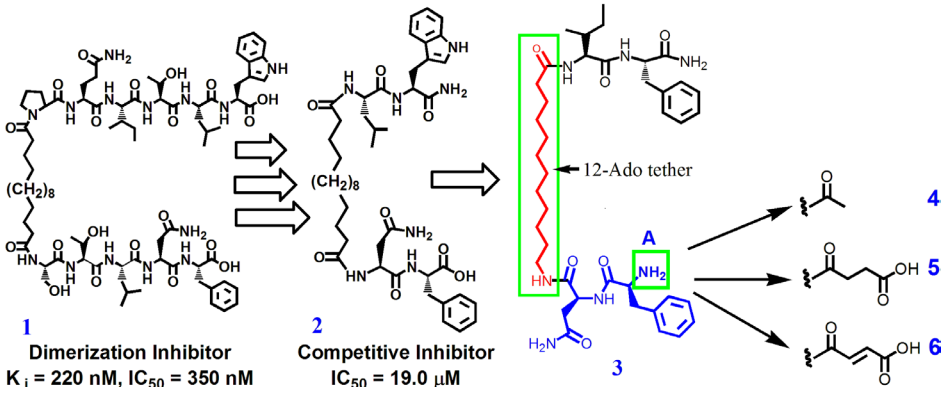

Fig. 1. Representative inhibitors used in this study.

the crude peptides were purified by RP-HPLC, analyzed by mass spectrometry, and quantified by amino acid analysis.

Four modifications (compounds **3**-**6**) were designed to determine which functional groups are important at position **A**. Percent inhibition of the agents was determined at various inhibitor concentrations (Table **1**). Functional modification at position **A** resulted in a significant change in activity. When comparing compound **2** to **3**, the decrease in potency by reversing the inhibitor direction may attribute to three features: 1) shortened tether length, 2) loss of the terminal acid functional group, and 3) disruption of β–sheet interaction between the agent and HIV-1 PR. Modification of the terminal amine (compound **3**) with an acetyl group (compound **4**) resulted in approximately two-fold decrease in potency. When the terminal acid functional group was recovered in compound **5**, inhibitory activity was increased by three-fold compared to compound **4**. However, the percent inhibition of the agent **5** was less than 50% up to 100 μM. By changing the functional group at position **A** from succinic acid (**5**) to maleic acid (**6**) the potency of agent **6** was increased dramatically and an IC_{50} value of 12 μM was obtained. Our binding model of the inhibitor **6**-PR complex showed that the maleic acid (Michael acceptor) of agent **6** is positioned 4.5 Å distance away from Cys **95** of HIV-1 PR. This data demonstrated the possibility that compound **6** may form a reversible, covalent bond with HIV-1 PR. Kinetic studies of **6** using the analysis developed by Zhang et al. [9] indicated that the inhibition observed occurred by the disruption of the protease dimer (K_i value of 4.9 μM).

*Table 1. Functional modified compounds at position **A** and their biological activities.*

Inhibitors	2	3	4	5	6
% Inhibition	ND[a]	< 35% at 100 μM	< 15% at 100 μM	< 50% at 100 μM	ND
IC_{50}	19.0 μM	ND	ND	ND	12.1 ± 0.4 μM
K_i	ND	ND	ND	ND	4.9 ± 0.1 μM

[a]*ND = not determined.*

In this study, we have demonstrated that the use of 12-Ado as crosslinking tether led to more potent inhibitors than compound **2,** and regained the ability to inhibit HIV-1 PR through a dissociative mechanism. Our binding model indicates the possibility that inhibitor **7** may form a reversible, covalent bond with HIV-1 PR.

Acknowledgments
We would like to acknowledge financial support from NIH (GM052739).

References

1. Oroszlan, S. and Luftig, R. B. *Curr. Top. Micro. Immunol.* **157**, 153-185 (1990).
2. Huff, J. R. and Kahn, J. *Advances in Protein Chemistry* **56**, 213-251 (2001).
3. Deeks, S. G., et al. *J. Am. Med. Assoc.* **227**, 145-153 (1997).
4. Bowman, M. J. and Chmielewski, J. A. *Biopolymers* **66**, 126-133 (2002).
5. King, R., et al. *Antiviral Res.* **28**, 13-24 (1995).
6. Zutshi, R., et al. *J. Am. Chem. Soc*. **119**, 4841-4845 (1997).
7. Shultz, M. D., et al. *Angew. Chem. Int. Ed.* **39**, 2710-2713 (2000).
8. Rink, H. *Tetrahedron Letters* **28**, 3787-3790 (1987).
9. Zhang, Z. Y., et al. *J. Biol. Chem.* **266**, 15591-15594 (1991).

Peptide Revolution: Genomics, Proteomics & Therapeutics
Michael Chorev & Tomi K. Sawyer (Editors)
American Peptide Society, 2003

CD Analysis of Structure and Lipid Interacting Property of Inhibitors of Proprotein Convertases

A. Basak, K. Beking, M. Chrétien and S. Basak

Regional Protein Chemistry Center, Diseases of Aging Program, Ottawa Health Research Institute, 725 Parkdale Ave, Ottawa, ON K1Y 4E9, Canada

Introduction

Activation of many biological proteins requires specific cleavages by the endoproteases proprotein convertases (PCs). PCs are Ca^{+2}-dependent subtilases that cleave at the consensus motif R/K/H-X-X/K/R-R↓, where X=any amino acid except Cys. PCs are implicated in many pathological conditions like tumor-genesis, neurological disorders, viral and bacterial infection [1]. This has generated a great deal of research interest in PC-inhibitors. Recently, we showed that peptides derived from prodomains inhibit PCs, although they often lack specificity [2]. We also demonstrated that attachment of dextroR_8 enhances cell permeability of PC-inhibitors [3]. Here we analyzed the secondary structures of these PC-inhibitors by circular dichroism (CD) [4] in various solvent, pH and phospholipid environments to study their effects in enzyme inhibition and membrane interaction.

Results and Discussion

We designed a number of inhibitors of Proprotein Convertases PC1, Furin, PC5 and PC7 (Table 1) based on their pro-domains and partner protein proSAAS [3] for PC1. These peptides inhibit cognate PCs, some with inhibition constants in low nM range. In addition we prepared several His to Ala mutants to determine the role of pH sensitive His in enzyme inhibition. We also attached a cell translocating peptide [dextroR_8] to the N-terminus of one of these inhibitors to enhance its cellular entry [3]. CD analysis of these peptides (Table 1, Figure 1) indicated a dominance of sheet and random structures in water (pH4-7) but not in TFE except for Furin$^{90\text{-}107}$ and PC1$^{55\text{-}6}$, both of which exhibited increased helices in either solvents. Interestingly, the cell permeable PC1-inhibitory pep #9 displayed an even higher content of sheet structure, which may possibly explain its enhanced cell translocating ability. Some correlation between enzyme inhibitory potency [3] and the content of sheet structure was noticed. Both pH and His to Ala mutation had minimal effects on secondary structures. As expected the cell permeable pep #9 showed strong interaction with a model phospholipid such as DGP (1,2-**d**ipalmitoyl rac-**g**lycero-3-**p**hosphocholine) as indicated by CD spectra in $CHCl_3$:MeOH (1:1) (Table 2**)**. Compared to pep #8 lacking R_8, its CD spectrum showed a strong shift of λ_{min} to lower wavelength upon interaction with lipid (Figure 2). Estimation by CD of secondary structural contents in presence of various amounts of a phospholipid indicated a significant enhancement in sheet structure of pep #9 and #10 in presence of excess lipid. In conclusion, a correlation is observed between sheet structure and enzyme inhibition potency. Moreover the cell permeable PC1-inhibitor exhibits increased lipid-interaction by CD, thus explaining its observed efficient delivery across the cell membrane.

Table 1. List of PC-inhibitory peptides and estimation of their secondary structures by CD.*

		Water				TFE			
Prodomain derived	Sequence	hx	s	t	r	hx	s	t	r
Pep#									
1 mPC1$^{39\text{-}62}$	NHYLFKHKSHPRRSRRSALHITKR	0	65	4	31	20	38	16	26
2 mPC1$^{39\text{-}62}$A^{40,45,48,58}	NAYLFKAKSAPRRSRRSALAITKR	0	13	29.5	59.5	43.5	31.5	0	25
3 mPC1$^{55\text{-}62}$	SALHITKR	22	26	0	52	25	29	0	46
4 mPC1$^{82\text{-}89}$A^{85}	SALAITKR	0	55.5	2.5	42	3.5	63.5	0	33
5 hPC5$^{71\text{-}80}$	QQVVKKRTKR	0	70	3	27	6.5	68	0	25.5
6 rPC7$^{95\text{-}104}$	EQRLLRRAKR	0	55.5	7.5	37	8	60.5	0	31.5
7 hFurin$^{66\text{-}83}$	EPQVQWLEQQVAKRRTKR	20.5	20	30.5	29	30.5	0	21	48.5
proSAAS derived									
8 hSAAS$^{234\text{-}246}$	VLGALLRVKRLE	0	67	0	33	19.5	28	14.5	38
Cell-permeable/control peptides									
9 R_8LnSAAS$^{234\text{-}246}$	R_8Ahx$_2$VLGALLRVKRLE	0	77	0	23	27	0	31	42
10 R_8Ln	R_8Ahx$_2$	4.5	82	2.5	11	0	82	2.5	15.5

**Estimated by "CD-estima" (Softwood Co), R=dextro-arginine, h=human, r=rat, m=mouse, Ln=Linker, Ahx=ε-amino hexanoic acid, hx=helix, s=sheet, t=turn, r=random.*

Table 2. Estimation of various secondary structural contents of cell permeable peptides in $CHCl_3$:MeOH (1:1) following interactions with the model phospholipid, DGP.

	Peptide:Phospholipid (DGP)											
	1:0				1:2				1:10			
	hx	s	t	r	hx	s	t	r	hx	s	t	r
Pep #8	16	33	20.5	30.5	14	38.5	17	30.5	19.5	26.5	25.5	28.5
Pep #9	13.5	45	18	23.5	13.5	40	18	28.5	5	70	4.5	20.5
Pep #10	0	81.5	1.5	17	0	83.5	0.5	16	1	84.5	0	14.5

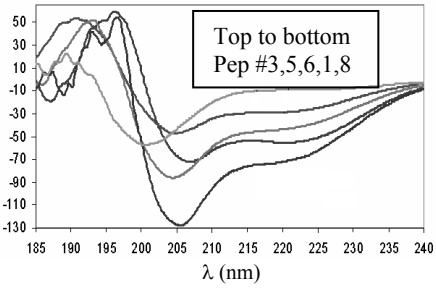

Fig. 1. CD Spectra of proPC peptides in TFE.

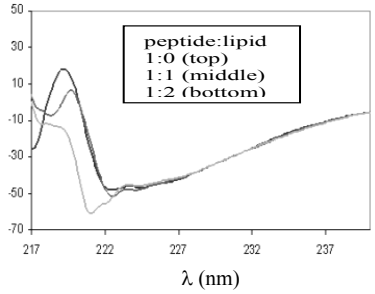

Fig. 2. Effect of phospholipid on CD of pept #9.

Acknowledgments

We acknowledge the financial support from CIHR and CFI, Canada.

References

1. Seidah, N. G. and Chrétien, M. *Brain Res*. **848**, 45-62 (1999).
2. Basak, A. and Lazure, C, *Biochem. J.* **373**, 231-239 (2003).
3. Basak, A., et al. In Lebl, M. and Hougten, R. (Eds.) *Peptides: The Wave of the Future (Proceedings of the 17th American Peptide Symposium),* APS, San Diego, 2001, pp. 558-560.
4. Johnson, Jr. W. C. *Protein Secondary Structure and Circular Dichroism: A Practical Guide, Proteins: Structure Function, and Genetics* **7**, 205-214 (1990).

Peptide Revolution: Genomics, Proteomics & Therapeutics
Michael Chorev & Tomi K. Sawyer (Editors)
American Peptide Society, 2003

Cellular Delivery and Design of Cell Transportable Inhibitors of Proprotein Convertases

A. Basak, F. Dong and S. Basak

Regional Protein Chemistry Center, Diseases of Ageing, Ottawa Health Research Institute, 725 Parkdale Avenue, Ottawa, ON K1Y 4E9, Canada

Introduction

Mammalian Proprotein Convertases (**PCs**) are Ca^{+2}-dependent serine proteases structurally related to bacterial subtilisin and yeast kexin. PCs cleave at the C-terminus of consensus motif **[R/K/H-X-X/K/R-R↓]**. They activate precursor proteins like growth factors, neuropeptides, hormonal peptides, transcription factors, bacterial toxins and viral glycoproteins and are linked to various pathologic conditions such as tumorigenesis, diabetes, neurological disorders, bacterial and viral infection [1]. PCs are thus considered as important therapeutic targets and as a result lot of research interest has focused on the development of PC inhibitors. A number of endogenous proteins of serpin (serine protease inhibitor) or other families such as α1-antitrypsin, α2-macroglobulin, turkey ovomucoid third domain, and eglin-C have been bioengineered to incorporate the recognition motif of PCs at the active site and thereby transform them into potent PC-inhibitors [2]. While significant progress has been achieved in macromolecule-based PC-inhibitors, little has been accomplished in small molecule PC-inhibitors. Such derivatives are more useful as biochemical and therapeutic agents because of their proteolytic stability and ease of preparation. However utilization of these molecules is often limited by the lack of their cell permeability. Recently various arginine, lysine and/or tryptophan-rich amino acid sequences have been shown to cross biological membranes efficiently and independently of transporters or specific reporters [3,4]. Attachment of such sequences to the N-terminus of a bioactive molecule may be an attractive approach for their cellular delivery. In fact we have recently demonstrated that dextro-R_8 when coupled to a PC1 inhibitor via a linker is capable of crossing the cell membrane and blocking PC1-mediated cleavage of POMC (pro-opiomelanocortin) into β-LPH (lypotropin hormone) [5]. Herein we have carried out further studies to examine the efficacy of various transporter peptides including the recently discovered pep-1 or pep-21 [4] as carrier for cellular delivery of small inhibitors of PC1 enzyme that resides in intracellular compartments. We have also tested their ability to block PC1-mediated proteolysis in cells.

Results and discussion

Design of cell transportable PC1-inhibitors: In earlier studies we showed that a 10-mer peptide (VLGALLRVKR) derived from the conserved region (235-244) of human/mouse proSAAS, a PC1-partner protein of granin family is a powerful and specific inhibitor of neuroendocrine convertase PC1 with inhibition constant of 51nM [5,6]. In order to enhance the cell permeability and bioavailability we have now attached via a spacer arm of 4-units of Ahx (ε-amino hexanoic acid), several cell transporter peptides such as pep-1 and its mutants, dextroR_8 and Tat^{48-64} [3] to the N-terminus of above PC1-inhibitor. Finally we incorporated a fluorescent tag at the N-terminus of the final peptides in order to monitor their cellular uptake (Table 1).

Syntheses were accomplished by Fmoc chemistry and acylating with 5-carboxy fluorescein at the last cycle [6].

Table 1: List of cell permeable fluorescent PC1-inhibitory and other peptides.

#	mts	Sequence	MW
1	Pep1	fl-K<u>ETW</u>W<u>E</u>TWWTEW<u>S</u>QPKKKRKV-Ahx$_4$-VLGALLRVKR	4763
2	Pep1-ES	fl-KETWW--TWWTEW--QPKKKRKV-Ahx$_4$-VLGALLRVKR	4547
3	Pep1-WS	fl-KET--WETWWTEW--QPKKKRKV-Ahx$_4$-VLGALLRVKR	4492
4	Pep1-E	fl-KETWW--TWWTEWSQPKKKRKV-Ahx$_4$-VLGALLRVKR	4634
5	Pep1-EE	fl-K--TWW--TWWTEWSQPKKKRKV-Ahx$_4$-VLGALLRVKR	4505
6	Pep1-TT	fl-KE--WWE--WWTEWSQPKKKRKV-Ahx$_4$-VLGALLRVKR	4561
7	Pep1	fl-KETWWETWWTEWSQPKKKRKV-Ahx$_2$-VLGALLRVKR	4537
8	R_8	fl-*RRRRRRRR*-Ahx$_2$-VLGALLRVKR	2954
9	none	fl-Ahx$_4$-VLGALLRVKR	1932
10	Tat$^{48-64}$	fl-GRKKRRQRRRPPQ-Ahx$_4$-VLGALLRVKR	3631

*fl=5-carboxy fluorescein, Ahx=ε-amino hexanoic acid, R=dextro-arginine, mts=**<u>m</u>**embrane **<u>t</u>**ransporter **<u>s</u>**equence; the deletion sites are indicated by underline.*

Effects on cellular PC1-mediated proteolysis: The designed peptide conjugates were tested *ex vivo* for their antiprotease activity in human pituitary AtT-20 cell line that contains PC1 and its substrate POMC. PC1 processes POMC to produce ACTH and β-LPH as initial products (Figure 1). Upon 6-hour incubation with 2-20μM peptides added exogenously to the cell media, these peptides block differentially the processing of POMC by PC1, as analyzed by Western blot on cell lysates using an antibody that recognizes both POMC and β-LPH. Pep-1 derived peptide#1 is most efficient as antiPC1 agent compared to Tat$^{48-64}$ peptide #10 or R_8 peptide #8. It exhibited >3-fold inhibition of POMC processing into βLPH compared to control under identical condition. It also blocks the above POMC processing ~2-fold better than that observed *ex vivo* with pro-SAAS expressing AtT-20 cells (Figure 2). Deletion of WS residues in Pep-1 led to a most significant loss in inhibition compared to peptides #5 and #6 suggesting their importance in interacting with cellular membrane (Figure 2). Both 4 and 2 units of Ahx are equally efficient as linker for cellular delivery since peptides #1 and #7 yielded similar results (*not shown*).

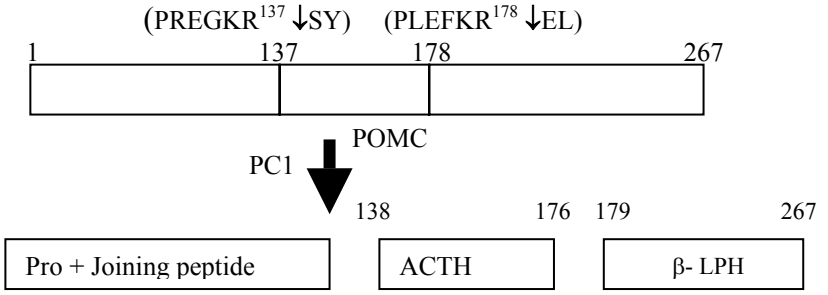

Fig. 1. Schematic diagram showing the PC1 cleavage sites of human <u>p</u>ro-<u>o</u>pio<u>m</u>elano<u>c</u>ortin (POMC).

Fig. 2. Western blot (Left Panel) and densitometric analysis (Right Panel) of AtT-20 cell lysates following 6-hour treatment with 20μM of different pep-1-derived PC1-inhibitory peptides Lanes 1=#1, 2=#5, 3=#6, 4=control, 5=AtT-20-SAAS cell line and 6=#3.

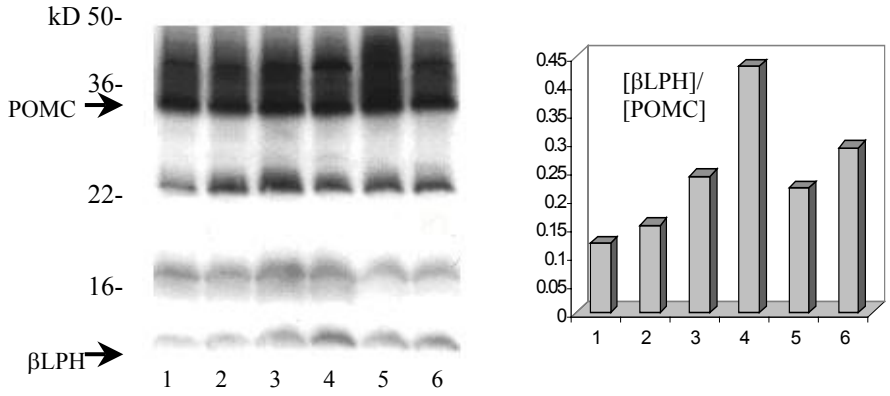

Cellular uptake: Both pep-1 derived fluorescent peptides #1 or 7 can efficiently cross AtT-20 cell membrane as they label most intracellular compartments compared to that observed with control peptide #9 that lacks the transportable peptide (Figure 3). A similar observation is also noted with R_8- and Tat^{48-64}-derived peptides #8 and #10.

In conclusion our data suggests that pep-1, dextroR_8 and Tat^{48-64} are all effective as cell carrier peptides for delivery of small PC1 and possibly other inhibitors across the cell membrane. Among these, pep-1 conjugated peptide is most efficient *ex vivo* PC1 inhibitor. Using the above strategy, study on the delivery of other PC-inhibitors such as those based on oxymethylene pseudopeptide is currently in progress.

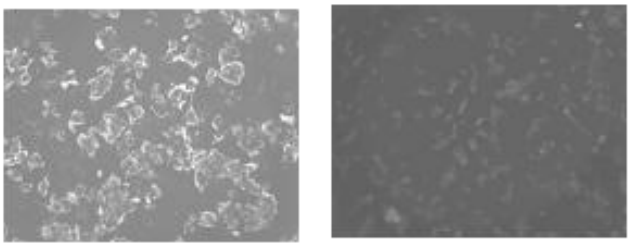

Fig. 3. Confocal microscopic image of AtT-20 cells following 6-hour incubation with 50μM fluorescent peptides. Left Panel: pep1-derived peptide #1 and Right Panel: control peptide #9.

Acknowledgment

CFI and Ottawa U for funding and Dr. M. Chrétien for support.

References

1. Seidah, N. G. and Chrétien, M. *Brain Res*. **848**, 45-62, (1999).
2. Fugere, M. and Day, R. *Curr. Pharm. Des.* **8**, 549-62, (2002).
3. Wright, L. R., Rothbard, J. B. and Wender, P. A. *Curr. Protein Pept. Sci.* **4,** 105-24, (2003).
4. Tayler, J. E and Patron, C. F. *Electrophoresis* **24,** 1331-1337, (2003).
5. Basak, A. et al. In Lebl, M. and Houghten, R. A. (Eds.) *Peptides: The Wave of Future, Proceedings 17th American Peptide Symposium,* APS, San Diego, pp. 558-560 (2001).
6. Basak, A. et al. *J. Biol. Chem*. **276**, 32720-8 (2001).

Peptide Revolution: Genomics, Proteomics & Therapeutics
Michael Chorev & Tomi K. Sawyer (Editors)
American Peptide Society, 2003

Immobilized Bivalent Inhibitors as Tools for the Affinity-based Isolation of Human Mast Cell Tryptases

Norbert Schaschke[1], Dusica Gabrijelcic-Geiger[2], Andreas Dominik[3] and Christian P. Sommerhoff[2]

[1]Max-Planck-Institut für Biochemie, D-82152 Martinsried, Germany; [2]Abteilung für Klinische Chemie und Klinische Biochemie in der Chirurgischen Klinik der LMU, D-80336 München, Germany; [3]Altana, D-78467, Konstanz, Germany

Introduction

Affinity chromatography is a powerful technique for the isolation and purification of proteins. In the particular case of proteases, reversible inhibitors are attractive ligands for the selective recognition and binding of the target enzyme. Recently, using a systematic distance scan, we identified a potent inhibitor of β-tryptases (**1**, K_i = 18 nM; see Figure 1) that interacts simultaneously with the negatively charged S1 pockets of two neighboring subunits of the tetrameric protease [1]. This unique inhibition mode allows for a selective recognition of this particular protease within the family of trypsin-like serine proteases and, thus, this bivalent inhibitor should be ideally suited as a ligand for an affinity-based isolation protocol of human mast cell tryptases.

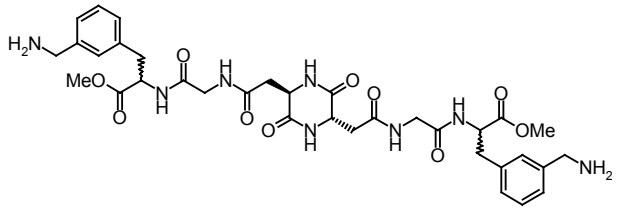

*Fig. 1. Structure of the bivalent inhibitor **1**.*

Results and Discussion

To immobilize the bivalent inhibitor **1** on a Sepharose-matrix, one of the amide nitrogens of the piperazine-2,5-dione scaffold was selected. The minimum length of the PEG-spacer to bridge the space between the anchoring point and the entrance of the central pore of β-tryptase was estimated from the docked inhibitor (*S*,*S*-diastereomer) to be ~ 20 Å. Therefore, to allow for an optimal interaction of the spacer-bound inhibitor with β-tryptase, a α,ω-diamino-PEG (M_r ~ 900) was selected. Finally, the methyl ester functions present in **1** were replaced by the corresponding methyl amides to allow for a regeneration of the affinity-matrix under basic conditions.

According to these design criteria, the bivalent inhibitor was synthesized and subsequently immobilized on NHS-activated Sehparose as shown in Figure 2. The modified scaffold was obtained by reacting cyclo-(D-Asp(OtBu)-L-Asp(OtBu)-) with $BrCH_2CO_2Bn$ in presence of Ag_2O [2] followed by cleavage of the *tert*-butyl ester groups using 95% aq TFA. The spacer-functionalized inhibitor was characterized by ESI-MS, and the data obtained are in full agreement with the structure. The concentration of the bound inhibitor was determined by quantitative amino acid analysis (0.5 μmol/mL swollen Sepharose).

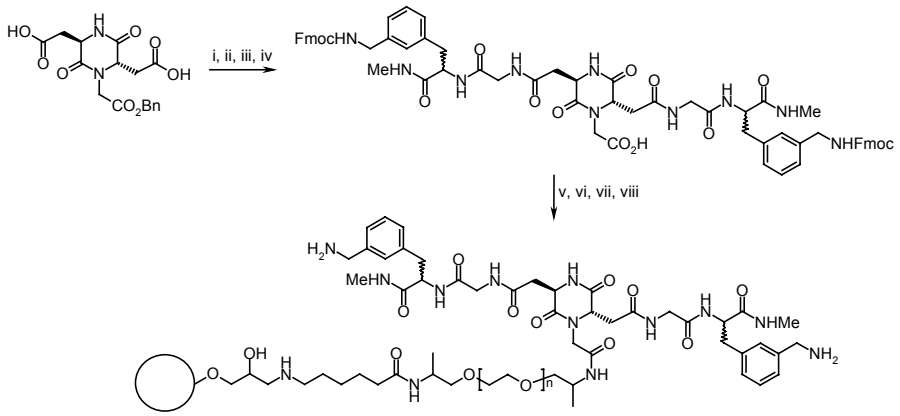

Fig. 2. Synthesis of the spacer-functionalized inhibitor and immobilization on a Sepharose-matrix. Reaction conditions: (i) H-Gly-DL-Phe(3-BocNH-CH_2)-NHMe/DIEA/EDC/HOBt, $CHCl_3$ (74%); (ii) 95% aq TFA, 0 °C → RT (88%); (iii) 10% Pd-C/H_2, MeOH (82%); (iv) Fmoc-OSu/$NaHCO_3$, dioxane/H_2O (2:1) (51%). (v) BocNH-CH(CH_3)-CH_2-(OCH_2CH_2)$_n$-OCH_2-CH(CH_3)-NH_2 (n = 12-18)/EDC/HOBt, $CHCl_3$ (83%); (vi) 95% aq TFA, 0 °C → RT (88%); (vii) a) NHS-activated Sepharose, iPrOH/0.2 M $NaHCO_3$-solution (1:9), b) 0.5 M ethanolamine, iPrOH; (viii) 5% piperidine/DMF.

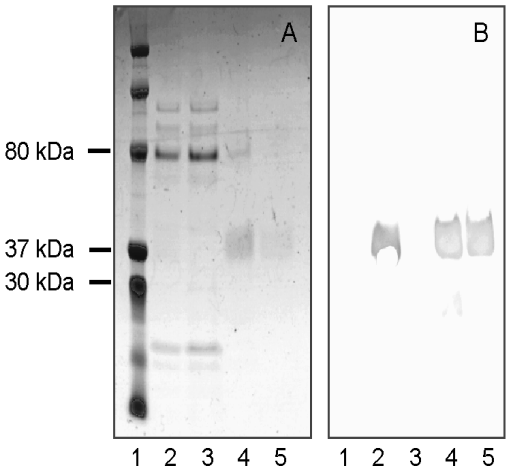

Fig. 3. Purification of β-tryptase by the inhibitor-functionalized Sepharose: (A) SDS-PAGE; (B) Western blot. Lane 1: molecular mass standards; Lane 2: partially purified β-tryptase from human lung tissue; Lane 3: flow-through, Lanes 4 and 5: eluted fractions.

To characterize the new affinity-matrix, partially purified β-tryptase derived from human lung tissue was used. As shown in Figure 3, the homogeneous protein fraction obtained by isocratic elution with Tris×HCl-buffer (50 mM, pH 7.6, containing 500 µg/mL heparin and 2 M NaCl) was identified as tryptase by Western blot analysis.

In conclusion, by using a structure-based design process we developed a novel affinity-matrix based on the bivalent interaction mode of the immobilized ligand with tryptases.

Acknowledgments

The study was supported by SFB 469 of the LMU Munich (Grants A2 and B6).

References

1. Schaschke, N., et al. *Bioorg. Med. Chem. Lett.* **12**, 985-988 (2002).
2. Falorni, M., Giacomelli, G., Nieddu and F. Taddei, M. *Tetrahedron Lett.* **38**, 4663-4666 (1997).

Peptide Revolution: Genomics, Proteomics & Therapeutics
Michael Chorev & Tomi K. Sawyer (Editors)
American Peptide Society, 2003

Cyclic Biphenyl Ether Tripeptides as Proteasome Inhibitors

Markus Kaiser[1], Alexander G. Milbradt[1], Christian Renner[1], Irmgard Assfalg-Machleidt[2], Michael Groll[1], Robert Huber[1] and Luis Moroder[1]

[1]Max-Planck-Institut für Biochemie, 82152 Martinsried; [2]Abt. Klinische Chemie und Biochemie, Ludwig-Maximilians-Universität, 80336 Munich, Germany

Introduction

TMC-95A is a cyclic tripeptide derivative, side-chain cross-coupled by an oxindole/phenol biaryl system (Figure 1, compound **1**) [1]. This secondary metabolite from *Apiospora montagnei* Sacc. TC 1093 was recognized as a highly selective and reversible inhibitor of proteasome, which binds to the active sites of the multienzyme complex via a network of hydrogen bonds between the β-type extended peptide moiety and the protein backbone [2]. Based on the X-ray crystallographic data, the markedly simplified analog **2** of the natural product was synthesized and was fount to retain most of its inhibitory activity [3]. The amino terminal *N*-(3-methyl)oxopentanoyl and C-terminal (*Z*)-(1-propenyl)amide groups were replaced by benzyloxycarbonyl and *n*-propylamide, respectively, and the highly oxidized form of the tryptophan could be reduced to the oxindolylalanine derivative which, however, proved to be essential for efficient ring closures of both the biaryl-containing linear precursor via the macrolactamization approach [3] and a suitable peptide derivative via intramolecular side-chain Suzuki cross-coupling [4].

According to the crystallographic analysis of the proteasome/TMC-95A complex, the main role of the biaryl system appears to be induction and stabilization of the extended peptide backbone conformation [2]. Since other biaryl systems such as biaryl ethers are known to exhibit the identical structuring properties when placed in i and i+2 positions of tripeptides [5], such structural modification of TMC-95A would further simplify the access to proteasome inhibitors. From modeling experiments of the possible 4,4´-, 3,4´ and 3,3´-biaryl ethers, the 3,4´-isomer appeared the most suitable to mimic the TMC-95A scaffold. Correspondingly, the biaryl ether compound **3**, shown in Figure 1, was synthesized to test the working assumption.

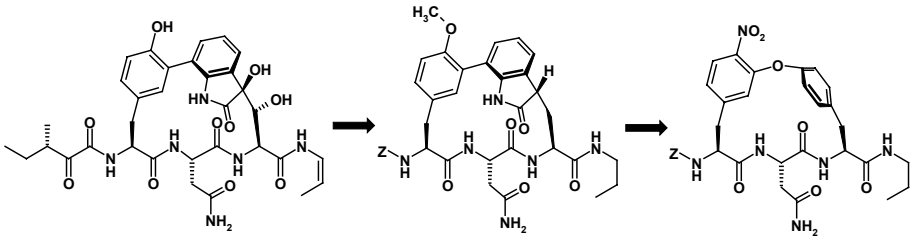

1 **2** **3**

*Fig. 1. Structure of the natural product TMC-95A (**1**), its simplified analog and (**2**) the mimetic compound **3** based on a biaryl ether system.*

Table 1. Inhibitory potencies of the proteasome inhibitors.

Inhibitor	K_i (μM)		
	Chymotryptic Activity	*Tryptic Activity*	*PGPH Activity*
Ac-Leu-Leu-Nle-H	1.4	364	≥ 2000
2	2.4	55	≥ 2000
3	5.5	74	≥ 2000

Results and Discussion

Among the various methods known for synthesis of biaryl ethers, the procedure of Beugelmans et al. [6] is based on the nucleophilic attack of the phenol on a fluorobenzol derivative activated by an *ortho*-nitro group. Since the phenolic group is fully solvent-exposed in the TMC-95A/proteasome complex, reaction of a Tyr residue as P2 on a (3-F,4-NO_2)-phenylalanine as P4 was selected for ring closure. The linear precursor was obtained in solution by coupling Z-Phe(3-F,4-NO_2)-OH with H-Asn-Tyr(TIPS)-NH(C_3H_7) via EDC/HOBt. Simultaneous deprotection of the Tyr residue and ring closure with TBAF followed by HPLC purification yielded **3** as analytically well characterized compound. A comparison of the inhibitory potencies of compounds **2** and **3** with the K_i values of the Ac-Leu-Leu-Nle-H as reference (Table 1) clearly revealed that binding affinities for the chymotryptic- and tryptic-like active sites of yeast proteasome were largely retained, thus confirming our hypothesis. To further investigate the structural effect of the biaryl ether system, a conformational analysis was performed on compound **3** and the resulting structure was compared to those of TMC-95A and its analog **2**. It observed that the peptide backbones are largely superimposable with the main deviation observable for the C-terminal 1-propenylamide group, which according to the X-ray analysis acts as P1 residue.

The results of this study confirm that the oxindole/phenol system of TMC-95A can be efficiently replaced by a biaryl ether system, which lends itself for solid phase synthesis of reversible proteasome inhibitors by replacement of the propylamine residue with amino acid derivatives.

Acknowledgments

The work was supported by Grants A2 and A6 of the SFB 469 of the Ludwig-Maximilians-University of Munich.

References

1. Koguchi, Y., Kohno, J., Nishio, M., Takahashi, K., Okuda, T., Ohnuki, T. and Komatsubara, S. *J. Antibiot.* **53**, 105-109 (2000).
2. Groll, M., Koguchi, Y., Huber, R. and Kohno, J. *J. Mol. Biol*. **311**, 543-548 (2001).
3. Kaiser, M., Groll, M., Renner, C., Huber, R. and Moroder, L. *Angew. Chem. Int. Ed*. **41**, 780-783 (2002).
4. Kaiser, M., Siciliano, C., Assfalg-Machleidt, I., Groll, M., Milbradt, A. G. and Moroder L. *Org. Lett.* **5**, 3435-3437 (2003).
5. Janetka, J. W., Raman, P., Satyshur, K., Flentke, G. R. and Rich, D. H. *J. Am. Chem. Soc.* **119**, 441-442 (1997).
6. Beugelmans, R., Bigot, A., Bois-Choussy, M. and Zhu, J. *J. Org. Chem.* **61**, 771-774 (1996).

Peptide Revolution: Genomics, Proteomics & Therapeutics
Michael Chorev & Tomi K. Sawyer (Editors)
American Peptide Society, 2003

Triple-Helical Peptide Ligand Dissection of Unique Melanoma Cell Signaling Pathways

Janelle L. Lauer-Fields, Mohammad Al-Ghoul, Diane Baronas-Lowell, Jeffrey A. Borgia and Gregg B. Fields

Dept. Chemistry & Biochemistry, Florida Atlantic University, Boca Raton, FL 33431, USA

Introduction

The metastatic process involves tumor cell adhesion to basement membrane components, such as type IV collagen, participation in the destruction of these constituents, and movement through them. These interactions are known to occur through several families of cell surface receptors, including the integrins and cell surface proteoglycan receptors (such as CD44). Ligand binding with receptors triggers a series of intracellular signaling events that ultimately result in the release of growth factors and proteases. Increased proteolysis eventually results in basement membrane degradation, liberation of cell surface receptors, and growth factor activation, all of which are often beneficial for tumor cell progression [1]. Triple-helical binding sites for the $\alpha1\beta1$, $\alpha2\beta1$, and $\alpha3\beta1$ integrins and CD44/chondroitin sulfate proteoglycan (CSPG) have been identified within type IV collagen [2-5]. One can use triple-helical ligands to link discrete receptor engagement with a specific signaling outcome by monitoring the downstream events of signaling pathways. In the present study, we have chosen matrix metalloproteinases (MMPs) as our initial targets of downstream signaling, due to their roles in matrix remodeling and growth factor release, and overall implication in tumor cell metastasis.

Results and Discussion

We constructed triple-helical peptide (THP) ligands for two melanoma cell receptors (Figure 1), and used these ligands to determine if the $\alpha2\beta1$ integrin and CD44/CSPG (a) have distinct MMP signaling pathways and (b) have signaling pathways affected by ligand triple-helical conformation and glycosylation. The $\alpha2\beta1$ integrin and CD44/CSPG ligands are derived from $\alpha1$(IV)402-413 and $\alpha1$(IV)1263-1277, respectively [4,5]. All triple-helical ligands were conformationally stable under assay conditions. Ligands were passively adsorbed onto non-tissue culture treated polystyrene plates/flasks. Highly metastatic human M14 melanoma cells were grown on each ligand in the absence of serum. RNA and conditioned media were collected at various time points and assayed for alterations in (a) mRNA levels (via RT-PCR), (b) protein content (via ELISA), and (c) enzyme activity (via zymography and modified ELISA utilizing fluorogenic substrates).

$\alpha2\beta1$ ligand C_{16}-$(GPP^*)_4$-GAP*GFP*GERGEK-$(GPP^*)_4$-NH_2
CD44 ligand C_{16}-$(GPP^*)_4$-GVKGDKGNPGWPGAP-$(GPP^*)_4$-NH_2

Fig. 1. Sequences of melanoma cell receptor ligands (P = 4-hydroxy-L-proline).*

Significant differences were observed with MMP targets, such as an increase in MMP-8 expression in response to the CD44 ligand only (Figure 2). Conversely, the $\alpha2\beta1$ integrin ligand alone modulated an increase in MMP-13 and MMP-14 (Figure 2). These results are indicative of specific activation sequences that tumor cells undergo

upon binding to select regions of basement membrane collagen. Conversely, MMP-1 is modestly increased by both ligands (Figure 2). While both receptors can induce the expression of collagenolytic proteases, only the α2β1 integrin affected MMP-14, an activator of other MMPs (such as MMP-2). Loss of triple-helical structure for either ligand, either partial or complete, significantly quenched cellular responses, as did single-site glycosylation of the α1(IV)1263-1277 region (data not shown).

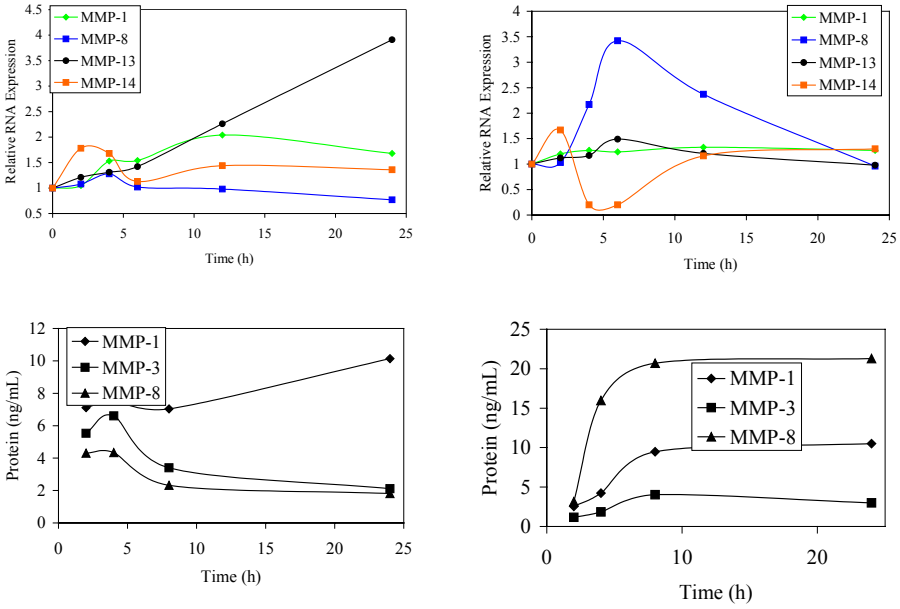

Fig. 2. mRNA (top panels) and protein (bottom panels) expression of MMP targets induced by ligands for the α2β1 integrin (left panels) and CD44/CSPG (right panels).

A modified ELISA assay utilizing a triple-helical fluorogenic substrate [6] quantified active enzyme (Figure 3). Higher levels of active MMP-1 were seen in response to α2β1 integrin ligation. In a separate assay, conditioned media were then either mixed with a selective triple-helical MMP-2/MMP-9 substrate [4] or assayed by gelatin zymography. Whereas mRNA results indicated no modulation of MMP-2, active enzyme was clearly upregulated (Figure 4). MMP-2 activation can be achieved via MMP-14 upregulation as well as TIMP modulation. We are not certain which pathway is being utilized in our system, but tests to elucidate the mechanism are ongoing.

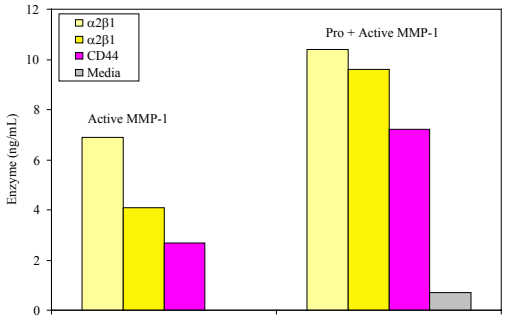

Fig. 3. Active MMP-1 expression.

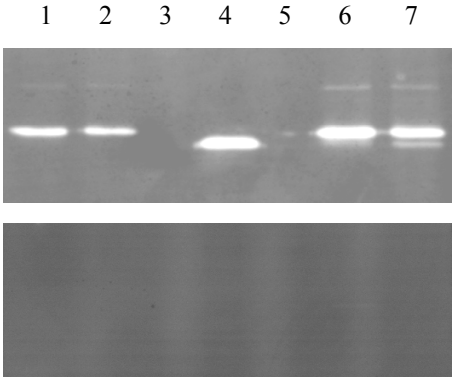

Fig. 4. Zymographic analysis of conditioned media from M14 cells grown for 12 or 24 h on the α2β1 ligand (lanes 2 and 7) or the CD44 ligand (lanes 1 and 6). Lane 4 contains MMP-2, while lanes 3 and 5 are empty. The bottom gel consists of the same samples run in the presence of 1,10-phenanthroline.

Triple-helical ligands for CD44 and the α2β1 integrin were found to promote expression of MMPs with differing downstream events. Linear constructs do not promote significant levels of MMP expression, further supporting the notion that triple-helical conformation selectively modulates cellular activity [7,8]. Clearly, different ligands produce different signaling outputs. Our ability to predict downstream events for discrete receptor ligation will improve our understanding of how individual cell surface receptors contribute to melanoma progression as well as aiding the design of new therapeutics.

Acknowledgments
The work was funded by the NIH (CA77402 and CA98799 to G.B. Fields).

References

1. Alessandro, R. and Kohn, E. C. *Clin. Exp. Metastasis* **19**, 265-273 (2002).
2. Miles, A. J., et al. *J. Biol. Chem.* **270**, 29047-29050 (1995).
3. Saccá, B., et al. *ChemBioChem* **9**, 904-907 (2002).
4. Lauer-Fields, J. L., et al. *J. Biol. Chem.* **278**, 18140-18145 (2003).
5. Lauer-Fields, J. L., et al. *J. Biol. Chem.* **278**, 14321-14330 (2003).
6. Lauer-Fields, J. L., et al. *Biochemistry* **40**, 5795-5803 (2001).
7. Lauer, J. L., Gendron, C. M. and Fields, G. B. *Biochemistry* **37**, 5279-5287 (1998).
8. Malkar, N. B., Lauer-Fields, J. L., Borgia, J. A. and Fields, G. B. *Biochemistry* **41**, 6054-6064 (2002).

Peptide Revolution: Genomics, Proteomics & Therapeutics
Michael Chorev & Tomi K. Sawyer (Editors)
American Peptide Society, 2003

Synthesis of $(Ac\text{-}XFRSLK)_2$ -Rhodamine 110

Xiao-He Tong and Anita Hong

AnaSpec, Inc., 2149 O'Toole Ave. # F, San Jose, CA 95131, USA

Introduction

Non-fluorescent bis-substituted peptide derivatives of rhodamine 110 (R110), which are intracellularly cleaved to green fluorescent mono-substituted R110 and free R110, proved to be more sensitive substrates for fluorometric assays [1]. Recent increasing awareness of the advantage of R110 derivatives in assay research has resulted in an interest in the synthesis of long chain R110 derivatives. Bis-substituted R110, such as $(dipeptide)_2$-R110 [2] and $(Z\text{-}DEVD)_2$-R110 [3], have been synthesized using sequential coupling method in solution phase. We have noted difficulty in the work-up stage if this method is employed for synthesis of long-chain bis-peptide-R110s. We have also noted difficulty in direct coupling short peptides to R110 to obtain products in good yield. Diwu's group also reported similar results when they attempted to directly couple protected Z-DEVD peptide to R110 [3].

Results and Discussion

Here we describe a novel synthetic strategy that greatly simplifies and increases the ability to construct long-chain bis-peptide-R110s. For the synthesis of the title compound, K_2-R110 was prepared by the reaction of R110 with 10-20 equiv. Fmoc-Lys(Boc)-OH and EDC in DMF/Pyridine, the Fmoc group was removed in Piperidine/ DCM (90%, Figure 1). The protected Ac-XFRSL peptide was easily coupled to $[Lys(Boc)]_2$-R110 to give protected $(Ac\text{-}XFRSLK)_2$-R110. Removal of the protected group was accomplished using TFA/H_2O/Phenol/DTT/Thioanisol (82.5:5:5:2.5:5) to give crude $(Ac\text{-}XFRSLK)_2$-R110 in good % yield.

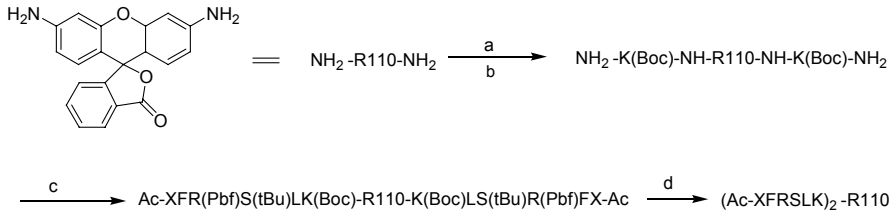

Fig. 1. Synthesis of $(Ac\text{-}XFRSLK)_2$ –R110. (a) Fmoc-Lys(Boc)-OH/EDC/Pyridine/DMF; (b) DCM/Piperidine (8:2); (c) Ac-XFR(Pbf)S(tBu)L-OH / HBTU/DIEA; (d) TFA/H_2O/ Phenol/Thioanisole/DTT.

After purification by RP-HPLC, we obtained pure $(Ac\text{-}XFRSLK)_2$-R110 (Figure 2). Using this method, we successfully synthesized other bis-peptide-R110 compounds, such as $(XXALRRASLKG)_2$-R110, $(XXYGAFKRRG)_2$-R110, $(XXLNR\text{-}TLSFAEPG)_2$-R110, and $[XX(pY)ANAARRG]_2$-R110.

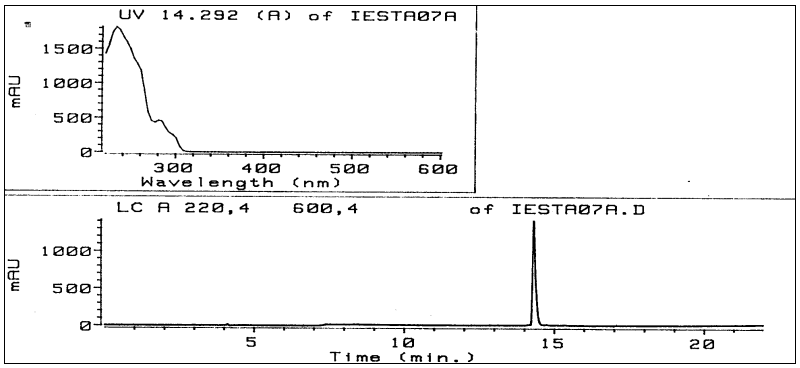

Fig. 2. RP-HPLC of (Ac-XFRSLK)$_2$-R110, A: 0.1% TFA/H_2O, B:0.09%TFA/MeCN; 1 ml/min, 10-70% B for 20 min.

References

1. Rothe, G., Klingel, S., Assfalg-M., I., Machleidt, W., Zirkelbach, C., Banati, R. B., Mangel, W. and Valet, G. *Biol. Chem. Hoppe-Seyler* **373**, 547-554 (1992).
2. Leytus, S. P., Patterson, W. L. and Mangel, W. F. *Biochem. J.* **215**, 253-260 (1983).
3. Liu, J., Bhalgat, M., Zhang, C., Diwu, Z., Hoyland, B. and Klaubert, D. H. *Bioorg. Med. Chem. Lett.* **9**, 3231 (1999).

Peptide Revolution: Genomics, Proteomics & Therapeutics
Michael Chorev & Tomi K. Sawyer (Editors)
American Peptide Society, 2003

Synthesis and Activity of a Novel Peroxidase Mimetic Peptide

Yali Liu,[1] Lili Guo,[2] Hui Yang,[1] Jingming Zhang,[2] Roger W. Roeske[2] and Wei Li[1]

[1]College of Life Science, Jilin University, Changchun, 130023, P.R. China; [2]Department of Biochemistry and Molecular Biology, Indiana University School of Medicine, Indianapolis, IN 46202, USA

Introduction

Cataracts are one of the most important causes of blindness. As our knowledge of the mechanism of oxidative damage in cataracts has evolved [1], anti-oxidants, especially peroxidase mimetics, have been used to develop agents to protect the eye and cure cataracts. Octapeptide MP-8, nonapeptide MP-9 (Figure 1 A), and undecapeptide MP-11 derived from cytochrome C are good mimics of peroxidase, whose anti-oxidative activities have been tested in cataract model experiments *in vitro* [2]. But the isolation and purification of these peptides from the proteolysis of cytochrome c is difficult, and they are also unstable, all of which hindered their clinical application [3]. Based on the molecular structure of peroxidase with heme as a prosthetic group and the structure of microperoxidase MP-9 [4], we designed a polypeptide DhHP-9 (Deuteroheamin-His-peptide amide: Dh-AAQAHTVEK-NH_2), by having histidine and deuterohaemin as peroxidase mimics (Figures 1B and 1C). The peroxidase-like activity of the mimics and their effect in protecting galactose-induced cataract *in vitro* were studied.

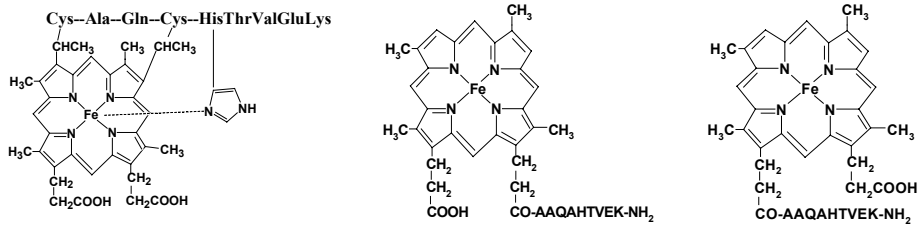

A B C

Fig. 1. Structures of the peroxidase mimics, A: MP-9; B and C are isomers of DhHP-9.

Results and Discussion

The nonapeptide DhHP-9 was synthesized using Fmoc chemistry on Fmoc-amide resin (0.68 mmol/g, 0.25mmole) in an ABI 431 peptide synthesizer. Deuterohaemin was incorporated into the peptide by coupling with Bop and HOBt. The resulting DhHP-9 is a mixture, probably equimolar, of the isomeric compounds B and C. Following deprotection and cleavage with TFA and anisole, the crude DhHP-9 was purified by C_{18}RP-HPLC (Vydac 218TP101550) with a gradient of 5-40% B (B: 70% CH_3CN in aq. 0.09% TFA). Purified DhHP-9 was identified by electron spray mass spectroscopy.

There were two concerns in the synthesis of the compound. First, the cleavage medium containing EDT was found to cause the loss of the Fe^{3+} ion from the deuterohaemin. The Fe^{3+} will be reduced to Fe^{2+} in the presence of ethanedithiol and be detached from the porphyrin ring in an acidic medium. The problem was avoided by

using TFA/anisole as cleavage/deprotection reagent. The second problem was formation of a bis-peptide compound (both the carboxyl groups of deuterohaemin attached to the nonapeptide). Since the dimer has only 13% of the activity of the monomer-DhHP-9, which probably is caused by competitive coordination of two histidines with one ferric ion, we have optimized the conditions for synthesis of the monomer. Our data suggests that resin with low degree of substitution favors the formation of the monomer product. The ratio of coupling reagent to deuterohaemin should be 1:1 (only half of the carboxyl group of the deuterohaemin would be activated).

Peroxidase enzymatic activity of DhHP-9 was measured by degrading H_2O_2 and tert-butyl hydroxyl radical in ascorbate-specific peroxidase test. The specific activity is 2.69×10^3 U/μmol with H_2O_2 as the substrate, which is 64% of the MP-9 activity under the same condition. The specific activity of DhHP-9 is 2.28×10^3 U/μmole with tert-butyl hydroperoxide as the substrate (1 U DhHP-9 can catalyze 1 μg ascorbate per minute). The enzyme activity of DhHP-9 increased with increasing DhHP-9 concentration and reached a maximum value, indicating that it obeys enzyme kinetics. In 0.5mM of ascorbate in 50mM PB, PH 7.0, dependence of reaction rate on H_2O_2 or on tert-butyl hydroperoxide was hyperbolic with Km 2.2μM and Km 56.8μM respectively, which showed Michaelis-Menten kinetics.

It has been shown that the catalytic site in peroxidase with heme as a prosthetic group consists of Fe^{3+} and His, while basic amino acids also contribute to the catalytic activities of the enzyme [5]. Our results showed that when His was replaced by Ala in DhHP-9, the enzymatic activity was reduced to 19% of the activity of DhHP-9. The loss of Fe^{3+} was also associated with the loss of the enzymatic activity. A Lys to Ala substitution slightly reduced the enzymatic activity, which suggests that Lys, although it contributes to the enzymatic activity, is not the primary residue responsible for the catalytic activity.

A cataract model of rat lens was generated by galactose induction, mimicking a type of cataract caused by diabetes. Microphotograph image showed significant inhibition of lens opacification by addition of DhHP-9, and the lenses could maintain transparency for a longer time. In contrast, in the absence of DhHP-9, the lens with galactose developed lens opacification, which eventually leads to maturity onset cataract.

References

1. Spector, A. *FASEB J.* **9**, 1173-1182 (1995).
2. Spector, A., et al. *Exp. Eye Res.* **65**, 457-470 (1997).
3. Aron, J., et al. *J. Inorg. Biochem*. **27**, 227-243 (1986).
4. Baldwin, D., Mabuya, M. and Helder, M. *S. Afr. J. Chem*. **40**, 2, 103-110 (1987).
5. David, A., Helder, M. and John, M. *FEBS Lett.* **183**, 2, 309-311 (1985).

Peptide Revolution: Genomics, Proteomics & Therapeutics
Michael Chorev & Tomi K. Sawyer (Editors)
American Peptide Society, 2003

Novel Potent Peptides that Regulate Phenoloxidase Activity

Takashi Sato, Chihiro Awada and Yoshimi Ogata

Department of Applied Biological Sciences, Saga University, Saga 840-8502, Japan

Introduction

Melanogenesis is considered to be crucial in insects for their growth and maintenance of life, such as sclerotization and tanning of cuticle during metamorphosis and also defense by clotting foreign pathogens with melanin and/or other biopolymers generated by oxidative condensation [1]. This cascade of reactions requires the activation of phenoloxidase (PO), which catalyzes an initial and rate-limiting step of complex reactions: oxidation of catecholamines to quinones. Activation of PO itself is also the final step of a long complex cascade that is triggered by exo-/endotoxins and also by hormonal stimulation. Although the mechanism of PO activation has been elucidated, regulation of activated PO that is necessary for protecting organs from excess and harmful oxidation is still unclear.

Recently, phenoloxidase inhibitor, POI, had been found in housefly pupae. POI is a novel 38 amino acid residues peptide that has a unique structure containing three disulfide bridges similar to several conus neuronal toxins [2] (Figure 1) and also contains a novel post-translational modification on Tyr^{32} (it is converted to DOPA [3,4-L-dihidroxy-phenylalanine] in the actual molecule). POI inhibits PO activity with *K*i value of 10^{-9}M to 10^{-10}M order in competitive manner [3] that is distinguishably more potent than native and synthetic inhibitors described to date.

However, the question still remains because the content of POI was found to be very little and not comparable to the total PO activity found *in vivo* even on the period when apparent PO activity is almost suppressed and the content of activated PO is found to be not changed in their amount analyzed by western-blot analyses.

In this study, to determine the actual regulating factor(s) for phenoloxidase *in vivo*, we performed affinity and extensive studies as described below to identify fractions containing comparable amounts of inhibitory activities for phenoloxidase.

POI H-AVTDNEIVPQ**C**LANGSK**C**YSHDV**CC**TKR**C**HN(Y)AKK**C**VT
ω-GVIA H-**C**KSOGSS**C**SOTSYN**CC**RS**C**NOYTKR**C**Y-NH_2

Fig. 1. Sequences of POI and ω-conotoxin GVIA from Conus geographs. The characters (Y) and O denote dopa and 4-trans-hydroxyprolyl residue, respectively.

Results and Discussion

Changes of apparent PO activities *in vivo*, in the housefly hemolymph, were reexamined from the very early stage of the larvae to the period of adult emergence. It was found that apparent activities of PO were dramatically changed from the undetectable levels in the early stage of larvae to the most prominent at the final instars of larvae, suggesting PO are strongly relating to the phenomena found in metamorphosis, in this stage cuticular tanning and sclerotization. The peak of *in vivo* PO activities are also found in the middle stage of the pupae as reported [4] and it was lost at the final stages in pupae and also in the periods of adult emergence. This supports the idea that the cascade reactions started by PO are correlated to the phenomena during their metamorphosis.

On the other hand, PO inhibitory activities *in vivo* were scanned for 11 days in the interval of 6 hr from hatching to adult emergence but for the periods when the activity dramatically changes are for 3 hr. Prior to assay for PO activities, the hemolymph was treated by two methods: PO mediated direct affinity process of hemolymph and solid extraction procedure (SEP) for peptides and small proteins. Interestingly, in both methods the apparent inhibitory activities were not found in the stages of larvae where prominent PO activities are observed. During the period in pupae, it makes two pinnacles of inhibitory activities sandwiching both ends of the second peak of apparent PO activity found in pupae. By considering together with the fact of western blot analyses, where the amounts of activated PO is not changed during this stage, the changes in PO activities in the periods of pupae are made by the difference in the level of the inhibitory activities co-expressed in the hemolymph. The values of inhibitory activities found there are about 600 U/100g samples which is comparable to or more than the apparent values of PO activities found at the time the second top of activities found (about 350 U/100g samples) which supports our hypothesis. The treatment of protein denaturalization of the crude extract when the apparent PO activities were not found generates another several hundreds units of inhibitory activity in the solution. Again, this suggests the loss of activity was caused by the formation of tight inert complex with PO and PO regulator(s). Moreover, another small peak of inhibitory activity was observed at the final stage of the pupae, and confirmed that the hemolymph at the time contains POI by further purification and molecular characterization.

Finally, to analyze and characterize all the components that act as the PO regulator(s) during their growth, we used the 'peptidome' approach employing extensive size exclusion HPLC followed by reverse phase separation. SEP treated samples for every 6 hr were two dimensionally analyzed. By these analyses, we found novel two PO regulating peptides with 42kDa and 8kDa, respectively, and intriguing changes of the peptide contents during these periods. Strikingly, expression of these two novel peptides corresponded to the former and the latter peaks sandwiching the second prominent of PO activity. Moreover, those two peptides inhibited PO with uncompetitive and non-competitive mechanism that is different manner of inhibition neither to POI nor to each other, suggesting these peptides are dictated various functions to regulate PO activity in vivo and those three peptides sharing complex roles to regulate multi-functional enzyme, PO, for each aspects of their activities.

Acknowledgments

The work was supported by Grants-in-Aid for Scientific Research from the Ministry of Education, Science and Culture of Japan, as well as SUNBOR GRANT from Suntory Institute for Bioorganic research.

References

1. Hopkins, T. L. *Science* **217**, 364-366 (1982).
2. Daquinag, A. C., Sato, T., Koda, H., Takao, T., Fukuda, M., Shimonishi, Y., Tsukamoto, T. *Biochemistry* **38**, 2179-2188 (1999).
3. Daquinag, A. C., Nakamura, S., Takao, T., Shimonishi, Y. and Tsukamoto, T. *Proc. Natl. Acad. Sci. U.S.A.* **92**, 2964-2968 (1995).
4. Hara, T., Tsukamoto, T., Maruta, K. and Funatsu, M. *Agric. Biol. Chem.* **53**, 1387-1393 (1989).

Peptide Revolution: Genomics, Proteomics & Therapeutics
Michael Chorev & Tomi K. Sawyer (Editors)
American Peptide Society, 2003

Methanethiosulfonyl Derivatives of Linear and Cyclic Peptides as Novel Reagents to Study Topology of Active Center Gorge of Acetylcholinesterase

Peteris Romanovskis[1], Terrone L. Rosenberry[2], Bernadette Cusack[2] and Arno F. Spatola[1]

[1]Department of Chemistry and the Institute for Molecular Diversity and Drug Design, University of Louisville, Louisville, KY 40292 USA; [2]Department of Neuroscience at Mayo Clinic, Jacksonville, FL 32224 USA

Introduction

Site-specific mutagenesis of H287C in the acetylcholinesterase (AChE) molecule has introduced a point on the enzyme surface where a covalent bond formed by thiol-specific reagents can be attached. Methanethiosulfonyl (MTS) compounds are known to interact rapidly and specifically with free thiol groups forming asymmetrical disulfides [1]. They may be designed to deliver and attach special R-S-groups to sulfhydryls according to:

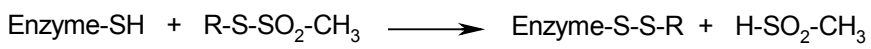

We seek AChE inhibitors that will bind to the *peripheral* site and exclude toxic organophosphorylating agents from the *acylation* site while interfering minimally with essential acetylcholine passage [2]. The goal of our work has been to design and build hybrid inhibitors that bind covalently to the mutated enzyme through the sulfhydryl group of Cys, but that remain tethered through a linker to a specific peripheral site inhibitor in order to study specific features of the mutated enzyme. Such compounds would consist of three parts: 1) an MTS-group that would interact with the H287C mutated AChE, 2) a peripheral site inhibitor of the enzyme, and 3) a linker of varying length that would connect each of these groups.

Results and Discussion

Our experiments have focused on: 1) the synthesis of MTS-tethered linkers; 2) evaluating the stability and versatility of MTS-modified compounds; and 3) finding conditions for the introduction of MTS-carrying tether groups onto the peptide molecule. Preliminary modeling data indicate that the ε-amino group of Lys could be a good candidate for the linker attachment.

We have synthesized 4-MTS-methyl-phenylacetic, 5-MTS-valeric, and 3-MTS-propionic acids from the corresponding ω-bromo-alkane acids and sodium methanethiosulfonate [1,3], and characterized them by RP-HPLC, H-NMR, MALDI-TOF MS and via their thiolation products with L-Cys [3]. Condensation of the MTS-acids with HONSu or HOPfp by DCC provided the corresponding –ONSu or –OPfp esters used to couple these residues to linker-derivatized AChE inhibitors: 9-amino-acridine [4] and 9-amino-1,2,3,4-tetrahydroacridine (tacrine) [5] and linear and cyclic peptides, using both solution-phase and SPPS methods. For example, reaction of 9-(7'-aminoheptyl)-amino-1,2,3,4-tetrahydroacridine with the –ONSu ester of 4-MTS-methyl-phenylacetic acid provided the desired 9-[(4-MTS-methyl-phenylacetyl)-7'-amidoheptyl]-amino-1,2,3,4-tetrahydroacridine. Similar condensation of 9-[N-ϒ-(ε -aminocaproyl)-ϒ-aminopropyl)-amino-acridine [4] with the –ONSu ester of 4-MTS-

methyl-phenylacetic acid provided the corresponding 4-MTS-methyl-phenylacetyl-derivative of aminocaproyl-aminopropyl-amino-acridine.

The cyclic peptides, presumed AChE peripheral site inhibitors, were obtained by on-resin cyclization [6]. Conversion of the cyclic peptides to their MTS-derivatives was performed as shown below (using c(Arg-3-AMB-Leu-Phe-Lys-Gln) as an example), where 3-AMB is 3-aminomethyl-benzoic acid.

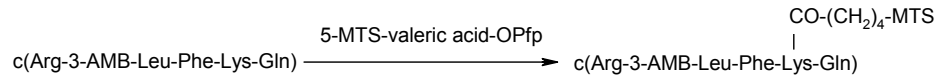

Similarly, we synthesized MTS-$(CH_2)_2$-CO-R, MTS-$(CH_2)_4$-CO-R, and MTS-CH_2-C_6H_4-CH_2-CO-R, where R = c(Arg-3-AMB-Leu-Phe-X-Gln) and X = Lys or D-Lys, (36.6 – 69.3% yield after purification by SPE).

The linear MTS-peptides with the MTS-group attached through the linker to the N-terminal amino group were obtained by SPPS on Wang resin using Fmoc-strategy.

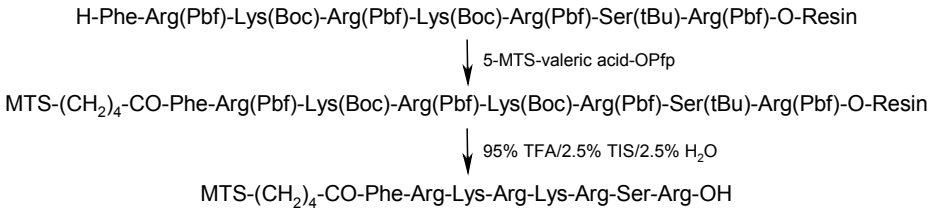

We also synthesized MTS-$(CH_2)_4$-CO-Gly-R, MTS-CH_2-C_6H_4-CH_2-CO-R, and MTS-CH_2-C_6H_4-CH_2-CO-Gly-R, where R = -Phe-Arg-Lys-Arg-Lys-Arg-Ser-Arg-OH (16.9-24.4% yield after purification by preparative RP-HPLC). All products were verified by HPLC and MALDI-TOF MS.

Preliminary data from the examination of the enzymatic activity of the MTS-tether-modified H287C AChE analogues indicate relatively short tethered cationic groups have only a small effect on the enzyme catalytic activity while longer-tethered cationic groups (with acridine and tacrine) profoundly block access to the peripheral site [7]. Studies of the MTS-tether-modified cyclic and linear peptides are in progress and will be reported elsewhere.

Acknowledgments

Funded by US Army/Mayo Clinic Grant, DAMD17-2-8019.

References

1. Bruice T. W. and Kenyon G. L. *J. Protein Chem.* **1**, 47-58 (1982).
2. Rosenberry T. L., Mallender W. D., Cusack B., Szegletes T., Romanvskis P., Spatola A. F. *Medical Defense Review, Proceedings of the USARMC Bioscience*, in press (2000).
3. Smith D. J., Maggio E. T. and Kenyon G. L. *Biochem.* **14**, 766-771 (1975).
4. Rosenberry T. L. and Scoggin D. M. *J. Biol. Chem.* **259**, 5643-5652 (1984).
5. Carlier P. R., Du D. M., et al. *Biorg. & Med. Chem. Lett.* **9**, 2335-2338 (1999).
6. Romanovskis P. and Spatola A. F. *J. Pep. Res.* **52**, 356-374 (1998).
7. Johnson J. J., Cusack B., Hughes R. F., McCullough E.H., Fauq A, Romanovskis, P., Spatola A. F. and Rosenberry T. L. *J. Biol. Chem.* **40**, 38948-38955 (2003).

Peptide Revolution: Genomics, Proteomics & Therapeutics
Michael Chorev & Tomi K. Sawyer (Editors)
American Peptide Society, 2003

Peptide Anticoagulants in a Rat Model of Disseminated Intravascular Coagulation

Sándor Bajusz, Éva Barabás, Irén Fauszt, Gabriella Szabó and Attila Juhász

IVAX Drug Research Institute, Ltd., H-1045 Budapest, Berlini u. 47-49, Hungary

Introduction

Disseminated intravascular coagulation (DIC) is a systemic thrombohemorrhagic disorder that occurs when monocytes or endothelial cells are activated by toxic substances and causes the appearance of thrombin and plasmin in the circulation. Plasmin degrades plasma proteins and thrombin induces coagulation, producing micro-clots that may cause multiorgan failure. In animal experiments, DIC is generally provoked by lipopolysaccharide (LPS) injection. In LPS-treated animals, anticoagulants like heparin and efegatran (N-Me-D-Phe-Pro-Arg-H) could increase lethality, while others, e.g. some P_3 analogues of efegatran, exhibited protective effect, which correlated with an *in vitro* activity profile, i.e. inhibition of clot-bound thrombin and factor Xa, anticoagulation in the APTT assay, and inhibition of plasmin and plasminogen activators. The most active analog was the P_3 D-cycloheptylalanine derivative, N-Me-D-cHpa-Pro-Arg-H (***1***). Analogues having Pab (4-aminomethyl-benzamidine) in place of Arg-H were not inhibitory against factor Xa and fibrinolytic enzymes and not clot-permeable, while melagatran (***R***: HO_2C-CH_2-D-Chg-Aze-Pab; Aze = azetidine-2-carboxylic acid), a related non-covalent anticoagulant, was found to have an activity profile similar to that of ***1*** [1]. Here we report on further analogues having D residues such as Chg and Hma (hexahydromandelic acid) at P_3 and Aze at P_2.

Results and Discussion

Table 1 presents the *in vitro* activities of ***1***, the leading compound of previous series, and its newly examined analogues ***2***-***5***; melagatran (***R***) is included as reference.

*Table 1. Inhibitory action of P_3-P_2-Arg-H, **1-5**, and melagatran (**R**) on plasma coagulation (A), thrombin (FIIa) and factor Xa (FXa) within plasma clots (B) and fibrinolytic enzymes (C)[a].*

No.	Inhibitor		A: CT_2, nM		B: IC_{50}, nM		C: LA_{50}, nM		
	P_3	P_2	TT	APTT	FIIa	FXa	PL	tPA	UK
1	N-Me-D-cHpa	Pro	118	315	118	102	16	14	18
2	N-Me-D-Chg	Aze	101	677	245	457	54	18	11
3	N-Me-D-Chg	Pro	104	875	180	426	32	12	16
4	D-Hma	Aze	93	988	172	182	197	255	212
5	D-Hma	Pro	124	788	270	193	238	330	270
R	Melagatran		30	500	175	360	38	68	102

[a] *A, CT_2: conc. needed to double the clotting time in the thrombin time (TT) and (activated partial thromboplastin time (APTT) assays. B, IC_{50}'s were determined in substrate assays. C, LA_{50}: conc. required to reduce the lytic area to 50% of the control on a fibrin-plate; PL, plasmin; tPA, tissue plasminogen activator; UK, urokinase.*

Table 2. Effect of anticoagulant peptides in a rat DIC model[a].

	% Survival rate at doses of 0.25, 0.75 and 1.5 mg/kg as indicated												
T	***C***		***1***			***2***		***3***	***4***	***5***		***R***	
	0	0.25	0.75	1.5	0.25	0.75	1.5	1.5	1.5	1.5	0.25	0.75	1.5
0	100	100	100	100	100	100	100	100	100	100	100	100	100
4	76	93	100	100	100	100	100	100	100	100	83	100	100
5	72	80	100	100	100	100	100	100	83	100	67	100	100
6	37	66	100	100	100	100	100	100	83	100	58	100	91
7	24	46	90	100	66	92	100	92	75	100	58	64	92
8	20	33	90	100	66	85	100	85	75	83	33	64	82

[a] *T, time in hours. C, control. Male rats were treated with an I.V. bolus of 30 mg/kg LPS (lethal dose). Test compounds were given as an initial bolus followed by an I.V. infusion for eight hours immediately after LPS. Mortality was recorded at 4, 5, 6, 7, and 8 hours post LPS.*

As compared to ***1***, ***2***-***4*** caused somewhat higher anticoagulation in the TT assay. ***2***, the Aze analog of **3**, turned to be the most inhibitory against UK. Analogs **2**-**5** inhibited clot-bound thrombin and factor Xa less efficiently than **1**, and **4**-**5** exhibited diminished inhibitory action against the fibrinolytic enzymes, <10% of the others.

Data of Table 2 indicate a potency order of ***2*** > ***1*** > ***R*** when comparing the survival rates observed at 0.25 mg/kg. The relatively high protective effect of ***2*** might stem from its improved inhibitory action on UK mentioned above (recent results have shown that UK plays a major contributory role of UK in LPS-induced disorder [3]). The protecting effect of ***2*** at 0.75 mg/kg is identical to that of ***3*** at 1.5 mg/kg, which may demonstrate that Aze is somewhat more favorable than Pro at P_2 when D-Chg resides at P_3. On the other hand, ***4*** with D-Hma-Aze as P_3-P_2 causes lower survival rate than ***5*** with D-Hma-Pro at the dose of 1.5 mg/kg. Otherwise, the somewhat high protective effect of ***5*** does not completely correlate with its antifibrinolytic activities being as moderate as those of ***4*** (C, Table 1).

In addition to DIC inhibitory peptidyl arginal ***1*** (N-Me-D-cHpa-Pro-Arg-H, GYKI-66430), a novel analog, ***2*** (N-Me-D-Chg-Aze-Arg-H, GYKI-66476), has been identified. Compound ***2*** proved to have slightly higher protective effect than ***1*** in the rat DIC model while showing somewhat moderate activities in all but one *in vitro* assay thought to be characteristic of DIC-inhibitory potential. The exception is the improved anti-UK activity that might result in the enhanced *in vivo* potency of ***2***. Thus, ***1*** and ***2*** may interfere with the events involved in DIC by different mechanisms.

References

1. Bajusz, S., et al. In Benedetti, E. and Pedone, C. (Eds.), *Peptides 2002 (Proceedings of the 27th European Peptide Symposium)*, Edizioni Ziino, Napoli, 2003, p. 430.
2. Bajusz, S. Patent application WO 03/016273 (2003).
3. Abraham, E., Gyetko, M.R., Kuhn, K., Arcaroli, J., Strassheim, D., Park, J.S., Shetty, S. and Idell, S. *J. Immunol.* **170**, 5644 (2003).

Peptide Revolution: Genomics, Proteomics & Therapeutics
Michael Chorev & Tomi K. Sawyer (Editors)
American Peptide Society, 2003

Solution Structure of a Cyclic Peptide, Subtilosin A, with Unusual Post-translational Modifications

Tara Sprules[1], Karen E. Kawulka[1], Ryan T. McKay[2], Pascal Mercier[3], Christopher M. Diaper[1], Peter Zuber[4] and John C. Vederas[1]

[1]Department of Chemistry; [2]National High Field NMR Centre (NANUC) and [3]Department of Biochemistry, University of Alberta, Edmonton, AB, T6G 2G2, Canada; [4]Department of Biochemistry and Molecular Biology, Oregon Graduate Institute of Science and Technology, Beaverton, OR 97006-8921, USA

Introduction

Bacteriocins are a group of extensively post-translationally modified antimicrobial peptides which are active against a broad range of pathogenic bacteria. They have important potential as food preservatives and for application in both veterinary and human medicine. Subtilosin A is a 34 amino acid bacteriocin isolated from *Bacillus subtilis*. Its post-translational modifications include the loss of a leader peptide, subsequent cyclization through the N- and C- termini and formation of three thioether crosslinks. The amino acid sequence of subtilosin A was initially deduced from the results of partial acid hydrolysis and amino acid sequencing [1]. Identification of the genes responsible for production of subtilosin [2] and the results of NMR studies [3] suggested that three thioether bridges, between cysteines 4, 7 and 13 and Phe22, Thr28 and Phe31, respectively, were present in mature subtilosin (Figure 1). We have established the identity of the thioether bridges and determined the solution structure of subtilosin using multi-dimensional NMR.

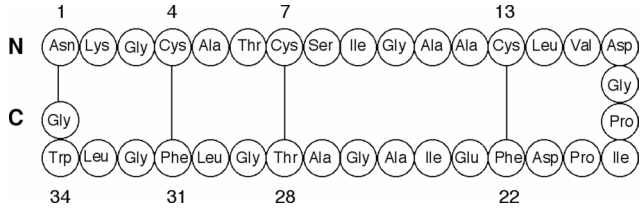

Fig. 1. Amino acid sequence and position of crosslinks in subtilosin A.

Results and Discussion

Universally [^{13}C-^{15}N]-enriched subtilosin A was purified from *B. subtilis* grown on a labelled peptone media generated from blue green algae (*Anabaena sp.*), which was grown on sodium [^{13}C]bicarbonate and sodium [^{15}N]nitrate [4]. Complete carbon, nitrogen and proton assignments were determined using standard two and three dimensional NMR experiments. These assignments indicated that Phe22 and 31 and Thr28 were fully substituted at their α-carbons, which were shifted downfield by approximately 10 ppm from random coil values. Synthesis of model compounds confirmed the chemical shifts observed were consistent with an unusual cysteine-α-carbon linkage. Inter-residue NOE correlations confirmed that the bridges were between Cys4 and Phe31, Cys7 and Thr28 and Cys13 and Phe22.

The stereochemistry of all the amino acids except the modified threonine and phenylalanines was confirmed to be L by desulfurization with nickel boride, acid hydrolysis to the amino acids and conversion to pentafluoropropanamide isopropyl esters for chiral GC MS analysis. The stereochemistry of the modified residues could not be unambiguously determined by chemical techniques. A series of NMR structures were therefore determined for each of the eight possible stereoisomers of subtilosin (i.e. D or L at each of the three substituted α-carbons). The NOE data matched the L-Phe22,D-Thr28,D-Phe31 stereoisomer most closely; this structure gave the lowest energy structures with the best r.m.s.d.

Subtilosin forms a twisted bowl-like conformation in methanol, with most of the sidechains pointing outwards (Figure 2). The thioether crosslinks hold the central portion of the polypeptide in a relatively rigid conformation, with more flexibility in the loops at the ends of the protein. The unique cysteine-α-carbon thioether linkages are essential for the antimicrobial activity. Desulfurization with nickel boride results in an inactive compound. The twisted conformation of subtilosin, with its outward pointing sidechains, is necessary for interaction with the cell membrane or surface receptors of sensitive bacterial strains.

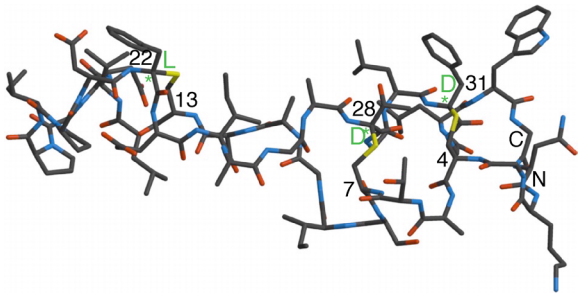

Fig. 2. Structure of subtilosin A. The positions and stereochemistries of the thioether linkages are indicated.

Acknowledgements

We thank Leon Lau and Liang-Zeng Yan (University of Alberta) for development of purification procedures for subtilosin A, James Hoyle for atomic emission analyses of isotopic content, and Leo Spyracopoulos for access to his computer system. This work was supported by CanBiocin Ltd. (Edmonton), the Natural Sciences and Engineering Research Council of Canada (NSERC), the Alberta Heritage Foundation for Medical Research, and the Canada Foundation for Innovation.

References

1. Babasaki, K., Takao, T., Shimonishi, Y. and Kurahashi, K. *J. Biochem. (Tokyo)* **98**, 585-603 (1985).
2. Zheng, G., Yan, L. Z., Vederas, J. C. and Zuber, P. *J. Bacteriol.* **181**, 7346-7355 (1999).
3. Marx, R., Stein, T., Entian, K. D. and Glaser, S. J. *J. Protein Chem.* **20**, 501-506 (2001).
4. Sailer, M., Helms, G. L., Henkel, T., Niemczura, W. P., Stiles, M. E. and Vederas, J. C. *Biochemistry* **32**, 310-318 (1993).

Peptide Revolution: Genomics, Proteomics & Therapeutics
Michael Chorev & Tomi K. Sawyer (Editors)
American Peptide Society, 2003

Synthesis and Biological Evaluation of Dimeric uPAR Antagonists and Somatostatin Analogs

A. Modlinger[1], M. Sukopp[1], M. Buergle[2], K. Wosikowski[2] and H. Kessler[1]

[1]Institut für Organische Chemie und Biochemie, Technische Universität München, Lichtenbergstr. 4, D-85747 Garching, Germany; [2]Wilex AG, D-81675 Munich, Germany

Introduction

Multivalent ligands can serve as potent inhibitors or effectors in biological processes and have shown higher binding affinities than their monomeric counterparts [1,2]. They can interact with receptors via many possible mechanisms, including chelate effect, subsite binding, statistical rebinding and steric stabilization. Moreover, they can induce receptor clustering. Recently, we have shown that multimeric RGD-peptides induce significantly higher tumor uptake than comparable monomeric peptides [3,4]. Herein we present the application of the multimeric concept to ligands for the receptor of urokinase plasminogen activator (uPAR) [5] and for somatostatin receptors (sstr) [6].

Results and Discussion

Recently we synthesized a series of cyclic nonapeptides, which mimic the structure and activity of the binding epitope of uPA to uPAR. Thus *cyclo*[21,29][D-Cys^{21}Cys^{29}]-uPA$_{21-30}$ (**1**) (Figure 1) was obtained displaying a relatively high uPAR binding activity in the nanomolar range [7]. The octapeptide **2** is a well known agonist of sstr2 and sstr5.

In order to dimerize **1**, structural modifications of the C- and N-terminus were carried out. Since maintenance of biological activity was observed when elongating the C-terminus we choose to link the active monomeric compound via the C-terminal Trp using different spacers and (ethylendioxy)-diethylamine as linker (Figure 2).

The capacity to inhibit uPA/uPAR interaction was assessed by LASER FACS analysis. We simultaneously determined the binding affinity of 1 in each assay.

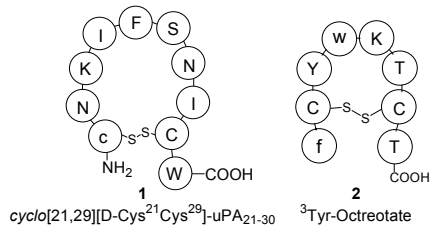

Fig. 1. Bioactive monomeric ligands.

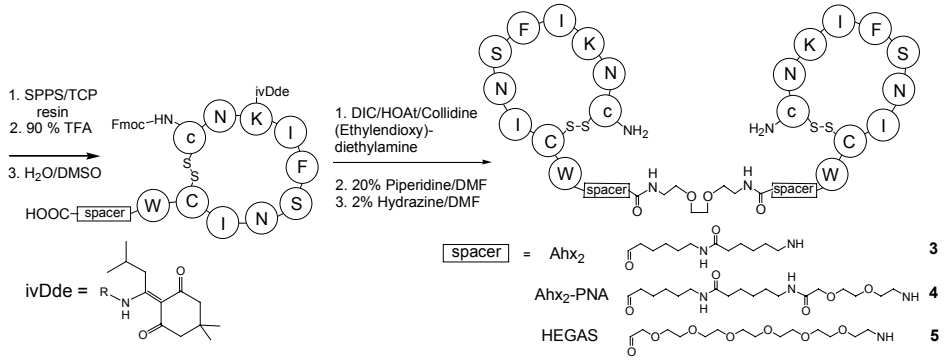

Fig. 2. Synthesis of dimeric uPAR antagonists.

Table 1. Binding affinities of dimers of 2.

	compound	Q=IC_{50}(compound)/ IC_{50} (1)
3	monomer Ahx_2	3.0
	dimer Ahx_2	1.5
4	monomer Ahx_2-PNA	3.1
	dimer Ahx_2-PNA	1.7
5	monomer HEGAS	1.5
	dimer HEGAS	2.4[a)]

[a)] *at concentrations >10 μM the peptide shows cell toxicity.*

Dimers **3** and **4** demonstrated an increase of binding affinity in the range of factor two. Hence, induced clustering of receptors is not very likely, as more than a two-fold increase due to cooperative effects was not observed. Dimer **5** revealed cell toxicity at concentrations higher than 10 mM probably due to polyethyleneglycol spacers, which could exhibit unfavourable interactions with cell membranes [8].

The multimeric concept was also applied to the somatostatin analog ^{3}Tyr-octreotate. In the key step N-terminal aminooxy functionalized ^{3}Tyr-octreotate 6 was chemoselective ligated to aldehydes 7 (Figure 3) to give oximes 8, 9 and 10. Compounds 8 and 9 will be radiolabeled with ^{125}I at ^{3}Tyr and PET studies will reveal whether these compounds show higher tumor uptakes than monomeric ones. Alternatively compound 10, bearing an additional Boc-protected aminooxy functionalization, could be chemoselective labeled with *p*-^{18}F-benzaldehyde. We consider these compounds as promising candidates for improved radionuclide diagnosis and therapy in sstr-positive tumors.

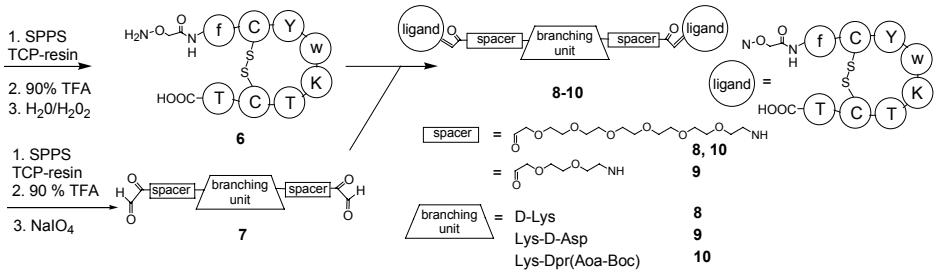

Fig. 3. Synthesis of dimeric somatostatin analogs.

Acknowledgments

The work was supported by the DFG Forschergruppe Radionuklidtherapie.

References

1. Gestwicki, J. E., et al. *J. Am. Chem. Soc.* **124**, 14922-14933 (2002).
2. Rao, J., et al. *Chem. Biol.* **6**, 353-359 (1999).
3. Thumshirn, G., Hersel, U., Goodman S. L., Kessler, H. *Chemistry Eur. J.* **9**, 2717-25, (2003).
4. Thumshirn, G., et al. *Biopolymers* **71**, 477 (2003).
5. Reuning, U., Kopitz, C., Kessler, H., Krüger, A., Schmitt, M., Magdolen, V., *Curr. Pharm. Design* **9**, 1529 (2003).
6. Froidevaux, S., Eberle, A.N.,*Biopolymers* **66**, 161-183 (2002).
7. Schmiedeberg, N., Schmitt, M., Rölz, C., Truffault, V., Sukopp, M., Bürgle, M., Wilhelm, O. G., Schmalix, W., Magdolen, V., Kessler H. *J. Med. Chem.* **45**, 4984-4994 (2002).
8. T. Minko, P. V. Paranjpe, B. Qiu, A. Lalloo, R. Won, S. Stein, P. J. Sinko *Cancer Chemother. Pharmacol.* **50**, 143-150 (2002).

Peptide Revolution: Genomics, Proteomics & Therapeutics
Michael Chorev & Tomi K. Sawyer (Editors)
American Peptide Society, 2003

Peptide-Based Near Infrared Optical Probes Specific for Matrix Metalloproteinases Activity Detection

Wellington Pham, Ralph Weissleder and Ching-Husan Tung

Center for Molecular Imaging Research, Massachusetts General Hospital
Harvard Medical School, 149, 13th Street, Charlestown, MA 02129, USA

Introduction

Molecular imaging has been proposed for detecting, characterizing and staging diseases. Disease is a phenotype of a chemical malfunction; detecting this abnormal pathway in the early stage of diseases is helpful for treatment. Tumor progression is a complicated and multi-step process in which a normal cell undergoes genetic alterations resulting in dysfunction of cell growth and differentiation. Many tumors have been shown to exhibit the over-expression of proteolytic enzymes, which can be an attractive target for molecular imaging. Especially, it has been suggested that matrix metalloproteinases (MMPs) mediate the invasion and metastatic spread of cancer cells. However, the specific role of each subtype of MMP is still not clear. It should be useful to develop novel MMP probes to study the specific function of each individual enzyme in the process of metastasis.

Imaging using a wavelength in the NIR spectrum (700-900 nm) can eliminate the interference from background biomolecules, thus enhancing the signal to noise ratio. In addition, the wavelength of NIR optical probes lies within the oscillation wavelength of a semiconductor laser. Therefore, it is suitable for imaging using a laser beam as a light source. Currently, there are a few commercial NIR dyes available for imaging. Due to scarcity and instability, the working scale of these dyes is in micrograms under a required mild condition. While labeling of a peptide with dyes via SPPS not only requires a large quantity of dyes, they also have to be stable in harsh organic maneuvers such as exposure of the dyes to different strong basic and acidic deprotection stages. In an effort to develop peptide-based NIR probes for MMPs imaging, we recently reported the development of NIR820 from a three-step reaction starting with Fischer indole synthesis between 4-hydrazinobenzoic acid and methyl isopropyl ketone. Alkylation of the indole ring with 1,4-butane sultone to increase the solubility feature of the dye in aqueous condition is followed by condensation with N-[(3-(anilinomethylene)-2-chloro-1-cyclohexen-1-yl)methylene]aniline [1]. The excellent chemical stability of this dye is compatible with SPPS. Moreover, the robust chemical purification using flash column chromatography allows us to obtain the dye in gram scale in a matter of hours. Combining with other commercially available fluorochromes, we are able to synthesize peptide-based MMP sensitive probes with distinct optical properties based on fluorescence resonance energy transfer (FRET) technology.

Results and Discussion

To demonstrate the usage of the dye, NIR820 was incorporated onto MMP-7 substrate via SPPS using standard HOBT/HBTU coupling reagents with extended coupling time in DMF. The labeled peptide was then cleaved and deported using 95% TFA. The NIR labeled peptide was confirmed by mass spectmetic analysis after purification by HPLC. NIR820 survived all reaction conditions and retained its excitation and emission at 790 and 820 nm respectively. At this stage, commercial thioreactive maleimide Cy5.5 was

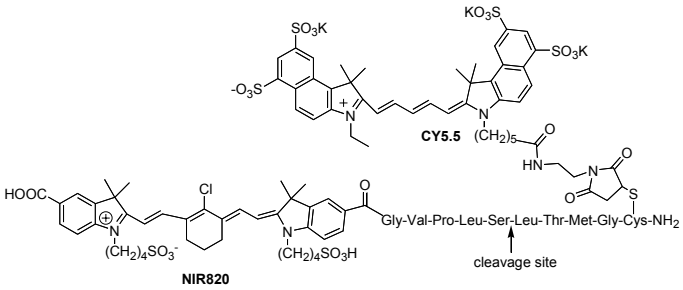

Fig. 1. Labeling of a MMP-7 peptide substrate with near infrared dyes. In this particular case, NIR820 is a quencher and Cy5.5 is a fluorescence emitter.

conjugated onto the peptide via cysteine moiety in 50 mM sodium acetate (pH 7.4) at room temperature. The product was purified by HPLC (Maldi-tof: 2814.99) (Figure 1).

Peptide-based probe specific for MMP-7 enzyme was tested in pH 7.4 buffer containing 50 mM Tris, 200 mM NaCl, 5 mM $CaCl_2$, 1μM $ZnCl_2$. A kinetic profile demonstrated that the maximum fluorescence signal was detected from 45 to 60 min of assay (Figure 2). Compared to the control experiment, the MMP-7 probe activates the enzyme with a nearly six-fold increase in the detected fluorescence signal. As expected, there is no change in signal in the presence of MMP-9 enzyme. Currently, we are combining NIR820 and other NIR fluorochromes with previously developed NIR quenchers [2-4] to prepare various MMP selective probes for *in vivo* imaging.

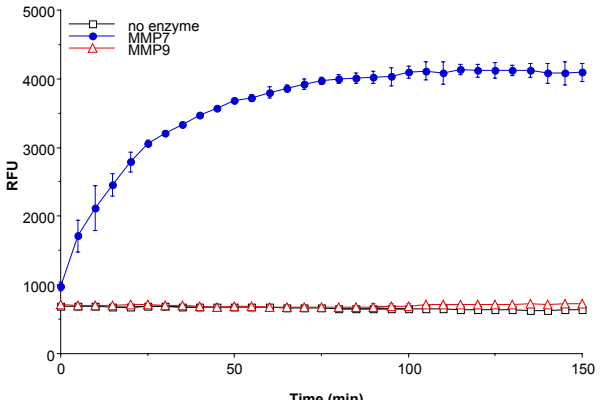

Fig. 2. Activation of MMP-7 probes with MMP-7 and MMP-9 enzymes.

Acknowledgments

The work was funded by NIH P50-CA86355, NSF BES-0119382 and ROI-CA 99385.

References

1. Pham, W., Weissleder, R. and Tung, C.-H. *Biocojug. Chem.* **14**, 1048-1051 (2003).
2. Pham, W., Weissleder, R. and Tung, C.-H. *Tetrahedron Lett.* **43**, 19-20 (2001).
3. Pham, W., Weissleder, R. and Tung, C.-H. *Angew. Chem. Int. Ed. Engl.* **41**, 3659 (2002).
4. Pham, W., Weissleder, R. and Tung, C.-H. *Tetrahedron Lett.* **44**, 3975 (2003).

Peptide Structure-Conformation-Function and Molecular Modeling

Peptide Revolution: Genomics, Proteomics & Therapeutics
Michael Chorev & Tomi K. Sawyer (Editors)
American Peptide Society, 2003

2D NMR Studies of Dynorphin A(1-13) in Solution: Potent κ Opioid Receptor Agonist

V. Renugopalakrishnan[1,2*], Shaw-Guang Huang[3] and M. Prabhakaran[2]

[1]*Children's Hospital, Harvard Medical School, Boston, MA 02115, USA;*
[2]*Dept of Biomedical Eng., Florida International Univ. FL 33199, USA;*
[3]*Dept of Chemistry, Harvard University, Cambridge, MA 02138, USA*

Introduction

Dynorphin A, a κ-selective opioid heptadecapeptide predominantly expressed in the brain, and has the sequence: (H)-Tyr-Gly-Gly-Phe-Leu-Arg-Arg-Ile-Arg-Pro-Lys-Leu-Lys-Trp-Asp-Asn-Glu (OH). Dynorphin A occupies an important place, in view of its unique sequence, hydrophilic nature, and the κ-receptor selectivity. Here we discuss the results of our structural studies on dynorphin A(1-13) in aqueous and in dimethyl sulfoxide solutions using 2D NMR spectroscopy and a model for 17 residue segement from the experimental results.

Results and Discussion

NMR studies were performed on a Bruker AM500 NMR spectrometer. 5 mg. of dynorphin A(1-13) was dissolved in 0.4 ml solvent giving - 8 mM concentration. Three different solvents were used in this study: 100% perdeuterated dimethyl sulfoxide, 100% perdeuterated water and an 80% H_2O/20% D_2O mixture. The magnetic field was locked on the deuterium resonance of the solvent. The data presented herein have taken water suppression into account. Two dimensional COSY and NOESY experiments were done using standard pulse sequences. For COSY experiments (90^o-t_1-90^o) 1024 points were used in the t_2 domain and at least 200 t_1 values were collected, which were later zero-filled to 512 points before performing the Fourier transformation in F_1 domain. For each t_1 value at least 32 transients were collected. For NOESY experiments (90^o-t_1-90^o-t_m-90^0) we have used similar parameters as in COSY experiments except that the number of transients for each t_1 value was increased to 128 or 256, and two different mixing times, 200 ms and 400 ms were used. The NOE data presented below corresponds to mixing time of 200 ms.

Many spin systems were recognized by the COSY experiments of dynorphin A(1-13). COSY spectrum of dynorphin A(1-13) in DMSO-D_6 is shown in Figure 1. A large number of NOE connectivities including those from intra-residue contacts and those from inter-residue contacts can be seen from this NOESY spectrum. Many intra-residue proton NOE connectivities were found in good agreement with the COSY connectivities. Some intraresidue proton NOE connectivities were found between non-scalar-coupled protons and should provide information on the side chain-conformations. The inter-residue NOE connectivities of $d_{\alpha N}$ and d_{NN} pairs are the most important elements for sequential assignment. Dynorphin A(1-13) contains Leu^5 enkephalin as the first five residues at the N-terminal. Except for Pro^{10}, the rest of the eight residues contain lengthy side chains. Leu^5 enkephalin has been widely studied using NMR as well as other physical methods and a number of different conclusions have been drawn on the conformation of the molecule. Most of the previous studies agreed that the Leu^5-enkephalin exhibits a β-turn structure involving hydrogen bonding. The addition of eight amino acids with long side chains to Leu^5 enkephalin may be expected to cause some perturbation to the conformation of Leu^5-enkephalin-

related sequence. We have found that there were no major variations in the chemical shifts of the first five residues. The upfield shift of Tyr^1 αCH from 3.60 ppm in Leu^5 enkephalin to 3.34 ppm in dynorphin A(1-13) indicates that a larger ring current shift is present at the Tyr^1 in dynorphin A(1-13) and implies that a tight β-turn structure is retained for the first 5 residues. We have also observed the $d_{\alpha N}$ and d_{NN} NOE's in these first 5 residues. An expanded slice of 2D NOESY spectrum of dynorphin A(1-13) in dimethyl sulfoxide-D_6 , shown in Figure 2.

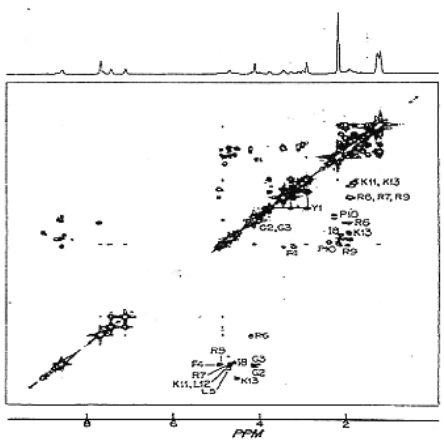

Fig. 1. COSY spectrum of dynorphin A(1-13) in DMSO-D_6.

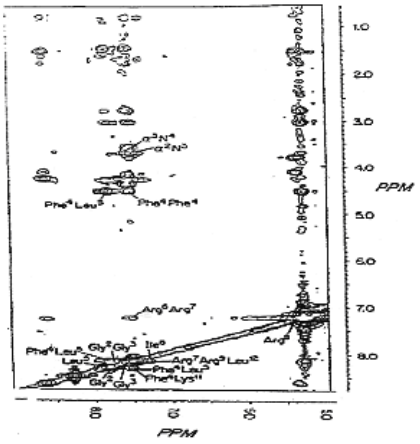

Fig. 2. 2D NOESY spectrum of dynorphin A(1-13) in DMSO-D_6.

Using the NMR data, we modeled the 17 residue segment using programs WHATIF and Insight (Accelrys) and the three D model is shown in Figure 3.

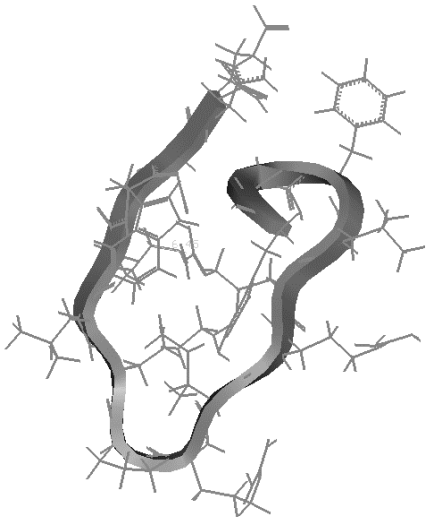

Fig. 3. A representative structure of dynorphin derived from NMR constraints.

Conclusion

2D NMR studies of dynorphin A(1-13) in DMSO-D_6 and in aqueous solution were carried out. In DMSO-D_6, dynorphin A(1-13) was found to contain a type I β-turn structure in the Leu^5-enkephalin segment at the N-terminal and most likely an extended structure at least up to Pro^{10} residue. The occurence of the β-turn rests on observed NOE contacts. A long-range NOE contact between Arg^6 and Lys^{13} causes a kink in the progression of the polypeptide backbone. Base on these findings we propose a molecular model for dynorphin A(1-13).

Peptide Revolution: Genomics, Proteomics & Therapeutics
Michael Chorev & Tomi K. Sawyer (Editors)
American Peptide Society, 2003

Effects of Arsenic(III) Binding on α-Helicity

Daniel J. Cline, Colin Thorpe and Joel P. Schneider

Department of Chemistry & Biochemistry, University of Delaware, Newark, DE, 19716 USA

Introduction

Cysteine is the second most uncommon naturally occurring amino acid, present in only 90% of all human proteins at a frequency of less than 2%. It is more prevalent in extracellular, excreted, and redox-active proteins where they are usually paired to form disulfide bridges. Interest in these disulfide containing proteins and, by extension, disulfide forming enzymes, has led to the development and use of many thiol reactive probes, including iodoacetamides, maleimides, symmetric disulfides, and organo-arsenical probes.

Arsenic-based probes are interesting in that they are reactive toward vicinal dithiols whereas the other probes are mono-reactive. Although arsenic has long been noted as a poison and/or carcinogen, surprisingly little is known about the effects of arsenic binding on protein structure. Herein, we develop several arsenic based probes for use in UV, fluorescence, and CD spectroscopies. In addition, we provide a thorough analysis of the structural effects these probes have on helical secondary structure.

Results and Discussion

$MeAs(OH)_2$ was a probe designed to be far-UV CD silent, and to bind dithiol containing peptides in 1:1 stoichiometry. Likewise, the *p*-Succinylamidephenyl arsenoxide (PSAO) probe was designed with a spectral handle so that upon binding a dithiol, its absorption maximum would red shift. Two *p*-Aminophenyl arsenoxide (PAO) derived fluorescent probes were synthesized from fluoroscein isothiocyanate and dansyl chloride. The dansyl-PAO was used to visualize the dithiol rich surface of reduced egg shell membranes, but could only be delivered in methanol; fluorescein-PAO overcame this limitation.

To investigate the effects of arsenic-based probes binding to proteins, we first used a simple α-helical model peptide, based on the marginally stable helical sequence first reported by Baldwin [2]. Cysteines residues were incorporated at the C-terminal end of the helix in positions about one turn of the helix, as well as in the center of the helix in the same relative positions. The purpose of using a marginally stable helix was so that by CD, the effects of the arsenic binding to the peptide would be emphasized. Binding either stabilizes or destabilizes helical structure; destabilization could mean populating the random coil state or an alternate conformation (Figure 1).

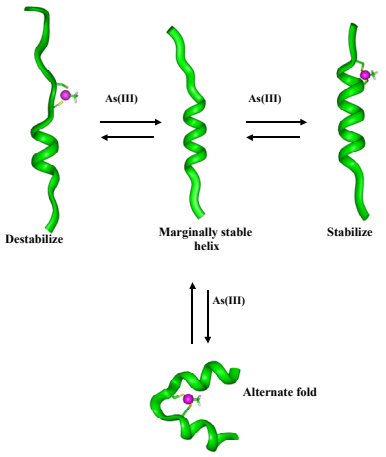

Fig. 1. Effects of arsenic (III) probe binding to helical peptides.

CD and binding results are shown below (see Table 1). Titrations with sub-stoichiometric portions of $MeAs(OH)_2$, as well as MALDI-MS data, demonstrate binding is 1:1 arsenic to peptide (data shown elsewhere [1]). While peptides with

cysteines in the i & i+1 and i & i+2 (peptides 1, 2, 5, and 6; see Table 1) show depopulation of the helical state with arsenic bound, peptides with cysteines in the i & i+4 positions (peptides 4 and 8) show an increase in helical signal. This increase was used to calculate pseudo pair wise interaction energies (ΔG_{pw}) between the cysteine side-chains, yielding values of -1.0 and -0.7 kcal/mole, respectively. These favorable side-chain interactions translate to an overall stabilization of the helical fold. However, arsenic bound to the peptides with cysteines arranged i & i+3 (peptides 3 and 7), while depopulating the helical state, populates another structure giving rise to a type B' CD signal, which is characteristic of some turn types. This alternate structure is very stable, retaining its signal up to 50º C. Binding studies were carried out as described [1], and PSAO shown to bind quickly (completely bound in less than 1 second for millimolar concentrations) and tightly (kD ~100nM), which agree with results found in Donoghue *et al.* [3] (Table 1).

Table 2. Results of structural and binding data for arsenic(III) probes to dicysteine containing, N-acetylated, C-amidated helical peptides. +/- standard error in ( ). values taken from reference [3].*

Peptide	Sequence	Cys-Cys Position	% Helix Apo	% Helix MeAs	ΔG_{pw}^{o}	K_d (nM)	k ($M^{-1}s^{-1}$)
1	YGGKAAAAKAAAAKACCA	i, i+1	20.8	14.3		74 (12)	14430 (230)
2	YGGKAAAAKAAAAKCACA	i, i+2	18.6	4.2		30 (19)	10970 (110)
3	YGGKAAAAKAAACKACAA	i, i+3	16.8	n/a		50 (20)	14250 (140)
4	YGGKAAAAKAAACKAACA	i, i+4	18.7	32.0	-1.0	198 (55)	14080 (120)
5	YGGKAAAAKACCAKAAAA	i, i+1	5.5	n/a		130 (19)	27670 (210)
6	YGGKAAAAKCACAKAAAA	i, i+2	6.8	n/a		15 (10)	21580 (290)
7	YGGKAAACKACAAKAAAA	i, i+3	7.8	n/a		88 (27)	23910 (300)
8	YGGKAAACKAACAKAAAA	i, i+4	9.6	20.6	-0.7	28 (6)	26550 (540)
9	YGGKAAAAKAAAAKAAAA	--	56.9	--		--	--
*	WCGPCK	i, i+4				1,420 (450)	--
*	WCGHCL	i, i+4				870 (270)	--
*	Thioredoxin	i, i+4				370 (180)	--

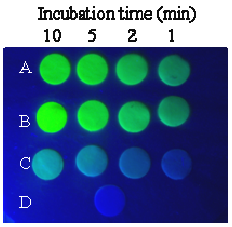

Fig. 2. Time-dependent dansyl-PAO treatment of egg shell membranes. A)reduced first with TCEP, then treated with probe B) co-treated with TCEP and probe C) unreduced membranes treated with probe D) no treatment.

Applications of the fluorescent arsenic probes are currently under investigation by this lab. Preliminary data suggest these probes will be useful for visualizing dithiol rich biopolymers such as the egg shell membrane (see Figure 2), as well as visualizing dithiol proteins in SDS-PAGE gels (not shown).

Acknowledgments

Funding: ACS PRF-G: 36376-G4 (JPS), NIH 26643 (CT) and Training Grant USPHS 1-T32-GM08550 to DJC.

References

1. Cline, D. J., Thorpe, C. and Schneider, J. P. *J. Am. Chem. Soc.* **125**, 2923-2929 (2003).
2. Marquese, S. and Baldwin, R. *Proc. Natl. Acad. Sci. U.S.A.* **84**, 8898-8902 (1987).
3. Donoghue, N., Yam, P. T. W., Jiang, X. M. and Hogg, P. J. *Pro. Sci.* **9**, 2436-2445 (2000).

Peptide Revolution: Genomics, Proteomics & Therapeutics
Michael Chorev & Tomi K. Sawyer (Editors)
American Peptide Society, 2003

3_{10}-Helix in Aib-Rich Peptides Containing Lactam-Bridged Side-Chains: Spectroscopic Characterization in TFE by CD and NMR

Elisabetta Schievano, Katiuscia Pagano, Stefano Mammi and Evaristo Peggion

Department of Organic Chemistry, University of Padova, Institute of Biomolecular Chemistry, CNR, Via Marzolo 1, 35131 Padova Italy

Introduction

It is well established that peptide sequences rich in Aib residues or, in general, in C^{α}-tetra-substituted amino acid residues, exhibit a strong tendency to fold into the 3_{10}-helical conformation [1,2]. It has been shown by different authors that the tendency of a peptide sequence to fold into the α-helical structure is enhanced when the side-chains of Glu(i)-Lys(i+4) are lactam-bridged [3,4]. Following the same rational the propensity of peptides rich in C^{α}-tetra-substituted amino acid residues to fold into the 3_{10}-helix is enhanced when lactam-bridged side-chains of Glu(i)-Lys(i+3) are introduced in the sequence. In a previous work [5] we have shown that Aib-rich oligomers with lactam-bridged side-chains Glu(i)-Lys(i+3) Ac-(Glu-Aib-Aib-Lys)$_n$–Ala-OH, with n= 1, 2 and 3, in aqueous solution containing sodium dodecylsulfate (SDS) micelles, tend to fold into the 3_{10}-helix. The conformational preference towards the 3_{10}-helical structure increases with chain elongation from monomer to trimer. However, the CD spectra do not match precisely the reported CD spectrum of the 3_{10}-helix [2]. In order to determine the effect of the solvent medium on the stability of this structure, in the present work we studied the conformational properties of the three oligopeptides in TFE by CD, NMR and molecular dynamics calculations.

Results and Discussion

The CD spectra of the three oligopeptides in TFE are shown in Figure 1. All spectra are characterized by a weak positive band at 220 nm and by a negative band around 200 nm. Upon chain elongation an increase in intensity and a red-shift of the negative band is observed. In the trimer the negative maximum is located at 200nm with molar

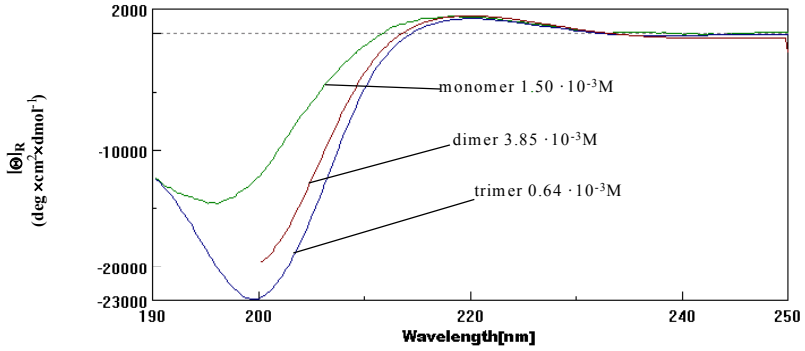

Fig. 1. CD spectra of the three oligopeptides in TFE; peptide concentrations are indicated in the spectra.

ellipticity $[\theta]_R$ value of – 15,000. These spectral characteristics are different from those previously observed in aqueous solution containing SDS micelles, and also do not match the reported CD spectrum of the 3_{10}-helix[2].

A detailed conformational characterization of the peptides was carried out by 2D-NMR spectroscopy. The spin systems of Lys, Glu and Ala residues of each peptide were identified using DQF-COSY and TOCSY spectra, while HMQC and HMBC experiments were used for the Aib residues. In the NOESY spectra all possible αH(i)-HN(i+2) connectivities typical of the 3_{10}-helix were observed in the three oligopeptides, while αH(i)-HN(i+4) connectivities typical of the α-helix are absent. The presence of the helical structure was confirmed by the temperature coefficients of the amide proton resonances. The conformational properties of the oligomers were further characterized by distance geometry and restrained molecular dynamics calculations. Superimposition of the ensembles of low energy structures indicate good convergence towards the 3_{10}-helical conformation in the three peptides.

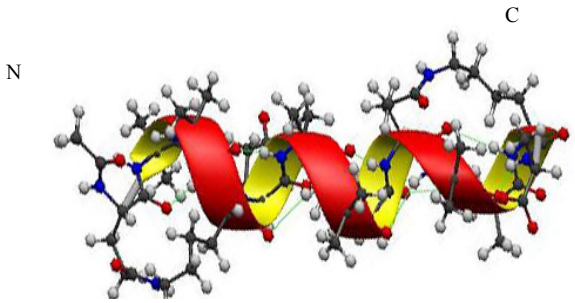

Fig. 2. One of the lowest energy structures of the trimer.

One of the lowest energy structures of the trimer is shown in Figure 2. The hydrogen bond pattern resulting from these calculations is completely consistent with the 3_{10}-helix. Comparison of CD and NMR results suggest that for each peptide we are dealing with an equilibrium system in which conformers with different helix contents are in fast exchange in the NMR time scale. The change of the CD spectrum observed upon chain elongation should therefore reflect the shift of the conformers towards an increasing population of helical molecules in the trimer. The CD spectrum of the trimer is different from those reported in the literature for the 3_{10}-helix. A possible reason for these differences could rest on a different equilibrium of the conformer populations of the various peptide sequences studied to date in different solvent systems.

References

1. Yoder, G., et al. *J. Am. Chem. Soc*. **119**, 10278-10285 (1997).
2. Toniolo, C., Polese, A., Formaggio, F., et al. *J. Am. Chem. Soc.* **118**, 2744-2745 (1996).
3. Felix, A. M., Heimer, E. P., Wang, C. T., et al. *Int .J. Pept. Protein Res*. **32**, 441-454 (1988).
4. Houston, M. E. Cannon, C. L., Kay, C. M. and Hodges, R. S. *J. Peptide Sci*. **1**, 274-282 (1995).
5. Schievano, E., Bisello, A., Chorev, M., Bisol, A., Mammi, S. and Peggion, E. *J. Am. Chem. Soc.* **123**, 2743-2751 (2001).

Peptide Revolution: Genomics, Proteomics & Therapeutics
Michael Chorev & Tomi K. Sawyer (Editors)
American Peptide Society, 2003

Amphipathic α-Helix Apolipoprotein A-I Peptide Models as Atheroprotective Probes: Design, Construction and Phospholipid/Cholesterol Interactions

Charalampos Alexopoulos, John Mitsios, Alexandros Tselepis, Maria Sakarellos-Daitsiotis and Constantinos Sakarellos

Department of Chemistry, University of Ioannina, Greece

Introduction

Human apolipoprotein A-I (ApoA-I), the major protein component of high-density lipoprotein (HDL), plays a crucial role in protecting against atherosclerosis and has the potential to form α-helical amphipathic structures, which interact with phospholipids [1]. Aiming at contributing to the development of potent atheroprotective agents, we present the design, construction, conformational and biological properties of two α-helix apoA-I peptide models, Ac-ESK(Palm)KELSKSW^{10}SEM^{13}LKEK(Palm)SKS-NH_2 (1) and Ac-ESK(Palm)KELSKSM^{10}SEW^{13}LKEK(Palm)SKS-NH_2 (2).

The concept for the design of the amphipathic α-helix apoA-I models is as follows: charged residues E and K are distributed along the molecule at positions i,i+3 or i,i+4 stabilizing the hydrophilic face of the helix through ionic interactions. Residues L, W and M, as well as the palmitoyl groups (Palm) covalently bound to K_3 and K_{17} side chains are expected to build up the opposite hydrophobic face. Moreover, the inclusion of M could serve as additional oxidant-scavenger for protecting LDL from irreversible oxidative damage. Serine at positions 2, 9, 11, 18 and 20 is presumed to constitute the interface of the spatially segregated opposite hydrophilic/hydrophobic interfaces of the helix.

Results and Discussion

The syntheses of the apoA-I peptide models were carried out on a Rink amide Resin following the Fmoc-strategy and an orthogonal protection (Fmoc-, Boc-, Alloc-). After completion of the syntheses the N-terminal amine groups were acetylated, the Alloc groups at positions 3 and 17 were removed under hydrostannolytic cleavage and the remaining Lys-$N^{\varepsilon}H$ groups were palmitoylated by palmitic anhydride. Peptides were isolated by applying programmed gradient elution (60/40-0/100) RP-HPLC with solvent A, H_2O/0.1% TFA and B, CH_3CN/0.1% TFA. Fractions 1A and 2A, eluted at ~35/65, correspond to the correct molecular mass by ESI-MS (expected M^+: 2648.19, found M^+: 2648.98), fractions 1B and 2B, eluted at ~30/70, correspond to a product with two additional acetyl-groups (expected M^+: 2648.19, found M^+: 2733.74), while fractions 1C and 2C, eluted at 0/100 correspond to a product with one additional palmitoyl-group (expected M^+: 2648.19, found M^+: 2888.14).

Table 1. Conformational characteristics of the apoA-I peptide models.

Lipid:chol:peptide molar ratio 80:4:1	$-[\Theta]_{222}$		α-helical content (%)	
	Peptide 1A	Peptide 2A	Peptide 1A	Peptide 2A
POPC:chol:peptide	7778.350	17868.535	22.44	51.55
DMPC:chol:peptide	8578.517	19458.872	24.75	56.13
DMPG:chol:peptide	12530.858	25947.380	36.15	74.85
EtOH	7210.848	20268.040	20.80	58.47

Taking into consideration that positive and negative charges of fractions B and C in both peptide models are detected by ESI-MS, the exact position of the acetyl and palmitoyl groups is under investigation by ^{1}H-NMR.

The conformational characteristics, by CD, of the reconstituted apoA-I peptide models in the presence of three phospholipids POPC, DMPC and DMPG are given in Table 1. It is concluded that peptide model 2A exhibits strong helical characteristics comparable with those of the apoA-I protein, while the helical content of 1A is significantly reduced. Upon addition of the phospholipid/cholesterol mixtures the helical content remains practically stable. It is of particular interest that the absence of a positive charge in DMPG substantially stabilizes the helical structure of both peptide models.

LDL (d=1.019-1.063 g/ml) was prepared from freshly isolated normolipidemic human plasma by sequential ultracentrifugation. Model peptides were used at concentration of 0.1 mM. LDL (100 μg protein/ml) was oxidized in the presence of 5μM Cu^{2+} for 4 hours at 37^{o}C and the sigmoidal oxidation curves, monitored at 234nm in the presence of apoA-I models, are depicted in Figure 1. Peptide model 2A significantly inhibits LDL oxidation (prolongation of the lag time by 65%), while 2B and 2C models completely prevent LDL oxidation. It is assumed that apoA-I peptides might be antiatherogenic by protecting LDL from oxidation and inhibiting the proatherogenic effects of oxLDL.

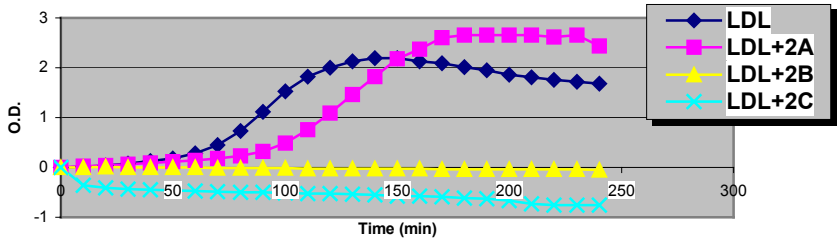

Fig. 1. Oxidation curve of LDL alone and in the presence of apoA-I peptide models.

The LDL-associated PAF-AH activity was measured by the trichloroacetic acid precipitation procedure before as well as at the end of oxidation In the absence of peptides the PAF-AH activity is reduced by 67.7% (from 59 to 19 nmol/mg protein/min). However, in the presence of the apoA-I models 2A and 2C the oxidation-induced enzyme inactivation is significantly inhibited (reduction by 44.1% and 54.2% respectively). Interestingly, the enzyme inactivation is completely inhibited in the presence of the apoA-I model 2B.

The reported findings confirm our initial concept and design mainly for the amphipathic α-helix model (2), which successfully mimics the conformational properties of the apoA-I protein, prevents LDL oxidation and inhibits the oxidation-induced inactivation of the potent anti-inflammatory and antiatherogenic enzyme PAF-AH. Thus, we concluded that the apoA-I model 2 is a potent atheroprotective candidate.

References

1. Reschly, E. J., Sorci-Thomas, M. G., Davidson, W. S., Meredith, S. C., Reardon, C.A. and Getz, G. S. *J. Biol. Chem*. **277**, 9645-9654 (2002).

Peptide Revolution: Genomics, Proteomics & Therapeutics
Michael Chorev & Tomi K. Sawyer (Editors)
American Peptide Society, 2003

Receptor-Bound Characteristics of MiniANP Analyzed by NMR, MM/MD, and the Use of Unusual Amino Acids

K. Sugase, M. Horikawa and M. Ishiguro

Suntory Institute for Bioorganic Research, Wakayamadai 1-1-1, Shimamto-cho, Mishima-gun, Osaka 618-8503, Japan

Introduction

MiniANP (**1**) (MCHFGGRMDRISCYR-NH_2), optimized by phage display, is an analogue of atrial natriuretic polypeptide (ANP). MiniANP (**1**) exhibits ANP-related activities such as regulation of blood pressure and the renin-angiotensin system [1]. MiniANP (**1**) binds selectively to natriuretic peptide receptor A (NPR-A), which is a transmembrane protein composed of approximately 1060 residues. Binding of miniANP (**1**) to NPR-A activates synthesis of cGMP. Since miniANP (**1**) is the smallest of ANP-related peptides, elucidation of the receptor-bound conformation will be useful for designing smaller non-peptide ligands.

We have investigated the receptor-bound characteristics of miniANP (**1**) analyzed by NMR and MM/MD, and the use of analogue peptides. Based on the characteristic conformation shown by the structural analysis, analogue peptides were designed as conformationally restricted ones, such as substitution of d-Ala for Gly or substitution of 4-(2'-guanidinoethyl)Pro (arginine-proline fused amino acid) for Arg, to facilitate the prediction of the receptor-bound conformation. Structural analysis of the analogue peptides along with their activity revealed that a turn-like conformation at residues 6 to 9 and close proximity between Phe^4 and Ile^{11} are important for the biological activity [2,3]. Moreover, upon binding to the receptor the position of the side-chain of Arg^7 was limited to approximately one-third of the whole conformationally accessible space.

Results and Discussion

First, we focused on the conformation of Gly^5-Gly^6, which was chosen as an indispensable region by phage display. Structural analysis by NMR and restrained MD suggested that positive ϕ angles for Gly^5 and Gly^6 are preferable in miniANP (**1**) when it forms both a turn-like conformation at residues 6 to 9 and the proximate pair Phe^4 and Ile^{11}. Since Phe^4, Ile^{11}, and Met^8 are the most important determinants of the activity they were preserved. Positive ϕ angles are typical for d-amino acids, and glycine is the only one among natural amino acids that can take a positive ϕ angle without unfavorable steric interaction. Thus, the necessity for the glycine in miniANP (**1**) may be ascribed to the positive ϕ angle formed upon binding. If this is the case, Gly^5 and/or Gly^6 may be substituted with appropriate d-amino acids without loss of the biological activity. To test this idea, [d-Ala^5]miniANP (**2**), [d-Ala^6]miniANP (**3**), and [d-Ala^5, d-Ala^6]miniANP (**4**) were synthesized, and their activity in the production of cGMP was examined. The activity of [d-Ala^5]miniANP (**2**) slightly increased compared to miniANP (**1**), but those of [d-Ala^6]miniANP (**3**) and [d-Ala^5, d-Ala^6]miniANP (**4**) decreased (Table 1). Solution structure of [d-Ala^5]miniANP (**2**) forms the turn-like conformation and the proximate Phe^4-Ile^{11} pair more clearly than miniANP (**1**) (Figure 1), but other analogues did not. Thus, the substitution of d-Ala^5 contributes to the formation of the turn-like conformation and the proximate pair Phe^4 and Ile^{11}, resulting in a higher bioactivity. The result also indicated that Gly^5 prefers a positive ϕ angle upon binding to the receptor.

Table 1. Biological activity of miniANP and analogue peptides.

Peptide	Relative activity[a]	Peptide	Relative activity
miniANP (**1**)	1.0	[4S-GEPro^7]miniANP (**5**)	0.42
[d-Ala^5]miniANP (**2**)	0.38	[4R-GEPro^7]miniANP (**6**)	1.5
[d-Ala^6]miniANP (**3**)	8.2	[Pro^7]miniANP (**7**)	18.7
[d-Ala^5, d-Ala^6]miniANP (**4**)	2.9		

[a]*Relative activity is calculated from* $EC50_{analogues} / EC50_{miniANP}$ *(1.5 ± 1.4 nM).*

Next, to determine the orientation of the side-chain of Arg^7, which is located at the *i+1* position of the turn-like conformation, upon binding to the receptor, (2S,4S)- or (2S,4R)-4-(2'-guanidinoethyl)proline (4S-GEPro and 4R-GEPro) was incorporated into miniANP (**1**). Since proline has a strong propensity to form a β-turn, GEPro can be used to stabilize the turn-like conformation without loss of the side-chain. Solution structures of both [4S-GEPro^7]miniANP (**5**) and [4R-GEPro^7]miniANP (**6**) formed a more stable β-turn than miniANP (**1**), and there was little conformational difference between those analogues. Therefore, the difference in the biological activity of the analogues may be ascribed to the chiral difference of GEPro. However, [4S-GEPro^7]miniANP (**5**) and [4R-GEPro^7]miniANP (**6**) were as potent as miniANP (**1**) (Table 1). The result suggested that the intersection region of the conformational spaces accessible to their guanidino group could be considered as the interaction site to bind to the receptor. Then, the conformationally accessible spaces of the guanidino group of 4S-GEPro, 4R-GEPro and arginine were mapped out systematically, and compared. The intersection region contained mainly the equatorial configuration of the guanidinoethyl group for 4S- and 4R-GEPro and Arg with an extended side chain (Figure 2). The volume size was one-third of the whole conformationally accessible space of Arg. Thirty-six conformations of Arg were included inside the intersection region; and at least one of those would bind to the receptor.

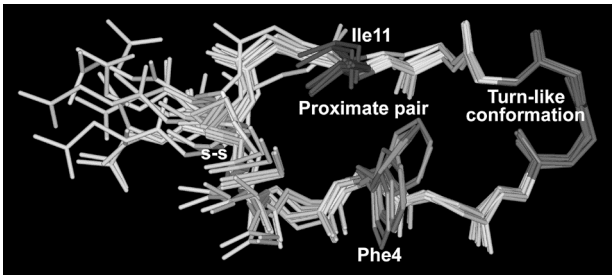

Fig. 1. NMR Structure of [d-Ala^5]miniANP.

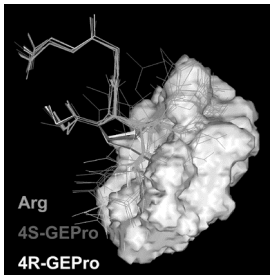

Fig. 2. Intersection region of the guanidino group.

Acknowledgments

This research was supported by the special coordination fund for the promotion of science and technology from the science and technology agency of Japan. We thank Mr. Katsuhiko Kitano and Ms. Masako Sugiyama (Daiichi Suntory Biomedical Research Co., Ltd) for measurement of the cGMP activity of the peptides.

References

1. Bing, L., et al. *Science* **270**, 1657-1660 (1995).
2. Sugase, K., et al. *J. Med. Chem.* **45**, 881-887 (2002).
3. Sugase, K., et al. *Bioorg. Med. Chem. Lett.* **12**, 1245-1247 (2002).

Peptide Revolution: Genomics, Proteomics & Therapeutics
Michael Chorev & Tomi K. Sawyer (Editors)
American Peptide Society, 2003

α,α-Dialkylated β-Hairpin Peptides: Design, Synthesis, and Conformational Analysis

Catherine L. Thomas[1], Marcus A. Etienne[1], Jia Wang[1], Vladimir Setnicka[2], Timothy A. Keiderling[2] and Robert P. Hammer [1]

[1]Department of Chemistry, Louisiana State University, Baton Rouge, LA 70803, USA
[2]Department of Chemistry, University of Illinois, Chicago, IL 6060, USA

Introduction

There are a number of diseases that are caused by the misfolding of proteins into fibrils, which consist of predominantly β-sheet secondary structure [1]. Also many protein-protein interactions are mediated by β-strands. Thus there has been an increased interest in understanding the factors that stabilize and destabilize β-sheet structures in proteins. Recently several groups have succeeded in making autonomously folding β-hairpin peptides, which serve as great models to study β-sheet structure [2].

Our group is studying the role that α,α-disubstituted amino acids (ααAAs) can play in stabilizing both the turn and the sheet portion of β-hairpin peptides. We hypothesized that ααAAs such as α-aminoisobutyric acid (Aib) and dipropylglycine (Dpg) might serve as excellent inducers of the type-I/I' β-turn (at the i + 1 position) due to their propensity to stabilize helical peptides resulting from their strong preference for gauche dihedral angles (±30-60°) [3]. We prepared several analogs of the Gellman peptide having Aib or Dpg in the i+1 position of the β-turn [4]. Two additional analogs, Dpg-3 and Dibg-3, have Dpg and diisobutylglycine (Dibg) respectively as substitutions for the third residue of the original Gellman sequence to determine if these amino acids could contribute to the stability of the extended structure (Figure 1 and Table 1).

Table 1. β-turn and R1/R2 substitutions.

Variant	β-turn	R^1/R^2
Gellman	DPro-Gly	iPr/H
A	Aib-Gly	iPr/H
B	Aib-Tyr	iPr/H
C	Ala-Gly	iPr/H
D	Ala-Tyr	iPr/H
E	Aib-DAla	iPr/H
F	Aib-DTyr	iPr/H
G	Dpg-Gly	iPr/H
Dpg-3	DPro-Gly	Pr/Pr
Dibg-3	DPro-Gly	iBu/iBu

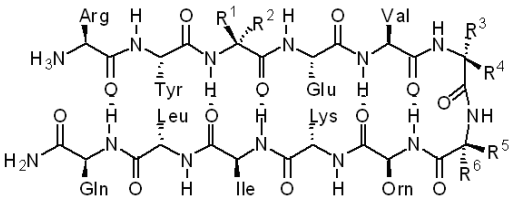

Fig. 1. Structure of Gellman Peptide.

The peptides were synthesized using automated protocols on a Pioneer peptide synthesizer. Four equivalents of each amino acid were used and activation was carried out using diisopropylethylamine (DIEA), TBTU and HOBt. PyAOP was used with

DIEA to activate the coupling of Aib, Dpg, to the Val residue that followed these two amino acids, and Dibg due to the difficulty of coupling. These couplings were also heated at 50 ºC and double coupled to aid in the incorporation of the residue. The peptides were then purified to homogeneity (>99% pure) by using reversed-phase HPLC analysis. Circular dichroism (CD), infrared (IR) spectroscopy, and vibrational circular dichroism (VCD) were used to determine the secondary structure of each peptide. Temperature studies were also done on some of the peptides to determine the stability of the secondary structure over a range of temperatures.

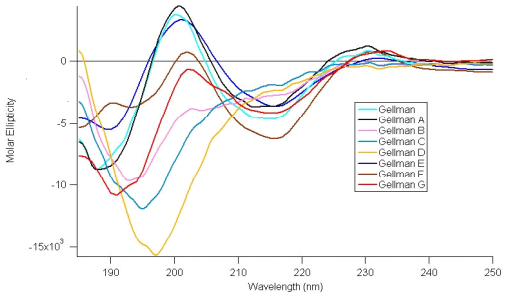

Fig. 2. CD spectra of combined Gellman compared to the original Gellman peptide.

Results and Discussion

The CD studies suggest that the Gellman variants A, E, F, and G (Figure 2), Dibg-3, and Dpg-3 (Figure 3) peptides may also contain a type-I' β-turn and β-sheet structure similar to that of the original Gellman peptide. It is possible that Gellman F and G variants are not as structured as Gellman A and E variants because their CD spectra do not posses the same intensity at the maximum and minimum points as variants A and E. IR and VCD results confirm the β-structure in the strands, and the maintenance of significant VCD at high temperatures, which suggests a stable turn structure for the Gellman A analog.

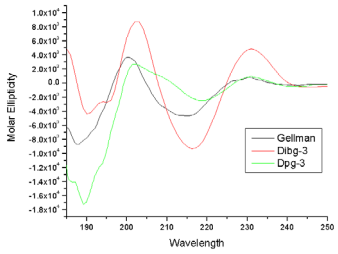

Fig. 3. CD spectra of Dibg-3 and Dpg-3 variants.

Future studies will include IR and VCD studies on these and other variants that appear to have a β-hairpin structure. Additionally NMR studies will be conducted to further analyze the secondary structure of the peptides.

Acknowledgments

We thank the National Institute on Aging of the National Institutes of Health (AG 17983) for financial support. We thank Pfizer for an Undergraduate Fellowship to Catherine L. Thomas.

References

1. Kelly, J. W. *Proc. Natl. Acad. Sci. U.S.A.* **95,** 930-932 (1998).
2. Gellman, S. H. *Curr. Opin.* **2,** 717-725 (1998).
3. Toniolo, C., Crisma, M., Fermaggio, F. and Peggion, C. *Biopolymers* **60,** 396-419 (2001).
4. Stanger, H. E. and Gellman, S. H. *J. Am. Chem. Soc.* **120,** 4236-4237 (1998).

Peptide Revolution: Genomics, Proteomics & Therapeutics
Michael Chorev & Tomi K. Sawyer (Editors)
American Peptide Society, 2003

Computational Design and Chemical Synthesis of a β-Sandwich Protein

Kai Fritzemeier and Wolfgang Haehnel

Institut für Biologie II / Biochemie, Albert-Ludwigs-Universität Freiburg, Schänzlestrasse 1, D-79104 Freiburg, Germany

Introduction

The concept of template assembled synthetic proteins (TASP) [1] provides a versatile basis for the design of synthetic proteins. It has been successfully used to synthesize several four-helix bundle proteins with different functions and cofactors [2]. A particular advantage is the possibility to bind helices or peptide building blocks in predetermined orientation to a specific position of the cyclic peptide template. This reduces the folding problem significantly, and the branched architecture increases the stability of the folded structure. The approach has been extended to combinatorial synthesis of small peptide libraries on cellulose support that was combined with spectroscopic screening of different properties such as Cu ligation, redox potential of a bound heme group or catalytic activity [3]. Here we present the first *de novo* design of a template-based modular protein (MOP) with β-sandwich structure. One challenge of this structure is the tight packing of the hydrophobic core which has to be rather uniform to ensure the correct length of the H-bonds between the β-strands. The packing of the amino acid side chains with the Global Minimum Energy Conformation (GMEC) can be aided by a dead end elimination (DEE) algorithm [4,5] and the rotamer library of amino acid side chain conformations.

Results and Discussion

Computational approach. The Protein Data Bank was screened for proteins with β-sandwich domains without disulfide bridge. We selected the structure of the eight-stranded antiparallel domain in the peptide binding protein adaptin 1BW8.PDB. From this we have taken the backbone coordinates of the strands only. Ends were connected by Pro-Gly turns to form four-stranded β-sheets. Three restraints were introduced by the design. (1) The β-sandwich should be assembled as a homodimer from two β-sheets with four antiparallel β-strands. This symmetric structure, not found in nature, implicates a *de novo* design and reduces the synthesis and coupling steps. (2) Trp should be placed at a favourable position for structural analysis by fluorescence measurements. (3) The amino acids in the hydrophobic core were limited to hydrophobic ones. For this backbone structure of an eight stranded β-sandwich protein with two antiparallel β-sheets, the DEE algorithm [4,5] and the non-bonding terms of the CHARMM force field have been used to pack the hydrophobic core from all possible side chain conformations (rotamers). The algorithm eliminates all rotamers that cannot be part of the GMEC. The branch and terminate algorithm [6] was then used to find the side chain assembly with the minimum non-bond energy calculated by the CHARMM forcefield. The best calculated hydrophobic core was selected for synthesis. The hydrophilic surface and hydrophobic edges of the proteins were rationally designed using statistical data of amino acid propensities and salt bridge orientation to minimize aggregation.

Synthesis and assembly. The novel concept is to couple four β-hairpins to the binding sites of a cyclic peptide template. Peptides were synthesized using standard Fmoc

chemistry and purified by RP-HPLC. The cyclic decapeptide contained four Cys residues orthogonally protected by Acm and Trt at diagonal positions. Different from previous templates [2], we have replaced one Ala by Asp to increase the solubility (Figure 1). The antiparallel strands were realised by coupling two of the hairpins with the bromoacetylated N-terminus and the other two with the bromoacetylated β-amino group of a C-terminal diaminopropionic acid (Dap) to the deprotected Cys. Dap and Ac were used as short linkers between the hairpins and the template, which provides a loop between the hairpins if the sequence of the template -CPGC- is included. The construct may be considered as an assembly of two β-sheets linked by the two residues Ala and Asp in the template. The sequences of the hairpins were (A) QKTIQPGSAKVTIK-Dap-NH_2 and (B) GELSIEWYPGSLTTQ-NH_2. The C-terminal Dap and the N-terminal Gly are included in Figure 1. Peptide (B) was not soluble in aqueous solution. Therefore we have switched the orientation of one of the two salt bridges between the two hairpins from A:K10 – B:E6 to A:E10 – B:K6. This resulted in a solubility of both hairpins sufficient for synthesis and assembly. This protein is termed beta-MOP-1. The ESI mass spectrum in Figure 2 shows the correct assembly and the purity.

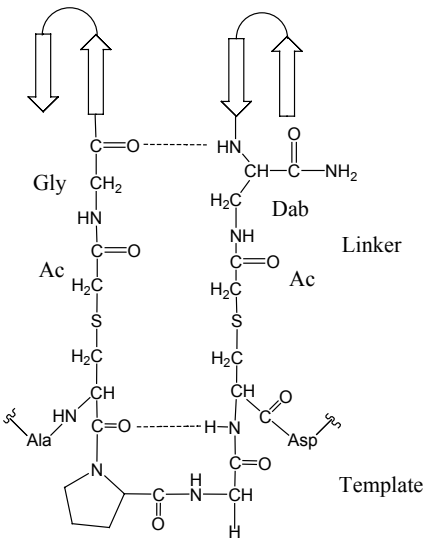

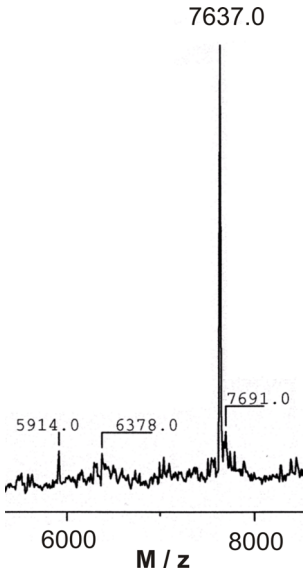

Fig. 1. β-Sandwich pepide structure. *Fig. 2. ESI mass spectrum of β-MOP-1.*

Properties. The circular dichroism spectrum (Figure 3) of the beta-MOP-1 protein in phosphate buffer confirms the β-sheet structure. It was water soluble. However, gel filtration showed an elution with the exclusion volume indicating aggregates in the range of 1000 kDa. Aggregation is one of the major problems of proteins with β-structures. Beta-MOP-1 has a total charge of –1, two salt bridges between the middle strands and L-Pro in the loops. To improve the turns we introduced D-Pro-Gly turns, more saltbridges at the surface, a Lys at the edges of the sandwich and an excess of 3 positive charges. First experiments with ultracentrifugation showed a diminished aggregation by more than one order of magnitude. The circular dichroism of this protein is shown in Figure 3 (MOP-2). The CD shows a shift to longer wavelength

when compared to MOP-1 but the minimum is typical for proteins with β-sheet structures [7].

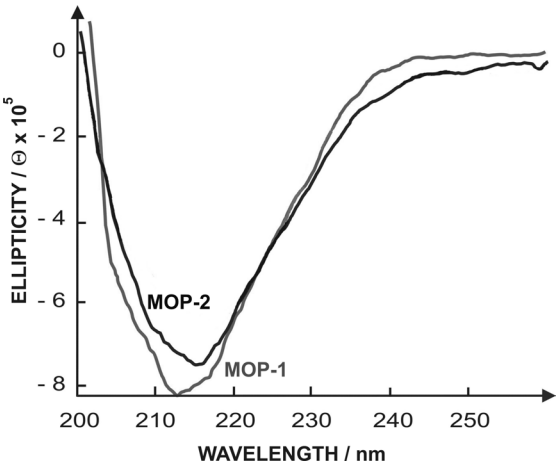

Fig. 3. Circular dichroism spectrum of β-MOP-1.

Conclusion

We have assembled a β-sandwich protein from two antiparallel four stranded β-sheets. This was achieved with a cyclic decapeptide template carrying only four Cys as binding sites by coupling four β-hairpin forming peptides. The side chains in the hydrophobic core were packed by a computational method using a given protein backbone. We believe that a precise packing of the core is essential for H-bond formation between the β-strands. The branched architecture of the template assembled synthetic protein (TASP) helps to overcome some of the problems in protein folding. Analytical ultracentrifugation showed a substantial decrease in the aggregation by rational improvement of the surface exposed amino acids.

Acknowledgments

The analytical ultracentrifugation was kindly performed by A. Lustig (Biozentrum Basel). We also thank VolkswagenStiftung and DFG for support.

References

1. Mutter, M., Vuilleumier, S. *Angew. Chem. Int. Ed*. **28** 535-554 (1989).
2. Rau, H. K. and Haehnel, W. *J. Am. Chem. Soc*. **120**, 468-476 (1998).
3. Rau, H. K., DeJonge, N. and Haehnel, W. *Angew. Chem. Int. Ed*. **39**, 250-253 (2000).
4. Desmet, J., DeMaeyer, M., Hazes, B. and Lasters, I. *Nature* **356**, 539-542 (1992).
5. Pierce, N. A., et al. *J. Comput. Chem*. **21**, 999-1009 (2000).
6. Gordon, B. and Mayo, S. L. *Structure* **7**, 1089-1098 (1999).
7. Johnson, W. C. *Proteins: Structure, Function and Genetics* **7**, 205-214 (1990).

Peptide Revolution: Genomics, Proteomics & Therapeutics
Michael Chorev & Tomi K. Sawyer (Editors)
American Peptide Society, 2003

Design and Conformational Analysis of Peptides Containing α,α-Disubstituted Amino Acid

Jia Wang, Yanwen Fu, Martha M. Juban and Robert P. Hammer

Department of Chemistry, Louisiana State University, Baton Rouge, LA 70803, USA

Introduction

$C^{\alpha,\alpha}$-Disubstituted amino acids (ααAAs) have been recognized as a means of introducing backbone conformational constraints in peptides. α,α-Dipropylglycine (Dpg) residues have been shown to adopt both extended and helical conformations, depending on peptide sequence, length, and environmental factors [1]. In this study several pentapeptides containing Dpg at alternating sequence positions and their L-norvaline (Nva) analogs were prepared, and their structures were studied by CD and NMR.

Results and Discussion

Incorporation of glutamic acid and lysine residues at each end of the peptides was designed to probe the potential conformational effect resulting from residue-residue side chain interactions. To further investigate the ααAAs impact on peptide backbone conformation, the L-norvaline (Nva) analogs were prepared (Dpg residues replaced by Nva). All peptides were prepared using Fmoc chemistry on Fmoc-PAL-PEG-PS resin as a solid support. All coupling reactions except the acetylation of the N-terminus of peptides were carried out using PyAOP as the coupling reagent.

Table 1. Primary sequences of Dpg and Nva peptides.

Dpg2	Ac-Glu-Dpg-Tyr-Dpg-Lys-NH_2	**Nva2**	Ac-Glu-Nva-Tyr-Nva-Lys-NH_2
Dpg5	Ac-Glu-Dpg-Thr-Dpg-Lys-NH_2	**Nva5**	Ac-Glu-Nva-Thr-Nva-Lys-NH_2
Dpg6	Ac-Glu-Dpg-Ala-Dpg-Lys-NH_2	**Nva6**	Ac-Glu-Nva-Ala-Nva-Lys-NH_2
Dpg7	Ac-Glu-Dpg-Val-Dpg-Lys-NH_2	**Nva7**	Ac-Glu-Nva-Val–Nva-Lys-NH_2

Except for Dpg2, CD of the Dpg and Nva peptides showed that most had minimal structure or random coil structure as indicated by weak CD signature bands (Dpg5, Nva2) or predominately large negative bands at ~195 nm (Dpg6, Dpg7, Nva5, Nva6 and Nva7) as shown in Figure 1.

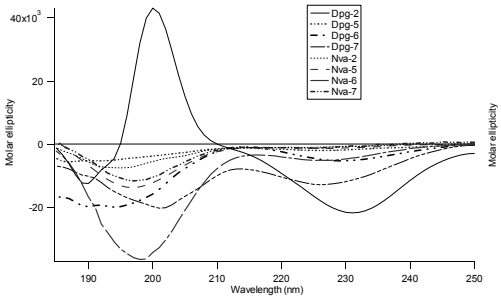

Fig. 1. CD spectra of Dpg2, Dpg5, Dpg6, Dpg7, Nva2, Nva5, Nva6 and Nva7 (100 μM peptide in 10 mM phosphate, pH 7.4, 20 °C).

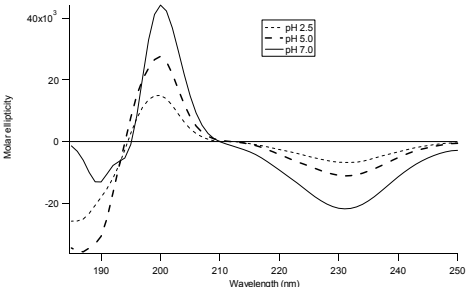

Fig. 2. CD spectra of Dpg2 in buffer with varying pH. Conditions: 100 μM peptide in 10 mM phosphate buffer, 20 °C.

In Dpg2 the intramolecular interaction between the side chains of glutamic acid and lysine may contribute to the stabilization of the β-turn structure. To examine this hypothesis, the CD of Dpg2 was carried out in three buffer solutions with different pH values (Figure 2). It was observed that Dpg2 possessed stronger CD bands in neutral solution, and there was a systematic reduction of molar ellipticity values for both positive and negative bands when the pH value was decreased. This result indicated a reduction of ordered structures at lower pH values presumably due to the titration of the charge-charge side chain interaction.

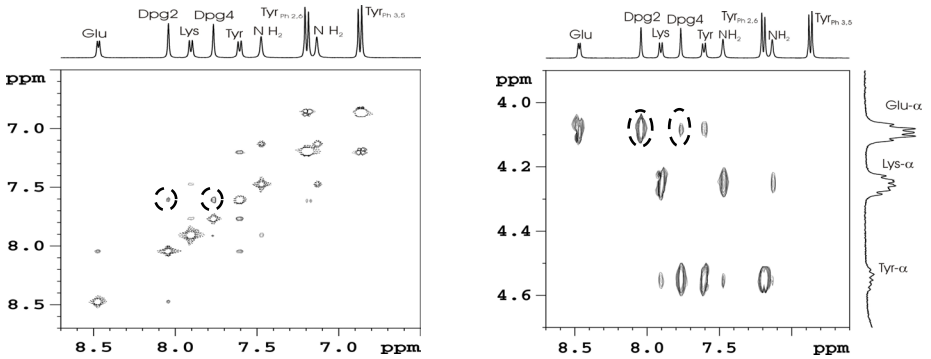

(a) (b)

Fig. 3. ROESY spectrum of Dpg2 (10 mM) in 30 mM phosphate buffer, pH 7.4 at 400MHz NMR, (a) amide-amide region; (b) amide-α hydrogen region.

In the ROESY spectrum of Dpg2, the crosspeaks of $d_{NN}(Dpg^2, Tyr^3)$ (Figure 3a) and $d_{\alpha N}(Glu^1, Dpg^2)$ (Figure 3b) indicate a type II β-turn structure with an intramolecular H-bonding between the acetyl carbonyl oxygen and the tyrosine NH. The crosspeaks of $d_{NN}(Tyr^3, Dpg^4)$ (Figure 3a) , $d_{\alpha N}(Glu^1, Dpg^4)$ (Figure 3b), and depressed temperature coefficient of the Dpg^4 NH suggested another β-turn in residue Glu^1-Dpg^4.

In conclusion, it is observed that Dpg2, Ac-Glu-Dpg-Tyr-Dpg-Lys-NH_2, adopts a β-turn structure in aqueous solution as determined by CD and NMR studies. The conformation of the Dpg peptides was affected by the whole sequence, and only the sequence of Dpg-Tyr-Dpg in the Dpg2 strongly favors the β-turn structure. The side chain interaction between the Glu and Lys plays an important role for the stabilization of the β-turn structure in the Dpg2.

Reference

1. Kaul, R., Banumathi, S., Velmurugan, D., Balaji Rao, R. and Balaram, P. *Biopolymers* **54**, 159-167 (2000).

Peptide Revolution: Genomics, Proteomics & Therapeutics
Michael Chorev & Tomi K. Sawyer (Editors)
American Peptide Society, 2003

An Encoding Method for One-bead One-compound Beta-turn Peptide and Peptidomimetic Libraries

Ruiwu Liu, Xiaobing Wang, Jan Marik and Kit S. Lam

Division of Hematology & Oncology, Department of Internal Medicine, UC Davis Cancer Center, University of California Davis, 4501 X Street, Sacramento, CA 95817, USA

Introduction

β-Turn peptides and peptidomimetics that bind to proteins may interrupt β-sheet formation and block protein-protein interactions. If these peptides contain unnatural amino acids (e.g. non-α-amino acids) or if their N-terminus is acylated, they will be more resistant to proteolysis. Using the "one-bead one-compound" (OBOC) combinatorial library method [1], millions of β-turn peptides or peptidomimetics can be synthesized and screened rapidly. However, there is no simple method to determine the chemical structure of these compounds. Mass spectrometry, although useful, cannot distinguish between amino acids with identical molecular masses. Furthermore, the compounds have to be cleaved off the bead prior to mass spectrometry analysis. We routinely use an automatic microsequencer (Edman chemistry) to sequence the individual peptide-bead. This method is convenient and reliable, and the individual peptide-bead can be sequenced directly without the need to cleave and recover the peptide from each bead. However, Edman chemistry requires that the peptide has only α-amino acids, and that the N-terminus is free. Therefore, there is a need to develop new methods to sequence peptide-beads containing non-sequenceable building blocks in certain positions or with their N-terminus blocked.

Results and Discussion

We recently reported a bi-layer bead encoding system for OBOC small molecule and peptidomimetic combinatorial libraries [2]. We have successfully used a similar strategy to encode two OBOC β-turn peptide and peptidomimetic libraries with non-sequenceable β-turn inducing amino acids in the middle of the peptide chain. One of these libraries has a free N-terminus, and the other has its N-terminus acylated by a number of different carboxylic acids. In these libraries, the library compounds (30% bead substitution) are present on the outer layer of the bead, and the coding tags (70% substitution) reside in the bead interior. The synthetic scheme for these two libraries is outlined in Figure 1. A split-mix synthesis approach [1] with Fmoc-chemistry and HOBt/DIC coupling were used in the construction of these libraries. Forty-nine α-amino acids (31 unnatural and 18 D-isomer of natural amino acids) were used in each cycle of coupling. After the first two amino acids (X_1 & X_2) were assembled on TentaGel resin and the Fmoc deprotected, the beads were topologically derivatized with Alloc on the outer layer leaving the amino group in the bead interior free [2]. This was achieved by first equilibrating the beads with water, followed by addition of AllocOSu (0.3 eq. to the beads) in a mixture of DCM/dimethyl ether (55/45, v/v) after the excess water was drained. The resulting bi-layer beads were split into eight aliquots, and a different coding α-amino acid (A_X) was coupled to the bead interior of each aliquot. The Alloc group on the outer layer was then removed with $Pd(PPh_3)_4/PhSiH_3$ and a corresponding β-turn inducing amino acid (A_{BT})was coupled to the outer layer of the beads in each of the bead aliquots. The beads were then combined and subject to another 2 cycles of amino acids coupling (X_3 & X_4) followed

by N-α-Fmoc deprotection. At this time, the bead library was split into two portions. One portion was subjected to side chain deprotection to form the first β-turn peptide library (EN-BT-01). The other portion was equilibrated with water and its outer layer derivatized with Fmoc (30%) according to the method described above. Boc-Lys(Dde) was coupled to the coding arm inside the beads. Fmoc in the testing arm and Dde in the coding arm were then removed in a single step by 2% hydrazine. The resin was divided into 49 portions in a 96-well plate (deep well). Forty-nine different carboxylic acids (each with 20 fold excess) pre-activated with HOBt/DIC were then added to the corresponding wells and incubated overnight. Both the N-terminus of the peptides at the outer layer and the ε-amino group of the lysine at the inner core were acylated at the same time. After side chain deprotection and thorough washing, the peptidomimetic library (EN-BT-02) was ready for screening. Positive beads from each of these two libraries can be sequenced directly with Edman chemistry. We have screened these libraries against a number of different biological targets and have identified several lead compounds for each of these targets.

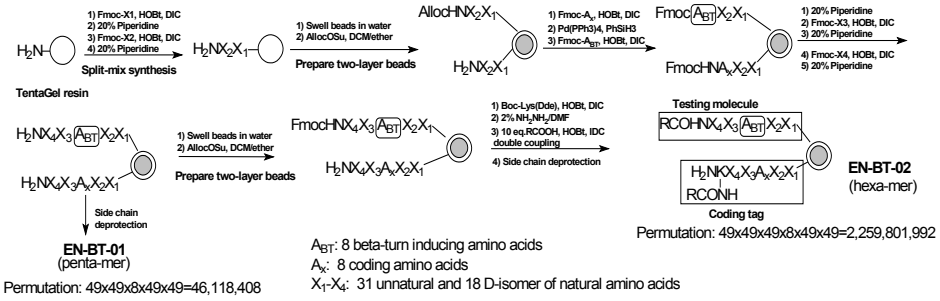

Fig. 1. A general synthetic and encoding scheme for OBOC peptide library with non-sequenceable building block and N-terminally blocked peptidomimetic library.

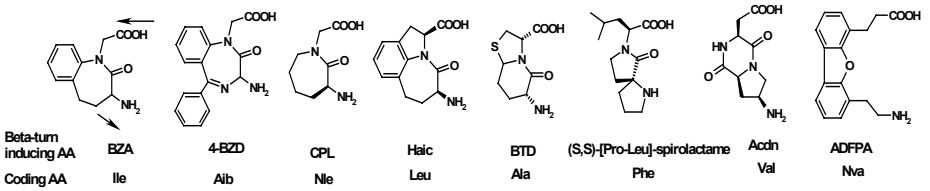

Fig. 2. Chemical structure of β-turn inducing amino acids and their corresponding coding amino acids.

Acknowledgments

The work was funded by NIH grants, R33CA86364 and R33CA89706, and the University of California Systemwide Biotechnology Research Program (Grant number: 2001-07).

References

1. Lam, K. S., et al. *Nature* **354**, 82-84 (1991).
2. Liu, R., Marik, J. and Lam, K. S. *J. Am. Chem. Soc*. **124**, 7678-7680 (2002).
3. Liu, R. and Lam, K. S. *Anal. Biochem*. **295***,* 9-16 (2001).

Peptide Revolution: Genomics, Proteomics & Therapeutics
Michael Chorev & Tomi K. Sawyer (Editors)
American Peptide Society, 2003

Synthetic Bivalent Inhibitors Based on the Bowman Birk Inhibitors: The BiKK Inhibitor

Agnès M. Jaulent and Robin J. Leatherbarrow

Department of Chemistry, Imperial College London, South Kensington Campus, London SW7 2AY, UK

Introduction

SFTI-1 is a small proteinaceous inhibitor isolated from sunflower seeds [1]. It presents striking similarities to a class of serine protease inhibitors called the Bowman Birk Inhibitors (BBIs) [2]. They both possess a nine-mer loop that is solely responsible for the interaction with the protease. The nine-mers' primary sequence and overall structure are strikingly similar. But SFTI-1 is however crucially different from the BBIs in its very small size and its ability to inhibit one protease only. Indeed, BBIs can be thought of as a large hydrophobic scaffold out of which projects two symmetrically spaced nine-mer loops, whereas SFTI-1 can be thought of as a nine-mer loop built onto the smallest of scaffolds. This is highlighted below where the scaffold of both proteins is represented in blue, and the reactive nine-mer loop in red.

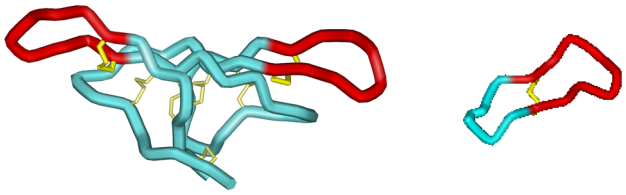

Fig. 1. A representative structure of a BBI protein (left) and SFTI-1 (right). Only the backbone can be seen. Blue represents the scaffold of the inhibitor, red its active loop, and yellow represents the disulfide bridges.

We wanted to synthesise bivalent inhibitors that would retain SFTI-1's high potency and small size, but that would resemble the BBIs in their dual ability to inhibit proteases.

BiKK is such an inhibitor. It has been designed by superimposing 2 nine-mer loops in such a way that it possesses a C2 symmetry axis between the 2 sulfur atoms. It is a 16-mer peptide that possesses a cyclic backbone as well as a disulfide bridge

Its synthesis, structure and enzymatic kinetics are presented and discussed.

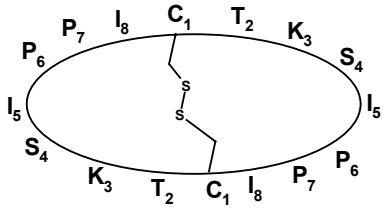

Fig. 2. A schematic representation of BiKK. The plain line shows the peptide backbone.

Results and Discussion

BiKK was synthesized on a pre-loaded chlorotrytil resin (Merck Biosciences) using standard Fmoc/tBu peptide synthesis on an ABI Apex 396 peptide synthesiser. After treatment of the resin-peptidyl with a mixture of AcOH/TFE/DCM (1:1:3) [3], the fully protected peptide was further cyclized using HOAT/HATU as coupling reagents [4]. The peptide was treated with TFA in order to deprotect its side-chains. The final cysteine oxidation step was performed by diluting the peptide in a 20% aqueous solution of DMSO containing 5% AcOH [5]. The peptide was then purified on C_{18} RP-HPLC (Waters) with a gradient of 0-80% CH_3CN in aq. 0.1% TFA. It was obtained with a 12% overall yield.

Table 1. Trypsin inhibitory assay results.

Inhibitor	Inhibition constant, K_i (nM)
BiKK	3.2
BBI protein	2.6
SFTI-1	0.3

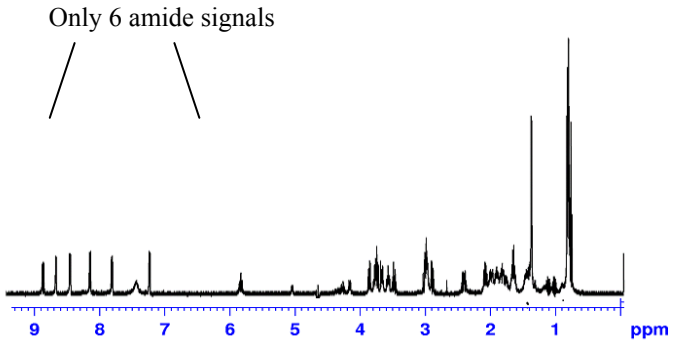

Fig. 3. ^1H NMR spectrum of BiKK.

BiKK's ^1H NMR confirms the fact that the peptide is symmetrical since only 6 instead of the 12 expected signals are present in the amide region.

BiKK is a very potent trypsin inhibitor with an inhibition constant in the nanomolar range. Although it is less potent than SFTI-1, it is as potent as its parent BBI protein while corresponding to a minimal design. Experiments are being currently undertaken in order to find out whether BiKK functions as a bivalent inhibitor and hits 2 trypsin molecules simultaneously.

Acknowledgments

This work was funded by the Chemistry Department at Imperial College London.

References

1. Luckett, S., Garcia, R. S., Barker, J. J., et al. *J. Mol. Biol.* **290**, 525-533 (1999).
2. Birk, Y. *Int. J. Pept. Protein Res.* **25,** 113-31 (1985).
3. Barlos, K., Chatzi, O., et al. *Int. J. Pept. Protein Res.* **37,** 513-520 (1991).
4. Descours, A., Moehle, K., Renard, A. and Robinson, J. A. *ChemBioChem* **3,** 318-23 (2002).
5.Tam, J. P., Wu, C. R., Liu, W. and Zhang, J. W. *J. Am. Chem. Soc.* **113,** 6657-6662 (1991).

Peptide Revolution: Genomics, Proteomics & Therapeutics
Michael Chorev & Tomi K. Sawyer (Editors)
American Peptide Society, 2003

Understanding β-Structure in Peptides and Proteins

Andrea G. Cochran, Nicholas J. Skelton and Melissa A. Starovasnik

Department of Protein Engineering, Genentech, Inc., 1 DNA Way,
South San Francisco, CA 94080, USA

Introduction

Determining the properties that govern β-sheet stability has been an active area of research for a number of years. Diverse features of sheet structure have been probed through mutagenesis studies (reviewed in [1]). These include contributions from intrinsic residue propensities at particular strand sites and from cross-strand residue pairing. In addition, much progress has been made in designing new sequences that can adopt β-folds [2–4]. Our own efforts in this area were prompted by the observation that certain peptide ligands selected by phage display were found to be remarkably well-structured as free peptides in solution [5–7]. Because these peptides were obtained from genetically-encoded libraries, they do not contain any D-residues or other synthetic modifications that are often used to enforce structure in short peptides. Despite this, several of these phage peptides can be heated to temperatures > 60 ˚C without any significant changes in their NMR spectra. Presumably, non-covalent interactions in these peptides contribute to the unusual conformational stabilities they exhibit. Several folds have been observed for phage peptides, examples of which are shown in Figure 1 (one of these is the "CX_8C" β-hairpin shown on the left). At the time we began this work, other examples of structured cyclic β-hairpins were few and generally contained in their turn sequences non-natural structure-promoting residues such as D-residues. We decided to investigate instead the contribution of individual strand residues to structural stability in this fold, with the goal of developing a scaffold for β-turn display. This idea is represented schematically in Figure 2. For maximum utility in phage selections, the turn region of the hairpin should be freely variable to any potential turn sequence. Therefore, in order to structure

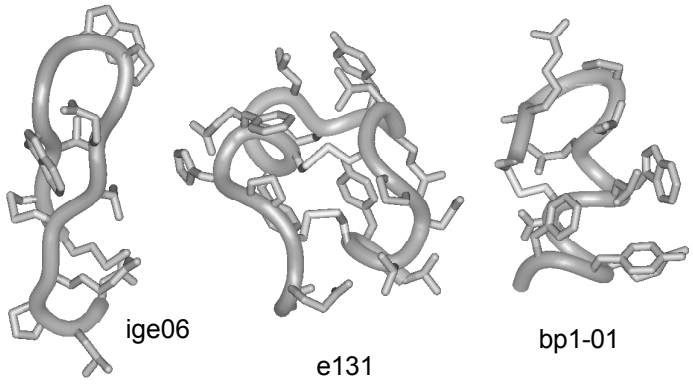

Fig. 1. Examples of structured peptides selected for target binding from phage-displayed libraries. Minimized-mean NMR structures are shown [5–7].

the turn, any energetic "cost" for the less favorable turns must be paid by particularly strong strand-strand interactions. Although there was at the time some published data on individual residue contributions to sheet stability, it was not clear whether these data would be applicable to β-hairpin design. We have since found that the amino acids preferred at the various hairpin strand positions are distinctive and not readily predicted from analysis of protein β-sheets. Data obtained from a cyclic hairpin model system were used to design surprisingly stable, linear folded hairpins and to reevaluate previous conclusions about the importance of side chain-side chain interactions to β-sheet stability.

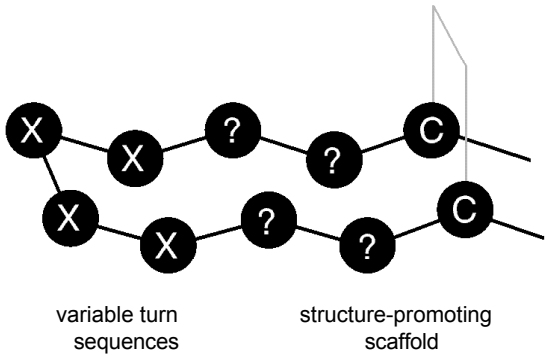

Fig. 2. Structured hairpin peptide scaffold for β-turn display.

Results and Discussion

Our initial experiments were directed at optimization of one non-hydrogen-bonded strand position in the model hairpin shown in Figure 3 [8]. We suspected that hydrophobic residues, especially leucine and phenylalanine, might be somewhat stabilizing; this idea was based on inspection of the residues surrounding disulfides in antiparallel β-sheets. However, the likely magnitude of any energetic contribution was difficult to estimate. We therefore synthesized peptides in which each of the 19 amino acids (excluding cysteine) was introduced into the guest site. The disulfide was both a structural element and a probe for stability: in redox buffer, the equilibrium between reduced and oxidized cysteines shifts as the disulfide-bonded peptide acquires structure [8, and references therein]. The ratio of reduced to oxidized peptide is readily quantified by HPLC, and relative equilibrium constants can be converted to relative free energy differences ($\Delta\Delta G$). This method is quite sensitive to small changes in stability (~30 cal mol^{-1}) but cannot be used to determine absolute stabilities (that is, the fraction of folded molecules).

The results of this initial study are shown in Figure 3. As we had thought likely, hydrophobic amino acids did tend to improve hairpin structural stability. However, we were very surprised to observe the unique contribution from a tryptophan substitution. This substitution promoted folding by $\geq$ 0.5 kcal mol^{-1} relative to any other amino acid, even other aromatic amino acids. This effect and the overall rank order of stabilities were not observed in other β-sheet model studies, nor do they reflect the composition of β-sheets in the Protein Data Bank. For example, some residues generally thought to promote β-sheet formation, most notably threonine, do not stabilize the model hairpin.

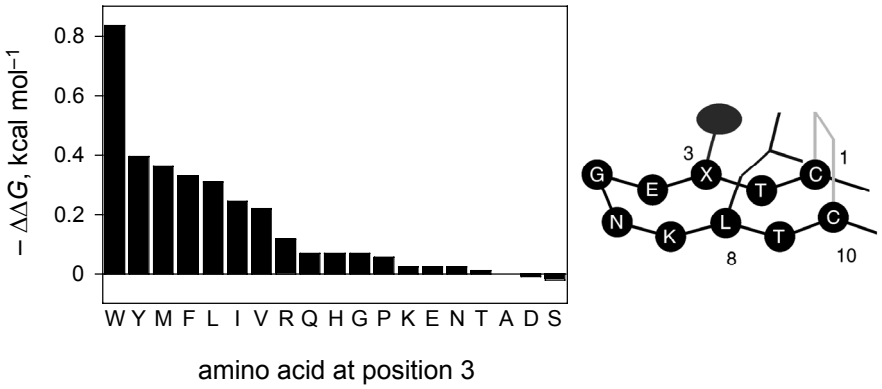

Fig. 3. Relative stabilities of β-hairpins with substitutions at sequence position 3. A cartoon representation of the β-haipin model host peptide (Ac-CTXEGNKLTC-NH$_2$) is shown at right.

Additional studies demonstrated that the stabilizing effect of tryptophan at position 3 did not depend on the turn sequence in the model peptide [8]. Furthermore, the energetic contributions of turns and the strand substitutions appeared to be independent (and strictly additive) in the model peptides. We then investigated hydrophobic residue subsitutions at the cross-strand non-hydrogen-bonding position 8 [9]. The rank order and relative stabilities were very similar to those observed for position 3 substitutions. In particular, tryptophan was significantly more stabilizing than any of the other hydrophobic amino acids. In contrast to what might be expected, it did not appear that introducing a cross-strand tryptophan pair added any stability beyond that attributable to the two single substitutions. Thus, despite the fact that the cross-strand tryptophan side chains are close enough to contact one another, the aromatic-aromatic side chain interaction does not appear to be energetically significant in this model system [9]. Nevertheless, the use of a non-hydrogen-bonding Trp-Trp pair did confer about 1.2 kcal mol^{-1} of stability improvement relative to a Leu-Leu pair.

Our next goal was to determine the most stabilizing residue combinations for the hydrogen-bonded cross-strand pair at positions 2 and 9 of our model hairpin [10]. Interestingly, in contrast to the non-hydrogen-bonded pair, we found that these positions were not equivalent. For example, while the aromatic residues were the most stabilizing substitutions at position 2, position 9 exhibited a strong preference for the branched hydrophobic residues Val and Ile. Once again, the effects could be quite dramatic; for example, the Val9 substitution improves stability by ~0.7 kcal mol^{-1} relative to the structurally very similar threonine [10]. Furthermore, the rank order of residue preferences did not closely resemble published β-propensity scales or statistical preferences in protein β-sheets. Instead it appears that these cyclic hairpin peptides, and perhaps all two-stranded antiparallel β-structures, have their own set of stability rules.

A summary of the scaffold optimization is shown in Figure 4, with our most useful scaffold is shown at the top. It includes the Trp-Trp non-hydrogen-bonded pair and the highly stabilizing Val9. Position 2 is chosen as His; although this is not the most stabilizing residue we found for this position, it does often improve peptide solubility relative to other aromatic residues. Overall, the final scaffold is about 2.2 kcal mol^{-1} more stable than the earlier version shown at bottom. We have found the final scaffold

to be generally effective in structuring turns taken from proteins, even relatively unstable turns containing β-bulges [11].

Ac-C**HW**EGNK**WV**C-NH_2	C_{eff} = 4100 mM
Ac-C**T W**EGNK**WT**C-NH_2	C_{eff} = 721 mM
Ac-C**T W**EGNK **L T**C-NH_2	C_{eff} = 210 mM
Ac-C**T L** EGNK **L T**C-NH_2	C_{eff} = 85 mM

Fig. 4. Optimization of the β-haipin scaffold. An early peptide with partial yet clearly discernible hairpin structure (based on NMR analysis) is shown at bottom, and the improved, highly stable final scaffold is shown at top. Cysteine effective concentrations (C_{eff}) are measured relative to glutathione.

The large number of peptides we have synthesized in our β-hairpin model series allow us to look for additive or non-additive contributions from different structural elements of the β-hairpin. Most typically, these questions are addressed through double mutant-cycles analyses (e.g., [12]). We have chosen instead to examine free energy correlations in different host backgrounds. This approach is drawn from classic physical organic chemistry and has been applied previously to protein mutagenesis data to separate "intrinsic" effects of substitutions on stability from those that are context dependent [13]. As described briefly above and in [8], we have found that stability changes upon strand substitution for host peptides with different turns correlate well, with close to unit slopes. In other words, despite the fact that a large overall increase in hairpin stability (0.5–1 kcal mol^{-1}) can be achieved by substituting a stronger reverse turn for the Gly-Asn sequence of the model peptide, the same stabilization is achieved for all the strand variants. This independent, additive behavior of the two structural elements (turn and strand site) is inconsistent with the idea that these might contribute *cooperatively* to hairpin stability.

In contrast, we have found evidence for cooperative behavior when comparing stability changes in host peptides with different strand sequences [9,10]. A striking example is shown in Figure 5 [10]. In this plot, free energy changes for position 3 substitutions are compared for the original model system (T2T9) and the more stable version (H2V9). There is a very good correlation between the two data sets. This may not be especially surprising, given that the side chain of residue 3 is on the opposite face of the hairpin from the side chains of residues 2 and 9 that differ between the two scaffolds. What is less expected is that the slope of the plot is ~2 instead of ~1. The free energy differences are thus amplified in the more structurally stable H2V9 background, suggesting that multiple strand substitutions can act synergistically, or cooperatively, to promote hairpin folding.

An additional example of the synergistic behavior described above was observed upon comparing stability changes for position 3 substitutions in peptides in which position 8 was also varied [9]. In this case, the variable host element (8) is on the same face as the guest residue (3), and the side chains potentially contact one another. Rather strikingly, stability changes were correlated for hydrophobic substitutions paired with Trp and those paired with Leu. A perfect correlation would suggest that interactions between the two side chains were exactly the same for Trp pairs as for Leu pairs. Given the different chemical properties of these two side chains, this would further suggest that the interactions must be energetically insignificant compared to the substitution

free energy differences. However, the correlation was not perfect. Instead, some scatter from the diagonal was observed [9]. This suggests that small (~0.1 kcal mol^{-1}) interaction energies may exist for some side chain-side chain contacts, yet overall, the trends are dominated by the single site effects (up to 1.4 kcal mol^{-1} in these experiments). Once again, the free energy differences were amplified in the more stable background (paired with Trp). An important consequence of this observation is that if one were instead to make only limited pair wise comparisons as in a double mutant-cycle analysis, the difference in slope would give rise to a potentially large apparent interaction energy [9]. In contrast, the linear free-energy correlations observed across larger series of peptides argue against this interpretation.

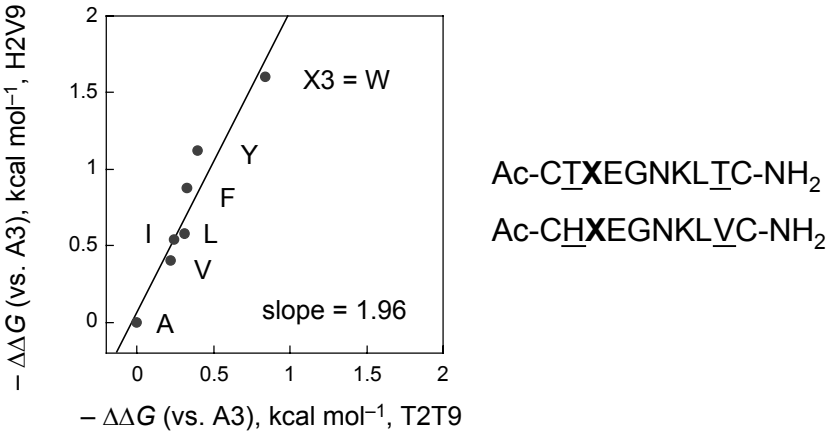

Fig. 5. Relative free energy differences for position 3 substitutions compared for two host backgrounds. The host peptides are shown at right. X represents the site of substitution, and the residues that differ between host peptides are underlined.

Our conclusion that specific side chain-side chain contacts contributed relatively little to β-hairpin stability did not agree with earlier conclusions in the β-sheet literature. We therefore decided to reinvestigate this question in the well-studied model system GB1, the B1 domain of Protein G [14–16]. GB1 consists of a single four-stranded β-sheet packed against an α-helix (Figure 6). It is thermally rather stable, undergoes a two-state unfolding transition, and is monomeric. Because of these favorable properties, many mutants of GB1 have been characterized thermodynamically. GB1 has served as a host protein for the determination of β-propensity scales (e.g., [14]) and for investigating pair interactions through double mutant-cycle analysis [15,16]. Interestingly, many pair interaction energies determined for GB1 are quite large (~1 kcal mol^{-1}) and similar in magnitude to the range of energies spanned by the propensity scales [15].

In our study, a large number of GB1 variants were examined simultaneously by phage display [17]. We prepared a library in which all 20 amino acids were allowed at each of the two surface positions 44 and 53 (Figure 6). A binding selection (to IgG Fc) was used to separate folded variants from unfolded variants. Importantly, the binding surface of GB1 is on the opposite face of the protein from the residue pair that was

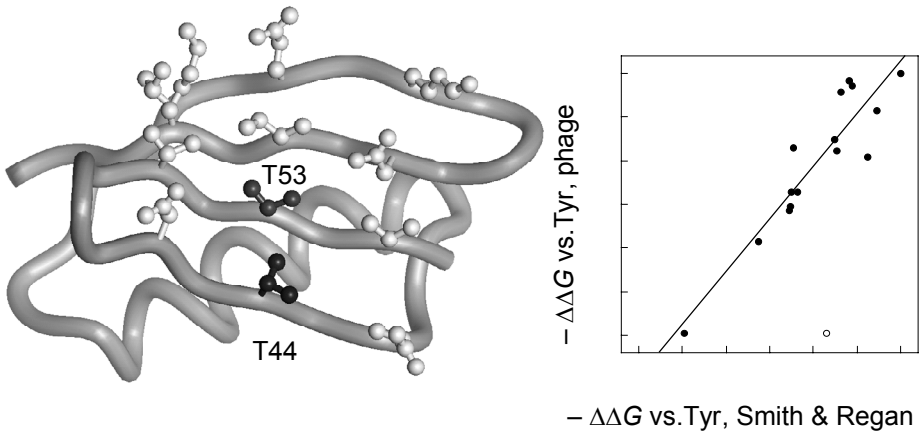

Fig. 6. Protein G (GB1) β-sheet model system. Residues varied in the GB1 phage library are noted (see text). At right is shown the correlation between statistical free energy differences (determined from recovery in a IgG Fc binding selection) and a published β-propensity scale derived from thermal stabilities of purified mutant proteins [14]. The data shown are for the interior strand position 53.

varied in the library. After three rounds of binding selection and phage amplification, all clones tested individually bound to the Fc target. A large number (1242) of GB1 mutant phage were sequenced and the distributions of amino acids at the two positions were examined. A key assumption is that these distributions reflect quantitatively the stability of the corresponding proteins. In order to test this idea, observed amino acid ratios were treated as equilibrium constants and converted to free energy differences. Since position 53 was the guest site in a previous mutagenesis study [14], it was possible to compare the phage-derived free energy differences to the true values for the same series of substitutions (Figure 6, right). Except for cysteine, which may impair display on phage, the phage sequence distributions correlate quite well with the propensity scale. This suggests that protein stability is in fact the dominant factor in the selection. Given this, it was possible to analyze statistically whether residue pairs were correlated in the phage data set. If particular side chain-side chain interactions enhanced sheet stability, one would expect to see those residue pairs overrepresented in the data compared to an unbiased pairing assumption. While some pairs did appear to be positively or negatively correlated in the phage clones, the majority appeared at frequencies close to those expected for unbiased pairing. In particular, hydrophobic-hydrophobic pairs were not overrepresented in the data, despite the fact that these pairs appeared to be quite stabilizing in earlier mutagenesis studies [15]. This discrepancy can be explained by anomalous properties of the alanine-substituted GB1 variants used as reference states in the double mutant-cycle analysis [17]. Taken together, the GB1 mutagenesis studies and the peptide model studies described above suggest that contributions from individual residues are more important to stability of β-structures than are specific side chain interactions, at least for those residues most common in β-sheets (aromatic and β-branched).

The idea that β-structures could be built around modular, stabilizing components was applied to the design of a well-folded, linear β-hairpin [18]. As described above, we had found tryptophan residues to be strongly stabilizing in non-hydrogen-bonded

bhpWW S **C** T**W**EGNK**W**T**C**K-NH_2

trpzip1 S**W**T**W**EGNK**W**T**W**K-NH_2

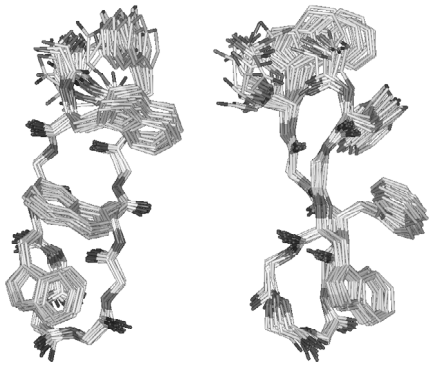

Fig. 7. Design of a stably folded linear β-hairpin [18]. A second tryptohan pair replaces the disulfide of the cyclic peptide bhpWW (left). The calculated NMR structure of trpzip1 is shown in two views at right.

strand positions. This suggested that it might be possible to use additional tryptophans to replace the cysteines in our cyclic model peptide (also occupying non-hydrogen-bonded strand sites). We therefore synthesized the peptide trpzip1 (Figure 7). Strikingly, trpzip1 underwent reversible and cooperative thermal denaturation and was monomeric. The structure of trpzip1 calculated from NMR data revealed an exceptionally well-defined structure for a short linear peptide. Interestingly, the strands of trpzip1 exhibited a pronounced twist, perhaps explaining the unusually strong preference for tryptophan in two-stranded hairpins compared to more extended sheets.

Another model β-hairpin is the C-terminal 16-residue peptide from Protein G (gb1 41–56, Figure 8). This peptide was shown through NMR studies to be partially folded

gb1, 41-56 GE**W**T**Y**DDATKT**F**T**V**TE

trpzip 4 GE**W**T**W**DDATKT**W**T**W**TE

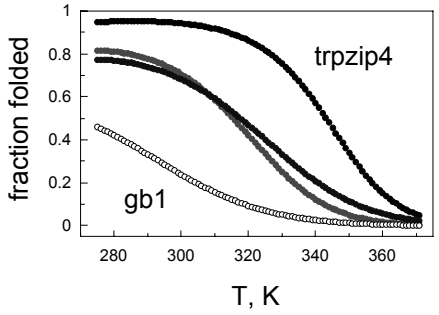

ΔG_{unf}, 25°C (kcal mol^{-1})

WWWW (tz4)	1.69
WYFW	0.57
WWWV	0.49
WYFV (gb1)	~ –0.6

Fig. 8. Comparison of the trpzip motif to the hydrophobic cluster of the GB1 C-terminal hairpin (a 16-residue peptide taken from GB1 [19] and depicted in the bottom half of the sheet shown in Fig. 6). The sequences of the synthetic peptides are shown at top. Thermal denaturation curves for gb1, trpzip4, and two intermediate peptides are shown, with the corresponding folding free energies (25 ˚C) shown at right. The melting temperature of trpzip4 is 73 ˚C [18].

at low temperatures [19]. Four hydrophobic residues that normally pack into the core of the intact domain were proposed to stabilize the hairpin. Intriguingly, three of these residues are aromatic, and all four occupy strand sites that are non-hydrogen-bonding in the structure of the hairpin within the intact domain (the structure of the hairpin itself cannot be determined with any confidence from the NMR data, since there is significant spectral overlap). In order to compare the trpzip motif to the gb1 hydrophobic cluster, we synthesized trpzip4 (Figure 8). Like trpzip1, trpzip4 was well-folded, undergoing reversible, apparent two-state denaturation. The folded structure was remarkably stable for such a short peptide; trpzip4 has an unfolding free energy of 1.7 kcal mol^{-1} at 25 ˚C. In contrast, the gb1 16-mer has an unfolding free energy < 0 kcal mol^{-1}, and its denaturation curve is much less cooperative than that of trpzip4. As we had expected, the successive addition of Trp pairs to the gb1 sequence produced increasingly stable folded hairpins. Each Trp pair stabilized the hairpin by ~1 kcal mol^{-1} compared to the original gb1 residue pair (Figure 8). Once again, trpzip4 adopted a highly twisted conformation [18].

Conclusions

From these studies, a consistent view of β-structural stability is beginning to emerge. Single-site residue preferences seem dominant, but it is clear that not all strand sites have the same preferences. Other structural features, such as degree of strand twist, are quite important to consider when designing sheets and hairpins.

Acknowledgments

We acknowledge contributions from Steve Russell, Tamas Blandl, Eleanor Park, Ricky Tong, Mark Distefano, and Bob McDowell to the work reviewed in this paper.

References

1. Smith, C. K. and Regan, L. *Acc. Chem. Res.* **30**, 153–161 (1997).
2. Struthers, M. D., Cheng, R. P. and Imperiali, B. *Science* **271**, 342–345 (1996).
3. Dahiyat, B. I. and Mayo, S. L. *Science* **278**, 82–87 (1997).
4. Kortemme, T., Ramírez-Alvarado, M. and Serrano, L. *Science* **281**, 253–256 (1998).
5. Nakamura, G. R., Starovasnik, M. A., Reynolds, M. E. and Lowman, H. B. *Biochemistry* **40**, 9828–9835 (2001).
6. Nakamura, G. R., Reynolds, M. E., Chen, Y. M., Starovasnik, M. A. and Lowman, H. B. *Proc. Natl. Acad. Sci. U.S.A.* **99**, 1303–1308 (2002).
7. Lowman, H. B., *et al. Biochemistry* **37**, 8870–8878 (1998).
8. Cochran, A. G., *et al. J. Am. Chem. Soc.* **123**, 625–632 (2001).
9. Russell, S. J. and Cochran, A. G. *J. Am. Chem. Soc.* **122**, 12600–12601 (2000).
10. Russell, S. J., Blandl, T., Skelton, N. J. and Cochran, A. G. *J. Am. Chem. Soc.* **125**, 388–395 (2003).
11. Blandl, T., Cochran, A. G. and Skelton, N. J. *Protein Sci.* **12**, 237–247 (2003).
12. Tatko, C. D. and Waters, M. L. *J. Am. Chem. Soc.* **124**, 9372–9373 (2002).
13. Predki, P. F., Agrawal, V., Brünger, A. T. and Regan, L. *Nat. Struct. Biol*. **3**, 54–58 (1996).
14. Smith, C. K., Withka, J. M. and Regan, L. *Biochemistry* **33**, 5510–5517 (1994).
15. Smith, C. K. and Regan, L. *Science* **270**, 980–982 (1995).
16. Merkel, J. S., Sturtevant, J. M. and Regan, L. *Structure* **7**, 1333–1343 (1999).
17. Distefano, M. D., Zhong, A. and Cochran, A. G. *J. Mol. Biol.* **322**, 179–188 (2002).
18. Cochran, A. G., Skelton, N. J. and Starovasnik, M. A. *Proc. Natl. Acad. Sci. U.S.A.* **98**, 5578–5583 (2001).
19. Blanco, F. J., Rivas G. and Serrano, L. *Nat. Struct. Biol*. **1**, 584–590 (1994).

Peptide Revolution: Genomics, Proteomics & Therapeutics
Michael Chorev & Tomi K. Sawyer (Editors)
American Peptide Society, 2003

Molecular Dynamic Investigation of the β-Turn Forming Nature of Tetra- and Hexapeptides

Attila Borics, Richard F. Murphy and Sándor Lovas

Department of Biomedical Sciences, Creighton University, Omaha, NE 68128, USA

Introduction

NMR- and CD-spectroscopic studies showed that the model sequences NPGQ [1], GKDG [2], DDKG [2], DEKS [3], VPAH [4], VPSH [4], SALN [5], SYPFDV [6] and SYPYDV [6] in N- and C-terminally blocked form, have a high propensity to adopt β-turn structure. However, other conformational families were also found, suggesting that tertiary interactions with neighboring polypeptide regions play an important role in stabilizing β-turns in proteins.

In this study, the β-turn forming tendency of the model sequences was studied using a protein database search, simulated annealing and molecular dynamics (MD).

Results and Discussion

The protein database search was done for the above sequences in a binary database of 1478 proteins, with less than 45% sequence similarity and a resolution of 3.5 Å or better, from the Brookhaven Protein Data Bank. For tetrapeptides, an additional residue (any) was added to each terminus in the search query, to facilitate successful secondary structure assignment to the fragments obtained by the DSSP method.

For repeated simulated annealing, the OPLS-AA force field and GB/SA solvation was used. One annealing cycle consisted of a 2000 ps equilibration period at 1050 K followed by 2000 ps exponential cooling to 50 K in 1 fs steps. 1000 resultant structures were then energy-minimized and ranked by their potential energies. The lowest energy structures of each sequence that adopted turn structure were then used as input for MD simulations.

MD simulations (25.1 ns) in the presence of SPC water molecules were carried out using the GROMOS96 force field at constant temperature (300 K) and pressure (1 bar), with 2 fs integration steps. For Coulomb interactions, both the twin range cut-off with reaction-field correction and the PME method were used. Coordinates were stored for evaluation after every 1000 steps having excluded the first 100 ps. Trajectories were analyzed using the DSSP secondary structure-assigning algorithm. Structures were clustered comparing peptide backbones with 0.1 nm RMSD cut-off.

While the number of fragments found in the database for each sequence is low, DSSP analysis shows that they occur mostly in the turns of protein backbones. Repeated simulated annealing and comparison of potential energies of resultant structures showed that β-turn conformation is highly favored for each sequence.

Analysis of trajectories obtained from MD simulations using the DSSP method shows a fluctuation between β-turn and unordered structure in most cases. No major differences were found between the results obtained using the different methods of the treatment of long-range electrostatic interactions. For tetrapeptides, the DSSP method recognized turn structures only but failed to assign bent or helical structure because of the insufficient length of the peptide chains. On the other hand, turn structure was assigned only when a hydrogen bond was present between the carbonyl oxygen of residue 1 and the amide nitrogen of residue 4. However, hydrogen bonding between the first and the last residue of the turn segment is a result of backbone conformation rather

Table 1. Results of clustering of the structural ensemble obtained from MD trajectories.

Sequence[a]	Number of clusters found		Population of the strongest cluster (%)	
	RF	PME	RF	PME
Ac-DDKG-NH_2	37	36	485 (19.3)	1194 (43.8)
Ac-DEKS-NH_2	30	24	988 (39.5)	1097 (43.9)
Ac-GKDG-NH_2	39	43	469 (18.8)	487 (19.5)
Ac-NPGQ-NH_2	16	12	1215 (48.6)	1447 (57.9)
Ac-SALN-NH_2	29	33	1010 (40.4)	941 (37.6)
Ac-VPaH-NH_2	11	11	1941 (77.6)	2061 (82.4)
Ac-VPsH-NH_2	10	11	2009 (80.3)	2014 (80.6)
Ac-SYPFDV-NH_2	94	97	506 (20.2)	351 (14.0)
Ac-SYPYDV-NH_2	74	74	662 (26.5)	581 (23.2)

[a]*D-amino acids are in lower case.*

than a requirement for β-turn structure. Analysis of the backbone dihedrals of structures along the trajectories may show that other structural elements such as bends and β-bridges are present. This is further supported by the results of clustering (Table 1) which show that some sequences can have more stable structures than could have been predicted from DSSP analyses of trajectories. The low number of clusters found for Ac-NPGQ-NH_2, Ac-VPAH-NH_2 and Ac-VPSH-NH_2 suggests higher conformational stability of these than of other peptides. The middle structure of the strongest clusters of Ac-NPGQ-NH_2 and Ac-VPAH-NH_2 adopts a β-turn, and of Ac-VPSH-NH_2, a bend. The high population of the strongest clusters also suggests high stability of these structures. These results are in good agreement with results of NMR and CD spectroscopic analyses of the peptides, where β-turn structure was found to be dominant, but other folded conformations were also found. Only minor differences between the clustering results were found when the different methods had been used for the calculation of long-range electrostatic interactions.

Acknowledgments
This work was supported by NIH-BRIN (1 P20 RR16469-01) and NSF-EPScOR (EPS-0091900) grants.

References

1. Carbone, F. R. and Leach, S. J. *Int. J. Pept. Protein Res.* **26**, 498-508 (1985).
2. Ishii, H., Fukunishi, J., Inoue, Y. and Chujo, R. *Biopolymers* **24**, 2045-2056 (1985).
3. Otter, A., Scott, P. G., Liu, X. H. and Kotovych, G. *J. Biomol. Struct. Dyn.* **7**, 455-476 (1989).
4. Imperiali, B., Fisher, S. L., Moats, R. A. and Prins, T. J. *J. Amer. Chem. Soc.* **114**, 3182-3188 (1992).
5. Santa, H., Peräkylä, M. and Laatikainen, R. *J. Biomol. Struct. Dyn.* **16**, 1033-1041 (1999).
6. Yao, J., Feher, V. A., Espejo, B. F., Reymond, M. T., Wright, P. E. and Dyson, H. J. *J. Mol. Biol*. **243**, 736-753 (1994).

Peptide Revolution: Genomics, Proteomics & Therapeutics
Michael Chorev & Tomi K. Sawyer (Editors)
American Peptide Society, 2003

Discovery and Applications of the Cyclotides: Circular Proteins from Plants

David J. Craik, Norelle L. Daly, Michelle L. Colgrave and K. Johan Rosengren

Institute for Molecular Bioscience, University of Queensland, Brisbane, Queensland, Australia, 4072

Introduction

The cyclotides [1,2] are a recently discovered family of circular mini-proteins that have a range of potential applications in drug design [3] and agriculture [4]. They are ~30 amino acids in size, contain a head-to-tail cyclized backbone and incorporate three disulfide bonds arranged in a cystine knot topology. We estimate that the family comprises at least several hundred proteins, with about 50 sequenced so far. This manuscript will describe the discovery of the cyclotides in plants, their structural characterization by NMR and their biophysical characterization. Their cyclic cystine knot motif makes the cyclotides exceptionally stable: they retain bioactivity after boiling and are resistant to enzymatic breakdown. Their stability and compact structure makes them an attractive framework for drug design applications.

The first reports of circular proteins in plants appeared in the mid-1990s, with the identification of viola peptide I, a hemolytic agent from *Viola arvensis* [5], the anti-HIV circulins from *Chassalia parvifolia* [6], the neurotensin antagonist cyclopsychotride A from *Psychotria longipes* [7], and kalata B1 from *Oldenlandia affinis* [8]. Soon after, a series of peptides from viola plants was identified [1,9], and the various peptides discovered to that point were recognized as part of a protein family that we named the cyclotides [1]. Additional members have been discovered in the last few years [10-15].

Although its primary sequence and circular backbone were not characterized at the time, kalata B1 had been discovered in the 1970s as a bioactive peptide in a native medicine used by women in the Congo region of Africa to accelerate labor and childbirth. Gran [16] reported that the women ingested a tea made by boiling the aerial parts of *O.affinis*, and in subsequent studies [17] noted that an apparent 30-amino acid peptide isolated from the plant was an active uterotonic agent [18]. The peptide was partially characterized at the time, but it was some 20 years later before it was established that the peptide contains 29 amino acid residues in a circular backbone [8].

Kalata B1 was the first cyclotide to be structurally characterized [8]. It is a compact mini-protein that incorporates a distorted triple-stranded β-sheet and several turns, as illustrated in Figure 1.

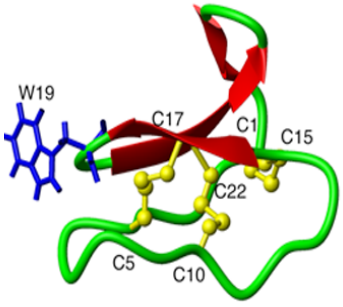

Fig. 1. Solution structure of kalata B1 determined using NMR spectroscopy [8,21]. The disulfide connectivities are shown in ball-and-stick representation between the conserved cysteine residues and highlight the knotted arrangement. The position of the triple-stranded β-sheet is indicated by arrows. An exposed tryptophan residue (W19) that forms part of a surface-exposed hydrophobic patch is highlighted.

Because of the resistance of the oxidized molecule to enzymatic cleavage it was not possible to determine its disulfide connectivity chemically, but NMR data suggested a I-IV, II-V, III-VI connectivity [8]. This arrangement of disulfide bonds forms a cystine knot in which an embedded ring formed by the first two disulfide bonds and their connecting backbone segments is penetrated by the third (i.e. III-VI) disulfide bond. Such a cystine knot motif is now well known in a wide variety of proteins, ranging from growth factors to toxins, and occurs in a wide range of organisms [19,20]. However, the cyclotides remain as the only example in which a cystine knot is embedded within a circular protein backbone, a motif that is referred to as the cyclic cystine knot (CCK) [1,19].

Although the structures of only a few cyclotides have been determined so far, their generally high sequence conservation suggests that all members will have a similar CCK motif. A schematic representation of the conserved residues superimposed onto the CCK structural framework is given in Figure 2 [21].

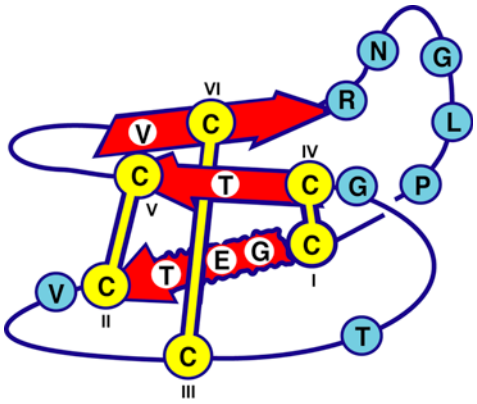

Fig. 2. Schematic illustration of the cyclotide framework. The amino acids that are conserved throughout most of the cyclotide family are indicated by circles and single-letter amino acid codes. Those residues surrounded by white circles are present in the core of the molecule; those outside are highlighted with shaded circles. Structural roles have been determined for many of the conserved residues [21]. The disulfide connectivities are shown by connections between the conserved cysteine residues and highlight the knotted arrangement. The framework may be thought of as comprising six loops between these conserved cysteines. The position of the triple-stranded β-sheet is indicated by arrows, with the arrow for the strand in loop 1, which is somewhat distorted, having jagged edges.

In the current study the factors contributing to the unique structures and exceptional stability of the cyclotides are examined. As much of the previous evidence for the exceptional stability of molecules from the cyclotide family was anecdotal it was of interest to systematically evaluate their stability to enzymatic, chemical and thermal perturbations, and to understand the structural basis for this stability.

Results and Discussion

Resistance to enzymatic degradation was examined first. Native kalata B1 was found to be completely impervious to proteolysis by endo Glu-C, as illustrated in Figure 3. By contrast, the reduced form was cleaved on the C-terminal side of the glutamic acid

residue to yield a linear product. Two acyclic permutants of kalata B1 in which residues from loops 5 and 6 had been removed were also examined and neither showed any signs of degradation. Similar results were obtained with a range of other enzymes, including trypsin and thermolysin. This evidence suggests that it is the knotted disulfide arrangement, and not just the cyclic backbone, that is primarily responsible for the enzymatic stability of kalata B1. Overall, the data show that the presence of the oxidized cystine framework and its attendant cystine knot provides a scaffold that stabilizes the peptides against digestion. Stability against exo-proteases has yet to be tested.

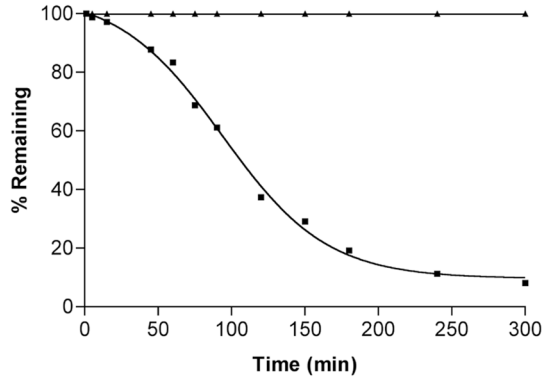

Fig. 3. Time course for the digestion of native, oxidized kalata B1 (▲) and reduced, alkylated kalata B1 (■). An enzyme: substrate ratio of 1:50 endoproteinase glu-C: peptide was used and the experiments were conducted at 37°C in 100 mM NH_4HCO_3 (pH 8.1). The resulting solutions were analyzed by LC/MS on an Agilent 1100 series HPLC coupled to an API Qstar mass spectrometer equipped with an electrospray ionisation source.

Digestion of reduced cyclotides with endo Glu-C is used in our standard protocol for sequencing of the cyclotides. As illustrated in Figure 2, there is a conserved Glu residue in the embedded ring of the cystine knot. Since there are rarely other Glu residues in cyclotide sequences convenient linear peptides representing the full cyclotide sequence are often obtained using this procedure.

The chemical stability, i.e. resistance to unfolding by denaturants such as guanidine hydrochloride (GdHCl), was investigated next. The fluorescence spectrum of kalata B1 (50 μM) alone was of low intensity with a maximum emission wavelength, λ_{max}, of 335 nm. This low intensity most likely reflects the exposed nature of the single Trp residue in kalata B1 shown in Figure 1. Upon addition of 6 M GdHCl, there was no significant change in either the fluorescence intensity or emission wavelength. The addition of dithiothreitol (DTT) followed by incubation at 37°C for 30 minutes resulted in a large and significant increase in the fluorescence intensity (approximately 5-fold) and the wavelength of maximum emission was red-shifted to ~345 nm. The kalata B1 solution containing both DTT and GdHCl was observed to yield fluorescence spectra that were similar in both intensity and emission maxima to the spectra of the free kalata B1. These data suggest that the Trp present in loop 5 is in a solvent-exposed environment in the native state as well as in the presence of GdHCl. The native conformation thus appears to be extremely resistant to chaotropes. However, when reduced, kalata B1 can adopt a conformation in which the Trp is partially buried, resulting in increased fluorescence intensity. Both analytical ultracentrifugation and mass spectrometry

showed no evidence of dimer or oligomer formation and thus the burial is hypothesized to be an intramolecular rearrangement.

The thermal denaturation of kalata B1 was studied by examining 1D ^{1}H-NMR spectra as a function of temperature. Spectra were acquired between 17°C and 97°C and again upon cooling to 37°C. Only slight changes to chemical shifts and/or peak widths were seen upon heating. The spectra recorded at high temperatures (greater than 67°C) contain peaks of lower intensity and some line broadening was observed, however, all signals were seen even at 97°C. Upon cooling back to 37°C, the 1D NMR spectrum was identical to the spectrum prior to heating, clearly showing the complete reversibility of any conformational process. In contrast, the NMR spectra resulting from the thermal titration of a control peptide lacking a cyclic backbone showed marked differences. Conotoxin PVIIA was utilized owing to its similar size (27 amino acids) and cystine knot connectivity to kalata B1. Above temperatures of 60°C, the amide proton peaks broadened and diminished in intensity substantially. Upon cooling to 37°C, the peaks in the spectra remained broad and did not recover to their initial intensity as occurred for kalata B1.

The effects of pH on the conformation of kalata B1 were determined by monitoring NMR spectra as a function of pH. While most backbone amide chemical shifts had a rather low sensitivity to pH, as exemplified by C10 in Figure 4, two residues were significantly affected, namely N11 and T12. The shifts of their amide protons titrated with an apparent pKa of ~3.5, but since they are non-ionizable protons this must reflect sensitivity to a nearby titrating residue. Inspection of the kalata B1 structure showed that this is due to a strong hydrogen bonding interaction with the conserved glutamic acid residue, E3, as illustrated in Figure 4A.

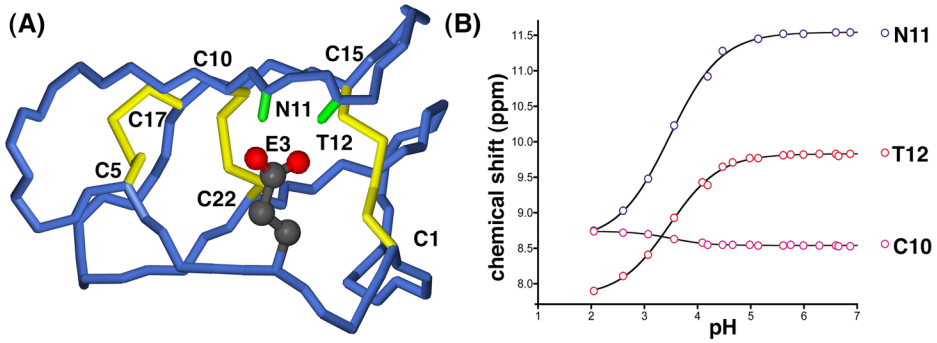

Fig. 4. Effects of pH on the amide proton chemical shifts of kalata B1. Most amides did not vary by more than 0.1 ppm over the pH range studied, as typified by C10. However, N11 and T12 were highly susceptible to pH. Panel A shows the hydrogen bonding interactions responsible for the pH profile in panel B.

Taken together, the various studies reported here show that the cystine knot is of crucial importance in the stability of the cyclotides. However, the cyclic backbone also plays a critical role, as without it the cystine knot may be irreversibly denatured at high temperature. The additional stability introduced by the cyclic backbone may be understood by considering graph theory representations of the cyclotides and linear cystine knot proteins, as illustrated in Figure 5.

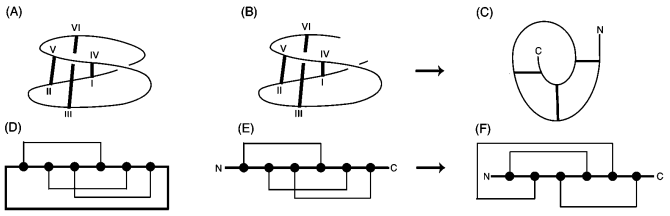

Fig. 5. Schematic representation of various cystine knot motifs (upper panel) and their corresponding graph theory representations (lower panel). A and D correspond to the CCK motif. B shows a linear cystine knot protein (e.g. conotoxin PVIIA) and E is the corresponding graph theory representation. Linear cystine knots may be topologically unwound, as shown in C and F [1].

Acknowledgments

Work in our laboratory on the cyclotides is supported by grants from the Australian Research Council (ARC). DJC is an ARC professorial fellow.

References

1. Craik, D. J., Daly, N. L., Bond, T. and Waine, C. *J. Mol. Biol.* **294**, 1327-1336 (1999).
2. Trabi, M. and Craik, D. J. *Trends Biochem. Sci.* **27**, 132-138 (2002).
3. Craik, D. J., Simonsen, S. and Daly, N. L. *Curr. Opin. Drug Dev.* **5**, 251-260 (2002).
4. Jennings, C., West, J., Waine, C., Craik, D. J. and Anderson, M. *Proc. Natl. Acad. Sci. U.S.A.* **98**, 579-591 (2001).
5. Schöpke, T., Hasan Agha, M. I., Kraft, R., Otto, A. and Hiller, K. *Sci. Pharm.* **61**, 145-153 (1993).
6. Gustafson, K. R., Sowder, R. C., II, Henderson, L. E., Parsons, I. C., Kashman, Y., Cardellina, J. H., II, McMahon, J. B., Buckheit, R. W., Jr, Pannell, L. K. and Boyd, M. R. *J. Am. Chem. Soc.* **116**, 9337-9338 (1994).
7. Witherup, K. M., Bogusky, M. J., Anderson, P. S., Ramjit, H., Ransom, R. W., Wood, T. and Sardana, M. *J. Nat. Prod.* **57**, 1619-1625 (1994).
8. Saether, O., Craik, D. J., Campbell, I. D., Sletten, K., Juul, J. and Norman, D. G. *Biochemistry* **34**, 4147-4158 (1995).
9. Göransson, U., Luijendijk, T., Johansson, S., Bohlin, L. and Claeson, P. *J. Nat. Prod.* **62**, 283-286 (1999).
10. Hallock, Y. F., Sowder, R. C. I., Pannell, L. K., Hughes, C. B., Johnson, D. G., Gulakowski, R., Cardellina, J. H. .I and Boyd, M. R. *J. Org. Chem.* **65**, 124-128 (2000).
11. Gustafson, K. R., Walton, L. K., Sowder, R. C. I., Johnson, D. G., Pannell, L. K., Cardellina, J. H. I. and Boyd, M. R. *J. Nat. Prod.* **63**, 176-178 (2000).
12. Broussalis, A. M., Göransson, U., Coussio, J. D., Ferraro, G., Martino, V. and Claeson, P. *Phytochemistry* **58**, 47-51(2001).
13. Bokesch, H. R., Pannell, L. K., Cochran, P. K., Sowder, R. C., II, McKee, T. C. and Boyd, M. R. *J. Nat. Prod.* **64**, 249-250 (2001).
14. Claeson, P., Göransson, U., Johansson, S., Luijendijk, T. and Bohlin, L. *J. Nat. Prod.* **61**, 77-81 (1998).
15. Hernandez, J. F., Gagnon, J., Chiche, L., Nguyen, T. M., Andrieu, J. P., Heitz, A., Trinh Hong, T., Pham, T. T. and Le Nguyen, D. *Biochemistry* **39**, 5722-5730 (2000).
16. Gran, L. *Medd. Nor. Farm. Selsk.* **12**, 173-180 (1970).
17. Sletten, K. and Gran, L. *Medd. Nor. Farm. Selsk.* **7-8**, 69-82 (1973).
18. Gran, L., Sandberg, F. and Sletten, K. *J. Ethnopharmacol.* **70**, 197-203 (2000).
19. Craik, D. J., Daly, N. L. and Waine, C. *Toxicon.* **39**, 43-60 (2001).
20. Craik, D. J. *Toxicon.* **39**, 1809-1813 (2001).
21. Rosengren, K. J., Daly, N. L. Plan, M. R, Waine, C. and Craik, D. *J. Biol. Chem*. **278**, 8606-8616 (2003).

Peptide Revolution: Genomics, Proteomics & Therapeutics
Michael Chorev & Tomi K. Sawyer (Editors)
American Peptide Society, 2003

Design of Novel Template Peptides to Mimic the Coiled Coil Conformation of the gp21 Envelope Subunit of HTLV-1 for the Induction of Neutralizing Antibodies

Roshni Sundaram[1], Sharad V. Rawale[2], Yiping Sun[4] and Pravin T.P. Kaumaya[1,2,3]

[1]Dept. of Microbiology, [2]Dept. of Obstetrics and Gynecology and [3]Center for Retrovirus Research, The Ohio State University, Columbus, OH 43210, USA;
[4]Corporate Research Division, Miami Valley Laboratories, The Proctor and Gamble Co., Cincinnati, OH 45253, USA

Introduction

Human T-cell Lymphotropic virus Type 1 (HTLV-1) is a retrovirus associated with adult T-cell leukemia and HTLV-1 associated myelopathy or tropical spastic paraparesis (HAM/TSP). The gp21 transmembrane (TM) subunit of the HTLV-1 envelope protein consists of a leucine-zipper like motif that forms a trimeric parallel coiled coil structure in the fusion activated state. This region is thought to undergo a conformational change following engagement of the host cell receptor by the surface gp46 subunit. This results in the exposure of the fusion peptide for successful completion of the fusion process [1]. We hypothesized that antibodies that are able to bind with high affinity to these transient conformations may be effective in arresting viral infection by interfering with the fusion process. The goal of the present study was to 1) design peptide immunogens that can mimic the gp21 triple helical coiled coil conformation and 2) to elicit antibodies to this folded conformation.

Results and Discussion

A core β-sheet template consisting of alternating Gly/Lys residues was synthesized such that the Σ sides of the lysine residues would allow for the simultaneous synthesis of the triple helical coiled coil sequence. This design was conceived to bring the three individual chains in close proximity to promote interactions between the hydrophobic residues to maximize the folding of the three strands into a coiled coil (Figure 1). To provide T-cell help for the induction of antibody responses, a promiscuous T-helper epitope from the tetanus toxoid (residues 580-599) was also included at the N-terminus [2]. A template peptide incorporating key mutations (V349L, I353L, N363L and I370L) at the *a* and *d* positions of the heptad repeat (designated CCR2T) was also synthesized to increase the potential for hydrophobic interactions and coiled coil formation. CD analysis of the constructs revealed that the Leu substituted template peptide showed a high helical content in aqueous medium that was concentration independent which did not increase upon the addition of TFE (Table 1). This indicated that the peptide was attaining its maximal helical potential in aqueous solution. In contrast, the wild type template peptide (designated WCCR2T) displayed high helicity only in the presence of 50% TFE. Hence leucine substitutions combined with a template design was essential for high helicity.

Both constructs were highly immunogenic in outbred mice and high titered antibodies were obtained against the template peptide (data not shown). Peptide antibodies were also tested for their ability to recognize native protein. As shown in Figure 2B antisera against the leucine substituted template peptide showed higher reactivity against the native protein as compared to the wild type template antisera.

These results indicated that the leucine substituted template peptide more closely mimicked the coiled coil gp21 conformation.

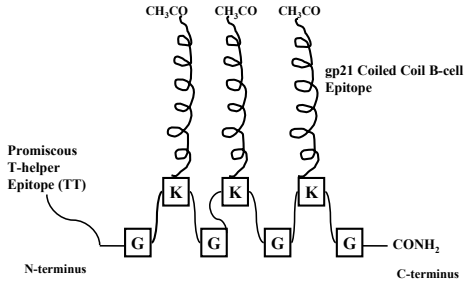

Fig. 1. Template design for synthesis of the coiled coil region of gp21 envelope subunit. Amino acids 347-374 corresponding to the coiled coil region was synthesized on a template of three Gly-Lys repeats (shown as boxed residues). A promiscuous T-helper epitope (TT) derived from tetanus toxoid was synthesized collinear with the template. The peptide was acetylated and amidated for greater stability.

Table 1: Concentration dependence analysis by circular dichroism.

Peptide (μM)	WCCR2T % helicity[a]		CCR2T % helicity	
	water	50% TFE	water	50% TFE
25	15.8	63	ND	ND
50	13.7	61.9	45.5	54.1
75	12.2	52.1	43.9	62.3
100	12.3	50.6	43.8	52.2

[a]*Helicity of peptides were calculated according to Chen's equation with reference to the mean. residue ellipticity of polylysine for a 100% helix* $(\theta)_{222}$ *= - 33000. ND = not determined.*

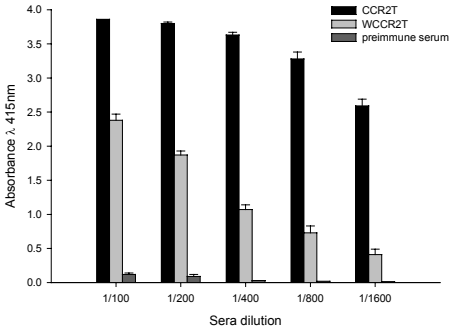

Fig. 2. Reactivity of CCR2T and WCCR2T antisera against native gp21 protein. Antisera against both template peptides were tested in a direct whole virus ELISA on plates coated with inactivated HTLV-1 viral lysate. Preimmune serum did not show any reactivity against whole viral lysate.

Acknowledgments

This work was supported by a NIH grant # A140302 to Pravin Kaumaya.

References

1. Rosenberg, A. R., et al. *J. Virol.* **71**, 7180-7186 (1997).
2. Kaumaya, P. T. P., et al. (1993) In Schneider, C. H. and Eberle, A. N. (Eds.), *Peptides 1992, Proceedings of the 22nd Eur. Pept. Symp.,* Escom Sci Publ., Leiden, pp. 139-141, (1993).

Peptide Revolution: Genomics, Proteomics & Therapeutics
Michael Chorev & Tomi K. Sawyer (Editors)
American Peptide Society, 2003

Importance of Hydrophobic Clusters on Protein Folding and Stability

Stephen M. Lu, Stanley C. Kwok and Robert S. Hodges

Department of Biochemistry and Molecular Genetics, University of Colorado Health Sciences Center, Denver, CO 80262, USA

Introduction

The α-helical coiled-coil is one of the simplest protein folds consisting of two intertwined α-helices. The coiled-coil motif is characterized by a heptad repeat of residues $(abcdefg)_n$, where residues in the *a* and *d* positions are typically hydrophobic and form the inter-chain helical interface. The contribution of numerous factors such as hydrophobicity, helical propensity, and electrostatic interactions (inter- and intrachain) have been extensively studied by our group [1-3]. Many natural coiled-coils such as tropomyosin (284 residues) have long stretches of hydrophobic residues in the hydrophobic core positions that are typically interspersed with hydrophilic/polar residues, which creates alternating clusters of stabilizing and destabilizing residues in the hydrophobic core.

Results and Discussion

In order to study the effect of hydrophobic residues in a stabilizing cluster, we designed and chemically synthesized several peptides that are two-stranded parallel disulfide-bridged α-helical coiled-coils with 60 residues per chain and favorable inter-chain electrostatics. These peptides contain the same composition (e.g., identical hydrophobicity in the hydrophobic core) but differ in the arrangement of stabilizing and destabilizing clusters of large hydrophobes (Figure 1). A cluster is defined for these peptides as three consecutive large hydrophobes (Ile or Leu) or three consecutive Ala residues in the hydrophobic core. Peptide P3 contains three stabilizing clusters while peptide P2 contains two stabilizing clusters through shuffling of an Ala and Ile residue.

P3 Ac-E**A**EA**L**KA-E**I**EA**L**KA-K**A**EA**A**EG-K**A**EA**L**EG-K**I**EA**L**EG-K**A**EA**A**EG-K**A**EA**L**EG-E**I**EA**L**KA-GGCY-Am
P2 Ac-E**A**EA**L**KA-E**A**EA**L**KA-K**I**EA**A**EG-K**A**EA**L**EG-K**I**EA**L**EG-K**A**EA**A**EG-K**A**EA**L**EG-E**I**EA**L**KA-GGCY-Am

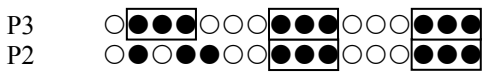

Fig. 1. Sequences and dot representation of peptides P3 and P2. Residues at position a and d are bolded. ● denotes Ile (at a) or Leu (at d) and ○ denotes Ala. Stabilizing clusters (three consecutive large hydrophobic residues in the core a and d positions) are indicated by boxes.

Peptide P3 was shown to be helical and fully folded with minima at 208 and 222 nm, while P2 was only partially folded and marginally stable at ambient conditions in benign buffer (50 mM phosphate, 100 mM KCl, pH 7) (data not shown). In order to study these peptides further, their stability was measured by thermal and chemical (urea) denaturation (Figure 2). P3 is substantially more stable than P2 (T_m=41.6°C vs. 23.1°C or $[urea]_{1/2}$=2.10 M vs. 0.65 M) and the free energy difference was calculated to be 2.1 kcal/mol.

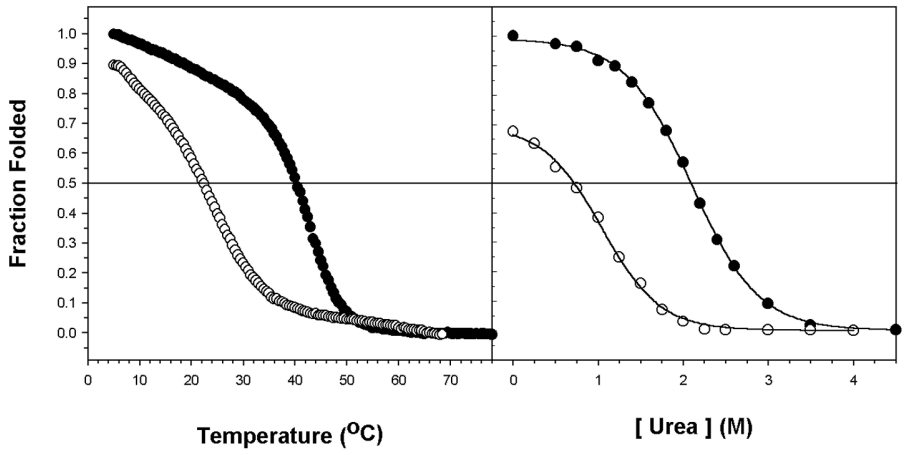

Fig. 2 Stability of P3 (closed circles) and P2 (open circles) by temperature (panel A) and chemical denaturation (panel B).

In order to further study the effect of hydrophobic residues in a stabilizing cluster, we designed another series of coiled-coils (Figure 3). Each peptide chain consists of two stabilizing clusters and a central cassette containing from zero to three large hydrophobic residues.

Ac-(EIEALKA)$_2$-KAEAAEG-KAEA**X**EG-K**X**EA**X**EG-KAEAAEG-KAEALEG-EIEALKA-GGCY-Am

Peptide	Schematic of Residues at *a* and *d* positions
1	O O O O O O O O O O O O O O O
2	O O O O O O O O O O O O O O O
3	O O O O O O O O O O O O O O O
4	O O O O O O O O O O O O O O O
5	O O O O O O O O O O O O O O O
6	O O O O O O O O O O O O O O O
7	O O O O O O O O O O O O O O O
8	O O O O O O O O O O O O O O O

*Fig. 3. Sequences of peptides used in this study. All peptides were oxidized and have identical sequences except for three residues indicated by **X**. A schematic representation of the hydrophobic core positions is shown by dots where O denotes Ile (at a) or Leu (at d) and* O *denotes Ala. The three **X** positions are indicated by the boxed region.*

The helical nature of the peptides was verified by circular dichroism (CD) spectroscopy. All peptides show canonical helical spectra in benign buffer and were essentially fully folded. The stability of each peptide was measured by thermal denaturation by monitoring the helical structure as a function of temperature (Figure 4).

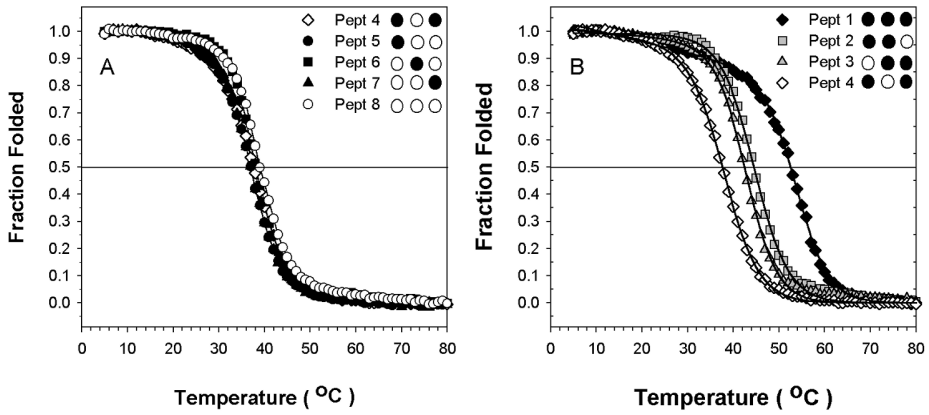

Fig. 4. Temperature denaturation profiles. Peptides 4-8 are shown in panel A while Peptides 1-4 are shown in panel B.

Peptide 1 was the most stable peptide of the series. This was expected as this sequence contains three stabilizing clusters of at least three consecutive hydrophobic residues in the *a* and *d* positions [4]. Peptides 2, 3 and 4 contain two hydrophobes in the cassette and therefore the same inherent hydrophobicity. Peptides 2 and 3 are notably more stable than Peptide 4 (Figure 4B). This suggests that there is a weak clustering effect of two adjacent hydrophobic residues in the hydrophobic core of coiled-coils. Even more surprising is that Peptide 4 (with two hydrophobes interspersed with an Ala) shows equivalent stability to the remaining peptides (with one hydrophobe in the cassette) (Figure 4A). We postulate that Peptide 8, with its nine consecutive alanine residues in the hydrophobic core, is a tightly packed coiled-coil in the cassette region. The addition of one large hydrophobic residue disrupts this packing, thus there is no gain in stability with increasing hydrophobicity in a core position. In fact, a single large hydrophobe is unable to overcome the loss in stability caused by disruption of the Ala packing. The free energy of unfolding can be calculated from urea denaturations (data not shown). Consider Peptide 8, 5, 2 and 1 (or Peptides 8, 7, 3 and 1) as a series from zero to three large hydrophobes in the cassette. There is no net gain in stability until we have two adjacent large hydrophobes in consecutive core positions ($\Delta\Delta G$=0.7 kcal/mol). Increasing the cassette from 2 to 3 hydrophobes leads to a non-additive increase in stability ($\Delta\Delta G$=1.3 kcal/mol), thus a clustering effect.

Acknowledgments
The work was funded by NIH grant R01GM61855.

References

1. Kohn, W. D., Kay, C. M. and Hodges, R. S. *J. Mol. Biol.* **267**, 1039-1052 (1997).
2. Wagschal, K., *et al. Protein Sci.* **8,** 2312-2329 (1999).
3. Tripet, B., *et al. J. Mol. Biol.* **300**, 377-402 (2000).
4. Kwok, S. C. and Hodges, R. S. *J. Biol. Chem.* **279**, 21576-21588 (2003).

Peptide Revolution: Genomics, Proteomics & Therapeutics
Michael Chorev & Tomi K. Sawyer (Editors)
American Peptide Society, 2003

Visual Molecular Recognition of cAMP with Azo-Bridged Cyclic Peptide Libraries

Martina Čížková[1], Martin Šafařík[2], Jaroslav Šebestík[3], Jan Hlaváček[2] and Ivan Stibor[3]

[1]DOC, FS Charles Univ., 128 43 Prague 2, Czech Republic; [2]IOCB, Academy of Sciences 166 10 Prague 6 - Czech Republic and [3]ICT in Prague, 166 28 Prague 6, Czech Republic

Introduction

cAMP plays an important role in cell signaling processes, such as second messenger of intracellular events in mammals and first messenger of intercellular events in Dictyostelium discoideum. A visual and/or fluorescence based indicator of cAMP in living cells may serve as a suitable diagnostic tool for cell signal kinetic measurement. In the field of supramolecular chemistry, macro-cyclic receptors have been extensively investigated as host compounds that may be functionalized with dye to induce specific visual recognition for target guest molecules [1]. Although the design of receptor molecules for target ones has made tremendous progress, it is still difficult to design *de novo* a host for a distinct guest. A biomimetic approach by preparing receptor libraries follows the combinatorial strategy of the nature that is demonstrated successfully in the immune system. The aims of this study have been the transfer of azo-coupling-cyclization reaction from solution phase [2] to polymer carrier and its utilization in dye library synthesis.

Results and Discussion

General formulas for our library were designed according to computer assisted molecular modeling of cAMP-macrocyclic peptide complexes, where the main rule applied was macrocycle cavity fitting (Figure 1). Several different approaches to mini-library synthesis and screening were investigated more or less unsuccessfully. The first one, an adaptation of a previously described method was based on Positional Scanning Libraries methodology, was carried out for five amino acids (Lys, Gln, Asp, Gly and Ser) and led to a set of 15 sublibraries which contains 125 compounds altogether (Figure 2). Unfortunately, none of the compounds recognized cAMP in buffer solution (pH = 6.8). We suppose that it is due to lack of hydrophobic amino acids such as Ile, Leu, Val and Phe in our mini-library. Soluble polymer support (PEG6000) was chosen for the second approach, in which cyclization on carrier was tested, but library was lost by unexpected hydrolysis during the cyclization step. The third approach, based on a one-bead-one-compound library, is still under development although suitable support SPOCC1000 [3] was already synthesized.

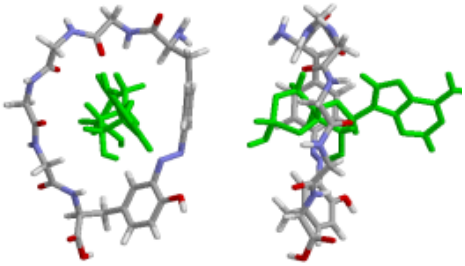

*Fig. 1. Here is shown the complex of cAMP with cyclic-azo(H-Pap-Gly-Gly-Gly-Gly-Tyr-OH) obtained by MM/PM3 calculation (B3LYP/6-31G**). View through macrocycle is on the left side and after 90 deg. rotations along y-axis on right. The host peptide may possess both cis and trans backbone configuration on azo bond shifting absorption maxima in UV/VIS spectra.*

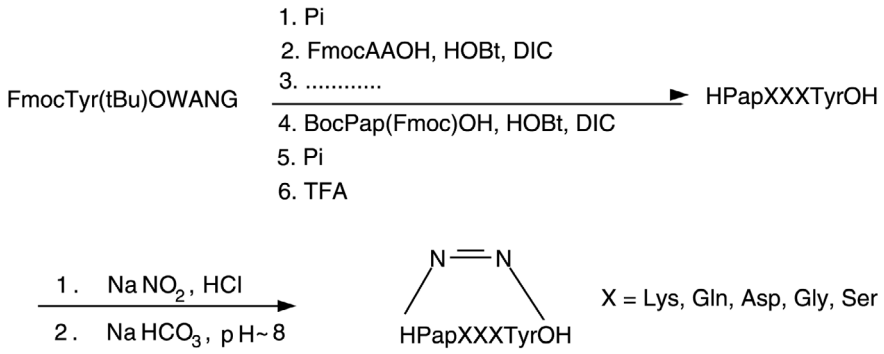

Fig. 2. Scheme of mini-library synthesis by Fmoc/tBu strategy.

Acknowledgments

I would like to thank the 18th APS organizing committee and sponsors for their travel grant. QM calculations were carried out on a PC cluster of METACentrum in CR. This work was supported by a project of Acad. Sci. CR no. Z 4055905 and a grant of GA CR no. 203/02/1379.

References

1. Tsubaki, K., Hayashi, N., Nuruzzaman, M., Kusumoto, T. and Fuji, K. *Org. Lett.* **3**, 4067 (2001).
2. Fridkin, G. and Gilon, G. *J. Pept. Res.* **60**, 104 (2002).
3. Rademann, J., Grøtli, M., Meldal, M. and Bock, K. *J. Am. Chem. Soc.* **121**, 5459 (1999).
4. http://www.gaussian.com/ and cited literature.

Peptide Revolution: Genomics, Proteomics & Therapeutics
Michael Chorev & Tomi K. Sawyer (Editors)
American Peptide Society, 2003

Organic Functionalization of Carbon Nanotubes with Peptides

D. Pantarotto,[1,2] C. D. Partidos,[1] J. Hoebeke,[1] J. -P. Briand,[1] M. Prato[2] and A. Bianco[1]

[1]*Institute of Molecular and Cellular Biology, UPR 9021 CNRS, 67084 Strasbourg, France;*
[2]*Department of Pharmaceutical Sciences, University of Trieste, 34127 Trieste, Italy*

Introduction

Carbon nanotubes (CNTs) are constituted of graphene sheets rolled-up into a tubular form. The potential applications of CNTs in medicinal chemistry are becoming of great interest given their capacity to form supramolecular complexes with macromolecules like proteins and oligosaccharides [1,2]. The main difficulty to integrate such materials into biological systems derives from their lack of solubility in physiological solutions. The chemical derivatization of carbon nanotubes has resulted in an efficient method to increase their solubility and to make their manipulation easier [3]. The synthesis and potential use of the first water soluble single-walled functionalized carbon nanotubes showed that it is possible to derivatize them further by coupling single N-protected amino acids [4] and bioactive peptides [5]. The immobilization of peptides on carbon nanotubes may find several interesting applications, including delivery of candidate vaccine antigens.

Results and Discussion

The method of functionalization of CNTs is based on the 1,3-dipolar cycloaddition of azomethine ylides, generated by condensation of an α-amino acid and an aldehyde. The CNTs are suspended in DMF, together with an excess of *para*formaldehyde and an appropriate modified amino acid. The heterogeneous reaction mixture is heated at 130 °C for 4 days. After work-up, a brown-colored solid is obtained. The functionalized single-walled carbon nanotube (SWNT) **1** (Scheme 1) shows water solubility higher than 20 mg/ml. Different chemical entities were then covalently attached to the free amine function of tube **1**. Protected amino acids like Fmoc-Gly-OH or Boc-Lys(Boc)-OH were first coupled to optimize the reaction conditions. The amino acid-based CNTs **2** and **3** were structurally characterized by homo- and hetero-nuclear NMR, FT-IR spectroscopy and electron transmission microscopy. This represents the first step towards the synthesis of bioactive peptide-carbon nanotube conjugates.

Two different methods of linking bioactive peptides to SWNTs were chosen: i) the fragment condensation of fully-protected peptides, thus obtaining conjugate **6**; and ii) the selective chemical ligation for conjugates **4** and **5**. For the fragment condensation approach we have chosen the N-terminal and side-chain protected sequence KGYYG, prepared in turn by solid-phase synthesis. For peptide conjugation onto carbon nanotubes using chemoselective ligation, we have chosen a B-cell epitope from foot-and-mouth disease virus (FMDV), corresponding to the 141-159 region of the viral envelope protein VP1. The SWNTs **1** were first derivatized with N-succinimidyl 3-maleimidopropionate and then the Ac-Cys-FMDV peptide was linked to the maleimido moiety of the wires, affording CNT **4**. CNT **3** was used to create the double branched peptide-nanotube conjugate **5** using the same strategy.

To check the immunological reactivity of the FMDV peptide coupled to carbon nanotubes, its recognition by a peptide specific antibody was studied by surface plasmon resonance and ELISA.

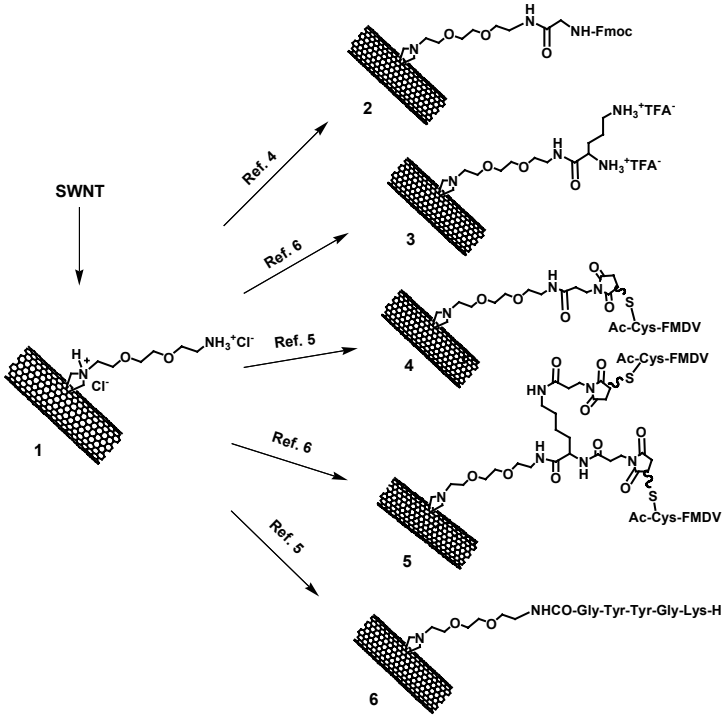

Scheme 1. Covalent functionalization of carbon nanotubes.

These experiments showed that the peptide linked to CNTs retained its conformational characteristics for antibody recognition [5]. Furthermore, biological studies performed *in vivo* demonstrated that the bis-conjugate **5** elicited higher antibody titers than the mono-conjugate **4** and the free peptide. However, significant virus neutralizing capacity was observed only by the antibodies induced by the mono-conjugate **4** [6]. This highlights: 1) the potential of carbon nanotubes for vaccine delivery, and 2) the importance of antigen presentation *in vivo* for the induction of antibodies with the right specificity.

References

1. Chen, R. J., Zhang, Y., Wang, D. and Dai, H. *J. Am. Chem. Soc*. **123**, 3838-3839 (2001).
2. Star, A., Steuerman, D., Heath, J. R. and Stoddard, J. F. *Angew. Chem. Int. Ed*. **41**, 2508 (2002).
3. Hirsch, A. *Angew. Chem. Int. Ed.* **41**, 1853-1859 (2002).
4. Georgakilas, V., *et al. Chem. Commun.* 3050-3051 (2002).
5. Pantarotto, D., *et al. J. Am. Chem. Soc.* **125**, 6160-6164 (2003).
6. Pantarotto, D., Partidos, C. D., Hoebeke, J., Brown, F., Kramer, E., Briand, J.- P., Muller, S., Prato, M. and Bianco, A. *Chem. Biol*. **10**, 961-966 (2003).

Peptide Revolution: Genomics, Proteomics & Therapeutics
Michael Chorev & Tomi K. Sawyer (Editors)
American Peptide Society, 2003

Structural and Biological Studies of a Penetratin-Linked Gas C-Terminal Peptide

Anna M. D'Ursi[1], S. Albrizio[2], L. Giusti [3], M. Mazzoni, E. Novellino[2] and P. Rovero[1]

[1]Dip. Scienze Farmaceutiche, University of Salernoy; [2]Dip. Chimica Farmaceutica e Toss. University of Naples "Federico II", Italy; [3] Dipartimento di Psichiatria, Neurobiologia, Farmacologia e Biotecnologie, Università di Pisa, Pisa, Italy

Introduction

The C-terminal domain of the heterotrimeric G protein α-subunits plays a key role in selective activation of G proteins by their cognate receptors. We have recently shown that peptides derived from the C-terminal portion of the $G\alpha_s$ subunit are endowed with biological properties similar to those of the whole α-subunit. In particular, among a series of varying length peptides, the 21-mer $G\alpha_s$(374-394) (Figure 1) shows the most significant biological activity, preventing G_s activation by the A_{2A} adenosine receptor [1,2]. Penetratin is the third helix from the N-terminal of *Antennapedia* homeodomain that possesses traslocation properties similar to those of the entire homeodomain. It is able to translocate oligopeptides and oligonucleotide into living cells and thus it has been proposed as an universal intracellular delivery vehicle [3]. We synthesized $G\alpha_s$(374-394) covalently linked to the penetratin sequence (A42). The biological activity and the spectroscopic structural investigation were performed in order to correlate the penetrating capacity of the peptide to its structural peculiarities.

A42 RQLKIWFQNRRMKWKKRVFNDCRDIIQRMHLRQYELL

Fig. 1. Sequences of A42. Penetratin and $G\alpha_s$(374-394) fragments are colored in red and in blue respectively.

Results and Discussion

Biological assays. To test the vector properties of penetratin, the effects of A42 peptide on adenylyl cyclase stimulated by agonist activation of A_{2A} adenosine receptors in intact PC12 cells were evaluated. The effect of NECA stimulated adenylyl cyclase activation was significantly ($P < .001$) inhibited by the addition of 300 μM A42 peptide by approximately 90% whereas the control peptide had no major effect on NECA-stimulated adenylyl cyclase activity leading to 8% stimulation of cAMP production. These data show that the linking of $G\alpha_s$(374-394) to the penetratin does not affect the inhibition capacity of G protein fragment, but moreover it endows the $G\alpha_s$(374-394) with an internalizing property so that it is active in intact cells.

NMR analysis. A whole set of 1D and 2D ^1H homonuclear NMR spectra was acquired on a Bruker DRX 600 at 300 K. Water/sodium dodecylsulphate (SDS) mixture was used as solvent. SDS micelles solution is known as a membrane mimetic environment, and in particular here it is able to reproduce the biological compartment where the vector properties of the penetratin can be explicated. Complete assignments of the proton spectra of A42 were obtained by standard procedures using DQF-COSY, TOCSY and NOESY experiments and with the aid of the SPARKY software package.

A qualitative analysis of NOE sequential and medium range connectivities of A42 shows the presence of many NH_i-NH_{i+1} and several critical $CH\alpha_i$/ NH_{i+2} $CH\alpha_i$/ NH_{i+3}

and $CH\alpha_i$/ $CH_2\beta_{(i+3)}$. This pattern of NOE effects is consistent with the presence of a well ordered structure encompassing the entire peptide sequence.

Three-dimensional structures were calculated by simulated annealing in torsion angle space, on the basis of 536 NOE restraints, using DYANA software package. Among 200 calculated structures, the 50 with the lowest value of target function were subjected to further minimization procedure by Discover module of InsightII [MSI]. All calculated conformers show two different α-helical regions including residues 3-10 and 18-35, respectively (RMSD, calculated on heavy atoms of residues 3 – 10, = 1.04; RMSD, calculated on heavy atoms of residues 18 – 35, = 0.92).

The analysis of the side chain conformations shows that in the region of A42 corresponding to the $G\alpha_s$ portion, hydrophobic and hydrophilic surfaces can be identified (Figure 2a). The side chains relative to the penetratin segment can be clustered in a hydrophobic area localized at the N terminal of the peptide (Figure 2b). The arrangement of the side chain confirm the previous data relative to the NMR studies of $G\alpha_s$ peptides [2]. As previously demonstrated, the side chains are rightly oriented so that the interactions fundamental for the coupling of the G protein fragment to the receptor can take place. On the other hand, the cluster of hydrophobic residues at the N-terminal region of the penetratin region, promoting the hydrophobic interaction with the membrane by-layer, explains the vector properties of the penetratin.

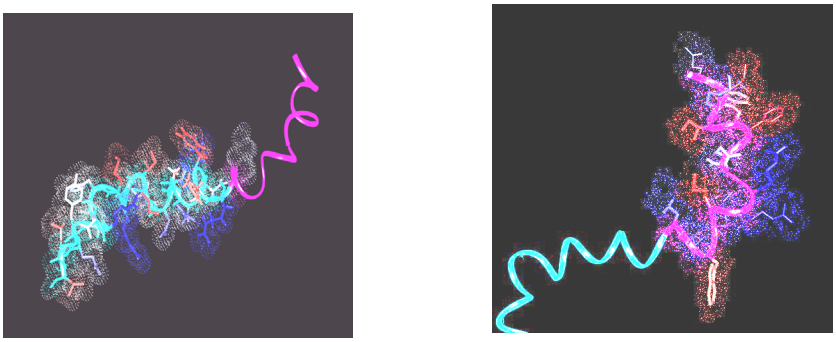

Fig. 2. NMR structure of A42 in SDS/water solution. Regions relative to Penetratin and Gαs(374-394) are highlighted with pink and cyan ribbons respectively. Gαs(374-394)(a) and penetratin (b) molecular surfaces are colored according to the hydrophobic character of amino acid side chains (blue/hydrophilic, red/hydrophobic).

References

1.Mazzoni, M.R., Taddei, S., Giusti, L., Rovero, P., Galoppini, C., D'Ursi, A. M., Albrizio, S., Triolo, A., Novellino, E., Greco, G. and Lucacchini, A. *Molec. Pharmacol* **58**, 226-236 (2000).

2. D'Ursi, A.M., Albrizio, S., Greco, G., Mazzeo, S., Mazzoni, M. R., Novellino, E. and Rovero, P. *J. Peptide Science **8**,* 576-588, (2002).

3. D. Derossi, A. H. Joliot, G. Chassaing and A. Prochiantz. *J. Biol. Chem.* **269**, 10444–10450 (1994).

Peptide Revolution: Genomics, Proteomics & Therapeutics
Michael Chorev & Tomi K. Sawyer (Editors)
American Peptide Society, 2003

Structural Analysis of Nanomolar Quantities of Marine Neuropeptides Using 2D-NMR Methods

Elena Matei[1], Fred Pflueger[1], Aldo Franco[1], Herminsul Cano[1], David Mora[1] and Frank Mari[1,2]

[1]Department of Chemistry & Biochemistry and [2]Center for Molecular Biology & Biotechnology, Florida Atlantic University, 777 Glades Rd., Boca Raton, FL 33431, USA

Introduction

Cone snails are venomous and predatory marine mollusks whose venom is composed of a cocktail of neuropeptides (conopeptides). Conopeptides have been recognized as potential neuropharmacological agents; however, limited amounts of single components are usually obtained at the end of elaborated separation schemes. Conopeptides contain highly modified polypeptide chains and they are often difficult to synthesize. In order to aid the characterization of conopeptides directly from their original sources, we have resorted to the use of NMR methods using a nano-NMR probe that employs magic angle spinning to obtain high resolution spectra for small volume samples (HR-MAS). We have been able to obtained a good quality 3D structure of α-conotoxin GI using only 30 nanomoles of the peptide. Here we present the results from the NMR characterization of nanomolar quantities of GI and several other conopeptides. The limits of detection and other analytical parameters associated with the use of the nano-NMR probe in conopeptide research are evaluated.

Results and Discussion

Cone snail venom is a complex mixture of modified peptides. After a laborious separation procedure, nanomolar quantities of native conopeptides are usually obtained. For this study, we have selected three samples: i) 30 nmoles of synthetic α-Conotoxin GI (ECCNPACGRHYSC; 2–7, 3–13), a competitive antagonist for the vertebrate muscular nicotinic acetylcholine receptor isolated from the venom of *C. geographus*' ii) 190 nmoles of bru-1, a 23-residue peptide with three disulfide bonds isolated from *Conus Brunneus*; and iii) 1 nmole of gla-1, a novel 8-residue conopeptide from *Conus gladiator*.

The nano-NMR spectra of these conopeptides were acquired on a Varian Inova 500 MHz (PFG equipped, 3RFs, WF generators) NMR spectrometer using a nano *g*HX NMR probe. The nano-NMR probe achieves higher relative sensitivity by placing whole sample inside the coil [1] and by eliminating the resulting lineshape distortions by spinning the sample at the magic angle [2]. We have obtained high quality 1D- ^{1}H and 2D-TOCSY spectra down to 1 nmole of the novel conopeptide gla-1. Two natural abundance heteronuclear experiments, *g*HSQC ^{15}N of bru-1 and *g*DEPT-HSQC ^{13}C of bru-1 @ 25^{o}C, were obtained with excellent S/N ratios. The 2D-NOESY NMR spectra of GI gave strong NOE interactions at t = 0°C. The α-conotoxin GI, a well-characterized conopeptide, was used as a model compound to optimized all NMR parameters. Using ~30 nmol of this conopeptide, we obtained sufficient structural information to ascertain the secondary structure of GI and enough constraints to determine its 3D structure.

The sequence-specific assignments and interproton distance constraints of 30 nanomoles of α-Conotoxin GI were derived with the combined use of ES-TOCSY and and wg-NOESY spectra. Spectra were processed using NMRpipe.

Most of the NOE correlations expected for 3_{10} helix secondary structure elements [3], including $d_{NN}(i,i+1)$, $d_{NN}(i,i+2)$, $d_{\alpha N}$, $d_{\beta N}$ or $d_{\alpha\beta}(i,i+3)$, were observed throughout the peptide structure, from Pro^5 to Arg^9. A number of 167 (95 intra-residues, 52 inter-residues, 20 long distance) NOE proton connectivities were identified. The 3D-structures were generated using XPLOR ver3.851, using a dynamical simulated annealing algorithm. We generated 100 structures, using embedding and optimization steps. Fifty of these structures, which best satisfy the experimental restraints, were further refined by energy minimization (10000 conjugated gradient steps and 20000 descent steps) under the cvff force field. The final 32 "nano"- structures were retained on the basis of the agreement with the experimental data and the low potential energy. The first structure in this assembly, which is closest to the average coordinates of the ensemble, was chosen as a representative conformer and used for structural illustration (Figure 1).

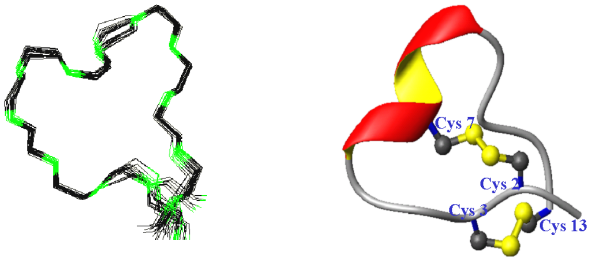

Fig. 1.A. Backnone representation of the best 32 nano-structures superpositions of GI; B. Ribbon representation of the closest structure of GI, of the average structure.

The RMSD value (0.47Å for backbone, 1.06Å all non-hydrogen atoms) for the superposition of these structures (Figure 1), reveals a very good quality of the structure, comparable with the structure of α-Conotoxin GI solved by Gehrmann et al. in 1998 (0.16Å for backbone, 1.27Å for all non-hydrogen atoms) [4]. The structure is characterized by the presence of a 3_{10} helix between residues 5 to 9 that is stabilized by the Cys^2- Cys^7 and Cys^3 – Cys^{13} disulfide bonds.

The nano NMR solution structure that we have determined for this conopeptide is in close agreement with the X-ray structure and previous NMR structures determined using micromolar quantities of GI. The nano-NMR methodologies described here can be used for analysis of other conopeptides and in cases where only limited quantities of modified peptides are available.

Acknowledgements

This work was supported by the Florida Sea Grant College Program.

References

1. Paul A. Keifer. L. Baltusis, D. M. Rice, A. A. Tymiak and J. N. Shoolery, *J. Mag. Res*. **A 119**, 65-75 (1996).
2. T. M. Barbara, *J. Magn. Reson*. **A 109**, 265-269 (1994).
3. Callihan D., West J., Surat K., K. Schweitzer B. I. and Logan, T. M. J. *J. Mag. Res.* ***B*** **112**, 82-85 (1996).
4. John Gerhrmann, Paul F. Alewood and David J. Craik, *J. Mol. Biol*. **278**, 401-415 (1998).

Peptide Revolution: Genomics, Proteomics & Therapeutics
Michael Chorev & Tomi K. Sawyer (Editors)
American Peptide Society, 2003

Solution Structure of α-Conotoxin OmIA, a Neuronal Toxin Specific for the α4β4 Subunit Interface of Neuronal Nicotinic Acetylcholine Receptor

Seung-Wook Chi, Do-Hyoung Kim and Kyou-Hoon Han

Proteome Analysis Laboratory, Division of Genomics and Proteomics, Korea Research Institute of Bioscience and Biotechnology, Yusong P. O. Box 115, Daejon, Korea

Introduction

The nicotinic acetylcholine receptors (nAChRs) are a well-studied family of ligand-gated ion channels comprising a diverse set of molecular subtypes [1]. Less well understood and more diverse are the neuronal nAChRs that assemble in exogenous expression systems with a general composition of (*m*)2(*n*)3, where *m* = 2-6 and *n* = 2-4, or (7)5 [2,3]. Small peptide toxins of *Conus* origin known as the α- and αA-Conotoxins are highly useful tools for exploring ligand-nAChR interactions [4,5]. A well-defined subgroup of α-Conotoxins, referred to as the α4/7 subfamily, are antagonists of neuronal and muscle nAChRs. The α4/7 subfamily contains two disulfide bonds like the α3/5 subfamily but has a different spacing between the disulfide bonds. Structural comparison among various nAChR ligands is one way of identifying important residues or pharmacophores involved in receptor binding.

Table 1. Sequence and receptor subtype specificity of α4/7 sub-family conotoxins.

Name	Sequence	Specificity
α4/7 subfamily		
EI	R D O **C** **C** Y H P T **C** N M S N P Q I **C** *	α1/δ
MII	G **C** **C** S N P V **C** H L E H S N L **C** *	α3/β2, α6/β2, α6/β4
PnIA	G **C** **C** S L P P **C** A A N N P D Y **C** *	α3/β2
PnIB	G **C** **C** S L P P **C** A L S N P D Y **C** *	α7/α7
AuIB	G **C** **C** S Y P P **C** F A T N P D **C** *	α3/β4
EpI	G **C** **C** S D P R **C** N M N N P D Y **C** *	α3/β2, α3/β4
OmI	G **C** **C** S H P A **C** N V N N P H I **C** G *	α4/β4

Results and Discussion

A high-resolution three-dimensional structure of a potent neuronal nicotinic acetylcholine receptor antagonist from *Conus omaria*, α-conotoxin OmIA, has been determined by nuclear magnetic resonance spectroscopy and restrained molecular dynamics. The α-conotoxin OmIA consists of 17 amino acid residues, GCCSHPACNVNNPHICG and belongs to the α4/7 subfamily, but with an additional C-terminal amidated glycine residue. This toxin represents the first α4β4 subtype specific antagonist of nicotinic acetylcholine receptor. The overall molecular fold of α-conotoxin OmIA is "ω-shaped" (Figure 1). As the other members of α4/7 subfamily it contains an α-helix comprised of residues His^{5}-Asn^{12}. Backbone rmsd with other α4/7

members such as EI, MII, and PnIA is less than 1 Å. The structure of α-conotoxin OmIA is well-determined with a backbone and a heavy atom root mean square deviation (for residues 2-16) of 0.36 Å and 0.75 Å, respectively, with all the residues belonging to most favored or allowed regions in Ramachandran map. Structural comparison with α-conotoxin AuIB that targets the α3β4 neuronal subtype [6] suggests potential residues that might be important for the α4β4 selectivity of α-conotoxin OmIA as well as those that might be responsible for the α3β4 specificity of α-conotoxin AuIB (Figure 2).

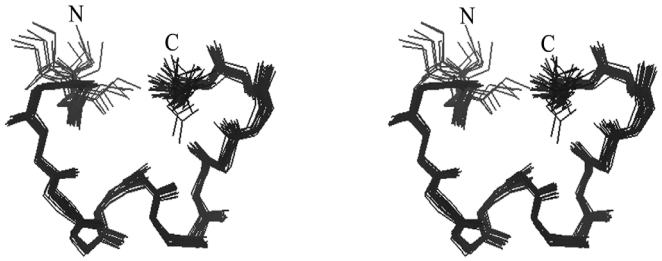

Fig. 1. A stereo view of the final 20 structures for α-conotoxin OmIA.

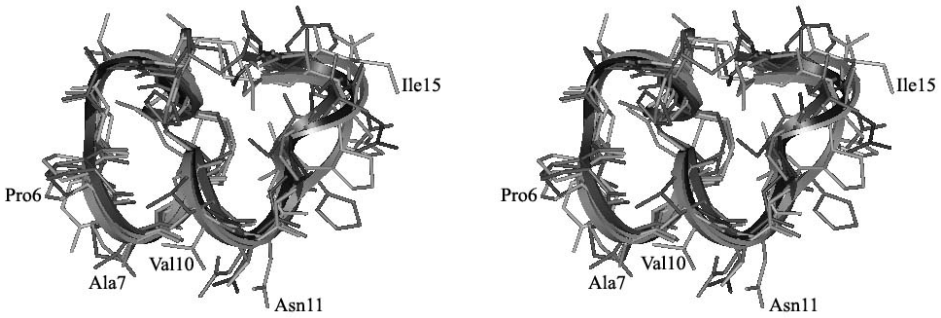

Fig. 2. Superposition of four α-conotoxins OmIA, MII, AuIB, and PnIA.

Acknowledgments

The present work has been supported by a grant from KRIBB Research Initiative Program and a grant NSM0140233 from the Ministry of Science and Technology of Korea (to K. H.).

References

1. Karlin, A. and Akabas, M. H. *Neuron* **15**, 1231-1244 (1995).
2. Sargent, P. B. *Annu. Rev. Neurosci.* **16**, 403-433 (1993).
3. McGehee, D. S. and Role, L. W. *Annu. Rev. Physiol.* **57**, 521-546 (1995).
4. Olivera, B. M., Rivier, J., Clark, C., Ramilo, C. A., Corpuz, G. P., Avogadie, F. C., Mena, E. M., Woodward, S. R., Hillyard, D. R. and Cruz, L. J. *Science* **249**, 257-263 (1990).
5. McIntosh, J. M., Santos, A. D. and Olivera, B. M. *Annu. Rev. Biochem*. **68**, 59-88 (1999).
6. Cho, J. H., Mok, K. H., Olivera, B. M., McIntosh, J. M., Park, K.-H. and Han, K.-H. *J. Biol. Chem.* **275,** 8680-8685 (2000).

Peptide Revolution: Genomics, Proteomics & Therapeutics
Michael Chorev & Tomi K. Sawyer (Editors)
American Peptide Society, 2003

Cyclic Proline Peptides as Privileged Reverse-Turn Templates

Ye Che and Garland R. Marshall

Center for Computational Biology; Department of Biochemistry and Molecular Biophysics, Washington University School of Medicine, St. Louis, MO 63110, USA

Introduction

Cyclic peptides bind multiple, unrelated classes of receptors with high affinity, and are considered to be privileged structures due to their high content of reverse-turn motifs. Of all residues, proline plays a crucial rule affecting the conformations of reverse-turn motifs [1-3]. Cyclic tetraproline (*DLDL*) is a potential template as synthetic routes to chimeric prolines containing chiral 3-, 4- or 5-substituents are abundant. Cyclo(*DLDL*)-Pro_4 was previously prepared in Rothe group [4] with *ctct*- and *tctc*-amide conformers, showing conformational interconversions at 80°C in water and 45°C in DMF. Here, we analyzed the length effects on conformations of cyclic peptides, and interconversion pathways for cyclo(*DLDL*)-Pro_4.

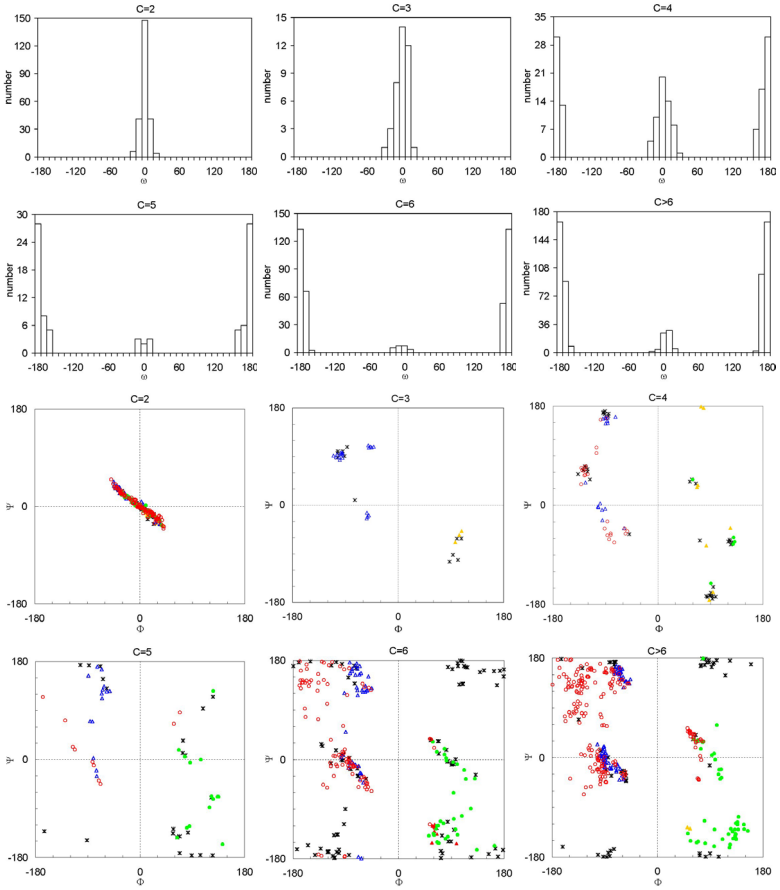

Fig. 1. The distribution of cis/trans-amide bonds and (ϕ,ψ) backbone torsions.

Results and Discussion

230 cyclic peptides containing 2 to 10 residues were analyzed for distribution of *cis*/*trans* amide bonds and (ϕ, ψ) backbone torsions (Figure 1). Cyclic dipeptides or tripeptides have exclusively *cis*-amide conformations and unfavorable (ϕ, ψ) values. Cyclic pentapeptides and longer have predominately *trans*-amide conformation and favorable (ϕ, ψ) values. Cyclic tetrapeptides are in the transition zone.

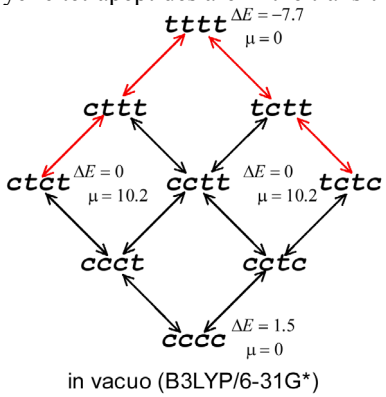

Fig. 2. The conformational energies of cyclo(DLDL)-Pro$_4$ in vacuo and water calculated using DFT method; The interconversion pathway (ctct↔cttt↔tttt↔tctt↔tctc) was determined with Elber's PATH algorithm and high-temperature dynamic simulations.

The entire potential energy surface of cyclo(*DLDL*)-*Pro*$_4$ was scanned using a basin-hopping method, followed by an exhaustive Monte Carlo search with OPLS and AMBER all-atom force fields *in vacuo* or with the GB/SA solvation model. The *ctct*- or *tctc*-amide conformers (crystal structures) with a large dipole are the most stable in water, while the all-*trans*-amide conformer with minimal dipole is much more stable *in vacuo*. A B3LYP/6-31G* DFT calculation showed that the all-*trans*-amide conformer is 7.7 kcal/mol more stable than the *ctct*-amide conformer *in vacuo*. This suggests that the all-*trans*-amide conformer should be experimentally observed under appropriate conditions (Figure 2). With Elber's PATH algorithm and high-*T* dynamic simulation, we determine an interconversion pathway: *ctct*↔*cttt*↔*tttt*↔*tctt*↔*tctc* (Figure 3).

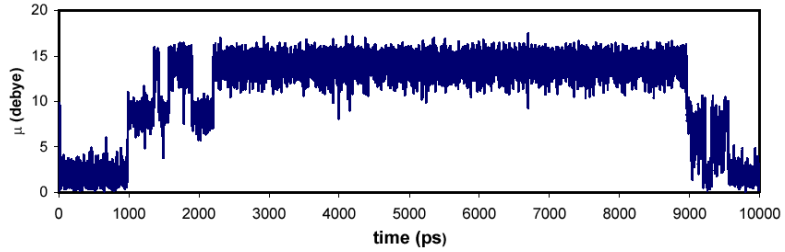

Fig. 3. 10ns molecular dynamics trajectory of cyclo(DLDL)-Pro$_4$ at 1,000K in CHCl$_3$ (AMBER).

Acknowledgments

The work was supported by NIH grant GM53630.

References

1. Chalmers, D. K. and Marshall, G. R. *J. Am. Chem. Soc.* **117**, 5927-5937 (1995).
2. Takeuchi, Y. and Marshall, G. R. *J. Am. Chem. Soc.* **120**, 5363-5372 (1998).
3. Zhang, W. J., *et al. J. Am. Chem. Soc.* **125**, 1221-1235 (2003).
4. Mastle, W., *et al. Biopolymers* **28**, 161-174 (1989).

Peptide Revolution: Genomics, Proteomics & Therapeutics
Michael Chorev & Tomi K. Sawyer (Editors)
American Peptide Society, 2003

Synthesis and Ca^{2+} Interactions of Model Amphipathic Cyclic Peptides in Detergents

Day Gates[1], Jack Rostas[2], Victor Bailey[2] and Maria Ngu-Schwemlein[1]

[1]Chemistry Department, and [2]Biomedical Science Department, University of South Alabama, Mobile, AL 36688, USA

Introduction

Chemosensors for the detection of metal ions with high selectivity and specificity have wide applications in environmental chemistry and the medical sciences [1,2]. Peptide-based chemosensors form an interesting class of sensors and have been designed for the detection of some metal ions [3] whereby the donor atoms for metal ion complexation resides within the peptide and ion binding modifies the emission properties of intrinsic or extrinsic fluorophores. Recent studies showed that self-assembling of sensor components in surfactant aggregates enables complexing Cu(II) with resultant quenching of entrapped dyes [4]. We are interested in extending this strategy to incorporate amphiphatic cyclic peptides tagged with an intrinsic fluorophore into inert detergent micelles to form a comicellar assemblage. This will improve solubilization of the peptide and its metal ion complex. Additionally, a stable assembly of peptide ion sensor with detergent micelles may be a useful approach towards the design of remote sensing chemosensors. To characterize the structural properties of amphipathic peptides and their metal ion interactions in detergents, two model amphipathic cyclic peptides were designed. Peptides containing alternating heterochiral sequences generally exhibit a greater tendency to adopt ring-like antiparallel β-sheets [5] and are also more stable under a variety of conditions compared to their homochiral analogues. We have designed c[Leu-D-Leu-Leu-D-Xaa-(Lys-D-Lys)$_2$], where Xaa = Leu (**1**) or Trp (**2**), to study the secondary structural preferences of amphipathic cyclic peptides in detergent assembly, and their interactions with Ca^{2+}.

Results and Discussion

Cyclo[(Leu-D-Leu)$_2$-(Lys-D-Lys)$_2$ was synthesized by solution phase peptide fragment coupling using N_α-*t*-Boc and O_α-phenacyl ester protecting group strategy. Head-to-tail cyclization was conducted using PyBOP/DIPEA in DMF. The side chain 2-Cl-CBZ protecting groups were removed by catalytic hydrogenation over Pd/C, and the crude peptide was purified by C_4 RP-HPLC (Vydac 214TP54) with a gradient of 20-45% CH_3CN/IPA containing 0.1% TFA. Cyclo[(Leu-D-Leu-Leu-D-Trp-(Lys-D-Lys)$_2$ was purchased from SynPep, Inc.

Circular dichroism (CD) was used to study the conformational preferences and Ca^{2+} binding properties of these model amphipathic cyclooctapeptides in the presence of dodecylphospho-choline (DPC), lysophosphatidic acid (LPAP) and sodium dodecylsulfate (SDS). Peptide **1** exhibited little persistent secondary structure in water and both peptides showed very low binding affinity for Ca^{2+} in water. However, their interactions with Ca^{2+} increased in the presence of detergents. Both peptides formed considerable secondary structure in the presence of micellar detergents or Ca^{2+} (Figure 1). Titration of the peptides in micellar detergents with Ca^{2+} indicates that they exhibited a relatively greater propensity for Ca^{2+} interactions, which leads to the formation of well defined secondary structures (antiparallel β structure) (Figure 2).

The Ca^{2+} binding constant of peptide **2** in DPC is in the 10^2 M^{-1} range and is relatively higher than peptide **1**. The variable temperature CD studies also showed that these interactions are reversible.

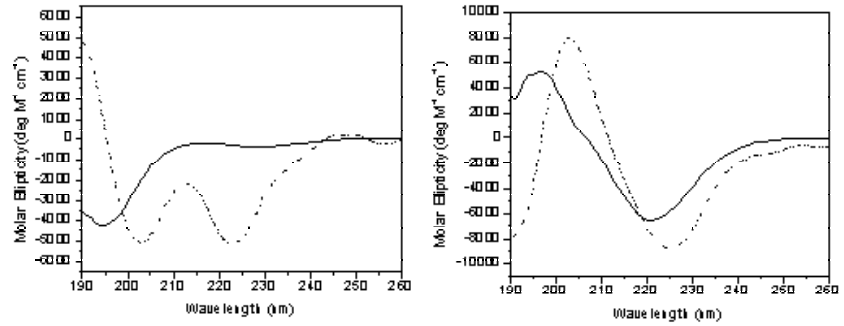

*Fig. 1. CD spectra of **1** (–) and **2** (- - -) in water (left); and of **1** (–) (with Ca^{2+}) and **2** (- - -) in DPC (right).*

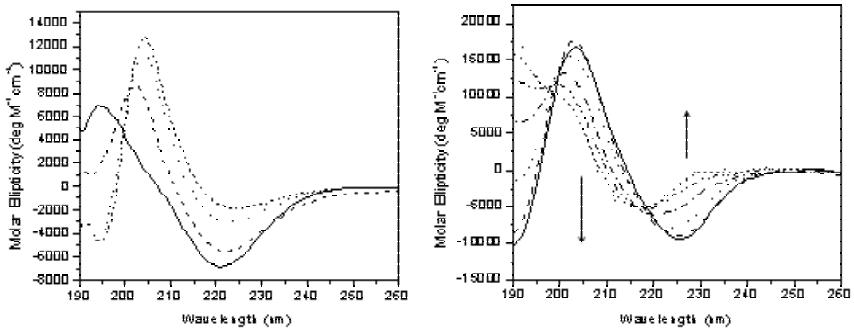

*Fig. 2. CD spectra of **1** in various detergents containing Ca^{2+}: no detergent (–), 10 mM DPC (•••), 5 mM DPC/1 mM LPAP (---), and 5 mM DPC/1 mM SDS (-•-) (left); and of **2** in DPC following titrations with 1:5, 1:10, 1:20, 1:30, 1:40, 1:50 peptide to Ca^{2+} ratios.*

These results indicate that these amphipathic peptides adopt a β sheet structure in the presence of DPC, which has a greater propensity for Ca^{2+} interaction. Interaction with Ca^{2+} is enhanced in the presence of anionic detergents, LPAP and SDS. To understand the structural properties of amphipathic peptides in micelles and their metal ion interactions, the fluorescence of Trp in peptide **2** will be studied, as well as interactions with other metal ions. The results from these studies will be useful in designing optimal metal ion binding moieties on amphipathic cyclic peptides for the attachment of a suitable fluorophore for specific signal transduction.

Acknowledgments
We acknowledge support from the grant NSF RUI CHE 0301097.

References

1. Bargossi, C., et al. *Coordination Chemistry Reviews* **208**, 17-32 (2000).
2. Czarnik, A. W. *In Fluorescent Chemosensors for Ion and Molecular Recognition*; Czarnik, A.W., Ed.; ACS Sym. Series 538; ACS: Washinghton, DC, 1993; and references therein.
3. Torrado, A., Imperiali, B. *J. Org. Chem*. **61**, 8940-8948 (1996).
4. Berton, M., Mancin, F., et al. *Langmuir* **17**, 7521(2001).
5. Rapaport H., Kim H. S., Kjaer K., Howes P. B., Cohen S., Als-Nielsen J., Ghadiri M. R., Leiserowitz L. and Lahav M. *J. Am. Chem. Soc.* **121**, 1186-1191 (1999).

Peptide Revolution: Genomics, Proteomics & Therapeutics
Michael Chorev & Tomi K. Sawyer (Editors)
American Peptide Society, 2003

Conformational Preferences and Biological Activity of Short Peptides Containing (E)-Dehydrophenylalanine

Rafal Latajka[1], Michal Jewginski[1], Malgorzata Pawelczak[2], Maciej Makowski[2] and Pawel Kafarski[1,2]

[1]Institute of Organic Chemistry, Biochemistry and Biotechnology, Wroclaw University of Technology, Wybrzeze Wyspianskiego 27, 50-37- Wroclaw, Poland; [2]Institute of Chemistry, University of Opole, Oleska 48, 45-052 Opole, Poland

Introduction

Dehydroamino acids play a catalytic role in the active sites of some yeast and bacterial enzymes [1] and also occur in a variety of peptide antibiotics of bacterial origin, including the lantibiotics [2] (nisin, subtilin, epidermin) and more highly modified peptides.

Dehydroamino acid residues in peptides have been found to influence the main-chain and side-chain dramatically, due to the presence of $C^{\alpha}=C^{\beta}$ double bond [3]. Therefore, their presence in a peptide chain produces remarkable conformational consequences. Dehydroalanine adopted a roughly planar conformation with *trans* orientation for the ψ and φ torsions and induced an inverse γ-turn in the preceding residue [1]. Dehydrophenylalanine exerts a β-turn conformation in tetrapeptides and 3_{10}-helical conformation in the case of peptides with longer main-chain [4]. It suggests that dehydroamino acid residues exert a powerful conformational influence, independent on other constraints.

The main function of cathepsin C (dipeptidyl-peptidase I) is protein degradation in lysosymes, but it is also found to participate in the activation of neuraminidase and proenzymes of serine proteinases [5]. Since dehydroamino acids are quite reactive and various thiol nucleophiles are known to add to their double bonds, short dehydropeptides might act as alkylating inhibitors of this enzyme. For this reason we have undertook synthesis of peptides containing ΔAla and ΔPhe residues. Unfortunately derivatives of ΔAla and Δ(Z)Phe acted only as a substrates of cathepsin C and their activity and solution conformations were comparable with their saturated counterparts [6,7].

Results and Discussion

Next target of our investigation is group of peptides containing (E)-dehydrophenylalanine. The conformational preferences of Boc-Gly-Δ(E)Phe-Phe-pNA, Boc-Gly-Δ(E)Phe-Gly-Phe-pNA and Gly-Δ(E)Phe-Gly-Phe-pNA were investigated by means of NMR and molecular mechanic calculations. In the case of NMR measurements besides two-dimensional techniques, we have investigated dependence of amide protons chemical shifts on temperature and solvent polarity. The most interesting result for temperature-dependent spectra was obtained for tripeptide. When temperature increased from 295K to 310K in the place of singlet from *p*-nitroanilide amide proton we have observed two signals and a change of chemical shift with temperature for only one of them. It suggested equilibrium between two conformers in which one of them is stabilized by an intermolecular hydrogen bond involving the amide proton of *p*-nitroanilide.

In the case of Boc-Gly-Δ(E)Phe-Gly-Phe-pNA, based on solvent polarity dependence, we could assume that the conformation of this peptide is stabilized by a hydrogen bond involving the amide proton of Gly(3).

Based on the results of two-dimensional NMR measurements (ROESY) and semi-empirical calculations using GAUSSIAN, we have obtained the conformational preferences of these dehydropeptides. All investigated compounds adopted conformations that were stabilized by intermolecular hydrogen bonding.

Table 1. Substrate activity of investigated peptides.

peptide	Michaelis constant K_M [mM]	V_{max} [μmol/min]
Gly-Phe-pNA	3.1	0.0136
Gly-Gly-Δ(E)Phe-Phe-pNA	4.3	0.0604
Gly-Δ(E)Phe-Gly-Phe-pNA	2.3	0.0079
Gly-Δ(Z)Phe-Gly-Phe-pNA	7.8	0.0022
Gly-Gly-Δ(Z)Phe-Phe-pNA	7.8	0.00003
Gly-Phe-Gly-Phe-pNA	22.5	0.0007

Preliminary enzymatic studies have shown that all investigated peptides exerted unexpectedly good substrate activity (Table 1) towards cathepsin C isolated from bovine spleen. As seen from Table 1 the affinities of (E)-dehydropeptides are higher then these observed for model peptides and comparable with that found for Gly-Phe-pNA, the standard synthetic substrate of the enzyme. The most interesting result is very high value of V_{max} observed for Gly-Gly-Δ(E)Phe-Phe-pNA, in contast with the analogue containing (Z)-dehydrophenylalanine residue. Better substrate activity of (E)-dehydropeptides is in good agreement with results obtained from conformational studies.

References

1. Palmer, D. E., Pattaroni, C., Nunami, K., Chadha, R. K., Goodman, M., Wakamiya, T. Fukase, K., Horimoto, S., Kitazawa, M., Fujita, H., Kubo, A. and Shiba, T. *J. Am. Chem. Soc*. **114**, 5634-5642 (1992).
2. Allgaier H., Jung G., Werner R. G., Schneider U. and Zahner H. *Angew. Chem*. **97**, 1052-1054 (1985).
3. Pieroni, O., Fissi, A., Jain, R. M. and Chauhan, V. S. *Biopolymers* **38**, 141-156 (1996).
4. Patel, S. M., Currie Jr., J. O. and Olsen, R. K. *J. Org. Chem*. **38**, 126-128 (1973).
5. Turk, B., Dolenc, I., Turk, V., In Barret A. J. (Ed.), *Handbook of Proteolytic Enzymes,* Academic Press (1998).
6. Makowski, M., Pawelczak, M., Latajka, R., Nowak, K. and Kafarski P. *J. Peptide Sci.* **7**, 141-145 (2001).
7. Latajka, R., Lisowski M., Picur, B., Panek, J., Makowski, M., Lis, T. and Kafarski, P. submitted to *New J. Chemistry.*

Peptide Revolution: Genomics, Proteomics & Therapeutics
Michael Chorev & Tomi K. Sawyer (Editors)
American Peptide Society, 2003

Controlled Assembly of Carbon Nanotubes in Aqueous Solution with Designed Peptides

Gregg R. Dieckmann[1], Alfonso Ortiz-Acevedo[1], Alan B. Dalton[2], Joselito Razal[1,2], Jian Chen[3], Edgar Muñoz[2], Inga H. Musselman[1], Ray H. Baughman[1,2] and Rockford K. Draper[4]

[1]Department of Chemistry, The University of Texas at Dallas, 2601 North Floyd Road, Richardson, TX 75083-0688, USA; [2]NanoTech Institute, The University of Texas at Dallas, 2601 North Floyd Road, Richardson, TX 75083-0688, USA; [3]Zyvex Corporation, 1321 North Plano Road, Richardson, TX 75081-2426, USA; [4]Department of Molecular and Cell Biology, The University of Texas at Dallas, 2601 North Floyd Road, Richardson, TX 75083-0688, USA

Introduction

Single-walled carbon nanotubes (SWNTs) are graphite sheets rolled into seamless cylinders with diameters of 0.7 nm to 1.5 nm and lengths in the micron range. Carbon nanotubes, which have novel electrical and mechanical properties and high surface-to-volume ratios, are potentially useful for applications such as nanosized field effect transistors, sensors, and artificial muscles. While there is intense interest in exploiting the novel properties of carbon nanotubes in both nanoscale and large scale devices, their extreme hydrophobicity and insolubility in most solvents make them difficult to organize into useful geometries. Here we describe the coating and solubilization of SWNTs using designed and chemically synthesized amphiphilic peptides, and demonstrate that the polypeptides organize the nanotubes into ordered fibrous arrays [1].

Results and Discussion

A 29-residue peptide named nano-1, designed to form an amphiphilic α-helix, is based on the previously characterized peptide CoilV_aL_d [2]. Specific design features of nano-1, which contains the amino acid sequence Ac-E(VEAFEKK)(VAAFESK)(VQAFEKK)(VEAFEHG)-$CONH_2$, include: (1) a primary sequence containing a repeating heptad designated $(a\ b\ c\ d\ e\ f\ g)_n$, where positions *a* and *d* contain

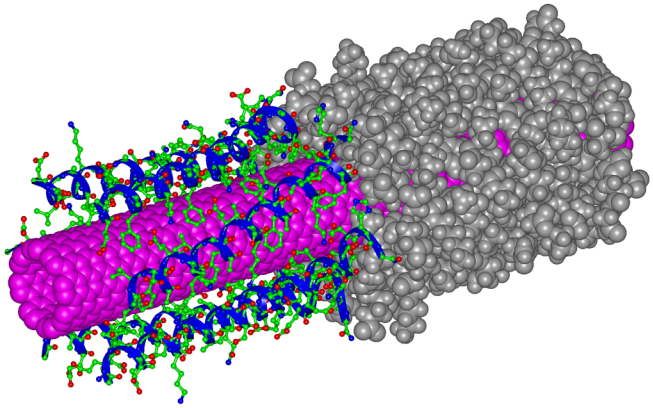

Fig. 1. Model of nano-1 wrapping a carbon SWNT. Left side shows 6 helices in ball-and-stick representation, with the backbone highlighted by blue ribbons. Right side shows 6 helices in CPK representation. The carbon atoms of the SWNT represented as pink spheres.

hydrophobic residues (Val and Phe, respectively) and the other positions are more hydrophilic [3]; (2) acetylation and amidation of the N- and C-termini, removing charges from the termini; (3) polar residues in positions *e* and *g* to favor helix/helix interactions once peptides associate with nanotubes; and (4) oppositely charged polar residues in positions *b* and *f* to favor interactions between helices from different peptide/nanotube complexes. Nano-1 was produced using standard solid phase peptide synthetic methods [4].

A model illustrating the potential interactions between several folded nano-1 molecules and a single SWNT is provided in Figure 1. Circular dichroism reveals that nano-1 adopts an α-helical conformation in aqueous solution which is dependent upon peptide concentration, suggesting that the peptide associates to form helical aggregates. Nano-1 effectively disperses either unpurified HiPco [5] or pulsed laser vaporization (PLV) [6] SWNTs in water to form homogeneous black dispersions (Figure 2). These dispersions are stable at room temperature for variable time periods, depending on peptide/nanotube ratios, sonication times, etc. (at least 12 weeks under some conditions). Thermogravimetric analysis of dispersions with saturating levels of SWNTs reveals that nanotubes are present up to 0.7 mg mL^{-1}, indicating high levels of solubilization. The structures present in the dispersions (and in the fibrillar precipitates that eventually form from the dispersions) have been studied by transmission electron microscopy (TEM). At low resolution, a reticulated network of peptide and SWNTs is observed in the dispersion, and at high resolution, the orientation of SWNTs parallel to the axis of fibers in the reticulum is evident (Figure 3).

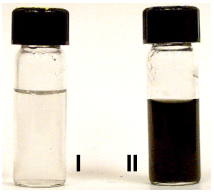

Fig. 2.(I) water with SWNTs. (II) Nano-1/SWNT dispersion. Both samples sonicated and filtered.

The peptide/SWNT dispersions have been extensively characterized by Raman spectroscopy. A prominent feature in the Raman spectrum of SWNTs is the radial breathing mode in the 160 to 300 cm^{-1} region associated with a symmetric movement of all carbon atoms in the radial direction (there are no prominent Raman active modes for the peptide in this region). Peptide/SWNT dispersions show shifts of the radial breathing modes by more than 9 cm^{-1} to higher frequencies, strongly suggesting that the peptide intercalates between a high percentage of the SWNTs in the raw material, coating and separating the nanotubes. Orientation-dependent measurements, performed using polarized Raman scattering, demonstrate a strong correlation of the modes associated with SWNTs with the long axis of the peptide/nanotube microfibers, indicating that the nanotubes are highly oriented along the axis of the microfibers.

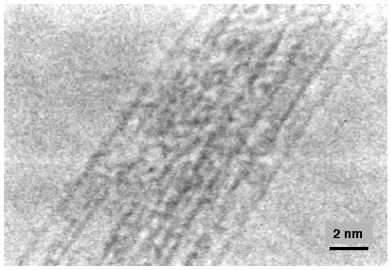

Fig. 3. High resolution TEM image of nano-1/SWNT composite.

The morphology of the peptide/SWNT composites can be manipulated by changing solution conditions to perturb the self-assembly properties of nano-1. The strength of charge-charge interactions, and hence the formation of higher-order structures, are manipulated by controlling the ionic strength of the solution through addition of NaCl. Increasing NaCl concentrations causes peptide-coated SWNTs to visibly assemble into

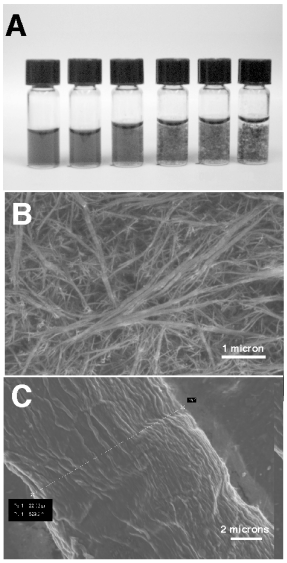

Fig. 4. (A.) Photograph of nano-1/SWNT dispersion mixed with different NaCl concentrations (left to right: 0 mM NaCl, 40 mM, 60 mM, 80 mM, 120 mM, 160 mM). (B) SEM image of fibers formed from nano-1/SWNT dispersion. (C) SEM image of fibers formed from nano-1/SWNT dispersion in presence of 40 mM NaCl.

larger structures, with the extent of aggregation dependent on NaCl concentration (Figure 4A). Scanning electron microscopy (SEM) has been used to characterize the resulting materials. Fiber diameters vary from ~100 nm (no NaCl) to ~20 μm (40 *mM* NaCl) (Figs. 4B and C). Raman spectra confirm the presence of SWNTs in the NaCl-induced fibers and show similar changes in the radial breathing modes as those observed in the peptide/SWNT dispersions, suggesting the presence of peptide-coated SWNTs in the salted fibers. We have also modulated the formation of peptide/nanotube solids through the addition of the amphiphilic molecule N,N-dimethylformamide (DMF). The solids, which form after 24 hours, contain long interwound strands of thin ribbon-like fibrils 30 to 75 nm wide (based on SEM) with extensively aligned nanotubes (high-resolution TEM) (Fig. 5). Altogether, these data demonstrate that designed peptides can be used to coat, solubilize, and induce the assembly and alignment of SWNTs into higher order structures.

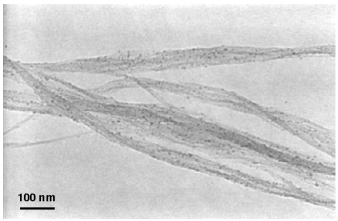

Fig. 5. High resolution TEM image of ribbons formed from nano-1/SWNT dispersion in presence of 0.0015% (by volume) DMF.

Acknowledgments

This research was supported by The Robert A. Welch Foundation [AT-1326 (IHM), AT-1448 (GRD)], the Texas Advanced Research Program [009741-0026-1999 (GRD)], and a University of Texas at Dallas Special Faculty Development Assignment (RKD).

References

1. Dieckmann, G. R., et al. *J. Am. Chem. Soc.* **125**, 1770-1777 (2003).
2. Ogihara, N. L., et al. *Prot. Sci.* **6**, 80-88 (1997).
3. McLachlan, A. D. and Stewart, M. *J. Mol. Biol.* **98**, 293-304 (1975).
4. Bodanszky, M. *Peptide Chemistry: A Practical Approach*. 2nd Ed., Springer-Verlag, New York (1993).
5. Nikolaev, P., et al. *Chem. Phys. Lett.* **313**, 91-97 (1999).
6. Thess, A., et al. *Science* **273**, 483-487 (1996).

Peptide Revolution: Genomics, Proteomics & Therapeutics
Michael Chorev & Tomi K. Sawyer (Editors)
American Peptide Society, 2003

Role of Disulfide Bonds in the Folding of Prouroguanylin and Heat-stable Enterotoxin

Yuji Hidaka[1], Len Ito[2] and Hiroshi Yamaguchi[2]

[1]Institute for Protein Research, Osaka University, Suita, Osaka 565-0871, Japan; [2]School of Science and Technology, Kwansei Gakuin University, Sanda, Hyogo 669-1337, Japan

Introduction

Uroguanylin, an endogenous ligand of guanylyl cyclase C, is initially secreted in the form of a prohormone, prouroguanylin, and then processed into the mature, bioactive form. We previously reported that the mature form, uroguanylin, does not possess the requisite information to permit native disulfide pairing, and that the propeptide in the precursor protein, prouroguanylin, functions as an intramolecular chaperone, thus permitting the correct folding of the mature peptide [1,2].

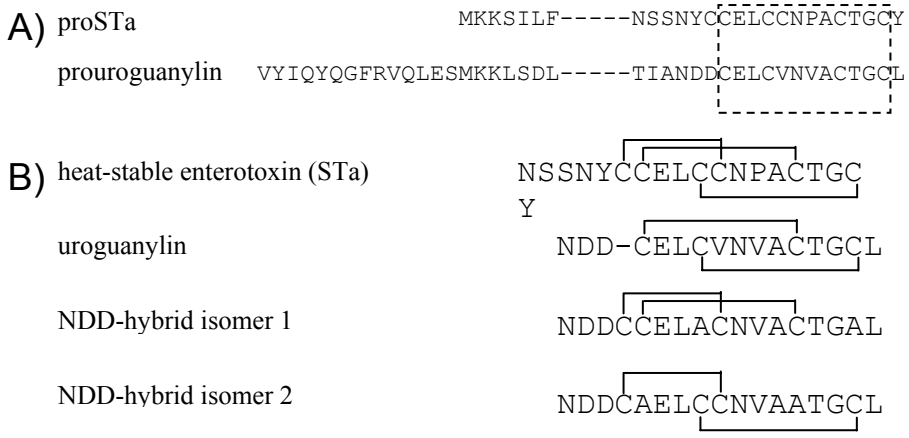

Fig. 1. A) Sequences of pro-heat stable enterotoxin (STa) and prouroguanylin. B) Mature peptides and hybrid isomers of uroguanylin and STa. Solid lines represent disulfide bonds.

Heat-stable enterotoxin (STa) produced by enterotoxigenic *E. coli*, an exogenous ligand of guanylyl cyclase C, shares a high homology to uroguanylin, as shown in Figures 1A and 1B [3]. However, STa possesses one additional disulfide bond and is able to fold into the native conformation without the assistance of the propeptide region. This raises a number of questions: 1) how STa folds into its native conformation without the assistance of the propeptide, 2) what roles do each of the disulfide bonds in uroguanylin and STa play in the folding process, and 3) Can propeptide of uroguanylin stabilize the bioactive form of STa-type disulfide pairing.

To address these problems, we prepared a series of hybrid disulfide isomers of uroguanylin and STa, as shown in Figure 1B, and examined their folding. In addition, hybrid disulfide isomers of prouroguanylin and STa were prepared in order to examine the chaperone function of the propeptide of uroguanylin.

Results and Discussion

To estimate the role of each of the disulfide bonds of uroguanylin and STa, we first introduced the additional disulfide bond contained by STa into the corresponding

position of uroguanylin, based on homology alignment, and eliminated one disulfide bond, resulting in the production of the hybrid disulfide isomers (ND-hybrid isomers), NDCCELACNVACTGCAL and NDCAELCCNVAATGCL. After reduction of the disulfide bonds, the peptides were folded under the several sets of conditions that normally permit disulfide bond formation to occur. Neither of the above peptides underwent selective disulfide bond formation as readily as native uroguanylin. This suggests that two disulfide bonds are not sufficient to stabilize the bioactive conformation of the peptides, and that three disulfide bonds are required to cooperatively stabilize the tertiary structure of STa.

To investigate the chaperone function of the propeptide in prouroguanylin, the hybrid disulfide isomers, containing the propeptide of uroguanylin, were prepared and their folding was examined. However, the introduction of the propeptide into the N-terminus of each of the hybrid peptides had no significant effect on folding or the disulfide bond formation, suggesting that the propeptide did not function as an intramolecular chaperone in the folding of these hybrid peptides. This result implies that the propeptide of uroguanylin is not capable of stabilizing STa-type disulfide pairing and conformation. However, the possibility that the propeptide is not able to interact with the mature region cannot be excluded, since a mutation frequently affects the tertiary structure of a peptide. Therefore, we realigned the sequences of uroguanylin and STa, and inserted a gap in the N-terminal region of uroguanylin (Figure 1B). In this case, an additional Asp residue was retained at the N-terminal region of the hybrid disulfide isomers of uroguanylin (Figure 1B).

The NDD-hybrid isomers 1 and 2 did not undergo selective disulfide bond formation as readily as the above isomers (ND-hybrid isomers). However, when the propeptide region of uroguanylin was introduced into the N-termini of the NDD-hybrid isomer 1, native disulfide pairing occurred exclusively, suggesting that the propeptide functions as an intramolecular chaperone in the folding of NDD-hybrid isomer 1. This clearly indicates that the propeptide of uroguanylin possesses the ability to regulate the conformation of the mature peptide. Therefore one can speculate that the propeptide recognizes the bioactive conformation of peptide hormones and regulates the folding of the mature hormone in the precursor protein.

In conclusion, three disulfide bonds of STa function cooperatively to stabilize the conformation of STa, resulting in the production of the bioactive form. The propeptide of uroguanylin possesses the ability to recognize the conformation of the bioactive form of the hybrid peptide and permits its selective folding into the native tertiary structure of the mature peptide.

Acknowledgments

The use of the facility at the Radioisotope Research Center at Osaka University is gratefully acknowledged.

References

1. Hidaka, Y., Ohno, M., Hemmasi, B., Hill, O., Forssmann, W.- G. and Shimonishi Y. *Biochemistry* **37**, 8498-8507 (1998).
2. Hidaka, Y., Shimono, C., Ohno, M., Okumura, N., Adermann, K., Forssmann, W.- G. and Shimonishi, Y. *J. Biol. Chem.* **275**, 25155-25162 (2000).
3. Kita, T., Smith, C. E., Fok, K. F., Duffin, K. L., Moore, W. M., Karabatsos, P. J., Kachur, J. F., Hamra, F. K., Pidhorodeckyj, N. V., Forte, L. R. and Currie, M. G. *Am. J. Physiol.* **266**, F342-348 (1994).

Peptide Revolution: Genomics, Proteomics & Therapeutics
Michael Chorev & Tomi K. Sawyer (Editors)
American Peptide Society, 2003

Pseudopeptide Foldamers. The Homo-oligomers of 4(*S*)-Oxazolidineacetic Acid, 2-Oxo (Oxac)

C. Tomasini[1], G. Luppi[1], S. Oancea[2], F. Formaggio[2] and C. Toniolo[2]

[1]Department of Chemistry "G. Ciamician", Alma Mater Studiorum, University of Bologna, 40126 Bologna, Italy; [2]Institute of Biomolecular Chemistry, CNR, Department of Organic Chemistry, University of Padova, 35131 Padova, Italy

Introduction

The synthesis of conformationally constrained amino acids is an important tool for the preparation of oligomers that assume a well defined secondary structure. We have recently described the synthesis of oligomers of L-Oxd [1, 2] and L-pGlu [3] and we have demonstrated that these molecules fold in ordered structures characterized by a *semi*-extended helical conformation. As part of this project, we report here a straightforward synthesis of 4(*S*)-oxazolidineacetic acid, 2-oxo benzyl ester (H-Oxac-OBzl), a β-amino acid derivative, the preparation of its homo-oligomers up to the tetramer level by solution methods, and their conformational analysis in structure supporting solvents.

Results and Discussion

By reaction with Ac_2O under microwave irradiation, Z-L-Asp-OH was transformed into the corresponding internal anhydride, which was then reduced to the lactone **1** with $NaBH_4$ in dry THF. Then, **1** was treated with Cs_2CO_3 in water and acetone for 4 hours at reflux to obtain the cesium carboxylate salt **2** in high yield, which was transformed into H-D-Oxac-OBzl **3** by reaction with benzyl bromide in DMF. After flash chromatography, **3** was obtained pure in 45% overall yield from Z-L-Asp-OH [4].

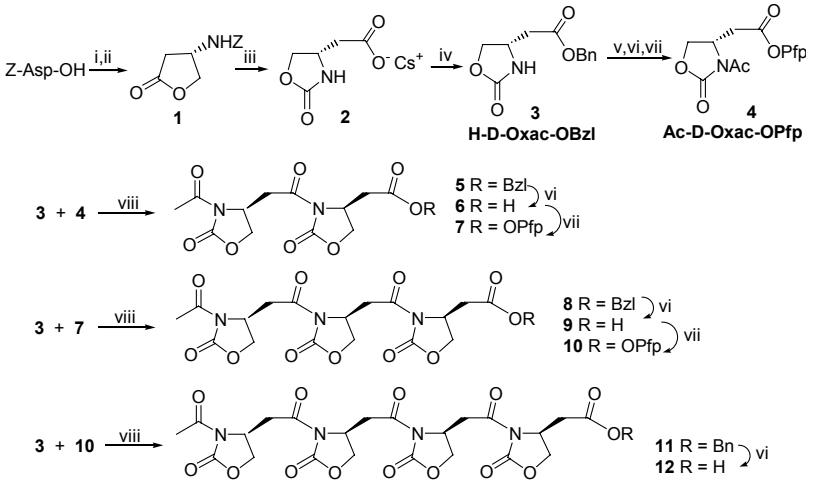

Scheme 1. Reagents and Conditions: (i) Ac_2O (3 equiv.), microwave, 1 min; (ii) $NaBH_4$ (1.1 equiv.), dry THF, r. t., 16 h; (iii) Cs_2CO_3 (3 equiv.), H_2O/acetone (3:1 ratio), 4 h, reflux; (iv) BzlBr (1.1 equiv.), DMF, r.t., 16 h; (v) AcCl (1.5 equiv.), DIEA (2 equiv.), DMAP (0.1 equiv.), dry DMF, r.t., 16 h; (vi) H_2 (3 atm.), C/Pd, MeOH, r.t., 2 h;(vii) $CF_3CO_2C_6F_5$ (1.1 equiv.), pyridine (1.1 equiv.), dry DMF, 2 h, r.t.; (viii) DIEA (4 equiv.), dry DMF, r.t., 16 h.

The homo-oligomers Ac-(D-Oxac)$_n$-OBzl **5**, **8** and **11** were obtained, respectively, by coupling the pentafluorophenyl esters **4**, **7** and **10** with H-D-Oxac-OBzl **3** in the presence of a base (DIEA). The preferred conformation of this pseudopeptide series in structure-supporting solvents was investigated by FT-IR absorption, ^{1}H NMR and CD techniques.

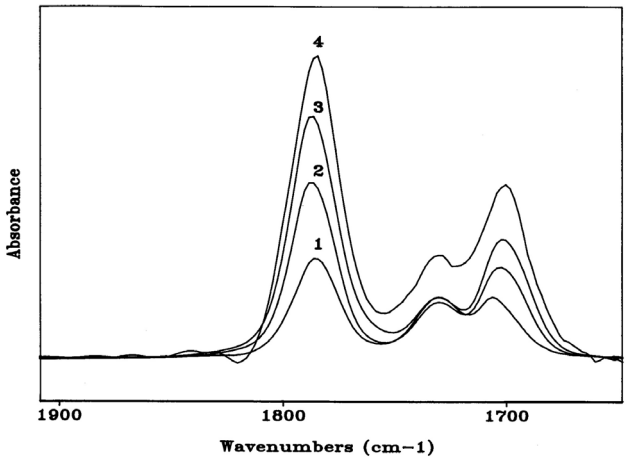

Fig. 1. Infrared absorption spectra of the Ac-(D-Oxac)$_n$-OBzl (n = 1-4) homo-oligomers in the 1900-1650 cm^{-1} region in $CDCl_3$ solution (conc.: 1 mM).

The far-UV CD spectra of the oligomeric D-Oxac free acids exhibit a strong positive Cotton effect centered near 205 nm in both methanol and water. No evidence of splitting of the acylurethane chromophore is observed. In the C=O stretching region the IR absorption spectra of the oligomeric benzyl esters in $CDCl_3$ solution (Figure 1) show two acylurethane bands at about 1785 and 1700 cm^{-1} in addition to the ester band near 1730 cm^{-1}. As the main chain increases, there is no evidence of any dramatic change in either band positions or intensities. The chemical shift of the β-CH proton in the ^{1}H NMR spectra of the oligomeric benzyl esters in $CDCl_3$ solution is slightly different for the C-terminal unit (4.74 - 4.78 ppm) as compared to the N-terminal and internal units (all clustered at 4.84 - 4.85 ppm). None of these signals is sensitive to the addition of DMSO. In conclusion, this novel, acylurethane-based, foldameric structure, if appropriately functionalized, can be considered as a promising template for a variety of applications.

References

1. Lucarini, S. and Tomasini, C. *J. Org. Chem.* **66**, 727-732 (2001).
2. Tomasini, C., Trigari, V., Lucarini, S., Bernardi, F., Garavelli, M., Peggion, C., Formaggio, F. and Toniolo, C. *Eur. J. Org. Chem.* 259-267 **(**2003).
3. Bernardi, F., Garavelli, M., Scatizzi, M., Tomasini, C., Trigari, V., Crisma, M., Formaggio, F., Peggion, C. and Toniolo, C. *Chem. Eur. J.* **8**, 2516-2525 (2002).
4. Luppi G., Villa M. and Tomasini C. *Org. Biomol. Chem.* 247-250 (2003).

Peptide Revolution: Genomics, Proteomics & Therapeutics
Michael Chorev & Tomi K. Sawyer (Editors)
American Peptide Society, 2003

C^{α}-Methyl Norvaline Foldamers

Fernando Formaggio[1], Marco Crisma[1], Claudio Toniolo[1], Quirinus B. Broxterman[2], Bernard Kaptein[2], Catherine Corbier[3], Michele Saviano[4], Pasquale Palladino[4] and Ettore Benedetti[4]

[1]Institute of Biomolecular Chemistry, CNR, Department of Organic Chemistry, University of Padova, 35131 Padova, Italy; [2]DSM Research, Life Sciences, Advanced Synthesis and Catalysis, P.O. Box 18, 6160 MD Geleen, The Netherlands; [3]Laboratory of Crystallography, ESA 7036, University Henry Poincaré – Nancy I, 54506 Vandoeuvre-lès-Nancy, France; [4]Institute of Biostructures and Bioimaging, CNR, Interuniversity Research Center on Bioactive Peptides, University of Naples "Federico II", 80134 Naples, Italy

Introduction

Recent interest in peptides based on C^{α}-methylated α-amino acids stems from their capability to induce significant restraints on the backbone conformational freedom [1]. In this connection the conformational preferences of homo-oligomers based on C^{α}-methylated α-amino acids with a linear, saturated aliphatic side chain of increasing length particularly attracted our attention. The experimental results obtained so far convincingly support our view that the Aib and Iva residues are strong β-turn and 3_{10}-helix formers (depending on peptide main-chain length), much more efficient than their C^{α}-unmethylated parent amino acids. However, in terms of screw sense bias Aib is achiral, thereby forming isoenergetic, equally probable, enantiomeric, right- and left-handed, homo oligomeric 3_{10}-helices. Iva is chiral, but the small difference (one carbon atom only) between the two aliphatic substituents on its C^{α}-atom does allow the formation of only a relatively limited, although sizable, excess of one 3_{10}-helix screw sense over the other in its homo-oligomers (likewise protein amino acids, the L-residue gives a predominantly right-handed helix).

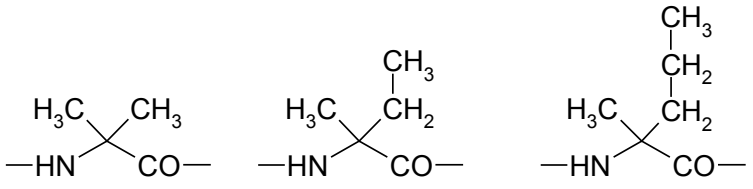

Aib Iva (αMe)Nva

In this work we expanded the investigation of this sub-class of C^{α}-methylated α-amino acids to the terminally protected homo-oligomeric series $[L\text{-}(\alpha Me)Nva]_n$ (n=2-6,8).

Results and Discussion

In this study, we successfully synthesized in solution a series of sterically hindered homo-oligomers based on L-(αMe)Nva, produced by DSM Research, to the octamer level using either the step-by-step or the segment condensation approach. Furthermore, the results of our solution conformational analysis, combined with those extracted from

the crystal-state X-ray diffraction study, strongly confirm our published preliminary findings [2] that (αMe)Nva has a remarkable propensity for β-turn and 3_{10}-helix formation. This conclusion strictly parallels those already reported for other C^{α}-methylated α-amino acids [1]. As for the relationship between (αMe)Nva α-carbon chirality and the screw sense of the turn/helix that is adopted by its peptides, the X-ray diffraction data available unambiguously support the contention that this structural property is analogous to that exhibited by protein amino acids, *i.e.,* L-amino acids fold into right-handed turns/helices.

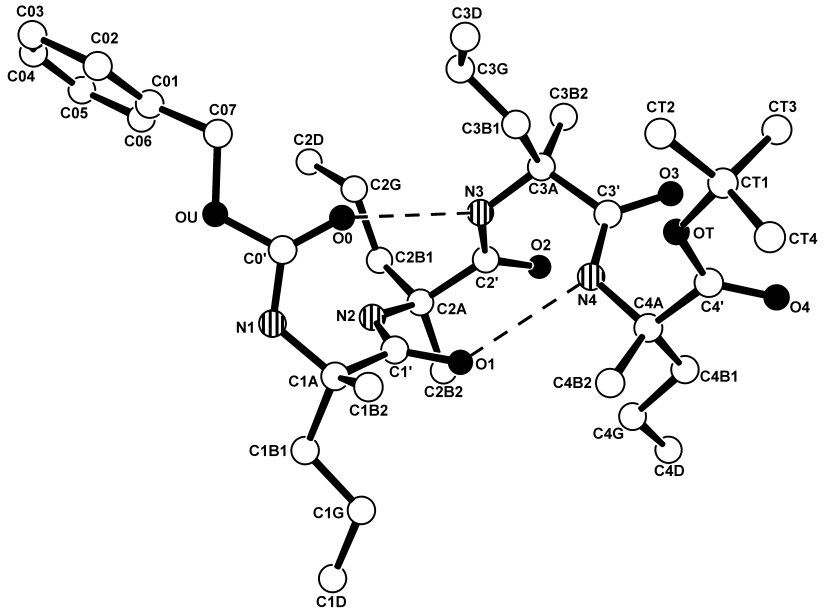

Fig.1. X-Ray diffraction structure of Z-[L-(αMe)Nva]$_4$-OtBu. The terminally protected homo-tetramer is folded in a right-handed, incipient 3_{10}-helical structure.

In our view L-(αMe)Nva homo-oligomers represent an excellent series, the best among those based on C^{α}-methylated α-amino acids with a linear, saturated aliphatic side chain, for application as a set of rigid, foldameric spacers in physicochemical investigations.

References

1. For a recent review-article, see: Toniolo, C., Crisma, M., Formaggio, F. and Peggion, C. *Biopolymers (Pept. Sci.)* **60**, 396-419 (2001).
2. Moretto, A., Peggion, C., Formaggio, F., Crisma, M., Toniolo, C., Piazza, C., Kaptein, B., Broxterman, Q. B., Ruiz, I., Díaz-de-Villegas, M. D., Galvez, J. A. and Cativiela, C. *J. Pept. Res.* **56**, 283-297 (2000).

Peptide Revolution: Genomics, Proteomics & Therapeutics
Michael Chorev & Tomi K. Sawyer (Editors)
American Peptide Society, 2003

Structure-Activity Studies of *cis*-γ-Amino-L-Proline Oligomers: Probing the Relationship between Conformational Stability and Cellular Internalization Capacity

Josep Farrera-Sinfreu[1], Ernest Giralt[1], Miquel Pons[1], Susana Castel[2], Fernando Albericio[1] and Miriam Royo[1]

[1]Barcelona Science Park-University of Barcelona; [2]Scientific and Technical Service, University of Barcelona, E-08028 Barcelona, Spain

Introduction

Oligomeric organic molecules are known to give a wide range of new secondary structures. In recent years, β- and γ-peptides have been studied intensively and many types of new structures have been reported [1]. β-Peptides also have been studied successfully as antimicrobials [2], hormone like peptides [3] and Trojan carriers [4]. Herein, we report the synthesis of a new family of γ-peptides as well as its NMR structural studies and preliminary structure–internalization capacity relationship studies in a new family of γ-peptides, the *cis*-γ-amino-L-proline hexamers. We have synthesized peptides with different type of linkages between the side chain and the γ-peptide backbone, obtaining two different families: the two types of linkages evaluated are the amide, which gave N^{α}-acyl-γ-peptides, and the amine, which gave N^{α}-alkyl-γ-peptides.

Results and Discussion

Synthesis of the N^{α}-alkyl-γ-hexapeptides and the N^{α}-acyl-γ-hexapeptides were carried out on solid phase using an Fmoc/Boc synthetic strategy on a MBHA resin. The elongation of the peptidic backbone was carried out with the protected amino acid [(2S,4S)-Fmoc-4-amino-1-Boc-pyrrolidine-2-carboxylic acid, [Fmoc-(2S,4S)-Abpc]] with a common coupling method, DIPCDI with HOBt and monitored by the ninhydrin test. The side chains of N^{α}-acyl-γ-peptides were introduced using the corresponding carboxylic acids and the same coupling reagents used above, and were followed by the chloranil test, which detects secondary amines. For N^{α}-alkyl-γ-peptides, the alkyl group was introduced by reductive amination using the corresponding aldehyde and $NaBH_3CN$. This strategy allows the synthesis of the homo-oligomeric γ-peptides with the same side chain at all monomers and hetero-oligomeric γ-peptides with different side chains at all monomers (Figure 1).

NMR and CD were chosen to study the conformational preferences of these peptides in aqueous solution. CD patterns observed in three solvents (H_2O, MeOH and TFE) for the two different γ-peptides families comprised from the aminoproline monomer are different. Whereas N^{α}-acyl hexamers show a spectrum with two minima around 215 and 205 nm and one minimum at ca. 190 nm in all three solvents, the N^{α}-alkyl family only show one maximum at ca. 190 nm in H_2O, but when the solvent is TFE, a minimum also appears at ca. 215 nm. These differences between families suggest that the structure found for the N^{α}-alkyl family in TFE is the same as that found in the N^{α}-acyl family in all three solvents.

Strong overlap of signals in NMR spectra in aqueous solution of these peptides prevents the sequential assignment of the backbone protons. Nevertheless, peptide **2** has been studied extensively. The observation of NOEs between protons located in

opposite faces of the proline ring in peptide **2** was taken as evidence of inter-residue interactions. The suggested regular structure can be described as a series of turns in which the two amide bonds connected to the α and γ positions of each proline are in the same plane, which is perpendicular to the average plane of the proline rings. In this structure, protons α and γ of prolines i and i+2 are close, explaining some of the observed NOEs. However, by assuming that *N*- and *C*-proline terminal rings can rotate around their last amide bonds ($H_\alpha C_\alpha$:C'O and $C'N_\gamma$:$C_\gamma H_\gamma$ respectively) we can understand the other observed NOEs.

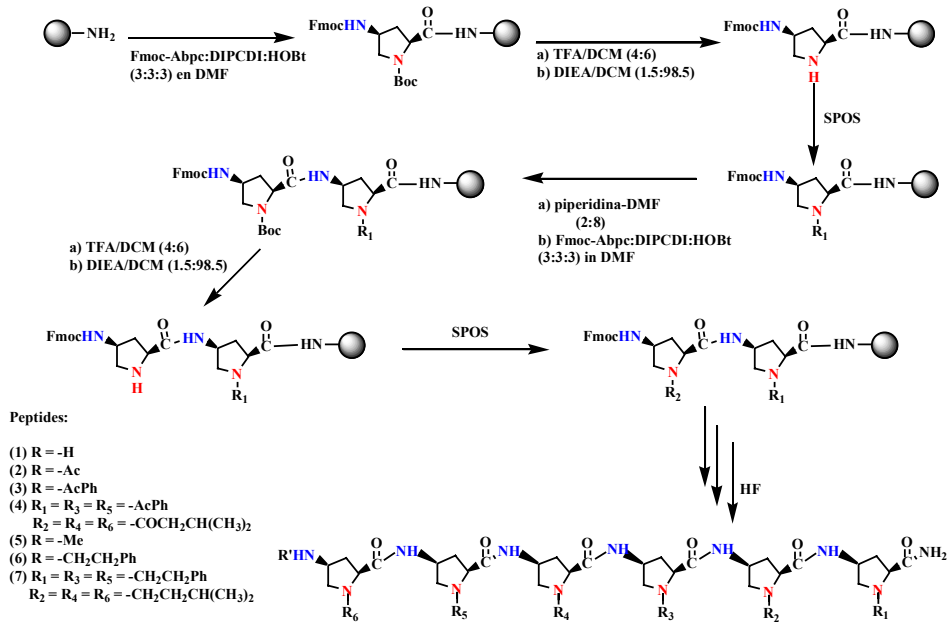

Fig. 1. Synthesis scheme of N^{α}-acyl and N^{α}-alkyl peptides.

These peptides were tested as carriers for drug delivery. Peptides were labeled with a fluorescent probe (5(6)-carboxyfluorescein) in the N^{γ}-terminal group using the same synthetic strategy described above. Quantification of internalization and cytotoxicity studies have performed and supplemented with confocal images. Cytotoxicity studies demonstrated that these peptides are not toxic even at high concentrations. Quantification using both fluorimetry and cytometry techniques determined that all of these peptides can be internalized by the COS-1 cell line. Interestingly, different uptake mechanisms and different localizations at the subcellular level were found for different peptides. For example, peptide **7** was accumulating in the nucleus.

References

1. Hill, D. J. *et al*. *Chem. Rev.* **101**, 3893 (2001).
2. Raguse, T. L. *et al*. *J. Am. Chem. Soc.* **124**, 12774 (2002).
3. Gademann, K. *et al*. *J. Med. Chem.* **44**, 2460 (2001).
4. Rueping, M. *et al*. *Chem. Bio. Chem.* **257** (2002).

Peptide Revolution: Genomics, Proteomics & Therapeutics
Michael Chorev & Tomi K. Sawyer (Editors)
American Peptide Society, 2003

Helix Formation in Oligomers of γ-Amino Acids (γ-Peptides)

Carsten Baldauf, Robert Günther and Hans-Jörg Hofmann

Institute of Biochemistry, Faculty of Biosciences, Pharmacy and Psychology,
University of Leipzig, Talstrasse 33, D-04103 Leipzig, Germany

Introduction

The imitation of native peptides by peptidomimetics is a field of outstanding interest. Since the functions of native peptides and proteins are based on definite three-dimensional structures with characteristic secondary structure elements, the designed compounds have to realize comparable structural and electronic properties. It is an old idea to improve the properties of native peptides by substitution of one or several unnatural amino acids for the α-amino acid constituents in the sequence. In recent years, it has been shown that the formation of characteristic secondary structures is also possible in sequences which are completely composed of unnatural amino acids, as for instance β- and γ-amino acids. The greater number of conformational degrees of freedom in the monomer constituents in comparison to α-amino acids does not prevent secondary structure formation, as previously assumed. It increases only the number of secondary structure alternatives, since definite conformers exist for the rotation around each single bond of the backbone. In particular the research on β-peptides has promoted the foldamer concept, which goes far beyond biologically relevant macromolecules [1,2].

In this study, we offer an overview of all periodic secondary structures in γ-peptides with hydrogen bonding between the peptide bonds. Figure 1 shows the basic possibilities for the formation of hydrogen-bonded pseudocycles C_x in forward and backward direction along the sequence.

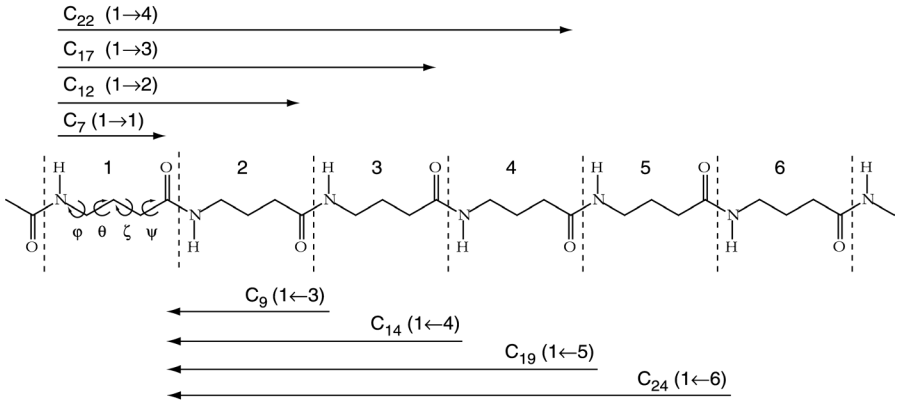

Fig. 1. Possible periodic hydrogen bonding patterns in γ-peptides.

A pool of 36,000 periodic hexamer structures, which was generated by systematic variation of the backbone torsion angles φ, θ, ζ and ψ in steps of 30°, was screened for candidates with the hydrogen bonding patterns in Figure 1. The obtained candidates were subjected to geometry optimizations at the HF/6-31G* and DFT/B3LYP levels of

ab initio MO theory, respectively. The solvent influence was estimated by a polarizable continuum model (PCM/6-31G*).

Results and Discussion

As the result of the systematic search, minimum conformations were found for all hydrogen bonding patterns in Figure 1 up to 24-membered hydrogen-bonded pseudocycles. The elongated backbone of the γ-amino acid constituents of the γ-peptides in comparison to the α- and β-amino acid constituents of α- and β-peptides leads to the following consequences:

i) It enables the realization of the same hydrogen bonding pattern for several conformational backbone alternatives. Thus, at least two structural alternatives occur for each size of the pseudocycles.

ii) Optimum arrangements for hydrogen bonding can already be realized in the smaller hydrogen-bonded cycles. Thus, the stability tends to increase in direction of the periodic structures with nearest neighbor interactions.

iii) Only the nearest neighbor structures can be derived from the conformers of the monomer constituents, which is impossible for the larger helices.

In Figure 2, the three most stable structures and their characteristics are presented. The most stable H_{14}^{I} conformer corresponds to the 2.6_1-helix suggested by the groups of Seebach and Hanessian [3,4]. The strongly related nearest neighbor structure H_9^{I} is a helical structure, whereas nearest neighbor structures of α- or β-peptides are still more sheet- or ladder-like.

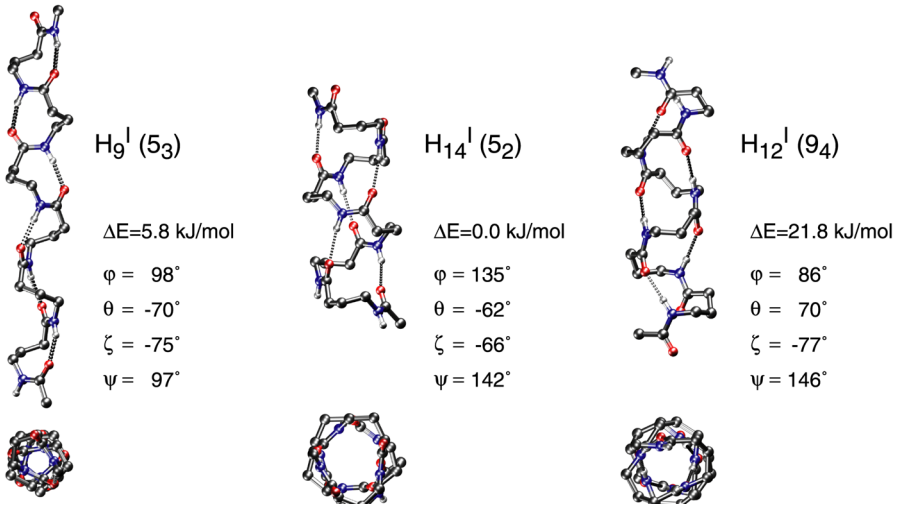

Fig. 2. Most stable helices in γ-peptides (H_{14}^{I}: E_T = -1956.361656 a.u.).

Acknowledgments

This work was supported by DFG (Projekt HO 2346/1 and SFB 610).

References

1. Gellman, S. H. *Acc. Chem. Res.* **31**, 173-180 (1998).
2. Hill, D. J., Mio, M. J., Prince, R. B., Hughes, T. S. and Moore, J. S. *Chem. Rev.* **101**, 3893-4011 (2001).
3. Hintermann, T., Gademann, K., et al. *Helv. Chim. Acta* **81**, 983-1002 (1998).
4. Hanessian, S., et al. *J. Am. Chem. Soc.* **120**, 8569-8570 (1998).

Peptide Revolution: Genomics, Proteomics & Therapeutics
Michael Chorev & Tomi K. Sawyer (Editors)
American Peptide Society, 2003

Vinylogous γ-Amino Acids as Building Blocks for Foldamers

Carsten Baldauf, Robert Günther and Hans-Jörg Hofmann

Institute of Biochemistry, Faculty of Biosciences, Pharmacy and Psychology,
University of Leipzig, Talstrasse 33, D-04103 Leipzig, Germany

Introduction

It has been shown that γ-peptides are able to form stable secondary structures. In comparison to α- and β-peptides, the elongated backbone of the γ-amino acid residues favors hydrogen bonding between nearest neighbor peptide bonds, even if helices with a larger size of the hydrogen-bonded pseudocycles are still possible. An interesting idea to support the formation of helices with larger pseudocycles is the introduction of a *trans*-double bond between the C(α) and C(β) atoms of the γ-amino acid constituents, which rigidifies the backbone in these vinylogous γ-amino acids and excludes conformations with nearest neighbor hydrogen bonding (1←3 and 1→1 interactions) in the peptides from the conformational space (Figure 1).

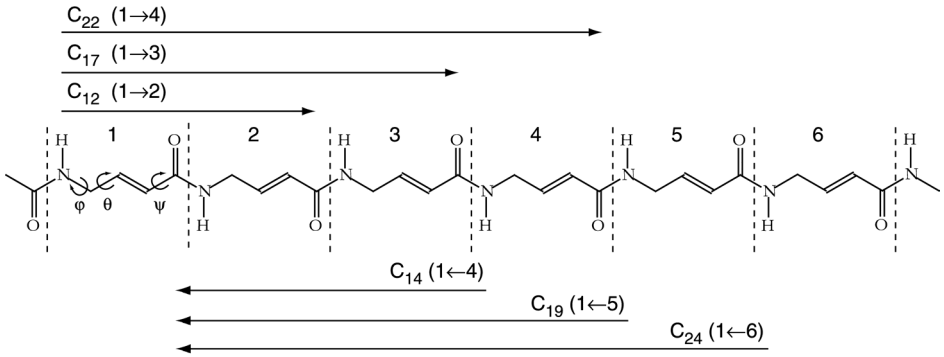

Fig. 1. Possible periodic hydrogen bonding patterns in trans vinylogous γ-peptides.

To give an overview on the possible periodic structures with hydrogen bonding patterns according to Figure 1, we analyzed a pool of about 9,000 periodic hexamer conformations generated by a systematic variation of the torsion angles φ, θ and ψ in steps of 30°. The corresponding candidates were subjected to *ab initio* geometry optimizations (HF/6-31G* and B3LYP/6-31G*).

Results and Discussion

As a consequence of the rigidity of the backbone, periodic structures with nearest neighbor hydrogen bonds like C_7 and C_9 could not be localized as minimum conformations. Even periodic structures forming the larger C_{12} pseudocycles are still impossible. Beginning with pseudocycles C_{14}, helices have been found in hexamers up to pseudocycles C_{24}. As expected, the structural variety of the vinylogous γ-peptides is restricted in comparison to the γ-peptides. With the exception of C_{22}, only one helix representative exists for each pseudocycle size. In the vinylogous γ-peptides, the H_{19} and H_{22}^1 helices (Figure 2) are more stable than H_{14}, which predominates in γ-peptides, although the latter has more hydrogen bonds for the same sequence length.

A detailed view on the structures forming larger rings like C_{22} or C_{24} reveals interesting structural properties. The corresponding helices represent tubes with a large inner diameter. Such structures, as for instance the rather stable H_{22}^{I} conformer, could be important for the design of channels or nanostructures (Figure 3).

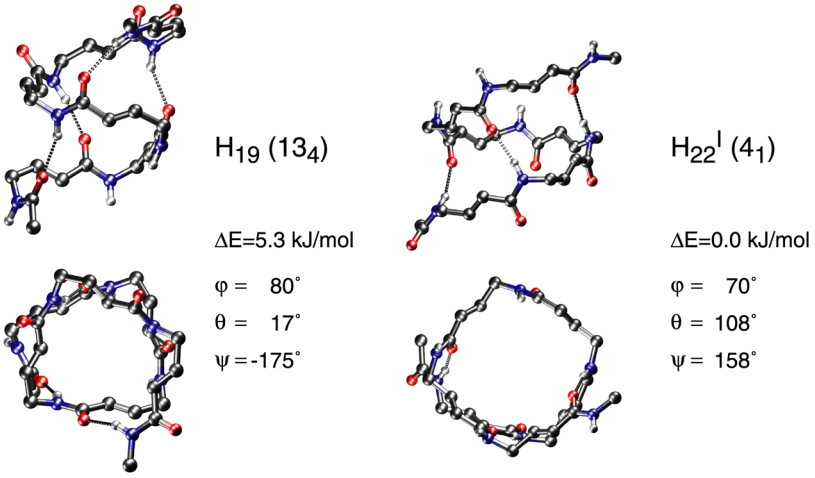

*Fig. 2. Most stable helices in trans vinylogous γ-peptides (**H_{22}^{I}**: E_T= -1949.211533 a.u.).*

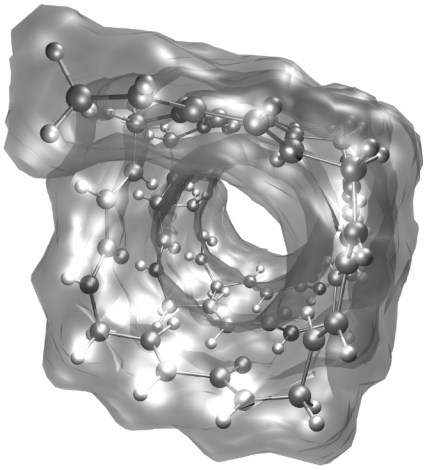

Fig. 3. Model of an undecamer H_{22}^{I} as channel or nanotube.

Contrary to the effects of a *trans* double bond in γ-amino acids, *cis* double bonds should support the formation of smaller, preferably nearest neighbor pseudocycles.

Acknowledgments
This work was supported by DFG (Projekt HO 2346/1 and SFB 610).

Peptide Revolution: Genomics, Proteomics & Therapeutics
Michael Chorev & Tomi K. Sawyer (Editors)
American Peptide Society, 2003

Role of Intramolecular Hydrogen Bonds on the Electron Transfer Rate in Structurally Defined Peptides

Fernando Formaggio[1], Alessandro Moretto[2], Sabrina Antonello[2], Flavio Maran[2] and Claudio Toniolo[1]

[1]Institute of Biomolecular Chemistry, CNR, Department of Organic Chemistry, University of Padova, 35131 Padova, Italy; [2]Department of Physical Chemistry, University of Padova, 35131 Padova, Italy

Introduction

Long-range electron transfer (ET) in proteins relies on the efficiency of the peptide chains to support charge transfer processes. Therefore, understanding how the electron tunneling between a donor (**D**) and an acceptor (**A**) separated by model peptide bridges takes place is an important issue. Although various studies have outlined interesting features of these ET processes, there are still aspects that remain elusive. The effect of the secondary structure is one of them, mostly because of the poor conformational control of the peptide bridges so far employed and/or the absence of intramolecular hydrogen bonding due to the extensive use of Pro residues.

We have recently engaged in research aimed at unraveling the ET dynamics across well-defined peptide bridges. The peptides of choice were Aib homo-oligomers, which are known for their propensity to form rigid 3_{10}-helices because of steric hindrance at the α-carbon and the resulting restricted torsional freedom [1].

Results and Discussion

By using well established electrochemical methodologies we studied the dissociative ET from the **D** end (the phthalimido radical anion donor) of the Aib homo-peptides **1** (Scheme 1) to their **A** end (the peroxide group) [2]. The observed *n*-dependence of the ET rate constant indicates that an increase in the number of Aib units, and therefore in the stability of the 3_{10}-helical structure, results in a more efficient **D**···**A** electron coupling. The trend observed is thus ascribed to an active role played by the intramolecular hydrogen bonds on the ET process. The case of peptide **1** ($n = 3$), illustrated in Figure 1, well-exemplifies this conclusion in that the ET rate increases with respect to those of peptides **1** ($n = 2$ and 1) despite the fact that the **D**···**A** distance would be greater by 2.3 and 3.2 Å, respectively.

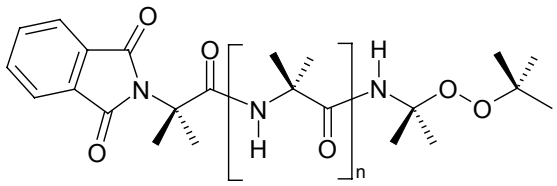

1 (n = 0-6)

*Scheme 1. Chemical structure of **1** (see text for discussion).*

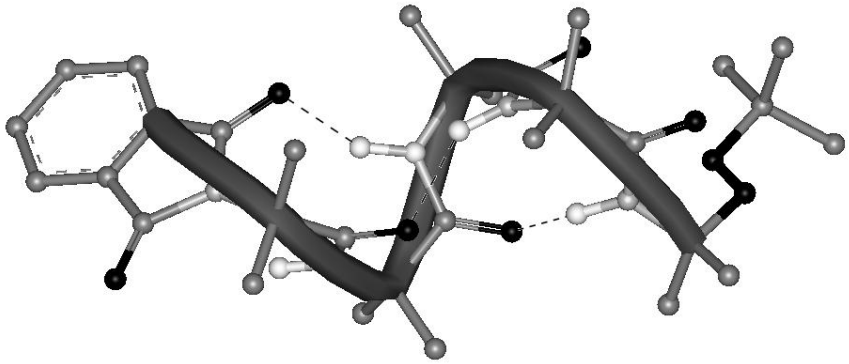

*Fig.1. The peculiar situation which develops for **1** (n = 3) where the same peptide group (between residues 2 and 3) is hydrogen bonded to both **D** and **A**, thereby establishing a particularly efficient ET shortcut.*

The main ingredient that contributes to showing the important effect of the intramolecular hydrogen bonds on the ET rate is the propensity of Aib homo-peptides to form a well-defined and rigid structure. Our study is the first electrochemical investigation of **D**–(peptide bridge)–**A** systems in solution and also the first investigation of a dissociative ET across peptides [3]. We are currently working to alter the energies of the **D**, bridge, and **A** components.

References

1. For a recent review-article, see: Toniolo, C., Crisma, M., Formaggio, F. and Peggion, C. *Biopolymers (Pept. Sci.)* **60**, 396-419 (2001).
2. Moretto, A., De Zotti, M., Scipionato, L., Formaggio, F., Crisma, M., Toniolo, C., Antonello, S., Maran, F. and Broxterman, Q. B. *Helv. Chim. Acta* **85**, 3099-3112 (2002).
3. Antonello, S., Formaggio, F., Moretto, A., Toniolo, C. and Maran, F. *J. Am. Chem. Soc.* **125**, 2874-2875 (2003).

Peptide Revolution: Genomics, Proteomics & Therapeutics
Michael Chorev & Tomi K. Sawyer (Editors)
American Peptide Society, 2003

A Structural Study of a Series of Conformationally Restricted Hexapeptides

Basilio Pispisa[1], Lorenzo Stella[1], Mariano Venanzi[1], Antonio Palleschi[1], Michel Wakselman[2], Jean-Paul Mazaleyrat[2], Ferdinando Fomaggio[3] and Claudio Toniolo[3]

[1]Department of Chemical Sciences and Technologies, University of Roma Tor Vergata, 00133 Roma, Italy; [2]SIRCOB, UMR CNRS 8086, Bât. Lavoisier, Université de Versailles, 78035 Versailles, France; [3]Istituto di Chimica Biomolecolare, C.N.R., Dipartimento di Chimica Organica, Università di Padova, 35131 Padova, Italy

Introduction

Protein-protein and protein-nucleic acid interactions are important naturally-occurring processes [1], involving helical portions of both partners. This explains the current interest in both model peptides containing amino acids with a high helical propensity, such as $C^{\alpha,\alpha}$-disubstituted Gly residues, and the study of conformational equilibria to which they undergo. A rapid identification of the most relevant 3D-structural features of peptides in solution is thus a significant aspect of their investigation, and time-resolved fluorescence spectroscopy represents a valuable tool in tackling this problem, provided that the compounds under study carry appropriate chromophores [2]. This is the case for a series of linear hexapeptides of general formula Boc-B-A_r-T-A_m-O*t*Bu, where A is L-Ala or Aib (α-aminoisobutyric acid), B is (R)-Bin, a binaphthyl-based $C^{\alpha,\alpha}$-disubstituted Gly residue, T is Toac, a nitroxide spin-labeled $C^{\alpha,\alpha}$-disubstituted Gly, and r + m = 4. These peptides are denoted as B-T/r-m, to emphasize the different position of Toac with respect to that of the Bin fluorophore in the amino acid sequence, as shown in Scheme 1. Their structural features were investigated in methanol solution by fluorescence, transient absorption, IR and CD spectroscopies, as well as molecular mechanics calculations.

r = 0, m = 4 (Ala-Aib-Aib-Ala): **B-T/0-4**

r = 1 (Aib), m = 3 (Ala-Aib-Ala): **B-T/1-3**

r = 2 (Aib-Ala), m = 2 (Aib-Ala): **B-T/2-2**

r = 3 (Aib-Aib-Ala), m = 1 (Ala): **B-T/3-1**

Scheme 1. Structures of hexapeptides.

Results and Discussion

The rigidity of the B-T donor-acceptor pair and of the Aib-rich backbone is primarily responsible for the finding that the hexapeptides examined populate very few conformers in methanol solution. By comparing the experimental and theoretical results, the type of secondary structure (right-handed 3_{10}-helix) attained by these peptides in solution was determined, a result not easily achievable when the CD and NMR data are not diagnostic, as in the present case. In addition, the lack of conformational mobility allowed us to investigate the influence of the interchromophoric distance and orientation on the photophysics of B-T/r-m peptides. Dynamic quenching of the excited singlet state of binaphthyl by Toac was successfully

interpreted by the Förster energy transfer model, provided that the mutual orientation of the chromophores is taken into account. This implies that interconversion among conformational substates, which involves puckering of the Toac piperidine ring, is slow on the time scale of the transfer process, i.e., slower than 5 ns. According to molecular mechanics results, the puckering of Toac piperidine ring controls the interprobe distance in the compounds investigated. This, in turn, affects their photophysics, so that a peculiar behaviour is observed. The conformations exhibiting a center-to center distance > 6 Å exhibit long-range dipolar interactions, leading to singlet-singlet energy transfer, while short-range exchange interactions are primarily involved in the conformers with < 6 Å, leading to both non-fluorescent species and highly populated triplet states via an enhanced intersystem crossing process. Among the computed deepest energy structures, there is only one low-energy conformer for each peptide examined, except B-T/1-3, exhibiting a NO·-naphthalene center-to-center distance < 6 Å, which might be assigned to the non-fluorescent complex. In the case of B-T/1-3, the steric arrangement of Toac and Bin in the low-energy conformers is such as to prevent the occurrence of any instantaneous process between the chromophores, because they are lie on the opposite side of the 3_{10}-helix. This is shown in Figure 1, where the sterically most favored structure is illustrated. In the same Figure, the hypothetical non-fluorescent complex of B-T/3-1 is also shown for comparison, whose theoretical population is 56%. In this case, the NO·-naphthalene center-to-center distance is 5.2 Å. The overall results emphasize the versatility of fluorescence experiments in 3D-structural studies in solution.

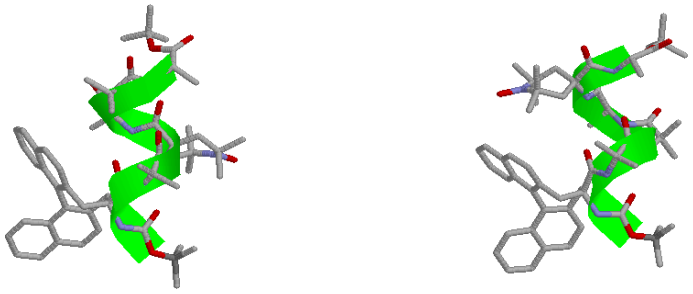

Fig. 1. The sterically most favored structures of B-T/3-1 (left) and B-T/1-3 (right). The ribbon shows the 3_{10}-helical peptide backbone.

Acknowledgments

The financial support of the Italian Research Council (CNR) is acknowledged.

References

1. Hecht, S. M. *Bioorganic Chemistry: Peptides and Proteins* Oxford Univ. Press (1998).
2. Pispisa, B., Palleschi, A., Stella, L., Venanzi, M., Mazzuca, C., Formaggio, F., Toniolo, C. and Broxterman, Q. B. *J. Phys. Chem. B.* **106**, 5733-5738 (2002).

Peptide Revolution: Genomics, Proteomics & Therapeutics
Michael Chorev & Tomi K. Sawyer (Editors)
American Peptide Society, 2003

Solution Structure of Daptomycin

Kenneth S. Rotondi[1] and Lila M. Gierasch[1,2]

[1]Department of Biochemistry & Molecular Biology and [2]Department of Chemistry University of Massachusetts-Amherst, Amherst, MA 01003, USA

Introduction

Daptomycin is a 13-residue anionic lipopeptide antibiotic effective against gram-positive bacteria ($^{1}W^{D}NDTGOD^{D}ADG^{D}SmEKyn^{13}$) and is derived from a fermentation product of *Streptomyces roseosporus*. The lipopeptide is cyclized by an ester linkage between the sidechain of Thr4 and the carboxy-terminal kynurenine (Kyn) residue, while a decanoyl chain caps the amino-terminal Trp1. Daptomycin contains a number of unusual amino acids including ornithine, methylglutamate (mE) and kynurenine, as well as several D-amino acids. The linear three-residue tail and lipid N-cap distinguishes the lipopeptide antibiotic family from other cyclic peptide antibiotics such as gramicidin. Bactericidal activity of daptomycin correlates with dissipation of membrane potential and requires calcium [1], but the details of its mechanism of action are as yet poorly understood. The observation that Ca^{2+} enhances the hydrophobicity of daptomycin suggests that insertion into the lipid membrane is involved in the mode of action [2]. Peptide antibiotics that target the membrane represent a bactericidal mode that is orthogonal to small molecule antibiotics. Indeed, targets of daptomycin have shown no indication of spontaneous resistance [3]. By understanding the biologically active conformation, the so-called pharmacophore, therapeutically superior analogues can be produced through structure-based drug design.

The solution structure of daptomycin will provide a starting point for understanding the conformational propensities of the daptomycin molecule, such as the conformational changes induced by the presence of Ca^{2+} and lipid membranes. Extensive use of proton NMR data provides information on interproton distances (nuclear Overhauser effects, nOes) and intramolecular hydrogen bonding (NH temperature coefficients, $\Delta\delta/\Delta T$). Daptomycin samples were analyzed at concentrations between 1 and 4mM, pH 5.3, 20mM phosphate, 10% D_2O in H_2O. No concentration dependence of NMR signals was observed. NOESY spectra were collected at 10°C with mixing times of 50, 100, 150, 200, 250 and 300ms. The nOe buildup curves were linear through 300ms, indicating that spin diffusion is not occurring during this time period. Molecular dynamics simulations were run with a cvff forcefield [4](no cross terms, no Morse potentials). Restraint energies for nOe derived distances were 20-30 kcal/mol*Å^2.

Results and Discussion

Generation of Qualitative Structure: The NMR evidence suggests that the backbone conformation of daptomycin in solution is well defined with little conformational fluctuation. The fingerprint region of a NOESY spectrum with a mixing time of 300ms displays a number of non-sequential nOes (Figure 1), including structurally significant nOes between Asp7αH-mE12NH and Kyn13αH-Gly5NH. These trans-annular nOes, along with those between Orn6αH and mGlu12α,β, and γ protons (Figure 2) indicate the presence of a hairpin-like structure in the daptomycin ring.. The strongest sequential NN nOe is between Asp9 and G10 (Figure 2) and suggests the presence of a turn centered around ^{D}Ala8-Asp9. This is confirmed by the relatively strong diagnostic

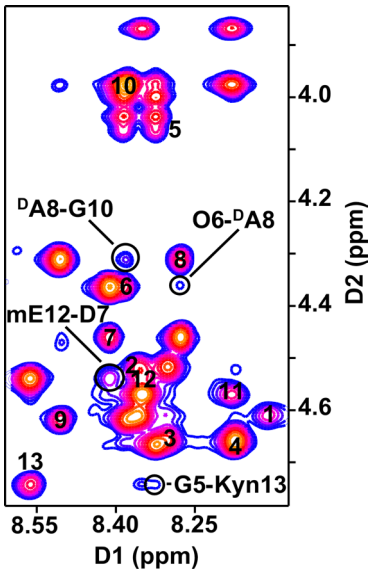

Fig. 1. Daptomycin NOESY NH-Hα region, t_m=300ms, 10°C, with structurally significant nOes circled.

i,i+2 nOe between ^{D}Ala8αH and Gly10NH (Figure 1). The Δδ/ΔT values for daptomycin are generally low (Figure 2) and suggest that both internal h-bonds and mainchain-sidechain via the anionic groups screen these amide groups, enhancing lipophilicity. Several amides have very low Δδ/ΔT values (>2) and are thus well screened from bulk solvent. Two of these, Gly5 and Gly10 (0.4 and 1.8 ppb/°C, respectively) are at the ends of the hairpin and likely participate in cross-strand hydrogen bonds. Notably, the amide proton of Gly5 displays the lowest Δδ/ΔT value in the molecule. The low Δδ/ΔT value for Gly10 provides further evidence for a β-turn in the sequence, ^{7}D^{D}ADG^{10}. The ^{D}Ala residue at the second position of the turn strongly suggests that it is a type II' turn, as this turn type requires the second residue to occupy a positive dihedral ϕ angle. Specific nOes between the aromatic sidechains of Trp1 and Kyn13 imply their interaction forms a hydrophobic cluster. Furthermore, nOes among the protons of the deconoyl N-cap and the aromatic rings of Trp1 and Kyn13 indicate their close spatial proximity, providing further evidence for a hydrophobic cluster in daptomycin. The close interaction of the aliphatic chain with the aromatic systems results in chemical shifts to the aliphatic protons; the atypical, perturbed chemical shifts have precluded specific assignment of the aliphatic tail. The low Δδ/ΔT values for Asp3 and Thr4 are possibly due to their sequestration from bulk solvent from the nearby aromatic residues and aliphatic tail. The NOESY spectrum contains a clear NN Asp7-Kyn13 nOe (Figures 2 and 3) that indicates that the hairpin structure is disrupted.

Structure Refinement: The nOes and hydrogen bonds were used as restraints in molecular dynamics to generate a family of structures consistent with the data. A total of 33 nOes, 11 greater than i,i+4, were used in modeling the daptomycin solution structure. The hydrogen bond acceptor for Gly5 was assigned to mGlu12 based on a nearly regular hairpin structure with a pseudo β-turn centered about Kyn13-Thr4. The interproton distances were quantified using the intensity of the nOe between the Trp1 indole and H7 protons, which have a fixed

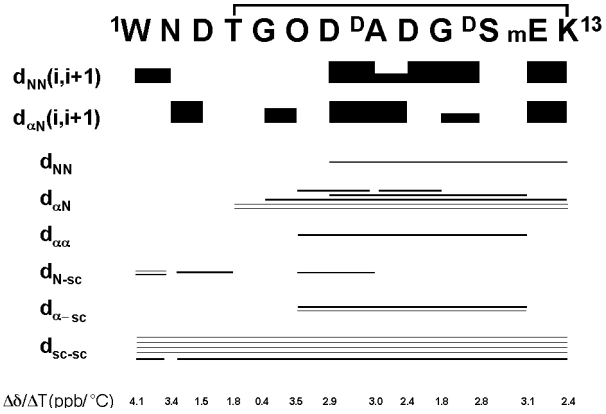

Fig. 2. The sequential and non-sequential nOes of daptomycin and the amide temperature coefficients. The intensity of the nOe is reflected in the thickness of the line.

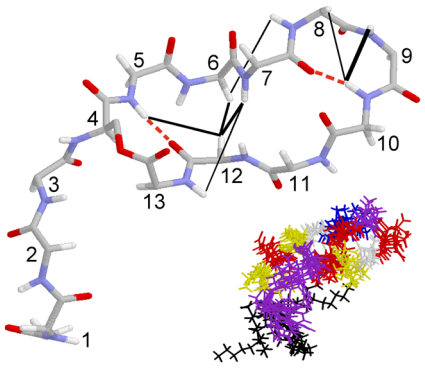

Fig. 3. Backbone depiction of the representative structure of daptomycin showing structurally significant nOes as solid lines and h-bonds as dashed lines.

separation of 2.8Å. Due to the nature of the nOe and the NMR timescale, the distances calculated were converted into restraints with no penalty for interproton distances 1Å less than the calculated distance, with an upper limit of 5Å. In the case of calculated distances greater than 4Å the upper distance was allowed to exceed 5Å. This occurred six times, with no restraint greater than 5.5Å.

A model of daptomycin was built in InsightII (Accelrys), and the structure was energy minimized and subjected to molecular dynamics at temperatures descending from 600 to 298K, with a progressive increase in the restraint energies to their full force at 298K. The simulation continued at 298K with full restraints, followed by energy minimization. The process was repeated to produce a family of 10 structures (Figure 3). With one exception the backbone RMSD of the structures with respect to the average structure are less than 1.3Å, and six are less than 1Å. The outlier was discarded and the remaining family of structures is shown in Figure 3 along with a representative of the conformational family. It had the lowest RMSD from the average structure (0.53), and no restraint violations greater than 0.1Å in the ring and one in the tail. The total restraint energy in this structure is 5.0 kcal/mole.

Several features of the daptomycin solution structure suggest a mechanism for activity. The cluster of hydrophobic elements suggests that this end of the hairpin is buried in the lipid bilayer. Two Asp residues and the mGlu residue dominate the cluster of polar residues at the opposite end of the hairpin resulting in an anionic character in this region of the molecule. The dependence of daptomycin on calcium could be explained by the charge neutralization on the polar end due to Ca^{2+} binding. Initial experiments with physiological concentrations of Ca^{2+} (~50mM) show a significant increase in tendency of daptomycin to aggregate under these conditions. This result is in accord with observations indicating that Ca^{2+} is necessary for membrane insertion. The lack of specific restraints in the aliphatic N-cap portion of the molecule results in considerable structural divergence. However, given the conformational flexibility of this portion of the molecule, it is not unreasonable to assume that, beyond the tendency to associate with the aromatic cluster, there is no single conformation adopted by the aliphatic chain in solution. Daptomycin with its aliphatic tail fully extended is ~40Å long, which is sufficient to severely disrupt the membrane integrity.

Acknowledgments

This work was funded by CUBIST Pharmaceuticals.

References

1. Alborn, W. E., Allen, N. E. and Preston, D. A. *Antimicrob. Agents Chemoth.* **35**, 2282 (1991).
2. Silverman J. A., *et al. Antimicrob. Agents Chemoth*. **45**, 1799 (2001).
3. Silverman, J. A., Perlmutter, N. G. and Shapiro, H. M. *Antimicrob. Agents Chemoth.* In Press.
4. Dauber-Osguthorpe, P., *et al. Proteins: Struct. Funct. Gen*. **4**, 31 (1988).

Peptide Revolution: Genomics, Proteomics & Therapeutics
Michael Chorev & Tomi K. Sawyer (Editors)
American Peptide Society, 2003

One Good Turn Deserves Another: Regular Turns in Peptide and Nucleic Acid Templates

Christian Lehmann
University of Lausanne, ICO-BCH, CH-1015 Lausanne, Switzerland

Introduction

"…Previous discussions of self-duplication have usually involved the concept of a template, or mould... Our model of deoxyribonucleic acid is in effect, a pair of templates." [1]

How far reaching these sentences pronounced 50 years ago by Watson and Crick will have proven to be manifest in the times to come might have only deemed by themselves. Nevertheless, convincing evidence has now been presented for the impact of template control, and this not only in the world of nucleic acids, but also in the world of peptides and proteins. In fact, the structure of the *N*-terminal tandem domain of the GCN4 transcription factor in complex with its operator DNA [2] proves through one single crystal structure (Figure 1) the interplay of template interactions in the transcriptional control of gene expression.

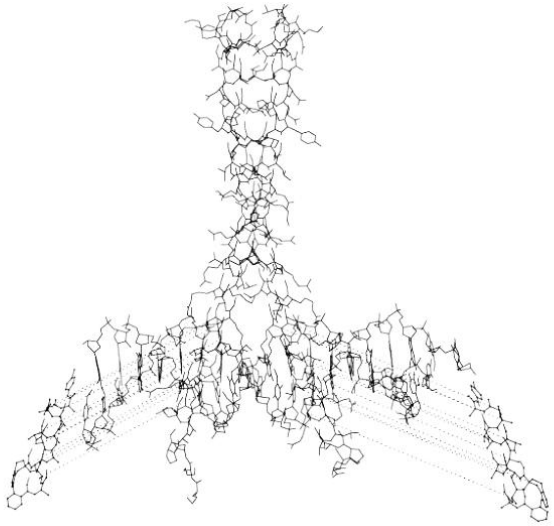

Fig. 1. Illustration of biomolecular template interactions in the complex of N-terminal leucine-zipper GCN4 with its parent operator DNA. Besides tertiary structure DNA-interstrand template pairing as well as tertiary structure peptide coiled-coil template pairing, the principle of secondary structure template α-helix induction through circularized N-cap peptidomimetics (Helix Induction Templates HIT, cf. [3,4,6]) is demonstrated.

The structural basis of regular peptide α-helix induction through secondary structure templates having been established [3,4], further studies accentuate low-molecular weight mimetics of transcription factors [5,6] as well as the extension of microstructural regular turn templates into partially constrained nucleic acid analogues. In this contribution we further feature a particular kind of chirosensitive nucleic acid, the bicyclo[3.2.1]amide nucleic acid [7].

Results and Discussion

The observation of a remarkable CD mirror image switch associated with homoduplex formation of bicyclo[3.2.1]amide nucleic acid as well as with heteroduplexes involving *L*-DNA and *L*-RNA ([7] and ref. cited therein) lead us to undertake a systematical conformational analysis [5,8] of the amide-related norbornane-based nucleic acid constitution involved.

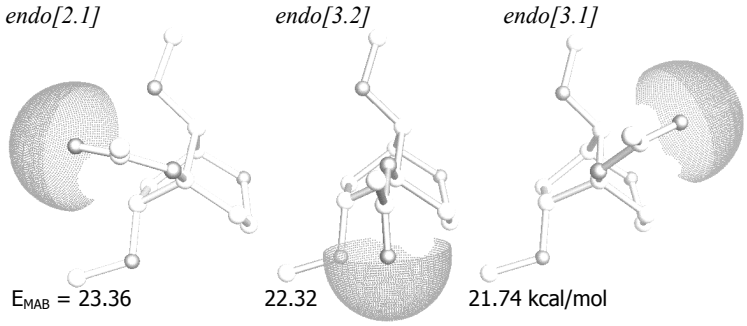

Fig. 2. Conformational analysis of bridgehead amide orientations in bicyclo[3.2.1]amide-NA.

As obtained for the isolated backbone-amide moiety, two out of the three major amide conformers as depicted in Figure 2, notably the two energy minimal orientations, do allow interresidual regular β-turn-like strand-propagation. In dependence of the amide-norbornane interlocking, a *left-* and a right-handed helical pitch is induced, for the *CO-endo[3.2]* and the *CO-endo[3.1]* respectively (Figure 3), both allowing intrastrand amide-H-bonding to link the phosphate-sugar backbone in a contiguously chiral sense.

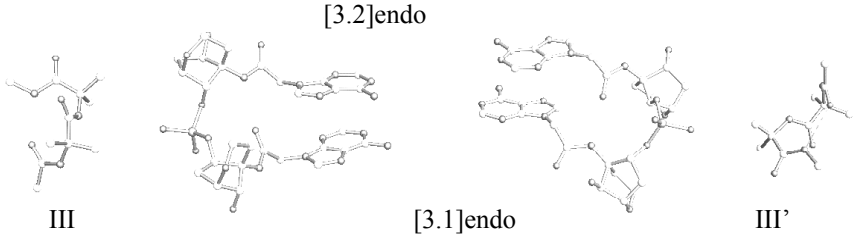

Fig. 3. Left- and Right-handed one-step pitches related by interresidual NA-β-turns; for comparison the regular peptidic types III and III'(mirror) β- turns are juxtaposed.

The basic regular peptide (φ,ψ)-structure elements characterized as belonging to the 3^{10}- or alpha-helical conformational regions α_R in the Ramachandran map according to conventional nomenclature [9] in congruency with the classification obtained by reduction from occurrences in representative protein structures [10], can thus be introduced into backbone restrained nucleic acid constitutions. When such regular arrays are perpetuated as in purely peptidic oligomers (e.g., the regular β-III/3_{10} as described in [11,12]), particular helical structures are adopted and have been characterized by their CD spectral relationship, depending on the chirality of their base-pairing strands. We therefore may extend the concept of conformationally restricted β-turn topologies into amide related phosphate backbone topologies allowing a number of

important applications in the field of antisense RNA, functional genomics and towards inhibitors of a broad range of polymerases such as HIV-polymerase [13].

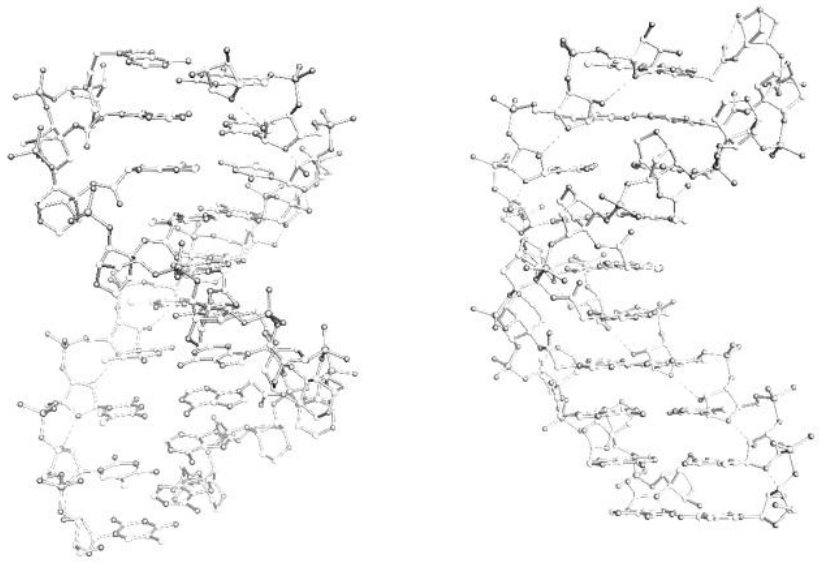

*Fig. 4. Molecular models of left- and right-handed duplexes of bicyclo[3.2.1]amide Nucleic Acid with enantio-*L*-RNA and the natural right-handed* R*-RNA respectively [7].*

References

1. Watson, J. D. and Crick, F. H. C. *Nature* **171**, 966 (1953).
2. Ellenberger, T. E., Brandl, C. J., Struhl, K. and Harrison, S. C. *Cell* **71**, 1223 (1992).
3. Lehmann, C. in Obrecht, D., Altorfer, M., Robinson, J. A. *Adv. Med. Chem.* **4**, 47/50 (1999).
4. Obrecht, D., Altorfer, M., Bohdal, U., Daly, J., Huber, W., Labhardt, A., Lehmann, C., Müller, K., Ruffieux, R., Schönholzer, P., Spiegler, C. and Zumbrunn, C. *Biopolymers* 42, 575-626 (1997).
5. Lehmann C., in *Peptides: The Wave of the Future*, *Proceedings of the 2nd International /17thAmerican Peptide Symposium*, San Diego, California, U.S.A. June 9-14, 2001, Lebl, M. and Houghten, R. A. Eds., 415-417 (American Peptide Society, 2001).
6. Lehmann, C., in *Peptides 2002*, *Proceedings of the 27th European Peptide Symposium*, Sorrento, Italy, August 31 – September 6, 2002, Benedetti, E. and Pedone, C. Eds., 380/1 (Editione Ziino, European Peptide Society, 2002).
7. Ahn, D.-R., Egger, A., Lehmann, C., Pitsch, S., Leumann, C. J. *Chem. Eur. J.* 8, 5312 (2002).
8. Lehmann, C. *Chimia* **54**, 391/469 (2000).
9. Barlow, D. J. and Thornton, J. *J. Mol. Biol.* **201**, 601 (1988).
10. Richardson, J. S. *Adv. Prot. Chem.* **34**, 167 (1981).
11. Karle, I. L., Rav, R. B., Prasad, S. and Balaram, P. *J. Am. Chem. Soc.* **116**, 10355 (1994).
12. Bavoso, A., Benedetti, E., Di Blasio, B., Pavone, V. Pedone, C., Toniolo, C. and Bonora, G. M. *Proc. Natl. Acad. Sci. U.S.A.* **83**, 1988 (1986).
13. Steitz, T. A., Smerdon, S. J., Jäger, J. and Joyce, C. M. *Science* **266**, 2022 (1994).

Peptide Revolution: Genomics, Proteomics & Therapeutics
Michael Chorev & Tomi K. Sawyer (Editors)
American Peptide Society, 2003

Molecular Modeling of Opioidmimetics Containing the Dmt-Tic-Bid Pharmacophores and Docking with the δ-Opioid Receptor

Sharon D. Bryant[1], Severo Salvadori[2], Remo Guerrini[2], Gianfranco Balboni[3], Yunden Jinsmaa[1] and Lawrence H. Lazarus[1]

[1]Peptide Neurochemistry Section, Laboratory of Computational Biology and Risk Assessment, NIEHS, RTP, NC 27709, USA; [2]Department of Pharmaceutical Sciences and Biotechnology Center, University of Ferrara, I44100, Ferrara, Italy; [3]Department of Toxicology, University of Cagliary, 109126, Cagliary, Italy

Introduction

One of the most intriguing new design motifs that has emerged recently in the opioid field involves the pharmacophores 2'6'-dimethyltyrosine (Dmt) and 1,2,3,4-tetrahydroisoquinoline-3-carboxylic acid (Tic). In fact, the incorporation of Dmt into the sequence of opioid peptides resulted in dramatic effects, exemplified by as much as 8500-fold increases in δ-opioid receptor affinity and changes in bioactivity profiles. For example, deltorphin, a δ-receptor agonist, displayed μ-receptor agonist bioactivity after substitution of Dmt for Tyr; similarly, dynorphin A (1-11), a κ-agonist, displayed κ-antagonist/δ-antagonist properties [1]. Furthermore, δ-opioid receptor agonism appeared consistently after the incorporation of 1H-benzimidazole-2-yl (Bid) into the sequence Dmt-Tic peptides [1]. This study utilized two structurally related ligands with diverse bioactivity profiles to investigate potential interactions between the δ-opioid receptor and ligands containing the Dmt, Tic and Bid pharmacophores.

Results and Discussion

The synthesis and receptor binding profiles of the peptides listed in Table 1 have been reported elsewhere [2,3]. Molecular modeling of H-Dmt-Tic-NH-CH(CH_2-Bid)-COOH and H-Dmt-Tic-NH-CH_2-Bid(CH_2-COOH) was based on x-ray structural data reported for H-Dmt-Tic-NH-1-adamantane, a μ-agonist and weak δ-agonist, and *N,N*-$(CH_3)_2$-Dmt-Tic-NH-1-adamantane, a δ-antagonist and weak μ-agonist, [4] and conformational searching of the unique C-terminal substitutions, CH(CH_2-Bid)-COOH and CH_2-Bid(CH_2-COOH) [5]. Unique conformations were arranged into clusters for each compound. Representative conformations from each cluster for the agonist

Table 1. Bioactivity of peptides containing the Dmt, Tic and Bid pharmacophores.

Peptide	Functional Bioactivity (nM)[a]		
	MVD		GPI
	IC_{50}	*Ke*	IC_{50}
H-Dmt-Tic-NH(*R*)CH(CH_3)-Bid	0.026 ± 0.03	-	6.36 ± 0.7
H-Dmt-Tic-NH-CH(CH_2-Bid)-COOH	0.015 ± 0.003	-	1558 ± 153
H-Dmt-Tic-NH-CH_2-Bid(CH_2-COOH)	-	0.27 ± 0.015	3193 ± 402
H-Dmt-Tic-NH-CH_2-CH_2-Bid	-	4.78 ± 0.37	107.5 ± 11.4 [b]

[a]*Data from Balboni et al. [2].* [b]*Data from Balboni et al.[3].*

compound are displayed in Figure 1. The representative conformations were docked into a computationally derived δ-opioid receptor. The receptor was modeled based on x-ray structural data of bovine rhodopsin [6]. Bovine rhodopsin was selected as the parent structure for two reasons: 1) like the δ-opioid receptor it has seven transmembrane regions that span the cell membrane and it couples G-proteins and 2) no other experimental data on the structures of the δ–, μ– or κ-opioid receptors were available.

Docking of the agonist compounds resulted in two regions of binding with the δ-opioid receptor model. One involved receptor residues, Tyr56, Gln105, His301, Tyr129, Trp274 forming interactions with the backbone carbonyl and hydroxyl groups of Dmt, the N-terminal amine, and the C-terminal carboxylic acid of the ligand models. The aromatic rings of Tic and Bid were aligned with Trp274. Another region included receptor residues Arg192, Tyr129, and His278 which formed interactions with the hydroxyl group of Dmt, the N-terminal amine; Tic was oriented toward the aromatic pocket defined by several receptor residues such as, Trp274, Phe270 and Phe222. In contrast, low energy conformers of the antagonist derivatives displayed interactions in only one region of the receptor, similar to the mechanism described for the agonist analogues involving Arg192, Tyr129 and His278. Although mutagenesis studies involving the δ-opioid receptor have indicated that there is not a direct interaction between Asp128 and opioid ligands [7], the docking of Dmt-Tic-Bid pharmacophoric models show that interactions can easily form between the agonist models and Asp128.

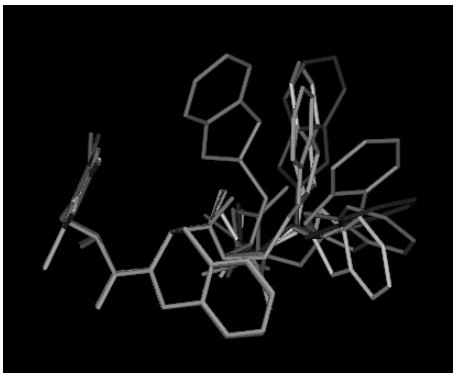

Fig. 1. Superimposition of six low energy structures of H-Dmt-Tic-NH-CH(CH_2-Bid)-COOH, a δ-opioid receptor agonist. Hydrogen atoms are not displayed.

Further studies are in progress to investigate the binding mechanism of δ-opioid receptor agonists and antagonists containing the Dmt, Tic and Bid pharmacophores.

Acknowledgments
The work was funded by the Division of Intramural Research at NIH.

References

1. Bryant, S. D., et al. *Biopolymers (Pept. Sci.)* **71**, 86-102 (2003).
2. Balboni, G., et al. *J. Med. Chem.* **45**, 5556-5563 (2002).
3. Balboni, G., et al. *J. Med. Chem.* **45**, 713-720 (2002).
4. Bryant, S. D., et al. *J. Med. Chem.* **45**, 5506-5513 (2002).
5. Models were computed using software from Accelrys Inc. http://www.accelrys.com/sim/
6. Palczewski, K., T. et al. *Science* **289**, 739-745 (2000).
7. a) Befort, K., L. Tabbara, S. Bausch, C. Chavkin, C. Evans and B. L. Kieffer, Mol. Pharmacol. 49 (1996) 216. b) Befort, K., C. Zilliox, D. Filliol, S. Yue and B. L. Kieffer, *J. Biol. Chem.* **274** (1999) 18574.

Peptide Revolution: Genomics, Proteomics & Therapeutics
Michael Chorev & Tomi K. Sawyer (Editors)
American Peptide Society, 2003

Molecular Dynamics Simulations of BNP Binding to the NPRA Receptor Dimer

B.C. Wilkes[1], A. De Léan[2] and P.W. Schiller[1,2]

[1]Chemical Biology and Peptide Research, Clinical Research Institute of Montreal, 110 Pine Avenue West, Montreal, H2W 1R7, Canada. [2]Department of Pharmacology, University of Montreal, C.P. 6128 Succursale Centre-ville, Montreal, H3C 3J7, Canada

Introduction

The natriuretic peptide receptor A (NPRA) is a member of the membrane bound guanylyl cyclase family of receptors and binding of the natuiuretic peptide ANP to NPRA results in signal transduction through cyclic GMP production. Natriuretic peptides counterbalance the renin-angiotensin system by lowering blood pressure and increasing natriuresis and diuresis. These receptors are constitutively noncovalently dimeric through interaction of both the extracellular and intracellular domains. ANP analogs containing photoaffinity labels at both ends of the peptide were shown to specifically crosslink the receptor dimer, indicating that the peptide must be interacting with both subunits of the receptor [1]. It has been suggested that the initial activation step involves a conformational change in the extracellular juxtamembrane region of this receptor [2].

The X-ray crystal structure of the unbound form of the NPRA receptor was reported as a V shaped dimer [2]. However, the ANP binding region of each monomer in the V shaped dimer was on the lateral face of each monomer in a position not easily amenable to simultaneous contact of ANP with both subunits. A more recent crystal structure of the NPRC receptor dimer with CNP bound was reported [3]. NPRC is the clearance receptor and is not involved in guanyl cyclase activation. CNP and BNP are related members of the ANP family. The CNP-bound NPRC receptor dimer is an A-shaped dimer with the dimerization interface in the membrane-distal lobe, and contains a single CNP molecule within the intersubunit cleft interacting with both receptor subunits. Subsequently, the A-shaped dimer was recognized in the original unbound form of the NPRA crystal structure.

Results and Discussion

We were able to reconstruct the A-shaped form of the NPRA receptor in the unbound form from the original crystal structure. We also constructed the probable bound form of this receptor by replacing each NPRC monomer in the CNP bound NPRC dimer with an NPRA monomer. The bound and unbound forms of this receptor differ in the distance between the membrane-proximal domains of the two forms and therefore in the size of the intersubunit cleft of the dimer. There is an approximately 13 angstrom increase in the distance between the open unbound form and the closed bound form of the NPRA dimer (Figure 1).

Next we inserted the NMR derived solution structure of BNP [4] into these two models of the NPRA receptor dimer. The structure of BNP has been determined by NMR spectroscopy in a membrane-like environment. It is a compact, folded structure stabilized by hydrophobic forces. Using previously determined contact points, including Met173 and His195 of the receptor and the N- and C-termini of the ligand, we manually docked BNP to both the open-unbound and closed-bound form of the

NPRA receptor until reasonable steric complementarity was obtained. These complexes were minimized, and molecular dynamics simulations were performed.

In the case of the open-unbound form of the NPRA dimer, BNP bound to only one of the monomers of the dimer because the distance between the two monomers was too large for the ligand to contact both of the monomers in the complex at the same time. In the case of the closed-bound form of the receptor, BNP fit nicely in the space previously occupied by CNP in the original CNP-NPRC complex. In both cases, the resulting contacts between BNP and the receptor were in agreement with other studies suggesting the close proximity of several amino acid residues of the receptor and of ANP [5, 6]. Each complex was minimized and 100 ps molecular dynamics simulations were performed.

When BNP was bound to the open form of NPRA, BNP induced a 13 angstrom closure of the receptor dimer to a form close to that of the closed form of NPRA. Each monomer of the receptor consists of two major domains linked by a peptide sequence acting as a hinge, allowing the membrane-proximal domains of the dimer to close around the ligand (arrows in Figure 1). In the absence of a ligand, the open form of NPRA remained essentially unchanged after the simulation. Interestingly, the closed form of the NPRA receptor remained closed whether a ligand was present or absent. Taken together, these results support the A-shaped dimer conformation of NPRA that is activated by binding to its ligand, followed by closure of the ligand-receptor dimer complex.

Fig. 1. Models of the NPRA receptor. Left panel represents the open, unbound form and the right panel represents the closed, BNP bound form of the receptor.

References

1. Rondeau, J.- J., McNicoll, N., Gagnon, J., et al. *Biochemistry* **34**, 2130-2136 (1995).
2. Lui, B., Meloche, S., McNicoll, N., Lord, C. and De Léan, A. *Biochemistry* **28**, 5599-5605 (1989).
3. van der Akker, F., Zhang, X., Miyagi, M., Huo, X., Misono, K. S. and Yee, V. C. *Nature* **406**, 101-104 (1999).
4. He, X.- L., Chow, D.- C., Martick, M. M. and Garcia, K. C. *Science* **293**, 1657-1662 (2001).

Carpenter, K. A., Wilkes, B. C., De Léan, A., Fournier, A. and Schiller, P. W., *Biopolymers* **42**, 37-48 (1997).

5. Wilkes, B. C., De Léan, A., Carpenter, K. A. and Schiller, P. W. In Lebl, M. and Houghten, R. A., Eds. *Peptides: The Wave of the Future (Proceedings of the 17th American Peptide Symposium),* American Peptide Society, San Diego, 2001, pp. 900-901.

Peptide Revolution: Genomics, Proteomics & Therapeutics
Michael Chorev & Tomi K. Sawyer (Editors)
American Peptide Society, 2003

The Symmetries in Changes of Conformational Equilibria Thermodynamic Parameters Made by Structure Modifications in Peptides

Boleslaw Picur

Faculty of Chemistry, Wroclaw University, 14 F. Joliot-Curie Str., 50-383 Wroclaw, Poland

Introduction

The special property of processes taking place in living organisms is synchronization. This involves cis/trans isomerization and peptide bond disruption (deacylation), among other modifications, switch the activities of the components in signal transduction cascades enabling communication in cells.

Results and Discussion

Shannon and Weaver mathematically investigated the communication process [1] (see Figure 1a). Their scheme, however, does not contain a important factors from a physical point of view with respect to relations between energy states of components acted in signal transmission. These relations are introduced on Figure 1b. As it is seen on Figure 1b the relations of symmetry are required for the energy states of transmitter and receiver. Similar relation is seen for the receiver before and after the signal transmission. I have expected to found in natural sources the isomeric or modified peptides with above symmetries and I have isolated from seed of *Linum ussitatissimum* the forms of cyclic nonapeptide CLB1 and CLB2 both of sequence cyclo (PPFFVIMLI). These two isomers reveal the opposite thermal effects in CD spectra [2]. It strongly suggests that this pair of isomeric peptides might to be represent the component of signal cascade before (T_0) and after (T_1) signal transmission (see Figure 1b). The spectroscopical data for CLB1 and CLB2 indicate that observed isomerism is caused by cis / trans switch of Met amide bond. This result encouraged me to investigate the influence of chemical modifications on the conformational equilibriums of the side chain of Met residue in model compounds with cis and trans amide bonds (Figure 2a). I have used the "energy level method" [3]. As it is seen in first line of frames (Figure 2b) the Met residue with both trans amide bonds has the mostly populated ***g-*** conformation. This conformation occupies the lowest enthalpy level while the ***t*** form the highest one. This is in opposition to the levels connected to entropy changes (expressed as $-\Delta Sx298$ values). Similar analysis can be done for conformational transitions on Cα-Cβ bond in methionine with cis amide bonds. As it is seen in the second line of frames the effects here are symmetrical to these observed for *trans* amide containing compound. This indicate that *cis/trans* isomerisation of amide bond "switch over" both enthalphy and entropy of conformational levels. The third line of frames present Met with free amino group. This case can give new insight to the "N-terminus rule" [4]. There are no changes in conformational equilibrium visible at the range from 230 K to 330 K. This is giving $\Delta H=0$ and opposite relations in entropic energy levels in comparison to these observed for the first line of frames. The most special case is presented in the last line of frames at Figure 2b. I have discovered that N-formamide moiety in fMet containing peptides is perpendicularly twisted. According to my best knowledge no reports are known for the perpendicularly twisted formamides. All investigated formamides (with fLeu, fVal, fPhe) in at approximate population of 99% appear in this form.

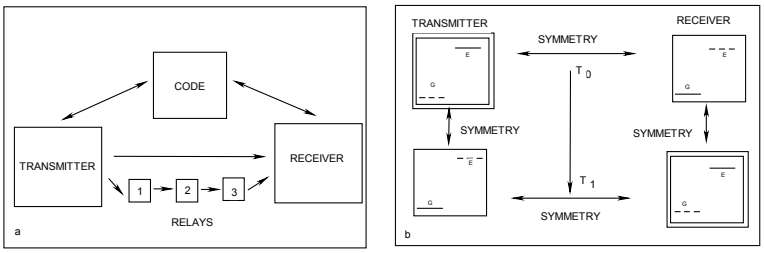

Fig. 1. (a) The communication scheme; and (b) levels changes for transmission.

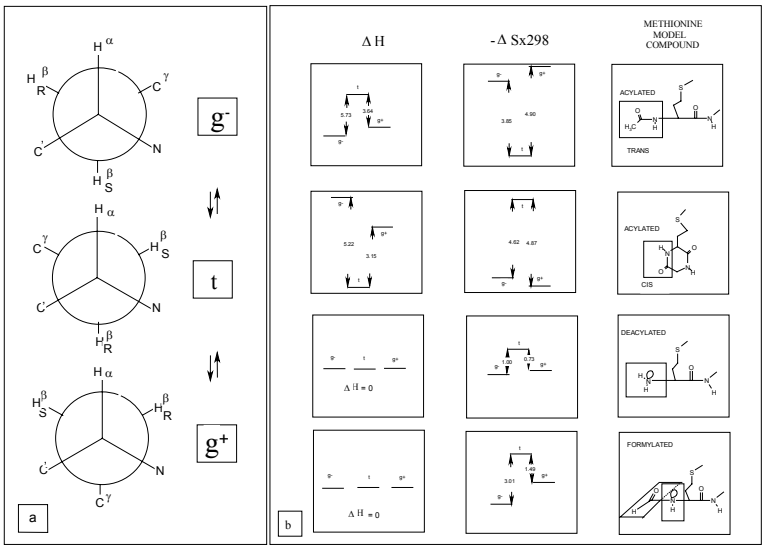

Fig. 2. (a) The conformational transitions on the Cα-Cβ bond at methionine residue; and (b) the conformational energy dependence on the state of methionine nitrogen atom.

Conclusions

The obtained thermodynamical characteristics for conformational equilibriums on methionine residue indicate that cis/trans isomerization and acylation/deacylation create symmetrical changes for conformational equilibriums on the Cα-Cβ bond. The presented symmetry relations are strongly required for living organisms as exemplified by fMet (appears in chemotactic peptides as well as was chosen as the starting residue in *Procariota*) which adopts the perpendicularly twisted form.

Acknowledgements

This work was financially supported by a KBN grant No. 3T09A03618. The Jelfa Pharmaceutical Company S.A. is also greatly appreciated for support this presentation.

References

1. Shannon, C. E., Weaver, W. in *Mathemathical Theory of Communication*, Urbana, (1949).
2. Brzezicka, A., Chliszcz, P., Lisowski, M., Olejarnik, M., Spiewak, K., Siemion, I. Z., Picur B. in *"Chemistry to Agriculture",* Velke Losiny 2001, Czech Republic, pp. 182-187.
3. Jablonski, A. *Nature* **131**, 839 (1933).
4. Bartel, B., Wunning, I. and Varshavsky A. *EMBO J.* **9**, 3179-3189 (1990).

Peptide Revolution: Genomics, Proteomics & Therapeutics
Michael Chorev & Tomi K. Sawyer (Editors)
American Peptide Society, 2003

Tripeptides as Model Systems to Understand the Random Coil Conformation of Peptides and Proteins: Ionized Tri-aspartate and Tri-Glutamate in Water

Reinhard Schweitzer-Stenner[1*], Fatma Eker[2], Cao Xiaolin[3] and Laurence Nafie[3]

[1]Department of Chemistry and [2]Department of Biology, University of Puerto Rico, Río Piedras Campus, P.O. Box 23346, San Juan, PR 00913; USA [3]Department of Chemistry, Syracuse University, Syracuse, NY 13244, USA

Introduction

Ample evidence has been provided in the last years that even small peptides with two or three amino acid residues adopt stable conformations in water [1-5]. This finding is at variance with the conventional view that these biopolymers sample the entire allowed region of the Ramachandran space [6]. Recently, we have developed an experimental and theoretical concept, which utilizes the amide I signal in polarized visible Raman, IR and vibrational circular dichroism (VCD) spectra of tripeptides in solution to determine the dihedral angle of the central amino acid residue. Thus, tri-alanine was found to adopt two conformations in water, namely a very extended β-strand-like (ϕ=-165^o, ψ=150^o) and a polyproline II-like (PPII, ϕ=-60^o, ψ=150^o) structures [4,5]. The latter was identified as an important motif in the unfolded states of many proteins and peptides [7]. Tri-serine exhibits a similar structural propensity, but with a higher population of the extended conformation, which is predominantly occupied by tri-valine[4, 6]. Surprisingly the fully ionized state of tri-lysine was found to adopt a left-handed turn conformation [4, 8], which was interpreted to result from Coulomb interactions between the positively charged residues. If this notion is correct, one can expect similar conformations for peptides with other ionizable side chains. This prompted us to investigate the structure of tri-aspartate (DDD) and tri-glutamate (EEE) in D_2O at pD 7.

The two amide I modes of a tripeptide are coupled via transition dipole and through bond coupling [8]. The corresponding excitonic states are written as:

$$|\chi_-\rangle = \cos\nu|\chi_1\rangle - \sin\nu|\chi_2\rangle$$
$$|\chi_+\rangle = \sin\nu|\chi_1\rangle - \cos\nu|\chi_2\rangle \qquad (1)$$

The parameter ν describes the degree of mixing between the unperturbed states $|\chi_1>$ and $|\chi_2>$. This can be determined from the intensity ratio $R_{iso}=I_{iso}/I^+_{iso}$ of the amide I isotropic Raman scattering. The anisotropic intensity ratio $R_{aniso}=I_{aniso}/I^+_{aniso}$ was used to determine the angle between the peptide normals. The corresponding intensity ratio R_{IR} was employed to obtain the angle between the amide I transition dipole moments. These two geometric parameters were finally used to determine the dihedral angles between the two peptide groups. To check the validity of the analysis, the VCD amide I signal was calculated for the obtained structure and compared with the experiment [4].

Table 1. Spectral and geometric parameter obtained for DDD and EEE at neutral pD.

	DDD	*EEE*
R_{iso}	0.47	0.36
R_{aniso}	1.1	1.03
R_{IR}	1.19	1.05
ρ_-[a]	0.17	0.25
ρ_+[a]	0.11	0.11
$\psi[^o]$	150^o	160^o
$\phi[^o]$	-65^0	-60^0

[a]*depolarization ratios of the out-of-phase (-) and (+) in-phase combination of amide I.*

Results and Discussion

Figure 1 exhibits the amide I' band region in the isotropic, anisotropic, IR and VCD spectra of DDD in D_2O at pD 7. The solid lines result from a self-consistent spectral decomposition. The (IR and Raman) intensity ratios and depolarization ratios relevant for the structure analysis are listed in Table 1. Two pairs of dihedral angles are consistent with the experimental data, namely (ϕ=-125°, ψ=170°) and (ϕ=-85°, ψ=145°). We calculated the VCD spectra for both conformations and found that only the latter reproduce the experimental signal in the amide I^+ region (Figure 1). The overestimation of the amide I^- signal most likely stems from an intrinsic rotational contribution to this mode due to a non-vanishing magnetic transition dipole moment [4]. From our analysis we can therefore conclude that ionized DDD predominantly adopts a PPII-like conformation. This is supported in principle by the corresponding electronic CD spectrum (data not shown), which clearly reflects a left-handed structure although the spectral composition looks somewhat different from the classical PPII spectrum [8].

We have also measured and analyzed the amide I' region in the Raman, IR and VCD spectra of EEE at neutral pD (data not shown). A single-conformer analysis again yields a PPII conformation with ϕ=-60° and ψ=160°. Our data therefore strongly suggest that charged side chains have a high propensity for PPII. This result is somewhat at variance with our earlier finding that KKK adopts a left handed turn structure with its coordinates in the upper right square of the Ramachandran plot. This prompted us to revisit the spectroscopic data of this peptide and, indeed, we identified another structure, which explains our spectroscopic data. Its coordinates are in close proximity to the classical PPII; the corresponding conformation can best be described as an i+1 type II β-turn conformation. A more detailed analysis and discussion of the structure of peptides with charged side chains will be described in a future studies.

Taken together our studies corroborate the use of vibrational spectroscopy as a tool for the quantitative structure analysis of short peptides. These and our earlier data provide conclusive evidence for peptides adopting stable structures in solution, in contrast to conventional wisdom. In concrete terms our data show that, in line with the classical hypothesis of Tiffany and Krimm [9], PPII must be considered as a main motif conformation of the so-called random coil state of peptides and proteins.

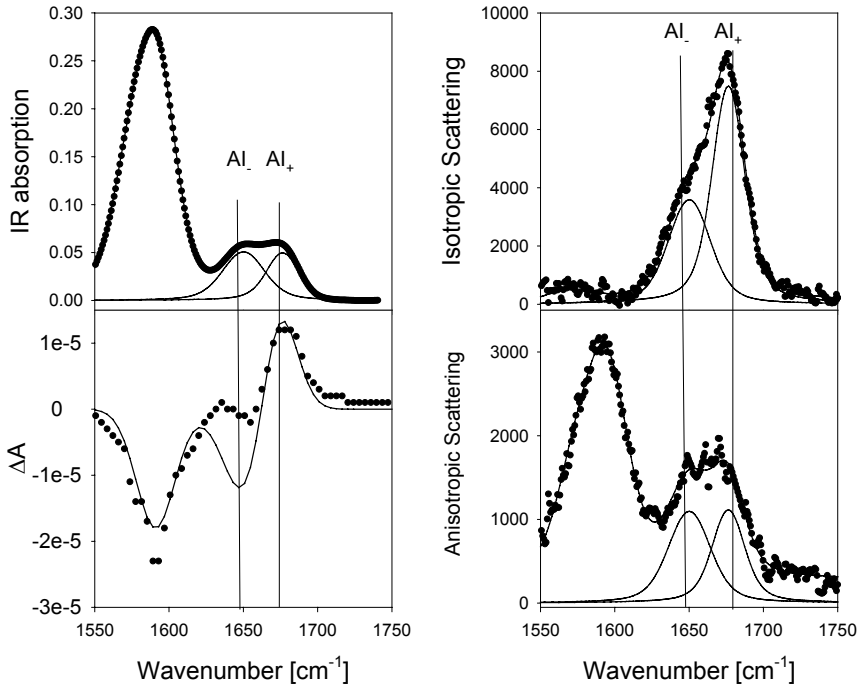

Fig. 1. IR, isotropic and anisotropic Raman and VCD spectra of the amide I' region of DDD. The Raman spectra were measured with 442 nm excitation. The solid lines result from the spectral decomposition (IR, Raman) and from a simulation on the basis of the obtained peptide structure.

Acknowledgments

Financial support was provided from the NIH-COBRE II grant for the Center for Research in Protein Structure, Function and Dynamics (P20 RR16439-01), from the NIH-SCORE grant (S06 GM008102-3052) and from the Fondos Institucionales para la Investigación of the University of Puerto Rico (20-02-2-78-514).

References

1. Han, W.- G., et al. *J. Phys. Chem. B.* **101**, 8595-2602 (1998).
2. Woutersen, S. and Hamm. *J. Phys. Chem. B.* **104**, 11316-11320 (2000).
3. Eker, F., Cao, X., et al. *J. Am. Chem. Soc.* **124**, 14330-14341 (2003).
4. Shi, Z., Olson, C. A., Rose, G. D., Baldwin, R. L. and Kallenbach, N. R. *Proc. Natl. Acad. Sci. U.S.A.* **99**, 9190-9195 (1982).
5. Eker, F., Cao, X., Nafie, L. and Schweitzer-Stenner, R. *J. Phys. Chem. B.* **107**, 358-365 (2003).
6. Wütrich, K. Billeter, M. and Braun. W. J. *J. Mol. Biol.* **180**, 715-724 (1984).
7. Siligardi, G. and Drake, A. F. *Biopolymers* **37**, 281-292 (1995).
8. Eker, F., Griebenow, K. and Schweiter-Stenner, R. *J. Am. Chem. Soc.* **125**, 8178-8185 (2003).
9. Tiffany, M. L. and Krimm, S. *Biopolymers* **6**, 1767-1770 (1968).

Peptide Revolution: Genomics, Proteomics & Therapeutics
Michael Chorev & Tomi K. Sawyer (Editors)
American Peptide Society, 2003

Analysis of Peptide β-Sheet Models Using Chemical Shift Deviations

Niels H. Andersen, R. Matthew Fesinmeyer and F. Michael Hudson

Department of Chemistry, University of Washington, Seattle, WA 98195, USA

Introduction

Designed β hairpins and double hairpins (three-stranded sheets) are currently the best models for β-sheet formation. With the exception of trpzip systems and peptides with D-Pro-Gly at the turn locus, all designed hairpins in the literature are less than 50% folded in water. Due to the problems with NOE interpretation at low fold populations, there have been instances of assignments of different hairpin registers to very similar sequences. This combination of circumstances prompted us to determine the chemical shift characteristics of the three most common types of hairpins so that chemical shifts can be used to determine both preferred register and fold population. Our nomenclature for these systems is ". . (S-2)(S-1)-turn-(S+1)(S+2). . ", with the turn residues set off by hyphens and numbered T1, T2, etc.

Results and Discussion

Our studies focused on NMR-monitored mutational and melting studies of four series of β-sheet models: KKZTVSI-XG-KKITVSA (where Z = Y or L, X=D- or L-Pro, N, or G), the corresponding [4:4] hairpins (KKYTVSX-PATG-KKITVSA), a literature [3:5]-hairpin (SEIYSN-PDG-TWTVSA) [1], and a series of mutants of the second hairpin of the protein G B1 domain. Key data from the first series are shown in Figure 1.

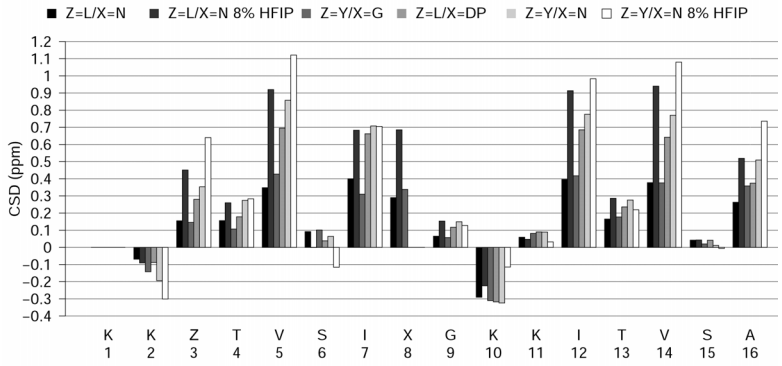

Fig. 1. HN CSDs along the sequence of KKZTVSI-XG-KKITVSA as the hairpin population increases. The effect of HFIP addition is shown for the Z=L/X=N and Z=Y/X=D-P systems; the latter provides the 100%-folded standard.

In the [2;2]-hairpin series, the Z = Leu peptides display lower hairpin populations (smaller CSDs); but the same pattern of CSDs. This indicates that these shifts are the result of backbone, rather than ring-current, effects. Throughout, the chemical shifts for the inwardly directed Hα's (S+/-2,4) move increasingly downfield as the hairpin population increases, with CSDs of 0.9 – 1.0 ppm reflecting 100% folding. For reasons that are not yet clear, those in the C-terminal strand are somewhat smaller in magnitude. The cross-strand H-bonded HNs are shifted downfield by a similar amount, with the exception of the S+1 HN, which is shifted upfield. These patterns are also observed for [3:5]- and [4:4]-hairpins. In [2:2]-hairpins, the HN of the first residue of

the turn consistently displays a downfield shift. The [4:4] hairpin loop is characterized by very large upfield shifts for HNs at T3 and S+1.

The strands of KKYTVSX-PATG-KKITVSA display alignment with the same strand register as the corresponding [2:2]-hairpins when X = His or Asp. The 2nd hairpin of the protein G B1 domain [2], GEWTYD-DATK-TFTVTE, has a Lys at the position that has positive φ,ψ angles. WT GB1 peptide is 40% folded at 5 ºC based on our chemical shift criteria. Core structures incorporating the PATG loop produced GB1 analogs of greatly enhanced stability.

GEWTYN-PATG-KFTVTE	(Tm = 48 ºC)
KKWTYN-PATG-KFTVQE	(Tm = 58 ºC)
KKYTWN-PATG-KWTVQE	(Tm = 67 ºC)
KKWTWN-PATG-KWTWQE	(Tm = 82 ºC)

The same analysis methods were also employed to probe the cooperativity of 3-stranded sheet formation using a series of turn-1 mutants of the Schenck-Gellman model [3]. In the original model both turns were D-Pro-Gly; the responses to mutations at the first turn locus appear in Figure 2. Destabilization of the locus by mutating the T1 position from D-Pro to Gly to L-Pro results in loss of structure-indicating deviations in the first strand, however hairpin CSDs are still observed for the second and third strand even in the most-destabilized system. In particular, note the change in CSDs on the central strand: HN positions (residues 10, 12) that become exposed on fraying of the first hairpin display more dramatic changes in deviation magnitude than those of neighboring residues (11, 13), which maintain intramolecular H-bonds with the third strand. While CSDs are equilibrium measures, they do suggest that folding of the 3-stranded sheet is not fully cooperative. A similar study of the second turn locus resulted in formation of a hairpin between the first and second strands and a disordered third strand. It seems unlikely that fully-cooperative folding would result if neither turn was destabilized.

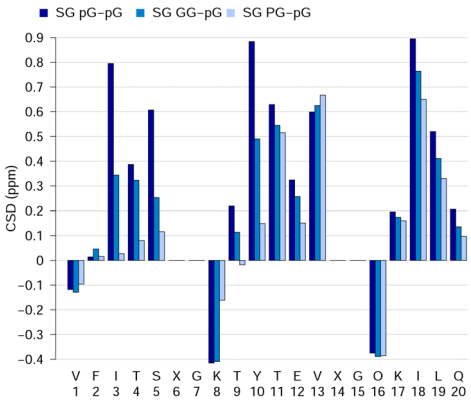

Fig. 2. HN CSDs for the Schenck-Gellman peptide model of a 3-stranded sheet and two mutants in which the first turn (residues 6 and 7) has been destabilized.

Proton chemical shift deviations are under-utilized in the structural studies of peptide hairpins and sheets: unlike other methods, they provide a residue-level profile of structure and are competent for study of ensembles ranging from 10 to 80% folded. Their application, however, requires sequence, temperature, and solvent corrected random coil values. Our CSD calculation method has been compiled into a web-based application, available via our website: http://andersenlab.chem.washington.edu/CSDb.

Acknowledgments

Supported by the grants from the U.S. NSF (CHE-0315361) and NIH (GM-59658).

References

1. de Alba, E., Rico, M. and Jimenez, M. A. *Prot. Sci.* **8**, 2234-2244 (1999).
2. Blanco, F. J., Rivas, G. and Serrano, L. *Nat. Struct. Bio.* **1**, 584-590 (1994).
3. Schenck, H. L. and Gellman, S. H. *J. Am. Chem. Soc.* **120**, 4869-4870 (1998).

Peptide Revolution: Genomics, Proteomics & Therapeutics
Michael Chorev & Tomi K. Sawyer (Editors)
American Peptide Society, 2003

Photodimerization in Peptides for High-Density Optical Data Storage

Rolf H. Berg[1] and P. S. Ramanujam[2]

[1]The Danish Polymer Centre; [2]Optics and Fluid Dynamics Department; Risø National Laboratory, DK-4000 Roskilde, Denmark

Introduction

It is believed that organic materials will be used extensively in future data storage systems. Presently, optical storage technology suffers from an absence of practical organic materials that apply to the next generation of commercially available laser diodes, namely the blue ones that operate between 400 and 500 nm. Looking further into the future, ultra-high density optical storage will move towards the use of even shorter wavelengths.

Photodimerization may be useful for high capacity optical storage in the blue and UV spectra [1]. Here, we have attached photodimerizable chromophores to a short DNO peptide developed for optical storage at visible wavelengths [2]. Experiments have been performed with anthracene and thymine dipeptides at 360 and 257 nm, respectively. The photoinduced change in absorption has been found to be stable both at room temperature, as well as at elevated temperatures. Very good optical quality films can be fabricated.

Results and Discussion

To test the general idea, an ornithine-glycine based peptide containing two neighbouring anthracene side chains (DNO-717, Figure 1) was assembled by standard solid-phase synthesis. A film prepared from the resulting peptide was then irradiated with 360 nm from a krypton ion laser for 60 s. Figure 2 shows the change in the absorption spectrum before and after irradiation. "Bits" recorded at this wavelength have been read out at the same wavelength at reduced intensity for more than 400 cycles without any noticeable deterioration.

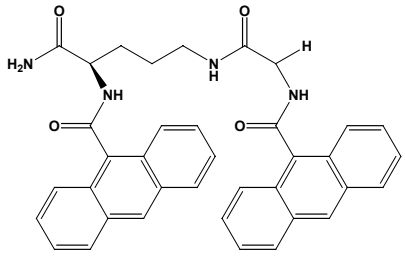

DNO-717

Fig. 1. Ornithine-glycine based peptide functionalized with anthracene side chains.

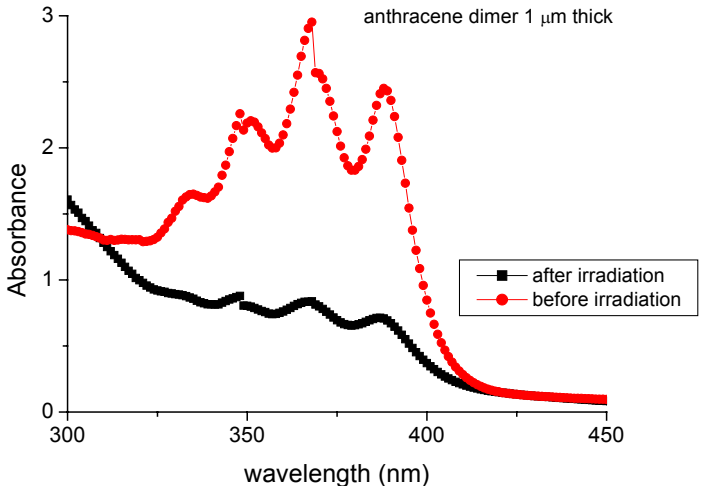

Fig. 2. Photodimerization of anthracenes attached to an Orn-Gly peptide backbone.

It is known that thymine can dimerise via ($2\pi + 2\pi$) cycloaddition on exposure to 266 nm. Photodimerisation of thymine monomers attached to alkyl chains have been proposed as photoresists [3]. A series of thymine containing peptides with varying number of methylene groups in the backbone (based on Dap-Gly, Dab-Gly, Orn-Gly and Lys-Gly, respectively) were prepared and investigated. Films have been made from these peptides and have been irradiated at 248 nm from an excimer laser. The backbone plays a significant role in the photodichroic process. There seems to be a critical backbone length for effective dimerization with an optimum around 6 bonds between the side chains (Orn-Gly). In this case, the absorbance decreases dramatically from approximately 3.0 before irradiation to less than 0.5 after irradiation. The dimers have proved to be extremely stable, withstanding temperatures of greater than 100° C for extended periods of time.

Plane wave gratings have been fabricated in thin films with thymine at 257 nm and in anthracene containing films at 360 nm. The gratings have been stable at room temperature for several years, and have been stable at 100 °C for several days. The materials have also been found to be capable of recording gray levels.

Acknowledgments
The work was funded in part by an STVF grant from the Danish Research Council.

References

1. Tomlinson, W. J., Chandross, E. A., Fork, R. L., Pryde, A. and Lamola, A. A. *Appl. Opt.* **11**, 553-548 (1972).
2. Berg, R. H., Hvilsted, S. and Ramanujam, P. S. *Nature* **383**, 505-508 (1996).
3. Wulff, D. L and Fraenkel, G. *Biochem. Biophys. Acta* **51**, 332 (1961).

Peptide Revolution: Genomics, Proteomics & Therapeutics
Michael Chorev & Tomi K. Sawyer (Editors)
American Peptide Society, 2003

Segmental Isotopic Labeling of RNA Polymerase for NMR Studies

Edmund C. Schwartz[1], Alexander Shekhtman[2], Seth A. Darst[3], David Cowburn[2] and Tom W. Muir[1]

[1]Laboratory of Synthetic Protein Chemistry and [3]Laboratory of Molecular Biophysics, The Rockefeller University, New York, NY 10021; [2]New York Structural Biology Institute, New York, NY 10021 USA

Introduction

The central role of RNA polymerase in biology makes it the subject of much study. Bacterial RNA polymerase is made up of a 4 subunit core enzyme and a regulatory subunit, known as the σ subunit. The σ subunit is required for promoter recognition and also aids in melting the DNA to facilitate transcription. Recent crystal structures have provided insight into the role that the σ subunit plays in transcription, but the first ~100 residues of the subunit had to be removed to allow crystallization [1,2]. The truncated region known as region 1.1 prevents the free subunit from binding DNA. We are using segmental isotopic labeling of the *Thermotoga maritima* σ^A subunit for NMR studies to both determine the structure of region 1.1 and to elucidate the mechanism of DNA binding autoinhibition.

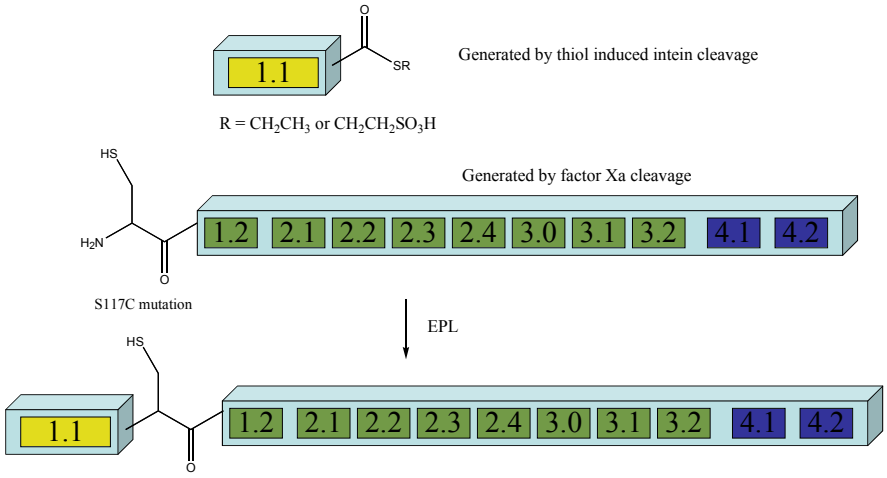

Fig. 1. Synthetic strategy for segmental isotopic labeling.

Regions 4.1 and 4.2, the C-terminus of the σ subunit, are responsible for recognizing and binding the –35 region of the promoter [3]. An earlier study attempted to determine the mechanism of autoinhibition by labeling region 4.2 with ^{15}N and ^{13}C [4]. This labeled protein was fused with the rest of the subunit both with and without region 1.1 through expressed protein ligation (EPL). A change in the NMR spectra of region 4.2 in the presence and absence of region 1.1 would suggest a direct interaction between the two regions. However, no significant difference was seen between the two spectra. The most likely explanation for this observation is that region 1.1 interacts with a region of σ other than region 4.2, for example, regions 4.1 or 3.0.

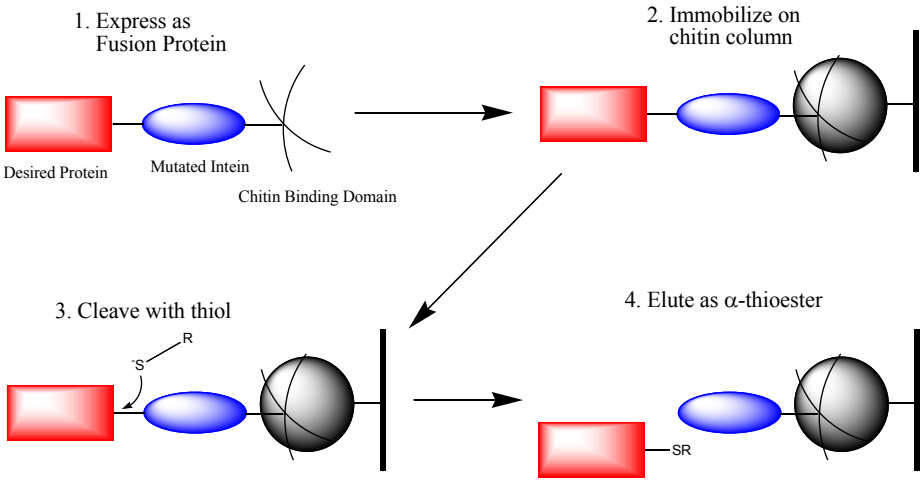

Fig. 2. Expression and purification scheme for labeled N-terminus.

To answer this question, we decided to label region 1.1 to determine the structure of region 1.1 on its own and then to ligate it to the rest of the σ subunit to determine the mechanism of autoinhibition (Figure 1). Region 1.1 was expressed in minimal media containing only ^{15}N and ^{13}C and purified as depicted in Figure 2. NMR spectra obtained indicate an ordered, helical structure (data not shown).

Regions 1.2-4.2 were expressed in unlabeled media. The two proteins were combined with regions 1.2-4.2 in vast excess. A new species that migrated in an SDS gel as an ~45 kDa product was observed which is consistent with the generation of the full length σ subunit.

Spectra of the segmentally labeled protein will soon be obtained. This will provide a solution structure of region 1.1 in the context of the whole subunit and hopefully also give insight into the mechanism of autoinhibition by providing information on where, if anywhere region 1.1 contacts the DNA binding sites.

Acknowledgments

The work was funded by the National Institutes of Health.

References

1. Murakami, K. S., Masuda, S. and Darst, S. A. *Science* **296**, 1280-1284 (2002).
2. Murakami, K. S., Masuda, S., Campbell, E. A., Muzzin, O. and Darst, S. A. *Science* **296.** 1285-1290 (2002).
3. Murakami, K. S. and Darst, S. A. *Curr. Op. Struct. Bio.* **13.** 31-39 (2003).
4. Camarero, J. A., Shekhtman, A., Campbell, E. A., Chlenov, M., Gruber, T. M., Bryant, D. A., Darst, S. A., Cowburn, D. and Muir, T. W. *Proc. Nat. Acad. Sci. U.S.A.* **99.** 8536-8541 (2002).

Peptide Revolution: Genomics, Proteomics & Therapeutics
Michael Chorev & Tomi K. Sawyer (Editors)
American Peptide Society, 2003

Role of Aromatic Residues in the Structure and Biological Activity of the Small Cytokine, Growth-Blocking Peptide (GBP)

Masahito Tada[1], Tomoyasu Aizawa[2], Mineyuki Mizuguchi[1], Katsutoshi Nitta[2], Yoichi Hayakawa[3] and Keiichi Kawano[1]

[1]Faculty of Pharmaceutical Sciences, Toyama Medical and Pharmaceutical University, Toyama 930-0194, Japan; [2]Division of Biological Sciences, Graduate School of Science, Hokkaido University, Sapporo 060-0810, Japan; and [3]Institute of Low Temperature Science, Hokkaido University, Sapporo 060-0819, Japan

Introduction

Growth-blocking peptide (GBP) was first identified as a growth factor that retards the larval development of the armyworm, *Pseudaletia separata*, parasitized by the parasitoid wasp, *Cotesia kariyai* [1, 2]. Injection of GBP into non-parasitized armyworm larvae during the last larval instar retards larval growth and causes a delay in pupation [3, 4]. Recently, GBP has been shown to demonstrate multifunctionality: cell proliferation, stimulation of immune cells (plasmatocytes) and paralysis [5]. GBP homologous peptides have been identified from other lepidopteran species and, based on their consensus amino-terminal sequences (Glu-Asn-Phe-), have been conveniently designated as the ENF peptide family [6]. Although each of these peptide family members was originally identified as a unique biological active peptide [1, 7-9], it has since been demonstrated that some exert multiple activities, such as larval retardation, plasmatocyte-stimulation, and paralysis [6, 10, 11]. Therefore, it seems reasonable to categorize the ENF family peptides as a cytokine family primarily found in insects.

GBP exhibits a strong mitogenic activity on cultured cells, such as insect Sf9 and human keratinocytes. Interestingly, GBP and epidermal growth factor (EGF) are more or less equivalent with respect to their cell proliferation activity in keratinocyte cells [5]. Recent studies have indicated that GBP binds directly to EGF receptors in keratinocytes and phosphorylates their tyrosine residues as EGF upon stimulating mitogenesis of keratinocyte cells [12]. Structural analyses of GBP as well as other ENF peptides using NMR spectroscopy have revealed that they consist of a core region with a striking similarity to the C-terminal β-loop domain of EGF and short disordered N- and C-termini [13-15]. A previous study demonstrated that the minimal structure of GBP-maintaining mitogenic activity is 2-23 GBP, whereas that with plasmatocyte stimulating activity is 1-22 GBP [13]. Further, the GBP mutants having a Glu, Leu or Asn residue at Asp16 lost their mitogenic activity but retained approximately 50% of their plasmatocyte stimulating activity. Based on these results, we conclude that specific residues in the structured and unstructured domains of GBP contribute differently to the biological activities of GBP.

The present studies focused on the three aromatic amino acid residues (Phe3, Tyr11, and Phe23) in the GBP molecule (Figure 1), since these residues are highly conserved among the ENF family peptides. We constructed eight types of point-mutated GBP variants at the aromatic residues and analyzed the relationship between their biological activities and structures.

GBP EN<u>F</u>SGGCVAG<u>Y</u>MRTPDGRCKPT<u>F</u>YQ

Fig. 1. Amino acid sequence of GBP.

Results and Discussion

The results of the hemocyte-stimulating assays of GBP mutants indicate that Phe3 is the key residue in this activity: Ala- or Tyr- replacement resulted in significant loss of the activity, but Leu- replacement did not. The replacements of other aromatic residues had minimal effect on activity. On the other hand, NMR analysis of the mutants suggested that Tyr11 is a key residue for maintaining the core structure of GBP. Surprisingly, the Y11A mutant maintained its biological activity although its native-like secondary structure was disordered (Figure 2-A). Detailed analyses of the ^{15}N-labeled Y11A mutant by hetero-nuclear NMR spectroscopy showed that the native-like β-sheet structure of Y11A was induced by the addition of 2,2,2-trifluoroethanol (TFE) (Figure 2-B). The results suggest that Y11A has a tendency to form a native-like structure, and this property may give the Y11A mutant native-like activity.

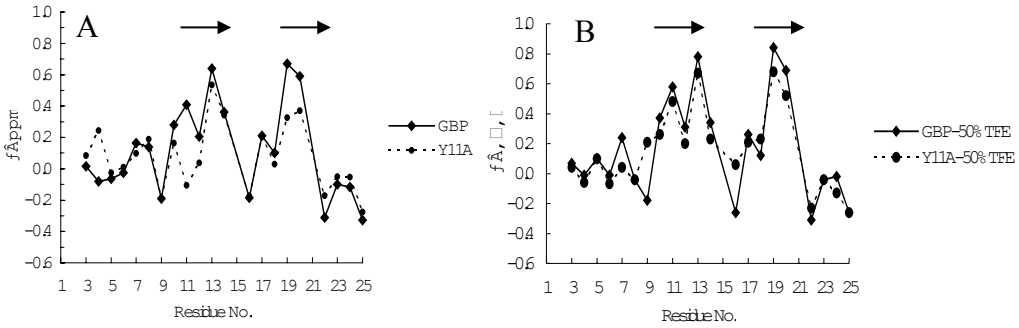

Fig. 2. Chemical shift differences of α-protons of amino acid residues in native GBP and Y11A in TFE solvent. The differences in chemical shift defined as δ(GBP or mutant)- δ(random coil) are plotted. Arrows indicate β-sheet regions. A, In water solution. B, In 50% TFE solvent.

Acknowledgments

This study was supported by the Program for the Promotion of Basic Research Activities for Innovative Biosciences (PROBRAIB), Japan.

References

1. Hayakawa, Y. *J. Biol. Chem.* **265,** 10813-10816 (1990).
2. Hayakawa, Y. *J. Biol. Chem.* **266,** 7982-7984 (1991).
3. Hayakawa, Y. and Yasuhara, Y. *Insect Biochem. Mol. Biol.* **23,** 225-231 (1993).
4. Hayakawa, Y. *J. Insect. Physiol.* **41,** 1-6 (1995).
5. Hayakawa, Y. and Ohnishi, A. *Biochem. Biphys. Res. Commun.* **250,** 194-199 (1998).
6. Strand, M. R., Hayakawa, Y. and Clark, K. D. *J. Insect Physiol.* **46,** 817-824 (2000).
7. Skinner, W .S., *et al. J. Biol. Chem.* **266,** 12873-12877 (1991).
8. Clark, K.D., Pech, L. L. and Strand, M. R. *J. Biol. Chem.* **272,** 23440-23447 (1997).
9. Furuya, K., *et al. Peptides* **20,** 53-61 (1999).
10. Wang, Y., Jiang, H. and Kanost, M. R. *Insect Biochem. Mol. Biol.* **29,** 1075-1086 (1999).
11. Aizawa, T., *et al. J. Biol. Chem.* **276,** 31813-31818 (2001).
12. Ohnishi, A., Oda, Y. and Hayakawa, Y. *J. Biol. Chem.* **276,** 37974-37979 (2001).
13. Aizawa, T, *et al. J. Biol. Chem.* **274,** 1887-1890 (1999).
14. Volkman, B. J., *et al. J. Biol. Chem.* **274,** 4493-4496 (1999).
15. Yu-X. -Q., Prakash, O. and Kanost, M. R. *J. Pept. Res.* **54,** 256-261 (1999).

Peptide Revolution: Genomics, Proteomics & Therapeutics
Michael Chorev & Tomi K. Sawyer (Editors)
American Peptide Society, 2003

Analysis of Structure and Metal Binding Properties of Secretoneurin and Related Peptides by CD and MALDI-MS

A. Basak[1], J. MacAulay[2] and V. Trudeau[2]

[1]Regional Protein Chemistry Center, Diseases of Ageing, Ottawa Health Research Institute, 725 Parkdale Ave, Ottawa, ON K1Y 4E9; [2]Department of Biology, University of Ottawa, Canada

Introduction

Secretoneurin (SN) is a highly conserved 33/34 amino acid neuropeptide that is generated from its precursor secretogranin-II (SgII), also called chromogranin-C by the proteolytic actions of proprotein convertase PC1 and carboxypeptidase-E. Recently we isolated SN from goldfish (gf) pituitary and showed that it is involved in the release of luteinizing hormone from pituitary [1]. Others have shown that SN stimulates dopamine release in rat brain and is involved in tumorigenesis [2]. Since binding of chromogranins to Ca^{+2} is partially responsible for their biological activities [3], we became interested to study the metal binding property and its effect on secondary structure of gfSN by circular dichroism (CD) and MALDI-mass spectrometry.

Results and Discussion

gfSecretoneurin (SN_{34}), located within the segment gfSgII$^{215\text{-}248}$ [^{215}TNENAAEEQ-YTPQKLATLQSVFEELSGIAASNANS^{248}] and a 15-mer peptide (SN_{15}) derived from its central region, gfSgII$^{223\text{-}237}$ [^{223}YTPQKLATLQSVFEE^{237}] as well some selected Ala-mutants (indicated by underline) were prepared. The mutation sites were chosen on the basis of modeling studies and the notion that charged and/or hydrophobic residues might play crucial roles on the metal binding and secondary structures that are considered crucial for biological function of SN_{34}. Among various alkali, alkaline earth and transition metal ions tested [4], mainly Cs^{+1} and to some extent Na^{+1}, K^{+1}, Cu^{+2} and Ca^{+2} ions bind with both SN_{34} and SN_{15}. Thus SN_{34} [molecular weight (mw)=3652] forms mono (major, mw=3785) and bis- (mw=3918) adducts upon incubation with CsCl (1:1 molar ratio) in 25mM Tris+25mM Mes, pH 7.0 at 37^0C (Figure 1A). A similar observation is also noted with SN_{15} (mw=1652), which forms mainly a mono Cs-adduct under identical conditions (Figure 1B). The optimal pH for Cs-binding is 5-7. At pH <4 or >8, no noticeable binding is observed. The results indicated that SN_{34} binds to Cs^{+1} via amino acids located at the central region gfSgII$^{223\text{-}237}$. MS data on various SN_{15}-mutants indicated that Glu-14 is most crucial for its binding, since its substitution by Ala led to a ~7-fold decrease in bound form while replacement of hydrophobic residues at positions 6 or 12 resulted in only ~1.8-2 fold decrease in Cs-adduct formation. The substitution of Glu-15 had only marginal effect.

Despite differences in Cs^{+}-binding ability, the secondary structures of SN_{15} and $SN_{15}A_{14}$ in water at pH 7 are quite similar to one another. Thus, based on analysis by CD spectra using contin and CD estima programs, they exhibit helix (hx)=0%, turn (t)=5-20%, β-sheet (s)=0-5% and random (r)=75-95% conformations. This differs significantly from that of SN_{34} which under identical conditions exhibited hx=2%, t=8%, s=40% and r=50%. Upon binding with Cs^{+1} all peptides showed changes in their

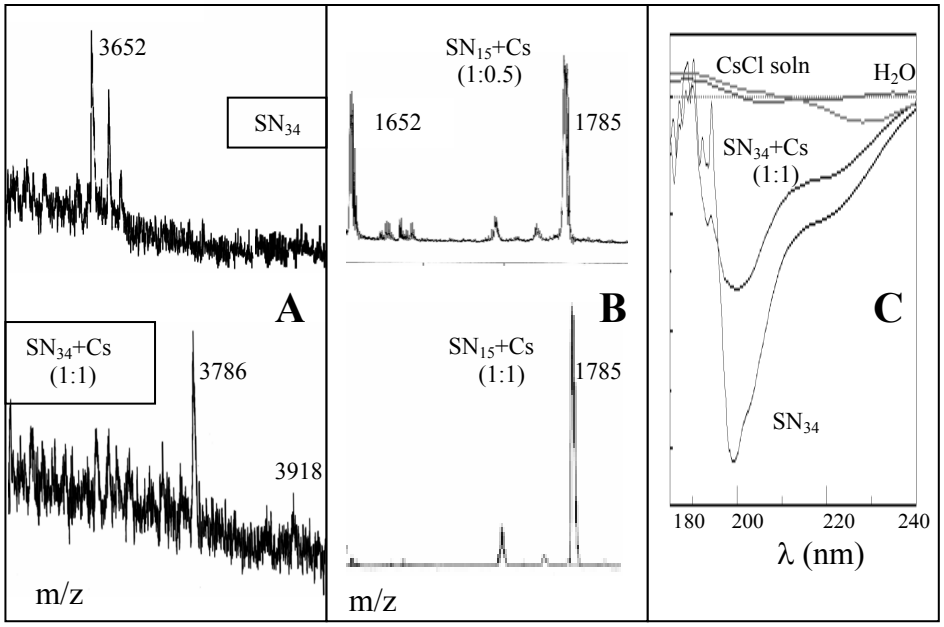

Fig. 1. Panel A: MALDI-MS of SN_{34} in absence (top) and presence of equimolar (bottom) amount of Cs^{+1} ion. Panel B: MALDI-MS of SN_{15} in presence of half (top) and equimolar (bottom) amounts of Cs^{+1}. Panel C: CD spectra of SN_{34} in absence and presence of equimolar amount of Cs^{+1} ion.

CD spectra, with SN_{34} being the one maximally affected. Based on analysis of CD spectra, SN_{34} exhibited a loss of sheet and increase in helix and turn structures (Figure 1C). Although the biological significance of Cs-binding of SN is unclear, alteration of its biological activity through interactions with endogenous ions such as Cu^{+2}, Ca^{+2} or K^{+1} may have important implications in normal and pathological conditions [4].

Acknowledgments

This work was funded by grants from Ottawa University (interfaculty), NSERC and CFI, Canada.

References

1. Blazquez, M., Bosma, P. T., Chang, J. P., Docherty, K. and Trudeau, V. L. *Endocrinology* **139**, 4870-4880, (1998).
2. Fischer-Colbrie, R., Laslop, A. and Kirchmair, R. *Progress In Neurobiology* **46**, 49-70, (1995).
3. Samia, M., Larivière, K. E., Basak, A. and Trudeau, V. L. 14th International Congress of Comparative Endocrinology, Sorrento (Napoli), Italy, May 26-30, p 655-661, (2001).
4. Dreost, I. E. and Smith, R. M (Eds.) *Neurobiology of the Trace Elements* Humana Press, (1983).

Peptide Revolution: Genomics, Proteomics & Therapeutics
Michael Chorev & Tomi K. Sawyer (Editors)
American Peptide Society, 2003

Effect of 4-Fluoroproline in the X-Position on the Stability of the Collagen Triple Helix

Jonathan A. Hodges[1] and Ronald T. Raines[1,2]

[1]Department of Biochemistry; [2]Department of Chemistry; University of Wisconsin–Madison, Madison, WI 53706, USA

Introduction

Collagen consists of three polypeptide chains that fold into a triple helix. Each natural chain contains many repeats of the sequence: XaaYaaGly, in which a third of the Xaa and Yaa residues are (2*S*)-proline (Pro). The pucker of a proline ring can be influenced by electronegative substituents, such as the hydroxyl in the naturally occurring residue, (2*S*,4*R*)-4-hydroxyproline (Hyp) [1,2]. This effect is stereoelectronic, as it depends on the configuration and electron-withdrawing ability of the substituent. In particular, the *gauche* effect exerted by an electron-withdrawing 4*R* substituent stabilizes the C^{γ}-exo pucker, and that by a 4*S* substituent stabilizes the C^{γ}-endo pucker. The degree of stabilization is likely to be greatest for fluorine, the most electronegative of atoms.

The thermal stability of the triple helix is increased by replacement of proline in the Yaa position with Hyp [3] and, to a greater degree, (2*S*,4*R*)-4-fluoroproline (Flp) [4]. Molecular modeling of a triple helix of $(ProProGly)_{10}$ strands has suggested that Pro in the Xaa position prefers to adopt a C^{γ}-endo pucker, whereas Pro in the Yaa position prefers a C^{γ}-exo pucker [5]. This pattern has been observed in a crystalline $(ProProGly)_{10}$ triple helix [6]. The pyrrolidine ring pucker influences the range and distribution of the ϕ and ψ main-chain dihedral angles of Pro, and can fix those dihedral angles for optimal packing of the triple helix. Increasing the preference for the desired C^{γ}-exo conformation in the Yaa position by inclusion of either Hyp or Flp decreases the entropic penalty for triple-helix formation. Likewise, Hyp and Flp increase the preference of the ω main-chain dihedral angle for the *trans* ($\omega = 180°$) conformation [7]. Because all peptide bonds in collagen are *trans*, preorganization of ω by Hyp and Flp decreases the entropic penalty for triple-helix formation.

Results and Discussions

Can triple-helix stability be increased by fixing the ring pucker of proline in the Xaa position? We synthesized peptides with both diastereomers of 4-fluroproline in the Xaa position [8]. Circular dichroism spectroscopy indicates that only $(flpProGly)_7$, where flp refers to (2*S*,4*S*)-4-fluoroproline, forms a stable triple helix at 5 °C. During thermal denaturation, $(flpProGly)_7$ exhibits a cooperative transition characteristic of a triple helix (Figure 1). The midpoint of this transition is at 33 °C. The linear decrease in elipticity by $(FlpProGly)_7$ is characteristic of the unfolding of a single polypeptide chain. Sedimentation equilibrium experiments confirm that $(FlpProGly)_7$ but not $(flpProGly)_7$ is a monomer at 4 °C, whereas both peptides are monomers at 37 °C.

Apparently, stereoelectronic effects can operate adventitiously (or deleteriously) in the Xaa position of collagen. There, flp is able to preorganize the ϕ and ψ dihedrals as in a triple helix without encountering the steric conflicts that appear to plague (2*S*,4*S*)-4-hydroxyproline (hyp) in this position [6,9]. Moreover, the 4*S* substituent in the Xaa position has limited access to solvent, thus making fluoro better suited than hydroxyl to occupy this position. Altogether, the gain in stability upon replacing hyp with flp in the Xaa position exceeds that of replacing Hyp with Flp in the Yaa position (Figure 1).

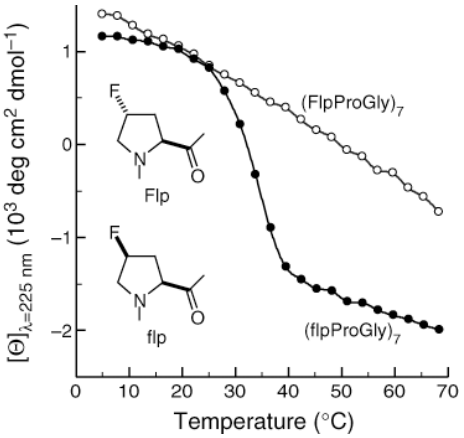

	T_m (°C)	
Xaa/Yaa	$(XaaProGly)_7$	$(ProYaaGly)_7$
Flp	no helix [8]	45 [7]
Hyp	no helix [10]	36 [7]
Pro	6–7 [11]	6–7 [11]
Hyp	no helix [9]	no helix [9]
flp	33 [8]	no helix [7]

Fig. 1. (Left) Thermal denaturation curves determined by measuring molar elipticity at 225 nm as a function of temperature [8]. (Right) Effect of 4-hydroxyproline (Hyp and hyp) and 4-fluoroproline (Flp and flp) diastereomers on the conformational stability of a collagen triple helix with $(XaaYaaGly)_7$ strands. "No helix" refers to T_m < 5 °C. Results with Hyp in the Xaa position and hyp in both the Xaa and Yaa positions are for $(XaaYaaGly)_{10}$ strands.

Because the stability of $(flpProGly)_7$ exceeds that of $(FlpProGly)_7$, the preorganization of ϕ and ψ in the Xaa position is more important than is the preorganization of ω [8]. This constraint could be less important for proline-poor regions of the triple helix, in which a non-proline residue occupies the Xaa or Yaa position. The structure of a collagen mimic indicates that proline-rich and proline-poor regions have a distinct triple-helical twist [12], which suggests that the factors that control stability could differ for these regions. Indeed, replacement of proline in the Xaa position with Hyp does increase the stability of a proline-poor region [13].

Hence, the conformational stability of collagen can be enhanced by stereoelectronics effects. We anticipate that the rational use of stereoelectronic effects could be used to enhance the conformational stability of other proteins as well.

Acknowledgments

This work was supported by grant AR44276 (NIH). J.A.H. was supported by postdoctoral fellowship AR48057 (NIH).

References

1. DeRider, M. L., *et al. J. Am. Chem. Soc.* **124**, 2497–2505 (2002).
2. Improta, R., Benzi, C. and Barone, V. *J. Am. Chem. Soc.* **123**, 12568–12577 (2001).
3. Sakakibara, S., *et al. Biochim. et Biophys. Acta* **303**, 198–202 (1973).
4. Holmgren, S. K., *et al*. *Nature* **392**, 666–667 (1998).
5. Improta, R., *et al. J. Am. Chem. Soc.* **124**, 7857–7865 (2002).
6. Vitagliano, L., *et al. Biopolymers* **58**, 459–464 (2001).
7. Bretscher, L. E., *et al. J. Am. Chem. Soc.* **123**, 777–778 (2001).
8. Hodges, J. A. and Raines, R. T. *J. Am. Chem. Soc.* **125**, 9262-9263 (2003).
9. Inouye, K., Sakakibara, S. and Prockop, D. J. *Biochim. Biophys. Acta* **420**, 133–141 (1976).
10. Inouye, K., *et al. Arch. Biochem. Biophys.* **219**, 198–203 (1982).
11. Shaw, B. R. and Schurr, J. M. *Biopolymers* **14**, 1951–1985 (1975).
12. Kramer, R. Z., *et al. Nat. Struct. Biol.* **6**, 454–457 (1999).
13. Bann, J. G. and Bächinger, H. P. *J. Biol. Chem.* **275**, 24466–24469 (2000).

Peptide Revolution: Genomics, Proteomics & Therapeutics
Michael Chorev & Tomi K. Sawyer (Editors)
American Peptide Society, 2003

Synthesis and Calcium Binding of Oligomeric Tropoelastin Analogs

Hiroaki Kodama[1], Shuhei Ueno[1], Satoshi Osada[1], Iori Maeda[2], Kouji Okamoto[2] and Michio Kondo[3]

[1]*Department of Chemistry, Saga University, Saga, Saga 840-8502, Japan;*
[2]*Kyushu Institute of Technology, Iizuka, Fukuoka 820-8502, Japan; and*
[3]*Nishikyushu University, Kanzaki, Saga 842-8585, Japan*

Introduction

Elastin, the core protein of the elastic fiber, is formed by cross-linking of tropoelastin that is a soluble precursor protein of elastin [1,2]. Aqueous solutions of soluble elastins, α-elastin, tropoelastin, and synthetic model peptides are clear and homogeneous at below room temperature, but on heating to body temperature or above the solutions become turbid *in vitro*. This process is called "coacervation" and is a reversible process based on intra and/or intermolecular hydrophobic interaction [3,4].

The hydrophobic regions of Tropoelastin contain distinct peptide repeating sequences. Among these peptide sequences, the pentapeptide Val-Pro-Gly-Val-Gly (VPGVG) repeating sequence is thought to largely contribute to the elastic function [5]. We have previously reported the synthesis and cation bindings of polypentapeptide H-(Val-Pro-Gly-Val-Gly)$_n$-Val-OMe (PPP) [6,7]. In the present study, to develop the tropoelastin-like peptides for the investigation of cation binding by spectroscopic studies, we synthesized dimeric analogs of pentapeptide (DPP-N) and their corresponding monomeric peptides (PP-N) by solid-phase method (Figure 1).

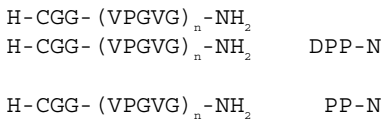

Fig. 1. Structures of synthetic tropoelastin analogs, dimeric pentapeptide (DPP-N) and monomeric pentapeptide (PP-N). N denotes the numbers of amino acid residues.

Results and Discussion

Peptide Synthesis and Purification. Peptide synthesis was carried out through a stepwise solid-phase peptide synthesis utilizing Fmoc-chemistry on Rink-amide resin. Fmoc amino acid was activated with HBTU-HOBt in the presence of DIEA. Coupling reaction using a 10-fold excess of amino acids was carried out for 30 min. The Fmoc group was removed by piperidine. After chain elongation, the resin was treated with TFA. Dimerization was carried out by air-oxidation, monitored by HPLC. The thiol group of monomeric peptides was protected by acetoamide methyl group to avoid the unexpected dimerization though the formation of disulfide bond. The precipitated peptide by the addition of cold ether was purified by preparative HPLC. Homogeneities and structures of the peptides were confirmed by analytical HPLC, amino acid analysis and MALDI-TOF MS.

Secondary Structures. Conformational analysis of peptides was performed by CD spectroscopy. It was found that dimeric peptides took on highly ordered structures (Figure 2), and the structure of the peptides increases with an increase in chain-length. It was found that no significant changes of the CD spectra were observed on the addition of Na^+ and K^+ ions but Ca^{2+} and Mg^{2+} ions induced significant conformational

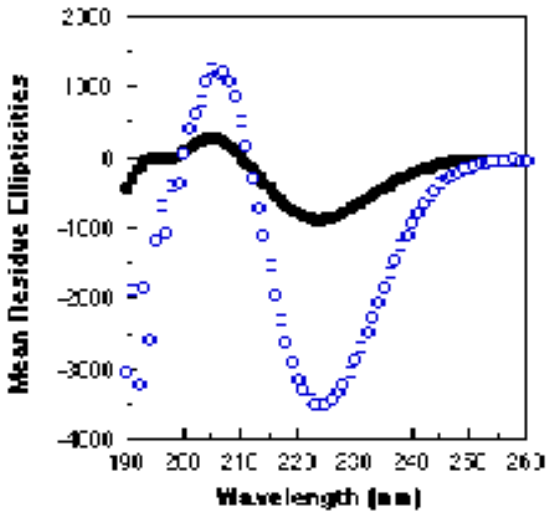

Fig. 2. CD spectra of synthetic tropoelastin analogs, DPP-30 (open circle) and PP-30 (close circle) in 97%TFE.

changes of the dimeric and monomeric oligopentapeptides. This result was compatible with the interaction of PPP and Ca^{2+} ion previously reported [6,7].

Coacervation Profiles. Coacervation was monitored as turbidity at 300 nm. Peptides were dissolved in H_2O (1 mg/ml). Turbidities which are caused by coacervation were not found for the dimeric peptides. Urry *et al.* reported that the coacevation of polypentapeptide occurs predominantly by intermolecular hydrophobic association [3]. In the present study, the chain lengths of dimers were not enough to make coacervates; however, the conformations of dimers were similar to those of PPP to interact specifically with calcium ions.

Acknowledgments

The authors wish to thank to Professor Seiji Ysuda and Dr. Hideki Ohba of AIST Kyushu (Tosu, Saga) for the MALDI-TOF MS measurements.

References

1. Ross, R., *J. Histochem. Cytochem*. **21**, 199-208 (1976).
2. Urry, D. W.,*Angew. Chem. Int. Ed. Engl*. **32**, 819-841 (1993).
3. Urry, D. W. *J. Protein Chem*. **7**, 1-34 (1988).
4. Vrhovski, B., Jensen, S. and Weiss, A. S. *Eur. J. Biochem*. **250**, 92-98 (1997).
5. Urry, D. W., Mitchell, L. W., Ohnishi, T. and Long, L. L. *J. Mol. Biol*. **96**, 101-107 (1975).
6. Kondo, M., Nakashima, N., Kodama, H. and Okamoto, K. *J. Biochem*. **101**, 89-94 (1987).
7. Kaibara, K., Akinari, K., Okamoto, K., Uemura, Y., Yamamoto, S., Kodama, H. and Kondo, M. *Biopolymers* **39**, 189-198 (1996).

Peptide Revolution: Genomics, Proteomics & Therapeutics
Michael Chorev & Tomi K. Sawyer (Editors)
American Peptide Society, 2003

Unique Structural Elements Profoundly Influence the Conformation of SOM230

Lukas Oberer[1], Gianluca Interlandi[2], Amedeo Caflisch[2], Günter Bovermann[1], Claus Ehrhardt[1] and Ian Lewis[1]

[1]Core Technologies and Transplantation Research Department, Novartis Pharma Basel
[2]Department of Biochemistry, University of Zürich

Introduction

The synthesis of Somatostatin (SRIF-14) peptide mimetics with uniformly high affinity to all of the sst1-5 receptors is a challenging goal for medicinal chemists. A rational approach has successfully lead to the discovery of SOM230 c-[(2-amino-ethyl-carbamoyl)-HyPro[1]-Phg[2]-D-Trp[3]-Lys[4]-(4-O-benzyl)-Tyr[5]-Phe[6]]. Since receptor binding sites and bound conformation structures of the ligands are unknown, 3D-structure determination of the ligands in solution and in crystalline form were made to improve understanding of structure / activity relationships. The 3D-structure determination of SOM230 in solution was made on the basis of NMR and molecular dynamics simulation. This allowed the comparison of the resulting structure with the structure of SMS201-995 a compound which is used for the treatment of acromegaly and certain gastrointestinal tumors (Figure 1).

SOM230 SMS201-995

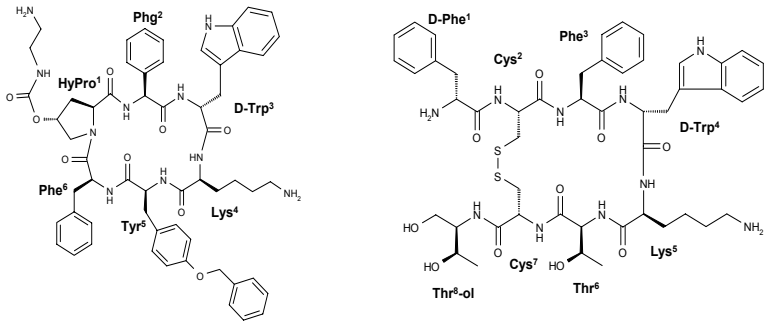

Fig. 1. Structures of SOM230 and SMS201-995.

Results and Discussion

The four structural backbone NOE's detected in the NOESY spectrum of SOM230 in H_2O were assigned to Phg[2]-NH/Phe[6]-α (medium), Phe[6]-α /HyPro[1]-α (medium to strong), Phg[2]-2',6'/ HyPro[1]-γ (weak), Tyr[5]-NH/Lys[4]-NH (strong), and the temperature coefficient of Phg[2]-NH indicated a hydrogen bond. The molecular dynamics simulations were performed with the program CHARMm (Axelrys all-hydrogen force field) and the initial conformation was generated from an NMR-structure of a similar peptide with a His instead of a Phg in position 2. The peptide was inserted into a cubical water box of 37.2A length containing 1728 molecules with periodic boundary conditions. Four simulations were performed. The total simulation time was 46ns (22 and 24ns for each simulation) and 36 ns (29ns and 7ns) at 300K and 330K, respectively. In the four simulations, all of the four experimentally measured NOE

distances are satisfied. The H bond between Phg^2-NH and Tyr^5-CO is present most of the time during the simulation (a distance cutoff of 2.7 A has been used). During one of the simulations at 300K, three clusters were found, using a cutoff of 1Å on the C-α atoms. The most populated cluster has a percentage of 73%, the second one 16% and the least populated one 11% (Figure 2A).

Structural comparison. The X-ray structure analysis of SMS201-995 reveals three structures in the crystalline state, only one of them corresponds to the structure observed in solution. This particular structure of SMS201-995 was superimposed with the calculated structure of SOM230. The backbones and the side chains of the β-turn forming D-Trp and Lys show an almost perfect match from Phg^2 to Tyr^5 in SOM230 and Phe^3 to Thr^6 in SMS201-995, respectively. The diaminoethylcarbamoyl-HyPro^1 lysine mimic has been found to be extended outwards from the cyclohexapeptide backbone and is pivotal in providing high affinity binding to sst1. The aromatic ring of Phg^2, covering roughly the volume of the corresponding Phe, could be responsible for the conservation and stability of the active backbone conformation of SOM230 and is contributing to exceptionally high affinity to sst5. In comparison, the SOM230 analog with His^2 instead of Phg^2 shows lower affinity to sst5. The 4'-O-benzyl-Tyr^5 side chain exceeds the space of the Thr^6 in SMS201-995 and has a distinctly different contribution to the binding of SOM230, resulting in a high affinity to sst3 and sst5. The backbone part of the second turn in SOM230, formed by Phe^6 and HyPro^1 is clearly displaced from the space of the disulfide bridge in SMS201-995.

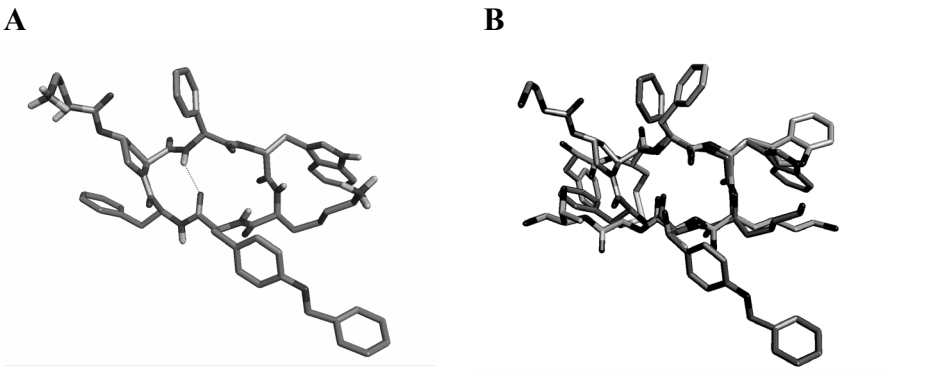

Fig. 2. Solution structure of SPM230 (A) and the superimposed structures of SOM230 (dark) and SMS201 (light) (B).

Acknowledgments
We are grateful to Claudio Dalvit for conformation studies on analogue compounds.

References

1. Lewis, I., Bauer, W., Albert, R., Chandramouli, N., Pless, J., Weckbecker, G. and Bruns, C. *J. Med. Chem.* **46**, 2334-2344 (2003).

Peptide Revolution: Genomics, Proteomics & Therapeutics
Michael Chorev & Tomi K. Sawyer (Editors)
American Peptide Society, 2003

Venom Proteomics & Drug Discovery

Reto Stöcklin, Sophie Michalet, Laure Menin, Philippe Bulet and Philippe Favreau

Atheris Laboratories, CH-1233 Bernex-Geneva, Switzerland

Introduction

The discovery of naturally occurring bioactive proteins usually relies on the initial observation of a particular biological activity of a crude sample. This is followed by purification and characterization of the compound responsible for such an activity. We have developed a backward strategy going from the structure to the function. Our complementary approach is based on a combination of bio-computing, proteomics and genomics. We have developed a unique biochemical and biological database on venomous animals [1], the venom components and the effect of these venoms that we can use to efficiently select a relevant animal or venom. Following this selection, we have set up a technical platform to isolate and characterize the bioactive compounds that includes: (i) genomics such as sequencing of cDNAs from venom glands and (ii) proteomics through a systematic identification and characterization of the venom components. To this end, we are using micro- or nano-technologies: (i) on-line liquid chromatography coupled to mass spectroscopy (LC-MS), (ii) tandem mass spectroscopy (MS/MS), and (iii) matrix assisted laser desorption/ionisation time-of-flight mass spectroscopy (MALDI-TOF-MS) for a direct analysis of crude venoms. This approach will be illustrated by three examples.

Results and Discussion

Conus textile crude venom was subjected to several experiments in order to characterize most of its constituents. Preliminary high resolution on-line LC-MS analysis of the crude venom allowed the detection of more than 150 peptides, most of them ranging from 1 to 3 kDa. The list of molecular masses detected in the *Conus* venom can be used as a chemotaxonomic specific marker for this particular *Conus* species, as is the case for snake or spider venoms [2]. Moreover, the data also enabled the detection of some post-translational modifications such as bromination through the particular isotopic pattern of the resolved spectra.

Interestingly, a specific molecular mass map of venoms can be obtained and used as a "molecular fingerprint" representative of the species to which the venomous animal belongs. These sets of data can further be compared to molecular masses calculated from described toxins having their sequences listed in our specialized protein databases. This allows easy targeting of potentially novel bioactive compounds for drug development. MALDI-TOF mass spectra of the high molecular mass range obtained with the venom of three snake species are illustrated in Figure 1. For all three analyses, the presence of complex and different phospholipase A2 profiles could be demonstrated. Many other proteins were also detected in the 7, 22-23 and 30 kDa mass ranges. A recent investigation on a scorpion venom revealed that the off-line MALDI-TOF-MS analysis of HPLC fractions can be an even more powerful method for searching for low abundant molecules in a highly complex mixture [3].

We have also analyzed crude venom from *Atractaspis microlepidota microlepidota*, looking for potentially novel endothelin-like toxins known as SRTX. Surprisingly, no SRTX in the 2.4 and 2.6 kDa mass range were detected but a series of some 20 masses

was detected around 2.8-3 kDa. These were submitted to *de novo* MS/MS amino acid sequencing. This analysis allowed direct C-terminal sequencing from LC-MS fractions, revealing a new family of 24 amino acid SRTX with an additional C-terminal "Asp-Glu-Pro" pattern that follows the typical 21 amino acid SRTX motif.

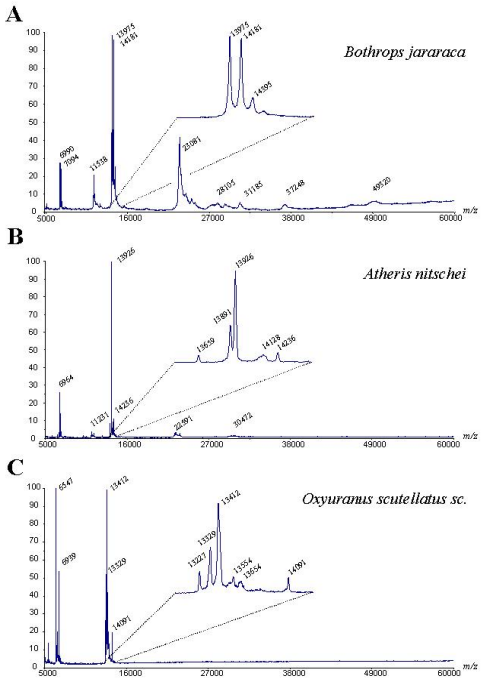

Fig. 1. MALDI mass spectra of the high molecular mass range obtained with snake venoms.

The different themes and techniques presented illustrate the diversity of approaches to the field of venom proteomics. Information such as venom mass fingerprints, *in vivo* biochemical processing, partial or complete amino acid sequence and post-translational modifications can easily be obtained offering new perspectives in protein toxicology.

Acknowledgments

We are grateful to Frédéric Ducancel, Robert Thai and André Ménez (DSV/DIEP, CEA-Saclay, France); Badia Amekraz, Christophe Moulin and Philippe Pierrard (DEN/DPC/SPCA, CEA-Saclay, France); Amos Bairoch (Swiss Institute for Bioinformatics), Denis Hochstrasser (University Hospital), Robin Offord (University Medical Center) and Keith Rose (GeneProt Inc.) in Geneva; as well as Guillaume Cretton and Sylvie Stöcklin from our laboratories.

References

1. Stöcklin, R. and Cretton, G. *Module 1:* "Snakes" - *Venomous snakes of the world* (CD-Rom). 2nd edition. Atheris Laboratories, Geneva, Switzerland. CD-Rom (2000).
2. Stöcklin, R., Mebs, D., Boulain, J. C., et al. *Methods Mol. Biol.* **146**, 317-335 (2000).
3. Pimenta, A. M. C., et al. *Rapid Commun. Mass Spectrom*. **15**, 1562-72 (2001).

Peptide Revolution: Genomics, Proteomics & Therapeutics
Michael Chorev & Tomi K. Sawyer (Editors)
American Peptide Society, 2003

Fusion of Small Dimerizer Sequence at The Terminal Ends of a Linear Random Coil Peptide Induces Conformational Switch

Tarikere L. Gururaja[1], Donald G. Payan[1] and D.C. Anderson[2]

[1]*Protein Chemistry Department, Rigel Pharmaceuticals Inc., South San Francisco, CA 94080;*
[2]*Institute for Molecula Biology, University of Oregon, Eugene, OR 97403, USA*

Introduction

Intracellular screens of constrained and/or cyclic peptide libraries for changes in cellular phenotype may identify novel functional peptides and their target proteins important in various disease processes. Unlike linear peptides, constrained and/or cyclic peptides have many valuable features, including enhanced stability to proteolysis and a restricted conformation space that can result in a higher binding affinity for cognate binding proteins [1]. In this context, we have previously shown that by incorporating a small dimerizer sequence, EFLIVKS and analogs at the terminal ends of a model 18-mer sequence derived from the protease contact loop of barley chymotrypsin inhibitor 2 (Ci2b) [2], significantly increases its proteolytic stability [3]. The proteolytic stability of the newly generated Ci2b dimerizer construct was found to be greater than the disulfide-cyclized 18-mer, which in turn is less readily proteolyzed than the linear 18-mer. The proteolytic resistance activity of dimerizer tagged-18-mer peptide was correlated to structural effects imparted by the dimerizer tag, which was further substantiated by conformational analysis. These results prompted us to further modify the original EFLIVKS dimerizer sequence, and investigate the effectiveness of the new dimerizer sequences in promoting better constraint of the peptide and, thus, modulating the activity.

In this study, we prepared several modified dimerizer sequences, which include EEEFLIVKKK, EEFLIVWKKS, KKFLIVKK, EEFLIVEE, KKKFLIVKKK, EEEFLIVEEE, KKKKKFLIVKKKKK and EEEEEFLIVEEEEE. The peptide constraining activity of these dimerizer peptides was examined by CD measurements after fusing them to the N- and C-termini of the 18-residue Ci2b model peptide. Overall, every new dimerizer sequences increased not only conformational stability as measured by *Tm's*, but also solubility of the dimerizer tagged-peptides generated.

18mer:	VGTIVTMEYRIDRTRSFV	(aa = 18, MW = 2143.49)
Dmr1:	EEEFLIVKKK-VGTIVTMEYRIDRTRSFV-EEEFLIVKKK	(aa = 38, MW = 4632.49)
Dmr2:	EEFLIVWKKS-VGTIVTMEYRIDRTRSFV-EEFLIVWKKS	(aa = 38, MW = 4664.42)
Dmr3:	KKFLIVKK-VGTIVTMEYRIDRTRSFV-EEFLIVEE	(aa = 34, MW = 4117.91)
Dmr4:	KKKFLIVKKK-VGTIVTMEYRIDRTRSFV-EEEFLIVEEE	(aa = 38, MW = 4632.49)
Dmr5:	KKKKKKKKKK-VGTIVTMEYRIDRTRSFV-EEEEEEEEEE	(aa = 38, MW = 4716.39)
Dmr6:	KKKKKFLIVKKKKK-VGTIVTMEYRIDRTRSFV-EEEEEFLIVEEEEE	(aa = 46, MW = 5661.65)

Fig. 1. Sequences of new generation dimerizer peptides.

Results and Discussion

Peptide constructs used in this study (Figure 1) were synthesized following classical Fmoc chemistry. All peptides were HPLC purified (C_{18} RP column) and their integrity was ascertained by MALDI-TOF MS analysis. Figure 2 shows the CD spectra of 18-mer insert alone derived from Ci2b as well as the dimerizer peptide (38mer, Dmr4)

recorded in phosphate buffer (pH 7.5) at 25 ˚C. It is very clear that the two peptides appear to possess different secondary structural content. The 18-mer showed a random coil structure characterized by a broad negative band around 200 nm, whereas the 38-mer (Dmr4) showed a mixture of β-sheet and β-turn structures, which is characterized by a broad negative band around 225 nm and a positive band around 195 nm. This variation in secondary structure populations in 18-mer versus 38-mer, attributed to the added dimerizer sequence such as KKKFLIVKKK and EEEFLIVEEE respectively, at N- and C-terminus of the 18mer insert may have caused the peptide to switch to a more ordered structure.

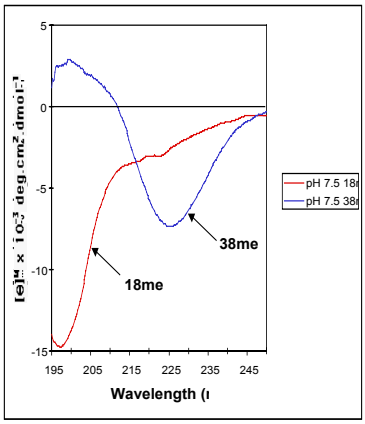

Fig. 2. CD profile of peptides.

Table 1. Structural stability data for dimerizer peptides.

Peptide	2˚ structure predicted*	2˚ structure found (CD)	Tm (˚C)
18mer	H=00%; B=72% C=22%; O=06%	Random coil	NA
Dmr1	H=13%; B=45% C=32%; O=10%	β sheet/turns	44.0˚ C (pH 4.5)
Dmr2	H=24%; B=37% C=31%; O=08%	β sheet/turns	46.6˚ C (pH 4.5)
Dmr3	H=21%; B=35% C=26%; O=18%	β sheet/turns	41.7˚ C (pH 4.5)
Dmr4	H=00%; B=72% C=22%; O=06%	β sheet/turns	50.0˚ C (pH 4.5)
Dmr5	H=29%; B=26% C=42%; O=03%	helix to random (pH dependent)	89.5 (pH 3.5) 26.6 (pH 7.0)
Dmr6	H=19%; B=35% C=35%; O=11%	β sheet/turns	25.5˚C (pH 7.0)

**Keys: H = helix; B = β sheet/turns; C = coil; O = other (analyzed using NPS@ bioinformatics website).*

A similar CD profile was obtained for most of the new generation dimerizer peptides used in this study (Table 1), except for the peptide, Dmr5. The conformation of this particular peptide was very dependent on pH of the buffer. At low pH (3.5), it showed helix conformation, at neutral pH it had mixture of β sheet/turns, but at high pH (10.0), it exhibited random coil structure, indicating the significance of ionic interactions involving charged side-chains. However, pH titration studies carried out for peptide constructs, Dmr1, Dmr2, Dmr3, Dmr4 and Dmr6 had no significant effect on their secondary structures determined by CD, implying the importance of the hydrophobic core **FLIV** in structure stabilization. On the other hand, thermal denaturation studies by CD showed a *Tm* in the range of 42 to 50˚ C for all except Dmr5**,** indicating good thermal stability for dimerizer tagged-peptides. Among all the new generation dimerizer peptides (Table 1), Dmr4 may be a good candidate for further complete structural studies utilizing NMR. The results from these studies implicate the potential application of these short dimerizer sequences in creating constrained peptide libraries *in vivo* for new drug target discovery.

Acknowledgments

Financial support from Rigel Pharmaceuticals Inc. is greatly appreciated.

References

1. Ladner, R. C. *Trends Biotechnol*. **13**, 426-430 (1995).
2. McPhalen, C. A. and James, M. N. *Biochemistry* **26**, 261-269 (1987).
3. Gururaja T. L., et al. *Chem. Biol.* **7**, 515-527 (2000).

Peptide Revolution: Genomics, Proteomics & Therapeutics
Michael Chorev & Tomi K. Sawyer (Editors)
American Peptide Society, 2003

Conformational Conversion of Prion Proteins: Role Synthetic PRP 173-195 Fibrillogenic Peptide

Barbara Tizzano[1], Daniela Marasco[1], Ettore Benedetti[1], Antonia De Capua[1], Pasquale Palladino[1], Carlo Pedone[1], Giuseppe Perretta[1], Filomena Rossi[1], Raffaele Ragone[2] and Menotti Ruvo[1]

[1]Dipartimento di Chimica Biologica, C.I.R.Pe.B., Università Federico II di Napoli and Istituto di Bioimmagini e Biostrutture, CNR, Via Mezzocannone 6, 80134 Napoli, Italy;
[2]Dipartimento di Biochimica e Biofisica, Seconda Università di Napoli, Via Costantinopoli 16, 80138 Napoli, Italy

Introduction

Transmissible spongiform encephalopathies, also known as prion diseases, are a group of unusual neurodegenerative disorders including Creutzfeldt-Jacob disease (CJD), new variant CJD, Gerstmann-Straussler-Scheinker syndrome (GSS) and fatal familial insomnia (FFI) in humans, as well as scrapie in sheep and bovine spongiform encephalopathy (BSE) in cattle[1,2]. They are characterized by progressive vacuolation of the neuropil, neuronal degeneration and gliosis. In almost all cases there is also a marked extracellular accumulation of an amyloidogenic conformer of the normal cellular prion protein (PrPC)[1-3], which is referred to as the scrapie isoforms PrP^{Sc}.

Spectroscopic data show that PrP^{C} is highly α-helical with the presence of a disulphide bridge between Cys^{179} and Cys^{214}, whereas PrP^{Sc} largely has a β-sheet structure [4] indicating that the conversion to PrP^{Sc} involves a major conformational transition. Solution NMR studies of recombinant prion protein from four species [5-8] gave similar, predominantly α-helical, monomeric folds, which were presumed to represent the PrP^{C} structure. Recently, the 2.0 Å resolution crystal structure of a recombinant human prion protein in a dimeric form has been reported [9]. This crystal structure provides the first high resolution view of a structural transition for the prion protein, revealing an unexpected three-dimensional (3D) domain swapping that may prove to be a mechanism for protein oligomerization with a conformational switch region located at the dimer interface.

The mechanism of PrP^{Sc} formation under physiological conditions is at present unknown; attempts to carry out *in vivo* conversion of PrP^{C} to PrP^{Sc} on a large scale have been unsuccessful. For this reason there have been studies to rationalize the behavior of the whole protein with peptide fragments. Various fragments have been shown to fold into α-helix- or β-sheet-rich conformation depending on the conditions under which they were prepared [10], suggesting that conformational lability could play a significant role in the conversion from PrP^{C} to PrP^{Sc}. Based on previous evidence on the behavior of small peptide sequences spanning the central region of the prion protein, we have investigated the secondary structure of N- and C-protected synthetic PrP (173-195), corresponding to the α2 helix of PrP, by far UV CD technique. Experiments suggest that the structural organization of the peptide depends on the solvent system employed, which could be related to the structural flexibility of the whole protein *in vivo*.

Results and Discussion

Carboxy-amidated and amino-acetylated PrP 173-195 was synthesized by manual Fmoc chemistry protocol using Rink-amide MBHA resin. Benzotriazole-1-yl-oxy-tris-pyrrolidino-phosphonium hexafluorophosphate (PyBop) 0.5 M in DCM and 2 M diisopropylethylamine (DIEA) in N-methyl pyrrolidone (NMP) were used as activators of carboxylic residues. The Fmoc-synthesized peptide was cleaved from the solid support by a trifluoroacetic acid (TFA) /triisopropylsilane (TIS)/water (9:0.5:0.5 v/v/v) mixture over the course of 90 min at room temperature.

The carboxy-amidated and amino-acetylated crude peptide corresponding to the sequence: Ac-Asn-Asn-Phe-Val-His-Asp-Cys-Val-Asn-Ile-Thr-Ile-Lys-Gln-His-Thr-Val-Thr-Thr-Thr-Thr-Lys-Gly-NH2 [henceforth called AcAmPrP(173-195)] was precipitated in ether, dissolved in water/acetonitrile (9:1 v/v) mixture, lyophilized and then purified by HPLC using an aqueous acetonitrile 0.1% TFA containing linear gradient. Peptide purity was confirmed by RP-HPLC and MALDI-TOF mass measurements.

Far UV CD spectra were recorded from 190 to 260 nm on a Jasco J-715 spectropolarimeter at 20°C, using 0.1 cm quartz cell containing about 0.1 mM peptide dissolved in 10 mM phosphate buffer (pH 7.3). The far UV CD spectrum of the AcAmPrP(173-195) peptide buffered aqueous solution exhibits a predominantly unordered conformation, whereas this behavior drastically changes upon addition of secondary structure-inducing agents. The titration with increasing amounts of SDS leads to a β-structured peptide. On the other hand, the use of an α-inducing agent (TFE) causes the helical arrangement of the peptide. This suggests that the peptide does not exhibit any intrinsic structural preference, because it is able to adopt a different conformation depending on solvent composition. This behavior could be partly responsible for the structural rearrangements that characterizes the transition from PrP^{C} to PrP^{Sc}. Using extrapolation procedures for obtaining equilibrium constants in the absence of any added agent, we are currently trying to characterize the whole system of conformational equilibria in which AcAmPrP(173-195) is involved.

Acknowledgments

The authors acknowledge M.I.U.R., Ministero dell'Istruzione, dell'Università e della Ricerca, PRIN 2000 program and the National Research Council (C.N.R.) of Italy for their support of this research.

References

1. Prusiner, S. B. *et al. Proc. Natl. Acad. Sci.* **95**, 13363-13383 (1998).
2. Horwich A. L. & Weissman J. S. *Cell* **89**, 499-510 (1997).
3. Pan K.- H. *et al. Proc. Natl. Acad. Sci. U.S.A.* **90**, 10962-10966 (1993).
4. Caughey B. W. *et al. Biochemistry* **30**, 7672-7680 (1991).
5. Riek R. *et al. Nature* **382**, 180-182 (1996).
6. Donne D. G. *et al. Proc. Natl. Acad. Sci. U.S.A.* **94**, 13452-13457 (1997).
7. Zahn R. *et al. Proc. Natl. Acad. Sci. U.S.A.* **97**, 145-150 (2000).
8. Lopez Garcia F. *et al. Proc. Natl. Acad. Sci. U.S.A.* **97**, 8334-8339 (2000).
9. Knaus K. J. *et al. Nature Structural Biology* **8**, 770-774 (2001).
10. Prusiner S. B. *et al. Cell* **38**, 127-134 (1984).

Peptide Revolution: Genomics, Proteomics & Therapeutics
Michael Chorev & Tomi K. Sawyer (Editors)
American Peptide Society, 2003

NMR Structure Investigation of α-MSH using TOAC Labeling

Renata de Freitas F. Vieira[1], Katya Sousa[2], Clóvis R. Nakaie[1*], Shirley Schreier[3], Paulo M. Bisch[2], Fábio C. L. Almeida[4] and Ana P. Valente[4]

[1]Departament of Biophysics, Federal University of São Paulo, Rua Três de Maio, nº 100, 04044-020, São Paulo, SP, Brazil; [2]Institute of Biophysics Carlos Chagas Filho, Federal University of Rio de Janeiro, Rio de Janeiro, RJ, Brazil; [3]Institute of Chemistry, Departament of Biochemistry, University of São Paulo, São Paulo, SP, Brazil; [4]Departament of Medical Biochemistry, Federal University of Rio de Janeiro, 21941-590, Rio de Janeiro, RJ, Brazil

Introduction

After the inception by our group of the use of TOAC (2,2,6,6-tetramethylpiperidine-1-oxyl-4-amino-4-carboxylic acid) amino acid for labeling peptide [1,2] or peptide-resin [3], this cyclic spin probe has been applied recently in a great variety of investigations encompassing many types of macromolecules. Extensive application of NMR to TOAC-containing molecules has been impaired partially by NMR resonance linebroadening effect due to the presence of the nitroxide moiety. This effect, however, can be of value for peptide conformational investigations since it seems to be sensitive to families of interconverting structures affecting the NOEs. In this study we examine the feasibility of combining the NMR method specifically to TOAC-containing peptides. The melanocyte stimulating hormone α-MSH was deliberately selected due to the fact that its Ac-TOAC^0-α-MSH analogue displayed fully activity even after the incorporation of the TOAC compound [4]. The studies with native and TOAC-labeled α-MSH were performed in different media and preliminarily CD experiments were also carried out in aqueous medium.

Results and Discussion

The structure of unlabeled α-MSH was recently evaluated in water and micelles of DPC and SDS by NMR [5]. Figure 1 shows the lowest energy structure calculated using NMR restraints in CNS_Solve.

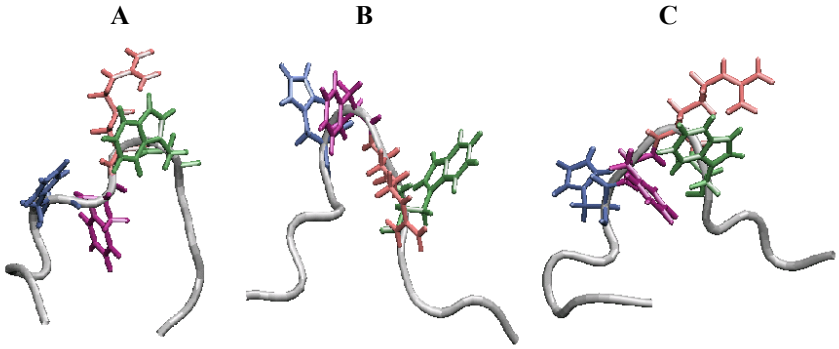

*Fig. 1. Lowest energy structures calculated using NMR restraints in CNS_Solve. The structures were obtained in (**A**) water, (**B**) dodecylphosphocholine micelles-DPC, and (**C**) sodium dodecyl sulfate micelles-SDS. Message sequence residues are His[6], Phe[7], Arg[8], Trp[9].*

α-MSH shows flexible structure as expected for a small peptide, due to the lack of long-range contacts. The NOEs observed were environment-dependent, larger in DPC than in SDS or in water. This is an indication of the varying flexibility presented by α-MSH in different environments. This can be a common feature of peptides that are highly flexible in water while the presence of an interface can restrain the peptide conformation. Next, the same experimental approach was applied to Ac-TOAC^0-α-MSH; the 1D hydrogen spectra indicated that α-MSH presented lower chemical shift dispersion in water than in SDS. Larger number of NOEs were detected in DPC medium. Otherwise the TOAC labeled analogue also displayed low dispersion in water and a slight line broadening. This effect is more pronounced in micelles.

The TOCSY spectra in different media depicted that there is a very small chemical shift difference between TOAC-labeled and unlabelled α-MSH, thus allowing the resonance assignment through the native peptide hormone in water and in SDS. Despite this similarity between both peptides, a small chemical shift difference is observed, as not all resonances are detected in the spectra of Ac-TOAC^0-a-MSH due to line broadening effect. It is noteworthy that this latter effect is markedly dependent on the environment. In DPC the strong line broadening completely impaired the spectral analysis while in SDS and water, one could still perform TOCSY and NOESY experiments.

The measurement of the longitudinal proton relaxation rate (T_1) [6] also allowed us to evaluate the effect of nitroxide probe on each region of the peptide sequence. The chemical shift values were greater the closer the amino acid residue was to the TOAC residue located at N-terminal position. In agreement with this finding, increased T_1 values were determined for protons of Lys^{11}, Pro^{12} and Val^{13} residues located at the peptide C-terminal region of the sequence. These NMR data are in agreement with preliminarily CD studies where an unordered conformation was detected for α-MSH and its TOAC-labeled analogue in aqueous solution. Otherwise in micelles (SDS and DPC), more folded structures are acquired by both melanotropic peptides.

Acknowledgments
This work was supported by FAPESP, FAPERJ and CNPq.

References

1. Nakaie, C. R., Goissis, G., Schreier, S. and Paiva, A. C. M. *Braz. J. Med. Biol. Res.* **14**, 173-180 (1981).
2. Nakaie, C. R., Schreier, S. and Paiva, A. C. M. *Bioch. Biophys. Acta* **742**, 63-71 (1983).
3. Marchetto, R., Schreier, S. and Nakaie, C. R. *J. Am. Chem. Soc*. **115**, 11042-11043 (1993).
4. Barbosa, S. R., Cilli, E. M., Lamy-Freund, M. T., Castrucci, A. C. M. and Nakaie, C. R. *FEBS Lett.* **446**, 45-48 (1999).
5. Sousa, K., Bisch, P. M., Almeida, F. C. L. and Valente, A. P. (submitted).
6. Hansen, D. F. and Led, J. J. *J. Magn. Reson.* **151**, 339-346 (2001).

Peptide Revolution: Genomics, Proteomics & Therapeutics
Michael Chorev & Tomi K. Sawyer (Editors)
American Peptide Society, 2003

Antimicrobial and Insecticidal Effects of Crude Extract Momosertatin from *Momordica cochinchinensis*

Dung Le Nguyen[1], Annie Heitz[2], Laurent Chiche[2], Jean-François Hernandez[3], Thi Ha Phan[4] and Tran Chau Pham[4]

[1]NSERM U376, CHU A. de Villeneuve, Montpellier, France; [2]CBS, Faculté de Pharmacie, Montpellier, France; [3]LAPP, CNRS UMR5810, Faculté de Pharmacie, Montpellier, France; [4]Center of Biotechnology, National University of Hanoi, Vietnam

Introduction

Momosertatin (Mos) is extracted from the seeds of *Momordica cochinchinensis* (MCo) which are very rich sources of trypsin inhibitors belonging to the squash knottins family (around 30 amino acid residues, cystine-knot with 3 disulfide bonds). Recently, three trypsin inhibitors (MCoTI-I, MCoTI-II and MCoTI-III) from MCo seeds have been characterized: MCoTI-III is a classical open chain while MCoTI-I and MCoTI-II are "cyclotides" (head-to-tail cyclized). The 3D structure of MCoTI-II has been reported [2,3] and the total synthesis of cyclic MCoTI-I described [4]. It is known that some plant cyclotides (kalata B1, circulin A, cyclopsychotride, etc.) exhibit a range of biological activities, i.e., uterotonic, anti-tumor, anti-HIV, insecticidal, antimicrobial activities [5]. These findings along with our knowledge in the use of MCo in traditional medicine, prompted us to search for insecticidal and antimicrobial properties of Mos.

Results and Discussion

Mos is prepared from dried, finely ground mature MCo seeds. Extraction is achieved with sodium acetate (20mM, pH 4.5) followed by centrifugation and G75 gel chromatography. Fractions showing anti-trypsin activities are pooled and lyophilized.

Insecticidal experiments were achieved in our laboratory and in vegetable fields targeting the larvae of *Spodoptera litura* and *Plutella xylostella*, two pest moths that severely affect commercial crops (cabbage, in particular) in Vietnam and many other countries. Laboratory assays were performed by evaluating the larvae mortality following feeding with cabbage leaves soaked in Mos aqueous solutions (Table 1).

Table 1. Insecticidal effects of Mos on S. litura and P. xylostella larvae (laboratory experiments).

LARVAE		% Mortality after Mos treatment[a]		
		3 days	5 days	7 days
Spodoptera litura	2nd instar	33.4	51.7	89.2
	3rd instar	27.2	46.1	76.7
Plutella xylostella	2nd instar	29.4	49.1	78.7
	3rd instar	25.7	42.5	73.6

[a]Experiments were carried out 3x, each with 20 (S. litura) and 50 (P. xylostella) larvae. Controls consisted of identical numbers of larvae fed with normal cabbage leaves; no mortality was observed in all control experiments.

In contrast, parcels (20m2) of cabbage fields were sprayed with Mos (400 liters per hectare, 4g Mos/l). The experiments were performed at Cooperative Mai Dich in Tu Liem district, Hanoi. After Mos spraying, the crop destruction extent was estimated and

the larvae mortality measured in comparison with data collected from "control" parcels sprayed with distilled water (Table 2).

Table 2. Insecticidal effects of Mos on S. litura and P. xylostella larvae[a].

LARVAE		% Mortality after Mos treatment[b]				
		Dosage (l/ha)	2 days	3 days	5 days	7 days
Spodoptera litura	2nd instar	400	11.5 (0)	32.1 (0)	51.6 (4.6)	72.6 (5.7)
	3rd instar	400	9.2 (0)	29.2 (0)	49.5 (3.2)	68.2 (3.8)
Plutella xylostella	2nd instar	400	8.6 (0)	28.2 (0)	29.4 (2.7)	71.1 (3.1)
	3rd instar	400	7.4 (0)	25.3 (0)	42.1 (2.2)	69.8 (2.8)

[a]*Field experiments;* [b]*Experiences were carried out thrice; values in brackets correspond to data collected on "control" cabbage parcels.*

Data from Tables 1 and 2 show that one week after Mos treatment, more than 75% larvae were destroyed. These results clearly indicate that Mos is an efficacious insecticide against these plant pests.

Antibacterial assays were performed *in vitro* according to a classical two stage radial diffusion procedure. Over 145 microorganisms were tested; the most interesting results were obtained with *Pseudomonas aeruginosa* isolated from burn wound pus. After 48h incubation, the wide colony-free zones surrounding the Mos-containing wells were clearly observed [6].

Studies are in progress in order to demonstrate the potential role of MCoTIs, the major polypeptidic components of Mos, and in particular the head-to-tail cyclic isoforms (MCoTI-I and II) which might represent the first cyclotides from Cucurbitaceae identified for their insecticidal and antimicrobial properties.

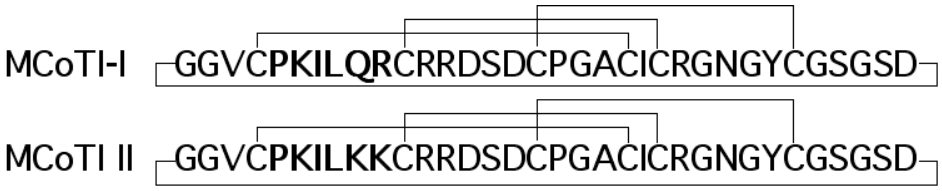

Fig. 1. Structures of MCoTI-I and MCoTI-II.

Acknowledgments

The authors gratefully thank the Institute for Plant Protection and the National Institute of Burns at Hanoi for their kind technical collaboration.

References

1. Hernandez, J.- F., et al. *Biochemistry* **39**, 5722-5730 (2000).
2. Le Nguyen, D., et al. In Benedetti, E. and Pedone, C. (Eds.) *PEPTIDES 2002 (Proceedings of the 27th European Peptide Symposium)*, Edizioni Zlino, Napoli, 2003, pp. 182-183.
3. Felizmenio-Quimio, M.- E., Daly, N.- L. and Craik, D.- J. *J. Biol. Chem.* **276**, 22875-22882 (2001).
4. Heitz, A., et al. *Biochemistry* **40**, 7973-7983 (2001).
5.For supplementary and up-to-date data, please visit websites http://www.cyclotide.com and http://knottin.cbs.cnrs.fr
6. Phan, T.H. *Masters Thesis in Microbiology, Proteinases from Pesudomonas N°1 isolated from burn wound pus – Effects of Momosertatin*, Hanoi National University, Vietnam (2000).

Peptide Revolution: Genomics, Proteomics & Therapeutics
Michael Chorev & Tomi K. Sawyer (Editors)
American Peptide Society, 2003

Effects of NOOPEPT in the Photochemically Induced Stroke Model

Galina A. Romanova[1], Tatjana A. Gudasheva[2], Rita U. Ostrovskaya[2] and Fatima M. Shakova[1]

[1]Institute of General Pathology and Pathophysiology, [2]Institute of Pharmacology, Russian Academy of Medical Sciences, 8 Baltijskaya, 125315, Moscow, Russia

Introduction

Cognition deficit is a typical symptom of stroke that occurs in 35% of patients. Because of the high frequency and severity of stroke the development of substances that might alleviate its consequences represents a clinical challenge of great importance. The data on the effectiveness of the standard cognition enhancer, Piracetam, in stroke are inconsistent and rather negative. N-phenylacetyl-L- prolylglycine ethyl ester (GVS-111, Noopept) was developed among other acetyl-proline-containing dipeptides as topological analogue of the cognition enhancer, piracetam [1]. According to our previous study Noopept demonstrates wide spectrum of cognition restoring effects in doses 0.1-1.0 mg/kg (effective doses of piracetam 200-500 mg/kg). Its advantage over longer peptides consists in high biological stability.

The aim of this study was to evaluate the effect of Noopept on general behaviour, passive avoidance performance and size of lesion in photochemically induced local cortical thrombosis, known to be the model of ischemic stroke [2].

Results and Discussion

Rat behaviour has been studied in a rectangular open field (46x46x19 cm) for 5 minutes automatically. This registration was followed by the acquisition and testing of passive avoidance in rats before and on the ninth day after photothrombosis of prefrontal cortex. Focal photothrombotic cortical infarction was induced in prefrontal cortex (Fr1 and Fr2) according to a stereotaxic atlas of rat brain [3]. Selection of the prefrontal cortex as the place of thrombotic lesion was based on the key role of this cortical area in the cognition. The rats were anaesthetized with chloralhydrate (300 mg/kg i.p.). After intravenous injection of the photosensitive dye Rose Bengal (40 mg/kg, 3% solution in saline), each rat was placed in stereotaxic frame and the scalp was incised. The skull was illuminated bilaterally with cold white light (air-cooled 24 V, 250 W halogen bulb) directed by the fibre-optic light-guide 3 mm diameter. To prevent heat-mediated brain damage the irradiated skull surface was irrigated with water (20ºC). Sham operated animals underwent the same procedure, except for Rose Bengal administration. Volumetric measurement of the infarcted cortical area in each rat performed after behavioural testing. Sections 100 microns thick were cut with vibratome throughout the whole rostro-caudal extent of infarcted area. The infarcted cortical area in each section was measured by digital planimetry, using the ASM Leitz analysing system. The total lesion volumes (V) were calculated by the formulae:$V=(\Sigma Sn)xd/a^2$, where "a" = the coefficient of the magnification of ASM Leitz system; "d" = the thickness of each slice in mm; "ΣSn" = the total sum of the infarcted areas in all sections.

All data are expressed as mean ± SEM. The difference between the preoperative and postoperative testings within one group was analyzed by means of Wilcoxon T-test. The pair-wise comparison between experimental groups was performed by Mann-Whitney U-test.

The photothrombosis of rat's prefrontal cortex provokes the selective deficit of passive avoidance performance. Locomotor activity, reactivity to external stimulii did not change either in lesioned, or in sham operated rats. Noopept treatment also did not change these parameters. Repetitive testing of the passive avoidance performance on day nine post operation revealed great differences between groups. Pairwise comparison of the data from sham operated rats and saline treated subjected to ischaemia animals showed that passive avoidance latency in second group is much shorter ($p<0.05$ in U-test). Rats subjected to ischaemic lesion and treated post-operatively with Noopept (at dose 0.5mg/kg/day i.p. firstly 1 hr after lesion, then daily for nine days after lesion with the last injection 15 min before the repetitive testing) demonstrated increase of passive avoidance latency comparing to ischaemic damaged saline treated rats ($p<0.01$ in U-test).

The effect of Noopept was also demonstrated in another shedule of the experiment. The acquisition of passive avoidance reflexes in rats took place after phototrombosis of prefrontal cortex, when Noopept (at the same dose) was administered for eight days before and three days during learning. In this case Noopept administered postoperatively, before the learning also improve the performance of passive avoidance comparing to ischaemic damaged saline treated rats ($p<0.05$ in U-test). Judging by the morphological assessment the treatment with Noopept causes statistically significant diminution of the volume of the lesioned cortical tissues, testifying to the neuroprotective effect. In saline treated rats, sacrificed on day nine after photothrombosis, the ischaemic lesion included central core of pan-necrosis, often with round cavities in the peri-infarction zone. In these rats the mean total volume of the focal ischaemic lesion was shown to be 6.2 ± 1.14 mm^3. In the group of rats treated with Noopept for 9 days after photothrombotic lesion the volume of infarction cortical area diminished to 3.03 ± 0.5 mm^3 ($p<0.01$ in U-test). The damaged area did not usually contain cavities in peri-infarction zone.

Present experiments provide evidence that Noopept being administered systemically possesses both cognition restoring and neuroprotective properties. The cognition restoring effect is probably based on the increase of the neocortical and hippocampal neuronal plasticity. Neuroprotective effect of Noopept is of the "cocktail" type: the substance combines the antioxidant activity with the ability to attenuate glutamate-provoked neurotoxicity and block voltage-antioxidant activity with the ability to attenuate glutamate-provoked neurotoxicity and block voltage-gated ionic channels, i.e., mitigates the main metabolic shifts involved in pathogenesis of brain ischaemia [4].

Acknowledgments
This work was supported by RBrF 03-04-49049.

References

1. Seredenin, S., Voronina, T., Gudasheva, T., Ostrovskaya, R., Rozantsev, G., Skoldinov, A., Trofimov, S., Halikas, J. and Garibova, T. Biologically Active N-Acylprolyldipeptides having Antiamnestic, Antihypoxic and Anorexigenic Effects. USP No 5,439,930. Aug. 8, (1995).
2. Watson, B., Dietrich, W., Busto, R., Wachtel, M., Ginsberg, M. *Ann. Neurol.* **17**, 497-504 (1985).
3. Paxinos, G. and Watson, Ch. *The Rat Brain in Stereotaxic Coordinates* 2d Ed., Academic Press Ltd. UK (1986).
4. Ostrovskaya, R., Romanova, G., Barskov, I., Shanina, E., Gudasheva, T., Victorov, I., Voronina, T. and Seredenin, S. *Behav. Pharmacol.* **10**, 549-553 (1999).

Peptide Revolution: Genomics, Proteomics & Therapeutics
Michael Chorev & Tomi K. Sawyer (Editors)
American Peptide Society, 2003

Effect of Chain Length on Coiled-Coil Stability: Decreasing Stability with Increasing Chain Length

Stanley C. Kwok and Robert S. Hodges

Department of Biochemistry and Molecular Genetics, University of Colorado Health Sciences Center, Denver, Colorado 80262, USA

Introduction

In nature, the coiled-coil motif is widely observed in more than 300 proteins involved in various cellular processes, e.g., gene regulation, vesicular transport, and viral entry into a host cell (reviewed in [1]). The coiled-coil domains of these proteins vary widely in length, from the short (less than 35-residue) DNA-binding domains to the greater than 1000-residue myosin coiled-coil rods of muscle proteins. This variance in size illustrates the diversity in function of coiled-coils despite the simple architecture. In this study, our goal was to examine the effect of chain length on coiled-coil stability when inserting heptad(s) that maintained the 3-4 hydrophobic repeat (Ala and Leu at positions ***a*** and ***d,*** respectively) but did not provide the optimal stabilization (Ala at position ***a***) in the hydrophobic core. The hypothesis was that increasing chain length does not necessarily increase protein stability, and the stability contribution of increasing chain length is dependent on the properties of the inserted heptad. Simply put, even with sufficient hydrophobic stabilization and attractive ionic forces, increasing chain length of the coiled-coil may still destabilize the fold without disrupting the overall α-helical secondary structure.

Results and Discussion

In order to study the effect of chain length on coiled-coil folding and stability, we designed and synthesized a series of peptides which are two-stranded parallel disulfide-bridged α-helical coiled-coils with 5, 6, 7 and 8 heptads. The A5 coiled-coil design provided two stabilizing hydrophobic clusters (three or more consecutive large hydrophobes, Ile and Leu, in positions ***a*** and ***d***), one at each end of the coiled-coil (Fig. 1). In addition, inter- and intra-chain ionic interactions between Lys and Glu further

Peptide Name	Peptide Sequence
A5	Ac-E**I**EA**L**KA-E**I**EA**L**KA-(K**A**EA**L**EG)$_2$-E**I**EA**L**KA-GGCY-am
A6	Ac-E**I**EA**L**KA-E**I**EA**L**KA-(K**A**EA**L**EG)$_3$-E**I**EA**L**KA-GGCY-am
A7	Ac-E**I**EA**L**KA-E**I**EA**L**KA-(K**A**EA**L**EG)$_4$-E**I**EA**L**KA-GGCY-am
A8	Ac-E**I**EA**L**KA-E**I**EA**L**KA-(K**A**EA**L**EG)$_5$-E**I**EA**L**KA-GGCY-am

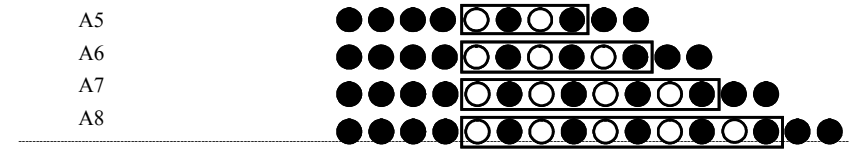

*Fig. 1 Nomenclature and schematics of coiled-coils with different chain lengths. The upper panel shows the sequences where the residues in positions **a** and **d** are bolded. The lower panel shows the **a** and **d** positions only where (•) denotes Ile at a or Leu at d and (o) denotes Ala.*

stabilize the α-helical structure. The Gly-Gly-Cys linker at the C-terminal forms a flexible linker for the formation of the disulfide bridge to eliminate the monomer-dimer equilibrium, thus making denaturation studies concentration independent.

Table 1 shows that the disulfide bridged coiled-coil A5 is dimeric, > 89% helical in benign conditions (50mM PO_4 (K_2HPO_4/KH_2PO_4), 100mM KCl, pH 7.0). The A5 coiled-coil provided sufficient stability ($T_{1/2}$ > 80 ^oC) to allow the ability to measure the effect of increasing chain length on coiled-coil stability.

We chose the heptad sequence K-A-E-A-L-E-G for insertion into the central region of the A5 coiled-coil to increase its chain length. This heptad maintains the continuous 3-4 hydrophobic repeat along the coiled-coil by placing an Ala and a Leu in the hydrophobic core positions ***a*** and ***d***, respectively. The leu-leu pair in the ***d*** position of the coiled-coil has been shown to contribute the most to protein stability, with an increase of 3.8 kcal/mol when compared to an Ala-Ala pair [2].

We chose the central region of the coiled-coil for chain length insertion because this region is most sensitive to substitution. We made three chain length coiled-coil analogs, A6, A7 and A8, denoting one, two and three heptad insertions, respectively (Figure 1). Circular dichroism was used to quantify the amount of helical secondary structure. At room temperature in benign conditions, all the disulfide-bridged analogs, A6, A7 and A8 were essentially fully folded α-helical coiled-coils, >88% helicity, with no significant difference relative to A5 (Table 1). Even in 50% TFE, no significant increase in helicity was observed for any of the chain length analogs; thus, the insertion of 7, 14 and 21 residues into our host coiled-coil did not disrupt the overall coiled-coil fold.

Table 1. Biophysical data for disulfide-bridged coiled-coil analogs with heptad inserts.

Peptide	$[\theta]_{222}$ Benign (deg•cm^2•dmol^{-1})	$T_{1/2}$ (^oC)	$[Urea]_{1/2}$ (M)	m (kcalmol^{-1}•M^{-1})
A5	-30,800	83.9	7.90	0.46
A6	-31,700	77.9	5.70	0.77
A7	-31,300	70.5	3.80	0.92
A8	-30,300	63.2	2.80	0.97

We further characterized the chain length analogs by thermal denaturation, and found that the stability of the analog decreased as chain length increased (Figure 2A). Indeed, there seemed to be a linear approximation relating the temperature midpoint, $T_{1/2}$, to coiled-coil length (Figure 2B). Even when the chain length analogs are non disulfide-bridged (i.e., in the reduced states), the linearity of decreasing stability versus chain length was observed (Figure 2B). Similar to the trend of decreasing stabilities revealed by thermal denaturation, progressive destabilization was observed in urea denaturation when the chain length was extended (Table 1). Parallel to the drop in protein stabilities, the *m* value, the slope term associated with unfolding, progressively increased as the transitions became more co-operative as chain length increased. The shortest and most stable A5 host protein had the highest $[Urea]_{1/2}$ (7.9 M) and $T_{1/2}$ (84^oC) but the shallowest slope *m* (0.46); in contrast, the longest coiled-coil has the lowest $T_{1/2}$ (63^oC) and $[Urea]_{1/2}$ (2.8 M) but the steepest slope *m* (0.97). The *m* value

has been implicated in the relative difference in hydrophobic surface area between the folded and the unfolded state. The observed difference in *m* value suggested that increasing the chain length might have affected the unfolded states, despite the fact that all the coiled-coil analogs are fully folded in benign medium.

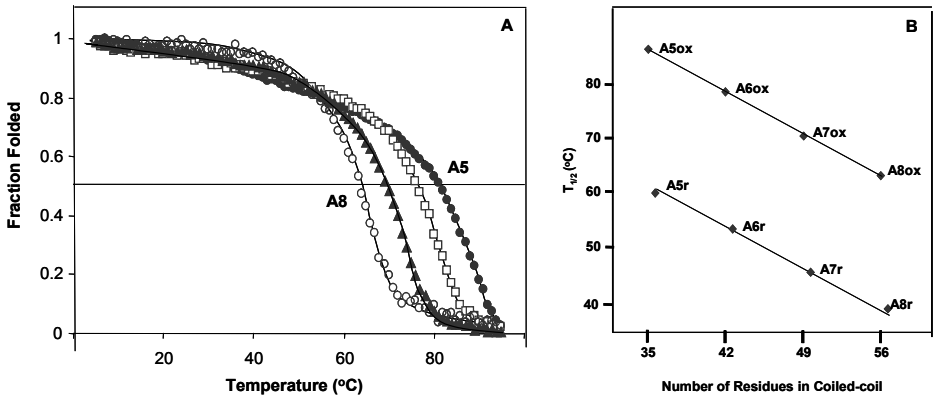

Fig. 2. Temperature denaturation profiles of peptides and relationships between stability and chain length of the oxidized and reduced coiled-coils.

Traditionally, increasing coiled-coil chain length has been synonymous with increasing protein stability. Intuitively, increasing the chain length of a coiled-coil while maintaining a continuous 3-4 hydrophobic repeat increases the number of favorable stabilizing contacts, and thus enhances stability. In fact, previous studies have clearly demonstrated the stabilization effect of increasing chain length, when heptads identical to the host coiled-coil were duplicated. However, these heptad sequences maintained excellent stabilizing residues in the ***a*** and ***d*** positions (i.e., Ile and Leu [3] and Val and Leu [4]) compared to Ala and Leu in the heptad insertion used in this study. In nature, a balance of regions of higher and lower stability is the determinant of protein function. The stable domains of a protein provide the necessary scaffold to maintain structure and integrity while allowing the flexible unstable regions to be involved in function. Take the example of the 284-residue protein, tropomyosin, on which we have previously reported the phenomenon of hydrophobic clustering in this molecule [5] which allows alternating regions of stability.

Further investigations into chain length, hydrophobic clustering, and hydrophobic density should provide new insights in the complexities of coiled-coil folding. In our model peptides, interpretation of our results shows that the introduction of one pair of favorable hydrophobic stabilizing interactions in the core per heptad did not have sufficient enthalpic stabilization to overcome the entropy of helical extension, and therefore the stability of the entire molecule decreased.

References

1. Burkhard, P., Stetefeld, J. and Strelkov, S. V. *Trends Cell Biol.* **11**, 82-88 (2001).
2. Tripet, B., Wagschal, K., Lavigne, P. and Hodges, R. S. *J. Mol. Biol.* **300**, 377-402 (2000).
3. Su, J. Y., Hodges, R. S. and Kay, C.M. *Biochemistry* **33**, 15501-15510 (1994).
4. Litowski, J. R. and Hodges, R. S. *J. Pept. Res.* **58**, 477-492 (2001).
5. Kwok, S. C. and Hodges, R. S. *J. Biol. Chem.* **278**, 35248-35254 (2003).

Intracellular Signaling, Metabolism and Gene Regulation Structure-Function

Peptide Revolution: Genomics, Proteomics & Therapeutics
Michael Chorev & Tomi K. Sawyer (Editors)
American Peptide Society, 2003

Inhibition of HuPrP106-26 Aggregation in Presence of dsDNA by Peptide Libraries

Jaroslav Šebestík[1], Lenka Borovičková[2], Jan Hlaváček[2] and Ivan Stibor[1]

[1]ICT in Prague, Technicka 5, Prague, 166 28 - Czech Republic; [2]IOCB, Academy of Sciences of the Czech Republic, Flemingovo nam. 2, Prague, 166 10 - Czech Republic

Introduction

Prion diseases are characterized by the accumulation of abnormal forms of the cellular prion protein (PrPC), termed PrPSc, in the brain. In contrast with the former, the PrPSc is partly resistant to digestion by protease due to enhanced content of beta-sheet conformation forming insoluble aggregates and amyloid fibrils. A peptide that includes residues 106-126 of human PrP (HuPrP106-126) has been shown to be highly amyloidogenic and is toxic to neurons *in vitro* [1,2]. Therefore, this peptide could represent a suitable model compound with properties of the infectious PrPSc. An active role of nucleic acids was found necessary for experimental transfer of bovine spongiform encephalopathy (BSE) infection to mice and for aggregation of HuPrP106-126 in solution [3]. Gc-rich-DNA which is known to bind 9-aminoacridines (Acr-NH_2) was found to induce polymerization of mouse PrPC more rapidly than other DNAs [4,5]. Intercalators change conformation of DNA and competitively cleave protein-DNA-complexes. Bis-intercalators have a higher binding constant to DNA than mono-intercalators. Design and syntheses of bis-intercalator peptide mini-libraries with 250 members that could influence HuPrP-DNA binding were already described [6]. The goal of present study was synthesis of the bigger library with 9826 members and development of assay for screening HuPrP106-26 aggregation.

Results and Discussion

We investigated aggregation assay based on facilitated precipitation of Congo Red dye from buffer solution, where amyloid-like structures accelerate dye precipitation. The faster aggregation of HuPrP, the earlier precipitation of Congo Red from solution occurs [7]. The syntheses of positional scan sublibraries with general formulas Acr-Gly-X1-X2-X3-$NHCH_2CH_2NH$-Acr (**A1**) and (Acr-Gly-X1-X2-X3-$NHCH_2$)$_2$ (**A2**) were carried out from 17 amino acids by Fmoc/tBu strategy on 3-formylindole resin with loaded N-Acridine-9-yl ethylene diamine in 51 syringe. Since solid phase bound amino acridines are not stable under basic conditions, DIC/HOBt was chosen as coupling agent. After cleavage with TFA and subsequent precipitation with ether, 51 sublibraries underwent the above-mentioned precipitation assay. In this library were compounds which are either inhibitors or activators of DNA facilitated aggregation (Figure 1). There are 28 sublibraries from 51 displaying anti-aggregation activity. Moreover, there are a few sublibraries delaying precipitation after non-DNA catalyzed prion peptide aggregation, i.e. with the higher positive value of precipitation time than that of those labeled with a minus sign. Relative low toxicity of sub-libraries was proved by MTT test on NG108-15 glioma/neuroblast. cells, which was carried out in 50-fold higher concentration of sub-libraries than that which is effective in anti-aggregation assay. We obtained a set of active non-toxic peptides with formulas **A1** and **A2**, where X1 stands for Tyr and Met; X2 is Tyr, Gly, Asn and Lys; and X3 stands for Gly and Asn. We suppose that these peptides with or without dsDNA can serve as a suitable model for anti-aggregation drugs design. Since prion protein binds DNA like

prion peptide, we suggested that intercalator-DNA complexes may affect prion peptide and prion protein aggregation.

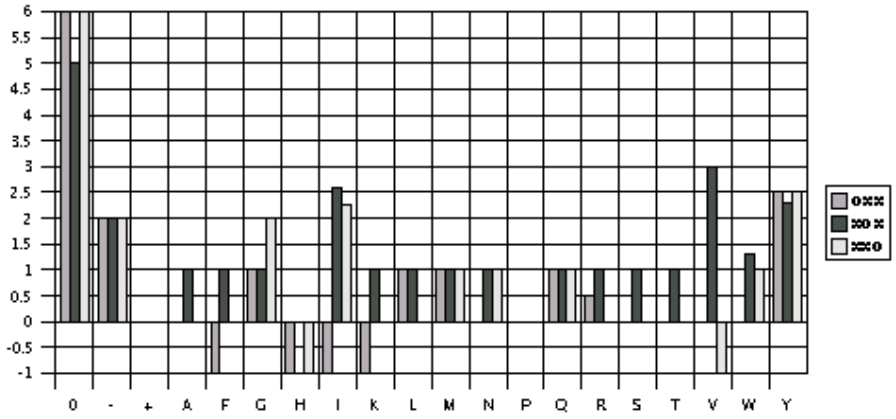

Fig. 1. Results from aggregation assay: ***O*** *stands for known amino acid and* ***X*** *for variable amino acid. Column labeled with plus shows DNA catalyzed aggregation time of HuPrP106-26 which was taken as arbitrary zero. Values higher than arbitrary zero stand for inhibitors of DNA catalyzed aggregation. When this number is higher then that in column labeled with minus sign, compound with DNA is inhibitor of prion aggregation itself.*

Acknowledgments

I would like to thank the 18th APS travel grant committee and sponsors for their travel grant. We are indebted to Dr. Jiřina Slaninová and her staff at IOCB AS CR for MTT tests, Prof. Milan Kodíček and his staff for MALDI-TOF-MS spectra, the Department of Structure Analysis at IOCB AS CR for IR, NMR, and FABMS spectra, and Dr. Stanislav Kmoch and Lenka Ondrová for lending a fluorescence scanner. This work was supported by a project of Acad. Sci. CR no. Z 4055905 and a grant of GA CR no. 203/02/1379.

References

1. Tagliavini, F., Prelli, F., Verga, L., Giaccone, G., Sarma, R., Gorevic, P., Ghetti, B., Passerini, F., Ghibaudi, E., Foroloni, G., Salmona, M., Bugiani, O. and Frangione, B. *Proc. Natl. Acad. Sci. U.S.A.* **90**, 9678, (1993).
2. Foroloni, G., Angeretti, N., Chiesa, R., Monzani, E., Salmona, M., Bugiani, O. and Tagliavini, F. *Nature* **362**, 543 (1993).
3. Nandi, P. K. *Arch. Virol.* **143**, 1251 (1998).
4. Nandi, P. K. and Leclerc, E. *Arch. Virol.* **144**, 1751 (1999).
5. Nandi, P. K., Leclerc, E., Nicole, J.-C. and Takahashi, M. *J. Mol. Biol.* **322**, 153161 (2002).
6. Šebestík, J., Hlaváček, J. and Stibor, I. In Benedetti, E. and Pedone, C. (Eds.) *Peptides 2002*, Edizioni Ziino, Napoli, Italy, p. 282. Napoli 2002.
7. Šebestík, J., Hlaváček, J. and Stibor, I. In Slaninova, J. (Ed.), *Collection Symposium Series*, Institute of Organic Chemistry and Biochemistry, Academy of Sciences of the Czech Republic, Prague **6**, 98-101 (2003).

Peptide Revolution: Genomics, Proteomics & Therapeutics
Michael Chorev & Tomi K. Sawyer (Editors)
American Peptide Society, 2003

Development of Peptides Able to Modulate the Interaction of AKAP121 with Mitochondria

Michele Saviano[1], Laura Zaccaro[1], Ettore Benedetti[1], Carlo Pedone[1], Annarita del Gatto[1], Antonio Feliciello[2], Adele Affaiatati[2] and Enrico V. Avvedimento[2]

[1]Istituto di Biostrutture e Bioimmagini, CNR and Dipartimento di Chimica Biologica, Università degli Studi di Napoli "Federico II", Napoli, 80134, Italy; [2]Dipartimento di Biologia e Patologia Molecolare e Cellulare, Università degli Studi di Napoli "Federico II", Napoli, 80131, Italy

Introduction

c-AMP is an important second messenger that regulates multiple cellular processes via the activation of the cAMP-dependent kinase A (PKA). Specific subcellular localization of PKA is achieved through binding to a family of scaffold proteins named A-kinase anchoring proteins (AKAPs) [1]. AKAP proteins bring PKA to different membrane and cellular organelles, thus mediating cAMP signaling events such as development, differentiation, cell survival and cell progression.

AKAP121 is able to localize PKA on mitochondria and endoplasmic reticulum and to mediate the protective effects of cAMP on cell survival. It has been demonstrated that the targeting of AKAP121 to the outer membrane of mitochondria, both in male germ cells and in transfected heterologous cells, is mediated by the first 30 N-terminal residues [2]. The AKAP121 mitochondrial targeting motif has been used as a model sequence to develop peptide and peptidomimetic molecules able to bind mitochondria and interfere positively or negatively with the biological activity of AKAP121 (see Figure 1).

AKAPWT Ac-*β*Ala-KKPLALPGMLALLGWWWFFSRKKβAla-NH_2
AKAP21 Ac-βAla-KKPLALPGMLALLGWWWFF**D**RKK-βAla-NH_2
AKAP20 Ac-βAla-KKPLALPGMLALLGWWWF**A**SRKK-βAla-NH_2
AKAP18 Ac-βAla-KKPLALPGMLALLGWW**A**FFSRKK-βAla-NH_2
AKAP17 Ac-βAla-KKPLALPGMLALLGW**A**WFFSRKK-βAla-NH_2

Fig. 1. Sequences of AKA121 analogs.

Results and Discussion

We have designed wild type and mutated peptides corresponding to the sequence encompassing the 10-30 MT domain of AKAP 121. To improve enzymatic stability and solubility, Lys and β-Ala residues were added to the N-terminus of the WT sequence. The designed peptides are reported in Figure 1. The mutated residues are underlined and indicated in bold.

The syntheses of all peptides were carried out using the Fmoc methodology. The peptides were obtained using Fmoc-PAL-PEG-PS as starting resin to obtain C-amidated sequences and were N-acylated on the resin at the end of the synthesis. The peptidyl-resins were treated with a mixture of TFA and scavengers to release the peptides from the resin. The crude products were purified by preparative RP-HPLC. The purity of the peptides was monitored by analytical RP-HPLC and the identity was confirmed by MALDI-TOF spectrometry.

To determine the effects of the synthesized peptides on cell survival, the PC12 pheochromocytoma cell line was analyzed. PC12 wild type cells were maintained in

DMEM supplemented with 10% heat-inactivated horse serum, 5% fetal bovine serum, 1 mM glutamine and 1% penicillin-streptomycin at 37°C and 5% CO2. After 5 hours the peptides were added at final concentration of 10 μM. Cell viability was assessed after 24 and 48 hours.

Since the wild type peptide did not show any significant effect on cell survival in normal growth conditions, we starved the cells from serum. Under these conditions, survival of the cells, assessed by propidium iodide staining and plating efficiency, was strictly dependent on the period of serum starvation. Exposure of cells to the wild type peptide induced a significant loss of plating efficiency and survival, most likely due to the inability of AKAP121 to bind the mitochondria. These effects were highly specific, since the four mutated peptides did not influence survival or plating efficiency of treated cells. Although some mutated peptides displayed significant differences (AKAP17, for example, induced some loss of viability in treated cells) relative to the other peptides, definitive proof of the critical residues awaits more quantitative data.

In conclusion, we have developed a new class of highly selective peptides that interfere with the biological function of the PKA scaffold protein AKAP121. Most likely, these peptides compete and inhibit anchoring of cAMP PKA to the outer wall of mitochondria and doing so, profoundly influence survival and reduce cAMP cytoprotective effects.

Acknowledgments

This work was supported by the M.I.U.R, Ministero dell'Istruzione, dell'Università e della Ricerca, and the National Research Council (C.N.R.).

References

1. Feliciello, A., Gottesman, M. E. and Avvedimento, V. E. *J. Mol. Biol.* **308**, 99-114 (2001).
2. Cardone, L, de Cristoforo, T., Affaitati, A., Grabi, C., Ginsberg, M. D., Saviano, M., Varrone, S., Rubin, C. S., Gottesman, M. E., Avvedimento, V. E. and Feliciello A. *J. Mol. Biol.* **320**, 663-675 (2002).

Peptide Revolution: Genomics, Proteomics & Therapeutics
Michael Chorev & Tomi K. Sawyer (Editors)
American Peptide Society, 2003

Synthesis of Heterodimeric Glycopeptide Hormone Containing Four Disulfide Bonds

H. Hojo[1], H. Nagasawa[2] and Y. Nakahara[1]

[1]*Department of Applied Biochemistry, Tokai University, Kanagawa 259-1292, Japan;*
[2]*Department of Applied Biological Chemistry, The University of Tokyo, Tokyo 113-8657, Japan*

Introduction

It has been found that sex differentiation in Crustacea is regulated by the androgenic gland hormone (AGH), which is isolated from male-specific organ, androgenic gland. Recently, the structure of AGH of terrestrial isopod *Armadillidium vulgare* was determined [1, 2]. Unlike the testosterone in mammals, this sex hormone is not a steroid but a peptide composed of two peptide chains crosslinked by disulfide bonds as shown in Figure 1. In addition, this peptide retains *N*-linked glycan at Asn^{A18}. The expression of recombinant AGH precursor by *E. coli* and baculovirus system showed that the glycosylation is essential for the AGH activity. The structure of carbohydrate is heterogeneous, which is composed of GlcNAc, Man, and Fuc [2], but at least the core structure of *N*-linked sugar, $Man_3GlcNAc_2$ is retained in common. To clarify the mechanism of sex differentiation by AGH, we chemically synthesized AGH carrying the core pentasaccharide unit.

Results and Discussion

The synthetic route for AGH carrying pentasaccharide unit is shown in Figure 2. The preparation of A chain was carried out by the ABI433A peptide synthesizer using FastMoc protocol. Three different cysteine-protecting groups, trityl (Trt), 4-methoxyphenylmethyl (Mpm), acetamidomethyl (Acm) groups, were employed to achieve the selective disulfide bond formation. The introduction of Asn^{18} was accomplished manually using 1.3 eq of Fmoc-Asn($Man_3GlcNAc_2Bn_{12}$) [3] by HATU. The coupling yield was about 60% judging from the HPLC analysis of the cleavage product of the resin sample. After the completion of chain assembly, the protected peptide resin **2** was treated with Reagent K for 2 h. The crude peptide was further treated with 1 M TMSBr in TFA at -10°C for 20 min to remove the benzyl groups of the carbohydrate portion. Without purification, the obtained peptide was air-oxidized to form intramolecular disulfide bond in 0.1 M $AcONH_4$ (pH 8). After HPLC purification, peptide **3** was obtained (8% yield based on the Glu on the initial resin). Then the Mpm group was converted to the thiol activating 2-pyridinesulfenyl group by 2,2-dipyridyl disulfide (DPDS) in TfOH-TFA at –10°C for 10 min. After HPLC purification, peptide **4** was obtained in 50% yield. The synthesis of the B chain was also carried out by the synthesizer. The protected peptide resin was treated with Reagent K and the crude

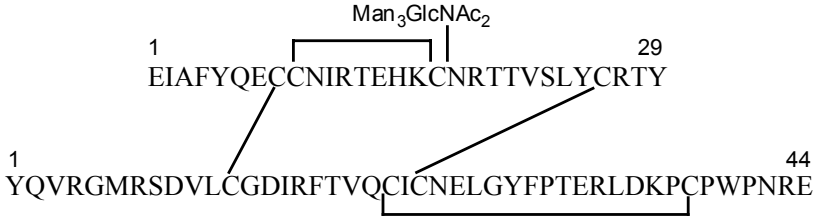

Fig.1. Structure of androgenic gland hormone carrying pentasaccharide unit 1.

peptide obtained was air-oxidized and purified by HPLC to obtain peptide **6** in 6% yield. Mpm group was removed by 1 M TfOH-TFA to give peptide **7** in 50% yield. Then the chain combination was carried out by adding peptide **7** into the solution of peptide **4** in 0.1M NH_4HCO_3. The product was purified by HPLC and peptide **8**, which retains three disulfide bonds, was obtained in 75% yield. The final disulfide bond was formed by the I_2 oxidation in aqueous methanol in the presence of hydrochloric acid at room temperature for 25 min. The reaction mixture was loaded on ion-exchange column and eluted by sodium chloride gradient. The main peak collected was desalted by HPLC and the desired AGH carrying the pentasaccharide unit **1** was obtained. The yield was 27%. The MALDI-TOF mass (found m/z: 9638.8, calcd for $(M+H)^+$ 9640.8 average) and the amino acid analyses ($Asp_{6.90}Thr_{5.42}Ser_{1.53}Glu_{8.34}Pro_{5.01}Gly_3Ala_{0.99}$ - $Cys_{0.83}Val_{4.23}Met_{0.92}Ile_{3.47}Leu_{3.85}Tyr_{4.87}Phe_{2.94}Lys_{2.05}His_{0.96}Arg_{7.76}$) confirmed that the expected peptide was successfully obtained. In conclusion, we succeeded in the synthesis of AGH carrying *N*-linked pentasaccharide by the solid-phase peptide synthesis and subsequent sequential disulfide bond formation reaction. The biological activity of this peptide is currently being studied.

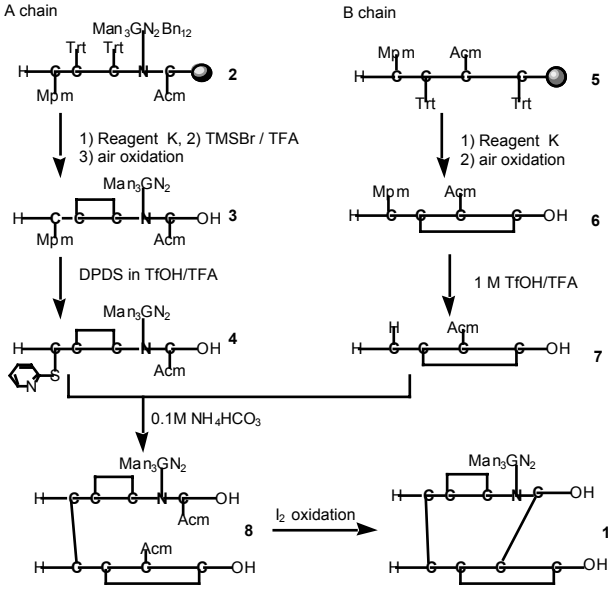

Fig. 2. Synthetic procedure for androgenic gland hormone.

References

1. Martin, G., Sorokine, O., Moniatte, M., Bulet, P., Hetru, C. and Dorsselaer, A.V. *Eur. J. Biochem*. **262**, 727-736 (1999).
2. Okuno, A., Hasegawa, Y., Ohira, T., Katakura, Y. and Nagasawa, H. *Biochem. Biophys. Res. Commun*. **264**, 419-423 (1999).
3. Matsuo, I., Nakahara, Y., Ito, Y., Nukada, T., Nakahara, Y. and Ogawa, T. *Bioorg. Med. Chem.* **3**, 1455-1463 (1995).

Peptide Revolution: Genomics, Proteomics & Therapeutics
Michael Chorev & Tomi K. Sawyer (Editors)
American Peptide Society, 2003

Peptidomimetic Design of Cyclic Grb2-SH2 Domain Antagonists not Relying on pTyr or its Mimics

Peter P. Roller[1], Peng Li[1], Manchao Zhang[2], Xiaodong Zhang[1], Ya-Qiu Long[3], Megan L. Peach[1], Marc Nicklaus[1], Hongpeng Liu[2] and Dajun Yang[2]

[1]Laboratory of Medicinal Chemistry, National Cancer Institute, NIH, Frederick, MD 21702, USA; [2]University of Michigan Cancer Center, School of Medicine, University of Michigan, Ann Arbor, MI 48109, USA; [3]Shanghai Institute of Materia Medica, Chinese Academy of Sciences, Shanghai, 200021, China

Introduction

The ErbB family of cellular receptors are essential mediators of cell proliferation and differentiation. Overexpression of these receptors predisposes cells to uncontrolled cellular proliferation, and thus to proliferative diseases, such as cancer. Extracellular signaling generates tyrosine phosphorylation of specific intracellular tyrosine regions. These Tyr phosphorylated regions provide docking sites for the binding of downstream signaling proteins. Two such proteins include the Grb2 and the Shc proteins, which facilitate the assembly of proteins that are responsible for cellular activation and cell proliferation pathways. The Grb2 adapter protein contains a structurally well characterized src homology two domain (SH2 domain) that binds to specific Tyr phosphorylated intracellular domains of the ErbB receptors and to other specific pTyr containing protein domains for assembly. Inhibition of the signaling protein assembly leads to the inhibition of the cell proliferative machinery. There have been a number of attempts to mimic the specific Tyr phosphorylated regions of receptors [1, 2], for use as competitive inhibitors of cellular signaling. Indeed, these agents show promise as potential antiproliferative agents [1, 2].

Early on, the Novartis group has shown by X-ray crystallography that specific phosphopeptides bound to the SH2 domain of Grb2 protein in a well defined turn conformation [3]. At the same time our collaborators used phage library methodology to discover an 11 amino acid long peptide that was disulfide cyclized through its two terminal cysteines [4]. Apparently, cyclization predisposed this peptide, termed **G1**, for fitting into the Grb2-SH2 domain binding pocket. Using this novel template we developed a redox stable analog, termed **G1TE** (Figure 1), that was non-phosphorylated, and exhibited Grb2-SH2 domain binding affinity, with an IC_{50} value of 20 μM, using Biacore binding affinity methodology [4]. Alanine scanning studies demonstrated the importance of amino acids Glu1, Tyr3, Asn5, and Met8 in the lead peptide [4, 5]. More recently, we have carried out extensive structural/activity studies, and the incorporation of a variety of peptidomimetically modified amino acid analogs, with the aim of substantially improving binding affinities without the use of tyrosine phosphate motifs [6, 7].

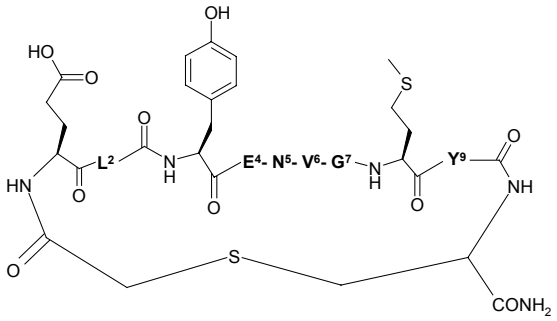

Fig. 1. Chemical structure of GITE.

Results and Discussion

We have carried out systematic structural modifications of the phage library derived cyclic peptide, G1TE, with the aim of discovering highly potent Grb2-SH2 domain antagonists. For synthesis of the various analogs, we used the PAL amide resin with an ABI 433A peptide synthesizer, utilizing s were N-terminally chloroacetylated. After resin cleavage and side-chain deprotection the peptides were cyclized under weakly basic condition [8]. Selected thioether cyclized peptides were oxidized to their sulfoxide analogs with 5% aqueous H_2O_2. ELISA assays were carried out in competitive binding assays, with the N-terminally biotinylated SHC phosphopeptide, DDPSpYVNVQ binding to the Grb2-SH2-GST fusion protein.

The unique feature of our lead generation was the discovery of glutamic acid in position 1 of G1TE. Our further structure activity studies revealed that Glu in this position is very sensitive to structural modifications [7]. Our previous SAR studies showed that the Glu at this side compensates for the absence of Tyr3 phosphorylation in retaining effective binding to the Grb2-SH2 domain. At the same time, non-phosphorylated Tyr3 is still a strong requirement. Replacement of Glu1 with γ-

Table 1. Binding affinity of G1TE analogs to Grb2-SH2 domain protein.

Peptide[b]	IC_{50} (μM)[a]
1, G1TE	> 100
2, G1TE (Gla1)	0.99 ± 0.09
3, G1TE (Gla1, Ach4)	0.54 ± 0.02
4, G1TE (Gla1, BCH4)	0.73 ± 0.34
5 G1TE (Gla1, Ach2, Ach4)	> 100
6, G1TE(Gla1, Ach4, NPG8)	0.31 ±0.10
7, G1TE(Gla1, Ach4, NPG8, Phe(4-NH_2)9)	0.24 ± 0.05
8, G1TE(Gla1, Ach4, NPG8)S=O-I (faster eluting)	0.075 ± 0.037
9, G1TE(Gla1, Ach4, NPG8)S=O-II (slower eluting)	0.75 ± 0.18

[a]*ELISA based binding assays were carried out, as described in [4].*

[b]*Gla: γ-carboxy-Glu; Ach: 1-amino-cyclohexylamine; NPG: neopentyl-glycine.*

carboxy-Glu generated a much more potent inhibitor, Peptide **2,** as tested by both Biacore and ELISA assays. Our molecular modeling studies support the structural interpretation of these results [6, 7, 9]. Therefore this peptide **2** forms the basis for the SAR studies presented here. Since previous structural work indicated that peptides fit into the Grb2-SH2 domain binding pocket in a turn configuration, we incorporated two turn-inducing amino acids, Ach and BCH, at position 4 of the peptide. G1TE(Gla1, Ach4) exhibited a promising inhibitory activity, with an IC_{50} value of 0.54 μM (Table 1). The beneficial effect was less well defined. We attempted to increase the length of turn conformation within G1TE by incorporating Ach in the 2 position (Peptide **5**). Additional turn induction at the N-terminal of the peptide, however, abrogated binding affinity. Apparently the conformational requirement for optimal binding affinity is considerably restricted.

The C-terminal region of G1TE consists of several hydrophobic amino acids, including Val6, Met8, and Tyr9. However, the thioether moiety of Met8 sidechain is susceptible to oxidation. Therefore, we replaced Met8 with various hydrophobic non-oxidizable amino acids. When Met8 was replaced with the small hydrophobic analog neopentyl-glycine, binding affinity was improved considerably, exhibiting an IC_{50} value of 310 nM for peptide **6**. Further improvements were made by incorporating the basic 4-amino-phenylalanine at the position 9, with additional improvement in activity.

Finally, a new approach was applied to impart conformational constraint by oxidizing the thioether linkage to its sulfoxide in G1TE(Gla1, Ach4, NPG) by hydrogen peroxide. Two HPLC separable stereoisomers were obtained, and one of these (Peptide **8**) possessed an IC_{50} value of 0.075 μM. The stereochemistry of chiral sulfoxide linkages was determined by CD methodology [10]. These peptides and the approach taken here provide exciting possibilities for developing a new class of inhibitors to the Grb2 mediated cellular signaling pathways.

References

1. Gay, B., Suarez, S., Caravatti, G., Furet, P., et al. *Int. J. Cancer* **83**, 235-241 (1997).
2. Wei, C. -Q., Gao, Y., Lee, K., Guo, R., et al. *J. Med. Chem.* **46**, 244-254 (2003).
3. Rahuel, J., Gay, B., Erdmann, D., Strauss, A, et al. *Nature Struct. Biol.* **3**, 586-589 (1996).
4. Oligino, L., Lung, F.- D. T., Sastry, L., et al. *J. Biol. Chem*. **272**, 29046-29052 (1997).
5. Lung, F.-D. T., Long, Y.- Q., King, C. R., et al. *J. Peptide Res.* **57**, 447-454 (2001).
6. Long, Y.- Q., Yao, Z.- J., et al. *Biochem. Biophys. Res. Commun.* **264**, 902-908 (1999).
7. Long, Y.-Q., Voigt, J.-H. and Lung, F.-D. T. *Bioorg. Med. Chem. Lett.* **9**, 2267-2272 (1999).
8. Lung, F.- D. T., King, C. R., Roller, P. P., et al. *Lett. Peptide Sci.* **6**, 45-49 (1999).
9. Li, P., Zhang, M., Long, Y.- Q., et al, *Bioorg. Med. Chem. Lett,* **13**, 2173-2177 (2003).
10. Kubec, R. and Musah, R. A., *Phytochemistry,* **58**, 981-985 (2001).

Peptide Revolution: Genomics, Proteomics & Therapeutics
Michael Chorev & Tomi K. Sawyer (Editors)
American Peptide Society, 2003

The Structure of a Cyclic Peptide Inhibitor of pp60$^{c\text{-}src}$

K. Kaluarachchi[1], J.W. Rice[1], W. Wang[2] and J.S. McMurray[2]

The University of Texas M. D. Anderson Cancer Center, Departments of [1]Experimental Therapeutics; [2]Neuro-Oncology, Houston, TX 77030, USA

Introduction

pp60c-src (Src) is the product of the *Src* oncogene and is the prototype enzyme for the Src-family of cytosolic protein tyrosine kinases (PTKs) [1]. Src participates in several signal transduction cascades, such as those initiated from binding of integrins and those originated from binding of growth factors such as PDGF to their receptors. Src and Src-family PTKs are activated during mitosis and are required for cell division. Src has been shown to have elevated kinase activity in cancers of the colon, breast, lung, stomach and other tissues, and antisense nucleotides directed to Src mRNA inhibit the growth of tumor cells in culture and in nude mouse xenograft models. Therefore, Src is a target for anti-tumor drug design [2].

Like all PTKs there are two areas on Src that are targets for drug design: the ATP binding site and the protein substrate binding site. Our work has focused on the discovery and development of inhibitors designed to compete with protein substrates. We developed a series of cyclic peptide inhibitors based on the sequence surrounding the autophosphorylation site of Src: Y^{416}, e.g., peptide **1** [3]. Replacement of Phe^{7} with 4-carboxyphenylalanine (4-Cpa) caused a dramatic increase in inhibition and a change in mode from mixed to competitive (peptide **2**, Table 1) [4]. Replacement of the tetrapeptide NEYA with 6-aminohexanoic acid led to the smaller peptide, **3**, which still retained competitive inhibition with protein substrate. To determine the structure of the competitive inhibitors, we studied them by NMR.

Table 1. Inhibition of Src with cyclic peptides.

Peptide	Sequence	*K*i (μM)	Inhibition mode
1	*cyclo*[DNEYAFFQfP]	150	mixed
2	*cyclo*[DNEYAF(4-Cpa)QfP]	0.85	competitive
3	*cyclo*[F(4-Cpa)QfPD(Ahx)]	24	competitive

4-Cpa = 4-carboxyphenylalanine, Ahx = 6-aminohexanoic acid.

Results and Discussion

Peptide **2** did not show any transannular or long distance NOEs and was thus considered to have no major conformations. Peptide **3** was studied in DMSO. The temperature dependence of the 4-Cpa NH was –1 ppb/deg, indicating that this proton is strongly shielded from solvent and likely resides in the interior of the ring, H-bonded to various atoms. The temperature dependence of the Gln NH is –3 ppb/deg, which also indicates shielding from solvent. Indeed there was an NOE interaction between these two protons. The remaining backbone NH protons appear to be dependent on temperature indicating exposure to solvent. The most exposed is D-Phe (-6.6 ppb/deg)By and large the coupling constants were unremarkable. The standard patterns one observes for Type I, I', II, and II' β-turns were not present. Whereas the NOEs and temperature dependence indicate that this peptide does exist in preferred

conformation(s), the temperature dependence and coupling constants suggest conformational averaging. NOE's were found between the NH of 4-Cpa[2] NH and those of Phe[1] and Asp[6]. Strong NOEs between the αCH of D-Phe and both of the δ-protons of Pro indicate a *trans* amide bond.

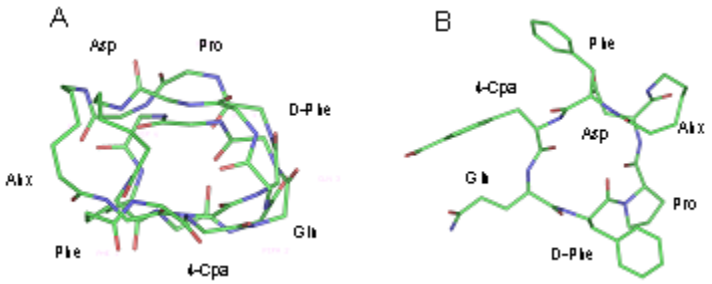

Fig. 1. Structures of peptide 3 from simulated annealing/molecular dynamics calculations.

Simulated annealing/molecular dymanics simulations were run using 58 NOE derived constraints and 20 structures were calculated starting with varying random number seeds. All structures had basically the same backbone conformation in which the 4-Cpa, Gln, D-Phe, and Pro residues exist in a reverse turn. For all 20 structures the rms deviation of the backbone was 3.3 Å. Three clusters were found with rms deviations of 2.0 Å or less. The backbone conformations are shown in Figure 1A. The Ahx residue was not constrained and found to occupy large conformation space, even within the clusters. As expected, the side chains experienced considerable rotation. An example of one structure is shown in Figure 1B.

The active region of decapeptide **2** was shown to be F-(4-Cpa)-QfPD [4]. It can be envisioned that in this relatively unstructured peptide residues from F-(4-Cpa)-QfPD could exist in a more extended, β-sheet like conformation, as observed in a peptide substrate of the insulin receptor kinase [5]. Analogs of **3** in which Ahx was replaced by Gly and Gaba were shown to be weaker inhibitors [4]. The NMR-derived structures suggest that the lower affinity of **3** may be due to important residues, e.g. QfPD, being forced out of optimum binding conformations by cyclization.

Acknowledgments
This work was funded by a grant from the National Cancer Institute, CA53617.

References

1. Brown, M. T. and Cooper, J. A. *Biochim. Biophys. Acta* **1287**, 121-149 (1996).
2. Levitzki, A. *Anti-Cancer Drug Design* **11**, 175-182 (1996).
3. McMurray, J. S., Budde, R. J. A., Ke, S., Obeyesekere, N. U. O., Wang, W., Ramdas, L. and Lewis, C. A. *Arch. Biochem. Biophys*. **355**, 124-130, (1998).
4. Wang, W., Ramdas, L., Sun, G., Ke, S., Obeyesekere, N. U., Budde, R. J .A. and McMurray, J. S. *Biochemistry* **39**, 5221-5228 (2000).
5. Hubbard, S. R. *EMBO J.* **16**, 5572-5581 (1997).

Peptide Revolution: Genomics, Proteomics & Therapeutics
Michael Chorev & Tomi K. Sawyer (Editors)
American Peptide Society, 2003

Synthetic Approaches to the Bioactive Marine Cyclodepsipeptide Halipeptin A

Assunta Napolitano[1], Ines Bruno[1], Luigi Gomez-Paloma[1], Raffaele Riccio[1], Nakia Maulucci[2], Carmela Della Monica[2], Irene Izzo[2] and Francesco De Riccardis[2]

[1]Dipartimento di Scienze Farmaceutiche; [2]Dipartimento di Chimica, Università di Salerno, Fisciano, 84084 (SA), Italy

Introduction

In the course of our on-going investigations on bioactive marine metabolites [1], we focused our attention on halipeptin A (**1**), a cyclodepsipeptide isolated, with halipeptin B (**2**), from the sponge *Haliclona* sp., which was collected in the waters off the Vanuatu Islands (Figure 1) [2]. Interestingly, halipeptin A shows a remarkable *in vivo* anti-inflammatory activity, causing a 60% reduction of edema in mice at the intraperitoneal dose of 0.3 mg/kg. A comparison of this value with those displayed in the same assay by indomethacin and naproxen (ED_{50} of 12 and 40 mg/kg, respectively) [3] indicates that halipeptin A is 40-130 times more potent than these standard anti-inflammatory drugs.

The remarkable biological activity of **1** gave rise to intriguing speculations on its possible origin, because compounds displaying anti-inflammatory activity typically belong to very different chemical classes, with only few reports of anti-inflammatory depsipeptides [4]. Chemically, halipeptin A is, in fact, a cyclodepsipeptide formed by a peptide moiety connected to a polyketide framework and characterized by the presence of common coded amino acid residues (2 x Ala) along with unusual units, such as the polysubstituted decanoic acid HTMMD, the *N*-Methyl-δ-hydroxyisoleucine (*N*Me-δOH-Ile) and the heterocyclic version of an α,α-disubstituted amino acid. Initially, the latter was incorrectly identified as a methyloxazetidine-carboxylic acid residue (OMCA), mainly on the basis of NMR and HRFABMS data. The isolation, from the same Vanuatu *Haliclona* species, of halipeptin C, a new minor related compound, derivative of halipeptin B bearing a *L*-*N*Me-Val in place of the *N*Me-δOH-Ile residue, gave us the opportunity to re-examine the spectral data of halipeptins. The HRESIMS data, acquired on superior instrumentation, were consistent with the presence of a methylthiazoline unit instead of the OMCA residue [5]. The synthesis of Δ^2-thiazoline fragment, along with the comparison of GIAO (gauge including atomic orbitals) calculated ^{13}C and ^{15}N NMR chemical shifts of four model compounds [6], allowed us to gather conclusive evidences for the structural revision of halipeptin A.

Results and Discussions

Considering the challenges posed by the complexity of halipeptin A molecular architecture, we examined the possibility of synthesizing a simplified analogue (**3**) of the natural product, with the hope that this analogue may also prove biologically active. In fact, synthetic access to this type of molecule may be helpful for the identification of new potential anti-inflammatory leads. Using solution techniques, we started with the reaction of the 2,2-dimethyl-3-hydroxy-propionic acid (a simplified version of the HTMMD) with the alaninamide, which was transformed into the 2-methyl-Δ^2-thiazoline unit by reaction with the (*R*)-2-methyl-cysteine methyl ester. For the synthesis of the Ala-*N*MeIle dipeptide (lower region of **3**) we employed Fmoc/t-Bu

chemistry, a HOBt/HBTU/NMM coupling and 2ClTrtCl-PS support, the latter chosen to avoid the N-demethylation of *N*Me-Ile, that could occur at the cleavage step in the highly acidic conditions required by working on other resins. Finally, we carried out the coupling of the depsipeptide (the upper emisphere of **3**) to the *N*Me-terminus of the dipeptide (the lower emisphere of **3**) anchored to the solid support, using CIP/HOBt activation, in order to promote coupling on the sterically hindered *N*Me-Ile and to minimize racemization at this level. A mild cleavage with AcOH/TFE/DCM (1:1:3) yielded our synthetic linear precursor, along with a minor product showing an increase of molecular weight of 18 Da (ESIMS spectra), a mass increment consistent with the hydrolitic opening of the thiazoline ring. Actually, subsequent investigations indicated that thiazoline ring opening is likely to occur during the HPLC purification step, due to the presence of acidic buffer (H_2O/CH_3CN each with 0.1% TFA).

In conclusion, as the synthetic strategy successfully yielded the desired linear precursor of **3**, we are currently working on the cyclization step to give rise to the first simplified model of halipeptin A. The model **3** may prove useful both for the optimization of the synthetic steps required for the total synthesis of halipeptin A and for assessing the relevance of its different structural units for exerting pharmacological activity.

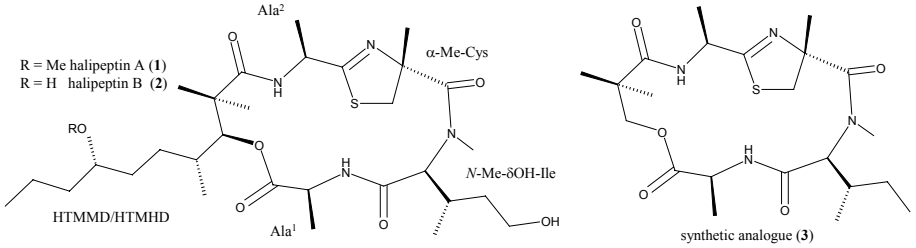

Fig. 1. Chemical structure of halipeptins A and B and of the halipeptin A synthetic analogue.

References

1. Napolitano, A., Bruno, I., Rovero, P., Lucas, R., Payà Peris, M., Gomez-Paloma, L. and Iccio, R. *Tetrahedron* **57**, 6249-6255 (2001); Napolitano, A., Bruno, I., Rovero, P., Lucas, R., Payà Peris, M., Gomez-Paloma, L. and R. Riccio *J. Peptide Sci.* **8**, 407-417 (2002).
2. Randazzo, A., Bifulco, G., Giannini, C., Bucci, M. R., Debitus, C., Cirino, G. and Gomez-Paloma, L. *J. Am. Chem. Soc.* **44**, 10870-10876 (2001).
3. Calhoun, W., Chang, J. and Carlson, R. P. *Agents Actions* **21**, 306-309 (1987).
4. Renner, M. K., Shen, Y. C., Cheng, X. C., Jensen, P. R., Frankmoelle, W., Kauffman, C. A., Fenical, W., Lobkovsky, E. and Clardy, J. *J. Am. Chem. Soc.* **121**, 11273-11276 (1999); Trischman, J. A., Tapiolas, D. M., Jensen, P. R., Dwight, R., Fenical, W., McKee, T. C., Ireland, C. M., Stout, T. J. and Clardy, J. *J. Am. Chem. Soc.* **116**, 757-758 (1994).
5. Della Monica, C., Randazzo, A., Bifulco, G., Cimino, P., Aquino, M., Izzo, I., De Riccardis, F. and Gomez-Paloma, L. *Tetrahedron Lett.* **43**, 5707-5710 (2002).
6. Ditchfield, R. *Mol. Phys.* **27**, 789 (1974); Barone, G., Gomez-Paloma, L., Duca, D., Silvestri, A., Riccio, R. and Bifulco, G. *Chem. Eur. J.* **8**, 3233-3239 (2000).

Peptide Revolution: Genomics, Proteomics & Therapeutics
Michael Chorev & Tomi K. Sawyer (Editors)
American Peptide Society, 2003

Toward the Synthesis of New Designed Analogues of the Marine Cyclodepsipeptide Jaspamide

Stefania Terracciano, Ines Bruno, Giuseppe Bifulco, Luigi Gomez-Paloma and Raffaele Riccio

Dipartimento di Scienze Farmaceutiche, Università di Salerno, Fisciano, 84084 (SA), Italy

Introduction

In recent years an increasing number of cytotoxic marine natural products have been found to target actin cytoskeleton, disrupting its organization. Since the actin cytoskeleton is involved in many vital cell functions, the identification of new agents interfering with its cellular activities may be relevant in therapeutic approaches to cancer and other human diseases [1]. In addition, such compounds represent useful tools in the investigation of actin organization, dynamics and functions. Among the actin-targeting natural products, jaspamide (**1**), also known as jasplakinolide (Figure 1), is a cyclodepsipeptide isolated from the marine sponge *Jaspis* sp. [2]. It has been found to possess an antiproliferative activity in the nanomolar range against acute myeloid leukemia and prostate carcinoma cells, due to the disruption of the actin cytoskeleton [3-4]. Jaspamide has been shown to induce actin polymerization *in vivo* and *in vitro* and to bind F-actin competitively with phalloidin [5]. In order to investigate the pharmacophor motif responsible for its biological activity, we have designed and synthetized seven simplified structural analogues of jaspamide, using a combination of solid phase and solution techniques (Figure 1). The design of such analogues has also taken into account structural similarities between jaspamide and other related macrocycles, such as doliculide, phalloidin, and chondramides, all these molecules seem to bind at the same site on F-actin [6].

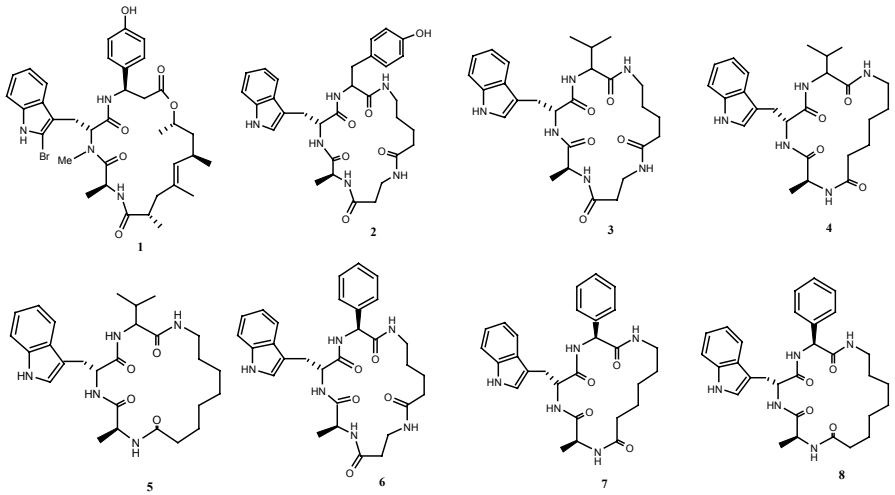

*Fig. 1. Chemical structures of jaspamide (**1**) and its analogues (**2-8**).*

Concerning the simplification of the jaspamide tripeptide unit, the rare amino acid (R)-2-bromoabrine has been replaced, in all analogues, by a common D-tryptophan, since SAR studies have shown that the bromine atom is not essential for bioactivity. Moreover, the (R)-β-tyrosine, originally present in the natural product, has been substituted by L-Tyr (analogue **2**), L-Val (analogues **3**-**5**) or by a L-Phg (analogues **6**-**8**). As concerning the polyketide chain of jaspamide, we envisaged that an isosteric replacement of the Δ^4-double bond with a peptide linkage gave rise to molecules with an entirely peptidic skeleton. The latter choice also allowed the exploration of the effects of the size of the macrocycle on biological activity, with analogues **2**, **3** and **6** keeping the 19-membered ring found in the reference product, while analogues **4, 7,** and **5**, **8** consisted of 16- and 18-membered rings respectively, in analogy to those of doliculide and chondramides.

Results and Discussion

The synthesis of all cyclopeptides was carried out by elongating the peptide chain on the solid phase and performing the cyclization in solution after the cleavage of the linear peptide from the resin. The linear sequence was synthetized using the Fmoc/ tBu chemistry on a PAC-PEG-PS resin for the analogue **2** and on a 2-chlorotrityl chloride-resin (ClTrt-Cl-resin) for all the other compounds. HOBt-HBTU in DMF was used for all coupling steps. For analogue **2**, the cleavage from the resin took place with TFA:H_2O (95:5), removing the side-chain protecting groups at the same time. The cyclization step was performed in all cases at a concentration of 10^{-4} M with HATU-DIEA in DMF/DCM. For analogues **3**-**8**, final deprotection (after cyclization) was obtained by treatment with TFA:H_2O:TIS (95:2.5:2.5). The crude cyclopeptides were then purified by a C18 RP-HPLC (Jupiter) using different gradients of aqueous CH_3CN with 0.1% TFA. All compounds have been characterized by ESI-MS and NMR spectroscopy.

The synthetized compounds are currently under pharmacological investigation.

References

1. Spector, I., Braet, F., Shochet, N. R. and Bubb, M. *Microsc. Res. Tech*. **47**, 18-37 (1999).
2. Zabriskie, T. M., Kocle, J. A., Ireland, C. M., Marcus, A. H., Molinsky, T. F., Faulkner, D. J., Xu, C. and Clardy, J. C. *J. Am. Chem. Soc*. **108**, 3123-3124 (1986).
3. Senderowic, A. M. J., Kaur, G., Sainz, E., Laing, C., Inman, W. D., Rodriguez, J., Cres, P. *et al., J. Natl. Cancer Inst.* **87**, 46-51 (1995).
4. Fabian, I., Shur, I., Bleiberg, I., Rudi, A., Kashman, Y. and Lishner, M. *Exp. Ematol*. **23**, 583-587 (1995).
5. Bubb, M. R., Senderowic, A. M. J., Sausville, E. A., Duncan, K. L. K. and Korn, E. D. *J. Biol. Chem*. **269**, 14869-14871 (1994).
6. Bai, R., Covell, D. G., Liu, C., Ghosh, A. K. and Hamel, E., *J. Biol. Chem.* **227**, 32165-32171 (2002).

Peptide Revolution: Genomics, Proteomics & Therapeutics
Michael Chorev & Tomi K. Sawyer (Editors)
American Peptide Society, 2003

Direct Translocation of Histone Molecules Across Cell Membrane

Elana Hariton-Gazal[1], Joseph Rosenbluh [2], Chaim Gilon[1] and Abraham Loyter[2]

[1]Department of Organic Chemistry; [2]Department of Biological Chemistry, The Hebrew University of Jerusalem, Jerusalem, 91904 Israel

Introduction

During the past few years, it became apparent that certain small molecular weight proteins are able to directly cross cell plasma membrane without the involvement of the endocytic pathway. A number of natural proteins or peptides such as the HIV-1 Tat or the Arginine Rich Motif (ARM) peptide derived from it, have been defined as cell penetrating proteins or peptides (CPP) due to their ability to translocate cell plasma membrane independently of transporters or specific receptors. Very recently, however, this concept was re-evaluated leading to the suggestion that the cellular accumulation of the HIV-1 Tat-ARM peptide – thus of any positively charged peptides - is due to internalization via endocytosis and not to direct penetration [1].

The histone octamer within the eukaryotic chromatin – composed of the four histone classes H2A, H2B, H3 and H4 - is surrounded by DNA molecules, which are electrostatically bound to it [2]. In spite of the extensive use of histones as a cell delivery system, very few studies have been conducted to elucidate the way by which these molecules are taken into animal cells. It was generally assumed that internalization of histones is mediated by the clatherin-coated pits and by the endocytic pathway [3-4].

Results and Discussion

The present work [5] demonstrates that histones are able to directly cross cell plasma membranes, not via endocytosis, and can be defined as new class of CPPs. Penetration of histones occurred under various conditions known to inhibit endocytosis: it was observed at 4ºC, was not competitively inhibited by the addition of molar excess of unlabelled histones, was not saturable and was an energy independent process as it was observed in ATP-depleted cells. Our studies with various inhibitors of microtubules, microfilaments and the Golgi apparatus ruled out the possibility that histones undergo endocytosis. The possible involvement of cell microtubules and microfilaments in the penetration of the histones as well as in their trafficking into the nucleoplasm was studied by the addition of Colchicine, Nocodazole and Cytochalasin D. The involvement of the ER/Golgi in the intra-cellular trafficking of the histones, especially into the cell nuclei, was studied by the use of Brefeldin-A (BFA). Even the combination of Nystatin and Sucrose did not inhibit the penetration process, completely ruling out the involvement of either clatherin or caveoloe-mediated endocytosis. None of these inhibitors had any effect on the internalization of the histones, nor on the pattern of their intracellular accumulation. This was observed using different and independent experimental systems: fluorescent microscopy observations with fixed and unfixed HeLa cells and a novel quantitative assay system using unfixed Colo-205 cells from which surface-bound histones were removed by neutralization. The view that the penetration of histone was not mediated by pinocytosis was also strengthened by our observations showing translocation into human lymphocytes. Further support for the claim that histones are able to directly translocate biological membranes was obtained by experiments showing penetration of histones into

phospholipid liposomes. The various histones differ in their ability to penetrate intact cells. H2A and H4 were the most effective while H2B and H3 were less potent (Figure 1).

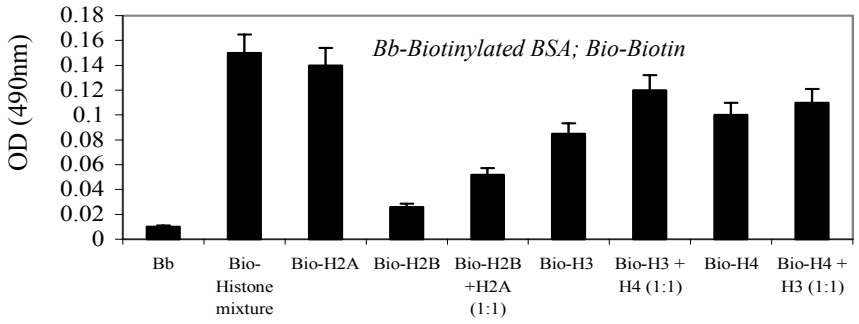

Fig. 1. Accumulation of biotinylated individual histones: quantitative estimation.

Molecules which have cell penetration ability are of potential use as carriers of drugs into cells. We have tested whether histones could carry covalently attached molecules into cells using histone-BSA constructs. Histone mixtures, as well as the histone H2A, were able to mediate the penetration of covalently attached BSA into intact cells (Figure 2). The addition of unlabelled histone mixture to the labelled histone-BSA conjugates stimulated the penetration of the labelled conjugate. Penetration of histone-BSA conjugates was distinguished by the same features that characterize the penetration of the histones, indicating that both the conjugates and histones are taken into the cells by the same route. Preliminary experiments also indicate that histones meditate the translocation of specific plasmids expressing the Luciferase gene attached to them. Utilization of such histone-DNA conjugates may open new possibilities for *in vivo* use of histones as a gene delivery system.

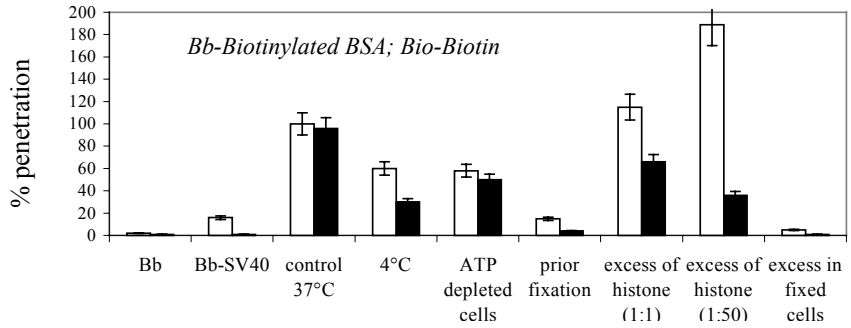

Fig. 2. Cellular and nuclear accumulation of Bb-histone conjugate within the Colo-205 cells – cytoplasm and nuclei.

References

1. Richard, J. P. *et al., J. Biol. Chem.* **278**, 585-590 (2003).
2. Luger, K. *et al*., *Nature* **389**, 251-260 (1997).
3. Ryser, H. J. P. and Hancock, R. *Science* **150**, 501-503 (1965).
4. Murphy, R. F., Jorgensen, E. D. and Cantor, C. R. *J. Biol. Chem.* **257**, 1695-1701 (1982).
5. Hariton-Gazal, E. *et al*. *J. Cell Sci.* **116**, 4577-4586 (2003).

Peptide Revolution: Genomics, Proteomics & Therapeutics
Michael Chorev & Tomi K. Sawyer (Editors)
American Peptide Society, 2003

Peptides as A New Family of Compounds with Estrogen-Like Activity

Roni Kasher[1], Batya Gayer[2], Tikva Kulik[2], Natarajan Venkatesh[1], Dalia Somjen[3], Mati Fridkin[4], Ephraim Katchalski-Katzir[1] and Fortune Kohen[2]

Departments of [1]Biological Chemistry, [2]Biological Regulation and [4]Organic Chemistry, Weizmann Institute of Science, Rehovot 76100, Israel, and [3]Institute of Endocrinology, Tel-Aviv Medical Center, Tel-Aviv University, 64239 Tel-Aviv, Israel

Introduction

The steroid hormone estradiol (E_2) regulates a diverse range of physiological processes, both within the reproductive system and outside it [1]. Estradiol mediates its effects via the nuclear estrogen receptor (ER), which functions as a ligand-activated transcriptional factor [2]. ER exists as two subtypes, ERα and ERβ. Both ERs interact either with the classical estrogen receptor element (ERE) or with activator protein (AP)-1 enhancer element [3]. The two ERs exhibit distinct tissue distribution patterns, and different binding-affinity profiles for estrogenic compounds [4].

E_2 and estrogenic compounds are currently being used in treatment of breast cancer, cardiovascular disease and osteoporosis. However, E_2 exerts detrimental effects on several pathological processes such as carcinoma of the breast and endometrium, which compromise the beneficial effects of E_2 in the bone [1]. Anti-estrogenic drugs that are currently used to treat breast carcinoma (e.g. tamoxifen) have agonistic activity in the endometrium therefore they might cause cancer of the endometrium. Accordingly, there is a strong need to develop selective estrogen receptor modulators (SERMs) with better tissue selectivity [5]. We suggest the development of peptides, as a new family of estrogenic chemicals that would have a potential of presenting new activity profiles. Furthermore, peptide mimetics of estradiol would allow facile preparation of combinatorial libraries from which new estrogen analogs with tissue selective profiles may be obtained.

Results and Discussion

A two-step approach was used to obtain a new family of estrogenic chemicals that are not related structurally to known estrogenic compounds: (a) Identification of a lead peptide that binds to ER with a low affinity using a random search method. A random search affords identification of new and independent family of ligands that are not based on known scaffolds. (b) Apply the systematic residue replacement approach presented in our previous study [6] to increase the affinity of the lead peptide to ER and obtain new peptides that are biologically active.

In the first step we used a monoclonal antibody against estradiol (mAb-E_2) to screen a 15-mer phage-display peptide library, and identified a linear peptide (LPALDPTKRWFFETK, peptide H5) that interacts specifically with mAb-E_2 (IC_{50} 1 μM) and recognizes ERα (IC_{50} of 0.5 mM) [7]. Peptide H5 activated transcription in ERα positive MCF-7 human breast cancer cells transfected with an estrogen-responsive-element (ERE)-luciferase construct. Moreover, it stimulated the specific activity of creatine kinase, an estrogen responsive enzyme, in rat tissues *in vivo*, an effect that was abolished by the selective ER antagonist raloxifene.

Subsequently, we determined the minimum sequence of the lead peptide H5 required for binding to mAb-E_2 and ER, by preparation of series of deleted peptides

derived from H5 that differ by one residue in length. The shortest peptide that bound mAb-E_2 was the tetramer WFFE, however, it did not recognize ERα or ERβ. The six-residue peptide KRWFFE (peptide 12) recognized both mAb-E_2 (IC_{50} of 1 μM) and ER (α and β; IC_{50} of 0.5 mM), a comparable binding to the original peptide H5.

In order to determine the importance of each amino-acid residue of peptide 12 for binding to mAb-E_2 and ER, Ala-screen was performed by preparing a series of 6 peptides in which each peptide represents one amino acid replacement by Ala. Residues Trp3, Phe4, Phe5 and Glu6 of peptide 12 were crucial for binding to mAb-E_2, whereas residues Lys1, and Arg2 were not important.

Next, we improved the binding potency of peptide 12 to mAb-E_2 and to ERs, using the systematic residue replacement approach [6]. Positions that are not important for binding to mAb-E_2 (positions 1 and 2 of peptide 12) were replaced by numerous amino acids, whereas positions that are important for binding (positions 3-6) were replaced only by amino acids of the same chemical nature.

A series of 34 peptides was prepared by systematic residue replacement of peptide 12. Peptides that were of special interest are listed in Table 1. A replacement of Lys1 by Val improved the binding affinity to mAb-E_2 (peptide 22, Table 1, IC_{50} of 15 nM), a two-fold increase in comparison to the parent peptide 12 (IC_{50} of 35 nM), and almost 2 orders of magnitude increase in comparison to the library-peptide H5. Interestingly, a substitution of Lys1 by Asp (reversed-charge substitution, peptide 27, Table 1) caused a dramatic loss of inhibition potency. Replacements in position 2 by Ser (peptide 36) or Pro (peptide 39) retained the inhibition of peptide 12, whether replacement of the same position by other amino acids caused loss of binding affinity (data not shown).

Table 1. Selected peptides obtained by systematic-single residue replacement of the parent peptide 12, and their binding affinities to mAb-E_2 and to ER.

Peptide no.	*Sequence*[a]	*mAb-E_2 binding (IC_{50}, μM)*[b]	*ERα binding (IC_{50}, μM)*[c]	*ERβ binding (IC_{50}, μM)*[c]
12	KRWFFE	0.035	400	400
22	**V**RWFFE	0.015	N.d.	N.d.
27	**D**RWFFE	>10	N.d.	N.d.
36	K**S**WFFE	0.040	(-)	N.d.
39	K**P**WFFE	0.045	500	>500

[a] *Residues in bold represent substitutions in peptide 12.* [b] *The inhibition of binding of E_2-ovalbumin europium conjugate to mAb-E_2.* [c] *The inhibition of binding of [^{3}H]-E_2 to ER.*

In an attempt to further increase the affinity of the synthetic peptides to mAb-E_2 and to ERs, we prepared peptides having two or three replacements concomitantly. The information obtained from the systematic single residue replacements indicated that Val may occupy position 1, Ser or Pro may be introduced to position 2 (Table 1), and Tyr may be introduced in positions 1 or 6. Peptides with two or three amino acid replacements are listed in Table 2.

Peptides 60 and 61 (Table 2), which have Val in position 1, recognized mAb-E_2 better than the parent peptide 12, with an IC_{50} of 6 nM. This inhibitory potency is better by almost three orders of magnitude than that of the 15-mer lead-peptide H5 (IC_{50} of 1 μM) described in our previous study [7]. Among peptides with high affinity to mAb-E_2

(60 and 61), only peptide 61 (Estrogen mimetic peptide-1, EMP-1) recognized ERs, with IC_{50} of 100 μM for ERα and 250 μM for ERβ.

Many of the peptides described here are partially insoluble in aqueous solutions, and are not compatible with the receptor-binding assay. An introduction of Lys or Asp at the amino or carboxy terminus of peptides 22, 55, and 61 yielded soluble analogs (data not shown). Among these soluble analogs only peptide 74 (EMP-2; see Table 2) maintained the receptor binding potency of its parent peptide EMP-1.

Table 2. Peptides obtained by multiple-residue replacement.

Pep no.	*Sequence*	*mAb-E_2 binding (IC_{50}, μM)*	*ERα binding (IC_{50}, μM)*	*ERβ binding (IC_{50}, μM)*
12	KRWFFE	0.035	400	400
60	**VP**WFFE	0.006	(-)	(-)
61 (EMP-1)	**VS**WFFE	0.006	100	250
63	**VS**WF**Y**E	0.2	N.d.	N.d.
67	**YS**WFF**Y**	20	N.d.	N.d.
74 (EMP-2)	**VS**WFFE**D**	0.030	200	125

Finally, we evaluated the estrogenic activity of peptides EMP-1 and EMP-2 *in vivo*. Peptide EMP-1 (0.5 mg/rat) caused an increase in the specific activity of creatine kinase, an estrogen-responsive gene, in all rat tissues examined (see Table 3). On the other hand, peptide EMP-2 induced activity only at the pituitary. Although differing by only one amino acid residue, peptide EMP-1 and EMP-2 possess different activity profiles in the tissues examined.

Table 3. Stimulation of the specific activity of creatine kinase by estrogen and by synthetic peptides in rat tissues in-vivo.

	Epiphysis (bone)	*Diaphysis (bone)*	*Uterus*	*Pituitary*
EMP-1 (6-mer)	⇑	⇑	⇑	⇑
EMP-2 (7-mer)	(-)	(-)	(-)	⇑
H5 (15-mer)	(-)	(-)	⇑	(-)
E_2	⇑	⇑	⇑	⇑

In conclusion, development of peptides as estrogenic compounds has tremendous importance since a new family of estrogenic chemicals would have a potential to present new activity profiles.

Acknowledgments

We wish to thank Aviva Kapitkovsky and Sara Rubinraut (Weizmann Institute of Science) for assistance in peptide synthesis.

References

1. Norman, A. W. and Litwack, G. In Litwack, G. (Ed.), *Estrogens and Progestins,* Academic Press, London, pp. 550-560 (1987).
2. McKenna, N. J. and O'Malley, B. W. *Ann. N. Y. Acad. Sci.* **949**, 3-5 (2001).
3. Evans, R. M. *Science* **240**, 889-95 (1988).
4. Kuiper, G. G., *et al*., *Endocrinology* **139**, 4252-63 (1998).
5. Jordan, V. C. *J. Med. Chem.* **46**, 883-908 (2003).
6. Kasher, R., *et al*., *Chem. Biol.* **8**, 147-55 (2001).
7. Venkatesh, N., *et al*., *Peptides* **23**, 573-80 (2002).

Peptide Revolution: Genomics, Proteomics & Therapeutics
Michael Chorev & Tomi K. Sawyer (Editors)
American Peptide Society, 2003

Macrocyclization in the Design of Tetrapeptide Mimetics that Display Potent Inhibition of Grb2 SH2 Domain Binding in Whole Cell Systems

Z.-D. Shi,[1] C.-Q. Wei,[1] X. Wang,[1] K. Lee,[1] H. Liu,[2] M. Zhang,[2] J. Vasselli,[3] L. R. Roberts,[4] K. M. Worthy,[4] M. J. Fivash,[4] R. J. Fisher,[4] D. P. Bottaro,[3] W. M. Linehan,[3] D. Yang[2] and T. R. Burke, Jr.[1]

[1]Laboratory of Medicinal Chemistry, CCR, NCI, NIH, Frederick, MD 21702, USA; [2]University of Michigan Medical School, Ann Arbor, MI 48109 USA; [3]Urologic Oncology Branch, CCR, NCI, NIH, Bethesda, MD 20892, USA, [4]Protein Chemistry Laboratory, SAIC-Frederick, Frederick, MD 21702 USA

Introduction

The growth factor receptor-bound protein 2 (Grb2) provides critical connectivity between growth factor receptor PTKs and downstream oncogenic Ras signaling. Grb2 SH2 domain-binding antagonists could potentially serve as therapeutics for a variety of cancers, including ErbB-2-dependent breast cancers and Met-dependent kidney cancers. Lead structures of type **1** have been reported by Novartis Corporation as high affinity Grb2 SH2 domain-binding inhibitors that take advantage of the preferred interactions of Grb2 SH2 domains with pTyr-Xxx-Asn containing peptides in type I β-bend conformations (Figure 1) [1]. We have previously reported analogues of **1** in which the pTyr residue has been replaced by mimetics such as **2** and **3** that vary in their phosphate-mimicking moieties and in their α-functionalities [2]. We have shown that appending a carboxyl group from the pTyr mimetic α-position can both increase binding affinity, presumably through favorable interactions with the αA2 Arg67 residue, and enhance activity in whole cell systems.

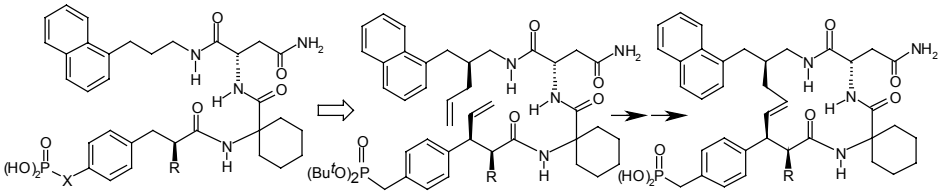

Fig. 1. Structures of open-chain and macrocyclic tetrapeptide-mimicking analogues.

In further work intended to enhance binding affinity through global conformational constraint, we designed macrocycles of type **6** and **7** that would be approached using ring-closing metathesis (RCM) of intermediates **4** and **5**. Ring closure of **4** was achieved using "first generation" Grubbs catalyst [3]. The resulting macrocyclic end product **6** showed a 100-fold increase in binding potency relative to the corresponding open-chain parent, validating the macrocycle design (Table 1) [4]. However, very poor efficacy was observed in whole cell preparations, presumably due to a lack of the critical pTyr mimetic α-carboxylic functionality. Therefore, attempts to introduce α-functionality were undertaken using RCM reactions on intermediates such as **5**. Unexpectedly, ring closure failed using first generation Grubbs catalyst, most probably

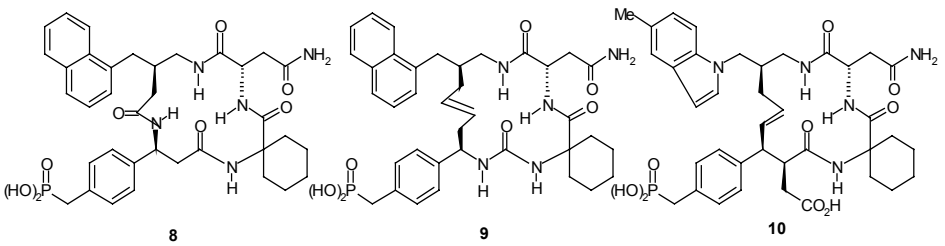

Fig. 2. Variations on macrocycles shown in Fig. 1.

due to steric crowding originating from the α-substituent. Reported herein is work directed toward introduction of needed α-functionality.

Results and Discussion

As an initial approach toward introducing α-functionality, macrocycles were prepared that either didn't rely on RCM ring closure (β-amino-containing **8**) or that afforded altered geometry at the α-position that might alleviate steric crowding (ureapeptido **9**) (Figure 2). Unfortunately, these modifications resulted in significant reductions in binding affinity relative to parent **6** (Table 1).

Utilizing a "second generation" Grubbs catalyst at elevated temperature, it was found that ring closure of α-substitutent-bearing analogues such as **5** could be achieved, leading to the preparation of fully functionalize macrocycles such as **7** [5]. In extracellular Grb2 SH2 domain-binding assays it was found that **7** exhibited significantly higher potency than the open-chain variant **2** as well as the equivalent macrocycle lacking an α-substitutent (**6**) (Table 1). Of equal importance, macrocycle **7** displayed markedly enhanced efficacy in whole cell systems as indicated by its ability to block association of Grb2 with activated erbB-2 PTK (Figure 3) and its antimitogenic effects in the ErbB-2 over-expressing breast cancer cell line MDA-MB-453 (Figure 4). This latter effect was not observed in MDA-MB-231 breast cancer cells, which are not mitogenically driven through the ErbB-2 system, indicating that effects in the MDA-MB-453 cells do not reflect simple cytotoxicity.

Table 1. Results of extracellular ELISA-based Grb2 SH2 domain binding assays[a].

Compound	IC_{50} (nM)	Compound	IC_{50} (nM)
2	20	**8**	8,000
6	20	**9**	650,000
7	1	**10**	K_D=0.062[b]

*[a]Experiments were performed as previously described [5]. [b]Obtained from plasmon resonance analysis of direct binding of **10** to Grb2 SH2 domain protein using Biacore.*

Additional aspects of the macrocycle **7** are amenable to further optimization. Based on the previous demonstration by Novartis that replacement of the naphthyl ring with a 5-methyl indolyl moiety resulted in affinity increases in open-chain mimetics [6], macrocycle **10** was prepared and shown to exhibit significantly enhanced potency.

Biacore analysis of direct binding of **10** to Grb2 SH2 domain protein provided a K_D value of 62 pM. *This value is currently the most potent yet reported for a synthetic binding antagonist against any SH2 domain*. In whole cell studies nearly complete inhibition of intracellular binding of Grb2 to activated erbB-2 was achieved at 30 nM concentrations (Fig. 3). Macrocycle **10** inhibits the erbB-2 dependent growth of MDA-

MB-453 breast cancer cells with an IC_{50} value of 0.6 μM, while being much less toxic to non-erbB-2 dependent breast cancer cells MDA-MB-231 (IC_{50} > 10 μM).

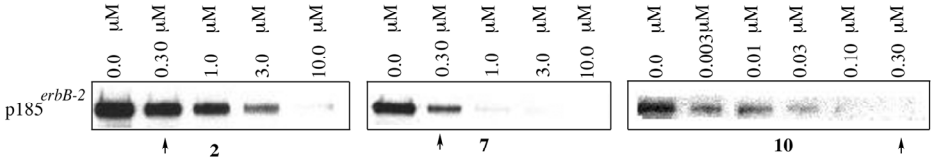

Fig. 3. Inhibition of Grb2 SH2 binding to erbB-2 in whole cells following extracellular administration of compounds at the indicated concentrations.

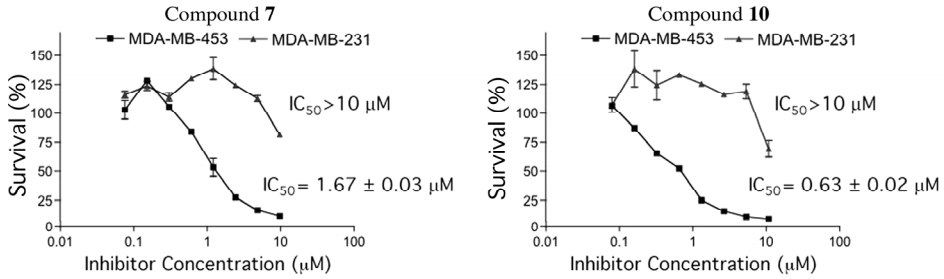

*Fig. 4. Antimitogenic effects of macrocycles **7** and **10** in MDA-MB-453 and MDA-MB-231 breast cancer cell lines.*

Macrocyclic tetrapeptide mimetics have been developed that exhibit potent inhibition of Grb2 SH2 domain binding in extracellular assays. When administered to whole cells certain of these agents are able to inhibit the binding of cytoplasmic Grb2 to activated erbB-2 at low nanomolar concentrations without prodrug derivatization or the use of carrier peptides. Promising antimitogenic effects against erbB-2 driven breast cancer cells provide evidence of the potential therapeutic utility of this class of signaling antagonist.

References

1. Furet, P.; Gay, B.; Caravatti, G.; GarciaEcheverria, C.; Rahuel, J.; Schoepfer, J.; Fretz, H. *J. Med. Chem.* **41**, 3442-3449 (1998).
2, Wei, C.-Q., Li, B., Guo, R., Yang, D. and Burke, T. R., Jr. *Bioorg. Med. Chem. Lett.* **12**, 2781-2784 (2002).
3. Gao, Y., Wei, C.- Q. and Burke, T. R., Jr. *Org. Lett.* **3**, 1617-1620 (2001).
4, Gao, Y., Voigt, J., Wu, J. X., Yang, D. and Burke, T. R., Jr. *Bioorg. Med. Chem. Lett.* **11**, 1889-1892 (2001).
5. Wei, C.- Q., Gao, Y., Lee, K., Guo, R., Li, B., Zhang, M., Yang, D. and Burke, T. R., Jr. *J. Med. Chem.* **46**, 244-254 (2003).
6. Schoepfer, J., Fretz, H., Gay, B., Furet, P., GarciaEcheverria, C., End, N. and Caravatti, G. *Bioorg. Med. Chem. Lett.* **9**, 221-226 (1999).

Peptide Revolution: Genomics, Proteomics & Therapeutics
Michael Chorev & Tomi K. Sawyer (Editors)
American Peptide Society, 2003

Potent Grb2-SH2 Domain Antagonists Discovered by Extensive SAR Studies

Peng Li[1], Megan L. Peach[1], Manchao Zhang[2], Hongpeng Liu[2], Dajun Yang[2], Marc Nicklaus[1] and Peter P. Roller[1]

[1]Laboratory of Medicinal Chemistry, National Cancer Institute, NIH, Frederick, MD 21702, USA; [2]Department of Biomedical Sciences; [2]School of Medicine, University of Michigan, Ann Arbor MI 48109, USA

Introduction

Intervention of the intracellular protein-protein interactions involving activated tyrosine kinase receptors and the Src homology 2 (SH2) domain of Growth factor receptor bound protein 2 (Grb2) [1] in the Ras signaling pathway is a conceptually attractive and contemporary approach to blocking human malignancy, since these interactions play significant roles in controlling mitogenic Ras signal transduction pathways that are activated or deregulated in cancer cells [2, 3]. Grb2-SH2 domain binding antagonists represent new therapeutics for the treatment of a variety of diseases including cancers [4]. Generally, the pTyr-X-Asn minimal binding motif is required for a high-affinity ligand binding to the Grb2-SH2 domain. Using phage-display techniques, we discovered a non-pTyr-containing cyclic peptide **G1** with moderate binding affinity from 10^7 different sequences [5]. To understand the structural basis for the high-affinity binding of these cyclic peptides to the Grb2-SH2 domain, we extensively studied herein the structure-activity relationship of G1TE analogs, with the aim at the development of potent Grb2-SH2 domain antagonists based upon this novel template (Scheme 1).

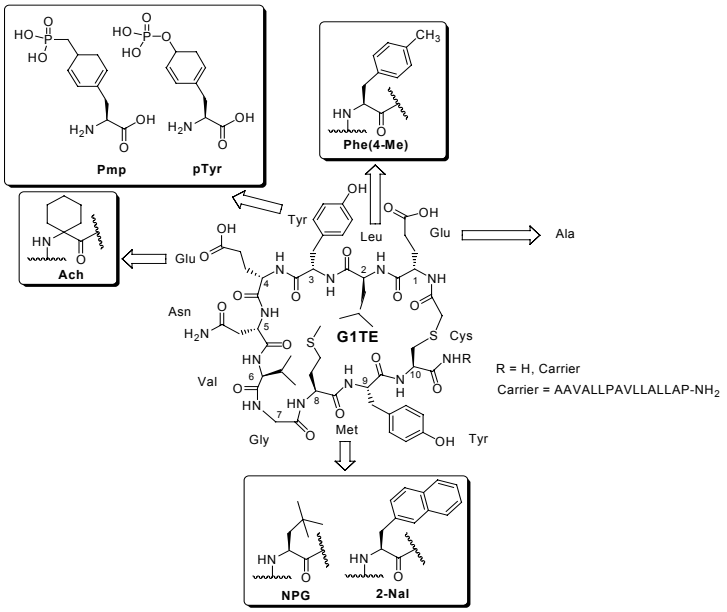

Scheme 1. Synthesis of G1TE analogs.

Table 1. Grb2-SH2 domain inhibitory activity of the G1TE analogs evaluated by ELISA assays.

Peptide	IC_{50} (μM)[a]
G1TE (lead)	> 100[b]
G1TE ($pTyr^3$)	0.14 ± 0.05
G1TE (A^1pTyr^3)	0.025 ± 0.009
G1TE ($A^1pTyr^3Ach^4$)	0.0038 ± 0.0001
G1TE ($A^1Pmp^3Ach^4$)	0.013 ± 0.001
G1TE($A^1Phe(4\text{-}Me)^2pTyr^3Ach^4Nal^8$)	0.0023 ± 0.0002
G1TE($A^1Pmp^3Ach^4Nal^8$)	0.0024 ± 0.0009
G1TE($A^1Pmp^3Ach^4NPG^8$)-carrier	0.013 ± 0.004

[a] *Values are means of at least three experiments, standard deviation is given.*

[b] *Biacore assay indicates that the parent compound G1TE exhibits inhibitory activity with an IC_{50} = 20 μM.*

Results and Discussion

Incorporation of phosphotyrosine or Phosphonomethylphenylalanine (Pmp) into the third position of G1TE analogs remarkably improves the binding affinity of these thioether-bridged cyclic peptides, as shown in Table 1. Since the Grb2-SH2 domain requires a peptide ligand to bind to it in a β-turn conformation, the more potent Grb2-SH2 antagonists were obtained when replacing Glu^4 with the turning-inducing amino acid 1-amino-1-cyclohexylic acid (Ach). The intramolecular hydrophobic packing of the amino acid residues in the second, eight and tenth positions of G1TE analogs considerably stabilizes the favorable conformation for these cyclic peptides binding to Grb2-SH2 protein. Consequently, incorporating Phe(4-Me) and NPG into the second and eighth positions of G1TE can further improve the inhibitory activity of G1TE analogs. Based upon these SAR studies, we are able to develop several very potent Grb2-SH2 inhibitors, such as the phosphatase-resistant G1TE($A^1Pmp^3Ach^4Nal^8$) with an IC_{50} = 2.4 nM, which is at least 40,000 times more potent than G1TE. These high-affinity Grb2-SH2 binding peptides, especially the carrier-conjugated peptide G1TE($A^1Pmp^3Ach^4NPG^8$)-carrier can cross cell membranes and effectively inhibit the association of the Grb2 with the $p185^{erbB2}$ complex in erbB2-overexpressing MDA-MA-453 cancer cells at a low micromolar concentration. Undoubtedly, these cyclic peptides are promising leads for the further development of pharmacokinetically improved therapeutic agents targeting Grb2-SH2 domain for the treatment of erbB2-related cancer.

References

1. Chardin, P., Cussac, D., Maignan, S. and Ducruix, A. *FEBS Lett.* **369**, 47-51 (1995).
2. Smithgall, T. E. *J. Pharmacol. Toxicol. Methods* **34**, 125-132 (1995).
3. Lowenstein, E. J., et al. *Cell* **70**, 431-442 (1992).
4. Garcia-Echeverria, C. *Curr. Med. Chem.* **8**, 1589-1604 (2001).
5. Oligino, L., Lung, F.- D. T., Sastry, L., Bigelow, J., Cao, T., Curran, M., Burke, T. R., Jr., Wang, S., Krag, D., Roller, P. P. and King, C. R. *J. Biol. Chem.* **272** 29046-29052 (1997).

Peptide Revolution: Genomics, Proteomics & Therapeutics
Michael Chorev & Tomi K. Sawyer (Editors)
American Peptide Society, 2003

Protein P2 from *Haemophilus influenzae*: The Role of its Surface Exposed Loops on the Mitogen-Activated Protein Kinase Cascade

Stefania Galdiero[1,4], Domenica Capasso[1,4], Mariateresa Vitiello[4], Marina D'Isanto[2], Erminia Di Niola[1,4], Simona Monti[1,4], Menotti Ruvo[1,4], Carlo Pedone[1,4] and Massimiliano Galdiero[3]

[1] Dipartimento di Chimica Biologica, Università degli Studi di Napoli Federico II & Istituto di Biostrutture e Bioimmagini, Via Mezzocannone 6, 80134 Naples, Italy; [2]Dipartimento di Patologia Generale, Facoltà di Medicina e Chirurgia, Seconda Università di Napoli, Via De Crecchio 7, 80138 Naples, Italy; [3]Dipartimento di Medicina Sperimentale, Facoltà di Medicina e Chirurgia, Seconda Università di Napoli, Via De Crecchio 7, 80138 Naples, Italy; [4]Centro Interuniversitario di Ricerca sui Peptidi Bioattivi, Via Mezzocannone 6, 80134 Naples, Italy

Introduction

Porin of nontypeable *Haemophilus influenzae* (NTHI) is one of the best characterized porins in terms of its functional characteristics. Sequence analyses of P2 genes indicate that the transmembrane regions are relatively conserved among strains, while considerable heterogenicity exists in the loop regions of the molecule. The activation of the inflammatory and immunological response is initiated by interactions with the bacterial cell or one of its components and involves the phosphorylation of the main signal transduction networks. In this study, we developed a model of protein P2 from *H. influenzae* type b (Hib) and investigated in detail which domains of the protein are involved in the signalling pathways.

Results and Discussion

As the three-dimensional structure has not yet been determined, we used molecular modeling techniques to generate a three-dimensional homology model of the porin starting from the X-ray structures of Phoe and Ompf from *Escherichia coli* [1], and Ompk36 from *Klebsiella pneumoniae.* The homology model enabled us to identify more precisely the structural as well as functional roles of individual residues and of loop regions. Despite low sequence identity, structurally known proteins of the porin family superimpose surprisingly well. Thus, we verified the signalling activity of the porin P2 from Hib and investigated in detail which domains of the protein are involved in signaling pathways. The protein P2 isolated from strain ATCC 9795 was able to induce tyrosine phosphorylation in U937 cells in a dose-dependent manner as demonstrated previously for THP-1 cells [2]. Thus, in our experiments we used protein concentrations of 0.13 nmol/mL.

We next examined the activation of MEK1-MEK2/MAPK pathway in untreated as well as Hib porin stimulated U937 cells. U937 cells (3 x 10^6 cells/mL) were treated with 0.13 nmol/mL (5 γ/mL) of porin. Cell lysates were prepared at different time points after the stimulation. The lysates obtained were immunoprecipitated with antibodies that specifically recognized the phosphorylated and nonphosphorylated forms of each enzyme. The results obtained in this study showed that porins from Hib are able to induce the activation of signaling pathway in U937 cells and we also identified one of the phosphorylation pathways that was activated through the MEK1-MEK2/MAPK cascade. The concentration of the stimuli used as well as porin from Hib activates, mainly but not exclusively, the JNK and p38 pathways. Peptides corresponding to the amino acid sequences of variable loop regions facing the cell exterior, and thus more probably involved in the initial interaction with the host cell,

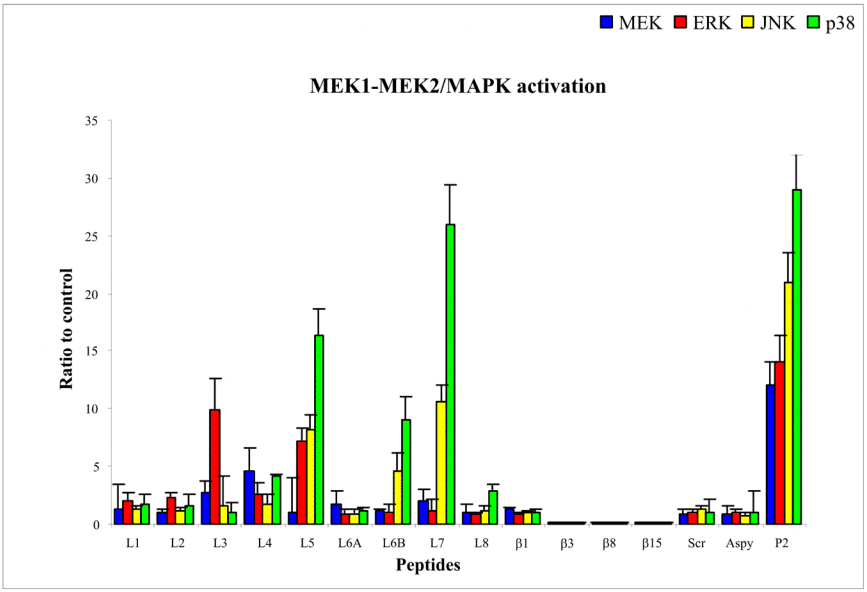

Fig. 1. MEK1-MEK2/MAPK activation in response to optimal doses and times for each peptide and for Hib. The ratio of each peptide to an unstimulated control is shown. The data are presented as an average from three separate experiments.

were synthesised. Peptide concentrations of 0.01 nmol/mL, 0.05 nmol/mL, 0.13 nmol/mL, 5.0 nmol/mL, 12 nmol/mL and 26 nmol/mL were assayed in our experiments (see Figure 1). As for the entire protein, signals from active peptide were visible by 3 min from the treatments with an activity peak at 10 min, which persists for at least 20 min thereafter and goes back to standard amounts by 60 min. Our results show that peptides corresponding to surface loops of protein P2 are able to activate the MEK1-MEK2/MAPK pathways. In particular, they are able to activate the MAPK pathway in a manner similar to the entire porin P2, thus confirming the validity of the proposed modeling.

In this study we showed that peptides corresponding to loop variable regions, not involved in structural functions, are mainly responsible for the activation of the MEK1-MEK2/MAPK signal transduction pathway. In particular, surface peptides corresponding to loops L5, L6 and L7, that in the model do not seem to have any obvious structural function, showed a prominent JNK and p38 activation. Our experiments are sufficient to determine which regions of the protein are involved in signal transduction, and thus, which regions should be subject to further analyses.

References

1. Cowan, S. W., et al. *Nature* **358**, 727-733 (1992).
2. Galdiero, M., et al. *FEMS Immunol. Med. Microbiol.* **13**, 121-130 (2001).

Peptide Revolution: Genomics, Proteomics & Therapeutics
Michael Chorev & Tomi K. Sawyer (Editors)
American Peptide Society, 2003

RDP58, A Rationally Designed Peptide, Inhibits Multiple Forms of Pathogenic Inflammation Through the Inhibition of p38MAPK and JNK

Suhasini Iyer[1], Ricardo Gonzalez[2], Jingsong Zhao[1], Mirella Lazarov[1], Ajith Welihinda[1], Roland Buelow[1], Alexis Te[2] and Timothy Fong[1]

[1]Department of Discovery Research, Sangstat Medical Corporation, Fremont, CA 94555, USA;
[2]Department of Urology, Weill Cornell Medical College, New York, NY 10021, USA

Introduction

To identify anti-inflammatory peptides with therapeutic potential, naturally occurring peptides were subjected to computer-assisted rational design based on a variable mapping approach [1], in which the biological activity of a learning set of isomeric forms of test peptides were analyzed using a nonlinear function of structural, topological, and molecular descriptors. Using a decapeptide derived from a class 1 major histocompatability protein shown to have non-allele specific immunosuppressive activity [2], RDP58 was identified from an initial learning set of peptides to have about 100-fold better activity and superior pharmacokinetics *in vivo* [3] .

RDP58 inhibits the over-production of tumor necrosis factor (TNF) α, interferon (IFN) γ, and IL12 in several animal models of inflammatory disease. Additionally, it up-regulates hemeoxygenase (HO-1) expression. Oral dosing of RDP58 is highly therapeutic in rodent models of colitis [4, 5], chemotherapy-induced diarrhea (CID), and spontaneous colitis in monkeys. RDP58 has recently been shown to significantly reduce clinical scores in patients with mild to moderate, active Ulcerative colitis in Phase II clinical studies and is currently in a Phase 1 safety study for CID.

Results and Discussion

Because RDP58 was identified based on *in vivo* and *in vitro* activity, we had no prior understanding of the molecular mechanism of action or molecular target for RDP58. Our data from co-immunoprecipitation studies of THP-1, Jurkat, and CaCo2 cells show that RDP58 inhibits the formation of the TRAF6-MyD88-IRAK (TRAFYK) complex, which is formed and initiates the intracellular signal transduction cascade after signaling through the Toll-like (TLR)/IL1 and TNFα receptor families. Disruption of TRAFYK formation inhibits the response to LPS, dsRNA, TNFα, IL1β, and other pro-inflammatory signals [6-8]. Inhibition of TRAFYK complex formation results in the inhibition of downstream phosphorylation and activation of p38MAPK and JNK. Both pathways are involved in the translational regulation of TNFα mRNA stability [9, 10] and regulation of transcription factors controlling expression of cytokine genes like IFNγ and IL2 [11]. These studies suggest that RDP58 may be used to treat inflammatory diseases by inhibiting the production and response to several pro-inflammatory stimuli and cytokines

Acute experimental cystitis was induced by transurethrally catheterizing mice and instilling LPS or SP. After 45 minutes, the bladders were drained and instilled with either distilled water (DW) or RDP58 (1mg/ml) for an additional 30 minutes. Twenty-four hrs after the RDP58 treatment, the bladders were removed for histopathological and cytokine production analysis. When given to LPS-exposed mice, RDP58 reduced PMN count by 83%, edema by 70%, and mast cell count by 45% (Table 1). RDP58 treatment *in vivo* significantly reduced TNFα production as well. Similar results were observed in studies using SP-induced inflammation.

Table 1. Histological analysis of RDP58 in experimental cystitis.

Treatment	PMN Count	Edema Grade	Mast Cell Count	TNFα pg/ml
Saline/DW	3.8 ± 0.8	0.1 ± 0.1	3.9 ± 0.5	0 ± 0
Saline/RDP58	3.6 ± 0.3	0 ± 0	3.0 ± 0.3	0 ± 0
LPS/DW	65.8 ± 7.9	2.7 ± 0.1	4.4 ± 0.7	25.9 ± 8.6
LPS/RDP58	11.5 ± 3.8*	0.8 ± 0.27*	2.4 ± 0.5	0 ± 2.5

** $p<0.05$ compared to LPS/DW group.*

In the bleomycin-induced pulmonary fibrosis model, RDP58 was tracheally instilled into the lungs to determine if RDP58 treatment can inhibit inflammation leading to fibrosis. A single instillation of RDP58 on Day 0 significantly decreased leukocyte infiltration and TNFα levels in bronchial lavage fluid at the peak of inflammation on Day 7 (Table 2). When given on Days 0, 7, 14, and 21, histological analysis showed that RDP58 significantly inhibited pulmonary fibrosis. Additionally, a single RDP58 administration on Day 0 or 7 only was also effective, indicating that RDP58 can be used to prevent or treat lung fibrosis.

Table 2. RDP58 inhibits pulmonary inflammation.

Treatment	PMN Count (x 10^{-4}/ml)	TNFα (pg/ml)
Control	3.6 ± 0.5	174 ± 30
Bleomycin only	46.9 ± 5.7	762 ± 139
Bleo + 0.25mg/kg RDP58	38.8 ± 3.9	237 ± 65*
Bleo + 0.5mg/kg RDP58	25.5 ± 5.9*	134 ± 72*
Bleo + 1.0mg/kg RDP58	14.5 ± 1.6*	162 ± 128*

** log mean compared to bleomycin only group ($p<0.05$).*

In summary, intravesical instillation of RDP58 inhibits polymorphonuclear (PMN) cell infiltration, bladder wall edema, and TNFα expression in a mouse model of inflammatory cystitis. Intratracheal instillation of RDP58 also significantly inhibits bleomycin induced PMN infiltration, and TNFα production in the lungs. These preclinical studies suggest that RDP58 may potentially be therapeutic in several other inflammatory diseases.

References

1. Grassy, G., et al. *Nature Biotechnol.* **16**, 748-752 (1998).
2. Cuturi, M. C., et al. *Transplantation* **59**, 661-669 (1995).
3. Iyer, S., Lahana, R. and Buelow, R. *Current Pharm. Design* **8**, p. 99-110 (2002).
4. Murthy, S., et al. *Inflamm Res.* **51**, 522-531 (2002).
5. Bourreille, A., et al. *Scand. J Gastroenterol.* **38**, 526-532 (2003).
6. Takeuchi, O., et al. *Int. Immunol*. **12**, 113-117 (2000).
7. Cao, Z., et al. *Nature* **383**, 443-446 (1996).
8. Suzuki, N., et al. *Nature* **416**, 750-756 (2002).
9. Kontoyiannis, D., et al. *Embo J.* **20**, 3760-2770 (2001).
10. Dumitru, C. D., et al. *Cell* **103**, 1071-1083 (2000).
11. Sullivan, K. E. *Immunol. Res.* **27**, 529-538 (2003).

Peptide Revolution: Genomics, Proteomics & Therapeutics
Michael Chorev & Tomi K. Sawyer (Editors)
American Peptide Society, 2003

Endeavors Toward a Specific Inhibitor for HDAC6

Tamaki Kato[1], Binoy Jose[3], Shinji Okamura[1], Yuko Sumida[3], Minoru Yoshida[2,3] and Norikazu Nishino[1,3]

[1]Graduate School of Life Science and Systems Engineering, Kyushu Institute of Technology, Kitakyushu, Japan; [2]RIKEN, Saitama 351-0198, Japan; [3]CREST Research Project, Japan Science and Technology Corp., Saitama, 332-0012, Japan

Introduction

The reversible acetylation of histone has a critical role in transcriptional regulation and the reversible acetylation of non-histone substrates is important for other cellular processes. Acetylation and deacetylation of histones are catalyzed by specific enzyme families, histone acetyl transferaces (HATs) and deacetylatses (HDACs), respectively. HDACs are integral nuclear enzymes that modulate the deacetylation of specific acetylated lysine residues. An increasing number of HDACs are being identified in different species, which are classified into different families. Structural differences among the members of each family suggest that it will be possible to develop specific inhibitors for each of these proteins, which would be useful for elucidating their individual cellular functions. Recent reports show that HDAC6 is a tubulin deacetylase [1]. A lysine residue at position 40 of α-tubulin is modified with an acetyl group. This reversible acetylation of α-tubulin is associated with microtubule stability. Based on the fact that α-tubulin is the target of HDAC6, we designed and synthesized a new inhibitor for HDAC6 using a cyclic hexapeptide cap group with the active sequence of α-tubulin (Figure 1) and aminosuberyl-ζ hydroxamic acid as the zinc binding functional group.

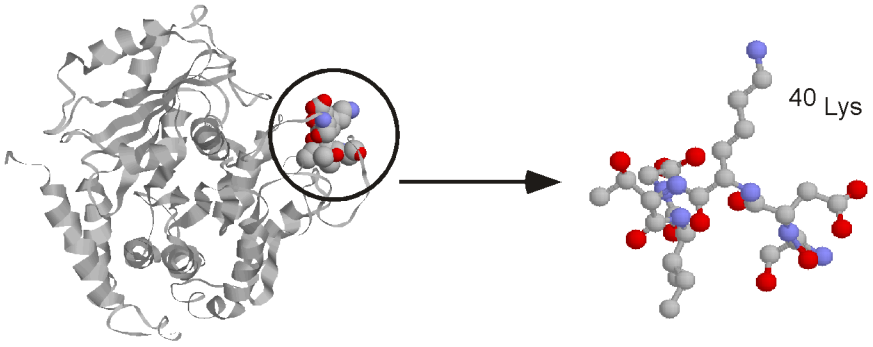

Fig. 1. Structure of α-tubulin and the enlarged view of amino acid residues from 38 to 43.

Results and Discussion

To study the conformation of the active sequence in the cyclic hexapeptide and compare it with that of tubulin sequence, we initially synthesized a substrate *cyclo*(Ser-Asp-Lys(Ac)-Thr-Ile-Gly). This compound was synthesized using the solid phase peptide method on oxime resin using Boc protection strategy with benzyl protected side-chains. The linear peptide was cyclized in DMF using HATU and side-chains were deprotected by catalytic hydrogenation. The cyclic hexapeptide was purified by HPLC and characterized by HR-FABMS and NMR. Next we synthesized the cyclic

hexapeptide inhibitor *cyclo*(Ser-Asp-Asu(NHOH)-Thr-Ile-Gly). The linear hexapeptide was synthesized using Barlos resin preloaded with Fmoc protected glycine on a synthesizer (Applied biosystems model 433A) by Fmoc strategy. The Fmoc amino acids used were Ile, Thr(tBu), Asu(OBzl), Asp(OtBu) and Ser(tBu) were, Asu is aminosuberic acid. The linear hexapeptide was cleaved from resin using acetic acid and cyclized in DMF using HATU as coupling agent and purified by column chromatography to yield 50% of cyclic hexapeptide. The benzyl ester was deprotected by catalytic hydrogenation and then coupled with hydroxylamine. The cyclic peptide was deprotected with TFA and purified by gel filtration (sephadex-LH 20) to yield the target compound in 96% yield. The cyclic hexapeptide is further purified by HPLC and characterized by HR-FABMS and ^{1}H NMR.

The cyclic hexapeptide inhibitor showed rather low inhibitory activity toward HDAC6 in comparison with the activity of the cyclic tetrapeptide-hydroxamic acid inhibitors (CHAPs) [2]. Conformational analysis of the cyclic hexapeptide by ^{1}H-NMR in DMSO-d_6 and MM calculation showed that the 3D-structure around the sequence containing the aminosuberyl residue in the cyclic hexapeptide differs from the crystal structure of the sequence containing Lys(Ac) in tubulin, as shown in Figure 2 [3]. Type I like β-turn was observed in this cyclic peptide, while type-II' like β-turn was observed in the tubulin crystal structure around Lys(Ac). This conformational difference may cause the low inhibitory activity of this cyclic peptide toward HDAC6.

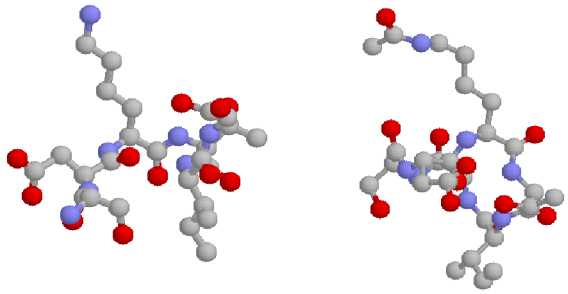

Fig. 2. Conformations of α-tubulin (from 38 to 43) and cyclic hexapeptide.

Acknowledgments

The work was funded by a research grant from the CREST Research Project, Japan Science and Technology Corporation.

References

1. Matsuyama, A., Shimazu, T., Sumida, Y., Saito, A., Yoshimatsu, Y., Seigneurin-Berny, D., Osada, H., Komatsu, Y., Nishino, N., Khochbin, S., Horinouchi S. and Yoshida, M. *EMBO J.* **21**, 6820-6831 (2002).
2. Komatsu, Y., Tomizaki, K., Tsukamoto, M., Kato, T., Nishino, N., Sato, S., Yamori, T., Tsuruo, T., Furumai, R., Yoshida, M., Horinouchi S. and Hayashi, H. *Cancer Res.* **61**, 4459-4466 (2001).
3. Nogales, E., Wolf, S. G. and Downing, K. H. *Nature* **391**, 199-203 (1998).

Peptide Revolution: Genomics, Proteomics & Therapeutics
Michael Chorev & Tomi K. Sawyer (Editors)
American Peptide Society, 2003

The Proteome and the Metabolome – A Structural Perspective

Irene Nobeli and Janet Thornton

EMBL – European Bioinformatics Institute, Wellcome Genome Campus,
Hinxton, Cambridge, CB10 1SD, UK

Introduction

Following whole genome sequencing, the general view within the biology community is that the time has finally come to move from studying the parts to studying the whole, from individual proteins to cell organization, and from reductionist biology to systems biology. Just as a complete list of the components in a car would be of little use in building one, the complete genome, and even complete proteome, is necessary but not sufficient for reconstructing a cell. The whole is bigger than the sum of its parts because the parts interact.

It is impossible to foresee all the benefits that may arise from having an integrated picture of how the cell works, but the following are areas that are likely to benefit the most: a) The fight against disease – from the understanding of how biochemical networks work, we shall be able to more successfully target the proteins responsible for a genetic or acquired malfunction, avoiding a detrimental effect on the rest of the network. It should be possible to design better drugs, which are non-toxic by predicting in advance the cross-reactivity of a drug. b) Protein function prediction - as new proteins are sequenced and their structures revealed, possible functions may be predicted, for example, by identifying the small molecules they are most likely to interact with, or even their role in a reaction network. c) Protein engineering – we shall be able to design new binding sites to achieve interaction with synthetic or natural ligands of our choice, and use them to perform new catalytic functions leading to synthesis of desired compounds (such as antibiotics).

In this paper, we briefly review, from a bioinformatics perspective, our knowledge of the proteome, the metabolome, and the networks which link them.

Results and Discussion

The proteome world

Advances in genome sequencing have resulted in an exponential increase of protein sequences available (in July 2003 there were over 940,000 translated sequences in TrEMBL, with less than one quarter of them predating the year 2000 [1]). New sequences not only have expanded our repertoire of known protein families, but, importantly, they have populated existing families, thus allowing for more reliable comparative sequence analyses. At the same time, the number of structures of proteins has increased dramatically (see Figure 1), although it is clearly far from catching up with the rate of sequence determination. Over 22,000 protein structures are already in the Protein Data Bank (PDB) [2], and structural genomics programs promise to deliver many more. Protein family classification schemes based on structural information have matured considerably in the last decade, and are now, at least partly, automated. CATH [3], SCOP [4], and Dali [5] are widely used by the bioinformatics community. It is now clear that there are a limited number of folds [6-8], that a few superfolds cover the majority of known protein structures, and that any future structures determined are most likely to belong to already known, rather than new, folds. Proteins can be clustered into homologous superfamilies. The members of such families have obvious structural similarities but their sequences may have diverged considerably, foiling our

attempts to detect their evolutionary relationship using sequence comparison methods. These evolutionary perspectives are unique to the molecules of the genome and proteome, and this has a number of implications when we try to relate the proteome to the small molecule world. Beyond sequence and structure analysis, the interactions of proteins are also currently under investigation. A recent explosion in efforts to correlate protein expression and function using microarray and proteome technologies is promising to deliver crucial information on how protein networks function, which proteins are likely to be co-expressed etc.

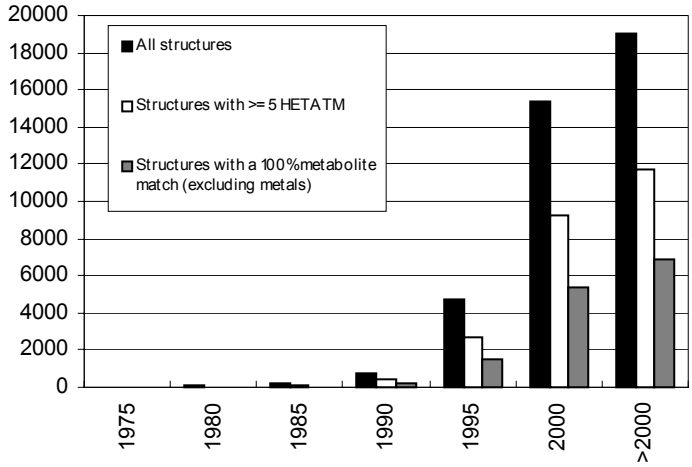

Fig. 1. The growth in the number of protein-ligand complexes (in white), and complexes where a HET group matches an EcoCyc metabolite (in grey, metals have been excluded) compared with the growth of all structures in the PDB (in black). A protein-ligand complex is defined here as a structure with at least 5 HETATM records, excluding water. Approximately one third of all structures contain no HETATM records (excluding water). The remaining two thirds contain some ligand group, with relatively few occasions (1613 of 13293) where only very small HET groups (such as metals) are present. The fraction of complexes versus all structures remains relatively unchanged over time.

In summary, we are experiencing an unprecedented increase in the data available about proteins, their sequences and structures. Can all this information be used to predict their function? One important observation derived from studying related proteins, is that proteins with very high sequence similarity (well above 50%) are likely to perform the same function, but proteins whose sequences have significantly diverged (even though they may share the same structure) often perform very different functions. For example, Todd et al. [9] have shown that in almost half of 167 homologous structural superfamilies, containing two or more enzymes, there is some variation in the enzyme function denoted by the Enzyme Commission (EC) number of their members. The fraction of such families increases to almost 70%, if sequence relatives are included (see Figure 2). Although often the variation is minor and restricted to the least significant digit of the EC classification, there are a number of cases where the EC number is not conserved at all across the family. Furthermore there are families that contain both enzymes and non-enzymatic proteins. Similar studies [10,11] have shown that, in the twilight zone of sequence similarity, variations in function are common. Moreover, difficulties in functional assignment are not only due to the inherent

difficulty arising from the continuum of sequence similarity values and the lack of clear cut-offs in going from protein sequence to function (directly or via structure). They are also due to the inevitable presence of human error in databases of protein functional annotation (inconsistency in the use of keywords, omissions etc) [10]. Such studies highlight the limitations of automated genome annotation, and suggest caution when interpreting homology-derived functional assignments.

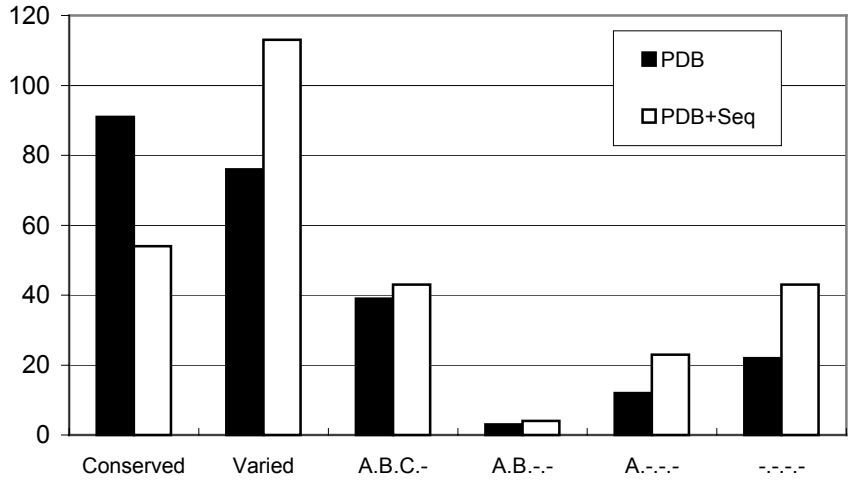

Fig. 2. Conservation of enzyme function as defined by EC number (x-axis). Shown in black is the conservation of EC number between CATH95 (hierarchical classification of protein domain structures, CATH. The four main levels of our classification are protein class (C), architecture (A), topology (T) and homologous superfamily (H)). representatives in 167 CATH homologous superfamilies containing two or more enzymes. In white is the conservation of EC number between all PF95 representatives within these superfamilies (i.e. sequence relatives included also).

It is common to observe a large variation of substrates among a homologous superfamily of enzymes. In some cases this variation is extreme, as in cytochrome P450 proteins that are known to bind surprisingly different substrates ranging from long-chain fatty acids to the tiny nitric oxide (Figure 3). The substrate - binding site complementarity means that substrate variation is directly related to binding site variation. Indeed, binding sites have been found to be less conserved than EC numbers [10], a fact that suggests that it is easier to evolve a binding site to bind a new substrate than to evolve a whole new catalytic mechanism, and hence a new function. In other words, chemistry rather than substrate specificity is likely to have dictated the path of evolution for enzymes. Support for this theory has come from earlier studies such as Gerlt and Babbitt's [12] who have shown that members of enzyme superfamilies, like the enolase or crotonase superfamilies, often retain the same strategy for stabilizing the transition state intermediate, even if the reaction involves different substrates and products. Similarly Teichmann *et al*. [13] have shown that, in the small molecule metabolic pathways of *E. coli*, conservation of the main substrate-binding site is not common among members of an enzyme family that are recruited across different pathways. Instead the catalytic mechanism and cofactor-binding properties are more commonly conserved.

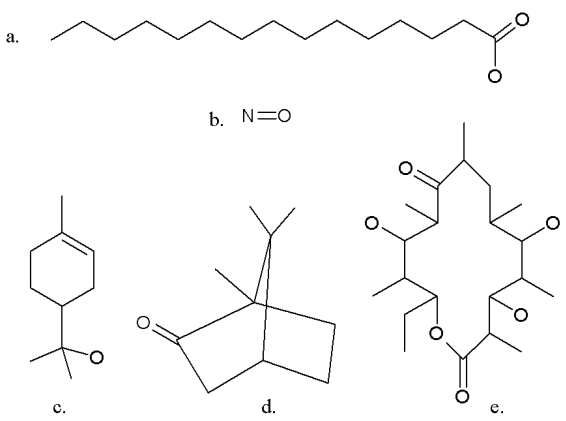

Fig. 3. A selection of substrates bound by enzymes belonging to the cytochrome P450 superfamily.

The promiscuity in substrate binding observed among homologous enzymes is an obstacle in our efforts to build a bridge that will connect the protein world to the small molecule world. Although proteins are large, they consist of a limited number of fragments (amino acids), exhibit a limited number of folds and their physical and evolutionary constraints have rendered possible the application of rigorous classification schemes (especially as a large number of examples became available). Small molecules on the other hand are not inherited and cannot be deconstructed into evolutionarily-related fragments analogous to protein domains. However, since the machinery (and chemistry) for making the small molecules is itself inherited, evolution may well be reflected in some way in their structure. Although we do not yet fully understand, to the level of prediction, how to correlate the structure of small molecules to their ability to bind a protein and perform a biological function, it is likely that chemoinformatics approaches to the metabolome will help elucidate the links between structure and function.

The small molecule world

In this section we move on from the proteome to the metabolome world, the word metabolome used here to represent "the full complement of metabolites of an organism", the definition being that of Mendes [7].

Interest in small molecules of biological importance has been traditionally the realm of the pharmaceutical industry, where research has focused primarily on synthetic ligands. Cognate (natural) ligands on the other hand are sometimes considered as starting scaffolds in the initial drug design steps, but interest in them rarely goes beyond assessing their similarity to drug candidates, with emphasis on the presence of pharmacophores and their interactions with the protein target. Relevant databases and software for exploring the small molecule space are almost all proprietary. With the notable exception of the National Cancer Institute (NCI) collection of databases [15], ligand information very often comes at a price. Cognate ligand information is even harder to access with the majority of valuable experimental data spread throughout the biochemical literature. Data on cognate ligands of diverse quantity and quality may be found in pathway- or enzyme-oriented databases such as KEGG's LIGAND [16], EcoCyc [17], and BRENDA [18] but there is currently no metabolite-centered database in the public domain. Moreover the data from existing databases can be inconsistent or

very difficult to retrieve. For example, as Wiittig and De Beuckelauer [19] have demonstrated in their review of metabolic pathway databases, a simple query for the compound ethanol not only returns a diverse set of results depending on the database (for example the number of reactions in which ethanol is supposed to participate varies widely), but in some cases it is not even possible to query compounds directly or exclusively (e.g. enzyme entries containing the word ethanol may be returned).

Interestingly, the variety of cognate ligands present in organisms is likely to be tiny in comparison to the chemical space of all possible compounds. A comparison of industrial drug-related databases with databases of known cognate ligands reflects this discrepancy: Highly diverse databases can contain up to a few hundreds of thousands of compounds, with high throughput screening databases often comprising an order of magnitude more. MDL's Screening Compounds Directory, for example, provides access to over 2 million unique chemicals [20] contrast, the KEGG database contains approximately 10,400 compounds from 96 organisms, EcoCyc lists 880 compounds for *E. coli* (March 2002). A quick graph-based [21,22] comparison of *E. coli* metabolites from EcoCyc with a subset of 4601 compounds found in various organisms in KEGG shows a minimum of one third of the compounds in the KEGG subset have at least 90% similarity to a compound found in *E. coli*. Hence the diversity of cognate ligands for these organisms is relatively limited (however, one should keep in mind that plants, which have been estimated to contain a total of up to 200,000 metabolites [23], are severely under-represented in the KEGG database). Although it is likely that the number of known cognate ligands will increase with the increasing number of organisms being investigated, it is also clear that it will always remain relatively small (compared with the number of ligands that can be synthesised in theory) reflecting the limited repertoire of biochemical pathways that evolution has produced.

In support of the suggestion that the set of known metabolites is rather homogeneous comes the observation that there are a limited number of scaffolds used in making cognate ligands. A preliminary study in our group showed that fewer than sixty fragments cover more than 90% of all atoms in a set of 745 small molecules obtained from EcoCyc. Moreover, certain fragments such as phosphates or ribose rings are so common that they represent 13% and 9% of all atoms in our dataset (see Figure 4 for more details).

Currently, there is an obvious lack of literature describing the metabolome and its properties as a whole. To describe and classify cognate ligands and their properties, we calculated a variety of molecular descriptors (using the free version of the program DRAGON [24]) for a dataset of 647 small molecules obtained from EcoCyc (for the remaining molecules either we do not have a connectivity table, or they were rejected by DRAGON). Almost 60% of the molecules in our dataset have molecular weight between 100 and 300. Their Moriguchi octanol-water partition coefficients (MlogP) are almost normally distributed around the most common values of -1 to 0 with only 2% having values greater than 4.15. Over 60% of them have fewer than 10 rotatable bonds. Expressed differently, the fraction of rotatable bonds varies between 0.2 and 0.4 for 66% of all molecules, the highest fraction observed being just over 0.5. The polar surface area (psa) calculated using the method of Ertl *et al*. [25] (a fragment-based approach that uses precalculated psa contributions) does not exceed 600 A^2 with 67% of all values lying between 50 and 200 A^2. These are, of course, *E. coli* molecules and there is no need for them to move in and out of the cell, so it is not surprising that 38% of them have a calculated psa larger than 140 A^2, a number suggested [26] as a limit above which compounds are poorly absorbed in humans. Finally, more than 77% of the molecules in our dataset have 5 or fewer hydrogen bond donors, and 71% have fewer

than 10 acceptors. The distribution of these descriptors allows us a quick overview of the *E. coli* metabolome. Interestingly, the Lipinski rule of 5 [27], which is obeyed by the majority of the set of drugs in the original study by Lipinski *et al*. [27], is also obeyed by our metabolites to a comparable extent. Of course the rule of 5 seems irrelevant here, since it was suggested as a rough estimate for rejecting drug candidates with poor solubility and permeability properties. However, drugs usually need to mimic the original substrates, and hence the above observation may reflect the target geometry and chemistry.

Ideally, we need a complete mapping between all proteins in a cell and their cognate ligands. Such a mapping will improve our understanding of the principles, which govern protein-ligand recognition, evolution and catalytic mechanisms. Despite all the databases available, even for *E. coli*, a mapping is currently not easy to derive, and is far from complete for most organisms, including humans. At the European Bioinformatics Institute (EBI), we are currently involved with the first task of classifying and clustering the metabolome using a variety of approaches. The most persistent observation from our clustering efforts is that the metabolome forms a

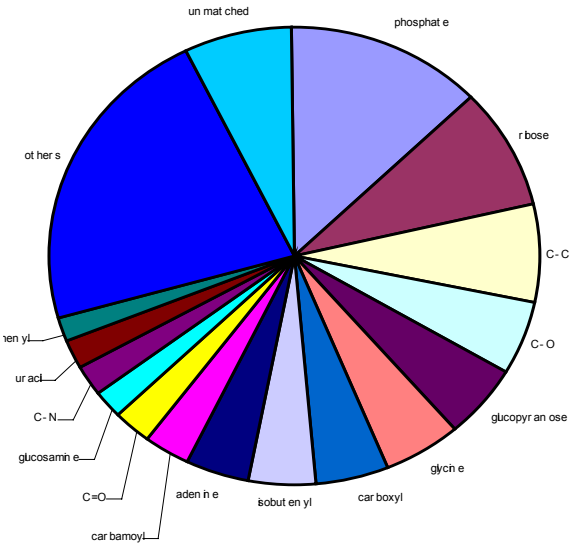

Fig. 4. Distribution of fragments in the E. coli metabolome (745 metabolites in total). The pie chart corresponds to the distribution of total number of atoms hit per fragment. Only the 15 most common fragments are shown in detail, remaining fragments are included in "others". The label "unmatched" corresponds to all atoms in the metabolites that could not be matched using our fragment definition.

continuum, with no "natural" cut-off to guide a hierarchical classification. The lack of clear-cut clusters in the metabolome makes it harder to see how these molecules map onto the relatively well characterized protein clusters. What complicates further this task, is that we cannot expect a one-to-one relationship between clusters of proteins and clusters of metabolites. In preliminary results we find that domain families are likely to exhibit different levels of promiscuity, and hence will be prone to different levels of cross-reactivity. Homologous superfamilies of the eightfold beta/alpha-barrel (TIM

barrel fold), for example, are extremely promiscuous, binding substrates from three quarters of the clusters produced in our classification.

In examples of pathways we find that the stepwise transformation of metabolites leads to high levels of similarity between substrate and product, except in the less common cases of a large rearrangement or addition. The average pairwise similarity score for the substrates in glycolysis is over 0.7 using fragment fingerprints and over 0.6 using graph matching, both values being substantially higher than the mean of the corresponding distributions for all metabolite pairwise scores.

Knowledge of the protein and small molecule worlds is of limited use, if we cannot reconstruct the biochemical networks that are responsible for the functioning of a cell. There has been an increased interest lately in the traditional biochemical pathways that have been known for decades, and this interest has resulted in a number of online databases (reviewed in reference 19) that cover mostly the metabolism of model organisms but that are slowly being extended to both non-metabolic reactions and a larger variety of organisms. However, many of our reconstructions of metabolic pathways at least, rely heavily on our knowledge of the *E. coli* metabolic network. As Cordwell [28] has argued in his study of three of the best-understood biochemical pathways in 17 microbial genomes, the *E. coli* models may have oversimplified our view of the rest of the world. If different organisms develop their own mechanisms for achieving similar goals, then inference by homology will be at best misleading, and such automated reconstructions of "known" pathways must always be experimentally verified. Going further, even the well-defined pathways of the past may prove too simplistic to incorporate the complexity of the highly connected cellular networks, and the notion itself of a pathway as an almost isolated list of reactions may hinder our understanding of how the many components of a cell are organized into well-tuned machinery.

The area of metabolomics is where the tools and knowledge in both bioinformatics and chemoinformatics will be required for interpretation of the data. From traditional physiology experiments to computer science methods, and organic chemistry mechanisms to X-ray crystallography, a variety of skills will be required for a full integration of the various "omics" into a true systems biology.

Acknowledgments

I. Nobeli acknowledges financial support from the Medical Research Council, in the form of a Special Training Fellowship in Bioinformatics.

References

1. TrEMBL version 24.2, statistics from www.ebi.ac.uk/trembl/index.html.
2. Berman, H. M., Westbrook, J., Feng, Z., Gilliland, G., Bhat, T. N., Weissig, H., Shindyalov, I. N. and Bourne, P. E. *Nucleic Acids Res.* **28**, 235-242 (2000).
3. Orengo, C. A., Michie, A. D., Jones, S., Jones, D. T., Swindells, M. B. and Thornton, J. M. *Structure* **5**, 1093-1108 (1997).
4. Murzin, A. G., Lo Conte, L., Ailey, B. G., Brenner, S. E., Hubbard, T. J. P. and Chothia, C. *J. Mol. Biol.* **247**, 536-540 (1995).
5. Holm, L. and Sander, C. *J. Mol. Biol.* **233**, 123-138 (1993).
6. Chothia, C. *Nature* **357**, 543-544 (1992).
7. Orengo, C. A., Jones, D. T. and Thornton, J. M. *Nature* **372**, 631-634 (1994).
8. Wolf, Y. I., Grishin, N. V. and Koonin, E. V. *J. Mol. Biol.* **299**, 897-905 (2000).
9. Todd, A. E., Orengo, C. A. and Thornton, J. M. *J. Mol. Biol.* **307**, 1113-1143 (2001).
10. Devos, D. and Valencia, A. *Proteins: Struct. Funct. Genet.* **41**, 98-107 (2000).
11. Wilson, C. A., Kreychman, J. and Gerstein, M. *J. Mol. Biol.* **297**, 233-249 (2000).

12. Gerlt, J. A. and Babbitt, P. C. *Curr. Opin. Chem. Biol.* **2**, 607-612 (1998).
13. Teichmann, S. A., Rison, S. C. G., Thornton, J. M., Riley, M., Gough, J. and Chothia, C. *J. Mol. Biol.* **311**, 693-708 (2001).
14. Mendes, P. *Brief. Bioinform.* **3**, 134-145 (2002).
15. http://dtp.nci.nih.gov/index.html.
16. Goto, S., Nishioka, T. and Kanehisa, M. *Bioinformatics* **14**, 591-599 (1998).
17. Karp, P. D., Riley, M., Saier, M. *et al., Nucleic Acids Res.* **30**, 56-58 (2002).
18. Schomburg, I., Chang, A. and Schomburg, D. *Nucleic Acids Res.* **30**, 47-49 (2002).
19. Wittig, U. and De Beuckelaer, A. *Brief Bioinform.* **2**, 126-142 (2001).
20. http://www.mdli.com/products/acdsc.html.
21. Krissinel, E. and Henrick, K., submitted for publication.
22. Number 4 Collaborative Computational Project. The CCP4 suite: programs for protein crystallography. *Acta Cryst.* **D50**, 760-763 (1994).
23. Fiehn, O. *Plant. Mol. Biol.* **48**, 155-171 (2002).
24. DRAGON: Software for the calculation of molecular descriptors, version 2.1. By Todeschini, R., Consonni, V. and Pavan, M. (http://www.disat.unimib.it/chm/Dragon.htm).
25. Ertl, P., Rohde, B. and Selzer, P. *J. Med. Chem.* **43**, 3714-3717 (2000).
26. Blake, J. F. *Curr. Opin. Biotech.* **11**, 104-107 (2000).
27. Lipinski, C. A., Lombardo, F., Dominy, B. W. and Feeney, P. J. *Adv. Drug. Deliv. Rev.* **23**, 3-25 (1997).
28. Cordwell, S. J. *Arch. Microbiol.* **172**, 269-279 (1999).

Peptide Revolution: Genomics, Proteomics & Therapeutics
Michael Chorev & Tomi K. Sawyer (Editors)
American Peptide Society, 2003

Synthesis and Application of Large Phosphopeptides from the Linker for Activation of T Cells (LAT) Protein

Hiroshi Yamaguchi[1], Jon C.D. Houtman[2], Lawrence E. Samelson[2] and Ettore Appella[1]

[1]Laboratory of Cell Biology and [2]Laboratory of Cellular and Molecular Biology, National Cancer Institute, NIH, Bethesda, MD, 20892, USA

Introduction

The formation of multiprotein complexes at receptors and adapter proteins is vital for the activation of intracellular signal transduction pathways. These proteins contain several association domains and binding motifs that allow for the formation of cooperative multiprotein complexes [1]. These complexes often have a defined stoichiometry and substantial *in vivo* binding specificity to individual motifs [1]. However, little has been done to clarify how cooperative interactions can enhance or inhibit complex formation at specific sites on receptors and adapter proteins. An adapter molecule critical for T-cell receptor (TCR)-mediated signal transduction is the linker for activation of T cells (LAT) protein [2,3]. Upon TCR activation, multiple tyrosine residues on LAT are phosphorylated [2], which allows for the direct binding of several SH2 domain-containing proteins, including Gads, Grb2 and PLC-γ [4]. LAT also indirectly associates with multiple proteins, such as Sos and SLP-76, following SH3 domain-mediated interactions with Grb2 and Gads, respectively [5]. LAT appears to form several multiprotein complexes, including a large complex with Gads, SLP-76 and PLC-γ [6]. To more fully examine the binding of LAT with various signaling proteins, we have synthesized large phosphopeptides derived from the region of *human* LAT that contain the binding sites for PLC-γ, Grb2 and the Gads/SLP-76 complex [5].

```
ADEDEDDYHN PG𝐘LVVLPDS TPATSTAAPS APALSTPGIR DSAFSMESID
D𝐘VNVPESGE SAEASLDGSR E𝐘VNVSQELH PG
```

Fig. 1. Sequence of a phosphopeptide derived from human LAT(120-201). Phosphorylated tyrosine residues at 132, 171 and 191 are denoted by a bold letter.

Results and Discussion

Analogues of LAT phosphopeptides corresponding to amino acid (120-201) were synthesized with various combinations of phosphorylated tyrosines at amino acids 132, 171 and/or 191, which are the *in vivo* binding sites on LAT for several SH2 domain-containing proteins (Figure 1).

During peptide synthesis, long peptide chains that are assembled on the resin matrix can form aggregates either with other peptide chains or with the polymer support. The formation of β-sheet structures may also result in incomplete solvation. Therefore, peptide synthesis of long and/or hydrophobic peptide requires several modifications such as changing solvent systems, resins, and coupling reagents. Thus, LAT phosphopeptides were synthesized by a stepwise Fmoc solid-phase method utilizing low-load polyethylene glycol polystyrene resin (Fmoc-Gly-PEG PS) and NMP as a solvent for all steps. Fmoc-amino acid was pre-activated with HBTU-HOBt in the presence of DIEA. Phosphotyrosine was incorporated as Fmoc-Tyr(PO_3H_2)-OH. All peptides were obtained in 56-67% yield based on the Fmoc-Gly-PEG PS resin. The peptides were purified to homogeneity using RP-HPLC on a C4 column eluted with 0.05% TFA in H_2O/CH_3CN. To confirm the molecular weight and tyrosine

phosphorylation status of the peptides, the phosphopeptides were treated with trypsin, as a specific endopeptidase for the two arginine residues present in LAT phosphopeptides. Each tryptic digest of the LAT peptides showed three peptide fragments, and MALDI-TOF mass spectrometry revealed that these fragments corresponded to amino acid residues (120-159), (160-189) and (190-201) of the sequence of each LAT phosphopeptide (Figure 2).

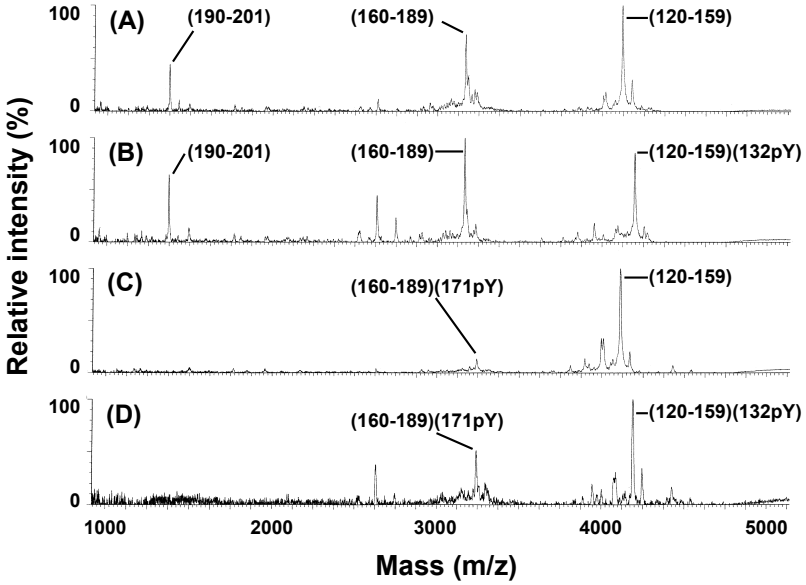

Fig. 2. MALDI-TOF mass spectra of the tryptic digests of LAT phosphopeptides. (A): LAT(120-201), (B): LAT(120-201)(132pY), (C): LAT(120-201)(171pY 191pY) and (D): LAT(120-201)(132pY 171pY 191pY).

Upon synthesis, the affinity of these peptides for the purified, recombinant PLC-γ and the Gads/SLP-76 complex was determined using isothermal titration calorimetry, a method that measures the affinity, stoichiometry and thermodynamic values of a binding reaction in a single experiment. Our data indicate that there are differences in affinity of the above proteins for specific LAT tyrosines. However, the association of the Gads/SLP-76 complex and PLC-γfor LAT tyrosine peptides does not appear to be solely driven by affinity [7].

References

1. Kuriyan, J. and Cowburn, D. *Annu. Rev. Biophys. Biomol. Struct.* **26**, 259-288 (1997).
2. Zhang, W., Sloan-Lancaster, J., Trible, R. P. and Samelson, L. E. *Cell* **92**, 83-92 (1998).
3. Tomlinson, M. G., Lin, J. and Weiss, A. *Immunol. Today* **21**, 584-591 (2000).
4. Samelson, L. E. *Annu. Rev. Immunol.* **20**, 371-394 (2002).
5. Zhang, W., Trible, R. P., Zhu, M., Liu, S. K., McGlade, C. J. and Samelson, L. E. *J. Biol. Chem.* **275**, 23355-23361 (2000).
6. Kane, L. P., Lin, J. and Weiss, A. *Curr. Opin. Immunol.* **12**, 242-249 (2000).
7. Houtman, J. C. D., Higashimoto, Y., Dimasi, N., Cho, S., Yamaguchi, H., Bowden, B., Regan, C., Malchiodi, E. L., Mariuzza, R., Appella, E. and Samelson, L. E. *Mol. Cell* submitted.

Peptide Revolution: Genomics, Proteomics & Therapeutics
Michael Chorev & Tomi K. Sawyer (Editors)
American Peptide Society, 2003

Binding Interactions of Phospho-Htc Peptide to c-Fgr SH2 Domain

Paolo Ruzza[1], Alessio Osler[1], Silvia Del Piero[1], Arianna Donella-Deana[2], AnnaMaria Brunati[2], Giuliano Siligardi[3], Rohanah Hussain[3], Andrea Calderan[1], Andrea Guiotto[1], Lorenzo A. Pinna[2] and Gianfranco Borin[1]

[1]C.N.R. Institute of Biomolecular Chemistry, Padova Unit, 35131 Padova, Italy;
[2]Department of Biological Chemistry, University of Padova, 35121 Padova, Italy;
[3]Pharmacy, King's College London, London SE1 9NN, UK

Introduction

Haematopoietic lineage cell-specific protein HS1 becomes Tyr-phosphorylated following B cell antigen receptor cross-linking. A prerequisite for *in vitro* phosphorylation of HS1 by Src-related tyrosine kinases is a previous phosphorylation of the protein by Syk tyrosine kinase. The Syk-phosphorylated tyrosines of HS1 become docking sites for the SH2 domain of the Src kinases, which secondarily phosphorylate the binding protein. In previous studies, we demonstrated that a peptide containing a Tyr replaced by its constraint [3S]-1,2,3,4-tetrahydroisoquinoline-7-hydroxy-3-carboxylic acid (Htc) was a highly selective substrate for Syk [1]. Here we show the usefulness of the replacement of Tyr by Htc for the development of peptides specifically interacting with Src SH2 domain. With this aim, we have synthesized peptides corresponding to the HS1 sequence phosphorylated by Syk replacing the phospho-Tyr (pTyr) residue by phospho-Htc (pHtc) (Figure 1). The interactions of the peptides with the SH2 domain of the Src-like kinase, c-Fgr, were analyzed by non-immobilized ligand interaction assay by CD (NILIA-CD).

HS1-pTyr H-Pro-Glu-Gly-Asp-pTyr-Glu-Glu-Val-Leu-Glu-OH
HS1-pHtc H-Pro-Glu-Gly-Asp-pHtc-Glu-Glu-Val-Leu-Glu-OH

Fig. 1. Sequences of HS1 phosphopeptides.

Results and Discussion

Synthetic peptides were synthesized by manual solid-phase technique on pre-loaded Wang (0.62 mmol/g) resins using Fmoc/HBTU chemistry. The N-terminal residue was protected with Boc. Tyr or Htc residues were first phosphytilated by treatment with di-*tert*-butyl-N,N-diisopropylphosphoramidide and then the phosphite esters were oxidized by m-chloroperbenzoic acid. Boc- and side chain protecting groups were left on during cleavage from the resin using TFA/water/anisole/TIS (95.0:0.5:2.5:2.0 v/v) for 1h. The crude peptides were purified by C_{18} RP-HPLC (Vydac 218TP1022) with a gradient of 13-22% CH_3CN in aq. 0.05% TFA.

The binding of HS1 phospho-peptides to c-Fgr HS2-GST conjugated domain was clearly determined by the CD changes either in the aromatic (near-UV) or in the back-bone (far-UV) spectral region. Upon peptide addition, the binding was monitored by the CD changes of the Trp side chains of the conjugated GST-SH2 (314 *aa*). The dissociation constant Kd was determined by analyzing the CD data at 294.4 nm using a nonlinear regression method [2]. The results show that the two peptides are equivalent and the Kd for the interaction of HS1-phosho-peptide to GST-SH2 is estimated 0.48±0.29 μM and 0.21±0.08 μM for the HS1-pTyr and the HS1-pHtc peptides, respectively (Figure 2). This study shows that the c-Fgr SH2 domain recognized the

phospho-Htc peptide as well as the natural parent phospho-Tyr peptide. The calculation of the Kd for the GST-SH2: phospho-peptide complexes did not yield satisfactory simulations. However, the fitting was successful by assuming a lower GST-SH2 concentration than that used in the titrations (Figure 2), indicating a stoichiometry of less than 1:1 molar ratio. This is consistent with association equilibrium with only the monomeric form of the conjugated GST-SH2 protein binding the phospho-peptides. It is interesting to note that the binding of the phospho-peptide induces a conformational change of the GST-SH2 conjugated protein reducing by about 20% its content of α-helical conformation (Figure 3).

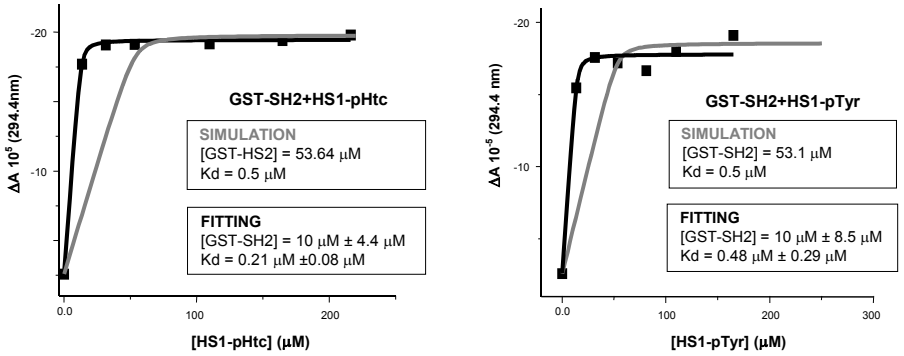

Fig. 2. Kd values of GST-SH2 binding interaction studies with HS1-pTyr and HS1-pHtc peptides determined analyzing the CD data at 294.4 nm using a nonlinear regression method [2].

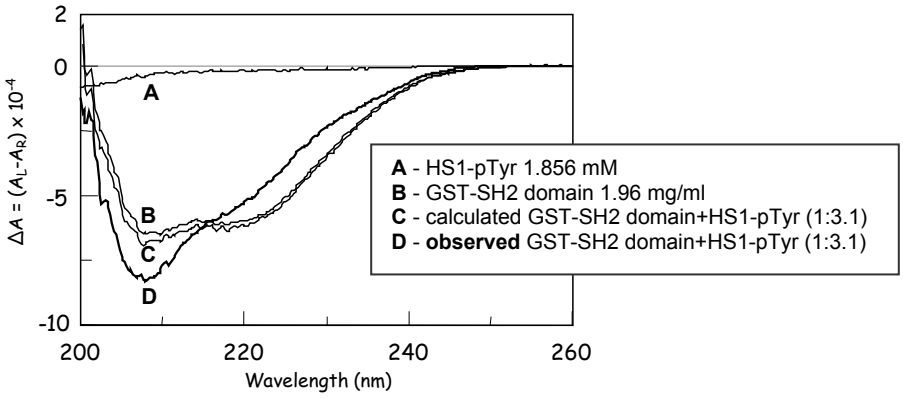

Fig. 3. Normalized far-UV CD spectra of GST-SH2 protein free and complex with HS1-pTyr.

Acknowledgments

The work was supported by the National Research Council (CNR) of Italy.

References

1. Donella-Deana, A., Ruzza, P., Cesaro, L., Brunati, A. M., Calderan, A., Borin, G. and Pinna, L. A. *FEBS Letters* **523**, 48-52 (2002).
2. Siligardi, G., Panaretou, B., Meyer, P., Singh, S., Woolfson, D. N., Piper, P. W., Pearl, L. H. and Prodromou, C. *J. Biol. Chem.* **277**, 20151-20159 (2002).

Peptide Revolution: Genomics, Proteomics & Therapeutics
Michael Chorev & Tomi K. Sawyer (Editors)
American Peptide Society, 2003

Fluorescence Detection of Conformationally-Restricted Oxy-Peptide Nucleic Acids/DNA hybrids

Mizuki Kitamatsu, Mamoru Saito, Takashi Nakai and Masahiko Sisido

Department of Bioscience and Biotechnology, Faculty of Engineering, Okayama University, Okayama 700-8530, Japan

Introduction

Peptide nucleic acids that contain a pyrrolidine ring and an ether linkage in the main chain (POPNAs) have been reported in our previous work (Figure 1) [1]. Of the four possible stereo configurations of the pyrrolidine ring, i.e., cis-L, trans-L, cis-D, and trans-D, the cis-L configuration was the optimum for hybridization with DNA and the trans-L was the optimum for hybridization with RNAs. The cis-L-POPNA-DNA hybrids show higher stability and sharper melting curves than the DNA-DNA counterparts. Further, cis-L-POPNA forms only duplex with DNA even under excess concentration of DNA. These characteristics of POPNA make it a promising candidate of DNA hunter for microarray analysis. However, for the POPNA microarray to be of practical use, a fluorescent probe that binds solely onto the duplexes has to be found. Among several minor-groove binders, $DiSC_2(5)$ has been known to form aggregates that causes visible color changes, when it is bound to DNA-DNA or to DNA-Nielsen-type PNA hybrids [2, 3]. In these cases, because of the aggregation, no fluorescence has been detected. Here, we report that the same cyanine dye exists as monomeric form and emits strong fluorescence when it binds to POPNA-DNA hybrids. This finding allows POPNA microarray to be a sequence-specific and highly sensitive tool for DNA analysis.

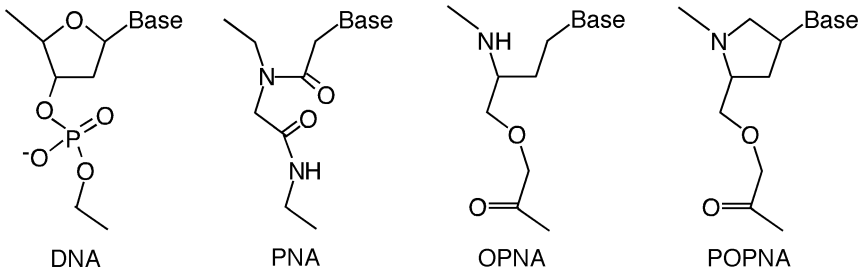

Fig. 1. Structures of DNA, Nielsen-type PNA, OPNA and POPNA.

Results and Discussion

All four nonamer (POPNA(A_9)s) formed hybrids with the complementary DNA (dT_9). The melting temperature was highest for cis-L-POPNA (35 ˚C) and was lowest for trans-L-POPNA(23 ˚C). Cis-D- and trans-D-POPNA-DNA had melting temperatures between cis-L-POPNA-DNA and trans-L-POPNA-DNA (30 and 31 ˚C, respectively).

When $DiSC_2(5)$ was added to POPNA(A_9)-dT_9 hybrids, the absorption and CD data indicated that the $DiSC_2(5)$ bound to cis-L-POPNA(A_9)-dT_9 and trans-L-POPNA(A_9)-dT_9 hybrid in a monomeric form, but did not bind to single-stranded POPNAs or DNAs (data not shown).

Figure 2 shows fluorescence spectra of $DiSC_2(5)$-cis-L-POPNA(A_9)-dT_9 (0.1:1:1) mixture at different temperatures, the excitation wavelength being 668 nm. At 50 ˚C,

where no hybridization takes place, the spectrum is identical to that of the dye in the absence of POPNA or DNA. Fluorescence intensity as well as the peak wavelength increased with the hybrid formation at low temperatures. Melting curves for cis-L- and trans-L-POPNA(A_9)-dT_9 hybrid were very clearly reproduced by the temperature dependence of fluorescence intensities of the cyanine dye. Strong fluorescence was detected neither for the single-stranded POPNAs and the DNA nor for the monomeric dye. These changes indicate that the dye bound to a hydrophobic site of the hybrid and not to monomeric DNA or POPNA.

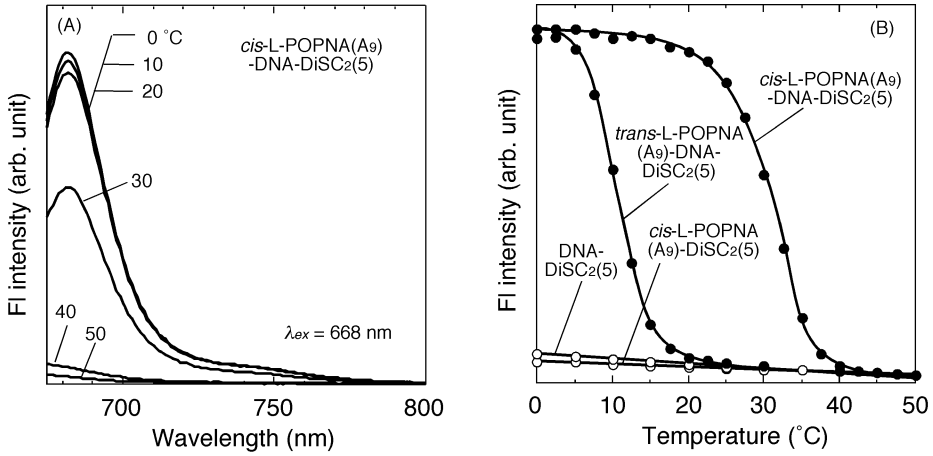

Fig. 2. Fluorescence spectra for $DiSC_2(5)$-cis-L-POPNA(A9)-dT9.

Table 1 shows ratios of fluorescence intensities of POPNA-DNA mixtures in the hybrid form (5 ˚C) and in the single stranded form (50 ˚C). Only full-match hybrids of cis-L- and trans-L-POPNA(A_9) with DNA showed significant fluorescence increase. Mismatch pairs of POPNA and DNA did not show the fluorescence increase. The sequence-specific fluorescence enhancement makes the POPNA array a promising candidate as a highly sensitive tool for DNA analysis.

Table 1. Ratios of fluorescence intensities of POPNA-DNA mixtures in the hybrid form and in the single stranded form.

	POPNA				OPNA		PNA	DNA
	L-		D-		L-	D-		
DNA	*cis*-	*trans*-	*cis*-	*trans*-				
dT_9	**44.6**	**46.0**	2.5	4.0	2.4	5.4	6.6	5.3
dT_4AT_4	1.6	1.9	2.7	2.4	2.7	1.3	2.8	2.2
dT_7AT	13.1	7.3	2.9	3.1	2.1	2.8	3.2	2.0

References

1. Shigeyasu, M., Kuwahara, M., Sisido, M. and Ishikawa, T. *Cheml. Lett.* **7**, 634-635 (2001).
2. Smith, J. O., Olson, D. A. and Armitage, B. A. *J. Am. Chem. Soc.* **121**, 2686-2695 (1999).
3. Seifert, J. L., Connor, R. E., Kushon, S. A., Wang, M. and Armitage, B. A. *J. Am. Chem. Soc.* **121**, 2987-2995 (1999).

Peptide Revolution: Genomics, Proteomics & Therapeutics
Michael Chorev & Tomi K. Sawyer (Editors)
American Peptide Society, 2003

Preparation of Fluorescent and Radiolabeled Peptide-PNA Conjugates for Imaging *bcl-2* Expression

Fabio Gallazzi[1], Fang Jia[2], Linda A. Landon[3], Nalini Shenoy[4], Geethapriya Sivaguru[2], Mark Hannink[3], Susan Z. Lever[4,5] and Michael R. Lewis[2,6,7]

[1]Molecular Biology Program; [2]Department of Veterinary Medicine and Surgery; [3]Department of Biochemistry; [4]Department of Chemistry; [5]University of Missouri Research Reactor Center; [6]Department of Radiology; and [7]Nuclear Science and Engineering Institute
University of Missouri-Columbia, Columbia, MO 65211, USA

Introduction

Advanced non-Hodgkin's Lymphoma (NHL) is incurable in 65% to 70% of patients, but response of newly diagnosed patients to conventional treatments, such as combination chemotherapy or external beam radiotherapy, is initially good. However, in later stages NHL patients often develop more aggressive disease that becomes resistant to radiation and chemotherapy. Results of long terms studies showed that bcl-2 protein is the only factor associated with increased relapse rate, reduced disease-free intervals, and poor overall survival. Consequently, non-invasive imaging of bcl-2 mRNA expression may aid in the identification of patient risk groups, that might respond better to targeted immunotherapy, radio-immunotherapy, or antisense therapy, all of which act to down-regulate bcl-2.

Following this working hypothesis, we have previously prepared radiometal-labeled anti-bcl-2 PNA conjugates, coupled to a cell-permeating peptide (PTD-4). These conjugates were shown to bind with high sensitivity, specificity, and stability to bcl-2 messenger RNA in cell-free systems [1]. We describe here the synthesis of a new class of anti-*bcl-2* and nonsense PNA conjugates for plasma stability and for fluorescence microscopy studies (Figure 1).

Results and Discussion

Because the critical basic residues of *retro-inverso* (r.i.) PTD-4 are in approximately the same three-dimensional configuration as in the parent sequence, it should retain cell-permeating activity and be resistant to proteolytic degradation. To test this hypothesis, we performed plasma stability studies of ^{111}In-labeled PTD-4- and r.i.PTD-4-anti-*bcl-2*-PNA. The results showed that the r.i. conjugate exhibited superior proteolytic stability, relative to the native, making the former a better candidate for subsequent *in vivo* evaluation of the radiolabeled peptide-PNA. However, prior to initiating these studies, the ability of r.i.PTD-4 to mediate cellular internalization needed to be evaluated.

Therefore, tetramethylrhodamine (TMR) conjugates were prepared. Digital scanning confocal fluorescence microscopy studies demonstrated that the *retro-inverso* analog of PTD-4 is active in membrane permeation and that the peptide mediates cellular internalization.

In order to make the synthetic procedure more flexible, we used Fmoc-Lys(DOTA) (synthesized in house) and Fmoc-Lys(TMR) (Molecular Probes), respectively, for the preparation of the radiolabeled and the fluorescent conjugates. The presence of TMR simplified the preparation of the conjugates, because the hydrophobic nature of the dye allows the direct preparative HPLC purification of the final conjugates. On the contrary, in case of the DOTA conjugates, it was necessary to proceed as previously described [1] to purify partially deprotected intermediates and then isolate fully

deprotected products. All conjugates were characterized by HPLC/ESI-MS, and all observed molecular ions were consistent with the structures of the desired products.

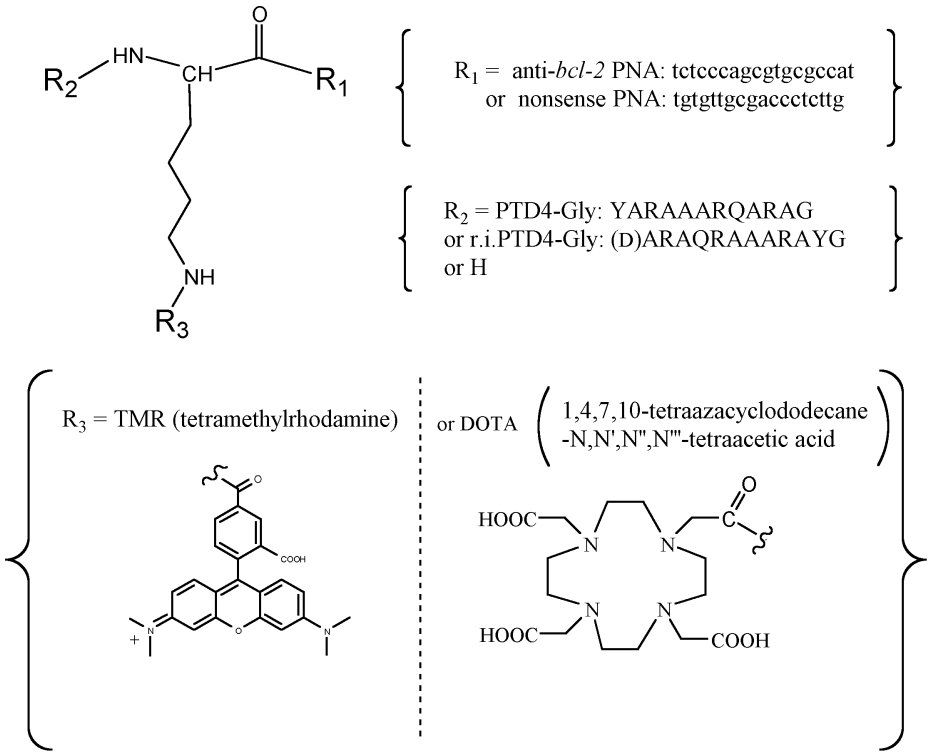

Fig. 1. Structure of the synthesized conjugates.

Acknowledgment
This work was supported by NIH Grant CA86290 (W.A. Volkert, PI) and a grant from the University of Missouri Research Reactor (to M.R.L.). The authors would like to acknowledge the Department of Veterans Affairs, for providing resources and the use of facilities at the Harry S Truman Memorial Veterans' Hospital in Columbia, MO, and the University of Missouri Research Reactor, for purchasing the Advanced ChemTech ACT Model 396 Omega Multiple Biomolecular Synthesizer used in this research.

References
1. Lewis et al. *Bioconjugate Chem.* **13**, 1176 (2002).

Peptide Revolution: Genomics, Proteomics & Therapeutics
Michael Chorev & Tomi K. Sawyer (Editors)
American Peptide Society, 2003

Solid Phase Synthesis of Tri-Peptide Derivatives of Kojic Acid Used as Tyrosinase Inhibitor

Hanyoung Kim, Jaehee Choi and Yoon-Sik Lee

School of Chemical Engineering, Seoul National University, Seoul 151-744 Korea

Introduction

Kojic acid has been used as a whitening agent in the cosmetics and food industry because of its tyrosinase inhibitory activity [1]. However, kojic acid is not stable enough for broad application. Furthermore, it has been reported recently that kojic acid may not be safe. In this study, we attempted to synthesize peptide-kojic acid conjugates, which are assumed to have longer storage stability, lower toxicity, and yet expected to be able to maintain their tyrosinase inhibitory activity. For this purpose, we prepared peptide-kojic acid libraries by solid-phase method and screened for tyrosinase inhibitory activity.

Results and Discussion

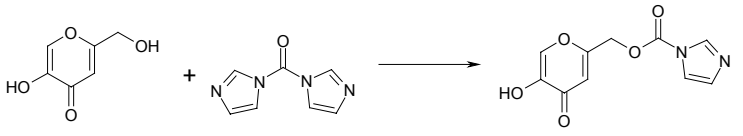

(1) (2) (3)

Scheme 1. Activation of kojic acid by carbonyldiimidazole.

For the coupling of kojic acid to the N-terminal of peptide library, kojic acid was activated by carbonyldiimidazole (CDI) (Scheme 1). We found that only the 2-hydroxymethyl group of kojic acid was activated by CDI, and the resulting compound (3) was precipitated as white powder (70%), leaving 5-hydroxy group of kojic acid, which is a key functional group for tyrosinase inhibition, untouched.

Peptide-kojic acid libraries (120 compounds) were synthesized by using Fmoc chemistry on Trityl (0.9 ~ 1.1 mmol/g) resins as shown in Scheme 2. The peptide

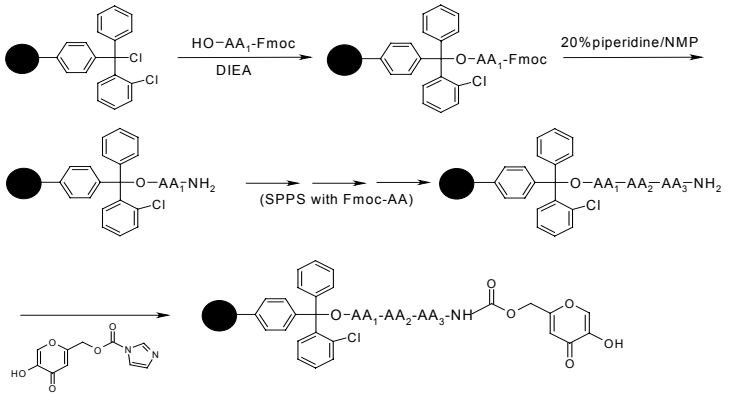

Scheme 2. Synthetic scheme of peptide-kojic acid libraries on Trityl resin.

products were isolated in pure form after treating the peptide-Trityl resin with reagent K, and leaving the filtrate to evaporate. The overall yields were 49-95%. We measured the tyrosinase inhibitory activities of products by the Mushroom tyrosinase inhibition assay method, and tested the activities of each peptide-kojic acid derivative in 10 μM solution. Next, we compared it with the activity of kojic acid (IC_{50} value of kojic acid for the inhibition of tyrosinase was 35 μM). We found that most of the peptide-kojic acids showed better inhibitory activity than pure kojic acid. Peptides derivatives with hydrophobic side chains, especially tyrosine-containing peptide derivatives (bold character sequences in Table 1) showed the best inhibitory activities. Such an outcome might be related to the hydrophobic pocket near the active site of tyrosinase [2]. We measured IC_{50} values of tyrosine-containing peptide-kojic acid derivatives, and found that several of them showed 100-150-fold stronger inhibitory activities than pure kojic acid. We also confirmed that peptide-kojic acid derivatives maintained their inhibitory activity for a longer than 15 days in open air at room temperature, while that of kojic acid only lasted for one day.

Table 1. The yields and tyrosinase inhibitory activities of selected peptide-kojic acid derivatives.

Inhibitor	% yield	% inhibition	Inhibitor	% yield	% inhibition	Inhibitor	% yield	% inhibition
YRG-KA	81	60	YWK-KA	91	68	YYF-KA	89	92
YKK-KA	89	67	YIF-KA	88	87	YWF-KA	94	95
YRK-KA	78	66	YRF-KA	91	90	YFF-KA	95	93

KA = kojic acid.

Table 2. IC_{50} values of selected peptide-kojic acid derivatives.

Inhibitor	IC50 (μM)	Inhibitor	IC50 (μM)	Inhibitor	IC50 (μM)
YRK-KA	7.92	YWK-KA	6.45	YWF-KA	0.24
YKK-KA	7.44	YYF-KA	0.39	YFF-KA	0.33

Through the toxicity test by MTT assay, we could confirm that most of the peptide-kojic acid derivatives are safe and that the toxicities are lower than kojic acid (Table 3).

Table 3. MTT assay results of selected peptide-kojic acid derivatives.

Sample	% Cell survive	Sample	% Cell survive	Sample	% Cell survive	Sample	% Cell survive
KA		YEK-KA		YRK-KA		YFF-KA	
1ppm	91.75	1ppm	98.38	1ppm	94.52	1ppm	91.62
10ppm	92.36	10ppm	98.78	10ppm	93.20	10ppm	94.66
100ppm	86.92	100ppm	100.81	100ppm	95.33	100ppm	104.36

Acknowledgments
The authors convey their appreciation to BK21 program and Amore Pacific Co. for their financial supports. The authors also thank Professor Sunny Kim of KyungHee University for the MTT assay.

References
1. Ohyama, Y. and Mishima, Y. *Fragrance J.* **6**, 55-58, (1990).
2. Yoshikane, K. and Hiroshi, T. *Bioorg. Med. Chem. Lett.* **6**, 1303-1308, (1996).

Peptide Revolution: Genomics, Proteomics & Therapeutics
Michael Chorev & Tomi K. Sawyer (Editors)
American Peptide Society, 2003

Tripeptide Inhibitors of *Yersinia* Protein-Tyrosine Phosphatase as Potential Leads for Therapeutic Development Against Plague

Kyeong Lee[1], Sang Uk Kang[1], Yang Gao[1], Zhu-Jun Yao[1], Jason Phan[2], Li Wu[3], Jiao Liang[3], David S. Waugh[2], Zhong-Yin Zhang[3] and Terrence R. Burke, Jr.[1]

[1]Laboratory of Medicinal Chemistry; [2]Macromolecular Crystallography Laboratory, CCR, NCI, NIH, NCI-Frederick, Frederick, MD 21702, US.; and [3]Department of Molecular Pharmacology, Albert Einstein College of Medicine, Bronx, NY 10461, USA

Introduction

The protein-tyrosine phosphatase (PTPase) "YopH" is a virulence factor of *Yersinia pestis*, the causative agent of plague. Potential use of *Yersinia* as a bioterrorism agent renders YopH inhibitors of therapeutic importance. Our strategy for discovery of novel PTPase inhibitors is based on the fact that pTyr residues play major roles in PTP substrate binding. Using a variety of non-hydrolyzable pTyr mimetics that were displayed in an EGFR-derived hexapeptide platform, we previously examined the inhibitory potencies against the human PTP1B [1]. The poor inhibitory potencies of certain of these pTyr mimetics were attributed to potentially restricted orientation within the PTP1B catalytic site incurred by extensive peripheral interactions of the hexapeptide structure. In an effort to develop leads for inhibition of YopH, we examined a similar set of pTyr mimetics in a truncated tripeptide platform 'Fmoc-Glu-Xxx-Leu-amide' (where Xxx = pTyr mimetic).

Results and Discussion

Table 1 shows the inhibitory potencies against YopH and PTP1B for the tripeptide series (**1**-**14**), along with the previous PTP1B inhibition data for hexapeptides (**HP**s) [1]. There are considerable discrepancies in PTP1B inhibitory potencies for pTyr mimetics arising from the peptide display platform. Some low affinity hexapeptide-expressed pTyr mimetics are found to exhibit high PTP1B affinity within the context of the tripeptide platform. A close concordance of YopH and PTP1B inhibitory potencies was observed for tripeptides containing Glu residues derivatized as their OBn esters (Table 1, **b** series). The corresponding peptides having Glu residues with unprotected carboxyl side chains (**a** series) also showed good PTP1B inhibitory potencies, however, these peptides uniformly exhibited poor YopH inhibitory potencies. This data indicates that the OBn ester is a key component of YopH recognition for these tripeptides. Of approximately 14 pTyr mimetics examined, several provided inhibition constants against YopH in the single digit micromolar range. It was of particular note that among the most potent analogues (e.g., **11b**, IC_{50} value of 1.8 μM) were those bearing a single anionic charge. This was encouraging, since enhanced cell membrane permeability would be expected to result from decreased charge. It is also of interest to examine effects of structural modifications to the N-terminal Fmoc group. Using peptide **11b** as a reference, N-Cbz (**11c**) and N-phenylethoxycarbonyl (**11d**) tripeptides were prepared. Both modifications resulted in significant reduction in binding affinity against YopH as well as PTP1B. One concern was that such inhibitors may potentially function by non-specific mechanisms. This was investigated using respresentative inhibitors. While failing to provide evidence of a non-specific promiscuous mode of inhibition, these studies did indicate that non-classical inhibition may be involved.

Table 1. Inhibitory potencies of synthetic peptides in YopH and PTP1B assays[a].

Xxx	No	R_1HN-Glu(OR_2)XxxLeu-amide **a** R_2 = H; R_1 = Fmoc, **b** R_2 = Bn; R_2 = Fmoc **c** R_2 = Bn; R_2 = Cbz, **d** R_2 = Bn; R_2 = Phenethyloxycarbonyl	Ac-Asp-Ala-Asp-Glu-Xxx-Leu-amide **HP**[c]
		YopH (IC_{50})	PTP1B (IC_{50})	PTP1B (IC_{50})
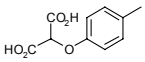	**1a**	>> 800	Ki = 29	10
	1b	82 +/- 16	116 +/- 20	
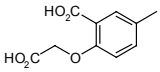	**2a**	> 100	54.7 +/- 15.3	19
	2b	10.5 +/- 3.9	8.3 +/- 2.1	
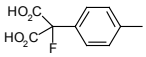	**3a**	>> 800	0.7	430
	3b	3.1 +/- 0.17	3.1 +/- 1.0	
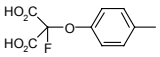	**4b**	2.9 +/- 0.4	1.5 +/- 0.5	1
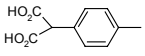	**5a**	>> 800	0.8	1,500
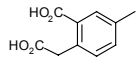	**6a**	>> 800	0.7	3,700
	6b	142 +/- 51	44 +/- 13	
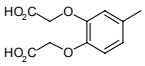	**7b**	19.4 +/- 3.3	19.4 +/- 3.6	800
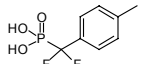	**8b**	5.2 +/- 2.2	1.41 +/- 0.25	0.1
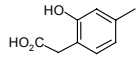	**9a**	>> 800	4	13,000
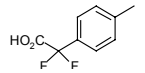	**10a**	>> 800	1.4	650
	10b	2.5 +/- 1.6	3.1 +/- 1.6	
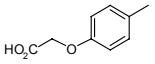	**11b**	1.8 +/- 1.0	2.9 +/- 1.3	12,00
	11c	119 +/- 14	72 +/- 14	
	11d	8.0 +/- 9.5	58.2 +/- 14.2	
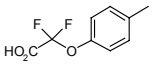	**12b**	1.94 +/- 1.26	3.8 +/- 1.8	ND[b]
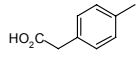	**13b**	2.38 +/ 1.44	4.6 +/- 1.8	2,500
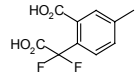	**14a**	287 +/- 74	> 50	ND[b]
	14b	53 +/- 16	139	

[a] *IC_{50} in μM,* [b] *Not Determined,* [c] *Previously reported [1].*

References

1. Gao, Y., *et al. Bioorg. Med. Chem. Lett.* **10**, 923-5031 (2000).

Peptide Revolution: Genomics, Proteomics & Therapeutics
Michael Chorev & Tomi K. Sawyer (Editors)
American Peptide Society, 2003

Interference with Protein-Protein Interactions in Signal Transduction

Frank J. Dekker, Nico J. de Mol, Marcel J.E. Fischer and Rob M.J. Liskamp

Department of Medicinal Chemistry, Utrecht Institute of Pharmaceutical Sciences, Utrecht University, PO Box 80.082, 3508 TB Utrecht, The Netherlands

Introduction

FcεRI-receptor activation in the mast cell may lead to excessive and undesired immune responses like asthma and hay fever. The Syk protein tyrosine kinase (p72syk) is an important protein in intracellular communication after FcεRI-receptor activation. The interaction between the Syk tyrosine kinase and the immunoreceptor tyrosine-based activation motif (ITAM) of the FcεRI receptor has a divalent character. Development of peptidomimetic molecular constructs that selectively interfere with this divalent interaction may provide valuable tools for biomolecular research and may represent a new class of therapeutic compounds.

Recently, we assembled a divalent Syk tandem SH2 domain binding construct by linking two monophosphorylated peptides with an oligoethylene glycol spacer resulting in construct **3** [1]. Application of a rigid spacer as is present in molecular construct **4** improved the affinity for the Syk tandem SH2 domain further [2]. This spacer was applied to assemble a construct with three parts: a) a binding site for the Syk tandem SH2 domain, b) a HIV TAT peptide, which facilitates translocation of peptides across the cell membrane [3] and c) a fluorescent label as presented in Scheme 1.

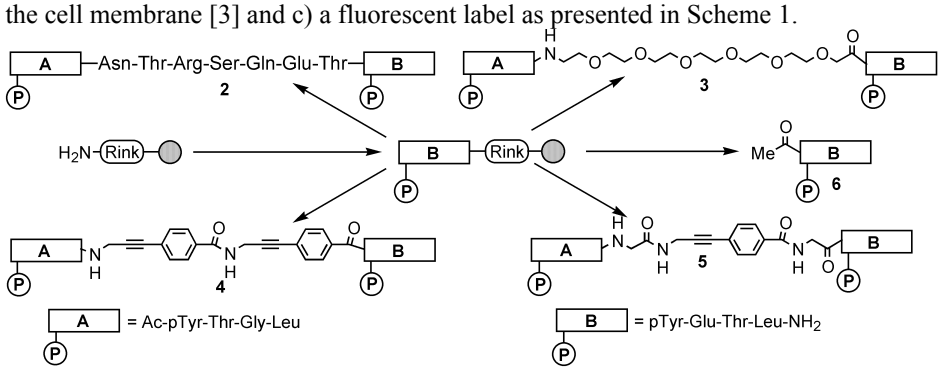

Scheme 1. Synthesis of the peptide molecular constructs as previously described [1,2].

Results and Discussion

Different spacers were designed in modeling studies based on the crystal structure of the ITAM peptide complexed with the Syk tandem SH2 domain. The designed peptide molecular constructs were assembled, purified and characterized (Scheme 1) [1,2]. Affinity for the Syk tandem SH2 domain was evaluated using a surface plasmon resonance assay (SPR) [1][2]. In Table 1 the 5000-fold difference in affinity between the monophosphorylated peptide **6** and the diphosphorylated peptide **2** is shown, which clearly demonstrates the magnitude of the divalency effect in this interaction. The construct with the ethylene glycol spacer **3** showed that a completly different spacer can replace the seven intervening amino acids between the interacting phosphotetra-

Table 1. Affinities of peptide/peptidomimetic constructs for the Syk tandem SH2 domains.

Compound	IC_{50} (μM)	K_d (μM)
2	0.13 ± 0.01	0.037
3	1.2 ± 0.2	0.34
4	0.1 ± 0.007	0.029
5	62 ± 12	4.0
6	570 ± 50	166

peptides of the ITAM peptide **2** [1]. Molecular construct **4** with the two rigid spacing building blocks showed a 10-fold increased affinity compared to construct **3** containing the flexible oligoethylene glycol spacer, thereby reaching an affinity that is equal to the affinity of the native diphosphorylated ITAM peptide **2**. Apparently, this construct has the proper geometry for optimal interaction with the Syk tandem SH2 domain, in which the rigidity possibly contributes to a more favorable entropy. The next step was construction of a molecule that constained a HIV-TAT peptide part, which might facilitate translocation of peptides acros the cell membrane (Figure 1). This construct will be used as a tool to interfere with Syk tandem SH2 domain signal-transduction in the intact mast cell, thus giving opportunities to investigate the role of this divalent interaction *in vivo*.

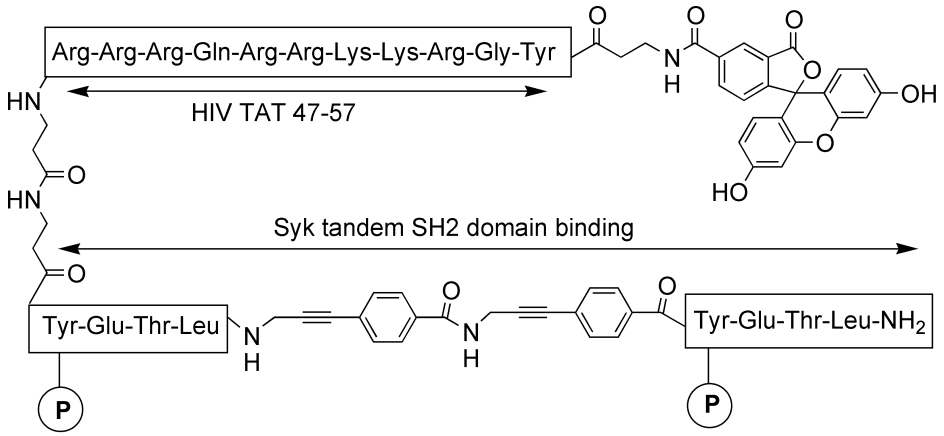

Fig. 1. Molecular construct consisting of three parts: a) a binding site for the Syk tandem SH2 domain, b) a HIV TAT peptide and c) a fluorescent label.

References

1. Dekker, F. J., de Mol, N. J., van Ameijde, J., Fischer, M. J. E., Ruijtenbeek, R., Redegeld, F. A. M. and Liskamp, R. M. J. *ChemBio. Chem.* **3**, 238-242 (2002).
2. Dekker, F. J., de Mol, N. J., Fischer, M. J. E. and Liskamp, R. M. J. *Bioorg. Med. Chem. Lett.* **13**, 1241-1244 (2003).
3. Dunican, D. J. amd Doherty, P. *Biolpoymers (Peptide Science)* **60**, 45-60 (2001).

Peptide Revolution: Genomics, Proteomics & Therapeutics
Michael Chorev & Tomi K. Sawyer (Editors)
American Peptide Society, 2003

Testing and Characterizing Focused Tyrosine Kinase Inhibitory Libraries

Györgyi Bökönyi[1], Eszter Schäfer[2], Edit Várkondi[2], Edit Z. Szabó[1], Frigyes Wáczek[2], Zsolt Székelyhidi[2], Péter G.Bánhegyi[2], György Mészáros[2], Dániel Erős[1], László Őrfi[3], Ákos Pap[2], Richárd E. Schwab[2] and György Kéri[1,2]

[1]Peptide Biochemistry Research Group of Hung Acad. Sci., Dept. of Med. Chem., Semmelweis Univ., Budapest, Hungary; [2]Cooperative Res. Centre, Semmelweis Univ., Budapest, Hungary; [3]Semmelweis Univ., Dept. of Pharm. Chem. Budapest, Hungary

Introduction

Our aim is to develop new peptido-mimetic compounds that inhibit tyrosine kinases by competing for the ATP-binding site in the catalytic domain. As a part of this research program we would like to characterize the efficacy of these compounds by testing them with an *in vitro* biochemical assay (LTS-low throughput screening) and an *in vitro* cell proliferation assay. Our most important target molecules are Epidermal Growth Factor (EGF)-RTK, Platelet Derived Growth Factor (PDGF)-RTK and Vascular Endothelial Growth Factor (VEGF)-RTK. Our aim was to characterize the efficacy of these compounds by testing them by relevant bioassays: *in vitro* cell proliferation assays, non-radioactive tyrosine kinase assays and by flow cytometry.

Results and discussion

We have synthesized a series of new potential protein tyrosine kinase (TK) inhibitory compounds which have been designed as focused libraries around a few core structures, like quinazolines, benzo[4,5]thieno[2,3-d]pyrimidines and 7H-Pyrrolo[2,3-d]pyrimidines. These ATP-binding site targeted molecules were screened for anti-proliferative activity and for apoptosis-inducing efficacy in different human tumor cell lines (e.g. A431) with the method of MB and MTT assay [1,2]. They were systematically tested against validated target molecules (EGF-R, VEGF-R2 and PDGF-R-α) in a non-radioactive ELISA-based tyrosine kinase assay using recombinant enzymes [3]. For QSAR analysis and pharmacophore model generation we have measured and calculated logP values of the compounds, logP being the most frequently utilized and most important physico-chemical parameter in such studies.

1. Cell proliferation test

This assay aimed to detect the anti-proliferative efficacy and toxicity of the inhibitor compounds. The assay was carried out on 96-well plates in A431 cell lines for 6 hours and 48 hours. Staining the cells after treatment with MB correlates with the cell number. The absorbancy measured after MTT treatment reflects the number of metabolically active cells. To evaluate the results, a factor called GIF (Growth Inhibition Factor) was introduced. Our anti-proliferative cellular assays seem to be stable and well reproducible after testing 300 compounds. Of the 100 compounds tested, 10% of the compounds showed better than 80% efficacy regarding growth inhibition accompanied with minimum *in vitro* toxicity.

2. Tyrosine kinase assay

Our aim was to set-up and characterize a non-radioactive TK assay platform to screen potential drug-candidate compound libraries designed against the ATP binding site of TK receptors. Recombinant EGF-R, PDGF-R-α and VEGF-R2 enzymes were derived

from baculovirus transfected insect-cell (Sf9) expression systems. In all cases, a synthetic substrate polyGluTyr and an ELISA-based detection system was used, targeting phosphorylated Tyr residues by a monoclonal antibody. The absorbance is measured with an ELISA Reader and correlates with the quantity of the phosphorylated substrate and thus enzyme activity. Following optimization and standardization based on individual determination of kinetic parameters and calculation of K_m values, a number of reference TK inhibitors were tested. In conclusion the present ELISA based non-radioactive TK assay offers a reproducible, sensitive and rapid method to measure TK activity and enables large-scale screening of TK inhibitors.

3. Flow cytometry

Screening tests provide binary data in terms of efficacy, which needs further characterization by more specific methods. In this paper we show different biological end-points of the action of "effective" structurally closely related compounds. Flow cytometry was used with various indicators of cell cycle and cell survival: Annexin V (early apoptosis), FLICA (general caspase activity), Calcein-AM (cell viability), and propidium iodide (membrane integrity and DNA content). A431 cells were treated with inhibitors for 0, 6, 16, 24 and 48 hours prior to analysis. zVAD.fmk was used as a general caspase inhibitor. Based on selective growth inhibitory properties, two compounds that induced dramatically different cellular morphology were selected. Analysis of apoptosis induction was based on Annexin-V and propidium iodide staining.

Summary

ELISA based non-radioactive TK assays offer reproducible, simple and rapid methods to measure kinase activity and enables large-scale screening of TK inhibitors. However, in our hands, methodological burdens seem to limit the sensitivity of ELISA-based approaches (relatively high background). In this respect ECL-based or fluorescent technologies seem to be superior on the "cost of the prize" of the assay.

Because of these difficulties, for prescreening we have worked out a strategy using A431 EGFR overexpressing cell lines in proliferation assays. The assay was carried out in two timepoints to distinguish between apoptotic and necrotic effect. The compounds were screened in core structure groups in order to select the best core structures for further synthetic work. The best compounds were further analyzed in EGF-RTK assay and in specific apoptotic assay with FACS. Analyzing the structures of several active inhibitors revealed that most of the potent compounds contained a condensed bicyclic heteroaryl moiety in which the pyrimidine ring seems to be an important element.

Acknowledgments

NKFP 1/47/2001 (MediChem), 1/2001 KKK NKFP 1/A/0020/2002 OTKA 32415.

References

1. Oliver, M. H. *et al*., *J. Cell. Sci*. **92**, 513-8 (1989).
2. Carmichael, J. *et al*., *Cancer Res.* **47**, 936-942 (1987).
3. Sigma, PTK-101.

Peptide Revolution: Genomics, Proteomics & Therapeutics
Michael Chorev & Tomi K. Sawyer (Editors)
American Peptide Society, 2003

The Development of Peptide-Based Inhibitors of Stat3α

Zhiyong Ren, David R. Coleman, Larry A. Cabell and John S. McMurray

Department of Neuro-Oncology; The University of Texas M. D. Anderson Cancer Center, Houston, TX 77030, USA

Introduction

Signal transduction and activator of transcription 3 (Stat3) is a member of the STAT family of latent, cytosolic transcription factors that directly relates signals from the plasma membrane to the nucleus [1]. Stat3 mediates IL-6 signals and has also been shown to participate in growth factor receptor cascades such as those originating from EGF. Downstream targets of Stat3 include bcl-x_L, a member of the bcl-2 family of anti-apoptotic proteins, cell cycle regulators such as cyclin D1 and $p21^{WAF1/CIP1}$, and other transcription factors including *c-myc* and *c-fos* [1,2]. Stat3 is recruited to phosphorylated receptors via its SH2 domain. It then becomes phosphorylated on Tyr^{705} by JAK kinases, Src, Abl, or the kinase activity of the receptor. Upon tyrosine phosphorylation, Stat3 forms a dimer in which the SH2 domain of one protein molecule binds to the $pTyr^{705}$ residue of the other and vice versa. The dimer migrates to the nucleus, binds to specific DNA sequences and initiates transcription. Aberrantly activated Stat3 has been observed in a variety of tumors. Antisense and dominant negative constructs have been shown to inhibit cell growth by increasing apoptosis and reducing progression through the cell cycle [3,4]. Thus Stat3 is an attractive target for anticancer drug development. To this end, we have embarked on a program to inhibit Stat3 signaling by inhibiting receptor docking and/or dimer formation by the use of phosphotyrosine-based peptidomimetics targeted to the SH2 domain.

To find a lead peptide, we synthesized a series of phosphotyrosyl-peptides based on sequences from known Stat3 docking sites on cytokine and growth factor receptors [5]. Of the 16 peptides screened, those with the canonical pYXXQ [6] sequence in general displayed the most activity. Interestingly, peptides with a Pro at pY+2 were even more active. Of the peptides tested, that from gp130 Tyr^{904} was the most active, exhibiting an IC_{50} value of 150 nM in electrophoretic mobility shift assays (EMSA) using recombinant, phosphorylated Stat3 and ^{32}P-labeled high affinity c-*fos sis* inducible element (hSIE). Thus, the lead peptide is Ac-pTyr-Leu-Pro-Gln-Thr-Val-NH_2, called 1.6 (Figure 1).

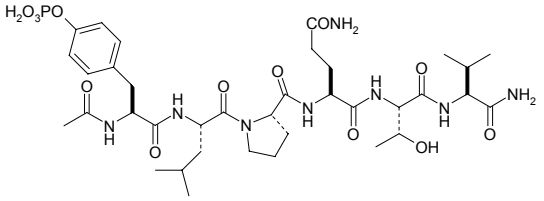

Fig. 1. The structure of the lead peptide, 1.6.

Truncation and alanine scanning showed that the C-terminal Val was unimportant and that Thr contributed modestly to binding. Gln was essential and Pro contributed greatly. Leu provided modest binding energy and on Tyr, phosphate was preferred over phosphonomethyl. Replacement of the phosphate with carboxyl or tetrazole groups abolished inhibition [6]. In this paper we will briefly probe the phosphopeptide

binding pocket of Stat3 with modifications to peptide 1.6 to find pharmacophores and gain information on the bioactive conformation.

Results and Discussion

SAR Studies. Further SAR studies were conducted at positions pY-1, pY+2, pY+3, and pY+4. EMSA assays were replaced with fluorescence polarization assays [7]. Small organic acids such as propionate and benzoate could replace the acetyl group at the pY-1 position; the Cbz group could not. Hydrophobic residues were substituted at pY+1. β-substituted amino acids and Phe were not tolerated, but Nle was.

To test for a *cis* or *trans* Leu-Pro bond in the bound conformation, the 2,2-dimethyloxazolidine proline mimic was incorporated into the peptide. NMR showed 74% *cis* Leu($\Psi^{Me,Me}$)Pro conformation. The IC_{50} value of 1.2 μM suggests that the Leu-Pro bond is in the *trans* conformation.

N^{ε}-methyl substitution on Gln was performed to reduce the polarity of the side chain. Ac-pTyr-Leu-Pro-Glu(OAll)-Thr(tBu) was synthesized on Rink resin. The allyl group was removed with standard palladium chemistry and the side chain of Glu was coupled to $MeNH_2 \cdot HCl$ or Me_2NH using DIC. Using pTyr without protection on the phosphate resulted in highly impure products. In contrast, the use of the bis(dimethylamino)phosphoramidate derivative, Tyr(OPO[NMe_2]$_2$) [8], resulted in clean crude products. Mono-or dimethyl substitution of the side chain amide of Gln destroyed the ability of the peptide to bind to Stat3.

Thr was replaced with various amines by first synthesizing Ac-Tyr(OPO[NMe2]2)-Leu-Pro-Glu-OAll on Rink resin, attaching via the side chain. The allyl group was removed and the amines were coupled to the C-terminus using DIC/HOBt. Disubstituted amides were >10-fold less active and monosubstituted amides were well tolerated.

The non-hydrolysable pTyr mimic, 4-phosphonodifuoromethylphenylalanine (F2Pmp), was incorporated into the peptide using the solid phase cross coupling reaction reported by Qabar [9]. Thus Ac-Phe(4-I)-Leu-Pro-Gln(Trt)-Thr(tBu) was assembled on Rink resin. The peptidyl resin was then treated with 20-fold excesses of $BrCdPO_3Et_2$ and CuCl in DMF at room temp for 4 days resulting in nearly quantitative conversion of Phe(4-I) to F2Pmp$(OEt)_2$. The ethyl groups were removed with TMSI. Not unexpectedly, the substitution of F2Pmp for pTyr reduced the activity (IC_{50} = 3.2 μM). The SAR studies are summarized in Figure 2.

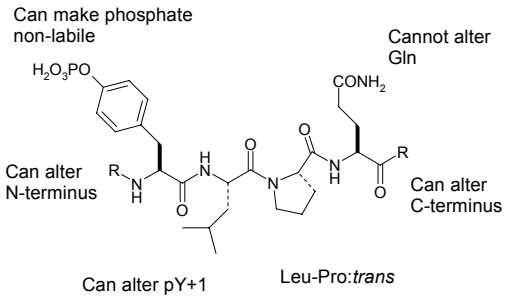

Fig. 2. Summary of SAR results.

Effect of C-terminal residues of Stat3α on peptide binding. Like all Stats, Stat3 is composed of cooperative DNA binding domain at the N-terminus, a 4-helix bundle

domain, a DNA binding domain, a linker region, a SH2 domain, and a transactivation domain at the C-terminus [1]. In the crystal structure of Stat3β dimer bound to DNA [10], residues 711-716 of each protein fold back onto the SH2 domain and form part of the binding surface of the reciprocal phosphopeptide sequence (Figure 3A). To test if this fold back region is important for peptide binding to Stat3 in solution, both full length Stat3 and a construct lacking residues from the C-terminal to the SH2 domain were assayed for binding to fluoresein tagged peptide 1.6 using FP. There was no appreciable difference in binding, suggesting that the SH2 domain in solution does not have residues 711-716 as part of its surface. Therefore we can use the isolated SH2 domain in molecular modeling studies.

Ac-pTyr-Leu-Pro-Gln-NH_2 was docked to the SH2 domain and minimized using Discover/insightII from Accelrys, Inc. The peptide formed the canonical "two pronged plug" interaction with Stat3 with the Leu-Pro in the *trans* conformation. This structure serves as a binding hypothesis and may lead to the discovery of small molecule Stat3 inhibitors.

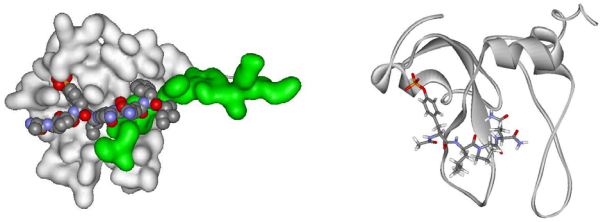

Fig. 3. A) From Stat3β showing "fold-back" region in green. B) Ac-pTyr-Leu-Pro-Gln-NH_2 docked to isolated Stat3 SH2 domain.

Acknowledgments

This work was funded by grants from the M. D. Anderson Cancer Therapeutics Development Program and the National Cancer Institute, CA16672.

References

1. Bromberg, J. and Darnell, J. E., Jr. *Oncogene* **19**, 2468-2473 (2000).
2. Bowman T., Garcia, R., Turkson, J. and Jove, R *Oncogene* **19**, 2474-2488 (2000).
3. Grandis, J. R., Drenning, S. D., Zeng, Q., Watkins, S. C., Melhem, M. F., Endo, S., Johnson, D. E., Huang, L., He, Y. and Kim, J. D *Proc. Natl. Acad. Sci. U.S.A.* **97**, 4227-4232 (2000).
4. Niu, G., Heller, R., Catlett-Falcone, R., Coppola, D., Jaroszeski, M., Dalton, W., Jove, R. and Yu, H *Cancer Res.* **59**, 5059-5063 (1999).
5. Ren, Z. Y. Cabell, L. A., Schaefer, T. S. and McMurray, J. S. *Bioorg. Med. Chem. Lett*. **13**, 633-636 (2003).
6. Stahl, N., Farruggella, T. J., Boulton, T. G., Zhong, Z., Darnell, J. E., and Yancopoulos, G. D. *Science* **267**, 1349-1353 (1995).
7. Lynch, B. A., Loiacono, K. A., Tiong, C. L., Adams, S. E. and MacNeil, I. A. *Anal. Biochem*. **247**, 77-82 (1987); b) Wu P., Brasseur M. and Schindler U. *Anal. Biochem.* **249,** 29-36 (1997).
8. Chao, H.- G. et al., *J. Org. Chem.* **60**, 7710 (1995), b) Ueki, M. et al., Bull. *Chem. Soc. Jpn*. **71**, 1887 (1998).
9. Qabar, M. N., Urban, J. and Kahn, M. *Tetrahedron* **53**, 11171-11178 (1997).
10. Becker, S., Gromer, B. and Muller, C. W. *Nature* **394**, 145-151 (1998).

Peptide Revolution: Genomics, Proteomics & Therapeutics
Michael Chorev & Tomi K. Sawyer (Editors)
American Peptide Society, 2003

Novel Neutrophil-Activating Peptides: Physiological Roles of Direct Activation of GTP-Binding Regulatory Proteins by These Peptides

Hidehito Mukai[1], Yuko Matsuo[1], Rie Kamijo[1] and Kaori Wakamatsu[2]

[1]Research Unit of Peptide Biosignal Engineering, Mitsubishi Kagaku Institute of Life Sciences, Machida, Tokyo 194-8511, Japan; [2]Department of Biochemical Sciences, Faculty of Engineering, Gunma University, Kiryu, Gunma 376-8515, Japan

Introduction

Neutrophils are a group of leukocytes involved in the innate defense system. They quickly infiltrate into injury sites, produce superoxide and digestive enzymes, and phagocytose toxic cell debris and infecting microorganisms. Transmigration of neutrophils is often observed immediately after tissue injury. Though some of chemokines such as interleukin 8 produced by surrounding tissues are known to induce migration and activation of neutrophils, they are synthesized, however, *after* the inflammatory stimulation. This suggests the presence of unknown neutrophil activating substances that promote rapid migration. In previous studies, we identified such a novel class of neutrophil-activating peptides, fCyt b and COSP-1 found in porcine hearts (Figure 1), and investigated their function in neutrophil-like differentiated HL-60 cells [1]. Based on these results, we have proposed novel mechanisms in an innate immuno-system in which digested peptides, such as fCyt b and COSP-1, produced by injured cells induce transmigration and activation of neutrophils to scavenge toxic cell debris [1]. Here we report our recent results about the effects of fCyt b and COSP-1 on primary neutrophils as well as differentiated HL-60 cells and about the biochemical activities of these peptides.

Results and Discussion

Previously, we demonstrated that porcine COSP-1 and fCyt b stimulate β-hexosaminid-ase (β-HA) release from differentiated HL-60 cells [1]. Because HL-60 cells are of human origin, we synthesized human homologs of COSP-1 (hCOSP-1) and fCyt b (hfCyt b) (Figure 1), and examined their effects on β-HA secretion and chemotaxis in differentiated HL-60 cells. hCOSP-1 and hfCyt b did induce the release and chemotaxis in a dose-dependent manner [EC_{50}'s for β-HA release being 3.5 x 10^{-6} M (hCOSP-1) and 6.3 x 10^{-8} M (hfCyt b); EC_{50}'s for chemotaxis being 3.9 x 10^{-7} M (hCOSP-1) and 7.9 x 10^{-9} M (hfCyt b)]. Notably, the concentrations of peptides needed

COSP-1 (C-terminal peptide of cytochrome c oxidase subunit VIII)

Porcine: Leu - Ser - Phe - Leu - Ile - Pro - Ala - Gly - Trp - Val - Leu - Ser - His -Leu - Asp - His - Tyr - Lys - Arg - Ser - Ser - Ala - Ala

Human: Val - Thr - Phe - Leu - Leu - Pro - Ala - Gly - Trp - Ile - Leu - Ser - His - Leu - Glu - Thr - Tyr - Arg - Arg - Pro - Glu

fCyt b (cytochrome b(1-15), N-terminal formylated)

Porcine: fMet - Thr - Asn - Ile - Arg - Lys - Ser - His - Pro - Leu - Met - Lys - Ile - Ile - Asn

Human: fMet - Thr - Pro - Met - Arg - Lys - Ile - Asn - Pro - Leu - Met - Lys - Leu - Ile - Asn

Fig. 1. Primary structures of porcine fCyt b and COSP-1 and their human homologs.

for chemotaxis were much lower than those needed for β-HA release stimulation, and the stimulation of chemotaxis was desensitized at the concentrations where the release is induced. Moreover, hCOSP-1 and hfCyt b stimulated the β-HA secretion in primary neutrophils purified from peripheral blood. These results suggest that neutrophils have monitoring systems for degraded peptides such as hCOSP-1 and hfCyt b, which allow them to remove toxic cell debris.

How these degraded peptides activate neutrophils? It is known that activators of neutrophils such as fMLP, complement 5a, and interleukin 8 stimulate neutrophils via the activation of Gi-type GTP binding regulatory proteins (G_i proteins) [3]. We therefore examined the effects of pertussis toxin (PTX), which ADP-ribosylates G_i proteins and renders them insensitive to stimulations, on β-HA release, chemotaxis, and an increase in cytosolic Ca^{2+} concentration ($[Ca^{2+}]_i$) in differentiated HL-60 cells. As shown in Figure 2, all stimulatory activities of hfCyt b and hCOSP-1 were completely inhibited by pretreatment with PTX, indicating that these peptides transmit signals in neutrophils via the activation of G_i proteins.

What are the receptors for the neutrophil-activating peptides? It has been demonstrated that G_i proteins can be stimulated by amphipathic peptides such as mastoparan [4]. We examined the effects of fCyt b and COSP-1 on purified G_i proteins and found that COSP-1 activated G_i proteins whereas fCyt b did not (data not shown). These results suggest that G_i proteins may act as 'receptors' COSP-1.

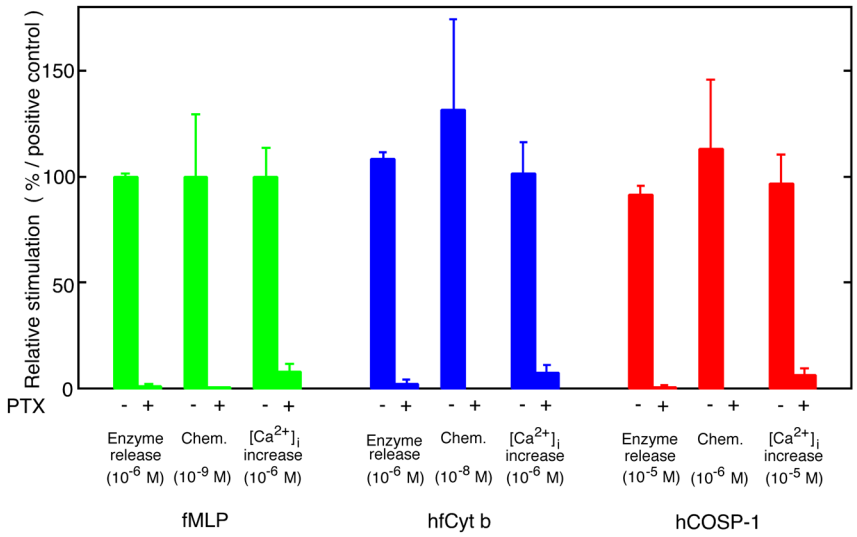

Fig. 2. Inhibitory effects of PTX on β-HA release, chemotaxis, and ($[Ca^{2+}]_i$ increase in differentiated HL-60 cells stimulated by fMLP, hfCyt b, and hCOSP-1. Differentiated HL-60 cells were incubated with 50 ng/ml of PTX for 18 h, and the cells were stimulated by fMLP, hfCyt b and hCOSP-1. The data expressed as the percentage relative to the stimulation in control untreated cells.

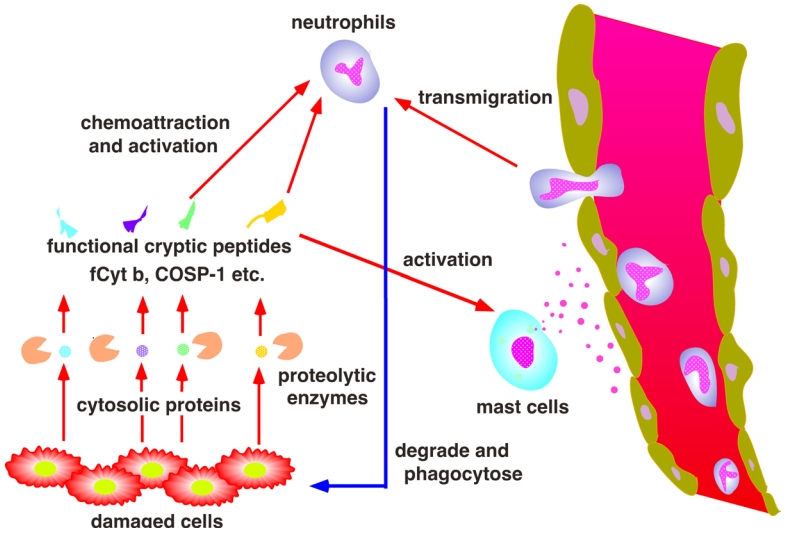

Fig. 3. Proposed mechanisms of acute inflammation involving functional cryptic peptides. Cytosolic proteins released from damaged cells are degraded by proteolytic enzymes, and some of them are maturated to become "functional cryptic peptides" having the ability to activate neutrophils in tissue injury sites. These peptides induce the transmigration of neutrophils from blood stream to the injury sites. During migration, neutrophils are not activated, but when they reach the injury sites, they are activated to scavenge toxic cell debris. Some of these peptides also activate mast cells to secrete histamine which helps in neutrophil transmigration.

Many proteins have amphipathic segments in their amino acid sequences, and we recently found that some of the peptide fragments of these proteins can in fact activate neutrophils to induce chemotaxis and β-HA release. In addition, such peptides including COSP-1 stimulated histamine release from rat peritoneal mast cells (Mukai, H., in preparation). We therefore named such peptides having 'cryptic' functions 'functional cryptic peptides'. The hypothetical mechanisms involving such functional cryptic peptides in an innate immuno-system are proposed in Figure 3. We are currently identifying such functional cryptic peptides using bioinformatic approach.

Acknowledgments

The work was supported by the grants from Mitsubishi Chemical Cooperation. The authors are indebted to many colleagues who gave us suggestions and advice including Drs. A. Sakai, T Sekiya, and M. Shibazaki.

References

1. Mukai, H., Hokari, Y., Seki, T., Nakano, H., Takao, T., Shimonishi, Y., Nishi, Y. and Munekata, E. In Lebl, M. and Houghten, R. A. (Eds.) *Peptides: The Wave of the Future* (*Proceedings of Second International and the Seventeenth American peptide Symposium),* American Peptide Society, San Diego, 2001, p. 1014-1015.
2. Chaplinski, T. J. and Niedel, J. E. *J. Clin. Invest.* **70**, 953-964 (1982).
3. Klinker, J. F., Wenzel-Seifert, K. and Seifert R. *Gen. Pharmac*. **27**, 33-54 (1996).
4. Higashijima, T., Uzu, S., Nakajima, T. and Ross, E. M. *J. Biol. Chem.* **263**, 6491-6294 (1988).

Peptide Revolution: Genomics, Proteomics & Therapeutics
Michael Chorev & Tomi K. Sawyer (Editors)
American Peptide Society, 2003

Ribonucleopeptide Receptors

Masaki Hagihara[1], Tetsuya Hasegawa[1], Shin-ichi Sato[2], Susumu Yoshikawa[1], Katsutoshi Ohkubo[1] and Takashi Morii[1,2]

[1]Institute of Advanced Energy, Kyoto University; [2]PRESTO, JST, Uji, Kyoto 611-0011, Japan

Introduction

Design of tailor-made receptors specific for desired molecules is a long-standing target for current chemistry and biology. Selection of functional RNAs from a randomized pool of RNA molecules successfully affords RNA aptamers that specifically bind to small molecules, and that have catalytic activities [1, 2]. Recent structural analyses of ribosomal RNA complex [3] revealed a remarkable diversity of the RNA-protein complexes, and suggested that its miniature analogue, a ribonucleopeptide (RNP), would serve as an excellent framework for the design of tailor-made receptors and enzymes. We have designed an ATP receptor that consists of an RNA subunit and a peptide subunit by means of a structure-based design approach and successive *in vitro* selection method [4]. The RNA subunit is designed to consist of two functional domains: an ATP binding domain with randomized nucleotides and an adjacent stem region that serves as a binding site for the RNA-binding peptide (Figure 1). The randomized nucleotide region was placed next to the HIV-1 Rev response element to enable the formation of ribonucleopeptide (RNP) pools in the presence of the Rev peptide. *In vitro* selection of RNA from the randomized pool afforded an RNP-receptor specific for ATP. The ATP-binding RNP did not share the known consensus nucleotide sequence for ATP aptamers, and completely lost its ATP-binding ability in the absence of the Rev peptide.

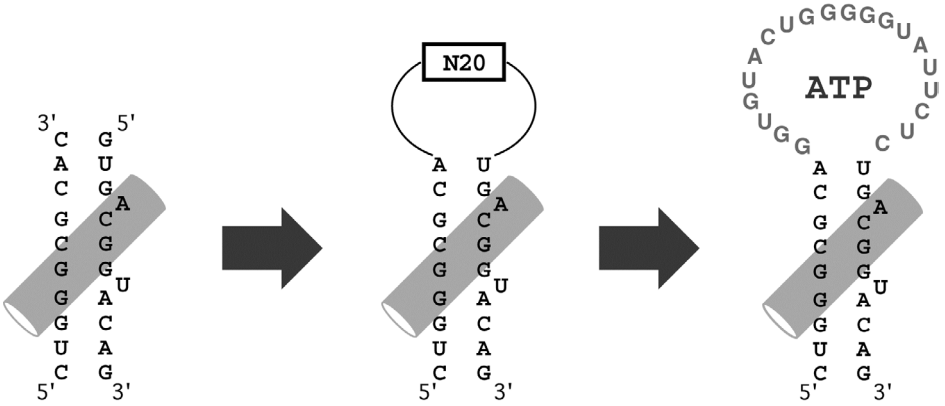

Ac-Rev	Ac-TRQARRNRRRRWRERQR-NH_2
Rev	H- TRQARRNRRRRWRERQR -NH_2
E-Rev	H- ETRQARRNRRRRWRERQR-NH_2
R-Rev	H- RTRQARRNRRRRWRERQR-NH_2

Fig. 1. A schematic representation showing the construction of ribonucleopeptide receptor (top, right) from Rev—RRE complex (top, left). Sequences of the peptide subunits of RNP20 are shown below.

Results and Discussion

Ribonucleopeptide complex was designed in a structure-based manner using the three-dimensional structure of the Rev Response Element (RRE) RNA and HIV-1 Rev peptide complex [5]. An RNA subunit, referred to as RRE20N, was designed to consist of two functionally separated regions, a possible ligand-binding region with 20 randomized nucleotides, and an adjacent stem region that served as a binding site for the Rev peptide (Figure 1). Ribonucleopeptide receptors for ATP were isolated from a pool of RNA sequences (4^{20}) by the *in vitro* selection method. In each round of selection, RNA pools were incubated with immobilized ATP in the presence of the Rev peptide (Ac-Rev), washed to remove unbound sequences, and then eluted with free ATP. The eluted fractions were collected, reverse transcribed, and applied to successive RT-PCR amplification to generate new DNA pools. DNA templates were transcribed and the resulting RNA pools were subjected to the next round of selection. After nine rounds of selective amplification in the presence of the Rev peptide, the fraction of RRE20N-peptide complex eluting with free ATP increased to 15 %. The RNA pool thus enriched in the presence of the Rev peptide, termed P9ATP, showed considerably lower ATP-binding activity (2 %) in the absence of the peptide.

Analysis of the nucleotide sequences of clones from P9ATP revealed three distinct consensus sequences. Among the 26 clones for P9, 15 revealed a 9-nucleotide consensus sequence 5'-GUGUA-UA-CU-3', denoted as class I. RNA clones from class I (P9ATP-02: 5'-GGUCUGGGCGCGGGUGUACUGGGGGUAUUCUCUGACGG-UACAGGCC-3') were transcribed from the respective DNA sequences, and tested for the ATP-binding activity. The fraction of RNA bound ATP was determined in the presence or absence of the Ac-Rev peptide. The class I RNA P9ATP-02 completely lost its ATP-binding activity in the absence of the peptide.

The N-terminal portion of the acetylated Rev peptide (Ac-Rev) was modified by removing the acetyl group (Rev), or by adding charged amino acids Arg (R-Rev) or Glu (E-Rev) to test an effect for ATP binding of class I RNP20. The RNP complexes of these peptides with the class I P9ATP-02 RNA were analyzed for the ATP-binding. RNP complexes with Rev and R-Rev showed higher affinity to ATP with equilibrium dissociation constants of 16 μM and 19 μM, respectively. Ribonucleopeptide with E-Rev bound ATP with slightly lower affinity (K_D = 38 μM) than the original Ac-Rev ribonucleopeptide did (K_D = 33 μM). Because the stability of these class I ribonucleopeptide P9-02 complexes judged by gel shift titration assay were similar to each other, these results suggest that the N-terminal region of Rev peptide participates in the formation of binding pocket for ATP.

The RNP20-Rev framework was next applied to construct an RNP receptor for N-acetyl glucosamine (GlcNAc). After 13 rounds of selective amplification (P13GNA), the fraction of RRE20N—Ac-Rev complex bound to GlcNAc increased to 8%. The RNA pool showed lower GlcNAc-binding activity (4%) in the absence of the Rev peptide.

Type 1	5'-CCCUCCGAUCUGAACGGGAG-3'
Type 2	5'-CACGGUUUUCGUUACCAUCA-3'
Type 3	5'-UCAGUACAAUAUAUGCGAGA-3'
Type 4	5'-UGCAGUGUUUACUGGUAGAA-3'
Type 5	5'-GGUAGAGGCAUUUUUGUCGC-3'

Fig. 2. Nucleotide sequences of the random region for the RNA subunit in RNP20 obtained for GlcNAc.

Analysis of the nucleotide sequences of clones from P13GNA revealed three distinct consensus sequences (Figure 2). Judging from the fraction bound to the ligand, the affinity of GlcNAc-binding RNP would be lower than ATP-binding RNP. However, the RNPs obtained from the selection with GlcNAc did not show any affinity to glucose.

These results indicate that RNP is obtained not only for ATP, but also for a small sugar derivative. Although the RNP receptor obtained by means of the RNA library exhibits moderate or low affinity to the ligand as observed for the case of GlcNAc, it would be possible to increase the affinity of RNP by modifying the N-terminal portion of the peptide subunit. The single amino acid subsutitution of the N-terminal Rev peptide increased the affinity of the ATP-binding RNP receptor. The ribonucleopeptide complex reported here consists of two subunits. It would be possible to assemble a larger number of binding units, i.e., by creating additional binding sites for a peptide within RNA. Such multi-subunit approaches using the ribonucleopeptide scaffold would create a new possibility for the design of small artificial receptors and enzymes with desired specificity and chemical activity.

Acknowledgments

This work was funded by PRESTO, JST and by the Grants-in-Aid for Scientific Research from the Ministry of Education, Science, Sports and Culture, Japan (No. 15030220) to T. Morii.

References

1. Osborne, S. E. and Ellington, A. D. *Chem. Rev*. **97**, 349-370 (1997).
2. Wilson, D. S. and Szostak, J. W. *Annu. Rev. Biochem*. **68**, 611-647 (1999).
3. Ban, N., Nissen, P., Hansen, J., Moore, P. B. and Steitz, T. A. *Science* **289**, 905-920 (2000).
4. Morii, T., Hagihara, M., Sato, S. and Makino, K. *J. Am. Chem. Soc.* **124**, 4617-4622 (2002).
5. Battiste, J. L., Mao, H., Rao, N. S., Tan, R., Muhandiram, D. R., Kay, L. E., Frankel, A. D. and Williamson, J. R. *Science* **273**, 1547-1511 (1996).

Peptide Revolution: Genomics, Proteomics & Therapeutics
Michael Chorev & Tomi K. Sawyer (Editors)
American Peptide Society, 2003

Deformation of One α-Helix Leads to S-S Bond Formation of YhhP

Toshimasa Yamazaki[1], Etsuko Katoh[1], Shizue Katoh[1], Yuki Tsunoda[1] and Takeshi Mizuno[2]

[1]Biochemistry Department, National Institute of Agrobiological Sciences, Tsukuba, Ibaraki 305-8602, Japan; [2]Laboratory of Molecular Microbiology, School of Agriculture, Nagoya University, Chikusa-ku, Nagoya 464-8601, Japan

Introduction

YhhP is a small *Escherichia coli* protein of 81 amino acid residues, implicated in cell division. YhhP shows no homology in primary sequence to any protein of known function. It is, however, of great interest that several hypothetical proteins homologous to YhhP are predicted to occur in a variety of microorganisms whose entire genome sequences have been completed. These proteins have a common sequence motif of CPxP, which may play a role in protein folding and/or function [1]. Our previous genetic and biological studies [2] have demonstrated that YhhP deficient (Δ*yhhP*) cells do not form normal colonies when grown on a rich medium (e.g. Luria-Bertani medium) containing a relatively low concentration of NaCl (< 1%), rather they form abnormally elongated filamentous cells longer than 10 μm in length. In addition, we identified that such defect was caused by impairment of the FtsZ-ring formation in the Δ*yhhP* cells, although the non-divided filamentous cells contained the FtsZ protein at a level comparable to that in the wild-type cells. Despite extensive studies detail biological function of this family of proteins is not known.

To gain insight into the structure and function of YhhP, we have previously determined its three-dimensional solution structure in the presence of DTT by NMR spectroscopy [3]. The structure revealed that YhhP (SH isoform) folds into a compact two-layered α/β-sandwich structure with a βαβαββ fold, comprising a mixed four-stranded β-sheet stacked against two α-helices, both of which are nearly parallel to the strands of the β-sheet. The CPxP motif is found to play a significant structural role in stabilizing the first helix as a part of the N-capping box that is characterized by a *cis* configuration of Cys19-Pro20 peptide bond, a hydrogen bond and several hydrophobic interactions within the motif. Thus, the more extended region of sequence LxCPxP was proposed to be a novel type of N-terminal α-helix capping box. Site-directed mutagenesis studies, using a series of point mutant proteins of YhhP, have revealed that the CPxP motif plays important roles in both structural stability of YhhP and cell division of *E. coli*, leading to the conclusion that the LxCPxP serves as a starting signal as well as a stabilizing element of α-helix.

During the course of our studies of YhhP, we have observed that in the absence of DTT, the SH isoform of YhhP is gradually converted into the S-S isoform even at lower temperature (4 °C). This is unexpected because in the SH isoform the two SH groups, one from Cys19 in the CPxP motif and the other from Cys56 in the middle of the second α-helix, are separated by 13 Å, and thus too far apart to readily form a disulfide bond. In this study, we have determined the three-dimensional structure of the S-S isoform of YhhP by NMR spectroscopy, and compared it to the previously determined structure of the SH isoform. In addition, we have characterized the internal dynamics of both the SH and S-S isoforms of YhhP using ^{15}N relaxation measurements. Structural and internal dynamics information was used to investigate the mechanism of this S-S bond formation.

Results and Discussion

Recombinant uniformly ^{15}N- and $^{15}N/^{13}C$-labeled YhhP proteins were expressed in *E. coli* grown in M9 minimum medium using the expression vector pET21b(+) and host bacterial strain BL21. The SH isoform of the protein was purified as described previously [2]. The S-S isoform was prepared by oxidative folding of the SH isoform in a 0.1 M Tris buffer (pH 8.7) containing 1 mM EDTA and reduce and oxidized glutathione, and purified by similar methods used for purification of the SH isoform but in the absence of DTT. The ratio of the protein and redox reagent was 1:100:10. NMR measurements for the SH isoform were carried out on a sample containing ca. 1 mM protein, 100 mM NaCl, 2 mM NaN_3 and 2 mM DTT in 10 mM potassium phosphate buffer (pH 7.1). NMR samples of the S-S isoform contained ca. 1 mM protein, 100 mM NaCl and 2 mM NaN_3 in 10 mM potassium phosphate buffer (pH 7.1). All NMR experiments were carried out at 25 °C on a Bruker DMX750 spectrometer. NMR signal assignments were obtained by a well-established sequence specific assignment strategy using triple resonance experiments. The backbone ^{15}N relaxation parameters comprising the ^{15}N longitudinal relaxation time T_1, transverse relaxation time T_2 and hetero-nuclear Overhauser enhancement ^{15}N-{^1H} NOE, were measured using HSQC type pulse sequences. The relaxation decay curves were sampled at seven relaxation delay points for T_1 and T_2 measurements. Because of their lower sensitivity, ^{15}N-{^1H} NOE experiments were performed three times, and the measured NOEs were averaged. Structures of the S-S isoform were calculated using the hybrid distance geometry-dynamical simulated annealing method as contained in X-PLOR 3.1.

The three-dimensional structures of the S-S and SH isoforms of YhhP, determined by NMR-derived distance and dihedral angle restraints, are shown in Figure 1. The S-S isoform assumes nearly the same 3D structure as the SH isoform with the exception of a lack of the second α-helix (residues 48-59), which contains the Cys56 residue. In fact, pairwise RMSD values for secondary structural regions (a three out of four β-strands, β1, β2 and β4, and α1-helix) of these two structures are less than 1 Å. The α2-helix of the SH isoform is converted into a long flexible loop upon the disulfide bond formation between Cys19 and Cys56. The pairwise RMSD values for backbone coordinates of this region are in a range from 3 to 13 Å. Note that amide signals from this region were severely exchange-broadened in the S-S isoform. These results suggest that structural conversion of YhhP from the SH isoform to the S-S isoform is achieved only by deformation of the second α-helix.

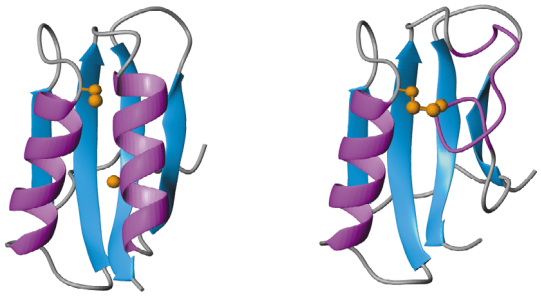

Fig. 1. Ribbon diagrams of the restrained minimized average structures of the SH (left) and S-S (right) isoforms of YhhP. Side-chain heavy atoms of Cys19 and Cys56 are shown as ball-and-stick models.

The ^{15}N relaxation parameters, T_1, T_2 and NOE, observed for the SH and S-S isoforms of YhhP are summarized in Figure 2. Most residues in the SH isoform show almost identical values in each of the three parameters with the exception of three sites, (1) Val30, (2) Met59-Glu60 and (3) Gly70-L71, indicating a well-ordered backbone structure and restricted internal motion. The Gly70-Leu71, located in the loop connecting the β3- and β4-strands, execute large amplitude motions on the ns-ps time scale while the Val30 and Met59-Glu60 at the C-termini of α1- and α2-helices, respectively, undergo slow internal motions affected by chemical exchange on the ms-μs time scale. In the case of the S-S isoform, many residues display significant internal motions and are classified into four regions. The Gly70-Leu71 execute large amplitude motions on the ns-ps time scale as in the SH isoform. Residues 48-64, a region unfolded upon the disulfide bond formation, are highly flexible as judged from elevated T_1 and decreased NOE values. Decreased T_2 values suggest that these residues are also affected by chemical exchange, probably as a consequence of configuration change around the S-S bond. This configuration change results in reduced T_2 values observed for the N-terminus of α1-helix (Cys19-Met24) and the end of β4-strand (Ile77-Gly80), close in space to the unfolded region. However, these two regions have well-ordered structures as in the SH isoform because observed T_1 and NOE values are almost identical between the two forms.

There is no significant difference in internal motion on the ms-ps time scale between α1- and α2-helices in the SH isoform (Figure 2). Thus, we investigated much slower motion measuring amide-proton-exchange rates. Although 8 NH(n+4) → CO(n) hydrogen bonds are expected for both α1- and α2-helices, only two residues of the latter have amide-proton-exchange lifetimes longer than 20 min while seven residues of the former have longer lifetimes, suggesting that α2-helix is less stable than α1-helix. We suspect that deformation of α2-helix, on the time scale longer than a second, may lead to structural conversion of YhhP from the SH isoform to the S-S isoform.

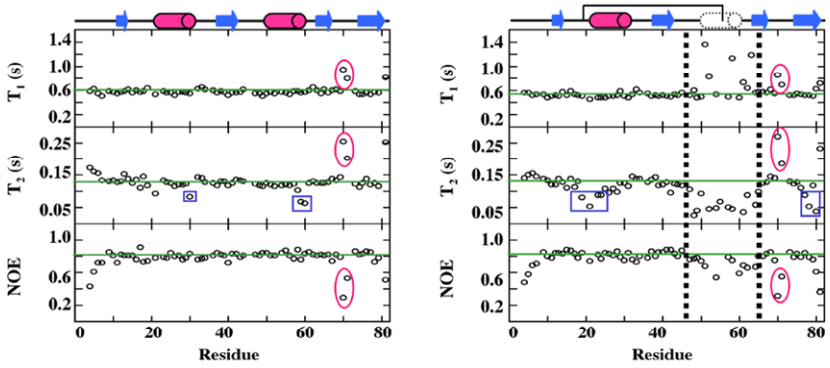

Fig. 2. Comparison of backbone ^{15}N relaxation parameters, T_1, T_2 and NOE, of the SH (left) and S-S (right) isoforms of YhhP.

Acknowledgments

The work was supported by the Bio-Oriented Technology Research Advancement Institution of Japan.

References

1. Yamashino, T., *et al., J. Bacteriol.* **180**, 2257-2261 (1998).
2. Ishii, Y., *et al., Biosci. Biotechnol. Biochem.* **64**, 799-807 (2000).
3. Katoh, E., *et al., J. Mol. Biol.* **304**, 219-229 (2000).

Receptor and Ion Channel Agonist/Antagonist Structure-Function

Peptide Revolution: Genomics, Proteomics & Therapeutics
Michael Chorev & Tomi K. Sawyer (Editors)
American Peptide Society, 2003

Structure and Function Studies of a Bicyclic Agouti-Related Protein (AGRP) Melanocortin-4 Receptor Antagonist

Andrzej Wilczynski[1], Xiang S. Wang[2], Rayna M. Bauzo[1], Ramanan Thirumoorthy[2], Zhimin Xiang[1], Arthur S. Edison[3], Nigel G. J. Richards[2] and Carrie Haskell-Luevano[1]

[1]Department of Medicinal Chemistry; [2]Department of Chemistry; [3]Department of Biochemistry and Molecular Biology, University of Florida, Gainesville, FL 32610, USA

Introduction

The melanocortin system consists of five receptors (MC1R-MC5R) and belongs to the GPCR family. Agouti-related protein (AGRP) is one of the two known naturally occurring antagonists of GPCRs, specifically the brain melanocortin receptors, MC3R and MC4R [1]. The cysteine-rich C-terminus of the AGRP has been identified as possessing nM antagonist activity equipotent to the full-length protein [1]. Thus, suggesting that the key structural and molecular recognition features are located in this domain. Previous studies showed that AGRPs RFF triplet (residues 111-113) are critical for the binding and antagonistic activity at the MC3R and MC4R. However, truncated synthetic analogs containing the active loop AGRP(109-118), have lower potency than that of the full-length C-terminal AGRP [2]. The recently determined NMR structure of AGRP(87-132) showed that the active loop is present in the form of a well-defined β-hairpin [3,4]. Truncated bicyclic AGRP fragments possessing nanomolar antagonist activity at melanocortin receptors have been previously reported [5]. Herein we present the synthesis, pharmacological characterization and NMR structure of a bicyclic analog of the AGRP:

AGRP(101-122) CUDPUATUYC**RFF**NAFCYCRKL U - α-aminobutyric acid

Additionally, theoretical model(s) of the bicyclic analog docked into the mouse MC4R is reported to narrow down possible NMR-based structural peptide families based on favorable ligand-receptor interactions.

Results and Discussion

Peptide synthesis was performed on the solid phase using standard Fmoc chemistry. Cyclization of the linear peptide was performed in solution. To ensure the correct disulfide pairing, the thiol groups were protected with acid-labile trityl groups and acetamidomethyl (Acm) groups.

Pharmacology. Table 1 summarizes functional and binding activity of the compound presented in this study.

Table 1. Functional and binding activity of the bicyclic analog.

		MC3R	MC4R
Binding activity	IC_{50}(nM)	100	20
Antagonist	K_i(nM)	170	30

^{1}H NMR structure. NOESY and TOCSY experiments were acquired at 30°C, pH=5.5 on a Bruker Avance 600 MHz spectrometer. Based upon these data, three-dimensional structures were calculated by restrained molecular dynamics (RMD) methods. RMD simulations and cluster analysis yielded five main families of structures. Each representative structure was docked into our mMC4R 3D model and the lowest energy binding value was obtained for the representative structure of the major family (78% of the total number of conformers). This approach eliminated the remaining possible NMR-based ligand structural families due to significant steric problems upon docking into the receptor. Superposition of this bicyclic hAGRP(101-122) peptide with corresponding residues from the high-resolution NMR structure of AGRP(87-132) [3,4] resulted in the lowest RMSD (1.4 Å) for the backbone atoms of the hAGRP(111-116) RFFNAF loop (Figure 1), suggesting that amino acids outside this AGRP(109-118) region are responsible for increasing ligand potency of AGRP at mMC4R.

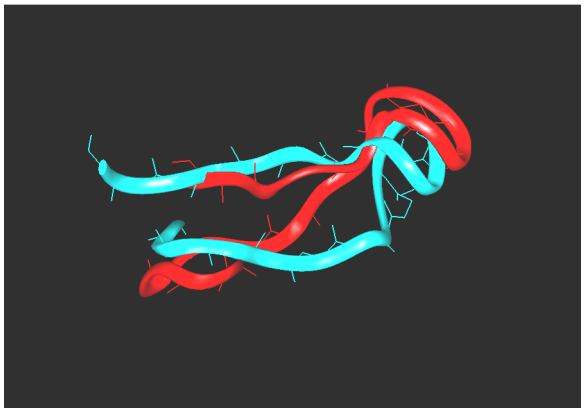

Fig. 1. Structural comparison of the bicyclic hAGRP(101-122) analog (light grey) presented in this study with corresponding residues from the previously reported high-resolution NMR structure of AGRP(87-132)[3] (dark grey).

Acknowledgments

The work was funded by NIH DK57080, DK64250 and Burroughs Welcome Career Award in Biomedical Sciences.

References

1. Ollmann, M. M., Wilson, B. D., Yang, Y. K., Kerns, J. A., Chen, Y., Gantz, I. and Barsh G. S. *Science* **278**, 135-138 (1997).
2. Tota, M. R., Smith, T. S., Mao, C. Macneil, T., Mosley, R. T., Van der Ploeg, L. H. and Fong, T. M. *Biochemistry* **38**, 897-904 (1999).
3. McNulty, G. C., Thompson, D. A., Bolin, K. A.,Wilken, J., Barsh, G. S. and Millhauser, G. L. *Biochemistry* **40**, 15520-7 (2001).
4. Jackson P. J., McNulty J. C., Yang Y. K., Thompson D. A., Chai B., Gantz I., Barsh G. S. and Millhauser G. L. *Biochemistry* **41,** 7565-72 (2002).
5. Jarosinski, M. A., Dodson, W. S., Harding, B. J., Hale, C., McElvain, M., Zamborelli, T. J., Lenz, T. M., Bennett, B. D., Marasco, J., Baumgartner, J., Liu, C.- F. and Carbon, E. W. *17th Am. Peptide Symp.* poster **322** (2001).

Peptide Revolution: Genomics, Proteomics & Therapeutics
Michael Chorev & Tomi K. Sawyer (Editors)
American Peptide Society, 2003

NMR Structure-Based Design of α-MSH Peptide Analogues

Jinfa Ying[1], Katalin E. Kövér[2], Xuyuan Gu[1], Guoxia Han[1], Josef Vagner[1], Minying Cai[1], Christopher M. Cabello[1], Chiyi Xiong[1], Junyi Zhang[1], Dev B. Trivedi[1], Malcolm J. Kavarana[1] and Victor J. Hruby[1]

[1]Department of Chemistry, University of Arizona, Tucson, AZ 85721, USA; [2]Department of Chemistry, University of Debrecen, H-4010 Debrecen, Hungary

Introduction

α-Melanocyte stimulating hormone (MSH) is an endogenous neuropeptide that is generated by post-translational processing and modification of the pro-opiomelanocortin (POMC) prohormone [1]. This hormone interacts with four of the five known melanocortin receptors (MC1R, MC3R, MC4R and MC5R), which belong to the superfamily of seven-helix transmembrane G-protein-coupled receptors (GPCRs). Its primary biological functions include skin pigmentation, erectile function, energy homeostasis, and control of feeding behavior, among others. Previous extensive studies led to identification of the core residues (His^6-D-Phe^7-Arg^8-Trp^9) in α-MSH and development of a number of conformationally constrained, biologically active α-MSH peptide analogues (*e.g.,* MTII, SHU9119, VJH085 and MK9 *etc*.) [2-4]. Due to the conformational constraints imposed by the macrocyclization of these peptides, their structures in solution can be readily studied by 2D NMR techniques and, more importantly, these solution NMR structures may be relevant to those in their receptor-bound state. The structural differences among these analogues may explain the differences in their biological activities, providing a rational basis for the further design of potent and selective agonists and antagonists for the various melanocortin receptors.

Results and Discussion

NMR samples of MTII and SHU9119 were prepared in 90% H_2O/10% D_2O solution containing 50 mM sodium acetate-d_3 and 1.0 mM NaN_3 with a peptide concentration of approximately 10 mM. Two dimensional TOCSY and ROESY spectra for each sample were acquired on a Bruker DRX-600 spectrometer at 25 °C and pH 4.5, using a combination of water flip-back and excitation sculpting pulse sequences for solvent suppression. The ^{1}H chemical shifts were assigned using standard methods [5].

Three dimensional structures were calculated using the torsion-angle dynamics simulated annealing protocol as implemented in the ARIA1.2 software interfaced with CNS 1.1. The intensities of ROESY cross peaks and the $^3J_{HN\text{-}H\alpha}$ derived ϕ torsion angles were used as the NMR constraints for structural calculations. The 20 structures with the lowest restraint energy were chosen to represent the solution structure for each peptide.

Analysis of the structures showed a β-turn structure spanning His^6 and D-Phe^7 in MTII. With respect to the pseudo-plane defined by the β-turn, it was found that the aromatic rings in both His^6 and D-Phe^7 adopted an equatorial-out orientation, while the side chains of Arg^8 and Trp^9 were oriented in axial positions but on the opposite surfaces of the turn structure. These observations are consistent with the previous prediction of the MTII structure based on the quenched molecular dynamics simulations [2]. The turn conformation in the lowest restraint energy structure of MTII best fits the criteria for type II and type V β-turn structures, as indicated from the low

backbone rmsd values (0.50 and 0.60 Å) obtained on superimposing MTII onto the model peptides with standard type II and type V structures, respectively.

For a structural comparison between SHU9119 and MTII, the lowest restraint energy structures of the two peptides were superimposed onto each other using the backbone heavy atoms of residues His^6, $D\text{-}Nal^7$/$D\text{-}Phe^7$, and Arg^8, giving an rmsd value of 0.41 Å (Figure 1). This suggested a similarity in the overall backbone conformations of the two ligands around the β-turn region observed in MTII. As evident from Figure 1, however, the backbone orientation of Nle^4 and Asp^5 of SHU9119 differs from that of MTII. This structural difference can be attributed to the stronger hydrophobic interactions between the side chains of Nle^4 and $D\text{-}Nal^7$ in SHU9119, as supported by the observation of several ROESY cross peaks between the side chain hydrogens in these two residues. As a result, the side chains of His^6 and Trp^9 in SHU9119 oriented at different positions in space from those in MTII, which may be responsible for the antagonist and agonist activities. In addition, a stronger hydrophobic cluster consisting of the side chains of Nle^4, $D\text{-}Nal^7$, and Trp^9 in SHU9119 was formed, which may lead to topographic differences between SHU9119 and MTII, and therefore provide further structural basis for their different biological functions.

The NMR structures of MTII and SHU9119 have been used as the structural target to design new ligands for melanocortin receptors. Synthesis and biological evaluation of the new peptide analogues are under investigation.

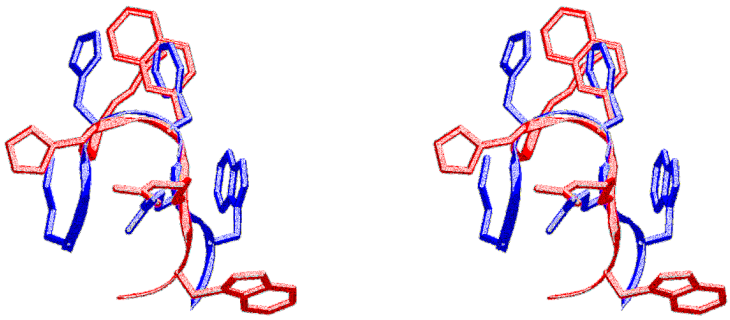

Fig. 1. Stereo plot of MTII (in blue) and SHU9119 (in red) superimposed using the backbone heavy atoms of residues His^6, $D\text{-}Nal^7$/$D\text{-}Phe^7$, and Arg^8.

Acknowledgments

The work was funded by the U. S. Public Health Service and by a travel grant from the MTA-OTKA-NSF U.S.-Hungary Cooperative Research Program.

References

1. Hruby, V. J. and Han, G. In *The Melanocortin Receptor*s, Cone, R. D. Ed., Humana Press: Totowa, NJ, pp 239-261 (2000).
2. Al-Obeidi, F. *et al. J. Am. Chem. Soc.* **111**, 3413-3416 (1989).
3. Hruby, V. J. *et al. J. Med. Chem.* **38**, 3454-3461 (1995).
4. Kavarana, M. *et al. J. Med. Chem.* **45**, 2644-2650 (2002).
5. Wüthrich, K. *NMR of Proteins and Nucleic Acids*, Wiley, New York (1986).

Peptide Revolution: Genomics, Proteomics & Therapeutics
Michael Chorev & Tomi K. Sawyer (Editors)
American Peptide Society, 2003

Design and Synthesis of Novel Antihypertensive Drugs

Thomas Mavromoustakos[1], Panagiota E. Roumelioti[2], Maria Zervou[1], Panagiotis Zoumpoulakis[1,2], Ioanna Kyrikou[1,2], Nektarios Giatas[2], Demetrios Gatos[2], Maria-Eleni P. Androutsou[2], Ioannis Papanastasiou[2], Anastasia Zoga[1,2,5], P.M. Minakakis[3], G. Kokotos[3], Demetrios Vlahakos[4], Eustathios Iliodromitis[5] and John Matsoukas[2]

[1]Institute of Organic and Pharmaceutical Chemistry, National Hellenic Research Foundation, 48 Vas. Constantinou Ave, 11635 Athens, Greece; [2] Department of Chemistry, University of Patras, 26500 Rio, Greece; [3]University of Athens, Department of Chemistry, Zographou 15771, Athens, Greece; [4]Aretaieo University Hospital, Division of Nephrology, Athens University, Medical School, 76 Vas. Sofias, Ave., 11528 Athens, Greece, School of Medicine; [5]Onassis Cardiac Surgery Center, 356 Sygrou Ave., Athens Greece

Introduction

Peptidomimetism is applied in medicinal chemistry in order to synthesize drugs devoid of the disadvantages of peptides. AT1 antagonists constitute a new generation of drugs for the treatment of hypertension designed and synthesized to mimic the C-terminal segment of Angiotensin II (Ang II) and to block its binding to AT1 receptors. In order to comprehend the molecular basis of hypertension, the conformational properties of Ang II and its derivatives have been explored as well as that of the AT1 antagonists belonging to SARTANs class of molecules. Such studies offer the possibility of revealing the stereoelectronic factors responsible for the bioactivity of AT1 antagonists and of applying rational design for the synthesis of new analogs with better pharmacological profiles and reduced development cost.

Results and Discussion

Two approaches were used in an attempt to design and synthesize novel AT1 antagonists. The first approach is based on losartan structural modifications while the second one uses pyrrolidinone as a template.

a. Derivatives of losartan. Various drug molecules structurally similar to losartan were synthesized. Among them V12 (Figure 1) was found to have similar biological effects as losartan. The positions of a butyl alkyl chain and hydroxymethyl substituents in the imidazole ring were interchanged in comparison to losartan. Based on the superimposition models such a substitution would optimize the spatial vicinity of the butyl chain with the isopropyl group of Ile^5. The imidazole ring of V12 is devoid of chlorine.

b. Derivatives that use a pyrrolidinone scaffold. An example of a simple molecule that possesses the characteristics of the C-terminal segment of Sarmesin and mimics its conformation is shown in Figure 1. More specifically, the aromatic side chains of Tyr^4 (OMe) and His^6 are mounted into a pyrrolidinone scaffold. The pyrrolidinone scaffold has already been used as a scaffold for the development of CCK peptide mimetics [1]. MM1 is the first lead compound and many others have been designed and are in the process of being synthesized. The antihypertensive activity of MM1 is significant (71% compared to losartan). MM1 has different structural features from losartan [2], thus introducing a new class of candidate antihypertensive drugs that uses a pyrrolidinone scaffold instead of the biphenyl ring. These molecules are advantageous over the known SARTANs in two respects: (a) they are easily synthesized and (b) their

structures are based on rational drug design. In addition, this class of molecules confirms the aromatic side-chain cluster model of Ang II and Sarmesin [3-5].

Reported results show that mimicry can lead to the rational design of drugs with better pharmacological profile. Understanding the stereoelectronic features responsible for activity in Ang II, Sarmesin and AT_1 antagonists will lead to new classes of molecules with certain advantages over the drugs currently existing in the market. From the reported models of Ang II in various environments there is no criterion for favoring a certain conformation. In our opinion a model has merit if it identifies the pharmacophores responsible for activity and helps in the design of new bioactive drugs. Our model [3] appears to be a useful one for the design of new AT1 antagonists.

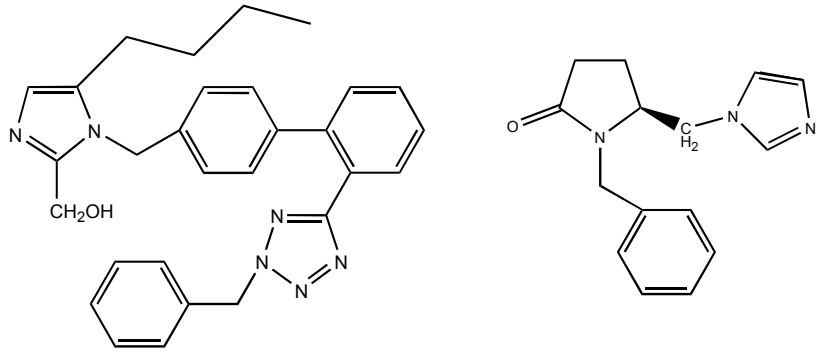

V 12 MM1

Fig. 1. Chemical structures of V12 and MM1.

Acknowledgments

The work was funded by GSRT (EPET II-EKVAN 115), Bilateral Collaboration of Greece-Slovenia (2001-2003, 2003-2005) EPAN-4.3. Dr. Panagiota Roumelioti was supported by the State Scholarship's Foundation (IKY).

References

1. Giannis, A. and Kolter, T. *Angew. Chem. Int. Ed. Engl.* **32**, 1244-1267 (1993).
2. Moutevelis-Minakakis, P., Gianni, M., Stougiannou, H., Zoumpoulakis, P., Zoga, A., Vlahakos, A. D., Iliodromitis, E. and Mavromoustakos, T. *Bioorg. Med. Chem. Letters* **13**, 1737-1740 (2003).
3. Matsoukas, J., Hondrelis, J., Keramida, M., Mavromoustakos, T., Makriyannis, A., Yamdagni, R., Wu, Q. and Moore, G. *J. Biol. Chem*. **269**, 5303-5312 (1994).
4. Matsoukas, J., Agelis, M., Wahhab, G., Hondrelis, A., Panagiotopoulos, J., Yamdagni, R., Wu, Q., Mavromoustakos, T., Maia, H. L. S., Ganter, R. and Moore, G. J. *J. Med. Chem*. **10**, 4660-4669 (1995).
5. Mavromoustakos T., Kolocouris, A., Zervou M., Roumelioti P., Matsoukas, J. and Weisemann, R. *J. Med. Chem*. **42**, 1714-1722 (1999).

Peptide Revolution: Genomics, Proteomics & Therapeutics
Michael Chorev & Tomi K. Sawyer (Editors)
American Peptide Society, 2003

Novel Angiotensin II Lactam Bridge Cyclic Analogues

Vani X. Oliveira Jr.[1], Alessandra Machado[2], Marcos A. Fázio[1], João B. Pesquero[1], Edson L. Santos[1], Cláudio M. C. Neto[1] and Antonio Miranda[1]

[1]Departamento de Biofísica, Universidade Federal de São Paulo, 04044-020; [2]Departamento de Bioquímica, Instituto de Química, Universidade de São Paulo, 05508-900, São Paulo, SP, Brasil

Introduction

Angiotensin II (A_{II}) is a potent natural hormone that plays an important role in blood pressure regulation. Conformational studies of A_{II} have been carried out using a variety of approaches including biological testing of conformationally constrained analogues. Many of these efforts were made in an attempt to establish the receptor-bound conformation. In our previous studies, we designed conformationally constrained analogues, scanning the whole A_{II} sequence with an i-(i+2) lactam bridge consisting of the Asp-X-Lys scaffold. They exhibited low agonistic activity except for cyclo(0-1a) [Asp^0, endo-(Lys^{1a})]-A_{II} (I) that showed similar activity to A_{II} [1]. Based on this peptide, we designed a new A_{II} agonist peptide series using D- or L-Asp, -Glu, -Orn and -Lys as bridgehead elements of the lactam bridge. We also designed an A_{II} antagonist series based on cyclo(3-5)[Sar^1,Asp^3,Lys^5]-A_{II} [2].

Results and Discussion

Peptides were synthesized by SPPS method on Merrifield resin, using the t-Boc strategy [3]. The cyclization of the peptides still attached to the resin were performed by using BOP as coupling reagent. Peptides were deprotected and cleaved from the resin by HF. They were purified by RP-HPLC and characterized by MS, AAA, CE and CD. The bioassays were performed using AT_1-receptor transfected cells suspension on a Cytosensor microphysiometer [4]. Agonistic activities of the peptides were compared to those effected by A_{II} at 10^{-7}M.]. Agonistic activities of the peptides were compared to those cause effected by A_{II} at 10^{-7} M. Antagonistic effects were determined at 10^{-6} and 10^{-7} M concentrations. All cyclic peptides (Table 1 and 2) presented a 20% increase in their agonistic activity in comparison with peptide (I) and were equipotent to A_{II}. Thus, we noticed that, independent of the bridgehead amino acid residue, their chirality and the size of the ring, no significant differences in the agonistic activities were observed. CD experiments showed that all A_{II} agonist analogues presented random

Table 1. Sequences and agonistic activities of the A_{II} cyclic analogues.

Nº	Sequences	Relative Potency[a]
I	Asp–Asp-Lys–Arg–Val–Tyr-Ile–His–Pro–Phe	87.1 ± 7.7
II	DAsp–Asp-Lys–Arg–Val–Tyr–Ile–His–Pro–Phe	99.9 ± 10.8
III	Asp–Asp-DLys–Arg–Val–Tyr–Ile–His–Pro–Phe	102.7 ± 8.9
IV	DAsp–Asp-DLys–Arg–Val–Tyr–Ile–His–Pro–Phe	94.8 ± 6.3
V	Glu–Asp-Lys–Arg–Val–Tyr–Ile–His–Pro–Phe	100.9 ± 5.1
VI	Glu–Asp-Orn–Arg–Val–Tyr–Ile–His–Pro–Phe	100.6 ± 7.7
VII	Asp–Asp-Orn–Arg–Val–Tyr–Ile–His–Pro–Phe	104.5 ± 14.5

[a]*Data reported as a percentage of the angiotensin II agonistic activity.*

Table 2. Sequences of the A_{II} antagonists analogues.

Nº	Sequences
VIII	Sar–Arg–Val–Asp–Tyr–Lys–Ile–His–Pro–Phe
IX	Sar–Arg–Val–Asp–Tyr–Orn–Ile–His–Pro–Phe
X	Sar–Arg–Val–Glu–Tyr–Lys–Ile–His–Pro–Phe
XI	Sar–Arg–Val–Glu–Tyr–Orn–Ile–His–Pro–Phe
XII	Sar–Arg–Asp–Tyr–Lys–Ile–His–Pro–Phe
XIII	Sar–Arg–Val–Asp–Tyr–Lys-His–Pro–Phe

conformations in water, but tend to adopt a turn conformation in SDS, TFE and methanol (data not shown). The antagonistic results (see Table 1 and Figure 1) showed that the analogues VIII to XII did not inhibit the A_{II} activity in the two different concentrations employed. On the other hand, the analogue XIII inhibited about 35% of the A_{II} response in both concentrations studied. When we compared the antagonistic activity of the analogues VIII and XIII, we observed that the potency increase could be due to the absence of the isoleucine residue that induces or stabilizes, in the receptor environment, a more favorable conformation. CD results showed that all antagonist analogues presented a tendency to adopt a β-turn type I structure in all conditions studied, i.e., methanol, TFE and SDS titrations (data not shown). These results suggest that the position of the lactam bridge in the A_{II} sequence is more important than the bridge length or chirality for recognition and binding to the A_{II} AT_1-receptor.

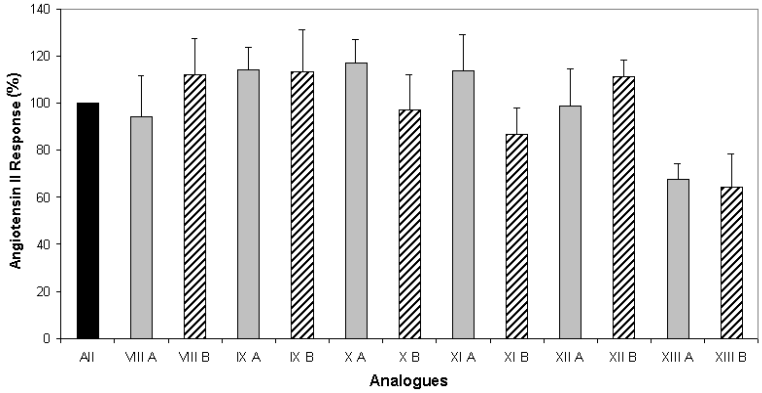

Fig. 1. Antagonistic effects of the analogues at 10^{-7} M (A) and 10^{-6} M (B) in the A_{II} response.

Acknowledgments

This work was supported by grants and fellowships from CNPq and FAPESP.

References

1. Oliveira Jr., V. X. et al. In Lebl, M. and Houghten, R. A. (Eds.) *Peptides: The Wave of the Future (Proceedings of the 17th American Peptide Symposium),* American Peptide Society, San Diego, 2001, pp. 723-724.
2. Plucinska, K. et al. *J. Med. Chem.* **36**, 1902-1913 (1993).
3. Miranda, A. et al. *J. Med. Chem.* **37**, 1450-1459 (1994).
4. Baptista, H. A. et al. *Mol. Pharmacol*. **62**, 1344-1355 (2002).

Peptide Revolution: Genomics, Proteomics & Therapeutics
Michael Chorev & Tomi K. Sawyer (Editors)
American Peptide Society, 2003

Shortcuts to Receptor Structures with Peptide Photoprobes: Angiotensin Receptors

Emanuel Escher, Maud Deraët, Jacqueline Pérodin, Marie-Ève Beaulieu, Lenka Rihakova, Martin Clément, Antony A. Boucard, Gaétan Guillemette, Richard Leduc and Pierre Lavigne

Department of Pharmacology, Faculty of Medicine, Université de Sherbrooke, 3001 12e Ave N, Sherbrooke, QC, J1H 5N4, Canada

Introduction

G-protein coupled receptors (GPCR) are among the most fascinating, challenging and promising drug targets. Contrary to many other drug targets with relatively abundant structural information, rational drug design for GPCR targets is very much in its infancy, if not in fetal state. Most drug targets have well characterized high resolution molecular structures, both in the free and ligand-bound state, derived from X-ray structure analysis and from protein NMR.

The only GPCR exception is the seminal bovine rhodopsin X-ray structure [1] and most, if not all, GPCR structural considerations are made on the rhodopsin template. The 3D-structures of the approximately 599 other GPCR in the human genome remain to be solved.

For most structural considerations on specific GPCR structures, classical structure-activity relationship (SAR) studies on the cognate ligands have been done for many decades and, more recently, site-directed mutagenesis studies have prevailed. These studies are however always of indirect nature, based on ligand affinity and/or on generation of intracellular signals. This has led to the creation of large amounts of contradictory conclusions, but also valuable insights.

More direct biochemical/biophysical methods have therefore been sought for many years, such as with reactive receptor probes. The present contribution intends to show avenues for such combined approaches that will ultimately lead to reasonably precise and accurate ligand-bound receptor structures and to the underlying mechanisms of receptor activation and signal transduction. This will not only permit more rational drug design for the already known drug targets and permit faster access to the necessary information on recently characterized GPCR [2] but also determine their activation mechanisms, important for new drug intervention in almost all areas of therapeutics, from cancer to infectious disease.

In recent years, several research groups, including ours, have determined peptide-ligand receptor contacts by photoaffinity labelling and subsequent biochemical analysis of the contact sites [3-5]. Several new analytical methods for this purpose were developed, in particular mass-spectrometry analysis [4]. We have utilized photoaffinity ligands for the angiotensin II (AngII) receptors AT_1 and AT_2 to determine multiple contact points, deduce general receptor structures, refine the ligand contacts through scanning approaches and find means to elucidate activation-related structural changes. In both receptors, AT_1 and AT_2, AngII analogous photolabels with *p*-benzoyl-phenylalanine (Bpa) residues, in either position 3 or 8, labelled receptor positions rather far apart. This allowed us to deduce spatial restrictions on the liganded GPCR structure compatible only with a ligand in an extended conformation reaching deep into the transmembrane domain (TM), and leading to nearly identical configurations for both AngII-bound AT_1 and AT_2 (Figure 1) [6].

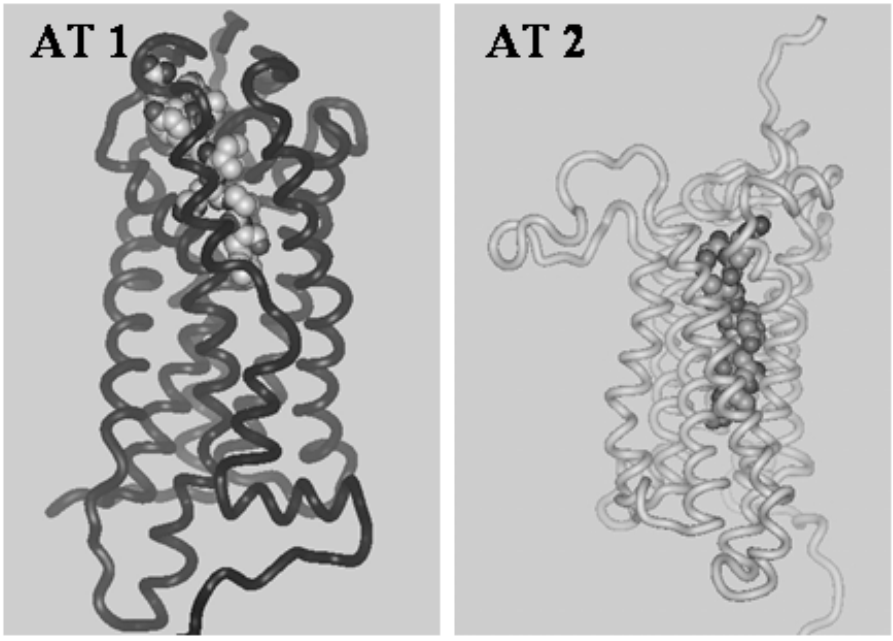

Fig. 1. Energy-minimized structures of liganded and β-rhodopsin homology modelled Ang II receptors. (2nd ECL of AT2 unfurled).

During the studies with Bpa photolabels, it was observed that Met residues were frequently the sites of label incorporation. Met-incorporation was an order of magnitude more frequent than the mean occurrence of Met in typical target proteins, suggesting a strong selectivity of photo-activated benzophenone towards the thioether of the Met-residue. This selectivity is probably due to a charge-transfer complex between the benzophenone radical and the thioether, leading to label incorporation into the ε-methyl or γ-methylene group of Met [7]. Based on this observation, we proposed the Methionine Proximity Assay (MPA): Introduction of Met-residues by site-directed mutagenesis into the target structure would thus, in the immediate proximity, "attract" and monopolize labelling. This mapping approach would permit scanning of the binding area of a given receptor for further contacts.

Results and Discussion

To refine the actual model of AT_1, MPA was carried out and a series of Met-mutated receptors was created for this purpose. Met-residues were introduced in discrete positions on all seven TM domains of hAT_1. According to the modelled ligand-receptor complex most of those residues had a distance of less than 8Å from the ligand photolabel position. Several of these residues had distances greater than 8Å; they were intended as obligatory negative controls. These mutant receptors were then photolabelled, partially purified and digested with cyanogen bromide. For all mutants except for F249M and W253M, labelling of the C-terminal fragment 285-334 was observed on residues similar to those labelled in the WT-hAT_1. This indicates that labelling of the non-Met contact at positions 293/294 remained dominant and occurred not on the presented "Met-bait". On the other hand, mutants F249M and W253M

produced ligand incorporation [8] indicating that labelling took place at those residues in these mutants and not on TM7. This result indicates a close proximity between the side-chain of the C-terminal photolabeling residue of the AngII analogue and TM7 and TM6 but greater distance from TM3 and TM2, as previously suggested. To be compatible with this result, the benzophenone ketone must be directed more towards TM7 but still facing TM6 as depicted in Figure 2. The most intriguing fact is the continuous accessibility on TM7 from residues 293 through 297, where all Met mutants gave ligand release. The most plausible explanation is a certain freedom of rotational movement of TM7, a hypothesis already outlined on rhodopsin [1].

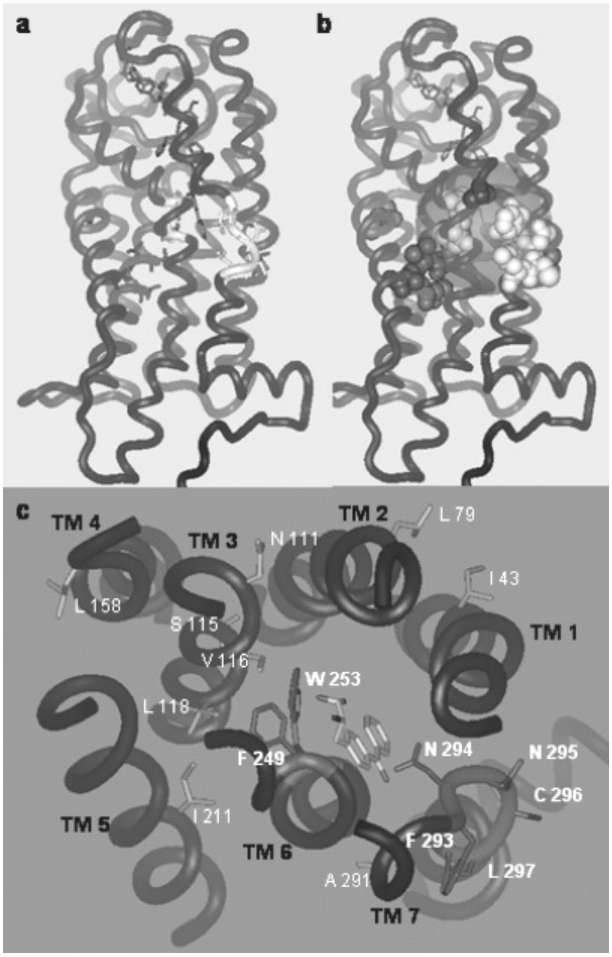

*Fig. 2. Panel **a)** Side-view of homology-modelled, energy minimized liganded AT_1. Panel **b)** 8 Å reaction sphere of Bpa residue with some MPA residues is shown. Panel **c)** Top view of the binding locus of the Bpa^8-residue in the helical bundle. MPA positive residues are in bold.*

Analyzing the water-accessible space of a receptor molecule is another way to learn its inner workings. For this particular purpose, a Cys mutagenesis strategy has been proposed designated as the Substituted Cysteine Accessibility Method (SCAM) (9). We have carried out such a Cys scan on TM7 and on the neighbouring portion of the 3rd extracellular loop from position 276 to 302 [10]. After treatment of these Cys mutants with the water-soluble cationic reagent methane thiosulfonylethylamine (MTSEA), water-accessible free cysteine sulfhydryl groups are disulfide aminated. Reduced ligand binding ([Sar[1],Ile[8]]AngII) was observed for several mutant/receptors (Figure 3A) after MTSEA treatment. The positions where important reagent-induced changes were observed are mostly above the area where MPA-positive mutants in TM7 (280-302) were found (only one position is located below the 280-302 sequence): SCAM positive - 277, 280,282, 283, 286-291 and 301; SCAM negative - 276, 278, 279, 281, 284, 285, 292-300, 302. MPA positive - 293-297; MPA negative - 290,291, and 300.

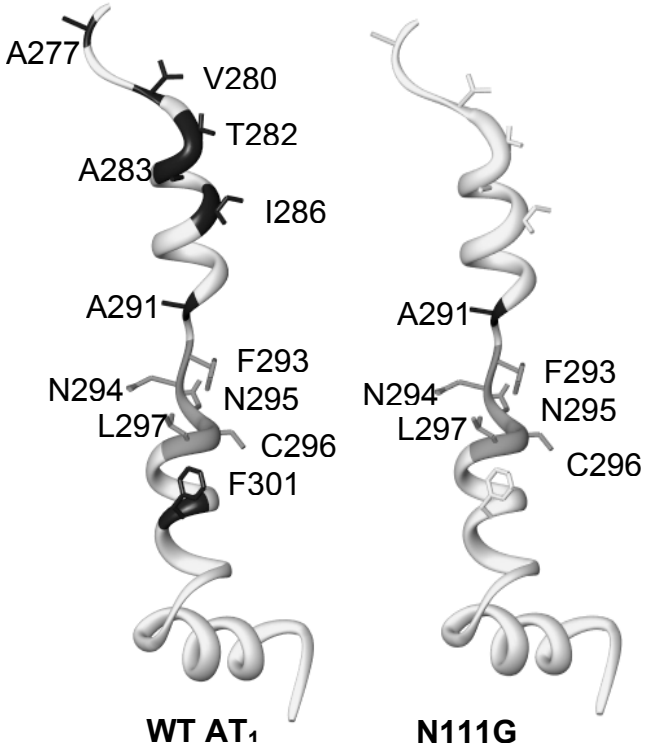

Fig. 3. Combination of MPA and SCAM analysis on TM7 of AT1 and N111G-AT1. SCAM-positive residues are dark grey, MPA-positive residues are light grey.

Two conclusions may be drawn from this observation: a) TM7 needs quite a lot of rotational flexibility to allow access of position 8 of the ligand to two continuous helix turns in TM7; and b) The upper part of TM7 (280-291) and the transmembrane-cytoplasmic interface (301) are water-accessible and interfere at several positions with ligand insertion after introduction of MTSEA.

Combining the receptor model created with molecular dynamics and energy minimization with the above-described observations from MPA and SCAM, it seems

that TM7, through its apparent rotational freedom, interacts in its whole length with the peptide ligand. The C-terminal residue of AngII is pointed towards TM7 and TM6, as seen in Figure 2C. These experiments were carried out on WT-hAT_1, and its respective Cys or Met mutants. In both cases, the employed ligands ([Sar^1,Bpa^8]AngII and [Sar^1,Ile^8]AngII) were of neutral antagonistic nature and therefore, the drawn conclusions apply to this inactive form of hAT_1.

In order to elucidate the changes occurring during receptor activation, those experiments were therefore repeated with the same ligands but on the constitutively active AT_1 mutant N111G [11]. The ligand used for the SCAM-analysis ([Sar^1,Ile^8]AngII) is a full agonist on N111G-AT_1 whereas [Sar^1,Bpa^8]AngII does not alter the considerable constitutive activity of N111G-hAT. The same series of X→M and X→C mutants was created on N111G-hAT_1. Most of those mutants retain constitutive activity. All Met-mutants from 293 through 297 in TM7 of N111G-hAT_1, again produced ligand release after photolabeling and CNBr cleavage, confirming a picture identical to the MPA carried on the non-constitutively active hAT_1. On the other hand, the SCAM analysis on the X→C mutants on N111G-hAT_1 produced a quite different picture insofar as only N111G,A291C produced inhibition of ligand binding after MTSEA modification.

Taken together, receptor activation of AT_1 necessitates a certain mobilization of the upper half of TM7 away from the receptor core but not in the area below position 290 where ligand contact remains apparently the same. The domain movement associated with receptor activation will need further investigation, in particular with fully agonistic photolabels and non-Met selective photoprobes in order to pinpoint the structural changes observed during receptor activation.

References

1. Ballesteros, J. and Palczewski, K. *Curr. Opin. Drug Discov. Devel.* **4**, 561-574 (2001).
2. Vanti, W. B., Nguyen, T., Cheng, R., Lynch, K. R., George, S. R. and O'Dowd, B. F. *Biochem. Biophys. Res. Commun.* **305**, 67-71 (2003).
3. Henry, L. K., Khare, S., Son, C., Babu, V. V., Naider, F. and Becker, J. M. *Biochemistry* **41**, 6128-6139 (2002).
4. Sachon, E., Bolbach, G., Chassaing, G., Lavielle, S. and Sagan, S. *J. Biol. Chem.* **277**, 50409-50414 (2002).
5. Perodin, J., Deraet, M., Auger-Messier, M., Boucard, A. A., Rihakova, L., Beaulieu, M. E., Lavigne, P., Parent, J. L., Guillemette, G., Leduc, R. and Escher, E. *Biochemistry* **41**, 14348-14356 (2002).
6. Deraet, M., Rihakova, L., Boucard, A., Perodin, J., Sauve, S., Mathieu, A. P., Guillemette, G., Leduc, R., Lavigne, P. and Escher, E. *Can. J. Physiol. Pharmacol.* **80**, 418-425 (2002).
7. Rihakova, L., Deraet, M., Auger-Messier, M., Perodin, J., Boucard, A. A., Guillemette, G., Leduc, R., Lavigne, P. and Escher, E. *J. Recept. Signal. Transduct. Res.* **22**, 297-313 (2002).
8. Clément, M., Rihakova, L., Deraët, M., Guillemette, G., Leduc, R. and Escher, E. In Chorev, M., and Sawyer, T. K. (Eds.) *Peptide Revolution: Genomics, Proteomics & Therapeutics, 18th American Peptide Symposium*, American Peptide Society, San Diego, pp. 578 (2004).
9. Javitch, J. A., Shi, L. and Liapakis, G. *Methods Enzymol.* **343**, 137-156 (2002).
10. Boucard, A. A., Roy, M., Beaulieu, M.- È., Lavigne, P., Escher, E., Guillemette, G. and Leduc, R. *J. Biol. Chem. jbcM305952200,* in press, (2003).
11. Noda, K., Feng, Y. H., Liu, X. P., Saad, Y., Husain, A. and Karnik, S. S. *Biochemistry* **35**, 16435-16442 (1996).

Peptide Revolution: Genomics, Proteomics & Therapeutics
Michael Chorev & Tomi K. Sawyer (Editors)
American Peptide Society, 2003

Synthesis and Evaluation of Substituted Benzophenone Photolabeling Amino Acids for the Methionine Proximity Assay

Martin Clément, Maud Deraët, Marie-Ève Beaulieu, Lenka Rihakova, Marie-Thérèse Bawolak, Gaétan Guillemette, Pierre Lavigne, Richard Leduc and Emanuel Escher

Departement of Pharmacology, Université de Sherbrooke, Sherbrooke, QC, J1H 5N4, Canada

Introduction

The C-terminal residue of angiotensin II (AngII) interacts with residues 293 and 294 of the 7th transmembrane element (TM) of the AngII receptor AT_1 [1]. This was shown by photoaffinity labeling with AngII analogues having a *p*-Benzoyl-L-phenylalanine (Bpa) residue in position 8. Since Bpa has pronounced selectivity for Met residues in the target structure [2], we used a Met substitution strategy on AT_1 to find further close contacts of this portion within the AngII binding pocket. We term this the Methionine Proximity Assay (MPA) [2].

To carry out such an MPA, Bpa analogues of reduced reactivity were created through electron-donating substituents (*p*-OMe, *m,p*-di-OMe, *p*-OH), substituted on the hAT_1 receptor and modeled based on the β–rhodopsin structure [3]. Several residues on all transmembrane (TM) segments within or above an 8 Å distance from the Bpa moiety. This 8 Å distance is the approximative reactivity radius of Bpa for the Met-residues in a given protein target. The following hAT_1 mutants were generated by site directed mutagenesis: N111M, S115M, V116M (TM3), F249M, W253M (TM6), F293M, N294M, N295M, C296M, L297M (TM7). All these residues were in an 8 Å radius in an AT_1 receptor model. As negative controls, a second series of mutants was created with Met outside the 8 Å radius: L43M (TM1), L79M (TM2), L118M (TM3), L158M (TM4), I211M (TM5) I290M, A291M, L300M(TM7). A Met-mutant with its side chain within the Met-selectivity radius of the Bpa moiety would then incorporate the photolabel and thus, abolish the non-Met labeling of TM7. Upon CNBr cleavage of the labeled receptor Met-labeling is evidenced by ligand release [1] and the appearance of corresponding receptor fragments, whereas TM7 labeling would produce the already reported 6.5 kDa fragment.

Results and Discussion

Several analogues of [Sar^1]AngII with modified Bpa residues were synthesized through Friedel-Craft acylation of methoxy-benzene [4] di-1,2-dimethoxy-benzene [5], direct alkylation either on a resin-bound glycine residue (-OMe, -di-OMe) or diethyl acetaminomalonate synthesis (-OH) [6], followed by solid phase peptide synthesis. After HF cleavage, peptides were separated by prep HPLC. The diastereomer identity was confirmed by a binding assay and peptide identity by MALDI-TOF MS. The affinity of all analogues was assessed on hAT_1 and all its Met mutants, showing close to 1nM affinity for [Sar^1]AngII and for all photolabeling analogues on native and most mutated hAT_1. In the case of mutants F249M and W253M, an affinity of ~5nM was observed for all peptides.

hAT_1 and its mutants were then photolabeled with all photoligands. [Sar^1,$OMeBpa^8$]AngII and [Sar^1, Bpa^8]AngII produced good to excellent labeling yield on all receptor mutants whereas [Sar^1,di-$OMeBpa^8$]AngII labeled only faintly W253M and N295M and not at all with respect to hAT_1 or the other receptor mutants. [Sar^1, $OHBpa^8$]AngII produced only non-specific labeling, presumably of BSA.

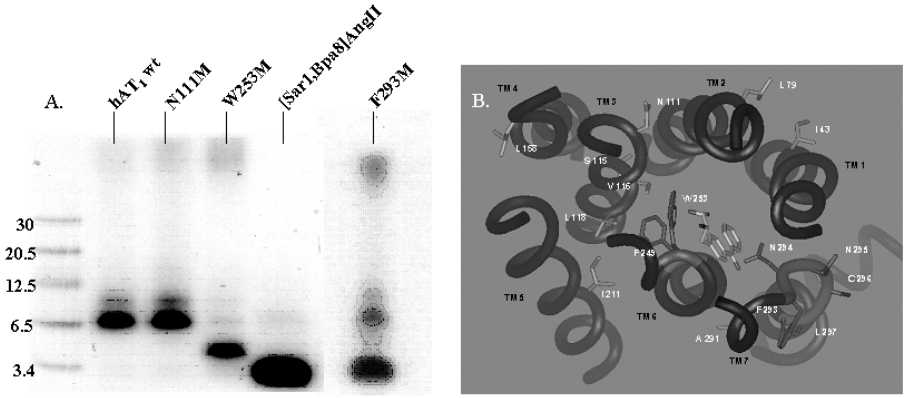

Fig. 1. A. CNBr cleavage of hAT_1 receptor and methionine mutants. B. Model of hAT_1receptor with photoligand [Sar[1],Bpa[8]]AngII within.

Isolation of the covalently labeled receptor complex was followed by CNBr digestion [1] and low molecular weight SDS-PAGE. From native hAT_1 a labeling 6.5kDa fragment was observed (285-334) [1] (Figure 1A), corresponding to TM7 and most of the intracellular C-terminal sequence. All receptors with mutants in TM1-5 produced the same 6.5kDa fragment, indicating that labeling took place on TM7 [1]. Mutants F249M and W253M, however, produced a new fragment at ~ 4 kDa, compatible with a new Met contact point within the fragment 249-284 (Figure 1A). A similar picture emerged with the 290-300 mutants in TM7 as expected: all mutants except I290M, A291M and L300M produced the corresponding fragments and ligand release.

These results confirm and improve the structural model of the AngII-hAT_1 interaction. MPA is a powerful tool to elucidate and refine GPCR structures. The C-terminal residue of AngII points deep into the transmembrane core towards TM6 and TM7 in particular, the latter having an important rotational freedom [7] (Figure 1B).

Acknowledgments
The work was supported by funds from CIHR to E. Escher.

References

1. Perodin, J., et al. *Biochem*. **48**, 14348-14356 (2002).
2. Rihakova, L., et al. *J. Recept. Signal Transduct. Res.* **22,** 297-313 (2002).
3. Palczewski, K., et al. *Science* **289**, 739-745 (2000).
4. Riggs, R. M, et al. *J. Med. Chem.* **30**, 1914-1918 (1987).
5. Parlow, J. J., Mischke, D. A. and Woodard, S. S. *J. Org. Chem*. **62**, 5908-5919, (1997).
6. Horner, M., *Chem. Ber*. **85**, 520-530 (1952).
7. Ballesteros, J. A., Shi, L. and Javitch J. A. *Mol. Pharmacol*. **60**, 1-19, (2001).

Peptide Revolution: Genomics, Proteomics & Therapeutics
Michael Chorev & Tomi K. Sawyer (Editors)
American Peptide Society, 2003

The Name Game: Use of Words Composed of Letters of the English Alphabet as a Source of Novel Bioactive Peptides

David Wade

Wade Research Foundation, 70 Rodney Avenue, Somerset, New Jersey 08873-2024, USA

Introduction

"The world hath noted, and your name is great…" (Othello, the Moor of Venice, by William Shakespeare).

The Name Game was a popular rock and roll song performed by the singer, Shirley Ellis, in 1965 [1]. The lyrics began: "Shirley, Shirley bo Birley Bonana fanna fo Firley, Fee fy mo Mirley, Shirley!...". In a variation of the name game strategy, this article proposes to use words that are composed of the letters of the English alphabet, such as surnames and given names, as a source of ideas for the design of novel, bioactive peptides [2].

This hypothesis was tested with a peptide that was designed to have an amino acid sequence corresponding to the name of the current Secretary of State of the United States, Colin Powell. The amino acid abbreviations shown in Table 1 were used as a guide. Assuming that the peptide would be capable of forming an α-helix, an amide group was included at the carboxyl terminal end of the peptide to reduce the helix dipole and stabilize helix formation. Due to the presence of a cysteine residue at the amino terminal end of the peptide, it has the ability to form dimers. Diagrams of the reduced and oxidized (dimeric) forms of COLINPOWELL are shown in Figure 1.

The peptide amide was custom synthesized in its reduced form by Bachem, and analyzed by Bachem for purity (HPLC and MS), amino acid composition and peptide content (amino acid analysis), and molecular weight (MS). The material was reanalyzed to verify purity, amino acid composition, peptide content, and molecular weight.

The reduced form of peptide amide was tested for bioactivity: (1) against Gram positive bacteria (*Staphylococcus aureus* and *Enterococci*) and (2) HSV-1, and in (3) coagulation and (4) chemotaxis assays.

Results and Discussion

The reduced form of peptide amide, COLINPOWELL, had no activity in the bacterial [3], viral [4], or coagulation [5] assays, but it caused chemotaxis of human monocytes and neutrophils [6]. Detailed bioactivity/biophysical test results for the reduced and oxidized forms of COLINPOWELL will be reported elsewhere.

There are at least three benefits to the use of words and names composed of letters of the English alphabet for designing new peptides: they provide a source of amino acid sequences that may not occur in nature, they might stimulate an interest in peptide research among the general public, and they may provide a new source of funding for peptide research.

Fig. 1. Reduced (left) and oxidized (right) forms of peptide amide, COLINPOWELL, showing the positions of charges. Net charges are +2 (reduced) and +4 (oxidized).

Table 1. Amino acids and their abbreviations[a].

Amino Acid	Abbreviations		Amino Acid	Abbreviations	
	3-Letter	1-Letter		3-Letter	1-Letter
Alanine	Ala	A	Asparagine	Asn	N
Aspartic acid or Asparagine	Asx (for Asp/Asn)	B	Ornithine	Orn	O
Cysteine	Cys	C	Proline	Pro	P
Aspartic acid	Asp	D	Glutamine	Gln	Q
Glutamic acid	Glu	E	Arginine	Arg	R
Phenylalanine	Phe	F	Serine	Ser	S
Glycine	Gly	G	Threonine	Thr	T
Histidine	His	H	Amino(iso)-butyric acid	Abu (Aib)	U
Isoleucine	Ile	I	Valine	Val	V
Isovaline	Iva	J	Tryptophan	Trp	W
Lysine	Lys	K	(unspecified)	Xaa	X
Leucine	Leu	L	Tyrosine	Tyr	Y
Methionine	Met	M	Glutamic acid or Glutamine	Glx (for Glu/Gln)	Z

[a]*Abbreviations from reference [7]. Amino acids that occur naturally in proteins include all those listed, except ornithine (Orn, O) and aminobutyric acid (Abu, U).*

Acknowledgments

Thanks to Ms. Sydney Wade, of Somerset, NJ, for reminding the author of the Name Game song and inspiring this work. The peptide was kindly donated by Mr. Steven Dola and Mrs. Rhea Dola, of Arlington, Virginia. Amino acid analysis was verified by Dr. Tomas Bergman and Ms. Marie Ståhlberg, Protein Analysis Center, Karolinska Institute, Stockholm, Sweden.

References

1. Ellison, S. and Chase, L., *The Name Game* © 1964.
2. Wade, D. *Chemistry Preprint Server*, http://preprint.chemweb.com/medichem/0301002 (2003).
3. Kuusela, P. Dept. of Bacteriology and Immunology, Haartman Institute, Helsinki University, FIN-00014 Helsinki, Finland, personal communication (2003).
4. Sällberg, M. Dept. of Clinical Virology, Huddinge University Hospital, 14186 Huddinge, Sweden, personal communication (2003).
5. Silveira, A. Atherosclerosis Research Unit, King Gustav V Research Institute, Karolinska Institutet, 17176 Stockholm, Sweden, personal communication (2003).
6. Yang, D. Basic Research Program, SAIC-Frederick, Inc., Center for Cancer Research, NCI at Frederick, NIH, Frederick, Maryland 21702-1201, USA, personal communication (2003).
7. IUPAC-IUB Joint Commission on Biochemical Nomenclature and Nomenclature Commission of IUBMB, In C. Liébecq (Ed.), *Biochemical Nomenclature and Related Documents*, 2nd ed., Portland Press, London, UK, pp. 39-69 (1992).

Peptide Revolution: Genomics, Proteomics & Therapeutics
Michael Chorev & Tomi K. Sawyer (Editors)
American Peptide Society, 2003

Beta-Methyl Substitution of the Cha Residue in Dmt-Tic-Cha-Phe Peptides Provides Highly Potent Delta Antagonists

Dirk Tourwé[1], Geza Tóth[2], Gunter Carlens[1], Csaba Tömböly[2], Antal Péter[3] and Peter W. Schiller[4]

[1]Department of Organic Chemistry, Vrije Universiteit Brussel, B-1050 Brussels, Belgium; [2]Biological Research Center; [3]University of Szeged, H-6701 Szeged, Hungary; [4]Clinical Research Institute of Montreal, Montreal, Quebec, H2W 1R7 Canada

Introduction

Since the discovery of the TIPP (H-Tyr-Tic-Phe-Phe) opioid peptide family as potent δ-antagonists, many new analogs have been prepared, leading to potent, stable and selective δ-antagonists and δ-agonists, and to mixed μ-agonists/δ-antagonists [1]. We have previously shown that the introduction of a β-methyl substituent in the Phe[3] side chain of TIPP strongly influences the activity profile [2]. The combination of Dmt[1] (2',6'-dimethyltyrosine) and β-MePhe[3] substitution led to δ-opioid ligands with subnanomolar potency [3]. It was also demonstrated that saturation of the Phe[3] residue to a Cha[3] (cyclohexylalanine) residue substantially increased δ-antagonist potency and δ selectivity [4]. We now present the *in vitro* opioid activity profiles of H-Dmt-Tic-Phe-Phe analogues containing the various β-MeCha stereoisomers in place of Phe[3].

Results and Discussion

The racemic *erythro* (2*S*,3*S* + 2*R*,3*R*) and *threo* (2*S*,3*R* + 2*R*,3*S*) β-MeCha stereoisomers were obtained from the corresponding β-MePhe stereoisomers [5] by hydrogenation at 60 psi H_2 and 50°C using PtO_2 catalysis in a Parr shaker, followed by Boc-protection and peptide synthesis on a Merrifield or MBHA resin. The stereoisomeric peptides were separated by preparative HPLC, and the absolute configuration of the βMeCha residue was determined after hydrolysis of the peptides and guanidinium thiocyanate (GITC) dramatization [6]. Their *in vitro* activities in the guinea pig ileum (GPI) and mouse vas defferens (MVD) assays (Table 1) showed that all except **6** have subnanomolar potencies as δ-opioid antagonists. The (2*S*,3*R*)β-MeCha[3] analog **1** is a weak partial μ-agonist and a potent δ-antagonist. This compound has the same profile as the corresponding Dmt-Tic-β-(2*S*,3*R*)β-MePhe-Phe-OH analog [3]. The Tyr-Tic-(2*S*,3*R*)β-MePhe-Phe-OH analog displays similar δ-antagonist potency (K_e = 0.192 nM), but has no μ-effect and, therefore, is more δ-selective [2]. Changing the C-terminal carboxylic acid in **1** to an amide in **5** did not alter the activity profile appreciably. All other stereoisomers displayed weak μ-antagonism. The (2*R*,3*S*)β-MeCha[3] analogs **2** and **6** are μ- and δ-antagonists showing moderate δ selectivity. In contrast, the corresponding (2*R*,3*S*)β-MePhe[3] analogs had been shown to be quite balanced partial μ-agonists/δ-antagonists in the GTPγS assay [3]. The (2*S*,3*S*)β-MeCha[3] analog **3** is a potent and selective (K_e^{μ}/K_e^{δ} = 4012) δ-opioid antagonist, similar to its (2*S*,3*S*)β-MePhe[3] analog [3].

In conclusion, saturation of the β-MePhe[3] aromatic ring to β-MeCha resulted in a new series of opioid peptides having subnanomolar δ-antagonist potency, and displaying either partial μ-agonist or μ-antagonist properties.

Table 1. In vitro opioid activities of [β-MeCha]^3-TIPP analogs.

Peptide	GPI (nM)	GPI (K_e, nM)[a]	MVD (K_e, nM)[b]
1. Dmt-Tic-[2*S*,3*R*-β-MeCha]-Phe-OH	146±28 (IC_{30})	-	0.810±0.149
2. Dmt-Tic-[2*R*,3*S*-β-MeCha]-Phe-OH	-	19.3±2.6	0.114±0.027
3. Dmt-Tic-[2*S*,3*S*-β-MeCha]-Phe-OH	-	967±31	0.241±0.051
4. Dmt-Tic-[2*R*,3*R*-β-MeCha]-Phe-OH	-	286±53	0.548±0.022
5. Dmt-Tic-[2*S*,3*R*-β-MeCha]-Phe-NH_2	108±17 (IC_{40})	-	0.677±0.045
6. Dmt-Tic-[2*R*,3*S*-β-MeCha]-Phe-NH_2		118±12	1.94±0.02

[a]*Determined against H-Tyr-(D)Ala-Phe-Phe-NH_2 (TAPP);* [b]*Determined against DPDPE.*

Acknowledgments

Supported by F. W. O. (Fund for Scientific Research Flanders), by AWI BIL00/52 grants, and by a U. S. National Institute on Drug Abuse grant (DA-04443).

References

1. Schiller, P. W., Weltrowska, G., Berezowska, I., Nguyen, T. M., Wilkes, B. C., Lemieux, C. and Chung, N. N. *Biopolymers (Pept. Sci.)* **51**, 411 (1999).
2. Tourwé, D., Mannekens, E., Diem, T. N., Verheyden, P., Jaspers, H., Tóth, G., Péter, A., Kertész, I., Török, G., Chung, N. N. and Schiller, P. W. *J. Med. Chem.* **41**, 5167 (1998).
3. Tourwé, D., Van Den Eynde, I., Piron, J, Carlens, G. Tóth, G., Ceusters, M., Jurzak, M., Heylen, L. and Meert, T. In Benedetti, E. and Pedone, C. (Eds.) *Peptides 2002 - Proceedings of the 27th European Peptide Symposium,* Edizioni Ziino, Napoli, Italy, pp. 310-311 (2002).
4. Schiller, P. W., Weltrowska, G., Nguyen, T. M., Lemieux, C., Chung, N. N., Zelent, B., Wilkes, B. C. and Carpenter, K. In Kaumaya, P. T. P. and Hodges, R. S. (Eds.) *Peptides: Chemistry, Structure and Biology - Proceedings of the 14th American Peptide Symposium,* Mayflower Scientific Ltd. Kingswinford, U.K. pp. 609-611 (1996).
5. Kataoka, Y., Seto, Y., Yamamoto, M., Yamada, T., Kuwata, S. and Watanabe, H. *Bull. Chem. Soc. Jpn.* **49**, 1081 (1976).
6. Péter, A., Tóth, G., Török, G. and Tourwé, D. *J. Chromatogr. A* **728**, 455 (1996).

Peptide Revolution: Genomics, Proteomics & Therapeutics
Michael Chorev & Tomi K. Sawyer (Editors)
American Peptide Society, 2003

BKM-570 and Its New Acyl-Amino Acid Amide Analogs for Lung and Prostate Cancer

Lajos Gera[1,4], Daniel C. Chan[2,4], Eunice J. York[1], Vitalija Simkeviciene[1,5], Adomas Vagonis[1,5], Daiva Bironaite[1,5], Paul A. Bunn, Jr.[2,4], Laimute Taraseviciene-Stewart[3] and John M. Stewart[1,2,4]

[1]Dept. of Biochemistry and Molecular Genetics, [2]Cancer Center, [3]Pulmonary Hypertension Center, Univ. of Colorado Health Sciences Center, Denver, CO 80262, USA; [4]Carcinex Inc., Boulder CO 80301, USA; [5]Inst. of Biochemistry, Dept. of Developmental Biology, Vilnius 2600, Lithuania

Introduction

Lung cancer is the leading cause of cancer–related death in men and women in most Western countries. The incidence of prostate cancer varies widely around the world, with by far the highest rates in the United States and Canada. The chemotherapeutic agents for lung cancer, such as cisplatin, paclitaxel, docetaxel, gemcitabine are highly toxic in patients. Although early stage prostate cancer can be treated by androgen ablation, once the tumors escape hormonal regulation there are no effective treatments. New therapeutic agents are needed for the treatment of both tumor types. We recently demonstrated the strong anticancer growth inhibitory effect of our potent bradykinin (BK) antagonist dimer (B9870) and its mimetics (BKM-638 and BKM-570) against small cell lung cancer (SCLC) cells in nude mouse xenografts [1]. BKM-570, a simple acyl-Tyr-amide and its derivatives also showed potent growth inhibition of prostate cancer cell line PC3 (IC_{50}:1.6 μM) *in vitro*. Therefore, we designed and synthesized new analogs of BKM-570 and tested them against lung and prostate cancer.

Results and Discussion

Peptides and mimetics were prepared using solution or solid phase methods, purified by HPLC and characterized by TLC, analytical HPLC, LDMS and amino acid analysis. Couplings were carried out in DMF using BOP or HATU as a coupling agent. Our lead compound, BKM-570, is a simple acyl-tyrosine amide derivative with 91% anticancer activity against SCLC [1] and with 65% activity against prostate cancer PC3 *in vivo*. Earlier studies using cultured tumor cell lines showed that a variety of non-steroidal anti-inflammatory drugs (NSAIDs) inhibited cell growth, caused cell cycle arrest, and induced apoptosis [2]. Therefore, we explored the incorporation of NSAIDs (aspirin, diclofenac, indomethacin, ketorolac, ketoprofen, and naproxen) into the acylating group position of BKM-570. These analogs showed encouraging growth inhibition *in vitro* against SCLC line SHP-77 and one of these (BKM-1376, Table 1) gave 44% growth inhibition of PC3 *in vivo*. Interestingly, replacement of the pentafluorocinnamoyl group of BKM-570 with a hydrophobic *trans*-retinoyl acylating group (BKM-1446) or substitution of the amide part (4-amino-2,2,6,6-tetramethylpiperidine) with an also hydrophobic piperazine derivative (BKM-1564, Figure 1) gave high growth inhibition (83% at 0.25 mg/kg/week) of PC3 tumors in nude mice. Based on this structure-activity study, probably using more hydrophobic building blocks is the way to develop more potent anti-cancer compound analogs of BKM-570 against prostate and lung cancer. Some of our compounds have higher growth inhibition (50-80%) against androgen-independent PC3 than standard anti-cancer drugs (cisplatin 39%, taxotere 42%) in our assays.

Table 1. Structures and activities of BK antagonists and mimetics.

Number	Structure	Biological Activity			
		GPI[a]	SCLC[b]	SHP-77[c]	PC3[c]
B9870	SUIM-(DR-R-P-Hyp-G-Igl-S-DIgl-Oic-R)$_2$	8.4	0.15	65	78
B10324	F5c-K-K-R-P-Hyp-G-CpG-S-DTic-CpG	--	--	86	43
BKM-570	F5c-OC2Y-Atmp	5.6	1.8	91	65
BKM-638	DDD-(DArg-Igl-Arg-Matp)$_2$	--	0.6	78	53
BKM-1376	Indo-OC2Y-Atmp	--	1.5	--	44
BKM-1446	Ret-OC2Y-Atmp	--	6.7	--	79
BKM-1564	F5c-OC2Y-*t*Cip	--	4.0	--	83
Cisplatin		--	--	60	39
Taxotere	(Docetaxel)	--	--	49	42

a. pA_2 for bradykinin antagonist activity on isolated guinea pig ileum. b. ED_{50} (μM) for cytotoxicity by MTT test for SHP-77 SCLC in vitro. c. Percent inhibition of growth of xenografts in nude mice. Compounds were injected i.p. at 5 mg/kg/day except for BKM-638, which was given at 1 mg/kg/day and BKM-1564, which was injected at 0.25 mg/kg/week. Cisplatin was administered as 4 weekly injections of 10 mg/kg. Taxotere was injected 8 mg/kg/week, three times. Abbreviations: Atmp, 4-amino-2,2,6,6-tetramethylpiperidine; CpG, α-cyclopentylglycine; DDD, dodecanedioyl; F5c, 2,3,4,5,6-pentafluorocinnamoyl; Hyp, trans-4-hydroxyproline; Igl, α-(2-indanyl)glycine; Indo, indomethacin; Matp, 4-(methylamino)-2,2,6,6-tetramethylpiperidine; Ret, trans-retinoyl; Tic: tetrahydroisoquinoline-3-carboxylic acid; OC2Y, O-(2,6-dichlorobenzyl)-tyrosine; Oic, octahydroindole-2-carboxylic acid; SUIM, suberimidyl; tCip, trans-1-cinnamylpiperazine.

These results suggest that certain of these peptides, B10324 (BK1 antagonist) and B9870 or their mimetics (BKM-638, BKM570 and BKM-1564) may be suitable candidates for commercial drug development for the treatment of both lung and prostate cancers.

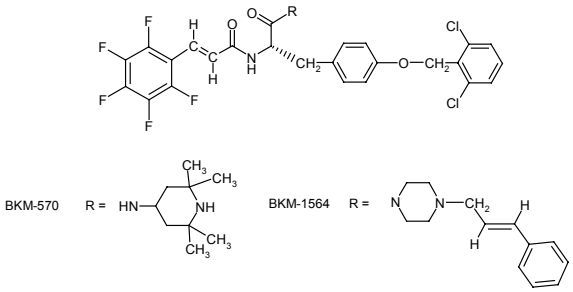

Fig. 1. BKM-570 (F5c-OC2Y-Atmp) and BKM-1564 (F5c-OC2Y-tCip).

Acknowledgments

This work was supported by NIH Grants HL-26284 and CA78154.

References

1. Stewart, J. M., Gera, L., et al. *Can. J. Physiol. Pharmacol.* **80**, 275-280 (2002).
2. Piazza, G. A., et al. *Cancer Res*. **57**, 2909-2915 (1997).

Peptide Revolution: Genomics, Proteomics & Therapeutics
Michael Chorev & Tomi K. Sawyer (Editors)
American Peptide Society, 2003

Identification of a Direct Interaction Between Calcitonin Peptide and its Receptor

Vi Pham, John D. Wade, Brooke W. Purdue and Patrick M. Sexton

Howard Florey Institute of Experimental Physiology and Medicine, The University of Melbourne, Victoria 3010, Australia

Introduction

Calcitonins (CTs) are 32 amino acid polypeptide hormones whose most recognized action is the inhibition of osteoclast-mediated bone resorption [1]. CTs, through their action on osteoclasts and to a lesser extent in the kidney, are widely used clinically in the treatment of bone-related disorders such as osteoporosis, Paget's disease and hypercalcemia of malignance [1,2]. However, the molecular basis for CT binding to its receptor (CTR), a class II family of G protein-coupled receptor, is not well defined. In this study we have developed a fully active salmon calcitonin analogue [$Arg^{11,18}$, Bpa^{19}]sCT, incorporating a photolabile *p*-benzoyl-L-phenylalanine (Bpa) into position 19 of the ligand for photoaffinity labeling of the human CTRa (hCTRa). Salmon CT (sCT) was chosen as the template molecule due to its wide use clinically, and its high affinity and efficacy at all CTRs [1-3].

Results and Discussion

Cross-linking of ^{125}I-[Bpa^{19}]sCT to intact COS-7 cells transiently expressing HA-hCTRa revealed a single radiolabeled band of ~ 72-kDa (Figure 1A, lane 2) which was shifted to ~ 51-kDa (Figure 1A, lane 3) after deglycosylation with Endo-F to remove carbohydrate. These bands are receptor-specific since they were completely inhibited by co-incubation with excess unlabeled sCT (10^{-7}M) (Figure 1A, lane 1).

The photolabeled HA-hCTRa was then digested with cyanogen bromide (CNBr), which cleaves at the C-terminus of methionine residues. Two specifically labeled bands were identified. One migrating at ~31-kDa and the other at ~8-kDa (Figure 1B, lane 1). Sequential deglycosylation with Endo-F followed by CNBr cleavage shifted the migration of the larger band to ~17-kDa, but did not alter the mobility of the 8-kDa fragment (Figure 1B, lane 2). Mutation of M^{133} to either leucine or alanine completely abolished the generation of the lower M_r band, with only a single prominent

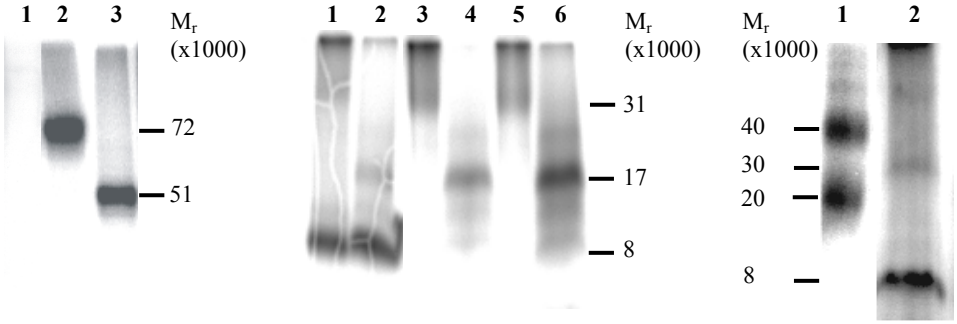

(A) 10% SDS-PAGE **(B)** 16.5% SDS-Tricine **(C)** 16.5% SDS-Tricine

Fig. 1. Photoaffinity cross-linking of ^{125}I-[Bpa^{19}]sCT to the HA-hCTRa transiently transfected into COS-7 cells. The autoradiograph is a representative of three independent experiments.

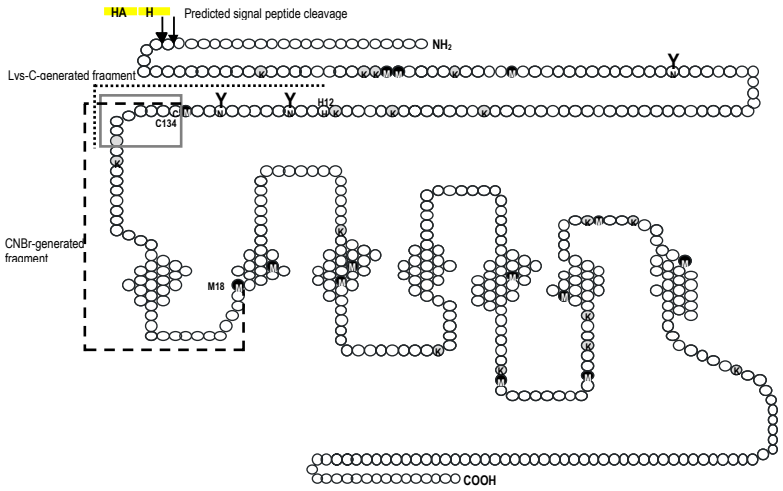

Fig. 2. Schematic diagram of the amino acid sequence of HA-hCTRa.

radiolabeled fragment formed following CNBr cleavage (Figure 1B, lanes 3-6). This band was equivalent to the larger M_r band seen with cleavage of the wild-type receptor and is consistent with incomplete digestion of this band around M^{133} site in the wild-type receptor. Thus, ^{125}I-[Bpa^{19}]sCT cross-links to a single CNBr-derived domain that is delimited by C^{134} and M^{187} (Figure 2).

To further refine and confirm the binding domain, the intact photolabeled HA-hCTRa was digested with endoproteinase Lys-C. Like the original CNBr digest, Lys-C cleavage yielded 2 radiolabeled bands, an approximately 20-kDa band, in addition to a higher M_r band presumably resulting from incomplete digestion (Figure 1C, lane 1). When treated with Endo-F, the electrophoretic mobility of the 20-kDa band shifted to 8-kDa, demonstrating that it is glycosylated (Figure 1C, lane 2). This is consistent with cross-linking to the region delineated by H^{121} and K^{141} (Figure 2). Taken together with the CNBr data, the results indicate that [Bpa^{19}]sCT cross-links specifically to a site contained within the small receptor region delimited by residues C^{134} and K^{141} of hCTRa (Figure 2), that is close to the border of transmembrane domain 1. The current study provides first constraint in defining the interface between sCT and its receptor and will contribute towards modeling of the calcitonin-receptor interface. Such knowledge will aid in the rational design of CT analogues with increased potency and improved selectivity for therapeutic purposes.

Acknowledgments

This study was funded by NHMRC project grant 145703. PMS is a NHMRC Senior Research Fellow and JDW is a NHMRC Principal Research Fellow.

References

1. Sexton, P. M., Findlay, D. M. and Martin, T. J. *Curr. Med. Chem.* **6**, 1067-1093 (1999).
2. Pondel, M. *Int. J. Exp. Pathol.* **81**, 405-422 (2000).
3. Purdue, B. W., Tilakaratne, N. and Sexton, P. M. *Receptors Channels* **8**, 243-255 (2002).

Peptide Revolution: Genomics, Proteomics & Therapeutics
Michael Chorev & Tomi K. Sawyer (Editors)
American Peptide Society, 2003

A Cyclic and Branched Peptide as a New Selective Ligand for the CCK_A Receptor

Ettore Benedetti[1], Giancarlo Morelli[1], Raffaella Della Moglie[1], Stefania De Luca[1], Michele Saviano[1] and Luigi Aloj[1]

[1]Dipartimento di Chimica Biologica, Centro Interuniversitario per la Ricerca sui Peptidi Bioattivi (CIRPeB) & Istituto di Biostrutture e Bioimmgini CNR – Via Mezzocannone 6, 80134 Napoli, Italy

Introduction

Small radiolabelled compounds such as peptides are quite attractive tools for the diagnosis of several different pathologies. Among the possible biological targets for radiolabelled compounds, the cholecystokinin receptors CCK_A-R and CCK_B-R are very promising due to their overexpression in many tumors [1]. These receptors belong to the GPCR superfamily and are localized in the cell membrane. Both CCK_A-R and CCK_B-R have been thoroughly investigated with the aim at characterizing the molecular basis of their interaction with the CCK peptide hormone. The structural characterization of the bimolecular complex of CCK8 with the 47-residue N-terminal extracellular arm of CCK_A-R was recently achieved by high-resolution NMR and computational refinement [2].

The starting point for the rational design of CCK8 peptidomimetic analogs was the NMR structure of the complex between CCK8 and the N-terminus of the CCK_A-R(1-47) receptor [2]. Relative to CCK8 (H-Asp^{26}-Tyr^{27}-Met^{28}-Gly^{29}-Trp^{30}-Met^{31}-Asp^{32}-Phe^{33}-NH_2) we substituted the Gly^{29} with a diaminopropionic acid (Dpr residue) to provide the opportunity of introducing a cyclic constraint, with the aim of stabilizing the bioactive conformation and increasing the enzymatic stability. At the same time the important residues for the CCK8 receptor interaction (i.e., Tyr^{27}-Met^{31} sequence) were conserved. Moreover, we needed to add one amino acid residue (Gly, Ala, Lys or β-Ala) at the CCK8 C-terminus to preserve the bioactive conformation. The introduction of the Ala residue, instead of the Gly residue, could increase the constrain of the cyclic structure. The choice of the Lys residue was dictated by the possibility of using its Nε amino group for binding a chelating agent, in order to obtain peptide conjugates able to coordinate radionuclide. Instead, the β-Ala residue was chosen to prepare an analogue characterized by the greater flexibility of the designed cyclic structure (Figure 1).

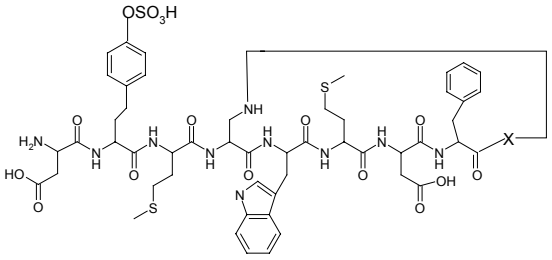

Fig. 1. Schematic view of the CCK8 analogs.

Results and Discussion

The cyclic peptides cyclo^{29,34}[Dpr^{29}, X^{34}]-CCK8 (Figure 1), were synthesized on solid-phase using Fmoc chemistry. The Fmoc-Tyr(SO_3H)-OH barium salt was incorporate in the peptide chain, in order to obtain sulfated peptides. The N-C cyclization reaction was performed in solution using DCM as a solvent and the PyBOP/DIPEA activation method.

The peptide conjugate cyclo^{29,34}[Dpr^{29}, Lys^{34}(DTPA-Glu)]-CCK8 (Figure 2) was synthesized on solid-phase using Fmoc chemistry and orthogonal protections on the two residues (Lys^{34} and Dpr^{29}) each containing two amino functions. The coupling of the DTPA-Glu pentaester, the chelating agent partially protected by *tert*-butyl groups, was very efficient: only two equivalents of the DTPA-Glu-pentaester, activated by HATU, were used to obtain a quantitative Lys side chain coupling (Figure 2).

Fig. 2. Sequence of the peptide conjugate.

The presence of many acidic functions on the chelating agent (Figure 2) increases the lability of the sulfate moiety on the Tyr side chain, indicating that the intramolecular carboxylic groups themselves could catalyse the desulfation process. A synthetic strategy has been developed for obtaining a N↔C cyclic peptide analogs containing the acid-labile sulfate group on a Tyr residue and a highly acidic chelating DTPA derivative. Using this strategy we could avoid prolonged acid treatments, in fact the sulfation reaction was performed on the fully deprotected compound by using the pyridine-SO3 complex. The conformational features of Cycle^{29,34}[Dpr^{29},Lys^{34}]-CCK8 have been determined by NMR spectroscopy in aqueous solution and in water containing DPC-d_{38} micelles. In DPC/water, the cyclic moiety adopts a "boat-shaped" conformation that is more compact than the one found in aqueous solution. A careful comparison of the NMR structure in DPC/water of the cyclic moiety with that from rational design shows that the turn conformation in the Trp^{30}-Met^{31} region is preserved (Figure 3). Preliminary binding studies on cell lines transfected with the CCK_A receptor indicate that the Tyr-Sulfate derivative of Cycle^{29,34}[Dpr^{29},Lys^{34}]-CCK8, displaces the natural ligand with an IC_{50} value of 15 mM.

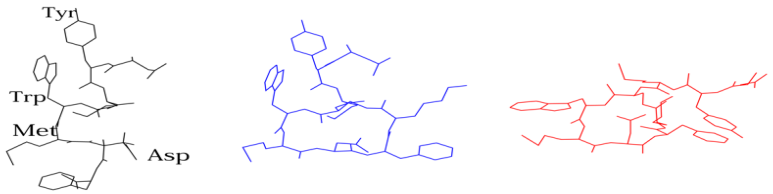

Fig. 3. NMR structure of Cycle^{29,34}[Dpr^{29},Lys^{34}]-CCK8 (right) compared with the CCK8 NMR structure (left) and its projected model (center).

References

1. Reubi, J. C., Shaer, J. C. and Waser, B. *Cancer Res.* **57**, 1377-1386 (1997).
2. Mierke, D. F. and Pellegrini, M. *Biochemistry* **38**, 1477-14783 (1999).

Peptide Revolution: Genomics, Proteomics & Therapeutics
Michael Chorev & Tomi K. Sawyer (Editors)
American Peptide Society, 2003

Interhelical Side Chain-Side Chain Hydrogen Bonds in Membranes: Capture Potential of Aspartic Acid vs. Glutamic Acid

Charles M. Deber, Mei Y. Choi, and Lia Cardarelli

Division of Structural Biology and Biochemistry, Research Institute, Hospital for Sick Children, 555 University Avenue, Toronto M5G 1X8; Department of Biochemistry, University of Toronto, Toronto M5S 1A8, Ontario, Canada

Introduction

This manuscript presents research excerpted from the Keynote Lecture given by Charles Deber at the 18th American Peptide Symposium. The Lecture first recognized the hallmarks of the peptide research field: synthesis (including peptide purification and characterization) and structure/spectroscopy – and how these have been employed to produce bioactive peptides, and to interpret their function and pharmacology. Then, the more recent contributions to peptide science of computational chemistry, molecular modeling, molecular biology, bioinformatics, genomics, and proteomics were discussed. As one example, site-directed mutagenesis now allows us to pinpoint the roles of individual amino acids as determinants of structure/function, with emphasis on what goes 'wrong' in disease states. This, in effect, refocuses a protein problem in terms of peptide chemistry, *i.e.*, the interactions of one or two specific side chains in a key context in a protein can determine whether or not disease occurs. With knowledge available at this level of detail, traditional synthesis and structural analysis can then help define the "molecular lesion" in conformational terms, thus surmounting a fundamental hurdle for drug development.

Peptide approaches to the molecular basis of membrane protein diseases

The biological function of membrane proteins is related to how they fold and assemble; defects often lead to disease. Protein-mediated human diseases linked to membrane proteins – indeed, to soluble proteins as well - can thus be viewed as biophysical events in which a mutation results in gain or loss of packing and/or electrostatic interactions critical for normal protein folding and function. But membrane proteins appear particularly susceptible to such events: numerous instances exist wherein a single mutation can incapacitate the entire protein. Understanding packing motifs and the interactions among helices within membranes is thus a valuable tool in clarifying the context - and the impact on function - of a mutation. As genetics research has progressed, an increasing number of human diseases, including cancer, diabetes, and cystic fibrosis have been ascribed to critical mutations in membrane proteins. However, little has been known about the structure/function relationships underlying these diseases, which is a necessary step in devising rational therapies. Our recent work has combined the approaches of peptide synthesis, molecular biology, and bioinformatics, to enable us to identify these interactions experimentally and relate their consequences to protein biology.

Protein segments generally span membranes in the form of transmembrane (TM) helices, each consisting of about 20 residues. Although 80% of the residues in TM helices are hydrophobic, the remaining 20% consists of such residues as Gln, Asn, Glu, Asp, Arg, Lys, Ser, Thr, Trp, and His, which must overcome barriers to membrane insertion. Our laboratory found that the concept of 'threshold hydrophobicity' can explain how polar residues occurring in an otherwise highly hydrophobic sequence can become membrane-inserted ([1] and references therein), but left unexplained the

question of why they would be incorporated into membranes in the first place. As all of these residues have polar side chain moieties, and occur on the average of 1-2 per TM helix, we speculated that native structures of multi-spanning membrane domains are stabilized by electrostatic crosslinks arising from side chain-side chain interhelical H-bonds. Some may be of modest strength - such as those between the -OH groups of two Ser residues - but others, *i.e.*, those involving residues with acidic protons, such as Asp or Glu, may participate in H-bonds that dominate the interactions between a given pair of transmembrane helices. Membrane proteins may therefore be vulnerable to loss of function either through loss of these latter crosslinks, or through gain of non-native crosslinks - which may 'lock' the protein into a conformation, which is misfolded and/or may interfere with the dynamics of protein function.

Our hypotheses about the role of membrane-embedded H-bonds was further tested by examining the membrane domain of CFTR – the cystic fibrosis transmembrane conductance regulator – a chloride channel which is the gene product defective in CF. Working with a database of hundreds of CF patients, which includes information on the nature of disease and the associated mutation, we observed that more than 50% of CF-phenotypic mutants that occur within the CFTR putative TM domain involve 'non-polar-to-polar' mutations. In turn, this suggested that the added polar side chain could lead to formation of non-native H-bonds in membranes that in turn could compromise the effectiveness of CFTR by disrupting the native fold of the protein. We accordingly addressed this question experimentally by preparation of model peptides (by expression in *E. coli* and/or by solid phase synthesis) in the form of 'helical hairpins' – helix-loop-helix constructs representing the minimum tertiary contact structure in membranes. Using a novel gel-shift assay devised by our lab, we can distinguish folded from unfolded hairpins, where formation of non-native inter-helical H-bonds folds the two helices into a compact, faster-migrating species. As described below, we undertook to design and test mutant hairpin libraries which 'walk' a polar residue in one helix through the vicinity of the polar partner residue to assess the 'capture range' of a potential H-bonding side chain. Given that membrane proteins are a disproportionately high percentage of pharmaceutical targets, while only a handful have been solved at high-resolution, information emerging from our studies could clarify key structural features of the target molecules.

The case for cystic fibrosis

Cystic fibrosis (CF) is the most prevalent genetic disease in North America, affecting one in two thousand births [2]. CF is caused by mutations to the membrane protein cystic fibrosis transmembrane conductance regulator (CFTR), resulting in malfunctions of the pancreas, lungs, sweat glands and reproductive organs [3,4]. The CFTR protein consists of 1480 residues arranged in 12 membrane spanning helices, two nucleotide-binding domains and a regulatory domain [5]. There are over 900 known mutations to CFTR, and approximately 100 of these mutations occur in membrane spanning regions. Many of the membrane spanning mutations involve apolar-to-polar amino acid substitutions that have the potential to form non-native hydrogen bonds [1].

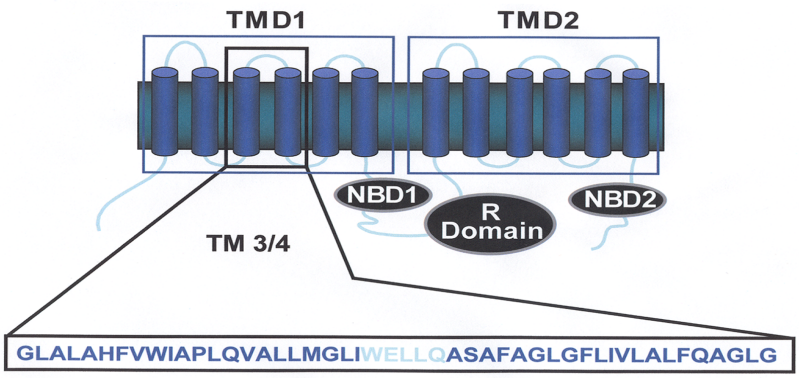

Fig. 1. Schematic representation of the proposed transmembrane protein CFTR with the amino acid sequence of the helix-loop-helix construct of TM 3/4 highlighted (Adapted from [5]).

One such mutant, V232D, is believed to result in an aberrant hydrogen bond formation between the mutant Asp and a wild type Gln (Q207) [1]. Thus, Therien *et al.* demonstrated that a wild type construct of the helix-loop-helix domain of the transmembrane (TM) segments three and four and the short hydrophilic loop that connects them, migrated more slowly in SDS-PAGE than the V232D mutant (Figure 2). After several variants and controls were examined, it was concluded that CF-phenotypic mutant V232D formed a tighter 'hairpin' structure stabilized by the non-native hydrogen bond. A tighter 'hairpin' structure is less retarded in the SDS-PAGE system and will migrate to a position that corresponds to an apparent molecular weight smaller than its actual mass, whereas the more open, rod-like structure of the wt construct will be impeded during migration. This can be further analyzed as an expression of the percent molecular weight decrease; a greater percent decrease corresponds to a faster migration, and therefore a tighter hairpin.

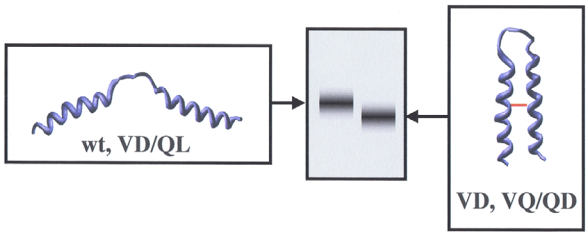

Fig. 2. Schematic representation of 'open' and 'closed' conformations of CFTR helical hairpins during migration in SDS-PAGE. The difference in migration rates provides a gel shift assay for hairpin folding. VD/QL indicates Q207 mutated to L. VQ/QD indicates switch of Q and D between helices 3 and 4.

Previous studies have shown that the native Q207 which resides on TM 3 has the ability to form a hydrogen bond to a mutant Asp at essentially any position along the helix of TM 4 and not only at the CF-phenotypic position of 232 [M.Y. Choi, L. Cardarelli, C.M. Deber, manuscript in preparation]. The mutant I231D of the TM 3/4 construct appears to migrate fastest in the SDS-PAGE system and is therefore thought to be at the optimum position for hydrogen bonding.

These results suggest that the energy of an inter-helical hydrogen bond between Asp and Gln is sufficient to drive the alternative alignment of the helices to satisfy the electrostatic link. In the present study, we have assessed the ability of Glu to substitute for Asp in an interhelical H-bond, and to probe the observable differences between the two amino acids in the context of the TM 3/4 construct. While Asp and Glu have similar side chain moieties, the Asp side chain carboxylic acid has a lower pKa than Glu (3.9 and 4.3 respectively) [6], which corresponds to aspartate's greater ability to participate in a hydrogen bond. The Asp side chain is also one methylene group shorter than the side chain of glutamate, with the consequence that the extra methylene in Glu potentially contributes to a greater degree of rotational ('entropic') freedom. As such, the less polar, longer and 'floppier' Glu side chain may therefore be expected to serve as a 'discriminator' of H-bond formation vs. the Asp residue when paired with wild type Gln 207 in TM 3.

Results and Discussion

The wild type TM 3/4 construct was cloned into a pET32a vector and was individually mutated to express glutamate mutations on TM 4 using the Stratagene Quikchange Mutagenesis kit (Figure 3). The vectors were transfected into *E. coli* BL21(DE3) cells and induced with IPTG. The constructs were expressed as thioredoxin fusion proteins, which contained two Histidine tags and an S-tag for Western blot analysis. Induced cells were lysed by sonication and the cell lysate was applied to a nickel affinity column [7]. The protein eluate was digested with thrombin to remove the thioredoxin moiety and purified by RP-HPLC using a water:isopropanol gradient of 5%-95% over 70 minutes and their identity confirmed by mass spectrometry. The purified peaks were lyophilized and resuspended in water or SDS solution and analyzed using circular dichroism (CD) spectroscopy and gel shift assays.

Mutant	Sequence	MW
Wt	KAMGLALAHFVWIAPL**Q**VALLMGLIWELLQASAFAGLGFLIVLALFQAGLGLE	9437 Da
F229E	KAMGLALAHFVWIAPL**Q**VALLMGLIWELLQASAFAGLG**E**LIVLALFQAGLGLE	9419 Da
I231E	KAMGLALAHFVWIAPL**Q**VALLMGLIWELLQASAFAGLGFL**E**VLALFQAGLGLE	9453 Da
V232E	KAMGLALAHFVWIAPL**Q**VALLMGLIWELLQASAFAGLGFLI**E**LALFQAGLGLE	9467 Da
L233E	KAMGLALAHFVWIAPL**Q**VALLMGLIWELLQASAFAGLGFLIV**E**ALFQAGLGLE	9453 Da
A234E	KAMGLALAHFVWIAPL**Q**VALLMGLIWELLQASAFAGLGFLIVL**E**LFQAGLGLE	9495 Da
L235E	KAMGLALAHFVWIAPL**Q**VALLMGLIWELLQASAFAGLGFLIVLA**E**FQAGLGLE	9453 Da
F236E	KAMGLALAHFVWIAPL**Q**VALLMGLIWELLQASAFAGLGFLIVLAL**E**QAGLGLE	9419 Da
Q237E	KAMGLALAHFVWIAPL**Q**VALLMGLIWELLQASAFAGLGFLIVLALF**E**AGLGLE	9438 Da

Fig. 3. Amino acid sequences of the wt and mutant constructs derived from transmembrane helices 3 and 4 from the CFTR membrane domain. When folded, H-bond formations may occur between Q207 and various E residues (bolded). Each construct also contains a C-terminal His-tag and an N-terminal S-tag (not shown).

The Glu mutant constructs each eluted from RP-HPLC between 64-68% isopropanol indicating a high relative hydrophobicity (Figure 4). The CD results indicate the construct had an α-helical secondary structure and was therefore properly inserted and folded in SDS micelles (Figure 4).

A

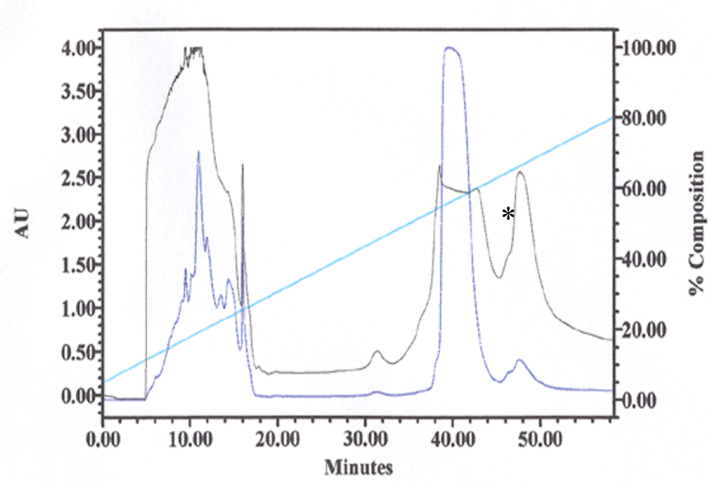

B

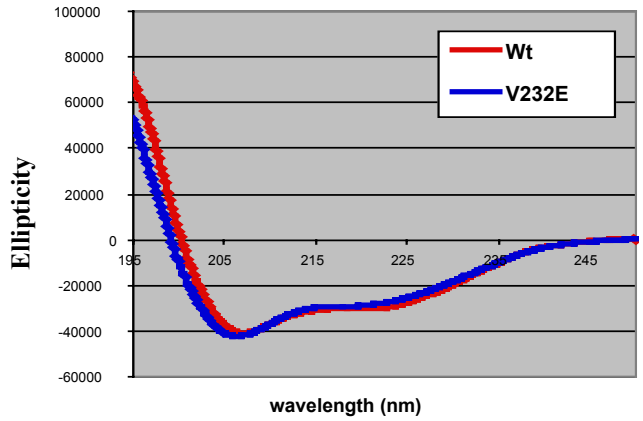

Fig. 4. (A) Representative RP-HPLC chromatogram for protein purification. The asterisk indicates the collected CFTR TM3/4 peak. (B) Circular dichroism spectra of the TM 3/4 wild type and V232E mutant. CD spectroscopy was performed in 1% SDS, Tris buffered solution.

The purified constructs were run on pre-cast Novex NuPAGE gels at least three times and their apparent molecular weight assessed and compared to the values of the corresponding D mutants and to wild type (Figure 5). Comparative gel shift analysis of the D and E mutants indicated that E was a weaker participant in the H-bond, irrespective of its position in TM 4, *i.e.*, each Asp mutant tested formed a tighter H-bond that its Glu mutant counterpart. However, seven out of eight E mutants did migrate faster than wild type, and do consequently form an H-bond, albeit a weaker one.

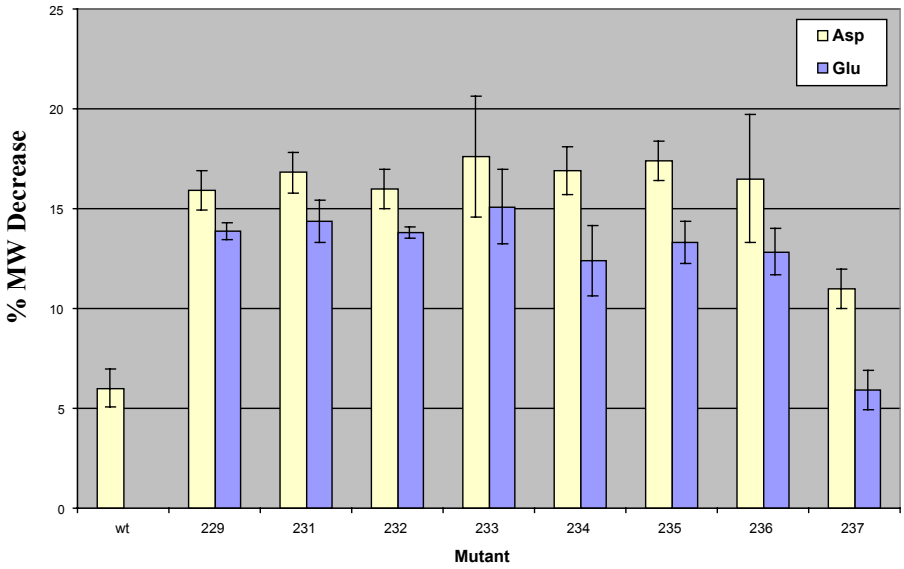

Fig. 5. Gel shift (SDS-PAGE) analysis of Asp and Glu mutant migration distances in CFTR TM3/4 constructs. Taller bars indicate a more tightly folded hairpin, and hence a stronger H-bond. White bars correspond to Asp mutants; gray bars correspond to Glu mutants.

As mentioned above, the degree of rotational freedom, pKa and side chain length likely all play a role in the differences between the migration rates of the D and E mutants. But which factor dominates the difference in the context of TM 3/4? It appears that the relative difference in migration rate between the D and E mutants is constant at each position tested. This difference appears to correlate to the less populated chance of finding the 'floppy' Glu side chain in the vicinity of its polar partner Q207. Even when within the required vicinity, *i.e*., at position 231, the E mutants are also less able to form a strong H-bond when compared to the D mutants, possibly due to their higher pKa value. It appears that length is not a strong issue in the decreased ability of Glu to participate in the H-bond, but that the slower migration is instead due to a combination of decreased polarity in conjunction with a larger degree of rotational freedom.

Besides V232D, Q237E is another CF-phenotypic mutant within TM 4. The Q237E mutant reverts to wild type migration, indicating complete loss of the hydrogen bond. This finding may be explained by a distance effect. When a Glu residue is close to Q207, it can overcome the rotational restrictions to the H-bond due to proximity. However, in the case of more distal positions, the rotational freedom of the Glu side chain may prevent the interaction, in effect rendering the Glu too difficult to 'capture'. In order to satisfy the polarity of the side chain in the membrane environment, the Glu side chain is most likely H-bonding to the TM 4 backbone in an intra-helical link. It will be of interest to observe the migration rate of constructs mutated to E at residues 238 and 239 to discover whether the loss of the H-bond is a distance effect or a residue-specific occurrence unique to position 237. The native Q237 has been observed to play a role in a hydrogen bond network [8] as well as mediate a hydrogen bond network for the more distal D mutants of TM 4 [in preparation].

Conclusions

This research suggests that apolar-to-polar mutations within membranes are not all alike, and may produce varying consequences. Even relatively similar side chains can exhibit nuanced differences in behavior in the same context, as seen in the relative migration rates of corresponding D and E mutants. The present approach of scanning mutagenesis can be used to compare the relative strength of association for each polar side chain, as well as to 'map' the folding patterns of wild type and mutant CFTR TM helices, and accordingly provides a means of assessing the molecular origins of CF and related diseases – a prerequisite for the development of therapies.

As such, the Keynote themes are anchored through use of some current tools to address the structural consequences of side chain-side chain interactions between transmembrane helices in phenotypic constructs of a membrane protein. The results provide an example of how, in an era of genomics and proteomics, peptide chemists/biologists are in a position to ask (and answer) bigger questions while using smaller molecules.

Acknowledgments

This work was supported, in part, by grants to C.M.D. from the Canadian Cystic Fibrosis Foundation (CCFF), and the Canadian Institutes of Health Research (CIHR). M.Y.C. is grateful for an award from the Hospital for Sick Children Research Training Committee. L.C. is a student research participant in the Samuel B. Lunenfeld Summer Student Research Program. The work described in the manuscript represents a portion of the broader research activity of this laboratory discussed in the Keynote Lecture, and C.M.D. wishes to thank all the members of his lab for their outstanding contributions to this research program.

References

1.Therien, A. G., Grant, F. E. M. and Deber, C. M. *Nature Str. Bio.* **8**, 597-601 (2001).
2. Ramsey, B. W. *N. Engl. J. Med.* **335**, 179-188 (1996).
3. Akabas, M. H. *et al.*, *J. Biol. Chem.* **275**, 3729-3732 (2000).
4. Gong, X *et al., J. Physiology* **540**, 39-47 (2002).
5. Riordan, J. R. *et al., Science* **245**, 1066-1073 (1989).
6. Stryer, L. *Biochemistry* 4th ed. (W.H. Freeman and Co., New York, 1995).
7. Therien, A. G. Glibowicka, M., and Deber, C. M. *Prot. Expr. Purif.* **25**, 81-86 (2002).
8. Partridge, A. W., Melnyk, R. A. and Deber, C. M. *Biochem.* **41**, 3647-3653 (2002).

Peptide Revolution: Genomics, Proteomics & Therapeutics
Michael Chorev & Tomi K. Sawyer (Editors)
American Peptide Society, 2003

A Simplified Model of the Interaction Between SDF-1 Chemokine and the CXCR4 Receptor

Pasquale Palladino[1], Antonia De Capua[1], Carlo Pedone[1], Raffaele Ragone[2], Filomena Rossi[1], Cristina Limatola[3], Davide Ragozzino[3] and Ettore Benedetti[1]

[1]Dipartimento di Chimica Biologica, C.I.R.Pe.B., Università Federico II di Napoli and Istituto di Bioimmagini e Biostrutture, CNR, Via Mezzocannone 6; 80134 Napoli, Italy; [2]Dipartimento di Biochimica e Biofisica, Seconda Università di Napoli, Via Costantinopoli 16; 80138 Napoli, Italy; [3]Dipartimento di Fisiologia Umana e Farmacologica Università La Sapienza di Roma, P.le A. Moro 5, 00185 Roma, Italy

Introduction

Chemokines belong to a family of small proteins involved in the inflammatory processes and in the chemoattraction of leukocytes [1]. Among chemokine receptors, CXC receptor 4 (CXCR4) and its natural ligand stromal-derived cell growth factor 1 (SDF-1 or CXCL12) have been highlighted for a role in human breast cancer metastasis and for syncytia-inducing form HIV-1 in CD^+ T-cell [2,3]. It has recently been observed in the CXC class of chemokines that important residues for receptor binding are located in the N-terminus and in the loop region following the two disulphide bridges (Figure 1). The solution structure of short N-terminal SDF-1 peptides [3] and other CXCR4 antagonists [4,5] suggests that the turn structure adopted by the N-terminus region may be important for recognition in receptor binding. In recent work we determined by fluorescence spectroscopy the apparent dissociation constant (Kd') of the bimolecular interaction between receptor- and ligand-derived synthetic peptides [6], which supports a simplified model for interaction of chemokine SDF-1 with the CXCR4 receptor. Now we show that the ERK1/2 phosphorylation is activated in a dose-dependent manner following stimulation of CHP100 cells with SDF-1-related peptides and that more than one site could assist receptor activation.

Results and Discussion

The chemokine fragment consisting of the N-terminal region of human SDF-1, SDF-1[1-17]: KPVSLSYRCPCRFFESH (A), and its analogue SDF-1[H-H]:

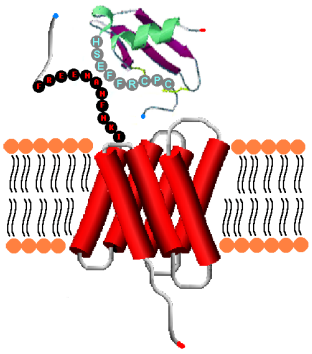

Fig. 1. A model for the interaction of chemokine SDF-1 with the CXCR4 receptor.

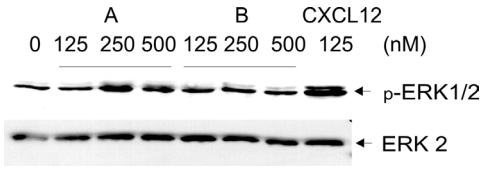

Fig. 2. Representative Western blot analysis of ERK1/2 phosphorylation: upper panel: anti phospho-ERK1/2, lower panel: anti ERK2 as a control for equal protein loading.

HSEFFRCPCRFFESH (B), both with the free amino- and carboxy-termini, were synthesized by solid phase peptide synthesis using standard F-moc protocol with PyBop or TBTU and HOBt as coupling reagents. For deprotection and cleavage, the fully protected peptide resins were treated with TFA containing TIS (2.5%) and water (2.5%) for 30 min at 4°C. Crude peptides were precipitated at 0°C with ether, liophilized by water and purified by HPLC using a linear gradient of CH3CN (0.1% TFA) in H2O (0.1% TFA). Mass spectra carried out on MALDI-TOF confirmed the product identity. Semi-confluent CHP100 human neuroepithelioma cells were serum-starved for 16-24 h, incubated for 1 h in Locke's buffer and stimulated with SDF-1 for different times. After stimulation, cells were lysed with hot sodium dodecylsulphate (SDS) sample buffer, boiled for 5 min and sonicated for 10 s on ice with a probe sonicator, and then centrifuged for 15 min at 15.000 x g in a microfuge. Protein contents were determined with a BCA protein assay kit (Pierce), and equal protein amounts from each sample were analyzed on 8.75% SDS polyacrylamide gel and electrophoretically transferred to nitrocellulose paper at 4°C for 2 h. Blots were incubated for 1 h with 5% non-fat dry milk or 3% bovine serum albumin to block non-specific binding sites and then incubated with specific antibodies. The immunoreactivity was detected with a chemiluminescent substrate (ECL). Relative band intensity was evaluated by densitometry (Scan Jet 4c HP) and software analysis (Jandel, Sigma Gel).

The expression of CXCR4 on CHP100 cells has already been described [7]. Figure 2 shows that an increase of ERK1/2 phosphorylation was observed (442% ± 26% of control values after 30 min), when CHP100 cells were stimulated with SDF-1, as previously described. When CHP100 cells were stimulated for the same time with peptides A and B and others SDF-1 analogues, ERK1/2 phosphorylation was activated in a dose-dependent manner, reaching the maximal value at 250 nM (mean of three different experiments ± SD), 190 ± 23% for peptide A and 140±13% for peptide B.

The linear SDF-1-related sequences: HSEFFRGGGRFFESH, GRFFESH and HRFFRFFRFFRFF, when tested in the same experiment, did not show any activity, thus highlighting the structural relevance of the CPC segment, which is exclusively present in peptides A and B. In particular, peptide B shows agonist activity, which is surprising in the light of literature data stressing the role played by the K and P amino acid residues in the N-terminal tract of the SDF-1 chemokine. Our preliminary results strongly support the possibility that more than one site could assist receptor activation [8].

Acknowledgments
The authors would like to thank Dr. Giuseppe Perretta and Mr. Leopoldo Zona for technical assistance.

References

1. Baggiolini, M. *J. Int. Med.* **250**, 91-104 (2001).
2. Muller, A. et al. *Nature* **410**, 50-56 (2001).
3. Elisseeva, E. L. et al. *The J. Biol. Chem.* **275**, 26799-26805 (2000).
4. Booth, V. et al. *J. Mol. Biol.* **327**, 329-334 (2003).
5. Ichiyama, K. et al *P.N.A.S.* **100**, 4185-4190 (2003).
6. Palladino, P. et al. *Prot. Pept. Lett.* **18**, 133-138 (2003).
7. Floridi, F. et al. *J. Neuroimmunol.* **135**, 38-46 (2003).
8. Sachpatzidis, A. et al. *J. Biol. Chem.* **278**, 896-907 (2003).

Peptide Revolution: Genomics, Proteomics & Therapeutics
Michael Chorev & Tomi K. Sawyer (Editors)
American Peptide Society, 2003

Synthetic Unnatural Chemokines: Probes of Receptor-Ligand Interactions and Inhibitors of HIV-1 Entry

Ziwei Huang[1], Santhosh Kumar[1], Chang-Zhi Dong[1], Dongxiang Liu[1], Shaomin Tian[1], Won-Tak Choi[1], Youli Wang[1], Vitaly Stepensky[1], Ying Li[1], Jing An[1], Navid Madani[2], Mark Cayabyab[2] and Joseph G Sodroski[2]

[1]Departments of Biochemistry and Chemistry, University of Illinois at Urbana-Champaign, Urbana, IL 61801, USA; [2]Department of Cancer Immunology and AIDS, Dana-Farber Cancer Institute, Harvard Medical School, Boston, MA 02215, USA

Introduction

The chemokine receptor CXCR4 is critical for many biological functions, such as B-cell lymphopoiesis, regulation of neuronal cell migration and vascular development [1]. In addition, CXCR4, together with another chemokine receptor CCR5, are two principal co-receptors for the cellular entry of the human immunodeficiency virus type 1 (HIV-1) [2]. The stromal cell-derived factor-1 (SDF-1α) is the only known natural ligand of CXCR4 and plays important roles in migration, proliferation, and differentiation of leukocytes. The viral macrophage inflammatory protein II (vMIP-II) encoded by human herpesvirus 8 is an antagonistic chemokine ligand of CXCR4. vMIP-II also interacts with other chemokine receptors such as CCR5 and CCR3 and inhibits HIV-1 entry mediated by these co-receptors.

CXCR4 and other chemokine receptors belong to the superfamily of seven transmembrane G-protein-coupled receptors (GPCRs) (reviewed in [3]). These membrane proteins transmit signals from extracellular ligands to intracellular biological pathways via heterotrimeric G-proteins and represent a major class of therapeutic targets for a wide variety of human diseases. As such, characterizing the mechanism of biological recognition between these receptors and their ligands is essential for understanding the physiological or pathological processes that they mediate and devising novel strategies for clinical intervention. In our recent studies of the structure-function relationship of the chemokine receptor-ligand interaction, we found that a synthetic 21-residue peptide derived from the N-terminus of vMIP-II, designated as V1, is a potent antagonist of CXCR4 and inhibits HIV-1 replication in $CXCR4^+$ T-cell lines [4,5]. Being highly amenable to chemical synthesis and modification, this V1 peptide prompted us to use chemically modified analogs of V1 as probes to study the molecular recognition of CXCR4-ligand complex. Since one important aspect of receptor-ligand interaction is the requirement of stereospecificity, here we synthesized an all-D-amino acid analog of V1 peptide, designated as DV1 [6] and studied its anti-viral activity and plausible structures in complex with the receptor CXCR4.

Results and Discussion

DV1, LGASWHRPDKCCLGYQKRPLP, displays strong binding and antagonistic activity toward CXCR4 with an IC_{50} value of 32 nM in competing with mAb 12G5 binding to CXCR4. In addition, due to the use of unnatural D-amino acids, DV1 is highly resistant to proteolytic degradation. Having shown that DV1 peptide is a potent CXCR4 antagonist and highly stable in biological conditions, we reasoned that it could inhibit the replication of CXCR4-dependent HIV-1 strains by blocking the entry of viruses via CXCR4 co-receptor. By measuring CAT activity in activated human PBMC infected

with a recombinant HIV-1 containing the HXBc2 envelope glycoproteins, we found that DV1 peptide was a potent inhibitor of infection. By contrast, a control mutant peptide DV1-L1A that contains a single alanine substitution at Leu-1 but substantially lost CXCR4 binding did not show any activity. The DV1 peptide was completely inactive in control experiments measuring CAT activity in $CCR5^{+}CD4^{+}$ Cf2Th cells infected with the dual-tropic 89.6 HIV-1 strain in which another chemokine receptor CCR5 mediates the viral entry. These data demonstrate that DV1 peptide is a selective inhibitor of HIV-1 co-receptor function of CXCR4 but not CCR5.

To determine the structural basis for DV1 activity, we studied the structure of DV1 peptide in solution by using 2D ^{1}H NMR. The DV1 peptide was found to adopt a turn-like structure over residues Trp5 - Pro8. With the DV1 solution structure as the starting conformation, we conducted computer simulations of the docking of the DV1 peptide into the CXCR4 model structure as published previously [7]. After energy minimization with molecular dynamics on the extra-cellular domains of CXCR4 and DV1 peptide, we found that the turn-like structure of DV1 was maintained in the DV1-CXCR4 complex structure and formed interactions with CXCR4 receptor (Figure 1). These results may provide the basis for designing more potent and smaller peptide or non-peptidic analogs that inhibit HIV-1 entry via CXCR4.

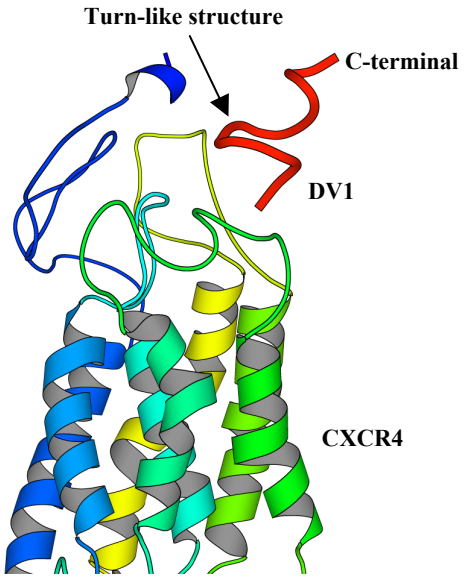

Fig. 1. A plausible structural model of the DV1-CXCR4 complex.

Acknowledgments

The work was supported by grants from the NIH.

References

1. Nagasawa, T., Hirota, S., Tachibana, K., Takakura, N., Nishikawa, S., Kitamura, Y., Yoshida, N., Kikutani, H. and Kishimoto, T. *Nature* **382**, 635-638 (1996).
2. Feng, Y., Broder, C. C., Kennedy, P. E. and Berger, E. A. *Science* **272**, 872-877 (1996).
3. Huang, Z. *Mini-Reviews Med. Chem.* **2**, 373-383 (2002).
4. Zhou, N., Luo, Z., Luo, J., Hall, J. W. and Huang, Z. *Biochemistry* **39**, 3782-3787 (2000).
5. Luo, Z., Fan, X., Zhou, N., Hiraoka, M., Luo, J., Kaji, H. and Huang, Z. *Biochemistry* **39**, 13545-13550 (2000).
6. Zhou, N., Luo, Z., Luo, J., Fan, X., Cayabyab, M., Hiraoka, M., Liu, D., Han, X., Pesavento, J., Dong, C. Z., Wang, Y., An, J., Kaji, H., Sodroski, J. G. and Huang, Z. *J. Biol. Chem.* **277**, 17476-17485 (2002).
7. Zhou, N., Luo, Z., Luo, J., Liu, D., Hall, J. W., Pomerantz, R. J. and Huang, Z. *J. Biol. Chem.* **276**, 42826-42833 (2001).

Peptide Revolution: Genomics, Proteomics & Therapeutics
Michael Chorev & Tomi K. Sawyer (Editors)
American Peptide Society, 2003

Enhanced Hepatic Clearance of Plasma Cholesterol and Inhibition of Atherosclerosis by an Apolipoprotein E-mimetic Peptide

David W. Garber[1], Himanshu Gupta[2], Shaila Handattu[1], Geeta Datta[1], Manjula Chaddha[1], M. N. Palgunachari[1], C. Roger White[2] and G. M. Anantharamaiah[1]

[1]Atherosclerosis Research Unit, Division of Gerontology and Geriatric Medicine; [2]Division of Cardiology; Department of Medicine, University of Alabama at Birmingham, Birmingham, AL 35294, USA

Introduction

Lipoproteins, which package and transport lipids throughout the body, are critical both for normal metabolism and in the development of disease processes such as atherosclerotic disease and stroke. The protein components of lipoproteins, called apolipoproteins, are largely responsible for the structure of lipoproteins, and control the metabolism of these particles through interactions with receptors, cofactors of enzymes, and modification of oxidative properties of the lipoproteins. A common structural motif of these apolipoproteins is the amphipathic α-helix. The class A amphipathic α-helix is characterized by distinct hydrophobic and hydrophilic faces, with positively-charged residues at the interface and negatively-charged residues on the center of the hydrophilic face [1].

Apolipoprotein (apo) E is an arginine-rich component of chylomicrons, very low density lipoprotein (VLDL), and intermediate density lipoprotein (IDL), and, to a lesser extent, high density lipoprotein (HDL). It is a ligand for the low density lipoprotein receptor (LDL-R), as well as for a number of related receptors involved in the metabolism of triglyceride-rich lipoproteins [2]. Apo E can be considered to have two major domains, an N-terminal four-helix-bundle receptor binding region, and a C-terminal lipid associating region. Based on this overall structure, we have designed a dual-domain peptide containing the putative receptor binding region of human apo E, residues 141-150 [3] and designated hE, and a lipid-associating amphipathic α-helical peptide, 18A [4], as shown in Figure 1. This peptide, called Ac-hE18A-NH_2, has both the N- and C-terminal residues blocked, and has a high lipid affinity as reflected by a surface exclusion pressure of 45 dynes/cm^2, compared with 30 dynes/cm^2 for 18A alone and 34 dynes/cm^2 for apo A-I (unpublished data courtesy of Dr. Michael C. Phillips).

Ac-hE18A-NH_2: Ac-**LRKLRKRLLR**DWLKAFYDKVAEKLKEAF-NH_2

*Fig. 1. Sequence of the dual-domain peptide, Ac-hE18A-NH_2. Residues 141-150 of human apo E are shown in **bold** text.*

Results and Discussion

In vivo and *in vitro* studies of Ac-hE18A-NH_2 have previously been reported [4]. As shown in Figure 2, when [^{125}I]Ac-hE18A-NH_2 was mixed with human plasma, peptide associated with VLDL and LDL at lower proportions. At the higher proportion, excess peptide was found in the HDL region and as free peptide. However, when analyzed with 2D polyacrylamide/agarose gel electrophoresis, peptide in the HDL region was not found in particles containing apo A-I (unpublished data), suggesting it may be forming a new HDL-sized particle. When the peptide was mixed with human VLDL

and re-isolated by ultra-centrifugation, apo E was displaced and the peptide remained with the VLDL. When mixed with human LDL, the positively charged peptide reduced the net negative charge on LDL, thus lowering its electrophoretic mobility on agarose gel.

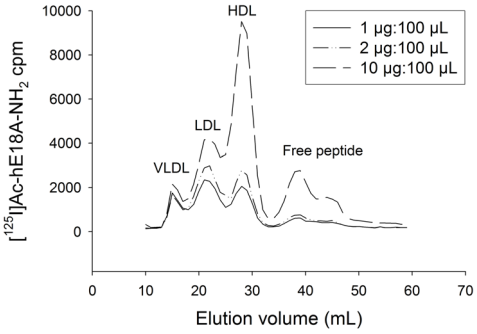

Fig. 2: In vitro mixing of [^{125}I]Ac-hE18A-NH$_2$ with human plasma at different proportions (Superose 6 size exclusion chromatography).

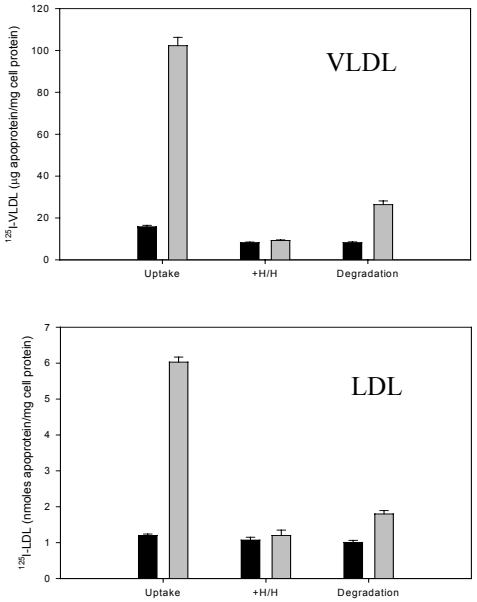

Fig. 3. Uptake and degradation of VLDL and LDL by Hep G2 cells. Black bars represent the lipoproteins and gray bars show the lipoproteins in presence of Ac-hE18A-NH$_2$. +H/H represents uptake in presence of heparinase/heparitinase.

In vitro studies of VLDL and LDL uptake were done in cell culture using human fibroblasts and HepG2 cells. In both cell types, the peptide enhanced the uptake of both LDL 5-fold and VLDL 6-fold (Figure 3). The peptide-enhanced uptake of the atherogenic lipoproteins was shown to be independent of the LDL-R pathway. Treatment with heparinase and the use of HSPG deficient cells indicated that this enhanced uptake was via the HSPG pathway. Degradation of the internalized lipoproteins was also enhanced 3-fold in the case of VLDL and 2-fold in the case of LDL.

The effects of injection of the peptide in several mouse models of dyslipidemia were studied. When injected intravenously into C57BL/6J mice fed an atherogenic diet, or into chow-fed apo E null mice, plasma cholesterol was rapidly reduced by up to 90%, and this reduction was maintained for six to eight hrs (Figure 4). The reduction was restricted to VLDL and IDL/LDL cholesterol; in no case was HDL cholesterol reduced (Figure 5). The rapidity of clearance suggests that the initial clearance involves binding of peptide-decorated lipoproteins to cell-surface proteoglycans, as was also suggested by *in vitro* studies, followed by a slower process of sequestration and internalization of the bound lipoproteins. When the peptide was incubated with human [^{125}I]VLDL or [^{125}I]LDL and injected into apo E null mice, the majority of the radioactivity was found in the liver at 5 hours after injection, and liver radioactivity was significantly

greater than that found in mice injected with [^{125}I]VLDL or [^{125}I]LDL incubated with saline.

In contrast to these two mouse models of dyslipidemia, injection of Ac-hE18A-NH_2 into LDL-R null mice fed either normal chow or a Western diet had no effect on plasma cholesterol. This was not due to the absence of the LDL receptor, as peptide injected into dual-knockout mice lacking both the LDL-R and apo E did reduce plasma cholesterol similarly to that seen in apo E null mice. *In vitro* mixing and *in vivo* injection experiments using [^{125}I]Ac-hE18A-NH_2 demonstrated that the peptide was unable to associate with the apo B containing lipoproteins of LDL-R null mice, perhaps due to higher surface pressures on the particles induced by apo B-100.

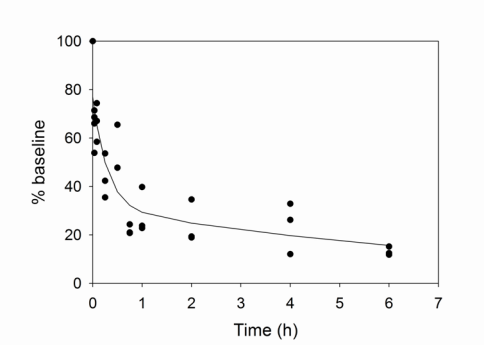

Fig. 4. Clearance of plasma cholesterol in apo E null mice injected intravenously with Ac-hE18A-NH_2 (100 μg). Data represent % remaining compared with pre-injection (baseline). Solid circles represent individual data points; the solid line represents data fitted to a biexponential equation.

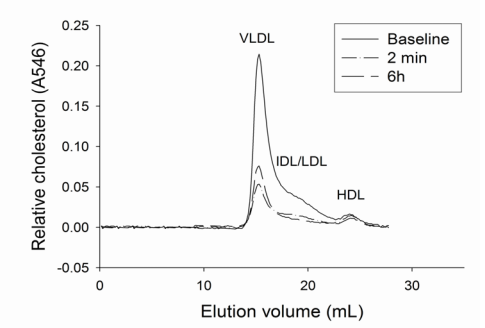

Fig. 5. Cholesterol profiles (Superose 6 size-exclusion chromatography) at different time points from a single apo E null mice injected intravenously with Ac-hE18A-NH_2 (100 μg).

An experiment was performed to assess the antigenicity of Ac-hE18A-NH_2 by injecting peptide three times per week for four weeks into C57BL/6J mice fed an atherogenic diet. No antibodies to the peptide could be detected.

These studies are currently being extended into rabbits fed an atherogenic diet, and Watanabe heritable hyperlipidemic (WHHL) rabbits. The effects of this peptide on atherogenesis and vascular function will be studied. Other studies underway are intended to understand the kinetics of binding and uptake of peptide-decorated lipoproteins, as well as the mechanisms for organ-specific targeting.

Acknowledgments

The work was funded by grants from NHLBI (R01-HL65663 and P01-HL34343) and from Phadros Inc.

References

1. Chung, B. H., et al. *J. Lipid Res.* **37**, 1099-1112 (1996).
2. Mahley, R. W. *Science* **240**, 622-630 (1988).
3. Zaiou, M., et al. *J. Lipid Res.* **41**, 1087-1095 (2000).
4. Anantharamaiah, G. M., et al. *J. Biol. Chem.* **260**, 10246-10255 (1985).

Peptide Revolution: Genomics, Proteomics & Therapeutics
Michael Chorev & Tomi K. Sawyer (Editors)
American Peptide Society, 2003

Development of CRF-R2 Selective Peptide Ligands

Doreen Wietfeld[1], Angelika Ehrlich[1], Reinhard Seifert[2], Klaus Fechner[1], Eberhard Krause[1], Michael Bienert[1] and Michael Beyermann[1]

[1]Forschungsinstitut für Molekulare Pharmakologie, D-13125 Berlin; [2]Institut für Biologische Informationsverarbeitung, Forschungszentrum Juelich, D-52425 Juelich, Germany

Introduction

Corticotropin releasing factor (CRF) is the principal neuroregulator of the mammalian pituitary-adrenal axis. As an important stress hormone it is involved in regulatory activities of both the central and peripheral systems. CRF has high homology in primary structure and shows functional similarity to the CRF-related peptides urocortin, urotensin I and sauvagine, all of which show activity on both CRF receptor subtypes, CRF-R1 and CRF-R2 as well. Urocortin-II has recently been described as the first CRF-R2 selective agonist [1].

CRF SQEPPISLD*LTFH*LLREVLEMTKADQLAQQAHSNRKLLDIA-NH_2
Ucn DDPPLSID*LTFH*LLRTLLELARTQSQRERAEQNRIIFDSV-NH_2
Utn NDDPPISID*LTFH*LLRNMIEMARNENQREQAGLNRKYLDEV-NH_2
Svg ZGPPISID*LSLE*LLRKMIEIEKQEKEKQQAANNRLLLDTI-NH_2

Ucn-II VILSLD*VPIG*LLRILLEQARYKAARNQAATNAQILAHV-NH_2

Fig. 1. Sequences of nonselective CRF-R1/R2 agonists CRF, urocortin (Ucn), urotensin (Utn) and sauvagine (Svg) in comparison with that of the CRF-R2 selective urocortin II (Ucn-II).

In order to understand the molecular basis of the Ucn-II selectivity on CRF-R2 we investigated Ucn and Ucn-II analogs, making systematic amino acid replacements within the underlined N-terminal tetrapeptide sequence (Figure 1), which is strikingly different in the two ligands. Syntheses were carried out on cellulose using the spot technique (~ 50 nmol/spot), and the products were analytically characterized by LC-MS after deprotection (TFA), cleavage from the support and dissolving in 50 µL of DMSO. Biological activities of analogs were determined by the use of an HTS assay (Figure 2), co-expressing CRF receptors and cAMP-gated ion channels in HEK cells and monitoring the calcium flux spectrofluorimetrically (Fluo-4, AM).

Results and Discussion

The screening assay used was evaluated with urocortin and urocortin-II on CRF-R1, -R2α and -R2β, showing the same rank order of potencies compared to those obtained by adenylate cyclase determination.

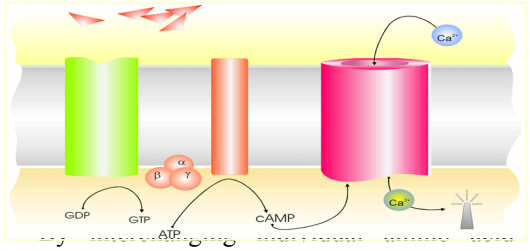

Fig. 2. Schematic description of the HTS assay used.

residues or short peptide sequences (3-5 aa) among CRF, Svg or Utn in which they are different (Figure 1), we did not find any subreceptor selectivity of those CRF analogs. Accordingly, incorporation of the corresponding amino acid residues of sauvagine or urotensin, which both show a increased activity at CRF-R2 compared to that of CRF, into CRF resulted in CRF analogs showing a low activity at CRF-R2 comparable to that of CRF itself (data not shown).

Most impressively, the replacement of *LTFH* in Ucn by the corresponding *VPIG* of Ucn-II led to a highly selective agonist on CRF-R2 (Figure 3), which exhibits no activity at CRF-R1.

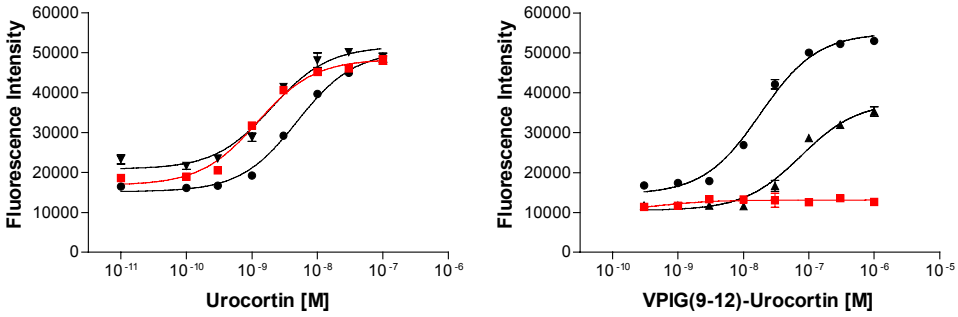

Fig. 3. Comparison of potencies of urocortin (■CRF-R1, ▼CRF-R2α, and ●CRF-R2β) and VPIG(9-12)-urocortin (■CRF-R1, ▲CRF-R2α, and ●CRF-R2β).

A positional scanning, replacing each position in the VPIG motif of VPIG(9-12)-Ucn by the other 19 proteinogenic amino acids, resulted in a set of 80 analogs. Only 5 out of the 80 analogs showed a high potency (at 10 nM) which were selectively acting on CRF-R2. The essential motif for this selective CRF-R2 activity was found to be VPXX, whereby X is a hydrophobic amino acid residue.

Surprisingly, while the individual amino acid residues of this tetrapeptide motif are essential for the CRF-R2 selective activity of the corresponding urocortin analogs, none of the individual amino acid residues within this motif where found to be essential for the high receptor selectivity and activity of urocortin-II. A corresponding positional scanning of the VPIG motif of Ucn-II showed that 56 out of 80 analogs of the set exhibited a CRF-R2 selective activity at a very low concentration (10 nM). Conclusively, our findings are clearly indicative for different receptor binding sites of the two agonists on CRF-R2.

Acknowledgments
The work was funded by a DFG grant (FOR 299/2-1).

References

1. Reyes, T. M., *et al., Proc. Natl. Acad. Sci. U.S.A.* **98**, 2843-2848 (2001).

Peptide Revolution: Genomics, Proteomics & Therapeutics
Michael Chorev & Tomi K. Sawyer (Editors)
American Peptide Society, 2003

Discovery of a Novel CXCR4 Antagonist Using Two Orthogonal Cyclic Peptide Libraries

Shinya Oishi[1], Ayumu Niida[1], Kenichi Hiramatsu[1], Satoshi Ueda[1], Takanobu Araki[1], Hirokazu Tamamura[1], Akira Otaka[1], Shuichi Kusano[2], Shigemi Terakubo[2], Hideki Nakashima[2], Zi-xuan Wang[3], Stephen C. Peiper[3] and Nobutaka Fujii[1]

[1]Graduate School of Pharmaceutical Sciences, Kyoto University, Sakyo-ku, Kyoto 606-8501, Japan; [2]St. Marianna University, School of Medicine, Miyamae-ku, Kawasaki 216-8511, Japan; [3]Department of Pathology, Medical College of Georgia, Augusta, GA 30912, USA

Introduction

Chemokines are a family of chemotactic cytokines. Among these, it has been shown that the stromal cell derived factor-1 (SDF-1)/CXCR4 receptor system is involved in the pathogenesis of cancer metastasis [1] and rheumatoid arthritis [2]. CXCR4 also acts as a co-receptor for the entry of HIV-1 virus into T-cells in acquired immune deficiency syndrome (AIDS) [3]. Therefore, CXCR4 antagonists are expected to be potential therapeutic agents against all of these diseases. We have developed a highly potent and selective CXCR4 antagonist, T140, through structure-activity relationship studies on an antimicrobial peptide, polyphemusin II (Figure 1) [4]. T140 is a 14-residue peptide, which possesses a number of basic residues and exhibits β-sheet-like structures. Recently, using alanine scanning, we identified four residues in T140 that are indispensable for bioactivity: Arg^2, Nal^3, Tyr^5 and Arg^{14}. These are all located in the side opposite to the β-turn element [5]. Meanwhile, it was difficult to ascertain the relative dispositions of these residues from conformational studies on T140 using structural calculations, since three residues are highly flexible and lie outside the macrocycle formed by the disulfide bond. This has made difficult the rational structure-based design of small molecule CXCR4 antagonists based on the structure of T140. In order to reduce the molecular size of T140, as well as to estimate proper orientations of these essential residues in the bioactive conformations, so they could be reproduced by using privileged structures, we developed novel CXCR4 antagonists containing these four pharmacophore residues.

T140 R**RX**C**Y**RKkPYRZC**R**

Fig. 1. Sequence of the highly potent CXCR4 antagonist, T140. k: D-lysine; X: L-3-(2-naphthyl)alanine; Z: L-citrulline; bold letters: essential residues for bioactivity.

Results and Discussion

Cyclic pentapeptides were utilized as molecular templates to disperse the four pharmacophore residues, since conformations of such peptides have been intensively investigated by many researchers. Potential libraries included 192 peptides that were designed from the four indispensable residues with an additional Gly residue for cyclization linkage. These libraries consist of combinations of 12 variations of amino acid sequence along with 16 types of chirality arrays (Figure 2). A limited number of peptides were first synthesized to identify required sequences for CXCR4 antagonism (conformation-based library, 12 sequences × 4 chirality arrays). On the basis of Kessler's research on cyclic RGD peptides [6], we selected two chirality arrays, which exhibited the respective II' β/γ arrangements, *cyclo*(-L-Xaa^1-Gly^2-L-Xaa^3-L-Xaa^4-D-

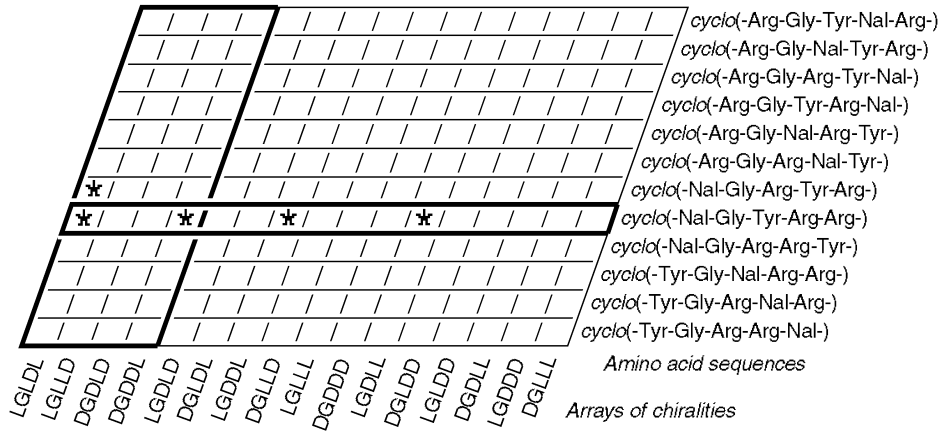

*Fig. 2. Two orthogonal libraries of cyclic peptides. Vertical box: conformation-based library; horizontal box: sequence-based library; *: key potent compounds; L: L-amino acids; D: D-amino acids; G: glycine.*

Xaa^5-) and *cyclo*(-L-Xaa^1-Gly^2-L-Xaa^3-D-Xaa^4-L-Xaa^5-), and their enantiomers. Synthesis of cyclic peptides was performed by parallel Fmoc-based synthesis on (2-Cl)-Trt resin with subsequent cyclization being achieved using diphenyl phosphorylazide. Biological activity was evaluated by assaying inhibition of [^{125}I]SDF-1 binding to CXCR4, and by an anti-HIV assay. In this first library, some peptides showed submicromolar potency. Interestingly, two peptides, FC008 and FC068, possess a common amino acid sequence, although differ in the chirality at positions 1 and 3. Therefore, based on FC008 and FC068 we designed two additional epimers at these positions and evaluated their activity. One of these latter peptides, FC092, exhibited more potent activity than that of FC068 (Table 1). Since this indicated that the Nal-Gly-Tyr-Arg-Arg sequence of the cyclic peptides could interact with the CXCR4 receptor, we extended the library to include a sequence-based array (1 sequence × 16 chirality arrays). Within this sequence-based library, FC131, *cyclo*(-L-Nal-Gly-D-Tyr-L-Arg-L-Arg-), which is an Arg^4 epimer of FC092, exhibited nearly identical biological activity as that of the parent peptide, T140. As such, a molecular size reduction of T140 was efficiently achieved through a distinctive sequential usage of two orthogonal libraries. It is notable that not only the amino acid sequence but also the chirality of the cyclic peptides seriously affects interactions with CXCR4.

Table 1. Biological activities of T140 and cyclic peptides.

Peptide	Sequence	IC_{50} (μM)[a]	EC_{50} (μM)[b]
T140	-	0.004	0.060
FC008	*cyclo*(-L-Nal-Gly-L-Tyr-D-Arg-L-Arg-)	0.1 – 1.0	4.3
FC068	*cyclo*(-D-Nal-Gly-D-Tyr-D-Arg-L-Arg-)	0.016	0.28
FC092	*cyclo*(-L-Nal-Gly-D-Tyr-D-Arg-L-Arg-)	0.008	0.11
FC131	*cyclo*(-L-Nal-Gly-D-Tyr-L-Arg-L-Arg-)	0.004	0.038

[a]IC_{50} values for the cyclic pentapeptides are based on inhibition of [^{125}I]SDF-1 binding to CXCR4 transfectants of CHO cells. [b]EC_{50} values are based on the inhibition of HIV-induced cytopathogenicity in MT-4 cells.

To characterize the bioactive conformations of FC131, ^{1}H-NMR measurements in DMSO and structural calculations were carried out. Small temperature coefficients of amide proton chemical shifts, which are derived from hydrogen bonding and can indicate limited solvent accessibility, were not observed. Simulated annealing molecular dynamics/energy minimization using dihedral angle and distance constraints derived from the ^{1}H-NMR data demonstrated that FC131 exhibits a nearly symmetrical pentagonal shape. Lack of hydrogen bonds indicated that these would have no contribution to the secondary substructures (Figure 3). Amide bond carbonyl oxygens, except for that between Nal^{1} and Gly^{2}, were oriented in opposite directions to that of the side chain of the respective following residues. These interrelated orientations corresponded to the observed strong NOE intensities: Gly^{2} H^{N}/D-Tyr^{3} H^{N}; Arg^{4} H^{N}/Arg^{5} H^{N}; Arg^{5} H^{N}/Nal^{1} H^{N}; Nal^{1} H^{α}/Gly^{2} H^{N}; and D-Tyr^{3} H^{α}/Arg^{4} H^{N}. We conclude that the characteristic orientations of amide bonds, which could potentially influence the interactions between ligands such as FC131 and CXCR4 receptor, depended on the amino acid chiralities.

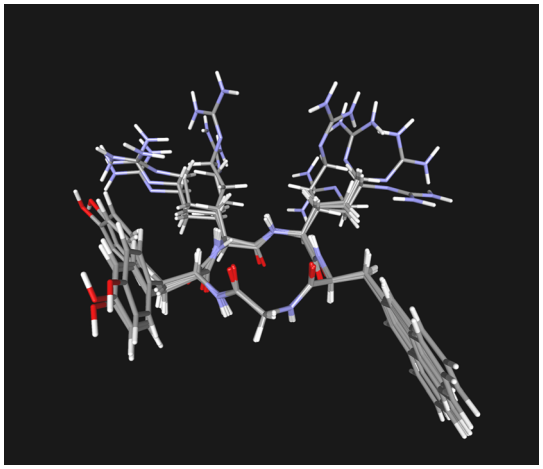

Fig. 3. Five overlaid structures by simulated annealing molecular dynamics/energy minimization (Insight II/Discover).

Acknowledgments

This work was supported by Health and Labour Sciences Research Grants (Research on HIV/AIDS) and Grant-in-Aid for Scientific Research from the Ministry of Education, Culture, Sports, Science and Technology of Japan.

References

1. Müller, A., *et al., Nature* **410**, 50-56 (2001).
2. Nanki, T., *et al., J. Immunol.* **165**, 6590-6597 (2000).
3. Feng, Y., Broder, C. C., Kennedy, P. E. and Berger, E. A. *Science* **272**, 872-877 (1996).
4. Fujii, N., Nakashima, H. and Tamamura, H., *Expert Opin. Investig. Drugs* **12**, 185-195 (2003).
5. Tamamura, H., *et al., Bioorg. Med. Chem. Lett.* **10**, 2633-2637 (2000).
6. Haubner, R., *et al., J. Am. Chem. Soc.* **118**, 7461-7472 (1996).

Peptide Revolution: Genomics, Proteomics & Therapeutics
Michael Chorev & Tomi K .Sawyer (Editors)
American Peptide Society, 2003

Design, Synthesis and Pharmacological Evaluation of Potential CXCR4 Chemokine Antagonist Peptides on Breast Cancer Cells

Xin Wang[1], Yan Wang[2], J.-P. Perchellet[2] and Sandra C. Vigil-Cruz[1]

[1]Department of Medicinal Chemistry, University of Kansas, Lawrence, KS 66045, USA;
[2]Division of Biology, Kansas State University, Manhattan, KS 66506, USA

Introduction

The cell-surface CXCR4 chemokine receptor is over-expressed in human malignant and metastatic breast cells but is essentially absent in normal breast tissue [1,2]. This receptor is speculated to play a crucial role in both the proliferation [1,3] and metastasis of breast tumor cells [2]. We were the first to report that small synthetic peptides derived from stromal cell-derived factor-1 (SDF-1) inhibited growth of breast tumor cells [4]. Our working hypothesis is that increasing CXCR4 receptor affinity of our analogues will enhance the anti-proliferative efficacy. To test this hypothesis, we designed, synthesized and assayed additional SDF-1 analogues for their ability to regulate breast tumor cell growth.

The design strategy of the SDF-1 analogues included N-terminal elongation of the SDF-1 fragment and utilizing ligand homodimers. A different Cys^9 homodimer has been shown to have modest affinity at CXCR4 [5], while the branched scaffold of the homodimer utilizes a Lys matrix and Ahx spacers to form a large surface area for ligand-receptor interaction. vMIP-II-(1-21) is a N-terminal fragment of a virally encoded chemokine with a CXCR4 affinity of 190 nM [6], while T140 amide is a polyphemusin analogue which has been reported to have increased metabolic stability [7]; both were included for comparison. The structure of the analogues is provided in Figure 1.

H-MKPVSLSYRFPAbuFFESH-NH_2
[Met^0,Phe^9,Abu^{11}]SDF-1-(1-17)NH_2

cyclo[Cys^9,$Cys^{9'}$]H-KPVSLSYRC-NH_2
Cys^9 SDF-1-(1-9) homodimer

H-$(KPVSLSYRFAhx)_2$-KAhx-NH_2
Branched SDF-1-(1-9) homodimer

H-LGASWHRPDKCCLGYQKRPLP-NH_2
vMIP-II-(1-21)NH_2

cyclo[$Cys^{4,12}$]H-RRNalCYRlPYRCitCR-NH_2
T140 amide

Fig. 1. CXCR4 analogues.

Results and Discussion

The peptides were prepared using a Fmoc/PyBOP protocol on a low-load PAL-PEG-PS resin, cleaved using TFA and scavengers and recovered using ether extraction and lyophilization. Intramolecular disulfide bridges were formed by DTT reduction followed by air oxidization in 0.1 mM ammonium bicarbonate, pH 8.0, whereas the intermolecular disulfide bond was formed using I_2 in HOAc-H_2O. The peptides were purified to >99% homogeneity using standard semi-preparative reverse-phase HPLC and characterized by mass spectrometry.

Radioligand binding assays were performed to determine CXCR4 receptor affinity (Table 1). As none of our SDF-1 analogues showed affinity for the CXCR4 chemokine receptor, the two high affinity literature analogues previously reported were selected for evaluation on T47-D breast tumor cell proliferation to examine the importance of CXCR4 for cell growth (Figure 2a). In these preliminary evaluations, neither of the high-affinity CXCR4 analogues appeared to modulate breast tumor growth, which was

surprising. As a result, we went one step further and evaluated the effect of monoclonal antibodies to SDF-1 and CXCR4 (Figure 2b) on breast cell proliferation, but neither antibody appeared to exert any significant effect on breast tumor cell growth.

Table 1. Affinity of peptide ligands.

Analogue	IC_{50} (nM)
SDF-1α	16.4 ± 0.6
$[Cys^9]$SDF-1-(1-9)NH_2 homodimer	> 10,000
Branched SDF-1 homodimer	> 10,000
$[Met^0,Phe^9,Abu^{11}]$SDF-1-(1-17)NH_2	> 10,000
vMIP-II-(1-21)NH_2	122.7 ± 0.6
T140 amide	1.2 ± 0.6

T47-D breast cancer cells express the CXCR4 chemokine receptor at a very low level which may be below that necessary to exert any significant effect on cell growth. Future studies will examine the DU-4475 cell line that expresses the CXCR4 receptor at an extremely high level and is more challenging to grow in culture and as such was not chosen for the initial evaluation. The analogues and monoclonal antibodies will also be evaluated for their ability to inhibit breast cancer metastasis.

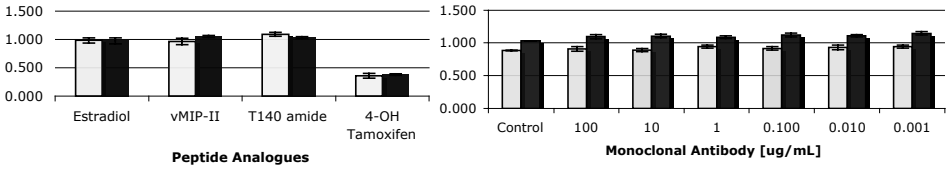

Fig. 2. a&b. Anti-proliferation activity of high affinity ligands and monoclonal antibodies.

Acknowledgments

The work was supported by the NIH COBRE Award 1P20RR15563, and matching support from the State of Kansas and the University of Kansas to S. Vigil-Cruz.

References

1. Sehgal, A., Ricks, S., Boyton, A. L., et al. *J. Surg. Oncol.* **69**, 239-248 (1998).
2. Müller, A., Homey, B., Soto, H., et al. *Nature* **410**, 50-56 (2001).
3. Sehgal, A., Kenner, C., Boyton, A. L., et al. *J. Surg. Oncol*. **69**, 99-104 (1998).
4. Condon, M. K., Sasiela, C. A., Brodie, A. H., and Vigil-Cruz, S. C. In *Peptides: The Wave of the Future*; Lebl, M. and Houghton, R. A. (Eds.) American Peptide Society: San Diego, CA, 801-802 (2001).
5. Loetscher, P., Gong, J.- H., Dewald, B., et al. *J. Biol. Chem.* **273**, 22279-22283 (1998).
6. Kledal, T. N., Rosenkilde, M. M., Coulin, F., et al. *Science,* **277**, 1656-1659 (1997).
7. Tamamura, H., Omagari, A., Hiramatsu, K., et al. *Bioorg. Med. Chem. Lett.* **11**, 1897-1902 (2001).

Peptide Revolution: Genomics, Proteomics & Therapeutics
Michael Chorev & Tomi K. Sawyer (Editors)
American Peptide Society, 2003

Synthesis of Branched Cyclic Peptide Analogs of Angiotensin II

Yuan Gao, Yun Wu, Wei-Jun Zhang and Garland R. Marshall

Department of Biochemistry and Molecular Biophysics, Washington University in St Louis, School of Medicine, 660 S Euclid, St Louis, MO 63110, USA

Introduction

Rational design of pharmaceuticals derived from naturally occurring peptides requires knowledge of peptide conformations within the ligand-receptor complex (the "receptor-bound" conformation). One approach to this problem is to employ cyclopentapeptides (CPPs) as "receptor probes" of the known 3D structures, which have been determined either by experimental or computational means. Specifically, conformational energy calculations suggested that the low-energy conformations of CPPs may mimic the receptor-bound conformations of active peptides.

The octapeptide angiotensin II (Asp^1-Arg^2-Val^3-Tyr^4-Ile/Val^5-His^6-Pro^7-Phe^8) is especially interesting for several reasons. First, it has been shown that residues indispensable for receptor binding and initiation of signal transduction are Tyr^4, His^6 and Phe^8 [1]. Second, a receptor-bound 3D model of AII has been developed earlier by molecular modeling and NMR spectroscopy [2]. Third, we have designed and synthesized different CPPs. Some of them exhibited good binding activities (K_D *ca*. 20 nM) and partial agonistic response at rabbit aorta [3]. All these considerations led us to continue the research on CPPs with different structures. Three types of branched cyclic peptides were devised based on our previous results (Figure 1).

cyclo(Xxx-Val-His-Asp(D-Phe)-Yyy), Xxx = Gly, D-Nle (Type I)
cyclo(Xxx-Val-His-D-Asp(D-Phe)-Yyy), Xxx = Gly, Nle (Type II)
cyclo(Dap(Xxx)-Val-His-D-Asp(D-Phe)-Yyy), Xxx = Val, Arg-Val (Type III)
*in all the compounds Yyy = Tyr, D-Tyr.

Fig. 1. Sequences of the devised branched cyclic peptides as angiotensin II mimics.

Results and Discussion

On-resin cyclization of branched cyclic peptides was difficult due to steric hindrance from branched segments. In strategy 1, the resin-linker moiety acted as an additional branch, so we adopted strategy 2 by linking a resin to one branch instead of the cyclic skeleton, trying to avoid steric hindrance in cyclization precursors (Figure 2).

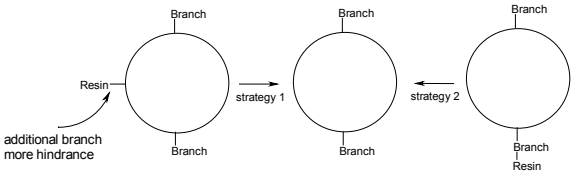

Fig. 2. Strategies to synthesize branched cyclic peptides.

Here, we report the synthesis of four two-branch cyclic peptides, which belong to Type III compounds. We failed to realize the cyclization when both of the branches had been assembled. The reason was assumed to be the high hindrance from one branch

(Fmoc-Val, or Cbz-Arg(Tos)-Val). So we changed the route by linking this branched segment after cyclization. Different reagent combinations were tried for the cyclization, and, HATU/HOAt/DIEA/DMF was found to be effective (Figure 3).

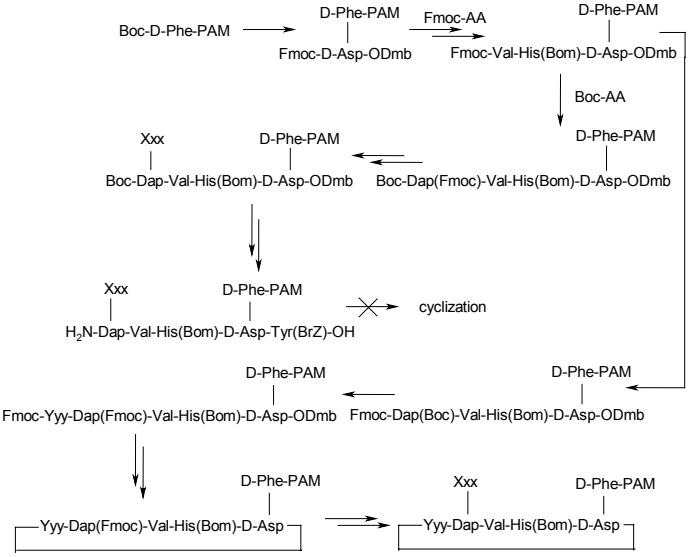

Fig. 3. Synthesis of Type III cyclic peptides. Xxx= Fmoc-Val, or Cbz-Arg(Tos)-Val. Yyy=Tyr(2,6-dichloro-Bz), or D-Tyr(2-bromo-Bz), cyclizaiton was in HATU/HOAt/DIEA 3:3:6 for 12-24 hr.

In this strategy (Figure 3), the linker-resin moiety did not act as additional steric hindrance. Instead, by linking resin to one branch, the distance between polystyrene and peptide skeletons was extended, which further facilitated on-resin cyclization.

Acknowledgments
We acknowledge NIH grant GM 53630 for partial support of this research.

References

1. (a) Nikiforovich, G. V. and Marshall, G. R. *Biochem. Biophys. Res. Commun.* **195**, 222-225 (1993), (b) de Gasparo, M., Catt, K. J., Inagami, T., Wright, J. W. and Unger, T. *Pharmacol. Rev.* **52**, 415-472 (2000).
2. Nikiforovich, G. V. and Marshall, G. R. *Biochem. Biophys. Res. Commun.* **286**, 1204-1211 (2001).
3. Nikiforovich, G. V., Linderberg, G., Kover, K. E., Ye, Y., Frandberg, P. A., Nyberg, F., Karlen, A., Hallberg, A. and Marshall, G. R. In Lebl, M. and Houghten, R. A. (Eds.) *Peptides: The Wave of the Future (Proceedings of the 17th American Peptide Symposium),* American Peptide Society, San Diego, 2001, pp. 917-918.

Peptide Revolution: Genomics, Proteomics & Therapeutics
Michael Chorev & Tomi K. Sawyer (Editors)
American Peptide Society, 2003

QSAR Analysis of Ring-Substituted Tyrosine Replacements at the N-Terminus of a Nonselective Deltorphin Analog

Deborah L. Heyl, Kutralanathan Renganathan, Malika N. Jayamaha, David W. Rodgers and Stephen E. Schullery

Department of Chemistry, Eastern Michigan University, Ypsilanti, MI 48197, USA

Introduction

The deltorphins show a remarkable selectivity for mammalian δ receptors and bind to these receptors to a far greater extent than any other known endogenous opioid peptides [1]. Hundreds of analogs of the various deltorphins have been synthesized to determine the precise nature of the binding interactions and the basis for receptor selectivity. Structure-activity relationship (SAR) studies of N-terminal residue suggest that the *L*-tyrosine is relatively intolerant to modification [2-4] and its spatial orientation is important [2]. It is theorized that Tyr^1 is involved in receptor recognition, and the *para*-orientation of the hydroxyl group is considered to be a required element in the binding pharmacophore [4]. In order to explore the function of the aromatic ring in Tyr side chain and, perhaps more importantly, the phenolic hydroxyl group, we have synthesized a series of 10 analogs in which substitutions were made to the Tyr ring of the parent compound Gly^4 deltorphin I/II (Tyr-*D*-Ala-Phe-Gly-Val-Val-Gly-NH_2) [1], which binds comparably tight to both the δ and μ receptors. The δ and μ receptor binding affinities of the single-substitution analogs were subjected to correlation and multiple regression QSAR analyses focused on the acid/base role of the Tyr^1 phenolic group. The roles of several other calculated quantum, solubility and geometric properties were also investigated.

Results and Discussion

Table 1 presents the experimental purity, molecular weight, and opioid binding affinities for each analog studied, along with the logarithms of the binding enhancement factors (log of the ratio of analog affinity to parent affinity, log E) used in the QSAR analyses. The hypothesis that Tyr plays a hydrogen bond donor role was tested by correlation/regression analyses of the binding dependence on pK_a of the Tyr ring-substituted analogs. QSAR data (Table 2) support a dual hydrogen bond donor/acceptor role for the Tyr^1 hydroxyl moiety, consistent with molecular modeling predictions reported for related model systems [5]. Analogs with less acidic hydroxyl groups exhibit stronger binding to opioid receptors, presumably by strengthening the less-favored hydrogen bond acceptor role of Tyr^1 after the first hydrogen bond (where Tyr^1 is a donor) is formed. Additional steric bulk in the Tyr^1 position strengthens μ binding, perhaps by either a ligand conformational effect or enhanced van der Waals interactions with the receptor site. The weaker steric effect for δ binding, although visually evident, is of borderline statistical significance. The stronger pK_a effect on δ than on μ binding results in an increase in δ selectivity with pK_a. While most modifications of Tyr^1 result in a reduction in opioid receptor binding affinity relative to the parent deltorphin, three of the analogs modified in position 1 displayed improved binding at both δ and μ receptors, along with increased δ selectivity: *o*-$MeTyr^1$, DMT^1, and TMT^1. The binding enhancements seen with these analogs are understandable in terms of the methyl groups' steric bulk and inductive effect on pK_a.

Table 1. Purity, mass and opioid receptor binding affinities of X^1Gly^4 Deltorphin I/II analogs.

X^1 Analog	Purity[a] (%)	Mol. Wt.	K_δ(nM)[b]	K_μ(nM)[b]	K_μ/K_δ	log E_δ	log E_μ
2,3,6-TMT	>99.9	753.8	0.42	0.78	1.86	1.733	1.473
o-Me-Tyr	98.7	725.8	7.0	6.1	0.87	0.511	0.580
2,6-DMT	98.1	739.8	15.6	17.6	1.13	0.163	0.120
Tyr	>99.9	711.8	22.7	23.2	1.02	0	0
m-Cl-Tyr	99.9	746.3	62	66.7	1.08	-0.436	-0.459
m-I-Tyr	99.8	837.5	209	95	0.45	-0.964	-0.612
m-OH-Tyr	99.7	727.8	248	241	0.97	-1.038	-1.017
3,5-Br_2-Tyr	99.5	869.5	1079	161	0.15	-1.677	-0.841
3,5-I_2-Tyr	99.5	963.3	1885	30.8	0.02	-1.919	-0.123
m-NO_2-Tyr	>99.9	756.5	>10,000	1322	<0.13	-2.644	-1.756

[a]*Purity of final product peptide as assessed by RP-HPLC peak integration at 230 nm.* [b]*Average values from three assays performed in triplicate (>10,000 nM indicates that less than 50% inhibition of the labeled [^{3}H]diprenorphine was reached at a peptide concentration of 10μM).*

Table 2. QSAR correlations for analogs [a].

QSAR Variable	log E_δ	log E_μ
pK_a	.903 (<.0005)	.706 (.023)
HOMO	.880 (.001)	.730 (.017)
LUMO	.859 (.001)	.712 (.021)
charge[b]	-.698 (.025)	-.553 (.097)
log P	.242	.529
polarizability	-.167	.229
area	-.055	.281
volume	-.055	.301
width	.111	.302
length	-.355	-.154

[a] *Significance levels (p-values) in parentheses.* [b] *Partial charge on oxygen atom of Tyr analog.*

Acknowledgments

The authors are grateful to Dr. Don Hansen, Jr. (Monsanto) for the methylated tyrosine analogs and to Dr. John Traynor at The University of Michigan for the binding assays.

References

1. Lazarus, L. H., et al. *Prog. Neurobiol.* **57**, 377-420 (1999).
2. Guerrini, R., Capasso, A., et al. *Eur. J. Pharmacol.* **302**, 37-42 (1996).
3. Schmidt, R., Menard, D., Mrestani-Klaus, C., et al. *Peptides* **18**, 1615-1621 (1997).
4. Lazarus, L. H., Salvadori, S., et al. *J. Med. Chem.* **35**, 1222-1227 (1992).
5. Mosberg, H. I. and Fowler, C. B. *J. Pept. Res*. **60**, 329-335 (2002).

Peptide Revolution: Genomics, Proteomics & Therapeutics
Michael Chorev & Tomi K. Sawyer (Editors)
American Peptide Society, 2003

New Paradigm for Drug Design: Overlapping Pharmacophores of Opioid and Cholecystokinin Ligands in the Design of New Compounds for the Treatment of Neuropathic Pain

Richard S. Agnes[1], Yeon S. Lee[1], Shou W. Ma[2], Peg Davis[2], Todd Vanderah[2], Jinfa Ying[1], Katalin Kövér[3], Josephine Lai[2], Frank Porreca[2] and Victor J. Hruby[1]

[1]Department of Chemistry, University of Arizona; [2]Department of Pharmacology, University of Arizona, Tucson, AZ 85705, USA; [3]Department of Chemistry, University of Debrecen, Hungary

Introduction

It is widely known that opioid receptor induced analgesia increases cholecystokinin (CCK) and CCK receptors in the central nervous system; and CCK, in turn, attenuates analgesia (i.e. CCK is an anti-opioid). These complex systemic changes and interactions between opioid and CCK receptor systems may play a role in neuropathic pain [1]. It also has been proposed that these types of diseases require a new paradigm in drug design in which the rational design of potential drugs for the treatment of disease is based on one ligand for multiple targets [2]. For the treatment of neuropathic pain, we have designed a single peptide which can interact with delta and/or mu opioid receptors as agonists and with CCK receptors as antagonists. The key feature of our design is to utilize the concept of overlapping pharmacophores of CCK and opioid ligands [3]. The resulting linear and cyclic disulfide analogues were tested for opioid agonist and CCK antagonist activities.

CCK-8	H-Asp-Tyr(SO_3H)-Met-Gly-Trp-Met-Asp-Phe-NH_2
DPDPE	H-Tyr-c[D-Pen-Gly-Phe-D-Pen]-OH
RSA504	H-Tyr-D-Nle-Gly-Trp-Nle-Asp-Phe- NH_2
RSA102C	H-Tyr-c[D-Cys-Gly-Trp-D-Cys]-Asp-Phe-NH_2
RSA101C	H-Tyr-c[D-Cys-Gly-Trp-Cys]-Asp-Phe-NH_2

Fig. 1. Sequences of CCK-8, DPDPE (δ-selective opioid agonist), and CCK/opioid synthetic peptide analogues.

Results and Discussion

Synthetic CCK/opioid peptide amides were synthesized manually using N^{α}-Fmoc chemistry on Rink amide resins. For cyclic disulfide analogues, RSA102C and RSA101C, side-chain to side-chain cyclization was achieved by air oxidation. Peptides were purified and characterized by RP-HPLC and mass spectrometry. Opioid agonist activity at delta and mu opioid receptors was determined by the ability of synthetic peptides to inhibit electrically induced tissue contractions at MVD and GPI tissues, respectively. CCK antagonist activity was determined by ability of the synthetic peptides to inhibit CCK-8 induced contractions at the unstimulated GPI/LMMP tissues.

Linear analogue RSA504, when compared to DPDPE, displayed increased CCK antagonist properties. To introduce a conformational constraint to the linear analogues and to mimic desirable properties of DPDPE, cyclic disulfides analogues were synthesized. Because modeling studies of RSA504 showed that the alkyl chains of D-Nle^2 and Nle^5 are oriented towards each other, positions 2 and 5 were used as sites of cyclization. Cyclic disulfide analogue c[D-Cys^2, D-Cys^5] RSA102C displayed

decreased activity at both opioid receptors when compared to RSA504, but the CCK antagonist activities increased ca. 8 fold (Table 1). When position 5 was substituted with L-Cys resulting in c[D-Cys^2, Cys^5] RSA101C, the opioid agonist properties increased significantly, displaying remarkable selectivity for the delta opioid receptors. Furthermore, the CCK antagonist activity increased dramatically, as well. The NMR structure of RSA101c shows a helical-like structure, which is similar to a structure of CCK-8 at CCK-A receptors [5] (Figure 2). This supports our initial hypothesis that opioid and CCK ligands have overlapping pharmacophores.

Table 1. Bioactivities of peptides.

Peptide	Opioid Agonist (IC_{50}, nM)		CCK Activity	
	MVD (δ)	*GPI (μ)*	*Agonist (EC_{50})*	*Antagonist (K_e, nM)*
DPDPE	2.2	6900	0% at 1 μM	0% at 1 μM
RSA504	23 ± 9.7	210 ± 52	0% at 1 μM	190 ± 80
RSA102C	120 ± 7.5	280 ± 9.1	0% at 1 μM	23 ± 9.1
RSA101C	0.45 ± 0.060	63 ± 5.5	0% at 1 μM	7.6 ± 2.3

This novel approach of a single peptide for multiple targets represents a new paradigm for drug design, particularly for pathological diseases, where systemic changes are taken into consideration.

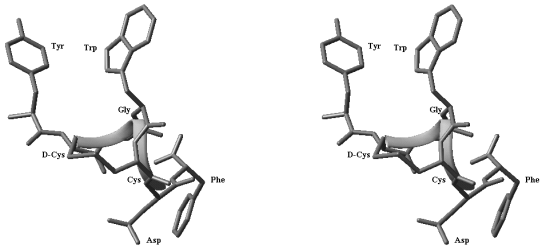

Fig. 2. NMR structure of RSA101C. The ribbon shows a helical-like peptide backbone.

Acknowledgments
The work was funded by NIDA Grant DA 12394. RSA thanks Pfizer for 2002 fellowship in Organic Chemistry. K.K. thanks the MTA-OTKA-NSF U.S.-Hungary Cooperative Research Program.

References

1. Stanfa, L., Dickenson, A., Xu, X. J. and Wiesenfeld-Hallin, Z. *Trends Pharmacol. Sci.* **15**, 65-66 (1994).
2. Hruby, V. J., Agnes, R. S., Lee, Y. S., Davis, P., Ma, S.- W., Lai, J. and Porreca, F., In Lebl, M. and Houghten, R. A. (Eds.) *Peptides: The Wave of the Future*, Kluwer, Dordecht, p. 969-970 (2001).
3. Hruby, V. J., Agnes, R. S., Davis, P., Ma, S. -W., Lee, Y. S., Vanderah, T., Lai, J. and Porreca, F. *Life Sciences* **73**, 699-704 (2003).
4. Slaninova, J., Knapp, R. J., Wu, J. J., Fang, S. N., Kramer, T., Burks, T. F., Hruby, V. J. and Yamamura, H. I. *Eur. J. Pharmacol*. **200**, 195-198 (1991).
5. Pellegrini, M. and Mierke, D. F. *Biochemistry* **38**, 14775-14783 (1999).

Peptide Revolution: Genomics, Proteomics & Therapeutics
Michael Chorev & Tomi K. Sawyer (Editors)
American Peptide Society, 2003

A New Series of Endothelin Receptor Antagonists

Ke-Liang Liu, Jun-Jun Dong, Bo Geng, Yuan-Jun Liang, Han Han Ping Wu, Mu-Gen Chi and Ze-Hui Gong

Beijing Institute of Pharmacology and Toxicology, Beijing 100850, China

Introduction

The endothelin (ET) is one of the most powerful vasoconstrictors. Two subtypes of ET receptors known as ET_A and ET_B have been cloned and characterized in animal and mammalian systems. Elevated ET levels have been noted in a variety of diseases including cerebral vasospasm, pulmonary hypertension, restenosis, myocardial infarction, renal failure, subarachnoid hemorrhage, and heart failure [1]. Now, the studies on ET receptor antagonists may lead to some new therapeutical agents for diseases induced by ET. Bosentan is the first drug of this kind of antagonists approved by FDA and has been used for treatment of pulmonary arterial hypertension [2]. The objective of our work was to get new structural endothelin receptor antagonists with high activity and selectivity and study the SAR of the new compounds.

Design and synthesis of ET receptor antagonists: The new series of ET receptor antagonists follow the general formula depicted Figure 1.

R-CO-AA_1-XAA_2-AA_3-OH

Where: R =

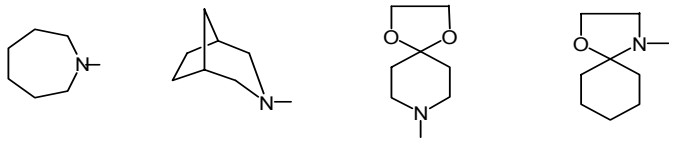

HIM ABO DAD CSO

AA_1 = Leu, Val, Ala, Pro, and alkyl unnatural amino acids

XAA_2 = D-Trp, substituted aromatic amino acids and non-amino acids

AA_3 = D-Trp, substituted aromatic amino acids

Fig. 1. The general structure of the antagonists.

R group showed crucial function in improving the selectivity and affinity to ET receptors. When the scissile amide bond (-CONH-) in a peptide was replaced with the ketomethylene (-$COCH_2$-) peptide bond surrogate, a series of pseudopeptides was obtained. These pseudopeptides were synthesized by a modified Szelke [3] reaction as described in Figure 2.

Results and Discussion

The antagonists were purified by HPLC and their structural integrity determined by MS-ESI. The bioactivities of these compounds were evaluated by inhibiting the ET-1-induced contraction of rat aorta; some of antagonists were more active than the positive control, BQ-485, reported by Itoh [4]. Results reporting this preliminary SAR study are listed in Table 1.

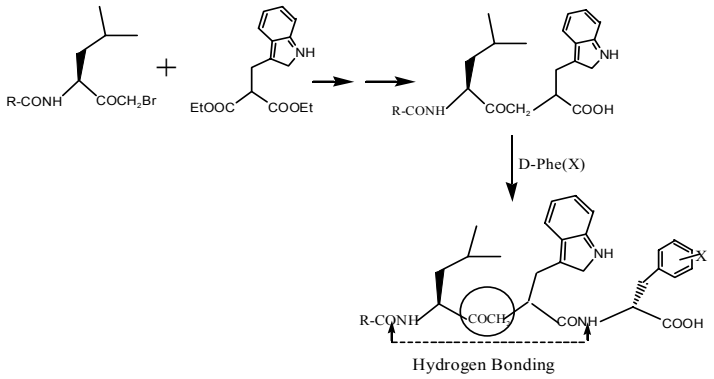

Fig. 2. The procedure for synthesizing pseudopeptides.

Table 1: Bioactivities of selected compounds (for structure of ENP002 see Figure 2).

Sample No.	Primary structure	IC_{50}(nM)[a]	γ[b]
BQ-485	HIM-CO-Leu-D-Trp-D-Trp-OH	3.40	0.960
ETP017	HIM-CO-Leu-D-Trp-D-Phe(4-F)-OH	50.0	0.932
ETP505	ABO-CO-Leu-D-Trp-D-Phe(4-F)-OH	8.74	0.980
ETP077	DAD-CO-Leu-D-Trp-D- Phe(4-F)-OH	1.23	0.926
ENP002	R=HIM, X=4-F	5.32	0.996
ETP037	HIM-CO-Leu-D-Trp-D-Phe(3,4-Cl_2)-OH	2.45	0.960
ETP022	HIM-CO-Leu-D-Trp-L-Phe(3,4-Cl_2)-OH	0.00	

[a]*IC_{50} was measured by inhibiting the ET-1-induced contraction of rat aorta (n=4).*[b]*γ is correlation coefficient.*

On the basis of this study, we can conclude: (i) If other components of tripeptides are kept unchanged, only replacing D-amino acid with L-amino acid at the C-terminal, such as ETP037 to ETP022, their activities showed great difference. (ii) When the second amide bond –CO-NH- was replaced with –CO-CH_2-, the activity was still preserved (compare antagonist ETP017 with ENP002). This pseudopeptide may be more resistant toward enzymatic degradation.

Acknowledgments
The work was funded by The National High Technology Research and Development Program of China (2001AA235021) and Drug Research and Development Program Beijing (H020220060190).

References
1. Hiroshi, M., Chiaki, F., Rikako, Y., *et al*. *Bioorg. Med. Chem.* **9,** 255-268 (2001).
2. Mealy, N. E., Bayès, M. and Freno, M. *Drugs of the Future* **26**, 1149-1154 (2001).
3. Szelke, M., Jones, D. M. and Hallett, A., *EP45665*(1982); *Chem. Abstr*. **97,** 39405 (1982).
4. Itoh, S., Sasaki, T., Ide, K., *et al*. *Biochem. Biophys. Res. Commun.* **195**, 969-975 (1993).

Peptide Revolution: Genomics, Proteomics & Therapeutics
Michael Chorev & Tomi K. Sawyer (Editors)
American Peptide Society, 2003

An Unexpected Modification of Histidine During the Preparation of Ghrelin

David L. Smiley, Steven Afendis, Melvin G. Johnson, Joseph V. Manetta, Xiliang Wang, Derrick R. Witcher and Lianshan Zhang

Lilly Research Laboratories, Indianapolis, IN 46285, USA

Introduction

Ghrelin has been identified as the endogenous ligand of the growth hormone secretagogue receptor, and is a gut-brain peptide with endocrine, orexigenic and gastrointestinal effects [1]. In order to further study its *in-vivo* pharmacology, significant quantities of the peptide are needed. A key step in the synthesis is the acylation of the Ser3 hydroxyl group which is essential for release of growth hormone [2]. Efforts to optimize the synthesis of ghrelin have included solid phase Fmoc/tBu-based protocols using O-trityl Ser in position 3 [3].

In an effort to further optimize the synthesis, we examined the effect of different acylation conditions to attach octanoic acid to the Ser3 hydroxyl group (Figure 1). When conducting the acylation using octanoic acid, dicyclohexylcarbodiimide in DMF/NMP and an equimolar amount of DMAP, we encountered a molecule that no longer behaved like native ghrelin. Here, we report the characterization of the new entity that had identical N-terminal sequence and mass spectral analyses compared to native ghrelin.

GSSFLSPEHQRVQQRKESKKPPAKLQPR

fragment	avg. mass:
(1-8)	823.9 + 126.2 (octanoyl)
(9-17)	1209.4
(18-28)	1250.5

Fig. 1. Sequence of native human ghrelin and expected Glu-C digest fragments.

Results and Discussion

The synthesis utilized Fmoc chemistry and hydroxybenzotriazole-activated single couplings on an ABI433A peptide synthesizer starting from 0.1mmole Rink amide resin (0.5mmol/g). The Ser in position 3 had O-trityl side chain protection and the N-terminal Gly was coupled as the Boc derivative. The peptidyl resin was given two 1 min treatments with 0.1%TFA/DCM/5%TIPS, and then neutralized with 5%DIEA/DCM. An acylation in DMF was carried out using 10 equiv. octanoic acid, DCC/NMP, and DMAP. After mixing at RT overnight, the resin was washed with DCM and cleaved for 2 hr using TFA/5%TIPS/2.5%thioanisole/2.5%MeOH. The ether precipitated product was purified over a 2.2x25cm Kromasil C18 with a gradient of 10-30% ACN in aq. 0.1%TFA. HPLC analysis (Zorbax C8) showed the synthetic product had a retention time of 4.25min compared with 5.05min for a commercial reference standard. Experimentally obtained masses were identical, as were N-terminal sequence analyses. Receptor activation via a FLIPR assay, however, showed the synthetic sample to be 100-fold less active (aprox.1000nM) than the reference standard. In order to determine the position of the octanoyl group, both samples were digested with Endoproteinase Glu-C and the solutions analyzed by Maldi-TOF (Figure 2).

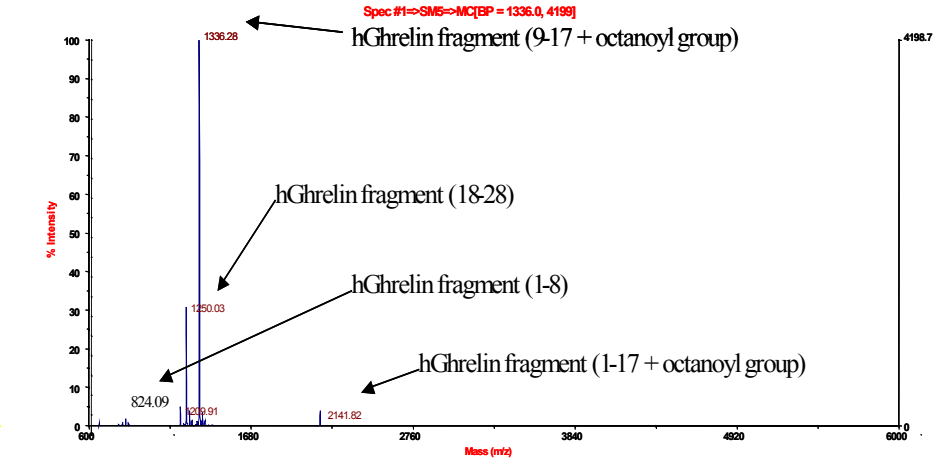

Fig. 2. endo-Glu-C digest analyzed by Maldi-TOF.

The data shows that the octanoyl group from the less active synthetic sample is no longer associated with the 1-8 fragment as in native ghrelin, but is now attached to the 9-17 fragment. Acylation of the histidine imidazole ring is known to occur at either N(1) or (N3) [4], and we propose that, under these conditions, an octanoylation at N(3) has occurred (Figure 3).

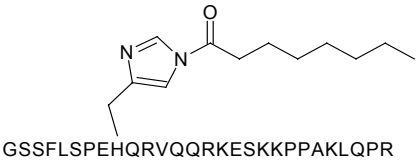

Fig.3. Proposed structure of His9 acylated ghrelin.

An acylation of a similar peptidyl resin (after a 45 min de-tritylation) using octanoic anhydride in DCM gave exclusively modification at the Ser3 hydroxyl. That product gave the expected endo-Glu-C digest fragments, co-eluted with commercial ghrelin, and was fully potent in the FLIPR assay. We believe that short periods of de-tritylation lead to deprotection of His(Trt) prior to Ser(OTrt), and that conducting the acylation in DMF/NMP may facilitate modification of the His side-chain. These data may also explain the isolation of bis-acylated products where both Ser3 and His9 were modified. We demonstrate here that the octanoylated His9 ghrelin analog has substantially less activity compared to native ghrelin.

References

1. Kojima, M., Hosada, D., Date, Y., et al. *Nature* **402**, 656 (1999).
2. Tschoep, M., Smiley, D. and Heiman, M., *Nature* **402**, 908 (2000).
3. Flora, D., Liu, M. Drane, J., Edwards, P. and Mayer J., In Lebl, M. and Houghten, R. (Eds.), *Peptides: The Wave of the Future, Proceedings, 2nd International and 17th American Peptide Symposium,* American Peptide Society, San Diego, p. 895 (2001).
4. Bundgarrd, H. and Moss, J., *Pharm. Res.* **7**, 895 (2001).

Peptide Revolution: Genomics, Proteomics & Therapeutics
Michael Chorev & Tomi K. Sawyer (Editors)
American Peptide Society, 2003

Misfolded Therapeutic Peptides Give Rise to Caspase-Mediated Cytotoxicity

Satomi Onoue[1,2], Keiichi Ohshima[3], Kazuhiro Debari[4], Keitatsu Koh[4], Takehiko Yajima[2] and Kazuhisa Kashimoto[1]

[1]Itoham Foods Inc., Moriya, Ibaraki 302-0104, Japan; [2]School of Pharmaceutical Sciences, Toho University, Funabashi, Chiba 274-8510, Japan; [3]Growth Factor Division, National Cancer Center Research Institute, Tsukiji, Tokyo 104, Japan; [4]Laboratory of Electron Microscopy, Showa University School of Medicine, Shinagawa, Tokyo 142-8555, Japan

Introduction

Glucagon is a polypeptide hormone that consists of 29 amino acid residues, and it is widely used for clinical diacrisis and treatment of hypoglycemia [1]. Water-insoluble glucagon is usually solubilized at acidic pH, however it forms gel-like fibrillar aggregates in dilute acid. Other therapeutic peptides such as insulin, GLP-1 analogue, and growth hormone also display conformational changes into ß-sheet-rich fibrils. These insoluble products are attributed to the formation of partially unfolded intermediates with an exposed hydrophobic region that drives the aggregation toward the pharmaceutically undesirable form. The generation of insoluble peptide/protein fibrils is well-confirmed in amyloidosis, complex disorders characterized by the polymerization and aggregation of normally innocuous and soluble proteins or peptides followed by extracellular insoluble fibrils with resistance to peptidases [2]. The pathologically-related amyloidogenic protein/peptide fibrils share a distinct conformational feature in the richness of the ß-sheet structure. In addition, there are similar characteristics of polarity, hydrophobicity, and the size of side-chain among certain segments containing 10–15 amino acid residues of amyloid-forming peptides such as insulin, ß-amyloid (Aß), and amylin. These factors are indicative of a consensus sequence as a recognition motif of Congo Red, a dye that is bound to amyloidogenic protein/peptide fibrils with ß-sheet dependency. Since there are similar neurotoxic effects of fibrils from pathologically-related peptides and non-pathologically-related peptides including glucagon, it is plausible that there is also a common toxic mechanism related to their secondary and macromolecular structures for different amyloid-forming proteins/peptides. Herein, to better understand the physicochemical and physiological properties of glucagon fibrils, we have characterized them using biological techniques including circular dichroism (CD), transmission electron microscopy, and ß-sheet-imaging probe. We demonstrate that glucagon fibrils possess the conformational properties and apoptotic signaling pathways by activating caspases as fibrils derived from pathologically-related peptides including Aß and prion. Here, we provide further insights into the associative behavior of glucagon, showing that its non-covalent aggregation is dependent on the dissolved conditions, especially its concentration.

Results and Discussion

Although glucagon exhibited a characteristic CD spectra for random coil conformation, a transition from random coil to ß-sheet structure was observed following a 24 h incubation at the concentration of over 5 mg/ml, indicating the generation of ß-sheet rich fibrils. Incubation of salmon calcitonin for 24 h also yielded the amyloid-like fibrils having an abundant ß-sheet structure, and about 10-fold higher concentration of

salmon calcitonin was required for its structural changes as compared to that of glucagon, suggesting that glucagon has high potential to yield amyloid-like fibrils.

We demonstrated the effect of aging period on aggregation with the use of Congo red-binding assay, turbidity analysis, and thioflavin T (ThT) assay. After 24 h incubation of glucagon, significant increases in turbidity and Congo red/ThT binding was confirmed, and the binding of Congo red and ThT to glucagon fibrils, aged at 5 mg/ml, was much higher than that binding to untreated glucagon. On the contrary, treatment of glucagon at low concentration (1 mg/ml) did not affect its physicochemical properties. These data indicate that aging at higher concentration (>5 mg/ml) accelerated the misfolding of glucagon, producing the fibrils readily.

To assess the cytotoxicity of glucagon fibril, PC12 and NIH-3T3 cells were exposed to aged or non-aged peptides (0.1–100 μM) for 72 h, and cell viability was determined by WST-8 assay. The results indicate that glucagon and salmon calcitonin fibrils are highly toxic to these cells, and aged prion protein fragment (PrP) and Aß also displayed the similar cytotoxicity toward PC12 cells [3,4]. Based on these findings, amyloid fibrils with ß-sheet structure were determined to be responsible for the cytotoxicity of aged glucagon or aged salmon calcitonin toward PC12 and NIH 3T3 cells. Although peptide fibrils including Aß, PrP and amylin were believed to be toxic to neurons or neuron-like cells, these results indicated that the toxicity of peptide fibrils is not specific to neuronal cells.

The caspase family of enzymes is a large group of proteases whose members have defined roles in apoptotic cell death. In particular, the activation of caspase-3 was confirmed in the apoptosis induced by many neurotoxic agents including nitric oxide, tumor necrosis factor-α, and cycloheximide. We previously reported that fibrillar aggregates of Aß and PrP were cytotoxic to PC12 cells [3,4], and that activation of caspase-3 is required for the commitment of these fibrils-induced apoptosis. The activation of caspase-3 is observed in the cytotoxicity of aged glucagon, and which was attenuated by the caspase-inhibitors, Ac-DEVD-CHO and Z-VAD-FMK. These findings, taken together with our previous reports, suggest that the fibril toxicity may be due to peptide accumulation at or near the cell surface in a conformation-specific manner rather than in a sequence-specific manner. Clarification of the exact mechanism should contribute to our understanding of amyloid-induced neurodegenerative diseases.

In conclusion, we demonstrate that misfolding of glucagon induced a conformational change to generate amyloid-like fibrils; this structural transition was accelerated at the high concentration of glucagon. Very importantly, we show that aggregated glucagon has an ability to cause the unexpected side-effects in the clinical use, due to its cytotoxicity mediated by activation of caspase-3. Upon our findings, staining with specific dyes for ß-sheet structure was a useful method to distinguish the contamination of aggregated forms in glucagon solution. This conformational analyses should be required in the manufacturing process of glucagon for clinical application in order to avoid undesirable side effects in peroral endoscopy, clinical treatment of hypoglycemia, and clinical diacrisis.

References

1. Rodbell, M. , *et al. Proc. Natl. Acad. Sci. U.S.A.* **68**, 909-913 (1971).
2. Glenner, G. G. *N. Eng. J. Med.* **302**, 1283-1292 (1980).
3. Onoue, S., *et al. Peptides* **23**, 1471-1478 (2002).
4. Onoue, S., *et al. FEBS Lett.* **522**, 65-70 (2002).

Peptide Revolution: Genomics, Proteomics & Therapeutics
Michael Chorev & Tomi K. Sawyer (Editors)
American Peptide Society, 2003

Long Acting Peptide (LAP^{TM}) Analogues of Glucagon-Like Peptide-1

Abdelkrim Habi[1], Daniel Abran[1], Krishna G. Peri[1], Patricia Brubaker[2] and Thierry Abribat[1]

[1]*Theratechnologies Inc., 2310 Alfred-Nobel Blvd, Montreal (Saint-Laurent), Quebec, H4S 2A4;*
[2]*University of Toronto, 1-King's College Circle, Toronto, Ontario, M5S 1A8, Canada*

Introduction

Glucagon-like peptide-1 (GLP-1), secreted by L-cells in the gastrointestinal tract following a meal, is a potent insulinotropic hormone. Both isoforms, GLP-1(7-37) and GLP-1(7-36)NH_2 (predominant in circulation), bind to a specific GLP-1 receptor (GLP-1R) on pancreatic beta-cells and augment cAMP formation, intracellular Ca^{2+} and glucose-stimulated insulin secretion. Furthermore, its effects include delay in gastric emptying, suppression of glucagon secretion and stimulation of beta cell biogenesis. GLP-1 is rapidly inactivated by dipeptidylpeptidase IV (DPP IV) in circulation. The potential of GLP-1 as a therapeutic agent in type II (non-insulin-dependent) diabetes mellitus is limited by its short *in vivo* half-life (2-4 minutes). DPP IV-resistant analogues of GLP-1 have been useful in controlling hyperglycemia in diabetic animals and humans. The objective of the present study was to apply the LAP^{TM} (Long Acting Peptide) technology to the development of a DPP IV-resistant derivative of GLP-1 that involved the covalent addition of a small rigidifying hydrophobic moiety to His^7 residue.

Materials and methods

Peptide Synthesis: GLP-1 analogues in this study were synthesized by solid-phase methodology on BHA resin using N-Fmoc-protected amino acids. The peptides were purified by preparative RP-HPLC. The purity (>95%) and the identity of the peptides were confirmed by analytical RP-HPLC and MALDI-TOF spectrometry. Exendin-4 was purchased from Phoenix Pharmaceuticals.

DPP IV proteolysis: DPP IV resistance was evaluated in *in vitro* assays (10 µg peptide incubated with 50 mU of enzyme in 10 mM Tris-HCl buffer pH 8.0 for 4 h) using purified DPP IV (Sigma). Residual peptide was quantified by RP-HPLC.

cAMP synthesis in RINm5F cells: Cells (50,000/well) cultured in 96-well plates were stimulated with peptides (10^{-12} M to 10^{-5} M) for 40 min in the presence of isobutylmethylxanthine (10^{-4} M). cAMP levels in the supernatants were determined by DPC radioimmunoassay (Amersham).

Animal studies: The peptides were tested in Sprague-Dawley rats (~ 300 g), CD-1 mice (~ 30 g), Zucker *fa/fa* rats (~ 500 g) and C57BL/ks *db/db* mice (~ 50 g) according to protocols approved by the institutional ethics committee. Blood glucose levels were measured using a glucometer (Acucheck) and insulin levels by RIA (Linco).

Oral glucose tolerance test (oGTT): Peptides in saline (10 µg per mouse; n=7) were injected in CD-1 mice ip 5 minutes prior to an oral glucose challenge (1 g /Kg). Blood glucose levels were measured for 120 min.

Intravenous (ivGTT) and intraperitoneal (ipGTT) glucose tolerance tests: Glucose was injected ip (1 g/kg) or iv (0.4 g/kg) in overnight-fasted Sprague Dawley rats (n=4 per group) just after injecting peptides (30 µg/kg) sc (ivGTT) or iv (ipGTT). Blood Glucose (for 240 min) and insulin (for 30 min) levels were measured.

Diabetic animal models: Overnight-fasted Zucker *fa/fa* rats and C57BL/ks *db/db* mice (n=6 per group) were fed for 30 minutes. Peptides (30 µg/kg in rats and 500 µg/kg in mice) were injected sc and blood glucose levels were measured for 2 h.

Table 1. Potency and efficacy of Exendin-4, GLP-1 and LAP™-GLP-1 analogues on cAMP production in RINm5F cells. Mean ± SEM; n = experiments.

Peptide	EC_{50} (nM)	E_{max} (pmol/mg protein)	n
GLP-1	2.2 ± 0.2	17.6 ± 2.6	16
Exendin-4	0.8 ± 0.3	21.5 ± 2.0	12
TH0115	16.8 ± 0.8	20.0 ± 2.4	8
TH0118	7.9 ± 0.3	25.1 ± 4.9	9
TH0272	20.6 ± 2.0	8.2 ± 2.1	6

Table 2. Relative efficacy of Exendin-4 and LAP™-GLP-1 analogues compared to GLP-1 on blood glucose (fold decrease) and insulin levels (fold increase) in animal models of hyperglycemia. AUCglc-area under the curve of glucose (mmol/L).

Peptide	[1]Acute insulin response (fold increase)	oGTT[2] AUC glc/2 h (fold decrease)	ivGTT[3] AUC glc/0.5h (fold decrease)	ivGTT[4] Peak insulin level at 2.5 min (fold increase)	ipGTT[5] AUC glc/4 h (fold decrease)	fa/fa rats[6] AUC glc/2h (fold decrease)	db/db mice[7] AUC glc/2h (fold decrease)
Exendin-4	ND	ND	1.50	1.82	2.10	ND	16.40
TH0115	1.76	1.91	1.47	0.71	2.35	0.40	4.66
TH0118	3.61	2.38	0.87	0.82	2.03	0.60	3.67
TH0272	3.06	1.70	0.82	0.71	ND	ND	ND

ND –Not determined.
[1]AUC of Plasma insulin levels for 30 min after peptide injection sc in 4-6 h fasted rats.
[2]AUC of blood glucose levels measured for 2 h in oGTT in normal mice.
[3]AUC of blood glucose levels for 30 min in ivGTT in normal rats.
[4]Peak plasma insulin levels at 2.5 min after injection of peptides in ivGTT in normal rats.
[5]AUC of blood glucose levels for 4 h in ipGTT in normal rats.
[6]AUC of blood glucose levels for 2 h in fed Zucker fa/fa rats.
[7]AUC of blood glucose levels for 2 h in fed C57BL/ks db/db mice.

Results and Discussion

Three LAP™-GLP-1 analogues were found to be DPP IV-resistant and showed superior or comparable efficacy compared to native GLP-1 in animal models of hyperglycemia. These analogues could be clinically useful towards achieving glycemic control in type II diabetic patients.

Peptide Revolution: Genomics, Proteomics & Therapeutics
Michael Chorev & Tomi K. Sawyer (Editors)
American Peptide Society, 2003

Design and Synthesis of Novel GLP-1 Analogs that have Significantly Improved *In Vivo* Activities

Jesse Z. Dong[1], Yeelana Shen[1], Jundong Zhang[1], John E. Taylor[1], Chee-Wai Woon[1], Barry Morgan[1], Steve Skinner[1], Michael Cawthorne[2], Michael Culler[1] and Jacques-Pierre Moreau[1]

[1]Biomeasure Incorporated/IPSEN Group, 27 Maple Street, Milford, MA 01757, USA;
[2]University of Buckingham, Buckingham, UK

Introduction

Glucagon-like peptide-1 (GLP-1) is an insulinotropic gluco-incretin secreted by the L-cells of the intestine in response to fat meals and carbohydrates [1]. It stimulates insulin secretion and inhibits glucagon release in a strictly glucose-dependent manner. GLP-1 also promotes insulin gene expression and proinsulin biosynthesis, induces pancreatic β-cell proliferation, slows gastric emptying and suppresses appetite. These unique properties make GLP-1 a potentially important treatment of type 2 diabetes. However, native GLP-1 is rapidly degraded by proteases *in vivo* and the short circulating half-life greatly hampers its clinical utility. In an effort to develop potent and enzymatically stable GLP-1 analogs, we have systematically investigated the structural elements in GLP-1 that influence its potency and enzymatic stability. Such structure-activity and structure-enzymatic stability relationship studies led to a novel series of potent human GLP-1 (hGLP-1) analogs that are highly resistant to enzymatic degradation.

Results and Discussion

The GLP-1 analogs were synthesized on MBHA resin using the *in situ* neutralization, fast Boc-chemistry [2]. The synthetic protocol included deprotection (100% TFA, 2 min) and coupling (HBTU/DIEA, 5 min). The total cycle time for addition of an amino acid residue was ~10 min. The peptides were cleaved from the resin by employing liquid hydrogen fluoride and the crude products were purified on a preparative RP-HPLC system.

Major conformational features of human GLP-1(7-36)NH_2 (hGLP-1(7-36)NH_2) are two amphiphilic α-helices that are connected by a linker region [3]. It is believed that the α-helices are critical for the ligand-receptor recognition. Furthermore, we hypothesized that the amphiphilic α-helical domains have membrane association properties, which facilitate the hormone-receptor interaction. Based on this hypothesis, hGLP-1(7-36)NH_2 analogs bearing $C^{\alpha,\alpha}$-disubstituted glycines, such as aminoisobutyric acid (Aib), 1-aminocyclopentane-1-carboxylic acid (A5c) and 1-aminocyclohexane-1-carboxylic acid (A6c), were designed to increase the stability of the α-helices and subsequently improve the membrane and receptor binding affinity. An example in this class of analogs is [Aib^8, $A6c^{32}$]hGLP-1(7-36)NH_2, which is about 2-fold more potent than native hGLP-1(7-36)NH_2 in *in vitro* receptor binding assays (peptide 1, Table 1).

It is well documented that dipeptidyl peptidase IV (DPP IV) rapidly degrades GLP-1 *in vivo* by cleaving the peptide bond between Ala^8 and Glu^9 at the N-terminus of the hormone [4]. To protect the amide bond from such cleavage, we replaced Ala^8 with N-methyl-D-alanine (N-Me-D-Ala), A5c, A6c or Aib [5]. These sterically hindered amino acids make the peptide bond between positions 8 and 9 less accessible to the enzyme, yielding analogs with greater DPP IV resistance (peptides 1, 3, 4 and 5, Table 1).

Substitution of (4-pyridylthio)acetic acid (Pta) for His residue at position 7 also produces a DPP IV resistant analog (peptide 6, Table 1). The DPP IV resistance of [Pta^7]hGLP-1(7-36)NH_2 is presumably due to its lack of amino functional group at the α-carbon, which is required for DPP IV cleavage [6].

Careful analysis of the degradation products of hGLP-1(7-36)NH_2 in rat, mouse and human plasmas using a LC-MS revealed that in addition to its susceptibility at the N-terminus to DPP IV degradation, the native hormone is also subjected to proteolysis at the C-terminus [7 and 8]. The peptide bond between Gly^{35} and Arg^{36} and the peptide bond between Lys^{34} and Gly^{35} were both extensively cleaved in the plasmas from these species. Our preliminary studies of incubating hGLP-1(7-36)NH_2 with individual plasma enzymes have indicated that plasma kallikrein and plasmin are likely among the enzymes responsible for the C-terminal degradation.

Table 1. hGLP-1 receptor binding affinity and rat plasma half-life.

Peptide	hGLP-1R[a] Ki (nM)	Rat plasma $T_{1/2}$ (h)	Sequence
hGLP-1(7-36)NH_2	1.09	0.84	
#1	0.56	6.74	[Aib^8, $A6c^{32}$]hGLP-1(7-36)NH_2
#2	0.81	1.12	[$A6c^{16,20}$]hGLP-1(7-36)NH_2
#3	1.13	4.35	[N-Me-D-Ala^8]hGLP-1(7-36)NH_2
#4	7.23	4.86	[$A5c^8$]hGLP-1(7-36)NH_2
#5	0.64	4.52	[Aib^8]hGLP-1(7-36)NH_2
#6	5.82	4.88	[Pta^7]hGLP-1(7-36)NH_2
#7	1.26	8.34	[Aib^8,β-Ala^{35}]GLP-1(7-36)NH_2
#8	1.39	17.6	[$Aib^{8,35}$, Phe^{31}]hGLP-1(7-36)NH_2

[a]*The assays were done in CHO-K1 cells expressing the human recombinant GLP-1 receptor.*

Knowing that the C-terminal peptide bonds are cleaved *in vivo*, we substituted the C-terminal Gly^{35} residue with Aib or β-alanine (β-Ala) with the goal of protecting the adjacent peptide bonds against enzymatic cleavage. The analogs bearing modifications at both positions 8 and 35, such as [$Aib^{8,}$ β-Ala^{35}]hGLP-1(7-36)NH_2 and [$Aib^{8,35}$, Phe^{31}]hGLP-1(7-36)NH_2 (peptides 7 and 8, Table 1), have much longer plasma half-life than the mono-substituted analog [Aib^8]hGLP-1(7-36)NH_2 (peptide 5, Table 1). The *in vitro* potency of [$Aib^{8,}$ β-Ala^{35}]hGLP-1(7-36)NH_2 is approximately equivalent to that of the native GLP-1 (K_i: 1.26 ± 0.158 nM *vs.* 1.093 ± 0.179 nM).

In normal Sprague-Dawley rats, administration of [$Aib^{8,}$ β-Ala^{35}]hGLP-1(7-36)NH_2 within the dose range of 0.03 to 0.3μg/kg enhances glucose-induced insulin secretion in a dose-dependent manner. It was observed that a 0.28μg/kg dose of [$Aib^{8,}$ β-Ala^{35}]hGLP-1(7-36)NH_2 produces enhanced glucose-induced insulin secretion that is equivalent to a 1μg/kg dose of native GLP-1. This increased efficacy is likely due to the enhanced enzymatic stability of [$Aib^{8,}$ β-Ala^{35}]hGLP-1(7-36)NH_2, resulting in an increased circulating half-life. When tested in the absence of elevated glucose, [$Aib^{8,}$ β-Ala^{35}]hGLP-1(7-36)NH_2 has no significant effect on insulin secretion, indicating that the gluco-incretin property of native GLP-1 is preserved.

In summary, hGLP-1(7-36)NH_2 analogs with modifications at both position 8 and 35 represent a new class of GLP-1 analogs that have substantially enhanced plasma half-live, while retaining full receptor potency and gluco-incretin properties of the native hormone. They are significantly more efficacious in stimulating glucose-dependent insulin secretion than native hGLP-1(7-36)NH_2 in vivo, presumably due to their greater enzymatic stability.

References

1. Mentlein, R., Gallwitz, B. and Schmidt, W. E. *Eur. J. Biochem.* **214**, 829-835 (1993).
2. Schnolzer, M., Alewood, P., Jones, A., Alewood, D. and Kent, S. B. H. *Int. J. Peptide Protein Res.* **40**, 180-193 (1992).
3. Thornton, K. and Gorenstein, D. G. *Biochemistry* **33**, 3532 (1994).
4. Deacon, C. F., et al. *J. Clin. Endocrinol. Metab.* **80**, 952-957 (1995).
5. Dong, J. Z., Shen, Y., Skinner, S., Morgan, B., Taylor, J. E., Culler, M., Woon, C.- W. and Moreau, J.- P. In Lebl, M. and Houghten, R. A. (Eds) *Peptides: The Wave of the Future*, (*Proceedings of the 2nd International and the 17th American Peptide Symposium),* American Peptide Society, San Diego, Kluwer, 2001, pp. 670-671.
6. Mentlein, R. *Regulatory Peptides* **85**, 9-24 (1999).
7. Dong, J. Z., Zhang, J., Zou, X., Shen, Y., Taylor, J. E., Culler, M., Woon, C.- W. and Moreau, J.- P. *J. Peptide Sci.* **8**, S148 (2002).
8. Dong, J. Z., Zhang, J., Zou, X., Shen, Y., Taylor, J. E., Culler, M., Woon, C.- W. and Moreau, J.- P. In Benedetti, E.and Pedone, C. (Eds), *Peptides 2002* (*Proceedings of the 27th European Peptide Symposium),* Edizioni Ziino, Napoli, 2003, pp. 88-89.

Peptide Revolution: Genomics, Proteomics & Therapeutics
Michael Chorev & Tomi K. Sawyer (Editors)
American Peptide Society, 2003

The Role of Residues 5-8 of Lamprey Gonadotropin-Releasing Hormone III in the Inhibition of Cancer Cell Growth

Krisztina Herédi-Szabó, Jeremiah Lubke, Richard F. Murphy and Sándor Lovas

Department of Biomedical Sciences, School of Medicine, Creighton University, Omaha, NE 68178, USA

Introduction

The decapeptide gonadotropin-releasing hormone (GnRH) acts on the pituitary to release FSH and LH. An isoform, lGnRH-III, from the sea lamprey has no endocrine activity in mammals even at high doses and directly suppresses sex hormone-dependent and -independent growth of breast and prostatic cancer cells *in vitro* [1]. The conserved structures, residues 1-4 and 9-10, in the GnRH isoforms are the most important for receptor binding and activation. The non-conserved residues are less critical for receptor binding and may reflect species specificity. The bioactive conformation of GnRHs has a β–turn at residues 5-8, whereas lGnRH-III has α–helical secondary structure [2]. This might play a role in the receptor binding properties of the peptides, thus giving another explanation for the unique biological activity of lGnRH-III.

In previous studies it was shown that modification of Lys at position 8 is well tolerated [3]. Here, residues 5-8 of lGnRH-III were systematically replaced with Ala (Figure 1) to reveal the residues important for the direct antiproliferative effect of lGnRH-III by testing effect of the synthetic analogs on growth of MDA-MB 231 breast and PANC-1 pancreatic cancer cell lines of human origin. Time-course experiments were carried out to determine the optimal length of the peptide treatment, while the sulphorhodamine B assay was used to detect the changes in protein content (directly proportional to cell number) after 3 days of peptide treatment. Binding of the analogs in competition with [^{3}H]lGnRH-III to receptors on isolated PANC-1 cell membrane was also examined.

GnRH	pGlu-His-Trp-Ser-Tyr-Gly-Leu-Arg-Pro-Gly-NH_2
lGnRH-III	pGlu-His-Trp-Ser-His-Asp-Trp-Lys-Pro-Gly-NH_2
[Ala^5]lGnRH-III	pGlu-His-Trp-Ser-**Ala**-Asp-Trp-Lys-Pro-Gly-NH_2
[Ala^6]lGnRH-III	pGlu-His-Trp-Ser-His-**Ala**-Trp-Lys-Pro-Gly-NH_2
[Ala^7]lGnRH-III	pGlu-His-Trp-Ser-His-Asp-**Ala**-Lys-Pro-Gly-NH_2
[Ala^8]lGnRH-III	pGlu-His-Trp-Ser-His-Asp-Trp-**Ala**-Pro-Gly-NH_2

Fig. 1. Sequences of lGnRH-III and the analogs synthesized.

Results and Discussion

Both the time-course experiment and the SRB assay showed that replacement of residues 5-7 resulted in complete loss of the biological activity (Table 1). Replacement of Lys^8 to Ala resulted in an analog that maintained biological activity comparable to that of the original peptide. In the time-course experiment both 10^{-5} M and 10^{-6} M [Ala^8]lGnRH-III significantly decreased the cell number. The findings for MDA-MB 231 and PANC-1 cell lines were similar.

In the receptor binding experiments, the lGnRH-III had an IC_{50} value about 10^{-7} M with both cell lines. Only [Ala^5]lGnRH-III and [Ala^8]lGnRH-III were able to displace [^{3}H]lGnRH-III (Table 1; Figure 2). Both peptides had an IC_{50} values about 10^{-5} M in

binding to PANC-1 cell membranes. In spite of its binding, [Ala^5]lGnRH-III did not have any biological activity.

The results revealed that Lys^8 of lGnRH-III is not important either for the biological activity or for receptor binding. Asp^6 and Trp^7 are important for both binding and growth inhibition. Though His^5 is not important in receptor binding, the corresponding analog showed no biological activity.

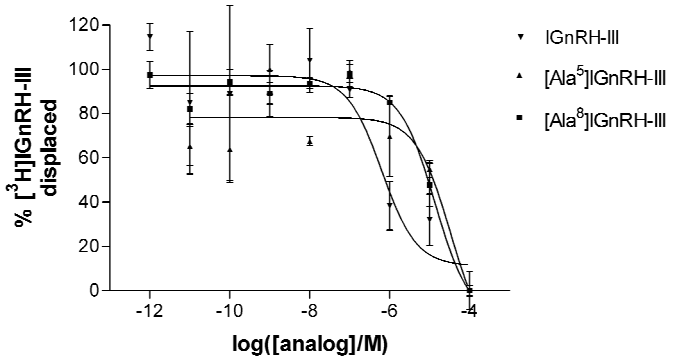

Fig. 2. Inhibition of [^{3}H]lGnRH-III binding to PANC-1 cell membrane.

Acknowledgments

The work was funded by NIH-BRIN (1 P20 RR16469-01) and NSF-EPScOR (EPS-0091900) grants.

References

1. Lovas, S., Palyi I., Vincze B., Horvath J., Kovacs M., Mezo I., Toth G., Teplan I. and Murphy R. F. *J. Peptide Res.* 5**2**, 384-389 (1998).
2. Watts, C. R., Mezei, M., Murphy, R. F. and Lovas, S. *J. Biomol. Struct. Dyn.* **18,** 733-748 (2001).
3. Pályi, I., Vincze, B., Lovas, S., Mezö, I., Pató, J., Kálnay, A., Turi, G., Gaál, D., Mihalik, R., Peter, I., Teplan, I. and Murphy, R. F. *Proc. Natl. Acad. Sci*. **96**, 2361-2366 (1999).

Peptide Revolution: Genomics, Proteomics & Therapeutics
Michael Chorev & Tomi K. Sawyer (Editors)
American Peptide Society, 2003

Native Chemical Ligation of Transmembrane Receptor Fragments of Ste2p

Vommina V. Suresh Babu[1], Jeffrey M. Becker[2] and Fred Naider[1]

[1]*Department of Chemistry, College of Staten Island/CUNY, New York 10314, USA;*
[2]*Department of Microbiology, University of Tennessee, Knoxville, TN 37996, USA*

Introduction

Ste2p (α-factor receptor) of *Saccharomyces cerevisiae* is a G protein-coupled receptor (GPCR) that upon binding the α-factor mating pheromone, transduces a signal resulting in growth arrest and gene regulation in preparation for sexual conjugation. Similar to other GPCRs, the 431-residue receptor contains seven hydrophobic putative transmembrane domains connected by extracellular and intracellular loops with its carboxyl terminal located intracellularly. The elucidation of the conformational and orientational states of regions of the Ste2p receptor in the membrane is crucial to reveal the molecular mechanism of ligand-receptor interaction and signal transduction. Fragments of the receptor are amenable to biophysical analysis using circular dichroism, nuclear magnetic resonance and infrared spectroscopies, and information concerning the structural tendencies of such fragments has been shown to be relevant to the structure and function of the cognate integral membrane protein.

The step-wise solid phase method, armed with an array of protecting groups and coupling strategies, has yielded impressive results in the chemical synthesis of globular proteins. On the other hand, its adaptability in the synthesis of even relatively short transmembrane peptide fragments (< fifty residues) required acrobatic efforts to obtain a few milligrams of homogeneous products [1]. Consequently, we have initiated a project to construct large fragments of Ste2p by native chemical ligation [2-4].

Results and Discussion

The C-terminal M7-13 α-thioester [290-302, PLSSMW(CHO)ATAANNA] was assembled following *in situ* neutralization and BOP activation employing manual, Boc-SPPS using a Boc-Ala-SCH_2CH_2CO-MBHA resin on a 0.1 mmol scale. The crude peptide was cleaved by treatment with HF-anisole (9.5:0.5) at 0°C for two h. Both T8 (S303C-S310G, CKTNTITG) and T37 (S303C-339, CKTNTITSDFT-TSTDRFYPGTLSSFQTDSINNDAKSS) N-Cys peptide fragments were synthesized by a machine-assisted solid phase method using HBTU activation/*in situ*, DIEA neutralization and a coupling protocol for Fmoc chemistry on a preloaded Wang resin. The crude peptides were cleaved using a TFA:PhOH:H_2O:$PhSCH_3$:EDT mixture. All three fragments, after purification by semi-preparative RP-HPLC, were found to be homogeneous and were characterized by MALDI-TOF MS.

Ligation between the α-thioester [$S(CH_2)_2CONH_2$ M7-13 and N-Cys terminal fragments T8 (S303C-S310G) and T37 (S303C-339) gave 21-residue and 50-residue Ste2p fragments, respectively. Because of the very hydrophobic nature of the transmembrane fragments, we used 30 % TFE in water. Both the N- and C-terminal fragments remained in this solution. A 10 % excess of the pure T8 or T37 fragment in 30% TFE in water was added to the M7-13 α-thioester fragment (2 mM) in 0.2 M sodium phosphate containing 6 M guanidinium hydrochloride at pH 7.5 in the presence of 3 equivalents of tris(carboxyethylphosphine). The ligation reaction was mediated by the addition of 3 % of thiophenol. The reaction, as monitored by analytical HPLC (Figure 1), was found to be complete in about 18 hr. The reaction mixture was

lyophilized and purified by semi-preparative HPLC. The yields of the final products as well as MALDI-TOF MS values obtained are given in the Table 1.

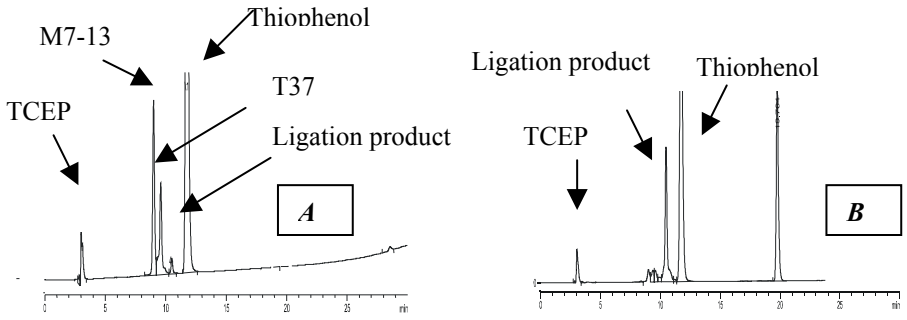

Fig. 1. Ligation between M7-13 α-thioester and T37 fragments of Ste2p; The ligation reaction was monitored by injecting 5 µl aliquots of the reaction solution on a C 18 column with a gradient of 10 % to 100 % acetonitrile versus water containing 0.025 % TFA, over 30 min. Detection was at 220 nm. The reaction is shown at (A) 45 min. and (B) 18 hr.

Table 1: Ste2p fragment sequences, ligation yield, molecular weight data.

Ste2p fragment sequence	Quantity of peptide used / obtained in			Molecular weight	
	mg	(mmole)	[% yield]	Found	Calcd.
M7-13 α-thioester (290-302)	2.2	(1.5)		1447.90	1448.60
T8 (S303C-310G)	1.9	(2.25)		836.42	835.95
[Cys303,G310]Ste2p 290-310 (21 residues)	2.1		[65 %][a]	2179.81	2180.41
M7-13 α-thioester (290-302)	1.5	(1.0)		1447.90	1448.60
T 37 (S303C-339)	6.0	(1.5)		4051.72	4051.60
[Cys303]Ste2p 290-339 (50 residues)	3.8		[62 %][a]	5487.00	5486.89

[a]*- yield is for ligation and HPLC purification.*

As judged by the molecular weights and HPLC purity successful ligation of various Ste2p fragments on a milligram scale was achieved. The isolated yields are suitable for detailed biophysical analyses on these receptor domains.

Acknowledgment
The work was funded by the grants GM-22086 and GM-22087 from NIH.

References

1. Naider, F., Arshava, B., Ding, F. X., Arevalo, E. and Becker, J. M. *Biopolymers* **60**, 334-350 (2001).
2. Zhang, L. and Tam, J. P. *J. Am. Chem. Soc.* **121**, 3311-3320 (1999).
3. Tam, J. P., Xu, J. and Eom, K. H. *Biopolymers* **60**, 194-205 (2001).
4. Dawson, P. In Goodman M. (Ed.-in-Chief), Houben-Weyl Methods of Organic Chemistry, New York: Thieme Stuttgart **22a**, pp. 621-641 (2002).

Peptide Revolution: Genomics, Proteomics & Therapeutics
Michael Chorev & Tomi K. Sawyer (Editors)
American Peptide Society, 2003

Development of Highly Potent and Selective Low Molecular Weight Agonists for the Human Orphan Receptor BRS-3

Horst Kessler[1], Dirk Weber[1] and Jochen Antel[2]

[1]Institut für Organische Chemie und Biochemie, Technische Universität München, Lichtenbergstrasse 4, 85747 Garching, Germany; [2]Solvay Pharmaceuticals GmbH, Hans-Böckler-Allee 20, 30173 Hannover, Germany

Introduction

Recent genomic research identified bombesin receptor subtype 3 (BRS-3) as a member of the bombesin receptor family by sequence comparison to the known bombesin receptors NMB-R and GRP-R [1,2]. BRS-3 belongs to the familiy of orphan G-protein-coupled receptors (GPCRs) with yet unclear physiological role and unknown natural ligand [3,4].

In order to find new molecular probes for BRS-3, we applied an extensive medicinal chemistry approach on the basis of the two known, unselective synthetic ligands nonapeptide **1** [5] and octapeptide **2** [6], which show agonist activity for all three BRS receptors (Figure 1).

Bombesin	pEQRLGNQWAVGHLM-NH_2
Nonapeptide (1)	fQWAVßAHFNle-NH_2
Octapeptide (2)	fQWAVGFpropylamide

*Fig. 1. Sequences of bombesin and synthetic BRS-3 ligands **1** and **2**.*

Ala- and D-amino acid scans were performed in order to determine the important amino acid residues for agonist activity and binding. Agonist activity was assessed in a functional cell assay (FLIPR-assay). Then, three independent strategies were pursued: (1) Peptides with C- and N-terminal deletions and substitutions were prepared in order to determine the minimal active fragment. (2) A combinatorial library of cyclic peptides with varying loop sizes was prepared. Loops were created by oxidative linkage of two inserted Cys or D-Cys, respectively. (3) Generation of a small molecule lead structure was attempted, assuming that the spatial distance of the important amino acids for agonist activity, as determined in the Ala-scans, is short in the bioactive conformation of the linear peptide **1**, these residues were combined on a small molecular scaffold. The results of these three different strategies are presented and discussed on the basis of a selected series of compounds.

Results and Discussion

Ala- and D-amino acid scans showed that Trp^8 and Phe^{13} are very important amino acids for receptor binding and functional activity at BRS-3 for both peptides **1** and **2** [7]. Additionally His^{12} plays an important role for functional activity for peptide **2**. Position 11 (β-Ala or Gly) showed a lower but still significant importance, whereas D-Phe^6 and Gln^7 were unimportant residues for functional activity.

Shortened Fragments and Substitutions. Deletion of the two N-terminal amino acids D-Phe^6 and Gln^7 or the C-terminal unit Nle^{14}-NH_2 was not possible without significant loss of activity, although these residues exhibited low importance in the previously conducted scans [7]. For position 11 in the N-terminal shortened fragment of peptide **1**, the activities decreased in the order β-Ala > GABA > Ala ≅ Gly [7]. These results

demonstrated that shorter BRS-3 agonists could not be obtained by simple deletion of C- or N-terminal amino acids and that peptides **1** and **2** already represent minimum active fragments.

Cyclic Peptides. Because of the lack of information about the exact spatial distance between the crucial amino acids Trp^{8} and Phe^{13}, a combinatorial approach for the introduction of a conformational constraint by means of cyclization where both stereochemistry and spacial distances would be varied simultaneously was considered (Figure2).

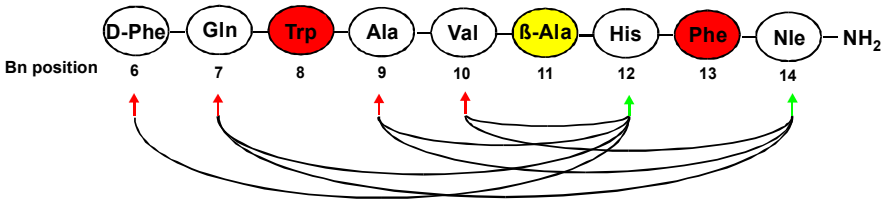

*Fig. 2. Combinatorial 'rolling loop scan' of **1**. Two amino acids at one time were replaced by Cys or D-Cys, respectively, except those with high (red-colored) and medium (yellow) significance for functional activity.*

Insertion of Cys and D-Cys, respectively, at each position generated four stereoisomers with different conformations for each possible loop size, which ranged from 3-9 amino acids. Synthesis of the linear percursors was carried out on Sieber amide resin; oxidative cyclization was carried out using a 50% aqueous DMSO (v/v) solution [8]. Unfortunately, none of the cyclic peptides had functional activity with EC_{50} > 10 µm. Due to the assumed high flexibility in both the linear and the cyclic peptides, an NMR-supported structure analysis leading to a more structure-based rational design was not considered feasible.

Small Molecule Lead Structure. Lead finding was successfully accomplished using a tetrapeptide which consisted of the three N-terminal amino acids of 1 and Phe-NH_2 [7]. Permutation of the stereoconfiguration of the two C-terminal amino acids Trp and Phe of this tetrapeptide yielded a four membered mini-library. Only one of these compounds, namely fQwF-NH_2 (**3**), showed low functional activity on BRS-3 (Table 1). Further investigations showed that all three aromatic residues of lead structure 3 were necessary for functional activity. Removal of the C-terminal amide was unfavorable, whereas removal of the Gln sidechain was tolerated as well as changes at the N-terminal configuration [7].

Systematic optimization of this lead structure by stepwise introduced C-and N-terminal modifications culminated in the development of a library of highly selective and potent peptidomimetics. Functional activity of the lead structure could be increased about 15-fold upon replacement of the Phe-NH_2 unit against 1-(2-Phenylethylamine) (Table 1, compound **4**) [8]. A 'biased' library of peptidomimetics with conserved C-terminal D-Trp-1-(2-Phenylethyl)amide moiety and structural variations on the N-terminal H-D-Phe-Gln unit was developed. It was demonstrated that N-terminal increase of lipophilicity by simple deletion of the aminofunction combined with removal of the Gln sidechain furnished selective BRS-3 agonists in the nanomolar range [9]. Furthermore, substitution of the H-D-Phe-Gln unit by peptoide monomers showed that the N-terminal peptide bond is not required for receptor activation [9]. Gln can further be replaced with azaglycine, leading to compounds with sub-nanomolar

Table 1. Functional potency of BRS-3 agonists (FLIPR-assay).

Compound	EC_{50} [nM]		
	NMB-R	*GRP-R*	*BRS-3*
fQWAVßAHFNle-NH_2 **1**	980 (770-1250)	9.4 (8.0-11)	62 (41-93)
FQWAVGFpropylamide **2**	n.d.[a]	n.d.[a]	220 (140-330)
fQwF-NH_2 **3**	inactive	17400 (17.0-17.8K)	10100 (8.2-12.3K)
fQw-1-(2-Phenylethyl)amide **4**	inactive	inactive	710 (590-860)
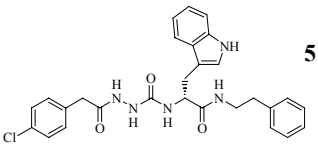 **5**	inactive	inactive	0.19 (0.06-0.58)

[a] *not determined.*

activities (Table 1, compound **5**). For azapeptides, too, a removal of the N-terminal peptide bond is possible [9]. The finding that also piperidine or piperazine can be incorporated suggests that a large number of different spacers are able to mimic the function of the former Gln at this position [9].

In summary this work describes the development of selective molecular probes for BRS-3, with assumingly improved pharmacokinetic properties, may help to understand the physiological role of this orphan receptor.

Acknowledgments
The authors gratefully acknowledge financial support by the Deutsche Forschungs-gemeinschaft.

References

1. Gorbulev, V., Akhundova, A., Büchner, H. and Fahrenholz, F. *Eur. J. Biochem.* **208**, 405-410 (1992).
2. Fathi, Z., Corjay, M. H., Shapira, H., Wada, E., Benya, R., Jansen, R., Viallet, J., Sausville, E. A. and Battey, E. F. *J. Biol. Chem.* **268**, 5979-5984 (1993).
3. Okhi-Hamazaki, H., Watase, K., Yamamoto, K., Ogura, H., Yamano, M., Yamada, K., Maeno, H., Imaki, J., Kikuyama, S., Wada, E. and Wada, K. *Nature* **390**, 165-169 (1997).
4. Lammerich, H.- P., Busmann, A., Kutzleb, C., Wendland, M., Seiler, P., Berger, C., Eickelmann, P., Meyer, M., Fossmann, W.- G. and Maronde, E. *PTC Int. Appl.* WO 02063305. (2002).
5. Mantey, S. A., Weber, H. C., Sainz, E. Akeson, M., Ryan, R. R., Pradhan, T. K., Searles, R. P., Spindel, E. R., Battey, J. F., Coy, D. H. and Jensen, R. T. *J. Biol. Chem.* **272**, 26062-26071 (1997).
6. Wu, J. M., Nitecki, D. E., Biancalana, S. and Feldman, R. I., *Mol. Pharmacol.* **50**, 1355-1363 (1996).
7. Weber, D., Berger, C., Heinrich, T., Eickelmann, P., Antel, J. and Kessler, H. *J. Peptide Sci.* **8**, 461-475 (2002).
8. Tam, J. P., Wu, C.- R., Liu, W. and Zhang, J.- W. *J. Am. Chem. Soc.* **113**, 6657-6662 (1991).
9. Weber, D., Berger, C., Eickelmann, P., Antel, J. and Kessler, H. *J. Med. Chem.* **46**, 1918-1930 (2003).

Peptide Revolution: Genomics, Proteomics & Therapeutics
Michael Chorev & Tomi K. Sawyer (Editors)
American Peptide Society, 2003

Synthesis and Cross-Linking of Photoactivateable Biotinylated Ligands of G Protein-Coupled Receptors

Hasmik Sargsyan[1], Cagdas D. Son[2], Jeffrey M. Becker[2] and Fred Naider[1]

[1]Department of Chemistry, College of Staten Island,CUNY, NY 10314, USA; [2]Department of Microbiology, University of Tennessee, Knoxville, TN 37996, USA

Introduction

G-protein-coupled receptors (GPCRs) constitute a large family of receptors, which regulate a wide variety of cellular functions. The yeast *Saccharomyces cerevisiae* embodies an ideal model system for the study of hormone-receptor interactions. The α-factor receptor (Ste2p) from *S. cerevisiae* belongs to the family of GPCRs that, upon binding of a ligand, transduce a signal via an associated guanine nucleotide binding protein (G protein). A number of agonistic analogs of α-factor (H-WHWLQLKPGQPMY-OH) containing the photoactivateable 4-benzoyl-L-phenylalanine (Bpa) group have been synthesized and characterized. Evidence for a specific contact region between Ste2p GPCR and its ligand has been obtained, supporting the concept that Bpa-α-factor probes and, especially their biotinylated derivatives might be highly useful in the mapping of the ligand binding site of this GPCR.

Results and Discussion

With the aim to complete a detailed mapping of the ligand binding site of Ste2p, the following series of photoactivateable, biotinylated analogs of α-factor were synthesized and characterized both chemically and biochemically:

H-BpaHWLQLK(Biot)PGQPNleY-OH
H-WHBpaLQLK(Biot)PGQPNleY-OH (1)
H-WHWLBpaLK(Biot)PGQPNleY-OH (2)
H-WHWQLK(Biot)BpaGQPNleY-OH (3)
H-WHWLQLK(Biot)PGQPNleBpa-OH (4)

Fig. 1. Sequences of photoactivateable, biotinylated analogs of α-factor. The Biot moiety is actually the ε-aminocaproic acid derivative of biotin attached to the ε-amine of Lys[7].

These analogs were designed to scan Bpa through the backbone of α-factor in positions 1,3,5,8, and 13. These positions were chosen because of their tolerance to substitution in comparison with wild type α-factor [1]. All analogs contained Lys^7, in order to enable biotinylation, Nle^{12} and Tyr^{13}, with the exception of analog (4), which contained Bpa^{13}.

N-α-Fmoc-protected α-factor analogs needed for the preparation of the corresponding biotinylated derivatives were synthesized by solid-phase peptide synthesis on an Applied Biosystems 433A peptide synthesizer starting with N-α-Fmoc-Tyr(OBu^t) - or N-α-Fmoc-Bpa-Wang resin (0.7 mmol/g). The last N-α-Fmoc group in the peptide was not deprotected after chain assembly. Peptides were cleaved from the resin using a cleavage cocktail containing TFA (10 ml), crystalline phenol (0.75 g), thioanisole (0.5 ml) and water (0.5 ml) at room temperature for 1.5 h. Fmoc-protected peptides (1-5) were purified by semipreparative RP-HPLC (Waters μ-Bondopack C_{18}) with a gradient of 20-60% of CH_3CN in aq. 0.1% TFA in 150 min),

lyophilyzed and used in the synthesis of their biotinylamidocaproate derivatives. N-α-Fmoc-protected analogues (1-4) were more than 99% homogeneous as determined by analytical RP-HPLC (Zorbax 300SB-C_{18}). Biotinylation at Lys^7 was accomplished using biotinyl-amidocaproate-N-hydroxysuccinimide ester in a mixture of DMF/ 50 mM $Na_2B_4O_7$, pH 9.5. After removal of the Fmoc group and isolation by RP-HPLC , high purity (>99 %) final products were obtained in 84-90% yield. The molecular weight of all synthesized peptides was confirmed by electro-spray MS analysis.

The biological activity of all photoactivateable α-factor analogs was determined using a growth arrest assay and receptor affinities were measured by competition with the binding of tritiated alpha-factor (^{3}H α-factor) to its receptor, Ste2p. Analogs 1, 2 and 4, containing Bpa in positions 3, 5 and 13, had agonistic activity in a growth arrest assay. In a competition binding assay analogs 1, 2, 3 and 4 exhibited 40 nM, 26 nM, 160 nM and 76 nM affinities, respectively, in comparison to 10 nM for the native ligand. Peptide with Bpa^8 did not give any detectable halos even at the highest concentration tested.

Crosslinking studies demonstrated that Bpa^1, Bpa^3 and Bpa^{13} were efficiently cross-linked to Ste2p; the biotin tag on the pheromone was detected by a NeutrAvidin-HRP conjugate on Western blots. The results of cross-linking with the receptor Ste2p revealed that all analogs tested give detectable biotin signals in the NeutrAvidin blot, although different intensities were obtained for the various ligands. The strongest biotin signal in crosslinking experiments was observed for analog (1) (Bpa^3) which, as mentioned above, has the highest affinity to the receptor. Surprisingly, peptide (4) with Bpa^{13} exhibited a very good signal despite its relatively low affinity for Ste2p.

The results obtained indicate successful crosslinking of members of this series into the α-factor receptor. Preliminary results indicate that Bpa^1- and Bpa^3-containing α-factor analogs crosslink to distinct sites in the receptor. Currently we are attempting to define these sites using mass spectrometry approaches. Determination of several crosslinks between the peptide and receptor will allow us to dock α-factor into the receptor-binding site and determine its biologically active structure.

Acknowledgments

The work was funded by Grants GM22086 and GM22087 from the NIH.

References

1. Henry, L. K., Khare, S., Son, C., Babu, S. V. V., Naider, F. and Becker, J. M. *Biochem.* **41**, 6128-6139 (2002).

Peptide Revolution: Genomics, Proteomics & Therapeutics
Michael Chorev & Tomi K. Sawyer (Editors)
American Peptide Society, 2003

Cyclic Melanocortin-4 Receptor Ligands: Conformational Analysis Using ^{1}H-NMR Spectroscopic Methodologies

Jerry Ryan Holder[1], Arthur S. Edison[2], Zhimin Xiang[1], Joseph W. Scott[1] and Carrie Haskell-Luevano[1]

[1]Department of Medicinal Chemistry and [2]Department of Biochemistry and Molecular Biology, University of Florida, Gainesville, FL, 32610, USA

Introduction

The melanocortin (MC) family of receptors is involved in a vast array of physiological functions including, but not limited to; energy homeostasis, feeding behavior, regulation of skin pigmentation, and erectile activity [1, 2]. The MC receptor family is composed of five isoforms identified to date, MC1R-MC2R, which are GPCRs that signal through the cAMP pathway [2]. The endogenous melanocortin peptide agonists are derived from post-translational processing of the POMC gene transcript, and all contain the His-Phe-Arg-Trp tetrapeptidyl sequence that is essential to receptor activation. The melanocortin peptides have been the subject of many structure activity studies aimed at increasing potency, stability, and receptor selectivity. There has also been considerable effort to discern the conformational and structural properties responsible for the observed biological activities of endogenous melanocortin peptides and synthetic analogues.

We have previously reported the activity of cyclic analogues of MTII [3] and SHU9119 [4], each modified at position seven, at the mouse MC4R and several mouse MC4 receptor mutants [5]. Additionally for this study, we have synthesized analogue **3** to complement the analysis of the cyclic ligands at the MC4R. The cyclic analogues (Table 1) exhibit pharmacology that varies from that of MTII (full agonist) and SHU9119 (antagonist). It was hypothesized that conformational differences may be responsible for the variation in MC4R functional activity. We report here the ^{1}H-NMR and molecular modeling analysis of the peptides employed to gain an understanding of the structural differences that exist between the 5 ligands.

Table 1. Sequences of MTII, SHU9119 and Analogues 1-3.

Peptide	Sequence
MTII	Ac-Nle-cyclo[Asp-His-***DPhe***-Arg-Trp-Lys]-NH_2
SHU9119	Ac-Nle-cyclo[Asp-His-***DNal(2')***-Arg-Trp-Lys]-NH_2
Analogue 1	Ac-Nle-cyclo[Asp-His-***DNal(1')***-Arg-Trp-Lys]-NH_2
Analogue 2	Ac-Nle-cyclo[Asp-His-***LNal(2')***-Arg-Trp-Lys]-NH_2
Analogue 3	Ac-Nle-cyclo[Asp-His-***LNal(1')***-Arg-Trp-Lys]-NH_2

Results and Discussion

The peptides MTII, SHU9119 and analogues **1-3** were synthesized using Boc chemistry on pMBHA (0.28 meq/g) resin in a manual reaction vessel equipped with a coarse glass frit. The peptides were deprotected and cleaved from resin using standard HF procedures and purified to homogeneity using semi-preparative RP-HPLC. The peptides were tested for agonist and antagonist activity using HEK-293 cells stably expressing mouse MC4R using the β–galactosidase reporter gene assay (Table 2). ^{1}H-NMR data were collected in 95%H_2O/D_2O solution on a Bruker spectrometer operating

at 500MHz. 1-D temperature titration data were collected over a range of 5ºC to 50ºC in 5ºC increments. 2-D ^{1}H-NMR data for the peptides were collected at 5ºC and 35ºC. Restrained molecular dynamics (RMD) simulations for the five peptides were performed with NMR derived NOE distance restraints using InsightII software (Molecular Simulations Inc., San Diego, CA).

The chemical shifts of each of the 5 peptides were assigned using standard TOCSY

Table 2. Functional activity of MTII, SHU9119 and analogues 1-3 at the mouse MC4R.

Peptide	Agonist	(MC4R)	Antagonist
	EC_{50} (nM)	Emax(%)	pA_2
MTII	0.033 ± 0.001	100	-
SHU9119	-	0	10.14
Analogue 1	0.338 ± 0.002	48	-
Analogue 2	48.2 ± 0.153	61	7.43
Analogue 3	111 ± 1.78	89	-

and ROESY strategies [6]. NMR chemical shifts are extremely sensitive to the electronic environment and thus provide useful probes into changes in molecular structure. Comparison of the backbone proton chemical shifts with reported random coil values indicate possible secondary structure formation in each of the peptides. Although the peptides are similar chemically, the functional activity at the MC4R varies considerably and analysis of the chemical shift patterns and amide temperature coefficients suggest conformational differences may exist between the 5 MC4R ligands. Following the 20ns RMD simulations, 201 energy minimized structures saved at equally spaced time points along the trajectory were analyzed. Comparison of backbone dihedral angles of the 201 structures indicates that the majority (>90%) fell into one main conformational family. Evaluation of the solution structures indicates that significant variations exist in the backbone conformation between each of the 5 peptides. Variations in the topographical orientation of the sidechains can also be seen. These structural differences may be responsible for the dissimilarity in functional activity of the peptides at the mouse MC4R.

Acknowledgments

The work was funded in part by NIH grant DK57080. Jerry Ryan Holder is recipient of the NIH/University of Florida Molecular Biophysics Initiative Biophysical Research Training Award and Carrie Haskell-Luevano is a recipient of a Burroughs Wellcome Career Award in the Biomedical Sciences.

References

1. MacNeil, D. J., *et al*. *Eur. J. Pharmacol.* **440**, 141-157 (2002).
2. Cone, R. D. (Ed.) *The Melanocortin Receptors* The Humana Press Inc, New Jersey, 2000.
3. Al-Obeidi, F*., et al. J. Med. Chem.* **32**, 2555-2561 (1989).
4. Hruby, V. J*., et al. J. Med. Chem.* **38**, 3454-3461 (1995).
5. Haskell-Luevano, C*., et al. Biochemistry* **40**, 6164-6179 (2001).
6. Wüthrich, K. (Ed.) *NMR of Proteins and Nucleic Acids,* Wiley and Sons, New York, 1986.

Peptide Revolution: Genomics, Proteomics & Therapeutics
Michael Chorev & Tomi K. Sawyer (Editors)
American Peptide Society, 2003

Stereochemical Inversion Studies of Monocyclic hAGRP(103-122) Peptide

Christine G. Joseph[1], Xiang S. Wang[2], Joseph W. Scott[1], Rayna Bauzo[1], Zhimin Xiang[1], Nigel G. Richards[2] and Carrie Haskell-Luevano[1]

Departments of Medicinal Chemistry[1] and Chemistry[2], University of Florida, Gainesville, FL 32610

Introduction

Agouti-related protein (AGRP) is one of two known endogenous antagonist of GPCRs. AGRP antagonizes the melanocortin-3 and 4 receptors (MC3R, MC4R) in the brain, and results in obesity when overexpressed [1]. The C-terminal domain of AGRP has been identified as possessing antagonistic properties at the melanocortin receptors equipotent to the full length peptide [1, 2], suggesting that the key structural and molecular recognition features are located in this domain. Structure-activity studies implicate the key amino acids motif to be Arg-Phe-Phe (111-113) of hAGRP important for activity [3].

There has been great interest in the MC4 receptor since it has been reported as being important in the regulation of feeding [4]. MC4R knockout mice exhibit hyperphagia and accelerated weight gain [4]. Both the MC3 and MC4 receptors are expressed in the brain, but the MC3 receptor involvement in the regulation of food intake is unclear. The MC3 receptor knockout mice exhibit increased fat mass but are not significantly overweight [5, 6], indicating that the MC3 and MC4 receptors may serve different roles in the regulation of weight and energy homeostasis.

Development of ligands that can discriminate between the MC3 and MC4 receptors may be of great therapeutic benefit for the treatment of obesity and its related diseases. Therefore, it is important to identify the molecular determinants of the ligands that enable MC3/MC4 receptor selectivity.

This study was undertaken to determine whether stereochemical conversion of a monocyclic hAGRP(103-122) template, Arg-Phe-Phe (111-113) residues would result in enhanced potency and/or MC3/MC4 receptor selectivity.

Results and Discussion

Four monocyclic analogues were synthesized by Fmoc solid phase peptide synthesis and tested for agonist activity at the mMC1 and mMC3-5 receptors and antagonist activity at the mMC3 and mMC4 receptors. Stereochemical inversion of L-Arg111 (**2**) and L-Phe113 (**4**) resulted in loss of antagonist activity at the mMC3 and mMC4 receptors, suggesting the importance of chirality at these amino acid residues (Table 1) for antagonism. The most notable result is seen with **4**, which became full agonist at both the mMC3 and mMC4 receptors.

Based on the functional results obtained, 3-D modeling of peptides **1**, **2** and 4 docked into the mMC4R was performed in attempts to explain why **2** and **4** are mMC4R agonists and **1** an antagonist (fig.1). Both L-Arg111 of **1** and **4** and D-Arg111 of **2** putatively interacts with the mMC4R in a negatively charged pocket formed by the MCR residues Glu92 (TM2), Asp114 (TM3) and Asp118 (TM3) [7]. However, the interaction of D-Arg111 with the ionic Asn115 (TM3) of mMC4R may be a key factor in converting the peptides with D-Arg111 from mMC4R antagonist to agonists. The Phe113 of **1** and **2** and D-Phe113 of **4** are observed to be interacting with an aromatic-

Table 1. Functional activity of monocyclic hAGRP(103-122) peptide analogues at the mMCRs.

ID	Peptide Sequence	Agonist EC_{50} (μM)		Antagonist pA_2	
		mMC3R	mMC4R	mMC3R	mMC4R
	MTII [8]	0.17 nM	0.040 nM		
	hAGRP (83-132)			8.9	9.4
1	DPAATAYc[CRFFNAFC]YARKL			6.2	6.9
2	DPAATAYc[C-DArg^{111}-FFNAFC]YARKL	>100	37.7		
3	DPAATAYc[CR-DPhe^{112}-FNAFC]YARKL			6.1	6.6
4	DPAATAYc[CRF-DPhe^{113}-NAFC]YARKL	13.7	3.70		

The mean from at least three independent experiments is presented. The pA_2 antagonist value was determined by Schild analysis (pA_2 = -log Ki) [9].

hydrophobic pocket consisting of the mMC4R Phe176 (TM4), Phe193 (TM5), Phe253 (TM6) and Phe254 (TM6) [7]; however, the D-Phe113 is interacting much more strongly with Phe176 (TM4) than Phe113. The strength of the hydrophobic interaction between D-Phe113 of **4** and mMC4R Phe176 (TM 4) may be participating in differentiating between mMC4R agonist and antagonist pharmacology.

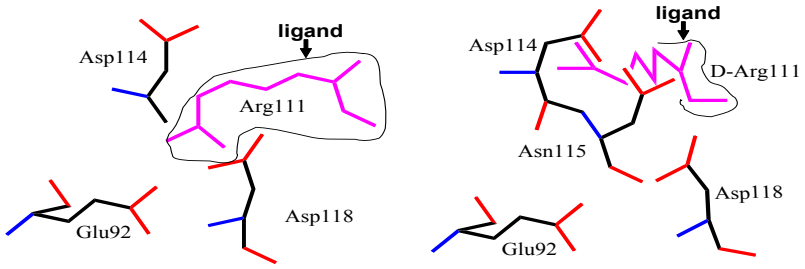

Fig. 1. Illustration of the hAGRP, Arg111 amino acid and stereoisomer interacting with the mMC4R residues located in the transmembrane putative binding domain.

Acknowledgments

This research was supported by NIH grants DK57080, DK64250, and Carrie Haskell-Luevano is a recipient of a Burroughs Wellcome Career Award.

References

1. Ollmann, M. M., et. al. *Science* **278**, 135-138 (1997).
2. Yang, Y. K., et. al. *Mol. Endo.* **13**, 148-155 (1999).
3. Tota, M. R., et. al. *Biochemistry* **38**, 897-904 (1999).
4. Huszar, D., et. al. *Cell* **88**, 131-141 (1997).
5. Butler, A. A., et. al. *Endocrinology* **141**, 3518-3521 (2000).
6. Chen, A. S., et. al. *Nat. Genet.* **26**, 97-102 (2000).
7. Haskell-Luevano C., Cone R. D., et. al. *Biochemistry* **40**, 6164-6179 (2001).
8. Al-Obeidi F., Castrucci A. M., et. al. *J. Med. Chem.* **32**, 2555-2561 (1989).
9. Schild H. O. *Brit. J. Pharmacol.* **2**, 189-206 (1947).

Peptide Revolution: Genomics, Proteomics & Therapeutics
Michael Chorev & Tomi K. Sawyer (Editors)
American Peptide Society, 2003

Long Chain Fatty Acid (LCFA) N-Acyl Derivatives of Melanocortin X-His-DPhe-Arg-Trp-NH_2 Tetrapeptides: Potency and Selectivity Alteration at mMCR System

Aleksandar Todorovic, Jerry R. Holder, Rayna M. Bauzo, Joseph W. Scott and Carrie Haskell-Luevano

Department of Medicinal Chemistry, University Florida, Gainesville, FL 32610, USA

Introduction

The melanocortin peptides make up a family of related hormones that are derived by posttranslational modification of the pro-opiomelanocortin (POMC) prohormone. Included in this agonist melanocortin family are: adrenocorticotropic hormone (ACTH), α-melanocyte-stimulating hormone (α-MSH), β-MSH and γ-MSH. The melanocortin receptor endogenous agonists contain a core sequence His-Phe-Arg-Trp, which has been implicated as important for a pharmacological response [1,2]. Melanocortin receptors belong to a super-family G-protein coupled receptors (GPCRs) and stimulate the cAMP signal transduction pathway. Five melanocortin receptors (MC1R-MC5R) have been identified to date [3]. The melanocortin system is implicated in many different physiological pathways: obesity, cognitive processes, erectogenic activity, melanogenesis, cardiovascular regulation and tanning.

The thirteen amino acid peptide, α-MSH, is posttranslationally modified at the N-terminus by acetylation and amidation at the C-terminus. This naturally occurring amide bond at α-MSH is thought to increase the stability of the peptide toward proteases [4]. Recently, we have performed a study examining the effect of addition of various aliphatic, cyclic or aromatic acyl groups to the N-terminus of the His-Phe-Arg-Trp-NH_2 tetrapeptide [5]. That study revealed that the potency of acylated tetrapeptides increased with the increasing chain length of the alkyl group. The study presented herein extends our previous observations and examines the influence of the alkyl chain length of long chain fatty acids (LCFA) at the N-terminus of the His-Phe-Arg-Trp-NH_2 tetrapeptide in regards to ligand potency and melanocortin receptor selectivity at the cloned mouse MCR's.

Results and Discussion

All peptides reported herein were synthesized using standard fluorenylmethyloxicarbonyl (Fmoc) chemistry. Introduction of the ocatnoyl moiety, peptide **3**, at the N-terminus of the X-His-DPhe-Arg-Trp-NH_2 significantly increases the potency at mMC1R (200-fold). Following this observation we hypothesized that introduction of longer LCFA may further increase MCR potency; however, a "point of diminishing returns" was expected to be reached by addition of LCFA, whereby the potency would begin to decrease due to steric hindrance. We observed two different trends (Table 1). 1)Introduction of various acyl groups at the N-terminus of the X-His-DPhe-Arg-Trp-NH_2 enhanced the mMC1R potency, as compared to peptide **1**. 2)Peptides having more than 10 carbon atoms in the acyl moiety were equipotent at mMC3R, as compared to the lead peptide **1**. The greatest preference for mMC1R versus the mMC3R (with >350-fold difference) was observed for the peptide **7**, which has 16 methylene units in the acyl residue. We postulate that the increase in ligand potency of the ligands presented herein, at the melanocortin receptors, and the potent pharmacology of peptides with high number of methylene units (> 12) attached at the N-terminus of the

Table 1. Functional agonist activity of N-acylated melanocortin tetrapeptides at the mouse MCR.

	N-terminal moiety on **X**-His-DPhe-Arg-Trp-NH_2	Cloned mouse melanocortin receptors				
		mMC1R		**mMC3R**		
		EC_{50} (nM)	*Fold Δ*	*EC_{50} (nM)*	*Fold Δ*	**MC1R vs. MC3R selectivity**
1	**–NH_2**	67	1.0	250	1.0	4
2	**-Acetyl**	50		170		3
3	**-Octanoyl**	0.3	-200	9.3	-30	30
4	**-Decanoyl**	3.3	-20	44	-6	13
5	**-Undecanoyl**	2.8	-20	100		35
6	**-Lauryl**	3.1	-20	170		55
7	**-Stearyl**	0.8	-80	280		350

*If a compound is more potent than a Peptide **1** the fold difference indicates a negative prefix. Only fold differences that are beyond experimental error (3-fold) are listed.*

X-His-DPhe-Arg-Trp-NH_2 may be related to the ligand-lipid interactions as previously proposed by R. Schwyzer [6].

Acknowledgments
This research was supported by NIH grant DK57080. Carrie Haskell-Luevano is a recipient of a Burroughs Wellcome fund Career Award in the Biomedical Sciences.

References
1. Hruby, V. J.; Wilkes, B. C., Hadley, M. E., Al-Obeidi, F., Sawyer, T. K. et. al. *J. Med. Chem.* **30***,* 2126-2130 (1987).
2. Haskell-Luevano, C., Holder, J. R., Monck, E. K. and Bauzo, R. M. *J. Med. Chem.* **44** ,2247-2252 (2001).
3. Cone, R. D., Lu, D., Koppula, S., Vage, D. I., Klungland, H., Boston, B., Chen, W., Orth, D. N., Pouton, C. and Kesterson, R. A. *Recent Prog. Horm. Res.* **51,** 287-317 (1996).
4. Castrucci, A. M., Hadley, M. E., Sawyer, T. K. and Hruby, V. J. *Comp. Biochem. Physiol. B* **78,** 519-524 (1984).
5. Holder, J. R., Marques, F. F., Xiang, Z., Bauzo, R. M. and Haskell-Luevano, C. *Eur. J. Pharmacol.* **462,** 41-52 (2003).
6. Sargent, D. F. and Schwyzer, R. *Proc. Natl. Acad. Sci. U.S. A.* **83,** 5774-5778 (1986).

Peptide Revolution: Genomics, Proteomics & Therapeutics
Michael Chorev & Tomi K. Sawyer (Editors)
American Peptide Society, 2003

Structurally Related Peptides, Peptoids, and Peptide-Peptoid Hybrids: Comparison of Agonist Activity at the Melanocortin MC4 Receptor

Jerry Ryan Holder, Rayna M. Bauzo, Joseph W. Scott, Zhimin Xiang and Carrie Haskell-Luevano

Department of Medicinal Chemistry, University of Florida, Gainesville, FL, 32610, USA

Introduction

Peptides are involved in a vast array of physiological functions; however optimization is often required to increase the stability, receptor selectivity, and biodistribution of a lead peptide prior to *in vivo* applications. Peptidomimetics are designed to emulate the pharmacophoric structural elements of a lead compound, aimed at improving and/or imparting properties desirable in the ligand [1]. Considerable effort has gone into developing non-peptide templates that provide all the interactions required for molecular recognition and signal transduction to occur. Peptoids (N-substituted glycine oligomers) have emerged as viable peptide surrogates with many improved properties over peptides [2]. Although potent ligands for GPCRs have been discovered from screening diverse libraries of peptoids [3], there is little information regarding the comparative activities of structurally similar peptides and peptoids at the cloned mouse melanocortin receptors. Herein we present the design, synthesis and pharmacological characterization of analogous peptides, peptoids, and peptide-peptoid hybrids at the mouse MC1R, MC3R-MC5R.

Novel melanocortin receptor ligands that possess enhanced biological properties, as compared with peptide ligands may prove to be beneficial for *in vitro*, and especially *in vivo,* characterization of this important receptor system. Based on the observation that novel ligands have been discovered from screening large diverse combinatorial collections of peptoid oligomers, investigations were initiated to determine if tetrameric N-substituted glycines could be modeled after melanocortin tetrapeptides and retain similar functional activity at the melanocortin receptors. The endogenous melanocortin agonists, adrenocorticotropic hormone (ACTH), α-melanocyte-stimulating hormone (α-MSH), β-MSH and γ-MSH, all contain a His-Phe-Arg-Trp tetrapeptidyl sequence (Table 1) that is essential for biological activity, and it is this sequence that was used to model our collection of peptoid and peptide-peptoid hybrid tetramers. Herein we present the design, synthesis and pharmacological characterization of analogous peptides, peptoids, and peptide-peptoid hybrids at the mouse MC4R.

Table 1. Primary Structure of Endogenous Melanocortin Agonists.

α-MSH	Ac-$S^1Y^2S^3M^4E^5$ **$H^6F^7R^8W^9$** $G^{10}K^{11}P^{12}V^{13}$-NH_2
γ-MSH	YVMG **$H^6F^7R^8W^9$** DRFG-OH
ACTH	SYSME **$H^6F^7R^8W^9$** GKPVGKKRRPVKVYPNGAEDSAEAFPLEF-OH
β-MSH	AEKKDEGPYRME **$H^6F^7R^8W^9$** GSPPKD-OH

Results and Discussion

Peptoid oligomers were synthesized using the submonomer approach outlined by Zuckerman and colleagues [2]. Peptide-peptoid hybrids were synthesized using a suitable combination of: 1) standard Fmoc solid phase peptide synthesis for amino acid residues; and 2) the submonomer approach for N-substituted glycine residues. All

peptoids and hybrids were synthesized in good yields and purified to homogeneity using semi-preparative RP-HPLC. Agonist assays were performed using HEK293 cells, stably expressing mouse MC4R, transfected with the CRE/β-galactosidase reporter gene [4]. Agonist EC_{50} values reported in Table 2 represent the mean of duplicate experimental data sets performed in three or more independent experiments.

Table 2. Functional Activity of Peptoids and Peptide-Peptide Hybrids at the mouse MC4R.

Compound	Sequence	MC4R EC_{50}(nM)
1	Ac-His-DPhe-Arg-Trp-NH_2*	17 ± 2.8
2	Ac-N**hHis**-DPhe-Arg-Trp-NH_2	880 ± 270
3	Ac-N**Phe**-DPhe-Arg-Trp-NH_2	260 ± 15
4	Ac-His-N**Phe**-Arg-Trp-NH_2	20%@100μM
5	Ac-His-DPhe-N**Arg**-Trp-NH_2	1100 ± 130
6	Ac-His-DPhe-Arg-N**hTrp**-NH_2	640 ± 92
7	Ac-N**hHis**-N**Phe**-N**Lys**-N**hTrp**-NH_2	27000±11000
8	Ac-N**Phe**-N**Phe**-N**hArg**-N**Nal(1')**-NH_2	NA
9	Ac-N**hHis**-N**Phe**-N**Arg**-N**hTrp**-NH_2	65%@100μM

*The concentration of compound at 50% maximum receptor stimulation (EC_{50}), or the % of receptor stimulation at the highest concentration of compound tested (relative to control). NA denotes that no agonist activity was observed at up to 100μM. *The peptide value has been previously reported [5] and is included herein for reference purposes.*

The peptoids initially synthesized (7-9) were far less potent than peptide 1 at the MC4R, or were completely inactive. To determine the degree of which the melanocortin tetrapeptide can be transformed into a peptoid without a significant decrease in activity, a "peptoid scan" was performed [6]. The DPhe residue (4), which is known to be very important for MC4R activity, was the most sensitive position to NSG substitution. The remaining His, Arg, and Trp positions (2,3,5, and 6) were moderately affected by NSG substitution of the amino acids, only resulting in a 15 to 65-fold decrease in MC4R activity. These data suggest that three of the "core" amino acids of melanocortin peptides may be replaced with peptoid residues, which may increase enzymatic stability or bioavailability, with the *caveat* that potency can be reduced at the MC4R.

Acknowledgments
The work was funded in part by NIH grant DK57080 and Carrie Haskell-Luevano is a recipient of a Burroughs Wellcome Career Award in the Biomedical Sciences.

References
1. Hruby, V. J. and Balse, P. M. *Curr. Med. Chem.* **7**, 945-970 (2000).
2. Zuckermann, R. N. K., Janice M.; Kent, Stephen B. H. and Moos, Walter H. *J. Am. Chem. Soc.* **114**, 10646-10647 (1992).
3. Zuckermann, R. N.*, et al. J. Med. Chem.* **37**, 2678-2685 (1994).
4. Chen, W.*, et al. Anal. Biochem.* **226**, 349-354 (1995).
5. Holder, J. R.*, et al. J. Med. Chem.* **45**, 2801-2810 (2002).
6. Ruijtenbeek, R.*, et al. Chembiochem.* **2**, 171-179 (2001).

Peptide Revolution: Genomics, Proteomics & Therapeutics
Michael Chorev & Tomi K. Sawyer (Editors)
American Peptide Society, 2003

A Novel AGRP-Melanocortin Peptide Chimeric Library

Krista R. Wilson, Andrzej M. Wilczynski, Joseph W. Scott, Rayna M. Bauzo and Carrie Haskell-Luevano

Department of Medicinal Chemistry, University of Florida College of Pharmacy, Gainesville, FL 32610, USA

Introduction

The Melanocortin pathway is made up of the melanocortin agonists, five GPCR receptors (MC1-5), and the only two known naturally occurring antagonists of the GPCRs, agouti (ASP) and agouti-related proteins (AGRP). The MC1R is expressed in melanocytes, monocytes, mast cells, and neutrophils, and is involved in skin pigmentation and inflammation [1]. It has been shown that subnM α-MSH analogues exhibit a potent anti-inflammatory effect in both *in vitro* and *in vivo* studies [1].

It is hypothesized that the amino acids Arg-Phe-Phe in the antagonist hAGRP [2-4] are mimicking the essential peptide Phe-Arg-Trp found in the endogenous agonist α-MSH. By substituting the agonist tetrapeptide sequence His-$_D$Phe-Arg-Trp into the antagonist AGRP template, a chimeric peptide is created that becomes a potent agonist of the melanocortin receptors (Figure 1). The AGRP-melanocortin chimeric peptide derivative AMW3-23 (Tyr-c[Asp-His-$_D$Phe-Arg-Trp-Asn-Ala-Phe-Dpr]-Tyr-NH_2) has been shown in our laboratory to be a potent melanocortin agonist, and is a novel peptide template.

This study involved the creation of a "focused" combinatorial library of peptides based on the **AMW3-23** template (Table 1). Each peptide contains a single amino acid substitution. The specific aim of this study was to see whether these substitutions would increase the potency of each compound compared to α-MSH at the mouse MC1R. Previous studies in our laboratory have identified unnatural amino acids that upon substitution drastically increase the potency of the ligand [5,6]. These residues were incorporated into this AMW3-23 template and pharmacology characterized at the mMC1R.

α-MSH: Ac-Ser-Tyr-Ser-Met-Glu-His-Phe-Arg-Trp-**Gly-Lys-Pro-Val-NH_2**
hAGRP (109-118): Tyr-c[Cys-Arg-Phe-Phe-**Asn-Ala-Phe-Cys]-Tyr-NH_2**
AMW3-23: Tyr-c[Asp-His-$_D$Phe-Arg-Trp-**Asn-Ala-Phe-Dpr]-Tyr-NH_2**

Fig. 1. Sequences of α-MSH, hAGRP (109-118), and AMW3-23, with substituted sequence in bold.

Results and Discussion

Substitution of Phe with (pI)$_D$Phe (peptide **8**), and Trp with Nal(2') (peptide **17**) and $_D$Nal(2') (peptide **18**) into AMW3-23 (peptide **1**, the template peptide) resulted in three compounds that showed equipotent activity with the template peptide. Generally, substitution at the Phe and Trp positions of AMW 3-23 with side chain moieties possessing large hydrophobic groups, resulted in a slight decrease in potency, and substitution with small hydrophilic or neutral groups resulted in a significant decrease in potency. Substitution at the His position of AMW3-23 resulted in decreased potency for each compound, and substitution at the AMW3-23 Arg position resulted in significantly decreased potency. (Table 1)

Previous studies have shown that modifications in the His-Phe-Arg-Trp sequence are tolerated relatively well at the MC1R in terms of ligand potency, except at the Trp position [6,7]. Substitution of Ala or His for Trp in the melanocortin tetrapeptide Ac-

His-$_D$Phe-Arg-Trp resulted in 200-fold decreased potency at the MC1R [7]. This suggests that the Trp side chain is important in peptide-receptor interactions [7]. In this study, substitution at the Trp position of AMW3-23 was consistent with previous data and serves to reinforce the hypothesis that modification of the His-Phe-Arg-Trp-NH_2 sequence is relatively well tolerated at the MC1R, as long as the hydrophobic receptor interactions at the Phe and Trp position are not disrupted.

Table 1. Functional activity of AGRP-melanocortin chimeras at the mMC1R.

Peptide	Structure	EC_{50} (nM)	Fold Difference
α- MSH	Ac-Ser-Tyr-Ser-Met-Glu-His-Phe-Arg-Trp-Gly-Lys-Pro-Val-NH_2	0.5	
hAGRP (109-118)	Tyr-c[Cys-Arg-Phe-Phe-Asn-Ala-Phe-Cys]-Tyr-NH_2	5100 [8]	
1	Y-c[Asp-His-$_D$Phe-Arg-Trp-Asn-Ala-Phe-Dpr]-Tyr-NH_2	0.2	1
2	Y-c[Asp-**Ala**-$_D$Phe-Arg-Trp-Asn-Ala-Phe-Dpr]-Tyr-NH_2	7.0	30
5	Y-c[Asp-**Atc**-$_D$Phe-Arg-Trp-Asn-Ala-Phe-Dpr]-Tyr-NH_2	680	3000
7	Y-c[Asp-His-**Pro**-Arg-Trp-Asn-Ala-Phe-Dpr]-Tyr-NH_2	10000	46000
8	Y-c[Asp-His-**(pI)$_D$Phe**-Arg-Trp-Asn-Ala-Phe-Dpr]-Tyr-NH_2	0.30	1
9	Y-c[Asp-His-**$_D$Nal(2')**-Arg-Trp-Asn-Ala-Phe-Dpr]-Tyr-NH_2	7.0	30
11	Y-c[Asp-His-**$_D$Bip**-Arg-Trp-Asn-Ala-Phe-Dpr]-Tyr-NH_2	4.0	20
12	Y-c[Asp-His-$_D$Phe-**Ala**-Trp-Asn-Ala-Phe-Dpr]-Tyr-NH_2	67	300
13	Y-c[Asp-His-$_D$Phe-**Lys**-Trp-Asn-Ala-Phe-Dpr]-Tyr-NH_2	1300	6200
15	Y-c[Asp-His-$_D$Phe-Arg-**Ala**-Asn-Ala-Phe-Dpr]-Tyr-NH_2	350	1500
16	Y-c[Asp-His-$_D$Phe-Arg-**Pro**-Asn-Ala-Phe-Dpr]-Tyr-NH_2	1000	4500
17	Y-c[Asp-His-$_D$Phe-Arg-**Nal(2')**-Asn-Ala-Phe-Dpr]-Tyr-NH_2	0.50	2
18	Y-c[Asp-His-$_D$Phe-Arg-**$_D$Nal(2')**-Asn-Ala-Phe-Dpr]-Tyr-NH_2	0.20	1
19	Y-c[Asp-His-$_D$Phe-Arg-**Bip**-Asn-Ala-Phe-Dpr]-Tyr-NH_2	11	50

Acknowledgments

This work was supported by NIH DK57080 and DK64250, and a Burroughs Wellcome Career Award in the Biomedical Sciences.

References

1. Herpin, T. F., Yu, G., Carlson, K. E., Morton, G. C, Wu, X., Kang, L, Tuerdi, H., Khanna, A., Tokarski, J. S., Lawrence, R. M. and Macor, J. E. *J. Med. Chem.* **46**, 1123-1126 (2003).
2. Yang, Y., Dickinson, C. J., Zeng, Q., Li, J. Y., Thompson, D. A. and Gantz, I. *J. Biol. Chem.* **274**, 14100-14106 (1999).
3. Haskell-Luevano, C, Sawyer, T. K., Trumpp-Kallmeyer, S., Bikker, J., Humblet, C., Gantz, I. and Hruby, V. J. *Drug Design & Discovery* **14**, 197-211 (1996).
4. Tota, M. R, Smith, T. S, Mao, C., MacNeil, T., Mosley, R. T, Van der Ploeg, L. H. T. and Fong, T. M. *Biochem*. **38**, 897-904 (1999).
5. Holder, J. R., Bauzo, R. M., Xiang, Z. and Haskell-Luevano, C. *J. Med. Chem.* **45**, 2801-2810 (2002).
6. Holder, J. R., Bauzo, R. M., Xiang, Z. and Haskell-Luevano, C. *J. Med. Chem.* **45**, 3073-3081 (2002).
7. Holder, J. R., et al. *J. Med. Chem.* **45**, 5736-5744 (2002).
8. Haskell-Luevano, C., et al. *Peptides* **21**, 683-689 (2000).

Peptide Revolution: Genomics, Proteomics & Therapeutics
Michael Chorev & Tomi K. Sawyer (Editors)
American Peptide Society, 2003

Structural Requirements for the Human MC4 Receptor Selectivity of Novel Cyclic MT-II Analogues

Alexander V. Mayorov, So-Yeop Han, Matthew R. Hammer, Minying Cai, Dev Trivedi and Victor J. Hruby

Department of Chemistry, 1306 E. University Blvd., University of Arizona, Tucson, AZ 85721, USA

Introduction

The human melanocortin receptors perform a number of important physiological functions, including regulation of feeding behavior and energy homeostasis, which has been shown to involve hMC3R and hMC4R receptors [1,2]. Recent findings that hMC4R antagonists promote feeding while agonists have a potent satiety-inducing effect suggest potential therapeutic applications for selective ligands at this receptor in treatment of feeding disorders such as obesity and anorexia. In addition, it has been suggested that the potential role of hMC3 receptor in the control of energy partitioning might provide a novel approach in the treatment of metabolic diseases [2]. Recent studies indicate that modification of the MT-II cyclic lactam template, through altering the size and rigidity of the lactam macrocycle, can result in diminished binding potency toward one or more of the melanocortin receptors, while binding at the receptor of interest can be retained, thus leading to enhanced receptor selectivity [3]. In our efforts to investigate the effects of hydrophobicity, bulk and size of the cyclic lactam bridge on the biological activity toward human melanocortin receptors, several novel MT-II analogues have been designed and synthesized.

Results and Discussion

MT-II, a superpotent but non-selective human melanocortin receptor agonist, along with potent non-selective antagonist SHU-9119, provided an excellent template for design of the more selective melanocortin ligands. The MT-II template in this study was modified to include a variety of dicarboxylic acid linkers between the α-amino group of histidine and the ε-amino group of lysine.

Earlier we reported the *o*-phthalic acid linker analogue (MK-6) [3], which exhibited some binding selectivity toward hMC4 receptor (Table 1). In order to determine the role of dihedral constraint of the linker versus its steric and hydrophobic effects we have synthesized the maleic acid linker analogues **V** and **VI**, as well as the *m*- and *p*-phthalic acid linker analogues (**I**-**IV**). *In vitro* competitive binding experiments (Table 1) showed that the analogues **V** and **VI** did not significantly discriminate between the different receptor subtypes, though the binding affinities at all the receptors were in the low nM range. It has also been determined that introduction of highly constrained rigid *m*- and *p*-phthalic acid linkers (analogues **I** and **III**) resulted in diminished binding potencies at hMC3 (290 nM and 204 nM respectively) and hMC5 (0.825 μM and 6.637 μM) receptors, while binding at hMC4R remained at the level comparable to that of MT-II (16 and 8 nM). However, in the *D*-Nal(2')-substituted analogues an overall increase in binding affinities was observed, whereas the receptor selectivity was less pronounced. Therefore, we suggest that hMC4 receptor selectivity requires not only the type of dihedral constraint provided by phthalic acid linkers, but also their steric bulk as well as hydrophobicity, which may introduce the topography favorable for hMC4R binding selectivity.

In addition to biological testing of the prepared analogues, molecular modeling experiments have been conducted, yielding some clues to the molecular determinants for binding and selectivity, as well as structure-activity relationships, observed for these peptides. For instance, Monte Carlo Multiple Minima [4,5] (MCMM)/Amber simulations performed on MT-II and SHU-9119 suggest that both peptides share a very similar backbone conformation, consistent with a non-hydrogen bonded β-sheet, as well as topography, which features nearly identical distances (6-8Å) between the side chains of His^3, $DPhe^4$ [or $DNal(2')^4$] and Trp^6 residues. It appears that these topographical features may be responsible for the high potency of both peptides. On the other hand, deviations from this "optimal" topography that computational experiments reveal for other reported hMC3/4 melanotropin ligands, such as MK1, MK7 and MK9, may be associated with the receptor selectivity observed for these MT-II analogues [3].

Acknowledgments
Financial support from grants from NIH and USPHS is gratefully acknowledged.

References

1. Yang, Y., Fong, T. M., Dickinson, C. J., Mao, C., Li, J. Y., Tota, M. R., Mosley, R., Van der Ploeg, L. H. T. and Gantz, I, *Biochemistry* **39**, 14900-14911 (2000).
2. Fan, W., Boston, B. A., Kesterson, R. A., Hruby, V. J. and Cone, R. D. *Nature* **385**, 165-168 (1997).
3. Kavarana M. J., Trivedi D., Cai M., Ying J., Hammer M., Cabello C., Grieco P., Han G., and Hruby V. J. *J. Med. Chem.* **45***,* 2644-2650 (2002).
4. Goodman, J. M. and Still, W. C. *J. Comput. Chem.* **12**, 1110-1117 (1991).
5. Chang, G., Guida, W. C. and Still, W. C. *J. Am. Chem. Soc.* **111**, 4379-4386 (1989).

Peptide Revolution: Genomics, Proteomics & Therapeutics
Michael Chorev & Tomi K. Sawyer (Editors)
American Peptide Society, 2003

Novel Ligands for Human Melanocortin Receptor Subtypes: Design, Synthesis and Structure-Activity Relationships

Magda Stankova, Minying Cai, Chris Cabello, Bridgette DeCot, Victor Krchnak Jr. and Victor J. Hruby

Department of Chemistry, University of Arizona, Tucson, AZ 85721,USA

Introduction

The pituitary hormones, melanotropins (MSHs) and corticotropin (ACTH) have been known for their role in skin pigmentation (α-MSH) and the secretion of corticosteroids (ACTH) for more then 50 years. In 1992-94, when the receptors for ACTH and α -MSH were cloned, three other receptor subtypes were discovered. Five receptor subtypes were named as the melanocortin 1, 2, 3, 4 and 5 receptor (MC1R-MC5R). They belong to the superfamily of G-protein coupled receptors, which are the largest group of transmembrane proteins. Pharmacological studies of melanocortin receptors revealed very broad physiological functions including energy homeostasis, food intake, sexual behavior, thermoregulation, anti-inflammatory effects, nerve regeneration, stimulation of learning, and memory. ACTH, α-, β-, and γ-MSH are the endogenous agonists for melanocortin receptors. All melanocortin ligands originate from a large protein, pro-opiomelanocortin (POMC), through post-translation processing. Due to the lack of selectivity of natural ligands, the exact biological effects of each melanocortin receptor cannot be determined. Potent and highly selective agonist and antagonist would make a pharmacological evaluation of the receptor subtypes more feasible The melanocortin receptors may serve as very important drug targets for treatment of obesity, anorexia, erectile dysfunction, melanoma tumors, drug abuse, and inflammation.

Results and Discussion

Significant contribution in synthesis of new melanocortin peptides has been made in Hruby's lab over last 20 years. The synthetic ligands such as NDP-MSH, MTII and SHU9119 [1-3] are extensively used for pharmacological evaluation of the melanocortin receptors around the world. As a continuation in the search for selective ligands we have synthesized and screened 36 novel cyclic peptides with the ring sizes varying from 15 to 30 atoms. The design is based on the primary structure of γ-MSH with stepwise truncation from the N-terminus (Table 1), which is more tolerated than truncation at the C-terminus. Macrocyclization was achieved by thioether bond formation in "side-chain to backbone" fashion (Figure 1).

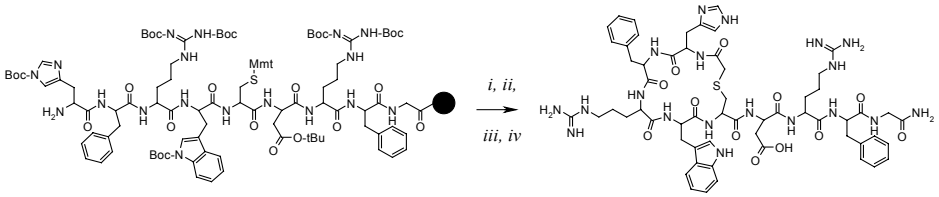

Fig. 1. Peptide cyclization on solid phase; i) $BrCH_2CO_2H$, DIC, DMF, ii) 2% TFA/DCM, iii) 5% DIEA/DMF, iv) 95% TFA.

In order to apply the sulfide bridge as a cyclization element, a cysteine residue has been introduced into the peptide sequence as a replacement of an amino acid or

inserted between two amino acids. All synthetic steps were completed on a solid support with Fmoc/*t*Bu strategy using Rink amide linker. First the linear peptide was capped with bromocarboxylic acid, then the monomethoxytrityl (Mmt) protecting group on the cysteine side-chain was selectively removed with 2% TFA in DCM. The peptide was cyclized in DMF in the presence of 5% N,N-diisopropylethylamine during 12 hours. The product was cleaved from solid phase by 95% TFA and purified by HPLC using an YMC C18 semipreparative column. Purity of the crude product was generally between 55-87 %.

Table 1. A subset of cyclic peptides.

#	*Primary structure*[a]	*Ring size*
γ- MSH	Tyr-Val-Met-Gly-His-Phe-Arg-Trp-Asp-Arg-Phe-Gly- OH	
1	Nle-Gly-His - Phe-Arg-Trp-Asp-Arg-Cys-Phe-Gly-NH_2	30
2	Nle-Gly-His - Phe-Arg-Trp-Asp-Cys-Arg-Phe-Gly-NH_2	27
3	Nle-Gly-His - Phe-Arg-Trp-Cys-Asp-Arg-Phe-Gly-NH_2	24
4	Gly-His - Phe-Arg-Trp-Asp-Cys-Arg-Phe-Gly-NH_2	24
5	Gly-His - Phe-Arg-Trp-Cys-Asp-Arg-Phe-Gly-NH_2	21
6	Gly-His-DPhe-Arg-Trp-Cys-Asp-Arg-Phe-Gly-NH_2	21
7	His - Phe-Arg-Trp-Asp-Cys-Arg-Phe-Gly-NH_2	21
8	His - Phe-Arg-Trp-Cys-Asp-Arg-Phe-Gly-NH_2	18
9	Phe-Arg-Trp-Asp-Cys-Arg-Phe-Gly-NH_2	18
10	Phe-Arg-Trp-Cys-Asp-Arg-Phe-Gly-NH_2	15

[a] *Cyclization occurs between sulfhydro group of a cysteine and bromoacetyl on N-terminal end via intramolecular thioether bond formation.*

All cyclic ligands have a carboxyamide at the C-terminus and a Met[3] was replaced with isosteric norleucine (Nle) to enhance the peptide stability in solution. From preliminary binding studies the cyclic peptides show activity at μM concentrations. Peptide # 3 with a 24-membered ring has an IC_{50} 76 nM at hMC1R with 20-fold selectivity over hMC3R, hMC4R and the hMC5R. The best ligand, peptide # 6 with a 21-membered ring and D-Phe[6] has an IC_{50} 11 pM at the hMC1R with a 10^6-fold selectivity over hMC3R, hMC4R and hMC5R. We have discovered highly active and selective ligand for the hMC1R. Further investigations are ongoing in our lab.

Acknowledgments
The work was supported by grants from the USPHS.

References

1. Sawyer, T. K., Sanfilippo, P. J., e*t al., Proc. Natl. Acad. Sci. U.S.A.* **77**, 5754-57-58. (1980).
2. Al-Obeidi, F., Castrucci, A. M. L., *et al., J. Med. Chem.* **32**, 2555-2561(1989).
3. Hruby, V. J., Dongsi, L., Sharma, S. D., *et al., J. Med. Chem.* **38**, 3454-3461 (1995).

Peptide Revolution: Genomics, Proteomics & Therapeutics
Michael Chorev & Tomi K. Sawyer (Editors)
American Peptide Society, 2003

Novel α-MSH/γ-MSH Hybrid Analogues that Lead to Selective Ligands for the Human MC1R and Human MC3R

Minying Cai, Magda Stankova, Christopher Cabello, Bridgette Decot, Alexander Mayorov, Dev Trivedi and Victor J. Hruby

Department of Chemistry, 1306 E. University Blvd., University of Arizona, AZ 85721, USA

Introduction

α-Melanocyte-stimulating hormone (α melanotropin, α-MSH, Ac-Ser-Tyr-Ser-Nle-Glu-His-Phe-Arg-Trp-Gly-Lys-Pro-Val-NH_2)**,** and γ-melanocyte-stimulating hormone (γ-melanotropin, γ-MSH H-Tyr-Val-Met-Gly-His-Phe-Arg-Trp-Asp-Arg-Phe-Gly-OH) belong to the family of melanotropin peptides derived by the posttranslational processing of the pro-opiomelanocortin (POMC) gene. The melanotropin peptides are known to have a broad spectrum of physiological actions, including regulation of pigmentation, thermoregulation, regulation of feeding behavior and erectile function [1]. To date, five melanocortin receptors (MCR) have been characterized and cloned and these all belong to the G protein coupled receptor (GPCR) family. The availability of cloned melanocortin receptor cell lines allows us to use high throughput screening and thus determine receptor selectivity for ligands.

A good number of potent but non-selective hMCR agonists and antagonists (e.g. MTII and SHU9119) have been reported in the literature [2], but potent and receptor-specific agonists and especially antagonists would be extremely valuable tools for determination of the physiological roles of the hMC1R, hMC3R, hMC4R and hMC5R. In our efforts to to produce such receptor-selective agonists/antagonists, we designed and synthesized a series of hybrid **α**-/**γ**-MSH analogues and determined their biological activities.

Result and Discussion

We recently reported that Nle^3 substituted C-terminal amidated analogue of γ-MSH considerably improves its binding affinity towards three melanocortin receptors subtypes (hMC3, hMC4, hMC5) [3]. Additionally, a D-amino acid scan of γ-MSH revealed that D-Trp^8 substitution resulted in a highly potent and hMC3R selective agonist [4]. Continuing further, we designed 10 analogues of γ-MSH by introducing D-Nal(2') in place of its core sequence residues His, Phe, Arg, Trp, which may lead to a better understanding of the possible stereo-chemical and topographical requirements of the side chain groups of each of the core amino acids for interaction with the various melanocortin receptors.

In vitro biological activity data (Table 1) shows that analogue **4**, in which the sterically bulky D-Nal(2')^8 is substituted for D-Trp^8, converts a hMC3R selective agonist to a hMC3R selective antagonist (IC_{50}=6nM). Furthermore, analogue **5**, which is a very potent and hMC1 receptor selective agonist (EC_{50}=3nM), is the first example of its kind reported in the literature. It seems that increasing the hydrophobicity of the parent analogue of Nle^3- γ-MSH amide by replacing Phe^6 and Trp^8 with D-Nal(2') and D-Trp (analogue **5**) leads to a very selective agonist of the hMC1 receptor. Similar observation were made in analogue **2**, which also is a hMC1 receptor agonist

(EC_{50}=55nM), when only D-Trp^{8} was substituted with D-Nal(2')^{8} resulting in a somewhat reduced hydrophobic environment. Hence, analogue **2** is not as selective as analogue **5**.

Table 1. Binding and intracellular cAMP accumulation of melanotropin analogues at the different human melanocortin receptors.

	hMC1R			**hMC3R**			**hMC4R**			**hMC5R**		
	IC_{50} nM	EC_{50} nM	% Max Eff.	IC_{50} nM	EC_{50} nM	% Max Eff.	IC_{50} nM	EC_{50} nM	% Max Eff.	IC_{50} nM	EC_{50} nM	% Max Eff.
1	1.2	70	100	73	516	38	45	65	76	327	389	73
2	20	55	120	32	13	28	350	2.6	14	654	246	46
3	0.7	2	87	6	N.A	/	6	36	100	4.5	195	67
4	1	8	63	25	141	60	17	29	130	11	410	88
5	0.3	3	70	5	303	6	6	634	18	3.5	N.A	6
6	60	80	100	622	1000	100	45	70	100	636	82	100
7	--	--	--	45	1.6	100	64	34	105	200	99	114
8	261	300	100	710	700	100	760	712	100	2200	550	100
9	--	--	--	6.7	0.33	100	600	100	99	340	82	97

IC_{50}=Concentration of peptide at 50% specific binding (N=4); EC_{50}=Effective concentration of peptide that was able to generate 50% maximal intracellular cAMP accumulation (N=4). The peptides were tested at a range of concentration (10^{-10}-10^{-5}M); N.A. no activity. Eff.: Effect.

1. H-Tyr-Val-Met-Gly-His-Phe-Arg-Trp-Asp-Arg-Phe-Gly-NH_2;
2. H-Tyr-Val-Nle-Gly-Pro-Phe-Arg-D-Nal(2')-Asp-Arg-Phe-Gly-NH_2;
3. H-Tyr-Val-Nle-Gly-His-D-Phe-Arg-D-Nal(2')-Asp-Arg-Phe-Gly-NH_2;
4. H-Tyr-Val-Nle-Gly-His-D-Phe-Arg-D-Trp-Asp-Arg-Phe-Gly-NH_2;
5. H-Tyr-Val-Nle-Gly-His-D-Nal(2')-Arg-D-Trp-Asp-Arg-Phe-Gly-NH_2;
6. Nle^{3} γ-MSH: H-Tyr-Val-Nle-Gly-His-Phe-Arg-Trp-Asp-Arg-Phe-Gly-OH;
7. Nle^{3} γ-MSH-NH_2: H-Tyr-Val-Nle-Gly-His-Phe-Arg-Trp-Asp-Arg-Phe-Gly-NH_2;
8. γ-MSH: H-Tyr-Val-Met-Gly-His-Phe-Arg-Trp-Asp-Arg-Phe-Gly-OH;
9. D-Trp^{8}- γ-MSH: H-Tyr-Val-Met-Gly-His-Phe-Arg-DTrp-Asp-Arg-Phe-Gly-OH

We conclude that analogue **5** is an important discovery, and this hMC1 receptor agonist can be used in *in-vivo* immunomodulation and anti-inflammatory effects, whereas analogue **3** (hMC3R antagonist) can be a good tool in studying feeding behavior and energy homeostatis.

Ackowledgments
This work was supported by a grant from the U.S. Public Health Service, Grant DK17420.

References

1. Wikberg, J. E. S., Muceniece, R., Mandrika, I., Prusis, P., Lindblom, J., Claes, P. and Skottner, A. *Pharmacol. Res.* **42**, 393-420 (2000).
2. Hruby, V. J. *Nat. Rev. Drug Discov.* **1**, 847-858 (2002).
3. Balse-Srinivasan, P. M., Grieco, P., et. al. *J. Med. Chem.* In Press (2003).
4. Grieco, P., Balse, P. M., Weinberg, D., MacNeil, T. and Hruby, V. J. *J. Med. Chem.* **43**, 4998-5002 (2000).

Peptide Revolution: Genomics, Proteomics & Therapeutics
Michael Chorev & Tomi K. Sawyer (Editors)
American Peptide Society, 2003

Synthesis and Evaluation of Leu-Enkephalin Analogues Containing Substituted β-Turn Bicyclic Dipeptide Mimetics

Chiyi Xiong, Junyi Zhang, Jinfa Ying and Victor J. Hruby

Department of Chemistry, University of Arizona, Tucson, AZ 85721, USA

Introduction

Previous studies on Leu-enkephalin (H-Tyr-Gly-Gly-Phe-Leu-OH) and related cyclic analogues have suggested that it adopts, predominantly, a β-turn centered at Gly^3-Phe^4 [1]. These studies also suggested that for opioid peptides, the turn position residues not only play a role of conformation restriction, but also are involved in direct interaction with receptor(s) [2]. Furthermore, our studies have indicated that the conformational requirements for optimal interaction with the μ and δ receptors differ in a subtle manner [3]. With these criteria in mind, we propose that conformationally restricted, substituted bicyclic β-turn dipeptide (BTD) mimetics with different stereochemical configurations would be a desirable peptidomimetic moiety. We report a flexible synthesis that allows for the preparation of diastereoisomers of Leu-enkephalin analogues containing substituted chiral β-turn bicyclic dipeptide mimetics.

Results and Discussion

The synthesis of 8-phenyl substituted thiaindolizidinone amino acids was accomplished using a convergent synthetic strategy shown in Scheme 1. The β-phenylcysteine derivatives (2*R*, 3*S*)-**2a** and (2*S*, 3*R*)-**2b**, were prepared according to our new protocol [4]. The doubly protected glutamic acid γ-aldehyde **1** was prepared according to a procedure previously described [5]. Aldehyde **1** was converted to a mixture of thiazolidines by condensation with the β-phenylcysteine derivative (2*R*, 3*S*)-**2a**, or (2*S*,3*R*)-**2b** in buffered aqueous ethanol. Sequential fluoride-mediate deprotection and cyclization of the resulting amino acids with the aid of carbodiimide coupling reagent resulted in clean formation of the bicyclic lactams **3a/3b-3c/3d** see Scheme 2) as epimers at the bridgehead. Incorporation of the 8-phenyl BTD into Leu-enkephalin and purification by RP-HPLC gave Leu-enkephalin analogues in a 9-15% overall yield.

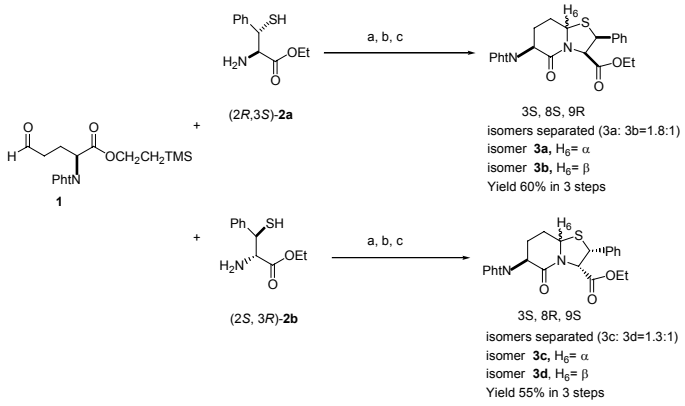

Scheme 1. Synthesis of 8-phenyl BTD.

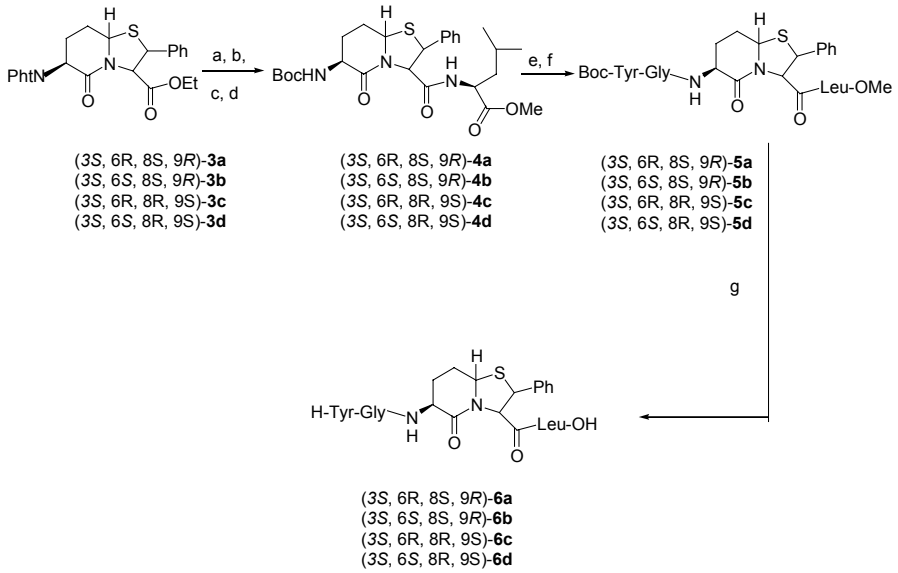

(*3S*, 6R, 8S, 9*R*)-**3a**
(*3S*, 6*S*, 8S, 9*R*)-**3b**
(*3S*, 6R, 8R, 9S)-**3c**
(*3S*, 6*S*, 8R, 9S)-**3d**

(*3S*, 6R, 8S, 9*R*)-**4a**
(*3S*, 6*S*, 8S, 9*R*)-**4b**
(*3S*, 6R, 8R, 9S)-**4c**
(*3S*, 6*S*, 8R, 9S)-**4d**

(*3S*, 6R, 8S, 9*R*)-**5a**
(*3S*, 6*S*, 8S, 9*R*)-**5b**
(*3S*, 6R, 8R, 9S)-**5c**
(*3S*, 6*S*, 8R, 9S)-**5d**

(*3S*, 6R, 8S, 9*R*)-**6a**
(*3S*, 6*S*, 8S, 9*R*)-**6b**
(*3S*, 6R, 8R, 9S)-**6c**
(*3S*, 6*S*, 8R, 9S)-**6d**

Reagent: a) BBr_3, DCM; b) Leu-OMe.HCl, BOP, HOBt, DIPEA, DMF; c) NH_2NH_2, EtOH, $CHCl_3$, H_2O; d) $(Boc)_2O$, THF, TEA; e) TFA, 0°C, 20min; f) Boc-Tyr-Gly-OH, HOBt, BOP, DIPEA, DMF; g) BBr_3, DCM, -10°C, 4h, 9-15% overall yield.

Scheme 2. Synthesis of Leu-enkephalin analogues containing the substituted chiral β-turn bicyclic dipeptide mimetics.

Compounds **6a-d** were evaluated in the isolated mouse vas deferens (MVD, for δ receptor) and guinea pig ileum (GPI, for μ receptor) bioassays. At 1uM concentration, Compounds **6a-c** showed 3.3%, 8.9%, 0% and 1% agonist activity for MVD respectively, and 2.9%, 2.6%, 4% and 4.6% agonist activity for GPI respectively. These correspond to a loss of potency of approximately three orders of magnitude compared with Leu-enkephalin, and suggest that the spatial distances and orientations of the two aromatic pharmacophores (Tyr^1 phenol group and Phe^4 phenyl group) in Leu-enkephalin are not properly positioned in topographical space in these analogues for high potency.

Acknowledgments
The authors thank the USPHS grants DA 06284 and DA 13449 for support.

References

1. Claridge, T. D. W., Christopher, H., Richard, J. K., Victor, L., Ian, A. N. and Christopher, J. S. *Bioorg. Med. Chem. Lett*. **6**, 485 (1996).
2. Nagai, U., Kazuki, S., Rika, N. and Rika, K. *Tetrahedron* **49**, 3577 (1993).
3. Mosberg, H., Hurst, I. R., Hruby, V. J., Gee, K., Yamamura, H. I., Galligan, J. J. and Burks, T. F. *Proc. Natl. Acad. Sci. U.S.A.* **80**, 5871 (1983).
4. Xiong, C., Wang, W., Cai, C. and Hruby, V. J. *J. Org. Chem*. **67,** 1399 (2002).
5. Bach, II, A., Markwalder, J. A. and Ripka, W. C. *Int. J. Peptide Protein Res*. **38**, 314(1991).

Peptide Revolution: Genomics, Proteomics & Therapeutics
Michael Chorev & Tomi K. Sawyer (Editors)
American Peptide Society, 2003

Using Diverse Topographical and Conformational Privileged Structures to Explore Selectivity in Melanocortin Receptors

Victor J. Hruby[1,2], Preeti Balse-Srinivasan[1], Paolo Grieco[1], Guoxia Han[1], Minying Cai[2], Dev Trivedi[1], Alexander Mayorov[1], Jinfa Ying[1] and Magda Stankova[1]

[1]Department of Chemistry; [2]Department of Biochemistry and Molecular Biophysics, University of Arizona, Tucson, AZ, USA

Introduction

To date, five subtypes of human Melanocortin receptors have been cloned. The ligands for these GPCR subtypes of receptors are the products from the processing of the protein from one gene, proopiomelanocortin (POMC). Interestingly, α-MSH appears to be the endogenous ligand for four of these receptors, the hMC1R, hMC3R, hMC4R and hMC5R, and as determined by SAR studies, it has been found that the tetrapeptide sequence –His-Phe-Arg-Trp-, is the primary pharmacophore [1]. This raises difficult questions in drug design, especially as to how we can design agonist, antagonist, and inverse agonist ligands that will be selective for only one of these subtypes of receptors. Yet, it is necessary to develop such selective ligands, since these ligands and receptors modulate many critical biological functions including: pigmentation, stress, feeding behavior, sexual behavior, immune response, and many others. Our working hypotheses to accomplish these goals is that since a common pharmacophore is used by these 4 receptor subtypes, selectivity can be achieved by proper conformational and topographical constraints imposed on a wide variety of peptide privileged structures. Indeed, we have found that by using a variety of known and new peptide scaffolds, highly potent and selective ligands can be obtained.

Results and Discussion

In previous studies, we designed a highly potent but non-selective cyclic ligand MT-II (Ac-Nle-c[Asp-His-D-Phe-Arg-Trp-Lys]NH_2) [2]. Appropriate conformational and topographical constraints of MT-II have led to highly potent and modestly selective agonists and antagonists. For example, replacing the His residue with the constrained cycloleucine, and D-Phe with D-Nal(2') (4, Table 1), leads to a modestly selective hMC4R antagonist. Though these and other constraints have provided interesting insights into the SAR, a major goal has been an examination of new templates. These include the following: 1) D-Nal(2') and D-Trp substituted α-MSH/γ-MSH analogues; 2) deltorphin/α-MSH chimeras [3]; 3) side chain-backbone cyclization via lactam bridge and variable rigid spacers [4]; 4) cyclic side chain-backbone structures via a thioether bridge; and 5) cyclic disulfides. A few examples of selective analogues developed by these methods are give in Table 1. α-MSH/γ-MSH hybrids have been very useful scaffolds. Two examples in Table 1 illustrate how this privileged scaffold, in conjunction with hydrophobic and chiral modifications in the tetrapeptide pharmacophore, can lead to a hMC1R selective agonist (2, Table 1) or a hMC4R agonist (5, Table 1). The use of side chain-backbone cyclizations via various bridges has become a powerful tool in the design of selective ligands for melanocortin receptors.

For example, use of a glutaric acid spacer (3, Table 1) in such analogues in conjunction with the D-Nal(2') substitution gives a potent hMC3R selective antagonist

Table 1. Novel peptide scaffolds for melanocortin receptors.

Target Receptor	Peptide	Template	IC_{50}/EC_{50}/Selectivity
hMC1R antagonist	1. c[CH_2-CO-Gly-His-D-Phe-Arg-Trp-Cys]-Asp-Arg-Phe-Gly-NH_2	Side Chain-Backbone Cyclization *via* Thioether Bridge	IC_{50}=0.1nM (MC1R); MC3R-20000x; MC4R-7000x; MC5R-5000x
hMC1R agonist	2. H-Tyr-Val-Nle-Gly-His-D-Nal(2')-Arg-D-Trp-Asp-Arg-Phe-Gly-NH_2	α-MSH/γ-MSH Hybrid	EC_{50}=3nM (MC1R); MC3R-100x; MC4R-200x; MC5R >1000x
hMC3R antagonist	3. c[CO-$(CH_2)_3$-CO-His-DNal(2')-Arg-Trp-Lys]-NH_2	Side Chain-Backbone Cyclization *via* Lactam Bridge	IC_{50}=6nM (MC3R); MC4R-40x; MC5R-4x; pA_2=10
hMC4R antagonist	4. AcNH-Nle-c[Asp-Cpe-D-Nal(2')-Arg-Trp-Lys]-NH_2	Side Chain-Side Chain Cyclization *via* Lactam Bridge	IC_{50}=0.51nM (MC4R); MC3R-200x; MC5R-32x; pA_2=8.0
hMC4R agonist	5. H-Tyr-Val-Nle-Gly-His-D-Nal(2')-Arg-Trp-Asp-Arg-Phe-Gly-NH_2	α-MSH/γ-MSH Hybrid	EC_{50}=23.9nM (MC4R); MC3R>1000x; MC5R>1000x
hMC5R antagonist	6. Ac-c[Cys-Glu-His-D-Phe-Arg-Trp-D-Cys]-Pro-Pro-Lys-Asp-NH_2	Side Chain-Side Chain Cyclization *via* Disulfide Bridge	IC_{50}=10nM (MC5R); MC3R-560x; MC4R>1000x

analogue. In a new series of side chain-backbone thioether bridged analogues such as 1 (Table 1), a highly potent and selective hMC1R antagonist was obtained. With these and other more rigid scaffolds that lead to selective analogues, we have performed extensive conformational analysis using 2D NMR and new computational methods to develop a comprehensive view of the stereostructural factors that are involved in selectivity. It is clear that highly selective agonists and antagonists for human melanocortin receptors are feasible, and this should greatly facilitate biological efforts to understand the many physiological roles of POMC ligands and their receptors, and to develop new drugs.

Acknowledgments
Supported by grants from the USPH Service.

References
1. Hruby, V. J. and Han, G. In Cone, R.D. (Ed.) *The Melanocortin Receptors,* Humana Press, Totawa, N.J. pp. 239-262 (2000).
2. Al-Obeidi, F. *et al., J. Am. Chem. Soc*. **111**, 3413-3416 (1989).
3. Han, G. *et al., J. Med. Chem*. **46**, 810-819 (2002).
4. Kavarana, M., *et al., J. Med. Chem*. **45**, 2644-2650 (2002).

Peptide Revolution: Genomics, Proteomics & Therapeutics
Michael Chorev & Tomi K. Sawyer (Editors)
American Peptide Society, 2003

Studies on Synthetic Analogs of the TM VI Segment of the MT_1 Melatonin Receptor

Andrea Calderan, Paolo Ruzza, Barbara Biondi, Andrea Guiotto, Alessio Osler and Gianfranco Borin

CNR - Institute of Biomolecular Chemistry, Padova Unit, Padova, Italy

Introduction

Melatonin (MLT) is a hormone mainly produced by the pineal gland in most vertebrate species, including humans. The physiological role of MLT is related to both chronobiology and modulation of the body hormonal milieu. MLT has also been shown to have powerful antioxidant properties acting as an efficient free radicals scavenger. Our attention is focused on the characterization of MLT interaction with its high affinity membrane-bound MT_1 receptor, which belongs to the GPCR superfamily [1].

A number of structure-activity relationships were identified and many studies have proposed molecular models of the putative MLT binding site in which residues belonging to the sixth transmembrane segment (TM VI) of the receptor are involved [2-6]. In particular, an aromatic interaction could take place between the indole ring of MLT and Phe^{247}, one of the three Phe residues present in TM VI [7]. In this work we examined the influence of the Phe^{247} residue on the interaction of TM VI with phospholipid membranes by means of CD and fluorescence spectroscopy studies.

Results and Discussion

The conformational behavior of TM VI synthetic peptide analogs, in which only one Phe residue is alternatively present (being the other two substituted with Ala), was compared with the native sequence structure. The four synthetic analogs utilized were constructed by adding eight Lys residues, four at N-terminus and four at C-terminus respectively, to peptides corresponding to the receptor TM sequence 244-264 in which Cys^{253} residue was replaced by Thr. Addition of Lys clusters greatly improves the peptide solubility and prevents its aggregation [8].

TMVI	H-KKKK**F**VV**F**VL**F**AITWAPLNLIGLIVKKKK-NH_2
TMVI-F1	H-KKKK**F**VV**A**VL**A**AITWAPLNLIGLIVKKKK-NH_2
TMVI-F2	H-KKKK**A**VV**F**VL**A**AITWAPLNLIGLIVKKKK-NH_2
TMVI-F3	H-KKKK**A**VV**A**VL**F**AITWAPLNLIGLIVKKKK-NH_2

Fig. 1. Sequences of synthetic analogs of sixth transmembrane segment (TM VI) of MT_1 receptor.

CD was used to examine the conformation of synthetic peptides in water, organic solvent (TFE), SDS micelles and both zwitterionic (net neutral, DMPC) and anionic (DMPG) phospholipid vesicles. In aqueous solution, all peptides adopt a random coil structure. In TFE and SDS micelles, all peptide spectra suggest a typical α-helical conformation. In DMPC, only TMVI adopts α-helical structure, whereas the other peptides are essentially random. In DMPG, the α-helical conformation characterizes the spectra of TMVI, TMVI-F1 and TMVI-F2, whereas in the TMVI-F3 spectrum a contribute of β-structures becomes evident (spectra not shown). Fluorescence was used to study the interactions of the synthetic peptides with lipid vesicles. An aqueous-phase quencher such as iodide can quench the fluorescence of tryptophan upon collision. In the presence of vesicles the % quenching varies as reported in Table 1. The spectra of unquenched peptides were recorded in the presence of KCl.

Table 1. Percentage quenching of Trp fluorescence by KI in different media.

Peptide	*Aq.*	*DMPC*	*DMPG*
TMVI	64	51	24
TMVI-F1	62	48	26
TMVI-F2	62	56	36
TMVI-F3	60	28	21

Trp fluorescence quenching of peptides by iodide indicates that the Trp residues are buried in DMPC and DMPG vesicles. For all the four peptides, the binding with anionic lipid vesicles appears to be tighter than that with zwitterionic lipid vesicles suggesting that electrostatic attractions play a crucial role in lipid-peptide interactions.

Taking advantage of the single Trp incorporated into the peptide sequences, the depth of this fluorophore can be detected by spin-labeled lipids. Trp fluorescence within a membrane can be quenched by doxyl stearate upon contact within 5 Å. The quenching within the bilayer is primarily static with a distance dependence, so that the highest quenching efficiency should be observed when the doxyl moiety is closest to Trp fluorophore [9]. The comparison of the peptide Trp emission in the presence of SUVs composed of DMPG/n-doxyl PC (molar ratio 9:1, n = 5, 12) with that in the presence of DMPG SUVs containing 10% DMPC is reported in Table 2.

Table 2. Percentage quenching of Trp fluorescence in SUVs containing spin-labeled lipids.

Peptide	5-doxyl	12-doxyl
TMVI	61	76
TMVI-F1	34	48
TMVI-F2	66	71
TMVI-F3	29	52

The results of fluorescence quenching experiments by doxyl-labeled lipids show that TMVI and TMVI-F2 closely interact with lipid bilayer. For these peptides the presence of a prevailing population of transbilayer peptide configuration is a reasonable hypothesis. Phe^{247} doesn't appear to have a significant influence on the peptide's conformational behavior, whereas this residue seems to play a role in the control of the peptide-lipid interactions.

Acknowledgments
Supported by MURST-CNR Biotechnology Program L. 95/95.

References

1. Reppert, S. M., Weaver and D. R. and Godson, C. *Trends Pharmacol. Sci.* **17**, 100-102 (1996).
2. Kokkola, T., et al. *Biochem. Pharmacol.* **65**, 1463-1471 (2003).
3. Jansen, J. M., et al. *Bioorg. Med. Chem.* **4**, 1321-1332 (1996).
4. Sudgen, D., Chong, N. W. S. and Lewis, D. F. V. *Br. J. Pharmacol.* **114**, 618-623 (1995).
5. Sicsic, S., et al. *J. Med. Chem.* **40**, 739-748 (1997).
6. Conway, S., et al. *Biochem. Biophys. Res. Comm.* **239**, 418-423 (1997).
7. Navajas, C., et al. *Eur. J. Pharmacol.* **304**, 173-183 (1996).
8. Liu, L.- P. and Deber, C. M. *Biopolymers (Peptide Sci.)* **47**, 41-62 (1998).
9. Liu, L.- P. and Deber, C. M. *Biochemistry* **36**, 5476-5482 (1997).

Peptide Revolution: Genomics, Proteomics & Therapeutics
Michael Chorev & Tomi K. Sawyer (Editors)
American Peptide Society, 2003

Opioid Peptide Analogues: Conformation and Pharmacological Properties of Synthetic Dermorphin and Deltorphin 1 Peptide-Peptoid Hybrids

Laura Biondi[1], Elisa Giannini[2], Fernando Filira[1], Marina Gobbo[1], Mauro Marastoni[3], Lucia Negri[2], Barbara Scolaro[1], Roberto Tomatis[3] and Raniero Rocchi[1]

[1]Department of Organic Chemistry, University of Padova, Institute of Biomolecular Chemistry, C.N.R., Section of Padova, Italy; [2]Department of Human Physiology and Pharmacology, University "La Sapienza" of Roma, Italy; [3]Department of Pharmaceutical Science, University of Ferrara, Italy

Introduction

Synthesis is described of new dermorphin and [D-Ala^2]-deltorphin 1 analogues in which tyrosine, phenylalanine and valine residues have been totally or partially substituted by the corresponding N-alkyl-glycine derivatives (Ntyr, Nphe and Nval, respectively) (Table 1).

All peptide-peptoid hybrids were characterized by analytical HPLC, optical rotation, amino acid composition and molecular weight determination. Structural investigations by CD measurements in different solvents and preliminary pharmacological experiments were carried out on the synthetic analogues.

Results and Discussion

Assembly of peptide-peptoid hybrids **I**–**VII** was performed on the Applied Biosystems Model 431 A Peptide Synthesizer, starting with Fmoc-Ser(tBu)- or Fmoc-Gly-Rink Amide MBHA resin [0.25 mmol scale, FastMoc methodology (HBTU/HOBt/DIEA), single acylation protocol]. For acylating the amino group of the N-alkylglycine residue, HATU was added as a solid to the cartridge containing the Fmoc-amino acid. The mixture was dissolved in DMF and the time of coupling was doubled (50 min). To prevent the possible intrachain aminolysis at the dipeptide stage [1], Fmoc-Tyr(tBu)-Pro-OH [2] was used in the first acylation step during the synthesis of **I** and **II**. When necessary peptide-peptoid analogues were further purified by semipreparative HPLC. CD Measurements were performed in H_2O, TFE and SDS aqueous solution, at 298 K, over 250-185 nm. The contribution from aromatic residues is prominent in the CD spectra of dermorphin analogues **I** and **II**, and the assignment of a prevailing secondary

Table 1. Amino acid sequences of dermorphin and [D-Ala^2]-deltorphin 1 analogues.

I	H-Ntyr-D-Ala-Phe-Gly-Tyr-Pro-Ser-NH_2	[Ntyr^1]-dermorphin
II	H-Tyr-D-Ala-Nphe-Gly-Tyr-Pro-Ser-NH_2	[Nphe^3]-dermorphin
III	H-Ntyr-D-Ala-Phe-Asp-Val-Val-Gly-NH_2	[Ntyr^1]-deltorphin 1
IV	H-Tyr-D-Ala-Nphe-Asp-Val-Val-Gly-NH_2	[Nphe^3]-deltorphin 1
V	H-Tyr-D-Ala-Phe-Asp-Nval-Val-Gly-NH_2	[Nval^5]-deltorphin 1
VI	H-Tyr-D-Ala-Phe-Asp-Val-Nval-Gly-NH_2	[Nval^6]-deltorphin 1
VII	H-Tyr-D-Ala-Phe-Asp-Nval-Nval-Gly-NH_2	[Nval^5,Nval^6]-deltorphin 1

structure could be questionable. The aromatic contribution is lower in the spectra of the deltorphin analogues, and the dichroic curves, in any solvent, indicate the predominance of random conformer populations with possible presence of type I and II β-turns. The more striking feature in the CD spectrum of **III** is the disappearance of the aromatic contribution at about 230 nm, which could be explained in terms of either achirality or high conformational freedom of the N-terminal residue. The binding of the synthetic compounds to opioid receptors was tested on crude membrane preparations from CHO cells stably transfected with the μ and δ receptors. The biological potency of the peptide-peptoid hybrids was compared with that of the μ-opioid receptor agonist dermorphin in guinea pig ileum (GPI) preparations and with that of the δ-opioid receptor agonist deltorphin 1 in mouse vas deferens (MVD) preparations. All substitutions produced a dramatic decrease in the affinity for both the μ- and δ-opioid receptors. Compounds **I**, **II**, **III** and **IV** are practically devoid of agonistic activity when evaluated on GPI and MVD preparations. Nval containing hybrids (**V**, **VI** and **VII**) behave as μ-opioid receptor agonists and elicit a dose-dependent analgesia (tail-flick test) when injected i.c.v. in rats. The analgesic effect shows a time course highly different from that of deltorphin 1. Preadministration (15 min) of naloxone significantly reduced or completely abolished the peptoid-induced antinociception. These results confirm that substitution of the valine residues produced μ-opioid receptor agonists. The kinetic of degradation of the synthetic analogues, in the presence of rat or human plasma, were compared with that of [Leu^5]-enkephalin used as the standard reference. Dermorphin and deltorphin 1 were also tested. Compounds **I** to **VII** were very resistant ($T_{1/2}$ > 360 min) to digestion by rat plasma enzymes. $T_{1/2}$ is 2.1 min for [Leu^5]-enkephalin and 190.6 and 131.6 min for dermorphin and deltorphin 1, respectively. In the presence of human plasma the degradation rate of all hybrids was essentially identical ($T_{1/2}$ > 360 min).

Acknowledgments
Financial support from MIUR (Cofin 2000 and 2002) and CNR of Italy is gratefully acknowledged.

References
1. Pedrose, E., Grandas, A., de La Heras, X., Eritia, R. and Giralt, E. *Tetrahedron Lett.* **27**, 743-746 (1986).
2. Negri, L., Lattanzi, R., Tabacco, F., Orrù, L., Severini, C., Scolaro, B. and Rocchi, R. *J. Med. Chem.* **42**, 400-404 (1999).
3. Jia, X., *et al., Appl. Environ. Microbiol.* **66**, 1928-1932 (2000).

Peptide Revolution: Genomics, Proteomics & Therapeutics
Michael Chorev & Tomi K. Sawyer (Editors)
American Peptide Society, 2003

A Potent Cyclic Opioid Peptide Antagonist Lacking an N-terminal Amino Group

Grazyna Weltrowska, Yixin Lu, Carole Lemieux, Nga N. Chung and Peter W. Schiller

Laboratory of Chemical Biology and Peptide Research, Clinical Research Institute of Montreal, Montreal, Quebec, Canada H2W 1R7

Introduction

2',6'-Dimethyl substitution of the Tyr[1] residue of opioid agonist peptides and deletion of the positively charged N-terminal amino group has recently been shown to represent a general structural modification to convert opioid peptide agonists into antagonists [1,2]. This conversion requires the syntheses of opioid peptide analogues containing 3-(2,6-dimethyl-4-hydroxyphenyl)propanoic acid (Dhp) in place of Tyr[1] [1]. For example, the cyclic enkephalin analogue Dhp-c[D-Cys-Gly-Phe(pNO$_2$)-D-Cys]NH$_2$ turned out to be a quite potent μ opioid receptor antagonist and a somewhat less potent δ and κ antagonist [1] (Tables 1 and 2). In the present paper, we examine the effect of β-methylation of Dhp[1] in Dhp-c[D-Cys-Gly-Phe(pNO$_2$)-D-Cys]NH$_2$ on the *in vitro* opioid activity profile.

Results and Discussion

β-Methylation of Dhp required the development of stereospecific syntheses of (3*S*)- and (3*R*)-3-methyl-3-(2,6-dimethyl-4-hydroxyphenyl)propanoic acid [(3*S*)- and (3*R*)-Mdp]. The key steps in these syntheses were the incorporation of the chiral auxiliary (4*S*)- or (4*R*)-4-phenyl-2-oxazolidinone into (*E*)-3-(4-*t*Boc-oxy-2,6-dimethylphenyl)-2-propenoic acid, followed by asymmetric methylation [3] with methylmagnesium bromide in ether at 0°C, whereby a diastereomeric excess (de) of 40-48% was achieved. Lowering the temperature (to -10°C or -25°C) or the use of 4-benzyl- or 4-diphenylmethyl substituted chiral auxiliaries resulted in lower stereoselectivity. Subsequent hydrolysis of the acyloxazolidinones and removal of the Boc group gave (3*S*)-Mdp and (3*R*)-Mdp. The target peptides were prepared by a combination of solid-phase and solution synthesis techniques.

In comparison with the Dhp-c[-D-Cys-Gly-Phe(pNO$_2$)-D-Cys]NH$_2$ parent peptide, the (3*S*)-Mdp[1]-analogue showed significantly higher μ-, δ- and κ- receptor binding affinities (Table 1). This result is in contrast to the observation made with the (2*S*,3*R*)-Tmt[1]-analogue of the δ agonist DPDPE (Tmt = 2',6'-dimethyl-β-methyltyrosine),

Table 1. Opioid receptor binding affinities of cyclic enkephalin analogues[a].

Compound	K_i^{μ}, nM	K_i^{δ}, nM	K_i^{κ}, nM
(3*S*)-Mdp-c[D-Cys-Gly-Phe(pNO$_2$)-D-Cys]NH$_2$	2.10	2.03	49.5
(3*R*)-Mdp-c[D-Cys-Gly-Phe(pNO$_2$)-D-Cys]NH$_2$	94.4	497	6970
Dhp-c[D-Cys-Gly-Phe(pNO$_2$)-D-Cys]NH$_2$	4.79	11.6	299
H-Dmt-c[D-Cys-Gly-Phe(pNO$_2$)-D-Cys]NH$_2$	0.247	0.704	3.77

[a]*Displacement of [^{3}H]DAMGO (μ-selective) and of [^{3}H]DSLET (δ-selective) from rat brain membrane binding sites, and of [^{3}H]U69,593 (κ-selective) from guinea pig brain membrane binding sites.*

Table 2. Antagonist potencies (K_e-values) of compounds in the guinea pig ileum (GPI) and mouse vas deferens (MVD) assays.

Compound	GPI		MVD
	K_e^{μ}, nM[a]	K_e^{κ}, nM[b]	K_e^{δ}, nM[c]
(3*S*)-Mdp-c[D-Cys-Gly-Phe(*p*NO_2)-D-Cys]NH_2	1.40	5.81	55.0
(3*R*)-Mdp-c[D-Cys-Gly-Phe(*p*NO_2)-D-Cys]NH_2	845	1630	3280
Dhp-c[D-Cys-Gly-Phe(*p*NO_2)-D-Cys]NH_2	3.68	22.6	63.0
H-Dmt-c[D-Cys-Gly-Phe(*p*NO_2)-D-Cys]NH_2[d]	IC_{50} = 0.541 nM		IC_{50} = 0.182 nM

[a]*Determined against TAPP (H-Tyr-D-Ala-Phe-Phe-NH_2).* [b]*Determined against U55,488.* [c]*Determined against DPDPE.* [d]*Agonist.*

which showed significantly lower μ and δ receptor binding affinities than [Dmt[1]]DPDPE (Dmt = 2',6'-dimethyltyrosine) [4,5]. Remarkably, the δ receptor binding affinity of (3*S*)-Mdp-c[D-Cys-Gly-Phe(*p*NO_2)-D-Cys]NH_2 (K_i^{δ} = 2.03 nM) is only three times lower than that of the agonist peptide H-Dmt-c[D-Cys-Gly-Phe(*p*NO_2)-D-Cys]NH_2 (K_i^{δ} = 0.704 nM), which contains a positively charged N-terminal amino group. In agreement with the receptor binding data, (3*S*)-Mdp-c[D-Cys-Gly-Phe(*p*NO_2)-D-Cys]NH_2 also showed higher μ-, δ- and κ-antagonist potencies than the Dhp[1]-parent in the functional assays (Table 2). In comparison with the (3*S*)-Mdp[1]-analogue, the diastereomeric (3*R*)-Mdp[1]-analogue displayed drastically lower binding affinities and antagonist potencies at all three receptors. This result is in agreement with observations that (2*S*,3*R*)-Tmt[1]-analogues of opioid agonist peptides generally show higher receptor binding affinities and higher agonist potencies than their corresponding (2*S*,3*S*)-Tmt[1]-analogues [4]. It thus appears that the stereochemical requirements of the 1-position side chain of β-methylated Dhp[1]-antagonist peptides and β-methylated Dmt[1]-agonist peptides for opioid receptor binding are the same.

Acknowledgments
The work was funded by the National Institute on Drug Abuse, NIH (grant DA-04443).

References

1. Schiller, P. W., Lu, Y., Weltrowska, G., Berezowska, I., Wilkes, B. C., Nguyen, T. M.- D., Chung, N. N. and Lemieux, C. In Lebl, M., Houghten, R. A. (Eds.) *Peptides: The Wave of the Future (Proceedings of the 2nd International Peptide Symposium/17th American Peptide Symposium)*, American Peptide Society, San Diego, CA, 2001, p. 676.
2. Lu, Y., Nguyen, T. M.- D., Weltrowska, G., Berezowska, I., Lemieux, C., Chung, N. N. and Schiller, P. W. *J. Med. Chem.* **44**, 3048-3053 (2001).
3. Ernesto, N., Russell, K. C. and Hruby, V. J., *J. Org. Chem.* **58**, 766-770 (1993).
4. Qian, X., Shenderovich, M. D., Kover, K. E., Davis, P., Horvath, R., Zawelska, T., Yamamura, H. I. Porreca, F. and Hruby, V. J., *J. Am. Chem. Soc.* **118**, 7280-7290 (1996).
5. Hansen, Jr., D. W., Stapelfeld, A., Savage, M. A., Reichman, M., Hammond, D. L., Haaseth, R. C. and Mosberg, H. I. *J. Med. Chem.* **35**, 684-687 (1992).

Peptide Revolution: Genomics, Proteomics & Therapeutics
Michael Chorev & Tomi K. Sawyer (Editors)
American Peptide Society, 2003

Dimerization of NPY-Receptors by Fluorescence Resonance Energy Transfer (FRET) in Living Cells

Annette G. Beck-Sickinger, Michaela Dinger, Robert Rennert, Ilka Böhme and Karin Mörl

Institute of Biochemistry, Faculty of Biosciences, Pharmacy and Psychology, University of Leipzig, 04103 Leipzig, Germany

Introduction

G-Protein-coupled receptors (GPCRs) represent a superfamily of proteins characterized by seven transmembrane alpha-helices that interact with a family of heterotrimeric GTP-binding proteins, referred to as G-proteins. GPCRs are found in a wide range of organisms, and many types of chemical messengers act through them, for example adrenalin, angiotensin or neuropeptide Y (NPY) [1]. Ligands for GPCRs are involved in a broad range of physiological functions and their malfunction is responsible for many diseases. Until recently GPCRs were thought to function as monomers. However, a growing number of studies suggest that they may exist as homo- and heterodimers [2,3]. The existence of homodimers has been shown for several GPCRs including ß2-adrenergic receptor, opioid receptors, metabotrobic glutamate receptor 5, m3 muscarinic receptor, vasopressin V2 receptor, somatostatin and dopamine receptors by Western blot analysis, crosslinking or immunoprecipitation.

In order to investigate the NPY/pancreatic polypeptide (PP) hormone family that bind to Y-receptors we used a different technique. We cloned fusion proteins consisting of an N-terminal receptor component (hY_1-, hY_2- hY_4- or hY_5-receptor) and a C-terminal variant of the green fluorescent protein (GFP). In total we used four different GFP analogues with different spectral characteristics to be suitable for fluorescence resonance energy transfer (FRET). Typical wavelengths for CFP (cyan fluorescent protein) and YFP (yellow fluorescent protein) are shown in Figure 1.

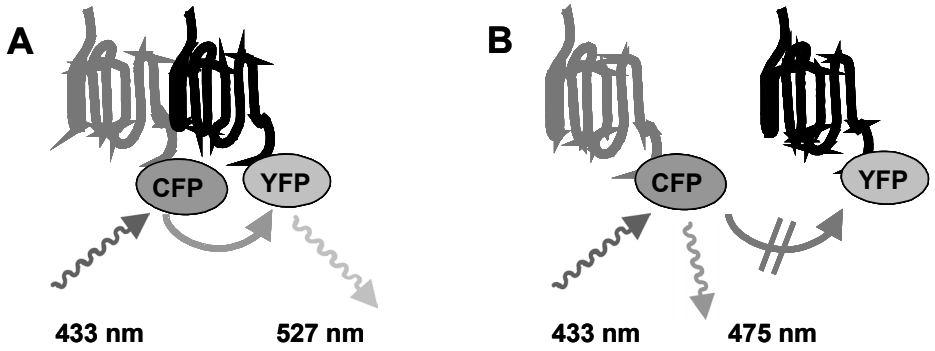

Fig. 1. Scheme of excitation and emission in the case of dimerized (A) fluorescence resonance energy transfer) or not dimerized (B) receptors.

Results and Discussion

To date, neuropeptide Y (NPY) receptors, which belong to the large family of G-protein coupled receptors and are involved in a broad range of physiological processes, are believed to act as monomers. Studies with the Y_1-receptor antagonist and Y_4-receptor agonist GR231118 which binds with a 250-fold higher affinity than its monomer, led to the first speculation that NPY-receptors can form homodimers [4]. In order to investigate this we first cloned the receptor fusion proteins. We generated fusion proteins of NPY receptors and green fluorescent protein or spectral variants of green fluorescent protein (cyan, yellow and red fluorescent protein), which can be used as FRET pairs [5]. We used the pEGFP-N1 vector and related vectors expressing the spectral variant of GFP, and applied the restricting site method after PCR amplification of Y-receptors. All constructs were characterized by restriction analysis and DNA sequencing. Plasmids were expressed in BHK (baby hamster kidney) and CHO (chinese hamster ovary) cells after lipofection.

Receptor fusion proteins were studied first by microscopy, including confocal laser scanning microscopy to investigate the receptor distribution on the membranes. Functionality of the receptor-fusion proteins were investigated by competition binding assays using commercially available ^{3}H-propionyl-NPY or ^{3}H-propionyl-PP [6] and by inhibition of forskolin stimulated cAMP production. Affinity and activity of all receptor constructs was maintained and comparable to the wild type receptors.

We used the fluorescence resonance energy transfer (FRET) to study homo- and heterodimerisation of the hY_1-, hY_2- hY_4- and hY_5-receptors in living cells. Two different FRET techniques, fluorescence microscopy and fluorescence spectroscopy, were applied. Furthermore photobleaching by CLSM was performed. All techniques clearly showed that the hY_1-, hY_2-, hY_4 and hY_5-NPY receptor subtypes are able to form homodimers and that the hY_1/hY_5 pair can form heterodimers. The dimerization is independent of the receptor expression level and only receptor subtype dependant, whereas $Y_4>Y_1,Y_5>Y_2$ was detected.

References

1. Beck-Sickinger, A. G. *Drug Discovery Today* **1**, 502-513 (1996).
2. Devi, L. A. *Trends Pharmacol. Sci.* **22**, 532-537 (2001).
3. Angers, S., Salahpour, A. and Bouvier, M. *Annu. Rev. Pharmacol. Toxicol.* **42**, 409-435 (2002).
4. Matthews, J. E., Jansen, M., Lyerly, D., Cox, R., Chen, W. J., Koller, K. J., and Daniels, A. J. *Regul. Pept*. **72**, 113-119 (1997).
5. Dinger, M. C., Bader, J. E., Kóbor, A. D., Kretzschmar, A. K. and Beck-Sickinger, A. G. *J. Biol. Chem.* **278**, 10562-10571 (2003).
6. Koglin, N., Lang, M. Rennert, R. and Beck-Sickinger, A. G. *J. Med. Chem*. in press (2003).

Peptide Revolution: Genomics, Proteomics & Therapeutics
Michael Chorev & Tomi K. Sawyer (Editors)
American Peptide Society, 2003

Replacement of the Tic Residue by Benzo-1,2,3,4-Tetrahydroisoquinoline-3-Carboxylic Acids in TIPP Peptides

Sylvia Van Cauwenberghe[1], José Martins[2], Mylene Gosselin[3], Lejla Hodzic[3], Sylvain Caron[3], Joanne Butterworth[3] and Dirk Tourwé[1]

[1]Department of Organic Chemistry, Vrije Universiteit Brussel, Pleinlaan 2, B-1050 Brussels; [2]Department of Organic Chemistry, NMR and Structure Analysis Unit, Universiteit Gent, Krijgslaan 281 S4, B-9000 Gent, Belgium; [3]Molecular Pharmacology Department, AstraZeneca R&D Montréal, 7171 Frédérick-Banting, Montréal (Ville St-Laurent), Québec, H4S 1Z9 Canada

Introduction

Peter Schiller developed H-Tyr-Tic-Phe-Phe-OH (TIPP), a potent and selective δ-opioid antagonist. Its δ-antagonist properties are related to the cyclic nature of the Tic residue. In the proposed bioactive conformation, the aromatic ring of Tic overlaps with the indole ring of the non-peptide δ-opioid antagonist naltrindole (NTI) [1]. In order to further probe the interaction of Tic with its receptor, the benzoTic series was designed by fusing an additional benzo ring to Tic and incorporating it into the TIPP sequence (Figure 1).

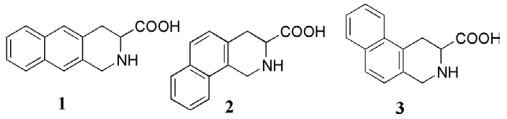

*Fig. 1. Benzo[g]Tic **1**, benzo[h]Tic **2**, benzo[f]Tic **3**.*

Results and Discussion

Molecular modeling of the tripeptides containing **1**-**3** was performed using the Sybyl software as described by Wilkes [1]. The low energy conformations of the tripeptides were calculated and analyzed for their similarity with NTI. The results showed that the compounds are promising ligands for the δ-opioid receptor (Figure 2). Compared to the two other isomers and to the native TIP the Tyr-benzo[g]Tic-Phe analogue shows major deviations of the tripeptide backbone versus NTI [1].

Fig. 2. Superimposition of NTI with low energy conformation of Tyr-benzo[g]Tic-Phe., Tyr-benzo[f]Tic-Phe and Tyr- benzo[g]Tic-Phe.

The synthesis of **1** and **2** was performed as described by C. Wang and H. I. Mosberg [2], whereas **3** was prepared by a cyclization of β-(1-naphthyl)alanine via the Pictet-Spengler reaction. The peptides were synthesized using the Boc solid phase strategy on a Merrifield resin. When **2** and **3** were incorporated in the tetrapeptide sequence, the correct peptides were obtained, but also substantial amounts of a side product having 2 mass units less than the correct peptide. The percentage of side product (measured by HPLC) formed during the reaction is shown in Table 1. The structure of these unexpected compounds was studied by 1D and 2D ^{1}H and ^{13}C NMR. It was shown that

tetrapeptide **8** was converted into the cyclic compound **12** (Figure 2). Apparently the methylene unit of the benzoTic residue was oxidized to an acyliminium intermediate, which was attacked by the Tyr-amine to give the cyclic compound.

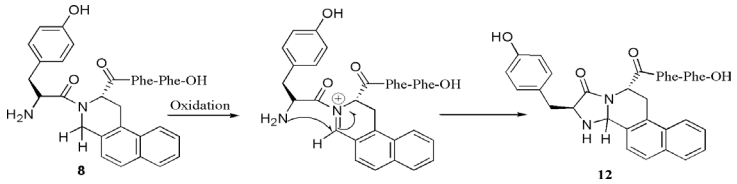

Fig. 3. Structure of side product 12.

All the tetrapeptides containing **1**-**3** as well as the side products **10**-**13** were tested for their binding and activity at the δ-opioid receptor (Table 1). The tetrapeptides **4**-**9** were tested in GTPγ[^{35}S] binding and did not activate the delta receptor up to concentrations of 90 μM. The addition of a benzene ring to the Tic residue leads to potent δ-opioid antagonists. Compared to the original TIPP none of the new analogs is more potent or selective. These results confirm that the exact distance and orientation of the Tyr/Tic aromatic rings is critical for δ-affinity.

Table 1. Yields and binding of tetrapeptides and side products.

Peptide		K_i (nM)[a]		
	%[b]	*DOR*	*MOR*	*KOR*
H-Tyr-Tic-Phe-Phe-OH **4** or **5**	/	0.13	5038	2769
H-Tyr-*rac*-benzo[g]Tic-Phe-Phe-OH **4** or **5**	100	5.4 or 132.7	742.6 or 690.1	5508 or >7300
H-Tyr-*L*-benzo[h]Tic-Phe-Phe-OH **6**	80	7.1	4883	6187
Side product **10**	20	2806.0	>9600	>7300
H-Tyr-*D*-benzo[h]Tic-Phe-Phe-OH **7**	45	28.6	837.2	1733
Side product **11**	55	337.0	129.1	>7300
H-Tyr-*L*-benzo[f]Tic-Phe-Phe-OH **8**	25	2.2	3131	>7300
Side product **12**	75	369.5	5365	>7300
H-Tyr-*D*-benzo[f]Tic-Phe-Phe-OH **9**	60	46.9	832.3	>7300
Side product **13**	40	104.9	4454	>7300

[a]Radioligands employed were [^{125}I]-Deltorphin II at delta, [^{125}I]-FK33824 at mu, and [^{125}I]-[D-Pro^{10}]-Dynorphin A[1-11] at kappa, [b]Percentage of correct peptide versus cyclic compound measured by HPLC (215 nm).

Acknowledgments
We thank Prof. Dr. H. Mosberg for the experimental details of the synthesis of **1**. This work was supported by grants of FWO and IWT.

References
1. Wilkes, B. C. and Schiller, P. W. *Biopolymers* **37**, 391-400 (1995).
2. Wang, C. and Mosberg, H. I. *Tetrahedron. Lett.* **36**, 3623-3626 (1995).

Peptide Revolution: Genomics, Proteomics & Therapuetics
Michael Chorev & Tomi K. Sawyer (Editors)
American Peptide Society, 2003

Synthesis, Purification, and Stabilization of a Myc/His Epitope Tagged Human δ Opioid Receptor

Scott M. Cowell[1], Isabel Alves[2], Eva Varga[3], Tadashi Okura[3], Padma Nair[1], Henry I. Yamamura[3] and Victor J. Hruby[1]

[1]Department of Chemistry; [2]Department of Biochemistry; [3]Department of Pharmacology
University of Arizona, Tucson, AZ, 85721, USA

Introduction

The study of novel drugs and characterization of the opioid receptor has historically been limited to *in vivo* studies. This limitation was partially overcome when the human δ opioid receptor (hDOR) was successfully transfected into CHO cell lines after the isolation of the correct cDNA plasmid, [1, 2] with thorough characterization and down regulation studies [3]. The cloning of the hDOR has a wide variety of applications in the areas of pharmacology and drug design, by providing adequate quantities of the receptor for experimentation.

In order to further characterize possible ligands for an hDOR, we have post-translationally modified the hDOR with a myc/His tag at the C-terminus of the receptor. We have now developed methods for the solubilization and purification of the receptor in a form that is stable for seven days.

Results and Discussion

Site-specific mutagenesis was used to modify the stop codon of the C-terminus so that the receptor DNA could be annealed into a pcDNA3 myc/his epitope tag (Invitrogen). The human δ opioid receptor was modified on the C-terminus. The stop codon was changed to an Xba1 site on the receptor via PCR and the sequence was placed into the pcDNA3 myc/his epitope tag. After insertion of the modified hDOR, a majority of the receptor sequence was replaced by wild type hDOR to prevent any possible DNA mismatches. The receptor was stably transfected into CHO cells and the DNA sequence was checked by sequencing.

Purification of the receptor started with solubilizing the cells in Tris-Cl buffer at pH=7.4 and homogenization using Teflon homogenizers (10 strokes). The cell was centrifuged at 42,000 rpm (160,000 X g) at 4 ^{o}C for 30 minutes. The upper layer was decanted and the membranes were solubilized in a buffer solution comprised of 25 mM Hepes, 0.5 M KCl, 30 mM of octylglucoside or 1% dodecylmaltoside at pH=7.4. Protease inhibitors specifically designed for metal chelating columns were used (SIGMA). After homogenization (15 strokes using a Teflon tube homogenizer), the solution was centrifuged at 42,000 rpm (160,000 X g) at 4 ^{o}C for 60 minutes.

The receptor was purified on a TALON Co^{+2} metal chelating column (Clontech), gentle mixing for 2 days on a rocker at 12 ^{o}C, and eluting with 25 mM Hepes, 0.5 M KCl, 30 mM octylglucosides and 100 mM imidazole buffer at pH. Subsequent purification involved passing the released receptor through a Sepharose column with deltorphin II bound. The receptor bound to the deltorphin II and was released with NTI. This step increased the purification of the receptor but also purified the only bioactive receptor.

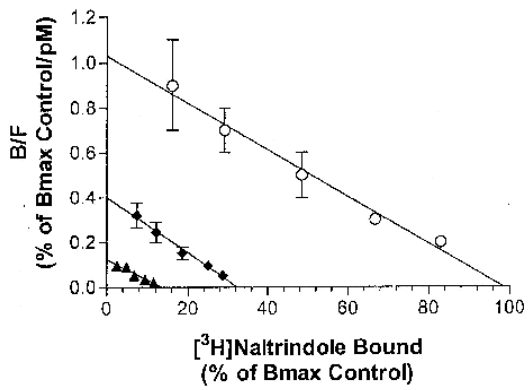

Fig. 1. Rosenthal plots of the saturation isotherms in epitope tagged hDOR.. Cells were preincubated with IMDM (control) (o) SNC80 (500nM) (▲) or DPDPE (500 nM) (♦) for 24h and then rinsed with IMDM (37 °C) three times. Saturation binding studies were performed using varying concentration of [^{3}H]naltrindole (0.03-0.5 nM). Each point represents the average ± the standard error of four determinations.

This solubilized receptor was characterized using standard pharmacological protocols and proved to share the same ligand binding affinities as the wild type receptor (Figure 1). The purity of the sample was confirmed using SDS-PAGE and immunoprecipitation. The purified receptor has subsequently been used for other projects including plasmon waveguide resonance (PWR) spectroscopy, a technique for measuring conformational changes to receptors with the addition of ligands. This purified sample has now been successfully used in various techniques such as PWR for the analysis of novel ligands and G-proteins.

Acknowledgments
The work was funded by a grant from the National Institute on Drug Abuse, USPHS.

References

1. H. I. Yamamura, W. R. Roeske, V. J. Hruby, E. V. Varga, G. Santoro, M. Nguyen, E. Babin, X. Li, L. Fang, E. Malatynska and R. J. Knapp, *Life Sciences* **54**, 463-469 (1994).
2. H. I. Yamamura, W. R. Roeske, S. Waite, X. Li, G. Santoro, R. J. Knapp, Y. Wang and E. Malatynska, *NeuroReport* **6**, 613-616 (1995).
3. W. R. Roeske, H. I. Yamamura, V. J. Hruby, K. Rice, S. Calderon, S. Saite, R. J. Knapp, Y. Yang and E. Malatynska, *J. Pharmaco. Experi. Therap.* **278**, 1083-1089 (1996).

Peptide Revolution: Genomics, Proteomics & Therapeutics
Michael Chorev & Tomi K. Sawyer (Editors)
American Peptide Society, 2003

Potent Antinociceptive Activity by a Novel Opioid, 3-(3'-Dmt-aminopropyl)-6-(4'-Dmt-aminobutyl)-5-methyl-2(1*H*)-pyrazinone

Yunden Jinsmaa[1], Yoshio Okada[2], Yuko Tsuda[2], Yusuke Sasaki[3], Akihio Ambo[3], Sharon D. Bryant[1] and Lawrence H. Lazarus[1]

[1]*National Institute of Environmental Health Sciences, Research Triangle Park, NC 27709, USA,*
[2]*Kobe Gakuin University, Nishiku, Kobe 651-2180, Japan,*
[3]*Tohoku Pharmaceutical University, Aoba-ku, Sendai 981-8558, Japan*

Introduction

All known μ-, δ- and κ-opioid peptides have a message domain, consisting of a N-terminal Tyr residue and a spacer (D-Ala, D-Met, Pro or Gly-Gly) between the Tyr and second aromatic ring (Phe or Trp), which is responsible for the binding to opioid receptors. The sequence C-terminal to the second aromatic ring is the address domain responsible for bioactivity. The studies on the design of opioid peptides showed that the substitution of Tyr at the message domain by 2',6'-dimethyl-L-tyrosine (Dmt) dramatically increased receptor affinity in numerous peptides and enhanced their antinociceptive effect [1,2]. Moreover, Dmt played a key role in the design of powerful opioidmimetics with agonist and antagonist activities [3,4].

Previously we showed that cyclization of dipeptidyl chloromethyl ketones gave pyrazinone derivatives which can be easily inserted into the opioid peptide sequence to give rise to a new family of opioidmimetic substances with selectivity for the μ-opioid receptor [5,6]. The pyrazinone ring may play a role in the address sequence due to the enhanced μ-opioid receptor affinity and bioactivity. On the basis of these results, we therefore synthesized new opioidmimetic substances containing *bis*-Dmt residue linked to the pyrazinone ring by Lys (K) or Orn (O) during synthesis**: 1** (3-(3'-Dmt-aminopropyl)-6-(4'-Dmt-aminobutyl)-5-methyl-2(1*H*)pyrazinone), **2** (3,6-*bis*-(3'-Dmt-aminobutyl)-5-methyl-2(1*H*)-pyrazinone)**, 3** (3,6-*bis*-(3'-Dmt-aminopropyl)-5-methyl-2(1*H*)-pyrazinone) and **4** (3-(4'-Dmt-aminobutyl)-6-(3'-Dmt-aminopropyl)-5-methyl-2(1*H*)pyrazinone). Compoud **1** bound with the highest affinity to μ-opioid receptors (K*i* = 0.025 nM), which was 1.7-4.4 times greater than the affinity of the other analogues and had the highest selectivity to μ-opioid receptors (μ/δ = 1,274). In this study, we examined *in vivo* activity of **1** using tail-flick (TF) and hot plate (HP) tests in mice following icv, sc and po administration.

Results and Discussion

Antinociception. Compound **1** (icv) showed spinal and supraspinal antinociception in mice, being 65-71-fold more potent than morphine (Figure 1A, C). Other compounds in this series, **2** and **3**, also exhibited potent antinociception, however, they were only 22-89% effective as **1** depending on the measurement test.

The antinociception induced by **1** was blocked by the non-selective opioid antagonist, naloxone, with same degree as that of morphine in both TF and HP tests, suggesting that the effect is mediated by μ-opioid receptors (Figure 1B, D).

Sc injection of **1** showed dose-dependent antinociception with a minimum effective dose (MED) of 1 mg/kg in both tests; it was equivalent to that produced by morphine in TF and was only 65% effective as morphine in HP test. Po administration of **1** exhibited antinociception with MED 10 and 30 mg/kg in TF and HP tests, respectively. Although the **1** was 65% as effective as morphine in the TF test, it did not reach the l

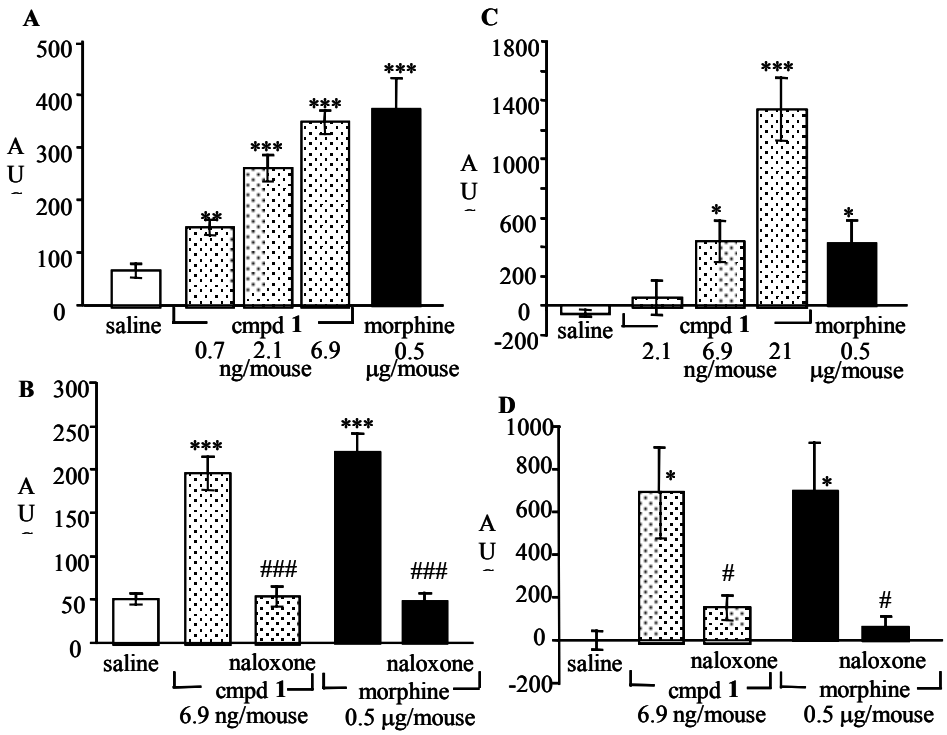

*Fig. 1. Effect of cmpd 1 (icv) on tail-flick(TF) and hot plate (HP) latencies in mice. A,C; AUC (area under the curve) in TF and HP tests, respectively. B,D; effect of naloxone (2 mg/kg sc) on TF and HP latencies of cmpd 1, respectively. ***p<0.001, **p<0.01, *p<0.05 vs saline group, ###p<0.001, #p<0.05, vs cmpd 1 or morphine group.*

level of morphine at 30 mg/kg; in the HP test, it had only 3% of the activity of morphine. Nonetheless, this result suggests that **1** was able to cross the gastrointestinal and blood-brain barriers to produce CNS-mediated analgesia.

Tolerance. To assess the development of tolerance, mice were injected sc with 3 mg/kg of 1 or morphine daily for 7 days and both TF and HP latencies were measured. Antinociception of 1 and morphine were significantly reduced, 56% and 51%, respectively, after daily (7 days) injection in TF, and 78% and 98%, respectively in HP test, suggesting that 1 is acting by the same mechanism as morphine.

References

1. Hansen, J. D. W., *et al*., *J. Med. Chem.* **35**, 684-687(1992).
2. Sasaki, Y., *et al., Chem. Pharm. Bull. (Tokyo)* **47**, 1506-159 (1999).
3. Salvadori, S., *et al*., *J. Med. Chem.* **40**, 3100-3108 (1997).
4. Bryant, S. D., *et al*., *Biopolymers (Peptide Sci.)* **71**, 86-102 (2003).
5. Okada, Y., *et al*., *Chem. Pharm. Bull. (Tokyo)* **46**, 1374-1382 (1998).
6. Okada, Y., *et al*., *Chem. Pharm. Bull. (Tokyo)* **47**, 1193-115 (1999).

Peptide Revolution: Genomics, Proteomics & Therapeutics
Michael Chorev & Tomi K. Sawyer (Editors)
American Peptide Society, 2003

ORL1 Receptor Agonists and Antagonists

A.K. Judd[1], D.J. Tuttle[1], A. Kaushanskaya[1], R.W. Jones[1], A. Sanchez[2], W. Polgar[3], T. Khroyan[3] and L. Toll[3]

[1]SynVax Inc. 1770 N. Research Park Way, North Logan, UT 84341, USA; [2]Protein and Nucleic Acid Facility, Beckmen Center, Stanford Medical Center, Palo Alto, CA 94305, USA; [3]SRI International, 333 Ravenswood Avenue, Menlo Park, CA 94025, USA

Introduction

Unlike the opioid receptors, and because of its recent discovery, structure-activity relationships leading to high affinity or agonist and antagonist activity for the family member ORL1 (OP4) are poorly understood. It has been suggested that high affinity agonists at the ORL1 receptor may be useful clinically for treatment of anxiety, whereas ORL1 receptor high affinity antagonists may have analgesic activity. We have designed a series of hexapeptides for ORL1 receptor with a broad range of *in vitro* efficacies. We also examined antinociceptive effects of a high affinity hexapeptide agonist. Recently, high throughput screening and classical and medicinal chemistry have led to the development of several high affinity and selective small molecule agonists and antagonists. Many of the Ac-RYYRWR-NH_2 analogs with modified amino acids, synthesized in our laboratory, maintained high affinity for ORL1 receptor. Modifications of the side chains produced variations in the efficacy of the compounds [1]. The peptide Ac-RY(3-Cl)YRWR-NH_2 was found to be the highest affinity compound with the highest efficacy in the [^{3}H]GTPγS binding assay. This compound, when administered intracerebroventricularly (ICV), appeared to be a nearly full agonist *in vivo*, as its ability to decrease tail flick latencies and reduce morphine induced analgesia was similar to that of nociceptin, the endogenous ligand. This compound, at its highest concentration (100 mg/kg), also attenuated morphine induced analgesia subsequent to subcutaneous administration.

Results and Discussion

Receptor binding studies were conducted on nociceptin/orphanin FQ (N/OFQ) and all the hexapeptide analogs. Binding was conducted on membranes prepared from CHO cells transfected with hORL1. The parent compound Ac-RRYRWR-NH_2 is a very high affinity compound with a Ki of 100 pM, similar to that of N/OFQ itself [2]. Many of the hexapeptide analogs with modified amino acids prepared in our laboratory maintained high affinity for ORL1 receptor. The peptide Ac-RY(3-Cl)YRWR-NH_2 was found to be the highest affinity compound. Each compound was also tested for functional activity *in vitro* by measuring stimulation of [^{35}S]GTPγS binding in membranes prepared from the hORL1-CHO cells. The results were compared to those of the endogenous peptide N/OFQ, which is a full agonist at ORL1, and thus by definition has 100% efficacy. The peptide Ac-RY(3-Cl)YRWR-NH_2 was found to have the highest efficacy in the [^{35}S]GTPγS binding assay. The peptide Ac-RY(3-Cl)YRWR-NH_2, when administered ICV alone, induced pro-nociception. This peptide appeared to be a nearly full agonist *in vivo,* as evidenced by its ability to increase tail-flick latencies (Figure 1). The peptide Ac-RY(3-Cl)YRWR-NH_2 dose-dependently reversed morphine-induced analgesia (Figure 2). The effect was similar to that of nociceptin, the endogenous ligand.

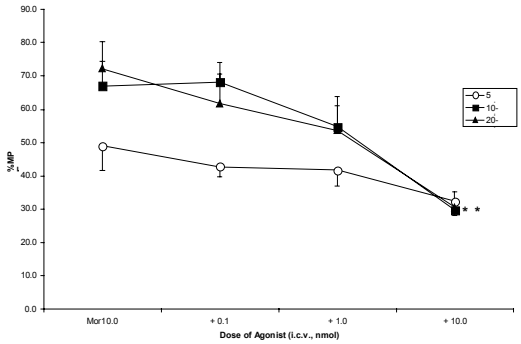

Fig. 1. Agonist 87-B dose-dependently reversed morphine-induced analgesia. An astrisk represents a significant difference from morphine alone.

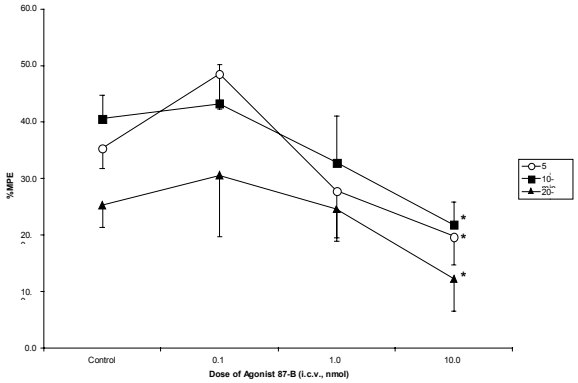

Fig. 2. Agonist 87-B administered alone induced pro-nociception. An astrisk represents a significant main effect from control values.

Conclusion

The high affinity agonist produced the same behavioral profile as the endogenous ORL1 agonist N/OFQ. These results suggest that modified hexapeptides may provide a template for longer lasting compounds with nociceptin-like activities and may produce clinically useful compounds for a variety of indications. Experiments with other agonists are in progress.

Acknowledgments

This work was supported by National Institute of Diabetes and Digestive and Kidney Diseases Grant DK55457 (to A. K. J.) and NIDA grant DA06682 (to L. T.).

References

1. Judd A. K., *et al*., *J. Peptide Res.* In Press.
2. Dooley, C. T., *et al*., *J. Pharmacol. Exp. Ther.* **283**, 735-741 (1997).

Peptide Revolution: Genomics, Proteomics & Therapeutics
Michael Chorev & Tomi K. Sawyer (Editors)
American Peptide Society, 2003

Bioactive N-terminal Undecapeptides Derived from Parathyroid Hormone: The Role of α-helicity

Alessandra Barazza[1], Nereo Fiori[2], Elisabetta Schievano[2], Stefano Mammi[2], Evaristo Peggion[2], Joseph M. Alexander[1], Michael Rosenblatt[1] and Michael Chorev[1]

[1]Division of Bone & Mineral Research, Beth Israel Deaconess Medical Center & Harvard Medical School, 330 Brookline Ave., Boston, MA 02215, USA; [2]Department of Organic Chemistry, University of Padova, Institute of Biomolecular Chemistry, CNR, Via Marzolo 1, 35131 Padova, Italy

Introduction

Parathyroid hormone (PTH) is an 84 amino acid peptide responsible for the regulation of calcium levels in blood and kidney [1]. The N-terminal (1-34) sequence is a fully active form of this hormone. *In vivo* it can reproduce all biological responses characteristic to the native intact PTH. Clinical studies have demonstrated PTH-(1-34) to be a powerful bone anabolic agent able to restore bone mineral density in postmenopausal women and to reduce fracture risk. Recently, recombinant human PTH(1-34), designated as FORTEO® (Triparatide), was approved by the FDA for treating osteoporosis in postmenopausal women who are at high risk for fractures.

NMR analyses of PTH(1–34) analogues in a variety of polar and non-polar solvents suggest that the N-terminal portion of PTH (from Ser^3 to Lys^{13}), known to be responsible for the activation of the receptor, contains a short helical segment. This N-terminal helix is connected to a more stable C-terminal α-helical segment (from Arg^{20} to Val^{31}), which contains the principal receptor binding domain, by a non-structured segment (from His^{14} to Glu^{19}).

Previously, enhancement of α-helicity in the PTH(1-14) and PTH(1-11) sequences yielded potent analogues of PTH(1-14)NH_2 [2]. This report presents our efforts to stabilize the structure and to increase the helical content of the short *h*PTH(1–11) sequence. We synthesised and characterized the following *h*PTH(1–11) analogues substituted in positions 1 and 3 by the following tetra-substituted amino acid residues: Aib, 1-aminocyclopentane-1-carboxylic acid (Ac_5c) and 1-aminocyclohexane-1-carboxylic acid (Ac_6c):
[Ac_5c^1,Aib ^{3}, Gln^{10}, Arg^{11}]-PTH(1-11)NH_2 (**I**); [Aib^1, Ac_5c^3, Gln^{10}, Arg^{11}]-PTH(1-11)NH_2 (**II**);
[Ac_6c^1, Aib ^{3},Gln^{10},Arg^{11}]-PTH(1-11)NH_2 (**III**); [Aib^1, Ac_6c^3, Gln^{10},Arg^{11}]-PTH(1-11)NH_2 (**IV**);
[$Aib^{1,3}$, Gln^{10}, Arg^{11}]-PTH(1-11)NH_2 (**V**).

Results and Discussion

The results of biological characterization, including efficacy in stimulating cAMP accumulation indicated that analogues **I** and **II** are active (10^{-7}-10^{-8} M), while analogues **III-V** are inactive ($\geq 10^{-3}$ M). The most potent analogue **I** exhibits biological activity 3500-fold higher than that of the native sequence PTH(1-11) and only 15-fold weaker that than of the full native sequence hPTH-(1-34). The CD spectra of the five analogues in aqueous solution containing 20% TFE (v/v) are shown in Figure 1. The CD results show a clear correspondence between biological activity and helical content of the peptides. Only the two bioactive peptides **I** and **II** exhibit the typical CD pattern of the α-helical conformation, with a helix content in the range 45-55%, estimated according to the method of Greenfield and Fasman. NMR experiments identify the amino acid

residues comprising the helical sequence. In analogues **I** and **II,** the chemical shift differences of αCH protons with respect to the corresponding random coil values identify a helical segment spanning the sequence Val^{2}-Met^{9}.

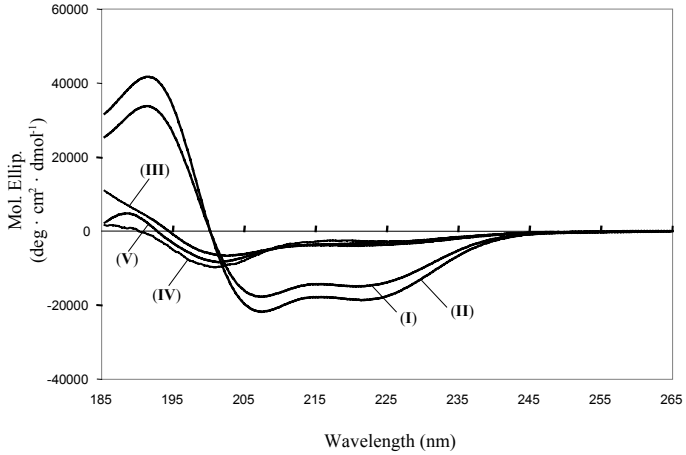

Fig. 1. CD spectra of the five analogues ın water containing 20% TFE at 50 μM peptide concentrations.

In the NOESY spectra, a number of αH(i)-HN(i+3), αH(i)-βH(i+3) connectivities and also one αH(i)-HN(i+4) connectivity typical of the α-helix were observed in the sequence 2-10 of analogues **I** and **II**. In the inactive analogues **III**-**V**, the tendency of the Ile^{5}-Met^{8} segment to fold into the helical structure is much weaker. In the inactive analogues, only three helical connectivities were observed. Superimposition of the ensembles of the low energy structures resulting from distance geometry and molecular dynamics calculations clearly indicated a much better convergence towards the helical structure of the active analogues compared to the inactive ones (Figure 2).

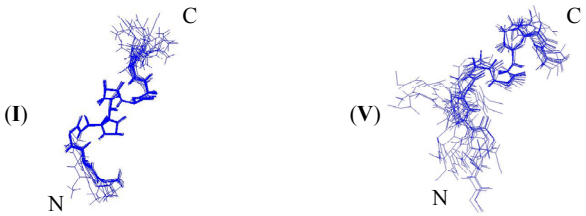

*Fig. 2. Superimposition of the ensembles of the lowest energy calculated structures of analogues **I** and **V**. Heavy backbone atoms of the sequences 3-9 and 5-8 were used in the superimposition, respectively.*

Taken together, these results stress the importance of the presence of a helical segment at the N-terminus of PTH (1-34) analogues on their biological activity.

References

1. Chorev, M. and Rosenblatt, M. In Bilezikian, J. P., Levine, M. A. and Markus, R. (Eds.) *Parathyroids,* Raven Press, N.Y., p. 139-156 (1994).
2. Shimizu, N., Guo, J. and Gardella, T. J. *J. Biol. Chem.* **276**, 49003-49012 (2002).

Peptide Revolution: Genomics, Proteomics & Therapeutics
Michael Chorev & Tomi K. Sawyer (Editors)
American Peptide Society, 2003

Carboxy Terminal Modifications of PTH-(1-34) that Confer Skin Protease Resistance and Retain Biological Potency

Krishna G. Peri, Annie Bergeron, Thuy Lam, Kim High and Thierry Abribat

Theratechnologies Inc., 2310 Alfred-Nobel Blvd, Montreal (Saint-Laurent), Quebec, H4S 2A4, Canada

Introduction

Parathyroid hormone (1-84), secreted by the parathyroid gland, is processed to release N- and C-terminal fragments in circulation. PTH is involved, along with calcitonin and vitamin D, in calcium homeostasis and displays potent anabolic and catabolic actions on cancellous bone. The actions of PTH are mediated by the PTHR1 and PTHR2 receptors. Though the role of PTHR1 in bone turnover, differentiation and function of osteoblasts, osteoclasts and osteocytes, and renal calcium handling is well known, the physiological role of PTHR2 is yet to be delineated. Even though, some of the actions of PTH(1-84) via PTHR1 are reproduced equipotently by the N-terminal truncated product, PTH(1-34), the physiological roles of the carboxy-terminal fragments of PTH(1-84) are not fully understood [1]. PTH has been shown to be a potent osteo-anabolic agent in animal models as well as in human clinical trials [2]. There is a great deal of interest in developing formulations containing PTH(1-34) and its derivatives for the anabolic therapy of postmenopausal osteoporosis.

The injectable formulations of PTH(1-34) [Eli Lilly & Co], intranasal, oral and inhalatory formulations are currently being developed. The route of administration poses different challenges for formulating the same compound due to the differences in absorption, degradation, bioavailability, pharmacokinetics, the metabolite composition of the circulating peptides, immunogenicity and other parameters. Transdermal delivery of peptides is an important administration route, due to the minimally-invasive nature of the procedures and the devices involved, as well as the ease of drug administration without the need for medical supervision. However, the issues facing transdermal delivery are very different compared to other drug delivery systems, due to the special challenges posed by the skin barrier to peptides and more particularly of this barrier towards peptides in view of the presence of skin proteases.

Proteolytic degradation could lead to a loss of potency of PTH (*in vitro* and *in vivo*), particularly in the case of shorter derivatives of PTH such as PTH(1-31). Degradation by skin proteases poses certain problems to the bioavailability of peptides such as PTH when administered transdermally. Degradation of PTH(1-34) takes place at the carboxy-terminal end, due to the action of skin carboxypeptidases. There thus remains a need to develop PTH derivatives that are resistant to skin proteases, and which can be used for transdermal administration.

The objective of this study is to produce modified derivatives of PTH(1-34) that exhibit increased resistance to proteases in skin extracts, and manifest applicability in the transdermal delivery of these peptides to patients diagnosed with bone loss, or more particularly, patients susceptible to bone loss.

Results and Discussion

PTH(1-34) and a series of PTH(1-34) derivatives amidated at the carboxy terminus (Figure 1) were produced, and their stability in hairless guinea pig (HGP) skin extracts and their potency to stimulate cyclic AMP synthesis in the human osteoblastic cell line,

SaOS2, were determined. PTH(1-34)OH was stable in human and HGP plasma for 2 h; on the other hand, it is rapidly degraded in HGP skin extracts with a half life of 19 min. The major metabolites of PTH(1-34) in HGP skin extracts were PTH(1-33) and, to a

PTH(1-34)-X	SVSEIQLMHNLGKHLNSMERVEWLRKKLQDVH-X
X = COOH	PTH(1-34) OH
X= $CONH_2$	PTH(1-34) amide
X = $CONHCH_2CH_2CH_3$	PTH(1-34) propylamide
X = $CONHCH_2CH_2CH_2Ph$	PTH(1-34) phenylpropylamide

Fig. 1 Sequence of native PTH(1-34) and synthetic PTH(1-34)analogs.

smaller extent, PTH(1-32). The incubation of PTH(1-34) and PTH(1-34) amide with skin extracts, over the indicated times, was conducted. Fractions containing the peaks were collected, lyophilized and the masses determined by MALDI-TOF. PTH(1-34) eluted at t = 25-26 minutes, whereas its major degradation product, having a mass corresponding to PTH(1-33), eluted at t = 17 minutes. PTH(1-34)NH_2 did not produce this metabolite following an incubation period of 30 min. Similar protection from skin proteases was observed for PTH(1-34) propylamide. The half-lives of the modified peptides in HGP skin extracts were: PTH(1-34)NH_2 25 min, PTH(1-34)NHpropyl 37 min; PTH(1-34)NHphenyl propyl 26 min. The carboxy modifications of PTH peptide did not affect their potency to stimulate cAMP synthesis in the human osteoblastic cell line, SaOS2 (Table 1), even though PTH(1-33) and PTH(1-32) were 10-fold less potent in this assay.

Table 1. In vitro efficacies of natural PTH and various PTH analogues in human osteoblast Saos-2 cells.

Compound	EC_{50} (nM)	n
PTH(1-34)	2.4	10
PTH(1-34)NH_2	3.1	6
PTH(1-34)propylamide	5.3	6
PTH(1-33)	19	4
PTH(1-32)	31	4

References

1. Whitfield, J. F., et al., *Medscape Women's Health eJournal* **5 (5)**, (2000), (http://www.medscape.com/viewarticle/408928).
2. Neer, R. M. et al., *New Engl. J. Med*. **344**, 1434-1441 (2001).

Peptide Revolution: Genomics, Proteomics & Therapeutics
Michael Chorev & Tomi K. Sawyer (Editors)
American Peptide Society, 2003

Synthesis of Conformationally Constrained PTH(1-14) Analogs

Ashok Khatri[1,2], Xiang-Chen Huang[1], Naoto Shimizu[1,2] and Thomas J. Gardella[1]

[1]Endocrine Unit, Massachusetts General Hospital and
[2]Harvard Medical School, Boston, MA 02114, USA

Introduction

Parathyroid hormone (PTH), an 84 amino acid polypeptide, is the major regulator of extracellular ionized calcium metabolism and binds to a class 2 GPCR expressed in bone and kidney. Synthetic PTH(1-34) is fully active and when administered by daily subcutaneous injection has anabolic effects on bone. Thus, PTH(1-34) is now being used to treat osteoporosis. An orally active PTH analog (peptidic or non-peptidic) would be desirable for this purpose, but, so far, no such compound has been described. The pharmacophore of native PTH is diffuse, with determinants of receptor-binding affinity and cAMP-signaling potency residing principally in the N- and C-terminal regions of PTH(1-34), respectively. N-terminal fragments of PTH are only weakly active {e.g. PTH(1-14)} or inactive {e.g. PTH(1-11)}. As part of our efforts to define and optimize the essential PTH pharmacophore, we have previously screened ~200 PTH(1-14) analogs for altered P1R activity, and these studies identified several activity-enhancing substitutions [1]. This work was facilitated by the capacity to synthesize the analogs on a multiple peptide synthesizer. In subsequent studies we found that substituting the constrained amino acid, Aib (α-aminoisobutyric acid) at positions 1 and 3 enhanced PTH(1-14) activity 100-fold, and when combined with the previous modifications, resulted in an analog, [$Aib^{1,3}$,Gln^{10},Har^{11},Ala^{12},Trp^{14}]PTH(1-14), that is 100,000-fold more potent than native PTH(1-14) and as potent as PTH(1-34) [2]. A similarly modified PTH(1-11) analog was also highly potent [2]. Based on these findings, we sought to explore the effects of other constrained amino acids at positions 1 and 3 of PTH(1-14) and shorter analogs on peptide activity [3]. Difficulties were encountered when we attempted to synthesize these constrained peptides on the multiple peptide synthesizer, compelling us to explore alternative synthesis modalities.

Results and Discussion

Preparation of previous non-constrained PTH(1-14) analogs on the multiple peptide synthesizer utilizing HBTU/HOBt/DIEA coupling chemistry resulted in crude products with >90% purity; these peptides could be assayed after a simple desalting step [1]. Attempts to prepare subsequent PTH(1-14) analogs containing Aib at various positions by this approach resulted, in some cases, in heterogeneous crude products that required extensive HPLC purification. Similar problems arose when we attempted to synthesize analogs substituted with other α,α-dialkyl amino acids (diethylglycine (Deg) and 1-amino-cyclopentane-1-carboxylic (Ac_5c) and 1-amino-cyclohexane-1-carboxylic acid (Ac_6c) at positions 1 and/or 3 on the multiple synthesizer, and in some cases we failed to obtain any desired product. We therefore turned to the large-scale synthesizer, and classical DCC/HOBt coupling chemistry. In most cases, this approach yielded high-quality crude products, which, after a single HPLC purification step, were fully homogenous.

Of the constrained analogs prepared so far, several (e.g. [Ac_5c^1,Aib^3,Gln^{10},Har^{11}, Ala^{12},Trp^{14}]PTH(1-14)NH_2 [3] and [Ac_5c^1,Aib^3,Gln^{10},Har^{11}]-PTH(1-11)NH_2) exhibited high signaling potencies when tested *in vitro* (increases in intracellular cAMP in

HKRK-B7 cells, Table 1) and *in vivo* (increases in plasma cAMP in mice). These peptides are among the most potent N-terminal PTH fragment analogs identified to date. We also obtained the shortest N-terminal PTH fragment analog for which both binding and cAMP signaling activities can be detected: [Ac_6c^1,Aib^3]PTH(1-9)NH_2.

Table 1 Functional properties of PTH analogs in HKRK-B7 cells.

Peptide[a]	IC_{50} (nM)[b]	EC_{50} (nM)[c]
[Tyr^{34}]PTH(1-34)NH_2	3.4	7.5
[Ac_5c^1,Aib^3,Gln^{10},Har^{11},Ala^{12},Trp^{14}]PTH(1-14)NH_2	24	0.15
[$Aib^{1,3}$,Gln^{10},Har^{11}]PTH(1-11)NH_2	2,600	5.7
[Ac_5c^1,Aib^3,Gln^{10},Har^{11}]PTH(1-11)NH_2	260	2.6
[Ac_6c^1,Aib^3]PTH(1-9)NH_2	240,000	110,000

We conclude that for the conformationally constrained PTH analogs studied here, the large-scale synthesis approach utilizing DCC/HOBt coupling chemistry is superior to the small-scale multiple peptide synthesis approach utilizing HBTU/HOBt/DIEA coupling chemistry. The results emphasize the need to optimize synthesis protocols for the incorporation of constrained amino acids into PTH oligopeptides. We are now trying to optimize such protocols for the multiple peptide synthesizer. The studies also show that the use of such constrained amino acids can help to define and minimize the essential PTH pharmacophore, which now appears to reside within the PTH(1-9) region of the hormone. The overall results suggest that this N-terminal domain binds to the extracellular loops/TM region of the P1R as an α-helix, since the α,α-dialkyl amino acids used in the study are known to promote helical structure. Extending these studies could provide new insights into the P1R binding and activation mechanisms and potentially facilitate the design of PTH mimetic compounds.

Acknowledgments
The work was funded by NIH grant DK11794.

References

1. Shimizu, M., Potts, Jr J. T. and Gardella, T. J. *J. Biol. Chem.* **275**, 21836-21843 (2000).
2. Shimizu, N., Guo, J. and Gardella, T. J. *J. Biol. Chem.* **276**, 49003-49012 (2001).
3. Shimizu, N. and Gardella, T. J. *J. Bone Miner. Res.* 17 suppl., S389-SU426 (2002)

Peptide Revolution: Genomics, Proteomics & Therapeutics
Michael Chorev & Tomi K. Sawyer (Editors)
American Peptide Society, 2003

Interactions of the Mid-Region of Parathyroid Hormone (1-34) with the Receptor Orient the Hormone for Receptor Activation

Angela Wittelsberger[1], Martina Corich[1], Byung-Kwon Lee[1], Alessandra Barazza[1], Dale F. Mierke[2], Michael Rosenblatt[1], and Michael Chorev[1]

[1]Division of Bone and Mineral Research, Beth Israel Deaconess Medical Center and Harvard Medical School, 4 Blackfan Circle, HIM 944, Boston, MA 02115; [2]Department of Chemistry and Molecular Pharmacology, Brown University, Providence, Rhode Island 02912, USA

Introduction

Parathyroid hormone (PTH) regulates calcium levels in blood through its action on bone and kidney. Elucidating the bimolecular interface between PTH and its cognate G protein-coupled receptor (PTH1-Rc) should yield insight into the basis of molecular recognition and the mechanism of ligand-mediated intracellular signaling. Such understanding in turn should aid the design of PTH-mimetic drugs and analogs for the treatment of osteoporosis, hypercalcemia of malignancy, and hyperparathyroidism [1]. From structure-activity studies, PTH-(1–34) contains two α-helical domains associated with specific functions: the N-terminal helix is required for activation of the receptor, and the C-terminal helix is responsible for receptor binding. Based on studies described in this report, this model now must be re-examined. We used photoaffinity scanning (PAS) to identify key ligand–receptor interactions for residues from the mid-region of PTH-(1–34), an unstructured domain subtended by the two α-helices. Four new analogs, containing a single photoreactive *p*-benzoyl-phenylalanine (Bpa) residue in position 11, 15, 18, or 21, were analyzed and their contact site on the receptor was determined.

Results and Discussion

For the design of the novel analogs, the hydrophobic residues Leu in positions 11 and 15, Met in position 18, and Val in position 21 were selected for replacement by the hydrophobic photoreactive Bpa residue. As in previous studies, several additional structural modifications were introduced into the bPTH sequence in order to make the Bpa-containing PTH analogs resistant to the chemical and enzymatic digestions carried out after crosslinking [2]. The purity of the four analogs exceeded 97%, as assessed by analytical RP-HPLC. Amino acid analysis and ESI-MS confirmed the structural integrity of the analogs.

The binding affinities of the novel Bpa-containing PTH analogs are summarized in Table 1. All four analogs showed binding affinities of the same order of magnitude as PTH-(1–34), indicating that receptor-binding was not diminished substantially by the introduction of the photoreactive Bpa residue in the positions chosen and crosslinking studies were not precluded. In addition, we determined the efficacy of these analogs in stimulating adenylyl cyclase activity. The EC_{50} values obtained are listed in Table 1 and indicate that the introduction of Bpa was accompanied with a slight to moderate reduction in potency compared to the parent PTH-(1–34). The greatest reduction in potency was observed with [Bpa^{18}]-PTH, which was 22-fold less potent than the parent PTH-(1–34). All analogs were full agonists, reaching the same maximal adenylyl cyclase stimulation as the parent PTH-(1–34). The radiolabeled PTH analogs crosslinked specifically and competitively to the PTH1-Rc stably expressed on HEK293 cells.

Table 1. Biological characterization and contact sites for the four new PTH analogs.

PTH analog*	Binding affinity IC_{50} (nM)	Adenylyl cyclase activity EC_{50} (nM)	Contact site Residue number
[Bpa^{11}]-PTH	9.0	7.0	[165-189]
[Bpa^{15}]-PTH	6.6	1.1	[183-189]
[Bpa^{18}]-PTH	10.0	22.0	[190-224]
[Bpa^{21}]-PTH	14.0	2.2	[165-189]
PTH	3.8	0.9	-

**Based on the sequence [$Nle^{8,18}$, $Arg^{13,26,27}$,Nal^{23},Tyr^{34}]-bPTH(1–34)NH_2.*

The purified radiolabeled ligand-receptor conjugates were analyzed extensively by chemical and enzymatic digestions to determine the sites of crosslinking. Chemical digestions carried out included treatment with cyanogen bromide and 2-(2'-nitrophenylsulfenyl)-3-methyl-3-bromoindolenine. Enzymatic digestions carried out for some of the analogs included treatment with endoproteinase Lys-C and endoproteinase Glu-C. Analysis of the digestive fragments by SDS-PAGE and comparison of the sizes of the products obtained with the theoretical restriction maps identified the fragment containing the crosslinking site for each analog and each digestion. The superposing region of the different fragments then yielded the contact site for each analog, as reported in the last column of Table 1.

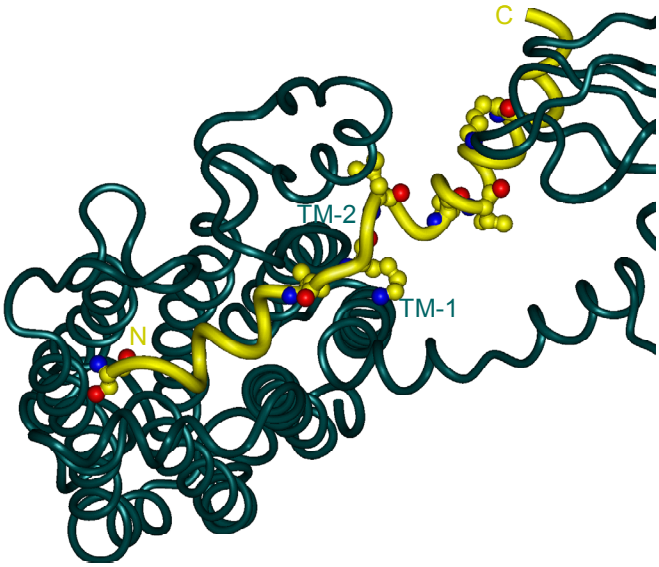

Fig. 1. Top view of the model showing the interaction between PTH and its receptor. The receptor is colored dark grey, whereas the ligand is light grey. Side chains are represented as ball and stick model for positions 1, 11, 13, 15, 18, 21, and 27 of PTH.

The experimentally-derived crosslinking sites were used as distance restraints in MD simulations. The molecular model of the PTH receptor was built as described previously [3]. In short, the starting conformation of the receptor was based on the X-ray structure of rhodopsin [4] and the structural features of fragments from the ectopic portion of TM–1 (transmembrane helix 1) and the juxtamembrane portion of the N-ECD (N-terminal extracellular domain), the ECL–1 (first extracellular loop), and the ECL–3 (third extracellular loop), as derived experimentally from previous NMR studies [5]. A target distance of 14 Å between α–carbons was chosen as restraint for the newly identified contact sites. In addition to the new contact sites for positions 11, 15, 18, and 21, previously identified contact sites for positions 1, 2, 13, and 27 of PTH were also applied [2,6,7]. The resulting model is represented in Figure 1. Note that this model is our current working model and that further refinement of the contact sites is required in order to increase the resolution of the ligand–receptor complex. However, we can already conclude that extensive contacts in the mid-region of PTH direct the activity domain of the ligand into its binding pocket on top of the seven helix bundle. Most significantly, the ligand traverses between the top of TM–1 and TM–2.

Therefore, we propose a three-step ligand–receptor interaction: First, a strong binding interaction between residues in the C-terminal helix in the ligand and the N-ECD of the receptor dominates. Unfortunately, this step is the least structurally characterized. Subsequently, the mid-region of PTH-(1–34) is directed towards the C-terminal part of the N-ECD. Extensive contacts here fix the hormone in the correct orientation to guide, in the final step, the N-terminal helix of the hormone into the binding groove on the extracellular surface of the seven transmembrane bundle, leading to receptor activation.

Acknowledgments

This research has been funded by NIH grant DK47940 to M.R. and post-doctoral fellowship stipends by the Deutscher Akademischer Austauschdienst (2001) and the Swiss National Science Foundation (2002) to A.W.

References

1.Chorev, M., Alexander, J. M. and Rosenblatt, M. In Bilezikian, J. P., Marcus, R. and Levine, M. A. (Eds.) *The Parathyroids, Second Edition*, Academic Press, San Diego, 2001, pp. 53-91.

2.Bisello, A., Adams, A. E., Mierke, D. F., Pellegrini, M., Rosenblatt, M., Suva, L. J. and Chorev, M., *J. Biol. Chem.* **273**, 22498-22505 (1998).

3.Rolz, C. and Mierke, D. F., *Biophys. Chem.* **89**, 119-128 (2001).

4.Palczewski, K., Kumasaka, T., Hori, T., Behnke, C. A., Motoshima, H., Fox, B. A., Le Trong, I., Teller, D. C., Okada, T., Stenkamp, R. E., Yamamoto, M. and Miyamo, M., *Science* **289**, 739-745 (2000).

5.Piserchio, A., Bisello, A., Rosenblatt, M., Chorev, M. and Mierke, D. F., *Biochemistry* **39**, 8153-8160 (2000).

6.Adams, A. E., Bisello, A., Chorev, M., Rosenblatt, M. and Suva, L. J., *Mol. Endocrinol.* **12**, 1673-1683 (1998).

7.Greenberg, Z., Bisello, A., Mierke, D. F., Rosenblatt, M. and Chorev, M., *Biochemistry* **39**, 8142-8152 (2000).

Peptide Revolution: Genomics, Proteomics & Therapeutics
Michael Chorev & Tomi K. Sawyer (Editors)
American Peptide Society, 2003

Hydrazide Linked Bifunctional Peptides for the Treatment of Pain

Yeon Sun Lee[1], Richard S. Agnes[1], Peg Davis[2], Shou-wu Ma[2], Josephine Lai[2], Frank Porreca[2] and Victor J. Hruby[1]

[1]Department of Chemistry; [2]Department of Pharmacology, University of Arizona, Tucson, AZ, 85721, USA

Introduction

Cholecystokinin (CCK) has been shown to reduce the analgesic effect of opioids at a number of CNS sites, particularly in the spinal cord, and also has been implicated in the development of opioid tolerance [1]. CCK receptor antagonists have been demonstrated to potentiate the antinociceptive actions of morphine and prevent morphine tolerance [2].

From this point of view, we hypothesized that a compound which has both antagonist and agonist activities at CCK and opioid receptors, respectively, would have the enhanced analgesic effects without tolerance. We therefore designed novel bifunctional peptides where both CCK and opioid pharmacophores are fused in one structure through a hydrazide linkage. For the opioid agonist pharmacophore, the half structure of biphalin was chosen and for the CCK antagonist pharmacophore, $CCK_{30\text{-}33}$ was selected and modified in different positions to optimize CCK activities while retaining opioid activities (Figure 1). The designed hydrazide linked peptides were prepared in good yields by solution phase synthesis using Boc/Bzl chemistry. Binding affinities and bioactivities of the synthesized bifunctional peptides for opioid and CCK receptors were determined by functional assays using previously described methods [3].

LYS201	H-Tyr-DAla-Gly-Phe-NH-NH-Phe-Asp-Nle-DTrp-Boc
LYS231	H-Tyr-DAla-Gly-Phe-NH-NH-Phe-Asp-Nle-DTrp-2-Adoc
LYS328	H-Tyr-DAla-Gly-Phe-NH-NH-Phe-Asp-NMeNle-DTrp-Boc
LYS322	H-Tyr-DAla-Gly-Phe-NH-NH-NMePhe-Asp-Lys(Cpac)-Trp-Ac

Fig. 1. Structures of hydrazide linked bifunctional peptides.

Results and Discussion

The synthetic strategy of the hydrazide linked peptides involved four key steps: i) first stepwise chain elongation starting from Phe^4-OEt; ii) hydrazine substitution; iii) second stepwise chain elongation on the tetrapeptide hydrazide; and iv) hydrogenation (Figure 2). During the chain elongation, peptide intermediates were isolated by crystallization from appropriate organic solvents or 5% $NaHCO_3$ solution with high purity, then deprotected by hydrogenation to give target peptides with more than 90% crude purity. These were purified by RP-HPLC to give pure (>98%) hydrazide linked peptides.

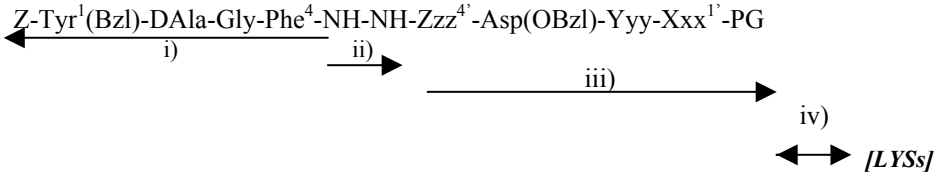

Fig. 2. Synthesis of hydrazide linked bifunctional peptides.

The synthesized peptides showed high binding affinities in the nM range at both δ and μ opioid receptors with slight δ selectivity and low, but very balanced binding affinities at CCK-A and CCK-B receptors in the μM range (Table 1). In functional assays δ opioid selectivity was increased, and no agonist activity was shown in the GPI assay (Table 2). **LYS201** with very low binding affinity (10 μM range) showed 6.5 nM antagonist activity in the GPI assay. As a lead compound, **LYS201** was modified in different positions to increase CCK activity. Interestingly, this modification resulted in not only an increase (up to 22-fold) for CCK-A and CCK-B binding affinities, but also greatly increased δ and μ opioid binding affinities (up to 70- and 26-fold, respectively). 2-Adoc group protection in the N-terminal position of the CCK pharmacophore in **LYS231** gave the highest binding affinities at CCK receptors. **LYS322**, where positions 2' and 4' are replaced with Lys(Cpac) [4] and NMePhe, respectively, showed a 10-fold increase in CCK binding affinities, and also very good opioid binding affinities (0.63 nM for the δ opioid receptor). This increase may be attributed to substitution of position 4'of CCK with NmePhe, a pharmacophore that is more relevant for opioid receptor recognition. From these structure-activity relationships, the hydrazide linker is considered to play a role in enabling a desirable conformation for opioid receptors more than for CCK receptors. Further CCK pharmacophore modifications affect not only CCK potency but also opioid potency, which suggest that the two pharmacophores are interrelated supporting either one conformation or two different conformations for both opioid and CCK receptors.

Table 1. Binding affinities of bifunctional peptides at opioid and CCK receptors.

Peptide	hDOR (nM)	rMOR (nM)	hCCK-A (nM)	hCCK-B (nM)
	[^{3}H]DPDPE	[^{3}H]DAMGO	[^{125}I]CCK$_8$	
LYS201	45	31	13,000	15,000
LYS231	3.4	16	570	930
LYS328	1.9	15	1,900	1500
LYS322	0.63	1.2	1,000	1700

Table 2. Functional assay results for bifunctional peptides at opioid and CCK receptors.

Peptide	Opioid (nM)		CCK GPI (nM)	
	MVD (δ)	GPI (μ)	agonist	antagonist
LYS201	24	460	0% at 1μM	6.5
LYS231	84	1,300	0% at 1μM	120
LYS328	42	0% at 1μM	0% at 1μM	None at 1 μM
LYS322	26	200	0% at 1μM	150

Acknowledgement
The work was supported by a grant from National Institute on Drug Abuse.

References
1. Wiesenfeld-Hallin, Z., *et al. Brain Res.* **848**, 78-89 (1999).
2. Lu, L, Huang, M., Liu, Z. and Ma, L. *NeuroReport* **11**, 829 (2000).
3. Hruby, V. J., *et al. Life Sci.* **73**, 679-704 (2003).
4. Sugg, E. E., *et al. J. Med. Chem.* **38**, 207-211 (1995).

Peptide Revolution: Genomics, Proteomics & Therapeutics
Michael Chorev & Tomi K. Sawyer (Editors)
American Peptide Society, 2003

Assembly of High-Affinity Insulin Agonists and Antagonists from Peptide Building Blocks

Lauge Schäffer[1], Søren Østergaard[1], Jane C. Spetzler[1], Thomas Hoeg-Jensen[1], Jakob Brandt[1], Gillian M. Danielsen[1], Renuka C. Pillutla[2], Renee E. Brissette[2], Ulla Ribel[1], Asser S. Andersen[1] and Neil I. Goldstein[2]

[1]Novo Nordisk A/S, Bagsvaerd, Denmark; [2]DGI Biotechnologies, Edison, New Jersey, USA

Introduction

As a prerequisite to creating an artificial molecule with insulin-like properties, we previously identified a number of peptides that bind to the insulin receptor [1]. Most of the peptides bound to two hot-spots on the receptor which are believed to be the same regions that insulin uses for binding to the receptor. In the present work we describe how these peptide building blocks can be assembled in various ways to yield both agonists and antagonists [2].

Results and Discussion

Insulin is thought to have two sites used for binding to its receptor. The simplest binding model, which will account for all the available binding data for receptor analogs and insulin analogs. implies that the insulin receptor also has two binding sites on each α-subunit. Activation of the receptor tyrosine kinase could then result from a conformational change in the receptor induced by crosslinking of the two α-subunits by insulin (Figure 1).

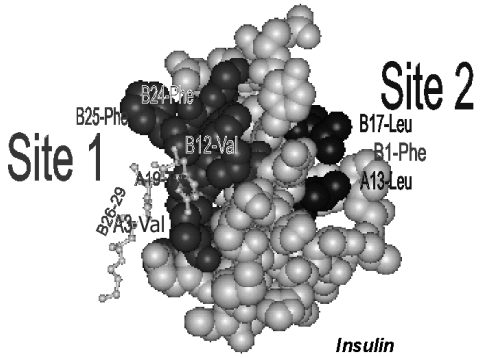

Fig. 1. Model of insulin receptor to study ligand binding.

Thus, to create an artificial molecule that would activate the insulin receptor by the same mechanism as insulin, requires a Site 1 binder and a Site 2 binder connected by an appropriate linker.

By panning of a phage display library of random 20-mer peptides against an insulin receptor construct, several hundred peptides were identified. Most peptides fell in five major groups based on their consensus motifs; the five groups were divided into two major families based on their cross competition. Binding experiments with various receptor constructs (not shown) indicate that the two peptide binding sites overlap with (but are not quite identical to) the sites used by insulin (Figure 2).

Site 1 binders:
Group 1: FHENFYDWFVRQVSKK
Group 6: KVRGFQGGTVWPGYEWLRNAAKK
Group 3: KDRAFYNGLRDLVGAVYGAWDKK

Site 2 binders:
Group 2: KWLDQEWAWVQCEVYGRGCPSKK
Group 7: KHLCVLEELFWGASLFGYCSGKK

Fig. 2. Examples of Site 1 and Site 2 binders (most important residues are underlined).

Further sequence optimization by secondary phage display libraries and synthetic bead libraries improved the affinity of the Site 1 peptides. As building blocks for assembly of dimers we chose GSLDESFYDWFERQLGKK as the Site 1 peptide (Kd for insulin competition $1.6*10^{-7}$ M) and EWLDQEWAWVQCEVYGRGCPSEE as the Site 2 peptide (Kd $4.9*10^{-7}$ M). In order to have a general method for generating peptide dimers in various orientations we used oxime chemistry. Best results were obtained with peptide aldehydes linked by bifunctional oxyamino-PEG (Scheme 1).

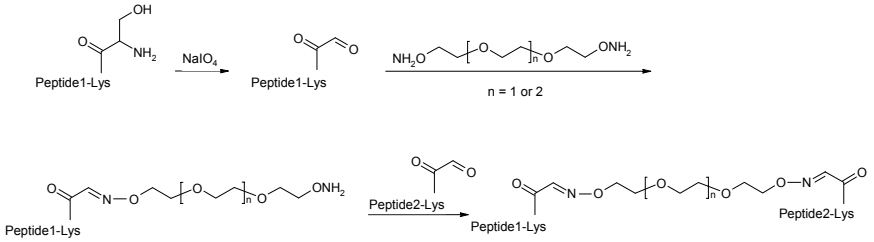

Scheme 1. Use of oxime chemistry to generate peptide dimers.

The aldehyde was generated by periodate oxidation of a serine, either in the N-terminus or on the side chain of a C-terminal lysine. A set of all four possible end-to-end heterodimers was prepared. All had affinities in the 1 nM range (>100 times better than the monomers) indicating that both sites contribute to binding. One was an antagonist, two were partial agonists and one was a full agonist (Scheme 2).

Scheme 2. Dimeric ligands types and functional properties.

Since the optimal orientation for agonism appeared to be Site2-Site1, we removed the linker and performed the subsequent optimization on single peptides containing both the Site 1 and the Site 2 sequence. The optimization was done using secondary phage display libraries and synthetic bead libraries. One such optimized Site2-Site1 peptide was S519 = SLEEEWAQVECEVYGRGCPSGSLDESFYDWFERQLG (Kd 20 pM = 40% of human insulin) which showed good activity both *in vitro* and *in vivo* (Figure 3).

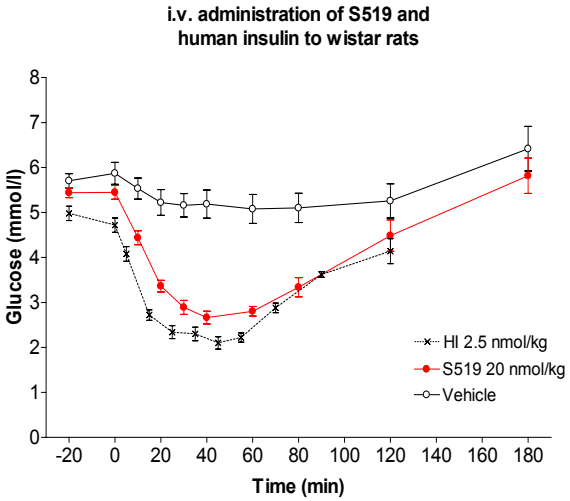

Fig. 3. In vivo activity of peptide S519.

Insulin mimetic peptides with receptor affinities close to that of the native hormone have been assembled from building blocks which bind to the same two sites used by insulin. An optimized peptide is about half the size of insulin and consists of a single peptide chain with one disulfide. The methods used could be applied to other receptor systems for which a peptide ligand would be desirable.

References

1. Pillutla, R. C., Hsiao, K. C., Beasley, J. R., Brandt, J., Østergaard, S., Hansen P. H., Spetzler J. C., Danielsen, G. M., Andersen, A. S., Brissette, R. E., Lennick, M., Fletcher P. W., Blume A. J., Schäffer, L. and Goldstein, N. I. *J. Biol. Chem.* **277**, 22590-22594 (2002).
2. Schäffer, L., Brissette, R. E., Spetzler, J. C., Pillutla, R. C., Østergaard, S., Lennick, M., Brandt, J., Fletcher, P. W., Danielson, G. M., Hsiao, K. C., Andersen, A. S., Dedova, O., Ribel, U., Hoeg-Jensen, T., Hansen, P. H., Blume, A. J., Markussen, J. and Goldstein, N. I. *Proc. Natl. Acad. Sci. U.S.A.* **100**, 4435-4439 (2003).

Peptide Revolution: Genomics, Proteomics & Therapeutics
Michael Chorev & Tomi K. Sawyer (Editors)
American Peptide Society, 2003

Restoring a Functionally Important Loop in MAdCAM-1, the Primary Ligand of $\alpha_4\beta_7$ Integrins

Gregory V. Nikiforovich and Garland R. Marshall

Department of Biochemistry and Molecular Biophysics,
Washington University, St. Louis, MO 63110, USA

Introduction

Rational design of selective peptide inhibitors of $\alpha_4\beta_7$ integrins [1,2] could be based on 3D structure of MAdCAM-1, whose fragment Leu^{41}-Asp^{42}-Thr^{43} (LDT) is required for binding $\alpha_4\beta_7$ integrins [3]. However, in the two X-ray structures available for MAdCAM-1 (PDB entries 1BQS [4] and 1GSM [5]), the highly flexible external loop 40-55 possesses dramatically different conformations (see Figure 1, left). Therefore, these two "snapshots" of the loop captured by the X-ray experiments are insufficient to use either conformation of LDT in MAdCAM-1 as a structural template; all plausible 3D structures of loop 40-55 in MAdCAM-1 have to be elucidated.

Results and Discussion

Geometrical closing of the loop consisted of stepwise elongation of the peptide backbone starting from residue 41 within the 3D structure of the MAdCAM-1 fragment 21-76 (the overlapped, nearly identical fragments of 1BQS and 1GSM), which lacked the loop in question. Elongation steps went from fragment 41-49 to 41-51 to 41-54. All combinations of local energetic minima in the Ramachandran map were considered for the initial fragment 41-49 as well as for fragments 50-51 and 52-54 which were added at the next two steps. At each elongation step, a system of limitations was imposed on the C^α-C^α distances within the growing fragment as well as on the distances between any C^α atom in the loop and any C^α atom in the rest of the molecule; C^α-C^α distances should be not less than 4 Å. One more distance limitation was that the end of the growing fragment should not be located too far from the target point, the C^α-atom in position 55, to ensure closure. In total, 304 conformers of the loop peptide backbone satisfied all constraints.

Energy calculations (the ECEPP/2 force field, see [6]) were then performed for the entire fragment 21-76, where the starting conformations of the non-loop fragments 21-40 and 54-76 were the same as in 1BQS/1GSM, and the starting conformations of the loop were the 304 structures satisfying the geometrical limitations. Fragment 21-76 contains two disulfide links connecting positions 25-72 and 29-76; nine additional constraints were incorporated into the energy calculations by weak parabolic potentials to keep the relative orientation of the non-loop fragments 21-40 and 54-76 the same as in the X-ray structures. Fifty structures of fragment 21-76 were found to possess low-energy (relative energy values, ΔE, were less than 30 kcal/mol). Out of these, 25 structures retained the starting spatial positions of the non-loop fragments 21-40 and 54-76 (rms differences with the X-ray structure calculated for C^α-atoms were less than 2 Å). The selected 25 low-energy conformations are depicted in Figure 1, right. They are almost equally distant from the spatial positions of loop 40-55 suggested by 1BQS and 1GSM (Figure 1, left). The loop conformations fall into two distinct clusters as to geometrical similarity of **LDT** (geometrical similarity here and below is defined as rms $\leq$ 1.0 Å, all backbone heavy atoms and C^β-atoms were considered).

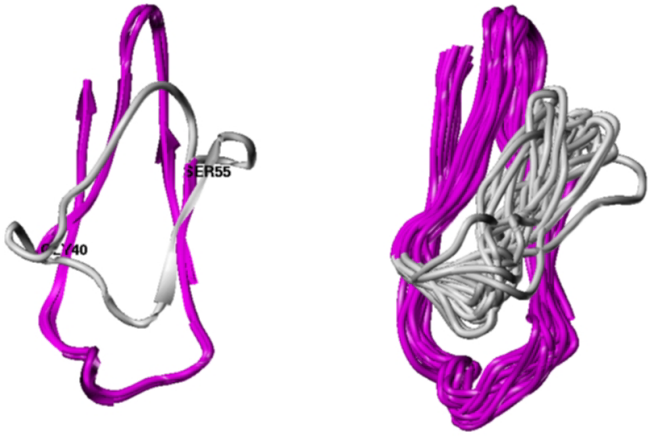

Fig. 1. Sketches of overlapping fragments 21-76 of 1BQS and 1GSM showing difference in 3D structures of loop 40-55 (left, the loop in light gray) and of the same fragments obtained by restoring low-energy conformations of the loop (right).

Rational design of selective peptide inhibitors of $\alpha_4\beta_7$ integrins, which involved mimicking the spatial arrangement of LDT in 1BQS, yielded *cyclo*(Leu[1]-Asp[2]-Thr[3]-Ala[4]-D-Pro[5]-Phe[6]), LDTApF, as the best compound showing an IC_{50} value of 292 μM in inhibition of $\alpha_4\beta_7$/MAdCAM interactions [1]. This value has been further improved to 61 μM by replacement of Phe by aza-Phe and Ala by Asp [2]. At the same time, the heptapeptide *cyclo*(Cys[1]-Arg[2]-Ser[3]-Asp[4]-Thr[5]-Leu[6]-Cys[7])-NH_2, CRSDTLC, which was selected from a random peptide-phage library, showed an IC_{50} value of 0.12 μM [7]. Energy calculations have found two clusters of low-energy conformers ($\Delta E \leq 10$ kcal/mol) for LDTApF and six clusters for CRSDTLC regarding geometrical similarity of fragments LDT and SDT, respectively. LDT in the first conformational cluster of the restored loop 40-55 was geometrically similar to LDT in one of the clusters of LDTApF and to SDT in one of the clusters of CRSDTLC; orientations of both compounds relative to MAdCAM-1 were rather similar. However, LDT in the second conformational cluster of the restored loop 40-55 was similar only to SDT in another cluster of CRSDTLC, and not to LDT in any of the LDTApF clusters. In the latter case, orientation of CRSDTLC was different and corresponded more closely to the general molecular shape of MAdCAM-1. This may explain why CRSDTLC inhibited binding of MAdCAM-1 to $\alpha_4\beta_7$ integrins significantly better than LDTApF.

Acknowledgments
The work was supported by NIH grant GM 53630.

References

1. Boer, J., *et al. J. Med. Chem.* **44**, 2586-2592 (2001).
2. Gottschling, D., *et al. ChemBio. Chem.* **3**, 575-578 (2002).
3. Viney, J. L., *et al. J. Immunology* **157**, 2488-2497 (1996).
4. Tan, K., *et al. Structure* **6**, 793-801 (1998).
5. Dando, J., *et al. Acta Crystallographica* **D58**, 233-241 (2002).
6. Galaktionov, S., Nikiforovich, G. V. and Marshall, G. R. *Biopolymers* **60**, 153-168 (2001).
7. Dubree, N. J. P, *et al. J. Med. Chem.* **45**, 3451-3457 (2002).

Peptide Revolution: Genomics, Proteomics & Therapeutics
Michael Chorev & Tomi K. Sawyer (Editors)
American Peptide Society, 2003

Synthesis of Membrane Active Peptides with a β-Helical Structure

Jyothi Thundimadathil, Lili Guo and Roger W. Roeske

Department of Biochemistry and Molecular Biology, Indiana University School of Medicine, Indianapolis, IN 46202, USA

Introduction

Living organisms depend on the transport of ions through cell membranes. The ion permeability of cell membranes is considered to be mediated by ion channels. Gramicidin A, which is a linear 15-residue peptide with alternating L and D residues, is the most well characterized membrane ion channel. The channel consists of two gramicidin units held in a head-head association by hydrogen bonds [1]. Due to the many studies on its structure and function, gramicidin is often cited as a model for the development of artificial ion channels. The design and synthesis of artificial channels are intended to both increase our understanding of natural ion channels and provide possible avenues to novel non-natural antimicrobials, drug delivery systems and biosensors. In 1971, a new helical conformation unique to polypeptide chains containing alternating L and D amino acid residues was proposed by Urry and independently by Ramachandran and Chandrasekharan [2]. These are regular helical structures in which individual amino acid residues have a local conformation equivalent to that in a β-pleated sheet and hence termed β-helices. The simplest member of this class of structures, the $\beta^6_{3,3}$ helix, has been suggested as the channel conformation of gramicidin A. Because of alternating peptide C=O directions, these helices are capable of forming head-head hydrogen bonded dimers through a formyl group at the N-terminus with uninterrupted structural continuity. Another higher member of this group, β^{12} helix, was proposed by Kennedy et al. in 1977 having a $(LLLD)_n$ configuration [3]. These β-helices are larger in diameter and would allow amino acid side chains in the interior of the helix, which can coordinate ions. So, N-formyl derivative of $(Leu\text{-}Ser\text{-}Leu\text{-}Gly)_6$ will have every serine side chain inside of the helix and would dimerize like gramicidin A. These peptides form ion channels in a lipid bilayer membrane system.

In the present study we designed and synthesized a similar peptide replacing most of the Gly- residues with D-Ala- and some Leu- residues with Arg- employing a solid phase Fmoc strategy. This resulted in a peptide which was much more soluble than Kennedy's peptide, which was soluble only in TFA. A typical peptide sequence is as follows: HCO-VSLGLSIAFSVAVSIAWSFARSRG-OH (molecular weight:2510), where all alanine residues are D-form. The peptide was found to be soluble in methanol (1 mg/mL), 70 % acetonitrile-30 % water-0.1% TFA system (1 mg/mL) and in DMSO (2 mg/mL). RP-HPLC purification was done on a C_4 column using gradient elution with 50 % aqueous methanol containing 0.1% TFA (A) and 100 % methanol containing 0.09 % TFA (B). The mass spectrum was recorded on a MALDI-TOF mass spectrometer. Also the desformylated and acetylated analogues of the above peptide were synthesized and characterized.

Results and Discussion

The synthetic peptides were examined for their ability to increase the conductance of a planar lipid bilayer membrane. Planar lipid bilayers were formed by painting a 2% solution of diphytanoylphosphatidyl choline (Avanti polar lipids Inc.) in decane over a small aperture between two chambers filled with electrolyte solutions. Peptide was added as a solution in methanol (2-5 μl of 1mg/mL solution) to cis and trans side of the chamber. The current signal was recorded at 1 KHz and sampled at 2 KHz using a

Bilayer Clamp-525C amplifier and Clampex 8.2 software. The data was smoothed with a digital filter at 500 Hz.

The conductance of DPPC membrane increased considerably after the formylated peptide (2×10^{-7}M) was introduced into the aqueous phase. However, the desformyl or acetyl analogues had no noticeable effect when added even at higher concentrations. The current through the membrane in the presence of formylated peptide was observed to fluctuate in discrete steps at different applied voltages indicating that the peptide forms ionic channels through the membrane (Figure 1). The relationship between channel current and membrane voltage is linear over a wide range of applied voltage.

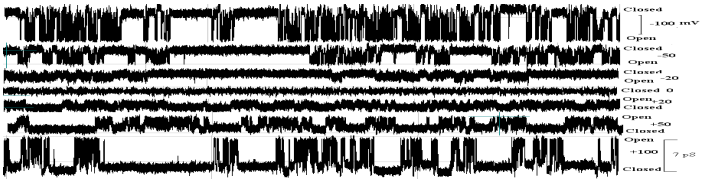

Fig. 1. Channel traces of the formylated peptide in 1M CsCl at different voltages.

The conductance of single channels measured under various conditions of electrolyte is summarized in Table 1. The selectivity for different ions in terms of conductance followed the order Cs>K>Na>Li, which is in accordance with the fact that cation movement through the channel is predominantly controlled by hydration energies. The channel lifetime varied inversely with the applied voltage indicating that the rate constant for the disruption of the channel increases with voltage.

Table 1. Single channel conductances (pS) at different electrolyte conditions.

Metal ions	Cs (.2M)	Cs (.5M)	Cs (1M)	K (1M)	Na (1M)	Li (1M)
pS	15±2.5	55±3.0	70±2.1	50±3.5	30±5.0	25±1.0
Cond.ratio	--	--	1.00	0.71	0.43	0.35

These results are consistent with a β-helical model proposed for this peptide. In this model serine hydroxyl groups are arrayed in the interior making it hydrophilic and this is important for ion coordination (Figure 2). This would not be possible in an α-helical model. Also, the formyl group is required for the dimer formation to get channel activity. Moreover, the higher unit conductance of this peptide compared to gramicidin A implies that the conformational mobility of serine side chains and the larger diameter of the channel are important factors.

Fig. 2. An axial view of the formylated peptide showing serine hydroxyl groups inside the pore and a ribbon model of β^{I2} helical dimmer.

Future studies will focus on the conformational studies of these types of peptides in a lipid bilayer environment, antimicrobial activity and also on the possible synthesis of β–helices with larger diameter.

References

1. Urry, D. *Proc. Natl. Acad. Sci. U.S.A*. **68**, 672-676 (1971).
2. Ramachandran, G. N. and Chandrasekharan, R. *Indian. J. Biochem. Biophys*. **9**, 1-11 (1972).
3. Kennedy, S. J., Roeske, R. W., et al. *Science,* **196**, 1341-1342 (1977).

Peptide Revolution: Genomics, Proteomics & Therapeutics
Michael Chorev & Tomi K. Sawyer (Editors)
American Peptide Society, 2003

Structure-Activity Relationships of a Novel Cyclic Dynorphin A Analog with Kappa Opioid Receptor Antagonist Activity

Matthew W. Leighty,[1] Thomas F. Murray[2] and Jane V. Aldrich[1]

[1]Department of Medicinal Chemistry, School of Pharmacy, University of Kansas, Lawrence, KS 66045, USA; [2]Department of Physiology and Pharmacology, College of Veterinary Medicine, University of Georgia, Athens, GA 30602, USA

Introduction

Our research focuses on the development of potent and selective peptide antagonists for kappa (κ) opioid receptors and examination of the structure-activity relationships (SAR) for antagonist activity at these receptors. Kappa opioid receptors represent potential pharmacological targets [1] and antagonists for these receptors have potential use in the treatment of opiate abuse [2].

We recently synthesized *cyclo*^{N,5}[Trp^{3,4},Glu^{5}]Dyn A-(1-11)NH_2, now known as cyclodyn, the first cyclic peptide antagonist for κ opioid receptors [3]. This novel cyclic analog of dynorphin A was designed based on the linear κ opioid receptor antagonist JVA-901, now called venorphin [4], and is cyclized through the N-terminus, encapsulating the "message" sequence [5] of the peptide. Continuing our efforts towards the development of selective peptide antagonists at κ opioid receptors, we synthesized a series of analogs of this novel lead peptide in order to explore its SAR.

(a) **Tyr-Gly-Trp-Trp-Leu-Arg-Arg-D-Ala-Arg-Pro-Lys-NH_2**

(b) **Tyr-Gly-Trp-Trp-Glu-Arg-Arg-Ile-Arg-Pro-Lys-NH_2**

Fig. 1. (a) [Gly^2]venorphin; (b) cyclodyn, the first cyclic peptide antagonist at κ opioid receptors.

Results and Discussion

The peptides were prepared as described previously [3] using an Fmoc protocol on a PAL-PEG-PS resin and the Pip (phenylisopropyl) ester for selective protection of Glu^5. Kappa opioid receptor affinities of the peptides were determined by radioligand binding assays using Chinese hamster ovary cells stably expressing κ opioid receptors.

Initial analogs prepared included alanine substituted peptides, analogs containing D-amino acids, and other selected derivatives (Table 1). The alanine scan, performed to determine which residues are key for binding to κ opioid receptors, suggested that the aromatic residues in positions 1 and 4 and the Arg^6 and Arg^7 residues of cyclodyn are important for interaction with κ opioid receptors. A D-amino acid scan within the cyclic region of cyclodyn was conducted in order to determine the effect of amino acid configuration in this region on binding affinity at these receptors. The results indicated that within the "message" sequence amino acids with the L-configuration are important for high κ opioid receptor affinity. The Phe^1 analog exhibited 3.7-fold lower affinity than cyclodyn, indicating that a phenolic side chain at position 1 of cyclodyn contributes to κ opioid receptor affinity. Replacement of Tyr^1 of cyclodyn with Dmt (2',6'-dimethyltyrosine) resulted in an analog that displayed equal affinity for κ opioid receptors; this is in contrast to the Dyn A analog dynantin [6], where incorporation of a Dmt analog at position 1 enhanced κ opioid receptor affinity. Decreasing the ring size

of cyclodyn by one methylene unit resulted in a dramatic decrease in binding affinity for κ opioid receptors, indicating the importance of ring size for high κ opioid receptor affinity. The SAR of cyclodyn is very different from that of its linear parent venorphin. In venorphin, the Trp in position 3 is critical for interaction at κ opioid receptors, but the aromatic residues at positions 1 and 4 are not [7]. This is in sharp contrast to the importance of Tyr^1 and Phe^4 in cyclodyn for κ opioid receptor affinity, which parallels the SAR of Dyn A [8]. This suggests that cyclodyn has a similar binding mode to κ opioid receptors as Dyn A while cyclodyn and venorphin appear to bind differently to these opioid receptors.

Additional pharmacological evaluation of analogs is ongoing and other analogs of cyclodyn are being prepared based on the results for these initial derivatives in order to further explore the SAR of this novel cyclic peptide.

Table 1. Kappa opioid receptor affinities of cyclodyn analogs.

Cyclodyn Analog	Ki (κ) ± S.E.M. (nM)	Cyclodyn Analog	Ki (κ) ± S.E.M. (nM)
Cyclodyn	26.8 ± 2.8	[D-Tyr^1]	45.2 ± 8.5
[Ala^1]	276 ± 17	[D-Ala^2]	227 ± 52
[Ala^2]	23.1 ± 1.8	[D-Trp^3]	168 ± 43
[Ala^3]	60.0 ± 2.9	[D-Trp^4]	328 ± 110
[Ala^4]	2260 ± 830	[Phe^1]	98.0 ± 5.0
[Ala^6]	434 ± 50	[Dmt^1]	23.4 ± 3.5
[Ala^7]	666 ± 63	[Asp^5]	400 ± 50

Acknowledgements
We would like to thank Dr. Xiuzhen Yan for performing the biological assays of the synthesized peptides. This research was supported by NIDA grant R01DA005195.

References

1. Aldrich, J. V. and Vigil-Cruz, S. C. In *Burger's Medicinal Chemistry and Drug Discovery* Abraham, D. (Ed.) John Wiley & Sons: New York, p. 329-481 (2003).
2. Rothman, R. B., Gorelick, D. A., Heishman, S. J., Eichmiller, P. R., Hill, B. H., Norbeck, J. and Liberto, J. G. *J. Subst. Abuse Treat.* **18**, 277-281 (2000).
3. Vig, B. S., Murray, T. F. and Aldrich, J. V. *J. Med. Chem.* **46**, 1279-1282 (2003).
4. Wan, Q., Murray, T. F. and Aldrich, J. V. *J. Med. Chem.* **42**, 3011-3013 (1999).
5. Chavkin, C. and Goldstein, A. *Proc. Natl. Acad. Sci. U.S.A.* **78**, 6543-6547 (1981).
6. Lu, Y., Nguyen, T. M.–D., Weltrowska, G., Berezowska, I., Lemieux, C., Chung, N. N. and Schiller, P. W. *J. Med. Chem.* **44**, 3048-3053 (2001).
7. Aldrich, J. V., Wan, Q. and Murray, T. F. In *Peptides: Chemistry and Biology*, Barany, G. and Fields, G., (Eds.) ESCOM, Leiden, p. 616-618 (2000).
8. Turcotte, A., Lalonde, J.–M., St.-Pierre, S. and Lemaire, S. *Int. J. Peptide Protein Res.* **23**, 361-367 (1984).

Peptide Revolution: Genomics, Proteomics & Therapeutics
Michael Chorev & Tomi K. Sawyer (Editors)
American Peptide Society, 2003

Multimeric Cyclic RGD Peptides with Improved Tumor Uptake for Tumor Targeting

G. Thumshirn[1], U. Hersel[1], T. Poethko[2], F. Rau[2], R. Haubner[2], M. Schwaiger[2], H.-J. Wester[2] and H. Kessler[1]

[1]Institut für Org. Chemie u. Biochemie, Technische Universität München, 85747 Garching, Germany; [2]Nuclear Medicine, Technische Universität München, 81675 Munich, Germany

Introduction

The αvβ3 integrin receptor plays an important role in several pathological processes like restenosis and tumor-induced angiogenesis. Cyclic RGD-pentapeptides have been developed as highly active and selective integrin ligands [1] and were used to prepare conjugates for tumor imaging by SPECT [2] and PET [3]. In order to improve tumor uptake and to obtain good tumor to background ratios, we synthesized mono- (**M**), di- (**D**) and tetrameric (**T**) cyclic RGD peptides and introduced a new strategy for ^{18}F-labeling.

Results and Discussion

The oxime ligation presents an elegant way to link totally unprotected aminooxy-functionalized peptides to any aldehyde under mild conditions. Our compounds (see Figure 1) were synthesized by SPPS using the TCP resin and applying Fmoc-strategy. To adapt the synthesis of our compounds to SPPS, we introduced the site for chemoselective oxime formation by using **1** as the starter amino acid. The branching unit for the multimeric compounds consists of L-lysine. The spacer was inserted by using Fmoc-heptaethylene glycol amino acid **2**. Finally the RGD moiety was attached by fragment coupling of *cyclo*(-R[Pbf]GD[tBu]fE-).[4] 4-[^{18}F]fluorobenzaldehyde was synthesized by displacement of NMe_3 by ^{18}F in 4-formyl-*N,N,N*-trimethylanilinium triflate using the $[K\subset2.2.2]^+/^{18}F^-$ system. The chemoselective oxime ligation (see Figure 2) of the deprotected peptides was carried out in a MeOH/water mixture acidified with TFA (pH 2.5) and the final purification was performed by radio-HPLC or SPE. Biodistribution studies at 1 h and 2 h p.i. with the ^{18}F-labelled monomer, dimer and tetramer were carried out in mice bearing an αvβ3-positive human M21 and the

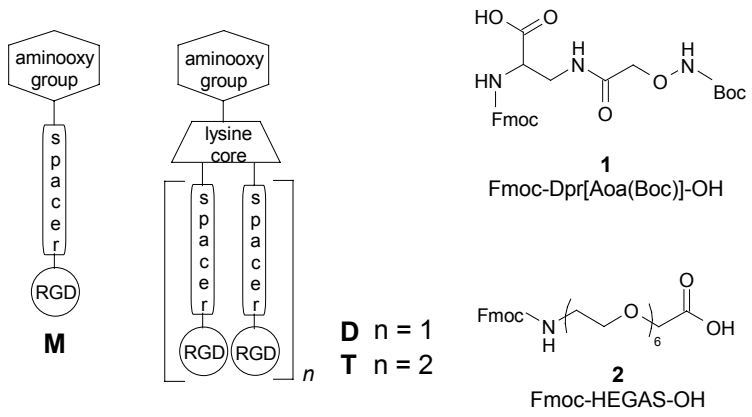

Fig. 1. Building blocks and general structure of the multimers for ^{18}F-labeling.

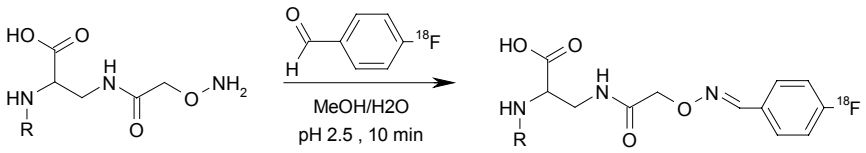

Fig.2. Chemoselective oxime ligation for ^{18}F-labeling of peptides.

αvβ3-negative M21L melanoma. Specifity of tumor uptake was studied after administration of 18 mg *c*(-RGDfV-)/kg.

No-carrier-added (n.c.a.) 4-[^{18}F]fluorobenzaldehyde can be prepared in less than 0.5 h using a SPE or radio-HPLC (RCY ~75 %). Peptide labelling was completed in 10 min (RCY 70-85 %, 0.5 mM) followed by HPLC-purification. Compared to the dimer, biodistribution studies show a faster clearance of the tetramer, while tumor uptake at 2 h p.i. was nearly identical (0.5±0.1 (M), 1.6±0.7 (D), 1.7±0.1%ID/g (T)). The highest tumor/non-tumor ratios were found for the tetramer (t/blood 14.0 (M), 12.4 (D), 21.3 (T); t/liver 1.0 (M), 10.1 (D), 19.8 (T); t/muscle 13.2 (M), 14.2 (D), 23.1 (T)). Metabolite analyses at 1 h revealed high stability for the monomer, and 83, 53, 57 and 28% intact tetramer in blood, liver, kidney and tumor, respectively.

The PET-images (see Figure 3) show the high accumulation of the tetrameric compound in the αvβ3-positive human M21 melanoma and the specifity of tumor uptake. Whether the improved tumor/non-tumor ratios are based on a cooperative effect has yet to be tested.

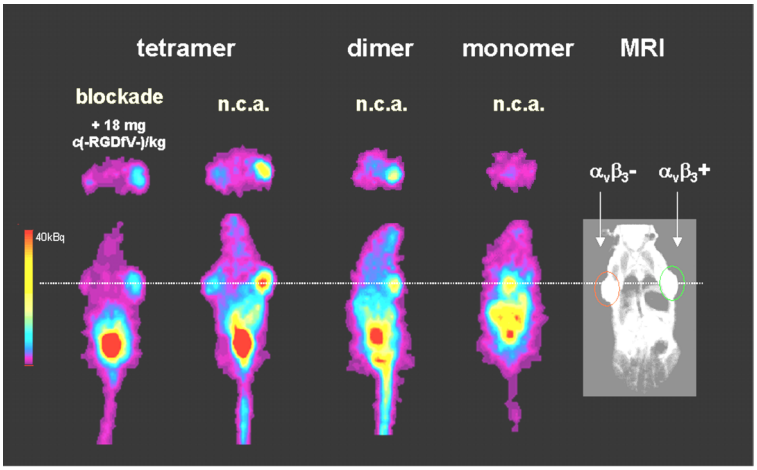

Fig. 3. PET Imaging of [^{18}F]RGD 90 min p.i.; n.c.a (no-carrier-added).

Acknowledgments

The work was supported by the DFG Forschergruppe Radionuklidtherapie.

References

1. Dechantsreiter, M. A., et al. *J. Med. Chem.* **42**, 3033-3040 (1999).
2. Haubner, R., et al. *J. Nucl. Med.* **40**, 1061-1071 (1999).
3. Haubner, R., et al. *Cancer Res.* **61**, 1781-1785 (2001).
4. Thumshirn, G., et al. *Chem. Eur. J.* **9**, 2717-2725 (2003).

Peptide Revolution: Genomics, Proteomics & Therapeutics
Michael Chorev & Tomi K. Sawyer (Editors)
American Peptide Society, 2003

Conformational Study of Na^+ Channel Inactivation Gate Peptides Interacting with Local Anesthetic Diphenyl Drugs Using NMR and Molecular Modeling

Bih-Show Lou[1], Ta-Hsien Lin[2] and Chi-Zen Lou[2]

[1]Center of General Education, Chang Gung University, Tao-Yuan, Taiwan, ROC; [2]Institute of Biochemistry, National Yang-Ming University, Taipei, Taiwan ROC

Introduction

The kinetics of recovery from Na^+ channel inactivation are crucial in determining the ability of the cell to fire repetitive action potentials [1]. In addition, many anesthetic and anticonvulsant drugs have been reported to dramatically slow the rate of recovery from inactivated Na^+ channels [2]. Therefore, understanding the molecular mechanism of local anesthetics and anticonvulsants, and the interactions of these drugs with Na^+ channel inactivation are of considerable physiological and pharmacological importance.

Previous studies [3] on the steady state effect and reaction kinetics in mixtures of inhibitory effect of different drugs with Na^+ channels are ascribable to the inhibition of Na^+ current by selective binding of diphenyl drugs to the inactivated channels. Such compounds can be roughly classified into three groups according to their effect on inactivated Na^+ channels. Group I (such as *phenytoin*) significantly bind to the inactivated but not in the resting channels. Group II (such as *diphenhydramine*) have higher affinity to the inactivated channel than group I drugs and may even have some binding to the resting channels. Group III (such as *phenylbutazone*) have little binding to either inactivated or resting channels. By comparing the group I and II drugs, which all bind to the inactivated channel, the diphenyl group is the only common structural motif, therefore their spatial orientation in two benzene rings is responsible for the selective binding to the inactivated Na^+ channel.

The local anesthetics have been proposed to relate to the Na^+ channel inactivation gate in rat brain type IIA Na^+ channel, which may function as a "hinged lid" model [4]. A cluster of hydrophobic amino acids, Ile-1488, Phe-1489, and Met-1490, within the intracellular linker between domain III and IV, occludes the transmembrane pore of Na^+ channel and stabilizes the inactivated state. An exploration of the key ligand groups of these drugs and their configuration binding with model peptide thus may provide important conformational information about the channel protein.

Results and Discussion

From our molecular modeling study, the structures of the predominant conformers of Group I, II and III drugs are plotted in Figure 1. The diphenyl groups of these drugs generally have similar spatial orientation between Group I (*phenytoin*) & II (*phenylbutazone*), though their chemical formula are different. On the other hand, the Group III (*phenylbutazone*) also with diphenyl, showed only minimal effect on the inactivated Na^+ channels. These structural data not only indicate that diphenyl groups play an essential role in selective binding to the inactivated Na^+ channels, but also demonstrate that the two phenyl groups must be arranged into appropriate configurations (stem bond angle ~110°, and center to center distance ~ 5 Å). Combining the results above, we then presume three roughly equally important structural determinants of these use-dependent Na^+ channel blockers, namely two

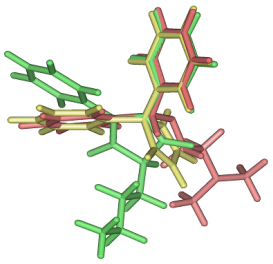

Fig. 1. Conformation comparion for Group I (yellow), Group II (red), Group III (green).

benzene rings and one linear tertiary amine chain. The binding site blockers can be suggested as following:

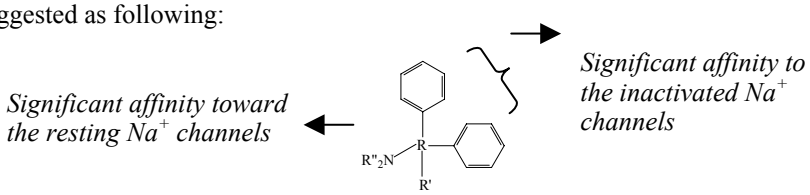

To investigate the expected π-stacking interaction between the inhibitor phenyl groups and receptors, we have synthesized a model peptide (BL-1: Ac-GGQDIFMTEEK-OH) corresponding to the linker part of rat brain type IIA Na^+ channel. BL-1 was synthesized by SPPS using Fmoc chemistry. NMR spectra of BL-1 in the presence of diphenyl drugs (such as phenytoin, and the peptide-drug molar ratio was 1:1) have been measured in both phosphate buffer and phospholipid bicelles (q = DMPC/DHPC = 0.5, and [BL-1]/[DMPC] ~ 3%) at Brucker 500 AMX and 300K. The typical bicelles consist of long chain phospholipids such as dimyristotl phosphocholine (DMPC) and a detergent such as dihexanoyl phospholcholine (DHPC). This model system serves to mimic biological membranes for the peptide-lipid interactions and is formed into the isotropic phase that is suitable for high-resolution NMR studies [5, 6].

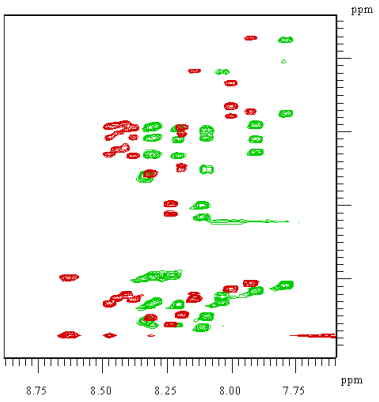

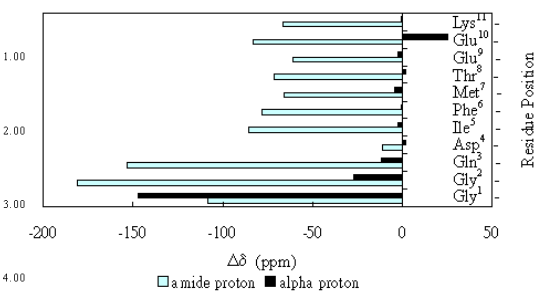

Fig. 3. Changes in chemical shifts (in units of hertz at 500 MHz) of the amino acid residues in BL-1 in phospholipid bicelles and in phosphate buffer. Delta $\delta = \delta_{in\ bicelles} - \delta_{in\ buffer}$

Fig. 2. NH region of z-fillig TOCSY spectra of BL-1 obtained in 100 mM phosphate buffer at pH 6.0 (red), and in phospholipid bicelles at pH 6.0 green).

Proton NMR spectra of BL-1 in phospholipid micelles in comparison with in phosphate buffer are presented in Figure 2, and the $\Delta\delta_{NH}$ and $\Delta\delta_{\alpha H}$ have been summarized in Figure 3. Because of a pronounced delta δ_{NH} and delta $\delta_{\alpha H}$, it is clear that the bicelles induced an α-helical conformation for Na^+ channel inactivated gate peptide, BL-1, which is unstructured in phosphate buffer. For bilayer-bound BL-1, the strongly hydrophobic environment of alkyl chains excludes water and may stabilize a bent helical structure by reducing the length and increasing the strength of the intramoelcular hydrogen bonds [5]. In addition, the local anesthetic drug, *phenytoin (DPH)*, caused a larger chemical shifts of BL-1 in phospholipid bicelles rather than in phosphate buffer (Figure 4) indicates its binding affinity with BL-1 is stronger once the α-helix is formed for BL-1. This agrees with α-helical conformation is bioactive structure for inhibitor-receptor interactions in Na^+ channel inactivated gate. The high-frequency shifts of BL-1 caused by DPH binding in Figure 4 can be explained as the electrostatic interaction between the positively charged tertiary ammonium of DPH and the negatively charged carboxyl group of Glu^9 and Glu^{10} or C-terminal. In addition, the remarkable chemical shift of the hydrophobic residues Phe^6 and Met^7 caused by DPH binding demonstrates that they are involved in inhibitor-receptor interaction. This result supports that IFM domain in III-IV linker for local anesthetic drug blocks the of Na^+ channel [4]. The phenyl protons of Phe^6 in Figure 5 shifted slightly to a higher frequency that is in contrast to the low-frequency shift of phenyl protons of DPH. This phenomenon indicates that the ring protons of Phe^6 locate at the side of DPH and that the DPH ring protons locate on the plane of Phe^6.

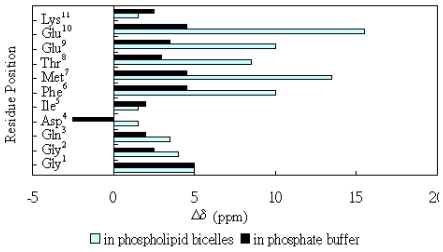

Fig. 4. Changes in amide protons chemical shifts (in units of hertz at 500 MHz) of the amino acid residues in BL-1 as a result of interaction with DPH drug in phospholipid bicelles (light blue), and phosphate buffer (black).

Delta $\delta_{NH} = \delta_{(BL\text{-}1+\ DPH)} - \delta_{(\ BL\text{-}1\ alone)}$

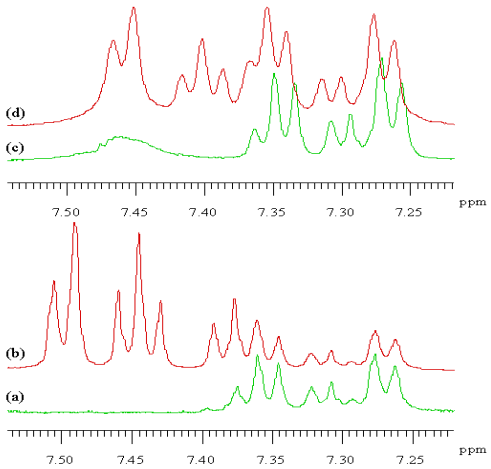

Fig. 5 ^{1}*H-NMR spectrum of the phenyl group protons of BL-1 (2mM) (a) alone in 100 mM phosphate buffer at pH 6.0 (b) with DPH (2mM) in buffer (c) alone in phopholipid bicelles at pH 6.0, and (d) with DPH in micelles.*

Acknowledgments

The work was funded by an NSC91-2320-B-182-054 grant to B.-S. Lou.

References

1. Armstrong, C. M. *Physiol Rev.* **61**, 644- 683 (1981).
2. Kuo, C.- C., Chen, R.- S., Lu, L. and Chen, R. C. *Mel. Pharmacol.* **51**, 1077-083(1997).
3. Kuo, C.- C., R.- C. Huang, and Lou, B.- S. *Mol. Pharmacol*. **57**, 135-143 (2000).
4. West, J. W., Patton, et al., *Proc. Natl. Acad. Sci. U.S.A.* **89**, 10910-10914 (1992).
5. Luchette, P.A., Vetman, T. N., et al., *J. Biochim. Biophys. Acta* 83-94 (2001).

Peptides and proteins folding
Michael Chorev & Tomi K. Sawyer (Editors)
American Peptide Society, 2003

Comparative Conformational Analysis of Neurokinin B and Selective NK3 Receptor Agonist

Gulshen A. Agaeva

Molecular Biophysics Laboratory, Department of Physics, Baku State University, Baku, 370148, Azerbaijan

Introduction

Neurokinin B (NKB), a decapeptideamide, is a member of the tachykinin family of peptides, characterized by a common carboxy terminal sequence of Phe-Xxx-Gly-Leu-Met-NH_2. Tachykinin peptides isolated in mammalian substance P, neurokinin A and neurokinin B and some of its analogues are the agonists at the distinct molecularly characterized receptor types, called neurokinin-1 NK-1, neurokinin-2 NK-2, and neurokinin-3 NK-3, respectively. They appear to be involved in many diverse biological processes such as smooth muscle contraction, blood pressure regulation, pain transmission and etc. The specific selectivity of neurokinins for these different types of receptor is certainly related to the conformational properties of these peptides. It is shown from constrained NKB analogues that the most selective for the NK3 type receptor is [Pro7]NKB with amino acid substitution of the valine residue in position 7 by proline (see Figure 1) [1]. To investigate the mechanism of the biological action of NKB and to identify structural features important for receptor NK-3 selectivity, a theoretical study of the spatial structure of NKB and its analog [Pro7]-NKB have been carried out using a molecular mechanics method.

Neurokinin B H-DMHDFF**V**GLM-NH_2
[Pro7]NKB H- DMHDFF**P**GLM-NH_2

Fig. 1. Sequences of neurokinin B and its synthetic analog with amino acid substitution of the valine residue in position 7 by prolin.

Results and Discussion

Semiempirical calculation of the whole NKB molecule were carried out based on the low-energy structures of its fragments. The conformational potential energy of the molecule is given as the sum of the independent contributions of nonvalent E_{nv}, electrostatic E_{el}, torsional interactions E_{tors} and hydrogen bonds. The obtained conformational space of the NKB under polar conditions has been classified into families with similar backbone form of the C-terminal heptapeptide. The optimal structures of NKB with relative energies in a sufficiently wide interval of 0-10 kcal/mol may be described by five families of low-energy conformations, possessing relatively conformational valid C-terminal heptapeptide and variable N-terminal fragments. The preferred α-helical structure of the NKB exhibits the most favorable dispersion contacts, and therefore may be expected to become the most preferred one in a strongly polar medium when electrostatic interactions do not play a significant role. Another favorable structure adopts a β-turn at the Asp4-Val7 level between two helical segments. In this conformation the distance between the C^{α} atoms of Asp4 and Val7 is found to be approximately 6.8Å, which indicates the presence of a β-turn. All these conformations are stabilized by networks of hydrogen bonds. The results from theoretical energy calculations indicate that the NKB is a relatively flexible molecule that can exist in several conformations.

Table 1. The geometrical and energetic parameters of two lowest conformations(1),(2) of the NKB and one preferred conformation (3) of its analog [Pro^7]NKB.

Amino acid residue	Conformation (φ,ψ,ω,χ1,χ2,χ3,χ4)		
	(1)NKB	(2)NKB	(3) [Pro7]NKB
Asp1	-39,-36,170,64,113	-39,-36,170,64,113	-39,-36,171,64,113
Met2	-83,-48,-176,-63 ,-57,178,180	-83,-52,-181,-63 ,-57,178,180	-84,-58,-181,-63, -57,178,180
His3	-79,-44,-180,-59,-91	-84,-55,-187,59,-92	-96,-48,-184,61,-87
Asp4	-58,-37,181,180,91	-88,171,182,60,99	-88,171,182,60,99
Phe5	-76,-34,182,180,90	-82,-60,174,-60,90	-81,-59,174,-61,90
Phe6	-66,-46,180,180,90	-138,132,180,-58,90	-137,130,179,-58,90
Val7(Pro7)	-79,-32,-84,175,59,59	-71,-36,-180,176,60,60	-35,-179
Gly8	-63,-39,-178	-58,-36,-180	-58,-35-179
Leu9	-82,-62,-174, 176, 64, 60,58	-88,-64,-173,175,64, 60,57	-87,-66,-173,175,65, 60,57
Met10	-91,-52,-181,-59,180, 180,180	-94,-53,-181,-60,180, 180,180	-95,-54,-181,-60,180, 180,180
Energetic parameters (kcal/mol)	E_{nv}= -58.5 E_{el}=5.0 E_{tors}=6.5 E_{tot}=-47.0	E_{nv}= -52.6 E_{el}=2.9 E_{tors}=5.7 E_{tot}=-44.0	E_{nv}= -51.8 E_{el}=-0.7 E_{tors}=4.9 E_{tot}=-47.7

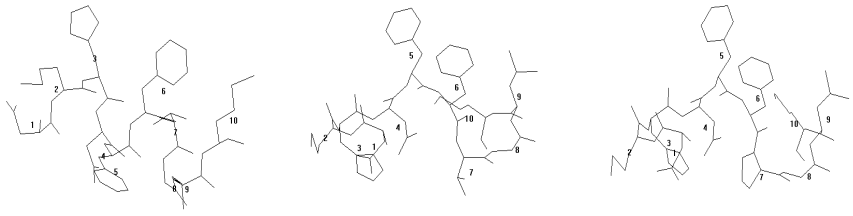

Fig. 2. The stereo pictures of two lowest energy structures of NKB [α-helical (1) and β-turn (2)] and one preferred conformation of [Pro7]NKB analog [structure with β-turn(3)].

Conformational analysis of [Pro7]NKB analog indicated that replacement of the valine with proline led to significant restriction of the parent molecule conformational possibilities, caused by the restricted rotation around the N-C^{α} bond of Pro. This conformationally constrained analog showed preference for only one conformational family with β-turn at the Asp4-Val7 level between two helical segments as obtained earlier for native NKB. The geometries, energies and stereo pictures of the preferred structures of NKB and [Pro7]NKB analog are presented in Table1 and Figure 2 respectively. Thus, knowledge and comparison of the conformational peculiarities of NKB and its constrained analog allowed the study of the influence of the substitution of Val with Pro on the three-dimensional structure of the native molecule by analysis of conformational energy as well as the determination of the conformation-receptor selectivity in these peptides.

References

1. Lavielle S., Chassaing G., et al., *Fundam.Clin.Pharmacol.* **4**, 257-268 (1990).

Peptide Revolution: Genomics, Proteomics & Therapeutics
Michael Chorev & Tomi K. Sawyer (Editors)
American Peptide Society, 2003

Novel PACAP Analogs that Selectively Bind to PACAP-I Receptor

Jesse Z. Dong, Yeelana Shen, John E. Taylor, Michael Culler and Jacques-Pierre Moreau

Biomeasure, Incorporated/IPSEN Group, 27 Maple Street, Milford, MA 01757, USA

Introduction

Pituitary adenylate cyclase-activating polypeptide (PACAP) is a neuropeptide belonging to the vasoactive intestinal peptide (VIP), secretin and glucagon family. It exists in two differently processed forms: PACAP38 and PACAP27, which have the same N-terminal 27 amino acids [1]. Both peptides bind to PACAP-I and PACAP-II receptors (PACAP-IR and PACAP-IIR). There is increasing evidence demonstrating that in animals PACAP38 has neuroprotective effects [2]. It has been suggested by different studies that systemic administration of PACAP38 may be clinically useful for reducing brain damage resulting from stroke [3]. Because the PACAP-II is associated with some undesirable *in vivo* effects, a PACAP38 analog that selectively binds to the PACAP-I receptor is desirable for development as a neuroprotective agent. Here we report novel PACAP38 analogs that selectively bind to PACAP-I receptor.

Results and Discussion

The solution conformational features of PACAP38 include an initial disordered domain at the N-terminus, an α-helical structure stretching from Ser^{9} to Val^{26}, and a short C-terminal α-helix between Gly^{28} and Arg^{34} [4] (Fig. 1). It is believed that the two α-, helices in PACAP38 are essential for the ligand-receptor interaction. Furthermore, we hypothesized that the α-helical domains have membrane association properties, which facilitate the hormone-receptor recognition. Therefore, it is important in the design of potent PACAP analogs to stabilize the α-helices by using certain structural elements. We took advantage of the α-helix promoting ability of the $C^{\alpha,\alpha}$-disubstituted glycines in our PACAP38 analog design. Most analogs bearing the $C^{\alpha,\alpha}$-disubstituted glycine substitutions, such as aminoisobutyric acid (Aib) and 1-aminocyclohexane-1-carboxylic acid (A6c), have improved receptor binding affinity on both PACAP-I and PACAP-II receptors (peptides 1, 2 and 3, Table 1). Interestingly, substitution of 1-aminocyclopentane-1-carboxylic acid (A5c) for valine at position 19 yielded a PACAP-I receptor selective ligand, [$A5c^{19}$]hPACAP(1-38)NH_2 (peptide 4, Table 1).

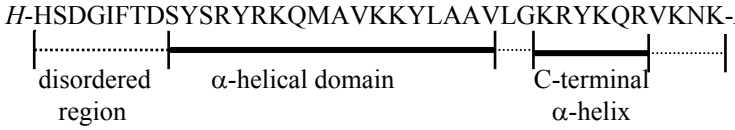

Fig. 1. PACAP38 sequence and conformational features.

During the course of developing PACAP-I receptor selective ligands, we were interested in the receptor binding functions of the structurally flexible hinge region (Leu^{27} and Gly^{28}) that links the two α-helical domains in PACAP38. It was discovered that the binding selectivity of PACAP38 analogs can be shifted in favor of the PACAP-I receptor by increasing the length of the hinge region. For example, replacement of Gly^{28} with 5-aminovaleric acid (Ava), which is three carbon atoms longer than Gly,

generated an analog that is 9.9-fold selective to PACAP-IR over PACAP-IIR (peptide 5, Table 1).

Table 1. Receptor binding affinity on hPACAP-I and hPACAP-II receptors.

Peptide	hPACAP-IR[a] Ki (nM)	hPACAP-IIR[a] Ki (nM)	Sequence
hPACAP(1-38)NH_2	1.21	4.05	
hPACAP(1-27)NH_2	1.76	2.16	
1	0.99	0.62	[A6c^{17}]hPACAP(1-38)NH_2
2	0.81	0.62	[Aib^{18,25}, A6c^{23}]hPACAP(1-38)NH_2
3	0.77	0.96	[Aib^{24}, A6c^{27}]hPACAP(1-38)NH_2
4	0.58	3.65	[A5c^{19}]hPACAP(1-38)NH_2
5	0.66	6.54	[Ava^{28}]hPACAP(1-38)NH_2

[a]*The assays were done in CHO-K1 cells expressing the human recombinant PACAP-I or PACAP-II receptor.*

Taken together, the PACAP-I receptor selectivity of PACAP38 analogs can be improved by modifying the residues inside either the N-terminal α-helix or the hinge region of the peptide. The analogs with such modifications also have higher receptor binding affinity to PACAP-I receptor than the native PACAP38.

References

1. Arimura, A. and Shioda, S. *Frontiers in Neuroendocrinology* **16**, 53 (1995).
2. Reglodi, D., Somogyvari-Vigh, A., Vigh, S., Maderdrut, J. L. and Arimura, A., *Ann N Y Acad. Sci*. **921**, 119 (2000).
3. Reglodi, D., Somogyvari-Vigh, A., Vigh, S., Kozicz, T., and Arimura, A., *Stroke* **31**, 1411 (2000).
4. Wray, V., Kakoschke, C., Nokihara, K.and Naruse, S. *Biochemistry* **32**, 5832-5841 (1993).

Peptide Revolution: Genomics, Proteomics & Therapeutics
Michael Chorev & Tomi K. Sawyer (Editors)
American Peptide Society, 2003

N-Methylated Analogs of the Receptor-Binding Region of Human Parathyroid Hormone (hPTH)

Jean-René Barbier, Susanne MacLean, James F. Whitfield and Gordon E. Willick

Institute for Biological Sciences, National Research Council, Ottawa, ON, Canada, K1A 0R6

Introduction

Parathyroid hormone is the major regulator of serum calcium in vertebrates and effects its actions through a receptor (PTHR1), principally located in bone, kidney, and intestinal cells. Many studies of this hormone have helped to establish the mechanism of its binding and activation of PTHR1, especially in its main receptor-binding sequence, residues 17-29 [1]. However, the backbone amide and carbonyl functions are important for defining the H-bonds that establish the binding energy and specificity of peptide hormones to their receptors and, to date, there have been no studies on their specific roles in PTHR1 activation. We performed a methylation scan of the hPTH(1-31)NH_2 sequence and report here on the effects of methylation, in turn, of residues 17-31. This region contains the principal receptor-binding region and includes an α-helix, between residues 17-29, and an amphiphilic helical region between residues 21-31. Methylation of the backbone NH groups affects the secondary structure of a peptide [2] and also its receptor specificity [3]. CD has been used to monitor the effects on secondary structure and its adenylyl cyclase activity has been measured in HKRK cells transfected to high density with the PTHR1.

Results and Discussion

Peptides were synthesized by the Fmoc protocol on an Applied BioSystems Pioneer Peptide Synthesizer, as described earlier [4]. The C-terminal Val was attached manually to the Tentagel-R support. Specific methylations were performed on-line using the protocol of Miller and Scanlan [5]. Fmoc-amino acid activation was performed with TBTU/HOBt, except immediately after methylation, where HATU replaced the TBTU. Particular difficulty was observed in coupling Fmoc-Arg-20(Pmc) to Me-α-NH_2-Val-21. In this case, the coupling solvent was replaced with DMSO with 2% triton-X100 and double-coupling was performed at 50 ^oC. CD spectra were measured with a JASCO J-600 spectropolarimeter at 20-23 ^oC in 25 mM sodium phosphate, pH 7.0, and the α-helical content estimated from the magnitude of the θ_{222} minimum [4]. AC-stimulating activities were determined in HKRK-B7 cells, derived from an LLC-PK1 porcine epithelial cell line, stably transformed with PTHR1 to about 10^6/cell [6], using a cAMP detection assay (cAMP direct Biotrak EIA, Amersham Biosciences).

Fig. 1. Sequence of hPTH(1-31)NH_2 showing the α-helical region (box) and amphiphilic helix (shaded).

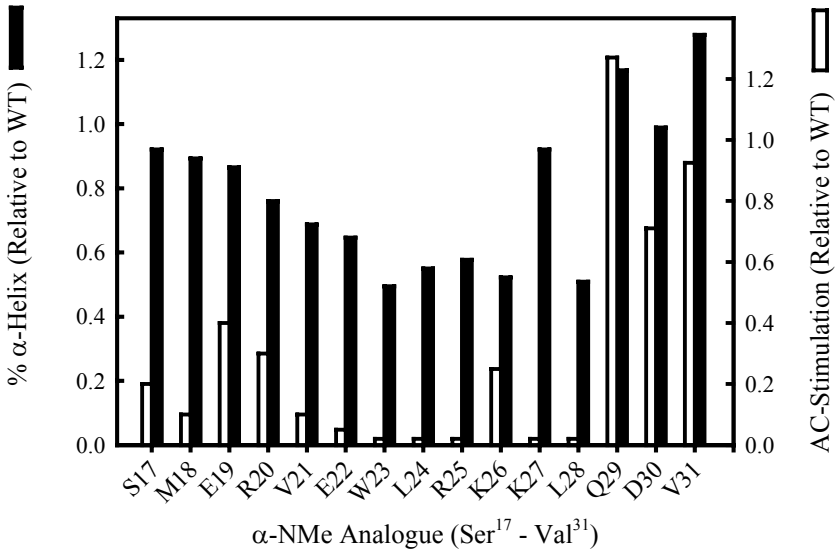

Fig. 2. Effects of specific α-N-methylations on structure and bioactivity of hPTH(1-31)NH_2.

The sequence of hPTH(1-31)NH_2 is shown in Figure 1. The hormone has an α-helix in the C-terminal region extending from residues 17-29 (boxed), and a helical amphiphilic region partially overlapping the helix and extending from residues 21 to 31.

Figure 2 summarizes the bioactivity and structure effects resulting from methylation of each residue. Except for the Gln-29 to Val-31 region, methylation lowers the amount of α-helix. The estimated α-helix actually is greater for the analogs methylated at either Gln-29 or Val-31 than for the unmodified hPTH. There is a pronounced loss of up to 50% of the secondary structure in the sequence Arg-20 to Leu-28, with the exception of Lys-27. There is a clear loss of some activity due to destabilization of the α-helix, but the loss of 95% of the activity when Glu-22, Trp-23, Leu-24, Arg-25, Lys-27, or Leu-28 are methylated points to a specific role of these backbone NH groups in determining the correct receptor-binding for AC-stimulating activity.

References

1. Morley, P., Whitfield, J. F. and Willick, G. E. *Curr. Med. Chem.* **6,** 1095-1106 (1999).
2. Chang, C. F. and Zehfus, M. H. *Biopolymers* **40,** 609-616 (1996).
3. Rajeswaran, W. G. *et al*., *J. Med. Chem.* **44,** 1305-11 (2001).
4. Barbier, J. R. *et al*., *J. Med. Chem.* **40,** 1373-1380 (1997).
5. Miller, S. C. and Scanlan, T. S. *J. Am. Chem. Soc.* **119,** 2301-2302 (1997).
6. Takasu, H., Guo, J. and Bringhurst, F. R. *J. Bone Miner. Res.* **14,** 11-20 (1999).

Peptide Revolution: Genomics, Proteomics & Therapeutics
Michael Chorev & Tomi K. Sawyer (Editors)
American Peptide Society, 2003

Are Neuropeptides of the NPY Family Recognized from the Membrane-Bound State?

M. Lerch[1], R. Bader[2] and O. Zerbe[1]

[1]*Insitute of Organic Chemistry, University of Zurich, 8057 Zurich, Switzerland ;*
[2]*Cavendish Laboratory, University of Cambridge, CB3 0HE United Kingdom*

Introduction

The concept that ligands, which target membrane-bound receptors, are recognized from the membrane-bound state dates back almost twenty years, when this idea was developed by Kaiser and Kezdy [1]. In their seminal paper they recognized that the active site of the receptor usually cannot accommodate more than five residues and that binding is usually mediated by a few stereospecific interactions between the ligand and the receptor. Many peptide hormones that are unstructured in solution fold into amphiphilic helices in a membrane-mimicking environment. From this observation, Kaiser and Kezdy developed the concept that these amphiphilic stretches serve to anchor the hormones onto the membrane from which they were recognized by the receptors.

Schwyzer *et al.* developed the ideas of Kaiser and Kezdy further into the membrane compartment model [2]. Their concept proposes that for many ligands membrane-association is an important event preceding receptor binding. Therefore, it is the membrane-bound conformation that is recognized by the receptor. Membrane-binding accumulates the ligands in the vicinity of the receptor, directs the molecules into the correct compartment and restricts the spatial search for the receptor to (lateral) two-dimensional diffusion. Moreover, conformations closed to the bioactive form are possibly induced. However, whether this model is valid or not is still under debate and we decided to study its applicability for peptides from the NPY family.

The NPY family of hormone peptides comprises the neuropeptide Y (NPY), the peptide YY (PYY) and the pancreatic polypeptide (PP). These C-terminally amidated peptides contain 36 amino acids residues. The hormones of the NPY family target a heterologous population of G-protein coupled receptors, the so-called Y receptors. So far, six different receptor subtypes have been identified from which the Y1, the Y2, the Y4 and the Y5 subtypes are cloned and pharmacologically best described. The Y receptors occur in the central and peripheral nervous systems as well as in the gastrointestinal tract. They are involved in the regulation of numerous pharmacologically highly important functions such as blood pressure, food intake and memory retention. Alanine scans performed on NPY at the human Y1 receptor indicated an essential role for the highly conserved residues Arg33 and Arg35 [3].

We have derived structural data of peptides from the NPY family using NMR spectroscopy. Three different strategies have been developed in order to decide whether the Schwyzer model is appropriate or not. The first two strategies are based upon the assumption that a couple of peptides that possess similar binding profiles at the receptor subtypes should display similar structures and dynamics in the particular environment from which they are recognized. Hence, we were looking for a couple of peptides which display high sequence similarity and similar binding affinities at the various Y receptor subtypes but have different structures in either the aqueous solution or in the micelle-bound state. In the second approach we were looking for peptides with very different binding profiles albeit very similar structures in one of the two

environments. In the third approach we were trying to rationalize receptor subtype specificity from structural features of the membrane-bound state.

In solution all peptides from this family of neurohormones display an amphiphilic α-helix that extends through the C-terminal half of the molecule. Differences occur in to what extent the helix extends through the C-terminal pentapeptide. In some peptides the less structured N-terminal half folds back onto the C-terminal α-helix (PP-fold).

In our structural studies, based upon distance restraints derived from NOE data, we were using dodecylphosphocholine micelles as a model for biological membranes. In order to decide whether the N-terminal half folds back onto the helix, measurements of the $^{15}N\{^{1}H\}$-NOE proved to be particularly helpful. Micelle integrating spin labels are utilized to determine the orientation of the peptides with respect to the micelle surface [4].

Results and Discussion

Two structural features have been proposed as important for receptor binding: the conformation of the C-terminal pentapeptide and the occurrence of the PP fold.

Figure 1 below depicts the values of the heteronuclear NOE for pNPY and bPP both in solution and in their micelle-bound states [5]. It adopts positive or negative values for rigid or flexible parts of the molecule, respectively.

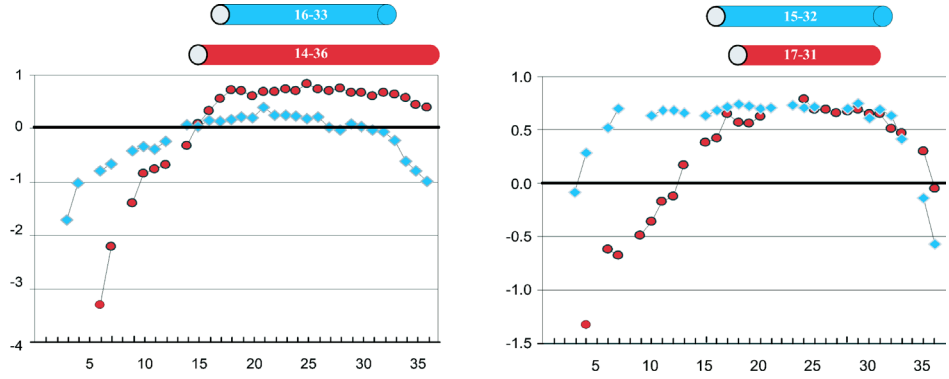

Fig. 1. Values of the $^{15}N\{^{1}H\}$ NOE for pNPY (left) and bPP(right). Diamonds (light gray) are used for data recorded for the peptides in solution, Circles (dark gray) for the micelle-bound peptides. The bars on top (light gray for solution and dark gray for micelle-bound) indicate the sequence over which the helix extends.

Clearly, bPP is backfolded [5], whereas the N terminus of NPY is fully flexible [4]. Upon binding to DPC micelles the N terminus is released, and the peptides bind in monomeric form to the micelle by inserting hydrophobic side chains into the hydrophobic interior and by partitioning of Tyr side chains into the water-membrane interface. Association of the N terminus with the micelle occurs for bPP but not for NPY.

NPY and PYY display high sequence similarity. Moreover, their binding profiles at the Y receptor subtypes are highly similar. Yet they differ largely in their solution structures. Whereas the N terminus of NPY is flexible in solution it is back-folded in PYY. In fact, the tertiary and quarterly structures of PYY are more similar to bPP than to NPY making NPY and PYY an ideal couple for our first strategy.

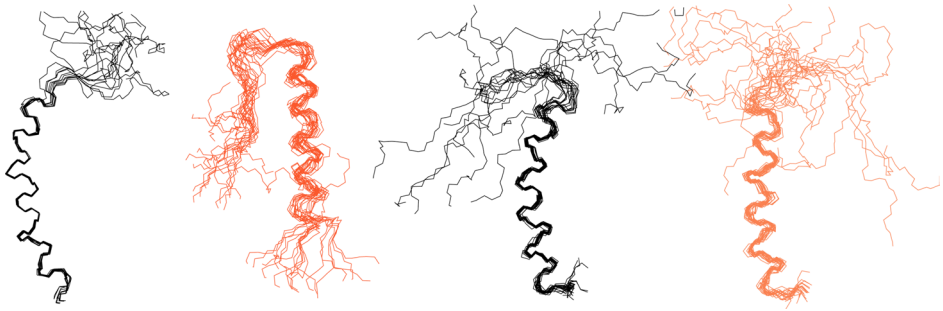

Fig. 2. Backbone presentation of the NMR ensemble of pNPY (black) and pPYY (gray) in aqueous solution (left) and the micelle-bound state (right). The sol'n structure of NPY was taken from [6].

In contrast, the structures of NPY and PYY in the micelle-bound state are almost identical whereas the conformation of bPP at the C terminus differs greatly. Therefore, this couple of peptides is more likely to be recognized from the membrane-bound state.

The chimera [$^{19\text{-}23}$hPP]-pNPY and [$^{19\text{-}23}$pNPY]-hPP present two peptides with dramatically altered receptor subtype specificities with respect to their parent peptides [7]. However, data on the hetereonuclear NOE indicate that no changes in their propensity to adopt the back-fold in solution are introduced through the mutations. In essence, the propensity for adopting the PP fold, the major structural feature by which the peptides differ *in solution*, seems to be uncorrelated to receptor binding.

Arg33 and/or Arg35 are proposed to be directly involved in binding to the Y receptors [3]. Moreover, mutagenesis studies have pointed out the importance of an Asp residue at the membrane-water interface of the E3 loop at the hY1 receptor [8]. Orientation of the two Arg residues with respect to the water-membrane interface may therefore be of crucial importance for initial recognition. We could demonstrate that for the Y5 selective peptide [Ala^{31},Pro^{32}]NPY the conformation in the C-terminal pentapeptide is different, and proposed that recognition of the particular receptor Asp residue at the water-membrane interface may be impaired at the other subtypes [9].

Acknowledgments

The work was financially supported by the ETH grants 0 20 439-97 and TH-39/00-3.

References

1. Kaiser, E. T. and Kezdy, F. J. *Science* **223**, 249-55 (1984).
2. Sargent, D. F. and Schwyzer, R. *Proc. Natl. Acad. Sci. U.S.A.* **83**, 5774-5778 (1986).
3. Beck-Sickinger, A. G., Wieland, H. A., et al. *Eur. J. Biochem.* **225**, 947-58 (1994).
4. Bader, R., Bettio, A., Beck-Sickinger, A. G. and Zerbe, O., *J. Mol. Biol*. **305**, 307-329 (2001).
5. Lerch, M., Gafner, V., Bader, R., et al. *J. Mol. Biol*. **322**, 1117-1133 (2002).
6. Monks, S. A., Karagianis, G., Howlett, G. J. and Norton, R. S. *J. Biomol. NMR* **8**, 379-390 (1996).
7. Cabrele, C., Wieland, H. A., Langer, M., Stidsen, C. E. and Beck-Sickinger, A. G. *Peptides* **22**, 365-378 (2001).
8. Walker, P., Munoz, M., Martinez, R. and Peitsch, M. C. *J. Biol. Chem*. **269**, 2863-2869 (1994).
9. Bader, R., Rytz, G., Lerch, M. Beck-Sickinger, A. G. and Zerbe, O. *Biochemistry* **41**, 8031-8042 (2002).

Peptide Revolution: Genomics, Proteomics & Therapeutics
Michael Chorev & Tomi K. Sawyer (Editors)
American Peptide Society, 2003

Chemical Synthesis of a Membrane Protein

Takeshi Sato, Yasuhiro Saito and Saburo Aimoto

Division of Organic Chemistry, Institute for Protein Research,
Osaka University, Osaka565-0871 Japan

Introduction

The biological importance of membrane proteins is emphasized in statistical analyses of the genomes that indicate about 30% of all open reading frames encode helix bundle membrane proteins [1]. However, compared with water-soluble proteins, research on membrane proteins is far behind. Sample preparation is a major problem in this area. As an alternative technique to obtain membrane proteins, other than using an expression system, a method for peptide synthesis should be taken into consideration. For synthesis of the segment containing TM region of the membrane protein, the first problem emerges in the step of the peptide chain elongation stage. β-branched amino acids that are commonly found in TM region are difficult to assemble. The hydrophobic nature of the TM region of membrane protein presents another serious problem, which makes the segments difficult to dissolve in aqueous solvents. As a result, the purification is hampered. Furthermore, while several ligation methods are successfully applied to synthesis of water-soluble protein, their application to membrane protein, especially one with multiple TM regions, is limited [2-4]. Nevertheless, chemical synthesis of membrane protein remains challenging. We report here two strategies aimed at a synthesis of a polytopic membrane protein. The first involves a preparation of a peptide thioester with TM region. The peptide thioester is designed to obtain a higher solubility to an aqueous solvent. Second, we introduced an –SH protecting group, which allows a compatibility of two ligation methods, the thioester method and native chemical ligation (NCL).

Results and Discussion

As a target for an examination of the synthesis, we selected opioid receptor-like 1 (ORL1) GPCR (Figure 1). A peptide thioester containing the 7th TM region of the protein [ORL1(288-328)–SR, –SR : $-SCH_2CH_2CO$-Gly-$(Arg)_5$-Leu] was synthesized by SPPS using Boc chemistry. The peptide thioester was designed to contain a sequence of five arginines (Arg-tag) at the C-terminal end. By the cation core of this Arg-tag, molecules themselves in a system must be dispersed. As a result, the separation was well-performed on RP-HPLC conditions, which we have previously introduced, to obtain highly pure ORL1(288-328)–SR. Comparatively, the purification of the peptide thioester without Arg-tag could not be accomplished.

Judging from the amino acid sequence, NCL should be our first choice for the ligation. Since the product is going to be a building block in further synthesis by the thioester method, the –SH group at the site of the coupling by NCL must be protected.

LGVQPSSETAVAILR*FCTALGYVNSCLNPILYAFL*DENFK**A-C**FRKFCCASALRRDVQVSDRVRSIAKDVALACKTSETVPRPA

Fig. 1 Amino acid sequence of ORL1(288-370). Putative TM region is shown in italics, and coupling site is shown in bold and a dash.

We performed a model experiment for the protection of the –SH group. As a result, it was found that $-S_2O_3^-$ can be used as a –SH protecting group in the thioester method,

which implies that the thioester method and NCL can be combined for synthesis of a single polypeptide. Next, ORL1(288-328)–SR was applied to a coupling reaction with ORL1(329-370) (C-tail). However, the coupling by NCL did not proceed to obtain the desired product under any conditions tested. Thus, our next choice was to use the thioester method for the coupling reaction. The building blocks that had been prepared for NCL coupling were converted to building blocks for the thioester method (Scheme 1). The $-S_2O_3^-$ group, designed for the combination of the thioester method and NCL, was also found to be stable during the preparation.

The segment condensation by the thioester method was examined. Under normal conditions, in the presence of silver chloride, 3,4-dihydro-3-hydroxy-4-oxo-1,2,3-benzotriazine (HOObt) and DIEA in dimethylsulfoxide, the coupling reaction did not proceed. By the addition of 3,4-dihydro-3-hydroxy-4-oxo-1,2,3-benzotriazine potassium salt, which controls the salt formation between N-terminal amino group and sulfonate, to the coupling mixture, the reaction proceeded to give the product Fmoc-[$Cys^{304,313,329}(S_2O_3)$,$Cys^{334,335,360}$(Acm)]ORL1(288-370).

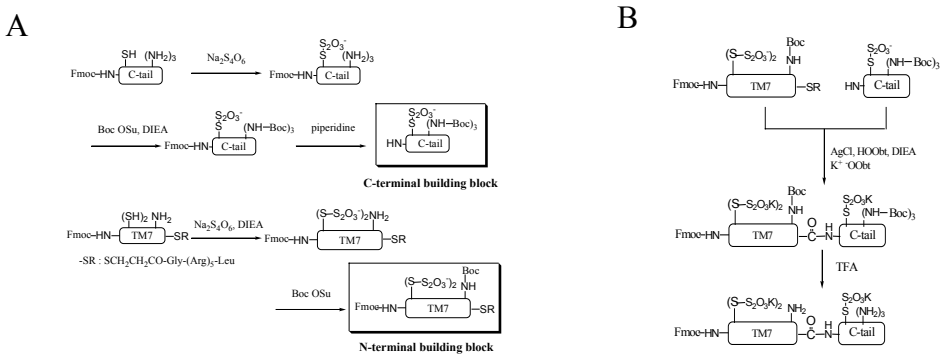

Scheme 1. Preparation of building blocks for the thioester method (A) and coupling reaction by the thioester method (B).

In conclusion, we showed that an addition of Arg-tag to a thioester moiety of a peptide thioester was effective for the purification. Also, the combination of the thioester method and NCL for a synthesis of a single polypeptide, ORL1, was found to be possible by using $-S_2O_3^-$ as a protecting group of –SH.

References

1. Wallin, E. and Heijne, V. G. *Protein Sci.* **7**, 1029-1038 (1998).
2. Sato, T., Kawakami, T., Akaji, K., Mochizuki, K., Fujiwara, T., Akutsu, H. and Aimoto, S. *J. Peptide Sci.* **8**, 172-180 (2002).
3. Kochendoerfer, G. G., Salom, D., Lear, J. D., Wilk-Orescan, R., Kent, S. B. H. and DeGrado, W. F. *Biochemistry* **38**, 11905-11913 (1999).
4. Valiyaveetil, F. I., MacKinnon, R. and Muir, T. W. *J. Am. Chem.Soc.* 124, 9113-9120 (2002).

Peptide Revolution: Genomics, Proteomics & Therapeutics
Michael Chorev & Tomi K. Sawyer (Editors)
American Peptide Society, 2003

Effect of RGD Peptides in *In Vivo* Model for Diabetic Retinopathy

Ralph-Heiko Mattern[1], Sergio Caballero[2], Amanda Omlor[1], Juerg F. Tschopp[1], Michael D. Pierschbacher[1] and Maria B. Grant[2]

[1]Integra LifeSciences Corporation Corporate Research Center, 11045 Roselle Street, San Diego, CA 92121, USA; [2]Department of Pharmacology, University of Florida, 1600 SW Archer Road, Gainesville, FL 32610-0267, USA

Introduction

Since the discovery of the cell adhesion sequence Arg-Gly-Asp (RGD) in fibronectin [1] it has been shown that the RGD sequence serves as a binding site of many adhesion proteins to integrin receptors [2]. The RGD sequence incorporated into small peptides can mimic these adhesion proteins and can regulate cell-cell and cell-matrix interaction. It has been demonstrated in early studies that the conformation of such peptides and the way the RGD portion is presented to the receptor have a tremendous influence on potency and integrin selectivity [3-6]. Several of the integrin receptors are very attractive targets for the design of drug candidates. The $\alpha 5\beta 1$ receptor is important for cell migration, tumor invasion and metastasis, and integrin $\alpha IIb\beta 3$ plays a major role in platelet aggregation. The $\alpha v\beta 3$ receptor has attracted considerable interest due to its possible involvement in osteoporosis, angiogenic disorders and cancer. The $\alpha v\beta 5$ receptor is involved in angiogenic events as well. RGD peptides that are selective for integrin receptors will enable us to elucidate the importance of these receptors for angiogenic events such as diabetic retinopathy. Diabetic retinopathy is the leading cause of blindness in the under 55 age group. The course of the disease is characterized by excessive angiogenesis in the vitreous and leakage of blood vessels into the vitreous, which subsequently causes loss of vision.

Table 1. Binding affinities of RGD-containing peptides to integrin receptors IC_{50} (nM).

Compound	$\alpha_v\beta_3$	$\alpha_v\beta_5$	$\alpha_5\beta_1$	$\alpha_{IIb}\beta_3$
1 c[RGDD(t-BuG)(Mamb)]	**3**	20	42	240
2 c[(Mpa)RGDD(t-BuG)C]-NH_2	**20**	210	390	70
3 G-c[(Pen)FRGDSFC]-A	2700	**46**	1800	3400
4 G-c[(Pen)RARGDNPC]-A	52	330	**2**	30
5 Ac-c[(Pen)Y(Me)ARGDN(Tic)C]-NH_2	**2**	**6**	**5**	190
6 c[RGDfV]	26	11	nt	960

Results and Discussion

The $\alpha v\beta 3$-specific peptides c[(Mpa)-Arg-Gly-Asp-Asp-(t-BuG)-Cys]-NH2 and c[Arg-Gly-Asp-Asp-(t-BuG)-(Mamb)] (compounds **1** and **2**), the $\alpha v\beta 5$–specific peptide Gly-c[(Pen)-Phe-Arg-Gly-Asp-Ser-Phe-Cys]-Ala (compound **3**), the $\alpha 5\beta 1$-specific peptide Gly-c[(Pen)-Arg-Ala-Arg-Gly-Asp-Asn-Pro-Cys]-Ala (compound **4**) and the potent but non-specific peptide Ac-c[(Pen)-Tyr(Me)-Ala-Arg-Gly-Asp-Asn-(Tic)-Cys]-NH2 (compound **5**) were synthesized and tested in *in vivo* and *in vitro* assays to study the effect of these peptides in angiogenesis models. Table 1 shows the binding affinities of the peptides to the integrin receptors in comparison with the c[RGDfV] peptide.

These peptides were tested in two *in vivo* models for angiogenesis, the mouse model of proliferative retinopathy (ROP) and the chick chorioallantoic membrane (CAM) assay. In the ROP assay the $\alpha v\beta 3$ specific peptides **1** and **2**, as well as the non-specific

peptide **5** show significant inhibition of angiogenesis at higher concentration (250ug IP). The $\alpha v\beta 3$ specific compound **1** exhibits the best inhibition of angiogenesis at the lower concentration of (25 ug IP). The $\alpha v\beta 5$ specific compound **3** does not significantly inhibit the growth of pre-retinal blood vessels at low or high concentration whereas the $\alpha 5\beta 1$ specific compound **4** demonstrates significant inhibition at high concentration but has no significant effect at the lower concentration.

The results obtained in the CAM assay also demonstrate that the peptides **1, 2, 3** and **5** inhibit FGF induced angiogenesis. The $\alpha 5\beta 1$ peptide **4** does not seem to have an effect in this particular assay. However, in this assay the angiogenesis is FGF-induced, which might overemphasize the involvement of the $\alpha v\beta 5$ receptor.

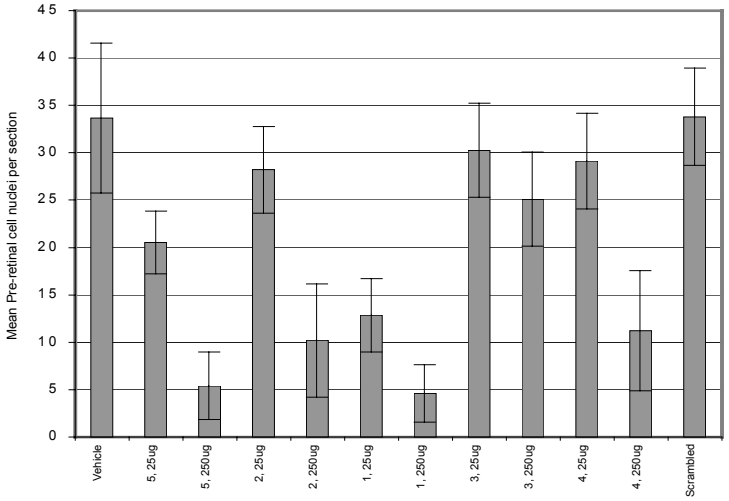

Fig. 1. Effect of RGD peptides on oxygen induced retinopathy.

Acknowledgments

We gratefully acknowledge financial support from the National Institutes of Health (DK51938-03).

References

1. Ruoslahti, E. and Pierschbacher, M. D. *Nature* **309**, 30-33 (1984).
2. Ruoslahti, E. and Pierschbacher, M. D. *Proc. Natl. Acad. Sci. U.S.A.* **81**, 5985-5988 (1984).
3. Pierschbacher, M. D. and Ruoslahti, E. *J. Biol. Chem.* **262**, 17294-17298 (1987).
4. Cheng, S., Craig, W. S. Mullen, D., Tschopp, J. F., Dixon, D. and Pierschbacher, M. D. In Hodges, R. S. and Smith, J. A. (Eds.) *Peptides: Chemistry, Structure and Biology (Proceedings of the 13th American Peptide Symposium),* Escom, Leiden, 1994, 384-386.
5. Ingram, R. T., Cardenas, J. Hessle, H., d'Avis, P., Mullen, D., Malaney, T. I., Minasyan, R., Paulson, G. O., Parker, J. and Pierschbacher, M. D. In *Transactions of the 24th Annual Meeting of the Society for Biomaterials,* Vol XXI, 1998, 196.
6. Cheng, S., Craig, W.S., Mullen, D. Tschopp, J. F., Dixon, D. and Pierschbacher, M. *J. Med. Chem.* **37**, 1-8 (1994).

Peptide Revolution: Genomics, Proteomics & Therapeutics
Michael Chorev & Tomi K. Sawyer (Editors)
American Peptide Society, 2003

Synthesis of Unusual RGD Cyclic Peptides Incorporating C $^{\alpha}$-Fluoromethylamino Acids, as Selective Inhibitors of $\alpha_v\beta_3$ Integrin

Alma DalPozzo, Minghong Ni and Laura Muzi

G. Ronzoni Institute for Chemical and Biochemical Research, 20133 Milano, Italy

Introduction

Cyclic peptides containing the RGD sequence are an exciting class of molecules showing a wide range of biological activities [1]. We sought to incorporate α-di- and trifluoromethylamino acids (Dfm- and Tfm-AAs) into the cyclic motif with the purpose of examining the effect on the conformation and activity. The discovery of $C^{\alpha,\alpha}$-disubstituted AAs and their propensity to induce secondary structures [2] has resulted in an increased interest in novel methods for their synthesis. Many efforts have been spent on the introduction of such hindered molecules into peptides, with variable success. However, in the case of α-Tfm- AAs, all methods known, so far, fail to afford acylation of the amino function, which, in addition to being sterically hindered is also deactivated by the polarizing effect of fluorine. While a number of methods, either chemical [3] or enzymatic [4], are available to introduce α-Dfm and Tfm-AAs in the N-terminal position of peptides, their incorporation in other positions still remains inaccessible, except for the less bulky α-Tfm-Ala. In fact, there is no knowledge of cyclic peptides containing these building blocks. Here we report the successful synthesis of RGD cyclic analogs containing one α-Tfm- or Dfm-AA in different positions of the ring:

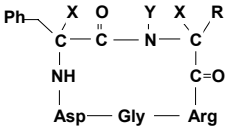

Where R=benzyl or isopropyl
X=H, CF_3 or CHF_2
Y=H or CH_3

Results and Discussion

A series of 5 analogs was prepared in good yields, following a method recently developed in our laboratories and utilizing N-protected AA-bromides as acylating agents of the amino function of α-fluoromethylamino acids [5]. Two different schemes of synthesis were applied, as exemplified below:

H-(R,S)-Tfm-Phe-OEt $\xrightarrow{i}$ Pht-D-Phe-Tfm-Phe-OEt $\xrightarrow{ii}$ Pht-D-Phe-Tfm-Phe-OH $\xrightarrow{iii, iv}$ Pth-D-Phe-Tfm-Phe-Orn(Cbz)-OH $\xrightarrow{v, vi}$ H-D-Phe-Tfm-Phe-Orn(Cbz)-Gly-OtBu $\xrightarrow{vii, viii,}$ TFA.H-AllGly-D-Phe-Tfm-Phe-Orn(Cbz)-Gly-OH $\xrightarrow{ix}$ c[AllGly-D-Phe-Tfm-Phe-Orn(Cbz)-Gly] $\xrightarrow{x, xi}$ c (Orn-Gly-Asp-D-Phe-Tfm-Phe) $\xrightarrow{xii, xiii}$ c [Arg-Gly-Asp-D-Phe-(R or S)-Tfm-Phe]

Scheme 1. Example of synthetic strategy.

(i), Pht-D-Phe-Br, collidine, DCM, r.t., 2 h; (ii), BBr_3, DCM, Δ, 2 h ; (iii), HCl.H-Orn(Cbz)-OtBu, HATU, DIEA, r.t., CH_3CN, 2h; (iv), TFA/DCM 1:1, r.t., 30 min; (v); HCl·H-Gly-OtBu, HOAT, DIEA, DCM, r.t., 2 h; (vi) ,1 N NH_2NH_2 in EtOH, reflux, 2.5 h; (vii), Fmoc-Allgly-OH, DCC, HOAT, DIEA, DCM, r.t., 1.2 h; (viii), piperidine, DCM ,r.t., 2h; (ix), TBTU, HOBT, DIEA 1% in DMF, 10 min; (x), $KMnO_4$ in H_2SO_4, acetone, r.t., 1 night; (xi), $HCOONH_4$, 10% Pd/C, DMF, AcOH; (xii), Pyrazole-carboxamidine, DIEA, MeOH, r.t. Ar, 1h; (xiii), Separation of R and S isomers by RP-HPLC, 34% CH_3CN in H_2O + 0.1% TFA.

Four out of the five analogs were obtained by the above procedure, with only minor modifications. However, the same method did not apply to the synthesis of the cyclopeptide containing N-Me-α-Tfm-Phe; this overhindered building block was incorporated following a modified method described in Scheme 2:

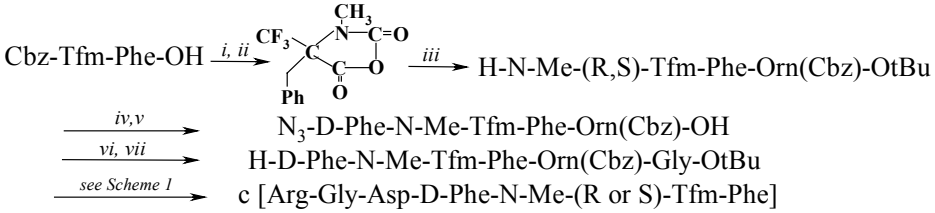

Scheme 2. Synthetic procedure for the incorporation of N-Me-α-Tfm-AAs.

(i), $SOCl_2$, reflux,1 night; (ii), NaH, MeI, DMF, 2h; (iii), HCl.H-Orn(Cbz)-OtBu, TEA, DCM, r.t., 70 h; (iv), N_3-D-Phe-Br, collidine, DCM, r.t., 1 night; (v), TFA/DCM 1:1,r.t., 1h; (vi), HCl.H-Gly-OtBu, DCC, HOAT, DIEA, DCM, r.t., 2h; (vii), $[Et_3NH][Sn(SPh)_3]$, CH_3CN, r.t., 1h.

A common feature of both syntheses is the acylation via a suitably N-protected bromide. The bromide was generated *in situ* by the brominating agent bromoenamine, following already published methods [5,6], and immediately used. Pht-Phe-Br could easily acylate the α-fluoromethyl-AA esters (see Scheme 1), but it proved inadequate for the N-Me-terminus of a dipeptide; in this case (see Scheme 2), only N_3-Phe-Br afforded the tripeptide, demonstrating azide superior to any other N-protecting group, probably due to its very small size [7]. Scheme 2 describes the N-methylation of the α–Tfm-Phe-OH; this was carried out by activation of the nitrogen through a Leuchs anhydride, which, in turn, accepts the nucleophilic attack of the next AA to give the dipeptide [8]. In both Schemes Allylgly and Orn were incorporated as precursors of Asp and Arg, respectively, in order to avoid some protection problems.

In conclusion, for the first time we succeeded in incorporating α-Tfm and N-Me-α-Tfm-AAs, ranging from Val, Asp, Phe and N-Me-Phe, into every desired position of linear and cyclic peptide chains. Strategic placement of these unusual building blocks represents a new approach to the design of biologically active peptides with potentially improved metabolic stability and bioavailability. Moreover, it is worth remarking that the incorporation of a fluoroalkyl group may be useful to increase the diversity of protein functions modifying the physical properties of protein-based materials.

Acknowledgments

This research was supported by Sigma-Tau, Rome, Italy.

References

1. Haubner, R., Finsinger, D. and Kessler, H. *Angew. Chem*. **36**, 1374-1389 (1997).
2. Toniolo, C. *Jannsen Chim. Acta* **11**, 10-16 (1993).
3. DalPozzo, A., Muzi, L., Moroni, M., et al., *Tetrahedron* **54**, 6019-6028 (1998).
4. Thust, S. and Koksch, B. *J. Org. Chem*. **68**, 2290-2296 (2003).
5. DalPozzo, A., Ni, M. H., Muzi, L, et al., *J. Org. Chem*. **67**, 6372-6375 (2002).
6. DalPozzo, A., Bergonzi, R. and Ni, M. H. *Tetrahedron Lett*. **42**, 3925-3927 (2001).
7. Meldal, M., Juliano, M. A. and Jansson, A. M. *Tetrahedron Lett*. **38**, 2531-2534 (1997).
8. Burger, K. and Hollweck, W. Synlett. 751-753 (1994).

Peptide Revolution: Genomics, Proteomics & Therapeutics
Michael Chorev & Tomi K. Sawyer (Editors)
American Peptide Society, 2003

Plasmon Waveguide-Resonance Spectroscopy: A New Method to Study GPCR Signal Transduction

Isabel D. Alves[1], Zdzislaw Salamon[1], Gordon Tollin[1,2] and Victor J. Hruby[1,2]

[1]Department of Biochemistry and Molecular Biophysics; [2]Department of Chemistry; University of Arizona, Tucson, AZ 85721, USA

Introduction

Understanding structure-function relationships and mechanisms of signal transduction in G-protein coupled receptors (GPCRs) is becoming increasingly important due in part to their central role as pharmacological targets. Their integral membrane nature and rather low natural abundance present many challenging problems. Using a recently developed technique, plasmon-waveguide resonance (PWR) spectroscopy, we have investigated structural changes accompanying the binding of ligands to the human δ-opioid receptor (hDOR) immobilized on a solid-supported lipid bilayer [1]. This highly sensitive technique can directly monitor changes in mass density, conformation and orientation occurring in such thin proteolipid films. Without requiring labeling protocols, PWR allows the direct determination of binding constants and other biophysical properties in a system that is very close to the receptor's natural environment. We have found that different classes of ligands induce different receptor conformational changes [2]. Using the same technology we have been able, for the first time, to directly measure the binding between the hDOR and its G-protein effectors in real time. We have found that both the affinity of the G- protein towards the receptor and the affinity of GTPγS towards the receptor-G protein complex are highly dependent on the nature of the ligand that is pre-bound to the receptor. This methodology provides a powerful new way of investigating transmembrane signaling.

Results and Discussion

We have incorporated the hDOR in a solid-supported lipid bilayer and monitored receptor conformational changes upon binding of agonists (peptide and non-peptide), antagonists, inverse agonists and partial agonists. Five distinctly different structural states of the receptor were observed upon binding of each of these classes of ligands. Ligand binding not only produced distinctive spectral changes, corresponding to different receptor conformational states, but also the formation of each state was characterized by very different kinetic properties. Binding constants, obtained by quantifying the extent of conformational change as a function of the amount of ligand bound, were in good agreement with published values determined by radiolabeling methods (Table 1). Using PWR we have, for the first time, directly monitor the interaction between G proteins (mixture from the brain containing $G_{i\alpha1}$, $G_{i\alpha2}$, $G_{i\alpha3}$, $G_{o\alpha}$ and the βγ subunits) and the hDOR prebound to agonist, antagonist or inverse agonist ligands. We have also monitored the PWR spectral changes obtained upon addition of GTPγS to the liganded receptor-G protein. Separate affinity constants were obtained for the G protein-receptor interaction as well as for the GTPγS interaction with the receptor-G protein complex, and those are given in Table 2. From these data, we can see that the affinity of the G protein to the receptor is highly dependent on the ligand that is pre-bound to the receptor. The highest affinity was observed when the receptor was bound to an agonist; the lowest when the receptor was bound to an antagonist; and

no binding was observed when the receptor was bound to an inverse agonist. We also have found direct evidence for the existence of an additional G-protein binding conformational state that corresponds to the unligated receptor. Furthermore, GTPγS binding to the receptor-G protein complex was only observed when the agonist was pre-bound. The results presented provide new insights into ligand-induced GPCR functioning and signal transduction events of the human δ-opioid receptor, and illustrate a powerful new protocol for drug development. Trafficking studies and other aspects of signal transduction such as receptor down-regulation are in progress.

Table1. Binding constants for the interaction between the hDOR and its ligands.

Ligands	K_d (nM)	
	p-pol. light	*s*-pol. light
DPDPE	14 ± 3	18 ± 5
pCl-DPDPE	2.94 ± 0.7	3.25 ± 0.8
Deltorphin II	0.88 ± 0.045	1.21 ± 0.3
SNC80	52 ± 6	57 ± 7
Tan 67	3.2 ± 1.2	3.7 ± 1.5
TIPP	1.1 ± 0.12	1.2 ± 0.1
NTI	0.025 ± 0.001	0.023 ± 0.004
Naloxone	8 ± 3	8 ± 1
TMT-L-Tic	2.5 ± 0.3	3.2 ± 0.2
Morphine	520 ± 30	*
Ethorphine	0.3 ± 0.08	0.26 ± 0.1

*Note: K_d values were obtained from plotting the resonance minimum position for the PWR spectra as a function of ligand concentration and fitting to the following hyperbolic function that describes the binding of a ligand to a receptor: $Y = (B_{max} \times X)/ (K_d + X)$. B_{max} represents the maximum concentration bound and K_d is the concentration of ligand required to reach half-maximal binding. *No net spectral shifts were obtained for this ligand using s-polarized light.*

Table 2. Binding constants for the interaction between G-proteins and the hDOR either unbound or prebound to agonist or antagonist.

Bound ligand	Agonist (DPDPE)		Antagonist (Naltrindole)		No ligand	
Polarization	*p*	*s*	*P*	*s*	*p*	*s*
$K_d^{G\text{-proteins}}$ (nM)	12 ± 2	10 ± 1	494 ± 48	509 ± 44	73 ± 9	52 ± 3
$K_d^{GTP\gamma S}$ (nM)	14 ± 2	13 ± 2	*	*	*	*

** No PWR spectral shifts were obtained upon addition of GTPγS up to 1 μM.*

Acknowledgments
Supported by grants from the USPHS and the National Science Foundation.

References
1. Salamon, Z. et al. *Biophys. J.* **79**, 2463-2472 (2000).
2. Salamon, Z. et al. *J. Pept. Res.* **60**, 322-328 (2002).

Peptide Revolution: Genomics, Proteomics & Therapeutics
Michael Chorev & Tomi K. Sawyer (Editors)
American Peptide Society, 2003

Novel, Potent, ORL-1 Receptor Agonist Peptides Containing α-Helix Promoting Conformational Constraints

Chongwu Zhang, Paul R. Blake, Shen Shan, Kenneth J. Valenzano and Donald J. Kyle

Purdue Pharma L.P. 6 Cedar Brook Dr. Cranbury NJ 08512, USA

Introduction

The ORL-1 receptor has been implicated in a wide variety of physiological and pathophysiological processes. Toward the goal of elucidating important features of the receptor-bound conformation of the endogenous ligand, nociceptin (NC), we recently reported [1] several conformationally constrained analogs, in which either a-aminoisobutyric acid (Aib) or N-methyl alanine was inserted as a replacement for the native Ala, either at position 7, 11 or 15. These conformational constraints, together with computational secondary structural predictions led us to propose a mostly helical bioactive conformation for NC (Fig. 1).

We have extended the study to the known, truncated, NC(1-13)-CONH2 with the goal of inserting conformational constraints into a shorter peptide. This might provide an opportunity to study the structure in solution using 2D NMR data as distance constraints. Three new peptides were prepared and tested for binding and functional activity at the human ORL-1 receptor.

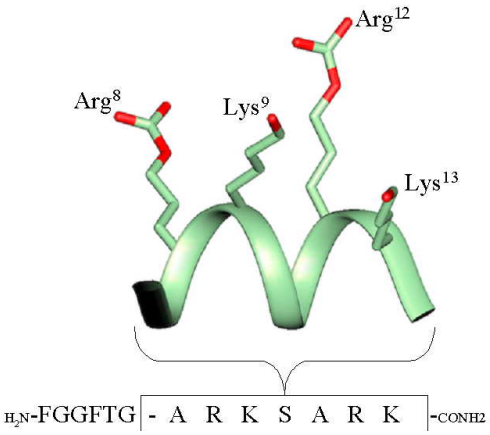

Fig. 1. Proposed helical conformation of NC(1-13)-CONH$_2$.

Results and Discussion

Peptides were prepared by Fmoc solid-phase synthesis. Fmoc-Rink amide resin resin was used to prepare the C-terminal amide. Double-couplings to the Aib residue was used. Peptides were deprotected and cleaved from the resin by reagent K (TFA:phenol:H_2O:thioanisole:1,2-ethanedithiol; 33:2:2:2:1). ORL-1 receptor assay methods is the same as previously described [1].

Table 1. Human ORL-1 In Vitro Assay Results.

Peptide Sequence	K_i (nM)	EC_{50} (nM)	E_{max}
NC H_2N-FGGFTG A RKS A RK LANQ-COOH	0.084 ± 0.014	0.182 ± 0.04	97.2 ± 2.5%
I H_2N-FGGFTG A RKS A RK- $COONH_2$	0.12 ± 0.03	0.44 ± 0.2	99 ± 1%
II H_2N –FGGFTG A RKS **(Aib)** RK- $COONH_2$	0.113 ± 0.012	0.45 ± 0.21	95 ± 5%
III H_2N –FGGFTG (Aib) RKS A RK- $COONH_2$	0.044 ± 0.007	0.17 ± 0.08	96 ± 4%
IV H_2N –FGGFTG **(Aib)** RKS **(Aib)** RK- $COONH_2$	0.048 ± 0.005	0.13 ± 0.04	83 ± 2%

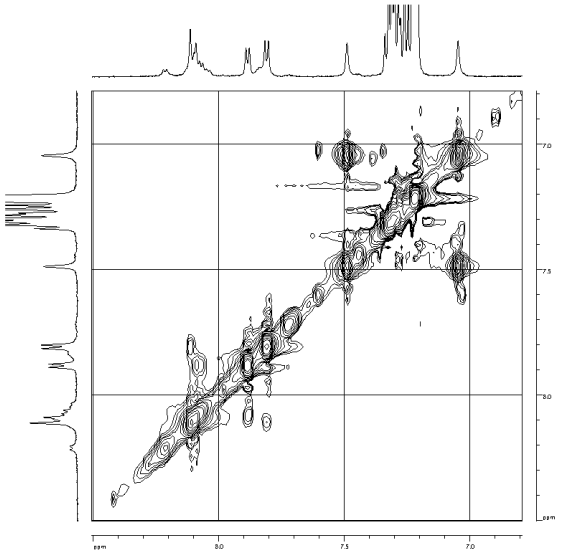

Fig. 2. 2DNOESY spectrum of ~6mg of H-F-G-G-F-T-G-Aib-R-K-S-Aib-R-K-NH_2 in 550ul of H_2O/10% D_20 pH 5.5. The data was acquired at 500MHz using a 350 msec Tm, 512 blocks and 64 transients/block.

In our previous study [1] our results show that NC peptides bearing a C-terminal amide are of higher affinity and greater potency than the corresponding C-terminal acid-containing peptides while on the other hand the C-terminal part of NC does not make a substantial energetic contribution to binding and conformational preference is minimal. We also demonstrated a high likelihood of a helical bioactive conformation spanning residues 7-15. In this work, we predicted that constraints incorporated into NC(1-13)-$CONH_2$ that impose a helical conformation should also improve potency. Moreover, since these peptides would be significantly shorter than those in our previous work, we might be able to experimentally confirm the secondary structure by NMR.

Our new data supports our hypothesis in that our doubly constrained NC(1-13)-$CONH_2$ peptide is approximately 3-fold more potent than the unconstrained parent. Moreover, several HN-HN cross peaks are detected in the amide region of the 2DNOESY spectrum. Although the resonances have not been assigned to date, they suggest the peptide may contain a helical region. The existence of HN-HN(i to i+1) NOEs are commonly used as a fingerprint for defining helical regions in proteins. In addition, the amide exchange rates vary, as depicted in the 1D (water presaturation) experiment plotted on the X & Y axis (above, variable amide intensities). This differential saturation suggests these amides undergo slower exchange rates with the bulk water (relative to other amide resonances in the peptide), and thus are less susceptible to saturation of the bulk water. Hydrogen bonding, solvent inaccessibility and low pH (<4) are the most common reasons for reduced exchange rates, suggesting some of the peptide amides are involved in H-bonding.

In summary we have improved the potency of NC(1-13)-$CONH_2$ 3-fold *in vitro* via the introduction of helix-promoting conformational constraints. In addition, our preliminary NMR analysis supports the proposal that the conformation of the peptide is helical.

References

1. Zhang, C., Miller, W., Valenzano, K. J. and Kyle, D. J. *J. Med. Chem*. **2002**, *45*, 5280-5286.

Peptide Revolution: Genomics, Proteomics & Therapeutics
Michael Chorev & Tomi K. Sawyer (Editors)
American Peptide Society, 2003

Synthesis and Pharmacological Activity of Novel Peptide Ligands for the NOP Receptor

Severo Salvadori[1], Remo Guerrini[1], Marina Zucchini[1], Giacomo Carrà[2], Daniela Rizzi[2], Domenico Regoli[2] and Girolamo Calo'[2]

[1]Department of Pharmaceutical Sciences and [2]Department of Experimental and Clinical Medicine, Section of Pharmacology, University of Ferrara, 44-100 Ferrara, Italy

Introduction

Nociceptin/orphanin FQ (N/OFQ: H-Phe-Gly-Gly-Phe-Thr-Gly-Ala-Arg-Lys-Ser-Ala-Arg-Lys-Leu-Ala-Asn-Gln-OH) mediates several biological functions by selectively activating a G protein coupled receptor (NOP). SAR studies on N/OFQ have established that Phe^1 and Phe^4 represent the critical residues of the peptide message domain (Phe^1-Gly^2-Gly^3-Phe^4) involved in the NOP receptor binding and activation, whereas the positively charged residues $Arg^{8,12}$, $Lys^{9,13}$, present in the address domain of the molecule, appear to be crucial for receptor occupation. Specific changes of the message sequence of N/OFQ led to the discovery of the NOP partial agonist [$Phe^1\Psi(CH_2$-NH)Gly^2]N/OFQ-NH_2, the pure antagonist [$Nphe^1$]N/OFQ-NH_2 (Nphe = N-benzyl glycine), and the highly potent agonist [(pF)Phe^4]N/OFQ(1-13)-NH_2 [1]. The importance of the positively charged amino acids in the address domain of the peptide was supported by the identification of [Arg^{14},Lys^{15}]N/OFQ, that is 10-fold more potent than the natural ligand [2]. Based on these findings, we have combined in the sequence of N/OFQ different modifications: Arg^{14}, Lys^{15} and (pF)Phe^4 which increase the agonist potency with those conferring partial agonist, $Phe^1\Psi(CH_2$-NH)Gly^2, or pure antagonist, $Nphe^1$, properties. The chemical structure of the compounds are listed in Table 1.

Table 1. Chemical structure of the peptides employed in this study.

#	*Compound*
1	N/OFQ-NH_2
2	[(pF)Phe^4]N/OFQ-NH_2
3	[Arg^{14},Lys15]N/OFQ-NH_2
4	[(pF)Phe^4,Arg^{14},Lys^{15}]N/OFQ-NH_2
5	[$Nphe^1$,Arg^{14},Lys^{15}]N/OFQ-NH_2
6	[$Phe^1\Psi(CH_2$-NH)Gly^2,(pF)Phe^4,Arg^{14},Lys^{15}]N/OFQ-NH_2

Results and Discussion

Peptides described here were prepared by solid-phase method on a PAL-PEG-PS-resin. The results of the pharmacological effects in the electrically stimulated mouse vas deferens are summarized in Table 2. In this pharmacological preparation the N/OFQ analogues 2-4 are full agonists with increasing potencies. [(pF)Phe^4]N/OFQ-NH_2, [Arg^{14},Lys^{15}]N/OFQ-NH_2, and [(pF)Phe^4,Arg^{14},Lys^{15}]N/OFQ-NH_2, were more potent than N/OFQ-NH_2 (pEC_{50} 8.27 and E_{max} 95 ± 2%). In particular, analogue 4, [(pF)Phe^4,Arg^{14},Lys^{15}]N/OFQ-NH_2, was 10-fold more potent than N/OFQ-NH_2. Compound 5 is an analogue of [$Nphe^1$]N/OFQ-NH_2, reported previously by us as the

first selective antagonist of the NOP receptor with a pK_b value of 6.3 in the mouse vas deferens [3]. The additional peptide sequence modification (Arg^{14}-Lys^{15}), made at the C-terminal of the [$Nphe^1$]N/OFQ-NH_2, led to about 10-fold increase of antagonist potency.

Phe^1-Gly^2 peptide bond modification gave the analogue [$Phe^1\Psi(CH_2$-$NH)Gly^2$]N/OFQ-NH_2 that, in the mouse vas deferens, mainly behaves as an antagonist with a pK_b value about 7 [3]. Combining the reduction of the Phe^1-Gly^2 peptide bond with (pF)Phe^4 and $Arg^{14}Lys^{15}$, as in compound 6, we obtained a highly potent NOP partial agonist with a pEC_{50} of 8.99 and a pK_b of 9.20.

In conclusion, this study demonstrated that chemical modifications such as $Phe^1\Psi(CH_2$-$NH)Gly^2$, $Nphe^1$, (pF)Phe^4 and $Arg^{14}Lys^{15}$ applied to the N/OFQ can be used alone or in combination for generating highly potent agonists, partial agonists and pure antagonists for the NOP receptor.

Table 2. Effects of N/OFQ-NH_2 analogues in the electrically stimulated mouse vas deferens.

#	*Agonist*		*Antagonist*
	pEC_{50} ($CL_{95\%}$)	E_{max}	pK_b ($CL_{95\%}$)
1	8.27 (8.11-8.43)	95 ± 2%	ND
2	8.59 (8.30-8.88)	92 ± 1%	ND
3	9.12 (8.93-9.31)	95 ± 1%	ND
4	9.36 (9.14-9.58)	94 ± 1%	ND
5	Inactive		7.24 (7.03-7.45)
6	8.99 (8.73-9.25)	53 ± 3%	9.20 (9.00-9.40)

The antagonistic properties of these compounds were tested using N/OFQ as agonist. For pEC_{50} and pK_b values the confidence limits 95% are given in brackets. ND = not determined since the compound behaves as a full agonist. Inactive up to 10 μM.

References

1. Salvadori, S., Guerrini, R., Calo, G. and Regoli, D. *Il Farmaco* **54**, 810-825 (2000).
2. Okada, K., Sujaku, T., Chuman, Y., *et al., Biochem. Biophys. Res. Com.* **278**, 493-498 (2000).
3. Guerrini, R., Calò, G., Bigoni, R., *et al., J. Med. Chem.* **43**, 2805-2813 (2000).

Peptide Revolution: Genomics, Proteomics & Therapeutics
Michael Chorev & Tomi K. Sawyer (Editors)
American Peptide Society, 2003

The Peptide Complementarity

Renata Zbozien-Pacamaj, Piotr Stefanowicz, Alicja Kluczyk, Marek Cebrat, Marek Lisowski and Ignacy Z. Siemion

Faculty of Chemistry, University of Wroclaw, 14 F. Joliot-Curie Str., 50-383 Wroclaw, Poland

Introduction

In 1969 Mekler formulated a hypothesis that a special kind of interaction should exist between the peptides coded by two complementary strands of DNA. In 1982 Root-Bernstein postulated that reading of complementary DNA strands in parallel 3'-5'– direction leads to antisense complementary peptides, composed of complementary amino acids. The amino acid pairs selected by such a procedure form the complexes when arranged in the β-ribbon conformation [1]. Few years ago we found that the genetic code can be arranged by a regular set of one-step mutations in a closed ring showing a clear periodicity in respect to the properties of coded amino acids (for the review see [2]). We showed that the same positions within the ring fragments belonging to A and U, and C and G families of codons, respectively, are occupied by "equivalent" codons, in which two first bases are complementary, and the third is exactly the same. This prompted us to the idea that equivalent codons may code the complementary amino acids. The amino acids complementarity patterns, resulted from this idea, are generally similar to those predicted by Root-Bernstein hypothesis. Both approaches, however, differ in two points. According to Root-Bernstein's hypothesis, Asn should form a pair with Leu, and Lys with Phe, whereas Tyr should interact with Ile and Met. On the contrary, according to our hypothesis, Asn should interact with Phe, Lys with Leu, and Tyr with Ile only.

Results and Discussion

We examined our approach using a series of peptides derived from the sequence of TGF-β_2 protein. However, the investigated series did not allow to decide, which of two approaches, our or Root-Bernstein's, is more suitable for determining complementary peptide sequence, because in this particular case both approaches resulted in the same prediction [3].

Such a possibility could be, however, realized for cyclolinopeptide A (c-LIILVPPFF- CLA) and its complementary peptides. According to our approach a linear nonapeptide, complementary to the CLA sequence, may have the following structure: KYYKQGGNN (peptide I), and the correspondent cyclic peptide: c-(KYYKQGGNN-) (peptide II), whereas Root-Bernstein's approach leads to the sequence NYYNQGGKK (peptide III). The tendency to form the complexes of peptide-"antipeptide" type was examined by us with the ESI-MS technique. We found that peptide I forms quite stable complex with CLA. Strong peaks at 1056.5 $(CLA+I+2H)^{+2}$ and 704.8 $(CLA+I+3H)^{+3}$are present in the mass-spectrum of the CLA-peptide I mixture. The separated peak, appearing at 704.8, splits in the collision-induced dissociation experiment into CLA and peptide I peaks (see Figure 1a). The amount of undissociated complex changes in parallel to the collision potential used (Figure 1b). The experiments showed that the stability of CLA-peptide I complex is comparable to that of YIGKTPKI-IIYTLC(Acm)GLYL pair (the most stable complex in the whole TGF-β_2 series). The "Root-Bernstein's" peptide III does not complex with CLA. In the presence of CLA the cyclic peptide II shows a very small peak of the $[CLA+II+2H]^{+2}$ complex, in addition to small peaks corresponding to $[2CLA+II+2H]^{+2}$

and $[2CLA+II+H+Na]^{+2}$ structures. The lowering of complexation ability of II, as compared with the linear sequence I, remains in a good agreement with our earlier statement that the folded conformation of the peptide is not suitable for the peptide-"antipeptide" complex formation [3]. However, the tendency to form "sandwiches" between CLA and peptide II is worth attention.

We also applied the antipeptide strategy to peptide VTKFYF from IL-1Ra and its analogue VTRFYF from Vaccinia virus protein [4]. It turned out that complexes of the antipeptides QWLNIN and QWANIN (our theory), and QWAKIK and QWAKIK (Root-Bernstein's theory) with their respective peptides could not be detected in the MS spectra, whereas the CD technique revealed that the complexation of the peptide VTKFYF is much more pronounced in the case of antipeptide created according to our theory than that of Root-Bernstein's. It is also interesting that the effects in CD spectra were more significant for IL-1 pairs than for the viral sequences, despite only one amino acid difference (Lys – Arg in peptides and Leu – Ala in antipeptides, respectively).

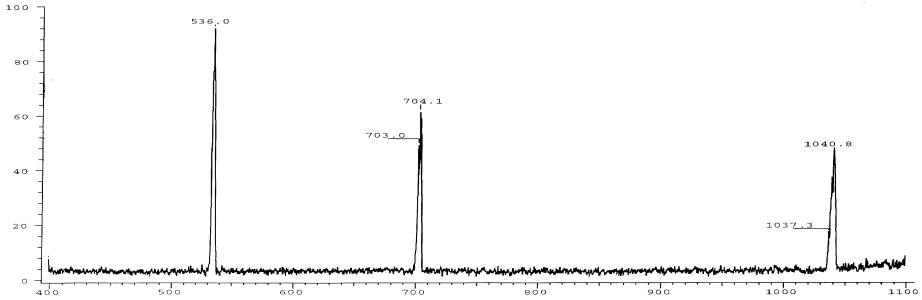

Fig. 1a. MS spectrum of a quite stable complex peptide I with CLA.

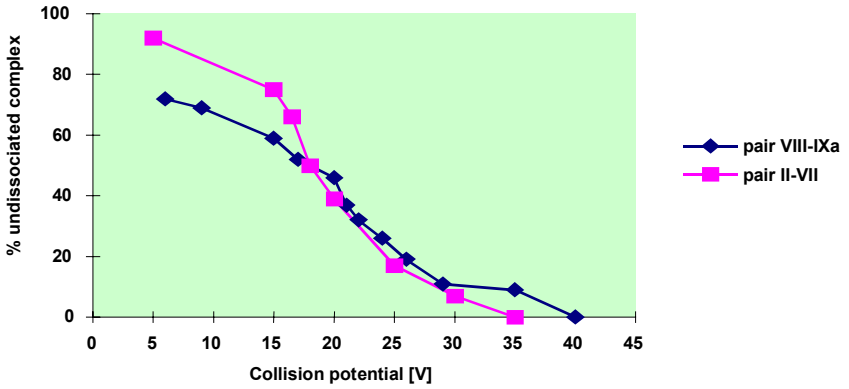

Fig. 1b. Collision –induced dissociation curves for heterodimer complexes.

References

1. Root-Bernstein, R. S., *J. Theor. Biol*. **94**, 885-894 (1982).
2. Siemion, I. Z., *Amino Acids* **8**, 1-13 (1995).
3. Siemion, I. Z., Zbozien-Pacamaj, R. and Stefanowicz, P., *J. Mol. Recognition* **14**, 1-12 (2001).
4. Kluczyk, A., Siemion, I. Z., Szewczuk, Z. and Wieczorek, Z., *Peptides* **23**, 823-834 (2002).

Peptide Revolution: Genomics, Proteomics & Therapeutics
Michael Chorev & Tomi K. Sawyer (Editors)
American Peptide Society, 2003

The Superior Therapeutic Potential of SOM230 Originates from Unique Structural Elements

Ian Lewis, Wilfried Bauer, Rainer Albert, Nagarajan Chandramouli, Janos Pless, Gisbert Weckbecker and Christian Bruns

Transplantation Department, Novartis Pharma Research, Basel, CH-4002, Switzerland

Introduction

A rational approach has successfully led to the discovery of SOM230, a novel, stable cyclohexapeptide somatostatin analogue which exhibits unique binding to four of the five human somatostatin receptors, sst1, sst2, sst3 and sst5, and consequently superior pharmacological properties [1-3]. The goal of this research was to discover a small, stable SRIF mimic exhibiting universal high affinity binding to sst1-5. This approach has been based on transposing functional groups from SRIF-14 **(1)** into reduced size, stable cyclohexapeptide templates.

	Structure	sst1	sst2	sst3	sst4	sst5
(1) SRIF-14	H-Ala-Gly-Cys-Lys-Asn-Phe-Phe-Trp-Lys-Thr-Phe-Thr-Ser-Cys-OH	9.4	10.1	9.6	9.1	9.3
(2) SMS201-995	H-DPhe-Cys-Phe-DTrp-Lys-Thr-Cys-Thr(ol)	6.7	9.3	7.9	6.0	8.2
(3) MK678	cyclo[MeAla-Tyr-DTrp-Lys-Val-Phe]	<6.0	10.1	7.5	<6.0	7.9
(4) L363,301	cyclo[Pro-Phe-DTrp-Lys-Thr-Phe]	6.2	9.2	6.9	<7.0	7.4
(5)	cyclo[HyPro-Phe-DTrp-Lys-Thr-Phe]	<6.0	9.7	6.7	<6.0	<6.0
(6)	cyclo[HyPro-Phe-DTrp-Lys-Tyr(Bzl)-Phe]	7.2	9.1	8.8	6.5	9.5
(7)	cyclo[MeSer-Tyr-DTrp-Lys-Tyr(Bzl)-Phe]	7.6	8.8	9.1	<7.0	9.7
(8)	cyclo[MeLys-Phe-DTrp-Lys-Tyr(Bzl)-Phe]	7.7	7.6	8.5	<7.0	9.2
(9)	cyclo[(diaminoethylcarb.)MeSer-Tyr-DTrp-Lys-Tyr(Bzl)-Phe]	7.8	9.1	8.5	<7.0	9.7
(10)	cyclo[(diaminoethylcarb.)HyPro-Phe-DTrp-Lys-Tyr(Bzl)-Phe]	8.4	8.7	9.1	6.3	9.4
(11)	cyclo[(acetyl-diaminoethylcarb.)HyPro-Phe-DTrp-Lys-Tyr(Bzl)-Phe]	7.6	8.3	9.1	6.2	9.8
(12)	cyclo[(4-trans-NH_2)Pro-Phe-DTrp-Lys-Tyr(Bzl)-Phe]	8.3	8.8	9.1	6.3	9.8
(13) SOM230	cyclo[(diaminoethylcarb.)HyPro-Phg-DTrp-Lys-Tyr(Bzl)-Phe]	8.2	9.0	9.1	<7.0	9.9

Results and Discussion

SRIF-14, the naturally occurring ligand, has been shown to exhibit high affinity binding to each of the five cloned somatostatin receptor subtypes, sst1-5 (Figure 1). SMS 201-995 **(2)**, introduced into clinical practice in 1987, exhibits only high affinity binding to sst2 and sst5, accompanied by intermediate affinity to sst3. MK678 **(3)** exhibits higher selectivity for sst2 accompanied by reduced affinity to sst5 and sst3 compared to SMS 201-995 **(2)**. The related cyclohexapeptide L363,301 **(4)**, in which, based on SRIF numbering, the NMeAla^6 of MK678 is replaced by the Pro^6 in combination with Phe^7 and Thr^{10}, replacing Tyr^7 and Val^{10}, provided a sst2 selective analogue albeit with reduced potency. Substitution of Pro^6 of **(4)** with HyPro^6 provided the very closely related cyclohexapeptide **(5)**, which exhibited enhanced potency and selectivity for sst2. This compound provided an important platform for our search for unique modifications transforming initial selectivity into high affinity binding to multiple ssts. An initial breakthrough emerged with the incorporation of Tyr(Bzl)^{10} into the cyclohexapeptide **(6)**, replacing Thr^{10}, which in combination with Phe^7 was designed to mimic Phe^6, Phe^7, Thr^{10} and Phe^{11} of SRIF-14 **(1)**. This substitution

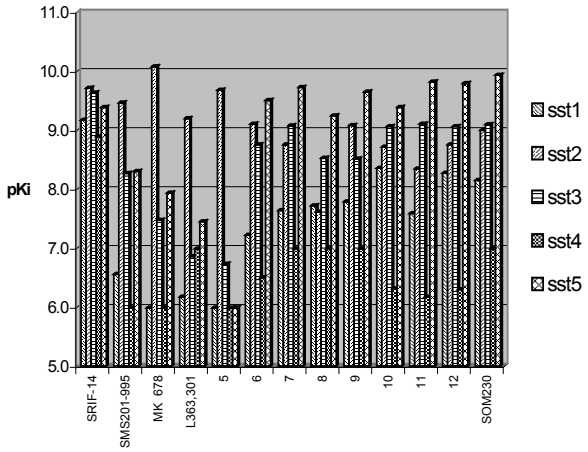

Fig. 1. Binding to SRIF Receptor Subtypes.

transformed the previously highly selective sst2 analogue into a cyclohexapeptide exhibiting high affinity for sst3 and sst5 in addition to sst2. Considering the influence of the rigid HyPro^6 ring, substitution with the more flexible NMeSer^6 provided a cyclohexapeptide **(7)** exhibiting increased affinity to sst1, sst3 and sst5 albeit accompanied with reduced affinity to sst2. Investigation of the incorporation of a flexible basic extension by replacement of the NMeSer^6 with NMeLys^6 **(8)** provided a very slight increase in sst1 affinity; however this was accompanied by a large reduction in sst2 affinity combined with reduced sst3 and sst5 affinities. Replacement of NMeLys^6 with the basic diaminoethyl extension attached to NMeSer^6 via a urethane linkage provided cyclohexapeptide **(9)**, for the first time exhibiting intermediate affinity binding to sst1 along with high affinity binding to sst2 and sst5, combined with continued high affinity binding to sst3. Further improvement in the sst1 affinity, along with improved sst3 affinity, could be obtained by attaching the basic diaminoethyl extension to the more rigid HyPro^6 via a urethane linkage providing cyclohexapeptide **(10)**, where good affinities to sst2 and sst5 were maintained. The importance of the basic extension was confirmed by capping the amino terminus with acetyl, providing analogue **(11)** where high affinities to sst2, sst3 and sst5 were maintained in the presence of dramatically reduced affinity to sst1. Alternative basic derivitization was investigated. Cyclohexapeptide analogue **(12)**, incorporating 4-aminoPro^6 was synthesized and exhibited high affinities to sst1, sst2, sst3 and sst5 comparable to **(10)**. However, the synthesis of the required 4-aminoPro^6 amino acid was considered to be much more cumbersome than the hydroxyProline urethane.

SOM230 **(13)**, derived from optimization of these structural elements, exhibits a novel somatostatin receptor binding profile with a 30- to 40-fold higher affinity to sst1 and sst5 than SMS 201-995. Initial Phase I clinical results demonstrate that the superior therapeutic potential of SOM230 originates from unique structural elements.

Acknowledgments

The technical support of S. Arnold, Ch. Bourquin, F. Kessler, J. Meisburger, C. Simeon and A. Stich are acknowledged.

References

1. Lewis, I., et al. In Lebl, M. and Houghten, R. (Eds.) *Peptides: The Wave of the Future,* American Peptide Society, San Diego, pp 718-720 (2001).
2. Bruns, C., Lewis, I., Briner, U., et al. *Eur. J. Endocrinol.* **146**, 707-716 (2002).
3. Lewis, I., Bauer, W., Albert, R., et al. *Med. Chem.* **46**, 2334-2344 (2003).

Peptide Revolution: Genomics, Proteomics & Therapeutics
Michael Chorev & Tomi K. Sawyer (Editors)
American Peptide Society, 2003

Sst_4-selectivity is Induced by L-Configuration at Position 8 in Somatostatin (SRIF) Octapeptides

Judit Erchegyi[1], Sandra Wenger[2], Beatrice Waser[2], Jean-Claude Schaer[2], Renzo Cescato[2], Christy R.R. Grace[1], Carl Hoeger[1], Steven C. Koerber[1], Roland Riek[1], Jean Claude Reubi[2] and Jean E. Rivier[1]

[1] The Clayton Foundation Laboratories for Peptide Biology, The Salk Institute for Biological Studies, La Jolla, CA, 92037, USA; [2]Department of Cell and Molecular Biology, University of Berne, Switzerland

Introduction

We recently found that the agonist des-$AA^{1,2,4,5,12,13}$-[$DCys^3$,Tyr^7,L-*threo*-β-Me2Nal^8]-SRIF (**2**) had comparable binding affinity to that of SRIF-28 (**1**) and >100-fold selectivity for sst_4 over the other four sst_s [1,2]. An N^{β}-methylated aminoglycine (Agl) scan led to the discovery of des-$AA^{1,2,4,5,12,13}$[L-Agl^7(NMe,benzoyl)]SRIF (**3**) with high sst_4 binding affinity and selectivity. The peptide with an L-amino acid at positions 7 and 8 showed greater selectivity than the same sequence with the L^7 and D^8 configurations [3]. Des-$AA^{1,2,4,5,12,13}$-SRIF (**4**), originally tested for its growth hormone release inhibiting ability [4], was further tested for binding affinity at the five sst_s and found to have high binding affinity and about 10-fold selectivity for sst_4. Based on these findings, we hypothesized that an L residue at position 8 and an optimized substitution at position 7 might direct selectivity towards sst_4.

Results and Discussion

We describe new, very potent and highly sst_4-selective SRIF analogs in Table 1. [Tyr^7]-**4 (5)** shows about 10-fold selectivity for sst_4 over the other receptors. An Aph^7

Table 1. Binding affinities (IC_{50}, nM) at the five human SRIF receptors.

	1 2 3 4 5 6 7 8 9 10 11 12 13 14					
SRIF:	**Ala-Gly-c[Cys-Lys-Asn-Phe-Phe-Trp-Lys-Thr-Phe-Thr-Ser-Cys]**					
	Compound	sst_1	sst_2	sst_3	sst_4	sst_5
1	Somatostatin-28	3.2	2.3	3.5	2.5	2.4
2	des-$AA^{1,2,4,5,12,13}$-[$DCys^3$,Tyr^7,L-*threo*-β-Me2Nal^8]SRIF	>10 K	339	664	3.5	668
3	des-$AA^{1,2,4,5,12,13}$-[L-Agl^7(NMe,benzoyl)] SRIF	>10K	>1000	403	5.4	>1000
4	des-$AA^{1,2,4,5,12,13}$-SRIF	5.3	130	13	0.7	14
5	des-$AA^{1,2,4,5,12,13}$-[Tyr^7]SRIF	27	54	22	1.3	63
6	des-$AA^{1,2,4,5,12,13}$-[Aph^7]SRIF	213	347	>1000	1.2	1000
7	des-$AA^{1,2,4,5,12,13}$-[Ala^7]SRIF	>1000	807	750	0.84	633
8	des-$AA^{1,2,4,5,12,13}$-[Ala^7,DTrp^8]SRIF	>1000	183	897	0.98	199
9	des-$AA^{1,4,5,12,13}$-[m$ITyr^2$,Ala^7]SRIF	>1000	>1000	1025	3.5	>1000
10	des-$AA^{1,2,4,5,12,13}$-[Ala^7,Ala^{11}]SRIF	>10 K	>1000	>1000	3.5	>1000

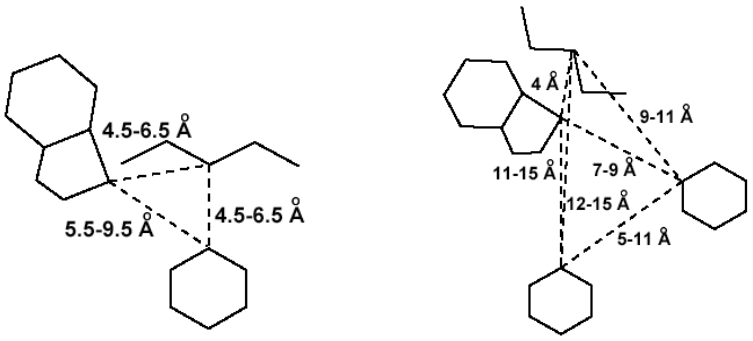

*Fig. 1. (**A**) Schematic drawing of the proposed pharmacophore for sst_4-selective SRIF analogs. The distances between Cγ of residue 8, Cγ of Lys^9 and Cγ of $Phe^{6/11}$ are displayed. (**B**) Schematic drawing of the proposed pharmacophore for sst_2/sst_5-selective SRIF analogs [7].*

substitution in **4** results in analog **6** with high binding affinity and about 200-fold selectivity for sst_4. Unpredictably, [Ala^7]-**4** (**7**) exhibited very high sst_4 binding affinity and selectivity (>600-fold). A Tyr extension and its iodination at the N-terminus in analog **9** were well tolerated with the retention of high sst_4-selectivity and binding affinity. Analog **9** could serve as a tracer for receptor binding or localization studies. All analogs, presented in Table 1, were synthesized with D-Trp at position 8 as well, but none of them was as selective as the corresponding L-Trp^8 analog (as exemplified with **8**), further sustaining our previous observation that a residue of L configuration at position 8 and an optimized substitution at position 7 favor sst_4-selectivity [5].

Figure 1 shows the comparison of the schematic drawings for a consensus sst_4-bioactive motif (**A**), identified with the help of these new sst_4-selective analogs by NMR spectroscopy [6], with the proposed pharmacophore for sst_2/sst_5-selective analogs (**B**) [7]. Although the backbone conformations are different, the side chains of Trp^8/DTrp^8/L-*threo*-β-Me2Nal^8, Lys^9 and either Phe^6 or Phe^{11} in all of the investigated sst_4-selective analogs are in a close spatial arrangement, almost at the same position in the binding motif and can be superimposed. These findings led to the discovery of analog **10** that also exhibits high sst_4 binding affinity and selectivity.

Acknowledgments

Studies were supported by NIH grants DK-50124 and DK 59953. We thank W. Low, R. Kaiser and D. Kirby for technical assistance and D. Doan for manuscript preparation.

References

1. Erchegyi, J., et al. In Benedetti, E. and Pedone, C. (Eds.) *Peptides 2002, Proceedings of the 27th Eur. Peptide Symp.* Edizioni Ziino, Napoli, Italy, 2002, pp 474-475.
2. Erchegyi, J., Penke, B., Simon, L., Michaelson, S., Wenger, S., Waser, B., Cescato, R., Schaer, J.- C., Reubi, J. C. and Rivier, J. Submitted (2003).
3. Rivier, J., Erchegyi, J., Hoeger, C., Miller, C., et al. Submitted (2003).
4. Vale, W., Rivier, J., Ling, N. and Brown, M. *Metabolism* **27**, 1391-1401 (1978).
5. Erchegyi, J., Waser, B., Schaer, J.- C., Cescato, R., et. al. Submitted (2003).
6. Grace, C. R. R., Erchegyi, J., Koerber, S. C., Reubi, J. C., et al. Submitted (2003).
7. Melacini, G., Zhu, Q., Ösapay, G. and Goodman, M. *J. Med. Chem.,* **40**, 2252-2258 (1997).

Peptide Revolution: Genomics, Proteomics & Therapeutics
Michael Chorev & Tomi K. Sawyer (Editors)
American Peptide Society, 2003

Design of Oxytocin Antagonists that are Strikingly More Potent and Selective in Human Receptor Assays than Atosiban

LingLing Cheng[1], Stoytcho Stoev[2], Maurice Manning[1], Nga C. Wo[2], W.Y. Chan[2], Hazel H. Szeto[2], Thierry Durroux[3], Bernard Mouillac[3] and Claude Barberis[3]

[1]Department of Biochemistry and Molecular Biology, Medical College of Ohio, Toledo, OH 43614, USA; [2]Department of Pharmacology, Weill Medical College of Cornell University, New York, NY 10021, USA; [3]INSERM U469, Endocrinologie moléculaire: Signalisation cellulaire et pathologie, Montpellier, France

Introduction

Premature birth is the major cause of neonatal morbidity and death [1]. Oxytocin antagonists have been studied extensively as potential therapeutic agents for the prevention of premature labor and delivery [2]. The oxytocin antagonist (OTA) atosiban ([1-deamino, D-Tyr(Et)^2,Thr^4]OVT) has been shown to be an effective tocolytic for the treatment of pre-term labor [3]. Atosiban is in fact the only OTA (peptide or nonpeptide) approved for clinical use under the tradename Tractocile in Europe [4]. Atosiban has however serious deficiencies as an OTA [5,6]. It is highly nonselective for OT receptors versus vasopressin (VP) V_{1a} receptors. In humans its affinity for V_{1a} receptors is 100 times greater than for OT receptors [6]. It is thus a strikingly more potent V_{1a} antagonist than an OTA in humans. We have shown that V_{1a} antagonism is an undesirable side effect in OTAs [7]. We recently reported a series of OTAs that are much more selective than atosiban in rat bioassays and in human receptor assays [8]. Here we report the synthesis and some pharmacological properties of the following six L-/D 2-Nal^2/2-Nal^2, OTAs (Nal = Naphthylalanine): **1** d$(CH_2)_5$[D-2-Nal^2,Thr^4,Tyr-NH$_2^9$]OVT, **2** d$(CH_2)_5$[2-Nal^2,Thr^4,Tyr-NH$_2^9$]OVT, **3** desGly-NH$_2$, d$(CH_2)_5$[D-2-Nal^2,Thr^4]OVT, **4** desGlyNH$_2$,d$(CH_2)_5$[2-Nal^2,Thr^4]OVT, **5** d$(CH_2)_5$[D-2-Nal^2,Thr^4,Eda^9]OVT, **6** d$(CH_2)_5$[2-Nal^2,Thr^4,Eda^9]OVT (Eda = ethylenediamine); all of which are much more potent and selective than atosiban in human receptor assays.

Results and Discussion

The pharmacological properties in rat bioassays and in human OT receptor (hOTR) binding assays of the six new OTAs and those of atosiban are presented in Table 1. In the rat, all six new OTAs exhibit *in vivo* anti-OT activity, as measured by their effective doses (EDs), in the same range as atosiban. All, however, exhibit significantly enhanced anti-V_{1a} potencies (EDs) compared to atosiban. Thus in the rat all six new OTA's are less selective for OT versus V_{1a} receptors than atosiban. By striking contrast, all six peptides exhibit enhanced affinities for the hOTR than atosiban. With K_i values in nM of 0.071; 0.152; 0.171 and 0.56, peptides **1-4** exhibit respectively, 577, 270, 240 and 73 times greater affinity for the hOTR than atosiban (K_i = 41 nM). All six new OTAs exhibit high affinities for the human V_{1a} receptor, with peptides **1** and **2** having V_{1a} receptor affinities in the same range as atosiban (K_i = 0.40 nM). However, because of their greatly enhanced affinities for the hOTR relative to atosiban, all six OTAs exhibit striking gains in selectivity for the hOTR versus the V_{1a} receptor relative to atosiban. Thus, peptides **1** to **6** exhibit, respectively, gains in selectivity of **1**=273, **2**=254, **3**=672, **4**=234, **5**=85 and **6**=81. Since all six peptides are both more potent and more selective OTAs than atosiban, they clearly possess a

superior and safer pharmacological profile as tocolytic agents than atosiban. These findings offer promising clues for the design of more potent and selective OTAs for development as potential tocolytic agents for the prevention of premature labor and as therapeutic agents for the diagnosis and treatment of tumors which express OT receptors [9].

*Table 1. L- and D-2-Nal[2] OT antagonists (**1-6**) are more potent and selective than atosiban in human receptor assays.*

Peptide[b]	Anti-OT *In vivo* (Rat)	Anti-V_{1a} *In vivo* (Rat)	hOTR Affinity	hOTR Affinity versus Atosiban	$hV_{1a}R$ Affinity	hOTR/ $hV_{1a}R$ Selectivity	hOTR/ $hV_{1a}R$ Selectivity versus Atosiban
	ED[a]	ED[a]	K_i (nM)		K_i (nM)		
Atosiban[b]	5.95[c]	48.5[c]	41[d]	1	0.40[d]	0.01	1
1	5.37	13.6	0.071	577	0.194	2.73	273
2	7.66	2.88	0.152	270	0.386	2.54	254
3	8.73	17.9	0.171	240	1.15	6.72	672
4	4.08	2.71	0.56	73	1.31	2.34	234
5	5.95	4.79	5.28	8	4.47	0.85	85
6	6.05	1.61	10.7	4	8.72	0.81	81

[a]The effective dose (ED) is defined as the dose (in nanomoles/kilogram) of antagonist that reduces the response to 2x units of agonist administered in the absence of antagonist. [b]For structures see text. [c]Data from [5]. [d]Data from [6]. hOTR = human oxytocin receptor. $hV_{1a}R$ = human vasopressin vasopressor receptor.

Acknowledgments

We thank Ms. Ann Chlebowski for expert help in the preparation of this manuscript. Supported by NIH Grant GM-25280 and the Institut National de la Santé et de la Recherche Médicale.

References

1. Norwitz, E. R., Robinson, J. M. and Challis, J. R. G. *N. Engl. J. Med.* **341**, 660-666 (1999).
2. Vatish, M. and Thornton, S. *Expert Opin. Ther. Patents* **12(9)**, 1403-1406 (2002).
3. Romero, R., Sibai, B. M., Sanches-Ramos, L., Valenzuela, G. J., Veille, J.-C., Tabor, B., Perry, K. G., Varner, M., Murphy, G., Lane, R., Smith, J., Shangold, G. and Creasy, G. W. *Am. J. Obstet. Gynecol.* **182**, 1173-1183 (2000).
4. *Pharmaceut. J.* **264(7100)**, 871 (2000).
5. Manning, M., Miteva, K., Pancheva, S., Stoev, S., Wo, N. C. and Chan, W. Y. *Int. J. Pept. Protein Res.* **46**, 244-252 (1995).
6. Barberis, C., Morin, D., Durroux, T., Mouillac, B., Guillon, G., Hibert, M., Tribollet, E. and Manning, M. *Drug News Persp.* **12**, 279-292 (1999).
7. Chan, W. Y., Wo, N. C. and Manning, M. *Am. J. Obstet. Gynecol.* **175**, 1331-1335 (1996).
8. Stoev, S., Cheng, L. L., Manning, M., Wo, N. C., Chan, W. Y., Durroux, T. and Barberis, C. in *Peptides*: *The Wave of the Future* (eds. M. Lebl and R. A. Houghton) *APS*, 699-700 (2001).
9. Cassoni, P., Sapino, A., Munaron, L., Deaglio, S., Chini, B., Graziani, A., Ahmed, A. and Bussolati, G. *Endocrinology* **142**, 1130-1136 (2001).

Peptide Revolution: Genomics, Proteomics & Therapeutics
Michael Chorev & Tomi K. Sawyer (Editors)
American Peptide Society, 2003

Design, Synthesis and Analysis of Single Chain Mimetics of Relaxin and Relaxin-Like Factor (INSL3)

Mark P. Del Borgo[1,2], Richard A. Hughes[2] and John D. Wade[1]

[1]Howard Florey Institute of Experimental Physiology and Medicine and [2]Department of Pharmacology, University of Melbourne, Victoria 3010, Australia

Introduction

Relaxin and INSL3 are 6kDa peptide hormone members of the insulin superfamily, comprising two chains (A and B) that are tethered together with two disulfide bonds. Relaxin is known to have a significant role in the maintenance of pregnancy and parturition by inhibiting uterine contractions, ripening the cervix and developing the mammary gland and nipple [1]. Recently however, relaxin has been shown to have other physiological effects in non-reproductive tissues and in both genders. It is a potent vasodilator acting through the nitric oxide pathway, an activator of angiogenesis by stimulating the expression of VEGF, and a potent antifibrotic by metabolising collagen [2]. The primary function of INSL3 is to initiate testis descent [3]. Another role is implicated by the recent finding [4] that the expression of INSL3 and its receptor is increased in patients with advanced thyroid carcinoma.

The receptors for relaxin and INSL3 (LGR7 and LGR8) are G-protein coupled receptors with large ectodomains containing many leucine-rich repeats [5]. INSL3 has been shown to bind and activate only LGR8, whereas relaxin can bind and activate both receptors although it binds LGR7 with greater affinity [6]. Crucial for relaxin binding to LGR7 is an Arg-X-X-Arg-X-X-X-Ile motif that is found on the B-chain α-helix of relaxin. The A-chain is thought to act as a structural support for the B-chain to maintain the α-helical structure and correct conformation.

A paucity of structure-function studies for INSL3 have resulted in little information regarding which residues are crucial for binding. However, due to the structural homology of all insulin family members and the sequence homology of relaxin and INSL3 of 50%, the INSL3 B-chain is predicted to contain a binding motif. For this reason, to prepare active mimetics of relaxin and INSL3, we undertook the preparation of single chain end-to-end cyclic analogues that were predicted by *in silico* analysis to retain native conformation.

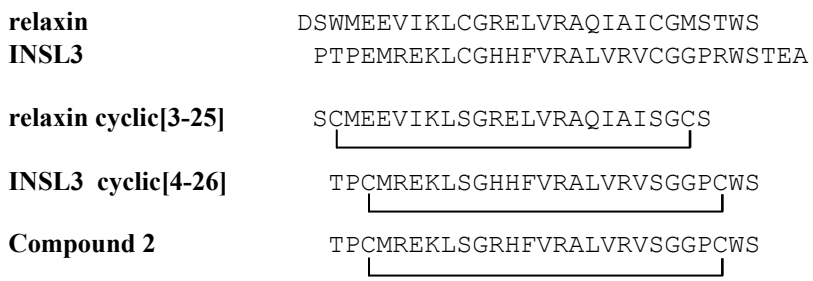

Fig. 1. Sequences of human relaxin and INSL3 B-chains and analogues.

Results and Discussion

Synthetic peptides corresponding to native relaxin and INSL3 B-chains, their cyclic analogues and an INSL3 B-chain analogue containing a relaxin point-mutated residue (Figure 1) were prepared by Fmoc-solid phase synthesis. Cyclization was by oxidation with aqueous DMSO [7] in good overall yields. High homogeneity of each peptide was confirmed by RP-HPLC and MALDI-TOF MS. CD spectroscopy showed that each cyclic analogue possessed significant α-helical propensity in both water and aqueous TFE (data not shown) indicating that simple disulfide cyclization promoted formation of significant native conformation.

Table 1. Receptor binding of relaxin and INSL3 analogues.

	IC_{50}	
	LGR7	**LGR8**
Relaxin (3-25)	n.b	n.b
INSL3 (4-26)	n.b	162 nM
Compound 2	n.b	485 nM

n.b: no binding.

All peptides were then assessed for binding to LGR7 and LGR8 (Table 1). Relaxin cyclo [3-25] did not bind to either receptor, suggesting that either the α-helical structure observed in the CD measurements does not correspond to the conformation required for biological activity, or there are other key residues required for the binding and activation not present in the peptide. In contrast, both INSL3 cyclo[4-26] and Compound 2 bind to LGR8 and antagonize the action of native INSL3. This result strongly suggests that, in the case of these compounds, the α-helix is important for ligand binding to the receptor but not in its activation. Further work is underway to produce second-generation analogues of the peptides with improved affinity for LGR7 and LGR8.

Acknowledgments

Work carried out at the Howard Florey Institute was supported by an Institute Block grant (reg. key # 983001) from the NHMRC of Australia. We are grateful for the advice of Ross Bathgate (HFI). We thank Laszlo Otvos, Jr. (The Wistar Institute, Philadelphia, USA) for CD spectroscopy.

References

1. Bryant-Greenwood, G. D. and Schwabe, C. *Endocrine Rev.* **15**, 5-26 (1994).
2. Ivell, R. and Einspanier, A. *Trends Endocrinol. Metab.* **13**, 343-348 (2002).
3. Zimmermann, S. *et al., Mol. Endocrinol.* **13**, 681-691 (1999).
4. Hombach-Klonisch, S. *et al*., *Int. J. Oncol*. **22**, 993-1001 (2003).
5. Hsu, S. Y., Nakabayashi, K., Nishi, S., Kumagai, J., Kudo, M., Sherwood, O. D. and Hsueh, A. J. *Science* **295**, 671-674 (2002).
6. Kumagai, J. *et al., J. Biol. Chem*. **277**, 31283-31286 (2002).
7. Spetzler, J. C., Rao, C. and Tam, J. P. *Int. J. Peptide Prot. Res*. **43**, 351-358 (1994).

Peptide Revolution: Genomics, Proteomics & Therapeutics
Michael Chorev & Tomi K. Sawyer (Editors)
American Peptide Society, 2003

Relaxin 3, a Novel Member of the Insulin Superfamily of Peptide Hormones

Ross A. Bathgate[1], Nicky F. Hanson[1], Feng Lin[1,2], Geoffrey W. Tregear[1] and John D. Wade[1]

[1]Howard Florey Institute, University of Melbourne, Victoria 3010, Australia, and [2]CRC for Cellular Growth Factors, The Walter and Eliza Hall Institute of Medical Research, Parkville, Victoria 3050, Australia

Introduction

Relaxin was first discovered in the early 1900's and has long been recognized to be a key hormone in the maintenance of pregnancy [1]. More recently, it has become clear that in higher animals including humans and primates, relaxin possesses a broader spectrum of biological actions. These include roles in the cardiovascular and central nervous systems as well as an essential role in normal tissue collagen turnover [2, 3].

Relaxin is a peptide hormone member of the insulin superfamily that is composed of two short chains (A and B) linked by disulphide bonds. Until recently, it was known there were two relaxin genes in the human, designated genes 1 and 2. Human Gene 1 (H1) relaxin is the product of a duplicated gene derived from human Gene 2 (H2) relaxin and is found only in higher primates. The H2 peptide is the principal product *in vivo,* is found in all mammals, and has constituted the primary focus of international research over the past 20 years. H2 relaxin has been isolated from human corpora lutea, pregnancy serum and seminal fluid and confirmed by sequence analysis and mass spectrometry (MS) to consist of a 24 residue A-chain and a 29 residue B-chain held together by three insulin-like disulfide pairs [4]. In an exciting new finding, our laboratory recently discovered a novel human Gene 3 (H3) relaxin, together with its mouse and rat equivalent, during a Celera and public genomic databases search [5].

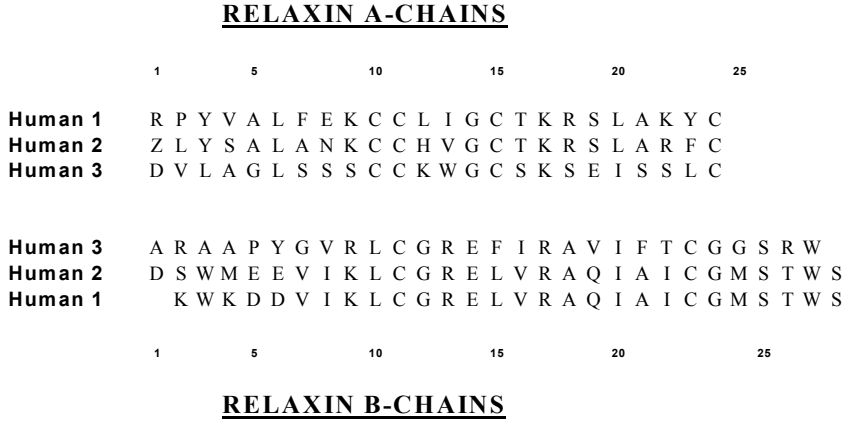

Fig 1. Primary structures of human Genes 1, 2 and 3 relaxins. Disulfide bonds: A10-15; A11-B11; A24-B23.

Curiously, whereas the primary structures of H2 relaxin vary significantly among the 20-plus different species (up to 60%), with the only invariant residues being the six cysteines that make up the insulin-like disulfides and 5 other residues including the two

arginines in the B-chains, in contrast, the known Gene 3 relaxin sequences show considerable species conservation but significant invariance compared to H1 and H2 relaxins (Figure 1). Recent studies have shown the H3 relaxin gene to be predominantly expressed in the brain; and mapping studies also indicate a highly developed network of relaxin genes 2 and 3 and relaxin receptor-expressing cells the brain organ, suggesting that relaxin peptides might have important roles in the central nervous system [6]. To further examine this possibility, we undertook the chemical synthesis and biological assay of H3 relaxin.

Results and Discussion

In contrast to H1 and H2 relaxins that can be prepared by simple yet efficient combination of the individual A- and B-chains in solution at high pH [7], H3 relaxin has thus far defied similar successful combination. H2 relaxin has been shown to fold via a hierarchic process along a redox-sensitive series of energy landscapes that is initiated by formation of the A-chain N-terminal α-helix [8]. In contrast, the N-terminal region of the H3 relaxin A-chain contains a stretch of three successive serines, which is predicted to be unfavourable for the formation of the α-helix and hence the process of chain combination. For this reason, recourse to regioselective disulfide bond formation methods was taken to prepare H3 relaxin. The two chains were each prepared separately by Fmoc-SPS using the following selective cysteine S-protection: Cys (A10, 15), Trt; Cys (A11, B11), Acm; Cys (A24), t-Bu, and Cys(B23), Trt. Following conventional TFA cleavage in the presence of scavengers, the intramolecular disulfide bond of the A-chain was formed by aeration and the Cys24 (t-Bu) displaced with S-Pyr by reaction with DPDS in TFMSA. Combination of the peptide with the B-chain occurred by thiolysis, after which the third and final disulfide bond between A11 and B11 was formed by iodolysis. Overall yield of synthetic H3 relaxin was low (*ca.* 3%) because of the losses incurred during repeated intermediate purification steps. The purity of the peptide was confirmed by MALDI-TOF MS (theory: 5511.4; found: 5516.2) and analytical RP-HPLC.

CD spectroscopy of the H3 relaxin in water exhibited a spectrum that was typical of repeated β-turns and loosened (3_{10}) helices (data not shown). Additionally, its helical content was significantly less than that of H2, clearly suggesting a different conformational structure. The synthetic H3 relaxin was shown to bind to and activate cAMP release from relaxin receptors on the human monocytic cell line THP-1, albeit with slightly lower affinity than human H1 or H2 relaxin [5]. Recently the relaxin receptor was cloned and shown to be the "orphan" receptor, leucine rich-repeat containing G-protein coupled receptor 7 (LGR7) [9]. We have now demonstrated that H3 relaxin clearly activates the LGR7 receptor (Figure 2), further proof of the identity of this receptor. Interestingly H2 relaxin was also shown to activate the related receptor LGR8 [9]. However, we have demonstrated that H3 relaxin does not activate the LGR8 receptor and that the LGR8 is actually the receptor for a related peptide hormone insulin-like peptide 3 (INSL3) [10]. Given that H3 relaxin, like the H2 peptide, contains an arginine cassette (R-X-X-X-R-X-X-I) within its B-chain that is known to be essential for relaxin receptor binding, its selectivity for LGR7 clearly reflects subtle differences in binding elements between the two relaxins. Further studies are currently underway to delineate this specificity. The availability of biologically active synthetic H3 relaxin will allow us to explore its functional roles in the central nervous system.

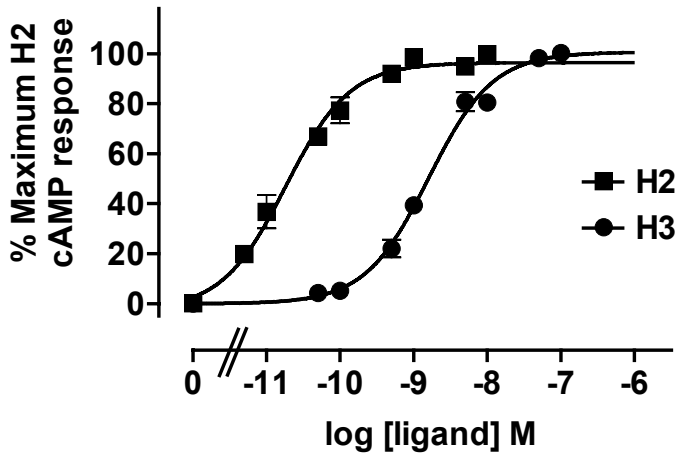

Fig. 2. Ability of H3 relaxin compared with H2 relaxin to stimulate cAMP accumulation in cells expressing the human relaxin receptor (LGR7). Data are expressed as mean ± SEM of the maximum response (%) to H2 relaxin.

Acknowledgments

Work carried out at the Howard Florey Institute was supported by an Institute Block grant (reg. key # 983001) from the NHMRC of Australia. We thank Laszlo Otvos, Jr. (The Wistar Institute, Philadelphia, USA) for CD spectroscopy.

References

1. Sherwood, O. D. In Knobil, E. and Neill, J. D. (Eds.) *The Physiology of Reproduction* Raven Press, New York, 1994, pp. 861-1009.
2. Kakouris, H., Eddie, L. W. and Summers, R. J., *Lancet*. **339**, 1076-1082 (1992).
3. Samuel C. S., Zhao C., Bathgate R. A. D., Bond C., Burton M. D., Parry L. J., Summers R. J., Tang,M. L. K., Amento, E. P. and Tregear, G. W. *FASEB J.* **17**,121-123 (2003).
4. Stults, J. T., Bourell, J. H., Canova-Davis, E., Ling, V. T., Laramee, G. R., Winslow, J. W., Griffin, P. R., Rinderknecht, E. and Vandlen, R. L. *Biomed. Environ. Mass Spectrom.* **19**, 655-64 (1990).
5. Bathgate, R. A. D., Samuel, C. S., Burazin, T. C. D., Layfield, S., Claasz, A. A., Reytomas, I. T., Dawson, N. F., Zhao, C., Bond, C., Summers, R. J., Parry, L. J., Wade, J. D. and Tregear, G.W**.** *J. Biol. Chem.* **277**, 1148-1157 (2002).
6. Burazin, T. C. D., Bathgate, R. A., Macris, M., Layfield, S., Gundlach, A. L. and Tregear, G. W. *J. Neurochem.* **82**, 1553-1557 (2002).
7. Wade, J. D. and Tregear, G. W. *Meths. Enzynol*. **289**, 637-646 (1997).
8. Tang, J-G., Wang, Z-H., Tregear, G.W. and Wade, J.D**.** *Biochemistry* **42**, 2731-2739, (2003).
9. Hsu, S. Y., Nakabayashi, K., Nishi, S., Kumagai, J., Kudo, M., Sherwood, O. D. and Hsueh, A. J. W. *Science* **295**, 671-674 (2002).
10. Sudo, S., Kumagai, J., Nishi, S., Layfield, S., Ferraro, T., Bathgate, R. A. D. and Hsueh, A. J. W. *J. Biol. Chem*. **278**, 7855-7862 (2003).

Peptide Revolution: Genomics, Proteomics & Therapeutics
Michael Chorev & Tomi K. Sawyer (Editors)
American Peptide Society, 2003

Non-Peptidic RGD Mimetics for Stimulated Cell Adhesion on Biomaterials

C. Dahmen[1], A. Meyer[1], B. Jeschke[2], A. Enderle[2], S. L. Goodman[3], B. Nies[2] and H. Kessler[1]

[1]Institut für Organische Chemie und Biochemie, Technische Universität München, Lichtenbergstr. 4, D-85747 Garching, Germany; [2]Biomet Merck BioMaterials GmbH; [3]Merck KGaA, Frankfurter Strasse 250, D-64271 Darmstadt, Germany

Introduction

Numerous linear and cyclic RGD peptides were used as a functional intermediate layer connecting different artificial material surfaces and cells to generate better interactions between them [1]. Immobilization of cyclic RGD peptides on poly-(methylmethacrylate) has shown improved osteoblast adhesion and accelerated ingrowth of bone implants *in vivo* [2]. Here we present the first αvβ3 integrin selective non-peptidic RGD mimetics tailored for surface immobilization on titanium.

Results and Discussion

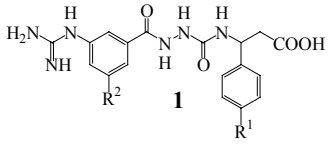

1

Fig. 1. Diacylhydrazines as non-peptidic RGD mimetics for surface immobilization.

Additional functional groups in structurally minimized diacylhydrazines (Figure 1) should allow coupling with anchor molecules for surface functionalization without loss of integrin ligand properties. The terminal guanyl and carboxyl groups are essential for receptor interaction, as is the non-alkylated aza-glycine [3]. Possible positions for linker connection are at the substituent of the β-amino acid (R^1) and at the aromatic spacer (R^2).

Docking studies were carried out to investigate this concept. Interactions of substituted ligands with the αvβ3 integrin headgroup, which was built up from the X-ray structure [4], were calculated using AutoDock 3.0 [5]. As shown in Figure 2, attachment of a linker at position R^1 or R^2 will not interfere with ligand binding. However, the distance from material surface to receptor has to be spanned with a sufficiently long spacer.

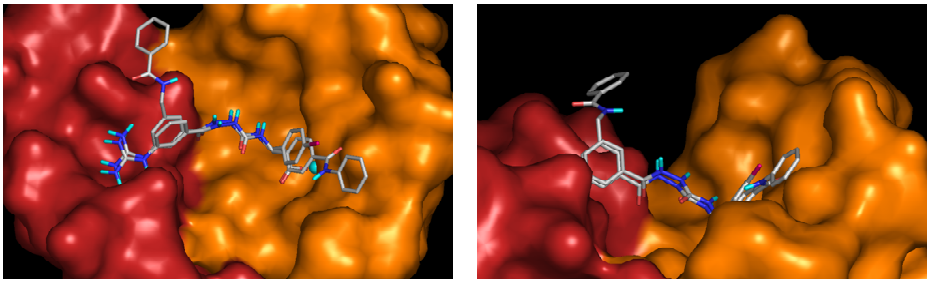

Fig. 2. Compound 1a/1b (1a: R1/R2 = CONH-C6H5 / H; 1b: R1/R2 = H / CH2NHCO-C6H5) modeled into the αvβ3 integrin headgroup.

Synthesis of the RGD mimetics was performed on solid phase with Fmoc-strategy as described previously [6]. After removal from resin by treatment with 20 % HFIP in DCM, **2** (R^1 = COOH) was modified with two linkers of different lengths to investigate

a possible spacer effect on cell adhesion. Therefore **2** was preactivated and coupled (HATU/HOAt/collidine) in solution with cysteamine yielding **4**, and a longer linear linker consisting of three ε-aminohexanoic acids and cysteine as anchor yielding **5**. Compounds **4** and **5** were obtained without loss of αvβ3 integrin ligand affinity and selectivity (Table 1).

Table 1. Ligand affinities of unanchored modified mimetics against different integrin subtypes.

Compound	R^1 R^2 = H	αvβ3	αvβ5	αvβ6	αIIbβ3
		IC_{50} / nM; inhibition at ligand concentration / nM			
2	COOH	16	10^4 (65 %)	10^3 (54 %)	10^4 (22 %)
3	CH_2NH_2	43	10^4 (48 %)	4.7	10^4 (12 %)
4	$CONH(CH_2)_2SH$	3.6	10^4 (83 %)	17	10^4 (77 %)
5	CO-Ahx_3-Cys	0.3	10^3 (51 %)	0.94	10^4 (48 %)

Ahx = ε-aminohexanoic acid.

The influence of immobilized **4** and **5** on MC3T3 mouse osteoblast adhesion was studied on titanium. The linker in **4** is too short to mediate any interactions, whereas **5** mediated cell adhesion in a concentration dependent way. As an osteoblast adhesion of 7% could be observed without any coating, cell adhesion increased up to 60% at a ligand concentration of 100 μM in the coating solution.

Substitution of residue R^2 by a long linker, as in **5**, resulted in compound **6** (Figure 3). No change of receptor affinity and selectivity could be obtained according to the result in the docking studies. Cell adhesion studies are in progress.

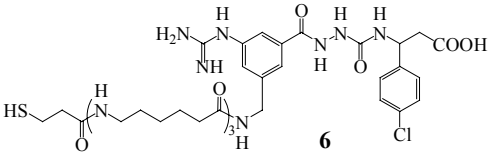

6

IC_{50} (αvβ3) = 0.009 nM
IC_{50} (αvβ5) = 10^3 nM (63 %)
IC_{50} (αvβ6) = 0.05 nM
IC_{50} (αIIbβ3) = 10^4 nM (75 %)

Fig. 3. Non-peptidic RGD mimetic with a long linker at position R^2 and receptor affinities of the soluble compound for different integrins.

αvβ3 integrin-selective RGD mimetics for surface immobilization have been synthesized for the first time. Based on results of ligand-receptor docking studies, two different possible linker positions have been investigated. All soluble mimetics showed high αvβ3 integrin affinity. Immobilized mimetics improved cell adhesion on titanium only, with a sufficiently long spacer between diacylhydrazine and surface to allow interaction between ligand and receptor.

References

1. Hersel, U., Dahmen, C. and Kessler, H. *Biomaterials* in press (2003).
2. Kantlehner, M., et al. *ChemBioChem* **1**, 107-114 (2000).
3. Gibson, C. et al. *J. Org. Chem.* **64**, 7388-7394 (1999).
4. Xiong, J.- P., Stehle, T., Zhang, R., Joachimiak, A., Frech, M., Goodman, S. L. and Arnaout, M. A. *Science* **296**, 151-155 (2002).
5. Morris, G. M., Goodsell, D. S., Halliday, R. S., Huey, R., Hart, W. E., Belew, R. K. and Olson, A. J. *J. Comput. Chem.* **19**, 1639-1662 (1998).
6. Sulyok, G. A. G., Gibson, C., et al. *J. Med. Chem.* **44**, 1938-1950 (2001).

Peptide Revolution: Genomics, Proteomics & Therapeutics
Michael Chorev & Tomi K. Sawyer (Editors)
American Peptide Society, 2003

Using Plasmon Waveguide Resonance (PWR) Spectroscopy to Directly Examine the Effects of Ligands on G-Protein Binding to Delta Opioid Receptors

Victor J. Hruby[1,2], Isabel Alves[2], Zdzislaw Salamon[2] and Gordon Tollin[1,2]

[1]Department of Chemistry; [2]Department of Biochemistry and Molecular Biophysics; University of Arizona, Tucson, AZ 85721, USA

Introduction

G-Protein Coupled Receptors (GPCRs) are found on virtually every cell type in animals including humans and are of central importance in intercellular communication. They are involved in many biological functions central to life and survival, and are the targets, or are involved in, the bioactivity of nearly 50% of all current drugs. Unfortunately, it has been difficult to examine the conformational and dynamic structures of GPCRs because of their low natural abundance in cells, their presence in anisotropic membrane environments, the difficulty in solubilizing them in a biologically active form, and the lack of a robust expression system.

We have developed a new biophysical method, plasmon waveguide resonance (PWR) spectroscopy [1,2], which makes it possible to study directly structural properties of GPCRs and other integral membrane proteins in lipid bilayers, to characterize changes in mass density, molecular orientation and light absorption characteristics of these biomembrane systems, and to monitor directly the thermodynamics and kinetics of binding processes and accompanying structural changes. These studies provide direct methods for determining binding constants and other biophysical properties of GPCRs interacting with ligands in a system that is very close to the receptor's natural environment. The native GPCRs, ligands and other compounds do not require labeling for these determinations. Using these methods, we have shown that agonists and antagonists of the human delta opioid receptor (hDOR) induce different conformational states in the receptor, which are also different from the unliganded receptor [3]. Furthermore, using the same methods, we have now been able for the first time to directly measure the binding of G-proteins to the liganded or unliganded delta opioid receptor in real time in an anisotropic membrane system. We report herein that the affinity of the G-proteins for the δ-opioid receptor is highly dependent on the nature of the ligand that is bound to the receptor, as is the affinity of GTPγS for the receptor-G-protein complex.

Results and Discussion

We have developed methods for obtaining highly purified and stable hDOR preparations using a His-*myc* tagged hDOR stably transfected into CHO cells, solubilizing the receptor in octylglucoside-containing buffer, and purifying the receptor on a Co^{+2}-chelating column followed by an affinity column. The purified solubilized receptor is stable for up to seven days. This receptor can be directly incorporated in solid-supported lipid bilayers in the PWR instrument. The process of formation of the lipid bilayer and incorporation of the receptor into the lipid bilayer can be monitored directly by PWR spectroscopy.

In order to examine G-protein-receptor interactions we first examined the effects of various classes of ligands (agonist, antagonists, inverse agonists, etc.) on the hDOR. In general, it was observed that *p*- and *s*-polarized light (light perpendicular and parallel to the plasmon-generating media, respectively) cause quite different PWR spectral

changes, such differences arising from the anisotropic properties of lipid bilayers. Binding constants were determined directly from experiments carried out at several concentrations, plotting the shifts in resonance as a function of concentration, and fitting the data to a hyperbolic binding isotherm. In the course of these experiments, we have found that agonist, antagonists, and inverse agonists binding to the hDOR each lead to unique structural changes: 1) Binding constants for a number of agonists, antagonists, inverse agonists, and partial agonists are very similar to those obtained using radiolabeled ligands and membrane preparations of the native receptor; 2) antagonists, agonists, and inverse agonists all give unique distinctive spectral changes, which correspond to different receptor conformational states. These states are very similar for all peptide agonists such as DPDPE, and all delta antagonists allowing one to distinguish between agonists, antagonists and inverse agonists without a need for second messenger studies.

We next turned our attention to examining directly the interactions of G-proteins with the delta opioid receptor. It is well known that G-protein interactions with GPCRs occur in intracellular domains of these receptors. Since G-proteins do not penetrate through membrane bilayers (nor do the peptide and peptidomimetic ligands) these studies required that agonist, antagonist and inverse agonist ligands be prebound to the receptor before the receptor is inserted into the membrane bilayer, and that some of the liganded (or unliganded) hDOR insert into the membrane bilayer with the intracellular domains located on the aqueous sample compartment side of the bilayers in the PWR instrument. Indeed, we have found this to be the case. Hence we have examined G-protein binding to the hDOR prebound with an agonist, antagonist or inverse agonist and unliganded, and determined affinity constants of G-proteins using first a mixture of the G-proteins: $G_{o\alpha}$, $G_{i\alpha1}$, $G_{i\alpha2}$, and $G_{i\alpha3}$ with the different liganded states, then carried out the same studies with purified individual G-proteins: $G_{o\alpha}$, $G_{i\alpha1}$, $G_{i\alpha2}$, and $G_{i\alpha3}$. In addition, we have examined the GTPγS/GDP exchange interaction with the liganded and unliganded receptor-G-protein complex. Binding of G-proteins to the agonist bound hDOR receptor occurs with high affinity, and addition of GTPγS to the hDOR-agonist-G-protein complex leads to potent binding affinities of GTPγS to the G-protein receptor. Other identical studies with the unoccupied hDOR, antagonist liganded hDOR, and the inverse agonist occupied hDOR (data not shown) show that the G-proteins bind to the receptor in the following order: agonists > unoccupied > antagonists >> inverse agonists. When the same experiments were done using pure separated G-proteins subunits: $G_{o\alpha}$, $G_{i\alpha1}$, $G_{i\alpha2}$, and $G_{i\alpha3}$ for the DPDPE-agonist bound hDOR or the unliganded receptor very interesting results are obtained as summarized in Table 1. In the agonist bound state, the G-proteins bind to the GPCR with up to 40-fold differences in binding affinities with $G_{o\alpha} > G_{i\alpha1} \approx G_{i\alpha3} > G_{i\alpha2}$. Interestingly, GTPγS binding to the individual G-proteins for unliganded receptors is virtually abolished except for very weak binding in the $G_{o\alpha}$ case (Table 1).

In summary, binding affinities of G-proteins to the hDOR are highly dependent on the ligand bound to the receptor, and different G-proteins bind with significantly different affinities to liganded or unliganded receptor. Furthermore, it is possible to monitor directly GDP/GTP exchange and determine binding affinities. Taken together, all of the studies reported clearly demonstrate that the hDOR exists in several conformational states, and that these states can change dramatically, depending on the ligand present, and the G-proteins that are involved. These results require the development of a more dynamic model of GPCR-mediated transduction. We will continue to examine in more detail this emerging picture of GPCR biological function by examination of the kinetics of these various interactions, development of

spectrospectic methods to more specifically define in structural terms the structural features that are affected by these multiple effects, and to continue to study by PWR spectroscopy the further downstream modulators of transduction.

Table 1. Binding affinities between the individual G-protein subtypes and the hDOR either unliganded or DPDPE-bound and between GTPγS and the receptor-G protein complex.

DPDPE bound								
G protein subtype	$G_{o\alpha}$		$G_{i\alpha1}$		$G_{i\alpha2}$		$G_{i\alpha3}$	
Polarization	*p*	*s*	*P*	*S*	*p*	*s*	*p*	*s*
$K_d^{Gprotein}$ (nM)	10 ± 1	9 ± 1	302 ± 24	306 ± 28	7 ± 1	7 ± 1	45 ± 5	41 ± 5
$K_d^{GTP\gamma S}$ (nM)	404 ± 37	394 ± 71	4.7 ± 0.3	3.7 ± 0.7	9.9 ± 0.5	8.3 ± 0.8	80 ± 11	83 ± 9
Unliganded receptor								
G protein subunit	$G_{o\alpha}$		$G_{i\alpha1}$		$G_{i\alpha2}$		$G_{i\alpha3}$	
Polarization	*p*	*s*	*P*	*S*	*p*	*s*	*p*	*S*
$K_d^{Gprotein}$ (nM)	20 ± 1.7	22 ± 1.8	79 ± 9	81 ± 8	598 ± 70	574 ± 70	95 ± 10	96 ± 10
$K_d^{GTP\gamma S}$ (nM)	1920 ± 177	1880 ± 219	*	*	*	*	*	*

** No PWR spectral shifts were obtained upon addition of GTPγS up to 5 μM.*

Acknowledgments
This work was supported by grants from the NSF and the USPHS.

References

1. Salamon, Z., Brown, M. F. and Tollin, G. *Trends Biochem. Sci.* **24**, 213-219 (1999).
2. Salamon, Z., *et al*., *Biophys. J*. **79**, 2463-2474 (2000).
3. Salamon, Z., Cowell, S., Hruby, V. J. and Tollin, G. *J. Peptide Res.* **60**, 322-328 (2002).

Peptide Revolution: Genomics, Proteomics & Therapeutics
Michael Chorev & Tomi K. Sawyer (Editors)
American Peptide Society, 2003

Silylated Amino Acid Containing Substance P Analogues

F. Cavelier[1], D. Marchand[1], J. Martinez[1], S. Lavielle[2] and S. Sagan[2]

[1]Laboratoire des Aminoacides, Peptides et Protéines, UMR-CNRS 5810, Université Montpellier II, CC19, 34095 Montpellier cedex 05, France; [2]Structure et Fonction de Molecules Bioactives, UMR-CNRS 7613, Universite Pierre et Marie Curie, boite courrier 182, 4, place Jussieu, 75252 Paris cedex 05, France

Introduction

The need to replace natural amino acids in peptides with nonproteinogenic counterparts in order to obtain new medicinal agents, exhibiting better binding to specific receptors and more potent inhibition of target enzymes has stimulated a great deal of innovation in synthetic methods. In addition, peptide activity is highly dependent on backbone conformation and three-dimensional orientation of amino acid side chains. Accordingly, induction of biologically active conformations in peptides is an important area of investigation that frequently entails utilization of constrained amino acids analogues [[1]], particularly cyclic amino acid residues. For these reasons, proline surrogates have been extensively investigated, mainly in order to modulate the proportion of *cis* and *trans* conformers. Moreover, replacing any amino acid with unnatural residues, presumably not recognized in the proteolytic enzymatic degradation process, should increase the bioavailability of the modified peptides.

Here we report the incorporation of non-natural amino acids containing a silicon atom, TMS-Ala and silaproline (Sip) [2] in substance P (SP) (Figure 1), and the evaluation of the affinity of the resulting peptide analogues for substance P binding sites. We also assessed the improvement of their stability towards enzymmatic degradation.

H-Arg^1-Pro^2-Lys^3-Pro^4-Gln^5-Gln^6-Phe^7-Phe^8-Gly^9-Leu^{10}-Met^{11}-NH$_2$

Fig. 1. Substance P sequence (SP).

Results and Discussion

Peptides were synthesized using Fmoc chemistry in a Perkin-Elmer ABI433A automatic synthesizer on a 0.25 mmol scale with Rink amide resin. The coupling reagent was a 0.45M solution of HBTU/HOBt. Deprotection cycles were carried out in piperidine/DMF (20/80) and monitored by conductimetry. Elongation was effected by single 30-min couplings in DMF with DIEA as a base. Final cleavage was carried out with 80% TFA and 20% anisole for 3 h. Peptide-resins were washed extensively with DMF, then dried *in vacuo*, dissolved in an acetonitrile-water mixture, and freeze-dried.

Binding assays on the two binding sites associated with the NK-1 receptor and second messenger assays were carried out on whole cells as previously described [3,4]. SP and [Pro^9]SP are taken as reference peptides of the more abundant (NK-1M) binding site, while [pGlu^6]SP(6-11) and [pGlu^6, Pro^9]SP(6-11) are selective peptides of the less abundant (NK-1m) binding site. Results are reported in Table 1.

A TmsAla residue has been incorporated in position 7 and/or 8 of SP, in place of Phe as recommended in literature [5]. The three resulting peptides (entries 8, 9 and 10) lost affinity for the two NK-1 binding sites, [TmsAla^8]SP being the more potent peptide with 50-fold and 10-fold lower affinity than SP for the NK-1M and NK-1m binding sites, respectively. The potency of these peptide analogues to stimulate second

messenger pathways follows, as generally observed, their affinity for the two binding sites. Indeed, with the exception of [TmsAla^{8}]SP, these SP analogues have no potency to stimulate both second messenger pathways. Similar results were obtained with the C-terminal hexapeptide analogue series (entries 5, 6 and 7).

Table 1. Binding and activity of peptides.

	peptide	NK-1M Ki, nM	cAMP EC50, nM	NK-1m Ki, nM	IP EC50, nM
1	(SP)	1.3 ± 0.4	8 ± 2	0.13 ± 0.02	0.7 ± 0.3
2	[Pro^{9}]SP	0.7 ± 0.2	10 ± 2	0.13 ± 0.02	0.7 ± 0.1
3	[pGlu^{6}]SP(6-11)	290 ± 10	850 ± 200	Not determined	4.0 ± 1.0
4	[pGlu^{6}, Pro^{9}]SP(6-11)	490 ± 10	5,200 ± 200	2.4 ± 0.5	2.7 ± 0.5
5	[pGlu^{6}, TmsAla^{7}]SP(6-11)	> 10,000	inactive	9,000 ± 250	> 10,000
6	[pGlu^{6}, TmsAla^{8}]SP(6-11)	> 10,000	inactive	2,200 ± 500	4,000 ± 1,000
7	[pGlu^{6}, TmsAla^{10}]SP(6-11)	2,000 ± 200	> 10,000	45 ± 10	27 ± 3
8	[TmsAla^{7}]SP	500 ± 120	> 10,000	800 ± 150	4,400 ± 1,200
9	[TmsAla^{8}]SP	63 ± 6	300 ± 40	1.5 ± 0.3	1.6 ± 0.4
10	[TmsAla$^{7, 8}$]SP	2,200 ± 600	inactive	5,700 ± 700	> 10,000
11	[pGlu^{6}, Sip^{9}]SP(6-11)	345 ± 75	27% (10,000) pK_B = 6.89 ± 0.08	0.87 ± 0.09	1.3 ± 0.3
12	[pGlu^{6}, (D)-Sip^{9}]SP(6-11)	1,245 ± 75	> 10,000	55 ± 2	40 ± 4
13	[Sip^{9}]SP	0.53 ± 0.06	30 ± 5 (75 ±5 %)	1.2 ± 0.2	5.0 ± 2.0

A silaproline has also been incorporated in place of proline in [Pro^{9}]SP or [pGlu^{6}, Pro^{9}]SP(6-11). NMR studies proved that replacement of Pro with Sip in model peptides did not affect their three-dimensional conformation [6]. Therefore, we could reasonably expect to retain binding affinity with such modification, while improving peptide stability towards enzyme digestion. Indeed, the affinity for NK-1M is not affected by incorporation of a Sip residue in [Pro^{9}]SP, however, the affinity for NK-1m is decreased by 10-fold (entry 13). The potency of [Sip^{9}]SP to stimulate cAMP production is similar to that of SP, but the efficacy (maximal response) is 75% that of SP or [Pro^{9}]SP. Nevertheless no antagonist property could be detected for that analogue. The analogue [Sip^{9}]SP was also a full agonist on PLC with a potency significantly lower than that of [Pro^{9}]SP, related to its binding affinity for NK-1m. The same modification in the C-terminal hexapeptide series (entry 11) results in an analogue with affinity slightly increasing for both binding sites. [pGlu^{6}, Sip^{9}]SP(6-11) is a full potent agonist in the PLC pathway but is a partial agonist in the cAMP one. Indeed, at 10 μM, the efficacy of this analogue is only 27% that of SP or [pGlu^{6}]SP(6-11). Moreover, this peptide analogue is an antagonist, although not very potent (pK_B = 6.89), of SP-stimulated cAMP accumulation. As expected, the analogue containing the (D)-Sip has decreased affinity for both binding sites (entry 12).

Finally the stability of the silaproline-containing SP analogue towards angiotensin-converting enzyme has been examined. Results show that after 1 hr incubation at 37°C, 80% of SP was degraded while [Pro^9]SP and [Sip^9]SP were not cleaved.

Conclusions

In conclusion, replacing Phe in position 7 or 8 of SP with TMS-Ala decreased its binding affinity and biological potency dramatically. In contrast, replacing Pro in position 9 with Sip leads to SP or C-terminal SP hexapeptide analogues retaining the whole affinity of the parent peptides. Moreover, in the C-terminal SP hexapeptide, replacement of Pro^9 with Sip led to a full agonist on the PLC pathway and a partial agonist on the adenylate cyclase one. This latter point underlines that silaproline is not only a proline mimetic but that it may also confer interesting pharmacological patterns to biologically active peptides.

References

1. (a) Babine, R. E. and Bender, S. L. *Chem. Rev*. **97**, 1359-1472 (1997). (b) Hruby, V. J. and Balse, P. M. *Curr. Med. Chem*. **7**, 945-970 (2000).
2. Vivet, B., Cavelier, F. and Martinez, J. *Eur. J. Org. Chem*., 807 (2000).
3. Sagan, S., Beaujouan, J.- C., Torrens, Y., Saffroy, M., Chassaing, G., Glowinski, J. and Lavielle, S. *Mol. Pharmacol*. **52**, 120-127 (1997).
4. Sagan, S., Karoyan, P., Chassaing, G., Lavielle, S. *J. Biol. Chem*. **274**, 23770-23776 (1999).
5. Weidmann, B. *Chimia*, 312-313 (1992).
6. Cavelier, F., Vivet, B., Martinez, J., Aubry, A., Didierjean, C., Vicherat, A. and Marraud, M. *J. Am. Chem. Soc*. **124**, 2917-2923 (2002).

Peptide Revolution: Genomics, Proteomics & Therapeutics
Michael Chorev & Tomi K. Sawyer (Editors)
American Peptide Society, 2003

Synthesis and Pharmacological Activity of Human Urotensin II Analogues Modified in Position 8

Remo Guerrini[1], Girolamo Calo'[2], Marina Zucchini[1], Valeria Camarda[2], Domenico Regoli[2] and Severo Salvadori[1]

[1]Department of Pharmaceutical Sciences; [2]Department of Experimental and Clinical Medicine, Section of Pharmacology, University of Ferrara, 44-100 Ferrara, Italy

Introduction

Human urotensin-II (U-II) is a cyclic undecapeptide (H-Glu-Thr-Pro-Asp-c[Cys-Phe-Trp-Lys-Tyr-Cys]-Val-OH) containing a disulphide bridge between Cys^5 and Cys^{10}. This peptide, isolated originally from fish urophyses [1], has been now identified in different species, including man [2]. The cyclic region c[Cys-Phe-Trp-Lys-Tyr-Cys] is fully conserved among species, suggesting that it may play a crucial role for biological activity. U-II was recognized as the natural ligand of an orphan G-protein coupled receptor, GPR14, now referred to as UT receptor [3]. This novel peptide/receptor system appears to be particularly involved in the regulation of cardiovascular homeostasis [4] and U-II exerts sustained contractile actions in isolated veins and arteries from different species. Recently Kinney *et al*. [5] proposed a model of U-II/UT receptor binding in which the interaction between the amine function of Lys^8 of the peptide and the carboxylic group of Asp^{130} of the UT receptor plays an essential role. In the present investigation, we describe the effects of substitution of position 8 in human U-II with natural and non-natural amino acids.

Results and Discussion

All the compounds were prepared by solid phase synthesis and pharmacologically evaluated in the rat aorta strips. In this preparation U-II (compound 1) induced a concentration dependent contraction with high potency but relatively small maximal effects. As shown in Table 1, substitution of Lys^8 with lipophilic amino acids (compounds 2 and 3) produced inactive peptides. Similar results were also obtained with hydrophilic but not basic residues (compounds 4-6), indicating that the basic character of the lysine side chain is essential for biological activity. Thus, the relative importance of the distance of the primary aliphatic amine from the peptide backbone has been investigated with compounds 7-9. [Orn^8]U-II produced a weak contraction (corresponding to about 20 % of the U-II maximal effect) of rat aorta strips only at micromolar concentrations: interestingly, it antagonized U-II effects showing a pA_2 value of 6.47. Similar results were obtained with compound 8 which, however, showed lower residual agonist activity (7 % of the U-II maximal effect) and potency (pA_2 5.51). On the other hand, further shortening of the amino acid side chain as in compound 9 produced a low potency (pEC_{50} 6.77) full agonist. Collectively, these data suggest that the positive charge of the primary aliphatic amine in position 8 and its relative spatial orientation is crucial for both receptor occupation and activation.

Table 1. Activities of U-II and [Xaa^8]U-II analogs in the rat aorta bioassay.

n°	Compound	Agonist		Antagonist
		pEC_{50} ($CL_{95\%}$)	**E_{max} (g)**	**pA_2 ($CL_{95\%}$)**
1	U-II	8.22 (8.06-8.38)	0.72 ± 0.06	ND
2	[Nle^8]U-II	Inactive		Inactive
3	[Leu^8]U-II	Inactive		Inactive
4	[Cit^8]U-II	Inactive		Inactive
5	[Gln^8]U-II	Inactive		Inactive
6	[(Ac)Lys^8]U-II	5.69 (5.39-5.99)	0.67 ± 0.11	ND
7	[Orn^8]U-II	10 µM: 0.15 ± 0.06		6.47 (6.23-6.71)
8	[Dab^8]U-II	10 µM: 0.05 ± 0.02		5.51 (5.32-5.70)
9	[Dap^8]U-II	6.77 (6.67-6.97)	0.66 ± 0.06	ND

ND = not determined since the compound behaves as a full agonist.
pEC_{50}: the negative logarithm to base 10 of the molar concentration of an agonist that produces 50% of the maximal possible effect.
pA_2: antagonist-potency calculated using the Gaddum-Schild equation.
$CL_{95\%}$: 95% confidence limits.
Emax: the maximal effect elicited by the agonist expressed as grams (g) of contraction.
Inactive: up to 10 µM.

References

1. Pearson D., Shively J. E. and Clark B. R., *et al*., *Proc. Natl. Acad. Sci. U.S.A.* **77**, 5021-5024 (1980).
2. Douglas S. A. and Ohlstein E. H. *Trends Cardiovasc. Med.* **10**, 229-237 (2000).
3. Douglas S. A. and Ohlstein E. H. *The IUPHAR compendium of receptor characterization and classification;* IUPHAR Media: London, pp 365-372 (2000).
4. Douglas S. A. *Curr. Opin. Pharmacol.* **3**, 159-167 (2003).
5. Kinney W. A., Almond Jr H. R., Qi J., Smith C. E., *et al*., *Angew. Chem. Int. Ed. Engl.* **41**, 2940-2944 (2002).

Peptide Revolution: Genomics, Proteomics & Therapeutics
Michael Chorev & Tomi K. Sawyer (Editors)
American Peptide Society, 2003

Mapping the N-terminal Contact of Urotensin II with its Receptor Using Peptide Photoprobes

Brian J. Holleran, Antony A. Boucard, Adrian Häberli, Klaus Klarskov, Richard Leduc and Emanuel Escher

Department of Pharmacology; Université de Sherbrooke, Sherbrooke, Qc, J1E 5N4, Canada

Introduction

Urotensin II (U-II) is a cyclic undecapeptide which has recently been shown to be the endogenous ligand of the G protein-coupled receptor (GPCR) GPR14, otherwise known as UT [1]. U-II is similar to peptides such as angiotensin II and endothelin-1 in that it may be implicated in the pathogenesis of cardiovascular diseases such as essential hypertension and heart failure. Our laboratory is interested in defining spatial orientation of the biological ligand within the binding pocket of peptidergic GPCRs. By introducing spatial constraints between distant residues of the receptor and homology modeling, the number of possible structures is narrowed down to a very few [2]. Spatial constraints can be experimentally determined by finding the points of contact between a peptide ligand and its receptor using multiple photoaffinity labelling e.g., with photoprobe radioligands incorporating *para*-benzoyl-*L*-phenylanaline (Bpa) at different positions within the peptide sequence. Using this approach, we have recently shown that the sixth residue of U-II is in close proximity to two adjacent Met residues within the fourth transmembrane domain of the rat UT (rUT) [3]. In order to determine ligand orientation and better define interactions within the binding pocket of UT, further contact points are needed. We have introduced Bpa into the N-terminal portion of U-II, since this portion of the ligand is highly heterogenous across species while still maintaining full biological properties.

U-II	NH_2-ETPDCFWK**Y**CV-OH
[Bpa^1]U-II	NH_2-**B**TPDCFWK**Y**CV-OH
[Bpa^2]U-II	NH_2-E**B**PDCFWK**Y**CV-OH
[Bpa^3]U-II	NH_2-ET**B**DCFWK**Y**CV-OH

Fig. 1. Sequences of urotensin II and synthetic photoprobes (**B** *= Bpa,* **Y** *=^{125}I labeled Tyr).*

Results and Discussion

We have generated a series of photoprobes incorporating the Bpa moiety in the first, second and third positions of U-II, namely [Bpa^1]U-II, [Bpa^2]U-II and [Bpa^3]U-II. These analogues incorporated ^{125}I on the tyrosine in the ninth position. Following transfection of the rUT cDNA in COS-7 cells, we determined that all three analogues had binding affinities similar to endogenous U-II and all three strongly photolabelled rUT in a specific manner. Each photolabeled complex was purified by SDS-PAGE, passively eluted from the gel and concentrated. Several biochemical analyses were carried out on each photolabeled complex in order to determine the region of contact between the Bpa moiety and the rUT receptor. Following V8 protease (Glu-C) cleavage of the ligand/receptor complex, a 17.5 kDa fragment corresponding to residues 148-286 of rUT was obtained for all three photoligands. We chose to focus on the [Bpa^2]U-II photolabeled complex. Arg-C cleavage generated a single 6.5 kDa fragment, which corresponded to residues 257-296 of rUT. By correlating both fragments obtained by

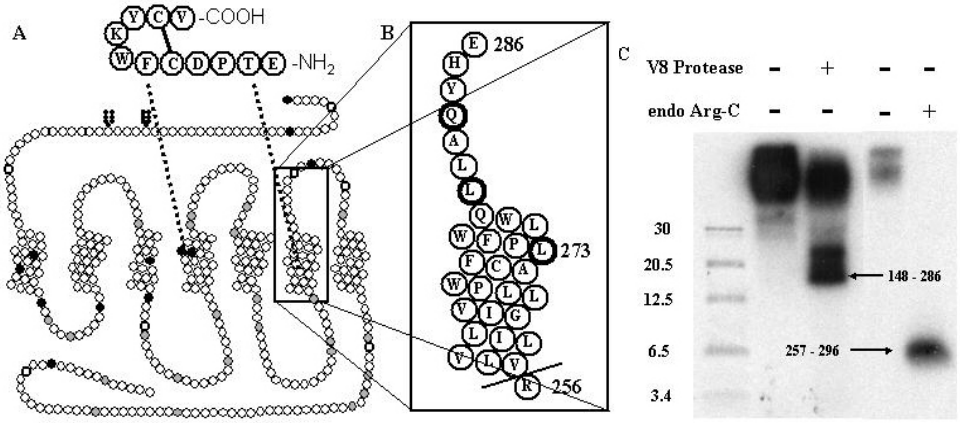

*Fig. 2. Labeling contents of U-II in rUT **A**. Schematic representation of rUT and U-II. Dotted lines connect rUT contact area to U-II. **B**. The box corresponds to the labeling sequence of [Bpa^2]U-II in TM6. Bold residues are the portions where Met mutations were carried out. **C**. SDS-PAGE of [Bpa^2]U-II labeled rUT.*

V8 protease and Arg-C cleavage, the minimal region that [Bpa^2]U-II photolabeled is the sequence encompassing 257-286 of rUT. This region comprises the sixth transmembrane element and the first part of the third extracellular domain. To further identify the exact contact point, we have generated mutants within this region by substituting the residues L273, L280 and Q283 with methionine. On the one hand, a new CNBr specific cleavage site is generated within the region allowing us to target a smaller minimal photolabeled sequence. On the other hand, we can take advantage of the property of methionine to release ligand upon CNBr cleavage if this methionine is the residue directly photolabeled [4]. However, we failed to observe ligand release by CNBr with these mutants, but were able to restrict ligand contact to the sequence 257-272 within the lower part of TM6. Generating new mutants of rUT within this region of interest should further narrow down the region and identify the residue that interacts with the second amino acid of U-II. Alternatively, we are currently applying photoprobes with affinity reporter groups for mass spectrometry analysis of labeled receptor fragments [5].

Acknowledgments
The work was funded by the Canadian Institutes of Health grant MOP-49438.

References

1. Maguire, J. J. and Davenport, A. P. *Br. J. Pharmacol.* **137**, 579-588 (2002).
2. Boucard, A. A., et al. *Biochemistry* **39**, 2662-2670 (2000).
3. Boucard, A. A., et al. *Biochem J.* **362**, 829-238 (2002).
4. Rihakova, L., et al. *J. Recept. Signal Transduct.* **22**, 297-313 (2002).
5. Sachon, E., et al. *J. Biol. Chem.* **277,** 50409-50414 (2002).

Peptide Revolution: Genomics, Proteomics & Therapeutics
Michael Chorev & Tomi K. Sawyer (Editors)
American Peptide Society, 2003

3D Structural Analysis of Urotensin-II Analogues in Membrane Mimetic Environment

Alfonso Carotenuto[1], Paolo Grieco[2], Pietro Campiglia[2], Ettore Novellino[2] and Paolo Rovero[1]

[1]Department of Pharmaceutical Sciences, University of Salerno, I-84084 Fisciano, Italy;
[2]Department of Pharmaceutical and Toxycological Chemistry, University of Naples, I-80131 Naples, Italy

Introduction

Urotensin II is an 11-amino acid vasoactive peptide found in different species, including humans, characterized by a highly conserved C-terminal cyclic heptapeptide portion. Recently, human Urotensin II (hU-II) was identified as the endogenous ligand of the orphan G-protein-coupled receptor GPR14 [1]. hU-II (H-Glu-Thr-Pro-Asp-cyclo[Cys-Phe-Trp-Lys-Tyr-Cys]-Val-OH) has been described as the most potent vasoconstrictor compound identified to date, probably involved in the regulation of cardiovascular homeostasis and pathology [2]. This knowledge indicates GPR14 as a potential target of novel therapeutic strategies related to the treatment of cardiovascular diseases, and underlines the importance of a clear understanding of hU-II structure-activity relationships. In view of these goals, we have previously analyzed the solution structure of hU-II in isotropic media and anisotropic membrane mimetic solutions [3]. In anisotropic media (water, DMSO/water, hexafluoroacetone (HFA)/water solutions) hU-II showed no evidence of ordered α-helix or β-sheet structures, while in SDS-micelles medium it adopts a well defined β-hairpin structure with a turn at positions Trp^7-Lys^8. To unravel the biological meaning of this 3D structure, we have investigated the conformational behavior in micelles of recently synthesized U-II analogues in which Cys 5 and/or 10 are replaced by Pen or hCys residues [4]. In particular, the following peptides were considered: a) the recently described **P5U** superagonist, where Cys residue in position 5 was replaced by Pen. This peptide showed higher affinity than hU-II at human cloned U-II receptors as well as higher activity in the rat thoracic aorta assay; b) an analogue in which both Cys^5 and Cys^{10} were substituted by Pen residues (compound **1**), which is almost as active as hU-II; c) analogue **2** (Cys^{10} replaced by Pen), whose activity dropped by two orders of magnitude; d) two analogues in which Cys^{10} or Cys^5 were substituted by hCys (compounds **3** and **4**, respectively), which resulted in both being very weakly active. The comparison of the 3D structures of these compounds with those of the parent peptides hU-II, and hU-II(4-11) may give interesting information about U-II active conformation.

Results and Discussion

The CD and NMR spectra of compounds hU-II(4-11), **P5U**, and **1**-**4** were run in aqueous SDS solution (200 mM). Almost complete ^{1}H NMR assignments were obtained by the combined use of DQF-COSY, TOCSY and NOESY spectra. A qualitative evaluation of the NOE connectivities showed that the active peptides hU-II(4-11), **P5U**, **1**, and **2** adopt a structured conformation in SDS solution. In fact, diagnostic NOE contacts and the shifts observed for CαH resonances compared to random coil peptides indicated that the structure of the region encompassing residues 4-11 consists of a β-hairpin with a turn at positions Trp^7-Lys^8, as observed for hU-II. Moreover, the observed upfield shifts for the side-chain protons of Lys^8 and the inter-chains NOE contacts indicate a close spatial position of these atoms to the aromatic

rings of Trp^7 and Tyr^9. The analysis of CD spectra confirmed the propensity of these active compounds to form strand and turn conformations. The inactive compounds **3** and **4** showed CD and NMR features different from those of **PU5**, **1** and **2**, indicating more flexible conformations. A structure calculation of these peptides were performed using NOE derived constraints and the standard protocol of the Dyana program. The best 10/100 Dyana calculated structures were then optimized unrestrained with the program DISCOVER (Molecular Simulation, Inc).

As expected from a qualitative analysis of the NMR data, in the anisotropic SDS micellar environment hU-II(4-11), the active peptides **P5U**, **1**, and **2** all adopt a well defined β-hairpin structure encompassing residues 4-11 with a distorted β-turn at Trp^7-Lys^8 positions. The side chains of residues 7-9 form a cluster. Interestingly, according to Flohr et al. [5] these side chains represent the hU-II pharmacophore. The different topochemical location of the Trp-Lys-Tyr triad side chains observed in **2**, compared to the corresponding ones in hU-II(4-11) and **P5U** (Figure 1), can explain the reduced activity of **2**, as compared to the parent peptide hU-II(4-11). Finally, calculated structures of the weakly active peptides **3** and **4** show lose of any propensity to the β-hairpin formation, indicating that this structural feature is essential to the interaction with the receptor. The above described results will serve as starting point for the development of novel peptide and non-peptide UT-II receptor agonists and/or antagonists.

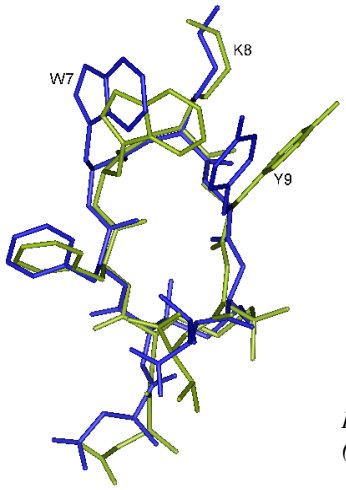

*Fig. 1. Superposition of **P5U** (black) and compound **2** (gray) representative structures.*

References

1. Ames, R. S. *et al., Nature* **401**, 282-286 (1999).
2. Douglas, S. A., and Ohlstein, E. H. *Trends Cardiovasc. Med.* **10**, 229-337 (2000).
3. Zampelli, E., Carotenuto, A., Grieco, P., Campiglia, P., Novellino, E. and Rovero, P. In Benedetti, E. and Pedone, C. (Eds.) *Peptides 2002 - Proceedings of the 27th European Peptide Symposium*, Edizioni Ziino, Napoli, Italy, pp. 926-927 (2002).
4. Grieco, P., Carotenuto, A., Campiglia, P., Zampelli, E., Patacchini, R., Maggi, C. A., Novellino, E. and Rovero, P. *J. Med. Chem.* **45**, 4391-4394 (2002).
5. Flohr, S., Kurz, M., Kostenis, E., Brkovich, A., Fournier, A. and Klabunde, T. *J. Med. Chem.* **45**, 1799-1805 (2002).

Peptide Revolution: Genomics, Proteomics & Therapeutics
Michael Chorev & Tomi K. Sawyer (Editors)
American Peptide Society, 2003

Development of New Urotensin-II Receptor Ligands

Pietro Campiglia[1], Alfonso Carotenuto[2], Riccardo Patacchini[3], Carlo A. Maggi[3], Ettore Novellino[1], Paolo Rovero[2] and Paolo Grieco[1]

[1]Dip. Chimica Farmaceutica e Toss., University of Naples "Federico II";
[2]Dip. Scienze Farmaceutiche, University of Salerno;
[3]Dip. Farmacologia, Menarini Ricerche, S.p.A. Firenze, Italy

Introduction

Urotensin II (hU-II), a potent vasoconstrictor, is found in diverse species, including human. The U-II C-terminal cyclic heptapeptide portion (CFWKYCV), which is essential for the biological activity, has been highly conserved in evolution from fish to mammals [1]. Several biological studies indicate that hU-II is the most potent mammalian peptide vasoconstrictor reported to date, and it appears to be involved in the regulation of cardiovascular homeostasis and pathology.

Recently, we have reported the first superagonist at a UT receptor (**P5U**) obtained replacing Cys^5 with Pen in hU-II-(4-11) sequence [2,3]. In order to elucidate the importance of the disulfide bridge in biological activity and in receptor interaction we synthesized new analogues where Cys^5 and Cys^{10} were replaced singularly with a residue of hCys (Figure 1). Also, to evaluate the contribution of disulfide bridge to the overall folding conformation and stability, we synthesized a thioether analogue of hU-II-(4-11) (Figure 1).

hU-II	H-Glu-Thr-Pro-Asp-[Cys-Phe-Trp-Lys-Tyr-Cys]-Val-OH
hU-II-(4-11)	H-Asp-[Cys-Phe-Trp-Lys-Tyr-Cys]-Val-OH
1	H-Asp-[hCys-Phe-Trp-Lys-Tyr-Cys]-Val-OH
2	H-Asp-[Cys-Phe-Trp-Lys-Tyr-hCys]-Val-OH
3	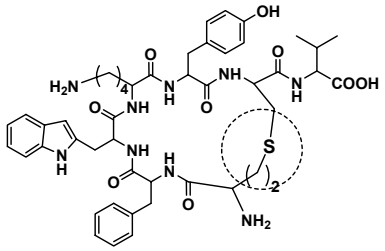

Fig. 1. Sequences of Urotensin-II and analogues synthesized.

Results and Discussion

The compounds were synthesized by solid phase peptide synthesis method using Fmoc chemistry. The disulfide bridge was obtained by potassium ferricyanide oxidation, using the syringe pump method. All final products were purified by semipreparative RP-HPLC. Analytical HPLC indicated a purity greater than 98%, and molecular weights were confirmed by HR-MS. The peptides were tested for their ability to induce efficacious contractions in the rat isolated thoracic aorta. Table 1 shows the biological activity of the hU-II-(4-11) analogues, **1** and **2**, in which Cys residues in positions 5 and 10 have been replaced singularly by hCys, and the thioether analogue, **3**.

Table 1. Contractile effects produced by h-Urotensin-II and derivatives in the rat isolated thoracic aorta.

Peptide	$-logEC_{50}$	*Emax (% of hU-II)*	*Emax (% of KCl)*
hU-II	8.48±0.02	100	56±5
hU-II-(4-11)	8.60±0.08	100	56±10
1	6.37±0.09	100	45±16
2	6.60±0.03	100	62±16
3	5.69±0.06	56±20	36±15

The preliminary pharmacological experiments show that compounds **1** and **2**, with hCys residues in position 5 and 10, respectively, are almost 2 logs less active when compared to hU-II, confirming that the nature of disulfide bridge is important for biological activity of this peptide. Interestingly, the thioether analogue resulted to be 3 logs less active suggesting that the disulfide bridge is an essential motif to evoke full activity (see Table 1).

The results obtained in this study will be used as a starting point for the development of novel ligands for the UT receptor.

References

1. Ames, R. S. *et al., Nature* **401**, 282-286 (1999).
2. Grieco, P., Carotenuto, A., Campiglia, P., Zampelli, E., Patacchini, R., Maggi, C. A., Novellino, E. and Povero, P. *J. Med. Chem.* **45**, 4391-4394 (2002).
3. Grieco, P., Carotenuto, A., Patacchini, R., Maggi, C. A., Novellino, E. and Rovero, P. *Bioorg. & Med. Chem.* **10**, 3731-3739 (2002).

Peptide Revolution: Genomics, Proteomics & Therapeutics
Michael Chorev & Tomi K. Sawyer (Editors)
American Peptide Society, 2003

Molecular Modeling of the Urotensin-II Receptor Complex

Paolo Grieco[1], Antonio Lavecchia[1], Pietro Campiglia[1], Teresa Lama[1], Paolo Rovero[2], Alfonso Carotenuto[2], Riccardo Patacchini[3], Carlo A. Maggi[3] and Ettore Novellino[1]

[1]Dip. Chimica Farmaceutica e Toss., University of Naples "Federico II"; [2]Dip. Scienze Farmaceutiche, University of Salerno; [3]Dip. Farmacologia, Menarini Ricerche, S.p.A. Firenze, Italy

Introduction

Urotensin-II is a neuropeptide "somatostatin-like" cyclic peptide which was originally isolated from fish spinal cords, and which has recently been cloned from human. Human U-II is composed of only 11 amino acids residues, while fish and frog U-II possess 12 and 13 amino acids residues, respectively. The cyclic region of U-II, which is responsible for the biological activity of the peptide, has been fully conserved from fish to human. Our recent structure-activity relationships studies performed on Urotensin-II have revealed that the peptide P5U is a superagonist at UT receptor [1-4]. The literature indicates that UT receptor as a potential target of novel therapeutic strategies related to the treatment of cardiovascular diseases and the discovery of UT receptor antagonists would help to elucidate the *in vivo* pharmacology, as well as afford potential therapeutic agents for the treatment of hypertension and heart failure. Here, we present a preliminary study of a model of human urotensin II receptor (*h*U-IIR) based on X-ray structure of rhodopsin [5] in an effort to establish the possible interactions between ligands known to date and the receptor.

Results and Discussion

To understand the activity of a series of *h*U-II derivatives synthesized in our laboratory, we modeled the complex of the most active compound P5U with a model of *h*U-IIR, known to be a G protein-coupled receptor. The model of *h*U-IIR was constructed through molecular modeling and molecular dynamics simulations, using the bovine rhodopsin crystal structure as a template for the seven transmembrane α-helices. The three extracellular loops were modeled on homologous loop regions in other proteins of known structure. The molecular simulations were carried out with the InsightII/Discover program package [6], selecting the CWFF force field [7]. The binding mode of P5U was analyzed by the program AUTODOCK [8] using standard parameters. From this simulation, the bound ligand was predicted to establish a number of favorable contacts within the *h*U-IIR binding site, and some of these interactions are shown in Figure 1. The residues that are involved in the closest contacts (Trp, Lys and Tyr), indicated to be important for ligand binding to the *h*U-IIR, are explicitly shown. In the receptor complex produced in these studies, the peptide ligand docks principally at the extracellular ends of TM-III, TM-V, TM-VI, and TM-VII of the receptor as well as EL-II and EL-III. Also, it is evident that the disulfide bridge may play an important role in biological activity in all Urotensin-II derivatives synthesized.

In summary, we have generated a model for the receptor-ligand complex. This model will be used to design other molecules that may fit in the binding pocket and act as agonists or antagonists.

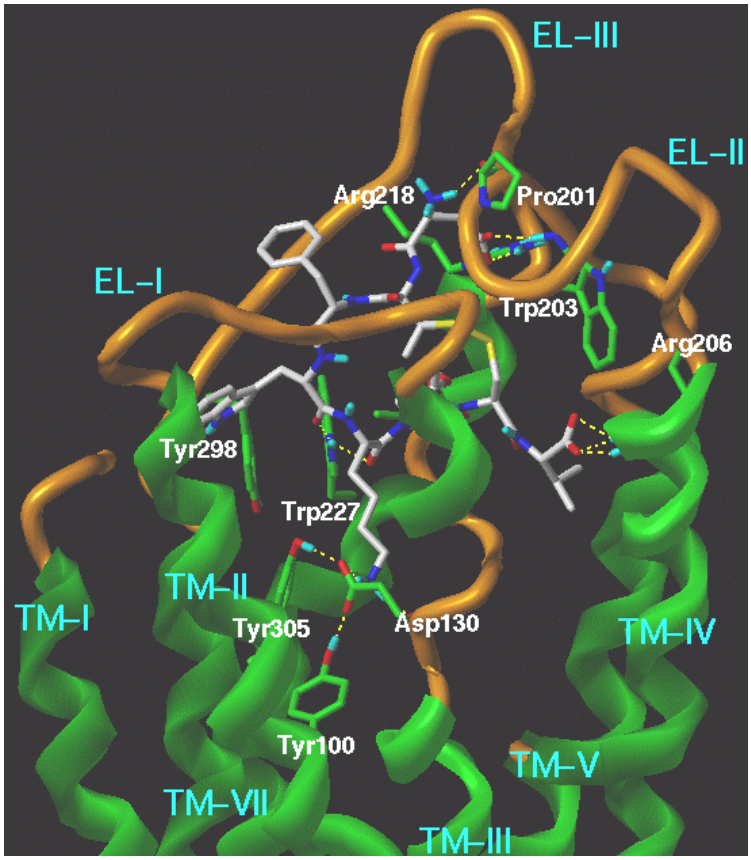

Fig. 1. Detailed view showing the orientation of P5U (by-atom) in the hU-IIR (green) binding site. The side chains of the hU-IIR residues that are involved in the closest contacts with the ligand are shown in stick representation. TM = transmembrane domain, IL = intracellular loop and EL = extracellular loop.

References

1. Ames, R. S. et al. *Nature* **401**, 282-286 (1999).
2. Douglas, S. A. and Ohlstein, E. H. *Trends Cardiovasc. Med.* **10**, 229-337 (2000).
3. Zampelli, E., Carotenuto, A., Grieco, P., Campiglia, P., Novellino, E. and Rovero, P. In Benedetti, E. and Pedone, C. (Eds.) *Peptides 2002 (Proceedings of the 27th European Peptide Symposium)* Edizinoni Ziino, Napoli, 2003, pp. 926-927.
4. Grieco, P., Carotenuto, A., Campiglia, P., Zampelli, E., Patacchini, R., Maggi, C. A., Novellino, E. and Rovero, P. *J. Med. Chem.* **45**, 4391-4394 (2002).
5. Palczewski, K., Kumasaka, T., Hori, T., Behnke, C. A., Motoshima, H., Fox, B. A., Le Trong, I., Teller, D. C., Okada, T., Stenkamp, R. E., Yamamoto, M., and Miyano, M. *Science* **289,** 739-745 (2000).
6. Insight II Molecular Modeling Package and Discover 2.2000 Simulation Package; MSI, Inc.: San Diego, CA.
7. Hagler, A. F., Lifson, S. and Dauber, P. *J. Am. Chem. Soc.* **101**, 5122-5130 (1979).
8. Morris, G. M., Goodsell, D. S., Halliday, R. S., Huey, R., Hart, W. E., Belew, R. K. and Olson, A. J. *J. Comput. Chem.* **19**, 1639-1662 (1998).

Peptide Revolution: Genomics, Proteomics & Therapeutics
Michael Chorev & Tomi K. Sawyer (Editors)
American Peptide Society, 2003

Structure-Activity Relationship and Bioactive Conformation of Prolactin Releasing Peptides (PrRPs), Ligand for a Potential Obesity Target

Waleed Danho, Joseph Swistok, Wajiha Khan, Theresa Truitt, Grazyna Kurylko, David Fry, David Greeley, Hongmao Sun, Mark Dvorozniak, Garry Mackie, Cheryl Spence and Robert Goodnow, Jr.

Roche Research Center, Hoffmann-La Roche Inc. Nutley, NJ 07110, USA

Introduction

Prolactin Releasing Peptide (PrRP) is a 31 amino acid peptide, H-Ser-Arg-Thr-His-Arg-His-Ser-Met-Glu-Ile-Arg-Thr-Pro-Asp-Ile-Asn-Pro-la-Trp-Tyr-Ala-Ser-Arg-Gly-Ile-Arg-Pro-Val-Gly-Arg-Phe-NH_2, discovered in 1998 as a ligand for the oGPCR10/hGR3 (Rat UHR-1) [1]. Since its original identification, PrRP has been shown to have many functions other than its weak effect on prolactin release, most prominently an anorexigenic activity. Intracerebroventricular (ICV) injection of PrRP inhibits food intake and body weight gain in rats without affecting water intake [2] Furthermore, PrRP neurons are located in regions that are known to be involved in regulation of food intake, a strong indication that PrRP has a physiological role to play in appetite and body weight control. Consequently, a potent PrRP agonist is regarded as potentially useful in the therapeutic approaches to obesity management.

The goal of this work is to identify the minimal sequence able to effect PrRP receptor agonism, and the critical amino acid residues responsible for agonist activity. In addition, NMR was used to study the conformational aspects of the PrRP peptides and define the positions of the key side chains involved in agonist activity. PrRP binds with high affinity (1 nM) to its receptor and stimulates calcium mobilization in CHOK1 cells stably transfected with the receptor. Previous studies revealed that PrRP(12-31) is equipotent to PrRP(1-31). Further N-terminal truncations reduce the affinity of the ligand although PrRP(25-41) is still able to compete for binding and behaves as an agonist [3].

Results and Discussion

75 analogues were synthesized by solid phase peptide synthesis. The peptides were tested in the functional cell-based assay for agonist activity in calcium flux assay with the FLIPR instrument. Figure 1 (A) illustrates that PrRP(25-31) still behaved as agonist with only two fold reduction of potency, confirming the results by Roland et al. [3]. Further deletion resulted in inactive peptides; however N-capping with Ac or pentyl restored the agonist activity with only 4 fold reduction of activity. Figure 1 (B) presents the Ala-scan, which indicates drastic reduction of agonist activity upon replacement of Arg26, Pro27, Val28, Arg30, or Phe31. Since the Ala scan proves the importance of Arg26 and Arg30, we substituted the Arg in both positions with Lys, Cit, 3-aminomethyl phenylglycine, 2-amino-4-guanidino-butyric acid and 2-amino-3-guanidino-propanoic acid [Figure 1 (C)]. The agonist activity was completely lost by such changes at position Arg30 and diminished at position 26. Arg26 can be replaced with Phe resulting in only a 4-fold reduction of agonist activity. Since the C-terminal portion is well defined, adopting one full helical turn preceded by a kink, it is important to determine the contribution of various NH group in stabilization of the structure. An N-methyl scan of PrRP(24-31) indicated that the NH groups of Gly29, Arg30, and

Phe31, play critical roles [Figure 1(D)]. N-methyl Ala in position 27 also causes reduction in activity.

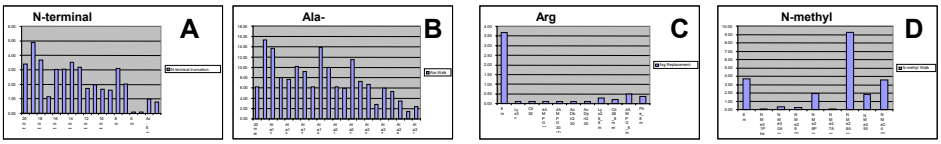

Fig. 1. PrRP-SAR summary (1/IC_{50} μM).

NMR studies: The solution structure of PrRP(12-31), as determined by NMR, reveals an L- shaped molecule. The N-terminal portion appears to be flexible and exhibits no regular type of secondary structure. The C- terminal portion is well defined and adopts a conformation consisting of one full helical turn preceded by a kink (Figure 2). This helical structure brings together the side chains of the important residues Arg26, Val28, and Phe31 to form a hydrophobic cluster. The side chain of the critical Arg30 points opposite to this cluster. In this structure the important residues are within 10-15 Å of each other (Figure 3).

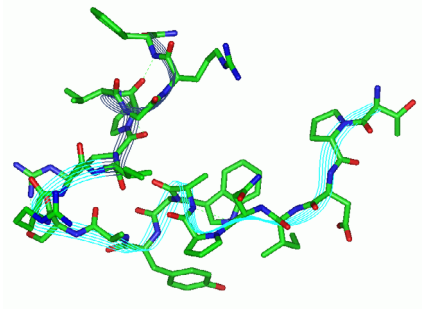

Fig. 2. Solution structure of PrRP(12-31).

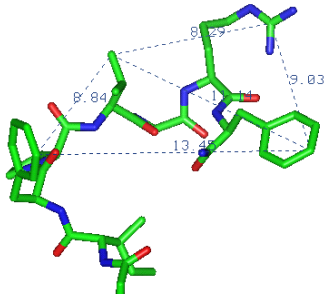

Fig. 3. Distances between key residues.

Conclusions

We identified the smallest agonist peptide fragment: Ac-Arg-Pro-Val-Gly-Arg-Phe-NH_2(26-31), as well as the critical amino acids responsible for agonist activity (Arg26, Pro27, Val28, Arg30, Phe31). It is clear that the C-terminal portion is well-defined and adopts a conformation consisting of one full helical turn preceded by a kink. This helical structure brings together the side chains of the important residues Arg/Phe26, Val28, and Phe31 to form a hydrophobic cluster. The side chain of the critical Arg30 points opposite to this cluster. The important residues are within 10-15 Å of each other. We have confirmed and reported the *in vivo* activity (ICV) reduction of food intake of PrRP(1-31), (12-31) and (25-31) [3].

References

1. Hinuma, S., Habata, Y., Fuji, R., Kawamata, Y., Hosoya, M., Fukusumi, S., Kitada, C., Masuo, Y., Asano, T., Matsmoto, H., Sekiguch, M., Kurokawa, T., Nishmura, O., Onda, H. and Fujino, M. *Nature* **393**, 272-276 (1998).
2. Lawrence, C. B., Celsi, F. Brennand, J. and Luckma, S. M. *Nat. Neurosci.* **3**, 645-646 (2000).
3. Roland, B., Sutton, S. W., Wilson, S. J., Luo, L., Pyati, J., Huvar, R., Erlander, M. G. and Lovenberg, T. W. *Endocrinology* **140,** 2736-2745 (1999).

Peptide Revolution: Genomics, Proteomics & Therapeutics
Michael Chorev & Tomi K. Sawyer (Editors)
American Peptide Society, 2003

Synthesis and Conformational Behavior of the First Extracellular Loop Peptide of a GPCR

Sanjay K. Khare[1], Boris Arshava[1], Jeffery M. Becker[2] and Fred R. Naider[1]

[1]*Department of Chemistry, College of Staten Island of CUNY, Staten Island, NY 10314, USA;*
[2]*Department of Microbiology, University of Tennessee, Knoxville, TN 37996, USA*

Introduction

The G protein-coupled receptor (GPCR) family is one of the largest and most diverse groups of eukaryotic proteins, is involved in many physiological processes, and is an attractive target for pharmacological intervention to modify these processes in normal and pathological states. Recently, the structure of rhodopsin was solved and opens new avenues to explore hidden facts about this class of integral membrane proteins [1]. Nevertheless, little information is available on the structure or function of extracellular loop peptides of GPCRs. A number of laboratories initiated investigations on peptides related to extracellular and intracellular loop regions of GPCRs, providing new information on the structure and the ligand binding sites of these receptors [2,3]. We reported that during the induction of the mating response pathway in *Saccharomyces cerevisiae,* the first extracellular loop of Ste2p, a peptide pheromone binding GPCR, plays an important role in the activation of the signal transduction pathway [4]. To understand more precisely the conformational changes and biological function of this GPCR loop, we carried out synthesis and biophysical studies of linear and constrained peptides corresponding to the first extracellular loop of Ste2p (residues 103-132, with two extra cysteine residue at both ends and a glycine at the C-terminal, **C**^{103}LSNYSSVTYALTGFPQFISR GDVHVYGAT ^{132}N**CG**).

Results and Discussion

Peptides were synthesized using a standard Fmoc/Bu^t procedure. Cyclization of the linear peptide was carried out using DMSO mediated oxidation. After RP-HPLC purification, products of over 99% homogeneity were isolated and characterized by ESI-MS (linear peptide, MW calcd: 3526.94; Found: 3527.47 and cyclic peptide, MW calcd: 3524.94; Found: 3525.54).

The goal of the synthesis of this peptide was to restrict the chain ends at a distance (10Å to 14Å) that corresponds to the distance calculated between the point at which the loop exits and enters the membrane based on the rhodopsin structure. CD and NMR studies on the linear peptide were performed in water and in membrane mimetic media, including aqueous trifluoroethanol and DPC micelles. The CD spectrum of linear and cyclic 33E1$^{103\text{-}132}$ peptides in water and DPC micelles showed that these molecules exhibited different degrees of structure in these solvents (Figure 1). As judged by the intensities of the characteristic double minima near 221 and 206 nm, both the linear and cyclic loop surrogates were partially helical in the presence of DPC micelles. In contrast, the 33E1$^{103\text{-}132}$ linear and constrained peptide were disordered in an aqueous medium. Due to poor solubility and aggregating tendency of this peptide in aqueous and several membrane mimetic environments, limited success was obtained using NMR spectroscopy. Further studies are in progress to reveal the detailed conformational behavior of these loop peptides.

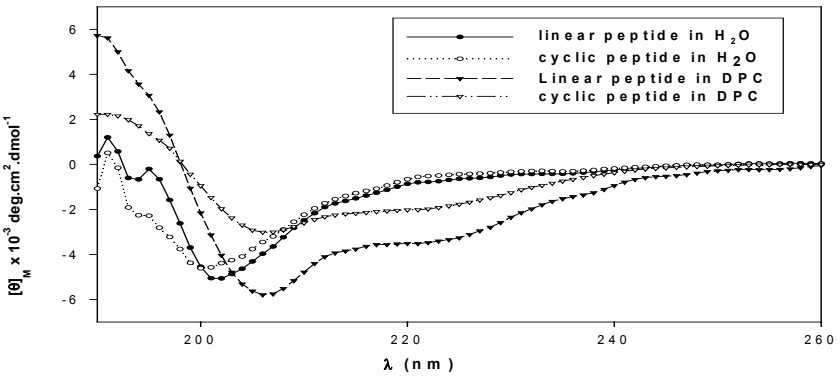

Fig. 1. CD of 33E1[103-132] linear and constrained peptides in water and DPC micelle at 25°C.

Acknowledgments

This work was supported by Grants GM 22086 and GM22087 from the National Institutes of Health

References

1. Palczewski, K., Kumasaka, T., Hori, T., Behnke, C. A., Motoshima, H., Fox, B. A., Trong, L. T., Tellar, D. C., Okada, T., Stenkamp, R. E., Yamamoto, M. and Miyano, M. *Science* **289**, 739-745 (2000).
2. Yeagle, P. L., Choi, G. and Albert, A. D. *Biochemistry* **40**, 11932-11937 (2001).
3. Giragossian, C. and Mierke, D. F. *Biochemistry* **40**, 3804-3809 (2001).
4. Akal-Strader, A., Khare, S. K., Xu, D., Naider, F. and Becker, J. M. *J. Biol. Chem.* **34**, 30581-30590 (2002).

Peptide Revolution: Genomics, Proteomics & Therapeutics
Michael Chorev & Tomi K. Sawyer (Editors)
American Peptide Society, 2003

Biosynthesis of the Sixth Transmembrane Domain of the S*accharomyces cerevisiae* α-Factor Receptor

Racha Estephan[1], Enrique Arevalo[1], Jeffrey M. Becker[2] and Fred Naider[1]

[1]Department of Chemistry, The College of Staten Island of the City University of New York, Staten Island, NY 10314, USA; [2]Department of Microbiology, University of Tennessee, Knoxville, TN 37996, USA

Introduction

GPCRs have been found in a wide range of organisms and they mediate cellular responses to extracellular signals such as physical stimuli, hormones, and neurotransmitters [1-5]. Analysis of the yeast α-factor mating pheromone receptor Ste2p indicates it is a member of the GPCR family. Mutation of Pro-258 in transmembrane domain (TM) 6 constitutively activates Ste2p [6, 7]. The P258L mutation is predicted to alter the structure of TM domain 6 (M6). Greater than 90% of all GPCRs contain a proline residue at a similar position in M6, suggesting that this aspect of receptor activation may be conserved in other receptors [7].

Wild-type and mutant (P258L) M6, Ste2p residues 238-270, were biosynthesized as fusion proteins using histidine-tagged TrpΔLE leader peptide as the N-terminus. The TrpΔLE directed the production of the fusion protein into inclusion bodies. The wild-type ^{15}N-labeled M6 fusion protein (^{15}N-M6FP) and the unlabeled constitutive mutant M6 fusion protein (M6FP(P258L)) were expressed, purified with HPLC, and then cleaved with cyanogen bromide (CNBr) at a methionine residue to remove the TrpΔLE. The cleaved fusion proteins were purified further with HPLC and the molecular weights of the ^{15}N-labeled M6 (^{15}N-M6) and unlabeled-M6(P258L) peptides were confirmed by mass spectrometry.

Results and Discussion

E. coli BL21(DE3)pLysS cells were transformed with pSW02 or pSW02M plasmids. pSW02 and pSW02M plasmids express wild-type and mutant M6FP(P258L), respectively. A single colony of the transformed cells was inoculated into 5 mL of LB medium containing ampicillin and chloramphenicol. The cells were allowed to grow at 37°C to late log phase (OD_{600} ~ 0.7). Two milliliters of the grown culture were then harvested at 6000 rpm for 3 min and inoculated into 250 mL of M9 minimal medium. The cells were grown overnight at 37°C to late log phase (OD_{600} ~ 0.7). Cells were then induced with 1 mM IPTG, incubated for 6 h, and harvested by centrifugation. Time course of expression was performed in order to optimize the time of expression.

The wild-type ^{15}N-M6FP containing M6 region of Ste2p (^{15}N-M6FP), which included the mutation Met250Ala and the addition of one non-natural lysine on each side of the natural sequence, exhibited decent expression properties (Figure 1). The ^{15}N-M6FP has a molecular weight of 17.542 kDa (Figure 1). The mutant M6FP(P258L) exhibited similar expression properties to those of the wild-type (data not shown). Biosynthesis, isolation, and purification of ^{15}N-M6FP were optimized to yield about 10 mg (> 90% homogeneous) of fusion protein/liter of bacterial culture in minimal medium. The TrpΔLE leader peptide was released from ^{15}N-M6FP by cleavage at a methionine residue with CNBr. The ^{15}N-M6FP cleavage was optimized and analyzed by RP-HPLC. Optimum cleavage of ^{15}N-M6FP was obtained with 1M CNBr for 24 hrs of cleavage at room temperature in the dark. After releasing the TrpΔLE, ^{15}N-M6 peptide was purified using a preparative C18 RP-HPLC column.

Cleavage of ^{15}N-M6FP yielded 1mg of ^{15}N-M6 peptide (> 90% homogeneous) / 8 mg of cleaved fusion protein. Its ^{15}N-edited HSQC spectrum indicated a uniform incorporation of the label throughout the peptide (data not shown). Biosynthesis of ^{15}N-labeled mutant (P258L) M6 peptide is being optimized.

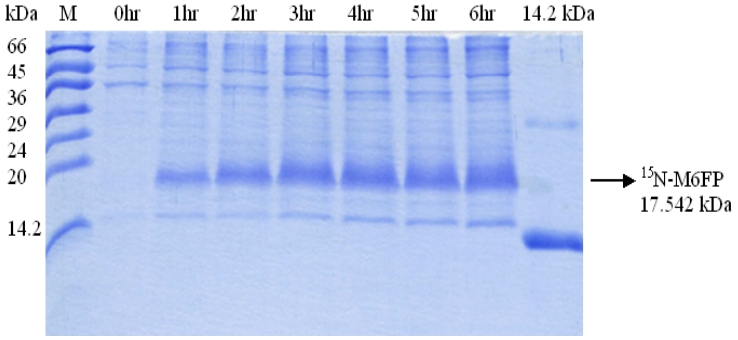

Fig. 1. SDS-PAGE of the expression of ^{15}N-labeled M6 fusion protein in Escherichia coli. *Lane 1 corresponds to molecular weight markers: 66, 45, 36, 29, 24, 20, 14.2 kDa. Lanes 2 through 8 correspond to the solubilized inclusion bodies of ^{15}N-labeled M6 fusion protein from 0-6 h expression. Lane 9 is a 14.2 kDa marker. The arrow indicates the expressed ^{15}N-labeled M6 fusion protein. The gel was stained with Coomassie dye.*

Acknowledgments

This work was supported by Grants GM22086, GM22087, and GM22086-27S1 from the National Institute of Health and by the New York City Louis Strokes Alliance for Minority Participation (NYC LS-AMP) in Research from the National Science Foundation.

References

1. Strader, C. D., Fong, T. M., Graziano, M. P. and Tota, M. R. *FASEB J.* **9**, 745-754 (1995).
2. Strader, C. D., Fong, T. M., Tota, M. R., Underwood, D. and Dixon, R. A. F. *Annu. Rev. Biochem.* **63**, 101-132 (1994).
3. Venter, J. C. and 284 others. *Science* **291**, 1304-1351 (2001).
4. Lander, E. S. and 248 others. *Nature* **409**, 860-921 (2001).
5. Baldwin, J. M. *The EMBO Journal* **12**, 1693-1703 (1993).
6. Dube, P. and Konopka, J. B. *Mol. Cell. Biol.* **18**, 7205-7215 (1998).
7. Konopka, J. B., Margarit, S. M. and Dube, P. *Proc. Natl. Acad. Sci. U.S.A.* **93**, 6764-6769 (1996).

Peptide Revolution: Genomics, Proteomics & Therapeutics
Michael Chorev & Tomi K. Sawyer (Editors)
American Peptide Society, 2003

Studies on the Cross-reactivity of Synthetic Oxytocin Receptors Prepared by Molecular Imprinting

Maria Kempe

Department of Cell and Molecular Biology, Biomedical Center, B12, Lund University, SE-221 84 Lund, Sweden

Introduction

Molecular imprinting is attracting a wide interest as a method for the production of nanostructured materials capable of molecular recognition. Molecularly imprinted polymers (MIPs) have found application as stationary phases for chromatographic separations and solid-phase extractions, *in vitro* antibody mimics, recognition elements in sensors, matrices for drug delivery, and catalysts of chemical reactions. The recognition sites are tailor-made *in situ* by self-assembly of functionalized monomer(s) and templates followed by copolymerization with cross-linkers to form a polymer network. The templates are subsequently extracted from the network, leaving recognition sites complementary in the positioning of functional groups and in shape. The sites recognize and rebind the template molecules upon exposure.

MIPs selective for oxytocin have previously been reported [1,2]. In this study, the cross-reactivity of these recognition sites was investigated.

Results and Discussion

MIPs were synthesized as previously described by radical bulk polymerization in acetonitrile with methacrylic acid as the functionalized monomer, trimethylolpropane trimethacrylate as the cross-linker, and Z-oxytocin as the template [2]. Competitive binding curves were determined in a radioligand binding assay using ^{3}H-labeled oxytocin and non-radioactive oxytocin and analogs as the competitors (Figure 1). EC_{50} values and cross-reactivities were calculated from these data (Table 1).

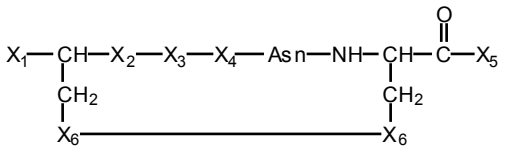

	Ligand	X_1	X_2	X_3	X_4	X_5	X_6
1	Oxytocin	H_2N	Tyr	Ile	Gln	Pro-Leu-Gly-NH_2	S
2	[Asu^{1,6}]-oxytocin	H	Tyr	Ile	Gln	Pro-Leu-Gly-NH_2	CH_2
3	AVP	H_2N	Tyr	Phe	Gln	Pro-Arg-Gly-NH_2	S
4	Atosiban	H	D-Tyr(Et)	Ile	Thr	Pro-Orn-Gly-NH_2	S
5	DDAVP	H	Tyr	Phe	Gln	Pro-D-Arg-Gly-NH_2	S
6	Tocinoic amide	H_2N	Tyr	Ile	Gln	NH_2	S
7	Z-[Abu^{1,6}]-oxytocin	Z-NH	Tyr	Ile	Gln	Pro-Leu-Gly-NH_2	CH_3

Fig. 1. Structure of oxytocin and analogs. Peptides 1-6 are cyclic. Peptide 7 is linear.

Table 1. EC_{50} values and cross-reactivities.

	Ligand	EC_{50} (μM)	Cross-reactivity (%)
1	Oxytocin	0.4	100
2	[Asu^{1,6}]-oxytocin	4.1	9.8
3	AVP	23.9	1.7
4	Atosiban	30.1	1.3
5	DDAVP	45.9	0.9
6	Tocinoic amide	169.8	0.2
7	Z-[Abu^{1,6}]-oxytocin	*No competition*	

As expected, oxytocin (**1**) was the best ligand for the MIP synthetic receptor. AVP (**3**) differs from oxytocin in residues 3 and 8 (Phe and Arg substitute Ile and Leu, respectively). Some cross-reactivity was observed when AVP was competing for the recognition sites. The des-amino analog DDAVP (**5**) contains D-Arg in position 8. The cross-reactivity of this compound was slightly lower than that observed for AVP.

Compared to oxytocin, Atosiban (**4**) lacks the N-terminal amino group, the Tyr in position 2 is of D-configuration and its side chain is protected by an ethyl ether, the 4th residue is Thr instead of Gln, and Orn replaces Leu in position 8. Some cross-reactivity was seen with Atosiban.

Tocinoic amide (**6**) is identical to the cyclic portion of oxytocin, but lacks the three residues at the C-terminal. Some cross-reactivity was observed when tocinoic amide was the competitor.

In [Asu^{1,6}]-oxytocin (**2**), the disulfide bridge has been replaced by an ethylene bridge and the N-terminal amino group is missing. This analog was a fairly good competitor to oxytocin for the MIP binding sites. In the linear peptide Z-[Abu^{1,6}]-oxytocin (**7**), the cysteines have been replaced by 2-aminobutyric acid. No competition was observed with this analog within the concentration range investigated. Hence, the cyclic structure of the ligand seems to be required for recognition by the oxytocin imprinted MIP.

Acknowledgments

This work was supported by the Swedish Research Council and the Swedish Foundation for Strategic Research (Individual Grant for the Advancement of Research Leaders).

References

1. Kempe, M. In Fields, G. B., Tam, J. P. and Barany, G. (Eds.) *Peptides for the New Millenium (Proceedings of the 16th American Peptide Symposium)* Kluwer Acadmic Publishers, Dordrecht, The Netherlands, 2000, 534-535.
2. Kempe, M. *Lett. Peptide Science* **7**, 27-33 (2000).

Peptide Revolution: Genomics, Proteomics & Therapeutics
Michael Chorev & Tomi K. Sawyer (Editors)
American Peptide Society, 2003

Does a π-Cation Interaction Stabilize the Rhodopsin-Bound Conformation of Transducin's Alpha-Subunit?

Matthew A. Anderson, Rieko Arimoto, Wei Sha and Garland R. Marshall

Department of Biochemistry and Molecular Biophysics, Washington University School of Medicine, St. Louis, MO 63110, USA

Introduction

The C-terminal undecapeptide of transducin's α-subunit, $G_t\alpha(340\text{-}350)$, has been shown to stabilize light-activated rhodopsin (R*) as does the whole G-protein transducin (G_t). From the TrNOE-determined structure of the R*-bound peptide [1], we observe that the ε-amino group of Lys^{341} is in close proximity (~3.1 Å) to the phenyl ring of Phe^{350} suggesting a possible π-cation interaction stabilizing the structure. To investigate this hypothesis, we synthesized a series of $G_t\alpha$-peptide analogs with various electron-withdrawing and electron-donating substituents on the phenyl ring of Phe^{350}. One set of peptide analogs contained a C-terminal carboxamide modification of Phe^{350} while another retained the carboxylate to determine the impact of an adjacent salt bridge.

Carboxylates:
H-Ile-Lys-Glu-Asn-Leu-Lys-Asp-Cys-Gly-Leu-Xxx-OH
Xxx = Tyr (**1**); Trp (**2**); Phe(*p*-F) (**3**); Phe(*p*-NH_2) (**4**); Phe(*p*-NO_2) (**5**); Cha (**6**)
Carboxamides:
H-Ile-Lys-Glu-Asn-Leu-Lys-Asp-Cys-Gly-Leu-Xxx-NH_2
Xxx = Phe(*p*-NO_2) (**7**); Phe(F_5) (**8**); Tyr (**9**); Tyr(Me) (**10**); 2-Nal (**11**); Phe(*p*-t-butyl) (**12**); Cha (**13**); Phe (**14**)

Fig. 1. Sequences for synthesized peptide analogs. (2-Nal = 2-napthylalanine).

Results and Discussion

Two series of α-peptide analogs with various substituents on the aromatic side-chain of Phe^{350} were synthesized: with electron-donating groups, i.e. Tyr (**1**,**9**), Phe(*p*-NH_2) (**4**), Trp (**2**), Tyr(Me) (**10**), and Phe(*p*-t-butyl) (**12**); with electron-withdrawing groups, i.e. Phe(*p*-F) (**3**), Phe(F_5) (**8**), and Phe(*p*-NO_2) (**5**,**7**); with an extended π-system, i.e. 2-Nal (**11**), and without a π–system, i.e. Cha (**6**,**13**). The proposed π-cation interaction involves an interaction between the side chain ε-NH_3^+ of Lys^{341} and the aromatic ring of Phe^{350}. If this interaction exists, varying the strength of this interaction should be observable in binding-affinity measurements. A stronger interaction would constrain the peptide into a more favorable binding conformation and stabilize the cation in the hydrophobic pocket of the binding site; a weaker interaction would have the opposite effect. Studies with the carboxylate series of analogs did not show the expected correlation between binding affinity and electronic effect. Instead, we observed a strong correlation with the hydrophobicity of the side chain at residue 350. Highly hydrophilic substituents lost affinity, i.e. Tyr (**1**) and Phe(*p*-NH_2) (**4**). Phe(*p*-F) (**3**), Trp(**2**), and Phe(*p*-NO_2) (**5**) retained affinity due to similar hydrophobic side chains. Cha (**6**) has the most hydrophobic side chain and showed a 1.5-fold increase in affinity over native peptide. These results indicated that the proposed π-cation interaction is not significantly contributing to the stability of the bound conformation of the peptide. A recent study by Bartoli and Roelens [2] has shown that the strength of the counter-

anion in a π-cation complex can effect the interaction energy between the π-system and a cation. The authors estimated that the free energy of a π-system with acetate as the counter ion is only 0.62 kcal/mol. Since we postulate that our binding-affinity assay allows us to observe a change in energy of approximately 1-2 kcal/mol, it is no surprise that the initial studies did not correlate binding affinity with aromatic electronic density.

Based on this information, we theorized that blocking the carboxylate of residue 350 as the carboxamide would allow us to observe the expected electronic character correlation with measured affinities. We synthesized a series of eight analogs with varying substituents on the aromatic ring of Phe[350] and a carboxamide at the C-terminus. The binding affinities of this series showed a positive correlation with the electronic character of the aromatic ring at residue 350 (Figure 2). Analogs with electron-withdrawing substituents Phe(*p*-NO_2) (**7**) and Phe(F_5) (**8**) retained only 53% and 38% of affinity respectively. Those analogs with electron-donating substituents had comparable or increased binding affinity over native peptide; Tyr (**9**), Tyr(Me) (**10**), and Phe(*p*-t-butyl) (**12**). 2-Nal (**11**) and Phe (**14**) displayed enhanced binding affinities of 1.66 fold and 1.97 fold respectively. Cha (**13**), the analog without a π-system also showed enhanced binding affinity of 2.09 fold.

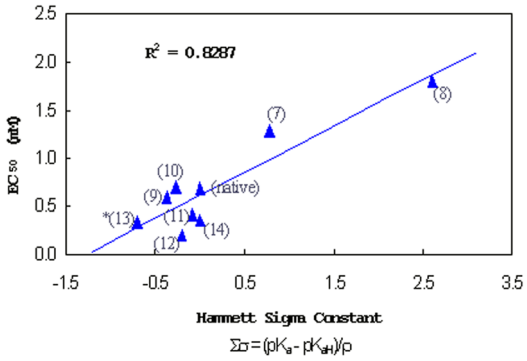

Fig. 2 Binding affinity vs. Electronic character of π-system. Hammett sigma constant values were calculated from experimental pKa values.

Analysis of these data leads us to conclude that a π-cation interaction is present in these analogs and can contribute to the stabilization of the bound conformation of the peptides as observed with the carboxamide analogs. However, it is evident that in the native peptide and the carboxylate series of analogs, the adjacent salt-bridge interaction between the carboxylate of Phe[350] and the ε-amine of Lys[341] significantly reduces the amount of stabilization provided by the π-cation complex. Further investigation of this phenomenon is underway with the synthesis of $G_t\alpha$(340-350) analogs lacking a carboxylate at the C-terminus.

Acknowledgments

The authors acknowledge support for this research from NIH grant EY12113.

References

1. Kisselev, O. G. et al. *Proc. Natl. Acad. Sci. U. S. A.* **95**, 4270-4275 (1998).
2. Bartoli, S. and Roelens, S. *J. Am. Chem. Soc.* **124**, 8307-8315 (2002).

Peptide Revolution: Genomics, Proteomics & Therapeutics
Michael Chorev & Tomi K. Sawyer (Editors)
American Peptide Society, 2003

Novel Peptide Therapeutic Approaches for Immune Tolerance

Stephanie D. Allen[1,2], Heike Bernert[2,3], Sharad V. Rawale[2], Anne M. VanBuskirk[4] and Pravin T.P. Kaumaya[1,2,5]

[1]The Ohio State Biochemistry Program; [2]Department of Obstetrics and Gynecology; [3]Department of Molecular Virology, Immunology, and Medical Genetics; [4]Department of Surgery; [5]Department of Molecular and Cellular Biochemistry, The Ohio State University, Columbus, OH 43210, USA

Introduction

There are currently over 80,000 people in the United States on the waiting list for an organ transplant. One of the most serious concerns facing patients that actually receive an organ transplant is the possibility of rejection after transplantation. Activated T cells predominantly mediate acute transplant rejection. Preventing or blocking T cell activation is the focus of much transplant research. Complete T cell activation requires two distinct signals. The first signal consists of the interaction between the T cell receptor (TCR) on the T cell, and the major histocompatibility complex (MHC) that contains the antigenic peptide on the antigen presenting cells (APC). The second signal comes from costimulatory molecules found on both the T cell and the APC. Most strategies attempt to block this second signal to force T cells into an anergic state, which inactivates the T cells and prevents a response to antigen stimulation [1].

One of the most well studied costimulatory pathways is the CD28:B7 pathway, with CD28 located on T cells and B7 located on APC. Traditionally, this pathway has been blocked by using antibodies or fusion proteins [2]. While these methods work, they also have potential side effects stemming from inherent immunogenicity, poor ability to penetrate tissue barriers, and the possibility for unwanted Fc receptor signaling. Peptide therapy offers a realistic solution to these side effects. By producing peptides mimicking the binding regions of costimulatory molecules, we are able to minimize the molecular weight and immunogenicity of the peptides. Previous studies by our laboratory have shown that a 20 residue peptide mimic of the CD28 peptide containing the conserved hexapeptide 'MYPPPY' motif is able to prevent disease induction and ameliorate established disease in the transgenic mouse model of multiple sclerosis [3]. We have developed peptide mimics with elongated half-lives by retro-inverso modifications of the peptide using D-amino acids to conserved overall peptide topology.

Results and Discussion

Table 1 depicts a summary of the peptides used in this study. The results of the *in vitro* half-life assay indicated that the ELCD28 synthesized with L-amino acids was degraded more rapidly than the RICD28 peptide synthesized with D-amino acids. This is an indication that the RICD28 peptide is resistant to proteolysis, and should have a longer half-life *in vivo*, circumventing one of the largest drawbacks to peptide therapy (Figure 1). To evaluate the ability of the CD28 peptides to block the activation of T cells by allogeneic challenge, the peptides were tested by a mixed lymphocyte reaction assay. In this assay, the Balb/c lymphocytes are irradiated to prevent proliferation, and C57BL/6 (B6) lymphocytes are allowed to respond to the antigenic stimulation of the Balb/c lymphocytes. Addition of our peptide to the mixture of cells determines the peptide's blocking ability. Our results show that both the EL- and the RICD28 have blocking ability *in vitro,* with percent reduction ranging from 22.3-84.6% at peptide

Table 1. Amino acid sequences of the synthetic CD28 and control peptides.

Abbreviation	Amino Acid Sequence
ELCD28	CH_3CO***L***[K-I-E-F-M-Y-P-P-P-Y-L-D-N-E-R-S-N-G-T-I]$CONH_2$
RICD28	CH_3CO***D***[I-T-G-N-S-R-E-N-D-L-Y-P-P-P-Y-M-F-E-I-K]$CONH_2$
RLCD28	CH_3CO***L***[I-T-G-N-S-R-E-N-D-L-Y-P-P-P-Y-M-F-E-I-K]$CONH_2$

L *and* ***D*** *refer to L and D amino acids, respectively.*

concentrations of 200 and 400 μM. This inhibition of *in vitro* alloreactivity is statistically significant ($p<0.05$) as determined by t-test.

The peptides have also been tested *in vivo*, in an allogeneic J558 tumor model. Mice were depleted of their $CD8^+$ T cells, forcing rejection into the CD4 pathway. J558 tumor cells were injected subcutaneuosly into syngeneic Balb/c and allogeneic B6 mice. B6 mice also received ELCD28, RICD28, or RLCD28 peptides (500μg i.v. on day of tumor injection). Tumor growth was monitored for 19 days. Large tumors progressively grew in all Balb/c mice. Only 1 of 4 control B6 mice grew a tumor >5mm in diameter, and was rejecting at the time of harvest. Two of 5 ELCD28, 2 of 5 RICD28 and all RLCD28 treated B6 mice grew tumors greater than 5mm in diameter. Interestingly, although RL CD28 treated mice grew tumors, these tumors were rapidly decreasing in size at the time of harvest. In the EL- and RI-CD28 treated groups, one tumor was rejecting and one progressivley growing at the time of harvest. Tumor rejection is typically mediated by $CD8^+$ T cells, but can also be mediated by $CD4^+$ T cells. By blocking the CD28-B7 pathway, rejection is stopped in CD8-depleted B6 mice. It is thought that antibody formation to the tumor cells may mediate ultimate rejection of the tumor, but this is still under investigation.

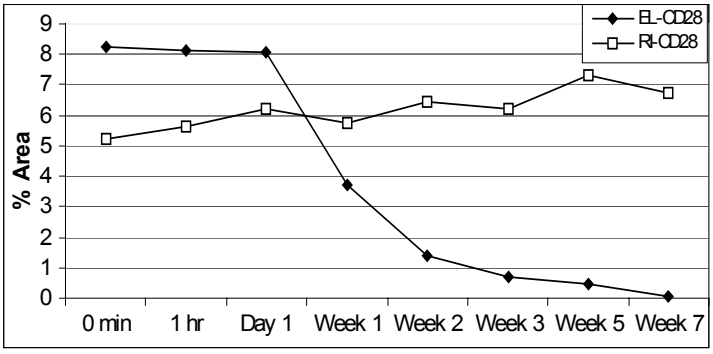

Fig. 1. Percent peak area over time.

Acknowledgements
The research is funded by NIH Grant AI 49875-01 to P.T.P.K.

References

1. Judge, T. A., Wu, Z., Zheng, X. G., Sharpe, A. H., et al. *J. Immunol.* **162**, 1947-1951 (1999).
2. Newell, K. A., He, G., Guo, Z., et al. *J. Immunol.* **163**, 2358-2362 (1999).
3. Srinivasan, M., Gienapp, I. E., et al. *J. Immunol.* **169**, 2180-2188 (2002).

Protein Aggregation
Substrate/Inhibitor
Structure-Function

Peptide Revolution: Genomics, Proteomics & Therapeutics
Michael Chorev & Tomi K. Sawyer (Editors)
American Peptide Society, 2003

Primary–Quaternary Structure Relationships Controlling Early Aβ Oligomerization

Gal Bitan, Marina D. Kirkitadze, Hilal A. Lashuel, Sabrina S. Vollers and David B. Teplow

Center for Neurologic Diseases, Brigham and Women's Hospital and Harvard Medical School, Boston, MA 02115, USA

Introduction

Assembly of the amyloid β-protein (Aβ) into neurotoxic oligomers and amyloid fibrils is a pathologic event which leads to the development of Alzheimer's Disease (AD). Aβ is produced from its precursor, the amyloid β-precursor protein (AβPP), by two sequential endoproteolytic events. Studies of structure–activity relationships among fibril assembly intermediates have revealed that many intermediates, ranging from dimers and trimers to protofibrils, are neurotoxic. These oligomers may, in fact, be the proximal effectors of neuropathogenesis in AD [1] (space limitations prevent us from citing all the appropriate references).

The predominant forms of Aβ found in brains of AD patients are 40 and 42 amino acids long (designated Aβ40 and Aβ42, respectively). Despite the small primary structure difference between them, i.e., the dipeptide Ile^{41}-Ala^{42}, the clinical and biophysical behaviors of the two Aβ alloforms are distinct. Oligomeric Aβ42 has been shown to be toxic at nanomolar levels to neuronal cells *in vitro*, whereas Aβ40 oligomers are significantly less toxic [2].

The biophysical characterization of Aβ oligomers has been difficult due to their metastable nature, and to co-existence of multiple oligomeric species. We have shown that the oligomer size distribution of Aβ could be effectively studied by using Photo-Induced Cross-linking of Unmodified Proteins (PICUP) [3]. Utilizing this methodology, we have recently shown that the oligomer size distributions of Aβ40 and Aβ42 were distinct [4]. Aβ40 exists as an equilibrium among monomer through tetramer, whereas Aβ42 preferentially forms pentamers and hexamer units (paranuclei) which self-associate into larger oligomers. Morphologic studies supported the differences between Aβ40 and Aβ42 found by PICUP [4]. Examination of the oligomer size distributions of Aβ(1-x) (x = 39-43) demonstrated that Ile^{41} was critical for formation of paranuclei and Ala^{42} was required for paranucleus self-association [4].

Results and Discussion

Here we sought to elucidate further the relationship between the primary structure of Aβ and its early oligomerization. Systematic substitution of Ile^{41} and Ala^{42} by smaller or larger residues revealed that the side-chain in position 41 was important both for formation of paranuclei and for their association into larger assemblies (Figure 1). Substitution of Ile^{41} by Gly yielded a distribution which was qualitatively similar to that of Aβ40 [3]. When Ile^{41} was substituted by Ala the distribution appeared to be a composite of Aβ40- and Aβ42-like distributions. Substitution of Ile^{41} by Val or Leu supported paranucleus formation but not self-association of paranuclei. Substitution of Ala^{42} by Gly or Val had little effect on formation of paranuclei. However, high molecular weight oligomers (~30-60 kDa) were not observed for [Gly^{42}]Aβ42, demonstrating a role for the methyl side-chain of Ala^{42} in the self-association of paranuclei. When the C-terminal carboxyl group was replaced by a carboxamide, a

substantial increase in the abundance of high molecular weight oligomers was seen. Thus, hydrophobic interactions involving the side-chains in residues 41 and 42 appear to be a driving force in the association of Aβ42 paranuclei into higher oligomers, whereas the C-terminal carboxylate anion moderates this assembly step.

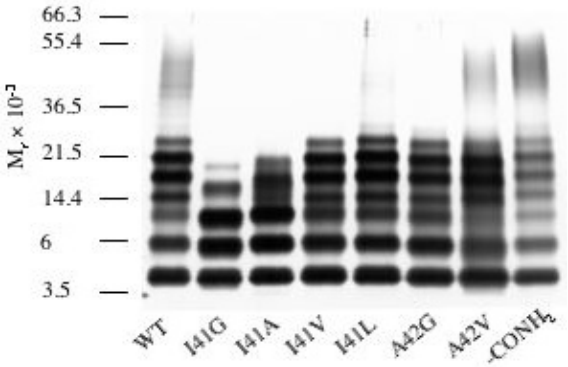

Fig. 1. Effects of C-terminus structure on paranucleus formation and assembly. PICUP was applied to LMW Aβ42 analogues containing the modifications Ile^{41}→Gly, Ile^{41}→Ala, Ile^{41}→Val, Ile^{41}→Leu, Ala^{42}→Gly, Ala^{42}→Val, or Aβ42-carboxamide. WT Aβ42 was used as control. Molecular weight markers are shown on the left.

Substitutions at or near the central hydrophobic cluster (CHC) of Aβ have been associated with cases of familial AD (FAD) [5]. The mechanism by which these substitutions cause disease is not well understood. To test whether FAD-related mutations alter early Aβ oligomerization we synthesized Aβ analogues, ending at both position 40 and position 42, containing the substitutions Ala^{21}→Gly (Flemish), Glu^{22}→Gly (Arctic), Glu^{22}→Gln (Dutch), Glu^{22}→Lys (Italian), and Asp^{23}→Asn (Iowa). To these five naturally occurring mutations we added the substitution Phe^{19}→Pro, which has been reported to arrest Aβ fibrillogenesis [6]. The peptides were cross-linked using PICUP and the oligomer size distributions analyzed by SDS-PAGE and silver staining (Figure 2).

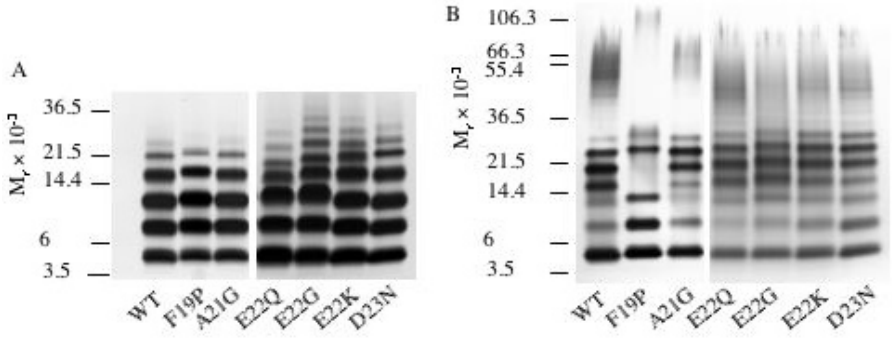

Fig. 2. Effects of central region structure on early Aβ assembly. Aβ40 (A) and Aβ42 (B) analogues were cross-linked and analyzed by SDS-PAGE/silver staining. Molecular weight markers are shown on the left of each panel.

Substitutions of the acidic residues Glu^{22} and Asp^{23} facilitated formation of higher order oligomers of Aβ40 but had little effect on Aβ42. In contrast, the substitutions of Phe^{19} or Ala^{21} altered the distribution of Aβ42. In particular, the distribution of paranuclei was narrower than for WT Aβ42 and higher order oligomers had apparent higher molecular weights. These results support the notion that Aβ40 and Aβ42

oligomerize through distinct mechanisms. Consequently, distinct residues affect each of these mechanisms.

Oxidation of Met^{35} in Aβ has been proposed to affect both Aβ toxicity [7] and Aβ oligomerization [8]. Here we examined the effect of Met oxidation on the oligomerization of both Aβ40 and Aβ42 using PICUP (Figure 3). Surprisingly, oxidation of Met^{35} in Aβ42 blocked paranucleus formation and produced oligomers indistinguishable in size (Figure 3) and morphology (data not shown) from those produced by Aβ40. Systematic structural alterations of the C_γ^{35}-substituent group revealed that its electronic nature, rather than its van der Waals volume, was the factor controlling oligomerization pathway choice. Thus, [Met^{35}(O)]Aβ42 and [$Met^{35}(O_2)$]Aβ42 produced similar oligomer size distributions, which were similar to the distribution produced by Aβ40. In contrast, when Met^{35} was substituted by norleucine (Nle) or by the bulky residue homoleucine (Hle) the observed distributions were similar to that of WT Aβ42.

Our data support the existence of distinct mechanisms controlling the initial oligomerization of Aβ40 and Aβ42. The N-terminal portion of Aβ and the charged residues Glu^{22} and Asp^{23} are particularly important for Aβ40 oligomerization, whereas Aβ42 oligomerization is most affected by the central residues Phe^{19} and Ala^{21}, and by the C-terminal residues Met^{35}, Ile^{41}, and Ala^{42}.

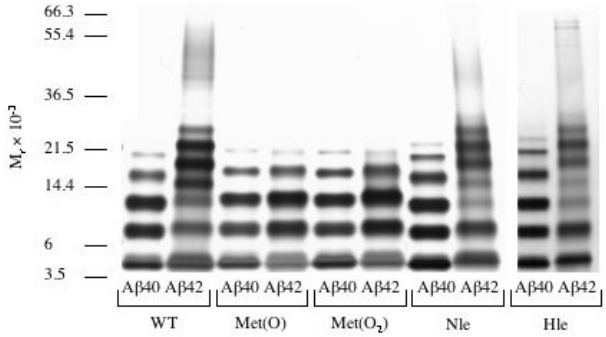

Fig. 3. Effects of residue 35 side-chain structure on Aβ oligomerization. PICUP was applied to Aβ40 and Aβ42 analogues containing the odifications Met^{35}→Met(O), Met^{35}→$Met(O_2)$, Met^{35}→Nle, and Met^{35}→Hle. WT Aβ40 and Aβ42 were used as controls.

Acknowledgments

This work was supported by grants AG14366, AG18921 and NS38328 from the National Institute of Health (DBT), by the Foundation for Neurologic Diseases (DBT) and by grant 1042312909A1 from The Massachusetts Alzheimer's Disease Research Center (GB).

References

1. Kirkitadze, M. D., Bitan, G. and Teplow, D. B. *J. Neurosci. Res.* **69**, 567-577 (2002).
2. Dahlgren, K. N., Manelli, A. M., Stine, W. B., Jr., Baker, L. K., Krafft, G. A. and LaDu, M. J. *J. Biol. Chem.* **277**, 32046-32053 (2002).
3. Bitan, G., Lomakin, A. and Teplow, D. B. *J. Biol. Chem.* **276**, 35176-35184. (2001).
4. Bitan, G., Kirkitadze, M. D., Lomakin, A., Vollers, S. S., Benedek, G. B. and Teplow, D. B. *Proc. Natl. Acad. Sci. U.S.A.* **100**, 330-335. (2003).
5. Teplow, D. B. *Amyloid: Int. J. Exp. Clin. Invest.* **5**, 121-142 (1998).
6. Wood, S. J., Wetzel, R., Martin, J. D. and Hurle, M. R. *Biochemistry* **34**, 724-730 (1995).
7. Butterfield, D. A. and Kanski, J. *Peptides* **23**, 1299-1309 (2002).
8. Palmblad, M., Westlind-Danielsson, A. and Bergquist, J. *J. Biol. Chem*. **277**, 19506-19510 (2002).

Peptide Revolution: Genomics, Proteomics & Therapeutics
Michael Chorev & Tomi K. Sawyer (Editors)
American Peptide Society, 2003

Conversion of a Natively Amyloidogenic Sequence into an Inhibitor of Amyloid Formation and Cytotoxicity Via Conformational Restriction

Aphrodite Kapurniotu[1], Andreas Buck[1], Marco Weber[1], Anke Schmauder[1], Thomas Hirsch[1], Jürgen Bernhagen[2] and Marianna Tatarek-Nossol[1]

[1]Laboratory of Bioorganic and Medicinal Chemistry; [2]Department of Biochemistry and Molecular Cell Biology, Institute of Biochemistry, University Hospital of the RWTH Aachen, D-52074 Aachen, Germany

Introduction

Alzheimer's disease (AD) is a fatal, neurodegenerative disease that currently affects about 20 million people worldwide. One characteristic feature of AD is the deposition of extracellular plaques in the brain. The AD plaques consist of fibrillar amyloid aggregates of the β-amyloid peptide (Aβ) [1]. Aβ is a 40 to 42 residue peptide which is present under normal and disease conditions in the cerebrospinal fluid and blood. Because Aβ aggregates are cytotoxic, the process of aggregation of Aβ into amyloid has been linked to the pathogenesis of AD. Aggregation of Aβ has been suggested to proceed via a transition of α-helical Aβ into β-sheets and may involve interactions between residues 18-20 of the Aβ amyloid core region. The α-helical region of Aβ is located in the extracellular, N-terminal sequence Aβ(1-28).

Several Aβ aggregation and amyloid formation inhibitory approaches have been investigated during the last 10 years [2]. Inhibition of β-sheet formation has resulted in inhibitors or modulators of Aβ amyloidogenesis and cytotoxicity. Importantly, it has been recently shown that an Aβ(10-35) cyclic analogue with a high barrier to a conformational transition did not form amyloid [3].

Herein we present a simple design strategy to convert a native amyloidogenic sequence into a non-amyloidogenic one that is able to interact with the former one and inhibit amyloid formation and cytotoxicity. This approach features the introduction of a cyclic conformational constraint into the amyloid core region of the amyloid forming sequence and is tested here on Aβ(1-28).

Results and Discussion

The design strategy aims to constrain into a non-β state the conformation of a sequence part of the amyloidogenic peptide that may be directly involved in the transition of the soluble conformeric state into aggregated β-sheets and in the self-recognition process. As, in the case of Aβ, the soluble amyloidogenic conformation has been suggested to contain an α-helix, the (i, i+4) side chain-to-side chain cyclization approach was applied, which is a well-known approach towards α-helical stabilization.

Aβ(1-28) is a conformationally flexible sequence that exists in α-helical state or as β-sheet amyloid aggregates. The transition of the helical part of Aβ(1-28) into β-sheets has been proposed to modulate Aβ(1-40(42)) amyloidogenesis. To constrain Aβ(1-28) in a non-β (i.e. an α-helical) state, we used a side chain-to-side chain lactam-bridged Lys^{i},Asp^{i+4} pair to generate cyclo^{17,21}-[Lys^{17},Asp^{21}]Aβ(1-28) (cyclo Aβ(1-28)) (Figure 1). To differentiate between the effects of the subsitutions alone versus the conformational restriction, the unconstrained [Lys^{17}, Asp^{21}]Aβ(1-28) (control Aβ(1-28)) was also synthesized and studied. The bridge was placed at residues 17 and 21 for

two reasons: a) the helix has been suggested to be located between residues 13 and 20, and b) Aβ-Aβ self-recognition involves interactions of the side chains of residues 18-20 (VFF), which correspond to an Aβ amyloid core region. Sequence VFF should thus remain intact to enable interactions of the designed analogues with Aβ. In addition, this sequence, via a conformational restriction, should be unable to form β-sheets as in amyloid aggregates.

Aβ(1-40) H-DAEFRHDSGYEVHHQKL**VFF**AEDVGSNKGAIIGLMVGGVV-OH
Aβ(1-28) H-DAEFRHDSGYEVHHQKL**VFF**A-EDVGSNK-OH

Cyclo Aβ(1-28) H-DAEFRHDSGYEVHHQKK**VFF**DEDVGSNK-OH
Control Aβ(1-28) H-DAEFRHDSGYEVHHQKK**VFF**DEDVGSNK-OH

Fig. 1. Sequences of Aβ(1-40), Aβ(1-28), cyclo^{17,21}-[Lys^{17}, Asp^{21}]Aβ(1-28) (cycloAβ(1-28)), and [Lys^{17}, Asp^{21}]Aβ(1-28) (controlAβ(1-28)). Residues 17 and 21 of Aβ(1-28) that were exchanged by K and D in the analogues are underlined and the Aβ amyloid core residues VFF are in bold.

The analogues were synthesized by both Boc- and Fmoc-SPPS using Fmoc/Ofm and Mtt/OPip (OPip, 2-phenylisopropylester), respectively, to temporarily protect the side chains of Lys^{17} and Asp^{21} and were purified by RP-HPLC. N-terminally biotinylated cyclo^{17,21}-[Aca^{0}, Lys^{17}, Asp^{21}]Aβ(1-28) was synthesized by Fmoc-SPPS.

FT-IR spectroscopy, atomic force microscopy (AFM), and congo red staining and polarization microscopy studies on the β-sheet and amyloidogenic propensities of cycloAβ(1-28), Aβ(1-28), and controlAβ(1-28) showed that cycloAβ(1-28) was devoid of β-sheet-forming potential and amyloidogenicity. By contrast, both Aβ(1-28) and control Aβ(1-28) formed β-sheet- and amyloid fibril-containing aggregates.

Kinetics of amyloid formation by Aβ(1-28), cycloAβ(1-28), and controlAβ(1-28) were next followed by far-UV CD spectroscopy under amyloidogenic conditions in combination with electron microscopy (EM). The conformation of Aβ(1-28) changed in a time-dependent manner from a mainly unordered one, at the start of the incubation, into a β-sheet conformation about 25 h later (225 μM peptide) (Figure 2). Insoluble fibrillar aggregates appeared immediately thereafter. ControlAβ(1-28) also formed β-sheets and amyloid aggregates. In strong contrast to Aβ(1-28), no conformational changes or precipitation were observed in the solution of cycloAβ(1-28) (450 μM peptide, observation time 8 days), and EM confirmed the absence of amyloid. Together, the above studies demonstrated that the introduced constraint in Aβ(1-28) resulted in an abolishment of its amyloidogenic properties. CD studies under helix-promoting conditions (10% TFE, pH 3) indicated that cycloAβ(1-28) had an increased α-helical propensity as compared to Aβ(1-28) and the control analogue and suggested that the lactam bridge might have contributed to an α-helix stabilization.

The interaction of cycloAβ(1-28) with Aβ(1-28) was next studied by CD in combination with EM. The CD spectrum of the mixture of cycloAβ(1-28) with Aβ(1-28) (each peptide at 450 μM) indicated the absence of β-sheet structure and markedly differed from the sum of the spectra of each peptide, which indicated that the two peptides interacted (Figure 2). Moreover, no time-dependent changes of the CD spectra were observed and no amyloid fibrils were detected by EM (observation time was 8 days), whereas Aβ(1-28) alone (at 450 μM) aggregated into β-sheets and insoluble amyloid between 2-6 h. A kinetic follow up of the aggregation process of Aβ(1-28) alone, versus the mixture of cycloAβ(1-28) with Aβ(1-28) via size exclusion chromatography indicated that interaction of the cyclic analogue might have resulted in

formation of heterodimers and/or that cycloAβ(1-28) might have interacted with and caused dissociation of Aβ(1-28) multimeric aggregates.

Aβ(1-28) amyloid aggregates were cytotoxic to the human glioblastoma/ astrocytoma cell line HTB14 according to the 3-[4,5-dimethylthiazol-2-yl]-2,5-diphenyltetrazolium bromide (MTT) reduction assay. In the presence of cycloAβ(1-28), however, Aβ(1-28) cytotoxicity was markedly reduced. Of note, cycloAβ(1-28) alone did not significantly affect cell viability.

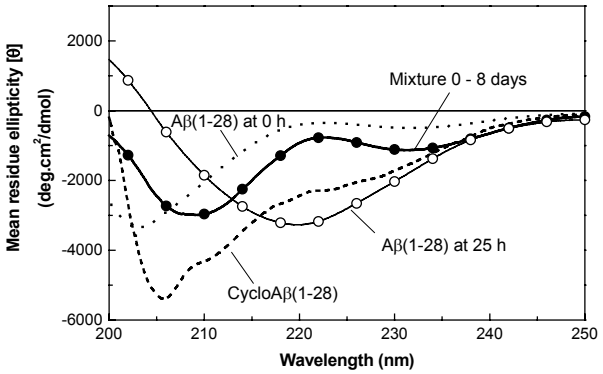

Fig. 2. Inhibitory effect of cycloAβ(1-28) on formation of β-sheet amyloid aggregates by Aβ(1-28) as assessed by CD [4]. Aβ(1-28) alone aggregated into β-sheets and insoluble amyloid after 25 h of incubation (225 μM peptide in phosphate buffer, pH 5.5, containing 100 mM NaCl and 30% ACN). In the presence of cycloAβ(1-28) (each peptide at 450 μM) no β-sheet or amyloid aggregate formation was observed up to 8 days.

Finally, first studies on the interaction of cycloAβ(1-28) with Aβ(1-40) were undertaken. Using an Aβ(1-40) pull down assay in combination with NuPAGE gel electrophoresis and Western blotting with anti-Aβ(1-40), Aβ(1-40) was found to strongly bind cycloAβ(1-28). EM clearly indicated that the cyclic peptide interfered with the amyloid formation pathway of Aβ(1-40) and led to a strong reduction of the amount of multimeric (mature) fibrillar aggregates.

Based on the above results, cycloAβ(1-28) [4] or other similarily constrained Aβ analogues may be suitable candidates or lead compounds for therapeutic or diagnostic applications in AD. Moreover, as common molecular principles may underly protein aggregation, amyloid formation and cytotoxicity in several of the amyloid-related diseases, the inhibitor design strategy that has been presented here for Aβ may be applied to the design of amyloid inhibitors for other diseases as well.

Acknowledgments

We thank M. Bergmann, K. Tenidis, and M. Waldner for HPLC purifications, J. Beck for synthesis of biotinylated peptides, and K. Sweimeh and R. Kayed for contributions to EM and CD experiments. This work was supported by a grant from the Fraunhofer Institute for Interfacial and Biological Engineering (Stuttgart, Germany).

References

1. Selkoe, D. J. *Physiol. Rev.*, **81**, 741-766 (2001).
2. Findeis, M. A. *Biochim. Biophys. Acta*. **1502**, 76-84 (2000).
3. Esler, W. P., Felix, A. M., Stimson, E. R., et al. *J. Struct. Biol*. **130**, 174-183 (2000).
4. Kapurniotu, A., Buck, A., Weber, M., et al. *Chem. & Biol*. **10**, 149-159 (2003).

Peptide Revolution: Genomics, Proteomics & Therapeutics
Michael Chorev & Tomi K. Sawyer (Editors)
American Peptide Society, 2003

Cu (II) Interaction with Amylin's Peptide Fragments

Angela Amoresano[3], Angela Flagiello[3], Giuseppe Impellizzeri[2], Antonio Magrì[1], Giuseppe Pappalardo[1], Piero Pucci[3] and Enrico Rizzarelli[1,2]

[1]C.N.R., Istituto di Biostrutture e Bioimmagini, Sez. di Catania, V.le A. Doria 6, Catania, Italy;
[2]Università di Catania, Dip. di Scienze Chimiche, V.le A. Doria 6, Catania, Italy;
[3]Università di Napoli, Dip. Chimica Organica e Biochimica, Via Cynthia 4, Napoli, Italy

Introduction

Amylin is the polypeptide responsible for the formation of amyloid deposits in 95% of patients affected by type II diabetes [1]. These deposits represent an integral part of type 2 diabetes mellitus pathology [2].

Human amylin: KCNTATCATQRLANFLVHSSNNFGAI LSSTNVGSNTY-NH_2 (hA)
Rat amylin: KCNTATCATQRLANFLVRSSNNLGPVLPPTNVGSNTY-NH_2 (rA)
Human amylin 17-29 (**1**): Ac-VHSSNNFGAI LSS-NH_2
Rat amylin 17-29 (**2**): Ac-VRSSNNLGPVLPP-NH_2
Rat amylin modified 17-29 (**3**): Ac-VHSSNNLGPVLPP-NH_2

Sequences of human and rat amylin and the 17-29 fragments studied in this work.

Human amylin (hA) forms fibrils *in vitro* [3] and is toxic to cultured pancreatic islet β-cells. In contrast, rat amylin (rA), which differs from hA by only six amino acid residues in the central region of the protein, (residues 18-29), does not form fibrils and is not toxic. Interest in the role played by various metals like Cu, Fe and Zn, has exponentially grown in recent years with respect to their involvement in the misfolded protein diseases which include Parkinson disease, Alzheimer's disease, amyotrophic lateral sclerosis and prion diseases [4]. Amyloid aggregates formation seems to be favoured by redox active and redox-inactive transition metal ions [5]. Recently, changes in Cu(II) concentration levels during the course of the type 2 diabetes has been found [6]. Here we report a comparative spectroscopic study (UV-Vis, CD and ESI-MS) on the Cu(II) complex formation with hA (17-29) **1** and rA (17-29) **2**. Furthermore, in order to get information on the geometry features of the complex species formed by Cu(II) and the peptide **1**, the peptide analogue **3** was synthesized. It corresponds to the region 17-29 of the rA in which the Arg residue has been replaced by the His residue. This mutation was introduced to obtain a water soluble model in which the potential Cu(II) binding site of the human fragment **1** is reproduced.

Results and Discussion

Due to the very low solubility in water of the system Cu(II)-**1** only ESI-MS spectra were carried out. Far UV CD spectra, recorded in the range between pH 5 and 10, indicate the presence of random coil structure in peptides **2** and **3**. Cu(II) complexation adds little structure formation: an inflection of a negative signal around 220 nm suggests the presence of bent chain conformation. However, the presence of strong negative ellipticity below 200 nm is indicative of the persistence of unstructured peptide chain. Visible CD spectra provided information about the donor atoms involved in Cu(II) complexation. In particular, the negative ellipticity observed in the

*Table 1. Spectroscopic data of peptides **1, 2** and **3**.*

pH	UV-Vis (ε)/cm^{-1} M^{-1}	CD ([θ])/deg cm^2 $dmol^{-1}$	ESI-MS m/z (%)
1			
7.5	--	--	718.2 (30) $[CuL]^{2+}$
9	--	--	1434.6 (10)$[CuL\text{-}1H]^{+}$; 718.4 (45) $[CuL]^{2+}$
2			
7.5	585 (60)	258 (390); 321 (74); 487 (14); 579 (-105)	1451.8 (10)$[CuL\text{-}1H]^{+}$; 727.0 (60) $[CuL]^{2+}$
9	565 (83)	256 (557); 314 (67); 488 (25); 568 (-150)	1451.8 (30)$[CuL\text{-}1H]^{+}$; 727.0 (100) $[CuL]^{2+}$
10	549 (80)	256 (667); 306 (62); 485 (43); 562 (-167)	--
3			
7.5	614 (85)	256 (1187); 334 (78); 610 (-213)	1434.5 (30)$[CuL\text{-}1H]^{+}$; 717.1 (93) $[CuL]^{2+}$
9	584 (108)	256 (933); 330 (34); 594 (-176)	1434.5 (50)$[CuL\text{-}1H]^{+}$; 714.3 (100) $[CuL]^{2+}$
10	565 (84)	330 (22); 476 (22); 569 (-179)	--

region expected for the *d-d* transition is typical of Cu(II)-peptide complexes in which only peptide nitrogens are present in the equatorial plane of the complexes.

In this respect, the presence of the CD signals at 320 nm and 330 nm, observed in the complexes of Cu(II) with peptide 2 and 3, confirm the involvement of deprotonate peptide nitrogens in metal complexation. These CD are in agreement with the ESI mass spectra carried out at pH=7.5. However, in the case of Cu(II)-peptide 3, the participation of the imidazole ring cannot be ruled out. Indeed, UV-Vis data agree with this hypothesis (see Table 1). Only above pH=9, UV-Vis blue shift indicates the increase of the number of nitrogen atoms (probably four) in the complex. Again, in the case of Cu(II)-peptide 3, UV-Vis data suggest the apical contribution of the imidazole nitrogen in the coordination environment up to pH=9. Interestingly, at pH=10, both the Cu(II) complexes show almost identical CD and UV-Vis parameters. This can be rationalized by admitting that in peptide 3 the imidazole ring is no longer engaged.

Acknowledgments
We thank C.N.R., University of Catania and MURST (PRIN 2001; project 2001031717_003 for financial support.

References

1. Sipe, J. D. and Cohen, A. S. *J. Struct. Biol.* **130***,* 88-98 (2000).
2. Kahn S. E., Andrikopoulos S. and Verchere, C. B. *Diabetes* **48**, 241-253 (1999).
3. Goldsbury, C. S., *et al., J. Struct. Biol.* **130***,* 217-231, (2000).
4. Bush, A. I. *Curr. Opin. Chem. Biol.* **4**, 184-191 (2000).
5. Bush A. I. and Tanzi, R. E. *Proc. Natl. Acad. Sci., U.S.A.* **99**, 7317-7319 (2002).
6. Zargar, A. H., *et al. Exp. Clin. Endocrinol. Diabetes* **108**, 397-400 (2000).

Peptide Revolution: Genomics, Proteomics & Therapeutics
Michael Chorev & Tomi K. Sawyer (Editors)
American Peptide Society, 2003

Inhibition of Amyloid Formation of Human Amylin

Dirk T.S. Rijkers[1], Jo W.M. Höppener[2], George Posthuma[3], Cornelis J.M. Lips[2] and Rob M.J. Liskamp[1]

[1]Department of Medicinal Chemistry, Utrecht Institute for Pharmaceutical Sciences, [2]Department of Internal Medicine and Endocrinology, University Medical Center Utrecht; [3]Department of Cell Biology, Center for Electron Microscopy, University Medical Center Utrecht, Utrecht University, PO Box 80082, 3508 TB Utrecht, The Netherlands

Introduction

Peptide-protein and protein-protein interactions are vital in cellular processes of healthy organisms, but they can also be detrimental or lethal to the organism. This has been shown in diseases where there is an uncontrolled aggregation leading to accumulation of, for example, protein fibrils and amyloidogenic plaques [1]. The most well-known diseases in this respect are Alzheimer's disease [2], and transmissible spongiform encephalopathies involving prions (scrapie, BSE, Creutzfeldt-Jakob disease [3]. Less known, but of increasing impact in view of the aging population in the Western world, is maturity onset diabetes (diabetes type II) [4]. The protein involved in this disease is amylin – islet amyloid polypeptide – (IAPP, see Figure 1). Amyloid deposits of fibrillar amylin in the pancreatic islets are cytotoxic for islet β-cells and are associated with the depletion of these cells that accompanies the progression of the disease [5].

Structure-activity studies have shown that amino acid residues 20-29 of amylin **1** are crucial for amyloid formation [6]. Moreover, a proline scan of this decamer has demonstrated that substitution of serine at position 28 by a proline residue efficiently reduces the capacity for amyloid formation [7]. This substitution is also present in mouse amylin, and this peptide does not form fibrillar assemblies.

We are interested in the design and synthesis of soluble β-sheet mimetics that interfere with amyloid fibril formation by inhibiting the assembly of β-pleated sheets. In a more molecular way we wanted our molecular constructs to be able to form hydrogen bonds with the β-chain of a starting or growing β-sheet; at the same time they should be incapable of accepting a subsequent β-chain for example as a result of their inability to form hydrogen bonds either by the absence of a hydrogen bond donor/acceptor or by a turn-like structure preventing proper alignment [8].

human IAPP H-K*C*NTATCATQRLANFLVHSSNNFGAILSSTNVGSNTY-NH_2
mouse IAPP H-K*C*NTATCATQRLANFLV**R**SSNN**L**G**PV**L**PP**TNVGSNTY-NH_2

Fig. 1. Sequences of human and mouse amylin (islet amyloid polypeptide); amylin contains a disulfide bridge that is formed between Cys2 and Cys7.

Results and Discussion

Recently we have shown that a single mutation of the amide bond at position 28 –either as an ester moiety or by *N*-alkylation– resulted in amylin(20-29) derivatives that did not form amyloid fibrils [8]. Although the absence of a single hydrogen bond donor has been found to be sufficient to retard its self-aggregation into fibrils, it is not efficient to inhibit amyloid fibrillogenesis of human IAPP or to disassemble preformed amylin(20-29) fibrils. Therefore, two novel amylin(20-29) derivatives have been synthesized in which the amide backbone has been modified at alternate positions (see Figure 2, compounds **2** and **3**).

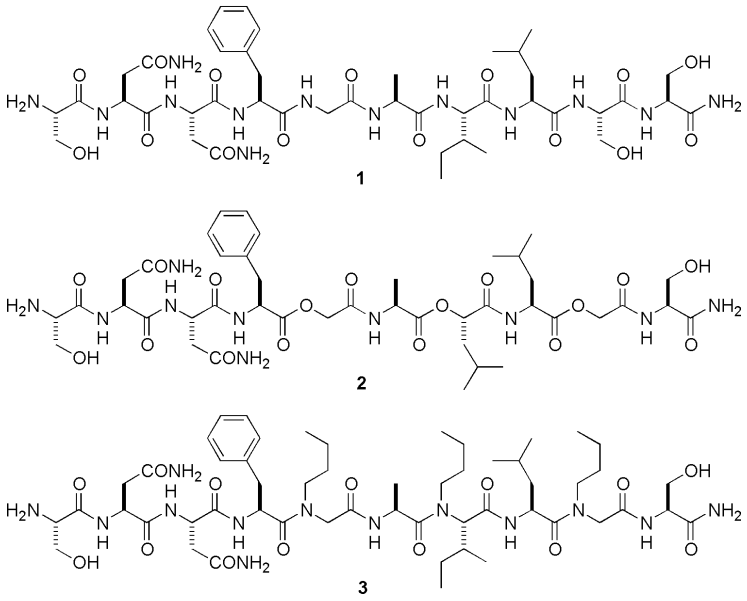

*Fig. 2. Chemical structures of amylin(20-29) **1**, the depsipeptide **2** and the N-alkylated peptide **3** as backbone-modified amylin derivatives.*

Compounds **2** and **3** were synthesized according to the solid phase protocol as described recently [8]. The most difficult step in the synthesis of **2** was the coupling of Fmoc-Ala-OH to the α-hydroxy functionality of L-leucic acid. Treatment with DIC/HOBt/DMAP for 24 hrs (two times) resulted in a coupling yield of 49%. The *N*-butyl glycine residues in **3** were introduced as their peptoid moieties. The next Fmoc amino acid was coupled to the secondary amine with HATU/HOAt in nearly quatitative yield. *N*-Butylation of the amino functionality of isoleucine at position 26 was carried out by using our site specific alkylation method [9]. The corresponding secondary amine was coupled to Fmoc-Ala-OH using HATU as coupling reagent in neat *sym*-collidine in 24% yield.

As expected, both peptides did not form amyloid fibrils as judged by electron microscopy. Preliminary results showed that **2** and **3** were not efficient inhibiting fibril growth of human amylin and/or resolubilizing preformed amylin(20-29) fibrils. Apparently, an additional molecular recognition motif linked to **2**/**3** is necessary to enhance the potency/affinity in the process of β-sheet disruption.

References

1. Rochet, J.- C. and Lansbury, Jr., P. T. *Curr. Opin. Struct. Biol.* **10**, 60-68 (2000).
2. Glenner, G. G. and Wong, C. W. *Biochem. Biophys. Res. Commun.* **122**, 1131-1135 (1984).
3. Prusiner, S. B. *Proc. Natl. Acad. Sci. U.S.A.* **95**, 13363-13383 (1998).
4. Cooper, C. J. S., *et al. Proc. Natl. Acad. Sci. U.S.A.* **84**, 8628-8632 (1987).
5. Höppener, J. W. M., Ahrén, B. and Lips, C. J. M. *N. Engl. J. Med.* **343**, 411-419 (2000).
6. Westermark, P., *et al. Proc. Natl. Acad. Sci. U.S.A.* **87**, 5036-5040 (1990).
7. Moriaty, D. F. and Raleigh, D. P. *Biochemistry* **38**, 1811-1818 (1999).
8. Rijkers, D. T. S. *et al. Chem. Eur. J.* **8**, 4285-4291 (2002).
9. Reichwein, J. F. and Liskamp, R. M. J. *Tetrahedron Lett.* **39**, 1243-1246 (1998).

Peptide Revolution: Genomics, Proteomics & Therapeutics
Michael Chorev & Tomi K. Sawyer (Editors)
American Peptide Society, 2003

Modulation of β-Amyloid 1-42 Aggregation by Other Aggregating Peptides

Lukasz P. Frankiewicz[1] and Aleksandra Misicka[1,2]

[1]*Faculty of Chemistry, Warsaw University, Warsaw, Poland;*
[2]*Medical Research Centre, Polish Academy of Sciences, Warsaw, Poland*

Introduction

One of the most common causes of senile dementia is Alzheimer's disease (AD). Formation of amyloid plaques and cerebrovascular deposits is the pathological characteristics of AD. β-Amyloid peptides (βA) derived from the amyloid precursor protein (APP) are the major components of the deposits. Amyloid peptides may consist of 39 to 43 amino acids in length, however the form 1-42 occurs predominantly in amyloid plaques [1,2]. It has been recognized that changes of conformation and aggregation of other types of proteins could cause other neurodegenerative diseases. The most studied recent example of this type is Creutzfeldt-Jakobs (CJ) disease which results from the aggregation of prions (PrP^{sc}).

Previously, we reported kinetic studies of interactions of β-amyloid peptide fragments (βA 22-35, βA 25-35) and prion fragment (PrP 109-126) [3]. The comparison of aggregation time of peptide fragments of βA and prion confirmed our previous hypothesis that in physiological conditions cross interaction of aggregating peptides may form metastable heterodimers which do not aggregate further because of uncomplementary hindrance.

In this communication, we describe the results of spontaneous aggregation kinetics of βA 1–42 and its combination with other aggregating short peptides. The selected sequences for our studies were chosen from the respective fragments responsible for aggregation of βA or PrP, namely two fragments of βA (βA 25–35 and βA 22–35) and two fragments of prion protein (PrP 113–126 and PrP 109–126) as shown in Figure. 1.

βA 1–42 – H-DAEFRHDSGYEVHHQKLVFFAEDVGSNKGAIIGLMVGGVVIA-NH_2
βA 25–35 – H-GSNKGAIIGLM-NH_2
βA 22–35 – H-EDVGSNKGAIIGLM-NH_2
PrP 113–126 – H-AGAAAAGAVVGGLG-NH_2
PrP 109–126 – H-MKHMAGAAAAGAVVGGLG-NH_2

Fig. 1. Sequences of βA 1 – 42 and short fragments of βA peptide and prion protein PrP.

Results and Discussion

β-Amyloid 1-42 was synthesized manually on MBHA resin (0.27 mmol/g) by standard Boc strategy with TBTU as the coupling reagent. 3 eq. (relative to resin loading) of BocAA, HOBt, TBTU and 6 eq. of DIPEA were used during synthesis. All peptides that are fragments of amyloid peptide (βA 25-35 and βA 22-35) and prion protein (PrP 109-126 and PrP 113-126) were synthesized on Rink - amide MBHA resin (0.6 mmol/g) by standard Fmoc strategy with HBTU or TBTU as the coupling reagent. 2 eq. (relative to resin loading) of FmocAA, HOBt, TBTU (or HBTU) and 6 eq. of DIPEA were used. Peptides were purified by semipreparative HPLC.

Stock solutions (0.01 mol/l) of β-amyloid and prion protein fragments were prepared by dissolving the appropriate amount of peptide in DMSO. Stock solution of β-amyloid 1-42 was prepared as above but its concentration was 0.005 mol/l.

According to the results of previous research which showed faster aggregation in PBS buffer than in TRIS buffer, we decided to follow the aggregation process only in PBS. 50 µl of βA 1-42 and 25 µl of each synthesized fragment were diluted in PBS to final a volume of 1 ml. Final content of DMSO was 30% to provide better solubility. The concentration of samples was 0.25 mmol/l regarding to each peptide in solution.

Kinetic studies were carried on analytical HPLC with diode array detector and Hamilton PRP-3 column. 0.05% TFA and ACN were used as eluents at the flow rate of 1 ml/min. The integration of βA 1-42 monomer peak was performed manually. Measurements of monomer peak area were taken at 0, 24, 48 and 96 hr intervals from initial injection. During the time of study, samples were incubated at 37°C. The value of peak area at point 0 was set as 100% of monomer content (Figure 2).

The results of present study are fully consistent with our hypothesis and preliminary findings. The βA 1-42 aggregation is significantly reduced in the presence of shorter fragments of βA4 or PrP. Shorter peptides of βA(25-35) or PrP (113-126) protect significantly better than βA4 versus slightly longer fragments of βA (22-35) or PrP (109-126). These data suggest the existing optimal properties of "protecting peptides" and provide rationale for further studies.

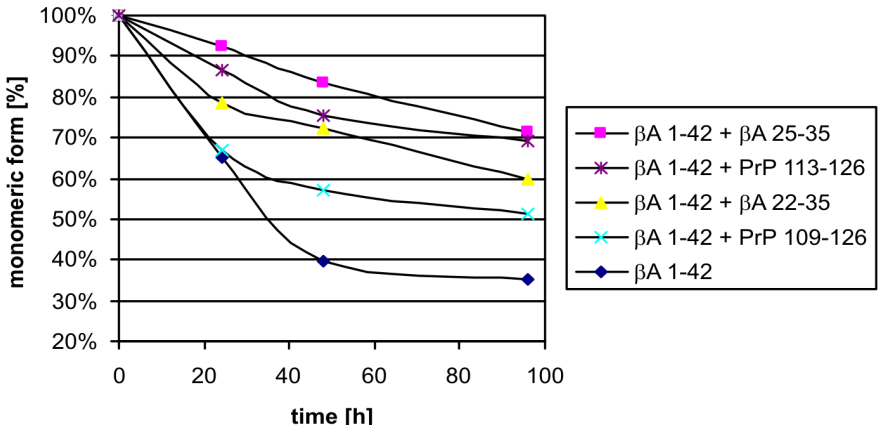

Fig. 2. Aggregation of βA 1-42 and with addition of other short aggregating peptides.

Acknowledgments

This work was partially supported by funds from Warsaw University. Lukasz P. Frankiewicz would like to thank the American Peptide Society for the travel grant to attend the 18th American Peptide Symposium

References

1. Snyder, S. W. et al., *Biophys. J.* **67**, 1216-1228 (1994).
2. Taylor, B. et al., *Journal of Protein Chemistry* **22**, 31-40 (2003).
3. Frankiewicz, L., Pulka, K., Lipkowski, A. W., Misicka, A. *LIPS* **9**, 77-81 (2002).

Peptide Revolution: Genomics, Proteomics & Therapeutics
Michael Chorev & Tomi K. Sawyer (Editors)
American Peptide Society, 2003

Inhibition of β-Amyloid Aggregation with $C^{\alpha,\alpha}$Disubstituted Amino Acid Containing Peptides

Marcus A. Etienne, Jed P. Aucoin, Yanwen Fu, Robin L. McCarley and Robert P. Hammer

Department of Chemistry, Louisiana State University, Baton Rouge, LA 70803, USA

Introduction

Alzheimer's disease (AD) is a degenerative disease that causes nerve impairment in the brain and loss of memory and mental functions. AD is characterized by the formation of protein aggregates that assemble into fibrillar structures. Many believe that the causative factor of AD is the proliferation of amyloid plaques, mostly consisting of the β-amyloid (Aβ) peptide [1-2]. It is known that $A\beta_{1\text{-}40}$ fibrils have β-sheet secondary structure. Figure 1 shows a β-strand peptide design in which alternating positions consist of α,α-disubstituted amino acids (ααAAs) having side chains larger than that of methyl groups and its interaction with Aβ. A key aspect to these novel β-strand mimics is that they allow interaction of the peptide with Aβ from only one hydrogen bonding face.

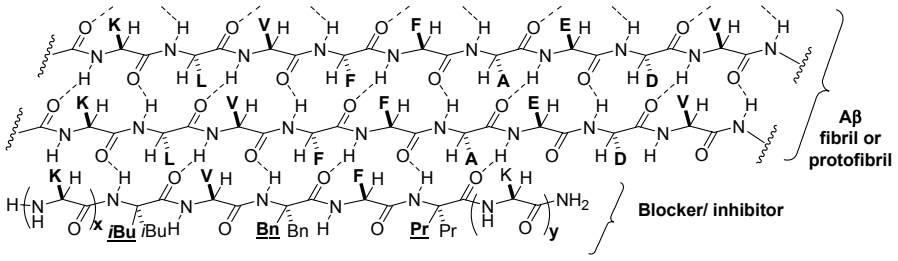

Fig. 1. Plausible interactions between β-sheet "blocker" and Aβ fibril.

It has been hypothesized that β-sheet "blockers" would inhibit protein aggregation and block amyloid fibril formation. ααAAs are widely used in peptide design because of their structure promoting effects. Incorporation of $C^{\alpha,\alpha}$disubstituded amino acids, such as dipropyl glycine (Dpg), diisobutyl glycine (Dibg), and dibenzyl glycine (Dbg), into the hydrophobic core of Aβ (KLVFF) are of particular interest due to their potential to adopt fully extended conformations [3], which may pre-dispose the ααAA containing peptides for interactions with Aβ assemblies or protofibrils.

Results and Discussion

Inhibitor peptides AMY-1, AMY-2, and Murphy [4] (Figure 2) were successfully synthesized according to protocols developed in our laboratory [5] and used to elucidate the mechanistic role of ααAAs on amyloidal aggregation.

Murphy	H-Lys-Leu-Val-Phe-Phe-$(Lys)_6$-NH_2
AMY-1	H-Lys-Dibg-Val-Dbg-Phe-Dpg-$(Lys)_6$-NH_2
AMY-2	H-$(Lys)_7$ -Dibg-Val-Dbg-Phe-Dpg-NH_2

Fig. 2. Peptide sequences of inhibitor peptides.

Surface tension measurements on the inhibitors alone show that AMY-1 and AMY-2 have critical micelle concentrations (cmc) of approximately 1mM. The Murphy inhibitor does not self assemble at concentrations greater than 10 μM. Circular dichroism (CD) of the inhibitors shows that all have a random coil structure.

Scanning force microscopy (SFM) results show that AMY-1 inhibits at a 1:1 ratio of Aβ:inhibitor (Figure 3). This result holds true over prolonged periods of time. Minimal amounts of aggregates were formed with AMY-1 in the presence of Aβ, but no fibrils resulted from these aggregates. Experimental results suggest that AMY-2 leads to the formation of large aggregates. This particular inhibitor is of interest because it appears to increase the rate of Aβ aggregation but, as in the case of AMY-1, no fibrils are present. The Murphy inhibitor forms only non-fibrillic aggregates.

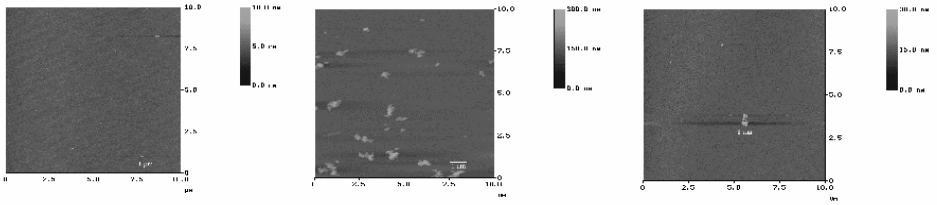

Fig. 3. SFM images of Aβ aggregates in the presence of a.) AMY-1 b.) AMY-2 c.) Murphy.

CD spectra of inhibitor peptides, in the presence of Aβ (1:1), indicate that the overall secondary structure of the inhibitors does not change over time. This suggests that these novel inhibitors are following a distinct pathway in their inhibition mechanisms. The CD results along with the SFM data suggest that these novel peptides are not blocking Aβ binding, which would result in the blocking of Aβ aggregation, but they are increasing the rate of aggregation of Aβ with non-fibrillic assemblies.

References

1. Gordon, D., Sciarretta, K. and Meredith, S. *Biochemistry* **40**, 8237-8245 (2001).
2. Omar, E., Sheridan, J., Sidera, C., Siligardi, G., Hussain, R., Haris, P. and Austen, B. *Biochemistry* **40**, 3449-3457 (2001).
3. Wysong, C., Yokum, T., McLaughlin, M. and Hammer, R. *CHEMTECH* **27,** 26-33 (1997).
4. Pallito, M., Ghanta, J., Heinzelman, P., Kiessling, L. and Murphy, R. *Biochemistry* **38,** 3570-3578 (1999).
5. Fu, Y. and Hammer, R. *Org. Lett.* **4,** 237-240 (2001).

Peptide Revolution: Genomics, Proteomics & Therapeutics
Michael Chorev & Tomi K. Sawyer (Editors)
American Peptide Society, 2003

Amyloid-Like Fibrils of Laminin-1 Peptides

Motoyoshi Nomizu[1], Shingo Kasai[1], Yukiko Ohga[1], Mayumi Mochizuki[1], Masanori, Yamada[1], Yuichi Kadoya[2] and Norio Nishi[1]

[1]Graduate School of Environmental Earth Science, Hokkaido University, Sapporo 060-0810, Japan; [2]Kitasato University School of Medicine, Sagamihara 228-8555, Japan

Introduction

Laminins, major components of basement membranes, are trimeric molecules composed of α, β, and γ chains [1]. Laminin-1 (α1β1γ1) has diverse biological activities, including promotion of cell adhesion, migration, neurite outgrowth, tumor metastasis, and angiogenesis [1]. Basement membrane components have been identified in senile plaques [2, 3]. Laminin-1 is over-expressed in the brains of both Alzheimer's and Down's syndrome patients [4]. Laminin and certain degradable fragments interact with β-amyloid proteins inhibit amyloid fibril formation and are present in Alzheimer's plaques [5]. These findings suggest that laminins are involved in amyloid-related diseases. Recently, using Congo red staining, X-ray diffraction, infrared spectroscopy, and electron microscopy, we found that an Ile-Lys-Val-Ala-Val (IKVAV)-containing active peptide A208 (AASIKVAVSADR), which promotes cell adhesion, neurite outgrowth, angiogenesis, collagenase IV production and tumor growth [6], forms amyloid-like fibrils composed of a cross-β conformation [7]. The IKVAV sequence interacts with a 110 kDa membrane-associated laminin-binding protein identified as β-amyloid precursor protein [8]. Interestingly, different amino acid substitutions of the IKVAV-containing peptide resulted in loss of cell binding and were unable to form fibrils, suggesting a relationship between biological activity and fibril formation [7].

Previously, we identified 60 cell adhesive peptides by screening 673 synthetic peptides covering the entire laminin-1 sequences (Figure 1) [9-12]. In this paper, using Congo red staining, we screened these 60 laminin-1-derived peptides and identified amyloidogenic sequences.

Results and Discussion

We have examined the amyloid-like fibril formation of 60 laminin-1-derived biologically active 12-mer synthetic peptides obtained from a library of 673 peptides (Figure 1). When the Congo red, which specifically binds to an amyloid structure [7], was incubated with the 60 active laminin-1 peptides, 13 peptides were stained with Congo red and caused a shift of the absorption peak at 486 nm to 540 nm. We also demonstrated that A208 showed cell attachment and neurite outgrowth activity only in the peptide-coated plate assay. Moreover, using various A208 analogs we demonstrated that the biological activity of A208 was closely related to the ability to form amyloid-like fibrils [7]. Therefore, we next evaluated the cell attachment activity of the 13 peptides, found to be active in the Congo red assay, in the peptide-coated and peptide-conjugated Sepharose bead assays. Five peptides (A119, A208, AG97, B133, and B160) showed cell attachment activity only in the peptide-coated plate assay (Figure 1). These 5 peptides also promoted neurite outgrowth in a dose-dependent manner. The other 8 peptides showed cell attachment activity in the both peptide-coated plate and peptide-conjugated Sepharose bead assay.

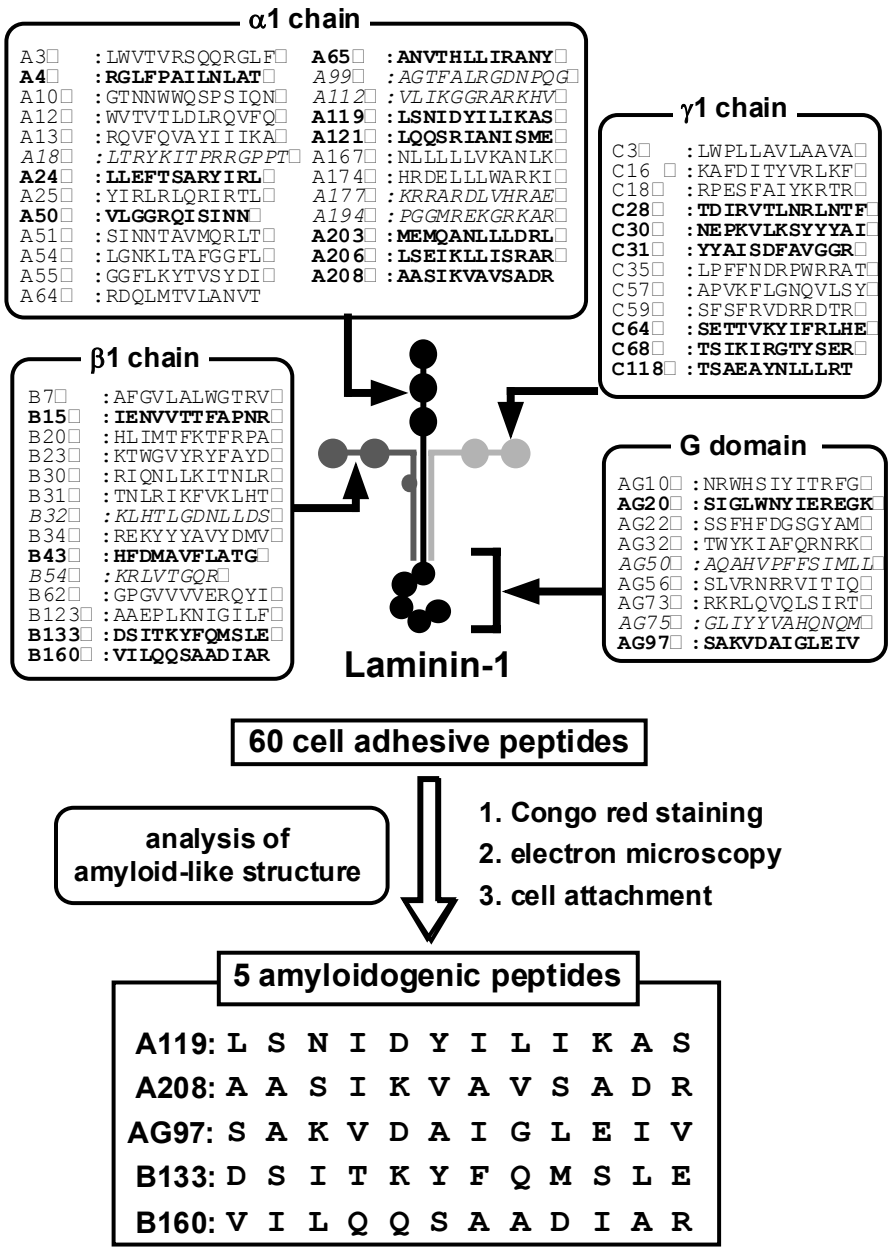

Fig. 1. Schematic diagram of identification of amyloidogenic peptides from 60 cell adhesive laminin-1 peptides. Chain localization of 60 cell adhesive peptides on laminin-1 is indicated [9-12]. Twenty-one peptides showed cell attachment activity only in the peptide-coated plate assay (bold), 9 peptides were active only in the peptide-conjugated Sepharose bead assay (italics), and 30 peptides promoted cell attachment in both assays (regular).

Based on the results, we focused on the peptides A208, A119, AG97, B133, and B160. The Congo red-stained solutions of these 5 peptides exhibited birefringence, suggesting that these peptides form amyloid-like structure and significantly bind to Congo red. Further, when the 5 peptides were analyzed by negative staining electron microscopy, all the peptides formed fibrillar structures. These results suggest that these peptides self-assemble and form amyloid-like fibrils.

Although amyloid fibril formation is generally related to diseases, including Alzheimer's disease, Parkinson's disease, type II diabetes, prion diseases, and systemic polyneuropathies, some proteins and peptides that are not related to diseases can also form amyloid fibrils [13]. Amyloid fibrils are deposited in the basement membrane matrix of the brain [14]. Laminin, type IV collagen, and heparan sulfate proteoglycans, which are the major components of basement membrane, have been localized within the senile plaques as punctate deposits [2, 3].

Several studies on amyloid fibril formation suggest that the interaction of specific amino acid residues contributes to the formation and stabilization of the amyloid fibrils [15]. Alignment of the sequences of the 5 amyloidogenic peptides derived from laminin-1 (Figure 1) did not identify any consensus sequences. All peptides have both basic and acidic amino acids, suggesting that charge interaction may be critical for fibril formation and/or stabilization of fibrils [15]. It has been proposed that aromatic amino acids are an important property for amyloid fibrils formation, but B208, AG97 and B160 have no aromatic residues. Aromatic amino acids may not be essential for amyloid fibril formation, but may accelerate fibril formation. Moreover, all 5 peptides contain polar side-chain amino acids (Ser and Thr) and β-branched hydrophobic amino acids (Ile and Val). The β-branched amino acids (Thr, Ile, and Val) may play a critical role in the self-assembly of the peptides into amyloid-like fibrils. Taken together, we conclude that both hydrophobic and electrostatic interactions may be necessary for amyloid-like fibril formation.

Previously, we showed that peptide A208 formed long fibrils composed of β-sheet structures [6]. Here, we identified 4 additional amyloidogenic peptides from the laminin-1-derived biologically active peptides. It is possible that the active peptide fragments of laminin form amyloid-like fibrils and play a critical role in its biological activity. Laminins and/or their degradative fragments may be involved in amyloid-related disease.

References

1. Colognato, H. and Yurchenco, P. D. *Dev. Dyn.* **218**, 213-234 (2000).
2. Perlmutter, L. S., Barron, E., Saperia, D. and Chui H. C. *J. Neurosci. Res.* **30**, 673-681 (1991).
3. Murtomaki, S., *et al*., *J. Neurosci. Res*. **32**, 261-273 (1992).
4. Palu, E. and Liesi, P. *J. Neurosci. Res*. **69**, 243-256 (2002).
5. Castillo, G. M., *et al*., *J. Neurosci. Res.* **62**, 451-462 (2000).
6. Nomizu, M., *et al*., *J. Biol. Chem.* **267**, 14118-14121 (1992).
7. Yamada, M., *et al*., *FEBS Lett.* **530**, 48-52 (2002).
8. Kibbey, M. C., *et al*., *Proc. Natl. Acad. Sci. U.S.A.* **90**, 10150-10153 (1993).
9. Nomizu, M., *et al*., *J. Biol. Chem.* **270**, 20583-20590 (1995).
10. Nomizu, M., *et al*., *J. Biol. Chem.* **272**, 32198-32205 (1997).
11. Nomizu, M., *et al*., *J. Biol. Chem.* **273**, 32491-32499 (1998).
12. Nomizu, M., *et al*., *Arch. Biochem. Biophys.* **378**, 311-320 (2000).
13. Rochet, J –C. and Lansbury, P. T. *Curr. Opin. Struct. Biol.* **10**, 60-68 (2000).
14. Inoue, S., Kuroiwa, M. and Kisilevsky, R. *Brain Res. Rev.* **29**, 218-231 (1999).
15. Tjernberg, L., *et al*., *J. Biol. Chem.* **277**, 43243-43246 (2002).

Peptide Revolution: Genomics, Proteomics & Therapeutics
Michael Chorev & Tomi K. Sawyer (Editors)
American Peptide Society, 2003

Mass Spectrometric Elucidation of an Amyloid Plaque-specific Epitope: Molecular Basis for Probing the Proteolytic Mechanism of Alzheimer's Amyloid Precursor Protein

Michael Przybylski[1], Roxana Cecal[1], Xiaodan Tian[1], JoAnne McLaurin[2], Marilena Manea[1], Raluca Stefanescu[1] and Peter St.George-Hyslop[2]

[1]Department of Chemistry, Laboratory of Analytical Chemistry, University of Konstanz, 78457 Konstanz, Germany; [2]Center for Research in Neurodegenerative Diseases, University of Toronto, Toronto, Ontario, Canada

Introduction

The accumulation of extracellular plaques containing the neurotoxic ß-amyloid peptide fragment Aß(1-42) of the ß-amyloid precursor protein (APP) as the major product, is one of the characteristics of Alzheimer's disease (AD). However, despite numerous recent studies on the involvement and role of ß- and γ-secretase [1], the molecular details of the pathophysiological degradation pathways of APP are still unclear. The identification of epitope structures of antibodies, using selective proteolytic digestion of antigen:antibody complexes (epitope excision) in combination with mass spectrometry, has been developed as a highly efficient molecular tool [2, 3]; analysis of epitopes specific for Aß and/or Aß precursor sequences, in principle, presents a molecular approach for probing the proteolytic APP pathway.

Immunization of transgenic mouse models of AD with Aß(1-42) has been shown to be effective to inhibit and disaggregate Aß-fibrils, and reduces both the AD-like neuropathology and memory impairments [4]. The mechanism underlying these therapeutic effects is as yet unclear. Using the epitope excision method in combination with high resolution Fourier-transform ion cyclotron resonance-mass spectrometry (FTICR-MS), we have identified a specific epitope recognized by the active antibodies as the N-terminal Aß(4-10) sequence [5]. The recognition specificity and properties of this epitope and derived peptides provide new lead structures both for AD vaccine development and for molecular diagnostic applications.

Results and Discussion

To identify both possible linear and conformational epitopes recognized by the therapeutically active antibodies, epitope excision of immobilized immune complexes followed by MALDI-TOF- and electrospray(ESI)-FTICR-MS was performed. IgG from Aβ(1–42)-immunised TgCRND8 mice (expressing the 670/671NL-human mutant APP [4]), IgG from control-immunized mice and commercial mouse (monoclonal) and rabbit (polyclonal) Aβ(1–42)-antibodies were immobilised in sepharose-microcapillaries, and exposed to a) Aβ(1–42) fibril aggregates; b) synthetic Aβ(1–42); and c) isolated amyloid plaques from TgCRND8 mouse brain tissue, and human AD plaques. The resultant antigen:antibody complexes were subjected to combinations of single and multiple digestions with trypsin, Lys-C, Glu-C, Asp-N protease and aminopeptidase M, followed by MALDI-TOF and FTICR-MS of trifluoroacetic acid-eluted epitope fractions (Figure 1). These studies identified Aβ(4–10) (FRHDSGY) as the specific minimal core epitope bound to the antibody with high affinity; in contrast no elution product was detected upon epitope excision of rat Aβ(1–42) (which has a different Aß(4-10) sequence), nor did antibodies from control mice yield detectable Aβ epitope. The epitope identified from human and mouse plaques was identical. In

contrast MALDI-MS analysis of intact monomeric Aß in plaques revealed a molecular distribution of most abundant Aß(1-42) together with less abundant (ca. 20 %) Aß(1-40) and Aß(1-38) in mouse plaque fibrils (Fig. 1), whereas human AD plaques showed most abundant Aß(1-40) and only low levels of Aß(1-42).

These results suggest that antibodies targeted to the specific Aß(4-10) recognition structure are effective modulators of Aß-induced neurotoxicity; they also demonstrate the efficiency of epitope excision/mass spectrometry as a molecular tool for epitope elucidation. Knowledge of the Aß- epitope recognized by therapeutically active antibodies provides the basis for the design of molecular mimics for vaccination, particularly, specific immunization antigens that are independant of the Aß(1-42) structure, aggregation propensity, and toxicity. Based on this epitope we have synthesised epitope-peptides comprising APP-precursor sequences beyond the ß-secretase cleavage site. ELISA studies of such peptides (see Figure 2) reveal: (i) substantially higher affinities to the therapeutically active antibodies compared to Aß(1-40), and (ii) significantly higher affinity of the peptide comprising the mutant APP sequence, EpAPP(661-687)NL compared to the peptide, APP(661-687)KM, suggesting a possible targeting of precursor APP molecules comprising the N-terminal Aß-epitope.

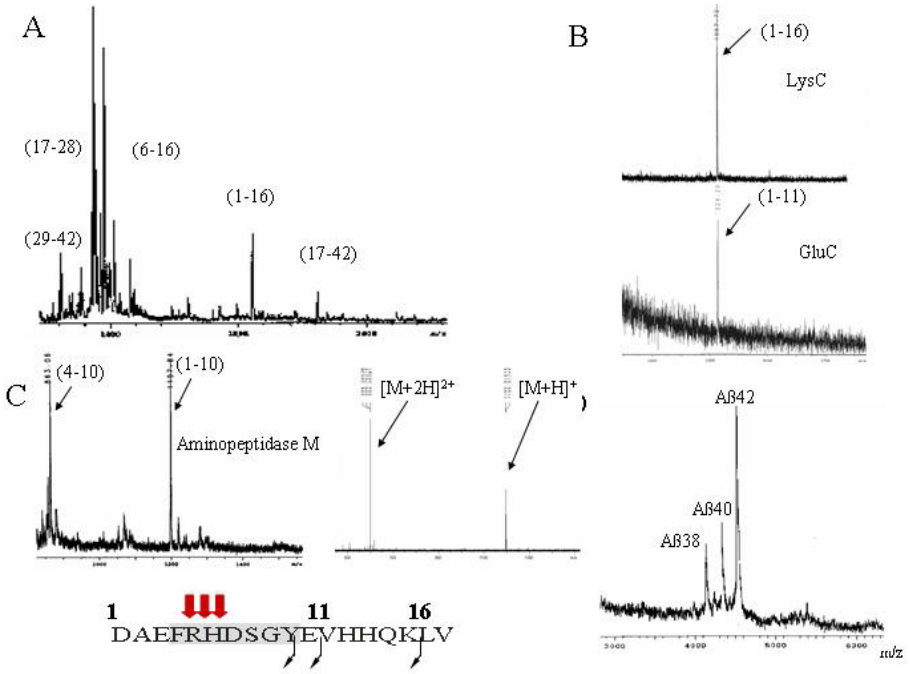

Fig. 1. MALDI-TOF- and FTICR-MS identification of Aß(4-10) epitope. A) MALDI-MS of Aß42 tryptic digest mixture. B) epitope excision and FTICR-MS using LysC and GluC protease. C) epitope-excision-MALDI- and ESI-MS from soluble plaques upon chymotypsin and ApaseM digestion. D) MALDI-MS of Aß peptides in mouse plaques. Thin and bold arrows denote accessible and shielded proteolytic sitesfound by epitope excision-MS, respectively.

CD spectra and molecular dynamics simulation of the N-terminal Aß(1-10) sequence suggest a flexible unstructured peptide (Figure 2). Such an unordered structure would be compatible with the presentation and accessibility of the epitope by the therapeutically active antibody in soluble Aß-oligomers and/or corresponding protofibrillary aggregates.

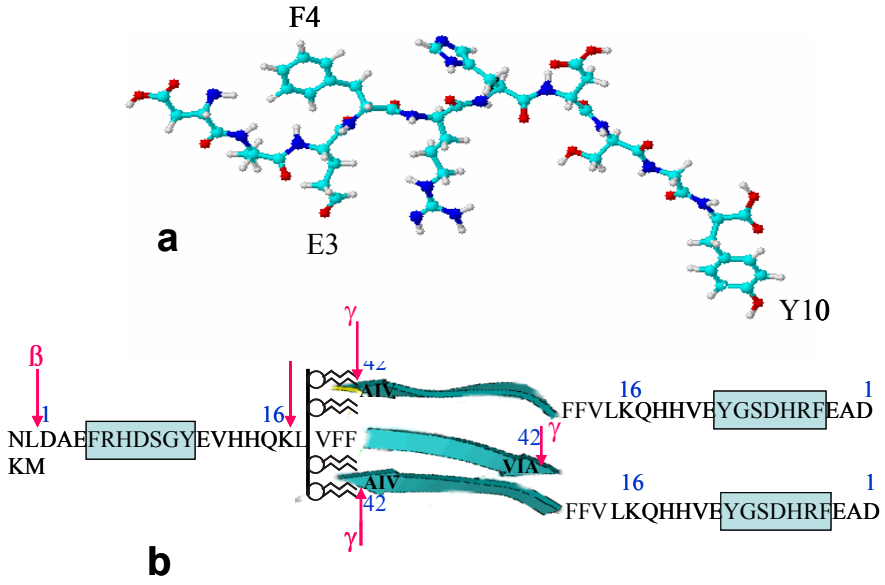

EpAPP(661-687)NL H-IKTEEISEV**NL**DAE***FRHDSGY***EVHHQK-COOH
EpAPP(661-687)KM H-IKTEEISEV**KM**DAE***FRHDSGY***EVHHQK-COOH

Fig. 2. (a), Molecular dynamics simulation of the Aß(1-10) epitope sequence; (b), model of protofibrillarAß-oligomers with accessible epitope, and synthetic Aß-epitope peptides comprising ß-secretase cleavage sites of human mutant (NL) and wild type (KM) APP. Molecular dynamics simulation was performed with the program Chemsketch with helical, ß-sheet and random conformations of single residues in Aß(1-10), using Hyperchem 6.0 and AMBER parameters. Sites of α-, ß- and γ-secretase cleavage of Aß(1-42) are denoted by arrows. Epitope sequences in synthetic peptides are denoted in bold italics.

Acknowledgments
This work was supported by grants from the Deutsche Forschungsgemeinschaft, Bonn, Germany.

References
1. Small, D. H, Mok, S. S. and Bornstein, J. C. *Nature Rev. Neurosci.* **2**, 595 (2001).
2. Macht, M., Fiedler, W., Kürzinger, K. and Przybylski, M. *Biochemistry* **35**, 15633 (1996).
3. Przybylski, M. et al. In Ens, W., Standing, K. G. and Chernusevich, I. V. (Eds.) *New Methods for the Study of Biomolecular Complexes*, Kluwer Acad. Publ., Dardrecht, 1998, pp. 17-43.
4. Janus, C. et al. *Nature* **408**, 979 (2000).
5. McLaurin, J., et al. *Nature Med.* **8**, 1263 (2002).

Peptide Revolution: Genomics, Proteomics & Therapeutics
Michael Chorev & Tomi K. Sawyer (Editors)
American Peptide Society, 2003

Expression of a Synthetic Gene Encoding Human Transthyretin in *Escherichia coli*

Kimiaki Matsubara, Mineyuki Mizuguchi and Keiichi Kawano

Faculty of Pharmaceutical Sciences, Toyama Medical and Pharmaceutical University, 2630 Sugitani, Toyama 930-0194, Japan

Introduction

Transthyretin (TTR) is a tetrameric protein with a total molecular mass of 55 kDa and 127 amino acid residues per subunit, and has a β-sheet rich structure. Although the mechanism is not fully understood at present, TTR misfolds into amyloid fibrils and causes amyloid diseases including senile systemic amyloidosis (SSA) and familial amyloid polyneuropathy (FAP). More than 80 different single-site mutants of TTR are known, and most of them are associated with FAP. Nevertheless, mutations are not an inherent requirement for amyloid fibril formation, for the reason that the wild-type TTR can form amyloid fibrils in middle-aged individuals, a condition known as SSA. Hence, the ability to form amyloid fibrils is an essential property of human TTR.

It has been reported that an expression system for TTR was constructed using *Escherichia coli*. First, Furuya *et al*. produced the Val30Met TTR variant using the pIN-III-ompA-1 system, which produced a fusion protein with an *E. coli* outer membrane protein A [1]. Second, Murrel *et al*. produced wild-type human TTR and five variant TTRs using the thermoinducible expression vector pCZ11 [2]. However, the level of expression in the previous systems was not high enough to produce large quantities of human TTR. To facilitate the research on amyloid formation, a high-expression system for the large-scale production of human TTR of a high quality is required. In this study, we constructed a high-level expression plasmid of human TTR using a fully synthetic gene, in which the codons were optimized for *E. coli*. Furthermore, in order to study the mechanism of amyloid fibril formation, four pathogenic mutant TTRs were produced by our expression system.

Results and Discussion

We have developed a procedure for the efficient expression and purification of human TTR fused to a six-histidine tag, using the expression vector pQE30 (QIAGEN). The recombinant human TTR was overexpressed in *E. coli* as a polyhistidine fusion protein and efficiently purified by single-step metal affinity chromatography. Our procedure has significant improvements over the previous methods because of the simplification of the purification protocol and the increase in the yield of the recombinant human TTR. We designed and constructed a synthetic gene based on the reported amino acid sequence of human TTR introducing frequently used *E. coli* codons. For highly expressed proteins, there is a strong correlation between the abundance of *E. coli* transfer RNAs and the occurrence of the respective codons in the protein genes [3]. The use of optimal codons for *E. coli* enabled the high-level expression of human TTR in *E. coli*. In this study, 130 mg of pure protein was obtained per 1 L of growth medium (Table 1). Moreover, the recombinant TTR fused to a polyhistidine tag formed a tetramer under physiological conditions and amyloid fibril formation under acidic conditions like the authentic human TTR. Therefore, our expression system provides a useful method for preparing a large amount of human TTR, and will facilitate the study of amyloidosis caused by the deposition of amyloid fibrils of human TTR.

Table 1. Purification of recombinant wild-type transthyretin from Escherichia coli.

Purification step	Total protein	Purity[a]
	(mg)	(%)
Supernatant after lysis[b]	44.3	45
Ni-NTA column eluate	13.6	99-100

[a]*The ratio of wild-type TTR to total protein was determined by gel scan.*

[b]*Fractions were collected from 100 ml initial volume of bacterial culture.*

Four pathogenic TTR variants, Val20Ile (V20I), Ser23Asn (S23N), Pro24Ser (P24S) and Ser112Ile (S112I) were produced by our expression system in order to study the mechanism of amyloid fibril formation. [4-7]. Quaternary structures of wild-type, V20I, S23N and S112I TTRs were investigated by analytical gel filtration chromatography. The chromatograms of V20I and S23N variants showed one peak with elution volume of 10.0 ml, corresponding to molecular mass of the tetramer. Interestingly, the S112I variant showed a peak corresponding to the molecular mass of 29 kDa. This result indicates that S112I TTR exists as a dimer under physiological conditions. In order to compare the relative amyloidogenicity of the S23N, P24S, S112I variants with wild-type TTR, we also investigated the amyloid fibril formation by turbidity and thioflavin-T binding assay. The S23N, P24S variants formed 4-fold more fibrils than wild-type TTR as judged by turbidity and 3-fold more as judged by thioflavin-T binding. However, using thioflavin-T binding assay, the extent of amyloid fibril formation for the S112I variant was similar to that of wild-type TTR. Therefore, our results indicate that the S23N and P24S variants are more amyloidogenic than the S112I variant.

Acknowledgments

This study was supported by grants from the Ministry of Education, Culture, Sports, Science and Technology of Japan; by Program for Promotion of Basic Research Activities for Innovative Biosciences (Japan); by National Project on Protein Structural and Functional Analyses; and by a grant from the Ministry of Agriculture, Forestry and Fisheries of Japan (Rice genome Project PR-4101).

References

1. Furuya, H., Nakazato, M., Saraiva, M. J., Costa, S. P., Sasaki, H., Matsuo, H., Goto, I. and Sakaki, Y. *Biochem. Biophys. Res. Commun*. **163**, 851-9 (1989).
2. Murrell, J. R., Schoner, R. G., Liepnieks, J. J., Rosen, H. N., Moses, A. C. and Benson, M. D. *J. Biol. Chem*. **267**, 16595-600 (1992).
3. Ikemura, T. *J. Mol. Biol.* **151**, 389-409 (1981).
4. Jenne, D. E., Denzel, K., Blatzinger, P., Winter, P., Obermaier, B., Linke, R. P. and Altland, K. *Proc. Natl. Acad. Sci. U.S.A*. **93**, 6302-6307 (1996).
5. Connors, L. H., Theberge, R., Skare, J., Costello, C. E., Falk, R. H. and Skinner, M. *Amyloid: Int. J. Exp. Clin. Invest*. **6**, 114-118 (1999).
6. Uemichi, T., Gertz, M. A. and Benson, M. D. *J. Med. Genet.* **32**, 279-281 (1995).
7. De Lucia, R., Mauro, A., Di Scapio, A., Buffo, A., Mortara, R., Orsi, L. and Schiffer, D. *Clin. Neuropathol*. **12**, S44 (1993).

Peptide Drug Delivery, Targeting and Biomaterials

Peptide Revolution: Genomics, Proteomics & Therapeutics
Michael Chorev & Tomi K. Sawyer (Editors)
American Peptide Society, 2003

Interactions Between Lipid Bilayer and pH-Triggered Amphiphilic Peptides

Hsienming Lee and Jean Chmielewski

Department of Chemistry, Purdue University, West Lafayette, IN 47906, USA

Introduction

Peptide and membrane interactions are very important in many pharmaceutical areas, such as peptide antibiotics [1], peptide-assisted liposomal drug delivery [2] and peptide-assisted gene delivery [3]. There are two major interactions between peptides and the lipid bilayer: electrostatic and hydrophobic [4]. Electrostatic and hydrophobic interactions act concertedly to promote the initial binding between the membrane and the membrane active peptide. For instance, positively charged antibiotic peptides facilitate initial binding to the membrane through electrostatic interactions. It is also known that amphiphilicity and α-helicity act to increase the membrane binding and membrane permeability [5].

In previous work, a membrane active peptide was designed, EALA1, to facilitate liposomal cargo unloading in cells [2]. The peptide was found to undergo a pH-dependent conformational switch from random coil to amphiphilic and helical upon acidification from neutral pH. Folate-targeted liposomes containing EALA1 were found to release their contents into the cytoplasm where pH is lower. In this system, the driving force bringing EALA1X peptide to the liposome membrane is mainly the hydrophobic force. Little electrostatic attraction, which is widely observed in the native systems such as NLS and antibiotic peptides, is used.

In order to develop a superior peptide-assisted liposomal drug delivery system, one needs to find a peptide sequence that is soluble and membrane inactive at neutral pH. At lower pH values, this peptide will switch its conformation and have a strong initial membrane binding that will increase the local peptide/membrane ratio. A higher peptide/lipid ratio should promote peptide-aggregated pore formation within the bilayer leading to cell membrane-liposome fusion, or liposome lysis.

EALA1X	NH_2-AALAEALAEALAEALAEALAEALAAAA-$CONH_2$
EALA5X	NH_2-AALAEALAEELLEALEELLAEALAAAA-$CONH_2$
EALA7X	NH_2-EALLEALAEALAEALAEALAEALAELA-$CONH_2$

To increase the helical switch, EALA5X was designed. EALA5X has more negative charge in physiological pH to destabilized helix formation in neutral pH (originally designed to prevent leakage in neutral pH). However, the membrane activity is less then EALA1X. Therefore, EALA7X was designed to have the same negative charge and the same hydrophobic residues although Glu and Leu are evenly distributed along the helix. EALA7X has membrane activity similar to EALA1X. Electrostatic interaction was also introduced into this liposome/peptide system by using cationic lipid containing liposome. The idea is to increase peptide/lipid interaction and we found that EALA7X is more effectively encapsulated in cationic liposome. Here, we demonstrate the new liposome formulation that contains 5% of cationic lipid 1,2-Dioleoyl-3-trimathylamonium-propane (DOTAP) and show that this liposome formulation helps increase lipid/peptide interactions.

Table 1. Helicity of EALA peptides in different environments measured by CD.

	pH = 7.5			pH = 6.0			pH = 5.0		
	Buffer	Neutral liposome	Cationic liposome	Buffer	Neutral liposome	Cationic liposome	Buffer	Neutral liposome	Cationic liposome
EALA1X	20%	30%	30%	25%	48%	53%	35%	65%	65%
EALA5X	13%	15%	20%	20%	40%	60%	55%	70%	70%
EALA7X	15%	28%	45%	25%	52%	70%	50%	70%	70%

Neutral liposomes contain 100% Egg phosphotidyl choline (PC). Cationic liposome contain 95% EggPC and 5% of cationic lipid 1,2-Dioleoyl-3-trimathylamonium-propane (DOTAP). Liposome size is 50 μm in diameter. Peptide concentration is 10 μM and lipid concentration is 1 mM.

Results and Discussion

The most important observation in the CD experiments is that peptide helicity can be induced by liposomes and different liposome compositions in pH 7.5 and pH 6.0 induce increase in helicity of each peptide to different extents (Table 1). In pH 7.5, EALA7X is much less helical in aqueous buffer. The helicity increased when peptide incubates with neutral liposome (hydrophobic force contribution) and helicity increasea even more in cationic liposome environment (hydrophobic + electrostatic interaction). EALA1X shows general peptide/liposome interaction, indicated by the fact that helicity increases in liposome environment but helicity does not differ in neutral or cationic liposome in pH 7.5. It could be that EALA1X has fewer Glu residues and therefore electrostatic interaction is not significant. EALA5X is highly random coiled in pH 7.5 with or without the presence of liposomes. It is probably that the Glu residues are too close to each other so that even when liposome and peptide bind together (the number of Glu in EALA5X is the same as EALA7X), the repulsion force between Glu residues is large enough to keep the peptide conformation in random coil. This repulsion force will decrease when pH drops and that is why we can observe the EALA5X become helical and can discriminate neutral and cationic liposome by showing higher helicity in cationic liposome solution. The helicity of all peptides in pH 5.0 are almost the same in both neutral and cationic liposome solutions but less helical in aqueous phase. This could be attributed to the fact that most of the Glu residues on all peptides are protonated and therefore lose the electrostatic interaction. The phenomena observered here in pH 7.5 also agree with the observation that EALA5X and EALA7X have higher encapsulation ratios compared to EALA1X in cationic liposome.

References

1.Shai, Y. *Biochem. Biophys. Acta -Biomem.* **1462**, 55-70 (1999).

2.Vogel, K., Lee, R. J., Low, P. S. and Chmielewski, A. J. *J. Am. Chem. Soc.* **118**, 1581-1586 (1996).

3 Zanta, M. A., Belguise-Valladier, P. and Behr, J. P. *Proc. Natl. Acad. Sci. U.S.A.* **96**, 91-96 (1999).

4. Zasloff, M. *Nature* **415**, 389-395 (2002).5. Turk, M. J., Reddy, J. A., Chmielewski, J. A. and Low, P. S. *Biochem. Biophys. Acta -Biomem.* **1559**, 56-68 (2002).

6. Parente, R. A., Nir, S. and Szoka, F. C. *Biochemistry* **29**, 8720-8728 (1990).

Peptide Revolution: Genomics, Proteomics & Therapeutics
Michael Chorev & Tomi K. Sawyer (Editors)
American Peptide Society, 2003

Application of Oligoarginine for the Delivery of Protein Complexes into Living Cells

Shiroh Futaki[1], Ikuhiko Nakase[1], Miki Niwa[1], Tomoki Suzuki[1], Daisuke Nameki[2], Ei-ichi Kodama[2], Masao Matsuoka[2] and Yukio Sugiura[1]

[1]Institute for Chemical Research, Kyoto University, Uji, Kyoto 611-0011, Japan;
[2]Institute for Virus Research, Kyoto University, Sakyo-ku, Kyoto 606-8507, Japan

Introduction

Arginine-rich peptides derived from human immunodeficiency virus (HIV)-1 Tat and Drosophila Antennapedia homeodomain protein have been reported to translocate through cell membranes quite easily and to be utilized as carriers for the intracellular delivery of various oligopeptides and proteins *in vitro* and *in vivo* [1]. The delivery of a 120 kDa protein, β-galactosidase in its active form, into the brain of a mouse was also reported using the Tat peptide as a carrier [2]. We have demonstrated that not only Tat-(48-60) and Antennapedia-(43-58) but also various arginine-rich basic peptides derived from RNA/DNA-binding proteins, such as HIV-1 Rev-(34-50), were membrane-permeable and have the ability to carry exogenous proteins into cells [3]. Octaarginine (R_8) showed similar ability. We report here the delivery of RNase S bearing an arginine-rich segment. RNase S is a non-covalent protein complex which is composed of the S-peptide (positions 1-20 of bovine pancreatic RNase A) and the S-protein (positions 21-124). We report here that this non-covalent protein complex can be introduced into living cells while retaining its activity.

Results and Discussion

The design of RNase S bearing an arginine-rich segment is illustrated in Figure 1. The S-peptide was conjugated with a membrane-permeable basic peptide such as HIV-1 Tat-(48-60), HIV-1 Rev-(34-50), and octaarginine composed of L- and D-arginines (R_8 and DR_8, respectively). The S-peptide and the S-protein do not retain RNase activity by themselves. But when mixed together, they fold into a complex and exert an RNase activity. The design of RNase S bearing the Rev-(34-50) segment was identical with the complex, which we previously showed to cleave an RNA corresponding to the Rev

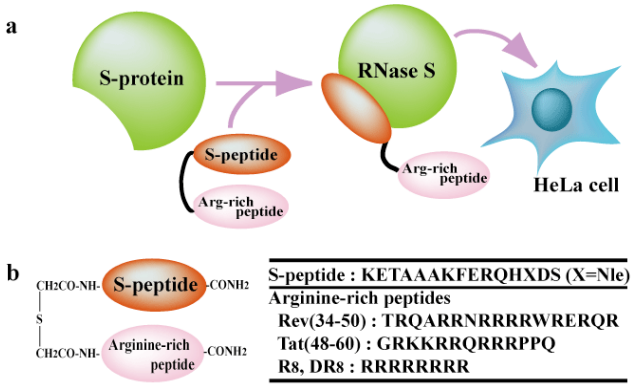

Fig. 1. The schematic representation of (a) the RNase S complexes bearing arginine-rich segments, and (b) amino acid sequence of S-peptide and basic peptides.

binding site (the Rev response element, RRE) [4]. The S-protein was labeled with the fluorescein-5-EX succinimidyl ester for microscopic observation.

Internalization of the RNase S complexes bearing these arginine-rich peptides was assessed using HeLa cells. The HeLa cells were incubated with a medium containing a protein complex (10 μM) at 37 °C for 3h. The cells were washed with PBS, soaked with fresh medium and subjected to confocal microscopic observation. Internalization of the complex was substantially recognized in all the cells treated with RNase S bearing the respective arginine-rich peptides. On the other hand, significant internalization was not observed for RNase S without the arginine-rich peptides. Note that the fluorescein probe was attached only on the S-protein, suggesting that the S-protein was internalized with retention of its complex structure.

The RNase S bearing the Rev segment has been shown to hydrolyze a single predominant position of the RNA stem-loop derived from the specific binding site for HIV-1 Rev protein. We have shown that these RNase S bearing an arginine-rich peptide translocate through cell membrane. These facts facilitated us to examine the anti-HIV activity of these complexes. The anti-HIV activity was determined in the multinuclear activated β-galactosidase indicator assay (MAGI assay). HIV-1 infection in HeLa CD4/LTR-β-Gal cells leads to the activation of the indicator β-galactosidase gene driven by Tat-LTR transactivation after 48 h of viral inoculation, which were ultimately seen as blue cells. Thus, in the MAGI assay, the anti-HIV activity, if exhibited at or before Tat protein formation during a virus life cycle, can be demonstrated by a decrease in the number of blue cells. The activity of the RNase S bearing the Rev, Tat, R_8 and DR_8 peptides, represented as the concentration that blocks HIV-1 replication by 50 % (EC_{50}), was 1.7, 2.9, 0.67, and 0.65 μM, respectively. The EC_{50} value of AZT under the same condition was 0.016 μM. Although the activity of the RNases was lower than that of AZT, the RNases exerted anti-HIV activity in the cells. On the other hand, significant suppression was not observed at 10 μM for the RNase S that does not contain an arginine-rich segment.

To determine the interaction stage of these RNase S complexes for one cycle of HIV replication, a time of drug addition experiment was conducted. The effect of RNase S bearing these arginine-rich peptides decreased slower than dextran sulfate (DS) and faster than MKC442. These results indicate that the action stage of these RNase S complexes should be between the adsorption of the virus on the cell surface and the start of reverse transcription. Details of the mechanisms of these RNase S complexes showing the anti-HIV activity have not been clarified at the present stage.

In this report, we have shown that RNase S bearing an arginine-rich peptide internalize into living cells to show anti-HIV activity. These results suggest that protein transduction using arginine-rich peptides occurs with retaining non-covalent protein complex structure. Such findings may help us to understand the mechanisms of transduction.

References

1. Waida, J. S. and Dowdy, S. F. *Curr. Opion. Biotechnol.* **13**, 52-56 (2002).
2. Schwarze, S. R., Ho, A., Vocero-Akbani, A. and Dowdy, S. F. *Science* **285**, 1569-1572 (1999).
3. Futaki, S., Suzuki, T., Ohashi, W., Yagami, T., Tanaka, S., Ueda, K. and Sugiura, Y. *J. Biol. Chem.* **276**, 5836-5840 (2001).
4. Futaki, S., Araki, M., Kiwada, T., Nakase, I. and Sugiura, Y. *Bioorg. Med. Chem. Lett.* **11**, 1165-1168 (2001).

Peptide Revolution: Genomics, Proteomics & Therapeutics
Michael Chorev & Tomi K. Sawyer (Editors)
American Peptide Society, 2003

In Silico Investigation of LogP Parameters of Amino Acids and Peptides Tethered to C-Alkylated Sugar Bioconjugates

Piotr A Mroz, Florence M. Brunel, K. Grant Taylor and Arno F. Spatola

Department of Chemistry, University of Louisville, Louisville, KY 40249, USA; Institute for Molecular Diversity and Drug Design, University of Louisville, Louisville, KY 40292, USA

Introduction

A new class of bioconjugates based on the C-alkylated sugar scaffold has been introduced by our group. [1] Peralkylation of the hydroxyl groups allows the preparation of the diverse series of polyetheral structure (Figure 1) with a wide range of *n*-octanol-water partition ability. In addition, replacement of exocyclic oxygen by carbon increases the stability of these bioconjugates in an acidic, basic or enzymatic environment. We report here an *in silico* study to better characterize the lipophilicity of this new class of bioconjugates and evaluate the predictive power of popular and commercially available computational packages.

Results and Discussion

For estimation of water solubility and the *n*-octanol-water partition coefficient (the most widely used indicator of the compounds lipophilicity and bioavailability) we used the Virtual Chemistry Laboratory [2] which provided results for the atom/fragment contribution methods such as CLOGP, ALOGPS, IA_LOGP, KOWWIN, and XLOGP [2]. In addition, for the series of single amino acids tethered to our primary bioconjugate (α-D-2,3,4,6-tetra-O-methyl-mannosylb acetic acid), the DFT based COSMO-RS [3] method in Dmol3, Cerius2 [4] program was used to calculate logarithm of the partition coefficients for *n*-octanol-water, hexane-water, benzene-water and diethylether-water systems; RP-HPLC was performed for comparison. We selected three amino acids that spanned extremes in their *n*-octanol-water partition coefficients: phenylalanine, lysine and histidine.

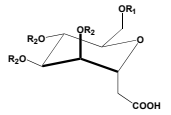

R_1 and R_2 = -CH_3, -CH_2CH_3, -CH_2CF_3

Fig. 1 Structure of α–D-2,3,4,6-(R_1,R_2) mannosyl acetic acid.

Table 1. Lipophilicity/hydrophobicity characteristic of single amino acids tethered to acetyl and α-D-2,3,4,6-tetra-O-methyl-mannosyl group.

STRUCTURE	R_t	Ex	**LogP** (atom/fragment contribution methods)					**log** of partition coefficients (DMOL3-COSMO-RS)			
	RP-HPLC	logP	*AlogPs*	*IA_logP*	*ClogP*	KOW *WIN*	*XlogP*	*oct./ wat.*	*hex./ wat.*	*benz./ wat.*	*Et_2O/ wat.*
Ac-**His**-NH_2	4.14	-1.70	-1.52	-1.64	-2.59	-1.80	-1.45	+0.23	-4.85	-2.68	-0.79
Ac-**Lys***-NH_2	4.14	-2.82	-0.94	-2.20	-1.90	-1.57	-0.97	+4.67	-4.04	-1.49	+6.82
Ac-**Phe**-NH_2	12.73	-0.04	+0.27	-0.13	-0.18	+0.13	+0.60	+1.54	-2.22	-0.34	+1.20
α–D-(OMe)$_4$Man(CH_2CO)-**His**-NH_2	8.87	N/A	-0.74	+0.72	-1.82	-3.15	-2.60	+3.50	-1.20	+1.32	+2.07
α–D-(OMe)$_4$Man(CH_2CO)-**Lys***-NH_2	8.78	N/A	-0.53	-0.49	-1.13	-2.92	-2.12	+7.64	+2.02	+4.37	+9.09
α–D-(OMe)$_4$Man(CH_2CO)-**Phe**-NH_2	19.53	N/A	+0.57	-0.57	+0.58	-1.22	-0.55	+3.84	+0.66	+2.78	+2.98

The increase in RP-HPLC retention time indicates that replacement of the N-terminal acetyl group by the methylated C-mannosyl acetic acid significantly increases its hydrophobicity (Table 1). This observation is consistent with the changes predicted by the DMOL3-COSMO-RS log of partition coefficients. It is also shown that different programs, which use the same methodology (atom/fragment contribution), can give dramatically different results regarding values of logP.

More importantly, they indicate opposite trends. The DMOL3 calculation, however, provides logP values, which are quite different from the reported experimental values. In these studies we were interested in the logP change trends due to the presence of C-alkylated sugar rather than in accurate prediction of its value, so that one may confidently conclude that the C-methylated sugar effectively increases lipophilicity of the investigated structure.

We postulate that mannosyl acetic acid can serve as a useful scaffold for this class of bioconjugates with a wide spectrum of logP values. In Table 2 we report average lipophilicity enhancement for the series of alkylated mannosyl acetic acid coupled with single amino aids relative to an acetyl group. It is important to note that this useful computational exercise can have only approximate and qualitative meaning. Relative to such a variety of results obtained, it is impossible to assign quantitative values for each bioconjugate without further experimental studies. In addition, studies with PERM-1 [5] coupled with a series of alkylated C-sugars indicate the complexity of the problem. It is impossible to correlate directly lipophilicity influence of our bioconjugates from single amino acid to peptides (Table 3). Importantly, these studies show that alkylated C-sugars can increase the lipophilicity of small peptides such as PERM-1 without drastically decreasing its water solubility.

Table 2. Average lipophilicity influence of series of alkylated mannosyl acetic acid.

C-sugar derivatives (X)	LogP(X-a.a.)-LogP(Ac-a.a)				
	AlogPs	*IA_logP*	*ClogP*	*KOWWIN*	***XlogP***
α–D-$(OMe)_4$Man(CH_2CO)-	0.50	1.21	0.77	-1.35	-1.15
α–D-(6-OEt,2,3,4-OMe).Man(CH_2CO)-	0.88	2.40	1.15	-0.86	-0.72
α–D-(6-$OEtF_3$,2,3,4-OMe) Man(CH_2CO)-	1.49	1.48	1.42	-0.44	0.28
α–D-$(OEt)_4$Man(CH_2CO)-	2.16	2.02	2.26	0.61	0.54
α-D-(6-$OEtF_3$,2,3,4-OEt) Man(CH_2CO)-	2.72	1.71	2.59	1.03	1.55
α-D-(2,3,4,6-$OEtF_3$)$_4$ Man(CH_2CO)-	4.17	5.29	3.38	2.28	4.55

Table 3. Lipophilicity and solubility prediction for series of alkylated mannosyl acetic acids tethered to cyclic nanopeptide PERM-I.

N-terminal attachments to PERM-I	logP					Solubility (S_w)	
	AlogPs	*IA_logP*	*ClogP*	KOWWIN	*XlogP*	*ALOGpS*	*IA_logS*
Ac	+0.08	+1.47	+0.41	-3.38	+0.22	28.43mg/L	1.79g/L
α-D-$(OMe)_4$Man(CH_2CO)-	+0.43	-0.41	+0.52	-3.51	-0.95	29.65mg/L	0.76g/L
α-D-(6-OEt,2,3,4-OMe) Man(CH_2CO)-	+0.64	-0.32	+0.91	-3.02	-0.53	27.41 mg/L	0.59 g/L
α-D-(6-$OEtF_3$,2,3,4-OMe) Man(CH_2CO)-	+1.06	-0.59	+1.17	-2.60	+0.47	27.38mg/L	1.12g/L
α-D-$(OEt)_4$Man(CH_2CO)-	+1.24	-0.20	+2.28	-1.55	+0.74	22.96mg/L	0.40g/L
α-D-(6-$OEtF_3$,2,3,4-OEt) Man(CH_2CO)-	+1.60	-0.18	+2.34	-1.13	+1.74	25.73 mg/L	25.32mg/L
α-D-(2,3,4,6-$OEtF_3$)$_4$ Man(CH_2CO)-	+2.86	N/A	+3.13	+0.12	+4.74	0.11g/L	N/A

References

1. Brunel, F. M., Leduc, A.- M., Mashuta, M. S., et al. *Lett. Pept. Sci.* **9**, 111-117 (2003).
2. (a) Tetko I. V., et al., *J. Chem. Inf. Comput. Sci.* **41**, 246-252 (2001); (b) Leo A. *Chem. Rev*. **93**, 1281-1306 (1993); (c) Meyland W. M., Howrd P. H., *J. Pharm. Sci*. **84**, 83-92 (1995); Wang R., Geo Y., Lai L., *Perspect. Drug Des.***19**, 47-56 (2000).
3. (a) Klamt A, Jonas V, Burger T, Lohrenz J. C. W. *J. Phys. Chem. A* **102**, 5074-5085 (1998); (b) Eckert F, Klamt A. *Ind. Eng. Chem. Res*. **40**, 2371-2378 (2001).
4. Accelrys Inc., Cerius2 Modeling Environment, Release 4.0, San Diego, Accelrys Inc., 1999.
5. Spatola, A. F., et al. In Lebl, M. and Houghten, R. A. (Eds.) *Peptides: The Wave of the Future,* American Peptide Society, San Diego, 2001, pp. 442-443.

Peptide Revolution: Genomics, Proteomics & Therapeutics
Michael Chorev & Tomi K. Sawyer (Editors)
American Peptide Society, 2003

Are Alkylated C-Sugars Useful as Solubility Buffers?

Florence M. Brunel, Amit K. Galande, Piotr A. Mroz, K. Grant Taylor and Arno F. Spatola

Department of Chemistry and the Institute for Molecular Diversity and Drug Design, University of Louisville, Louisville, KY 40292 USA

Introduction

A compound is a good drug candidate if it combines potent biological activity and suitable bioavailability. Many prospects lack acceptable solubility or their transport through biological membranes may not be efficient. One solution to modulate such properties is to introduce a bioconjugate, sometimes in the form of a prodrug. We have recently proposed the use of permethylated C-sugar derivatives as solubility modulators for enhancing peptide and non-peptide drug delivery [1, 2]. Our bioconjugate contains an acid or an amine functional group to allow easy attachment to a drug candidate. In one example, the amino acid analog was condensed to the N-terminus of an LXXLL-containing peptide [3]. The amide bond could be formed with either TFFH or BOP. The modified peptide showed interesting biological activity against a coactivator peptide/estrogen receptor α (K_i= 0.20 μM) and, even more significant was that its inhibitory activity with respect to estrogen receptor β actually increased compared to the parent molecule (0.27 μM vs. 0.39 μM) [2]. An ester derivative, introduced to illustrate the utility of the bioconjugate as a prodrug, was also formed by attaching the acid C-sugar to the side chain of a serine residue.

We assumed that the solubility (absolute and relative) of molecules attached to our bioconjugate would be improved. The absolute solubility is apparently enhanced: the solubility in different solvents (aqueous and organic) was shown to increase for a simple derivative such as leucine. More significantly, the infamously insoluble amino acid tyrosine saw its water solubility multiplied by a factor of at least 10.

Table 1. Comparison of the water solubility of two amino acids, neat or conjugated; the alkylated C-sugar is condensed to the N-terminal position in the case of leucine (amide) and on the phenol side-chain in the case of tyrosine (ester).

Amino Acid	Before conjugation (g/L)	After conjugation (g/L)	Minimum increase in solubility
Leucine (25 °C)	24[a]	>46	x 2
Tyrosine (21 °C)	421-427	4670-5250	x 10

[a] *literature value, Merck Index, 11th edition (1989).*

Results and Discussion

In a number of instances, relative solubility, studied by comparing retention times obtained from HPLC experiments, showed an increase in overall lipophilicity (Table 2). We initially postulated that introducing the C-sugar bioconjugate would have a buffer effect on a compound's solubility, but this seems not to be the case. The observed increases in lipophilicity, especially if accompanied with an improvement in absolute solubility, could nevertheless result in better transport through membranes, and potentially contribute to improved bioavailability.

Table 2. A comparison of RP-HPLC retention times for several amino acids with either N-terminal acetyl or alkylated C-sugar adducts.

Amino Acid	With the acetyl group	With the bioconjugate
Phenylalanine	12.73	19.53
Histidine	4.14	8.87
Lysine	4.14	8.78

We believe that the most useful application for our alkylated C-sugar may be in improving the solubility of compounds that are less suitable as drugs due to this factor. Many peptides and some pharmaceutical agents, such as the anticancer drug Taxol, are known to suffer from poor solubility. Future efforts will focus on modifying our alkylated C-sugars (base sugar, configuration, alkyl groups, and attachment modes) to assess their suitability in these applications.

References

1. Brunel, F. M., Taylor, K. G. and Spatola, A. F. *Tetrahedron Lett.* **2003**, 44, 1287-1289.
2. Brunel, F. M., Leduc, A. M., Mashuta, M., Taylor, K. G. and Spatola, A. F. *Lett. Pept. Sci.* **2003**, 9, 111-117.
3. Spatola, A. F., Leduc, A., Wittliff, J. L., Taylor, K. G. *Proceedings of the 17th American Peptide Symposium*, **2001** p. 442.

Peptide Revolution: Genomics, Proteomics & Therapeutics
Michael Chorev & Tomi K. Sawyer (Editors)
American Peptide Society, 2003

Conformation and Bioactive Properties of Novel Osteoblast-Adhesive Peptides for Biomaterial Design

Manuela Vacatello[1], Gabriella D'Auria[1], Lucia Falcigno[1], Romina Oliva[1], Carmen Bevilacqua[1], Monica Dettin[2], Maria T. Conconi[3], Roberta Gambaretto[2], Carlo Di Bello[2] and Livio Paolillo[1]

[1]Department of Chemistry, University "Federico II" of Naples, 80126 Naples, Italy;
[2]Department of Chemical Process Engineering, University of Padua, 35131 Padua, Italy;
[3]Department of Pharmaceutical Sciences, University of Padua, 35131 Padua, Italy

Introduction

Proactive dental/orthopedic biomaterials are designed to enhance and support osteoblast adhesion and growth [1]. The adhesion process is an early effect of tissue genesis before the osteoblasts proliferate and organize into a functional tissue, and therefore represents a crucial step for the complete implant integration. The osteoblasts use different ways to adhere, that is, integrin- [2] and proteoglycan- [3] mediated mechanisms. Both mechanisms involve interaction of these osteoblast receptors with consensus motives on extracellular matrix (ECM) proteins; namely the tripeptide RGD for integrin adhesion, and multibasic sequences for proteoglycan interaction. ECM proteins are involved in the adhesion process of different types of cells, including osteoblasts, and among them fibronectin and vitronectin are believed to have a primary role. The clinical use of these natural proteins to promote osteoblast adhesion is complicated due to their size, instability, insolubility and to the fact that the entire tertiary structure is needed for biological activity. A valid alternative is the employment of short peptide sequences, carrying the adhesive and growth motives, which are usually stable, soluble, obtainable in high quantities, with a good percentage of purity and at low costs.

The best known motif that promotes cell adhesion is the tripeptide RGD which is contained in many ECM molecules, including fibronectin and vitronectin. This active sequence has been extensively used to develop peptides capable of enhancing cell adhesion on biomaterials [4]. The second mechanism for cell adhesion to ECM proteins through cell surface proteoglycans [3] involves multibasic sequences of the type BBXB and BBBXXB [5] (X= Hydropatic residue, B= positively charged residue), also known as heparin-binding sites. Recent studies have demonstrated the essential role of this second mechanism in promoting osteoblast adhesion; in fact peptides incorporating the fibronectin heparin binding site and RGD cell-binding site enhanced the degree of rat calvarial osteoblast surface interaction and influenced the long term formation of mineralized ECM *in vitro* [6].

Vitronectin also expresses a primary heparin binding site localized in the 341-380 sequence [7]. This protein was shown to have an essential role for *in vitro* spatial distribution, attachment and spreading of osteoblasts [8], making it a good candidate for bone biomaterial design.

Here we report on the structural characterization via CD, NMR and computational methods of a series of novel peptides carrying heparin-binding sites mapped on the human vitronectin sequence in Figure 1.

^{339}MAPRPSLA**KKQR**F**RHRNRK**GYRSQRG^{364}

Fig. 1. Sequence 339-364 of human vitronectin.

The sequence reported here includes both the multibasic consensus sequences (shown in bold). The structural results will be discussed in relation to the exhibited adhesive activities towards osteoblasts *in vitro* [9].

Results and Discussion

The N-terminal 13-mer peptide, the C-terminal 14-mer peptide and two 9-mer peptides, linear and cyclic forms, derived from the vitronectin sequence, were synthesized by solid-phase methods using a fully automated peptide synthesizer via Fmoc chemistry.

The adhesion assay was carried out through conditioning of polystyrene plates with the peptides and then testing their adhesive activities toward osteoblasts from bone marrow of femora of adult Sprague-Dowley rats (for experimental see [9]). The results, displayed in Figure 2, were expressed as % of optical density and normalized over the amount of adsorbed peptide. The best adhesive activities were shown by the shorter sequences, in particular the cyclic 9-mer. The 9-mer peptides also showed the best adsorption properties on polystyrene.

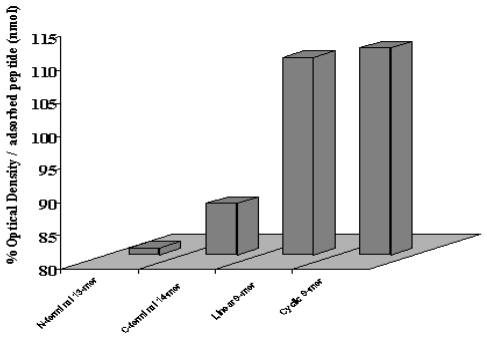

Fig. 2. Osteoblast adhesion assay on polystyrene plates.

CD spectra were recorded at room temperature on a Jasco Model J710 automatic recording circular dichrograph. Peptide concentration was 2.0×10^{-5} M. The spectra in 98% TFE showed a contribution of about 50% of flexible conformation and 50% of structure going from β-sheet to turn. Interestingly the linear 9-mer showed the same conformational features in different solvents.

The NMR analysis of the peptides was performed in TFE/H_2O 90:10 (v/v) at 11.7 T. A set of experimental constraints from NOE data were determined for structure calculations. One hundred conformers were calculated with the DYANA program [10] (REDAC strategy) and the best 30 DYANA structures were then subjected to restrained energy minimization by the AMBER 6.0 package [11]. The best 10 structures after AMBER refinement were selected to represent the peptide conformation.

This procedure was followed for all peptides except for the cyclic 9-mer peptide for which restrained molecular dynamics simulations were performed for structure calculation. The RMD simulation was carried out in vacuo at 300K, for 210 ps, with 0.5 fs time steps using the DISCOVER/INSIGHT package. Data recorded during the last 50 ps of the simulation were used for the statistical analysis.

The molecular models display overall flexible conformations, with more structurally defined segments 5 to 6 residues long, where the root mean square deviations on backbones fall from about 3.00 Å to around 1.15 Å. These segments

display extended-type structures and/or bendings. The more structurally defined areas involve the central parts of the peptides where most of the basic residues are located, except for the N-terminal 13-mer peptide, which in fact displays the basic residues in the more flexible C-terminal end.

A clearer insight into the conformational features that explain the exhibited adhesive activities is found in the spatial arrangement of the basic residues side chains. The orientation of the positively charged chains was tested against a model of heparin dodecasaccharide [12] with the INSIGHT program.

The results show that two requisites are essential: the clustering of basic residues on one face of the peptide, and the spacing between the charges. These results are in agreement with previous findings [5, 13]. We believe that the higher spacing between charges becomes particularly important for the interaction with the less sulfated glycosaminglycan heparan-sulfate.

References

1. Anselme, K. *Biomaterials* **21**, 667-681 **(**2000).
2. Puleo, D. A. and Bizios, R. *Bone* **12**, 271-276 (1991).
3. Dalton, B. A., McFarland, C. D., Underwood, P. A., and Steele, J. G. *J. Cell Sci*. **108**, 2083-2092 (1995).
4. Schaffner, P. and Dard, M. M. *CMLS Cell. Mol. Life Sci.* **60**, 119-132 (2003).
5. Cardin, A. D. and Weintraub, H. J. R. *Arteriosclerosis* **9**, 21-32 (1989).
6. Rezania, A. and Healy, K. E. *Biotechnol. Prog.* **15**, 19-32 (1999).
7. Suzuki, S., Pierschbacher, M. D., Hayman, E. G., Nguyen, K., Ohgren, Y.and Ruoslahti, E. *J. Biol. Chem.* **259**, 15307-15314 (1984).
8. Thomas, C. H., Mc Farland, C. D., Jenkins, M. L., Rezania, A., Steele, J. G. and Healy, K. E. *J. Biomed. Mater. Res.* **37**, 81-93 (1997).
9. Dettin, M., Conconi, M. T., Gambaretto, R., Pasquato, A., Folin, M., Di Bello, C. and Parnigotto, P. P. *J. Biomed. Mater. Res.* **60**, 466-471 (2002).
10. Güntert, P., Mumenthaler, C. and Wutrich, K. *J. Mol. Biol.* **273**, 283-298 (1997).
11. Case, D. A., Pearlman, D. A., Caldwell, J. W., Cheatham III, T. E., Ross, W. S., Simmerling, C. L., Darden, T. A., Merz, K. M., Stanton, R. V., Cheng, A. L., Vincent, J. J., Crowley, M., Tsui, V., Radmer, R. J., Duan, Y., Pitera, J., Massova, I., Seibel, G. L., Singh, U. C., Weiner, P. K. and Kollman P. A., AMBER 6, University of California, San Francisco (1999).
12. Mulloy, B., Forster, M. J., Jones, C. and Davies, D. B. *Biochem. J.*, **293**, 849-858 (1993).
13. Margalit, H., Fischer, N. and Ben-Sasson, S. A. *J. Biol. Chem.* **268**, 19228-19231 (1993).

Peptide Revolution: Genomics, Proteomics & Therapeutics
Michael Chorev & Tomi K. Sawyer (Editors)
American Peptide Society, 2003

Evolutionary Combinatorial Chemistry, a Novel Tool for SAR Studies on Peptide Transport Across the Blood-Brain Barrier 1. Design, *In Silico* Validation and First Peptide Generation

Meritxell Teixidó[1], Ignasi Belda[1,2], Sonia González[3], Míriam Fabre[3], Senén Vilaró[3], Josep M. Garrell[2], Xavier Roselló[4], Fernando Albericio[1,5] and Ernest Giralt[1,5]

[1]Biomedical Research Institute, Barcelona Science Park, Universitat de Barcelona; [2]Dept. Sistemes Intel.ligents, E. Eng. La Salle, Univ. Ramon Llull; [3]Advancell, Barcelona Science Park, Universitat de Barcelona; [4]Universitat Politècnica de Catalunya; [5] Dept. Química Orgànica, Universitat de Barcelona, Barcelona, E-08028, Spain

Introduction

Many peptides with therapeutic potential for treatment of Central Nervous System (CNS) disorders have recently been identified. Successful drug development requires efficient delivery to the site of action. Drugs directed towards targets in the CNS must overcome the blood-brain barrier (BBB). The BBB is a vital tool for the regulation of the internal environment of the brain. The BBB is formed at the level of the endothelial cells of the cerebral capillaries; these cells have tight junctions between them prohibiting any paracellular pathway between the cells. There is a great need for a systematic study of molecular structure and properties of peptide-based drugs that are able to pass through the BBB. No general tool to predict the transport of peptides across the BBB has been established, and there are many exceptions to the existing rules based on the few systematic studies which have been performed. The few available data are not representative in terms of diversity.

The novel approach, Evolutionary Combinatorial Chemistry, combines the selection and synthesis of biologically active compounds with artificial intelligence optimization methods. Genetic Algorithms (GA) are evolutive tools classified in the evolutive computational branch of Artificial Intelligence Science. They were first proposed in 1975 by Holland and are based on natural evolution as described by Darwin, wherein individuals with the highest degree of adaptation to an environment will have a greater chance of survival.

GA make individuals evolve, so individuals will increase their fitness step by step. A GA is composed of five stages: initialization (creation of the first generation), selection (selection of individuals who are going to be crossed-over to obtain the next generation), cross-over (mating between individuals who are going to be crossed over hence obtaining new individuals), mutation (change in the value of a gene) and elitism (percentage of intact individuals of the previous generation whom will be kept in the new one).

Once we have the fitness of the individuals of one generation, the GA will propose which are the individuals of next generation. The individuals are represented in a uniform way in all GA as a chromosome. A chromosome is a gene sequence in which each gene represents one of the solution parameters. Our GA works with chromosome (genotypes) that are sets of physico-chemical properties whereas the phenotypes are peptide sequences. The set of genes composing our chromosome are the physico-chemical properties believed to be relevant for the transport of peptides across the BBB. It is our hope that the GA will allow us to increase our knowledge about the genome of peptides able to cross the blood-brain barrier.

Table 1. GA optimized parameters.

Initialization	Geometry	%Replication	Crossover Probability	Parent Selection	
Random	*24x10*	*20*	*0.95*	*Fitness Ranking*	
Scaling	Crossover	Mutation Probability	Mutation	Parents in Crossover	Children in Crossover
Direct	*1-point Random*	*0.1*	*Random to all alleles*	*2*	*2*

Results and Discussion

Since genetic algorithms are highly configurable tools, the ideal configuration for our project was not known. Thus a meta-algorithm was designed to optimize our genetic algorithm. Also, the GA was optimized for this project. The optimized configuration of the GA for our project is shown in Table 1.

To obtain the fitness of the peptides, the permeability of the peptides through the BBB is determined using an *in vitro* BBB model. This model consists of two compartments that mimic the blood and the brain. The Bovine Brain Endothelial Capillary (BBEC) cells are grown on a filter and form tight junctions due to the presence of astrocites. The peptide is added to the apical compartment and samples are collected from both compartments at different times. This assay has been optimized using the following test peptides: RC-161, a Somatostatine analogue with passive diffusion *in vivo*, AVP 1-9, a Vasopresine fragment, also described in an *in vitro* BBB model that uses BBEC cells and Met5-Enk, described also to have transport in an *in vitro* BBB model that uses BBEC cells. The optimized parameters for the *in vitro* assay are shown in Table 2. The first generation of 24 peptides has already been synthesized.

Table 2. In vitro assay optimized parameters.

Cells	Medium	Sample Volume	Apical Volume	Basal Volume
BBEC	*Hanks Buffer*	*150 μL*	*1500 μL*	*3000 μL*
Time of analysis	Transwell surface	Initial Conc.	Cells/Transwell	Controls
90 min	*4.7 cm^2*	*1mM*	*40.000cel./Tw*	*TEER, Manitol-^{14}C, Inulina-^{3}H*

References

1. Pardridge, W. M. Peptide Drug Delivery to the Brain. Raven Press, New York (1991).
2. Holland, J. E. Adaptation In Natural and Artificial Systems; The University of Michigan Press: Ann Arbor, MI, (1975).
3. Weber, L. *Drug Discov. Today* **3**, 379-385 (1998).
4. Patel, S., Stott, I., Bhakoo, M. and Elliott, P. *Patenting evolved bactericidal peptides*. In Bentley, P. J. and Corne, D. W. (Eds.), *Creative Evolutionary Systems*, Morgan Kaufmann Publishers pp. 525-545 (2001).
5. Cecchelli, R., et al. *Advanced Drug Delivery Reviews* **36**, 165-178 (1999).

Peptide Revolution: Genomics, Proteomics & Therapeutics
Michael Chorev & Tomi K. Sawyer (Editors)
American Peptide Society, 2003

Structural Requirements for Non-Covalent Peptide-Mediated Cellular Delivery of siRNAs

Sébastien Deshayes, Nicole Van Mau, May C. Morris, Gilles Divita and Frédéric Heitz

CRBM-CNRS, FRE 2593, 1919, route de Mende, 34293 Montpellier, France

Introduction

We have compared the influence of the sequence and potentially of the conformational state of primary amphipathic carrier peptides on their ability to deliver small interfering RNA (siRNA) cargos into living cells. Here, we describe the behavior of four peptides with closely related sequences. The sequences are the following:

G-A-L-F-L-G-F-L-G-A^{10}-A-G-S-T-M-G-A-W-S-Q^{20}-P-K-K-K-R-K-V ***1***
G-A-L-F-L-G-F-L-G-A^{10}-A-G-S-T-M-G-A-W-S-Q^{20}-P-K-**S**-K-R-K-V ***2***
G-A-L-F-L-A-F-L-**A**-A^{10}-A-**L**-S-**L**-M-G-**L**-W-S-Q^{20}-P-K-K-K-R-K-V ***3***
L-F-L-G-**W**-L-G-A-A-G - W-S-Q - P-K-K-K-R-K-V ***4***

All peptides were N-acetylated and have a cysteamide group (NH-CH_2-CH_2-SH) at their C-terminus.

The parent peptide ***1*** results from the association of a hydrophobic sequence derived from the fusion sequence of gp41 of HIV1 (residues 1 to 17) [1] with a hydrophilic and positively charged nuclear localization sequence (NLS) (residues 21 to 27) [2] and separated by a linker in order to maintain the integrity of both domains [3-5]. Peptide ***2*** was obtained by substitution of a single lysine in the NLS by a serine with the aim to modify the final cellular localization [6]. Peptide ***3*** was designed on the basis of conformational criteria in order to check the possible influence of the conformation on the cellular internalization pathway. Peptide ***4*** highly resembles peptide ***1*** but with a shorter hydrophobic sequence aiming to minimizing the cost for chemical synthesis.

Results and Discussion

When labeled at their cysteamide C-terminus by a Lucifer Yellow probe the peptides show different cellular localizations. We focused on the two extreme situations generated by peptides ***1*** and ***3***. Peptide ***1***, which behaved similarly to ***2*** and ***4***, mainly localized to the nucleus. In contrast, peptide ***3*** could only be detected in the endosomes.

These cellular localizations are closely related to the conformational states of the peptides. In solution in pure water, the CD spectra indicate that peptide ***1***, which has a single minimum at 199 nm, is non-structured while ***3*** with two minima at 205 and 221 nm and a maximum near 195 nm, adopts, at least in part a helical conformation (Figure 1, left panel) [7]. In the presence of phospholipids, both these peptides still adopt different conformational states. FTIR spectra of peptides ***1*** and ***3*** obtained in the presence of various phospholipids reveal major Amide I band contributions at 1625 and 1655 cm^{-1}, respectively (Figure 1, right panel) [8,9]. Such positions for Amide I bands indicate that the peptides adopt, respectively, a β-sheet and an α-helical conformations in the presence of phospholipids, regardless of the nature of the lipid.

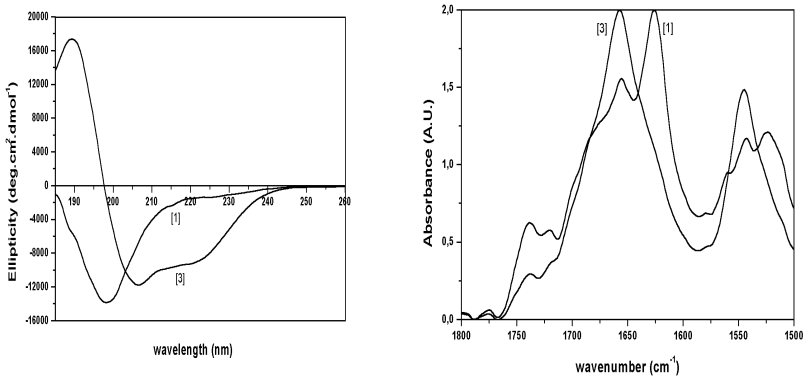

*Fig. 1. Left panel: Far UV CD spectra of peptides **1** and **3** in pure water. Right panel: FTIR spectra of peptides **1** and **3** in the presence of dioleoylphosphatidylcholine.*

All peptides were able to form complexes with siRNAs through non-covalent electrostatic interactions. The final localizations of the siRNA cargos delivered by the peptides are different from those of the free peptides. The peptide-driven intracellular delivery of a siRNA, designed to silence the GAPDH gene, was followed by measuring the biological activity of GAPDH and revealed a strong dependence on the vector sequence (Figure 2, left panel).

The data in Figure 2 clearly indicates that using peptides ***3*** and ***4***, no activity or only poor siRNA induced silencing activity is detected. When using ***1*** or ***2***, strong enhancement of the siRNA effect is observed however, with a slightly higher effect with peptide ***2***. Peptide ***1***, which contains a true NLS sequence, promotes a nuclear localization of the RNA, while peptide ***2*** promotes delivery into the cytoplasm [10]. Such localizations of the siRNA are in line with the induced downregulation. Indeed,

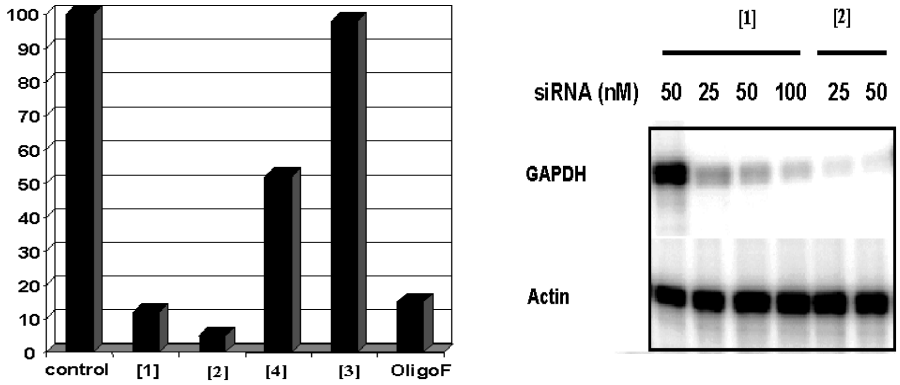

*Fig. 2. Left panel: induced biological responses of siRNA directed against GAPDH delivered into HeLa cells by peptides **1** to **4**. Oligofectamine (OligoF) was used as control. Right panel: Western blot analysis of peptide-mediated delivery of siRNA targeting the GAPDH gene using different concentrations of siRNA. Analysis was performed 30 h post-transfection. Actin was used as a control to normalize mRNA levels.*

the effects observed using peptide ***2*** account for a more rapid release of the siRNA in the cytoplasm, which improves and accelerates the biological response (Figure 2, right panel). The origin of the difference between the activity induced by the delivery mediated by ***1*** and ***2*** is not well understood. Is it due to a decrease in the stability of the siRNA – peptide complex arising from the Lys to Ser substitution and therefore from the difference of one positive charge between ***1*** and ***2***, or due to a modification of the target subcellular compartment caused by the modification of the NLS? This point is currently under investigation.

In conclusion, the present work shows that chemical modifications, which *a priori* can be considered as minor, are able to modify the final cellular localization of cell penetrating peptides. It appears that the conformational state of the hydrophobic sequence plays a crucial role, both in the localization and delivery efficiency. The existence of a helical structure appears to be unfavorable for endosomal-independent delivery and this criteria has to be taken into account when designing future peptide-mediated delivery systems. A1so, a severe shortening of the hydrophobic domain strongly reduces the delivery potency and thus, primary amphipathic cell penetrating peptides should contain a hydrophobic domain long enough to span the thickness of a membrane. As for the role of the NLS sequence, depending on whether the target has a nuclear or cytoplasmic localization, it can be slightly modified according to the target position in the cell.

Acknowledgments
The work was funded by the EU grant QLK2-CT-2001-01451.

References

1. Slepushkin, V. A. *et al*., *AIDS Res. Hum. Retroviruses* **8,** 9-18 (1992).
2. Goldfarb, D. S. *et al*., *Nature* **322,** 641-644 (1986).
3. Morris, M. C. *et al*., *Nucleic Acid Res*. **25,** 2730-2736 (1997).
4. Vidal, P. *et al*., *J. Membrane Biol*. **162,** 259-264 (1998).
5. Morris, M. C. *et al*., *Curr. Opin. Biotechnol*. **11,** 461-466 (2000).
6. Morris, M. C. *et al*., In Langel, U. (Ed.) *CRC Handbook*, CRC Press, pp. 93-113. (2002).
7. Chaloin, L. *et al*., *Biochemistry* **36,** 11179-11187 (1997).
8. Vié, V. *et al*., *Biophys. J.* **78,** 846-856 (2000).
9. Chaloin, et al., In Langel, U. (Ed.) *CRC Handbook*, CRC Press, pp.163-186 (2002).
10. Simeoni, F. *et al*., *Nucleic Acids. Res*. **31,** 2717-2724 (2003).

Peptide Revolution: Genomics, Proteomics & Therapeutics
Michael Chorev & Tomi K. Sawyer (Editors)
American Peptide Society, 2003

Development of Bioavailable Water-Soluble Prodrugs of Peptidomimetics: Importance of the Conversion Time for Higher Gastrointestinal Absorption of Prodrugs Based on Spontaneous Chemical Cleavage

Youhei Sohma, Yoshio Hayashi, Tomoko Ito, Hikaru Matsumoto, Tooru Kimura and Yoshiaki Kiso

Department of Medicinal Chemistry, Center for Frontier Research in Medicinal Science, Kyoto Pharmaceutical University, Yamashina-Ku, Kyoto 607-8412, Japan

Introduction

Despite the hope that HIV-1 protease inhibitors have generated in the treatment of AIDS, the sparing water-solubility of these inhibitors is one of the major drawbacks in oral administration, causing high pill burden and poor oral bioavailability (BA).

Our strategy of water-soluble prodrug development is dependent on an intramolecular chemical reaction, not an enzymatic reaction. The general structure of the prodrugs involves an auxiliary consisting of two units covalently and tandemly linked through the hydroxyl group of the parent HIV-1 protease inhibitor, KNI-727 (**1**, Table 1). Previous biological evaluation of several synthetic water-soluble prodrugs indicated that our strategy afforded not only a high water-solubility, but also the potential to control the conversion time by altering the auxiliary structures [1].

We herein describe the development of new auxiliaries that exhibited a wide range of constant conversion times, and the *in vivo* evaluation of prodrugs with those auxiliaries from a practical standpoint [2].

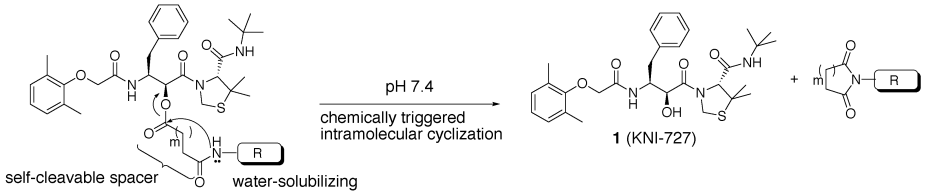

Results and Discussion

Time dependent drug release of synthesized prodrugs in PBS (pH 7.4) at 37˚C was monitored by HPLC (Table1). Prodrug **3**, which has a *N*-propyl group in place of the *N*-aminoethyl group group of **2**, exhibited about 70-fold slower conversion (15.3 h), despite the presence of the same succinic acid-based spacer. Based on the finding, it was postulated that the effect of this amino group on accelerated imide formation can be explained by neighboring-group participation, as shown in Figure 1-A and 1-B. Namely, the electron donative effect of this group is thought to activate the amide nitrogen atom through a five-membered ring intermediate, with consequent imide formation through an alternative five-membered ring intermediate for amidolysis of the ester bond. This hypothesis afforded the idea that the modification of the terminal amino group could influence the

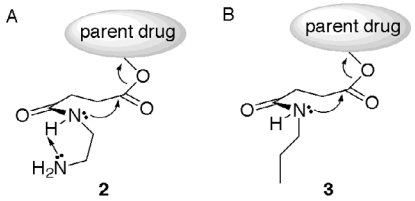

*Fig. 1. Proposed conversion mechanism of prodrugs **2** and **3**.*

Table 1. Water-solubility and converting time (PBS, pH 7.4) of the prodrugs.

			mg / mL	Ratio	(min)
1	-	-	$(5.5 \pm 0.3) \times 10^{-3}$	1	-
2	1	$-(CH_2)_2NH_2 \cdot HCl$	77.1 ± 4.5	14,018	12.7 ± 0.7
3	1	-propyl	$< (5.5 \pm 0.3) \times 10^{-3}$	-	922 ± 17.8
4	1	$-(CH_2)_2$-piperidinyl·HCl	47.8 ± 6.0	8,691	3.6 ± 0.1
5	1	$-(CH_2)_2$-morpholino·HCl	53.2 ± 1.8	9,673	40.3 ± 0.9
6	1	$-(CH_2)_3$-morpholino·HCl	73.6 ± 9.3	13,382	79.5 ± 2.0
7	2	$-(CH_2)_2$-morpholino·HCl	57.1 ± 6.0	10,382	2,056 ± 48.7
8	1	$-CH_2$-3-pyridyl·HCl	30.3 ± 5.8	5,509	35.4 ± 2.3
9	1	$-CH_2$-4-pyridyl·HCl	91.5 ± 2.5	16,636	34.9 ± 0.6

cyclization reaction of **2** and provide the diversified conversion times to the prodrugs.

The substitution with piperidine in prodrug **4** accelerated the conversion with $t_{1/2}$ values of 3.6 min. This $t_{1/2}$ value is shorter than that of **2**, which has an original amino group. In contrast, the 10-fold increase in the $t_{1/2}$ value of **5**, which has a morpholine as opposed to the piperidine of **4**, could be explained as an electron inductive effect by an oxygen atom at the 1-position of the morpholine structure. Moreover, the observed further extension of the $t_{1/2}$ value by the introduction of propyl morpholine in **6** was probably due to the reduced electron donative effect of the *tert*-amino group through an energetically less favorable six-membered ring intermediate formation. A similar extension of the $t_{1/2}$ value to **6** was observed in the introduction of a weaker base, i.e., pyridines, in prodrugs **8** and **9**.

To clarify the effect of these water-soluble prodrugs on the gastrointestinal absorption of the parent drug, intraduodenal (id) administration of the prodrugs was performed in rats. By analyzing the plasma concentration of parent **1** for 8 h after administration, a clear increase in the gastrointestinal absorption was observed in prodrugs **5** (23.1%), **8** (26.4%) and **9** (29.0%), with BA values, 1.5-1.9-fold higher than those obtained by the administration of parent drug **1** alone (15.8%). The other prodrugs showed similar or decreased BA values to parent drug **1** (5.4-17.5%).

In regards to the relationship between conversion time and gastrointestinal absorption, prodrugs **5**, **8** and **9**, which showed improved gastrointestinal absorption, all had a conversion time of approximately 35 min, even though the solubilizing moieties of these prodrugs were different (either morpholine or pyridine). In contrast, the prodrugs with conversion times of less than 10 min or greater than 80 min, did not show any improvement in BA, suggesting that the gastrointestinal absorption of parent drug **1** is dependent on the conversion time of the prodrugs, and that the conversion time to allow gastrointestinal absorption exists within relatively narrow limits.

Consequently, a water-soluble strategy allowing the conversion time to be controlled would improve the gastrointestinal absorption of sparingly soluble drugs. These findings will contribute to the future design of practical water-soluble prodrugs.

References

1. Matsumoto, H., et al. *Bioorg. Med. Chem. Lett*. **11**, 605-609 (2001).
2. Sohma, Y., et al. *J. Med. Chem*. **46**, 4124-4135 (2003).

Peptide Revolution: Genomics, Proteomics & Therapeutics
Michael Chorev & Tomi K. Sawyer (Editors)
American Peptide Society, 2003

Cyclic RGD-Peptides with Acidic-Anchors for Stimulated Cell Adhesion on Biomaterials

Jörg Auernheimer[1], Ulrich Hersel[1], Claudia Dahmen[1], Martin Kantlehner[1], Brigitte Jeschke[2], Anja Enderle[2], Berthold Nies[2], Simon L. Goodman[3] and Horst Kessler[1]

[1]Institut für Organische Chemie und Biochemie, Technische Universität München, Lichtenbergstr. 4, D-85747 Garching, Germany; [2]Biomet Merck BioMaterials GmbH; [3]Merck KGaA, Frankfurter Str. 250, D-64271 Darmstadt, Germany

Introduction

Cell-cell and cell-extracellular matrix (ECM) interactions are complex, highly regulated processes that play a crucial role in most fundamental cellular functions, including motility, proliferation, differentiation and apoptosis [1,2]. Mammalian mineralized tissues contain a variety of hydroxyapatite-binding proteins, which have definite hydroxyapatite-binding sites. One class of hydroxyapatite-binding sites is composed of phosphorylated amino acids (e.g.. phosphoserine pS, phosphotyrosine pY). Another consists of consecutive sequences of acidic amino acids (e. g. aspartic acid, glutamic acid) [3]. It was possible to stimulate cell adhesion on hydroxyapatite with a fusion peptide containing a hydroxyapatite-binding site from salivary statherin and the RGD peptide sequence from osteopontine [4].

Based on these findings we designed a set of peptides containing cyclic RGD-peptides of the type c(-RGDfX-), which have been developed as high affinity ligands for the αvβ3 integrins [5]. c(-RGDfK-) stimulates osteoblast adhesion and supports ingrowth of bone implants in vivo when immobilized on polymethylmethacrylat (PMMA) with an acrylamide anchor.[6] As anchoring groups for hydroxyapatite we used a set of acidic peptides consisting of glutamic acid and phosphoserine in different ratios.

Table 1. Set of different linker molecules containing c(-RGDfX-) as well as cyclic pentapeptides (18 - 20) (RGD: active peptide, RAD: inactive peptide). Succ = succinate spacer; Hegas = heptaethylene glycol amino acid.

c(-RGDfE-)-Hegas-EEEEE	1	c(-RGDfK-)-Succ-EpSEpSE	7	c(-RGDfE-)-EpSEpS	13
c(-RGDfE-)-Hegas-EEEEpS	2	c(-RADfK-)-Succ-EpSEpSE	8	c(-RGDfE-)-EEpSE	14
c(-RGDfE-)-Hegas-EEEpSpS	3	c(-RGDfE-)-GpSEpS	9	c(-RGDfE-)-EpSEpSE	15
c(-RGDfE-)-Hegas-EpSpSEE	4	c(-RGDfE-)-pSpS	10	c(-RGDf-pS-)	16
c(-RGDfE-)-Hegas-EepSpSpS	5	c(-RGDfE-)-pSEpS	11	c(-RGD-py-V-)	17
c(-RGDfE-)-Hegas-EEpS	6	c(-RGDfE-)-EpSpS	12	c(-RGD-py-pY-)	18

Results and Discussion

Cyclic pentapeptides (Table 1) were synthesized on TCP-resin using the Fmoc-strategy [7] in linear form as D(OtBu)fXR(Pbf)G - wherein X is K(Z) or E(OBzl) which allows the coupling of the head group to a spacer-anchor construct after cyclization and hydrogenation. Cyclization was performed with DPPA and $NaHCO_3$ in DMF [8]. The spacer-anchor constructs were also synthesized on TCP-resin according to the Fmoc-strategy. Phosphoserine was introduced as N-α-Fmoc-O-benzyl-phosphoserine. Fmoc-deprotection must be performed carefully to avoid elimination. The spacer-anchor fragments were coupled to the cyclic peptides with HATU / HOAt / collidine in DMF.

After deprotection with 95% TFA, containing TIPS as scavenger, peptides were purified by semi-preparative RP-HPLC (water/acetonitrile, 0.1% TFA).

Biological testing proved that αvβ3 integrin affinities of the conjugates of cyclic peptide and anchor are comparable with c(-RGDfX-), whereas the conjugates with c(-RADfX-) are inactive as expected. If in the cycle -f- is replaced by -py- (**17**) the activity is not affected, but replacement of -X- by -pS- (**16**) or -f-X- by -py-pS- (**18**) leads to total loss of activity.

ELISA tests showed peptide anchoring on hydroxyapatite needs at least one phosphoserine (**2**). Deletion of all phosphoserine (pS) leads to significantly inferior results (EEEEE **1**). Anchors with two pS (**3**, **4**) bound at lower concentrations better than the one with only one phosphoserine (**2**). Introduction of a third phosphoserine (**5**) into the anchor showed no additional effect (Figure 1).

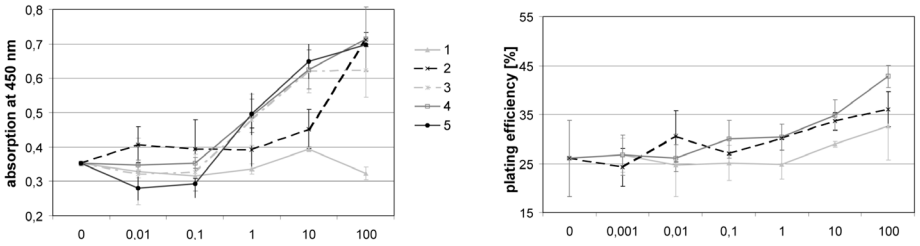

Fig. 1. Peptides with Hegas-spacer and increasing pS:E ratio in the anchor. Qualitative determination of bound peptide in dependence of peptide concentration in coating solution via ELISA (left). MC3T3 cell adhesion (right) on coated hydroxyapatite surface.

Peptides **9** - **15** showed that no spacer unit between the cyclic peptide and the anchoring group is necessary for effective cell adhesion.

Peptides in which one amino acid within the cycle was replaced by phosphoserine (**16**) or phosphotyrosine (**17**, **18**) showed no activity in both ELISA and cell adhesion tests.

A simple but very efficient method for the biofunctionalization of hydroxyapatite has been developed. The acidic anchors presented here allow the coating of calcium phosphate surfaces with c(-RGDfX-) peptides for stimulation of osteoblast adhesion. The anchors can easily be synthesized via SPPS using commercially available Fmoc-protected amino acids as starting materials.

References

1. Blau, H. M. and Baltimore, D. *J. Cell Biol.* **112**, 781 (1991).
2. Ruoslahti, E. and Obrink, B. *Exp. Cell. Res.* **227**, 1 (1996).
3. Fujisawa, R., Mizuno, M., Nodasaka, Y. and Kuboki, Y. *Matrix Biology* **16**, 21 (1997).
4. Gilbert, M., Shaw, W. J., Long, J. R., Nelson, K., et al. *J. Biol. Chem.* **275**, 16213 (2000).
5. Sulyok, G. A. G., Gibson, C., et al. *J. Med. Chem.* **44**, 1938 (2001).
6. a) Kantlehner, M., et al. *ChemBioChem.* **1**, 107 (2000).
   b) Kantlehner, M. et al. *Angew. Chem. Int. Ed.* **38**, 560 (1999).
7. a) Fields G. B. and Noble R. L. *Int. J. Pept. Protein Res.* **35**, 161 (1990).
   b) Carpino L. A., Sadat-Aalaee D., et al. *J. Am. Chem. Soc.* **112**, 9651 (1990).
8. Shioiri, T. Yamada, S. and Ninomiya, K. *J. Am. Chem. Soc.* **94**, 6203 (1972).

Peptide Revolution: Genomics, Proteomics & Therapeutics
Michael Chorev & Tomi K. Sawyer (Editors)
American Peptide Society, 2003

Lipid and Carbohydrate Based Macromolecules in Drug and Vaccine Delivery

Istvan Toth[1], Aniko Horvath[1], Joanne Blanchfield[1], Colleen Olive[2], Michael Good[2], Norbert Wimmer[1] and P. Elizabeth Rakoczy[3]

[1]School of Molecular and Microbial Sciences, University of Queensland; [2]Queensland Institute for Medical Research, Brisbane, Queensland, Australia; [3]Lions Eye Institute University of Western Australia Perth, WA, Australia

Introduction

To induce high antibody response when administering a low molecular weight synthetic peptide, conventionally it must be conjugated to a carrier protein (KLH, BSA). High antibody titres have been attained by coupling immunogenic peptides to a polylysine core, to form a multiple antigenic peptide (MAP). A good immune response was observed when the antigen was covalently coupled to a triacyl-S-glycerylcysteinyl (Pam_3Cys) construct. We have further refined this approach, by using a lipidic anchor moiety at the N-terminal of a polylysine system, to form a lipid-polylysine core-peptide (LCP).

Group A streptococci (GAS) are among the most common and widespread human pathogen. They cause a wide range of infections, including acute rheumatic fever, rheumatic heart disease and acute glomerulonephritis. Protection against GAS infection is mediated predominantly by opsonic antibodies directed against the surface M protein, the major virulence factor of GAS [1].

There is no human mucosal adjuvant system available for oral immunization. The LCP system works without the use of any conventional, toxic adjuvant. We have synthesized a library of Lipid-Core compounds, to which any potential peptide vaccine candidate can be conjugated, and the immunogenicity evaluated. Therefore the results of this study provide compounds as a basis for the development of many other synthetic peptide vaccines.

The positively charged dendritic LCP system is also capable of physically entrapping negatively charged molecules, including DNA sequences. Numerous antisense DNA sequences have been identified as potential new therapeutic agents but few have progressed into the clinic, due to (i) lack of absorption/uptake and (ii) rapid enzymatic breakdown. Our research addresses these major issues through a highly novel strategy involving ion pair formation of lipophilic dendrimer constructs with an oligonucleotide sequence ODN1 (5'AGGACCTGTCAATTCCGGTG). We have designed new dendrimer/ODN1 complexes, which reduce the production of vascular endothelial growth factor (VEGF). We aim to develop this complex as a drug to cure choroidal neovascularisation (CNV).

Results and Discussion

Immunoadjuvant: A series of LCP compounds containing a GAS peptide epitope from the bacterial surface M protein were synthesised. This peptide (p145: LRRDLDASREAKKQVEKALE) [2] is recognized by antibodies in the sera of most adults living in areas of high streptococcal exposure. The number of peptide sequences, the number, length and spacing of lipids were varied (Figure 1).

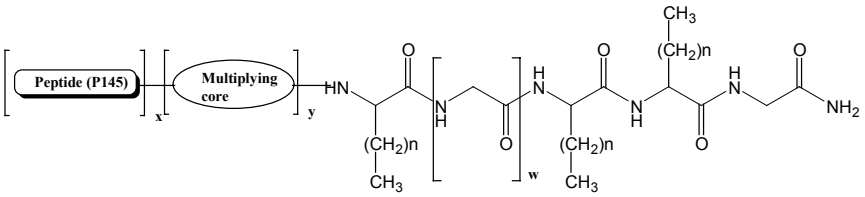

Fig. 1. The LCP system.

The most immunogenic construct contained the longest alkyl side chains (Figure 2). The number of lipoamino acids in the constructs affected the immunogenicity and spacing between the alkyl side chains increased immunogenicity. We observed up to 100-fold increase in immunogenicity of the LCP-p145 administered without any conventional adjuvant compared with p145 administered with CFA. The nature of the LCP construct also had an influence of the opsonic activity of antisera [1].

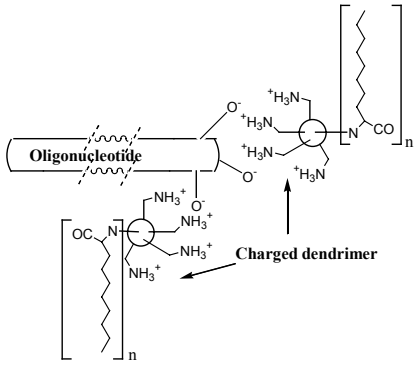

Fig. 2. ODN/Charged LCP complexes.

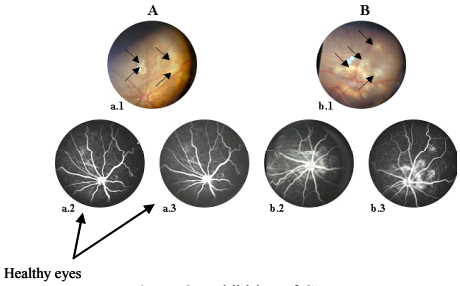

Figure 3: Inhibition of CNV

(a.1; b.1) laser lesions
(a.2) 1 month post injection (Den4/ODN1)
(a.3) 2 month post injection (Den4/ODN1)
(b.2) 1 month post injection (Den4)
(b.3) 2 month post injection (Den4)

Oligonucleotide delivery. We have demonstrated that the charged dendrimers were able to transport ODN-1 into cultured D407 cells, which in turn decreased VEGF expression significantly; the dendrimers alone had no effect on the expression of VEGF [2]. In addition, we have investigated the efficacy of dendrimer mediated delivery of ODN-1 *in vivo*. Fluorescein angiography indicated that the dendrimers were highly efficient at delivering an ODN into the retinal cells of rats and inhibit laser induced CNV (Figure 3). In addition, the complex formed with one of the dendrimers was able to persist for up to two months post injection. This study demonstrates that synthetic lipophilic charged dendrimers can be used for gene delivery and will be valuable tools in gene therapy.

References

1. Horváth, A., Olive, C., Wong, A., Clair, T., Yarwood, P., Good, M. and Toth, I. *J. Med. Chem.* **45**, 1387-1390 (2002).
2. Wimmer, N., Marano, R., Kearns, P., Rakoczy, E. P. and Toth, I. *Bioorg. Med. Chem. Letters* **12***,* 2635-2637 (2002).

Peptide Revolution: Genomics, Proteomics & Therapeutics
Michael Chorev & Tomi K. Sawyer (Editors)
American Peptide Society, 2003

Liposaccharides in Peptide Drug Delivery

Joanne Blanchfield[1], O. Paul Gallagher[1], Yasuko Koda[1], Paul Alewood[2], Richard Lewis[2] and Istvan Toth[1]

[1]School of Molecular and Microbial Sciences, University of Queensland, St. Lucia, QLD, Australia 4072. [2] Institute for Molecular Biosciences, University of Queensland, St. Lucia, QLD, Australia 4072

Introduction

The development of peptide based drugs is hampered by poor bioavailability as a result of low metabolic stability and poor membrane permeability. Our work has shown that incorporating lipids, in the form of lipoamino acids, and /or carbohydrate moieties into the peptide sequence can greatly improve their resistance to digestive enzymes and their absorption across the GI tract. Lipoamino acids are α-amino acids bearing an alkyl side chain that can vary in both length and degree of unsaturation. These lipids can be coupled to peptides at any point in the sequence using standard peptide coupling techniques in both solid or solution phase syntheses. Increasing the lipophilicity of a peptide has been shown to increase the passive diffusion across membranes and offer some protection against digestive enzymes. Coupling sugars to peptides maintains the water solubility and introduces the possibility of utilizing specific transporter molecules or target a drug to a specific organ or cell line.

Results and Discussion

Biodistribution studies The α-conotoxin MII (Figure 1) is a highly selective and potent inhibitor of the a3b2 subtype of the nicotinic acetylcholine receptor. Our previous work showed that coupling a C_{12}-lipoamino acid to this peptide (LMII Figure 1) significantly increased its Caco-2 cell permeability while having no effect on the receptor binding or inhibition [1].

MII = NH_2-G**C**C**C**SNPV**C**HLEHSN**C**-$CONH_2$
LMII = C_{12}Laa-G**C**C**C**SNPV**C**HLEHSN**C**-$CONH_2$
Disulphide bonds in both peptides: Cys2-Cys8, Cys3-Cys16

Fig. 1. The sequence of α-conotoxin MII and the Lipoamino acid conjugate, LMII.

Encouraged by these findings we examined the biodistribution of both MII and LMII after oral administration to male rats. Tritium labeled peptide (1mg per rat) was administered via oral gavage and after a given time the rats were destroyed and their organs removed, homogenized in buffer, digested using tissue solubilizer for 3 days,

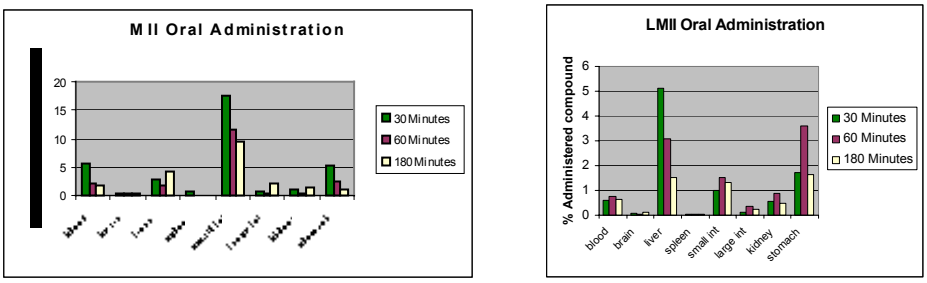

Fig. 2. Tissue distribution of MII and LMII following oral administration.

decolourised using bleach and finally the radioactivity determined by liquid scintillation counting (Figure 2).

Our results showed a shift in the distribution of the compounds. MII appears to accumulate predominately in the small intestine and stomach while the lipid analogue LMII appears to accumulate in the liver, the site of first-pass metabolism. We attribute the reduction of total levels of LMII detected to its lower water solubility which caused it to interact and bind to the food in the stomach of the animals.

Since the presence of the Laa did not appear to alter the peptide's GI tract permeability we decided to examine directly the permeability across the blood brain barrier. Labelled peptide (1mg) was injected into the jugular vein of each rat and the level of radioactivity in the blood, liver and brain determined over time (Figure 3).

The accumulation of the lipophilic peptide in the liver is even more pronounced in this experiment. Unfortunately, neither peptide was detected in the brain.

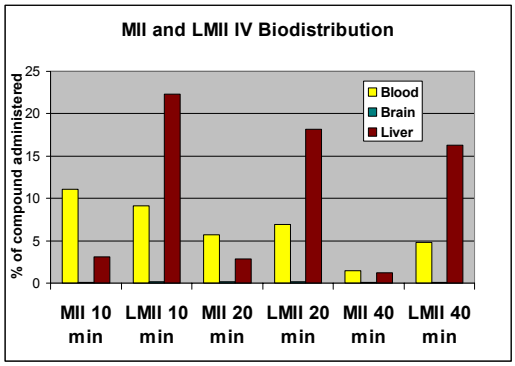

Fig. 3. Distribution of MII and LMII in the blood, brain and liver following jagular vein injection.

Conclusions

- A peptide the size of MII can cross the GI tract in significant levels (5%).
- Increasing the lipophilicity of MII significantly increases the accumulation (and presumably metabolism) in the liver but also decreases its solubility so it is absorbed more by the food within the stomach.
- The presence of one Laa is not sufficient to induce passage across the BBB.

In the future it may be necessary to combine sugar molecules with Laas to improve solubility and hopefully absorption and study the distribution of these liposaccharide conjugates.

Neuroactive peptides. Our liposaccharide delivery system is also being applied to the delivery of peptides across the blood brain barrier. Endomorphin 1 is an endogenous opioid peptide that exhibits the highest affinity and specificity for the morphine favored μ-opioid receptor. Our goal is to modify Endomorphin 1 (Tyr-Pro-Trp-Phe-NH_2) with lipoamino acids and sugars to increase its metabolic stability and passage across the blood brain barrier. Our first series of compounds have been generated by placing either a C_8, C_{12} or C_{18} Laa or a glucose residue on the N-terminus of the peptide. These compounds have been examined using the Caco-2 cell permeability assay to determine if any improvement in the absorption of the peptide was achieved. As yet, not peptide conjugate has shown a significant increase in permeability but this demonstrates the process by which we generate and assess peptide analogues to determine the most promising conjugates for *in vivo* examination.

References

1. Blanchfield, J., Dutton, J., Hogg, R., Craik, D., Adams, D., Lewis, R., Alewood, P. and Toth, I. *J. Med. Chem.* **46**, 1266-1272 (2003).

Peptide Revolution: Genomics, Proteomics & Therapeutics
Michael Chorev & Tomi K. Sawyer (Editors)
American Peptide Society, 2003

In Vivo Pharmacokinetic and Metabolic Studies of Peptide Drugs by MS and MS/MS

Reto Stöcklin, Philippe Favreau, Laure Menin, Philippe Bulet and Sophie Michalet

Atheris Laboratories, CH-1233 Bernex-Geneva, Switzerland

Introduction

Proteins are involved in major health problems and are widely used as diagnostics markers or therapeutic drugs. Our objective is to offer innovative tools and solutions to what we term the "post-proteomics era" focusing on technologies adapted for *in vivo* metabolic studies such as pharmacokinetics (PK) and pharmacodynamics (PK). New strategies were developed for fast, precise and sensitive measurements of peptide hormone levels in body fluids and tissues through the example of lutheinizing hormone-releasing hormone (LHRH) and analogues such as goserelin. Following a simple extraction protocol, with or without addition of an internal standard, an on-line liquid chromatography tandem mass spectroscopy equipment (LC-MS/MS) allows one to reach the low sub-pM detection. A second approach, using stable isotope labelled analogues and named isotope dilution assay (IDA), is illustrated with insulin. IDA provides accurate and sensitive measurements of protein levels with direct positive identification of the target protein or peptide by mass spectroscopy.

Results and Discussion

For the *in vivo* quantification of the analogue of LHRH, namely goserelin, we take advantage of the high resolution Q-TOF tandem mass spectrometer to precisely quantify the goserelin present in plasma samples. First, the goserelin $(M+2H^+)/2$ precursor ion was selected in MS1 (quadrupole), fragmented by CID and directed towards MS2 (TOF analyser with reflectron optics) where the intensity of its fragment ion at *m/*z 607.6 was measured during the chromatographic process. The use of a Q-TOF tandem mass spectrometer provides resolved mass spectra with *m/z* values of 607.6; 608.1 and 608.6 as illustrated in Figure 1A. Using an external calibration the lower limit of detection (LLOD) was 0.17 mg/l and the lower limit of quantification (LLOQ) close to 0.3 mg/l as illustrated in Figure 1B.

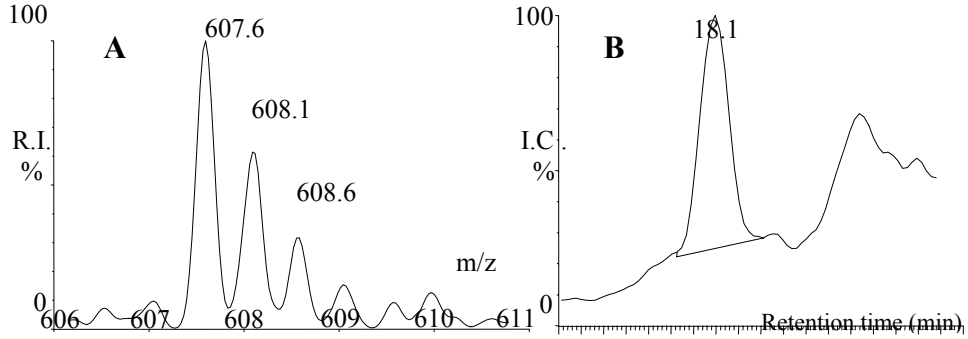

*Fig. 1. **A** high resolution mass spectrum at goserelin plasma concentration of 0.3 mg/l. **B** The ion currents (IC) of the major isotopic signals were summed and integrated for quantification of goserelin at a concentration of 0.3 mg/l in rat plasma.*

In fact, high resolution was essential for these measurements, as contaminating fragments generated by CID under the same MS/MS analytical conditions and with similar retention times appeared in the same *m/z* mass scale. They could be distinguished from goserelin only under high resolution as they are singly charged (specific isotopic motif). The use of a high resolution Q-TOF tandem mass spectrometer allowed us to avoid the problem of false positives due to contamination without sensitivity losses as compared to classical analyses on the Quattro II triple stage quadrupole instrument.

The second approach we used for *in vivo* quantification corresponds to the IDA assay. We developed this method using human insulin, a recombinant deuterated form as internal standard and a recombinant ^{15}N-labelled version as carrier. Following extraction from clinical serum plasma, analysis by electrospray ionization mass spectroscopy (ESI-MS) and quantification, the IDA was found to provide accurate and sensitive measurements of the insulin level.We also obtained a good correlation with standard immunoassay data, except in some samples where much lower values were obtained using IDA. This suggests an overestimation of insulin levels by immunoassay in some cases. As it is not subject to immunological interferences with insulin-related compounds, this new assay is relevant from the clinical point of view since it is not subject to any confusion related with hyperinsulinemia. In addition, IDA is not susceptible to errors arising from immunological cross-reactivity with closely related compounds (e.g. precursors, maturation or degradation fragments). IDA has also the advantage of not requiring any radioactive material. The measured molecular masses further allow an unambiguous identification of the target compound at sub-picomolar levels with a clear distinction between its endogenous or exogenous (injected) forms. Finally, IDA allows for simultaneous *in vivo* quantitative investigations on both native endogenous or injected compounds.

Acknowledgments
We are grateful to A. Bairoch (Swiss Institute for Bioinformatics), M. Fathi and D. Hochstrasser (University Hospital), R. Offord (University Medical Center) and K. Rose (GeneProt Inc.) in Geneva; A. Ménez (DSV/DIEP, CEA-Saclay, France), B. Amekraz, C. Moulin and P. Pierrard (DEN/DPC/SPCA, CEA-Saclay, France); as well as to G. Cretton, Y. Duchemin and S. Stöcklin from our laboratories.

References
1. Michalet, S., Favreau, P. and Stöcklin, R. *Clin. Chem. Lab. Med*. in press (2003).
2. Stöcklin et al., *Diabetes* **46**, 44-50 (1997).

Peptide Revolution: Genomics, Proteomics & Therapeutics
Michael Chorev & Tomi K. Sawyer (Editors)
American Peptide Society, 2003

Peptide Targeting of Daunomycin into Sensitive and Multidrug Resistant Tumors

Ferenc Hudecz[1], Judit Reményi[1], Tamás Hegedűs[2], Péter Kovács[3], Barbara Szabó[1], Balázs Sarkadi[2] and Dezső Gaál[4]

[1]Research Group of Peptide Chemistry, Hungarian Academy of Sciences, Eötvös L. University; [2]National Institute of Haematology and Immunology; [3]Department of Genetics, Cell and Immunobiology, Semmelweis Medical University; [4]National Institute of Oncology, Budapest, Hungary

Introduction

Anthracycline antibiotics like adriamycin (Adr) and daunomycin (Dau) continue to be essential components of first-line chemotherapy in the treatment of a variety of solid and hematological tumours [1]. However, their efficacy is frequently restricted by dose-limiting toxicities, including cardiotoxicity, myelosuppression and the selection of multiple mechanisms of cellular drug resistance (MDR). For eliminating/decreasing these side effects we have developed a new group of water-soluble drug-conjugates in which acid labile *cis*-aconytil derivative of Dau (cAD) is coupled to branched polypeptides, (poly[Lys-(DL-Ala$_m$-X$_i$)] (XAK) with amphoteric (X = Glu, EAK) or polycationic (X = Ser, SAK) character. Our earlier studies showed that the amphoteric cAD-EAK conjugate significantly increased the survival of L1210 leukemia bearing mice as compared to that of free drug [2]. This effect could be interpreted by favourable changes in pharmacokinetics (blood clearance and tissue distribution) of the conjugate versus free drug and/or by the altered cellular uptake mechanism [3,4].

In human tumors, the over-expression of ATP-dependent transporter proteins, like MDR1 and MRP1, are often responsible for the appearance of multidrug resistance [5]. Since Dau and Adr are substrates of these proteins the therapeutic effectiveness of the anthracyclines in resistant tumors is rather low. The application of inhibitors (e.g. verapamil, reversins) can decrease the activity of MDR transporters. Another approach could be the use of drug-peptide conjugates utilizing different cellular uptake routes. To this end we have performed a comparative study with cAD-EAK conjugate proved to be active against murine L1210 *in vivo*. We report here on the *in vitro* effect of this conjugate on sensitive (HL-60/sensitive) and MDR resistant (HL-60/MDR1 and HL-60/MRP1) human leukemia cell lines and also on results of the cAD-EAK as well as free Dau uptake experiments. Considering the importance of pH in certain mechanisms of cellular uptake of macromolecular conjugate we have also analyzed the kinetics of drug release under various conditions.

Results and Discussion

In this study we have prepared and characterized *cis*-aconytil-Dau containing conjugate with amphoteric polypeptide (cAD-EAK, M_w=80000, average degree of substitution = 5.4%) [6]. We have determined the release of the Dau from the cAD-EAK conjugate in buffer solution at various pH (pH = 3-7) using analytical RP-HPLC. The rate of the release of the drug from conjugate was time and pH dependent. For example at neutral pH (pH=7) 3.45% of the drug was liberated during 72h, while lowering the pH resulted in much more pronounced drug release (50% at pH 4 during 72h).

For cellular experiments, the multidrug resitance factor (f) of the tumor cells was first determined by quantitative calcein assay [7]. The following f values were obtained: f=0.13 for HL-60/sensitive cells, f=0.90 for the HL-60/MDR1 cells and

f=0.61 for the HL-60/MRP1 cells. The *in vitro* antitumor effect of the cAD-conjugate was investigated on these cell lines using MTT-assay. The cells were treated with Dau or cAD-EAK conjugate alone, or with Dau+verapamil and cAD-EAK+verapamil mixture. Dau was by two orders of magnitude more efficient on sensitive cells than on MDR1 cells (IC_{50} = 0.03 μM, vs. IC_{50} = 2.54 μM) (Figure 1A). Interestingly this difference was less pronounced when the effect of cAD-conjugates was compared (IC_{50} = 5.03 μM vs IC_{50} = 51.34 μM) (Figure 1B). The profile of the cytostasis curves of the Dau and of the Dau+verapamil mixture treated HL-60/sensitive cells was almost identical (IC_{50}=0.03 μM and 0.01 μM). But in HL-60/MRP1 and HL-60/MDR1 cells, the Dau+verapamil treatment resulted in decreased IC_{50} values as compared with those of Dau treatment. Similar tendency of antitumor effect was produced by cAD-EAK conjugate or cAD-EAK conjugate + verapamil mixture. However, verapamil had only little influence on the cytostasis of cAD-EAK conjugate in resistant cell lines.

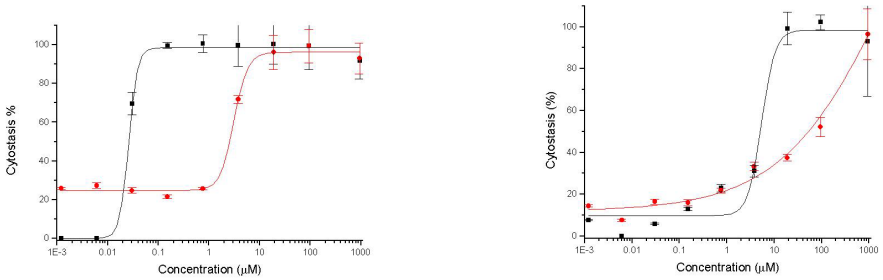

Fig.1. In vitro antitumor effect of Dau (A) and cAD-EAK conjugate (B) in HL-60/sensitive (f=0.13) (■) and HL-60/MDR1 (f=0.90 (●) cell lines).

The uptake of Dau and cAD-EAK conjugate was studied as a function of time and of temperature using FACS and confocal microscopy. We have also examined the drug uptake in ATP-depleted cells, and the effect of colchicin on the conjugate uptake. Cells were treated with Dau and cAD-EAK conjugate alone, or with Dau+verapamil and cAD-EAK+verapamil mixture. The comparison of the uptake of the Dau in the presence or in the absence of verapamil showed no significant differences in HL-60/sensitive cells. As expected in the presence of verapamil, an elevated free drug accumulation was observed by FACS in the case of both resistant cells, HL-60/MRP1 and HL-60/MDR1. In contrast, we did not find any marked changes between the curves corresponding to cAD-EAK conjugate or cAD-EAK conjugate + verapamil treated sensitive or resistant cells. The cAD-EAK conjugate accumulated not only in the sensitive but also in the drug resistant cell lines. We also found that the entering process of cAD-EAK conjugate was temperature dependent. More pronounced accumulation was detected at higher temperature. Comparison of data obtained in normal and in ATP-depleted cells showed that ATP is needed for the elevated uptake of the conjugate. In addition, colchicine decreased the uptake of cAD-EAK conjugate. These results show that the polypeptide attached drug enters not only the sensitive, but also the MDR resistant human leukemia cells. Results obtained so far indicate that the conjugate enter the cells by endocytosis.

In order to investigate the localization of Dau and cAD-EAK conjugate in HL-60/sensitive and resistant cell lines, confocal laser scanning microscopy study was performed. In these experiments the cells were incubated with Dau or cAD-EAK at a concentration of 2 μM (Dau content) for different periods of time. Data obtained with

HL-60/sensitive and HL-60/MDR1 cells after 3 h incubation are presented in Figure 2. Our results show that Dau can be mainly detected in the nucleus, while the cAD-EAK conjugate is present in the cytoplasm of HL-60/sensitive cells. Interestingly, in the HL-60/resistant cells, Dau as well as cAD-EAK conjugate, are visible in the cytoplasm. We also found differences in localization of cAD-EAK conjugate in HL-60/MRP1 cells.

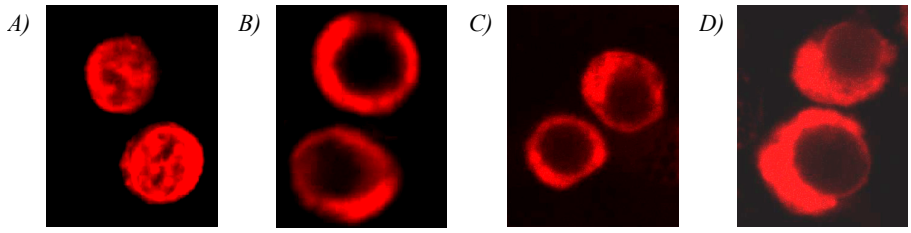

Fig. 2. Localization of Dau (2 μM) in HL-60/sensitive (f=0.13) (A) and in HL-60/MDR1 (f=0.90) (B) and of cAD-EAK conjugate (2 μM) in HL-60/sensitive (f=0.13) (C) and in HL-60/MDR1 (f=0.90) (D) cells (incubation: 3h).

Taken together these data suggest that Dau conjugated to polypeptide is effective against MDR resistant human leukemia cells *in vitro*. Experiments outlined above indicate that this construct is taken up by resistant cells perhaps by using endocytosis. Further studies are in progress to investigate the mechanism of drug release inside the cells.

Acknowledgments

This work has been supported by grants from the Ministry of Health (T01094/1999) and from the Hungarian Ministry of Culture (Medichem NFKP 1/047).

References

1. Lothstein, L., Israel, M. and Sweatman, T. W. *Drug Resist. Update* **4**, 169-177 (2001).
2. Gaál, D. and Hudecz, F. *Eur. J. Cancer* **34**, 155-161 (1998).
3. Takakura, Y. and Hashida, M. *Crit. Rev. Oncol. Hematol.* **18**, 207-231 (1995).
4. Duncan, R., Dimitrijevic, S. and Evagorou, E.G. *S.T.P. Pharma. Sci.* **6**, 237-263 (1996).
5. Bolhuis, H., van Veen, H. W., Poolman, B., Driessen, A. J. M. and Konings, W. N. *FEMS Microbiol. Rev.* **21,** 55-84 (1997).
6. Hudecz, F., Clegg, J. A., Kajtár, J., Embleton, M. I., Szekerke, M. and Baldwin, R. W. *Bioconjug. Chem.* **3**, 49-57 (1992).
7. Homolya, L., Holló, Z., Müller, M., Mechetner, E. B. and Sarkadi, B., *Br. J. Cancer* **73,** 849-855 (1996).

Peptide Revolution: Genomics, Proteomics & Therapeutics
Michael Chorev & Tomi K. Sawyer (Editors)
American Peptide Society, 2003

Characterization of Multicomponent Aggregate Containing a Bioactive Peptide and a Gd Complex

Antonella Accardo[1], Diego Tesauro[1], Paola Roscigno[2], Luigi Paduano[2], Eliana Gianolio[3], Giancarlo Morelli[1] and Ettore Benedetti[1]

[1]Department of Biological Chemistry, Via Mezzocannone, 6 Naples, I-80134, Italy;
[2]Department of Chemistry, Via Cynthia, Naples, I-80126, Italy;
[3]Department of Chemistry IFM, Via Giuria, 7 Turin, I-10125, Italy

Introduction

There is an increasing interest in developing new contrast agents in magnetical resonance imaging (MRI) with enhanced properties, such as high relaxivity of the paramagnetical gadolinium complex and selectivity for a specific biological target [1]. To reach the required local concentration of the contrast agent on the target tissue many carriers have been developed such as liposomes and other microparticulates, micelles, dendrimers, linear polymers, peptides or proteins, which have been all derivatized as the gadolinium complex [2]. Among these carriers, micellar aggregates, formed by amphiphilic molecules and structurally constituted by a hydrophobic core and a hydrophilic shell, have recently drawn much attention owing to their easily controlled properties and good pharmacological characteristics. Our aim is to prepare a mixed micelle formed by two different monomers, one containing a bioactive molecule (peptide) able to address the contrast agent on the specific biological target, and the other containing a chelating moiety able to form stable complexes with the metal of interest (gadolinium), both also presenting a lipophilic tail (Figure 1). The selected bioactive molecule is the natural CCK8 peptide able to selectively bind cholecistokinin receptors, which are overexpressed in a large amount of tumor lesions [3].

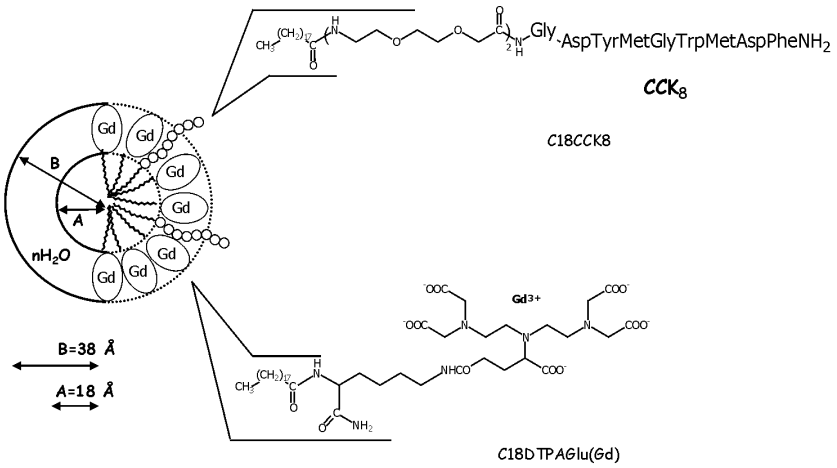

Fig. 1. The mixed micelle formed by two monomers: C18DTPAGlu(Gd) and C18CCK8; and the structural dimensions obtained by Small-Angle Neutron Scattering (SANS) technique.

Results and Discussion

Both monomers were synthetized in solid-phase. C18DTPAGlu was obtained by linkage of the nonadecanoic acid [$CH_3(CH_2)_{17}COOH$] to the α-NH_2 group of a Lys residue bearing the chelating agent (DTPAGlu-pentaester) on its ε-NH_2 group. After cleavage from the solid support, the fully deprotected compound was obtained in good yield. The Gd(III) complex, C18DTPAGlu(Gd), was obtained by adding stoichiometric amounts of $GdCl_3$ to the aqueous solution of the ligand at neutral pH.

C18CCK8 was obtained by sequential coupling in solid phase of the eight residues of CCK8, a Gly residue, two units of amino-3,6-dioxaoctanoic acid and the nonadecanoic acid. All micelle containing solutions were prepared by weighting, buffering the samples at pH=7.4 with 0,10 M phosphate and 34 mM NaCl. In the ternary solutions (C18DTPAGlu-C18CCK8-water or C18DTPAGlu(Gd)-C18CCK8-water) the imposed ratio between the two monomers was such to have an average of 3 peptide derivatives per micelle. C18DTPAGlu and C18DTPAGlu(Gd) show an anionic surfactant behaviour forming self-assembling micelles. Both are able to incorporate the C18CCK8 monomer to give mixed micelles. All systems were fully characterized (see Table 1). Surface tension measurements were performed in order to determine the critical micellar concentration (c.m.c.). The self-diffusion coefficients, D, were measured by the FT-PGSE-NMR technique, and the hydrodynamic radii of the aggregates, R_{app}, were calculated by Stokes-Einstein equation. Moreover, in order to evaluate the mean aggregation number of micelles, fluorescence quenching measurements were performed. The structural data (reported in Table 1) were obtained by Small-Angle Neutron Scattering (SANS) technique. Mixed micelles containing two different monomers – C18CCK8 and C18DTPAGlu (with or without gadolinium ions) – have been studied and structurally characterized.

In conclusion, the mixed aggregates contain 48 monomers per unit, 3 of them being the C18CCK8 units. The structural charecterization indicates a spheric arrangement of the micelles with an external shell of 20 Å and the inner core of 18 Å. Both the chelating agents (or the DTPAGlu(Gd) complexes) and the CCK8 peptides point toward the external surface as schematized in Figure 1. Relaxivity measurements indicate that the micellar aggregates, containing the Gadolinium complexes, show high relaxivity parameters (R_{1p} = 18.7 $mM^{-1}s^{-1}$) with a large enhancement with respect to the isolated DTPAGlu(Gd) complex (R_{1p} = 6.2 $mM^{-1}s^{-1}$).

Table1. Physico-chemical parameter of micellar aggregates.

	Cmc ($mol \cdot kg^{-1}$)	N_{agg}	R_{app}(Å)	Rint(Å)	charge	nH_2O	R_{1p} ($mM^{-1}s^{-1}$)
C18DTPAGlu-water	$5 \cdot 10^{-5}$	35	32	16	-10	90	
C18DTPAGlu(Gd)-water	$9 \cdot 10^{-5}$	35	36	16	-2	126	17.5
C18DTPAGlu-C18CCK8-water	$5 \cdot 10^{-5}$	50	36	18	-10	90	
C18DTPAGlu(Gd)-C18CCK8-water	$7 \cdot 10^{-5}$	48	38	18	-3	126	18.7

Acknowledgments

We thank Bracco Imaging spa (Milan, Italy) for DTPAGlu.

References

1. Aime, S., Botta, M., Fasano, M. and Terreno, E. *Chem. Soc. Rev*. **27**, 19 (1998).
2. Andrè, J. P., Toth, E., Fisher, H., Seelig, A., et al. *Chem. Eur. J*. **5**, 2977 (1999).
3. Reubi, J. C., Shaer, J. C. and Waser, B. *Cancer Res.* **57**, 1377 (1997).

Peptide Revolution: Genomics, Proteomics & Therapeutics
Michael Chorev & Tomi K. Sawyer (Editors)
American Peptide Society, 2003

Synthesis and Application of Functional Peptides for the Therapy of HPV Type 18 Positive Cervix Cancer Cells

Rüdiger Pipkorn[1], Klaus Braun[2], Waldemar Waldeck[3], Mario Koch[1] and Jürgen Debus[2]

[1]Central Peptide Synthesis Unit, DKFZ; [2]Clinical Cooperation Unit Radiooncology, DKFZ; [3]Department of the DNA Topology, DKFZ; German Cancer Research Center, DKFZ D-69120 Heidelberg, Germany

Introduction

The human papillomavirus (HPV) infection exhibits the most important risk factor for developing cervical cancer. The viral E6 protein binds to functional tumor suppressor gene p53 product and the E7 protein interferes with the function of the retinoblastoma gene product (Rb) resulting in a loss of function. Therefore the viral *E6/E7* genes are crucial targets. We tried to improve the radiosensitivity of cervical cancer cells by different peptide nucleic acids (PNAs) against the viral *E6/E7* target genes. The mixed-PNA leads to the reactivation of the Rb and repression of E2F-responsive genes. This increases cell dead after photon irradiation. Regulating the cell cycle is strongly sensible to viral E6 and E7 proteins. The two tumor suppressor genes (TSGs) are functionally intact in HeLa cells which suggest the reconstitution of *p53* and $p105^{RB}$ *genes* by PNAs. Therefore the *E6* and *E7* genes are optimal targets for anti-genetic strategies combined with photon-irradiation.

Material and Methods

The determination of the functional peptide fragments was realized by HUSAR, PDB biocomputing and the FASTA algorithm. Visualization and charactization were carried out by molecular modeling, mass spectroscopy (MS) and molecular imaging. Peptides were synthesized with the solid phase strategy using the Fmoc-method in a fully automated multiple synthesizer and purified by preparative HPLC on a reverse phase column. The material was characterized with analytical HPLC and laser desorption mass spectroscopy. The BioShuttle was composed by the two units Transmembrane-peptide and nuclear localization signal (NLS)-PNA respectively, according to the above strategy. HeLa cervix cancer cells were obtained from the DKFZ tumorbank. Cells were maintained at 37°C, 5% CO_2 in minimal essential medium (Joklik modified) containing 10% fetal bovine serum (FBS) and 2mM glutamine (GIBCO, Germany). 10 µl PNA/ml was added to culture in a final concentration of 0.1 nM 24 hours before irradiation. The point of time 0 hours in all plots means that cell were 24 hours in contact with PNA. Cells were irradiated with 6 MeV photons using a Linearbeschleuniger (Siemens).

Results and Discussion

The mixed-PNAs E6/7 inhibits the cell proliferation significantly. Without irradiation the PNA E6 alone is not able to interfere with cell growth. After photon-irradiation with 7.5 Gy the tumor cell proliferation was suppressed. PNAs E6, E7 and Random were also able to strengthen the effect of radiation treatment. The bimodal strategy: incubation with PNA E6/7 combined with photon-irradiation inhibits cell growth and leads to cell killing. The transport peptide-conjugate, labeled on both sides [the transport peptide (Figure 1), the conjugated NLS-peptide (Figure 2)] was detected after

1 h in the cytoplasm and a few minutes later in the cell nucleus suggesting a fast nuclear delivery.

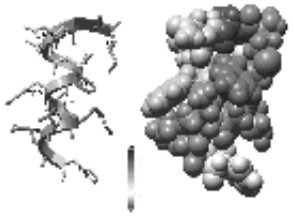

Fig. 1. Transport peptide.

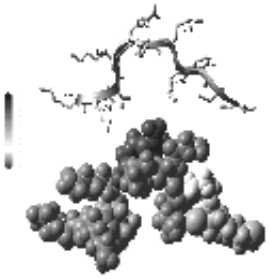

Fig. 2. Address peptide.

Fig. 3. Substance.

The BioShuttle transporter is a highly efficient system for the delivery of macromolecules into the cell nuclei of living cells at concentrations of 100 pM in the culture medium (Figure 4).

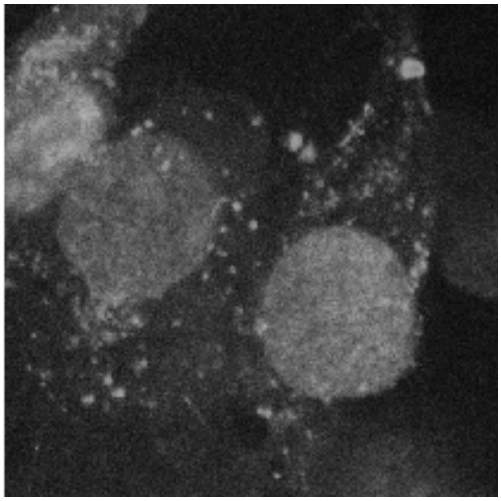

Fig. 4. Human prostate DU 145 cells, BioShuttle incubated; final concentration 100 pM incubation time 1 h.

With the BioShuttle transporter, we achieved non-membrane perturbing delivery into the cytoplasm. By help of the cleavable bonds the second part of the transport module (Figure 2) is liberated and delivered to the desired cell compartment.

We have demonstrated a very efficient nuclear transport of the fluorochrome as an example for any transportable substances or drugs (like peptide nucleic acids) (Figure 3).

References

1. Braun K., *et al*., *J Mol Biol.* **318**, 237-243 (2002).
2. Derossi D. *et al*., *Trends in Cell Biology* **8**, 84-87 (1998).
3. Kalderon D., *et al*., *Cell* **39**, 499-509 (1984).

Peptide Revolution: Genomics, Proteomics & Therapeutics
Michael Chorev & Tomi K. Sawyer (Editors)
American Peptide Society, 2003

Tat Peptide-Mediated Vectorization of Nucleic Acids

Eric Vivès[1], Thibault Michel[2], Françoise Debart[2], Jean-Philippe Richard[1], Kamran Melikov[3], Leonid Chernomordik[3], Jean-JacquesVasseur[2] and Bernard Lebleu[1]

[1]University Montpellier II, CNRS-UMR5124, 1919 Route de Mende, 34093 Montpellier Cedex 05, France; [2]University Montpellier II, CNRS-UMR5625, Pl. Eugène Bataillon, 34095 Montpellier Cedex 05, France; [3]NICHD, NIH, Bethesda, MD 20892, USA

Introduction

We recently proposed a reevaluation of the uptake mechanism of the cell penetrating peptide (CPP) derived from the Tat protein [1]. It was initially thought that this Tat peptide (as other CPPs used in this field such as Antennapedia or Penetratin peptide) was internalized through an energy-independent process. The high number of basic amino acids within the Tat sequence first favored a strong binding to the cell membrane (Figure 1), probably through the high number of anionic moieties exposed on the cell surface. Then the peptide is taken up by cell through the endocytosis pathway as shown by the characteristic punctuated pattern in the cell cytoplasm [1]. Moreover the strong initial binding of the peptide at the cell membrane induced an over-evaluation of the cell-associated signal during FACS quantification despite intensive washes. In addition, fixation procedures prior microscopy also induced an artifactual diffusion of the Tat peptide to the cell nucleus [1].

Despite evidences that the Tat peptide followed the endocytosis pathway, CPPs have been successfully used to deliver oligonucleotides (ONs) into cells. The effective delivery of these Tat bound ONs has been associated with the expected biological activity [2]. Therefore, these data support the use of CPPs for nucleic acid delivery.

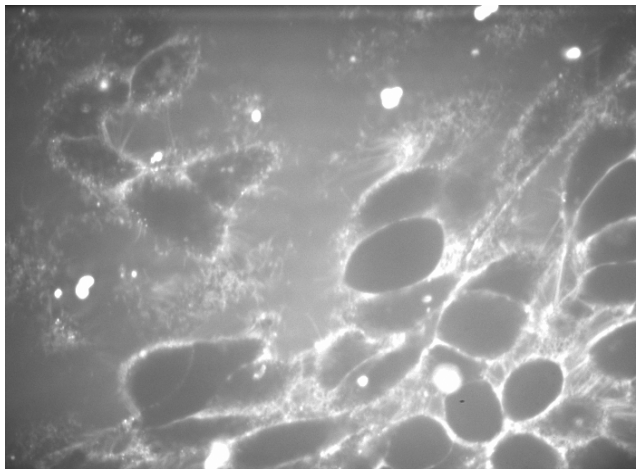

Fig. 1. HeLa cells were incubated for 30 min with fluorescein-maleimide labeled Tat peptide (1mM), washed three times with PBS (5min), and then observed by confocal fluorescence microscopy without any fixation. An important labeling of the cell membrane is revealed.

Results and Discussion

Although the cost of unmodified synthetic ON is relatively low, prices strongly increase when chemical modifications of ONs are required for allowing the final condensation to the peptide. These include several steps from a 5'-thiotrityl oligonucleotide usually obtained through ON synthesis. The first step corresponding to the deprotection of the trityl group was performed by a silver nitrate treatment, followed by precipitation of the silver with dithiothreitol (DTT). A gel filtration was required for recovering the reduced ON prior the activation of the thiol function with 2,2'-dipyridyl disulfide. Finally, the purified activated ON was coupled to the peptide. In order to obtain high yield of chimeric Tat-ON molecules easily, chemical activation/ligation has to be simplified.

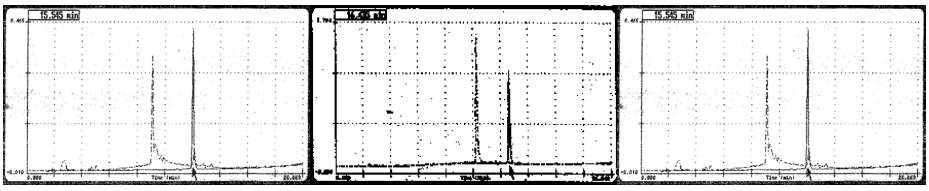

Fig. 2. "One step" activation was achieved for phosphodiester ONs (left) for phosphorothioate ONs (middle) and 2'OMe ONs (right). In each chromatogram, the activated-ON shows the lower retention time (left peak).

We first investigated the direct substitution of the thiotrityl of phosphodiester ON by the 2-nitrophenyl sulfenyl chloride (NpsCl) (Figure 2, left). Such substitution was inspired from the activation of Trt protected cysteine by 3-nitro-2-pyridinesulfenyl chloride in peptide synthesis [3]. However, phosphodiester ONs are expected to be strongly digested by cellular nucleases. Other ON analogues showing much higher stability are commercially avalaible. These include phosphorothioate ONs, where an oxygen of the phosphate group is replaced by a sulfur, and 2'-OMe, where the 2' position of the sugar is alkylated. The direct substitution of the thiotrityl of these analogues was shown to be fully effective under these conditions and led to the activated ONs.

Conclusion

The one step activation of three different ON analogues has been performed. This should improve the overall yields of ON-peptide chimera. Moreover the final condensation of the ONs to the CPP such as Tat (or Antennapedia) through a disulfide bridge formation should allow the release of the vectorized ONs once in the cytoplasmatic reductive environment.

Acknowledgments

The work was supported by funds from the CNRS and Association de la Recherche contre le Cancer (ARC).

References

1. Richard, J. P., *et al*., *J. Biol. Chem*. **278**, 585-590 (2003).
2. Astriab-Fisher, A., *et al.*, *Pharm. Res.* **19**, 744-54 (2002).
3. Matsueda, R., *et al*., *Chem. Lett.* 921- 924 (1982.

Peptide Combinatorial Libraries, Proteomics and Screening Methods

Peptide Revolution: Genomics, Proteomics & Therapeutics
Michael Chorev & Tomi K. Sawyer (Editors)
American Peptide Society, 2003

A Reassessment of the Role of Cys^8 in Annexin A2-tPA Interaction

Oriol Roda[1], Mari-Luz Valero[1], Cristina Chiva[1], Sandra Peiró[2], Francisco X. Real[1,2], Pilar Navarro[2] and David Andreu[1]

[1]Department of Experimental and Health Sciences, Pompeu Fabra University, and [2]Molecular and Cell Biology Unit, Municipal Institute of Medical Research, 08003 Barcelona, Spain

Introduction

Annexin A2 (AnxA2, also termed p36, calpactin 1 or lipocortin II) is known to be an important receptor for tissue-type plasminogen activator (tPA) in endothelial and other cell types, including tumor cells. For instance, both tPA and AnxA2 overexpression have been described in pancreatic cancer and related to malignant and invasive phenotypes. Conversely, inhibition of tPA activity has been associated with reduced invasiveness and in vivo tumorigenicity. Identifying tPA receptors in pancreatic cells and their involvement in tumorigenesis is thus a matter of considerable interest.

Interaction between tPA and its AnxA2 cellular receptor at the level of an hexapeptide (LCKLSL, residues 7-12 of AnxA2) has been proposed as a specific motif mediating tPA interaction, with the Cys^8 residue as particularly crucial for binding [1]. In an attempt to identify other amino acids that might be critical for the AnxA2-tPA interaction, we prepared a synthetic library derived from the consensus hexapeptide and screened its components as inhibitors.

Results and Discussion

On the basis of the original LCKLSL motif, the peptide library contained alterations in sequence (Gly, Ala and D-amino acid scans; conservative mutations of the Leu and Cys residues, randomization), stereochemistry (enantiomer and retroenantiomer versions), size, and availability of the thiol group. The peptides were individually assayed as AnxA2 competitors in a binding assay against recombinant biotinylated tPA using alkaline phosphatase-coupled streptavidin for detection. We found all peptides containing a free thiol group, regardless of size, sequence or structure, to be effective inhibitors of the AnxA2-tPA interaction [2]. Free Cys-containing peptides totally unrelated to the LCKLSL motif had a similar inhibitory effect while Cys-blocked peptides such as LC(Acm)KLSL were inactive. To determine whether binding of peptides to tPA, rather than to AnxA2, was required for the inhibition, peptides were directly added to (plate-bound) AnxA2, plates were washed and tPA was added. The results were similar to those above, strongly suggesting a direct interaction of AnxA2 with the peptides. These findings were completely paralleled by cell culture experiments, where the Cys-containing peptides also inhibited tPA binding to the surface of cultured human umbilical vein endothelial cells, in which AnxA2 is the main receptor for tPA.

We considered two possible explanations for the above facts: i) that tPA and AnxA2 interact with low affinity through the Cys^8 residue of AnxA2 and can therefore be relatively easily dissociated by moderate concentrations of thiol-containing molecules, or ii) that Cys^8 of AnxA2 readily engages in disulfide formation with our Cys-containing peptides (as it does with homocysteine, [1]), therefore rendering that residue unavailable for other interactions, such as tPA binding. To test these hypothesis, we analyzed by MALDI-TOF MS (data not shown) both untreated and peptide-treated AnxA2. Both LCKLSL and its homocysteine analogue caused increments in molecular mass of ca. 600 Da, compatible with the formation of a 1:1

complex between AnxA2 and the peptide. To further probe into the interaction, we separated the AnxA2-peptide reaction mixture by SDS-PAGE (10% acrylamide), excised the main Coomassie Blue spot and digested it with trypsin. The tryptic peptides were separated in a home-manufactured nanocolumn (15 cm × 75μm; 3μm, Zorbax C_{18} silica beads) interfaced to a Q-Star Pulsar mass spectrometer (Applied Biosystems) and eluted with a 5-65% water/acetonitrile gradient (200 nL/min) over 80 min. Peptide masses and sequences were determined by MS/MS using an information-dependent acquisition method. Sequence was determined for masses corresponding to the N-terminal tryptic peptide, with or without an attached LCK fragment. The results (Figure 1) clearly proved the specific binding of the Cys-containing peptide to the Cys^8 residue of AnxA2.

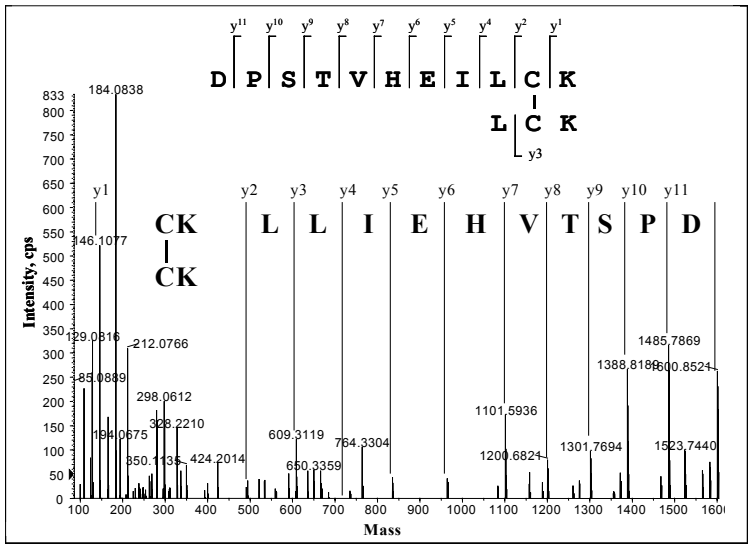

Fig. 1. MS-MS analysis of a tryptic peptide obtained from the reaction of recombinant AnxA2 and LCKLSL and corresponding to the N-terminal sequence of AnxA2. Ser^1 of AnxA2 is preceded by an Asp-Pro dipeptide resulting from N-terminal extension of the recombinant AnxA2 construct [1].

In summary, we have demonstrated that the previously held view of LCKLSL as a sequence-specific inhibitor of tPA-AnxA2 interaction [1] is inaccurate; rather, a free thiol group is all that seems to be required for inhibition. On the other hand, the precise nature of the tPA-AnxA2 interaction is still unclear and will require further work to be structurally elucidated.

References

1. Hajjar, K. A., Mauri, L., Jacovina, A. T., Zhong, F., Mirza, U. A., Padovan, J. C., and Chait, B. T. *J. Biol. Chem.* **273,** 9987–9993 (1998).
2. Roda, O., Valero, M. L., Peiró, S., Andreu, D., Real, F. X., and Navarro, P. *J. Biol. Chem.* **278**, 5702-5709, (2003).

Peptide Revolution: Genomics, Proteomics & Therapeutics
Michael Chorev & Tomi K. Sawyer (Editors)
American Peptide Society, 2003

Application of Topologically Segregated Bifunctional Beads to Construct Unique Combinatorial Bead Libraries

Xiaobing Wang, Li Peng, Ruiwu Liu and Kit S. Lam

Department of Internal Medicine, UC Davis Cancer Center, California 95817, USA

Introduction

The "one-bead-one-compound" (OBOC) combinatorial libraries can be constructed with a "split-and-mix" synthesis method such that each bead in the library only displays one single compound [1]. Upon biological screening, the positive beads can be physically isolated for structural determination. For peptide libraries, the peptide-bound beads can be individually sequenced with an automatic micro-sequencer using Edman chemistry. This necessitates that peptides of the library must have a free N-terminus and contain only α-amino acids as building blocks. There is a need to develop methods to overcome such limitations. We recently reported a novel encoding method on double-layer beads [2] for OBOC small molecule or peptidomimetic libraries, where the library compound resides on the outer layer of the bead and the coding tag remains in the bead interior. Such topologically segregated bi-layer beads can easily be prepared with a bi-phasic approach, and they can be applied to OBOC peptide libraries with structures that cannot be sequenced. Furthermore, the bi-functional beads can be used for the development of library beads with low substitution on the bead surface but normal substitution in the bead interior. The application of bi-layer bead approach on three unique combinatorial libraries is shown in Figure 1.

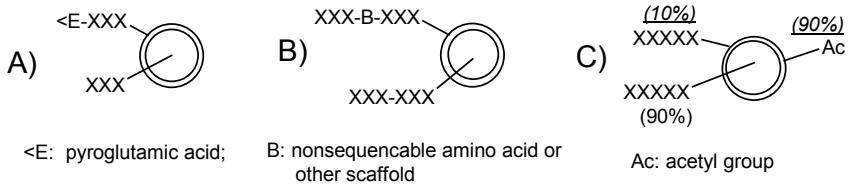

Fig. 1. Unique combinatorial libraries with library compounds on the bead surface and coding tags in the bead interior: A) N-terminal blocked; B) Middle-blocked; C) down-substituted testing library.

Results and Discussion

The three combinatorial libraries shown above were all synthesized on TentaGel resins (Scheme 1). **Library A:** Using "split-mix" synthesis method, a tri-peptide library was first synthesized. The library beads were then topologically segregated into double layers, in which the outer layer was protected with Fmoc and the interior was protected with Boc. Upon deprotection of Fmoc, pyroglutamic acid was coupled to the outer layer. Although pyroglutamic acid containing peptide is unsequenceable, the entire peptide sequence can be determined by sequencing the peptide tag in the bead interior. **Library B:** A tripeptide library was prepared. Then in the bi-layer segregation step, the outer layer of the bead was protected with Fmoc and the interior was protected with Alloc. After Fmoc-deprotection, a β-turn amino acid was added to the outer layer. The Alloc group was then removed with palladium chemistry and the Fmoc group deprotected. The remaining peptide was simultaneously assembled on both layers. When more than one β-turn amino acid was used in the library construction, all of them

were encoded with α-amino acids in the interior coding tag. In this way the un-sequenceable residue can be by-passed. **Library C:** A surface-down-substituted library was constructed by first preparing the bi-layer beads. The outer layer was then down-substituted with a homogeneous solution of Fmoc-Gly-OH and Ac-Gly-OH at a desired ratio. After Fmoc- and Alloc- deprotection, a pentapeptide library was assembled on the beads. This library enables one to screen a target protein at higher stringency (low concentration of ligands on the bead surface) while leaving enough peptides in the bead interior for microsequencing. **Results:** We randomly sequenced some beads obtained from each of the three libraries and were able to demonstrate that we can unambiguously determine the amino acid sequence of each peptide-bead. Because TentaGel beads can be segregated into bi-layers at any point during library synthesis, one can apply the OBOC combinatorial peptide library methods to many unsequenceable peptides or peptidomimetics.

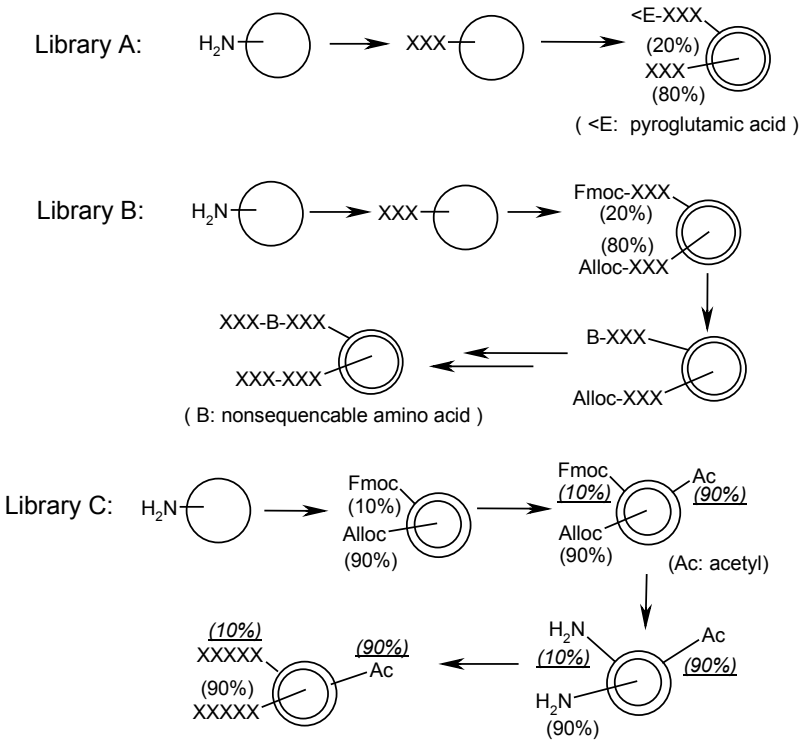

Scheme 1. Synthetic route of libraries A, B & C.

Acknowledgments
This work was funded by NIH R33CA-86364 and R33 CA-89706 grants.

References

1. Lam, K. S., Salmon, S. E., Hersh, E. M., Hruby, V. J., et al. *Nature* **354**, 6348 (1991).
2. Liu, R., Marik, J. and Lam, K. S. *J. Am. Soc. Chem*. **124**, 7678 (2002).

Peptide Revolution: Genomics, Proteomics & Therapeutics
Michael Chorev & Tomi K. Sawyer (Editors)
American Peptide Society, 2003

Minimalism Applied to a Hit to Lead Program

Marc Vendrell[1], Rubén Ventura[1], Fernando Albericio[1], Rosario González-Muñiz[2], Laura García de Diego[3], Cristina Carreño[3], Antonio Ferrer-Montiel[3,4] and Miriam Royo[1]

[1]Combinatorial Chemistry Unit, Barcelona Science Park, Barcelona, Spain;[2]Instituto de Química Médica, CSIC, Madrid, Spain; [3]DiverDrugs S.L., L'Hospitalet de LLobregat Barcelona, Spain; [4]Institute for Molecular and Cellular Biology, Universitas Miguel Hernández, Elche, Spain

Introduction

The most desirable binding characteristics of a good lead compound for protein targets depend largely on the physiochemical properties of the molecule. These characteristics are often not fully accomplished in molecules involved in drug discovery programs, especially when the structural requirements for the interaction of such compounds with their corresponding biological targets are unknown. One of the paradigms of medicinal chemistry is to increase the therapeutic index of these structures, converting them into lead molecules. Recent contributions to the literature suggest that leads suitable for further optimization by medicinal chemistry share some physiochemical properties [1]. Some of the most remarkable are: a relative polarity, low molecular weight (between 200 and 350), the existence of a single charge (secondary or tertiary amine preferred), the exclusion of chemically reactive functional groups, a relative lipophilicity and a number of H-bond acceptors (atoms of N and O) below 10. These properties should be compatible with the structural requirements needed in the interaction with the receptor. Our work is focused on the TRPV1 receptor, which has emerged as a key therapeutic target for inflammatory pain management [2]. Among the different groups of ligands recognized by this receptor, we are interested in non-competitive antagonists. Arginine rich hexapeptides (Figure 1) are good examples of this type of compounds and share some characteristics in their structure: (a) an aromatic region; (b) more than one positive charge; and (c) a lipophilic moiety.

Ac-Arg-Arg-Arg-Arg-Trp-Trp-$CONH_2$

Fig. 1. Structure of a TRPV1 non-competitive antagonist.

The objective of this project is to combine both types of requirements in order to achieve an improvement of the lead-like properties of these molecules without affecting their biological properties.

Results and Discussion

Previous studies established the guidelines to synthesize a first generation library of non-competitive antagonist for the TRPV1 receptor in which some hits with high affinity for the receptor were obtained [3]. Nevertheless, the toxicity that some compounds displayed required an improvement of their lead-like properties. This objective was accomplished by introducing three types of modifications into the tryptophan-(Nps) scaffold (Figure 2): 1) the exploitation of the charge distribution in the N-terminal end with different guanidines, amines or amides; 2) the study of the lipophilicity by linking different moieties to the C-terminal; and 3) the substitution of

the amide linkage for other motifs in order to reduce the molecular weight and minimize the peptidic character of the molecule.

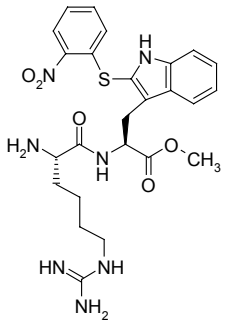

Fig. 2. Scaffold for further optimization.

The synthesis of a 40-compound library was carried out in solid-phase using Fmoc/Alloc chemistry on MBHA resin (0.7 mmol/g) and AM and BAL as handles. Cleavage of the products was developed with a mixture of TFA:H_2O:triethylsilane (TES) 90:5:5 and analyzed by LC-MS chromatography. Yields ranged from 50% to 80% and the grade of purity varied from 65% to 80%. The library is currently being tested biologically in order to obtain new non-competitive antagonists for the TRPV1 receptor.

References

1. Rishton, G. M. *Drug Discovery Today* **8**, 86-96 (2003).
2. Caterina, M. J. et al. *Annual Reviews of Neuroscience* **24**, 487-517 (2001).
3. Zaccaro, L. et al. In Benedetti, E. and Pedone, C. (Eds.) *Peptides 2002 (Proceedings of the 27th European Peptide Symposium), Edizioni Ziino, Napoli,* 2003, pp. 1024-5.

Peptide Revolution: Genomics, Proteomics & Therapeutics
Michael Chorev & Tomi K. Sawyer (Editors)
American Peptide Society, 2003

Is it Possible to Minimize the Toxicity of a Hit Compound Without Reducing its Activity?

Rubén Ventura[1], Marc Vendrell[1], Fernando Albericio[1], Rosario González-Muñiz[2], Laura de Diego[3], Cristina Carreño[3], Antonio Ferrer-Montiel[3,4] and Miriam Royo[4]

[1]Combinatorial Chemistry Unit, Barcelona Science Park, Barcelona, Spain; [2]Medicinal Chemistry Institute, CSIC, Madrid, Spain;[3]DiverDrugs S.L. L'Hospital de Llobregat, Barcelona, Spain; [4]Institute for Molecular and Cellular Biology, Universitas Miguel Hernández, Elche, Spain

Introduction

Pain is an unpleasant sensation primarily designed to avoid tissue damage. Although pain has been traditionally considered as a unique and homogeneous pathology, cumulative progress has established that pain is an extremely complex and dynamic process involving multiple, irrelated neurotransmitter/neuromodulator systems in the peripheral nervous system. Indeed, as many as 15 neurotransmitters have been implicated in diverse aspects of pain-processing pathways [1]. Two major types of pain are widely recognized, namely neuropathic and inflammatory. Nerve injury due to infection or autoimmune disease underlie the etiology of neuropathic pain. Inflammatory pain is produced in response to tissue damage.

The molecular components and mechanism involved in inflammatory pain transduction are now tarting to be unfolded. The identification and cloning of the TRPV1 channel represents a significant step in the clarification of its molecular mechanisms[2]. Because of its central implication in hyperalgesia, the TRPV1 receptor has emerged as a key therapeutic target for inflammatory pain management. TRPV1 is a nonselective cation channel with high Ca^{2+} permeability and belongs to the superfamily of cation channels with six transmembrane domains. Desensitization of the receptor in response to specific ligands has long been considered a promising therapeutic approach for the treatment of neuropathic pain and other pathological conditions involving C-fiber neurons. The challenge is to develop antagonists that preserve the physiological activity of the TRPV1 receptor while correcting over-active receptors. DD161515 and arginine rich hexapeptides (Figure 1) are good examples of this type of compound and share some structural characteristics.

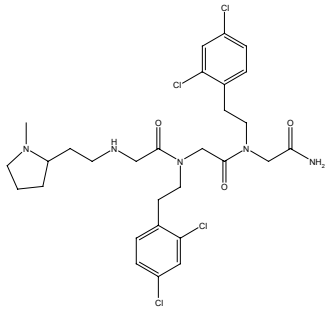

DD161515

Ac-Arg-Arg-Arg-Arg-Trp-Trp-$CONH_2$

Fig. 1. Structures of well-known vanilloid-related inhibitors.

Results and Discussion

Taking into consideration the structural requirements of the TRPV1 receptor and the fact that dipeptides derivatives containing the 2-[(*o*-nitrophenyl)sulfenyl] (Nps) tryptophan moiety (Figure 2) have antinociceptive activity (this dipeptide exhibited *in vivo* analgesic activity) [3], a previous library was designed and synthesized in the search of new compounds with yet higher biological activity and selectivity. In spite of the good biological results in terms of activity and selectivity, some of these dipeptides also have a high toxicity. Thus, there is increasing evidence that the existence of a high number of charges can induce negative effects in terms of toxicity [4].

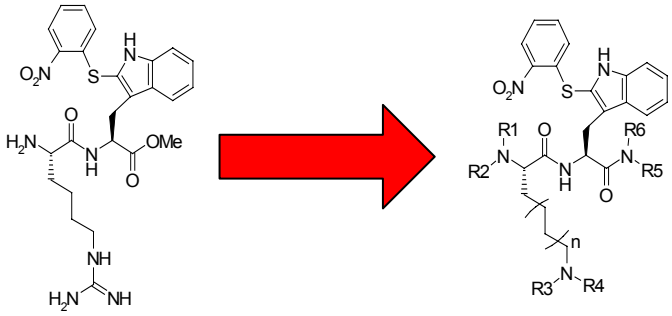

Fig. 2. Library of dipeptide derivatives containing Nps-tryptophan.

We have designed and synthesized a new library to explore the effect of the reduction of the number of charges in biological activity. Dipeptides were synthesized using Fmoc/Alloc chemistry on MBHA (0.7 mmol/g) resins and AM and BAL as handle. Several modifications were introduced to test the influence of the pKa of the molecule. The cleavage was carried out with a mixture of TFA:H_2O:triethylsilane (TES) 90:5:5. The crude peptides were concentrated with a Discovery Speedvac System, then dissolved in a mixture 50:50 of acetonitrile:water, and analyzed by HPLC (using a C_{18} Symmetry column) with a gradient of 0-100% CH_3CN in aq. 0.1% TFA. The compound purities are in the range of 60-80%.
Biological assays are currently being carried out.

References

1. Williams, M., Kowaluk, E. A. and Arneric, S. P. *J. Med. Chem*. **42**, 1481-1500 (1999).
2. Caterina, M. J. and Julius, D. *Annu. Rev. Neurosci*. **24**, 487-517 (2000).
3. García-López, M. T., Herranz R., González-Muñiz R., Naranjo, J. R., de Ceballos, M. L. and del Río J. *Peptides* **7**, 39-43 (1986).
4. Rishton, G. M. *Drug Discovery Today* **8**, 86-96 (2003).

Peptide Revolution: Genomics, Proteomics & Therapeutics
Michael Chorev & Tomi K. Sawyer (Editors)
American Peptide Society, 2003

The Combined Solid and Solution-Phase Synthesis of Small Molecular Libraries: The Evolution of the "Libraries from Libraries" Concept

Yongping Yu, John M. Ostresh and Richard A. Houghten*

Torrey Pines Institute for Molecular Studies, 3550 General Atomics Court, San Diego, California 92121, USA

Introduction

Combinatorial chemistry has emerged as a powerful methodology for the preparation of libraries of small organic compounds in order to accelerate the drug discovery process [1]. The generation of diverse chemical libraries using the "libraries from libraries" concept in conjunction with solid-phase and solution-phase methods is described. The central features of the approaches presented are the use of solid-phase synthesis methods for the generation of polyamines, which were used as starting material for the synthesis of triazepanes **1**, 1,5-disubstituted-2-aryliminoimidazolidines **2** and indolines **3**. Following cleavage from the resin with HF, the polyamine library was transformed to the corresponding nitrosamine library **4** in the solution-phase as an evolution of the "libraries from libraries" concept.

Results and Discussion

Starting from p-methylbenzhydrylamine (MBHA) resin, a Boc-amino acid (Boc-AA(R^1)-OH) was coupled to the resin. The Boc group was removed using 55% trifluoroacetic acid (TFA) in dichloromethane (DCM). The resulting primary amine was acylated with a wide range of commercially available carboxylic acids to provide the resin-bound acylated amino acid. The resin-bound di-amide was treated with borane in THF, resulting in the exhaustive reduction of the amides to yield resin-bound diamine **5**.

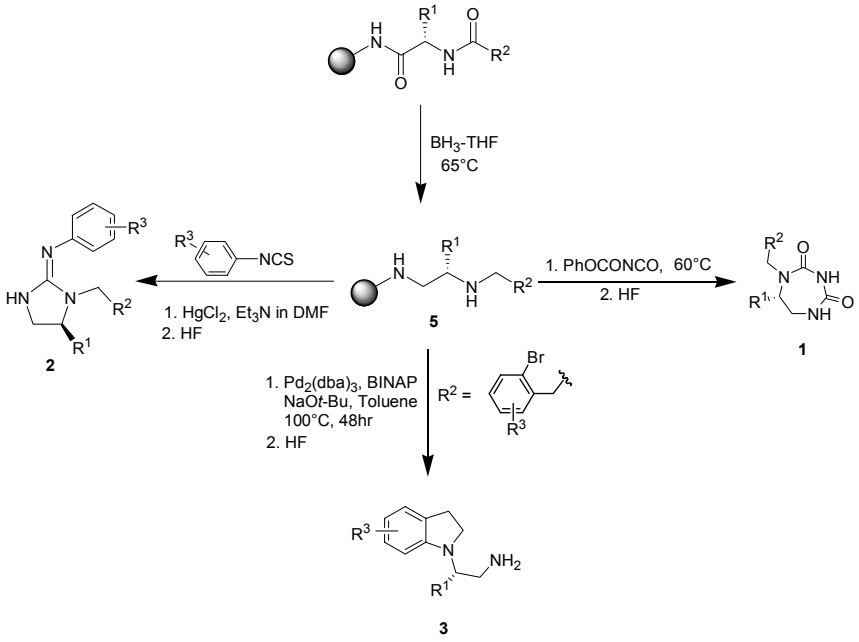

Resin-bound diamine **5** was then treated with phenyl isocyanatoformate in dimethylformamide to give the corresponding resin-bound 1,7-disubstituted-1,3,5-triazepane-2,4-dione **1** following cleavage [2]. The resin-bound diamine **5** was reacted with arylisothiocyanate in the present of the $HgCl_2$, Et_3N in anhydrous DMF at room temperature overnight and cleaved to afford the corresponding guanidines **2** [3]. When 2-bromophenyl acetic acid derivatives were used as R^2, the resin-bound diamine **5** yielded the corresponding disubstituted indolines **3** via palladium-catalyzed intramolecular cyclization and cleavage [4].

Due to instability of the N-N bond of the nitrosamine under HF cleavage conditions, we modified our "libraries from libraries" concept by first generating the triamines of interest from the corresponding resin-bound dipeptides. Following cleavage from the resin with HF, the polyamine library was reacted with ethyl nitrite in the solution phase to yield the desired nitrosamine library **4** in good yield and purity [5]. Excess ethyl nitrite was easily removed under vacuum. The approaches described enable the efficient syntheses of individual nitrosamines as well as mixture-based nitrosamine libraries.

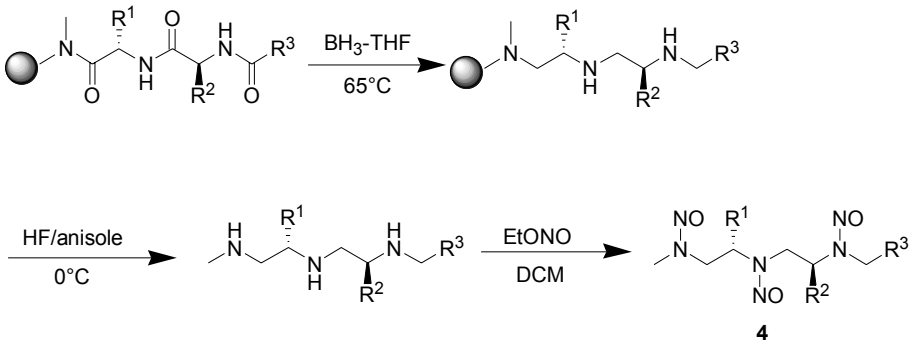

4

In summary, the work presented is a continuation of our efforts directed toward the synthesis of acyclic and heterocyclic compounds directly from amino acids and short peptides. Using the concept of "libraries from libraries," we have thus been able to generate individual small molecular compounds as well as a mixture-based small molecular library.

Acknowledgments

This work was supported by National Cancer Institute Grant No. CA78040 (Houghten).

References

1. (a) Jung, G. (Ed.) *Combinatorial Chemistry: Synthesis, Analysis, Screening*, Wiley-VCH: Weinheim, 1999. (b) Gordon, E. M., Kerwin, J. F. Jr. (Eds.) *Combinatorial Chemistry and Molecular Diversity in Drug Discovery*, John Wiley & Sons Ltd.: New York, 1998.
2. Yu, Y., Ostresh, J. M. and Houghten, R. A. *Organic Lett*. **3**, 2797 (2001).
3. Yu, Y., Ostresh, J. M. and Houghten, R. A. *J. Org. Chem.*, **67**, 3138 (2002).
4. Yu, Y., Ostresh, J. M. and Houghten, R. A. *Tetrahedron Lett*. **44**, 2569 (2003).
5. Yu, Y., Ostresh, J. M. and Houghten, R. A. *J. Org. Chem.* **68**, 183 (2003).

Peptide Revolution: Genomics, Proteomics & Therapeutics
Michael Chorev & Tomi K. Sawyer (Editors)
American Peptide Society, 2003

Combinatorial Neoglycopeptide Arrays for the Study of Peptide Resistance to Proteolysis

Michael R. Carrasco, Matthew D. Bernardina, Ryan T. Brown and Katherine A. Rawls

Department of Chemistry, Santa Clara University, Santa Clara, CA, 95053-0270, USA

Introduction

The chemoselective reaction of completely unprotected carbohydrates and peptides offers an attractive route for the synthesis of neoglycopeptide arrays. If a synthetic strategy allows reacting a single peptide with a variety of native sugars, then a small set of peptides can be reacted combinatorially with a group of sugars to produce a diverse array of neoglycopeptides. One such synthetic strategy utilizes aminooxy-derivatized peptides, which react chemoselectively in oxime-forming reactions with reducing sugars in mild aqueous conditions.

We recently reported a novel amino-oxy amino acid, *O*-(*N*-methyl)-aminohomoserine (Amh), for the synthesis of neoglycopeptides [1,2]. When incorporated into peptides, this amino acid can be chemoselectively glycosylated at the amino-oxy side chain. Importantly, the sugar adopts a cyclic conformation and remains close to the peptide backbone. These features enhance its ability to mimic natural glycopeptides and enable biologically relevant studies of how attached sugars modulate peptide structure and function. We are now using Amh-based neoglycopeptides to investigate the generally observed phenomenon of peptidic resistance to proteolysis conferred by glycosylation. Here we report preliminary data on the synthesis of the neoglycopeptide array for that study.

Results and Discussion

We based our neoglycopeptide array on the insulin-derived model peptide shown in Figure 1. This peptide has two unambiguous, well-studied protease cleavage sites: an endoproteinase Glu-C cleavage site between Glu21 and Arg22 and a trypsin cleavage site between Arg22 and Gly23. Our idea was to attach different sugars at different positions relative to the two cleavage sites. By studying the relative cleavage rates of the glycosylated peptides, we could determine how different factors — distance from the cleavage site, size of the sugar, etc. — contributed to the proteolytic resistance.

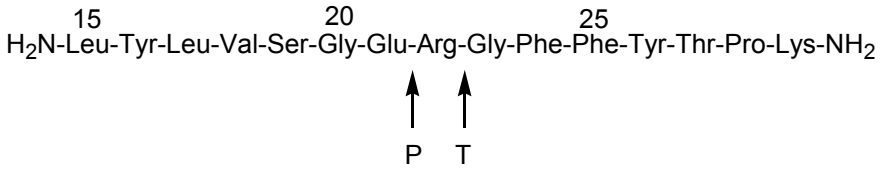

Fig. 1. Portion of the B-chain of insulin (with Cys19 to Ser substitution for easier handling). The residue numbers are those of the entire B-chain. ***T*** *indicates the tryptic cleavage site;* ***P*** *indicates the endoproteinase Glu-C cleavage site.*

The design for the neoglycopeptide array is shown in Figure 2. The four starting peptides, $\mathbf{A_1}$-$\mathbf{D_1}$, each have one Amh residue located near the cleavage sites. In the diagrammed, first generation array, each of these peptides is treated individually with D-glucose, lactose, and *N*-acetylglucosamine to quickly generate 12 neoglycopeptides,

[A-D]$_{2-4}$. Later iterations could both increase the number of peptides and variety of sugars to increase the size and diversity of the array.

Peptides **A_1-D_1** were synthesized using *in situ*-neutralization Boc chemistry [3] with MBHA (1.0 mmol/g, 0.1 g) resins and manual synthesis procedures. Following HF deprotection and cleavage with *p*-cresol as a scavenger, the crude peptides were dissolved in 25% CH_3CN in aq. 0.1% TFA and lyophilized. The peptides were purified to homogeneity by semi-preparative C_{18} RP-HPLC (Microsorb).

Glycosylation of the peptides proceeds efficiently in 0.1 M NaOAc, pH 4.0 buffer at 40 °C in 6-24 h as measured by ESI-MS. However, in contrast with the majority of our previous results with other peptides, we have had difficulty separating these neoglycopeptides from their non-glycosylated counterparts by standard RP-HPLC. Our current separation efforts are focused on a variety of alternative RP-HPLC conditions and other forms of chromatography, such as HILIC.

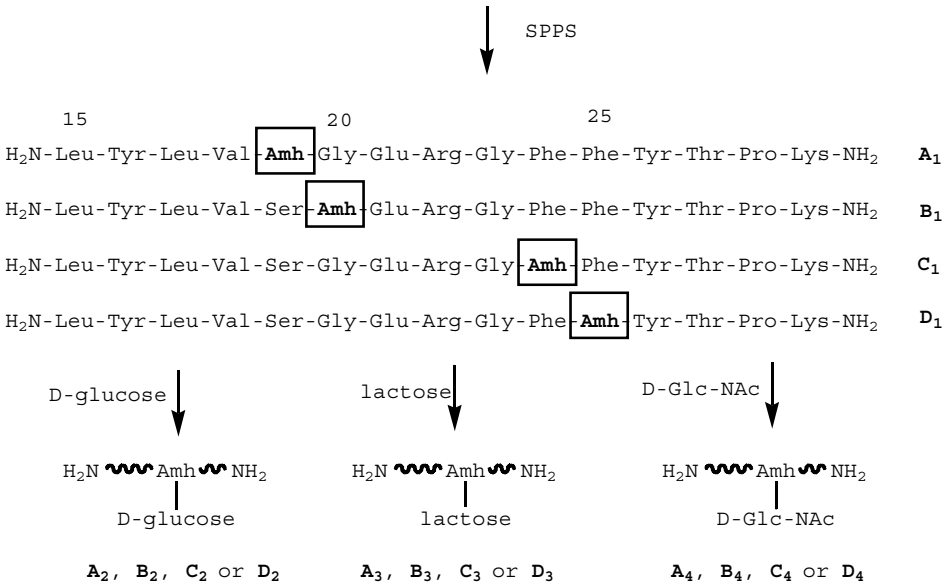

Fig. 2. Design of the neoglycopeptide array. Four Amh-derivatized peptides are synthesized, and each peptide is reacted with each sugar to create an array of 12 neoglycopeptides.

Acknowledgments

We gratefully acknowledge financial support from: the Camille and Henry Dreyfus Faculty Start-up Grant Program for Undergraduate Institutions; the NSF-REU grant CHE01-39527 and NSF-CAREER grant CHE01-34818; the Donors of The Petroleum Research Fund administered by the American Chemical Society; and an award to Santa Clara University Undergraduate Biological Sciences Education Program of the Howard Hughes Medical Institute.

References

1. Carrasco, M. R., et al., *Tetrahedron Lett.* **43**, 5727-5729 (2002).
2. Carrasco, M. R., Brown, R. T., et al. *J. Org. Chem.* **68**, 195-197 (2003).
3. Schnölzer, M., Alewood, P., Jones, A., Alewood, D. and Kent, S. B. H. *Int. J. Peptide Protein Res.* **40**, 180-193 (1992).

Peptide Revolution: Genomics, Proteomics & Therapeutics
Michael Chorev & Tomi K. Sawyer (Editors)
American Peptide Society, 2003

Solid-Phase Synthesis of 1,3,4-Thiadiazolium-2-Aminides

Joseph C. Kappel, T. Scott Yokum and George Barany

Department of Chemistry, University of Minnesota, Minneapolis, MN 55455, USA

Introduction

Combinatorial chemistry can be an important aspect of the drug discovery process, insofar as it facilitates the efficient synthesis of a large number of structurally related compounds [1]. These efforts often target small heterocyclic compounds due to their potential for desirable physical and biological properties, and the opportunity to introduce a wide degree of structural diversity [2]. Derivatives of 1,3,4-thiadiazoles are known antibacterial and antifungal agents [3]. In particular, 1,3,4-thiadiazolium-2-aminides (**1**) have been found to possess antimicrobial and antitumor properties [4]. Herein, we report a solid-phase strategy for the synthesis of 1,3,4-thiadiazolium-2-aminides in library fashion.

Results and Discussion

The synthesis began by loading three diverse aromatic aldehydes onto discrete PAL-PEG-PS resins. Separately, 1,4-disubstituted thiosemicarbazides **2** were prepared in solution by reacting substituted hydrazines (5 equiv with respect to the resin loading) with isothiocyanates (15 equiv with respect to the resin loading) in dioxane at 60 °C for 1 h. Six hydrazines and nine isothiocyanates were used in preparing a total of thirteen examples of **2**. Immediately following, the reaction solution containing crude **2** was transferred to a vessel containing the resin-bound aldehyde, plus trimethylsilyl chloride (5 equiv) in THF. The reaction was allowed to proceed for 2 h at 60 °C, giving the resin-bound cyclized product. Following cleavage with TFA–H_2O (19:1), the filtrate was concentrated, and the crude residue redissolved and purified over silica gel to give the title compounds **1** (Scheme 1).

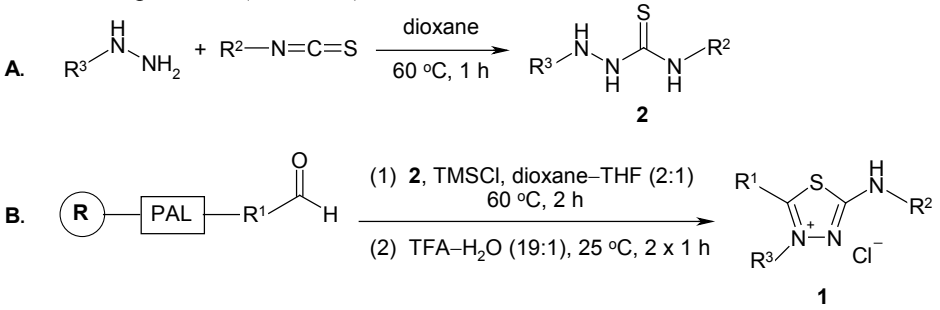

Scheme 1. (A) Solution synthesis of 1,4-disubstituted thiosemicarbazides. (B) Solid-phase synthesis of 1,3,4-thiadiazolium-2-aminides.

The structures of **1** were proven by elemental analysis, mass spectrometry, and ^{1}H NMR. Interestingly, an unanticipated oxidation must take place to account for the highly stable **1**, insofar as the simple condensation product **3** was expected by analogy to the literature synthesis of substituted 2,3-dihydro-3-phenyl-1,3,4-thiadiazoles (**4**) (Scheme 2).

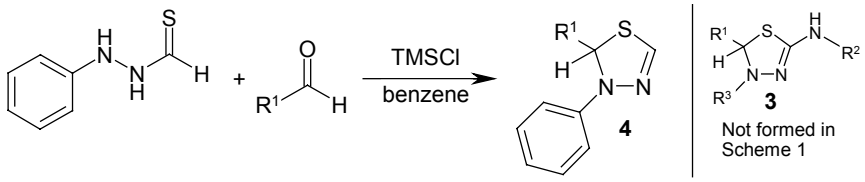

Scheme 2. Literature preparation of substituted 2,3-dihydro-3-phenyl-1,3,4-thiadiazoles [5].

In total, seventeen compounds were prepared in high purity (90-98%), as determined by HPLC analysis with monitoring at 220 nm. The isolated yields, determined following purification over silica gel, and calculated based on the substitution level of the starting resin, were moderate (53-74%) to good (77-94%) with one exception (38%), all with excellent initial purity. Electron-rich aromatic, electron-deficient aromatic, and aliphatic substituents were tolerated in both the hydrazine and isothiocyanate components.

In conclusion, we have described a solid-phase synthesis of 1,3,4-thiadiazolium-2-aminides. The compounds were generated in high purity and prepared in a concise two-step procedure from resin-bound aldehydes.

Acknowledgments

The work was supported by the National Institutes of Health (GM 42722).

References

1. (a) Gallop, M. A., Barrett, R. W., Dower, W. J., Fodor, S. P. A. and Gordon, E. M. *J. Med. Chem.* **37**, 1233-1251 (1994). (b) Gordon, E. M., Barrett, R. W., Dower, W. J., Fodor, S. P. A. and Gallop, M. A. *J. Med. Chem.* **37**, 1385-1401 (1994). (c) Pavia, M. R., Sawyer, T. K. and Moos, W. H. *Bioorg. Med. Chem. Lett.* **3**, 387-396 (1993). (d) Booth, R. J. and Hodges, J. C. *Acc. Chem. Res.* **32**, 18-26 (1999). (e) An, H. and Cook, P. D. *Chem. Rev.* **100**, 3311-3340 (2000).
2. (a) Thompson, L. A. and Ellman, J. A. *Chem. Rev.* **96**, 555-600 (1996). (b) Nefzi, A., Ostresh, J. M. and Houghten, R. A. *Chem. Rev.* **97**, 449-472 (1997). (c) Franzén, R. G. *J. Comb. Chem.* **2**, 195-214 (2000). (d) Krchňák, V. and Holladay, M. W. *Chem. Rev.* **102**, 61-91 (2002). (e) Horton, D. A., Bourne, G. T. and Smythe, M. L. *Chem. Rev.* **103**, 893-930 (2003).
3. (a) Dogan, H. N., Rollas, S. and Erdeniz, H. *Il Farmaco* **53**, 462-467 (1998). (b) Dogan, H. N., Duran, A., Rollas, S., Sener, G., Uysal, M. K. and Gülen, D. *Bioorg. Med. Chem.* **10**, 2893-2898 (2002). (c) Mamolo, M. G., Vio, L. and Banfi, E. *Il Farmaco* **51**, 71 (1996).
4. (a) Montanari, C. A., Amaral, A. T. D. and Giesbrecht, A. M. *Pharm. Sci.* **3**, 565-568 (1997). (b) Grynberg, N., Santos, A. C. and Echevarria, A. *Anti-Cancer Drugs* **8**, 88-91 (1997). (c) Silva, E. F., Canto-Cavalheiro, M. M., Braz, V. R., Cysne-Finkelstein, L., Leon, L. L. and Echevarria, A. *Eur. J. Med. Chem.* **37**, 979-984 (2002).
5. Matsubara, Y., Kitano, K., Tsutsumi, A., Yoshihara, M. and Maeshima, T. *Chem. Pharm. Bull.* **42**, 373-374 (1994).

Peptide Revolution: Genomics, Proteomics & Therapeutics
Michael Chorev & Tomi K. Sawyer (Editors)
American Peptide Society, 2003

Synthesis, Folding and Deconvolution of Combinatorial Peptide Libraries Based on α-Conotoxins: Generation of a Novel Ligand for α7 Nicotinic Acetylcholine Receptors

M. Ellison[1], J. Nielsen[2], B. Green[2], P. Buczek[2], M.J. McIntosh[1], B.M. Olivera[1] and G. Bulaj[1,2]

[1]Department of Biology, University of Utah, Salt Lake City, UT 84112;
[2]Cognetix, Inc. 421 Wakara Way, Salt Lake City, Utah 84108, USA

Introduction

α-Conotoxin ImI is a small bicyclic peptide antagonist of α7 nicotinic acetylcholine receptors (nAChRs). The affinity of α-ImI for the α7 nAChRs lies in the micromolar range, but this interaction is characterized by a very fast off-rate. This fast off-rate reduces the usefulness of this peptide as a research tool for studying α7 nAChRs. To improve properties of α-ImI, we employed a combinatorial approach to select an α-ImI-based peptide with significantly slower off-rate. Here we report the synthesis and deconvolution of four α-ImI-based combinatorial libraries, this resulted in identification of α-exoconotide 1, a conotoxin-derived peptide exhibiting at least 20-times slower off-rate from α7 nAChRs than α-ImI.

Results and Discussion

In order to produce an α-ImI-derived ligand with significantly slower off-rate than that of α-ImI, we produced four biased combinatorial libraries. The general strategy was to retain a portion of the α-ImI structure and to introduce a mix of several amino acids in a few positions of the peptide sequence. An example of such a library is shown in Figure 1A. In this library, only four positions within the first loop were randomly changed. Four libraries were synthesized using standard Fmoc chemistry. In each library, all cysteine residues were protected by trityl groups. To improve cyclization yields, we developed a cosolvent-assisted oxidative folding. Briefly, the peptide mixtures were cleaved from a solid support, purified by solid-phase extraction on a C18 resin and oxidized in a mixture of reduced and oxidized glutathione in the presence of 10% ethanol. Before testing their activities, the oxidized mixtures were further purified by solid-phase extraction.

Screening of the oxidized libraries against human α7 nAChRs revealed potential compounds with significantly slower off-rates. Iterative deconvolution of one of the libraries (shown in Figure 1A) resulted in discovery of a unique peptide antagonist of α7 nAChRs. The deconvoluted sequence, GCCRHRKCAWRC#, contained a large number of positively charged residues. This peptide, called α-exoconotide 1, exhibited at least 20-fold slower off-rate than α-ImI, as shown in Figure 1B.

Since the libraries were produced using random folding, we characterized the structure of the active component of the folding mixture. Interestingly, none of the three possible two-disulfide bond bridging patterns of α-exoconotide 1, when imposed by regioselective folding, generated a molecule with the slow off-rate observed with the random folding mixture. When analyzed by HPLC, the folding mixture of α-exoconotide 1 showed multiple folding species, one of them exhibiting the slow off-rate. MALDI-TOF analysis of the slow off-rate component of the folding mixture suggested the presence of a partially folded species. Alkylation of the peptide cysteine thiols with iodoacetamide and sequencing showed that a vicinal disulfide bridge was

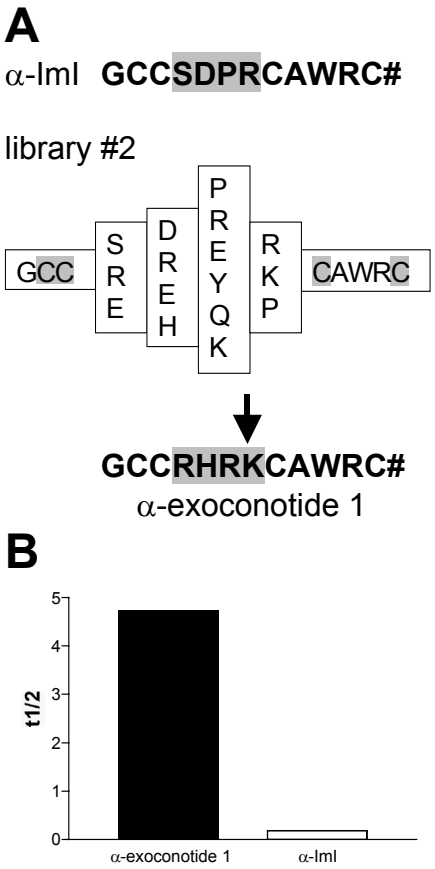

Fig. 1. A - α-conotoxin ImI was used to design several combinatorial libraries. Deconvolution of the library #2 resulted in identification of α-exoconotide 1, exhibiting at least 20 times slower off-rate than that of α-ImI. B – half time [min] of recovery of α7 nAChRs after response to 1 sec impulse of ACh in the presence of α-ImI or α-exoconotide 1.

formed between Cys 2 and Cys 3, whereas the other two cysteines were reduced. Indeed, analogs of α-exoconotide 1 with all possible disulfide-bridging patterns showed that the molecule with the vicinal bridge had the slowest off-rate.

Sasaki et al. described another example of improving properties of conotoxins, where a combinatorial approach and directed parallel synthesis were used to improve selectivity of ω-conotoxin MVIIC toward P/Q-type Ca channel [1]. In this work, a total number of 47 three-disulfide bonded analogs were synthesized; some of them retained the affinity for the P/Q channels, but had lower affinity toward N-type channels.

Our work presented here suggests that the combinatorial approach may be applicable to conotoxins, but the most active component of the library may not necessarily contain the native conotoxin fold. Thus, in addition to generating a novel diversity of conotoxin sequences, the combinatorial approach may select novel conformations preferred in binding to ion channels and receptors.

References

1. Sasaki T., et al. *FEBS Lett*. **466**, 125-129 (2000).

Peptide Revolution: Genomics, Proteomics & Therapeutics
Michael Chorev & Tomi K. Sawyer (Editors)
American Peptide Society, 2003

A Novel Encoding Method for "One-Bead One-Compound" Peptidomimetic and Small Molecule Combinatorial Libraries

Aimin Song[1], Jinhua Zhang[2], Carlito B. Lebrilla[2] and Kit S. Lam[2]

[1]Department of Internal Medicine, UC Davis Cancer Center, 4501 X Street, Sacramento, CA 95817, USA; [2]Department of Chemistry, University of California, Davis, CA 95616, USA

Introduction

In 1991, we first introduced the "one-bead one-compound" (OBOC) combinatorial library method [1]. With an on-bead screening assay, literally millions of compound-beads can be screened against specific molecular targets in a few days [1]. Peptide-beads can easily be microsequenced with Edman degradation, but structure determination of small molecule-beads is challenging. In an effort to continue to improve the OBOC technology, we have recently developed a novel, simple and efficient encoding method based on mass spectrometry (MS) for "one-bead one-compound" peptidomimetic and small molecule combinatorial libraries (Scheme 1). The topologically segregated bifunctional resin beads with orthogonal protecting groups in the outer and inner regions are first prepared according to our previous published procedure [2]. Prior to library synthesis, the inner region of each bead is derivatized with 3-4 different coding blocks (C^n) on a cleavable linker. Each functional group (X, Y and Z) on the scaffold (S) is encoded by an individual coding block containing a functional group (X', Y' and Z') with the same chemical reactivity. During library synthesis, the same building blocks (B^n) are coupled to the scaffold (outer layer of the bead) and the coding blocks concurrently. After screening, the coding tags in the positive beads are released and analyzed by MALDI-FTMS. The chemical structure of library compounds can be readily determined according to the molecular mass of the coding tags. The feasibility and efficiency of this approach was demonstrated by the synthesis and screening of a model library.

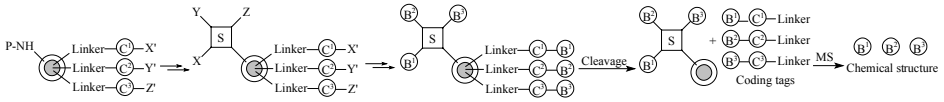

Scheme 1. General synthetic and encoding/decoding strategy of encoded libraries.

Results and Discussion

MALDI-FTMS was used for decoding due to its high resolution, high accuracy and high sensitivity. The topologicallly segregated bifunctional TentaGel resin beads were prepared using our published procedure [2]. The inner region (40%) was used for encoding. A simple and peptide-like linker (Scheme 2) was designed and synthesized.

A model small molecule library was synthesized and encoded (**1**, Scheme 3) [3]. Prior to the library synthesis, a randomly selected model compound (**1a**) was tested on the TentaGel resin beads with a cleavable linker in both of the outer and inner regions.

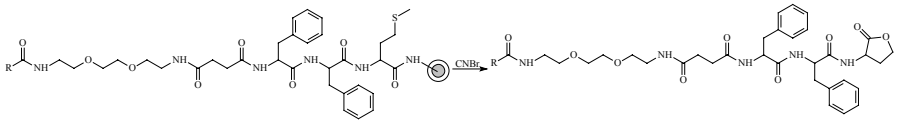

Scheme 2. Design of the cleavable linker.

The decoding result was consistent, indicating that the structures of library compounds can be reliably decoded. During the library synthesis, 37 amino acids, 51 primary amines and 86 nucleophiles were used as the first, second and third building blocks, respectively. A library containing 37×51×86 = 162,282 members was obtained. This library was screened for streptavidin binding ligands using an enzyme-linked colorimetric assay (Figure 1a) [4]. Four positive beads were isolated and analyzed with MALDI-FTMS (Table 1). The decoding results were clear and unambiguous (Figure 1b), indicating this encoding method is reliable and efficient.

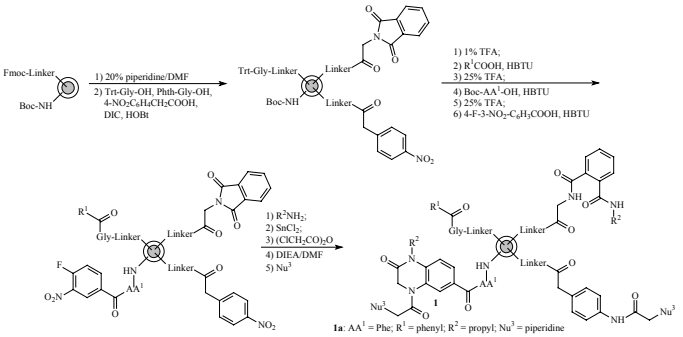

Scheme 3. Synthetic and encoding reactions of a model library.

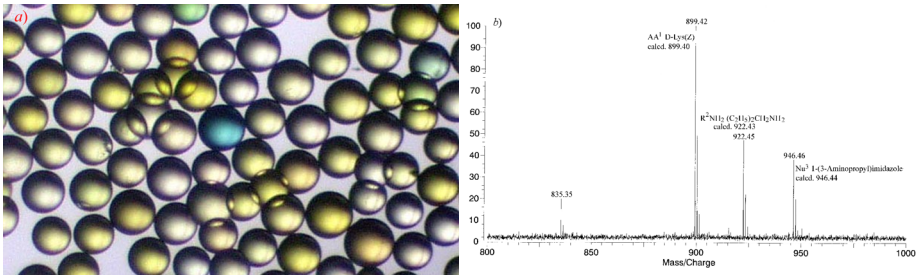

Fig. 1. Photomicrograph (a) of a positive bead (dark gray) from the screening and its MALDI-FTMS decoding spectrum (b).

Table 1. Decoding results of positive beads obtained from streptavidin binding assay.

AA^1	R^2NH_2	Nu^3
D-Lys(Z)	$(C_2H_5)_2CH_2NH_2$	1-(3-Aminopropyl)imidazole
D-Lys(Z)	2-Aminonorbornane	Histamine
Nipecotic acid	1-(3-Aminopropyl)-2-pyrrolidinone	1-Phenylpiperazine
Nipecotic acid	H-Glu(OEt)-OEt	4-Bromobenzylamine

Acknowledgments
The work was supported by NIH grants R33 CA-86364 and R33 CA-89706.

References

1. Lam, K. S. et al., *Nature* **354**, 82-84 (1991).
2. Liu, R., Marik, J. and Lam, K. S. *J. Am. Chem. Soc.***124**, 7678-7680 (2002).
3. Zaragoza, F. and Stephensen, H. *J. Org. Chem.* **64**, 2555-2557 (1999).
4. Lam, K. S. and Lebl, M. *Immuno. Methods* **1**, 11-15 (1992).

Peptide Revolution: Genomics, Proteomics & Therapeutics
Michael Chorev & Tomi K. Sawyer (Editors)
American Peptide Society, 2003

Characterizations of Peptides that Selectively Bind Neuroendocrine Differentiated Prostate Cancer Cells

Amanda M. Enstrom and Kit S. Lam

Department of Internal Medicine, UC Davis Cancer Center, 4501 X Street, Sacramento, CA 95817, USA

Introduction

Prostate cancer represents 30% of cancer in men. Neuroendocrine differentiation (NED) of prostate epithelial cancer cells has been linked to poor prognosis possibly contributed by androgen insensitivity of the NED cells [1, 2]. NED cells secrete factors promoting growth and differentiation in surrounding cancer cells [3, 4], suggesting a tumorogenic promoting mechanism. Therefore, the ability to target NE cells and halt signal transduction could decrease conversion to more malignant disease. Many cell surface receptors such as integrins are proximal to many cell signal transduction cascades and their expression becomes increasingly altered as the cancer progresses. "One-bead one-compound" (OBOC) peptide libraries [5, 6] have been screened for peptides that specifically bind NED prostate cancer cells. To accomplish this, we have employed prostate cancer cell models of NED, which are NED inducible using the cytokine interleukin-6 (IL-6) (Figure 1). Peptides identified through this process are currently being examined for any biological effects on the cells and their signaling. Many of these peptides show selectivity for prostate cancer over other cancer cell lines. The identification of peptides able to stimulate or inhibit specific cell signaling pathways could be useful in understanding the process of NED, as well as develop useful tools to diagnose, study, and possibly treat aggressive differentiated prostate cancer [7].

Through screening OBOC combinatorial all D-amino acid peptide-bead libraries, we identified 22 peptides that bind to human prostate cancer cell lines (DU145, PC3, and LNCaP). Some of these peptides appear to be relatively specific as they do not bind to hepatocytes and only bind weakly to ovarian cancer cells. Some of these peptides can bind and support cell growth. Some of them appear to stimulate cell migration. Work is currently underway to resynthesize 9 of these peptides for further characterization, and for development of reagent for flow cytometry and peptide-histochemical or peptide-fluorescent microscopy.

Results and Discussion

Peptide libraries have been constructed on 90 micron Tenta gel beads using the OBOC library approach [6]. A secondary library, with a unique D-amino acid motif identified from the primary screen, has also been constructed. A whole cell on-bead binding assay [8] has been used to identify peptides that bind to the surface of either the NED cells or the undifferentiated LNCaP prostate cancer cells. We have also used PC3 prostate cancer cells, an androgen insensitive line that has been demonstrated to NED. Peptide-beads with attached cells are isolated and stripped of cells. These beads can be re-washed and re-tested for binding specificity. This two-step approach isolates peptides specific to the differentiation state of the cells, as well as reduces the number of false positives. Promising peptides are resynthesized and tested against a variety of different cancer cells. Peptides appearing to have preferential binding to prostate cells will be later tested against normal prostate epithelial cells and prostate cancer biopsy specimens.

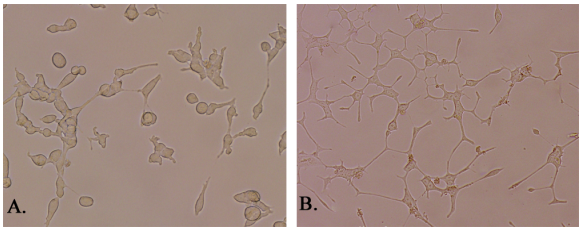

Fig. 1. (A) LNCaP cells (B) LNCaP cells displaying neuron like morphology after 4 days treatment with IL-6.

Several biological assays have been utilized to determine any effects the peptides have on the growth and differentiation of the prostate cells. To determine if the peptide-bead can bind and promote cell growth, cells are allowed to bind to the bead briefly (5 minutes), and all free cells removed. After overnight incubation, these beads are completely covered with tightly bound cells with cellular spreading (Figure 3). A modified cell migration assay demonstrated that when cells and beads are mixed in soft agar, after 96 hours, each bead is completely covered with the malignant cells, whereas the amount of residual cells in the agar matrix is sparse (Figure 4). This suggests that either these peptide beads are able to attract prostate cells, and/or the attached cells grow rapidly. Using anti phosphor-tyrosine antibody, we can compare the Western blots of lysate obtained from free cells and cells that attached to the beads. Peptides that elicit the most potent signaling in prostate cancer cells, will be further evaluated for the exact biochemical mechanism.

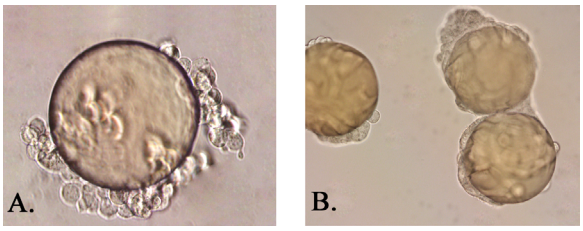

Fig. 2. Cell growth assay: NED LNCaP prostate cells incubated with a turned D-amino acid nanopeptide (P2), (A) after 5 minutes partially and loosely bound beads are moved to a dish with no free cells and (B) after 24 hours cell spreading and growth is visible.

Acknowledgments
The work was funded by NIH grants R33CA-86364 and R33 CA-89706.

References
1. Spiotto, M. T. and Chung, T. D. K., *Prostate* **42**, 186-195 (2000).
2. Bonkhoff, H., *Annals Oncol*. **12**, S141-S144 (2001).
3. di Sant'Agnese, P. A., *Cancer* **75**, 1850 (1995).
4. Cox, M. E., Deeble P. D., Lakhani S. and Parsons S. J., *Cancer Res*. **59**, 3821-3830 (1999).
5. Lam, K. S., Salmon, S. E., Hersh, E. M., et al. *Nature 354*, 82-84 (1991).
6. Lam, K. S., Lebl, M. and Krchnak, V., *Chem. Rev*. **97**, 411-448 (1997).
7. Aina, O. H., Sroka, T. C., Chen, M. L. and Lam, K. S., *Biopolymers* **66**, 184-199 (2002).
8. Lau, D. H., Guo, L., Liu, R., et al., *Biotech. Lett*. **24**, 497-500 (2002).

Peptide Revolution: Genomics, Proteomics & Therapeutics
Michael Chorev & Tomi K. Sawyer (Editors)
American Peptide Society, 2003

Increasing Diversity of One-bead One-compound Combinatorial Peptide Libraries Using Side-chain Derivatization

Ruiwu Liu and Kit S. Lam

Division of Hematology & Oncology, Department of Internal Medicine, UC Davis Cancer Center, University of California Davis, 4501 X Street, Sacramento, CA 95817, USA

Introduction

Peptides containing unnatural amino acids have unique structural properties and are more resistant to proteolysis. We have recently developed a sequencing method enabling us to determine the sequence of peptide beads containing many unnatural amino acids [1]. By incorporating unnatural amino acids, the diversity of peptide libraries can be greatly increased. However, unnatural amino acids are generally much more expensive than the standard eukaryotic amino acids. An important approach to increase the diversity of a peptide library is to derivatize the side-chains of common, but inexpensive amino acids such as lysine (Lys), α,β-diaminopropionic acid (Dpr), Phe(4-NH_2) and aspartic acid (Asp).

Results and Discussion

We have determined the retention times of a large number of derivatives of Lys, Dpr, Phe(4-NH_2) and Asp where their side-chains are derivatized with carboxylic acids, isocyanates, or amines (data not shown). To detect the more hydrophobic PTH-amino acid derivatives, we extend the elution gradient program for an additional 6 minutes prior to washing the column with 90% solvent B (Table 1). The first 18 minutes of the gradient profile are identical to the normal gradient. This ensures that the elution profile of all 20 PTH-natural amino acids remains unchanged and that they can be read automatically using the analysis program already installed in the protein sequencer. R2C (methyl piperidine/water/butanol/isopropanol) is used to replace R2B (methyl piperidine/water/methanol). This eliminates the phenylmethylthiocarbamate peak (an adduct of the original coupling reagent phenylisothiocyanate and methanol) allowing the PTH-amino acid derivative to be detected at this area.

Table 1. Comparison of normal and modified gradient program for Perkin Elmer/Applied Biosystem PTH-Amino acid elution.

Normal	Time (min)	0.0	0.3	0.4	18.0	18.5	21.5	22.0
	% B	6	6	16	43	90	90	50
Modified	Time (min)	0.0	0.3	0.4	18.0	24.5	27.5	28.0
	% B	6	6	16	43	90	90	50

The equipment parameters are as follows: column, Spheri-5 C-18 PTH Column, 5 μm, 2.1 x 220 mm; column temperature, 55 ℃; cartridge temperature, 48 ℃; flask temperature, 64 ℃. Reservoir A: 25 mL premix buffer added to 1 L solvent A3 (3.5 % v/v tetrahydrofuran in water). Reservoir B: 88 % acetonitrile/12 % isopropanol v/v (solvent B2).

By using orthogonal protecting groups, such derivatization can occur on beads during the library synthesis. Orthogonal protecting groups for NH_2 group can be Fmoc, Boc, Dde and Alloc. NO_2 can also be treated as a protected NH_2 group since it can be easily reduced to NH_2 by $SnCl_2$. The derivatization reactions are monitored with on-bead color detection methods such as ninhydrin test, chloranil test [2] or malachite

green test [3] for the detection of primary amine, aniline amine or carboxyl group, respectively.

To demonstrate the synthesis and application of amino acid derivatives, a 1,346,400-member "one-bead one-compound" (OBOC) tetra-peptide library containing derivatives of Dpr, Lys, Phe(4-NH_2) and Asp were constructed using a split-mix synthesis strategy (Figure 1). The library consists of 30 Dpr derivatives of isocyanates at the N_4 position, 30 Phe(4-NH_2) derivatives at the N_3 position and 44 Lys derivatives at the N_2 position. At N_1 position, a combination of 17 natural amino acids, 4 unnatural amino acids and 13 Asp derivatives of amines were used. The peptide bead-library was screened for streptavidin binding. Novel ligands with a high consensus motif were identified (Figure 2), e.g. all ligands contain Lys derivative of 2-pyrazinecarboxylic acid at N_2 position, and α-aminoisobutyric acid or valine at the N_1 position.

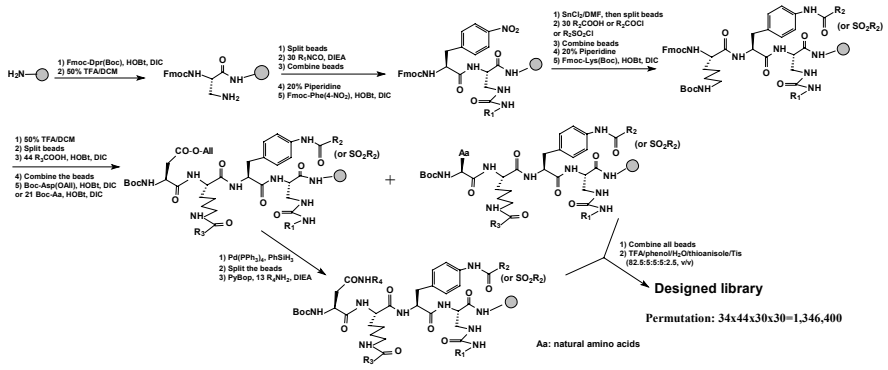

Fig. 1. Synthetic scheme of an OBOC tetra-peptide library containing unnatural amino acids derived from side-chain derivatization.

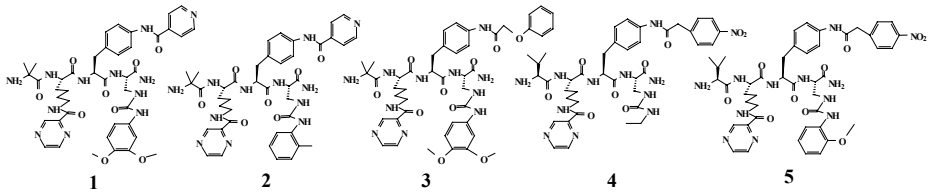

Fig. 2. Structure of streptavidin-binding ligands identified from library shown in Fig.1.

In summary, we now have the option of using any combination of the standard 20 natural amino acids, commercially available unnatural amino acids, or derivatized amino acids illustrated above to construct OBOC combinatorial peptide libraries, as long as these amino acids can be resolved on the HPLC of the microsequencer. The structural diversity of such libraries could be enormous even for short peptides.

Acknowledgments

The work was funded by grants NIH R33CA86364 and R33CA89706, and the University of California Systemwide Biotechnology Research Program (2001-07).

References

1. Liu, R. and Lam, K. S. *Anal. Biochem*. **295***,* 9-16 (2001).
2. Marik, J., Song, A. and Lam, K. S. *Tetrahedron Lett*. **44**, 4319-4320 (2003).
3. Attardi, M. E., Porcu, G. and Taddei, M. *Tetrahedron Lett*. **41**, 7391-7394 (2000).

Peptide Revolution: Genomics, Proteomics & Therapeutics
Michael Chorev & Tomi K. Sawyer (Editors)
American Peptide Society, 2003

A Novel Encoded High-Density Chemical Microarray Platform for Proteomics and Drug Development

Jan Marik, Qingchai Xu, Xiaobing Wang, Li Peng and Kit S. Lam

Division of Hematology & Oncology, Department of Internal Medicine, UC Davis Cancer Center, 4501 X Street, Sacramento, California 95817, USA

Introduction

Some of the early forms of combinatorial library methods were low density arrays, including the multi-pin system first described by Geysen [1], and the spot-synthesis method described by Frank [2]. In 1991, Fodor and coworkers reported the use of a light-directed, spatially addressable parallel chemical synthesis method to generate 1024 peptides on glass chip [3], the first high-density chemical microarray. Parallel synthesis methods were employed in the preparation of these peptide arrays. As a result, these arrays were spatially separable and addressable. About the same time, we described the use of a "split-mix" synthesis method to generate a random peptide library containing millions of peptide-beads, such that each bead displayed only one peptide entity [4]. These peptide-beads were screened simultaneously with an enzyme-linked colorimetric method and positive beads were isolated for structure determination [4,5]. If the library compound is an N-terminally free peptide, it can be microsequenced directly with Edman chemistry. If the library compound is a small molecule or a non-sequenceable peptide, it needs to be encoded (see below). This one-bead one-compound (OBOC) combinatorial peptide library can also be viewed as an ultra-high density peptide microarray that is spatially separable but not addressable.

In the last few years, protein and chemical microarrays have emerged as a very important tool for proteomic research. Similar to gene chips, chemical microarrays are prepared by immobilizing a large number of different chemical or biological molecules on the surface of a solid-support via (i) *in situ* synthesis [3], (ii) chemical ligation through a covalent bond [6], or (iii) non-covalent binding. Through spotting, proteins can be immobilized on solid support by covalent ligation or non-covalent binding to form a microarray. In contrast, short peptides or small molecule microarrays require covalent attachment because many of these compounds do not adsorb reliably to solid supports. Although peptide microarrays can be efficiently synthesized *in situ* on glass surface via photochemistry, synthesizing small molecule microarrays directly on the glass surface is problematic. Most investigators synthesize the small molecule compounds and then ligate them covalently to the solid support [7]. We have recently developed a novel microarray approach by covalently ligating the ligands to a biopolymer, such as human serum albumin or agarose, via chemoselective ligation chemistry. The ligand-biopolymers are then spotted onto the solid support (see below).

In spite of the intrinsic power of the OBOC combinatorial library method, it has not been widely practiced by most combinatorial chemists. This is particularly true with OBOC small molecule libraries because of the difficulty in deciphering the chemical structure of small molecule on one single bead. The chemical encoding techniques reported so far are rather tedious and not easily reproduced by other laboratories. However, we have recently described two novel chemical encoding methods using topographically segregated bifunctional beads [8,9]. In these methods, the outer layer of the bead is used for the synthesis of the library compound, and the inner core of the bead is used for the synthesis of the code. As a result, the coding arm will not interfere with the screening. One of our encoding systems uses α-amino acid containing

peptides as the coding tag. The side chains of these α-amino acids are derivatized by the building blocks at the same time when the small molecules library compounds are constructed on the outer layer of the bead. This peptide coding tag can be directly microsequenced with Edman chemistry [5] or released and decoded by mass spectroscopy [10]. The second coding system [9] is to link three to four coding blocks to the interior of the bead with methionine containing linkers. The functionality of the coding blocks is either similar or identical to those on the chemical scaffold of the library. During library synthesis, each building block will be incorporated into the scaffold and into the corresponding coding block simultaneously, thus eliminating many extra synthetic and washing steps. Positive beads are then isolated, treated with cyanogen bromide, and the releasate analyzed by MALDI-FT mass spectrometry. This latest MS based encoding system is highly robust and versatile, and can be readily applied by combinatorial chemists from other laboratories that have access to MALDI-FT mass spectrometer.

Another reason why the OBOC library method has not been widely used is because it cannot be readily applied to standard solution phase assays. Schreiber et al [11] expanded on the OBOC library methods [4,5] by developing releasable OBOC libraries in microtiter plates. To increase the amount of compound recovered from each bead after release, they used macrobeads (500μm). The compounds were then collected in microtiter plates and printed on glass slides to form chemical microarrays for biological evaluation. However, the capacity of macrobeads is very limited (<0.1 μmol/bead). Furthermore, the increased bead size leads to incomplete coupling due to limited reagent diffusion. To solve this problem, we have recently developed a novel solid support consisting of bead-aggregates (1-10 μmol/aggregate), on which a large number of compounds can be rapidly generated with the highly efficient "split-mix" synthesis method. These compounds, after release from the bead aggregates, can be fed into the

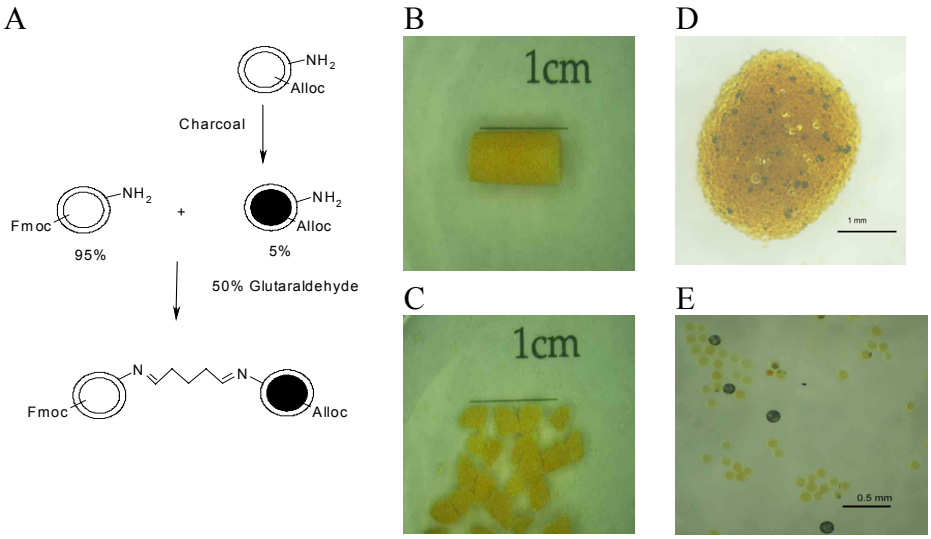

Fig. 1. (A) Preparation of the bead aggregates, (B) photomicrograph of freshly prepared bead aggregate block, (C) bead aggregate block cut into smaller pieces, (D) a bead aggregate after the 10 step synthesis, and (E) a crumbled bead aggregate with dark encoding beads and tan color compound beads.

standard solution phase high throughput screen, or ligated to a biopolymer and printed on solid support to form chemical microarrays. Positive spots or wells can be traced back to the mother plate where the encoded beads are isolated for decoding. The methodology and result of this highly efficient and economical chemical platform will be described below.

Results and Discussion

Novel encoded "one-aggregate one-compound" combinatorial libraries Our encoded bead aggregates consist of a mixture of two kinds of chemically orthogonal beads. The majority of the beads within the aggregate (e.g. 95-98%) bear the testing compound, which is released to the solution after the library synthesis is complete. The remaining 2-5% of the beads in the aggregate are colored (for easy retrieval at a later time) and contains the coding tag that can be decoded by Edman sequencing [8] or by MS [9]. The encoding method for the bead aggregate is very similar to our single bead encoding schemes outlined above. For single bead encoding, the testing compound resides on the bead surface and the coding tag resides in the bead interior. Similarly, for bead aggregate encoding, the testing compound resides in the majority of the beads within the aggregate, and the coding tag resides in a minority population of beads that are colored. Bead aggregates are formed by cross-linking these two populations of beads with glutaraldehyde.

The two kinds of spatially segregated bifunctional beads, one with 90% Fmoc-inside/10% NH_2-outside and the other with 90% Alloc-inside/10% NH_2-outside (Figure 1A), were prepared according to the procedure published by our laboratory [8]. The Alloc substituted beads swollen in DMF were treated with activated charcoal in water to yield black colored beads. The two populations of beads (tan and dark) were then mixed in ratio 95/5, washed with water and treated with 50% aqueous solution of glutaraldehyde and compressed for 30 minutes inside a 1mL syringe fitted with a frit on one end. The head of the syringe was removed, and the formed bead aggregate block was pushed out (Figure 1B). The bead aggregate block was then sliced to desirably sized pieces with a sharp razor blade (Figure 1C). Each aggregate shown in Figures 1C and D carried approximately 1μmol of compound according to the quantitative Fmoc substitution assay. Decoding of bead aggregates was accomplished by crumbling the bead aggregate (Figure 1D) gently with a spatula, and then retrieving the black encoded beads under a microscope with a hand-held micropipette (Figure 1E). The beads were then sent for structural determination. In principle, this bead retrieval step, as well as the sample preparation step for MS analysis, can all be automated.

Novel approach to chemical microarrays In this method, agarose (low melting temperature) is first chemically modified with a ketone. A synthetic peptide or small molecule ligand containing an aminooxy group is then conjugated onto the modified agarose at the ketone moiety via an oxime chemoselective ligation reaction. In this reaction, only the aminooxy group, but not the other free amines or sulfhydryl groups in the ligand, reacts with the ketone group in the agarose. The peptide-linked agarose solution melts above 60°C but gels at 25°C. Depending on the composition and type of agarose used, the melting and gelling temperature could vary. If diluted, it will not gel but will dry and stick onto the solid support. Figure 2 shows the chemistry of the peptide-agarose conjugate preparation. The peptide-agarose solutions are then spotted onto solid support (glass slide, polystyrene slide, or PVDF membrane) with an

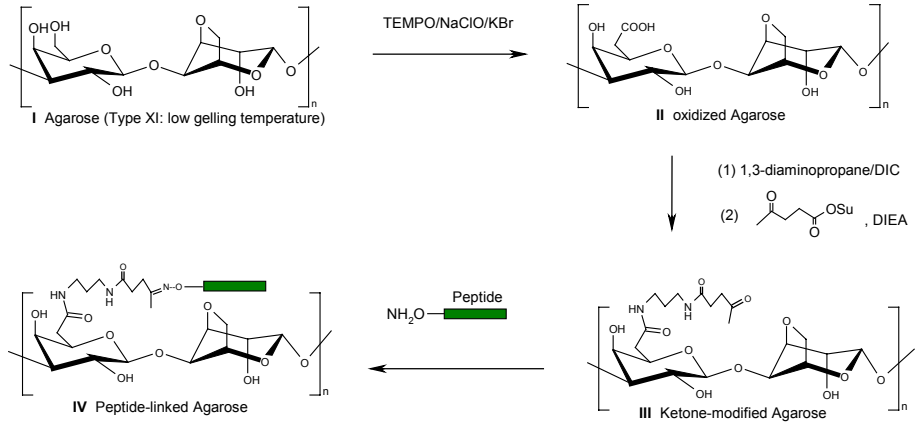

Fig. 2. Scheme for preparation of ketone-modified agarose and peptide-linked agarose.

automatic arrayer. After overnight drying, the peptide microarray is ready for biological studies.

For proof of concept, the above-mentioned one-aggregate one-compound method was used for the synthesis of a 25 member encoded small molecule library with two random positions: R_1 and R_2. The chemical structure of the library is shown in Figure 3. The α-amino group of the *p*-nitrophenylalanine was first acylated with 5 different carboxylic acids including d-biotin. The aromatic nitro group was then reduced with $SnCl_2$ and acylated with 5 other carboxylic acids, according to our published method [8]. The library compounds were then cleaved from the bead aggregates and conjugated to ketone-modified agarose via an oxime bond (Figure 2). The residual bead aggregates were washed and stored for subsequent decoding. The compound-agarose conjugates were printed on a PVDF membrane to form a microarray. The microarray was then incubated with streptavidin-alkaline phosphatase conjugate for one hour, washed and incubated with BCIP substrate for color development (Figure 3 B&C). The four corners of the microarrays plus the spot adjacent to the right-top corner were marked with d-biotin-agarose conjugate for microarray orientation and alignment.

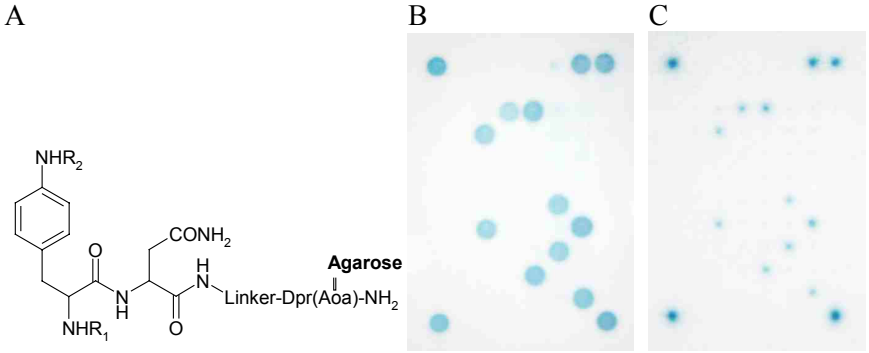

Fig. 3. (A) Chemical structure of small molecule ligands to be printed on PVDF membrane, (B) 300μm and (C) 100μm microarrays stained with Streptavidin-alkaline phosphatase conjugate.

Upon decoding, the 9 additional stained spots (Figure 3B) were all found to have d-biotin at the R_1 position. In another experiment, we used a similar microarray approach to print a number of different cell surface binding peptides on polystyrene slides and demonstrated that differential adhesion of intact cells to these peptide microarrays can be detected.

These experiments demonstrate that compound libraries can be prepared from encoded bead aggregates and that the chemical microarray system is working well. Because excess ligands, but equal amounts of ketone-modified agarose, are used in each of the chemoselective ligation reactions, the final concentrations of covalently linked ligands are identical in each microarray spot. This last but very important feature is unique for this microarray platform, and we believe this platform will be widely applied by investigators in the fields of proteomics and diagnostics.

Acknowledgments
The work was funded by R33CA99136, R33CA86364, and R33CA98116.

References

1. Geysen, H. M., Meloen, R. M. and Barteling, S. J. *Proc. Natl. Acad. Sci. U.S.A.* **81**, 3998 (1984).
2. Frank, R. *Tetrahedron* **48**, 9217 (1992).
3. Fodor, S. P. A., Leighton, R. J., Pirrung, M. S., Stryer, L., Lu, A. T. and Solas, D. *Science* **251**, 767 (1991).
4. Lam, K. S., Salmon, S. E., Hersh, E. M., Hruby, V. J., Kazmierski, W. M. and Knap, R. J. *Nature* **354**, 82 (1991).
5. Lam K. S., Lebl, M. and Krchnak, V. *Chem. Rev.* **97**, 411 (1997).
6. Falsey, J. R., Renil, M., Park, S., Li, S. and Lam, K. S. *Bioconjugate Chem.* **12**, 346 (2001).
7. Lam, K. S. and Renil, M. *Curr. Opin. Chem. Biol.* **6**, 353 (2002).
8. Liu, R., Marik, J. and Lam, K. S. *J. Am. Chem. Soc.* **124**, 7678 (2002).
9. Song, A., Zhang, J., Lebrilla, C. B. and Lam, K. S. *J. Am. Chem. Soc.* **125**, 6180 (2003).
10. Franz, A. H., Liu, R., Song, A., Lam, K. S. and Lebrilla, C. B. *J. Comb. Chem.* **5**, 125 (2003).
11. Blackwell, H. B., Perez, L. Stavenger, R. A., Tallarico, J. A., Eatough, E. C., Foley, M. A. and Schreiber, S. L. *Chem. Biol.* **8**, 1167 (2001).

Peptide Revolution: Genomics, Proteomics & Therapeutics
Michael Chorev & Tomi K. Sawyer (Editors)
American Peptide Society, 2003

Highly Flexible Assembly of Large Peptide Arrays Using a Novel Fully Automated SPOT-Robot

Johannes Zerweck, Thomas Ast, Stefan Guffler, Karsten Schnatbaum and Holger Wenschuh

Jerini Peptide Technologies, A Division of Jerini AG, Invalidenstr. 130, D-10115 Berlin, Germany

Introduction

The SPOT-synthesis concept has been described as a highly parallel synthesis technique to array large numbers of peptides, peptidomimetics and small organic molecules [1]. The compounds synthesized on planar membranes can directly be applied for solid phase screening assays [2] or alternatively be cleaved from the surfaces and used in cell-based assays in solution [3].

Despite the easy process of library generation by means of commercially available devices, speed and reproducibility of the operations are hampered by the semi-automated mode of these SPOT devices.

The present communication describes the development of a fully automated SPOT-system enabling the parallel synthesis of either 2,300 cleavable peptides for solution phase screening or 5,000 membrane bound peptides for solid phase screening (epitope mapping, receptor-ligand studies etc.).

Results and Discussion

The core piece of the system is a pivoted reaction/incubation tray carrying the membrane that was combined with a commercially available semi-automated ASP222 system. Main features of this computer-navigated tray are the capability of automated addition and removal of solvents and reagents, and the corrugated shape of its tray surface enabling efficient penetration and washing of the membrane. An elastic clamping fixture ensures a flexible and reliable mounting of membranes varying in shape and size (see Figure 1 for hardware configurations). The ability of the system to re-address the SPOTs in each synthesis step was shown, eliminating the possibility of cross-contamination between SPOTs. Additionally, a newly developed Windows-based software enables the implementation of complex coupling protocols and flexible washing steps.

The system was validated for both the automated and parallel assembly of 70,000 (2,300 per membrane) cleavable peptides and the synthesis of 100,000 membrane bound peptides (5,000 per membrane) for screening directly at the membrane. Many of the peptides were quality checked by LC-MS and found to be of equal quality compared to those synthesized on the semi-automated system.

Binding assays performed on substitutional analysis of well characterized epitopes revealed that binding patterns also corresponded well with previous results on other systems.

A comparative calculation of total synthesis time necessary to achieve library synthesis was performed for the semi vs. the fully automated system showing a decrease of the synthesis time by approx. 50%.

Compared to the commercial systems the automated version displays the following advantages:

- No manual steps necessary
- Faster and economical synthesis

- Very flexible coupling protocols due to modular software design
- Flexible reaction geometries, scales and numbers of peptides
- Highly parallel peptide synthesis (up to 2,300 cleavable peptides or 5,000 membrane bound peptides per batch)

Conclusively, the new system enables the high quality assembly of large peptide arrays in short timespans and in a fully automated manner.

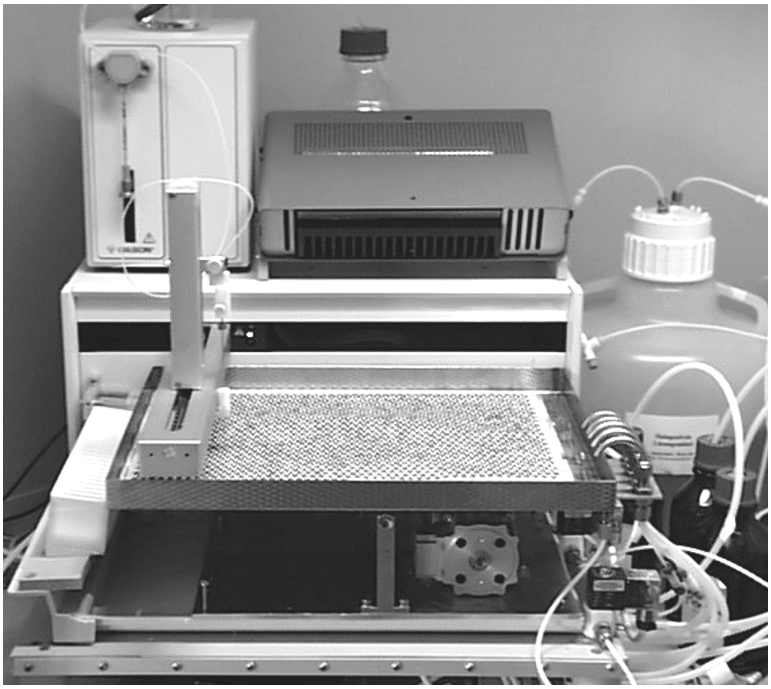

Fig. 1. Alignment of the automated SPOT-Robot.

References

1. Frank, R. *Tetrahedron* **48**, 9217-9232 (1992).
2. Reineke, U., Volkmer-Engert, R. and Schneider-Mergener, *J. Curr. Opin. Biotechnol.* **12**, 59-64 (2001) and refs. cited therein.
3. Wenschuh, H., Volkmer-Engert, R., Schmidt, M., Schulz, M., Schneider-Mergener, J. and Reineke, U. *Biopolymers* **55**, 188-206 (2000).

Peptide Revolution: Genomics, Proteomics & Therapeutics
Michael Chorev & Tomi K. Sawyer (Editors)
American Peptide Society, 2003

Peptide Libraries as a Tool for Studying Proteolytic Enzymes

Benjamin E. Turk and Lewis C. Cantley

Division of Signal Transduction, Department of Medicine, Beth Israel Deaconess Medical Center and Department of Systems Biology, Harvard Medical School, Boston, MA, 02215, USA

Introduction

Broadly speaking, proteolytic enzymes perform two functions: degradation and processing. Complete proteolytic degradation of proteins occurs during digestion, extracellular matrix breakdown, and in the targeted destruction of cytosolic proteins involved in cellular regulation. Though protein degradation can be a highly specific and regulated process, substrate recognition is largely independent of the cleavage site sequence. Conversely, protein processing involves limited proteolysis and is generally site-specific. Such limited cleavage can be an essential step in protein activation or deactivation and can occur either constitutively or in an inducible manner. As with many protein-modifying enzymes, substrate selection by proteases depends to a large extent on complementarity between the active site cleft of the enzyme and residues surrounding cleavage site within the substrate.

The cleavage site motif for a protease can be defined as the set of amino acid residues surrounding the scissile bond that are optimal or preferred for catalysis. Knowing such a cleavage site motif can be important for unraveling the biological function of a given protease. For example, knowing the sequences that a protease targets is helpful in mapping cleavage sites within protein substrates, and can guide the design of cleavage-resistant mutants for investigating the consequences of cleavage of a particular substrate. In addition, computer database searching with cleavage motif data can identify additional candidate substrates for a protease.

Proteases and peptidases are unique among protein-modifying enzymes in that the reactions they catalyze are irreversible. Consequently, multiple regulatory mechanisms are generally present to hold the activity of a given protease in check. Given the array of biological processes that are dependent on tightly regulated proteolytic activity, it is not surprising that misregulation of proteases can contribute to disease pathology. In addition, most pathogenic microorganisms carry proteases that are essential for their viability. Accordingly, a number of proteases are under investigation as possible drug targets. While inhibitors of HIV protease and angiotensin converting enzyme are already in widespread clinical use, drugs that target a growing set of other proteases—matrix metalloproteinases, methionine aminopeptidase, hepatitis C virus protease, the proteasome, rhinovirus 3C protease, caspase-1, neutral endopeptidase, thrombin and factor Xa among them—are currently in clinical trials for a number of indications. Cleavage site motif information can be invaluable to the development of protease-targeted drugs, as optimized model substrates enable high-throughput screening of chemical libraries to identify inhibitors [1]. Highly potent and specific inhibitors can also be prepared systematically by conjugating optimized substrate peptides to chemical groups that target catalytic residues at the protease active site [2]. Such inhibitors can act as lead compounds in drug discovery and can also be important tools for dissecting the biological function of a protease, as they provide a means for temporally controlled inactivation of the enzyme.

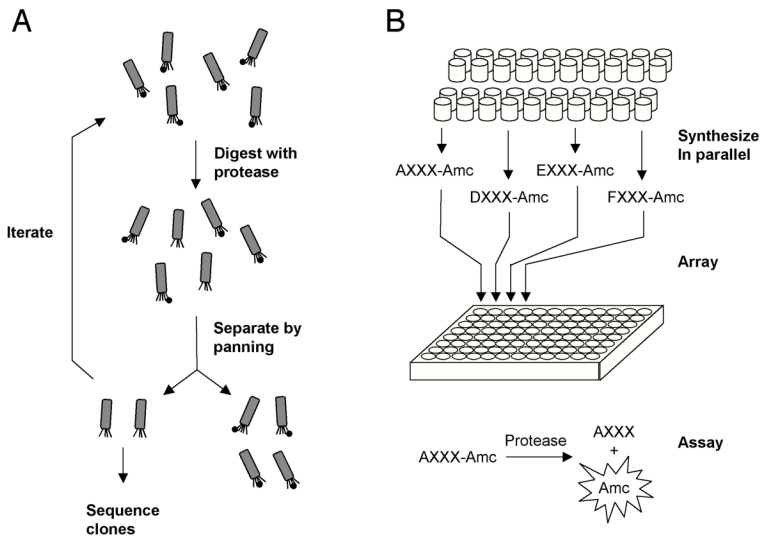

Fig. 1. Peptide library methods for determining protease cleavage specificity. A. Phage display. Clones are selected for loss of an epitope that occurs as a result of cleavage in an encoded randomized linker region. B. Positional scanning libraries. Cleavage is monitored by the increase in fluorescence of the aminomethylcoumarin (Amc) group that occurs upon hydrolysis.

Background

Conventionally, determining a protease cleavage motif is an arduous process involving the preparation of large numbers of peptide or mutant protein substrates and analyzing individually their cleavage efficiency. For proteases where no efficient substrates are known, such analysis is impossible, and even in the best cases only limited information can be obtained in practice due to the cost and labor involved. Peptide libraries provide a means for the simultaneous analysis of millions of peptide substrates, thus producing a truly exhaustive set of data.

Peptide library approaches in general involve either genetically-encoded libraries or chemically-synthesized libraries [3]. Among encoded library approaches, phage display methods are the most widespread and have been adapted to identification of protease substrates (Figure 1A). An epitope tag followed by a random peptide sequence is engineered into the amino terminus of a phage coat protein [4]. Treatment with the protease of interest results in loss of the epitope from phage particles bearing efficient peptide substrates, allowing selection by panning. The major advantage of phage display over other methods is that it can take advantage of cooperativity between subsites at the enzyme active site to reveal multiple distinct binding modes when they occur. However, the labor involved makes it difficult to perform phage display analysis in a high-throughput manner. Since the method provides a limited collection of efficient substrates, it is difficult to infer subtle preferences or residues that are strongly deselected at a particular subsite. Among synthetic peptide libraries, immobilized peptide methods using either "one bead-one peptide" libraries prepared by split-and-mix strategies or membrane-bound peptide arrays provide similar information

(a collection of good substrates), and therefore have similar advantages and disadvantages as phage display [5].

A breakthrough in synthetic peptide library approaches to proteases came with the development of general spatially-addressable positional scanning libraries designed for use with these enzymes (Figure 1B) [6]. Typically a collection of 80 distinct tetrapeptide mixtures is prepared by parallel synthesis. In each mixture, a single residue is fixed at one position with the remaining positions produced as degenerate mixtures. The peptides are conjugated at their carboxy-termini with a fluorophore that produces a large increase in fluorescence upon proteolytic release from the peptide. Cleavage of the entire set of peptide mixtures can therefore be analyzed simultaneously in a fluorescence plate reader. The main limitation of these libraries at this time is that they can only be used for enzymes that can cleave short tetrapeptide substrates, which is generally only true of serine and cysteine proteases. In addition, these libraries only provide information on selectivity amino terminal to the cleavage site.

An alternative strategy to the methods described is a mixture-based synthetic peptide library approach. Complex mixtures of peptides are cleaved followed by detection of the substrate component as a pool. One method of detection has been to use liquid chromatography-mass spectrometry, but analysis has been restricted to simple mixtures in which only one position is varied at a time [7]. The use of Edman degradation to quantify cleavage products was initially described for positions carboxy terminal to the cleavage site [8]. We have recently developed a general method based on Edman sequencing of peptide library mixtures that allows for extended cleavage site motifs (covering both sides of the scissile bond) to be determined [9]. Like other synthetic library methods, it is rapid, but also provides the general applicability found with phage display libraries. In addition, the method requires only a limited amount of custom synthesis (widely available on a fee-for-service basis) making it accessible to any standard biochemistry laboratory.

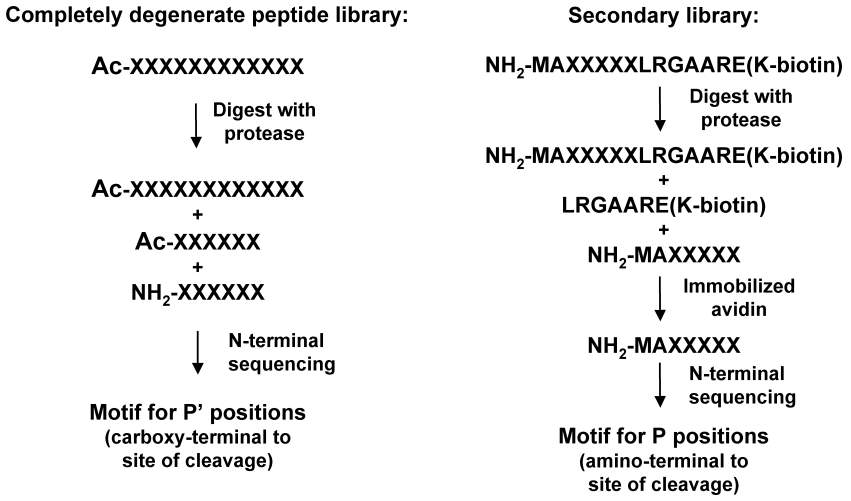

Fig. 2. Determining cleavage motifs with mixture-based peptide libraries. Figure is adapted from reference [9].

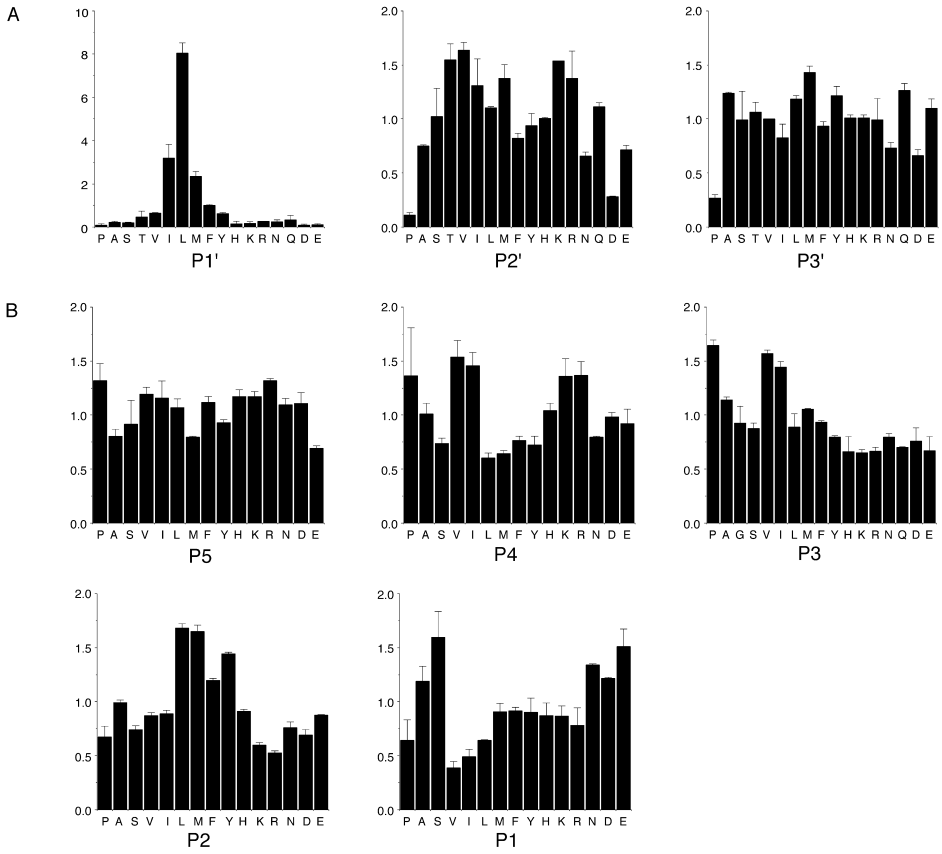

Fig. 3. MMP-7 cleavage selectivity determined using mixture-based libraries. Data represent the molar proportion of each amino acid residue present within an Edman sequencing cycle. Data are normalized to an average value of 1, so that values greater than one are positive selections and values less than 1 are negative selections. A. Primed side selectivity, using the random peptide dodecamer library Ac-XXXXXXXXXXXX. B. Unprimed side selectivity, using the library MAXXXXXLRGAAREK(biotin) for the P3 position and the library MGXXPXXLRGGGEEK(biotin) for the other positions. Figure is reprinted from reference [9].

Results and Discussion

By standard nomenclature, the positions surrounding the cleavage site are defined as the sequence Pn…P3-P2-P1-P1'-P2'-P3'…Pn', where cleavage occurs between the P1 and P1' positions. Our method (Figure 2) involves initially determining the motif for the so-called primed positions (downstream of the cleavage site) and subsequently determining the specificity at the unprimed positions (upstream of the cleavage site). We begin with a completely degenerate peptide library, typically a random peptide dodecamer. Each degenerate position has an equimolar mixture of the 19 natural amino acids excluding cysteine (which is excluded to avoid problems with disulfide formation). The dodecamer library is amino-terminally blocked with an acetyl group.

The library is partially digested with the protease of interest so that only the more efficient substrates within the mixture are cleaved. Most of the components of the mixture are uncleaved peptides that remain blocked at their amino termini. Likewise, the amino-terminal fragments of the reaction products are also blocked. The carboxy-terminal fragments present in the mixture, however, have a free amino terminus. The entire mixture is then subjected to automated amino-terminal Edman degradation-based sequencing, and only these carboxy-terminal fragments are detected on the sequencer. Some quantity of each of the 19 amino acid residues is present in each sequencing cycle. From the molar proportion of the various amino acids within a given cycle, we infer which residues are preferred by the protease at a given position downstream of the cleavage site. The data from the first sequencing cycle, for example, provides information regarding the P1' position; the second sequencing cycle provides information about the P2' position, and so on.

To determine the motif upstream of the cleavage site we design a secondary library in which the primed positions are fixed with the residues that are most strongly selected from the dodecamer library screen (Figure 2). The secondary library is biotinylated at its carboxy terminus, and the amino terminus is left free. As with the completely degenerate library, this secondary library is partially digested with the protease. The intact peptides and carboxy-terminal fragments in the reaction mixture retain the biotin tag, while the amino-terminal fragments have lost the tag. The mixture is treated with immobilized avidin to remove the biotinylated components, leaving only the amino-terminal fragments in solution. These fragments are subjected to Edman sequencing as before to provide the motif for the unprimed positions.

As an example, Figure 3A shows typical data generated using the method with matrix metalloproteinase-7 (MMP-7, also called matrilysin). As is apparent from casual inspection of the data, MMP-7 is most selective at the P1' position, immediately carboxy-terminal to the cleavage site, where the protease requires a hydrophobic residue and has a particular preference for leucine. At other positions downstream, the

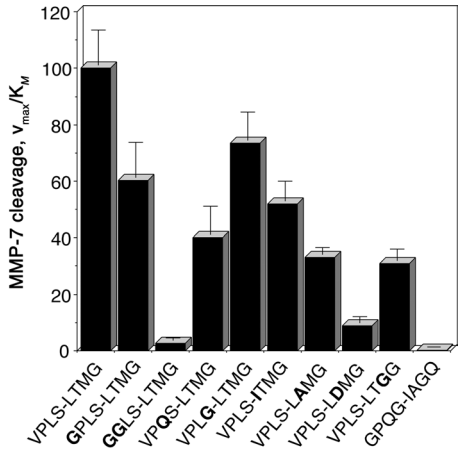

Fig. 4. The MMP-7 consensus peptide is optimal. Cleavage rates for the MMP-7 consensus peptide (far left), peptides with substitutions to the consensus (middle), and the collagen aI cleavage site-spanning peptide (far right) as determined by fluorescamine assay. Data were originally reported in reference [9].

Table 1. Selectivity data for six MMPs [91].

		Cleavage position						
Enzyme	Common name	P4	P3	P2	P1	P1'	P2'	P3'
MMP-7	Matrilysin	V (1.4)	P (1.6)	L (1.7)	S (1.8)	L (8.4)	V (1.7)	M (1.5)
		I (1.4)	V (1.6)	M (1.6)	E (1.6)	I (3.6)	T (1.7)	Y (1.3)
		R (1.3)	I (1.5)	Y (1.4)	N (1.3)	M (2.5)	I (1.5)	Q (1.3)
					A (1.3)		M (1.5)	
							K (1.5)	
MMP-1	Collagenase-1	V (1.4)	P (2.3)	M (1.5)	S (2.2)	M (4.9)	M (1.7)	A (2.0)
				Y (1.4)	N (1.8)	I (3.8)	I (1.5)	G (1.8)
				L (1.4)	A (1.8)	L (3.1)	K (1.4)	S (1.6)
				E (1.4)			R (1.3)	
MMP-2	Gelatinase A	I (1.4)	P (1.7)	V (1.3)	S (1.9)	L (4.2)	R (1.5)	S (2.2)
		V (1.3)	V (1.6)	A (1.3)	G (1.4)	M (2.8)	Y (1.5)	A (2.1)
			I (1.5)		A (1.4)	I (2.6)	K (1.4)	G (2.1)
					E (1.3)	Y (1.9)	M (1.4)	
						F (1.8)	I (1.4)	
MMP-9	Gelatinase B	V (1.3)	P (2.5)	L (1.6)	S (1.8)	L (3.4)	R (1.4)	S (1.9)
			V (1.6)	Y (1.3)		M (2.6)	T (1.4)	A (1.8)
						I (2.6)	Y (1.4)	G (1.6)
						Y (2.1)	V (1.3)	
						F (1.3)	I (1.3)	
MMP-3	Stromelysin-1	K (1.6)	P (2.5)	F (1.5)	S (1.6)	M (3.5)	M (1.9)	M (1.6)
		V (1.4)	V (1.4)	Y (1.5)	E (1.4)	I (2.9)	K (1.8)	A (1.3)
		I (1.4)	I (1.4)	L (1.4)		L (2.5)	I (1.7)	
		R (1.4)		M (1.3)		Y (2.4)	R (1.6)	
				A (1.3)		F (2.1)		
MMP-14	MT1-MMP	I (1.6)	P (2.0)	X	S (1.8)	L (3.5)	R (1.4)	M (1.4)
		K (1.4)	V (1.4)		A (1.4)	I (2.2)	K (1.3)	A (1.4)
		V (1.3)				M (2.2)	Y (1.3)	
		D (1.3)				Y (1.4)		
						F (1.4)		

enzyme is less selective, but still has subtle preferences for particular residues (for example methionine at the P3' position). In order to determine the selectivity amino-terminal to the cleavage site, a secondary library with the sequence MAXXXXXLRGAAREK(biotin) was generated, fixing the preferred leucine and arginine at the P1' and P2' positions, respectively. Using this library, we observed significant selectivity for MMP-7 only at the P3 position (where the enzyme prefers proline, valine and isoleucine), despite literature precedent indicating more subtle preferences at other positions. The reason that selectivity was observed at only one site is likely to be because the library is cleaved at sites other than the intended X-L bond to a significant degree (approximately 30% of the cleavage appears to be so "misdirected"). This increases the background noise in the sample from peptide fragments that are out of register with those arising from the major cleavage site, thus making weaker selections difficult to detect. To circumvent this problem, a tertiary library was prepared with the sequence MGXXPXXLRGGGEEK(biotin), which fixes the selected proline residue at the P3 position. When digested with MMP-7, over 90% of this library was cleaved at the intended bond, allowing us to determine the selectivity at the other positions upstream of the cleavage site (Figure 3B). These selections include a preference for hydrophobic residues at the P2 position and for smaller residues at the P1 position. Our experimentally determined MMP-7 motif was in good agreement with prior available literature on the selectivity of this protease [11]. To further validate our motif, we prepared a consensus peptide substrate and found it to be efficiently cleaved by MMP-7 when compared to a peptide that spans the MMP cleavage site in collagen α_1-I (Figure 3). As anticipated, substitution of any residue in the consensus peptide for another residue was found to decrease cleavage efficiency. Analysis of a series of peptides also indicated that the rank order of the selections at a given position determined using the peptide libraries was also observed in the context of the individual consensus peptide.

Because the mixture-based approach is rapid, it lends itself well to screening large numbers of proteases. In addition to MMP-7, we also determined the cleavage motif for five other MMPs (Table 1). As a family, MMPs appear to share common features in their cleavage selectivity. All of them prefer hydrophobic amino acids at the P1' position, though some of the enzymes, termed "deep pocket" MMPs, are better able to accommodate aromatic residues at that position. All of the MMPs profiled prefer proline at the P3 position. Though there is a general selection for hydrophobic residues at P2, the particular residues that are selected vary from enzyme to enzyme. Thus the method has the capability of distinguishing between even closely related enzymes.

Armed with a complete set of data regarding the cleavage specificity for a protease, one has the potential to use this information to identify novel protein substrates that may be critical effectors of the protease *in vivo*. The Scansite program (scansite.mit.edu) allows users to enter matrices of data derived from peptide library experiments [12]. These matrices are used to search protein sequence databases for matches to the data and a list of "hits" is produced, akin to searching with BLAST or other sequence-matching programs. Searching the protein databases in this manner with our MMP data identified a number of potential novel substrates. One of these proteins, the brain-specific chondrotin sulfate proteoglycan neurocan was identified as a possible MMP-2 substrate. Interestingly, neurocan is known to undergo developmentally-regulated proteolytic processing, and the predicted cleavage site in neurocan was identical to its *in vivo* processing site [13]. Accordingly, we found that MMP-2 can indeed process neurocan *in vitro* (Figure 5), thus substantiating our ability to predict protein substrates using peptide library data. Interestingly, several of the

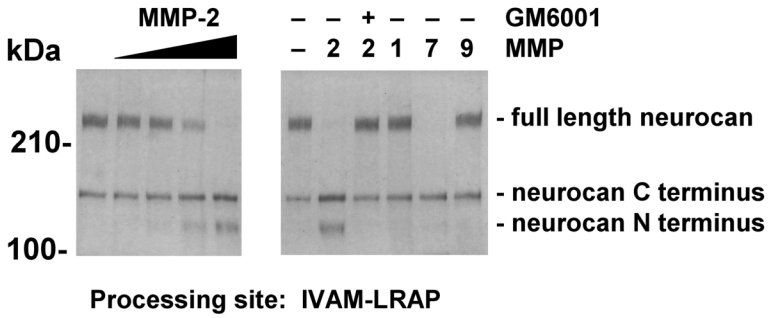

Fig. 5. Cleavage of neurocan by MMP-2. The gel shows purified rat brain neurocan (a mixture of the full length protein and the carboxy-terminal fragment) and its cleavage products as detected by silver stain. Catalytic amounts of MMP-2 cleave neurocoan in a dose-dependent manner (left). Cleavage is blocked by the MMP inhibitor GM6001, and equimolar amounts of other MMPs do not cleave neurocan site-specifically (right).

amino acid residues at the neurocan cleavage site that were selected from our peptide library work were not previously known to be preferred by MMP-2.

Conclusions

Mixture-based libraries have been used as a general method for defining the specificity of protein modifying enzymes and protein interaction domains. With specific modifications to the technique, we have now adapted these methods for use with proteases. We and others have now used this method to profile roughly 20 proteases, including serine, aspartyl, and metalloproteases, indicating that this method is indeed broadly applicable. In the case of MMPs a small set of libraries could be used to provide useful information that distinguished between even closely related members of a single protease family. Thus the method should become even more useful with the expansion of protease families that has accompanied genome sequencing efforts.

Acknowledgments

The work was funded by the National Institutes of Health. B. Turk is a Leukemia and Lymphoma Society Special Fellow.

References

1. Knight, C. G. *Meth. Enzymol*. **248**, 18-34 (1995).
2. Barrett, A. J. and Salvesen, G., (Eds.) *Proteinase Inhibitors,* Elsevier (Amsterdam) 55-298 (1986).
3. Turk, B. E. and Cantley, L. C. *Curr. Opin. Chem. Biol*. **7**, 84-90 (2003).
4. Matthews, D. J. and Wells, J. A. *Science* **260**, 1113-1117 (1993).
5. Meldal, M., Svendsen, I., et al. *Proc. Natl. Acad. Sci. U.S.A.* **91**, 3314-3318 (1994).
6. Backes, B. J., Harris, J. L., Leonetti, F., et al. *Nature Biotechnol.* **18**, 187-193 (2000).
7. Berman, J., et al. *J. Biol. Chem*. **267**, 1434-1437 (1992).
8. Birkett, A. J., et al. *Anal. Biochem*. **196**, 137-143 (1991).
9. Turk, B. E., Huang, L. L., et al. *Nature Biotechnol*. **19**, 661-667 (2001).
10. Turk, B. E. and Cantley, L. C. *Methods* in press.
11. Smith, M. M., Shi, L. and Navre, M. *J. Biol. Chem*. **270**, 6440-6449 (1995).
12. Yaffe, M. B., Leparc, G. G., Lai, J., et al. *Nature Biotechnol.* **19**, 348-353 (2001).
13. Rauch, U., et al. *J. Biol. Chem.* **267**, 19536-19547 (1992).

Peptide Revolution: Genomics, Proteomics & Therapeutics
Michael Chorev & Tomi K. Sawyer (Editors)
American Peptide Society, 2003

Novel Tools and Applications in Parallel Peptide Synthesis

O.J. Kreuzer[1], M. Birringer[1], K. Zarse[1], J. Henkel[2], F. Bier[2], M. Thürk[3]and W. Zinsser[4]

[1]peptides&elephantsGmbH; [2]Fraunhofer Institut für Biomedizinische Technik Abteilung Molekulare Bioanalytik & Bioelektronik, Arthur-Scheunert-Alle 114-116, 14558 Bergholz-Rehbrücke, Germany; [3]CPI/Creative Pharma International, Hannah-Vogt-Str. 1, 37085 Göttingen, Germany [4]Zinsser Analytic, Eschborner Landstraße 135, 60489 Frankfurt, Germany

Introduction

Since the development of the solid phase peptide synthesis in 1963 by Robert Bruce Merrifield [1] and the development of the first peptide synthesizer in 1966, different automatic systems for the synthesis of peptides had been built up [2,3,4]. The development of the combinatorial strategies to synthesize complex mixtures of peptides (peptide libraries) was inspired by the concept of selection, as verified by nature. This combinatorial strategy followed by a high throughput screening on biological systems is nowadays the most used process in drug discovery [5]. For this reason the development of the parallel peptide synthesis was nearly stopped ten years ago. The multiple pin method in 1984 [6], the spot synthesis in 1990 [7] and the light-directed, spatially addressable parallel synthesis in 1991 [8] were the latest technology developed for parallel synthesis. Since the human genome project was finished, the proteome project has been started. The identification of disease relevant proteins leads to the question of the active region in the protein. Epitope mapping of proteins is one possible method to identify these regions. Hundreds of individual peptides will be needed for one Epitope mapping [9]. The systematic characterization of peptide hormones using alanine walk or substitution analysis are newly used techniques for rational drug design [10]. Modern biotech companies like CPI/Creative Pharma Int. offers a computational approach to medical drug design. A combination of experimental and in silico optimization of peptides leads in a cyclic discovery process to new proposals. For each new method a variety of individual soluble peptides are needed.

Results and Discussion

Therefore we developed the next generation of multiple peptide synthesizer. On the base of a pipetting robot we consequently followed the principle of the "lab hand" (Figure 1A). Each building block is stored in an individual cartridge. The robot hand picks up the cartridge (Figure 1B) and delivers the reagents to the reaction vessels.

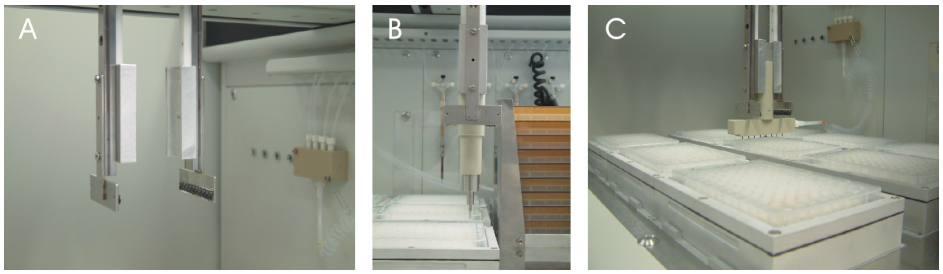

Fig. 1. The " Lab hand" (A) picks up cartridges (B) or other tools like a rinse comb (C).

The reaction takes place in multititer plates. Following the Fmoc-Strategy, nine 96-well plates can be handled in one run to synthesize 864 peptide amides in parallel, 2µmol scale within in 30h. The washing and deprotecting solutions will be delivered by a manifold the robot picks up (Figure 1 C). The plates are stored on nine evaporation station that can be individually exhausted. The robot learns the position of each building block cartridge while scanning a 2-dimensional barcode on top of each cartridge.

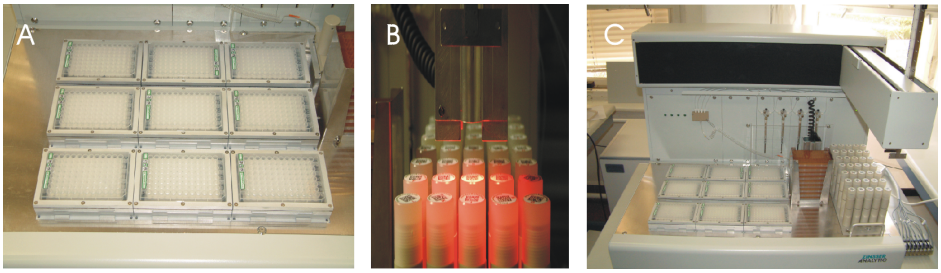

Fig. 2. Nine individual evaporation stations store nine Mikrotiter plates (A). The "Lab Hand" picks up a barcode reader to learn the position of each building block (B). A complete view of the system (C).

A complex software program enables the user to plan a peptide library, to set up the synthesis and to organize output data such as the sequence information, the molecular mass, the plate position and an additional barcode on the Mikrotiter plates. In conclusion this is the first peptide synthesizer that allows one to synthesize 864 peptide amides in parallel within 30 hours. This novel tool allows the researcher to synthesize individual libraries to address a variety of questions like finding active epitopes in proteins, analyzing peptide hormones systematically, and using peptide libraries for drug discovery.

Acknowledgments

The work was funded by an EEF grant from the BMBF Marc Birringer and Oliver Kreuzer via the German Institute of Human Nutrition.

References

1. Merrifield, R. B. *J. Am. Chem. Soc.* **85**, 2149-2154 (1963).
2. Schnorrenberg, G. and Gerhardt, H., *Tetrahedron* **45**, 7759-7764 (1989).
3. Gausepohl, H. et al. In Yanaihara, N. (Ed.), *Peptide Chemistry, Proc. 2JSPC*., ESCOM, Leiden, p. 107-109 (1992).
4. Hogan, J. C. Jr. *Nat. Biotechnol.* **15**, 328-330 (1997).
5. Geysen, H. M., Meloen, R. H. and Barteling, S. J. *Proc. Natl. Acad. Sci. U.S.A.* **81**, 3998-4002 (1984).
6. Frank, R. *Tetrahedron* **48**, 9217-9232 (1992).
7. Fodor, S. P., Read, J. L., Pirrung, M. C., Stryer, L., Lu, A. T. and Solas, D. *Science* **251**, 767-773 (1991).
8. Appel, J. R., Campbell, G. D., Buencamino, J., Houghten, R. A. and Pinilla, C. *J. Peptide Res.* **52**, 346-355 (1998).
9. Bruns, C., Lewis, I., Briner, U., Meno-Tetang, G. and Weckbecker, G. *Eur. J. Endocrinol.* **146**, 707-716 (2002).
10. Bhargava, S., et al. *J. Mol. Recognit*. **15**, 145-153 (2002).

Peptide Revolution: Genomics, Proteomics & Therapeutics
Michael Chorev & Tomi K. Sawyer (Editors)
American Peptide Society, 2003

Design, Synthesis, and Study of Peptides Able to Recognize Hydrophilic Protein-Surface Patches

Marc Martinell[1], Xavier Salvatella[1], Ignasi Belda[1], Xavier Llorà[4], Jose J. Pastor[1], Marta Vilaseca[3], Margarida Gairí[3] and Ernest Giralt[1,2]

[1]Institut de Recerca Biomèdica, Parc Científic de Barcelona-UB, Barcelona, Spain; [2]Departament de Química Orgànica, Universitat de Barcelona, Spain; [3]Serveis Científico-Tècnics, Universitat de Barcelona, Spain; [4]Illinois Genetic Algorithms Lab, National Center for Supercomputing Applications, University of Illinois at Urbana Champaign, USA

Introduction

Both from a basic science perspective as well as from a drug design point of view, there is no doubt that proteins can be considered as privileged targets for binding of small ligands. In this context the design of ligands able to disrupt protein-protein interactions is emerging as an even more relevant issue [1]. However, the design of protein-surface binders and, specially, the design of ligands able to bind tightly and selectively to *hydrophilic* protein-surface patches is a very challenging task. In the last years we have been trying to get some insight in the principles that govern these molecular recognition processes using peptides as models for the entire protein receptors [2-5]. Protein-protein interactions are usually mediated through large areas, ca. 600 square Å that have complementary shape and charge. So, in our opinion, medium-size peptide compounds can be very appropriate candidates to modulate this kind of interaction. Of course, before a generalized use of peptides as therapeutic agents can be accomplished, the bioavailability and biodisposability issues must be solved. Importantly, there are very recent and spectacular advances in this area. We report here the general approach that is currently used in our laboratory for the design of new peptides able to recognize protein-surface patches. This approach is based on three consecutive steps: *i)* peptide-ligand *design; ii)* solid-phase *synthesis* of strongly focused *peptide libraries*; and *iii)* ligand *screening*. We illustrate this approach with examples derived from the design and synthesis of a series of peptide ligands able to recognize a highly hydrophilic patch located at the surface of the tetramerization domain of the tumor suppressor protein p53. The design of the lead peptides has been assisted by molecular modeling. The structure has been refined using a combinatorial approach. The interactions have been studied by the combined use of fluorescence spectroscopy, NMR and surface plasmon resonance.

Results and Discussion

Peptide-ligand design: Peptide ligands are currently designed in our laboratory using two different approaches. Our first approach combines chemical knowledge, common sense and the use of molecular dynamics-simulated annealing calculations. In the case of p53 tetramerization domain such an approach has led to the ligand **Ac-AGAAGWARGRARSR–NH_2** that is able to recognize a tetra-anionic patch at the surface of the protein.

The second approach makes use of virtual screening using evolutionary algorithms. Virtual screening emerges nowadays as a very efficient tool for *in silico* screening of large libraries. This virtual screening can be used as an efficient 'filter' to select promising candidates before undertaking the real screening in the laboratory. In spite of the impressing increase in efficiency of the available virtual screening methods, the *exhaustive screening* of the huge chemical space defined by all the medium size

possible peptide-candidates is nowadays an unachievable goal. In this context we have found that evolutionary algorithms, combined with docking routines, are very powerful tools for peptide-ligand design. Figure 1 shows a schematic view of our general procedure for the evolution of peptide ensembles. We start with an ensemble of n randomly generated different peptides. Their 'fitness', *i.e.* their affinity for a predetermined surface-patch from a given protein, is assessed using docking algorithms. This allows ranking the peptides ensemble according to their fitness. Then the evolutionary algorithm generates a new ensemble of peptides that are generated from the previous one using criteria as elitism and operations as mutations or crossover. We have evaluated four different computational approaches: conventional Darwinist genetic algorithms, Lamarckian genetic algorithms, population based incremental learning, and Bayesian optimization algorithms.

The best results were obtained using Lamarckian genetic algorithms.

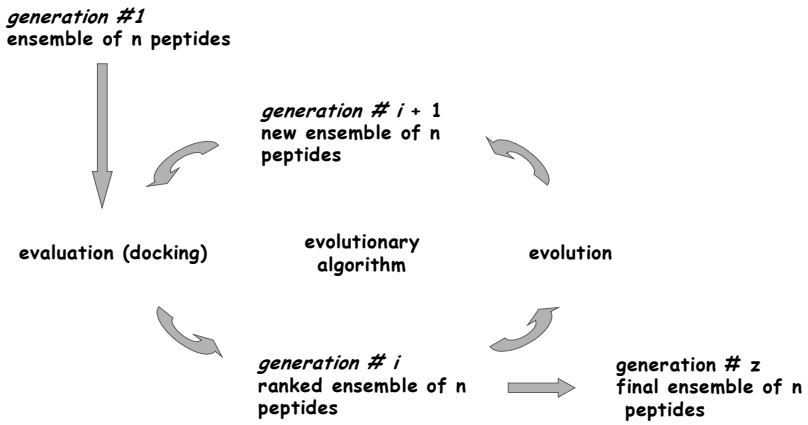

Fig. 1. Use of evolutionary algorithms for the design of protein-surface peptide binders.

*Solid-phase synthesis of strongly focused peptide libraries:*The lead peptides generated at the design steps are synthesized and optimized preparing strongly focused libraries. We use two different approaches. In those cases where the screening for binding properties is performed in solution, we optimize the lead by parallel solid-phase synthesis. An example of such an optimization process is shown in Figure 2. The different basic residues of a basic ligand are systematically replaced by other residues containing basic side-chains.

When the screening is made in solid-phase we prefer to use a solid-phase synthetic strategy that combines the use of the N-[(9-hydroxymethyl)-2-fluorenyl] succinamic acid (HMFS) handle and the amino-PEGA resin [6]. The screening is normally carried out by fluorescence and the positive beads are deconvoluted via cleavage of the peptide-resin bond with morpholine in DMF followed by sequencing of the peptide by MS.

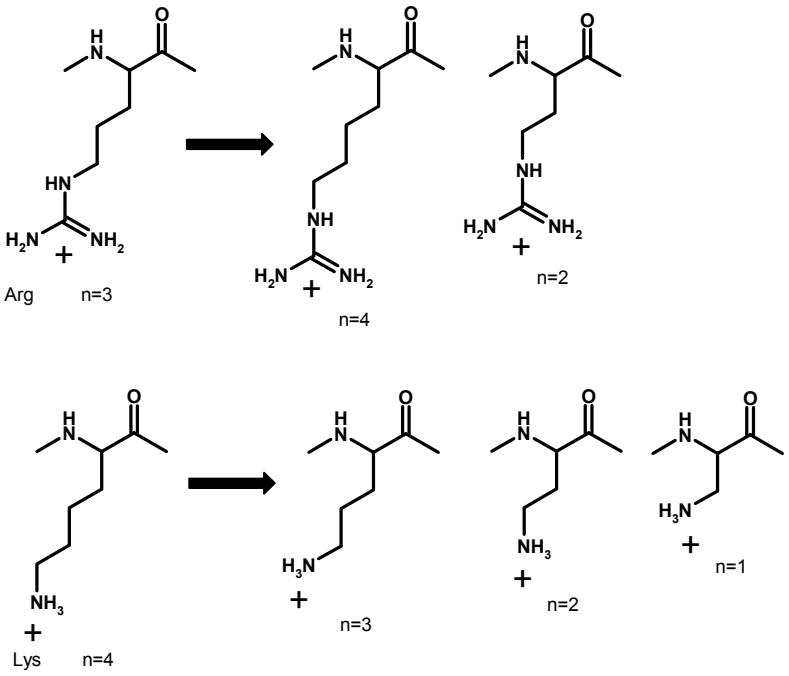

Fig. 2. Example of a focused peptide library that incorporates amino acid residues with different length basic side-chains.

Ligand screening: Fluorescence spectroscopy, surface plasmon resonance and NMR are the three basic tools that we use to study the interactions between peptides and proteins. Each approach has advantages and disadvantages. Fluorescence spectroscopy requires the presence of a fluorescent probe either in the ligand or in the protein. Surface plasmon resonance requires a careful case-by-case optimization. NMR is very flexible and can be used either with small and medium-size proteins (chemical shift perturbation) or much larger targets (saturation transfer difference). However NMR is more difficult to apply to very flexible ligands.

Acknowledgments

This work was supported by MCYT-FEDER(Bio2002-2301) and Generalitat de Catalunya (CeRBa and SGR).

References

1. Berg, T., *Angew. Chem. Int. Ed*. **42**, 2462-2481 (2003).
2. Peczuh, M. W., Hamilton, A. D., Sánchez-Quesada, J., de Mendoza, J., Haack, T. and Giralt, E. *J. Am. Chem. Soc*. **119**, 9327-9328 (1997).
3. Haack, T., Peczuh, M. W., Salvatella, X., Sánchez-Quesada, J., de Mendoza, J., Hamilton, A. D. and Giralt, E. *J. Am. Chem. Soc.* **12**, 11813-11820 (1999).
4. Salvatella, X., Peczuh, M. W., Gairí, M., Jain, R. K., Sánchez-Quesada, J., de Mendoza, J., Hamilton, A. D. and Giralt, E. *Chem. Commun.* **15,** 1399-1400 (2000).
5. Orner, B., Salvatella, X., Sánchez-Quesada, J., de Mendoza, J., Giralt, E. and Hamilton, A. D. *Angew. Chem. Int. Ed.* **41**, 117-119 (2002).
6. Pastor, J. J., Fernández, I., Rabanal, F. and Giralt, E. *Org. Lett*. **4**, 3831-3833 (2002).

Peptide Revolution: Genomics, Proteomics & Therapeutics
Michael Chorev & Tomi K. Sawyer (Editors)
American Peptide Society, 2003

Chirality-Based Isotope Labeling in Library of Substrates (CHILLS) to Screen for Enzyme Preference by Mass Spectrometry

Laszlo Prokai[1], Stanley M. Stevens, Jr.[1] and Katalin Prokai-Tatrai[2]

[1]Department of Medicinal Chemistry; [2]Department of Pharmacology and Therapeutics; University of Florida, Gainesville, FL 32610, USA

Introduction

Combinatorial chemistry has become a powerful tool for the discovery and optimization of ligands that bind to a variety of enzymes and protein receptors. On the other hand, screening of combinatorial mixtures for efficient catalysis [1,2] (e.g., identification for the optimal substrates of an enzyme) has been a considerably more challenging problem. This is mainly because measuring directly and accurately the interaction that occurred between the enzyme and the substrate/product(s) in a catalytic event [during which the enzyme binds to a substrate, converts the substrate into product(s), and then dissociates from the product(s)] is practically impossible. In the case of identifying optimal enzyme substrates, the challenge also lies partly in the separation/identification of the individual compounds from a complex mixture of potential substrates and reaction products. The use of liquid chromatography – mass spectrometry (LC/MS) may circumvent this problem, but quantitative data obtained by this method without rigorous and labor-intensive method development are generally unreliable.

We report a novel methodology for the rapid identification of optimal enzyme substrates from a combinatorial library by mass spectrometry. By this method, we have overcome the problem of poor/unreliable quantitative data by an approach we call chirality-based isotope labeling for a library of substrates (CHILLS) that does not fall short to such limitations, since we exploit the inherent stereospecificity of enzymes in determining optimal substrates. Additionally, the CHILLS method generates accurate results compared to typical screening approaches that require specific and tedious method development, since the CHILLS library already contains a structurally similar internal reference for each individual library component to quantitate the progress of the enzymatic reaction by LC/MS.

Results and Discussion

The specific example presented here relates to the substrate specificity of a peptidylglycine α-amidating (PAM) enzyme involved in the C-terminal amidation of Gly-extended prohormones [3]. A control library Ac-Arg-Gln-Leu-(Xaa)-Gly-OH (where Xaa represents Phe, Tyr, Trp, Ile, Leu, Val, or Pro) was prepared by solid-phase peptide synthesis using Fmoc-chemistry and the split-and-mix method [4]. ESI-MS characterization and correlation with simulated mass distribution confirmed the presence of practically equimolar concentrations of the expected peptides in the combinatorial mixture. The CHILLS approach was evaluated by synthesizing a mixture of selectively labeled (Ac/d_3-Ac)-Arg-Gln-Leu-(Xaa/D-Xaa)$_{1\text{-}6}$-Gly-OH by the split-and-mix method, where equivalent amounts of the resin-bound Ac-Arg-Gln-Leu-(Xaa)$_{1\text{-}6}$-Gly-OH and d_3-Ac-Arg-Gln-Leu-(D-Xaa)$_{1\text{-}6}$-Gly-OH were mixed only before cleaving the peptide mixture from the resin. (Acetic anhydride-d_6 is commercially available to allow for an affordable isotope labeling.)

The standard enzyme assay [5] was carried out at 37 °C by adding 450 U of the enzyme (PAM, 18 µl from the 25,000 U/ml stock solution purchased from Unigene,

Fairfield, NJ) into the pre-incubated solution of 100 mM MES/KOH, pH 6.0, 1.5 mM sodium ascorbate, 0.001% (v/v) Triton X-100, 30 mM KCl, 30 mM KI, 1μM CuSO4, 100 μg/ml catalase and CHILLS (1 mM of total substrate concentration). Aliquots were taken at regular time periods and added to 100 μl ice-cold aqueous 10% (v/v) acetic acid to stop the reaction. The sample was then desalted (C18 ZipTip), lyophilized, and reconstituted in 0.5% acetic acid prior to LC-MS analysis. When samples were removed from the incubation for the screening of the control [d_3-Ac-Arg-Gln-Leu-(D-Xaa)$_{1\text{-}6}$-Gly-OH] library, the stopping solution contained 20 μM internal standard (trigonellyl-Tyr-D-Ala-Gly-Phe-D-Leu-OH). A MicroPro gradient solvent delivery system (Eldex Laboratories, Napa, CA, USA) providing a flow rate of 10 μL/min and a quadrupole ion trap instrument (LCQ, ThermoFinnigan, San Jose, CA) operating with electrospray ionization (ESI) were used for the LC/MS analyses. Gradient reversed-phase LC separation was performed on a 15 cm x 0.5 mm i.d. Targa C18 column (Higgins Analytical, Mountain View, CA, USA).

As shown in Figure 1, CHILLS combined with LC/MS required no tedious assay development while producing kinetic profiles for the enzymatic reaction superior to those of a control procedure. The optimal substrate for PAM in the library we synthesized was Ac-Arg-Gln-Leu-Phe-Gly-OH; i.e., PAM preferentially amidated Phe.

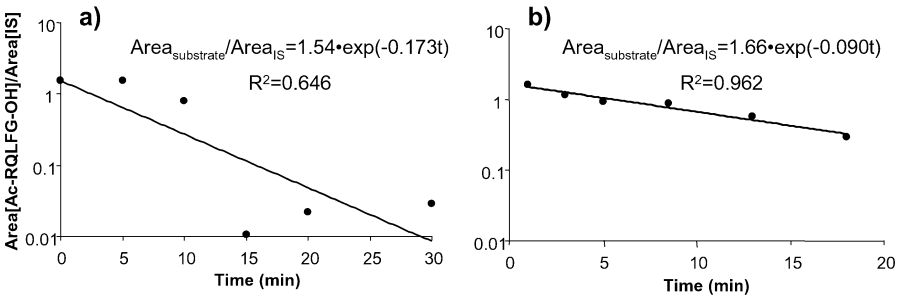

Fig. 1. A typical substrate concentration versus time profile measured by LC/ESI-MS using a) single internal standard for all substrates in the mixture of the control library and b) isotope-labeled D-analogue substrate isomer as the internal standard (IS) from CHILLS.

Acknowledgments
The work was funded by the NIH grant MH59360 to L. Prokai.

References

1. Ecker, D. J. and Crooke, S. T. *Bio-Technol.* **13**, 351-360 (1995).
2. Williard, X. *et al. Eur. J. Med. Chem.* **31**, 87-98 (1996).
3. Eipper, B. A. *et al. Annu. Rev. Neurosci.* **15**, 57-85 (1992).
4. Furka, A. *et al. Int. J. Pept. Protein Res.* **37**, 487-493 (1991).
5. Kulathila, R. *et al. Arch. Biochem. Biophys.* **311**, 191-195 (1994).

Peptide Antibiotic, Anticancer, Antiviral and Antifungal Structure-Function

Peptide Revolution: Genomics, Proteomics & Therapeutics
Michael Chorev & Tomi K. Sawyer (Editors)
American Peptide Society, 2003

Membrane Binding and Antibacterial Activity of Cecropin-Mellitin Hybrid Peptides

Kalpana Bhargava and Jimmy B. Feix

Department of Biophysics, Medical College of Wisconsin, Milwaukee, WI 53226, USA

Introduction

Cecropins are among the most potent of the antibiotic peptides identified to date. Originally isolated from the moth *Hyalophora cecropia* [1,2], this family of peptides contains between 33 and 37 residues and includes a highly basic amino-terminal domain and a relatively hydrophobic C-terminal domain [3]. Previous work has described a series of chimeric cecropin-mellitin peptides with potent antibacterial activity that are significantly shortened relative to the parent peptides [4-6]. These hybrid peptides, 15 to 26 residues in length, retain the strong, broad-spectrum antimicrobial activity of full-length cecropins, yet lack the hemolytic activity associated with mellitin [4-6].

Although it is generally accepted that the interaction of antimicrobial peptides with membranes is a key factor in their biological activity, the precise physical characteristics that govern potency and selectivity remain unclear. With a goal to further understand the mechanism of action for cecropin-mellitin hybrid peptides, we have prepared a series of synthetic analogs of CM15 (composed of first 7 residues of cecropin and residues 2-9 of mellitin) (Figure 1) containing single cysteine substitutions, modified the cysteine with nitroxide spin label, and used Electron paramagnetic resonance (EPR) site-directed spin labeling (SDSL) to characterize peptide-membrane interactions.

Cecropin AD	Ac-K W K L F K K I D K V G Q R V R D A V I S A G P A V A T V A Q A T A L A K-NH_2
CM15	Ac-K W K L F K K I G A V L K V L-NH_2
CM15-C12	Ac-K W K L F K K I G A V ***C*** K V L-NH_2
CM16-C9	Ac-K W K L F K K I ***C*** G A V L K V L-NH_2
CK7-C12	Ac-K W K K F K K I G K V ***C*** K V L-NH_2

Fig. 1. Primary sequences of peptides. Sites modified from the original CM15 sequence are underlined. Cysteine labeling sites are shown in italics.

Results and Discussion

In this study we have introduced cysteine at sites that are relatively hydrophobic in the native peptide. All the cysteine containing analogs of CM15 peptide were synthesized by standard Fmoc solid phase peptide synthesis on a rink amide MBHA resin. Peptides were purified on reverse-phase C8 HPLC column. All the peptides were spin-labeled by incubation with a 10-fold molar excess of the cysteine-specific methanethiosulfonate spin label (1-oxo-2,2,5,5-tetramethylpyrroline 3-methylmethane thiosulfonate (MTSL). Excess label was removed by HPLC on a C8 column. Purity of all the peptides was checked by analytical HPLC and the molecular mass was determined by MALDI-TOF mass spectrometry. The antibacterial activity of these peptides was tested against Gram-negative (*E. coli* and *Pseudomonas araginosa*) and

Gram-positive (*Staphylococcus aureus*) bacteria and their binding affinity determined for liposomes composed of neutral (POPC) and negatively charged (POPS/POPC) synthetic liposomes.

Molar partition coefficients for CM15-C12, CM16-C9 and CK7-C12 with liposomes composed of POPC:10%POPS were $1.8x10^4$, $5.1x10^4$ and $1.2x10^3$ M^{-1}, respectively. These results were comparable to that previously determined for full-length cecropin AD [7].

Cysteine containing CM15 peptides and their spin-labeled analogs retained antibacterial activity against both gram-negative and gram-positive bacteria (Table 1), indicating that attachment of nitroxide label to the cysteine site in peptides resulted in no loss in antibacterial activity. The peptide CK7-C12, designed to optimize the amphipathic distribution of side chains in a membrane environment, has antibacterial activity as good or better than the parent peptide despite a lower binding affinity for model membranes. Conversely, CM16-C9, which has increased hydrophobicity relative to CM15, has diminished antibacterial activity despite enhanced membrane binding (Table 1).

Table 1. Antibacterial activity of Peptides.

Peptide	Antibacterial Activity, MIC(μM)[a]		
	E. coli	*P. aeruginosa*	*S. aureus*
CM15-C12	0.6	2.1	7.9
CM15-C12-MTSL	1.5	5.5	12
CM16-C9	2.7	45	5.5
CM16-C9MTSL	3.2	24	20
CK7-C12	3.0	1.6	3.6
CK7-C12-MTSL	1.6	1.2	2.9

[a]*Minimum inhibitory concentration (MIC) was determined by a Zone-inhibition assay on agarose plate.*

References

1. Steiner, H., Hultmark, D., Engstrom, A., Bennich, H. and Boman, H. G. *Nature* **292**, 246-248 (1981).
2. Hultmark, D., Steiner, H., Rasmuson, T. and Boman, H. G. *Eur. J. Biochem*. **106**, 7-16 (1980).
3. Fink, J., Boman, A., Boman, H. G. and Merrifield, R. B. *Int. J. Pep. Prot. Res*. **33**, 412-421 (1989).
4. Andreu, D., Ubach, J., Boman, A., Wahlin, B., Wade, D., Merrifield, R. B. and Boman, H. G. *FEBS Lett*. **296**, 190-194 (1992).
5. Boman, H. G., Wade, D., Boman, I. A., Wahlin, B. and Merrifield, R. B. *FEBS Lett*. **259**, 103-106 (1989).
6. Wade, D., Andreu, D., Mitchell, S. A., Silveira, A. M., Boman, A., Boman, H. G. and Merrifield, R. B. *Int. J. Pep. Prot. Res*. **40**, 429-436 (1992).
7. Mchaourab, H. S., Hyde, J. S. and Feix, J. B. *Biochemistry* **33**, 6691-6699 (1994).

Peptide Revolution: Genomics, Proteomics & Therapeutics
Michael Chorev & Tomi K. Sawyer (Editors)
American Peptide Society, 2003

Interaction of Cationic Antimicrobial Peptides with Vesicles Mimicking the Outer Membrane of Gram-Negative Bacteria

Marina Gobbo[1], Laura Biondi[2], Fernando Filira[1,2] and Raniero Rocchi[1,2]

[1]Institute of Biomolecular Chemistry of C. N. R.- Section of Padova; [2]Department of Organic Chemistry, University of Padova, I-35131 Padova, Italy

Introduction

Gram-negative bacteria have two cell envelope membranes. The outer membrane, presenting in its outer leaflet the strongly negatively charged lipopolysaccharides (LPS), is an ideal target for the initial binding of antimicrobial cationic peptides. Several studies suggest that some antimicrobial peptides, such as magainin, cecropin and polymixin, can throw disorder in the LPS supramolecular structure, interacting with lipid A, the glycolipid membrane component of the LPS [1]. Some antimicrobial peptides do not have such a dramatic effect on the morphology of the outer membrane, however they reach the cytoplasmatic membrane or different bacterial targets.

In order to study the interactions between LPS and antimicrobial cationic peptides, LPS vesicles [2] or liposomes doped with LPS or lipid A [3] have been used as a model of the bacterial outer membrane. Owing to the heterogenicity among various LPS preparations, the results of detailed biophysical studies, carried out in these systems, are difficult to compare. Recently, we synthesized two simple, structurally well defined lipid A analogues [4] shown in Figure 1. GL1 and GL2 were used to build up mixed phosphatidylcholine (PC) vesicles, presenting glycosidic head groups on the outer surface.

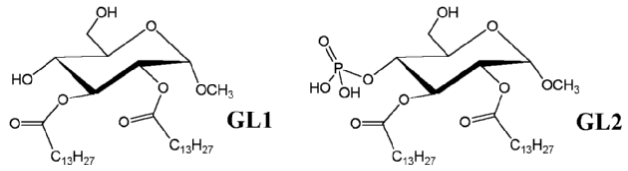

Fig. 1. Glycolipid analogues of lipid A.

These model membranes should allow one to distinguish the contribution of the sugar and of the phoshate group to the interaction between lipid A and antimicrobial cationic peptides.

We have previously reported [4] how these model membranes affect the conformation of some antimicrobial peptides: **magainin 2**, representative for α-helical membrane active peptides, and **apidaecin** and **drosocin**, two insect Pro-rich peptides, whose killing mechanism is not mediated by disruption of the membrane integrity [5] (Figure 2). This report will focus on the effect of these peptides on the barrier property of PC bilayers containing either neutral glicolipid GL1 or anionic glycolipid GL2. The peptide induced permeabilization of PC/dimyristoyl phosphatidylglycerol (DMPG) vesicles was also tested for comparison.

Magainin 2	H-GIGKFLHSAKKFGKAFVGEIMNS-OH
Apidaecin Ib	H-GNNRPVYIPQPRPPHPRL-OH
Drosocin	H-GKPRPYSPRP(GalNAcα)TSHPRPIRV-OH

Fig. 2. Sequences of antimicrobial peptides.

Results and Discussion

The perturbation induced by the peptides on the model membranes was evaluated by the leakage of a fluorescent dye, calcein, entrapped inside large unilamellar vesicles (LUVs) [3] of different composition: PC-GL1 (2/1 molar ratio), PC-GL2 (2/1 or 1/2 molar ratio) and PC-DMPG (2/1 or 1/2 molar ratio). As an example, the profiles of calcein leakage, 5 min after the peptide addition, as a function of the peptide/lipid ratio (lipid concentration 50 μM) are shown in Figure 3. Apidaecin and drosocin showed a negligible leakage activity at any PC/glycolipid ratio, similar to that reported for phosholipid bilayers [6]. On the contrary, the α-helical peptide magainin was able to permeabilize both neutral and anionic glycolipid membranes, showing the maximum activity against bilayers containing acidic phospholipids. Apparently, the high affinity of magainin for anionic vesicles only depends on stronger electrostatic interactions. However, as evidenced by measurements carried out on vesicles with lower PC/anionic lipid ratio (1:2), maganain was much more effective to permeabilize GL2-rich than DMPG-rich bilayers, suggesting that other properties, in addition to the membrane charge, could determine the leakage of dye from LUVs.

In conclusion, the susceptibility of these model glycolipid membranes to different groups of cationic antimicrobial peptides closely resembles that of simple phosholipid bilayers and, in keeping with the CD data [4], it depends on the ability of the peptides to adopt an amphipathic structure in the membrane environment.

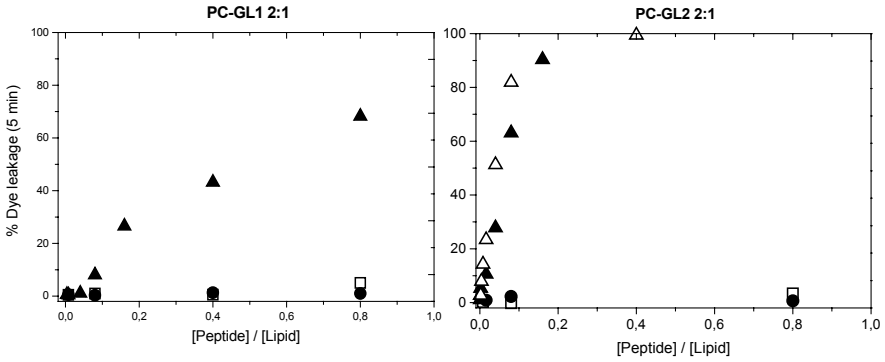

Fig. 3. Profiles of calcein release from LUVs of different composition, at 37˚C. Squares: apidaecin Ib, circles: drosocin, solid triangles: magainin 2, open triangles: magainin 2 against PC-DMPG (2:1) LUVs.

Acknowledgments

Financial support from MIUR (Cofin 2002) and CNR of Italy is gratefully acknowledged.

References

1. De Lucca, A. J., Jacks, T. J. and Brogden, K. A. *Mol. Cell. Biochem.* **151**, 141- 148(1995).
2. Brandenburg, K. and Seydel, U. *Biochim. Biophys. Acta* **1069**, 1-4 (1991).
3. Matsuzaki, K., Sugishita, K. and Miyajima, K. *FEBS Lett.* **449**, 221-224 (1999).
4. Gobbo, M., et al. In Benedetti, E., Pedone, C. (Eds.) *Peptides 2002 (Proceedings of the 27th European Peptide Symposium),* Edizioni Ziino, Napoli, 2003, pp. 760-761.
5. Otvos, L. Jr *J.Peptide Sci.* **6**, 497-511 (2000).
6. Gobbo, M., Biondi, L., Filira, F., Gennaro, R., et al. *J. Med. Chem.* **45**, 4494-4504 (2002).

Peptide Revolution: Genomics, Proteomics & Therapeutics
Michael Chorev & Tomi K. Sawyer (Editors)
American Peptide Society, 2003

Structure-Function Studies of Antimicrobial and Endotoxin Neutralizing Peptides

Sylvie E. Blondelle[1], Roman Jerala[2], Marta Lamata[3], Ignacio Moriyon[3], Klaus Brandenburg[4], Jörg Andrä[4], Massimo Porro[5] and Karl Lohner[6]

[1]Torrey Pines Institute for Molecular Studies, San Diego, CA, USA; [2]National Institute of Chemistry, Slovenia; [3]Medical School of the University of Navarra, Spain; [4]Center for Medicine and Biosciences, Borstel, Germany; [5]BiosYnth Srl., Siena, Italy; [6]Institute for Biophysics and X-ray Structure Research, Austrian Academy of Sciences, Graz, Austria

Introduction

In addition to the rapid emergence of multi-resistant bacteria, classical antibiotics may release endotoxin during the process of killing bacteria thus promoting endotoxic shock [1], claiming hundreds of thousands of lives yearly. To respond to the urgent need for antibiotics with novel mechanisms of action and for effective compounds to combat sepsis, we have designed antibiotic and anti-septic drug candidates by modification of a host defense peptide, a fragment of human lactoferrin (LF11, FQWQRNIRKVR-NH_2) with hydrophobic groups. A set of peptides was prepared by inserting hydrophobic groups varying in length and nature of their chains at either terminus. The antimicrobial activities of peptides against a panel of strains and their cellular toxicity were compared. Information on the peptide conformation in solution and upon interaction with membrane mimetic environments and LPS, and the effects the peptides may have on membrane mimetic systems were also investigated.

Results and Discussion

LF11 belongs to an amphipathic α-helical region of lactoferrin that is distinct from the site of iron binding and that represents part of the LPS binding region (residues 28-34) [2]. As shown by NMR, LF11 forms a well-defined hydrophobic core when bound to LPS, allowing the basic residues to interact with the phosphate groups of LPS, the side chain of Phe-1 close to the aliphatic chains of lipid A, and Trp-3 at the interface between polar and nonpolar groups of the lipid A. The structure in anionic micelles forms a loop, which contains a kink at the N-terminus, positioning the hydrophobic chains towards the nonpolar interior of the micelles, and the basic groups spread around at the polar surface, interacting with anionic headgroups.

Derivatization of LF11-homoserine lactone derivative (LF12) with alkylamines of varying hydrocarbon chain lengths showed that the addition of a C12 alkyl chain to LF12 led to the largest increase in antimicrobial potency, LPS binding and neutralizing activity compared to LF11 [3]. Further studies were then performed on a derivative of LF11 having a lauryl group at the N-terminus (C12-LF11). Neither LF11 nor C12-LF11 exhibited toxicity toward HeLa cells at 500 μg/ml (MTT assay) or hemolytic activity against human red blood cells at 100 μg/ml. As compared to LF11, C12-LF11 shows increased antimicrobial activity against several Gram-negative and Gram-positive bacteria determined by the microdilution method in Mueller-Hinton broth according to the NCCLS guidelines (Table 1).

The interactions of LF11 and C12-LF11 with LPS were analyzed using the deep rough mutant LPS from Salmonella minnesota (R595). Both peptides were able to neutralize the LPS induced production of TNFα by mononuclear cells as well as macrophages. The peptide/LPS affinity was rather similar for both peptides, as evidenced by the displacement of ^{45}Ca from LPS monolayers (Figure 1). However,

Table 1. Antimicrobial activity of peptides.

Bacteria	Minimum Inhibitory Concentration (μg/ml)[a]		
	LF11	**C12-LF11**	**Polymyxin B**
Escherichia coli (ATCC 25922)	256	64	0.5
Acinetobacter baumanii (10817/01 CUN)	>256	64	0.25
Bordetella bronquiseptica (10844/99 CUN)	128	8	0.125
Neisseria meningitides (10827/01 CUN)	>256	64	16
Staphylococcus aureus (ATCC 25923)	>256	128	8
Streptococcus pyogenes (ATCC 19615)	>256	64	8

[a]*MIC is the minimum inhibitory conc. where bacterial growth was not observed at 18h.*

C12-LF11 was much more efficient to compensate for the surface charge of LPS aggregates, a prerequisite for LPS neutralization, indicating that C12-LF11 inserts into the hydrophobic core of LPS aggregates.

Microcalorimetry showed that LF11 only negligibly affects the phase behavior of negatively charged dipalmitoyl-PG and zwitterionic dipalmitoyl-PE model membranes, while C12-LF11 strongly decreases the main transition temperature and the cooperativity of both lipids, and abolishes the pretransition around 33°C, as confirmed by wide-angle X-ray diffraction experiments. While LF11 only binds to the lipid surface, C12-LF11 inserts into the hydrophobic core of the membrane, which is consistent with its enhanced antimicrobial activity.

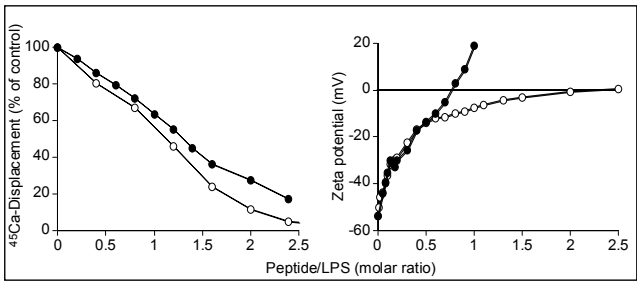

Fig. 1. Displacement of 45Ca2+ from LPS RE monolayers (left) and surface charge compensation of LPS RE aggregates (right) by LF11 (●) and C12-LF11 (○).

Acknowledgments

This study has been carried out with financial support from the Commission of the European Communities, specific RTD programme "Quality of Life and Management of Living Resources", QLK2-CT-2002-01001 "Antimicrobial endotoxin neutralizing peptides to combat infectious diseases". It does not necessarily reflect its views and in no way anticipates the Commission's future policy in this area.

References

1. Periti, P. and Mazzei, T. *J. Chemother.* **10**, 427-448 (1998).
2. Elass-Rochard, *et al. Biochem. J.* **312**, 839-845 (1995).
3. Majerle, A., Kidric, J. and Jerala, R. *J. Antimicrob. Chemother.* **51**, 1159-1165 (2003).

Peptide Revolution: Genomics, Proteomics & Therapeutics
Michael Chorev & Tomi K. Sawyer (Editors)
American Peptide Society, 2003

Fluorescent Analogs of Trichogin GA IV: A New Insight into the Mechanism of Membrane Permeabilization

Basilio Pispisa[1], Emanuela Gatto[1], Claudia Mazzuca[1], Antonio Palleschi[1], Lorenzo Stella[1], Mariano Venanzi[1], Fernando Formaggio[2] and Claudio Toniolo[2]

[1]Dipartimento di Scienze e Tecnologie Chimiche, Università di Roma Tor Vergata, 00133 Rome, Italy; [2]Istituto di Chimica Biomolecolare, C.N.R., Dipartimento di Chimica Organica, Università di Padova, 35131 Padova, Italy

Introduction

Trichogin GA IV is the main component of a family of natural antibiotic and membrane-active linear peptides, called lipopeptaibols, having the following sequence:

n-Oct-Aib-Gly-Leu-Aib-Gly-Gly-Leu-Aib-Gly-Ile-Lol

n-Oct being n-octanoyl and Lol leucinol. In order to characterize the mode of action of this peptide, a series of analogs, carrying fluorescent probes (energy transfer donor-acceptor pairs) in different positions along the peptide sequence, have been synthesized [1]. Steady-state and time resolved fluorescence, IR and CD spectroscopies, as well as molecular mechanics calculations [2], were employed to investigate the structural features of these trichogin analogues in solution and in model membrane (LUV = large unilamellar vesicle). The aim of the work was to elucidate the yet undefined mechanism of membrane perturbation by this class of antimicrobial peptides.

Results and Discussion

Fluorescent analogues, in which FMOC substitutes the octanoyl chain, show higher permeabilizing activity than the natural peptide, as illustrated in Figure 1, where the fractional release of a fluorescent dye entrapped into the inner core of ePC:Cho 1:1 vesicles is caused by the permeabilizing activity of micromolar concentrations of FMOC analogues.

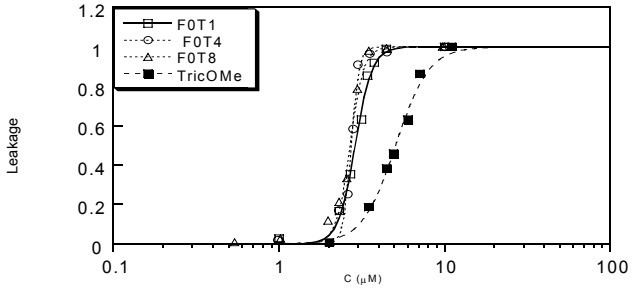

Fig. 1. Fractional release of carboxyfluorescein in ePC:Cho 1:1 as a function of concentration of several FMOC analogues and trichogin GA IV.

The binding of the peptide analogues to the lipid phase is determined by complex chemical equilibria, involving not only the monomeric form, but also small peptide aggregates both in solution and in the membrane. Furthermore, fluorescence quenching experiments, using iodide as an external quencher, indicate that the trichogin analogs partition between the surface and the interior of the lipid phase. In the latter case, the

molecules are inaccessible to the quencher, so that the Stern-Volmer plot is curved downward.

Quenching experiments using several lipids functionalized by bromine quenchers at different positions along the lipid chain confirm the idea that the trichogin analogs are located into the lipid phase. A significant correlation between the membrane activity and the fraction of aggregated peptides in the lipid phase is observed, thus suggesting that the latter species are responsible for the liposome permeabilization. This is illustrated in Figure 2, where the initial rate of carboxyfluorescein release as a function of a trichogin analog concentration fairly correlates with the fraction of aggregated species.

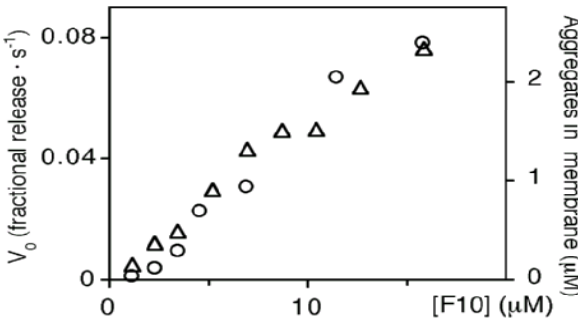

Fig. 2. Initial rate of fractional release of carboxyfluorescein in ePC:Cho 1:1 (left- hand axis) and fraction of aggregated species (right-hand axis) as a function of concentration of an FMOC analog of trichogin GA IV.

As far as the mechanism of liposome perturbation is concerned, both light scattering measurements and fluorescence microscopy experiments on LUVs show that membrane permeabilization is not due to liposome disruption. Moreover, experiments of dye release from liposomes above or below the lipid phase transition temperature allowed us to rule out, at least in the range of peptide/lipid ratio examined, an ion-carrier mechanism. Additional measurements involving the release of markers of different sizes show that molecules with a diameter of about 4 nm are released to a minor extent.

All these results rule out both an ion-carrier and a detergent-like action and suggest the formation of a transmembrane pore as the most likely mechanism of permeabilization.

Acknowledgments

This research was financially supported by MIUR-2002.

References

1. Stella, L., Mazzuca, C., Palleschi, A., Venanzi, M., Formaggio, F., Toniolo, C., Moroder, L. and Pispisa, B. In Benedetti, E. and Pedone, C. (Eds.) *Peptides 2002 (Proceedings of the 27th European Peptide Symposium),* Edizioni Ziino, Napoli, 2002, p. 894.
2. Pispisa, B., Palleschi, A., Mazzuca, C., Stella, L., Valeri, A., Venanzi, M., Formaggio, F., Toniolo, C. and Broxterman, Q. B., *J. Fluoresc.* **12**, 213-217 (2002).

Peptide Revolution: Genomics, Proteomics & Therapeutics
Michael Chorev & Tomi K. Sawyer (Editors)
American Peptide Society, 2003

SAPD: Synthetic Antibiotic Peptides Database

David Wade[1] and Jukka Englund[2]

[1]Wade Research Foundation, 70 Rodney Avenue, Somerset, New Jersey 08873, USA;
[2]Research and Development Unit, National Library of Health Sciences, FIN-00290
Helsinki University, Helsinki, Finland

Introduction

The problem of microbial resistance to antibiotics has been acknowledged for over a half century. Nobel Laureates in Medicine who have received awards for the development of antibacterial agents (G. Domagk, for prontosil, 1939; A. Fleming, for penicillin, 1945; S.A. Waksman, for streptomycin, 1952) all devoted substantial portions of their Nobel lectures to the problem of microbial resistance to the their antibiotics [1]. Recently, the phenomenon has become acute and it is now generally recognized that the worldwide epidemic of antibiotic resistant microbes may even threaten the ability of the medical profession to treat infectious diseases. Statements such as the following are no longer uncommon: "Mutation of organisms to produce antibiotic resistance is undoubtedly going to outstrip availability of new antibiotics in the near future" [2]. Consequently, there is an urgent need for the development of new antibiotic agents and new strategies to treat microbial diseases. All of the tools of modern science will have to be utilized if humanity is not to succumb to this epidemic. Two of the most useful tools developed during the 20th century were the computer and the Internet.

One potential source of new antibiotics, or at least of lead compounds for the development of new antibiotics, is the gene-encoded peptide antibiotics that were discovered during the last 35 years [3]. These new antibiotics have been found in a wide variety of living organisms, hundreds have been isolated, and they are thought to be a previously unrecognized form of innate immunity. A search of Medline from 1966 to the present reveals a nearly exponential increase in the number of publications containing the words, "anti-bacterial, -biotic, -fungal, or -microbial peptide" in their titles or abstracts, and it is currently over 500 per year [4]. This increase is mostly due to research on the new gene-encoded peptide antibiotics. For every naturally occurring peptide antibiotic, many synthetic derivatives can be developed, and thousands have already been created through the use of solid phase peptide synthesis technologies. The amino acid sequences of all of these peptides, natural and synthetic, along with their biological properties, represent a vast goldmine of data for use in the future development of new antibiotics.

Researchers need easily available sources of organized data on existing antibiotics to help guide the development of new therapeutic agents. In the developed world, general access to computers and the Internet provides a nearly ideal method for the rapid dissemination of such data. Prior to 2001, there were two databases for naturally occurring antibiotics, the Antimicrobial Sequences Database (AMSDb; http://www.bbcm.univ.trieste.it/~tossi/pag1.html) for gene encoded peptides and the Peptaibol Database (PD; http://www.cryst.bbk.ac.uk/peptaibol/home.shtml) for peptides that generally have a fungal origin. A database for synthetic antibiotic peptides, the SAPD, was established in 2001 and is available on the Internet (http://oma.terkko.helsinki.fi:8080/~SAPD). The SAPD is stored on the server of TERKKO, the Finnish National Library of Health Sciences, Helsinki, Finland, and it maintained by the voluntary efforts of the database organizers and users. The goals of

Table 1. SAPD users are located in many countries[a].

Australia	Costa Rica	Hungary	Kuwait	South Africa
Austria	Denmark	Iceland	Mexico	Spain
Belgium	Egypt	India	Netherlands	Sweden
Canada	Finland	Israel	New Zealand	Switzerland
Chile	France	Italy	Norway	Taiwan
China	Germany	Japan	Poland	United Kingdom
Colombia	Greece	Korea	Slovenia	USA

[a]*Information supplied voluntarily by users.*

the database organizers are to provide information that will complement that which is available in the AMSDb and PD, and, hopefully, to speed the development of new antibiotics. At the present time, the AMSDb, PD, and SAPD contain 804, 307, and 250 entries, respectively. However, it is anticipated that as SAPD development progresses, the number of entries in the SAPD will greatly exceed those of the AMSDb and PD combined, due to the greater number of amino acid sequences accessible through synthetic chemistry as compared to those available in nature (e.g., peptides can be synthesized entirely from D amino acids).

All three databases are freely available for use by researchers worldwide. In order to access the SAPD, a new user must provide only his/her name and e-mail address, and create a login name. They then receive a temporary password that enables them to access the database. This simple registration information helps the database organizers keep track of database usage for statistical and funding purposes.

Results and Discussion

Over 300 users from at least 35 countries have registered to access the SAPD (Table 1), and users other than the database organizers have recently begun to contribute entries (e.g., tables of peptides that have entered clinical trials). Both of these developments are taken as positive indicators for continued expansion of the SAPD, since it has been in existence for less than two years, and it has fewer entries and is less elaborate than either the AMSDb or PD.

As the number of entries in the SAPD increases, new features will be added to enhance its usefulness to antibiotics researchers (e.g., links to web sites outside of the SAPD). It is hoped that the SAPD, AMSDb and PD will facilitate the development of many new therapeutic agents to help solve the current crisis caused by antibiotic resistant microorganisms.

Acknowledgments

The authors thank Helsinki University and the Academy of Finland for continued support of SAPD development.

References

1. The Nobel Foundation web site, http://www.nobel.se (2003).
2. Paterson, D. L. *Crit. Care Med.* **31**(1), S25-28 (2003).
3. Boman, H. G. *Immuno.l Rev.* **173**, 5-16 (2000).
4. Wade, D. and Englund, J. *Protein Peptide Lett.* **9**, 53-57 (2002).

Peptide Revolution: Genomics, Proteomics & Therapeutics
Michael Chorev & Tomi K. Sawyer (Editors)
American Peptide Society, 2003

Generation of Novel Vancomycin–Type Glycopeptide Antibiotics by Mutasynthesis

Stefan Weist[1], Bojan Bister[1], Oliver Puk[2], Daniel Bischoff[1], Stefan Pelzer[2], Wolfgang Wohlleben[2] and Roderich D. Süssmuth[1]

[1]Institute of Organic Chemistry, University of Tübingen, Auf der Morgenstelle 18, D-72076 Tübingen; [2]Institute of Microbiology & Biotechnology, University of Tübingen, Auf der Morgenstelle 18, D-72076 Tübingen, Germany

Introduction

Vancomycin is the most prominent glycopeptide antibiotic being used in clinical treatment for severe staphylococcal infections for more than 40 years. In 1997, the first case of a staphylococcal infection with diminished sensitivity against vancomycin was reported. Since then, vancomycin-resistant enterococci (VRE) and methicillin-resistant *Staphylococcus aureus* strains (MRSA) have become a serious threat to human health.

The ongoing search for glycopeptide derivatives with an altered or a new structure to encounter vancomycin-resistant bacterial strains has put forth a vast number of novel synthetic or semisynthetic approaches. Considerable work on the alteration of the vancomycin structure has been done in the last years.

The vancomycin structure is representative of a whole class of antibiotics comprising several hundred compounds. Important work was done on structure elucidation and on biosynthesis studies, as well on the total synthesis, which was accomplished independently by the groups of Evans, Nicolaou and Boger.

The structure of the vancomycin-type glycopeptide antibiotics consists of a glycosylated tricyclic heptapeptide essentially built up from unusual aromatic amino acids. The two 3-chloro-β-hydroxytyrosines at amino acid position 2 and 6 are a crucial structural feature since they span two (C-*O*-D, D-*O*-E) of the three rings cyclized in the aromatic side chains (Figure 1). A member of the vancomycin family is balhimycin, which is produced by *Amycolatopsis balhimycina*. The investigation of balhimycin biosynthesis is serving our groups as a model system to study vancomycin-type glycopeptide antibiotic biosynthesis. By generation of mutants in *A. balhimycina* and subsequent structure elucidation of the gene products we were able to identify the order of the oxidative cyclization steps performed by three oxygenases leading to the vancomycin aglycon [1].

Moreover, we are interested in the biosynthesis of the unusual amino acid building blocks, 4-hydroxyphenylglycine (Hpg), 3,5-dihydroxyphenylglycine (Dpg) [2], and 3-chloro-β-hydroxytyrosine (Cht) [3].

In this contribution, we present the application of a method known as mutasynthesis [4], combining chemical synthesis of aromatic amino acid building blocks together with genetically engineered bacterial strains producing hitherto unknown compounds with promising antibacterial properties. The lack of the chlorine atoms in natural vancomycin results in 5-10 times loss of antibiotic activity [5]. Therefore, the halogen atoms at the two Cht moieties were considered as an interesting target for structural modifications of the heptapeptide core. Actually, total synthesis does not allow accomplishing this task within a reasonable period of time.

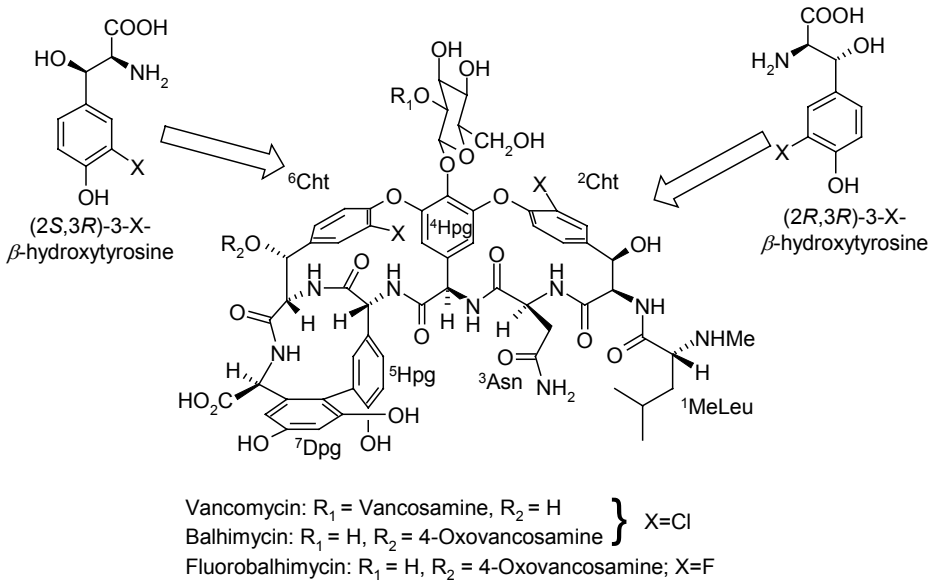

Fig. 1. Structure of the glycopeptide antibiotics balhimycin and vancomycin with the central building block 3-chloro-β-hydroxytyrosine and structure of the mutasynthetically generated fluorobalhimycin.

Results and Discussion

Using methods of molecular biology, a mutant deficient in Cht biosynthesis was generated. Lacking the two Cht side-chain bridging moieties (Figure 1), the *bhp* mutant strain is not able to produce balhimycin. We thought supplementation of the mutant with synthetic analogues of Cht to be a promising way to achieve novel balhimycin derivatives thus bypassing the deficiency of the mutant. A synthetic strategy towards Cht derivatives was developed. To provide both of the diastereomeric Cht configuration isomers we employed a racemic and an enantioselective synthesis route via aldol reaction of a glycine synthon with a 3-substituted 4-hydroxybenzaldehyde. Having tested a set of Cht analogues, we found that supplementation with 3-fluoro-*β*-hydroxytyrosine resulted in restored antibiotic activity of the *bhp* mutant culture filtrate. After fermentation and isolation of the novel active antibiotic, structure was elucidated by means of high resolution FTICRMS and 2D-NMR. Thus we could prove the assumed structure to be the fluorine analogue of balhimycin [6].

In further supplementation assays, the culture filtrate showed antibiotic activity if 2-fluoro-*β*-hydroxytyrosine, 3,5-difluoro-*β*-hydroxytyrosine or 3-methyl-*β*-hydroxy-tyrosine was used. The presence of corresponding fluorobalhimycins was confirmed by LCMS experiments. From the above studies we conclude that employing the mutasynthetic approach we were able to generate three novel fluorinated core structures (Figure 1).

Current work focuses on the structure elucidation of these novel vancomycin type glycopeptides as well as on the extension of the mutasynthetic approach to other aromatic amino acids of the vancomycin aglycon i.e. 4-hydroxyphenylglycine and 3,5-dihydroxyphenylglycine (Dpg). Recent experiments have shown that alteration of the

core structure at position 7 (Dpg) of vancomycin-type glycopeptide antibiotics is also possible using a mutant being deficient in Dpg biosynthesis supplemented with synthetic Dpg analogues.

In summary, we present a method for the introduction of structural variety into the heptapeptide core of vancomycin-type glycopeptide antibiotics combining methods of molecular biology and chemical synthesis.

Acknowledgments
The work of R. D. S. was funded by an Emmy Noether fellowship (SU 239/2-1) by the DFG.

References

1. a) Bischoff, D. *et al. Angew. Chem. Int. Ed.* **40**, 1693-1696 (2001); b) Bischoff, D. *et al. Angew. Chem. Int. Ed.* **40**, 4688-4691 (2001).
2. Pfeifer, V. *et al. J. Biol. Chem.* **42**, 38370-38377 (2001).
3. Puk, O. *et al. Chem. Biol.* **9**, 225-235 (2002).
4. Rinehart. K. L. *et al. Pure Appl. Chem.* **49**, 1361-1384 (1977).
5. Bister, B., Bischoff, D., Süssmuth, R. D. *et al., ChemBio. Chem.* **4**, 649-662 (2003).
6. Weist S., Bister, B., Bischoff D., Süssmuth, R. D. *et al. Angew. Chem. Int. Ed.* **41**, 3383-3385 (2002).

Peptide Revolution: Genomics, Proteomics & Therapeutics
Michael Chorev & Tomi K. Sawyer (Editors)
American Peptide Society, 2003

Solution Structure of an Antifungal Peptide, Scarabaecin, from the Rhinoceros Beetle

Hikaru Hemmi[1], Jun Ishibashi[2], Tetsuya Tomie[3] and Minoru Yamakawa[2]

[1]National Food Research Institute, Tsukuba, Ibaraki 305-8642, Japan; [2]National Institute of Agrobiological Sciences, Tsukuba, Ibaraki 305-8634, Japan; [3]Biological Research Laboratories, Nissan Chemical Industries, Ltd., Shiraoka, Saitama 349-0294, Japan

Introduction

Antibacterial and antifungal peptides/polypeptides play an important role in insect immune systems [1,2]. To date, a large number of antibacterial peptides have been isolated from insects [3,4]. However, only a few antifungal peptides/polypeptides from insects have been reported. In these antifungal peptides/polypeptides, drosomycin [5], heliomicin from *Heliothis virescens* [6], termicin from *Pseudacanthotermes spininger* [7], and thanatin from *Podisus maculiventris* [8] are demonstrated to have disulfide bonds in the molecule.

In the course of our study on insect antifungal peptides for the development of transgenic rice plants, we identified a novel cysteine-containing antifungal peptide from the coconut rhinoceros beetle *Oryctes rhinoceros*. Here we report the amino acid sequence, antimicrobial activity, chitin-binding property, and the solution structure of the antifungal peptide designated scarabaecin.

Results and Discussion

Scarabaecin was purified from the hemolymph of the coconut rhinoceros beetle. The deduced amino acid sequence of scarabaecin from cDNA was shown to have an open reading frame consisting of 66 amino acid residues. As a result of the amino acid sequencing of the mature portion, it was found that there are two peptides (36 amino acid residues for major component and 38 amino acid residues for minor component, Figure 1). Synthetic scarabaecin showed strong antifungal activity against phytopathogenic fungi such as *Pyricularia oryzae*, but weak antifungal activity against an insect pathogenic fungus, *Bauberia bassiana.* This peptide showed no activity against bacteria except a pathogenic bacterium, *Staphlococcus aureus*. Scarabaecin also showed chitin binding activity (K_d = 1.315μM). Amino acid sequences were compared focusing on putative chitin-binding domains among scarabaecin and some chitin-binding proteins in invertebrates and plants. The results suggest that scarabaecin is a new member of chitin-binding antimicrobial proteins even though this peptide has no overall sequence similarity to chitin-binding proteins.

Major component ELPKLPDDKVLIRSRSNCPKVWNGFDCKSPFAFS
Minor component DAELPKLPDDKVLIRSRSNCPKVWNGFDCKSPFAFS

Fig. 1. Amino acid sequence of scarabaecin.

The solution structure of scarabaecin was determined from two dimensional ^{1}H NMR spectroscopy and hybrid distance geometry/simulated annealing calculation. The results showed that scarabaecin is comprised of a two-stranded antiparallel β-sheet linked by a type-I β-turn (residues 23 – 30) and a short helical structure (residues 31 – 34). The backbone conformation of the putative chitin-binding domain (residues 18 – 36) was compared with those of the corresponding regions identified as chitin-binding

domain in hevein, plant chitin-binding protein [9], and tachycitin, invertebrate chitin-binding protein [10]. The results indicated that the backbone conformation of the putative chitin-binding domain in scarabaecin shared a significant structural similarity with those in hevein and tachycitin. Therefore, it was confirmed that scarabaecin belongs to the family of chitin-binding antimicrobial proteins even though scarabaecin has no overall sequence similarity to other chitin-binding proteins. Moreover, the 3D structure-based sequence alignment of chitin-binding domains between scarabaecin and some chitin-binding proteins in invertebrates and plants suggests that the residues of Asn25, Phe27, and Phe35 in scarabaecin are critical for chitin-binding.

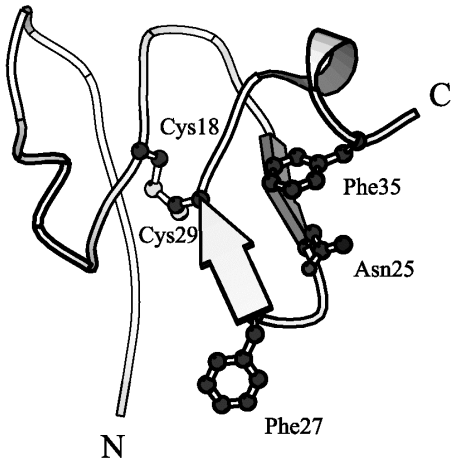

Fig. 2. The lowest energy structure of scarabaecin among all the calculated structures. Disulfide bridges and putative functional residues are shown as ball-and-stick model. This figure was generated using Molscript [11].

Acknowledgments

The work was supported in part by the Program for Promotion of Basic Research Activities for Innovative Biosciences of the Bio-Oriented Technology Research Advancement Institute, Japan, and by a grant (Insect Technology Program), MAFF, Japan.

References

1. Hoffman, J. A., Kafatos, F. C., et al. *Science* **284**, 1313-1318 (1999).
2. Bulet, P., Hetru, C., et al. *Dev. Comp. Immunol*. **23**, 329-344 (1999).
3. Yamakawa, M. and Tanaka, H. *Dev. Comp. Immunol*. **23**, 281-289 (1999).
4. Hetru, C., Hoffman, D. and Bulet, P. In Brey, P. T. and Hultmark, D. (Eds.) Molecular Mechanisms of Immune Responses in Insects, Chapman & Hall, London, p. 40-66 (1998).
5. Fehlbaum, P., Bulet, P., Michaunt, L., et al. *J. Biol. Chem*. **269**, 33159-33163 (1994).
6. Lamberty, M., Ades, S., Uttenweiler-Joseph, S., et al. *J. Biol. Chem*. **274**, 9320-9326 (1999).
7. Lamberty, M., Zachary, D., Lanot, B. et al. *J. Biol. Chem*. **276**, 4085-4092 (2001).
8. Fehlbaum, P., Bulet, P., et al. *Proc. Natl. Acad. Sci. U.S.A*. **93**, 1221-1223 (1996).
9. Anderson, N. H., Cao, B., Rodriguez-Romero, A. and Arreguin, B. *Biochem*. **32**, 1407-1422 (1993).
10. Suetake, T., Tsuda, S., Kawabata, S., et al. *J. Biol. Chem*. **275**, 17929-17932 (2000).
11. Kraulis, P. J. *J. Appl. Crystallogr*. **24**, 946-950 (1991).

Peptide Revolution: Genomics, Proteomics & Therapeutics
Michael Chorev & Tomi K. Sawyer (Editors)
American Peptide Society, 2003

Small Analogues of Lysozyme with Antibacterial Properties

Xavier Doisy, Dan Ifrah, Trine S. Neerup and Paul R. Hansen

Chemistry Department, The Royal Veterinary and Agricultural University, DK-1871 Frederiksberg C, Copenhagen, Denmark

Introduction

There is a great need for new antibiotics as resistance in bacteria is becoming a dramatic problem both in community and hospital environments. This urgent quest is directed toward antibiotics with a new mode of action. Antimicrobial peptides and proteins belong to such a class and have a promising potential.

Lysozyme is a small sized enzyme (14.4 KDa, 129 amino acids) [1] widely distributed in living organisms. This basic protein is implicated in many biological processes antimicrobial activity. This activity is due to two different mechanisms: a) an enzymatic antimicrobial activity targeting gram positive bacteria, and b) an antimicrobial activity against gram positive and negative bacteria due to a domain located in the loop structure at the upper lip of the enzymatic site. This active helix-loop-helix motif has been obtained by clostripain digestion of lysozyme [2]. The C-terminus nonamer **1** (Table 1) obtained is more active than the N-terminus fragment and displays a higher activity on gram positive bacteria than on gram negative bacteria [3]. Using this sequence **1** as a lead structure, we have synthesized small peptide analogues with antimicrobial activity. The selectivity towards bacterial versus mammalian cells has been explored, as well as the specificity for gram positive versus gram negative bacteria.

Results and Discussion

All peptides were manually synthesized by standard solid phase peptide synthetic methods using Fmoc chemistry. The following protecting groups were used on the amino acid side chains: Boc for Trp and Lys, Pbf for Arg, and Trt for Asn. The resin used was Tentagel S RAM (50 mg, loading 0.24 mmol/g), which upon cleavage yielded the corresponding peptides amidated on the *C*-terminus. The following coupling conditions were used: Fmoc-AA-OH/TBTU/HOBt/DIPEA (3:3:3:4.5) in NMP with double coupling (40 + 20 mn). Cleavage of the peptides from the resin was achieved using 0.5 ml of TFA/TES/H_2O (95:2.5:2.5) for 2 h. The peptides were then precipitated and washed with cold diethyl ether, and centrifuged. The resulting white pellets were dissolved in 10% acetic acid-water and freeze-dried. The peptides were purified by RP-HPLC, their mass confirmed with MALDI-TOF and LC-MS, and their sequence with amino acid analysis.

The MIC was determined with the broth microdilution assay on *Escherichia coli* (ATCC 25922) and *Staphylococcus aureus* (ATCC 25923) with ampicilline as internal standard. Triplicate serial two-fold dilutions of the peptides were made, ranging from 64 µg/ml to 2 µg/ml, and assayed on an average bacterial concentration of 4.10^6 cfu/ml. The MIC values obtained were then corrected with the results from amino acid analysis.

The haemolytic activity of the peptides was assessed on fresh human erythrocytes. Serial two-fold dilutions of the peptides were made, ranging from 250 µg/ml to 1.95 µg/ml. After incubation 1h at 37°C and centrifugation, absorbance of the supernatant was read at 415 nm. Percentage of haemolysis was calculated as (A_{415}peptide –

Table 1. Antibacterial and haemolytic activity of peptides.

Peptide	*S. aureus*	*E.coli*	Haemolysis[a]
1 RAWVAWRNR-NH_2	>67.8	>67.8	5.5%/265
2 KAWVAWKNK-NH_2	>32	>32	6.1%/125
3 RAWVAWRRR-NH_2	>92.2	92.2	1.9%/360
4 RAFVAFRNR-NH_2	>38.4	>38.4	5.4%/150
5 RVWVVWRNR-NH_2	13.4	13.4	7.3%/105
6 RVWLVWRNR-NH_2	30.1	30.1	6.2%/235
7 RLWLLWRNR-NH_2	32	16	5.4%/250
8 RAWLAWRNR-NH_2	>68.5	>68.5	1.0%/267
9 RAWFAWRNR-NH_2	64	32	0%/250

[a]*Percentage of haemolysis per μg of peptide.*

A_{415}PBS)/(A_{415}1% Triton X-100 – A_{415}blank) x 100, and the value was corrected with the results from amino acid analysis.

We arbitrarily set a cut off maximum value of 64 μg/ml for our bacteriological assay. Our results (Table 1) showed that replacing the following amino acids was unsuccessful: 1) the three Arg in peptide **1** with Lys (**2**), despite the different pKa and hydrogen bond patterns of the side chains; 2) Asn (**1**) with Arg (**3**), despite an increase in the overall net positive charge (nevertheless, a slight discrimination between gram positive and negative bacteria was noticed); 3) the two Trp (**1**) with another aromatic amino acid: Phe(**4**); and 4) Val (**1**) with the more lipophilic Leu (**8**).

Improvements in the MIC values were satisfactorily noticed when the following replacements were made in peptide **1**: 1) Ala and Val (**1**) replaced respectively with the more lipophilic Val and Leu (**6**); 2) Ala and Val (**1**) both replaced with the more lipophilic Leu (**7**); 3) Val (**1**) replaced with the aromatic and lipophilic Phe (**9**); and 4) both Ala (**1**) replaced with the more hindered and lipophilic Val (**5**), with a MIC value for both gram positive and negative bacteria culminating at 13.4 μg/ml.

In conclusion, using the C-terminus nonamer **1** from the active helix-loop-helix motif of lysozyme as a lead structure, we were able to obtain peptides with a better antimicrobial activity. Indeed, some of these peptides displayed a better MIC value and an altered selectivity towards gram positive and negative bacteria. Discrimination between gram positive and negative bacteria was achieved for peptides **7** and **9**, reversing the natural trend of lysozyme to preferentially target gram positive bacteria. This was achieved by altering the delicate balance between hydrophilic and lipophilic side chain residues. Furthermore, the haemolysis assay showed that all these peptides retained their exquisite selectivity towards bacterial membranes.

Acknowledgments

We thank Ms. Jette Petersen for performing the amino acid analysis. Support from the Danish Research Council (grant 9900234) and the Augustinus Foundation is gratefully acknowledged.

References

1. Fleming, A. *Proc. Roy. Soc. London* **93B**, 306-317 (1922).
2. Ibrahim, H. R., *et al J. Agric. Food Chem.* **44**, 1416-1423 (1996).
3. Ibrahim, H. R., Thomas, U. and Pellegrini, A. *J. Biol. Chem.* **276**, 43767-43774 (2001).

Peptide Revolution: Genomics, Proteomics & Therapeutics
Michael Chorev & Tomi K. Sawyer (Editors)
American Peptide Society, 2003

Effects of Glycine and Alanine Substitutions on Activity and Selectivity in Amphipathic β-Sheet Antimicrobial Peptides

Jack Blazyk, Yi Jin, Janet Hammer, Michelle Pate, Adam Bobbey, Jessica Mellinger and Erik Zmuda

Department of Biomedical Sciences, Ohio University College of Osteopathic Medicine, Athens, OH 45701, USA

Introduction

The dramatic rise in the resistance of virulent microorganisms to antibiotics in current use has heightened interest in new antimicrobial agents. Over the past 15 years, we have gained a much greater understanding of the innate host defense systems in organisms ranging from bacteria to humans. A key element in these systems, particularly in lower organisms, is the production of small antimicrobial peptides, a process often triggered by infection [1]. A wide variety of such peptides has been intensively investigated over the past decade. A great deal of effort has focused on how these peptides function at the molecular level and whether the native peptides or their derivatives may be useful in fighting bacterial infection.

Recently we tested a new design in which the amino acid sequence of a linear cationic peptide had the potential to form an amphipathic β-sheet instead of an α-helix [2]. Our model β-sheet peptide, $(KIGAKI)_3$-NH_2, possessed equivalent antimicrobial activity to that of an analogous peptide with amphipathic α-helical properties, but appeared to have greater selectivity for bacterial vs. mammalian plasma membranes, suggesting a potential selective advantage for amphipathic β-sheet peptides. The substitution of a single Ile by Trp resulted in significant changes in lytic activity [3].

We have studied $(KL)_5K$-NH_2 peptides with Trp replacing one Leu. These peptide had excellent antimicrobial activity. W_2-KL-11 had high hemolytic activity, while that of W_4-KL-11 was somewhat lower. Here, we examined two peptide families consisting of (1) single Ala replacements for Leu in W_4-KL-11 and (2) single Gly replacements for either Lys or Leu in W_2-KL-11 (see sequences below).

W_4-KL-11	KLKWKLKLKLK-NH_2	W_2-KL-11	KWKLKLKLKLK-NH_2
A_2,W_4-KL-11	K**A**KWKLKLKLK-NH_2	G_1,W_2-KL-11	**G**WKLKLKLKLK-NH_2
W_4,A_6-KL-11	KLKWK**A**KLKLK-NH_2	W_2,G_3-KL-11	KW**G**LKLKLKLK-NH_2
W_4,A_8-KL-11	KLKWKLK**A**KLK-NH_2	W_2,G_4-KL-11	KWK**G**KLKLKLK-NH_2
W_4,A_{10}-KL-11	KLKWKLKLK**A**K-NH_2	W_2,G_5-KL-11	KWKL**G**LKLKLK-NH_2
		W_2,G_6-KL-11	KWKLK**G**KLKLK-NH_2
		W_2,G_7-KL-11	KWKLKL**G**LKLK-NH_2
		W_2,G_8-KL-11	KWKLKLK**G**KLK-NH_2
		W_2,G_9-KL-11	KWKLKLKL**G**LK-NH_2
		W_2,G_{10}-KL-11	KWKLKLKLK**G**K-NH_2
		W_2,G_{11}-KL-11	KWKLKLKLKL**G**-NH_2

Results and Discussion

Changes in antimicrobial and hemolytic activity resulting from these modifications are shown in Table 1. The substitution of a single Leu by Ala in W_4-KL-11 resulted in a substantial decrease in hemolytic activity for the four analogs. The antimicrobial activity of A_2,W_4-KL-11 was as at least as potent as the parent compound. The substitution of a single Lys or Leu by Gly in W_2-KL-11 resulted in more complex effects. Replacements at positions 1 or 3 were more hemolytic than W_2-KL-11.

Table 1. Antimicrobial and hemolytic activity of modified compounds.

Peptide	Minimum Inhibitory Concentration (μg/ml)				
	E. coli ATCC 25922	*S. aureus* ATCC 29213	*P. aeruginosa* ATCC 27853	% Hemolysis at 100 μg/ml	% Hemolysis at 250 μg/ml
W_4-KL-11	4	4	4	12	47
A_2W_4-KL-11	2	4	4	0	4
W_4A_6-KL-11	4	8	8	0	1
W_4A_8-KL-11	4	16	16	0	0
W_4A_{10}-KL-11	4	8	16	0	9
W_2-KL-11	1	2	2	61	87
G_1W_2-KL-11	2	2	4	85	99
W_2G_3-KL-11	2	4	4	69	100
W_2G_4-KL-11	4	16	32	0	0
W_2G_5-KL-11	4	4	4	13	64
W_2G_6-KL-11	4	16	64	0	0
W_2G_7-KL-11	2	4	4	10	45
W_2G_8-KL-11	4	16	32	0	0
W_2G_9-KL-11	2	4	4	28	72
W_2G_{10}-KL-11	2	4	8	5	23
W_2G_{11}-KL-11	4	8	16	40	88

Replacements at positions 4, 6 or 8 were nonhemolytic, while other replacements resulted in intermediate levels of hemolysis. All of the Gly-containing peptides possessed good antimicrobial activity vs. *E. coli*. The three nonhemolytic analogs were much less effective vs. *S. aureus* and *P. aeruginosa*. All of these analogs, like other antimicrobial peptides with amphipathic β-sheet character, induced more leakage in large unilamellar vesicles containing a mixture of PG and PE rather than PC as the neutral lipid component. The A-containing derivatives of W_4-KL-11 were generally less effective at inducing leakage in mixed lipid vesicles. In contrast, the Gly-containing derivatives of W_2-KL-11 were much more effective at inducing leakage.

A_2W_4-KL-11 was comparable to W_4-KL-11 in antimicrobial potency and much lower in hemolytic activity. W_2G_7-KL-11 and W_2G_{10}-KL-11 were close to W_2-KL-11 in antimicrobial activity, but much less hemolytic. It therefore appears that simple modifications such as single alanine and glycine replacements can enhance the selectivity of linear amphipathic β-sheet antimicrobial peptides.

Acknowledgments
The work was funded by NIH Grant AI047165 to J. Blazyk.

References

1. Maloy, W. L., and Kari, U. P. *Biopolymers* **37**, 105-122 (1995).
2. Blazyk, J., Weigand, R., et al. *J. Biol. Chem.* **276**, 27899-27906 (2001).
3. Jin, Y., Mozsolits, H., Hammer, J., et al. *Biochemistry* **42**, 9395-9405 (2003).

Peptide Revolution: Genomics, Proteomics & Therapeutics
Michael Chorev & Tomi K. Sawyer (Editors)
American Peptide Society, 2003

Structure of Horseshoe Crab Antimicrobial Peptide, Tachyplesin I, in Dodecylphosphocholine Micelles

Mineyuki Mizuguchi[1], Shinichi Kamata[1], Shun-ichiro Kawabata[2] and Keiichi Kawano[1]

[1]Faculty of Pharmaceutical Sciences, Toyama Medical and Pharmaceutical University, Toyama 930-0194, Japan; [2]Department of Biology, Graduate School of Sciences, Kyushu University, Fukuoka 812-8581, Japan

Introduction

In 1988, an antimicrobial peptide, tachyplesin I, was found in the Japanese horseshoe crab (*Tachypleus tridentatus*) hemocytes [1]. Its isopeptides, tachyplesin II and polyphemusins I and II, have also been found in the hemocytes of *T. tridentatus* and the American horseshoe crab (*Limulus polyphemus*) [2]. The tachyplesin family peptides are composed of 17 or 18 amino acid residues with two disulfide bonds and a carboxyl-terminal arginine α-amide [2]. Tachyplesins and polyphemusins inhibit the growth of both Gram-negative and positive bacteria at low concentrations [1,2]. It has been shown that tachyplesin I increases the K^+ permeability of *Staphylococcus aureus* and *Escherichia coli* cells, concomitantly reducing cell viability. Tachyplesin exhibits a strong capacity to bind with lipopolysaccharide in the outside of the outer membrane in *E. coli*, thus, this peptide effectively disrupts the outer membrane structure and easily penetrates the cytoplasmic membrane. This peptide also enhances the permeability of human erythrocytes, although the concentration range required for this effect is significantly higher than that used with the bacteria [3]. Determination of the tachyplesin structure in water and bound to model membranes should not only reveal the conformational changes upon binding to the membrane, but may also give an indication of how the membrane is disrupted. Therefore, we have determined the structure of tachyplesin I in the presence and absence of dodecylphosphocholine (DPC) micelles using two-dimensional (2D) ^{1}H NMR spectroscopy.

Results and Discussion

Tachyplesin I was isolated from acid extracts of *T. tridentatus* hemocytes, as described previously [1]. 2D NMR spectra of tachyplesin I were obtained at 30°C and pH 3.6 in the presence and absence of 60 mM DPC micelles. The proton resonance assignments were performed as described previously [4]. Spin systems were identified in the TOCSY and DQF-COSY spectra, and sequential assignments were made by $d_{\alpha N}(i,i+1)$ and $d_{NN}(i,i+1)$ NOEs. The ^{1}H-resonance of all of the main chain atoms, except for the backbone amide proton of the N-terminal Lys1, and most of the side chain atoms of tachyplesin I were unambiguously assigned. The structures of tachyplesin I in the absence and presence of DPC micelles were calculated using 66 and 80 NOE-based distance restrains, respectively. The 10 dihedral ϕ angle restraints and 6 hydrogen bond restraints were used as additional restraints for the calculations of the structure in water. Figure 1A shows the ensemble of 30 NMR structures of tachyplesin I best fitted for all atoms of the converged region (Cys3-Tyr13). A root-mean-square deviation (RMSD) of the peptide backbone in water (0.10 ± 0.07 Å for residues 3-13) is considerably better than in DPC micelles (0.41 ± 0.14 Å for residues 3-13). The residues near the N- and C-terminus are poorly defined for both structures. Figure 1B shows the ribbon representation of tachyplesin structures in water and in the DPC

micelles. Tachyplesin I in water is comprised of two strands (strand-1 and -2 are composed of Trp2-Cys7 and Cys12-Arg17, respectively) and type II β-turn (Tyr8-Ile11), and is similar to that reported previously [5,6]. The β-sheets are stabilized by two disulfide bonds: Cys3-Cys17 and Cys7-Cys12. The backbone structure in water adopts a twisted antiparallel β-sheet structure. The interactions with the DPC micelles result in slight structural changes of tachyplesin I. The backbone structure in the DPC micelles also has the antiparallel β-sheet, i.e., the strand-1 and -2 are composed of Phe4-Tyr8 and Ile11-Arg15, respectively. However, tachyplesin I in DPC lacks the twist in the β-sheet and adopts an extended β-sheet structure, which is due to the different NOE connectivities observed in the β-sheet region (Figure 1).

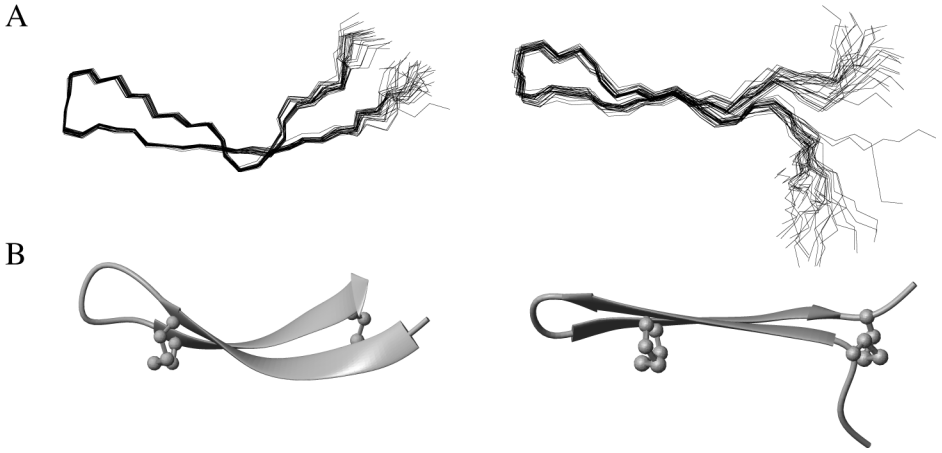

Fig. 1. Calculated structure of tachyplesin I in water (left) and in the DPC micelles (right). (A) Superposition of the 30 polypeptide backbones. (B) Ribbon representation of the energy-minimized average structure. The disulfide-bonds are shown by balls and sticks.

The orientation of tachyplesin I bound to the DPC micelles may be possibly deduced from the structural changes upon binding to the micelles. Two binding models for tachyplesin I bound to DPC micelles may be plausible for interpreting our experimental data: the β-sheet orientation perpendicular or parallel to the plane of the micelle surface. The structure of tachyplesin I in water shows that the hydrophobic side chains locate in the concave surface around Tyr13 and the basic Arg side chains in the turn and β-sheet of the molecule. The phenol ring of Tyr13 is partially covered with the side chain of Arg15 in water (Figure 2A). The side chain of Arg15 is, however, rotated away from the phenol ring of Tyr13 in the structure bound to DPC micelles, exposing the Tyr13 side chain to the solvent or micelle molecules (Figure 2B). These observations suggest that the side chain of Tyr13 is buried in the membrane, since the exposed hydrophobic side chain preferably interacts with hydrocarbon chains rather than with the ionic surfaces of the membrane. In water, the side chains of Arg5 and Arg14 extend from one side of the β-sheet plane and the side-chain of Arg9 sticks out from the loop (Figure 2A). The side chains of these hydrophilic basic residues are folded near the backbone upon binding to the membrane, making the structure compact (Figure 2B). Therefore, the residues of Arg5, Arg9 and Arg14 fold the basic ionic side chains into compact shape in the DPC micelles, and thus, may be buried in the

micelles. These observations suggest that the residues on both sides of the β-sheet plane and the head loop region are buried in the DPC micelles. Therefore, the most plausible model for tachyplesin I bound to DPC micelles is that the β-sheet penetrates the membrane with perpendicular orientation with respect to the plane of the membrane surface. Moreover, the β-sheet of tachyplesin I is extended in the structure bound to the DPC micelles (Figure 1). The extended β-sheet structure may be caused by the perpendicular orientation with respect to the plane of the membrane surface. The extended β-sheet is favorable for the peptides to penetrate the phospholipid bilayer, and burial of the amphiphilic peptide probably results in perturbation of the membrane organization.

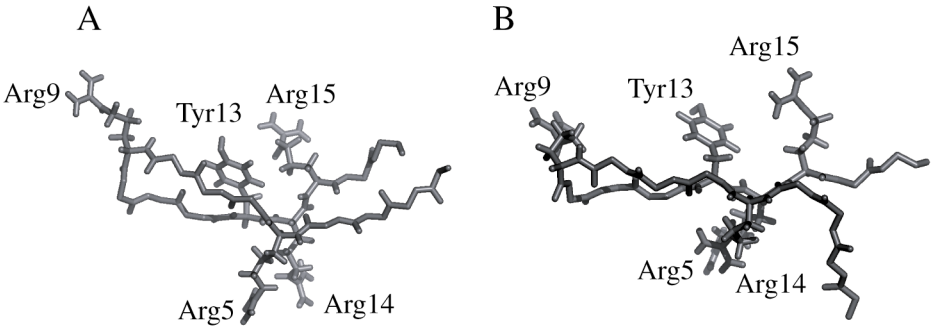

Fig. 2. Structure of tachyplesin I in water (A) and DPC micelles (B). Side-chains of Arg5, Arg9, Tyr13, Arg14 and Arg15 are shown.

Acknowledgments

This work was supported by a grant from the Program for Promotion of Basic Research Activities for Innovative Biosciences (PROBRAIN).

References

1. Nakamura, T., Furunaka, H., Miyata, T., Tokunaga, F., Muta, T., Iwanaga, S., Niwa, M., Takao, T. and Shimonishi, Y. *J. Biol. Chem*. **263**, 16709-16713 (1988).
2. Miyata, T., Tokunaga, F., Yoneya, T., Yoshikawa, K., Iwanaga, S., Niwa, M., Takao, T. and Shimonishi, Y. *J. Biochem. (Tokyo)*. **106**, 663-668 (1989).
3. Katsu, T., Nakao, S. and Iwanaga, S. *Biol. Pharm. Bull*. **16**, 178-181 (1993).
4. Wüthrich, K. *NMR of Proteins and Nucleic Acids* Wiley-Interscience, New York, (1986).
5. Kawano, K., Yoneya, T., Miyata, T., Yoshikawa, K., Tokunaga, F., Terada, Y. and Iwanaga, S. *J. Biol. Chem*. **265**, 15365-15367 (1990).
6. Tamamura, H., Kuroda, M., Masuda, M., Otaka, A., Funakoshi, S., Nakashima, H., Yamamoto, N., Waki, M., Matsumoto, A., Lancelin, J.M., Kohda, D., Tate, S., Inagaki, F. and Fujii, N. *Biochim. Biophys. Acta* **1163**, 209-216 (1993).

Peptide Revolution: Genomics, Proteomics & Therapeutics
Michael Chorev & Tomi K. Sawyer (Editors)
American Peptide Society, 2003

From Innate Immunity to *De Novo* Designed Antimicrobial and Anticancer Diastereomeric Peptides

Yechiel Shai

Department of Biological Chemistry Weizmann Institute of Science, Rehovot, 76100 Israel

Introduction

Water-membrane soluble protein and peptide toxins are used in the defense and offense systems of all organisms including plants and humans. A major group includes gene-encoded antimicrobial peptides, which serve as part of the innate immunity that complements the highly specific cell-mediated immune response [1-3]. In higher organisms they are mainly produced on epithelial surfaces and in phagocytic cells. The increasing resistance of bacteria to conventional antibiotics stimulated the isolation and characterization of many antimicrobial peptides for potential use as new target antibiotics. Strains of bacteria already exist that are resistant to all available drugs [4]. The finding of thousands of antimicrobial peptides with variable lengths and sequences, all of which are active *in vitro* at micromolar concentrations, which is their biological concentration at the sites of infection, suggests a general mechanism, as well as a common target which was found to be the bacterial membrane [5,6]. Interestingly, peptides that share similar structures either selectively kill bacteria or are non-selective and kill both bacteria and mammalian cells [7].

Results and Discussion

How do antimicrobial peptides recognize their target cell? In contrast to conventional antibiotics, most antimicrobial peptides disrupt and permeate the target cell membrane and inflict damage hard to fix, making it hard for the bacteria to become resistant [7,8]. Compared to normal mammalian cells in which the outer leaflet is composed predominantly of zwitterionic phosphatydilcholine (PC) and sphingomyelin phospholipids, the bacterial membrane (predominantly PE/PG) as well as their outer surface (lipopolysacharides, and techoic acid) are negatively charged. Since antimicrobial peptides are positively charged, they bind preferentially to the negatively charged surface of bacteria [9-11]. Many studies revealed a correlation between the capacity of antimicrobial peptides to bind and permeate phospholipid membranes with different composition and their biological function.

How do antimicrobial peptides permeate the phospholipid membrane? In order to interact and insert into the target membrane, antimicrobial peptides must undergo substantial conformational changes. In water, their overall structure needs to be hydrophilic. However, upon interaction with membranes they must expose a hydrophobic region to the lipidic constituent of the membrane. Two general mechanisms have been proposed: The barrel-stave and the carpet mechanisms (Figure 1).

Pore Formation via the Barrel Stave Mechanism: In early studies, most of the antimicrobial peptides found had an amphipathic helical structure suggesting that they form transmembrane pores, presumably via a "barrel-stave" mechanism (Figure 1 Panel A') [12], mainly because they induced single channels in planar lipid membranes. Peptides that act via the barrel-stave mechanism must fulfill several criteria: (i) Their interaction with the membrane should be triggered mainly by hydrophobic interactions. (ii) They need to self-associate in the membrane. (iii) A minimal length of ~22 amino acids is required to transverse the lipid bilayers with α-helical peptides, or ~8 amino acids if the peptide adopts a β-sheeted structure. (iv) Only

a few of transmembrane pores are required to dissipate the transmembrane potential in cells. We found that these criteria hold only for non-cell selective lytic peptide [13-19].

Membrane permeation via the Carpet Mechanism: Based on many studies with antimicrobial peptides we have proposed an alternative mechanism we termed the "carpet" or a detergent-like mechanism [20,21]. The steps involved in the carpet mechanism are described in the legend to Figure 1. According to the carpet mechanism peptides are in contact with the phospholipid head group throughout the entire process of membrane permeation. Based on the above, the major advantage of the carpet mechanism is that many peptides can fulfill its criteria, which indeed explains why thousands of peptides can kill bacteria regardless of their length, sequence and the specific amino acids that compose them. The carpet mechanism has been used to describe the mode of action of many other antimicrobial peptides (reviewed in [7,10]).

Studies on the morphology of bacteria after treatment with antimicrobial peptides demonstrate the breakdown of the bacterial membrane as proposed by the carpet model (Figure 1 A-C) [22-24].

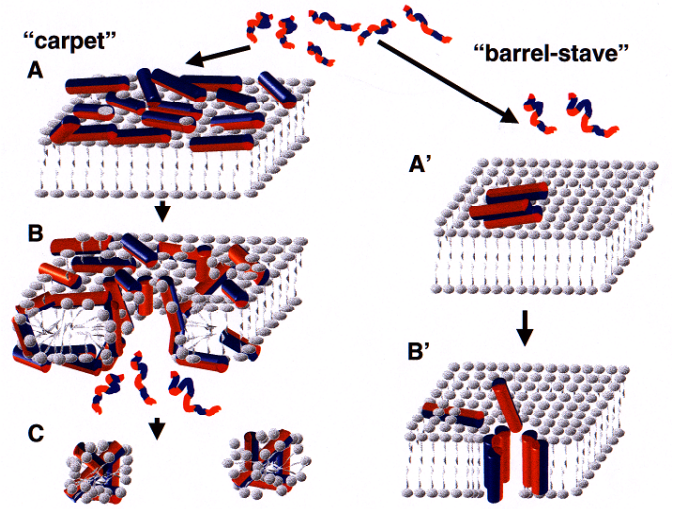

Fig. 1. A cartoon illustrating the barrel-stave (to the right) and the carpet (to the left) models. In the carpet model the peptides are bound to the surface of the membrane with their hydrophobic surfaces facing the membrane and their hydrophilic surfaces facing the solvent (step A). When a threshold concentration of peptide monomers is reached, the membrane is permeated and transient pores can be formed (step B), a process that can also lead to membrane disintegration (step C). In the barrel-stave model peptides first assemble on the surface of the membrane (step A'), then insert into the lipid core of the membrane following recruitment of additional monomers (step B').

Transformation from a barrel stave to a carpet mechanism is accompanied by cell selective activity. Several studies supported the carpet mechanisms as the mode of action of non-hemolytic antimicrobial peptides. These include: (i) Incorporation of D-amino acids within α-helical pore forming peptides, such as pardaxin and melittin, which act via the barrel-stave mechanism, abolished their lytic effect towards mammalian cells but preserved antimicrobial activity. This was concomitant with a change in their mode of action to a carpet mechanism [22,23]. (ii) Short diastereomeric peptides composed of only lysine (as a source of positive charges) and leucine (as a source of hydrophobic amino acids) were shown to possess potent antibacterial activity

but not hemolytic acitivity [24]. (iii) Cyclization of linear amphipathic α-helical peptides preserved their potency to permeate membranes [25,26]. (iv) Drastic sequence alteration of diastereomers of amphipathic α-helical peptides preserved their ability to permeate membranes and to kill bacteria [27]. Overall, it seems that whenever there is an appropriate balance between hydrophobicity and a net positive charge the peptides are active on bacteria. However, activity also depends on other parameters, such as the volume of the molecule, its aggregation state in solution and membrane, and its ability to coassemble in the membrane-bound state. The carpet model was successful because it allowed developing a novel family of diastereomeric antibacterial peptides. The unique properties of this family, such as controlled enzymatic degradation, stability in serum and in whole blood, and the drastic changes that can be done to their sequences, make them promising candidates for the treatment of infectious diseases. Indeed recent studies in our laboratory demonstrated their effectiveness to combat bacterial infection following intravenous administration (unpublished results).

Table 1 shows for example the sequences of a series of diastereomeric peptides with a different ratio between Lys and Leu, and their antimicrobial and hemolytic activity (at 50 μM). In contrast to the non-hemolytic activity of the diastereomers shown in Table 1, the all L-amino acid parental peptides of the diastereomers listed in the first three rows are 100% hemolytic at 50 μM. Furthermore, whereas all L-amino acid peptides lost their activity in serum, the diastereomers remained fully active.

Anticancer activity of diastereomeric antimicrobial peptides. The high toxicity of most chemotherapeutic drugs and their inactivation by multidrug resistance phenotypes, has led to an extensive search for drugs with new modes of action. Antimicrobial peptides are promising candidates. Cancer cell membranes maintain higher transmembrane potentials and have a higher content of anionic phospholipids on their outer leaflet compared to normal cells. Many antimicrobial peptides therefore preferentially disrupt prokaryotic and cancer cell membranes rather than eukaryotic membranes [28]. A few studies demonstrated the potential of antimicrobial peptides to efficiently lyse cancer cells [29,30]. However, direct intravenous administration was not reported due to the limitation of the use of all L-amino acid lytic peptides. We designed short cationic diastereomeric peptides composed of D and L leucines, lysines, and arginines that have selective toxicity toward cancer cells (see for example Table 2) [31,32]. One of these peptides, with the sequence KL**L**RLL**KK**L**L**RL**L**LK ($K_4R_2L_9$) (bold and underlined amino acids are the D enatiomers) significantly inhibited lung metastasis formation in mice (86%) with no detectable side effects (Figure 2). The

Table 1. Antibacterial activity of diastereomeric antimicrobial peptides with different ratio between K and L.

Peptide sequence and designation	Minimum Inhibitory Concentration (MIC) (μM)[a]				Hemolysis at 50 μM (%)
	E. Coli D21	*A. Calcoacetcus AC11*	*P. Aeruginosa ATCC-27853*	*B. Subtiis ATCC6051*	
K_3L_9-KLLLLKLLLK	9	20	125	1	30
K_4L_8-KLLLKLLLKLLK	3.5	4	10	0.5	2
K_5L_7-KLLLKLKLKLLK	7	20	10	2	0
K_5L_7-KKLLKLKLKLKK	80	200	>200	100	0
Dermaseptin (36 aa)	6	3	25	4	0

[a]*MIC is the minimum peptide conc. where bacterial growth was not observed at 18h.*

ability of $K_4R_2L_9$ to depolarize the transmembrane potential of cancer cells at the same rate (within minutes) and concentration (3 μM), at which it shows biological activity, suggests a killing mechanism that involves plasma membrane perturbation. Confocal microscopy experiments verified that the cells died as a result of acute injury, swelling and bursting, suggesting necrosis. The simple sequence of the peptide, its high solubility, substantial resistance to degradation and inactivation by serum components might make it a good candidate for future anticancer treatment.

Table 2. Anticancer activity (IC_{50} in μM) of a diastereomeric antimicrobial peptide with cancer and non cancer NIH-3T# cells.

Compound	Breast MCF-7	*Colon* HT-29	*Lung* A-549	*Melanoma* SK-MEL-5	*Prostate* PCL-3	*NIH-3T3*
$K_4R_2L_9$	3.3	2.2	1.4	1.2	1.6	30
5-fluorouracil	13	40	87	85	51	ND

ND – Not determined.

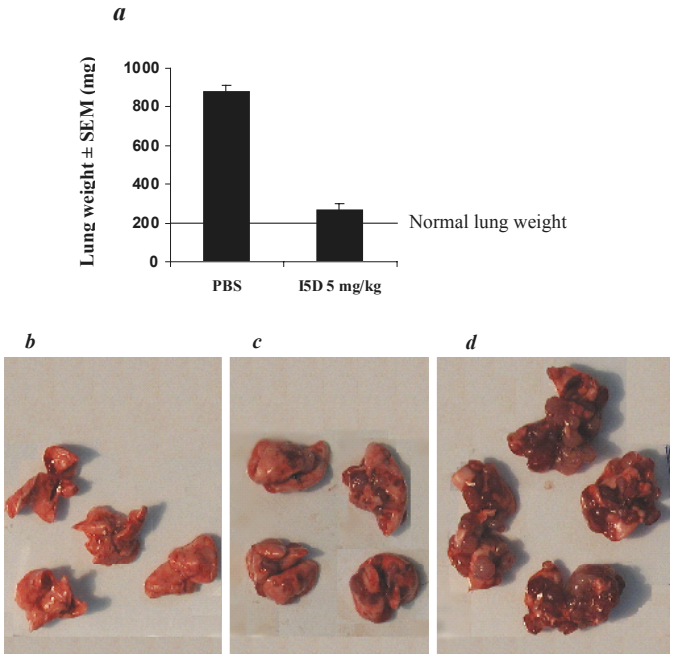

Fig. 2. Reduction in lung metastatic load in C57BL/6 mice treated with $K_4R_2L_9$. **a,** *The lung weight of D122 lung tumor-bearing mice treated with the peptide or vehicle control.* P<*0.005,* t-*test. The horizontal line indicates the average level of normal lung weight (178 mg).* **b,** *Lungs of normal mice.* **c-d,** *Lungs of mice injected with D122 lung tumor and treated with the peptide (panel* **c***) or vehicle control (panel* **d***).*

References

1. Boman, H. G., Faye, I., Gudmundsson, G. H., Lee, J. Y. and Lidholm, D. A. *Eur. J. Biochem.* **201**, 23-31 (1991).
2. Hoffmann, J. A., Kafatos, F. C., Janeway, C. A. and Ezekowitz, R. A. *Science* **284**, 1313-1318 (1999).
3. Zasloff, M. *Nature* **415**, 389-395 (2002).
4. Wong, A. H., Wenzel, R. P. and Edmond, M. B. *Am. J. Infect. Control* **28**, 277-281 (2000).
5. Matsuzaki, K. *Biochim. Biophys. Acta* **1462**, 1-10 (1999).
6. Shai, Y. *Biochim. Biophys. Acta* **1462**, 55-70 (1999).
7. Shai, Y. *Biopolymers* **66**, 236-248 (2002).
8. Hancock, R. E. and Diamond, G. *Trends Microbiol.* **8**, 402-410 (2000).
9. Matsuzaki, K. *Biochim. Biophys. Acta* **1376**, 391-400 (1998).
10. Oren, Z. and Shai, Y. (1998) *Biopolymers* **47**, 451-463 (1998).
11. Tossi, A., Sandri, L. and Giangaspero, A. *Biopolymers* **55**, 4-30 (2000).
12. Christensen, B., Fink, J., Merrifield, R. B. and Mauzerall, D. *Proc. Natl. Acad. Sci. U.S.A.* **85**, 5072-5076 (1988).
13. Shai, Y., Bach, D. and Yanovsky, A. *J. Biol. Chem.* **265**, 20202-20209 (1990).
14. Rapaport, D. and Shai, Y. *J. Biol. Chem.* **266**, 23769-23775 (1991).
15. Rapaport, D. and Shai, Y. *J. Biol. Chem.* **267**, 6502-6509 (1992).
16. Strahilevitz, J., Mor, A., Nicolas, P. and Shai, Y. *Biochemistry* **33**, 10951-10960 (1994).
17. Shai, Y. *Toxicology* **87**, 109-129 (1994).
18. Gazit, E., Bach, D., Kerr, I. D., Sansom, M. S., Chejanovsky, N. and Shai, Y. *Biochem. J.* **304** (Pt 3), 895-902 (1994).
19. Shai, Y. and Oren, Z. *Peptides* **22**, 1629-1641 (2001).
20. Pouny, Y., Rapaport, D., Mor, A., Nicolas, P. and Shai, Y. *Biochemistry* **31**, 12416-12423 (1992).
21. Gazit, E., Boman, A., Boman, H. G. and Shai, Y. *Biochemistry* **34**, 11479-11488 (1995).
22. Shai, Y. and Oren, Z. *J. Biol. Chem.* **271**, 7305-7308 (1996).
23. Oren, Z. and Shai, Y. *Biochemistry* **36**, 1826-1835 (1996).
24. Oren, Z., Hong, J. and Shai, Y. *J. Biol. Chem.* **272**, 14643-14649 (1997).
25. Oren, Z. and Shai, Y. *Biochemistry* **39**, 6103-6114 (2000).
26. Unger, T., Oren, Z. and Shai, Y. *Biochemistry* **40**, 6388-6397 (2001).
27. Papo, N., Oren, Z., Pag, U., Sahl, H. G. and Shai, Y. *J. Biol. Chem.* **277**, 33913-33921 (2002).
28. Chan, S. C., Hui, L. and Chen, H. M. *Anticancer Res.* **18**, 4467-4474 (1998).
29. Baker, M. A., Maloy, W. L., Zasloff, M. and Jacob, L. S. *Cancer Res.* **53**, 3052-3057 (1993).
30. Ellerby, H. M., Arap, W., Ellerby, L. M., Kain, R., Andrusiak, R., Rio, G. D., Krajewski, S., Lombardo, C. R., Rao, R., Ruoslahti, E., Bredesen, D. E. and Pasqualini, R. *Nat. Med.* **5**, 1032-1038 (1999).
31. Papo, N., Shahar, M., Eisenbach, L. and Shai, Y. *J. Biol. Chem.* **278**, 21018-21023 (2003).
32. Papo, N. and Shai, Y. *Biochemistry **42,** 9346-9354* (2003).

Peptide Revolution: Genomics, Proteomics & Therapeutics
Michael Chorev & Tomi K. Sawyer (Editors)
American Peptide Society, 2003

Putative Intracellular Targets of the PR-rich Antimicrobial Peptide Bac7

Elena Podda[1], Marco Scocchi[1], Giuseppina Mignogna[2], Donatella Barra[2], Fulvio Micali[1], Andrea Mazzoli[1] and Renato Gennaro[1]

[1]Department of Biochemistry, University of Trieste, Trieste, I-34127, Italy;
[2]Department of Biomedical Sciences, La Sapienza University, Roma, I-00185, Italy

Introduction

Cationic antimicrobial peptides (AMPs) are ubiquitous in nature and are among the key players in host defense against infection. They show significant diversity in sequence and structure, and can be divided into two groups. Members of the first group represent the vast majority of AMPs and act by permeabilizing bacterial membranes, those of the second group appear to inactivate bacteria without significant membrane permeabilization probably by binding to putative intracellular targets. The Pro- and Arg-rich peptides from mammals are members of the second group. They are derived from precursors belonging to the cathelicidin family and have linear structures characterized by the presence of tandem repeats. Among the PR-rich peptides identified in leukocytes, the 60-residue Bac7 has a modular structure comprising an Arg clustered region at the N-terminus, followed by three identical tandem repeats of a tetradecamer [1]. In contrast with membrane active peptides, for which no significant effect of chirality was observed, all-D enantiomers of the PR-rich peptides were poorly active or inactive [1,2]. A mechanism of action based on the interaction with stereospecific intracellular targets is a possible explanation of this behavior [2]. Following this observation, the present study was aimed at identifying peptides derived from Bac7 that will act as putative bacterial ligands and their localization in the bacterial cells. Thus, the 1-35 N-terminal fragment of Bac7, whose activity is comparable to that of the parent peptide, and its enantiomer all-D Bac7(1-35), which shows a remarkably lower antimicrobial activity [3], were studied.

Bac7 <u>RRIRPRPPRLPRPRPRPLPFPRPGPRPIPRPLPFP</u>RPGPRPIPRPLPFP
RPGPRPIPRPL

Scheme1. Amino acid sequence of Bac7. Its N-terminal fragment Bac7(1-35) is underlined.

Results and Discussion

In order to identify Bac7-intracellular molecular targets, a Cys residue was added to the C-terminus of the fully active Bac7(1-35) fragment (Scheme 1) to allow its immobilization to a specific support and obtain an affinity matrix. An *E. coli* ML-35 lysate, obtained by sonication of the bacterial cells, was then loaded to the above matrix. After extensive washing of the column, proteins were eluted at low pH, and analyzed by SDS-PAGE. When the lysate was loaded in a low ionic strength buffer, a large number of proteins were retained by the affinity matrix. To identify the proteins that bound with high affinity, the lysate was added to the column in a buffer containing 1 M NaCl and 0.1% TritonX-100. Under these conditions, the number of retained proteins decreased and six major bands and a few minor bands were identified by SDS-PAGE. This interaction has been considered specific, as the same proteins were not retained by a matrix prepared with the all-D Bac7(1-35) fragment. The six major proteins have been purified by SDS-PAGE and analyzed by N-terminal sequencing and/or

Table 1. Proteins from E. coli lysate retained by all-L Bac7(1-35) affinity matrix.

Apparent MW (SDS-PAGE)	Protein MW (Da) / pI	Protein identified
100 k	116,351 / 5.28	*β-Galactosidase*
70 k	68,983 / 4.83	*Chaperone protein DnaK*
52 k	51,772 / 5.26	*Glutamine synthetase*
40 k	38,712 / 4.81	*Glycerol dehydrogenase*
38 k	36,150 / 6.87	*Transcription activator CysB*
18 k	19,424 / 4.77	*Ferritin 1*

mass spectrometry. Comparing the isolated sequences with the completed *E. coli* genome database identified the proteins reported in Table 1. It remains to determine whether Bac7(1-35) is able to inhibit the biological activity of any of these proteins and if this possible inhibition plays a determinant role for the antimicrobial activity of Bac7. In addition, the localization of the Bac7(1-35) fragment in the bacterial cells was investigated using immunogold labeling electron microscopy. *E. coli* ML-35 cells were exposed to 10 μM concentration of the peptide for 30 min, prepared by standard methods to obtain thin sections, and then treated with affinity-purified polyclonal anti-Bac7 antibodies and a secondary gold-conjugated antibody. The peptide was found mainly localized into the cytoplasm of the cells and only marginally associated to the membranes that maintained a normal morphology. It appeared irregularly distributed in the cytoplasm with areas of high concentration, possibly corresponding to cellular structures (Figure 1). This suggests that Bac7 penetrates the bacterial membrane without major perturbation, as already observed for mammalian cells [4,5]. It is anticipated that these studies will allow the identification and validation of novel bacterial targets for the design of effective antibiotics.

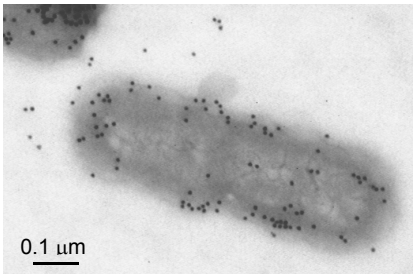

Fig. 1. Localization of Bac7(1-35) in E. coli ML-35 by immunoelectron microscopy.

References

1. Gennaro, R., Zanetti, M., Benincasa, M., Podda, E., Miani, M. *Curr. Pharm. Des.* **8**, 763-778 (2002).
2. Cudic, M. and Otvos, L. Jr. *Curr. Drug Targets* **3**, 101-106 (2002).
3. Podda, E., et al. In Benedetti, E. and Pedone, C. (Eds.) *PEPTIDES 2002, Proceedings of the 27th Eur. Peptide Symp.* Edizioni Ziino, Napoli, Italy, 2000, 586-587.
4. Tomasinsig, L., et al. In Benedetti, E. and Pedone, C. (Eds.) *PEPTIDES 2002, Proceedings of the 27th Eur. Peptide Symp.* Edizioni Ziino, Napoli, Italy, 2000, 910-911.
5. Sadler, K., Eom, K. D., Yang, J.L., Dimitrova, Y., Tam, J.P. *Biochemistry* **41,** 14150-14157 (2002).

Peptide Revolution: Genomics, Proteomics & Therapeutics
Michael Chorev & Tomi K. Sawyer (Editors)
American Peptide Society, 2003

Pyrularia pubera Thionin: A Single Residue Mutation Enhances Antimicrobial Activity

Miquel Vila-Perelló[1], Andrea Sánchez-Vallet[2], Antonio Molina[2] and David Andreu[1]

[1]Department of Experimental and Health Sciences, Pompeu Fabra University, 08003 Barcelona, Spain; [2]Department of Biotechnology, ETSIA, Polytechnic University of Madrid, 28040 Madrid, Spain

Introduction

Antimicrobial peptides are considered one of the most ancient evolutionary weapons developed by almost all organisms to fight microbial infections [1]. Thionins are the first family of cystein-rich plant peptides for which antimicrobial activity was demonstrated *in vitro* and a defensive role was postulated [2]. Despite sequence differences, thionins share essentially the same 3D structure, mainly consisting in two antiparallel α-helices and a β-sheet stabilized by three or four disulfide bonds. Thionins are highly basic, with an amphipathic distribution of their polar and non-polar residues, which is related to their ability to disrupt microbial membranes. *Pyrularia pubera* thionin is remarkable for the presence of a unique Asp at position 32, instead of the consensus Arg found in almost other thionins with the same disulfide pattern. In order to evaluate the effect of the Asp^{32} and the ensuing loss of cationic character on the activity of this peptide, we synthesized both the native sequence and its Arg (D32R) analogue. The disulfide pattern of almost all thionins (Figure 1) has been established by homology from X-ray structures of other plant defensins due to the inability to characterize their Cys connectivities by the classical means of proteolysis and MS analysis. We report here how the disulfide pattern of PpTH can be assigned by the novel method of partial reduction and cyanylation [3].

Fig. 1. Amino acid sequence alignment (A) and disulfide pattern (B) of thionins, types I and II.

Results and Discussion

We have efficiently synthesized both PpTH and its D32R analogue by Fmoc/tBu solid phase protocols using Trt as the protecting group for all the eight Cys residues. Peptides were cleaved from the resin, deprotected by TFA acidolysis (cocktail K) and purified by RP-HPLC. The octathiols thus obtained were submitted to oxidative folding under optimized conditions (high dilution, Ar atmosphere, in the presence of denaturants and thiol/disulfide reshuffling agents). This methodology has been proven to be suitable for the synthesis of large multiple disulfide-containing peptides and

allowed us to isolate the folded peptides in a combined (folding/purification) yield of 40% and 33% (Pp-TH and D32R, respectively) [4].

CD spectra in aqueous solution of both PpTH and PpTH(D32R) are consistent with a mainly α-helical conformation. Furthermore thermal denaturating experiments showed the helical pattern to be fully preserved between 5 and 80ºC, and only slight variations were observed in pH titration experiments, thus demonstrating a very compact folding for these thionins.

We have achieved disulfide bond characterization by the methodology of partial reduction and cyanylation. PpTH was partially reduced under optimized conditions (TCEP, pH 3) such that the major products obtained were isoforms where only a single disulfide had been reduced, and the nascent sulfhydryl groups were *in situ* cyanylated with 1-cyano-(4-dimethylamino)pyridinium. Singly reduced and cyanylated peptides were separated by RP-HPLC, cleaved with aqueous ammonia (pH 12) and completely reduced. When the resulting peptide mixture was analyzed by MALDI-TOF MS, the fragments resulting from alkaline hydrolysis were directly relatable to the location of the Cys residues originally paired before partial reduction, thus allowing to establish the connectivity of the four disulfides: a Cys^{3}-Cys^{43}, Cys^{4}-Cys^{33}, Cys^{12}-Cys^{31}, Cys^{16}-Cys^{27} pattern was found. Identical results were obtained for both natural and synthetic PpTH, thus confirming their identity and demonstrating the feasibility of this method for disulfide bond determination in thionins.

Interestingly, in the D32R analogue the Asp-by-Arg replacement has a much lower impact on the 3D structure (27% loss in helicity at 207 nm) than on the antimicrobial activity against Gram-negative bacteria (Table 1). This effect can be reasonably explained by the increased cationicity of the Arg-containing peptide, cationic character being well known to improve the activity of antimicrobial peptides. Overall, the findings suggest that even compact and complex structures such as thionins are susceptible to improvement of their activity by simply structural modifications.

Table 1. EC_{50} (μM) against Gram positive (C. michiganensis), Gram negative (R. meliloti and X. campestris) and fungi (P. cucumerina). N.A. not active at concentration<19μM.

	Pp-TH(natural)	Pp-TH(synthetic)	Pp-TH(D32R)
C. michiganensis	0.48	0.48	0.39
R. meliloti	N.A.	N.A.	3.3
X. campestris	3.1	2.9	1.1
P. cucumerina	0.7	0.8	1.2

References

1. Zasloff, M. *Nature* **415**, 389-395 (2002).
2. García-Olmedo, F., Molina, A., Alamillo, J. M. and Rodríguez-Palenzuela, P. *Pept. Sci.* **47**, 479-491 (1998).
3. Qi, J., Wu, J., Somkuti, G.A. and Watson, J. T., *Biochemistry* **40,** 4531-4539 (2001).
4. Vila-Perelló, M., Sánchez-Vallet, A., García-Olmedo, F., Molina, A., and Andreu, D. *FEBS Lett.* **536**, 215-219 (2003).

Peptide Revolution: Genomics, Proteomics & Therapeutics
Michael Chorev & Tomi K. Sawyer (Editors)
American Peptide Society, 2003

Development of Orally Active Antibacterial Peptide Derivatives that Kill Resistant Urinary and Respiratory Tract Pathogens

Laszlo Otvos, Jr.[1,3], Daniel J. Weiner[2], David E. Johnson[4] and Mare Cudic[1,3]

[1]The Wistar Institute and [2]Institute for Human Gene Therapy, The University of Pennsylvania, 3601 Spruce Street, Philadelphia, PA 19104, USA; [3]Chaperone Technologies, 801 Mockingbird Lane, Audubon, PA 19403, USA; [4]University of Maryland School of Medicine, 10 North Greene Street, Baltimore MD 21201, USA

Introduction

The incidence of serious bacterial and fungal infection is increasing despite remarkable advances in antibiotic chemotherapy. High levels of antibacterial resistance have been found in wild rodents that probably have never been exposed to antibiotics, suggesting that more careful use of conventional antibiotics may not be enough to reduce antibiotic resistance [1]. It is not an overstatement to claim that one of the most serious and urgent topics of the health-care industry today is the rapid development of antibacterial compounds that kill bacteria in a manner completely different from those utilized by the currently marketed antimicrobial compounds. No new type of antimicrobial drug was approved for human therapy in the last 20 years [2]. Thus, the search is on for a novel type of agent that acts on a new target, which has not yet experienced selective pressure in the clinical setting [3]. Such a target should be essential to the growth and survival of bacteria, and sufficiently different from similar macromolecules in the human host. Derivatives of native proline-rich antibacterial peptides exhibit these required features.

We have earlier reported that pyrrhocoricin, a peptide originally isolated from the European sap-sucking bug *Pyrrhocoris apterus*, is non-toxic to eukaryotic cells and healthy mice, has good *in vitro* activity against model bacterial strains and when administered intravenously *in vivo*, can protect mice from systemic *Escherichia coli* challenge [4]. Although pyrrhocoricin is toxic to infected animals at a high dose (50 mg/kg), pyrrhocoricin derivatives in which the peptide is protected from exopeptidase cleavage lack this high dose toxicity and show improved protease resistance while maintaining the *in vitro* and *in vivo* efficacies. Native pyrrhocoricin, similar to drosocin and apidaecin, other medium-sized proline-rich antibacterial peptides from insects, kills the sensitive species by binding to the 70 kDa bacterial heat shock protein DnaK at the D-E helix region [5], preventing the frequent movements of the multihelical lid over the conventional peptide-binding pocket and thereby inhibiting chaperone-assisted protein folding [5]. Remarkably, pyrrhocoricin does not bind to either the full-sized human equivalent protein Hsp70 or the analogous D-E helix fragments of human Hsp70.1 or mouse Hsp70.2, indicating the potential of this peptide as a drug lead to treat human or animal infections [6].

Results and Discussion

Earlier studies with lactoferricin, another cationic antimicrobial peptide, give suggestions for the optimal therapeutic application of the pyrrhocoricin-based peptide family. Lactoferricin is shown to be active in a mouse urinary tract infection (UTI) model when administered orally [7]. In general, UTI are always prime targets for antimicrobial peptides because cationic antimicrobial peptides are cleared through the kidney [8], and therefore the drug is concentrated at the desired site of action. The

other promising therapeutic area where a peptide-based drug can be of significant use is the treatment of respiratory tract infections (RTI). Bovine lactoferricin given intravenously to mice 24 hr before intravenous infection with *E. coli* reduces the lethality caused by the bacteria mostly in the kidneys and lungs [9].

First we studied the efficacy of pyrrhocoricin, and its two designed dimer derivatives (Table 1) against clinical RTI pathogens *in vitro* (Table 2). The designed dimers, especially the Pip-pyrr-MeArg analog, containing an additional N-terminal positive charge known to improve efficacy against *Pseudomonas aeruginosa* [10], showed remarkable activity when the growth medium was adjusted to suit peptide antibiotics. Especially noteworthy is the efficacy against *P. aeruginosa* 2192, a strain isolated from a cystic fibrosis patient. These encouraging *in vitro* results prompted the study of the efficacy of the dimeric peptides *in vivo*. Mice were infected intranasally with *H. influenzae* H233 and the Chex-pyrr-MeArg dimer was added after 4 hr at a single 20 mg/kg dose via the same intranasal route. After removing and homogenizing the lungs, the bronchoalveolar lavage (BAL) and the lung were analyzed for viable bacteria. After peptide addition, the viable bacterial count was reduced by 11% and 57% in the lung and in the BAL, respectively [11].

Table 1. Pyrrhocoricin derivatives used in the current study.

Pyrrhocoricin: H-Val-Asp-Lys-Gly-Ser-Tyr-Leu-Pro-Arg-Pro-Thr-Pro-Pro-Arg-Pro-Ile-Tyr-Asn-Arg-Asn-NH_2

Chex-pyrr-MeArg dimer: (H-Chex-Asp-Lys-Gly-Ser-Tyr-Leu-Pro-Arg-Pro-Thr-Pro-Pro-Arg-Pro-Ile-Tyr-Asn-MeArg-Asn)$_2$-Dab-NH_2

Pip-pyrr-MeArg dimer: (H-Pip-Asp-Lys-Gly-Ser-Tyr-Leu-Pro-Arg-Pro-Thr-Pro-Pro-Arg-Pro-Ile-Tyr-Asn-MeArg-Asn)$_2$-Dab-NH_2

Table 2. In vitro efficacy of antimicrobial peptides against clinical respiratory tract pathogens. Amoxicillin is used as a control conventional antibiotic.

Strain	IC_{50} in μM			
	Chex-pyrr-MeArg dimer	Pip-pyrr-MeArg dimer	Pyrrhocoricin	Amoxicillin
P. aeruginosa 10	resistant	10	resistant	resistant
P. aeruginosa 2192	2	1	resistant	resistant
H. influenzae H233	14	14	1	<0.1
H. influenzae H338	10	10	5	0.2
H. influenzae 119	1	3	0.3	0.5
M. catarrhalis BC1	10	10	resistant	<0.1
K. pneumoniae K1	7	5	10	resistant

From the UTI strains, the Pip-pyrr-MeArg dimer killed all eight clinical *E. coli* and three *Klebsiella pneumoniae* strains we studied in the sub-low micromolar concentration range. Almost all control antibiotics, including the currently leading trimethoprim-sulfametoxazole combination for UTI in the clinics, remained without activity against two or more of these bacterial strains. In a mouse ascending UTI

model with the human pyelopnehritis-originated *E. coli* CFT073 as pathogen, two doses of intravenous, subcutaneous or oral treatment with the Pip-pyrr-MeArg derivative reduced the bacterial counts in the kidneys, bladder and urine to varying levels. Statistically significant elimination or reduction of bacteria compared to untreated animals was observed at dual intravenous or subcutaneous doses of 0.4 or 3 mg/kg, respectively [12]. Less successful was the oral therapy, although the mean bacterial counts of the positive tissues after treatment with 3 mg/kg peptide were reduced from 4.6×10^5 to 9×10^4 cfu/ml in the urine, from 3.7×10^5 to 5.6×10^4 cfu/gram in the bladder and from 2.4×10^5 to 7.2×10^4 cfu/gram in the kidneys. Serial passage of the same *E. coli* strain in the presence of sublethal doses of the designed peptide failed to generate resistant mutants. In addition, the dimer was non-toxic to the kidney-originated COS-7 cells up to the highest 500 μM concentration studied. These data warrant further preclinical development of the Pip-pyrr-MeArg dimer in UTI in hospital and nursing home settings where the resistance rate to current antibiotics, including fluoroquinolones, is the highest and continuously rising.

Acknowledgments
The authors acknowledge the financial support from the Commonwealth Universal Research Enhancement Program, Pennsylvania Department of Health. This work was supported by NIH grants AI055174 and DK64477.

References
1. Gilliver, M. A., Bennett, M., Begon, M., Hazel, S. M. and Hart, C. A. *Nature* **401**, 233-234 (1999).
2. Tan, Y.-T., Tillett, D. J. and McKay, I. A. *Mol. Med. Today* **6**, 309-314 (2000).
3. Goldman, R. C. and Gange, D. *Curr. Med. Chem*. **7**, 801-820 (2000).
4. Otvos, L., Jr., Bokonyi, K., Varga, I., Otvos, B. I., Hoffmann, R., Ertl, H. C. J., Wade, J. D., McManus, A. M., Craik, D. J. and Bulet, P. *Protein Sci*. **9**, 742-749 (2000).
5. Kragol, G., Lovas, S., Varadi, G., Condie, B. A., Hoffmann, R. and Otvos, L. Jr. *Biochemistry* **40**, 3016-3026 (2001).
6. Kragol, G., Hoffmann, R., Chattergoon, M. A., Lovas, S., Cudic, M., Bulet, P., Condie, B. A., Rosengren, K. J., Montaner, L. J. and Otvos, L., Jr. *Eur. J. Biochem.* **269**, 4226-4237 (2002).
7. Haversen, L. A., Engberg, I., Baltzer, L., Dolphin, G., Hanson, L. A. and Mattsby-Baltzer, I. *Infect. Immun*. **68**, 5816-5823 (2000).
8. Lupetti, A., Welling, M. M., Pauwels, E. K. J. and Nibbering, P. H. *Lancet. Infect. Dis.* **3**, 233-239 (2003).
9. Zagulski, T., Lipinski, P., Zagulska, A. and Jarzabek, Z. *Int. J. Exp. Pathol*. **79**, 117-123 (1998).
10. Bencivengo, A.-M., Cudic, M., Hoffmann, R. and Otvos, L., Jr. *Lett. Pept. Sci*. **8**, 201-209 (2001).
11. Cudic, M., Condie, B. A., Weiner, D. J., Lysenko, E. S., Xiang, Z. Q., O, I., Bulet, P. and Otvos, L., Jr. *Peptides* **23**, 271-283 (2002).
12. Cudic, M., Lockatell, C. V., Johnson, D. E. and Otvos, L., Jr. *Peptides* **24,** 807-820 (2003).

Peptide Revolution: Genomics, Proteomics & Therapeutics
Michael Chorev & Tomi K. Sawyer (Editors)
American Peptide Society, 2003

Super Adhesive Peptides and Bacterial Adhesion

Yanlei Liu[1], Kit S. Lam[2], Xiaobing Wang[2], Ruiwu Liu[2], Frank Ventimiglia[3] and Joseph W. Leung[1, 4]

[1]C.W. Law Biofilm Laboratory and [4]Divisions of Gastroenterology and [2] Hematology & Oncology; University of California, Davis Medical Center, CA 95817, USA; [3]Department of Anatomy, Physiology and Cell Biology; University of California Davis, CA 95616, USA; [4]Section of Gastroenterology, VA Northern California Health Care System, CA 95655, USA

Introduction

The research of bacterial adhesion and its significance involves a large field covering different aspects of nature and human life, such as marine science, soil and plant ecology, food industry, and most importantly, the biomedical field [1]. The exact mechanisms by which bacteria adhere to animate or inert surfaces still remain unclear. Attachment may be mediated by nonspecific physical or specific ligand-receptor interaction. Several mechanisms may be involved in microbial attachment including electrostatic interaction [2], hydrophobic interaction [3], covalent bonding [4] or partial covalent bond formation between the microorganism and hydroxyl groups on the surface. The strength of the attachment and the binding force changes with different environment and varies between different microbial species, as well as the surface or fluid properties. The goal of this research is to apply the "one-bead-one-compound" (OBOC) combinatorial library method [5] to identify peptide ligands involved in early bacterial attachment and adhesion using the high-throughput screening approach.

Results and Discussion

Method: A random penta-peptide library composed of D-amino acids was first synthesized on TentaGel resins using the OBOC combinatorial library approach. 150,000 peptide beads were then incubated with 10^8 *E.coli* stained with fluorescent dye at 37°C for 30 min. Bacterial attachment was observed as an adherent layer on the bead surface under fluorescent microscopy. Positive beads were harvested and the peptide sequences were identified by automatic micro-sequencer. Peptides with consensus sequences from the positive beads were re-synthesized in large quantities. Bacterial attachment to the selected peptides was tested using clinical strains of *E.coli, Klebsiella oxytoca, Pseudomonas aeruginosa, Citrobacter, Staphylococcus epidermis, Streptococcus sp., Bacillus sp.* and *Enterococcus faecalis,* to evaluate the binding

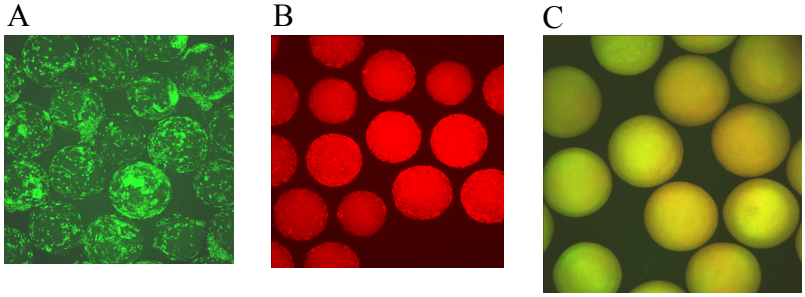

Fig. 1. CSLM image of E.coli (A) and E. faecalis (B) attachment on peptide beads, and anti-bacterial attachment on peptide beads as control (C) after half an hour incubation.

specificity of the selected peptides. *Results:* Fifty-six peptide beads exhibited strong binding to bacteria in 30 minutes and 19 peptide beads were harvested. Eleven beads were sequenced by the microsequencer. Subsequent binding assay showed that these peptides can strongly bind to *E.coli, K. oxytoca, P. Aeruginosa, S. epidermis, E. faecalis, Bacillus sp. Streptococcus, and Citrobacter* in 30 min as seen under confocal laser scanning microscope (Figure 1A, B & C). These results indicated that the eleven peptides could be potent ligands for attachment of commonly isolated clinical bacteria. Out of the 11 peptides, 10 were positively charged and may favor the adhesion of negatively charged bacteria. *Significance:* Super adhesive peptides may facilitate the study of bacterial biofilm by serving as ligands of specific conformational receptor for bacterial attachment. These peptides may also allow the dynamic study of bacteria/surface interaction in biofilm formation. Moreover, these strong binding peptides may be applied in biofiltration system for the waste treatment by the use of the filter material grafted with the peptides.

Acknowledgments

The work was supported by the C. W. Law Biofilm Research Fund and NIH R33CA-86364, R33 CA-89706 grants.

References

1. Costerton, J. W., Lewandowski, Z. and Caldwell, D. E. *Annu. Rev. Microbiol*. **49**, 711-745 (1995).
2. Jucker, B. A., Jarms, H. and Zejmder, A. J. *J. Bacteriol*. **178**, 5472-5479 (1996).
3. Mafu, A. A., Roy, D. and Goulet, J. *Appl. Environ. Microbiol*. **57**, 1969-1973 (1991).
4. Dalton, H. M., March, P. E. *Curr. Opin. Biotechnol*. **9**, 252-255 (1998).
5. Lam, K. S., et al. *Nature* **354**, 82-84 (1991).

Peptide Revolution: Genomics, Proteomics & Therapeutics
Michael Chorev & Tomi K. Sawyer (Editors)
American Peptide Society, 2003

The Anti-HIV-1 Activity of Cyclic α-Defensins is Not Affected by Deleting Cystine

Hua Li, Qitao Yu, Jin-Long Yang and James P. Tam

Department of Microbiology and Immunology, University of Vanderbilt, Nashville, TN 37232, USA

Introduction

Defensins are a family of antimicrobial peptides abundant in immune cells. They are found in white blood cells, especially neutrophils, intestinal Paneth cells and barrier epithelial cells that engage in host defense. All defensins are cysteine-rich and cationic peptides, typically containing 29 to 35 amino acids and a characteristic six-cystine motif that interconnects three intramolecular disulfide bonds. The cystine motif of α-defensins is formed by the SS-pairings of Cys1-Cys6, Cys-2-Cys4 and Cys3-Cys5 [1]. Several α-defensins, such as the defensins from humans, rabbits, guinea pigs and rats, have been shown to have anti-HIV-1 activity [2-3]. Since the mechanism is poorly defined, we investigated whether the anti-HIV-1 activity of defensins is related to the highly conserved structure with the six-cystine linked disulfide bond. Here, we report our synthesis and antiviral property of cyclic analogs of rabbit α-defensin with and without disulfide bonds.

Results and discussion

α-Defensins contain three disulfide bonds and are circularly permutated by an end-to-end, $Cys^{3,31}$, disulfide bond. The circulins provide precedents and incentives for designing α-defensin analogs with end-to-end cyclic structures. Synthesis of cyclic defensin started from Boc-Leu-thiopropionyl-MBHA resin; the peptide thioester was assembled using a standard DCC/HOBt coupling protocol in an Applied Biosystems 430A synthesizer [4]. In this study, four cyclic analogs of rabbit neutrophils peptide-1

Table 1. Amino acid sequence and HIV-1 inhibitory activity of cyclic α-defensin peptides.

Peptide	Amino Acid Sequence	Disulfide bond number	IC50 (μM)
CA33A	VVGACRRALCLPRERRAGFCRIRGRIHPLCGRR	2	1.3
CA33B	VVGACRRALGLPRERRAGFCRIRGRIHPLGGRR	1	2.4
CL33B	VVGAGRRALGLPRERRAGFGRIRGRIHPLGGRR	0	3.1
CF(1)33	VVGAGRRALGLPRERRAGFCRIRGRIHPLGGRR	0	4.1
Human α-defensin	ACYCR I PACIAGERRYGTCIYQGRLWAICC	3	>10

(NP-1), named CA33A, CA33B, CL33B and CF(1)33, were designed and prepared. In these analogs, we replaced one or more disulfide bonds in natural NP-1 with two glycines and the free N- and C-terminus with a covalently linked peptide bond (Table 1).

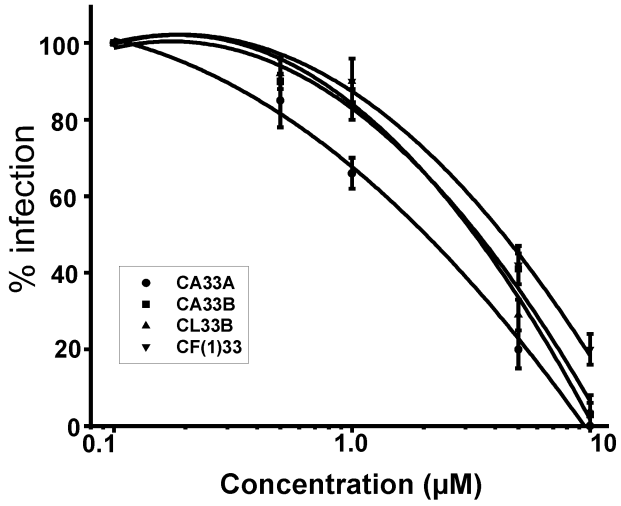

Fig. 1. Dose-response inhibition of cyclic α-defensins on infection of R9 HIV-1 viruses in cells.

The inhibitory effect of cyclic rabbit defensin analogs on HIV-1 infection was determined by a single-cycle MAGI assay [5]. Virus R9, T-cell-tropic strain, was employed in this study. P4R5 cells were transactivated by the HIV-1 tat protein induced expression of the *Escherichia coli* β-galactosidase gene from the HIV-I long-terminal repeat. All of the cyclic rabbit α-defensin analogs inhibited the infection of R9 HIV-1. Table 1 shows their 50% inhibitory concentrations (IC_{50}) which range from 1-5 μM. Loss of disulfide bonds in the cyclic α-defensin structure did not result in a significant change in the anti-HIV-1 activity. All cyclic α-defensin analogs with 0-2 disulfide bonds are equally potent. Comparison between the cyclic analogs with the human α-defensin-1 revealed that these peptides are more potent than the human α-defensin-1, whose IC_{50} is >10 μM. Our results show that the cystine-bond in cyclic α-defensin is not essential for anti-HIV-1 activity.

Acknowledgments
The work was funded by NIH Grants CA36544 and AI46164.

References

1. Lehrer, R. I. and Ganz, T. *Current Opin. Immunol.* **14,** 96-102 (2002).
2. Nakashima, H., Yamamoto, N., Masuda, M. and Fujii, N. *AIDS* **7**, 1129 (1993).
3. Zhang, L., Yu, W., He, T., Yu, J., Caffrey, R. E., Dalmasso, E. A., Fu, S., Pham, T., Mei, J., Ho, J. J., Shang, W., Lopez, P. and Ho, D. D. *Science* **298**, 995-1000 (2002).
4. Yu, Q., Lehrer, R. I. and Tam, J. P. *J. Biol. Chem.* **275**, 3943-3949 (2000).
5. Pirounake, M., Heyden, N. A. and Ratner, L. *J. Virol. Meth.* **85**, 151-161 (2000).

Peptide Revolution: Genomics, Proteomics & Therapeutics
Michael Chorev & Tomi K. Sawyer (Editors)
American Peptide Society, 2003

Identification of T-Cell Epitopes Using SPOT-Synthesized Peptides

Mathias Streitz, Bernhard Aÿ, Florian Kern and Rudolf Volkmer-Engert

Institut für Medizinische Immunologie, Charité-Universitätsmedizin Berlin, Schumannstr. 20-21, 10098 Berlin, Germany

Introduction

The CD8 T-cell response is an essential part of the cell-mediated immune response against human cytomegalovirus (HCMV). Known T-cell epitopes could potentially be useful for designing therapies against HCMV. Unfortunately, most CD8 T-cell epitopes have so far been identified in two HCMV proteins. The identification of all CD8 T-cell stimulating peptides within the whole CMV proteome is an interesting model to establish strategies for the study of T-cell responses against large numbers of proteins.

Positionally addressable parallel nano-synthesis on continuous cellulose membranes (SPOT synthesis) is an extensively used tool for the fast synthesis of thousands of matrix-bound peptides [1-3]. For screening large amounts of soluble peptides with respect to T-cell induction, a previously established PBMC-based assay may be used [4]. Unfortunately, due to chemical problems the efficient, reproducible and automatic assembly of cleavable peptides in SPOT-synthesis is limited in the formation of the ester bond between C-terminal amino acid and the hydroxy-functions of the cellulose. However, the C-terminal carboxy-function (free acid) is essential for T-cell stimulation since it is a prerequisite for efficient external class-I MHC loading [4]. Therefore, we developed a novel strategy based on the principle of the SPOT concept that yields peptides with a free C-terminus. This modification allows the production of very large numbers of peptides that are suitable for direct class-I MHC loading and thus ex-vivo CD8 T-cell stimulation.

Results and Discussion

Initially, known CD8 T-cell stimulating nonamer sequences with different C-terminal alterations (acid, amid, glycin amide) were tested for T-cell stimulation in order to determine the optimal C-terminal peptide function and peptide concentration. Peptides at a concentration between 0.1 – 1 µg/ml (106 PBMC) bearing a non-modified C-terminus resulted in the best stimulation. To expand the T-cell epitope mapping [5] to all the peptides derived from the HCMV, a high throughput synthesis approach is necessary. To map all CD8 T-cell epitopes of the HCMV about 66,000 nonamer-peptides bearing a C-terminal carboxy-function was synthesized. We have recently reported a method for the parallel synthesis of cleavable peptides on cellulose membranes using special linker molecules [6]. This approach, however, is affected by relatively time-consuming preparation of the linker molecules and of the modified cellulose membranes. Therefore, we determined that an alternative strategy, whereby (i) each cellulose membrane was acylated with the first amino acid and (ii) the HCMV-derived nonamere peptides were sorted according to the C-terminal amino acid, could solve the synthetic problem. The elimination of repeated nonamer sequences in the complete HCMV proteome is one advantage to sorting the peptides according to their C-terminal amino acid. Acylation of the cellulose membranes with the different amino acids was achieved using CDI as an activation reagent [7]. The coupling yields vary from 200 to 1700 nmol/cm^2 depending on the amino acid used. As a next step the peptides bearing the same C-terminal amino acid were synthesized according to the standard SPOT-synthesis protocol. Up to 1,200 peptides were synthesized in parallel on

a cellulose membrane and the synthesis quality was determined by HPLC-MS using an array of 20 peptides on each membrane.

The peptides were released from the membrane by hydrolysis with a dilute solution of sodium hydroxide yielding an amount of about 50 µg peptide/spot (0.25 cm^2). Pools of up to 100 peptides were used for the screening of the CD8 T-cell stimulation (epitope identification). Before cleavage from the membrane the pools were created as described in [4]. In a first attempt 24 peptide pools were screened in parallel whereby the responses of the stimulated T-cells were detected by flow-cytometry (see Figure 1). In the next step, we screened 5,000 peptides in parallel in a number of lymphocytes samples from different HCMV-positive donators. Using the technique described here, we identified unknown HCMV-epitopes and confirmed published epitopes of different HLA-types. The mapped epitopes will be verified by an assay with peptides synthesized on solid phase support.

In conclusion we have shown that our approach - the combination of SPOT synthesis with an intelligent generation of peptide pools and computing - is an efficient tool for the synthesis of large numbers of peptides that can be used for identification of T-cell epitopes.

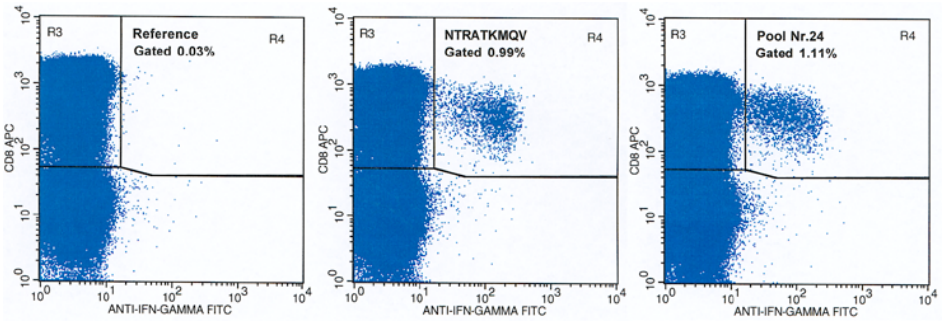

Fig. 1. T-cell response in flow diagrams. left: reference (unstimulated sample); center: IFN-g-positive response (region R4) with a known stimulating peptide and right: IFN-g-positive response (region R4) with one peptide pool.

References

1. Frank R. *Tetrahedron* **48,** 9217 (1992).
2. Wenschuh H., Volkmer-Engert R., Schmidt M., Schulz M., Schneider-Mergener J. and Reineke U. *Biopolymers* **55,** 188-206 (2000).
3. Reineke U., Volkmer-Engert R. and Schneider-Mergener *J. Curr. Opin. Biotechnol.* **12**, 59-64 (2001).
4. Hoffmeister B., Kiecker F., Tesfa L., Volk H. D., Picker L. J. and Kern F. *Methods* **29**, 270-281 (2003).
5. Kern F., Surel I.P., Brock B., Freistedt H., Radtke A., Scheffold A., Blasczyk R., Reinke P., Schneider-Mergener J., Radbruch A., Walden P. and Volk H.D. *Nature Med*. **4**, 975-978 (1998).
6. Licha K., Bhargava S., Rheinländer C., Becker A., Schneider-Mergener J. and Volkmer-Engert R. *Tetrahedron* **41,** 1711 (2000).
7. Epton R. (Ed.) *Innovation and Perspectives in Solid Phase Synthesis & Combinatorial Libraries*, Mayflower, Kingswinford, 2000, p.337.

Peptide Revolution: Genomics, Proteomics & Therapeutics
Michael Chorev & Tomi K. Sawyer (Editors)
American Peptide Society, 2003

Approaches to the Reconstruction of a Discontinuous Binding Site

Judit Villén[1], Ricard A. Rodríguez-Mias[2], Ernest Giralt[2], Francisco Sobrino[3,4] and David Andreu[1]

[1]Department of Experimental and Health Sciences, Universitat Pompeu Fabra, Barcelona, Spain; [2]Parc Científic de Barcelona, Universitat de Barcelona, Spain; [3]CISA-INIA, Valdeolmos, Madrid, Spain; [4]CBMSO, CSIC-UAM, Cantoblanco, Madrid, Spain

Introduction

Functional features of continuous antigenic sites have been successfully achieved with linear peptides. However, more stringent structural requirements are needed for a good mimicry of discontinuous sites, defined by residues distant in sequence but spatially close, as is the case with the majority of binding sites. A certain level of mimicry of this kind of sites is possible if: i) the 3D structure of the antigen is known, and ii) the residues involved in antigenic recognition are identified. These data can be used to build a peptide construct that displays the antigenically relevant residues and their environment in a native-like orientation.

Here we report our results in this direction, using as a model foot-and-mouth disease virus (FMDV), an economically very important animal pathogen. Three antigenic sites have been defined on the surface of the virus by experiments with mAb-resistant mutants [1]. We focused our attention on discontinuous site D, located on the junction of capsid proteins VP1, VP2 and VP3, and developed two different approaches for the design and reconstruction of the epitope and their functional evaluation as peptide vaccine candidates.

Results and Discussion

Our initial design was a heterotrimeric construction [2] in which critical amino acids and their adjoining environments were connected through a polyPro spacer between VP2 and VP3 (antiparallel fragments) and a disulfide bond between VP1 and VP3 (parallel). The connections were placed far from the surface, aiming for minimal distortion. Two mutations to Pro in the VP1 fragment were also made to reinforce incipient polyPro structure. Several analogues with different lengths of the polyPro spacer were also screened by molecular dynamics simulations [3]. This analysis suggested peptide D8 and four Dn analogues (with n = 2, 4, 7, 10 Pro residues in the spacer, Figure 1A) as candidates. The peptides were made from two fragments: one

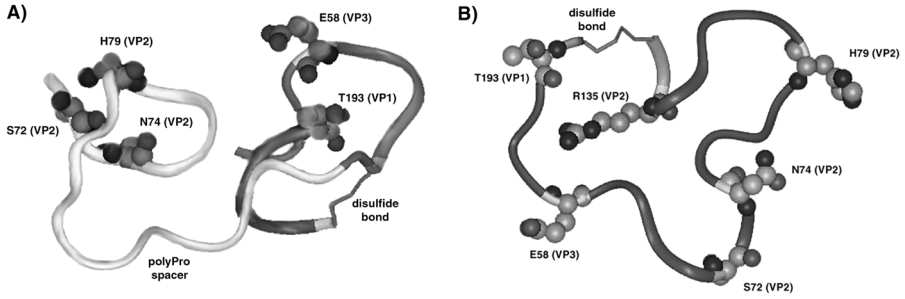

Fig. 1. Design of peptides reproducing discontinuous site D of FMDV: A) heterotrimeric constructions, B) surface mimics. Critical residues are represented in CPK.

(DnA) prepared by Fmoc chemistry and comprising the VP2 and VP3 regions, separated by the polyPro spacer; another (DnB) representing the VP1 segment and prepared using Boc chemistry. Directed heterodisulfide formation (0.1 M peptides, 0.01 M HOAc, pH 4.5, 25 ºC, 2 h) between DnA and DnB was promoted by using Npys as Cys-protecting-activating group on the DnB fragment.

A second generation of peptides was designed as surface mimics, in which highly exposed loops on the antigenic site D region were assembled into a cyclic peptide structure (Figure 1B). In addition to the critical amino acids defining the epitope, other residues such as Arg135 (VP2), involved in heparan sulfate cell receptor interaction [4], were included. The main difference, derived from the cyclic nature of the mimic, was the surface location of the connecting segments. Four analogues providing different levels of flexibility at the non-native disulfide region were tested. The peptides were obtained from linear precursors (made by Fmoc chemistry) by air oxidation under high dilution conditions (25 μM peptide, pH 8.0, 25 ºC, 4-16 h).

Both designs were tested for antigenicity, immunogenicity in guinea pigs and protection against the viral pathogen, as a preliminary step toward their incorporation into a multicomponent fully synthetic vaccine.

The heterotrimeric constructions failed to bind site D mAbs, but induced high antibody titers in guinea pigs. Specific binding of antisera to site D of FMDV was demonstrated by competition with site D mAbs. Moderate reduction of viral infectivity in cell culture was also achieved (Figure 2A). Finally, some animals vaccinated with D8 were protected against the disease. Minor differences between Dn analogues were found but on the whole the length of the polyPro spacer was not a significant issue.

The cyclic peptides were recognized by site D-specific mAbs in ELISA, a finding further confirmed by STD-NMR binding experiments [5]. In guinea pigs, the peptides elicited antibodies with higher neutralization levels (Figure 2B) than the Dn series. Animals were fully protected against FMD or showed delayed appearance of lesions.

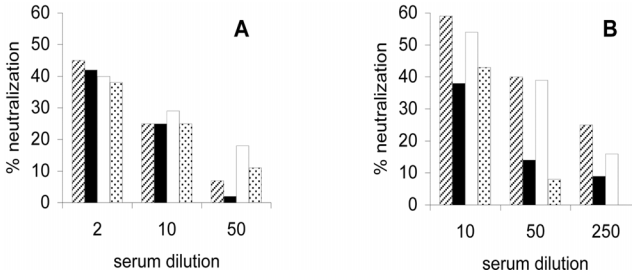

Fig. 2. Neutralization in cell culture for A) heterotrimeric peptide D4 and B) surface mimic cD2.

In conclusion, while only the surface mimics were able to bind site D mAbs, both designs induced protective responses, thus proving that functional reproduction of discontinuous sites is possible by structure-assisted design of antigenic site mimics.

Acknowledgments

This work was funded by the Spanish Ministry of Science and Technology (BIO2002-04091).

References

1. Lea, S., *et al. Structure* **2**, 123-139 (1994).
2. Borràs, E., Giralt, E. and Andreu, D. *J. Am. Chem. Soc.* **121**, 11932-11933 (1999).
3. Villén, J., *et al. Chembiochem.* **3**, 175-182 (2002).
4. Fry, E. E., *et al. EMBO J.* **18**, 543-554 (1999).
5. Johnson, M. A., Rotondo, A. and Pinto, B. M. *Biochemistry* **41**, 2149-2157 (2002).

Peptide Revolution: Genomics, Proteomics & Therapeutics
Michael Chorev & Tomi K. Sawyer (Editors)
American Peptide Society, 2003

Inhibition of Antimicrobial Peptides by Exopolysaccharides of Lung Pathogens

Monica Benincasa, Maura Mattiuzzo, Yury Herasimenka, Paola Cescutti, Roberto Rizzo and Renato Gennaro

Department of Biochemistry, Biophysics and Macromolecular Chemistry, University of Trieste, Trieste, I-34127, Italy

Introduction

Cystic fibrosis (CF) is a severe genetic disease characterized by an incidence of 1:2500 live births in the Caucasian population and an average life expectancy of about 30 years. The gene responsible for CF encodes the CFTR (cystic Fibrosis transmembrane conductance regulator) protein, which is involved in chloride transport. The most serious clinical symptom of the disease is the chronic microbial colonization of the major airways by opportunistic and non-opportunistic bacteria. This causes severe pulmonary infections, which are the major cause of morbidity and mortality in CF patients [1, 2].

Two models have been proposed to explain microbial colonization of CF affected lungs. One model states that hyper-adsorption of fluid by the airway surface epithelium leads to a lower than normal surface liquid. The reduced volume leads in turn to under-hydrated mucus and to impaired mucociliary clearance. These changes contribute to the establishment of an environment in the airway that favors bacterial colonization of the lungs. The second model states that the salt content in the airway fluid in CF patients is higher than normal, and thus inhibits the salt-sensitive activity of the antimicrobial peptides (e.g., LL-37 and defensins) that are released in this fluid and are thought to play a major defense role against inhaled microbes [3].

Antimicrobial peptides are widespread in living organisms as part of the innate immune defenses. In mammals, major sources of these peptides are circulating leukocytes and epithelial cells of skin and mucosal surfaces. Phagocytes store peptides that belong to the defensin and the cathelicidin families [4].

We have investigated the effect of exopolysaccharides produced by lung pathogens on the antimicrobial activity of peptides either present in the airway surface liquid of humans (e.g., LL-37 and the β-defensins hBD-1 and hBD-3), or from other sources (SMAP-29 from sheep and PG-1 from pigs), to establish their involvement in the poor defense reaction of the CF affected lung and thus explain infection persistence.

The study was carried out using peptides that differ by sequence and molecular conformation: the α-helical peptides LL-37 and SMAP-29, and the β-sheet peptides PG-1, with two disulfide bridges, and hBD-1 and hBD-3, with three disulfide bridges.
Exopolysaccharides produced by bacteria that cause pulmonary infections and characterized by different negative charge densities were chosen for these studies: alginate (Alg), produced by *Pseudomonas aeruginosa,* the polysaccharides BTS3, BTS7 and BTS13, produced by three clinical isolates of *Burkholderia cepacia*, and the polymer K40, produced by *Klebsiella pneumoniae*. *P. aeruginosa* and *B. cepacia* are opportunistic bacteria infecting CF patients, while *K. pneumoniae* is responsible for secondary infections in patients affected by chronic pulmonary diseases [5].

Results and Discussion

The presence of bacterial exopolysaccharides at 0.1-1.0 mg/ml inhibits the antimicrobial activity of LL-37, hBD-3, SMAP-29, and PG- 1 in a dose-dependent manner, as shown by increases ranging from 2- to 64-fold of the relative MIC values, as determined by the microdilution susceptibility test. The peptides are differently inhibited by the exopolysaccharides: Alg exerts the strongest inhibition towards LL-37 and hBD-3, whereas PG-1 and SMAP-29 are better inhibited by K40 and BTS7, respectively. Conversely, the low antimicrobial activity of hBD-1 prevented the possibility to test the inhibitory effect of the exopolysaccharides on this peptide.

To further investigate the effect of the exopolysaccharides on the activity of the peptides, time killing and permeabilization kinetics assays were performed. These experiments confirmed the results of the microdilution susceptibility tests. The time killing assays show that the bactericidal activities of LL-37, SMAP-29, and PG-1 are inhibited by K40 and Alg. Conversely, BTS7 exerts moderate inhibitory effects on the killing kinetics of these peptides only at high concentration (1 mg/ml). Similarly, the permeabilization kinetics of *E. coli* ML-35 inner membrane by SMAP-29 and LL-37 is strongly inhibited by the presence of Alg and K40, whereas BTS7 has little or no effect. The membranolytic activity of PG-1 is completely inhibited by the presence of K40, slowed down by Alg and poorly affected by BTS7.

The interaction of the α-helical antimicrobial peptides with the bacterial exopolysaccharides was investigated by CD spectroscopy. These peptides show a disordered conformation in aqueous buffer (with the possible exception of LL-37, which displays a modest helical content under this condition), and assume an α-helical structure, or an increase in its content, in the presence of a membrane-mimicking environment. CD studies carried out with LL-37 and SMAP-29 show that K40 is the most effective helical inducer, followed by Alg. Conversely, BTS7 is ineffective in this respect, in keeping with the negligible inhibition exerted by this exopolysaccharide on the antimicrobial activity of the peptides. This data suggest that the structure of the polysaccharides plays a role in defining the secondary conformation of the peptides and that their interaction is not merely based on the charge density of the polysaccharide, which ranks in the following order Alg > BTS7 > K40.

Based on the above results, we suggest that the inhibitory effect of the bacterial exopolysaccharides on the activity of antimicrobial peptides expressed in the human lung (e.g., LL-37 and defensins) might contribute to the persistence of pulmonary infections in CF patients.

References

1. Saiman, L., Tabibi, S., Starner, T. D., Gabriel, P. S., Winokur, P. L., Jia, H. P., Mc Cray Jr., P. B. and Tack, B. F. *Antimicrob. Agents Chemother.* **45**, 2838-2844 (2001).
2. Wine, J. J. *J. Clin. Invest.* **103**, 309-312 (1999).
3. Bals, R., Weiner, D. J. and Wilson, J. M. *J. Clin. Invest.* **103**, 303-307 (1999).
4. Gennaro, R. and Zanetti, M. *Biopolymers* **55**, 31-49 (2000).
5. Govan, J. R. W. and Deretic, V. *Microbiol. Rev.* **60**, 539-574 (1996).

Peptide Revolution: Genomics, Proteomics & Therapeutics
Michael Chorev & Tomi K. Sawyer (Editors)
American Peptide Society, 2003

Structural Study of the HIV-1 gp160 Cleavage Site by Native and Modified Sequences: Role of Site Specific Mutations

Lucia Falcigno[1], Romina Oliva[1], Gabriella D'Auria[1,2], Massimiliano Maletta[1], Manuela Vacatello[1], Monica Dettin[3], Antonella Pasquato[3], Carlo Di Bello[3] and Livio Paolillo[1]

[1]Department of Chemistry, University "Federico II" of Naples, 80126 Naples, Italy; [2]Institute of Biostructures and Bioimaging, CNR, 80134 Naples, Italy; [3]Department of Chemical Process Engineering, University of Padua, 35131 Padua, Italy

Introduction

Gp160 is a HIV-1 envelope glycoprotein precursor, which is activated by proteolytic cleavage to give the two mature envelope glycoproteins gp120 and gp41, playing a key role in the virus-host cell fusion. Thus, gp160 cleavage is a prerequisite for virus infectivity. The proteolytic activation of gp160 is performed by furin and other precursor convertases (PCs) at the carboxyl side of the sequence R508-E-K-R511 (site 1) [1]. To date, no structure or model is available for a large sequence around the gp160 cleavage site. Moreover, no PDB structure is available for furin or other PCs. The conformational features acting in the gp160 molecular recognition by proteolytic enzymes remain to be clarified.

We approached the problem by studying the structure-activity relationship in a series of analogues mapped on the gp160 processing site. The peptides are native or modified to exhibit specific secondary structures at the N-terminal of the gp160 site 1 [2,3]. Here, we report the activity and conformation of three 23-mer peptides (Table 1).

Table 1. Sequences and biological activities of potential substrate peptides.

	Sequence	% Cleavage[b]
	Nomenclature[a]: P4 P3 P2 P1 P1' P2'	
1	D[1]PKGVTVTVTvtVTR P K R↓A VGIG[23]	91
2	D[1]PKGVTVTVTvtVTR E K R↓A PGIG[23]	13
3	D[1]PKGVTVTVTvtVTR P K R↓A PGIG[23]	40

[a] *For nomenclature at cleavage site see Schecter and Berger [4].*
[b] *After 1 h of incubation by furin.*

The N-terminal sequence contains a pair of D-residues to disrupt its propensity to ordered structure [5]. At the C-terminal, it is followed by the gp160 native sequence R508-G516, where proline mutations have been inserted at positions P3 and/or P2', sites which were not studied previously.

Results and Discussion

All three analogues were characterized by NMR in a TFE/H_2O (90/10 v/v) solution. Analogues **1** and **3** exhibit the same chemical shifts for all the protons in the sequence D1-R15, and have a striking similarity to analogue **2** in the C-terminal region R18-G23. A set of preliminary structures was obtained by means of the DYANA program [6], then energy refined by the AMBER program [7] using interproton distances from

NOEs as conformational restraints. The best 10 structures were then selected as representative of the solution conformation for each analogue. All the analogues show a quite similar structure at the N-terminal side consisting in one distorted α-helix turn on residues T6-V9, in fair agreement with the negative deviations of αCH chemical shifts with respect to random coil values [8]. Analogues **1** and **3** exhibit a similar extended conformation in the C-terminal region, while analogue **2** shows a non-canonical bending from K17 to G21.

The average molecular models for all three peptides were docked to the furin catalytic site built by homology in order to investigate the exposure/accessibility of their cleavage sites to the enzyme catalytic region. A rigid docking was performed taking advantage of the presence of a canonical inhibitor in the furin substrate channel. The backbone of four residues around the peptide cleavage point (P3-P1') was superimposed on the backbone of the corresponding residues in the homology modeled inhibitor eglin-c [2].

A suitable peptide docking onto the furin catalytic region was obtained for analogue **1**. Residues at the cleavage site present a very good fit with the corresponding segment in the modeled eglin-c, which also exhibits an analogous extended conformation. Proline at P3 introduces constraints on the dihedral angles of the adjacent residues P4-P2' toward the expected values for recognition, in agreement with the Bode and Huber model [9]. Therefore, the proline mutation at P3 should allow the substrate to lose less entropy while assuming the correct orientation, explaining the high cleavage efficiency.

The lower activities of analogues **2** and **3** are probably due to a balance between the entropic gain from Pro20, and the loss of a specific interaction required in position P2'. Indeed, a proline at P2', although less efficiently than at P3, induces the correct dihedrals of extended conformation on P2-P2' residues, and particularly on the Ala residue at P1'. Therefore, according to the Bode and Huber model [9], the proline mutation at P2' could be structurally favored, although to a lesser extent than at P3. However, the proline mutation at P2' seems to be enthalpically disadvantageous, as hydrophobic interactions between a Val residue at P2' and the furin subsite S2' are lost.

References

1. Moulard, M. and Decroly, E. *Biochim. Biophys. Acta* **1469**, 121-132 (2000).
2. Oliva, R., Leone, M., Falcigno, L., D'Auria, G., Dettin, M., Scarinci, C., Di Bello, C. and Paolillo, L. *Chem. Eur. J.* **8**, 1467-1473 (2002).
3. Oliva, R., Falcigno, L., D'Auria, G., Dettin, M., Scarinci, C., Pasquato, A., Di Bello, C. and Paolillo, L. *ChemBioChem*. **4**, 727-733 (2003).
4. Schechter, I. and Berger, A. *Biochem. Biophys. Res. Commun.* **27**, 157-162 (1967).
5. Krause, E., Beyermann, M., Fabian, H., Dathe, M., Rothermund, S. and Bienert, M. *Int. J. Peptide Protein Res.* **48**, 559-568 (1996*)*.
6. Güntert, P., Mumenthaler, C. and Wüthrich, K. *J. Mol. Biol.* **273**, 283-298 (1997).
7. Case, D. A., Pearlman, D. A., Caldwell, J. W., *et al*. *AMBER 6*, University of California, San Francisco (1999).
8. Wishart, D. S., Sykes, B. D. and Richards, F. M. *J. Mol. Biol.* **222**, 311-333 (1991).
9. Bode, W. and Huber, R. *Eur. J. Biochem.* **204**, 433-451 (1992).

Peptide Revolution: Genomics, Proteomics & Therapeutics
Michael Chorev & Tomi K. Sawyer (Editors)
American Peptide Society, 2003

Structural Investigation of the HIV-1 Envelope Glycoprotein gp160 Cleavage Site: Solution Conformation of a 41-mer Peptide

Romina Oliva[1], Lucia Falcigno[1], Gabriella D'Auria[1,2], Diego Gargiulo[1], Monica Dettin[3], Antonella Pasquato[3], Carlo Di Bello[3] and Livio Paolillo[1]

[1]Department of Chemistry, University "Federico II" of Naples, 80126 Naples, Italy; [2]Institute of Biostructure and Bioimaging, CNR, 80134 Naples, Italy; [3]Department of Chemical Process Engineering, University of Padua, 35135 Padua, Italy

Introduction

The infection process of the HIV virus requires the entry of viral genome into the target cell [1]. The virus penetration is triggered by the binding between the envelope viral glycoproteins and cell receptors [2]. The virus surface glycoprotein gp120 is anchored to the virus envelope via noncovalent interactions with the transmembrane protein gp41. In the early phase of HIV-1 penetration, gp120 binds to the CD4 receptor on the host cell with a high affinity. An additional interaction between gp120 and a chemokine receptor, such as CCR5 or CXCR4, is also required so that the gp120-CD4 binding may eventually evolve into a fusion event [3]. It was proposed that the gp120 receptor binding induced conformational change results in an exposure of the N-terminal sequence of gp41 (fusion peptide). This in turn, is believed to initiate the fusion by insertion into the cell membrane [4,5].

The two mature HIV-1 envelope glycoproteins gp120 and gp41 are generated from the common precursor gp160 (160 KDa). gp160 is synthesized as an inactive precursor in the endoplasmic reticulum [6,7] and, after oligomerization to a trimeric form, it is cleaved to produce the noncovalent $(gp120\text{-}gp41)_3$ trimeric complex, which characterizes the infectious viral particles [1]. Consequently, the proteolytic cleavage of the HIV-1 gp160 protein plays a key role in the virus-host cell fusion and eventually in the virus replication.

The sequence of human gp160 (856 residues) is known [8]. However, to date, no 3D structure is available for the entire gp160 protein. Furthermore, while the 3D structure of gp120 (complexed to CD4 receptor) [9] and a model for gp41 (built by homology from SIV gp41 structure) [10] are known, no 3D structure has been reported for a large gp160 sequence (493-539) which, interestingly, includes the processing site (Figure 1). Indeed, our aim to fill this gap.

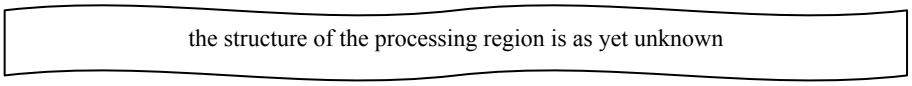

493-PLGVAPTKAKRRVVQREKRAVIGIGALFGFLGAAGSTMGAASMTLTV-539

Fig. 1. Sequence 493-539 of HIV-1 gp160.

Proteolytic activation of the HIV-1 gp160 is selectively performed by furin or other precursor convertases (PCs) [11] at the carboxyl site of the multibasic sequence R^{508}EKR (site 1) in spite of the presence of another consensus motif K^{500}AKR (site 2) a few residues upstream [12]. In order to clarify the structural basis of the gp160/furin recognition, we have previously analyzed the activity and conformational properties of a synthetic 19-mer peptide, namely p498, spanning the gp160 sequence from P^{498} to

G^{516}, thus containing both the primary and secondary furin concensus sites [13]. p498 is properly digested by furin at site 1, suggesting that in this gp160 fragment the structural features required for enzyme recognition are preserved. On the basis of the solution structural analysis of p498, we have hypothesized a possible role of a N-terminal helix, enclosing site 2, in regulating the exposure and accessibility to the gp160 physiological cleavage site proximal to the C-terminal loop. In order to further investigate the possible role of the specific secondary motifs flanking the gp160 cleavage site, we have analyzed the structure-activity relationships of a series of modified analogues incorporating a model sequences known to adopt helix or random structures at the N-terminal side [14,15].

Here we report the structural characterisation by CD, NMR and computational methods of a larger synthetic sequence reproducing the native gp160 region L494-S534. This sequence, namely wt-41, contains both the secondary and primary furin concensus sites and interestingly contains the segment, which works in gp41 as a fusion peptide.

Results and Discussion

CD spectra of wt-41, obtained in pure water or in mixtures of up to 98% trifluoroethanol (TFE) in water, outline the presence of a helical structure. The helical structure starts to form at 40% TFE. The NMR analysis was performed in TFE/H_2O 90:10 (v/v). The NOE pattern and the proton chemical shift deviations from random coil values [9] point to a helical conformation in the N-terminal region of the peptide from T^{499} to R^{508}. In the C-terminal region a well-defined helix is found from L^{518} to A^{526}. A set of 363 NOE data (190 intra-residual, 89 sequential and 65 long-range, including 52 constraints characteristic of helical structure) was used for structure calculations.

LGVAPTKAKRRVVQREKRAVIGIGALFGFLGAAGSTMGAAS

Fig. 2. Schematic representation of secondary structure elements found for wt-41.

Wt-41 covers almost the entire 494-539 gp160 region for which till now, no 3D structure was available. With regard to the processing site, the wt-41 NMR data, supported by preliminary structure calculations, show that site 1 is placed in an exposed loop while site 2 is incorporated in a helical structure (Figure 2). We suggest that this structural pattern exhibited by p498 as well as by the larger wt-41, is also operative in gp160, and may justify the furin selectivity for site 1. Furthermore, by comparing wt-41 with the 23-mer peptide reproducing gp120 C-terminal side [16] (PDBCode:1MEQ) and with the model obtained for gp41 N-terminal side [17] (PDBCode:1ERF), two more points can be stressed.

The former structure, 1MEQ, which spans the gp120 sequence V^{489}-R^{511} (C5 domain) and ends up with site 1, was found by us to form a helical conformation. From our results we find that this motif is not pre-existent in gp160. Its occurrence may result from a site 1 conformational re-arrangement following the cleavage event itself.

The latter structure, 1ERF, which reproduces the gp41 sequence A^{512}-S^{534}, shows the entire fusion peptide in helical conformation. In our wt-41 structure, the fusion

peptide adopts a shorter helical structure before the cleavage. Indeed, our data are in accordance with the gp160 secondary structure prediction that, for the segment A^{512}-I^{515}, located at the C-terminal side of site 1, predicts the absence of a regular secondary structure.

Our preliminary wt-41 molecular model suggests the gp160 processing region to be globally arranged in a helix-loop-helix structure. In particular, wt-41 shows the physiological site 1 exposed in a loop. This is in accordance with the structure typically found for proteolysis sites that when exposed to the solvent and protruding from the protein surface, are easily approachable by the processing enzyme.

References

1. Turner, B. G. and Summers, M. F. *J. Mol. Biol.* **285**, 1-32 (1999).
2. Weber, J. N. and Weiss, R. A. *Sci. Am.*, **259**, 100-109 (1988).
3. Chapham, P. R. and Weiss, R. A. *Nature* **388**, 230-231 (1997).
4. Carr, C. M. and Kim, P. S. *Cell* **73**,823-832 (1993).
5. Bentz, J. *Biophys. J.* **78**, 227-245 (2000).
6. Klenk, H. D. and Garten, W. *Trends Microbiol.* **2**, 39-43 (1994).
7. Stein, B. S. and Engleman, E. G. *J. Biol. Chem.* **265**, 2640-2649 (1990).
8. Reitz, M. S. *et al*. *AIDS Res. Hum. Retroviruses* **10**, 1143-1155 (1994).
9. Kwong, P. D. *et al. Nature* **393**, 648-659 (1998).
10. Caffrey, M. *et al. Biochim. Biophys. Acta* **1536**, 116-122 (2001).
11. Hallenberger S. *et al*. *Nature* **360**, 358-361 (1992).
12. Moulard, M. and Decroly, E. *Biochim. Biophys. Acta* **1469**, 121-132 (2000).
13. Oliva, R. *et al*. *Chem. Eur. J.* **8**, 1467-1473 (2002).
14. Oliva, R., Falcigno, L., D'Auria, G. Dettin, M., Scarinci, C., Pasquato, A., Di Bello, C. and Paolillo, L., *ChemBioChem.* **4**, 727-733 (2003).
15. Oliva, R. *et al*. In Benedetti E. and Pedone C. (Eds.), *Peptides 2002, Proceedings of the 27th Eur. Peptide Symp.* Edizioni Ziino*, Napoli, Italy, 2002,* pp.734-735.
16. Guilhaudis, L., Jacobs, A. and Caffrey, M. *Eur. J. Biochem.* **269**, 4860-4867 (2002).
17. Gordon, L. M. *et al. Biochim. Biophys. Acta* **1559**, 96-120 (2002).

Peptide Revolution: Genomics, Proteomics & Therapeutics
Michael Chorev & Tomi K. Sawyer (Editors)
American Peptide Society, 2003

Dendrimeric ε–Peptides: A Novel Design of Antimicrobials

Qitao Yu, Chengwei Wu, Jin-Long Yang and James P. Tam*

Department of Microbiology and Immunology, Vanderbilt University,
A5119 Medical Center North, Nashville, TN 37232 USA

Introduction

Antimicrobial peptides constitute an important part of innate defense mechanisms. More than 500 antimicrobial peptides have been identified and thousands have been synthesized in the search of a therapeutic agent. Dendrimeric peptides are biopolymers with unusual architectures. They consist of a multi-arm scaffold (core) and an array of branching peptides. In our previous studies, we found that a dendrimeric peptide consisting of second-generation Lys scaffold (K2K) with four residues peptide branches on each arm display a broad activity spectrum against 10 test microbes in both low and high salt assays [1]. In this paper, we describe the development of δ- and ε-dendrimers as novel antimicrobial structures.

Results and Discussion

Different forms of dendrons and dendrimeric peptides were prepared using two amino acids, Lys or Orn, as peptide backbones for scaffolds. The δ- or ε-dendrimers contained, respectively, the δ- or ε-peptide scaffolds that included δ-tetrapeptide **3** and δ-pentapeptide **4,** as well as ε-tetrapeptide **5** ande-pentapeptide **6** (Figure 1). They were compared with the cascade α/δ-dendrimer **1** and α/δ-dendrimer **2** with the Orn_2Orn (α-and δ-peptide) and Lys_2Lys (α- and ε-peptides) scaffolds, respectively. The remaining amino groups of these di-amino-acid derived dendrimers not used for the scaffolds were tethered to a functionalized side chain. A tetrapeptide R4, Arg-Leu-Tyr-Arg, was used as this side-chain peptide. This side-chain peptide consisted of a BHHB motif (B = basic and H = hydrophobic amino acids) and an equal contribution of positively charged and bulky hydrophobic amino acids. The R4 peptide also contained the topological motifs of a family of cystine-stabilized β-stranded antimicrobial peptides that included protegrins, tachyplesins and theta defensin [2-4].

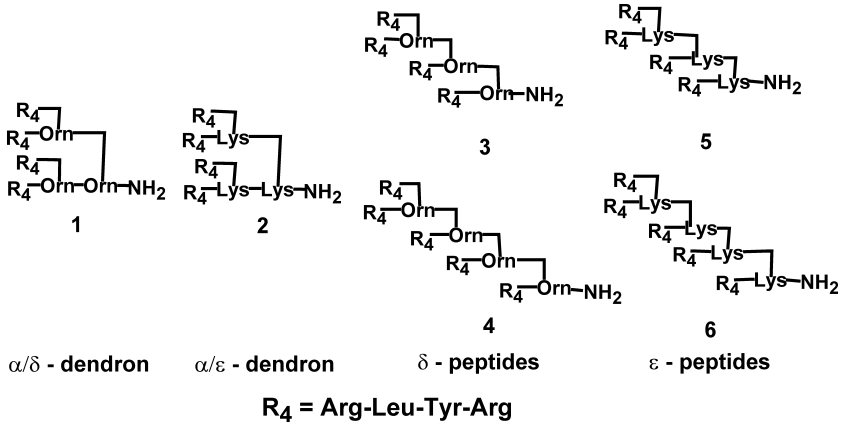

Fig. 1. Schematic representation of α/δ-, α/ε-dendrons and δ–, ε-peptides.

The cascade dendrons **1** and **2** were prepared using Fmoc chemistry. The δ– and ε-dendrimeric peptides **3-6** were prepared by a combination of Boc and Fmoc chemistries, with the δ- and ε-scaffold assembled by the Fmoc chemistry and the side-chain R4 peptides by the Boc chemistry (Figure 2).

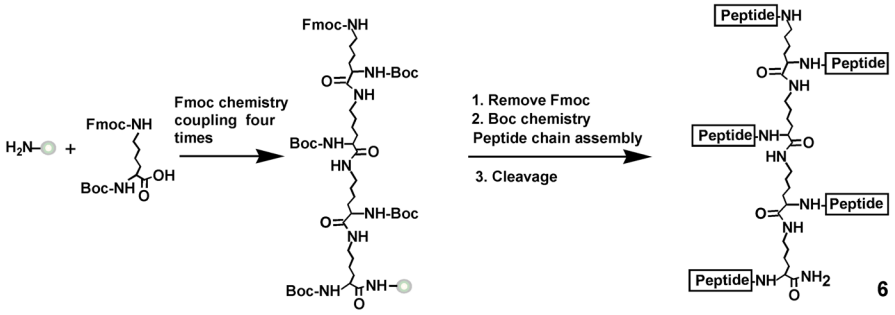

*Fig. 2. Synthetic scheme of ε-peptide **6.***

These linear δ- and ε-dendrimeric peptides represent novel peptide scaffolds and provide new structures. With repeating methylene units, they may be less rigid and more flexible than common α-peptide; the lipid-like backbones of the peptides may also contribute to the amphipathicity for their activities. When assayed against 10 test organisms under both low- and high-salt conditions, these dendrimers exhibit contrasting activity profiles, potent antimicrobial activity and salt sensitivity. The ε- and α/ε-dendrimers using Lys as scaffolds display potent and broad-spectrum activity against 10 test organisms under both low- and high-salt conditions. In ε-dendrimers, a ε-scaffold with three repeating ε-peptide bonds is sufficient for high antimicrobial activity. In contrast, the corresponding δ-dendrimers with Orn as scaffolds are many-fold less potent and are salt sensitive to certain bacteria and, particularly, totally inactive against *E. faecalis*. Our results provide a new approach to the design of bioactive peptides based on the diversity of scaffold structures.

Acknowledgments
This work was supported in part by US Public Health Service grants, CA 36544 and AI46164.

References

1. Tam, J. P., Lu, Y-A. and Yang, J-L. *Eur. J. Biochem.* **269**, 923-932 (2002).
2. Nakamura, T., Furanaka, H., Miyata, T., Tokunaga, F., Muta, T., Iwanaga, S., Niwa, M., Taokao, T. and Shimonishi, Y. *J. Biol. Chem.* **263**, 16709-16713 (1998).
3. Lehrer, R. I., Rosenman, M., Harwing, S. S., Jackson, R. and Eisenhauer, P. *J. Immunol. Med.* **137**, 167-173 (1993).
4. Tang, Y.- Q., Yuan, J., Osapay, K., Tran, D., Miller, C. J., Ouellette, A. J. and Selsted, M. E. *Science* **286**, 498-502 (1999).

Peptide Revolution: Genomics, Proteomics & Therapeutics
Michael Chorev & Tomi K. Sawyer (Editors)
American Peptide Society, 2003

Membrane Permeable ε-Peptides

Khee Dong Eom, Jin-Long Yang and James P. Tam

Department of Microbiology and Immunology, Vanderbilt University, Nashville, TN 37232, USA

Introduction

Previous work in our laboratory focused on peptide chimeras containing both α- and ε-peptides [1-3]. The ε-peptides are Lys isopeptides and present a new class of amphipathic peptides (Figure 1). In the well folded α-peptides, their amphipathicity is due to side chains that cluster hydrophilic and hydrophobic functional groups rigidified by the structured backbones. In contrast, the amphipathicity of the ε-peptide is contributed by the hydrophobic backbone, and enhanced by adding an α-amino acid to their amino groups as side chains. The intramolecular hydrogen-bonding of ε-peptide differs from that of α-peptide, and can lead to different folded structures because of their backbone flexibility and adaptability to form loops or turns [4].

Here we report on the synthesis and membrane-active properties of ε-peptides and ε-peptide chimeras, $(\varepsilon\text{-Lys})_n$, $\varepsilon\text{-(Arg)}_n$, $\varepsilon\text{-(Leu)}_n$, and $\varepsilon\text{-(Tyr)}_n$, where n = 4-10 (Fig. 1).

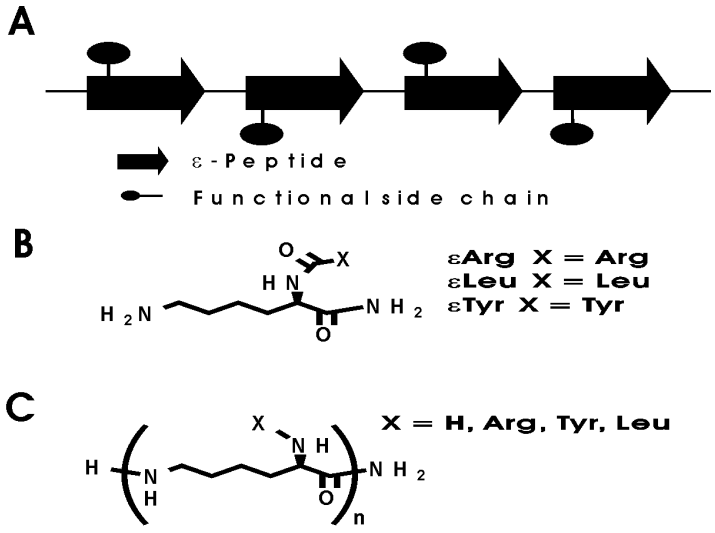

Fig. 1. Schematic diagram of (A) ε-peptides, (B) ε-amino acids and (C)ε-peptide chimeras.

Results and Discussion

ε-Peptides (Figure 1) with or without side-chain attachments of selected amino acids at their α-amines were prepared by a stepwise solid-peptide synthesis on MBHA (0.62 mmol/g) resins in high yields. Boc-Lys(Fmoc) was used as a building block for ε-peptide. The terminal ε–amines were capped by Boc-Lys(2-Cl-Z) or a fluoresceinated compound. A double-coupling protocol was required when the monomers units were > 7 (n = 7, Figure 1). The N-terminal Boc-groups were removed by TFA. Following HF cleavage with anisole scavenger, the ε-peptides dissolved in water were purified by C_{18} RP-preparative HPLC, and confirmed by MALDI mass spectrometry. Longer ε-peptides with n > 6 required an additional hour compared to the normal 1-hr HF cleavage time. Antimicrobial activity was determined by a radial diffusion assay.

Their membrane-permeability activity was determined by confocal microscopy collected from emission wavelengths at 488 nm with a 510-550 band-pass filter after fixation and 30 min incubation on HeLa cells.

Antimicrobial assays were performed in three different organisms: Gram-negative and Gram-positive bacteria as well as fungi, under both low- and high-salt conditions containing 100 mM NaCl. Low antimicrobial activity against *E. coli* (MICs 19 μM) of ε-peptides was observed when n > 7 at low-salt conditions, but not at high-salt conditions. The increase of antimicrobial activity was moderate (MIC, 4.6 μM) even when n = 10. Similar antimicrobial profiles were observed against Gram-positive bacteria such as *S. aureus* and fungi such as *C. albicans*. However, this ε-peptide series (MICs 30-112 μM, n > 7) retained low antimicrobial activity against *C. albicans* in high salt conditions. The ε-$(Leu)_n$ series displayed nearly identical profiles as the ε-peptides, suggesting the addition of Leu as side chains in this limited oligomeric series does not contribute to either the amphipathic or antimicrobial characters the ε-peptides.

In contrast, ε-peptides such as ε-$(Arg)_n$ with a cationic charged amino acid Arg tethered to the side chains of ε-peptide backbone were amphipathic and showed potent antimicrobial activity. Low antimicrobial activity (MIC, 3.4 μM) against *E. coli* was observed when n = 4, and the potency increased steadily with MIC values < 1 μM when n = 6 in low-salt conditions. They retained most of their activity under high-salt conditions. The ε-$(Arg)_n$ peptides were less potent against *S. aureus* and *C. albicans,* but displayed similar antimicrobial profiles as those against *E. coli*. Unexpectedly, the ε-$(Tyr)_n$ series behaved similar to the ε-$(Arg)_n$ series, albeit showing a lower potency in pairwise comparison. For example, against *E. coli* the MIC value of ε-$(Tyr)_6$ is 4.1 μM compared to 0.9 μM of ε-$(Arg)_6$. However, they are equally potent when n = 7, display MIC values of about 0.6 μM. Our results suggest that the antimicrobial activity of ε-peptides depends on a balance of side-chain hydrophobicity and hydrophilicity in addition to the contribution by the hydrophobic ε-peptide backbone. Our study on the membrane-permeability of these four series ε-peptides is incomplete but appears to correlate well with their antimicrobial properties. This correlation has also been observed in our structure-function study of dendrimers, dendrons, and other antimicrobial peptide mimetics. In summary, our results provide useful information for designing novel ε-peptides with membrane-active properties.

Acknowledgments

The work was supported in part by NIH grants CA36544 and AI46164.

References

1. Tam, J. P., et al. *Proc. Natl. Acad. Sci. U.S.A.* **86**, 9084-9088 (1989).
2. Jones, N. A., et al. *Biochim. Biophys. Acta* **1517**, 1-18 (2000).
3. Szókán, Gy., et al. *Biopolymers* **42**, 305-318 (1997).
4. Woll, M. G., et al. *J. Am. Chem. Soc.* **123**, 11077-11078 (2001).

Peptide Revolution: Genomics, Proteomics & Therapeutics
Michael Chorev & Tomi K. Sawyer (Editors)
American Peptide Society, 2003

Structure-Activity Relationship Study of the Fragment 33-61 of α-Chain Bovine Hemoglobin

Alessandra Machado[1], Maurício L. Sforça[2], Sirlei Daffre[3], Antonio Miranda[4], Alberto Spisni[2], Thelma A. Pertinhez[2] and M. Terêsa M. Miranda[1]

[1]Depto. Bioquímica, IQ, Universidade de São Paulo, 05508-900, São Paulo, SP; [2]Centro de Biologia Molecular Estrutural, Lab. Nacional de Luz Síncroton; [3]Depto. Parasitologia, ICB, Universidade de São Paulo; [4]Depto. Biofísica, Universidade Federal de São Paulo, Brasil

Introduction

The peptide FLSFPTTKTYFPHFDLSHGSAQVKGHGAK corresponds to fragment 33-61 of the α-chain of bovine hemoglobin (Hb 33-61). It was isolated from gut contents of the cattle tick *Boophilus microplus* and found to be active in micromolar concentration against Gram-positive bacteria and fungi [1]. Recently, 3D structure of the amidated form of Hb 33-61 (Hb 33-61*a*) in SDS micelles has been determined by ^{1}H-NMR. The results indicated that its C-terminal portion adopts an α-helical fold while the remaining part of the peptide presents turns connected by flexible loops [2]. In order to determine the structural requirements for the antifungal activity of Hb 33-61, we synthesized its N- and C-terminally truncated fragments and studied their conformational behavior by CD and NMR spectroscopies.

Results and Discussion

The peptide syntheses were carried out manually by SPPS using Boc chemistry. Hb 33-61*a* and Hb 33-52*a* were built on pMBHA resin while Hb 33-61, Hb 48-61 and Hb 40-61 were assembled on PAM resin. The resulting peptidyl-resins were treated with HF/scavengers to yield the crude peptides. After purification by preparative RP-HPLC, the final compounds were characterized by RP-HPLC (purities higher than 98%), amino acid analysis and ESI-MS. Antifungal activity was determined by a liquid growth inhibition assay against *C. albicans* [1]. As shown in Table 1, Hb 33-61*a* was 16-fold more active than Hb 33-52*a,* revealing that its C-terminal portion is crucial for the activity expression. Hb 33-61*a* was also 8-fold more active than Hb 33-61, which is in accordance with previous reports of antimicrobial activity enhancement by C-terminal amidation [3]. Since Hb 33-61 was slightly less active than Hb 40-61 and Hb 48-61 was inactive up to 100 μM, we concluded that Hb 40-61 presents the minimum structural requirements for the activity against *C. albicans*. CD experiments were performed on a Jasco J-810 spectropolarimeter. Hb 33-61*a*, Hb 33-61 and the truncated fragments showed random coil conformation in aqueous solution. In zwitterionic LPC micelles they presented structural behavior that was not well-defined while in negative SDS micelles they acquired elements of secondary structure. TFE was used for the estimation of the peptide helical contents (Table 1) [4]. A good correlation between helical content and the biological activities was observed. 2D ^{1}H-NMR spectra of Hb 48-61 and Hb 40-61 in 200 mM SDS-d_{25} were acquired using a Varian INOVA 500 spectrometer at 300 K. COSY, TOCSY, NOESY and ROESY experiments were done for spin system identification and structure determination. Energy minimization and molecular dynamics were carried out on an Octane2 Silicon Graphics workstation using DYANA and DISCOVER software. Figure 1a shows the 3D structure of Hb 48-

Table 1. Antifungal activity and helical content of the peptides.

Peptide	*Sequence*	*MIC(μM)*	*Helical content (%)*
Hb 33-61*a*	FLSFPTTKTYFPHFDLSHGSAQVKGHGAK-NH_2	3.12-6.25	24.2
Hb 33-52*a*	FLSFPTTKTYFPHFDLSHGS-NH_2	50.0-100.0	0.0
Hb 33-61	FLSFPTTKTYFPHFDLSHGSAQVKGHGAK-OH	25.0-50.0	9.5
Hb 40-61	KTYFPHFDLSHGSAQVKGHGAK-OH	12.5-25.0	19.5
Hb 48-61	LSHGSAQVKGHGAK-OH	n.d.[a]	9.9

[a]*not detected at concentration up to 100 μM.*

61 in solution. The observation of medium range $d_{\alpha N}(i, i+3)$ and intense range $d_{NN}(i, i+1)$ NOEs indicated the presence of a helical fold spanning residues S52-G59. In addition, the observation of $d_{\alpha N}(i, i+2)$ NOEs spanning residues G57-K61, together with $d_{NN}(i, i+2)$ NOEs, suggested the presence of a possible turn in that region. Figure 1b shows that Hb 40-61 presented a helical structure spanning residues S52-A60. This is in agreement with the presence of medium range $d_{\alpha N}(i, i+3)$ and $(i, i+4)$ and the intense range $d_{NN}(i, i+1)$ NOEs. The $d_{NN}(i, i+1)$ NOEs, as well as $d_{\alpha N}(i, i+2)$ and $(i, i+3)$, led to the identification of turns spanning residues K40-P43 and S49-G51, respectively. These results indicated that the helical content is important, but not crucial, for the expression of antifungal activity of the peptides studied. Indeed, the global folding displayed by the Hb 40-61 in 200 mM SDS (Figure 1b) is similar to that of the corresponding portion in Hb 33-61*a*.

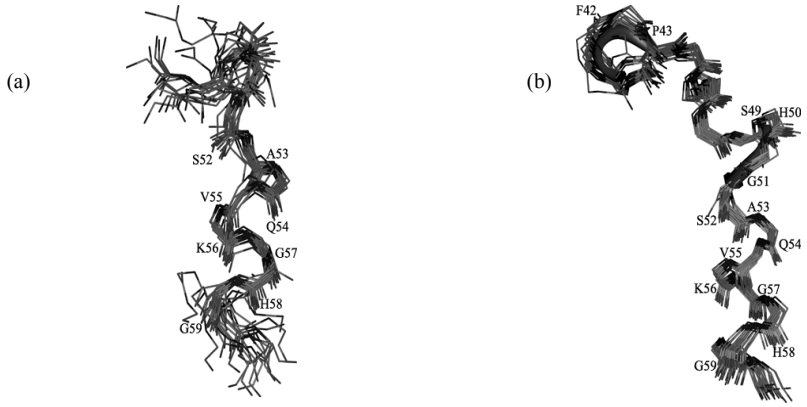

Fig. 1. The 3D NMR-derived solution structures of Hb 48-61 (a) and Hb 40-61 (b) in the presence of SDS micelles. The superimposition has been made for residues S49-G59 (backbone RMSD = 0.73 ± 0.19) and T41-G59 (backbone RMSD = 0.52 ± 0.23), respectively.

Acknowledgments

The authors are grateful to FAPESP and CNPq for the grants and fellowships.

References

1. Fogaça, A. C., Silva Jr., P. I., et al. *J. Biol. Chem.* **274**, 25330-25334 (1999).
2. Sforça, M. L., Pertinhez, T. A., Figueredo, R. C. R., Oyama Jr., S., Miranda, M. T. M., Miranda, A., Daffre, S. and Spisni, A. *in preparation*.
3. Shalev, D. E., Mor, A. and Kustanovich, I. *Biochemistry* **41**, 7312-7317 (2002).
4. Ganz, P. J., Lyu, P. C., Manning, M., Woody, R. W. and Kallenbach, N. R. *Biopolymers* **31**, 1605-1614 (1991).

Peptide Revolution: Genomics, Proteomics & Therapeutics
Michael Chorev & Tomi K. Sawyer (Editors)
American Peptide Society, 2003

Conformational Studies of Gomesin Analogues

Marcos A. Fázio[1], Sirlei Daffre[2], M. Terêsa M. Miranda[3] and Antonio Miranda[1]

[1]Depto. de Biofísica, UNIFESP, 04044-020; [2]Depto. de Parasitologia, ICB-USP, 05508-900, [3]Depto. de Bioquímica, IQ-USP, 05508-900, São Paulo, São Paulo, Brasil

Introduction

Gomesin is a cationic antimicrobial peptide isolated from hemocytes of the Brazilian spider *Acanthoscurria gomesiana*. It contains four cysteines performing two disulfide bridges, being effective against Gram-positive and Gram-negative bacteria strains and yeast such as *M. luteus*, *E. coli* and *C. albicans* (MIC< 0.64 μM). This peptide carries two post-translational modifications: cyclization of the N-terminal glutamine into a pyroglutamic acid (Z) and amidation of the C-terminal arginine [1]. As such, it shows sequence similarity to tachyplesin, polyphemusin, androctonin and protegrin. NMR studies have shown that the structure of gomesin consists of a well-resolved two-stranded antiparallel β-sheet connected by a noncanonical β-turn [2]. The aim of this work was to study the importance of the secondary structure on the activities of this potent antimicrobial peptide. Thus, we synthesized the native peptide, D-gomesin and variants that lack one or both disulfide bridges. Their activities were evaluated against the microorganisms cited above [3].

Results and Discussion

Gomesin and their analogues shown in Table 1 were synthesized by the SPPS using the t-Boc strategy on a MBHA-Resin. After full deprotection and cleavage from the resin in anhydrous HF (2 hours at 0°C), the crude peptides were cyclized by air oxidation at pH 6.8 to 7.0 during 48 hours at 5ºC. Cyclizations were monitored by LC/ESI-MS. The crude compounds were purified by RP-HPLC and characterized by LC/ESI-MS, CE and AAA. Conformational studies were performed by CD spectroscopy in different media such as 70% methanol, 70% TFE and 10 mM SDS. The spectra of gomesin obtained in these environments showed a negative band at 205 nm and a positive at 232 nm characteristic of β-hairpin structure [4]. D-gomesin showed to be equipotent to the native peptide and, as expected, its CD spectrum displayed a mirror image of the L-enantiomer. Linear peptide **III** presented a significative decrease (2-32-fold) on its antimicrobial activity in the strains tested. Its CD spectra in TFE (Figure 1A) revealed

Table 1. Sequences of gomesin and of the synthetic peptides.

Nº	Peptide	Sequence
I	Gomesin (Gm)	ZCRRLCYKQRCVTYCRGR-NH_2
II	D-Gomesin	**ZCRRLCYKQRCVTYCRGR**-NH_2
III	[$Ser^{2,6,11,15}$]-Gm	ZSRRLSYKQRSVTYSRGR-NH_2
IV	[$Cys^{2,15}$ / $Ser^{6,11}$]-Gm	ZCRRLSYKQRSVTYCRGR-NH_2
V	[$Ser^{2,15}$ / $Cys^{6,11}$]-Gm	ZSRRLCYKQRCVTYSRGR-NH_2

Bold letters correspond to D-amino acids.

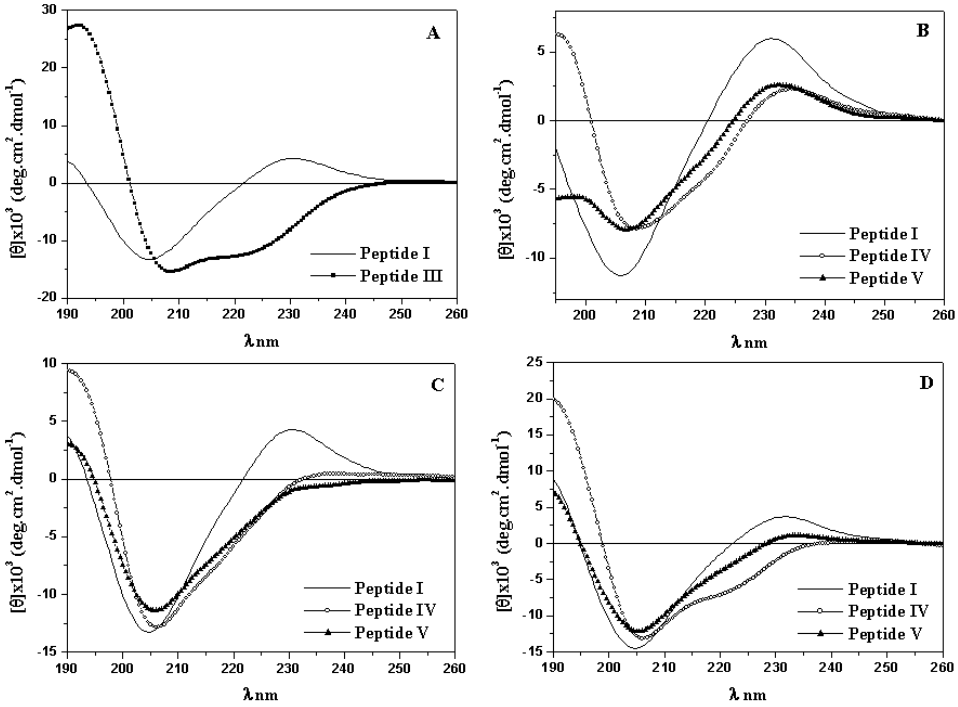

Fig. 1. CD spectra: A) Linear peptide in 70% TFE; B, C and D) Monocyclic analogues in 70% methanol, 70% TFE and 10 mM SDS, respectively.

α-helical conformation while in methanol and SDS micelles indicated unordered and β-sheet structure, respectively (data not shown). Therefore, the absence of the disulfide constraints allowed peptide **III** to adopt different conformations in the environment employed. Peptides **IV** and **V** showed to be just 2-4-fold less active than gomesin. Their CD spectra in methanol (Figure 1B) and TFE (Figure 1C) showed that both analogues have the tendency to assume β-turn structure since they present a negative band at 205 nm [5]. CD spectrum of peptide **IV** in SDS (Figure 1D) presented typical shape of coexisting structures, in this case unordered and β-turn structure. The spectrum of peptide **V** in the same medium showed to be similar to that of gomesin although with lower ellipticity intensities. Thus, these results suggested that the spatial amino acids distribution, the presence of at least one disulfide bridge and the β-hairpin conformation presented by gomesin are crucial elements for its antimicrobial activity.

Acknowledgments

This work was supported by grants and fellowships from CNPq and FAPESP.

References

1. Silva Jr., P. I., Daffre, S., and Bulet, P. *J. Biol. Chem.* **275**, 33464-33470 (2000).
2. Mandard, N., Bulet, P., Caille, A., et al. *Eur. J. Biochem.* **269**, 1190-1198 (2002).
3. Fázio, M. A. et al. In Lebl, M. and Houghten, R. A. (Eds) *Peptides: The Wave of the Future* (*Proceedings of the 17th APS)*, American Peptide Society, San Diego, 2001, p. 495.
4. Heller, W. T., Waring, A. J., Lehrer, R. I. and Huang, H. W. *Biochemistry* **37**, 17331-17338 (1998).
5. Perczel, A., Hollósi, M., Foxman, B. M. and Fasman, G. D. *JACS* **113**, 9772-9784 (1991).

Peptide Revolution: Genomics, Proteomics & Therapeutics
Michael Chorev & Tomi K. Sawyer (Editors)
American Peptide Society, 2003

Small L- and D-Amino Acid Peptides Antagonize HIV-1 Replication

César Boggiano and Sylvie E. Blondelle

Torrey Pines Institute for Molecular Studies, San Diego, CA 92121, USA

Introduction

A number of reports have now not only demonstrated the potential of human immunodeficiency virus type 1 (HIV-1) peptide antagonists as drug candidates, but also the flexibility of peptides to specifically antagonize separate steps of the HIV-1 life cycle. In particular, clinical trials have shown that the 36-amino acid long peptide T20 corresponding to a region of HIV-1 glycoprotein gp41 provides significant viral suppression and immunologic benefit as part of a background antiretroviral regimen [1]. Since attachment and membrane fusion are the first steps in HIV-1 infection process, therapeutic approaches involving the inhibition of HIV-1 mediated membrane fusion are gaining importance. In the present study, synthetic peptide combinatorial libraries (SCLs) were used as sources to generate novel peptide antagonists of HIV-1 replication of both X4 and R5 viruses via blockage of HIV-1 Env mediated fusion process.

In particular, a L-amino acid nonapeptide SCL (free C- and N-terminus) and a D-amino acid decapeptide SCL (N-acetylated and C-amidated), both in a positional scanning (PS) format [2] which allows the determination of key functionalities at all diversity positions in a single screening assay, were used in these studies. All 20 L- or D-amino acids were inserted at the defined positions ("O" positions), while L- or D-cysteine was omitted from the mixture positions ("X" positions) in order to avoid polymerization. The L-amino acid nonapeptide SCL was made up of nine separate sublibraries, each containing 20 mixtures for a total of 180 separate mixtures to be tested, each sublibrary containing the same total 3.4×10^{11} nonapeptide sequences present in the entire library. The D-amino acid decapeptide PS-SCL was made up of 10 sublibraries, each containing the same 6.5×10^{12} individual decapeptides.

Results and Discussion

All mixtures of the L-amino acid nonapeptide PS-SCL and D-amino acid decapeptide PS-SCL were assayed for their ability to inhibit HIV-1 Env fusogenic activity in two assay systems mimicking X4 (T-cell line tropism) and R5 (macrophage tropism) infection [3,4]. Based on the two screening profiles in the X4 and R5 systems, 44 L-amino acid nonapeptides were generated: 32 from a direct deconvolution of the screening profile in the X4 system peptides (LA series) and 12 from a selected amino acid combination from active mixtures in R5 having different chemical character (LB series). Similarly, 55 D-amino acid decapeptides were generated: 16 from a direct deconvolution of the screening profile in the X4 system (DA series), 22 from a selected amino acid combination from other active mixtures in X4 and different chemical character (DB series), and 17 from a selected amino acid combination based on the screening results in the R5 system (DC series).

Thirty-four of the forty-four L-amino acid nonapeptides inhibited the HIV-1 Env-mediated membrane fusion using the X4 co-receptor with IC_{50} values lower than 10μM, while none of them exhibited activity greater than 50% inhibition at 50μM when using the R5 co-receptor. Similarly, none of the D-amino acid decapeptides selected based on the X4 screening results exhibited activity greater than 50% inhibition at 40μM in the Env mediated fusion assay using the CCR5 co-receptor,

Table 1. Inhibition of HIV-1 entry.

Peptide	% Inhibition[a]			
	JC2 (X4)	JRFL (R5)	ADA (R5)	VSV
Ac-wiceyiywdd-NH_2 (16μM)	31	7	58	28
Ac-rrmyrriyrr-NH_2 (3μM)	28	94	78	17

[a]*Inhibition is measured by detection of emission light using a luciferase substrate.*

while seventeen of these peptides had IC_{50} values lower than 10μM in the Env mediated fusion assay that uses CXCR4 co-receptor. In agreement with the library screening results, the most active L- or D-amino acid peptides in the X4 system was derived from the direct deconvolution of the most active mixtures in that system. In contrast, 15 of the 17 D-amino acid decapeptides selected based on the R5 screening results exhibited similar activity in the two fusion assay systems (R5 and X4) with IC_{50} values lower than 10μM.

The most active peptides were assayed for inhibition of replication of the X4 HIV-1 laboratory strain IIIb (X4), two R5 HIV-1 strains, a laboratory strain JRCSF (R5) and a clinical isolate resistant to AZT AB28 (R5), and a dual tropic virus SF2(X4R5). Among the L-amino acid nonapeptides, only NWEIWMECL-OH showed inhibitory activity at concentration lower than 50μM. In contrast, all of the D-amino acid decapeptides tested showed inhibitory activity of replication with IC_{50} between 5 and 30μM (Figure 1), which is in the same range as the inhibitory effect of the membrane fusion.

All peptides were found to be specific to HIV-1 as shown in an entry assay using defective HIV-1 NL4-3 pseudotyped with Envs from different HIV-1 strains [5]. Thus, the viruses carry a reporter gene for luciferase replacing nef and are pseudotyped with different viral Envs, which restrict the viruses to a single cycle of replication. While inhibition was observed for specific HIV-1 pseudotyped viruses, none of the peptides inhibited the entry of virions pseudotyped with amphotropic vesicular stomatitis virus (VSV) Env (Table 1).

A possible mechanism of action for the peptide inhibitors is through blockade of HIV gp120/CD4/coreceptor interaction. The most active peptides were tested for inhibition of receptor recognition and analyzed by flow cytometry using three

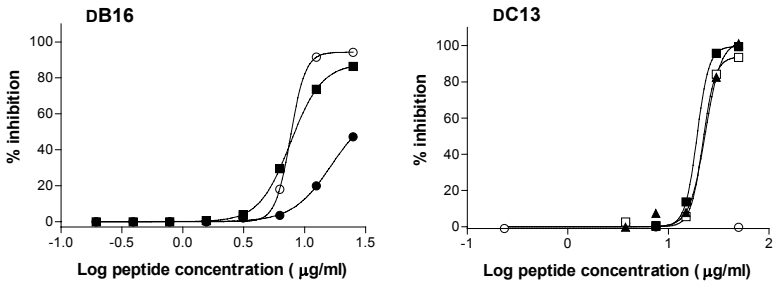

Fig. 1. Inhibition of HIV-1 replication by two representative D-amino acid decapeptides: (■) IIIb (X4), (□) SF2 (X4), (▲) SF2 (R5), (■) JRCSF (R5), and (○) AB28 (R5) viruses.

monoclonal antibodies (mAb) specific for CD4, CCR5 and CXCR4. Each mAb can block the replication of HIV-1 disrupting the interaction between gp120 and the cellular receptor. The inhibition of the chemotactic response of CCRF-CEM cells to the physiological CXCR4 agonist SDF-1α [6] was also examined. Only peptides from the DC series were able to block the recognition of a CXCR4 mAb. Thus, while those arginine-rich peptides were found to abrogate the recognition of the antibody 12G5 αCXCR4 and chemotaxis induced by SDF-1α, no direct correlation can be drawn between the ability to block CXCR4 recognition and inhibition of HIV-1 replication. Since the N-terminal domains of CXCR4 and CCR5 are rich in anionic amino acids and sulfated tyrosines, which participate in gp120 recognition, one can envision such cationic peptides as interacting with the co-receptor N-terminal regions, resulting in inhibition of HIV gp120/CD4/coreceptor interaction.

Acknowledgments

The authors thank Dr. Berger at the National Institute of Allergy and Infectious Diseases for providing the vaccinia virus constructs, Dr. Landau for providing the molecular clone of HIV-1 NL4-3 and *env* plasmids, and Dr. Mosier at the Scripps Research Institute for providing the HIV-1 isolates. This research was supported in part by Universitywide AIDS Research Program grant #R 98 TPI 064, and by National Institute of Dental and Craniofacial Research grant #RO1 DE12923.

References

1. Lazzarin, A., Clotet, B., Cooper, D., Reynes, J., Arasteh, K., Nelson, M., Katlama, C., Stellbrink, H. J., Delfraissy, J. F., Lange, J., Huson, L., DeMasi, R., Wat, C., Delehanty, J., Drobnes, C. and Salgo, M. *N. Engl. J. Med.* **348**, 2186-2195 (2003).
2. Pinilla, C., Appel, .R., Blanc, P. and Houghten, R. A. *Biotechniques* **13**, 901-905 (1992).
3. Nussbaum, O., Broder, C. C. and Berger, E. A. *J. Virol.* **68,** 5411-5422 (1994).
4. Boggiano, C., Reixach, N., Pinilla, C. and Blondelle, S. E. *Biopolymers (Peptide Sci.)* **71**, 103-116 (2003).
5. Connor, R. I., Chen, B. K., Choe, S. and Landau, N. R. *Virology* **206**, 935-944 (1995).
6. Hesselgesser, J., Liang, M., Hoxie, J., Greenberg, M., Brass, L. F., Orsini, M. J., Taub, D. and Horuk, R. *J. Immunol.* **160**, 877-883 (1998).

Peptide Revolution: Genomics, Proteomics & Therapeutics
Michael Chorev & Tomi K. Sawyer (Editors)
American Peptide Society, 2003

Structure-Function Relationship of Peptide Analogues of Gaegurin 4, an Antimicrobial Peptide Isolated from a Korean Frog

Hyung-Sik Won and Bong-Jin Lee

National Research Laboratory (MPS), College of Pharmacy, Seoul National University, San 56-1, Shillim-Dong, Kwanak-Gu, Seoul 151-742, Korea

Introduction

Antimicrobial peptides are an integral part of the non-specific immune defence system [1]. It is becoming clear that antimicrobial peptides are an important component of the innate defenses of all species [2]. It has been shown that peptide-lipid interactions leading to membrane permeation play a role in their activity [3]. A number of peptides with a broad-spectrum of antimicrobial activities have been isolated from the skin of various amphibians, and six antimicrobial peptides, named gaegurins (GGNs), were also isolated from the skin of a Korean frog, *Rana rugosa* [4]. Such peptides with no or little hemolytic activity are considered as target molecules for the development of new antibiotic or anticancer agents by peptide engineering. Out of the six gaegurins, GGN4 has the longest length (37 residues) and is the most abundant in the frog skin. GGN4 adopts a random structure in an aqueous solution, but adopts a helical conformation consisting of two amphipathic α-helices (residues 2-10 and 16-32) in membrane-mimetic environments [5]. In the present study, as part of an effort to discovery a target molecule with lower molecular mass for potential peptide antibiotics, the structure-function relationships of several GGN4 analogues with C-terminal truncations were analyzed by CD, NMR and fluorescence spectroscopy.

Results and Discussion

The C-terminal 14 residue truncated GGN4 ($\Delta^{24\text{-}37}$ GGN4) showed no significant biological activity. Surprisingly, D16W-$\Delta^{24\text{-}37}$ GGN4 showed antimicrobial activity comparable to that of native GGN4 and less hemolytic activity. Neither K15W nor D16F substitution restored the antimicrobial activity as effective as that by D16W substitution. This suggests that position 16 is the most effective position for a single tryptophanyl substitution to increase the antimicrobial activity of the C-terminally truncated GGN4, and that the introduced single Trp would have an amino-acid specific role in the biological action of the peptide. Based on the CD spectra, all of the peptides showed a common conformational change from a random-coil in aqueous solution to an α-helix in membrane-mimetic solvents (50% TFE/water, 5 mM DPC micelles, and 10 mM SDS micelles). Among the 23-residue analogues, the most active analogue, D16W-$\Delta^{24\text{-}37}$ GGN4, showed the most stabilized helical content, indicating the functional importance of the helical stability. The tryptophan fluorescence emission spectra of D16W-$\Delta^{24\text{-}37}$ GGN4 showed a blue shift of 13 nm, from 357 nm in water to 344 nm in SDS micelles, with a concurrent decrease of the peak intensity by about 13%. Particularly, the large blue shift of more than 10 nm indicates that the Trp residue (W16) of D16W-$\Delta^{24\text{-}37}$ GGN4 anchors into the hydrophobic core of the SDS micelle

The NMR structure (Figure 1) of $\Delta^{24\text{-}37}$ GGN4 in 50% TFE/water showed a well-ordered N-terminal α-helix (I2~K11), but the other parts (G12~Q23) showed no significant secondary structure. In contrast, D16W-$\Delta^{24\text{-}37}$ GGN4 showed a structure with stable long α-helix: I2~V18 in 50% TFE/water and I2~G20 in 300 mM SDS micelles. This indicates that the W16 would stabilize the potential helical propensity [5] of the previous loop region (residues 11-15) as well as the C-terminal helix

destabilized by truncation. The helical structures of D16W-$\Delta^{24\text{-}37}$ GGN4 showed typical amphipathic characteristics (Figure 1). Thus, it can be deduced that the positively charged hydrophilic side would easily recognize and bind to the negatively charged membrane surface of microorganisms. Indeed, in the NOESY spectra, the observed intra-residue NOEs between the side-chain H^{ε} and H^{ζ} atoms of Lys residues, which could not be observed in TFE/water mixture, indicated that the lysine sidechains are immobilized in SDS micelles. The C-terminally more lengthened α-helical structure in SDS micelles than that in 50% TFE also suggests a possible electrostatic interaction between the K19 and the SDS micelles. In contrast, the observed intermolecular NOE cross-peaks between the SDS methylene protons and the peptide backbone amide and aromatic ring protons of the F9, V13, and W16 residues, suggested that the non-polar residues in the hydrophobic face of D16W-$\Delta^{24\text{-}37}$ GGN4 would contact the core region of SDS micelles by hydrophobic interactions.

In both 50% TFE/water and SDS micelles, the W16 residue was located at the hydrophobic-hydrophilic interface of the amphipathic helix (Figure 1). This location would be advantageous to facilitate the amphipathic interaction between the peptide and the membrane surface, since the Trp sidechain is amphiphilic in nature. The orientation of the Trp side chain from the helical axis was quite different between the two conditions, despite the well-converged backbone conformation; i.e., the W16 sidechain slanted toward the hydrophilic face in 50% TFE, while toward the hydrophobic face in SDS micelles. As the SDS micelle more closely mimics the amphiphilic environment of a biological phospholipid bilayer than TFE does, this difference in orientation seems to imply the anchoring role of the residue in the membrane-binding process of D16W-$\Delta^{24\text{-}37}$ GGN4.

Altogether, the present results not only contribute to a better understanding of the structure-activity relationships of a group of antimicrobial peptides with a linear amphipathic α-helix, but also suggest that the D16W-$\Delta^{24\text{-}37}$ GGN4 could be considered as a potential target molecule for new peptide antibiotics. In addition, from the present results, the utility of a tryptophan insertion can be proposed for peptide engineering to enhance the helical propensity and/or membrane-interacting ability.

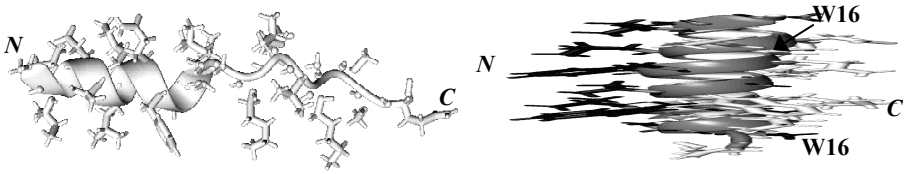

Fig. 1. Ribbon presentation of the refined average structure. Left: Δ24-37 GGN4 in 50% TFE/water. Right: Superimposed structure of D16W Δ24-37 GGN4 in 50% TFE (backbone and W16 sidechain colored in white) and in SDS micelles (backbone in gray, W16 and hydrophobic sidechains in black, and hydrophilic sidechains in white).

Acknowledgments

This work was supported by National Research Laboratory Program (M1-0203-00-0075) from Korea Institute Science & Technology Evaluation and Planning.

References

1. Park, S. H., et al. *Biochem. J.* **368,** 171-182 (2002).
2. Park, S., et al. *FEBS Lett.* **507,** 95-100 (2001).
3. Won, H.- S., et al. *Eur. J. Biochem.* **269,** 4367-4374 (2002).
4. Park, J. M., Jung, J. E. and Lee, B. *Biochem. Biophys. Res. Commun.* **205,** 948-954 (1994).
5. Park, S.- H., et al. *Eur. J. Biochem.* **267,** 2695-2704 (2000).

Peptide Revolution: Genomics, Proteomics & Therapeutics
Michael Chorev & Tomi K. Sawyer (Editors)
American Peptide Society, 2003

Fragments of HIV GAG Polyproteins Expressing Affinity to Opioid Receptors

Andrzej W. Lipkowski[1], Piotr Kosson[1], Aleksandra Misicka[2], Daniel B. Carr[3], Victor J. Hruby[4], Masaaki Yoshikawa[5], Fanni Toth[6] and Geza Toth[6]

[1]Medical Research Centre, 02103 Warsaw, Poland; [2]Department of Chemistry, Warsaw University, 02093 Warsaw, Poland; [3]New England Medical Center, Boston, MA, USA; [4]Department of Chemistry, University of Arizona, Tucson, AZ 85721, USA; [5]Kyoto University, Uji, Japan; [6]Biological Research Center, Szeged, Hungary

Introduction

The current consensus mechanism for HIV entry into host cells (e.g., T cells) involves an interaction between the virus and the CD4 receptor, the chemokine "co-receptors" [1]. Nevertheless, increasing evidence indicates that HIV infects cells such as neurons that lack CD4 receptors and/or established co-receptors. These observations prompted us to search for alternative cell membrane receptors to which the virus may bind and thereby enter cells. The distribution of opioid receptors in immunocytes and neurons overlaps well with targets that may be infected by HIV. In addition, some data indicates a partially protective effect of opioid ligands on HIV infection [2,3]. Therefore, opioid receptors might be considered as a potential target for HIV. In our general screening of intraprotein sequences that may interact with opioid receptors, motifs with the general formula ...-AA-Tyr-AA2-Arg/Lys-Trp/Phe-... have been identified as potential opioid receptor ligands [4]. Screening of protein sequence databases disclosed a match between this sequence and intraprotein fragments of p24 GAG protein. Interestingly, mutations within this fragment preserve affinity for opioid receptors (Table 1).

Table 1. Opioid-like motifs identified in p24 protein of HIV-1, HIV-2 and SIV viruses (located in GAG protein apr 255).

Peptide Motif	Virus strain
GEIYKRWIILG	GAG_HV1A2; HV1BI; HV1B5; HV1BR; HV1C4; HV1H2; HV1J3; HV1JR; HV1LW; HV1N5; HV1ND; HV1OY; HV1PV; HV1RH; HV1W2; HV1Y2
GEIYKRWIIVG	GAG_HV1EL
GDIYKRWIILG	GAG_HV1MA
GDIYRRWIILG	GAG_HV1U4
GNIYRRWIQIG	GAG_HV2BE; HV2CA; HV2D1; HV2G1; HV2KR; HV2SB;
GNIYRRWIQLG	GAG_HV2D2; SIVM1; SIVMS; SIVS4; SIVSP
GSIYRRWIQIG	GAG_HV2ST;
GAIYRRWIILG	GAG_SIVA1; SIVAG; SIVAT
GDVYRRWVILG	GAG_SIVCZ
GNIYRRWIQLR	GAG_SIVMK
GTIYKSWIILG	GAG_SIVGB

Results and Discussion

Peptide library synthesis: Libraries of analogs of intraprotein fragments were synthesized (Table 1). To simulate the intraprotein location of these sequences, Gly(1) and Gly(11) were replaced with acetyl and amide groups, respectively.

Molecular modeling: In parent p24 proteins the selected opioid fragment lies within an α-helix. Therefore, we performed molecular modeling of selected fragments that possess an alpha-helical structure. We observed that all these motifs share the common feature that two basic amino acids follow tyrosine, and so may adopt conformations that place the phenol group of tyrosine in a classical opioid "tyramine-like topographical construct". The basic group on the side chains of the amino acid residues following tyrosine may serve to enhance the recognition of κ receptors.

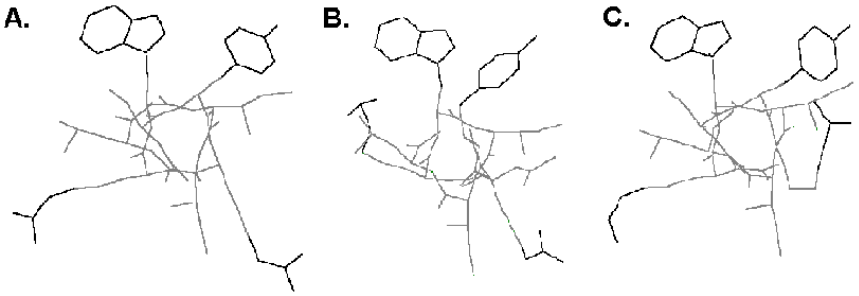

Fig. 1. Ac-SYRRWIIL-NH2 in common alpha helical structure (A), and possible "opioid" topography Y-R^{+2} (B) and Y-R^{+1} (C) .

Opioid receptor binding: All the synthesized peptides have affinity for μ opioid receptors in rat brain homogenates in the 0.5 -1.5 micromolar range, and lacked affinity for δ receptors up to 50 μM.

Stimulation of [^{35}S]GTP binding: Two of the synthesized peptide analogues, Ac-AIYRRWIILK-NH_2 (**I**) and Ac-SYRRWIIL-NH_2 (**II**), have been examined for stimulation of [^{35}S]GTP binding. Both peptides were active, indicating that they are opioid agonists (Figure 2A). Surprisingly the stimulatory effect was not reversed with naloxone (Figure 2B), suggesting that they activate other, non-opioid receptors as well.

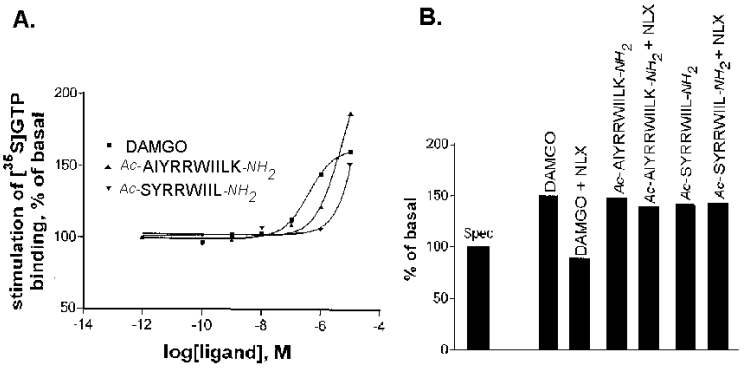

Fig. 2. The stimulation of [35S]GTP binding assay.

Antinociceptive assay: Because of their low solubility, peptides **I** and **II** were tested intrathecally (i.t.) as a peptide/cyclodextran complex. Single i.t. doses of 5 ug of each peptide possessed significant antinociceptive activity in the rat tailflick assay.

Current agents for HIV therapy are not uniformly effective. In addition, the currently accepted model of infection fails to account for infection of cells (e.g., neurons) that lack CD4 and/or coreceptors. The present results suggest that peptide motifs within p24 proteins may interact with opioid and likely other, unidentified neuromembrane receptors. P24 protein has been identified in the serum of HIV-positive individuals. Serum concentrations of this protein may correlate better with disease progression [5] than does the HIV viral load assayed by shell protein levels. Others have shown that p24 protein alone may form a capsid containing RNA [6, and references cited therein]. Keeping in mind the parsimonious processes evolved by viruses, an alternative mechanism for HIV infection may be envisaged. We hypothesize that, in parallel with the formation of fully developed HIV viruses, capsids of p24 proteins with RNA may be formed and released. Because of their higher sensitivity to environmental conditions, capsids p24 are probably unable to spread disease between individual hosts. Nevertheless, they are stable enough to effectively penetrate (potentially with greater effectiveness than the full HIV virus) various tissues within the host organism. Because the recognition elements on the p24 capsid protein differ from those of the full HIV virus, the former may interact with distinct membrane receptors that are inaccessible to the latter. Because the p24 capsid is smaller than whole virus, the simple mechanisms of pinocytosis/endocytosis may suffice for its internalization within host cells. A key question to be answered is at which stage of viral replication the RNA-laden capsids are formed and/or released.

Our hypothesis implies that inhibition of host cell recognition sites other than those for HIV shell (p120) proteins may offer a useful strategy for drug therapy not only of HIV/AIDS, but also for other conditions (e.g., some cancers) that result from retroviral infection. Finally, we believe that our findings provide a novel rationale for inclusion of opioid-like ligands within the arsenal of components for multidrug treatment of HIV/AIDS.

References

1. Kilby J. M. and Eron, J. J. *N. Engl. J. Med*. **348**, 2228-2238 (2003).
2. Tang, J. L., Lipkowski, A. W. and Specter, S. *Int. J. Immunopharmacol*. **20**, 457-466 (1998).
3. Peterson, P. K., Gekker, G., Lokensgoral, J. R., Bidlack, J. M., Chang, A. C., Fang, X. and Portoghese, P. S. *Biochem. Pharmacol*. **61**, 1145-1151 (2001).
4. Misicka, A., Lachwa, M., Carr, D. B., Hruby, V. J., Yoshikawa, M. and Lipkowski, A. W. In Okada, Y. and Lazarus, L. H. (Eds.) *Proceedings of Opioid Mimetic Analgesics 2002,* Kobe Gaikuim University, Kobe, 2002, p. 53-54.
5. Ofori, H., Prokop, J. and Jagodzinski, P. P. *Biomed. Pharmacother*. **57**, 15-19 (2003).
6. Gross, I., Hohenberger, H., Wilk, T., Wiegers, K., Grattinger, M., Muller, B., Fuller, S. and Krausslich, H. G. *EMBO J*. **19**, 103-113 (2000).

Peptide Revolution: Genomics, Proteomics & Therapeutics
Michael Chorev & Tomi K. Sawyer (Editors)
American Peptide Society, 2003

Dimeric Analogs of the Immunosuppressory Fragment of HLA-DR

Zbigniew Szewczuk[1], Monika Biernat[1], Marcin Dyba[1] and Michal Zimecki[2]

[1]Faculty of Chemistry, University of Wrocaw, 50-383 Wrocaw, Poland; [2]Institute of Immunology and Experimental Therapy PAS, 53-114 Wrocaw, Poland

Introduction

Our previous studies revealed that the nonapeptide fragment of human histocompatibility antigens (HLA) class DR, located in the β 164-172 loop with the VPRSGEVYT sequence, suppresses the immune response [1]. The sequence is located on the loop of the molecule exposed toward the solvent and, therefore, may be involved in interactions with other proteins. We suggest that the loop may serve as a functional epitope on the HLA class II surface for intermolecular binding. The possible mechanism of biological action of the synthesized peptides is connected to specific interference of adhesion between HLA class II molecules and their coreceptors [2,3]. It has been postulated that oligomerization of the coreceptors is required for stable binding to class II HLA [4]. On the basis of the crystal dimeric structure of HLA-DR [5], we designed and synthesized molecules able to induce the putative coreceptors dimerization, which consist of two VPRSGEVYT sequences linked through their C-termini by spacers of different length (Figure 1).

I. (H-VPRSGEVYT***GGGG)$_2$K-NH$_2$*** (31)
II. (H-VPRSGEVYT***GGGGG)$_2$K-NH$_2$*** (37)
III. (H-VPRSGEVYT***GGGGGG)$_2$K-NH$_2$*** (43)
IV. H-VPRSGEVYT***GGGGGG-NH$_2$***

*Fig. 1. Synthetic dimeric analogs of the immunomodulatory fragment of HLA-DR molecules (**I-III**) and their monomeric counterpart containing six glycine residues at C-terminus (**IV**). The linker structure is given in bold; numbers of atom in linker are in brackets-counting only the atoms contributing to the length of the linker.*

Results and Discussion

The bivalent analog should consist of two monomers covalently linked by a spacer with sufficient length to allow for positioning in the same orientation as in the superdimers. Therefore, we began the design by examining the three-dimensional structure of the superdimers [5] (Figure 2A). To quickly determine the optimal linker length, we decided to synthesize a series of dimeric analogs containing linkers of various lengths. Whereas compound **I** contains a 31-atom linker, which is too short to orient the suppressors in the same position as in the crystal structure, its analogs **II** and **III** possess sufficient length of the linkers (Figure 2B and 2C). The 43-atom linker in compound **III** seems even longer than necessary, although flexible enough to orient the peptides more precisely, and without any distortion.

Peptides were prepared by manual solid-phase techniques. The peptide was assembled on the solid support, using standard Fmoc procedure. The first amino acid attached to the MBHA-Rink Amide resin (0.55mmol/g) was di-Fmoc-Lys in case of dimeric compounds. Successive amino acids were coupled simultaneously to the α and ε-amino groups of the lysine residue.

The synthesized peptides were investigated for their activities in the humoral and cellular immune responses. Their potencies were compared to that of cyclosporine

(CSA). Dimeric peptides **II** and **III** exhibited higher potencies than their linear counterpart **IV**. The immunosuppressory activity of the dimeric peptides depended on their linker length. Both in humoral and cellular immune response, the shorter linker dimeric analog **I** exhibited the weakest potency in the series, although slightly higher than that of its monomeric analog **IV.** The longer linker analogs (**II** and **III)** were very active immunosuppressants, more effective than CSA. CD spectra of compounds **I**–**IV** were similar to each other, suggesting that dimerization has little effect on stabilization of their structure in water solution. The unstructured conformation of the linker may enable the orientation the immunosuppressory peptides in a desired position.

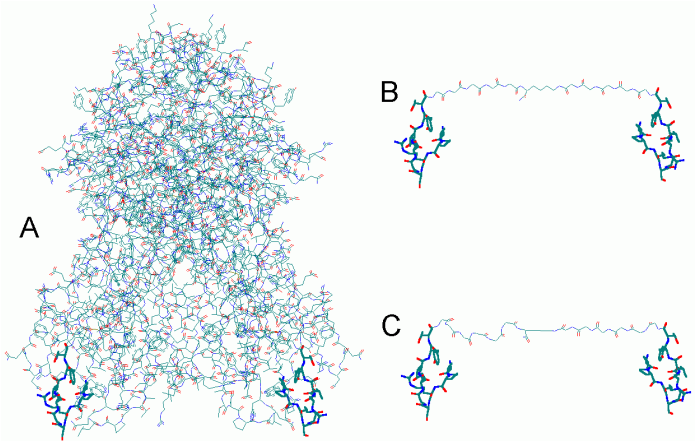

Fig. 2. ***A.*** *View of the superdimer of human class II histocompatibility antigen HLA-DR. The β164-172 loops with the immunosuppressive sequences (VPRSGEVYT) are in bold.* ***B.*** *Peptide contains a 37-atom linker that is able to span the distance between the carbonyl groups of* $Thr^{\beta 172}$ *as in the superdimer structure.* ***C****.43-atom linker is longer than necessary and may have conformational flexibility to orient the VPRSGEVYT loops in the same position as in the crystal structure.*

Our results demonstrate that the immunosuppressive activity of β 164-172 fragment of HLA-DR is enhanced by its dimerization. The linker length affects the immunosuppressory effects.

Acknowledgments

This work was supported by Grant No. 6P05A 013 21 from the State Committee for Scientific Research (KBN, Poland).

References

1. Szewczuk, Z., Wilczyński, A., Stefanowicz, P., Fedorowicz, W., Siemion, I. Z. and Wieczorek, Z. *Molec. Immunol*. **36**, 525 (1999).
2. Szewczuk, Z., Buczek, P., Stefanowicz, P., Krajewski, K., Siemion, I. Z. and Wieczorek, Z. *Acta Biochim. Polon.* **48**, 121-130 (2001).
3. Szewczuk, Z., Wilczyński, A., Dyba, M., Petry, I., Siemion, I. Z. and Wieczorek, Z. *Peptides* **21**, 1849-1858 (2000).
4. Sakihama, T., Smolyar, A. and Reinherz, E. L. *Proc. Natl. Acad. Sci. U.S.A.* **92**, 6444 (1995).
5. Brown, J. H., Jardetzky, T. S., Gorga, J. C.,Stern, L. J., Urban, R. G., Strominger, J. L. and Wiley, D. C. *Nature* **364**, 33-39 (1993).

Peptide Revolution: Genomics, Proteomics & Therapeutics
Michael Chorev & Tomi K. Sawyer (Editors)
American Peptide Society, 2003

Indolicidin Analogs with Potent Antibacterial Activity

Trine S. Neerup, Xavier Doisy, Dan Ifrah and Paul R. Hansen

Chemistry Department, The Royal Veterinary and Agricultural University,
1871 Frederiksberg C, Copenhagen, Denmark

Introduction

Indolicidin is a 13-residue antimicrobial peptide amide, H-ILPWKWPWWPWRR-NH_2, **1**, isolated from the cytoplasmic granules of bovine neutrophils [1]. The peptide is active against Gram-positive and Gram-negative bacteria, protozoa, fungi, and HIV. To investigate the importance of tryptophan in the antibacterial activity of indolicidin, we prepared peptide analogs (Figure 1) in which Trp-residues in positions 4, 6, 8, 9 and 11 were replaced with a single unnatural amino acid or *N*-substituted glycine (peptoid). The analogs were tested for antibacterial activity against *S. aureus* ATCC 25923 and *E. coli* ATCC 25922, using a broth microdilution assay modified from the method of Hancock [2]. Indolicidin and ampicillin were used as controls.

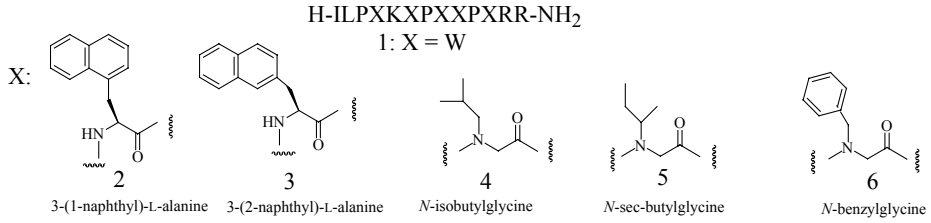

Fig. 1. Indolicidin analogs containing non-proteinogenic amino acid replacements used in this study.

Results and Discussion

Synthesis of Trp-replaced indolicidin analogs was accomplished manually, using a Tenta Gel S RAM resin and Fmoc solid-phase peptide chemistry.

Compounds **1**-**3**: Amino acids (4 equiv.) were coupled using DIPCDI (4 equiv.) and HOBt (4 equiv.) for 30 minutes. The resin was washed and drained and a 1hr recoupling was performed. Following synthesis, the peptide resins were washed, dried and cleaved using TFA:H_2O:triisopropylsilane.

Compounds **4**-**6**: Prepared as described above, except amino acids Pro^3, Lys^5, Pro^7, Pro^{10} (5 eq.), were coupled using HATU (5 eq.) and DIEA (10 eq.) in NMP for 2hr, followed by a 1hr recoupling step. The peptoid monomers replacing Trp in positions 4, 6, 8, 9 and 11 were coupled by adding 0.6 M bromoacetic acid (10 eq.) in NMP and 3.2 M DIPCDI (12.8 equiv). After 30 min a recoupling was performed. Following washing with NMP the side chain was introduced by nucleophilic substitution in NMP of the halide with a primary amine (40 equiv.) and agitated for 2hr. Cleavage from the resin was preformed as above. All indolicidin analogs were purified by preparative HPLC and characterized by LC-MS.

Table 1. Antibacterial activity of indolicidin and analogs.

	Compound	Minimum Inhibitory Concentration (μM)	
		S. aureus ATCC 25923	*E. coli* ATCC 25922
1	Indolicidin	2.0	4.0
2	[(3-(1-naphthyl) -L-Ala) ^{4,6,8,9,11}] indolicidin	1.2	4.6
3	[(3-(2-naphthyl) -L-Ala) ^{4,6,8,9,11}] indolicidin	1.2	2.3
4	[(*N*-(*iso*-butyl) Gly) ^{4,6,8,9,11}] indolicidin	> 41	> 41
5	[*N*-(*sec*-butyl) Gly) ^{4,6,8,9,11}] indolicidin	> 41	> 41
6	[(*N*-benzyl Gly) ^{4,6,8,9,11}] indolicidin	20.9	20.9

The most active of the indolicidin analogs containing tryptophan to naphthylalanine substitutions was compound **3**, [3-(2-naphthyl)-L-Ala)^{4,6,8,9,11}] indolicidin.

This analog was more active against *S. aureus* than against *E. coli,* with MIC values of 1.2 μM (2.3 μg/ml) and 2.3 μM (4.6 μg/ml), respectively. However, the related derivative **2** displayed the same activity as compound **3** against *S. aureus*, but was less active against *E. coli,* with MIC value of 4.6 μM (9.3 μg/ml). This may be explained in terms of steric hindrance. The 2-naphthyl ring is pushed further away from the extended peptide backbone as compared to the 1-naphthyl derivative, and enables the 2-naphthyl derivative to penetrate deeper into the outer membrane of *E. coli.* The aromatic side chain of both naphthyl derivatives are of similar size to that of tryptophan but possesses no hydrogen bonding ability. The finding that [(3-(2-naphthyl) -L-Ala) ^{4,6,8,9,11}] indolicidin (**3**) is more active than indolicidin indicates that the hydrogen bonding ability is not essential for antibacterial activity. The most active of the indolicidin analogs containing tryptophan to *N*-glycine derivative replacements, compounds **4**-**6**, was compound **6**, [*N*-benzyl Gly) ^{4,6,8,9,11}] indolicidin with MIC value of 20.9 μM (35.8 μg/ml) against both *S. aureus* and *E. coli.* The [(*N*-benzyl Gly) ^{4,6,8,9,11}] indolicidin derivative showed some activity but was still more than 8 times less active than parent indolicidin. The corresponding [(*N*-(*iso*-butyl) Gly) ^{4,6,8,9,11}] indolicidin compound **4** and [(*N*-(*sec*-butyl) Gly) ^{4,6,8,9,11}] indolicidin compound **5** did not display any significant antibacterial activity. These data suggest that all-tryptophan replacements with an aliphatic peptoid side-chain result in loss of antimicrobial activity.

In conclusion, we found that tryptophan is not essential in the antibacterial activity of indolicidin, which is in agreement with Subbalakshmi [3]. More active analogs than indolicidin were obtained by replacing tryptophan with unnatural aromatic amino acids.

Acknowledgments

We thank Ms. Jette Petersen, and Charlotte D. Sørensen for skillful technical assistance. Supported by the Danish Research Council grant number 9900234, Augustinus Foundation, Frimodt-Heineke Foundation and Dana Lim.

References

1. Selsted, M. E. *et al. J. Biol. Chem*. **267**, 4292-4295 (1992).
2. http://cmdr.ubc.ca/bobh/MIC.htm.
3. Subbalakshmi, C. *et al. Biochem. Biophys. Res. Comm*. **274**, 714-716 (2000).

Peptide Revolution: Genomics, Proteomics & Therapeutics
Michael Chorev & Tomi K. Sawyer (Editors)
American Peptide Society, 2003

MS PepKit: The First Diagnostic Test to Follow-up Multiple Sclerosis

Anna M. Papini[1], Barbara Mulinacci[1], Alfonso Carotenuto[2], Bruno Bonetti[3], Giuseppina Sabatino[1], Elisa Peroni[1], Francesca Nuti[1], Maria C. Alcaro[1], Maria C. Pozo-Carrero[4], Benedetta Mazzanti[1], Marta Pazzagli[4], Luca Massacesi[5], Luca Battistini[6], Mario Chelli[1], Paolo Rovero[2] and Francesco Lolli[5]

[1]Laboratory of Peptide Chemistry & Immunology, Dipartimento di Chimica Organica "Ugo Schiff", and CNR-ICCOM, Università di Firenze, I-50019 Sesto Fiorentino (FI), Italy; [2]Dipartimento di Scienze Farmaceutiche, Università di Salerno, I-84084 Fisciano (SA), Italy; [3]Clinica Neurologica, Azienda Ospedaliera di Verona, I-37134 Verona, Italy; [4]C.S.F. S.r.l., I-50124 Firenze, Italy; [5]Azienda Ospedaliera Careggi, and Dipartimento di Scienze Neurologiche e Psichiatriche, Università di Firenze, I-50134 Firenze, Italy; [6]Istituto di Ricovero e Cura a Carattere Scientifico (IRCCS), Fondazione Santa Lucia, Unità di Neuroimmunologia, I-00179 Roma, Italy

Introduction

Multiple Sclerosis (MS) is the most known neurological disease of the CNS. It is an inflammatory, demyelinating disease, which affects young adults of Northern Europe and Northern America with a definite relationship with latitude. In the world there are about 2 million patients with MS. In the United States there are about 350,000 patients with MS, including approximately 200 new cases per week. It is not a life-shortening disease with huge social costs estimated around $2.5 billion in the United States.

Because of the high variability of the disease course and of the different responses to therapeutic treatments, it is more and more accepted that MS is not a single disease, but rather a group of diseases in which demyelination is mediated by different pathogenic mechanisms.

We focused our research on the characterization of the disease subgroup in which demyelination is mediated by autoantibodies (auto-Abs). This pathogenic mechanism seems to correlate with relapsing-remitting MS (RR-MS), one of the most common MS disease course. In recent years, the role of auto-Abs in the pathogenesis of MS has been reevaluated. In a recent study, anti-myelin Abs have been shown to be important as predictors of the disease [1]. In particular glycoproteins and glycolipids are important components of myelin because glycosyl moieties are exposed at the surface of myelin, and therefore more susceptible to Ab attacks. Moreover, it is well known that glycosylation plays an important role in other autoimmune diseases such as rheumatoid arthritis [2].

Results and Discussion

We have previously reported that [Asn^{31}(Glc)]hMOG(30-50), a glycopeptide derived from an immunodominant epitope of myelin oligodendrocyte glycoprotein (MOG), glycosylated with a β-D-glucopyranosyl moiety on Asn at position 31 (native site of glycosylation of MOG), was able to detect high Ab titers in MS patients by solid phase indirect non-competitive ELISA (SP-ELISA). Moreover the Ab titer correlated with the disease activity [3]. The first insight that Asn(Glc), but not the MOG sequence, was important for Ab recognition was obtained by the conformational analysis of the

glycopeptide hMOG(30-50), in comparison with its unglycosylated counterpart. In fact, no significant differences were observed between the structures of the two peptides [4].

We subsequently synthesized a de novo designed glycopeptide, termed CSF114(Glc), containing the same amino acid residues as [Asn^{31}(Glc)]hMOG(30-50), but characterized by a β-hairpin secondary structure able to expose at the best Asn(Glc) on the tip of the β-turn.

It was definitively assessed that Asn(Glc) was the minimal epitope responsible for the auto-Ab recognition by competitive ELISA on anti-CSF114(Glc) Abs, using the CSF114-type glycopeptides of a focused library based on glycosyl amino acids diversity as inhibitors. Moreover the importance of the β-hairpin structure for the best exposition of the minimal epitope was demonstrated by SP-ELISA and competitive ELISA of the glycopeptides of a focused library based on structural diversity [5]. Therefore, CSF114(Glc) was selected as the best synthetic antigen able to detect the highest Ab titer, by SP-ELISA, in a 40% of MS patients sera, possibly corresponding to the subgroup of MS in which demyelination is antibody mediated.

Based on these data, we developed the first prototype of the diagnostic test, MS PepKit, based on SP-ELISA, able to detect pathogenic auto-Abs in MS patients sera [6]. An extensive validation study was completed in June 2003, on a total of 690 sera of MS patients followed longitudinally in comparison to blood donors (BD) and patients affected by inflammatory neurological diseases of the CNS, and by other autoimmune diseases (OAD). In particular, we examined a first group of 30 untreated RR-MS patients followed for 2 years every 6 months, for a total of 150 sera, with a parallel evaluation of the clinical relapses. We observed that IgG Ab titers of relapsing MS patients showed variations in the Ab titer during the observation period compared to remitting patients (Figure 1). The second group of 15 RR-MS patients has been followed with monthly blood tests for 3 years, the first 6 months with no therapeutic treatment, and parallel magnetic resonance imaging (MRI) lesions and clinical relapse evaluations.

In Figure 2 is a representative case from which we can see a high IgG level before MRI detectable lesions and clinical relapses were diagnosed. Moreover, the Ab titer lowers during the therapeutic treatment applied.

In conclusion, positive Ab titers for anti-CSF114(Glc) IgM can be detected in 40% RR-MS sera compared to < 5% BD, and OAD. The anti-CSF114(Glc) IgM Abs, detected in MS patients sera, are characterized by higher affinity compared to control sera. Finally in an RR-MS subgroup, high anti-CSF114(Glc) IgG Abs correlated with clinical relapses.

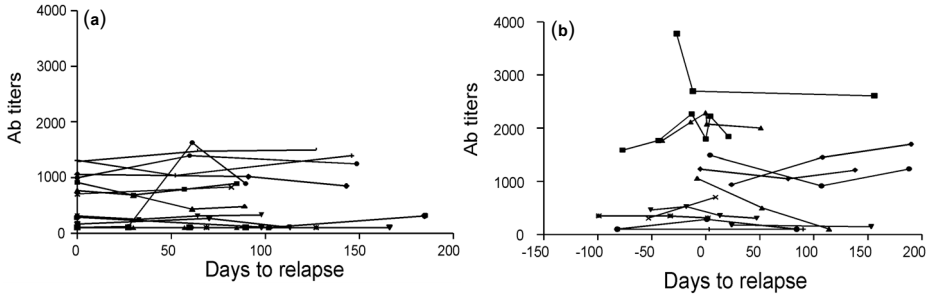

Fig. 1. Anti-CSF114(Glc) Ab titer in relapsing (a) and remitting (b) MS patients.

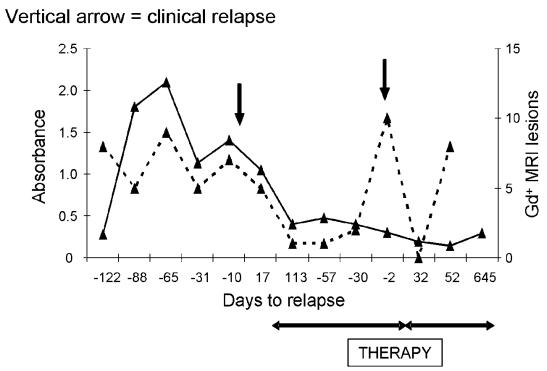

Fig. 2. Anti-CSF114(Glc) IgG in a representative RR-MS patient in parallel with MRI and clinical relapses evaluation.

Therefore, the MS PepKit is a reliable test to detect anti-CSF114(Glc) Abs correlating with clinical relapses. MS PepKit can be proposed as a diagnostic and prognostic test to follow-up the disease course of a subgroup of MS patients, most likely characterized by antibody mediated demyelination, to guide the best therapeutic treatment.

References

1. Antel, J.P. and Bar-Or, A. *N. Engl. J. Med.* **349**, 107-109 (2003).
2. Delves, P.J. *J. Autoimmunity* **27**, 239-253 (1998).
3. Mazzucco, S., Matà, S., Vergelli, M., Fioresi, R., Nardi, E., Mazzanti, B., Chelli, M., Lolli, F., Ginanneschi, M., Pinto, F., Massacesi, L. and Papini, A. M. *Bioorg. Med. Chem. Lett.* **9**, 167-172 (1999).
4. Carotenuto, A., D'Ursi, A.M., Nardi, E., Papini, A. M. and Rovero, P. *J. Med. Chem.* **44**, 2378-2381 (2001).
5. Lolli, F., Mulinacci, B., Carotenuto, A., Bonetti, B., Sabatino, G., Zipoli, V., Mastrangelo, E., Mazzanti, B., Pazzagli, M., Alcaro, M. C., Peroni, E., Marconi, S., Pozo-Carrero, M. C., Nuti, F., Battistini, L., Chelli, M., Rovero, P., Papini. A. M., manuscript submitted (2003).
6. Papini, A. M., Rovero, P., Chelli, M., Lolli, F., *Eur. Pat. Appl.* (2002), EP02-06767 20020619. Priority: IT 2001-FI114 20010622.

Peptide Revolution: Genomics, Proteomics & Therapeutics
Michael Chorev & Tomi K. Sawyer (Editors)
American Peptide Society, 2003

Structural Studies and Sequence Homology Investigations of the Guinea Pig Myelin Basic Protein (MBP) Epitope 74-85 Analogues

Andreas G. Tzakos[1], Patrick Fuchs[2], Nico A.J. van Nuland[2], Anastasios Troganis[3], Theodore Tselios[4], Spyros Deraos[4], George Deraos[4], Dimitrios Gatos[4], Ioannis P. Gerothanassis[1], Alexandre M.J.J. Bonvin[2] and John Matsoukas[4]

[1]Department of Chemistry, University of Ioannina, Ioannina Greece; [2]Bijvoet Center for Biomolecular Research Utrecht, the Netherlands; [3]Department of Biological Applications and Technologies, University of Ioannina, Greece; [4]Department of Chemistry, University of Patras, Patras 265 00, Greece

Introduction

Experimental autoimmune encephalomyelitis (EAE), an animal model of multiple sclerosis (MS), is induced in susceptible animals by immunodominant determinants of myelin basic protein (MBP) [1-4]. In order to characterize the molecular features of antigenic sites, which are important for designing EAE suppressing molecules, we carried out structural studies. We report NMR experimental data in conjunction with molecular dynamic simulations of the potent linear dodecapeptide epitope of the guinea pig MBP, Gln^{74}-Lys^{75}-Ser^{76}-Gln^{77}-Arg^{78}-Ser^{79}-Gln^{80}-Asp^{81}-Glu^{82}-Asn^{83}-Pro^{84}-Val^{85} (MBP$_{74\text{-}85}$), and its antagonist analogue Ala^{81}MBP$_{74\text{-}85}$.

Results and Discussion

Structure in Aqueous Solution: The MBP$_{74\text{-}85}$ epitope adopts a compact S-shaped conformation in aqueous solution with RMSDs of 0.90 ± 0.25 Å for the backbone N,

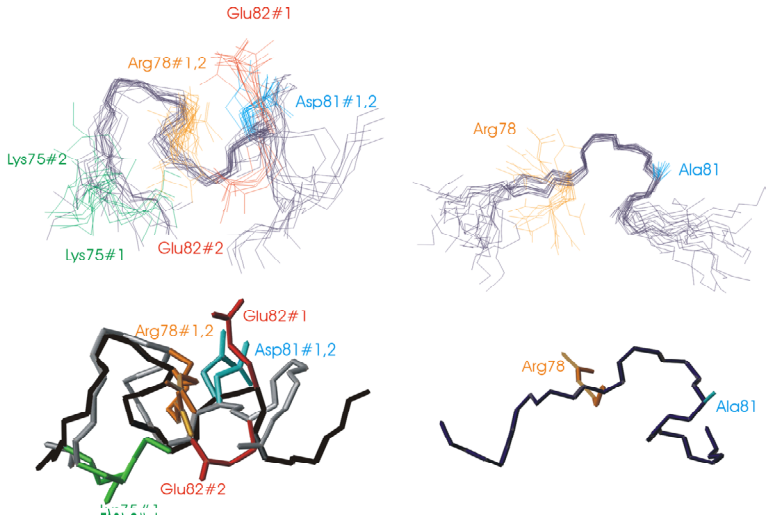

[A] **[B]**

Fig. 1. An ensemble of 20 3D structures of the agonist (A) and the antagonist (B), linear analogues of MBP$_{74\text{-}85}$, in aqueous solution. The lower thicker trace corresponds to a representative conformer whose structure is closest to the average structure of the ensemble.

C^{α}, C' atoms and 2.05 ± 0.55 Å for all heavy atoms for the mean structure of the Lys^{75} – Glu^{82} fragment. A characteristic feature of this ensemble of structures is the presence of two conformational families with different orientations of the side-chain of Glu^{82}. The $Ala^{81}MBP_{74-85}$ variant seems to adopt a more open U-shaped loop conformation of residues Arg^{78}–Ala^{81}. The RMSDs from the mean structure for the Lys^{75}–Glu^{82} fragment are 0.95 ± 0.40 Å and 2.65 ± 0.75 Å for backbone N, C^{α}, C' atoms and all heavy atoms, respectively.

Structure in DMSO Solution: The MBP_{74-85} epitope adopts a rather compact conformation with RMSDs of 1.05 ± 0.40 Å and 2.05 ± 0.60 Å for backbone N, C^{α}, C' atoms and all heavy atoms respectively for the mean structure of the Lys^{75}–Glu^{82} fragment. The $Ala^{81}MBP_{74-85}$ antagonist in DMSO adopts a less compact conformation than the MBP_{74-85} epitope with RMSDs from the mean structure for the Lys^{75}–Glu^{82} fragment of 1.90 ± 0.55 Å and 3.40 ± 0.80 Å for backbone N, C^{α}, C' atoms and all heavy atoms, respectively. The two peptides exhibit significantly different side-chain and backbone conformations in both H_2O and DMSO solutions. The agonist MBP_{74-85} adopts a compact conformation due to electrostatic interactions of Arg^{78} with the side-chains of Asp^{81} and Glu^{82}. Side-chain of Arg^{78} is, therefore, "locked" in a well-defined conformation, perpendicular to the peptide backbone that may be easily accessible for the action of enzymes. These electrostatic interactions are, however, absent in the case of the antagonist Ala^{81} MBP_{74-85}, resulting in a high flexibility of the side-chain of Arg^{78}. Sequence alignment of the 74-85 sequence of guinea pig with the same region of MBP's from other species [5], reveals high conservation of Gln^{74}, Lys^{75}, Ser^{76}, Arg^{78}, Asp^{81}, Glu^{82}, Asn^{83}, Pro^{84}, Val^{85} (numbers according to the guinea pig species). The studied segment of the guinea pig MBP_{74-85}, which lacks His^{77} – Gly^{78} that is present in the bovine MBP, has been reported to be much more encephalitogenic.

From the above findings it may be concluded that the positively charged residue Arg^{78} plays a significant role first, in the stabilization of the local microdomains (epitopes) of the integral protein; second, in a number of post-translational modifications relevant to multiple sclerosis such as the conversion of charged arginine residues to uncharged citruline and third, in the formation of the trimolecular T-cell receptor (TCR) –MBP_{74-85} –MHC II complex.

Acknowledgments

Financial support from the Greek General Secretary of Research and Technology (EPET II 15, PENED 1999) is gratefully acknowledged. The 750 MHz spectra were recorded at the SONNMR Large Scale Facility in Utrecht, which is funded by the 'Access to Research Infrastructures Programme of the European Union' (HPR1-CT-1999-00005). We also thank the SONNMR Large Scale Facility for the use of the computational facilities. Dr. T. Tselios was supported by the State Scholarship's Foundation (IKY).

References

1. Martin, R., McFarland, H. F. and McFarlin, D. E. *Annu. Rev. Immunol.* **10**, 153-187 (1992).
2. Steinman, L. *Cell* **85**, 299-302 (1996).
3. Kursula, P. *Int. J. Mol. Med*. **8**, 475-479 (2001).
4. Tselios, T., Probert, L., Daliani, I., Matsoukas, E., Troganis, A., Gerothanassis, I. P., Mavromoustakos, T., Moore, G. and Matsoukas, J. *J. Med. Chem.* **42**, 1170-1177 (1999).
5. Deber, C. M. and Reynolds, S. J. *Clin. Biochem.* **24**, 113-134 (1991).

Peptide Revolution: Genomics, Proteomics & Therapeutics
Michael Chorev & Tomi K. Sawyer (Editors)
American Peptide Society, 2003

Peptide Strategies for Suppression of EAE

Stephanie D. Allen[1,2], Sharad V. Rawale[2], Caroline C. Whitacre[4] and Pravin T.P. Kaumaya[1,2,3,4]

[1]The Ohio State Biochemistry Program; [2]Department of Obstetrics and Gynecology; [3]Department of Molecular and Cellular Biochemistry; [4]Department of Molecular Virology, Immunology, and Medical Genetics, The Ohio State University, Columbus, OH 43210, USA

Introduction

Multiple sclerosis (MS) is a debilitating disease that affects over 400,000 people in the United States alone. MS is caused by activated, autoreactive T cells that enter the central nervous system (CNS) and attack the myelin sheath that surrounds the nerves [1]. For full activation of T cells, two signals are needed. The first signal comes from the interaction between the T cell receptor (TCR) on the T cell and the major histocompatibility complex (MHC) containing the antigenic peptide on the antigen presenting cell (APC). The second signal involves the interaction between costimulatory molecules on both the T cell and the APC. Studies have shown that both interactions need to take place to avoid the T cell undergoing anergy [2]. The most widely studied costimulatory interaction is between CD28 on the T cell and B7 on the APC, although many more costimulatory molecules have been discovered and are being researched.

Strategies for immune intervention have focused on the blockade of the costimulation interactions, traditionally by blocking antibodies or fusion proteins. But this strategy is associated with several potential problems, including the inherent immunogenicity of these molecules, poor penetration across tissue barriers, and the potential for unwanted signaling via Fc receptors. Peptide therapy offers a simple solution to all of these potential problems. We have previously shown that a 20 residue peptide of CD28 that incorporates the conserved hexapeptide 'MYPPPY' motif can prevent disease induction and ameliorate established disease in the Experimental Autoimmune Encephalomyelitis (EAE) mouse model of MS [3]. We have developed novel peptide mimics of the ligand binding regions of CD40 and CD40L by retro-inverso modifications of the parent peptides synthesized using D-amino acids to preserve peptide topology and lead to increased peptide stability *in vivo*.

Results and Discussion

The peptide mimics ELCD40, ELCD40L and RICD40L have been used in the following studies. A proliferation assay was performed to test the blocking abilities of our CD40L peptide mimics *in vitro*. TCR transgenic $CD4^+$ T cells specific for the NAc1-11 portion of the MBP molecule were incubated with MBP, NAc1-11, or anti-CD3. The peptide mimics were added to test their suppressive abilities. Both ELCD40L and RICD40L showed significant suppression against both MBP and NAc1-11. Suppression was also observed at the higher peptide concentrations in the wells treated with both anti-CD3 and the CD40L peptides. Blockade of the CD40-CD40L pathway prevents the upregulation of B7-1 and B7-2 on the APC, as well as blocking the production of IL-12. IL-12 is known to help activate T cells, specifically T_H1 $CD4^+$ T cells

The peptide mimics were also tested in the EAE model. Mice were immunized with MBP in CFA containing *Mycobacterium tuberculosis*, pertussis toxin, and peptide on day of sensitization. As EAE is a relapsing/remitting disease, mice were observed

from disease onset through the first relapse of the disease. Mice treated with ELCD40 and ELCD40L peptides both showed less severe disease scores as compared to the sensitized only and vehicle treated groups (Figure 1). This indicates that the peptides are able to block the CD40-CD40L costimulation pathway, most likely reducing the amount of IL-12 produced, which would reduce the number of $T_H1^+CD4^+$ T cells, leading to the observed, less severe disease symptoms.

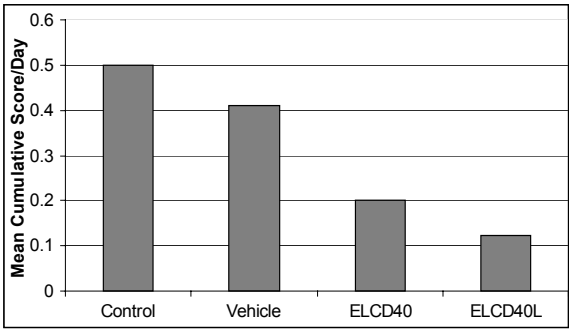

Fig. 1. B10.PL mice were sensitized with MBP in CFA, and given pertussis toxin on day of sensitization and Day 2. Animals also received 500µg peptide i.v. on day of sensitization. Mean cumulative score is calculated by the cumulative clinical score/mouse divided by days observed. This was then averaged per group.

We also compared the efficacy of our peptide constructs against blocking antibodies anti-CD28 and anti-B7-1, and fusion proteins CD28Ig and CTLA-4Ig. A proliferation assay was performed as above, with peptides and antibodies being added in the appropriate amounts. With the exception of CTLA-4Ig, the rest of the blocking agents showed similar blocking capabilities (Figure 2).

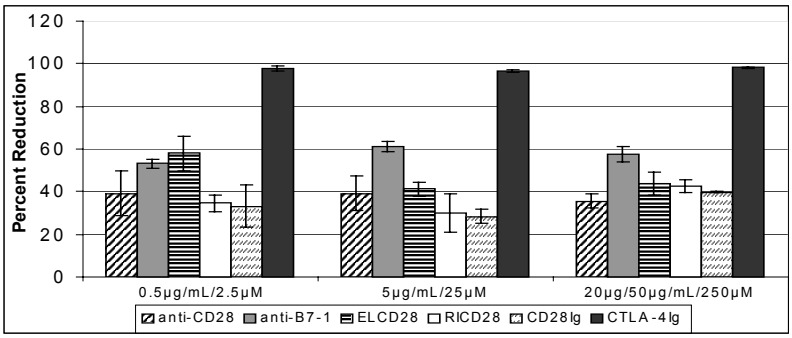

Fig. 2. Comparison of suppressive effects of the CD28 blocking antibody 37.51, B7-1 blocking antibody 16-10A1, CD28Ig, CTLA-4Ig and our EL- and RICD28 peptides. Percent reduction was calculated by the following formula: Percent Reduction=100-(100(T+APC+ Ag+Pep/T+APC+Ag)).*

References

1. Noseworthy, J. H., Lucchinetti, C., Rodriguez, M. and Weinshenker, B. G. *New Engl. J. Med.* **343**, 938-952 (2000).
2. Girvin, A. M., Dal Canto, M. C. and Miller, S. D. *J. Autoimmunity* **18**, 83-94 (2002).
3. Srinivasan, M., Gienapp, I. E., Stuckman, S. S., Rogers, C.J., Jewell, S. D., Kaumaya, P. T. and Whitacre, C. C. *J. Immunol.* **169**, 2180-2188 (2002).

Peptide Revolution: Genomics, Proteomics & Therapeutics
Michael Chorev & Tomi K. Sawyer (Editors)
American Peptide Society, 2003

The Temporin/VesCP (T/V)-Like Family of Bioactive Peptides

David Wade

Wade Research Foundation, 70 Rodney Avenue, Somerset, New Jersey 08873-2024, USA

Introduction

During the past quarter century, a new category of antibiotics has been discovered in nature, the gene-encoded peptide antibiotics. These molecules have a wide range of bioactivities in addition to their antibiotic properties. One of the most prolific sources of these peptides has been the skin secretions of amphibians [1]. The most studied genus has been the Ranid frogs, of which it has been estimated that there are about 250 species worldwide [2]. In 1996, it was reported that a group of 10 small, linear, highly hydrophobic, and cationic peptide amides had been isolated from the skin secretions of the European frog, *Rana temporaria*, and these peptides were named, temporins [3]. These and other frog skin peptides were noted to be structurally similar to 8 chemotactic peptides isolated from the venom of wasps, mostly of the genus, *Vespa* (the VesCPs) [4, 5]. A search of the literature revealed that several other peptides that had been isolated from the skin secretions of frogs also had strong structural resemblance to the temporins and VesCPs [6]. An ambiguous consensus sequence was derived from 30 frog skin peptides, and it was shown to be a good predictor of the sequences of temporin-like peptides subsequently isolated from the skin secretions of additional frog species [2, 6, 7]. The newly isolated peptides enabled a refinement of the consensus sequence for frog skin temporin-like peptides [8].

To date, a total of 48 temporin/VesCP (T/V)-like peptides have been isolated from the skin secretions of 13 species of Ranid frogs and the venoms of 8 species of Vespid and other wasps. Unambiguous consensus sequences for these peptides are shown in Table 1. Both the frog and wasp consensus peptides are linear, have an average length of 13 amino acids (AAs), are highly hydrophobic (61-69% hydrophobic residues), have a net charge of +2 at pH 7, and are amidated at their C-terminal ends. The positions of the positive charges in the T/V-like peptides are at the N-terminal end (all peptides) and most frequently at internal positions 7 (most wasp peptides) or 11 (most frog peptides) (Table 2). The charge at position 7 of wasp peptides has been shown to be essential for the ability of these peptides to release histamine from mast cells [10].

Figure 1 shows the frequency with which each AA residue of each consensus sequence occurs in its respective position within the peptides used to derive the consensus sequences. This is expressed as the percent certainty of finding that residue at that position in the peptides used to derive the consensus sequences. If these molecules are thought of as undergoing an evolutionary process, then residues found at positions 2, 3, 9, 13, and 14 (the C-terminal amide group) seem to have stabilized (percent certainty $\geq$ 80%) whereas residues 1, 4-7 and 10-12, which contain the two sites of positive charge, still seem to be in a state of evolutionary flux.

It is likely that T/V-like peptides have a high α-helical content in a hydrophobic environment, such as the interior of a biological membrane. CD experiments have shown 7 T/V-like peptides (TA, TB, TD, TH, TL, Crabrolin, and I-CP) to be α-helical in micellar or TFE solutions [3, 4, 11-14]. NMR experiments also showed a T/V-like analog, [Lys^7]I-CP, to be α-helical from position 3 (Pro) to the C-terminus (85% helix) [15]. Based on this evidence, hypothetical secondary structures for the consensus sequences are shown below, where italicized and underlined residues are within the α-helix. Helical wheel diagrams show that both sequences are amphipathic.

Table 1. Consensus sequences for Temporin/VesCP (T/V)-like peptides isolated from the skin secretions of frogs and the venoms of wasps[a].

Consensus Peptide	Amino Acid Sequence[b,c]	N.C.[d]	%H[e]
Frog (40 peptides)	F-L-P-L-I-A-S-L-L-S-K-L-L-am	+2	69
Wasp (8 peptides)	F-L-P-I-I-G-K-L-L-G-G-L-L-am	+2	61
Combined F+W (48)	F-L-P-L/(I)-I-A/(G)-S-L-L-S-K/(G)-L-L-am	+2	69

[a]From references [6] and [8]; [b]all peptides are amidated at their carboxyl terminal ends; [c]letters in parentheses at positions 4, 6, and 11 are the second most frequently occurring residues at these positions; [d]net charge at pH 7; [e]percent of hydrophobic residues based on Kyte and Doolittle scale of hydropathicity [9].

Table 2. Positions and types of charged residues within T/V-like peptides[a].

Pos. (+)	48	0	0	0	0	0	18	2	0	4	21	0	0
Position	1	2	3	4	5	6	7	8	9	10	11	12	13
Neg. (-)	0	0	0	0	0	0	0	0	0	0	1	0	0

[a]Numbers indicate the number of occurrences of the charge at that position when all T/V-like peptides are aligned as shown in Table 1.

Table 3. Biological properties exhibited by various T/V-like peptides.

Antimicrobial	Histamine release	Lysosomal enzyme release
Anti-tumor	(mast cells)	(neutrophils)
Chemotaxis	Lipid vesicle binding	Superoxide generation
(monocytes and neutrophils)	leakage and lysis	(neutrophils)
Hemolysis (erythrocytes)		Vasorelaxation

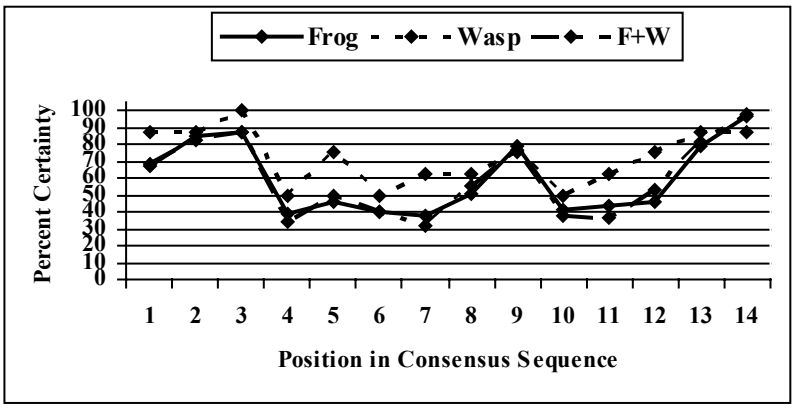

Frog: F-L-P-L-I-A-S-L-L-S-K-L-L-am Wasp: F-L-P-I-I-G-K-L-L-G-G-L-L-am

Fig. 1. Percent certainty of the identity of each AA at each position in the consensus sequences.

VesCPs were the first of the T/V-like group of peptides to be discovered, and the properties of chemotaxis, histamine and lysosomal enzyme release, and superoxide generation were studied (Table 3). The frog skin peptides were discovered later, and studies concentrated mostly on their antibiotic properties. There have been only a few studies where the antibiotic properties of the wasp peptides, or the chemotactic properties of frog peptides, were studied. In these few studies the wasp peptides were found to exhibit properties of the frog peptides and vice versa [11, 16, 17].

One temporin, temporin A, has been the subject of extensive SAR studies using synthetic analogs, and it was found that most of the structural features present in the peptide (helicity, amphipathicity, presence of positive charge within the sequence, presence of the C-terminal amide group, chirality, etc.) were all important for the peptide's various bioactivities [16, 17]. These studies indicated that the probable mechanism of action of T/V-like peptides on bacteria was a simple, nonchiral, hydrophobic interaction with membrane lipids. The α-helical form of T/V-like peptides is 22 Å long, and they could span a 45 Å thick microbial bilayer membrane by stacking interactions. Ion channels could be formed from cylindrical bundles of ≥ 3-4 such stacked, parallel α-helices with a central pore for transmembrane ion movement.

Results and Discussion

Secretion to the environment of structurally similar molecules by widely divergent species, such as the T/V-like peptides of frogs/wasps, is not a unique phenomenon. It has also been found to occur with pheromones produced by elephants and moths [18].

The skin secretions of only 13 (5%) of the estimated 250 species of Ranid frogs have been examined, but there seems to be little variation in the AA sequences of the 40 T/V-like peptides found so far. These particular AA sequences seem to be almost optimized for whatever function(s) are intended for them in nature, indicating that they may be in the final stages of an evolutionary process. The defensive types of properties discovered for these peptides may be their main functions in nature, but there may be other, as yet unknown, functions. The embryological origin of the tissues producing these peptides is the ectoderm, which also differentiates into the nervous system. It is possible that these peptides may have neurological properties.

References

1. Simmaco, M., et al. *Biopolymers (Peptide Science)* **47**, 435-450 (1998).
2. Isaacson, T., et al. *Peptides* **23**, 419-425 (2002).
3. Simmaco, M., et al. *Eur. J. Biochem.* **242**, 788-792 (1996).
4. Nakajima, T., et al. *Biopolymers* **25**, S115-S121 (1986).
5. Simmaco, M., et al. *Biochim. Biophys. Acta* **1033**, 318-323 (1990).
6. Wade, D., et al. *Protein Peptide Lett*. **7**, 349-357 (2000).
7. Kim, J. B., et al. *J. Peptide Res*. **58**, 349-356 (2001).
8. Wade, D. *Internet J. Chem*. 5, article 5 (2002) [Full text article available at web address: http://www.ijc.com:8000/articles/2002v5/94/front.page.html.]
9. Kyte J., et al. *J. Mol. Biol.* **157**, 105-132 (1982).
10. Nagashima, K., et al. *Biochem. Biophys. Res. Commun.* **168**, 844-849 (1990).
11. Krishnakumari, V., et al. *J. Peptide Res*. **50**, 88-93 (1997).
12. Mangoni, M.L., et al. *Eur. J. Biochem*. **267**, 1447-1454 (2000).
13. Wade, D., et al. *FEBS Letts*. **479**, 6-9 (2000).
14. Zhao, H., et al. *J. Biol. Chem*. **277**, 25170-25177 (2002).
15. Shimada, I., et al. *Biochem. Biophys. Res. Commun*. **168,** 596-603 (1990).
16. Wade, D., et al. *Protein Peptide Lett.* **9**, 533-543 (2002).
17. Yang, D, et al. *Letters Peptide Sci*. submitted (2003).
18. Kelly, D. R. *Chemistry and Biology* **3**, 595-602 (1996).

Peptide Revolution: Genomics, Proteomics & Therapeutics
Michael Chorev & Tomi K. Sawyer (Editors)
American Peptide Society, 2003

Tissue Specific Peptide Pools: Fine Tuning of Cell Proliferation Rate in Cell Cultures and Tissues

Olga V. Sazonova[1], ElenaYu. Blishchenko[1], Konstantin V. Leontiev[1], Sergei V. Khaidukov[1], Evgeny I. Amchislavsky[2], Ella A. Starikova[2], Dmitry I. Sokolov[2], Irina S. Freidlin[2], Oleg N. Yatskin[1], Marina M. Philippova[1], Andrei A. Karelin[1] and Vadim T. Ivanov[1]

[1]Shemyakin-Ovchinnikov Institute of Bioorganic Chemistry, Russian Academy of Sciences, 117997 Moscow V-437, Russia; [2]Institute of Experimental Medicine, Russian Academy of Medical Sciences, 197376 St. Petersburg, Russia

Introduction

Screening of peptides fragments of functional proteins from various mammalian tissues and comparative analysis of peptide sets from various sources resulted in formulation of the concept of tissue-specific peptide pools [1]. Activity of over 100 peptides from tissue extracts were studied in tumor cells [2]. It was found that 23% were inactive, 55% inhibited cell proliferation, 13% stimulated cell proliferation, and 9% showed both effects depending on concentration. We suggested that the main function of this class of peptides is regulation of cell proliferation [2]. The majority of endogenous tissue specific peptides are derived from hemoglobin. The study of the peptides obtained from the erythrocyte lysate and the supernatant of primary culture of erythrocytes showed that most intraerythrocyte peptides stimulate tumor cells proliferation or exhibit both growth stimulatory and growth inhibitory effects as depending on concentration [3]. It was found that 84% of secreted peptides were antiproliferative, which could stand for the dominance of the inhibitory peptides in tissue extracts. Comparing the data on peptide location and peptide activity, we suggested that peptide pool composition could reflect the tissue state (ratio of dividing, dying and functioning cells) and its action could be directed at restoration of normal state in case of deviations from homeostasis.

In this work we: (1) obtained new data on the ratio of bioactive peptides in the lysate and the supernatant of tumor cells; (2) modeled the action of the peptide pools in cell cultures using two-peptide and whole peptide pool models; and (3) obtained new data on the action of individual peptides.

Results and Discussion

Activity of the peptides obtained from transformed murine myelomonocytes WEHI-3 lysate and supernatant was studied and compared to the results obtained earlier for erythrocyte culture. Figure 1 shows that, as with erythrocytes, significant part of the peptides found in WEHI-3 lysate stimulate cell proliferation, which confirms the intracellular origin of proliferative peptides found in tissues. In contrast to the peptides released by the erythrocytes, the components secreted by WEHI-3 cells stimulate tumor cell proliferation. These results are consistent with literature data on proliferative activity of the compounds released by tumor cells [4].

The basic way of pool activity regulation could be the interaction between proliferative and antiproliferative pool components. More than 80% of antiproliferative pool components studied so far belong to four structural groups (β-globin (32-41) fragments (hemorphins), β-actin (75-90) and (68-77) fragments and a family of 3-4 membered acidic peptides, [5]) They effectively inhibit proliferation in a large number of tumor cell lines, in transformed endothelial cells, and are several fold less active in

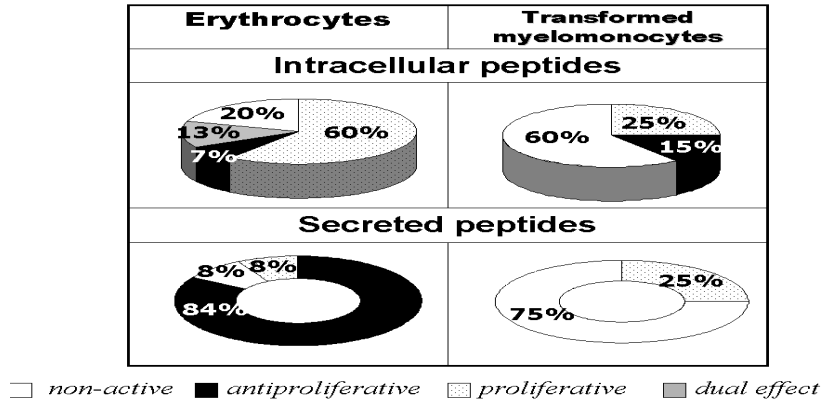

Fig. 1. The ratio of active and non-active peptides in lysate and supernatant of cell cultures.

normal cells [6]. The common pattern of their activity in tumor cells is the induction of reversible cell cycle arrest accompanied by temporary resistance of the cells to the further action of the peptide. We found that peptides belonging to different structural groups do not induce additive effect, which might indicate common molecular targets in the signal transduction.

As reported earlier, α-globin (134-141) and α-globin (137-141) exhibit reliable proliferative effect in tumor and normal cells [7]. Recently, we found that α-(137-141) is not active in WEHI-3 cells, and that both peptides inhibit PC-12 rat pheochromocytoma cell growth. The latter is consistent with the mechanism of action proposed for α-(137-141), i.e., the increase of Ca^{2+} influx through L-type channels [7]; according to literature data, cytotoxity in PC-12 cells is associated with that process [8]. The action of peptides α-(134-141), α-(137-141) and α-(2-32) also depends on culturing conditions. All peptides are most active in cases of FBS deficit (<0,1%) independent of the initial cell density. At optimal FBS (10%) supply, α-(134-141) is active at all cell densities, α-(137-141) effect is cell density dependent and α-(2-32) is not active. α-(137-141) is inactive at 0% of FBS (not tested for other peptides). α-(2-32) restores normal cell proliferation in FBS-supplied medium after pre-incubation with epirubicin, while peptides from the α-(133-141) segment are inactive. Thus, the activity of peptides exhibiting proliferative effect depends on cell type, serum concentration, cell density and presence of growth inhibitory agents.

Peptides whose effect shifts to opposite with the change of their concentration are cleaved from α-(1-32) and α-(12-25) hemoglobin segments [9]. Being inactive in the presence of 10% FBS, in FBS-deficient medium the former peptides stimulate tumor cell proliferation at high concentration and inhibit at low; for the latter the opposite dependence is observed. In concentrations found in tissues the peptides are inactive. Due to such peptides, pool activity could be regulated not only by the change of the individual peptides ratio, but also by the simultaneous change of the content of all peptides comprising the pool. The activity of the peptides with dual effects and "proliferative" peptides is probably associated with stress conditions and not realized in norm.

The effect of two peptides with opposite effects applied together was studied in L929 tumor cells. The proliferative α-globin-(137-141) was tested in pair with three antiproliferative peptides. As reported earlier, with valorphin (α-globin (33-39)) the proliferative effect of α-(137-141) was detected only in the case of its 100-fold

prevalence; at equimolar ratio of the peptides the effect of valorphin was reduced two fold [2]. With β-actin (68-77), at equimolar ratio no effect was observed; otherwise, the reduced effect of the peptide prevailing in the mixture was detected. The representative of short acidic peptides, Pep. 11.2 inhibited the effect of α-(137-141) even in case of 100-fold prevalence of the latter. These results confirm that the overall effect of a tissue peptide pool could be affected by the change of the ratio of the individual peptides.

To model the action of the total peptide pools, the activity of low molecular fraction from renal extract was tested in tumor cells. In the presence of 10% FBS the extract was inactive in a broad range ($5x10^{-7}$- 1 mg/ml) of concentrations. At FBS deficit, weak proliferative effect was observed at $5x10^{-3}$ (25±4%) and $5x10^{-7}$ (21±12%) mg/ml concentration and the inhibitory effect - at $5x10^{-5}$ mg/ml (35±15%). These shifts of activity resemble the shifts observed for peptides with dual effect. The contribution of peptides with dual effect and of proliferative peptides in case of FBS deficit is most likely since their activity is associated with stress conditions. Both in FBS-supplied and FBS-deficient medium, further increase of the extract concentration results in strong inhibition of proliferation (78-100% for 0,5–1,65 mg/ml). We have also found that the elevation of the level of a single antiproliferative peptide *in vivo* leads to tumor suppression. In mice inoculated with M3 melanoma cell suspension, the representative of short acidic peptides, Pep. 11.2, (1 mg/kg, 3 injections at days 0, 6, 12) decreased the tumor volume by 40% as compared to control group (0,9% NaCl aqueous solution). Thus, only when significantly raising all pool components or one antiproliferative peptide level is an antiproliferative effect achieved. We believe that at lower concentration ranges corresponding to endogenous situation the pool could work as a stabilizing factor. It agrees with the normalizing properties of such polypeptide preparations as Actovegin, Cerebrolysin, etc.

The data obtained allows us to propose that the peptide pool activity is regulated both by the shifts in peptide ratio and by the change of the overall level of pool components. These changes in turn could be caused by the alteration of tissue homeostasis, i.e., change of the ratio of dying/live cells or increase of abnormal cells number, for instance in the case of cancer.

References

1. Karelin, A., et al. *FEBS Lett.* **428**, 7-12 (1998).
2. Ivanov, V., et al. *J. Pept. Sci*. **9**, 553-562 (2003).
3. Ivanov, V., et al. *Pure & Appl. Chem.* **70**, 67-74 (1998).
4. Gilmour, L., et al. *Clin. Cancer Res*. **8**, 3933-3942 (2002).
5. Elgjo, K., Reichelt, K. and Gembitsky, D. *Prog. Mol. Subcell. Biol.* **20**, 143-159 (1998).
6. Blishchenko, E., et al. *J. Pept. Sci.* **8**, 438-452 (2002).
7. Sazonova, O., et al. *Prot. Pept. Lett.* **10**, 1-10 (2003).
8. Gibson, G., Toral-Barza, L. and Zhang, H. *J. Neurochem*. **69**, 603-611 (1997).
9. Ivanov, V., et al. *Pure Appl. Chem.* **72**, 355-363 (2000).

Peptide Revolution: Genomics, Proteomics & Therapeutics
Michael Chorev & Tomi K. Sawyer (Editors)
American Peptide Society, 2003

Metastin: Synthesis and Distribution in the Rat Medulla Oblongata and Spinal Cord

Jun Yang[1], G. Cristina Brailoiu[2], Siok L. Dun[2], Jaw-Kang Chang[1] and Nae J. Dun[2]

[1]Phoenix Pharmaceuticals, Inc. Belmont, CA 94002; [2]Department of Pharmacology, James H. Quillen College of Medicine, East Tennessee State University, Johnson City, TN 37614, USA

Introduction

Metastin is a novel peptide first isolated from the human placenta and proposed to be the endogenous ligand for the G protein-coupled receptor GPR54 or AXOR12, or OT7T175 [1-3]. Metastin is encoded by the human metastasis suppressor gene, KiSS-1 [1,4,5], whose expression has been reported in the human central nervous system, with the highest level in the basal ganglia, hypothalamus and hippocampus, and low levels in the medulla oblongata and spinal cord [2]. Recently, the mouse homologues of KiSS-1 peptide and its G protein-coupled receptor were identified and characterized [6]. The expression of metastin receptors has also been described in the human and rat nervous system, with a pattern similar to that of metastin [1,2,7]. Here, the chemical synthesis of metastin and the distribution of metastin-immunoreactivity in the rat medulla oblongata and spinal cord are described.

Materials and Methods

1. Synthesis of human metastin: Using the C/S Bio Automatic Peptide Synthesizer and *p*-methylbenzhydrylamine (pMeBHA) as the solid-support (0.32mM/g of resin), the human metastin (GTSLSPPPES SGSRQQPGLS APHSRQIPAP QGAVLVQREK DLPNYNWNSF GLRF-NH_2) was synthesized by the solid-phase method. Ten molar excess Fmoc-protected amino acids and the coupling reagent, HBTU in DMF were used to incorporate the corresponding amino acids onto the resin. The reaction time was 30 min at room temperature. The side chain protected groups used in the whole process were: Arg(Tos), Ser(t-Bu), Asn(Trt), Tyr(t-Bu), Asp(t-Bu), Lys(Boc), Glu(t-Bu), Gln(Trt) and Thr(t-Bu). Deprotection of the Fmoc-group was carried out for 20 min with 20% piperidine in DMF. After 54 cycles of synthesis, the protected peptide-pMBHA was treated with 40% TFA in CH_2Cl_2 with 1% indole for 20 min.

2. Hydrogen fluoride (HF) cleavage of protected peptide resin: The protected peptide resin was cleaved by HF (10ml/g of resin) with anisole (1ml/g of resin) and DMS (0.1ml/g of resin) at 0ºC for 1 h. After evaporation under vacuum to dryness, the reaction mixture was washed well with anhydrous ether. The peptide was dissolved in water and CH_3CN, and filtered. The filtrates were combined and lyophilized to yield the desired crude peptide (1.65g of crude peptide, 88% yield based on 0.32mM capacity of resin).

3. Purification of human metastin: A part of the crude peptide (150mg) was dissolved in 0.1% TFA solution and loaded onto a semi-preparative C-18 HPLC column (Vydac, 5μm, 300A, 4.6mm ID x 250mm L). The peptide was eluted with linear gradient (6ml/min) using 0.1% TFA and 60% CH_3CN in 0.1% TFA as the initial and final buffer, respectively. Pure fractions were collected based on analytical HPLC (purity of 95%) and lyophilized to afford pure metastin (26mg, yield 17%). Mass spectrum (Kompact, MALDI 1) showed a single molecular ion with a mass of 5857.22 (M.W. 5857.51).

4. Synthesis and purification of metastin(45-54)-NH_2: The synthesis and purification of metastin(45-54)-NH_2, YNWNSFGLRF-NH_2, was performed as described above for the synthesis of metastin. With 53% yield, the peptide showed a single peak by analytical HPLC and correct molecular ion of 1302.39 (M.W. 1302.44).
5. Synthesis and purification of metastin(1-25): The synthesis of metastin (1-25), GTSLSPPPESSGSRQQPGLSAPHSR, was carried out by using 0.5mM/g of Boc-Arg(Tos)-Merrifield resin with Boc-chemistry. HF cleavage of the peptide resin, Gly-Thr(Bzl)-Ser(Bzl)-Leu-Ser(Bzl)-Pro-Pro-Pro-Glu(cHex)-Ser(Bzl)-Ser(Bzl)-Gly-Ser(Bzl)-Arg(Tos)-Gln-Gln-Pro-Gly-Leu-Ser(Bzl)-Ala-Pro-His(Tos)-Ser(Bzl)-Arg(Tos)-resin and purification of the crude peptide were performed as described in the process of metastin. Pure peptide (30% yield) showed a single peak on HPLC and correct molecular ion of 2519.2 (M.W. 2517.70).
6. Immunohistochemistry: A breeding colony of Sprague-Dawley rats from Harlan (Indianapolis, IN) was established in the Division of Laboratory Animal Facility, East Tennessee State University. Animal protocols were reviewed and approved by the University Animal Care and Use Committee. Coronal medulla oblongata and transverse spinal cord sections were processed for metastin-immunoreactivity (MTS-LI) by means of the standard avidin-biotin complex procedures, as described previously [8-10]. The metastin-antiserum, a rabbit polyclonal (Phoenix Pharmaceuticals, Inc.), was raised against the metastin fragment (45-54)-NH_2, Cys0 (human) (C^{45}YNWNSFGLRF^{54}). The antiserum exhibits 100% cross-reactivity with metastin (45-54)-NH_2 (human), metastin (1-54) (human), and RFamide-related peptide-1 (human).

Results and Discussion
The total synthesis and purification of human metastin (1-54)-NH_2, and its related C-terminal (45-54)-NH_2 and N-terminal (1-25) fragments were performed and accomplished by the solid-phase method (Figure 1).

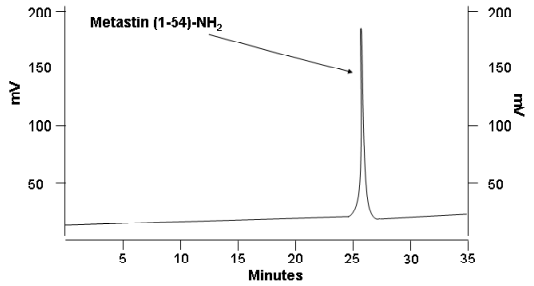

Fig. 1. Analytical HPLC of purified human metastin show single peak.

With the use of an antiserum against metastin fragment (45-54)-NH_2, MTS-LI was detected in the brainstem and spinal cord of Sprague-Dawley rats (Figure 2). In the rat medulla oblongata, MTS-LI neurons were present in the nucleus of the solitary tract (Sol) (Figure 2B-C) and caudo-ventrolateral reticular nucleus at the level at/or caudal to the area postrema (AP). Labeled fibers and a few labeled perikarya were detected in the Sol rostral to the area postrema (Figure 2A). Numerous MTS-LI fibers and occasionally a few lightly labeled somata were present in the spinal trigeminal tract

(sp5) and in the lateral reticular nucleus (LRt) (Figure 2C). Scattered fibers were seen in the ambiguus nucleus, raphe obscurus, raphe pallidus, gigantocellular reticular nucleus, intermediate reticular nucleus and medullary reticular field. In the spinal cord, dense networks of MTS-LI fibers and few lightly labeled somata were present in the superficial layers of the dorsal horn of every segment (Figure 2D). The pattern of MTS-LI distribution suggests a role in autonomic and sensory neural signaling for this novel peptide.

Medulla oblongata or spinal cord sections showed no immunoreactivity when processed with metastin-antiserum pre-absorbed with the peptide (45-54)-NH_2.

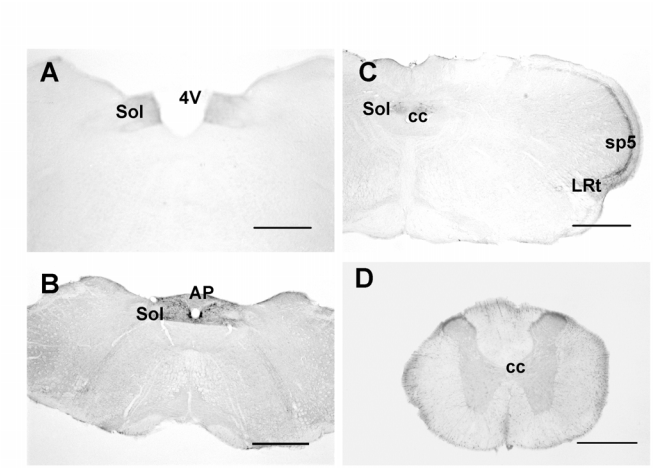

Fig. 2. Photomicrographs of rat medulla oblongata and spinal cord sections labeled with metastin-antiserum.

Acknowledgments

The work was funded by NIH Grants NS18710 and NS39646 from the Department of Health and Human Services.

References

1. Kotani, M., *et al*. *J. Biol. Chem*. **276**, 34631-34636 (2001).
2. Muir, A. I*., et al*. *J. Biol. Chem*. **276**, 28969-28975 (2001).
3. Ohtaki, T., *et al*. *Nature* **411**, 613-617 (2001).
4. Lee, J. H., *et al*. *J. Natl. Cancer Inst*. **88**, 1731-1737 (1996).
5. Lee, J. H. and Welch, D. R. *Int. J. Cancer* **71**, 1035-1044 (1997).
6. Stafford, L. J., *et al*. *Cancer Res*. **62,** 5399-5404 (2002).
7. Lee, D. K., *et al*. *FEBS Lett*. **446**, 103-107 (1999).
8. Dun, N. J., *et al*. *Neuroscience* **54**, 845-857 (1993).
9. Dun, S. L., *et al*. *J. Chem. Neuroanat*. **23**, 123-132 (2002).
10.Dun S. L., *et al*. *Neurosci. Lett.* **335**, 197-201(2003).

Peptide Dendrimer, Epitope and Vaccine Structure-Function

Peptide Revolution: Genomics, Proteomics & Therapeutics
Michael Chorev & Tomi K. Sawyer (Editors)
American Peptide Society, 2003

An Irreversible Inhibitor of a VIP-Hydrolyzing Antibody

Gita Bhatia, Yogesh Bangale, Hiroaki Taguchi, Robert Dannenbring, Stephanie Planque, Sangeeta Karle, Sudhir Paul and Yasuhiro Nishiyama

Chemical Immunology and Therapeutics Research Center, Department of Pathology and Laboratory Medicine, University of Texas–Houston Medical School, 6431 Fannin, Houston, TX 77030, USA

Introduction

Previous studies have documented the proteoytic character of antibodies (Abs) found in certain diseases, including VIP-hydrolyzing Abs (VIPase Abs) from asthma [1], autoimmune thyroiditis and systemic lupus erythematosus patients and lupus-prone *Fas*-defective mice [2]. Proteolytic Abs can interfere with the biological actions of target polypeptide antigens more severely than ordinary Abs, since a single catalyst molecule can permanently inactivate multiple antigen molecules. This feature is hypothesized to distinguish pathogenic from benign autoantibodies. Selective inhibitors are promising means to identify the pathophysiological functions of proteolytic Abs and potentially ameliorate their biological actions. We report herein the first inhibitor capable of selective covalent binding to VIPase Abs guided by classical noncovalent antigen-Ab interactions.

Results and Discussion

The inhibitor (3) consists of the diphenyl phosphonate moiety placed on the side-chain of Lys20 and biotin at the *C*-terminus of VIP (Fig 1). Cleavage of VIP on the *C*-terminal side of Lys20 by a monoclonal Ab to VIP and polyclonal Abs from asthma patients has been reported previously [3]. Serine protease-like nucleophiles in

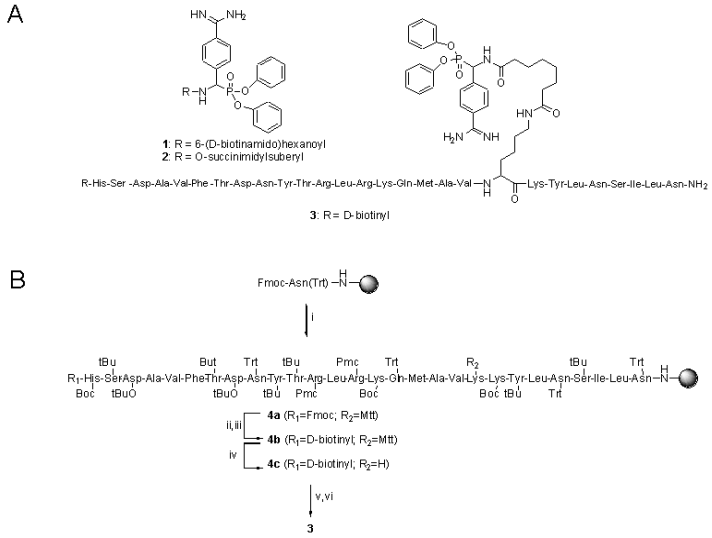

*Fig. 1. (A) Structures of **1**–**3**. (B) Synthetic scheme for **3**. (i) Fmoc-solid-phase peptide synthesis; (ii) 20% piperidine in DMF; (iii) D-biotin, PyBOP, HOBt, DIEA in DMF; (iv) 1% TFA in CH_2Cl_2; (v) **2**, 0.1 mM DIEA in DMF; (vi) TFA, thioanisole, phenol.*

proteolytic Abs are hypothesized to recognize the reactive phosphonate within the context of noncovalent epitope recognition including neighboring amino acids of VIP. Location of the phosphonate on the Lys side-chain serves as a test of the hypothesis that Ab nucleophiles capable of backbone peptide bond cleavage enjoy sufficient flexibility to recognize spatially neighboring electrophiles. Irreversible 3-binding by monoclonal VIPase IgG (clone c23.5) [3] determined by denaturing electrophoresis occurred preferentially in the L-chain subunit (Fig 2A) consistent with observations that this subunit contains the catalytic nucleophile. The c23.5 L-chain binding rate of 3 was superior to that of phosphonate 1 devoid of the VIP sequence. 3–IgG binding was inhibited by VIP and diisopropyl fluorophosphate, indicating that the covalent interaction of 3 with the serine protease-like active site is facilitated by the VIP sequence. The proteolytic activity of the recombinant L-chain of IgG c23.5 [4] measured using a model amide substrate was inhibited by 3 with potency superior to 1. Similarly, 3 inhibited the cleavage of VIP by a polyclonal IgG autoantibody preparation (HS-2) (Fig 2B). As HS-2 IgG contains several Ab subspecies and cleaves VIP at multiple peptide bonds [5], the near-complete inhibition of catalysis by 3 supports the model of alternate ground state complexes in which the Ab nucleophile can be placed in register with different peptide bonds of VIP. These results indicate that the selective VIPase Ab inhibitor reported here can be employed to delineate the pathophysiological role of VIPase Abs and may serve as a model compound in the development of novel therapies for proteolytic Ab-related disorders.

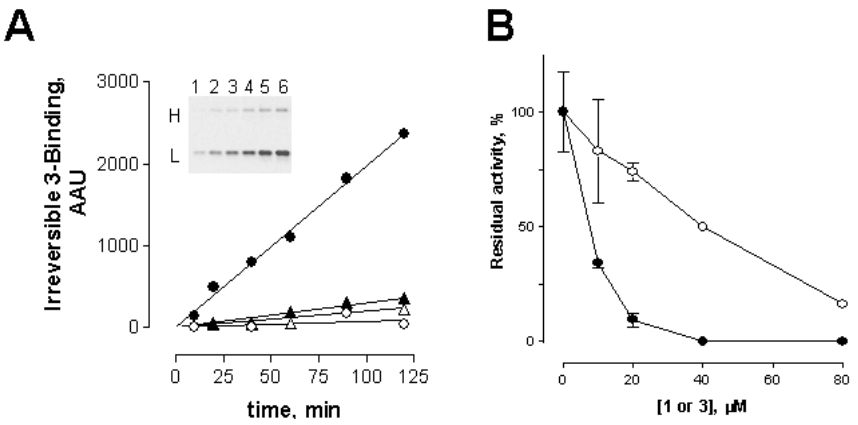

Fig. 2. (A) ***3****-Binding by VIPase c23.5 IgG and control UPC10 IgG. IgG (1 μM) treated with* ***3*** *(10 μM) for various time were subjected to reducing SDS gel electrophoresis. Inset shows the streptavidin–HRP-stained blot. Intensities of biotin-containing bands were determined by densitometry.* M*, c23.5 L-chain;* O*, c23.5 H-chain;* F*, UPC10 L-chain;* G*, UPC10 H-chain. (B) Inhibition of HS-2 IgG-catalyzed* ^{125}*I-VIP cleavage by* ***1*** *and* ***3****. Data are means (S.D.).*

References

1. Paul, S., et al. *Science* **244**, 1158-1162 (1989).
2. Bangale, Y., et al. *FASEB J.* **17**, 628-635 (2003).
3. Paul, S., et al. *J. Biol. Chem.* **267**, 13142-13145 (1992).
4. Gao, Q. S., et al. *J. Biol. Chem.* **269**, 32389-32393 (1994).
5. Paul, S., et al. *J. Biol. Chem.* **266**, 16128-16134 (1991).

Peptide Revolution: Genomics, Proteomics & Therapeutics
Michael Chorev & Tomi K. Sawyer (Editors)
American Peptide Society, 2003

Bacterial and Mammalian Cell Penetration of Polycationic Antibacterial Peptides: Potential Utility as Drug Delivery Vehicles

Mare Cudic[1,2], Georgia Deliyannis[3], David C. Jackson[3] and Laszlo Otvos Jr.[1,2]

[1]The Wistar Institute, 3601 Spruce Street, Philadelphia, PA 19104, USA; [2]Chaperone Technologies, 801 Mockingbird Lane, Audubon, PA 19403, USA; [3]Department of Immunology and Microbiology, University of Melbourne, Parkville, Victoria 3052, Australia

Introduction

Epithelial tissues represent a major barrier through which molecules can be absorbed. The phospholipid bilayer of the plasma membrane of epithelial cells is considered the major factor restricting the free movement of substances from the lumen to the bloodstream through the transcellular pathway [1]. While hydrophobic and small molecules can penetrate this system, cell membranes are almost impermeable to large hydrophilic biopolymers such as most peptides [2]. Peptides can be smuggled into cells by utilizing active transport, passive transport or particle delivery. As carriers for passive delivery, highly cationic peptides, just like cationized proteins, are generally able to interact electrostatically with negatively charged phospholipids and then insert into model membranes of planar bilayers or liposomes [3]. The cationic proline-rich peptide pyrrhocoricin enters not only bacteria, but mouse macrophages as well [4], yet pyrrhocoricin derivatives show no toxicity *in vitro* and *in vivo* [5]. Therefore, if chimeras of pyrrhocoricin-based antibacterial peptides and peptidic drug leads were made, such chimeras would be expected to undergo an enhanced cellular uptake, and would be expected to be potentially more efficacious *in vivo*.

Results and Discussion

We studied the uptake of pyrrhocoricin and its most potent dimeric analog into bacteria, as well as human dendritic cells and fibroblasts. Native pyrrhocoricin efficiently entered the susceptible organism *Escherichia coli*, the non-susceptible bacterium *Staphylococcus aureus* and human peripheral blood mononuclear cells. The lack of antibacterial activity against *S. aureus* is due to altered sequence of the target protein DnaK compared to susceptible strains, such as *E. coli* [4]. Although pyrrhocoricin cannot kill this bacterium, the positive entry into *S. aureus* indicates that novel antibacterial peptide analogs can be developed that retain the residues responsible for bacterial cell entry but feature domains capable of binding to altered versions of the target protein DnaK. This also suggests that the pyrrhocoricins can deliver cargo into cells. However, native pyrrhocoricin failed to enter fibroblasts as opposed to the designed Pip-pyrr-MeArg dimmer, which penetrated all cell types studied. One potential reason why our pyrrhocoricin dimer shows improved mammalian cell penetration properties and is absorbed after oral administration [5] is the large number of positive charges. Alternatively, the explanation may rest in the backbone protection. It has been reported that N-methylation enhances membrane permeation by passive diffusion [6].

To test our hypothesis that the Pip-pyrr-MeArg dimer can deliver unrelated peptides into target cells, we synthesized two peptide constructs. In the first chimera, the NPK^d peptide, a major histocompatibility complex protein (MHC) class I epitope [7] was attached to the N-terminus of the Pip-pyrr-MeArg dimer. Our selection as a test

peptidic hormone was the 7-36 fragment of the glucagon-like peptide 1 (Glp-1). Peptide Glp-1 is an important glucoincretin hormone that is secreted from intestinal L cells in response to nutrient ingestion [8]. Since the N-terminus of Glp-1 can be freely substituted, in this design, the carrier dimer was placed at the C-terminus of the chimera. First we wanted to make sure that by being part of the constructs, the building constituents retained their intended biological activities, which were bacterial cell penetration of the Pyp-pyrr-MeArg dimer, MHC class I activity of the NPK^d epitope, and insulin secretion of the Glp-1 fragment. The Pip-pyrr-MeArg dimer without any peptide cargo killed the *E. coli* JC7623 cell line with an IC_{50} value of 1 μM (Table 1). Some reduction in the antibacterial activity (IC_{50} of 4 μM) was observed when the NPK^d epitope was added. However, the bacterial cell penetrating ability of the Pip-pyrr-MeArg dimer was not significantly compromised when two copies of the NPK^d epitope were attached, and suggested that the pyrrhocoricin derivative would be able to deliver the antigenic cargo into mammalian cells as well. In contrast, no bacterial killing was observed in the case of the Dimer-Glp-1 chimera. While the epitope-dimer chimera fully retained the antigenic properties of the MHC class I fragment, the dimer-Glp-1 chimera did not induce any insulin production either *in vitro* using a HIT-1 hamster islet tumor cell line or *in vivo* during an oral glucose tolerance test in mice. The epitope-dimer chimera indeed penetrated mammalian cells as indicated by 2- to 3-fold increase in the activation of surface markers HLA-DR, CD86, and CD83 when incubated with human monocyte-derived dendritic cells. This construct also induced a vigorous T-cell response in Balb/c mice. Detailed analysis of the immunogenic properties of the epitope-dimer construct will reveal the utility of the pyrrhocoricin analogs in subunit vaccine development.

Table 1. 50% inhibitory concentration (IC_{50} in μM) of peptide chimeras against E. coli JC7623.

Pip-pyrr-MeArg dimer	1
Epitope-dimer chimera	4
Dimer-Glp-1 chimera	>40

Acknowledgments

The authors acknowledge the financial support from the Commonwealth Universal Research Enhancement Program, Pennsylvania Department of Health. This work was supported by NIH grants AI055174 and DK64477.

References

1. Wong, A. and Toth, I. *Curr. Med. Chem.* **8**, 1123-1136 (2001).
2. Kompella, U. B. and Lee, V. H. *Adv. Drug Deliv. Rev*. **46**, 211-245 (2001).
3. Lehrer, R. I., Barton, A., Daher, K. A., Harwig, S. S. L., Ganz, T. and Selsted, M. E. *J. Clin. Invest*. **84**, 553-561 (1989).
4. Kragol, G., Hoffmann, R., Chattergoon, M. A., Lovas, S., Cudic, M., Bulet, P., Condie, B. A., Rosengren, K. J., Montaner, L. J. and Otvos, L., Jr. *Eur. J. Biochem.* **269**, 4226-4237 (2002).
5. Cudic, M., Lockatell, C. V., Johnson, D. E. and Otvos, L., Jr. *Peptides* **24,** 807-820 (2003).
6. Burton, P. S., Conradi, R. A., Hilgers, A. R., Ho, N. F. H. and Maggiora, L. L. *J. Controlled Release* **19**, 87-98 (1992).
7. Deliyannis, G., Jackson, D. C., Ede, N. J., Zeng, W., Hourdakis, I., Sakabetis, E. and Brown, L. E. *J. Virol*. **76**, 4212-4221 (2002).
8. Xiao, Q., Giguere, J., Parisien, M., Jeng, W., St-Pierre, S. A., Brubaker, P. L. and Wheeler, M. B. *Biochemistry* **40**, 2860-2869 (2001).

Peptide Revolution: Genomics, Proteomics & Therapeutics
Michael Chorev & Tomi K. Sawyer (Editors)
American Peptide Society, 2003

Synthetic Peptides in the Form of Dendrimers Retain Biological Activity and Become Resistant to Proteases

C. Falciani[1], B. Lelli[1], L. Lozzi[1], Y. Runci[1], A. Pini[1], P. Neri[1], M.G. De Montis[2], A. Tagliamonte[2] and L. Bracci[1]

[1]Department of Molecular Biology, Via Fiorentina; [2]Department of Neuroscience, University of Siena, Via A. Moro 4, 53100 Siena, Italy

Introduction

Selective agonists or antagonists of natural peptides are extremely useful for the investigation of peptidergic systems and are also potential therapeutic agents [1]. However, the use of peptides as therapeutic drugs has largely been limited by their short half-life *in vivo*. Degradation of peptides is mainly due to protease and peptidase activity, and peptide pharmacokinetic is the bottleneck in development of new peptide drugs.

To increase peptide half-life, many strategies, involving different levels of chemical modification, are possible [2,3]. The introduction of D-amino acids, or pseudo amino acids and the replacement of the peptide bond are the most common strategies to increase peptide stability. However, these modifications may profoundly alter peptide activity. Alternatively, peptidomimetic molecules can be developed by the synthesis of conformationally restricted compounds, in which the peptide is constrained in order to reproduce the active conformation. The resulting structures are mostly non-peptide molecules, more resistant to degrading enzymes.

In general, peptide molecules have the advantage of good specificity and high selectivity and the disadvantage of poor metabolic stability and limited distribution. Although non-peptide molecules have better stability and pharmacokinetics, they may have very different specificity and affinity to natural peptides.

In this study we report results suggesting that synthesis of bioactive peptides in Multiple Antigen Peptide (MAP) [4] dendrimeric form, can result in increased half-life, due to acquired resistance to protease and peptidase activity.

We previously reported that the tetrameric MAP form of the peptide mimotope p6.7 and its high affinity analogues pDD and pDDD, which compete with the nicotinic receptor (nAchR) for binding α-bungarotoxin, a snake neurotoxin, efficiently neutralize toxin lethality in mice, unlike the corresponding monomeric sequences. This happens despite the nearly identical K_A and IC_{50} of MAPs and monomeric peptides, and their similar *in vitro* activity [5,6]. In the particular case of mimotopes of the nicotinic receptor toxin-binding site, MAP has no polyvalent-interaction-associated advantage with respect to the corresponding monomeric peptide, which could explain its much greater *in vivo* activity. Indeed, MAP acts as a soluble competitor of the receptor, binding a soluble monomeric toxin. Its much higher efficiency *in vivo* with respect to the monomeric peptide is therefore presumably due to a pharmacokinetic advantage, such as different clearance, or resistance to peptidase and protease activity.

In order to verify this possibility, we examined the stability of the monomeric and MAP mimotopes in human plasma and serum and in the presence of trypsin and chymotrypsin.

Results and Discussion

We previously produced synthetic peptides mimicking the snake neurotoxin binding site of the nicotinic receptor and found that the *in vivo* efficiency of these mimotopes reflects their affinity and IC_{50} only when they are synthesized in MAP form [5,6]. The efficacy of the tetrameric peptides *in vivo* could not be ascribed to any kinetic or thermodynamic effect and seemed therefore related to differences in pharmacokinetic behavior.

To verify this possibility, we compared the stability of monomeric and tetrabranched peptide mimotopes in human plasma and serum. Monomeric and tetrabranched peptides were incubated with human plasma or serum for 2 or 24 hours and the mixture was analyzed by HPLC and mass spectrometry (MS) to monitor the presence of monomeric and MAP peptides.

As a general rule, peptides that were cleaved in plasma within 2 hours were also cleaved in serum in the same time. Those resistant in serum after 24 hours were also resistant in plasma (Table 1).

Table 1. Proteolytic stability of monomeric and MAP peptides. The absence (NO) or presence (YES) of peptides, refers to the intact peptide sequences as detected by HPLC and MS.

Peptide	Plasma		Serum	
	2 h	24 h	2 h	24 h
p6.7	NO	NO	NO	NO
MAPp6.7	YES	YES	YES	YES
pDD	YES	NO	NO	NO
MAPpDD	YES	YES	YES	YES
pDDD	YES	NO	NO	NO
MAPpDDD	YES	YES	YES	YES

Monomeric peptide mimotopes (p6.7, pDD and pDDD) were completely transformed within 2 hours in serum and MS detected fragments derived from proteolytic cleavage in the HPLC eluted material. Conversely, tetrabranched forms of the same peptides were still detected after 24 hours in plasma and serum.

As an example, we report in Figure 1 HPLC chromatograms and MALDI-ToF spectra of p6.7 and MAP p6.7 after incubation in plasma or serum: in panel A analysis of p6.7 after incubation in plasma for 2 hours is shown. HPLC eluted material was collected from 21 to 26 min (24 min is the retention time of uncleaved p6.7) and analysed by MS. Instead of the intact peptide, fragments of proteolytic cleavage were found. In panel B analysis of MAP p6.7 after incubation in serum for 24 hours is shown: HPLC eluted material was collected from 23 to 30 min (26 min is the retention time of uncleaved MAP p6.7) (bottom) and analysed by MS (top). The uncleaved sequence was still present.

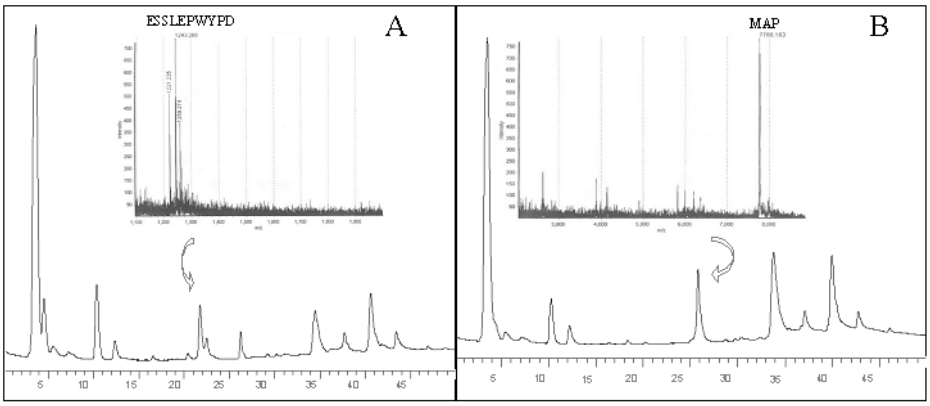

Fig. 1. HPLC and MALDI-ToF of p6.7 and MAP p6.7 after incubation in plasma or serum.

Residual activity of monomeric and MAP mimotope peptides after incubation in serum or plasma for 24 hours was measured. Incubation for 2 hours in human plasma or serum increased the IC_{50} of monomeric peptides by at least 3 Log, whereas MAP peptides retained their inhibition power after 24 hours (Figure 2).

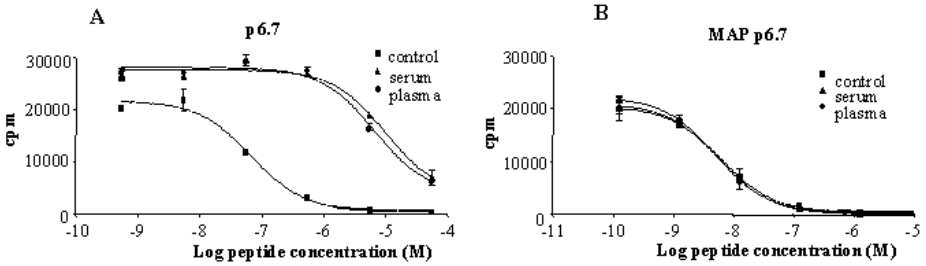

Fig. 2. (A) Monomeric peptide p6.7 ability to inhibit nAchR α-bgt binding decreased of about 3 Log. (B) MAP p6.7 maintained the same IC_{50} after incubation in plasma or serum for 24 hours. Similar results were obtained with pDD and pDDD.

The increased stability of dendrimeric peptides was also confirmed with purified proteases. Tetrabranched mimotopes MAP p6.7, MAP pDD and MAP pDDD were not cleaved by trypsin in 24 hours, whereas their corresponding monomers were proteolysed within 2 hours, except for peptide p6.7, which was still detectable. Most monomeric and MAP peptide mimotopes were degraded by chymotrypsin after 2 hours of incubation. However, the MAP form of the peptide pDDD was still found after 24 hours of incubation.

Acknowledgments
This work was supported by grants lo LB by Italian Ministry of Education, University and Research (MIUR).

References

1. Hruby, V. J. *Nat. Rev. Drug Discov*. **11**, 847-858 (2002).
2. Adessi, C. and Soto, C. *Curr. Med. Chem*. **9**, 963-978 (2002).
3. Goodman, M., Zapf, C. and Rew, Y. *Biopolymers* **60**, 229-245 (2001).
4. Tam, J. P. *Proc. Natl. Acad. Sci. U.S.A.* **85**, 5409-5413 (1988).
5. Bracci, L. *et al. Biochemistry* **41**, 10194-10199 (2002).
6. Lozzi, L. *et al. Chem. Biol*. **10**, 411-417 (2003).

Peptide Revolution: Genomics, Proteomics & Therapeutics
Michael Chorev & Tomi K. Sawyer (Editors)
American Peptide Society, 2003

Design and Synthesis of Porphyrin Centered Dendritic Poly(L-Lysine)

Louis A. Watanabe[1], Katsunori Kontani[2], Tamaki Kato[2] and Norikazu Nishino[2]

[1]Faculty of Engineering, Kyushu Institute of Technology, Kitakyushu, 804-8550, Japan,
[2]Graduate School of Life science and Systems Engineering, Kyushu Institute of Technology, Kitakyushu, 808-0196, Japan

Introduction

Antenna chlorophylls are important photoreceptors in photosynthesis. They play a role of antenna that absorb energy from light, and transmit to the reaction center chlorophyll by excitation energy transfer between molecules. High energy transfer efficiency of this process is due to the appropriate arrangement of the chlorophyll molecules in the antenna complex. In order to develop an artificial light-harvesting antenna system, we synthesized dendritic poly(L-lysine)s containing a large number of free base- and Zn(II)-porphyrins near the surface in scramble fashion [1], hemisphere fashion [2] and double strata fashion [3] with free base and zinc porphyrin ratio up to 1:4 or 4:1. In this work, we proposed to synthesize dendritic poly(L-lysine)s with free base and zinc porphyrin ratio of 1:8 or 8:1 and a porphyrin at the center of the dendrimer molecule. Thus, we designed and synthesized free base- and Zn(II)-porphyrin centered dendritic poly(L-lysine)s (Fb1/Zn8)K4 and (Zn1/Fb8)K4 using 5,10,15,20-tetrakis(4-aminophenyl)porphyrin (TAP).

Results and Discussion

The dendrimer (Fb1/Zn8)K4 was synthesized using symmetrical acid anhydride method starting from TAP(Fb) and Boc-Lys(Boc)-OH. After deprotection of Boc group using TFA, the product was coupled with Por(Zn) by HATU-HOAt method to give (Fb1/Zn8)K4. The dendrimer (Zn1/Fb8)K4 was also synthesized using the same method described above starting from TAP(Fb) and Fmoc-Lys(Fmoc)-OH. Then, zinc ion was introduced to the TAP using zinc acetate. After deprotection of the Fmoc group using piperidine, the product was coupled with Por(Fb) by HATU-HOAt method to yield (Zn1/Fb8)K4 (Figure 1).

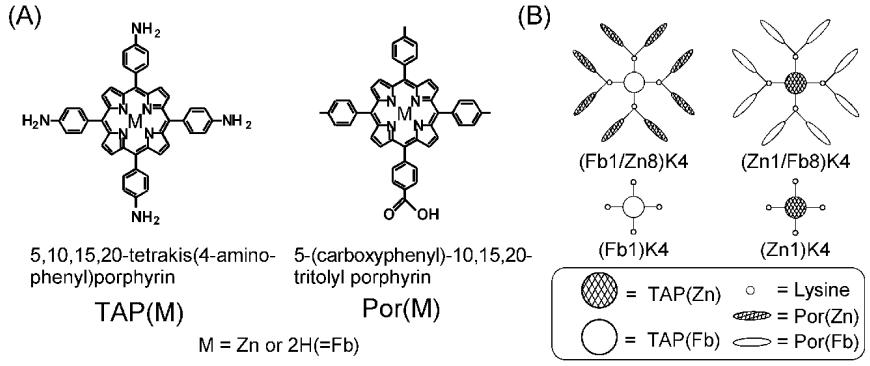

Fig. 1. (A) Structure of porphyrin derivatives. (B) Illustration of dendrimers.

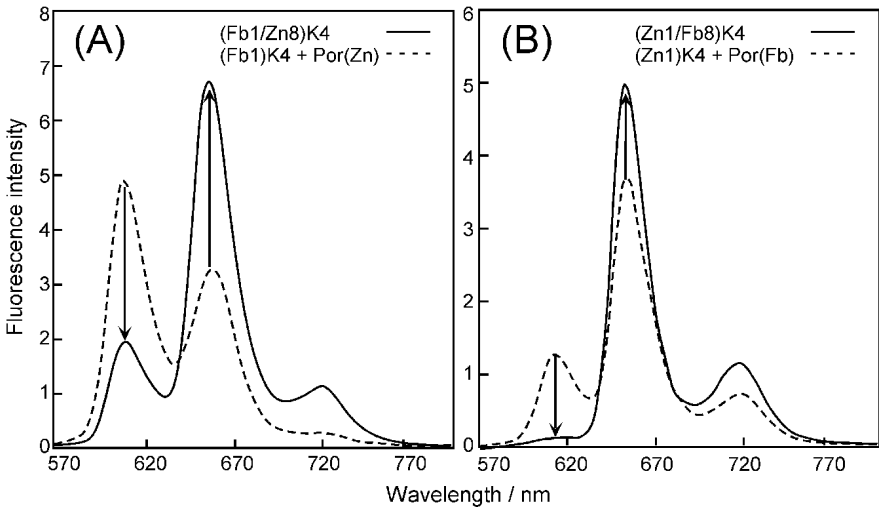

Fig. 2. Fluorescence spectra of denderimers in DMF. Excitaion at 560 nm.
(A) [(Fb1/Zn8)K4] = 8 mM, [(Fb1)K4] = 1 mM, [Por(Zn)] = 8 mM
(B) [(Zn1/Fb8)K4] = 8 mM, [(Zn1)K4] = 1 mM, [Por(Fb)] = 8 mM

The dendrimer (Fb1/Zn8)K4) was subjected to fluorescence measurements with reference to a mixture of (Fb1)K4 and eight equivalents of Zn(II)-porphyrin in DMF. Upon excitation at 560 nm for Q band of Zn(II)-porphyrin, the emission at 610 nm from Zn(II)-porphyrin was significantly quenched. Instead, emission from free base-porphyrin at 660 nm and 720 nm increased significantly. Most interestingly, extent of decrease in the emission at 610 nm and the extent of increase in emission at 660 nm were almost identical. This fact suggests that energy transfer occurred quantitatively. Fluorescence measurement for (Zn1/Fb8)K4 was also performed and compared with (Fb1/Zn8)K4 (Figure 2). The energy transfer efficiency of the dendrimers (Fb1/Zn8)K4 and (Zn1/Fb8)K4 were estimated as 60% and 90%, respectively. From this we concluded that the presence of large numbers of free-base porphyrins in the dendrimer compared with zinc porphyrins give higher energy transfer efficiency.

Acknowledgments
We thank the Ministry of Education, Culture, Sports, Science and Technology for a research grant (13450380).

References

1. Kato, T., Uchiyama, M., Maruo, N., Arai, T. and Nishino, N. *Chem. Lett.* 144-145 (2000).
2. Maruo, N., Uchiyama, M., Kato, T., Arai, T., Akisada, H. and Nishino, N., *Chem. Commun.* 2057-2058 (1999).
3. Watanabe, L. A., Uchiyama, M., Oniki, Y., Kato, T., Arai, T., Nishino, N., In Lebl, M., Houghten, R. A. (Eds.) *Peptides: The Wave of the Future (Proceedings of the 17th American Peptide Symposium)*, American Peptide Society, San Diego, 2001, p. 526.

Peptide Revolution: Genomics, Proteomics & Therapeutics
Michael Chorev & Tomi K. Sawyer (Editors)
American Peptide Society, 2003

Property and Antibacterial Activity of Dendritic and Linear Cationic Peptides

Haruhiko Aoyagi, Akira Hirano, Takuro Niidome and Tomomitsu Hatakeyama

Department of Applied Chemistry, Faculty of Engineering, Nagasaki University, Nagasaki 852-8521, Japan

Introduction

Cationic antibacterial peptides often act on bacterial cell membranes and suppress generation of tolerant bacteria because of their induction of rapid death of bacteria [1]. Such peptides are expected to be useful candidates as new drugs. In this connection, much attention has been concentrated on finding peptides with strong antibacterial activity but no hemolytic activity, because the hemolytic activity is undesirable in terms of practical use of peptides as drugs. Dendritic cationic peptides have been reported to show higher antibacterial activity but lower hemolytic activity than the corresponding linear peptides [2]. In this study, to confirm whether this finding is generally applicable to any cationic antibacterial peptides, some dendritic and linear model peptides (Figure 1) were synthesized. A sequence of LARL was selected as a unit, because we previously found that Ac-$(LARL)_3$-$NHCH_3$ had strong antibacterial activity [3]. In $L4_3$ and $L4_4$, the LARL units are aligned in tandem, which can take an α-helical structure. $L4_3$-PG and $L4_4$-PG also contain the LARL sequence, but formation of the α-helical structure is prevented by a PG sequence. $D4_3$ and $D4_4$ have the LARL sequence dendritically attached. Properties and biological activities of the synthetic peptides were then investigated.

$L4_3$: H-$(LARL)_3$-NH_2 $L4_4$: H-$(LARL)_4$-NH_2
$L4_3$-PG : H-LARL-PG-LARL-PG-LARL-NH_2
$L4_4$-PG : H-LARL-PG-LARL-PG-LARL-PG-LARL-NH_2
$D4_3$: $(H\text{-}LARL)_2$-K-NH-$(CH_2)_6$-NH-LRAL-H
$D4_4$: $(H\text{-}LARL)_2$-K-NH-$(CH_2)_6$-NH-K-$(LRAL\text{-}H)_2$

Fig. 1. Structures of synthetic peptides.

Results and Discussion

Dendritic and linear peptides were prepared using Fmoc-amino acids by the solution method and the solid phase method, respectively, and the final products were identified by mass spectrometry. To examine the secondary structure of the peptides CD measurements were performed in a buffer (pH 7.4) and in the presence of egg PC or egg PC / egg PG (3:1) vesicles. The peptides, except $L4_3$ and $L4_4$, were random under all the conditions, whereas $L4_3$ and $L4_4$ considerably took an α-helix structure in the presence of lipid vesicles.

Antibacterial activity of the peptides was examined using two Gram-positive bacteria and two Gram-negative bacteria (Table 1). The activity of $D4_3$ was 64 μM against all the bacteria, while $D4_4$ had moderate activity of 8-16 μM. However, their activities were weaker than those of the corresponding linear peptides. This result is different from the reported one [2]. $L4_3$-PG and $L4_4$-PG had no or weak activity. It is noteworthy that dendritic peptides had no hemolytic activity even at a peptide concentration of 100 μM, whereas $L4_3$ and $L4_4$ showed the activity of 100% at 100 μM and 5 μM, respectively. Calcein leakage mediated by the peptides from calcein-

Table 1. Antibacterial activities of the peptides.

	Minimum inhibitory concentration (μM)[a]						
	$L4_3$	$L4_4$	$L4_3$-PG	$L4_4$-PG	$D4_3$	$D4_4$	GS[b]
S. aureus IFO 12732	1	1	>64	64	64	8	1
B. subtilis IFO 3134	1	1	>64	64	64	8	1
E. coli ATCC 43827	4	16	>64	>64	64	16	8
P. aeruginosa ATCC 27853	4	16	>64	>64	64	16	8

[a] *Method, liquid based assay; medium, tryptic soy broth medium (pH 7.4); inoculum size* 10^4 *cells/ml.* [b]*GS is gramicidin S.*

entrapped vesicles was measured to examine the peptide-lipid interaction. Leakage activities of $D4_3$ and $D4_4$ for egg PC vesicles were much weaker than those of $L4_3$ and $L4_4$. In the case of egg PC / egg PG (3:1) vesicles, exact measurement for $D4_3$ and $D4_4$ could not be done because of formation of some turbidity. All of the peptides showed to some extent outer membrane permeability. On the other hand, their inner membrane permeabilities were different from one another (Figure 2).The order of inner membrane permeabilities of the peptides was roughly parallel to that of their antibacterial activities. This result suggests that the targeting site of the peptides might be bacterial cell membrane. In conclusion, the present study indicates that dendritic cationic peptides have favorable characteristics as antibiotics.

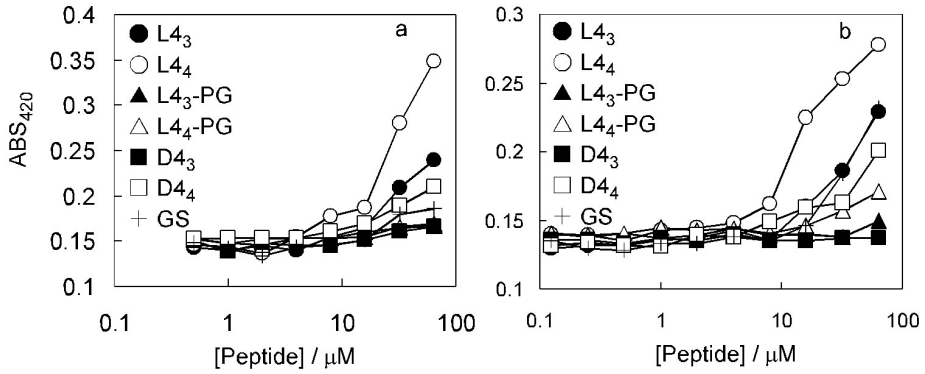

Fig. 2. Inner membrane permeabilization by peptides assessed by o-nitrophenyl β-D-galacto-pyranoside (ONPG) uptake in B. subtilis (a) and E. coli (b). Time, 30 min; [ONPG] = 25 μM.

Acknowledgments

This work was supported by a Grant-in-Aid from the Ministry of Education, Science, Sports and Culture of Japan.

References

1. Saberwal, G. and Nagaraj, R. *Biochim. Biophys. Acta* **1197**, 109-131 (1994).
2. Tam, J. P., Lu, Y. -A. and Yang, J. -L. *Eur. J. Biochem.* **269**, 923-932 (2002).
3. Lee, S., Mihara, H., Aoyagi, H., Kato, T., Izumiya, N. and Yamasaki, N. *Biochem. Biophys. Acta* **862**, 211-219 (1986).

Peptide Revolution: Genomics, Proteomics & Therapeutics
Michael Chorev & Tomi K. Sawyer (Editors)
American Peptide Society, 2003

Introduction of Disulfide Bond Pairing into a HER-2 B-Cell Epitope Improves Tumor Cell Binding and Antitumor Activities of Peptide Antibodies

Kenneth D. Lute[2], Naveen Dakappagari[1], Shard Rawale[1] and Pravin T.P. Kaumaya[1,2,3]

[1]Department of Obstetrics and Gynecology; [2]Integrated Biomedical Sciences Graduate Program; [3]Arthur G. James Comprehensive Cancer Center, The Ohio State University, Columbus, OH 43210, USA

Introduction

Human Epidermal Growth Factor Receptor-2 (HER-2) is a member of the EGFR family of receptor tyrosine kinases, participating in cellular proliferation and differentiation. HER-2 over-expression is associated with markedly aggressive forms of several cancers, including breast, ovarian and colon. Although passive immunotherapies such as HERCEPTIN® have produced promising results, a therapeutic approach capable of inducing active specific immunity would prove to be highly advantageous, offering enhanced protection at a lower cost. In order to overcome tolerance and induce an active immune response to self-antigens, our approach entails designing B cell epitopes as chimeric constructs incorporating promiscuous T_H cell epitopes for eliciting high titer antitumor antibodies. Constructs are designed using computer-aided analysis to predict antigenic determinants within target proteins. The antitumor properties of these epitope vaccines are characterized by immunizing transgenic and FVB/n mice and assessing tumor burden in a challenge model. Additionally, we also characterize the properties of the elicited antibodies using several *in vitro* assays.

In previous studies we reported the superior antitumor properties of the linear B-cell epitope HER-2 MVF628-647 in a mouse tumor challenge model [1]. Since conformational epitopes are likely to offer improved vaccine efficacy by increasing immune cross-reactivity and antitumor responses, we redesigned this epitope to incorporate two native disulfide pairings. We employed a strategy described by Soll end coworkers in which both pairings are made in a single-step fashion in solution [2]. This technique allowed us to generate a selectively oxidized epitope in which the four cysteines were optimally paired by using differential cysteine protection. The resulting construct was characterized by reversed-phase HPLC and the degree of oxidation was determined by treatment with a thiol-reactive biotinylating agent and subsequent ESI-MS analysis.

Results and Discussion

B-cell epitopes were synthesized colinearly with a promiscuous T-helper epitope using Fmoc chemistry on a Milligen/Biosearch 9600 peptide synthesizer (Bedford, MA). To allow for directed disulfide pairing differential cysteine protection was utilized. Following purification and characterization the immunogenicity of the constructs were determined by direct ELISA (Table 1). The linear and cyclized peptides produced similar antibody titers in ICR mice, but there was a clear increase in the immunogenicity of cyclized versus linear constructs in FVB/n mice. To determine the ability of peptide antibodies to cross-react with native protein, we utilized flow cytometry. Our results indicate that the peptide antibodies raised to the cyclized

Table 1. Antitumor activity of peptide antibodies.

Peptide Antibody	*Immunogenicity*[a]	*Cross-reactivity*[b]	*Anti-tumor activity*[c]
MVF 626-649 SS	+++	+++	+++
MVF 626-649 NC	+++	++	++

[a]*Immunogenicity was determined by measuring antibody titers from sera of immunized animals.*
[b]*The ability of peptide antibodies to recognize native protein was determined by flow cytometry.*
[c]*Anti-tumor activity was measured by the ability of peptide antibodies to induce IFN-γ release.*

peptide demonstrate greater than a five-fold increase in binding affinity (Table 1). Additionally, we investigated whether peptide-antibody coated tumor cells could induce the release of the antitumor cytokine interferon-γ from human peripheral blood mononuclear cells (Table 1).

Substantial IFN-γ release was observed following treatment with antibodies raised against the cyclized construct, with slightly less witnessed for those raised against the linear construct. Taken together these preliminary studies demonstrate the importance of conformational epitopes in vaccine design.

Acknowledgments
The work was funded by a National Cancer Institute, #CA 84356-01A1 grant to P.T.P. Kaumaya.

References
1. Dakappagari, N. K., et al. *Cancer Res.* **60**, 3782-3789 (2000).
2. Soll, R. and Beck-Sickinger, A. *J. Peptide Sci.* **6**, 387-397 (2000).

Peptide Revolution: Genomics, Proteomics & Therapeutics
Michael Chorev & Tomi K. Sawyer (Editors)
American Peptide Society, 2003

Conformational and Conserved Epitope of gp120 Exposed During Viral Fusion in HIV-Vaccine Design

Kristen Sadler, Yi-An Lu, Khee Dong Eom, Ying Zhang and James P. Tam

Department of Microbiology and Immunology, Vanderbilt University, Nashville, TN 37212, USA

Introduction

Recent figures show that the HIV/AIDS epidemic is rampant—the number of people living with HIV/AIDS reached 42 million in 2002 [1]. While highly active antiretroviral therapy has been effective, the need for a prophylactic and/or therapeutic vaccine is urgent. However, antibodies directed against one isolate are typically poorly neutralizing or not cross-reactive amongst other HIV-1 isolates. In order to generate a broadly active vaccine we are investigating the vaccine potential of a conserved region of protein gp120. Protein gp120 plays a major role in infection: HIV-1 entry into host cells is initiated by a high-affinity interaction between gp120 and host CD4, followed by binding of the activated gp120 to a chemokine coreceptor. The conformational and conserved region known as the bridging sheet, located between the V2 and V3 loops of gp120 [2], is critical to both CD4 and coreceptor interactions. Therefore, antibodies specific for the bridging sheet can potentially inhibit one of the earliest stages of infection. This study aimed to design and synthesize peptides mimicing the bridging sheet of HIV-1 gp120 and to examine peptide immunogenicity, particularly the induction of anti-peptide antibodies recognizing and binding viral proteins and virions.

Results and Discussion

A series of 10 peptides (β4A through β4J) was assembled that incorporated residues from the four non-continuous strands, denoted as β2, β3, β20 and β21 which make up the bridging sheet of HIV gp120. All peptides were constrained by cysteine knots or disulphide bonds to maintain conformation. Each peptide differed either in strand synthesis order or in the number and position of disulphide bonds. Figure 1 shows diagrammatic representations of two such peptides, β4A and β4H.

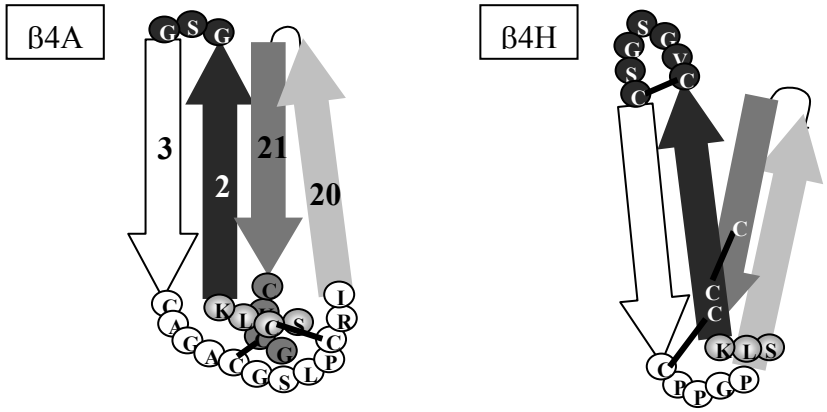

Fig. 1. Schematic of two peptides designed to mimic gp120 bridging sheet. Four β-strands shown as arrows; connecting residues shown as circles; disulphide bonds shown as solid lines.

The immunogenicity of each peptide was ascertained through inoculation of guinea pigs and assay of resultant antisera for antibodies capable of binding to peptides and recombinant proteins (Table 1). Eight of the 10 peptides tested were good immunogens with high anti-peptide antibody titres resulting from inoculation. However, only three peptides, β4A, β4G and β4H, were found to induce antibodies capable of binding to gp120 and gp160 with significant titre. The lack of anti-protein responses detected in the remainder of samples are likely due to the absence of B cell epitopes shared by immunogen and antigen. The more tightly constrained peptides tended to induce higher anti-protein antibody titres.

Table 1. Immunogenicity and antigenicity of synthetic peptides based on gp120 bridging sheet.

Immunizing peptide	Anti-peptide titre (log_{10})	Anti-gp120 titre (log_{10})	Anti-gp160 titre (log_{10})
β4A	4.8[a]	3.7	3.9
β4B	5.4	2.4	2.2
β4C	4.0	<2	2.1
β4D	2.9	2.3	ND[b]
β4E	3.0	2.1	<2
β4F	1.3	<2	ND
β4G	4.7	<2	3.0
β4H	4.9	3.5	3.8
β4I	4.1	<2	<2
β4J	5.7	<2	<2

[a]*Titres expressed as reciprocal of serum dilution that equaled four times the absorbance value of wells lacking serum.* [b]*Not determined. Limiting volumes precluded use in assay.*

To further characterize the anti-peptide antibodies, antisera were tested by immunostaining for binding to HIV-infected cells. P4 cells expressing CCR5 were incubated with various M-tropic viral strains (BAL, NL-36, R9) for 72h prior to fixing and addition of antisera. Antibody binding was detected with anti-guinea pig Ig-fluorescein conjugate and visualized by fluorescent microscopy. All antibody samples tested bound to infected cells regardless of viral strain used (data not shown). This result highlights the potential of the bridging sheet as a vaccine candidate due to the broad specificity of the antibodies induced. The subtle differences in protein binding detected using the ELISA are not reflected in the immunostaining results, thus emphasizing the value of the ELISA for vaccine candidate evaluation.

Anti-peptide antisera collected from animals inoculated with β4A, β4G and β4H were tested for their ability to inhibit the gp120-CD4 interaction *in vitro*. It was found that antibodies induced by inoculation with β4G and β4H prevented CD4 from binding to gp120. Currently, anti-peptide antisera are being assayed for ability to inhibit viral infection *in vitro*. These results will be used to optimize peptide structure in order to produce the next generation of potential vaccine candidates.

Acknowledgments

We thank Dr. Jin-Long Yang and Yoana Dimitrova for technical assistance and Dr. Christopher Aiken for provision of virus samples. This work was supported by NIH grant AI46174.

References

1. www.unaids.org/epidemic_update.
2. Kwong, P. D. et al. *Nature* **393**, 648-59 (1998).

Peptide Revolution: Genomics, Proteomics & Therapeutics
Michael Chorev & Tomi K. Sawyer (Editors)
American Peptide Society, 2003

Multiepitope Analysis of the HIV-1 gp41-Specific Immune Response Using a Panel of Constrained and Unconstrained Peptides

Elisabetta Bianchi[1], David Opalka[2], Paolo Ingallinella[1], William Schleif[3], Michael McElhaugh[3], Renee Danzeisen[3], Romas Geleziunas[3], Michael Miller[3], Debra Eckert[4], David Bramhill[4], Joseph Joyce[3], James Cook[3], William Magilton[3], Gennaro Ciliberto[1], John Shiver[3], Mark Esser[2] and Antonello Pessi[1]

[1]IRBM P. Angeletti, Via Pontina Km 30.600, 00040 Pomezia (Rome) Italy; [2]Merck Research Laboratories, Wayne, PA 19087, USA; [3]Merck Research Laboratories, P.O. Box 4, West Point, PA 19486, USA; [4]Merck Research Laboratories, Rahway, NJ 07065, USA

Introduction

Much effort is devoted to the development of a safe and effective vaccine against HIV. Many studies demonstrated that HIV-infected individuals can produce neutralizing antibodies. The HIV envelope glycoproteins gp120 and gp41 mediate virion attachment and fusion and are the prime targets for the humoral response. A few broadly neutralizing antibodies, targeting conserved regions in gp41 and gp120, have been developed. However, the development of vaccine candidates capable of eliciting a broadly reactive humoral immune response has been unsuccessful to date.

In order to map the dominant, subdominant and potentially immunologically silent regions of gp41, we developed a multiplexed antibody-binding and mapping assay to characterize the specificity, breadth and magnitude of the antibody response in sera from HIV-infected individuals. The HIV-1 positive sera were also evaluated using infectivity inhibition assays to determine whether there was any correlation between the neutralization potency and the antigen-reactivity profile.

Results and Discussion

The multiplexed Luminex epitope-mapping technology was employed to rapidly characterize the HIV envelope-specific antibody response. The antigen panel included recombinant gp41, gp120 as well as peptides covering different regions of gp41 as shown in Figure 1: the fusion peptide region (FP), the polar region (PR), the N-heptad,

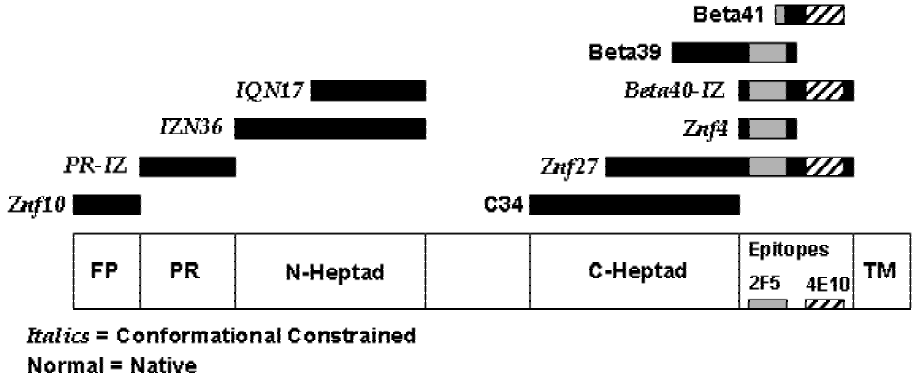

Fig. 1. HIV gp41 antigens used for the multiplex epitope mapping assay.

the C-heptad regions and the 2F5/4E10/Z13 neutralizing antibody epitopes from the tryptophan rich region (Trp-rich). Some of these peptides represented portions of gp41 as linear native sequences, such as C34, Beta39, Beta41. Other peptides were conformationally constrained through the use of presentation scaffolds, by grafting gp41 sequences on to the helical portion of a Cys2-His2 zinc finger domain to be displayed as helical epitopes [1]: ZnF4 (helical 2F5 epitope), ZnF10 (helical FP), ZnF27 (helical C-heptad and unconstrained Trp-rich region). Other gp41 regions were fused to designed, soluble trimeric coiled coil motifs such as IZ [2]: PRIZ, Beta40IZ. We also tested IQN17 [3], IZN36 [2] and gp41 5-Helix [4] and 6-Helix to characterize the immune response to the proposed pre-fusion and fusion intermediates. Overall, this panel of peptides was aimed not only at representing a scan of the gp41 primary sequence, but also at presenting the same sequences in different conformations.

The specificity of the epitope mapping assay was first tested using three HIV-1 monoclonal antibodies reactive to known gp41 and gp120 epitopes, i.e., mAb2G12, mAb2F5 and mAb4E10, against a subset of the gp41 peptides and recombinant proteins.

The epitope mapping assay was then used to characterize antibody responses in HIV-1-infected individuals. The results confirmed that HIV infected individuals have very high titers to gp41 and specific to many regions across gp41, while titers to gp120 are generally much lower. We also observed the highest titers for 5-helix and 6-helix suggesting that antibodies may recognize the fusion complex. The analysis revealed that many individuals have a broad, high titer antibody response to the N-heptad, C-heptad and the 2F5-4E10 regions and medium titer antibody response to the fusion peptide and polar regions. In general we found that many of the individuals' sera had antibodies that recognized all of the peptides and recombinant proteins, suggesting that there are no immunologically silent regions in HIV-1 gp41.

We next wanted to determine whether there was a correlation between the antigen reactivity profile of the sera and their neutralization potency. Towards this end, we tested the sera in two different neutralization assays, in single-cycle infectivity assay (using HIV-1_{HXB2}) and in multicycle infectivity assay (using HIV-1_{MN}). According to their neutralization potency the sample sera were grouped in low, medium and high titer samples. The sera neutralization potency titers were then compared to the corresponding antibody titers for gp120, each of gp41 peptides and the sum of the titers to all the gp41 peptides.

Despite the high antibody titer responses, we found no significant correlation between the specificity, breadth or magnitude of the IgG antibody response and the neutralization potency of the sera.

These results suggest that HIV-1 infected individuals make broad, high-titer responses to many regions of gp41, including the pre-fusion and fusion intermediates. However these antibodies are unable to interfere with the fusion process. Overall the data suggest that most gp41 regions are inaccessible to antibodies and that viral debris is eliciting the gp41 specific humoral response.

References

1. Bianchi. E, et al. In Benedetti, E. and Pedone, C. (Eds.) *Peptides 2002 (Proceedings of the 27th European Peptide Symposium)*, Edizioni Ziino, Napoli, 2003, pp. 682-683.
2. Eckert, D. M. and Kim, P. S. *Proc. Natl. Acad. Sci. U.S.A.* **98**, 11187-11193 (2001).
3. Eckert, D. M., Malashkevich, V. N., Hong, L. H., Carr, P. A. and Kim, P. S. *Cell* **99**, 103-115 (1999).
4. Root, M. J., Kay, M. S. and Kim, P. S. *Science* **291**, 884-898, (2001).

Peptide Revolution: Genomics, Proteomics & Therapeutics
Michael Chorev & Tomi K. Sawyer (Editors)
American Peptide Society, 2003

Structural Analysis of the Epitope of the Anti-HIV-1 mAb 2F5 Yields Insights into the Mechanism of Neutralization and into the HIV-1 Fusion Process

Antonello Pessi[1], Gaetano Barbato[1], Paolo Ingallinella[1], William H. Hurni[2], Michael D. Miller[2], Gennaro Ciliberto[1], Riccardo Cortese[1], Renzo Bazzo[1], John W. Shiver[2] and Elisabetta Bianchi[1]

[1]IRBM P. Angeletti, Via Pontina Km 30.600, 00040 Pomezia (Rome) Italy and
[2]Merck Research Laboratories, P.O. Box 4, West Point, PA 19486, USA

Introduction

Fusion of human immunodeficiency virus (HIV) with the host cell is mediated by the gp41 subunit (Figure 1) of the envelope glycoprotein gp160 [1]. Only three broadly neutralizing antibodies have been identified, which bind to gp41: 2F5, Z13 and 4D10. Their epitopes are all concentrated in a small region, close to the transmembrane domain (Figure 1). In addition to being the preferred target for neutralization, this region is essential for fusion to occur. Deletions within this segment may completely abrogate fusogenicity. Moreover, this region contributes to the potency of the FDA-approved fusion inhibitor T-20 (Figure 1), and shows inhibitory activity on its own. And finally, the region is strictly conserved in the majority of otherwise highly variable HIV isolates.

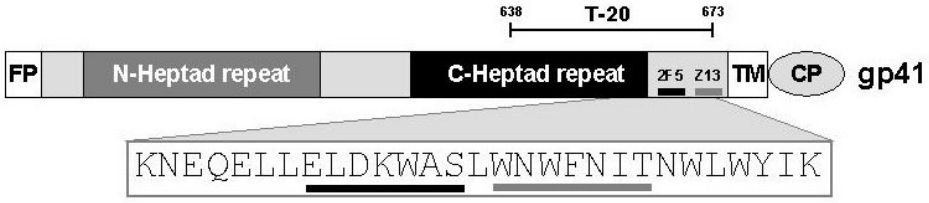

Fig. 1. Schematic representation of gp41, the fusogenic subunit of the HIV envelope glycoprotein gp160. The boxed sequence (residues 655-683) corresponds to the region of interest for this work. Indicated are the locations of the epitopes of the broadly neutralizing mAbs 2F5 and Z13, and of the fusion inhibitor T-20. FP, fusion peptide, TM, transmembrane, CP, cytoplasmic.

While structural studies are available of peptides encompassing the membrane-proximal region, the results of these studies are contradictory. Shibli *et al.* showed that residues 665-683 fold in dodecyl phosphocholine micelles as a single α-helix parallel to the membrane surface [3]. Biron *et al*. showed that the central part of a peptide, spanning residues 659-671, assumes a 3_{10} helical conformation in aqueous solution [4]. By contrast, the crystal structure of a Fab fragment of mAb 2F5, in complex with a peptide corresponding to the core epitope ELDKWAS, shows the latter in a type I β-turn conformation [5].

The evidence supporting two different secondary structures for the same region could be reconciled, if a *conformational transition* between them were occurring as part of the fusion mechanism. We sought support for this hypothesis by a detailed structural study of the 2F5 epitope region.

Results and Discussion

Using a competitive ELISA assay [6] we found that the epitope must include between 13-15 amino acids (residues 659-671 or -673), instead of the previously found [2,5] core heptapeptide ELDKWAS [7].

Alanine scanning experiments, performed on longer C-peptides, have shown that none of the alanine substitutions, either upstream or downstream from the core DKW triad, severely reduced binding. On the contrary, binding was completely abolished by substitution of any one of the D/K/W residues [6]. This suggested to us that the increase in binding affinity was not due to additional contacts, but rather to structural stabilization. Accordingly, NMR showed that, while peptide ELDKWAS is too flexible to allow detection of any preferred conformation, in the longer peptides some structural elements were being stabilized, as argued by the chemical shift dispersion and the $^{3}J_{HN\text{-}\alpha H}$ coupling constants. Based on solubility and lower tendency to aggregation, the 13-aa peptide ELLELDKWASLWN appeared as the best candidate for subsequent analysis.

The peptide was present in solution as a complex mixture of conformers. A convenient way to draw reliable conclusions in these situations is to focus on the *local* structural elements, shared by multiple conformers, and perform a statistical analysis of the relative conformer populations [7]. This is the key feature of our previously developed method NAMFIS (Nmr Analysis of Molecular Flexibility in Solution) [8]. NAMFIS clusters all conformers whose local conformation in a defined region is similar, *irrespective of their structure in other regions.*

A detailed analysis of the NAMFIS results is reported elsewhere [7]. The key finding of our study was that the increase in binding affinity parallels the stabilization of specific local and global conformational propensities, absent in the shorter epitope. In particular, we found that:

(i) The central DKW turn is the locally dominant structure, *also in the absence of the antibody*. The molar fraction of the conformer population with identical ($rmsd_{N,C\alpha,C',O} \leq 0.1$Å) or very similar ($0.1$Å $\leq rmsd_{N,C\alpha,C',O} \leq 0.2$Å) backbone structure to the 2F5-bound conformation [5] is in the range of 0.78-0.88;

(ii) The turn is embedded in a set of conformers, which represent intermediate forms between a partially bent structure, with extended termini, and a fully helical structure;

(iii) These conformations are linearly encoded in the sequence itself, rather than dependent on other parts of the envelope structure.

Establishment of the intrinsic conformational propensities of the 2F5 epitope domain allowed us to rationalize a series of previous observations, and to assign a more active role to the membrane-proximal region during HIV fusion [7]. The proposed structural model of the conformational transition is illustrated in Figure 2.

This model also offers an explanation for the neutralization mechanism of mAb 2F5. By binding to the turn structure, as shown by X-ray [5], the antibody would prevent the required conformational transition to the extended and then helical structure, and would thus stall fusion. This hypothesis is compatible with the knowledge that 2F5 does not block viral attachment, but rather interferes with a subsequent step in viral fusion [9]. Moreover, the 2F5 epitope becomes inaccessible following CD4 binding, suggesting that it may indeed undergo a conformational change.

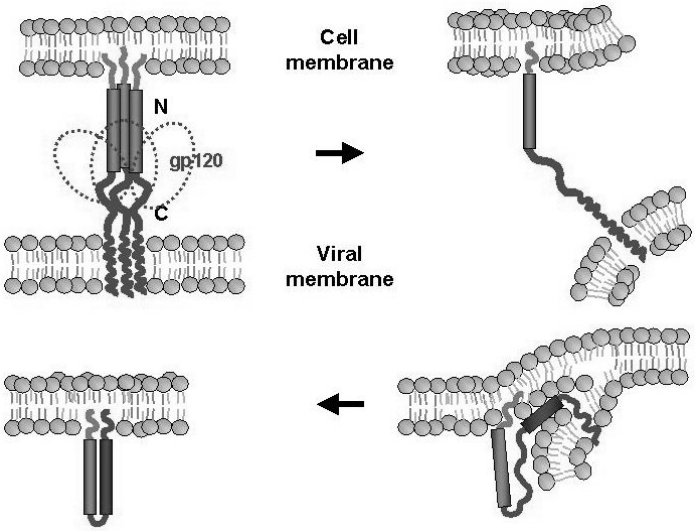

Fig. 2. Proposed model for the conformational transition of the 2F5 epitope region, from a closed (β-turn) conformation to an extended and then to a helical structure, either a 3_{10} helix or an α-helix. We favor the helical structure, which is depicted parallel to the plane of the membrane, to be a α-helix, since the peculiar distribution of the indispensable Trp residues on both faces of the helix would allow this region to interact with both *membranes, this way driving the juxtaposition of the viral and cellular membranes during the late stages of fusion.*

We envisage further application of the strategy utilized here to the study of analogous viral domains, whose function requires a controlled level of flexibility, and which therefore do not easily lend themselves to crystallographic studies.

Acknowledgments

We thank P.S. Kim, X. Liang, J. Joyce, D.M. Eckert, U. Koch, B. Gatti and M. Finotto.

References

1. Weissenhorn, W., Dessen, A., Harrison, S. C., Skehel, J. J. and Wiley, D. C. *Nature* **387**, 426-430 (1997); Chan, D. C., Kim, P. S. *Cell* **93**, 681-684 (1998).
2. Muster, T., Steindl, F., Purtscher, M., Trkola, A., Klima, A., Himmler, G., Ruker, F. and Katinger, H., *J. Virology* **67**, 6642-6647 (1993); Zwick, M. B., Labrjin, A. K., Wang, M., Spenlehauer, C., Saphire, E. O., Binley, J. M., Moore, J. P., Stiegler, G., Katinger, H., Burton, D. R. and Parren, P. W. H. I. *J. Virol*. **75**, 10892-10905 (2001).
3. Schibli, D. J., Montelaro, R. C. and Vogel, H. J. *Biochemistry* **40**, 9570-9578 (2001).
4. Biron, Z., Khare, S., Samson, A. O., Hayek, Y., Naider, F. and Anglister, J. *Biochemistry* **41**, 12687-12896 (2002).
5. Pai, E. F., Klein, M. H., Chong, P. and Pedyczak, A., WIPO patent WO-00/61618 (2002).
6. Joyce, J. G., Hurni, W. M., Bogusky, M. J., Garsky, V. M., Liang, X., Danzeisen, R. C., Miller, M. D., Shiver, J. W. and Keller, P. M. *J. Biol. Chem*. **277**, 45811-45820 (2002).
7. Barbato, G., Bianchi, E., Ingallinella, P., Hurni, W. H., Miller, M. D., Ciliberto, G., Cortese, R., Bazzo, R., Shiver, J. W. and Pessi, A. *J. Mol. Biol*. **30,** 1101-1115 (2003).
8. Cicero, D. O., Barbato, G. and Bazzo, R. *J. Am. Chem. Soc.* **117**, 1027-1033 (1995).
9. Ugolini, S., Mondor, I., Parren, P. W., Burton, D. R., Tilley, S. A., Klasse, P. J. and Sattenau, Q. J. *J. Exp. Med*. **186**, 1287-1298 (1997).

Peptide Revolution: Genomics, Proteomics & Therapeutics
Michael Chorev & Tomi K. Sawyer (Editors)
American Peptide Society, 2003

Novel Design of Thiol-Containing Lactam-Bridge Constraints for Immune Presentation of the ELDKWAS Epitope from gp41 in the Type-I β-Turn Conformation Recognized by mAb 2F5

Yu Tian[1], Edward Arnold[1,2], Gail F. Arnold[1,2] and John W. Taylor[1]

[1]Department of Chemistry and Chemical Biology, Rutgers University, Piscataway, NJ 08854, USA; [2]Center for Advanced Biotechnology and Medicine, Piscataway, NJ 08854, USA

Introduction

MAb 2F5 is an HIV-1 neutralizing human monoclonal antibody that recognizes a continuous linear epitope, LELDKWASL, in the membrane-proximal ectodomain of the envelope glycoprotein gp41 [1]. Crystallographic studies of the 2F5-bound peptide h-ELDKWAS-oh indicate that the antibody-bound epitope adopts a type-I β-turn conformation centered around the KW sequence [2]. Analog studies indicate that the DKW sequence is most critical for antibody recognition, and that the terminal residues in the LELDKWASL sequence, L^1 and L^9, are also required for high-affinity binding. However, L^3 and S^8 are more tolerant of certain types of substitution [3]. Direct attempts to use linear peptide haptens to elicit a 2F5-like neutralizing response to this epitope have failed, possibly because the epitope was incorrectly presented to the immune system. To address these problems, we have synthesized a series of conformationally constrained analogs of this neutralizing epitope that are cyclized through side-chain linkages and are designed to be compatible with the reported conformation of the 2F5-bound epitope. Some of these side-chain linkages have been designed to incorporate thiol groups within their structures. These thiol-containing bridges serve a dual role. First, they constrain those residues that are most critical for 2F5 recognition in the appropriate β-turn conformation. Second, they substitute for the thiol groups that are more customarily placed at the N or C terminus of a peptide hapten and used for conjugation to a protein carrier. The placement of the hapten-carrier linkage within the constraining bridge is a novel approach that is intended to focus the immune response on all of the structural and conformational features of the β-turn epitope that determine its high affinity for mAb 2F5 (Figure 1).

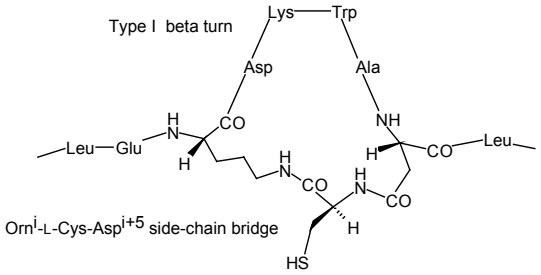

Fig. 1. A side-chain bridged LELDKWASL analog designed for immune presentation of this neutralizing epitope as a type-I β-turn on a protein carrier.

Results and Discussion

The peptides listed in Figure 2 were synthesized by Fmoc or Boc solid-phase methods and purified to apparent homogeneity. Peptides were then assayed in their thiol-protected forms for their relative affinities for 2F5 in competitive ELISAs (Table 1). A

comparison of the Lys^9-Asp^{14} side-chain bridged analog, Lac1, with its isosteric acyclic analog, Iso1, showed that this cyclization constraint enhanced the affinity of the epitope for the antibody. Furthermore, peptides constrained by Orn^9-to-Asp^{14} side-chain bridges with Gly or L-Cys inserts had even higher antibody binding affinities.

Lac1 Ac-*cyclo*(Lys^9,Asp^{14})-CNEQELLEKDKWADL-nh_2
Iso1 Ac-CNEQELLE-Nle-DKWANL-nh_2
Gly linker Ac-*cyclo*(Orn[Gly]^9,Asp^{14})-CNEQELLE-Orn(G)-DKWADL-nh_2
L-Cys linker Ac-*cyclo*(Orn[L-Cys]^9,Asp^{14})-NEQELLE-Orn(C)-DKWADL-nh_2
D-Cys linker Ac-*cyclo*(Orn[D-Cys]^9,Asp^{14})-NEQELLE-Orn(*C*)-DKWADL-nh_2

Fig. 2. Structures of side-chain bridge constrained and unconstrained LELDKWASL analogs.

Table 1. Antibody binding affinities and immunogenicities of peptides.

Peptide	Affinity for mAb 2F5[a]		Serum titer[a]
	IC_{50} (nM)	*Relative potency (%)*	*Dilution factor (to IC_{50})*
Lac1	38 ± 5	190	13,400 ± 2000
Iso1	71 ± 13	100	3000 ± 800
Gly linker	20 ± 5	360	29,800 ± 14,000
L-Cys linker	6.1 ± 1.6	1200	12,600 ± 3800
D-Cys linker	41 ± 9	170	8300 ± 2500

[a]*ELISAs were performed using biotin-LELDKWASL-nh_2 on streptavidin-coated plates.*

Peptides were coupled *via* their thiol groups to maleimide-derivatized KLH, and these preparations were used to inoculate guinea pigs (n=3 for each peptide). All of the challenged animals responded, but the antisera raised against the bridge-constrained analogs all gave titers (measured by binding to LELDKWASL) that were higher than those of the sera raised against the unconstrained Iso1 peptide hapten (Table 1). Furthermore, competitive ELISAs showed that the antisera raised against the bridge-constrained peptides had binding specificities for linear and cyclized peptides that were similar to those of mAb 2F5, whereas antisera raised against the unconstrained analog, Iso1, failed to recognize conformationally constrained peptides (not shown). These results show that lactam conformational constraint of the 2F5 epitope can produce a strong focused immune response with recognition specificities for the β-turn conformation that are similar to those of 2F5, and that placement of a thiol group within the bridge constraint for linkage of the hapten to a carrier protein is also effective.

Acknowledgments
This work was supported by NIH R21 grants AI45316 (JWT) and AI45353 (GFA).

References

1. Muster, T., Steindl, F., Purtscher, M., Trkola, A., Klima, A., Himmler, G., Ruker, F. and Katinger, H. *J. Virol.* **67**, 6642-6647 (1993).
2. Pai, E. F., Klein, M. H., Chong, P. and Pedyczak, A. *World Intellectual Property Organization* (http://www.wipo.org) patent WO-00/61618 (2000).
3. Tian, Y., Ramesh, C. V., Ma, X, Naqvi, S., et al. *J. Peptide Res.* **59**, 264-276 (2002).

Peptide Revolution: Genomics, Proteomics & Therapeutics
Michael Chorev & Tomi K. Sawyer (Editors)
American Peptide Society, 2003

Induction of Protective CTL Responses in HLA-A*0201 Transgenic Mice Against HTLV-1 Recombinant Vaccinia Virus Using a Multivalent CTL Epitope Peptide Construct

Roshni Sundaram[5], Sharad V Rawale[1], Naveen Dakappagari[1], Don Young[5], Christopher M Walker[4], Steven Jacobson[6] and Pravin T.P. Kaumaya[1,2,3]

[1]Dept. of Obstetrics and Gynecology; [2]Center for Retrovirus Research; [3]Dept. of Microbiology; [4]Dept. of Pediatric; [5]Dept. of Biostatistics, The Ohio State University, Columbus, OH 43210; [6]Viral Immunology Section, NINDS, National Institutes of Health, Bethesda, MD 20892, USA

Introduction

Human T-cell Lymphotropic Virus Type 1 (HTLV-1) is the causative agent of a chronic inflammatory disorder HTLV-1 associated Myelopathy or Tropical Spastic Paraparesis (HAM/TSP) and a very aggressive T-cell malignancy called Adult T-cell Leukemia (ATL) [1]. Cytotoxic T-lymphocytes have been implicated to be important for the clearance of chronic viral infections. The use of multiple epitopes would be more beneficial than single epitopes to achieve broad population coverage and tackle the issue of CTL escape mutants. Recently, we reported a novel strategy to deliver multiple epitopes into the same antigen presenting cell for simultaneous priming of multi-specific CTLs [2]. In this report we have investigated the effect of individual epitope orientation within the multiepitope construct on the processing efficacy of each epitope by 20s proteasome. Furthermore, we also tested the protective efficacy of our multiepitope peptide vaccine approach in HLA-A*0201 transgenic mice [3] against challenge with recombinant vaccinia virus expressing the Tax protein of HTLV-1. The results of these experiments are discussed in the context of immunotherapeutic approaches against HTLV-1.

Results and Discussion

Four variants of a multiepitope construct consisting of three immunogenic epitopes from the Tax protein of HTLV-1 were synthesized as one colinear sequence separated by double Arginine residues in tandem (Figure 1). Each of these constructs were digested *in vitro* using 20s immunoproteasome and also tested for their immunogenicity in HLA-A*0201 transgenic mice. We observed that the construct with the highest rate of digestion was also the most immunogenic for each of the three intended epitopes *in vivo*. The construct designated 236 had the highest rate of digestion with complete substrate turnover at the earliest 12 hour time point of digestion and was also the most immunogenic for all three intended epitopes (Table 1). In contrast, the 632, 362 and 326 constructs had slower rates of digestion that corresponded to lower immunogenicities for each intended epitope. Thus, the rate of digestion was influenced by the amino acid sequence of each construct, which varied depending on the relative positioning of each epitope. It is therefore imperative to optimize the positioning of individual epitopes when designing multiepitope constructs. The most rapidly digested construct was used to vaccinate groups of HLA-A*0201 transgenic mice in conjunction with a promiscuous T-helper epitope from tetanus toxoid (amino acids 947-967). Upon challenge with Tax recombinant vaccinia virus the vaccinated mice showed a statistically significant decrease in viral replication as compared to naïve mice or mice that were mock vaccinated with the promiscuous T-

helper epitope alone (Table 2). These results may have implications in the development of immunotherapeutic strategies against HTLV-1.

Fig.1. Design of the multiepitope CTL peptide construct.

Table 1. Summary of rate of digestion and immunogenicity of each intended epitope for each of the four multiepitope variants. Tax_{11-19} (LLFGYPVYV) is designated 2, $Tax_{178-186}$ (QLGAFLTNV) is designated 3 and $Tax_{306-315}$ (HLLFEEYTNI) is designated 6.

Construct	**20s Immunoproteasome digestion[a]**			**Immunogenicity (IFN-γ release)[b]**		
	Tax 11-19	**Tax 178-186**	**Tax 306-315**	**Tax 11-19**	**Tax 178-186**	**Tax 306-315**
236	+	+	+	++	+++	+++
632	-	-	-	++	+++	-
362	+	-	-	+	-	-
326	+	+	-	+	+	+

[a]*The four peptide constructs were digested for 12 hrs and the digested samples were analyzed by capillary liquid chromatography-nanospray tandem mass spectrometry. Relative abundance of each individual epitope is indicated as +/- (+++ > ++ >+).*
[b]*Immunogenicity of each construct was determined by the ability of splenocytes from HLA-A*0201 transgenic mice immunized with each construct to secrete IFN-γ in response to target cells coated with each individual epitope in a 24 hr culture.*

*Table 2. 236 vaccine induced protection in HLA-A*0201 transgenic mice against challenge with recombinant vaccinia virus expressing Tax protein. Values presented are mean $log_{10} \pm$ standard error of pfu/ovaries of groups of treated mice.*

Treatment	**Average vaccinia titer (Log_{10} pfu/ovary)**
236 immunized	8.75 ± 0.38*
Mock immunized control	12.23 ± 0.57
Naïve control	12.7 ± 0.4

** statistically significant reduction in viral titers ($p<0.0001$).*

Acknowledgments
This work was supported by an NIH grant to P. Kaumaya. We thank Dr. Francois Lemonnier for providing us with breeding pairs of the HLA-A*0201 transgenic mice.

References
1. Bangham, C. R. *J. Clin. Pathol.* **53**, 581-586 (2000).
2. Sundaram, R., Sun, Y., Walker, C. M., Lemonnier, F. A., Jacobson, S. and Kaumaya, P. T. *Vaccine* **21**, 2767-2781 (2000).
3. Pascolo, S., Bervas, N., Ure, J. M., Smith, A. G., Lemonnier, F. A., and Perarnau, B. *J. Exp. Med.* **185**, 2043-2051 (1997).

Peptide Revolution: Genomics, Proteomics & Therapeutics
Michael Chorev & Tomi K. Sawyer (Editors)
American Peptide Society, 2003

Totally Synthetic Lipopeptides as Self-Adjuvanting Contraceptive Vaccines

Weiguang Zeng, Yuk Fai Lau, Lorena E. Brown and David C. Jackson

Cooperative Research Center for Vaccine Technology, Department of Microbiology & Immunology, The University of Melbourne, Parkville, Victoria, Australia 3010

Introduction

One of the problems of using peptides as vaccine candidates is their generally weak immunogenicity unless inoculated with a potent adjuvant such as complete Freund's adjuvant (CFA). Of the many adjuvants currently available many are toxic or ineffective. Lipids and lipopeptides have been shown to be capable of adjuvanting otherwise weak immunogens. Tripalmitoyl-S-glyceryl cysteine (Pam3Cys) [1], a synthetic version of the N-terminal moiety of *E. coli* lipoprotein, has been shown to be capable of stimulating virus-specific cytotoxic T cell (CTL) responses against influenza virus-infected cells and to elicit protective antibodies against foot-and-mouth disease when coupled to a CTL epitope and to a B cell epitope, respectively [1,2]. Recently Pam2Cys, an analogue of Pam3Cys, has been synthesized [3] and shown to correspond to the lipid moiety of MALP-2, a macrophage-activating lipopeptide isolated from mycoplasms lacking cell walls [4].

Results and Discussion

Various peptides with or without lipid moiety were synthesized (Table 1). The peptides consist of a collinear CD4+ T helper cell epitope from the L chain of influenza virus hemagglutinin (represented in Table 1 as [T]) and a B cell epitope, which is luteinizing hormone-releasing hormone (LHRH) (represented in Table 1 as [B]). The lipid moiety is either tripalmitoyl-S-glyceryl cysteine (Pam3Cys) or dipalmitoyl-S-glyceryl cysteine (Pam2Cys) attached at two different positions within the peptides to produce linear or branched configurations of lipopeptides. We found that these two configurations of lipopeptide result in markedly different solubilities; better solubility was most evident in those cases where lipid was placed at the approximate center of the molecule.

Table 1. HPLC elution and mass characteristics of the peptide vaccines.

Peptide construct	HPLC retention time (min)	Expected mass (Da)	Experimentally determined mass (Da)
[T]-[B]	26.3	2957.1	2957.3
[T]-Lys-[B]	26.0	3085.5	3084.7
Pam3Cys-Ser-Ser-[T]-[B]	51.5	4022.4	4020.8
Pam2Cys-Ser-Ser-[T]-[B]	41.8	3785.1	3785.5
Pam2Cys-[T]-[B]	40.7	3609.3	3605.7
[T]-Lys(Pam2Cys)-[B]	40.7	3739.5	3739.6
[T]-Lys(Pam3Cys)-[B]	50.4	3977.4	3969.5

Antibody (Ab) titres and the fertility status of animals were determined following two doses of vaccines. Three of these lipopeptides, Pam2Cys-Ser-Ser-[T]-[B]. [T]-Lys(Pam3Cys)-[B], and [T]-Lys(Pam2Cys)-[B], when administered subcutaneously in saline, induced high levels of anti-LHRH Ab (Table 2). In fact, Ab titres induced after two doses of these lipopeptides were comparable to those obtained with non-lipidated

peptides [T]-[B] and [T]-Lys-[B] when they were administered in CFA. The two soluble branched lipopeptides [T]-Lys(Pam3Cys)-[B] and [T]-Lys(Pam2Cys)-[B] induced 10- to 100-fold higher levels of anti-LHRH Ab following the primary inoculation than did the other less soluble lipopeptide constructs (Table 2). The fertility study shows that none of the mice that received the two branched lipopeptides in saline or the non-lipidated in CFA became pregnant. Ab levels were followed up to 6 months after the second dose of peptide vaccine. The titres of anti-LHRH Ab present in the lipopeptide-primed mice and also in those mice that were primed with non-lipidated peptide administered in CFA maintained similar levels. A second fertility study was carried out three months following the second inoculation of vaccine and yielded similar results to the 2-weeks postimmunization trial (Table 2).

Table 2. Anti-LHRH antibody titres and incidence of pregnancy following inoculation with peptide constructs. Mice were inoculated twice at week 0 and at week 4 with lipidated peptides in saline and the non-lipidated peptides in CFA at 20 nmole/mouse. ELISA assays were conducted to measure the antibody titres in the serum samples as described [5].

Inoculum	Mean anti-LHRH titres (log_{10}) weeks following second dose					Incidence of pregnancy	
	4 weeks	6 weeks	11 weeks	14 weeks	24 weeks	2 weeks after 2nd Dose	13 weeks after 2nd Dose
[T]-[B]	4.18	4.92	4.32	4.28	4.06	0/5	0/5
[T]-Lys-[B]	4.62	4.70	4.36	4.24	4.12	0/5	0/5
Pam3Cys-Ser-Ser-[T]-[B]	2.40	3.36	3.12	3.04	2.78	2/5	0/5
Pam2Cys-Ser-Ser-[T]-[B]	2.70	4.78	3.96	3.80	3.52	1/5	2/5
Pam2Cys-[T]-[B]	1.46	4.24	3.38	3.34	3.18	2/5	3/5
[T]-Lys(Pam2Cys)-[B]	3.36	4.68	3.96	3.94	3.78	0/5	0/5
[T]-Lys(Pam3Cys)-[B]	3.42	4.48	4.18	4.06	3.86	0/5	0/5
Saline	1.0	1.0	ND	ND	ND	5/5	3/5

References

1. Deres, K., *et al*. *Nature* **342**, 561-564 (1989).
2. Wiesmuller, K. H., Bessler, W. G. and Jung, G. *Int. J. Peptide Protein Res.* **40,** 255-226 (1989).
3. Metzger, J. W. *et al*., *J. Peptide Sci.* **3**, 184-190 (1995).
4. Muhlradt, P. F. *et al*., *J. Exp. Med.* **185**, 1951-1958 (1997).
5. Zeng, W., *et al*. *J. Immunol.* **169**, 4905-4912 (2002).

Peptide Revolution: Genomics, Proteomics & Therapeutics
Michael Chorev & Tomi K. Sawyer (Editors)
American Peptide Society, 2003

The Matrix-Scan: A Micro Array of Peptide Constructs Mimicking Discontinuous Sites

Wim M. M. Schaaper, Jerry W. Slootstra, Wouter C. Puijk, Evert van Dijk, Johannes P. M. Langedijk, Rob H. Meloen and P. Timmerman

Pepscan Systems B.V., P.O. Box 2098, NL-8203AB Lelystad, The Netherlands

Introduction

The concept behind the Matrix-Scan is to use peptide constructs that mimic discontinuous interaction sites. A single part of an interaction site usually does not have sufficient affinity to the binding partner to allow its detection. Therefore, the different parts of the discontinuous interaction site are combined into a single molecule. The Matrix-Scan uses large arrays of peptide constructs that contain all combinations of overlapping peptide sequences derived from a protein. These peptide constructs are covalently linked with a functionalized polypropylene surface and can be made up by two or more peptides in all kinds of spatial orientations. Consequently, in these arrays we use peptides as building blocks to reconstruct different parts of interaction sites that are normally (far) apart in the linear sequence of the protein.

Previously, we have shown results of a Matrix-Scan of human Follicle Stimulating Hormone (FSH), tested against a set of 20 anti-FSH monoclonal antibodies [1,2]. We found that discontinuous epitopes could be defined accurately for most monoclonal antibodies, and that the results match very well with the reported X-ray structure of the closely related human Chorionic Gonadotropin (HCG) in combination with two antibody Fv fragments, specific for the α- and β-subunit [3].

In this presentation, we tested a commercially available monoclonal antibody (MCA19) that binds HCG and the β-HCG subunit, but gives no cross-reaction with human LH, FSH, and TSH. Antibodies that can distinguish between these hormones are commercially interesting products; however up to now no knowledge about the interaction site has been available. A scan with single overlapping 12-mer peptides did not reveal the binding site; however, the Matrix-Scan showed binding with three sequences in different peptide constructs, each of them containing two of these sequences. The interaction site could thus be defined and explains the difference in specificity of the mAb between HCG and LH.

Results and Discussion

Monoclonal antibody MCA19 was tested in a Pepscan against overlapping 12-mer peptides from the α- and β–subunit of HCG (results not shown). This scan showed many peaks, and only at high dilution of the mAb, peptide 142 (from the β3 loop) could be identified as a possible part of the interaction site.

A Matrix-Scan was synthesized as reported before [1] by coupling of peptides from the HCG sequence in all combinations using ligation chemistry. In this Matrix-Scan, odd numbered peptides were coupled at the square areas and even numbered peptides were coupled on these peptide-squares as dots, generating an array of all peptide combinations. Cysteines were replaced by alanine. Testing MCA19 in this Matrix-Scan, we found strong interactions (see Figure 1) for the constructs combining peptide 49 (VQKNVTSESTAA, α2-loop) with peptides 136-146 (VVANYRDVRFESIRLP-GAPRGV, β3-loop), peptide 91 (RPINATLAVEKE, β1-loop) with peptides 136-146 (VVANYRDVRFESIRLPGAPRGV, β3-loop) and peptide 141 (RDVRFESIRLPG, β3-loop) with peptides 46-52 (TMLVQKNVTSESTAAVAK, α2-loop) or peptides 94-98

(NATLAVEKEGAPVAIT, β1-loop). Some interaction was also found with peptides 186-192 (DHPLTADDPRFQDSSSSK, C-terminus β subunit.

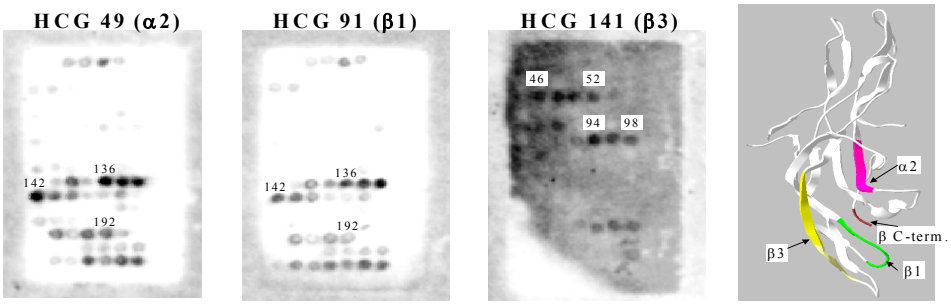

Fig. 1. A selection of reactive parts from the Matrix-Scan of HCG against MCA19. At the whole surface of the rectangles the first peptide (peptides 49, 91 and 141) is bound, the dots represent a second set of peptides, ligated to the first one. Several peptide combinations show binding (explanation in text). The location of the reactive sequences is shown in the X-ray model of HCG at the right: peptides 136-146 = β3 loop, peptides 94-98 = β1 loop, peptides 186-192 = C-terminus of β subunit and peptides 46-56 = α2 loop.

In the X-ray model of HCG [3] these sequences are located in the same area and are likely to form the interaction site of MCA19 with HCG. Only the sequence of peptides 46-52, in the α-subunit of HCG (and possibly the C-terminus of the β-subunit), is located too far from the other reactive sequences. Its reactivity could be explained by sequence similarity with the reactive sequence in the β3 loop (KNVTSES <=> RDVRFES). Although the most reactive sequences are identical for HCG and LH, the difference in specificity of MCA19 for these hormones can be explained by mutations in the β3 loop spanning peptides 136-152. The first mutation in this sequence is N => T in VVCNYR (in peptide 136), the second is N =>D in GAPRGVNP (in peptide 152). A third mutation (YA =>FP in VVSYAV, peptide 160) is close under the interaction site. The second possibility (N =>D) seems the most likely, since this amino acid is exposed and it drastically changes the electrostatic surface of the protein in this area.

We conclude that using a Matrix-Scan of HCG, three different sequences were defined that are part of the discontinuous antigenic site of MCA19; these sequences could not be found by simple linear scanning methods. Further, we could explain the specificity of the antibody for HCG by a mutation in the sequence of LH, located in the middle of the interaction site.

Acknowledgments

Part of this work was supported by Bit/Eureka project SYNMIC-FSH (E1255811).

References

1. Schaaper, W. M. M., *et al.* In Benedetti, E. and Pedone, C. (Eds.), *Peptides 2002*, Edizioni Ziino, Napoli, Italy, p. 1008-1009 (2002).
2. Timmerman, P., *et al. J. Mol. Div.* in prep.
3. Tegoni, M., *et al. J. Mol. Biol.* **289**, 1375-85 (1999).

Peptide Revolution: Genomics, Proteomics & Therapeutics
Michael Chorev & Tomi K. Sawyer (Editors)
American Peptide Society, 2003

Synthetic Peptide Vaccine Strategies for the Enhancement of Cytotoxic T-Cell Responses

Naveen K. Dakappagari[1], Roshni Sundaram[1], Sharad Rawale[1], and Pravin T. P. Kaumaya [1,2,3,4,5]

Departments of [1]Obstetrics and Gynecology; [2]Medical Biochemistry; [3]Microbiology, [4]Molecular Virology, Immunology and Genetics; [5]Arthur G. James Comprehensive Cancer Center, The Ohio State University, Columbus, OH 43210 USA

Introduction

Human Epidermal Growth Factor Receptor, HER-2 is a proto-oncogene overexpressed in approximately 30% of breast, ovarian and colon cancer patients. Hyperexpression of HER-2 is associated with poor clinical prognosis and resistance to conventional forms of cancer therapy. Although, increased expression of HER-2 activates host immune response against the antigen, the natural immune response is usually too weak to control disease progression. We hypothesized that a multi-component vaccine designed to effectively boost both cellular and humoral arms of the host immune responses against HER-2 would selectively counteract and eliminate the growth of the cancer cells. We previously demonstrated that a synthetic peptide vaccine (MVF HER-2 628-647) was capable of preventing the development of mammary tumors in > 80% HER-2/neu transgenic mice [1]. MVF HER-2 628-647 primarily induces antibody response against HER-2. To broaden the scope and effectiveness of this B-cell epitope vaccine, we have now explored various peptide vaccine strategies capable of eliciting robust cytotoxic T cell (CTL) responses.

Results and Discussion

We have used a library of synthetic nonameric peptides predicted to bind the HLA-A0201 molecule with high affinity to screen for CTL responses in HLA-A0201 transgenic mice that have been immunized with DNA encoding the entire HER-2 protein. This screening identified a set of naturally processed epitopes. When the HLA-A0201 transgenic mice were immunized with these naturally processed peptide epitopes, only a subset of epitopes (369, 435 & 789) activated CTL responses. Based on this finding, we designed a multiepitope peptide containing epitopes 369, 435 & 789, each epitope separated from the other by double arginine spacers. Arginine containing peptides and proteins were found to be preferentially processed by the cellular proteosomes, therefore, we speculated that incorporating arginine residues would prevent formation of junctional epitopes. As expected, arginine containing multi-epitope peptides were efficiently digested to release individual epitopes when incubated with the proteosomes *in vitro* [2]. In addition, to deliver this novel multiepitope peptide directly into the cytoplasm of cells for loading onto the MHC class I pathway, we have made use of novel amphipathic peptide carrier (designated 'chariot), which is capable of making hydrophobic contacts with the large peptides and delivering the peptide cargo into cells [3].

The formation of chariot-multiepitope complex was confirmed by ion exchange chromatography and the delivery of multiepitope epitope peptide into mature dendritic cells by chariot was confirmed by flow cytometry. Most importantly, when HLA-A0201 transgenic mice were immunized with either chariot-multiepitope complex or multiepitope peptide alone, the chariot-multiepitope complex enhanced the CTL

responses by four- to six-fold compared with multiepitope vaccine alone. These results are summarized in Table 1.

Table 1. Differences in the activities of multiepitope vaccine and chariot-multiepitope vaccine complex.

Activity	*Multiepitope Vaccine*	*Chariot - Multiepitope Vaccine complex*
Complex Formation (retention times in min)	***12:53 (Vaccine alone)*** 11:38 (Chariot alone)	***15:52 (Complex)***
Intracellular Delivery (cells positive by flow cytometry)	***26.8%***	***51.8%***
CTL Response (% Lysis)		
Epitope 369	10.8	***44.5***
Epitope 435	7.8	***58.4***
Epitope 789	3.0	***5.7***

Conclusions

We believe that it is possible to activate robust CTL responses through a systematic approach that involves identification of naturally processed epitopes, functional vaccine design and delivery of the vaccine into the appropriate cellular compartments.

Acknowledgements

This work was supported by a grant from National Cancer Institute (# CA 84356) to P.T.P.K.

References

1. Dakappagari, N. K., Douglas, D. B., Triozzi, P. L., Stevens, V. C. and Kaumaya, P. T. *Cancer Res.* **60,** 3782 (2000).
2. Sundaram, R., Sun, Y., Walker, C. M., Lemonnier, F. A., Jacobson, S. and Kaumaya, P. T. *Vaccine* **21,** 2767 (2003).
3. Morris, M. C., Depollier, J., Mery, J., Heitz, F. and Divita, G. *Nat. Biotechnol.* **19,** 1173 (2001).

Peptide Revolution: Genomics, Proteomics & Therapeutics
Michael Chorev & Tomi K. Sawyer (Editors)
American Peptide Society, 2003

Effects of a Specific Peptide Bond Replacement on a *Plasmodium falciparum* Protein Primary Processing

José Manuel Lozano[1], Diana R. Tovar[1], Luz M. Salazar[1], Marisol Ocampo[1,2], Fanny Guzmán[1] and Manuel Elkin Patarroyo[1,2]

[1]Fundación Instituto de Inmunología de Colombia (FIDIC), Carrera 50 No. 26-00, Bogotá, Colombia; [2]Universidad Nacional de Colombia, Bogotá, Colombia

Introduction

Malaria, representing one of the world's most important public health problems, is a lethal, infectious disease, resulting in 300-500 million clinical cases and more than two million deaths per year, mainly amongst children in developing countries [1]. The majority of deaths from malaria are due to *Plasmodium falciparum*, the disease's most virulent causative agent. Vaccination is considered to be an approach which would complement other strategies for the prevention and control of malaria [2]. The development of an effective malaria vaccine has thus become a major challenge for biomedical research.

MSP-l is the most characteristic intraerythrocyte stage antigen. MSP-1 is a 195 kDa glycoprotein, which is proteolytically processed into 83 kDa, 42 kDa, 33 kDa and 19 kDa fragments. Significant experimental evidence has involved MSP-l with the red blood cell (RBC) invasion process, constituting the rationale for deve1oping MSP-l based malarial vaccines [3-4] (Figure 1).

Different sets of pseudopeptide analogues from naturally processed *Plasmodium falciparum* MSP-1 sequences were thus designed and synthesized to afford 20-mer reduced amide $\Psi[CH_2NH]$ surrogates so as to assess a peptide bond's role in molecular structure modulation and its biological significance. Evidence supporting molecular competition between MSP-1 pseudopeptides and actual protein is discussed, as well as the potential use of these novel molecules as possible malarial vaccine components.

Searching for the next generation of malaria vaccines, detection of high activity binding peptides (HABPs) from protein malaria parasites to RBCs constitutes a novel approach for such a purpose. In that direction several malaria antigens have been assessed and subsequently rationally modified to afford novel malaria vaccine candidates [5-7]. A second approach consisting of replacing peptide bonds with $\Psi[CH_2\text{-}NH]$ isoster bonds of critical RBCs binding residues has also been explored for obtaining novel malaria-derived pseudopeptides [8-9]. The use of site-directed malaria pseudopeptides also constitutes a pathway to potentially obtaining blockers of malaria proteases.

Results and Discussion

MSP-1 site-directed designed reduced amide pseudopeptides effectively interfered with the malaria parasite invasion process of RBCs as shown in Figure 2. In panel A the effect of peptide bond replacement in the Sub-1 putative hydrolysis motif is displayed. S-V and V-T peptide bonds are critical for MSP-1 primary processing.

In a similar way, K-L and R-Y peptide bonds in the MSP-1 fourth region play a critical role for the secondary protein process, as it can be seen in Figure 2, panel D.

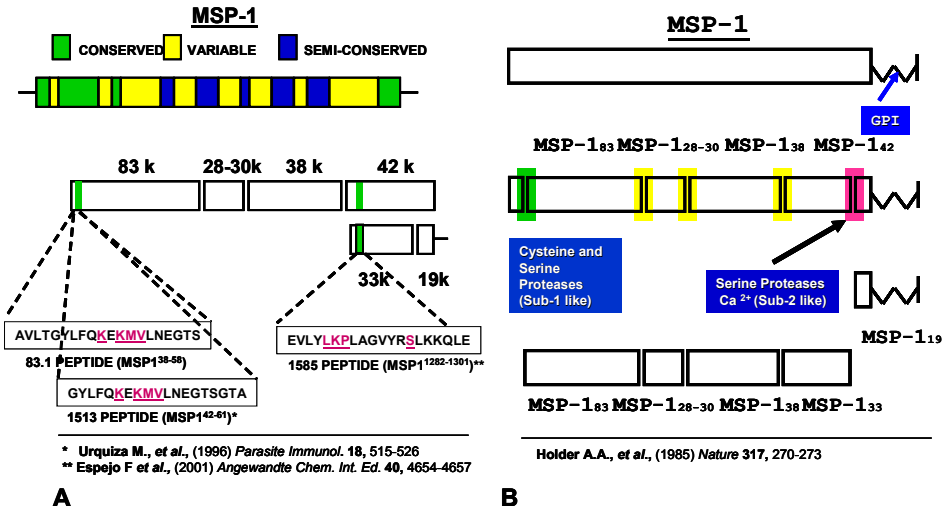

Fig. 1. Approaches for peptide selection. A) MSP-1 (Merozoite Surface Protein-1), HABPs and B) Enzyme hydrolysis-target motifs on the MSP-1.

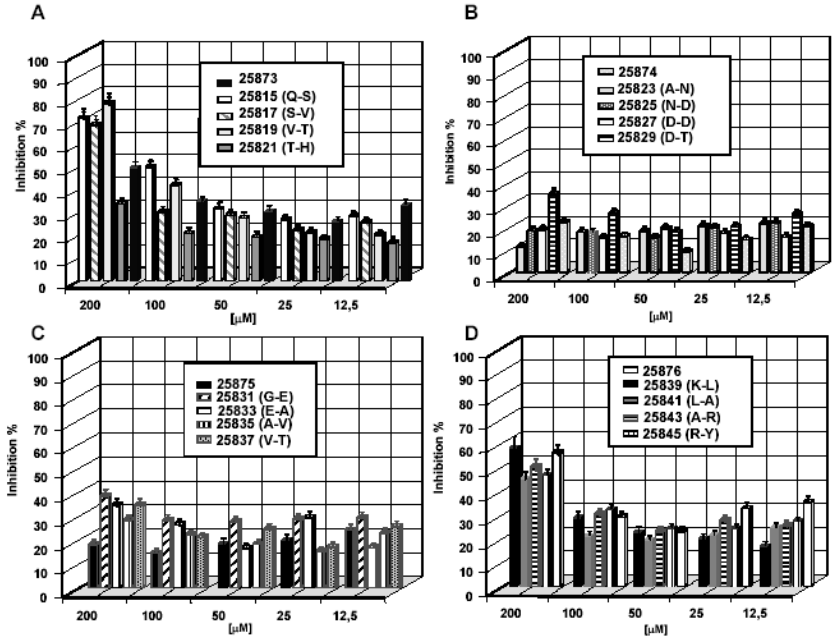

Fig. 2. Inhibition of P. falciparum invasion of RBCs by site-directed MSP-1 Ψ[CH_2NH] pseudopeptides. A) First region, B) Second region, C) Third region and D) Fourth region.

Specific peptide bonds from regions 1 and 3 are also critical for the *P. falciparum* intraerythrocyte survival as shown in Figure 3.

As demonstrated, site-directed reduced amide pseudopeptides have potential therapeutic application for the prevention and control of malaria.

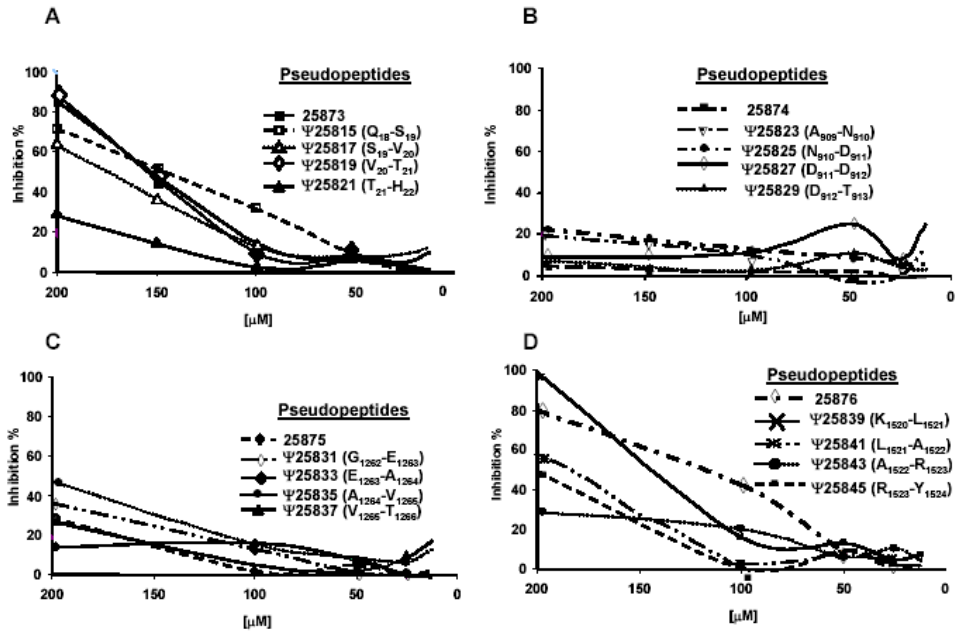

Fig. 3. P. falciparum intraerythrocyte inhibition by site-directed MSP-1 Ψ[CH_2NH] pseudopeptides. A) First region, B) Second region, C) Third region and D) Fourth region.

Acknowledgments
This work was supported by the Colombian Ministry of Public Health.

References

1. Tropical Disease Research: Progress Thirteenth Programme Report of the UNDP/World Bank/WHO Special Programme for Research and Training in Tropical Diseases, Geneva, pp 40-61 (1997).
2. Graves, P., Gelband, H. and Garne, P. *Parasitol. Today* **14**, 219 (1998).
3. Holder, A., Lockyer, M. J. and Odink, K. G. *Nature* **317**, 270-273 (1985).
4. Urquiza, M., Rodriguez, L., Suarez, J., Guzmán, F., Ocampo, M., Curtidor, H., Segura, C., Trujillo, E. and Patarroyo, M. E. *Parasite Immunol*. **18**, 505-526 (1996).
5. Espejo, F., Cubillos, M., Salazar, L. M., Guzmán, F., Urquiza, M., Ocampo, M., Silva, Y., Rodríguez, R., Lioy, E. and Patarroyo, M. E. *Angew. Chem. Int. Ed*. **40**, 4654-4657 (2001).
6. Cubillos, M., Espejo, F., Purmova, J., Martinez, J. and Patarroyo M. E. *Proteins* **50**, 400-409 (2003).
7. Salazar, L. M., Alba, M., Torres, M. H., Pinto M., Cortés, X., Torres, L., and Patarroyo, M. E. *FEBS Lett.* **527**, 95-100 (2002).
8. Lozano, J. M., Espejo, F., Diaz, D., Salazar, L. M., Rodríguez, J., Pinzón, C., Calvo, J. C., Guzmán, F. and Patarroyo, M. E. *J. Peptide Res*. **52**, 457-469 (1998).
9. Lozano, J. M., Alba, M. P., Vanegas, M., Silva, Y., Torres-Castellanos, J. L. and Patarroyo, M. E. *Biol. Chem*. **384**, 71-82 (2003).

Peptide Revolution: Genomics, Proteomics & Therapeutics
Michael Chorev & Tomi K. Sawyer (Editors)
American Peptide Society, 2003

Phosphorylated Antigenic Determinants of the La/SSB Autoantigen and Their Contribution as Potential Targets of the Autoimmune Response in Patients with Sjogren's Syndrome

Dimitrios Rokas[1], Eugenia Panou-Pomonis[1], Constantinos Sakarellos[1], Nicolas Coudevylle[2], Manh-Thong Cung[2], Athanassios G. Tzioufas[3], Haralampos M. Moutsopoulos[3] and Maria Sakarellos-Daitsiotis[1]

[1]Department of Chemistry, University of Ioannina, 45110 Ioannina, Greece; [2]Laboratoire de Chimie-Physique Macromoleculaire, UMR 7568 CNRS-INPL, 54001 Nancy, France; [3]Medical School, University of Athens 11527, Greece

Introduction

The autoimmune response in patients with Sjogren's Syndrome (SS) is mainly directed against four discrete B cell epitopes 145-164, 289-308, 349-368 of La/SSB, a conserved cellular phosphoprotein of 47KD [1]. Among the four, well-defined phosphorylation sites of La/SSB, two are located within the 349-368 epitope (Thr-362 and Ser-366), one within 301-318 (Thr-302) and the fourth one between them (Ser-325). In recent years, phosphorylation of proteins has been proposed as the most important post-translational event that may potentiate the autoimmune response by altering the immunogenicity, the conformation and the cell distribution of the phosphorylated proteins, resulting thus in the breakdown of the immune tolerance [2].

With the aim to investigate the potential role of phosphorylation in the conformational characteristics and the autoimmune response of the La/SSB epitopes in SS patients sera, we have synthesized and studied the phosphorylated epitopes (359-368)-P:Ac-GKKT(PO_3H_2)KFAS(PO_3H_2)DD-NH_2, (346-368)-P: Ac-AQPGSGKGKV-QFQGKKT(PO_3H_2)KFAS(PO_3H_2)DD-NH_2 and (301-318)-P: Ac-VT(PO_3H_2)WEVLE-GEVEKEALKKI-NH_2, with respect to their non-phosphorylated counterparts. Epitope (359-368)-P derives from specific hydrolysis of the Gln^{358}-Gly^{359} bond under stress conditions.

Results and Discussion

The syntheses of the phosphorylated La/SSB epitopes were carried out using Fmoc-chemistry, solid-phase synthesis procedure and Rink Amide AM resin, whereas the Boc-chemistry and the 4-methyl-benzydrylamine resin (MBHA) was used for the syntheses of the non-phosphorylated epitopes. Peptides were purified by HPLC and the molecular masses were confirmed by ESI-MS.

The ELISA assays clearly indicate that anti-La/SSB antibodies are much more strongly recognized by the phosphorylated epitopes, in comparison to their counterparts. One could hypothesize that, at least for epitope 346-368, which is a minor T cell epitope, phosphorylation does not dramatically affect its binding to MHC II and consequently phosphorylated residues point away from the MHC groove. Confocal laser scanning microscopy experiments of the phosphorylated epitopes bearing the fluorescein tag suggest that phosphorylated epitopes can easily penetrate into the cytosol but remain outside of the nucleus. Therefore, under specific conditions, phosphorylated epitopes could reach the cytoplasmic membrane and be seen by the immune system.

Fig. 1. The superimposed K_2KTK_5 backbone atoms of the non-phosphorylated and phosphorylated 359 - 368 peptides correspond to 0.4Å rmsd for the N-terminal segment.

Peptides were studied by ^{1}HNMR in H_2O/D_2O 95/5 v/v at pH 6. The non-phosphorylated (359-368) peptide exhibits some NOE correlations, essentially for the $K_2K_3T_4K_5$ sequence, including the intense NN(K_3, T_4) NOE cross-peak suggesting the possible presence of a β-turn at the N-terminal $G_1K_2K_3T_4$. In addition to the continuous intense NOE connectivities between successive amide protons for the $T_4K_5F_6A_7S_8$ sequence of the phosphorylated (359-368)-P, numerous medium range βN(i, i+2) and some αN(i, i+2), γN(i, i+2), and βN(i, i+3) NOE correlations were also detected in the $K_3TKFASDD_{10}$. These latter NOEs argue in favor of a folded structure, whereas the βN(i, i+2) consecutive connectivities are diagnostic of an α helix.

Energy minimization and molecular dynamics calculations with a simulated annealing protocol were applied. The best fit for the superimposed peptide backbones of the non-phosphorylated (359-368) peptide gave an RMSD of 0.36Å for the $K_2K_3T_4K_5F_6$. The φ and ψ angles of residues K_3(-65°, -9°), T_4(-74°, -50°) and K_5 (-96°, -63°), estimated by the MD consecutive β-turns stabilized by the $K_5NH \rightarrow K_2CO$ (80% occurrence), $F_6NH \rightarrow$ simulation, are compatible with the presence of a distorted β_{III}-turn (38% occurrence) in the $K_2K_3T_4K_5$ and an α-turn (34% occurrence) in the $K_2K_3T_4K_5F_6$ sequences. The best fit for the superimposed peptide backbones gave an RMSD of 0.32Å for the $K_2K_3T_4(PO_3H_2)K_5F_6A_7S_8(PO_3H_2)$ segment. The ϕ and ψ angles of residues K_3(-58°, -11°), T_4(-52°, -21°), K_5(-45°, -39°), F_6(-54°, -33°) and A_7(-93°, -32°), estimated by MD, fit better with 3_{10}-helix (-49°, -26°) rather than with α-helix (-57°, -47°). This structure comprises four K_3CO(14% occurrence), $A_7NH \rightarrow T_4CO$ (42% occurrence), $S_8NH \rightarrow K_5CO$ (16% occurrence) and one α-turn stabilized by the $S_8NH \rightarrow T_4CO$ (40% occurrence) hydrogen bonding. The helix formation of the (359-368)-P in aqueous solution is probably due to the simultaneous presence of the two phosphate groups at the i and i+4 positions, which however do not interact with each other. It is assumed that the phosphorylated peptide is much more structured than the non-phosphorylated one (Figure 1). The latter assumption holds true for the other two pairs of epitopes.

In conclusion, it seems likely that phosphorylation induces significant modifications in the immunogenicity, the conformation and the cell distribution of the self-epitopes. In fact, neo-self antigens are created and viewed as "foreign" to which the immune system has never been exposed or tolerized in the periphery.

References

1. Yiannaki, E. E., Tzioufas, A. G., Bachmann, M., Hantoumi, J., Tsikaris, V., Sakarellos-Daitsiotis, M., Sakarellos, C. and Moutsopoulos, H. M. *Clin. Exp. Immunol.* **112**, 152-158 (1998).
2. Doyle, H. A. and Mamula, M. J. *Trends Immunol.* **22**, 443-449 (2001).

Peptide Revolution: Genomics, Proteomics & Therapeutics
Michael Chorev & Tomi K. Sawyer (Editors)
American Peptide Society, 2003

Ligand Binder Arrays

Michael J. Taussig

Technology Research Group, The Babraham Institute, Cambridge CB2 4AT, England

Introduction

'Classical' proteomics is the art of analyzing complex protein mixtures using 2-dimensional gel electrophoresis (2DE) and mass spectrometry to identify protein composition and changes in protein expression in tissues and fluids [1,2]. While this will doubtless remain a method of choice for the foreseeable future, 2DE has its limitations, particularly for profiling proteins expressed at very low levels, and is not well suited to high sample throughput. This has led to the adoption of new array-based tools to monitor protein expression changes quantitatively, accurately and at high throughput. These tools include protein, cell and tissue arrays [3-6].

Ligand binders for proteome analysis

To make use of genome information to characterize the proteome, whether on arrays or by other means, will require a comprehensive collection of 'ligand binders' against all the proteins. Ligand binders are fundamental tools for monitoring protein profiles and determining protein function. The most familiar are antibodies, but there are also the newer developments of protein scaffolds and nucleic acid aptamers. However, there is clearly a problem of scale to be confronted: to produce binders against the proteins encoded by the ~30,000 genes in the human genome would in itself be daunting, but the existence of alternative splicings and post-translational modifications means that there may be more than 10 times that number of individual protein species in the proteome. While the long-term aim should be to cover all the members of the proteome, there is an immediate need for a collection of binders against all human gene products as a reference resource. As well as protein expression analysis, such a collection will be used in protein isolation, biomarker discovery, diagnostics and therapeutics. At least one project to develop such a collection is already under way [7].

Ligand binder microarrays

Ligand binder or capture microarrays are currently receiving intense interest and are one of the most active areas emerging in biotechnology [3,4,8,9]. They are solid-phase assay systems using immobilized binding reagents (antibodies, scaffolds, aptamers), usually on surfaces such as glass slides but may also be on beads or mass spectrometry plates. The assays are highly parallel and often highly miniaturized. Their advantages include speed and automation, sensitivity and economy of samples and reagents. In principle, such arrays can be used to quantitate many proteins simultaneously using very small volumes of complex mixtures such as plasma or tissue extracts, making them ideally suited to protein expression profiling and diagnostics applications.

There are several important technical issues and choices in ligand binder array technologies. They include the nature of the binder molecules; obtaining global expression of protein targets against which the binders will be raised; the chemistry of coupling proteins to different surfaces; conditions for effective ligand binding; and the sensitivity and range of detection systems. Crucial considerations are the specificity, affinity and cross-reactivity of the binders; their correct folding and functionality when immobilized on the array; signal to noise ratio of different surfaces; and the sensitivity, accuracy and dynamic range of detection methods. Given the diversity of proteins with

respect to physicochemical properties, one of the major problems is to determine solution conditions such that all target proteins in a complex mixture would be bound and quantitated on the array under identical assay conditions. Hoheisel and colleagues have recently reviewed methods for optimising binding to antibody arrays [10]. Moreover, analyte concentrations in biological samples vary over a c. 10^8-fold range, so sensitivity may be tailored through different affinities of the capture reagents.

Protein detection on arrays

There are several means for detection of ligand binding, including direct labeling with fluors, 'sandwich' labelling, and label free detection. The principal requirements are for optimal sensitivity and specificity, with low backgrounds and high signal to noise. Where labels are used, fluorescence is popular and highly sensitive. Samples can be labeled directly, e.g. with Cy dyes, or indirectly detected in sandwich assays. Direct labeling of targets allows for 2-colour assays to carry out comparison between two different samples in expression profiling [11]; however, the label modifies the protein and lacks the benefit of dual recognition. Sandwich assays address the problem of specificity through use of a second, labeled binder and are the best way to detect moderately low abundance proteins such as cytokines. Label free methods, which do not alter the protein, include mass spectrometry, surface plasmon resonance and atomic force microscopy. A general principle is that for maximum specificity, it is important to provide two levels of specific recognition in the array. This is achieved by sandwich assays, by coupled binding and crosslinking using 'photoaptamers' [22], and in label free systems by mass spectrometry to identify the protein definitively. A further solution to the problem of cross-reactivity, proximity ligation, is described below.

Varieties of ligand binder

More than one type of ligand binder is applicable to arrays. The molecules available include antibodies and recombinant single chain fragments and single domains, as well as engineered protein scaffolds, based on particular protein frameworks and usually chosen for stability and expression [12]. Nucleic acid aptamers are also a source of high affinity binders against many proteins, with some distinct advantages in production and amplification [13].

Monoclonal antibodies (mAbs) are generally the first choice for arrays, where accurate quantitation and defined specificity against native proteins is essential, but polyclonals are not ruled out when they can be purified and made ligand specific [7]. Polyclonals are attractive as multi-epitope reagents that are efficient and inexpensive to produce. In both cases, selection of antibodies for lack of cross reactivity is critical to array specificity. Protein scaffolds are domains that can be engineered for specificity and affinity binding against different ligands. Their desirable properties are generally small size, stability in harsh conditions, absence of glycosylation or disulphide bridges, capacity to be engineered for variability and selected for ligand binding, and good prokaryotic expression. These properties are seen with, among others, lipocalins [14], fibronectin domains [15], protein A domains [16] and CTLA-4 [17]. Where possible, a human origin is important for potential therapeutic applications. Selection of scaffold variants is generally by library display methods.

Anticalins are a novel class of ligand binder proteins with tailored specificities derived from the lipocalin scaffold [14]. Their tertiary structure comprises a single domain of a β-barrel with four loops at one end forming the entrance to a binding pocket. Anticalins with high affinity and specificities for peptides and proteins have been prepared using targeted mutagenesis and phage display. Affibody molecules [16]

are a scaffold of a very different structure to antibodies as they do not have a barrel structure or loops for engineering. They are based on a domain of *Staph. aureus* Ig-binding protein A, well known as an affinity reagent for IgG purification. Protein A has a triple helical structure and affibodies residues on the face of the molecule that recognizes Fc are mutated, so that a rigid scaffold structure is used as the basis of randomized mutation. Although published examples are mostly of a relatively low (micromolar) affinity, higher affinities are obtainable from large display libraries. Recently a structure of a bound affibody complex was determined and shows similarity in buried area and number of interactions to an antigen-antibody interface [18].

Linking ligand binders and nucleic acids

Nucleic acids are being employed at various levels of the protein array process:

a. In the selection and evolution of binders from molecular libraries, nucleic acids can be either the binders themselves, as in the case of aptamers selected by the SELEX procedure [13], or the protein-encoding templates for *in vitro* display selection procedures such as ribosome display and mRNA display, in which a physical link is established between the nucleic acid (genotype) and the protein (phenotype) [19-21].

b. It is possible to make protein-binding arrays directly from DNA or RNA, either as the recently developed photoaptamer arrays [22] or as 'self-assembling' protein arrays which make use of DNA hybridization to localize protein-mRNA fusions [23]. We have developed a cell free method for making protein arrays from arrayed DNA (protein *in situ* arrays, PISA) [24].

c. DNA is a uniquely specific, amplifiable 'tag' which can be used in highly sensitive protein detection, either to prime rolling circle amplification to detect ligands bound to the array [25] or in the method of proximity ligation where oligonucleotide tags on pairs of ligand binders are specifically ligated before amplification, providing an additional layer of specificity [26, 27].

Aptamers

Aptamers are single-stranded nucleic acid ligand binders, either ssDNA or RNA, with properties of protein binding similar to those of antibodies [13]. They have an unexpectedly high affinity, some being 100pM or better. One drawback is that it has proven difficult to obtain aptamers against different epitopes on the same protein, as required by sandwich assays. In the more recently developed photoaptamer technology [22], photoreactive nucleotides are introduced by replacing thymine or uracil bases with bromodeoxyuridine, so that the aptamer is capable of covalent cross-linking when bound to its target and exposed to light. The specific requirement for precise crosslinking provides additional specificity as well as permanence. On photoaptamer arrays to detect proteins, covalent binding increases signal to noise by enabling stringent washing procedures, and bound protein is detected with a general stain.

Protein-mRNA linkage: Ribosome display and mRNA display

Two methods have been described for linking protein to its encoding mRNA at the end of translation. In 'ribosome display', the protein and mRNA remain together in the translation complex of nascent protein, ribosome and mRNA [19,20], whereas in 'mRNA display', the protein and mRNA become covalently attached as an mRNA-protein fusion via a puromycin bridge [21, 28]. In both methods, the proteins are made by cell free synthesis, and both have been used for selection of specific ligand binders from large libraries. For input, these methods use PCR-generated DNA without cloning and because bacterial transformation is avoided, there is the potential for creating very

large libraries (>10^{12} members). The systems are appropriate for continuous mutation and selection of proteins (e.g. evolution and engineering of ligand binders) in a cell free manner.

Protein *in situ* arrays (PISA)

While antibodies can generally be purified from natural sources such as hybridomas, problems with bacterial expression mean that there are advantages in cell free production of engineered molecules from DNA using *in vitro* systems. We have developed a cell free protein array synthesis method termed 'protein *in situ* array' (PISA) and demonstrated its applicability to production of ligand binder arrays [24]. The protein is made directly from DNA, either in solution or immobilized, and carries a novel double hexahistidine tag. The protein is synthesized in wells or on other surfaces which are precoated with the immobilizing agent, e.g. Nickel NTA; thus as each protein is made it simultaneously becomes fixed to the surface after translation and the other material can be washed away. By multiplexing, it is possible to go in a single step from PCR DNA to protein array. This has the advantages of avoiding bacterial cloning or expression systems, and the need to purify the ligand binder protein separately.

Proximity ligation and the 'cross-reactivity problem' for multiplexed arrays

Undoubtedly, a major problem, which will be encountered when using large numbers of ligand binders simultaneously, is cross-reactivity. High multiplexing and specificity have to be combined and, with thousands of possible targets in an expression profiling experiment, cross-reactivity will lead to potentially disastrous false-positives. This problem has been addressed by Landegren and colleagues using the novel proximity ligation method [26,27]. This technique combines protein recognition with DNA-based hybridization and amplification. Two (or more) binders selected against the same target are coupled to oligonucleotides as probes and used to give dual (or triple) recognition of the target. The detection system involves specific ligation of the probes by DNA ligase, following their hybridization by a specific connector oligonucleotide, with an absolute requirement for the probes to be bound concurrently onto the same target molecule. Amplification of the ligated oligonucleotides is used to generate the signal, either from PCR or rolling circle amplification. Compared with a regular sandwich assay, the requirement for proximal binding of pairs of probes, combined with the generation of a signature DNA sequence, makes proximity ligation immensely specific, combining as it does immunological recognition with specific base pair hybridisation and DNA amplification. In effect, DNA is used to measure proteins by artificial 'reverse translation'. The reaction can be carried out multiplexed either in solution or on an array. Nucleic acid aptamers are particularly advantageous for the assay because they are easily extended with the additional DNA sequence at the 5' and 3' ends, as shown using aptamers against PDGF [26]. Recently, more generally available mono- and polyclonal antibodies have also been shown to be suitable as proximity ligation reagents (Gullberg et al. submitted). In concentration terms, proximity ligation and ELISA have similar sensitivities, but since the former can be carried out as a homogeneous solution assay in volumes of 1μl, it is far more sensitive in absolute amount. The reaction can be multiplexed using individual zip codes that are identified on a tag array. In the solid phase version, ligand binders would be immobilized on a solid support and the ligation of proximity probes performed in the same way as a sandwich assay and amplified by rolling circle amplification.

Conclusions

Ligand binder microarrays will be applied to biological research problems, discovery of biomarkers and complex protein profiling, with the aim of making maximal use of genome information to detect, quantify and characterise all relevant proteins in health and disease. There will be important applications in profiling cancer cells, to define cancer subtypes from their characteristic 'protein signatures', leading to tools for early diagnosis based on multiple marker profiles. In order to create a profiling chip on which every protein in the proteome could be measured, binders will be needed not only against the protein products of each of the ~30,000 genes in the human genome, but also against splice variants and post-translational modifications. In time, a collection of such binders will be an invaluable resource of reference molecules for arrays as well as many other applications.

Acknowledgements

I am grateful to Professor Ulf Landegren for comments on the manuscript. Work at the Babraham Institute is supported by the Biotechnology and Biological Sciences Research Council.

References

1. Wilkins M. R. et al. (Eds.) Proteome Research: New Frontiers in Functional Genomics. Springer-Verlag (Berlin) (1997).
2. James P. (Ed.) Proteome Research: Mass Spectrometry. Springer Verlag (Berlin) (2001).
3. MacBeath, G. *Nat. Gen*. suppl. **32**, 526-532 (2003).
4. Cutler, P. *Proteomics* **3**, 3-18 (2003).
5. Wu, R. Z., Bailey, S. N. and Sabatini, D. M. *Trends Cell Biol.* **12**, 485-8 (2002).
6. Mousses, S. et al. *Curr. Opin. Chem. Biol.* **6**, 97-101 (2002).
7. Agaton, C. et al. *Mol. Cell Proteomics* **2**, 405-414 (2003).
8. Lal, S. P., Christopherson, R. I. and dos Remedios, C. G. *Drug Dis. Today* **7**, S143-149 (2002).
9. Kusnezow, W. and Hoheisel, J. D. *Biotechniques* Dec. Suppl.14-23 (2002).
10. Kusnezow, W. et al. *Proteomics* **3**, 254-264 (2003).
11. Haab, B. B., Dunham, M. J. and Brown, P. O. *Genome Biol.* **2**, 4.1 – 4.13 (2001).
12. Ladner, R. C. and Ley, A. C. *Curr. Opin. Biotechnol*. **12**, 406-410 (2001).
13. Brody, E. and Gold, L. *Rev. Mol. Technol*. **74**, 5-13 (2000).
14. Skerra A. *J. Biotechnol.* **74**, 257-275 (2001).
15. Xu L et al. *Chem. Biol.* **9**, 933-942 (2002).
16. Nord, K. et al. *Nat. Biotechnol.* **15**, 772-777 (1997).
17. Hufton, S. E. et al. *FEBS Lett*. **475**, 225-231 (2000).
18. Hogbom M. et al. *Proc. Nat. Acad. Sci. U.S.A.* **100**, 3191-3196 (2003).
19. He, M. and Taussig, M. *J. Nucleic Acids Res.* **24**, 5132-5134 (1997).
20. Hanes J. and Pluckthun A. *Proc. Nat. Acad. Sci. U.S.A.* **94**, 4937-4942 (1997).
21. Roberts, R. W. and Szostak, J. W. *Proc. Nat. Acad. Sci. U.S.A.* **94**, 12297-12302 (1997).
22. Petach, H. and Gold, L. *Curr. Opin. Biotechnol.* **13**, 309-314 (2002).
23. Weng, S. et al. *Proteomics* **2**, 48-57 (2002).
24. He, M. and Taussig, M. *J. Nucl. Acids Res.* 29:E73 (2001).
25. Schweitzer, B. et al. *Nat. Biotechnol*. **20**, 359-365 (2002).
26. Fredriksson, S. et al. *Nat. Biotechnol*. **20**, 473-477 (2002).
27. Gullberg, M. et al. *Curr. Opin. Biotechnol.* **14**, 82-86 (2003).
28. Takahashi, T. T. et al. *Trends Biochem. Sci* **28**, 159-165, (2003).

Peptide Revolution: Genomics, Proteomics & Therapeutics
Michael Chorev & Tomi K. Sawyer (Editors)
American Peptide Society, 2003

T Cell Immunogenecity of Synthetic Oligopeptides with 91-105 Epitope Core and Ala Flanks of 16 kDa Protein of Mycobacterium Tuberculosis

Szilvia Bosze[1], Nadia Caccamo[2], Zsuzsa Majer[3], Francesco Dieli[2], Gábor Mezo[1] and Ferenc Hudecz[1]

[1]Research Group of Peptide Chemistry, Hungarian Academy of Sciences, Eötvös L. University Budapest 112, POB 32, H-1518, Hungary, [2]Department of Biopathology, University of Palermo, Corso Tukory, 211 Palermo 90134, Italy, [3]Department of Organic Chemistry, Eötvös Loránd University, Budapest 112, POB 32, H-1518, Hungary

Introduction

The 16kDa protein of *Mycobacterium tuberculosis* provokes specific immune response, therefore related epitope peptides can be considered as potential diagnostics and subunit vaccines. The presence of several antigenic regions containing murine as well as human T-cell epitopes have been reported [1, 2]. In our previous study the functional human T-cell epitope 91-104 within the 91-110 region was determined [3]. Based on these results we selected the 91-105 region for detailed analysis. Two groups of peptides were prepared: a) N- and C-terminal alanine elongated variants of the 91-104 epitope and b) 91/92-104 peptides with aspartic acid at position 92. With these peptides we have: 1) analyzed the role of flanking regions (the amino acid residues on both sides of the core region); and 2) established primary structure–conformation correlation of T-cell stimulatory peptides.

Results and Discussion

Eight peptides corresponding to the ^{91}SEFAYGSFVRTVSLP^{105} region were prepared by solid phase synthesis on MBHA resin (1.04 mequiv/g) using Boc/Bzl strategy. Amino acids were coupled with the HOBt/DCC coupling method using 3 molar excess over the capacity of the resin in DMF/DCM 1:4 (v/v). The homogeneity and the primary structure of peptides were checked by analytical RP-HPLC, amino acid analysis, and ESI-MS (data not shown). The solution conformation of peptides was studied by CD spectroscopy. Spectra were recorded in water, in trifluoroethanol (TFE) and in water: TFE mixture (1:1, v/v). The T-cell stimulatory activity of the compounds was investigated using *in vitro* assays (proliferation and IFN-γ production) on the 91-110 epitope specific human T-cell clones [4]. Studies with BV2+ clones showed that peptide ^{92}EFAYGSFVRTVSL^{104} was mainly inactive. In contrast the peptide Ac-^{92}EFAYGSFVRTVSL^{104} initiated IFN-γ production, while peptide *A*^{93}FAYGSFVRTVSL^{104} with alanine at the position 92 was not effective on most clones. Peptides containing ^{92}E and elongated with alanine residues (*A*^{92}EFAYGSFVRTVSL^{104}*A*, *AA*^{92}EFAYGSFVRTVS^{103}*A* and *A*^{92}EFAYGSFVR-TVS^{103}*AA*) were active on human T-cell clones. Peptides with ^{92}*D* (^{91}S*D*FAYGSFVRTVSL^{104}, Ac-^{92}*D*FAYGSFVRTVSL^{104} and ^{92}*D*FAYGSFVR-TVSL^{104}) were not capable of inducing IFN-γ production. These data suggest that the glutamic acid at position 92 is highly important for the activity of synthetic peptides.

Conformation studies indicated that peptide ^{91}SEFAYGSFVRTVSLP^{105} adopts helical conformation in TFE (Figure 1). The absence of serine residue at position 91 did not result significant comformational change in the spectrum (data not shown).

The helix content (calculated according to $[\Theta m_{MR}]_{222}$/-39000 [5]) of the alanine elongated active peptides (A^{92}EFAYGSFVRTVSL^{104}A, AA^{92}EFAYGSFVRTVS^{103}A and A^{92}EFAYGSFVRTVS^{103}AA, 36%, 44% and 40%, respectively) is markedly higher as compared to the native ^{91}SEFAYGSFVRTVSLP^{105} peptide (29%) (Figure 1).

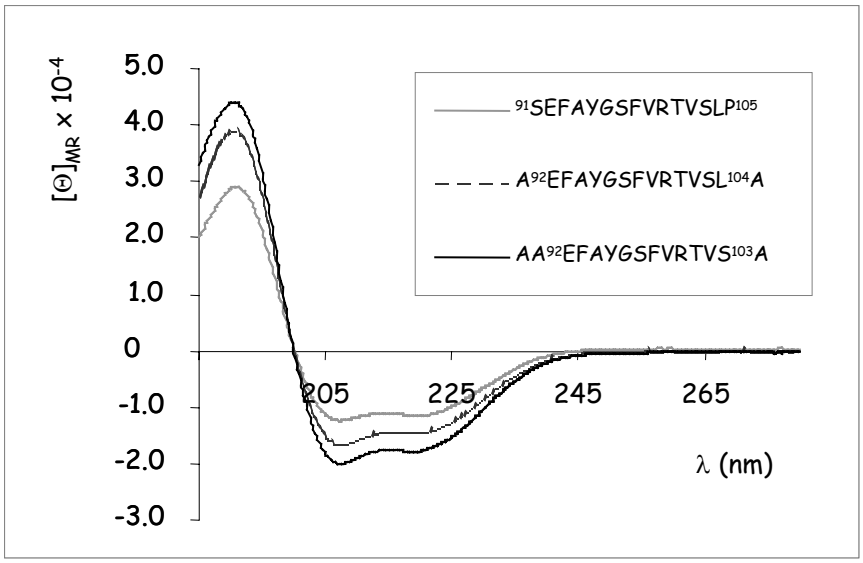

Fig. 1. CD spectra of peptides in TFE.

The spectra of peptides with aspartic acid at position 92 indicate similarly ordered conformation in TFE (helical content ranges from 40-45%). We concluded that the alanine elongation of epitope core 92-103/104 at the N- and C-terminii resulted in peptides active on human T-cell clones. This can be due to the fact that the alanine residues can stabilise the helical conformation of the 92-103/104 region.

Acknowledgments
These studies were supported by grants from COST Chemistry Action (D13/0007/00), Hungarian Research Fund (OTKA No. T037719 and F 034886) and from Ministry of Culture (FKFP 0153/2001).

References

1. Bogdán, K.A. et al. In Epton, R. (Ed.) *Innovation and Perspectives in Solid phase Synthesis*, Mayflower Worldwide, Birmingham, 1996, p. 329.
2. Friscia, G., et al. *Clin. Exp. Immunol.* **102**, 53-57 (1995).
3. Bosze, Sz., et al. In Benedetti, E. and Pendone C. (Eds.) *Peptides 2002 (Proceedings of the 27th European Peptide Symposium),* Edizioni Ziino, Napoli, 2003, pp. 512-513.
4. Jurcevic, S., et al. *Clin. Exp. Immunol.* **105**, 416-421 (1996).
5. Kallenbach, N. R., Lyu, P. and Zhou, H. In Fasman, G. D. (Ed.), *CD and the Conformational Analysis of Biomolecules*, Plenum Press, London, 1996, pp. 201-251.

Peptide Revolution: Genomics, Proteomics & Therapeutics
Michael Chorev & Tomi K. Sawyer (Editors)
American Peptide Society, 2003

Solubility and CTL Activity of Elongated Hydrophobic Peptide Epitopes

Christine Klinguer-Hamour, Liliane Goetsch, Maryline Lokteff, Marie-Claire Bussat, Aline Blaecke, Alexandra Gonzales, Jean-François Haeuw, Nathalie Corvaia and Alain Beck

Centre d'Immunologie Pierre Fabre, 5 Avenue Napoléon III, BP 497, F74164 Saint-Julien-en-Genevois cedex, France

Introduction

Many peptides corresponding to cytotoxic T cell epitopes have been identified and several have been investigated in clinical trials as anti-cancer or anti-infectious vaccine candidates. Most of the HLA-A2 binding epitopes like ELA melanoma-associated decapeptide (MART-1(26-35)A27L) [1] or Flu-M1 (58-66) influenza A matrix protein derived nonapeptide [2] are very hydrophobic. They require the addition of organic solvent like DMSO, which is not an ideal vehicle for the solubilization of a pharmaceutical product. We have synthesized derivatives of ELA and Flu-M1 peptides and have investigated their solubility in phosphate buffer saline (PBS). Their ability to bind to T2 cells was then evaluated, as well as their potency to generate CTL responses in HLA-A2/Kb transgenic mice, when mixed with P40, a *Klebsiella pneumoniae* derived adjuvant protein [3,4].

Results and Discussion

Synthetic peptides ELA, FluM1 and 94 derivatives were synthesized using Fmoc chemistry on Wang resins (Novabiochem, Switzerland) in a multiple peptide synthesizer (Advanced Chemtech ACT348, USA). The ELA and FluM1 derivatives consisted in addition to the epitopes an insert of a single residue or a cluster (2-5 amino acids) of the same residue (D, E, S, T, N, Q, K, H, R) either at the N- or C-terminus of the peptides. Following TFA deprotection and cleavage with TIS, phenol and thioanisole as scavengers, the crude peptides were lyophilized, and then dissolved in 5% aqueous acetonitrile. They were analyzed by C_{18} RP-HPLC (Vydac 218TP, 5 μm, 250x4.6 mm) with a gradient of 10-80% CH_3CN in aq. 0.1% TFA, and by mass spectrometry (ES-MS). The crude peptides below 85% homogeneity were purified by RP-HPLC.

Peptide solubility assays were performed in triplicate. The HPLC peak areas of peptides in PBS (10 mg/ml) were calculated and compared to those obtained with totally soluble peptides in DMSO. This allowed the quantification of soluble peptide in PBS. Addition of at least three Lys or Arg residues either at N- or C-terminus of the peptides increased their solubility in PBS from 0.5 up to 10 mg/ml and from 1.7 up to 10 mg/ml for FluM1 and ELA, respectively (Table 1). None of the other amino acid residues added at the N- or C-terminus of FluM1 or ELA was able to increase their solubility.

Evaluation of the ability of peptides to stabilize HLA-A2 molecules at the surface of T2 cells was carried out by FACS analysis as previously described [5]. All the peptide derivatives soluble in PBS (Table 1) were able to bind to T2 cells.

Table 1. Solubility in PBS of FluM1 and ELA peptides and their derivatives.

Peptide	Sequence	Solubility (mg/ml) [a]
	GILGFVFTL	0.5 ± 0.2
3K-FluM1	KKKGILGFVFTL	11.4 ± 0.4
4K-FluM1	KKKKGILGFVFTL	9.4 ± 0.3
FluM1-4K	GILGFVFTLKKKK	7.3 ± 0.3
4R-FluM1	RRRRGILGFVFTL	8.8 ± 0.9
ELA	ELAGIGILTV	1.7 ± 01
4K-ELA	KKKKELAGIGILTV	11.5 ± 0.3
ELA-4K	ELAGIGILTVKKKK	10.9 ± 0.5
4R-ELA	RRRRELAGIGILTV	9.9 ± 0.2

[a] *as determined by HPLC.*

PBS soluble peptides (Table 1). Which were able to bind to T2 cells, were assayed for CTL activity. All ELA and FluM1 peptides derivatized with Lys or Arg clusters were as potent as the parent peptides to induce a CTL response in HLA-A2/Kb transgenic mice (e.g 4R-ELA in Figure 1). These results are striking considering the fact that the acetyl or pyroglutamyl forms of ELA were completely unable to bind T2 cells and failed to induce a CTL response in HLA-A2/Kb transgenic mice [1].

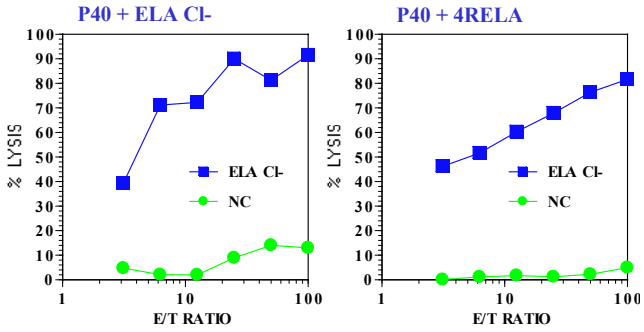

Fig. 1. CTL activity induced in HLA-A2/Kb transgenic mice by P40+ELA/4R-ELA.

From these studies, we can conclude that elongation of HLA-A2 peptide epitopes either by Arg or Lys allows both aqueous solubilization and conservation of the specific cytotoxic potency of the parent hydrophobic peptides. These properties make these new hydrophilic HLA-A2 pro-epitopes more suitable for pharmaceutical development as vaccine candidates.

References

1. Beck, A., *et al. J. Peptide Res.* **57**, 528-538 (2001).
2. Plotnicky, H., *et al. Virology* **309**, 320-329 (2003).
3. Jeannin, P., *et al. Nat. Immunol.* **1**, 502-509 (2000).
4. Beck, A., *et al. Biologicals* **29**, 293-298 (2001).
5. Burrows, S. R., *et al. J. Virol.* **64**, 3974-3976 (1990).

Peptide Revolution: Genomics, Proteomics & Therapeutics
Michael Chorev & Tomi K. Sawyer (Editors)
American Peptide Society, 2003

Identification of Potential Vaccine T Cell Epitopes Based on Computer Selected Sequences

Leo Kei Iwai[1,3,4], Márcia Yoshida[4], Maria A. Shikanai-Yasuda[4], Maria A. Juliano[5], Jurgen Hammer[7], Luiz Juliano[5], Jorge Kalil[1,2,3], Luiz R. Travassos[6] and Edecio Cunha-Neto[1,2,3]

[1]Lab. Immunology, Heart Institute (Incor) and [2]Disc. Clin. Immunol. Allergy, University of São Paulo Medical School; [3]Inst. Investigation in Immunology, Millenium Institutes, Brazil; [4]Dept. Infect. Paras. Dis, University of São Paulo, Brazil; [5]Dept. Biophysics and [6]Dept. Microbiol. Immunol. Parasitol., UNIFESP, Brazil; [7]Dept Gen Info Science, Hoffmann-La Roche Inc, Nutley, NJ, USA

Introduction

Vaccines based on synthetic peptides allow the focus of immune response toward carefully chosen epitopic regions. Immunization of inbred mice with single peptides from the immunodominant antigen gp43 afforded protection against challenge with *Paracoccidioides brasiliensis* [1], the most prevalent systemic mycosis in Latin America. However, T cell recognition of individual synthetic peptides by a population of genetically distinct individuals is often limited. Thus, the major challenge of a peptide-based vaccine is the identification of a "promiscuous" epitope that could bind to several HLA alleles that may cover the majority of the population [2]. With the aid of the TEPITOPE algorithm which predicts binding of peptide sequences to a matrix of 25 different HLA class II molecules with high avidity [3,4], we selected five 15-mer sequences from gp43 of *P. brasiliensis* (Figure 1). Peptides were tested on proliferation assays with PBMC from 29 non-anergic PCM patients and 6 normal individuals.

gp43 (45-59)	H-IGGWLLLEPWISPSV-NH_2
gp43 (94-109)	H-TEDDFKNIAAAGLNHV-NH_2
gp43 (106-120)	H-LNHVRIPIGYWAVNP-NH_2
gp43 (283-298)	H-IDQHVKLACSLPHGRL-NH_2
gp43 (181-195)	H-QTLIAIHTLAIRYAN-NH_2

Fig. 1. Sequences of synthetic peptide derived from the gp43 of P. brasiliensis selected by TEPITOPE algorithm predicted to bind with multiple HLA molecules.

Results and Discussion

Among 29 PCM patients tested, 23 individuals recognized at least one peptide whereas none of the normal individuals recognized any of the tested peptides. Peptide gp43(181-195) was recognized by 48% of the patients (Figure 2); the combination of this peptide with gp43(45-59), gp43(95-109) and gp43(283-298) increased the coverage up to 79%. Similarly, 6/8 (75%) patients responded to a peptide pool (1 μM each) with the same contents (Table 1).

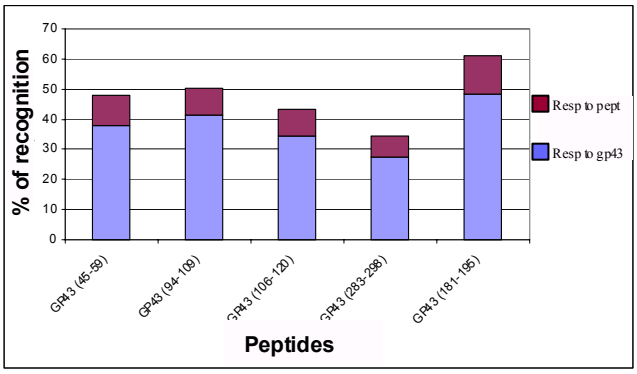

Fig. 2. Frequency of responders to peptides tested in proliferation assay with PBMC of 29 treated and healed nonanergic PCM patients among responders to peptides (dark) and gp43 (gray).

Table 1. Patient group PBMC proliferative response to gp43 peptides selected by TEPITOPE and their pool. Positive stimulation index values (SI ≥ 2) are marked with X.

Group	Peptide					Pool	gp43	PHA
	45-59	95-109	106-120	181-195	283-298			
#1	-	-	-	**X**	-	-	**X**	**X**
#2	-	-	-	**X**	-	**X**	**X**	**X**
#3	-	**X**	-	**X**	-	**X**	**X**	**X**
#4	-	**X**	-	-	-	**X**	**X**	**X**
#5	-	-	-	-	-	-	-	**X**
#6	**X**	-	-	-	-	**X**	**X**	**X**
#7	-	-	-	-	-	**X**	**X**	**X**
#8	-	-	-	**X**	-	**X**	**X**	**X**

The results show that TEPITOPE is an important tool for selection of potential immunodominant epitopes with potential usage in peptide based vaccine or immunodiagnostic tools, and that pooling of additional promiscuous epitopes may increase responsiveness and coverage.

Acknowledgments
The work was supported by grant 99/15319-6 from São Paulo State Science Funding Agency (FAPESP).

References

1. Taborda, C. P. *et al. Infect. Immun.* **66**, 786-793 (1998).
2. Cunha-Neto, E. *Braz. J. Med. Biol. Res.* **32**, 199-205 (1999).
3. Hammer, J. *et al. J. Exp. Med.* **180**, 2353-2358 (1994).
4. Hammer, J., Sturniolo, T. and Sinigaglia, F. *Adv. Immunol*. **66**, 67-100 (1998).

Peptide Revolution: Genomics, Proteomics & Therapeutics
Michael Chorev & Tomi K. Sawyer (Editors)
American Peptide Society, 2003

Structure-Activity Relationship Study of Glycopeptide Antigens Recognizing Specific Autoantibodies in Multiple Sclerosis

Barbara Mulinacci[1], Francesca Nuti[1], Giuseppina Sabatino[1], Mario Chelli[1], Alfonso Carotenuto[3], Paolo Rovero[3], Benedetta Mazzanti[1], Marta Pazzagli[1,4], Francesco Lolli[2] and Anna M. Papini[1]

[1]Laboratory of Peptide Chemistry & Immunology, Dipartimento di Chimica Organica "Ugo Schiff", and CNR-ICCOM, Università di Firenze, I-50019 Sesto Fiorentino (FI), Italy; [2]Azienda Ospedaliera Careggi, and Dipartimento di Scienze Neurologiche e Psichiatriche, Università di Firenze, I-50134 Firenze, Italy; [3]Dipartimento di Scienze Farmaceutiche, Università di Salerno, I-84084 Fisciano (SA), Italy; [4]C.S.F. S.r.l., I-50124 Firenze, Italy

Introduction

The glycopeptide CSF114(Glc) [1], containing a β-D-glucopyranosyl residue linked to an Asn residue, is the first synthetic antigen able to detect specific antibodies (Abs) by solid phase noncompetitive indirect ELISA (SP-ELISA) on sera of patients affected by Multiple Sclerosis (MS). The Ab titre correlates with disease activity. CSF114(Glc) displayed a well-defined conformational preference in solution characterized by a β-hairpin motif [2] with the minimal epitope Asn(Glc) at the tip of the β-hairpin structure.

Results and Discussion

We sought to optimize synthetic autoantigens to be used in immunoenzymatic assays in solid phase, working with the minimal glycopeptide sequence and with the β-hairpin conformation of the antigen. Confirmation that the β-hairpin structure was crucial for the exposition of the minimal epitope was obtained by the analysis, by SP-ELISA and by competitive ELISA, using a small focused library of glycopeptides based on structural diversity (Table 1).

Table 1. Focused library of glycopeptides to test for β-hairpin structure.

Peptide	Sequence
CSF114(Glc) (**1**)	TPRVERN(Glc)GHSVFLAPYGWMVK
[Asn^{7}(Glc)]CSF114 (1-14) (**2**)	TPRVERN(Glc)GHSVFLA
[Asn^{7}(Glc)]CSF114 (2-13) (**3**)	PRVERN(Glc)GHSVFL
[Asn^{6}(Glc)]Trpzip2 (**4**)	SWTWEN(Glc)GKWTWK
[Asn^{7}(Glc)]MBH12 (**5**)	RGKWTYN(Glc)GITYEGR
[Asn^{7}(Glc)]MBH36 (**6**)	RGKYTYN(Glc)GITYEGR
[Thr^{9}]CSF114(Glc) (**7**)	TPRVERN(Glc)GTSVFLAPYGWMVK
Ac-*c*[Dap5,Asp10]CSF114(Glc) (**8**)	Ac-TPRV-*c*[Dap-RN(Glc)GHD]VFLAPYGWMVK
[Asn^{7}(Glc)] Scramble CSF114 (**9**)	LAKVSYN(Glc)FRMETRVGWHPVGP
Scramble CSF114 (**9'**)	LAKVSYNFRMETRVGWHPVGP

The auto-Ab titre of glycopeptides **2** and **3** [CSF114(Glc) shortened sequences at both termini] was evaluated by SP-ELISA. IgG Abs in MS patients over control negative sera were not detected using the glycopeptides **2** and **3**. Far-UV CD spectra and preliminary NMR studies confirmed the structure of the synthesized glycopeptides. In particular, glycopeptide **4** [3] has a structural motif, the tryptophan zipper, that greatly stabilizes the β-hairpin conformation in short peptides in aqueous solution; **5** and **6** [4] have aromatic residues that may stabilize the β-hairpin conformation in aqueous solution. The glycopeptide **7** reproduces one of the glycosylation consensus sequences (NGT) typical of N-glycoproteins, and **8** is a cyclic peptide with a conformational constraint around the glycosylation site. Scramble CSF114(Glc) (**9**) and the corresponding unglycosylated sequence **9'** were designed to avoid any secondary structure, maintaining the glycosylation site at position 7. We previously reported the Ab titre by SP-ELISA to the glycopeptides **4**–**9**, and to the unglycosylated peptide **9'** [5]. Increased IgG titres over control sera were detected only for glycopeptides **5**–**8**, as well as for CSF114(Glc), but not for the glycopeptides **4** and **9** (scrambled sequence), and for the corresponding unglycosylated sequence **9'**. At variance, we have now demonstrated by competitive ELISA that both glycopeptides **2**–**8** [including the CSF114(Glc) shortened sequences], and scrambled sequence **9** displayed an affinity for MS auto-Abs similar to CSF114(Glc) (**1**), while the corresponding unglycosylated sequences had a very low affinity. These results can be interpreted assuming that the scrambled glycopeptide **9** is not able to expose at the best the epitope Asn(Glc) in the solid-phase conditions of the SP-ELISA, but it is able to inhibit the Abs binding when used in inhibition experiments in solution because it contains the minimal epitope. We can also assume that the length of the synthetic antigen is fundamentally particularl for the coating of the antigen to the polystyrene of the ELISA plate. In conclusion, all the glycopeptides containing the minimal epitope Asn(Glc) inhibit anti-CSF114(Glc) Abs in competitive ELISA independently from the length of the peptide sequence. To date, the glycopeptide CSF114(Glc) is the most effective synthetic antigen to identify auto-Abs in MS patients by SP-ELISA to follow the disease activity and specifically guide therapeutic treatments [6].

References

1. Papini, A. M., Rovero, P., Chelli, M. and Lolli, F. *Glycopeptides, their preparation and use in the diagnosis or therapeutic treatment of multiple sclerosis.* Eur. Pat. Appl. (2002), EP02-06767 20020619. Priority: IT 2001-FI114 20010622.
2. Carotenuto, A., Di Fenza, A., Nardi, E., Papini, A. M., and Rovero, P. In: Lebl, M. and Houghten, R. A. (Eds.) *Peptides: The Wave of the Future*, San Diego, 2001, p. 340-341.
3. Cochran, A. G., Skelton, N. J., Starovasnik, M. A. *Proc. Natl. Acad. Sci. U.S.A.* **98**, 5578-5583 (2001).
4. Pastor, M., Lopez de la Paz, M., Lacroix, E., Serrano, L. and Pérez-Payà, E. *Proc. Natl. Acad. Sci. U.S.A.* **99,** 614-619 (2002).
5. Mulinacci, B., Peroni, E., Sabatino, G., Mazzanti, B.; Pazzagli, M., Pozo-Carrero, M. C., Chelli, M., Carotenuto, A., Rovero, P., Lolli, F. and Papini, A. M. In: Benedetti, E. and Pedone, C. (Eds.) *Peptides 2002*, Editions Ziino, Napoli, Italy, p. 388-389.
6. Lolli, F., Mulinacci, B., Carotenuto, A., Bonetti, B., Sabatino, G., Zipoli, V., Mastrangelo, E., Mazzanti, B., Pazzagli, M., Alcaro, M. C., Peroni, E., Marconi, S., Pozo-Carrero M. C., Nuti, F., Battistini, L., Chelli, M., Rovero, P. and Papini, A. M. *"A glycopeptide designed to identify, isolate, and characterize autoantibodies in Multiple Sclerosis"*, manuscript submitted.

Author Index
Subject Index

1010

Abel,P.W. 143
Abran,D. 623
Abribat,T. 623, 675
Accardo,A. 818
Adan,R.A.H. 213
Afendis,S. 619
Affaitati,A. 497
Afonin,S. 19
Agaeva,G.A. 698
Agnes,R.S. 615, 682
Agricola,I. 183
Aimoto,S. 707
Aizawa,T. 468
Albericio,F. 125, 319, 437, 800, 831, 833
Albert,R. 721
Albrizio,S. 416
Alcaro,M.C. 17, 49, 942
Aldrich,J.V. 691
Alewood,P. 811
Alexander,J.M. 673
Alexopoulos,C. 377
Al-Ghoul,M. 350
Allen,S.D. 760, 947
Almeida,F.L. 484
Aloj,L. 588
Alves,I. 667, 734
Alves,I.D. 713
Ambo,A. 669
Ambulos,N.P. 65
Amchislavsky,E.I. 952
Amin,N. 33
Amiri,P. 315
Amoresano,A. 771
An,J. 599
Anantharamaiah,G. 601
Andersen,A.S. 684
Andersen,N.H. 462
Anderson,D. 480
Anderson,L.L. 252
Anderson,M.A. 758
Andrä,J. 877
Andreu,D. 827, 902, 913
Andrews,G.C.
Androutsou,M.P. 569
Andrus,D. 215
Antel,J. 632
Antonello,S. 443
Aoki,M. 331
Aoyagi,H. 970
Appella,E. 127, 534
Appleby,T. 33
Arad,G. 181
Araki,T. 606
Arevalo,E. 754
Arimoto,R. 758
Arnold,E. 981
Arnold,G.F. 981
Assfalg-Machleidt,I. 348
Ast,T. 854
Aucoin,J.P. 777
Auernheimer,J. 807
Avvedimento,E.V. 497
Awada,C. 357

Bachovchin,W.W. 321
Bader,R. 704
Baidakova,L.K. 55
Bailey,V. 424
Bain,S. 33
Bajusz,S. 361
Bakelaar,F.T. 57
Balasubramaniam,A. 79
Balboni,G. 453
Baldauf,C. 439, 441
Balse-Srinivasan,P. 655
Banda,P.W. 153
Bang,D. 242
Bangale,Y. 961
Bánhegyi,P.G. 548
Bann,J.G. 233
Barabás,É. 361
Baranski,T.J. 252
Barany,G. 59, 87, 317, 839
Barazza,A. 673, 679
Barbato,G. 978
Barberis,C. 725
Barbier,J. 702
Barlos,K. 240
Baronas-Lowell,D. 350
Barra,D. 900
Barthe,P. 260
Basak,A. 341, 343, 470
Basak,S. 341, 343
Battistini,L. 942
Bauer,W. 721
Baughman,R.H. 428
Bauzo,R. 639
Bauzo,R.M. 565, 641, 643, 645
Bawolak,M. 578
Bazzo,R. 978
Beaulieu,M. 573, 578
Beck,A. 1003
Becker,J.M. 635, 754
Beck-Sickinger,A.G. 113, 254, 663
Beking,K. 341
Belda,I. 800, 866
Bélec,L. 179
Bellanger,L. 260
Benedetti,E. 435, 482, 497, 588, 597, 818
Benincasa,M. 915
Berditchevskaia,M. 19
Berg,R.H. 464
Bergeron,A. 675
Berlicki,L. 310
Bernardina,M.D. 837
Bernhagen,J. 768
Bernhard,A. 911
Bevilacqua,C. 797
Beyermann,M. 113, 604
Bhargava,K. 873
Bhatia,G. 961
Bhatia,M.B. 47
Bianchi,E. 976, 978
Bianco,A. 414
Bienert,M. 113, 604
Bier,F. 864
Biernat,M. 938
Bifulco,G. 508
Biondi,B. 657
Biondi,L. 659, 875
Bironaite,D.-. 584
Birringer,M. 864
Bisch,P.M. 484
Bischoff,D. 883
Bister,B. 883
Bitan,G. 765
Blaecke,A. 1003
Blake,P.R. 715
Blanchfield,J. 811
Blanchfield,J.T. 809
Blaney,E.J. 313
Blazyk,J. 890
Blishchenko,E.Y. 952
Blondelle,S.E. 877, 930
Blum,E.S. 269
Boas,U. 108
Bobbey,A. 890
Boden,O. 229
Boggiano,C. 930
Böhme,I. 663
Boisguerin,P. 141
Bökönyi,G. 548
Bols,L. 147
Bonetti,B. 75, 942

Bonewald,L.F. 65
Bongaarts,R. 147
Bonvin,A.M. 945
Booth,H. 89
Borgia,J.A. 350
Borics,A. 155, 400
Borin,G. 536, 657
Borovickova,L. 495
Bosze,S.E. 1001
Bottaro,D.P. 515
Botti,P. 71, 235
Boucard,A.A. 573, 742
Bovermann,G. 476
Boyd,J.G.
Bracci,L. 965
Brailoiu,G.C. 955
Bramhill,D. 976
Bramlett,K.S. 198
Brandenburg,K. 877
Brandi,A. 77
Brandt,J. 684
Brask,J. 125
Braun,K. 820
Briand,J. 414
Brissette,R.E. 684
Brouwer,A. 147
Brouwer,A.J. 210
Brown,D.A. 313
Brown,L.E. 985
Brown,R.T. 837
Broxterman,Q.B. 98, 137, 435
Brubaker,P. 623
Brunati,A. 536
Brunel,F. 198, 793, 795
Bruno,I. 506, 508
Bruns,C. 721
Bryant,S.D. 453, 669
Buck,A. 768
Buczek,P. 841
Buelow,R. 522
Buergle,M. 365
Bulaj,G. 841
Bulet,P. 478, 813
Bunn, Jr.,P.A. 584
Burgess,K. 205
Burke, Jr.,T.R. 544
Burke,T.R. 515
Burris,T.P. 198
Bussat,M. 1003
Butterworth,J. 665
Byk,G. 91, 104

Caballero,S. 709
Cabell,L.A. 550
Cabello,C. 649, 651
Cabello,C.M. 567
Caccomo,N. 1001
Caflisch,A. 476
Cai,M. 567, 647, 649, 651, 655
Calderan,A. 536, 657
Calò,G. 717, 740
Calvo,J.C. 163
Camarda,V. 740
Camarero,J.A. 111, 248
Campiglia,P. 17, 194, 744, 746, 748
Cano,H. 418
Cantley,L.C. 856
Cao,X. 459
Capasso,D. 520
Cardarelli,L. 590
Carell,T. 265
Carlens,G. 582
Carotenuto,A. 744, 746, 748, 942, 1007
Carr,D.B. 935
Carrà,G. 717
Carrasco,M.R. 837
Carreño,C. 831, 833
Casallanovo,F. 250
Castel,S. 437
Cava,M. 315
Cavelier,F. 119, 737
Cawthorne,M. 625
Cayabyab,M. 599
Cebrat,M. 186, 719
Cecal,R. 782
Cescato,R. 723
Cescutti,P. 915
Chaddha,M. 601
Chan,D.C. 584
Chan,W. 725
Chance,W.T. 79
Chandramouli,N. 721
Chang,E. 227
Chang,J. 955
Chang,L. 196
Che,Y. 422
Chelli,M. 17, 49, 75, 77, 942, 1007
Chen,J. 428
Chen,Y. 151
Cheng,L. 725
Chernomordik,L. 822
Chiche,L. 486
Chiva,C. 827
Chmielewski,J.A. 227, 292, 337, 339, 789
Choi,J. 542
Choi,M.Y. 590
Choi,W. 599
Chopra,N. 242
Chorev,M. 673, 679
Chretien,M. 341
Christensen,J.B. 108
Chung,N.N. 661
Ciliberto,G. 976, 978
Cizkova,M. 412
Clément,M. 573, 578
Cline,D.J. 373
Cochran,A.G. 392
Coleman,D.R. 550
Colgrave,M.L. 402
Conconi,M.T. 797
Contillo,L.G.
Cook,J. 976
Corbier,C. 435
Cordero,F.M. 77
Corich,M. 679
Cortese,R. 978
Corvaïa,N. 1003
Costa,S.P.G. 85
Costa-Neto,C.M. 571
Courtney,J.C. 157
Coutinho,F.B. 133
Cowell,S.M. 667
Craik,D.J. 402
Crisma,M. 51, 98, 137, 435
Cudic,M. 904, 963
Culler,M. 625, 700
Cunha-Neto,E. 1005
Cusack,B. 359
Czaplewski,C. 333
Czerwinski,A. 59

Daffre,S. 926, 928
Dahmen,C. 732, 807
Dakappagari,N. 983
Dakappagari,N.D. 972
Dakappagari,N.K. 989
DalPozzo,A. 711
Dalton,A.B. 428
Daly,N.L. 402
Danho,W. 750
Danielsen,G.M. 684
Dannenbring,R. 961
Danzeisen,R. 976

Darlak,K. 59
Darlak,M. 59
Datta,G. 601
D'Auria,G. 797, 917, 919
David,R. 254
Davis,P. 615, 682
De Riccardis,F. 506
De Bont,D.B.A. 210
De Capua,A. 482, 597
De Jong,R. 210
De Lean,A. 455
De Luca,S. 588
de Mol,N.J. 546
De Montis,M.G. 965
de Visser,P.C. 115
de Yoreo,J.J. 111, 248
Debari,K. 621
Debart,F. 822
Deber,C.M. 590
Debus,J. 820
DeCot,B. 649
Decot,B. 651
DeGrado,W.F. 3
Dekker,F.J. 546
Del Borgo,M.P. 727
Del Gatto,A. 497
Del Piero,S. 536
del Río,X. 173
Del Valle,J.R. 202
Deliyannis,G. 963
Della Moglie,R. 588
Della Monica,C. 506
Deraët,M. 131, 573, 578
Deraos,G.N. 945
Deraos,S.N. 945
Deshayes,S. 802
Dettin,M. 797, 917, 919
Dettwiler,J.E. 179
Di Bello,C. 797, 917, 919
Di Niola,E. 520
Diaper,C.M. 363
Dieckmann,G.R. 428
Dieli,F. 1001
Diez,A. 173
Dinger,M. 663
D'Isanto,M. 520
Divita,G. 802
Doisy,X. 888, 940
Dominik,A. 346
Donella-Deana,A. 536
Dong,C. 599
Dong,F. 343
Dong,J.Z. 625, 700
Drag,M. 310
Draper,R.K. 428
Dreznjak,D. 106
Drijfhout,J.W. 115
Dun,N.J. 955
Dun,S.L. 955
Durroux,T. 725
D'Ursi,A.M. 416
Dvorozniak,M. 750
Dyba,M. 938

Eckert,D. 976
Edison,A.S. 565, 637
Eggen,I.F. 57
Ehrhardt,C. 476
Ehrlich,A. 604
Eisenstein,E. 65
Eker,F. 459
El Hafi,R. 173
Ellison,M. 841
Enderle,A. 732, 807
Ene,C. 155
Englund,J. 881
Enstrom,A.M. 845
Eom,K. 924, 974
Erchegyi,J.C. 723
Erdélyi,M. 102, 190
Eros,D. 548
Escher,E. 131, 573, 578, 742
Esser,M. 976
Estephan,R. 754
Etienne,M.A. 381, 777

Fabre,M. 800
Falciani,C. 965
Falcigno,L. 797, 917, 919
Falconer,R.A. 73
Farkas,Ö. 61
Farrera-Sinfreu,J. 437
Fauszt,I. 361
Favreau,P. 478, 813
Fázio,M.A. 571, 928
Fechner,K. 604
Feix,J.B. 873
Feliciello,A. 497
Fernandes,S.M. 313
Ferrer-Montiel,A. 831, 833
Fesinmeyer,R.M. 462
Fields,G.B. 95, 350
Filip,S.V. 119
Filippov,D.V. 115
Filira,F. 659, 875
Fillion,D. 131
Fillon,Y. 227
Fiori,N. 673
Fischer,M.J. 546
Fisher,R.J. 515
Fivash,M.J. 515
Flagiello,A. 771
Florian,K. 911
Fong,T.C. 522
Formaggio,F. 51, 98, 137, 433, 435, 443, 445, 879
Forns,P. 173
Fowler,E. 65
Fraga,S.M.B. 31
Franco,A. 418
Frankiewicz,L.P. 775
Freidlin,I.S. 952
Fridkin,M. 139, 512
Fritzemeier,K. 383
Fry,D. 750
Fu,Y. 386, 777
Fuchs,P. 945
Fuerst,P. 307
Fujii,M. 165
Fujii,N. 331, 606
Furet,P. 307
Fushman,D. 248
Futaki,S. 791

Gaál,D. 815
Gabrijelcic-Geiger,D. 346
Gaertner,H. 71, 235
Gairí,M. 866
Galande,A.K. 129, 198, 795
Galaud,F. 188
Galdiero,M. 520
Galdiero,S. 520
Gallagher,O.P. 811
Gallazzi,F. 540
Gambaretto,R. 797
Gangadhar,B.P. 79
Gao,Y. 27, 196, 544, 611
Garavelli,M. 223
Garber,D.W. 601
García de Diego,L. 831, 833
Garcia,M. 173
Garcia-Echeverria,C. 307
Gardella,T.J. 677
Garelli,A. 223
Gargiulo,D. 919
Garrell,J.M. 800
Gates,D. 424
Gatos,D. 240, 569, 945
Gatto,E. 879

Gaucher,A. 98
Gayer,B. 512
Gazal,S. 43, 181
Geleziunas,R. 976
Gellerman,G. 43
Gennaro,R. 900, 915
Gera,L. 584
Gerothanasis,I.P. 945
Getun,I.V. 317
Geysen,J. 147
Giannini,E. 659
Gianolio,E. 818
Giantsidis,J. 33
Giatas,N. 569
Gierasch,L.M. 447
Gillies,R.J. 117
Gilon,C. 43, 181, 510
Giralt,E. 173, 437, 800, 866, 913
Giriat,I. 269
Gispen,W. 213
Giusti,L. 416
Glaser,R.W. 19
Glukhov,E. 181
Gobbo,M. 659, 875
Göbel,M.W. 229
Goetsch,L. 1003
Gogoll,A. 102, 190
Goldstein,N.I. 684
Gomez-Monterrey,I. 194
Gomez-Paloma,L. 506, 508
Gonçalves,M.T. 31
Gonzales,A. 1003
Gonzalez,R.R. 522
González,S. 800
González-Muñiz,R. 831, 833
Good,M. 809
Goodman,M. 202
Goodman,S.L. 732, 807
Goodnow,R. 750
Gosselin,M. 665
Goszczynski,T. 186
Goulas,S. 240
Grace,C.R.R. 723
Grant,M.B. 709
Greeley,D. 750
Green,B. 841
Greiner,G. 183
Grieco,P. 17, 194, 655, 744, 746, 748
Groll,M. 348
Gross,D.E. 45
Grzonka,Z. 23
Gu,X. 215, 567
Guagnano,V. 307
Guerrini,R. 453, 717, 740
Guffler,S. 106, 854
Guillemette,G. 573, 578
Guiotto,A. 536, 657
Günther,R. 439, 441
Guo,L. 355, 689
Gupta,H. 601
Gururaja,T.L. 480
Guzmán,F. 163, 991

Haas,E. 91
Haberli,A. 742
Habi,A. 623
Hack Joo,K. 93
Hackel,B.J. 111
Haehnel,W. 265, 303, 383
Haeuw,J. 1003
Hagihara,M. 556
Hahn,M.E. 267
Hammer,J. 890, 1005
Hammer,M.R. 647
Hammer,R.P. 381, 386, 777
Han,G. 567, 655
Han,K. 420
Han,S. 647
Handattu,S. 601
Handl,H.L. 117
Hannink,M. 540
Hansen,P.R. 888, 940
Hansford,K.A. 176
Harding,J.R. 89
Hariton-Gazal,E. 510
Hasegawa,T. 556
Haskell-Luevano,C. 565, 637, 639, 641, 643, 645
Hatakeyama,T. 970
Haubner,R. 693
Hayakawa,Y. 468
Hayashi,Y. 67, 805
Hazan,K. 181
Heged?s,T. 815
Heinze,J. 303
Heitz,A. 486
Heitz,F. 802
Hellwig,P. 303
Hemmi,H. 886
Henkel,J. 864
Herasimenka,Y. 915
Herédi-Szabó,K. 628
Hernandez,J. 486
Hersel,U. 693, 807
Heyl,D.L. 313, 613
Hidaka,Y. 431
High,K. 675
Hiramatsu,K. 606
Hirano,A. 970
Hiromichi,N. 499
Hironobu,H. 499
Hirsch,T. 768
Hirschmann,R. 217
Hlavacek,J. 412, 495
Ho,N. 121, 325
Hodges,J.A. 472
Hodges,R.S. 123, 145, 149, 151, 301, 409, 490
Hodzic,L. 665
Hoebeke,J. 75, 414
Hoeger,C. 723
Hoeg-Jensen,T. 684
Hoeppener,J.WM. 773
Hoesl,C. E. 39
Hofmann,H. 439, 441
Holder,J.R. 637, 641, 643
Holleran,B.J. 742
Hong,A. 21, 353
Horikawa,M. 379
Horvath,A. 809
Houghten,R.A. 39, 63, 835
Houtman,J.C.D. 534
Hruby,V.J. 45, 117, 200, 215, 567, 615, 647, 649, 651, 653, 655, 667, 682, 713, 734, 935
Huang,S. 371
Huang,X. 677
Huang,Z. 599
Hubbell,W.L. 252
Huber,R. 348
Hudecz,F. 815, 1001
Hudson,F.M. 462
Hughes,R.A. 727
Hurni,W.H. 978
Hussain,R. 536
Huttunen,H.K. 244
Hyuk-Kwang,J. 93
Hyun Jin,L. 93

Ichihara,K. 21
Ifrah,D. 888, 940
Iliodromitis,E. 569
Imbach,P. 307
Impellizzeri,G. 771
Ingallinella,P. 976, 978
Ingenito,R. 106

Interlandi,G. 476
Iori,M. 474
Ishibashi,J. 886
Ishida,H. 165
Ishiguro,M. 379
Ishimaru,M. 169
Ito,L. 431
Ito,T. 805
Ittah,V. 91
Ivanov,V.T. 55, 952
Iwai,L.K. 1005
Iyer,S. 522
Izzo,I. 506

Jablonkai,I. 335
Jackson,D.C. 963, 985
Jacobson,S. 983
Janmey,P.A. 333
Jaulent,A.M. 390
Jayamaha,M.N. 613
Jeannotte,G. 176
Jensen,K.J. 108, 125
Jerala,R. 877
Jeschke,B. 732, 807
Jessing,M. 108
Jewginski,M. 426
Jia,F. 540
Jin,Y. 890
Jinsmaa,Y. 453, 669
Johnson,C.
Johnson,D.E. 904
Johnson,J. 65
Johnson,M.G. 619
Jois,S.D. 79
Jones,R. 671
Jose,B. 323, 524
Joseph,C.G. 639
Joyce,J. 976
Juban,M.M. 386
Judd,A. 671
Juhász,A. 361
Juliano,L. 1005, 1005
Juliano,M.A. 1005

Kabha,E. 104
Kadoya,Y. 779
Kaempfer,R. 181
Kafarski,P. 310, 426
Kaiser,M. 348
Kalászi,A. 61
Kalil,J. 1005
Kaluarachchi,K.K. 504
Kalutkiewicz,K. 147
Kamata,S. 892
Kamijo,R. 553
Kang,S. 544
Kantlehner,M. 807
Kao,J.L -K. 233
Kappel,J.C. 87, 839
Kaptein,B. 137, 435
Kapurniotu,A. 768
Karelin,A.A. 952
Karle,S. 961
Karlén,A. 190
Kasai,S. 779
Kasher,R. 512
Kashimoto,K. 621
Katchalski-Katzir,E. 512
Kato,T. 323, 524, 968
Katoh,E. 559
Katoh,S. 559
Katsutoshi,O. 556
Kaumaya,P.T.P. 407, 760, 947, 972, 983, 989
Kaushanskaya,A. 671
Kavarana,M.J. 567
Kawabata,S. 892
Kawano,K. 468, 785, 892
Kawulka,K.E. 363
Keiderling,T.A. 381
Keliang,l. 617
Kempe,M. 756
Kent,S.B.H. 242
Kéri,G. 548
Kessler,H. 365, 632, 693, 732, 807
Khaidukov,S.V. 952
Khan,W. 750
Khatri,A. 65
Khatri,A.J. 677
Khroyan,T. 671
Khullar,L. 313
Kim,H. 542
Kimura,T. 67, 169, 327, 805
Kirkitadze,M.D. 765
Kiso,Y. 67, 805
Kit,L.S. 907
Kitamatsu,M. 538
Klarskov,K. 742
Klinguer-Hamour,C. 1003
Klose,A. 113
Kluczyk,A. 719
Koch,M. 820
Koda,Y. 811
Kodama,E. 791
Kodama,H. 474
Koerber,S.C. 723
Koh,K. 621
Koh,Y. 331
Kohen,F. 512
Kokotos,G. 569
Kontani,K. 968
Kosson,P. 935
Kostanyan,I.A. 55
Kouji,O. 474
Kovács,P. 815
Kover,K. 615
Kover,K.E. 567
Krajewski,K.A. 329
Krause,E. 604
Krchnak,V.Jr. 649
Krebs,A. 229
Kretsinger,J. 256
Kreuzer,O.J. 864
Kruijtzer,J.A.W. 213
Kuenzel,S. 183
Kulik,T. 512
Kumar,S. 599
Kurylko,G. 750
Kusano,S. 606
Kutateladze,T.G. 301
Kwok,S.C. 409, 490
Kyakuno,M. 165
Kyle,D.J. 715
Kyrikou,I. 569

Laborde,P. 188
Lai,J. 615, 682
Lai,J.H. 321
Lam,K.S. 100, 388, 829, 843, 845, 847, 849
Lam,T. 675
Lama,T. 748
Lamata,M. 877
Lanci,D. 223
Landon,L.A. 540
Lang,M. 307
Langedijk,J.P. 987
Lankiewicz,L. 23
Lashuel,H.A. 765
Latajka,R. 426
Lau,D.H. 100
Lau,Y. 985
Lauer-Fields,J.L. 350
Lavecchia,A. 748
Lavielle,S. 737
Lavigne,P. 573, 578
Law,E. 47
Lazarov,M. 522

Lazarus,L.H. 453, 669
Le Clainche,L. 263
Leatherbarrow,R.J. 390
Leben,R. 141
Lebleu,B. 822
Lebrilla,C.B. 843
Leduc,R. 573, 578, 742
Lee,B. 679, 933
Lee,D.L. 149
Lee,H. 789
Lee,K. 315, 515, 544
Lee,S. 167
Lee,Y. 542, 682
Lee,Y.S. 615
Lehmann,C. 450
Leighty,M.W. 691
Lejeune,V. 119
Lelli,B. 965
Lemieux,C. 661
Leontiev,K.V. 952
Leopold,M.F. 153
Lerch,M. 704
Leung,J.W. 907
Lever,S.Z. 540
Levy,R. 181
Lewis,C. 47
Lewis,I. 476, 721
Lewis,M.R. 540
Lewis,R. 811
Li,H. 290, 909
Li,P. 501, 518
Li,W. 265, 303, 355
Li,X. 292
Li,Y. 599
Liang,J. 544
Liepina,I. 333
Lima,G.H. 192
Limatola,C. 597
Lin,T. 695
Lindquist,R.N. 315
Linehan,W.M. 515
Lipkin,V.M. 55
Lipkowski,A.W. 935
Lips,C.J.M. 773
Liskamp,R.M.J. 147, 210, 213, 546, 773
Lisowski,M. 186, 719
Liu,B. 167
Liu,D. 599
Liu,H. 501, 515, 518
Liu,R. 388, 829, 847, 907
Liu,Y. 355, 907
Lively,M.O. 65
Liwo,A. 333, 333
Llorà,X. 866
Lohner,K. 877
Lokteff,M. 1003
Lolli,F. 75, 77, 942, 1007
Long,D. 59
Long,Y. 329, 501
Longobardo,L. 194
López,P. 173
Lou,B. 695
Lou,C. 695
Lovas,S. 155, 400, 628
Lowik,D.W.P.M. 210
Loyter,A. 510
Lozano,J.M. 163, 991
Lozzi,L. 965
Lu,S.M. 409
Lu,Y. 159, 661, 974
Lubell,W.D. 37, 176, 179, 188
Lubke,J. 628
Ludwig,V. 229
Luppi,G. 223, 433
Lute,K.D. 972

Ma,S. 682
Ma,S.W. 615
MacAulay,J. 470
Machado,A. 192, 571, 926
Machova,Z. 254
Mackie,G. 750
MacKinnon,R. 276
MacLean,S. 702
Madani,N. 599
Maeda,K. 331
Maggi,C. 746, 748
Magilton,W. 976
Magrì,A. 771
Maia,H.L.S. 31, 85
Maillere,B. 260
Majer,Z. 1001
Makowski,M. 426
Maletta,M. 917
Malkinson,J.P. 53, 73
Mammi,S. 375, 673
Manea,M. 782
Manetta,J.V. 619
Manganiello,S. 235
Manning,M. 725
Mant,C.T. 123, 145, 149
Maran,F. 443
Marasco,D. 482
Marastoni,M. 659
Marchand,C. 329
Marchand,D. 737
Marcotte,F. 176
Mari,F. 95, 418
Maria,Z. 569
Marik,J. 100, 388, 849
Marshall,G.R. 27, 196, 252, 422, 611, 687, 758
Martin,L. 260
Martinell,M. 866
Martinez,J. 119, 737
Martins,J.C. 665
Massacesi,L. 942
Matcham,G. 47
Matei,E. 418
Matola,T. 335
Matsoukas,J.M. 569, 945
Matsubara,K. 785
Matsumoto,H. 805
Matsuo,Y. 553
Matsuoka,M. 791
Mattern,R. 709
Mattiuzzo,M. 915
Maulucci,N. 506
Mavromoustakos,T. 569
Maw,H. 321
Mayorov,A. 651, 655
Mayorov,A.V. 647
Mazaleyrat,J. 51, 98, 445
Mazur,S. 127
Mazzanti,B. 75, 77, 942, 1007
Mazzoli,A. 900
Mazzoni,M. 416
Mazzuca,C. 879
McCarley,R.L. 777
McElhaugh,M. 976
McIntosh,M.J. 841
McKay,R.T. 363
McLaughlin,M.L. 29, 35, 83, 135
McLaurin,J. 782
McMurray,J.S. 504, 550
Mechulam,A. 260
Mehok,A.R. 145
Melandri,F. 51
Melendez,R.E. 37
Melikov,K. 822
Mellinger,J. 890
Meloen,R.H. 987
Menez,A. 260
Menin,L. 478, 813
Mercier,P. 363

Mészáros,G. 548
Meyer,A. 732
Mezo,G. 1001
Micali,F. 900
Michalet,S. 478, 813
Michel,T. 822
Michio,K. 474
Mierke,D.F. 679
Mignogna,G. 900
Mihara,H. 258
Milbradt,A.G. 41, 348
Miller,M. 976
Miller,M.D. 978
Minakakis,P. 569
Miranda,A. 192, 571, 926, 928
Miranda,M.M. 192, 926, 928
Misicka,A. 775, 935
Mitchell,A.R. 111
Mitsios,J. 377
Mitsuya,H. 331
Mizuguchi,M. 468, 785, 892
Mizuno,T. 559
Mochizuki,M. 779
Modlinger,A. 365
Molina,A. 902
Monjardet,V. 263
Monnee,M.C.F. 210
Monti,S. 520
Mootz,H.D. 269
Mora,D. 95, 418
Moreau,J. 625, 700
Moree,W.J. 210
Morelli,G. 588, 818
Moretto,A. 443
Morgan,B. 625
Morii,T. 556
Moriyon,I. 877
Mörl,K. 663
Moroder,L. 41, 81, 348
Morris,M.C. 802
Mouillac,B. 725
Mroz,P. 795
Mroz,P.A. 793
Mueller,M.M. 81
Mueller,S. 183
Muir,T.W. 267, 269, 276
Mukai,H. 553
Mulinacci,B. 77, 942, 1007
Munoz,E. 428
Murphy,R.F. 155, 400, 628
Murray,T.F. 691
Musiol,H.J. 81
Musselman,I.H. 428
Mutter,M. 225
Muzi,L. 711

Nafie,L. 459
Naider,F. 630, 635, 752, 754
Nair,P. 667
Nakai,T. 538
Nakaie,C.R. 133, 250, 484
Nakase,I. 791
Nakashima,H. 606
Nakazato,T. 165
Nameki,D. 791
Napolitano,A. 506
Navarro,P. 827
Ndungu,J.M. 45
Neerup,T.S. 888, 940
Nefzi,A. 39, 63
Negri,L. 659
Nelson,R. 47
Nemoto,Y. 167
Neri,P. 965
Neves,M.S. 133
Ngu-Schwemlein,M. 424
Nguyen,L. 486
Ni,M. 711
Nicklaus,M. 501, 518
Nielsen,J.S. 841
Nies,B. 732, 807
Niida,A. 606
Niidome,T. 970
Nijenhuis,W.A.J. 213
Nikiforovich,G.V. 233, 687
Nishi,N. 779
Nishino,N. 323, 524, 968
Nishio,H. 169
Nishiuchi,Y. 169, 327
Nishiyama,Y. 961
Nitta,K. 468
Niwa,M. 791
Nobeli,I. 526
Nokihara,K. 258
Nomizu,M. 779
Noorani,M. 307
Noort,D. 115
Novellino,E. 17, 194, 416, 744, 746, 748
Nuland,N.A. 945
Nuti,F. 77, 942, 1007

Oancea,S. 51, 98, 433
Oberer,L. 476
Ocampo,M. 991
Ogata,Y. 357
Oguz,U. 35, 83
Ohga,Y. 779
Ohshima,K. 621
Oishi,S. 165, 606
Ojima,T. 258
Okada,Y. 669
Okamura,S. 524
Okura,T. 667
Oldfield,S.P. 115
Oliva,R. 797, 917, 919
Olive,C. 809
Oliveira Jr.,V.X. 571
Olivera,B.M. 841
Omlor,A. 709
Ono,S. 25
Onoue,S. 621
Opalka,D. 976
Orfi,L. 548
Ortiz-Acevedo,A. 428
Oschkinat,H. 141
Osler,A. 536, 657
Østergaard,S. 684
Ostresh,J.M. 835
Otaka,A. 331, 606
Ottoboni,T. 315
Otvos, Jr.,L. 904, 963
Otvos,L.Jr. 155
Overduin,M.J. 301
Overkleeft,H.S. 115

Paduano,L. 818
Pagano,K. 375
Paiva,A.C.M. 250
Palgunachari,M. 601
Palladino,P. 435, 482, 597
Palleschi,A. 445, 879
Pantarotto,D. 414
Paolillo,L. 797, 917, 919
Paolini,I. 77
Pap,Á. 548
Papanastasiou,I. 569
Papini,A.M. 17, 49, 75, 77, 942, 1007
Pappalardo,G. 771
Partidos,C.D. 414
Pasquato,A. 917, 919
Pasternak,A. 186
Pastor,J.J. 866
Patacchini,R. 746, 748
Patarroyo,M.E. 163, 991
Pate,M. 890
Patiny,L. 225

Paul,S. 961
Pawelczak,M. 310, 426
Payan,D.G. 480
Pazzagli,M. 75, 77, 942, 1007
Peach,M.L. 501, 518
Pedone,C. 482, 497, 520, 597
Peggion,E. 375, 673
Peiró,S. 827
Pellois,J. 267
Pelzer,S. 883
Peng,L. 829, 849
Pennington,M.W. 69
Perchellet,J. 609
Pereira-Lima,S.M.M.A.. 85
Peri,K.G. 623, 675
Pérodin,J. 573
Peroni,E. 75, 942
Perrault,D. 147
Perretta,G. 482
Pertinhez,T.A. 926
Pesquero,J.B. 571
Pessi,A. 976, 978
Péter,A. 582
Petersen,A. 57
Pflueger,F. 95, 418
Pham,T.T. 486
Pham,V. 586
Pham,W. 367
Phan,H.T. 486
Phan,J. 544
Philippova,M.M. 952
Picur,B. 186, 457
Pierschbacher,M.D. 709
Pillutla,R.C. 684
Pini,A. 965
Pinna,L.A. 536
Pinyol,E. 173
Pipkorn,R. 820
Piró,J. 173
Pisarewicz,K. 95
Pispisa,B. 445, 879
Planque,S. 961
Pless,J. 721
Pochan,D.J. 256
Podda,E. 900
Poethko,T. 693
Polchaninoff,M.
Poletti,E.F. 133
Polgar,W. 671
Pommier,Y. 329
Pons,M. 437
Popa,T.V. 123
Poreddy,A. 196
Porreca,F. 615, 682
Porro,M. 877
Posthuma,G. 773
Pozo-Carrero,M. 49, 77
Pozo-Carrero,M.C. 942
Prabhakaran,M. 371
Prato,M. 414
Pretzel,D. 183
Price,E. 33
Prokai,L. 869
Prokai-Tatrai,K. 869
Przybylski,M. 782
Pucci,P. 771
Puijk,W.C. 987
Puk,O. 883
Pulak,R. 147
Purdue,B.W. 586

Ragone,R. 482, 597
Ragozzino,D. 597
Raines,R.T. 472
Rajagopal,K. 256
Rakoczy,E. 809
Ramanujam,P.S. 464
Rana,H. 47
Rau,F. 693
Rawale,S. 972, 989
Rawale,S.V. 407, 760, 947, 983
Rawls,K.A. 837
Razal,J. 428
Real,F.X. 827
Regoli,D. 717, 740
Reissmann,S. 183
Reményi,J. 815
Remmer,H.A. 65
Ren,Z. 550
Renganathan,K. 613
Renner,C. 41, 348
Rennert,R. 663
Renugopalakrishnan,V. 371
Reubi,J. 723
Reyes,C. 163
Ribel,U. 684
Riccio,R. 506, 508
Rice,J.S. 504
Richard,J. 822
Richards,N.G. 565, 639
Riek,R. 723
Rihakova,L. 573, 578
Rijkers,D.T.S. 210
Rijkers,D.T.S. 773
Ritter,M. 303
Ritter,N. 65
Rivier,J.E. 723
Rizzarelli,E. 771
Rizzi,D. 717
Rizzo,R. 915
Roberts,L.R. 515
Rocchi,R. 659, 875
Roda,O. 827
Rodgers,D.W. 613
Rodionov,I.L. 55
Rodríguez-Mias,R.A. 913
Roesel,J. 307
Roeske,R.W. 355, 689
Rofman,I. 91
Roller,P.P. 329, 501, 518
Romanelli,A. 269
Romanova,G.A. 488
Romanovskis,P. 359
Rombouts,F. 176
Roscigno,P. 818
Roselló,X. 800
Rosenberry,T. 359
Rosenblatt,M. 673, 679
Rosenbluh,J. 510
Rosengren,K. 402
Rossi,F. 482, 597
Rostas,J. 424
Rotondi,K.S. 447
Roumelioti,P.E. 569
Roumestand,C. 260
Rovero,P. 49, 75, 416, 744, 746, 748, 942, 1007
Royo,M. 437, 831, 833
Rubiralta,M. 173
Ruchala,P. 186
Rudolf,V. 911
Runci,Y. 965
Ruvo,M. 482, 520
Ruzza,P. 536, 657

Sabatino,G. 49, 942, 1007
Sadler,K. 974
Safarik,M. 412
Sagan,S. 737
Saito,M. 538
Saito,Y. 707
Sakarellos,C. 377
Sakarellos-Daitsiotis,M. 377, 994
Salamon,Z. 713, 734
Salazar,L.M. 163, 991
Salvadori,S. 453, 717, 740

Salvatella,X. 866
Samelson,L.E. 534
Sanchez,A. 671
Sánchez-Vallet,A. 902
Santos,E.L. 571
Sargsyan,H. 635
Sarkadi,B. 815
Sasaki,M. 67
Sasaki,Y. 669
Sato,S. 556
Sato,T. 357, 707
Satoshi,O. 474
Saviano,M. 435, 497, 588
Sazonova,O.V. 952
Schaaper,W.M. 987
Schaer,J. 723
Schafer,E. 548
Schäffer,L. 684
Schaschke,N. 346
Scherf,T. 139
Schievano,E. 375, 673
Schiller,P.W. 455, 582, 661
Schleif,W. 976
Schmauder,A. 768
Schmidt,M. 183
Schnatbaum,K. 854
Schneider,J.P. 256, 373
Schneider-Mergener,J. 141
Schreier,S. 133, 250, 484
Schullery,S.E. 613
Schütt,M.H. 41
Schwab,R.E. 548
Schwaiger,M. 693
Schweitzer-Stenner,R. 459
Scocchi,M. 900
Scolaro,B. 659
Scott,J.W. 637, 639, 641, 643, 645
Searcey,M. 53
Sebestik,J. 412, 495
Seifert,R. 604
Sekedat,M. 276
Seo,E.S. 246
Setnicka,V. 381
Sexton,P.M. 586
Sforça,M.L. 926
Sha,W. 758
Shai,Y. 895
Shan,S. 715
Shekhtman,A. 269
Shen,Y. 625, 700
Shenoy,N. 540
Sheriff,S. 79
Sherman,J.C. 244
Sherman,J.S. 246
Shi,Z. 515
Shikanai-Yasuda,M.A. 1005
Shimizu,N. 677, 677
Shiver,J. 976
Shiver,J.W. 978
Shuhei,U. 474
Sicherl,F. 161
Siemion,I.Z. 719
Siligardi,G. 536
Silva,E.H. 133
Simkeviciene,V. 584
Singh,S. 69
Singleton,D.H. 157
Sisido,M. 294, 538
Sivaguru,G. 540
Skelton,N.J. 392
Skinner,S. 625
Slomczynska,U. 196
Slootstra,J.W. 987
Smiley,D.L. 619
Smith, III,A.B. 217
Smith,D.D. 143
Smith,N.D. 202
Smith,S.O. 252
Sobrino,F. 913
Sodroski,J.G. 599
Sohma,Y. 67, 805
Sokolov,D.I. 952
Somjen,D. 512
Sommerhoff,C.P. 346
Son,C.D. 635
Song,A. 843
Sousa,K. 484
Spatola,A.F. 59, 129, 198, 359, 793, 795
Spence,C. 750
Spetzler,J.C. 684
Spisni,A. 926
Sprules,T. 363
St.George-Hyslop,P. 782
Stankova,M. 215, 649, 651, 655
Starikova,E.A. 952
Starovasnik,M.A. 392
Stefanescu,R. 782
Stefanowicz,P. 186, 719
Stella,L. 445, 879
Stepensky,V. 599
Stephen,P.C. 606
Sternberg,U. 183
Stevens,S.M. 869
Stewart,J.M. 584
Stibor,I. 412, 495
Stöcklin,R. 478, 813
Stoev,S. 725
Stout,B. 47
Streitz,M. 911
Stricher,F. 260
Suessmuth,R.D. 883
Sugase,K. 379
Sugiura,Y. 791
Sukopp,M. 365
Suleske,R.T. 157
Sumida,Y. 323, 524
Sun,H. 750
Sun,Y. 407
Sundaram,R. 407, 983, 989
Suzuki,M. 258
Suzuki,T. 791
Swistok,J. 750
Szabó,B. 815
Szabó,E.Z. 548
Szabó,G. 361
Székelyhidi,Z. 548
Szeto,H.H. 725
Szewczuk,Z. 938
Szymanska,A. 23

Tada,M. 468
Tagliamonte,A. 965
Taguchi,H. 961
Takada,K. 327
Takahashi,M. 258
Takahashi,N. 67
Talele,T.T. 29, 135
Tam,J.P. 159, 280, 290, 909, 922, 924, 974
Tamamura,H. 331, 606
Tamiya,E. 258
Taraseviciene-Stewart,L. 584
Tarnawski,L. 186
Tatarek-Nossol,M. 768
Taussig,M.J. 996
Taylor,C.K. 143
Taylor,G. 793, 795
Taylor,J.E. 625, 700
Taylor,J.W. 981
Te,A.E. 522
Teixidó,M. 800
Ten Kortenaar,P.B.W. 57
Teplow,D.B. 765
Terakubo,S. 606
Terracciano,S. 508
Teruya,K. 127

Tesauro,D. 818
Thirumoorthy,R. 565
Thomas,C.L. 381
Thornton,J.M. 526
Thorpe,C. 373
Thumshirn,G. 693
Thundimadathil,J. 689
Thurk,M. 864
Tian,Q. 21
Tian,S. 599
Tian,X. 782
Tian,Y. 981
Timmerman,P. 987
Tizzano,B. 482
Todorovic,A. 641
Toll,L. 671
Tollin,G. 713, 734
Tomasini,C. 223, 433
Tomatis,R. 659
Tomboly,C. 582
Tomie,T. 886
Tong,X. 21, 353
Toniolo,C. 51, 98, 137, 433, 435, 443, 445, 879
Torres,A.G. 163
Toth,F. 935
Toth,G. 582, 935
Toth,I. 809, 811
Toulemonde,N. 98
Tourwe,D. 582
Tourwé,D. 665
Tovar,D.R. 991
Travassos,L.R. 1005
Trent,J.O. 198
Trigari,V. 223
Tripet,B. 145, 301
Trivedi,D. 647, 651, 655
Trivedi,D.B. 567
Troganis,A. 945
Trudeau,V. 470
Truitt,T. 750
Tschopp,J.F. 709
Tselepis,A. 377
Tselios,T.V. 945
Tsubery,H. 139
Tsuda,Y. 669
Tsunemi,M. 327
Tsunoda,Y. 559
Tulla-Puche,J. 317
Tung,C. 121, 325, 367
Turk,B.E. 856
Turpin,O. 225
Tuttle,D. 671
Tzakos,A.G. 945

Ueda,S. 606
Ulrich,A.S. 19
Umezaki,M. 25
Usui,K. 258

Vacatello,M. 797, 917
Vagner,J. 117, 215, 567
Vagonis,A. 584
Valente,A.P. 484
Valenzano,K.J. 715
Valenzuela,F. 59
Valero,M. 827
Valiyaveetil,F. 276
van Boom,J.H. 115
Van Cauwenberghe,S. 665
van der Marel,G.A. 115
van Dijk,E. 987
Van Eps,N. 252
van Helden,M. 115
Van Mau,N. 802
Van Osta,P. 147
van Zoelen,D.J. 115
VanBuskirk,A.M. 760
Vanderah,T. 615
Varga,E. 667
Várkondi,E. 548
Vasselli,J. 515
Vasseur,J. 822
Vázquez,J. 319
Veas,F. 260
Vederas,J.C. 363
Venanzi,M. 445, 879
Vendrell,M. 831, 833
Venkatesh,N. 512
Ventimiglia,F. 907
Ventura,R. 831, 833
Ver Donck,K. 147
Vidal,A. 63
Vidaud,C. 260
Vieira,R.F. 484
Vigil-Cruz,S.C. 609
Vila-Perelló,M. 902
Vilaró,S. 800
Vilaseca,M. 866
Villain,M. 71, 235
Villén,J. 913
Vita,C. 260, 263
Vitiello,M. 520
Vives,E. 822
Vlahakos,D. 569
Volkmer-Engert,R. 141
Vollers,S.S. 765
von Eggelkraut-Gottanka,R. 113
Vors,J. 119

Wáczek,F. 548
Wade,D. 580, 881, 949
Wade,J.D. 586, 727, 729
Wadhwani,P. 19
Wakamatsu,K. 553
Wakselman,M. 51, 98, 445
Waldeck,W. 820
Walker,C.M. 983
Waner,J.M. 313
Wang,A. 47
Wang,J. 381, 386
Wang,W. 504
Wang,X. 388, 515, 609, 619, 829, 849, 907
Wang,X.S. 565, 639
Wang,Y. 599, 609
Wang,Z. 606
Waser,B. 723
Watanabe,L.A. 968
Waugh,D.S. 544
Weber,D. 632
Weber,M. 768
Weber,M.E. 196
Weckbecker,G. 721
Wegner,K. 23
Wei,C. 515
Weiner,D.J. 904
Weintraub,S.T. 65
Weissleder,R. 325, 367
Weist,S. 883
Welihinda,A. 522
Weltrowska,G. 661
Wenger,S. 723
Wenschuh,H. 106, 854
Weonu,C. 93
Wessleder,R. 121
Wester,H. 693
Whitacre,C.C. 947
White,C. 601
Whitfield,J.F. 702
Wietfeld,D. 604
Wilczynski,A. 565
Wilczynski,A.M. 645
Wilkes,B.C. 455
Willick,G.E. 702
Wilson,K.R. 645
Wimmer,N. 809
Witcher,D.R. 619

Wittelsberger,A. 225, 679
Witter,R. 183
Wittliff,J.L. 198
Wittmann,V. 161
Wo,N.C. 725
Wohlleben,W. 883
Won,H. 933
Wood,J.M. 301
Woodhouse,D.P. 89
Woodward,C. 317
Woon,C. 625
Worthy,K.M. 515
Wosikowski,K. 365
Wright,K. 51, 98
Wu,C. 922
Wu,L. 544
Wu,W. 321
Wu,Y. 27, 196, 233, 611

Xavier,G.C. 192
Xiang,Z. 565, 637, 639, 643
Xiong,C. 200, 567, 653
Xu,J. 167
Xu,Q. 849
Xuyuan,G. 45

Yajima,T. 621
Yamada,M. 779
Yamaguchi,H. 431, 534
Yamakawa,M. 886
Yamamura,H.I. 667
Yamasaki,T. 331
Yamazaki,T. 559
Yang,D. 501, 515, 518
Yang,H. 355
Yang,J. 290, 909, 922, 924, 955
Yao,Z. 544
Yatskin,O.N. 952
Ying,J. 45, 567, 615, 653, 655
Yokum,S.T. 839
York,E.J. 584
Yoshiaki,N. 499
Yoshida,M. 323, 524, 1005
Yoshikawa,M. 935
Yoshikawa,S. 556
Yoshimura,K. 331
You Seok,H. 339
Young,D. 983
Young-Deug,K. 93
Yu,Q. 290, 909, 922
Yu,Y. 835

Zaccaro,L. 497
Zarse,K. 864
Zarzarova,V. 176
Zbozien-Pacamaj,R. 186, 719
Zeng,Q. 325
Zeng,W. 985
Zerbe,O. 704
Zerweck,J. 854
Zhang,C. 715
Zhang,J. 200, 355, 567, 625, 653, 843
Zhang,L. 619
Zhang,M. 501, 515, 518
Zhang,W. 27, 196, 611
Zhang,X. 501
Zhang,Y. 974
Zhang,Z. 544
Zhao,J. 522
Zhao,L. 337
Zhou,Y. 321
Zimecki,M. 938
Zimmermann,J. 307
Zinsser,W. 864
Ziora,Z. 67
Zmuda,E. 890
Zoetewey,D.L. 301
Zoga,A. 569
Zoumpoulakis,P. 569
Zuber,P. 363
Zucchini,M. 717, 740

1,3,4-thiadiazoles 839
16 kDa protein 1001
2,5-diketopiperazines 17
20S proteasome 307
2D NMR 371
2-methylalanine 186
3-10-helix 51, 137, 435
4-amino-N-methylproline 186
4-Base codon 294
4-fluoro-phenylglycine 19
4-methoxytrityl resin 240
5-FAM-SSSSSSSSSS-OH 21
9-aminoacridines 495

ab initio MO theory 439, 441
Acetylcholine 420
Acetylcholinesterase 359
Acridoalanine 23
Actin 508
Acylation 619, 641
Adenylyl 702
Adhesion 907
Adhesive peptides 797
Affinity chromatography 346
Affinity separation 25
Affinity-binding assay 147
Aggregation 495, 775
Agonist 698, 746
Agonists of ORL1 receptor 671
AGRP 565, 639, 645
Aib 27
Aib-Rich Peptides 375
AKAP121 497
Ala scan 628
Alkylations 135
Alpha carbon-sulfur bond 363
Alpha helix 246
Alpha, alpha-dialkyl glycines 85
Alpha, alpha-Disubstituted amino acid 386
Alpha-conotoxin MII 811
Alpha-Helicity 373
Alpha-MSH 484, 567, 651
Alpha-tubulin 524
Alzheimer 765
Alzheimer's disease 768
Amide bond formation 278
Amino acid 29
Amino acid labeling 31
Amino protecting group 33
Aminoboronic acids 315
Aminoisobutiric acid 443
Aminolactams 173
Aminophosphonates 310
Aminopyrrole 176
Amphipathic 890
Amphipathic peptides 424, 802
Amphipatic helix 377
Amphiphilic peptide 789
Amylase 313
Amylin 771, 773
Amylodial aggregation 777
Amyloid 621, 765, 771, 773, 779, 785
Analog 698
Analogues 888
Analytical standards 65
Androgenic gland hormone 499
Angiotensin II 131, 569, 571, 573, 578
Angiotensin receptor 573, 578
AngiotensinII 611
Anion Binding 165
Anionic ion-pairing reagents 123
Annexin 2 N-terminus 827
Antagonist 565, 582, 740
Antagonists of ORL1 receptor 671
Antibacterial 895
Antibacterial activity 970
Antibacterial peptides 873, 875, 940
Antibiotic 179, 447, 877, 883, 895, 949
Antibiotic peptides 879, 881
Antibody 407, 996, 1007
Anticancer peptide 895
Anticoagulants 361
Anti-estradiol 512
Antifungal activity 926
Antifungal peptide 886
Anti-HIV-1 909
Anti-inflammatory 506
Antimicrobial 888, 890, 904, 922
Antimicrobial activity 924
Antimicrobial peptide 3, 19, 892, 895, 900, 902, 928
Antinociception 669
Antiobiotic 928
Antiparallel 301
Antiproliferative 307, 508, 548
Antisepsis 877
Antitumor effect 815
ApoA-I peptide model 377
Apolipoproteins 601
Apoptosis 548
Aptamer 996
Arginine-rich peptide 791
Arg-tag 707
Arsenic(III)-based probe 373
Arylhydrazide linker 111

Aspartate 590
Aß4-10 vaccine epitope 782
Assembly 684, 765
Asymmetric Hydrogenation 202
AT1 Receptor 569
Atherosclerosis 601
Atrial natriuretic peptide 379
Atropoisomers 98
Auperantigen antagonists 181
Aureobasidin 179
Autoantibodies 75
Autoimmunity 994
Automated waste collection 157
Axial chirality 98
Azabicyclo[4.3.0]nonane amino acid 200
Azabicycloalkane amino acids 45
Aza-peptide 35, 37
Aza-Wittig 39
Azo compounds 31
Azobenzene 41

Backbone 702
Backbone amide linker (BAL) 125
Backbone cyclic peptidomimetics 181
Backbone cyclization 43
Bactenecins 900
Bacteria 907
Bacterial Transcription 248
Bacteriocin 363
BAL 108
B-cell epitope 407
Bcl-2 540
Bead-sorting 147
Behavior 488
Benzophenone 742
Benzophenone (Bpa) 131
Beta amyloid 775
Beta amyloid peptide 768
Beta helical peptide 689
Beta-amyloid 777
Beta-hairpin 381, 462
Beta-hairpin scaffolds 392
Beta-hairpin-glycopeptides 1007
Betaine analog 315
Beta-ketolactam of amino acids 104
Beta-sandwich 383
Beta-sheet 381, 437
Beta-structures 392
Beta-turn 381, 386, 400, 437, 653, 981
Beta-turn analogue 200
Beta-turn peptidomimetics 388
BHMT 315
Biaryl ether 348
Bicyclic 45
Bicyclic beta-turn dipeptide 215
Bicyclic dipeptide mimetics 653
Bifunctional beads 829
Bifunctional peptides 682
Binding affinity 723
Bioactive conformation 750
Bioactive peptide 580
Bioavailability 793, 795
Biocatalysis 47
Biological activity 390, 582, 597, 727
Biomaterial 732, 797, 807
Bioremediation 263
Biosensor 263
Biotinylated ligands 635
Bis-peptide R110 353
Bivalent 346
Bivalent inhibitor 390
Blood clot 325
Blood-brain barrier 79, 800
Boc/Bzl strategy 55
Bombesin receptor 632
BOP reagent 119
Bovine hemoglobin 926
Bpa analogs 635
BPTI 317
Bradykinin antagonist 584
Brain 729
Brainstem 955
Branch 611
Breast cancer 609
Bridge 129
Bsmoc 33
BTC 43
Building unit 43

C alpha-fluoromethylamino acids 711
C alpha-tetrasubstituted 51, 98
Calcitonin 586
Calcitonin receptor 586
CAMP 412
Cancer 628
Capillary electrophoresis 123
Carbon nanotubes 414, 428, 428
Carrier peptides 802
Caspase 621
Caspase-3 333
Caspase-3 probe 121
Catalytic activity 183
Catalytic antibody 961
Catalytic efficiency 292
Cataract 355
Cathelicidins 900

Cathepsin C 426
Cationic micellar solution 294
Cavitand 246
Cavitein 246
CCK antagonist 682
CCK8 588
CCK8 peptide 818
CD spectroscopy 377, 381, 386, 1001
CD28:B7-1 760
CD40:CD40L 947
Cell adhesion 732, 807
Cell attachment 779
Cell division 559
Cell penetrating peptide 822
Cell transportable inhibitors 343
Cellular delivery 802
CFTR 590
CGRP 143
Chaperone 233
Chemical ligation 113, 235
Chemical protein synthesis 242
Chemical shift 462
Chemoinformatics 526
Chemokine 597, 599, 606, 609
Chemokine receptor 930
Chemokines MCP-1 & Rantes 153
Chemoselective ligation 837
Chemosensor 424
Chemotaxis 580
Chimera 645, 963
Chiral 47
Chiral auxiliary 135
Chiral auxillary 69
Chitin binding 886
Chloroform-phenol mixed solvent 169
Cholecystokinin 615
Cholesterol 601
Chromogranin 470
Circular dichroism 163, 250, 341, 375, 424, 470, 482, 879, 928
Circular proteins 402
CLEAR-OX 59
Coacervation 474
Coiled-coil 292, 301, 407, 409, 490
COLINPOWELL 580
Collagen 350, 472
Combinatorial array 837
Combinatorial chemistry 205, 229, 319, 831, 833
Combinatorial library 147, 835, 841, 930
Combinatorial mixture 869
Complex formation 183
Compound libraries 839
Computational design 383
Conformation 250, 333, 375, 414, 426, 439, 441, 476, 480, 698, 715, 945
Conformational analysis 416, 433, 450, 524, 673, 744
Conformational restriction 571, 655, 768, 981
Conformational search 61
Conjugate 25
Conopeptides 95
Conotoxin 418, 420, 841
Consensus sequence 949
Constrained amino acid 35
Constrained peptides 976
Constrained pseudopeptides 173
Conus venom 478
Convergent solid-phase synthesis 169
Convergent synthesis 240
Conversion time 805
Copper 771
Copper salts 106
Correlation 61
Costimulation 760, 947
Coupling reagents 49
Cpg 69
CPP 510
CPS 269
Crambin 242
CRF analogs 604
Cross interaction 775
Cross-reactivity 756
Crowned amino acids 51
C-sugar 793, 795
C-terminal modified peptide 108
C-terminus 27
CTL epitope 983
Cucubitaceae 486
Curtius rearrangement 29
CXCR4 599
CXCR4 antagonist 606
CXCR4 receptor 609
CXCR4 receptor agonist 597
Cyanine dye 538
Cyclic 647
Cyclic amphipathic peptides 149
Cyclic defensin 909
Cyclic hexapeptide 524
Cyclic peptide 41, 53, 186, 402, 412, 422, 424, 501, 504, 518, 588, 611, 691
Cyclic RGD-peptid 807
Cyclic sulfamidates 188
Cyclic tetrapeptide 323
Cyclization 17, 49

Cyclodepsipeptide 506, 508
Cyclolinopeptide A 719
Cyclopentylglycine 69
Cyclosporin 225
Cyclotide 486
Cyclotides 402
Cysteine analogs 202
Cysteine proteases 319
Cystic fibrosis 915
Cystine-bond 909
Cytotoxic agents 307

Database 881
Daunomycin 815
De novo design 3, 117, 244, 246, 256, 409, 428, 428
Defensins 915
Dehydropeptides 426
Delivery 822
Delta antagonist 665
Delta opioid receptor 453, 713
Deltorphin 613
Denatured state 233
Dendrimer 965, 968
Dendritic bioactive peptide 970
Dendron 922
Density functional theory 422
Depsipeptide 53
Designed peptide 258
Desulfurization 129
Diabetes 709
Diagnostic test 942
Diamine 188
Diazirine (Tdf) 131
DIC 361
Differentiation 55
Diketopiperazine 43
Dimeric analogs 938
Dimeric peptides 329
Dimerization inhibitor 337
Dimerization of receptors 663
Dimerizer 480
Dimers 365
DioRaSSP 57
Dipeptide 45
Dipeptide isostere 331
Dipeptidyl peptidase 321
Dipeptidyl peptidase resistance 623
Diphenyl drugs 695
Direct penetration 510
Discontinuous epitope 987
Disruption of the protease dimer 339
Disulfide 313
Disulfide bond 59, 59, 373, 418, 431, 499, 559, 746
Disulfide heterodimer 913
Disulfide pairing 902
Divalency 546
Dmt 453
DNA 538
DNA binding 53
DNO 464
Downregulation 802
D-peptides 930
Dpg and Nva peptide 386
DPP IV 321
Drug delivery 437, 675, 789, 809, 811, 820
Drug design 260, 569, 615
Druglikeness 833
Dyes 31
Dynorphin 371
Dynorphin A 691

E2-mimetic peptides 512
Edman sequencing 847
Electron transfer 265, 443
Elements 476
Encoding method 388, 843
Endocytosis 510
Endoproteolysis 343
Endothelin antagonists 617
Endothelin-like toxin 478
Endotoxin neutralizing 877
Energy transfer 968
English words 580
Enkephalin analogues 661
Enterobacteriaceae 904
Enzyme Inhibitor 307, 315, 323, 341, 343
Enzyme substrate 869
Epitope 963
Epitope mapping 911, 976
Epitope rebuilding 913
Epitope structure 978
Epitope vaccine 972
EPL 269, 466
Epsilon-peptide 922, 924
Epsilon-peptide chimera 924
ESI-MS 771
Esr study 133
Estrogen 198
Estrogen receptor 512
Evolutionary algorithms 866
Exopolysaccharides 915
Experimental Autoimmune Encephalomyelitis 947

Expressed protein ligation 248, 254
Extracellular loop 752

Factor XIII 325
Fatty acids 641
FC131 606
Fibril 779
Flavin 265
Flexible linker 117
Flexible molecules 61
Fluorescence 121, 325
Fluorescence label 254
Fluorescence spectroscopy 538
Fluorescent probe 23
Fluoresence Energy Resonance Transfer 663
Fluorinated analogs 63
Fluoroalkylbenzyl 115
Fluoroalkylsulphonyl 115
Fluoroproline 472
Fluorous HPLC 115
Fmoc 65, 67, 111, 113, 235
Fmoc-Cyclopentylglycine 69
Fmoc-iminosugars 77
Fmoc-Ser(tBu)-OH 21
Fmoc-Ser(Trt)-OH 21
Foldamers 210, 433, 435, 437, 439, 441, 445
Folding 431, 841
Foot-and-mouth disease virus 913
Forster distance 23
Four helix bundle 303
Fragment 926
Fragment coupling 167
Freidinger Lactam 188
FRET 91, 327
Functional peptides 820
Furin 917
Fusion peptide 919

G protein 250, 553
G protein peptides 416
G protein-coupled receptors 586
Gaegurin 4 933
GAG 935
Gamma-MSH 651
Gastrointestinal absorption 805
GBP 468
Gelsolin 333
Gelsolin domains 333
Gene delivery 809
Genetic algorithm 800
GGN4 analogues 933
Ghrelin 619
GLP-1 321, 625
Glucagon 621
Glucagon-like peptide-1 623, 625
Glutathione 335
Glutathione S-transferase 335
Glycine ligation 71
Glycopeptide 73, 75, 77, 79, 499, 793, 795, 883, 942
Glycoside 73
Glycoside scaffolds 217
Glycosyl amino acids 77
Glycosylation 79
Gomesin 928
Gonadotropin-releasing hormone 628
Gp120 974
Gp160 917, 919
Gp41 976, 981
GPCR 630, 635, 704, 752, 754
GPCR receptor ligands, BRS-3 632
G-protein 252
G-protein coupled receptor 573, 713, 734
Grb2-SH2 518
Grb2-SH2 domain 501, 515
Green fluoresence protein 663
Growth-blocking 468
GSH isoster 335
Guanidine compounds 81
Guanidinylation 81
Guanylin 167

Haemophilus influenzae 520
Hairpin 190
H-bonds 590
HCG 987
HCTU 49
HDAC6 524
Helical peptides 155, 428, 428
Helix 625, 700
Heme 265
Hemolytic 890, 970
Her-2 972
Heterocycles 839
Heterodisulfide 827
High activity binding protein 991
High density microarray 849
High temperature 192
High throughput synthesis 854
Histidine imidazole ring 619
Histone 510
Histone deacetylase 323
HIV 919, 935, 974, 976, 978
HIV antagonist 930

HIV Inhibitor 260
HIV integrase 329
HIV protease 331
HIV vaccine 260, 981
HIV-1 337
HIV-1 entry 290, 599
HIV-1 inhibitors 280
HIV-1protease dimerization inhibitor 339
HIV-1protease inhibitor 805
Homeostasis 952
Housefly 357
Htc residue 536
HTLV-1 407, 983
Human calcitonin gene related peptide 37
Human interleukin-8 254
Human lactoferrin 877
Human receptor 725
Hydrazide linked 682
Hydrazines 37, 83
Hydrazino amino acid 35, 83
Hydrogels 256
Hydrogen bonds 443
Hydrophobic clusters 409
Hydrophobic core 292
Hydrophobic peptide 67, 1003
Hydrophobic peptide purification 67
Hydrophobic peptide synthesis 67
Hydroxyvaline 95
Hyperglycemia 623
Hypothalamus 955

Imaging 325
Imidazolinones 85
Immunogenicity 972
Immunology 911
Immunosuppressors 938
In vitro selection 556
In vivo treatment 904
Indolicidin analogs 940
Induced chirality 98
Inflammation 522
Inhibitor 313, 317, 335, 357, 359, 495, 515, 518, 542, 768, 961
Innate immunity 553
Insecticide 486
Insulin 684
Insulin superfamily 729
Integrase 337
Integrin 196, 687, 693, 709, 732, 807
Intein-fusion 276
Internet 881
Interstitial cystitis 522
Intracellular delivery 791, 989
Intramolecular chaperone 431
Ion channels 689
IR spectroscopy 459
Isocratic RP-HPLC 145
Isoquinolines 665
Isotope dilution assay 813
Isotopic labelling 89

JNK 522

K opioid receptors 691
Kojic aicd 542

La/SSB epitopes 994
Labeled peptides 91
Lactam bridge 192, 571
Lactamization 192
Laminin 779
Large scale 57
Large-scale synthesis 65
LAT 534
LC-MS 478
LC-MS/MS 813
L-cystathionine 329
LDL antioxidant 377
Lead optimization 831, 833
Leadlikeness 831
Leu-enkephalin 653
Leu-enkephalin analogues 215
LHRH 813, 985
Library 412
Ligand-receptor interaction 573
Ligation 106, 159
Linear Peptide 480
Linker 87, 108
Lipid A analogues 875
Lipid interaction 341, 657
Lipids 809
Lipoamino acid 811
Lipopeptide 447, 985
Liposaccharides 811
Liposome 789
Liposomes 875
Liquid chromatography - mass spectrometry 869
L-lanthionine 329
L-N-Boc-N-methyl-b-hydroxyvaline 179
Local anesthetic drugs 695
Losartan 569
LPPS 93
Lung cancer 584
Lung pathogens 915
Lysine cyclic peptides 87

Lysozyme 888

MAb 2F5 978
Magainin 875
Magnetic resin 100
Malaria vacines 991
MALDI-TOF MS 359
Manufacture 47
MAP 965
MAP-Kinase 520
Mass spectrometry 782, 843
Matrix metalloprotease 350, 367
Matrix-Scan 987
MC4R 643
MeAla 715
Melanocortin 213, 565, 637, 639, 641, 643, 645, 647
Melanocortin 649
Melanocortin receptor 651
Melanoma 350
Melanotropin peptide 200
Melanotropins 655
Melatonin receptor 657
Membrane 704, 789
Membrane permeability 879, 924, 970
Membrane protein 707
Membrane transport 963
Metabolites 526
Metabolome 526
Metal binding peptide 470
Metal chelation 263
Metal complex 196
Metastasis 955
Methionine 87
Methionine sulfoxide 145
Methyl-(L)-DOPA 51
Methylation 702
Methyleneamino bond 194
MHC fragments 938
MHC II 89
Microarray 258
Microwave 102
Microwave synthesis 17, 194
Mimetic 45, 584, 684
Mimic 721
Mitochondria 497
Mitochondrial 553
Mixed Micelles 818
MM/MD 379
Mmt-Cysteine 91
Modification 227
Modulators 198
Molecular Design 165
Molecular dynamics 400, 447, 455
Molecular imprinting 756
Molecular mechanics 445
Molecular modeling 310, 371, 450, 453, 455, 665, 679, 687, 748
Molecular transporter 121
Momosertatin 486
Mouse vas deferens 717
MRI contrast agent 818
MSH analogues 655
MS-MS sequencing 827
MTII 637
Multicomponent reaction 104
Multi-drug resistance 331
Multiepitope 989
Multimer 693
Multimeric interaction 117
Multiple disulfide 902
Multiple fragments 71
Multiple peptide synthesizer 677
Multiple sclerosis 77, 942, 945, 947
Multivalent 983
Mutagenesis 578
Mutasynthesis 883
Mutational analysis 276
Myc/His tagged 667
Myelin basic protein 945

Na+ channel inactivation 695
N-alkylated peptides 773
Nano-NMR 95
Native chemical ligation 111, 240, 242, 248, 630
Natriuretic peptides 455
Near infrared spectroscopy 367
Neoglycopeptide 837
Neuroendocrine differentiation 845
Neurokinin B 698
Neuronal toxin 420
Neuropathic pain 615
Neuropeptide Y 704
Neuroprotective 700
Neurotrophins 205
Neutrophil 553
Nickel complex 135
Nicotinic receptors 841
NILIA-CD 536
Nitrosoamines 83
N-linked pentasaccharide 499
N-methylation 27
NMP 143
NMR 141, 163, 190, 301, 375, 379, 386, 390, 416, 426, 447, 457, 462, 466, 468,

484, 504, 565, 637, 695, 704, 744, 797, 886, 892, 917, 919, 945, 978
NMR peptide-resin structure 153
NMR structure determination 567
Nociceptin 715
Nociceptin/orphanin FQ 717
Non-coded amino acids 137, 229, 435
Non-Hodgkin's lymphoma 540
Nonnatural mutagenesis 294
Non-sequenceable amino acid 388
Noopept 488
NOP receptor ligands 717
Novel design 922
Novel methodology 215
N-protected amino acid bromides 711
NPY receptor 663
NPY receptor antagonist 79
Nsc-amino acids 93
N-substituted glycines 213
Nuclear magnetic resonance 418
Nuclear medicine 588
Nuclease activity 55
Nucleic acid peptidomimetica 450

Obesity 643, 750
OBOC Libraries 843
Octapeptides 723
Oligoimides 433
Oligomer 765
Oligonucleotide 822
Oligosaccharide mimetics 161
One-bead one-compound 388, 829, 845, 847, 907
Opioid 453, 582, 613, 615, 665, 715
Opioid affinity 935
Opioid antagonists 661
Opioid mimetics 669
Opioid peptide 371, 659, 661
Opioid receptor 659, 667
Optical data storage 464
Optical probe substrate 367
Organocuprate reagents 319
ORL1 receptor 671
Orphan receptor ligand 632
Osmolyte refolding 317
Oxac 433
Oxazolidinone 223
Oxazolinium intermediate 85
Oxime ligation 693
Oxytocin 756
Oxytocin antagonist 725
P. brasiliensis gp43 1005
P24 capsid 935
P38MAPK 522
P53 (303-393) 127
P5U 748
PACAP 700
Pain 682
Pam2Cys 985
Parallel peptide synthesis 864
Parallel synthesis 856
Parathyroid 702
Parathyroid hormone 673, 675, 677, 679
Partially folded 317
Passive delivery 963
P-BOP reagent 119
PC12 621
PDZ domain 141
Penthionine 129
Peptide aldehydes 361
Peptide analogs 601, 917
Peptide antagonist 609, 717
Peptide antibiotics 933
Peptide antigens 75, 1007
Peptide array 987
Peptide bond surrogates 991
Peptide complementarity 719
Peptide conformation 457, 459, 657
Peptide coupling 119
Peptide cyclization 139
Peptide design 567
Peptide engineering 933
Peptide fragment 250
Peptide hormone analog 677
Peptide labeling 31
Peptide library 61, 327, 604, 827, 845, 854, 856, 864, 866
Peptide ligation 121, 278
Peptide nucleic acid 538, 540
Peptide screening 854
Peptide secondary structure 151
Peptide self-association 149
Peptide solubilization 1003
Peptide standards 123
Peptide structure 418
Peptide synthesis 19, 21, 57, 106, 108, 137, 435, 474, 630, 659, 691, 707, 740
Peptide thioester 111, 113, 240, 707
Peptide transport 800
Peptide vaccine 983, 989, 1005
Peptide-ligand design 866
Peptidome 357
Peptidomimetic 3, 37, 161, 176, 179, 181, 186, 188, 190, 194, 196, 198, 200, 202, 205, 210, 213, 217, 227, 501, 515, 582, 632, 773

Peptidosulfonamides 210
Peptoid 643, 659
Peptoid-peptide hybrids 213
Peroxidase mimetic 355
Pharmacokinetic studies 813
Phenoloxidase 357
Phosphopeptide 534, 536, 546, 550
Phosphorylation 127, 994
Photoactivation 267
Photoaffinity crosslinking 679
Photoaffinity labeling 586
Photochemistry 190
Photoisomerization 41
Photolabeling 131, 578, 742
Photothrombosis 488
Pi-cation 758
Pituitary adenylate cyclase-activating polypeptide 700
Plague 544
Plant peptides 902
Plasmon waveguide resonance 713
PLE 29
PNA 820
Poly(L-lysine) 968
Polyethyleneglycol 25
Polymer-bound oxidant 59
Polymers 133
Polypeptide chain length 490
Polypeptide conjugate 815
Polyproline II 459
Porphyrin 968
Positional scanning libraries 856
Posttranslational modification 95
Potassium channel KcsA 276
Potency 641
Potent and selective 725
Pp60c-src 504
Precipitation 25
Preparative RP-HPLC 145
Prion 482, 495
Prion protein fragments 775
Priviledged scaffold 196
Pro-CTL epitope 1003
Pro-drug 225
Prokineticin 2 169
Prolactin releasing peptide 750
Proliferation 952
Proline 227, 422
ProP 301
Proprotein convertase 341, 343
Pro-rich peptides 900
Prostate cancer 584, 845
Protease 965
Protease inhibitor 321, 331, 346
Protease specificity 327
Protease substrate 353
Proteasome inhibitor 348
Protecting group 235
Protein and peptide engineering 260, 263
Protein array 996
Protein chip 258
Protein design 244, 265, 303
Protein folding 242, 409, 490, 559
Protein inhibitors 310
Protein ligation 252, 267
Protein loops 687
Protein mimetics 280, 290
Protein P2 520
Protein photocaging 267
Protein splicing 269
Protein stability 490
Protein synthesis 235, 244, 278
Protein tyrosine phosphatase 544
Protein-protein interaction 205, 550, 866
Proteolytic enzymes 856
Proteome 526
Proteomics 478, 849
Pseudomimetics 217
Pseudopeptide 183, 223
Pseudoproline 223, 225
PTH 673, 677
PTH1 receptor 679
PTyr mimetic 544
Purification 667
PWR 734
Pyrazinone 669
Pyrrhocoricin 904
Pyrrolo-proline 176
Pyrrolo-pyrimidine 176

QM/MM 412
QSAR 613
Quinone 303
Quinoprotein 303

Radiolabeled 540
Raman spectroscopy 459
Rapid solid phase peptide synthesis 143
Rat aorta stris assay 740
Rational design 687
Receptor 198, 556
Receptor binding 455
Receptor selective analogues 655
Receptor Ste2p 635
Receptor subtype selective ligands 604
Receptor subtypes 649

Redox potential 41
Reduced peptide bonds 991
Reference standards 65
Regioselective 972
Regular helix turn 450
Relaxin 727, 729
Relaxin-like factor 727
Resin-bound 81
Resins 133
Retinopathy 709
Reversed-phase HPLC 123, 149
Reverse-turn 422
Reversing the southern peptide 339
RGD 709
RGD cyclic peptides 711
RGD mimetics 732
Rhodamine 353
Rhodopsin 252, 758
Rigid peptides 443
RNA 556
RNA polymerase 248, 466
RNA-ligands 229
RP-HPLC 151
Ruthenium 165
Saccharomyces cerevisiae 752
Safety-catch 127
Sample displacement 145
SAPD 881
SAR 518, 617, 750, 926
SAR of Angiotensin II 571
Scaffold 996
Screening 869
SDF-1 597
SDS-PAGE 742
Secondary structure 163, 258, 439, 441, 462, 474
Secretoneurin 470
Segmental labeling 466
Selectivity 647
Self assembly 428, 428
Self replication 292
Semisynthesis 276
SH2 domain 534, 536, 550
SHU9119 637
Side reaction 139
Side-chain derivatization 847
Side-chain mimetic 727
Signal transduction 515, 546, 713
Signaling inhibitor 501
Silaproline 737
Silylated amino acids 737
Sjogren's Syndrome 994
Skin proteases 675
Slow-binding 310
Solid phase 102
Solid phase support 215
Solid phase synthesis 17, 49, 53, 63, 73, 87, 89, 100, 115, 117, 125, 194, 729
Solid state 19F-NMR 19
Solid support 91
Solubility 793, 795
Solubilizing entity 225
Solution phase 57
Solution structure 886
Solvation 133
Solvents 143
Somatostatin 365, 721
Somatostatin analogs 723
Spinal cord 955
Spirobicyclic ring 104
Spontaneous chemical cleavage 805
SPOS 839
Spot synthesis 141, 159, 854, 911
SPPS 27, 55, 102, 153
Src 504
ß-amyloid 782
ß-sheet 890
Sst4-selectivity 723
Stability 965
Stat3 550
Staudinger ligation 278
Ste2p 752, 754
Stereoelectronics 472
Stereospecificity 599
Stroke model 488
Structural 476
Structural determination in solution 445
Structural studies 744
Structure 402, 420, 892
Structure-activity relationship 628, 649, 671
Structure-based design 1007
Stylostatin 1 173
Substance P analogues 737
Substituted prolines 202
Subtilosin A 363
Sugar amino acids 161
Sugar diamino acids 161
Superdimer of MHC Class-II 938
Superior Antagonist 725
Supported reagent 119
Supra-molecular self-assembly 256
Suzuki coupling 229
Syk tandem SH2 domain 546
Symmetrical anhydride 35
Synthesis 102, 348, 480, 506, 508

Synthesis of acridoalanine 23
Synthesis of N-protected amino acids 33
Synthetic antigen 942
Synthetic epitope peptide 1001
Synthetic peptide 163, 355
Synthetic protein 383
Synthetic receptor 756
Synthetic vaccines 913

T cell epitope 1005
T140 606
T20 290
Tachyplesin 892
Tandem ligation 280
Targeting 815
Tat 822
T-cell 911
T-cell response 1001
Technology 147
Temperature profiling 149
Temperature selectivity 151
Template assembled protein 383
Temporin 949
Tendamistat 313
TEPITOPE algorithm 1005
Tetra-substituted a-amino acids 673
TFE 468
TGF-b2 719
Therapeutic 721
Therapeutic antibody 782
Therapeutic apheresis 75
Thermodynamics 457
Thiaindolizidinone 653
Thiazolidine 71
Thioester 106, 125, 159
Thioester condensation 127
Thioether 129, 363
Thiol capture 280
Thiolation 359
Thiosugar 73
Three helix 290
Time-resolved fluorescence 445, 879
Tissue-specific peptide pool 952
TMC-95A 348
TOAC 484
Tolerance 669, 760
Toxic shock syndrome 181
Transdermal delivery 675
Transducin 758
Transgenic mice 989
Transition metal ions 183
Transition state isosteres 210
Transmembrane 590
Transmembrane domain 754
Transmembrane peptide fragments 630
Transmembrane segment 657
Transplantation 760
Transthyretin 785
Trimethylsilylalanine 737
Triple helix 472
Triple-helical peptide 350
Trithioortho ester 125
TRNA aminoacylation, non-enzymatic 294
Tropoelastin 474
Trp 155
Tryptase 346
Tryptophan 940
Tumor 952
Turn 223
Turn mimetics 173
Twisted formamides 457
Type II diabetes 623, 625
Tyrosinase 542
Tyrosine 613
Tyrosine analogues 661
Tyrosine kinase 548

Ugi reaction 85
Unique 476
Unnatural 227
Unnatural amino acids 47, 165, 379, 847
Uroguanylin 167, 431
Urokinase 365
Urotensin II 740, 742, 744, 746, 748
UT receptor 748
UV CD 155
UV monitoring Fmoc deprotections 153

Vaccine 809, 974, 985
Vancomycin 883
Vasoactive intestinal peptide 961
Vasoconstrictors 617
VCD spectroscopy 459
VesCP 949
Vibrational circular dichroism 155
Vitronectin 797

Waste Handling 157

X-Cys ligation 159
X-ray structures 137

Yersinia pestis 544
YhhP 559

Zn/HCl reduction 83